

AERONAUTICS

NINETEENTH ANNUAL REPORT

OF THE

NATIONAL ADVISORY COMMITTEE

FOR AERONAUTICS

1933

INCLUDING TECHNICAL REPORTS
Nos. 441 to 474



UNITED STATES
GOVERNMENT PRINTING OFFICE
WASHINGTON: 1934

LETTER OF SUBMITTAL

TO THE CONGRESS OF THE UNITED STATES:

Pursuant to the act of March 3, 1915, which established the National Advisory Committee for Aeronautics, I submit herewith the Nineteenth Annual Report of that Committee for the fiscal year ended June 30, 1933.

The attention of the Congress is invited to the opening pages of the Committee's report giving the major reasons for the recent improvements in the speed and efficiency of airplanes for military and civil uses. The principal underlying cause of this remarkable progress has been the efficient functioning of the National Advisory Committee for Aeronautics in coordinating and planning for the research needs of aviation, civil and military, and in conducting the necessary fundamental scientific researches to serve the needs of all agencies.

I concur in the Committee's opinion that the continuous prosecution of fundamental research in aeronautics is essential to the national defense and to the future of air transportation upon a sound economic basis.

FRANKLIN D. ROOSEVELT.

THE WHITE HOUSE,
January 12, 1934.

LETTER OF TRANSMITTAL

NATIONAL ADVISORY COMMITTEE FOR AERONAUTICS,
Washington, D.C., December 15, 1933.

MR. PRESIDENT:

In compliance with the provisions of the act of Congress approved March 3, 1915 (U.S.C., title 50, sec. 153), I have the honor to transmit herewith the Nineteenth Annual Report of the National Advisory Committee for Aeronautics for the fiscal year ended June 30, 1933.

The past year has to an unprecedented degree witnessed the application by the Army, the Navy, and the aircraft industry of the cumulative results of years of fundamental research conducted by this Committee to meet the needs of military and civil aviation. It saw greater improvement in the speed of aircraft and in economy of operation than has been made in any single year since the war.

Higher speeds have introduced new problems into a heavily crowded program of investigations. The Committee is energetically prosecuting a comprehensive research program to serve all needs, and is confident that continued support of its work will continue to yield results of immeasurable military value and of economic value greatly in excess of its annual appropriations. The independent status of the Committee has been the most vital factor in its success and is essential to its continued efficient functioning.

Respectfully submitted.

JOSEPH S. AMES, *Chairman.*

THE PRESIDENT,
The White House, Washington, D.C.

TECHNICAL REPORTS

	Page
No. 441. A Flight Investigation of the Spinning of the NY-1 Airplane with Varied Mass Distribution and other Modifications, and an Analysis Based on Wind-Tunnel Tests. By Nathan F. Schudder.....	37
No. 442. A comparison Between the Theoretical and Measured Longitudinal Stability Characteristics of an Airplane. By Hartley A. Soulé and John B. Wheatley.....	53
No. 443. Pressure-Distribution Measurements on the Hull and Fins of a 1/40-Scale Model of the U.S. Airship <i>Akron</i> . By Hugh B. Freeman.....	67
No. 444. Wind-Tunnel Research Comparing Lateral Control Devices Particularly at High Angles of Attack. VI-Skewed Ailerons on Rectangular Wings. By Fred E. Weick and Thomas A. Harris.....	81
No. 445. Working Charts for the Determination of the Lift Distribution Between Biplane Wings. By Paul Kuhn.....	93
No. 446. Airfoil Section Characteristics as Affected by Protuberances. By Eastman N. Jacobs.....	109
No. 447. Static Thrust of Airplane Propellers. By Walter S. Diehl.....	125
No. 448. Improved Apparatus for the Measurement of Fluctuations of Air Speed in Turbulent Flow. By W. C. Mock, Jr., and H. L. Dryden.....	131
No. 449. Wing Characteristics as Affected by Protuberances of Short Span. By Eastman N. Jacobs and Albert Sherman....	155
No. 450. The Calculation of Take-Off Run. By Walter S. Diehl.....	163
No. 451. The Drag of Two Streamline Bodies as Affected by Protuberances and Appendages. By Ira H. Abbott.....	171
No. 452. General Potential Theory of Arbitrary Wing Sections. By T. Theodorsen and I. E. Garrick.....	177
No. 453. The Estimation of Maximum Load Capacity of Seaplanes and Flying Boats. By Walter S. Diehl.....	211
No. 454. Photomicrographic Studies of Fuel Sprays. By Dana W. Lee and Robert C. Spencer.....	215
No. 455. Penetration and Duration of Fuel Sprays from a Pump Injection System. By A. M. Rothrock and E. T. Marsh..	241
No. 456. The Aerodynamic Forces and Moments Exerted on A Spinning Model of the NY-1 Airplane as Measured by the Spinning Balance. By M. J. Bamber and C. H. Zimmerman.....	249
No. 457. Maneuverability Investigation of an O3U-1 Observation Airplane. By F. L. Thompson and H. W. Kirschbaum..	263
No. 458. Relative Loading on Biplane Wings. By Walter S. Diehl.....	275
No. 459. The N.A.C.A. Full-Scale Wind Tunnel. By Smith J. De France.....	291
No. 460. The Characteristics of 78 Related Airfoil Sections from Tests in the Variable-Density Wind Tunnel. By Eastman N. Jacobs, Kenneth E. Ward, and Robert M. Pinkerton.....	299
No. 461. Interference on an Airfoil of Finite Span in an Open Rectangular Wind Tunnel. By Theodore Theodorsen.....	355
No. 462. Tests of Nacelle-Propeller Combinations in Various Positions with Reference to Wings. III-Clark Y Wing—Various Radial-Engine Cowlings—Tractor Propeller. By Donald H. Wood.....	359
No. 463. The N.A.C.A. High-Speed Wind Tunnel and Tests of Six Propeller Sections. By John Stack.....	399
No. 464. Negative Thrust and Torque Characteristics of an Adjustable-Pitch Metal Propeller. By Edwin P. Hartmen....	421
No. 465. Determination of the Theoretical Pressure Distribution for Twenty Airfoils. By I. E. Garrick.....	433
No. 466. Aircraft Power-Plant Instruments. By Harcourt Sontag and W. G. Brombacher.....	447
No. 467. The Experimental Determination of the Moments of Inertia of Airplanes. By Hartley A. Soulé and Marvel P. Miller.....	501
No. 468. The Interference Between Struts in Various Combinations. By David Biermann and William H. Herrnstein, Jr..	515
No. 469. Increasing the Air Charge and Scavenging the Clearance Volume of a Compression-Ignition Engine. By J. S. Spanogle, C. W. Hicks, and H. H. Foster.....	525
No. 470. The N.A.C.A. Tank—A High-Speed Towing Basin for Testing Models of Seaplane Floats. By Starr Truscott..	535
No. 471. Performance of a Fuel-Injection Spark-Ignition Engine Using a Hydrogenated Safety Fuel. By Oscar W. Schey and Alfred W. Young.....	557
No. 472. Wind-Tunnel Tests on Combinations of a Wing With Fixed Auxiliary Airfoils Having Various Chords and Profiles. By Fred E. Weick and Robert Sanders.....	567
No. 473. Strength Tests of Thin-Walled Duralumin Cylinders in Compression. By Eugene E. Lundquist.....	585
No. 474. Nomenclature for Aeronautics. By National Advisory Committee for Aeronautics.....	603

NATIONAL ADVISORY COMMITTEE FOR AERONAUTICS

HEADQUARTERS, NAVY BUILDING, WASHINGTON, D.C.

LABORATORIES, LANGLEY FIELD, VA.

Created by act of Congress approved March 3, 1915, for the supervision and direction of the scientific study of the problems of flight. Its membership was increased to 15 by act approved March 2, 1929. The members are appointed by the President, and serve as such without compensation.

JOSEPH S. AMES, Ph.D., *Chairman*,
President, Johns Hopkins University, Baltimore, Md.

DAVID W. TAYLOR, D.Eng., *Vice Chairman*,
Washington, D.C.

CHARLES G. ABBOT, Sc.D.,
Secretary, Smithsonian Institution.

LYMAN J. BRIGGS, Ph.D.,
Director, Bureau of Standards.

ARTHUR B. COOK, Captain, United States Navy,
Assistant Chief, Bureau of Aeronautics, Navy Department.

BENJAMIN D. FOULOIS, Major General, United States Army,
Chief of Air Corps, War Department.

HARRY F. GUGGENHEIM, M.A.,
Port Washington, Long Island, N.Y.

ERNEST J. KING, Rear Admiral, United States Navy,
Chief, Bureau of Aeronautics, Navy Department.

CHARLES A. LINDBERGH, LL.D.,
New York City.

WILLIAM P. MACCRACKEN, Jr., Ph.B.,
Washington, D.C.

CHARLES F. MARVIN, Sc.D.,
Chief, United States Weather Bureau.

HENRY C. PRATT, Brigadier General, United States Army,
Chief, Matériel Division, Air Corps, Wright Field, Dayton,
Ohio.

EUGENE L. VIDAL, C.E.,
Director of Aeronautics, Department of Commerce.

EDWARD P. WARNER, M.S.,
Editor of Aviation, New York City.

ORVILLE WRIGHT, Sc.D.,
Dayton, Ohio.

GEORGE W. LEWIS, *Director of Aeronautical Research*

JOHN F. VICTORY, *Secretary*

HENRY J. E. REID, *Engineer in Charge, Langley Memorial Aeronautical Laboratory, Langley Field, Va.*

JOHN J. IDE, *Technical Assistant in Europe, Paris, France*

TECHNICAL COMMITTEES

AERODYNAMICS
POWER PLANTS FOR AIRCRAFT
MATERIALS FOR AIRCRAFT

PROBLEMS OF AIR NAVIGATION
AIRCRAFT ACCIDENTS
INVENTIONS AND DESIGNS

Coordination of Research Needs of Military and Civil Aviation

Preparation of Research Programs

Allocation of Problems

Prevention of Duplication

Consideration of Inventions

LANGLEY MEMORIAL AERONAUTICAL LABORATORY

LANGLEY FIELD, VA.

Unified conduct for all agencies of
scientific research on the fundamental
problems of flight.

OFFICE OF AERONAUTICAL INTELLIGENCE

WASHINGTON, D.C.

Collection, classification, compilation,
and dissemination of scientific and
technical information on aeronautics.

NINETEENTH ANNUAL REPORT

OF THE

NATIONAL ADVISORY COMMITTEE FOR AERONAUTICS

WASHINGTON, D.C., November 14, 1933.

To the Congress of the United States:

In accordance with the act of Congress approved March 3, 1915, which established the National Advisory Committee for Aeronautics, the Committee submits herewith its nineteenth annual report for the fiscal year 1933.

Continued progress.—It is gratifying to the Committee to report that the past year was notable as witnessing the greatest advance in airplane performance and efficiency accomplished in any single year since the Great War. This is largely the cumulative result of years of organized scientific research conducted by this Committee and of the practical application of the results by the Army, the Navy, and the aircraft industry.

Result of sound governmental policy.—In the opinion of the Committee aeronautical development in the United States is certainly abreast, and, in certain particulars, in advance of the development in any other country. This is the result of long-continued sound governmental policy in supporting fundamental aeronautical research. It began with legislation 18 years ago which established the National Advisory Committee for Aeronautics as an independent Government establishment "to supervise and direct the scientific study of the problems of flight," and has been continued through generous appropriations to this Committee. Thus one central governmental organization, with the active cooperation of the War, Navy, and Commerce Departments and of the aircraft industry, supplies the research needs of aviation. By this policy of coordination, results of greatest value to aeronautics are obtained with prevention of duplication and waste. Supplementing this policy, there is effective application of the results of the Committee's researches in the experimental and development laboratories of the Army and Navy.

Comprehensive researches serve all needs.—The research programs of the Committee are formulated largely by the various technical subcommittees whose membership embraces all governmental agencies concerned. A large part of the Committee's research programs consists of specific requests of the Army and

Navy air organizations. The latter depend upon the Committee for the scientific study and investigation of fundamental problems necessary for the improved design of military and naval aircraft. Aircraft manufacturers and operators also rely upon the Committee for fundamental data, and the Committee broadens its military and naval researches to obtain as much fundamental information as possible in order to meet the needs of civil and commercial aviation. In this the Committee is assisted by the cooperation of the Aeronautics Branch of the Department of Commerce and by an annual conference with representatives of the aircraft industry, held at the research laboratories at Langley Field, Va.

Facilities for fundamental research.—The Committee has recognized its responsibility in shaping the progress of aeronautics and, with the far-sighted support of the Congress, has anticipated the research needs of aviation and developed at Langley Field, Va., the best-equipped aeronautical research laboratory in the world. This one central laboratory is known as the Langley Memorial Aeronautical Laboratory and is operated under the single and direct control of the Committee. The fundamental researches approved by the Committee are conducted at that laboratory, where there are combined under ideal conditions facilities for laboratory investigations and for researches on airplanes in flight. Much of the equipment there is original and ingenious and permits investigations that give results not obtainable in any other country. The development of this laboratory represents in itself an accomplishment in which the Congress and the country may take pride, for the excellence of its product has gained for the United States an advantageous position among the progressive nations in the development of aeronautics.

Results of research.—Speed is still the most important single factor in increasing the relative importance of aircraft for national defense and in extending their use for commercial purposes. Primarily as a direct result of the Committee's researches there have been great increases in speed and efficiency during the past year, which have opened a new era in the development of both military and commercial aircraft. The in-

crease in the speed of multiengine airplanes, military and commercial, from 1932 to 1933 has approximated 40 to 60 percent with practically the same engine power. This development is one of the outstanding contributions of the Committee, the major factors being:

(1) The National Advisory Committee for Aeronautics engine location and cowling. (The results of the cowling research were published in 1928. The results of the engine location research were issued confidentially to the Army, Navy, and industry in 1930, and were kept confidential until 1932, when the first American airplanes embodying the principles had been designed and actually constructed.)

(2) The development by the Army, the Navy, and the industry of reliable retractable landing gears.

(3) Increased horsepower with same size and weight of engines, involving increased revolutions per minute, higher compression ratio, improved fuels, and improved cylinder cooling.

(4) The development by the Army, the Navy, and the industry of satisfactory controllable-pitch propellers.

(5) The development by the Committee of new and more efficient wing sections.

(6) Improved streamlining and use of wing flaps, assisted by the Committee's researches.

A great increase in the high speed of an airplane would ordinarily be accompanied by a dangerous increase in its landing speed. This presented a problem of devising means of increasing the lift and drag of the wing to permit landing at a lower speed, without attendant loss of control. Increased safety in the operation of aircraft will result primarily from reduction in landing speeds with retention of adequate control. Toward this end the Committee has conducted researches on a number of high-lift devices, some of which are now in use. Others under investigation hold promise of further progress in retaining adequate control at lower landing speeds.

Research pays.—It is essential to national defense and to American air commerce that the United States

strive to keep abreast or ahead of other nations in the technical development of both military and commercial aviation. The researches of the Committee lead to material improvement in the performance, efficiency, and safety of aircraft. No money estimate can be placed on the value of superior performance of aircraft in warfare, for aerial supremacy is quite likely to be ultimately decisive of a war; nor can a money estimate be placed on the indeterminable savings in life and property due to improved safety in the operation of both military and civil aircraft. The value in dollars and cents of improved efficiency in aircraft resulting from the Committee's work can, however, be fairly estimated. For example, the results of six researches completed by the Committee within the last few years, when applied to airplanes equal in number to those in use during 1932, show that savings in money alone will be made possible in excess annually of the total appropriations for the Committee since its establishment in 1915.

In the opinion of the Committee the continued development of aviation is vital to our national security and defense. Aviation is also becoming an increasingly important factor as an agency of transportation. Its continued development holds possibilities for the growth of a large industry, creating new sources of wealth, new fields of employment, and new outlets for the energies of the American people. The Committee is of the opinion that the most essential fundamental activity of the Government in aeronautics is the continuous prosecution of well-organized and coordinated scientific research. Continuous fundamental research is absolutely vital in the last analysis, as it underlies the effectiveness of the air arms of the national defense, the stability of the aircraft industry, and the prospect of ultimate success of air transportation upon a sound economic basis. The Committee accordingly recommends continuation of its work in the fields of pure and applied research on the fundamental problems of flight.

PART I

REPORTS OF TECHNICAL COMMITTEES

In order to carry out effectively its principal function of the supervision, conduct, and coordination of the scientific study of the problems of aeronautics, the National Advisory Committee for Aeronautics has established under the executive committee four main technical committees—the committees on aerodynamics, power plants for aircraft, materials for aircraft, and problems of air navigation—and under these committees, eight subcommittees. These technical committees prepare and recommend to the executive committee programs of research to be conducted in their respective fields, and as a result of the nature of their organization, which includes representation of the various agencies concerned with aeronautics, they act as coordinating agencies, providing effectively for the interchange of information and ideas and the prevention of duplication. The membership of these committees and subcommittees is listed in part II.

The committees on aerodynamics and power plants for aircraft have direct control of the aerodynamic and aircraft-engine research, respectively, conducted at the Committee's laboratory at Langley Field, and of special investigations conducted at the Bureau of Standards. The greater part of the research under the supervision of the committee on materials for aircraft is conducted by the Bureau of Standards. The experimental investigations in aerodynamics, aircraft power plants, aircraft materials, and air-navigation problems undertaken by the Bureau of Aeronautics of the Navy, the Army Air Corps, the Bureau of Standards, and other Government agencies are reported to these four committees.

REPORT OF COMMITTEE ON AERODYNAMICS SUBCOMMITTEE ON AIRSHIPS

In order that the committee on aerodynamics may be kept in close touch with the latest developments in the field of airship design and construction and that research on lighter-than-air craft may be fostered and encouraged, a subcommittee on airships has been organized under the committee on aerodynamics.

The subcommittee has kept in close touch with the airship investigations under way at the Langley Memorial Aeronautical Laboratory. The program of airship work at the laboratory includes the study in the full-scale wind tunnel of the forces on a large airship model at large angles of pitch and of yaw. In cooperation with the Bureau of Aeronautics of the Navy, the Committee has also obtained information on the speed and deceleration on the full-size airship *Macon*.

LANGLEY MEMORIAL AERONAUTICAL LABORATORY

LANDING SPEED AND SPEED RANGE.—The speed of both military and commercial airplanes has increased very markedly during the past year. This increase in speed has been accomplished partly through an increase of engine power, but mainly through the reduction of drag. The low drag, while advantageous in obtaining high speed, is disadvantageous in that it limits the gliding angle which can be obtained at low speed, and makes necessary a very long flat approach to a landing. The higher maximum speeds have also been accompanied by a tendency to use heavier wing loadings, and the landing speeds have increased to what seems to be the practical limit. Under these adverse landing conditions, devices for increasing the maximum lift coefficient and also the drag at the high angles of attack have been of great interest.

Flap modifications.—The committee's work on split flaps has been continued during the past year. These flaps have now been used on several airplanes, either in the simple form or in the Alfaro-Zap form, in which the flap is moved to the rear as well as deflected downward. In response to the demand for more detailed information in regard to their aerodynamic effect and in regard to the air loads on the flaps, further tests have been made in the 7- by 10-foot wind tunnel. The air loads on the flaps have been measured for the purpose of supplying information on which to compute the structural strength needed and the forces required to deflect them (report in preparation). The results of these tests showed that the division of the total lift between the split flaps and the wing was little affected by flap deflection in the ordinary flight range, although the division of the total drag was greatly affected by flap deflection. The normal-force coefficient was also greatly affected by flap deflection, the coefficient for the flap alone reaching a value of approximately 1.40 at the angle of attack and flap deflection for maximum lift.

Another investigation was made in the 7- by 10-foot tunnel to determine the effect on the aerodynamic characteristics of partial-span split flaps located at various positions along the wing span (Technical Note No. 472). The results showed that as the flap is cut away from the tip, the loss in lift is small at first, but becomes substantial if sufficient flap is removed to allow room for ordinary ailerons. If the flap is cut away from the center, the loss starts more rapidly, being in the neighborhood of 8 or 10 percent for the cut-out usually found necessary for structural reasons.

Full-scale tests with simple split flaps have been made with a parasol monoplane both in the full-scale tunnel and in flight, with flaps 20 percent of the wing chord in width extending over the outer 90 percent of the wing span. The full-scale lift, drag, and pitching-moment coefficients for the airplane were found in the full-scale tunnel both with the horizontal tail surfaces in place and with them removed (Technical Note No. 475). The value of $C_{L_{max}}$ was increased from 1.47 to 2.09 by deflecting the flap, the stalling angle being the same in both cases. These results agree well with the model results obtained in the 7- by 10-foot tunnel with regard to the effect of the flap. The computed landing speed of the airplane was reduced from 51 miles per hour to 41.9 miles per hour by the use of the flaps.

The flight tests, the model tests in the 7- by 10-foot tunnel, and the full-scale wind-tunnel tests all showed that the control force required to displace a simple split flap is undesirably great. A series of wind-tunnel tests is now in progress to study the effectiveness of various methods of reducing the hinge moments of these flaps.

A year ago the highest lift coefficient obtained by the Committee with any kind of flap device was 3.17, obtained with the Fowler flap. During the past year attempts have been made to obtain still higher lift coefficients. First, a slot was added to the leading edge of the Fowler-type wing, but only a slight increase in lift coefficient resulted. A special slot having a slot of good airfoil section was then developed and this in its best location gave a maximum lift coefficient with the Fowler-type flap of 3.62 (Technical Note No. 459). Then still another slot was added, a fixed slot near the trailing edge of the basic wing, which gave a slight additional increase to 3.76, a total increase of about 200 percent above the value for the wing with all devices retracted. The investigation of the plain Fowler-type flap is being continued in the 7- by 10-foot wind tunnel to find the relative characteristics with Fowler flaps of various sizes and to determine the loadings on the flaps.

Wind-tunnel tests have also been made with a flap consisting of an auxiliary airfoil pivoted at the rear of the main wing as proposed by Wragg. The auxiliary airfoil is located so that a slot is formed between the two wings in a manner somewhat similar to that of the Fowler-type flap, but the auxiliary is not retracted into the main wing. This arrangement with a 15 percent auxiliary airfoil gave a maximum lift about the same as that obtained with a simple split flap.

Fixed auxiliary airfoils.—Last year a fixed auxiliary airfoil had been developed which gave an increased lift coefficient and an increased speed range, and which was thought advantageous particularly because it had no moving parts (Technical Report No. 428). Flight tests were made with the auxiliary airfoil mounted on

a small parasol monoplane (Technical Note No. 440). At that time the investigation had included only one size of auxiliary airfoil and only one auxiliary airfoil section. The results seemed sufficiently promising to make it worth while to test auxiliary airfoils of other sizes and airfoil sections, and several sizes with three different sections have now been tested in a sufficient number of positions with respect to the main wing to determine the best arrangement (Technical Report No. 472). None of these has been found to be definitely superior in all respects to the original, although a decidedly lower minimum drag was obtained with a symmetrical section. The highest values of the maximum lift coefficients and the speed range criterion, $C_{L_{max}}/C_{D_{min}}$, were obtained with auxiliary airfoils with chords 11 to 15 percent of the main wing chord, although those as small as 7.5 percent of the main wing chord gave nearly the same values as the larger sizes.

Tailless airplanes.—Wind-tunnel tests were made of a model wing having an aspect ratio of 3 and a tapered plan form with a straight trailing edge (Technical Note No. 463). The Clark Y airfoil section was used throughout the entire span, with no washout. A constant-chord trailing-edge flap was used for longitudinal balance and control moments. The simple wing with no washout or change of basic section along the span had aerodynamic characteristics well suited for use on tailless airplanes. A higher lift coefficient was obtained with the full-span flap deflected as a unit to give longitudinal balance than with either the inner or outer portions of the flap deflected separately. Further tests are being made with the same basic model having a fixed auxiliary airfoil mounted ahead of the leading edge for the purpose of increasing the maximum lift coefficient and improving the balance characteristics.

CONTROLLABILITY.—The Committee's work on lateral control has been continued during the past year along two main lines. First, the search has been continued for a lateral-control device that is completely satisfactory throughout the entire speed range, including angles of attack above the stall. More recently the work has been concentrated on lateral-control devices suitable for wings equipped with flaps or other high-lift devices along their entire spans. During the past year some of the control devices that the wind-tunnel investigation showed to be promising have been tried on an airplane in flight, with the result that considerable information has been obtained about the characteristics to be desired in a good lateral-control device, but it was found that each of the single lateral-control devices when tested in flight had at least one undesirable feature. One interesting point brought out by the flight and wind-tunnel tests was that the yawing effect of the ailerons as observed by the pilots corresponded to the yawing moments as measured

about wind axes, and not about body axes as had previously been thought. The flight tests also brought out the fact that the yawing moments caused by the ailerons are relatively unimportant in cruising and in high-speed flight, but are of critical importance at the angles of attack near and above the stall.

Conventional ailerons.—The investigation in the 7- by 10-foot wind tunnel has been extended to include conventional ailerons of various shapes and sizes, with differential movements and with balance arrangements, on wings of various plan forms (Technical Reports Nos. 419, 422, 423, and 444, and Technical Notes Nos. 445, 449, and 451). In all the tests the ailerons of wide-chord and short-span dimensions gave reasonably high values of rolling moment at the high angles of attack definitely above the stall, whereas the narrower ailerons gave substantially lower values above the stall. It therefore seemed that the short wide ailerons might give at least fair control at angles of attack above the stall. The wind-tunnel tests showed, however, that while some conventional aileron arrangements had positive yawing moments with respect to the body axes, all gave adverse yawing moments with respect to the wind axes at high angles of attack, regardless of the differential motion, or of such balancing arrangements as the Frise type. When tested in flight none of the conventional ailerons, whether of long narrow or of short wide form, regardless of the differential motion used, gave control above the stall. From these results it seems that with conventional ailerons the secondary features, the adverse yawing moments, and the aggravation of the stall by the down-going aileron over its portion of the wing, become more important at high angles of attack than the direct rolling moment given by the ailerons.

Wind-tunnel tests have been made with conventional ailerons on a slotted wing (Technical Note No. 443), and flight tests have been made on the lateral-control characteristics of a low-wing monoplane equipped with both slots and flaps, the flaps being confined to the inner portion of the span to allow room for conventional slotted ailerons (Technical Note No. 478). The results of these tests showed that the rolling-moment coefficients obtained were about the same regardless of whether the slots were open or closed, or whether the flaps were up or down, all of which is in accordance with the results of the wind-tunnel tests. In fact, the rolling moments measured in flight agreed very well with the rolling moments measured on similar ailerons under static conditions in the wind tunnel when the rolling action of the airplane was taken into account in the computations.

If conventional ailerons are used on wings with flaps, whether of the plain or split variety, a part of the span of the flap must in most cases be sacrificed. One arrangement has been devised in which ordinary ailerons are used with a full-span split flap by retract-

ing the flap into the wing ahead of the ailerons. With this arrangement, in order to bring the flap into the most favorable position when deflected it is moved to the rear as well as downward. Wind-tunnel tests have shown that reasonably satisfactory rolling and yawing moments are obtained by the conventional ailerons with the flap deflected. With the flap retracted the conventional ailerons operate in the normal manner. A special wing having this arrangement is now being fitted to a parasol monoplane for flight tests.

External ailerons.—A wind-tunnel investigation has been completed on external ailerons composed of separate airfoils attached to but apart from the main wing. The external ailerons were tried in positions all around the main wing, but particularly in four regions: (1) In front of and below the leading edge; (2) above the nose portion; (3) above the trailing edge; and (4) below the trailing edge of the main wing. The ailerons in front of and below the leading edge were found to give reversal of control at low angles of attack. In the region above the forward portion of the wing the ailerons had rolling and yawing moment characteristics somewhat similar to those of spoilers, the rolling-moment coefficients increasing in magnitude as the angle of attack was increased to and through the stall. For the ailerons above the trailing edge the characteristics were similar to those of conventional ailerons except for the yawing moments, which were better. When mounted behind and below the trailing edge, the external ailerons could be used as lift flaps if deflected downward together. If deflected differentially they acted like ordinary ailerons with unusually large adverse yawing moments.

The most favorable location for control at high angles of attack up to well above the stall appeared to be just above the nose portion of the main airfoil, a short distance back from the leading edge. Flight tests have been made on external ailerons in this position with two different types of deflection, in both of which the ailerons were moved one at a time. With one type of deflection the trailing edge was moved up only, and with the other type the trailing edge was moved down only, these opposite deflections being selected because the wind-tunnel tests showed that moving the aileron in either direction from a critical neutral position reduced the lift on the adjacent portion of the wing.

When tested in flight these ailerons had a lag, or delayed action, when given the deflection in which the trailing edge was moved downward, but they were free from lag when the trailing edge was given the individual upward deflection. In the ordinary flying range the acceleration in roll was found to be only about half as great as that obtained with ordinary ailerons of approximately the same size, but the final rate of roll was greater than that obtained with ordinary ailerons. The latter condition was not consid-

ered advantageous by the pilots. The ailerons gave moderate control at the angles of attack above the stall. As has been found with all external ailerons tested in flight, however, the control force was high at the high speeds, even with the aileron hinge axis moved as far back as possible without resulting in overbalance at low speed. The work dealing with external ailerons is still in progress and the reports of the tests are not yet completed.

Floating tip ailerons.—A wind-tunnel investigation has been completed of floating tip ailerons having various airfoil sections, hinge axis locations, and end-plate arrangements, on rectangular wings; on straight wings with single and multiple floating tip ailerons of narrow chord; and on tapered wings with 2° of taper (Technical Report No. 424 and Technical Note No. 458). In general, the floating tip ailerons gave reasonably satisfactory values of rolling moment at all angles of attack, practically zero values of yawing moment about wind axes, and a reduction in the unstable autorotational moments, but they also gave poor airplane performance characteristics, especially in regard to climb. The most promising of the floating tip ailerons seem to be those on wings of extreme taper. In this case, very light control forces are required and it would seem that there should be no great reduction in airplane performance if the span of the fixed part of the wing is sufficient for the rate of climb desired.

Upper-surface ailerons.—These ailerons are used with split flaps and are formed by deflecting the upper trailing-edge portions of the wing above the split flaps. They are deflected upward individually. Both wind-tunnel and flight tests showed that, while moderate rolling control can be obtained at angles of attack below the stall with the flap either deflected or retracted, if simple unbalanced upper-surface ailerons are used the control forces required are excessively high even though the ailerons have a narrow chord. Reports on both the wind-tunnel and flight tests are in preparation. Work is now being carried on in the 7- by 10-foot tunnel to investigate the possibility of obtaining a suitable reduction of hinge moment by means of proper hinge location and aileron profile.

Spoilers.—Various spoiler arrangements have been tested both in the wind tunnel (Technical Note No. 415 and Technical Report No. 439) and in flight (report in preparation). These spoilers consisted essentially of plates and surfaces arranged to project from the upper surface of a portion of the wing in order to reduce the lift over that portion. The spoilers located near the nose of the wing gave control at angles of attack above the stall, but, unfortunately, below the stall they had a definite lag or delayed action due to an initial but imperceptible tendency to roll in the wrong direction. The time from the deflection of the control to the start of the roll in the desired direction averaged about one half

second. The lag was found in flight with each of the three forms of spoiler tested, the first being a flap set in the upper surface and hinged at the front edge, the second a retractable spoiler projecting out through a slot in the upper surface of the wing, and the third the retractable spoiler cut to saw-tooth form. These results seem to eliminate the simple spoiler located in the forward portion of the wing as a satisfactory lateral-control device when used by itself, but, if control above the stall is of sufficient importance, a satisfactory arrangement free from lag can apparently be obtained by the proper combination of spoilers and ordinary ailerons. The spoilers can be arranged to reduce the aileron hinge moments if desired, either by means of their location or their connecting linkage.

In regard to control at angles of attack above the stall, the flight tests have shown that the lateral instability above the stall may be so violent as to eliminate the possibility of handling the airplane satisfactorily even with an effective lateral control. Considering this condition it seems that even for occasional emergency use control above the stall may be of slight value unless it is accompanied by stability.

If the spoilers are moved sufficiently far back along the chord of the wing there is no doubt that the lag can be eliminated. Unfortunately, as the spoiler is moved back its effectiveness in giving control at angles of attack above the stall is lost. The present plans are to continue flight tests to find the most forward spoiler location free from lag. Tests are now under way with the retractable-type spoilers near the trailing edge of the wing. In this position they might well be called "retractable ailerons", for they give approximately the same rolling and yawing moments as the upper-surface ailerons but with the advantage of very low control forces, for with this device the hinge moments can be made practically zero.

Aerodynamic balancing of control surfaces.—Considerable interest has been centered during the past year on means of balancing the forces required to operate the various control surfaces of an airplane. An investigation has been made in the 7- by 10-foot tunnel on a model wing with ailerons and balanced surfaces of various kinds. Hinge moments and rolling and yawing moments, as well as the general performance with the various arrangements, were measured. One type of balancing arrangement investigated consisted of flat plates or tabs attached to the trailing edge of the ailerons and deflected various amounts. Another type of tab was formed by deflecting the trailing-edge portion of the aileron itself. The latter type proved more effective and complete servo-control could be obtained for moderate aileron deflections when the inset tab was 20 percent of the aileron chord and covered the entire aileron span. The hinge moments for large aileron deflections, however, were greater with the tabs than without. Further work is in progress

with inset tabs and horn-and-paddle-type balances on ailerons, and with inset tabs on rudders and elevators also.

STABILITY.—A theoretical study of stability, based on the theory of small oscillations, is being made with a view to making possible the rational prediction of the stability characteristics of an airplane by simple means.

Effect of wing-tip shape.—A wind-tunnel investigation of the effect of wing-tip shape on lateral stability is in progress. Tests have been made with tips having rectangular and curved plan forms, and with the tip in front curved upward and downward different amounts. The tests include 6-component force and moment measurements at several angles of yaw, as well as rotation tests at zero yaw. The results show the effect of tip shape on general performance and on four of the lateral-stability factors—damping in roll, and variation of the rolling moment, yawing moment, and cross-wind force with sideslip. It was found that the rectangular tips gave higher values of the rolling and yawing moments due to sideslip than the curved tips, while the damping in roll was about the same for all of the tips tested.

Effective dihedral.—A detailed wind-tunnel investigation is being made to determine the effects of dihedral on lateral stability and on general performance. In the 7- by 10-foot wind tunnel tests are being made with wing models having various amounts of the span deflected upward to give dihedral. The results obtained to date indicate that a dihedral angle only in the outer 25 percent of the wing is quite effective in producing rolling moments due to sideslip up through large angles of attack. In addition to the wind-tunnel investigation qualitative flight tests are being made in which the lateral stability is being found for a parasol monoplane with dihedral angles ranging from 0° to 9° .

LANDING.—The cinematographic apparatus developed for studying the motion of airplanes in flight close to the ground, particularly in landings, has been utilized in an investigation of glide landings in gusty air. The airplane used in this investigation was equipped with unusually long shock-absorber struts. In the tests with the elevator held stationary, for the worst case recorded the attitude of the airplane varied from 14° nose up to 9° nose down, and the rate of descent varied from 28 feet per second to 4 feet per second, while the airplane was descending from 550 feet to 350 feet. At the present time a paper is being prepared in which the results of this investigation will be presented, together with the results of an investigation of the variation in wind speeds close to the ground.

The above-mentioned apparatus has also been used in investigations of the relative efficiency of two types of long-stroke shock-absorber struts, and of the landing characteristics of an autogiro. The latter investi-

gation was undertaken at the request of the Aeronautics Branch, Department of Commerce, to provide data for use in the formulation of design rules.

TAKE-OFF.—A comparatively simple method of calculating the length of take-off run has been developed from the assumption of a linear variation in net accelerating force with air speed. This method has been published during the year in Technical Report No. 450.

A flight investigation was made to determine the effect of automatic slots and plain flaps on take-off, the tests being made with a small low-wing monoplane. The take-off run was materially reduced with slots but not with flaps, the magnitude of the effects being dependent to some extent on the gross weight. The difference in the effects of the two devices lay principally in the fact that the flaps increased the drag throughout the take-off run and thereby retarded the acceleration, whereas the slots had no appreciable deleterious effect during the preceding ground run.

Further information on the effect of flaps on take-off run is available from tests in the full-scale tunnel on a small parasol monoplane. Calculations based on the power characteristics with a 95-horsepower engine and a fixed-pitch propeller indicated that a slight reduction in the calculated take-off run would be obtained with a flap depression of about 27° , but because of the poor climb with the flaps down, the total take-off distance required to clear an obstacle 100 feet high would be greatly increased for flap settings greater than 20° and would not be appreciably improved by lower settings.

In an attempt to calculate the take-off run from known airplane and propeller characteristics it was found that no one value for the coefficient of ground friction would give satisfactory agreement with the experimental data for all take-off conditions. A study is being made of the influence of various factors on take-off.

The recent perfection of several types of controllable propellers has increased the interest in methods of computing the possible performance of such propellers. A report has been prepared pointing out some of the methods to be used in such calculations making use of data previously published by the Committee. The report (Technical Note No. 484) also shows the possibility of increasing the performance of some airplanes.

In the computation of the propeller performance of airplanes, particularly of seaplanes, it has been found that the information previously published in Technical Report No. 350 was not complete enough in the low-speed range for the calculation of the available thrust of the propeller. The original data have been recomputed, a new coefficient being used, and the results are being presented in a new report in the form of charts which will be useful to designers in computing the low-speed characteristics of propellers.

When retractable landing gears are used on a low-wing monoplane the question arises how the lift coefficient of the wing is affected by the open wheel wells in the lower surface of the wing when the landing gear is extended and how the time for taking off may be affected. In order to furnish information on this point, the Committee was requested by the Army Air Corps to make tests in the full-scale tunnel on a Lockheed Altair airplane. It was found that the wheel openings in the lower side of the wing have a negligible effect upon the lift and take-off of the airplane. The results are given in Technical Note No. 456.

MANEUVERABILITY.—A report on the maneuverability of an observation airplane, an investigation undertaken at the request of the Bureau of Aeronautics, Navy Department, has been published (Technical Report No. 457). Consideration has been given to the development of a criterion for maneuverability based on the results of previous tests.

SPINNING.—Intensive research on the problem of the spin has been continued both in flight and in the vertical tunnel, the latter having been in regular operation throughout the past year (Technical Report No. 456). Attention has been concentrated largely on the factors affecting the steady spin and recovery from it, for the ultimate purpose of insuring in the design of airplanes that proper recovery will be obtained, or that the steady spin will be entirely prevented.

A paper has been published on the effect of sharp leading edges on the spin (Technical Note No. 447). There has also been published a paper (Technical Note No. 468) on the results of a study of the influence of the various factors affecting the steady spin. In this study the predicted influence of various modifications in airplane design features were correlated with the results of flight tests as reported from numerous sources. An analysis of the results obtained in a flight investigation conducted on a small biplane, of the effect of control setting and mass distribution on the steady spin, has been completed and a paper on this subject is now being prepared. It was found that in general the observed effect of extensive changes in mass distribution could be predicted by utilizing the knowledge already available from previous theoretical and experimental studies of the problem.

There are rather conclusive indications that provision of sufficient damping yawing moments offers the most effective method of eliminating bad spinning characteristics, and several researches designed to provide additional information on the amount of yawing moment desired and the method of securing it effectively have been carried out or are now in progress. An investigation conducted in the vertical tunnel to determine the effect on spinning characteristics of locating the stabilizer and elevator in several fore-and-aft

positions and also in two vertical positions has been completed and a paper on the results has been published (Technical Note No. 474). The results indicate that a very favorable increase in yawing moment is obtained by a high and/or a rearward position of the horizontal tail surfaces.

In the same connection the spinning characteristics of a biplane of the fighter type have been investigated in flight with various modifications to improve the effective fin area. In its original condition this airplane would occasionally fail to recover when the controls were manipulated in accordance with the normal procedure for recovery. The character of the spin was first improved to an extent that made it safe for spinning by the addition of considerable fin area above the fuselage, a modification that could be readily incorporated in the existing airplanes of that type. The investigation was then continued to determine the effect of raising the stabilizer, a modification that was expected to prove very beneficial, on the basis of previous studies in the vertical tunnel. In tests now completed a very marked improvement in the character of the spin has been brought about by raising the stabilizer to the top of the vertical fin. At the present time the effect of an intermediate stabilizer position is being investigated, such a position being more readily adaptable to structural design requirements than the extreme upper position.

The flight investigation with this airplane has been very closely correlated with tests in the vertical tunnel on a model of the same airplane primarily for the purpose of determining the extent to which agreement might be expected between model and flight spinning tests, and possibly of deriving factors for converting model spinning results to full scale. The model data have not yet been completely analyzed.

A third research concerned with the yawing moments contributed by various parts of the airplane in spins is now being carried out in flight on a small biplane previously used for mass-distribution studies. The lateral forces on the fin, rudder, and fuselage are being determined by pressure-distribution measurements, and at the same time the spinning motion is determined so that resultant moments can be computed. The yawing moment developed by the remainder of the airplane, chiefly the wings, is then found.

At the request of the Army Air Corps, three models of special pursuit airplanes were tested in the vertical tunnel for prediction of their spinning characteristics. It is interesting to note that the characteristics as measured compared favorably with what had been predicted on the basis of previous tests with other models on the spinning balance.

An experimental method for determining the moments of inertia of airplanes for use chiefly in spinning studies has been used by the Committee for several years. Essentially, the method consists in

suspending the airplane so that it can oscillate as a pendulum. Refinements in the method have been made from time to time, some of them being of fundamental importance. A report has been published (Technical Report No. 467) describing the procedure followed in these experiments, particularly the method employed in correcting for effects of the ambient air.

AERODYNAMIC INTERFERENCE AND DRAG.—The broad basic investigation of aerodynamic interference and drag previously undertaken has been continued through the year. The investigation is intended to determine where and under what conditions interference effects may be of importance, and how adverse interferences between airplane parts may be reduced and favorable interferences utilized. The work is advantageously divided among various sections of the laboratory.

Wing-fuselage interference.—An extensive investigation dealing largely with interference effects between the fuselage and the wing has been in progress during the year in the variable-density wind tunnel. The tests are made at a high value of the Reynolds Number, and deal with combinations of variously shaped fuselages and wings in different relative positions. A large part of the test program has been carried out and the results are being analyzed, but the investigation has not progressed sufficiently far to warrant the drawing of conclusions.

The best means of determining interference effects is by measurements on actual airplanes in the full-scale wind tunnel where the tests can be made with and without the slipstream, and where flow surveys can be made behind the airplane. Two investigations of this nature have been undertaken during the year. Wing-fuselage interference and buffeting were investigated on a low-wing monoplane displaying excessive drag and tail buffeting at high angles of attack, successive modifications being made, including the addition of variously formed fillets at the juncture of the wing and fuselage, the installation of a National Advisory Committee for Aeronautics engine cowl, the use of short-span auxiliary airfoils, and provision for reflexing the trailing edge of the wing. Preliminary results of this investigation have been published in Technical Note No. 460.

A more complete report is in preparation in which will be shown surveys of the flow about the tail surfaces with and without power and with the various modifications mentioned. A special survey apparatus described previously was used for this work. It was found that the fillets, either alone or in combination with the National Advisory Committee for Aeronautics cowl, reduced the buffeting and interference to unobjectionable magnitudes at angles of attack up to the stall. The best results were obtained by the use of fillets together with the National Advisory Committee for Aeronautics cowl.

Another full-scale investigation of wing-fuselage interference on a YO-31A airplane is in progress in the full-scale tunnel. A mock-up of this airplane, which was originally built with a gull wing, has been arranged for the installation of wings in three positions representing a high-wing, a mid-wing, and a low-wing monoplane and in the latter position a full cantilever wing will be tested as well as the braced wing used in the other positions. Both force tests and pressure-distribution measurements will be made for the whole series of tests and these, taken with air-flow measurements at the tail and engine power data, will give a complete picture of the effects of wing-fuselage interference on this particular airplane. The part of the investigation dealing with the gull wing has now been completed and the results are being analyzed while the next wing arrangement is being set up.

Wing-nacelle propeller research.—The extensive program of research on the mutual influences of wing, nacelle, and propeller has been continued in the propeller-research tunnel. Investigation of nacelles with tandem propellers, of nacelles with pusher propellers, and of nacelles with tractor propellers on biplane wings has been completed. A large number of supplementary tests correlating these investigations with the investigations of tractor propellers on nacelles and monoplane wings have also been made. Reports covering these various parts of the investigation are now in preparation.

The effect of the shape and size of the wing on the mutual interference has been investigated by means of tests on a wing of Clark Y section and smaller chord for comparison with the earlier tests with a thick wing of large chord. Results of this investigation have been published as Technical Report No. 462. The general conclusion drawn from the investigation is that a completely cowled tractor nacelle located ahead of the leading edge of the wing is the best arrangement. The tandem-nacelle arrangement suffered largely from the high drag of the engine nacelle. The same is true of the pusher nacelle arrangement; in fact, the pusher part of the nacelle or nacelle adjacent to the pusher propeller appears to be the undesirable feature in both the pusher and tandem arrangements. None of these arrangements approaches the efficiency of the best tractor-nacelle arrangement. There appear to be good grounds for supposing that an arrangement consisting of an engine located ahead of the leading edge of the wing in a National Advisory Committee for Aeronautics cowled nacelle and an extension shaft carried to the trailing edge of the wing with the propeller located at the end will have high efficiency. Tests are soon to be made with this arrangement.

Most of the preceding tests have been made with nacelles for air-cooled radial engines. The liquid-cooled airplane engine has not been overlooked; some tests have been made to determine the propulsive

efficiency and the interference effects of a liquid-cooled engine nacelle and a wing. The tests made thus far indicate that the largest drag-producing component of the nacelle of the ordinary type is the radiator, which is normally exposed below the nacelle. A test was also made with a radiator completely surrounding the engine and enclosed within a nacelle of circular cross section, giving an outward shape similar to that of an air-cooled engine nacelle. The results of this test indicated that the drag of the usual liquid-cooled installation could be considerably reduced by such an arrangement.

The great mass of data obtained on wing-nacelle-propeller effects in the propeller-research tunnel was obtained on wings of 15-foot span, aspect ratio 3, with a propeller of 4-foot diameter. If the propeller-nacelle interference extends more than about two diameters outboard of the thrust axis, then the effect is incompletely measured on such a small-span wing. In order to check this possibility, the same nacelle-propeller combination has been tested in the full-scale wind tunnel in three positions relative to a wing of the same chord and section whose span was progressively decreased from 30 to 25, to 20, and finally to 15 feet. Forces, propeller characteristics, and pressure distribution were measured and a preliminary comparison shows the effect of span to be not so large as to invalidate the test results on short spans. The results of these tests in the full-scale tunnel are being prepared for publication.

Drag of landing gears.—It has been realized for some time that the drag of the landing gear constitutes in many cases a large part of the total drag of the airplane. That manufacturers of airplanes are cognizant of this fact is witnessed by the numerous installations of retractable landing gears in recent airplanes. The additional weight and the mechanical complexity have retarded the general adoption of retractable landing gears. That these difficulties are being surmounted is attested by the numerous installations of retractable gears in recent designs, but the use of nonretractable gears in several high-performance airplanes indicates the need for more information on the possibilities of reducing the drag and the unfavorable interference effects.

An investigation of the drag of landing gears has recently been completed in the propeller-research tunnel. In this investigation a full-size airplane fuselage was mounted on the balance and a large number of landing gears were attached to this fuselage and the drag determined. The drag of the complete landing gear as thus determined was supplemented by tests on component parts which were made in the 7- by 10-foot wind tunnel (Technical Report No. 468). About 20 types of landing gears were investigated which, with numerous variations, brought the total number of tests to over 100. A number of styles of wheels

and wheel fairings and fairings between wheels and struts were tried, so that the whole research constituted a fairly complete study of landing-gear effects. The final report including analysis and design studies has been completed.

It was found that landing gears of the older types without any particular streamlining and having very high drag can be greatly improved by installing fillets between the struts and wheels and fairings over the wheels. Of the newer types, the cantilever-type gear had a fairly low drag but the lowest drag was obtained with a gear protruding vertically below the wing and completely faired in. With this type the drag was reduced to about 13 pounds for the landing gear at 100 miles an hour. It was also found that, as far as drag is concerned, the various types of wheels, such as high-pressure, low-pressure, and streamlined wheels, have relatively small effect on the total drag, but that interference effects between wheels and adjacent members is much more important. Taken all together, it appears that the drag for the exposed landing gear can be reduced to a point where its effect even on the high-performance airplane will be relatively small and the consequent complication of retractable gears can be avoided in a number of instances.

Cowling.—The very general adoption of the National Advisory Committee for Aeronautics cowling and its importance for high-speed flight have pointed to the desirability of further research to establish more trustworthy design data. An extensive systematic investigation has accordingly been undertaken, consisting of three parts: (1) the cooling requirements of an air-cooled engine, to be established by the power plants division; (2) the best cowling arrangement to obtain the necessary cooling with minimum drag, to be established by model tests in the 7- by 10-foot tunnel; (3) verification of the results from parts (1) and (2) by cowling tests on full-size engines in the propeller-research tunnel.

Part (1) is in progress by the engine research division. Part (2) is in progress in the 7- by 10-foot tunnel, and includes the effect of changes in the front opening, the rear opening, the size of the nacelle, the camber of the leading part of the cowling, and the effect of different types of leading edge. The investigation has not been carried far enough to warrant definite conclusions.

Propeller drag.—For those airplanes whose functions require that they be dived at terminal velocity, the accurate prediction of this velocity is of importance. Since the propeller may offer considerable drag in fast dives and since it exerts a controlling influence on the engine speed, the Committee was requested by the Bureau of Aeronautics, Navy Department, to make an investigation to determine the quantitative nature of these effects to the end that precise estimates of the terminal velocity could be made. This investigation included flight dive tests

and wind-tunnel propeller tests. During the past year the information has been analyzed and a report prepared (Technical Report No. 477), which presents the results in a form readily usable for the quantitative determination of the influence of the propeller on the terminal velocity and engine speed. Some of the propeller tests were extended to include the negative thrust range of operation applicable to this condition of flight, and the results have been given in Technical Report No. 464.

Use of the smoke tunnel and the high-speed tunnel.—The smoke tunnel and the high-speed tunnel have been employed in connection with interference studies. Investigations in the smoke tunnel, however, have been made primarily to study its utility for such researches. For example, the air flow was examined about a model on which was simulated a windshield of the forward-sloping V-type as used on some transport airplanes. Observations of the smoke flow indicated a large wake. The windshield was then altered until a form was reached which gave a more satisfactory flow. The actual drags of the original and final windshields were then compared by tests at a large value of Reynolds Number in the variable-density tunnel. The results confirmed the deductions from the observations in the smokeflow tunnel in that they showed the original windshield to have an excessive drag and the final form less than half that of the original.

Another investigation of particular interest was started in the smoke tunnel and continued in the high-speed tunnel. In the smoke tunnel the flow about a streamline wire (lenticular section) model was observed to indicate a relatively high drag. The flow was found to be improved by the addition of small round wires on the surface of the streamline wire to form a longitudinal protuberance on either side of the section contour somewhat behind the leading edge. Various sizes and positions of the protuberance were investigated. Later the investigation was continued in the high-speed tunnel where full-scale wires could be tested at full speed, and the drag accurately measured. A streamline wire of nominal size, 0.5 inch with round wires of 0.003-inch diameter soldered along its surfaces to form the protuberance, at certain speeds showed a drag reduction due to the protuberances of more than 40 percent.

Effects of surface roughness.—The question sometimes arises as to the effect of surface roughness on the aerodynamic characteristics of a wing, and two investigations of a minor nature have been conducted on this subject during the year. Tests were made in the variable-density wind tunnel on a number of airfoils of the National Advisory Committee for Aeronautics 0012 section on which the character of the surface was changed from a rough to a very smooth finish. Measurable adverse effects were found to be

caused by small irregularities in airfoil surfaces which might ordinarily be overlooked. These results were published in Technical Note No. 457.

An investigation of the effect of rivet heads on the characteristics of a 6- by 36-foot Clark Y metal airfoil was carried out in the full-scale tunnel and the results published in Technical Note No. 461. The effect of conventional brazier-head rivets on the drag of the wing was found to be large, and an investigation of various types of flush rivets is next to be undertaken.

AIRFOILS.—Theory of wing sections.—A report on the aerodynamic potential theory of wing sections (Technical Report No. 452) has been prepared in which is presented a unified rigorous treatment of the general theory of monoplane wing sections of any shape. The numerous special cases that have been previously treated in the aerodynamic literature are reduced to special cases of the general theory, which permits a clearer perspective of the entire field of wing theory. A comparison of the predicted theoretical pressures with experimental work for the National Advisory Committee for Aeronautics M6 airfoil at 12 different angles of attack presents a striking illustration of the value of the theory. In a later report (Technical Report No. 465) application of the general theory is made to 20 conventional or selected airfoils. The theoretical distribution of pressure at lift coefficients of 0, 0.5, 1.0, and 1.5 is presented graphically. Analysis and discussion of the results show clearly that many of the aerodynamic properties and characteristics of airfoils are explainable and predictable on the basis of the theoretical pressure-distribution curves.

Investigation of airfoil shape.—The systematic investigation of airfoil characteristics as affected by variations of the airfoil shape has been continued in the variable-density tunnel and a report (Technical Report No. 460) has been prepared covering the tests under comparable conditions of 78 related airfoils.

The tests were made primarily to investigate airfoil characteristics as affected by variations of the section thickness and the mean-line form. One of the objects of investigating a wide variety of related airfoils, aside from supplying data to facilitate the choice of the most satisfactory airfoil for a given application, was to determine the trends with changes of shape that might be followed in order to design new shapes having better characteristics. The most promising possibility of improvement was found to be with those airfoils which have the position of the maximum camber well forward. A number of sections of this type have therefore been developed from the original family with the expectation of finding new sections that give a reasonably high maximum lift without an excessively large pitching-moment coefficient.

Among the 78 related airfoils considered in the published report are some having thickness forms differing from the basic one, notably those having leading

edges blunter and sharper than the basic leading edge. The consideration that the airfoil profile must enclose an efficient structure, however, dictates the investigation of other thickness forms. With single-spar construction, for example, an airfoil section having the maximum thickness well forward may be desirable. On the other hand, for wings like the Fowler variable-area wing a deep rear spar may be required. A thickness form having the maximum thickness farther back than $0.3c$ may then be desirable. Furthermore, various thickness forms have never been studied under conditions corresponding to full-scale airplane wings. Some thickness forms, such as one having the maximum thickness at $0.4c$, which appears from tests in the high-speed tunnel to be better than the basic one at very high speeds, may in flight be more efficient aerodynamically.

Scale effect.—The results of airfoil tests in the variable-density tunnel and in the full-scale tunnel as well as indications from flight tests show that a rather large variation of airfoil characteristics with the Reynolds Number is to be found within the range of values of the Reynolds Number encountered in flight. Data from tests of an airfoil at only one value of the Reynolds Number cannot therefore be considered adequate, but must be supplemented by some knowledge of the changes produced by varying the value of the Reynolds Number from that of the test.

The Reynolds Numbers common to modern flight lie in the range between 2,000,000 and 20,000,000. Airfoil results from wind-tunnel tests have been available only up to a Reynolds Number of about 3,000,000, obviously indicating that an extension of airfoil characteristics further into the flight range is highly important. The characteristics of the Clark Y airfoil were therefore measured in the full-scale tunnel over a range of Reynolds Number from 350,000 to 5,600,000 at maximum lift, and from about 350,000 to 9,000,000 at minimum drag. This wide range was obtained by testing four similar metal airfoils with spans of 12, 24, 36, and 48 feet at velocities from 30 to 118 miles per hour.

The maximum lift coefficient for the Clark Y airfoil shows a steady rise in value with increase in Reynolds Number while the minimum drag coefficient shows a decrease in value with increase in scale. A report is in preparation indicating the variation of the airfoil characteristics with Reynolds Number, and making available for design purposes these large-scale data.

Tapered airfoils.—Other work on airfoils includes routine tests or the tabulation and analysis of data requested by the military services, or by the Department of Commerce. Some of these investigations have dealt with tapered airfoils rather than airfoil sections. Several tapered airfoils were tested in the variable-density tunnel at the request of the Army Air Corps to provide data for inclusion in the handbook of instruc-

tions for airplane designers. In connection with the investigation of tapered airfoils a technical note (no. 483) has been prepared presenting in short form for convenient use by designers the theoretical pitching-moment characteristics of tapered wings having various plan forms and having sweepback and twist. The information is applicable to the design of wings for ordinary airplanes as well as tailless airplanes.

Compressibility effects.—A technical report has been published (no. 463) giving a description of the high-speed tunnel and an account of the tests of a series of six commonly used propeller sections, showing the effects of compressibility at air speeds up to 85 percent of the velocity of sound. The investigation of the effects of compressibility has been further extended during this year to include a study of the important variations of airfoil shape. Eleven related symmetrical airfoils have been tested over a wide speed range to determine the effects of variations in the leading-edge radius, the thickness, and the location of the maximum ordinate, as well as the effects of compressibility. The analysis of these results is now nearing completion and it is indicated that the best position for the maximum ordinate is 40 percent of the chord aft of the leading edge. The effects of variations in the leading edge radius on minimum profile drag for airfoils 9 percent thick are negligible for values of the radius less than $0.0089c$.

The results of this investigation were used to determine a thickness distribution for use in the development of cambered airfoils. Three cambered airfoils were tested; one of these, the National Advisory Committee for Aeronautics 216 airfoil, is superior at high speeds to both the Clark Y and R.A.F. 6 propeller airfoils having the same thickness. This airfoil is 9 percent thick; its maximum ordinate is at 40 percent of the chord aft of the leading edge, and its leading-edge radius is $0.0022c$ (approximately one quarter the usual value for the National Advisory Committee for Aeronautics family airfoils). The mean camber line corresponds to that of the National Advisory Committee for Aeronautics 24 series.

A detailed investigation of the drag of fundamental shapes—circular, elliptical, and prismatic cylinders—is now in progress. The tests are being conducted over a speed range extending up to approximately 65 percent of sound velocity. Drag tests of cylinders of various sizes show remarkably close agreement when the results for the lower speeds are plotted against Reynolds Number and the results for all the circular cylinders are in excellent agreement as to the speed (0.4 sound velocity) at which the compressibility effects become of first importance.

Boundary-layer control.—A number of investigations have been made in previous years, both by the Committee and elsewhere, showing rather startling effects of the use of blowers to suck air in through slots

in the surface of a wing or to blow it out. Most of these investigations have been made on relatively small models, and trustworthy results have been difficult of attainment because of the smallness of the models and because the amount of auxiliary apparatus required and the method used for attaching it to the model necessitated numerous corrections. An investigation is now in progress in the propeller-research tunnel in which a large model is used with the blower in the wing itself. In addition to the measurements of lift and drag, apparatus has been installed for measuring the thickness of the boundary layer and the pressure distribution over the wing. The power input to the motor is, of course, measured also. Although it is realized that the use of a blower for suction or pressure is not now attractive from a practical standpoint, it is believed the results will provide a definite contribution to our knowledge of the boundary-layer characteristics of the wing.

JET-BOUNDARY INVESTIGATION.—The unique possibility of obtaining results in the full-scale tunnel for direct comparison with flight results made it important to investigate all factors which might tend to cause a discrepancy between the wind-tunnel and flight results. That the limited boundary of a wind-tunnel jet causes a change in the aerodynamic characteristics of a body tested therein is well known, and at the time this tunnel was put in operation there was no theoretical correction factor available for this type of jet. An investigation was therefore undertaken to determine experimentally the jet-boundary correction factor. The results have verified in a very satisfactory manner the theoretical factor for this jet which became available during the progress of the work.

The procedure consisted in measuring the characteristics of geometrically similar airfoils graded in size from large to small and then in extrapolating plots of these measured characteristics to simulate the condition of a finite wing in space. A preliminary study of the test data indicated an apparent contradiction of the general theory of jet boundary. After further investigation this discrepancy was clarified when a distortion of the velocity field in front of the airfoil, caused principally by the wake from the body carried around through the return passage, was shown to be responsible. A close agreement was shown to exist between the characteristics of several airplanes as measured in flight and in the tunnel when the jet-boundary correction and the correction for wake effect or blocking were applied. The results of this investigation are being prepared for publication as a technical report. The theory for an airfoil of finite span in an open rectangular wind tunnel has been covered in Technical Report No. 461.

STRUCTURAL LOADING.—The studies of the flight loads on airplane structures which have been made in the past 3 years have resulted in a marked advance in

knowledge of this subject. These investigations have been continued, either to add to the existing statistical data on some phases of the subject or to pursue further the underlying principles of phenomena not yet clearly understood.

Load factors.—Four airplanes have been used in an investigation of the relation between control forces and acceleration in pulling out of fast dives. A theoretical study of this relation has also been made to determine the possibility of utilizing a stick-force formula in load-factor estimates. The results of these investigations indicate (1) that the stick force has no appreciable influence on the probable applied load factor in those cases where the forces are within the pilot's strength, (2) that the pilot's opinion of the control "heaviness" and maneuverability of the airplane may be greatly influenced by a number of qualities of the airplane not directly related to the stick force, and (3) that stick-force formulas are untrustworthy for estimating probable applied load factors.

A statistical study of applied load factors and corresponding air speeds has been in progress on a number of airplanes under actual operating conditions, for which a special type of instrument has been developed. The instrument records acceleration and air speed, and has been named the "V-G recorder." A number of these instruments have been in constant use throughout the past year on various military and naval aircraft, commercial transport airplanes, and a few privately owned airplanes. The data being collected cover the loadings experienced in normal operation, ranging from the conditions corresponding to violent maneuvers to those resulting from atmospheric gusts. Although the data so far accumulated are insufficient to justify final conclusions, a very considerable advance has been made in knowledge of the loading conditions to which airplanes are subjected. Among several interesting points which have developed in regard to the loads resulting from gusty air, perhaps the most impressive was a load factor of 5.2 applied by a gust on an airplane cruising at 190 miles per hour. This value, while unusual, illustrates the possibility of large gust loads in rare instances. Assuming a sharp-edge gust, the gust velocity for this case was computed to be 40 feet per second.

Load distribution.—Several questions relating to the problem of load distribution have been given attention during the year. Since the preparation of Technical Report No. 445, which presents working charts for the determination of the lift distribution between biplane wings, further study of this subject has resulted in Technical Report No. 458. The influence of the fuselage has been evaluated from pressure-distribution tests made on two conventional biplanes in flight. This latter information may easily be used in conjunction with the charts for the pure cellule.

Studies have also been made of the influence of biplane interference on the moment coefficients of the individual wings and on the span-load distribution. In regard to the moment coefficients, it has been found that the biplane effect is completely overshadowed by other influences such as surface roughness, imperfect profiles, and experimental error. The span-load distribution does not appear to be appreciably influenced by biplane interference.

Experimental pressure-distribution investigations have been continued on an observation airplane and a diving bomber. The results have not yet, however, been completely analyzed.

FIELD OF VIEW.—The field of view from an airplane cockpit or cabin is generally classified arbitrarily by the occupant as "good" or "poor." An investigation has been started to establish a suitable criterion by which to rate airplanes in this respect. An apparatus has been developed for measuring the extent of the view from any seat in an aircraft and several service-type airplanes have already been mapped. A report now in preparation will give data from a sufficient number of representative airplanes to make possible the development of a criterion for determining relative fields of view.

RAIN-VISION WINDSHIELD.—An investigation has been completed in the 7- by 10-foot tunnel on a full-scale model of a cabin fuselage for the purpose of exploring the possibilities of obtaining satisfactory vision through open windows under conditions of rain and fog. The rain was simulated by a controlled spray located upstream from the fuselage. Tests were made with openings of various forms directly forward and to the side, which resulted in a side-window arrangement which is inclined inward to give straight forward vision and which can be completely opened without the entrance of even large drops of rain. A report is in preparation describing the tests and giving the proportions of the successful design.

SOURCES OF NOISE IN AIRCRAFT.—The fundamental research on the source and character of propeller noise has been continued. During the past year the work has been confined to a study of model propellers. The noise from such propellers has been analyzed and is found to consist in general of two groups of sounds. One group consists of a musical note whose frequency is connected with the speed of rotation, with its train of harmonics. The other group is composed of much higher frequencies, nonmusically related, which are undoubtedly generated by the shedding of vortices from the trailing edge of the blades. The effect of changes in tip speed and angle of attack upon these two types of sound has been investigated. The manner in which the ear responds to noises of this sort, together with several possible methods of estimating loudness, has been studied.

VIBRATION RESEARCH.—Tests with an airplane in floating suspension excited by a sinusoidal force were continued, the response of the fuselage and wings to the various frequencies being studied. In the particular airplane it was found that a large response occurred near the normal operating speed of the engine. In order to facilitate the observation of vibrations on all points of an airplane structure, a new instrument has been developed which permits instantaneous readings, obviating laborious preparations and precautions. A number of flight tests have been performed for the purpose of identifying vibrations of pure aerodynamic origin. Preliminary tests on a biplane disclosed considerable disturbances of irregular type in the range of 400 to 650 per minute. These disturbances could only be observed at diving speeds or above the stalling angle; no vibrations that could be attributed to aerodynamic forces were recorded in normal flight conditions.

ROTATING-WING AIRCRAFT.—Because of the possibility of obtaining sustentation with little or no forward speed and the consequent possibility of safe flight at low speeds, continued attention has been given during the past year to three promising types of rotating-wing aircraft.

The first is the familiar autogiro in which the rotor axis is vertical, the rotation of the rotor occurs automatically as a result of air forces acting on the rotor blade, and lift on opposing blades is equalized by a flapping motion of the blades. Investigations have been made of the various elements controlling the performance of this type of machine, and one such investigation, which consisted of determining the rotor blade motions and the division of load between the rotor and the fixed wing, has been completed and described in Technical Report No. 475. The results of this investigation served two purposes: (1) The measured loads on the fixed wing have aided in the formulation of design rules for the fixed wings of this type of aircraft, and (2) the load on the rotor correlated with the measured blade motion has provided data needed for a theoretical study of rotor characteristics, the results of which are now being prepared for publication. A brief investigation of the vibrations occurring in a 3-blade autogiro has also been completed, and flight tests are in progress for the purpose of determining the effect of the incidence of the fixed wings on the rotor characteristics and on performance in general.

The second type of rotating wing being investigated, the gyroplane, is similar in general principle to the autogiro, but is fundamentally different in regard to its rotor operation, in that opposite blades of the rotor are rigidly connected and lift on these blades is equalized by oscillation about an axis parallel to the blade span. A theoretical analysis of this type of machine has been completed and is now in preparation for publication.

The third type being investigated, the cyclogiro, derives its lift and thrust from a power-driven rotor consisting of several blades rotating about an axis parallel to the lateral axis of the aircraft. A theoretical analysis of the cyclogiro has been completed and a simplified aerodynamic theory of the machine has been prepared and published (Technical Note No. 467). The analysis indicates that the aerodynamic principles are sound, that hovering flight, vertical climb, and a reasonable forward speed may be expected with a reasonable expenditure of power, and that autorotation in a gliding descent is available in the event of engine failure.

The studies on all three types of rotating-wing aircraft are being continued mainly in the form of wind-tunnel investigations principally for the purpose of improving the rotor characteristics of the autogiro and gyroplane and confirming the soundness of the principles involved in the cyclogiro.

AIRSHIPS.—Airship work has been confined to some miscellaneous activities such as cooperation with the Army in speed trials with the *TC-11* and *TC-13* airships, cooperation with the Navy in speed and deceleration tests with the U.S. airship *Macon*, and the amplification of previous reports to the Navy giving data obtained in the trial flights with the U.S. airship *Akron*.

SEAPLANES.—A description of the National Advisory Committee for Aeronautics tank, or seaplane channel, has been prepared and issued as Technical Report No. 470. Reference is made in the report to the important items of equipment and the satisfactory behavior of the rubber tires, the towing carriage, and the towing gear. The research program has followed quite closely the program outlined in last year's report. Although emphasis has been placed on investigations which have immediate application, the addition of wave suppressers has greatly expedited the carrying out of the research program.

Effects of variation in dimensions and form of hull on take-off of flying boats.—The effects of variation in dimensions are being studied by tests of a series of five models derived from a parent form by systematic variations in dimensions. The five models were investigated according to the general method in which the resistance, rise, and trimming moment of the model are determined at various fixed trims over a range of speeds. The results show that the performance of the parent model could be improved by changing its form to give a longer and flatter forebody. A new forebody was made and tested with the original afterbody, and the improved model equals in performance the best flying-boat hull. Tests of two models, nos. 11 and 11A, are described in Technical Notes Nos. 464 and 470.

Observation of the behavior of the models of hulls tested suggested the possibility of improving perform-

ance by a radical change in the form of the main step. A model was prepared in which the step was much deeper than usual and was pointed in plan form instead of square across the hull. This model, no. 22, showed a general performance much superior to the previous model. These results will be issued as a technical note and it is hoped that a full-scale test of this form may be made to determine its behavior under operating conditions.

A model of a flying-boat hull having one form of stub wings or sponsons to provide lateral stability was investigated. Other forms of sponsons have been made for tests with the same main hull, and in view of the later development of this type of lateral stabilization, it is planned to extend the application to hulls of other shapes.

Floats for seaplanes.—In order to obtain information regarding the performance of a good high-speed seaplane float, tests were made of a model of a float used on the Macchi racer of 1926. As a result of the tests a float designed to be an improvement of this float and to be used as a parent of future series was tested. This model showed a marked improvement over the Macchi float. The results of the two tests are compared in Technical Note No. 473.

Fundamental information regarding planing surfaces.—For a large part of the take-off run of the seaplane, that part of the weight of the craft not supported by the wings is supported by the hydrodynamic reaction of the water on the bottom of the float or boat. By testing surfaces that skim along the top of the water simulating only the bottom of a float, much valuable fundamental information can be obtained. A series of tests of planing surfaces consisting of flat surfaces at 0° , 10° , 20° , and 30° dihedral has been completed, and the results are being prepared for issue as a technical note. A series of somewhat similar models consisting of two surfaces with transverse curvature set at various dihedrals is being constructed for use in further tests. It is also planned to test surfaces with fore and aft curvature at a later date.

The results of the tests of these models may make possible the separation of the pure planing phenomena from the other factors encountered in tests of complete models and thus give valuable clues as to the proper form of bottoms.

Frictional resistance of boat surfaces.—Frictional resistance of those surfaces of a boat hull which are exposed to the passing water has not been determined for speeds from 30 to 60 miles per hour. The surfaces for a series of tests of frictional resistance, with their supporting gear, are completed, and the surfaces for another series nearly ready for investigation.

Specific tests for Government agencies.—A number of investigations specifically requested by the Bureau of Aeronautics have been conducted. An investigation

of methods for the control of spray was made on a model of a Navy flying boat. It was found that the addition of spray strips gave some improvement, but in this particular case not as much as was desired.

At the request of the Army Air Corps, extensive tests were made of models of the hull of an amphibian flying boat to obtain information as to the water performance of the craft with various modifications.

BUREAU OF STANDARDS

WIND-TUNNEL INVESTIGATIONS.—The aerodynamic activities of the Bureau of Standards have been conducted in cooperation with the National Advisory Committee for Aeronautics.

Apparatus for measuring turbulence.—Because of the considerable weight and bulk of the present equipment for making turbulence measurements the possibilities of developing a light and easily portable type of instrument are being investigated. The problem is being attacked by two principal methods: first, by simplification of the present hot-wire type of apparatus by eliminating the batteries, and, second, by the direct measurement of forces on bodies such as spheres and cylinders.

Computation of boundary-layer flow.—A comparison has been made of the boundary-layer flow computed by the approximate method developed by Pohlhausen with the more exact solutions which have been published for several special cases. Approximate methods of the type suggested by Pohlhausen are useful in giving a picture of the flow in many cases, but their range of application is limited. A modification of Pohlhausen's method has been developed which extends the range of application and a comparison of the flow computed by this method with that of more exact solutions shows that the range of application has been increased at the expense of some decrease in the accuracy of the approximation. A paper describing the methods used in the computations has been prepared.

Cup anemometers.—An investigation of the effects of turbulence on the speed indications given by the ordinary hemispherical cup anemometer has been completed. When disturbances in the air stream were produced by a turbulence screen consisting of a wire net on which were loosely fastened small metal tags, the normal rate of the anemometer was found to be considerably increased. A systematic investigation has been made of the effects of roughening the outer surfaces of the cups.

AERONAUTIC INSTRUMENT INVESTIGATIONS.—The work on aeronautic instruments was conducted in cooperation with the National Advisory Committee for Aeronautics and the Bureau of Aeronautics of the Navy Department and included the investigations and the instrument development outlined below.

Temperature coefficient of elastic moduli.—The results of this investigation were published in the Bureau of Standards Journal of Research (R.P. 531) in March 1933.

Lubricants for instrument mechanisms.—The essential requirements of a lubricant for aircraft instruments include long life and operation at low temperatures. Mineral oils spread and therefore do not have a long life in the bearing. On the other hand, animal or vegetable oils do not spread but gum more or less slowly. An investigation was initiated to determine the characteristics of the oils available, including those with antioxidants, with a view to the preparation of specifications based on the performance of the best lubricant. Tests are being made on samples of about 40 oils. In addition to the customary tests given lubricants, each sample is being given two tests, the results of which it is hoped to correlate: (a) An accelerated oxidation test, and (b) a life test. The apparatus for the life test consists of a bank of 50 watch balance wheels, 3 or 4 of which are lubricated with the same oil, which are kept in oscillation by a suitable electromechanical device. The condition of the lubricant in each balance wheel is checked from time to time by measuring and comparing the time for the amplitude of the freely oscillating balance wheel to decrease from a given initial to final value.

Reports on aircraft instruments.—A report on aircraft power plant instruments, including descriptions of, and performance data on, tachometers, thermometers, pressure gauges, fuel-quantity gauges, and fuel-flow indicators was completed and will be published as Technical Report No. 466. Considerable progress has been made on two reports similar in scope on blind-flying instruments and on altitude instruments.

New instruments.—A number of new instruments were developed and constructed. These developments include the following:

A superheat meter of the resistance type has been completed and installed in the metal-clad airship ZMC-2. With this type a marked reduction in weight is obtained and a more rugged indicator can be used as compared with the thermocouple type.

An alarm which operates when the indication of carbon monoxide exceeds 0.02 percent has been developed and added to the M.S.A. carbon monoxide indicator.

An instrument was developed to indicate the level of the liquid air in the helium purifier apparatus. The level is indicated by the differential effect in the alternating currents from two external coils produced by a float in the liquid carrying a soft iron plunger.

An air-speed meter of the commutator-condenser type, the propeller and commutator unit of which are designed for mounting on an airplane strut, was completed.

A fundamental modification has been made in the venturi fuel flow-meter which in the usual form has been found to be unsatisfactory on airplanes. Air instead of gasoline is used as the medium by which the differential pressure developed by the venturi tube is transmitted to the indicator in the cockpit. The differential pressure developed by the venturi tube is transmitted to two flexible elements the differential action of which controls a valve regulating the suction within an air chamber. This suction is transmitted to the indicator. Several designs have been prepared and one instrument constructed which is ready for flight tests.

REPORT OF COMMITTEE ON POWER PLANTS FOR AIRCRAFT

LANGLEY MEMORIAL AERONAUTICAL LABORATORY

COMPRESSION-IGNITION ENGINES.—The advantages claimed for the compression-ignition engine of reduced fuel consumption and the maintenance of power at altitude have been substantiated by recent flight tests of several compression-ignition aircraft engines. The power output per cubic inch of displacement of compression-ignition engines, however, is still inferior to that of conventional aircraft engines. The results obtained from an investigation of the performance of compression-ignition engines with boosting have shown that the increase in engine power with boosting is considerably less than that obtained with the carburetor engine. The research of the Committee has indicated that the method which holds the greatest promise for increasing the performance of the compression-ignition engine is to operate the engine on the two-stroke cycle. The investigation of the factors controlling the performance of a high-speed two-stroke-cycle single-cylinder compression-ignition engine has resulted in the attainment of a power output per unit of displacement which is 27 percent greater than that obtained with present commercial aircraft engines.

Fuel spray characteristics.—The attainment of efficient combustion in compression-ignition engines is dependent upon the distribution of the fuel sprays within the combustion chamber. Previous investigations of the Committee have shown that with fuel injected from round-hole orifices the greater part of the fuel is concentrated in the spray core. The effect on fuel-spray distribution of breaking up the core of fuel sprays has been investigated by injecting a small quantity of air at high pressure with the fuel oil. Spark photographs of the fuel sprays and measurements of the diameters of the oil drops in the spray showed that the use of the compressed air gave improved distribution and atomization of the fuel spray. An injection system incorporating this principle of fuel distribution was constructed and tested on a single-cylinder engine having a vertical-disk form of combustion chamber. The engine performance with the combined hydraulic and air injection system was not

improved over that obtained with hydraulic injection except at high air-fuel ratios. The results obtained from the engine-performance tests indicated that with conventional hydraulic-injection pressures the atomization of the fuel was sufficient to result in good combustion. Additional methods of improving fuel distribution are to be investigated.

The penetration and distribution of fuel sprays following the cut-off of injection have been investigated with the National Advisory Committee for Aeronautics spray-photography apparatus. The object of the investigation was to obtain new knowledge concerning the distribution of fuel sprays for time intervals as great as 0.05 second after the cut-off of injection. The effects of air density, injection pressure, and air velocity counter to the fuel spray, on the spray distribution have been investigated. The results show that air-flow velocities from 15 to 25 feet per second directed counter to the fuel spray are very effective in distributing the fuel spray after injection cut-off, provided the fuel is well broken up during the injection process. The effect of these low air velocities on the spray core during injection is negligible.

Pintle-type fuel-injection nozzles have been used as a possible means of obtaining increased spray distribution. During the year spark photographs have been taken of fuel sprays from pintle nozzles. An analysis of the photographs shows that the angle of the spray from the pintle nozzle is approximately that of a spray from a round orifice and that the angle of the pintle has only a small effect on the spray angle. The penetration of the spray tip is comparable to that obtained with round-hole orifices. The results of this investigation are presented in Technical Note No. 465.

Injection-system characteristics.—A fuel-injection system has been developed to give a high rate of fuel discharge and to give discharge characteristics that do not vary with engine speed. The energy for injecting the fuel is supplied from a high-pressure reservoir at the pump in which the pressure is built up previous to the injection of fuel into the engine. The injection of the fuel is caused by the sudden opening of a pressure relief valve, which permits a hydraulic pressure wave to be transmitted through the injection tube to the injection valve. Injection of the fuel continues until the intensity of the pressure wave drops below the injection-valve closing pressure. With this injection system the period required for the injection of full-load fuel quantity for an engine having a bore of 5 inches and a stroke of 7 inches and operating at a speed of 1,500 revolutions per minute is only 10 crank degrees. This injection system is being used to determine the effect of the rate of fuel injection on the performance of compression-ignition engines.

An investigation has been made to determine the effect of placing a reservoir between the fuel-injection pump and the injection tube connecting the pump to

the injection valve. The results show that the rates of fuel injection can be changed considerably by the use of such a reservoir and that the chattering of injection valve stems when a large discharge orifice is used can be prevented by using a reservoir of the correct volume.

Combustion in compression-ignition engines.—Although progress has been made toward decreasing the weight-power ratio of compression-ignition engines, the best ratio obtained is still excessive when compared with that of present-day spark-ignition aircraft engines. The decrease of this ratio is dependent upon an increase in the combustion efficiency of compression-ignition aircraft engines. The National Advisory Committee for Aeronautics spray-combustion apparatus has been used to determine the effect of the time for mixture formation on the course of combustion. The compression ratio used in the investigation was 12.7. In the preliminary tests the ignition of the fuel at a definite time in the cycle was insured by using an electric spark. The factors investigated were injection-advance angle, engine-coolant temperature, engine speed, and spark timing and location. Indicator cards were obtained with an optical engine indicator; continuous photographic records were taken of the movement of the combustion zone. These data showed the course of the combustion to be a function of the temperature and pressure to which the fuel had been subjected previous to the ignition of the air-fuel mixture. At low air temperatures it was found that the rates of combustion varied with the volatility of the fuel, but at high air temperatures this relationship did not exist and the rates depended to a greater extent on the chemical nature of the fuel. The results of this investigation are being prepared for publication as a technical report.

The rapid rate of pressure rise and high maximum cylinder pressures obtained in compression-ignition engines are detrimental to smooth engine operation. The rate of pressure rise and maximum cylinder pressure are influenced by the time required for the fuel after injection to absorb heat from the compressed air in the cylinder. Preliminary investigations conducted with a cam-operated fuel-injection pump and a diaphragm-loaded fuel-injection valve showed that preheating the fuel to 330° F. before injection reduced the ignition lag and the maximum cylinder pressure. For higher fuel temperatures the injection of the fuel became erratic. A conventional injection system has been modified so that it functions independently of the temperature of the fuel. Bench tests conducted with the injection system showed satisfactory operating characteristics for fuel temperatures of 900° F. The engine performance obtained with this injection system is being determined with the system installed in a compression-ignition engine having a high-velocity air flow for distributing the fuel spray.

Information relating to the composition of the fuel used, the air-fuel ratio, carbon monoxide content, and fuel wasted because of incomplete combustion may be readily obtained from an analysis of the exhaust gas from internal-combustion engines. Research has been conducted from five different engines to determine the relationship between hydrogen, methane, and carbon monoxide in the exhaust of four-stroke cycle engines using a large number of hydrocarbon fuels. It was determined that a linear relation existed between the carbon monoxide and the hydrogen found in the exhaust gas from engines using hydrocarbon fuels. A small amount of methane was found to be always present in the exhaust gas, but the amount was independent of the air-fuel ratio and of the hydrogen-carbon ratio of the fuel. These determined relationships and the use of the Ostwald combustion diagram make available all the information of a complete exhaust-gas analysis when any two factors (carbon monoxide content, carbon dioxide content, air-fuel ratio) are known. The investigation has been reported in Technical Report No. 476.

Hydrogen as an auxiliary fuel for compression-ignition engines.—The designers of airships are of the opinion that the successful commercial airship must be powered with compression-ignition engines. The use of compression-ignition engines reduces the fire hazard and makes it possible to operate over a wide range of engine speeds with low specific fuel consumptions. Additional lift and a reduction in weight of the water-recovery apparatus used with helium would be obtained in commercial airships by the use of hydrogen stored within the helium cells. Since the hydrogen required to lift a given weight of fuel contains a quantity of heat energy equal to 20 percent of the heat energy of the fuel, it would be desirable to utilize this energy in driving the airship by burning the hydrogen in the engines.

The Committee has conducted a research to determine the quantity of hydrogen that can be mixed with the inlet air and burned in a compression-ignition engine. A single-cylinder compression-ignition engine operating at a speed of 1,500 revolutions per minute was used in this investigation. The engine was operated at compression ratios of 13.4 and 15.6. The results indicated that a sufficient quantity of hydrogen could be burned with all useful fuel-oil quantities to compensate for the increase in lift due to the consumption of the fuel oil. Quantities of hydrogen from 5 to 14 percent of the inducted air by volume could be burned, depending upon the engine conditions. More power could be obtained from the engine when the composite fuel was used. At light loads the thermal efficiency was less than that obtained with fuel oil alone, but at full load the efficiency was greater with the composite fuel. The engine could be stopped by shutting off the supply of liquid fuel, since it was found

impossible to ignite the hydrogen-air mixture by compression. A report of this investigation is being prepared for publication.

Combustion-chamber investigation—Integral type with no effective air flow.—The results of the investigation made to determine the effects of scavenging the clearance volume and boosting on the performance of a compression-ignition engine with an integral combustion chamber having no effective air flow have been published as Technical Report No. 469. This research, conducted at a compression ratio of 12.6, has been extended to include the determination of the engine performance obtained at compression ratios of 10.5 and 15.0. The engine-operating characteristics were found to be quite different at these compression ratios. At a compression ratio of 10.5 starting is difficult and the ignition lag under standard test conditions is more than one third longer than that obtained at a compression ratio of 15.0. The rate of pressure rise at the lower compression ratio as determined from indicator cards is nearly double the corresponding values obtained at a compression ratio of 15.0. Starting was easier at the higher compression ratio and operation smoother, with more uniform explosion pressures.

Combustion-chamber investigation—Prechamber type with high-velocity air flow.—Progressive changes made to the shape of the prechamber and of the connecting passage have resulted in an 18 percent increase in the brake horsepower developed by a single-cylinder compression-ignition engine when operating with the theoretical full-load fuel quantity and with an engine speed of 1,500 revolutions per minute. The results of previous investigations indicated that improvement in performance was the result of intensification of the air flow, and the first change in shape was the use of a passage tangential to the spherical chamber instead of the radial passage that had been used for the purpose of symmetry in previous investigations. The tangential passage caused a forced rotation of the sphere of air in the chamber which persisted during injection and combustion of the fuel and improved the engine performance. The tangential passage was tested as a straight passage and also as a tapered flared passage. Best results were obtained with a passage slightly flared at the cylinder and tapered toward the prechamber.

As a further means of intensifying the air flow, the auxiliary chamber shape was changed from a sphere to a disk with rounded edges to eliminate the comparatively low-velocity air at the poles of the rotating sphere. This change in shape was effective in increasing the engine power. Changes in the direction of the connecting passage in an attempt to produce an air swirl in the cylinder seemed to have no beneficial effect. The use of three passages diverging from the cylinder, however, resulted in smoother engine operation, although the performance was slightly inferior to that obtained with the single passage. An increase

in the fuel-spray penetration obtained by increasing the length-diameter ratio of the injection-valve orifice from 2.5 to 6.0 resulted in a slight increase in power output.

Two-stroke cycle investigation.—The use of the compression-ignition engine as a power plant for airplanes is dependent upon obtaining a power output per cubic inch of displacement comparable to that obtained with the conventional spark-ignition aircraft engine. A method of increasing the power output of compression-ignition engines is to operate engines of this type on the two-stroke cycle. The factors affecting the performance of a two-stroke-cycle compression-ignition engine are being investigated with a single-cylinder water-cooled engine having a 4.625-inch bore and a 7-inch stroke, and operating at a maximum speed of 1,800 revolutions per minute. The factors investigated include the distribution of the fuel spray, the scavenging air pressure, the engine speed, and the injection timing. The variation in fuel-spray distribution was obtained by varying the size, number, and arrangement of the fuel-valve orifices and the number and position of the fuel-injection valves.

Based on the results of these tests a single injection valve having a three-orifice nozzle was selected for continuing the tests. With increase in the scavenging air pressure the brake mean effective pressure increased linearly to 152 pounds per square inch at a pressure of 3 pounds per square inch and a speed of 1,250 revolutions per minute. Performance tests at variable speed emphasized the importance of obtaining proper scavenging and charging of the engine cylinder. A description of the two-stroke-cycle test engine and the results of the preliminary engine tests are being prepared for publication.

FIRE HAZARD IN AIRCRAFT—Hydrogenated safety fuels.—The investigation of the engine performance obtained with a hydrogenated safety fuel injected into the engine cylinder has been continued, a fuel having a flash point of 125° F. and an octane number of 95 being used. The performance of a single-cylinder liquid-cooled engine has been determined with the hydrogenated safety fuel for compression ratios of 5.85 and 7.0, valve timings giving 30° and 130° overlap, inlet pressures from atmospheric to 5 pounds per square inch boost pressure, and engine speeds from 1,250 to 2,200 revolutions per minute. The best results were obtained by locating the single injection valve between the two exhaust valves so as to direct the fuel spray horizontally across the combustion chamber against the incoming air. The duration of fuel injection was from 60 to 70 crankshaft degrees and the start of injection from 70° to 90° after top center on the suction stroke. At a compression ratio of 7.0, a valve overlap of 130 crank degrees, a speed of 1,750 revolutions per minute, and a boost pressure of 1 pound per square inch, the brake mean effective

pressure obtained was 175 pounds per square inch and the corresponding fuel consumption 0.50 pound per brake horsepower per hour. In general, for similar conditions the power obtained with the safety fuel was equal to that obtained with gasoline, although the fuel consumption with the safety fuel was 5 percent greater. The investigation has been described in Technical Report No. 471.

INCREASE IN ENGINE POWER—*Increase in engine speed.*—The two principal methods of increasing the power output of conventional aircraft engines are to increase the brake mean effective pressure and to increase the engine rotative speed. The performance obtained with the Committee's single-cylinder test engines has been limited to maximum speeds of 2,200 revolutions per minute. In order to extend the investigation on boosting to higher boost pressures and higher engine speeds, a single-cylinder liquid-cooled test engine has been designed and constructed to operate at a maximum speed of 3,000 revolutions per minute and a maximum explosion pressure of 1,500 pounds per square inch. A system of gear-driven counterweights is used to balance the engine. The test engine has been assembled and motoring tests of the engine are in progress.

COWLING AND COOLING OF AIRCRAFT ENGINES—*Cooling properties of finned surfaces.*—The demand for engines of higher power and the general use of the National Advisory Committee for Aeronautics cowling or of ring cowlings on airplanes has necessitated a study of all possible methods for improving the cooling of air-cooled engines. An investigation to determine the effect of fin pitch, fin width, and average fin thickness on the temperature distribution in and the heat dissipation from steel cylinders having tapered fins has been completed. The range of fin pitches investigated was from 0.1 to 0.6 inch, the range of fin widths from 0.37 to 1.47 inches, and the range of average fin thickness from 0.04 to 0.27 inch. The cylinder diameter was maintained constant at 4.5 inches. The range of air speeds investigated was from 30 to 150 miles per hour. The experimental data obtained have been used as the basis for the development of a method for determining fin dimensions permitting the use of a minimum of material for a range of conditions of heat transfer, air flow, and fin materials. The results of the investigation will be made available in technical reports now in preparation.

Research has been conducted with several finned specimens enclosed by a shroud. A blower was used for supplying the cooling air and a Durley orifice box for measuring the air quantity. In these tests the effects on the heat transfer from the finned cylinder to the cooling air of a range of air densities from 0.0476 to 0.072 pound per cubic foot, cooling air temperatures from 113° F. to 192° F., and air speeds from 10 to 150 miles per hour have been investigated. For the

cylinders tested the cooling was found to be proportional to the mass flow of the air raised to the 0.45 power.

The use of deflectors for directing the cooling air to the rear of the cylinder, thus increasing the amount of finned surface in contact with the cooling air, has been investigated with an electrically heated finned specimen mounted in a wind tunnel. In these tests it was found that the cylinder temperatures in the rear could be reduced 25 percent by the use of a sheet-metal deflector in contact with the fin tips. The best results were obtained with this deflector when the front edge of the deflector was from 70° to 90° from the front of the cylinder and the rear opening was large enough not to restrict the air flow. A duct about 3 inches long connected to the rear of the deflector appreciably improved the cooling. Welding the deflector to the fins increased the finned surface that dissipated heat to the air stream and appreciably reduced the cylinder temperatures. This investigation is to be extended to include tests of the more promising deflector and cylinder combinations at a range of air speeds from 50 to 200 miles per hour.

The design of the National Advisory Committee for Aeronautics cowling could be placed on a more rational basis if the minimum quantity of air required to cool satisfactorily a given design of engine cylinder and the pressure differences available for forcing the air through the cowling in flight were known. The minimum quantity of air required to cool satisfactorily a conventional design of engine cylinder is being determined with a single-cylinder test engine. The cylinder is shrouded and the cooling air supplied by a blower. The quantity of cooling air and the pressure drop through the cowling are being measured for a wide range of engine-operating conditions. The effect of varying the shape of the entrance and exit openings in the cowling on the quantity of air and pressure drop through the cowling are being investigated by the aerodynamics division by means of models of the cowling mounted in a wind tunnel.

Two-row radial engine.—At the request of the Bureau of Aeronautics, Navy Department, the Committee has determined the effect of air speed, engine power, and engine speed on the temperature distribution obtained with a two-row radial engine installed in a service airplane. The airplane was tested in flight and in the full-scale wind tunnel. The temperature distribution over the engine was investigated by means of 47 small-diameter wire thermocouples and two recording pyrometers. Thirty of these thermocouples were used to determine the temperature distribution over two representative cylinders, one in the front row and one in the rear. The effect on the cooling of the attitude of the airplane and of the number of propeller blades was also investigated.

INSTRUMENTS—Hub dynamometer.—The National Advisory Committee for Aeronautics hub dynamometer has been designed to measure and photographically record the torque developed by an aircraft engine in flight. During the past year work has been directed toward improving the torque-cell diaphragms. The original diaphragms machined from bar stock have been replaced by diaphragms machined from die forgings. Flight tests made with the dynamometer for a range of altitudes from sea level to 15,000 feet gave very encouraging results. The engine power as determined in flight was in good agreement with the calculated engine power obtained by correcting the sea-level brake horsepower for the pressures and temperatures at altitude. The temperature of the liquid in the torque cells was found to be the same as the free-air temperature and this fact will simplify the correction for temperature at high altitudes.

Engine indicators.—The increasing demand for pressure records from spark-ignition and compression-ignition engines requires that the precision and reliability of the pressure-recording apparatus be increased. Modifications of the Farnboro engine indicator used by the laboratory have been continued and the pressure element will now operate continuously under desirable engine-operating conditions. The length of service of the disk has been increased by eliminating the arcing at the disk and seats. The low-pressure portion of the engine cycle is being studied with the aid of a stroboscopic valve, designed primarily for obtaining gas samples from an engine cylinder.

A new optical indicator which records photographically the variation in pressure with time has been developed for use with the National Advisory Committee for Aeronautics spray combustion apparatus. The large windows in the combustion apparatus permit the use of a diaphragm having a diameter of 2 inches. The measured frequency of the diaphragm, mirror, and mirror staff is approximately 9,000 vibrations per second.

BUREAU OF STANDARDS

Altitude tests of aircraft engines.—Altitude tests of a Curtiss D-12 engine, in which the jacket water outlet temperature was varied over a range of nearly 70° C., showed that friction decreases and fuel economy improves at all altitudes as the temperature of the jacket water is increased. At sea level and low altitudes the power output decreases with increasing jacket-water temperature, but at high altitudes the brake horsepower increases on account of the predominant effect of the decrease in friction. A report of these tests will be published as a technical note.

Pistons giving compression ratios of about 6, 7, and 8 were obtained from the Army Air Corps for use in studying the effect of compression ratio upon the varia-

tion of horsepower with exhaust pressure, and the runs at one compression ratio have been completed.

Phenomena of combustion.—A detailed study was made of the effect of water vapor on the speed of flame in space in equivalent mixtures of carbon monoxide and oxygen at low pressures. Among numerous results of this investigation it was found in particular that, for low-pressure explosions of these gases, a moderate increase in the amount of water vapor was sufficient to double the flame speed, and that the greater the pressure of the active constituents the greater was the accelerating action. These facts indicate that the control of the water-vapor content in mixtures of carbon monoxide and oxygen is very important in any investigation involving measurement of flame speed. Provisions were made for adequate control of this factor in new apparatus which has been built for continuing the study of gaseous explosive reactions.

Combustion in an engine cylinder.—Measurements have been made of the variations during combustion in the intensity and spectral distribution of the radiant energy (to 11 μ) emitted by the flame at two widely separated points in the engine combustion chamber and under a variety of operating conditions. The series of filters used in obtaining spectral distributions for the engine flames was used also in making supplementary observations of the radiation from a black-body furnace at different temperatures and from burner flames of diverse fuels.

Preliminary analysis of these data indicates that the great bulk of the energy radiated by the engine flame is in the infrared and exhibits strongly under all conditions the characteristic emissions of water vapor and carbon dioxide, while radiant energy from incandescent carbon is relatively weak and insufficient to serve as a basis for estimating flame temperature. Although total radiation varies greatly during an engine cycle and considerably for different operating conditions, spectral distribution shows little change over a wide range of conditions. In a normal explosion, radiation begins to increase upon arrival of visible flame under a window and continues to rise for 20° or more of crank movement thereafter, which indicates that reactions producing highly active molecules of water vapor and carbon dioxide continue to a considerably greater depth behind the flame front and for a longer period in a given unit of charge than is generally supposed. In a knocking explosion, these reactions apparently are completed much more rapidly after inflammation in that part of the combustion chamber which is remote from the spark plug.

Pressures and temperatures in aircraft engines.—A pressure element of the balanced-diaphragm type has been constructed for use on the C.F.R. research engine. The design incorporates certain experimental features which may prove useful in attaining the high degree of

simplicity and compactness necessary to the construction of a reliable combination spark plug and pressure element for aircraft-engine use. Maximum diaphragm diameter and provision for adjusting the zero reading while the indicator is on the engine also were incorporated in the present element to give high accuracy in studying low-pressure phenomena, while the passages between the diaphragm and the engine combustion chamber were made very short to prevent distortion of the peaks of the indicator diagrams.

Ignition research.—The ignition laboratory has been engaged in various confidential investigations for the Bureau of Aeronautics, Navy Department. Further work has been done on the problem of measuring the electrical characteristics of the spark discharge and a paper on the character of spark discharges is being prepared for publication in the Bureau of Standards Journal of Research. An improved type of low-capacitance ignition cable has been developed which overcomes one of the main objections to shielding from the ignition standpoint. Apparatus has been devised for comparing the effectiveness of different types of shielding as regards radio reception. The study of hydrocarbon oxidation has been continued and a method has been perfected for obtaining photographic records of the changes in absorption which occur during a single engine cycle when a beam of light is passed through the combustion chamber of an engine.

Detonation rating of aviation gasolines.—The C.F.R. Motor Method, which is in general use for the knock rating of motor fuels, has been recommended for use in rating commercial aviation gasolines pending the adoption of a C.F.R. Aviation Method. A program of multicylinder engine tests to ascertain how much tetraethyl lead or benzol in certain typical base fuels is required to match the detonation characteristics of three reference fuels (rated, respectively, 73, 80, and 87 octane number by the C.F.R. Motor Method) has been adopted and the tests will be made by the Bureau of Standards in cooperation with four engine manufacturers. Each of the five laboratories will use representative commercial or military aircraft engines and the average performance of the diverse test fuels will give a basis for developing a suitable laboratory method of rating aviation gasolines.

Ice formation in the induction systems of aircraft engines.—A study of the relation of fuel volatility to ice formation in the induction systems of aircraft engines was undertaken in December and is nearly completed. The fuels used included three conventional aviation gasolines, selected to cover the commercial volatility range, and three aviation natural gasolines, differing widely in volatility. Small-scale tests at sea level and at altitude, using a thermally insulated carburetor through which conditioned air was drawn by means of a Nash pump, showed that it was possible to predict quite accurately the atmospheric conditions

under which a fuel would cause ice formation in the carburetor from a knowledge of the distillation curve of the fuel and the supplied air-fuel ratio. Full-scale tests with a Curtiss D-12 engine mounted in the altitude chamber verified the results obtained in the small-scale tests, ice being formed at the same venturi temperatures in each case within a few degrees.

REPORT OF COMMITTEE ON MATERIALS FOR AIRCRAFT

SUBCOMMITTEE ON METALS

Intercrystalline embrittlement of sheet duralumin.—A report entitled "The Weathering of Sheet Aluminum Alloys Used in Aircraft", which summarizes the results of exposure tests of 5 years' duration has been prepared for publication as a technical report. The tests in which were obtained the data upon which the report is based were conducted upon both commercial alloys and special compositions by exposing them continuously to the weather at three locations: Washington, D.C.; Hampton Roads, Va.; and Coco Solo, Canal Zone. The resulting changes in the tensile properties as determined at intervals of several months during the duration of the tests have been used as the principal measure of the corrosive effect by comparison with the corresponding properties of similar materials carefully stored under noncorrosive conditions. The change in the product of tensile strength and elongation expressed as a percentage of the original was found to be very useful for this purpose. All specimens after corrosion were examined as to the character of any corrosive attack which had occurred and its relation to the microstructure.

In addition to showing the useful life which may be expected of the various materials under different climatic conditions, the investigation has clearly established a number of important facts relating to (a) the underlying causes of intercrystalline embrittlement of duralumin, (b) the most desirable method of heat treatment for developing reliable material having the high strength required, and (c) the dependability and usefulness of various protective coatings and surface treatments.

Numerous advances have been made in the development of light alloys since the exposure tests referred to above were started. Early in the year a second series of tests intended to cover a 5-year period was started. The general plan is similar to that of the tests just completed, with a few improvements, however, prompted by the first series. Considerable progress has already been made in the testing of the specimens removed at 3-month and 6-month intervals from the racks. The materials included in the tests represent 19 aluminum-base alloys and 9 magnesium-base alloys. Fifteen hundred specimens have been used at each test location. Fourteen methods for

surface treatment and 12 different types of coatings are represented. Close cooperation has been given by the manufacturers of the materials as well as of the various coating materials which form a part of the test.

Exposure tests of magnesium and magnesium alloys.—Observations on materials in sheet form and as thin castings exposed continuously to the weather have been continued. The average change in tensile strength of the sheet material after 4½ years' exposure to the weather at Washington was of the order of 15 percent. Most of the surface coatings failed within 1½ years. Outstanding exceptions were aluminum-pigment spar varnish and an "acid-seal" coating on a red-lead primer. With the completion of the 5-year period, all of the specimens will have been tested and a report will be prepared. As part of the new series of exposure tests mentioned above, various magnesium alloys have been included. These will furnish information on the dependability of the materials under seacoast conditions.

Protection of duralumin, anodic oxidation.—The practical value of treating the surface of duralumin parts by an anodic oxidation process is now generally recognized and specified in airplane construction. Study of the various electrolytic methods used for this purpose has been continued and has resulted in improving and simplifying the method considerably. A number of modifications of the usual chromic-acid solution have been developed and progress has been made in the explanation of the deterioration of the electrolytic bath during use, whereby the surface oxide film formed in treatment of successive lots is less and less effective. Close contact with the Naval Aircraft Factory has been maintained.

Airplane propellers—Aluminum alloy.—The continued sporadic failure of propeller blades constitutes a serious problem to aircraft. During the year 8 aluminum alloy blades, 4 with hub failures and 4 with blade failures, were studied. All were fatigue fractures. Those at the hub originated at the periphery approximately in line with the trailing edge. The metallurgical examination did not reveal any significant defects in material nor heat treatment. Stresses associated with the method of clamping the blades in the steel hub appear to have more bearing on the hub failures than defective material.

Failures in the blade itself, beyond the hub, originated on the flat side of the blade, the fractures being suggestive of a coarsely crystalline brittle metal. Ordinarily fatigue fractures in aluminum alloys have a comparatively smooth surface. Preliminary experiments have indicated that fatigue cracks formed in the aluminum alloy blades by a few thousand cycles of reversed stresses greatly in excess of the fatigue limit were similar in appearance to those formed in the blades that failed in service.

In the examinations of the metals of the failed blades two rather unusual types of metallographic markings within the structure of individual grains were discovered, one being a veined structure and the other criss-cross or "slip-line" markings. The cause and significance of these markings have not yet been determined. Both have been eliminated by suitable heat treatment and neither appears to have a marked effect upon the tensile properties of the material.

Airplane propellers—Steel.—Examination of the fracture of a failed welded steel propeller revealed a fatigue fracture, associated with a defect in the weld on the leading edge. Other portions of the welds in this blade and some other similar blades showed defects of various sorts. A study was made of nondestructive methods applicable to the inspection of such blades. The use of a magnetic powder dusted on the magnetized blades was considered to be most practicable. It was found that this method revealed some defects which were not shown by an X-ray examination.

A thorough study was made of hollow welded steel blades furnished by the manufacturer and a detailed report prepared describing the necessary technique to be employed and illustrating the patterns formed by the various defects. This report was intended for the use of inspectors in routine inspection in the field and in the manufacturer's plant. The information was supplied to the Aeronautics Branch of the Department of Commerce, the Army Air Corps, and the Bureau of Aeronautics of the Navy.

SUBCOMMITTEE ON AIRCRAFT STRUCTURES

Inelastic behavior of duralumin and alloy steels in tension and compression.—A procedure has been developed for the determination of the stress-strain properties in compression of sheet and thin-walled structures. In this test a number of coupons are cut from the material and placed together like leaves in a book. Buckling of the outer leaves is prevented by a number of steel studs inserted between the specimen and an auxiliary frame. The preliminary tests indicate that values for a yield point can be obtained which can be repeated by different observers and, in the case of coupons cut from tubing, compared with values obtained in the test of tubes with a length-radius ratio of about 15.

End fixation of struts.—The laboratory work on round normalized or annealed chromium molybdenum steel, duralumin, and high-strength stainless-steel tubing has been completed. Formulas similar to those by Orrin E. Ross published in Technical Note No. 306 of the National Advisory Committee for Aeronautics have been developed, which represent with a good degree of accuracy the relation between the column strengths and the geometric properties of Navy standard steel tubes and S.A.E. standard duralumin tubes passing Navy Department specifications for the tubing tested. From these formulas curves have been drawn

giving the axial load which can be carried by any standard tube of any free length up to 200 times the slenderness ratio or 200 inches, whichever is the smaller.

Friedrich Bleich's method of designing compression members with elastically restrained ends has been extended so that it is now possible in trusses to design such members against buckling in the plane of the truss with considerably greater accuracy than before. The method consists essentially, after making a preliminary design, in assuming as freely supported the far ends of all members meeting at either end of a member to be designed finally, and then determining the free length of the latter. A nomographic chart has been worked out which materially assists in this determination. When the free length has been found, the rest is merely a matter of selecting the proper section, either by the use of the appropriate column formula, or from the corresponding load-free-length curves.

Torsional strength of tubing.—The report on the torsional strength of chromium molybdenum steel tubing, which has been prepared in manuscript form, is being held in abeyance awaiting the results of the parallel program on 17ST duralumin tubes.

The experimental part of this latter program has been completed. Tubes of the following sizes are included: 1-inch diameter, 0.018 to 0.120 inch thick; 1-inch diameter, 0.022 to 0.220 inch thick; and 2-inch diameter, 0.022 to 0.220 inch thick. Torsion tests were made on tubes 20 inches and 60 inches long of each size; tensile and hardness tests were also made on tubes of each size.

It is planned to present the results of these tests as soon as they have been analyzed as the second part of a report on torsional strength of tubing, thus including in one report tubing of the two materials principally used in aircraft design.

Strength of riveted joints in aluminum alloy.—The majority of the testing fixtures and the heat-treating equipment have been constructed for this investigation. Tests have been made to determine the effect of hole and plate clearances in double-shear tests of the rivet stock. Tests have been started to determine the optimum driving pressure for a given rivet size, plate thickness, and grip, but these have not yet progressed far enough for definite conclusions to be given.

Vibration tests of propellers.—This investigation was undertaken in cooperation with other agencies of the Government in an attempt to gain a clearer understanding of propeller failures in flight. Most propeller failures are found to proceed from typical fatigue cracks which in turn must be due to high periodic stresses. The source and nature of these stresses are not known. It is not clear whether they are due to resonance vibrations of large amplitude superimposed on the steady stress due to the centrifugal forces or whether they are due to purely forced vibrations.

No answer to these questions can be expected until it has been shown whether or not either resonance vibrations or forced vibrations of sufficient amplitude can be maintained in a propeller to cause failure. It was therefore decided to begin the investigation by developing a method of exciting vibrations of controllable frequency and amplitude in the propeller, of measuring the stresses set up during this vibration, and, if possible, of producing fatigue failures.

Of the various methods considered the following was successful in accomplishing its purpose. A direct-current motor has its armature connected across an alternating-current source of variable frequency while its field is excited by a steady direct current; the rotor of the motor then performs torsional vibrations of the frequency of the armature current and an amplitude that may be controlled by controlling the field current or the impressed alternating voltage. This torsional vibration is transmitted through the shaft of the rotor to the propeller blades, which are mounted in a hub at the end of this shaft in the same way as an airplane propeller is connected to the crankshaft of its driving engine. The propeller executes a forced vibration, which becomes large whenever the impressed frequency coincides with one of its natural frequencies.

In the new equipment, which was installed after preliminary tests had shown the method to be practical, the impressed frequency may be varied from 10 to 180 cycles per second. As the frequency was increased gradually from its lowest value the first resonance vibration was observed between 30 and 40 cycles; the propeller blade vibrated approximately as a cantilever beam fixed at the hub end; a careful determination of the stress distribution in this mode was made, using 2-inch Tuckerman optical strain gages having a special heavy knife edge to reduce inertia effects. The stresses were found to vary linearly with the deflection of the tip of the blade. This result was utilized in making fatigue tests on eight propeller blades. The blades were run at a given tip amplitude, corresponding to a maximum stress amplitude given from the strain-gage measurements, until failure occurred. This failure took place in each of the eight blades by the formation of a crack at a point close to the observed stress maximum, which was 20 to 30 inches from the center of the hub of the propeller. The results were plotted on a diagram of logarithmic stress versus number of cycles to failure. However, the number of points was not sufficient to draw definite conclusions. The torque amplitude causing failure was of the order of 100 ft.-lb.

As the frequency was increased beyond the point corresponding to the fundamental described above, a torsional resonance vibration of the whole propeller about the driving shaft was passed at around 50 cycles, and finally at around 110 to 130 cycles a further bending vibration of the individual blades was reached, this time with a node about 9 inches from the tip.

The stress distribution for the mode was obtained for one blade and showed a maximum a few inches from the node.

The experimental investigation has been paralleled by a theoretical analysis. The stress distribution in a propeller of given design vibrating with its fundamental frequency was calculated by a method of successive iteration first applied to propellers by Hansen and Mesmer (Z.F.M., vol. 23, 1933). This gave a close check with the observed frequency and with the stress distribution obtained by the Tuckerman gages. The same method has been modified to compute the natural mode, frequency, and stress distribution due to the first harmonic with node near the tip.

The Matériel Division of the Army Air Corps has conducted a study of the resonant-vibration frequencies of propeller blades, using entirely different methods and equipment. The results of this investigation have been published (Air Corps Technical Report No. 3891), and show in general that the failures of propellers were due to the coinciding of the resonant-vibration frequencies of the propeller blades with the engine-explosion frequencies.

Airship girders and airship structural members.—A number of column tests have been made on two experimental and two production plate airship girders of aluminum alloy fabricated by the Goodyear-Zeppelin Corporation. These tests were made in the large Emery testing machine. The specimens were placed in the machine to simulate as nearly as practicable flat end columns. The lowest maximum load recorded for any of the specimens taken from the production girders was 27,450 pounds for a column 103.4 inches long. The determinations of the areas of the chord members are in progress.

Specimens of the original German duralumin lattices and channels from the airship *Los Angeles* have been submitted at intervals throughout the year. The results of the tensile tests on lattice and channel material do not suggest that there has been any appreciable progress in corrosion during the last year. In no piece tested was the corrosion sufficient to lower the strength of the ship.

A number of specimens of thin sheet Alclad cut from the hull plating of the airship *MC-2* have been tested in tension. The results of these tests do not suggest an appreciable deterioration as a result of corrosion. No hull specimen showed ultimate strengths of less than 54,900 pounds per square inch or elongations less than 15 percent.

The investigation of the stresses in wire loops has been continued. Studies have been made of the fractures of bulkhead fork wires. These fractures are attributed to fatigue. A satisfactory procedure for determining the residual stresses in wire helixes has been obtained. The determination of these stresses is proceeding as opportunity affords.

Flat plates under normal pressure.—The analysis of results from a detailed test of a 5 by 5 by 0.02 inch duralumin plate with clamped edges led to the following tentative conclusions:

The only known theory which gives a roughly adequate picture of the behavior of a plate of this type is that of Foepl. The distribution of median plane stresses is roughly the same as that given by Foepl; that of the bending stresses is very different. The magnitude of the maximum total stress which occurs at the middle of the edge of the plate is 10 to 20 percent higher than that predicted by Foepl.

By the application of Foepl's theory it can be shown that all curves of pressure versus center deflection obtained from tests of square plates of a given material with fixed edges can be reduced to one curve if the pressures are divided by the fourth power of the ratio of the thickness of the plate to its width, and the center deflection by the thickness alone. This curve was computed for square duralumin plates with logarithmic paper and it was found that all the observed curves when reduced come fairly close to this curve throughout the elastic range.

A number of stainless-steel plates have been tested under normal pressure; they showed the same behavior qualitatively as the duralumin plates reported on above.

Following a lead from an article in Z.V.I., vol. 26, 1932, a varnish was developed which cracked under a tensile strain from 1.3 to 2.3 10^{-3} in./in. corresponding to stress well below the yield point for duralumin. Rectangular duralumin plates were coated with this varnish and the formation of the definite strain pattern that developed as each plate was subjected to increasing normal pressure was followed; this strain pattern showed directly the extent to which the clamping at the short ends affected the stress distribution and it also showed the curve near the edges along which the surface strains reversed from compression to tension.

Strength of welded joints in tubular members for aircraft.—Tests have been completed on the majority of specimens of the second series of this investigation. A series of 216 butt-welded tensile specimens in chromium molybdenum plate 0.0325 inch to 0.1875 inch thick has been tested to determine the strengths obtainable in joints heat-treated after welding for three types of welding: The standard procedure using low-carbon rod; welding with chromium molybdenum rod; and "carburizing flux" welding.

Joints made by these three methods and tested without having been heat-treated had about the same tensile strength. Of the heat-treated welds those made by the standard procedure showed less tensile strength than the chromium molybdenum and the carburizing flux welds. The last type showed somewhat higher tensile strengths for all heat-treated specimens

of 0.0325 inch thickness and in general for all the thicknesses tested, except at the lowest drawing temperature, 500° F.

Tests made on T-joints in both carbon and chromium molybdenum steel tubing of 1.5 inches outside diameter by 0.058-inch wall, show the inserted-gusset type of reinforcement to be the best considering strength, stiffness, weight, and ease of welding.

Tests are being continued on tubular joints heat-treated after welding and on joints made in thin-walled tubing of 1.5 inches outside diameter by 0.020-inch wall.

TEMPORARY SUBCOMMITTEE ON RESEARCH PROGRAM ON MONOCOQUE DESIGN

STRESSED-SKIN, OR MONOCOQUE, STRUCTURES.—During the past year, research on stressed-skin, or monocoque, structures for aircraft has consisted largely of fundamental studies concerning the strength and behavior of skin and stiffeners. Where possible, such phases of the general subject have been summarized in useful form for the designer.

In order that the industry and others interested in research on stressed-skin structures may be kept informed regarding the work of the subcommittee, a brief summary of the minutes of each meeting is prepared for circulation. These minutes record the suggestions that are made from time to time regarding problems suitable for research (in other than Government laboratories).

The subcommittee is now preparing a chart showing the present status of research on stressed-skin structures. Accompanying the chart will be a bibliography and brief discussion of the most authoritative literature on the various phases of the subject.

Research on thin-walled cylinders.—Last year the Committee published a preliminary report on the strength of thin-walled cylinders in torsion. This year a more complete report on the same subject is being published under the authorship of Dr. L. H. Donnell of the California Institute of Technology (Technical Report No. 479). In the recent report, all the available test data on thin-walled cylinders in torsion are included and the results correlated with theory.

A report on the strength of thin-walled cylinders in compression is now in the process of publication (Technical Report No. 473). In this report all the available test data are included, together with the results of tests made by the Committee and by the California Institute of Technology. The results of the tests are presented in nondimensional form and discussed in connection with existing theory.

A report on the strength of thin-walled cylinders in pure bending is also in process of publication (Technical Note No. 479). In this report no consideration is given to theory but the results are

presented in nondimensional form for comparison with the results of similar tests in compression published in Technical Report No. 473. The important conclusion regarding the strength of thin-walled cylinders in bending is that the stress on the extreme fiber at failure as calculated by the ordinary theory of bending is from 30 to 80 percent greater than the compressive strength at failure for thin-walled cylinders of the same dimensions.

A report on the strength of thin-walled cylinders of circular section subjected to combined transverse shear and bending is in progress. This report also covers work which is largely experimental, but the results are presented in nondimensional form and compared with the results of torsion and bending tests previously reported. The tests show that, for large values of the ratio of moment to radius-shear (M/rV), the cylinder fails in bending and the stress on the extreme fiber at failure, as calculated by the ordinary theory of bending is equal to the stress on the extreme fiber at failure for a cylinder of the same dimensions in pure bending. For small values of M/rV , the cylinder fails in shear and the maximum shearing stress at failure as calculated by the ordinary beam theory is approximately equal to the shearing stress at failure for a cylinder of the same dimensions in torsion (pure shear). For intermediate values of M/rV , there is a transition from failure by bending to failure by shear that is accompanied by a reduction in strength. In calculating the strength of the cylinder, this reduction in strength may be allowed for by a proper consideration of the dispersion of the results of the tests on thin-walled cylinders in pure bending.

Strength tests on thin-walled truncated cones and thin-walled cylinders of elliptic section have been completed. The results of these tests will be published later.

Research on strength of stiffeners.—After the airplane division of the Ford Motor Co. suspended operations last year a large portion of the engineering data accumulated from its researches on various types of structural elements was made available to the committee. As a portion of these data revealed that valuable information regarding local failure in stiffeners could be obtained, it is now being condensed for issuance in one or more reports. The reports as finally published will include design charts with the critical stresses plotted against the proper dimensions of the stiffener sections.

Research on strength of stiffened skins.—In collaboration with Professor Niles of Stanford University, the Committee is preparing for publication a general report summarizing all the tests made to date on the compressive strength of corrugated sheet. The data for use in this report have been assembled from various sources, including the Army, the Navy, aircraft manufac-

turers, and the Massachusetts Institute of Technology. In this report the strength of corrugated sheet for the various types of failure will be presented in chart form correlated with the column curve for the material. Consideration will also be given to the effect of pitch-line curvature on the strength of corrugated sheet and the effect of nonuniform spacing of transverse rings on the column strength of the corrugations.

During the past year the Committee published a report on the compressive strength of flat and slightly curved sheet and stiffener combinations (Technical Note No. 455). In this report the accuracy of three methods based upon various assumptions for calculating the compressive strength of flat sheet and stiffener combinations was compared. The method based upon mutual action of the stiffener and on effective width of sheet as a column gave the best agreement with the results of tests. The investigation of the effect of small curvature presented in the report resulted in the conclusion that the compressive strength of curved panels is, for all practical purposes, equal to the strength of flat panels except for thick sheet where nonuniform curvature throughout the length of the panel may cause the strength of a curved panel to be as much as 10 to 15 percent less than the strength of a corresponding flat panel.

Design of rings.—During the past year the Committee published two reports on the stress analysis of rings (Technical Notes Nos. 444 and 462). By use of the formulas and charts presented in these reports the designer is relieved of the necessity of making a least-work analysis when calculating the stresses in circular and elliptic rings for the majority of loading conditions that are likely to be imposed on the main frames of a monocoque fuselage. The study is being extended to an analysis of the forces that act upon the intermediate rings between the main rings of monocoque fuselages.

Design of beams having thin webs in diagonal tension.—During the past year a study was made and a report prepared (Technical Note No. 469) summarizing the essential formulas for the design of diagonal tension field beams; that is, beams with very thin webs, the theory of which was developed by Professor Wagner of Germany. The purpose of this report was to present in condensed form a brief summary of the fundamental principles and useful formulas for the specific use of the designer.

SUBCOMMITTEE ON METHODS AND DEVICES FOR TESTING AIRCRAFT MATERIALS AND STRUCTURES

The Committee has continued the work on the survey of methods and devices for testing aircraft materials and structures, with a view to publication of the material in a series of reports dealing with various phases of the testing of aircraft materials and structures. At the request of the Subcommittee on Aircraft Structures, priority is being given to a special report on extensometers which is being prepared for publication.

SUBCOMMITTEE ON MISCELLANEOUS MATERIALS

Development of fire-resistant dope for aircraft.—The available cellulose esters and synthetic resins were investigated to ascertain their relative values in rendering dopes for airplane wing fabric nonflammable. None of the resins studied gave satisfactory tautness. Cellulose acetate dope was found to be the most satisfactory fire-resistant material of all the products examined. Additional protection is obtained by impregnating the fabric with an aqueous solution of a boric acid-borax mixture before applying the cellulose acetate dope. Fabric fireproofed and doped in this manner is not ignited by lighted matches, cigarettes, redhot nails, nor burning gasoline. The amount of fireproofing salt mixture required on the cloth is approximately 5 percent of the total weight of the doped fabric.

REPORT OF COMMITTEE ON PROBLEMS OF AIR NAVIGATION

In response to the need for the coordination of scientific research being conducted by a number of different agencies, both within and without the Government, on the problems of air navigation, the National Advisory Committee for Aeronautics has established a committee on problems of air navigation, with members representing the principal agencies concerned with the development of aids to air navigation.

In order to cover effectively the large and varied field of research and development on problems of air navigation, the following subcommittees have been organized under the committee on problems of air navigation: subcommittee on instruments and subcommittee on meteorological problems.

PART II

ORGANIZATION AND GENERAL ACTIVITIES

ORGANIZATION

The National Advisory Committee for Aeronautics is composed of 15 members appointed by the President and serving as such without compensation. The law provides that the members shall include 2 representatives each from the War and Navy Departments and 1 each from the Smithsonian Institution, the Weather Bureau, and the Bureau of Standards, together with not more than 8 additional persons "who shall be acquainted with the needs of aeronautical science, either civil or military, or skilled in aeronautical engineering or its allied sciences." One of these eight is a representative of the Aeronautics Branch of the Department of Commerce. Under the rules and regulations governing the work of the Committee as approved by the President the chairman and vice chairman of the committee are elected annually.

On July 12, 1933, President Roosevelt appointed Dr. Lyman J. Briggs a member of the committee to succeed Dr. George K. Burgess, whose death on July 2, 1932, had been noted in the preceding annual report. Dr. Briggs had succeeded Dr. Burgess as director of the Bureau of Standards, and his membership on the Committee is as a representative of that Bureau.

The first vacancy occurring during the past year was caused by the tragic death of Rear Admiral William A. Moffett, United States Navy, Chief of the Bureau of Aeronautics, Navy Department, who was killed in the destruction by storm of the airship *Akron* on April 4, 1933. For 12 years he had served on this Committee faithfully and with great distinction. His outstanding service as a member was his uniform sincerity in fostering truly cooperative efforts in order to prevent duplication in the field of fundamental research in aeronautics. His colleagues adopted resolutions mourning his loss and testifying to the enduring value of his great work for the development of aviation for national defense.

Rear Admiral Ernest J. King, United States Navy, succeeded Admiral Moffett as Chief of the Bureau of Aeronautics, and on July 19, 1933, he was appointed by President Roosevelt to succeed Admiral Moffett as a member of this Committee.

A second vacancy during the year was caused by the resignation on November 9, 1933, of Dr. William F. Durand, who was one of the original members appointed by President Wilson in 1915. Dr. Durand had served as chairman of the Committee in 1916 and

1917. He resigned because his residence on the Pacific coast made it difficult for him to attend meetings frequently, and was succeeded as a member of the Committee by Mr. Eugene L. Vidal, Director of Aeronautics, Department of Commerce.

The executive offices of the Committee, including its offices of aeronautical intelligence and aeronautical inventions are located in the Navy Building, Washington, D.C., in close proximity to the air organizations of the Army and Navy.

The office of aeronautical intelligence was established in the early part of 1918 as an integral branch of the Committee's activities. It is the designated depository for scientific and technical data on aeronautics secured from all parts of the world. The material is classified, cataloged, and disseminated.

To assist in the collection of scientific and technical data, the Committee maintains a technical assistant in Europe with headquarters at the American Embassy in Paris.

CONSIDERATION OF AERONAUTICAL INVENTIONS

In accordance with act of Congress approved July 2, 1926, as amended by act approved March 3, 1927, the Committee passes upon the merits of aeronautical inventions and designs submitted to any branch of the Government and submits reports thereon to the Aeronautical Patents and Design Board, consisting of Assistant Secretaries of the Departments of War, Navy, and Commerce. That board is authorized, upon the favorable recommendation of the Committee to "determine whether the use of the design by the Government is desirable or necessary and evaluate the design and fix its worth to the United States in an amount not to exceed \$75,000."

The work of considering aeronautical inventions and designs submitted is under the supervision of the committee on aeronautical inventions and designs.

SUBCOMMITTEES

The executive committee has organized a number of standing committees, with subcommittees, for the purpose of supervising its work in their respective fields. The four technical committees on aerodynamics, power plants for aircraft, materials for aircraft, and problems of air navigation, and their subcommittees supervise and direct the aeronautical research conducted by the Advisory Committee and coordinate the investigations conducted by other agencies. Their work has been described in part I.

The organization of the committees and subcommittees under the executive committee is as follows:

COMMITTEE ON AERODYNAMICS

Dr. David W. Taylor, chairman.
 Dr. L. J. Briggs, Bureau of Standards.
 Theophile dePort, Matériel Division, Army Air Corps, Wright Field.
 Lt. Comdr. W. S. Diehl (C.C.), United States Navy.
 Dr. H. L. Dryden, Bureau of Standards.
 Richard C. Gazley, Aeronautics Branch, Department of Commerce.
 Maj. C. W. Howard, United States Army, Matériel Division, Air Corps, Wright Field.
 George W. Lewis, National Advisory Committee for Aeronautics (ex officio member).
 Dr. Charles F. Marvin, Weather Bureau.
 Lt. Comdr. Donald Royce (C.C.), United States Navy.
 Hon. Edward P. Warner, editor of Aviation.
 Dr. A. F. Zahm, Division of Aeronautics, Library of Congress.

SUBCOMMITTEE ON AIRSHIPS

Hon. Edward P. Warner, editor of Aviation, chairman.
 Starr Truscott, National Advisory Committee for Aeronautics, vice chairman.
 Dr. Karl Arnstein, Goodyear-Zeppelin Corporation.
 Commander Garland Fulton (C.C.), United States Navy.
 Maj. William E. Kepner, United States Army, Matériel Division, Air Corps, Wright Field.
 George W. Lewis, National Advisory Committee for Aeronautics (ex officio member).
 Ralph H. Upson, Ann Arbor, Mich.

COMMITTEE ON POWER PLANTS FOR AIRCRAFT

Hon. William P. MacCracken, Jr., chairman.
 George W. Lewis, National Advisory Committee for Aeronautics, vice chairman.
 Henry M. Crane, Society of Automotive Engineers.
 Prof. Harvey N. Davis, Stevens Institute of Technology.
 Dr. H. C. Dickinson, Bureau of Standards.
 Carlton Kemper, National Advisory Committee for Aeronautics.
 Lt. Comdr. F. M. Maile, United States Navy.
 Lt. E. M. Powers, United States Army, Matériel Division, Air Corps, Wright Field.
 Prof. C. Fayette Taylor, Massachusetts Institute of Technology.

COMMITTEE ON MATERIALS FOR AIRCRAFT

Dr. L. J. Briggs, Bureau of Standards, chairman.
 Prof. H. L. Whittemore, Bureau of Standards, vice chairman and acting secretary.
 S. K. Colby, Aluminum Co. of America.
 Lt. Alden R. Crawford, United States Army, Matériel Division, Air Corps, Wright Field.
 Lt. N. A. Draim (C.C.), United States Navy.
 Warren E. Emley, Bureau of Standards.
 Commander Garland Fulton (C.C.), United States Navy.
 Dr. H. W. Gillett, Battelle Memorial Institute.
 C. H. Helms, National Advisory Committee for Aeronautics.
 Dr. Zay Jefferies, American Magnesium Corporation.
 J. B. Johnson, Matériel Division, Army Air Corps, Wright Field.
 George W. Lewis, National Advisory Committee for Aeronautics (ex officio member).
 H. S. Rawdon, Bureau of Standards.

E. C. Smith, Republic Steel Corporation.
 G. W. Trayer, Forest Products Laboratory.
 Starr Truscott, National Advisory Committee for Aeronautics.
 Hon. Edward P. Warner, editor of Aviation.

SUBCOMMITTEE ON METALS

H. S. Rawdon, Bureau of Standards, chairman.
 Dr. H. W. Gillett, Battelle Memorial Institute.
 Dr. Zay Jefferies, American Magnesium Corporation.
 J. B. Johnson, Matériel Division, Army Air Corps, Wright Field.
 George W. Lewis, National Advisory Committee for Aeronautics (ex officio member).
 E. C. Smith, Republic Steel Corporation.
 Starr Truscott, National Advisory Committee for Aeronautics.
 Prof. H. L. Whittemore, Bureau of Standards.

SUBCOMMITTEE ON AIRCRAFT STRUCTURES

Starr Truscott, National Advisory Committee for Aeronautics, chairman.
 Capt. Howard Z. Bogert, United States Army, Matériel Division, Air Corps, Wright Field.
 C. P. Burgess, Bureau of Aeronautics, Navy Department.
 Richard C. Gazley, Aeronautics Branch, Department of Commerce.
 Charles Ward Hall, Hall-Aluminum Aircraft Corporation.
 Lt. Lloyd Harrison (C.C.), United States Navy, Naval Aircraft Factory.
 George W. Lewis, National Advisory Committee for Aeronautics (ex officio member).
 Lt. Comdr. R. D. MacCart (C.C.), United States Navy.
 Charles J. McCarthy, Chance Vought Corporation.
 Prof. J. S. Newell, Massachusetts Institute of Technology.
 J. A. Roché, Matériel Division, Army Air Corps, Wright Field.
 Dr. L. B. Tuckerman, Bureau of Standards.

TEMPORARY SUBCOMMITTEE ON RESEARCH PROGRAM ON MONOCOQUE DESIGN

George W. Lewis, National Advisory Committee for Aeronautics, chairman.
 Capt. Howard Z. Bogert, United States Army, Matériel Division, Air Corps, Wright Field.
 Richard C. Gazley, Aeronautics Branch, Department of Commerce.
 Eugene E. Lundquist, National Advisory Committee for Aeronautics.
 Lt. Comdr. R. D. MacCart (C.C.), United States Navy.
 Dr. L. B. Tuckerman, Bureau of Standards.

SUBCOMMITTEE ON METHODS AND DEVICES FOR TESTING AIRCRAFT MATERIALS AND STRUCTURES

Henry J. E. Reid, National Advisory Committee for Aeronautics, chairman.
 Capt. Howard Z. Bogert, United States Army, Matériel Division, Air Corps, Wright Field.
 Lt. Lloyd Harrison (C.C.), United States Navy, Naval Aircraft Factory.
 George W. Lewis, National Advisory Committee for Aeronautics (ex officio member).
 Eugene E. Lundquist, National Advisory Committee for Aeronautics.
 R. L. Templin, Aluminum Co. of America.
 G. W. Trayer, Forest Products Laboratory.
 Dr. L. B. Tuckerman, Bureau of Standards.

SUBCOMMITTEE ON MISCELLANEOUS MATERIALS

C. H. Helms, National Advisory Committee for Aeronautics, chairman.

Dr. W. Blum, Bureau of Standards.

C. J. Cleary, Matériel Division, Army Air Corps, Wright Field.

Warren E. Emley, Bureau of Standards.

George W. Lewis, National Advisory Committee for Aeronautics (ex officio member).

J. E. Sullivan, Bureau of Aeronautics, Navy Department.

G. W. Trayer, Forest Products Laboratory.

P. H. Walker, Bureau of Standards.

G. P. Young, Matériel Division, Army Air Corps, Wright Field.

COMMITTEE ON PROBLEMS OF AIR NAVIGATION

Hon. William P. MacCracken, Jr., chairman.

Dr. L. J. Briggs, Bureau of Standards.

Lloyd Espenschied, American Telephone and Telegraph Co.

Maj. Gen. B. D. Foulois, United States Army, Air Corps, War Department.

Paul Henderson, National Air Transport, Inc.

Capt. S. C. Hooper, United States Navy, Director of Naval Communications, Navy Department.

Dr. J. C. Hunsaker, Massachusetts Institute of Technology.

George W. Lewis, National Advisory Committee for Aeronautics (ex officio member).

Col. Charles A. Lindbergh.

Rex Martin, Aeronautics Branch, Department of Commerce.

Dr. Charles F. Marvin, Weather Bureau.

Lt. J. P. W. Vest, United States Navy, Hydrographic Office, Navy Department.

Eugene L. Vidal, Director of Aeronautics, Department of Commerce.

Charles J. Young, R.C.A. Victor Co., Inc.

SUBCOMMITTEE ON INSTRUMENTS

Dr. L. J. Briggs, Bureau of Standards, chairman.

Marshall S. Boggs, Aeronautics Branch, Department of Commerce.

Dr. W. G. Brombacher, Bureau of Standards.

C. H. Colvin, Society of Automotive Engineers.

Capt. A. F. Hegenberger, United States Army, Matériel Division, Air Corps, Wright Field.

Dr. A. W. Hull, General Electric Co.

Carl W. Keuffel, Keuffel and Esser.

George W. Lewis, National Advisory Committee for Aeronautics (ex officio member).

Lt. C. D. McAllister, United States Army, Matériel Division, Air Corps, Wright Field.

Henry J. E. Reid, National Advisory Committee for Aeronautics.

Lt. L. D. Webb, United States Navy.

Charles J. Young, R.C.A. Victor Co., Inc.

SUBCOMMITTEE ON METEOROLOGICAL PROBLEMS

Dr. Charles F. Marvin, Weather Bureau, chairman.

W. R. Gregg, Weather Bureau.

Dr. W. J. Humphreys, Weather Bureau.

Dr. J. C. Hunsaker, Massachusetts Institute of Technology.

George W. Lewis, National Advisory Committee for Aeronautics (ex officio member).

Lt. F. W. Reichelderfer, United States Navy, Naval Air Station, Lakehurst.

Dr. C. G. Rossby, Massachusetts Institute of Technology.

Eugene Sibley, Aeronautics Branch, Department of Commerce.

Capt. Alfred H. Thiessen, United States Army, Signal Corps, War Department.

COMMITTEE ON AIRCRAFT ACCIDENTS

Hon. Edward P. Warner, editor of Aviation, chairman.

George W. Lewis, National Advisory Committee for Aeronautics.

W. Fiske Marshall, Aeronautics Branch, Department of Commerce.

Lt. Comdr. A. C. McFall, United States Navy.

Lt. Samuel P. Mills, United States Army, Air Corps, War Department.

Capt. Max F. Schneider, United States Army, Air Corps, War Department.

Lt. H. B. Temple, United States Navy.

COMMITTEE ON AERONAUTICAL INVENTIONS AND DESIGNS

Dr. David W. Taylor, chairman.

Capt. Arthur B. Cook, United States Navy.

Dr. Charles F. Marvin, Weather Bureau.

Brig. Gen. Henry C. Pratt, United States Army, Matériel Division, Air Corps, Wright Field.

John F. Victory, secretary.

COMMITTEE ON PUBLICATIONS AND INTELLIGENCE

Dr. Joseph S. Ames, chairman.

Dr. Charles F. Marvin, Weather Bureau, vice chairman.

Miss M. M. Muller, secretary.

COMMITTEE ON PERSONNEL, BUILDINGS, AND EQUIPMENT

Dr. Joseph S. Ames, chairman.

Dr. David W. Taylor, vice chairman.

John F. Victory, secretary.

LANGLEY MEMORIAL AERONAUTICAL LABORATORY

The Committee's laboratory is located on the Army flying field, known as "Langley Field, Va.", on ground set aside by the War Department for the Committee's use. The laboratory is subject to the military police fire, and sanitary regulations governing the post, but is otherwise under the exclusive and direct control of the Committee. The Committee's research work is conducted without interference with military operations at the field, and there is a splendid spirit of cooperation which has materially aided the Committee in its work.

As many of the Committee's fundamental researches are based upon requests received from the Army and Navy for the investigations of particular problems there has been full cooperation on the part of the Army and Navy in placing at the Committee's disposal airplanes, engines, and accessories needed for research purposes.

The Committee's laboratories comprise 11 buildings and a paid research staff of 260 employees.

ANALYSIS OF AIRCRAFT ACCIDENTS

A standard procedure for the analysis of aircraft accidents proposed by the committee on aircraft accidents, approved by the executive committee, and published as Technical Report No. 357, is followed by the War, Navy, and Commerce Departments. Uniformity in interpretation of the Committee's plan is

secured through meetings of the committee on aircraft accidents, which includes in its membership representatives of the War, Navy, and Commerce air organizations. The result is to render accident statistics comparable and thus through the accurate determination of the causes of accidents to be enabled to take appropriate measures for the reduction of accidents due to such causes.

TECHNICAL PUBLICATIONS OF THE COMMITTEE

The Committee has four series of publications, namely, technical reports, technical notes, technical memorandums, and aircraft circulars.

The technical reports present the results of fundamental research in aeronautics. The technical notes are mimeographed and present the results of short research investigations and the results of studies of specific detail problems which form parts of long investigations. The technical memorandums are mimeographed and contain translations of important foreign aeronautical articles. The aircraft circulars are mimeographed and contain descriptions of new types of foreign aircraft.

The following are lists of the publications issued:

LIST OF TECHNICAL REPORTS ISSUED DURING THE PAST YEAR

- No.
441. A Flight Investigation of the Spinning of the NY-1 Airplane with Varied Mass Distribution and Other Modifications, and an Analysis Based on Wind-Tunnel Tests. By Nathan F. Scudder, National Advisory Committee for Aeronautics.
 442. A Comparison between the Theoretical and Measured Longitudinal Stability Characteristics of an Airplane. By Hartley A. Soulé and John B. Wheatley, National Advisory Committee for Aeronautics.
 443. Pressure-Distribution Measurements on the Hull and Fins of a 1/40-Scale Model of the U.S. Airship *Akron*. By Hugh B. Freeman, National Advisory Committee for Aeronautics.
 444. Wind-Tunnel Research Comparing Lateral Control Devices, Particularly at High Angles of Attack. VI—Skewed Ailerons on Rectangular Wings. By Fred E. Weick and Thomas A. Harris, National Advisory Committee for Aeronautics.
 445. Working Charts for the Determination of the Lift Distribution between Biplane Wings. By Paul Kuhn, National Advisory Committee for Aeronautics.
 446. Airfoil Section Characteristics as Affected by Protuberances. By Eastman N. Jacobs, National Advisory Committee for Aeronautics.
 447. Static Thrust of Airplane Propellers. By Walter S. Diehl, Bureau of Aeronautics, Navy Department.
 448. Improved Apparatus for the Measurement of Fluctuations of Air Speed in Turbulent Flow. By W. C. Mock, Jr., and H. L. Dryden, Bureau of Standards.
 449. Wing Characteristics as Affected by Protuberances of Short Span. By Eastman N. Jacobs and Albert Sherman, National Advisory Committee for Aeronautics.
 450. The Calculation of Take-Off Run. By Walter S. Diehl, Bureau of Aeronautics, Navy Department.
 451. The Drag of Two Streamline Bodies as Affected by Protuberances and Appendages. By Ira H. Abbott, National Advisory Committee for Aeronautics.

- No.
452. General Potential Theory of Arbitrary Wing Sections. By T. Theodorsen and I. E. Garrick, National Advisory Committee for Aeronautics.
 453. The Estimation of Maximum Load Capacity of Seaplanes and Flying Boats. By Walter S. Diehl, Bureau of Aeronautics, Navy Department.
 454. Photomicrographic Studies of Fuel Sprays. By Dana W. Lee and Robert C. Spencer, National Advisory Committee for Aeronautics.
 455. Penetration and Duration of Fuel Sprays from a Pump Injection System. By A. M. Rothrock and E. T. Marsh, National Advisory Committee for Aeronautics.
 456. The Aerodynamic Forces and Moments Exerted on a Spinning Model of the NY-1 Airplane as Measured by the Spinning Balance. By M. J. Bamber and C. H. Zimmerman, National Advisory Committee for Aeronautics.
 457. Maneuverability Investigation of an *O3U-1* Observation Airplane. By F. L. Thompson and H. W. Kirschbaum, National Advisory Committee for Aeronautics.
 458. Relative Loading on Biplane Wings. By Walter S. Diehl, Bureau of Aeronautics, Navy Department.
 459. The N.A.C.A. Full-Scale Wind Tunnel. By Smith J. DeFrance, National Advisory Committee for Aeronautics.
 460. The Characteristics of 78 Related Airfoil Sections from Tests in the Variable-Density Wind Tunnel. By Eastman N. Jacobs, Kenneth E. Ward, and Robert M. Pinkerton, National Advisory Committee for Aeronautics.
 461. Interference on an Airfoil of Finite Span in an Open Rectangular Wind Tunnel. By Theodore Theodorsen, National Advisory Committee for Aeronautics.
 462. Tests of Nacelle-Propeller Combinations in Various Positions with Reference to Wings. III—Clark Y Wing—Various Radial-Engine Cowlings—Tractor Propeller. By Donald H. Wood, National Advisory Committee for Aeronautics.
 463. The N.A.C.A. High-Speed Wind Tunnel and Tests of Six Propeller Sections. By John Stack, National Advisory Committee for Aeronautics.
 464. Negative Thrust and Torque Characteristics of an Adjustable-Pitch Metal Propeller. By Edwin P. Hartman, National Advisory Committee for Aeronautics.
 465. Determination of the Theoretical Pressure Distribution for Twenty Airfoils. By I. E. Garrick, National Advisory Committee for Aeronautics.
 466. Aircraft Power-Plant Instruments. By Harcourt Sontag and W. G. Brombacher, Bureau of Standards.
 467. The Experimental Determination of the Moments of Inertia of Airplanes. By Hartley A. Soulé and Marvel P. Miller, National Advisory Committee for Aeronautics.
 468. The Interference between Struts in Various Combinations. By David Biermann and William H. Herrnstern, Jr., National Advisory Committee for Aeronautics.
 469. Increasing the Air Charge and Scavenging the Clearance Volume of a Compression-Ignition Engine. By J. A. Spanogle, C. W. Hicks, and H. H. Foster, National Advisory Committee for Aeronautics.
 470. The N.A.C.A. Tank. A High-Speed Towing Basin for Testing Models of Seaplane Floats. By Starr Truscott, National Advisory Committee for Aeronautics.
 471. Performance of a Fuel-Injection Spark-Ignition Engine Using a Hydrogenated Safety Fuel. By Oscar W. Schey and Alfred W. Young, National Advisory Committee for Aeronautics.

No.

472. Wind-Tunnel Tests on Combinations of a Wing with Fixed Auxiliary Airfoils Having Various Chords and Profiles. By Fred E. Weick and Robert Sanders, National Advisory Committee for Aeronautics.
473. Strength Tests of Thin-Walled Duralumin Cylinders in Compression. By Eugene E. Lundquist, National Advisory Committee for Aeronautics.
474. Nomenclature for Aeronautics. By National Advisory Committee for Aeronautics.

LIST OF TECHNICAL NOTES ISSUED DURING THE PAST YEAR

No.

432. Drag Tests of 4/9-Scale Model Engine Nacelles with Various Cowlings. By Ray Windler, National Advisory Committee for Aeronautics.
433. The Pressure Distribution Over a Standard and a Modified Navy Elliptical Wing Tip on a Biplane in Flight. By Richard V. Rhode, National Advisory Committee for Aeronautics.
434. Influence of Several Factors on Ignition Lag in a Compression-Ignition Engine. By Harold C. Gerrish and Fred Voss, National Advisory Committee for Aeronautics.
435. The Effect of Clearance Distribution on the Performance of a Compression-Ignition Engine with a Precombustion Chamber. By C. S. Moore and J. H. Collins, Jr., National Advisory Committee for Aeronautics.
436. The Effect of Connecting-Passage Diameter on the Performance of a Compression-Ignition Engine with a Precombustion Chamber. By C. S. Moore and J. H. Collins, Jr., National Advisory Committee for Aeronautics.
437. The Pressure Distribution Over a Long Elliptical Wing Tip on a Biplane in Flight. By Richard V. Rhode, National Advisory Committee for Aeronautics.
438. The Gaseous Explosive Reaction at Constant Pressure—Further Data on the Effect of Inert Gases. By F. W. Stevens, Bureau of Standards.
439. Meteorological Conditions During the Formation of Ice on Aircraft. By L. T. Samuels, Weather Bureau.
440. Flight Tests to Determine the Effect of a Fixed Auxiliary Airfoil on the Lift and Drag of a Parasol Monoplane. By Hartley A. Soule, National Advisory Committee for Aeronautics.
441. Rolling, Yawing, and Hinge Moments Produced by Rectangular Ailerons (Correlating Technical Reports Nos. 298, 343, and 370). By R. H. Heald, Bureau of Standards.
442. Jet Propulsion with Special Reference to Thrust Augmentors. By G. B. Schubauer, Bureau of Standards.
443. Wind-Tunnel Research Comparing Lateral Control Devices, Particularly at High Angles of Attack. Part VII—Handley Page Tip and Full-Span Slots with Ailerons and Spoilers. By Fred E. Weick and Carl J. Wenzinger, National Advisory Committee for Aeronautics.
444. Working Charts for the Stress Analysis of Elliptic Rings. By Walter F. Burke, University of Michigan.
445. Wind-Tunnel Research Comparing Lateral Control Devices, Particularly at High Angles of Attack. Part VIII—Straight and Skewed Ailerons on Wings with Rounded Tips. By Fred E. Weick and Joseph A. Shortal, National Advisory Committee for Aeronautics.
446. Estimation of the Variation of Thrust Horsepower with Air Speed. By Shatswell Ober, Massachusetts Institute of Technology.

No.

447. The Effect on Lift, Drag, and Spinning Characteristics of Sharp Leading Edges on Airplane Wings. By Fred E. Weick and Nathan F. Seudder, National Advisory Committee for Aeronautics.
448. Effect of Aileron Displacement on Wing Characteristics. By R. H. Heald, Bureau of Standards.
449. Wind-Tunnel Research Comparing Lateral Control Devices, Particularly at High Angles of Attack. Part IX—Tapered Wings with Ordinary Ailerons. By Fred E. Weick and Carl J. Wenzinger, National Advisory Committee for Aeronautics.
450. Mercerization of Cotton for Strength with Special Reference to Aircraft Cloth. By J. B. Wilkie, Bureau of Standards.
451. Wind-Tunnel Research Comparing Lateral Control Devices, Particularly at High Angles of Attack. Part X—Various Control Devices on a Wing with a Fixed Auxiliary Airfoil. By Fred E. Weick and Richard W. Noyes, National Advisory Committee for Aeronautics.
452. The Importance of Auto-Ignition Lag in Knocking. By E. S. Taylor, Massachusetts Institute of Technology.
453. Experiments with a Counter-Propeller. By E. P. Lesley, Stanford University.
454. The N.A.C.A. Combustion Chamber Gas-Sampling Valve and Some Preliminary Test Results. By J. A. Spanogle and E. C. Buckley, National Advisory Committee for Aeronautics.
455. Comparison of Three Methods for Calculating the Compressive Strength of Flat and Slightly Curved Sheet and Stiffener Combinations. By Eugene E. Lundquist, National Advisory Committee for Aeronautics.
456. The Aerodynamic Effect of a Retractable Landing Gear. By Smith J. DeFrance, National Advisory Committee for Aeronautics.
457. The Aerodynamic Characteristics of Airfoils as Affected by Surface Roughness. By Ray W. Hooker, National Advisory Committee for Aeronautics.
458. Wind-Tunnel Research Comparing Lateral Control Devices, Particularly at High Angles of Attack. Part XI—Various Floating Tip Ailerons on Both Rectangular and Tapered Wings. By Fred E. Weick and Thomas A. Harris, National Advisory Committee for Aeronautics.
459. Wind-Tunnel Tests on Model Wing with Fowler Flap and Specially Developed Leading-Edge Slot. By Fred E. Weick and Robert C. Platt, National Advisory Committee for Aeronautics.
460. Full-Scale Wind-Tunnel Research on Tail Buffeting and Wing-Fuselage Interference of a Low-Wing Monoplane. By Manley J. Hood and James A. White, National Advisory Committee for Aeronautics.
461. The Effect of Rivet Heads on the Characteristics of a 6- by 36-Foot Clark Y Metal Airfoil. By Clinton H. Dearborn, National Advisory Committee for Aeronautics.
462. Formulas for the Stress Analysis of Circular Rings in a Monocoque Fuselage. By Roy A. Miller, Consolidated Aircraft Corporation, and Karl D. Wood, Cornell University.
463. Aerodynamic Tests of a Low Aspect Ratio Tapered Wing with Various Flaps, for Use on Tailless Airplanes. By Fred E. Weick and Robert Sanders, National Advisory Committee for Aeronautics.
464. A Complete Tank Test of a Model of a Flying-Boat Hull—N.A.C.A. Model No. 11. By James M. Shoemaker and John B. Parkinson, National Advisory Committee for Aeronautics.

- No.
465. Some Characteristics of Sprays Obtained from Pintle-Type Injection Nozzles. By E. T. Marsh and C. D. Waldron, National Advisory Committee for Aeronautics.
466. Engine Performance with a Hydrogenated Safety Fuel. By Oscar W. Schey and Alfred W. Young, National Advisory Committee for Aeronautics.
467. Simplified Aerodynamic Analysis of the Cyclogiro Rotating-Wing System. By John B. Wheatley, National Advisory Committee for Aeronautics.
468. A Study of Factors Affecting the Steady Spin of an Airplane. By Nathan F. Scudder, National Advisory Committee for Aeronautics.
469. A Summary of Design Formulas for Beams Having Thin Webs in Diagonal Tension. By Paul Kuhn, National Advisory Committee for Aeronautics.
470. A Complete Tank Test of a Model of a Flying-Boat Hull—N.A.C.A. Model No. 11-A. By John B. Parkinson, National Advisory Committee for Aeronautics.
471. A Complete Tank Test of a Model of a Flying-Boat Hull—N.A.C.A. Model No. 16. By James M. Shoemaker, National Advisory Committee for Aeronautics.
472. The Effect of Partial-Span Split Flaps on the Aerodynamic Characteristics of a Clark Y Wing. By Carl J. Wenzinger, National Advisory Committee for Aeronautics.

LIST OF TECHNICAL MEMORANDUMS ISSUED DURING THE PAST YEAR

- No.
687. Methods for Facilitating the Blind Landing of Airplanes. By M. Heinrich Gloeckner. From *Zeitschrift für Flugtechnik und Motorluftschiffahrt*, June 24, 1932.
688. Speed and Pressure Recording in Three-Dimensional Flow. By Dr. F. Krisam. From *Zeitschrift für Flugtechnik und Motorluftschiffahrt*, July 14, 1932.
689. The Problem of Tire Sizes for Airplane Wheels. By Franz Michael. From *Zeitschrift für Flugtechnik und Motorluftschiffahrt*, July 14, 1932.
690. Transmission of Heat from a Flat Plate to a Fluid Flowing at a High Velocity. By Luigi Crocco. From *L'Aerotecnica*, February 1932.
691. Some Ideas on Racing Seaplanes. By Giovanni Pegna. From *Rivista Aeronautica*, June 1932.
692. Methods of Recording Rapid Wind Changes. By A. Magnan. From *Jahrbuch No. 4 (1929) des Forschungsinstitutes der Rhön-Rossitten-Gesellschaft*.
693. The Testing of Airplane Fabrics. By Karl Schraivogel. From *Zeitschrift für Flugtechnik und Motorluftschiffahrt*, August 27 and September 14, 1932.
694. Combustion of Gaseous Mixtures. By R. Duchene. From *Publications Scientifiques et Techniques du Ministère de l'Air*, No. 11, Service des Recherches de l'Aéronautique.
695. Automatic Stability of Airplanes. By Fr. Haus. From *L'Aéronautique*, May, June, July, and August 1932.
696. The Problem of the Propeller in Yaw with Special Reference to Airplane Stability. By Franz Misztal. From *Abhandlungen aus dem Aerodynamischen Institut an der Technischen Hochschule Aachen*, No. 11, 1932.
697. The 'D.V.L. Gliding-Angle Control (W. Hübner Design). By Walter Hübner and Wilhelm Pleines. From *Zeitschrift für Flugtechnik und Motorluftschiffahrt*, August 12, 1932.
698. Dynamic Breaking Tests of Airplane Parts. By Heinrich Hertel. From *Zeitschrift für Flugtechnik und Motorluftschiffahrt*, August 14 and August 28, 1931.

- No.
699. The Process of Separation in the Turbulent Friction Layer. By E. Gruschwitz. From *Zeitschrift für Flugtechnik und Motorluftschiffahrt*, June 14, 1932.
700. Increasing the Volumetric Efficiency of Diesel Engines by Intake Pipes. By Hans List. From *Mitteilungen aus den technischen Instituten der Staatlichen Tung-Chi Universität*, Report No. 4, April 1932.
701. The Effect of a Gap between Elevator and Stabilizer on the Static Stability and Maneuverability about the Lateral Axis in Flight. By Walter Hübner. From *Zeitschrift für Flugtechnik und Motorluftschiffahrt*, June 14, 1932.
702. Determination of Inherent Stresses by Measuring Deformations of Drilled Holes. By Josef Mathar. From *Archiv für das Eisenhüttenwesen* (Communication from the Aachen Aerodynamic Institute), 1932-33.
703. Take-Off and Propeller Thrust. By Martin Schrenk. From *Zeitschrift für Flugtechnik und Motorluftschiffahrt*, November 14, 1932.
704. Scale Effect of Model in Seaplane-Float Investigations. By W. Sottorf. From *Zeitschrift für Flugtechnik und Motorluftschiffahrt*, December 28, 1932.
705. The Critical Shear Load of Rectangular Plates. By Edgar Seydel. From *Zeitschrift für Flugtechnik und Motorluftschiffahrt*, February 14, 1933.
706. Knowledge Gained from Practical Experience in the Designing of Aircraft Engines. By Oskar Kurtz. From *Zeitschrift für Flugtechnik und Motorluftschiffahrt*, December 14 and December 28, 1932.
707. Experiments with Needle Bearings. By Pericle Ferretti. From *Rivista Aeronautica*, October 1932.
708. Flight-Test Data on the Static Fore-and-Aft Stability of Various German Airplanes. By Walter Hübner. From *Zeitschrift für Flugtechnik und Motorluftschiffahrt*, January 28, 1933.
709. Future Problems of Soaring Flight (Report of 1932 Rhön Soaring Contest). By Walter Georgii; and Systematic Observations of Local Cumuli. By Roland Eisenlohr. From *Zeitschrift für Flugtechnik und Motorluftschiffahrt*, March 14, 1933.
710. Tests for the Elimination of Tail Flutter. By Curt Biechteler. From *Zeitschrift für Flugtechnik und Motorluftschiffahrt*, January 14, 1933.
711. Pressure Rise, Gas Vibrations, and Combustion Noises During the Explosion of Fuels. By Professor Wawrzyniok. From *Automobiltechnische Zeitschrift*, February 10 and March 10, 1933.
712. The Schneider Trophy Contest. By Alfred Richard Weyl. From *Zeitschrift für Flugtechnik und Motorluftschiffahrt*, August 12 and August 27, 1932.
713. Behavior of Vortex Systems. By A. Betz. From *Zeitschrift für angewandte Mathematik und Mechanik*, June 1932.
714. A Simple Method for Increasing the Lift of Airplane Wings by Means of Flaps. By Eugen Gruschwitz and Oskar Schrenk. From *Zeitschrift für Flugtechnik und Motorluftschiffahrt*, October 28, 1932.
715. Pressure and Frictional Resistance of a Cylinder at Reynolds Numbers 5,000 to 40,000. By L. Schiller and W. Linke. From *Zeitschrift für Flugtechnik und Motorluftschiffahrt*, April 13, 1933.
716. Development of the Rules Governing the Strength of Airplanes. By H. G. Küssner and Karl Thalau. Part I—German Loading Conditions Up to 1926. From *Luftfahrtforschung*, June 21, 1932.

- No.
717. Development of the Rules Governing the Strength of Airplanes. By H. G. Küssner and Karl Thalau. Part II—Loading Conditions in Germany (Continued), England, and the United States. From *Luftfahrtforschung*, June 21, 1932.
718. Development of the Rules Governing the Strength of Airplanes. By H. G. Küssner and Karl Thalau. Part III—Loading Conditions in France, Italy, Holland, and Russia—Aims at Standardization. From *Luftfahrtforschung*, June 21, 1932.
719. Dimensions of Twin Seaplane Floats. By L. Meyer. From *Association Technique Maritime et Aeronautique*, May 1933.
720. Recent Results of Turbulence Research. By L. Prandtl. From *Zeitschrift des Vereines Deutscher Ingenieure*, February 4, 1933.
721. Results of Extended Tests of the Focke-Wulf F 19a "Ente", a Tail-First Airplane. By Walter Hübner. From *Zeitschrift für Flugtechnik und Motorluftschiffahrt*, April 28 and May 13, 1933.
722. Guide Vanes for Deflecting Fluid Currents with Small Loss of Energy. By G. Kröber. From *Ingenieur-Archiv*, 1932.
723. An Airfoil Spanning an Open Jet. By J. Stüper. From *Ingenieur-Archiv*, 1932.

LIST OF AIRCRAFT CIRCULARS ISSUED DURING THE PAST YEAR

- No.
172. The Messerschmidt M. 29 Touring Airplane (German). A Two-Seat Cantilever Monoplane. From information furnished by the manufacturers, and from *Zeitschrift für Flugtechnik und Motorluftschiffahrt*, October 14, 1932.
173. Nieuport-Delage 590 Military Airplane (French). A Two-Place High-Wing Cantilever Monoplane. From *Revue de la Société Générale Aéronautique*, October 1932.
174. The D.H. "Dragon Moth" Commercial Airplane (British). A Twin-Engine Six-Passenger Biplane. From *The Aeroplane*, December 21, 1932; and *Flight*, December 22, 1932.
175. Heinkel He 64 c Sport Airplane (German). A Two-Seat Low-Wing Cantilever Monoplane. From data furnished by the manufacturers.
176. The Caudron P.V. 200 Touring Airplane (French). An All-Metal Amphibian Monoplane. From *L'Aéronautique*, December 1932, January 1933; and from information furnished by the manufacturers.
177. The Boulton and Paul P. 64 Mail-Carrier. A Two-Engine All-Metal Biplane. From *The Aeroplane*, April 5, 1933.
178. The Airspeed "Courier" Commercial Airplane (British). A Low-Wing Cantilever Monoplane. From *The Aeroplane*, March 22, 1933.
179. The Westland "Wallace" General-Purpose Airplane (British). An All-Metal Biplane. From *Flight*, May 4, 1933.
180. The Dewoitine D. 500 Pursuit Airplane (French). An All-Metal Cantilever Low-Wing Monoplane. From data furnished by the manufacturers.
181. The Shackleton-Murray SM-1 Light Airplane. A Two-Place High-Wing Monoplane. From *The Aeroplane*, May 17, 1933.
182. The Hanriot-Biche 110 C1 Airplane (French). An All-Metal Low-Wing Pursuit Monoplane. By Rene Rabion. From *Les Ailes*, March 30, 1933; and *L'Aéronautique*, May 1933.

- No.
183. Heinkel He 70 Commercial Airplane (German). A Seven-Seat Cantilever Low-Wing Monoplane. From data furnished by the manufacturers; and *Luftwacht*, March 1933.

FINANCIAL REPORT

The general appropriation for the National Advisory Committee for Aeronautics for the fiscal year 1933, as carried in the Independent Offices Appropriation Act approved June 30, 1932, was \$900,000. In accordance with provisions of the Economy Acts affecting personal services, furlough and compensation deductions amounting to \$72,586 were made during the fiscal year. The amount expended and obligated was \$827,186, itemized as follows:

Personal services.....	\$600, 043. 86
Supplies and materials.....	38, 309. 12
Communication service.....	1, 877. 83
Travel expenses.....	10, 256. 30
Transportation of things.....	1, 545. 12
Furnishing of electricity.....	29, 565. 29
Rent of office (Paris).....	960. 00
Repairs and alterations.....	17, 872. 08
Special investigations and reports.....	45, 200. 00
Equipment.....	81, 556. 65
Expenditures.....	827, 186. 25
Unobligated balance.....	227. 70
Furlough and compensation deductions.....	72, 586. 05
Total, general appropriation.....	900, 000. 00

The appropriation for printing and binding for 1933 was \$15,000, of which \$14,983 was expended.

The sum of \$6,780.82 was collected by this Committee during the fiscal year 1933, for scientific services furnished private parties, and this amount was deposited in the Treasury to the credit of Miscellaneous Receipts.

The appropriations for the current fiscal year 1934 are \$676,000 for general expenses and \$19,000 for printing and binding.

On August 23, 1933, a severe storm inundated Langley Field and 9 of the 11 Committee laboratories were flooded with salt water, reaching a maximum depth of 5 feet in the full-scale wind tunnel. Damage also resulted to the walls of several structures from the battering effect of waves and debris from Chesapeake Bay, backed by winds of hurricane intensity.

The Committee had previously obtained an allotment of \$200,000 from the Public Works Administration for needed items of construction and repair. Immediately after the storm the Public Works Administration authorized the expenditure of as much of the \$200,000 as might be necessary to repair the storm damage. This prompt action made it possible to minimize the direct and consequential damages. The cost of such emergency repairs was \$47,944, and

an additional allotment of this amount was subsequently made by the Public Works Administration for this purpose.

CONCLUSION

The Committee is grateful to the President and to the Congress for the liberal support that has been given to its work. It is proud of the contributions it has made to the progress of American aeronautics. It is glad to have the opportunity thus to make further contributions to the progress of civilization, for the history of the human race shows that man's

progress has kept pace with improvements in transportation. Each improvement in the performance, efficiency, and safety of aircraft increases the relative importance of aviation to the national defense, and hastens the advent of the era when air travel will grow with increased safety and flourish on a sound economic basis.

Respectfully submitted.

NATIONAL ADVISORY COMMITTEE
FOR AERONAUTICS,
JOSEPH S. AMES, *Chairman*.

REPORT No. 441

A FLIGHT INVESTIGATION OF THE SPINNING OF THE NY-1 AIRPLANE WITH VARIED MASS DISTRIBUTION AND OTHER MODIFICATIONS, AND AN ANALYSIS BASED ON WIND-TUNNEL TESTS

By NATHAN F. SCUDDER

SUMMARY

This report presents the results of an investigation of the spinning characteristics of the NY-1 naval training biplane. The results of flight tests and an analysis based on wind-tunnel test data are given and compared. The primary purpose of the investigation was the determination in flight of the effect of changes in mass distribution along the longitudinal axis, without change of mass quantity or centroid. Other effects were also investigated, such as those due to wing loading, center-of-gravity position, dihedral of wings, control setting, and the removal of a large portion of the fabric from the fin and rudder. The wind-tunnel test results used in the numerical analysis were obtained in the 7 by 10 foot wind tunnel through an angle-of-attack range of 90° .

The effect of varied mass distribution was to decrease the angle of attack and the linear and angular velocities, as ballast was moved from the center of gravity to the nose and tail of the airplane, without shift of centroid. Moderate changes in wing loading and dihedral of the wings and comparatively large changes in center-of-gravity position have small effects on the spin under the conditions of the tests. Different settings of ailerons and elevator altered the nature of the spin but did not bring about recovery, which was effected only by the rudder. The tests showed that full-down deflection of the elevator alone increased the rate of rotation, indicating that recoveries could best be made by using the rudder before moving the elevator down. Removal of a large portion of the fin and rudder covering (above the stabilizer and elevator) had no appreciable effect on the spin. A reasonable agreement was obtained between flight results and a numerical analysis, although the method of the analysis neglected many of the minor factors that usually are thought to influence the spin.

INTRODUCTION

The control of the spinning of airplanes is one of the important unsolved problems of the general subject of safety in flying. It has been the subject of many

researches in recent years, some of which are listed in the bibliography appended to this report. In these investigations the problem has been attacked from several theoretical and experimental aspects. On the theoretical side, analyses of the conditions for equilibrium in the steady spin, stability in the spin, the effect of control forces, and the effect of several important airplane characteristics have been made. The experimental investigations include flight tests with airplanes, tests with free-flying models, and tests in wind tunnels of models of airplanes or airplane parts. During the course of the present investigation, results have appeared in the literature on spinning that effectively illuminate some of the important features of spinning; however, the problem will require much more quantitative and extensive data before a satisfactory solution can be evolved.

The National Advisory Committee for Aeronautics has been engaged for some time in a comprehensive investigation of spinning. One phase of the investigation has been a quantitative determination of the motion of airplanes during spins both in their normal conditions and after various significant changes in the properties of the airplane have been made. The first step in this work was the development of a satisfactorily accurate method of making measurements, which was reported in reference 1. The present report deals with the application of this method to a study of the spinning characteristics of the NY-1 airplane, the first to be studied extensively. The principal effect studied was that of changes in mass distribution along the longitudinal axis, but the effects of some minor aerodynamic changes were determined also.

In order to furnish a logical basis for studying the intricately related flight results, an analysis of the spin based on wind-tunnel measurements on a model was made. The wind-tunnel data employed were obtained with a stationary balance, and some of the moments were computed by the strip method. The method of analysis was the same as that followed in reference 2.

of the individual containers were inversely proportional to their distances from the center of gravity. This arrangement made it possible to transfer ballast from the center of gravity to the nose and tail without altering the center-of-gravity position of the ballast. Latches and doors operated by a lever in the cockpit were provided on the front and rear containers so that their contents might be emptied quickly in a spin should an emergency requiring it arise. Such a necessity never occurred during the tests. Mass carried in these containers was used in determining the effect of different mass distributions with no change of center of gravity and for determining that of changes of center of gravity with changes of mass distribution.

The initial moments of inertia of the airplane with its test equipment installed were obtained by means of swinging tests. The virtual mass of the airplane under the conditions of the swinging tests was used in determining the moments of inertia, but no effort was made to compute the moments of inertia for the virtual mass corresponding to the air density and flow conditions of the spin, since the values thus computed would differ from the measured values by entirely negligible amounts.

Modifications were made to the airplane for the purpose of investigating the effect of changing the dihedral of the wings and the area of the empennage parts. The normal wing dihedral angles of 2.25° for the upper wing and 3.00° for the lower wing were changed to 0° for the upper and 1.25° for the lower, and to 4.17° for the upper and 4.60° for the lower wing. These modifications were accomplished by varying the lengths of the landing and the flying wires with no changes in the length of the struts. The resultant effect of these changes in the shape of the wing cellule can be readily appreciated by reference to Figure 1, in which the normal rigging is shown. The modifications to the empennage were accomplished by the removal of fabric covering to the extent shown in Figure 2. All of the fin covering and portions of the rudder and elevator covering were removed. The purpose of this modification to the empennage was to find to what degree the spinning characteristics of this airplane could be attributed to its unusually large tail surfaces.

Tests of the effect of control setting were made by recording steady spins with the ailerons fully deflected in each direction, in contrast to the neutral setting for all other tests, and with the elevator hard down instead of hard up. In making these tests, entry was effected in the usual manner, and after the spin had been started the control element was eased into the position for which the test was to be made. When steady motion had developed, the records were taken in the usual manner.

The instrument installation was essentially the same as that described in reference 1, consisting principally of three electrically driven gyroscopic angular-velocity

recorders, a 3-component accelerometer, and a sensitive altimeter. The quantities necessary for a complete determination of the motion of the airplane were measured with these instruments. For most of these tests the accelerometer was housed in an insulated box (all tests numbered higher than 40) that was held at constant temperature by a thermostatically controlled electric heater. Control of the operating temperature of this instrument eliminated temperature-effect errors and obviated the necessity for frequent changes of damping oil with changes of air temperature.

The accelerometer was placed as close to the center of gravity as possible, which was within a distance of 0.25 foot. Corrections to the accelerometer readings were not at first considered necessary, but after the flight tests had been completed it was thought advisable to make the correction to obtain forces acting at the center of gravity, especially because some of the tests



FIGURE 2.—Tail of the NY-1 airplane with fabric removed

involved changes in the center-of-gravity position. In order to make the correction, the coordinates of the accelerometer elements were needed, and in the absence of complete data the distances were estimated from partial data.

The method of making the flight tests and computing the results was the same as that described in reference 1 with the exception of the computation of the accelerometer-position correction just mentioned and that the virtual mass was used in computing the moments of inertia given in this report while it was not considered in the computations of reference 1.

RESULTS

Before presenting the results of the tests reported herein, a list of the symbols appearing in the text or tables which are not sufficiently defined on the covers of the report is given with definitions. A more extensive table of symbols and definitions may be found in the appendix of reference 1.

X'' , Y'' , Z'' , forces along ground axes.

p, q, r , components of angular velocity about airplane axes (based on the thrust line).

α , angle of attack referred to airplane X axis.

β , angle of sideslip (positive for outward sideslip).

ΔM , moment about airplane Y axis acting on propeller.

ΔN , moment about airplane Z axis acting on propeller.

$\Lambda = \frac{\Omega b}{2V}$, spin coefficient (Ω , resultant angular velocity).

C_x , tangential-force coefficient (airplane axes).

C_z , normal-force coefficient (airplane axes).

All the records were made at a mean standard altitude of 3,000 feet, hence the value of ρ used in computing the moment coefficients was 0.002176 slug per cubic foot. This value was used for all the other computations made in the investigation.

The data are presented completely in numerical form in Tables I, II, and III. Table I gives the results measured with instruments, Table II gives the condition of the airplane at the time of the spin, and Table III gives the results computed from records and the constants applying to the airplane.

Table II shows that for some flights ballast was placed in the rear ballast holder for the purpose of moving the center of gravity of the airplane rearward. This condition does not correspond to the ordinary condition for an airplane with its center of gravity farther aft than normal, because the stabilizer was not adjustable and changes in rigging were not made to balance the airplane "hands off." The external shape of the airplane was thus unaltered and the changes in the spin were the result of changes in center-of-gravity position and mass distribution only.

Pitching moments about the initial center-of-gravity position were used in computing all pitching-moment coefficients. This required adding the moment of the ballast (taking effect of accelerations into account) to the other moments (gyroscopic moment of the airplane and of the propeller) for the cases in which "tail-heavy" conditions of loading were used.

The center-of-gravity position is given as percentage mean chord in Table II. This mean chord was taken as the chord in the plane of symmetry midway between the upper and lower wing roots, with leading and trailing ends on lines joining the corresponding edges of the upper and lower wings, and having an incidence midway between that of the upper and lower wings.

PRECISION

The precision of the instrumental measurements was equivalent to that stated in reference 1 with the exception of the vertical-velocity measurements, in which the error may have been as much as 5 percent instead of 3 percent, the previously stated limit of error. This larger limit of error was indicated by the spread of measured vertical-velocity values and an occasional

evidence of sticking in the altimeter movement. Fluctuations of pressure in the cockpit may have been a contributory source of error.

Corrections for the distance of the accelerometer elements from the center of gravity were made as mentioned previously, using values for the coordinate of the elements estimated from partial data. The maximum error in these values was not in excess of 0.15 foot, and the resulting error in acceleration corrections was negligible.

The timer was tested on a turntable under conditions comparable to those of the spin and its operation and accuracy were found to be unaffected by rotation and acceleration.

A check on the accuracy of the angular-velocity recorders in most of the spins was obtained by timing 10 or 15 turns of the spin from the ground. The average angular velocity thus obtained agreed in general within 3 percent of the average angular velocity recorded by the instruments. This agreement is probably as close as the limits of accuracy of the timing.

The values in column 4 of Table III are indicative of the precision of the angular-velocity and acceleration records taken as a whole. These values (vertical force at the *c. g.*) should be 1 *g* in a steady spin, and it may be seen that the results deviate only slightly except in a few cases, notably for tests 51 and 52. The deviation in these latter tests was caused by lack of damping oil in the dashpot of the longitudinal element of the accelerometer, but since the maximum error of 0.1 *g* noted in the value of the longitudinal force causes only a small error in most of the results computed from the records, they were not discarded.

Moments of inertia of the airplane were not in error more than 1 percent, as stated in reference 3. This estimation of the precision is further supported by more recent tests to be reported soon. The determinations of weights of the airplane at the time of the spin were likewise not in error more than 1 percent.

The limits of error of the fundamental measurements may be summarized as follows: Angular velocity, 3 percent for each component; acceleration, 0.05 *g* except in a few extreme cases which fell within 0.1 *g*; interval of altitude, 5 percent; time, 2 percent; weight, 1 percent; moments of inertia, 1 percent.

DISCUSSION OF RESULTS

The tests were planned to show the effect of changes of single factors of the airplane properties on the spin as far as this was physically possible without major modifications to the airplane. For instance, it was not practicable to move the center of gravity aft other than by placing ballast at the tail, and this was accompanied by a large change in the moments of inertia. The results are further complicated by incidental factors, such as asymmetry of rigging or shape of the airplane. These tests and experience with other airplanes indicated that right and left spins were not

comparable, even with the motor idling slowly or stopped. Tests such as those reported herein should therefore be made in one direction of spin only or in parallel series of tests in each direction of spin. In general, the former course was followed in these tests. One should bear in mind, therefore, that conclusions drawn from the results later discussed might have been slightly different if the spins had been made in both directions for each condition tested.

Angle of attack.—This airplane spins at moderately high angles of attack. Throughout the tests the angle of attack varied through a range of 10° (46° – 56°) for the left spins. The range of angles of attack for the right spins was about 12° (39° – 51°). In comparison, values have been observed with other airplanes that have shown the value of angle of attack to range from 30° to 70° in extreme cases.

Angle of sideslip.—The angle of sideslip for the normal left spins was zero or very small. For the normal right spins this angle was positive (outward) and of moderate magnitude (5° to 8°). Considering this in relation to the angle of attack, it is noted that relatively small angles of attack, as for the right spins, are associated with positive sideslip (outward), whereas the larger angles of attack of the left spins were associated with zero (or very small) angles of sideslip.

Effect of wing loading.—The only important changes in spin characteristics brought about by a change from 8.2 to 10.0 pounds per square foot wing loading were increases in linear velocity and angular velocity. The pertinent tests are tabulated for comparison in Table IV.

TABLE IV

Group	Test Nos.	$\frac{W}{S}$		V		Ω	
		Lb./ft. ²	Increase	Ft./sec.	Increase	Rad./sec.	Increase
A	16, 17, 18	8.2	Per cent	80.4	Per cent	2.46	Per cent
B	29, 30, 31	10.0	22.0	91.4	13.5	2.76	12.2
C	45, 46	10.0	22.0	83.6	4.0	2.65	7.7

Test groups A and B, when compared, show that the velocity along the flight path and the angular velocities both vary roughly as the square root of the wing loading. Reference to the simplified equations of motion given in the latter part of this report and consideration of the changes in angle of attack (see Table III) show that these results compare satisfactorily with the theory. The lack of agreement between the groups of tests B and C (Table IV) may be partly due to error in measurement of vertical velocity, but it is undoubtedly due in considerable measure to the difference in the spins, as shown by the fact that the angle of attack for the tests of group B was 50.6° and for group C it was 51.4° . The reason for this difference in spins is not known, other than that these groups of tests were separated in time by several months and some unno-

ticed changes in the airplane, such as changes in the condition of the fabric, may have occurred. Tests 45 and 46, therefore, should be omitted in the discussion of the effect of wing loading.

Effect of mass distribution.—Change in mass distribution produced by moving ballast from the center of gravity to the nose and tail caused a decrease in rate of rotation, decrease in angle of attack, negligible change in sideslip angle, and a decrease in glide-path angle. These effects are to be seen by comparing tests 29, 30, 31 with tests 19, 20, 21. The averages of the values mentioned above for the two groups of tests are tabulated in Table V with the values of the spin radii. (Table II gives ballast and moments of inertia for these tests.)

TABLE V

Test Nos.	Ballast position	Ω	α	β	γ	Radius
		Rad./sec.	$^\circ$	$^\circ$	$^\circ$	Feet
29, 30, 31	At c. g.	2.76	50.6	-2.0	-83.2	3.5
19, 20, 21	At nose and tail	2.21	47.0	.4	-81.5	6.3

The effect of this mass distribution change on the ease of recovery was practically negligible. There were indications, however, that if any difference existed it was a tendency toward easier recovery for the spins with ballast at the nose and tail than for the spins with all ballast at the center of gravity, the same method of manipulating the controls being used in both cases.

Effect of moving the center of gravity aft.—The effect of a rearward position of the center of gravity with respect to its normal position can not be seen directly from these tests, because, on account of the limited ballast-carrying capacity of the airplane, appreciable displacement of the center of gravity could be accomplished only by putting ballast in the tail, and such procedure changes the moments of inertia more extensively than it changes the center-of-gravity position. The test results therefore show directly the effect of putting ballast in the rear end of the fuselage and indirectly the effect of the rearward position of the center of gravity. For the purpose of comparing results, the characteristics for the pertinent groups of tests are tabulated in Table VI. (Table II gives ballast and moments of inertia.)

TABLE VI

Group	Test Nos.	Ballast position	c. g., per cent mean chord	Ω	α	β	γ	Radius
				Rad./sec.	$^\circ$	$^\circ$	$^\circ$	Feet
A	29, 30, 31	c. g.	25.8	2.76	50.6	-2.0	-83.2	3.5
B	19, 20, 21	Nose and tail	25.8	2.21	46.9	.4	-81.5	6.3
C	32, 33, 34	Tail and c. g.	34.5	2.18	49.6	.9	-80.8	6.2
D	35, 36, 37	Tail and c. g.	40.0	1.74	48.0	1.1	-79.4	10.0

As may be seen from Table II, groups B and C represent about equal increases of moments of inertia

(group B having slightly greater values than C) and, in regard to moments of inertia, are comparable. The moments of inertia for group D are much greater than for those of any of the other tests.

The effect of placing a large amount of ballast in the tail of the airplane as shown by a comparison of these data was a large decrease in rate of rotation, slight decrease in angle of attack, slight change in sideslip (in outward sense), and a large increase of radius of spin. The ease of recovery with ballast in the tail was the same as in the normal condition. Similar results have been observed in other airplanes, but the same results probably would not be found with all airplanes. Pilots should not conclude from these results that it is safe to place ballast or luggage in the rear part of the fuselage, unless tests have been made to prove the point.

Conclusions concerning the effect of the center-of-gravity position alone without any mass-distribution effect can not be drawn from the flight results with any certainty. It is evident from the flight results that with this airplane the rearward position of the center of gravity had very little effect; however, the exact nature of whatever effect there may have been can not be determined. Reference to the analysis given in the Analysis of Model Test Data shows that little effect would have resulted from the rearward displacement of the center of gravity, and that there might have been a slight decrease in angle of attack and rate of rotation.

Effect of dihedral of wings.—The effect of dihedral of the wings may be seen from Table VII. (Table II gives amounts of ballast and moments of inertia.)

TABLE VII

Test No.	Dihedral		Ω	α	β	γ	Radius	
	Lower wing	Upper wing						
57, 58, 60, 61, 62...	°	°	Rad./sec.	°	°	°	Feet	} c. g. at 25.8 per cent mean chord, no ballast.
16, 17, 18	1.25	0	2.42	54.3	1.1	-82.8	4.1	
76, 77, 78	3	2.25	2.46	48.5	1.0	-82.1	4.6	
	4.6	4.17	2.56	50.7	0	-82.9	4.0	
63, 64, 65, 35, 36, 37	1.25	0	1.71	55.6	3.3	-80.1	8.6	} c. g. at 40 per cent mean chord and full ballast.
66, 68, 69	3	2.25	1.74	48.0	1.1	-79.4	10.0	
	4.6	4.17	1.89	51.2	1.8	-80.3	8.1	

The effect of dihedral is evidently very small, but these results indicate that an increase of wing dihedral causes a slight increase in angular velocity. The recovery from spins was not noticeably affected by the changes of dihedral employed in the tests.

Effect of decreased area of empennage elements.—Tests 76, 77, 78 were made with fabric stripped from elements of the empennage as described above, and they will be compared with tests 16, 17, 18 in Table VIII. The ballast conditions in these two groups of tests were not identical, as may be seen in Table II, but differed only by the weight and moment of inertia of the ballast containers, which were in place in the

airplane for the tests with the empennage altered but not for the tests 16, 17, 18 in which the empennage was in its normal condition. Aside from this small difference of ballast, the conditions of the tests involve no changes other than the change in empennage area. There was no appreciable difference in the ease of recovery for these two groups of tests.

TABLE VIII

Test Nos.	Condition of empennage	Ω	α	β	γ	Radius
		Rad./sec.	°	°	°	Feet
16, 17, 18	Normal	2.46	48.5	1.0	-82.1	4.6
76, 77, 78	Part of fabric removed	2.50	49.4	-1.6	-82.2	4.4

The values in Table VIII show that the spins with the fabric removed were practically the same as those with the airplane in its normal condition. This result leads to the conclusion that the air forces on the area from which the fabric was removed were normally small during the spin and, since the ease of recovery was not affected, the conclusion must apply also to the forces acting on these areas during recovery. Considering the forces that produced recovery (and recovery was effected mainly by means of the rudder with this airplane), the facts that very little fabric was removed from the rudder below the elevator, and that the ease of recovery was about the same for both groups of tests show that the important part of the rudder must have been the portion below the elevator where the air flow was unobstructed. A further conclusion that may be drawn is that since the actual area of the rudder which was effective was small, the yawing moment required to effect recovery, or at least the initial stages of the recovery must have been small.

Effect of control setting.—The effect of control setting may be seen in Table IX which shows results for right spins.

TABLE IX

Test Nos.	Control variation from normal ¹	Ω	α	β	γ	Radius
		Rad./sec.	°	°	°	Feet
6, 7, 8	None	2.48	42.4	8.0	-80.9	5.7
9	Ailerons with spin	2.91	47.7	-8.7	-82.8	3.5
12	Ailerons against spin	2.56	51.5	14.7	-82.6	4.0
13	Elevator down	3.17	40.3	16.2	-82.0	4.0

¹ The controls were deflected in the manner stated in the table to the extreme limit of their ranges.

In general, it is noted that aileron deflection causes a pronounced change in the nature of the spin, especially with respect to the angle of sideslip. The changes in the sideslip angle of the spin are undoubtedly related to the effect of aileron deflection on rolling moment due to rolling, but since many other factors are involved in the change of aerodynamic properties caused by aileron deflection, more complete data will be needed before the results may be completely understood.

stood. Several characteristics other than sideslip angle were affected by aileron deflection, especially angle of attack and rate of rotation, which were both increased by aileron deflection in either sense.

The airplane had no tendency to recover as a result of aileron deflection, but undoubtedly the aileron setting must influence recovery indirectly, because of the difference in the nature of the spins produced. No tests on this subject were made.

The effect of aileron deflection on the spins of several other airplanes was noted during the course of the investigation and considerable difference in results was observed for the different airplanes. Because both the rolling moments and the yawing moments introduced by aileron deflection influence the spin, as will be seen in the analysis given later in this report, it is evident that the many variations of proportions and arrangements of ailerons occurring on different airplanes (especially on biplanes) would result in a wide variation of behavior.

Test results and experience indicate that conventional ailerons offer little promise for effective control of the spin; however, as in most cases some effect may be obtained, there is no reason why pilots should not avail themselves of this aid after experimenting with their particular airplanes to find the best conditions for recovery.

Downward deflection of the elevator produced an increase in angular velocity as shown in Table IX (right spins) and also in Table X giving results for left spins. For the right spins, downward deflection of the elevator produced a large increase in outward sideslip. In other respects the effect of downward elevator deflection is the same as for the left spin with normal center-of-gravity position discussed in the following paragraphs.

The effect of deflecting the elevator downward for left spins is shown by the results given in Table X for two mass-distribution and center-of-gravity conditions. The ballast used and moments of inertia are given in Table II.

TABLE X

Test Nos.	c. g., per cent mean chord	Elevator setting	Ω	α	β	γ	Radius
			Rad./sec.	°	°	°	Feet
29, 30, 31	25.8	Up-----	2.76	50.5	-2.0	-83.2	3.5
53, 54, 56	25.8	Down-----	3.42	47.7	5.0	-82.9	2.8
35, 36, 37	40.0	Up-----	1.74	48.0	1.1	-79.4	10.0
49, 51, 52	40.0	Down-----	2.48	49.5	1.2	-81.7	5.3

The most evident effect of putting the elevator down in all the tests made in the investigation was an increase in angular velocity, and this was accompanied by a small decrease in angle of attack; in fact, with the center of gravity in a rearward position the angle of attack increased when the elevator was put down. This result led to the expectation that possibly a more

rapid recovery from the spin could be effected by holding the elevator up during the first part of the recovery and putting it down later instead of immediately as is usually recommended. Accordingly, a few flight tests were made to compare the usual method of recovery with a method in which the elevator was held up at first until the rotation had been practically stopped by means of the rudder. The number of turns and altitude required for recovery were determined for both methods by simple observations, and no great difference in number of turns or altitude required was found. The NY-1 airplane was not particularly well suited for these tests, however, because it would recover normally in 1 to 1½ turns; an airplane requiring many turns for recovery would have shown the effect of this method of control manipulation much more clearly.

ANALYSIS OF MODEL TEST DATA

At present there are not sufficient data available to make an exact numerical analysis including all the factors affecting the spin; however, approximate methods utilizing wind-tunnel model tests have been devised which are very helpful, and which in some cases give results surprisingly consistent with flight measurements. A computation of the characteristics of the spin by one of these methods would be of especial interest when applied to an airplane for which accurate flight data were available, and therefore wind-tunnel measurements were made on a model of the airplane used in the above-described flight investigation to be used for a numerical analysis.

Fuchs and Schmidt have reported (reference 2) a method of analyzing spins that is logical and as complete as practicable with the data available. Other somewhat similar methods have been reported, but their method is best suited to this study and was used almost without change, except that the conventional symbols and axes of the National Advisory Committee for Aeronautics were employed.

MODEL TESTS

A 1/12-scale model of the airplane was tested in the 7 by 10 foot open-throat wind tunnel, which, with its balance and test procedure, is described in reference 4. Measurements of lift, drag, and pitching moment were made over a range of from 0° to 90° angle of attack (referred to *X* body axis) and all appropriate corrections, except tunnel-wall corrections, were made. The tunnel-wall correction is of no importance for these tests, since it is relatively small at very high angles of attack. Three positions of the elevator were tested for the complete model. For the tests of the wing cellule a center section was inserted in the lower wing where the fuselage formerly had been. The wing cellule was then tested through the same angles as those for the complete model. All coefficients were computed on

the basis of the area of the wing cellule with the lower wing carried through. Moment coefficients were referred to the center of gravity. The results of the model tests are presented as curves in Figure 3. The normal and tangential force curves were computed from the wing cellule alone and are given in Figure 4.

CALCULATIONS

The preliminary assumptions employed in the method outlined by Fuchs and Schmidt were that

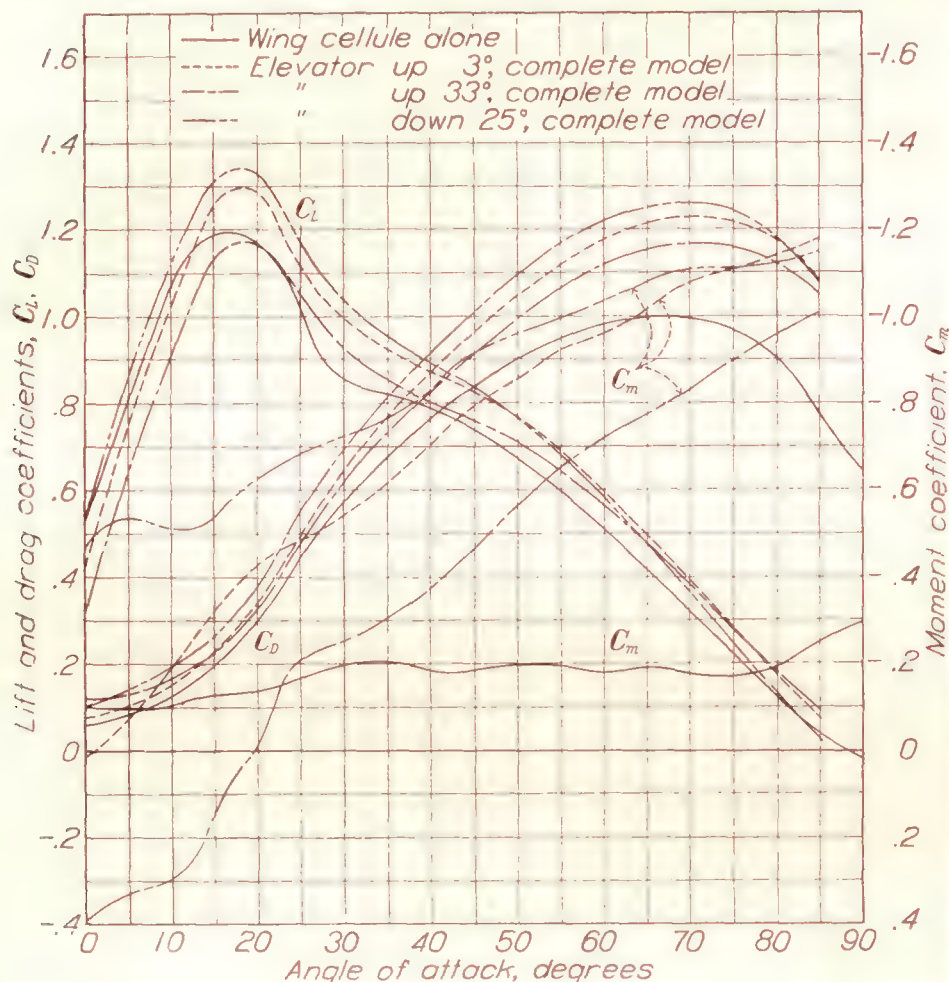


FIGURE 3.—Aerodynamic characteristics of a 1/12-scale model of the NY-1 airplane and of the wing cellule alone

lift, drag, and lateral force were not seriously affected by moderate degrees of sideslip; that lift, drag, and pitching moment were not affected seriously by small rates of rotation; and that rolling and yawing moments were affected by sideslip of 20° or less only in a manner that would correspond to some particular aileron setting with no sideslip. Some of these assumptions lead to negligible errors; others, as for example the assumption that lift, drag, and pitching moments are not affected by rotation, lead to small errors, but the necessity of assuming that rolling moment due to sideslip must be counterbalanced by a certain amount of aileron moment is indeed unfortunate when a study of a particular spin is to be made. An assumption that sideslip had no effect on the rolling moments would be untenable for values of sideslip of 10° or 20°, as may be seen from the results of reference 5.

When the method of Fuchs and Schmidt was applied to the left spins of the NY-1 airplane, it was improved in three particulars: (1) The airplane was known to spin with no sideslip (or a very small degree of side-

slip) with the controls in the normal setting for the spin, which eliminates errors from sideslip in the most important spin to be studied; (2) the pitching moment due to pitching as determined by approximation was found to be about equal to the pitching moment exerted on the propeller measured in the flight tests for left spins, making it possible to simplify the equations by dropping the terms for both of these factors; and (3) the moments of inertia of this airplane were known from actual measurement.

The yawing moment of the fuselage and empennage due to yawing is a factor of considerable importance and one concerning which the information available is meager. The importance of this factor is indicated by two results of the flight tests: First, the tests indicated that all of the vertical surface of the empennage above the stabilizer and elevator was practically ineffective during the spin; and, second, it was found that the airplane would not remain in a spin if the rudder was neutralized while the elevator was still held hard up as for a spin. Since the effective area of the rudder was evidently small, the change in yawing moment that destroyed the spinning equilibrium was small, which points to the importance of even a small moment. On the other hand, wind-tunnel tests made in England and at this laboratory have shown that for rectangular-section fuselage the magnitude and sense of the yawing moments (due to yaw or yawing)

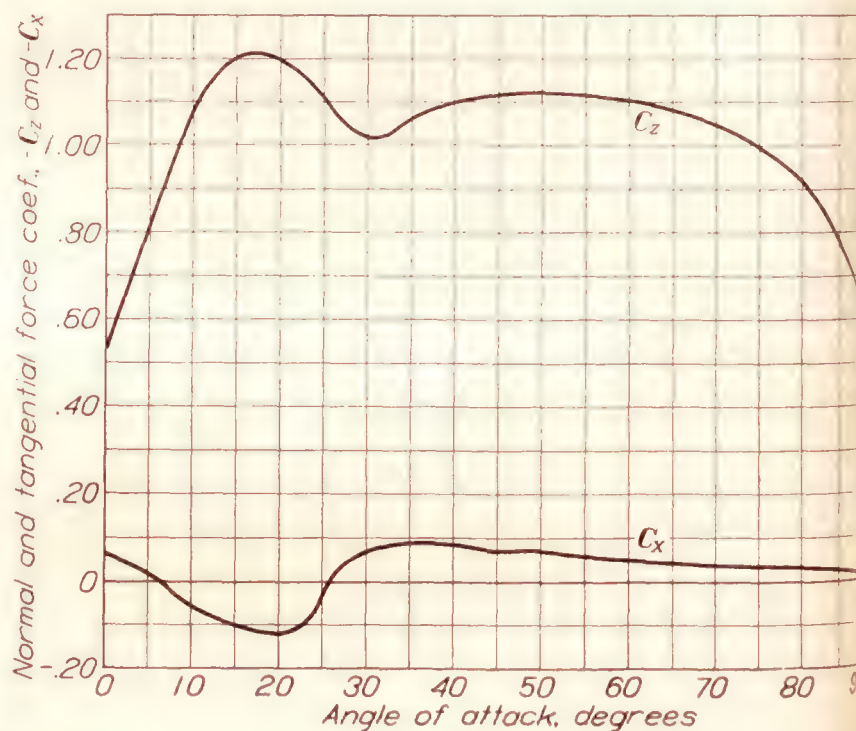


FIGURE 4.—Normal-force and tangential-force curves for the 1/12-scale model NY-1 wing cellule alone

high angles of attack were so much dependent upon details of shape that a method of approximation was practically out of the question. Thus, in spite of the importance of an exact knowledge of this factor, about the only course left open in the question was to assume that the yawing moment of the fuselage and empennage due to yawing was zero.

The rolling and yawing moments of the wing cellule due to rolling and yawing, computed by the strip method, are not exact when a finite number of strips

are employed, but the accuracy of this type of computation is certainly within the limits of the errors of the assumptions required for other parts of the analysis. These wing rolling and yawing moments were equated to the gyroscopic rolling and yawing moments acting on the airplane, since the rolling and yawing moments of the other parts of the airplane were taken to be zero. The rolling moment of the fuselage and empennage may be seen to be negligible from a consideration of their shapes; the reason for assuming the yawing moment of the fuselage and empennage to be zero was discussed in the foregoing paragraph.

The computation of the quantities necessary in the analysis of a spin is based on the following six equations of motion, which are the simplified forms of the general equations given in reference 6 for the case of zero sideslip.

Equilibrium of forces:

Path axis:

$$-W \sin \gamma - C_D q S = 0 \quad (1)$$

Lift axis:

$$m V \Omega \cos \gamma \sin \phi + W \cos \gamma \cos \phi - C_L q S = 0 \quad (2)$$

Axis \perp to path and lift axes:

$$m V \Omega \cos \gamma \cos \phi + W \cos \gamma \sin \phi = 0 \quad (3)$$

(Ω is positive for right spins.)

Equilibrium of moments, incorporating the above-mentioned simplifications:

$$-(B-C) qr = L \quad (4)$$

$$-(C-A) rp = M \quad (5)$$

$$-(A-B) pq = N \quad (6)$$

The values of p , q , and r , the angular velocities about the airplane body axes (assumed to coincide with the principal axes, which in many cases is exactly true, and is very nearly true in all others) were determined in terms of the resultant angular velocity and attitude angles, as follows:

$$p = -\Omega (\cos \gamma \cos \phi \sin \alpha + \sin \gamma \cos \alpha).$$

$$q = \Omega (\cos \gamma \sin \phi).$$

$$r = \Omega (\cos \gamma \cos \phi \cos \alpha - \sin \gamma \sin \alpha).$$

Solving (1) for V after substitution of $\frac{1}{2} \rho V^2$ for q :

$$V = \sqrt{\frac{-2W \sin \gamma}{C_D \rho S}} \quad (7)$$

Taking $\rho = 0.002176$ slug per cubic foot (3,000 feet altitude), $W = 2,910$ pounds (full ballast total weight), $S = 291$ square feet (area with wing extended through fuselage):

$$V = 95.5 \sqrt{\frac{-\sin \gamma}{C_D}}$$

Solving (2) and (3) for Ω :

$$\Omega = \sqrt{\frac{C_L^2 S^2 \rho^2 V^2}{4 m^2 \cos^2 \gamma} - \frac{g^2}{V^2}} \quad (8)$$

which, with the constants combined, becomes:

$$\Omega = g \sqrt{(1.18 \times 10^{-8}) \frac{C_L^2 V^2}{\cos^2 \gamma} - \frac{1}{V^2}} \quad (9)$$

Solving (3) for ϕ :

$$\phi = \tan^{-1} \left(\frac{V \Omega}{g} \right) \quad (10)$$

Because analytic expressions could not be obtained for the variation of lift and drag as a function of α , the solution could only be obtained by a semigraphical method. Therefore, choosing the values of $\gamma = -80^\circ$ and $\gamma = -86^\circ$, velocities along the flight path were computed for the whole range of angle of attack and plotted in Figure 5. Then values of Ω were computed and plotted in Figure 6 for $\gamma = -80^\circ$, -82° , -85° , -86° , and finally values of angle of bank ϕ were computed and plotted in Figure 7. These quantities made it possible to compute values of p , q , and r in terms of α with γ as a parameter. (Figs. 8 to 10.)

With the values of p , q , and r computed it was possible to evaluate the expressions:

$$C_{l_w} = \frac{1}{V^2 S b} \sum_{y=-\frac{b}{2}}^{y=\frac{b}{2}} \left(C_z(\alpha + \Delta\alpha, V + \Delta V) \left(\frac{V + \Delta V^2}{\cos \Delta\alpha} \right) \right) c y \Delta y,$$

and

$$C_{n_w} = -\frac{1}{V^2 S b} \sum_{y=-\frac{b}{2}}^{y=\frac{b}{2}} \left(C_x(\alpha + \Delta\alpha, V + \Delta V) \left(\frac{V + \Delta V^2}{\cos \Delta\alpha} \right)^2 \right) c y \Delta y$$

in which $\Delta V = r y$ and $\Delta\alpha = \tan^{-1} \frac{p y}{V + \Delta V}$ and C_z and C_x are taken from the curves (fig. 4) of normal and tangential force coefficients of the wing cellule alone. As mentioned previously, the rolling and yawing moments of the wing cellule are set equal to the total aerodynamic rolling and yawing moments:

$$C_{l_w} = C_l$$

$$C_{n_w} = C_n$$

The actual computation of these two moments was made by using four strips on either side of the plane of symmetry.

The computed values of p , q , and r and the moments of inertia determined by measurement were used to compute the gyroscopic moments.

Figures 11 to 13 are curves of computed aerodynamic and gyroscopic moments about the three axes plotted in terms of angle of attack and for the several values of glide path. It is evident that in considering any one of these sets of three figures, equilibrium of moments might exist for any of the intersections of aerodynamic and gyroscopic moment curves corresponding to the same glide-path angle. However, it is necessary that equilibrium exist about all three moment axes simultaneously for a steady state of motion (spinning), and consequently only those intersections which occur for the same glide-path angle and angle of attack on the three charts of moments corresponded to an actual steady spin. Curves of glide-path angle and angle of

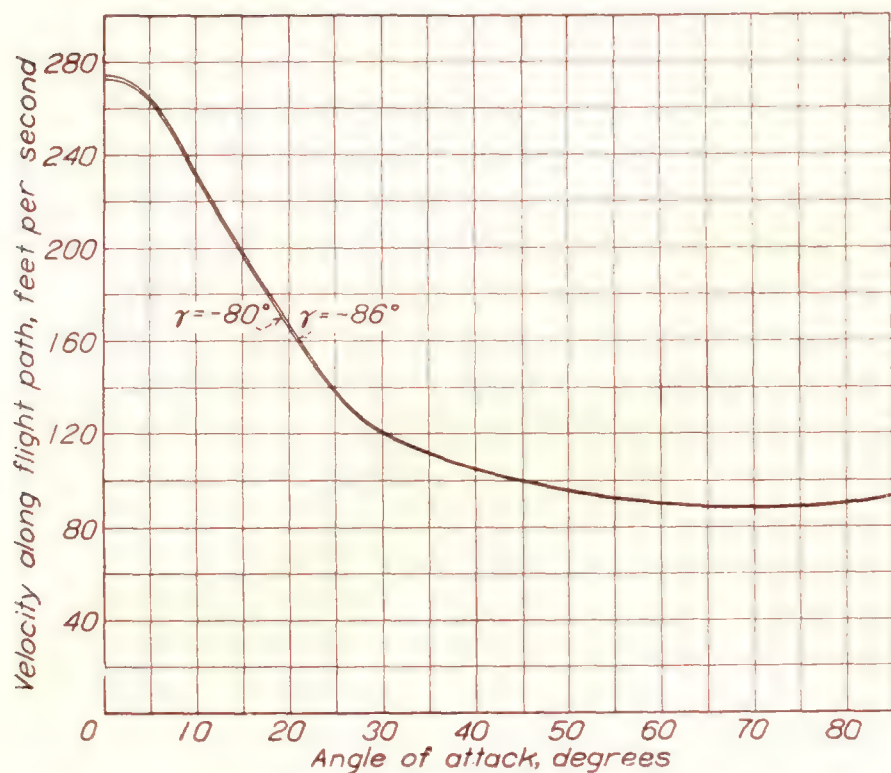


FIGURE 5.—Computed velocity along flight path, elevator up 33°, ballast at c. g.

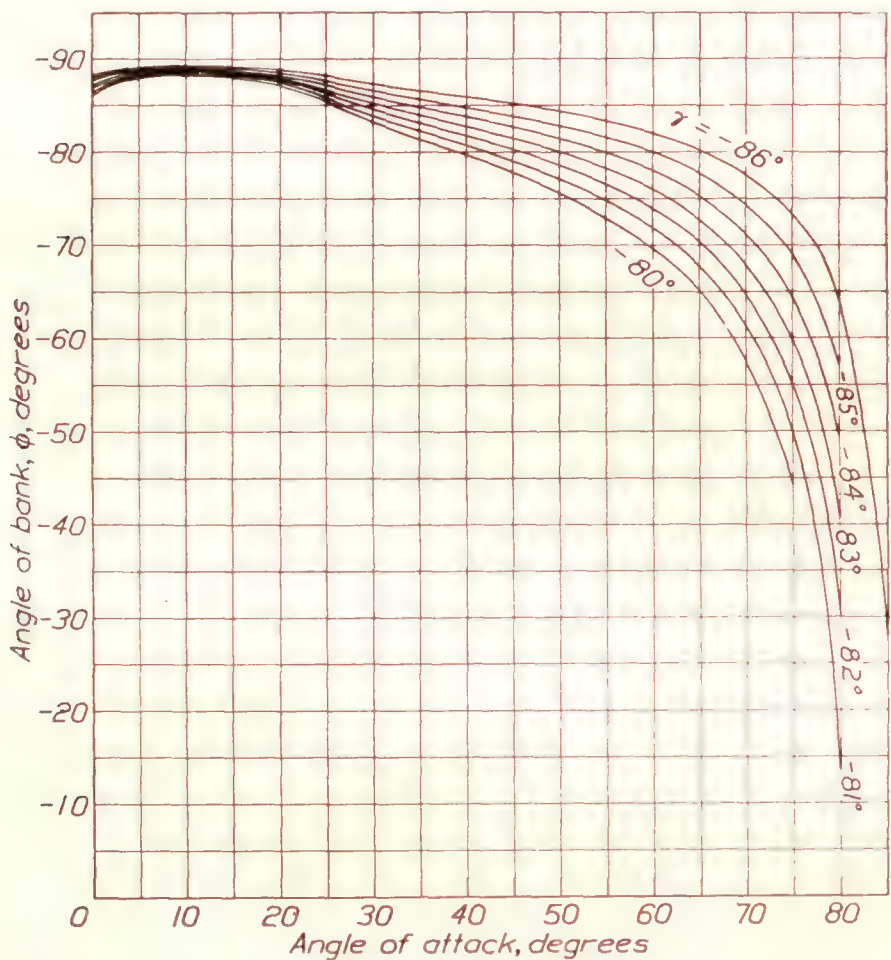


FIGURE 7.—Computed angle of bank, elevator up 33°, ballast at c. g.

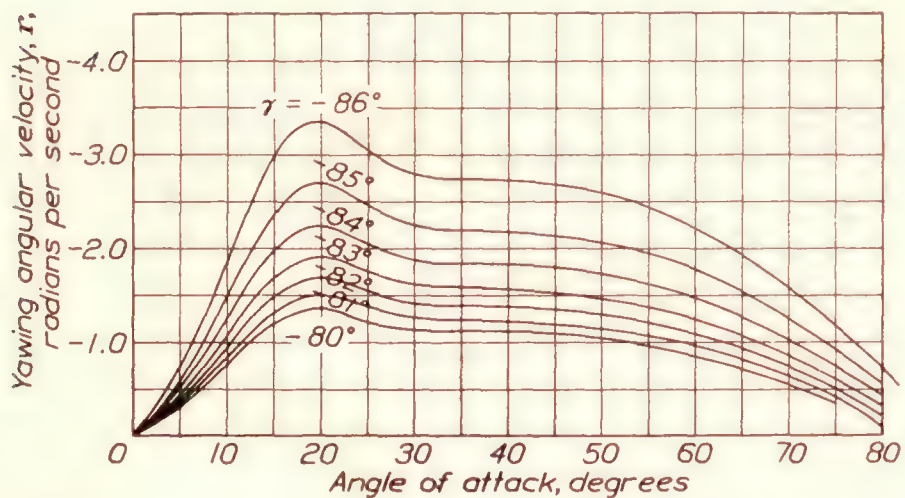


FIGURE 10.—Computed yawing angular velocity, elevator up 33°, ballast at c. g.

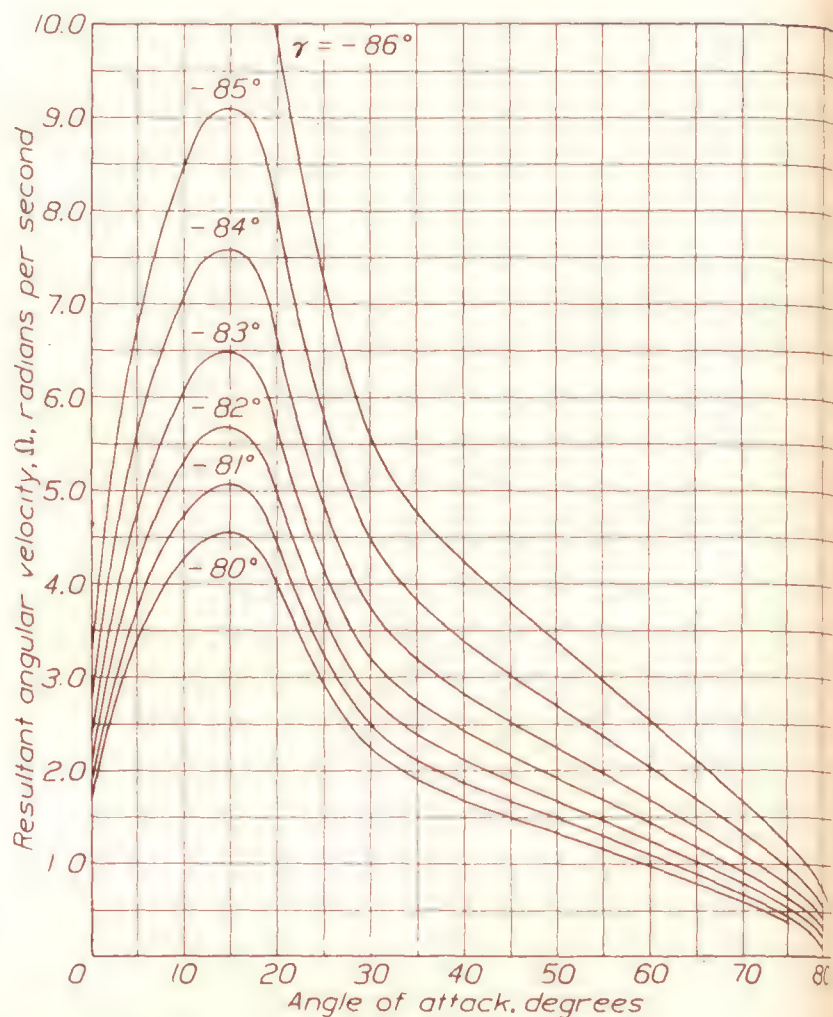


FIGURE 6.—Computed resultant angular velocity, elevator up 33°, ballast at c. g.

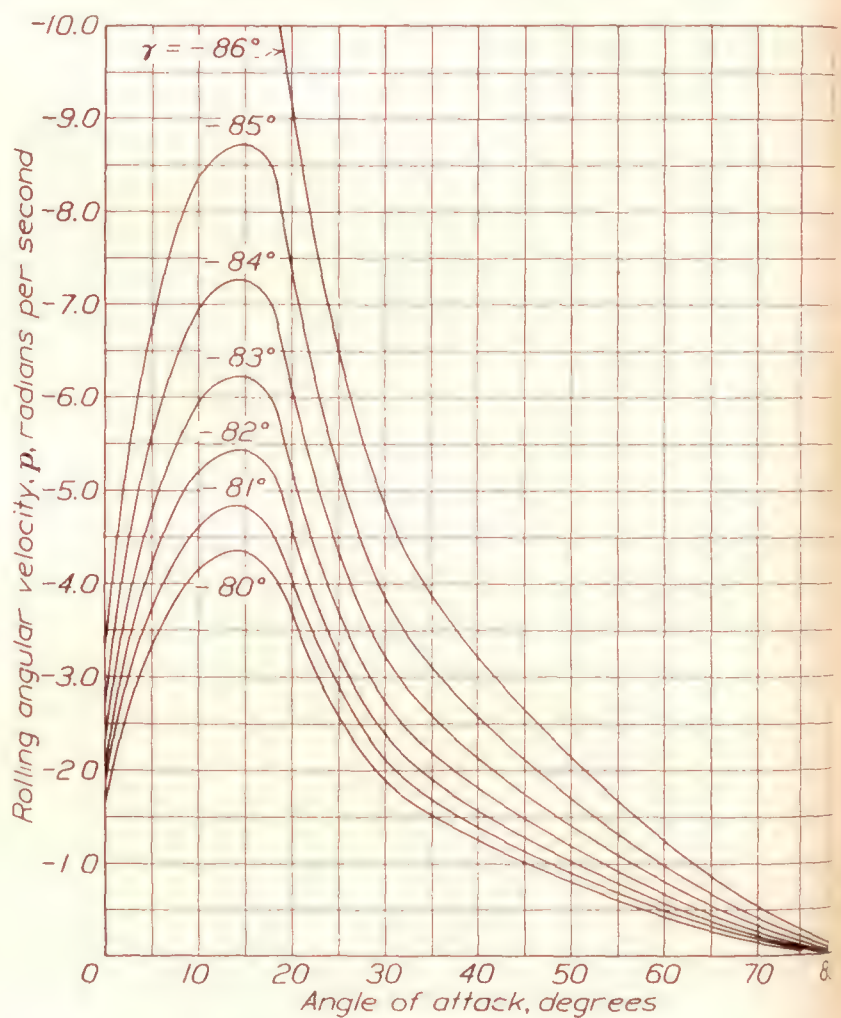


FIGURE 8.—Computed rolling angular velocity, elevator up 33°, ballast at c. g.

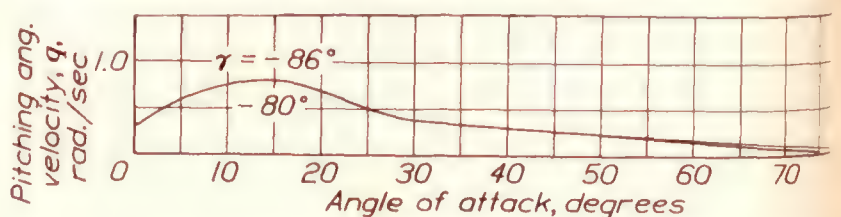


FIGURE 9.—Computed pitching angular velocity, elevator up 33°, ballast at c. g.

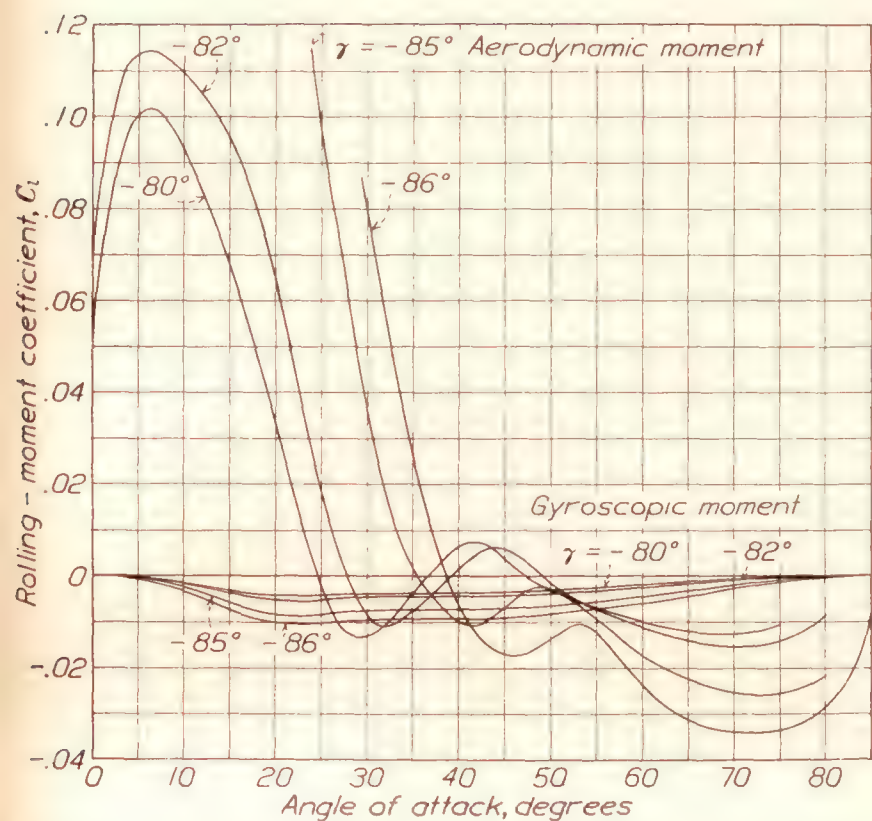


FIGURE 11.—Computed aerodynamic and gyroscopic rolling-moment coefficients, elevator up 33°, ballast at c. g.

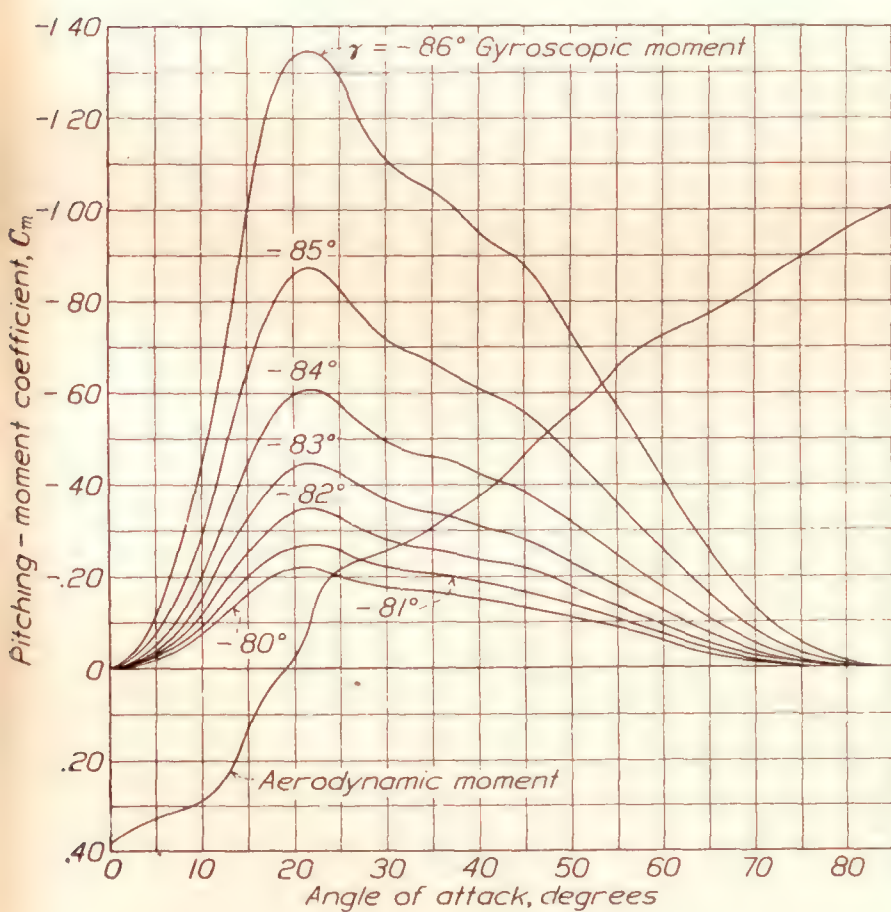


FIGURE 12.—Computed aerodynamic and gyroscopic pitching-moment coefficients, elevator up 33°, ballast at c. g.

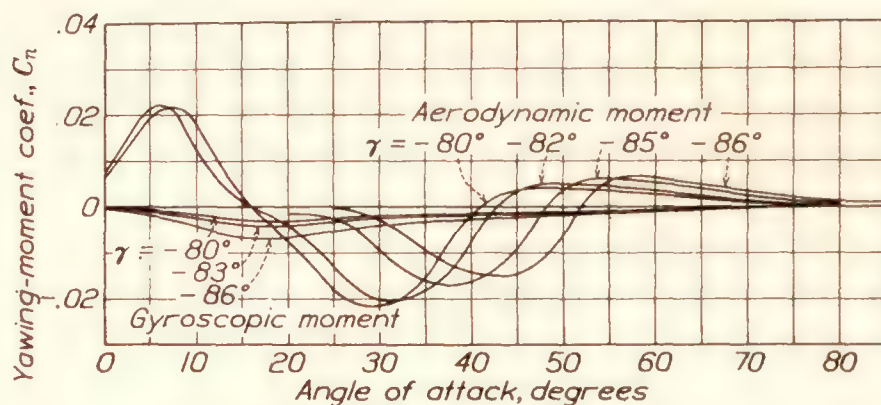


FIGURE 13.—Computed aerodynamic and gyroscopic yawing-moment coefficients, elevator up 33°, ballast at c. g.

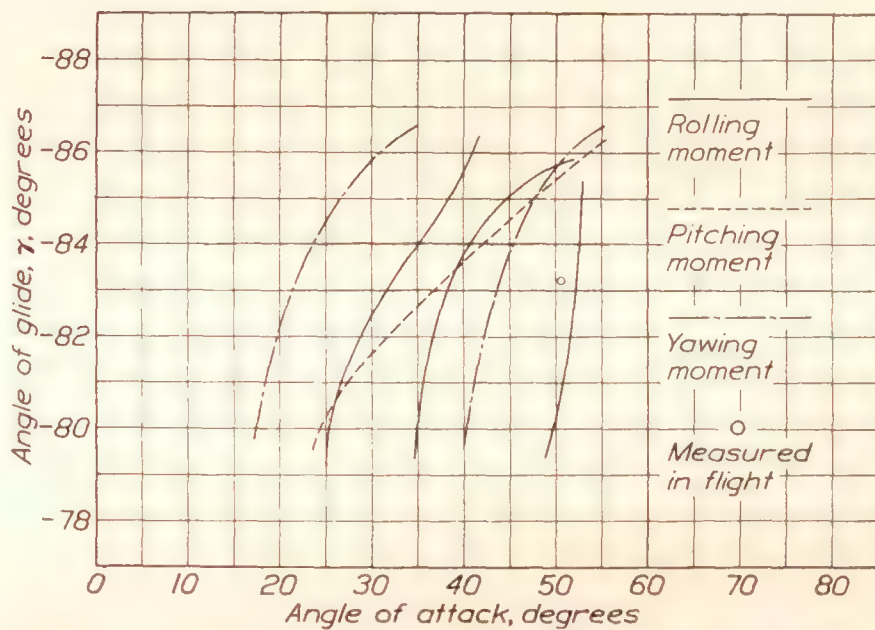


FIGURE 14.—Equilibrium of three moments, elevator up 33°, ballast at c. g.

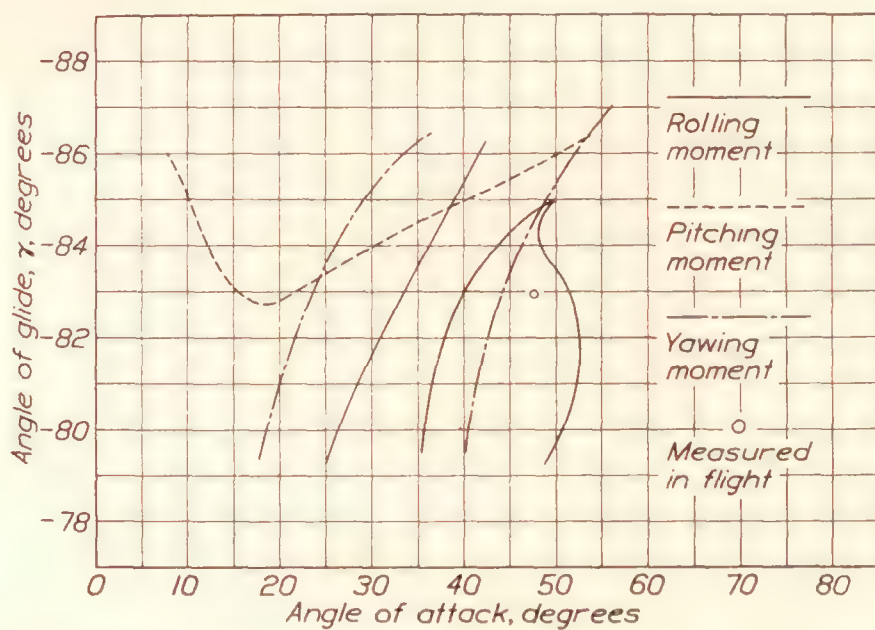


FIGURE 15.—Equilibrium of three moments, elevator down 25°, ballast at c. g.

attack, at which equilibrium of moments occurs for each of the three moments, are given in Figure 14. The curves of Figure 15 were obtained by a similar computation based on the model test with elevator down. Interesection of the three curves for rolling, pitching, and yawing moments at one point in these

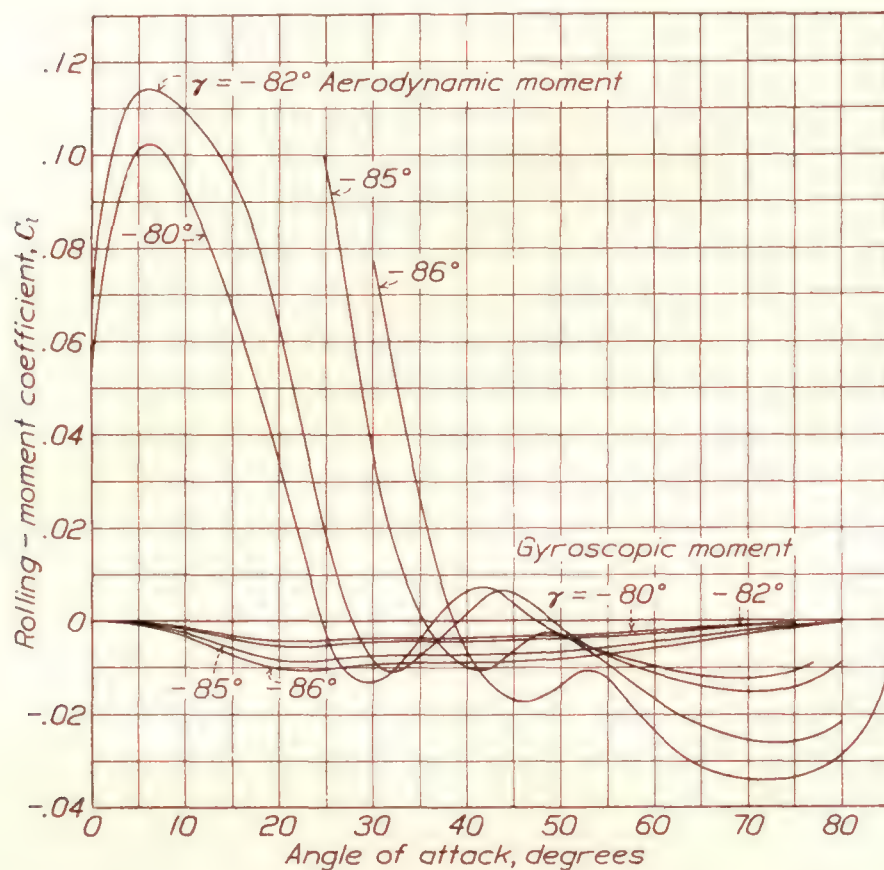


FIGURE 16.—Computed aerodynamic and gyroscopic rolling moments, elevator up 33°, ballast at nose and tail

charts would represent the conditions for a steady spin.

Thus far in the computations, only one ballast condition has been used. Computation of equilibrium conditions for other ballast conditions may be readily made employing most of the data already computed. It is obviously true in this computation

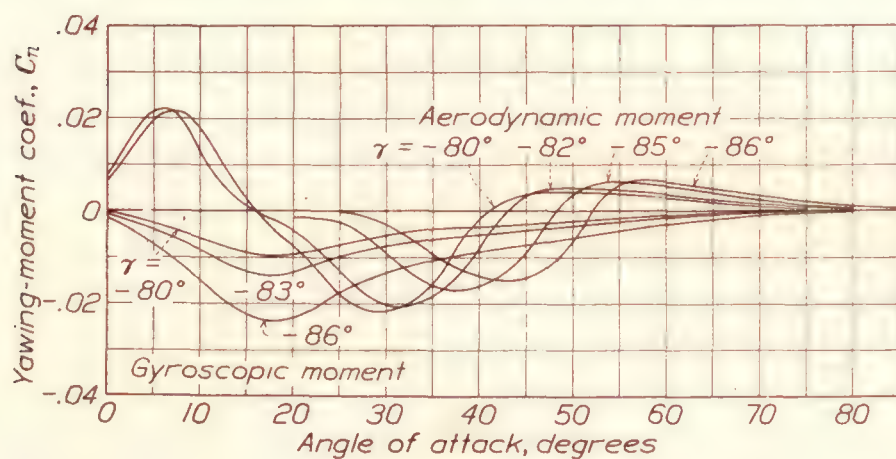


FIGURE 18.—Computed aerodynamic and gyroscopic yawing moments, elevator up 33°, ballast at nose and tail

that changes in ballast conditions do not change the aerodynamic quantities in any way so long as the weight remains constant. Therefore, the only computation necessary will be a determination of the gyroscopic moments, which is a relatively simple matter since the only new values will be those of moments of inertia. In cases in which the center of gravity was moved aft by placing unbalanced ballast in the tail of the airplane, the moment of the ballast

under the existing conditions of linear acceleration referred to the center-of-gravity position of the origin computations, should be included with the gyroscopic moments.

A computation of the equilibrium state was made for one ballast condition other than that of the con

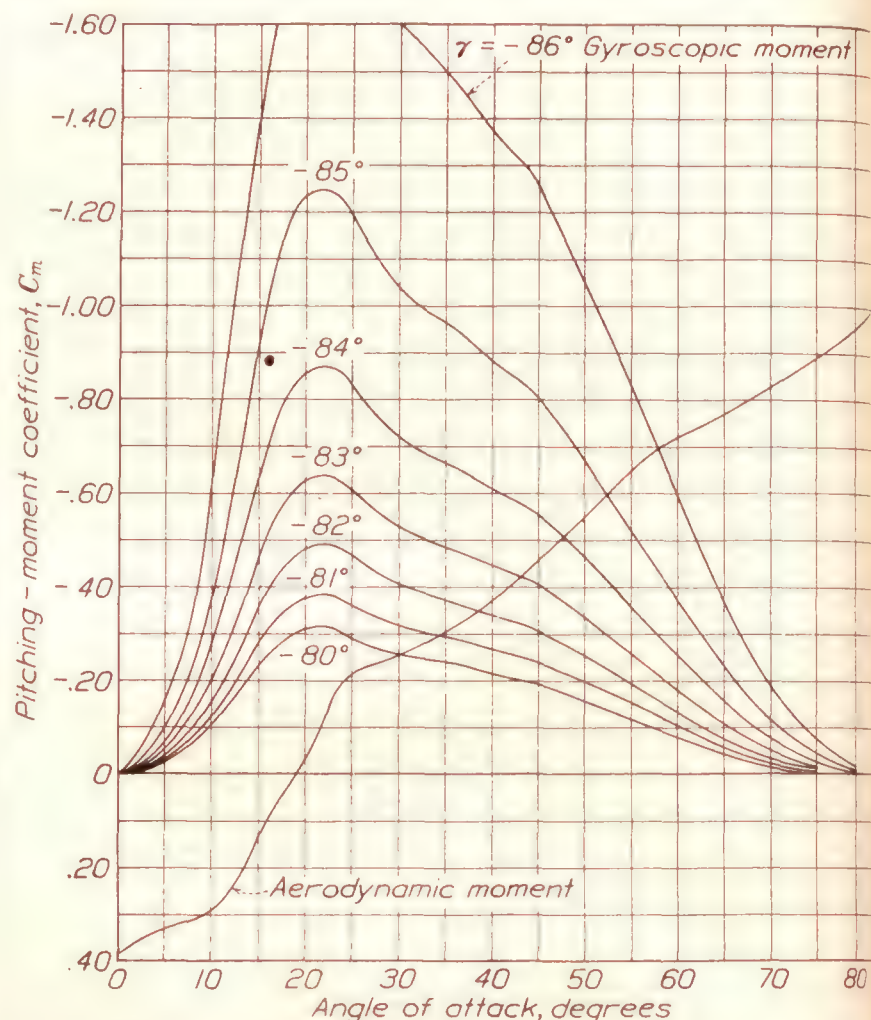


FIGURE 17.—Computed aerodynamic and gyroscopic pitching moments, elevator up 33°, ballast at nose and tail

putations already described. This was for the case that the ballast was placed in the nose and tail and therefore corresponded to the moments of inertia for flight tests, 19, 20, and 21. The results are shown in Figures 16 to 19.

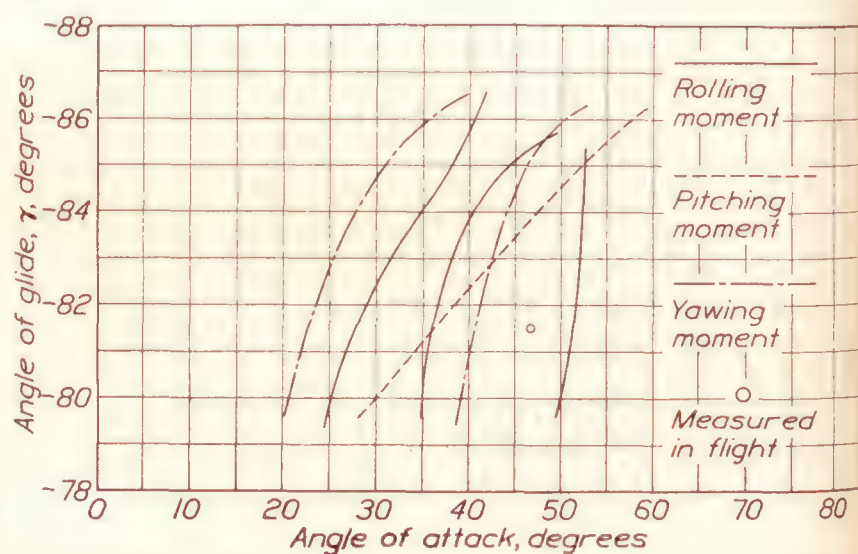


FIGURE 19.—Equilibrium of three moments, elevator up 33°, ballast at nose and tail

DISCUSSION OF COMPUTED RESULTS

A comparison of the flight results with the results of this numerical analysis discloses gratifying agreement when there is no sideslip. For the condition of ballast at the center of gravity and elevator up (fig. 15) the curves come very close to an intersection indicating equilibrium. The point plotted is the measured value

of angle of attack and glide-path angle from the flight tests. The major discrepancy between this flight result and the computed results is a $2\frac{1}{4}^\circ$ difference in glide-path angle. This difference, it is believed, is to be attributed to an interference effect in the wind-tunnel measurements. The model support employed for the tests was not particularly suitable for measurements at high angles of attack; force measurements (not published) on the same model in another tunnel indicate that the measurements presented herein are a few per cent too low. A study of the equations has shown that if the forces measured on the model were too small, all the computed curves would be shifted to unduly high values of glide-path angle, but that their form would not be seriously affected.

A further study of the results (fig. 14) shows that the intersection of the yawing and pitching moment equilibrium curves would occur at a slightly higher angle of attack if a small negative yawing moment were assumed in addition to that computed for the wings by the strip method. Such a moment could easily have arisen in the flight tests from the rudder, especially as the pilot reported that a moderate force on the rudder pedal was required to hold the rudder hard over for the spin. Finally, whatever slight shifting of the rolling-moment equilibrium curve may be required to cause it to pass through the intersection of the other two curves would correspond to differences in rolling moments smaller than the limits of error in the computation, or to the additional rolling moment caused by a very small degree of sideslip. Thus it is seen that, although the conditions for equilibrium were not obtained exactly and the flight results did not correspond exactly with the computed values, the lack of agreement was small enough to be readily explained.

The moment-equilibrium curves failed to intersect for the condition of elevator down, but the discrepancy is explained when it is noted that outward sideslip was recorded in the flight tests for both right and left spins. Since the computations did not take rolling moment due to sideslip into account, equilibrium of all moments should not be obtained by the computation. It may be seen, however, in a qualitative way, by inspecting Figures 23 to 26, that rolling moment due to outward sideslip would shift the rolling moment equilibrium curve upward toward larger values of glide-path angle, which would reasonably be expected to result in a condition of complete equilibrium. Since outward sideslip was recorded in the flight tests, there was undoubtedly a positive yawing moment due to air forces acting on the vertical tail surfaces which was not taken into account. Such a moment would have shifted the yawing-moment equilibrium curve toward larger values of angle of attack, a correction that would make the computed results agree more closely with the flight results.

Comparison of flight and computed results for changes of mass distribution (fig. 18) shows the same

trend in the computed results as in the flight results, but equilibrium of the computed curves was not indicated. In order to obtain equilibrium corresponding to the flight results, negative yawing and negative rolling moments must be added to the computed moments. Such moments could easily have resulted from some of the several factors not taken into account in the analysis. In spite of this lack of indicated equilibrium, however, it is clear that the trend of the computed value is the same as for the values measured in flight.

The equilibrium curves show only one intersection in the high angle-of-attack range for a particular condition of the airplane, and this was confirmed by flight tests. The orientation of the three moment-equilibrium curves, however, suggests that equilibrium at low angles of attack (in the region of 20° to 30°) may be possible. Spinning experience with this airplane has not indicated definitely that a spin is or is not possible at such a low angle of attack, but during this investigation the only maneuver approximating the low angle-of-attack spin was a maneuver inadvertently obtained in a few instances, which the pilot described as a steep spiral. The control forces and air speed were reported to build up to very high magnitudes and the maneuver was always terminated before a steady state was reached. The pilot's sensations were reported as very different from those in a spin. An extension of the numerical analysis to low values of α and γ and further flight tests would yield interesting information on this subject.

This method of analysis, or any equivalent method, may be considered perfectly general; its only limitations are the limitations of accuracy or knowledge of the data necessary for the computations. All the effects of the many complex details of aerodynamic shape, mass distribution, and other similar factors could be easily taken into account in this type of analysis, but at present data are not available for many of the factors that might be worth including. When it becomes possible to measure the resultant moments and forces on a model while executing a motion that simulates the full-scale spin, much of the uncertainty of the results will be removed. A special balance is now being perfected by the National Advisory Committee for Aeronautics for making these measurements.

CONCLUSIONS

The following conclusions were based on the results of these tests and computations.

1. Moderate increases in wing loading produced only the expected slight increases in angular velocity and linear velocity.

2. The change in mass distribution produced by moving ballast from the center of gravity to the nose and tail of the airplane without shift of centroid caused a decrease in rate of rotation, decrease in angle of

attack, negligible change in sideslip angle, and a decrease in glide-path angle. Recovery was perhaps slightly easier in this condition than with normal mass distribution.

3. The effect on the steady spin of moving the center of gravity aft without changes in stabilizer setting was small. Ballast placed in the tail of the airplane produced almost the same changes in the spin as ballast placed in the nose and tail with no change in center-of-gravity position.

4. The effect of moderate changes in dihedral of the wing cellule was small.

5. Removal of the covering from the fin and part of the rudder of this airplane did not materially affect the spin.

6. Displacement of the ailerons during a steady spin caused large changes in sideslip angle and several other minor changes, but no tendency to recover.

7. Full-down displacement of elevator caused an increase of angular velocity. With the center of gravity in its forward position, angle of attack was decreased and outward sideslip was produced, but with ballast in the tail the angle of attack increased and sideslip remained the same.

8. A numerical analysis based on static wind-tunnel measurements and strip computations gave results that checked the results of flight measurements very closely considering the assumptions necessary. The charts constructed in the analysis aided materially in studying the various characteristics of the spin, but with the data available at present, an analysis such as this for an airplane of unknown spinning characteristics would not always lead to useful results.

LANGLEY MEMORIAL AERONAUTICAL LABORATORY,
NATIONAL ADVISORY COMMITTEE FOR AERONAUTICS,
LANGLEY FIELD, VA., June 18, 1932.

REFERENCES

1. Soulé, H. A., and Scudder, N. F.: A Method of Flight Measurement of Spins. T. R. No. 377, N. A. C. A., 1931.

2. Fuchs, R., and Schmidt, W.: The Steady Spin. T. M. No. 630, N. A. C. A., 1931.

3. Miller, Marvel P., and Soulé, Hartley A.: Moments of Inertia of Several Airplanes. T. N. No. 375, N. A. C. A., 1931.

4. Harris, Thomas A.: The 7- by 10-Foot Wind Tunnel of the National Advisory Committee for Aeronautics. T. R. No. 412, N. A. C. A., 1932.

5. Knight, Montgomery, and Wenzinger, C. J.: Rolling Moments Due to Rolling and Yaw for Four Wing Models in Rotation. T. R. No. 379, N. A. C. A., 1931.

6. Fuchs, R., and Hopf, L.: Aerodynamik, Handbuch der Flugzeugkunde, Band II; 1922. R. C. Schmidt and Co., Berlin, W. 62.

BIBLIOGRAPHY

Baranoff, Alexander: Einige Ergebnisse von Rechnungen über den Übergang eines Flugzeugs ins Trudeln. Jahrbuch 1928, D. V. L., Seiten 205-208.

Baranoff, Alexander: Beitrag zur Frage der Stabilität der Trudelbewegung. Jahrbuch 1929, D. V. L., Seiten 175-182.

Fuchs, R.: Mathematical Treatise on the Recovery from a Flat Spin. T. M. 591, N. A. C. A., 1930.

Fukatsu, R.: On the equilibrium of the Steady Spinning of Aeroplanes. Read before the Fifth International Air Congress at the Hague, 1930.

Gates, S. B., and Bryant, L. W.: The Spinning of Airplanes. R. & M. No. 1001, British A. R. C., Oct., 1926.

Gates, S. B.: Spinning Experiments on a Single Seater Fighter, Part II, Full-Scale Spinning Tests. R. & M. No. 1278, British A. R. C., 1929.

Irving, H. B., and Batson, A. S.: Spinning of a Model of the Fairey III-F Seaplane. R. & M. No. 1356, British A. R. C., 1930.

Irving, H. B., and Stephens, A. V.: Safety in Spinning. Jour. Roy. Aero. Soc., March, 1932.

Sutton, H. A.: Airplane Spinning Characteristics. Air Corps Information Circular No. 613, February 15, 1928. Effect of Cellule Arrangement on the Rate of Autorotation Calculated by the "Strip" Method. Air Corps Information Circular No. 609, February 1, 1928.

Wright, K. V.: Experiments on the Spinning of a Bristol Fighter Aeroplane. R. & M. No. 1261, British A. R. C., May, 1929.

TABLE I. INSTRUMENT DATA

Test No.	Components of angular velocity, (rad./sec.)			Components of acceleration (g)			Vertical velocity, ft./sec.
	<i>p</i>	<i>q</i>	<i>r</i>	$\frac{X}{m}$	$\frac{Y}{m}$	$\frac{Z}{m}$	
1R ¹	1.45	0.076	1.78	-0.0236	-0.0375	1.37	86.1
2R.....	1.70	.126	1.67	-.0329	-.0333	1.42	92.1
3R.....	1.64	.120	1.81	-.0260	-.0351	1.40	93.4
5R.....	1.68	.060	1.76	-.0472	-.0379	1.39	83.3
7R.....	1.90	.041	1.57	-.0222	-.0433	1.56	89.8
8R.....	1.75	-.001	1.81	-.0076	-.0340	1.41	84.8
9R.....	1.82	.787	2.13	-.0010	.0565	1.38	80.1
12R.....	1.60	-.325	1.97	-.0083	-.0806	1.34	80.6
13R.....	2.40	-.453	2.02	-.0277	-.1158	1.64	89.9
16L.....	-1.58	.291	-1.86	-.0202	.0268	1.31	78.9
17L.....	-1.58	.291	-1.86	-.0100	.0251	1.30	82.9
18L.....	-1.58	.286	-1.88	-.0100	.0335	1.29	76.9
19L.....	-1.48	.258	-1.60	-.0867	-.0182	1.36	92.5
20L.....	-1.46	.378	-1.57	-.0468	-.0173	1.35	96.5
21L.....	-1.45	.286	-1.72	-.0720	-.0061	1.34	94.2
22L.....	-1.44	.251	-1.70	-.0284	.0049	1.27	85.6
23L.....	-1.44	.300	-1.71	-.0376	.0043	1.28	83.2
24L.....	-1.50	.455	-1.84	-.0464	-.0322	1.36	86.7
25L.....	-1.59	.413	-1.99	-.0408	-.0011	1.34	91.1
27L.....	-1.61	.369	-1.87	-.0437	.0006	1.36	85.3
28L.....	-1.61	.410	-1.92	-.0366	-.0234	1.31	87.4
29L.....	-1.68	.437	-2.12	-.0202	-.0328	1.20	97.3
30L.....	-1.71	.350	-2.14	-.0189	-.0192	1.33	91.4
31L.....	-1.72	.370	-2.12	-.0218	-.0286	1.36	85.8
32L.....	-1.37	.333	-1.71	-.1157	-.0218	1.26	80.4
33L.....	-1.34	.289	-1.66	-.110	-.0060	1.31	85.5
34L.....	-1.34	.306	-1.61	-.107	.0189	1.33	88.7
35L.....	-1.11	.276	-1.33	-.0916	.0059	1.44	95.3
36L.....	-1.14	.291	-1.31	-.0951	.0135	1.35	99.0
37L.....	-1.16	.290	-1.37	-.116	-.0334	1.37	95.3
42L.....	-1.40	.279	-1.72	-.0702	.0171	1.29	91.7
43L.....	-1.41	.323	-1.75	-.0783	-.0173	1.34	93.8
44L.....	-1.38	.302	-1.76	-.0796	-.0024	1.31	92.4
45L.....	-1.63	.295	-2.10	-.0377	.0051	1.28	85.1
46L.....	-1.58	.332	-2.08	-.0369	-.0039	1.29	82.2
47L.....	-1.03	.255	-1.42	-.123	-.0210	1.25	89.1
48L.....	-1.06	.240	-1.40	-.129	-.0008	1.30	84.9
49L.....	-1.54	.317	-1.87	-.223	-.0220	1.38	92.1
51L.....	-1.55	.304	-1.88	-.215	-.0394	1.31	91.3
52L.....	-1.65	.297	-1.90	-.226	-.0693	1.31	93.2
53L.....	-2.28	.057	-2.61	-.104	-.0052	1.39	72.1
54L.....	-2.25	.308	-2.56	-.100	-.0023	1.40	76.5
56L.....	-2.33	.023	-2.44	-.106	.0028	1.43	82.1
57L.....	-1.42	.266	-1.90	-.0164	-.0155	1.31	83.4
58L.....	-1.38	.258	-1.95	-.0122	-.0049	1.35	76.6
60L.....	-1.33	.249	-2.06	-.0123	.0078	1.28	76.3
61L.....	-1.37	.235	-1.98	-.0178	.0123	1.28	78.3
62L.....	-1.32	.249	-2.02	-.0103	.0188	1.15	82.3
63L.....	-.92	.166	-1.48	-.123	.0083	1.24	85.0
64L.....	-.92	.207	-1.43	-.130	.0006	1.25	84.0
65L.....	-.95	.209	-1.39	-.112	.0029	1.25	89.6
66L.....	-1.16	.255	-1.50	-.142	.0170	1.28	92.0
68L.....	-1.13	.265	-1.51	-.138	-.0055	1.24	85.4
69L.....	-1.12	.240	-1.42	-.130	-.0121	1.29	95.6
70L.....	-1.56	.294	-1.99	-.0112	-.0065	1.31	80.2
71L.....	-1.58	.368	-2.01	-.0103	-.0177	1.30	85.3
72L.....	-1.58	.271	-1.99	-.0159	.0070	1.30	87.9
76L.....	-1.56	.283	-1.90	-.0089	.0081	1.27	82.1
77L.....	-1.56	.287	-1.89	-.0162	.0083	1.31	79.9
78L.....	-1.57	.500	-1.95	-.0091	-.0156	1.33	84.9

¹ Letter R is right-hand spin; letter L is left-hand spin.

TABLE II.—PROPERTIES OF AIRPLANE

Test No.	Wt. during spin, pounds	Ballast, pounds			Moment of ellipsoid constants				c. g. position, per cent mean chord	Changes to external dimensions or controls of airplane
		Front	c. g.	Rear	A	B	C	τ^1		
					<i>Slug ft.²</i>	<i>Slug ft.²</i>	<i>Slug ft.²</i>	$^{\circ}$		
1R	2,306	0	0	0	2,300	2,470	3,863	-0.3	25.8	None.
2R	2,366	0	0	0	2,300	2,470	3,863	-0.3	25.8	None, but motor was stopped.
3R	2,390	0	0	0	2,300	2,470	3,863	-0.3	25.8	Do.
5R	2,377	0	0	0	2,300	2,470	3,863	-0.3	25.8	Do.
6R	2,391	0	0	0	2,300	2,470	3,863	-0.3	25.8	None.
7R	2,391	0	0	0	2,300	2,470	3,863	-0.3	25.8	None.
8R	2,391	0	0	0	2,300	2,470	3,863	-0.3	25.8	None.
9R	2,385	0	0	0	2,300	2,470	3,863	-0.3	25.8	Ailerons with spin. ²
12R	2,377	0	0	0	2,300	2,470	3,863	-0.3	25.8	Ailerons against spin.
13R	2,354	0	0	0	2,300	2,470	3,863	-0.3	25.8	Elevator down.
16L	2,388	0	0	0	2,300	2,470	3,863	-0.3	25.8	None.
17L	2,390	0	0	0	2,300	2,470	3,863	-0.3	25.8	None.
18L	2,394	0	0	0	2,300	2,470	3,863	-0.3	25.8	None.
19L	2,900	343	0	93	2,330	3,427	4,814	2.5	25.8	None.
20L	2,923	343	0	93	2,330	3,427	4,814	2.5	25.8	None.
21L	2,911	343	0	93	2,330	3,427	4,814	2.5	25.8	None.
22L	2,930	243	131	62	2,314	3,151	4,547	2.1	25.8	None.
23L	2,930	243	131	62	2,314	3,151	4,547	2.1	25.8	None.
24L	2,900	243	131	62	2,314	3,151	4,547	2.1	25.8	None.
25L	2,900	114	291	31	2,308	2,879	4,288	1.6	25.8	None.
27L	2,911	114	291	31	2,308	2,879	4,288	1.6	25.8	None.
28L	2,917	114	291	31	2,308	2,879	4,288	1.6	25.8	None.
29L	2,916	0	436	0	2,298	2,607	4,026	.9	25.8	None.
30L	2,916	0	436	0	2,298	2,607	4,026	.9	25.8	None.
31L	2,916	0	436	0	2,298	2,607	4,026	.9	25.8	None.
32L	2,916	0	359	77	2,295	3,124	4,546	0	34.5	None.
33L	2,910	0	359	77	2,295	3,124	4,546	0	34.5	None.
34L	2,898	0	359	77	2,295	3,124	4,546	0	34.5	None.
35L	2,904	0	301	135	2,293	3,494	4,918	0	40.0	None.
36L	2,898	0	301	135	2,293	3,494	4,918	0	40.0	None.
37L	2,904	0	301	135	2,293	3,494	4,918	0	40.0	None.
42L	2,919	343	0	93	2,330	3,427	4,814	2.5	25.8	None.
43L	2,907	343	0	93	2,330	3,427	4,814	2.5	25.8	None.
44L	2,919	343	0	93	2,330	3,427	4,814	2.5	25.8	None.
45L	2,901	0	436	0	2,298	2,607	4,026	.9	25.8	None.
46L	2,937	0	436	0	2,298	2,607	4,026	.9	25.8	None.
47L	2,907	0	301	135	2,293	3,494	4,918	0	40.0	None.
48L	2,919	0	301	135	2,293	3,494	4,918	0	40.0	None.
49L	2,907	0	301	135	2,293	3,494	4,918	0	40.0	Elevator down.
51L	2,890	0	301	135	2,293	3,494	4,918	0	40.0	Do.
52L	2,901	0	301	135	2,293	3,494	4,918	0	40.0	Do.
53L	2,907	0	436	0	2,298	2,607	4,026	.9	25.8	Do.
54L	2,919	0	436	0	2,298	2,607	4,026	.9	25.8	Do.
56L	2,901	0	436	0	2,298	2,607	4,026	.9	25.8	Do.
57L	2,491	0	0	0	2,284	2,593	4,026	.9	25.8	Dihedral, lower wing, decreased from 3° to 1.25°. ³
58L	2,505	0	0	0	2,284	2,593	4,026	.9	25.8	Do.
60L	2,477	0	0	0	2,284	2,593	4,026	.9	25.8	Do.
61L	2,483	0	0	0	2,284	2,593	4,026	.9	25.8	Do.
62L	2,489	0	0	0	2,284	2,593	4,026	.9	25.8	Do.
63L	2,921	0	301	135	2,293	3,494	4,918	0	40.0	Do.
64L	2,919	0	301	135	2,293	3,494	4,918	0	40.0	Do.
65L	2,919	0	301	135	2,293	3,494	4,918	0	40.0	Do.
66L	2,896	0	301	135	2,293	3,494	4,918	0	40.0	Dihedral, lower wing, increased from 3° to 4.6°.
68L	2,913	0	301	135	2,293	3,494	4,918	0	40.0	Do.
69L	2,907	0	301	135	2,293	3,494	4,918	0	40.0	Do.
70L	2,495	0	0	0	2,284	2,593	4,026	.9	25.8	Do.
71L	2,495	0	0	0	2,284	2,593	4,026	.9	25.8	Do.
72L	2,495	0	0	0	2,284	2,593	4,026	.9	25.8	Do.
76L	2,501	0	0	0	2,284	2,593	4,026	.9	25.8	Fabric stripped from empennage.
77L	2,495	0	0	0	2,284	2,593	4,026	.9	25.8	Do.
78L	2,495	0	0	0	2,284	2,593	4,026	.9	25.8	Do.

¹ Angle between X body axis and X^{IV} principal axis.² "Ailerons with spin" is aileron deflection such that in normal flight the airplane would be caused to roll in the direction of the rolling of the spin.³ Dihedral values given are for the lower wing; interplane struts were not changed.

TABLE III COMPUTED DATA

Test No.	Ω	R (g)	Z'' (g)	Radius	V	γ	α	β	L	M	N	ΔM	ΔN	Bal- last mo- ment	C_l	C_m	C_n	Λ
	Rad./sec.			Feet	Ft./sec.	°	°	°	Lb.-ft.	Lb.-ft.	Lb.-ft.	Lb.-ft.	Lb.-ft.	Lb.-ft.				
1R	2.29	1.37	1.048	5.4	86.9	-82.1	50.2	16.0	189.6	-4,009.2	18.7	438	-19	0	0.00237	-0.342	0.00000	0.454
2R	2.39	1.43	.974	5.9	93.1	-81.7	43.8	5.2	295.1	-4,453.7	36.3	411	-31	0	.00321	-.336	.00006	.443
3R	2.45	1.40	1.015	5.1	94.3	-82.6	47.2	4.5	305.2	-4,651.2	33.4	446	30	0	.00324	-.343	.00004	.448
5R	2.43	1.39	.971	5.4	84.4	-81.6	45.7	6.9	146.3	-4,614.3	17.0	433	17	0	.00194	-.414	.00000	.497
6R	2.46	1.47	.979	5.9	87.4	-80.8	42.3	6.8	230.4	-4,710.6	30.1	411	24	0	.00285	-.408	.00007	.485
7R	2.46	1.56	.974	6.4	91.2	-80.2	39.1	8.8	89.4	-4,636.4	13.1	386	10	0	.00101	-.378	.00004	.465
8R	2.52	1.41	1.011	5.0	85.7	-81.6	45.7	8.4	-2.9	-4,966.7	-.35	446	3	0	-.00004	-.444	-.00003	.507
9R	2.91	1.38	1.021	3.5	80.7	-82.8	47.7	-8.7	2,347.4	-6,059.7	242.0	524	194	0	.0340	-.613	.00070	.622
12R	2.56	1.34	1.039	4.2	81.4	-82.6	51.5	14.7	-891.6	-4,880.6	-87.8	485	79	0	-.0127	-.479	-.00013	.542
13R	3.17	1.65	1.043	4.1	90.8	-82.0	40.3	16.2	-1,283.4	-7,587.3	-184.3	497	112	0	-.0147	-.622	-.00083	.602
16L	2.46	1.31	.974	4.6	79.7	-82.0	48.3	1.1	-758.7	-4,603.8	-78.0	-458	72	0	-.0113	-.575	-.00223	.533
17L	2.46	1.30	.975	4.6	83.7	-82.4	48.5	.7	-756.9	-4,595.9	-77.6	-459	72	0	-.0102	-.521	-.00201	.507
18L	2.47	1.29	.973	4.5	77.7	-82.0	48.5	1.3	-752.0	-4,636.8	-76.5	-462	70	0	-.0118	-.609	-.00229	.549
19L	2.20	1.36	.937	6.6	92.5	-81.0	46.4	2.2	-551.5	-5,926.3	-439.7	-395	64	0	-.00609	-.534	-.00557	.411
20L	2.18	1.35	.947	6.6	96.5	-81.5	45.7	-1.6	-787.6	-5,708.6	-633.2	-386	93	0	-.00800	-.472	-.00636	.390
21L	2.27	1.34	.968	5.8	94.2	-82.0	48.8	.7	-656.6	-6,287.7	-479.3	-424	70	0	-.00700	-.546	-.00585	.395
22L	2.24	1.27	.949	5.4	85.6	-81.8	48.7	1.7	-577.3	-5,532.4	-314.6	-419	62	0	-.00745	-.586	-.00486	.453
23L	2.26	1.28	.944	5.4	83.2	-81.5	48.6	.8	-693.0	-5,554.3	-378.2	-420	74	0	-.00947	-.623	-.00618	.468
24L	2.42	1.36	1.01	5.0	86.7	-82.0	49.3	-2.9	-1,131.2	-6,240.2	-597.7	-452	112	0	-.0142	-.643	-.00893	.481
25L	2.58	1.34	1.01	4.3	91.1	-83.1	50.1	-2.4	-1,133.4	-6,349.6	-388.8	-490	102	0	-.0129	-.595	-.00559	.490
27L	2.49	1.36	.989	4.8	85.3	-81.9	47.9	-.5	-941.5	-5,988.8	-347.8	-459	90	0	-.0122	-.640	-.00569	.504
28L	2.54	1.31	.972	4.4	87.4	-82.7	48.9	-2.1	-1,085.4	-6,172.8	-389.2	-473	101	0	-.0134	-.629	-.00605	.501
29L	2.74	1.20	.924	3.3	97.3	-84.7	50.9	-3.9	-1,302.1	-6,195.0	-231.0	-524	118	0	-.0130	-.513	-.00348	.486
30L	2.76	1.32	1.018	3.6	91.4	-83.8	50.5	-1.1	-1,047.5	-6,368.6	-188.5	-526	86	0	-.0118	-.596	-.00310	.521
31L	2.76	1.36	1.032	3.7	85.8	-83.1	50.0	-.9	-1,098.3	-6,348.6	-200.9	-521	91	0	-.0141	-.674	-.00375	.554
32L	2.21	1.27	.905	5.8	80.4	-80.8	50.2	.5	-808.2	-5,245.5	-376.8	-420	82	1,457	-.0119	-.796	-.00673	.475
33L	2.16	1.32	.945	6.3	85.5	-80.8	49.9	1.4	-683.6	-5,033.8	-322.5	-410	71	1,505	-.00886	-.686	-.00510	.436
34L	2.12	1.33	.939	6.8	88.7	-80.7	48.8	.8	-701.6	-4,859.7	-339.7	-397	75	1,527	-.00845	-.622	-.00500	.413
35L	1.75	1.44	1.033	10.5	95.3	-78.9	48.4	1.9	-524.3	-3,868.9	-367.3	-328	68	2,900	-.00547	-.564	-.00454	.318
36L	1.76	1.35	.942	10.0	99.0	-79.7	47.2	.1	-543.6	-3,933.1	-398.9	-323	72	2,718	-.00525	-.513	-.00455	.308
37L	1.82	1.37	.963	9.5	95.3	-79.5	48.5	1.2	-565.7	-4,173.1	-403.3	-337	71	2,758	-.00590	-.578	-.00495	.350
42L	2.23	1.29	.947	5.7	91.7	-82.1	49.7	.7	-640.9	-6,054.1	-450.2	-423	69	0	-.00721	-.556	-.00584	.421
43L	2.27	1.34	.987	5.7	93.8	-82.1	50.0	-.3	-809.3	-6,661.8	-526.3	-430	80	0	-.00870	-.582	-.00651	.417
44L	2.26	1.31	.976	5.6	92.4	-82.2	50.9	0	-712.3	-6,133.3	-480.8	-434	74	0	-.00789	-.556	-.00614	.422
45L	2.67	1.28	.982	3.7	85.1	-83.2	51.3	.3	-867.6	-5,957.7	-151.1	-517	72	0	-.0113	-.646	-.00291	.542
46L	2.64	1.29	.996	3.8	82.2	-83.0	51.6	-.3	-968.7	-5,739.4	-165.8	-512	82	0	-.0136	-.668	-.00347	.554
47L	1.77	1.26	.931	8.7	89.1	-80.1	52.4	1.5	-517.3	-3,828.7	-314.9	-350	63	2,528	-.00618	-.612	-.00451	.344
48L	1.77	1.30	.947	9.2	84.9	-79.0	51.3	3.1	-477.6	-3,895.7	-305.1	-344	59	2,618	-.00628	-.688	-.00479	.361
49L	2.45	1.40	.918	5.6	92.1	-81.4	49.7	1.2	-847.3	-7,603.5	-588.6	-460	78	2,778	-.00948	-.921	-.00746	.460
51L	2.46	1.32	.870	5.3	91.4	-81.7	50.0	1.2	-817.2	-7,674.2	-567.2	-462	75	2,638	-.00929	-.930	-.00730	.466
52L	2.54	1.33	.839	5.1	93.2	-81.9	48.7	1.3	-804.4	-8,248.1	-590.7	-467	73	2,638	-.00879	-.944	-.00726	.471
53L	3.47	1.39	.976	2.6	72.1	-82.7	48.8	6.3	-208.1	-10,350.4	-40.9	-642	14	0	-.00380	-.1528	-.00100	.832
54L	3.43	1.41	.985	2.8	76.5	-82.9	48.1	1.9	-1,103.8	-10,015.6	-218.0	-630	76	0	-.0178	-.1314	-.00475	.773
56L	3.37	1.43	.960	3.0	82.1	-82.9	46.4	6.7	-80.0	-9,823.6	-17.1	-600	6	0	-.00113	-.1117	-.00325	.710
57L	2.38	1.31	1.034	4.5	83.4	-82.5	52.3	1.0	-716.8	-4,721.9	-119.1	-467	66	0	-.00972	-.538	-.00251	.493
58L	2.40	1.35	1.085	4.4	76.6	-82.0	53.5	1.8	-712.6	-4,733.5	-112.7	-479	64	0	-.0115	-.642	-.00284	.540
60L	2.46	1.28	1.061	3.8	76.3	-83.0	56.0	1.1	-725.6	-4,831.1	-104.8	-506	61	0	-.0118	-.662	-.00269	.556
61L	2.42	1.28	1.034	4.1	78.3	-82.7	54.2	1.7	-659.4	-4,798.8	-101.9	-487	58	0	-.0102	-.622	-.00247	.534
62L	2.43	1.15	.951	3.6	82.3	-84.0	55.6	0	-711.6	-4,726.4	-104.5	-497	61	0	-.00991	-.558	-.00231	.509
63L	1.75	1.25	.983	8.1	85.0	-80.4	56.8	4.1	-347.8	-3,560.5	-182.8	-364	41	2,497	-.00456	-.642	-.00294	.355
64L	1.71	1.26	.971	8.7	84.0	-79.7	55.6	3.2	-421.9	-3,465.9	-230.4	-352	51	2,518	-.00567	-.649	-.00378	.353
65L	1.70	1.26	.966	9.0	89.6	-80.2	54.3	2.6	-415.3	-3,466.0	-237.7	-342	51	2,518	-.00490	-.569	-.00341	.328
66L	1.91	1.29	.926	7.9	92.0	-80.5	51.3	1.8	-545.2	-4,559.4	-353.4	-369	63	2,578	-.00610	-.640	-.00466	.360
68L	1.90	1.25	.904	7.7	85.4	-80.1	51.8	1.7	-568.2	-4,464.9	-358.9	-372	65	2,497	-.00740	-.725	-.00552	.385
69L	1.83	1.30	.928	8.7	95.6	-80.4	50.6	2.0	-486.9	-4,189.4	-323.3	-349	59	2,597	-.00751	-.563	-.00590	.331
70L	2.55	1.31	1.014	4.1	80.2	-82.6	50.9	.7	-828.6	-5,445.3	-144.7	-489	72	0	-.0122	-.665	-.00318	.548
71L	2.58	1.30	1.006	3.9	85.3	-83.1	50.7	-1.4	-1,046.7	-5,581.7	-183.5	-494	91	0	-.0136	-.603	-.00356	.523
72L	2.55	1.30	1.002	4.1	87.9	-83.2	50.5	.7	-760.0	-5,500.5	-124.7	-489	67	0	-.00928	-.559	-.00246	.500
76L	2.47	1.27	.967	4.3	82.1	-82.6	49.6	.8	-761.9	-5,184.9	-138.7	-467	70	0	-.0107	-.606	-.00292	.520
77L	2.47	1.31	.993	4.5	79.9	-82.0	49.3	1.3	-767.1	-5,176.5	-141.0	-465	71	0	-.0113	-.636	-.00313	.533
78L	2.55	1.33	1.013	4.3	84.9	-82.6	49.4	-4.1	-1,376.7	-5,372.3	-248.0	-480	123	0	-.0180	-.586	-.00486	.519

1 Positive angle is sideslip outward; negative is sideslip inward.

REPORT No. 442

A COMPARISON BETWEEN THE THEORETICAL AND MEASURED LONGITUDINAL STABILITY CHARACTERISTICS OF AN AIRPLANE

By HARTLEY A. SOULÉ and JOHN B. WHEATLEY

SUMMARY

This paper covers an investigation of the application of the theory of dynamic longitudinal stability, based on the assumption of small oscillations, to oscillations an airplane is likely to undergo in flight. The investigation was conducted with a small parasol monoplane for the fixed-stick condition. The period and damping of longitudinal oscillations were determined by direct measurements of oscillations in flight and also by calculation in which the factors that enter into the theoretical stability equation were determined in flight. A comparison of the above-mentioned characteristics obtained by these two methods indicates that the theory is applicable to the conditions encountered in flight.

The investigation was extended to determine the feasibility of calculating the stability characteristics from basic data of the type that would be available to a practicing designer. The results of this phase of the work show that for the power-off condition the agreement between the actual and predicted stability characteristics was reasonably satisfactory, except perhaps when the predicted stability is close to neutral. For the power-on condition the stability can not be predicted owing to the present lack of information concerning slipstream effects. Further progress in a solution of the problem of longitudinal stability depends largely on increasing the knowledge of these effects.

INTRODUCTION

With each new airplane design, the designer is confronted with the problem of attaining some, although not a definitely established, degree of longitudinal dynamic stability. The theory utilized in this problem has been evolved and published in various standard works such as those of Bryan, Bairstow, Cowley and Levy, and Glauert. This theory involves the basic assumption of small deviations from the steady state and the application of numerous data relating to the airplane. The theory is not widely applied in design, probably because an acceptable (although not necessarily the most desirable) degree of dynamic stability is often attained by the application of simple rules developed from experience, and also because the theory is fairly complex and its validity has not been clearly demonstrated. New designs, however, are fre-

quently found to possess decidedly objectionable stability characteristics. Furthermore, it is quite probable that the stability characteristics of many airplanes could be considerably improved. Owing to the lack of knowledge concerning the factors that tend to produce dynamic stability and the relative importance of these factors, the nature of the changes necessary for improvement is not generally understood. Thus there has arisen the need for a comprehensive study of the problem to ascertain the validity of the theory, to determine in what respects, if any, it requires modification, and to establish thereby the procedure by which the designer can predict the stability characteristics of an airplane from basic data. An additional phase of the problem arises from the fact that the most desirable degree of stability is not definitely established. The solution to this phase probably should be obtained by determining the degree of dynamic longitudinal stability possessed by airplanes that have very good flying characteristics.

For the reasons mentioned above, an investigation of the dynamic longitudinal stability of an airplane in flight with and without power was undertaken. The results of the investigation, as reported herein, are divided into two parts. The first deals with checking the validity of the basic assumption of small deviations from the steady state against the actual conditions encountered in flight. The second deals with the calculation of stability from basic data and the comparison between calculated and test results. The flight tests required by the investigation were made with a small parasol monoplane. No attempt was made in the present case to establish the most satisfactory degree of dynamic longitudinal stability.

THEORY OF STABILITY

GENERAL PRINCIPLES

As previously mentioned, the classical theory of the stability of small oscillations, its application to the airplane, and the development of the equation of dynamic longitudinal stability are completely covered in the various works on the subject. The standard form of the stability biquadratic, however, is given in dimensional units and is very difficult to handle. Glauert

has developed a nondimensional form for the equation (reference 1) which is more convenient in application and which greatly simplifies the analysis of the longitudinal stability. This nondimensional form has been used in the present case.

For convenience of reference, the transformation from the dimensional to the nondimensional form of the stability equation is given in the appendix using the absolute system of units. As explained therein, only the long-period, lightly damped oscillation is considered. The nondimensional expression for the period of this oscillation is

$$T_1 = \frac{2\pi}{\sqrt{\frac{E}{C} - \left(\frac{DC - BE}{2C^2}\right)^2}}$$

and that for the damping coefficient is

$$\zeta_1 = -\frac{1}{2} \left(\frac{D}{C} - \frac{BE}{C^2} \right)$$

where

$$B = -m_q - x_u - z_w$$

$$C = z_w m_q + z_w x_u + m_q x_u - z_u x_w - \mu m_w$$

$$D = \frac{1}{2} \mu m_u C_L + \mu m_w x_u + \frac{1}{2} C_L \tan \theta_o \mu m_w + m_q (z_u x_w - x_u z_w) - x_w \mu m_u$$

and

$$E = \frac{1}{2} \mu C_L \tan \theta_o (x_w m_u - x_u m_w) + \frac{1}{2} \mu C_L (m_w z_u - m_u z_w)$$

If the damping coefficient is negative, the motion is stable; that is, the oscillations are damped; and if it is positive the motion is unstable.

The terms x_u , x_w , z_u , z_w , m_u , m_w , and m_q are the nondimensional derivatives (or derivative coefficients), and μ is a parameter. As noted in the appendix the length l on which m_u , m_w , m_q , and μ are based can be chosen arbitrarily. The length used throughout this paper is the distance from the center of gravity to the rudder post. The terms C_L and θ_o refer to the initial condition.

The above expressions for the period and damping can be readily converted to the dimensional form for comparison with experimental data by introducing the factor $\frac{\rho V S}{m}$

$$T = T_1 \frac{1}{\rho V S m}$$

and

$$\zeta = \zeta_1 \frac{\rho V S}{m}$$

where T and ζ are the period and the damping factor, respectively, in dimensional form.

THE RESISTANCE DERIVATIVES IN TERMS OF FUNDAMENTAL AIRPLANE CHARACTERISTICS

The terms x_u , x_w , C_L , θ_o , z_u , z_w , m_u , m_w , m_q , and the parameter μ must be evaluated for an analysis of the dynamic longitudinal stability. The manner in which

most of the derivatives can be expressed in terms of the fundamental airplane characteristics will now be shown. Because of the marked change produced by the propeller in the stability derivatives, the derivatives will be first discussed for the power-off condition, then for the power-on condition.

Power-off.—A basic assumption for this case is that with the propeller idling the V/nD ratio for the propeller remains constant for small changes in V . The assumed initial conditions is a steady glide with the propeller operating at the V/nD of zero effective thrust.

In the appendix it is shown that for the power-off condition $x_u = -C_D$; similarly, it can be shown that $z_u = -C_L$ and $m_u = \frac{C_m c}{l}$.

These expressions for x_u and z_u apply when C_D and C_L are taken as the over-all drag and lift coefficients of the airplane. As the airplane is in the steady gliding condition C_m is zero and consequently $m_u = 0$.

It is noted at this point for later reference, that in actual gliding flight with throttled engine the propeller, in general, develops a small effective thrust, T , which may have an appreciable effect on the term x_u . In this case

$$X = T - D = C_T \rho V^2 D^2 - C_D \frac{1}{2} \rho V^2 S$$

and for constant V/nD

$$x_u = \frac{2C_T D^2}{S} - C_D = -C_D'$$

where C_D' is the effective drag coefficient of the airplane-propeller combination.

The velocity w introduces a change in the magnitude and direction of the resultant velocity. The change in magnitude, however, is a second order effect and can be neglected. The change of angle causes a change in the flight-path angle. Then

$$X_w = \frac{dX}{dw} = \frac{dX}{d\theta} \frac{d\theta}{dw}$$

$$\tan \theta = \frac{w}{V} \text{ and } \frac{d\theta}{dw} = \frac{1}{V}$$

for a small angular displacement θ

$$X = -C_D \frac{\rho V^2}{2} S \cos \theta + C_L \frac{\rho V^2}{2} S \sin \theta$$

as θ is small, $\cos \theta = 1$ and $\sin \theta = \theta$

Also, it may be assumed that θ equals the change in α . Then

$$x_w = -\frac{1}{2} \frac{dC_D}{d\alpha} + \frac{1}{2} C_L$$

By a similar procedure it is found that

$$z_w = -\frac{1}{2} \frac{dC_L}{d\alpha} - \frac{1}{2} C_D$$

The term m_w is given by the expression

$$m_w = \frac{1}{2} \frac{c}{l\eta} \frac{dC_m}{d\alpha}$$

The coefficient m_q of the moment derivative M_q is a basic characteristic of the airplane comparable with C_L , C_D , and C_m . The expression for this coefficient is simply

$$m_q = M_q / \rho S V l^2 \eta$$

The term " M_q " can be determined from calculations by the method described later in the paper, or by direct measurement with a model or full-sized airplane.

The foregoing discussion shows that a complete theoretical analysis of the dynamic longitudinal stability for the power-off condition can be readily made from basic data. The basic data required for a complete determination of the power-off stability characteristics can be summarized as follows:

Wing area.

Mass of the airplane.

A characteristic length, l (here taken as the distance from the center of gravity to the rudder post).

Moment of inertia about the Y axis.

Lift, drag, pitching moment, and rotary derivative coefficient as functions of angle of attack.

Power-on.—As already pointed out, the propeller, because of its thrust and slipstream, causes considerable change in the stability derivatives. In the first place the propeller, when operating at a positive thrust, must have a distinct series of stability derivatives of its own which are additive to those of the airplane. (Reference 2.) It is very probable that the majority of these, particularly those depending on angular velocity, are negligible. The variation of longitudinal force or thrust with velocity, however, must be considered. Besides the derivatives of the propeller, there is a large change produced in the stability derivatives of the airplane because of relatively high velocity of the slipstream flowing over the central portion of the wings and over the fuselage and tail. The increase of drag due to this effect need not be considered when the propeller characteristics are based on effective thrust.

Our present knowledge of the character of the flow behind a propeller does not permit a satisfactory prediction of the effect of the slipstream on the stability, although the experiments discussed later show the magnitude of the effects on some of the derivatives for this particular airplane. The following discussion of the power-on derivatives will be carried as far as our present knowledge of the propeller effects allows.

A basic assumption in this case is that the propeller torque remain constant. The assumed initial condition is steady level flight.

The thrust now varies with velocity so that we have

$$x_u = \frac{1}{\rho S V} \frac{dT}{dV} - C_D$$

As T is here taken as the effective thrust, C_D is the same as for the power-off condition. An expression for $\frac{dT}{dV}$ in terms of generalized propeller characteristics has been derived by Glauert (reference 2) for the assumption of constant torque. This expression is

$$\frac{dT}{dV} = -\frac{2T}{V} \frac{r^2 (2a - 3r + r^3)}{(1 - r^2)(2a + r^3)}$$

where

a is a constant = 1.325

and r is the ratio of V/nD of the initial condition to V/nD for zero thrust.

Consideration of Glauert's expression shows that, although the term $\frac{dT}{dV}$ varies considerably with changes

in r over the normal speed range, the term is always small relative to C_D . Consequently, it is permissible to evaluate the term on the basis of the average value of r . Then we can write

$$\frac{dT}{dV} = -\frac{2T}{V} K$$

$$\frac{1}{\rho S V} \frac{dT}{dV} = -C_D K$$

since the thrust equals the drag when the angle of attack of the thrust line is neglected. Then

$$x_u = -C_D(1 + K)$$

The form of the expression for z_u is the same as for the power-off but, owing to the previously mentioned slip stream effect, the lift coefficient at a given angle of attack is in reality not the same as in the power-off condition. Actually

$$z_u = -C_L' = -(C_L + \Delta C_L)$$

where ΔC_L represents the effects of the slipstream and the thrust component on the lift coefficient. The term ΔC_L can not be satisfactorily evaluated. The experiments discussed later show that at least in this particular case this term is not negligible.

The principal difficulty in the evaluation of the power-on stability derivatives pertains to the moment derivatives. Both the thrust and slipstream effects enter into these terms. The thrust moment is introduced because in the general case the line of action of the propeller does not pass through the center of gravity. The action of the slipstream is more complex. The change of lift coefficient of the wings is accompanied by a change of downwash angle which in turn produces a change of angle of attack at the tail. In

addition to the change of angle of flow at the tail, the velocity there is increased. As the variation of the angle and velocity at the tail with a change in the airplane's velocity is not known, it is impossible to evaluate m_u . That m_u is not zero for the power-on condition is demonstrated by the change of balance that takes place when power is applied and the V/nD of the propeller changed from that for zero thrust to some other value. The factors that complicate the solution of m_u also enter into m_w . The moment derivative m_q is less complex and varies from the power-off derivative essentially because of the relatively greater velocity over the tail for the power-on condition.

Attempts were made to evaluate the derivatives m_u , m_w , and m_q for the power-on condition on the basis of assumed flow over the tail. Although reasonable agreement was obtained for the damping and period calculated from computed values of these derivatives,

from the type of data obtainable before the airplane is constructed. Complete measurements were made for the power-off condition. For the power-on condition only the derivatives depending on C_L and C_D were determined as it is impossible to measure the moment derivatives for this condition.

THE AIRPLANE

The airplane used in the investigation was a Doyle O-2, a small parasol monoplane. (Figs. 1 and 2.) The dimensions required in the study of longitudinal stability are given in the following table:

Weight	1,290-1,340 lb.
Moment of inertia about Y axis (B)	673 slug ft. ²
Wing dimensions:	
Span	30.0 ft.
Chord	5.50 ft.
Area	159.5 sq. ft.
Airfoil section	Clark Y.



FIGURE 1.—Front view of Doyle O-2 airplane

so many arbitrary assumptions had to be made in their evaluation that it is not considered worth while to include either the methods used to compute the derivatives or the results of the calculations made with them.

EXPERIMENTAL STABILITY

Flight tests were made with the airplane utilized in this investigation to determine the stability derivatives previously discussed and also to determine the period and damping of oscillations in flight by direct measurements. These data served two purposes. By comparing the period and damping found by direct measurements with the period and damping calculated from derivatives obtained from flight data, it was possible to test the applicability of the theory. Also, by comparing the derivatives and stability characteristics obtained from flight data with those calculated from basic data for the airplane elements, as explained later, it was possible to test the precision with which stability can be predicted

Center-of-gravity position:

Below chord	23.4 in., 36.0 per cent chord.
Rear of L. E.	22.4 in., 34.0 per cent chord.
Above thrust line (<i>h</i>)	12.0 in.
Horizontal tail surface:	
Span	9.0 ft.
Area	18.7 sq. ft.
Airfoil section	Flat plate.
Distance from c. g. to rudder post (<i>l</i>)	11.8 ft.
Engine	LeBlond, 60 hp
Propeller pitch-diameter ratio	0.60
Wing loading	8.09-8.40 lb./sq. ft.
Power loading	21.5-22.3 lb./hp

INSTRUMENTS

The instruments used during the flights were:

- Air-speed recorder.
- Recording inclinometer.
- Timer.
- Control-position recorder.
- Angular-velocity recorder.
- Angle-of-attack recorder.

All the instruments are photographic recording. Detailed descriptions of the air-speed recorder, inclinometer, timer, control-position recorder, and angular-velocity recorder are given in references 3, 4, 5, 6, and 7, respectively. The angle-of-attack recorder is a recent development. It consists of a light wind vane, free to rotate about an axis parallel to the Y axis of the

angle was obtained from the angle of attack and inclination of the X axis. The lift and effective drag coefficients were deduced from the wing area, dynamic pressure, and components of weight parallel and perpendicular to the glide path, the effective drag coefficient being the drag coefficient of the airplane-propeller combination. In addition to the above-mentioned



FIGURE 2.—Side view of Doyle 0-2 airplane

airplane, mounted about a chord length ahead of the wing at the outboard strut fitting. The motion of the vane is transmitted through the supporting tube by a fishline to the recording mechanism. The vane and recording mechanism are so placed in relation to one another that when the vane is in the desired position the recording mechanism may be embedded in the wing so as not to disturb the flow. A schematic sketch of the angle-of-attack recorder is shown in Figure 3.

FLIGHT PROCEDURE

Preliminary flights.—Preliminary to the main flight tests it was necessary to calibrate the air-speed system and the angle-of-attack recorder in flight. For this purpose a trailing Pitot-static tube, a second air-speed recorder, and an indicating statoscope were added. The air-speed system was calibrated against the trailing Pitot-static tube suspended 70 feet below the wing. The angle-of-attack recorder was calibrated against the inclinometer in the airplane during steady level flight. The calibrations were made over the complete speed and angle-of-attack range.

Determination of C_L and C_D .—Lift and drag coefficients for the power-off condition were determined in glides with the throttle closed. The dynamic pressure, angle of attack, and inclination of the X axis were recorded directly in glides. The gliding

items, the average altitude, engine speed, and air temperature were noted during each glide.

Lift coefficients for the power-on condition were obtained by recording dynamic pressure and angle of attack in a series of level-flight runs. The true drag coefficients for this condition were deduced from the results of the glide tests by correcting the effective drag coefficient for the calculated drag of the idling pro-

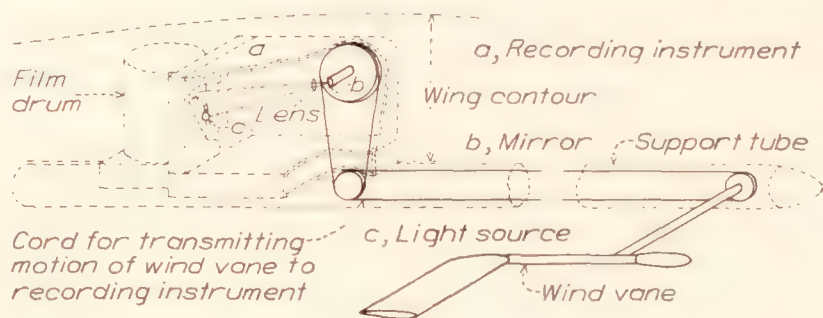


FIGURE 3.—Schematic sketch of the angle-of-attack recorder

PELLER. The thrust coefficients required in these calculations of propeller drag were determined from the actual V/nD of the propeller in each glide and a curve of calculated propeller characteristics.

Determination of C_m .—The static pitching moment was obtained from the results of glide tests in which a known pitching moment was applied. The pitching moment was applied by a sliding weight mounted so that its position could be controlled from the pilot's

cockpit. A 100-pound lead weight was mounted on a steel tube in the front cockpit and was fitted with a control and locking device so that it could be locked at the center of gravity and at various known distances from the center of gravity. (Figs. 4 and 5.)

The airplane was first glided with the weight at the center of gravity at a given air speed and with the elevator held stationary. Records were made of the air speed, angle of attack, and elevator position. The elevator position was recorded to make certain that the elevator angle remained constant during the runs. Subsequent records were made with the weight moved to a new position and with the original elevator angle.



FIGURE 4.—The installation of the sliding weight in the front cockpit

This procedure was repeated until the entire normal range of angle of attack with one elevator position was covered. Difficulty experienced in maintaining a constant elevator angle was obviated by providing a stop on the control column.

The static pitching moments were calculated from the weight and position of the sliding mass reduced to coefficient form and plotted against angle of attack. The moment-coefficient curve was obtained for only one elevator setting. In the application of these results to the calculation of stability the assumption was made that a change of elevator angle produces a constant difference in the ordinates over the entire extent of the curve.

Determination of m_q .—The damping coefficient due to rotation for the power-off condition was determined by studying the motion of the airplane during pitching oscillations in glides. The pitching oscillations were set up from an initially steady state by a fore-and-aft movement of the stick after which the stick was returned to its original position. Continuous records of the angular velocity in pitch, air speed, angle of attack, and elevator angle were obtained during a portion of the steady glide and an ensuing period of several seconds. Angular acceleration was deduced from recorded angular velocity by graphical differentiation. The resultant pitching moment acting on the airplane



FIGURE 5.—The pilot's cockpit showing crank for moving the sliding weight

at any given instant was calculated from the acceleration and the moment of inertia of the airplane about the Y axis. The pitching moment caused by the rotation was found by deducting the static component from the resultant and was then reduced to coefficient form. The static component of the resultant pitching moment for a given instantaneous angle of attack was found by referring to the angle of attack in the initial steady state, the curve of static pitching-moment coefficient against angle of attack previously established, and the recorded air speed for the same instant. As the static pitching moment is zero in a steady glide the reference to the angle of attack of the initial steady condition provided a means of determining the shift

in ordinates of the curve of static moment coefficient against angle of attack corresponding to any given elevator position. The static pitching-moment coefficient for any given elevator position and angle of attack was thereby readily established. Values of m_q for the power-off condition were calculated in the above-described manner for various angles of attack throughout the range of normal flight.

Determination of period and damping coefficients.—

The period and the damping coefficient were determined by direct measurements of the oscillation characteristics in flight at the same altitude as that at which the previously mentioned tests were made. These direct measurements were made both for the power-off and power-on conditions. As u , w , and θ are interdependent variables, the periods of their va-

$$\zeta = \frac{2}{T} \log_e \left(\frac{V_3 - V_2}{V_1 - V_2} \right)$$

where

ζ , damping factor.

T , period, in seconds.

V_1 , V_2 , V_3 , true air speed in feet per second at two successive maximums and the intervening minimum.

PRECISION OF MEASUREMENTS

Frequent check calibrations were made of the instruments used in the flight tests. Appreciable errors caused by faulty operation or changed calibration of the instruments were thereby eliminated. The effect of lag in the angular-velocity recorder was eliminated by a correction determined in laboratory tests. Probably the most serious source of error in the results was

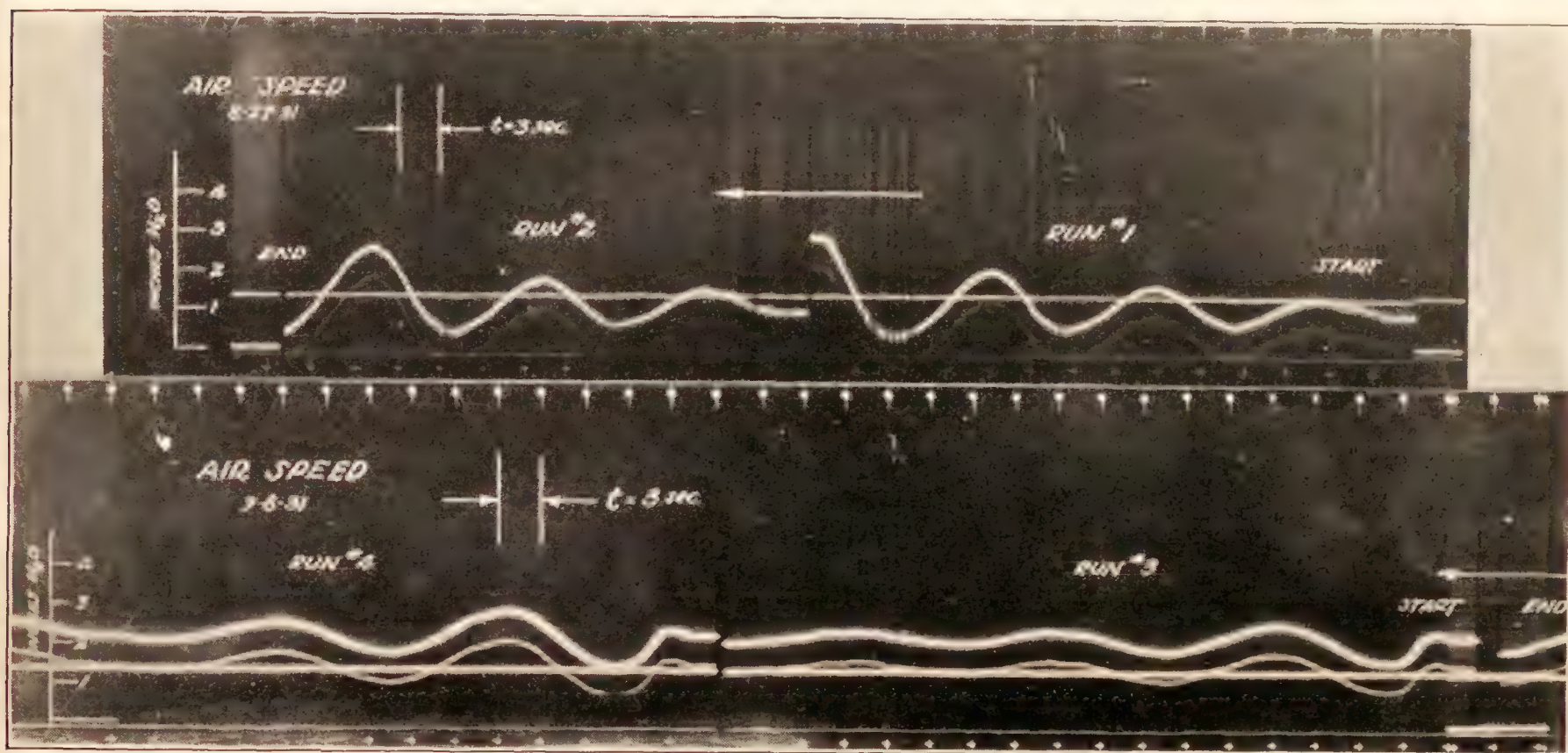


FIGURE 6.—Typical records of air speed during oscillations

riations with time are necessarily the same, although the variations may not be in phase with each other. Consequently, the period and damping could be determined by studying the behavior of only one variable. Air speed was chosen as the one most convenient for study. The tests were made by setting up oscillations in the manner previously described and obtaining records of air speed for at least one complete oscillation. Sample records are shown in Figure 6. The records designated Runs 1 and 2 illustrate an unstable condition experienced with power-on at initial angles of attack of 16.5° and 15.0° , respectively; and those designated Runs 3 and 4 illustrate a stable condition with power-off at an initial angle of attack of 4.8° .

The period of the oscillation was found by the time interval between two consecutive points of maximum velocity. The damping coefficient is given with sufficient accuracy by the approximate relation

introduced by the limitations of accuracy in determining angular accelerations by graphical differentiation of the angular-velocity records. Wide record lines caused by instrument vibration were a contributing cause to inaccuracies in evaluating records. The effect of accidental errors was considerably reduced, however, by obtaining two or three repeat runs for each test condition and expressing the results as faired curves. Following is a list showing the estimated limits of accuracy for the various items measured and derived from flight tests:

Experimental quantity	Precision
C_L (except at L_{max})	± 2 per cent to ± 5 per cent.
C_{Lmax}	± 10 per cent.
C_D	± 2 per cent to ± 8 per cent.
C_m	± 5 per cent.
m_q	± 20 per cent.
ζ	± 10 per cent.
Period	± 5 per cent.

CALCULATED STABILITY

In most cases it is desirable to complete an analysis of the stability of a proposed airplane design before construction. For such an analysis there are at hand standard basic data regarding the aerodynamic characteristics of the airplane elements from which the aerodynamic characteristics of the complete airplane can be calculated. In an advanced stage of the design there may also be available results of wind-tunnel tests on a model of the airplane from which the flight characteristics of the airplane can be more accurately predicted than from data for the airplane elements. In the present case an analysis of the dynamic longitudinal stability of the airplane used in the flight tests has been made by utilizing only basic data for the airplane elements; i. e., wing airfoil characteristics, parasite drag of nonlifting elements, and tail-plane characteristics neglecting interference effects and assuming a tail efficiency of 1.

It will be assumed at the outset that the design has been carried to such a point that certain principal features of the airplane have been tentatively adopted. These features include the weight, the wing profile, area, dimensions, and arrangement with respect to the center of gravity; the horizontal tail-plane profile, area, dimensions, and position relative to the center of gravity and to the wings; and the over-all length and height, including the landing gear. In order to study the longitudinal stability it is then necessary to find in addition the moment of inertia about the Y axis and the lift, drag, static pitching-moment and rotary pitching-moment coefficients as a function of angle of attack.

The moments of inertia of the airplane used in these tests had previously been measured (reference 8); consequently, the moment of inertia about the Y axis was available for the calculations. In general, this moment of inertia will not be known and must be estimated. It may be determined from the summation of small elements. This method, however, besides requiring long and tedious calculations, is not likely to prove very accurate. Probably the most convenient and accurate method is that given in reference 8 in which there are given the results of accurate measurements of the moments of inertia of several airplanes representative of different wing arrangements. From these results there have been derived nondimensional coefficients based on the weight and over-all dimensions. The suggested procedure is to choose the coefficients of the airplane most nearly similar to the projected design and to obtain the moments of inertia of the projected design by multiplying the nondimensional coefficients by the appropriate factors.

Curves of C_L and C_D for the complete airplane were obtained by consideration of the airfoil characteristics as determined in tests at large scale in the variable-density wind tunnel, and of the probable effect

of the other airplane elements. The lift coefficient for the airfoil, after correction to the aspect ratio of the actual wing, were assumed to apply to the complete airplane. To the drag coefficients of the airfoil were added an estimated drag coefficient representing the effect of the fuselage and engine, landing gear, and exposed struts. The parasite-drag coefficient was assumed to remain constant at all angles of attack.

The static pitching-moment coefficient was obtained by first constructing a vector diagram of the wing resultant force at a constant air speed. On the diagram the center of gravity of the airplane was spotted in its correct position in relation to the wing chord. The moment of the wing about the center of gravity was then computed with the data obtained from the diagram. As the moment of the parasite drag about the center of gravity was assumed to be zero, the only other moment was derived from the tail. The downwash angle at the tail was computed from the equation developed by Diehl (reference 9) employing the constant recommended by Reid (reference 10) for general use,

$$\epsilon = 60/R(x+1)^{-0.38}(y+1)^{-0.23}C_L$$

where x and y are the horizontal and vertical distance of the tail plane behind and below the wings in units of chord length. The angle of attack of the tail was corrected for the downwash from the wing. Next the slope of the lift-coefficient curve for the tail plane was estimated by consideration of the airfoil section at the same aspect ratio. The tail moment about the center of gravity was then calculated for the same velocity for the wing, from the slope of the tail lift-coefficient curve, angle of attack of the tail, the tail area, and the moment arm. This moment was added algebraically to the moment of the wing and the resultant moment reduced to coefficient form.

The coefficient m_q of the rotary derivative was calculated directly from the tail characteristics. The assumption was made that the damping of rotation of the tail is not materially augmented by the damping of the other parts of the airplane and that the total damping can be taken as equal to that of the tail. The equation used for the calculation of m_q may be derived as follows: Let the change in angle of attack of the tail caused by the angular velocity q be $\Delta\alpha_T$

$$\Delta\alpha_T = w_T/V_T$$

now

$$w_T = lq$$

and

$$V_T = \{V^2 + (lq)^2\}^{1/2}$$

Let M_T be the change in moment of the tail caused by the angular velocity q then

$$M_T = l^2 q \frac{dC_{L_T}}{d\alpha_T} S_T \frac{\rho}{2} \{V^2 + (lq)^2\}^{1/2}$$

as lq is small compared to V the term $(lq)^2$ may be neglected

$$M_q = \frac{dM_T}{dq} = l^2 \frac{\rho V}{2} S_T \frac{dC_{LT}}{d\alpha_T}$$

and

$$m_q = \frac{M_q}{\rho V S l^2 \eta} = \frac{1}{2} \frac{S_T}{S} \frac{1}{\eta} \frac{dC_{LT}}{d\alpha_T}$$

RESULTS AND DISCUSSION

The results of the investigation are given in Figures 7 to 16, inclusive. The lift and drag curves of the airplane are given on Figure 7, showing the power-off curves obtained both from flight tests and from calculations. The experimental power-on curves of lift and drag are given for comparison. In Figure 8 the experimental and calculated curves of pitching-moment coefficients are plotted. Figures 9, 10, 11, 12, and 13 show the stability derivatives computed from the data of the two previous figures, and Figure 14 gives the experimental and calculated curves of the stability derivative m_q . In Figure 15 are plotted curves of period and damping obtained from the experimental and calculated stability derivatives and points representing the actual measured period and damping. Faired curves are given in Figure 16 to show the difference in the measured stability characteristics power-off and power-on. It should be noted that all results are given for an air density of 0.00217 slug per cubic foot which corresponds to an altitude of 3,000 feet in a standard atmosphere.

For the determination of the validity of the assumption of small oscillations in dealing with the stability it is obviously necessary that the disturbances during which the actual period and damping were measured should have been large enough to represent actual average conditions that the airplane is expected to meet in normal flight. An inspection of the air-speed records obtained during the oscillations showed variations in magnitude as great as 30 miles per hour during the course of several of the runs and average deviations in excess of 20 miles per hour. The amplitudes of these oscillations are thought to be great enough to be regarded as representative of conditions following a disturbance produced by the roughness of the air.

The nature of the agreement between the theory and experiment is shown on Figure 15 where the curves of period and damping coefficients as calculated from the experimental derivatives are shown with the points representing the measured values of the same items obtained from the oscillation tests. It can be seen that although none of the points actually fall on the theoretical curve of damping coefficient they are dispersed about equally on either side of the curve. The dispersion of the points is probably caused to a large extent by unsteady air conditions affecting the airplane during the time the records were made. The agreement obtained indicates that the theory

is satisfactory for use in analysis of the longitudinal stability characteristics of airplanes.

For the prediction of stability characteristics it is essential that not only can the stability characteristics be calculated from the derivatives but also that the derivatives can be calculated with the necessary degree of accuracy. The degree of accuracy with which the stability derivatives can be calculated is shown by a comparison of the calculated and experimental curves for the power-off condition in Figures 7 to 14. The curves of lift coefficient and associated derivatives show fair agreement except at the stall. The calculated drag curve differs from that obtained in gliding flight by an amount that is approximately equal to the drag attributed to the idling propeller and consequently is in fair agreement with the curve for the power-on condition. This discrepancy, which is brought about by the neglect of the drag of the idling propeller, is reflected in x_u and x_w where the disagreement is proportional to that for C_d . The greatest discrepancy between the calculated and experimental derivatives is in C_m and m_w and is probably caused by a nonelliptical lift distribution and interference effects at high angles, with the result that the calculated downwash angles are in error. With m_q the agreement is fair.

The results of the computations of period and damping from the calculated derivatives are of interest notwithstanding the relatively poor agreement in m_w which seemingly has no serious effect on the final result. The curves of the calculated period and damping coefficient show the same general trend as those computed from the experimental derivatives, though the damping curve is offset an appreciable amount. The calculated values for the damping are smaller than the true values for this case. The comparison indicates that predicted results would often be useful where more exact data are lacking. Without the assurance of better accuracy than that attained in the present case, however, it seems evident that predicted results showing close to neutral stability should not be interpreted too literally. In this connection it should be noted that much better accuracy can probably be attained if model test data are available for the analysis.

Aside from the principal results of the report there are other points of interest that have been brought out. The most important of these is the marked difference in the stability characteristics between the power-off and power-on conditions. (Fig. 16.) The stability for the power-on condition is generally less than with power-off. A portion of this difference can be attributed to the difference in flight path. Supplementary calculations made show, however, that the difference in flight path accounts for very little of the difference and that the larger part must be attributed to slipstream effects. It will be further noticed that the

curvature of the power-on damping coefficient curve is reversed at high angles of attack and with a very slight change of angle the damping coefficient becomes

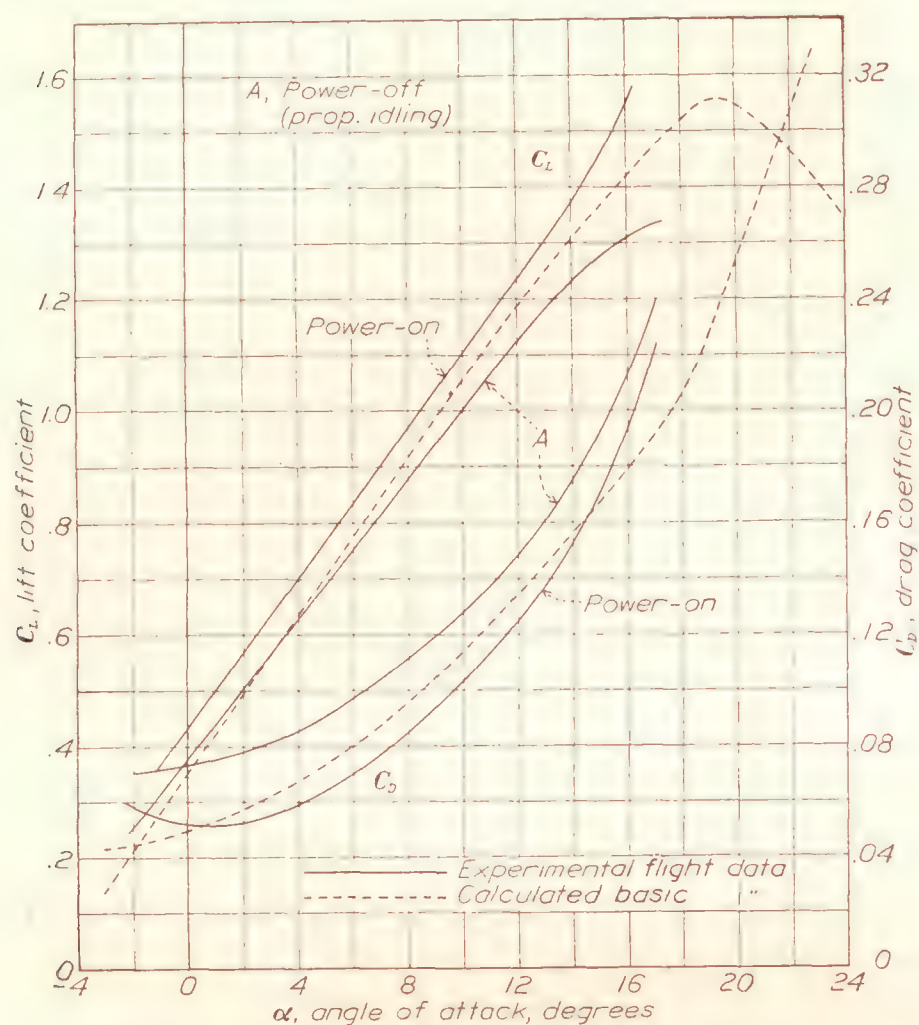


FIGURE 7.—Lift and drag coefficients of Doyle 0-2 airplane

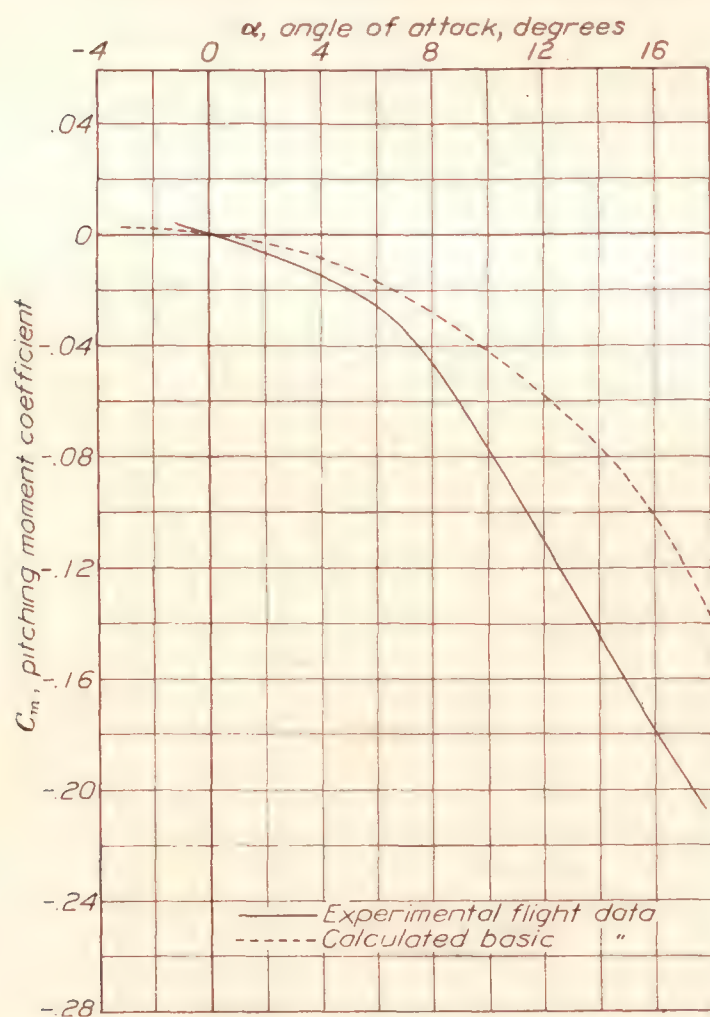


FIGURE 8.—Static pitching-moment coefficient of Doyle 0-2 airplane

positive, i. e., the motion becomes unstable. This change of curvature can not be explained by making allowance for the effect of the thrust and must be dependent on the slipstream effect. Another demonstration of the slipstream effect is shown on Figure

7 by the high maximum lift coefficient for the power-on condition. Both of these phenomena illustrate the need for further study of the flow behind the propeller

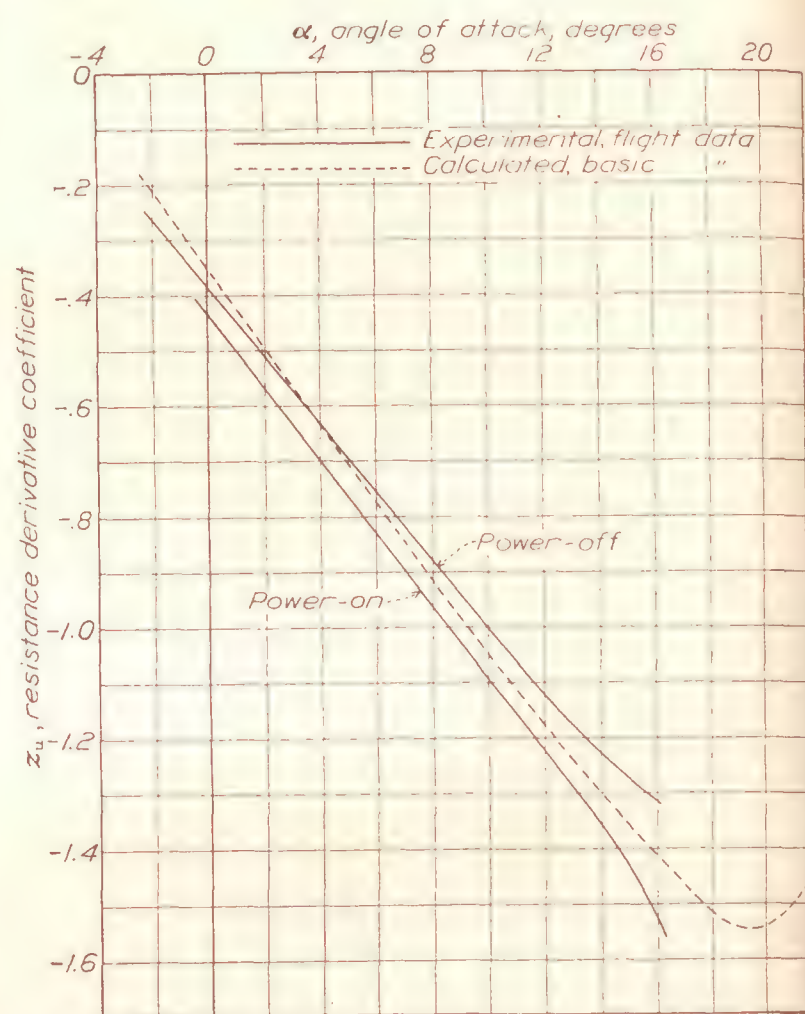


FIGURE 9.—Resistance-derivative coefficient z_u of Doyle 0-2 airplane

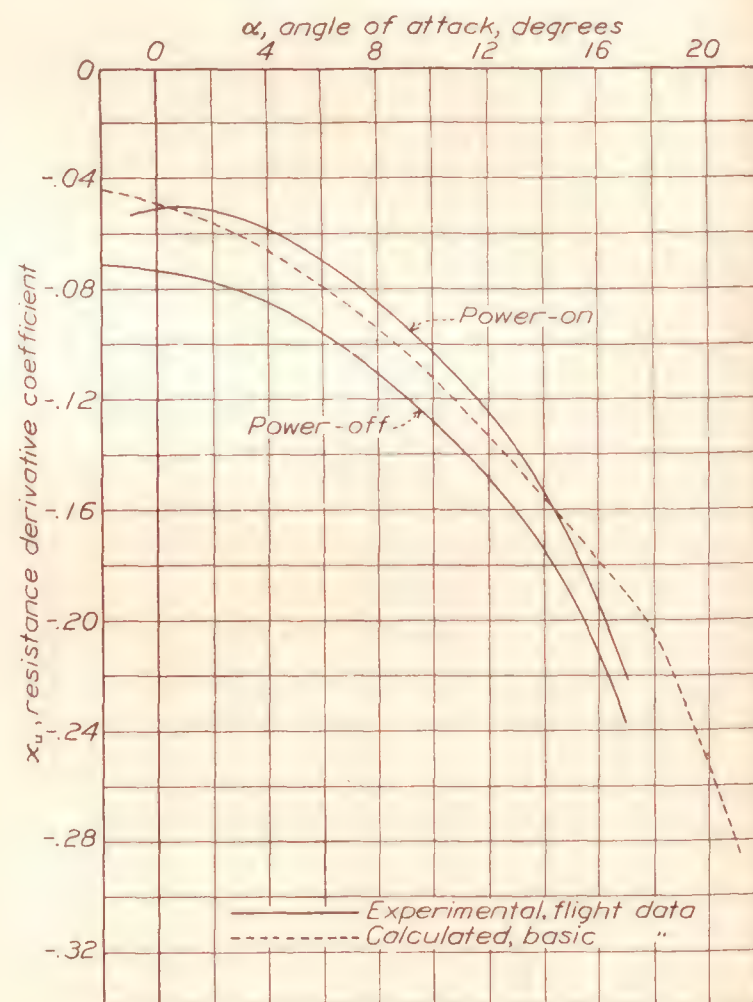


FIGURE 10.—Resistance-derivative coefficient x_u of Doyle 0-2 airplane

The present investigation was made with a fixed stick, that is, a fixed elevator setting. This condition represents the case in which the stabilizer is set to the desired condition of flight and the pilot keeps the elevator in a constant position in spite of slight tendencies

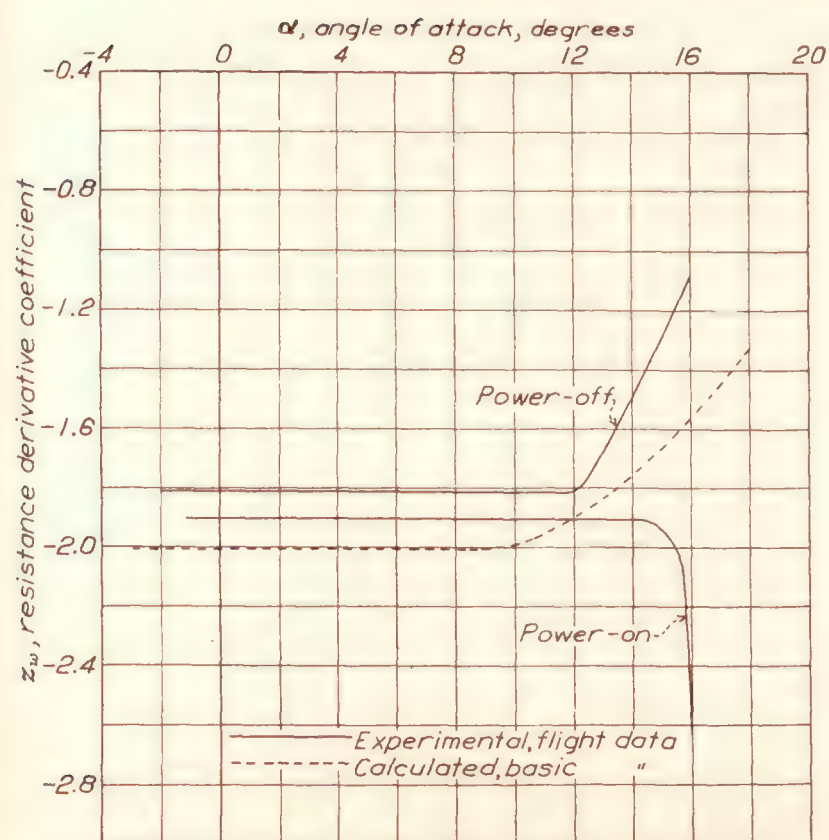
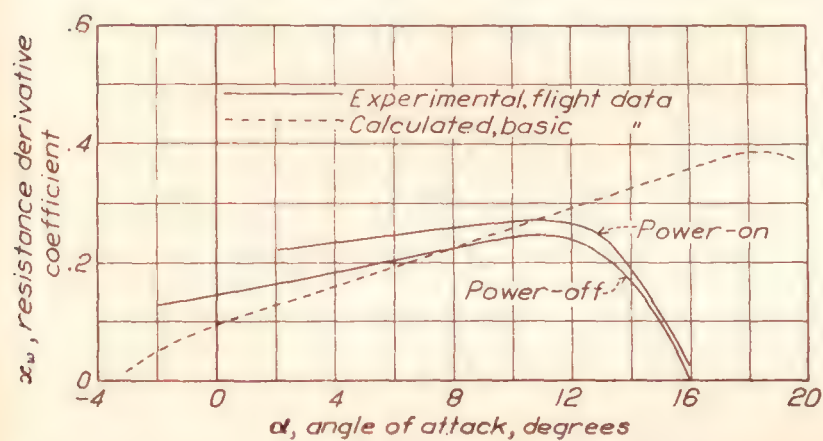
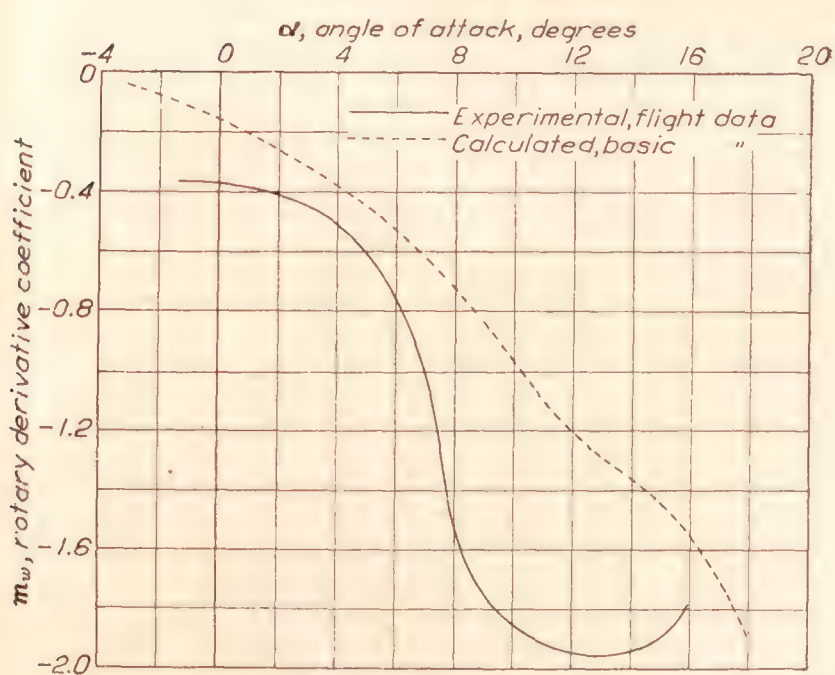
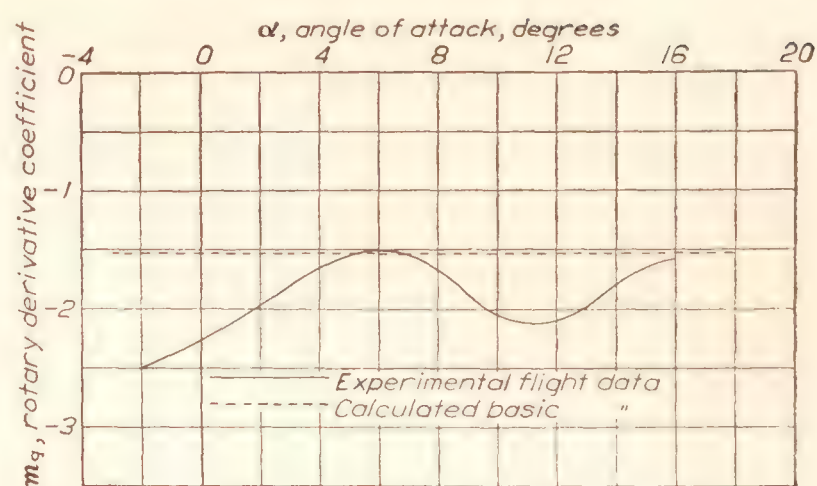
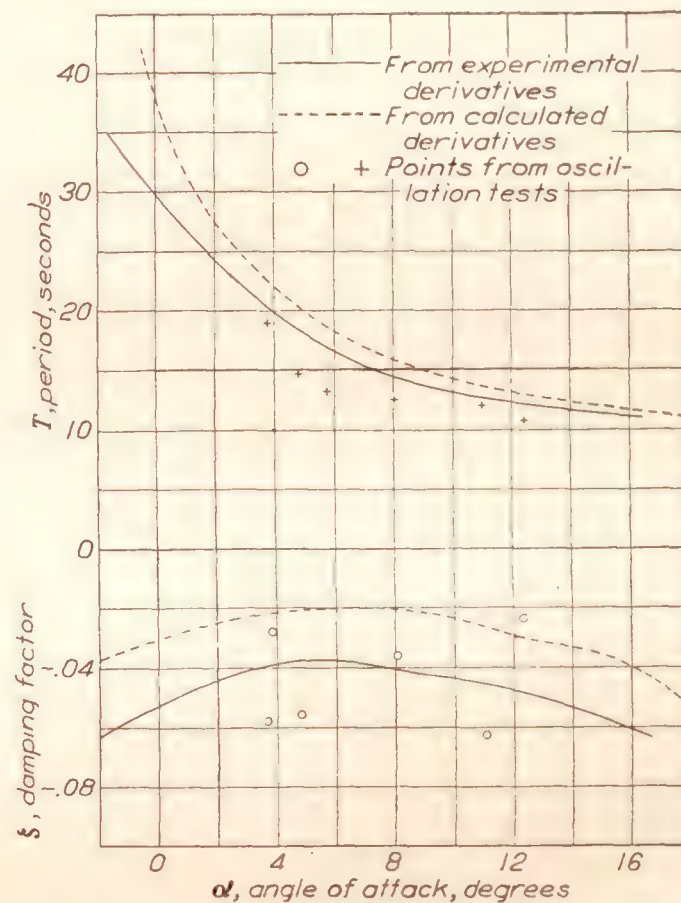

 FIGURE 11.—Resistance-derivative coefficient z_w of Doyle 0-2 airplane

 FIGURE 12.—Resistance-derivative coefficient x_w of Doyle 0-2 airplane

 FIGURE 13.—Rotary-derivative coefficient m_x of Doyle 0-2 airplane

 FIGURE 14.—Rotary-derivative coefficient m_q of Doyle 0-2 airplane


FIGURE 15.—The period and damping coefficient for the power-off condition of Doyle 0-2 airplane

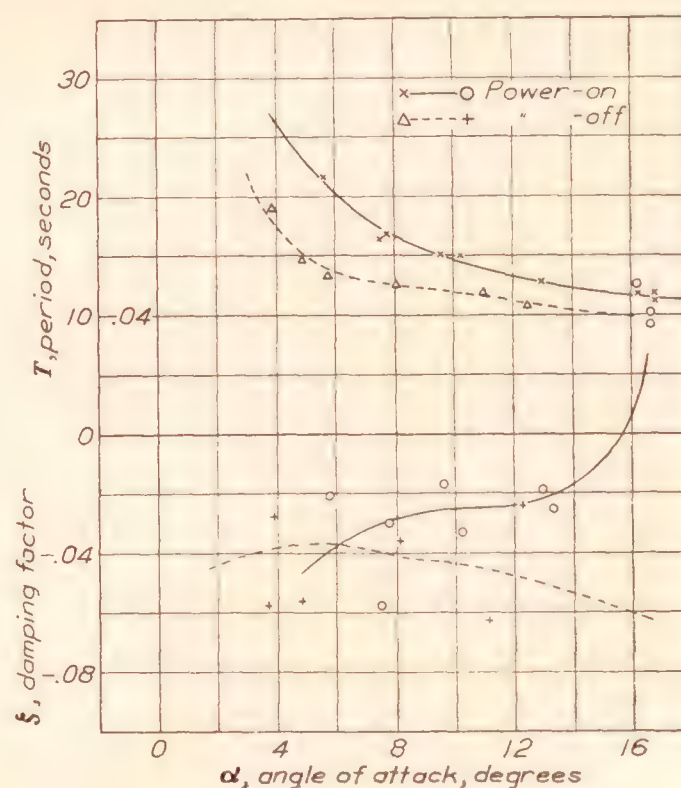


FIGURE 16.—Comparative curves of the measured period and damping coefficient for the power-off and power-on conditions of Doyle 0-2 airplane

encies to fluctuate about the zero stick-force position. Another condition that might well be investigated is the case of free elevators as in that case the stability then attained determines whether or not the airplane can be flown hands-off.

CONCLUSIONS

The following conclusions are based on the results of the study of the dynamic longitudinal stability of the airplane used in this investigation:

1. The theory of longitudinal stability based on the assumption of small oscillations is satisfactory for practical studies of the longitudinal stability of airplanes.

2. The calculation of stability for the power-off condition from basic data is practicable and gives

sufficient information to be of value in regard to the stability of new designs, though the results should not be interpreted too literally if they show the stability to be close to neutral.

3. There is not enough knowledge at present concerning the effect of the slipstream on the various factors upon which the stability of the airplane depends to warrant calculations for the power-on condition.

LANGLEY MEMORIAL AERONAUTICAL LABORATORY,
NATIONAL ADVISORY COMMITTEE FOR AERONAUTICS
LANGLEY FIELD, VA., *June 24, 1932.*

APPENDIX

DEVELOPMENT OF NONDIMENSIONAL STABILITY EQUATION

The dimensional form of the equation of the longitudinal biquadratic, as given in the various works on stability, can be expressed as a determinant.

$$\begin{vmatrix} m\lambda - X_u & -X_w & -\lambda X_q + W \cos \theta_o + \lambda m w_o \\ -Z_u & m\lambda - Z_w & -\lambda Z_q + W \sin \theta_o - \gamma m u_o \\ -M_u & -M_w & \lambda^2 B - \lambda M_q \end{vmatrix} = 0 \quad (1)$$

where the subscript zero refers to the initial values of the variables and the derivatives are in terms of total force and moment rather than force and moment per unit mass. The nondimensional form was first suggested by the consideration

$$X = -C_D \rho^{1/2} S V^2$$

where the symbols have their usual significance.

$$\begin{aligned} X_u &= dX/dV = -C_D \rho S V \\ X_u/\rho S V &= -C_D = x_u \end{aligned}$$

where x_u is the nondimensional form of the derivative X_u .

By similar reasoning, the coefficients of the other derivatives can be obtained and will be found to be

$$\begin{aligned} z_u &= Z_u/\rho S V \\ x_w &= X_w/\rho S V \\ z_w &= Z_w/\rho S V \\ x_q &= X_q/\rho S V l \\ z_q &= Z_q/\rho S V l \\ m_u &= M_u/\rho S V l \eta \\ m_w &= M_w/\rho S V l \eta \\ m_q &= M_q/\rho S V l^2 \eta \end{aligned}$$

where $\eta = B/ml^2$ and l = a characteristic length.

The choice of the length l is arbitrary. The distance from the center of gravity to the rudder post is considered suitable for a study of longitudinal stability.

Substituting for the dimensional derivatives in equation (1) and replacing

$$W \cos \theta_o \text{ by } \frac{1}{2} C_L \rho S V^2$$

and

$$W \sin \theta_o \text{ by } \frac{1}{2} C_L \rho S V^2 \tan \theta_o$$

the following is obtained

$$\begin{vmatrix} m\lambda - x_u \rho S V & -x_w \rho S V & -\lambda x_q \rho S V l + \frac{1}{2} C_L \rho S V^2 + \lambda m w_o \\ -z_u \rho S V & m\lambda - z_w \rho S V & -\lambda z_q \rho S V l + \frac{1}{2} C_L \rho S V^2 \tan \theta_o - \lambda m u_o \\ -m_u \rho S V l \eta & -m_w \rho S V l \eta & \lambda^2 m l^2 \eta - m_q \rho S V l^2 \eta \end{vmatrix} = 0$$

Replace

$$\lambda \text{ by } \lambda_1 \rho S V / m$$

and cancel all factors common to every member of a line or column

$$\begin{vmatrix} \lambda_1 - x_u & -x_w & -\lambda_1 x_q \rho S l / m + C_L / 2 + \lambda_1 w_o / V \\ -z_u & \lambda_1 - z_w & -\lambda_1 z_q \rho S l / m + \frac{1}{2} C_L \tan \theta_o - \lambda_1 u_o / V \\ -m_u & -m_w & -\lambda_1^2 \rho S l / m - \lambda_1 m_q \rho S l / m \end{vmatrix} = 0$$

In any steady state, using the wind axes, w_o will be zero and u_o equals V . Then introducing the parameter

$$\mu = m / \rho S l$$

the determinant can be written

$$\begin{vmatrix} \lambda_1 - x_u & -x_w & \frac{1}{2} C_L \mu - \lambda_1 x_q \\ -z_u & \lambda_1 - z_w & \frac{1}{2} C_L \mu \tan \theta_o - \mu \lambda_1 - z_q \lambda_1 \\ -m_u & -m_w & \lambda_1^2 - m_q \lambda_1 \end{vmatrix} = 0 \quad (2)$$

In practice it has been found that x_q and z_q are terms of the second order with respect to the other derivatives and consequently are hereafter neglected.

The biquadratic obtained from the nondimensional determinant, which is of similar form to that obtained from the dimensional form, is

$$\lambda_1^4 + B \lambda_1^3 + C \lambda_1^2 + D \lambda_1 + E = 0$$

where

$$B = -m_q - x_u - z_w$$

$$C = z_w m_q + z_w x_u + m_q x_u - z_u x_w - \mu m_w$$

$$D = \frac{1}{2} \mu m_u C_L + \mu m_w x_u + \frac{1}{2} C_L \mu m_w \tan \theta_o + m_q (z_u x_w - x_u z_w) - x_w \mu m_u$$

$$E = \frac{1}{2} \mu C_L (x_w m_u - x_u m_w) \tan \theta_o + \frac{1}{2} \mu C_L (m_w z_u - m_u z_w)$$

Stability is assured if Routh's discriminant $R = BCD - D^2 - B^2 E$ and each of the coefficients are positive. For a more detailed analysis of the character of the motion following a disturbance, the complete solution of the equation is found. This analysis can be made by an approximate factorization of the biquadratic into two quadratics

$$\begin{aligned} \lambda_1^2 + B \lambda_1 + C &= 0 \\ \lambda_1^2 + \left(\frac{D}{C} - \frac{BE}{C^2} \right) \lambda_1 + \frac{E}{C} &= 0 \end{aligned}$$

of which the first represents a short-period, heavily damped oscillation, and the second a long-period, lightly damped oscillation.¹ It is with the lightly damped oscillation that instability is most likely to occur and therefore it is usually only necessary to investigate this phase. The solution for λ_1 from the second quadratic is

$$\lambda_1 = -\frac{1}{2} \left(\frac{D}{C} - \frac{BE}{C^2} \right) \pm \sqrt{\left(\frac{DC - BE}{2C^2} \right)^2 - \frac{E}{C}}$$

¹ The accuracy of this approximate factorization, which depends on the relative values of the constants, was found satisfactory in the present case by reversing the operation with the appropriate numerical values of the constants substituted in the equations.

The motion is periodic only when the term represented by the radical is imaginary, and for this condition the period in nondimensional units is

$$T_1 = \frac{2\pi}{\sqrt{\frac{E}{C} - \left(\frac{DC - BE}{2C^2}\right)^2}}$$

The term $-\frac{1}{2}\left(\frac{D}{C} - \frac{BE}{C^2}\right)$ is the constant part of the

logarithmic decrement of damping and is called the damping coefficient ζ_1 . If the damping coefficient is negative, the motion is stable; that is, the oscillations are damped; and if the damping coefficient is positive, the motion is unstable.

For comparison with the values obtained through the measurements in flight of the period and damping coefficient, it is necessary to convert the solution of λ_1 to the dimensional form. This conversion can be easily made by the introduction of the factor $\rho VS/m$.

REFERENCES

1. Glauert, H.: A Non-Dimensional Form of the Stability Equations of an Aeroplane. R. & M. No. 1093, British A. R. C., 1927.
2. Glauert, H.: The Stability Derivatives of an Airscrew. R. & M. No. 642, British A. C. A., 1919.
3. Norton, F. H.: N. A. C. A. Recording Air Speed Meter. T. N. No. 64, N. A. C. A., 1921.
4. Coleman, Donald G.: N. A. C. A. Flight-Path-Angle and Air-Speed Recorder. T. N. No. 233, N. A. C. A., 1926.
5. Brown, W. G.: The Synchronization of N. A. C. A. Flight Records. T. N. No. 117, N. A. C. A., 1922.
6. Ronan, K. M.: An Instrument for Recording the Position of Airplane Control Surfaces. T. N. No. 154, N. A. C. A., 1923.
7. Reid, H. J. E.: A study of Airplane Maneuvers with Special Reference to Angular Velocities. T. R. No. 155, N. A. C. A., 1922.
8. Miller, Marvel P., and Soulé, Hartley A.: Moments of Inertia of Several Airplanes. T. N. No. 375, N. A. C. A., 1931.
9. Diehl, Walter S.: The Determination of Downwash. T. N. No. 42, N. A. C. A., 1921.
10. Reid, Elliott G.: Applied Wing Theory. McGraw-Hill, 1932, p. 196.

REPORT No. 443

PRESSURE-DISTRIBUTION MEASUREMENTS ON THE HULL AND FINS OF A 1/40-SCALE MODEL OF THE U. S. AIRSHIP "AKRON"

By HUGH B. FREEMAN

SUMMARY

This report presents the results of measurements of pressure distribution conducted in the propeller-research wind tunnel of the National Advisory Committee for Aeronautics on a 1/40-scale model of the U. S. airship "Akron" ("ZRS-4"). The pressures, which were measured simultaneously at nearly 400 orifices located at 26 stations along one side of the hull, were recorded by two photographic multiple manometers placed inside the model. The hull pressures were measured both with and without the tail surfaces and the control car for eight angles of pitch varying from 0° to 20° and at air speeds of approximately 70 and 100 miles per hour. The pressures were also measured at approximately 160 orifices on one horizontal fin for the above speeds and pitch angles and for nine elevator angles.

The integrated transverse forces and the integrated moments about the center of buoyancy were in good agreement with the forces and moments measured on the balances in the force tests. The pressural drag of the hull was found to be practically zero within the accuracy of the tests. The pressure forces on the after portion of the hull in the presence of the tail surfaces were found to contribute more than 40 per cent of the total fin moments measured in the force tests. Negative pressures as great as seven times the dynamic pressure of the undisturbed air stream were measured on the leading edge of the horizontal fin at the 20° pitch angle with 20° down elevator.

INTRODUCTION

A knowledge of the pressure distribution over airship forms is of interest primarily to the airship designer in determining the stresses in the hull structure, the most important of which are due directly or indirectly to the aerodynamic forces on the hull. Experimental pressure-distribution results are also useful in checking theoretical methods of calculating the pressures on streamline forms, in checking the forces and moments measured on the balances in wind-tunnel tests and, indirectly, in computing the frictional forces on the surface of the hull. Previous measurements of pressure distribution on good streamline shapes at 0° pitch angle have shown that the

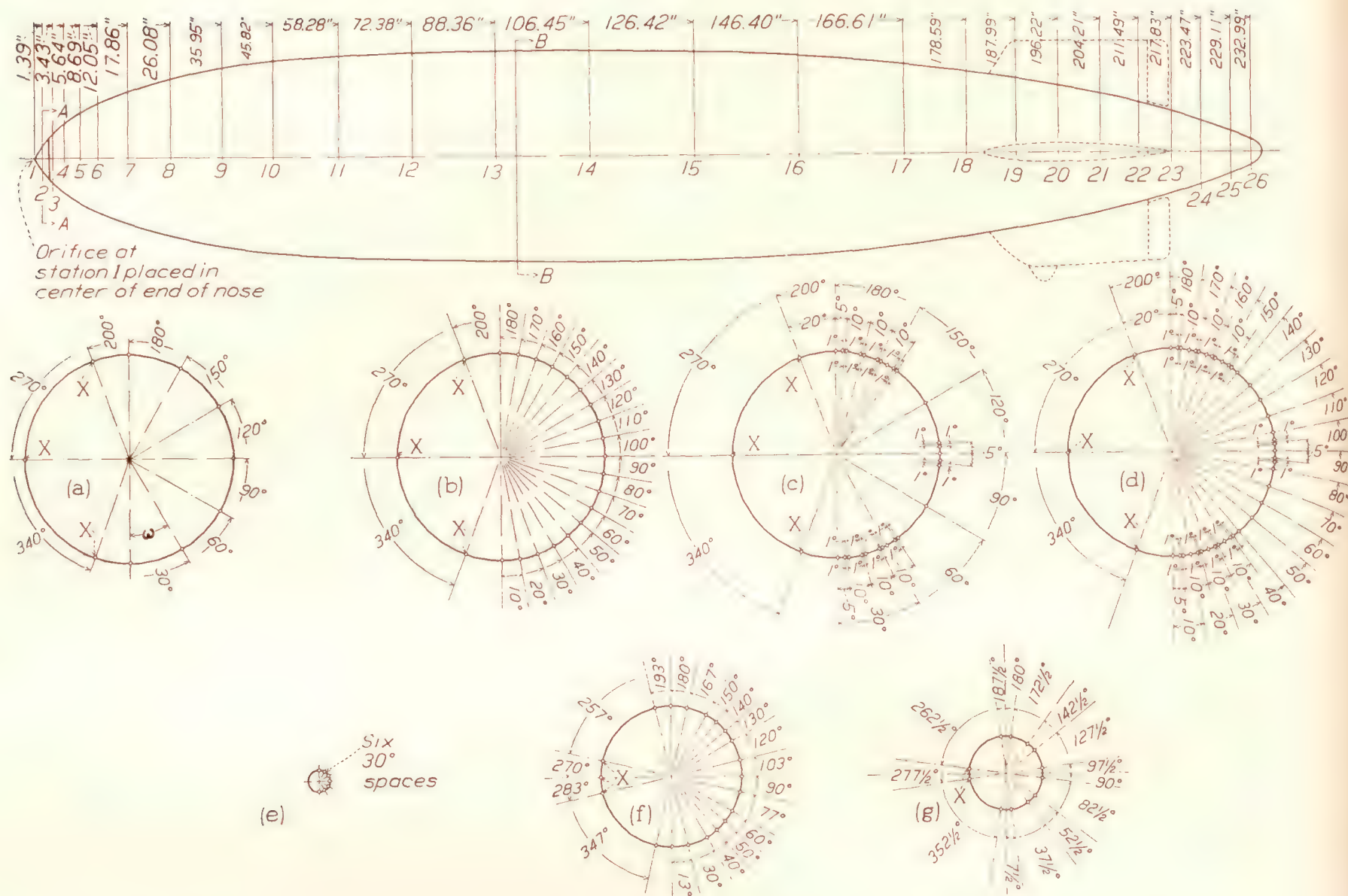
resultant of the normal forces on the hull is practically zero; whereas, the tangential or frictional forces constitute nearly the entire drag of the hull.

The subject tests are a part of a program of research undertaken at the request of the Bureau of Aeronautics, Navy Department, on a 1/40-scale model of the U. S. airship *Akron* (ZRS-4), with the object of determining: (1) The forces and pitching moments on the bare hull and on the hull fitted with two different sets of tail surfaces, (2) the elevator forces and hinge moments, and (3) the pressure distribution over the hull and fins. This program was later extended to include (4) the measurement of total head in the boundary layer at ten stations on the hull. The results of (1) and (2) are presented in reference 1, those of (3) are the subject of the present report, and the results of the boundary-layer tests are given in reference 2.

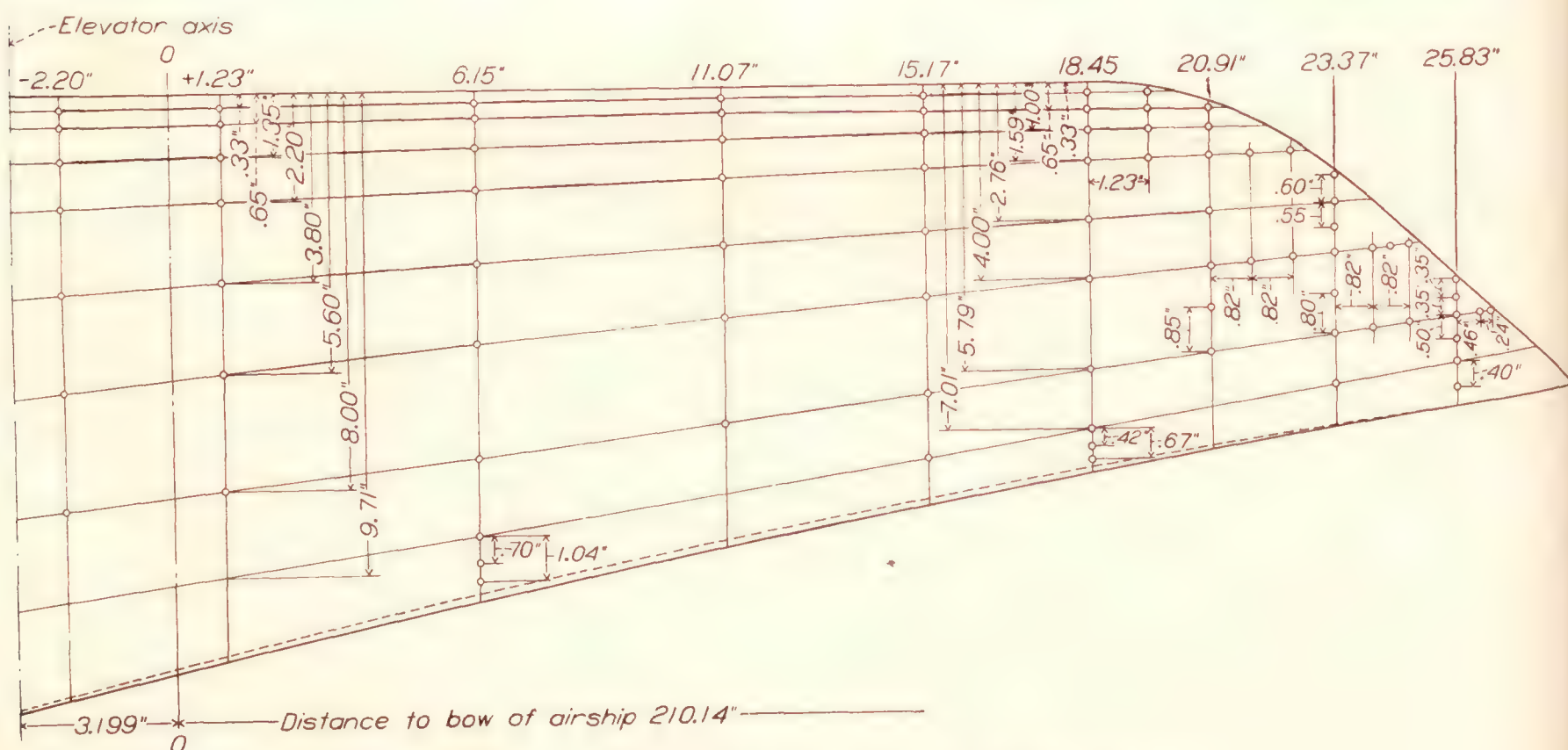
The unusually large size of the model, 19.62 feet in length and 3.33 feet in maximum diameter, allowed the tests of pressure distribution to be conducted at a larger Reynolds Number than has previously been obtained in model tests of a similar nature. The large model also permitted the multiple manometers, which record simultaneously 400 pressures, to be installed inside the model, thus greatly expediting this work. The tests were conducted in the 20-foot propeller-research wind tunnel of the National Advisory Committee for Aeronautics and were completed in July, 1931.

APPARATUS AND TESTS

The model, built in the shops of the Washington Navy Yard, is of hollow wooden construction having 36 sides over the fore part of the hull fairing into 24 sides near the stern. The length of the hull is 19.62 feet, the maximum diameter 3.33 feet, and the fineness ratio 5.9. The principal dimensions of the hull and fins are given in Table I. Four hundred pressure orifices, distributed among 26 stations, were placed along one side of the hull. The location of the stations and the distribution of the orifices around the hull are shown in Figure 1. The orifices, $\frac{1}{32}$ inch in diameter, were drilled into circular brass plates $\frac{1}{2}$ inch in diameter set into and flush with the surface of the hull. The

FIGURE 1.—Location of orifices for the pressure measurements on a 1/40 scale model of the *Akron*

- (a) Typical sections in direction "B-B" at stations 3, 4, 6, 10, 14, and 16 showing radial locations of orifices in hull. Three orifices marked "x" placed at stations 4 and 6 only
- (b) Typical sections in direction "B-B" at stations 7, 9, 11, 13, and 15 showing radial location of orifices in hull. Three orifices marked "x" placed at station 7 only. Orifices marked "z" at station 11 omitted
- (c) Typical sections in direction "B-B" at stations 8 and 12 showing radial location of orifices in hull. Three orifices marked "x" placed at station 8 only.
- (d) Typical sections in direction "B-B" at stations 5 and 17 showing radial location of orifices in hull. Three orifices marked "x" placed at station 5 only.
- (e) Section "A-A" showing radial location of orifices at station 2
- (f) Typical sections in direction "B-B" at stations 8 to 21 inclusive, showing radial location of orifices in hull. Three orifices marked "x" placed at station 21 only.
- (g) Typical sections in direction "B-B" at stations 22 to 26 inclusive, showing radial location of orifices in hull. Two orifices marked "x" placed at stations 22 and 23 only,



location of the fin orifices is given in Figure 2. The fin shown is of the Mark-II type, which is described in detail in reference 1.

The orifices were connected inside the hull to two photographic-recording multiple manometers of the type shown in Figure 3. Each manometer consisted of 200 glass tubes placed about the periphery of a drum, a long incandescent light bulb for making the exposures placed at the center of the drum, a reservoir to which the lower ends of the tubes were connected by means of a circular brass header, and a box which contained the photostat paper and the mechanism for changing the paper after each exposure. The photostat paper, wound initially on spool A, was passed around the metering spool B and then around the outside of the glass tubes on the drum and back into the box, and was wound on the spool C, which was driven by an electric motor. The metering spool was geared to a mechanism that broke the electric circuit and stopped the motor when the proper length of paper had been metered out to encircle the drum.

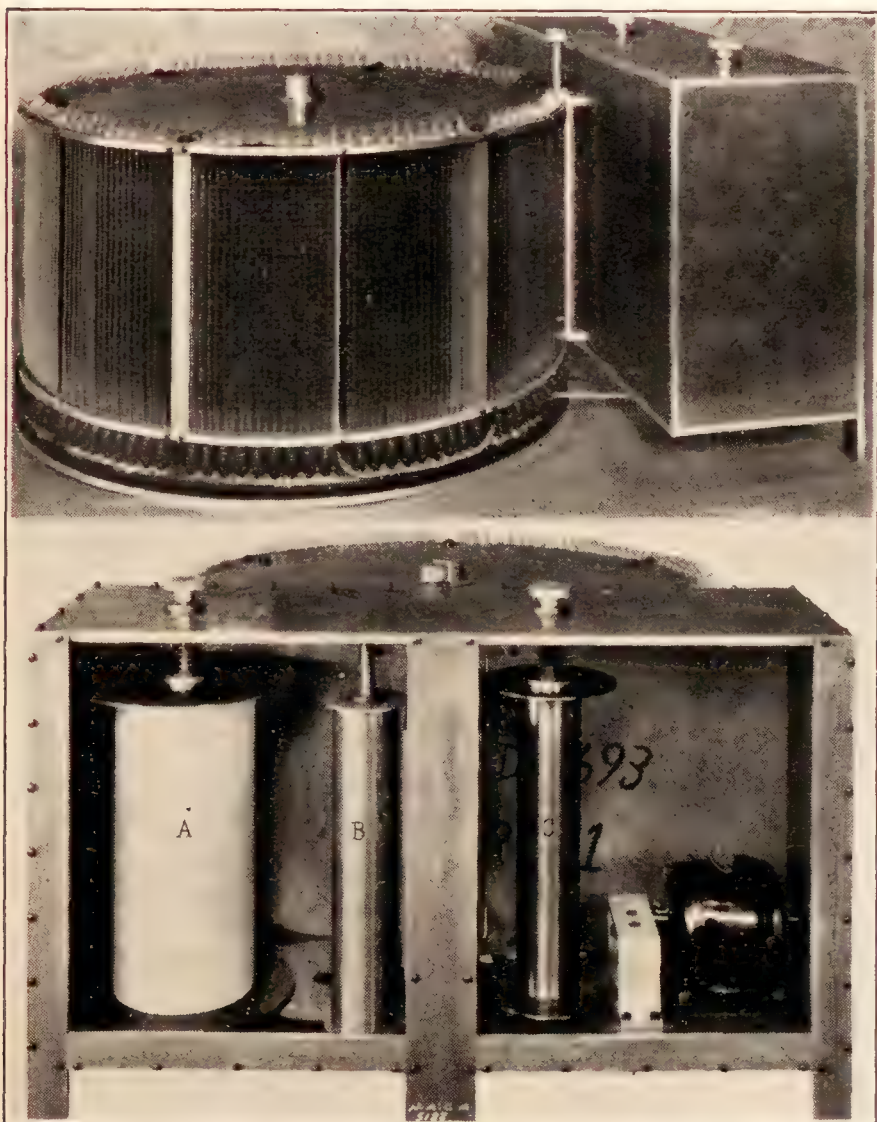


FIGURE 3.—Photographic-recording multiple manometer used for recording pressures on the 1/40-scale model *Akron*

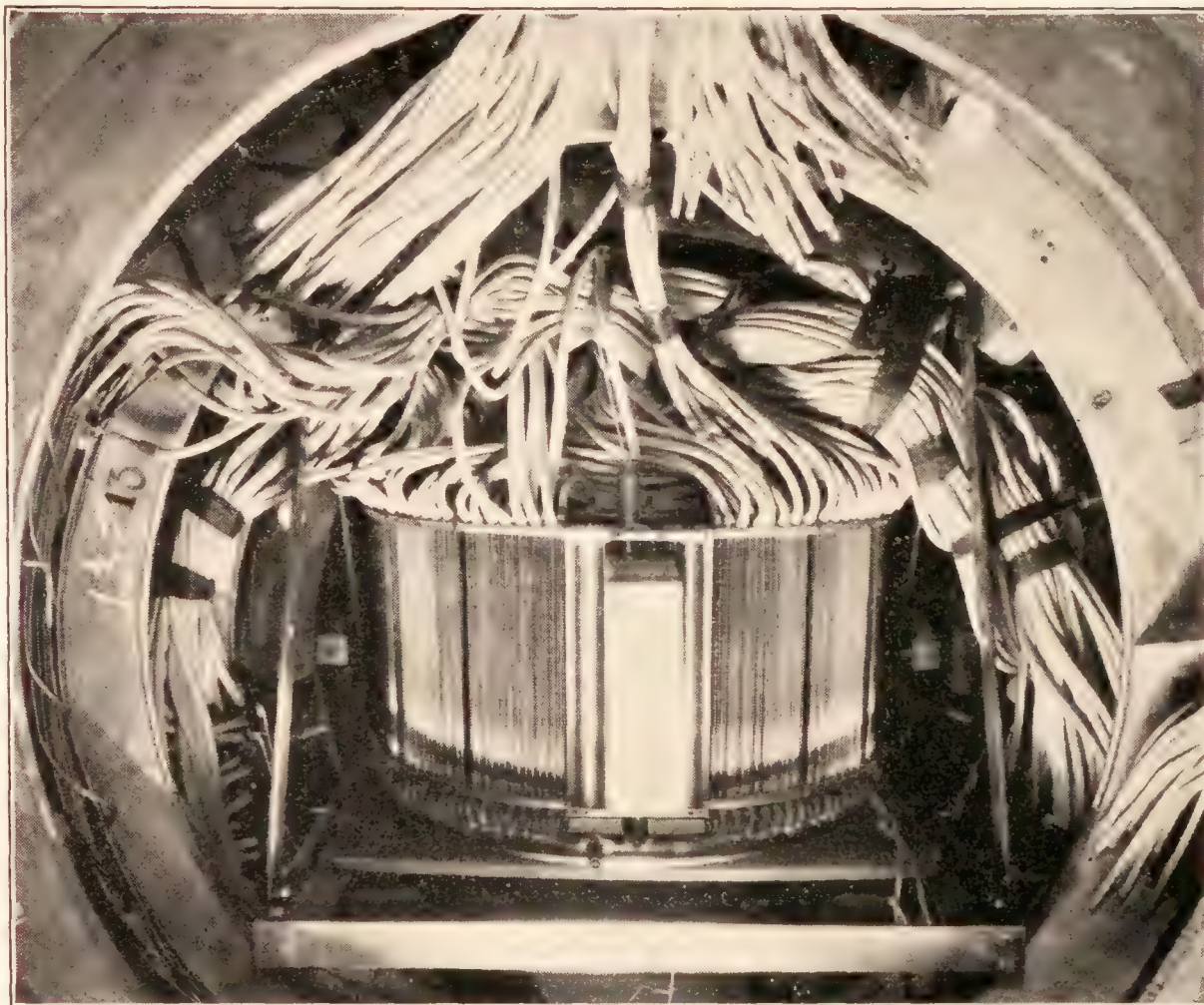


FIGURE 4.—Manometer installation within the hull of 1/40-scale model *Akron*

The manometers were mounted inside the model on cradles, which were free to swing about a horizontal axis at right angles to the longitudinal axis of the hull, thus allowing the manometers to remain level for the various angles of pitch. (Fig. 4.) In order to provide a reference line on the records, six of the glass tubes spaced equidistant about the circumference of the drums were connected, together

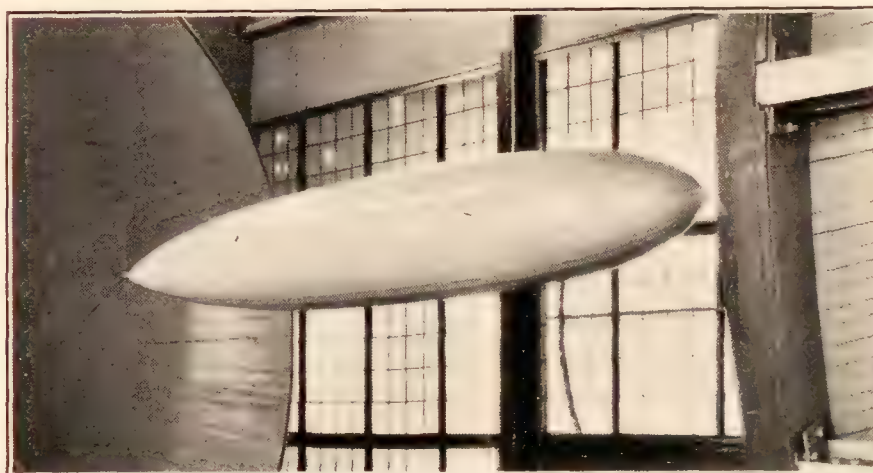


FIGURE 5.—The 1/40-scale model *Akron* mounted in the 20-foot propeller-research wind tunnel

with the reservoirs, to the reference pressure, which for these tests was the static pressure in the test chamber.

Two simultaneous records, one from each manometer, gave a complete diagram of the pressure distribution over one side of the hull at one angle of pitch and at one wind speed. The capacity of the manometers was 18 exposures. Thus, complete diagrams for nine angles of pitch and two wind speeds could be obtained in one run of about 30 minutes duration.

The method of mounting the model in the wind tunnel is shown in Figure 5, and is described in detail in reference 1.

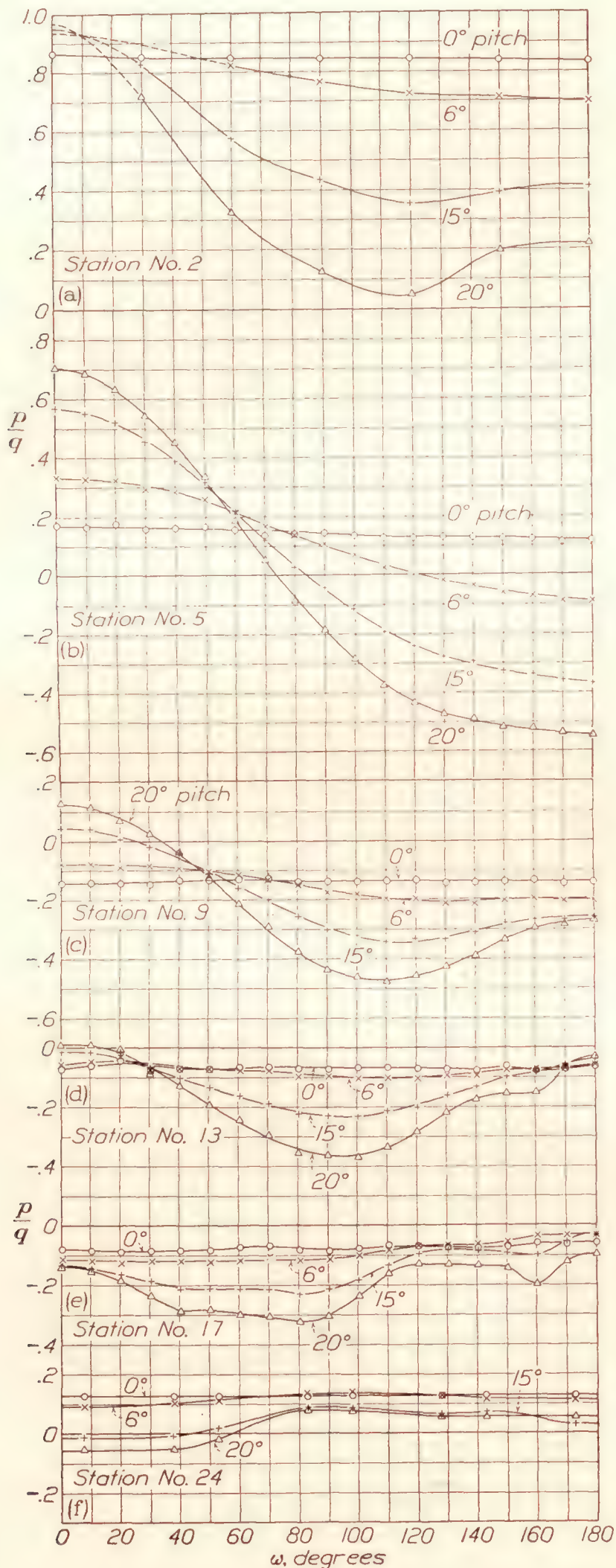


FIGURE 6.—Observed point pressures on bare hull at several stations for four angles of pitch of the 1/40-scale model Akron

The pressure distribution was measured (1) on the bare hull at nine angles of pitch ($\theta = -3^\circ, 0^\circ, 3^\circ, 6^\circ, 9^\circ, 12^\circ, 15^\circ, 18^\circ, 20^\circ$) and at air speeds of approximately 70 and 100 miles per hour, (2) on the hull with

fins and control car at the above pitch angles and speeds and for three elevator angles ($\delta = 0^\circ, 20^\circ$, and -20°), and (3) on one horizontal fin at the above angles of pitch and air speeds and for nine elevator angles ($\delta = -20^\circ, -15^\circ, -10^\circ, -5^\circ, 0^\circ, 5^\circ, 10^\circ, 15^\circ$, and 20°).

Because of the limited head (about 9 inches) that could be recorded by the manometers, which did not allow the low pressures on the suction side of the leading edge of the fin to be measured with the manometers containing alcohol, these pressures were measured in a separate test with the manometers containing mercury.

PRECISION OF MEASUREMENTS

The following sources of error affect the accuracy of the measured pressures:

- Shrinkage of the photographic records.
- Errors in measurements of the manometer deflections.
- Oscillation of the manometers.
- Fluctuations in the velocity and direction of the air stream.

The errors from a were found, in general, to be less than 1 per cent and those from b are believed to be within ± 1 per cent. The combined errors due to a, c, and d, estimated from a comparison of the pressures over the nose of the hull from different test records were of the order of ± 2.5 per cent. The portion of these errors contributed by the oscillation of the manometers is believed to be small except for the high-speed, high-pitch-angle condition when the model was observed to be quite unsteady. Additional small errors may have been introduced owing to the fact that some of the orifices had pulled into the surface slightly. The relative accuracy of the point pressures for any particular test, is best shown by the plots of the observed values presented in Figure 6. The scattering of the values from a mean curve is small.

RESULTS AND DISCUSSION

Because of the great mass of observed and derived data obtained in the present tests, it has been necessary to limit the results presented here to relatively few data representative of the whole.

The results have been presented in terms of the dynamic pressure q of the air stream and have been corrected for the difference between the local static pressure in the air stream and the reference pressure. This correction consisted simply of subtracting from the pressures at any section of the model the static pressure of the air stream, measured in the absence of the model, at the corresponding position along the axis of the tunnel. This correction should reduce the pressure of the stagnation point at the nose of the hull with the model at 0° pitch, to a value equal to the dynamic pressure q . The mean value of p/q for this station (where p is the pressure) obtained from eight different tests was 1.005.

The variation in static pressure along the hull, measured in the absence of the model, is given in the following table:

a/L	0.0	0.1	0.2	0.3	0.4	0.5	0.6	0.7	0.8	0.9	1.0
p/q	.032	.025	.020	.017	.015	.013	.011	.010	.010	.011	.013

where a is the axial distance from the nose of the model, L is the length of the model, and p is the static pressure at any point on the axis.

The observed values of the point pressures on the bare hull are presented in Table II and are plotted in

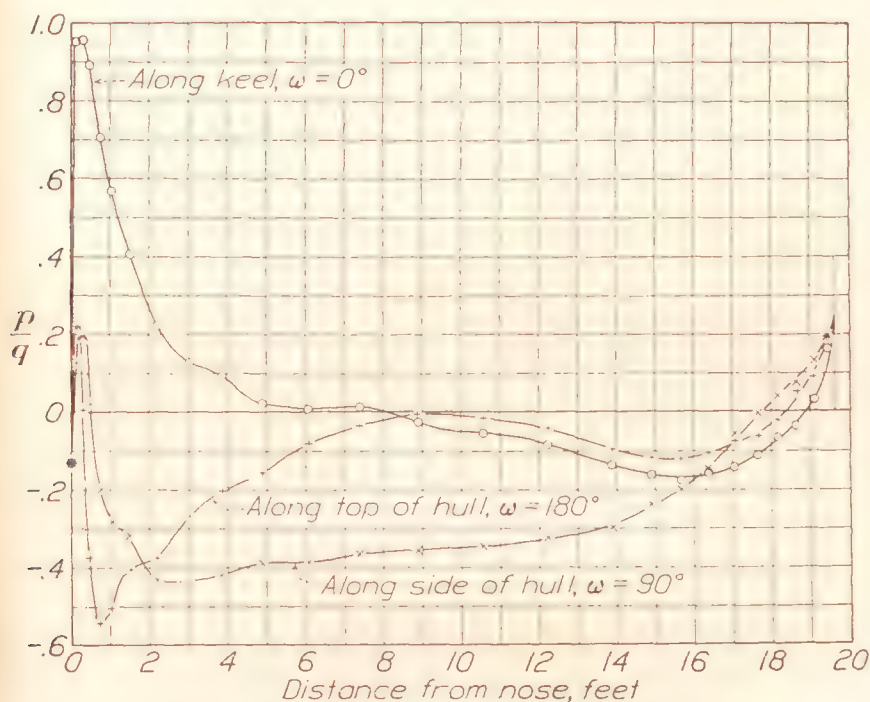


FIGURE 7.—Longitudinal distribution of pressure along three longitudinals of the bare hull of 1/40-scale model Akron. Pitch angle $\theta = 20^\circ$

Figure 6 for six stations and for four angles of pitch against the angular displacement ω of the orifices from the bottom center line of the hull. The longitudinal distribution of pressure along the hull at $\omega = 0^\circ, 90^\circ$, and 180° , for an angle of pitch of 20° , is

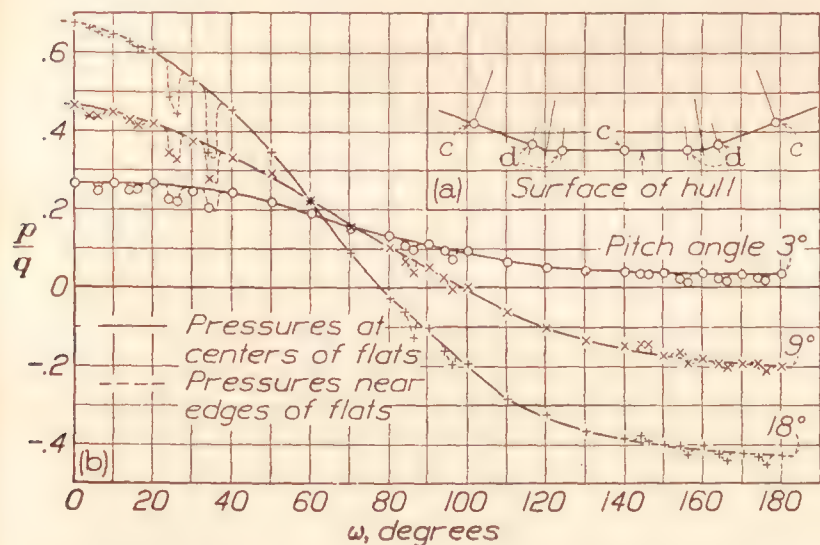


FIGURE 8.—Effect of polygonal form on the distribution of pressures at station 5 on 1/40-scale model Akron. c=orifices at centers of flat sides of hull. d=orifices 1° from edges of flat sides of hull

given in Figure 7. The values were taken from curves such as those given in Figure 6.

The effect of the polygonal form of the hull upon the pressure distribution around the hull is shown in Figure 8. Figure 8 (a) shows a typical layout of the orifices located near the corners of the polygonal hull. Figure 8 (b) shows the pressures measured at station 5

plotted against the angle ω . Continuous curves have been drawn through the pressures measured at the centers of the flats and broken lines through the pressures measured near the edges of the flats. In general, the pressures at the corners are slightly lower

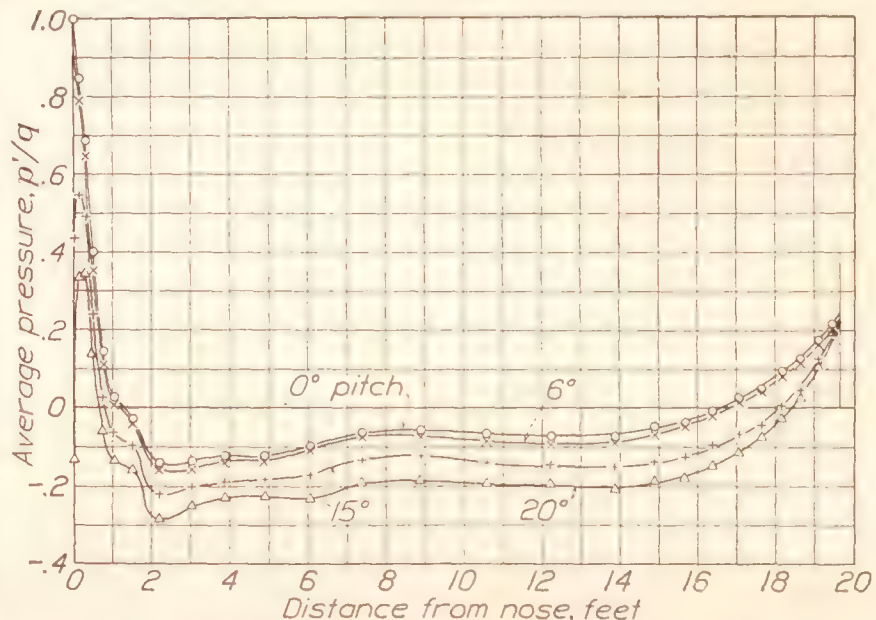


FIGURE 9.—Average pressures on bare hull of 1/40-scale model Akron for four angles of pitch

than those at the center. The difference is greatest on the lower side of the hull in the range of the values of ω between 20° and 40° . In this range the difference increases with both the angle of pitch and the angle of displacement from the keel. The maximum effect shown occurs at $\omega = 34^\circ$ for the 18° angle of pitch

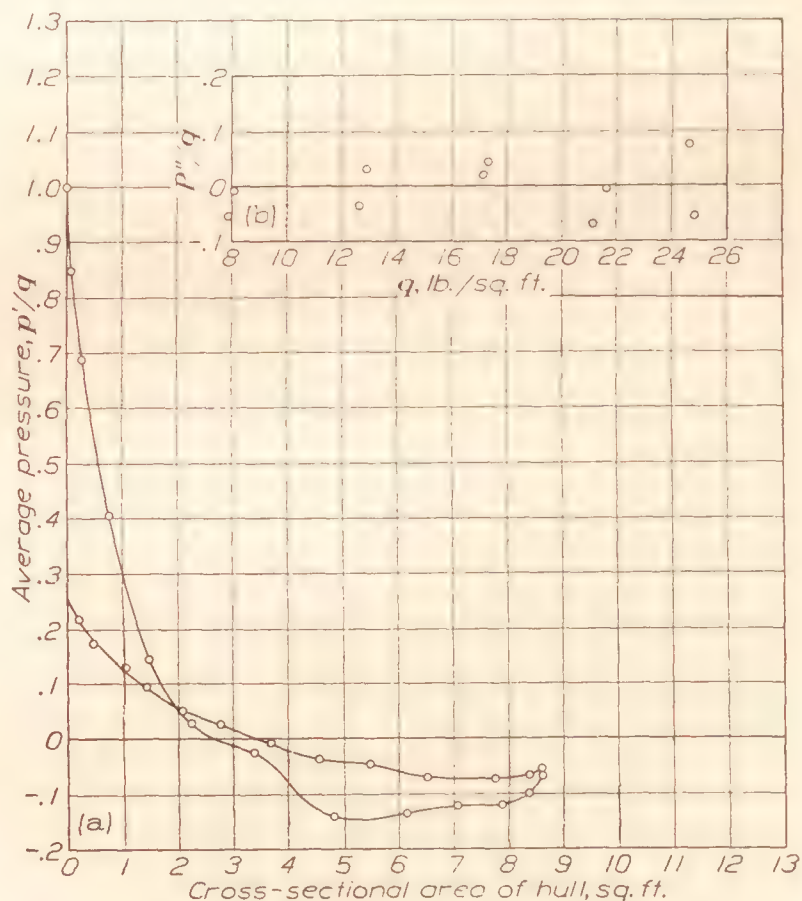


FIGURE 10.—(a) Average pressures plotted against cross-sectional area. (b) Longitudinal force on bare hull of 1/40-scale model Akron. Pitch angle $\theta = 0^\circ$

where the pressure near the corner is about 30 per cent less than that at the center. The trend of the results indicates that the maximum effect occurs at a still higher value of ω , probably around 45° , where there were no orifices at the corners. The results for the stations numbered 8, 12, and 17 were similar to

those shown for station 5, except that the magnitude of the effect was somewhat smaller.

The average pressure at any station, considering the hull as a body of revolution, is given by the equation (reference 3)

$$p' = \frac{1}{2\pi} \int_0^{2\pi} p \, d\omega \quad (1)$$

or, for the present case, if it be assumed that the pressure diagrams are symmetrical on the two sides of the hull, the average pressure is given by

$$p' = \frac{1}{\pi} \int_0^{\pi} p \, d\omega$$

The average pressures, obtained by integrating graphically curves such as those given in Figure 6, are

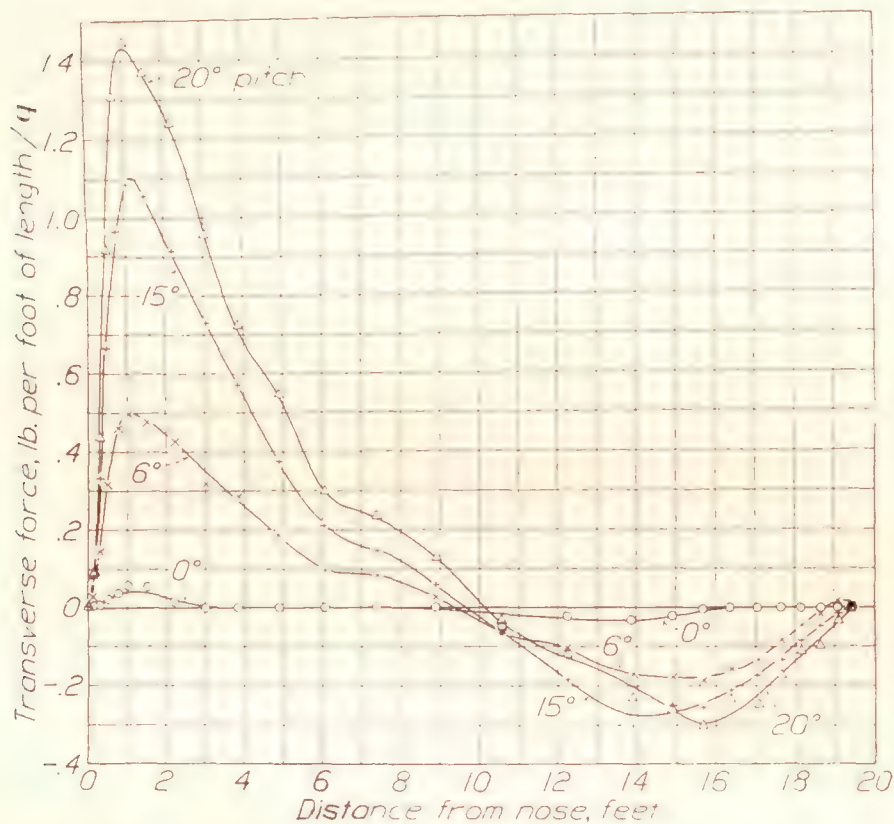


FIGURE 11.—Transverse force per foot of length on the bare hull of the 1/40 scale model Akron

presented in Table III and are plotted for four angles of pitch in Figure 9.

The pressure at station 7, which is approximately 1.5 feet from the bow, appears to be high in relation to those of the neighboring stations and causes an irregularity in the curves of average pressures. This characteristic, which appears in all the tests, could not be satisfactorily explained. It was thought perhaps to be due to an irregularity in the model. A careful check of the form of the hull in this region, however, showed the actual ordinates to be in close agreement with those specified and the form to be fair. Another possible explanation of the distortion of the curves in this region was the fact that many of the orifices at this station were not exactly flush with the surface, but had pulled into the surface slightly. An inspection of the pressures measured at station 7 at orifices that were flush with the surface showed that these pressures were slightly lower than the mean curve, but only by an average amount of $p/q = 0.015$, a value too small to remove the hump in the curve.

The longitudinal force or, for 0° angle of pitch, the pressural drag is given by the equation

$$P'' = \int_{\theta_1}^{\theta_2} p' \, dA$$

where A is the area of cross section of the hull. The integral was evaluated by integrating graphically the area under the curve of the average pressure plotted against the cross-sectional area of the hull. (Figure 10 (a).) The pressural drag for ten observations made at five air speeds is plotted in Figure 10 (b) against the dynamic pressure of the air stream. The scattering of the values is probably due to errors in the measurements and in the graphical computation, which involves the subtraction of two approximately equal areas, very small errors in the pressures causing relatively large errors in the integrated results. The plotted values fall about a mean line which is coincident with the axis of the abscissa, indicating that within

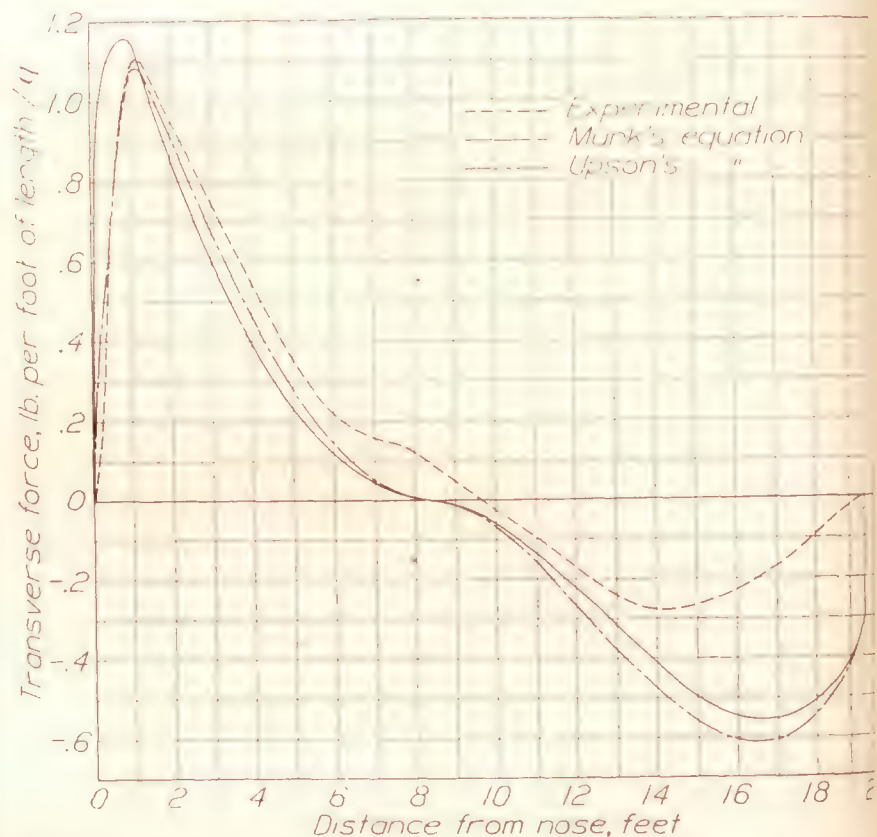


FIGURE 12.—Computed and experimental transverse forces on the bare hull of the 1/40 scale model Akron. $\theta = 15^\circ$

the accuracy of these tests the pressural drag is so small it may be considered zero. However, this result is also dependent upon the accuracy of the correction for the variation in static pressure along the hull. Without this correction the pressural drag amounts to about 21 per cent of the measured drag of the hull.

The longitudinal forces for the various angles of pitch are given in Table IV and compared to the longitudinal forces obtained from the force measurements. Here, as in the case for 0° angle of attack the values of the integrated forces are small and quite erratic.

The transverse force, in a vertical plane through the longitudinal axis of the hull, for any station is given by the equation

$$f = \frac{dF}{dx} = \int_0^{2\pi} p r \cos \omega \, d\omega \quad (2)$$

where F is the total transverse force, x is the distance from the nose of the hull measured along the longitudinal axis, and r is the radius of the hull. The values of f determined graphically are given in Table V, and are plotted for four angles of pitch in Figure 11. The existence of the small transverse forces at the 0° angle of pitch indicates either that the air flow was not strictly axial or that the model was not exactly symmetrical. The curve for the 15° angle of pitch is re-

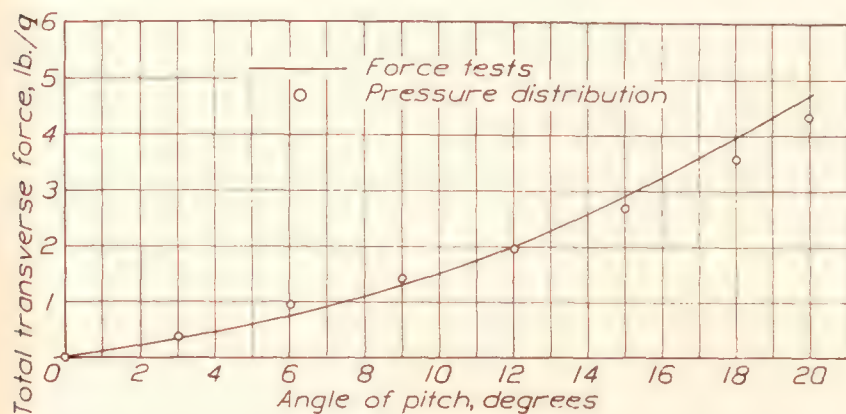


FIGURE 13.—Comparison of total transverse forces obtained from pressure distribution and from force tests on the bare hull of 1/40-scale model Akron

plotted in Figure 12 and compared to the transverse forces computed from Munk's equation (reference 4)

$$f = \frac{dF}{dx} = \frac{dA}{dx} q (k_2 - k_1) \sin 2\theta$$

where A is the cross-sectional area of the hull

θ is the angle of pitch

k_2 and k_1 are the coefficients of additional mass of air transversely and longitudinally, respectively,

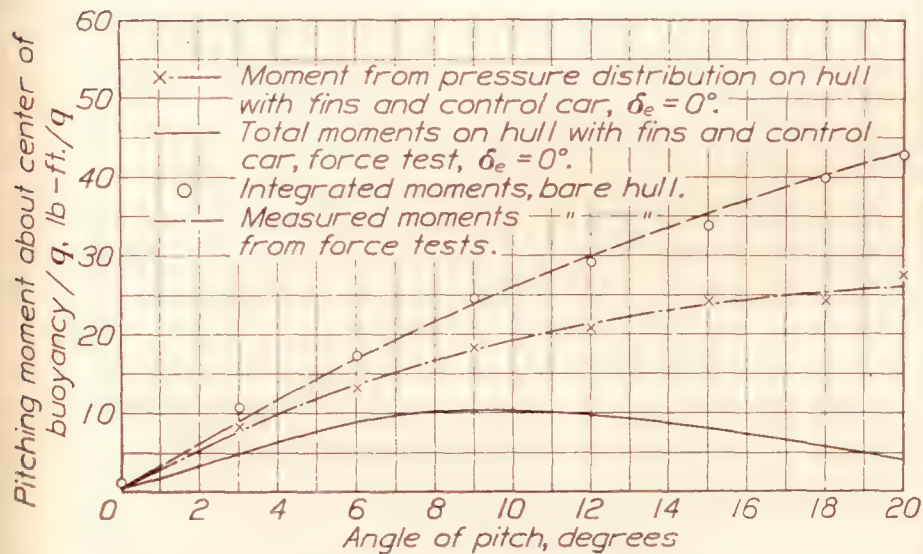


FIGURE 14.—Comparison of pitching moments obtained from pressure distribution and from force tests on 1/40-scale model Akron

and also from the alternative form of this equation due to Upson and Klikoff (reference 5)

$$f = \frac{dF}{dx} = \frac{dA}{dx} q \cos^2 \alpha \sin 2\theta$$

where α is the inclination of the surface of the hull to the longitudinal axis. The latter equation, as has been found in previous experiments, gives somewhat better agreement over the fore part of the hull than the former.

The total transverse forces on the hull, which were obtained by integrating the areas under curves such as those in Figure 11, are plotted against angle of pitch in Figure 13 and compared to the values computed from the lift and drag taken from the force tests. (Reference 1.) The integrated values are in fairly good agreement with the measured forces at the low angles of pitch but are somewhat lower than the measured forces at the high angles. These results are what would be expected as the integrated values do not take into account the frictional forces, which at the high

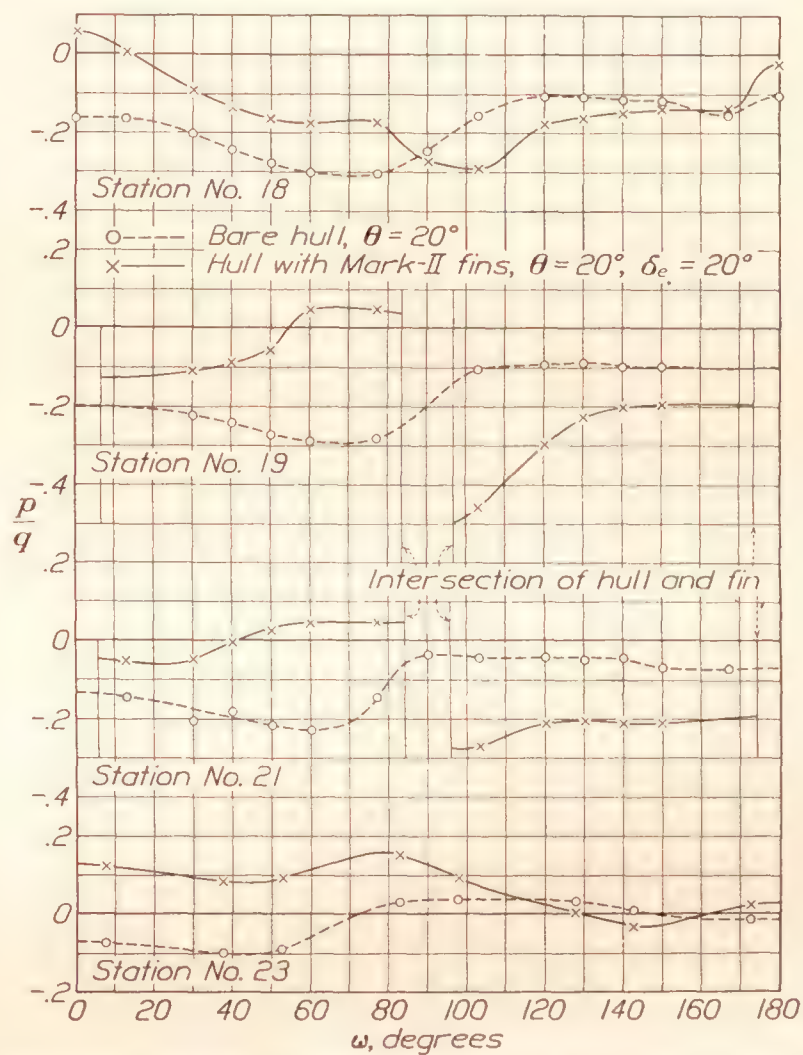


FIGURE 15.—Comparison of point pressures on the after portion of the hull of the model Akron with and without tail surfaces

angles of pitch have appreciable components normal to the hull axis.

The moment about the center of buoyancy was computed in two parts—(1) the moment due to the transverse force, and (2) the moment due to the longitudinal force. The first part (M_1) was obtained by taking the moment of the area of the transverse force curves (fig. 11) about the center of buoyancy by means of a mechanical integrator. The second part is given by

$$M_2 = \frac{1}{2\pi} \int_{\theta_1}^{\theta_2} f dA \quad (4)$$

where A is the cross-sectional area of the hull. This equation was solved graphically by plotting f determined from equation (3) for the different stations against the corresponding cross-sectional area and integrating the area under the resulting curve. The moments due to the longitudinal forces amount to about 4 per cent of the total and are in the opposite

direction to those due to the transverse forces. The total moment is then

$$M = M_1 + M_2$$

Figure 14 (upper curve) shows the integrated moments for the various angles of pitch compared to the mo-

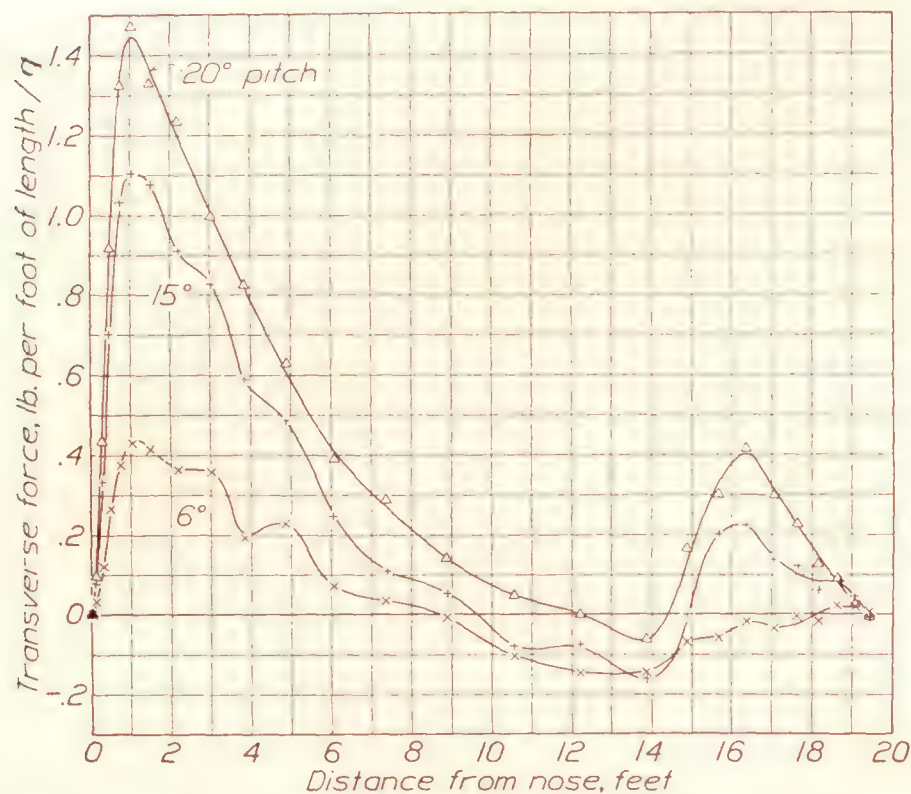


FIGURE 16.—Transverse force per unit length on the hull of 1/40-scale model Akron with the control car and tail surfaces in place. Elevator angle $\delta_e = 0^\circ$

ments determined by the force tests. In general, the two sets of results are in very close agreement.

The influence of the fins and control car upon the pressure distribution over the hull is shown in Figures 15 to 17, inclusive. The point pressures observed at

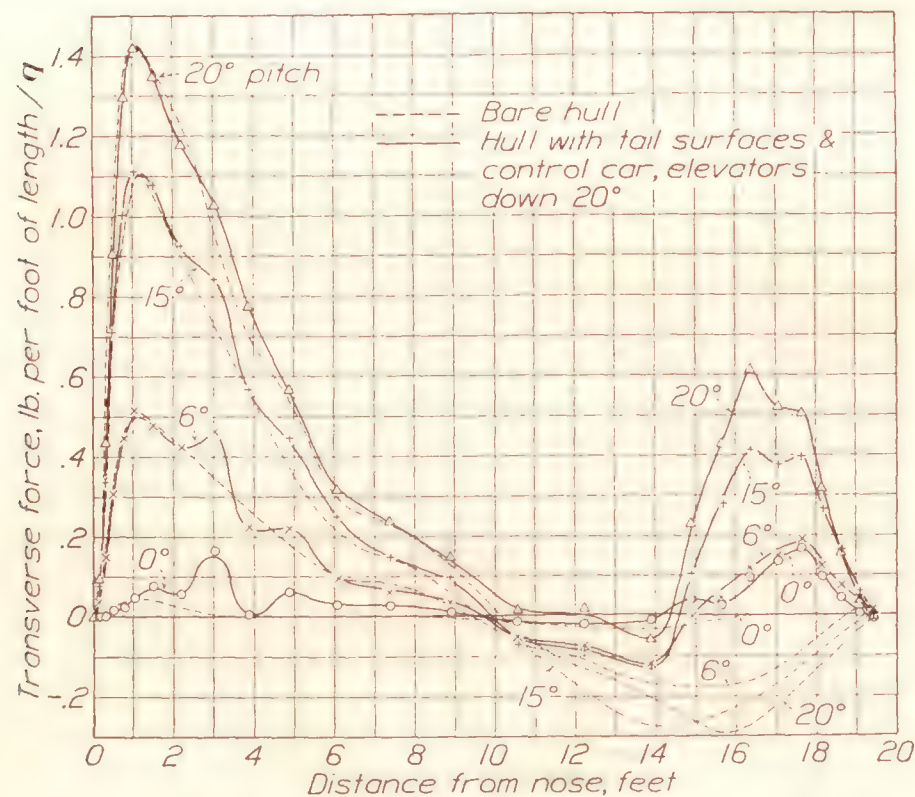


FIGURE 17.—Comparison of transverse forces on the hull of the 1/40-scale model Akron with and without control car and tail surfaces

four stations in the vicinity of the fins are shown in Figure 15 for the 20° pitch angle and compared to the pressures on the bare hull. The greatest change in the point pressures due to the presence of the fins occurs, as was to be expected, in the vicinity of the leading edges of the fins which are just forward of station 19.

The transverse forces on the hull with the fins in place are presented in Tables VI, VII, and VIII, and are shown for several angles of pitch in Figure 16 for an elevator angle δ_e of 0° . Figure 17 shows the transverse forces when the elevators were down 20° . For comparison, the curves for the bare hull are replotted on the same diagram. The influence of the tail surfaces on these forces on the after portion of the hull is very marked, the forces being of equal or greater magnitude than those on the bare hull but acting in the opposite direction. The influence of the control car

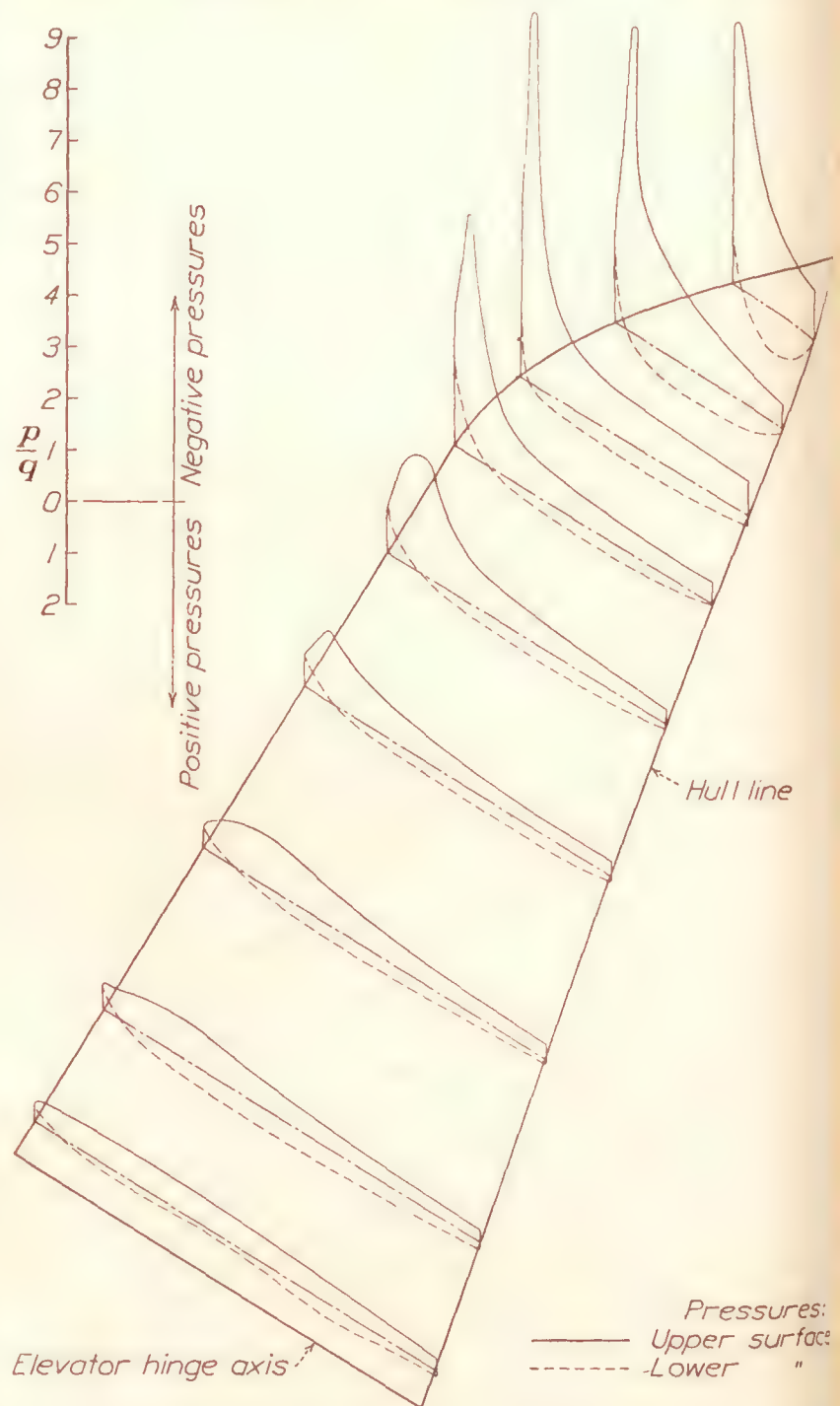


FIGURE 18.—Pressure distribution on horizontal fin surface of the 1/40-scale model Akron. Pitch angle $\theta = 20^\circ$. Elevator angle $\delta_e = 20^\circ$

on the transverse forces over the fore part of the hull is also quite pronounced, especially at the low angles of pitch.

The integrated pitching moments on the hull, with the fins and control car in place, are compared in Figure 14 with the moments on the bare hull and with the total pitching moments of the hull with the fins and control car obtained from the force tests. The difference between the upper curve and the lower one for any particular angle of pitch, represents the total moment due to the fins. The difference between the upper curve and the intermediate one represents the

portion of the moment due to the influence of the fins and control car on the pressural forces on the hull. The latter forces are seen to contribute more than 40 per cent of the total fin moment. The large magnitude of the fin action of the hull suggests the possibility of augmenting this effect and thereby increasing the effectiveness of the fin surfaces, and also of distributing the forces more widely over the after portion of the hull. In this connection, it would be of interest to test the airship model with eight tail surfaces instead of four, the four additional fins to be placed on the 45° diameters of the hull and the total fin area to be the same as

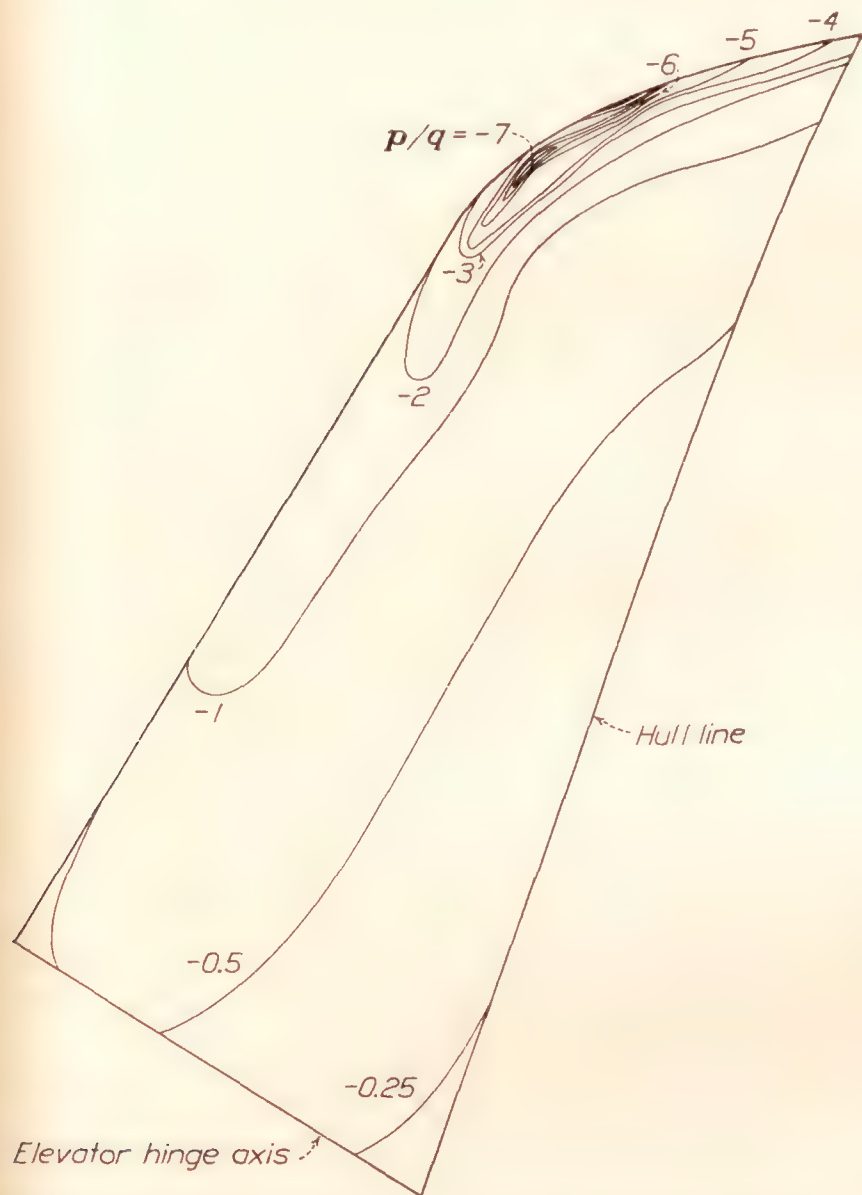


FIGURE 19.—Pressure contours on negative pressure side of horizontal fin surface of the 1/40-scale model Akron. Pitch angle $\theta = 20^\circ$. Elevator angle $\delta_e = 20^\circ$

before. With this fin arrangement and with the model at an angle of pitch, the pressure decrease over the top of the hull and the pressure increase over the bottom of the hull due to the influence of the tail surfaces should produce much larger components in the vertical plane than the present fins. The fin action of the hull should be increased, whereas the forces on the fins should be decreased, thus shifting the greater part of the fin forces directly onto the hull. The ZMC-2 metal-clad airship actually has a system of eight tail surfaces similar to that described above, except that the fins are all shifted around the hull by $22\frac{1}{2}^\circ$.

The results of the measurements of the fin pressures are presented in Figures 18, 19, and 20. The isometric chart in Figure 18 shows the pressures over the fin for the 20° angle of pitch and 20° down elevator.

The maximum negative pressure recorded was on the leading edge and amounted to seven times the dynamic pressure of the undisturbed air stream. Figure 19 shows the pressure contours on the suction side of the fin for the same pitch and elevator angles. The integrated normal-force coefficients

$$C_N = \frac{\text{normal force on fin}}{qS}$$

where S is the area of the fin, are plotted in Figure 20 against the elevator angle for the various pitch angles tested. The variation of the normal-force coefficient with the elevator angle is approximately linear over the range of angles from elevators down 20° to elevators up 15° . The elevators apparently lose much of

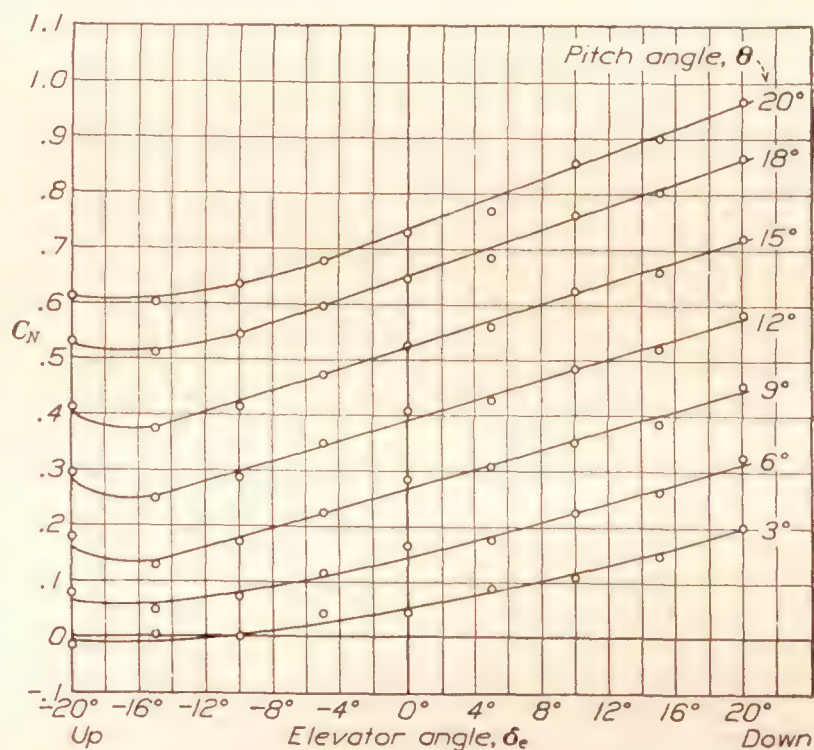


FIGURE 20.—Normal-force coefficients for horizontal fin surfaces on the 1/40-scale model Akron

their effectiveness when deflected upward 20° , the normal-force coefficient for this elevator angle being about the same as with the elevators up 10° .

CONCLUSIONS

1. The integrated transverse forces and the moments about the center of buoyancy were found to be in good agreement with the forces and moments determined in the force tests.

2. The pressural drag of the hull at 0° pitch was found to be practically zero, within the accuracy of the tests.

3. The fin action of the after portion of the hull in the presence of the tail surfaces was found to contribute more than 40 per cent of the total fin moment measured on the balances.

4. Negative pressures as great as seven times the dynamic pressure of the undisturbed air stream were measured on the leading edge of the horizontal fin at the 20° pitch angle with 20° down elevator.

LANGLEY MEMORIAL AERONAUTICAL LABORATORY,
NATIONAL ADVISORY COMMITTEE FOR AERONAUTICS,
LANGLEY FIELD, VA., June 28, 1932.

REFERENCES

1. Freeman, Hugh B.: Force Measurements on a 1/40-Scale Model of the U. S. Airship "Akron." T. R. No. 432, N. A. C. A., 1932.
2. Freeman, Hugh B.: Measurements of Flow in the Boundary Layer of a 1/40-Scale Model of the U. S. Airship "Akron." T. R. No. 430, N. A. C. A., 1932.
3. Jones R.: The Distribution of Normal Pressures on a Prolate Spheroid. R. & M. No. 1061, British A. R. C., 1925.
4. Munk, Max M.: The Aerodynamic Forces on Airship Hulls. T. R. No. 184, N. A. C. A., 1924.
5. Burgess, C. P.: Airship Design. The Ronald Press Co. (1927). p. 95.

TABLE I

DIMENSIONS OF MODEL U. S. S. "AKRON"

[Scale=1/40]

Distance from nose length	Radius (circum- scribed circle)	
<i>a/L</i>	<i>Inches</i>	
0	0	
0.02	4.95	Length, 19.62 feet.
.05	9.96	Volume, 115.0 cubic feet.
.10	14.20	
.15	16.65	
.20	18.39	Total horizontal tail surface area (square feet):
.25	19.12	<div><div>Mark-I</div><div>5.074</div></div>
.30	19.61	<div><div>Mark-II</div><div>4.590</div></div>
.35	19.85	
.40	19.90	Elevators (including balance vanes) square feet:
.45	19.90	<div><div>1.004</div><div>0.932</div></div>
.50	19.80	
.55	19.59	Elevator balance vanes square feet:
.60	19.12	<div><div>0.234</div><div>0.220</div></div>
.65	18.46	
.70	17.50	Elevator chord length (feet):
.75	16.15	<div><div>c=0.410</div><div>c=0.369</div></div>
.80	14.44	
.85	12.29	Location of elevator axis:
.90	9.61	<div><div><i>a/L</i>=0.9090</div><div><i>a/L</i>=0.9059</div></div>
.95	6.52	Center of buoyancy:
1.00	0	<div><div><i>a/L</i>=0.464</div></div>
		Leading edge of control car:
		<div><div><i>a/L</i>=0.1555</div></div>
		Length of control car=1.238 (feet).

TABLE II. 1/40-SCALE MODEL U. S. S. "AKRON"

OBSERVED PRESSURES p/q

BARE HULL

[100 m. p. h. approximately]

Station No.	ω	Angle of pitch, θ							
		0°	3°	6°	9°	12°	15°	18°	20°
1	Nose.		1 0.967	1 0.900	0.785	0.682	0.434	0.098	-0.132
	0	0.866	1.934	1.956	1.975	1.983	1.990	1.985	1.960
	30	.853	1.891	1.901	1.890	.865	.829	.783	.720
	60	.849	.850	.826	.771	.695	.575	.451	.330
2	90	.846	.825	.769	.674	.596	.432	.262	.128
	120	.844	.799	.728	.606	.519	.353	.164	.049
	150	.840	.786	.716	.601	.519	.393	.284	.197
	180	.834	.770	.700	.589	.521	.413	.294	.220
	0	.702	.779	.834	.888	1.920	1.944	1.962	1.970
	30	.698	.749	.800	.838	.822	.836	.854	.837
	60	.681	.699	.712	.713	.661	.619	.579	.515
3	90	.681	.668	.625	.576	.499	.396	.291	.190
	120	.681	.633	.563	.474	.399	.275	.144	.043
	150	.678	.599	.513	.404	.329	.206	.067	-.014
	180	.681	.590	.505	.389	.312	.200	.079	.004
	0	.414	.507	.580	.674	.704	.774	.845	1.878
	30	.417	.480	.550	.627	.625	.676	.733	.737
	60	.408	.433	.465	.489	.446	.436	.433	.390
4	90	.393	.370	.346	.325	.416	.177	.103	.024
	120	.386	.312	.238	.162	.080	-.032	-.150	-.245
	150	.382	.279	.180	.077	-.003	-.115	-.250	-.358
	180	.376	.254	.158	.032	-.052	-.160	-.290	-.373

1 Value taken from faired curve.

TABLE II. 1/40-SCALE MODEL U. S. S. "AKRON"—C

OBSERVED PRESSURES p/q

BARE HULL

[100 m. p. h. approximately]

Station No.	ω	Angle of pitch, θ							
		0°	3°	6°	9°	12°	15°	18°	20°
	0	.170	.257	.332	.434	.477	.567	.652	.700
	10	.164	.247	.330	.429	.466	.550	.633	.680
	20	.177	.244	.324	.416	.440	.552	.595	.630
	30	.158	.219	.294	.374	.386	.455	.505	.540
	40	.160	.217	.282	.349	.342	.389	.428	.450
	50	.165	.211	.260	.310	.288	.318	.341	.350
	60	.152	.184	.215	.249	.210	.216	.202	.180
	70	.134	.148	.167	.184	.135	.116	.082	.040
	80	.140	.131	.132	.129	.068	.024	-.038	-.080
5	90	.142	.123	.102	.085	.015	-.046	-.115	-.180
	100	.136	.098	.070	.032	-.040	-.117	-.206	-.280
	110	.126	.073	.023	-.035	-.103	-.195	-.301	-.370
	120	.125	.056	-.001	-.076	-.148	-.242	-.353	-.430
	130	.131	.055	-.018	-.105	-.176	-.280	-.393	-.470
	140	.128	.041	-.035	-.131	-.199	-.297	-.415	-.490
	150	.123	.025	-.063	-.163	-.233	-.330	-.446	-.520
	160	.121	.018	-.071	-.176	-.244	-.340	-.453	-.520
	170	.111	.003	-.086	-.198	-.266	-.360	-.471	-.540
	180	.112	-.002	-.091	-.203	-.275	-.372	-.478	-.550
	0	.049	.132	.201	.288	.338	.433	.508	.580
	30	.056	.117	.183	.250	.270	.336	.386	.410
6	60	.037	.074	.101	.121	.093	.097	.075	.060
	90	.035	.028	.005	-.017	-.077	.134	-.210	-.270
	120	.003	-.047	-.095	-.174	-.232	-.316	-.417	-.490
	150	.008	-.070	-.142	-.234	-.287	-.366	-.462	-.510
	180	-.004	-.077	-.152	-.242	-.300	-.372	-.452	-.500
	0	-.027	.043	.107	.171	.222	.305	.372	.400
	10	-.003	.058	.122	.184	.232	.306	.367	.380
	20	-.015	.043	.104	.161	.200	.270	.321	.330
	30	-.029	.025	.084	.131	.155	.211	.251	.270
	40	-.017	.034	.080	.117	.124	.159	.176	.190
	50	-.010	.034	.067	.087	.080	.098	.089	.100
	60	-.018	.015	.034	.042	.017	.017	-.016	-.020
	70	-.027	-.001	.006	.004	-.034	-.053	-.109	-.150
	80	-.030	-.021	-.028	-.046	-.091	-.126	-.194	-.240
7	90	-.011	-.019	-.031	-.063	-.113	.163	.241	.280
	100	-.018	-.041	-.063	-.113	-.164	.226	.314	.370
	110	-.044	-.071	-.103	-.166	-.217	.283	.377	.440
	120	-.051	-.096	-.133	-.208	-.254	.325	.419	.480
	130	-.030	-.081	-.119	-.198	-.241	.305	.394	.440
	140	-.047	-.103	-.149	-.228	-.269	.330	.416	.480
	150	-.046	-.103	-.153	-.229	-.268	.323	.396	.430
	160	-.066	-.134	-.183	-.254	-.296	.345	.404	.430
	170	-.044	-.109	-.159	-.227	-.268	.317	.369	.400
	180	-.049	-.119	-.169	-.239	-.283	.331	.377	.400
	0	-.139	-.092	-.041	.014	.058	.124	.199	.220
	4	-.144	-.097	-.044	.009	.054	.120	.189	.210
	6	-.144	-.097	-.044	.008	.052	.120	.186	.210
	14	-.142	-.097	-.044	.006	.046	.105	.162	.180
	16	-.137	-.096	-.044	.006	.042	.100	.156	.170
	24	-.139	-.099	-.057	-.021	.004	.045	.081	.100
	26	-.134	-.097	-.059	-.029	-.014	.015	.036	.060
	30	-.132	-.097	-.061	-.031	-.017	.010	.033	.040
	34	-.148	-.113	-.082	-.064	-.062	-.047	-.033	-.040
	36	-.149	-.113	-.087	-.071	-.079	-.074	-.081	-.080
	60	-.130	-.106	-.094	-.086	-.109	-.113	-.147	-.160
	84	-.132	-.134	-.151	-.182	-.234	-.283	-.374	-.430
	86	-.146	-.155	-.172	-.206	-.257	-.314	-.402	-.460
	90	-.137	-.147	-.166	-.199	-.246	-.293	-.379	-.430
	94	-.151	-.167	-.194	-.244	-.294	-.366	-.461	-.510
	96	-.154	-.175	-.204	-.251	-.302	-.370	-.462	-.510
	120	-.136	-.175	-.207	-.269	-.309	-.366	-.447	-.500
	144	-.149	-.198	-.264	-.302	-.336	-.389	-.467	-.530
	146	-.163	-.212	-.251	-.317	-.351	-.404	-.481	-.530
	150	-.171	-.223	-.261	-.319	-.351	-.395	-.459	-.500
	154	-.144	-.197	-.232	-.296	-.326	-.369	-.430	-.470
	156	-.158	-.210	-.246	-.301	-.330	-.369	-.417	-.440
	164	-.158	-.210	-.246	-.294	-.321	-.352	-.381	-.400
	166	-.158	-.210	-.247	-.296	-.321	-.352	-.381	-.400
	174	-.164	-.215	-.252	-.297	-.322	-.352	-.375	-.390
	176	-.163	-.213	-.251	-.297	-.321	-.350	-.369	-.380
	180	-.156	-.205	-.244	-.286	-.314	-.345	-.364	-.380
	0	-.147	-.117	-.080	-.042	-.005	.042	.106	.120
	10	-.144	-.115	-.079	-.040	-.005	.040	.093	.110
	20	-.149	-.128	-.090	-.057	-.032	.007	.046	.060
	30	-.150	-.120	-.087	-.062	-.044	-.020	.005	.020
	40	-.137	-.119	-.094	-.077	-.069	-.060	-.052	-.040
	50	-.137	-.123	-.105	-.100	-.114	-.114	-.134	-.140
	60	-.134	-.127	-.119	-.122	-.147	-.162	-.207	-.220
	70	-.128	-.128	-.129	-.137	-.175	-.201	-.262	-.280
	80	-.144	-.148	-.159	-.179	-.225	-.260	-.337	-.360
	90	-.140	-.160	-.179	-.210	-.259	-.305	-.390	-.420
	100	-.140	-.165	-.185	-.229	-.274	-.325	-.409	-.440
	110	-.140	-.175	-.200	-.250	-.292	-.347	-.426	-.460
	120	-.137	-.175	-.200	-.252	-.290	-.338	-.412	-.450
	130	-.147	-.190	-.215	-.262	-.295	-.335	-.399	-.430
	140	-.144	-.186	-.212	-.250	-.283	-.313	-.365	-.400
	150	-.140	-.180	-.204	-.238	-.267	-.286	-.324	-.360
	160	-.139	-.178	-.199	-.230	-.255	-.270	-.290	-.320
	170	-.149	-.188	-.210	-.234	-.259	-.270	-.277	-.290
	180	-.145	-.181	-.205	-.229	-.252	-.261	-.264	-.270
	0	-.125	-.107	-.075	-.045	-.023	.017	.075	.090
	30	-.109	-.093	-.072	-.055	-.045	.030	.010	.020
	60	-.120	-.111	-.110	-.113	-.148	-.165	-.205	-.220

TABLE II. 1/40-SCALE MODEL U. S. S. "AKRON"—Con.

OBSERVED PRESSURES p/q

BARE HULL

[100 m. p. h. approximately]

Station No.	ω	Angle of pitch, θ							
		0°	3°	6°	9°	12°	15°	18°	20°
11	0	-.143	-.133	-.111	-.091	-.075	-.045	.005	.011
	10	-.107	-.095	-.075	-.055	-.040	-.009	.029	.032
	20	-.111	-.105	-.081	-.065	-.058	-.038	-.003	-.006
	30	-.124	-.116	-.106	-.105	-.110	-.115	-.121	-.122
	40	-.124	-.114	-.098	-.090	-.086	-.076	-.065	-.061
	50	-.123	-.114	-.111	-.118	-.136	-.150	-.176	-.188
	60	-.136	-.131	-.136	-.148	-.185	-.209	-.260	-.282
	70	-.121	-.121	-.128	-.146	-.188	-.222	-.285	-.319
	80	-.111	-.111	-.125	-.143	-.190	-.224	-.291	-.334
	100	-.111	-.131	-.156	-.200	-.243	-.292	-.381	-.441
	110	-.116	-.136	-.156	-.201	-.238	-.286	-.360	-.411
	120	-.123	-.144	-.163	-.208	-.238	-.286	-.346	-.386
	130	-.136	-.156	-.173	-.208	-.230	-.266	-.320	-.342
	140	-.131	-.149	-.161	-.190	-.209	-.230	-.271	-.282
	150	-.143	-.158	-.168	-.184	-.203	-.210	-.235	-.242
	160	-.121	-.139	-.143	-.156	-.173	-.173	-.191	-.295
	170	-.138	-.158	-.171	-.175	-.185	-.173	-.175	-.173
	0	-.100	-.094	-.079	-.065	-.057	-.034	.001	.007
12	4	-.091	-.085	-.072	-.057	-.052	-.024	.010	.010
	6	-.093	-.087	-.072	-.057	-.052	-.025	.003	.010
	14	-.091	-.087	-.072	-.059	-.057	-.037	.003	-.010
	16	-.103	-.094	-.080	-.072	-.070	-.052	-.034	-.032
	24	-.103	-.095	-.088	-.087	-.090	-.087	-.087	-.085
	26	-.103	-.095	-.090	-.094	-.104	-.101	-.129	-.124
	30	-.191	-.087	-.077	-.065	-.092	-.102	-.120	-.121
	34	-.118	-.117	-.122	-.132	-.155	-.172	-.225	-.229
	36	-.105	-.099	-.099	-.110	-.134	-.154	-.194	-.202
	60	-.098	-.094	-.100	-.119	-.152	-.179	-.222	-.253
	84	-.105	-.112	-.134	-.172	-.229	-.285	-.390	-.445
	86	-.105	-.110	-.134	-.174	-.230	-.287	-.390	-.452
	90	-.096	-.107	-.124	-.162	-.203	-.255	-.343	-.393
	94	-.100	-.107	-.125	-.175	-.229	-.288	-.397	-.460
	96	-.103	-.118	-.132	-.184	-.237	-.295	-.403	-.464
	120	-.105	-.118	-.132	-.174	-.200	-.241	-.305	-.337
	144	-.105	-.118	-.124	-.160	-.175	-.204	-.250	-.256
	146	-.108	-.122	-.127	-.162	-.175	-.201	-.240	-.246
	150	-.101	-.112	-.115	-.140	-.152	-.161	-.193	-.199
13	154	-.103	-.112	-.117	-.138	-.150	-.157	-.188	-.194
	156	-.103	-.109	-.110	-.124	-.139	-.142	-.172	-.179
	164	-.106	-.109	-.107	-.112	-.124	-.112	-.140	-.141
	166	-.103	-.107	-.104	-.107	-.119	-.109	-.132	-.129
	174	-.103	-.105	-.102	-.102	-.110	-.096	-.107	-.095
	176	-.101	-.100	-.100	-.100	-.109	-.092	-.095	-.087
	0	-.070	-.065	-.055	-.050	-.040	-.016	.008	.010
	10	-.060	-.055	-.048	-.040	-.037	-.015	.005	.009
	20	-.041	-.068	-.032	-.055	-.030	-.015	-.005	-.003
	30	-.077	-.073	-.072	-.075	-.083	-.080	-.088	-.090
	40	-.070	-.070	-.068	-.078	-.093	-.102	-.128	-.132
	50	-.072	-.071	-.073	-.097	-.120	-.139	-.187	-.197
	60	-.067	-.068	-.073	-.102	-.135	-.165	-.227	-.247
	70	-.067	-.070	-.078	-.103	-.152	-.190	-.266	-.296
	80	-.072	-.082	-.100	-.133	-.182	-.227	-.318	-.356
	90	-.072	-.083	-.097	-.137	-.185	-.231	-.321	-.366
	100	-.069	-.087	-.102	-.132	-.178	-.232	-.310	-.371
	110	-.069	-.087	-.102	-.137	-.172	-.217	-.290	-.337
	120	-.072	-.095	-.105	-.137	-.160	-.206	-.256	-.287
	130	-.074	-.095	-.095	-.120	-.138	-.165	-.189	-.221
14	140	-.079	-.102	-.092	-.107	-.122	-.135	-.161	-.179
	150	-.065	-.080	-.072	-.078	-.090	-.100	-.135	-.159
	160	-.082	-.090	-.077	-.075	-.087	-.088	-.126	-.154
	170	-.074	-.082	-.070	-.063	-.072	-.060	-.072	-.068
	180	-.065	-.073	-.062	-.053	-.062	-.043	-.038	-.033
	30	-.057	-.069	-.061	-.062	-.072	-.071	-.082	-.088
	60	-.059	-.071	-.074	-.099	-.134	-.161	-.225	-.251
	90	-.059	-.082	-.101	-.124	-.176	-.225	-.309	-.357
	120	-.059	-.081	-.094	-.113	-.136	-.171	-.216	-.237
	150	-.063	-.074	-.066	-.071	-.081	-.091	-.136	-.168
	180	-.054	-.059	-.046	-.037	-.042	-.024	-.014	-.007
	0	-.076	-.092	-.087	-.082	-.082	-.069	-.044	-.052
	10	-.081	-.099	-.094	-.089	-.090	-.077	-.060	-.065
	20	-.073	-.089	-.085	-.085	-.092	-.082	-.075	-.082
	30	-.092	-.109	-.111	-.119	-.135	-.139	-.153	-.160
	40	-.095	-.100	-.100	-.110	-.134	-.147	-.173	-.185
	50	-.081	-.099	-.100	-.119	-.149	-.169	-.216	-.232
	60	-.081	-.100	-.104	-.132	-.165	-.198	-.256	-.286
	70	-.069	-.085	-.094	-.119	-.159	-.199	-.266	-.294
	80	-.085	-.105	-.117	-.146	-.194	-.237	-.318	-.355
15	90	-.074	-.100	-.109	-.139	-.185	-.233	-.303	-.349
	100	-.069	-.090	-.101	-.132	-.172	-.218	-.281	-.319
	110	-.062	-.080	-.087	-.117	-.149	-.186	-.235	-.259
	120	-.069	-.085	-.092	-.119	-.134	-.168	-.186	-.202
	130	-.073	-.085	-.084	-.102	-.110	-.131	-.144	-.160
	140	-.057	-.069	-.065	-.069	-.084	-.099	-.124	-.143
	150	-.067	-.070	-.064	-.069	-.082	-.082	-.122	-.152
	160	-.059	-.064	-.052	-.054	-.059	-.085	-.137	-.165
	170	-.073	-.072	-.055	-.052	-.055	-.055	-.055	-.055
	180	-.049	-.052	-.035	-.022	-.032	-.010	-.012	-.018
	0	-.077	-.098	-.098	-.101	-.104	-.098	-.081	-.086
	30	-.083	-.101	-.105	-.118	-.134	-.138	-.153	-.158
	60	-.084	-.101	-.111	-.140	-.176	-.210	-.270	-.293
	90	-.079	-.098	-.110	-.138	-.181	-.223	-.287	-.323
	120	-.083	-.096	-.096	-.115	-.121	-.148	-.165	-.165
	150	-.070	-.068	-.059	-.053	-.074	-.088	-.165	-.201
	180	-.060	-.053	-.038	-.023	-.031	-.016	-.031	-.046

TABLE II. 1/40-SCALE MODEL U. S. S. "AKRON"—Con.

OBSERVED PRESSURES p/q

BARE HULL

[100 m. p. h. approximately]

Station No.	ω	Angle of pitch, θ							
		0°	3°	6°	9°	12°	15°	18°	20°
17	0	-.079	-.103	-.114	-.125	-.153	-.154	-.129	-.159
	4	-.079	-.103	-.110	-.125	-.153	-.154	-.130	-.137
	6	-.084	-.112	-.117	-.134	-.143	-.140	-.137	-.149
	10	-.084	-.110	-.119	-.135	-.147	-.147	-.142	-.154
	14	-.096	-.125	-.134	-.157	-.173	-.181	-.183	-.194
	16	-.083	-.107	-.117	-.134	-.150	-.150	-.152	-.168
	20	-.088	-.115	-.124	-.145	-.163	-.167	-.169	-.185
	24	-.091	-.115	-.130	-.157	-.180	-.187	-.214	-.227
	26	-.091	-.117	-.132	-.167	-.199	-.214	-.251	-.268
	30	-.083	-.102	-.117	-.147	-.173	-.187	-.226	-.238
	34	-.084	-.105	-.120	-.151	-.177	-.194	-.231	-.248
	36	-.084	-.105	-.120	-.154	-.187	-.214	-.268	-.285
	40	-.084	-.105	-.119	-.154	-.187	-.214	-.269	-.289
	50	-.084	-.107	-.122	-.154	-.183	-.214	-.266	-.285
	60	-.074	-.098	-.117	-.149	-.182	-.214	-.273	-.302
	70	-.067	-.087	-.104	-.135	-.170	-.214	-.278	-.309
	80	-.083	-.100	-.119	-.151	-.185	-.231	-.294	-.327
	84	-.083	-.100	-.119	-.154	-.187	-.249	-.321	-.361
	86	-.091	-.117	-.134	-.167	-.208	-.261	-.330	-.369
18	90	-.084	-.102	-.115	-.147	-.180	-.217	-.266	-.302
	94	-.077	-.093	-.109	-.139	-.173	-.217	-.268	-.304
	96	-.077	-.092	-.104	-.137	-.172	-.217	-.264	-.300
	100	-.079	-.090	-.100	-.129	-.153	-.184	-.209	-.240
	110	-.067	-.077	-.080	-.102	-.117	-.134	-.135	-.161
	120	-.072	-.077	-.075	-.087	-.092	-.100	-.109	-.132
	130	-.074	-.070	-.067	-.073	-.077	-.084	-.109	-.114
	140	-.079	-.070	-.067	-.070	-.073	-.084	-.109	-.136
	144	-.081	-.073	-.067	-.070	-.080	-.087	-.110	-.137
	146	-.077	-.068	-.060	-.065	-.077	-.087	-.120	-.148
	150	-.074	-.067	-.055	-.063	-.080	-.094	-.120	-.146

TABLE II. 1/40-SCALE MODEL U. S. S. "AKRON"—Con.

OBSERVED PRESSURES p/q

BARE HULL

[100 m. p. h. approximately]

Station No.	ω	Angle of pitch, θ							
		0°	3°	6°	9°	12°	15°	18°	20°
22	127 $\frac{1}{2}$.053	.063	.067	.050	.030	.009	.002	-.018
	142 $\frac{1}{2}$.053	.063	.066	.042	.015	-.001	-.010	-.032
	172 $\frac{1}{2}$.053	.063	.066	.032	.000	-.037	-.053	-.062
23	7 $\frac{1}{2}$.095	.073	.050	.009	-.018	-.044	-.054	-.073
	37 $\frac{1}{2}$.096	.076	.063	.021	-.013	-.049	.068	-.101
	52 $\frac{1}{2}$.096	.081	.066	.036	.012	-.038	.051	-.090
	82 $\frac{1}{2}$.096	.096	.098	.080	.069	.046	.056	.030
	97 $\frac{1}{2}$.096	.099	.100	.083	.066	.050	.061	.036
	127 $\frac{1}{2}$.098	.099	.100	.080	.062	.048	.050	.031
	142 $\frac{1}{2}$.089	.094	.095	.066	.046	.029	.028	.009
	172 $\frac{1}{2}$.089	.094	.088	.046	.012	-.018	-.012	-.014
	7 $\frac{1}{2}$.127	.109	.091	.053	.016	-.014	-.036	-.054
24	37 $\frac{1}{2}$.127	.114	.101	.070	.045	-.008	-.021	-.054
	52 $\frac{1}{2}$.127	.117	.113	.086	.072	.019	.019	-.019
	82 $\frac{1}{2}$.127	.129	.130	.115	.101	.085	.095	.075
	97 $\frac{1}{2}$.127	.133	.133	.116	.101	.085	.093	.075
	127 $\frac{1}{2}$.127	.129	.128	.103	.084	.066	.066	.055
	142 $\frac{1}{2}$.127	.123	.116	.096	.076	.070	.068	.055
	172 $\frac{1}{2}$.127	.119	.113	.066	.036	.029	.063	.053
	7 $\frac{1}{2}$.172	.168	.166	.142	.108	.072	.042	.022
	37 $\frac{1}{2}$.172	.170	.170	.156	.143	.104	.095	.064
25	52 $\frac{1}{2}$.172	.170	.177	.164	.149	.145	.134	.116
	82 $\frac{1}{2}$.172	.172	.177	.164	.148	.147	.140	.136
	97 $\frac{1}{2}$.172	.172	.171	.162	.148	.142	.136	.131
	127 $\frac{1}{2}$.172	.165	.166	.152	.136	.131	.120	.120
	142 $\frac{1}{2}$.172	.163	.159	.149	.135	.132	.132	.126
	172 $\frac{1}{2}$.172	.160	.146	.115	.111	.132	.146	.136
	7 $\frac{1}{2}$.215	.216	.216	.210	.199	.198	.190	.174
	37 $\frac{1}{2}$.215	.214	.213	.196	.174	.196	.203	.197
	52 $\frac{1}{2}$.215	.212	.206	.190	.174	.190	.203	.194
26	82 $\frac{1}{2}$.215	.209	.201	.185	.169	.181	.197	.196
	97 $\frac{1}{2}$.215	.206	.198	.183	.167	.185	.195	.192
	127 $\frac{1}{2}$.215	.206	.198	.186	.177	.195	.197	.196
	142 $\frac{1}{2}$.215	.206	.198	.186	.182	.198	.203	.196
	172 $\frac{1}{2}$.215	.202	.201	.201	.202	.206	.211	.197

TABLE III-A

1/40-SCALE MODEL U. S. S. "AKRON"

AVERAGE PRESSURES— p'/q ¹

BARE HULL

 $\theta=0^\circ$

Station No.	Cross-sectional area	q , lb./sq. ft.				
		8.0	12.7	18.2	21.4	24.7
1	Sq. ft.					
2	0	1.001	1.005	1.003		0.842
3	.05	.848	.853	.849	0.852	.673
4	.27	.681	.678	.687	.688	.387
5	.75	.390	.378	.391	.390	.127
6	1.51	.130	.122	.134	.128	.017
7	2.22	.013	.015	.018	.014	-.036
8	3.40	-.053	-.041	-.035	-.036	-.036
9	4.83	-.155	-.150	-.146	-.153	-.155
10	6.11	-.148	-.140	-.146	-.152	-.150
11	7.06	-.127	-.128	-.130	-.131	-.128
12	7.87	-.125	-.125	-.130	-.127	-.130
13	8.36	-.105	-.100	-.105	-.103	-.104
14	8.60	-.068	-.066	-.073	-.070	-.072
15	8.60	-.057	-.058	-.061	-.060	-.063
16	8.40	-.065	-.075	-.075	-.073	-.076
17	7.76	-.072	-.077	-.076	-.073	-.079
18	6.54	-.076	-.078	-.077	-.071	-.073
19	5.60	-.051	-.052	-.052	-.049	-.052
20	4.55	-.031	-.033	-.033	-.030	-.037
21	3.68	.000	-.001	-.005	-.003	-.010
22	2.85	.029	.033	.024	.032	.024
23	2.07	.055	.058	.050	.057	.048
24	1.45	.087	.094	.087	.097	.091
25	.98	.119	.122	.120	.130	.125
26	.47	.163	.166	.166	.176	.169
26	.18	.205	.208	.207	.214	.212

¹Values in each column are a mean of two independent observations

TABLE III-B

AVERAGE PRESSURES $-p'/q$

BARE HULL

[$q=25.2$ lb./sq. ft.]

Station No.	Angle of pitch— θ						
	3°	6°	9°	12°	15°	18°	20°
1		0.942	0.840	0.682	0.434	0.098	-.0.132
2	0.830	.793	.717	.656	.544	.455	.332
3	.671	.649	.609	.553	.490	.409	.340
4	.376	.358	.337	.288	.240	.193	.138
5	.127	.111	.096	.058	.028	-.024	-.059
6	.024	.014	-.003	-.039	-.061	-.103	-.137
7	-.031	-.034	-.055	-.077	-.098	-.137	-.157
8	-.150	-.160	-.178	-.199	-.221	-.261	-.286
9	-.150	-.157	-.170	-.189	-.202	-.236	-.254
10	-.131	-.138	-.150	-.173	-.192	-.211	-.232
11	-.132	-.133	-.150	-.178	-.184	-.212	-.229
12	-.101	-.104	-.129	-.156	-.171	-.217	-.233
13	-.078	-.075	-.097	-.114	-.132	-.172	-.195
14	-.076	-.075	-.087	-.108	-.123	-.170	-.189
15	-.090	-.087	-.100	-.120	-.144	-.176	-.197
16	-.090	-.092	-.103	-.125	-.149	-.185	-.198
17	-.087	-.090	-.113	-.131	-.153	-.188	-.210
18	-.060	-.069	-.092	-.113	-.140	-.170	-.190
19	-.042	-.049	-.075	-.101	-.129	-.147	-.180
20	-.016	-.018	-.048	-.070	-.098	-.123	-.149
21	.022	.018	-.013	-.034	-.065	-.088	-.114
22	.048	.039	.011	-.016	-.046	-.054	-.075
23	.088	.083	.055	.032	.004	.000	-.025
24	.125	.114	.088	.068	.045	.041	.025
25	.169	.165	.153	.137	.128	.115	.106
26	.210	.205	.192	.180	.196	.202	.196

TABLE IV

1/40-SCALE MODEL U. S. S. "AKRON"

LONGITUDINAL FORCE— P'/q

θ degs.	Pressure distribution ¹	Force tests	θ degs.	Pressure distribution ¹	Force tests
3	0.007	0.459	15	0.047	0.346
6	.064	.443	18	-----	.256
9	.001	.430	20	-----	.158
12	.025	.398			

¹ Mean of two speeds.

TABLE V

1/40-SCALE MODEL U. S. S. "AKRON"

TRANSVERSE FORCE PER FOOT LENGTH— f/q

BARE HULL

[$q=25.2$ lb./sq. ft.]

Station No.	Angle of pitch— θ						
	3°	6°	9°	12°	15°	18°	20°
1	0	0	0	0	0	0	0
2	.014	.027	.047	.062	.076	.073	.090
3	.078	.146	.220	.255	.331	.404	.435
4	.184	.319	.470	.537	.666	.835	.918
5	.287	.461	.665	.770	.966	1.177	1.307
6	.305	.498	.735	.879	1.088	1.290	1.443
7	.280	.475	.715	.844	1.051	1.242	1.366
8	.269	.426	.650	.771	.913	1.104	1.239
9	.144	.317	.477	.585	.730	.858	.957
10	.162	.285	.390	.481	.570	.694	.720
11	.093	.189	.290	.340	.371	.528	.544
12	.078	.096	.165	.211	.206	.293	.298
13	.067	.081	.070	.107	.144	.160	.232
14	-.005	.028	.030	.046	.058	.065	.128
15	-.091	-.066	-.094	-.103	-.069	-.066	-.037
16	-.090	-.106	-.125	-.180	-.187	-.154	-.123
17	-.103	-.174	-.259	-.279	-.301	-.268	-.234
18	-.100	-.181	-.265	-.268	-.254	-.266	-.263
19	-.120	-.184	-.262	-.254	-.254	-.299	-.304
20	-.101	-.158	-.209	-.221	-.216	-.245	-.239
21	-.077	-.137	-.178	-.187	-.175	-.209	-.250
22	-.046	-.087	-.105	-.137	-.137	-.149	-.174
23	-.027	-.046	-.046	-.051	-.088	-.101	-.116
24	-.014	-.018	-.001	-.026	-.049	-.090	-.100
25	.001	.016	.006	.004	.017	-.038	-.035
26	.006	.008	.007	.005	-.001	-.003	-.001

TABLE V—Continued
1/40-SCALE MODEL U. S. S. "AKRON"—Con.
[$q=12.5$ lb./sq. ft.]

Station No.	Angle of pitch— θ						
	3°	6°	9°	12°	15°	18°	20°
1	0	0	0	0	—	—	0
2	.018	.044	.043	.061	—	—	.095
3	.074	.150	.191	.266	—	—	.437
4	.183	.326	.413	.571	—	—	.895
5	.274	.459	.615	.822	—	—	1.309
6	.300	.496	.677	.898	—	—	1.423
7	.308	.475	.650	.869	—	—	1.379
8	.272	.447	.596	.806	—	—	1.296
9	.159	.344	.440	.606	—	—	1.031
10	.156	.274	.386	.456	—	—	.848
11	.071	.162	.224	.306	—	—	.662
12	.066	.103	.117	.227	—	—	.367
13	.060	.093	.084	.169	—	—	.276
14	-.002	.023	.021	.032	—	—	.151
15	-.080	-.066	-.110	-.105	—	—	-.009
16	-.106	-.110	-.132	-.158	—	—	-.112
17	-.111	-.182	-.265	-.244	—	—	-.184
18	-.122	-.178	-.261	-.291	—	—	-.211
19	-.145	-.211	-.254	-.222	—	—	-.281
20	-.097	-.175	-.204	-.206	—	—	-.251
21	-.084	-.141	-.176	-.159	—	—	-.222
22	-.038	-.101	-.108	-.114	—	—	-.164
23	-.015	-.035	-.028	-.029	—	—	-.136
24	-.003	-.009	.006	.002	—	—	-.110
25	.021	.025	.031	.018	—	—	-.055
26	.005	.014	.014	.008	—	—	-.009

TABLE VI
1/40-SCALE MODEL U. S. S. "AKRON"
TRANSVERSE FORCE PER FOOT LENGTH— f/q
ON HULL WITH TAIL SURFACES AND CONTROL CAR
[Elevators neutral; $q=25.2$ lb./sq. ft.]

Station No.	Angle of pitch— θ						
	3°	6°	9°	12°	15°	18°	20°
1	0	0	0	0	0	0	0
2	.012	.031	.048	.066	.079	.077	.096
3	.055	.123	.204	.268	.333	.354	.432
4	.144	.269	.428	.571	.702	.783	.916
5	.164	.377	.625	.831	1.033	1.127	1.330
6	.217	.440	.716	.885	1.104	1.232	1.470
7	.251	.416	.686	.871	1.077	1.198	1.360
8	.211	.367	.568	.759	.909	1.008	1.232
9	.301	.360	.574	.654	.829	.937	.995
10	.078	.194	.363	.490	.587	.650	.823
11	.182	.231	.262	.327	.484	.493	.630
12	.039	.071	.160	.165	.245	.339	.389
13	.028	.035	.046	.107	.107	.183	.286
14	.007	-.009	-.012	-.009	.051	.109	.139
15	-.055	-.105	-.111	-.139	-.080	-.039	.046
16	-.070	-.147	-.180	-.156	-.077	-.086	.000
17	-.079	-.141	-.141	-.208	-.168	-.135	-.069
18	-.043	-.069	-.068	-.046	.000	.115	.164
19	-.085	-.057	-.005	.083	.198	.287	.299
20	-.037	-.018	.021	.133	.221	.361	.412
21	-.024	-.036	.005	.097	.136	.252	.299
22	-.009	-.002	.024	.101	.120	.194	.227
23	-.010	-.017	.014	.069	.058	.103	.124
24	.006	.021	.057	.055	.082	.072	.090
25	.006	.017	.050	.043	.026	.023	.023
26	-.001	.007	.021	.015	-.006	.000	-.006

[Elevators neutral; $q=12.5$ lb./sq. ft.]

Station No.	Angle of pitch— θ						
	3°	6°	9°	12°	15°	18°	20°
1	0	0	0	0	0	0	0
2	.016	.037	.044	.068	.078	.086	.094
3	.075	.154	.195	.268	.346	.378	.417
4	.177	.338	.424	.582	.703	.788	.874
5	.231	.469	.613	.841	1.025	1.133	1.258
6	.268	.488	.692	.906	1.150	1.230	1.377
7	.288	.472	.660	.872	1.065	1.217	1.310
8	.206	.409	.575	.765	.891	1.013	1.150
9	.288	.373	.571	.655	.819	.889	.922
10	.068	.236	.333	.470	.597	.610	.739
11	.169	.211	.222	.338	.460	.495	.561
12	.027	.114	.156	.229	.232	.339	.291
13	.000	.021	.053	.095	.114	.146	.186
14	.007	.011	-.019	.035	.081	.086	.137
15	-.053	-.110	-.101	-.114	-.039	-.032	.046
16	-.077	-.110	-.145	-.154	-.066	-.092	-.029
17	-.071	-.141	-.135	-.180	-.157	-.101	-.075
18	-.053	-.096	-.056	-.039	.024	.081	.144
19	-.085	-.081	.005	.071	.179	.304	.316
20	-.026	-.023	.006	.102	.224	.332	.377
21	-.036	-.027	.001	.099	.154	.236	.300
22	.000	-.015	.031	.082	.113	.178	.214
23	-.013	-.002	.028	.057	.070	.094	.106
24	.005	.021	.058	.062	.070	.066	.079
25	.005	.022	.050	.054	.037	.028	.013
26	.000	.008	.015	.013	-.001	-.002	-.009

TABLE VIII
1/40-SCALE MODEL U. S. S. "AKRON"

TRANSVERSE FORCE PER FOOT LENGTH— f/q ON HULL WITH TAIL SURFACES AND CONTROL CAR

[Elevators 20° up]

Station No.	$q=12.8$ lb./sq. ft.				$q=22.8$ lb./sq. ft.			
	θ				θ			
	0°	6°	15°	20°	0°	6°	15°	20°
1	0	0	0	0	0	0	0	0
2	-.003	.035	.077	.098	-.001	.031	.068	.090
3	-.003	.137	.350	.422	-.007	.135	.314	.421
4	.012	.303	.740	.903	.008	.305	.671	.924
5	.014	.468	1.068	1.296	.029	.454	.963	1.320
6	.015	.505	1.177	1.391	.039	.503	1.042	1.383
7	.051	.506	1.111	1.337	.022	.518	1.010	1.299
8	.026	.416	.955	1.128	.016	.433	.851	1.143
9	.114	.411	.834	.958	.123	.434	.734	.900
10	-.027	.211	.555	.715	-.023	.228	.477	.682
11	.036	.169	.442	.542	.055	.173	.362	.513
12	.023	.099	.280	.321	.032	.064	.149	.293
13	.023	.053	.097	.197	.039	.060	.046	.172
14	.000	.005	.012	.174	.002	.002	.007	.148
15	-.039	-.059	-.048	.069	-.023	-.091	-.119	.064
16	-.011	-.112	-.165	.018	-.024	-.159	-.165	-.004
17	-.055	-.152	-.166	-.036	-.069	-.164	-.212	-.109
18	-.020	-.074	.000	.206	-.028	-.087	-.030	.148
19	-.112	-.110	.178	.338	-.086	-.071	.152	.270
20	-.111	-.085	.152	.320	-.067	-.070	.140	.318
21	-.149	-.109	.088	.212	-.080	-.108	.083	.259
22	-.134	-.138	-.025	.066	-.164	-.125	-.016	.084
23	-.089	-.066	-.028	.021	-.081	-.029	-.040	.062
24	-.035	-.008	.028	.028	-.032	-.020	-.053	.026
25	.001	.016	.048	.024	-.009	.033	.047	.015
26	.003	.012	.008	-.002	-.010	.018	.011	-.003

TABLE VII
1/40-SCALE MODEL U. S. S. "AKRON"
TRANSVERSE FORCE PER FOOT LENGTH— f/q ON HULL WITH TAIL SURFACES AND CONTROL CAR

[Elevators 20° down]

Station No.	$q=12.8$ lb./sq. ft.				$q=22.8$ lb./sq. ft.			
	θ				θ			
	0°	6°	15°	20°	0°	6°	15°	20°
1	0	0	0	0	0	0	0	0
2	-.001	.035	.084	.093	.001	.037	.079	.094
3	-.003	.142	.348	.421	.000	.150	.333	.433
4	.008	.303	.717	.897	.017	.309	.709	.906
5	.022	.441	1.000	1.247	.023	.445	1.000	1.293
6	.048	.496	1.104	1.432	.047	.518	1.112	1.418
7	.058	.477	1.096	1.379	.076	.480	1.075	1.346
8	.043	.412	.902	1.199	.057	.422	.921	1.176
9	.143	.442	.829	1.080	.164	.461	.842	1.023
10	-.021	.196	.567	.770	.002	.224	.565	.770
11	.029	.204	.417	.573	.060	.220	.441	.561
12	.023	.101	.206	.353	.028	.094	.245	.312
13	.018	.067	.116	.255	.028	.060	.146	.234
14	-.007	.032	.065	.123	.007	.035	.095	.142
15	-.034	-.073	-.062	.032	-.018	-.057	-.075	.014
16	-.031	-.174	-.090	-.009	-.022	-.079	-.088	.013
17	-.034	-.091	-.143	-.061	-.012	-.125	-.135	-.061
18	.052	.013	.092	.252	.041	.000	.102	.227
19	.008	.064	.308	.431	.024	.042	.279	.426
20	.064	.113	.434	.650	.096	.118	.410	.610
21	.120	.131	.393	.516	.133	.145	.373	.514
22	.155	.192	.382	.512	.168	.190	.395	.503
23	.087	.122	.275	.317	.096	.122	.265	.313
24	.050	.075	.164	.167	.046	.075	.163	.151
25	.005	.044	.049	.044	.005	.046	.058	.033
26	-.006	.011	.001	-.005	-.007	.011	.000	-.003

REPORT No. 444

WIND-TUNNEL RESEARCH COMPARING LATERAL CONTROL DEVICES, PARTICULARLY AT HIGH ANGLES OF ATTACK

VI—SKEWED AILERONS ON RECTANGULAR WINGS

By FRED E. WEICK and THOMAS A. HARRIS

SUMMARY

This report covers the sixth of a series of investigations in which various lateral control devices are compared with particular reference to their effectiveness at high angles of attack. The present report deals with flap-type ailerons hinged about axes having an angle with respect to the leading and trailing edges of the wing. Tests were made on four different skewed ailerons, including two different angles of skew and two sizes of ailerons. At the high angles of attack, all the skewed ailerons tested were slightly inferior with respect to rolling and yawing moments to straight ailerons having the same span and average chord. Computations indicate that the skewed ailerons are also inferior with respect to hinge moments.

INTRODUCTION

This report is the sixth of a series giving the results of an investigation in which it is hoped to compare all types of lateral control devices which have been satisfactorily used or which show reasonable promise of being effective. In this program it is planned first to test the various types of ailerons and other control devices on rectangular wings of aspect ratio 6. Later the best of these control devices are to be tested on wings of different shape. In the entire series the various devices are to be subjected to the same program of wind-tunnel tests which, it is thought, include all the factors directly connected with lateral control and stability that can be satisfactorily handled in a routine manner in a wind tunnel. The tests are designed to show the relative merits of the various control devices in regard to lateral controllability, lateral stability, and general usefulness. They include regular 6-component force tests with the control devices both neutral and deflected various amounts, rotation tests in which the model is rotated about the tunnel axis and the rolling moment measured, and free rotation tests showing the range and rate of autorotation. Because of the large effect of yaw on lateral stability, the tests are made not only at 0° yaw, but also with an angle of yaw of 20° , which represents the conditions in a fairly severe sideslip.

Part I of this series (reference 1) dealt with three different sizes of ordinary ailerons. One of these ailerons was of a medium size taken from the average of a number of conventional airplanes, one was extremely short and wide, and the other was extremely long and narrow. All the ailerons were proportioned to give approximately equal controllability at angles of attack below the stall and with equal up-and-down deflection. The results were analyzed to show the relative merits of the three sizes of ailerons when set in the above manner and also in accordance with two differential movements, and with upward movement only.

Other work that has been done in this series is reported in references 2, 3, 4, and 5.

The present report covers similar tests on skewed ailerons. Previous tests made by the Army Air Service on skewed ailerons had shown them to give higher rolling moments than straight ailerons at high angles of attack on a certain wing model. (Reference 6.) These tests indicated that the best angle of skew was about 8° or 10° , with 20° as the maximum giving beneficial results. The present tests included ailerons with 10° and 20° skew, both angles being tried on ailerons of two different sizes, one having the same span and average chord dimensions as the medium-sized ailerons of Part I and the others the same as the short, wide ailerons of Part I. These ailerons were tested on a rectangular wing only, but skewed ailerons will be later tested on wings with other plan forms.

APPARATUS AND METHODS

Wind tunnel.—The 7- by 10-foot wind tunnel of the National Advisory Committee for Aeronautics, which is being used throughout the entire investigation, has an open jet and a single closed return passage. The tunnel, together with the regular balance and associated apparatus, is described in detail in reference 7.

Models.—Inasmuch as previous tests (reference 1) had shown that the moments caused by both right and left ailerons could be found separately and added together to give the total effect of both with a satisfactory accuracy, the present tests were made with

the right aileron only. All four ailerons were tested on one 10- by 60-inch laminated mahogany Clark Y wing model, which had a removable portion in the right rear corner as indicated in Figure 1. Four

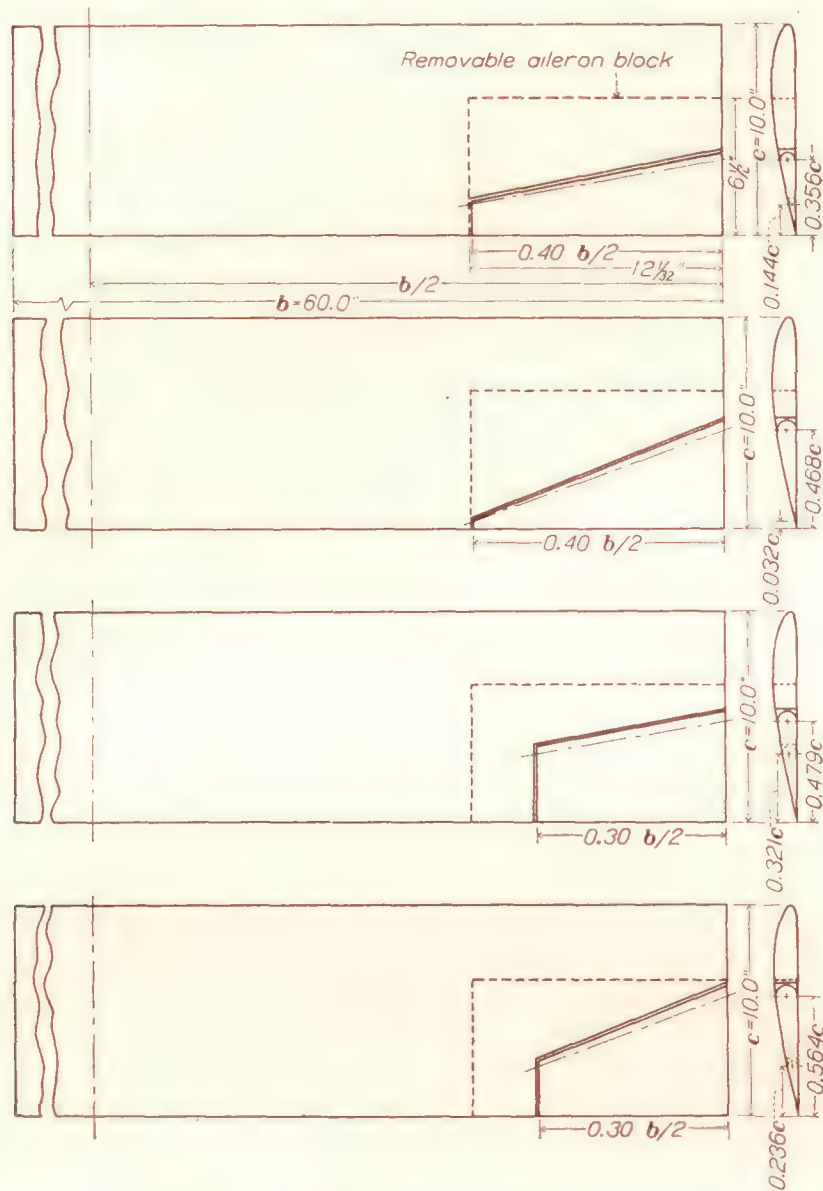


FIGURE 1.—Diagram of wings showing details of ailerons

different models of this portion of the wing were made, each containing one of the four ailerons.

Tests.—This series of tests was conducted in accordance with the standard procedure and at the dynamic pressure and Reynolds Number employed throughout the present research on lateral control. (See reference 1.) The dynamic pressure was 16.37 pounds per square foot, corresponding to a speed of 80 miles per hour at sea level under standard atmospheric conditions, and the Reynolds Number based on the 10-inch wing chord was 609,000.

Aileron movements.—From tests with the single ailerons deflected upward and downward various amounts, data were obtained from which the results were computed for four aileron movements: The equal up-and-down, average differential, extreme differential, and up-only movements. These movements were the same as those used in Part I. (Reference 1.) The relative up-and-down displacements with the two differential movements are given in Table I and the assumed linkages to obtain all of the movements in Figure 2. The deflection of the skewed ailerons was measured in a plane perpendicular to the hinge axis,

and is slightly greater than the projected angle deflection in a longitudinal plane.

Accuracy.—The accuracy of the results present in this report is the same as that obtained in Part I. It is considered satisfactory at all angles of attack except in the burbled region between 20° and 25° when the rolling and yawing moments are relative unreliable due to the critical, and often unsymmetric condition of the burbled air flow around the wing.

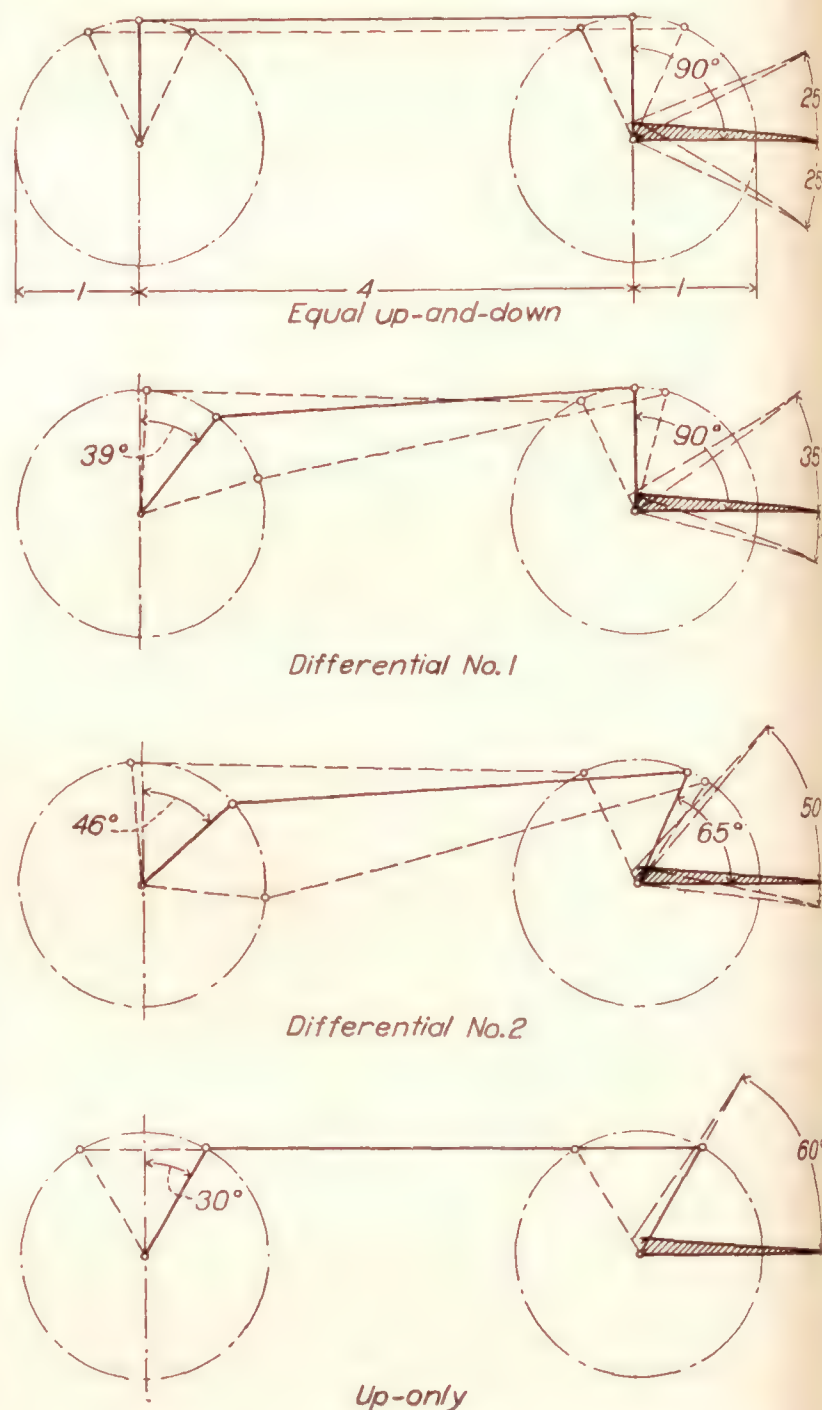


FIGURE 2.—Aileron linkage systems. Assumed maximum deflections

RESULTS

Coefficients.—The results are given in the form absolute coefficients of lift and drag and of rolling and yawing moments:

$$C_L = \frac{\text{lift}}{qS}$$

$$C_D = \frac{\text{drag}}{qS}$$

$$C_l' = \frac{\text{rolling moment}}{qbS}$$

$$C_n' = \frac{\text{yawing moment}}{qbS}$$

where S is the total wing area, b is the wing span, and q is the dynamic pressure. The coefficients as given above are obtained directly from the balance and refer to the wind (or tunnel) axes. In special cases in the discussion where the moments are used with reference to body axes the coefficients are not primed. Thus the symbols for the rolling and yawing moment coefficients about the body axes are C_l and C_n .

Tables.—The complete detailed results of the present tests are given in Tables II to XIII.

Table II contains the following data for the unyawed wing with the 40 per cent semispan ailerons having a 10° angle of skew:

1. C_L and C_D with zero aileron deflection.

2. C_l' and C_n' for each aileron setting. Table III gives similar data for the same aileron with the wing at -20° yaw, and Table IV with the wing at $+20^\circ$ yaw.

Tables V, VI, and VII are similar to Tables II, III, and IV, respectively, but cover the results for the 40 per cent semispan aileron having 20° skew; Tables VIII, IX, and X cover the wider 30 per cent semispan ailerons with 10° skew, and Tables XI, XII, and XIII the 30 per cent semispan ailerons with 20° skew.

DISCUSSION IN TERMS OF CRITERIONS

For a comparison of the different lateral control arrangements, the results of the tests are discussed in terms of criterions, which are explained in detail in Part I and briefly in the following paragraphs. By use of these criterions a comparison of the effect of the different control devices on the general performance, the lateral controllability, and the lateral stability may be made. The values of the criterions summarizing the results of the present tests are given in Table XIV, and the values for the standard and the short, wide ailerons of Part I (no skew) are included for comparison.

GENERAL PERFORMANCE

The values of the three criterions used in connection with the general performance of the wing, the maxi-

mum lift coefficient, the speed-range ratio $\frac{C_{Lmax}}{C_{Dmin}}$, and

the climb criterion $\frac{L}{D}$ at $C_L = 0.70$, are not appreciably

affected by ordinary ailerons, so these values are approximately the same for the various cases tested.

LATERAL CONTROLLABILITY

Rolling criterion.—The rolling criterion upon which the effectiveness of each of the aileron arrangements is judged is a figure of merit that is designed to be proportional to the initial acceleration of the wing tip that follows a deflection of the ailerons from neutral, regardless of the air speed or the plan form

of the wing. Expressed in coefficient form for a rectangular monoplane wing, the criterion is

$$RC = \frac{C_l}{C_L}$$

where C_l is the rolling-moment coefficient about the body axis due to the lateral controls. The value of this expression that has been found to represent satisfactory control is approximately 0.075. A more detailed explanation of the derivation of RC and of its more general form, which is applicable to any wing plan form, is given in Part I.

The comparison of the various ailerons and movements is given in Table XIV for four representative angles of attack: 0° , 10° , 20° , and 30° . The 0° angle represents the high-speed attitude; $\alpha = 10^\circ$ represents the highest angle of attack at which entirely satisfactory control with ordinary ailerons can be obtained; $\alpha = 20^\circ$ is the condition of greatest lateral instability and is probably about the greatest obtainable angle of attack in a steady glide with most present-day airplanes; and finally, $\alpha = 30^\circ$ is given only for a comparison with controls for possible future types of airplanes.

At $\alpha = 0^\circ$, all the ailerons gave values of RC greatly in excess of that considered necessary.

At $\alpha = 10^\circ$, the ailerons with 10° skew gave slightly higher values of RC for most of the assumed aileron movements than the straight ailerons having the same average chord, but the ailerons with 20° skew gave lower values.

At $\alpha = 20^\circ$, the 40 per cent semispan ailerons, both with 10° and with 20° skew, gave substantially lower values of RC than the straight ailerons of the same span and average chord. The same is true for the 30 per cent semispan aileron with 20° skew, but the 30 per cent semispan aileron with 10° skew gave values nearly as high as the straight ailerons of the same span and average chord.¹

At $\alpha = 30^\circ$, none of the ailerons gave values of RC approaching the assumed satisfactory one.

Lateral control with sideslip.—If a wing is yawed appreciably, a rolling moment is set up that tends to raise the forward tip. The magnitude of this rolling moment is always greater at very high angles of attack than the available rolling moment due to ordinary ailerons. The highest angle of attack at which the aileron can balance the rolling moment due to 20° yaw is tabulated for all the arrangements tested as a criterion of control with sideslip. As previously men-

¹ Owing to the fact that the wing with 40 per cent chord by 30 per cent semispan straight ailerons (reference 1) had a lift coefficient at an angle of attack of 20° that was about 9 per cent lower than the other Clark Y wings of this series of tests, the values of RC are correspondingly higher for that condition. A rigorous comparison of the results at an angle of attack of 20° can not, therefore, be made with this wing, but on the basis of later tests with the same size aileron on another wing, it seems that a reasonable comparison can be made with the present data on skewed ailerons if the values of RC for the short, wide, straight aileron given in Table XIV are reduced by 9 per cent. If that is done the values will be very slightly higher than those for the 30 per cent semispan aileron with 10° skew.

tioned, 20° yaw represents the conditions in a fairly severe sideslip. Table XIV shows that the lateral control against the effect of 20° sideslip is maintained up to approximately the same angle of attack with all of the combinations tested.

Yawing moment due to ailerons.—The desirable yawing moment due to ailerons depends to some extent upon the type of airplane that is being considered. For highly maneuverable military or acrobatic machines complete independence of the controls as they affect turning moments about the various body axes is a desirable feature. On the other hand, for large transport airplanes or for machines to be operated by relatively inexperienced pilots, a favorable yawing moment of proper magnitude would be an appreciable aid to safe flying at high angles of attack. Finally, it is obvious that a yawing moment tending to retard the high wing when the airplane is banked is never desirable.

The yawing moments obtained with the skewed ailerons follow closely those for the straight ailerons having the same span and average chord, the adverse values being slightly higher in general for the skewed ailerons at angles of attack above the stall. The maximum adverse yawing moments for the equal up-and-down movement and for both differential movements were greater with all of the skewed ailerons tested, but could be overcome by an average rudder.

LATERAL STABILITY

Inasmuch as the skewed ailerons do not affect the shape of the wing to an appreciable extent when neutral, they have no appreciable influence on the lateral stability, and the values of the criteria on this subject are considered the same as those for the wings with the straight ailerons. The criteria for lateral stability are given in Table XIV and explained in reference 1. The rolling moments tending to make the wings autorotate (C_{λ}) depend in a very critical manner on the exact profile of the airfoils and are sometimes quite different for two airfoils made to the same design. The two examples given in Table XIV represent the extremes of this variation.

CONTROL FORCE REQUIRED

The hinge moments were not measured for the skewed ailerons, the rolling and yawing moment tests having shown them inferior to straight ailerons. Since it is approximately true that the hinge moment of an aileron varies as the square of the chord, however, it is to be expected that the hinge moments would be slightly higher for skewed than for straight ailerons of the same span and average chord. This condition has been substantiated by computations made by integrating values of the hinge moment for different unit chords obtained from data given in reference 8. These approximate computations showed that for equal up-and-down deflection of 25°, the total hinge moment

of the 40 per cent semispan ailerons with 10° skew should be about 9 per cent higher and with 20° skew about 18 per cent higher than the values for the straight ailerons.

CONCLUSIONS

At the high angles of attack, all the skewed ailerons tested were slightly inferior to the straight ailerons having the same span and average chord with respect to both the rolling and yawing moments produced. Computations indicate that they are also inferior with respect to the control force required.

LANGLEY MEMORIAL AERONAUTICAL LABORATORY,
NATIONAL ADVISORY COMMITTEE FOR AERONAUTICS,
LANGLEY FIELD, VA., July 12, 1932.

REFERENCES

1. Weick, Fred E., and Wenzinger, Carl J.: Wind-Tunnel Research Comparing Lateral Control Devices, Particularly at High Angles of Attack. I—Ordinary Ailerons on Rectangular Wings. T. R. No. 419, N. A. C. A., 1932.
2. Weick, Fred E., and Noyes, Richard W.: Wind-Tunnel Research Comparing Lateral Control Devices, Particularly at High Angles of Attack. II—Slotted Ailerons and Frise Ailerons. T. R. No. 422, N. A. C. A., 1932.
3. Weick, Fred E., and Wenzinger, Carl J.: Wind-Tunnel Research Comparing Lateral Control Devices, Particularly at High Angles of Attack. III—Ordinary Ailerons Rigged Up 10° when Neutral. T. R. No. 423, N. A. C. A., 1932.
4. Weick, Fred E., and Harris, Thomas A.: Wind-Tunnel Research Comparing Lateral Control Devices, Particularly at High Angles of Attack. IV—Floating-Tip Ailerons on Rectangular Wings. T. R. No. 424, N. A. C. A., 1932.
5. Weick, Fred E., and Shortall, Joseph A.: Wind-Tunnel Research Comparing Lateral Control Devices, Particularly at High Angles of Attack. V—Spoilers and Ailerons on Rectangular Wings. T. R. No. 439, N. A. C. A., 1932.
6. Morse, A. L.: Aileron Effectiveness. Information Circular No. 454, Airplane Engineering Division, U. S. Air Service, 1924.
7. Harris, Thomas A.: The 7- by 10-Foot Wind Tunnel of the National Advisory Committee for Aeronautics. T. R. No. 412, N. A. C. A., 1931.
8. Monish, B. H.: Effect of Variation of Chord and Span of Ailerons on Hinge Moments at Several Angles of Pitch. T. R. No. 370, N. A. C. A., 1930.

TABLE I
SIMULTANEOUS AILERON DISPLACEMENTS WITH
ASSUMED DIFFERENTIAL ARRANGEMENTS

Angles measured about aileron axis

Average differential (No. 1)		Extreme differential (No. 2)	
Upward displacement	Downward displacement	Upward displacement	Downward displacement
Degrees	Degrees	Degrees	Degrees
0	0	0	0
10	8.5	10	7
20	13	20	12
30	15	30	14
35	15	40	11.5
		50	7

TABLE II

FORCE TEST. 10- BY 60-INCH CLARK Y WING WITH 10° SKEWED AILERONS 25 PER CENT AVERAGE c BY 40 PER CENT $b/2$. YAW=0°. R. N.=609,000. VELOCITY=80 M. P. H.

δ_A up	δ_A down	α	-5°	-3°	0°	4.5°	10°	12°	14°	15°	16°	18°	20°	22°	25°	30°	40°	50°	60°
AILERONS LOCKED-NEUTRAL																			
0°	0°	C_L	0.004	0.143	0.354	0.700	1.061	1.180	1.256	1.278	1.246	1.245	1.198	1.132	0.827	0.862	0.802	0.718	0.598
0°	0°	C_D	.018	.017	.022	.045	.089	.108	.131	.145	.171	.201	.247	.283	.425	.531	.714	.879	1.050
UP ONLY																			
10°	10°	C_L'			0.020		0.021						0.006			0.006	0.003		
10°	10°	C_n'			-.001		-.004						-.006			-.004	-.004		
20°	20°	C_L'			.036		.042						.021			.015	.007		
20°	20°	C_n'			.001		-.005						-.011			-.009	-.007		
25°	25°	C_L'			.044		.049	0.048	0.048		0.043	0.045	.030	0.024	0.006	.015	.011		
25°	25°	C_n'			.003		-.004	-.006	-.007		-.009	-.012	-.013	-.013	-.008	-.009	-.009		
30°	30°	C_L'			.048		.051						.033			.025	.015		
30°	30°	C_n'			.004		-.004						-.012			-.011	-.010		
35°	35°	C_L'			.053		.057	.055	.054		.051	.050	.035	.031	.011	.022	.019		
35°	35°	C_n'			.006		-.002	-.004	-.006		-.007	-.009	-.011	-.012	-.006	-.009	-.012		
40°	40°	C_L'			.059		.061						.039			.023	.021		
40°	40°	C_n'			.008		-.001						-.010			-.007	-.011		
50°	50°	C_L'			.063		.039	.057	.036		.064	.030	.044	.036	.008	.013	.011		
50°	50°	C_n'			.012		.002	.000	-.002		-.004	-.006	-.008	-.008	-.002	-.004	-.006		
60°	60°	C_L'			.039		.075	.075	.074		.071	.039	.053	.042	.008	.012	.011		
60°	60°	C_n'			.015		.005	.003	.000		-.002	-.005	-.006	-.006	-.001	-.004	-.005		
80°	80°	C_L'			.076		.034						.062			.018	.010		
80°	80°	C_n'			.019		.009						-.003			-.005	-.007		
DOWN ONLY																			
7°	7°	C_L'			-.015		-.012	-.012	-.011		-.007	-.010	-.003	-.001	-.007	-.001	-.001		
7°	7°	C_n'			.001		.003	.003	.004		.004	.004	.005	.004	.004	.002	.003		
8½°	8½°	C_L'			-.018		-.015						-.005			.001	-.001		
8½°	8½°	C_n'			.002		.004						.006			.003	.004		
10°	10°	C_L'			-.021		-.017						-.007			-.002	-.001		
10°	10°	C_n'			.003		.005						.007			.004	.004		
11½°	11½°	C_L'			-.025		-.019						-.009			-.004	-.002		
11½°	11½°	C_n'			.003		.006						.008			.005	.005		
12°	12°	C_L'			-.025		-.019						-.007			-.004	-.001		
12°	12°	C_n'			.004		.007						.008			.005	.006		
13°	13°	C_L'			-.027		-.021						-.007			-.002	-.002		
13°	13°	C_n'			.004		.007						.009			.003	.006		
14°	14°	C_L'			-.029		-.024						-.006			-.001	-.002		
14°	14°	C_n'			.005		.008						.010			.006	.007		
15°	15°	C_L'			-.031		-.024	-.023	-.021		-.017	-.012	-.006	.001	-.038	-.001	-.002		
15°	15°	C_n'			.005		.008	.009	.009		.010	.010	.010	.007	.037	.006	.007		
20°	20°	C_L'			-.037		-.030						-.005			-.001	-.001		
20°	20°	C_n'			.007		.013						.013			.008	.010		
25°	25°	C_L'			-.041		-.036	-.035	-.033		-.028	-.020	-.005	.007	-.006	-.001	-.001		
25°	25°	C_n'			.009		.015	.016	.017		.018	.017	.014	.039	.011	.010	.011		
35°	35°	C_L'			-.046		-.044						-.010			.003	.002		
35°	35°	C_n'			.015		.021						.017			.014	.015		

TABLE III

FORCE TEST. 10- BY 60-INCH CLARK Y WING WITH 10° SKEWED AILERONS 25 PER CENT AVERAGE c BY 40 PER CENT $b/2$. YAW=-20°. R. N.=609,000. VELOCITY=80 M. P. H.

δ_A up	δ_A down	α	-5°	0°	5°	10°	12°	14°	15°	16°	18°	20°	22°	25°	30°	40°	50°	60°
AILERONS LOCKED—NEUTRAL																		
0°	0°	C_L	-0.014	0.305	0.635	0.946	1.044	1.123	1.145	1.162	1.179	1.178	0.972	0.912	0.914	0.817	0.758	0.642
0°	0°	C_D	.020	.022	.042	.078	.094	.114	.123	.133	.168	.218	.350	.421	.545	.681	.882	1.045
0°	0°	C_L'	-.002	-.006	-.006	-.006	-.015	-.020	-.026	-.032	-.055	-.078	-.102	-.104	-.035	-.057	-.048	-.044
0°	0°	C_n'	.001	.001	.002	.004	.006	.008	.010	.011	.014	.016	.023	.039	.049	.042	.046	.054
UP ONLY																		
25°	-----	C_L'	-----	0.046	-----	0.042	0.048	0.048	-----	0.048	0.061	0.050	0.039	0.031	0.013	-0.002	-----	-----
25°	-----	C_n'	-----	.003	-----	-.005	-.007	-.003	-----	-.010	-.011	-.014	-.023	-.022	-.017	-.006	-----	-----
35°	-----	C_L'	-----	.057	-----	.054	.061	.051	-----	.062	.064	.065	.091	.075	.019	.012	-----	-----
35°	-----	C_n'	-----	.007	-----	-.003	-.005	-.007	-----	-.010	-.012	-.015	-.018	-.037	-.025	-.010	-----	-----
50°	-----	C_L'	-----	.067	-----	.068	.075	.075	-----	.076	.079	.076	.071	.092	.031	.026	-----	-----
50°	-----	C_n'	-----	.015	-----	-.003	.000	-.003	-----	-.006	-.008	-.011	-.028	-.036	-.024	-.008	-----	-----
60°	-----	C_L'	-----	.064	-----	.074	.082	.085	-----	.085	.089	.083	.098	.090	.035	.026	-----	-----
60°	-----	C_n'	-----	.015	-----	.007	.004	.001	-----	-.002	-.004	-.008	-.027	-.035	-.023	-.013	-----	-----

TABLE IV

FORCE TEST. 10- BY 60-INCH CLARK Y WING WITH 10° SKEWED AILERONS 25 PER CENT AVERAGE *c* BY 40 PER CENT *b*/2. YAW=20°. R. N.=609,000. VELOCITY=80 M. P. H.

δ_A up	δ_A down	α	-5°	0°	5°	10°	12°	14°	15°	16°	18°	20°	22°	25°	30°	40°	50°	60°
		AILERONS LOCKED-NEUTRAL																
0°	0°	C_L	0.003	0.318	0.646	0.956	1.057	1.130	1.148	1.166	1.181	1.176	0.942	0.914	0.908	0.815	0.752	0.629
0°	0°	C_D	.019	.022	.043	.080	.096	.116	.125	.136	.171	.222	.353	.424	.523	.679	.872	1.021
0°	0°	C_l'	.008	.012	.013	.017	.021	.027	.032	.039	.063	.081	.106	.107	.097	.060	.052	.047
0°	0°	C_n'	-.001	-.002	-.003	-.006	-.008	-.011	-.012	-.014	-.017	-.022	-.031	-.045	-.055	-.048	-.054	-.063
		DOWN ONLY																
	7°	C_l'		-0.013		-0.010	-0.009	-0.009		-0.007	-0.008	-0.006	-0.003	-0.003	-0.001	-0.002		
	7°	C_n'		.002		.003	.003	.004		.003	.003	.004	.003	.004	.003	.004		
	15°	C_l'		-.026		-.020	-.020	-.019		-.016	-.013	-.013	-.006	-.007	-.003	-.004		
	15°	C_n'		.004		.007	.007	.008		.007	.006	.007	.008	.008	.007	.008		
	25°	C_l'		-.036		-.033	-.033	-.030		-.027	-.025	-.019	-.009	-.010	-.006	-.004		
	25°	C_n'		.007		.013	.014	.015		.014	.012	.013	.013	.014	.012	.013		

TABLE V

FORCE TEST. 10- BY 60-INCH CLARK Y WING WITH 20° SKEWED AILERONS 25 PER CENT AVERAGE *c* BY 40 PER CENT *b*/2. YAW=0°. R. N.=609,000. VELOCITY=80 M. P. H.

δ_A up	δ_A down	α	-5°	-4°	-3°	0°	4 5°	10°	12°	14°	15°	16°	18°	20°	22°	25°	30°	40°	50°	60°
		AILERONS LOCKED-NEUTRAL																		
0°	0°	C_L	0.005	0.076	0.151	0.360	0.700	1.060	1.173	1.250	1.253	1.244	1.243	1.170	1.117	0.803	0.858	0.790	0.713	0.600
0°	0°	C_D	.018	.016	.017	.022	.045	.088	.108	.130	.146	.165	.201	.245	.283	.418	.540	.706	.890	1.053
		UP ONLY																		
10°		C_l'				0.015		0.015						0.003			0.001	0.000		
10°		C_n'				-.001		-.003						-.005			-.004	-.003		
20°		C_l'				.030		.031						.015			.008	.005		
20°		C_n'				.000		-.004						-.010			-.007	-.007		
25°		C_l'				.038		.038	0.040	0.038		0.036	0.034	.022	0.021	0.010	.013	.010		
25°		C_n'				.002		-.004	-.005	-.006		-.008	-.009	-.011	-.011	-.008	-.008	-.009		
30°		C_l'				.042		.044						.028			.015	.012		
30°		C_n'				.003		-.004						-.011			-.009	-.010		
35°		C_l'				.047		.049	.051	.050		.048	.048	.033	.032	.015	.018	.015		
35°		C_n'				.005		-.002	-.004	-.005		-.007	-.010	-.011	-.012	-.007	-.008	-.010		
40°		C_l'				.049		.052						.038			.016	.014		
40°		C_n'				.007		-.001						-.010			-.007	-.008		
50°		C_l'				.052		.058	.058	.056		.055	.056	.050	.037	.020	.019	.016		
50°		C_n'				.010		.003	.001	-.001		-.003	-.005	-.007	-.008	-.004	-.005	-.006		
60°		C_l'				.056		.063	.065	.065		.064	.065	.048	.037	.020	.019	.012		
60°		C_n'				.013		.006	.005	.003		.001	-.001	-.003	-.004	-.001	-.002	-.006		
80°		C_l'																		
80°		C_n'																		
		DOWN ONLY																		
	7°	C_l'				-0.011		-0.013	-.011	-0.011		-0.009	-0.009	-0.005	-0.001	0.001	0.000	-0.001		
	7°	C_n'				.001		.003	.004	.004		.005	.005	.005	.004	.003	.002	.003		
	8 1/2°	C_l'				-.016		-.014						-.009			-.007	-.005		
	8 1/2°	C_n'				.002		.004						.006			.005	.005		
	10°	C_l'				-.018		-.017						-.009			-.006	-.005		
	10°	C_n'				.002		.005						.008			.005	.008		
	11 1/2°	C_l'				-.021		-.020						-.010			-.006	-.005		
	11 1/2°	C_n'				.003		.006						.009			.006	.006		
	12°	C_l'				-.022		-.020						-.010			-.006	.002		
	12°	C_n'				.003		.006						.009			.006	.007		
	13°	C_l'				-.023		-.023						-.012			-.007	-.006		
	13°	C_n'				.003		.007						.010			.006	.007		
	14°	C_l'				-.024		-.023						-.012			-.007	-.006		
	14°	C_n'				.004		.007						.010			.007	.007		
	15°	C_l'				-.026		-.025	-.023	-.024		-.021	-.008	-.010	.000	-.003	-.006	-.005		
	15°	C_n'				.004		.008	.009	.010		.011	.011	.010	.007	.006	.007	.007		
	20°	C_l'				-.032		-.032						-.008			-.007	-.006		
	20°	C_n'				.005		.012						.013			.009	.010		
	25°	C_l'				-.035		-.035	-.034	-.032		-.028	-.015	-.008	.004	-.002	-.006	-.005		
	25°	C_n'				.008		.014	.015	.016		.018	.018	.015	.009	.010	.011	.013		
	35°	C_l'				-.041		-.040						-.014			-.005	-.005		
	35°	C_n'				.010		.017						.016			.014	.015		

TABLE VI

FORCE TEST. 10- BY 60-INCH CLARK Y WING WITH 20° SKEWED AILERONS 25 PER CENT AVERAGE *c* BY 40 PER CENT *b*/2. YAW=-20°. R. N.=609,000. VELOCITY=80 M. P. H.

δ_A up	δ_A down	α	-5°	0°	5°	10°	12°	14°	15°	16°	17°	18°	20°	22°	25°	30°	40°	50°	60°
		AILERONS LOCKED-NEUTRAL																	
0°	0°	C_L	-0.002	0.312	0.637	0.944	1.040	1.118	1.144	1.167	-----	1.178	1.168	0.966	0.917	0.912	0.818	0.759	0.642
	0°	C_D	.019	.021	.042	.079	.096	.115	.125	.137	-----	.169	.221	.348	.422	.525	.687	.886	1.053
	0°	$C_{l'}$	-.001	-.003	-.004	-.008	-.012	-.018	-.024	-.030	-----	-.052	-.076	-.102	-.104	-.091	-.056	-.048	-.044
	0°	$C_{n'}$.002	.002	.002	.005	.006	.008	.010	.012	-----	.014	.016	.022	.040	.049	.044	.048	.055
		UP ONLY																	
25°	-----	$C_{l'}$	-----	0.035	-----	0.036	0.036	0.037	-----	0.037	-----	0.038	0.038	0.033	0.027	0.011	0.006	-----	-----
25°	-----	$C_{n'}$	-----	.002	-----	-.005	-.007	-.009	-----	-.011	-----	-.011	-.014	-.019	-.022	-.016	-.010	-----	-----
35°	-----	$C_{l'}$	-----	.046	-----	.048	.049	.051	-----	.051	-----	.052	.052	.046	.040	.023	.012	-----	-----
35°	-----	$C_{n'}$	-----	.005	-----	-.004	-.006	-.008	-----	-.011	-----	-.012	-.015	-.024	-.027	-.023	-.013	-----	-----
50°	-----	$C_{l'}$	-----	.058	-----	.064	.065	.067	-----	.068	-----	.069	.070	.063	.055	.038	.021	-----	-----
50°	-----	$C_{n'}$	-----	.013	-----	.001	-.002	-.004	-----	-.008	-----	-.009	-.014	-.025	-.027	-.025	-.015	-----	-----
60°	-----	$C_{l'}$	-----	.062	-----	.071	.073	.075	-----	.076	-----	.078	.077	.069	.061	.044	.028	-----	-----
60°	-----	$C_{n'}$	-----	.020	-----	.006	.004	.000	-----	-.004	-----	-.005	.010	-.020	-.025	-.023	-.016	-----	-----

TABLE VII

FORCE TEST. 10- BY 60-INCH CLARK Y WING WITH 20° SKEWED AILERONS 25 PER CENT AVERAGE *c* BY 40 PER CENT *b*/2. YAW=20°. R. N.=609,000. VELOCITY=80 M. P. H.

δ_A up	δ_A down	α	-5°	0°	5°	10°	12°	14°	15°	16°	17°	18°	20°	22°	25°	30°	40°	50°	60°
		AILERONS LOCKED-NEUTRAL																	
0°	0°	C_L	0.000	0.328	0.699	0.955	1.053	1.130	1.153	1.168	-----	1.181	1.174	0.936	0.912	0.901	.0812	0.747	0.631
	0°	C_D	.018	.021	.043	.080	.096	.115	.125	.138	-----	.172	.224	.356	.422	.520	.677	.871	1.035
	0°	$C_{l'}$.010	.013	.015	.019	.023	.028	.034	.042	-----	.065	.082	.107	.109	.097	.060	.052	0.047
	0°	$C_{n'}$	-.001	-.001	-.003	-.006	-.008	-.011	-.012	-.014	-----	-.017	-.022	-.031	-.044	-.055	-.048	-.053	-.063
		DOWN ONLY																	
7°	7°	$C_{l'}$	-----	-0.010	-----	-0.011	-0.010	-0.009	-----	-0.008	-----	-0.008	-0.005	-0.003	-0.004	-0.002	-0.003	-----	-----
7°	7°	$C_{n'}$	-----	.001	-----	.003	.003	.004	-----	.003	-----	.003	.003	.003	.003	.002	.004	-----	-----
15°	15°	$C_{l'}$	-----	-.021	-----	-.021	-.020	-.019	-----	-.019	-----	-.016	-.012	-.007	-.009	-.004	-.005	-----	-----
15°	15°	$C_{n'}$	-----	.003	-----	.007	.008	.009	-----	.008	-----	.007	.008	.007	.007	.006	.008	-----	-----
25°	25°	$C_{l'}$	-----	-.031	-----	-.033	-.033	-.032	-----	-.031	-----	-.027	-.021	-.011	-.012	-.005	-.007	-----	-----
25°	25°	$C_{n'}$	-----	.007	-----	.014	.015	.017	-----	.016	-----	.013	.014	.012	.013	.012	.013	-----	-----

TABLE VIII

FORCE TEST. 10- BY 60-INCH CLARK Y WING WITH 10° SKEWED AILERONS 40 PER CENT AVERAGE c_b
30 PER CENT $b/2$. YAW=0°. R. N.=609,000. VELOCITY=80 M. P. H.

δ_A up	δ_A down	α	-5°	-3°	0°	4.5°	10°	12°	14°	15°	16°	18°	20°	22°	25°	30°	40°	50°	60°
AILERONS LOCKED—NEUTRAL																			
0°	0°	C_L	0.008	0.149	0.363	0.700	1.068	1.176	1.260	1.255	1.240	1.241	1.163	1.117	0.793	0.845	0.808	0.716	0.600
0°	0°	C_D	.016	.016	.020	.043	.087	.108	.130	.148	.166	.199	.246	.281	.419	.538	.727	.881	1.045
UP ONLY																			
10°	10°	C_l'			0.018		0.023						0.006			0.001	0.000		
10°	10°	C_n'			-.001		-.004						-.006			-.003	-.003		
20°	20°	C_l'			.037		.040						.025			.002	.004		
20°	20°	C_n'			.002		-.005						-.011			-.005	-.007		
25°	25°	C_l'			.044		.048	.047	.046	.043	.047		.034	.020	.009	.007	.008		
25°	25°	C_n'			.004		-.004		-.008		-.011	-.012	-.013	-.008	-.007	-.007	-.008		
30°	30°	C_l'			.048		.055						.042			.009	.011		
30°	30°	C_n'			.006		-.002						-.012			-.008	-.009		
35°	35°	C_l'			.053		.065	.055	.054		.064	.064	.052	.037	.018	.016	.016		
35°	35°	C_n'			.009		.000	-.003	-.005		-.007	-.009	-.012	-.014	-.009	-.009	-.012		
40°	40°	C_l'			.059		.071						.059			.019	.019		
40°	40°	C_n'			.012		.002						-.010			-.009	-.012		
50°	50°	C_l'			.065		.081	.083	.082		.082	.083	.070	.050	.034	.018	.027		
50°	50°	C_n'			.016		.007	.005	.003		.000	-.003	-.005	-.008	-.007	-.005	-.011		
60°	60°	C_l'			.072		.087	.089	.091		.092	.094	.079	.052	.043	.026	.017		
60°	60°	C_n'			.021		.012	.010	.008		.006	.004	.001	-.001	-.003	-.003	-.008		
80°	80°	C_l'			.062		.071						.054			.014	.010		
80°	80°	C_n'			.018		.009						.001			.001	-.005		
DOWN ONLY																			
7°	7°	C_l'			-.014		-.012	-.011	-.009		-.007	-.007	-.005	-.013	-.000	-.001	-.001		
7°	7°	C_n'			.002		.004	.004			.005	.005	.005	.005	.003	.003	.003		
8½°	8½°	C_l'			-.017		-.014						-.005			.001	.003		
8½°	8½°	C_n'			.002		.004						.006			.003	.005		
10°	10°	C_l'			-.020		-.016						-.004			.001	.000		
10°	10°	C_n'			.003		.005						.007			.004	.005		
11½°	11½°	C_l'			-.022		-.017						-.005			.002	.000		
11½°	11½°	C_n'			.003		.006						.007			.004	.005		
12°	12°	C_l'			-.023		-.018						-.004			.002	.000		
12°	12°	C_n'			.003		.006						.008			.004	.005		
13°	13°	C_l'			-.025		-.021						-.005			.003	.000		
13°	13°	C_n'			.004		.008						.009			.005	.006		
14°	14°	C_l'			-.026		-.022						-.002			.002	.000		
14°	14°	C_n'			.004		.008						.009			.005	.007		
15°	15°	C_l'			-.027		-.023	-.023	-.022		-.018	-.003	-.006	-.010	.001	.001	.000		
15°	15°	C_n'			.005		.009	.010	.011		.012	.012	.010	.008	.007	.006	.008		
20°	20°	C_l'			-.033		-.029						.002			.004	.001		
20°	20°	C_n'			.007		.013						.011			.007	.010		
25°	25°	C_l'			-.039		-.033	-.033	-.030		-.027	-.007	-.004	-.004	.004	.005	.001		
25°	25°	C_n'			.012		.016	.018	.018		.020	.018	.014	.010	.010	.009	.013		
35°	35°	C_l'			-.044		-.037						-.005			.010	.004		
35°	35°	C_n'			.016		.022						.017			.012	.017		

TABLE IX

FORCE TEST. 10- BY 60-INCH CLARK Y WING WITH 10° SKEWED AILERONS 40 PER CENT AVERAGE c_b
30 PER CENT $b/2$. YAW=-20°. R. N.=609,000. VELOCITY=80 M. P. H.

δ_A up	δ_A down	α	-5°	0°	5°	10°	12°	14°	15°	16°	18°	20°	22°	25°	30°	40°	50°	60°
AILERONS LOCKED—NEUTRAL																		
0°	0°	C_L	-0.008	0.311	0.639	0.938	1.043	1.114	1.139	1.155	1.174	1.175	0.984	0.922	0.908	0.816	0.760	0.642
0°	0°	C_D	.019	.022	.042	.078	.095	.111	.124	.134	.166	.214	.346	.413	.525	.681	.879	1.057
0°	0°	C_l'	-.001	-.003	-.005	-.009	-.013	-.019	-.024	-.030	-.053	-.075	-.103	-.105	-.093	-.057	-.047	-.044
0°	0°	C_n'	.002	.002	.002	.005	.006	.008	.010	.011	.013	.016	.021	.038	.048	.042	.047	.055
UP ONLY																		
25°	25°	C_l'		0.042		0.042	0.043	0.042	0.042	0.042	0.045	0.043	0.039	0.032	0.021	0.005		
25°	25°	C_n'		.004		-.005	-.006	-.008	-.009	-.010	-.011	-.014	-.021	-.024	-.022	-.010		
35°	35°	C_l'		.060		.061		.061		.063	.062	.057	.049	.037	.037	.011		
35°	35°	C_n'		.010		-.001		-.008		-.011	-.015	-.025	-.028	-.027	-.015			
50°	50°	C_l'		.070		.088	.090	.090		.090	.094	.093	.086	.074	.060	.020		
50°	50°	C_n'		.021		.009	.005	.002		-.001	-.005	-.010	-.021	-.029	-.030	-.018		
60°	60°	C_l'		.069		.103	.104	.106		.108	.113	.110	.102	.089	.074	.032		
60°	60°	C_n'		.024		.019	.015	.011		.007	.004	-.002	-.015	-.024	-.028	-.019		

TABLE X

FORCE TEST. 10- BY 60-INCH CLARK Y WING WITH 10° SKEWED AILERONS 40 PER CENT AVERAGE c BY 30 PER CENT $b/2$. YAW=20°. R. N.=609,000. VELOCITY=80 M. P. H.

δ_A up	δ_A down	α	-5°	0°	5°	10°	12°	14°	15°	16°	18°	20°	22°	25°	30°	40°	50°	60°
AILERONS LOCKED—NEUTRAL																		
0°	0°	C_L	0.002	0.326	0.653	0.962	1.059	1.128	1.157	1.175	1.188	1.178	0.980	0.915	0.890	0.808	0.750	0.630
0°	0°	C_D	.017	.022	.043	.080	.098	.115	.125	.138	.172	.222	.357	.421	.521	.673	.869	1.037
0°	0°	C_l'	.010	.013	.015	.019	.024	.028	.034	.043	.064	.083	.095	.109	.096	.061	.053	.048
0°	0°	C_n'	-.001	-.001	-.003	-.006	-.008	-.011	-.012	-.014	-.017	-.021	-.030	-.045	-.054	-.048	-.054	-.064
DOWN ONLY																		
	7°	C_l'		-.012		-.011	-.011	-.010		-.010	-.007	-.005	0.010	-.004	-.003	-.004		
	7°	C_n'		.001		.003	.003	.004		.004	.003	.003	.002	.004	.003	.006		
	15°	C_l'		-.025		-.022	-.024	-.022		-.021	-.016	-.013	.008	-.007	-.003	-.005		
	15°	C_n'		.004		.008	.009	.010		.010	.008	.008	.006	.009	.007	.009		
	25°	C_l'		-.039		-.038	-.040	-.036		-.034	-.026	-.016	.004	-.010	-.003	-.005		
	25°	C_n'		.011		.019	.020	.021		.020	.015	.015	.012	.015	.012	.014		

TABLE XI

FORCE TEST. 10- BY 60-INCH CLARK Y WING WITH 20° SKEWED AILERONS 40 PER CENT AVERAGE c BY 30 PER CENT $b/2$. YAW=0°. R. N.=609,000. VELOCITY=80 M. P. H.

δ_A up	δ_A down	α	-5°	-3°	0°	4.5°	10°	12°	14°	15°	16°	18°	20°	22°	25°	30°	40°	50°	60°
AILERONS LOCKED—NEUTRAL																			
0°	0°	C_L	0.022	0.164	0.372	0.700	1.069	1.178	1.249	1.247	1.244	1.243	1.164	1.102	0.795	0.838	0.804	0.707	0.589
0°	0°	C_D	.017	.016	.022	.046	.093	.112	.134	.152	.171	.207	.245	.281	.424	.535	.721	.857	1.053
UP ONLY																			
10°		C_l'			0.017		0.016	0.016	0.016		0.013	0.013	0.003	0.004	0.002	0.001	0.000		
10°		C_n'			.000		-.003	-.004	-.004		-.005	-.005	-.005	-.005	-.003	-.003	-.004		
20°		C_l'			.033		.035		.034	.031	.033	.033	.023	.021	.008	.010	.005		
20°		C_n'			.001		-.005		-.007	-.007	-.008	-.010	-.010	-.012	-.007	-.007	-.008		
25°		C_l'			.041		.043	.041	.041		.039	.039	.028	.025	.008	.009	.006		
25°		C_n'			.003		-.004	-.005	-.006		-.008	-.010	-.011	-.012	-.007	-.008	-.009		
30°		C_l'			.049		.051	.051	.050		.050	.050	.041	.037	.015	.015	.012		
30°		C_n'			.006		-.002	-.004	-.006		-.008	-.010	-.012	-.013	-.009	-.010	-.011		
35°		C_l'			.053		.059	.059	.057		.056	.055	.043	.040	.015	.016	.014		
35°		C_n'			.008		-.002	-.003	-.005		-.007	-.010	-.011	-.013	-.009	-.010	-.012		
40°		C_l'			.058		.067	.066	.066		.066	.066	.057	.049	.023	.021	.020		
40°		C_n'			.011		.001	-.002	-.003		-.006	-.008	-.011	-.012	-.010	-.010	-.014		
50°		C_l'			.069		.079	.078	.078		.077	.077	.062	.054	.030	.024	.026		
50°		C_n'			.017		.006	.004	.001		-.002	-.004	-.006	-.008	-.007	-.008	-.013		
60°		C_l'			.070		.087	.087	.088		.087	.087	.070	.061	.036	.029	.024		
60°		C_n'			.020		.013	.010	.008		.005	.002	.000	-.002	-.002	-.004	-.011		
80°		C_l'																	
80°		C_n'																	
DOWN ONLY																			
	7°	C_l'			-.011		-.008	-.009	-.009		-.009	-.008	-.001	0.000	0.002	0.001	0.000		
	7°	C_n'			.002		.004	.004	.005		.005	.006	.006	.005	.004	.004	.004		
	8½°	C_l'			-.013		-.011	-.012	-.011		-.008	-.011	-.009	.000	.001	.001	-.001		
	8½°	C_n'			.003		.004	.005	.006		.006	.007	.006	.005	.004	.003	.004		
	10°	C_l'			-.015		-.013	-.014	-.014		-.012	-.001	-.003	.000	.002	.002	.000		
	10°	C_n'			.003		.006	.006	.007		.007	.008	.007	.006	.004	.004	.004		
	11½°	C_l'			-.016		-.016	-.017	-.016		-.015	-.002	.000	.001	.002	.002	.000		
	11½°	C_n'			.003		.006	.007	.008		.009	.009	.008	.006	.004	.005	.005		
	12°	C_l'			-.018		-.017	-.018	-.017		-.015	-.003	-.004	.001	.002	.002	.000		
	12°	C_n'			.004		.007	.007	.009		.009	.009	.008	.006	.005	.005	.005		
	13°	C_l'			-.019		-.020	-.021	-.019		-.016	-.004	.004	.001	.003	.002	-.001		
	13°	C_n'			.004		.008	.009	.009		.010	.010	.009	.007	.005	.005	.006		
	14°	C_l'			-.020		-.020	-.021	-.020		-.016	-.004	-.003	.001	.002	.002	.000		
	14°	C_n'			.004		.008	.009	.010		.011	.011	.009	.007	.005	.005	.007		
	15°	C_l'			-.022		-.023	-.023	-.022		-.018	-.005	-.003	.002	.002	.003	.000		
	15°	C_n'			.005		.009	.010	.011		.012	.012	.010	.007	.006	.006	.007		
	20°	C_l'			-.027		-.028	-.028	-.027		-.022	-.005	-.003	.005	.004	.003	.000		
	20°	C_n'			.007		.013	.014	.015		.016	.015	.012	.009	.007	.008	.010		
	25°	C_l'			-.033		-.032		-.031	-.031	-.026	-.007	.001	.006	.005	.004	.001		
	25°	C_n'			.010		.016		.018	.019	.020	.017	.014	.010	.009	.009	.011		
	30°	C_l'			-.039		-.037	-.037	-.035		-.029	-.018	-.003	.006	.007	.007	.002		
	30°	C_n'			.013		.019	.020	.021		.023	.021	.016	.012	.011	.012	.015		

TABLE XII

FORCE TEST. 10- BY 60-INCH CLARK Y WING WITH 20° SKEWED AILERONS 40 PER CENT AVERAGE *c* BY PER CENT *b*/2. YAW=−20°. R. N.=609,000. VELOCITY=80 M. P. H.

δ_A up	δ_A down	α	−5°	0°	5°	10°	12°	14°	16°	17°	18°	20°	22°	25°	30°	40°	50°	60°
		AILERONS LOCKED—NEUTRAL																
0°	0°	C_L	0.006	0.326	0.651	0.948	1.048	1.109	1.152	1.168	1.166	1.164	0.953	0.914	0.896	0.819	0.754	0.639
0°	0°	C_D	.018	.022	.044	.080	.097	.115	.137	.152	.172	.220	.350	.423	.526	.692	.881	1.048
0°	0°	C_l'	−.002	−.004	−.005	−.009	−.013	−.019	−.033	−.042	−.055	−.078	−.104	−.105	−.089	−.057	−.048	−.043
0°	0°	C_n'	.001	.001	.002	.005	.006	.009	.012	.013	.014	.017	.025	.041	.049	.044	.048	.055
		UP ONLY																
25°	25°	C_l'		0.037		0.036	0.037	0.036	0.038		0.039	0.047	0.043	0.033	0.016	0.003		
25°	25°	C_n'		.003		−.006	−.007	−.008	−.011		−.012	−.015	−.020	−.025	−.020	−.012		
35°	35°	C_l'		.052		.053	.053	.052	.053		−.055	−.054	−.048	−.038	−.025	−.008		
35°	35°	C_n'		.007		−.004	−.006	−.008	−.011		−.013	−.016	−.025	−.029	−.026	−.016		
50°	50°	C_l'		.071		.077	.076	.078	.080		.079	.082	.072	.065	.046	.018		
50°	50°	C_n'		.019		.003	.001	−.002	−.006		−.009	−.013	−.026	−.031	−.030	−.021		
60°	60°	C_l'		.081		.091	.092	.093	.096		.097	.098	.089	.080	.061	.025		
60°	60°	C_n'		.029		.012	.008	.005	.001		−.003	−.009	−.022	−.029	−.029	−.019		

TABLE XIII

FORCE TEST. 10- BY 60-INCH CLARK Y WING WITH 20° SKEWED AILERONS 40 PER CENT AVERAGE *c* BY PER CENT *b*/2. YAW=20°. R. N.=609,000. VELOCITY=80 M. P. H.

δ_A up	δ_A down	α	−5°	0°	5°	10°	12°	14°	16°	17°	18°	20°	22°	25°	30°	40°	50°	60°
		AILERONS LOCKED—NEUTRAL																
0°	0°	C_L	0.017	0.337	0.663	0.965	1.067	1.136	1.177	1.194	1.185	1.177	0.935	0.903	0.894	0.803	0.744	0.628
0°	0°	C_D	.017	.021	.044	.081	.098	.118	.141	.157	.175	.225	.353	.421	.523	.681	.879	1.042
0°	0°	C_l'	.009	.013	.015	.018	.022	.028	.042	.054	.055	.083	.107	.107	.096	.058	.052	.041
0°	0°	C_n'	−.001	−.002	−.003	−.006	−.008	−.010	−.014	−.015	−.017	−.022	−.031	−.050	−.054	−.046	−.052	−.061
		DOWN ONLY																
	7°	C_l'		−0.010		−0.009	−0.010	−0.010	−0.010		−0.008	−0.005	−0.003	−0.003	−0.001	0.000		
	7°	C_n'		.002		.003	.004	.004	.005		.004	.005	.004	.005	.004	.004		
	15°	C_l'		−.021		−.022	−.023	−.022	−.022		−.019	−.016	−.007	−.007	−.003	−.002		
	15°	C_n'		.004		.009	.010	.011	.011		.010	.010	.008	.010	.008	.009		
	25°	C_l'		−.034		−.036		−.045	−.034		−.032	−.028	−.023	−.009	−.010	−.002	−.002	
	25°	C_n'		.009		.017		.019	.019		.018	.016	.016	.014	.016	.012	.012	

TABLE XIV.—CRITERIONS SHOWING RELATIVE MERITS OF AILERONS

ASSUMED RIGHT AILERON UP AND LEFT AILERON DOWN

Subject	Criterion	Straight ailerons 25 per cent chord by 40 per cent semispan (assumed standard size)				10° skewed ailerons 25 per cent average chord by 40 per cent semispan				20° skewed ailerons 25 per cent average chord by 40 per cent semispan			
		Stand-ard 25° up, 25° down	Differ-ential No. 1 35° up, 15° down	Differ-ential No. 2 50° up, 7° down	Up only 60°	Stand-ard 25° up, 25° down	Differ-ential No. 1 35° up, 15° down	Differ-ential No. 2 50° up, 7° down	Up only 60°	Stand-ard 25° up, 25° down	Differ-ential No. 1 35° up, 15° down	Differ-ential No. 2 50° up, 7° down	Up only 60°
Wing area or minimum speed. Speed range Rate of climb	Maximum C_L ----- Maximum C_L /minimum C_D ----- L/D at $C_L=0.70$ ----- } $\delta_A=0^\circ$	1.270 79.4 15.9	1.270 79.4 15.9	1.270 79.4 15.9	1.270 79.4 15.9	1.278 74.7 15.6	1.278 74.7 15.6	1.278 74.7 15.6	1.278 74.7 15.6	1.253 76.4 15.6	1.253 76.4 15.6	1.253 76.4 15.6	1.253 76.4 15.6
Lateral controllability	$RC \alpha=0^\circ$ ----- $RC \alpha=10^\circ$ ----- $RC \alpha=20^\circ$ ----- $RC \alpha=30^\circ$ -----	.204 .076 .038 .017	.202 .074 .051 .005	.214 .074 .055 .002	.196 .072 .054 .002	.240 .082 .035 .026	.238 .077 .039 .032	.221 .075 .041 .018	.194 .069 .044 .014	.204 .071 .031 .031	.204 .070 .041 .032	.179 .065 .048 .024	.155 .058 .040 .021
Lateral control with side-slip.	Maximum α at which ailerons will balance C_l' due to 20° yaw.	20°	20°	21°	22°	19°	20°	20°	21°	18°	19°	20°	20°
Yawing moments due to ailerons: (+) Favorable; (-) unfavorable.	$C_{n_A} \alpha=0^\circ$ ----- $C_{n_A} \alpha=10^\circ$ ----- $C_{n_A} \alpha=20^\circ$ ----- $C_{n_A} \alpha=30^\circ$ -----	-.007 -.004 -.010 -.008	.002 b-.003 b-.002 b-.007	.010 b-.002 b-.001 b-.006	.016 -.018 -.013 b-.004	-.007 -.005 -.013 -.008	.001 b-.003 a-.002 c-.009	.010 c-.003 b-.001 b-.005	.015 a-.007 -.018 b-.004	-.006 b-.003 -.005 c-.014	.002 b-.003 b-.002 c-.009	.009 b-.003 b-.002 c-.009	.013 a-.001 -.017 a-.001 -.014 -.008 b-.003
Lateral stability ($\delta_A=0^\circ$)	α for initial instability in rolling ----- α for initial instability at $p'b/2V=0.05$: Yaw=0° ----- Ditto: Yaw=20° ----- Maximum unstable C_{n_A} at $p'b/2V=0.05$: Yaw=0° ----- Ditto: Yaw=20° -----	18° 17° 11° .048 .093	18° 17° 11° .048 .093	18° 17° 11° .048 .093	18° 17° 11° .048 .093								

Subject	Criterion	Straight ailerons 40 per cent chord by 30 per cent semispan				10° skewed ailerons 40 per cent average chord by 30 per cent semispan				20° skewed ailerons 40 per cent average chord by 30 per cent semispan			
		Stand-ard 25° up, 25° down	Differ-ential No. 1 35° up, 15° down	Differ-ential No. 2 50° up, 7° down	Up only 60°	Stand-ard 25° up, 25° down	Differ-ential No. 1 35° up, 15° down	Differ-ential No. 2 50° up, 7° down	Up only 60°	Stand-ard 25° up, 25° down	Differ-ential No. 1 35° up, 15° down	Differ-ential No. 2 50° up, 7° down	Up only 60°
Wing area or minimum speed. Speed range Rate of climb	Maximum C_L ----- Maximum C_L /minimum C_D ----- L/D at $C_L=0.70$ ----- } $\delta_A=0^\circ$	1.258 78.5 15.9	1.258 78.5 15.9	1.258 78.5 15.9	1.258 78.5 15.9	1.260 80.3 16.3	1.260 80.3 16.3	1.260 80.3 16.3	1.260 80.3 16.3	1.249 78.5 15.2	1.249 78.5 15.2	1.249 78.5 15.2	1.249 78.5 15.2
Lateral controllability	$RC \alpha=0^\circ$ ----- $RC \alpha=10^\circ$ ----- $RC \alpha=20^\circ$ ----- $RC \alpha=30^\circ$ -----	.226 .078 .046 .019	.234 .084 .058 .025	.226 .083 .073 .026	.202 .076 b.074 .022	.229 .078 .037 .011	.220 .082 .053 .024	.216 .085 .064 .024	.197 .078 .064 .028	.199 .072 .029 .016	.200 .077 .044 .023	.214 .080 .054 .030	.187 .078 .057 .032
Lateral control with side-slip.	Maximum α at which ailerons will balance C_l' due to 20° yaw.	19°	20°	22°	25°	19°	20°	21°	22°	19°	19°	20°	21°
Yawing moments due to ailerons: (+) Favorable; (-) unfavorable.	$C_{n_A} \alpha=0^\circ$ ----- $C_{n_A} \alpha=10^\circ$ ----- $C_{n_A} \alpha=20^\circ$ ----- $C_{n_A} \alpha=30^\circ$ -----	-.007 -.006 -.007 -.010	.005 b-.002 b-.003 b-.008	.016 a-.001 a-.002 b-.007	.021 -.026 -.029 a-.003	-.008 -.006 -.013 -.013	.004 b-.003 b-.002 b-.009	.014 b-.003 b-.002 b-.008	.021 a-.001 -.028 a-.004	-.006 b-.003 -.006 c-.014	.003 b-.003 b-.003 c-.009	.014 b-.003 a-.003 b-.009	.020 a-.001 -.028 a-.004 -.010 a-.004 -.010 a-.002
Lateral stability ($\delta_A=0^\circ$)	α for initial instability in rolling ----- α for initial instability at $p'b/2V=0.05$: Yaw=0° ----- Ditto: Yaw=20° ----- Maximum unstable C_{n_A} at $p'b/2V=0.05$: Yaw=0° ----- Ditto: Yaw=20° -----	18° 17° 12° .022 .085	18° 17° 12° .022 .085	18° 17° 12° .022 .085	18° 17° 12° .022 .085								

a to f Where the maximum yawing moment occurred below maximum deflection, the letters indicate the deflection of the up aileron as follows: a=10°, b=15°, c=20°, d=25°, e=30°, f=40°.

* RC has a minimum value of 0.066 at $\alpha=17^\circ$ and a maximum of 0.074 at $\alpha=22^\circ$.

^ RC=0.064 at $\alpha=17^\circ$ and 0.094 at $\alpha=22^\circ$.

REPORT No. 445

WORKING CHARTS FOR THE DETERMINATION OF THE LIFT DISTRIBUTION BETWEEN BIPLANE WINGS

By PAUL KUHN

SUMMARY

In this report are presented empirical working charts from which the distribution of lift between wings; viz, the fraction of the total lift borne by each, can be determined in the positive lift range for any ordinary biplane cellule whose individual wings have the same profile. The variables taken directly into account include airfoil section, stagger, gap/chord ratio, decalage, chord ratio, and overhang. It is shown that the influence of unequal sweep-back and unequal dihedral in upper and lower wings may be properly provided for by utilizing the concepts of average stagger and average gap/chord ratio, respectively. The effect of other variables is discussed, but they have not been included in the charts either because their influence was obviously small or because insufficient data existed to make possible a complete determination of their influence. All available pertinent biplane data were analyzed in establishing the charts, and in some cases theoretical relationships were utilized to establish qualitative tendencies.

INTRODUCTION

The importance of the knowledge of lift distribution is too well known to require much comment. If the structural design of airplanes is to be improved by using methods of stress analysis more refined than those now in use, the applied loads must be known to a higher degree of accuracy.

The determination of the lift distribution between biplane wings is only one phase of the problem of applied loads that has not been satisfactorily solved. The reason lies largely in the absence of a satisfactory biplane theory and in the absence of sufficiently extensive coordinated test data. For instance, the method of determining the lift distribution between biplane wings now recommended by the Department of Commerce (reference 1), is based exclusively on tests of the R. A. F. 15 airfoil, whereas there is considerable evidence that the lift distribution changes with the airfoil section. Furthermore, the recommended rules for determining the effect of overhang and unequal chords are based on inadequate assumptions. Rules in use by the Army and Navy at the time of writing are even more sketchy and incomplete than those in use by the Department of Commerce.

For the above reasons, an analysis of all available biplane test data has been made at the request of the Aeronautics Branch, Department of Commerce, with a view toward further refinement of the method for determining the lift distribution between biplane wings. The present report gives the results of the analysis.

The results are summarized and condensed into working charts from which the lift distribution may be obtained in the positive lift range for any ordinary biplane whose upper and lower wings have the same airfoil section. If C_{L_u} , C_{L_l} , and C_{L_b} denote the lift coefficients, respectively, for the upper wing, lower wing, and their biplane combination, each coefficient can be determined from the other two. In this report the lift distribution is arbitrarily characterized by the ratio $C_{L_u}/C_{L_b} \equiv R$, and is given as a function of the following variables: Stagger, gap/chord ratio, decalage, chord ratio, overhang, and airfoil section. Other variables, such as tip shape, aspect ratio, dihedral, fuselage interference, and scale effect were neglected either because their influence was obviously small or because insufficient data were available to take them properly into account.

METHOD OF PROCEDURE

The procedure followed in arriving at the working charts involved: (1) An examination of available test data bearing on the problem, in which certain of the data were selected as a basis; (2) a comparison of the selected test data with biplane theories; (3) a selection of the most important variables to be included in the charts; and (4) construction of the charts, which were finally based largely on the test data, although certain qualitative relationships were established by the theory.

Test data.—A complete list of references to the test data used in the analysis is given at the end of the report. The test data consist of results from pressure-distribution and force measurements. It was found, where comparable results were available, that the pressure-distribution data were only slightly inferior in accuracy to the force data. Both kinds of data were therefore used.

Comparison of test data from different sources showing the effect of a given variable indicated, in general, a

reasonably good agreement. There were, however, three exceptions—the tests reported in references 2, 3, and 4. Reference 2 presents the results of tests on biplanes composed of R. A. F. 6c airfoils. Because the R. A. F. 6c airfoil is now obsolete and because these tests were made before the technic of wind-tunnel testing was well advanced, reference 2 was discarded.

Reference 3 presents the results of extensive tests with the R. A. F. 19 airfoil. This airfoil, although only moderately thick, has an excessive camber and is known to be subject to large scale effects. For that reason, and also because such abnormal airfoils are not commonly used, the results of reference 3 were given no consideration in the analysis.

The results given in reference 4 show a bad scattering in some respects, and the tests were made in such a manner that it is difficult to compare the results with any others. Reference 4 was therefore not used.

Biplane theories.—Although theories of the biplane are plentiful, only Millikan's theory (reference 5) was used, as it is the most complete. This theory was found to be much superior to the older theories, but it was not found to check the experimental data sufficiently well in all cases to serve as a basis for the quantitative determination of the lift distribution. In view of its complexity, attempts to introduce empirical correction factors were considered inadvisable. The theory was therefore used only in certain cases to establish qualitative trends where insufficient data were available to accomplish that result. When adequate data were at hand, the results of calculation by Millikan's theory were not used.

The variables of the problem.—Although the ultimate object of this analysis was to establish a basis for the determination of the lift distribution between the wings of actual biplanes, an insufficient number of tests in which the influence of such factors as the fuselage and slipstream was present were available to permit such a result. By far the most of the data available were obtained from tests on wind-tunnel models in which the fuselage and propeller were absent. For this reason, the problem was considered from two points of view: First, that of the cellule (which is defined here as the combination of two superposed or approximately superposed wings without fuselage); and second, that of the biplane (which is here defined as the cellule plus appurtenances, such as the fuselage, that make up the complete airplane).

Analysis of the data indicated that the distribution of lift between the wings of a cellule is appreciably affected by the following variables: Decalage, stagger, gap/chord ratio, airfoil section, overhang, and chord ratio. Of minor importance are unequal sweepback and unequal dihedral in upper and lower wings. These factors can be dealt with by using an average stagger and average gap/chord ratio, respectively. The influence of tip shape, equal dihedral in both wings, and equal sweepback in both wings is assumed

to be negligible. Aspect ratio is probably of small importance within its usual practical limits, and it has also been assumed to be of negligible importance. In unusual designs involving very small aspect ratios, special consideration may, however, be necessary.

The charts.—The charts include the variables listed in the preceding paragraph as having an appreciable influence on the lift distribution. They are arranged in sequence as follows: First, a basic chart (fig. 19, Appendix) which gives R against C_{Lb} for cellules having gap/chord and chord ratios of 1, no overhang, and no decalage; second, a chart (fig. 20, Appendix) giving correction factors for gap/chord ratios other than 1; third, a chart (fig. 21, Appendix) giving correction factors for decalage other than zero; and fourth, a chart (fig. 22, Appendix) giving correction factors for overhang. These factors are to be multiplied by or added to the basic curves to correct for gap/chord ratio, decalage, and overhang, as discussed in the report and detailed in the Appendix. No chart is given for chord ratios other than 1, but means for taking them into account are indicated. The above arrangement and content of the charts are somewhat arbitrary, but they appeared to be logical after an inspection of the data. A discussion of the derivation of these charts in the light of the test data and Millikan's theory follows.

DISCUSSION OF CELLULE DATA AND DERIVATION OF THE CHARTS

The basic chart.—Figure 1 shows a series of experimental R curves for two sets of cellules with gap/chord ratio of 1 having 0° stagger and 30° stagger with different airfoil sections. Comparison of the curves, particularly for 30° stagger, shows that the lift distribution may be taken as a function of the sum of mean camber and thickness, where the mean camber is the camber of the mean line and is measured from the chord subtending the mean line.

An explanation is necessary regarding the Clark Y points. The R curve derived from the tests of reference 6 was found to be somewhat out of place on the camber-thickness scale. This discrepancy was believed to be due to the fact that the individual airfoils used in the cellule had different monoplane characteristics on account of slight differences in the ordinates of the two airfoils. (See reference 5.) Millikan's theory was therefore used in this case. Its validity for the purpose was first established by comparing the experimental Clark Y results with the theoretical R values that were computed using the monoplane characteristics of the experimental airfoils. A close agreement was found up to a biplane lift coefficient of 0.9. This agreement was considered evidence that the theory was correct in this case. Two R values for the Clark Y were therefore recomputed on the basis of monoplane characteristics obtained on an accurate model in the variable-density tunnel (reference 7), and

these values were used to represent the Clark Y cellule with 30° stagger in Figure 1.

Figure 2 shows the experimental points for two airfoils at 0°, 15°, and 30° stagger. The curves shown for 0° and 30° are taken directly from the basic chart. The curves for 15° were obtained from the basic chart by straight-line interpolation between the curves for 0° and 30°, i. e., by halving the difference in ordinates; it is therefore apparent that straight-line interpolation for stagger is sufficiently accurate. This conclusion is supported by other test data.

The same figure shows a number of points obtained by using the present design rules. (Reference 1.) They show the errors that are due to basing rules on R. A. F. 15 tests only.

It will be seen in Figure 1 that at 0° stagger the value of R does not appear to be a clearly defined function of the sum of camber and thickness as in the case of 30° stagger. However, the total variation in R for different airfoils at 0° stagger is considerably smaller than at 30° stagger, so that errors involved by assuming that R is still a function of this sum are hardly larger than the experimental errors.

At negative stagger there are very few data (references 6 and 8) other than R. A. F. 15 data in existence. They indicate that at low and medium biplane lift coefficients a single curve adequately represents the tests, and that the difference in airfoil section makes itself felt only near the stalling point.

The basic chart was therefore drawn up (see Appendix, fig. 19), giving the lift-distribution curves for equal span, equal chord cellules with gap/chord ratio of 1 and without decalage as functions of the sum of camber and thickness for staggers of -30°, 0°, and 30°. The chart is based on test results given in reference 6 and references 8 to 16, inclusive.

The gap/chord factor chart.—In Figure 3 three sets of R curves are shown for airfoils at different gap/chord ratios. They suggest the possibility of obtaining the R curves for gap/chord ratios other than 1 by multiplying the R curves of the basic chart by correction factors that depend on the biplane lift coefficient and on the stagger. On the basis of all applicable test data (references 6, 8, and 14), correction-factor curves were derived for a gap/chord ratio of 0.75. These curves are shown in Figure 20. (See Appendix.) It was found that for a stagger of 30° straight lines served the purpose. For 0° it was found necessary to replace the straight lines at lower lift coefficients by curves.

On account of lack of data the factors for -30° stagger were obtained by symmetrical inversion from the factors for 30°. There is no theoretical justification for this procedure, but the resulting factors are well confirmed by test data for the R. A. F. 15 airfoil at two gap/chord ratios. The only applicable test data available for a thick airfoil (fig. 4) do not show more than a fair agreement with the derived factors,

but there is not sufficient information available to attempt refinement of the procedure.

For gap/chord ratios between 1 and 0.75 the gap/chord factors may be obtained by straight-line interpolation. A word of caution is necessary here regarding extrapolation of the gap/chord factor chart. The Göttingen 133 airfoil, with a camber-thickness sum of 12.85 at a gap/chord ratio of 0.67 and 37° stagger, which represents extrapolation both for stagger and gap/chord ratio, shows fair agreement (fig. 8, decalage=0°), but the Clark Y with a camber-thickness sum of 15.4 at a gap/chord ratio of 0.5 shows a large discrepancy at 0° stagger (not illustrated). Consequently, extrapolation to gap/chord ratios below approximately 0.65 is hazardous, particularly for airfoils with a camber-thickness sum of 13.0 or more.

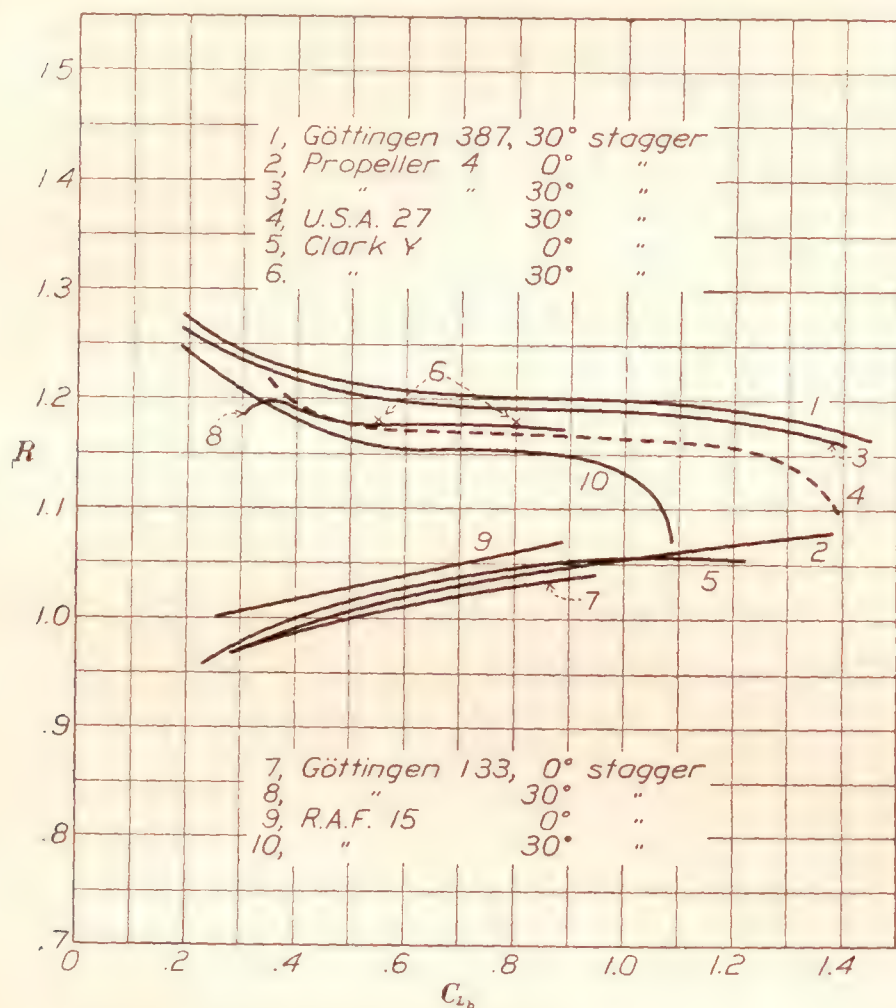
If it be assumed that for a gap/chord ratio of 3 the biplane interference has disappeared, then $R=1$ for this gap/chord ratio and larger ones. This result may be used to obtain R curves for gap/chord ratios larger than 1 by interpolating lineally between the R curve for a gap/chord ratio of 1 (and for the given stagger) and between the R curve for the gap/chord ratio of 3, which is $R=1$ regardless of stagger. The R curves obtained by this method of interpolation agree reasonably well with the test data.

Figure 4 shows experimental points and R curves derived from the charts for the U. S. A. T. S. 5 at 0°, 30°, and -30° stagger and at a gap/chord ratio of 0.9. Figure 5 similarly compares the experimental points and R curves from the charts for the Clark Y at three values of stagger and at a gap/chord ratio of 0.75. The relatively large disagreement at 33¼° stagger may be attributed, in part, to the differences between the upper and lower wings of the Clark Y cellule mentioned in the discussion of the basic chart.

The decalage-factor chart.—Figures 6, 7, and 8 show the results of some tests on cellules with varying amounts of decalage. From these and similar tests (reference 6, 9, and 14), decalage-factor curves have been derived (see Appendix, fig. 21) in a manner similar to that by which the gap/chord factor curves were obtained. The decalage-factor curves are not, however, straight lines. The decalage factors are seen to depend on the gap/chord ratio and the stagger, but not on the airfoil section. No test results are available at negative stagger, so no curves could be given for this case.

In Figure 8 the discrepancy between the experimental points and the R curves determined by using the charts is larger than in the cases shown in Figures 6 and 7. Examination of the figure shows, however, that the discrepancies are systematic and are due to the fact that the basic curve for 0° decalage is too high at low and medium lift coefficients. It should be pointed out, too, that the basic curve for this case was extrapolated from the charts both for stagger and gap/chord ratio.

When dealing with the influence of gap/chord ratio it was assumed that R is always 1 for a gap/chord ratio of 3. If there is no biplane interference, R depends on the ratio of the angles of attack of upper wing and cellule (average of upper and lower) and on the slope of the monoplane lift curve. Assuming for the latter an average value of 0.075, it was possible to draw the decalage-factor curve for a gap/chord ratio of 3 (any stagger) which can be used to obtain factors for gap/chord ratios larger than 1 by straight-line interpolation. This relation is expressed by curve 5, Figure 21.



Airfoil.....	{ Göttingen 387	Propeller 4	U. S. A. 27	Clark Y	Göttingen 133	R. A. F. 15
Maximum mean camber, per cent chord.....	5.9	5.7	5.4	3.8	4.6	2.6
Maximum thickness, per cent chord.....	15.1	12.7	11.0	11.7	8.1	6.4
Gap/chord ratio.....	1.0	1.0	1.0	1.0	1.0	1.0
Chord ratio.....	1.0	1.0	1.0	1.0	1.0	1.0
Decalage, degree.....	0	0	0	0	0	0
Percentage overhang.....	0	0	0	0	0	0
Reference.....	13	13	13	5, 6	14	8, 10, 11, 12

FIGURE 1.—Experimental lift-distribution curves for biplane cellules

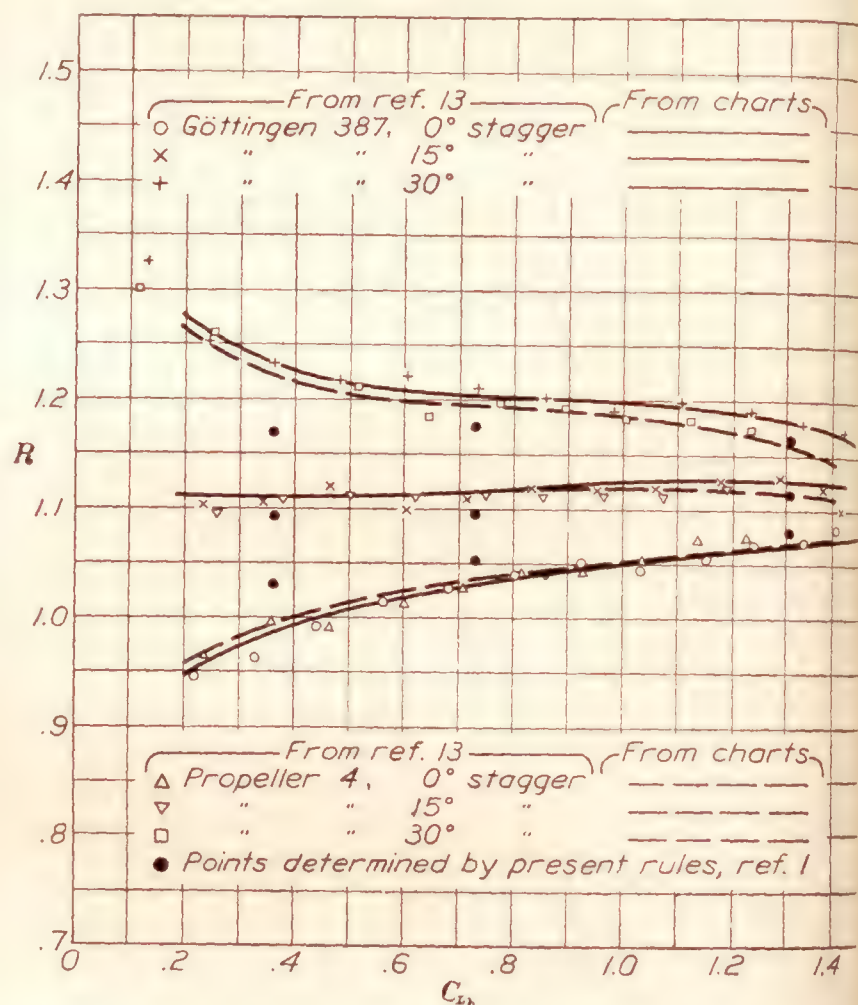
The overhang-factor chart.—Comparison of the experimental curves for the Clark Y with varying overhang (fig. 9) shows that except possibly for very low lift coefficients, the effect of overhang is to shift the R curve vertically by amounts proportional to the percentage of overhang, where percentage of overhang

is defined as $\frac{\text{upper span} - \text{lower span}}{\text{upper span}} \times 100$. At first

glance this does not seem to hold for negative overhang at low lift coefficients. There is, however, a possibility that an error of $\frac{3}{4}^\circ$ decalage may have existed in the test set-up which would account for the apparent

discrepancy between the results at positive and negative overhang. For this reason it was assumed that in all cases the change in R is proportional to the amount of overhang. Figure 22 (see Appendix) shows the derived overhang factors.

It will be noticed that Figure 22 requires the overhang factor to be multiplied by the chord ratio. This rule is based on the consideration that the effect of overhang is due chiefly to a change in aspect ratio of one of the wings. If one wing has a smaller chord and consequently a larger aspect ratio, the effect caused by



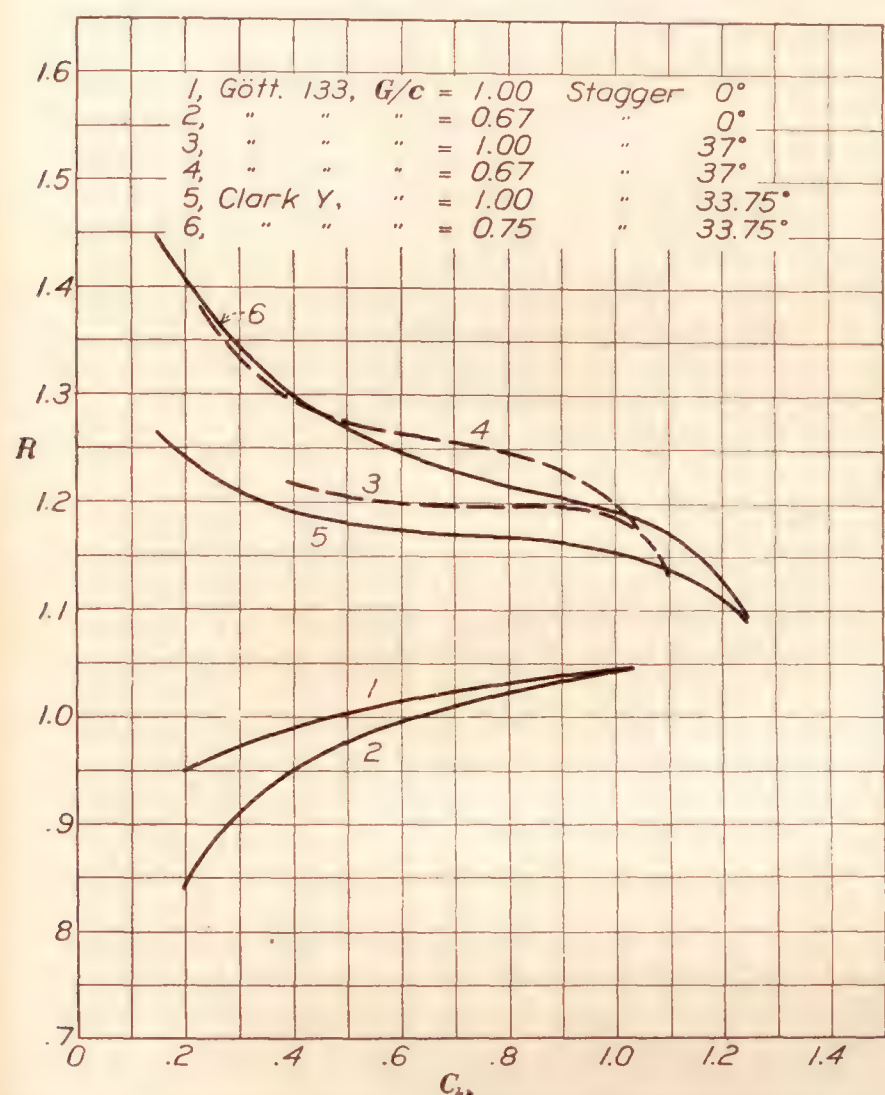
Airfoil.....	{ Göttingen 387	Propeller 4
Maximum mean camber, per cent chord.....	5.9	
Maximum thickness per cent chord.....	15.1	
Gap/chord ratio.....	1.0	
Chord ratio.....	1.0	
Decalage, degree.....	0	
Percentage overhang.....	0	
Reference.....	13	

FIGURE 2.—Lift distribution in cellules with Göttingen 387 and Propeller 4 airfoils

changing its aspect ratio will be less. The variation of the overhang factor with stagger is based on simple aerodynamical considerations and is at least partly substantiated by test data. (Fig. 10.)

The influence of chord ratio.—If an equal-chord cellule be compared with a cellule having the lower chord smaller than the upper (assuming the upper wing to be the same in both cases), a qualitative consideration of the changes indicates that the ratio R of the unequal-chord cellule will be nearer 1 than in the equal-chord cellule. The same effect is produced by increasing the gap/chord ratio of the equal-chord cellule. It seems possible, therefore, to treat the unequal-chord case by introducing an effective gap/chord ratio

At the same time, however, the question of stagger must be considered. The stagger has been measured in the past at the leading edges, the quarter-chord points, the one-third chord points, and the half chord points. Some of these points were chosen merely for convenience, others with some aerodynamical reasoning. Examination of the curves from references 17 and 18 (fig. 10) suggested that the stagger should be measured at points even farther back. The three-quarter chord points were chosen as convenient reference points. When this was done and when an effective gap/chord



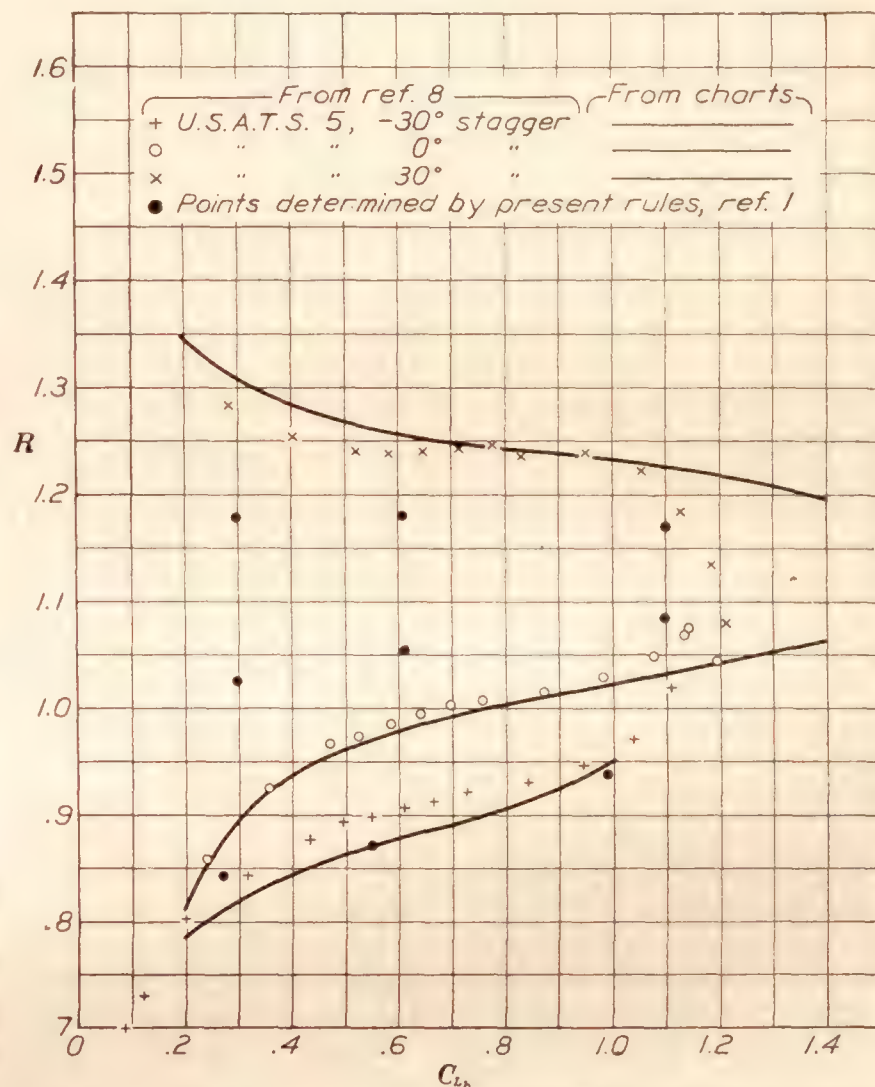
Airfoil.....	Göttingen 133	Clark Y
Maximum mean camber, per cent chord.....	4.6	3.8
Maximum thickness, per cent chord.....	8.1	11.7
Chord ratio.....	1.0	1.0
Decalage, degree.....	0	0
Percentage overhang.....	0	0
Reference.....	14	6

FIGURE 3.—Change in lift-distribution curves due to change in gap/chord ratio

ratio based on the actual gap and the lower chord was used, the charts were found to check the few test results available. (Fig. 10 and fig. 11, decalage = 0°, taken from references 17, 18, 19, and 20.)

In the absence of test data at larger staggers, basic curves were calculated by the Millikan theory; from these R curves were obtained for certain unequal-chord biplanes with a chord ratio of 2 by interpolation. These curves are shown in Figure 12. The same unequal-chord biplanes were then computed directly, also by means of Millikan's theory; the results are shown by the symbols on the figure and are seen to check the curves quite well.

The same procedure was followed with biplanes having a chord ratio of 1:2 inasmuch as there were no test data available for cells in which the lower wing had the larger chord. The results, also shown in Figure 12, are seen to check well at negative stagger, but not quite so well at large positive stagger. Because the degree of accuracy of the theory is uncertain, these calculations can serve only as weak evidence, but they tend to strengthen the conviction that the proposed method of measuring an effective stagger and an effective



Airfoil.....	U. S. A. T. S. 5
Maximum mean camber, per cent chord.....	5.4
Maximum thickness, per cent chord.....	17.5
Gap/chord ratio.....	.9
Chord ratio.....	1.0
Decalage, degree.....	0
Percentage overhang.....	0
Reference.....	8

FIGURE 4.—Comparison of experimental points with curves from charts for U. S. A. T. S. 5 airfoil

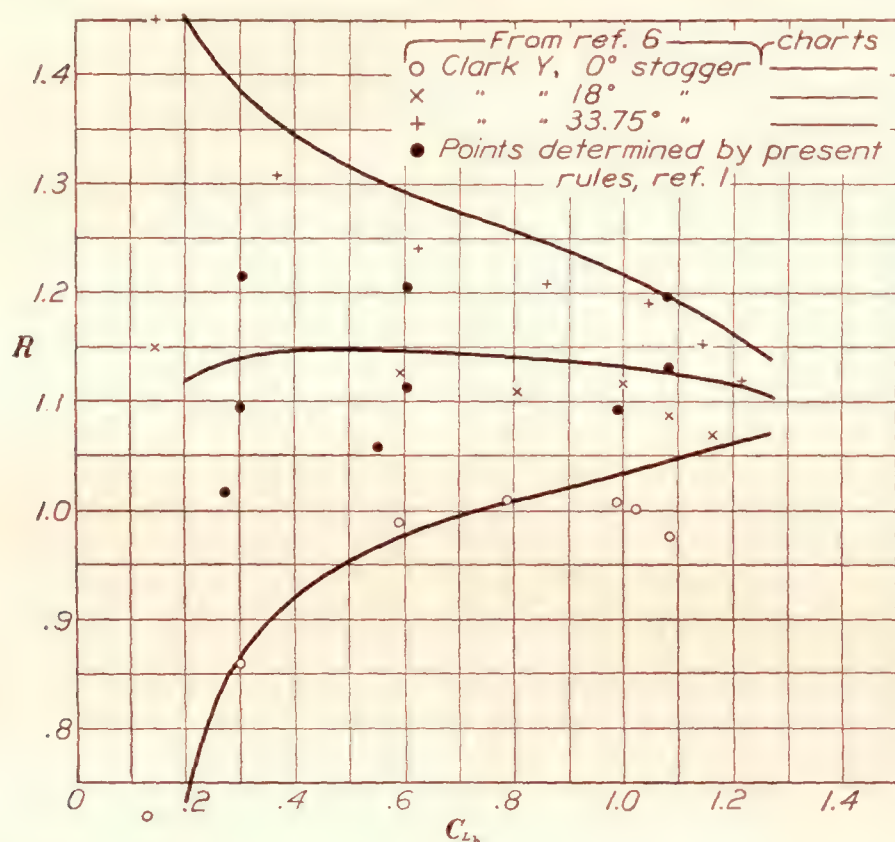
tive gap/chord ratio gives a fair approximation for the lift distribution.

Minor factors.—As has been stated before, the influence of equal dihedral and sweepback on both wings can probably be entirely neglected. For the case of unequal dihedral, the lift distribution can be obtained, with small error, by assuming no dihedral and measuring the gap at a section including the centroid of the semicellule. For practical purposes, any convenient section may be used for measuring the gap, since the differences in the lift distribution with slight changes in gap are very small at normal gap/chord ratios.

Unequal sweepback can be taken into account by measuring the stagger at the centroid of the semicellule. Experimental evidence of the validity of this procedure is shown in Figure 13.

The influence of tip shape is probably negligible, as indicated by the fact that almost all the data were consistent even though they represent airfoils with square tips, semicircular tips, and raked tips.

The influence of increasing the aspect ratio above 6 up to the practical limit probably has not much influence on the lift distribution. One test at aspect ratio 5.6 (reference 21) shows no variation from the others, but it is probable that for aspect ratios below



Airfoil.....	Clark Y
Maximum mean camber, per cent chord.....	3.8
Maximum thickness, per cent chord.....	11.7
Gap/chord ratio.....	.75
Chord ratio.....	1.0
Decalage, degree.....	0
Percentage overhang.....	0
Reference.....	6

FIGURE 5.—Comparison of experimental points with curves from chart for Clark Y airfoil

this there will be a rapidly increasing influence. However, such cases are rare.

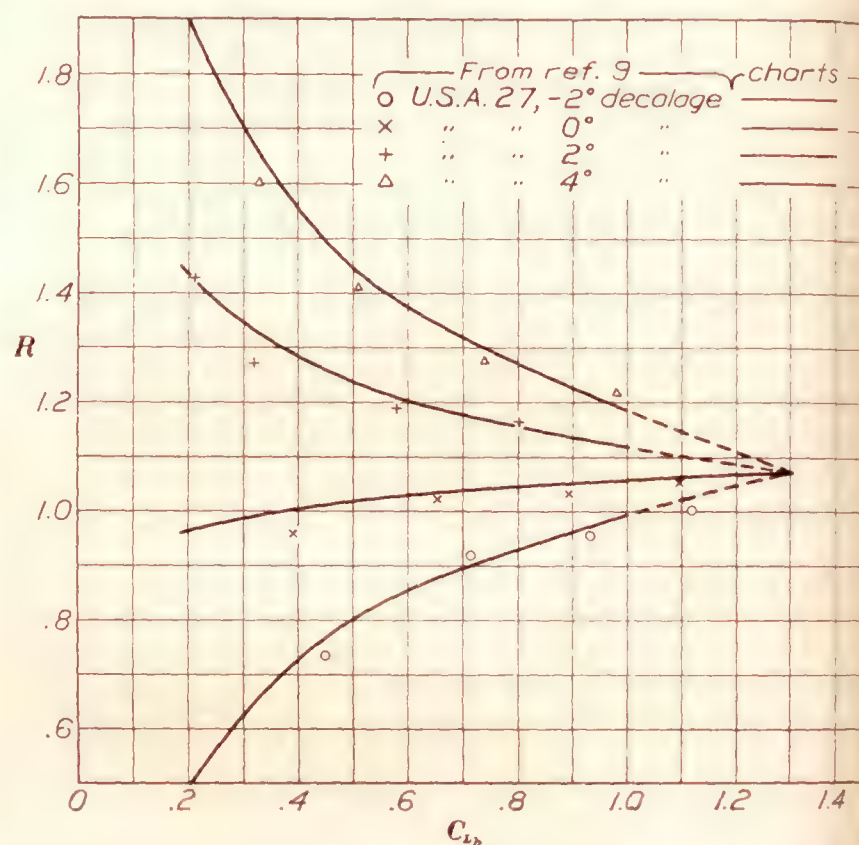
PRECISION OF THE CHARTS

It must be borne in mind that the charts are based on tests of airfoils having a flat lower surface or only a moderate degree of lower camber. They should therefore be used only for such airfoils. As a matter of interest, curves are shown for a widely different type of airfoil. (Fig. 14.)

Between $C_{Lb}=0.3$ and approximately 90 to 95 per cent C_{Lmax} the deviation of experimental points from the R curves of the working charts is generally less than 0.03 except in cases involving decalage. Below $C_{Lb}=0.3$ the error increases rapidly and at $C_{Lb}=0.2$ is

in a number of cases about 0.10. At $C_{Lb}=0.2$, however, an error in decalage of 0.2° in the test set-up will cause an error in R of about 0.05. Since 0.2° was about the limit of accuracy of the decalage setting in most of the wind-tunnel tests forming the basis of this analysis and since decalage is not the only source of error, discrepancies of 0.10 between the R curves and experimental data at $C_{Lb}=0.2$ are not surprising. Below $C_{Lb}=0.2$ the test results scatter so badly that the curves were discontinued at this point.

As the burbling point depends on the Reynolds Number and other factors besides the airfoil, the R curves are unreliable near this point. They should



Airfoil.....	U. S. A. 27
Maximum mean camber, per cent chord.....	
Maximum thickness, per cent chord.....	
Gap/chord ratio.....	
Chord ratio.....	
Stagger, degree.....	
Percentage overhang.....	
Reference.....	

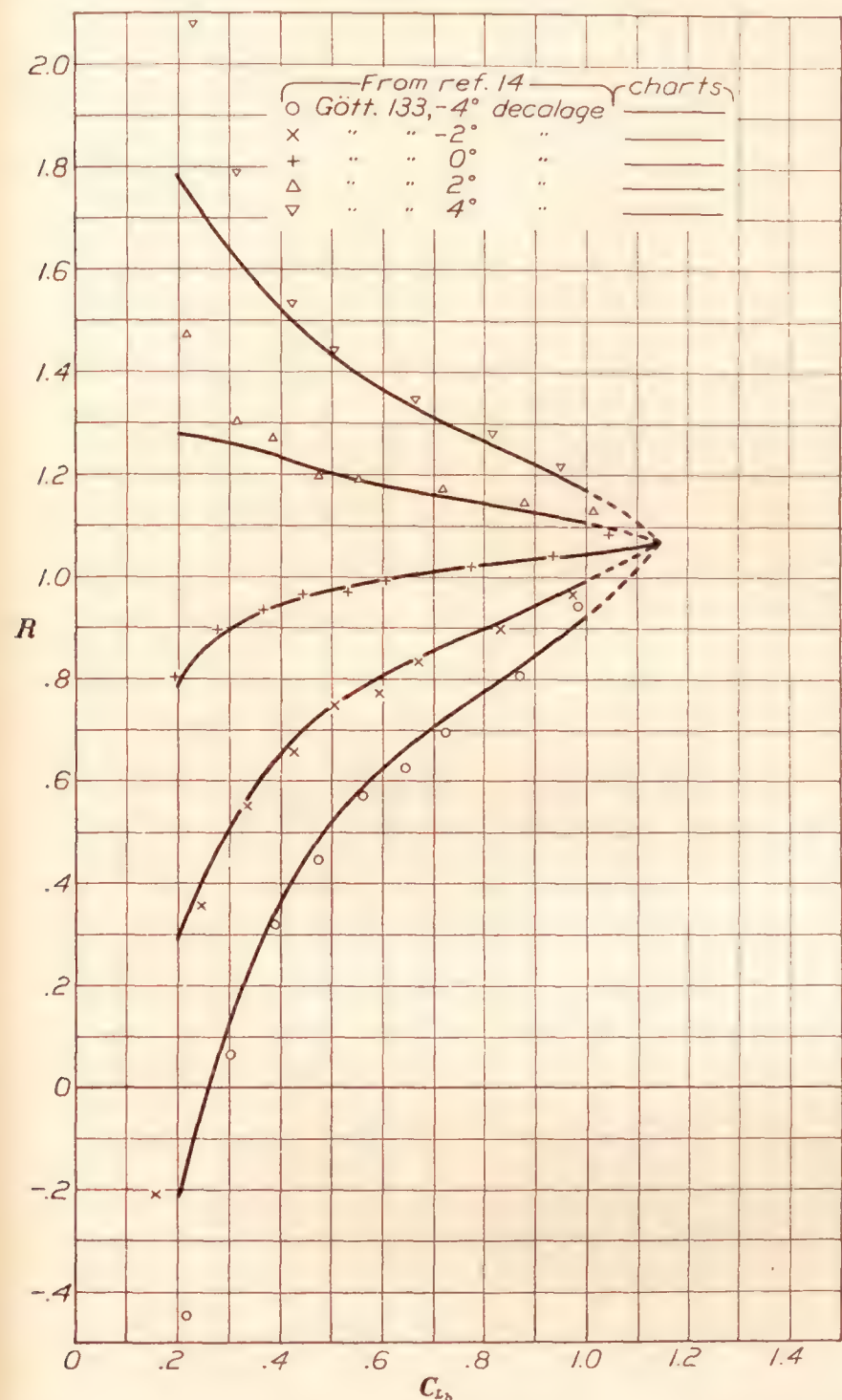
FIGURE 6.—Effect of decalage on U. S. A. 27 airfoil

not be relied on above 90 per cent C_{Lmax} where C_{Lmax} taken, if possible, from wind-tunnel tests on a comparable biplane combination. If such tests are unavailable, the termination of the curves may be used as a rough indication of the burbling point. The U. S. A. T. S. 5 burbled considerably sooner than the chart would indicate (fig. 4), but for most tests the curves gave a good approximation practically up to the experimental burbling point.

The accuracy of curves obtained by means of the decalage factors is somewhat lower than the general accuracy of the curves involving no decalage. The maximum deviation of experimental points may be taken as about 0.05 for decalage up to 6° and between $C_{Lb}=0.3$ and $0.95 C_{Lmax}$.

APPLICATION OF THE CHARTS TO COMPLETE BIPLANES

The model biplane.—Aerodynamic investigators have realized that it is important to test not only component parts of the airplane, but also the complete assembly, since interference effects may be very large. Numerous tests of this type have been made for other



Airfoil.....	{Göttingen 133
Maximum mean camber, per cent chord.....	4.6
Maximum thickness, per cent chord.....	8.1
Gap/chord ratio.....	.67
Chord ratio.....	1.0
Stagger, degree.....	0
Percentage overhang.....	0
Reference.....	14

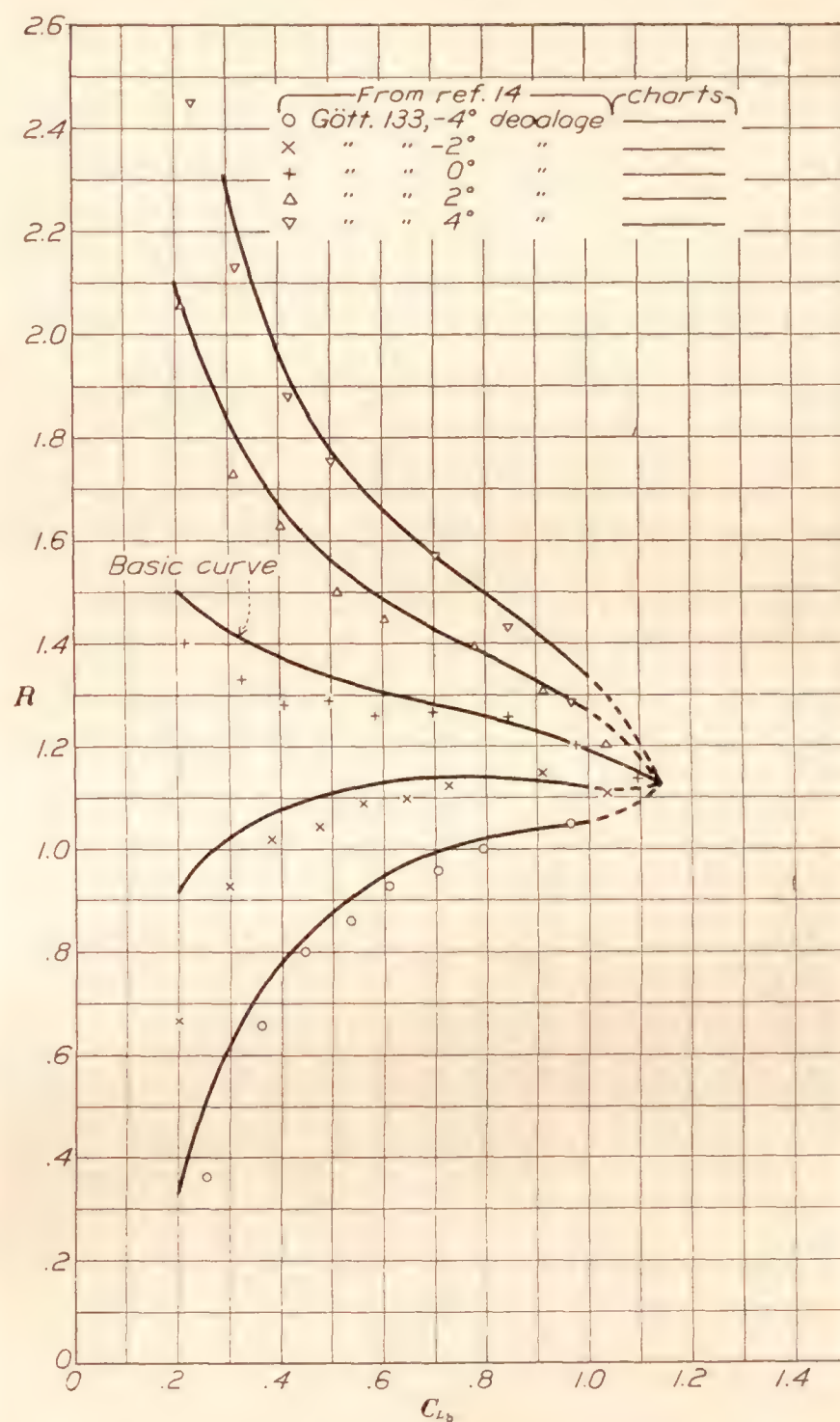
FIGURE 7.—Effect of decalage on Göttingen 133 airfoil

purposes, but only a single test is available where the complete model with fuselage was tested to obtain the loads on the upper and the lower wing separately.

This test, reported in reference 22, shows a very considerable influence of the fuselage. (Fig. 15.) The value of R is approximately 14 per cent higher than predicted from the chart. The span-load curves for the lower wing in this case show a very marked

falling off toward the center line of the airplane. This effect is probably somewhat larger than would ordinarily be expected because a rather large opening existed between the root of the wing and the fuselage.

Tests on the influence of a fuselage on the wings of a low-wing monoplane (reference 23) have shown that even without such a gap at the root of the wing, a

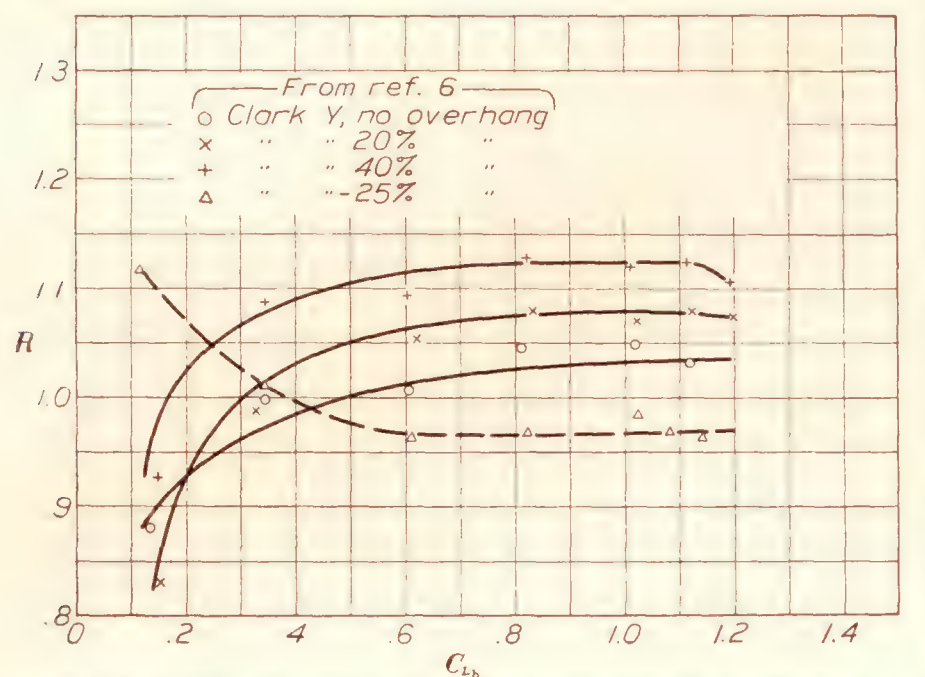


Airfoil.....	{Göttingen 133
Maximum mean camber, per cent chord.....	4.6
Maximum thickness, per cent chord.....	8.1
Gap/chord ratio.....	.67
Chord ratio.....	1.0
Stagger, degrees.....	37
Percentage overhang.....	0
Reference.....	14

FIGURE 8.—Effect of decalage on Göttingen 133 airfoil

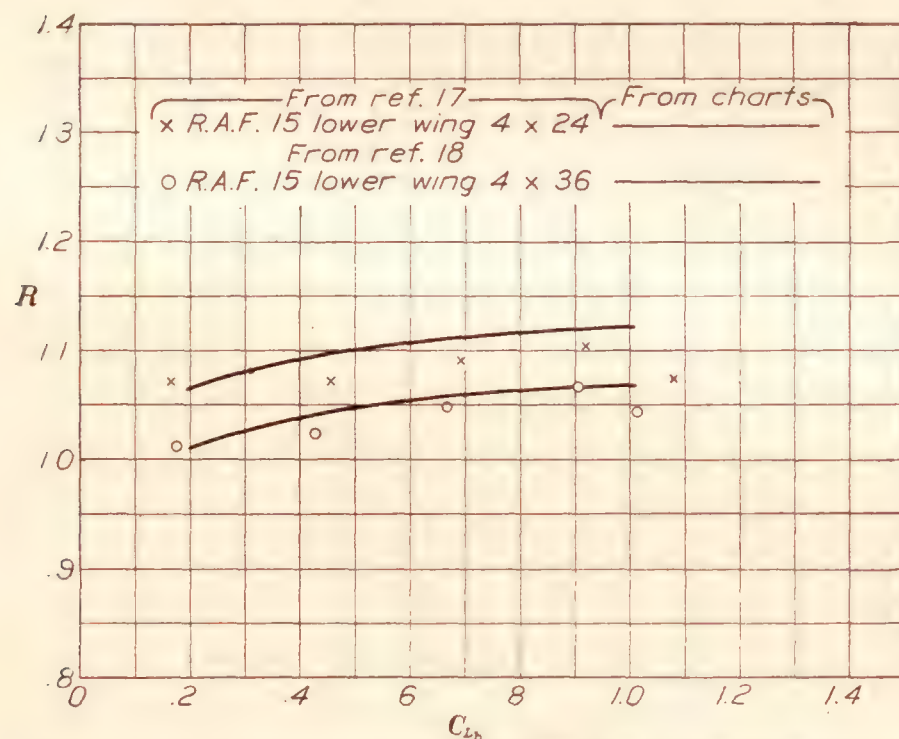
very marked reduction of the lift may occur. Figure 16, which was derived from data given in reference 23, shows the curve of lift coefficient against angle of attack for different types of fuselages attached to the wing; for unfavorable fuselage shapes as much as 20 per cent of the lift may be lost due to interference from the fuselage. It should be noted, too, that the

lift used is the total lift of the combination, whereas the reference area is the wing area; consequently, the decrease in lift coefficient on the wing itself is even larger than indicated on the figure. Such an effect



Airfoil.....	Clark Y
Maximum mean camber, per cent chord.....	3.8
Maximum thickness, per cent chord.....	11.7
Gap/chord ratio.....	1.0
Chord ratio.....	1.0
Stagger, degree.....	0
Decalage, degree.....	0
Reference.....	6

FIGURE 9.—Experimental lift distribution on cellule with overhang



Airfoil.....	R. A. F. 15	R. A. F. 15
Upper wing.....	6 by 36	6 by 36
Lower wing.....	4 by 36	4 by 24
Gap, inches.....	4.5	4.5
Stagger, degrees at L. E.....	20	20
Decalage, degree.....	0	0
Reference.....	18	17

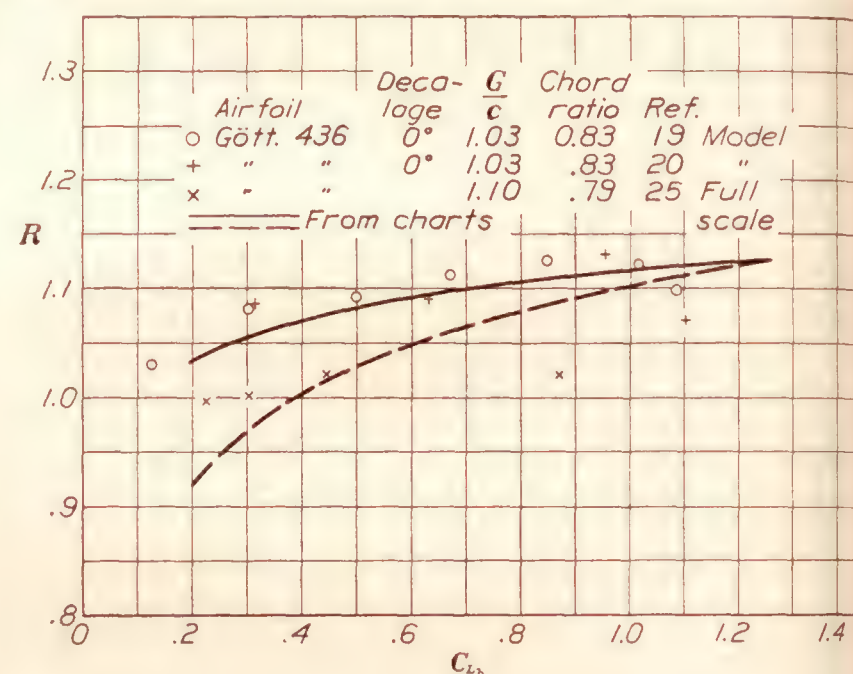
FIGURE 10.—Lift distribution for unequal-chord biplanes with and without overhang

might be considered to be comparable to conditions on the lower wing of a biplane. An opposite effect may be expected on the upper wing.

The influence of the fuselage will be extremely difficult to predict, because it depends so much on the

fairing of the wing root into the fuselage, the size and shape of windshields, the gap between the fuselage and upper wing, and other factors. The lack of tests on complete biplane models is to be very much deplored.

The full-scale biplane.—The oldest complete pressure-distribution tests were made on the MB-3 pursuit airplane. (Reference 24.) This airplane has very unusual feature in that the upper wing has washout of 3° , while the lower wing has a washin of 1° . In the computation of the R curve for this airplane was assumed that it would be sufficiently accurate to use the average incidence for each wing, resulting in decalage of 2° . However, it is evident that this assumption can give only a rough approximation, particularly at low angles of attack. Figure 17 shows



Airfoil.....	Göttingen 436	Götting 436
Maximum mean camber, per cent chord.....	3.9	3.9
Maximum thickness, per cent chord.....	11.2	11.2
Gap/chord ratio.....	1.1	1.1
Chord ratio.....	.79	.79
Stagger (approximate).....	0	0
Percentage overhang.....	29.75	29.75
Reference.....	25	18

FIGURE 11.—Lift distribution on PW-9 airplane

a comparison of the experimental points with the curve. The agreement at high lift coefficients is fair, particularly considering the fact that the pressure distribution measurements are made with only a very few orifices per rib. The agreement at low lift coefficients is very much poorer, as was expected. The dotted lines show the lift distribution at the maximum load during pull-ups from dives. As no time histories were given, the biplane lift coefficient at which these maximum loads occurred could not be computed.

A more comprehensive and more detailed series of measurements was made on the PW-9. (Reference 25.) It is mentioned in this reference that the airplane had an accident that caused, later on, frequent change in rigging, of which no continuous record was kept. The deviations of the experimental points from the R curve at high and intermediate speeds could be explained by $\frac{1}{2}^\circ$ of decalage. (Fig. 11.) This possibility

ity is made plausible by a close examination of the photograph of the airplane that shows that the right upper wing, on which the measurements were made, had less incidence than the left upper wing. However, the true explanation of the discrepancy is probably to be found largely in the differences in lift distribution due to the slipstream.

Figure 18 shows a series of points obtained from the time histories of mild pull-ups with power off. It will be seen that these points group much more closely around the R curve, the influence of the slipstream

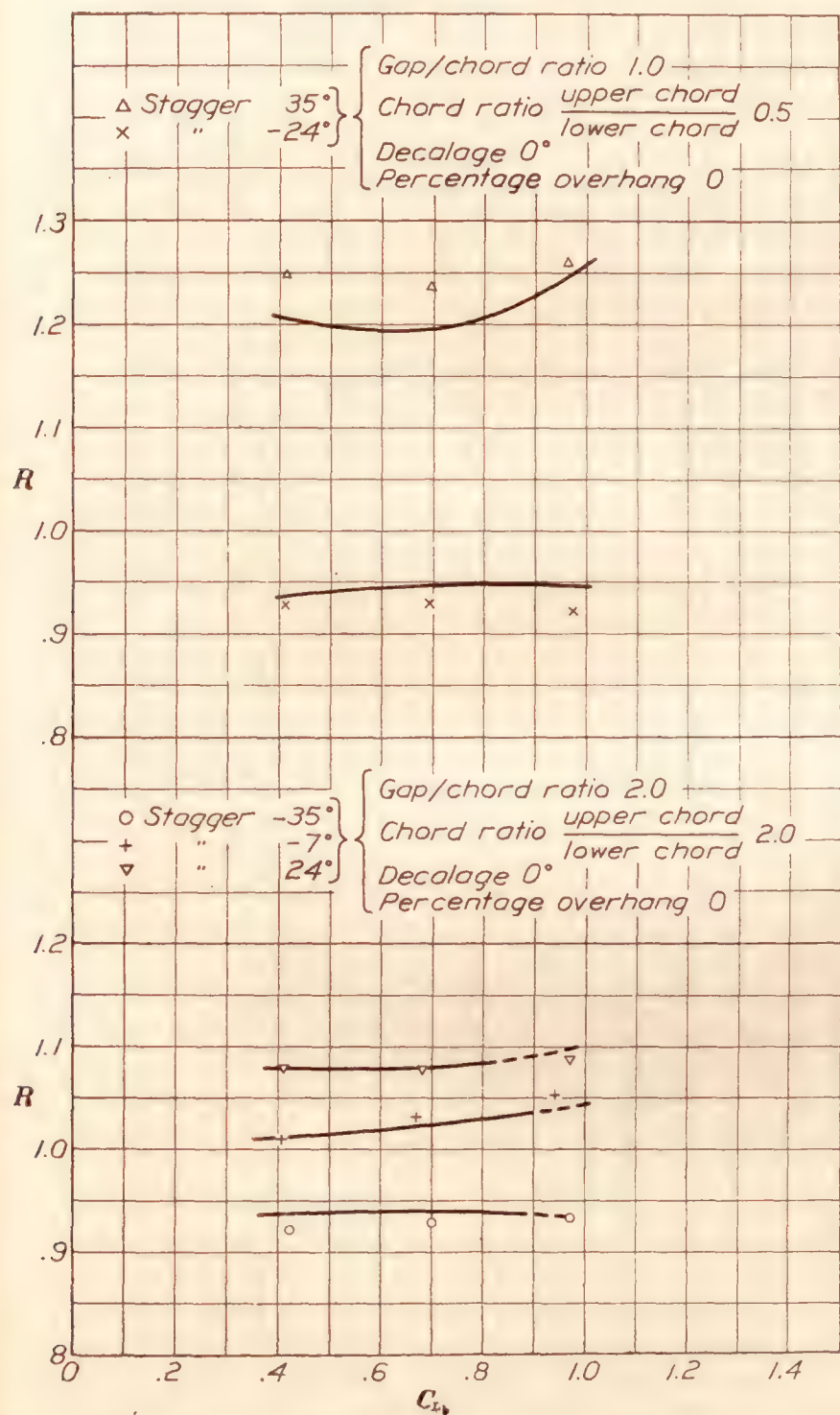
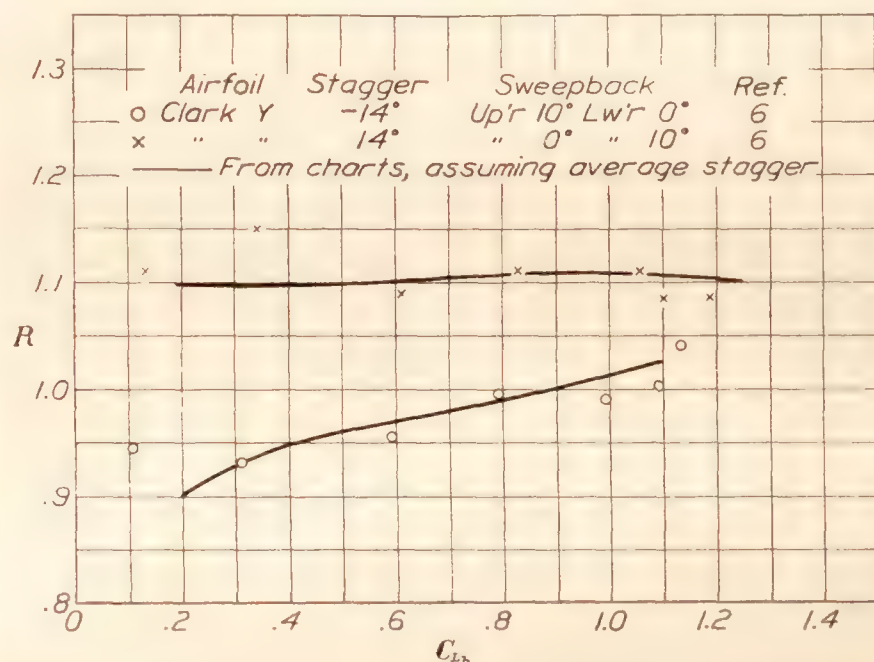


FIGURE 12.—Lift distribution for unequal-chord biplanes by Millikan's theory being smaller in this case. Another peculiarity, however, appears on this chart; that is, a number of points are beyond the range of biplane lift coefficients which are obtained in steady flight or in the wind tunnel. This phenomenon, which is more pronounced in abrupt pull-ups, is discussed in reference 25, where it is pointed out that the increased maximum lift coefficient occurs mainly on the upper wing and is probably caused by the high rate of change of angle of attack. Recently, wind-tunnel tests have been made in Germany (reference 26) in which the angle of attack

was increased suddenly by changing the direction of the air stream. A formula is given for the increase in lift coefficient as a function of chord, speed, and rate of change of angle of attack. The formula, applied to the PW-9 tests, gives maximum values for the increase in maximum lift coefficient which are, in general, only about half as great as the observed values. The higher coefficients obtained in the PW-9 pull-ups, however, might be expected as a result of the fact that the Reynolds Number in the pull-ups was more than twice as great as that in level flight.

More attention should be given this subject in future research to determine how the critical loads depend on the maximum lift coefficient of the pitching wing.

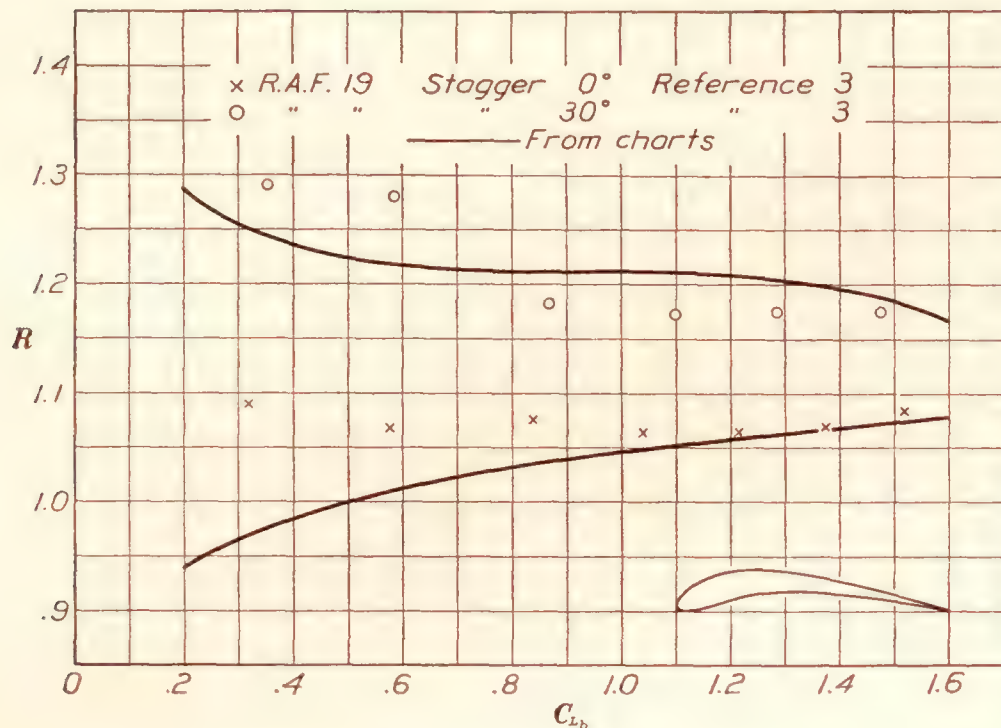


Airfoil	Clark Y
Maximum mean camber, per cent of chord	3.8
Maximum thickness, per cent of chord	11.7
Gap/chord ratio	1.0
Chord ratio	1.0
Decalage, degree	0
Percentage overhang	0

FIGURE 13.—Validity of average stagger assumption for unequal sweepback in upper and lower wings

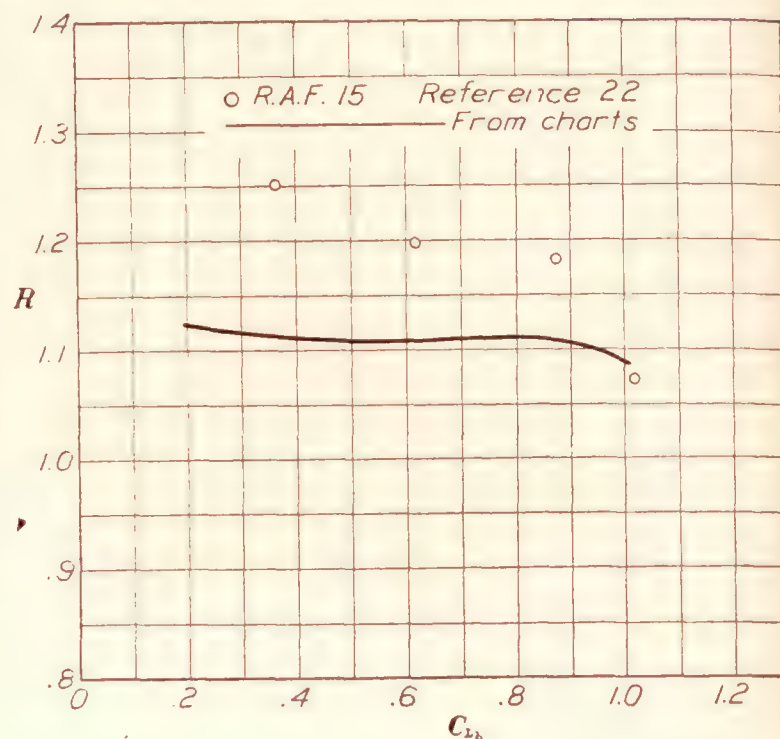
RECOMMENDATIONS

As far as our knowledge of the cellule is concerned, tests are desirable on the following doubtful points: (1) Effect of unequal chords; (2) effect of unequal chords in combination with overhang and decalage (unequal-chord tests should include cellules with the upper wing having the smaller chord); (3) effect of gap/chord ratio below 1, using airfoils of different thicknesses and cambers. In one otherwise excellent series of tests an attempt was made to evaluate this effect by making only one test at a gap/chord ratio of 0.5, which is probably below any practical dimension. The argument was that such a test would show in an exaggerated way the influence of low gap/chord ratios. This argument seems unsound, for, at such low gap/chord ratios, so many other factors begin to exert an influence that it is difficult to draw any general conclusions from such an experiment.



Airfoil.....	R. A. F. 19
Maximum mean camber, per cent of chord.....	10.52
Maximum thickness, per cent of chord.....	9.9
Gap/chord ratio.....	1.0
Chord ratio.....	1.0
Decalage, degree.....	0
Percentage overhang.....	0
Reference.....	3

FIGURE 14.—Lift distribution on a cellule with R. A. F. 19 airfoil



Airfoil.....	R. A. F. 15
Maximum mean camber, per cent of chord.....	17.5
Maximum thickness, per cent of chord.....	17.5
Gap/chord ratio.....	1.0
Chord ratio.....	1.0
Stagger.....	0
Decalage.....	0
Percentage overhang.....	0
Reference.....	22

FIGURE 15.—Lift distribution on a B. E. 2C airplane model

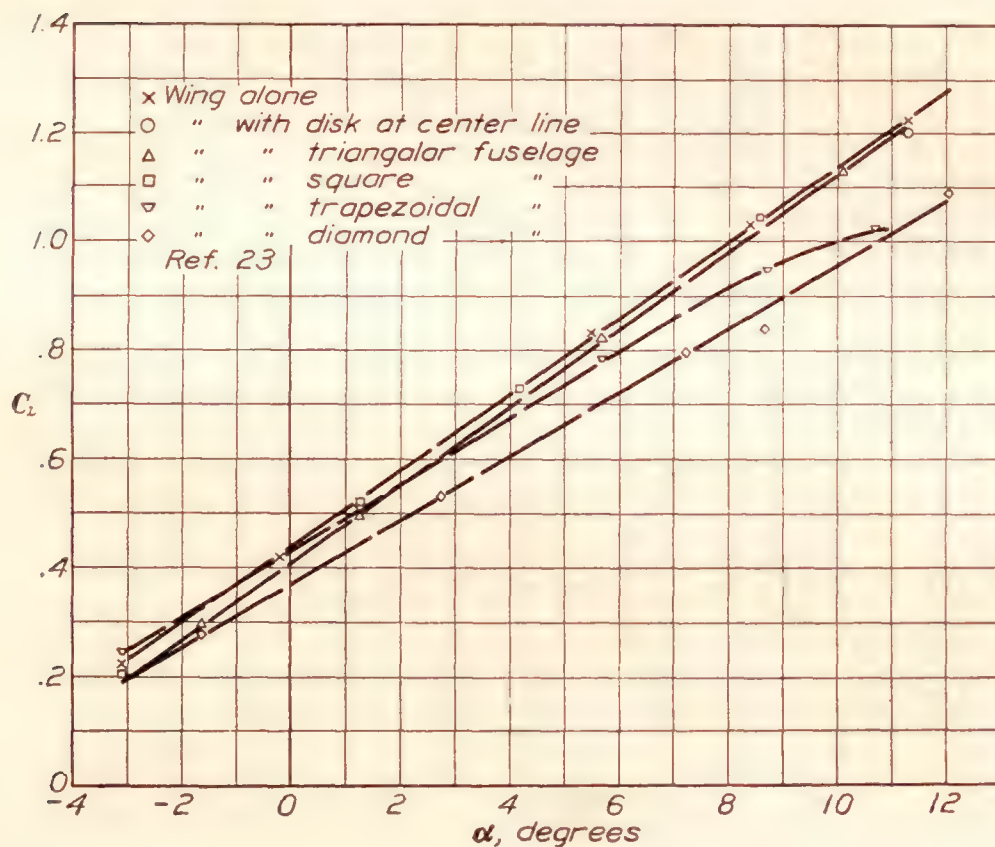
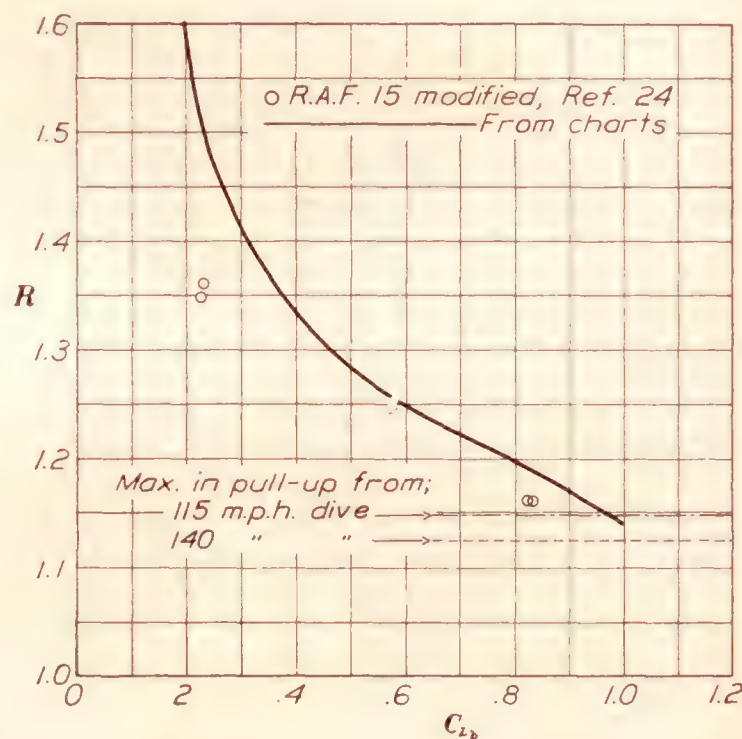
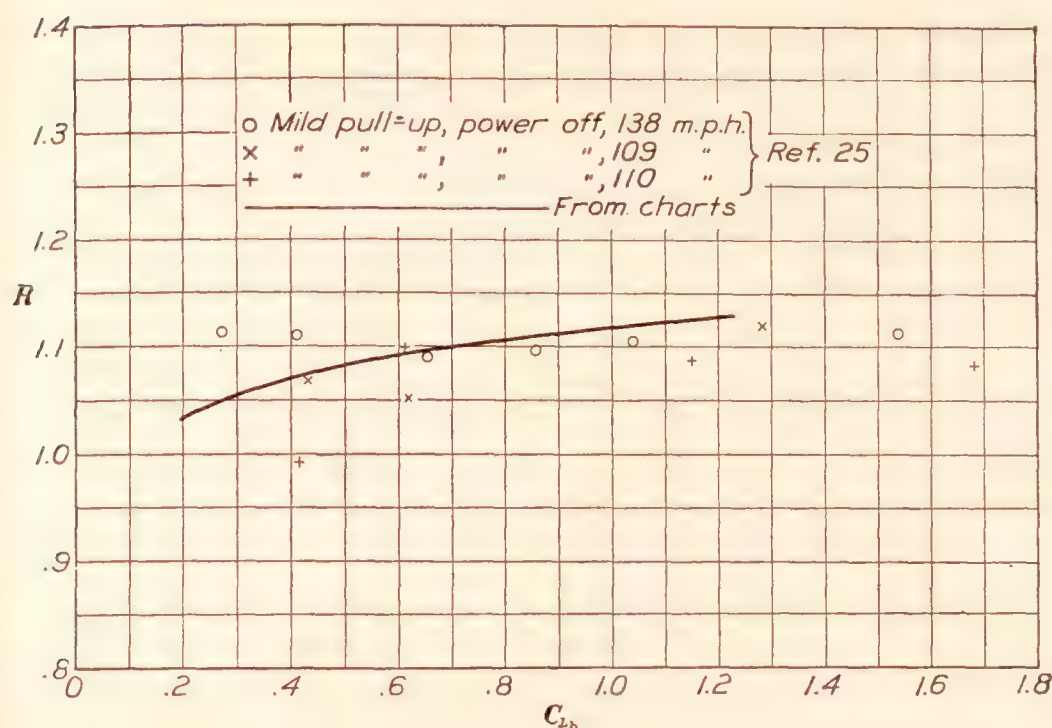


FIGURE 16.—Influence of fuselage shape on lift of low-wing monoplane



Airfoil.....	R. A. F. 15 (modified)
Maximum mean camber, per cent of chord.....	17.5
Maximum thickness, per cent of chord.....	17.5
Gap/chord ratio.....	1.0
Chord ratio.....	1.0
Stagger, degree.....	0
Decalage, degrees.....	0
Percentage overhang.....	0
Reference.....	24

FIGURE 17.—Lift distribution on MB-3 airplane



Airfoil.....	{ Göttingen 436
Maximum mean camber, per cent of chord.....	3.9
Maximum thickness, per cent of chord.....	11.2
Gap/chord ratio.....	1.1
Chord ratio.....	.79
Stagger, degree (approximate).....	0
Decalage.....	
Percentage overhang.....	29.75
Reference.....	25

FIGURE 18.—Comparison of predicted and experimental lift distribution on the PW-9 airplane

No information at all is available on the important subject of biplane lift distribution in inverted flight. Some tests should be made at negative lift up to the maximum negative lift coefficient.

Design rules should take into account possible variations in decalage caused by errors or arbitrary changes in rigging. In view of the fact that lack of data prevented the establishment of correction factors for decalage at negative stagger, the decalage correction for 0° stagger may be applied to allow for rigging changes in biplanes having negative stagger until test data become available.

The influence of interferences, particularly that caused by the fuselage, should be studied more extensively. The effects of fuselage interference should be recognized in formulating design rules for the load distribution between biplane wings. Such effects might be tentatively included in the allowance for accidental positive decalage.

LANGLEY MEMORIAL AERONAUTICAL LABORATORY,
NATIONAL ADVISORY COMMITTEE FOR AERONAUTICS,
LANGLEY FIELD, VA., *July 11, 1932.*

APPENDIX

USE OF THE CHARTS

The fundamental idea of the charts is, briefly, that one chart gives the lift-distribution, or R , curve for the basic biplane; that is, the equal-span, equal-chord biplane without decalage, and with a gap/chord ratio of 1. The other charts give correction factors that are multiplied by or added to the basic curves to take account of decalage, overhang, and gap/chord ratios other than 1.

The important characteristics of the biplane are listed below in the sequence in which they appear in the determination of the R curve:

- (1) Airfoil section.
- (2) Gap/chord ratio.
- (3) Chord ratio.
- (4) Stagger.
- (5) Decalage.
- (6) Overhang.

(1) The airfoil is taken into account by selecting the proper curve for the sum of camber and thickness. This applies to the basic chart (fig. 19) and to the gap/chord factor chart (fig. 20).

(2) The gap/chord ratio is taken into account:

(a) For gap/chord ratios less than 1, by multiplying corresponding ordinates of the basic R curve and of the proper gap/chord factor curve. (Fig. 20.) The method of interpolating to find the proper gap/chord factor curve is explained under the subhead Interpolation of Factors.

(b) For gap/chord ratios greater than 1, by interpolating linearly between the R curve for the gap/chord ratio of 1 and the R curve for the gap/chord ratio of 3, which is $R = 1$.

(c) The gap/chord factors are used only for the staggers for which they are given; viz, 30° , 0° , and -30° . If the biplane has any other stagger, say 17° , it is necessary to find the R curves for 0° and 30° stagger at the given gap/chord ratio and to interpolate between these two R curves to obtain the R curve for 17° stagger.

(3) If the chord ratio differs from 1, an effective gap/chord ratio, which is the actual gap divided by the chord of the lower wing, is used.

(4) The stagger used is an effective stagger measured in degrees between the line connecting the three-quarter chord points and a perpendicular to the chord of the upper wing in a plane containing the centroid of the semicellule. This method of measuring stagger must be borne in mind in the case of unequal-chord biplanes.

The R curve for a stagger other than 30° , 0° , or -30° is obtained by straight-line interpolation. For 17° for instance, the R curves are drawn for 0° and 30° and the curve for 17° is found by linear interpolation between them.

The end points of the 0° and -30° curves are connected by a straight line to determine the end points of curves for negative stagger; otherwise the procedure is the same as for positive stagger.

(5) Decalage is provided for by multiplying corresponding ordinates of the basic curve and of the proper decalage-factor curve. (Fig. 21.) The interpolation for finding the proper decalage-factor curve is explained under the subhead Interpolation of Factors. For C_{Lb} greater than 1.0, the end of the R curve is faired into the end of the basic curve as indicated by dotted lines in Figures 6, 7, and 8.

(6) Overhang is provided for by adding to the R curve the overhang correction from Figure 22 after all other corrections have been made.

INTERPOLATION OF FACTORS

(1) **Gap/chord factor.**—The gap/chord factor chart gives the factor curves for a gap/chord ratio of 0.75. From these, the factor curve for a gap/chord ratio between 0.75 and 1 is obtained by linear interpolation remembering that the factor is 1 for a gap/chord ratio of 1.

(2) **Decalage factors.**—There are two cases—

(a) $G/c < 1$:

For example let $G/c = 0.8$; stagger = 17° .

In Figure 21, between the F_d curve for ($G/c = 1.0$, stagger = 0°) and the F_d curve for ($G/c = 0.75$, stagger = 0°), interpolate to obtain the F_d curve for ($G/c = 0.8$, stagger = 0°).

Between the F_d curve for ($G/c = 1.0$, stagger = 30°) and the F_d curve for ($G/c = 0.75$, stagger = 30°), interpolate to obtain the F_d curve for ($G/c = 0.8$, stagger = 30°).

Between the F_d curve for ($G/c = 0.8$, stagger = 0°) and the F_d curve for ($G/c = 0.8$, stagger = 30°) interpolate to obtain the F_d curve for ($G/c = 0.8$, stagger = 17°).

(b) $G/c > 1$:

Let $G/c = 1.25$; stagger = 17° .

Between the F_d curve for ($G/c = 1.0$, stagger = 0°) and the F_d curve for ($G/c = 1.0$, stagger = 30°) interpolate to obtain the F_d curve for ($G/c = 1.0$, stagger = 17°).

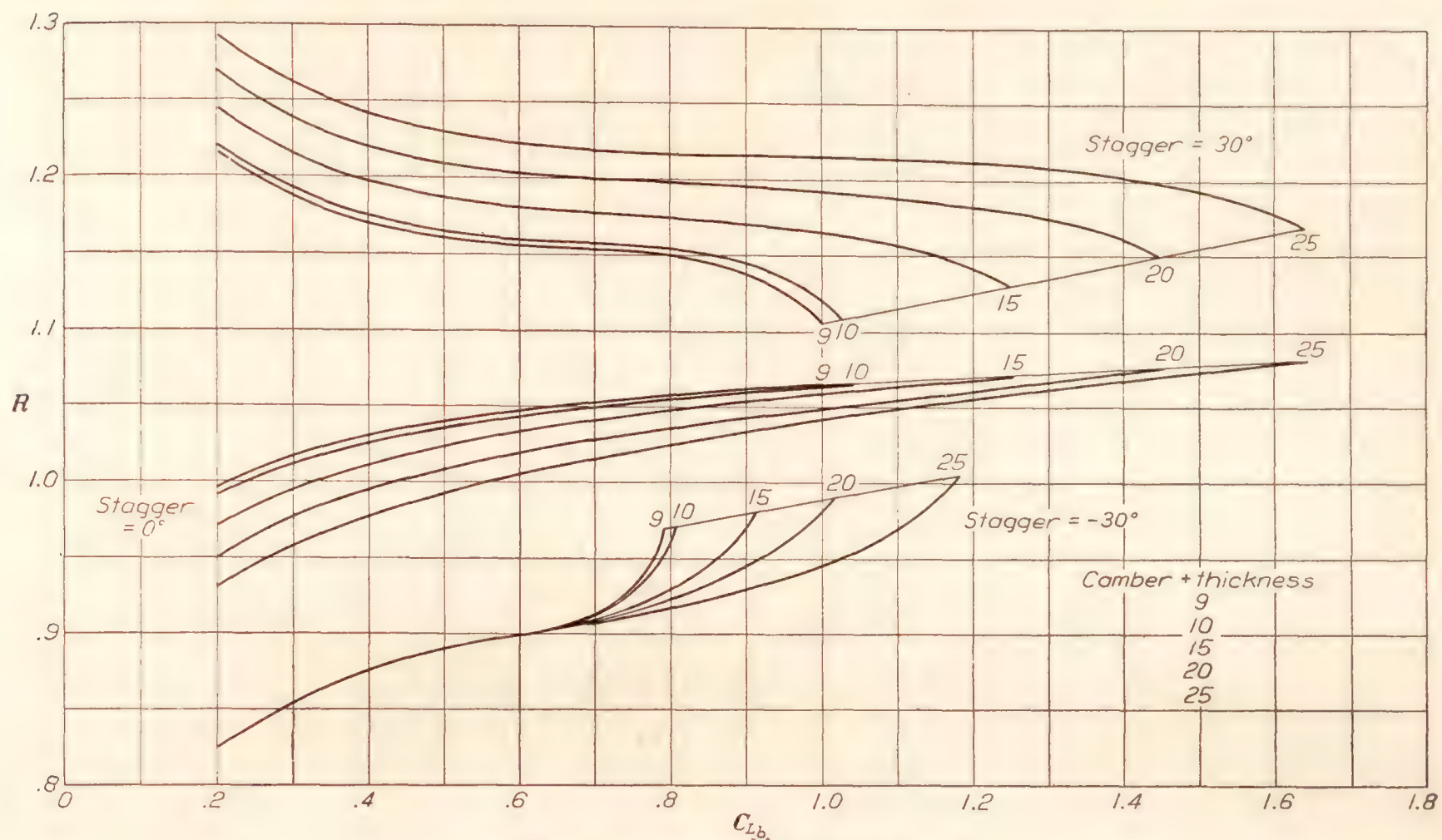
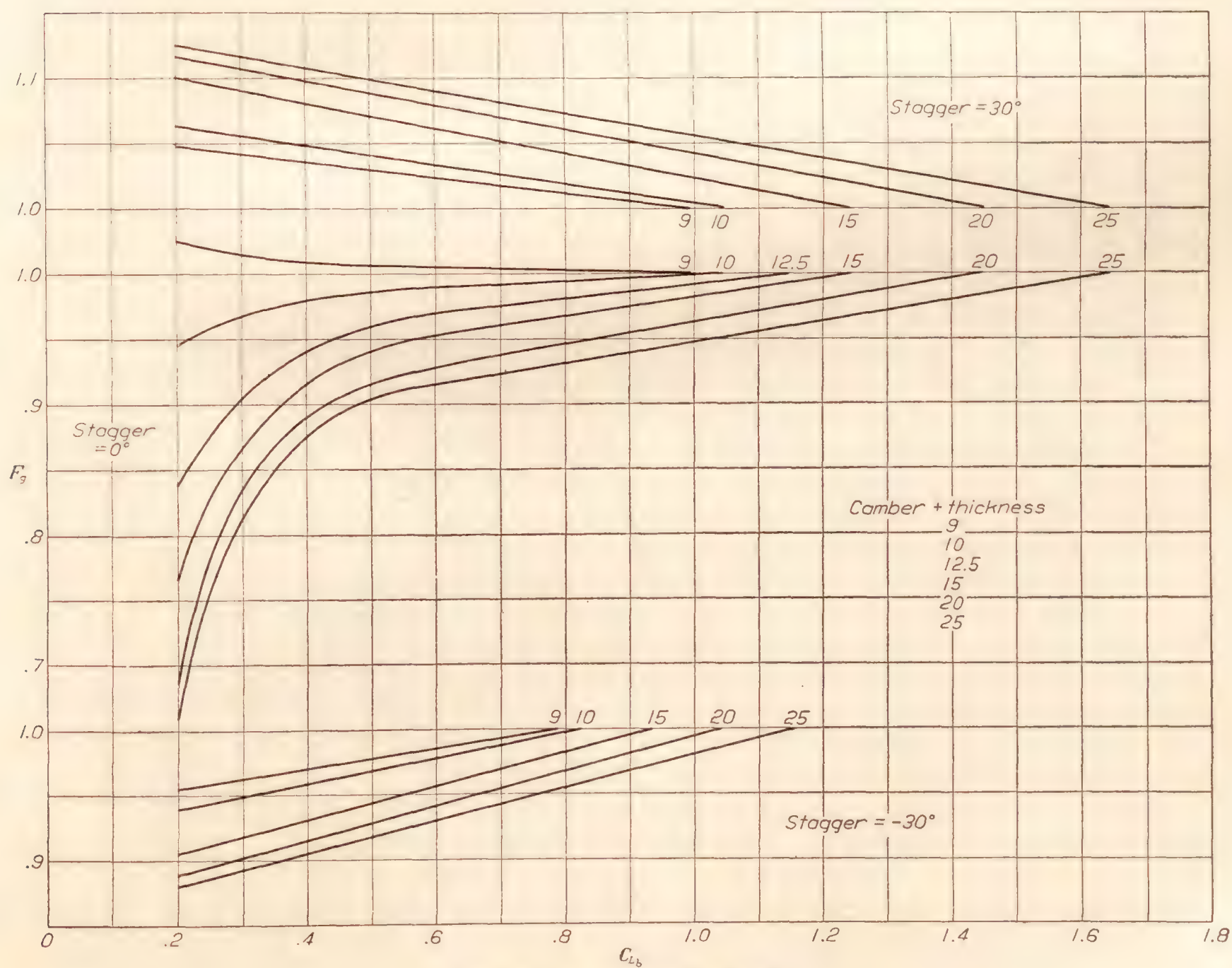


FIGURE 19.—Basic lift-distribution chart for biplanes

FIGURE 20.—Gap/chord factors. $G/c=0.75$

Between the F_d curve for ($G/c=1.0$, stagger= 17°) and the F_d curve for ($G/c=3$) interpolate to obtain the F_d curve for ($G/c=1.25$, stagger= 17°).

Example.—The following is an example of the procedure for finding R against C_{L_b} in the most general case.

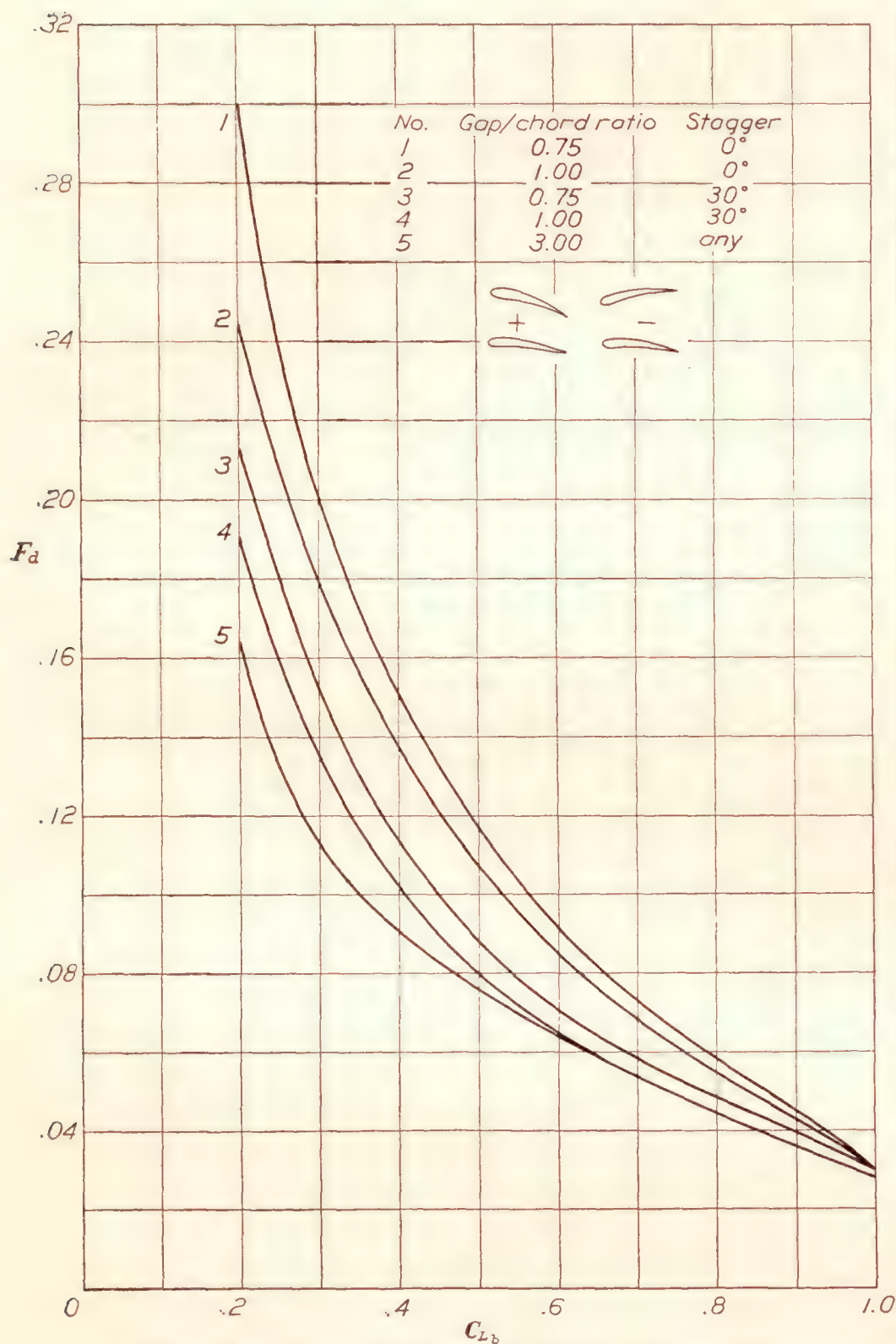


FIGURE 21.—Decalage factors $= (1+d \times F_d)$ F_d from chart. d =decalage in degrees

DATA

Airfoil—Clark Y
 Camber + thickness: 15.5.
 Span, upper: 40 ft.
 Span, lower: 30 ft.
 Chord, upper: 7 ft.
 Chord, lower: 5 ft.
 Gap: 4.5 ft.
 Stagger: 13° (measured at the three-quarter chord points).
 Decalage: 1.5° .
 Gap/chord ratio: 0.9.
 The following list explains the significance of each item in Table I and tells how it is obtained.

(1) R values for $G/c=1$, (camber + thickness) = 15.5, stagger = 30° from Figure 19.

(2) R values for stagger = 0° .

(3) G/c factor for (camber + thickness) = 15.5, stagger = 30° , $G/c=0.75$ from Figure 20.

(4) G/c factor for stagger = 30° , $G/c=0.9$ by interpolation; (4) $= 1 + [(3) - 1] \times \frac{0.1}{0.25}$.

(5) G/c factor for (camber + thickness) = 15.5, stagger = 0° , $G/c=0.75$ from Figure 20.

(6) G/c factor for (camber + thickness) = 15.5, stagger = 0° , $G/c=0.90$ by interpolation from (5); (6) $= 1 - [1 - (5)] \times \frac{0.1}{0.25}$.

(7) R values for $G/c=0.9$, stagger = 30° ; (7) $= (1) \times (4)$.

(8) R values for $G/c=0.9$, stagger = 0° ; (8) $= (2) \times (6)$.

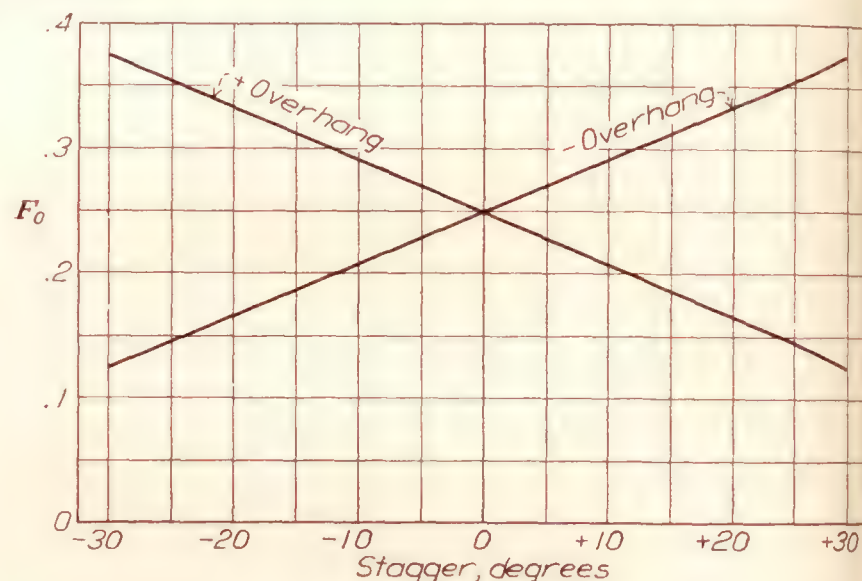


FIGURE 22.—Overhang factors.

$$\text{Overhang correction} = F_o \times \frac{\text{upper span} - \text{lower span}}{\text{upper span}} \times \frac{\text{smaller chord}}{\text{larger chord}}$$

(9) Difference between R values, (7) and (8).

(10) $= (9) \times \frac{13}{30}$ (interpolating for stagger).

(11) R values for $G/c=0.9$, stagger = 13° ; (11) $= (8) + (10)$.

(12) Decalage factors, F_d , for $G/c=0.9$, stagger = 0° by interpolating in ratio $\frac{0.1}{0.25}$ between F_d curves for $G/c=1$, stagger = 0° and $G/c=0.75$, stagger = 0° on Figure 21.

(13) Decalage factors for $G/c=0.9$, stagger = 30° obtained in a manner similar to (12).

(14) Difference between (12) and (13).

(15) $= (14) \times \frac{13}{30}$ (interpolating for stagger).

(16) F_d values for $G/c=0.9$, stagger = 13° ; (16) $= (13) + (15)$.

(17) Complete decalage factor for 1.5° decalage; (17) $= 1 + 1.5 \times (16)$.

(18) R values for $G/c=0.9$, stagger = 13° , decalage = 1.5° ; (18) $= (11) \times (17)$.

(19) Overhang correction from Figure 22 $= 0.197 \times \frac{10}{40} \times \frac{5}{7} = 0.035$.

(20) Final R values by adding (19) to (18).

TABLE I.—Calculation of typical *R* curve

Cl_b	0.2	0.4	0.6	0.8	1.0	1.26
Item No.:						
(1)-----	1.247	1.199	1.183	1.177	1.167	1.131
(2)-----	.968	1.008	1.030	1.044	1.056	1.071
(3)-----	1.102	1.083	1.063	1.044	1.025	1.000
(4)-----	1.041	1.033	1.025	1.017	1.010	1.000
(5)-----	.758	.913	.950	.965	.980	1.000
(6)-----	.903	.965	.980	.986	.992	1.000
(7)-----	1.299	1.239	1.213	1.197	1.179	1.131
(8)-----	.875	.973	1.010	1.029	1.048	1.071
(9)-----	.424	.266	.203	.168	.131	.060
(10)-----	.184	.115	.088	.073	.057	.026
(11)-----	1.059	1.088	1.098	1.102	1.105	1.097
(12)-----	.266	.142	.086	.057	.029	-----
(13)-----	.199	.106	.067	.046	.029	-----
(14)-----	.067	.036	.019	.011	.000	-----
(15)-----	.029	.016	.008	.005	.000	-----
(16)-----	.228	.122	.075	.051	.029	-----
(17)-----	1.342	1.183	1.112	1.076	1.043	1.000
(18)-----	1.421	1.288	1.221	1.186	1.153	1.097
(19)-----	$0.197 \times \frac{40-30}{40} \times \frac{5}{7} = 0.035$					-----
(20)-----	1.456	1.323	1.256	1.221	1.188	1.132

REFERENCES

1. Aeronautics Branch, Dept. of Commerce: Relative Lift Distribution in Any Biplane. Aero. Bull. No. 14, July 1, 1929.
2. Pannell, J. R., and others: Experiments on Models of Biplane Wings. R. & M. No. 196, British A. C. A., 1915.
3. Carroll, J. A., and Bradfield, F. B.: Model Tests of R. A. F. 19 Wing Section as a Biplane. R. & M. No. 648, British A. C. A., 1919.
4. Anon.: Études Systématiques Sur les Biplans. Résultats d'essais effectués, en 1922, à l'Institut Aérotechnique de St. Cyr. French Tech. Service of Aero., Mars, 1923.
5. Millikan, Clark B.: An Extended Theory of Thin Airfoils and Its Application to the Biplane Problem. T. R. No. 362, N. A. C. A., 1930.
6. Noyes, Richard W.: Pressure Distribution Tests on a Series of Clark Y Biplane Cellules with Special Reference to Stability. T. R. No. 417, N. A. C. A., 1932.
7. Jacobs, Eastman N., and Anderson, Raymond F.: Large Scale Aerodynamic Characteristics of Airfoils as Tested in the Variable-Density Tunnel. T. R. No. 352, N. A. C. A., 1930.
8. Munk, Max M.: The Air Forces on a Systematic Series of Biplane and Triplane Cellule Models. T. R. No. 256, N. A. C. A., 1927.
9. Mock, Richard M.: The Distribution of Loads between the Wings of a Biplane Having Decalage. T. N. No. 269, N. A. C. A., 1927.
10. Cowley, W. L., and Levy, H.: The Contribution of the Separate Planes to the Forces on a Biplane. R. & M. No. 589, British A. C. A., 1919.
11. Cowley, W. L., and Lock, C. N. H.: Biplane Investigation with R. A. F. 15 Section R. & M. No. 774, British A. R. C., 1921.
12. Cowley, W. L., and Jones, L. J.: Biplane Investigation with R. A. F. 15 Section. Part II. R. & M. No. 857, British A. R. C., 1922.
13. Parkin, J. H., Shortt, J. E. B., and Cade, J. G.: Biplane Investigation. Aero. Research Paper No. 19, Univ. Toronto Bull. No. 7, 1927, pp. 181-221.
14. Munk, Max M.: Beitrag zur Aerodynamik der Flugzeugtragorgane. T. B., Band II, 1918.
15. Irving, H. B., Powell, C. H., and Jones, C. N.: The Distribution of Pressure on the Upper and Lower Wings of a Biplane. R. & M. No. 355, British A. C. A., 1917-18.
16. Bryant, L. W., and Jones, C. N.: Biplane Effect on R. A. F. 15 Wing Section. R. & M. No. 366, British A. C. A., 1917.
17. Irving, H. B., and Batson, A. S.: The Distribution of Pressure over a Biplane with Wings of Unequal Chord and Span. R. & M. No. 997, British A. R. C., 1925.
18. Batson, A. S., Halliday, A. S., and Maidens, A. L.: The Distribution of Pressure over a Monoplane and a Biplane with wings of Unequal Chord and Equal Span. R. & M. No. 1098, British A. R. C., 1927.
19. Fairbanks, A. J.: Pressure Distribution Tests on PW-9 Wing Models Showing Effects of Biplane Interference. T. R. No. 271, N. A. C. A., 1927.
20. Loeser, Oscar E., jr.: Pressure Distribution Tests on PW-9 Wing Models from -18° through 90° Angle of Attack. T. R. No. 296, N. A. C. A., 1929.
21. Pressure Distribution on Model FE-9 Wings. R. & M. No. 347, British A. C. A., 1917.
22. Batson, A. S., and Nixon, H. L.: Pressure Distribution over the Wings of, and Force Measurements on, a Model B. E. 2C Biplane with Raked Wing Tips. R. & M. No. 891, British A. R. C., 1923.
23. Muttray, H.: Investigation of the Effect of the Fuselage on the Wing of a Low-Wing Monoplane. T. M. No. 517, N. A. C. A., 1929.
24. Norton, F. H.: Pressure Distribution over the Wings of an MB-3 Airplane in Flight. T. R. No. 193, N. A. C. A., 1924.
25. Rhode, Richard V.: The Pressure Distribution over the Wings and Tail Surfaces of a PW-9 Pursuit Airplane in Flight. T. R. No. 364, N. A. C. A., 1930.
26. Kramer, Max: Increase in the Maximum Lift of an Airplane Wing due to a Sudden Increase in its Effective Angle of Attack Resulting from a Gust. T. M. No. 678, N. A. C. A. 1932.

REPORT No. 446

AIRFOIL SECTION CHARACTERISTICS AS AFFECTED BY PROTUBERANCES

By EASTMAN N. JACOBS

SUMMARY

The drag and interference caused by protuberance from the surface of an airfoil have been determined in the N. A. C. A. variable-density wind tunnel at a Reynolds Number of approximately 3,100,000. The effects of variations of the fore-and-aft position, height, and shape of the protuberance were measured by determining how the airfoil section characteristics were affected by the addition of the various protuberances extending along the entire span of the airfoil. The results provide fundamental data on which to base the prediction of the effects of actual short-span protuberances. The data may also be applied to the design of air brakes and spoilers.

INTRODUCTION

The ideal airplane, aerodynamically, may be considered as one having only the drag due to skin friction and the minimum induced drag associated with its lift. Prof. B. M. Jones in England has shown that actual airplanes fall far short of such an ideal. Interference effects, it seems, must be blamed for a considerable part of the energy wasted in producing the turbulence associated with the comparatively large drag of actual airplanes.

The National Advisory Committee for Aeronautics has planned a series of investigations dealing with the subject of aerodynamic interference. The investigations will, it is hoped, lead to the discovery of the cause of the serious adverse effects and will provide data that may be applied to the solution of practical problems of design. An examination of present-day airplanes, both military and commercial, has led to the belief that a considerable part of the adverse interference arises from small projecting objects, such as fittings, tubes, wires, rivet heads, lap joints, butt straps, filler caps, inspection plates, and many other projections from the main surfaces that may be considered together as protuberances. A systematic investigation of protuberances differently formed and variously located should indicate the relative magnitude of such effects and also show the effect of disturbing the flow in the boundary layer about otherwise streamline bodies.

Some early investigations of boundary-interference effects were originated by Prandtl at Göttingen in 1914

to study the effects of a small ring protruding from the surface of a sphere. Large negative, or favorable, interference effects were observed at certain values of the Reynolds Number because the turbulence produced by the protuberance changed the character of the boundary layer so as to delay the separation of the flow from the surface, thus producing a smaller turbulent wake and a smaller drag. Similar experiments have more recently been performed by Ower in England with streamline bodies. (Reference 1.) At low values of the Reynolds Number, when the flow in the boundary layer of the body is to a considerable extent laminar, protuberances from the forward portions of the body cause a transition from the laminar to the turbulent state of flow in the boundary layer with a resulting increase of drag. This effect is not of great practical significance, however, because the flow in the boundary layer of full-scale bodies is probably, in any event to a large extent, of the turbulent type. It is advisable, therefore, to make investigations involving boundary-interference effects at large values of the Reynolds Number if they are to be of the greatest practical value.

Tests have been made in the variable-density wind tunnel at large values of the Reynolds Number to determine the effects of protuberances from the surface of a streamlined body of revolution. The results have not yet been published. The present report deals with another phase of the investigation; that is, the effects on airfoil *section* characteristics of protuberances extending along the entire span from the airfoil surface. A succeeding report will consider the effects on *wing* characteristics of protuberances extending only over portions of the wing span. The tests with which the present report deals were made in the N. A. C. A. variable-density wind tunnel during March, 1932.

The N. A. C. A. 0012 airfoil section was employed throughout the investigation and the dynamic scale of the tests was maintained approximately the same throughout (Reynolds Number 3,100,000). The effects of variations of the position, size, and shape of the protuberance were measured by determining how the airfoil section characteristics were affected by the addition of the various protuberances.

TESTS

The N. A. C. A. variable-density tunnel and the methods employed for airfoil testing in the tunnel are described in detail in reference 2. These tests were made in the usual way, measuring the lift, drag, and pitching moments on a 5 by 30 inch duralumin airfoil mounted in the air stream so that the angle of attack could be varied. The model mounting differed in one respect from that described in reference 2. Instead of using a sting attached to the lower surface of the airfoil as part of the airfoil support, a special sting was employed that was attached near the trailing edge of the airfoil. As the airfoil has symmetrical sections, it was thus possible to make the airfoil and sting assembly symmetrical about the plane of the airfoil chords.

A section of the airfoil employed, the N. A. C. A. 0012 (reference 3), is shown in Figure 1. The protuberances were placed in the slots shown, the posi-

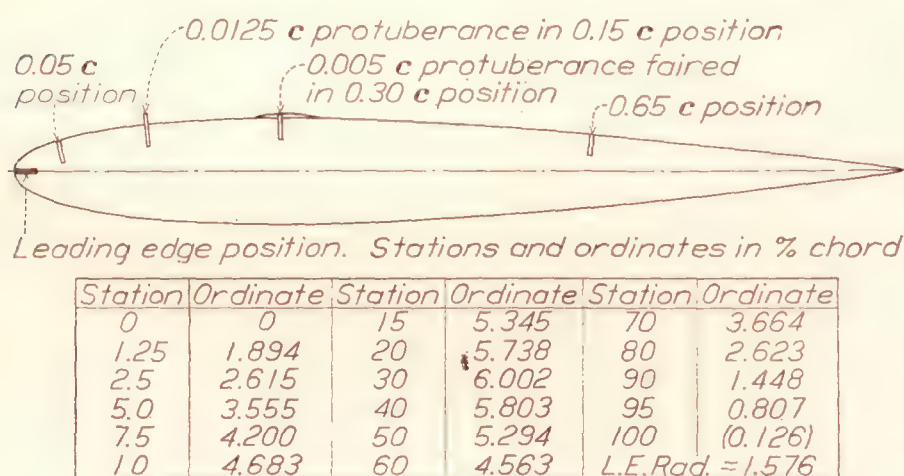


FIGURE 1.—N. A. C. A. 0012 airfoil showing protuberances

tions being: Directly at the leading edge; 5 per cent of the chord behind the leading edge; 15 per cent (approximately the front spar position); 30 per cent (maximum ordinate position); and 65 per cent (approximately the rear spar position). The protuberances were placed only on the upper side of the symmetrical airfoil, but the effect of each on the lower surface was determined by testing the airfoil through the negative angle-of-attack range.

The protuberance consisted of a strip of sheet duralumin having the desired height placed in one of the slots indicated in Figure 1 in such a way as to extend along the entire span of the model. The form that will be referred to as the faired protuberance was produced, as indicated in Figure 1, by forming over the protuberance a plaster-of-Paris fairing the cross section of which approximated a small half airfoil section on the surface of the main airfoil. The slots in the airfoil when not in use were filled with duralumin strips carefully filed to the surface and polished to present a continuous smooth surface. The protuberance was used in only one slot at a time, starting with the highest protuberance $0.0125c$, and then reducing the height consecutively to $0.0050c$, $0.0020c$, and in some cases to $0.0010c$ and $0.0004c$, by filing off the top of the projecting strip.

The characteristics of the airfoil without protuberances—that is, with all slots filled—were measured twice during the progress of the investigation as a check on the consistency of the results.

For comparison with the results obtained at negative angles of attack, average curves for the negative-angle runs on the plain airfoil have been used. These differ slightly from the corresponding positive-angle curves because of asymmetrical support interference. When the protuberance was in the leading-edge position the tests were made at both positive and negative angles of attack, but average curves have been used to present the results. Thus the various curves presenting the results for the plain airfoil do not agree exactly. Furthermore, they should not be expected to agree with other tests of the same airfoil, because the tare-drag correction applied throughout this investigation did not allow for the lower drag of the special airfoil sting employed.

RESULTS AND DISCUSSION

The results are presented by means of curves of the lift coefficient C_L , profile-drag coefficient C_{D_o} , moment coefficient about a point one-quarter of the chord behind the leading edge $C_{m_{c/4}}$, and the angle of attack for infinite aspect ratio α_o . The results are thus presented as airfoil section characteristics. The most important results, those corresponding to the various heights and positions of the protuberance, are presented in Figures 2 to 10. Attention should be here called to the fact, however, that the characteristics thus presented should not be used with precise strip method calculations as though they were true infinite-aspect-ratio characteristics, but should be considered as average section characteristics deduced from the test data by the methods described in reference 2. Differences between these section characteristics and the true ones may probably be neglected as long as all the sections of the rectangular wing that was tested were operating at effective angles of attack within the range of approximately normal lift curve slope. Their use is also partly justified by the fact that approximately correct results for a full-span protuberance on a wing of normal aspect ratio are obtained from them when the simple aspect-ratio corrections (reference 2) are applied.

Protuberance position.—The results for the largest protuberance ($0.0125c$) in the various positions on the airfoil surface are shown in Figure 11. Considering first the effects of the protuberance on the lift at low angles of attack, it will be seen that the effect of the protuberance is to decrease the lift slightly for all upper-surface positions and to increase it slightly for all lower-surface positions. As regards the lift at higher angles of attack and the maximum value of the lift, the protuberances on the lower surface have little effect, whereas the adverse effect of those on the upper

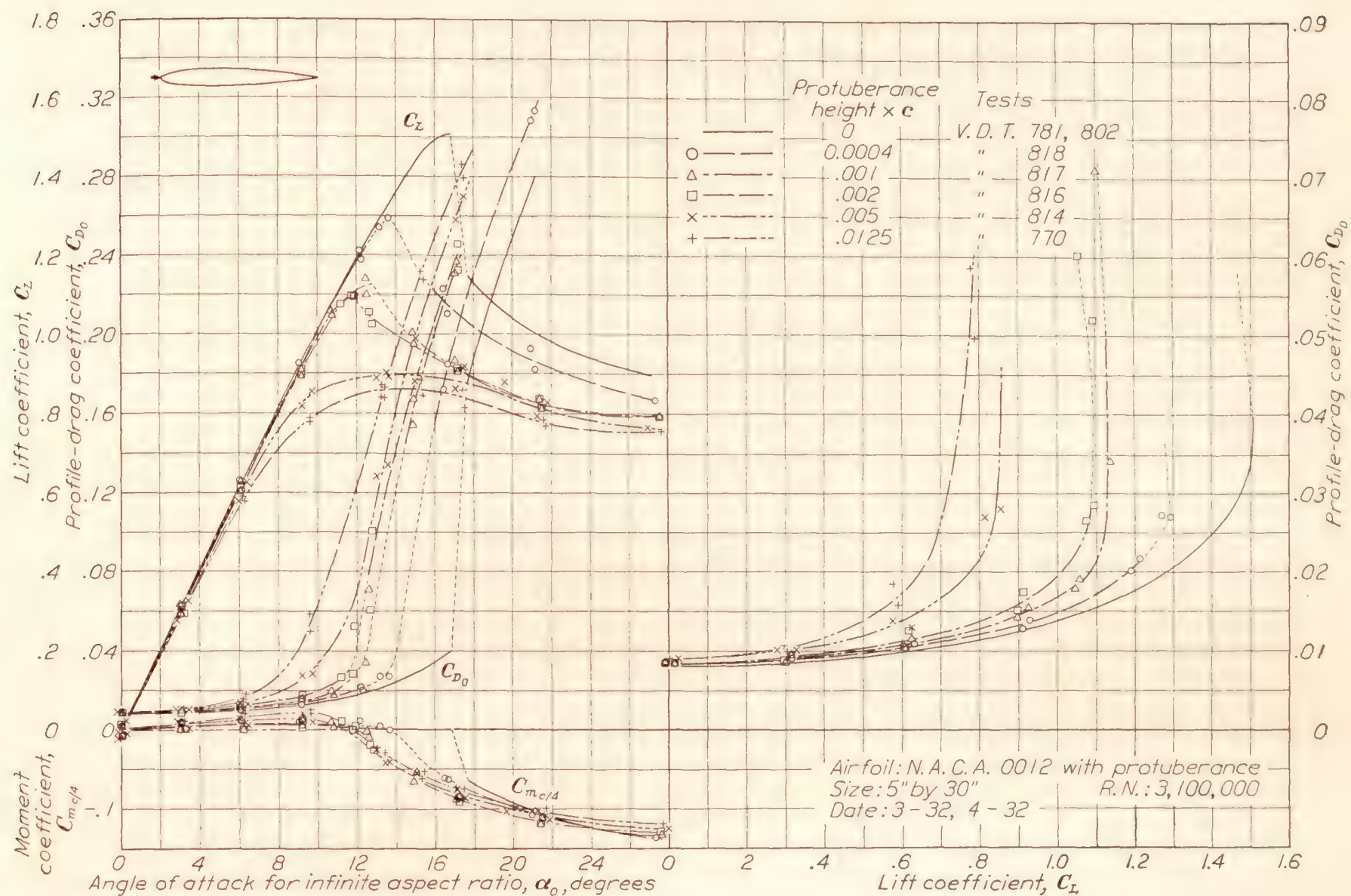


FIGURE 2.—Section characteristics for various protuberance heights. Protuberance on leading edge (position indicated by arrow)

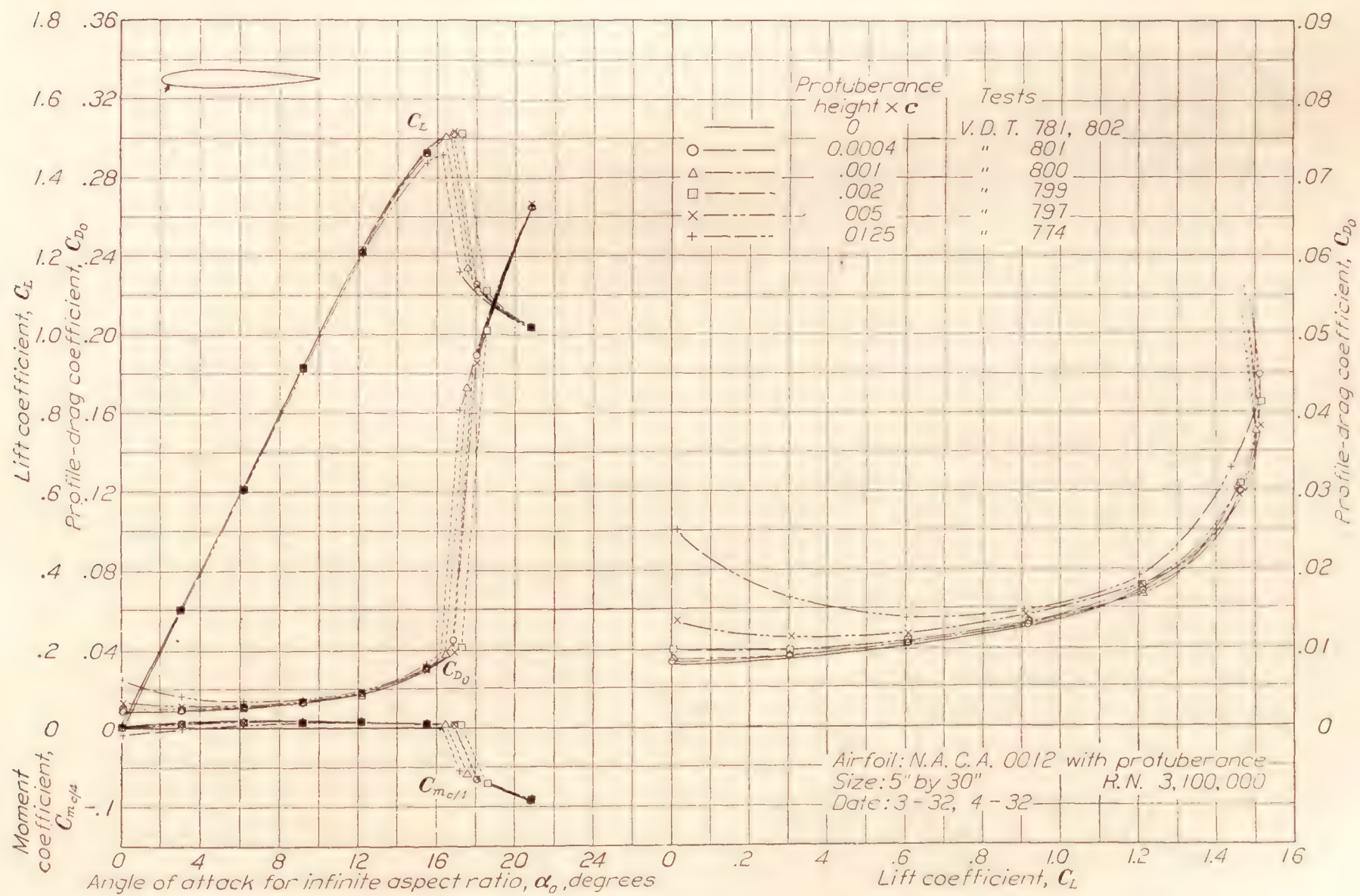


FIGURE 3.—Section characteristics for various protuberance heights. Protuberance on lower surface, 0.05c behind leading edge (position indicated by arrow)

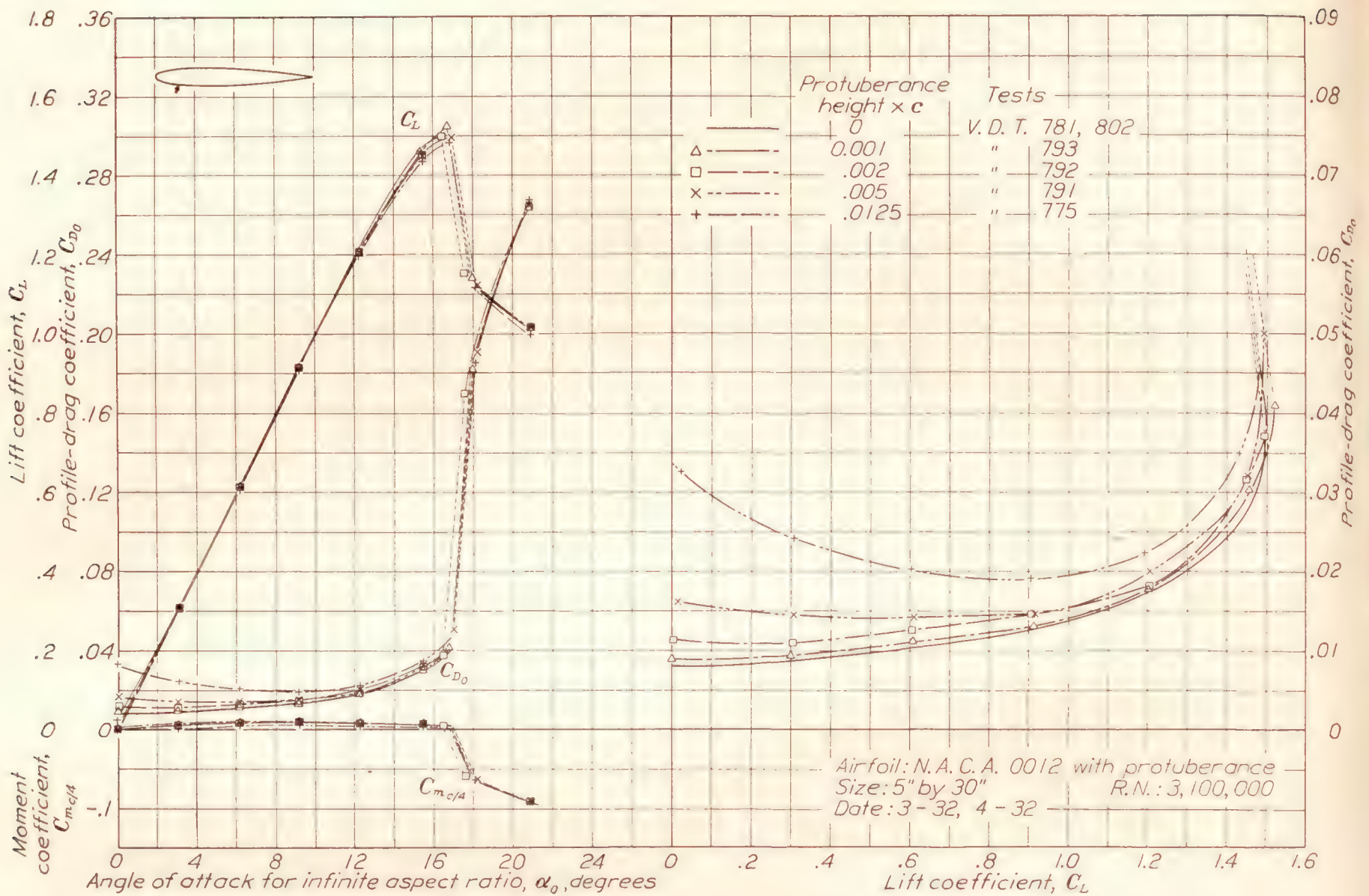


FIGURE 4.—Section characteristics for various protuberance heights. Protuberance on lower surface, 0.15c behind leading edge (position indicated by arrow)

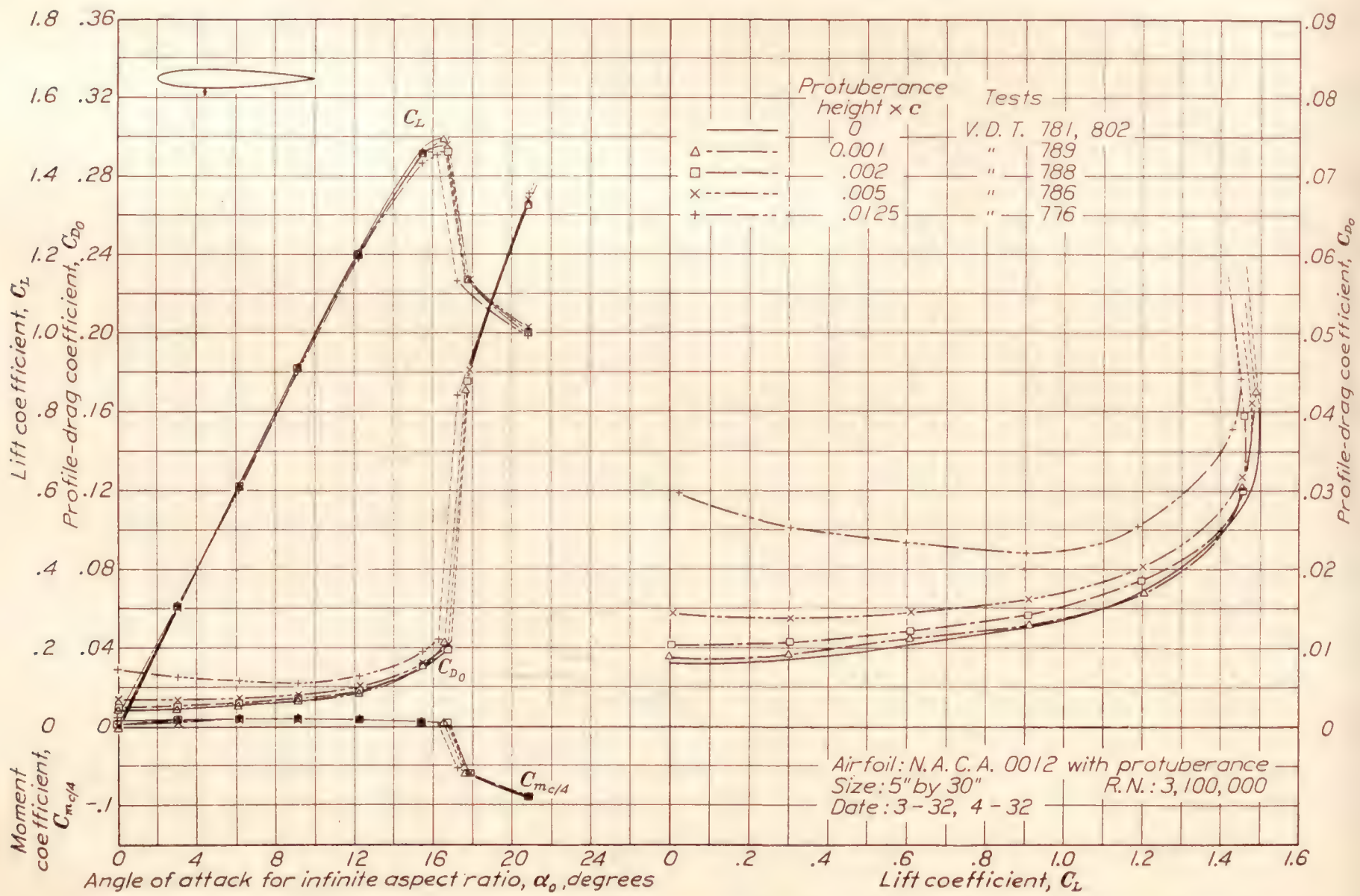
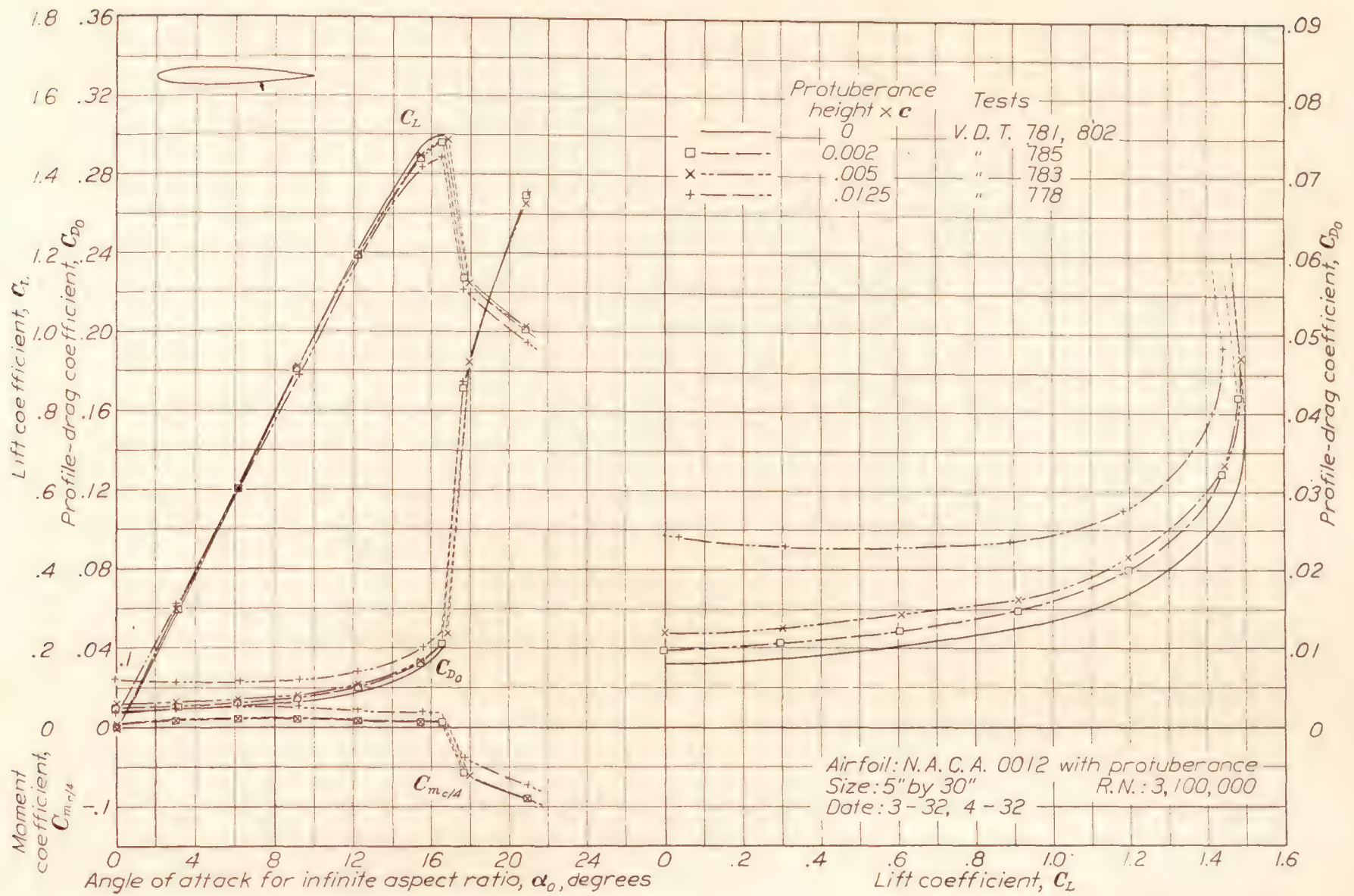
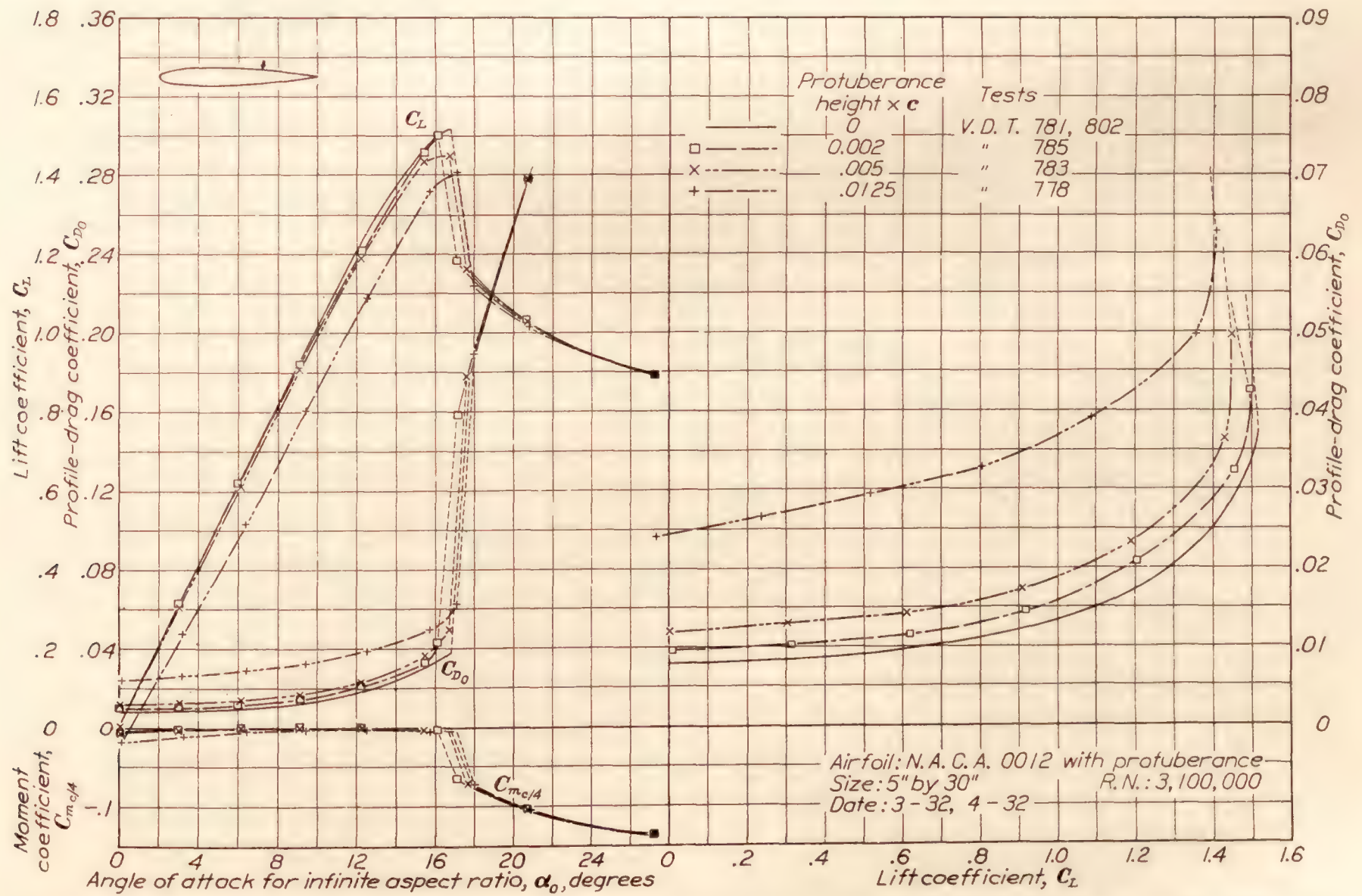


FIGURE 5.—Section characteristics for various protuberance heights. Protuberance on lower surface, 0.30c behind leading edge (position indicated by arrow)

FIGURE 6.—Section characteristics for various protuberance heights. Protuberance on lower surface, $0.65c$ behind leading edge (position indicated by arrow)FIGURE 7.—Section characteristics for various protuberance heights. Protuberance on upper surface $0.65c$ behind leading edge (position indicated by arrow)

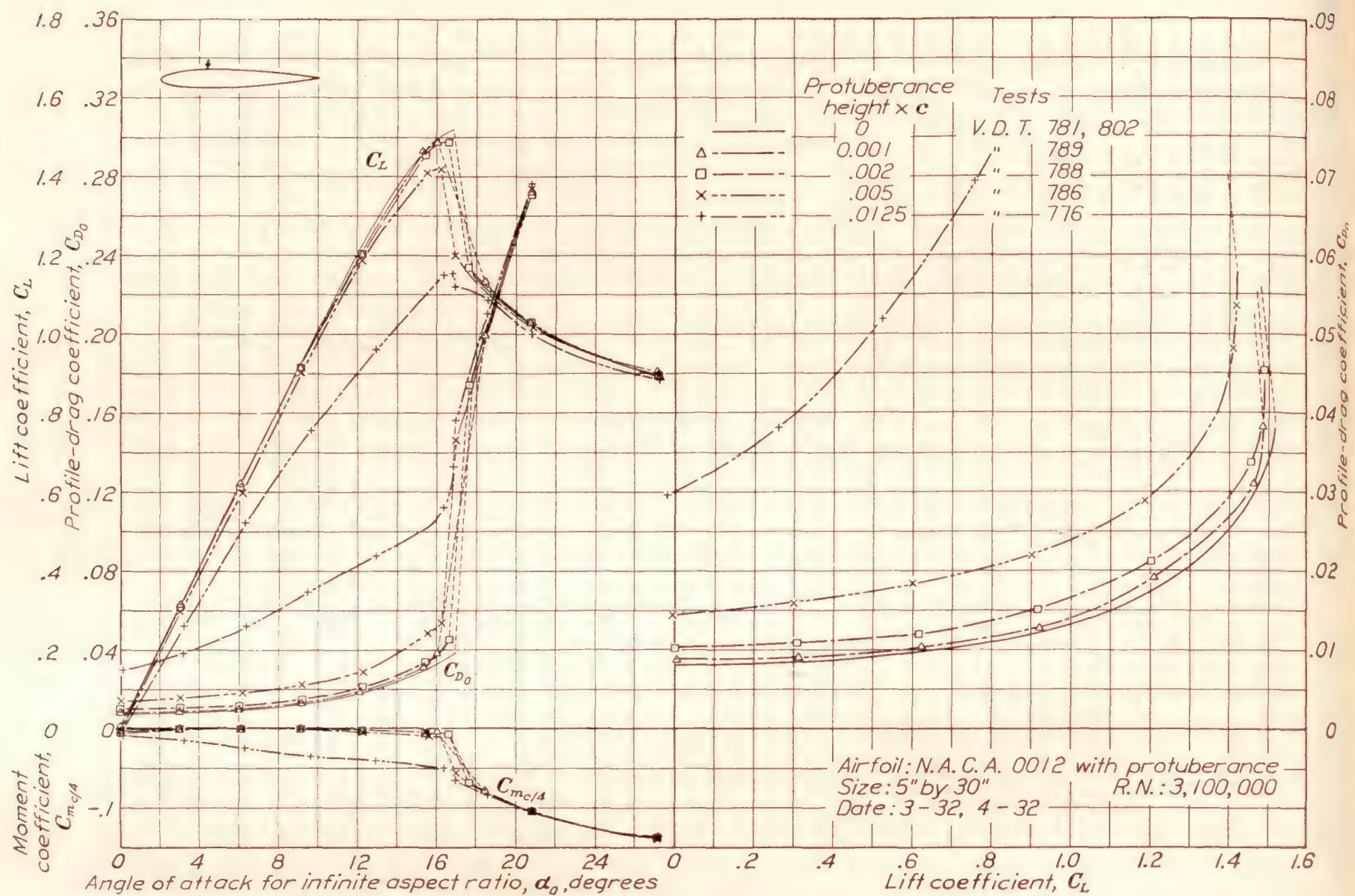


FIGURE 8.—Section characteristics for various protuberance heights. Protuberance on upper surface, 0.30c behind leading edge (position indicated by arrow)

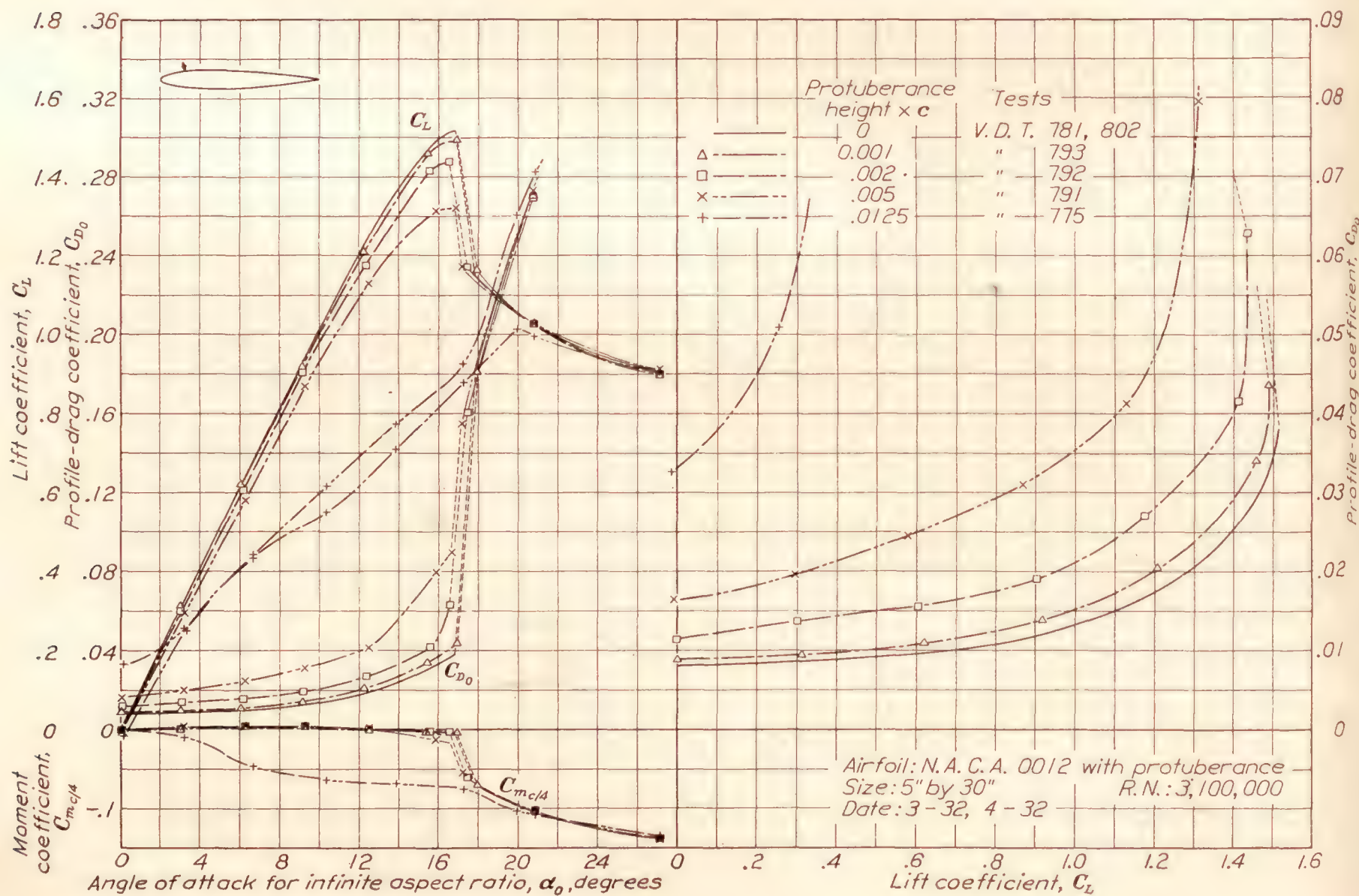


FIGURE 9.—Section characteristics for various protuberance heights. Protuberance on upper surface, 0.15c behind leading edge (position indicated by arrow)

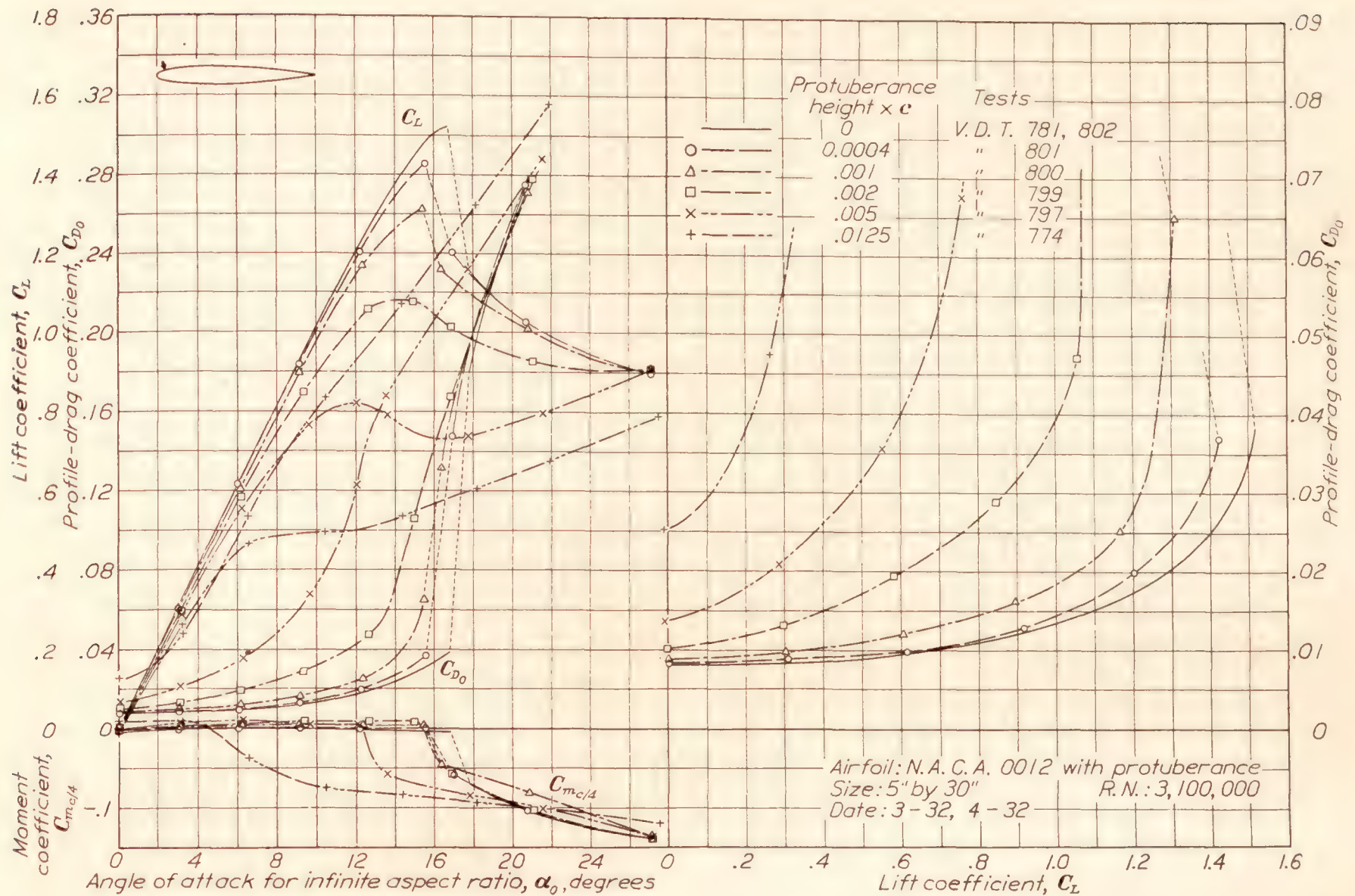


FIGURE 10.—Section characteristics for various protuberance heights. Protuberance on upper surface, 0.05c behind leading edge (position indicated by arrow)

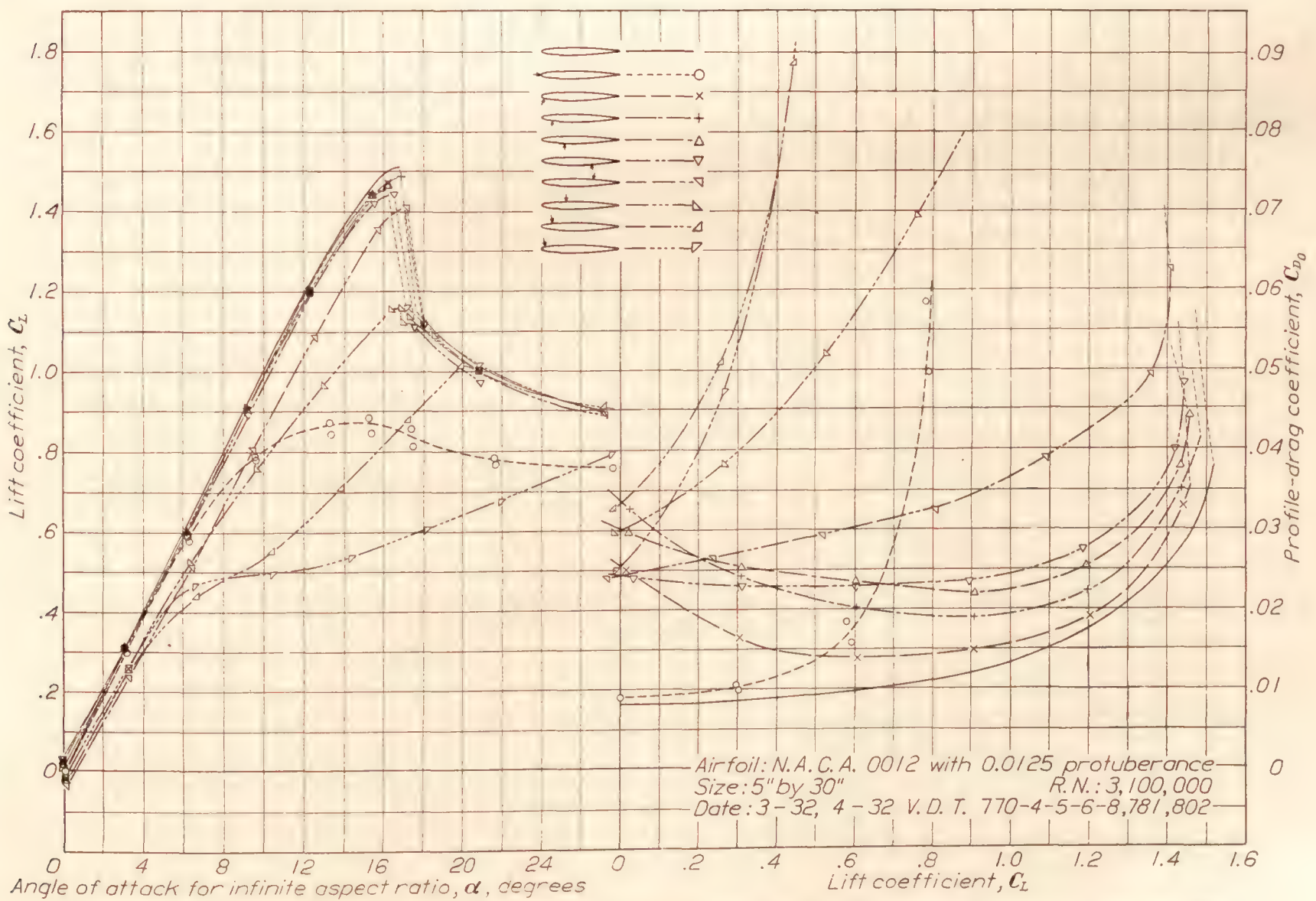


FIGURE 11.—Section characteristics for various protuberance positions. Height of protuberance: 0.0125c (positions indicated by arrows)

surface becomes increasingly serious as the protuberance approaches a point near the leading edge.

Considering now the effect of the protuberance on the drag, it will be seen from the plots of the profile-drag coefficient in Figure 11 that the effect is drastic for any position of the protuberance and attitude of the airfoil except for the nose position at low angles of

attack is shown by the curves in Figures 2 to 10. These figures give complete test data for the various protuberance positions and heights. The effect on the drag of varying the height, however, is shown more advantageously in Figure 12, where the profile drag coefficients corresponding to $C_L = 0$ and $C_L = 0.5$ are plotted against protuberance height. Straight lines repre-

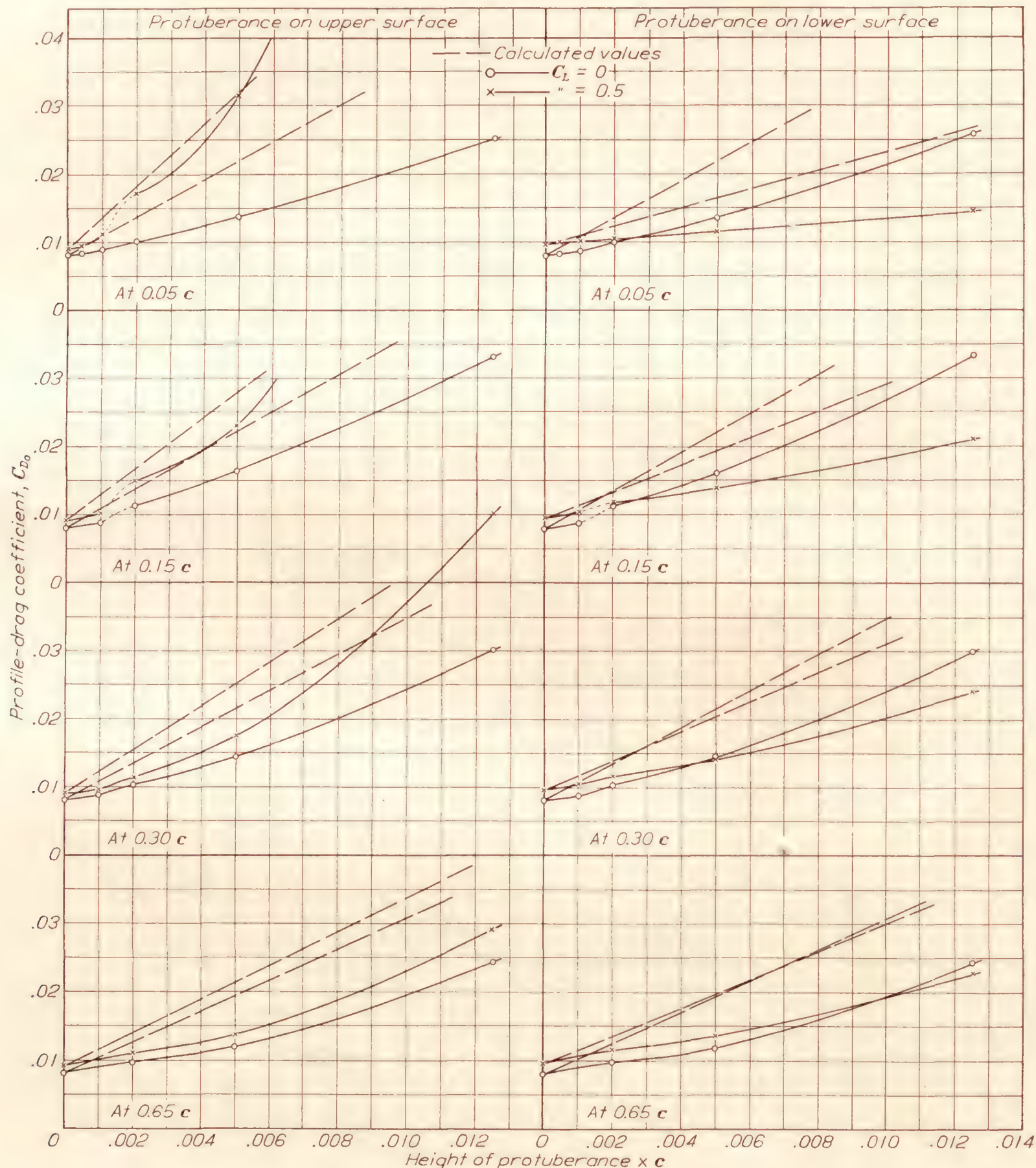


FIGURE 12.—Variation of drag with protuberance height

attack and the lower-surface positions behind the nose at the higher angles of attack. The protuberances in the most critical positions, on the upper surface near the leading edge, produce very large increases of the profile drag even at comparatively low angles of attack.

Protuberance height.—The effect on the airfoil characteristics of varying the height of the protuber-

ance is shown by the curves in Figures 2 to 10. These figures give complete test data for the various protuberance positions and heights. The effect on the drag of varying the height, however, is shown more advantageously in Figure 12, where the profile drag coefficients corresponding to $C_L = 0$ and $C_L = 0.5$ are plotted against protuberance height. Straight lines repre-

sents a calculated variation in drag with protuberance height are also included for comparison. The calculated lines were obtained by computing the additional profile drag due to the protuberance from the formula

$$\Delta C_{D0} = C_D (V'/V)^2 h/c$$

C_D is the drag coefficient of the protuberance based on

its frontal area. Weiselsberger (reference 4) gives the drag coefficient for flat plates of very large aspect ratio as approximately 2. The value 2 was therefore used for the calculations. The term $(V'/V)^2$ represents the square of the ratio of the local velocity at the airfoil surface at the position of the protuberance to the free-stream velocity. Values of this ratio calculated by the method of reference 5 are given in Table I for the positions on the surface corresponding to those of the protuberance. The ratio h/c is the ratio of the protuberance frontal area to the airfoil area. In other words, ΔC_{D_0} is the drag the plate would be expected to have expressed as a coefficient based on airfoil area neglecting the interference of the plate on the flow over the airfoil and the effects of the reduced velocity in the boundary layer of the airfoil on the drag of the plate. The lines plotted in Figure 12, obtained by adding ΔC_{D_0} to the profile drag of the wing without protuberance, are of value for comparison with the actual experimental curves.

TABLE I.—RESULTS OF CALCULATIONS OF VELOCITY AT SURFACE OF N. A. C. A. 0012 AIRFOIL

Station, per cent c	5	15	30	65
$\left(\frac{V \text{ at airfoil}}{V \text{ undisturbed stream}}\right)^2$ for $C_L=0$	1.38	1.41	1.36	1.14
$\left(\frac{V \text{ at airfoil}}{V \text{ undisturbed stream}}\right)^2$ on upper surface for $C_L=0.5$	2.29	1.89	1.61	1.24
$\left(\frac{V \text{ at airfoil}}{V \text{ undisturbed stream}}\right)^2$ on lower surface for $C_L=0.5$68	.98	1.06	1.03

A comparison of the lines with the experimental curves indicates that four regions may be considered as the protuberance height is increased.

The first is that region extending from $h=0$ to approximately $h=0.001c$, where the rate of increase of drag with protuberance height is low as compared with that indicated by the lines representing the calculated values. The relatively slow increase of drag with protuberance height in this region is probably due to the fact that the protuberance is in the low-velocity part of the wing boundary layer. Even in this region, however, the drag should not be considered as negligible, as shown by the fact that the drag increase due to the $0.001c$ protuberance expressed as a drag coefficient based on the free-stream dynamic pressure and the protuberance frontal area is in no case less than 0.7 at $C_L=0$.

The forward positions particularly show a second region extending from approximately $0.001c$ to $0.002c$ where the drag increases rapidly with protuberance height. In this region the protuberance is probably producing serious disturbing effects on the airfoil boundary layer. From a practical standpoint, it is therefore concluded that a special effort should be made to eliminate from a wing surface protuberances that exceed a height of $0.001c$. On a wing of 70-inch chord this height corresponds to 0.07 inch, or little more than one-sixteenth inch.

In the third region the curves tend to become parallel to the calculated lines. The actual drag influences, however, are much smaller than the calculated ones.

Some of the curves show a fourth region where the protuberance produces a marked interference with the flow over the airfoil. This region is not shown by any of the curves corresponding to $C_L=0$, and only by those corresponding to $C_L=0.5$ for the protuberance positions on the upper surface forward of the $0.65c$ position. Very rapid increases of drag with protuberance height are indicated in this region for protuberances higher than $0.005c$. The conclusion is that protuberances extending from the upper surface forward of the maximum-thickness position, having a height greater than $0.005c$, should be particularly avoided. These protuberances may, however, have a useful application as spoilers or air brakes.

For the estimation of the drag due to protuberances in connection with practical applications, a simpler method of calculating the drag due to protuberances based on the data given in the following table will probably be more satisfactory than the previous discussion. In the table are presented the important results at a lift coefficient of 0.2 corresponding to high-speed flight. The results are given as coefficients of drag due to the protuberance, the coefficients being based on the protuberance frontal area and the free-stream dynamic pressure, so that the drag due to a protuberance may be obtained simply as the product of the protuberance frontal area, dynamic pressure, and the coefficient from the following table:

COEFFICIENTS OF DRAG DUE TO PROTUBERANCE BASED ON PROTUBERANCE FRONTAL AREA ($C_L=0.2$)

per cent c behind leading edge	Height in terms of chord	0.0004	0.001	0.002	0.005	0.0125
5 upper surface.....	1	1.1	1.8	1.9	2.4	2.4
15 upper surface.....		.8	2.3	2.0	2.9	2.9
30 upper surface.....		.7	1.2	1.5	2.2	2.2
65 upper surface.....			.9	.9	1.4	1.4
5 lower surface.....	1	.6	.7	.7	.8	.8
15 lower surface.....		.8	1.2	1.3	1.5	1.5
30 lower surface.....		.7	1.1	1.1	1.5	1.5
65 lower surface.....			1.0	.8	1.2	1.2

As a rule, the drag due to most of the protuberances investigated could be roughly estimated as equal to or greater than the product of the protuberance frontal area and the free-stream dynamic pressure. A lower drag results from protuberances on the leading edge or near the leading edge on the lower surface, and from other small protuberances, but the rule may be found useful. The higher drags may be seen from the table to correspond to protuberances having a height of $0.002c$ or more, particularly when they are on the forward portion of the upper surface.

As a practical application, consider a $\frac{1}{32}$ -inch thick butt strap at a position on the upper surface $0.05c$

behind the leading edge extending along the span of a wing having a 70-inch chord and a 35-foot span, the frontal area of the protuberance is then 0.091 square feet. If the velocity is 200 miles per hour, the dynamic pressure for standard air is 102.32 pounds per square foot. Applying the above rule, or taking the coefficient 1 from the preceding table, the drag is estimated as 102 times 0.091, or 9.3 pounds. The corresponding power consumption at the speed considered would be approximately 5 horsepower.

The effects on maximum lift of the protuberances of various heights are also shown in Figures 2 to 10. The effect can be seen more easily, however, from the curves of Figure 13 representing the variation of maximum lift with protuberance height for the various positions

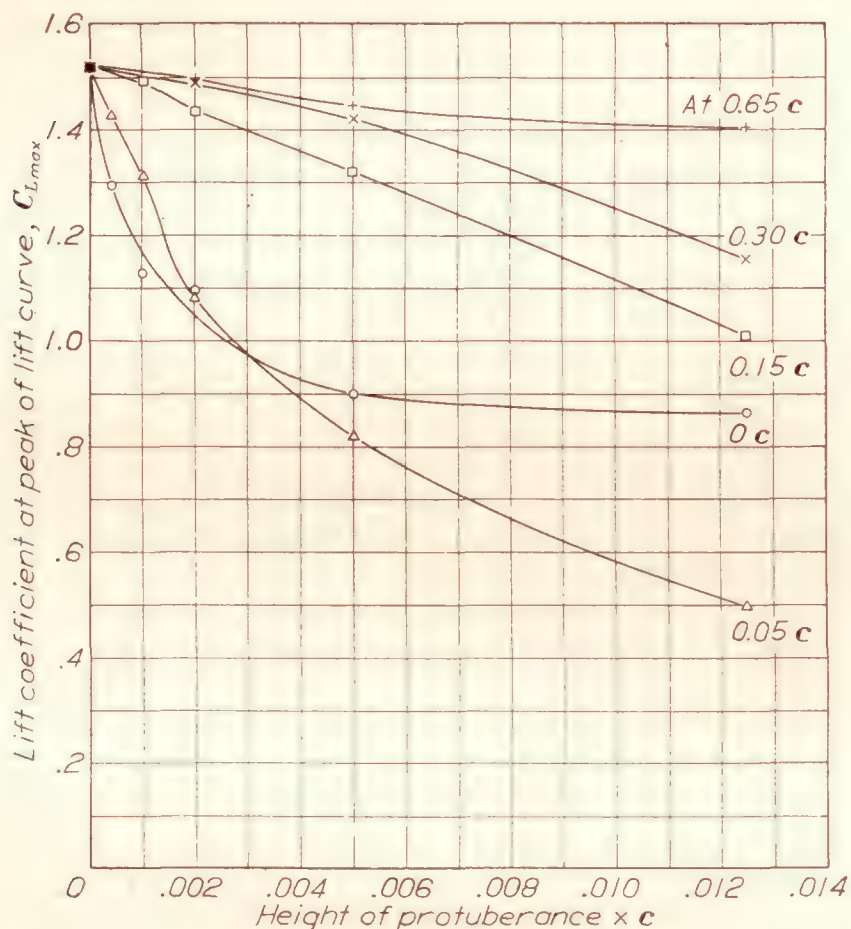


FIGURE 13.—Variation of maximum lift with protuberance height. Protuberance on upper surface

on the upper surface of the airfoil. It will be remembered that the protuberance on the lower surface produced only a slight change in the maximum lift coefficient. Figure 13 indicates that the loss of maximum lift due to the protuberance is nearly proportional to the protuberance height except for the positions near the leading edge on the upper surface. For these positions the small protuberances produce disproportionately large effects. In the nose position the protuberance having a height of only $0.0004c$ reduced the maximum lift by approximately 15 per cent. This protuberance was so small that it might rather be classed as a surface roughness. Because considerable difficulty was experienced in forming it, the shape of the protuberance was not maintained exactly as desired. Sections of the airfoil nose, including the protuberance, were measured after the protuberance had been reduced in height to $0.0004c$. The results of these measurements for four sections are shown in

Figure 14 to a scale corresponding approximately to full scale for medium-size airplanes. The general conclusion that may be drawn from this phase of the investigation is that the airfoil leading edge must be smooth and fair if high maximum lift coefficients are to be obtained.

Fairing.—The effects of fairing the $0.005c$ protuberance are shown in Figures 15 to 23. Each figure presents the airfoil section characteristics corresponding to one protuberance position for the plain airfoil, the airfoil with the normal $0.005c$ protuberance, and the airfoil with the faired protuberance.

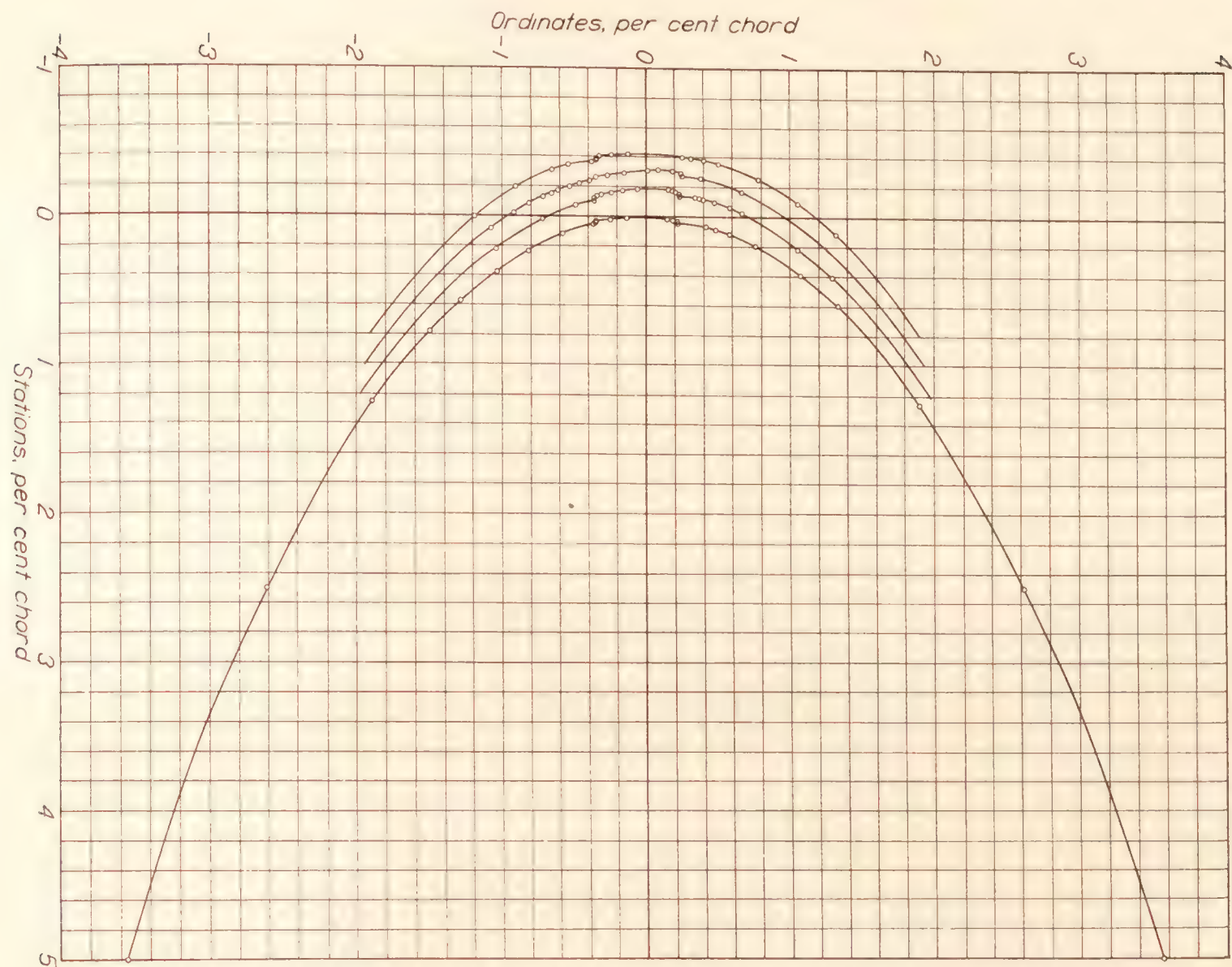
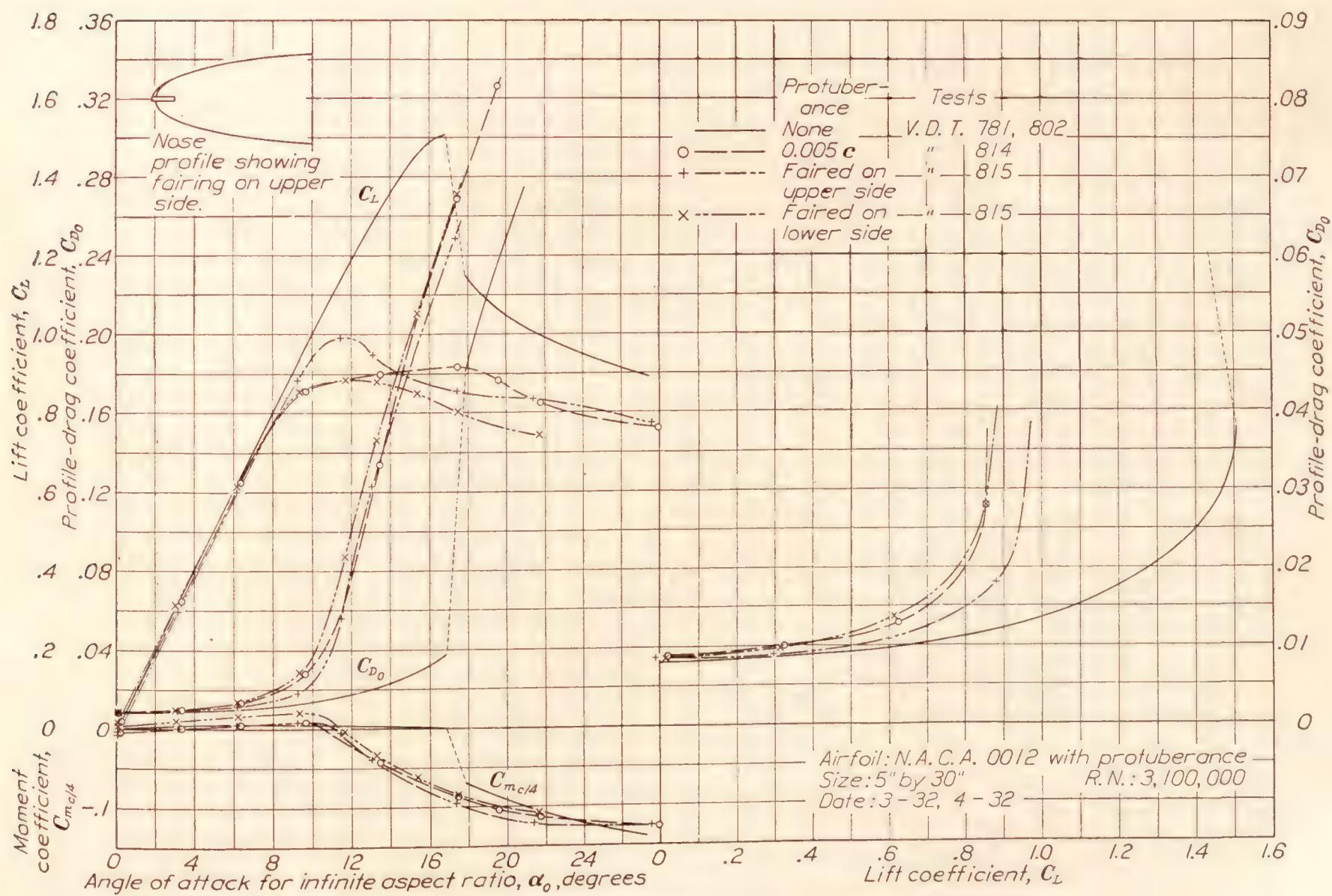
The results showing the effects on drag of fairing the protuberances are shown by the profile-drag curves at the right of each figure. It is concluded from these results that the adverse drag effects of the protuberance may be greatly reduced but not entirely eliminated by employing a simple fairing over the protuberance as shown in Figure 1.

As regards the adverse effects of the protuberance on the maximum lift, it may be concluded that they can be practically eliminated by a simple fairing of the type employed except where the protuberance is near the leading edge. With the protuberance in the leading-edge position, it is obvious that a suitably formed fairing would eliminate the adverse effects. In this position, therefore, the fairing was applied to only one side of the protuberance. These results, which are presented in Figure 15, indicate that the fairing has little effect when it is employed on only one side of the protuberance. For the first position behind the leading edge on the upper surface the simple fairing employed apparently was not adequate, as the full value of maximum lift coefficient (fig. 23) was not regained after the fairing had been applied.

CONCLUSIONS

The following conclusions of immediate practical value may be drawn from the results in regard to the effects of full-span protuberances.

1. For most of the unfaired protuberances investigated except those very near the leading edge, the drag resulting from the addition of the protuberance could be roughly estimated as equal to or greater than the product of the free-stream dynamic pressure and the protuberance frontal area.
2. The greater drag increases may result from protuberances the height of which exceeds $0.001c$, particularly when the protuberances are from points along either surface forward of the maximum-thickness position.
3. Very large increases of drag may result from the interference of a protuberance having a height exceeding $0.005c$ if it is on the forward portion of the upper surface of the profile.
4. A simple fairing over the protuberance greatly reduces but does not entirely eliminate the adverse effect.


 FIGURE 14.—Nose profile, measured at four representative stations along span, showing $0.0004c$ protuberance at leading edge

 FIGURE 15.—Effect of fairing upper side or lower side of $0.005c$ protuberance on leading edge

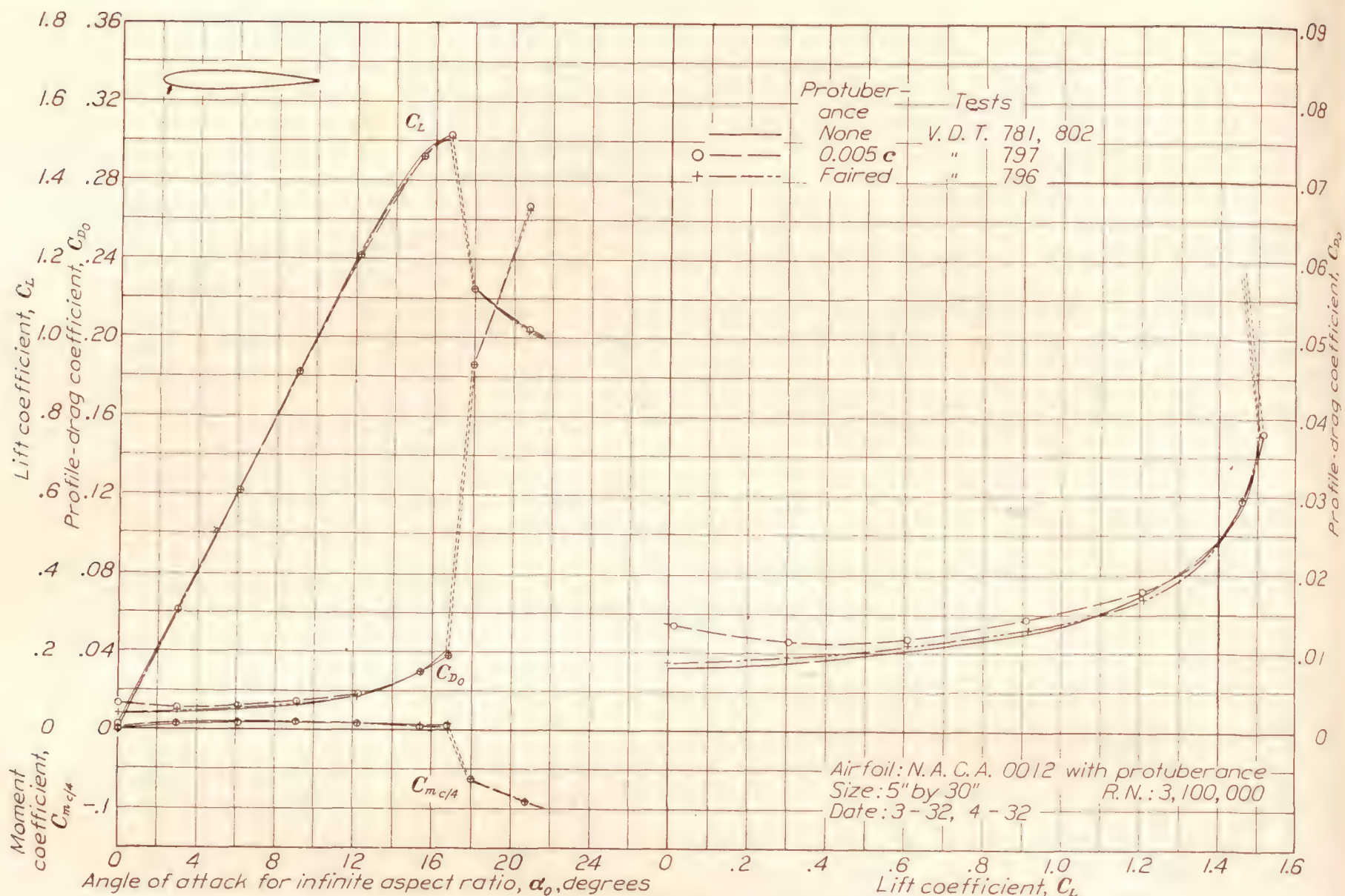


FIGURE 16.—Effect of fairing 0.005c protuberance on lower surface, 0.05c behind leading edge (position indicated by arrow)

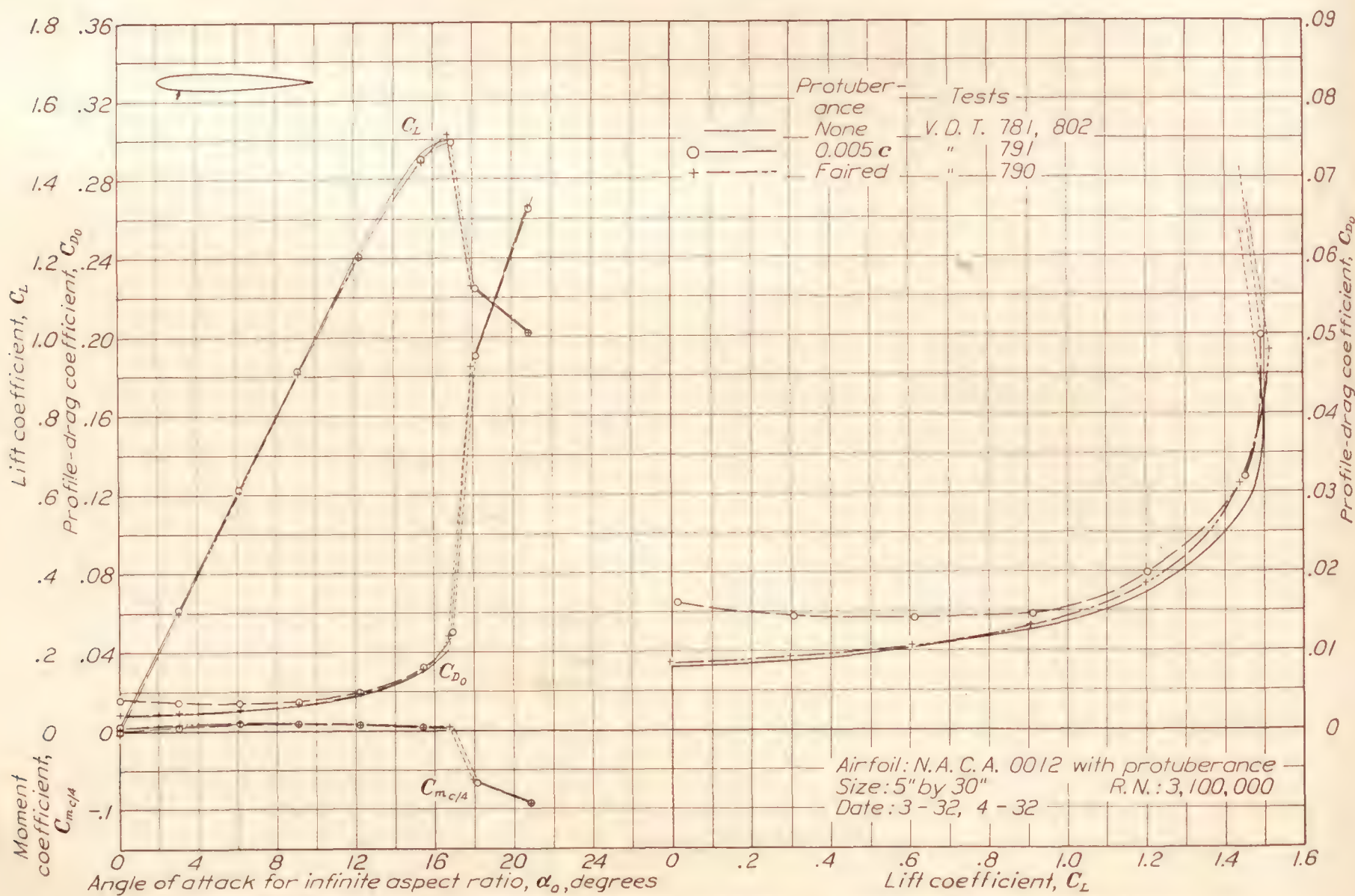


FIGURE 17.—Effect of fairing 0.005c protuberance on lower surface, 0.15c behind leading edge (position indicated by arrow)

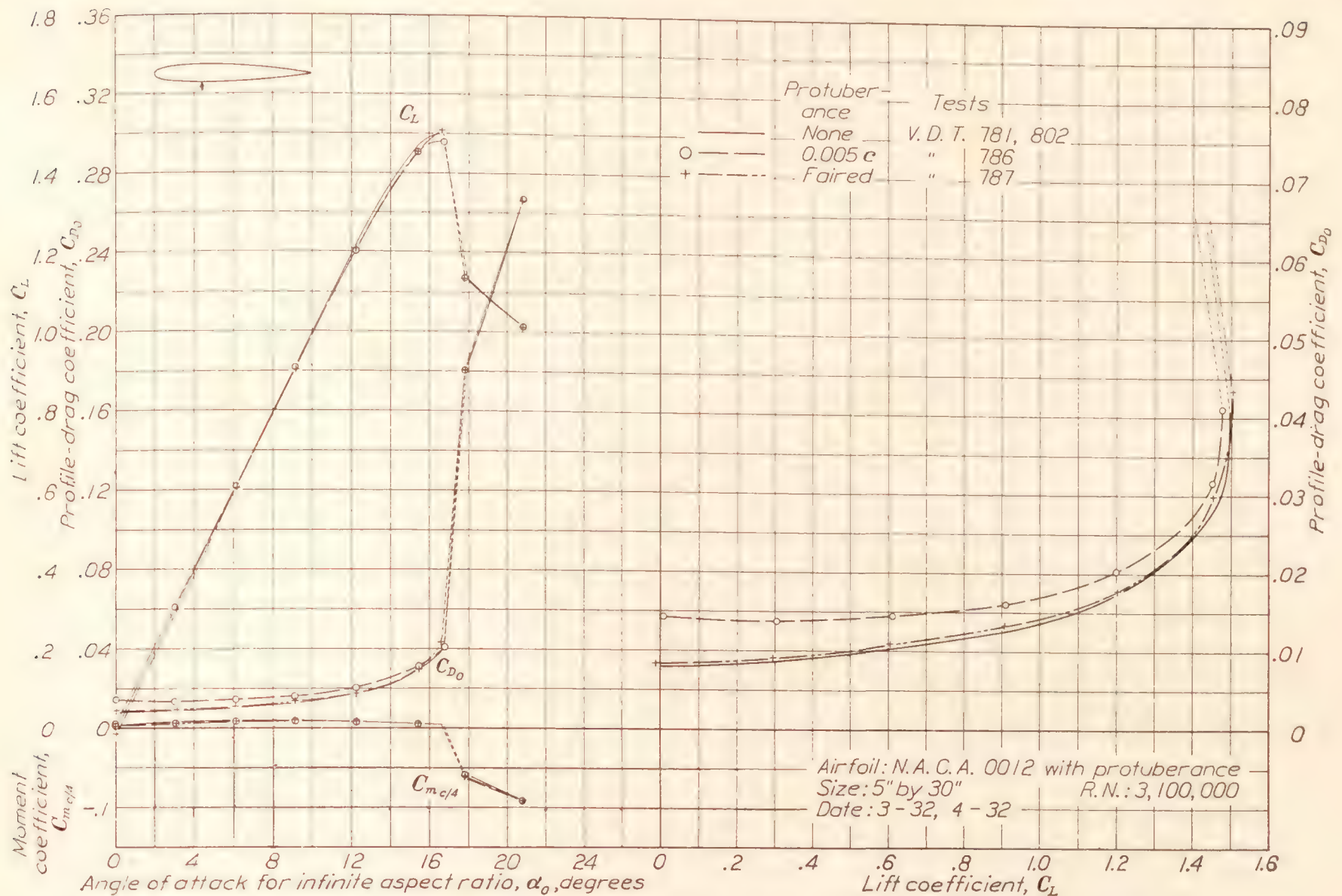


FIGURE 18.—Effect of fairing 0.005c protuberance on lower surface, 0.30c behind leading edge (position indicated by arrow)

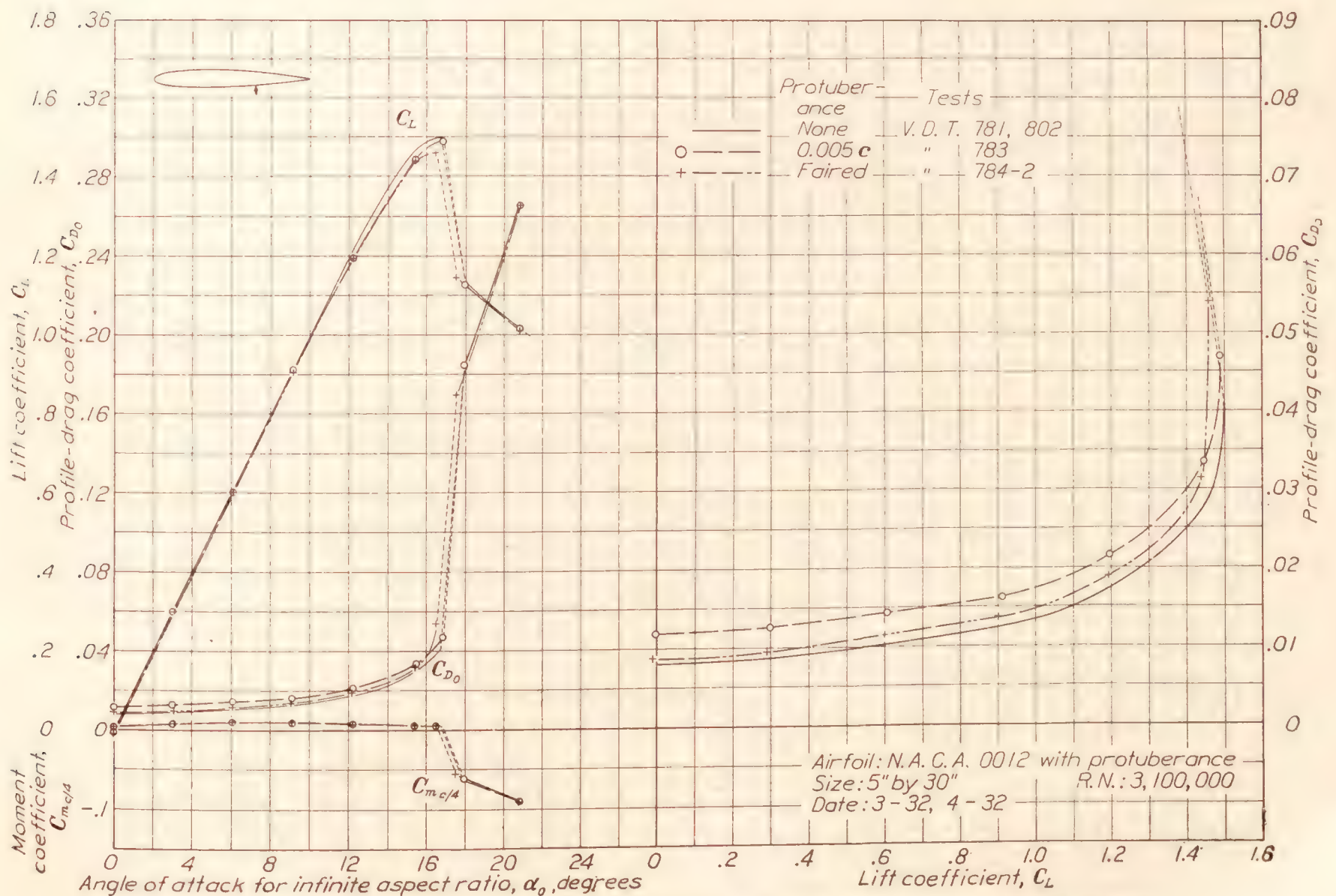


FIGURE 19.—Effect of fairing 0.005c protuberance on lower surface, 0.65c behind leading edge (position indicated by arrow)

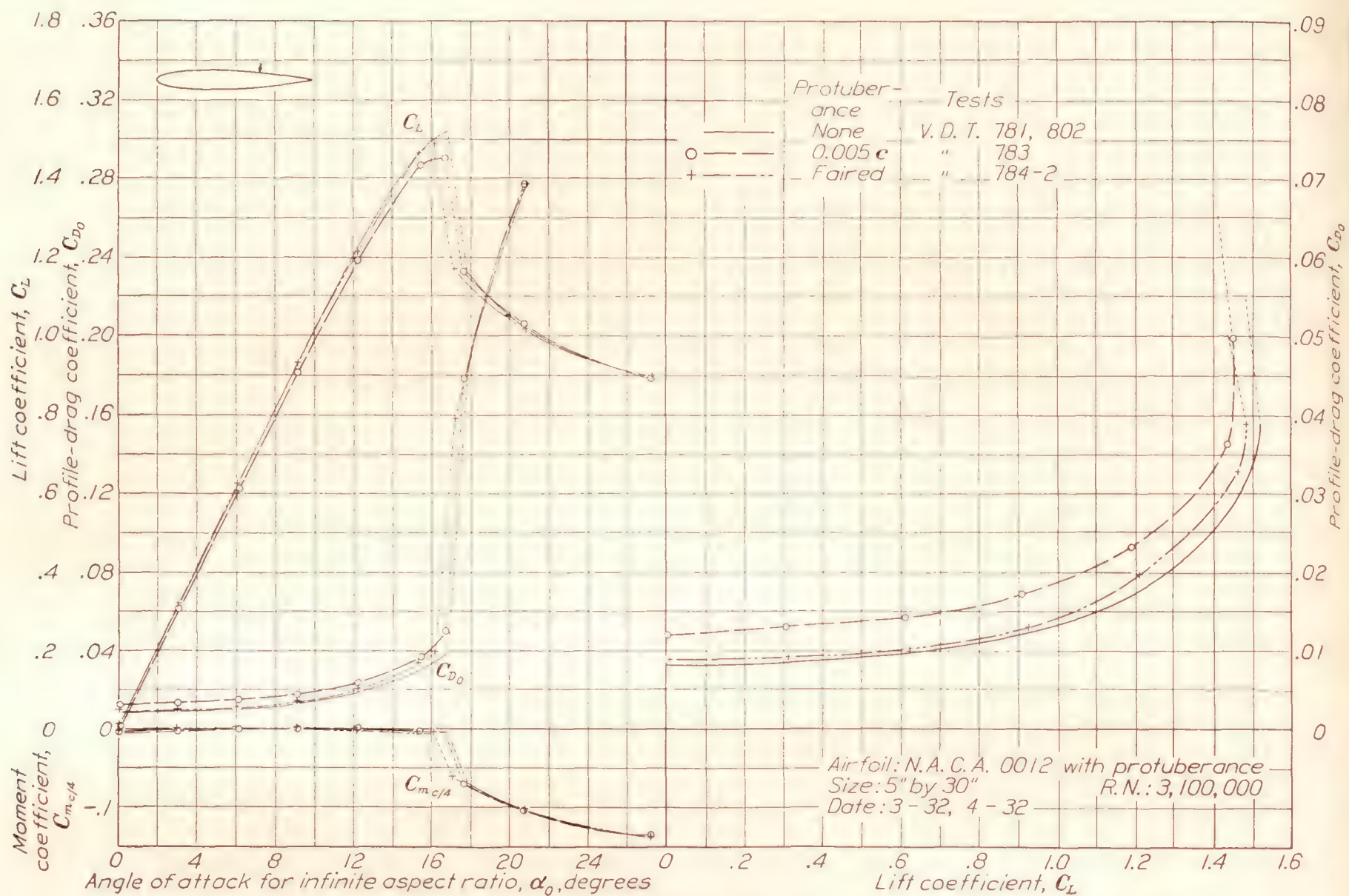


FIGURE 20.—Effect of fairing 0.005c protuberance on upper surface, 0.65c behind leading edge (position indicated by arrow)

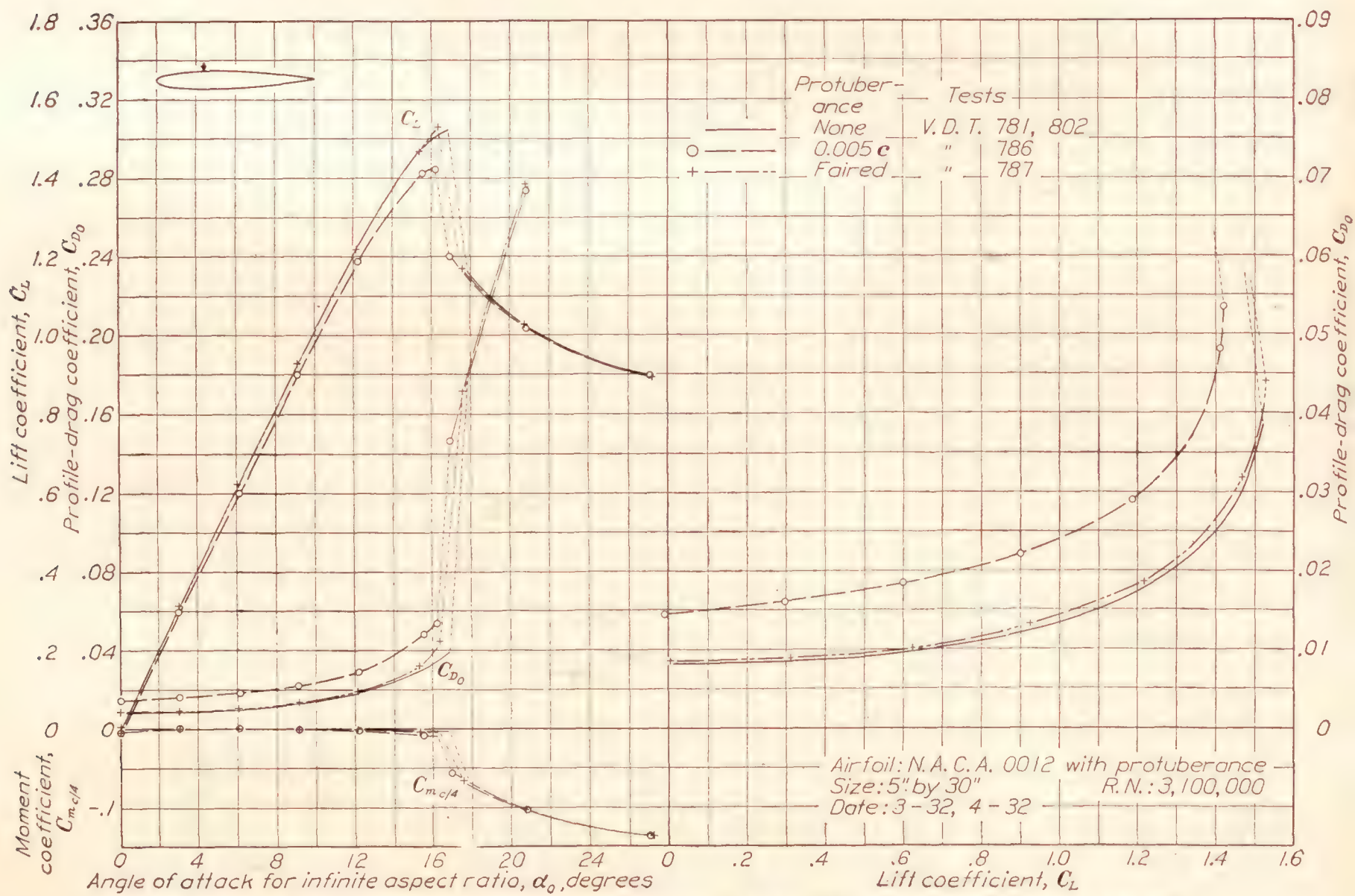


FIGURE 21.—Effect of fairing 0.005c protuberance on upper surface, 0.30c behind leading edge (position indicated by arrow)

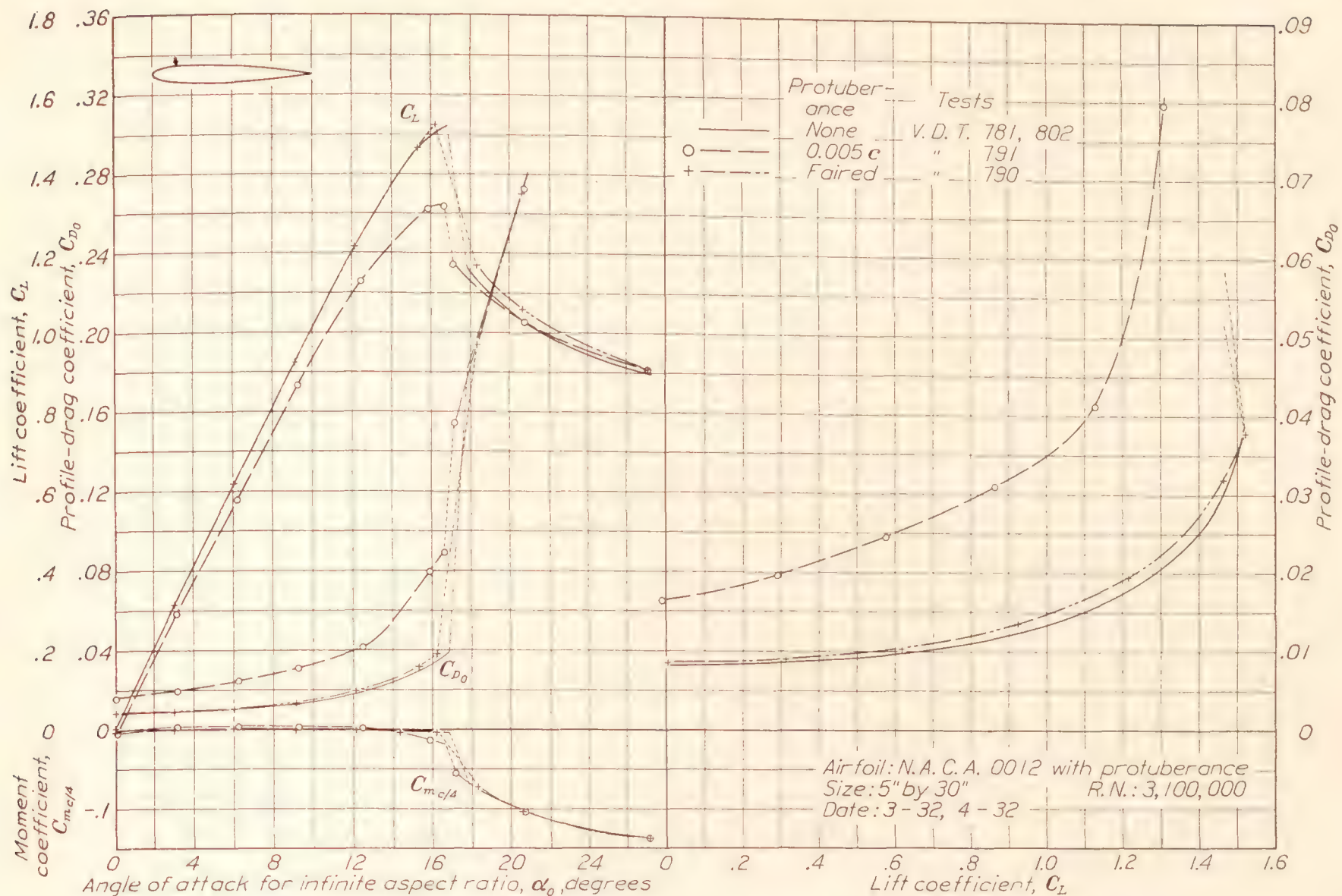


FIGURE 22.—Effect of fairing 0.005c protuberance on upper surface, 0.15c behind leading edge (position indicated by arrow)

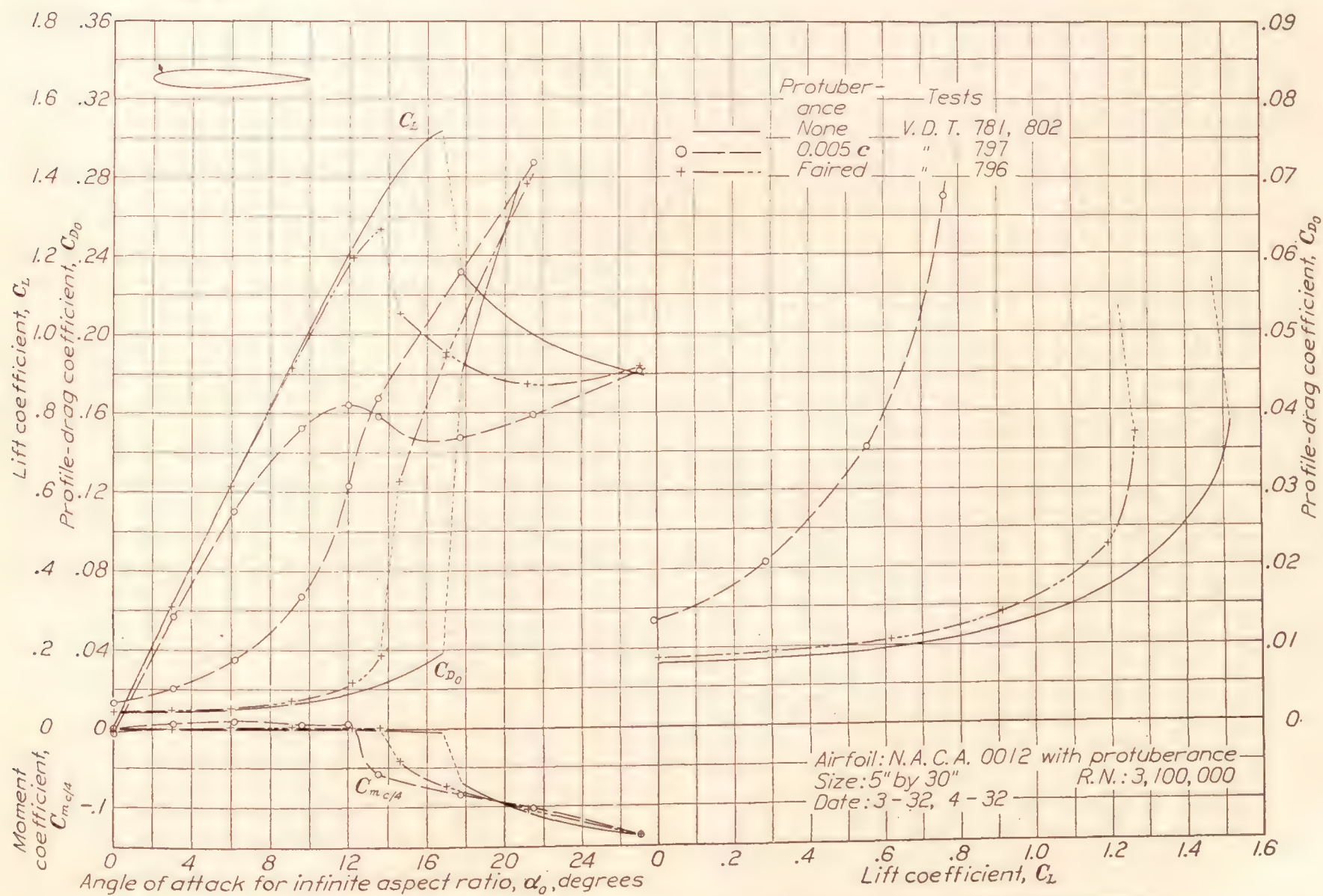


FIGURE 23.—Effect of fairing 0.005c protuberance on upper surface, 0.05c behind leading edge (position indicated by arrow)

5. The effect of a protuberance on the maximum lift is unimportant when the protuberance is on the lower surface, but becomes very important, even for a protuberance so small that it would ordinarily be classed as a surface roughness, as the position approaches the leading edge along the upper surface.

LANGLEY MEMORIAL AERONAUTICAL LABORATORY,
NATIONAL ADVISORY COMMITTEE FOR AERONAUTICS,
LANGLEY FIELD, VA., *July 11, 1932.*

REFERENCES

1. Ower, E.: Interference. Roy. Aero. Soc. Jour., July, 1932, pp. 531-77.
2. Jacobs, Eastman N., and Abbott, Ira H.: The N. A. C. A. Variable-Density Wind Tunnel. T. R. No. 416, N. A. C. A., 1932.
3. Jacobs, Eastman N.: Tests of Six Symmetrical Airfoils in the Variable-Density Wind Tunnel. T. N. No. 385, N. A. C. A., 1931.
4. Wieselsberger, C., and Betz, A.: Ergebnisse der Aerodynamischen Versuchsanstalt zu Göttingen. Oldenbourg (München), 1923. II Lieferung, pp. 33-34.
5. Theodorsen, T.: Theory of Wing Sections of Arbitrary Shape. T. R. No. 411, N. A. C. A., 1931.

REPORT No. 447

STATIC THRUST OF AIRPLANE PROPELLERS

By WALTER S. DIEHL

SUMMARY

Static thrust data from more than 100 airplane propeller tests are collected from various sources and combined in working charts, from which the static thrust coefficient K_{T_0} in the equation

$$T_0 = \frac{K_{T_0} \times \text{b. hp}}{\text{r. p. m.} \times \text{diam.}}$$

may be readily determined. The available data cover practically all types of propellers and are in good agreement. For extreme pitch ratios, or for very low and for very high blade settings, the values of K_{T_0} are shown to deviate considerably from the generally used linear relations based on data at moderate pitch ratios.

INTRODUCTION

The static thrust of a propeller was formerly of interest only in connection with proposed helicopter designs, but the advent of very high powers and corresponding high performance in recent airplane designs have made it necessary to consider the static thrust as a design factor. At present the chief applications of accurate static thrust data are in the calculation of nosing-over moments and the estimation of take-off runs.

The available methods of calculating static thrust are based on constants derived from Durand and Lesley's tests on wooden propellers. (Reference 4.) It is the purpose of this report to revise the constants and to extend the methods to include recent data on adjustable metal propellers.

Warner shows in reference 1 that the thrust per horsepower is obtained by division, from the coefficients

$$C_T = \frac{T}{\rho n^2 D^4} \quad (1)$$

and

$$C_P = \frac{P}{\rho n^3 D^5} \quad (2)$$

giving

$$\frac{T}{P} = \frac{C_T}{C_P} \frac{1}{nD}$$

or

$$T = \frac{C_T}{C_P} \frac{P}{nD} \quad (3)$$

In Chapter XIV of reference 2, Mr. Warner states: "It can be shown from propeller theory that the static thrust per horsepower for a propeller is equal to a constant divided by the product of the r. p. m. of the propeller and its diameter, and experiments by Durand have shown that the average value of the constant ranges from 49,000 for propellers designed to work normally at a value of V/nD of 1.1 up to 79,000 when V/nD for maximum efficiency is 0.5 — — —. The variation of the coefficient is approximately linear between the points given."

In reference 3 the author gives the static thrust formula

$$T_0 = 6,000 \left(18.7 - 9.5 \frac{p}{D} \right) \frac{\text{b. hp}}{(\text{r. p. m.}) \times D} \quad (4)$$

Where T_0 is the static thrust in pounds, p/D is the nominal pitch/diameter ratio and D is the diameter in feet. The value of the constant in equation (4) was based on Durand and Lesley's data and is substantially identical with Warner's values as quoted above.

It will be shown that the static thrust coefficient K_{T_0} in the equation

$$T_0 = \frac{K_{T_0} \times \text{b. hp}}{(\text{r. p. m.}) \times D} \quad (5)$$

can be determined with fair accuracy for any propeller from data usually available or readily obtained.

DURAND AND LESLEY'S TESTS

In Table V of reference 4, Durand and Lesley give the "standing thrust and power" for 67 propellers. These include a number of variations in blade section and blade form that are of academic interest only, since practically all propellers now in use are in the $S_1 F_2$ class. Table I lists the essential data including the static thrust coefficient K_{T_0} for all of the $S_1 F_2$ propellers. K_{T_0} is found from the relation

$$K_{T_0} = 33,000 \frac{C_T'}{C_P'}$$

the conversion factor 33,000 being required for the units of b. hp and r. p. m. in equation (5).

The values of K_{T_0} are plotted against p/D on Figure 1. The dashed line on this figure corresponds to equation (4) and may be represented by

$$K_{T_0} = 112,400 - 57,000 \frac{p}{D} \quad (6)$$

or

$$K_{T_0} = 57,000 \left(1.97 - \frac{p}{D} \right) \quad (6a)$$

both of which are identical with equation (4).

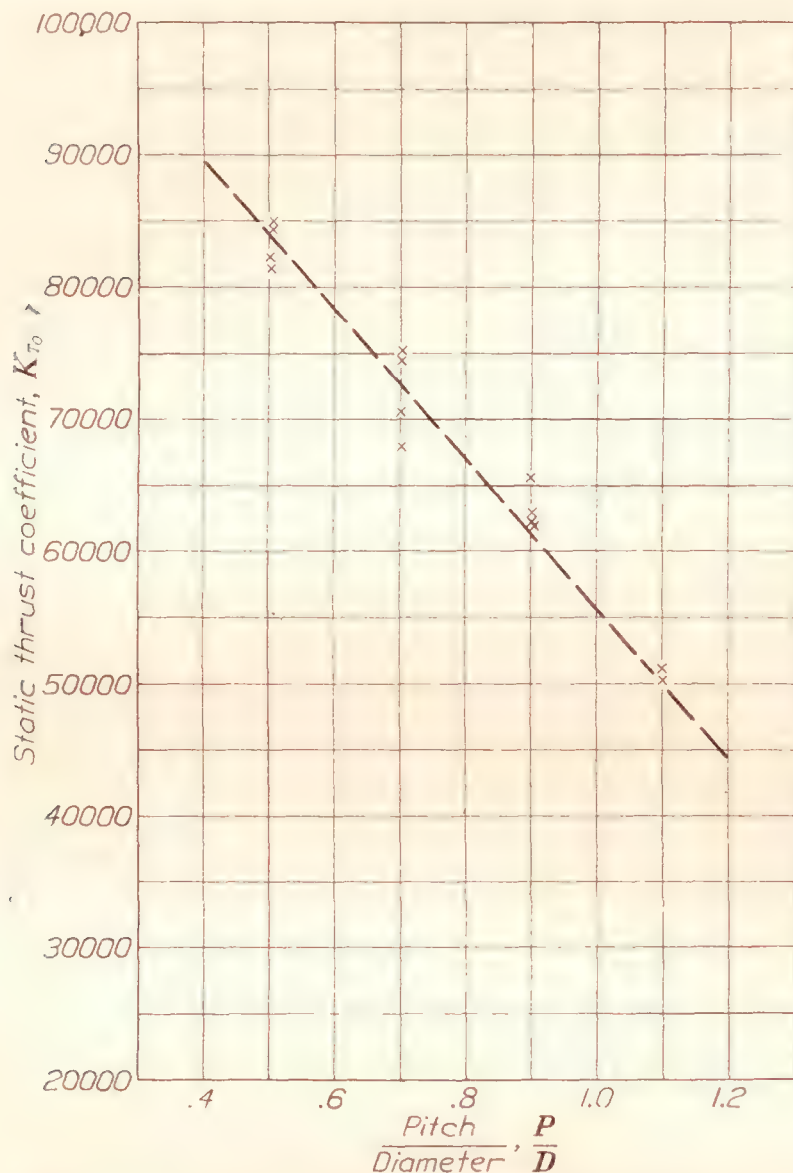


FIGURE 1.—Static thrust coefficients for 2-blade wooden propellers. Durand and Lesley's tests. N. A. C. A. Technical Report No. 30

N. A. C. A. TESTS

Three series of systematic tests on adjustable blade metal propellers have been made by the National Advisory Committee for Aeronautics in the propeller research tunnel at Langley Field. (References 5, 6, and 7.) Static thrust data from these reports are given in Tables II to V, inclusive, and the values of K_{T_0} are plotted against blade setting at $0.75 R$ in Figure 2. There is a considerable scattering of the points probably due to fuselage interference effects and to the method of obtaining the static values of C_T and C_P by extrapolation but the trend of the variation is well defined. It is of considerable interest to note the reduction in static thrust at high pitch angles for propellers with the Clark Y section. This characteristic, which may be due to an early stalling of the blade sections, has been observed in flight tests to such an extent that a separate curve is apparently required

for these propellers. As shown by the data from Technical Report No. 351 (reference 6), given in Table III, cutting off the tips to reduce the diameter does not appreciably affect the static thrust coefficient.

BRITISH TESTS

A very complete investigation of propeller characteristics is covered by Reports and Memoranda No. 829 of the British Aeronautical Research Committee. (Reference 8.) Static thrust data from this report are given in Tables VI and VII. The former covers propellers having constant pitch along the blade, while the latter have the variable pitch distribution obtained with the usual blade adjustment. Values of K_{T_0} are plotted against blade angle at $0.75 R$ on Figure 3. The data are usually consistent due to care exercised in eliminating interference and fall very close to the three curves, the one for two blades being identical with that given on Figure 2.

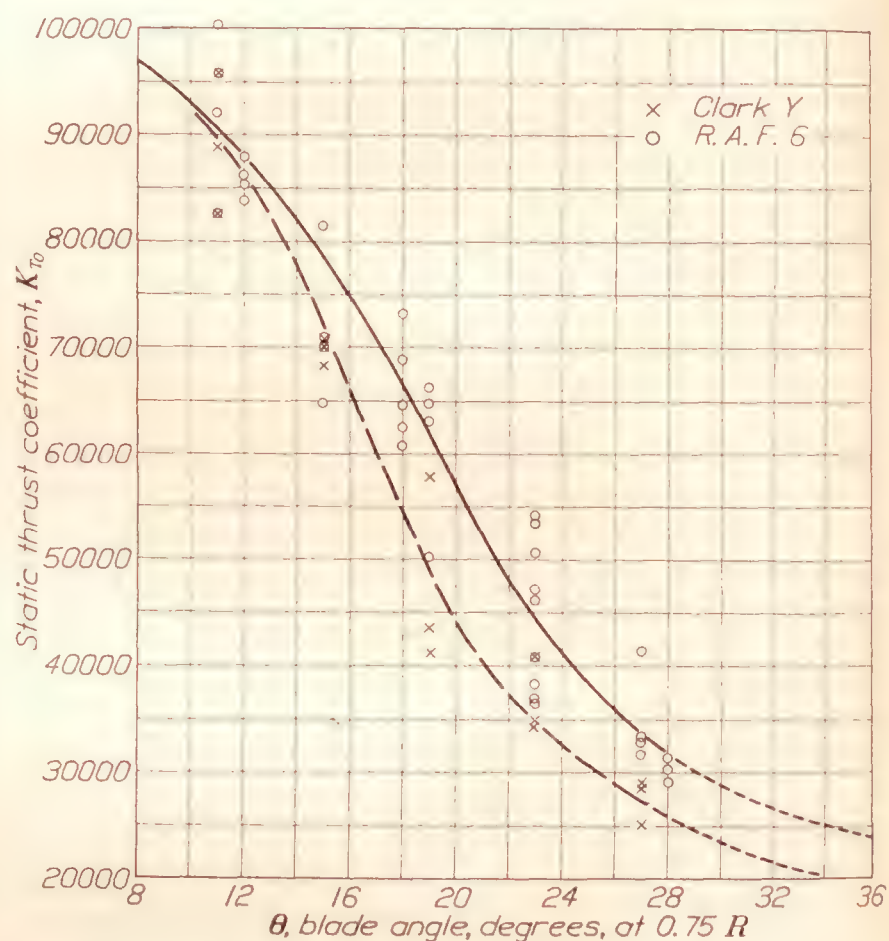


FIGURE 2.—Static thrust coefficients for adjustable blade metal propellers

THE CALCULATION OF STATIC THRUST

For any given set of design conditions the static thrust may be calculated from equation (5):

$$T_0 = \frac{K_{T_0} \times (\text{b.hp})}{(\text{r.p.m.}) \times (\text{diam.})} \quad (5)$$

the proper value of K_T being obtained from Figures 1, 2, or 3. In the case of adjustable blade metal propellers it is common practice to specify the blade setting in terms of the blade angle at the 42-inch radius. Figure 4 has been prepared for obtaining blade angles at $0.75 R$ from the values at the 42-inch radius, for conventional pitch distributions. This curve gives the correction $\Delta\theta$ to be added to or subtracted from the

blade angle at the 42-inch radius to obtain the blade angle at the 0.75 R .

In design studies it is more convenient to work with the V/nD for maximum efficiency than with the blade angle. Figure 5 is a plot of K_{T0} against V/nD for maximum efficiency, using the data from Tables I to VII. The points appear to fall nearer to regular curves than when p/D or θ is used as the base.

In using equation (5), the full rated b.hp and r.p.m. may be used without appreciable error since the ratio b.hp/r.p.m. is substantially constant for full-throttle operation.

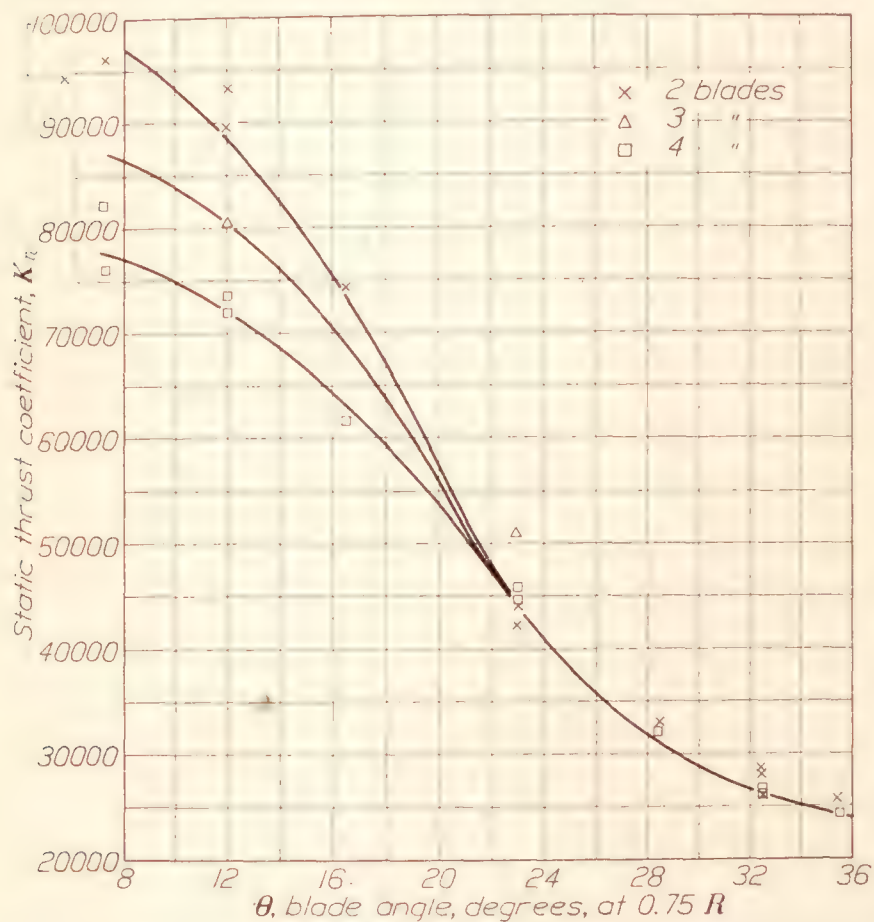


FIGURE 3.—Static thrust coefficients for metal propellers. British tests, R. & M. No. 829

CONCLUSIONS

A study of the collected data leads to the following conclusions:

1. In general, narrow blades give a higher static thrust coefficient than wide blades.
2. Thin blades appear to give a higher static thrust coefficient for low pitch setting and less static thrust at high pitch settings than thick blades.
3. Blade section may be very important in determining the static thrust coefficient at high pitch settings.
4. There is a decrease in the static thrust coefficient due to the use of 3 or 4 blades at low pitch settings but the curves converge into one curve at and above a blade setting of 23° at 0.75 R .
5. The effect of gearing an engine is to reduce the propeller r. p. m., to increase the diameter, and to increase the pitch or blade angle required. With large reduction ratios the effect of the increased diameter and the reduction in K_{T0} corresponding to the increased pitch may more than offset the effect of the change in r. p. m., and thus reduce the static thrust.

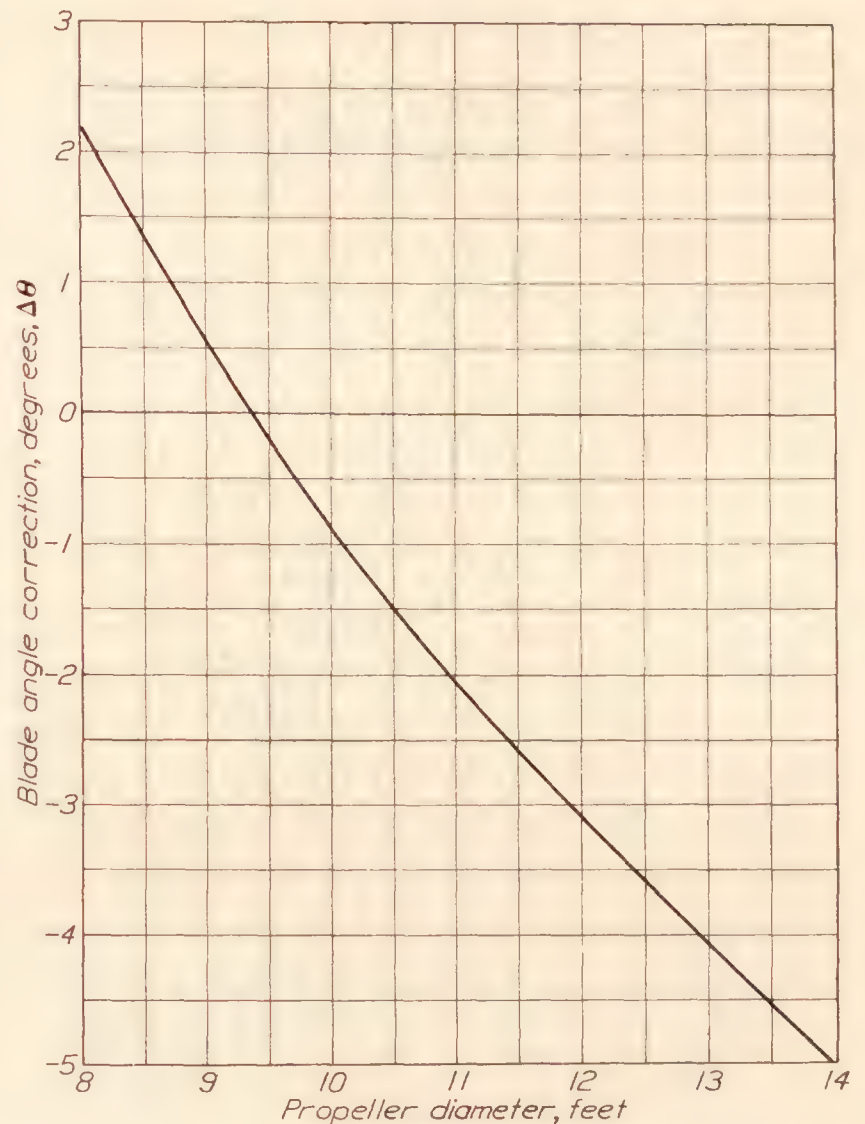


FIGURE 4.—Correction for obtaining blade angle at 0.75 radius from blade setting at 42" station. Positive (+) values of $\Delta\theta$ to be added to setting at 42" station, negative (−) values to be subtracted to get blade angle at 0.75 radius. Example: For 10 ft. dia. Prop. $\Delta\theta = -0.9^\circ$, $\theta_{0.75R} = \theta_{42"} - 0.9^\circ$

6. The variable pitch propeller will give a large increase in static thrust coefficient when the available blade setting change is sufficient to attain blade angles of 12° or less.

BUREAU OF AERONAUTICS,

NAVY DEPARTMENT,

WASHINGTON, D. C. Sept., 1932.

REFERENCES

1. Warner, Edward P.: The Problem of the Helicopter. T. N. No. 4, N. A. C. A., 1920.
2. Warner, Edward P.: Airplane Design-Aerodynamics. (Chapter XIV.) McGraw-Hill Book Co., Inc., New York City, 1927.
3. Diehl, W. S.: Engineering Aerodynamics. The Ronald Press Co., 1928.
4. Durand, W. F., and Lesley, E. P.: Experimental Research on Air Propellers-II. T. R. No. 30, N. A. C. A., 1920.
5. Weick, Fred E.: Full-Scale Wind-Tunnel Tests of a Series of Metal Propellers on a VE-7 Airplane. T. R. No. 306, N. A. C. A., 1929.
6. Wood, Donald H.: Full-Scale Wind-Tunnel Tests of a Propeller with the Diameter Changed by Cutting Off the Blade Tips. T. R. No. 351, N. A. C. A., 1930.
7. Freeman, Hugh B.: Comparison of Full-Scale Propellers Having R. A. F.-6 and Clark Y Airfoil Sections. T. R. No. 378, N. A. C. A., 1931.
8. Fage, A., Lock, C. N. H., Howard, R. G., and Bateman, H.: Experiments with a Family of Airscrews Including the Effect of Tractor and Pusher Bodies. Part I. Experiments with the Family of Airscrews Mounted in Front of a Small Body. R. & M. No. 829, British A. R. C., 1922.

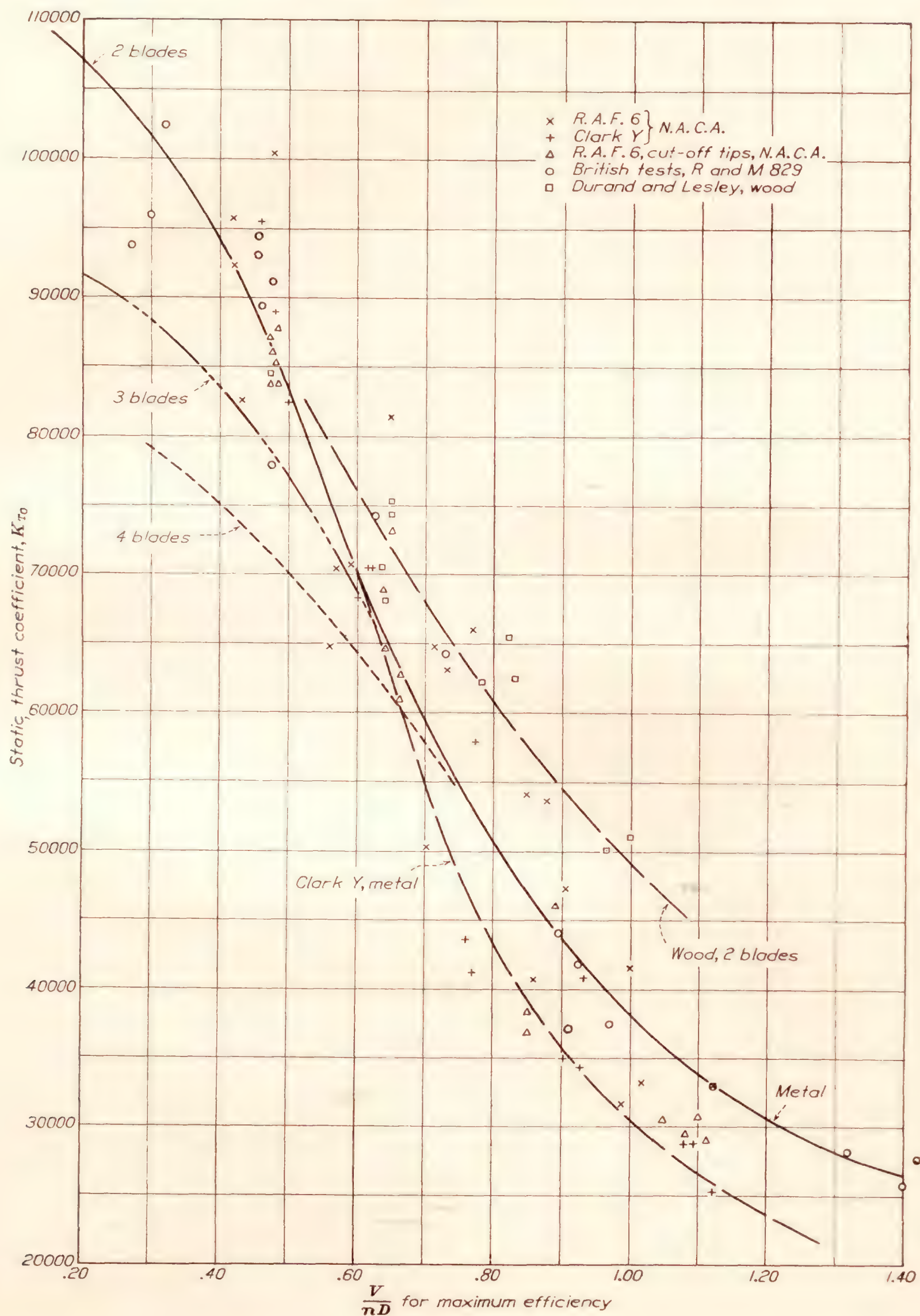


FIGURE 5.

TABLE I

STATIC THRUST COEFFICIENTS FOR WOODEN PROPELLERS—DATA FROM DURAND AND LESLEY'S TESTS, TABLE V, N. A. C. A. TECHNICAL REPORT NO. 30

Prop. No.	$\frac{b}{D}$	$\frac{p}{D}$	Maximum efficiency		Thrust coefficient $C_T' = \frac{T_0}{\rho p n^2 D^4}$	Power coefficient $C_P' = \frac{P_0}{\rho p n^3 D^5}$	Static thrust coefficient $K_{T_0} = 33000 \frac{C_T'}{C_P'}$
			η_m	V/nD for η_m			
3	0.075	0.9	0.810	0.83	0.0160	0.00840	62800
4	.100	.9	.798	.78	.0195	.01035	62200
7	.075	.7	.778	.65	.0149	.00662	74300
8	.100	.7	.759	.63	.0164	.00769	70400
11	.075	.5	.708	.49	.0120	.00470	84300
12	.100	.5	.670	.47	.0122	.00490	82100
15	.075	.9	.804	.82	.0168	.00848	65400
16	.100	.9	.803	.80	.0188	.01000	61900
19	.075	.7	.781	.65	.0137	.00601	75100
20	.100	.7	.772	.64	.0164	.00800	67700
23	.075	.5	.699	.48	.0112	.00435	84800
24	.100	.5	.680	.47	.0121	.00491	81400
82	.075	1.1	.834	1.00	.0158	.01021	51000
83	.100	1.1	.818	.96	.0189	.01248	50000

TABLE II

STATIC THRUST COEFFICIENTS FOR METAL PROPELLERS N. A. C. A. TESTS, TECHNICAL REPORT NO. 306

Blade setting at $0.75R\theta$	Static thrust coefficient C_{T_0}	Static torque coefficient C_{P_0}	$\frac{V}{nD}$ for η_m	Static thrust coefficient K_{T_0}
11°	0.079	0.026	0.48	100300
15°	.094	.038	.65	81400
19°	.101	.050	.77	66200
23°	.096	.067	.91	47200
27°	.099	.098	1.13	33000

TABLE III

STATIC THRUST COEFFICIENTS FOR ADJUSTABLE METAL PROPELLERS WITH CUT-OFF TIPS N. A. C. A. TESTS, TECHNICAL REPORT NO. 351

Diameter D feet	Blade angle at $0.75R$ θ	Static values		Maximum efficiency		Static thrust coefficient K_{T_0}	$\frac{b}{D}$
		C_{T_0}	C_{P_0}	η_m	V/nD for η_m		
10.0	12	0.066	0.026	0.733	0.48	83700	0.0803
	17	.091	.041	.790	.65	73200	
	23	.080	.072	.819	.85	36700	
	28	.089	.101	.836	1.08	29000	
9.5	12	.080	.031	.714	.48	85200	.0845
	17	.096	.046	.771	.63	68900	
	23	.096	.083	.808	.85	38200	
	28	.108	.118	.822	1.05	30200	
9.0	12	.093	.035	.705	.48	87700	.0892
	17	.102	.052	.759	.64	64600	
	23	.110	.100	.791	.87	36300	
	28	.114	.125	.810	1.05	30100	
8.5	12	.098	.037	.689	.47	87400	.0945
	17	.116	.063	.756	.66	60700	
	23	.126	.090	.785	.89	46100	
	28	.134	.153	.800	1.11	28900	
8.0	12	.099	.038	.675	.47	86000	.1005
	17	.127	.067	.740	.66	62500	
	23	.149	.097	.772	.92	50600	
	28	.148	.159	.780	1.10	30700	

TABLE IV

STATIC THRUST COEFFICIENTS FOR ADJUSTABLE PITCH PROPELLERS WITH NAVY STANDARD SECTION (MODIFIED R. A. F.-6) N. A. C. A. TESTS, TECHNICAL REPORT NO. 378

Camber ratio	Blade setting at $0.75R$ θ	C_{T_0}	C_{P_0}	Maximum efficiency		Static thrust coefficient K_{T_0}
				η_m	V/nD for η_m	
0.06	°					
	11	0.081	0.028	0.700	0.42	95600
	15	.083	.039	.753	.57	70400
	19	.102	.067	.795	.70	50100
	23	.113	.092	.810	.86	40500
	27	.111	.112	.820	1.02	33300
.08	11	.081	.029	.680	.42	92000
	15	.080	.041	.740	.56	64700
	19	.098	.050	.780	.71	64700
	23	.102	.062	.805	.85	54100
	27	.115	.120	.820	.99	31600
.10	11	.075	.030	.660	.43	82400
	15	.088	.041	.732	.59	70900
	19	.101	.053	.782	.73	63000
	23	.106	.065	.802	.88	53600
	27	.116	.092	.805	1.00	41500

TABLE V

STATIC THRUST COEFFICIENTS FOR ADJUSTABLE PITCH PROPELLERS WITH CLARK Y SECTION N. A. C. A. TESTS, TECHNICAL REPORT NO. 378

Camber ratio	Blade setting at $0.75R$ θ	C_{T_0}	C_{P_0}	Maximum efficiency		Static thrust coefficient K_{T_0}
				η_m	V/nD for η_m	
0.06	°					
	11	0.081	0.028	0.725	0.46	95600
	15	.081	.039	.777	.60	68200
	19	.106	.085	.802	.77	41100
	23	.114	.108	.815	.90	34800
	27	.097	.110	.820	1.08	28800
.08	11	.078	.029	.750	.48	88800
	15	.083	.039	.795	.62	70400
	19	.074	.056	.810	.76	43500
	23	.088	.085	.820	.93	34100
	27	.105	.120	.826	1.09	28800
.10	11	.075	.030	.746	.50	82400
	15	.085	.040	.778	.62	70400
	19	.091	.052	.802	.77	57800
	23	.098	.079	.813	.93	40900
	27	.086	.113	.828	1.12	25100

TABLE VI

STATIC THRUST COEFFICIENTS FOR METAL PROPELLERS DATA FROM BRITISH A. R. C. R. & M. NO. 829

Data from Table No.	Blades			Pitch diam. $\frac{p}{D}$	Maximum efficiency		Static data		Static thrust coefficient K_{T_0}
	No.	Width diam.	Blade angle at $0.75R$		η_m	V/nD for η_m	Thrust coefficient K_{T_0}'	Torque coefficient K_{Q_0}	
		$\frac{b}{D}$	θ						
6(1)	2	0.082	7 15	0.3	0.545	0.300	0.0622	0.00341	95900
6(2)	4	.082	7 15	.3	.446	.288	.0928	.00638	76400
6(3)	2	.082	12 0	.5	.734	.456	.0910	.00514	93000
6(4)	4	.082	12 0	.5	.630	.480	.1400	.01003	73300
6(5)	2	.082	16 30	.7	.780	.624	.1145	.00811	74200
6(6)	4	.082	16 30	.7	.725	.623	.1860	.0159	61500
6(7)	2	.082	23 0	1.0	.85	.928	.1200	.0151	41700
6(8)	4	.082	23 0	1.0	.84	.945	.2180	.0257	44500
6(9)	2	.082	32 30	1.5	.867	1.400	.1330	.0269	25900
6(10)	4	.082	32 30	1.5	.865	1.370	.2440	.0489	26200
6(11)	3	.082	12 0	.5	.664	.465	.1210	.0792	80200
6(12)	3	.082	23 0	1.0	.852	.955	.1827	.01888	50800
6(13)	2	.123	23 0	1.0	.842	.967	.1953	.01835	55800
6(14)	2	.0615	23 0	1.0	.875	.970	.0861	.01210	37400
6(15)	4	.0615	23 0	1.0	.837	.920	.1550	.0214	38000
6(16)	2	.041	23 0	1.0	.882	.910	.0536	.00760	37000
6(17)	3	.041	23 0	1.0	.865	.933	.0780	.01130	36200
6(18)	4	.041	23 0	1.0	.855	.950	.1000	.01490	35200
6(19)	6	.041	23 0	1.0	.807	.893	.1395	.02113	34700
6(20)	2	.123	12 0	.5	.668	.475	.1140	.00769	77900
6(21)	2	.0615	12 0	.5	.738	.456	.0727	.00415	94700
6(22)	4	.0615	12 0	.5	.658	.465	.1224	.00816	78900
6(23)	2	.041	12 0	.5	.758	.477	.0500	.00288	91200
6(24)	3	.041	12 0	.5	.684	.455	.0692	.00423	85900
6(25)	4	.041	12 0	.5	.665	.455	.0867	.00561	81200
6(26)	6	.041	12 0	.5	.613	.434	.1135	.00813	73500

TABLE VII

STATIC THRUST COEFFICIENTS FOR ADJUSTABLE PITCH METAL PROPELLERS—DATA FROM BRITISH A. R. C. R. & M. NO. 829

Data from Table No.	Blades			Pitch diam. $\frac{P}{D}$	Maximum efficiency		Static data		Static thrust coefficient K_{T_0}
	No.	Width diam.	Blade angle at $0.75R$		η_m	V/nD for η_m	Thrust coefficient K_{T_0}'	Torque coefficient K_{Q_0}	
		$\frac{b}{D}$	θ						
			$^{\circ}$						
7 (1)	2	0.082	7 15	0.33	0.551	0.320	0.0659	0.00338	102500
7 (2)	2	.082	12 0	.51	.715	.460	.0950	.00558	89400
6 (5)	2	.082	16 30	.70	.780	.624	.1145	.00811	74200
7 (3)	2	.082	23 0	1.00	.853	.896	.1235	.01475	44000
7 (4)	2	.082	28 30	1.25	.886	1.127	.1332	.02096	33300
7 (5)	2	.082	32 30	1.45	.896	1.424	.1383	.0255	28400
7 (6)	2	.082	35 30	1.64	.885	1.583	.1445	.0293	25900
7 (7)	2	.082	34 15	1.52	.837	1.320	.1458	.0271	28200
6 (1)	2	.082	7 15	.30	.545	.300	.0622	.00341	95900
7 (8)	2	.082	5 30	.28	.445	.272	.0586	.00328	93900
6 (9)	2	.082	32 30	1.40	.867	1.400	.1330	.0269	25900
7 (9)	4	.082	7 15	.33	.480	.312	.0987	.00631	82200
7(10)	4	.082	12 0	.51	.637	.480	.1393	.01022	71600
6 (6)	4	.082	16 30	.70	.725	.623	.1860	.0159	61400
7(11)	4	.082	23 0	1.00	.805	.896	.2245	.02585	45600
7(12)	4	.082	28 30	1.25	.847	1.136	.2330	.0379	32300
7(13)	4	.082	32 30	1.45	.855	1.286	.2395	.0471	26700
7(14)	4	.082	35 30	1.64	.882	1.560	.2470	.0534	24300

REPORT No. 448

IMPROVED APPARATUS FOR THE MEASUREMENT OF FLUCTUATIONS OF AIR SPEED IN TURBULENT FLOW

By W. C. MOCK, Jr., and H. L. DRYDEN

SUMMARY

This paper describes recent improvements in the design of the equipment associated with the hot-wire anemometer for the measurement of fluctuating air speeds in turbulent air flow, and presents the results of some experimental investigations dealing with the response of the hot wire to speed fluctuations of various frequencies. Attempts at measuring the frequency of the fluctuations encountered in the Bureau of Standards' 54-inch wind tunnel are also reported. The design of the amplifying and compensating equipment for use with the hot wire is treated briefly. In addition, the difficulties encountered in the use of such apparatus and the precautions found helpful in avoiding them are discussed. The work was carried out at the Bureau of Standards with the cooperation and financial support of the National Advisory Committee for Aeronautics.

INTRODUCTION

Theoretical investigations of turbulence such as those formulated by Reynolds (reference 1), by Lorentz (reference 2), and by Burgers (reference 3) emphasize the need for experimental data on the fluctuations of air speed found in turbulent air flow. The most promising instrument for such measurements is the hot-wire anemometer, which we believe

to have been first suggested for this use by E. Huguenard and his coworkers. (Reference 4.) In two earlier papers (references 5 and 6) the equipment developed at the Bureau of Standards has been described, and the application of the equipment illustrated by a study of the effects of turbulence in wind-tunnel measurements. Within the last two years, the equipment has been greatly improved as to uniformity of response to fluctuations of various frequencies. It was felt desirable to describe the improved apparatus and to place on record such parts of our experience as might be valuable to other laboratories engaged in similar investigations.

The paper is divided into four parts, each of which is self-contained and may be read independently. Part I treats the response of the hot-wire anemometer to speed fluctuations, giving a recapitulation of the theory developed in a previous paper, describing methods of compensating for the lag of the wire, and experimental determinations of the performance of the wire and the compensating circuit. Part II deals with the design of amplifiers for use in turbulence measurements. Part III describes improvements in the Bureau of Standards' apparatus made since the publication of references 5 and 6. Part IV gives an account of some experiments on the frequency distribution of the speed fluctuations in a wind tunnel.

REPORT No. 448

IMPROVED APPARATUS FOR THE MEASUREMENT OF FLUCTUATIONS OF AIR SPEED IN TURBULENT FLOW

IN FOUR PARTS

PART I

RESPONSE OF THE HOT-WIRE ANEMOMETER TO SPEED FLUCTUATIONS

GENERAL THEORY

The hot-wire anemometer, as used for measurements of speed fluctuations, consists essentially of a platinum wire, of small diameter and short length, placed in the air stream with its long dimension perpendicular to the direction of the mean flow, and heated to a suitable temperature by means of an electrical current. Fluctuations in the speed of the air stream produce fluctuations in the temperature of the wire and hence in its resistance. The changes in voltage drop across the wire may be amplified by means of vacuum-tube amplifiers, and finally measured by means of a thermocouple-actuated milliammeter indicating the square root of the mean square of their magnitudes. If the changes in resistance are negligible as compared to the total resistance in the heating circuit, so that the current remains constant, the fluctuation in the voltage drop will be proportional to the fluctuation in resistance. For special purposes, such as examination of the wave form of the fluctuations, a cathode ray oscillograph may be used as the final measuring instrument. Vacuum-tube voltmeters may also be used if the fluctuations are periodic and of known wave form, otherwise their use will introduce errors.

Unfortunately for the simplicity of the measurements, the fluctuating voltage drop across the hot-wire anemometer is neither proportional in amplitude nor in phase with the speed fluctuations. When the speed is decreasing rapidly the electrical current heating the wire is unable to supply sufficient energy to raise the temperature of the wire at the required rate. Conversely, when the speed is increasing rapidly, the supply of heat energy possessed by the wire retards its cooling. In other words, the hot-wire anemometer has a lag which causes the fluctuating voltage drop to be less in magnitude and to lag in phase behind the voltage drop which would correspond under equilibrium conditions to the instantaneous speed, by an amount which increases as the rapidity of the speed fluctuation increases.

The theory of the behavior of a hot wire when subjected to speed fluctuations, either periodic or irregular, has been developed in a previous paper (reference 5) and need not be repeated in full here. It suffices to state that the response of the hot wire is characterized by a time constant M , related to the physical properties of the wire and the operating conditions in the following manner:

$$M = \frac{4.2\rho A^2 s (\bar{T} - T_0)}{i^2 r_0}$$

where

T_0 = room or air temperature.

\bar{T} = average temperature of the hot wire.

A = cross-sectional area of the hot wire.

s = the specific heat of air, 0.037 cal. per g per degree C., approximately.

i = the heating current.

ρ = density of the wire, 21.37 g/cm³ for platinum.

r_0 = resistivity of the wire at temperature T_0 = approximately 0.000012 ohm-cm, for platinum at the usual room temperature.

For periodic fluctuations the action of the hot wire is to produce a fluctuating voltage drop equal in amplitude to

$$\frac{1}{\sqrt{1 + M^2 \omega^2}}$$

times the amplitude of the fluctuating voltage drop that would correspond under equilibrium conditions to the speed fluctuation, and lagging behind the speed fluctuation, in phase, by the angle, $\alpha = \tan^{-1} M \omega$, where M is the time constant of the hot wire as defined above, and ω is 2π times the frequency of the velocity fluctuations.

For irregular fluctuations, the voltage fluctuation corresponding to the speed fluctuation under equilibrium conditions may be expanded in a Fourier series, the effect on each component of the series computed as

for a periodic fluctuation, and the results added to give the response of the wire.

From the form of the expression for the reduction of amplitude, it is evident that the hot-wire anemometer becomes very insensitive at any but the lowest frequencies. Improvement in the performance in this respect may be obtained by reducing the diameter of the wire used, but even with the smallest sizes, 0.003 to 0.015 mm, the use of which is attended by considerable practical difficulty, the performance remains inadequate if the higher frequencies thought to exist in the speed fluctuations are to be reproduced in their true relation to the lower frequencies.

The performance of a typical hot-wire anemometer (diameter 0.0167 mm) is illustrated by Table I.

TABLE I

Frequency cycles per second	ω	$\frac{1}{\sqrt{M^2\omega^2+1}}$	$\tan^{-1} M\omega$
1	6.3	1.000	1.4
5	31.4	.992	7.2
10	62.8	.970	14.1
20	125.7	.893	26.7
50	314.2	.636	51.5
75	471.2	.469	62.0
100	628.3	.370	68.3
200	1,256.6	.195	78.7

$M=0.004$, $r_s=0.000012$, $\rho=21.37$, $s=0.037$, $\bar{T}-T_0=120^\circ$ C., $A=2.2\times 10^{-6}$, $i=0.2$ ampere.

COMPENSATION CIRCUITS FOR REDUCING THE LAG ERROR

A graphical correction for the amplitude reduction and phase lag of the hot-wire anemometer is possible (reference 5) if an oscillogram, or similar record, of the fluctuation is available and the fluctuation is small. In practice, however, the complexity of the oscillogram makes such a method so laborious as to be impractical. Furthermore, the condition that the fluctuation be small does not always obtain.

The expressions given for the amplitude reduction and phase lag of the hot-wire anemometer are identical in form with those expressing the magnitude and phase of the current relative to the impressed voltage in a circuit containing inductive reactance and resistance. It should therefore be possible to introduce somewhere in the apparatus associated with the hot-wire anemometer an electrical distortion, having an equal but opposite effect, in such a way as to eliminate the lag errors. This method was suggested in an earlier paper. (Reference 5.)

The method adopted for introducing this compensating distortion consists essentially of the use of a voltage-dividing circuit (fig. 1) made up of an inductance L and a resistance R_1 in series and connected across the load resistor R_L of one of the vacuum tubes in the amplifier in such a manner that the grid circuit of the following vacuum tube is connected across the inductance. In series with the inductance L , and in

that part of the voltage divider feeding the following vacuum tube, is a resistance R_2 used for adjustment of the time constant L/R_2 which must be made equal to the time constant M of the hot wire. Designating by R_0 the resistance of the load resistor R_L in parallel with the internal alternating current resistance of the vacuum tube out of which the circuit works, it is readily seen that the ratio of the voltage applied to the

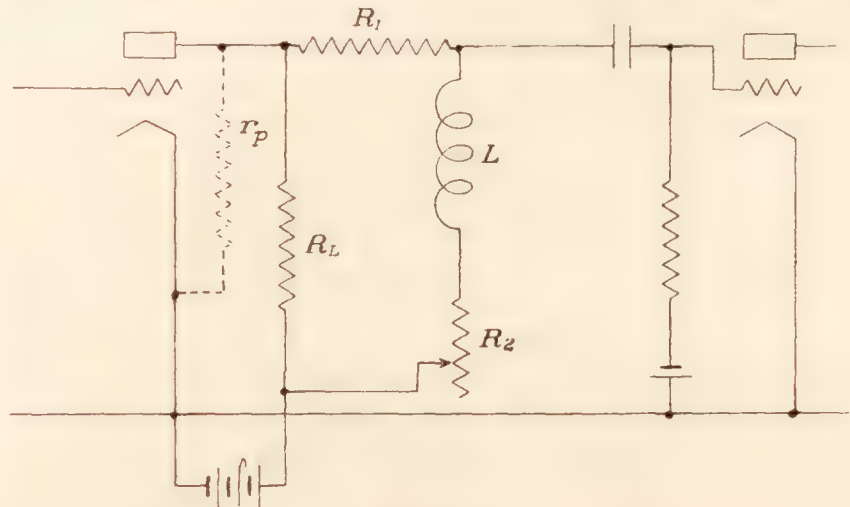


FIGURE 1

grid circuit of the following tube to the voltage drop across the plate resistor R_L is equal to

$$\frac{R_2 + j\omega L}{R_0 + R_1 + R_2 + j\omega L}$$

To give the desired compensation, the ratio should be proportional to $R_2 + j\omega L$, the factor of proportionality not containing ω , and L/R_2 should equal the time constant M of the wire. As explained more fully in reference 5, the sensitivity of the apparatus is reduced by the compensating circuit in the ratio

$$\frac{R_2}{R_0 + R_1 + R_2}$$

and the error in compensation at a given frequency depends primarily on the factor

$$\frac{L}{R_0 + R_1 + R_2}$$

For an error of 1 per cent in amplitude, $\frac{\omega L}{R_0 + R_1 + R_2}$ must be as small as 0.14, or the error factor must be as small as $\frac{0.14}{\omega}$. The frequency at which the error reaches 1 per cent is equal to 0.14 divided by 2π times the error factor.

In 1930 a similar circuit (fig. 2) was described by Ziegler. (Reference 8.) The practical equivalence of this circuit and that in use at the Bureau of Standards is made evident by a consideration of the impedance to alternating currents presented by condensers and inductances. The capacity C across the resistance R_1' (fig. 2) offers an impedance $Z_c = \frac{1}{2\pi fC}$. This impedance decreases with increasing frequency and thus decreases the voltage drop across R_1' , allowing a

greater voltage to be passed on to the grid of the following vacuum tube. The inductance L in the Bureau of Standards circuit offers an impedance $Z_L = 2\pi fL$, which increases as the frequency increases and thus increases the voltage impressed across the grid circuit of the following vacuum tube. The effect in each case is directly proportional to the frequency and the results are equivalent.

By the process used in deriving the corresponding expressions for the inductance type of compensating circuit it may be shown that in Ziegler's arrangement

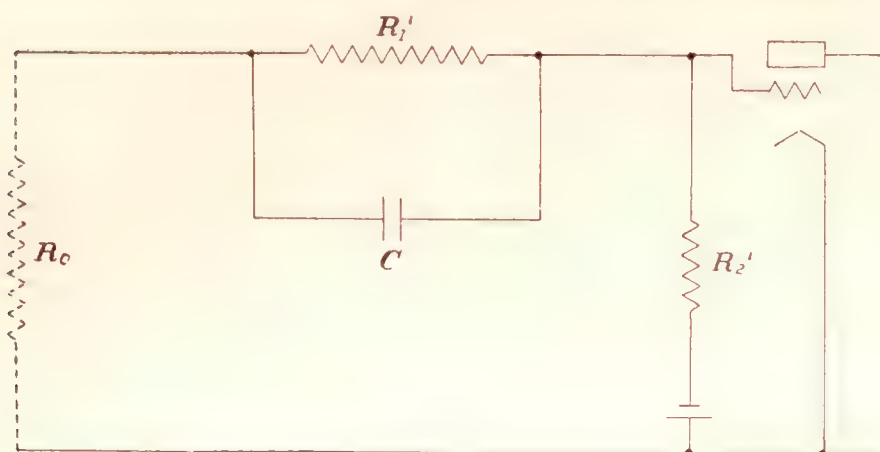


FIGURE 2

the sensitivity is reduced by the compensating circuit in the ratio

$$\frac{R_2'}{R_0 + R_1' + R_2'}$$

the error factor is

$$\frac{CR_1'(R_0 + R_2')}{R_0 + R_1' + R_2'}$$

and the time constant, which must be equal to the time constant of the hot wire is CR_1' , where R_0 is the impedance out of which the system works.

The relative performance of the two circuits may be examined by substituting in the expressions for the attenuation, error, and time constant of the inductance compensation circuit typical values of inductance and resistance as used at the Bureau of Standards, equating the values of attenuation and time constant thus obtained to the equivalent expressions for the capacity compensation circuit, substituting various appropriate values of R_0 and R_1' , and finally solving for C , R_2' and the value of the error factor. This operation is carried out below, and the results presented in Table II.

$$\begin{aligned} L &= 10.87 \text{ henrys.} \\ R_0 &= 100,000 \text{ ohms.} \\ R_1 &= 1,000,000 \text{ ohms.} \\ R_2 &= 3,000 \text{ ohms.} \end{aligned}$$

Attenuation equals

$$\frac{R_2}{R_0 + R_1 + R_2} = 0.00272$$

Time constant equals

$$\frac{L}{R_2} = 0.003623$$

Error factor equals

$$\frac{L}{R_0 + R_1 + R_2} = 0.00000985$$

Equating values of attenuation and time constant thus obtained to corresponding expressions for the capacity compensation circuit,

$$\text{Attenuation} = \frac{R_2'}{R_0 + R_1' + R_2'} = 0.00272$$

$$\text{Compensation} = CR_1' = 0.003623$$

and solving for C , R_2' and the error factor for $R_1' = 1,000$, 10,000, 100,000, and 1,000,000 ohms when $R_0 = 10$ ohms and again when $R_0 = 100,000$ ohms, we obtain the results of Table II.

TABLE II

R_1' ohms	$R_0 = 10$ ohms			
	$C \mu f$	R_2' ohms	error factor	Frequency for 1 per cent error c. p. s.
1,000	3.623	2.755	0.00004560	489
10,000	.3623	27.30	.00001346	1,653
100,000	.03623	272.8	.00001021	2,182
1,000,000	.003623	2,727.4	.00000989	2,252
	$R_0 = 100,000$ ohms			
	$C \mu f$	R_2' ohms	error factor	Frequency for 1 per cent error c. p. s.
1,000	3.623	275.5	0.003575	6.2
10,000	.3623	300.0	.003292	6.8
100,000	.03623	545.5	.001816	12.3
1,000,000	.003623	3,000.2	.0003381	65.8

Examination of the data thus obtained leads to the following conclusions: First, in order to obtain an error factor comparable with that of the inductance type of circuit, 0.00000985, R_0 must be small, thus precluding the possibility of working the capacity compensation system in the plate circuit of one of the amplifying vacuum tubes; second, R_1' should be large for best results. The fact that the circuit may not be used in a vacuum-tube plate circuit leads to a practical difficulty in that if it is employed ahead of the amplifier, as is the case in Ziegler's apparatus (reference 7), the fluctuating voltage from the hot wire is attenuated by the compensating circuit, and may reach the amplifier at a voltage level near that of the tube noises originating in the first amplifying tube. If this happens, amplification increases the tube noises from the first tube in the same proportion as the fluctuating voltage, and since they are so nearly equal, their separation is difficult. Further, the presence of tube noise may introduce spurious frequencies into the voltage fluctuations. The advantage of a compensating circuit that can be used in the middle of the amplifier is that the fluctuating voltage from the hot wire reaches the first tube unattenuated and therefore at a considerably higher level than the noises originating there. The proportion between tube noises and voltage fluctuation

tuation then remains the same, regardless of any subsequent amplification or attenuation. Compensation following the amplifying apparatus is difficult, practically, because such a system would require the voltage fluctuations to be built up to a level too high to be conveniently handled in the vacuum tubes ordinarily available if the output, after being subjected to the attenuation of the compensation circuit, is to remain large enough to operate any ordinary measuring instrument.

EXPERIMENTAL INVESTIGATIONS OF THE PERFORMANCE OF THE HOT-WIRE ANEMOMETER AND THE COMPENSATION CIRCUIT

The performance of the hot-wire anemometer and the compensating system has been investigated experimentally by two methods.

The first method (reference 5) consisted of placing the suitably mounted hot wire in an air stream and imparting a simple harmonic motion to it by mechanical means, the direction of the motion being parallel to the direction of the air flow. The hot wire was oscillated at several frequencies with amplitudes so chosen that the product of frequency and amplitude, and therefore the maximum speed, remained constant. A detailed discussion of the result obtained from those tests is given in reference 5. Briefly, it was found that over the range of frequencies investigated, 0 to 60 c. p. s., the results showed good agreement with the theory, and the action of the compensating circuit was found to be satisfactory.

In 1931, H. Doetsch and P. V. Mathes (reference 8) made a similar investigation and reported good agreement with the earlier work at the Bureau of Standards.

Attempts to extend this method of investigation to higher frequencies by mounting the hot-wire anemometer on one prong of an electrically driven tuning fork met with failure because the fine platinum wire was broken by the large inertia forces set up when any useful amplitude of oscillation, at high frequency, was obtained.

A less direct but more practical method has been described by Ziegler. (Reference 7.) In this method changes in the electrical resistance of the hot wire are produced by a small alternating electric current of known magnitude and frequency superposed on the direct heating current instead of by fluctuations of air speed. For small changes in resistance, the theory of the response to resistance changes produced by changes in the current is identical with that for resistance changes produced by changes in the rate of cooling. The change in resistance is measured as a function of the frequency, the alternating component of the current in the wire being maintained constant. Some measurements by this method have been made at the Bureau of Standards.

The circuit of Figure 3 was used to introduce the alternating current into the wire and to measure the

resulting changes in the resistance of the wire as a function of frequency. It consists simply of a Wheatstone bridge of which one arm R_1 is the hot-wire anemometer. The battery ($E=12$ volts) in series with the regulating resistance R_b , supplies the necessary heating current to maintain the hot wire at the proper average temperature.

The bridge is first balanced both for direct and alternating current when the hot wire is replaced by a resistor whose resistance is equal to the mean resistance of the hot wire and does not vary with the current. The hot wire is then substituted for this resistor. When the small alternating current is applied, it produces an alternating change in the resistance of the hot wire, unbalancing the bridge. The magnitude of the fluctuation of the resistance of the hot wire may be computed from the voltage drop applied to the amplifier and the sensitivity of the bridge. The equilibrium values may be obtained by direct experiment, measuring the resistance of the wire for different heating

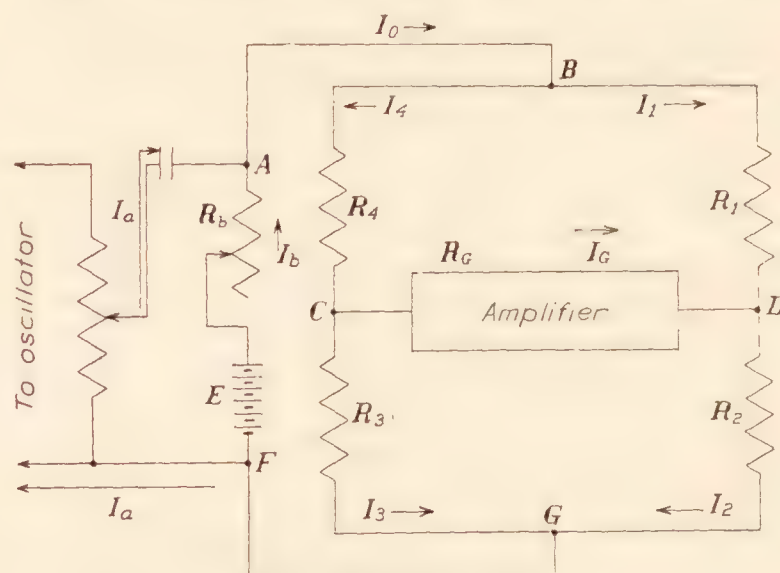


FIGURE 3

currents, using a galvanometer as the indicating instrument for the bridge.

The alternating current was supplied from an audio-frequency vacuum-tube oscillator through a condenser which isolated the oscillator from the bridge, as far as direct current is concerned. The oscillator was a General Radio Co. type 377-B instrument, having a frequency range of 25 to 70,000 c. p. s. with excellent wave form when working into a suitable load impedance, and a power output of about 100 milliwatts, sufficient for the purpose of the tests.

Because of the great bulk of the amplifier and the difference between the capacities of the two sides of the input circuit to ground, it was found desirable to house the amplifier in a metal cage and to place a Wagner ground to the cage across the input terminals. A small slide rheostat (potentiometer) of 25,000 ohms resistance was found satisfactory, the ends of the winding being connected to the two input terminals and the variable point to the cage. The variable point was so adjusted that reversing the bridge current and reversing the amplifier terminals gave the minimum effect.

A number of difficulties were encountered, not mentioned by Ziegler, and perhaps not met with by him because of suitable choice of the bridge constants. It seems desirable to discuss the performance of the combined a. c.-d. c. bridge in a little detail to indicate the nature of the difficulties and how they may be avoided.

Application of Kirchhoff's laws for the continuity of the current at junction points **A, B, C, G**, and for the voltage relations in circuits **BCDB, CGDC**, and **ABCGFA** gives the following seven equations for determining the seven unknown currents, I_a being measured.

$$\begin{aligned} I_b + I_a &= I_0 \\ I_1 + I_4 &= I_0 \\ I_3 + I_g &= I_4 \\ I_2 + I_3 &= I_0 \\ I_4 R_4 + I_g R_g - I_1 R_1 &= 0 \\ I_3 R_3 - I_2 R_2 - I_g R_g &= 0 \\ I_4 R_4 + I_3 R_3 + I_b R_b &= E \end{aligned}$$

Since it is desired to hold the alternating current in the wire constant, and only I_a can be readily measured, the first thing of interest is the relation between I_1 and I_a . Solution of the above equations for I_1 gives

$$I_1 = \frac{(E + I_a R_b) (R_g R_3 + R_g R_4 + R_2 R_4 + R_3 R_4)}{Y + R_g X}$$

where

$$Y = R_1 R_2 R_3 + R_1 R_2 R_4 + R_1 R_3 R_4 + R_2 R_3 R_4 + R_b R_1 R_2 + R_b R_1 R_3 + R_b R_2 R_4 + R_b R_3 R_4$$

and

$$X = R_1 (R_b + R_3 + R_4) + R_b R_2 + R_b R_3 + R_b R_4 + R_2 R_3 + R_2 R_4.$$

R_g , the resistance of the input circuit of the amplifier is quite large as compared with the values of the other resistances in the bridge. Introducing this fact, we find

$$I_1 = \frac{(E + I_a R_b) (R_3 + R_4)}{X}$$

The resistance R_1 of the hot wire is not constant, but fluctuates with the current. Let us place $R_1 = \bar{R}_1 + r$, where \bar{R}_1 is the mean value and the departure r is a function of I_1 . Introducing the value of R_1 in X , we find $X = \bar{X} + (R_b + R_3 + R_4) r$ when \bar{X} is the value of X with \bar{R}_1 substituted for R_1 . Thus

$$I_1 = \frac{(E + I_a R_b) (R_3 + R_4)}{\bar{X} + (R_b + R_3 + R_4) r} \quad (1)$$

Since r is a function of I_1 and also of the frequency, the relation between I_1 and I_a is not independent of the frequency and is far from simple in the general case. Keeping I_a constant does not keep I_1 constant.

However, $\frac{I_a R_b}{E}$ and $\frac{(R_b + R_3 + R_4) r}{\bar{X}}$ will be small if

I_a is small. Treating them as small quantities whose squares and products may be neglected, equation (1) may be written

$$I_1 = \frac{E(R_3 + R_4)}{\bar{X}} + \frac{I_a R_b (R_3 + R_4)}{\bar{X}} - \frac{E(R_3 + R_4) (R_b + R_3 + R_4) r}{\bar{X}^2} \quad (2)$$

The first term in equation (2) is the direct current through the wire which we shall call I_{dc} . The second term is the main alternating current through the wire, proportional to I_a . The third term represents the fluctuation in current through R_1 due to the variation of R_1 . To secure a simple relation between I_1 and I_a , it is desirable to make this last term negligible. The ratio of the last term to the second is

$$\begin{aligned} & \frac{E (R_b + R_3 + R_4) r}{I_a R_b \bar{X}} \\ \text{or,} \quad & \frac{I_{dc} \left(1 + \frac{R_b}{R_3 + R_4} \right) r}{I_a R_b} \quad (3) \end{aligned}$$

Since r and I_a are not in phase, the direct ratio can not be taken. Placing $I_a = \bar{I}_a e^{j\omega t}$ and $r = \bar{r} e^{j(\omega t - \alpha)}$ the ratio (3) becomes

$$\frac{I_{dc} \left(1 + \frac{R_b}{R_3 + R_4} \right) \bar{r} e^{-j\alpha}}{\bar{I}_a R_b} \quad (4)$$

The importance of the choice of suitable values of the bridge resistances in reducing the ratio (3) is best illustrated by two numerical examples.

Assuming the reasonable value of $M = 0.0041$, and a frequency of 25 c. p. s., we will consider first a bridge having the following values of resistances, $\bar{R}_1 = 7.60$ ohms, $R_2 = R_3 = 7.58$ ohms, $R_4 = 7.60$ ohms, $R_b = 22.44$ ohms, and $\bar{r} = 0.053$ ohms, a 12-volt heating battery being used, and \bar{I}_a made 0.005 ampere. Then,

$$\begin{aligned} I_{dc} &= \frac{(15.18) 12}{911.71} \\ &= 0.1998 \text{ ampere,} \end{aligned}$$

and the ratio (4) of the alternating current caused by the resistance variation to the main alternating current through the hot wire is

$$\frac{0.1998 \left(1 + \frac{R_b}{R_3 + R_4} \right) \bar{r} e^{-j\alpha}}{0.005 R_b} = 0.339 e^{-j\alpha}.$$

Next, consider a bridge having the same direct current through the same hot wire, and the following values of resistance $R_b = 44.52$ ohms, $R_1 = 7.60$ ohms, $R_2 = 7.60$ ohms, $R_3 = 900$ ohms, $R_4 = 900$ ohms, M and ω having the same values as in the first example. Then, it may be shown, that $I_{dc} = 0.1998$ ampere as before. Also, from a consideration of the second term of (2), the alternating current in the wire is increased by a factor of 1.97. The value of r is therefore taken to be 0.053×1.97 or 0.104, i. e., as proportional to the alternating current, an assumption which experiment shows to be reasonable when the

alternating current is small as compared to the direct heating current. The ratio of the alternating current caused by the resistance variation to the main alternating current through the hot wire is then $0.096 e^{-j\alpha}$, which is less than one-third the value for the bridge arrangement of the first example.

The current I_1 is very nearly in phase with I_a when r is small, and the resistance variation lags the current I_1 by the phase angle $\tan^{-1} M\omega$ where M is the time constant of the hot wire. Hence α is approximately $\tan^{-1} M\omega$ or for the above examples $\tan^{-1} 0.0041 \times 2\pi \times 25 = \tan^{-1} 0.64$ or 32.6° . Even with the second bridge arrangement, the alternating current due to resistance variation is 8 per cent of the main alternating current at a frequency of 25 c. p. s. With increasing frequency, \bar{r} decreases in magnitude and α increases so that the effect disappears. Hence an experimental procedure which holds I_a constant permits variations of the alternating component of I_1 of approximately 8 per cent.

Solution of the bridge equations for $I_g R_g$ with R_g large leads to the result:

$$I_g R_g = \frac{(E + I_a R_b)(R_2 R_4 - R_1 R_3)}{X} \quad (5)$$

or introducing $\bar{R}_1 + r$ for R_1 , assuming the bridge to be balanced as to \bar{R}_1 , i. e., $R_2 R_4 = \bar{R}_1 R_3$, and neglecting $I_a R_b$ as compared to E and $(R_b + R_3 + R_4) r$ compared to \bar{X} , we find

$$I_g R_g = \frac{E R_3 r}{\bar{X}} \quad (6)$$

Introducing I_{ac}

$$I_g R_g = \frac{I_{ac} R_3 r}{R_3 + R_4} \quad (7)$$

Equation (7) gives the relation between the voltage across the amplifier input and the resistance variation r . It is seen that the sensitivity may be increased by making R_3 large in relation to R_4 . However, this procedure requires R_2 to be increased in order to preserve the balance of the bridge which in turn requires I_1 to flow through a large resistance. This is impractical because of the large battery required to supply the heating current. A good compromise between sensitivity and battery size is obtained when R_3 and R_4 are equal, the sensitivity then being one-half the theoretical maximum.

When designing a bridge for use with both alternating and direct current it is essential to make all resistances as nearly noninductive as is possible. In the instance of R_2 , R_3 , and R_4 this presents no greater problem than that of constructing the resistances according to one of the several methods known to give satisfactory results over the range of frequencies involved, roughly 0 to 10,000 c. p. s. The solution is not so simple in the case of R_1 because this arm of the bridge contains the hot wire, which must of necessity be mounted in the wind tunnel and connected to the

remainder of the apparatus by leads of considerable length. The inductance of these leads may be of great importance.

The alternating current potential across R_1 (main term only) is

$$\frac{R_1(R_3 + R_4)(I_a R_b)}{\bar{X}} = \frac{I_{ac} I_a R_b R_1}{E} \quad (8)$$

and the voltage being measured is, from equation (7),

$$I_g R_g = \frac{I_{ac} R_3 r}{R_3 + R_4} \quad (9)$$

It is evident that any inductive reactance in the R_1 branch of the bridge, such as that due to the inductance L_e of the long leads to the hot wire, will cause the current in the wire to lag behind the voltage (8); in other words, the voltage (8) will lead the current by the phase angle $\tan^{-1} \frac{\omega L_e}{R_1}$. The quadrature voltage component leading the current in the wire will be

$$\frac{\omega L_e I_{ac} I_a R_b}{E} \quad (10)$$

since $\frac{\omega L_e}{R_1}$ is small. At high frequencies, the change in resistance of the wire lags the current in the wire by nearly 90° , and hence is nearly in quadrature. The ratio of the quadrature component due to the inductance of the leads to the measured voltage is therefore approximately

$$\frac{\omega L_e R_b (R_3 + R_4) I_a}{R_3 r E} \quad (11)$$

and the voltages are in opposite phase so that the effect is to reduce the measured voltage.

The magnitude of the effect of lead reactance is shown by the following example.

Assuming as probable values, $R_3 + R_4 = 2,000$ ohms, $R_3 = 1,000$ ohms, $R_b = 85$ ohms, $L_e = 10^{-5}$ henrys, $E = 12$, $\bar{I}_a = 0.005$, $\omega = 6,280$, ratio (11) becomes $\frac{0.00222}{\bar{r}}$ and if $\bar{r} = 0.00222$ which is a reasonable value at the frequency considered, the ratio of the quadrature voltage to the voltage we wish to measure is 1.00. Since the amplifier amplifies and measures the sum of the two voltages, which are in opposite phase, an error of 100 per cent is introduced, the input voltage to the amplifier being reduced to zero.

Equation (11) indicates that the error caused by the inductive reactance of the leads to R_1 may be reduced by decreasing R_b , a remedy that does not meet the requirements for low ratio of alternating current due to resistance variation to main alternating current. (Equation 4.) An alternative remedy is to balance out the effect of the inductance L_e in the R_1 arm of the bridge by one of two ways: (1) the use of a capacity of proper magnitude across R_3 , or (2) the use of an inductance of magnitude equal to $\frac{L_e R_2}{R_1}$ in the R_2 arm

of the bridge. The latter is the easier solution, and the method employed was to mount R_2 on the end of a pair of leads exactly similar to those in the R_1 arm. Then, since $R_1 = R_2$, and the inductance in the two arms is equal, the quadrature voltages balance each other.

The alternating current balance of the bridge may be checked experimentally by substituting a resistance in the R_1 branch equal to the resistance of the hot wire, but independent of temperature. The bridge is then balanced to the direct current, in the usual manner, and alternating voltage from the audio-frequency oscillator applied. If no alternating voltage appears across the amplifier input under these conditions, the bridge is balanced with respect to alternating current.

Figure 4 shows the results of a test on the uncompensated hot-wire anemometer in still air. The input voltage to the amplifier is plotted against frequency,

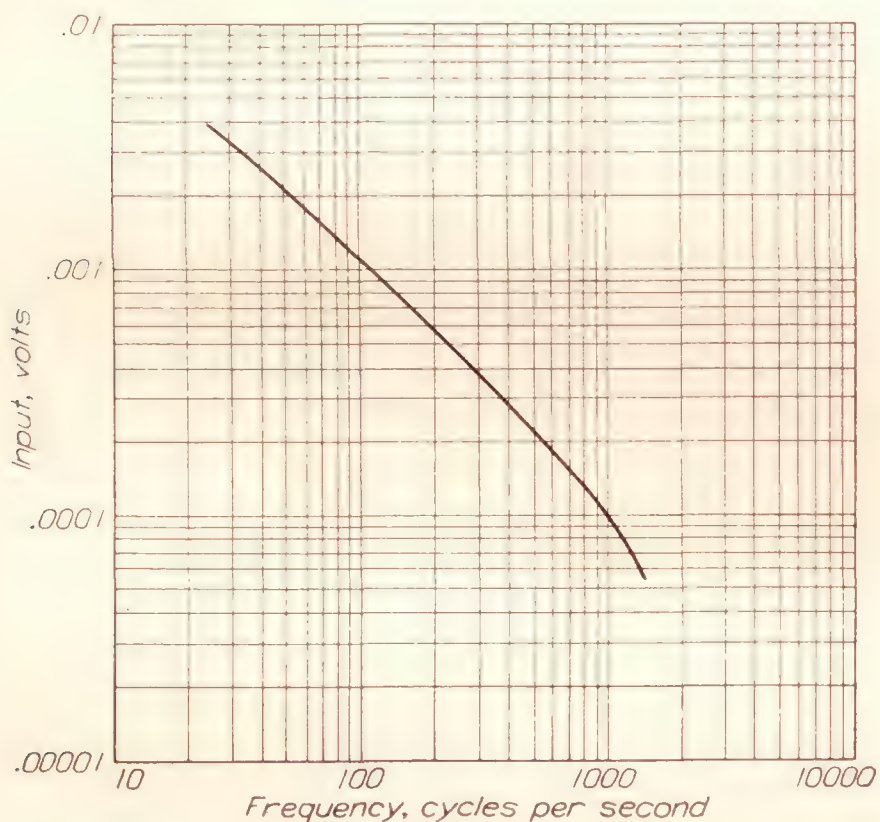


FIGURE 4

the alternating current applied to the bridge being held constant. The procedure followed in making this test was first to adjust the heating current to the proper value by means of R_b . The bridge was then balanced by adjusting R_2 until no direct potential appeared across the amplifier input terminals, using a sensitive direct-current galvanometer as the indicating instrument, since the amplifier was not suitable for direct-current indication. An alternating current of 0.005 ampere was then applied to the bridge, the frequency being varied from 25 to 10,000 c. p. s. Readings of the amplifier output were taken at each frequency. By means of the calibration data, the corresponding input voltages were computed.

The theoretical result of this test would be a curve such that the input voltage was inversely proportional to $\sqrt{1 + M^2\omega^2}$. Over the higher frequency range where $M^2\omega^2$ is large compared to 1, the relation between input voltage and frequency would be expected to be linear

and in the lower frequency range where $M^2\omega^2$ is comparable in magnitude to 1 the curve should be concave downward. The actual result of the test is seen to be identical with the theoretical from 25 to 700 c. p. s. Above 700 c. p. s. the response is less than the theoretical, partly because of some decrease of the amplifier output at the higher frequencies, but largely because the balancing of the inductance of the leads to the hot wire was not perfect, being limited by the sensitivity of the amplifier.

Figure 5 illustrates the results obtained from a test on the hot-wire anemometer working into the compensated amplifier. In this case the wire was placed in the air stream of the wind tunnel. The compensation was set at the value computed from the relation

$$\frac{L}{R_2} = M = \frac{4.2 \rho A^2 S (\bar{T} - T_0)}{i^2 r_v}$$

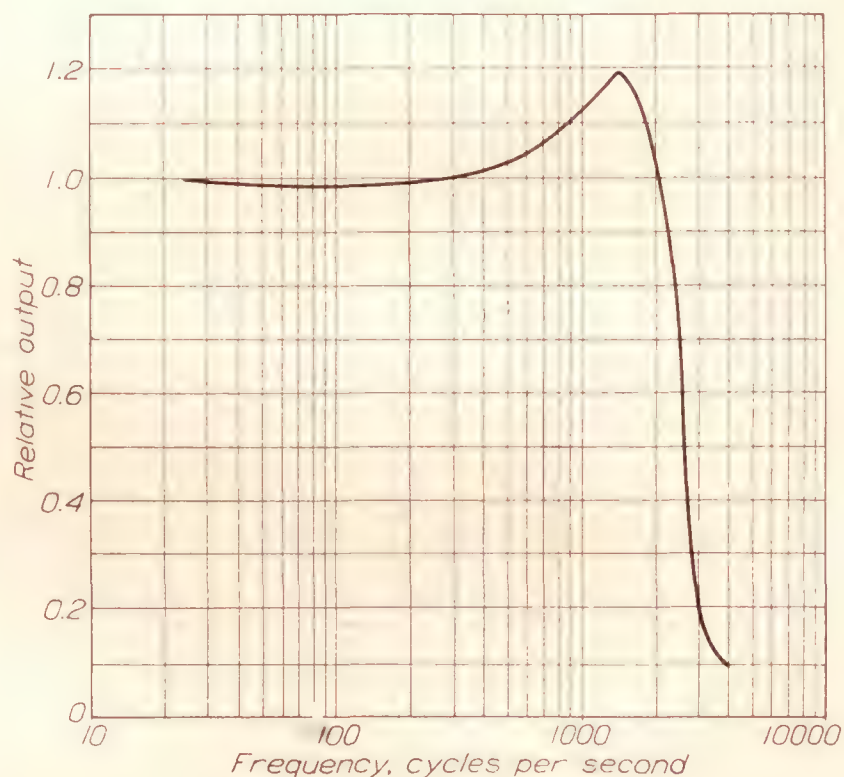


FIGURE 5

From 25 c. p. s. to 430 c. p. s. the compensation brings the output of the hot wire and amplifier combination to within 2 per cent of the ideal value represented by the ordinate 1.0, i. e., the value representing a response independent of the frequency. Above 430 c. p. s. the ratio of the actual to the ideal response increased to a maximum of 1.19 at 1,500 c. p. s. This rise is due to the fact that the coil used in the compensating circuit has unavoidable distributed capacity, as well as the desired inductance, and therefore acts as a tuned circuit resonating at about 1,500 c. p. s. The impedance of an inductance with distributed capacity does not increase directly with frequency, as does the reactance of a pure inductance, but acts rather as though the inductance had been replaced by an equivalent inductance

$$L_e = \frac{L}{1 - \omega^2 LC}$$

where C represents the distributed capacity. For this reason, it is very desirable to reduce the distributed

capacity of the compensating inductance to the lowest possible value and thus reduce the dependence of L_c on frequency.

To summarize, our experiments and those of Ziegler have shown that the theory of the lag of the wire is valid for frequencies up to perhaps 1,000 per second. Verification at higher frequencies is difficult because of the increased sensitivity required and the effects

of the inductance of the several members of the bridge. Since the theory of the lag is shown to be correct, the required performance of the compensating circuit is readily computed. The actual performance may be tested by applying known a. c. voltages of varying frequency. The degree with which the required performance can be met is illustrated in Figure 11, given later.

REPORT No. 448

IMPROVED APPARATUS FOR THE MEASUREMENT OF FLUCTUATIONS OF AIR SPEED IN TURBULENT FLOW

PART II

THE DESIGN OF AMPLIFIERS FOR USE IN TURBULENCE MEASUREMENTS

The fluctuating voltage drop produced by the action of the speed fluctuations in the free stream of a wind tunnel on the hot-wire anemometer is of the order of a few thousandths of one volt and therefore, for convenience in measurement, must be amplified. The vacuum-tube amplifier is the only practical instrument available for this purpose.

Vacuum-tube amplifiers for turbulence measurement must meet several general requirements in the matter of performance. First, they must give sufficient amplification of the available input voltage to operate suitable measuring instruments. Second, they must be free from amplitude distortion; that is, the output must be directly proportional to the input. Third, they should, for a given fixed input voltage, give a constant output, regardless of the frequency of the input voltage, throughout the range of frequencies involved in turbulence measurement.

The first requirement, in the present state of the art at least, means that a suitable amplifier must be one with several stages of amplification. The second requirement means simply that care must be exercised to supply the proper grid and plate potentials to each vacuum tube, so that it will operate on the straight portion of its grid-voltage plate-current curve, and to so choose the tube and its operating conditions that the maximum expected grid voltage swing will neither carry the grid potential from the straight part of the curve nor cause the grid to become positive and draw current. The third requirement, namely, that the amplifier response be independent of frequency in the range of frequencies involved is the most difficult to satisfy, principally because of the first requirement. The construction of a multi-stage amplifier necessitates some method of coupling the tubes together so that the amplified voltage from one vacuum tube may be applied to the grid of the following tube for further amplification. To make this connecting circuit independent of frequency entails considerable difficulty.

There are several interstage coupling systems that may be used over the range of frequencies in which we are interested, and each has certain advantages as well as disadvantages, the discussion of which requires some consideration of the theory of vacuum tubes as amplifiers.

The action of a vacuum tube in amplification is determined by the relations between instantaneous currents and voltages in both input and output circuits. When a steady voltage is impressed on the grid circuit of a vacuum tube, no grid current flows if the grid is negative with respect to the filament. If an alternating voltage is then applied, an alternating current will flow in the grid circuit because of the path offered by the internal grid-filament capacity of the tube, and also in the plate circuit because of the grid-plate capacity. The power thus supplied is dissipated as heat in the resistances of the circuits and must be reduced to the lowest possible level in order to maintain a high efficiency in the amplifier.

The performance of circuits containing vacuum tubes may be computed by assuming that the tube impresses a voltage of μE_g , μ being the amplification factor and E_g the alternating grid voltage, in a circuit consisting of the external impedance Z_0 , and the internal alternating current impedance r_p of the tube under the operating conditions. Hence, the alternating component of the plate current I_p is given by the relation

$$I_p = \frac{\mu E_g}{r_p + Z_0} \quad (10)$$

The alternating voltage E_p across the load circuit is the product of the alternating plate current and the load impedance, that is,

$$I_p Z_0 = E_p = \left(\frac{Z_0}{r_p + Z_0} \right) \mu E_g \quad (11)$$

Since $\frac{E_p}{E_g}$ is the voltage amplification A of the tube and load combination, we may write

$$A = \mu \left(\frac{Z_0}{r_p + Z_0} \right) \quad (12)$$

Equation (12) is of considerable importance in amplifier design in that it shows the effect of load impedance Z_0 , on the voltage amplification. It is seen that Z_0 should be made as large as possible, in order to obtain the maximum gain in voltage. The increase in amplification is rapid until Z_0 becomes some 5 or 10 times as large as r_p . As Z_0 is increased beyond that point, however, comparatively little gain in amplification is obtained.

The four types of interstage couplings that are commonly used are transformer coupling, impedance-capacity coupling, direct coupling, and resistance-capacity coupling. They are illustrated schematically in Figures 6-a, b, c, and d, respectively.

Figure 6a represents the essentials of the common transformer coupled audio-frequency amplifier, which derives its name from the fact that an iron-cored transformer is used to couple the plate circuit of vacuum tube A to the grid circuit of vacuum tube B. The alternating voltage E_g applied to the grid of tube A appears in the output circuit as a voltage μE_g in series with the internal alternating current impedance of the tube r_p , and the primary impedance of the

The advantage of the transformer coupled amplifier is obviously the effect of n in increasing the amplification. The disadvantage, where extreme uniformity of response at a wide range of frequencies is necessary, as in turbulence measurement, lies in the fact that Z_0 , being the impedance of a circuit consisting essentially of inductance and some resistance, is a function of the frequency, varying directly with frequency if the resistance is negligible. Since Z_0 varies with frequency, so does the amplification according to the relation expressed by equation (13). Therefore, if uniform response over any range of frequencies is desired, it can be obtained only by making Z_0 extremely large with respect to r_p at the lowest frequency of the

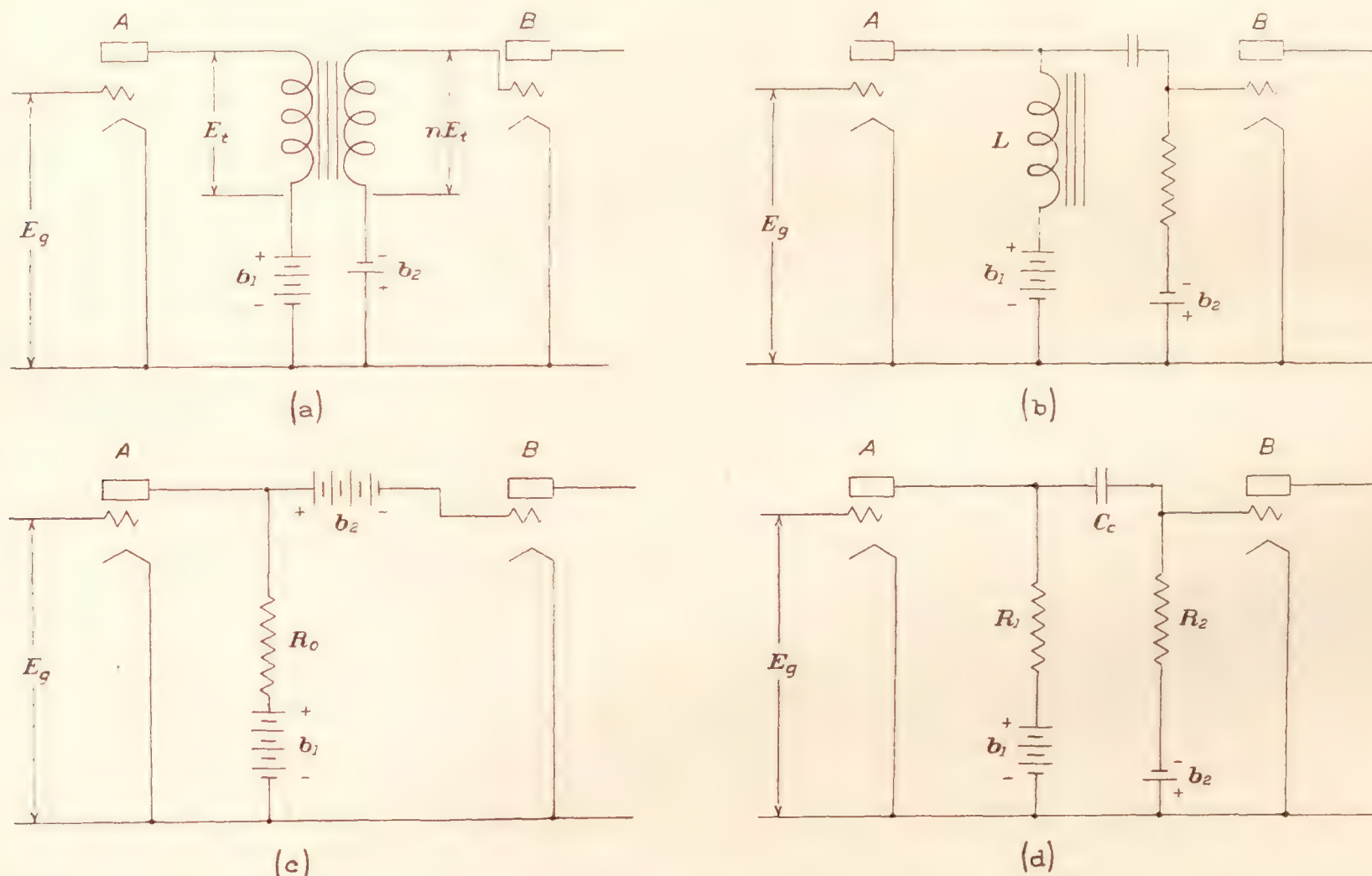


FIGURE 6

transformer T . The voltage E_g thus causes an alternating current to flow through the transformer primary impedance, producing an alternating voltage drop E_t across the transformer primary and inducing an alternating potential nE_t across the transformer secondary, where n is the voltage ratio of the transformer, equal to the turns ratio if the input impedance of tube B is nonreactive and very high, and the transformer is free from all losses and flux leakage. The amplification of tube A and transformer T is then

$$A = \frac{nE_t}{E_g},$$

or n times equation (12); that is,

$$A = \frac{n\mu Z_0}{r_p + Z_0} \quad (13)$$

where Z_0 is the impedance of the transformer primary.

desired range. Since this lowest frequency may be only a few c. p. s., the practical difficulty in constructing a transformer having a large enough impedance for satisfactory operation is very great. A further practical difficulty arises from the fact that the construction of such a transformer requires a primary winding of many turns and hence considerable distributed capacity. This distributed capacity, in conjunction with the capacity between the elements of the associated vacuum tubes, forms a parallel tuned circuit with the transformer inductance. If the resonant frequency of this tuned circuit lies in or near the range of frequencies over which the amplifier is to be used, the impedance Z_0 will be greatly increased at and near resonance with consequent nonuniformity of amplification. If the transformer is so designed that the resonant effect does not occur, the distributed capacity will still make itself felt in the form of a

marked reduction of impedance, and loss of amplification at frequencies above a few thousand c. p. s., because of its shunting effect on the transformer impedance.

From the above discussion, it is seen that the transformer-coupled amplifier experiences considerable difficulty in meeting the requirements for a successful turbulence measuring instrument. As far as is known to us, it is impossible to obtain suitable transformers for such an amplifier.

The impedance-capacity coupled amplifier of Figure 6b may be considered as a special case of transformer coupling in which the voltage ratio n , is unity. It lacks the principal advantage of the transformer coupled type, namely, the possibility of amplification due to transformer voltage ratios greater than one, and possesses the same disadvantages of frequency dependence and distributed capacity effects.

Figure 6c is the basic circuit of the amplifier first used at the Bureau of Standards for turbulence measurements. (Reference 5.) It is a member of a large family of essentially similar amplifiers known as direct coupled. The load impedance Z_0 , is a simple nonreactive resistor and therefore independent of frequency. Hence, theoretically at least, this type of coupling gives uniform action regardless of frequency, and is operable even at zero frequency. Practically, this performance is not obtained because of the shunting effect of the stray capacities of the wiring, and the interelectrode capacities of vacuum tubes A and B. These capacities which, as will be shown later, may be quite appreciable in magnitude, are all in parallel with each other and the load resistor R_0 . Then since the impedance Z_0 of the load circuit consisting of R_0 and C in parallel is at frequency f ,

$$Z_0 = \frac{1}{\sqrt{\frac{1}{R_0^2} + (2\pi fC)^2}} \quad (14)$$

it is at once evident that Z_0 decreases with increasing frequency, and that the amplification factor A is

$$A = \mu \frac{1}{r_p \sqrt{\frac{1}{R_0^2} + (2\pi fC)^2} + 1} \quad (15)$$

The amplification decreases with increasing frequency. The loss in amplification at high frequencies is seen to be a function of the capacity C . Unfortunately, the value of C is comparatively large in the direct coupled amplifier of the type illustrated because of the large capacity to ground of battery b_2 , which is used to maintain the grid of tube B at the proper negative potential with respect to the filament.

In use it was found that the direct-coupled amplifier gave uniform response from zero to a few hundred c. p. s. only. For this reason, and also because of the fact that in the direct-coupled amplifier slight variation of the voltage of any battery, or the constants

of any component of the system, caused amplified shifting of the grid and plate potentials of all the following vacuum tubes, making the amplifier subject to drifting, and difficult of adjustment, the use of the direct coupling was abandoned in favor of resistance-capacity coupling.

The resistance-capacity method of coupling is illustrated by Figure 6d. It differs from the direct coupling of Figure 6c only in that a condenser C_c is placed in the connection between the plate of vacuum tube A and the grid of vacuum tube B, the latter being held at the required negative potential by battery b_2 through R_2 .

The purpose of the condenser C_c , is to insulate the grid of tube B from the positive plate potential of tube A, while allowing the amplified alternating voltage across the load resistor R_1 of tube A to be impressed on the grid of tube B. The use of a large grid battery at a high potential above the filament, such as battery b_2 of Figure 6c is then unnecessary. By doing away with this battery a large portion of the shunting capacity which makes the direct-coupled amplifier unsuitable for use at frequencies greater than 100 or 200 c. p. s., is eliminated with consequent improvement in performance. A further advantage realized by the use of resistance-capacity coupling, in preference to direct coupling, is that the condenser C_c , localizes the effect of variation of battery voltages to the tube or tubes connected to that battery, thereby eliminating the general shift of operating voltages and difficulty of adjustment characteristic of direct-coupled systems.

The disadvantage of resistance-capacity coupling is that C_c is reactive and therefore its impedance is dependent on the frequency. That this disadvantage may be obviated by proper design, and in some particulars even turned to advantage, may be shown from an elementary consideration of the circuit theory.

Neglecting, for the present, the effect of the vacuum-tube interelectrode capacities, the load impedance of a resistance-capacity coupled amplifier consists of R_1 (fig. 6d) in parallel with the circuit formed by R_2 with C_c in series. The alternating grid voltage for vacuum tube B is taken from across R_2 . At low frequencies, where the reactance of C_c is large compared to the resistance of R_2 , that part of the alternating voltage across R_1 which is impressed on the grid of vacuum tube B is small, being zero at zero frequency. As the frequency is increased the reactance of C_c decreases, and when it becomes negligible compared to R_2 the maximum amplification results. The amplification is then independent of frequency and the load impedance of tube A is essentially equal to the resistance of R_1 and R_2 in parallel.

From the above it follows that two items must be considered in the design of the coupling circuit namely, C_c must be large so that good amplification

may be obtained at low frequencies, and R_2 should be large in proportion to R_1 so that the load impedance of vacuum tube A and hence the amplification may be as high as possible.

Unfortunately, the use of a high capacity at C_c and a high resistance at R_2 also results in a circuit of large time constant $C_c R_2$. If a momentary surge or overload of the amplifier causes the grid of tube B to become positive the amplifier will become inoperative, or "block" for a length of time equal to that required for the positive charge to leak off from C_c through R_2 . The time required for this leakage is proportional to the time constant of the coupling circuit. To reduce

lected in the discussion of coupling condenser and grid resistor size. Here it is the magnitude of the unavoidable interelectrode capacities, and the somewhat avoidable stray capacity between grid, plate, and filament wiring that controls the performance.

Figure 7a is the simplified schematic diagram of a 2-stage resistance-capacity coupled amplifier, with the interelectrode capacities shown as dotted lines. Let us investigate the effect of these capacities on the performance of the amplifier at high frequencies.

If we assume that the mean grid potentials of vacuum tubes A and B are negative so that the grid to filament resistances of the tubes are high, and that E_g ,

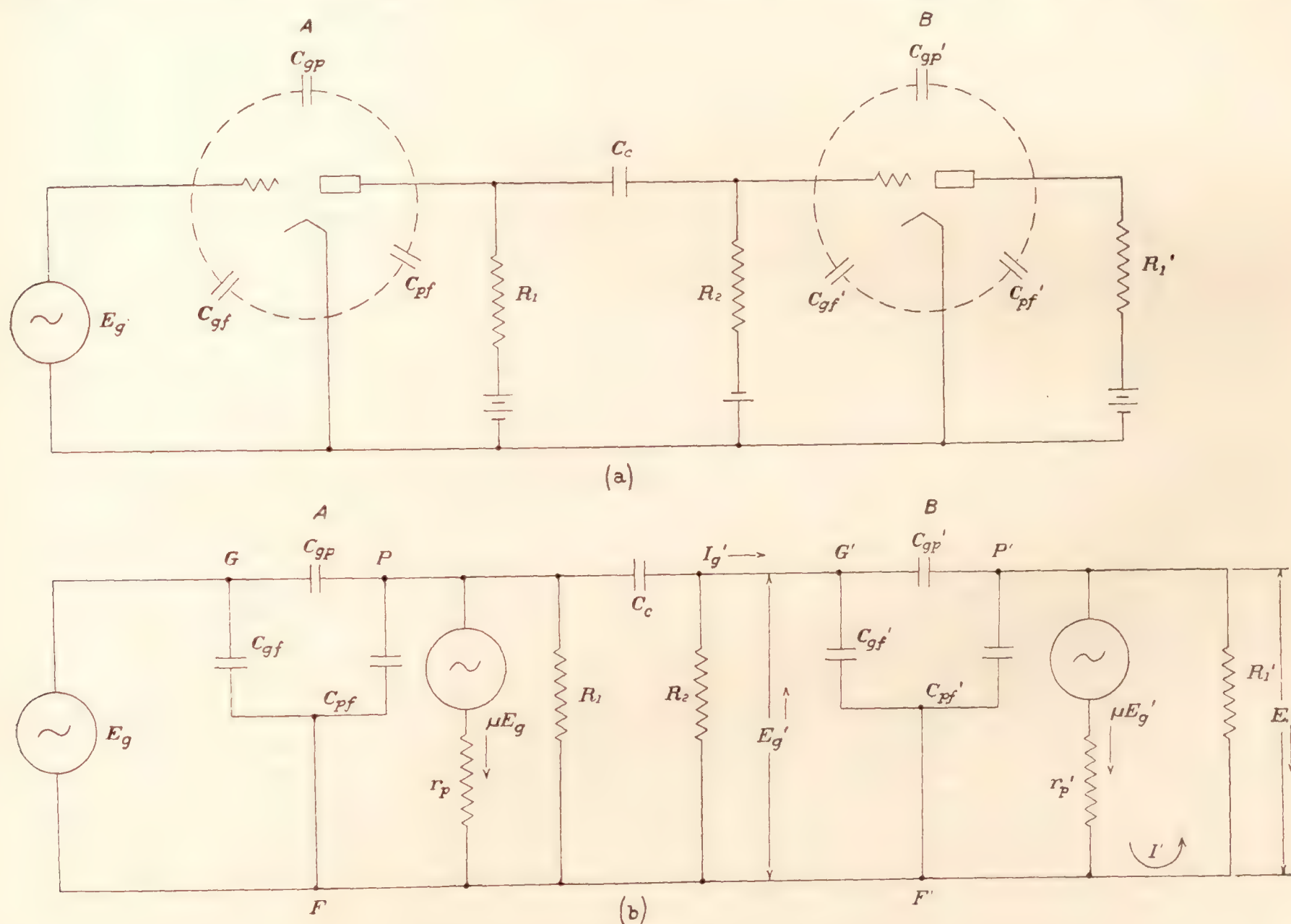


FIGURE 7

this effect to a practical minimum, it is necessary to reduce the time constant either by reducing C_c with resultant loss of amplification at low frequencies, or by reducing R_2 with consequent loss of amplification at all frequencies. The latter alternative, if employed, necessitates the use of a large number of stages in order to obtain the desired amplification, which leads to serious practical difficulties. We are therefore forced to reduce C_c , fixing its value to obtain a compromise between loss of amplification at low frequencies and the degree of sluggishness to be tolerated in the amplifier.

The response of a resistance-capacity coupled amplifier to high frequencies is determined by factors neg-

the applied alternating grid voltage, is small, we may represent the circuit of Figure 7a by the equivalent network of Figure 7b. E_g represents a small alternating input voltage; G , P , and F the grid, plate, and filament, respectively, connected by the interelectrode capacities C_{gf} , C_{gp} , and C_{pf} , r_p the internal alternating-current impedance of the vacuum tube; R_1 the plate-circuit load resistor; C_c the coupling condenser; and R_2 the grid-circuit resistor of the following tube. The amplifying action of the tube is represented by the alternating voltage μE_g , introduced into the plate circuit in series with r_p . Since the plate current increases as the grid becomes more positive μE_g is in opposite phase to E_g .

The exact solution of the network of Figure 7b requires the solution of 17 simultaneous equations and will not be given here. The most important effect with many types of vacuum tubes is due to the shunting effect of the network to the right of R_2 , especially to the current flowing in the condenser C_{gp}' . The voltage across this condenser is readily seen to be $E_g' + E'$ where E' is the voltage across the plate resistor R_1' of the second tube. In computing E' for an amplifier used at audio-frequencies, it is permissible as a first approximation to neglect the current flowing through C_{gp}' and C_{pf}' in comparison with I' , since at audio-frequencies the impedances of the interelectrode capacities are large compared with the rest of the network. Then, considering the circuit farthest to the right,

$$I' = \frac{\mu E_g'}{r_p' + R_1'}$$

and

$$E' = I' R_1' = \frac{\mu R_1'}{r_p' + R_1'} E_g'$$

The voltage across the condenser C_{gp}' is therefore

$$E_g' \left(1 + \frac{\mu R_1'}{r_p' + R_1'} \right)$$

or since $\frac{\mu R_1'}{r_p' + R_1'}$ is the voltage amplification A of tube B, $E_g' (1 + A)$. The current flowing through C_{gp}' is therefore $j 2 \pi f C_{gp}' E_g' (1 + A)$.

The voltage applied to the network to the right of R_2 is E_g' . Hence the apparent impedance of the condenser C_{gp}' is

$$\frac{1}{j 2 \pi f (1 + A) C_{gp}'} \quad (16)$$

or the effect is as if the capacity of this condenser were increased by the factor $(1 + A)$.

An exact solution of the network would give a still lower shunting impedance because of the effects of C_{gf} , C_{pf} , C_{pf}' , C_{gp} , and C_{gf}' . C_{pf}' , C_{gf} , C_{pf}' , and C_{gf}' are approximately fixed for any conventional assembly of commercially available tubes and associated components, $C_{pf} + C_{gf}$ being of the order of $30 \mu\mu f$. With $R_1 = 250,000$, a capacity of this magnitude produces a one per cent reduction of the effective plate impedance at a frequency of 3,010 cycles per second, account being taken of the fact that the shunting current is in quadrature with the plate current. With $R_1 = 100,000$, a 1 per cent reduction occurs at a frequency of about 7,540 cycles per second.

When the effects of $(1 + A) C_{gp}'$ are included, we find that frequency errors become large at still lower frequencies. Consider the two amplifiers which have been used at the Bureau of Standards. In the first using UX240 tubes with $R_1 = 100,000$ ohms, C_{gp} is about $10 \mu\mu f$ and A about 20. The effective shunting capacity is $21 \times 10 + 30 = 240 \mu\mu f$. Appreciable errors are introduced at frequencies as low as 900 cycles per second. In the second using the UY224 screen-grid

tubes, with $R_1 = 250,000$ ohms, C_{gp} is only $0.015 \mu\mu f$, and A about 80. The effective shunting capacity is about $80 \times 0.015 + 30 = 31.2 \mu\mu f$. Appreciable errors are introduced only above a frequency of about 2,860 cycles.

The calculations given above correspond fairly well to the actual performance of the two amplifiers. The effect of the shunting capacity is frequently overlooked in the design of resistance-capacity coupled amplifiers.

Another factor having an important effect on the performance at high frequencies as illustrated in part in the preceding calculations is the relation between the shunting capacity and the external plate impedance. If, at a certain high frequency C_s , the shunting capacity has 10 times the impedance of R_1 , its effect will be much less than if, at the same frequency, and with the same shunting capacity, R_1 is increased until its impedance is, say, one-half that of C_s . The effect is further complicated in practice because increase in R_1 will cause increased amplification, according to the relation expressed by equation (12), which in turn results in increased effective shunting capacity, making the difference between the impedance of C_s and the impedance of R_1 still smaller than if R_1 alone had been increased. The modern practice of using very high values of R_1 in order to obtain high amplification per stage must therefore be avoided if good uniformity of response over a wide range of frequencies is necessary. Conversely, if unduly low values of R_1 are employed, in an effort to improve the range of uniform response, the amplification per stage will be so reduced that the number of stages necessary to obtain the required amplification may become excessive.

The objection to a large number of stages is two-fold. First, the difficulty in operation and adjustment of the complete amplifier increases much faster than the number of stages. Second, the actual improvement in uniformity of response obtained may be of slight consequence, even though the performance of each individual stage is improved, because the addition of each similar stage amplifies the nonuniformity of the previous stages. For example, if we have a 2-stage amplifier giving a voltage gain of 100 per stage at some low frequency and 50 per stage at 10,000 c. p. s., the over-all gain of the two stages at the low frequency will be 10,000, and at 10,000 c. p. s., 2,500. If we then reduce R_1 with the object of improved performance, until the voltage gain per stage becomes 10 at the low frequency and 7.5 at the high frequency of 10,000 c. p. s., it will be necessary to use four stages to obtain the same over-all gain at the low frequency as in the previous instance, and the over-all gain at 10,000 c. p. s. will be 3,160. The over-all performance is seen to be improved slightly but not to the same extent as the performance of the individual stages, and probably not enough to compensate for the operational difficulties introduced by the addition of two stages.

REPORT No. 448

IMPROVED APPARATUS FOR THE MEASUREMENT OF FLUCTUATIONS OF AIR SPEED IN TURBULENT FLOW

PART III

IMPROVEMENTS IN THE BUREAU OF STANDARDS APPARATUS

The assembly of equipment at the Bureau of Standards for measurement of turbulence consists of five parts: (1) The wire itself; (2) a Wheatstone bridge for accurate measurement of the resistance of the wire at room temperature; (3) an apparatus with suitable switching arrangements for supplying the wire with heating current, measuring the heating current, measuring the voltage drop across the wire at various air speeds for calibration purposes, and finally transferring the fluctuating voltage drop across the wire to the amplifier input; (4) a suitable amplifying system, including the requisite compensation for the amplitude reduction and phase angle lag of the wire; and (5) a final measuring instrument. The earlier forms of the apparatus are described in references 5 and 6; it is assumed that the reader is familiar with them. Those references also give in detail the method of calibration and the method of computing the magnitude of the speed fluctuation.

THE WIRE

The wire itself has undergone little modification since its first use at the Bureau of Standards. It is generally a platinum wire about 0.75 to 1.0 centimeter in length and 0.017 millimeter in diameter, electrically welded to a suitable mounting. Some of the first hot wires were soldered to their mountings but this practice was soon abandoned because of the uncertain contact between wire and support. The welds joining the platinum wire to the prongs of the supports should be inspected with a low-power microscope, or a good jeweler's eyeglass. A good uniform weld is easily identified. No other kind will be found satisfactory.

It has been found advisable to anneal each new wire before use by passing sufficient current through it to cause it to glow a dull red. If the wire is to be used tightly stretched, as when working in the boundary layer of a flat plate or other body, this annealing process should be conducted with the wire tight but must not be continued for more than a few minutes. Undue prolongation of the annealing of such a wire usually leads to a greatly shortened life. The wire when heated tends to soften, as is desired, but tension tends to stretch and harden it again. If the annealing

is continued for a long time, the wire becomes considerably elongated and weakened, breaking soon after being put in service. Measurements of the turbulence in the free stream of the wind tunnel do not require that the wire be under tension; therefore wires for this use may be annealed for longer periods without detrimental effect on their life. Fifteen to thirty minutes is probably quite sufficient for proper annealing.

Proper annealing tends to reduce the magnitude of the changes in the room-temperature resistance of the wire which often take place during the course of a set of observations. Thus, the accuracy of the data obtained is increased and the labor of the computations decreased. Since the resistance of the wire is seldom the same after a run as before, it is advisable to measure it carefully immediately before and after completing the observations.

The age of the wire has been found to have an effect on the results obtained. In one case the use of a wire several months old increased the readings several per cent in comparison with those obtained with a new wire. This action is believed to be due to some change in the character or condition of the surface of the wire, perhaps accumulation of dirt, and may not occur everywhere. It is believed to be the best policy to change the wire frequently and avoid any possibility of this effect.

EQUIPMENT FOR MEASURING MEAN VOLTAGE DROP

The third item of the equipment, the heating-current measurement, control, and voltage-drop measurement apparatus, together with the switching circuits, remains the same as that described in previous reports (references 5 and 6), except that the mechanical arrangement has been considerably improved, with resultant increase in convenience of operation.

THE AMPLIFIER

The amplifier has undergone several modifications since the publication of references 5 and 6. The amplifier described in reference 5 consisted of four stages, using UX240 vacuum tubes, direct coupled as in Figure 6c, and an output stage consisting of one UX171 vacuum tube. While this arrangement proved

usable over the range of frequencies between zero and one or two hundred c. p. s., it was subject to drifting, and difficult to maintain in the proper operating condition. It sometimes happened that the change in calibration of the amplifier during the course of taking a set of observations was so great that the observations had to be discarded. For these reasons the use of this amplifier was discontinued and the amplifier described in reference 6 was constructed. This amplifier differed from the former principally in the use of resistance-capacity coupling instead of the original direct-coupling system. This change resulted in a great improvement in the constancy of performance of the apparatus by eliminating the drifting and general uncertainty of operation over any extended period of time. Furthermore, the range of frequencies over

In 1930 work was started on an improved amplifier. The schematic circuit diagram of the fifth and final arrangement (fig. 8) indicates that basically it is the same as the amplifier of reference 6. The differences are in the details and components employed.

The first difference of note is the use of the more modern UY224 tetrode vacuum tubes in place of the earlier UX240 triodes. These tubes have two advantages: First, the voltage amplification factor is much higher, permitting a voltage amplification per stage of 60 to 80 under the conditions of operation existing in the present amplifier; second, due to the use of a screening, or shielding grid between the control grid and plate, the internal capacity between grid and plate is reduced from the $10 \mu\mu f$ of the UX240 type to $0.015 \mu\mu f$, resulting in a reduction of the total shunting

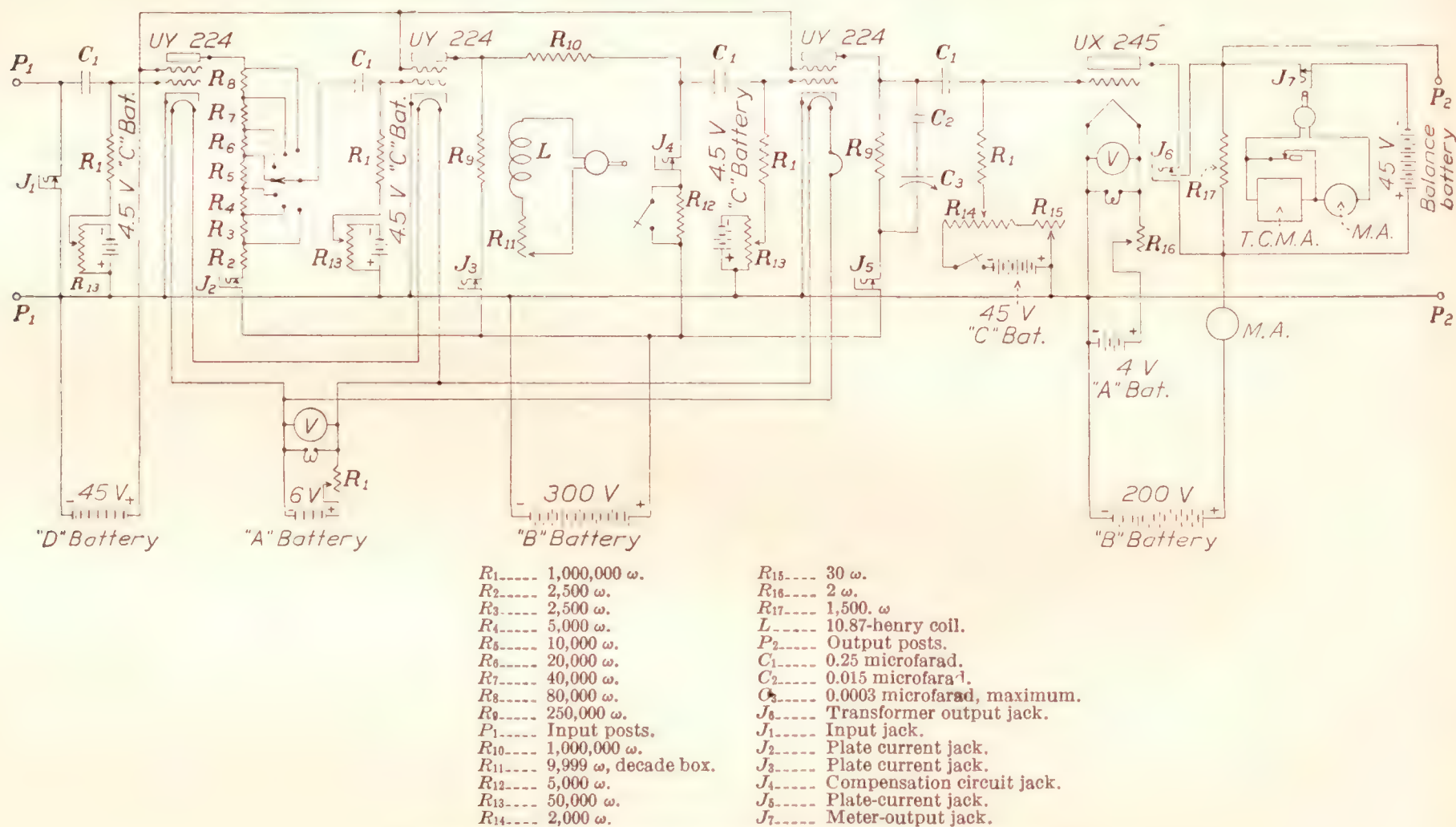


FIGURE 8.—Circuit of audio-frequency amplifier for turbulence measurement

which uniform response was obtained was substantially increased, because of the reduction in shunting capacity effected by dispensing with the large grid bias battery. (See b_2 of fig. 6c.) The coupling capacities used were $2 \mu f$ mica condensers of high quality, and together with the 1 megohm grid resistors formed a coupling circuit having a time constant of 2 seconds. This large coupling capacity permitted uniform response to frequencies as low as 1 c. p. s. or less, but the 2-second time constant caused some inconvenience because of the long time required for the amplifier to unblock after being subjected to a momentary overload, such as often occurs in the use of the apparatus. The tubes employed were the UX240 type, and the voltage amplification per stage was about 20.

capacity from $240 \mu\mu f$, to $31.2 \mu\mu f$ with consequent increase in the range of uniform response. A further improvement in operation resulting from the use of the UY224 vacuum tube, with its considerably higher voltage amplification is that the number of stages exclusive of the output stage has been reduced from four to three. This reduction in the number of stages, together with the use of stages having superior individual performance with respect to uniformity of response, results in still greater over-all improvement in uniformity.

In the 4-stage amplifiers of references 5 and 6, control of the over-all amplification was obtained by means of taps on the plate resistor of the first tube and a switching arrangement for cutting out one stage. In the present 3-stage amplifier the amplification control

consists of a greater number of taps on the plate resistor of the first tube, and no provision is made for cutting out a stage of amplification. The plate-resistor taps are so arranged that each step reduces the amplification to half that of the previous step. There are 7 such steps in the control and the amplification may be varied over a range of 64 to 1.

Another important modification in the present apparatus consists of the substitution of coupling condensers of $0.25 \mu f$ capacity for those of $2.0 \mu f$ previously used. This change results in nonuniformity of response at frequencies below 25 c. p. s.,¹ but increased uniformity of response at the higher frequencies because of the reduced bulk and stray capacity of the condensers. Also, the performance with respect to blocking is greatly improved, since with 1-megohm grid resistors the time constant of the coupling circuit has been reduced to 0.25 second from the 2.0 seconds of the previous amplifier.

The input of the earlier amplifiers (references 5 and 6) was directly to the grid of the first vacuum tube. In the present amplifier (fig. 8) this has been changed by the insertion in the first grid circuit of a condenser of the same capacity as the coupling condensers. This change increases the ease of operation by insulating the grid of the first vacuum tube from the hot wire as far as direct current is concerned, making exact balancing of the direct current voltage drop across the wire less necessary than before. In the previous amplifiers any unbalance in the direct current voltage drop was transmitted directly to the grid of the first tube, changing the grid voltage thereof, and hence changing the operating conditions of the tube. In the presence of large speed fluctuations, it is difficult to obtain exact balance of the direct current voltage drop, therefore the use of the condenser input has a practical advantage in that it confines any error resulting from incorrect balance to the measurement of the mean voltage across the wire, avoiding further errors due to changes in the condition of operation of the amplifier from that for which the calibration was made.

The UX171 output vacuum tube used in the earlier amplifiers has been replaced in the newer equipment by the UX245 type. This tube was chosen because of its higher transconductance; that is, a greater change in plate current for a given change in grid voltage. Since the measuring instrument generally used is a current-measuring device, this change results in an increase in the sensitivity of the output stage of the amplifier. Further increase in the sensitivity of this stage has been secured by abandoning the use of a potentiometer across the balancing battery to adjust the voltage necessary to balance out the direct-current potential drop across the plate resistor of the output tube. This direct-current potential drop must be balanced

in order that the a. c. milliammeter shall read only the alternating current, but the use of a potentiometer across the balancing battery introduces resistance in series with the measuring instrument and reduces the sensitivity. In the improved amplifier this effect is avoided by choosing a suitable balancing voltage and then adjusting the voltage drop across the output tube plate resistor until it is equal to the balancing battery voltage. The adjustment is made by changing the plate and grid voltages of the output tube. Fortunately, it is found that if the balancing-battery voltage is 45 volts and the plate voltage 200 volts, proper operating conditions are obtained when the plate current of the output tube is adjusted to the 30 m. a. necessary for balance.

Vacuum-tube amplifiers while essentially simple in principle, require constant vigilance to insure satisfactory operation. Constancy of calibration is seldom attained. It is most closely approximated when constant watch is kept on the voltage of all batteries associated with the amplifier. The amplifier must in general be calibrated before and after every set of observations, and the simplest method is to apply a known voltage to the input, under standard conditions, and measure the output current. The amplifier used at the Bureau of Standards is provided with a 5,000-ohm resistor, R_{12} of Figure 8, in series with the compensating circuit, and normally shortcircuited by a switch. When it is desired to calibrate the amplifier the compensating coil and resistance L and R_{11} , are removed from the circuit and the shortcircuiting switch across R_{12} opened. The amplification control R_2 to R_8 , is then set on the fourth step, a resistance of 2 ohms placed across the amplifier input, an alternating current of 2 milliamperes of frequency 500 c. p. s. passed through this resistance, and the output current read. The output current normally obtained is about 3 milliamperes with the present amplifier. If the output is found to be below normal the voltage of all batteries is checked. If no low voltage is found the next step advisable is a check on the operating conditions of each of the three screen-grid tubes. This check is made by inserting a milliammeter in each plate circuit in turn and noting the plate current. A voltmeter and a potentiometer are then connected so that a known grid voltage may be applied to each tube and a curve of plate current versus grid voltage obtained under the conditions of plate and screen-grid voltage and plate-resistor resistance existing in that stage. If the operating plate current as first measured lies within the straight portion of the curve, the stage is in the proper operating condition. If it does not, the trouble is localized and the individual components must be examined. Since these are few in number the trouble is usually easily located. The usual sources of trouble are the plate resistor of the stage under consideration and the coupling condenser of the preceding stage.

¹ The computed error is less than 5 per cent at 10 cycles per second.

Considerable difficulty has been experienced in obtaining suitable plate resistors. It is found that their resistance sometimes increases greatly with age, often becoming extremely high. If this happens, the operating conditions in the stage are upset with consequent loss of amplification. Less frequently the coupling condensers give trouble due to leakage. Any current leakage through the coupling condenser flows through the grid resistor of the following stage, producing a voltage drop tending to make the grid more positive, thus disturbing the operating conditions of the tube. In extreme cases the grid voltage may be so changed that the tube becomes saturated, because of insufficient negative grid voltage, and altogether ceases to amplify. The coupling condenser following the compensation circuit is the one most likely to give trouble because it is subjected to almost the full 300 volts of the plate battery, whereas the other coupling condensers are at a voltage lower than 300 volts by the voltage drop through the plate resistors. The use of the highest grade condensers available is strongly recommended. Infrequently the above examination of the defective stage will disclose no faults in the components. If this is the case the tube itself is probably defective and must be replaced. Faulty tubes, however, are quite rare according to our experience. Some considerable differences may be noticed between the characteristics of tubes nominally of the same type. This is especially true of the UY224 tetrodes, but if care is taken to adjust the grid voltage to the proper value for best operation they will generally be found to give the same performance.

Another item in the amplifier that sometimes gives trouble is the imperfection of wire connections. Whenever possible, all connections should be soldered with a good rosin flux solder. Acid or paste fluxes should never be used because of the corrosion and leakage caused by spattering of the flux when heat is applied. Those connections, such as switches, jacks, and vacuum-tube sockets, which may not be soldered must be frequently inspected and cleaned.

COMPENSATION CIRCUIT

The arrangement of the compensation circuit has been changed slightly from that of the earlier amplifiers. Reference to Figure 8 shows that the compensating inductance and resistance L and R_{11} , are not placed directly in the plate circuit of the vacuum tube in series with the plate resistor, as in the previous amplifiers, but, together with the one megohm resistance R_{10} , form a voltage dividing circuit in parallel with the plate resistor R_9 . This system is essentially the same as the earlier one of inserting L and R_{11} in series with R_9 so that R_9 performs the function of R_{10} , but offers the advantage that R_{10} may be made as large as desired, with consequent reduction of the phase error of the circuit (reference 5), without materially

affecting the amplification of the tube preceding the compensating circuit. In the original arrangement, since the plate battery voltage is fixed by practical considerations R_9 , which also acts as R_{10} , may not be increased indefinitely without reduction of the amplification because of the reduction of the plate voltage as R_9 becomes larger. This reduction in the amplification takes place before R_9 has become as large as might be desired from the standpoint of reducing the errors of compensation.

The compensating inductance L , used in the present equipment is the result of extended efforts to improve the action of the former coil. Reduction of the distributed capacity was the major problem involved, and the solution adopted consisted of winding the coil in three equal sections separated somewhat and connected in series. The finished coil has a length to diameter ratio of about 1.0, an inductance of 10.87

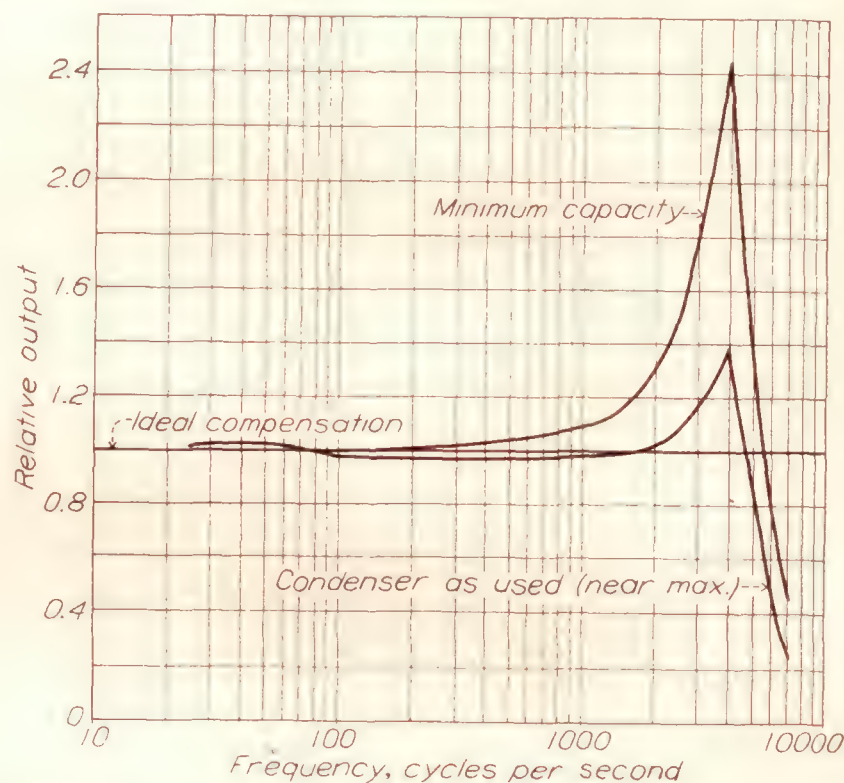


FIGURE 9.—Effect of variable condenser across third tube-load resistance on compensation

henrys, and a resistance of 713 ohms. This coil was found to have sufficient distributed capacity to cause resonance at 4,000 c. p. s., whereas the coil formerly used resonated at 1,500 c. p. s., a considerable improvement even in view of the fact that the inductance of the coil is some 5 per cent lower than that of the original coil.

The presence of the resonant frequency in the range of frequencies over which measurements were desired led to a further modification in the new apparatus not found in the old. This modification is the addition of the shunting condensers C_2 and C_3 (fig. 8), across the plate resistor of the last tube but one. The purpose of these condensers is to introduce a reduction of response at the high frequencies to compensate for the increase in impedance of the compensating coil at and near the resonant frequency. The first condenser C_2 , in series with the variable condenser C_3 , is merely

a protective device. Since the plate current of the next to the last tube is 0.001 ampere and the plate resistor has a resistance of 250,000 ohms, a voltage drop of 250 volts exists across the plate resistor. If the plate resistor is accidentally short-circuited, as has happened during adjustment when C_3 alone was used, the grid of the last tube is subjected to a transient voltage change of 250 volts, with results that are sometimes disastrous. For this reason the condenser C_2 was inserted in series with C_3 to prevent accidental short circuiting of C_3 from short circuiting the plate resistor.

By careful adjustment of the capacity of the shunting condenser C_3 it was found possible considerably to improve the action of the compensating circuit. Figure 9 presents the results of tests with two condenser settings. The horizontal line of ordinate 1.0 represents the ideal of uniform response of the hot wire plus compensated amplifier. The curve labeled "minimum capacity" is the response obtained when the variable capacity C_3 is set at its minimum value. The curve

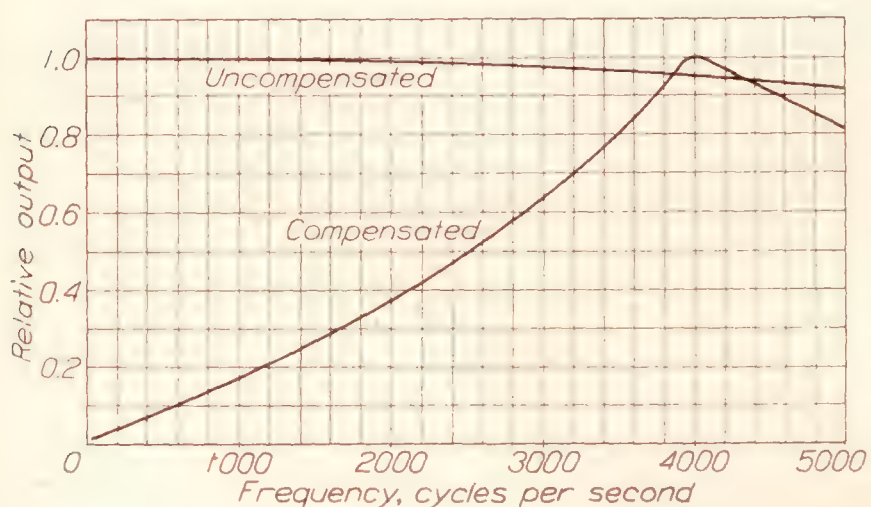


FIGURE 10.—Frequency characteristic of amplifier alone. In each instance the curve is plotted on the basis of maximum output=1.0. The actual maximum output compensated is 121.5 times the uncompensated maximum output

marked "condensers as used" is the best condition obtained as a result of several trial settings of C_3 . With the condenser set at minimum the response is within 2 per cent of the ideal from 25 c. p. s. to 300 c. p. s., an improvement over the previous amplifiers and compensators, but with the condenser set as used, the response is within 2 per cent of the ideal from 25 c. p. s. to 2,000 c. p. s., a very considerable improvement in performance.

The curves of Figure 7 were made by applying a known alternating voltage to the amplifier, measuring the output at various frequencies, and multiplying by $\frac{1}{\sqrt{1+M^2\omega^2}}$ the amplitude reduction factor of the hot wire. Therefore, they represent the combined performance of the hot wire and the compensated amplifier. Figure 10 shows the performance of the amplifier alone; that is, without the effect of the hot wire. It is seen that the response of the uncompensated amplifier is within 2 per cent of uniform from 25 to 3,000 c. p. s. and falls off only 8 per cent at 5,000

c. p. s. The second curve shows the output of the compensated amplifier, plotted relative to 1.0 as the maximum, for convenience. Actually the maximum of the compensated curve is 122 times the maximum of the uncompensated. The compensated curve is seen to rise almost uniformly to 4,000 c. p. s. Above 4,000 c. p. s. it falls again because of the rapidly decreasing impedance of the compensating circuit above its resonant frequency.

In Figure 11 the performance of the hot wire, the amplifier, and the compensating circuit are summarized. The curve marked "amplifier distortion" is the performance of the uncompensated amplifier, as in Figure 10; the curve marked "uncompensated" represents the performance obtained by using the hot wire with the uncompensated amplifier, to the same scale; and the curve marked "compensated" is the performance resulting from the combination of hot wire and compensated amplifier also to the same scale. The "compensated" curve is seen to be within 2 per cent

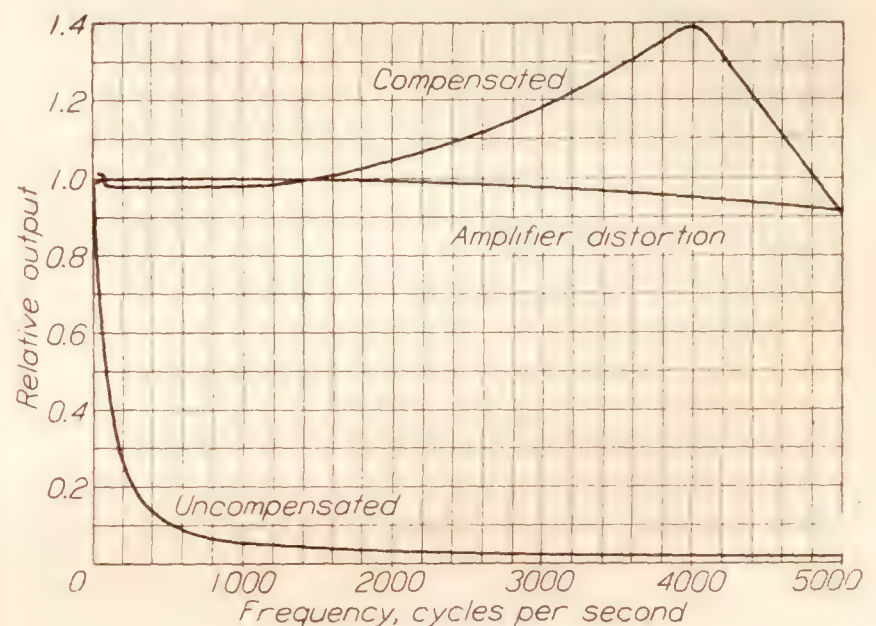


FIGURE 11.—Frequency characteristic of amplifier and hot wire

of the ideal, represented by the ordinate 1.0, from 25 to 2,000 c. p. s. This is the performance of the amplifier as now used. It is to be especially noted that the output of the amplifier does not fall below the ideal until 5,000 c. p. s. is reached, thus insuring that any high frequencies existing in the turbulent air flow will make their presence felt in the observations.

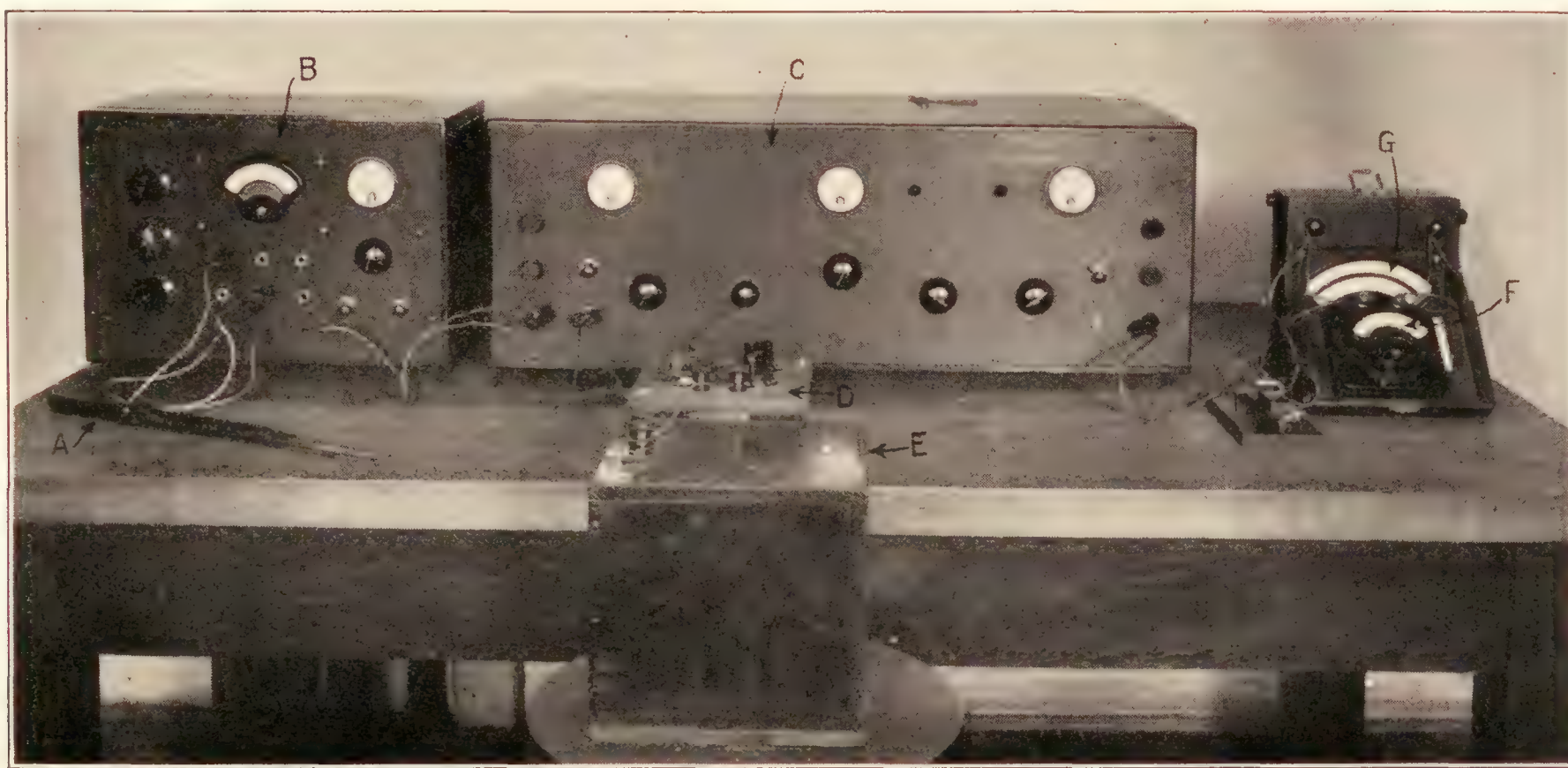
FINAL MEASURING INSTRUMENT

The fifth section of the measuring assembly, namely, the final measuring instrument, remains, in general, the 0 to 5 m. a. thermocouple milliammeter used in all previous work. Reference to Figure 8 will show that it is normally short-circuited by a key or switch. This has been found necessary because of the frequency with which disturbances large enough to burn out the meter occur. It is very essential to avoid making any adjustments in the amplifier or associated equipment, or even touching any portion of the input circuit, when the meter is not shortcircuited. Otherwise, a burned-out milliammeter is almost certain to result. As a

further precaution, a direct-current milliammeter is connected in series with the thermocouple instrument to indicate whether or not the balance of the direct-current voltage drop across the amplifier output resistor is correct. If this meter does not read zero the balance is imperfect and must be adjusted before removing the short-circuit from the thermocouple milli-

reduce the sensitivity because of the resistance introduced in series with the meter.

The thermocouple milliammeter has been supplemented for some purposes by a General Radio cathode-ray oscillograph. The oscillograph is found very useful for visual inspection of the wave form and has been used with a moving-film camera for making permanent



- A. Support for the hot wire.
- B. Controls, measuring instruments and switching circuits for power supply to the hot wire, and for measurement of mean air speed.
- C. Amplifier.
- D. Resistance R of compensating circuit.
- E. Inductance L of compensating circuit.
- F. Direct-current milliammeter.
- G. Thermocouple actuated alternating-current milliammeter.

FIGURE 12.—Turbulence-measuring apparatus (batteries not shown)

ammeter. The direct-current milliammeter is also a useful indicator of the magnitude of the slower fluctuations in the turbulence. If the reading of the direct-current milliammeter is fluctuating more than one or two milliamperes it is unsafe to put the thermocouple milliammeter in the circuit.

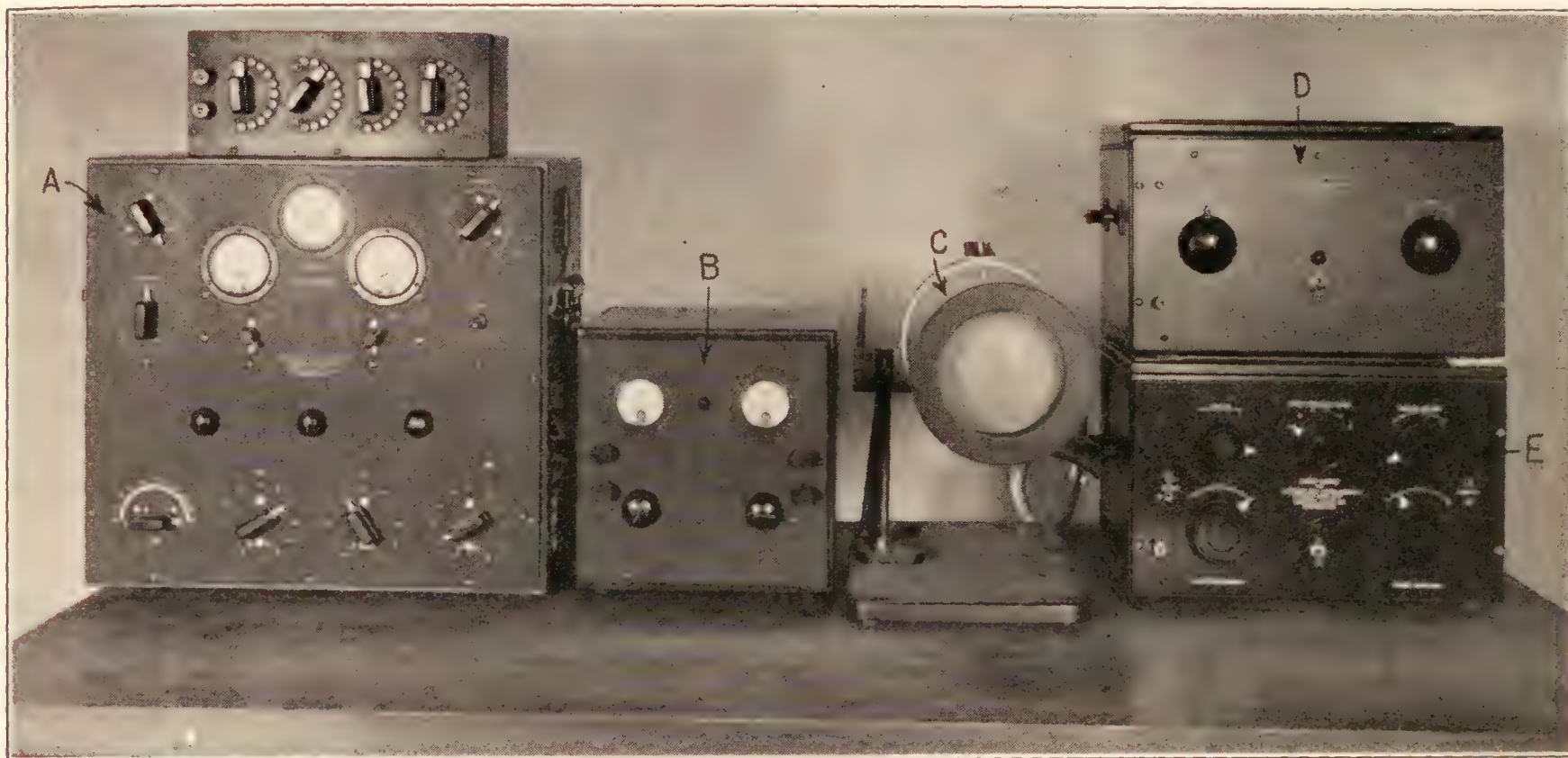
We have not been able to find suitable fuses to protect this meter, which do not at the same time greatly

records. It is also useful for checking the performance of the amplifier by comparing the shape of an amplified sinusoidal voltage wave with the original. The cathode-ray oscillograph may also be used as a visual check on the accuracy of the compensation according to the method of Ziegler. (Reference 9.)

Since the output of the main amplifier is insufficient to operate the cathode-ray tube from the low levels of

turbulence found in the free stream of the wind tunnel, an additional stage of amplification is employed. This consists of a single RCA247 pentode vacuum tube, resistance-capacity coupled to the main amplifier, and working into a load resistor of 7,000 ohms, with plate and screen-grid voltages of 250 and 200 volts, respectively. Under these conditions the voltage gain of the

visual observation the time axis is supplied by a revolving or rocking mirror, while for permanent records the moving-film camera is used. It has been found that a film speed of approximately one foot per second may be used under the usual conditions of spot brightness and film sensitivity. The film employed to date has been regular Eastman negative motion-picture



A. Audio-frequency oscillator for calibrating and studying the distortion the amplifier.
B. Single-stage amplifier for use with cathode-ray oscillograph.

C. Cathode-ray oscillograph tube.
D. Power-supply unit for cathode-ray oscillograph.
E. Time-axis apparatus for cathode-ray oscillograph.

FIGURE 13.—Auxiliary equipment for use with turbulence-measuring apparatus

stage is about 11 and the permissible grid swing is about 22 volts; hence an output peak voltage swing of as much as 132 volts may be obtained. One pair of the two sets of deflecting plates of the cathode ray tube is connected across the output resistor of the pentode amplifier through a $1.0\mu f$ condenser and the cathode-ray beam thus deflected by the alternating voltage appearing across the output resistor. For

film. It is thought that the use of the newer and extremely sensitive panchromatic films might permit higher film speeds.

The wire mounting, amplifier, etc. (without batteries), are shown in Figure 12, and the audio-frequency oscillator, cathode-ray oscillograph tube, and auxiliary equipment in Figure 13.

REPORT No. 448

IMPROVED APPARATUS FOR THE MEASUREMENT OF FLUCTUATIONS OF AIR SPEED IN TURBULENT FLOW

PART IV

EXPERIMENTAL DETERMINATION OF THE FREQUENCY DISTRIBUTION OF THE SPEED FLUCTUATIONS

The question of the frequencies present in the speed fluctuations is one of great interest. Knowledge of the range of frequencies involved would be of help in the design of the compensating circuit, and might throw much needed light on the nature of turbulence.

In 1931 several attempts were made to determine the frequencies present in the fluctuations in the free stream of the Bureau of Standards 54-inch wind tunnel. In the first of these experiments an amplifier was used, which passed a narrow band of frequencies, the location of which in the audio-frequency spectrum could be controlled. It was thought that by means of this arrangement it might be possible to compare the amplifier outputs at various settings of the band circuit and obtain some information regarding the distribution of the energy of the fluctuations with frequency.

The amplifier used for this purpose was one of several stages of resistance-capacity coupled UY224 vacuum tubes preceded by one stage in which the load circuit consisted of a fixed inductance L , and a variable capacity C , in parallel, instead of the plain resistance load used in the following stages. This inductance-capacity parallel circuit resonates at a frequency

$$f_r = \frac{1}{2\pi \sqrt{LC}} \quad (17)$$

neglecting the small effect of the resistance R , of the coil having the inductance L . At the resonant frequency the circuit presents an impedance,

$$Z_r = \frac{L}{RC} \quad (18)$$

At frequencies much different from that of resonance the impedance is very low. Since the inductance-capacity circuit acts as the load circuit of the vacuum tube with which it is associated, the amplification obtained in that tube is given by equation (12) where Z_0 is the impedance of the inductance-capacity combination, and the effect of interelectrode capacities is neglected. The amplification is very low at all fre-

quencies except those at and near the resonant frequency f_r . By varying the capacity C , the resonant frequency may be shifted as desired, and by connecting the amplifier to the hot wire in the usual manner and taking output readings at several settings of the capacity C , some qualitative information regarding the frequency distribution in the speed fluctuation may be obtained. Quantitative data is not easily obtained by this method for two reasons. First, the amplification at resonance depends on the relation between L and C , as expressed by equation (18), and since C is variable the amplification will be different for each setting of C . The selectivity or sharpness of the resonant circuit may be defined as the fractional change in impedance for a given change in either C or L at resonance, which may in turn be shown to be equal to the ratio of the inductive reactance to the resistance of the inductance; that is, $\frac{2\pi f_r L}{R}$. Therefore, the selectivity, or width of the band of frequencies amplified, depends on the frequency of resonance.

The first difficulty, that of unequal amplification at each of the various capacity settings, may be more or less easily remedied by calibrating the amplifier at each of the various condenser settings and making appropriate corrections to the outputs obtained.

The second difficulty, that of unequal selectivity of the system, is not so easily corrected. The method of correction employed consisted of plotting the response of the amplifier against frequency for each of the condenser settings and measuring the area under the curves thus obtained, between certain limits of frequency. These areas were then used as the basis of a correction to be applied to the output readings.

The effectiveness of the highly selective amplifier was checked experimentally by introducing a pronounced and definite frequency into the turbulence by means of mounting the hot wire in the wake of a round rod placed in the wind tunnel with its axis perpendicular to the direction of the flow. It was found possible to detect the frequency of the eddies in the wake of the rod quite easily by properly tuning

the inductance-capacity circuit. Furthermore, the frequency measured corresponded closely with the frequency computed from the velocity of flow and diameter of rod according to the well-known relation

$$f = 0.18 \frac{V}{D}.$$

When the hot wire was placed in the free stream of the wind tunnel no definitely predominant frequency or frequencies could be detected, but by comparing the corrected experimental results with theoretical results predicted on the basis of various arbitrary distributions of frequency it was concluded that the turbulence was mainly of low frequency and the energy was probably distributed in some such manner as 90 per cent between 25 and 500 c. p. s., and 10 per cent between 500 and 1,000 c. p. s. No conclusions could be drawn regarding frequencies much below 25 c. p. s., because the amplifier was inoperative in that frequency range.

The second attempt to determine the frequency distribution in the turbulence arose from the desire to eliminate the effect of the unequal selectivity, and the rather unsatisfactory correction for it. Use was made of an apparatus for sound analysis developed by Theodorsen. (Reference 10.)

Briefly, the operation of Theodorsen's apparatus is dependent on the fact that the energy loss in an ohmic resistance through which a complex current wave flows is equal to the sum of the energy losses due to the harmonic components of the complex wave, except in the case in which there are two components of the same frequency in phase with each other, in which instance the energy loss is increased by a certain amount. Practical use is made of this principle by causing the complex wave to flow in a hot wire through which an alternating current of sine wave form and controllable frequency also flows. When the controlled wave is adjusted to the same frequency as that of any component of the complex wave the energy dissipated in the hot wire in the form of heat is increased or decreased relative to the dissipation due to the sum of the component losses, depending on the phase relationship. The temperature of the hot wire rises or falls, resulting in a change in resistance, and therefore in the voltage drop, which may be amplified and recorded. The principal advantage of this system of frequency is its great and uniform selectivity. All components of the complex wave are detected with equal selectivity and their effects are proportional to their amplitudes.

The successful use of Theodorsen's apparatus depends on the existence in the complex wave form of components constant in frequency; otherwise it would be impossible to set the controlled wave to the same frequency as the component.

When an attempt was made to analyze the complex wave resulting from the amplified and compensated effect of the wind-tunnel turbulence on the hot-wire anemometer by means of the apparatus described above, entirely negative results were obtained. This we believe to be due to the absence from the turbulence of any components sufficiently constant in frequency to be detected by the very selective apparatus.

The third, and perhaps most definitely successful attack on the frequency distribution problem was made by the use of a cathode ray oscillograph. Using this instrument, with its auxiliary amplifier, on the output of the compensated amplifier, moving film records were made of the turbulence in the free stream of the wind tunnel. The speed of the moving film being known, it was possible to count the number of velocity fluctuations occurring in a given length of the record or, if advisable, to make a harmonic analysis.

Records were made using a hot wire of 2 mm length, in place of the usual 1 cm type, in the hope that the shorter wire might exhibit a better response to the high frequencies. There is some evidence that the physical dimensions of the higher frequency velocity fluctuations may be so small as to cause their effect to cancel out over the 1 cm length of the longer wire. Measurements made with long and short wires alternately indicated very little, if any difference, however, in the mean amplitude of the fluctuations.

The greatest number of maxima found in the moving-film records was in every instance between 300 and 400 per second, including those records made when using the 2 mm wire. Since, as shown by Figure 11, the performance of the amplifier and compensator is entirely adequate for the reproduction of frequencies up to 5,000 c. p. s., and the records show no trace of reversals of higher frequency than 300 or 400 per second, it seems quite permissible to conclude that reversals of greater frequency than 400 c. p. s. either do not exist in the turbulence or are so small in effect as to be unnoticeable, even under the favorable conditions existing in the apparatus. This conclusion is in agreement with the qualitative data as to frequency distribution derived from the experiments with the inductance-capacity tuned selective amplifier.

Since the fluctuations are not sinusoidal, the reproduction of frequencies much higher than the frequency of the reversals is necessary correctly to reproduce the wave form.

Unfortunately, because of the limited illumination available, and the necessity of using a rather high film speed in order to record any high frequencies that might exist in the turbulence, the records obtained were too faint for satisfactory half-tone reproduction, and therefore could not be included in this report. They were, however, quite satisfactory for their original purpose of supplying data regarding the wave form of the fluctuation.

ACKNOWLEDGMENT

We wish to acknowledge the assistance of Mr. S. S. West in the construction and operation of much of the apparatus and of Mr. B. H. Monish in the preparation of photographic records.

BUREAU OF STANDARDS,
WASHINGTON, D. C., *Sept., 1932.*

REFERENCES

1. Reynolds, Osborne: On the Dynamical Theory of Incompressible Viscous Fluids and the Determination of the Criterion. Phil. Trans. Roy. Soc., Vol. 186, Part I, 1895.
2. Lorentz, H. A.: Abhandlungen über Theoretische Physik, Leipzig, p. 43, 1907.
3. Burgers, J. M.: Versl. Kon. Akad. v. Wetensch., Amsterdam, Vol. 26, p. 582, 1923.
4. Huguenard, E., Magnan, A., and Planiol, A.: A Method for the Instantaneous Determination of the Velocity and Direction of the Wind. T. M. No. 264, N. A. C. A., 1924.
5. Dryden, H. L., and Kuethe, A. M.: The Measurement of Fluctuations of Air Speed by the Hot-Wire Anemometer, T. R. No. 320, N. A. C. A., 1929.
6. Dryden, H. L., and Kuethe, A. M.: Effect of Turbulence in Wind Tunnel Measurements. T. R. No. 342, N. A. C. A., 1930.
7. Ziegler, M.: The Application of the Hot-Wire Anemometer for the Investigation of the Turbulence of an Airstream. Versl. d. Kon. Akad. v. Wetensch., Amsterdam, vol. 33, p. 723, 1930.
8. Doetsch, H., and v. Mathes, P.: Über Schwankungsmessungen im Aachener Windkanal. Abh. Aerodyn. Inst. Aachen, No. 10, p. 22, 1931.
9. Ziegler, M.: A Complete Arrangement for the Investigation, the Measurement and the Recording of Rapid Airspeed Fluctuations with Very Thin and Short Hot Wires. Versl. Kon. v. Wetensch., Amsterdam, Vol. 34, p. 663, 1931.
10. Theodorsen, Theodore: A New Principle of Sound Frequency Analysis. T. R. No. 395, N. A. C. A., 1931.

REPORT No. 449

WING CHARACTERISTICS AS AFFECTED BY PROTUBERANCES OF SHORT SPAN

By EASTMAN N. JACOBS and ALBERT SHERMAN

SUMMARY

The drag and interference caused by short-span protuberances from the surface of an airfoil have been investigated in the N. A. C. A. variable-density wind tunnel at a Reynolds Number of approximately 3,100,000, based on the chord length of the airfoil. The effects of variations of the protuberance span length, span position, and shape were measured by determining how the wing characteristics were affected by the addition of the various protuberances.

The results indicate that the central sections of a rectangular wing are more sensitive to the addition of protuberances than the outer sections. A very short protuberance in the midspan position may cause a disproportionately large reduction in maximum lift. At low values of the lift coefficient the drag due to the protuberances increases approximately as the total length for protuberances of equal height, but at higher lift coefficients induced interference effects appear so that short-span protuberances produce disproportionately large drag increases. An example is included to show how airfoil theory and a knowledge of the section characteristics may be applied to estimate induced interference effects. The adverse effects of protuberances are shown to be greatly reduced by simple fairings.

INTRODUCTION

The National Advisory Committee for Aeronautics is conducting in the variable-density wind tunnel a series of fundamental investigations dealing with aerodynamic interference. The investigations will, it is hoped, lead to the discovery of the sources of adverse interference effects and provide data that may be applied to the solution of practical problems of design. Some of the investigations deal with the effects of protuberances from the surfaces of bodies. The data obtained from these investigations are applicable to the prediction of the effects of projecting objects such as fittings, tubes, wires, rivet heads, joints, filler caps, and inspection plates protruding from the main surfaces.

Variations of the height and the chord position of protuberances extending along the entire span of an airfoil have been investigated to determine how the airfoil section characteristics are affected. These re-

sults have been published. (Reference 1.) Tests have also been made to investigate the effects of protuberances from the surface of a body of revolution. (Reference 2.) Because the protuberances found on actual airplane wings usually extend over only short portions of the span, it is necessary to consider the effects of short-span protuberances. The investigation with which this report deals was therefore made to study the effects of short-span protuberances and to form a basis for the practical application of the airfoil section data reported in reference 1.

Most of the present investigation was confined to the effects of protuberances of one height at one position along the chord of a symmetrical airfoil section. The variables considered were the protuberance length along the span, position along the span, and the number and shape of the protuberances. The generality of the results was tested by investigating the effects on the aerodynamic characteristics of a cambered airfoil of protuberances simulating lift or landing-wire fittings of a type sometimes found on airplanes. The tests were made during March and April, 1932.

TESTS

The tests necessary for this investigation were made in the N. A. C. A. variable-density wind tunnel at one value of the Reynolds Number, approximately 3,100,000. This tunnel and the methods employed for testing are described in detail in reference 3. The tests herein reported were made in the usual way except that the symmetrical airfoil used with most of the tests was provided with the special mounting described in reference 1.

For most of the tests a standard 5 by 30 inch duralumin airfoil having the symmetrical N. A. C. A. 0012 section (reference 1) was used. This airfoil was tested with different protuberance arrangements in order to determine the effects of varying the protuberance span length, span position, and shape. The various protuberances were of one height, 0.0125*c*, and were placed on the upper surface of the airfoil at the single position on the profile shown in Figure 1, 0.05 of the chord behind the leading edge. A strip of metal to form the protuberances was placed in the slot shown in Figure 1, which extended along the

entire span of the airfoil. The portions of the strip which were not needed to form protuberances were carefully filed to the airfoil surface and polished to present a continuous smooth surface. Protuberances having various lengths were thus formed at the mid-span position by progressively filing off the ends of the

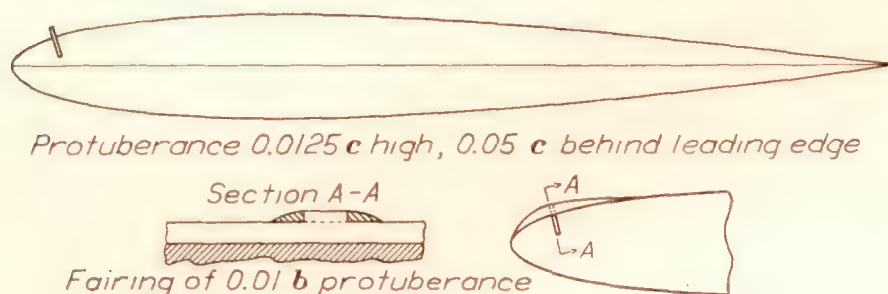


FIGURE 1.—N. A. C. A. 0012 profile showing protuberances

remaining protuberance. The airfoil was also tested with short protuberances placed at positions along the span corresponding approximately to those of the interplane struts on single-bay and two-bay biplanes. The protuberances that will be referred to as faired protuberances were produced, as indicated in Figure 1, by forming over the protuberance a plaster-of-Paris

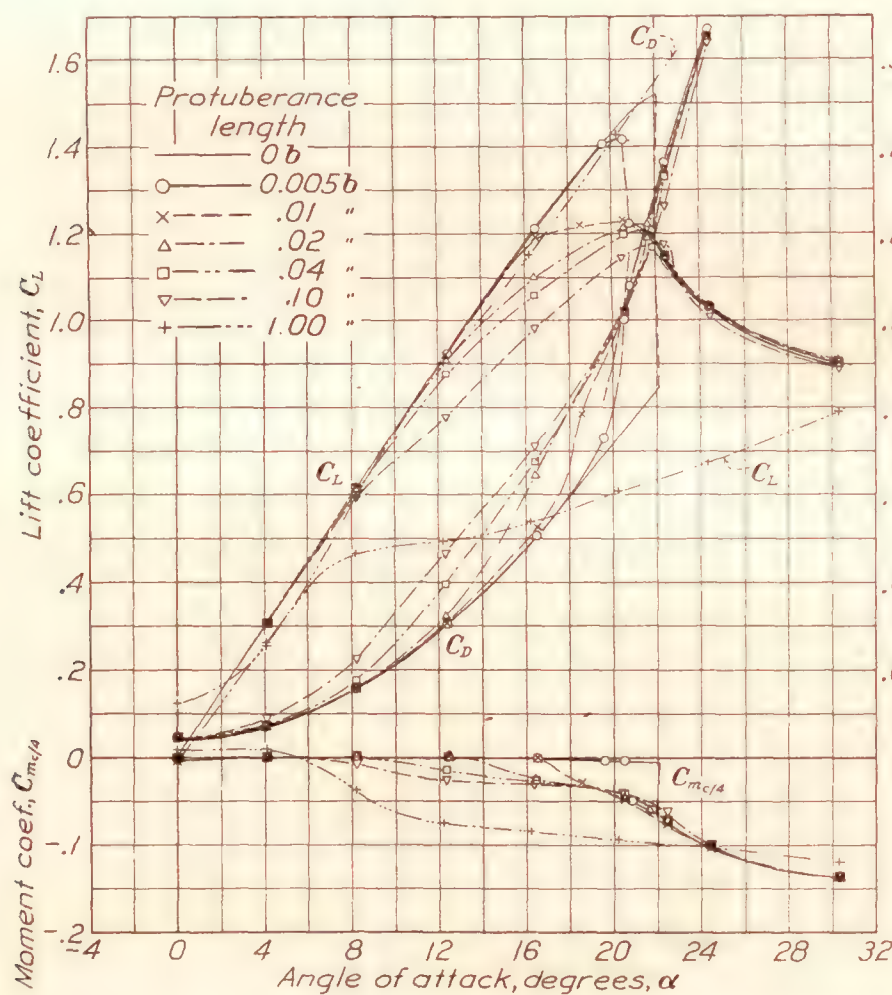


FIGURE 3.—The characteristics of an airfoil having a protuberance on the upper surface at mid span

fairing, the cross section of which approximated a small half-airfoil section on the surface of the main airfoil.

Two tests were also included of an N. A. C. A. 4412 airfoil with protuberances simulating the interplane wire fittings sometimes found on single and two bay biplanes. These protuberances and their arrangement on the airfoil are shown in Figure 2.

RESULTS

The results are presented in the form of curves of lift coefficient C_L , drag coefficient C_D , and moment coefficient about a point on the chord one-quarter of

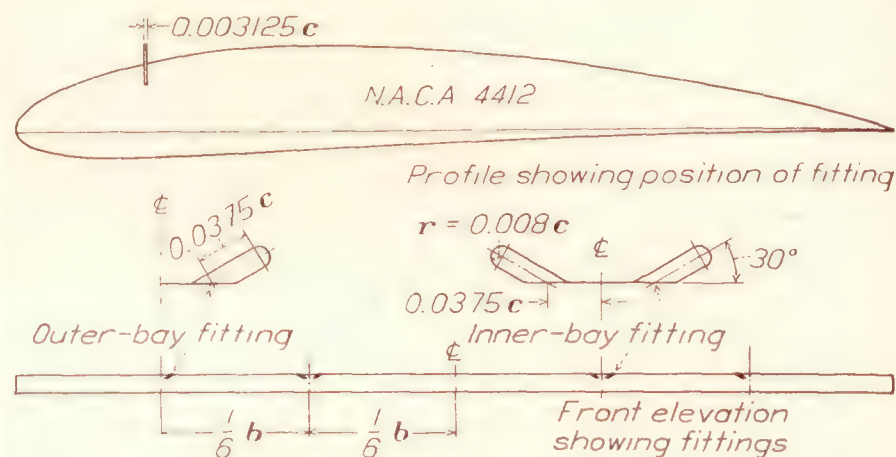
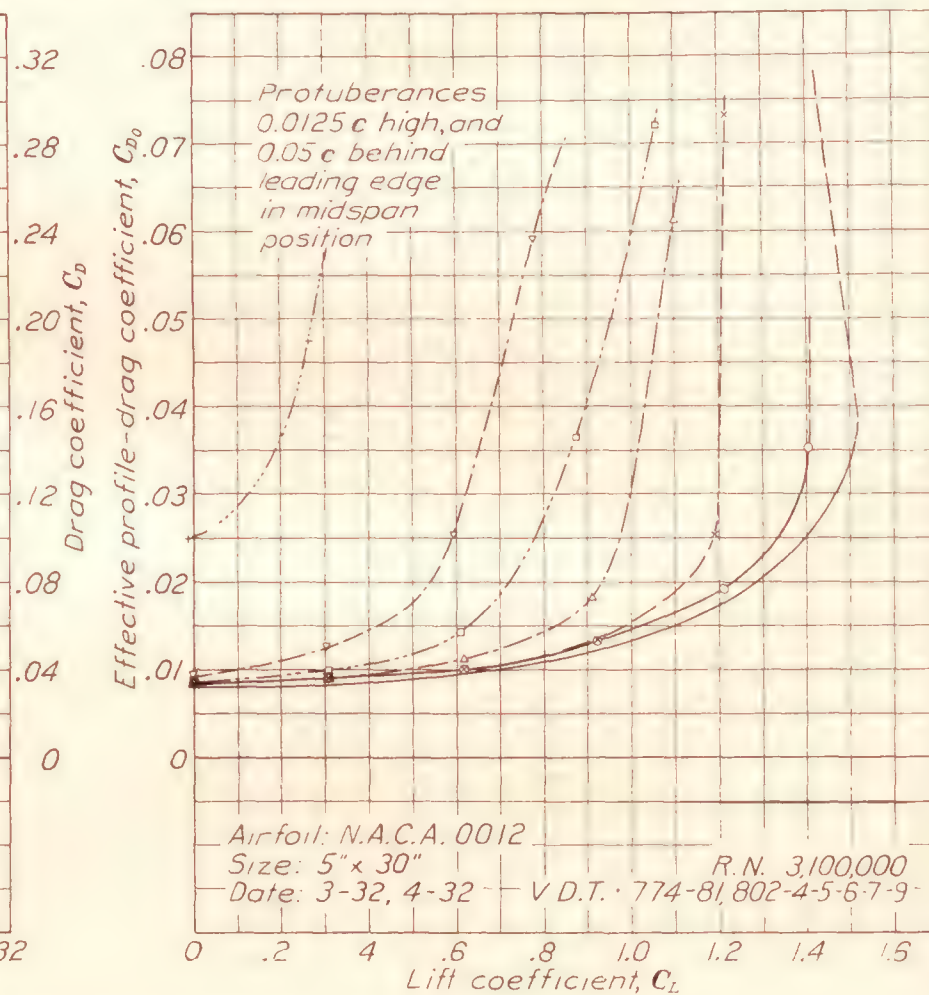


FIGURE 2.—Fitting arrangements on N. A. C. A. 4412 airfoil

the chord behind the leading edge $C_{m_{c/4}}$ plotted against angle of attack. These results, which are corrected for tunnel-wall effects (reference 3), thus represent the characteristics of an airfoil of aspect ratio 6. Curves are also given representing the effec-



tive profile-drag coefficient C_{D_0} plotted against the lift coefficient C_L . The effective profile-drag coefficient is that obtained by deducting from the total drag coefficient the usual induced-drag coefficient of a rectangular airfoil of aspect ratio 6. (Reference 3.) The effective profile drag therefore includes any additional induced drag due to the protuberance over that of a plain rectangular airfoil operating at the same lift coefficient.

DISCUSSION

Protuberance length.—The results obtained by varying the protuberance length are shown in Figure 3. The characteristics of the airfoil with midspan protuberances of various lengths between one-tenth span ($0.10b$) and five one-thousandths span ($0.005b$) are compared in this figure with the characteristics of the plain airfoil and the characteristics of the airfoil having the full-span protuberance, taken from reference 1. The variation of drag and maximum lift with protuberance length, however, is shown more advantageously in Figure 4 where the effective profile-drag coefficients, corresponding to various angles of attack, and the maximum lift coefficient are plotted against protuberance length.

Referring to the curve in Figure 4 representing the variation of the maximum lift coefficient with protuberance length, it will be seen that as the protuberance length is increased from zero the maximum lift at first drops very sharply, then at an approximately constant rate. Apparently, a protuberance of length $0.01b$ is sufficiently large to disturb the entire flow over the central portion of the airfoil at large angles of attack.

The curves of effective profile-drag coefficient in Figure 4 indicate that at the small angles of attack which correspond to the small lift coefficients the additional drag due to the protuberance is approximately proportional to the protuberance length. The effect of a short-span protuberance on the drag of a wing at very low lift coefficients may therefore be approximated from the section characteristics of an airfoil with a full-span protuberance. At higher angles of attack corresponding to higher lift coefficients, however, the moderately short protuberances produce disproportionately large adverse effects. These effects may be attributed in part to an additional drag resulting from induced interference. The increase in induced drag caused by the protuberance over that of a plain rectangular airfoil appears on the plot as an increased effective profile drag.

Induced interference.—Short-span protuberances that reduce the lift coefficients of the airfoil sections near the center of a rectangular wing tend to increase the departure from the elliptical span load distribution, and thus to increase the induced drag. This effect is said to be due to induced interference. If the aerodynamic characteristics of all the sections of a wing are known, airfoil theory may be applied to estimate its span load distribution, and hence the induced interference drag.

The span load distribution for a wing having a short-span protuberance may be approximated as follows: For a given angle of attack of the wing, a more or less arbitrary curve is drawn representing a span load

distribution that is thought to approximate the true one. From this assumed span load distribution, the downwash is found at a number of stations along the span. The effective angle of attack at each station is then obtained as the difference between the geometric angle of attack at the station and the downwash angle. From the effective angle of attack at each station and the experimentally determined airfoil section characteristics for the section at that station, the lift coefficient for the section at each station is obtained. A check span load distribution is thus derived, from which,

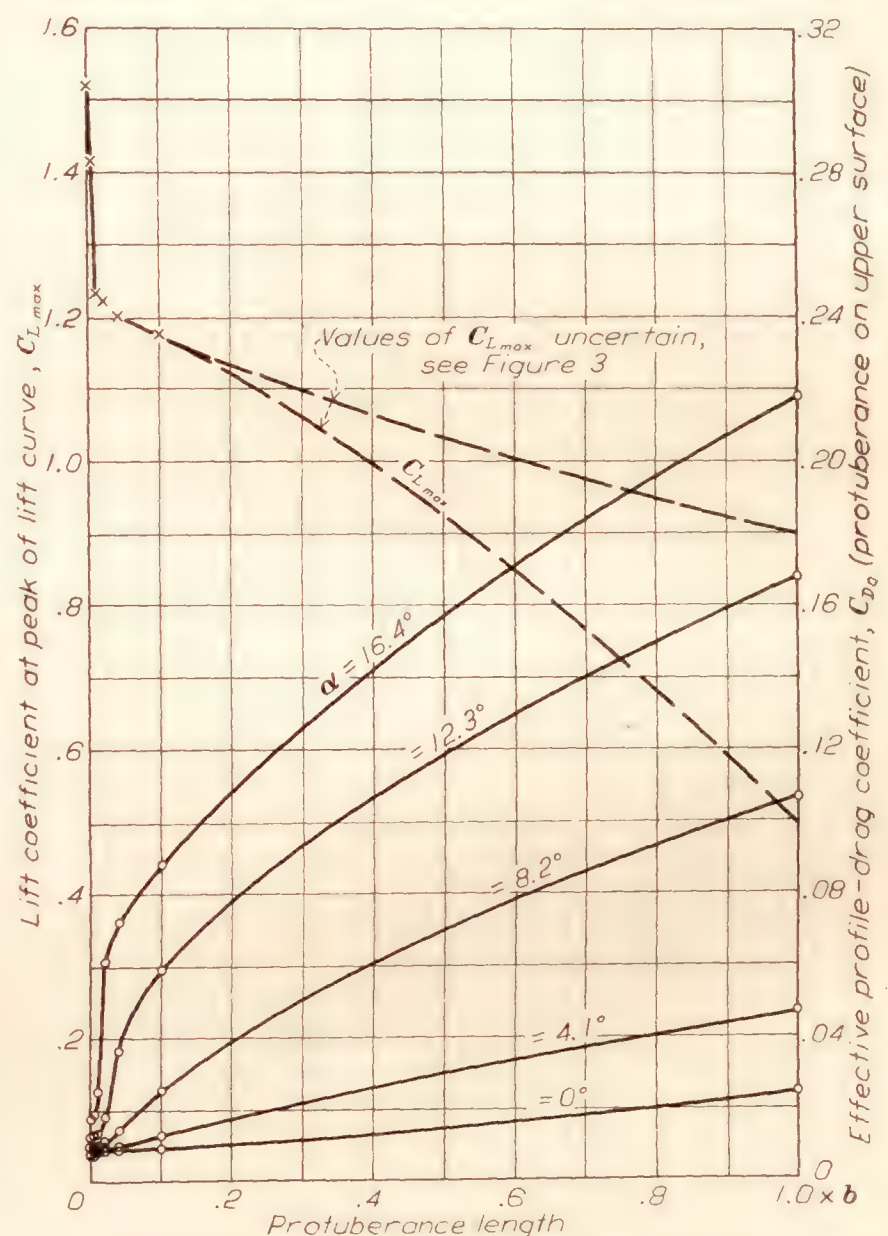


FIGURE 4.—Variation of lift and drag with protuberance length

together with the span load distribution curve originally assumed, a more nearly accurate span load distribution curve may be estimated. Thus, a curve approximating the actual span load distribution may be determined, as shown in Figure 5, by continuing the process through successive approximations until a check distribution is reached that agrees with the assumed curve from which it was derived.

Figure 5 illustrates the application of this method to the approximation of the span load distribution for the N. A. C. A. 0012 airfoil with the $0.10b$ protuberance in the midspan position for an angle of attack of 15° . Figure 6 shows some of the results.

In the derivation of the check span load distribution, the following equation for the downwash w_1 at any station y_1 was used:

$$w_1 = \frac{1}{4\pi} \int_{-s}^s \frac{dK}{y_1 - y} dy \quad (\text{Reference 4})$$

where K is the circulation at any point along the span, y is the distance of any point out from the center line along the span, and s is the length of the semispan. This equation was put in a more convenient form by

tion for the downwash to the more useful form:

$$\frac{w_1}{V} = \frac{c}{8\pi} \int_{-s}^{y_1-\Delta} \frac{\frac{dC_L}{dy} dy}{y_1 - y} + \frac{c}{8\pi} \int_{y_1+\Delta}^s \frac{\frac{dC_L}{dy} dy}{y_1 - y} + \frac{c}{8\pi} \left[\left(\frac{dC_L}{dy} \right)_{y_1-\Delta} - \left(\frac{dC_L}{dy} \right)_{y_1+\Delta} \right]$$

where Δ is a small distance as compared with the span. The first two terms were integrated graphically. The third term resulted from evaluating

$$\frac{c}{8\pi} \int_{y_1-\Delta}^{y_1+\Delta} \frac{\frac{dC_L}{dy} dy}{y_1 - y}$$

after expressing the span load distribution between the limits $y_1 - \Delta$ and $y_1 + \Delta$ by the equation $C_L = a + by + cy^2$, the constants a , b , and c being expressed in terms of the slopes of the span load distribution curve at $y = y_1 - \Delta$ and $y = y_1 + \Delta$.

Difficulties resulting from uncertainty in regard to the exact form of the loading curve along the portions of the span near the ends of the protuberance were avoided by calculating independently the downflow resulting from those portions of the lift grading curve. The downflow resulting from each small portion of the curve between $y = h - \Delta$ and $y = h + \Delta$, where h is the value of y at the ends of the protuberance, was evaluated approximately by considering the downflow to be induced by a finite vortex at $y = h$, the strength of which is the difference between the vorticity at $y = h - \Delta$ and $y = h + \Delta$. This part of the downflow at the station y_1 due to each vortex is then given by

$$\frac{w_1}{V} = \frac{c}{8\pi} \frac{C_{Lh-\Delta} - C_{Lh+\Delta}}{h - y_1}$$

When working through the successive approximations shown in Figure 5, the method was found to require some care and judgment in order to converge rapidly to an acceptable solution. The judgment was required for the estimation of each succeeding approximate loading curve from considerations of the character of the preceding loading curve and its check distribution. It was noticed, in developing this method, that the use of the check distribution as the succeeding approximation might lead to successively divergent loading curves.

From the span load distribution, the lift coefficient C_L and the induced-drag coefficient C_{Di} were calculated from the following equations (reference 4):

$$C_L = \frac{1}{2s} \int_{-s}^s C_L dy$$

$$C_{Di} = \frac{1}{2s} \int_{-s}^s \frac{w}{V} C_L dy$$

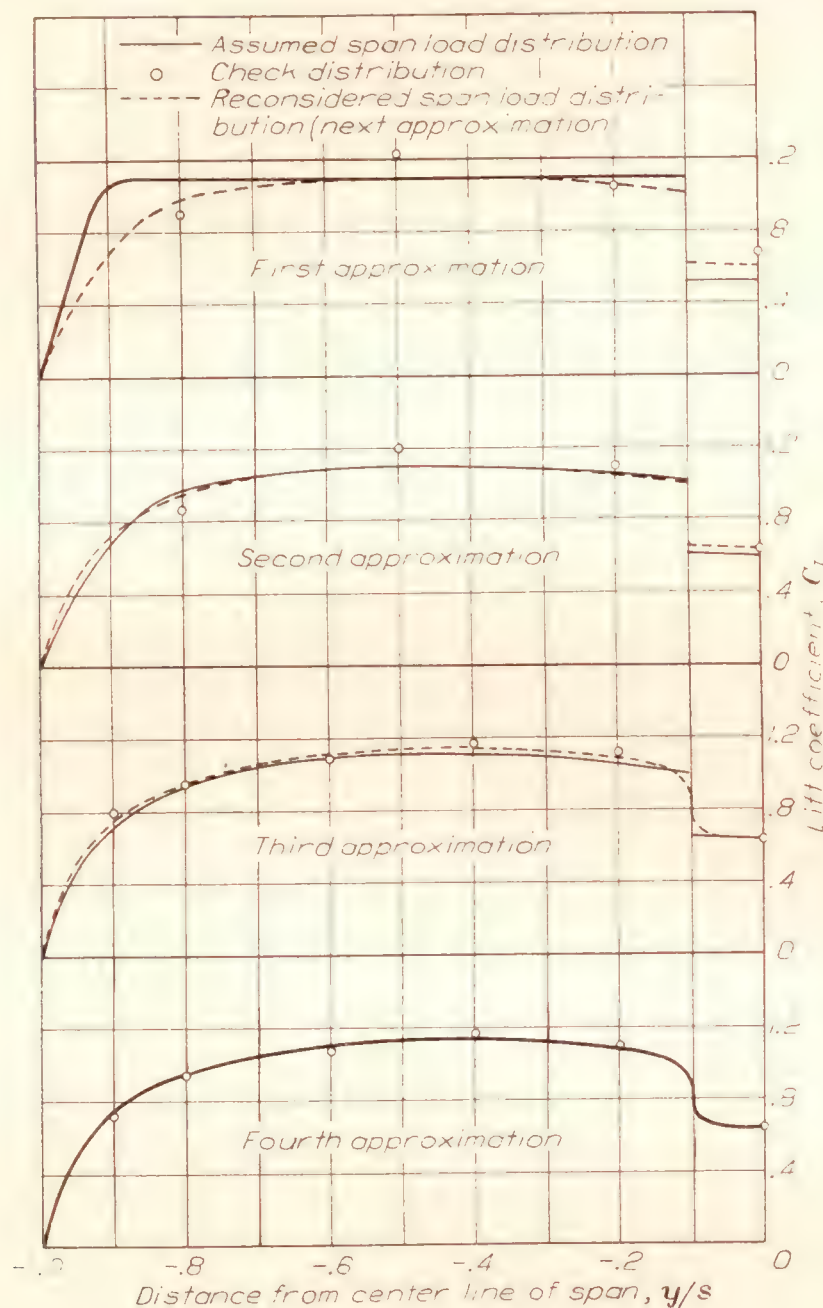


FIGURE 5.—Approximation of span load distribution for a wing with 0.10b protuberance at midspan position. $\alpha = 15^\circ$

substituting $\frac{C_L}{2} cV$ for K where c is the chord length and V is the free-stream velocity, thus:

$$\frac{w_1}{V} = \frac{c}{8\pi} \int_{-s}^s \frac{\frac{dC_L}{dy} dy}{y_1 - y}$$

However, because $\frac{dC_L}{dy}$ approaches infinity as y approaches y_1 , $\frac{w_1}{V}$ was determined by expanding the equa-

The value of C_L calculated for this example was 0.97 as compared with the test value of 0.91, the discrepancy being 7 per cent.

The calculated C_{D_i} was 0.0670, which corresponds to an increase of 26 per cent over that of the wing without a protuberance at the same lift coefficient.

The total drag coefficient of the wing was calculated as follows: The average values of effective angle of attack for the portions of the wing with and without the protuberance were found from Figure 6(c) to be 20.5° and 9.9° , respectively. At these effective angles of attack, the profile-drag coefficients for the corresponding airfoil sections were read from the section characteristics in reference 1. They were 0.296 and 0.0125, respectively. They were each multiplied by the portions of the span their corresponding profiles occupied (0.1 and 0.9) and added to the calculated induced-drag coefficient to obtain the total calculated drag coefficient. The value obtained was 0.108, which was 14 per cent low as compared with the test value of 0.1250.

The differences between the calculated and the experimentally determined values may be due in part to the fact that the section characteristics used in the computations are average section characteristics derived from tests of rectangular airfoils of normal aspect ratio and not true infinite aspect ratio characteristics. Such calculations may be of value, nevertheless, in connection with the interpretation of experimental results, and should also be of assistance in predicting certain interference effects.

Protuberance arrangements.—The results of the tests of the airfoil with the short protuberances at various positions along the span are presented in Figures 7 and 8. It is evident from the lift curves that protuberances distributed along the span away from the center have a smaller adverse effect on the maximum lift than a protuberance of the same total length at center span. The greater effect of the protuberance at the center might be expected, because the central sections of a rectangular airfoil near maximum lift operate at higher effective angles of attack than the outer sections. Protuberances near the center therefore tend to start the burble at a lower angle of attack.

Considering now the effects of the distributed protuberances on the drag in the range of the lift coefficient corresponding to high-speed flight, the results of Figures 7 and 8 indicate that the additional drag due to the protuberances depends approximately directly on their total length. Although this agrees with the results of Figure 4, from which it was concluded that the additional drag was proportional to the protuberance length, it should be mentioned here that all the results tend to indicate that at very low lift coefficients protuberances of length $0.01b$ or less may produce relatively larger than proportional adverse effects. If very short protuberances do produce serious disturbing effects, such objects as small protruding rivet heads on

an airplane wing might be expected to reduce substantially the performance of the airplane. Full-scale tests should therefore be made to investigate the effects of a large number of such short-span protuberances.

The effect of the distributed protuberances on the drag at higher values of the lift coefficient might be estimated by applying the airfoil theory previously described as applied to a midspan protuberance. Experimental results (figs. 7 and 8) indicate, as might be expected, that the distributed protuberances do not increase the drag at higher lifts as much as a single protuberance of the same total length at the center of the airfoil.

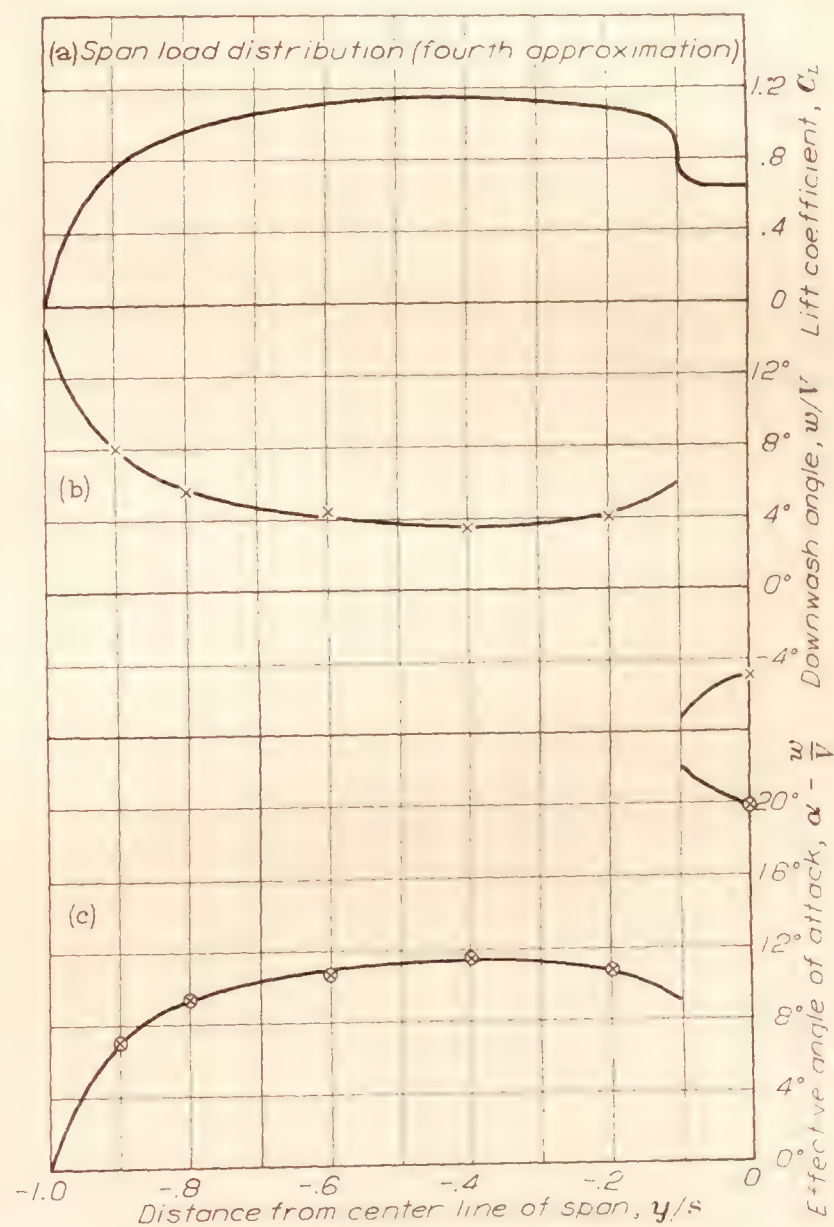


FIGURE 6.—Results of interference calculated for a wing with $0.10b$ protuberance at midspan position. $\alpha = 15^\circ$

Practical applications.—From practical considerations, it is desirable to know whether or not the adverse effects of protuberances may be eliminated by fairing them into the wing surface, and if the effects of actual protuberances can be predicted from the results of tests of these simplified protuberances. The results shown in Figure 8 indicate that the adverse effects of short-span protuberances may be largely eliminated within the working range of angles of attack by applying simple fairings as shown in Figure 1. The maximum lift of the airfoil with the faired protuberances, however, was not so high as that of the plain airfoil. The results in reference 1, dealing with the fairing of full-span protuberances, indicated that the adverse effect of a

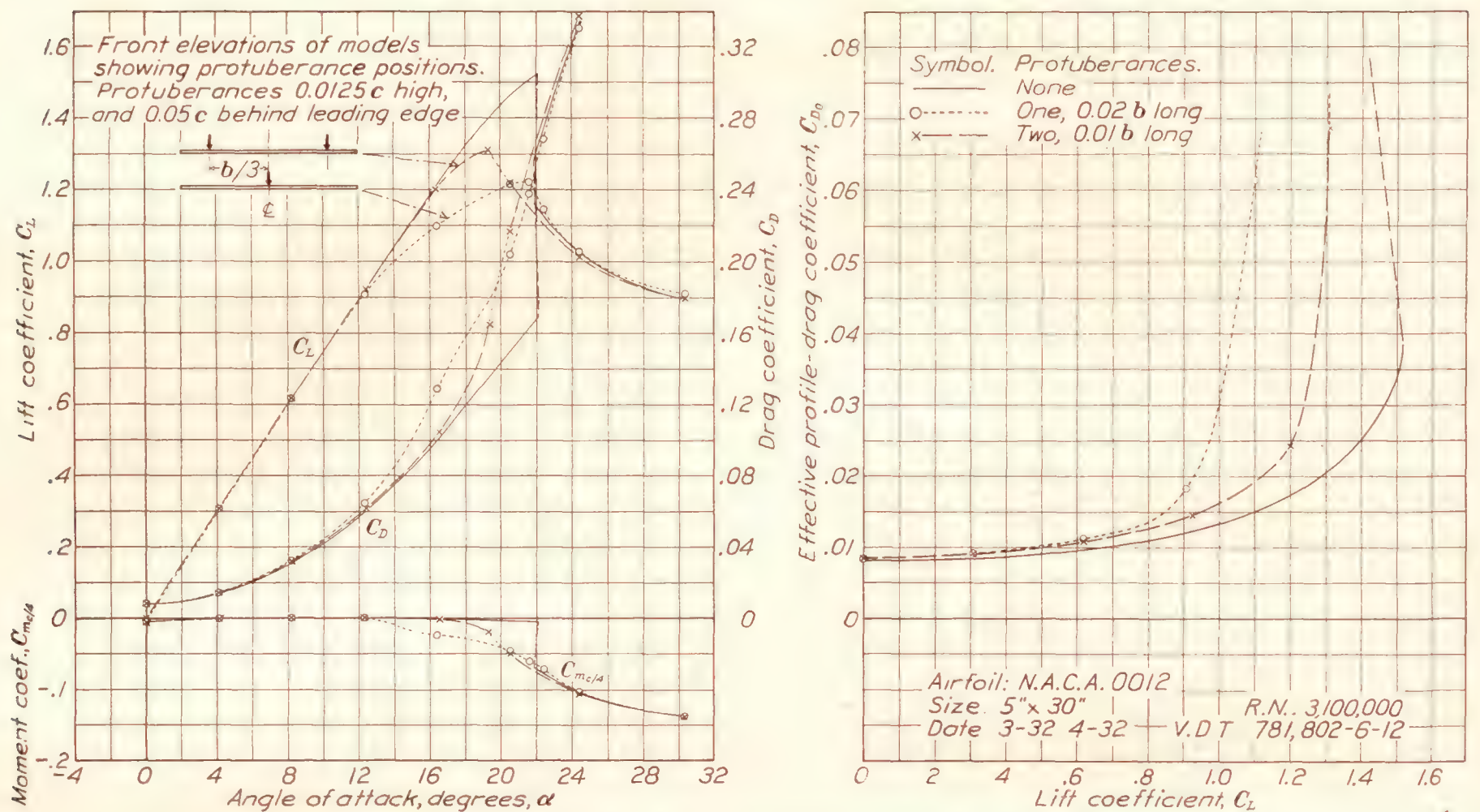


FIGURE 7.—The characteristics of an airfoil with protuberance arrangements having same total length on upper surface

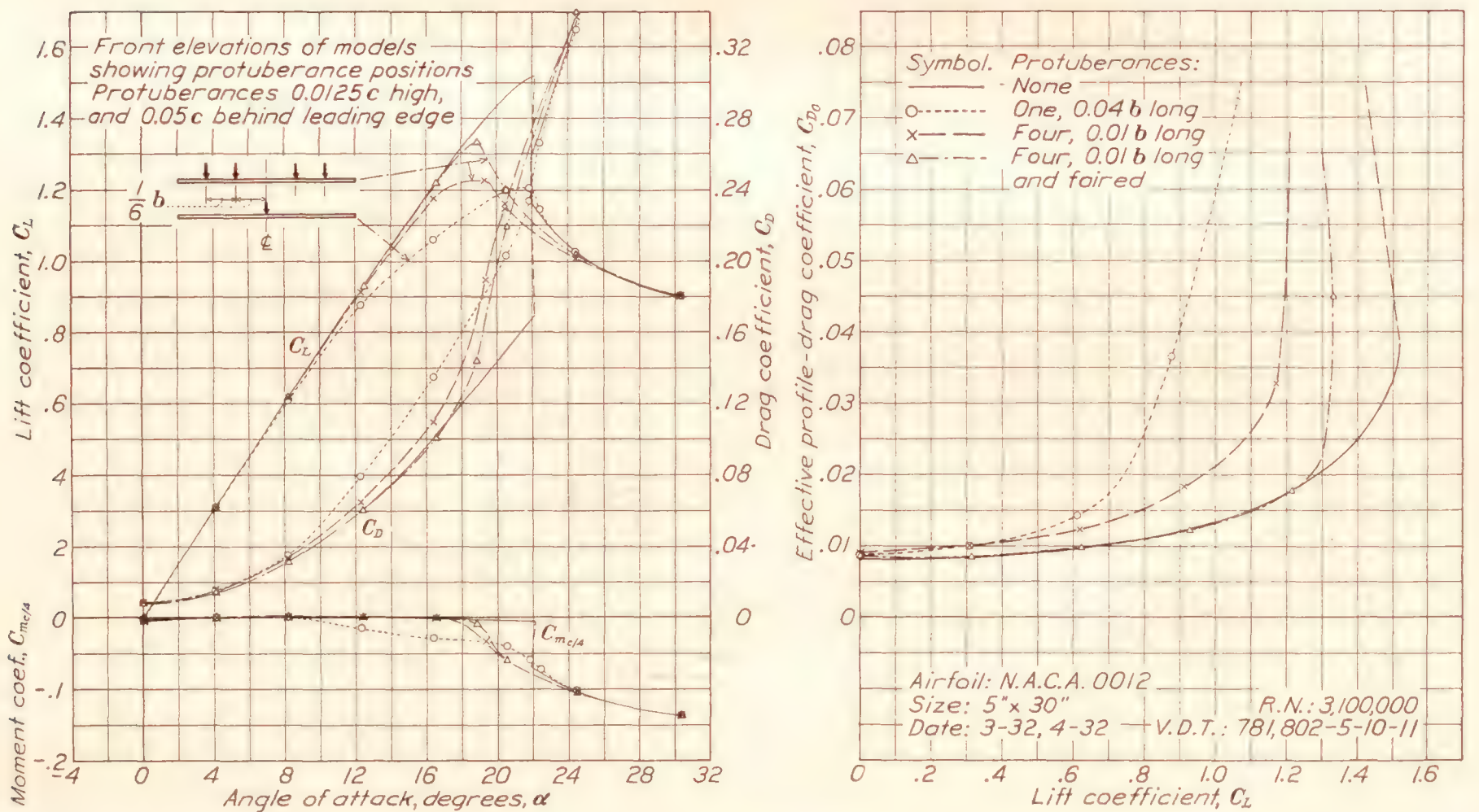


FIGURE 8.—The characteristics of an airfoil with various protuberance arrangements having same total length on upper surface

protuberance on maximum lift was practically eliminated by a simple fairing unless the protuberance was very near the leading edge. In all probability, therefore, fairings over short-span protuberances from positions on the wing near or behind the front-spar position would also eliminate any adverse effects on the maximum lift coefficient.

The applicability of the results to a practical instance of a wing with protuberances was investigated by testing an airfoil having the N. A. C. A. 4412 section with protuberances simulating lift or landing-wire fittings. (Fig. 2.) The results of these tests are presented in Figure 9. They indicate that within the usual flying range of lift coefficients, the protuberances

coefficient is found to be 0.0366. Then if the fittings are considered as occupying the portions of the span between the extremities of each projection, the portion of the span occupied by the two outer-bay fittings is $0.019b$, and by the outer-bay and inner-bay fittings is $0.056b$. Then applying the conclusion that the effect of short-span protuberances at low lifts is proportional to the total length of the protuberances, the increase in drag coefficient resulting from the two outer-bay protuberances is found to be 0.0007, and for the outer and inner-bay protuberances, 0.0020. The agreement between these predicted drag increases and those shown by the test results in Figure 9, 0.0008 and 0.0020, respectively, is good.

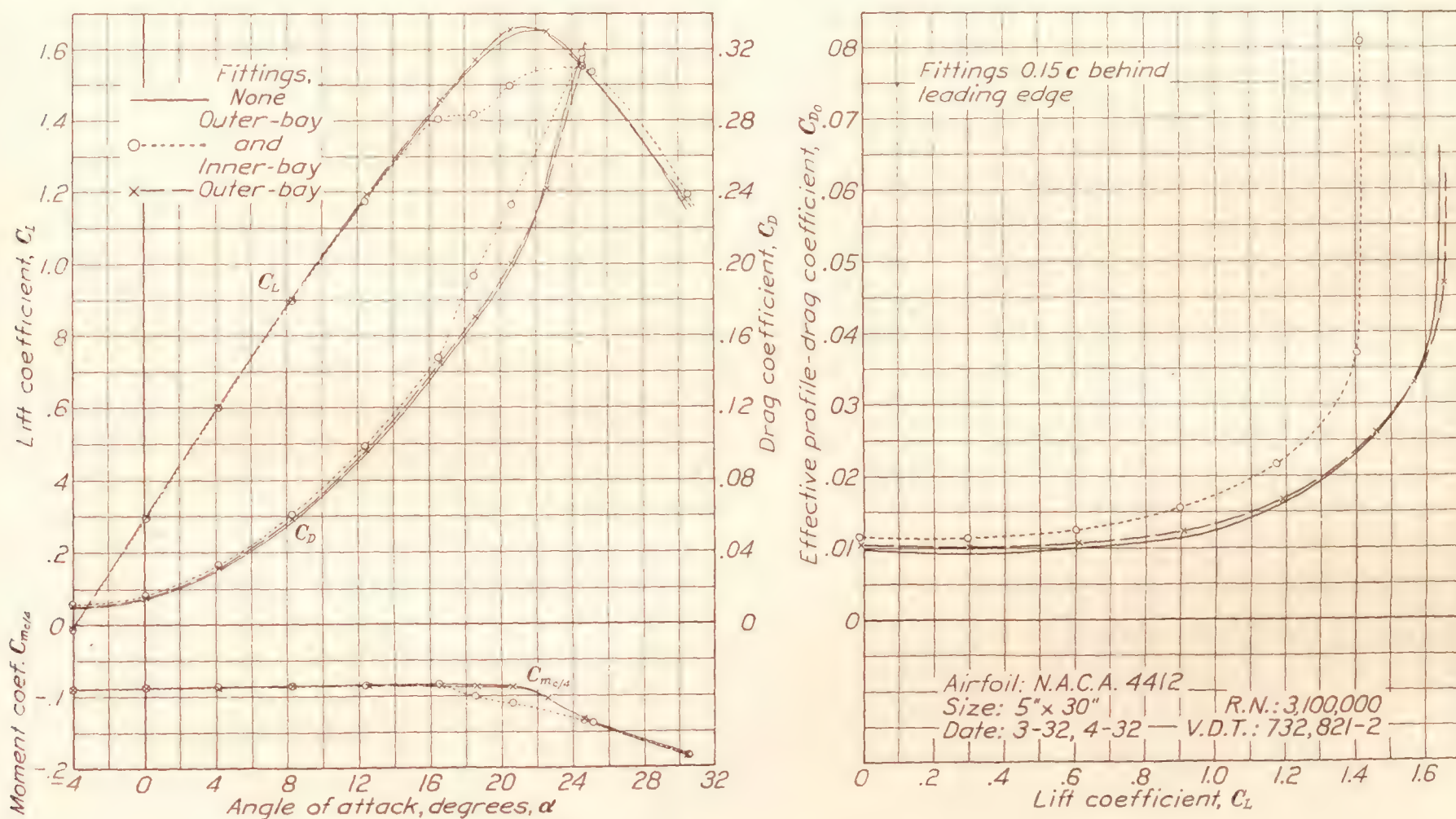


FIGURE 9.—N. A. C. A. 4412 airfoil with various fitting arrangements on upper surface

produce no marked loss of lift and therefore no marked induced interference, although at very high lifts the inner-bay fittings do show an effect on the lift. The drag curve then shows a definite interference-drag effect. The effect of protuberances on the drag of a wing, from the practical designer's standpoint, is of greatest importance in the high-speed range of lift coefficients where the induced interference effects may be neglected. In this range, the drag due to the fittings would be approximated as follows: The increase in profile drag due to a protuberance of equivalent height, and at the same position along the chord as the fittings (0.15c behind the leading edge), is taken from the section characteristics of reference 1. If the equivalent height of the fitting is taken as 0.0125c (the average height is 0.0124c) and a value of the lift coefficient of 0.2 is assumed, the increase in profile-drag

CONCLUSIONS

1. At low values of the lift coefficient corresponding to the high-speed flight condition, the effect on drag of partial-span protuberances is approximately proportional to their total length. This conclusion, however, may not apply to a large number of very small protuberances, such as rivet heads, on an airplane wing. Full-scale tests should be made to investigate the effects of a multiplicity of small protuberances.

2. At higher values of the lift coefficient induced interference effects may become important if the protuberance is of the type that alters the airfoil section lift. Under these conditions short-span protuberances may produce disproportionately large effects, which for rectangular wings are greatest when the disturbing protuberances are near the midspan position.

3. Small protuberances near the midspan position may produce serious adverse effects on the maximum lift coefficient.

4. A simple fairing over a small protuberance practically eliminates its adverse effects.

LANGLEY MEMORIAL AERONAUTICAL LABORATORY,
NATIONAL ADVISORY COMMITTEE FOR AERONAUTICS,
LANGLEY FIELD, VA., *October 24, 1932.*

REFERENCES

1. Jacobs, Eastman N.: Airfoil Section Characteristics as Affected by Protuberances. T. R. No. 446. N. A. C. A., 1932.
2. Abbott, Ira H.: The Drag of Two Streamlined Bodies as Affected by Protuberances and Appendages. T. R. No. 451, N. A. C. A., 1932.
3. Jacobs, Eastman N., and Abbott, Ira H.: The N. A. C. A. Variable-Density Wind Tunnel. T. R. No. 416, N. A. C. A., 1932.
4. Glauert, H.: The Elements of Aerofoil and Airscrew Theory. Cambridge University Press (London), 1926.

REPORT No. 450

THE CALCULATION OF TAKE-OFF RUN

By WALTER S. DIEHL

SUMMARY

A comparatively simple method of calculating length of take-off run is developed from the assumption of a linear variation in net accelerating force with air speed and it is shown that the error involved is negligible. The run formula is reduced to

$$S = \frac{K_s V_s^2}{\left(\frac{T_1}{W}\right)}$$

Where V_s is the take-off speed, T_1 is the initial net accelerating force, W is the gross weight and K_s a coefficient depending only on the ratio of initial to final net accelerating force. Detailed instructions are given for application of the formula and for the calculation of all factors involved.

INTRODUCTION

Exact calculations may be made for the distance run during the take-off of a landplane if sufficient data are available on propeller, engine, and airplane characteristics, and if some assumption is made regarding the pilot's technique. The calculations are necessarily laborious since the relations are such that step-by-step integration is required. In most cases lack of exact data on power plant and airplane prevents an exact calculation even if such were desired, while for all practical purposes a close approximation is all that is needed.

A number of formulas and methods have been proposed and used extensively in the past for calculating take-off runs. Most of these methods are based on average thrusts obtainable with the power plants formerly in use, and under favorable conditions gave satisfactory results. However, the advent of high performance has brought about changes in propeller design, for example, that greatly affect the take-off run so that a complete revision is required to accommodate the new variables.

The present study is concerned with the development of a method suitable for routine take-off calculations in the Bureau of Aeronautics of the Navy Department. Such a method, to be satisfactory, was required to be reasonably simple without neglecting any important variable. The method derived in this or has been in use long enough to justify consider-

able confidence in its validity. All attempts to obtain a more simple method have resulted in unsatisfactory reliability. While the method here presented is intended as a practical approximation to a difficult problem, it is highly probable that greater accuracy would have no significance in view of lack of definite knowledge regarding basic data.

Unless otherwise specified the take-off run is to be the run required to attain a given air speed in a calm; lb.-ft.-sec. units will be used.

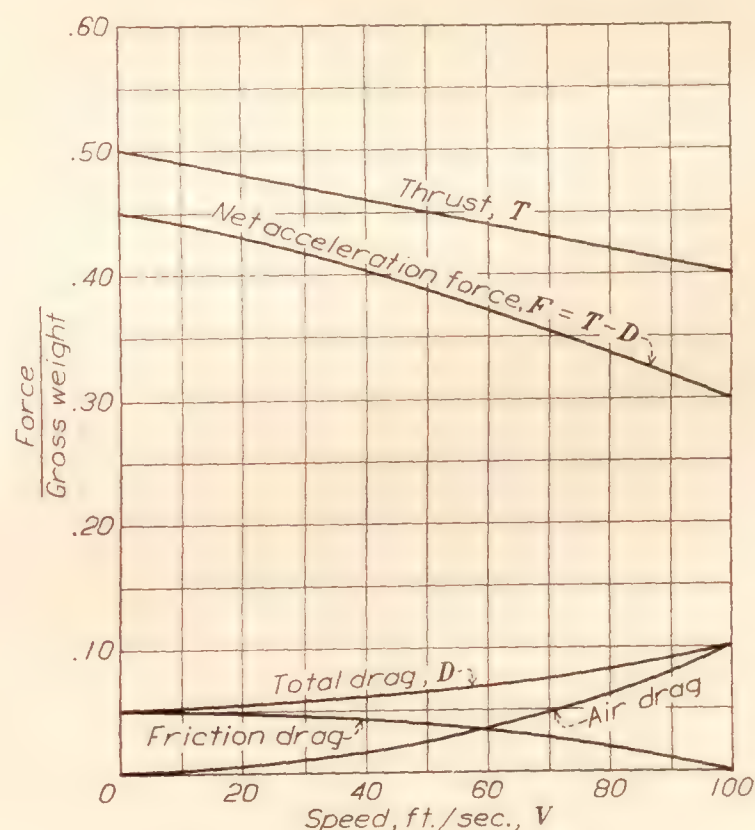


FIGURE 1.—Forces acting during take-off run

GENERAL CALCULATION OF TAKE-OFF RUN

The major forces acting on the airplane during take-off are thrust, air drag, and friction drag. In the simplest case, at constant angle of attack, the air drag will vary as the square of the air speed and the friction drag will vary with the load on the wheels. The net accelerating force will then be the difference between the thrust and the total drag as indicated on Figure 1. For convenience, the forces may be reduced to unit values by dividing each by the gross weight.

In general the take-off may be considered to consist of three stages: A short initial period during which the tail is raised to normal position, a relatively long

period of acceleration at a substantially constant angle of attack and a short period during which the angle is increased for take-off. It is possible for the third stage to be partially or wholly suppressed, depending on the airplane characteristics and pilot's efforts. If a definite sequence be assumed, the corresponding curves for air drag and friction drag may be determined. The variation of thrust with air speed may be calculated from engine and propeller test data. The normal tendency is for the thrust to decrease slightly with increase in speed and with a substantially linear relation, as indicated on Figure 1. In some cases, however, the thrust may remain constant, or even increase with air speed.

Assuming that the thrust and the drag are known as a function of air speed, the calculation of take-off run is made as illustrated by Figure 2 and Table I. The

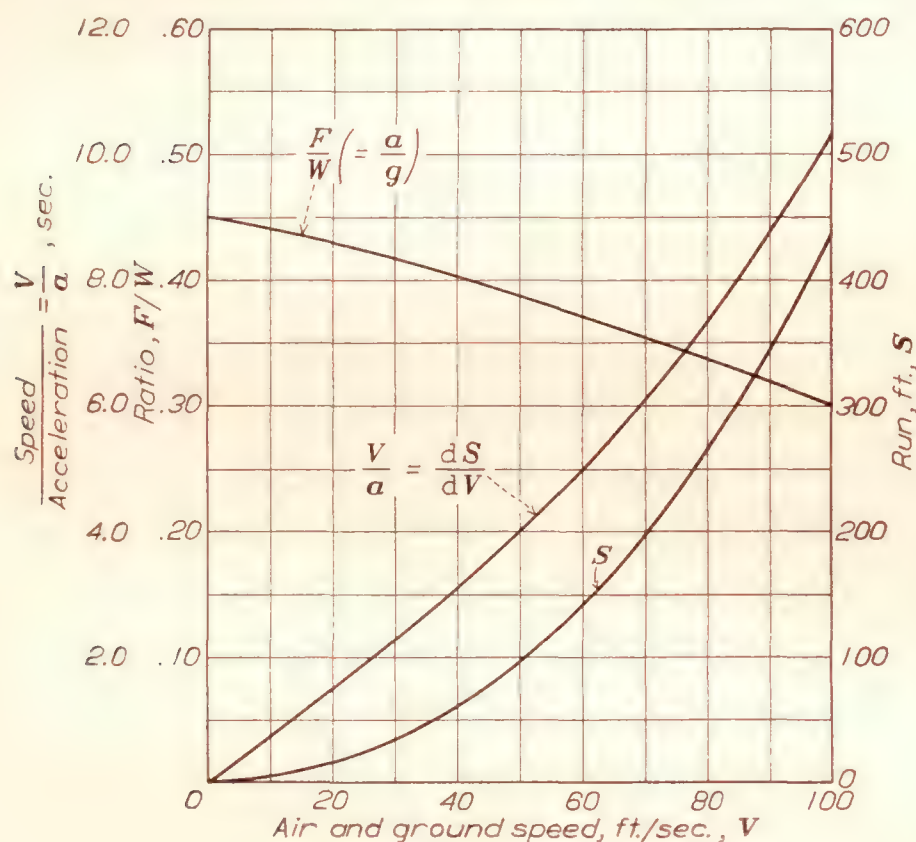


FIGURE 2

curve of net accelerating force F/W in Figure 2 is the same as that in Figure 1. The acceleration is given by

$$a = g \left(\frac{F}{W} \right) \quad (1)$$

$$\text{Since } V = \frac{dS}{dt} \text{ and } a = \frac{dV}{dt}$$

$$\frac{V}{a} = \frac{dS}{dV}; \quad (2)$$

if $\frac{V}{a}$ is plotted against V as in Figure 2 the area under the curve is proportional to the run S . This area may be found by any convenient method, such as by a planimeter, the trapezoidal rule or Simpson's rule. The trapezoidal rule used in Table I is ordinarily the simplest method. By this method the area under a curve, between any number of equally spaced ordinates, is equal to the product of the sum of the inside ordinates plus one-half of the end ordinates, by the

spacing between the ordinates. It is usually given in the form

$$A = (\frac{1}{2}y_1 + y_2 + y_3 + \dots + \frac{1}{2}y_n) \Delta X$$

where $y_1, y_2, y_3, \dots, y_n$ are the ordinates of the curve equally spaced at the distance ΔX apart.

EQUATION FOR TAKE-OFF RUN

An extended analysis of calculated take-off runs in comparison with observed runs leads to the following conclusions:

1. The effects of thrust variation, gross weight, take-off air speed, and wind speed predominate to such an extent that in practice all other variables may be neglected.
2. The effect of normal variations in power is so great that considerable latitude is allowable in simplifying assumptions.

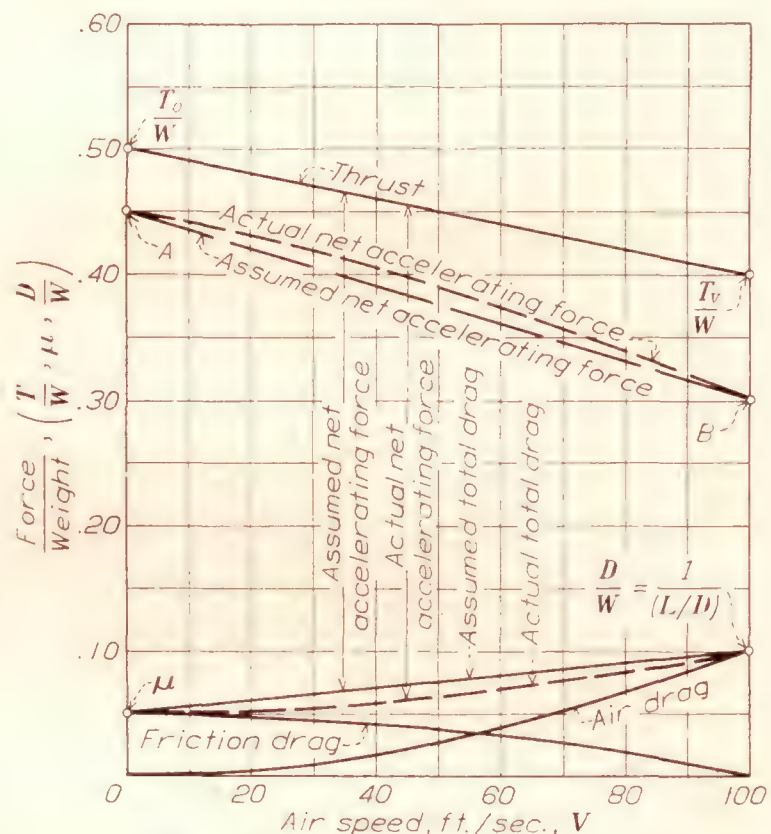


FIGURE 3.—Major forces acting during take-off run

3. The effect of thrust variation from the static condition to take-off is of such primary importance that proper allowance must be made for the propeller characteristics.
4. The effects of wind speed and actual take-off speed are best handled in the form of corrections to the run required to attain stalling speed in a calm.

The most promising method of simplifying the calculations appears to be in the assumption that the net accelerating force varies linearly with air speed as indicated on Figure 3. The calculations of Table II, based on this assumption, shows a run of 448.8 feet, as compared with 439.3 feet obtained in Table I. This is an error of less than 2.2 per cent, for what may be considered an average case. Such an error is entirely negligible in comparison with the uncertainty in power or propeller characteristics, and the variation in piloting.

With the assumption of a linear variation in net accelerating force the relations are as shown on Figure 3. The thrust per pound varies from T_o/W at the start, T_o being the static thrust, to T_v/W at take-off, T_v being the thrust at take-off speed V . The total drag per unit weight varies from $\mu = f/W$ at the start to $\frac{D}{W} = 1/\left(\frac{L}{D}\right) = \frac{D}{L}$ at the take off. The net accelerating force per unit weight at the start is

$$\frac{T_1}{W} = \frac{T_o}{W} - \mu \quad (3)$$

The net accelerating force at take-off is

$$\frac{T_F}{W} = \frac{T_v}{W} - \frac{D}{L} \quad (4)$$

Since the net accelerating force varies linearly with air speed it follows that

$$\frac{F}{W} = \frac{T_1}{W} \left(1 - K \frac{V}{V_s}\right) \quad (5)$$

where $(1-K)$ is the ratio of the final to the initial accelerating force. That is,

$$(1-K) = \frac{T_F}{T_1} \text{ or } K = \frac{T_1 - T_F}{T_1}.$$

The resulting equation of motion is

$$\frac{dV}{dt} = g \frac{F}{W} = g \frac{T_1}{W} \left(1 - K \frac{V}{V_s}\right) \quad (6)$$

or

$$\frac{V dV}{\left(1 - K \frac{V}{V_s}\right)} = g \frac{T_1}{W} dS \quad (7)$$

Integrating this gives

$$S = \frac{1}{g \left(\frac{T_1}{W}\right)} \left[-\frac{V V_s}{K} - \left(\frac{V_s}{K}\right)^2 \log \left(1 - K \frac{V}{V_s}\right) \right] \quad (8)$$

For take-off at speed V_s equation (8) reduces to

$$S = \frac{V_s^2}{g \frac{T_1}{W}} \left[\frac{1}{K} \left(-1 - \frac{1}{K} \log (1-K)\right) \right] \quad (9)$$

The term within the brackets on the right hand side of equation (9) depends only on the ratio of the final net thrust to the initial net thrust T_F/T_1 . Hence we may write

$$S_o = \frac{K_s V_s^2}{\left(\frac{T_1}{W}\right)} \quad (10)$$

where S_o is the total run to attain the speed V_s in a calm and $K_s = \frac{1}{g} \left[\frac{1}{K} \left(-1 - \frac{1}{K} \log (1-K)\right) \right]$.

Calculated values of K_s are given in Table III and plotted on Figure 4.

In order to use equation (10), the static thrust and

the thrust at take-off speed must be known. Methods for calculating the thrust will be given.

TIME REQUIRED FOR TAKE-OFF

In some cases the time required for take-off is of importance. This may be obtained from equation (6) written in the form

$$\frac{dV}{1 - K \frac{V}{V_s}} = g \frac{T_1}{W} dt \quad (6a)$$

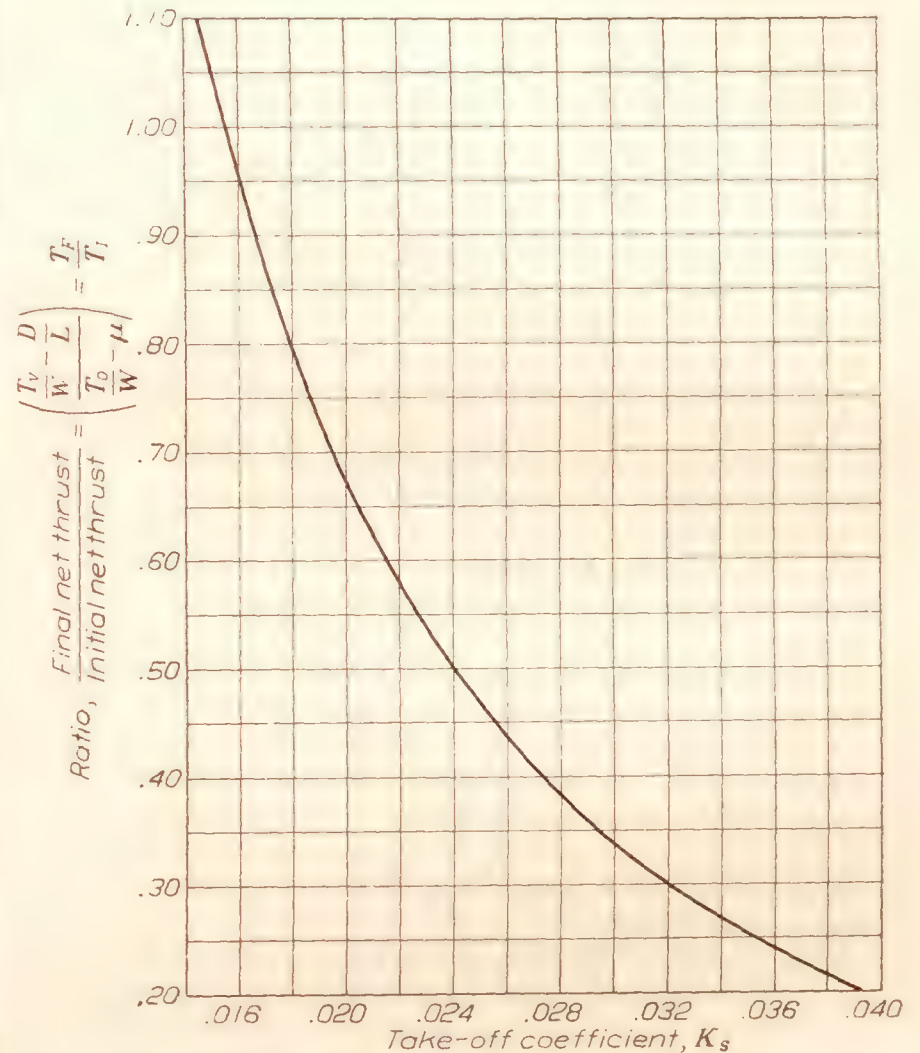


FIGURE 4.—Take-off run in a calm

$$S_o = \frac{K_s V_s^2}{\left(\frac{T_o}{W} - \mu\right)} \text{ ft.}$$

V_s = take-off air speed—ft./sec.
 T_o = static thrust—pounds.
 W = gross weight—pounds.
 μ = coefficient of traction.

from which, by integration

$$t = \frac{-V_s}{gK \left(\frac{T_1}{W}\right)} \log \left(1 - K \frac{V}{V_s}\right) \quad (11)$$

For time to take-off speed $V = V_s$, this becomes

$$t = \frac{-V_s}{g \left(\frac{T_1}{W}\right)} \left[\frac{1}{K} \log (1-K) \right] \quad (12)$$

As in equation (9), the term in the brackets depends only on the ratio of the net thrusts. Hence

$$t_o = \frac{K_s V_s}{\left(\frac{T_1}{W}\right)} \quad (13)$$

where t is the time in seconds to attain the take-off speed V_s (in ft./sec.) in a calm and $K_t = \frac{-1}{9K} \log (1 - K)$.

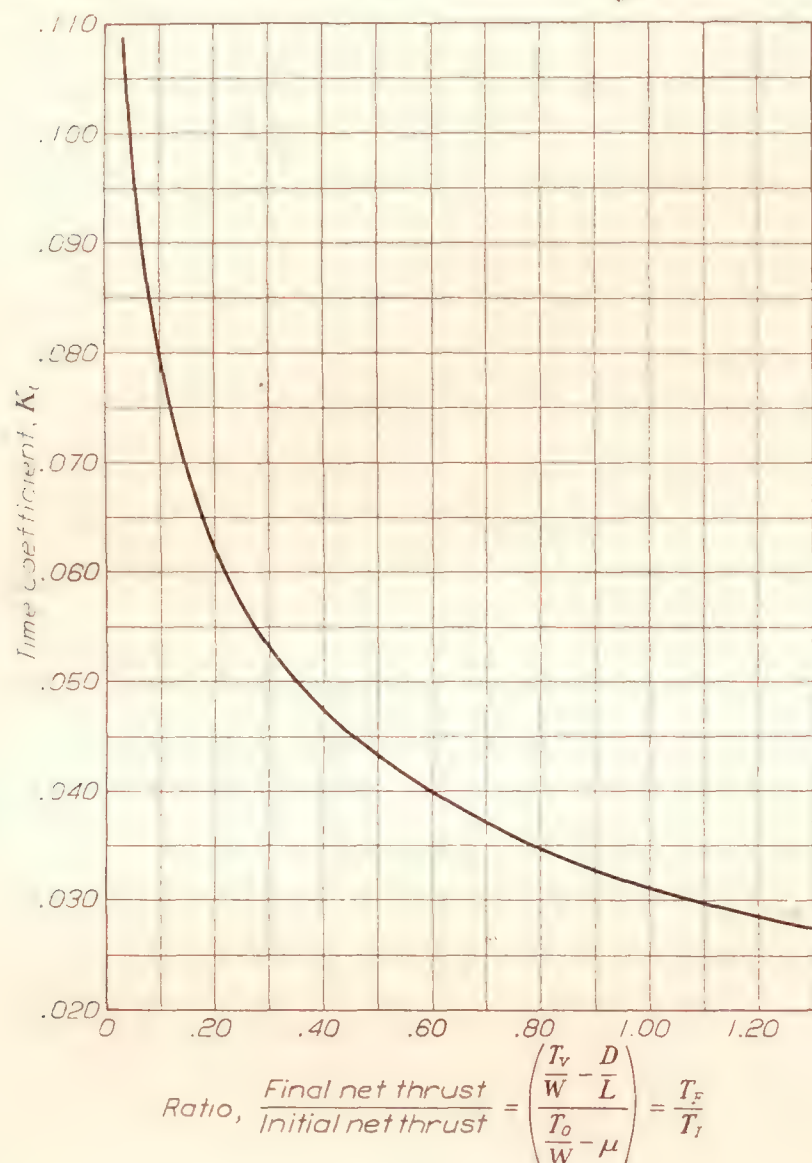


FIGURE 5.—Coefficient for time to take-off

$$t_{sec} = \frac{K_t V_s}{\left(\frac{T_I}{W} \right)}$$

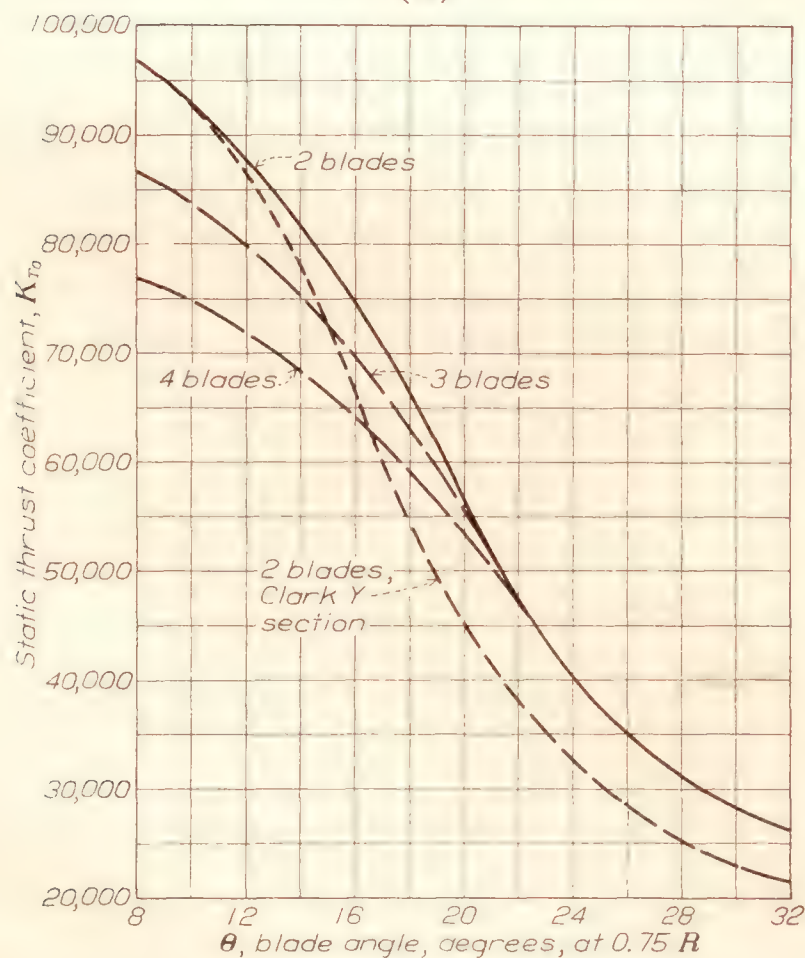


FIGURE 6.—Static thrust coefficient

Calculations for K_t are given in Table III and K_t is plotted as a function of the ratio T_F/T_I on Figure 5.

INITIAL NET ACCELERATING FORCE

The initial net accelerating force per unit weight is defined by equation (3)

$$\frac{T_1}{W} = \frac{T_o}{W} - \mu \quad (3)$$

In reference 4 it is shown that the static thrust may be calculated by the equation

$$T_o = \frac{K_{T0} \times \text{b. hp}}{\text{r. p. m.} \times D}$$

The static thrust coefficient K_{T0} may be plotted as a function of blade angle at $0.75 R$ as in Figure 6.

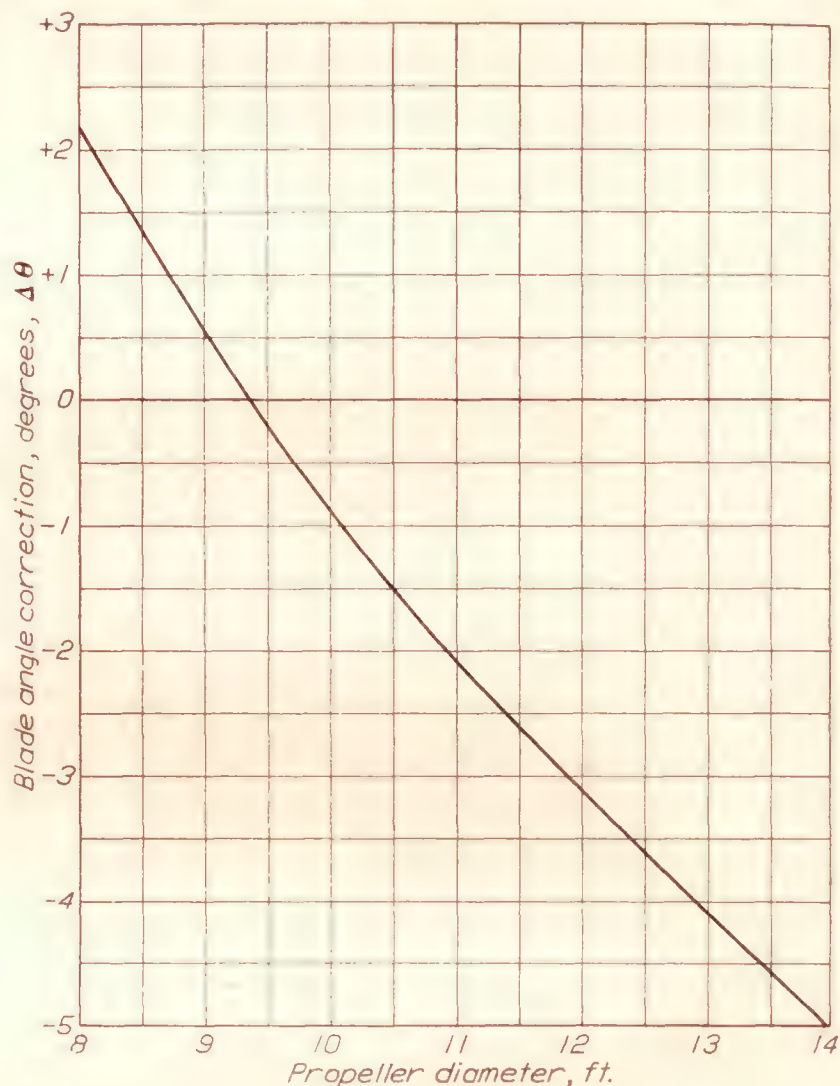


FIGURE 7.—Correction for obtaining blade angle at 0.75 radius from blade setting at 42" station. Positive (+) values of $\Delta\theta$ to be added to setting at 42" station, negative (−) values to be subtracted, to get blade angle at 0.75 radius.

Example: For 10 ft. dia. prop.

$$\Delta\theta = -0.9^\circ$$

$$\theta_{0.75R} = \theta_{42''} - 0.9^\circ$$

Since it is common practice to adjust or read the blade angle at a given station regardless of the propeller diameter, a correction must be applied to obtain the setting at $0.75 R$. Figure 7 gives the correction $\Delta\theta$ to convert the blade angle at the 42-inch station to the corresponding value at $0.75 R$. The 42-inch station is 75 per cent of 56 inches, so that the correction is zero for a diameter of 9 feet 4 inches. For diameters less than 9.33 feet the $0.75 R$ station will therefore lie inboard of the 42-inch station and consequently will have greater blade angles, i. e., $\Delta\theta$ is positive. For diameters greater than 9.33 feet the $0.75 R$ station blade setting will be less than at the 42-inch station, i. e., $\Delta\theta$ is negative.

K_{T_0} may also be plotted against the V/nD for maximum efficiency as in Figure 8. In design studies it is probably more convenient to use V/nD than blade angle. Under normal conditions the two methods give identical results, but in general the blade angle is slightly preferable owing to the practice of setting the pitch instead of changing diameter to obtain the desired revolutions.

The coefficient of traction μ must be selected according to ground conditions. It varies from about 0.02 for a smooth surface such as a concrete runway or a flight deck to as much as 0.30 for a sandy surface. In the absence of exact data, the following values may be used:

Smooth deck or hard surface	$\mu=0.02$
Good field, hard turf	$\mu=0.04$
Average field, short grass	$\mu=0.05$
Average field, long grass	$\mu=0.10$
Soft ground, gravel or sand	$\mu=0.10$ to 0.30

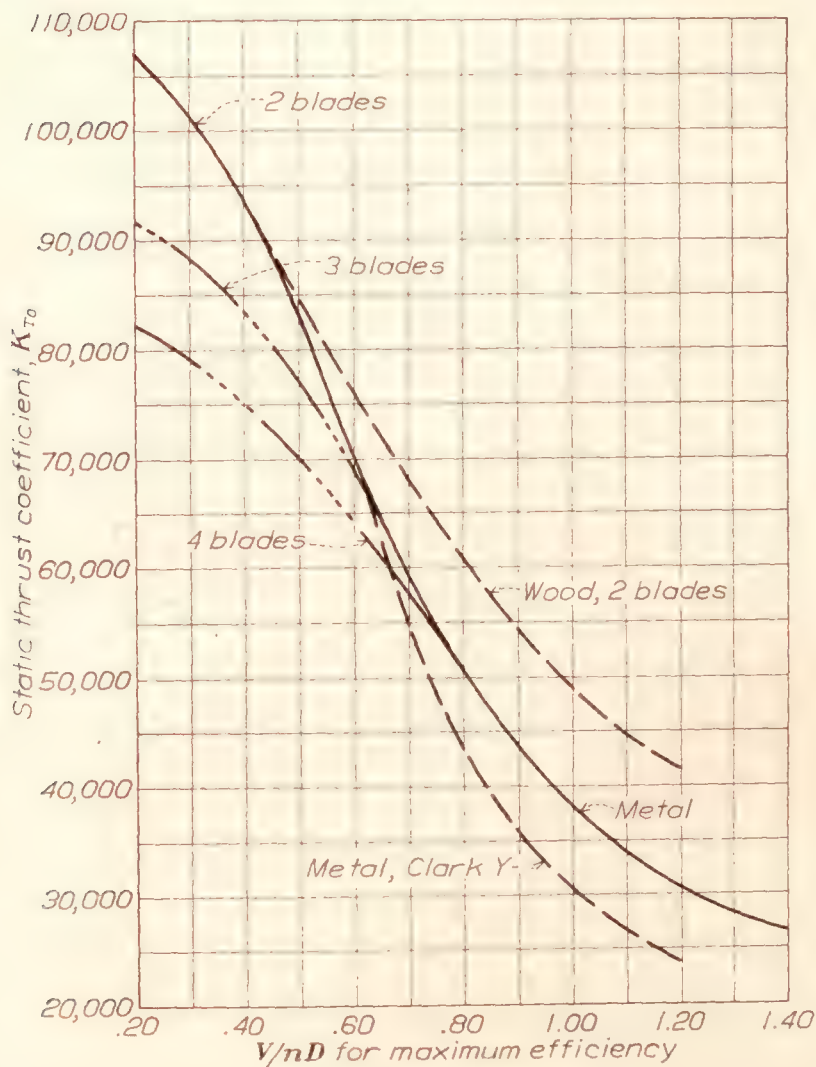


FIGURE 8.—Static thrust coefficient

FINAL NET ACCELERATING FORCE

The final net accelerating force per unit weight is defined by equation (4)

$$\frac{T_F}{W} = \frac{T_v}{W} - \frac{D}{L} \quad (4)$$

where T_v is the thrust at take-off speed and D/L is the ratio of drag to lift.

T_v may be obtained from the thrust horsepower at take-off speed V_s by the use of Figure 9, which is a plot of $t.hp/t.hp_m$ against V/V_m . The thrust horsepower at take-off speed is the product of the maximum $t.hp$ by the ratio $t.hp/t.hp_m$ from the curve, or

$$t.hp = t.hp_m \times \frac{t.hp}{t.hp_m} \quad (15)$$

The corresponding thrust is given by

$$T_v = \frac{550 \text{ t.hp}}{V_{f.p.s.}} \quad (16)$$

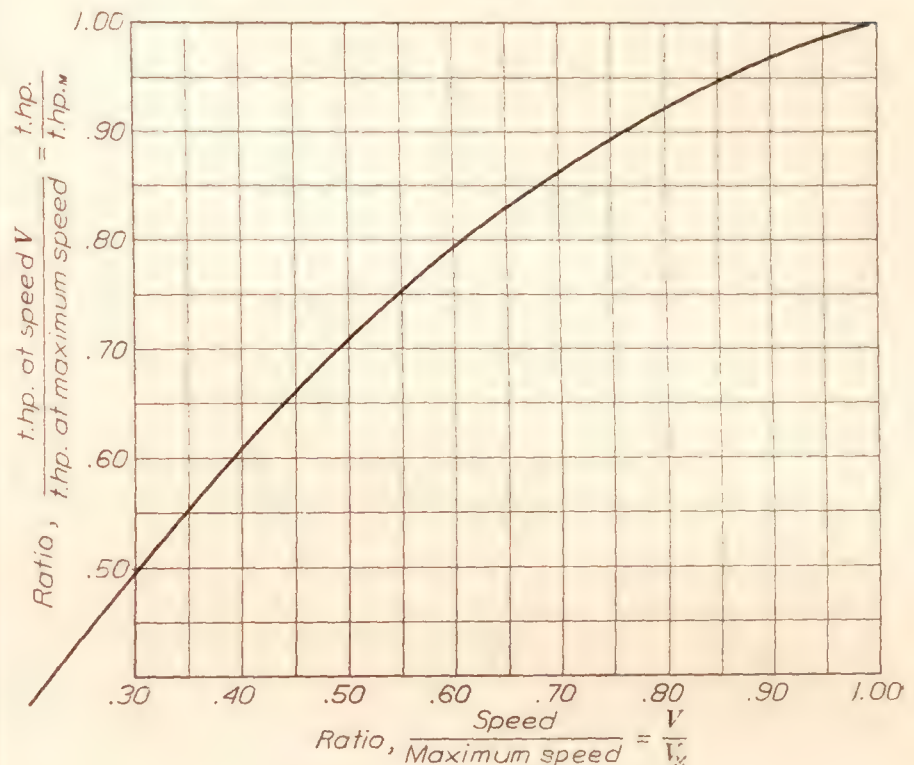


FIGURE 9.—General full-throttle t.hp. curve

The value of D/L may be taken as the reciprocal of the maximum value of L/D for the airplane, which is usually known. Figure 10 is a plot of $(L/D)_{max}$ as a function of aspect ratio and total parasite coefficient

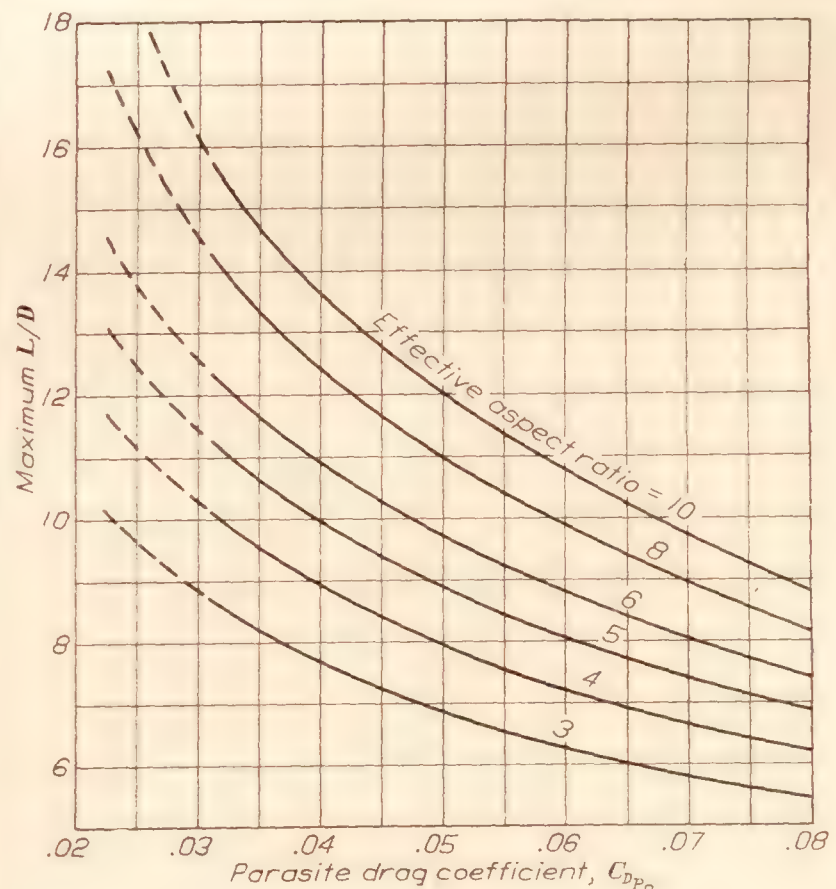


FIGURE 10

C_{DP_0} for use in estimating $(L/D)_{max}$. The total parasite coefficient C_{DP_0} includes the wing profile drag.

EFFECT OF WIND ON TAKE-OFF RUN

While the effect of wind may be obtained directly from the integrated equations of motion, it is always

more convenient to apply a correction to the run in a calm. Analysis of a series of take-off runs under various assumed conditions shows that a single curve (fig. 11) is sufficient to give the correction factor. In Figure 11 the ratio of the run S_w in a wind V_w to the run S_o in a calm is plotted against the ratio of

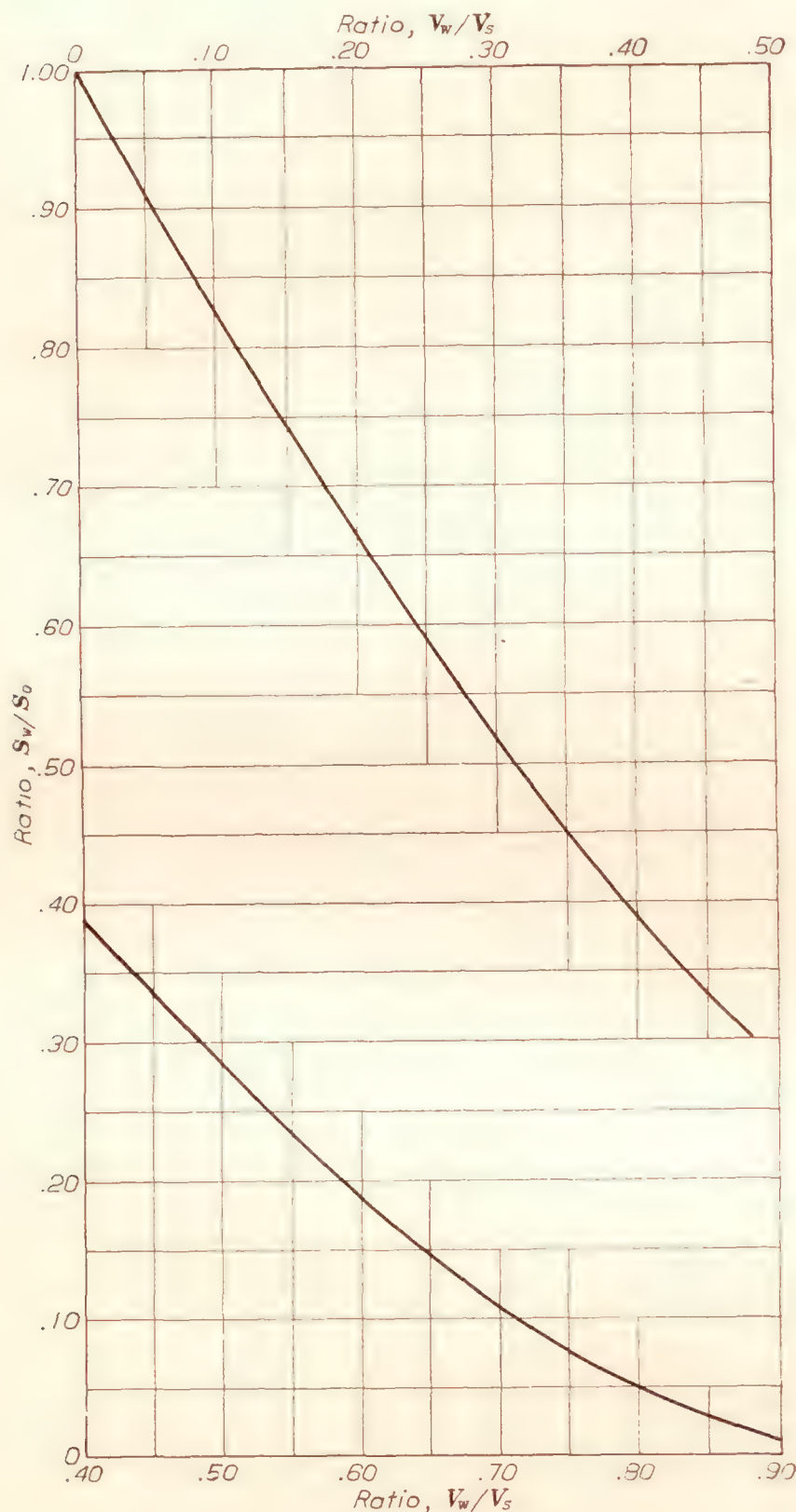


FIGURE 11.—Effect of wind on take-off run

wind speed V_w to the take-off speed V_s . When the run in a calm is known, the run in any wind is

$$S_w = S_o \times \frac{S_w}{S_o} \quad (17)$$

the value of S_w/S_o being read from Figure 11 for the value of V_w/V_s corresponding to the desired V_w .

EFFECT OF CHANGES IN WEIGHT AND TAKE-OFF SPEED

The effect of a change in weight is to change both the take-off coefficient K_s and the take-off speed V_s . Since W/V_s^2 is assumed constant

$$\frac{S_1}{S_2} = F \left(\frac{W_1}{W_2} \right)^2 \quad (18)$$

where F is a correction factor to allow for the variation in K_s . Figure 12 gives F as a function of W_1/W_2 and T_F/T_I . It will be noted that for small changes in weight (± 25 per cent) and for normal values of T_F/T_I (i. e., 0.60 to 1.00) the value of F may be taken as unity for most purposes, the average error probably being of the order of 3 per cent.

When the stalling speed is varied, with weight held constant, there will be a slight change in the ratio T_F/T_I and a corresponding change in K_s . In general these changes are negligible so that for all practical purposes

$$\frac{S_1}{S_2} = \left(\frac{V_{s1}}{V_{s2}} \right)^2 \quad (19)$$

INSTRUCTIONS FOR CALCULATION OF TAKE-OFF RUN

In general the use of equation (10) requires the following steps:

1. Obtain the static thrust coefficient K_{T_o} from Figure 6 or Figure 8 and calculate the static thrust T_o using equation (14);
2. Divide the static thrust by the gross weight, and subtract the proper value of the coefficient of traction μ to obtain the initial net accelerating force per unit weight $\frac{T_I}{W}$ (equation (3));
3. Calculate the thrust available at take-off speed T_v using the method described above, equations (15) and (16) with Figure 9, and divide T_v by the gross weight;
4. Calculate or estimate the maximum L/D of the airplane (using Figure 10, if necessary) and subtract the reciprocal from T_v/W to obtain the final net accelerating force per unit weight T_F/W (equation (4));
5. Take the ratio of T_F/T_I and read the corresponding value of the take-off coefficient K_s from Figure 4.
6. Calculate the take-off run in a calm, using this value of K_s with equation (10);
7. Apply corrections as required; for wind using equation (17) with Figure 11, or for a different gross weight using equation (18) with Figure 12.

An example of a calculation for take-off run, showing method of tabulating work, is given in Table IV.

BUREAU OF AERONAUTICS,
NAVY DEPARTMENT,
WASHINGTON, D. C., Sept., 1932.

REFERENCES

1. Wood, R. McKinnon, and Bradfield, F. B.: The Distance Required to Take Off an Aeroplane. R. & M. No. 680, British A. R. C., 1920.
2. Rolles, B. H., and Stevens, H. L.: The Effect of Wind, Weight, and Atmospheric Conditions (Including Semi-Tropical Conditions) on the Distance to Take Off and Land an Aircraft. R. & M. No. 1172, British A. R. C., 1928.
3. Warner, Edward P.: Airplane Design-Aerodynamics. McGraw-Hill Book Co., Inc., New York City, 1927.
4. Diehl, Walter S.: Static Thrust of Airplane Propellers. T. R. No. 447, N. A. C. A., 1932.

TABLE I

CALCULATED TAKE-OFF RUN USING NET ACCELERATING FORCE SHOWN ON FIGURE 2

Air speed V ft./sec.	Net accelerating force $\frac{F}{W}$	Acceler- ation a ft./sec. ²	$\frac{V}{a}$ $\frac{dS}{dV}$	$\Sigma \left(\frac{V}{a} \right)$	Distance run S ft.
0	0.4500	14.48	0	0	0
10	.4395	14.13	0.71	0.35	3.5
20	.4280	13.77	1.45	1.43	14.3
30	.4155	13.36	2.25	3.28	32.8
40	.4020	12.92	3.09	5.95	59.5
50	.3875	12.46	4.01	9.50	95.0
60	.3720	11.97	5.02	14.02	140.2
70	.3555	11.43	6.12	19.59	195.9
80	.3380	10.87	7.35	26.32	263.2
90	.3195	10.27	8.76	34.38	343.8
100	.3000	9.65	10.35	43.93	439.3

TABLE II

CALCULATED TAKE-OFF RUN USING ASSUMED
LINEAR NET ACCELERATING FORCE SHOWN ON
FIGURE 3

Air speed V ft./sec.	Net ac- celerating force $\frac{F}{W}$	Acceler- ation a ft./sec. ²	$\frac{V}{a}$ $\frac{dS}{dV}$	$\Sigma \left(\frac{V}{a} \right)$	Distance run S ft.
0	0.450	14.48	0	0	0
10	.435	13.98	0.71	0.35	3.5
20	.420	13.50	1.48	1.45	14.5
30	.405	13.02	2.30	3.34	33.4
40	.390	12.55	3.19	6.08	60.8
50	.375	12.06	4.14	9.75	97.5
60	.360	11.59	5.18	14.41	144.1
70	.345	11.10	6.30	20.15	201.5
80	.330	10.62	7.53	27.06	270.6
90	.315	10.13	8.88	35.27	352.7
100	.300	9.65	10.35	44.88	448.8

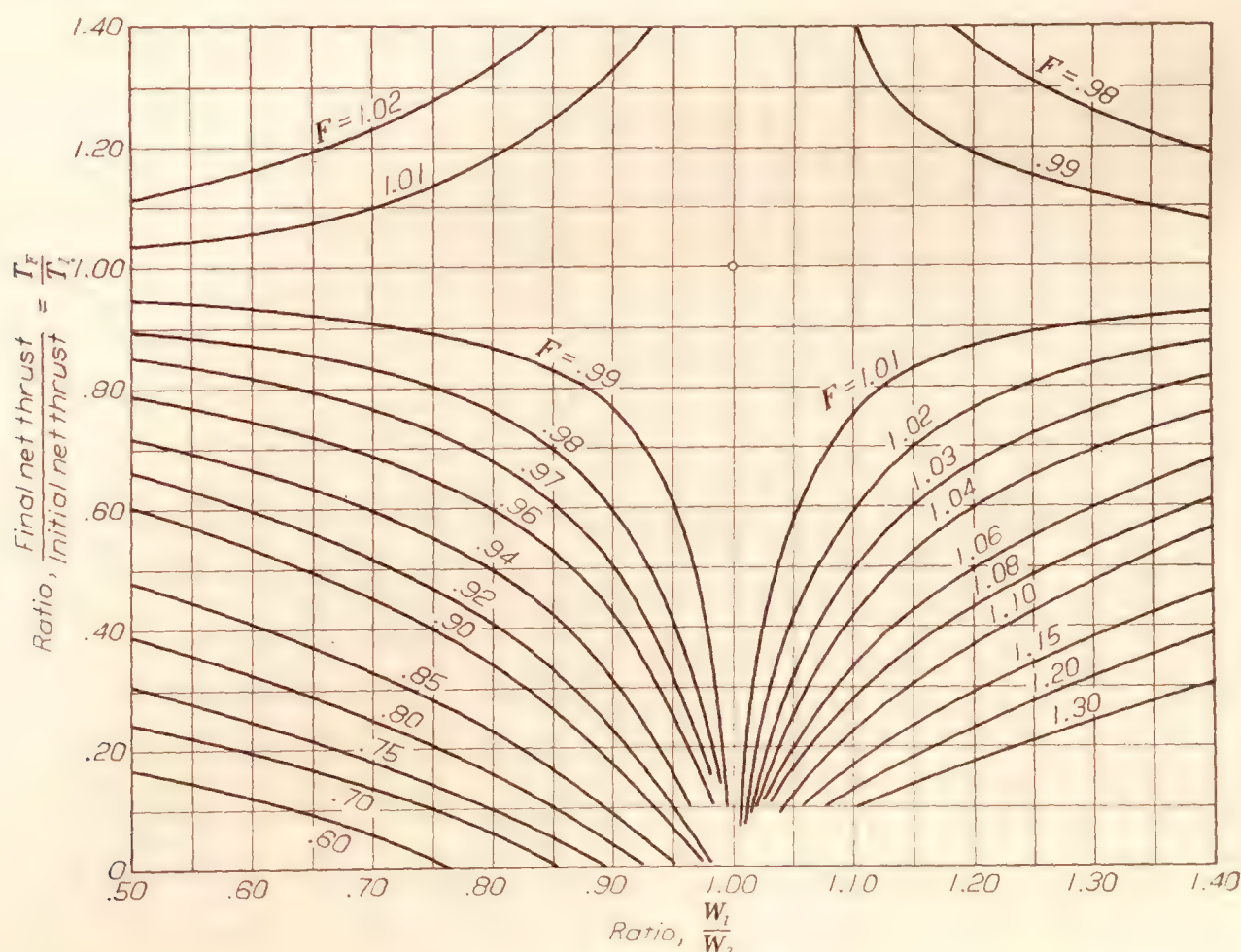


FIGURE 12.—Effect of weight on take-off run

$$\frac{S_1}{S_2} = F \left(\frac{W_1}{W_2} \right)^2$$

TABLE III
CALCULATION FOR K_s AND K_t

$\frac{T_P}{T_I}$ = $(1-K)$	K	$\log(1-K)$	$\frac{\log(1-K)}{K^2}$ A	$\frac{1}{K}$ B	$\frac{F}{-B-A}$	$\frac{K_s}{F}$ $=\frac{F}{g}$	$\frac{-\log(1-K)}{K}$	$\frac{K_t}{-\log(1-K)}$ $=\frac{K_t}{gK}$
1.30	-.30	0.262364	2.915159	-3.3333	0.41817	0.01300	0.8745	0.02718
1.20	-.20	.182321	4.558036	-5.0000	.44196	.01374	.9116	.02833
1.10	-.10	.095310	9.531021	-10.0000	.46898	.01458	.9531	.02962
1.05	-.05	+.048790	19.51606	-20.0000	.48394	.01504	.9758	.03033
1.00	0	0			(.50000)	(.01554)	(1.0000)	.03108
.95	+.05	-.051293	-20.51732	+20.0000	.51732	.01609	1.0259	.03189
.90	.10	-.105360	-10.53603	10.0000	.53603	.01666	1.0536	.03275
.85	.15	-.162519	-7.223053	6.66667	.55639	.01729	1.0835	.03368
.80	.20	-.223143	-5.578587	5.0000	.57859	.01798	1.1157	.03467
.75	.25	-.287682	-4.602912	4.0000	.60291	.01874	1.1507	.03577
.70	.30	-.356675	-3.963053	3.3333	.62972	.01957	1.1889	.03695
.60	.40	-.510826	-3.192659	2.5000	.69266	.02153	1.2771	.03969
.50	.50	-.693147	-2.772589	2.0000	.77259	.02401	1.3863	.04309
.40	.60	-.916291	-2.545252	1.6666	.87859	.02731	1.5272	.04747
.30	.70	-1.203973	-2.457087	1.428571	1.02852	.03197	1.7200	.05346
.20	.80	-1.609438	-2.514746	1.25000	1.26475	.03931	2.0118	.06253
.10	.90	-2.302585	-2.842695	1.1111	1.73158	.05382	2.5584	.07952

TABLE IV
EXAMPLE OF CALCULATIONS FOR TAKE-OFF RUN

		Remarks
Airplane type.....	Biplane	
Gross weight W lb.....	3,000	
b. hp/prop. r.p.m.....	400/1900	
Wing area S sq. ft.....	250	
Wing loading W/S lb./sq. ft.....	12.00	
Wing section.....	Clark Y	
Maximum lift coefficient C_L	1.50	
Stalling speed V_s ft./sec.....	82	
Maximum speed V_m ft./sec.....	220	
Propeller diameter D ft.....	9.0	
V/nD77	
η_m80	
t.hp $_m$	320	$=\eta_m \times \text{b.hp.}$
Propeller blade setting $42'' R$	20.0°	Setting given.
Propeller blade setting $0.75 R$	20.5°	Figure 7.
Propeller blade section, or design.....	normal	
Static thrust coefficient K_{T_0}	53,000	Figure 6 or Figure 6.8.
Static thrust $T_0 = \frac{K_{T_0} \times \text{b.hp.}}{\text{r.p.m.} \times D}$	1,240	Equation (14).
$\frac{T_0}{W}$413	

TABLE IV
EXAMPLE OF CALCULATIONS FOR TAKE-OFF RUN—
Continued

		Remarks
$\frac{T_1}{W} = \left(\frac{T_0}{W} - \mu \right)$ $\mu = .02$393	Equation (3).
Ratio V_s/V_m373	
t.hp/t.hp at V_s578	From Figure 9.
t.hp at V_s	185	Equation (15).
Thrust at V_s T_s	1,240	Equation (16).
$\frac{T_s}{W}$413	
Maximum L/D	9.0	See Figure 10.
$\frac{T_P}{W} = \left(\frac{T_s}{W} - \frac{D}{L} \right)$302	Equation (4).
Ratio T_P/T_I770	
Take-off run coefficient K_s0183	From Figure 4.
Run $S_0 = \frac{K_s V_s^2}{(T_P/W)}$ ft.....	313	Equation (10).
Wind velocity V_w ft./sec.....	40	
Ratio V_w/V_s49	
Ratio S_w/S_0295	From Figure 11.
S_w ft.....	92	Equation (17).

REPORT No. 451

THE DRAG OF TWO STREAMLINE BODIES AS AFFECTED BY PROTUBERANCES AND APPENDAGES

By IRA H. ABBOTT

SUMMARY

Two airship models were tested in the N. A. C. A. variable-density wind tunnel to determine the drag coefficients at zero pitch, and the effect of fins and cars and of flat and streamline protuberances located at various positions along the hull. During the investigation the stern of one model was rounded off to produce a blunter shape. The extreme range of the Reynolds Number based on the over-all length of the models was from 1,300,000 to 33,000,000.

At large values of the Reynolds Number the streamline protuberance affected the drag very little, and the additional drag caused by the flat protuberance was less than the calculated drag of the protuberance alone. The fins and cars together increased the bare-hull drag about 20 per cent.

INTRODUCTION

The National Advisory Committee for Aeronautics is conducting in the variable-density wind tunnel an extensive investigation of aerodynamic interference. The investigation deals in part with the effects of protuberances from the surfaces of otherwise streamline bodies. Tests have been made (reference 1) to study the effects on the characteristics of wings and airfoil sections of protuberances from the surface of an airfoil. The part of the investigation dealt with in this report is the study of the interference of protuberances from the surfaces of streamline bodies of revolution.

The desirability of making such interference tests in the variable-density wind tunnel where large values of the Reynolds Number may be obtained is apparent from consideration of the boundary-layer theory. (Reference 2.) If wind-tunnel tests of airship models are made in the usual range of relatively small Reynolds Numbers where neither the laminar nor the turbulent condition of the boundary layer is predominant, the type of flow existing in the boundary layer over a large portion of the surface is dependent upon the turbulence of the air stream. The drag coefficients thus obtained have no simple relation to the full-scale coefficients; in fact, those obtained for the same model at the same Reynolds Number but in different wind tunnels vary greatly. (References 2 to 6.) If a

protuberance is attached to a model tested in this range of Reynolds Numbers, the additional turbulence created by the protuberance may cause the line of transition between the laminar and turbulent boundary layers to move upstream with a resulting increase in the drag coefficient. The nature of the interference between the body and the protuberance in this case is obviously different than that which occurs when the boundary layer is almost completely turbulent. The data obtained at large values of the Reynolds Number in this investigation are accordingly expected to be more applicable than those previously obtained at small values of the Reynolds Number to the solution of design problems, such as the determination of the drag of fittings, radiators, water-recovery apparatus, and other objects projecting from fuselages and airship hulls.

A study of the effects of protuberances was planned to be made during a previous investigation of the aerodynamic characteristics of airship models. (Reference 4.) The drag of the models, however, was found to vary with the surface roughness which, with the wooden models used in the investigation, could not be maintained constant under the conditions of temperature and pressure in the variable-density wind tunnel.

An attempt to measure the relatively small differences in drag due to protuberances was accordingly considered inadvisable. To obviate the difficulty the Goodyear-Zeppelin Corporation furnished a simplified metal model of the U. S. airship *Akron*. The tests on this model were delayed by extensive alterations of the variable-density wind tunnel. Meanwhile the U. S. Army Air Corps requested tests of a model of a proposed metal-clad airship. The two models were tested in January, 1931. The drag coefficients at zero pitch, and the additional drag due to flat and streamline protuberances, and to fins and cars were determined. The extreme range of Reynolds Numbers obtained in these tests was from about 1,300,000 to 33,000,000.

APPARATUS AND METHOD

The two airship models of aluminum alloy used in this investigation are designated models A and M, respectively.

Model A was a simplified model of the U. S. airship *Akron* with circular cross sections. The length of this model was 37.39 inches and the fineness ratio was 5.9. The measured ordinates are given in Table I. The surface of this model was very smooth. No fins and cars were furnished. During the investigation the stern of this model was altered to a blunter shape, the

During the course of the investigation the surface of this model was polished for a distance of 6 inches aft of the bow, and later was polished all over. This model was equipped with one control and four motor cars, and with two sets of tail surfaces, one set having six and the other eight fins. The arrangements of the fins and cars are shown in Figures 2a and 2b.

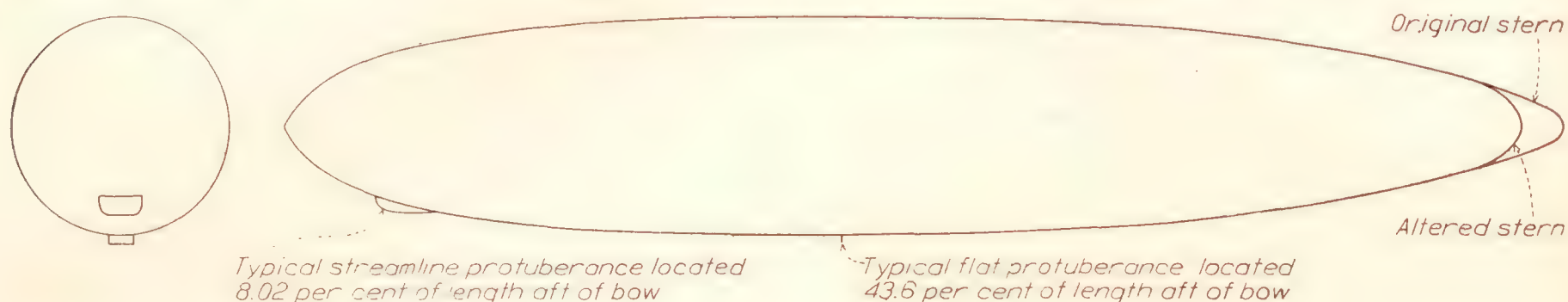
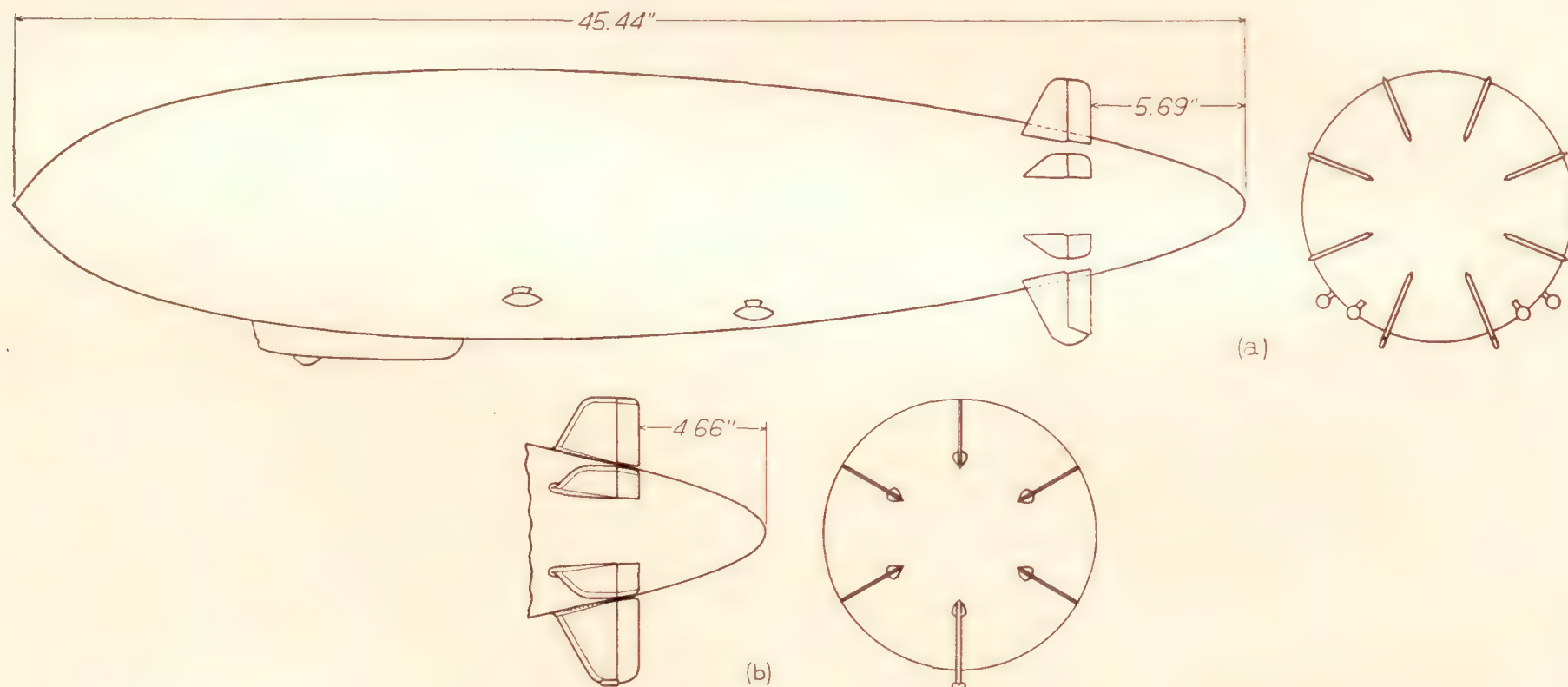


FIGURE 1.—Outlines of model A with original and altered sterns showing typical flat and streamline protuberances

ordinates of which are given in Table I. Figure 1 is an outline drawing of the model showing the two sterns.

Model A was tested with a flat-plate protuberance having a width of 11.8 per cent and extending 3.9 per cent of the maximum diameter of the model from the surface. This protuberance was successively attached to the model perpendicular to the surface at 8.02, 17.4, 30.7, 43.6 (near maximum ordinate), 63.5, and 82.2 per cent of the length of the model aft of the bow. Further tests were made with the flat protuberance faired to

The tests were made in the variable-density wind tunnel, which is described in reference 7. The mounting of the model on the auxiliary drag balance was similar to that described in reference 3, except that four partly shielded round wires were used to support the model instead of three streamline wires, and that a 45° linkage was used instead of a bell crank to transmit the force of a counterweight. Figure 3 is a photograph of model M mounted in the tunnel. The distances from the downstream edge of the entrance



FIGURES 2 a and b.—Outline of model M showing arrangement of fins and cars (a) 8 fins (b) 6 fins

form a streamline protuberance located successively at 8.02, 30.7, and 63.5 per cent of the length aft of the bow. The outlines of the protuberances in typical positions on the hull are shown in Figure 1.

Model M was a model of a proposed metal-clad airship. The length of this model was 45.44 inches and the fineness ratio was 4.5. The ordinates are given in Table II. This model had a machined surface showing very small circumferential tool or finishing marks.

cone to the bows of models A and M when mounted for tests were 12 and 10 inches, respectively.

The results were corrected for the drag of the support wires, the effect of the static pressure gradient along the axis of the tunnel, and the effect of the tunnel walls. The wire drag was computed (reference 8), and was checked by testing model A successively with two sizes of wires. The interference between the rear support wires and the fins of model M was found to be

negligible by testing this model with the rear support wires in two positions. The static pressure gradients were measured at all tank pressures (reference 7) for the determination of the horizontal buoyancy correction, which was computed for each pressure by a process of graphical integration. As this correction showed small inconsistent variations with tank pressure, an average correction was used for all pressures. The tunnel-wall correction was computed from the formulas given in reference 9.

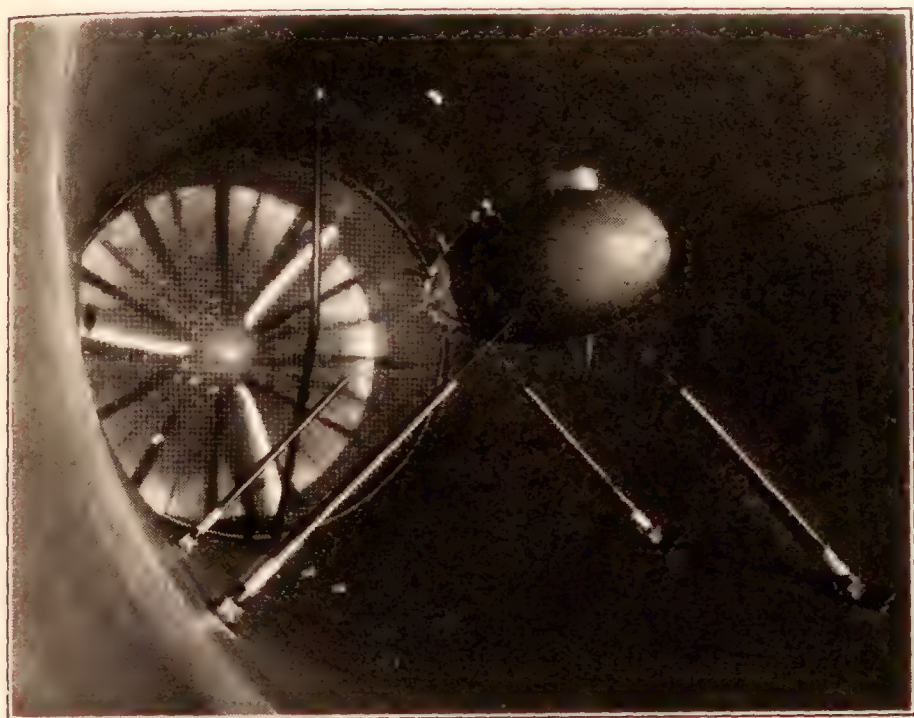


FIGURE 3.—Photograph of model M with fins and cars mounted for test in the variable-density wind tunnel

PRECISION

The variation in check points indicates the accidental error of the gross force measurements to be about ± 1 per cent of the net bare-hull drag. The error of the balance calibration may be as large as ± 2 per cent at the small Reynolds Numbers and ± 1 per cent at the large ones.

The drag coefficients of model A as determined from successive tests with support wires 0.0155 and 0.0240 inch in diameter were the same within the accuracy of the tests. The precision of the tare-drag correction is accordingly believed to be within ± 3 per cent of the net bare-hull drag. No reliable estimate of the error in the horizontal buoyancy correction can be made, but the result of this error is believed to be small because this correction was only about 5 and 10 per cent, respectively, of the net bare-hull drags of models A and M. The tunnel-wall correction was very small and the error in this correction is believed to be negligible.

Disregarding the error in the horizontal buoyancy correction, the possible error in the results is ± 6 per cent. As the inaccuracies of corrections do not affect the precision of the values obtained for the additional drags of protuberances and appendages, these values

are believed to be precise to about ± 1 per cent of the net bare-hull drags.

RESULTS AND DISCUSSION

The results are presented in the form of drag coefficients which are defined as $C_D = \frac{D}{q(\text{Vol.})^{\frac{2}{3}}}$ and are

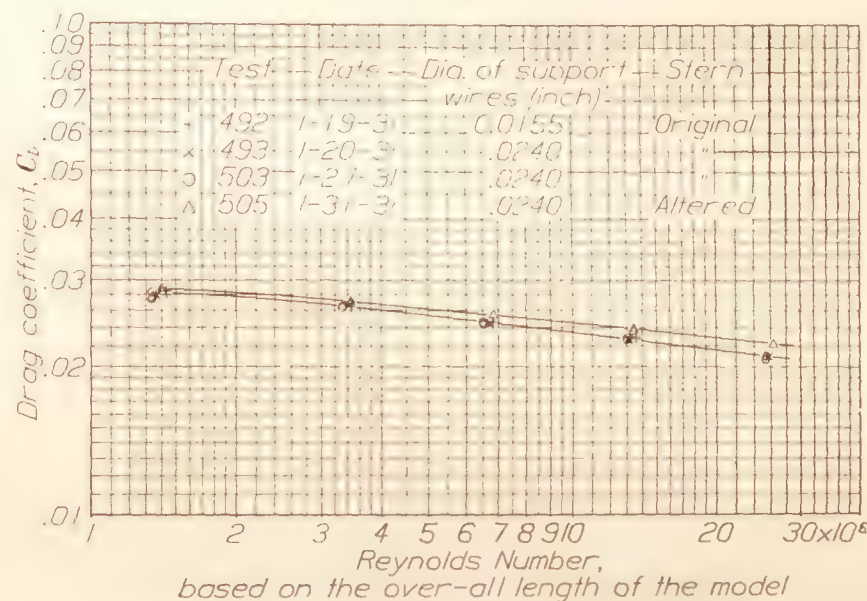


FIGURE 4.—Drag coefficients of model A

Tested in the N. A. C. A. variable-density wind tunnel. Volume=0.472 cu. ft. (Vol.)^{2/3}=0.606 sq. ft. Length=37.39 in. Bare hull with original and altered sterns. Drag coefficient and Reynolds Number of altered model based on original volume and length. Results corrected for wire drag, horizontal buoyancy, and tunnel-wall effect.

plotted as functions of Reynolds Number. The Reynolds Numbers are based on the lengths of the models.

Bare-hull drags.—The bare-hull drags of models A and M are presented in Figures 4 and 5. The figures show that the curves of drag coefficients are nearly straight lines when plotted on logarithmic scales

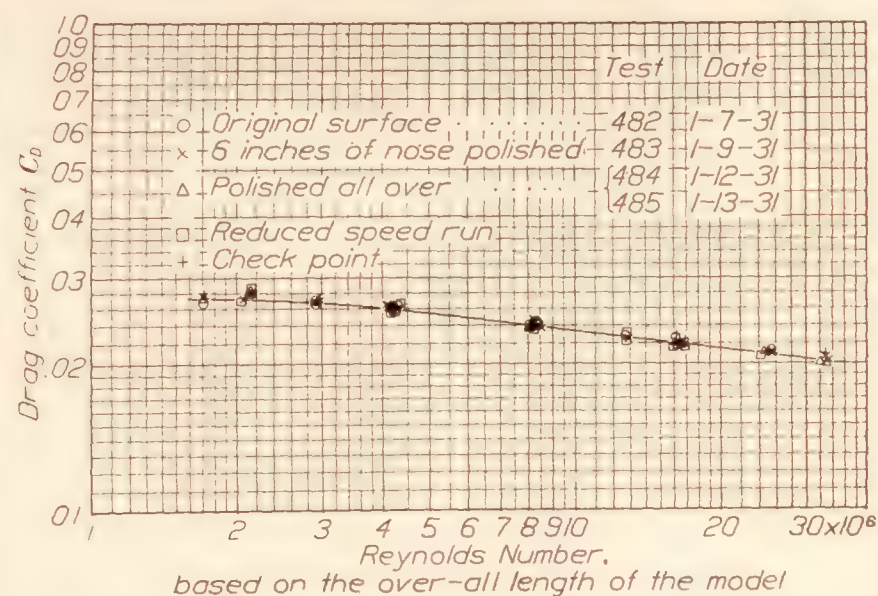


FIGURE 5.—Drag coefficients of model M

Tested in the N. A. C. A. variable-density wind tunnel. Bare hull. Volume=1.291 cu. ft. (Vol.)^{2/3}=1.186 sq. ft. Length=45.44 in. Support wires=0.0240 in. dia. Results corrected for wire drag, horizontal buoyancy, and tunnel-wall effect.

against the Reynolds Number. It will be seen from Figure 5 that the drag coefficient of model M is the same, within the accuracy of the tests, at a given value

of the Reynolds Number irrespective of the combination of air speed and density used to give that Reynolds Number. A comparison of the results obtained for model A with those obtained for different models of the same airship in different tunnels is given in reference 10.

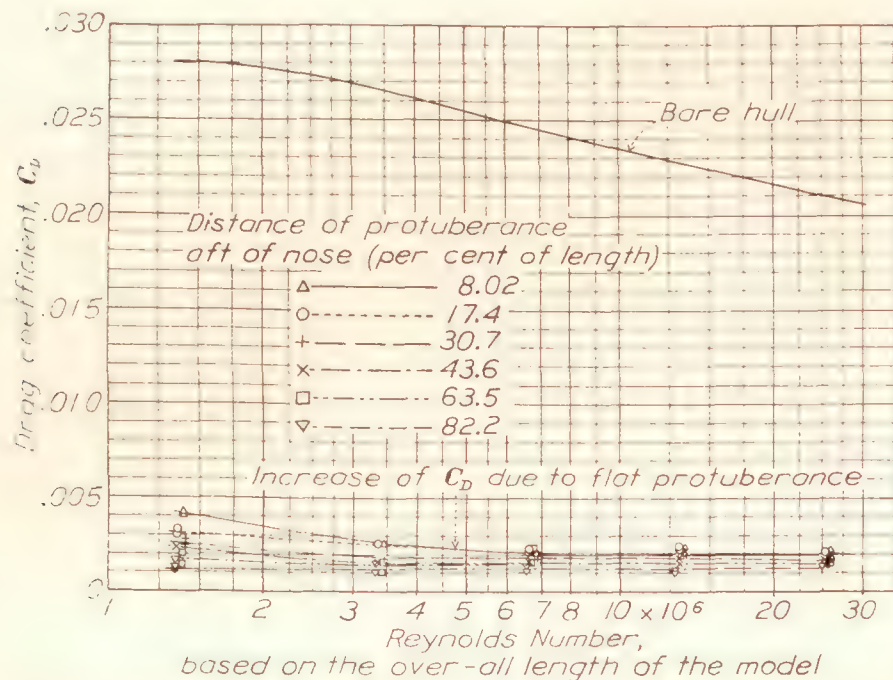


FIGURE 6.—The increase of drag coefficient of model A resulting from a flat protuberance located in various positions along the hull

Effect of blunt stern.—The drag coefficients of model A with the altered stern, which was considerably blunter than the original one (fig. 1), are presented in Figure 4. At the highest values of the Reynolds Number the drag is about 5 per cent higher with the altered stern than with the original one. It will be noticed that the rate of decrease of the drag coefficient with increasing values of the Reynolds Number is less for the model with the altered stern than for the original model.

Effect of flat protuberances.—The additional drag coefficients due to a flat protuberance located at various positions along the hull of model A are plotted against the Reynolds Number in Figure 6. At the highest values of the Reynolds Number the additional drag due to the protuberance in any position is less than the drag of the protuberance alone as calculated from flat-plate data. (Reference 11.) This fact indicates that at large values of the Reynolds Number any increase of drag resulting from the effect of the protuberance on the flow over the hull need not be considered.

Figure 6 shows a fairly consistent decrease in the additional drag due to the protuberance as its position varies from bow to stern. This variation is in the direction that would be expected, since the protuberance when located near the stern may be in a region of lower velocity than when located near the bow. It is interesting to note how well this effect can be predicted from boundary-layer and pressure-distribution data.

The apparent drag coefficients of the protuberance as located in the various positions have been calculated using the measured additional drags due to the protuberance, and the average dynamic pressures of the air streams in which the protuberance was placed. These average dynamic pressures were determined graphically from pressure-distribution and boundary-layer data obtained at a Reynolds Number of 18,000,000. (Reference 12.) The calculated drag coefficients of the protuberance are tabulated in Table III. As expected, these calculated coefficients show less variation with the position of the protuberance than the measured additional drags. The calculated drag coefficients of the protuberance are much lower than the usual flat-plate coefficients (reference 11), indicating the presence of favorable additional interference that was not considered in the above calculations. The values of the calculated drag coefficients of the protuberance apply directly only to flat-plate protuberances in contact with the hull, and may be considerably different from coefficients similarly obtained for flat plates near, but not in contact with, the hull.

Effect of streamline protuberances.—The additional drag coefficients due to streamline protuberances are plotted against the Reynolds Number in Figure 7 for three positions along the hull of model A. It will be noted that the additional drag due to these protuber-

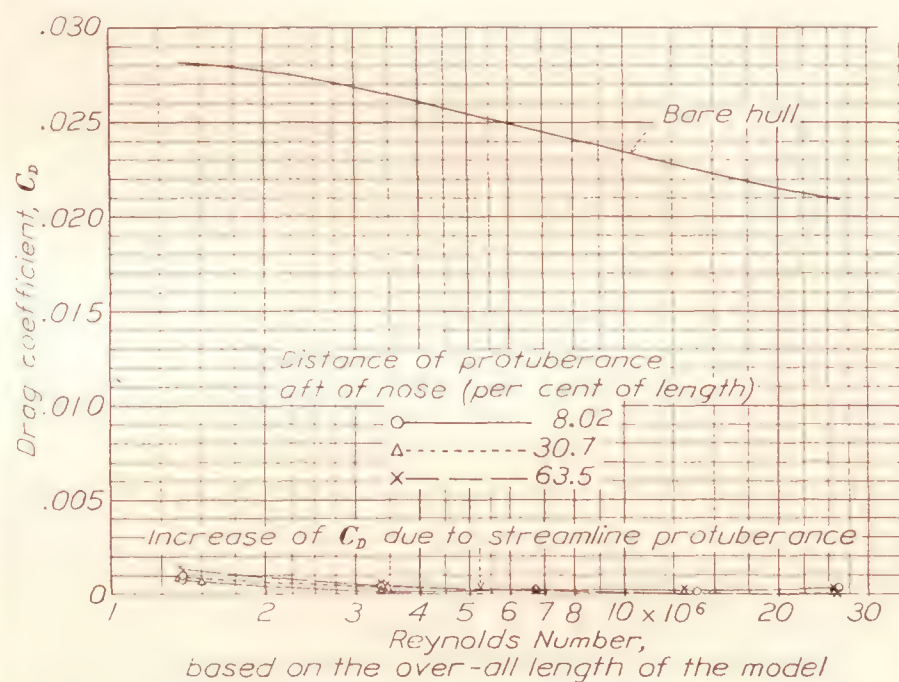


FIGURE 7.—The increase of drag coefficient of model A resulting from a streamline protuberance located in various positions along the hull

ances is very small at the high values of the Reynolds Number.

Effect of fins and cars.—The additional drag coefficients for each group of fins and of fins and cars on model M are plotted against the Reynolds Number in Figure 8. The increase of drag coefficients due to the six and eight fin groups is about 8 and 11 per cent, respectively, of the bare-hull drag. The low drag of the six-fin group was originally thought to be due to

interference between the fins and the rear support wires, which were located nearly in the planes of two of the fins. The tests were therefore repeated with the rear support wires moved, but the results checked those previously obtained.

No data are available to permit the computation of the average dynamic pressure of the flow over the fins; therefore the drag coefficients of the fins have been computed using the measured additional drag due to them, the dynamic pressure of the stream with no model present, and the fin areas. These drag coeffi-

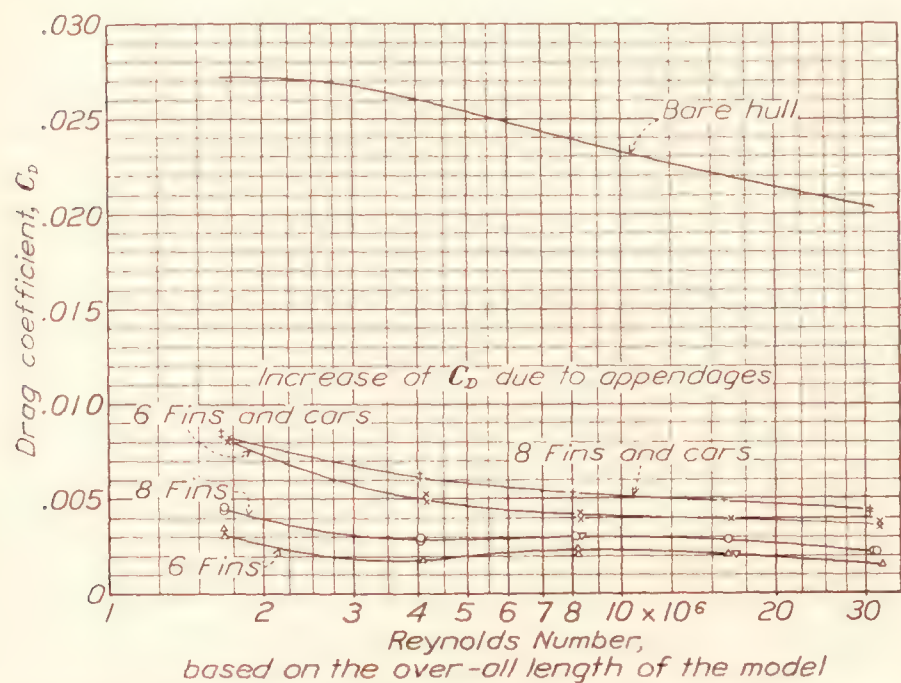


FIGURE 8.—The increase of drag coefficient of model M resulting from fins and cars

cients were found to be 0.0073 and 0.0088 for the six and eight fin groups, respectively, at the highest value of the Reynolds Number obtained. These values are approximately the same as the minimum drag coefficients of thin symmetrical airfoils. (Reference 13.) The fin sections, however, were not of good streamline form, and hence it is probable that there was a favorable interference effect.

The additional drag due to the cars with either set of fins at the highest values of the Reynolds Number was equal to about 10 per cent of the bare-hull drag. The drag coefficient of the cars based on the sum of their maximum cross-sectional areas and the dynamic pressure of the air stream with no model present has been computed from the measured additional drag due to the cars. This drag coefficient was about 0.12 at the largest values of the Reynolds Number obtained which were about 1,200,000 and 5,600,000 for the motor and control cars, respectively. This drag coefficient is about 50 per cent larger than that for good streamline bodies at the same Reynolds Numbers. (Reference 4.) Part of this difference may be due to interference between the hull and cars, but it is probable that the relatively poor streamline forms of the

cars as compared with the airship models of reference 4 accounts for most of the difference. It will be noted that there is an apparent error in the test at the lowest value of the Reynolds Number (fig. 8), because the results of this test show an appreciable difference in the additional drag due to the cars with the different sets of fins.

Effect of surface roughness.—The drag coefficients obtained for model M with its original surface, with the surface polished for a distance of 6 inches aft of the bow, and with the surface polished all over are plotted in Figure 5. The drag coefficients agree within the accuracy of the tests. The previous tests which showed large effects of surface roughness on the drag coefficient were made with models whose surfaces were much rougher than those of the present tests. (Reference 4.)

CONCLUSIONS

The results reported in this paper are significant in showing that the addition to a streamline body of revolution of flat and streamline protuberances of the size tested does not result in adverse interference effects at large values of the Reynolds Number. Accordingly, no large adverse interference effects would be expected to result from variations of the shape of the protuberance. It is probable, however, that the removal of the protuberance from the hull to form a body or plate separated from the hull by a small gap would modify the interference to an appreciable extent.

LANGLEY MEMORIAL AERONAUTICAL LABORATORY,
NATIONAL ADVISORY COMMITTEE FOR AERONAUTICS,
LANGLEY FIELD, VA., September 26, 1932.

REFERENCES

1. Jacobs, Eastman N.: Airfoil Section Characteristics as Affected by Protuberances. T. R. No. 446, N. A. C. A., 1932.
2. Dryden, H. L., and Kuethe, A. M.: Effect of Turbulence in Wind Tunnel Measurements. T. R. No. 342, N. A. C. A., 1930.
3. Higgins, George J.: Tests of the N. P. L. Airship Models in the Variable Density Wind Tunnel. T. N. No. 264, N. A. C. A., 1927.
4. Abbott, Ira H.: Airship Model Tests in the Variable Density Wind Tunnel. T. R. No. 394, N. A. C. A., 1931.
5. Millikan, Clark B.: The Boundary Layer and Skin Friction for a Figure of Revolution. Trans. A. S. M. E., Jan. 30, 1932, pp. 29-43.
6. Ower, E.: Interference. Jour. R. A. S., July, 1932, pp. 531-77.

7. Jacobs, Eastman N., and Abbott, Ira H.: The N. A. C. A. Variable-Density Wind Tunnel. T. R. No. 416, N. A. C. A., 1932.

8. De Foe, George L.: Resistance of Streamline Wires. T. N. No. 279, N. A. C. A., 1928.

9. Lock, C. N. H.: The Interference of a Wind Tunnel on a Symmetrical Body. R. & M. No. 1275, British A. R. C., 1929.

10. Freeman, Hugh B.: Force Measurements on a 1/40-Scale Model of the U. S. Airship Akron. T. R. No. 432, N. A. C. A., 1932.

11. Warner, Edward P.: Airplane Design, Aerodynamics. McGraw-Hill Book Co., 1927.

12. Freeman, Hugh B.; Measurements of Flow in the Boundary Layer of a 1/40-Scale Model of the U. S. Airship Akron. T. R. No. 430, N. A. C. A., 1932.

13. Jacobs, Eastman N.: Tests of Six Symmetrical Airfoils in the Variable Density Wind Tunnel. T. N. No. 385, N. A. C. A., 1931.

TABLE I
MEASURED ORDINATES OF MODEL A

Station, measured from bow	Ordinates	
	With original stern	With altered stern
<i>Inches</i>	<i>Inches</i>	<i>Inches</i>
0.000	0.000	0.000
.250	.414	.414
.500	.726	.726
1.000	1.167	1.167
2.000	1.752	1.752
4.000	2.384	2.384
6.000	2.744	2.744
8.000	2.963	2.963
10.000	3.083	3.083
14.000	3.187	3.187
18.000	3.179	3.179
22.000	3.071	3.071
26.000	2.826	2.826
30.000	2.304	2.304
32.500		1.830
33.000		1.717
33.500		1.598
34.000	1.476	1.473
34.500		1.344
34.750		1.267
35.000		1.173
35.250		1.055
35.500		.905
35.750		.651
36.000		.314
36.180		.000
36.600	.658	
37.100	.421	
37.350	.204	
37.390	.000	

TABLE II
MEASURED ORDINATES OF MODEL M

Station, measured from bow	Ordinates
<i>Inches</i>	<i>Inches</i>
0.000	0.000
.250	.402
.500	.728
1.000	1.291
2.000	2.123
4.000	3.123
6.000	3.745
8.000	4.194
10.000	4.513
12.000	4.738
14.000	4.888
18.000	4.992
22.000	4.907
26.000	4.654
30.000	4.239
34.000	3.679
36.000	3.336
38.000	2.949
40.000	2.496
42.000	1.966
43.000	1.643
44.000	1.256
44.500	1.002
44.750	.856
45.000	.691
45.250	.455
45.438	.000

TABLE III
DRAG COEFFICIENTS OF FLAT PROTUBERANCES
ON MODEL A

$$C_{D_p} = \frac{D_p}{q_a S}$$

Where q_a is the average local dynamic pressure and S is the area of the protuberance
Reynolds Number of model A based on the over-all length of the model, 18,000,000

Location of protuber- ance, per cent of length of model A aft of nose	C_{D_p}
8.02	0.88
8.02	.84
17.4	.84
17.4	.84
30.7	.75
30.7	.75
43.6	.75
43.6	.70
63.5	.79
63.5	.79
63.5	.70
63.5	.75
82.2	.75
82.2	.75

REPORT No. 452

GENERAL POTENTIAL THEORY OF ARBITRARY WING SECTIONS

By T. THEODORSEN and I. E. GARRICK

SUMMARY

This report gives an exact treatment of the problem of determining the 2-dimensional potential flow around wing sections of any shape. The treatment is based directly on the solution of this problem as advanced by Theodorsen in N. A. C. A. Technical Report No. 411. The problem condenses into the compact form of an integral equation capable of yielding numerical solutions by a direct process.

An attempt has been made to analyze and coordinate the results of earlier studies relating to properties of wing sections. The existing approximate theory of thin wing sections and the Joukowski theory with its numerous generalizations are reduced to special cases of the general theory of arbitrary sections, permitting a clearer perspective of the entire field. The method not only permits the determination of the velocity at any point of an arbitrary section and the associated lift and moments, but furnishes also a scheme for developing new shapes of preassigned aerodynamical properties. The theory applies also to bodies that are not airfoils, and is of importance in other branches of physics involving potential theory.

INTRODUCTION

The solution of the problem of determining the 2-dimensional potential flow of a nonviscous incompressible fluid around bodies of arbitrary shape can be made to depend on a theorem in conformal representation stated by Riemann almost a century ago, known as the fundamental theorem of conformal representation. This theorem is equivalent to the statement that it is possible to transform the region bounded by a simple curve into the region bounded by a circle in such a way that all equipotential lines and stream lines of the first region transform respectively into those of the circle. The theorem will be stated more precisely in the body of this report and its significance for wing section theory shown—suffice it at present to state that if the analytic transformation by which the one region is transformed conformally into the region bounded by the circle is known, the potential field of this region is readily obtained in terms of the potential field of the circle.

A number of transformations have been found by means of which it is possible to transform a circle into

a contour resembling an airfoil shape. It is obviously true that such *theoretical* airfoils possess no particular qualities which make them superior to the types of more empirical origin. It was probably primarily because of the difficulty encountered in the inverse problem, viz, the problem of transforming an airfoil into a circle (which we shall denote as the direct process) that such artificial types came into existence. The 2-dimensional theoretical velocity distribution, or what is called the flow pattern, is known only for some special symmetrical bodies and for the particular class of Joukowski airfoils and their extensions, the outstanding investigators¹ being Kutta, Joukowski, and von Mises. Although useful in the development of airfoil theory these theoretical airfoils are based solely on special transformations employing only a small part of the freedom permitted in the general case. However, they still form the subject of numerous isolated investigations.

The direct process has been used in the theory of thin airfoils with some success. An approximate theory of thin wing sections applicable only to the mean camber line has been developed² by Munk and Birnbaum, and extended by others. However, attempts³ which have been made to solve the general case of an arbitrary airfoil by direct processes have resulted in intricate and practically unmanageable solutions. Lamb, in his "Hydrodynamics" (reference 1, p. 77), referring to this problem as dependent upon the determination of the complex coefficients of a conformal transformation, states: "The difficulty, however, of determining these coefficients so as to satisfy given boundary conditions is now so great as to render this method of very limited application. Indeed, the determination of the irrotational motion of a liquid subject to given boundary conditions is a problem whose exact solution can be effected by direct processes in only a very few cases. Most of the cases for which we know the solution have been obtained by an inverse process; viz, instead of trying to find a value of ϕ or ψ which satisfies [the Laplacian] $\nabla^2\phi=0$ or $\nabla^2\psi=0$ and given boundary conditions, we take some known solution of these differential equations

¹ See bibliography given in reference 9, pp. 24, 84, and 583.

² Cf. footnote 1.

³ See Appendix II of this paper.

and inquire what boundary conditions it can be made to satisfy."

In a report (reference 2) recently published by the National Advisory Committee for Aeronautics a general solution employing a direct method was briefly given. It was shown that the problem could be stated in a condensed form as an integral equation and also that it was possible to effect the practical solution of this equation for the case of any given airfoil. A formula giving the velocity at any point of the surface of an arbitrary airfoil was developed. The first part of the present paper includes the essential developments of reference 2 and is devoted to a more complete and precise treatment of the method, in particular with respect to the evaluation of the integral equation.

In a later part of this paper, a geometric treatment of arbitrary airfoils, coordinating the results of earlier investigations, is given. Special airfoil types have also been studied on the basis of the general method and their relations to arbitrary airfoils have been analyzed. The solution of the inverse problem of creating airfoils of special types, in particular, types of specified aerodynamical properties, is indicated.

It is hoped that this paper will serve as a step toward the unification and ultimate simplification of the theory of the airfoil.

TRANSFORMATION OF AN ARBITRARY AIRFOIL INTO A CIRCLE

Statement of the problem.—The problem which this report proposes to treat may be formulated as follows. Given an arbitrary airfoil⁴ inclined at a specified angle in a nonviscous incompressible fluid and translated with uniform velocity V . To determine the theoretical 2-dimensional velocity and pressure distribution at all points of the surface for all orientations, and to investigate the properties of the field of flow surrounding the airfoil. Also, to determine the important aerodynamical parameters of the airfoil. Of further interest, too, is the problem of finding shapes with given aerodynamical properties.

Principles of the theory of fluid flow.—We shall first briefly recall the known basic principles of the theory of the irrotational flow of a frictionless incompressible fluid in two dimensions. A flow is termed "2-dimensional" when the motion is the same in all planes parallel to a definite one, say xy . In this case the linear velocity components u and v of a fluid element are functions of x , y , and t only.

The differential equation of the lines of flow in this case is

$$v \, dx - u \, dy = 0$$

⁴ By an airfoil shape, or wing section, is roughly meant an elongated smooth shape rounded at the leading edge and ending in a sharp edge at the rear. All practical airfoils are characterized by a lack of abrupt change of curvature except for a rounded nose and a small radius of curvature at the tail.

and the equation of continuity is

$$\frac{\partial u}{\partial x} + \frac{\partial v}{\partial y} = 0 \text{ or } \frac{\partial u}{\partial x} = -\frac{\partial v}{\partial y}$$

which shows that the above first equation is an exact differential.

If $Q = c$ is the integral, then

$$u = \frac{\partial Q}{\partial y} \text{ and } v = -\frac{\partial Q}{\partial x}$$

This function Q is called the stream function, and the lines of flow, or streamlines, are given by the equation $Q = c$, where c is in general an arbitrary function of time.

Furthermore, we note that the existence of the stream function does not depend on whether the motion is irrotational or rotational. When rotational its vorticity is

$$\zeta = \frac{\partial v}{\partial x} - \frac{\partial u}{\partial y} = \frac{\partial^2 Q}{\partial x^2} + \frac{\partial^2 Q}{\partial y^2}$$

which is twice the mean angular velocity or "rotation" of the fluid element. Hence, in irrotational flow the stream function has to satisfy

$$\frac{\partial^2 Q}{\partial x^2} + \frac{\partial^2 Q}{\partial y^2} = 0 \quad (2')$$

Then there exists a velocity potential P and we have

$$\left. \begin{aligned} \frac{\partial P}{\partial x} &= u = \frac{\partial Q}{\partial y} \\ \frac{\partial P}{\partial y} &= v = -\frac{\partial Q}{\partial x} \end{aligned} \right\} \quad (1)$$

The equation of continuity is now

$$\frac{\partial^2 P}{\partial x^2} + \frac{\partial^2 P}{\partial y^2} = 0 \quad (2)$$

Equations (1) show that

$$\frac{\partial P}{\partial x} \frac{\partial Q}{\partial x} + \frac{\partial P}{\partial y} \frac{\partial Q}{\partial y} = 0$$

so that the family of curves

$$P = \text{constant}, \quad Q = \text{constant}$$

cut orthogonally at all their points of intersection.

For steady flows, that is, flows that do not vary with time, the paths of the particles coincide with the streamlines so that no fluid passes normal to them. The Bernoulli formula then holds and the total pressure head H along a streamline is a constant, that is

$$\frac{1}{2} \rho v^2 + p' = H$$

where p' is the static pressure, v the velocity, and ρ the density. If we denote the undisturbed velocity at infinity by V , the quantities $p' - p'$ by p , and $\frac{1}{2} \rho V^2$ by q , the Bernoulli formula may be expressed as

$$\frac{p}{q} = 1 - \left(\frac{v}{V} \right)^2 \quad (3)$$

The solutions of equations (2) and (2'), infinite in number, represent all possible types of irrotational motion of a nonviscous incompressible fluid in two dimensions. For a given problem there are usually certain specified boundary conditions to be satisfied which may be sufficient to fix a unique solution or a family of solutions. The problem of an airfoil moving uniformly at a fixed angle of incidence in a fluid field is identical with that of an airfoil fixed in position and fluid streaming uniformly past it. Our problem is then to determine the functions P and Q so that the velocity at each point of the airfoil profile has a direction tangential to the surface (that is, the airfoil contour is itself a streamline) and so that at infinite distance from the airfoil the fluid has a constant velocity and direction.

The introduction of the complex variable, $z = x + iy$, simplifies the problem of determining P and Q . Any analytic function $w(z)$ of a complex variable z , that is, a function of z possessing a unique derivative in a

each real functions of x and y . Suppose now in the xy complex plane there is traced a simple curve $f(z)$. (Fig. 1.) Each value of z along the curve defines a point w in the w plane and $f(z)$ maps into a curve $f(w)$ or $F(z)$. Because of the special properties of analytic functions of a complex variable, there exist certain special relations between $f(z)$ and $F(z)$.

The outstanding property of functions of a complex variable analytic in a region is the existence of a unique derivative at every point of the region.

$$\frac{dw}{dz} = \lim_{z \rightarrow z'} \frac{w - w'}{z - z'} = \rho e^{i\gamma}$$

or

$$dw = \rho e^{i\gamma} dz$$

This relation expresses the fact that any small curve zz' through the point z is transformed into a small curve ww' through the point w by a magnification ρ and a rotation γ ; i. e., in Figure 1 the tangent t will coincide in direction with T by a rotation $\gamma = \beta - \alpha$.

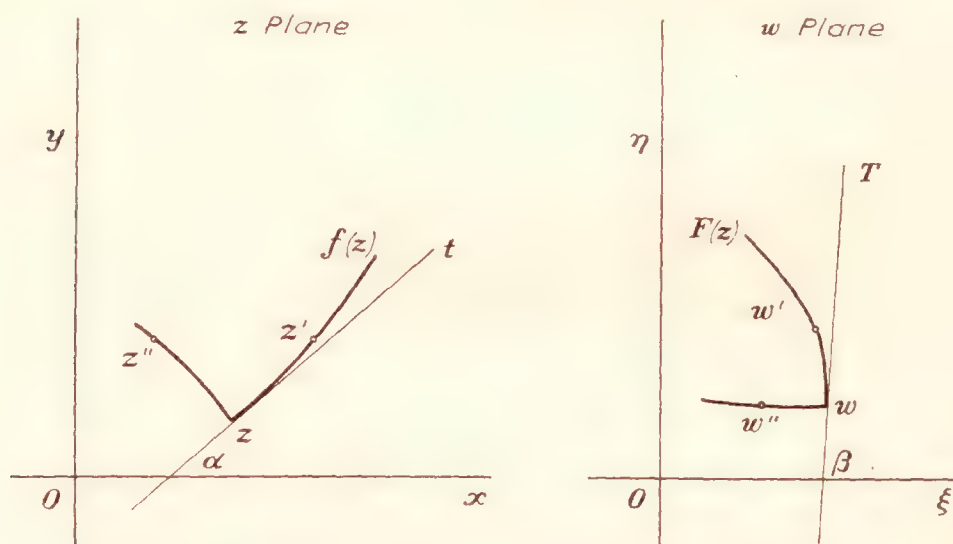


FIGURE 1.—Conformal property of analytic functions

region of the complex plane, may be separated into its real and imaginary parts as $w(z) \equiv w(x + iy) = P(x, y) + iQ(x, y)$, determining functions P and Q which may represent the velocity potential and stream function of a possible fluid motion. Thus, analytic functions of a complex variable possess the special property that the component functions P and Q satisfy the Cauchy-Riemann equations (eq. (1)), and each therefore also satisfies the equation of Laplace (eq. (2)). Conversely, any function $P(x, y) + iQ(x, y)$ for which P and Q satisfy relations (1) and (2) may be written as $w(x + iy) \equiv w(z)$. The essential difficulty of the problem is to find the particular function $w(z)$ which satisfies the special boundary-flow conditions mentioned above for a specified airfoil.

The method of conformal representation, a geometric application of the complex variable, is well adapted to this problem. The fundamental properties of transformations of this type may be stated as follows: Consider a function of a complex variable $z = x + iy$, say $w(z)$ analytic in a given region, such that for each value of z , $w(z)$ is uniquely defined. The function $w(z)$ may be expressed as $w = \xi + i\eta$ where ξ and η are

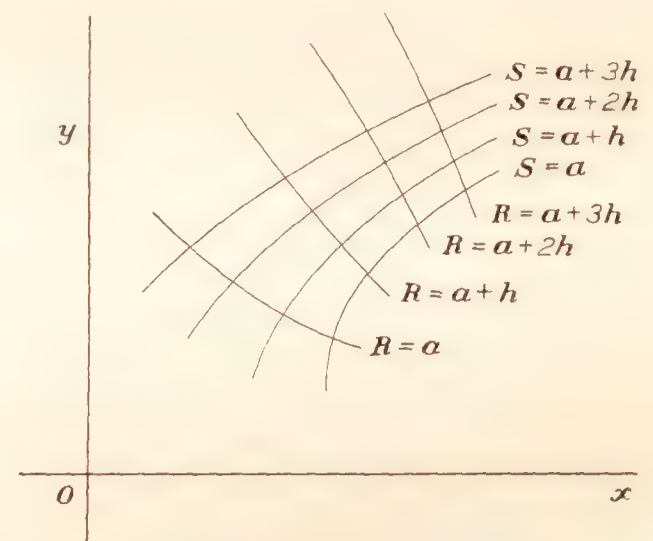


FIGURE 2.—Orthogonal network obtained by a conformal transformation

This is also true for any other pair of corresponding curves through z and w , so that in general, angles between corresponding curves are preserved. In particular, a curve zz'' orthogonal to zz' transforms into a curve ww'' orthogonal to ww' .

It has been seen that an analytic function $f(z)$ may be written $P(x, y) + iQ(x, y)$ where the curves $P = \text{constant}$ and $Q = \text{constant}$ form an orthogonal system. If then $f(z)$ is transformed conformally into $f(w) = P(\xi, \eta) + iQ(\xi, \eta)$ that is into $f[w(z)] \equiv F(z) = R(x, y) + iS(x, y)$, the curves $P(x, y) = \text{constant}$, $Q(x, y) = \text{constant}$ map into the orthogonal network of curves $R(x, y) = \text{constant}$, $S(x, y) = \text{constant}$. (Fig. 2.) If the magnification $\left| \frac{dw}{dz} \right| = \rho$ is zero at a point w , the transformation at that point is singular and ceases to be conformal.

We may use the method of conformal transformations to find the motion about a complicated boundary from that of a simpler boundary. Suppose $w(z)$ is a function which corresponds to any definite fluid motion in the z plane, for instance, to that around a circle. Now if a new variable ζ is introduced and z set equal

to any analytic function of ζ , say $z=f(\zeta)$, then $w(z)$ becomes $w[f(\zeta)]$ or $W(\zeta)$ representing a new motion in the ζ plane. This new motion is, as has been seen, related to that in the z plane in such a way that the streamlines of the z plane are transformed by $z=f(\zeta)$ into the streamlines of the ζ plane. Thus, the contour into which the circle is transformed represents the profile around which the motion $W(\zeta)$ exists. The problem of determining the flow around an airfoil is now reduced to finding the proper conformal transformation which maps a curve for which the flow is known into the airfoil. The *existence* of such a function was first shown by Riemann.

We shall first formulate the theorem for a simply connected region⁵ bounded by a closed curve, and then show how it is readily applied to the region external to the closed curve. The guiding thought leading to the theorem is simple. We have seen that an analytic function may transform a given closed region into another closed region. But suppose we are given two separate regions bounded by closed curves—does there exist an analytic transformation which transforms one region conformally into the other? This question is answered by Riemann's theorem as follows:

Riemann's theorem.—The interior T of any simply connected region (whose boundary contains more than one point, but we shall be concerned only with regions having closed boundaries, the boundary curve being composed of piecewise differentiable curves [Jordan curve], corners at which two tangents exist being permitted) can be mapped in a one-to-one conformal manner on the interior of the unit circle, and the analytic⁶ function $\zeta=f(z)$ which consummates this transformation becomes *unique* when a given interior point z_0 of T and a direction through z_0 are chosen to correspond, respectively, to the center of the circle and a given direction through it. By this transformation the boundary of T is transformed uniquely and continuously into the circumference of the unit circle.

The unit circle in this theorem is, of course, only a convenient normalized region. For suppose the regions T_1 in the ζ plane and T_2 in the w plane are transformed into the unit circle in the z plane by $\zeta=f(z)$ and $w=F(z)$, respectively, then T_1 is transformed into T_2 by $\zeta=\Phi(w)$, obtained by eliminating z from the two transformation equations.

In airfoil theory it is in the region external to a closed curve that we are interested. Such a region can be readily transformed conformally into the region internal to a closed curve by an inversion. Thus, let us suppose a point z_0 to be within a closed curve B whose

external region is Γ , and then choose a constant k such that for every point z on the boundary of Γ , $|z-z_0|>k$. Then the inversion transformation $w=\frac{k}{z-z_0}$ will transform every point in the external region Γ into a point internal to a closed region Γ' lying entirely within B , the boundary B mapping into the boundary of Γ' , the region at infinity into the region near z_0 . We may now restate Riemann's theorem as follows:

One and only one analytic function $\zeta=f(z)$ exists by means of which the region Γ external to a given curve B in the ζ plane is transformed conformally into the region external to a circle C in the z plane (center at $z=0$) such that the point $z=\infty$ goes into the point $\zeta=\infty$ and also $\frac{df(z)}{dz}=1$ at infinity. This function can be developed in the external region of C in a uniformly convergent series with complex coefficients of the form

$$\zeta-m=f(z)-m=z+\frac{c_1}{z}+\frac{c_2}{z^2}+\frac{c_3}{z^3}+\dots \quad (4)$$

by means of which the radius R and also the constant m are completely determined. Also, the boundary B of Γ is transformed continuously and uniquely into the circumference of C .

It should be noticed that the transformation (4) is a normalized form of a more general series

$$\zeta-m=a_0+a_{-1}z+\frac{a_1}{z}+\frac{a_2}{z^2}+\dots$$

and is obtained from it by a finite translation by the vector a_0 and a rotation and expansion of the entire field depending on the coefficient a_{-1} . The condition $a_{-1}=1$ is necessary and sufficient for the fields at infinity to coincide in magnitude and direction.

The constants c_i of the transformation are functions of the shape of the boundary curve alone and our problem is, really, to determine the complex coefficients defining a given shape. With this in view, we proceed first to a convenient intermediate transformation.

The transformation $\zeta=z'+\frac{a^2}{z'}$.—This initial transformation, although not essential to a purely mathematical solution, is nevertheless very useful and important, as will be seen. It represents also the key transformation leading to Joukowski airfoils, and is the basis of nearly all approximate theories.

Let us define the points in the ζ plane by $\zeta=x+iy$ using rectangular coordinates (x, y) , and the points in the z' plane by $z'=ae^{\psi+i\theta}$ using polar coordinates (ae^{ψ}, θ) . The constant a may conveniently be considered unity and is added to preserve dimensions. We have

$$\zeta=z'+\frac{a^2}{z'} \quad (5)$$

⁵ A region of the complex plane is simply connected when any closed contour lying entirely within the region may be shrunk to a point without passing out of the region. Cf. reference 3, p. 367, where a proof of the theorem based on Green's function is given.

⁶ Attention is here directed to the fact that an analytic function is developable at a point in a power series convergent in any circle about the point and entirely within the region.

and substituting $z' = ae^{\psi+i\theta}$

we obtain $\zeta = 2a \cosh(\psi + i\theta)$

or $\zeta = 2a \cosh \psi \cos \theta + 2ia \sinh \psi \sin \theta$

Since $\zeta = x + iy$, the coordinates (x, y) are given by

$$\begin{cases} x = 2a \cosh \psi \cos \theta \\ y = 2a \sinh \psi \sin \theta \end{cases} \quad (6)$$

If $\psi = 0$, then $z' = ae^{i\theta}$ and $\zeta = 2a \cos \theta$. That is, if P and P' are corresponding points in the ζ and z' planes, respectively, then as P traverses the x axis from $2a$ to $-2a$, P' traverses the circle $ae^{i\theta}$ from $\theta = 0$ to $\theta = \pi$, and as P retraces its path to $\zeta = 2a$, P' completes the circle. The transformation (5) then may be seen to map the entire ζ plane external to the line $4a$ uniquely into the region external (or internal) to the circle of radius a about the origin in the z' plane.

Let us invert equations (6) and solve for the elliptic coordinates ψ and θ . (Fig. 3.) We have

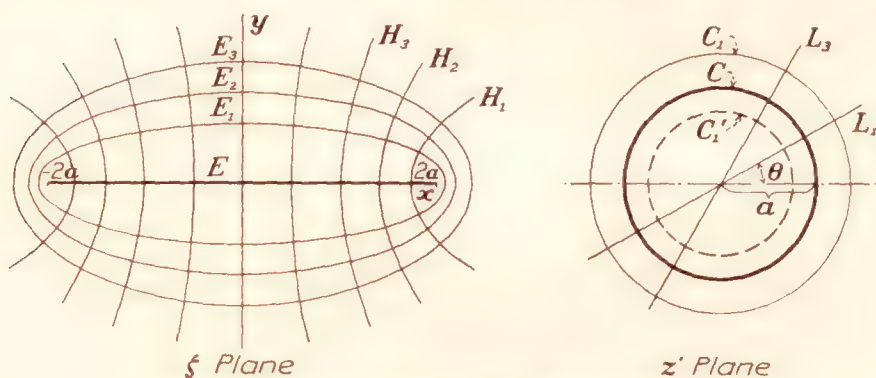


FIGURE 3.—Transformation by elliptic coordinates

$$\cosh \psi = \frac{x}{2a \cos \theta}$$

$$\sinh \psi = \frac{y}{2a \sin \theta}$$

and since $\cosh^2 \psi - \sinh^2 \psi = 1$

$$\left(\frac{x}{2a \cos \theta}\right)^2 - \left(\frac{y}{2a \sin \theta}\right)^2 = 1$$

or solving for $\sin^2 \theta$ (which can not become negative),

$$2 \sin^2 \theta = p + \sqrt{p^2 + \left(\frac{y}{a}\right)^2} \quad (7)$$

where

$$p = 1 - \left(\frac{x}{2a}\right)^2 - \left(\frac{y}{2a}\right)^2$$

Similarly we obtain

$$\left(\frac{x}{2a \cosh \psi}\right)^2 + \left(\frac{y}{2a \sinh \psi}\right)^2 = 1$$

or solving for $\sinh^2 \psi$

$$2 \sinh^2 \psi = -p + \sqrt{p^2 + \left(\frac{y}{a}\right)^2} \quad (8)$$

We note that the system of radial lines $\theta = \text{constant}$ become confocal hyperbolas in the ζ plane. The circles $\psi = \text{constant}$ become ellipses in the ζ plane with major axis $2a \cosh \psi$ and minor axis $2a \sinh \psi$. These orthogonal systems of curves represent the potential lines and streamlines in the two planes. The foci of these two confocal systems are located at $(\pm 2a, 0)$.

Equation (8) yields two values of ψ for a given point (x, y) , and one set of these values refers to the correspondence of (x, y) to the point (ae^ψ, θ) external to a curve and the other set to the correspondence of (x, y) to the point $(ae^{-\psi}, -\theta)$ internal to another curve. Thus, in Figure 3, for every point external to the ellipse E_1 there is a corresponding point external to the circle C_1 , and also one internal to C_1' .

The radius of curvature of the ellipse at the end of the major axis is $\rho = 2a \frac{\sinh^2 \psi}{\cosh \psi}$ or for small values of ψ , $\rho \cong 2a\psi^2$. The leading edge is at

$$2a \cosh \psi \cong 2a \left(1 + \frac{\psi^2}{2}\right) \cong 2a + \frac{\rho}{2}.$$

Now if there is given an airfoil in the ζ plane (fig. 4), and it is desired to transform the airfoil profile into a curve as nearly circular as possible in the z' plane by using only transformation (5), it is clear that the axes of coordinates should be chosen so that the airfoil appears as nearly elliptical as possible with respect to the chosen axes. It was seen that a focus of an elongated ellipse very nearly bisects the line joining the end of the major axis and the center of curvature of this point; thus, we arrive at a convenient choice of origin for the airfoil as the point bisecting the line of length $4a$, which extends from the point midway between the leading edge and the center of curvature of the leading edge to a point midway between the center of curvature of the trailing edge and the trailing edge. This latter point practically coincides with the trailing edge.

The curve B , defined by $ae^{\psi+i\theta}$, resulting in the z' plane, and the inverse and reflected curve B' , defined by $ae^{-\psi-i\theta}$, are shown superposed on the ζ plane in Figure 4. The convenience and usefulness of trans-

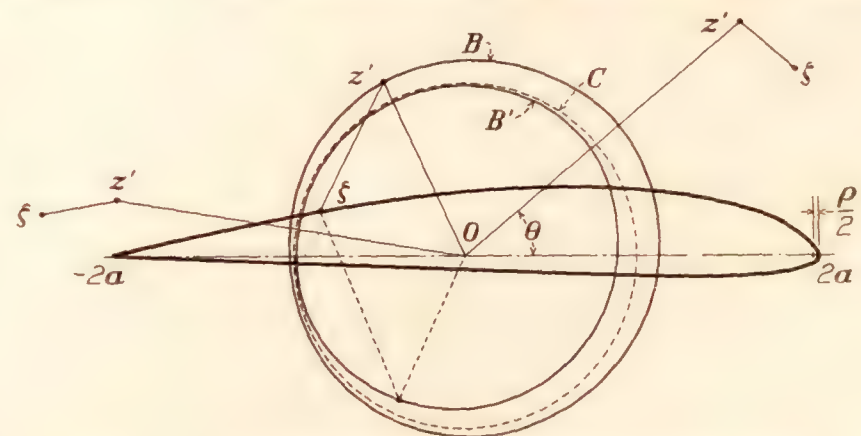


FIGURE 4.—Transformation of airfoil into a nearly circular contour

formation (5) and the choice of axes of coordinates will become evident after our next transformation.

The transformation $z' = ze^{\sum_{n=0}^{\infty} \frac{c_n}{z^n}}$.—Consider the transformation $z' = ze^{f(z)}$ where $f(z) = \sum_{n=0}^{\infty} \frac{c_n}{z^n}$. Each exponential

term $e^{\frac{c_n}{z^n}}$ represents the uniformly convergent series

$$1 + \frac{c_n}{z^n} + \frac{1}{2!} \left(\frac{c_n}{z^n}\right)^2 + \cdots + \frac{1}{m!} \left(\frac{c_n}{z^n}\right)^m + \cdots \quad (9)$$

where the coefficients $c_n = A_n + iB_n$ are complex numbers. For $f(z)$ convergent at all points in a region external to a certain circle, z' has a unique real absolute value $|z|e^{1/(z)}$ in the region and its imaginary part is definitely defined except for integral multiples of $2\pi i$. When $z = \infty$, $z' = ze^{c_0}$. The constant $c_0 = A_0 + Bi_0$ is then the determining factor at infinity, for the afieid t infinity is magnified by e^{A_0} and rotated by the angle B_0 . It is thus clear that if it is desired that the regions at infinity be identical, that is, $z' = z$ at infinity, the constant c_0 must be zero. The constants c_1 and c_2 also play important rôles, as will be shown later.

We shall now transform the closed curve $z' = ae^{\psi+i\varphi}$ into the circle $z = ae^{\psi_0+i\varphi}$ (radius ae^{ψ_0} , origin at center) by means of the general transformation (reference 2)

$$z' = ze^{\sum_{n=1}^{\infty} \frac{c_n}{z^n}} \quad (10)$$

which leaves the fields at infinity unaltered, and we shall obtain expressions for the constants A_n , B_n , and ψ_0 . The justification of the solution will be assured by the actual convergence of $\sum_{n=1}^{\infty} \frac{c_n}{z^n}$, since if the solution exists it is unique.

By definition, for the correspondence of the boundary points, we have

$$z' = ze^{\psi-\psi_0+i(\theta-\varphi)} \quad (10')$$

Also

$$z' = ze^{\sum_{n=1}^{\infty} (A_n + iB_n) \frac{1}{z^n}}$$

Consequently

$$\psi - \psi_0 + i(\theta - \varphi) = \sum_{n=1}^{\infty} (A_n + iB_n) \frac{1}{z^n}$$

where

$$z = ae^{\psi_0+i\varphi}$$

On writing $z = R(\cos \varphi + i \sin \varphi)$ where $R = ae^{\psi_0}$, we have

$$\psi - \psi_0 + i(\theta - \varphi) = \sum_{n=1}^{\infty} (A_n + iB_n) \frac{1}{R^n} (\cos n\varphi - i \sin n\varphi)$$

Equating the real and imaginary parts of this relation, we obtain the two conjugate Fourier expansions:

$$\psi - \psi_0 = \sum_{n=1}^{\infty} \left[\frac{A_n}{R^n} \cos n\varphi + \frac{B_n}{R^n} \sin n\varphi \right] \quad (11)$$

$$\theta - \varphi = \sum_{n=1}^{\infty} \left[\frac{B_n}{R^n} \cos n\varphi - \frac{A_n}{R^n} \sin n\varphi \right] \quad (12)$$

From equation (11), the values of the coefficients $\frac{A_n}{R^n}$, $\frac{B_n}{R^n}$, and the constant ψ_0 are obtained as follows:

$$\frac{A_n}{R^n} = \frac{1}{\pi} \int_0^{2\pi} \psi \cos n\varphi d\varphi \quad (a)$$

$$\frac{B_n}{R^n} = \frac{1}{\pi} \int_0^{2\pi} \psi \sin n\varphi d\varphi \quad (b)$$

⁷ Unless otherwise stated, ψ and θ will now be used in this restricted sense, i. e., as defining the boundary curve itself, and not all points in the z' plane.

$$\psi_0 = \frac{1}{2\pi} \int_0^{2\pi} \psi d\varphi \quad (c)$$

The evaluation of the infinite number of constants as represented by equations (a) and (b) can be made to depend upon an important single equation, which we shall obtain by eliminating these constants from equation (12).

Substitution of (a) and (b) for the coefficients of equation (12) gives

$$(\theta - \varphi)' = \frac{1}{\pi} \sum_{n=1}^{\infty} \left[\cos n\varphi' \int_0^{2\pi} \psi(\varphi) \sin n\varphi d\varphi - \sin n\varphi' \int_0^{2\pi} \psi(\varphi) \cos n\varphi d\varphi \right]$$

where $\psi(\varphi) = \psi$ and $(\theta - \varphi)'$ represents $\theta - \varphi$ as a function of φ' , and where φ' is used to distinguish the angle kept constant while the integrations are performed. The expression may be readily rewritten as

$$\begin{aligned} (\theta - \varphi)' &= \frac{1}{\pi} \sum_{n=1}^{\infty} \int_0^{2\pi} \psi(\varphi) (\sin n\varphi \cos n\varphi' - \cos n\varphi \sin n\varphi') d\varphi \\ &= \frac{1}{\pi} \sum_{n=1}^{\infty} \int_0^{2\pi} \psi(\varphi) \sin n(\varphi - \varphi') d\varphi \end{aligned}$$

But

$$\sum_{n=1}^{\infty} \sin n(\varphi - \varphi') = \frac{1}{2} \cot \frac{\varphi - \varphi'}{2} - \frac{\cos(2n+1) \frac{(\varphi - \varphi')}{2}}{2 \sin \frac{\varphi - \varphi'}{2}}$$

Then

$$\begin{aligned} (\theta - \varphi)' &= \lim_{n \rightarrow \infty} \left\{ \frac{1}{2\pi} \int_0^{2\pi} \psi(\varphi) \cot \frac{\varphi - \varphi'}{2} d\varphi \right. \\ &\quad \left. - \frac{1}{2\pi} \int_0^{2\pi} \psi(\varphi) \frac{\cos(2n+1) \frac{(\varphi - \varphi')}{2}}{\sin \frac{\varphi - \varphi'}{2}} d\varphi \right\} \end{aligned}$$

The first integral is independent of n , while the latter one becomes identically zero.

Then finally, representing $\varphi - \theta$ by a single quantity ϵ , viz $\varphi - \theta \equiv \epsilon \equiv \epsilon(\varphi)$, we have

$$\epsilon(\varphi') = -\frac{1}{2\pi} \int_0^{2\pi} \psi(\varphi) \cot \frac{\varphi - \varphi'}{2} d\varphi \quad (13)$$

By solving for the coefficients in equation (12) and substituting these in equation (11) it may be seen that a similar relation to equation (13) holds for the function $\psi(\varphi)$.

$$\psi(\varphi') = \frac{1}{2\pi} \int_0^{2\pi} \epsilon(\varphi) \cot \frac{\varphi - \varphi'}{2} d\varphi + \frac{1}{2\pi} \int_0^{2\pi} \psi(\varphi) d\varphi \quad (14)$$

The last term is merely the constant ψ_0 , which is, as has been shown, determined by the condition of mag-

nification of the z and z' fields at infinity. The corresponding integral $\frac{1}{2\pi} \int_0^{2\pi} \epsilon(\varphi) d\varphi$ does not appear in

equation (13), being zero as a necessary consequence of the coincidence of directions at infinity and, in general, if the region at infinity is rotated, is a constant different from zero.

Investigation of equation (13).—This equation is of fundamental importance. A discussion of some of its properties is therefore of interest. It should be first noted that when the function $\psi(\varphi)$ is considered known, the equation reduces to a definite integral. The function $^8 \epsilon(\varphi)$ obtained by this evaluation is the "conjugate" function to $\psi(\varphi)$, so called because of the relations existing between the coefficients of the Fourier expansions as given by equations (11) and (12). For the existence of the integral it is only necessary that $\psi(\varphi)$ be piecewise continuous and differentiable, and may even have infinities which must be below first order. We shall, however, be interested only in continuous single-valued functions having a period 2π , of a type which result from continuous closed curves with a proper choice of origin.

If equation (13) is regarded as a definite integral, it is seen to be related to the well-known Poisson integral which solves the following boundary-value problem of the circle. (Reference 3.) Given, say for the z plane a single-valued function $u(R, \tau)$ for points on the circumference of a circle $w = Re^{i\tau}$ (center at origin), then the single-valued continuous potential function $u(r, \sigma)$ in the external region $z = re^{i\sigma}$ of the circle which assumes the values $u(R, \tau)$ on the circumference is given by

$$u(r, \sigma) = \frac{1}{2\pi} \int_0^{2\pi} u(R, \tau) \frac{r^2 - R^2}{R^2 + r^2 - 2Rr \cos(\sigma - \tau)} d\tau$$

and similarly for the conjugate function $v(r, \sigma)$

$$v(r, \sigma) = \frac{1}{2\pi} \int_0^{2\pi} v(R, \tau) \frac{r^2 - R^2}{R^2 + r^2 - 2Rr \cos(\sigma - \tau)} d\tau$$

These may be written as a single equation

$$u(r, \sigma) + iv(r, \sigma) = f(z) = \frac{1}{2\pi} \oint_C f(w) \frac{z+w}{z-w} dw$$

where the value $f(z)$ at a point of the external region $z = re^{i\sigma}$ is expressed in terms of the known values $f(w)$ along the circumference $w = Re^{i\tau}$. In particular, we may note that at the boundary itself, since $i \frac{e^{i\sigma} + e^{i\tau}}{e^{i\sigma} - e^{i\tau}} = \cot \frac{(\sigma - \tau)}{2}$, we have

$$u(R, \sigma) + iv(R, \sigma) = -\frac{i}{2\pi} \int_0^{2\pi} [u(R, \tau) + iv(R, \tau)] \cot \frac{(\sigma - \tau)}{2} d\tau,$$

which is a special form of equations (13) and (14).

The quantity ψ is immediately given as a function of θ when a particular closed curve is preassigned, and this is our starting point in the direct process of transforming from airfoil to circle. We desire, then, to find the quantity ψ as a function of φ from equation (13), and this equation is no longer a definite integral but an

integral equation whose process of solution becomes more intricate. It would be surprising, indeed, if anything less than a functional or integral equation were involved in the solution of the general problem stated. The evaluation of the solution of equation (13) is readily accomplished by a powerful method of successive approximations. It will be seen that the nearness of the curve $ae^{\psi+i\theta}$ to a circle is very significant, and in practice, for airfoil shapes, one or at most two steps in the process is found to be sufficient for great accuracy.

The quantities ψ and ϵ considered as functions of φ have been denoted by $\psi(\varphi)$ and $\epsilon(\varphi)$, respectively. When these quantities are thought of as functions of θ they shall be written as $\bar{\psi}(\theta)$ and $\bar{\epsilon}(\theta)$, respectively.

Then, by definition

$$\begin{aligned} \bar{\psi}(\theta) &\equiv \psi[\varphi(\theta)] \\ \bar{\epsilon}(\theta) &\equiv \epsilon[\varphi(\theta)] \end{aligned} \quad (15)$$

Since $\varphi - \theta = \epsilon$, we have

$$\left. \begin{aligned} \theta(\varphi) &= \varphi - \epsilon(\varphi) \\ \varphi(\theta) &= \theta + \bar{\epsilon}(\theta) \end{aligned} \right\} \quad (16)$$

We are seeking then two functions, $\psi(\varphi)$ and $\epsilon(\varphi)$, conjugate in the sense that their Fourier series expansions are given by (11) and (12), such that $\psi[\varphi(\theta)] = \bar{\psi}(\theta)$ where $\bar{\psi}(\theta)$ is a *known* single-valued function of period 2π .

Integrating equation (13) by parts, we have

$$\epsilon(\varphi') = \frac{1}{\pi} \int_0^{2\pi} \log \sin \frac{\varphi - \varphi'}{2} \frac{d\psi(\varphi)}{d\varphi} d\varphi \quad (13')$$

The term $\log \sin \frac{\varphi - \varphi'}{2}$ is real only in the range $\varphi = \varphi'$ to $\varphi = 2\pi + \varphi'$, but we may use the interval 0 to 2π for φ with the understanding that only the real part of the logarithm is retained.

Let us write down the following identity:

$$\begin{aligned} \log \sin \frac{\varphi - \varphi'}{2} &\equiv \log \sin \frac{\theta - \theta'}{2} \\ &+ \log \frac{\sin \frac{(\theta + \bar{\epsilon}_1) - (\theta + \bar{\epsilon}_1)'}{2}}{\sin \frac{\theta - \theta'}{2}} + \log \frac{\sin \frac{(\theta + \bar{\epsilon}_2) - (\theta + \bar{\epsilon}_2)'}{2}}{\sin \frac{(\theta + \bar{\epsilon}_1) - (\theta + \bar{\epsilon}_1)'}{2}} \\ &+ \dots + \log \frac{\sin \frac{(\theta + \bar{\epsilon}_k) - (\theta + \bar{\epsilon}_k)'}{2}}{\sin \frac{(\theta + \bar{\epsilon}_{k-1}) - (\theta + \bar{\epsilon}_{k-1})'}{2}} + \dots \\ &+ \log \frac{\sin \frac{(\theta + \bar{\epsilon}_n) - (\theta + \bar{\epsilon}_n)'}{2}}{\sin \frac{(\theta + \bar{\epsilon}_{n-1}) - (\theta + \bar{\epsilon}_{n-1})'}{2}} + \log \frac{\sin \frac{(\theta + \bar{\epsilon}) - (\theta + \bar{\epsilon})'}{2}}{\sin \frac{(\theta + \bar{\epsilon}_n) - (\theta + \bar{\epsilon}_n)'}{2}} \end{aligned} \quad (17)$$

where in the last term we recall that $\theta + \bar{\epsilon}(\theta) = \varphi(\theta)$; and where it may be noted that each denominator is the

⁸ This function will be called "conformal angular distortion" function, for reasons evident later.

numerator of the preceding term. The symbols $\bar{\epsilon}_k$ ($k=1, 2, \dots, n$) represent functions of θ , which thus far are arbitrary.⁹

Since by equation (15) $\bar{\psi}(\theta) \equiv \psi[\varphi(\theta)]$ we have for corresponding elements $d\theta$ and $d\varphi$

$$\frac{d\psi(\varphi)}{d\varphi} d\varphi = \frac{d\bar{\psi}(\theta)}{d\theta} d\theta$$

Then multiplying the left side of equation (17) by $\frac{1}{\pi} \frac{d\psi(\varphi)}{d\varphi} d\varphi$ and the right side by $\frac{1}{\pi} \frac{d\bar{\psi}(\theta)}{d\theta} d\theta$ and integrating over the period 0 to 2π we obtain

$$\begin{aligned} \epsilon[\varphi(\theta')] \equiv \bar{\epsilon}(\theta') &= \frac{1}{\pi} \int_0^{2\pi} \log \sin \frac{\theta - \theta'}{2} \frac{d\bar{\psi}(\theta)}{d\theta} d\theta + \dots \\ &+ \frac{1}{\pi} \int_0^{2\pi} \log \frac{\sin \frac{(\theta + \bar{\epsilon}_k) - (\theta + \bar{\epsilon}_k)'}{2}}{\sin \frac{(\theta + \bar{\epsilon}_{k-1}) - (\theta + \bar{\epsilon}_{k-1})'}{2}} \frac{d\bar{\psi}(\theta)}{d\theta} d\theta + \dots \\ &+ \frac{1}{\pi} \int_0^{2\pi} \log \frac{\sin \frac{(\theta + \bar{\epsilon}(\theta)) - (\theta + \bar{\epsilon}(\theta))'}{2}}{\sin \frac{(\theta + \bar{\epsilon}_n) - (\theta + \bar{\epsilon}_n)'}{2}} \frac{d\bar{\psi}(\theta)}{d\theta} d\theta \quad (18) \end{aligned}$$

where $k=1, 2, \dots, n$.

We now choose the arbitrary functions $\bar{\epsilon}_k(\theta')$ so that

$$\bar{\epsilon}_0(\theta') = 0$$

and

$$\bar{\epsilon}_k(\theta') = \frac{1}{\pi} \int_0^{2\pi} \log \sin \frac{(\theta + \bar{\epsilon}_{k-1}) - (\theta + \bar{\epsilon}_{k-1})'}{2} \frac{d\bar{\psi}(\theta)}{d\theta} d\theta \quad (19)$$

where $k=1, 2, \dots, n$.

Equation (18) may then be written

$$\bar{\epsilon}(\theta') = \bar{\epsilon}_0 + \bar{\epsilon}_1 + (\bar{\epsilon}_2 - \bar{\epsilon}_1) \dots + (\bar{\epsilon}_n - \bar{\epsilon}_{n-1}) + (\bar{\epsilon} - \bar{\epsilon}_n) \quad (20)$$

or

$$\bar{\epsilon}(\theta') = \lambda_1 + \lambda_2 + \dots + \lambda_n + \lambda$$

where $\lambda_k(\theta') = \bar{\epsilon}_k - \bar{\epsilon}_{k-1}$ and is in fact the k^{th} term of equation (18). The last term we denote by λ .

From equation (19) we see that the function $\bar{\epsilon}_k(\theta')$ is obtained by a knowledge of the preceding function $\bar{\epsilon}_{k-1}(\theta')$. For convenience in the evaluation of these functions, say

$$\bar{\epsilon}_{k+1}(\theta') = \frac{1}{\pi} \int_0^{2\pi} \log \sin \frac{(\theta + \bar{\epsilon}_k) - (\theta + \bar{\epsilon}_k)'}{2} \frac{d\bar{\psi}(\theta)}{d\theta} d\theta$$

we introduce a new variable φ_k defined by

$$\varphi_k(\theta) = \theta + \bar{\epsilon}_k(\theta) \quad (k=1, 2, \dots, n)$$

Then

$$\bar{\epsilon}_{k+1}[\theta(\varphi'_{k+1})] \equiv \epsilon^*_{k+1}(\varphi'_k)$$

$$= \frac{1}{\pi} \int_0^{2\pi} \log \sin \frac{(\varphi_k - \varphi'_k)}{2} \frac{d\bar{\psi}[\theta(\varphi_k)]}{d\varphi_k} d\varphi_k \quad (21)$$

From the definition of φ_k as

$$\varphi_k(\theta) = \theta + \bar{\epsilon}_k(\theta)$$

we may also define the symbol $\epsilon_k(\varphi_k)$ by

$$\theta(\varphi_k) = \varphi_k - \epsilon_k(\varphi_k)$$

where

$$\bar{\epsilon}_k(\theta) \equiv \epsilon_k[\varphi_k(\theta)]$$

It is important to note that the symbols $\bar{\epsilon}_k$, ϵ_k , ϵ_k^* denote the same quantity considered, however, as a function of θ , φ_k , φ_{k-1} , respectively.

The quantities $(\bar{\epsilon}_k - \bar{\epsilon}_{k-1})$ in equation (20) rapidly approach zero for wide classes of initial curves $\bar{\psi}(\theta)$, i. e., $\bar{\psi}[\theta(\varphi_k)]$ very nearly equals $\bar{\psi}[\theta(\varphi_{k+1})]$ for even small k 's. The process of solution of our problem is then one of obtaining successively the functions $\bar{\psi}(\theta)$, $\bar{\psi}[\theta(\varphi_1)]$, $\bar{\psi}[\theta(\varphi_2)]$, \dots , $\bar{\psi}[\theta(\varphi_n)]$ where $\bar{\psi}[\theta(\varphi_n)]$ and $\bar{\epsilon}_n[\theta(\varphi_n)]$ become more and more "conjugate." The process of obtaining the successive conjugates in practice is explained in a later paragraph. We first pause to state the conditions which the functions φ_k are subject to, necessary for a one-to-one correspondence of the boundary points, and for a one-to-one correspondence of points of the external regions, i. e., the conditions which are necessary in order that the transformations be conformal.

In order that the correspondence between boundary points of the circle in the z plane and boundary points of the contour in the z' plane be one-to-one, it is necessary that $\theta(\varphi)$ be a monotonic increasing function of its argument. This statement requires a word of explanation. We consider only values of the angles between 0 and 2π . For a point of the circle boundary, that is, for one value of φ there can be only one value of θ , i. e., $\theta(\varphi)$ is always single valued. However, $\varphi(\theta)$, in general, does not need to be, as for example, by a poor choice of origin it may be many valued, a radius vector from the origin intersecting the boundary more than once; but since we have already postulated that $\bar{\psi}(\theta)$ is single valued this case can not occur, and $\varphi(\theta)$ is also single valued. If we decide on a definite direction of rotation, then the inequality $\frac{d\theta}{d\varphi} \geq 0$ expresses

the statement that as the radius vector from the origin sweeps over the boundary of the circle C , the radius vector in the z' plane sweeps over the boundary of B and never retraces its path.

The inequality

$$\frac{d\theta}{d\varphi} = 1 - \frac{d\epsilon(\varphi)}{d\varphi} \geq 0$$

corresponds to

$$\frac{d\epsilon(\varphi)}{d\varphi} \leq 1$$

Also, the condition

$$\frac{d\varphi}{d\theta} = 1 + \frac{d\bar{\epsilon}(\theta)}{d\theta} \geq 0$$

corresponds to

$$\frac{d\bar{\epsilon}(\theta)}{d\theta} \geq -1$$

⁹ The symbol $(\theta + \bar{\epsilon}_k)'$ represents $\theta' + \bar{\epsilon}_k(\theta')$ and is used to denote the same function of θ' that $\theta + \bar{\epsilon}_k(\theta)$ is of θ . The variables θ and θ' are regarded as independent of each other

Multiplying $\frac{d\theta}{d\varphi}$ by $\frac{d\varphi}{d\theta}$ we get

$$\left(1 - \frac{d\epsilon(\varphi)}{d\varphi}\right) \left(1 + \frac{d\bar{\epsilon}(\theta)}{d\theta}\right) = 1$$

This relation is shown in Figure 5 as a rectangular

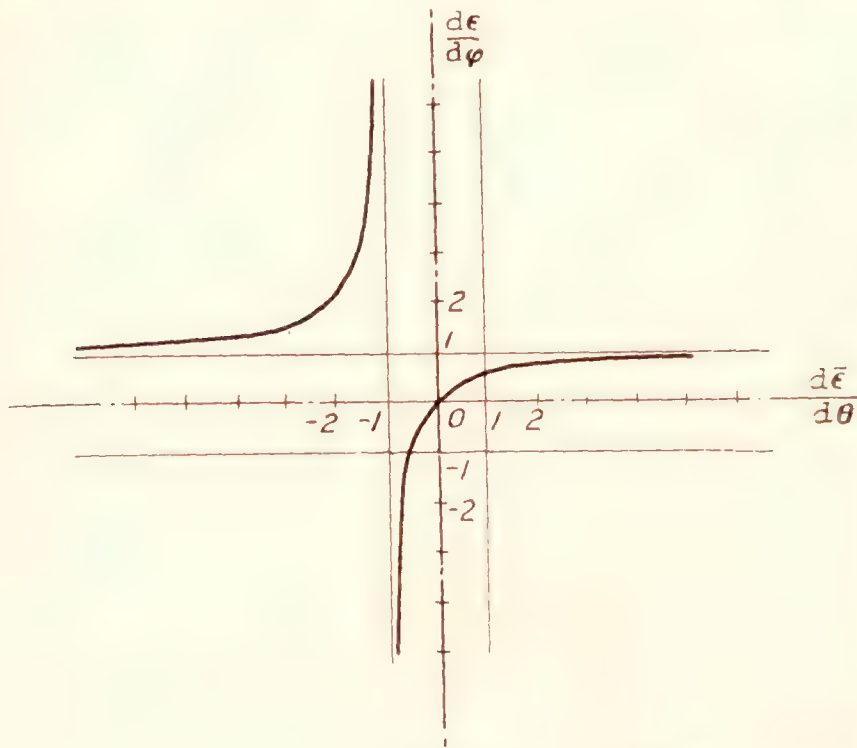


FIGURE 5.—The quantity $\frac{d\epsilon}{d\varphi}$ as a function of $\frac{d\bar{\epsilon}}{d\theta}$

hyperbola. We may notice then that the monotonic behavior of $\varphi(\theta)$ and $\theta(\varphi)$ requires that $\frac{d\epsilon}{d\varphi}$ remain on the lower branch¹⁰ of the hyperbola, i. e.,

$$-\infty \leq \frac{d\epsilon}{d\varphi} \leq 1 \quad (22)$$

It will be seen later that the limiting values

$$\frac{d\epsilon(\varphi)}{d\varphi} = 1, \frac{d\epsilon(\varphi)}{d\varphi} = -\infty \left(\text{i. e., } \frac{d\bar{\epsilon}}{d\theta} = \infty, \frac{d\bar{\epsilon}}{d\theta} = -1 \right)$$

correspond to points of infinite velocity and of zero velocity, respectively, arising from sharp corners in the original curve.

The condition for a one-to-one conformal correspondence between points of the external region of the circle and of the external region of the contour in the z' plane may be given (reference 5, p. 98 and reference 6, Part II) as follows: There must be a one-to-one boundary point correspondence and the derivative of

the analytic function $z' = ze^{\sum_{n=1}^{\infty} \frac{c_n}{z^n}}$ given by equation (10) must not vanish in the region. That is, writing $g(z)$

for $\sum_{n=1}^{\infty} \frac{c_n}{z^n}$ we have

$$\frac{dz'}{dz} = e^{g(z)} \left(1 + z \frac{dg(z)}{dz} \right) \neq 0 \text{ for } |z| > R \text{ or since}$$

the integral transcendental function $e^{g(z)}$ does not vanish in the entire plane, the condition is equivalent to

$$z \frac{dg(z)}{dz} \neq -1 \text{ for } |z| > R$$

By equation (10') we have on the boundary of the circle, $g(Re^{i\varphi}) = \psi - \psi_0 - i\epsilon$, and

$$\begin{aligned} z \frac{dg(z)}{dz} &= Re^{i\varphi} \frac{d[\psi(\varphi) - i\epsilon(\varphi)]}{iRe^{i\varphi} d\varphi} \\ &= -\frac{d\epsilon(\varphi)}{d\varphi} - i \frac{d\psi(\varphi)}{d\varphi} \end{aligned}$$

the first term on the right-hand side being real and the last term a pure imaginary. We have already postulated the condition

$$-\infty \leq \frac{d\epsilon}{d\varphi} \leq 1$$

as necessary for a one-to-one boundary point correspondence. Now by writing $z = \xi + i\eta$ and $z \frac{dg(z)}{dz} =$

$P(\xi, \eta) + iQ(\xi, \eta)$, we note that $\frac{d\epsilon(\varphi)}{d\varphi}$ gives the boundary values of a harmonic function $P(\xi, \eta)$ and therefore this function assumes its maximum and minimum values on the boundary of the circle itself. (Reference 3, p.

223.) Hence $z \frac{dg(z)}{dz}$ can never become -1 in the external region, i. e., $\frac{dz'}{dz}$ can never vanish in this region.

At each step in the process of obtaining the successive conjugates we desire to maintain a one-to-one correspondence between θ and φ_k , i. e., the functions $\theta(\varphi_k)$ and $\varphi_k(\theta)$ should be monotonic increasing and are hence subject to a restriction similar to equation (22), viz,

$$-\infty \leq \frac{d\epsilon_k}{d\varphi_k} \leq 1 \quad (22')$$

The process may be summed up as follows: We consider the function $\bar{\psi}(\theta)$ as known, where $\bar{\psi}(\theta)$ is the functional relation between ψ and θ defining a closed curve $ae^{\bar{\psi}+i\theta}$. The conjugate of $\bar{\psi}(\theta)$ with respect to θ is $\bar{\epsilon}_1(\theta)$. We form the variable $\varphi_1 = \theta + \bar{\epsilon}_1(\theta)$ and also the function $\bar{\psi}[\theta(\varphi_1)]$. The conjugate of $\bar{\psi}[\theta(\varphi_1)]$ with respect to φ_1 is $\epsilon^*_2(\varphi_1)$ which expressed as a function of θ is $\bar{\epsilon}_2(\theta)$. We form the variable $\varphi_2 = \theta + \bar{\epsilon}_2(\theta)$ and the function $\bar{\psi}[\theta(\varphi_2)]$. The conjugate of $\bar{\psi}[\theta(\varphi_2)]$ is $\epsilon^*_3(\varphi_2)$, which as a function of θ is $\bar{\epsilon}_3(\theta)$, etc. The graphical criterion for convergence is, of course, reached when the function $\bar{\psi}[\theta(\varphi_n)]$ is no longer altered by the process. The following figures illustrate the method and exhibit vividly the rapidity of convergence. The numerical calculations of the various conjugates are obtained from formula I of the appendix.

In Figure 6, the $\bar{\psi}(\theta)$ curve represents a circle referred to an origin which bisects a radius (obtained from an extremely thick Joukowski airfoil) (see p. 200) and has numerical values approximately five times greater than occur for common airfoils. The $\psi(\varphi)$ curve is known independently and is represented by the dashed curve. The process of going from $\bar{\psi}(\theta)$ to $\psi(\varphi)$ assuming $\psi(\varphi)$ as unknown is as follows: The function $\bar{\epsilon}_1(\theta)$, the conjugate function of $\bar{\psi}(\theta)$, is found.

¹⁰ The values of the upper branch of the hyperbola arise when the region internal to the curve $ae^{\psi+i\theta}$ is transformed into the external region of a circle, but may also there be avoided by defining $\epsilon = \varphi + \theta$ instead of $\varphi - \theta$.

The quantity ψ is then plotted against the new variable $\varphi_1 = \theta + \bar{\epsilon}_1(\theta)$ (i. e., each point of $\bar{\psi}(\theta)$ is displaced horizontally a distance $\bar{\epsilon}_1$) and yields the curve $\bar{\psi}[\theta(\varphi_1)]$. (Likewise, $\bar{\epsilon}_1(\theta)$ is plotted against φ_1 yielding $\epsilon_1(\varphi_1)$.)

is drawn at P' . This process yields the function $\bar{\epsilon}_2(\theta)$. The quantity ψ is now plotted against the new variable $\varphi_2 = \theta + \bar{\epsilon}_2(\theta)$ (i. e., each point of $\bar{\psi}(\theta)$ is displaced horizontally a distance $\bar{\epsilon}_2$) giving the function $\bar{\psi}[\theta(\varphi_2)]$.

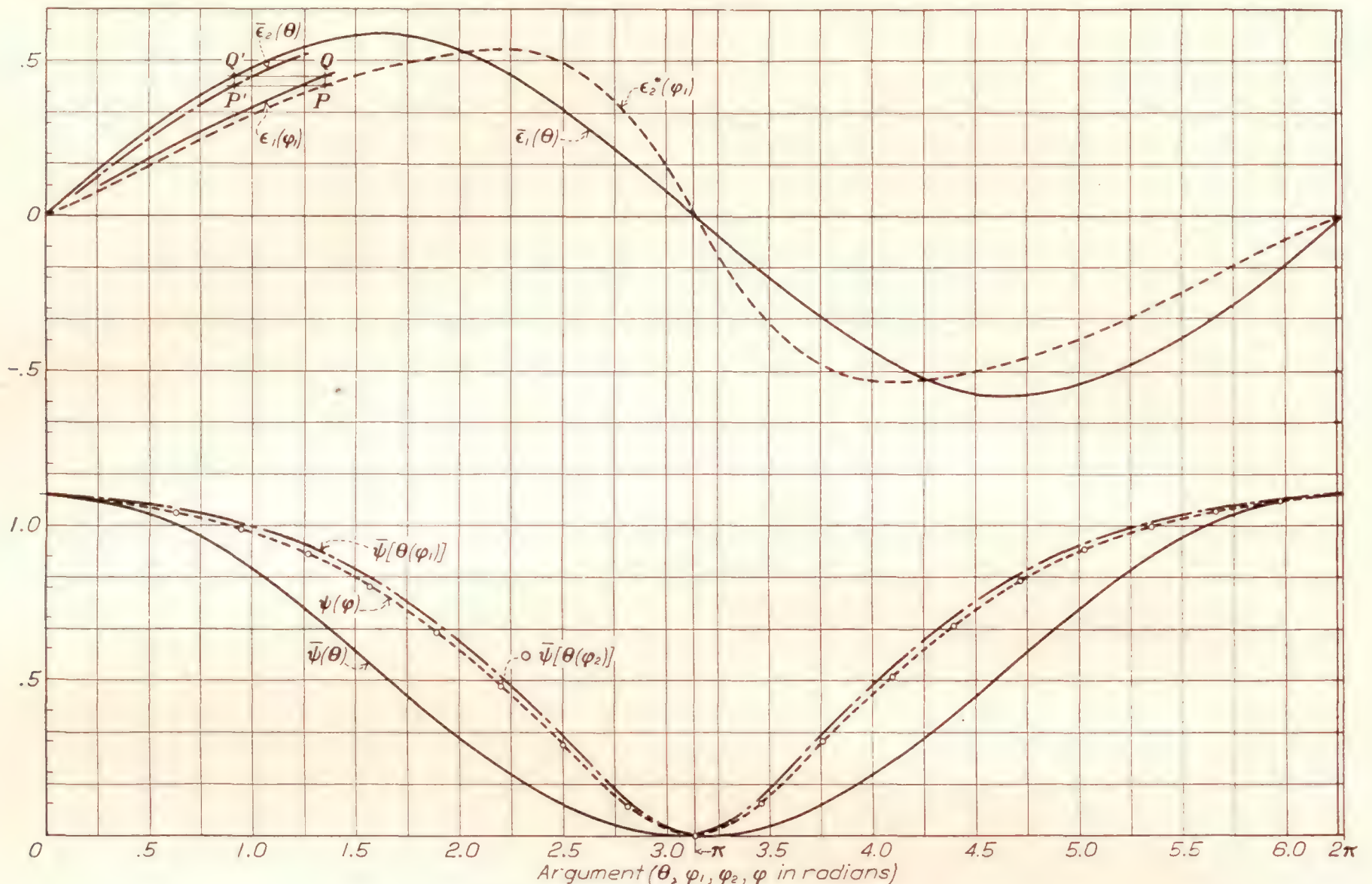


FIGURE 6.—The process of obtaining successive conjugates

The function $\epsilon_2^*(\varphi_1)$ is now determined as the conjugate function of $\bar{\psi}[\theta(\varphi_1)]$. This function expressed as a function of θ is $\epsilon_2^*[\varphi_1(\theta)] \equiv \bar{\epsilon}_2(\theta)$. It is plotted as follows:

This curve is shown with small circles and coincides with $\psi(\varphi)$. Further application of the process can yield no change in this curve. It may be remarked

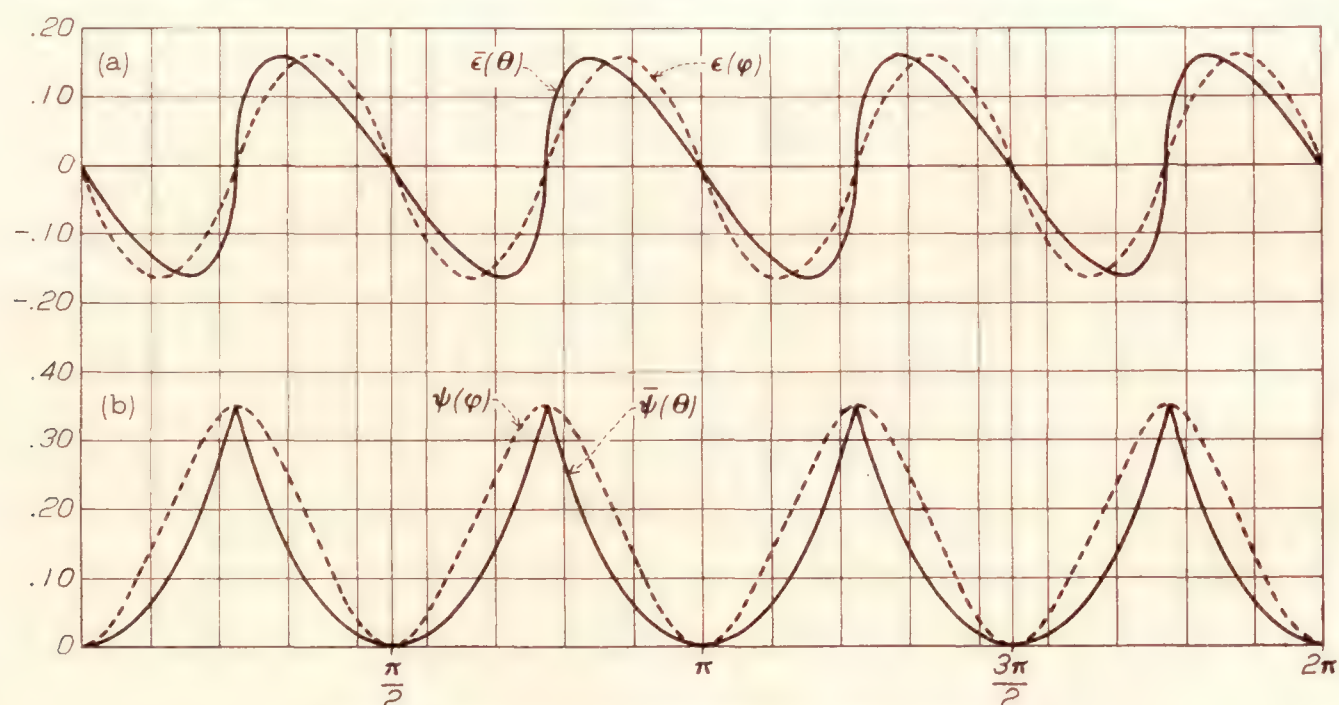


FIGURE 7.—Process applied to transforming a square into a circle

At a point P of $\epsilon_2^*(\varphi_1)$ and Q of $\epsilon_1(\varphi_1)$ corresponding to a definite value of φ_1 one finds the value of θ which corresponds to φ_1 by a horizontal line through Q meeting $\bar{\epsilon}_1(\theta)$ in Q' ; for this value of θ , the quantity ϵ_2 at P

here that for nearly all airfoils used in practice one step in the process is sufficient for very accurate results.

As another example we shall show how a square (origin at center) is transformed into a circle by the

method. In Figure 7 the $\bar{\psi}(\theta)$ curve is shown, and in Figure 8 it is reproduced for one octant.¹¹ The value is $\bar{\psi}(\theta) = \log \sec \theta$. The function $\bar{\psi}[\theta(\varphi_1)]$ is shown dashed; the function $\bar{\psi}[\theta(\varphi_2)]$ is shown with small crosses; and $\bar{\psi}[\theta(\varphi_3)]$ is shown with small circles. The solution $\psi(\varphi)$ is represented by the curve with small triangles and is obtained independently by the known transformation (reference 3, p. 375) which transforms the external region of a square into the external region of the unit circle, as follows:

$$w(z) = \int_{z_0}^z \frac{\sqrt{z^4 - 1}}{z^2} dz = z \left[1 + P\left(\frac{1}{z}\right) \right]$$

where $P\left(\frac{1}{z}\right)$ denotes a power series. Comparing this with equation (10), we find that $\psi(\varphi)$ except for the constant ψ_0 is given as the real part of $\log \left[1 + P\left(\frac{1}{z}\right) \right]$ evaluated for $z = e^{i\varphi}$, and that $\epsilon(\varphi)$ is given as the negative of the imaginary part. It may be observed in Figure 8 that the function $\bar{\psi}[\theta(\varphi_3)]$ very nearly

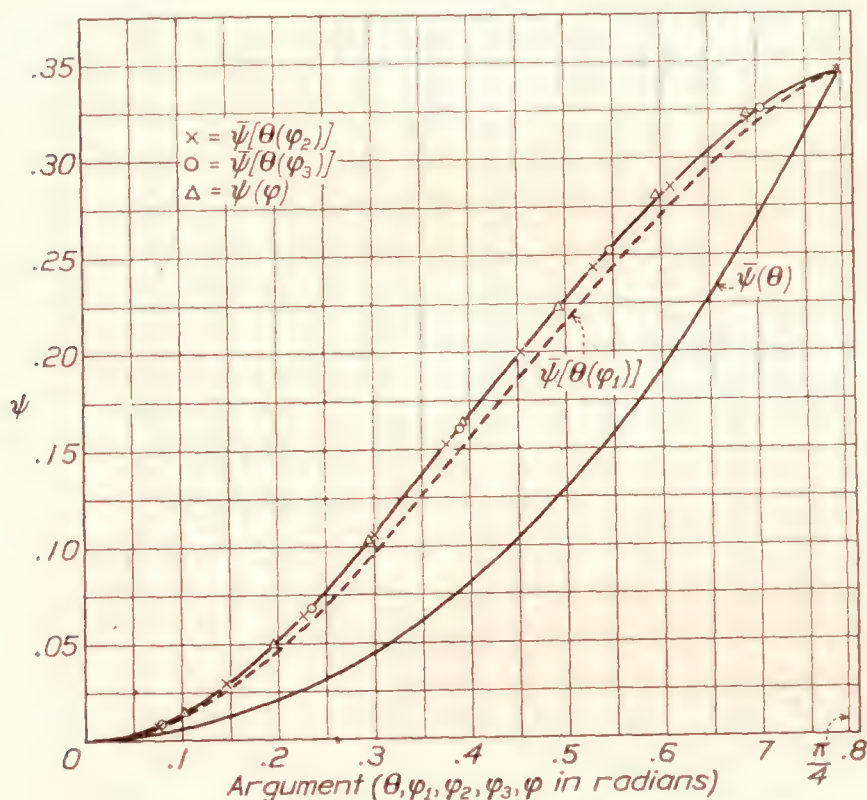


FIGURE 8.—Process applied to transforming a square into a circle

equals $\psi(\varphi)$. The functions $\epsilon(\varphi)$ and $\bar{\epsilon}(\theta)$ are shown in Figure 7 (a); we may note that at $\varphi = \frac{\pi}{4}$, which corresponds to a corner of the square, $\frac{d\epsilon}{d\varphi} = 1$ or also, $\frac{d\bar{\epsilon}}{d\theta} = \infty$.

¹¹ Because of the symmetry involved only the interval 0 to $\frac{\pi}{4}$ need be used. The integral in the appendix can be treated as

$$\begin{aligned} \epsilon(\varphi') &= -\frac{1}{2\pi} \int_0^{2\pi} \psi(\varphi) \cot \frac{\varphi - \varphi'}{2} d\varphi \\ &= -\frac{2}{\pi} \int_0^{\frac{\pi}{4}} \psi(\varphi) [\cot 2(\varphi - \varphi') - \cot 2(\varphi + \varphi')] d\varphi \end{aligned}$$

It may be remarked that the rapidity of convergence is influenced by certain factors. It is noticeably affected by the initial choice of $\bar{\epsilon}_0(\theta)$. The choice $\bar{\epsilon}_0(\theta) = 0$ implies that θ and φ are considered to be very nearly equal, i. e., that $ae^{\psi+i\theta}$ represents a nearly circular curve. The initial transformation given by equation (5) and the choice of axes and origin were adapted for the purpose of obtaining a nearly circular

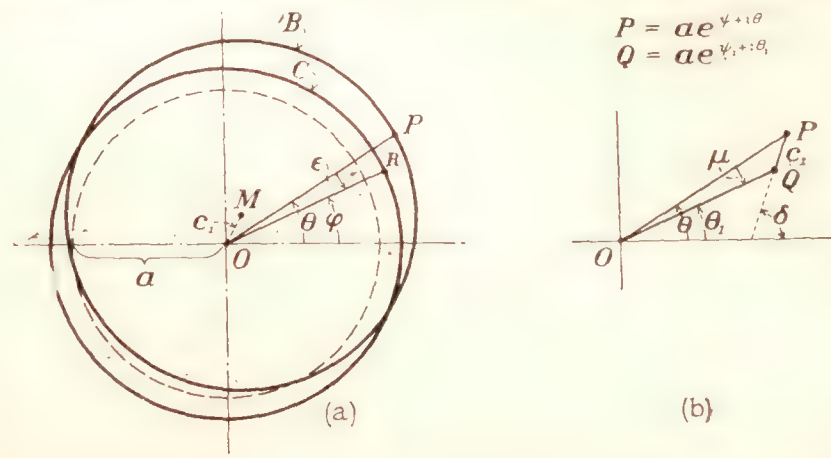


FIGURE 9.—Translation by the distance OM

curve for airfoil shapes. If we should be concerned with other classes of contours, more appropriate initial transformations can be developed. If, however, for a curve $ae^{\psi+i\theta}$ the quantity $\epsilon = \varphi - \theta$ has large values, either because of a poor initial transformation or because of an unfavorable choice of origin, it may occur that the choice $\bar{\epsilon}_0(\theta) = 0$ will yield a function $\epsilon_1(\varphi_1)$ for which $\frac{d\epsilon_1}{d\varphi_1}$ may exceed unity at some points, thus violating condition (22'). Such slopes can be replaced by slopes less than unity, the resulting function chosen as $\bar{\epsilon}_0(\theta)$ and the process continued as before.¹² Indeed, the closer the choice of the function $\bar{\epsilon}_0(\theta)$ is to the final solution $\bar{\epsilon}(\theta)$, the more rapid is the convergence. The case of the square illustrates that even the relatively poor choice $\bar{\epsilon}_0(\theta) = 0$ does not appreciably defer the convergence.

The translation $z_1 = z + c_1$.—Let us divert our attention momentarily to another transformation which will prove useful. We recall that the initial transformation (eq. (5)) applied to an airfoil in the ζ plane gives a curve B in the z' plane shown schematically in Figure 9(a). Equation (10) transforms this curve into a circle C about the origin O as center and yields in fact small values of the quantity $\varphi - \theta$. We are, however, in a position to introduce a convenient transformation, namely, to translate the circle C into a most favorable position with respect to the curve B (or vice versa). These qualitative remarks admit of a mathematical formulation. It is clear that if the curve B itself happens to be a circle¹³ the vector by which the circle C should be translated is exactly the distance between centers. It is readily shown that

¹² The first step in the process is now to define $\varphi_0 = \theta + \epsilon_0(\theta)$ and form the function $\bar{\psi}[\theta(\varphi_0)]$. The conjugate function of $\bar{\psi}[\theta(\varphi_0)]$ is $\epsilon^*_0(\varphi_0)$ which expressed as a function of θ is $\bar{\epsilon}_1(\theta)$, etc.

¹³ See p. 200.

then equation (10) should contain no constant term. We have

$$z' = ze^{\sum_{n=1}^{\infty} \frac{c_n}{z^n}} \quad (10)$$

$$= z \left(1 + \frac{c_1}{z} + \frac{1}{2!} \left(\frac{c_1}{z} \right)^2 + \dots \right) \left(1 + \frac{c_2}{z^2} + \dots \right) \times \\ \left(1 + \frac{c_3}{z^3} + \dots \right) \text{ etc.} \\ = z \left(1 + \frac{k_1}{z} + \frac{k_2}{z^2} + \dots \right) \quad (10a)$$

where ¹⁴

$$k_1 = c_1 \\ k_2 = c_2 + \frac{c_1^2}{2} \\ k_3 = c_3 + c_2 c_1 + \frac{c_1^3}{6} \\ \dots \dots \dots$$

It is thus apparent that if equation (10) contains no first harmonic term, i. e., if

$$c_1 = A_1 + iB_1 = \frac{R^2 \pi}{\pi} \int_0^{2\pi} \psi e^{i\varphi} d\varphi = 0,$$

the transformation is obtained in the so-called normal form

$$z' = z_1 + \frac{d_1}{z_1} + \frac{d_2}{z_1^2} + \dots \quad (23)$$

This translation can be effected either by substituting a new variable $z_1 = z + c_1$, or a new variable $z_1' = z' - c_1$.

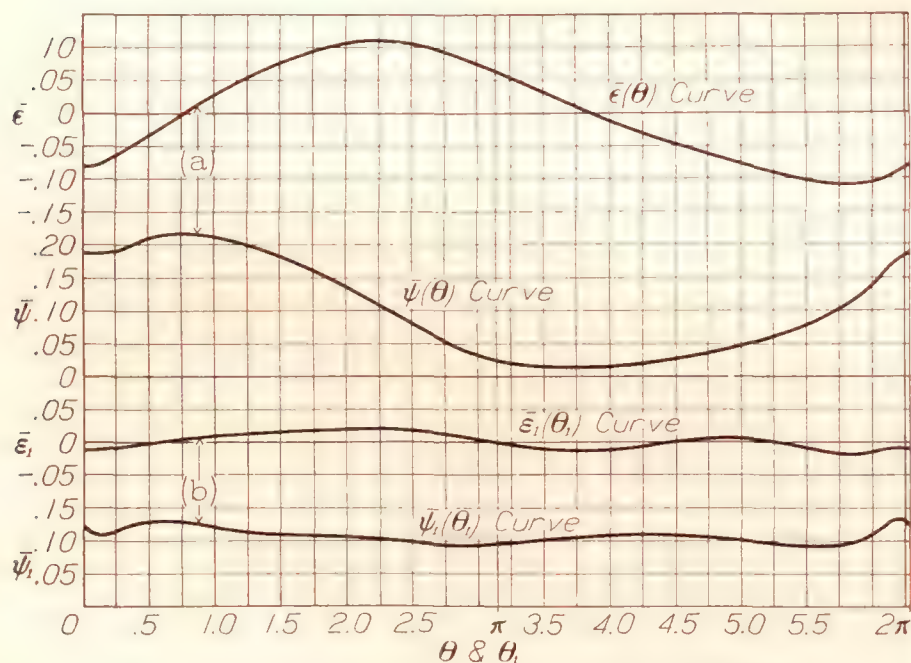


FIGURE 10.—The $\bar{\psi}(\theta)$ and $\bar{\psi}_1(\theta_1)$ curves (for Clark Y airfoil)

This latter substitution will be more convenient at this time. Writing

$$z_1' = ae^{\psi_1 + i\theta_1}, \quad c_1 = ae^{\gamma + i\delta}, \quad \text{and} \quad z' = ae^{\psi + i\theta}$$

we have

$$ae^{\psi_1 + i\theta_1} = ae^{\psi + i\theta} - ae^{\gamma + i\delta}$$

The variables ψ_1 , and θ_1 , can be expressed in terms of ψ , θ , γ , and δ . In Figure 9(b), P is a point on the B

curve, i. e., $OP = ae^{\psi}$, PQ represents the translation vector $c_1 = ae^{\gamma + i\delta}$, OQ is $ae^{\psi_1 + i\theta_1}$, and angle POQ is denoted by μ . Then by the law of cosines

$$e^{2\psi_1} = e^{2\psi} + e^{2\gamma} - 2e^{\psi}e^{\gamma} \cos(\theta - \delta) \quad (a)$$

and by the law of sines

$$\sin \mu = \frac{e^{\gamma} \sin(\theta - \delta)}{e^{\psi_1}}$$

$$\text{or} \quad \theta_1 = \theta + \mu = \theta + \tan^{-1} \frac{e^{\gamma - \psi} \sin(\theta - \delta)}{1 - e^{\gamma - \psi} \cos(\theta - \delta)} \quad (b)$$

In Figure 10 are shown the $\bar{\psi}(\theta)$ and $\bar{\epsilon}(\theta)$ curves for the Clark Y airfoil (shown in fig. 4) and the $\bar{\psi}_1(\theta_1)$ and $\bar{\epsilon}_1(\theta_1)$ curves which result when the origin is moved from 0 to M . It may be noted that $\bar{\epsilon}_1(\theta_1)$ is indeed considerably smaller than $\bar{\epsilon}(\theta)$. It is obtained from

$$(\varphi - \theta_1)' = -\frac{1}{2\pi} \int_0^{2\pi} \psi_1(\varphi) \cot \frac{\varphi - \varphi'}{2} d\varphi$$

and the constant ψ_0 is given ¹⁵ by

$$\psi_0 = \frac{1}{2\pi} \int_0^{2\pi} \psi_1(\varphi) d\varphi$$

The combined transformations.—It will be useful to combine the various transformations into one. We obtain from equations (5) and (10) an expression as follows:

$$\zeta = 2a \cosh \left(\log \frac{z}{a} + \sum_{n=1}^{\infty} \frac{c_n}{z^n} \right) \quad (24)$$

or we can also obtain a power series development in z

$$\zeta = c_1 + z + \frac{a_1}{z} + \frac{a_2}{z^2} + \frac{a_3}{z^3} + \dots \quad (25)$$

where ¹⁶

$$a_n = k_{n+1} + a^2 h_{n-1}$$

The constants k_n may be obtained in a convenient recursion form as

$$k_1 = c_1 \\ 2k_2 = k_1 c_1 + 2c_2 \\ 3k_3 = k_2 c_1 + 2k_1 c_2 + 3c_3 \\ 4k_4 = k_3 c_1 + 2k_2 c_2 + 3k_1 c_3 + 4c_4 \\ \dots \dots \dots$$

The constants h_n have the same form as k_n but with each c_i replaced by $-c_i$ (and $h_0 = 1$). It will be re-

¹⁵ The constant ψ_0 is invariant to change of origin. (See p. 200.) It should be remarked that the translation by the vector c_1 is only a matter of convenience and is especially useful for very irregular shapes. For a study of the properties of airfoil shapes we shall use only the original $\epsilon(\varphi)$ curve. (Fig. 10(a).)

¹⁶ By equations (5) and (10) we have

$$\zeta = ze^{\sum_{n=1}^{\infty} \frac{c_n}{z^n}} + \frac{a^2}{z} e^{-\sum_{n=1}^{\infty} \frac{c_n}{z^n}}$$

The constant k_n is thus the coefficient of $\frac{1}{z^n}$ in the expansion of $e^{\sum_{n=1}^{\infty} \frac{c_n}{z^n}}$ and the constant

h_n the coefficient of $\frac{1}{z^n}$ in the expansion of $e^{-\sum_{n=1}^{\infty} \frac{c_n}{z^n}}$. For the recursion form for k_n see Smithsonian Mathematical Formulæ and Tables of Elliptic Functions, p. 120.

¹⁴ These constants can be obtained in a recursion form. See footnote 16.

called that the values of c_n are given by the coefficients of the Fourier expansion of $\psi(\varphi)$ as

$$\frac{c_n}{R^n} = \frac{1}{\pi} \int_0^{2\pi} \psi(\varphi) e^{in\varphi} d\varphi \text{ where } R = ae^{\psi_0}$$

and

$$\psi_0 = \frac{1}{2\pi} \int_0^{2\pi} \psi(\varphi) d\varphi$$

The first few terms of equation (25) are then as follows:

$$\zeta = z + c_1 + \frac{c_2 + \frac{c_1^2}{2} + a^2}{z} + \frac{c_3 + c_2c_1 + \frac{c_1^3}{6} - c_1a^2}{z^2} + \dots \quad (25')$$

By writing $z_1 = z + c_1$, equation (25) is cast into the normal form

$$\zeta = z_1 + \frac{b_1}{z_1} + \frac{b_2}{z_1^2} + \dots \quad (26)$$

The constants b_n may be evaluated directly in terms of a_n or may be obtained merely by replacing $\psi(\varphi)$ by $\psi_1(\varphi)$ in the foregoing values for a_n .

The series given by equations (25) and (26) may be inverted and z or z_1 developed as a power series in ζ . Then

$$z(\zeta) = \zeta - c_1 - \frac{a_1}{\zeta} - \frac{a_2 + a_1c_1}{\zeta^2} - \frac{a_1c_1^2 + 2a_2c_1 + a_3 + a_1^2}{\zeta^3} \dots \quad (27)$$

and

$$z_1(\zeta) = \zeta - \frac{b_1}{\zeta} - \frac{b_2}{\zeta^2} - \frac{b_3 + b_1^2}{\zeta^3} \dots \quad (28)$$

The various transformations have been performed for the purpose of transforming the flow pattern of a

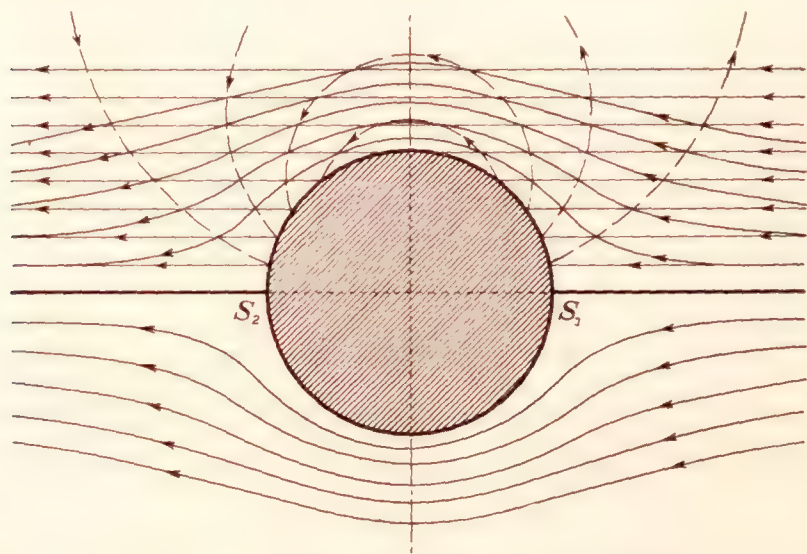


FIGURE 11.—Streamlines about circle with zero circulation (shown by the full lines) $Q = -V \sinh \mu \sin \varphi = \text{constant}$

circle into the flow pattern of an airfoil. We are thus led immediately to the well-known problem of determining the most general type of irrotational flow around a circle satisfying certain specified boundary conditions.

The flow about a circle.—The boundary conditions to be satisfied are: The circle must be a streamline of flow and, at infinity, the velocity must have a given magnitude and direction. Let us choose the ξ axis as corresponding to the direction of the velocity at

infinity. Then the problem stated is equivalent to that of an infinite circular cylinder moving parallel to the ξ axis with velocity V in a fluid at rest at infinity.

The general complex flow potential¹⁷ for a circle of radius R , and velocity at infinity V parallel to the x axis is

$$w(z) = -V \left(z + \frac{R^2}{z} \right) - \frac{i\Gamma}{2\pi} \log \frac{z}{R} \quad (29)$$

where Γ is a real constant parameter, known as the

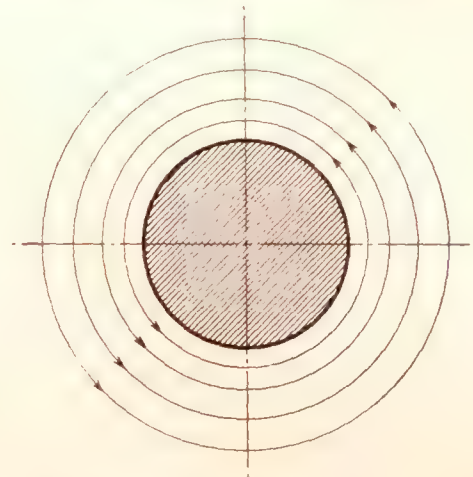


FIGURE 12.—Streamlines about circle for $V=0$ $Q = -\frac{\Gamma}{2\pi}\mu = \text{constant}$

circulation. It is defined as $\oint v_s ds$ along any closed curve inclosing the cylinder, v_s being the velocity along the tangent at each point.

Writing $z = Re^{\mu+i\varphi}$ and $w = P + iQ$, equation (29) becomes

$$w = -V \cosh(\mu + i\varphi) - \frac{i\Gamma}{2\pi}(\mu + i\varphi) \quad (29')$$

$$\text{or} \quad \left. \begin{aligned} P &= -V \cosh \mu \cos \varphi + \frac{\Gamma}{2\pi} \varphi \\ Q &= -V \sinh \mu \sin \varphi - \frac{\Gamma}{2\pi} \mu \end{aligned} \right\}$$

For the velocity components, we have

$$\frac{dw}{dz} = u - iv = -V \left(1 - \frac{R^2}{z^2} \right) - \frac{i\Gamma}{2\pi z} \quad (30)$$

In Figures 11 and 12 are shown the streamlines for the cases $\Gamma=0$, and $V=0$, respectively. The cylinder experiences no resultant force in these cases since all streamlines are symmetrical with respect to it.

The stagnation points, that is, points for which u and v are both zero, are obtained as the roots of $\frac{dw}{dz} = 0$. This equation has two roots.

$$z_0 = \frac{i\Gamma \pm \sqrt{16\pi^2 R^2 V^2 - \Gamma^2}}{4\pi V}$$

and we may distinguish different types of flow according as the discriminant $16\pi^2 R^2 V^2 - \Gamma^2$ is positive, zero, or negative. We recall here that a conformal transformation $w=f(z)$ ceases to be conformal at points where $\frac{dw}{dz}$ vanishes, and at a stagnation point the flow divides and the streamline possesses a singularity.

¹⁷ Reference 4, p. 56 or reference 5, p. 118. The log term must be added because the region outside the infinite cylinder (the point at infinity excluded) is doubly connected and therefore we must include the possibility of cyclic motion.

The different types of flow that result according as the parameter $\Gamma^2 \gtrless 16\pi^2 R^2 V^2$ are represented in Figure 13. In the first case (fig. 13 (a)), which will not interest us later, the stagnation point occurs as a double point in the fluid on the η axis, and all fluid within this streamline circulates in closed orbits around the circle, while the rest of the fluid passes downstream. In the second case (fig. 13 (b)), the stagnation points are together at S on the circle $Re^{i\varphi}$ and in the third case (fig. 13 (c)) they are symmetrically located on the circle. We have noted then that as Γ increases from 0 to $4\pi RV$ the stagnation points move downward on

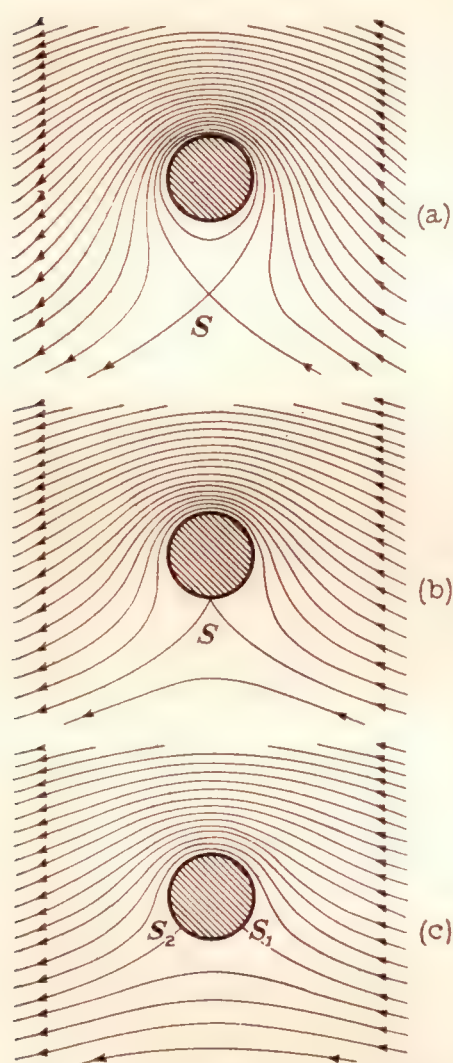


FIGURE 13.—Streamlines about circle [from Lagally—Handbuch der Physik Bd. VII] $Q = V \sinh \mu \sin \varphi - \frac{\Gamma}{2\pi} \mu = \text{constant}$ (a) $\Gamma^2 > 16\pi^2 R^2 V^2$ (b) $\Gamma^2 = 16\pi^2 R^2 V^2$ (c) $\Gamma^2 < 16\pi^2 R^2 V^2$

the circle $Re^{i\varphi}$ from the ξ axis toward the η axis. Upon further increase in Γ they leave the circle and are located on the η axis in the fluid.

Conversely, it is clear that the position of the stagnation points can determine the circulation Γ . This fact will be shown to be significant for wing-section theory. At present, we note that when both Γ and $V \neq 0$ a marked dissymmetry exists in the streamlines with respect to the circle. They are symmetrical about the η axis but are not symmetrical about the ξ axis. Since they are closer together on the upper side of the circle than on the lower side, a resultant force exists perpendicular to the motion.

We shall now combine the transformation (27) and the flow formula for

the circle equation (29) and obtain the general complex flow potential giving the 2-dimensional irrotational flow about an airfoil shape, and indeed, about any closed curve for which the Riemann theorem applies.

The flow around the airfoil.—In Figure 14 are given, in a convenient way, the different complex planes and transformations used thus far. The complex flow potential in the z plane for a circle of radius R origin at the center has been given as

$$w(z) = -V \left(z + \frac{R^2}{z} \right) - \frac{i\Gamma}{2\pi} \log z \quad (29)$$

where V , the velocity at infinity, is in the direction of the negative ξ axis. Let us introduce a parameter to

permit of a change in the direction of flow at infinity by the angle α which will be designated *angle of attack* and defined by the direction of flow at infinity with respect to a fixed axis on the body, in this case the axis $\varphi = 0$. This flow is obtained simply by writing $ze^{i\alpha}$ for z in equation (29) and represents a rotation of

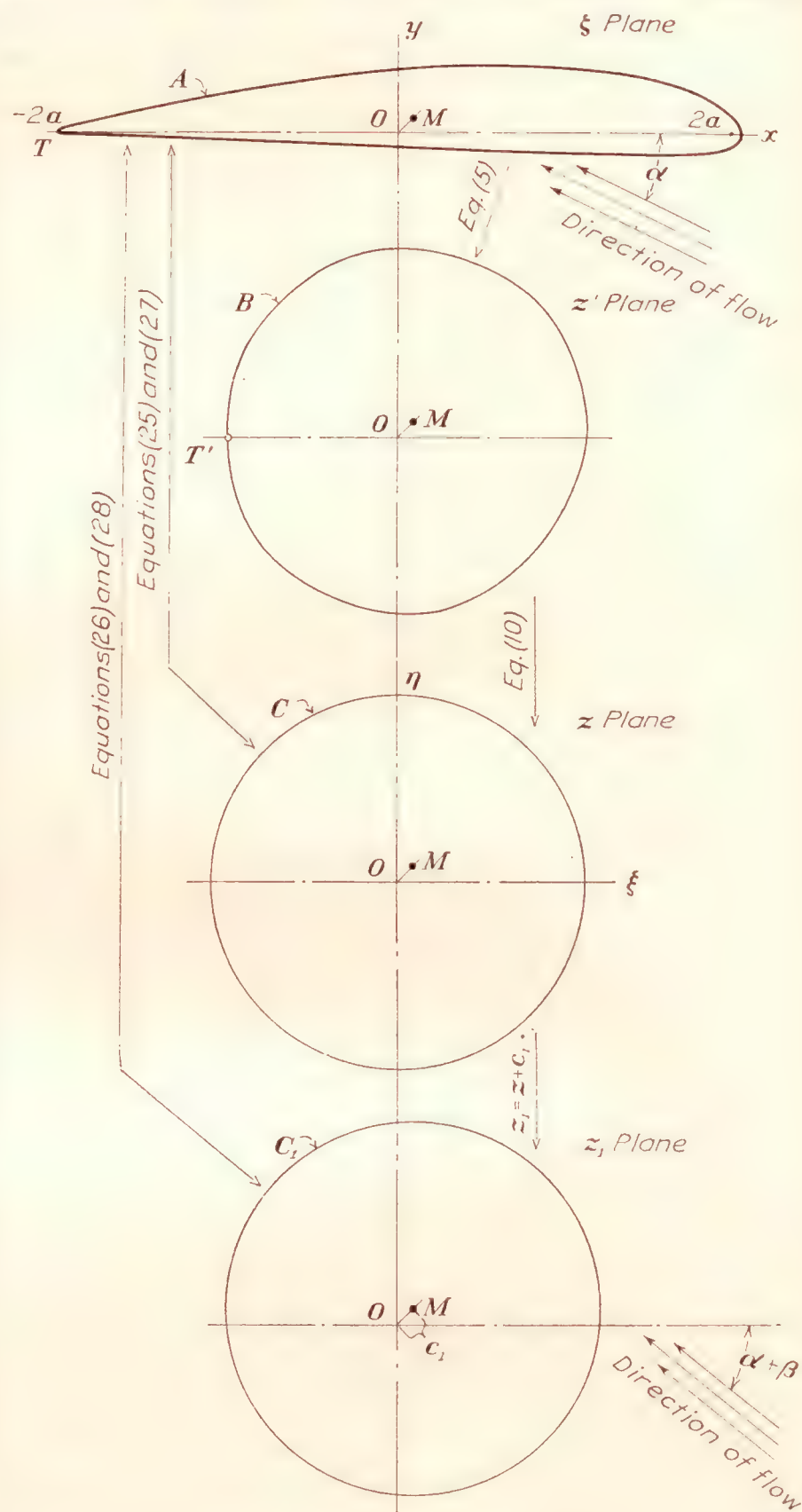


FIGURE 14.—The collected transformations

the entire flow field about the circle by angle α . We have

$$w(z) = -V \left(ze^{i\alpha} + \frac{R^2}{z} e^{-i\alpha} \right) - \frac{i\Gamma}{2\pi} \log z \quad (31)$$

$$\begin{aligned} \frac{dw}{dz} &= u - iv \\ &= -Ve^{i\alpha} \left(1 - \frac{R^2}{z^2} e^{-2i\alpha} \right) - \frac{i\Gamma}{2\pi z} \end{aligned} \quad (32)$$

Since a conformal transformation maps streamlines and potential lines into streamlines and potential lines,

we may obtain the complex flow potentials in the various planes by substitutions. For the flow about the circle in the z_1 plane, z is replaced by $z_1 - c_1$

$$w(z_1) = -V \left[(z_1 - c_1)e^{i\alpha} + \frac{R^2 e^{-i\alpha}}{(z_1 - c_1)} \right] - \frac{i\Gamma}{2\pi} \log(z_1 - c_1) \quad (31')$$

$$\frac{dw}{dz_1} = -Ve^{i\alpha} \left[1 - \frac{R^2 e^{-2i\alpha}}{(z_1 - c_1)^2} \right] - \frac{i\Gamma}{2\pi(z_1 - c_1)} \quad (32')$$

For the flow about the B curve in the z' plane, z is replaced by $z(z')$ (the inverse of eq. (10a)) and for the flow about the airfoil in the ζ plane z is replaced by $z(\zeta)$ from equation (27)

$$W(\zeta) = -V \left[z(\zeta)e^{i\alpha} + \frac{R^2}{z(\zeta)}e^{-i\alpha} \right] - \frac{i\Gamma}{2\pi} \log z(\zeta) \quad (33)$$

$$\frac{dW}{d\zeta} = \left[-Ve^{i\alpha} \left(1 - \frac{R^2 e^{-2i\alpha}}{[z(\zeta)]^2} \right) - \frac{i\Gamma}{2\pi[z(\zeta)]} \right] \frac{dz(\zeta)}{d\zeta} \quad (34)$$

The flow fields at infinity for all these transformations have been made to coincide in magnitude and direction.

At this point attention is directed to two important facts. First, in the previous analysis the original closed curve may differ from an airfoil shape. The formulas, when convergent, are applicable to any closed curve satisfying the general requirements of the Riemann theorem. However, the peculiar ease of numerical evaluations for streamline shapes is noteworthy and significant. The second important fact is that the parameter Γ which as yet is completely undetermined is readily determined for airfoils and to a discussion of this statement the next section is devoted. It will be seen that airfoils may be regarded as fixing their own circulation.

Kutta-Joukowski method for fixing the circulation.—All contours used in practice as airfoil profiles possess the common property of terminating in either a cusp or sharp corner at the trailing edge (a point of two tangents). Upon transforming the circle into an airfoil by $\zeta = f(z)$, we shall find that $\left| \frac{dz}{d\zeta} \right|$ is infinite at the trailing edge if the tail is perfectly sharp (or very large if the tail is almost sharp). This implies that the numerical value of the velocity $\left| \frac{dw}{dz} \right| \left| \frac{dz}{d\zeta} \right| = |v|$ is infinite (or extremely large) provided the factor $\left| \frac{dw}{dz} \right|$ is not zero at the tail. There is but one value of the circulation that avoids infinite velocities or gradients of pressure at the tail and this fact gives a practical basis for fixing the circulation.

The concept of the ideal fluid in irrotational potential flow implies no dissipation of energy, however large the velocity at any point. The circulation being a measure of the energy in a fluid is unaltered and independent of time. In particular, if the circulation is zero to begin with, it can never be different from zero.

However, since all real fluids have viscosity, a better physical concept of the ideal fluid is to endow the fluid with infinitesimal viscosity so that there is then no dissipation of energy for finite velocities and pressure gradients, but for infinite velocities, energy losses would result. Moreover, by Bernoulli's principle the pressure would become infinitely negative, whereas a real fluid can not sustain absolute negative pressures and the assumption of incompressibility becomes invalid long before this condition is reached. It should then be postulated that nowhere in the ideal fluid from the physical concept should the velocity become infinite. It is clear that the factor $\left| \frac{dw}{dz} \right|$ must then be zero at the trailing edge in order to avoid infinite velocities. It is then precisely the sharpness of the trailing edge which furnishes us the following basis for fixing the circulation.

It will be recalled that the equation $\frac{dw}{dz} = 0$ determines two stagnation points symmetrically located on the circle, the position of which varies with the value of the circulation and conversely the position of a stagnation point determines the circulation. In this paper the x axis of the airfoil has been chosen so that the negative end ($\theta = \pi$) passes through the trailing edge. From the calculation of $\epsilon = \varphi - \theta$ (by eq. (13)) the value of φ corresponding to any value of θ is determined as $\varphi = \theta + \epsilon$, in particular at $\theta = \pi$, $\varphi = \pi + \beta$, where β is the value of ϵ at the tail and for a given airfoil is a geometric constant (although numerically it varies with the choice of axes). This angle β is of considerable significance and for good reasons is called the angle of zero lift. The substance of the foregoing discussion indicates that the point $z = Re^{i(\pi+\beta)} = -Re^{i\beta}$ is a stagnation point on the circle. Then for this value of z , we have by equation (32)

$$\frac{dw}{dz} = -Ve^{i\alpha} \left(\frac{1 - R^2 e^{-2i\alpha}}{z^2} \right) - \frac{i\Gamma}{2\pi z} = 0$$

or

$$\begin{aligned} \Gamma &= -2\pi R V i e^{i(\alpha+\beta)} (1 - e^{-2i(\alpha+\beta)}) \\ &= 4\pi R V \left(\frac{e^{i(\alpha+\beta)} - e^{-i(\alpha+\beta)}}{2i} \right) \\ &= 4\pi R V \sin(\alpha + \beta) \end{aligned} \quad (35)$$

This value of the circulation is then sufficient to make the trailing edge a stagnation point for any value of α . The airfoil may be considered to equip itself with that amount of circulation which enables the fluid to flow past the airfoil with a minimum energy loss, just as electricity flowing in a flat plate will distribute itself so that the heat loss is a minimum. The final justification for the Kutta assumption is not only its plausibility, but also the comparatively good agreement with experimental results. Figure 15 (b) shows the streamlines around an airfoil for a flow satisfying the Kutta condition, and Figures 15 (a) and 15 (c) illus-

trate cases for which the circulation is respectively too small and too large, the stagnation point being then on the upper and lower surfaces, respectively. For these latter cases, the complete flow is determinable only if, together with the angle of attack, the circulation or a stagnation point is specified.

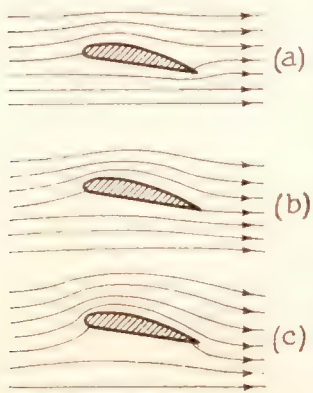


FIGURE 15.—(a) Flow with circulation smaller than for Kutta condition; (b) flow satisfying Kutta condition; (c) flow with circulation greater than for Kutta condition

Velocity at the surface.—The flow formulas for the entire field are now uniquely determined by substituting the value of Γ in equations (33) and (34). We are, however, in a position to obtain much simpler and more convenient relations for the boundary curves themselves. Indeed, we are chiefly interested in the velocity at the

surface of the airfoil, which velocity is tangential to the surface, since the airfoil contour is a streamline of flow. The numerical value of the velocity at the surface of the airfoil is

$$v = \sqrt{v_x^2 + v_y^2} = |v_x - iv_y| = \left| \frac{dw}{d\zeta} \right| = \left| \frac{dw}{dz} \right| \cdot \left| \frac{dz}{dz'} \right| \cdot \left| \frac{dz'}{d\zeta} \right|$$

We shall evaluate each of these factors in turn. From equations (32 and (35)

$$\frac{dw}{dz} = -Ve^{i\alpha} \left(1 - \frac{R^2}{z^2} e^{-2i\alpha} \right) - \frac{i4\pi RV \sin(\alpha + \beta)}{2\pi z}$$

At the boundary surface $z = Re^{i\varphi}$, and

$$\frac{dw}{dz} = -Ve^{i\alpha} (1 - e^{-2i(\alpha + \varphi)}) - 2iVe^{-i\varphi} \sin(\alpha + \beta)$$

or

$$\begin{aligned} \frac{dw}{dz} &= -Ve^{-i\varphi} [(e^{i(\alpha + \varphi)} - e^{-i(\alpha + \varphi)}) + 2i \sin(\alpha + \beta)] \\ &= -2iVe^{-i\varphi} [\sin(\alpha + \varphi) + \sin(\alpha + \beta)] \end{aligned}$$

and

$$\left| \frac{dw}{dz} \right| = 2V[\sin(\alpha + \varphi) + \sin(\alpha + \beta)] \quad (36)$$

In general, for arbitrary Γ we find that

$$\left| \frac{dw}{dz} \right| = 2V \sin(\alpha + \varphi) + \frac{\Gamma}{2\pi R} \quad (36')$$

To evaluate $\left| \frac{dz}{dz'} \right|$ we start with relation (10)

$$z' = ze^{\sum_{n=1}^{\infty} \frac{c_n}{z^n}}$$

At the boundary surface

$$z' = ze^{\psi - \psi_0 - i\epsilon} \text{ where } \epsilon = \varphi - \theta \text{ and } z = ae^{\psi_0 + i\varphi}$$

$$\frac{dz'}{dz} = \frac{z'}{z} \left(1 + z \frac{d(\psi - i\epsilon)}{dz} \right)$$

$$= \frac{z'}{z} \left(1 + \frac{d(\psi - i\epsilon)}{id\varphi} \right) \quad (37')$$

$$= \frac{z'}{z} \left(\frac{\frac{d\varphi}{d\theta} - \frac{d\bar{\epsilon}}{d\theta} - i \frac{d\bar{\psi}}{d\theta} \right) = \frac{z'}{z} \left(\frac{1 - i \frac{d\bar{\psi}}{d\theta}}{1 + \frac{d\bar{\epsilon}}{d\theta}} \right)$$

$$\text{Then } \left| \frac{dz'}{dz} \right| = e^{\psi - \psi_0} \sqrt{\frac{1 + \left(\frac{d\bar{\psi}}{d\theta} \right)^2}{1 + \frac{d\bar{\epsilon}}{d\theta}}} \quad (37)$$

By equation (5)

$$\zeta = z' + \frac{a^2}{z'}, \text{ and at the boundary } z' = ae^{\psi + i\theta}, \text{ or}$$

$$\zeta = 2a \cosh(\psi + i\theta)$$

$$\begin{aligned} \frac{d\zeta}{dz'} &= 2a \sinh(\psi + i\theta) \frac{d(\psi + i\theta)}{dz'} \\ &= 2 \sinh(\psi + i\theta) e^{-(\psi + i\theta)}. \end{aligned}$$

$$\begin{aligned} \text{Then } \left| \frac{d\zeta}{dz'} \right|^2 &= 4e^{-2\psi} (\sinh^2 \psi \cos^2 \theta + \cosh^2 \psi \sin^2 \theta) \\ &= 4e^{-2\psi} (\sinh^2 \psi + \sin^2 \theta) \end{aligned}$$

$$\text{and } \left| \frac{d\zeta}{dz'} \right| = 2e^{-\psi} \sqrt{\sinh^2 \psi + \sin^2 \theta} \quad (38)$$

Then finally

$$\begin{aligned} v &= \left| \frac{dw}{d\zeta} \right| = \left| \frac{dw}{dz} \right| \cdot \left| \frac{dz}{dz'} \right| \cdot \left| \frac{dz'}{d\zeta} \right| \\ &= \frac{V[\sin(\alpha + \varphi) + \sin(\alpha + \beta)] \left(1 + \frac{d\bar{\epsilon}}{d\theta} \right) e^{\psi_0}}{\sqrt{(\sinh^2 \psi + \sin^2 \theta) \left(1 + \left(\frac{d\bar{\psi}}{d\theta} \right)^2 \right)}} \quad (39) \end{aligned}$$

In this formula the circulation is given by equation (35). In general, for an arbitrary value of Γ (see equation (36')), the equation retains its form and is given by

$$v = \frac{V \left[\sin(\alpha + \varphi) + \frac{\Gamma}{4\pi R V} \right] \left(1 + \frac{d\bar{\epsilon}}{d\theta} \right) e^{\psi_0}}{\sqrt{(\sinh^2 \psi + \sin^2 \theta) \left(1 + \left(\frac{d\bar{\psi}}{d\theta} \right)^2 \right)}} \quad (40)$$

For the special case $\Gamma = 0$, we get

$$v = \frac{V \sin(\alpha + \varphi) \left(1 + \frac{d\bar{\epsilon}}{d\theta} \right) e^{\psi_0}}{\sqrt{(\sinh^2 \psi + \sin^2 \theta) \left(1 + \left(\frac{d\bar{\psi}}{d\theta} \right)^2 \right)}} \quad (41)$$

Equation (40) is a general result giving the velocity at any point of the surface of an arbitrary airfoil section, with *arbitrary* circulation for any angle of attack α . Equation (39) represents the important special case in which the circulation is specified by the Kutta condition. The various symbols are functions only of the coordinates (x, y) of the airfoil boundary and expressions for them have already been given. In Tables

I and II are given numerical results for different airfoils, and explanation is there made of the methods of calculation and use of the formulas developed.

We have immediately by equation (3) the value of the pressure p at any point of the surface in terms of the pressure at infinity as

$$\frac{p}{q} = 1 - \left(\frac{v}{V}\right)^2$$

Some theoretical pressure distribution curves are given at the end of this report and comparison is there made with experimental results. These comparisons, it will be seen, within a large range of angles of attack, are strikingly good.¹⁸

GENERAL WING-SECTION CHARACTERISTICS

The remainder of this report will be devoted to a discussion of the parameters of the airfoil shape affecting aerodynamic properties with a view to determining airfoil shapes satisfying preassigned properties. This discussion will not only furnish an illuminating sequel

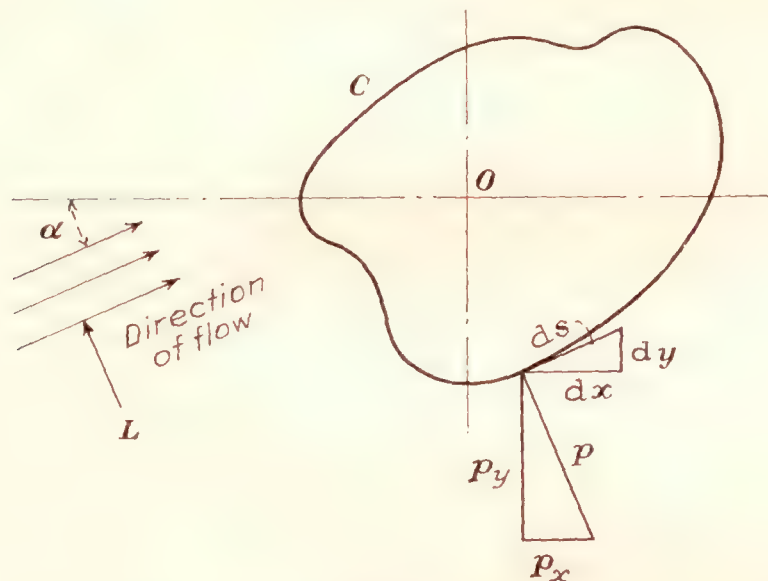


FIGURE 16.

to the foregoing analysis leading to a number of new results, but will also unify much of the existing theory of the airfoil. In the next section we shall obtain some expressions for the integrated characteristics of the airfoil. We start with the expressions for total lift and total moment, first developed by Blasius.

Blasius' formulas.—Let C in Figure 16 represent a closed streamline contour in an irrotational fluid field. Blasius' formulas give expressions for the total force and moment experienced by C in terms of the complex velocity potential. They may be obtained in the following simple manner. We have for the total forces in the x and y directions

$$P_x = - \int_C p_x ds = - \int_C p dy$$

$$P_y = \int_C p_y ds = \int_C p dx$$

$$P_x - iP_y = - \int_C p(dy + idx)$$

The pressure at any point is

$$p = p_o - \frac{1}{2}\rho v^2$$

Then,

$$P_x - iP_y = \frac{\rho}{2} \int_C v^2 (dy + idx)$$

$$= \frac{i\rho}{2} \int_C \frac{dw}{dz} \frac{d\bar{w}}{d\bar{z}} d\bar{z}$$

where the bar denotes conjugate complex quantities. Since C is a streamline, $v_x dy - v_y dx = 0$. Adding the quantity

$$i\rho \int_C (v_y + iv_x)(v_x dy - v_y dx) = 0$$

to the last equation, we get.¹⁹

$$\begin{aligned} P_x - iP_y &= \frac{i\rho}{2} \int_C (v_x - iv_y)^2 (dx + idy) \\ &= \frac{i\rho}{2} \int_C \left(\frac{dw}{dz}\right)^2 dz \end{aligned} \quad (42)$$

The differential of the moment of the resultant force about the origin is,

$$\begin{aligned} dM_o &= p(x dx + y dy) \\ &= R. P. \text{ of } p[x dx + y dy + i(y dx - x dy)] \\ &= R. P. \text{ of } p z d\bar{z} \end{aligned}$$

where "R. P. of" denotes the real part of the complex quantity. We have from the previous results

$$d(P_x - iP_y) = -i p d\bar{z} = \frac{i\rho}{2} \left(\frac{dw}{dz}\right)^2 dz$$

$$\text{Then } dM_o = -R. P. \text{ of } \frac{\rho}{2} \left(\frac{dw}{dz}\right)^2 z dz$$

$$\text{and } M_o = -R. P. \text{ of } \frac{\rho}{2} \int_C \left(\frac{dw}{dz}\right)^2 z dz \quad (43)$$

Let us now for completeness apply these formulas to the airfoil A in the ζ plane (fig. 14) to derive the Kutta-Joukowski classical formula for the lift force. By equation (32) we have

$$\frac{dw}{dz} = -Ve^{i\alpha} - \frac{i\Gamma}{2\pi z} + \frac{R^2 Ve^{-i\alpha}}{z^2}$$

and by equation (25)

$$\frac{d\zeta}{dz} = 1 - \frac{a_1}{z^2} - \frac{a_2}{z^3} - \dots$$

Then

$$\begin{aligned} \frac{dw}{d\zeta} &= \frac{dw}{dz} \cdot \frac{dz}{d\zeta} \\ &= -Ve^{i\alpha} - \frac{i\Gamma}{2\pi z} + (R^2 Ve^{-i\alpha} - a_1 Ve^{i\alpha}) \frac{1}{z^2} + \dots \end{aligned}$$

¹⁸ Cf. Blasius, H: Zs. f. Math. u. Phys. Bd. 58 S. 93 and Bd. 59 S. 43, 1910. Similarly,

$$P_x + iP_y = -\frac{i\rho}{2} \int_C \left(\frac{dw}{dz}\right)^2 \frac{d\bar{z}}{dz}$$

a less convenient relation to use than (42).

Note that when the region about C is regular the value of the integral (42) remains unchanged by integrating about any other curve enclosing C .

¹⁹ A paper devoted to more extensive applications to present-day airfoils is in progress.

and

$$\left(\frac{dw}{d\zeta}\right)^2 = A_0 + \frac{A_1}{z} + \frac{A_2}{z^2} + \dots$$

where

$$A_0 = V^2 e^{2i\alpha}$$

$$A_1 = iV e^{i\alpha} \frac{\Gamma}{\pi}$$

$$A_2 = -2R^2 V^2 + 2a_1 V^2 e^{2i\alpha} - \frac{\Gamma^2}{4\pi^2}$$

Then

$$\begin{aligned} P_x - iP_y &= \frac{i\rho}{2} \int_A \left(\frac{dw}{d\zeta}\right)^2 d\zeta \\ &= \frac{i\rho}{2} \int_C \left(\frac{dw}{d\zeta}\right)^2 \frac{d\zeta}{dz} dz \\ &= \frac{i\rho}{2} (2\pi i A_1) \\ &= -ie^{i\alpha} \rho V \Gamma \end{aligned}$$

Therefore

$$\begin{cases} P_x = \rho V \Gamma \sin \alpha \\ P_y = \rho V \Gamma \cos \alpha \end{cases}$$

and are the components of a force $\rho V \Gamma$ which is perpendicular to the direction of the stream at infinity. Thus the resultant lift force experienced by the airfoil is

$$L = \rho V \Gamma \quad (44)$$

and writing for the circulation Γ the value given by equation (35)

$$L = 4\pi R \rho V^2 \sin(\alpha + \beta) \quad (45)$$

The moment of the resultant lift force about the origin $\zeta = 0$ is obtained as

$$\begin{aligned} M_0 &= R. P. \text{ of } -\frac{\rho}{2} \int_A \left(\frac{dw}{d\zeta}\right)^2 \zeta d\zeta \\ &= R. P. \text{ of } -\frac{\rho}{2} \int_C \left(\frac{dw}{d\zeta}\right)^2 \zeta \frac{d\zeta}{dz} dz \\ &= R. P. \text{ of } -\frac{\rho}{2} \int_C \left(A_0 + \frac{A_1}{z} + \frac{A_2}{z^2} + \dots\right) \times \\ &\quad \left(c_1 + z + \frac{a_1}{z} + \frac{a_2}{z^2} + \dots\right) \left(1 - \frac{a_1}{z^2} + \dots\right) dz \\ &= R. P. \text{ of } -\frac{\rho}{2} 2\pi i (\text{coefficient of } z^{-1}) \\ &= R. P. \text{ of } -\frac{\rho}{2} 2\pi i (A_2 + A_1 c_1) \end{aligned}$$

or, M_0 is the imaginary part of $\pi\rho(A_2 + A_1 c_1)$. After putting ²⁰ $c_1 = me^{i\delta}$ and $a_1 = b^2 e^{2i\gamma}$ we get

$$M_0 = 2\pi\rho V^2 b^2 \sin 2(\alpha + \gamma) + \rho V \Gamma m \cos(\alpha + \delta) \quad (46)$$

The results given by equations (44) and (46) have physical significance and are invariant to a transforma-

tion of origin as may be readily verified by employing equations (26) and (32') and integrating around the C_1 circle in the z_1 plane. It is indeed a remarkable fact that the total integrated characteristics, lift and location of lift, of the airfoil depend on so few parameters of the transformation as to be almost independent of the shape of the contour. The parameters R , β , a_1 , and c_1 involved in these relations will be discussed in a later paragraph.

We shall obtain an interesting result ²¹ by taking moments about the point $\zeta = c_1$ instead of the origin. (M in fig. 17.) By equation (25) we have,

$$\zeta - c_1 = z + \frac{a_1}{z} + \frac{a_2}{z^2} + \dots$$

and by equation (43)

$$\begin{aligned} M_M &= R. P. \text{ of } -\frac{\rho}{2} \int_A \left[\frac{dw}{d(\zeta - c_1)}\right]^2 (\zeta - c_1) d\zeta \\ &= R. P. \text{ of } -\frac{\rho}{2} \int_C \left(A_0 + \frac{A_1}{z} + \frac{A_2}{z^2} + \dots\right) \times \\ &\quad \left(z + \frac{a_1}{z} + \frac{a_2}{z^2} + \dots\right) \left(1 - \frac{a_1}{z^2} + \dots\right) dz \\ &= R. P. \text{ of } -i\pi\rho A_2 \end{aligned}$$

or

$$M_M = 2\pi b^2 \rho V^2 \sin 2(\alpha + \gamma) \quad (47)$$

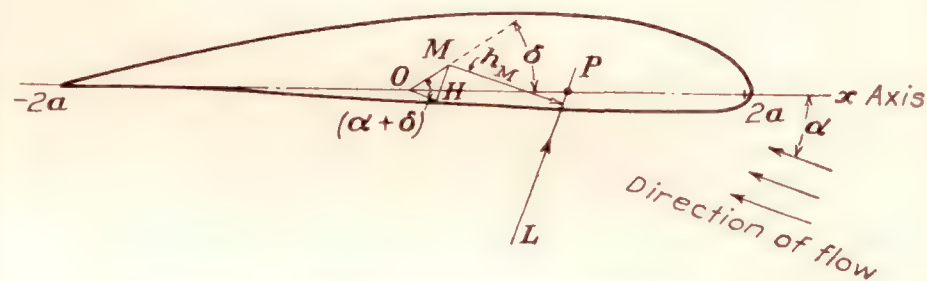


FIGURE 17.—Moment arm from M onto the lift vector

This result could have been obtained directly from equation (46) by noticing that $\rho V \Gamma$ in the second term is the resultant lift force L and that $Lm \cos(\alpha + \delta)$ represents a moment which vanishes at M for all values of α . (In fig. 17 the complex coordinate of M is $\zeta = me^{i\delta}$, the arm OH is $m \cos(\alpha + \delta)$.) The perpendicular h_M from M onto the resultant lift vector is simply obtained from $M_M = Lh_M$, as

$$h_M = \frac{b^2 \sin 2(\alpha + \gamma)}{2R \sin(\alpha + \beta)} \quad (48)$$

The intersection of the resultant lift vector with the chord or axis of the airfoil locates a point which may be considered the center of pressure. The amount of travel of the center of pressure with change in angle of attack is an important characteristic of airfoils, especially for considerations of stability, and will be discussed in a later paragraph.

²⁰ It may be recalled that $c_1 = \frac{R^2 \pi}{\pi} \int_0^{2\pi} \psi(\varphi) e^{i\varphi} d\varphi$ and $a_1 = a^2 + \frac{c_1^2}{2} + c_2$. (See eq. (25').)

²¹ First obtained by R. von Mises. (Reference 6.) The work of von Mises forms an elegant geometrical study of the airfoil.

The lift force has been found to be proportional to $\sin (\alpha+\beta)$ or writing $\alpha+\beta=\alpha_1$

$$L=4\pi\rho R V^2 \sin \alpha_1 \quad (49)$$

where α_1 may be termed the absolute angle of attack. Similarly writing $\alpha + \gamma = \alpha_2$

$$M_M = 2\pi b^2 \rho V^2 \sin 2\alpha_2 \quad (50)$$

With von Mises (reference 6, Pt. II) we shall denote the axes determined by passing lines through M at angles β and γ to the x axis as the first and second axes of the airfoil, respectively. (Fig. 18.) The directions of these axes alone are important and these are fixed with respect to a given airfoil. Then the lift L is proportional to the sine of the angle of attack with respect to the first axis and the moment about M to

If this moment is to be independent of α , the coefficients of $\sin 2\alpha$ and $\cos 2\alpha$ must vanish.

Then

$$b^2 \cos 2\gamma = Rr \cos (\beta + \sigma)$$

and

$$b^2 \sin 2\gamma = Rr \sin(\beta + \sigma)$$

Hence,

$$r = \frac{b^2}{R} \text{ and } \sigma = 2\gamma - \beta$$

Then if we move the reference point of the moment to a point F whose radius vector from M is $\frac{b^2}{R}e^{i(2\gamma-\beta)}$, the moment existing at F is for all angles of attack constant, and given by

$$M_F = 2\pi\rho b^2 V^2 \sin 2(\gamma - \beta) \quad (51)$$

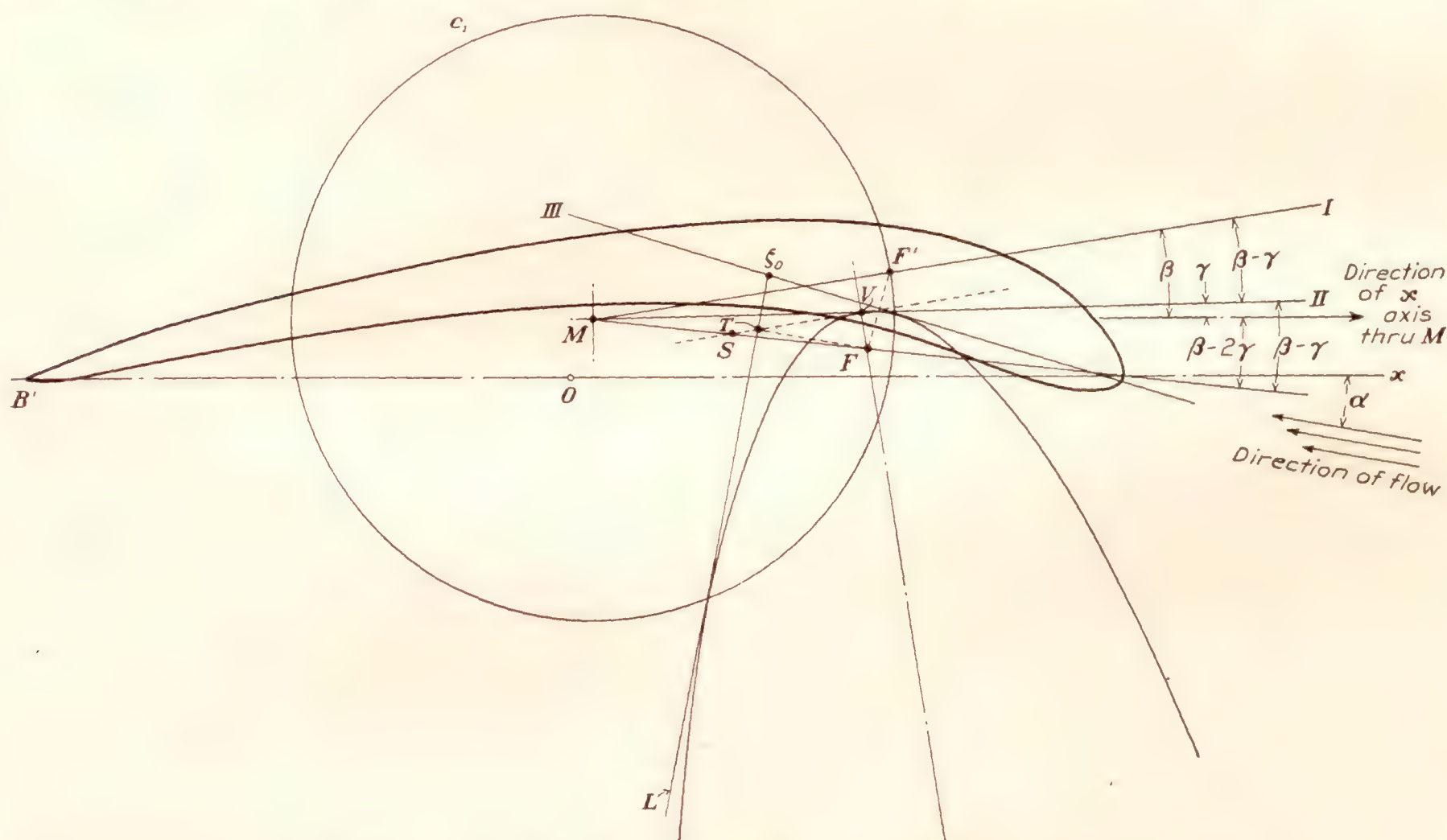


FIGURE 18.—Illustrating the geometrical properties of an airfoil (axes and lift parabola of the R. A. F. 19 airfoil)

the sine of twice the angle of attack with respect to the second axis.

From equation (47) we note that the moment at any point Q whose radius vector from M is $re^{i\sigma}$, is given by

$$M_p = 2\pi\rho b^2 V^2 \sin 2(\alpha + \gamma) - Lr \cos (\alpha + \sigma)$$

Let us determine whether there exist particular values of r and σ for which M_Q is independent of the angle of attack α . Writing for L its value given by equation (45),

$$M_{\theta} = 2\pi\rho b^2 V^2 \sin 2(\alpha + \gamma) - 4\pi\rho RrV^2 \sin(\alpha + \beta) \cos(\alpha + \sigma)$$

And separating this trigonometrically

$$M_Q = 2\pi\rho V^2[(b^2 \cos 2\gamma - Rr \cos(\beta + \sigma)) \sin 2\alpha + (b^2 \sin 2\gamma - Rr \sin(\beta + \sigma)) \cos 2\alpha - Rr \sin(\beta - \sigma)]$$

It has thus been shown that with every airfoil profile there is associated a point F for which the moment is independent of the angle of attack. A change in lift force resulting from a change in angle of attack distributes itself so that its moment about F is zero.

From equation (47) it may be noted that at zero lift (i. e., $\alpha = -\beta$) the airfoil is subject to a moment couple which is, in fact, equal to M_F . This moment is often termed "diving moment" or "moment for zero lift." If M_F is zero, the resultant lift force must pass through F for all angles of attack and we thus have the statement that the airfoil has a constant center of pressure, if and only if, the moment for zero lift is zero.

The point F , denoted by von Mises as the focus of the airfoil, will be seen to have other interesting properties. We note here that its construction is very

simple. It lies at a distance $\frac{b^2}{R}$ from M on a line making angle $2\gamma - \beta$ with respect to the x axis. From Figure 18 we see that the angle between this line and the first axis is bisected by the second axis.

The arm h_F from F onto the resultant lift vector L (h_F is designated FT in Figure 18; note also that FT , being perpendicular to L , must be parallel to the direction of flow; the line TV is drawn parallel to the first axis and therefore angle $VT F = \alpha + \beta$) is obtained as

$$h_F = \frac{M_F}{L} = \frac{-b^2 \sin 2(\beta - \gamma)}{2R \sin(\alpha + \beta)}$$

or setting

$$h = \frac{b^2}{2R} \sin 2(\beta - \gamma)$$

$$h_F = -\frac{h}{\sin(\alpha + \beta)} \quad (52)$$

But h_F is parallel to the direction of α , and the relation $h = -h_F \sin(\alpha + \beta)$ states then that the projection of h_F onto the line through F perpendicular to the first axis is equal to the constant h (h is designated FV in the figure) for all angles of attack. In other words, the pedal points T determined by the intersection of h_F and L for all positions of the lift vector L lie on a straight line. (The line is determined by T and V in fig. 18.) The parabola is the only curve having the property that pedal points of the perpendiculars dropped from its focus onto any tangent lie on a straight line, that line being the tangent at the vertex. This may be shown analytically by noting that the equation of L for a coordinate system having F as origin and FV as negative x axis is

$$x \sin \alpha_1 + y \cos \alpha_1 = h_F = -\frac{h}{\sin(\alpha + \beta)}$$

By differentiating with respect to $\alpha_1 = \alpha + \beta$ and eliminating α_1 we get the equation of the curve which the lines L envelop as $y^2 = 4h(x + h)$. From triangle FVS in Figure 18, it may be seen that the distance $MF = \frac{b^2}{R}$ is bisected at S by the line TV ; for, since $FV = h = \frac{b^2}{2R} \sin 2(\gamma - \beta)$ and angle $FSV = 2(\beta - \gamma)$, then $SF = \frac{b^2}{2R}$. It has thus been shown that the resultant lift vectors envelop, in general, a parabola whose focus is at F and whose directrix is the first axis. The second axis and its perpendicular at M , it may be noted, are also tangents to the parabola being, by definition, the resultant lift vectors for $\alpha = -\gamma$ and $\alpha = \frac{\pi}{2} - \gamma$, respectively.

If the constant h reduces to zero, the lift vectors reduce to a pencil of lines through F . Thus a constant center of pressure is given by $h = 0$ or $\sin 2(\beta - \gamma) = 0$ which is equivalent to stating that the first and second axes coincide. The lift parabola opens downward when the first axis is above the second axis ($\beta > \gamma$); it reduces to a pencil of lines when the two axes are

coincident ($\beta = \gamma$) and opens upward when the second axis is above the first ($\beta < \gamma$).

W. Müller²² introduced a third axis which has some interesting properties. Defining the complex coordinate ζ_0 as the centroid of the circulation by

$$\Gamma \zeta_0 = \int_A \zeta \left(\frac{dw}{d\zeta} \right) d\zeta$$

and using equations (25) and (32) one obtains

$$\zeta_0 - c_1 = x_0 + iy_0$$

where

$$\left. \begin{aligned} x_0 &= \frac{1}{2 \sin(\alpha + \beta)} \left[R \sin \alpha + \frac{b^2}{R} \sin(\alpha + 2\gamma) \right] \\ y_0 &= \frac{1}{2 \sin(\alpha + \beta)} \left[R \cos \alpha - \frac{b^2}{R} \cos(\alpha + 2\gamma) \right] \end{aligned} \right\} \quad (53)$$

The equation of the lift vector lines referred to the origin at M and x axis drawn through M is

$$x \cos \alpha - y \sin \alpha = \frac{b^2 \sin(\alpha + \gamma)}{2R \sin(\alpha + \beta)} \quad (54)$$

and it may be seen that the point (x_0, y_0) satisfies this equation. The centroid of the circulation then lies on the lift vectors. By elimination of α from equation (53) one finds as the locus of (x_0, y_0)

$$\begin{aligned} 2x_0 \left[R \cos \beta - \frac{b^2}{R} \cos(\beta - 2\gamma) \right] + 2y_0 \left[R \sin \beta \right. \\ \left. + \frac{b^2}{R} \sin(\beta - 2\gamma) \right] = R^2 - \frac{b^4}{R^2} \end{aligned} \quad (55)$$

which is the equation of a line, the third axis, and proves to be a tangent to the lift parabola. Geometrically, it is the perpendicular bisector of the line FF' joining the focus to the point of intersection of the first axis with the circle. (Fig. 18.)

The conformal centroid of the contour.—It has already been seen that the point M has special interesting properties. The transformation from the airfoil to the circle having M as center was expressed in the normal form and permitted of a very small $\epsilon(\varphi)$ curve. (See p. 188.) It was also shown that the moment with respect to M is simply proportional to the sine of twice the angle of attack with respect to the second axis. We may note, too, that in the presentation of this report the coordinate of M , $\zeta = c_1$ $= \frac{R}{\pi} \int_0^{2\pi} \psi e^{i\varphi} d\varphi$, is a function only of the first harmonic of the $\psi(\varphi)$ curve.

We shall now obtain a significant property of M invariant with respect to the transformation from airfoil to circle. We start with the evaluation of the integral

$$\int_A \zeta \left| \frac{dz}{d\zeta} \right| ds$$

²² Reference 7, p. 169. Also Zs. für Ang. Math. u. Mech. Bd. 3 S. 117, 1923.

Airfoils having the same first, second, and third axes are alike theoretically in total lift properties and also in travel of the center of pressure, i. e., they have the same lift parabola.

where A is the airfoil contour, ds the differential of arc along A , and $\left|\frac{dz}{d\zeta}\right|$, as will be recalled, is the magnification factor of the transformation $\zeta=f(z)$ mapping airfoil into circle; i. e., each element ds of A when magnified by $\left|\frac{dz}{d\zeta}\right|$ gives dS the differential of arc in the plane of the circle, i. e., $|dz|$. Then we have,

$$\begin{aligned} \int_A \zeta \left|\frac{dz}{d\zeta}\right| ds &= \int_C \zeta(z) |dz| \text{ and by equation (25),} \\ &= \int_C \left(c_1 + z + \frac{a_1}{z} + \frac{a_2}{z^2} + \dots\right) |dz| \\ &= \int_0^{2\pi} \left(c_1 + Re^{i\varphi} + \frac{a_1}{R} e^{-i\varphi} + \frac{a_2}{R^2} e^{-2i\varphi} + \dots\right) R d\varphi \\ &= 2\pi R c_1 \\ &= c_1 \int_C dS = c_1 \int_A \left|\frac{dz}{d\zeta}\right| ds \end{aligned}$$

Then

$$c_1 = \frac{\int_A \zeta \left|\frac{dz}{d\zeta}\right| ds}{\int_A \left|\frac{dz}{d\zeta}\right| ds} \quad (56)$$

The point M of the airfoil is thus the conformal centroid obtained by giving each element of the contour a weight equal to the magnification of that element, which results when the airfoil is transformed into a circle, the region at infinity being unaltered. It lies within any convex region enclosing the airfoil contour.²³

ARBITRARY AIRFOILS AND THEIR RELATION TO SPECIAL TYPES

The total lift and moment experienced by the airfoil have been seen to depend on but a few parameters of the airfoil shape. The resultant lift force is completely determined for a particular angle of attack by only the radius R and the angle of zero lift β . The moment about the origin depends, in addition, on the complex constants c_1 and a_1 or, what is the same, on the position of the conformal centroid M and the focus F . The constants c_1 and a_1 were also shown (see footnote 20) to depend only on the first and second harmonics of the $\epsilon(\varphi)$ curve. Before studying these parameters for the case of the arbitrary airfoil, it will be instructive to begin with special airfoils and treat these from the point of view of the "conformal angular distortion" [$\epsilon(\varphi)$] curve.

Flow about the straight line or flat plate.—As a first approximation to the theory of actual airfoils, there is the one which considers the airfoil section to be a straight line. It has been seen that the line of length $4a$ is obtained by transforming a circle of radius a , center at the origin, by $\zeta = z + \frac{a^2}{z}$. The region ex-

ternal to the line $4a$ in the ζ plane maps uniquely into the region external to the circle $|z|=a$. A point Q of the line corresponding to a point P at $ae^{i\theta}$ is obtained by simply adding the vectors $a(e^{i\theta} + e^{-i\theta})$ or completing the parallelogram $OPQP'$.

For $\psi=0$, we have from equation (6)

$$\begin{aligned} x &= 2a \cosh \psi \cos \theta = 2a \cos \theta \\ y &= 2a \sinh \psi \sin \theta = 0 \end{aligned}$$

Then the parameters for this case are $R=a$, $\beta=0$, $a_1=a^2$ (i. e., $b=a$, $\gamma=0$), and M is at the origin O . Taking the Kutta assumption for determining the circulation we have,

$$\left. \begin{aligned} \text{the circulation,} & \quad \Gamma = 4\pi a V \sin \alpha \\ \text{the lift,} & \quad L = 4\pi a \rho V^2 \sin \alpha \\ \text{moment about } M, & \quad M_M = 2\pi a^2 \rho V^2 \sin 2\alpha \\ \text{position of } F \text{ is at } z_F &= c_1 + \frac{b^2}{R} e^{i(2\gamma-\beta)} = a \end{aligned} \right\} \quad (57)$$

Since $\beta=\gamma$, we know that the travel of the center of pressure vanishes and that the center of pressure is at

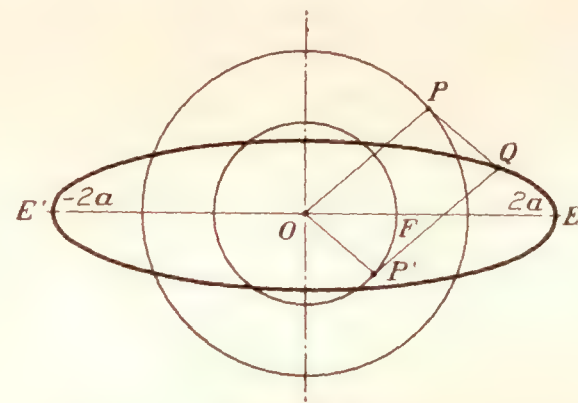


FIGURE 19.

F or at one-fourth the length of the line from the leading edge. The complex flow potential for this case is

$$w(\zeta) = -V \left[z(\zeta) e^{i\alpha} + \frac{a^2}{z(\zeta)} e^{-i\alpha} \right] + \frac{i\Gamma}{2\pi} \log z(\zeta) \quad (58)$$

where $z(\zeta) = \frac{\zeta}{2} \pm \sqrt{\left(\frac{\zeta}{2}\right)^2 - a^2}$ is the inverse of equation (5). Since $\psi(\varphi) = \epsilon(\varphi) = 0$ for this case, equation (39) giving the velocity at the surface reduces to

$$v = V \left[\frac{\sin\left(\frac{\varphi}{2} + \alpha\right)}{\sin \frac{\varphi}{2}} \right] \text{ for } \Gamma = 4\pi a V \sin \alpha,$$

and by equation (41) $v = V \left(\frac{\sin(\varphi + \alpha)}{\sin \varphi} \right)$ for $\Gamma = 0$.

Flow about the elliptic cylinder.—If equation (5) is applied to a circle with center at the origin and radius ae^ψ , the ellipse (fig. 19)

$$\frac{x^2}{(2a \cosh \psi)^2} + \frac{y^2}{(2a \sinh \psi)^2} = 1$$

is obtained in the ζ plane and the region external to this ellipse is mapped uniquely into the region external to the circle. The same transformation also transforms this external region into the region internal to the inverse circle, radius $ae^{-\psi}$. We note that a point

²³ Cf. P. Frank and K. Lowner, Math. Zs. Bd. 3, S. 78, 1919. Also reference 5, p. 146.

Q of the ellipse corresponding to P at $ae^{\psi+i\theta}$ is obtained by simply completing the parallelogram $OPQP'$ (fig. 19) where P' now terminates on the circle $ae^{-\psi}$. The parameters are obtained as $R=ae^{\psi}$, $\beta=0$, $a_1=a_2$, M is at the origin O . Then, assuming the rear stagnation point at the end of the major axis,

$$\begin{aligned}\Gamma &= 4\pi ae^{\psi} V \sin \alpha \\ L &= 4\pi \rho ae^{\psi} V^2 \sin \alpha \\ M_M &= 2\pi a^2 \rho V^2 \sin 2\alpha\end{aligned}$$

Since $\beta=\gamma$, the point F is the center of pressure for all angles of attack and is located at $z_F=ae^{-\psi}$ from O or a distance ae^{ψ} from the leading edge. The quantity

$$\frac{EF}{EE'} = \frac{ae^{\psi}}{2a(e^{\psi}+e^{-\psi})} = \frac{\cosh \psi + \sinh \psi}{4 \cosh \psi} = \frac{1}{4}(1 + \tanh \psi)$$

represents the ratio of the distance of F from the leading edge to the major diameter of the ellipse.

The complex flow potential is identical with that given by equation (58) for the flat plate, except that the quantity a^2 in the numerator of the second term is replaced by the constant $a^2 e^{2\psi}$. Since $\psi(\varphi) = \text{constant}$, $\epsilon(\varphi) = 0$ and equation (39) giving the velocity at each point of the surface for a stagnation point at end of major axis becomes

$$v = V \frac{[\sin(\varphi + \alpha) + \sin \alpha] e^{\psi}}{\sqrt{\sinh^2 \psi + \sin^2 \varphi}} \quad (59)$$

and for zero circulation by equation (41)

$$v = V \frac{\sin(\varphi + \alpha) e^{\psi}}{\sqrt{\sinh^2 \psi + \sin^2 \varphi}} \quad (59')$$

Circular arc sections.—It has been shown that the transformation $\zeta = z + \frac{a^2}{z}$ applied to a circle with center at $z=0$ and radius a gives a straight line in the ζ plane, and when applied to a circle with center $z=0$ and radius different from a gives an ellipse in the ζ plane. We now show that if it is used to transform a circle with center at $z=is$ (s being a real number) and radius $\sqrt{a^2+s^2}$, a circular arc results. The coordinates of the transform of the circle C in the ζ plane are given by equation (6) as

$$\begin{aligned}x &= 2a \cosh \psi \cos \theta \\ y &= 2a \sinh \psi \sin \theta\end{aligned}$$

A relation between ψ and θ can be readily obtained. In right triangle OMD (fig. 20), $OM=s$, angle $OMD=\theta$, and recalling that the product of segments of any chord through O is equal to a^2 , $OD = \frac{1}{2}(OP - OP_1) = a \frac{(e^{\psi} - e^{-\psi})}{2} = a \sinh \psi$. Then $s \sin \theta = a \sinh \psi$, and from the equation for y , $y = 2s \sin^2 \theta$. Eliminating both θ and ψ in equation (6) we get

$$x^2 + \left(y + \left(\frac{a^2 - s^2}{s} \right) \right)^2 = \left(\frac{a^2 + s^2}{s} \right)^2 \quad (60)$$

the equation of a circle; but since y can have only positive values, we are limited to a circular arc. In fact, as the point P in Figure 20 moves from A' to A on the circle, the point Q traverses the arc $A_1' A_1$ and as P completes the circuit AA' the arc is traversed in the opposite direction. As in the previous cases, we note that the point Q corresponding to either P or to the inverse and reflected point P' is obtained by completing the parallelogram $OPQP'$. We may also note

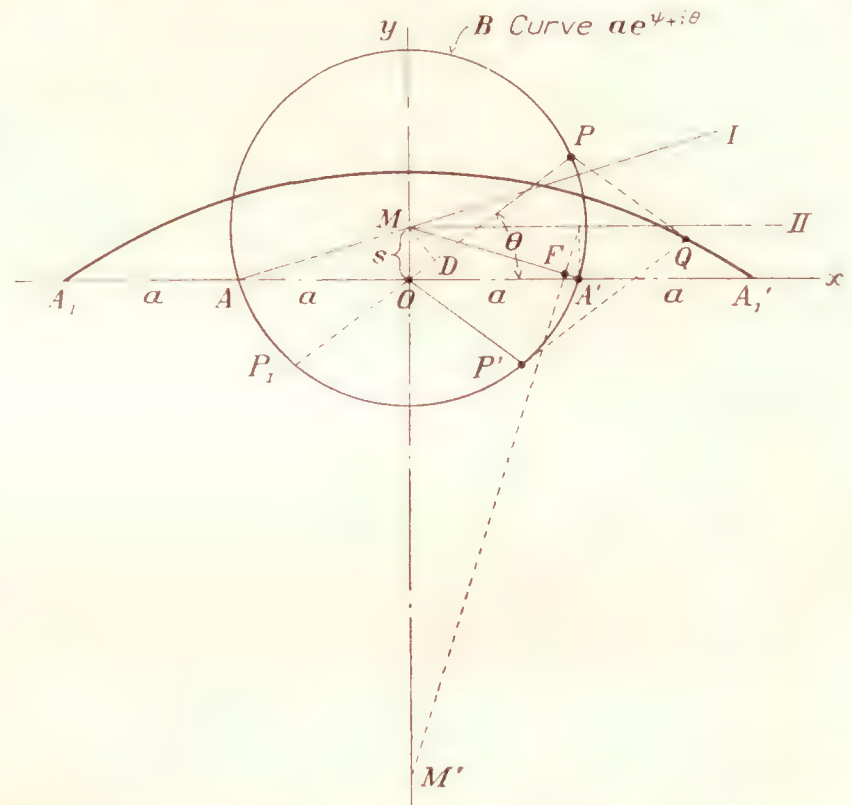


FIGURE 20.—The circular arc airfoil

that had the arc $A_1 A_1'$ been preassigned with the requirement of transforming it into the circle, the most convenient choice of origin of coordinates would be the midpoint of the line, length $4a$, joining the end points. The curve B then resulting from using transformation (5) would be a circle in the z' plane, center at $z'=is$, and the theory developed in the report could be directly applied to this continuous closed B curve.

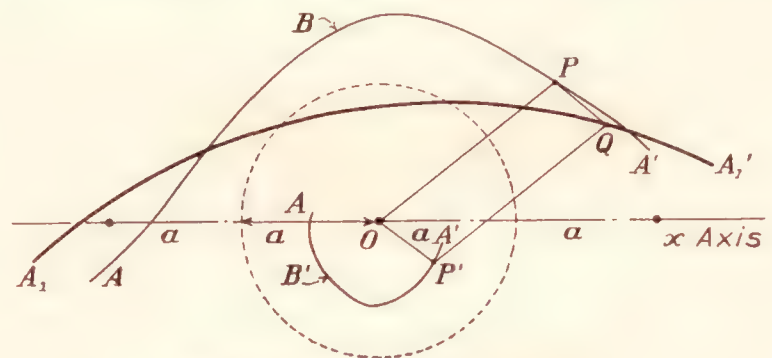


FIGURE 21.—Discontinuous B curve

Had another axis and origin been chosen, e. g., as in Figure 21, the B curve resulting would have finite discontinuities at A and A' , although the arc $A_1 A_1'$ is still obtained by completing the parallelogram $OPQP'$.

The parameters of the arc $A_1 A_1'$ of chord length $4a$, and maximum height $2s$ are then, $R = \sqrt{a^2 + s^2}$, $\beta = \tan^{-1} \frac{s}{a}$. The focus F may be constructed by erecting a perpendicular to the chord at A' of length s

and projecting its extremity on MA' . The center M' of the arc also lies on this line.

The infinite sheet having the circular arc as cross section contains as a special case the flat plate, and thus permits of a better approximation to the mean camber line of actual airfoils. The complex flow potential and the formulas for the velocity at the surface for the circular arc are of the same form as those given in the next section for the Joukowski airfoil, where also a simple geometric interpretation of the parameters ϵ and ψ are given.

Joukowski airfoils.—If equation (5) is applied to a circle with center at $z=s$, s being a real number, and with radius $R=a+s$, a symmetrical Joukowski airfoil (or strut form) is obtained. The general Joukowski airfoil is obtained when the transformation $\zeta = z + \frac{a^2}{z}$ is applied to a circle C passing through the point $z=-a$ and containing $z=a$ (near the circumference usually), and whose center M is not limited to either the x or y axes, but may be on a line OM inclined to the axes. (Fig. 22.) The parametric equations of the shape are as before

$$\left. \begin{aligned} x &= 2a \cosh \psi \cos \theta \\ y &= 2a \sinh \psi \sin \theta \end{aligned} \right\} \quad (6)$$

Geometrically a point Q of the airfoil is obtained by adding the vectors $ae^{\psi+i\theta}$ and $ae^{-\psi-i\theta}$ or by completing the parallelogram $OPQP'$ as before, but now P' lies on another circle B' defined as $z=ae^{-\psi-i\theta}$, the inverse and reflected circle of B with respect to the circle of radius a at the origin (obtained by the transformation of reciprocal radii and subsequent reflection in the x axis). Thus $OP \cdot OP' = a^2$ for all positions of P , and OP' is readily constructed. The center M_1 of the circle B' may be located on the line AM by drawing OM_1 symmetrically to OM with respect to the y axis. Let the coordinate of M be $z=is+de^{i\beta}$, where d , s , and β are real quantities. The circle of radius a , with center M_0 at $z=is$, is transformed into a circular arc through A, A_1' which may be considered the mean camber line of the airfoil. At the tail the Joukowski airfoil has a cusp and the upper and lower surfaces include a zero angle. The lift parameters are

$R = \sqrt{a^2 + s^2} + d$, $\beta = \tan^{-1} \frac{s}{a}$, $a_1 = a^2 = b^2 e^{2i\gamma}$ or $b = a$ and $\gamma = 0$. Since $\gamma = 0$, the second axis has the direction of the x axis. The focus F is determined by laying off the segment $MF = \frac{a^2}{R}$ on the line MA' . This quantity, it may be noted, is obtained easily by the following construction. In triangle MDC' , $MD = R$, MC' and MC are made equal to a , then CF drawn parallel to DC' determines $MF = \frac{a^2}{R}$. The left parabola may be now determined uniquely since its directrix AM and focus F are known.

It may be observed that if it is desired to transform a preassigned Joukowski profile into a circle, there exists a choice of axis and origin for the airfoil such that the inverse of transformation (5) will map the airfoil directly into a circle. This axis is very approximately given by designating the tail as $(-2a, 0)$ and the point midway between the leading edge and the center of curvature of the leading edge as $(+2a, 0)$ the origin then bisecting the line joining these points.

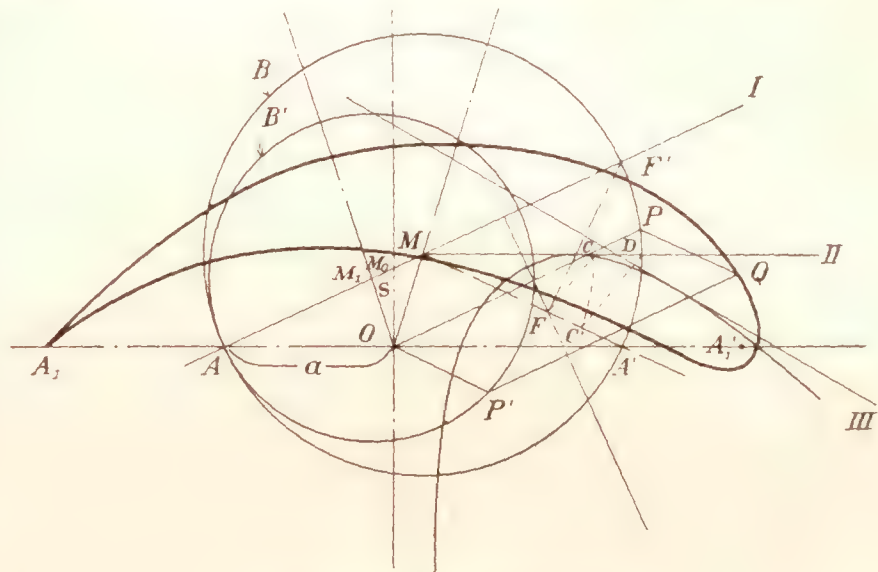


FIGURE 22.—The Joukowski airfoil

The complex potential flow function for the Joukowski airfoil is

$$w(\zeta) = -V \left[g(\zeta) e^{i\alpha} + \frac{R^2 e^{-i\alpha}}{g(\zeta)} \right] + \frac{i\Gamma}{2\pi} \log g(\zeta) \quad (61)$$

where

$$g(\zeta) = \frac{\zeta}{2} \pm \sqrt{\left(\frac{\zeta}{2}\right)^2 - a^2 - m}$$

By equation (39) we have for the velocity at the surface

$$v = \frac{V[\sin(\alpha + \varphi) + \sin(\alpha + \beta)] \left(1 + \frac{d\bar{\epsilon}}{d\theta}\right) e^{\psi_0}}{\sqrt{(\sinh^2 \psi + \sin^2 \theta) \left(1 + \left(\frac{d\psi}{d\theta}\right)^2\right)}}$$

This formula was obtained by transforming the flow around C into that around B and then into that around A . Since we know that B is itself a circle for this case, we can simply use the latter two transformations alone.

We get

$$v = \frac{V[\sin(\alpha + \varphi) + \sin(\alpha + \beta)]e^\psi}{\sqrt{\sinh^2 \psi + \sin^2 \theta}} \quad (62)$$

That these formulas are equivalent is immediately evident since the quantity

$$\frac{e^{\psi_0 - \psi} \left(1 + \frac{d\bar{\epsilon}}{d\theta} \right)}{\sqrt{1 + \left(\frac{d\bar{\psi}}{d\theta} \right)^2}}$$

is unity being the ratio of the magnification of each arc element of C to that of B . (See eq. (37).)

A very simple geometrical picture of the parameters ϵ and ψ , exists for the cases discussed. In Figure 23 the value of ϵ or $\varphi - \theta$ at the point P is simply

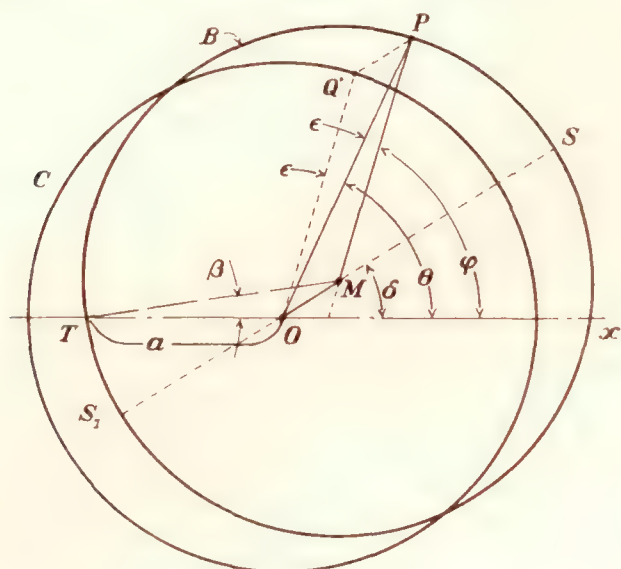


FIGURE 23.—Geometrical representation of ϵ and ψ for Joukowski airfoils

angle OPM , i. e., the angle subtended at P by the origin O and the center M . The angle of zero lift is the value of ϵ for $\theta = \pi$; i. e., $\epsilon_{\text{Tail}} = \beta = OTM$. In particular, we may note that $\epsilon = 0$ at S and S_1 which are on the straight line OM . Consider the triangle OMP , where $OP = ae^\psi$, $MP = R = ae^{\psi_0}$, $\frac{OM}{MP} = \rho$, angle $OPM = \epsilon$; also, $MOX = \delta$, $MOP = \theta - \delta$, $OMP = \pi - (\varphi - \delta)$. Then by the law of cosines, we have

$$e^{2(\psi - \psi_0)} = 1 + 2\rho \cos(\varphi - \delta) + \rho^2$$

or

$$\psi - \psi_0 = \frac{1}{2} \log (1 + 2\rho \cos(\varphi - \delta) + \rho^2) \quad (63)$$

$$= \sum_1^{\infty} (-1)^{n-1} \frac{\cos n(\varphi - \delta)}{n} \rho^n$$

and by the law of sines

$$\sin \epsilon = \frac{\rho \sin(\varphi - \delta)}{(1 + 2\rho \cos(\varphi - \delta) + \rho^2)^{1/2}}$$

or

$$\begin{aligned} \epsilon(\varphi) &= \tan^{-1} \frac{\rho \sin(\varphi - \delta)}{1 + \rho \cos(\varphi - \delta)} \\ &= \sum_1^{\infty} (-1)^{n-1} \frac{\sin n(\varphi - \delta)}{n} \rho^n \end{aligned} \quad (64)$$

We see that, as required, the expressions for the “radial distortion” $\psi(\varphi)$ and the “angular distortion” $\epsilon(\varphi)$ are conjugate Fourier series and may be expressed as a single complex quantity

$$\begin{aligned} (\psi - \psi_0) - i\epsilon &= \sum_1^{\infty} \frac{(-1)^{n-1}}{n} \rho^n e^{-in(\varphi - \delta)} \\ &= \log [1 + \rho e^{-i(\varphi - \delta)}] \end{aligned}$$

It is evident also that the coefficient for $n=1$ or the “first harmonic term” is simply $\rho e^{i\delta}$ and a translation by this quantity brings the circle C into coincidence with B as was pointed out on page 187.

The constant $\psi_0 = \frac{1}{2\pi} \int_0^{2\pi} \psi d\varphi$ is readily shown to be

invariant to the choice of origin O , as long as O is within B . We have

$$\begin{aligned} \frac{1}{2\pi} \int_0^{2\pi} \psi d\varphi &= \frac{1}{2\pi} \int_0^{2\pi} \frac{1}{2} \log (1 + 2\rho \cos(\varphi - \delta) + \rho^2) e^{2\psi_0} d\varphi \\ &= \frac{1}{2\pi} \int_0^{2\pi} \left(\psi_0 + \sum_1^{\infty} (-1)^{n-1} \frac{\cos n(\varphi - \delta)}{n} \rho^n \right) d\varphi = \psi_0 \end{aligned}$$

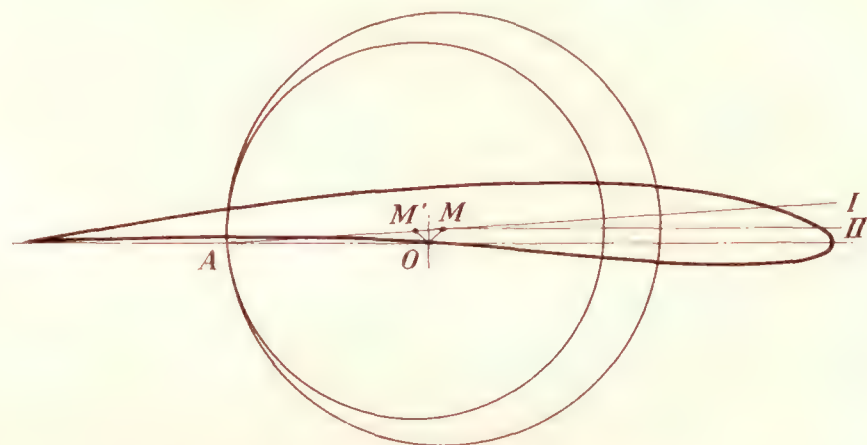


FIGURE 24.—The Joukowski airfoil $\rho=0.10$, $\delta=45^\circ$

Figure 24 shows the Joukowski airfoil defined by $\rho=0.10$ and $\delta=45^\circ$, and Figure 25 shows the $\bar{\psi}(\theta)$, $\psi(\varphi)$, $\bar{\epsilon}(\theta)$, and $\epsilon(\varphi)$ curves for this airfoil.

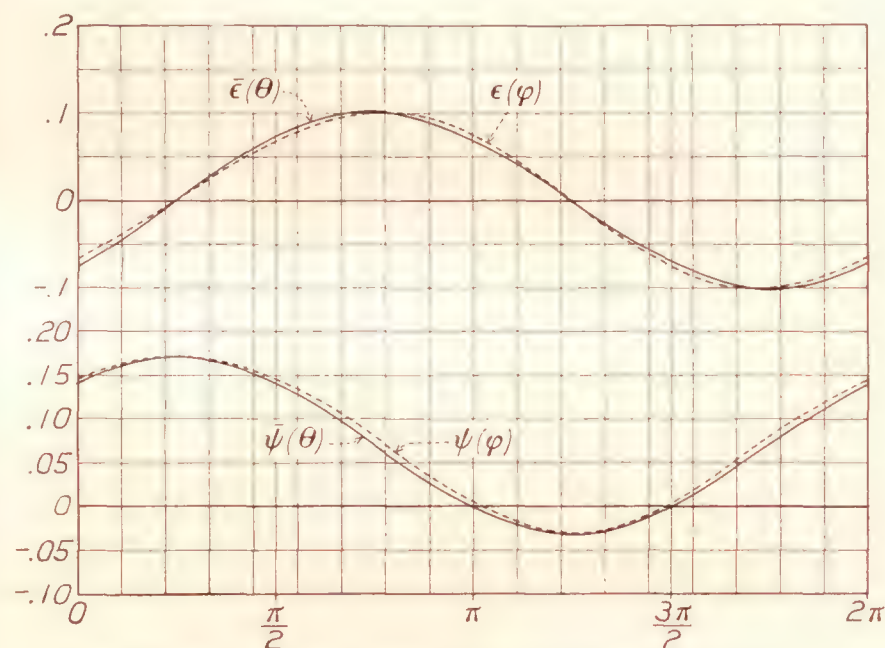


FIGURE 25.—The $\bar{\epsilon}(\theta)$ and $\bar{\psi}(\theta)$ curves for the airfoil in Figure 24

Arbitrary sections.—In order to obtain the lift parameters of an arbitrary airfoil, a convenient choice of coordinate axes is first made as indicated for the Joukowski airfoil and as stated previously. (Page 181.) The curve resulting from the use of transformation (5) will yield an arbitrary curve $ae^{\psi+i\theta}$ which will, in general, differ very little from a circle. The inverse and reflected curve $ae^{-\psi-i\theta}$ will also be almost circular. The transition from the curve $ae^{\psi+i\theta}$ to a circle is reached by obtaining the solution $\epsilon(\varphi)$ of equation (13). The method of obtaining this solution as already given converges with extreme rapidity for nearly circular curves.

The geometrical picture is analogous to that given for the special cases. In Figure 26 it may be seen that a point Q on the airfoil (N. A. C. A. -M6) corre-

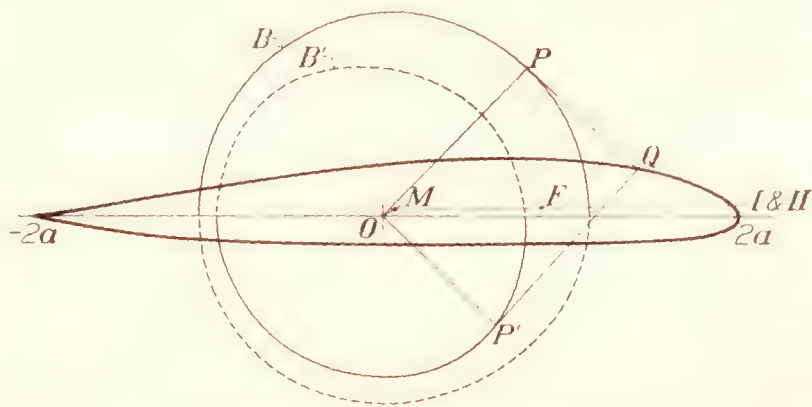


FIGURE 26.—The N. A. C. A. -M6 airfoil

sponding to P on the B curve (or P' on the B' curve) is obtained by constructing parallelogram $OPQP'$. The $\bar{\psi}(\theta)$ and $\bar{\epsilon}(\theta)$ curves are shown in Figure 27 for this airfoil. The complex velocity potential and the expression for velocity at the surface are given respec-

The method used for arbitrary airfoils is readily applied to arbitrary thin arcs or to broken lines such as the sections of tail surfaces form approximately. In Figure 26 the part of the airfoil boundary above the x axis transforms by equation (5) into the two discontinuous arcs shown by full lines, while the lower boundary transforms into the arcs shown by dashed lines. If the upper boundary surface is alone given (thin airfoil) we may obtain a closed curve $ae^{\psi+i\theta}$ only by joining the end points by a chord of length $4a$ and choosing the origin at its midpoint.²⁵ The resulting curve has two double points for which the first derivative is not uniquely defined and, in general, it may be seen that infinite velocities correspond to such points.

At a point of the $\bar{\psi}(\theta)$ curve corresponding to a mathematically sharp corner, there exist two tangents, that is, the slope $\frac{d\bar{\psi}(\theta)}{d\theta}$ is finitely discontinuous. The

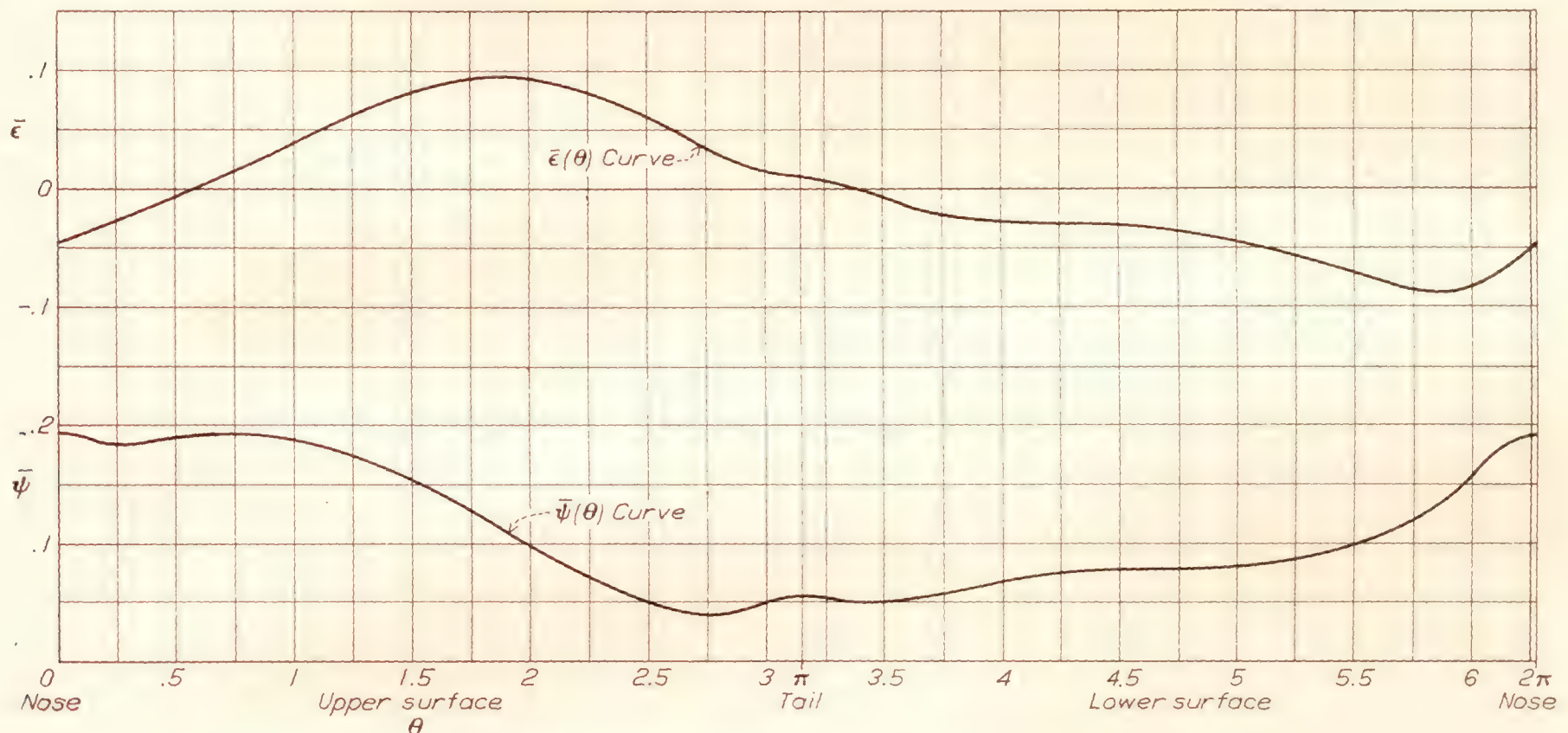


FIGURE 27.—The $\bar{\epsilon}(\theta)$ and $\bar{\psi}(\theta)$ curves for the N. A. C. A. -M6 airfoil

tively by equations (33) and (39). The lift parameters are

$$R = ae^{\psi_0}, \beta = \epsilon_{tail} \text{ (at } \theta = \pi), M \text{ is at } z = c_1 = \frac{R}{\pi} \int_0^\pi \psi(\varphi) e^{i\varphi} d\varphi$$

and F is at $z = c_1 + \frac{a_1}{R}$ where a_1 is given in equation (25').

The first and second axes for the N. A. C. A. -M6 airfoil are found to coincide and this airfoil has then a constant center of pressure at F . Figures 28 (a) to 28 (l) give the pressure distribution (along the x axis) for a series of angles of attack as calculated by this theory and as obtained by experiment.²⁴ Table I contains the essential numerical data for this airfoil.

²⁴ The experimental results are taken from test No. 323 of the N. A. C. A. variable-density wind tunnel. The angle of attack α substituted in equation (39) has been modified arbitrarily to take account of the effects of finite span, tunnel-wall interference, and viscosity, by choosing it so that the theoretical lift is about 10 per cent more than the corresponding experimental value. The actual values of the lift coefficients are given in the figures.

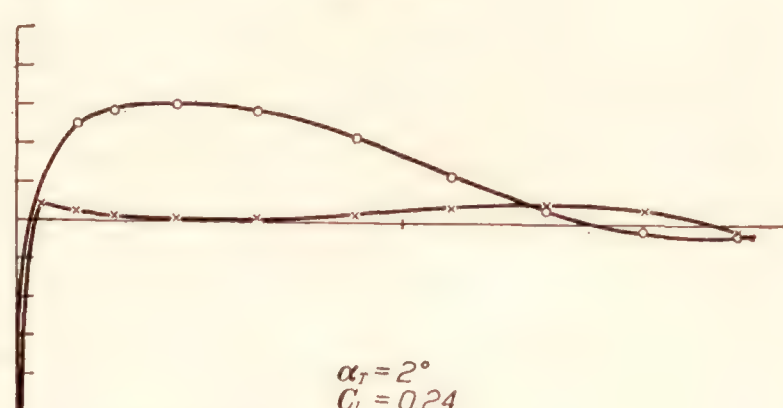
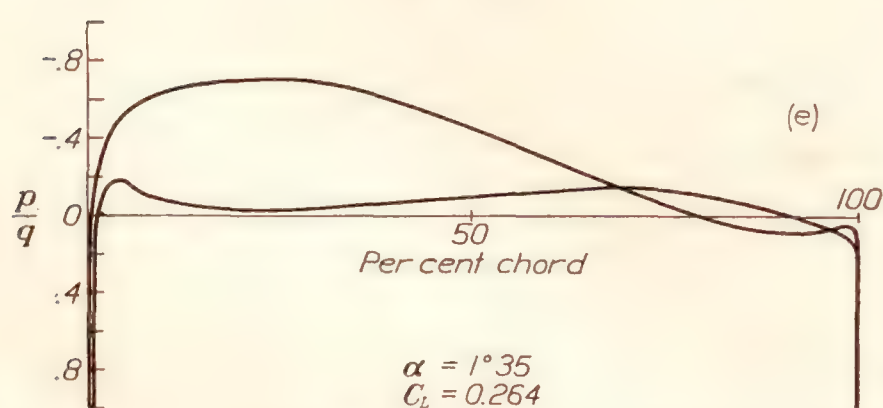
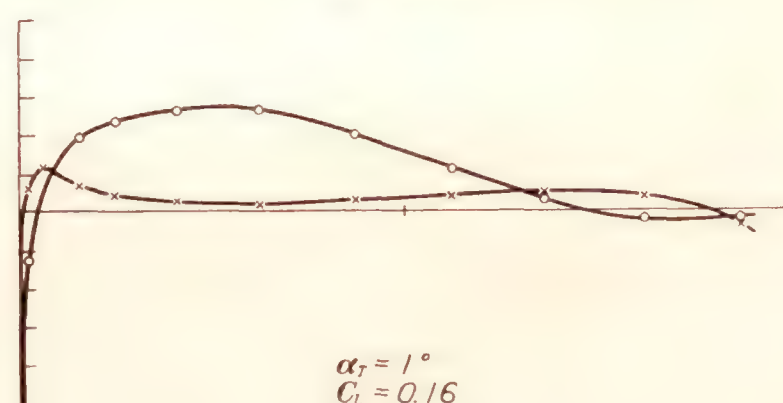
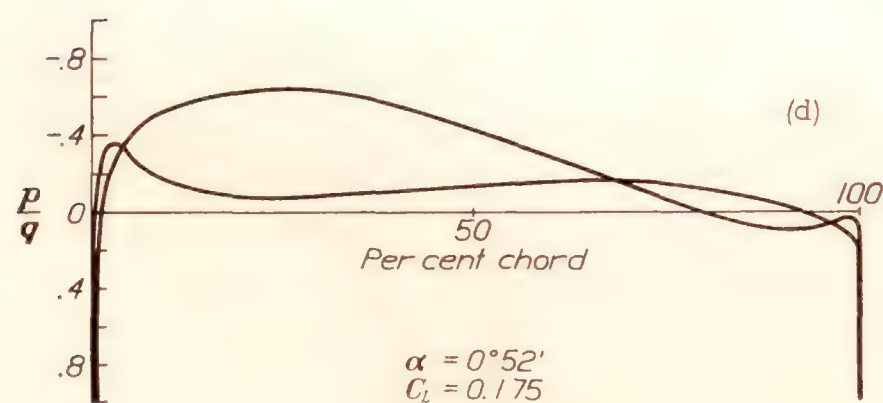
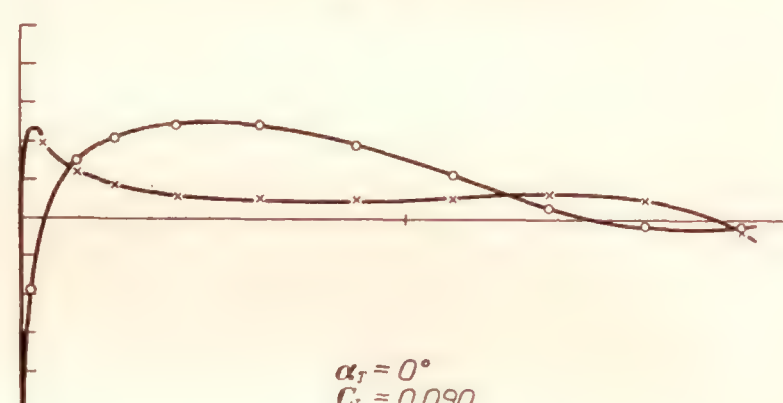
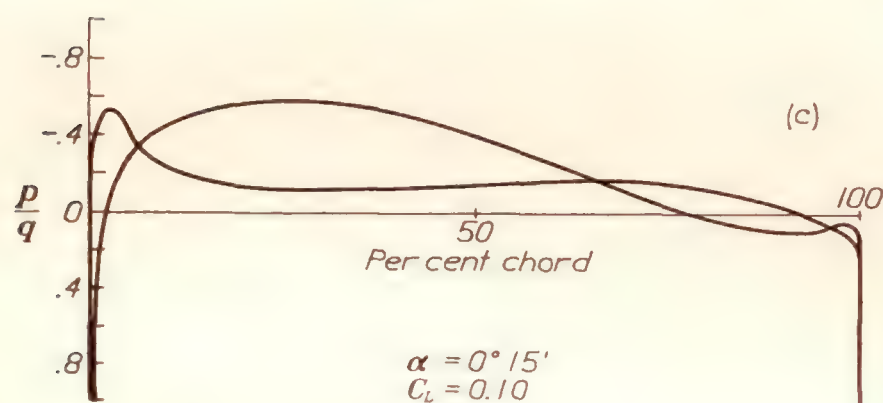
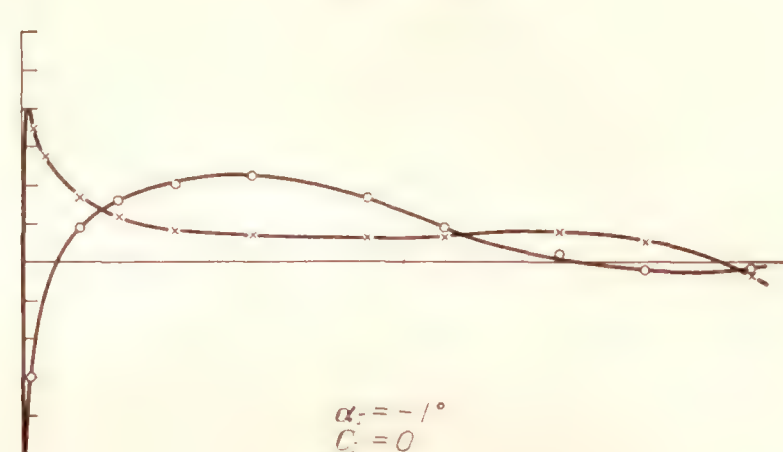
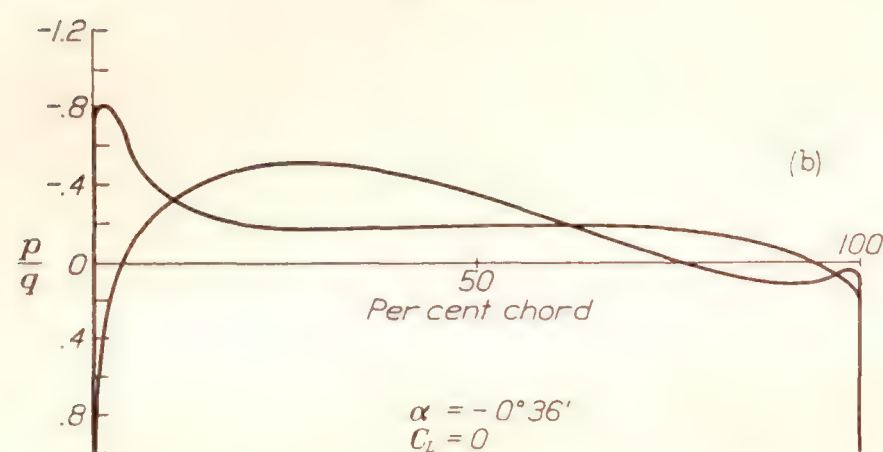
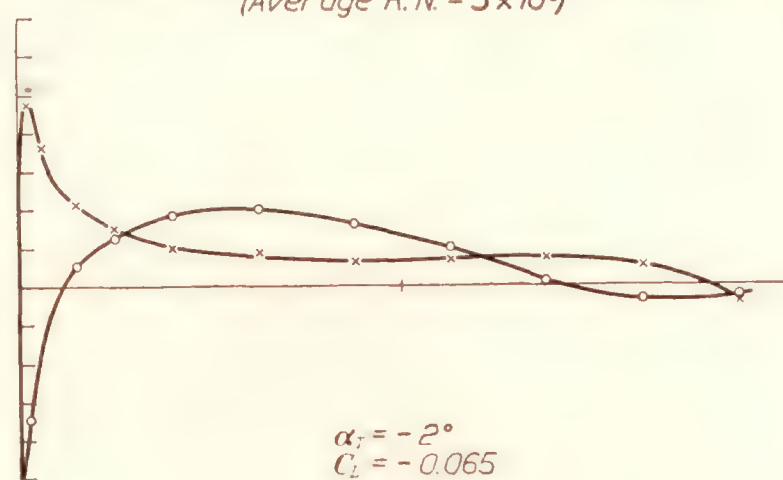
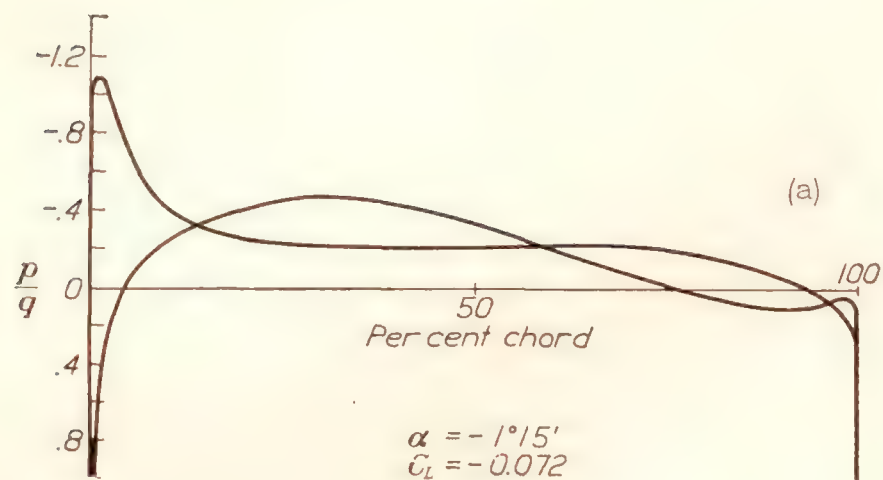
curve $\bar{\epsilon}(\theta)$ must have an infinite slope at such a point for according to a theorem in the theory of Fourier series, at a point of discontinuity of a F. S., the conjugate F. S. is properly divergent. This manifests itself in the velocity-formula equation (39) in the factor $\left(1 + \frac{d\bar{\epsilon}}{d\theta}\right)$ which is infinite at these sharp corners. For practical purposes, however, a rounding of the sharp edge, however small, considerably alters the slope $\frac{d\bar{\epsilon}(\theta)}{d\theta}$ at this point.

Ideal angle of attack.—A thin airfoil, represented by a line arc, has both a sharp leading edge and a sharp trailing edge. The Kutta assumption for fixing the circulation places a stagnation point at the tail for all angles of attack. At the leading edge, however,

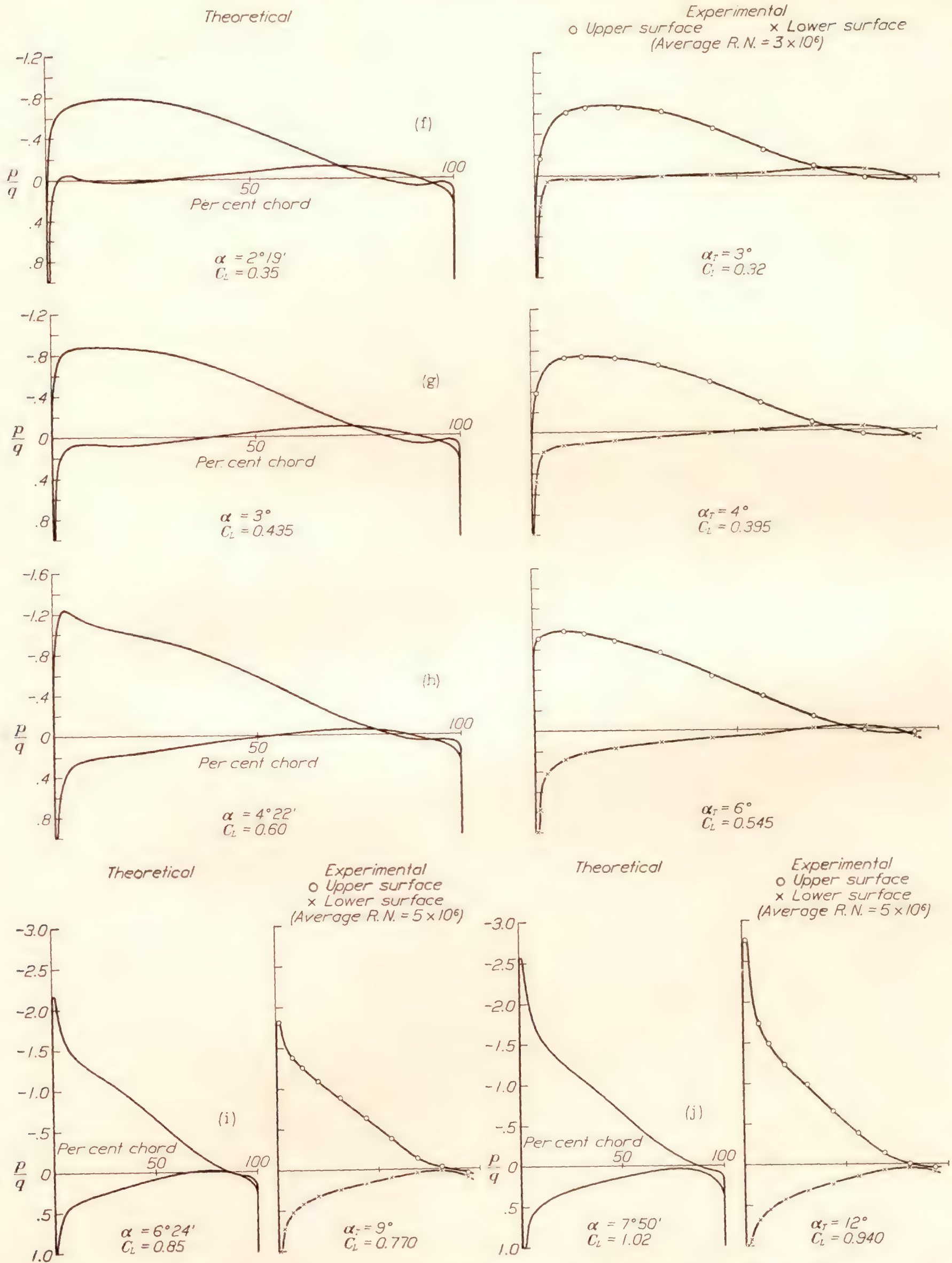
²⁵ Note that $\bar{\psi}(\theta + \pi) = -\bar{\psi}(\theta)$ for this case.

Theoretical

Experimental

o Upper surface x Lower surface
(Average $R.N. = 3 \times 10^6$)

FIGURES 28 a to e.—Theoretical and experimental pressure distribution for the M6 airfoil at various angles of attack



FIGURES 28 f to j.—Theoretical and experimental pressure distribution for the M6 airfoil at various angles of attack

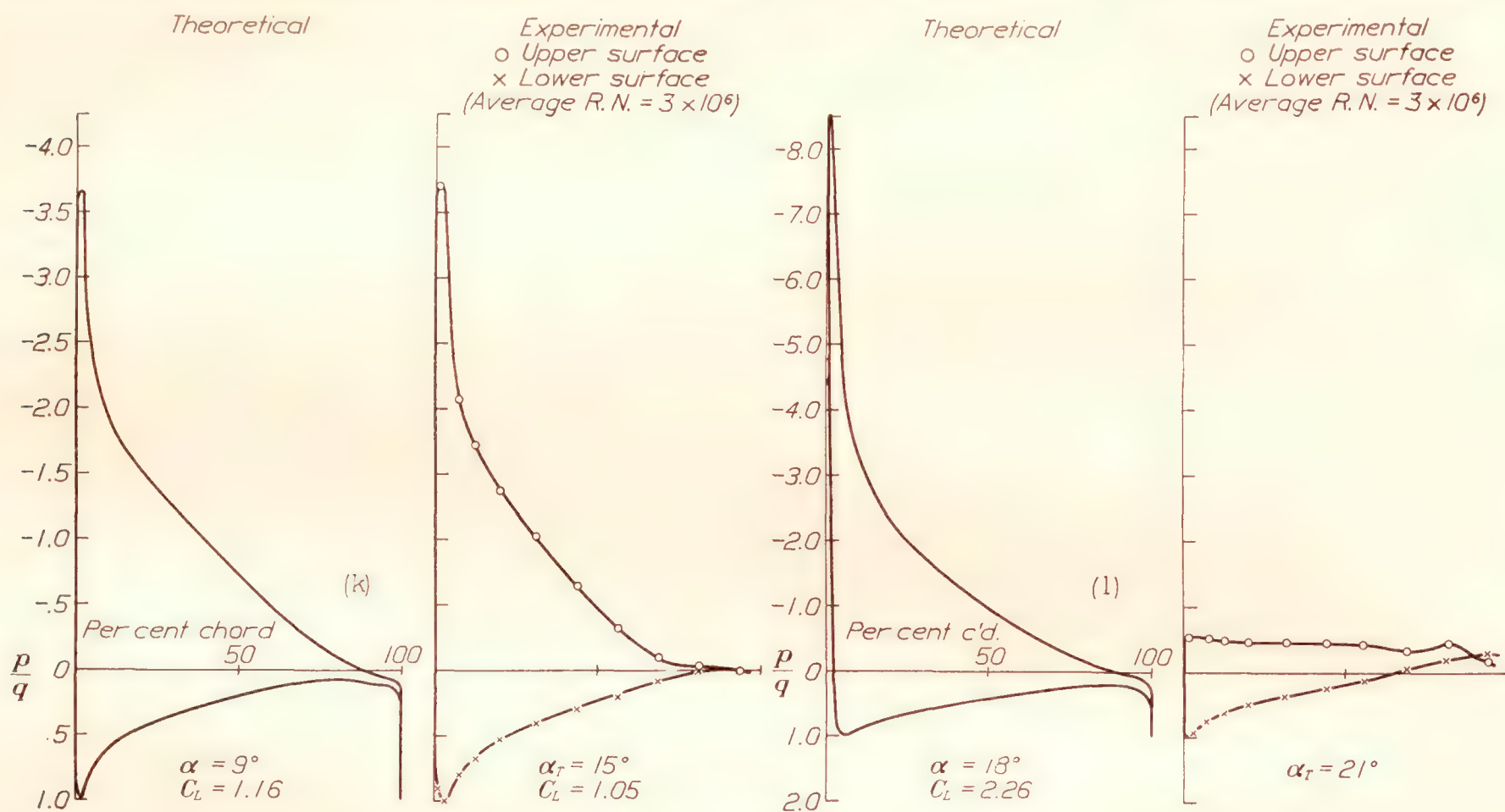
the velocity is infinite at all angles of attack except one, namely, that angle for which the other stagnation point is at the leading edge. It is natural to expect that for this angle of attack in actual cases the frictional losses are at or near a minimum and thus arises the concept of "ideal" angle of attack introduced by Theodorsen (reference 8) and which has also been designated "angle of best streamlining." The definition for the ideal angle may be extended to thick airfoils, as that angle for which a stagnation point occurs directly at the foremost point of the mean camber line.

The lift at the leading edge vanishes and the change from velocity to pressure along the airfoil surface is usually more gradual than at any other angle of attack.

of this function, one can determine airfoil shapes of definite properties. The $\epsilon(\varphi)$ function, which we have designated conformal angular distortion function, will be seen to determine not only the shape but also to give easily all the theoretical aerodynamic characteristics of the airfoil.

An arbitrary $\epsilon(\varphi)$ curve is chosen, single valued, of period 2π , of zero area, and such that $-\infty \leq \frac{d\epsilon}{d\varphi} \leq 1$.

These limiting values of $\frac{d\epsilon}{d\varphi}$ are far beyond values yielding airfoil shapes.²⁷ The $\psi(\varphi)$ function, except for the constant ψ_0 , is given by the conjugate of the Fourier expansion of $\epsilon(\varphi)$ or, what is the same, by evaluating equation (14) as a definite integral. The



FIGURES 28 k to l.—Theoretical and experimental pressure distribution for the M6 airfoil at various angles of attack

The minimum profile drag of airfoils actually occurs very close to this angle. At the ideal angle, which we denote by α_I , the factor $[\sin(\alpha + \varphi) + \sin(\alpha + \beta)]$ in equation (39) is zero not only for $\theta = \pi$ or $\epsilon = \epsilon_T = \beta$ but also for $\theta = 0$ or $\epsilon = \epsilon_N$. We get

$$\alpha_I + \epsilon_N = -(\alpha_I + \epsilon_T) \text{ or } \alpha_I = -\frac{(\epsilon_N + \epsilon_T)}{2} \quad (65)$$

CREATION OF FAMILIES OF WING SECTIONS

The process of transforming a circle into an airfoil is inherently less difficult than the inverse process of transforming an airfoil into a circle. By a direct application of previous results we can derive a powerful and flexible method for the creation of general families of airfoils. Instead of assuming that the $\bar{\psi}(\theta)$ curve is preassigned (that is, instead of a given airfoil), we assume an arbitrary $\psi(\varphi)$ or $\epsilon(\varphi)$ curve²⁸ as given. This is equivalent to assuming as known a boundary-value function along a circle and, by the proper choice

constant ψ_0 is an important arbitrary²⁸ parameter which permits of changes in the shape and for a certain range of values may determine the sharpness of the trailing edge.

We first obtain the variable θ as $\theta(\varphi) = \varphi - \epsilon(\varphi)$, so that the quantity $\bar{\psi}$ considered as a function of θ is $\bar{\psi}(\theta) = \bar{\psi}[\varphi(\theta)]$. The coordinates of the airfoil surface are then

$$\begin{aligned} x &= 2a \cosh \psi \cos \theta \\ y &= 2a \sinh \psi \sin \theta. \end{aligned} \quad (6)$$

²⁷ For common airfoils, with a proper choice of origin, $\left| \frac{d\epsilon}{d\varphi} \right| < 0.30$.

²⁸ For common airfoils ψ_0 is usually between 0.05 and 0.15. The constant ψ_0 is not, however, completely arbitrary. We have seen that the condition given by equation (22) is sufficient to yield a contour free from double points in the z' plane. We may also state the criterion that the inverse of equation (5) applied to this contour shall yield a contour in the ζ plane free from double points. Consider the function $\bar{\psi}(\theta)$ for θ varying from 0 to π only. The negative of each value of $\bar{\psi}(\theta)$ in this range is considered associated with $-\theta$, i. e., $\pi \leq \theta \leq 2\pi$. Designate the function thus formed from $\theta = 0$ to 2π by $\bar{\psi}(\theta)^*$. Then $\bar{\psi}(\theta)^*$ represents a line arc in the ζ plane, i. e., the upper surface of a contour. [See footnote 25.] Then for the entire contour to be free from double points it is necessary that the lower surface should not cross the upper, that is, the original $\bar{\psi}(\theta)$ curve for θ varying from π to 2π must not cross below $\bar{\psi}(\theta)^*$.

²⁹ Subject to some general restrictions given in the next paragraph.

The velocity at the surface is

$$v = V \frac{[\sin(\alpha + \varphi) + \sin(\alpha + \beta)] e^{\psi_0}}{\sqrt{(\sinh^2 \psi + \sin^2 \theta) \left[\left(1 - \frac{d\epsilon}{d\varphi}\right)^2 + \left(\frac{d\psi}{d\varphi}\right)^2 \right]}} \quad (39')$$

and is obtained by using equation (37') instead of (37) in deriving (39). The angle of zero lift β is given by

$$\varphi(\theta) = \theta + \bar{\epsilon}(\theta) \text{ for } \theta = \pi, \text{ i. e., } \varphi(\pi) = \pi + \beta.$$

The following figures and examples will make the process clear. We may first note that the most natural method of specifying the $\epsilon(\varphi)$ function is by a Fourier series expansion. In this sense then the elementary types of $\epsilon(\varphi)$ functions are the individual terms of this expansion.

29(h) to 29(t). In particular, the second harmonic term may yield S shapes, and by a proper combination of first and second harmonic terms, i. e., by a proper choice of the constants A_1 , A_2 , δ_1 , and δ_2 in the relation

$$\epsilon(\varphi) = A_1 \sin(\varphi - \delta_1) + A_2 \sin(2\varphi - \delta_2)$$

it is possible to fix the focus F of the lift parabola as the center of pressure for all angles of attack.²⁹ The equation

$$\epsilon(\varphi) = 0.1 \sin(\varphi - 60^\circ) + 0.05 \cos 2\varphi$$

represents such an airfoil and is shown in Figure 29(u).

The general process will yield infinite varieties of contours by superposition of sine functions; in fact, if



FIGURE 29.—Airfoils created by varying $\epsilon(\varphi)$

Consider first the effect of the first harmonic term

$$\epsilon(\varphi) = A_1 \sin(\varphi - \delta_1), \quad \psi_0 = c$$

In Figures 29(a) to 29(g) may be seen the shapes resulting by displacing δ_1 successively by intervals of 15° and keeping the constants $A_1 = 0.10$ and $\psi_0 = 0.10$. The first harmonic term is of chief influence in determining the airfoil shape. The case $\epsilon(\varphi) = 0.1 \sin(\varphi - 45^\circ)$ is given detailed in Table II. (This airfoil is remarkably similar to the commonly used Clark Y airfoil.) The entire calculations are characterized by their simplicity and, as may be noted, are completely free from the necessity of any graphical evaluations or constructions.

The effect of the second and higher harmonics as well as the constant ψ_0 may be observed in Figures

the process is thought of as a boundary-value problem of the circle, it is seen that it is sufficiently general to yield every closed curve for which Riemann's theorem applies.

LANGLEY MEMORIAL AERONAUTICAL LABORATORY,
NATIONAL ADVISORY COMMITTEE FOR AERONAUTICS,
LANGLEY FIELD, VA., November 4, 1932.

²⁹ This is accomplished as follows: We seek to determine the constants A_1 , A_2 , δ_1 , and δ_2 so that $\beta = \gamma$, where γ is obtained from equation (25') as $a_1 = b^2 e^{2i\gamma} = a^2 + \frac{c_1^2}{2} + c_2$ and we may note that $\frac{c_1}{a e^{\psi_0}} = A_1 e^{i\delta_1}$ and $\frac{c_2}{a^2 e^{2\psi_0}} = A_2 e^{i\delta_2}$. These relations are transcendental; however, with but a few practice trials, solutions can be obtained at will. Addition of higher harmonics will yield further shapes having the same center of pressure properties if β is kept unchanged.

APPENDIX

I. EVALUATION OF THE INTEGRAL.

$$\epsilon(\varphi') = -\frac{1}{2\pi} \int_0^{2\pi} \psi(\varphi) \cot \frac{\varphi - \varphi'}{2} d\varphi \quad (13)$$

$$= \frac{1}{\pi} \int_0^{2\pi} \frac{d\psi(\varphi)}{d\varphi} \log \left| \sin \frac{\varphi - \varphi'}{2} \right| d\varphi \quad (13')$$

The function $\psi(\varphi)$ is of period 2π and is considered known. (Note that the variables φ and φ' are replaced by θ and θ' , φ_1 and φ_1' , φ_2 and φ_2' , etc., in equation (21) and that the following formula is applicable for all these cases.)

A 20-point method for evaluating equation (13) as a definite integral gives

$$\epsilon(\varphi') \cong -\frac{1}{\pi} \left[a_0 \frac{d\psi(\varphi)}{d\varphi} + a_1(\psi_1 - \psi_{-1}) + a_2(\psi_2 - \psi_{-2}) + \dots + a_9(\psi_9 - \psi_{-9}) \right]_{\varphi=\varphi'} \quad (I)$$

where

$$\psi_1 = \text{value of } \psi(\varphi) \text{ at } \varphi = \varphi' + \frac{\pi}{10}$$

.

$$\psi_n = \text{value of } \psi(\varphi) \text{ at } \varphi = \varphi' + \frac{n\pi}{10}$$

$$(n = 1, -1, 2, -2, \dots, 9, -9).$$

and the constants a_n are as follows: $a_0 = \frac{\pi}{10} = 0.3142$; $a_1 = 1.091$; $a_2 = 0.494$; $a_3 = 0.313$; $a_4 = 0.217$; $a_5 = 0.158$; $a_6 = 0.115$; $a_7 = 0.0884$; $a_8 = 0.0511$; and $a_9 = 0.0251$.

This formula may be derived directly from the definition of the definite integral. The 20 intervals¹ chosen are $\varphi - \frac{\pi}{20}$ to $\varphi + \frac{\pi}{20}$, $\varphi + \frac{\pi}{20}$ to $\varphi + \frac{3\pi}{20}$, etc.

It is only necessary to note that by expanding $\psi(\varphi)$ in a Taylor series around $\varphi = \varphi'$ we get

$$\frac{1}{2} \int_{\varphi'-s}^{\varphi'+s} \psi(\varphi) \cot \frac{\varphi - \varphi'}{2} d\varphi \cong -2s \left[\frac{d\psi(\varphi)}{d\varphi} \right]_{\varphi=\varphi'}$$

where the interval $\varphi' - s$ to $\varphi' + s$ is small. And, in general,

$$\frac{1}{2} \int_{\varphi_1}^{\varphi_2} \psi(\varphi) \cot \frac{\varphi - \varphi'}{2} d\varphi$$

is very nearly

$$-\psi_A \log \left| \frac{\sin \frac{\varphi - \varphi_2}{2}}{\sin \frac{\varphi - \varphi_1}{2}} \right|$$

where the range $\varphi_2 - \varphi_1$ is small and ψ_A is the average value of $\psi(\varphi)$ in this range. The constants a_n for the 20 divisions chosen above are actually

$$a_n = \log \left| \frac{\sin \pi \frac{2n+1}{40}}{\sin \pi \frac{2n-1}{40}} \right| \quad (n = -9, \dots, +9)$$

As an example of the calculation of $\bar{\epsilon}(\theta)$ we may refer to Table I and Figures 26 and 27 for the N. A. C. A. -M6 airfoil. From the $\bar{\psi}(\theta)$ curve (fig. 27) we obtain the 20 values of ψ and $\frac{d\bar{\psi}}{d\theta}$ for 20 equal intervals of θ .

For the airfoil (fig. 26) we get the following values:

(Upper θ surface)	ψ	$\frac{d\bar{\psi}}{d\theta}$	(Lower θ surface)	ψ	$\frac{d\bar{\psi}}{d\theta}$
0 (nose)	0.192	0.000	$\frac{11\pi}{10}$	0.049	-0.002
$\frac{\pi}{10}$.185	.027	$\frac{12\pi}{10}$.057	.050
$\frac{2\pi}{10}$.192	.000	$\frac{13\pi}{10}$.071	.030
$\frac{3\pi}{10}$.189	-.030	$\frac{14\pi}{10}$.077	.011
$\frac{4\pi}{10}$.174	-.064	$\frac{15\pi}{10}$.079	.000
$\frac{5\pi}{10}$.146	-.095	$\frac{16\pi}{10}$.082	.016
$\frac{6\pi}{10}$.110	-.114	$\frac{17\pi}{10}$.090	.039
$\frac{7\pi}{10}$.077	-.086	$\frac{18\pi}{10}$.111	.091
$\frac{8\pi}{10}$.052	-.066	$\frac{19\pi}{10}$.150	.154
$\frac{9\pi}{10}$.041	.025	2π (nose)	.192	.000
π (tail)	.055	.000			

The value of ϵ at the tail (i. e., the angle of zero lift) is, for example, using formula I

$$\begin{aligned} \epsilon = & -\frac{1}{\pi} \left[\frac{\pi}{10} \times 0 \right. \\ & + 1.091(.049 - .041) \\ & + .494(.057 - .052) \\ & + .313(.071 - .077) \\ & + .217(.077 - .110) \\ & + .158(.079 - .146) \\ & + .115(.082 - .174) \\ & + .0884(.090 - .189) \\ & + .0511(.111 - .192) \\ & \left. + .0251(.150 - .185) \right] = .0105 \end{aligned}$$

¹ Reference 2, p. 11, gives a 10-point method result.

The value of ϵ for $\theta = \frac{3\pi}{10}$, for example, is obtained by a cyclic rearrangement. Thus,

$$\begin{aligned} \epsilon = & -\frac{1}{\pi} \left[\frac{\pi}{10} (-0.030) \right. \\ & + 1.091(.174 - .192) \\ & + .494(.146 - .185) \\ & + .313(.110 - .192) \\ & + .217(.077 - .150) \\ & + .158(.052 - .111) \\ & + .115(.041 - .090) \\ & + .0884(.055 - .082) \\ & + .0511(.049 - .079) \\ & \left. + .0251(.057 - .077) \right] = .0347 \end{aligned}$$

The 20 values obtained in this way form the $\bar{\epsilon}_1(\theta)$ curve, which for all practical purposes for the airfoil considered, is actually identical with the final $\bar{\epsilon}(\theta)$ curve.

II. NOTES ON THE TRANSFORMATION.

$$\zeta = f(z) = c_1 + z + \frac{a_1}{z} + \frac{a_2}{z^2} + \dots \quad (4')$$

There exist a number of theorems giving general limiting values for the coefficients of the transformation equation (4), which are interesting and to some extent useful. If $\zeta = f(z)$ transforms the external region of the circle C of radius R in the z plane, into the external region of a contour A in the ζ plane in a one-to-one conformal manner and the origin $\zeta = 0$ lies *within* the contour A (and $f'(\infty) = 1$) then the area S inclosed by A is given by the Faber-Bieberbach theorem as ²

$$S = R^2 \pi - \sum_{n=1}^{\infty} \frac{n|a_n|^2}{R^{2(n+1)}}$$

Since all members of the above series term are positive, it is observed that the area of C is greater than that inclosed by any contour A in the ζ plane (or, at most, equal to the area inclosed by A if A is a circle).

This theorem leads to the following results

$$|a_1| \leq R^2 \quad (a)$$

$$|c_1| \leq 2R \quad (b)$$

Let us designate the circle of radius R about the conformal centroid M as center as C_1 (i. e., the center is at $\zeta = c_1$; this circle has been called the "Grundkreis" or "basic" circle by von Mises). Then since $\frac{|a_1|}{R}$ represents the distance of the focus F from M , the relation (a) states that the focus is always within C_1 . In fact, a further extension shows that if r_0 is the radius of the largest circle that can be inclosed within A , then F is removed from C_1 by at least $\frac{r_0^2}{R}$.

From relation (b) may be derived the statement that if any circle within A is concentrically doubled in radius it is contained entirely within a circle about M as center of radius $2R$. Also, if we designate by c the largest diameter of A (this is usually the "chord" of the airfoil) then the following limits can be derived:

$$R \geq \frac{1}{4}c$$

$$R \leq \frac{1}{2}c$$

These inequalities lead to interesting limits for the lift coefficient. Writing the lift coefficient as

$$C_L = \frac{L}{\frac{1}{2}\rho V^2 c}$$

where by equation (45) the lift force is given by

$$L = 4\pi R \rho V^2 \sin(\alpha + \beta)$$

we have

$$2\pi \sin(\alpha + \beta) \leq C_L = \frac{8\pi R}{c} \sin(\alpha + \beta) \leq 4\pi \sin(\alpha + \beta) \quad (II)$$

The flat plate is the only case where the lower limit is reached, while the upper limit is attained for the circular cylinder only. We may observe that a curved thin plate has a lift coefficient which exceeds $2\pi \sin(\alpha + \beta)$ by a very small amount. In general, the thickness has a much greater effect on the value of the lift coefficient than the camber. For common airfoils the lift coefficient is but slightly greater than the lower limit and is approximately $1.1 \times 2\pi \sin(\alpha + \beta)$.

Another theorem, similar to the Faber-Bieberbach area theorem, states that if the equation $\zeta = f(z)$ transforms the internal region of a circle in the z plane into the internal region of a contour B in the ζ plane in a one-to-one conformal manner and $f'(0) = 1$ (the origins are within the contours) then the area of the circle is less than that contained by any contour B . This theorem, extended by Bieberbach, has been used in an attempt to solve the arbitrary airfoil.³ The process used is one in which the area theorem is a criterion as to the direction in which the convergence proceeds. Although theoretically sound, the process is, when applied, extremely laborious and very slowly convergent. It can not be said to have yielded as yet really satisfactory results.

III. LOCATION OF THE CENTER OF PRESSURE FOR AN ARBITRARY AIRFOIL

It is of some interest to know the exact location of the center of pressure *on the x axis* as a function of the angle of attack. In Figure 30, O is the origin, M the conformal centroid, L the line of action of the lift force for angle of attack α . Let us designate the

² Müller, W., Zs. f. angew. Math. u. Mech. Bd. 5 S. 397, 1925.
Höhdorf, F., Zs. f. angew. Math. u. Mech. Bd. 6 S. 265, 1926.
Also reference 5, p. 185.

³ For details of this and following statements see reference 5, p. 100 and p. 147, and also reference 6, Part II.

TABLE I
N. A. C. A.—M6
UPPER SURFACE

Per cent <i>c</i>	<i>y</i> in per cent <i>c</i>	<i>x</i>	<i>y</i>	$\sin 2\theta$	$\sinh 2\psi$	θ radians	ψ	ϵ	$\frac{d\psi}{d\theta}$	$\frac{d\epsilon}{d\theta}$	<i>k</i>	$\varphi=\theta+\epsilon$
0	0	2.037	0.000	0.000	0.0373	0.000	0.192	−0.0457	0.000	0.085	6.280	−2 37
1.25	1.97	1.986	.0796	.0465	.0341	.217	.184	−.0276	−.010	.080	4.249	10 52
2.50	2.81	1.936	.1135	.0941	.0342	.312	.184	−.0205	.009	.080	3.368	16 41
5.0	4.03	1.835	.163	.187	.0354	.447	.187	−.0098	.022	.080	2.557	25 4
7.5	4.94	1.734	.200	.275	.0363	.551	.189	−.0015	.022	.080	2.163	31 31
10	5.71	1.633	.231	.357	.0373	.640	.192	.0063	.020	.085	1.929	37 3
15	6.82	1.431	.276	.507	.0375	.792	.193	.0188	−.009	.095	1.660	46 27
20	7.55	1.229	.305	.636	.0366	.923	.190	.0310	−.031	.100	1.498	54 38
30	8.22	.825	.332	.835	.0330	1.153	.181	.0549	−.066	.107	1.324	69 11
40	8.05	.421	.325	.957	.0276	1.361	.165	.0717	−.085	.088	1.220	82 7
50	7.26	.017	.293	1.000	.0215	1.571	.146	.0856	−.100	.060	1.166	94 55
60	6.03	−.387	.244	.963	.0154	1.764	.124	.0932	−.100	.025	1.152	106 25
70	4.58	−.791	.185	.845	.0101	1.975	.100	.0920	−.100	−.029	1.167	118 28
80	3.06	−1.195	.124	.645	.0059	2.209	.077	.0828	−.088	−.056	1.302	131 19
90	1.55	−1.599	.063	.363	.0027	2.495	.052	.0617	−.067	−.085	1.687	146 30
95	.88	−1.801	.036	.191	.0016	2.690	.040	.0410	−.035	−.080	2.340	156 28
100	.26	−2.003	.000	.000	.0030	3.142	.055	.0105	.000	−.027	19.83	180 36

LOWER SURFACE

0	0	2.037	0.000	0.000	0.0373	6.283	0.192	−0.0457	0.000	0.085	6.280	−2 37
1.25	1.76	1.986	−.071	.0425	.0297	6.075	.172	−.0781	.133	.120	4.615	−16 21
2.50	2.20	1.936	−.089	.0844	.0234	5.989	.152	−.0850	.160	.050	3.525	−21 43
5.0	2.73	1.835	−.110	.173	.0176	5.855	.132	−.0882	.133	−.010	2.510	−29 35
7.5	3.03	1.734	−.122	.259	.0144	5.749	.120	−.0850	.109	−.045	2.025	−35 28
10	3.24	1.633	−.131	.342	.0125	5.659	.112	−.0811	.080	−.057	1.764	−40 24
15	3.47	1.431	−.140	.494	.0099	5.505	.099	−.0723	.069	−.067	1.466	−48 44
20	3.62	1.229	−.146	.626	.0085	5.371	.092	−.0637	.057	−.067	1.307	−55 54
30	3.79	.825	−.153	.831	.0070	5.136	.084	−.0516	.025	−.052	1.156	−68 39
40	3.90	.421	−.158	.956	.0065	4.924	.081	−.0421	.008	−.036	1.098	−80 17
50	3.94	.017	−.159	1.000	.0063	4.712	.079	−.0350	.000	−.029	1.081	−91 59
60	3.82	−.387	−.154	.963	.0062	4.518	.0785	−.0310	.010	−.013	1.120	−102 53
70	3.48	−.791	−.141	.845	.0058	4.307	.076	−.0300	.019	.000	1.211	−114 55
80	2.83	−1.195	−.114	.645	.0050	4.074	.071	−.0295	.036	−.011	1.370	−128 14
90	1.77	−1.599	−.072	.363	.0035	3.788	.059	−.0235	.044	−.040	1.769	−144 16
95	1.08	−1.801	−.044	.191	.0025	3.594	.050	−.0140	.020	−.067	2.368	−154 50
100	.26	−2.003	.000	.000	.0030	3.142	.055	.0105	.000	−.027	19.83	−179 24

TABLE II
 $\epsilon(\varphi)=0.1 \sin (\varphi-45^{\circ}) \quad \psi_0=0.10 \quad \beta=\epsilon(\pi)=0.0657=3^{\circ} 47'$
UPPER SURFACE

φ		ϵ	θ		ψ	$\frac{d\epsilon}{d\varphi}$	$\frac{d\psi}{d\varphi}$	$\cosh \psi$	$\sinh \psi$	$\cos \theta$	$\sin \theta$	$\frac{x}{2}$	$\frac{y}{2}$	<i>k</i>
Degrees	Radians		Radians	Degrees										
0	0.0000	−0.0707	0.0707	4 3	0.1707	0.0707	0.0707	1.0146	0.1715	0.9975	0.0703	1.0121	0.0121	6.3941
5	.0873	−.0643	.1516	8 41	.1766	.0766	.0643	1.0156	.1775	.9885	.1510	1.0039	.0268	5.1215
10	.1745	−.0574	.2319	13 17	.1819	.0819	.0574	1.0166	.1826	.9733	.2298	.9895	.0420	4.0960
15	.2618	−.0500	.3118	17 52	.1866	.0866	.0500	1.0175	.1877	.9518	.3068	.9685	.0576	3.3602
20	.3491	−.0423	.3914	22 26	.1906	.0906	.0423	1.0182	.1918	.9243	.3816	.9411	.0732	2.8421
25	.4363	−.0342	.4705	26 57	.1940	.0940	.0342	1.0189	.1952	.8914	.4532	.9082	.0885	2.4704
30	.5236	−.0259	.5495	31 29	.1966	.0966	.0259	1.0194	.1979	.8528	.5223	.8693	.1034	2.1892
35	.6109	−.0174	.6283	36 0	.1985	.0985	.0174	1.0198	.1998	.8090	.5878	.8250	.1174	1.9746
45	.7854	.0000	.7854	45 0	.2000	.1000	.0000	1.0201	.2013	.7071	.7071	.7213	.1423	1.6689
55	.9599	.0174	.9425	54 0	.1985	.0985	−.0174	1.0198	.1998	.5878	.8090	.5994	.1616	1.4709
70	1.2217	.0423	1.1794	67 35	.1906	.0906	−.0423	1.0182	.1918	.3813	.9244	.3882	.1773	1.2859
80	1.3963	.0574	1.3389	76 43	.1819	.0819	−.0574	1.0166	.1826	.2298	.9733	.2336	.1777	1.1233
90	1.5708	.0707	1.5001	85 57	.1707	.0707	−.0707	1.0146	.1715	.0706	.9975	.0716	.1711	1.1717
100	1.7453	.0819	1.6634	95 18	.1574	.0574	−.0819	1.0124	.1581	−.0924	.9957	−.0935	.1574	1.1586
110	1.9199	.0906	1.8293	104 49	.1423	.0423	−.0906	1.0101	.1428	−.2557	.9368	−.2583	.1381	1.1756
125	2.1817	.0985	2.0832	119 22	.1174	.0174	−.0985	1.0069	.1177	−.4904	.8715	−.4933	.1026	1.2727
135	2.3562	.1000	2.2562	129 16	.1000	.0000	−.1000	1.0050	.1002	−.6329	.7742	−.6361	.0776	1.4088
150	2.6180	.0966	2.5214	144 28	.0741	−.0259	−.0966	1.0028	.0742	−.8138	.5812	−.8161	.0431	1.8306
160	2.7925	.0906	2.7019	154 48	.0577	−.0423	−.0906	1.0017	.0577	−.9048	.4258	−.9063	.0246	2.4584
170	2.9671	.0819	2.8852	165 19	.0426	−.0574	−.0819	1.0009	.0426	−.9673	.2538	−.9682	.0108	4.0496
180	3.1416	.0707	3.0709	175 57	.0293	−.0707	−.0707	1.0004	.0293	−.9975	.0706	−.9979	.0021	13.4411

LOWER SURFACE

0	0.0000	−0.0707	0.0707	4 3	0.1707	0.0707	.0707	1.0146	0.1715	0.9975	0.0706	1.0121	0.0121	6.3941
−5	−.0873	−.0766	−.0107	−0 37	.1643	.0643	.0766	1.0135	.1650	.9999	−.0103	1.0134	−.0018	7.1236
−10	−.1745	−.0819	−.0926	−5 18	.1574	.0574	.0819	1.0124	.1581	.9957	−.0924	1.0030	−.0146	6.3827
−15	−.2618	−.0866	−.1752	−10 2	.1500	.0500	.0866	1.0113	.1506	.9847	−.1742	.9958	−.0262	5.0338
−20	−.3491	−.0906	−.2585	−14 49	.1423	.0423	.0906	1.0101	.1428	.9368	−.2557	.9766	−.0365	3.9225
−25	−.4363	−.0940	−.3423	−19 37	.1342	.0342	.0940	1.0090	.1346	.9420	−.3357	.9505	−.0452	3.1489
−30	−.5236	−.0966	−.4270	−24 28	.1259	.0259	.0966	1.0079	.1262	.9102	−.4142	.9174	−.0523	2.6077
−35	−.6109	−.0985	−.5124	−29 21	.1174	.0174	.0985	1.0069	.1177	.8716	−.4901	.8776	−.0577	2.2203
−45	−.7854	−.1000	−.6854	−39 16	.1000	.0000	.1000	1.0050	.1002	.7742	−.6329	.7781	−.0634	1.7161
−55	−.9599	−.0985	−.8614	−49 21	.0826	−.0174	.0985	1.0034	.0827	.6514	−.7587	.6536	−.0627	1.4164
−70	−1.2217	−.0906	−1.1311	−64 48	.0577	−.0423	.0906	1.0017	.0577	.4258	−.9048	.4235	−.0522	1.1650
−80	−1.3963	−.0819	−1.3144	−75 19	.0426	−.0574	.0819	1.0009	.0426	.2535	−.9373	.2537	−.0412	1.0763
−90	−1.5708	−.0707	−1.5001	−85 57	.0293	−.0707	.0707	1.0004	.0293	.0706	−.9975	.0706	−.0292	1.0322
−100	−1.7453	−.0574	−1.6879	−96 43	.0181	−.0819	.0574	1.0002	.0181	−.1170	−.9931	−.1170	−.0180	1.0270
−110	−1.9199	−.0423	−1.8776	−107 3	.0094	−.0906	.0423	1.0000	.0094	−.3021	−.9533	−.3021	−.0090	1.0616
−125	−2.1817	−.0174	−2.1643	−124 1	.0015	−.0985	.0174	1.0000	.0015	−.5594	−.8289	−.5594	−.0012	1.2136
−135	−2.3562	.0000	−2.3562	−135 0	.0000	−.1000	.0000	1.0000	.0000	−.7071	−.7071	−.7071	.0000	1.4209
−150	−2.6180	.0259	−2.6439	−151 29	.0034	−.0259	.0034	1.0000	.0034	−.8787	−.4774	−.8787	−.0016	2.1106
−160	−2.7925	.0423	−2.8348	−162 25	.0094	−.0906	−.0423	1.0000	.0094	−.9533	−.3021	−.9533	−.0028	3.3501
−170	−2.9671	.0574	−3.0245	−173 18	.0181	−.0819	−.0574	1.0002	.0181	−.9932	−.1167	−.9934	−.0021	8.6641
−180	−3.1416	.0707	−3.2123	−184 3	.0293	−.0707	−.0707	1.0004	.0293	−.9975	+.0706	−.9979	+.0021	13.4411

REPORT No. 453

THE ESTIMATION OF MAXIMUM LOAD CAPACITY OF SEAPLANES AND FLYING BOATS

By WALTER S. DIEHL

SUMMARY

It is shown that the relation between the gross load W and the time for take-off t of seaplanes and flying boats is of the form

$$W_m = W + K \frac{b \cdot \text{hp}}{t}$$

Where W_m is the maximum possible load corresponding to infinite value of t , $b \cdot \text{hp}$ is the total brake horsepower and K is a constant. Data from four tests give $K=140$.

This equation supplies a method of calculating time for take-off with any load, or vice versa, when the time for one load is known.

INTRODUCTION

The maximum load that can be taken into the air by a seaplane or flying boat is a matter of general interest and, in some cases, of considerable importance. It may be obtained either by calculation or by direct experiment. However, the calculation requires model basin data not always available, while the direct determination with gradually increased loads is often out of the question, due to the time and expense involved. Consequently, very little data are available on the ability of seaplanes to take off with heavy loads. This paper is concerned with the study of take-off data and the development of a simple method for the estimation of maximum load.

GRAPHICAL SOLUTION FOR MAXIMUM LOAD

Observed times for take-off with a progressive increase in gross weight are given in Table I. These data are for a typical flying boat fitted with two engines developing 540 b.hp each, according to calibration tests. The conventional plot of take-off time against gross weight is given in Figure 1.

A test was also made on another flying boat substantially identical with the above except that it was fitted with two calibrated engines developing 620 b.hp each, and the time for take-off was found to be 30 seconds with a gross load of 17,184 pounds. This point is also plotted on Figure 1. The question then arises as to what is the maximum load that can be taken off with the second flying boat. It is obvious that the plotting method used in Figure 1 is unsatisfactory for this purpose.

A study of the various methods of plotting indicates that the use of the reciprocal of the time for take-off

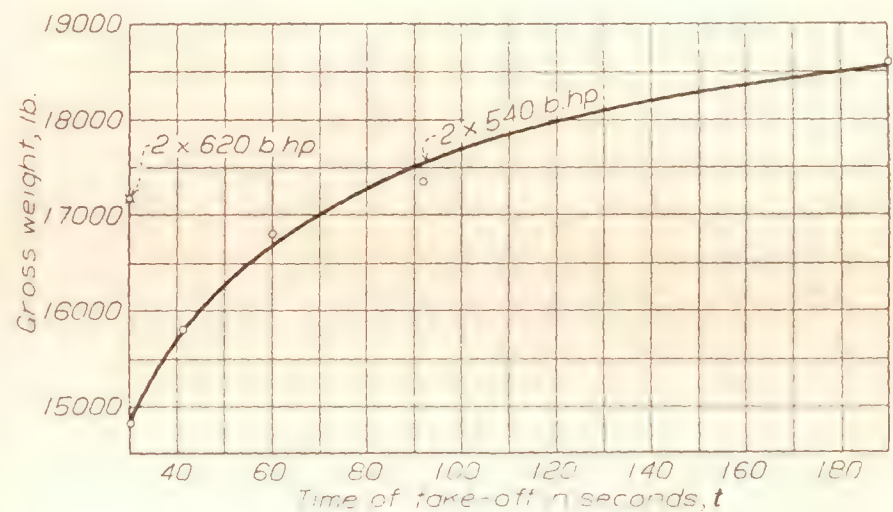


FIGURE 1.—Observed time for take-off of flying boats

should give a curve intercepting the weight axis at the limiting weight and that the use of power loading in-

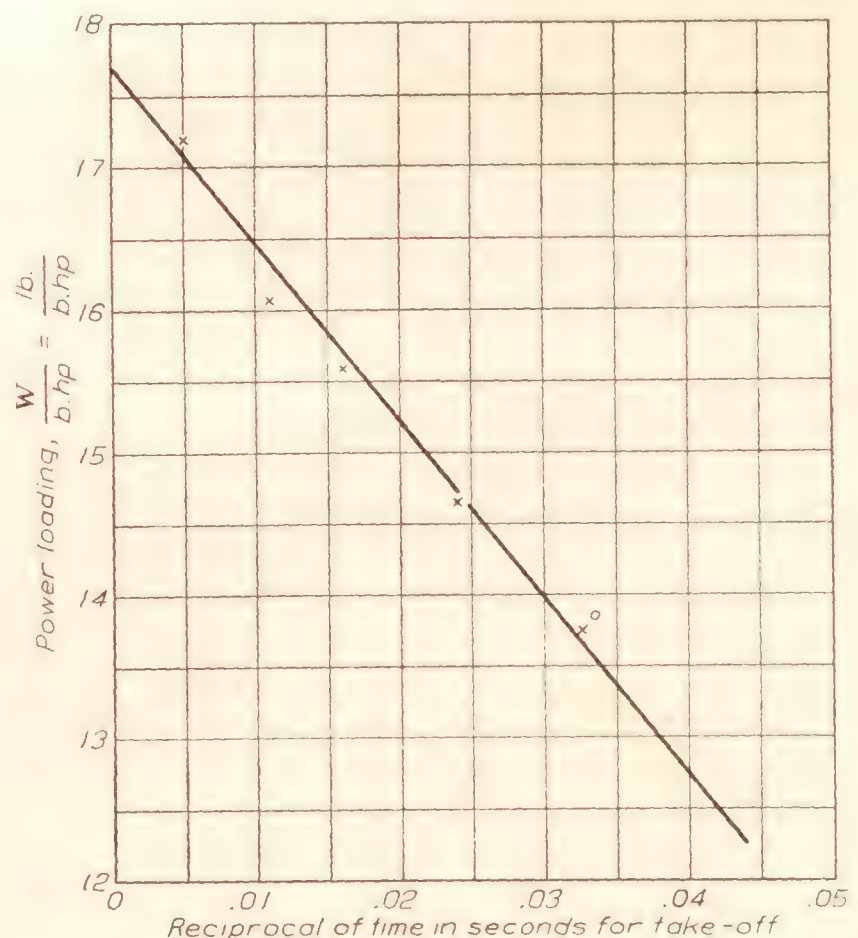


FIGURE 2.—Take-off curve for flying boats

stead of weight would make the plot more general. When plotted in this manner, as in Figure 2, the data from Table I lie on or very near to a straight line as

does the single point from the second test. If this relation is general it supplies a very simple method of determining the maximum load from a single take-off since the straight line is represented by an equation of the form

$$\left(\frac{W_m}{b. hp}\right) = \left(\frac{W}{b. hp}\right) + \frac{K}{t} \quad (1)$$

Where t is the time in seconds for take-off with the power loading $\left(\frac{W}{b. hp}\right)$, $\left(\frac{W_m}{b. hp}\right)$ is the power loading for the maximum load that can be taken off and K , the slope of the line, is a load constant.

The maximum possible load would be

$$W_m = b. hp \times \left(\frac{W_m}{b. hp}\right) \quad (2)$$

DETERMINATION OF LOAD CONSTANT K

Table II contains take-off data for two flying boats. Table III contains take-off data for the short "Singapore I" as given in Tables I and II of Reports and Memoranda No. 1411 of the British Aeronautical Research Committee. (Reference 1.) All of these data are plotted on Figure 3, and the points are found to lie on lines of the same slope giving $K=140$. This slope differs slightly from that obtained from a single set of test data in Figure 2, where K would appear to be about 125. The tests on the "Singapore," Table III, if taken alone would indicate a value of about 150

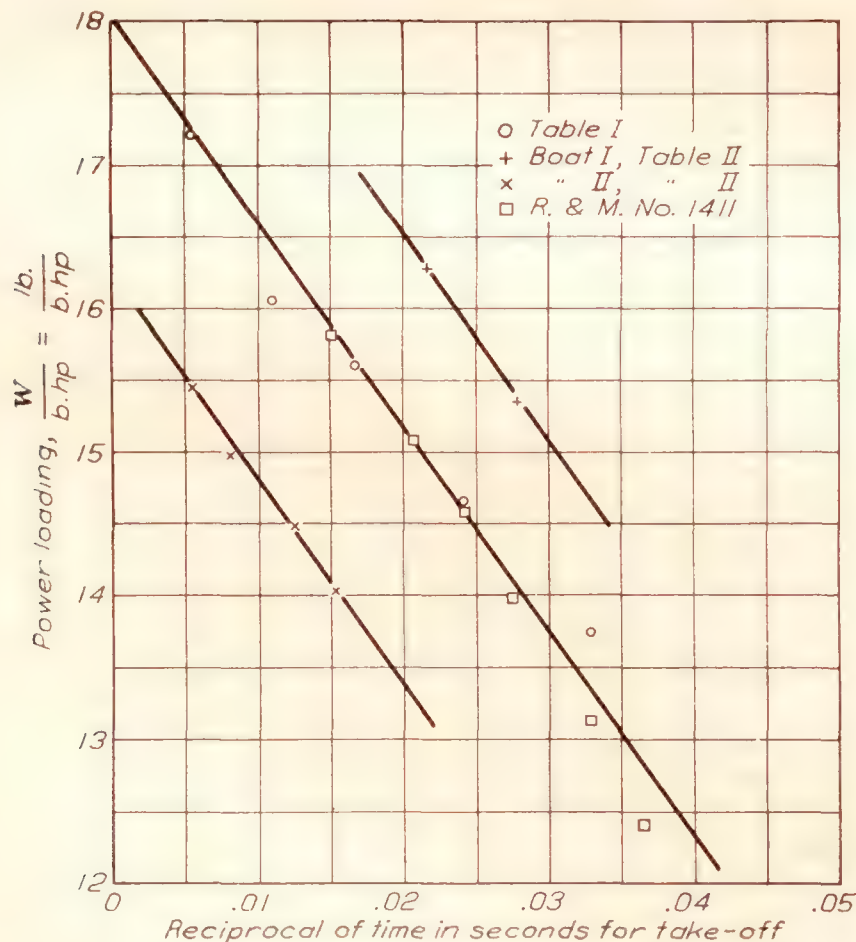


FIGURE 3.—Take-off curves for flying boats

for K . The value of $K=140$ in Figure 3 obviously fits the two sets of data combined and gives good agreement with the data from Table II as well. The relation of equation (1) therefore becomes

$$\left(\frac{W_m}{b. hp}\right) = \left(\frac{W}{b. hp}\right) + \frac{140}{t} \quad (3)$$

or

$$\left(\frac{W}{b. hp}\right) = \left(\frac{W_m}{b. hp}\right) - \frac{140}{t} \quad (3a)$$

The vertical displacement of the lines in Figure 3 is due to differences in propulsive efficiency and total resistance. Flying boat No. I of Table II has very low drag due to good hull lines and ample wing surface of high aspect ratio. Flying boat No. II of the same table has considerably more hull and wing drag with the addition of an excessive amount of parasite resistance. The flying boats of Tables I and III are quite similar except for size. The locations of the lines on Figure 3 are in accordance with these conditions.

It would be desirable to use thrust power, $t. hp$, instead of brake horsepower, $b. hp$, in equation (1), if the propeller efficiency were readily obtained. However, the differences would be small with modern designs and the probable improvement does not appear to justify the increased difficulty in practical use.

ESTIMATION OF MAXIMUM LOAD

Equation (3) supplies a very simple method for estimation of the maximum load that can be taken off by a seaplane or flying boat. All that is required is a single timed take-off with a known gross load. Substitution of this observed take-off time and the corresponding power loading $\frac{W}{b. hp}$ into equation (3) gives the maximum power loading corresponding to infinite time. The gross load is then found from equation (2) if desired, but this is of academic interest only. The practical limit may be set according to conditions at, say, 60 seconds or 120 seconds, and equation (3a) solved for the corresponding power loading.

It is of interest to check the indications of Figure 3 against observed or calculated data. In the tests given in Figure 1, the maximum load appears to be approximately 19,000 pounds. The calculated maximum loads substituting the take off time and power loading for each run into equation (3), are given in Table IV. The values range from 19,000 to 19,800 pounds, a maximum deviation of about 4 per cent from the actual value. This means that the maximum load could have been predicted within 4 per cent by the first run or within about 2 per cent from any of the succeeding runs.

In a similar manner the total resistance curves given on Figure 1 of reference 1 indicate that the limiting load for the "Singapore I" is just less than 30,000, while the calculated maximum loads for each run of Table III, as given in Table V range from 28,750 to 29,600 pounds. This is less than 4 per cent deviation, or about the same accuracy as shown by Table IV. As might be expected, the greatest deviation occurs

at the light loads. In using this method it appears desirable that a load giving a run of about 50 seconds to 60 seconds be used if maximum accuracy is to be attained.

Multiplying both sides of equation (3) by b . hp gives

$$W_m = W + \frac{140 \text{ b. hp}}{t} \quad (4)$$

this gives the maximum load W_m directly when the value of t is known for a given weight. For example, assume that the time for take-off is 35 seconds with a gross load of 15,000 pounds and 1,000 b. hp. Then by substitution in equation (4)

$$W_m = 15,000 + \frac{140 \times 1000}{35} \\ = 19,000 \text{ pounds.}$$

This is the maximum possible load for an unlimited run in a calm. A more practical problem is to find the load that can be taken off in a specified time, say, 60 seconds. If this load is designated the service load W_s and the specified maximum time by t_s , the substitution in equation (4) gives

$$W_s = W_o + 140 \text{ b. hp} \left(\frac{1}{t_o} - \frac{1}{t_s} \right) \quad (5)$$

t_o being the observed take-off time with the load W_o . Using the values $t_o = 35$ sec., $W_o = 15,000$ pounds, and b . hp = 1,000 from the example above it is found, for $t_s = 60$

$$W_s = 15,000 + 140 \times 1,000 \left(\frac{1}{35} - \frac{1}{60} \right) \\ = 16,667 \text{ pounds.}$$

If the specified maximum time is $t_s = 120$ sec.

$$W_s = 15,000 + 140 \times 1,000 \left(\frac{1}{35} - \frac{1}{120} \right) \\ = 17,833 \text{ pounds.}$$

BUREAU OF AERONAUTICS,
NAVY DEPARTMENT,
WASHINGTON, D. C., Sept., 1932.

REFERENCES

1. Coombes, L. P., and Read, R. H.: The Effect of Various Types of Lateral Stabilizers on the Take-Off of a Flying Boat. R. & M. No. 1411, British A. R. C., 1932.
2. Diehl, W. S.: Engineering Aerodynamics, Chapter XV. The Ronald Press Co., Inc., New York City, 1928.

TABLE I.—OBSERVED TAKE-OFF DATA ON A FLYING BOAT

(Tests by Patrol Plane Squadron 7-F)

Run No.	Gross weight W lb.	Power loading $\frac{W}{b \text{ hp}}$	Time to take off t sec.	Reciprocal of time to take off $\frac{1}{t}$	Remarks
1-----	14,824	13.75	30.5	0.0328	4-knot wind.
2-----	15,808	14.65	41.4	.0241	5-knot wind.
3-----	16,825	15.60	60.3	.0166	2-knot wind.
4-----	17,350	16.05	92.0	.0109	2-knot tail wind.
5-----	18,600	17.20	190.0	.0053	4-knot cross wind. Plane had to be taken into shoal water to get on step.
6-----	18,991	17.50	-----	-----	Did not get off after getting on step under same conditions as in run 5.

TABLE II.—OBSERVED TAKE-OFF DATA ON TWO FLYING BOATS

Type	Gross weight W lb.	Power loading $\frac{W}{b \text{ hp}}$	Time to take off t sec.	Reciprocal of time to take off $\frac{1}{t}$	Remarks
I-----	19,945	15.35	36	0.0278	2×650 b. hp. Tests at Anacostia Naval Air Station. 2×535 b. hp. Tests in glassy water at Naval Aircraft Factory.
	21,145	16.26	46	.0217	
	15,000	14.03	65	.0154	
II-----	15,500	14.50	80	.0125	
	16,000	14.96	123	.0081	
	16,500	15.42	180	.0055	

TABLE III.—TAKE-OFF DATA FROM TABLES I AND II OF BRITISH A. R. C. R. & M. No. 1411

Gross weight W lb.	Power loading $\frac{W}{b \text{ hp}}$	Time for take-off t sec.	Reciprocal of time for take-off $\frac{1}{t}$	Remarks
20,350	12.38	27.5	0.0364	1,645 b. hp, gear ratio 0.477. 4-blade propeller: P=12.0 ft. D=12.5 ft.
21,580	13.12	30.5	.0328	
23,000	13.98	36.3	.0275	
24,000	14.58	41.3	.0242	
24,800	15.07	48.0	.0208	
26,000	15.80	66.0	.0151	

TABLE IV.—CALCULATED MAXIMUM LOADS FOR TAKE-OFF

Using Observed Data from Table I with Equation (3)

t sec.	$\frac{140}{t}$	$\left(\frac{W}{b \text{ hp}} \right)$	$\left(\frac{W_m}{b \text{ hp}} \right)$	W_{max}
30.5	4.59	13.75	18.34	19,800
41.4	3.38	14.65	18.03	19,500
60.3	2.32	15.60	17.92	19,400
92.0	1.52	16.05	17.57	19,000
190.0	.74	17.20	17.94	19,400

TABLE V.—CALCULATED MAXIMUM LOADS FOR TAKE-OFF

Using Observed Data from Table III with Equation (3)

Time for take-off t sec.	$\frac{140}{t}$	$\left(\frac{W}{b \text{ hp}} \right)$	$\left(\frac{W_m}{b \text{ hp}} \right)$	W_{max}
27.5	5.10	12.38	17.48	28,750
30.5	4.60	13.12	17.72	29,150
36.3	3.86	13.98	17.84	29,350
41.3	3.39	14.58	17.97	29,600
48.0	2.92	15.07	17.99	29,600
66.0	2.12	15.80	17.92	29,500

REPORT No. 454

PHOTOMICROGRAPHIC STUDIES OF FUEL SPRAYS

By DANA W. LEE and ROBERT C. SPENCER

SUMMARY

A large number of photomicrographs of fuel sprays were taken for the purpose of studying the spray structure and the process of spray formation. They were taken at magnifying powers of 2.5, 3.25, and 10, using a spark discharge of very short duration for illumination. Several types and sizes of nozzles were investigated, different liquids were used, and a wide range of injection pressures was employed. The sprays were photographed as they were injected into a glass-walled chamber in which the air density was varied from 14 atmospheres to 0.0013 atmosphere.

Within the range investigated, the photomicrographs support the theory advanced by Dr. R. A. Castleman, jr., to explain the atomization of liquid fuels in carburetors and in injected sprays. With injected sprays, the fuel leaves the nozzle as an unbroken column, is ruffled, and then torn into small, irregular ligaments by the action of the air. The ligaments are then quickly drawn up into drops by the surface tension of the fuel. Turbulent fuel flow accelerates the disintegration of the fuel jet by ruffling its surface close to the orifice, but has relatively small disintegrating power in itself. When other factors are kept constant the degree of disintegration of the jet increases with the distance from the nozzle, the air density, the fuel velocity, or the fuel turbulence, but decreases with an increase of fuel viscosity, surface tension, or nozzle orifice diameter.

INTRODUCTION

More rapid and uniform mixing of the fuel and air in the combustion chambers of fuel-injection engines is essential if the combustion process is to be controlled and higher specific outputs obtained. Accordingly, many experiments have been made to determine the general shape, the rate of growth, the final drop size, and the fuel distribution of sprays from various types of nozzles. However, the study of the manner in which the fuel is divided into the millions of small drops which constitute a fuel spray has hitherto been handicapped by a scarcity of direct experimental evidence. Some investigators have discussed the process of spray formation with particular emphasis on vibrations and turbulent flow within the nozzle. (See references 1 and 2.) Others have been most interested in the effects of the forces which result from the rela-

tive motion between the fuel and the air. (See references 3, 4, 5, and 6.)

The investigation described in this report was made to study the formation of fuel sprays by means of instantaneous photomicrographs, and to determine the effect of various design and operating factors on the characteristics of the sprays. The experiments were conducted during the early part of 1932 by the National Advisory Committee for Aeronautics at Langley Field, Va.

APPARATUS AND TEST PROCEDURE

A microscope with camera attachment was used to take photomicrographs at a magnifying power of 10 and a large camera with a short focus lens was used for magnifications of 2.5 and 3.25.

The illumination for photographing the sprays was supplied by a spark from the electrical circuit shown in

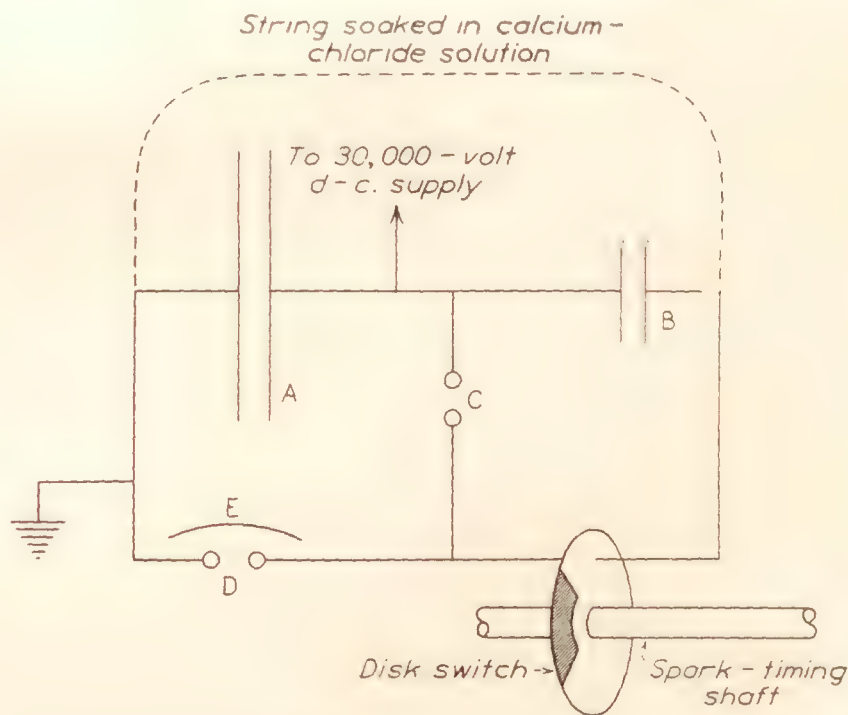


FIGURE 1.—Circuit used to produce illuminating sparks of short duration

- A. Main condenser.
- B. Auxiliary condenser.
- C. Auxiliary spark gap.
- D. Illuminating spark gap.
- E. Reflector.

Figure 1. The principle of this circuit is as follows: The condensers A and B are charged to a high potential by a transformer and a rectifying tube. When the switch controlling the discharge is closed, the small condenser B discharges across the auxiliary spark

gap **C**, ionizing the air in the gap and greatly lowering its resistance. Condenser **A** then discharges across both gaps **C** and **D**; the light from gap **D** is used to photograph the spray, that from gap **C** being shielded from the camera lens. The duration of the illuminating discharge in circuits of this type is of the order of 10^{-7} second, provided that the resistance of the connecting wires is low. (See reference 7.) In this case, the capacities of the condensers **A** and **B** were about 0.01 and 0.001 microfarad, respectively. They were charged to about 30,000 volts and the connecting copper wires were about 0.16 inch in diameter and as short as practicable.

When taking photomicrographs, the spark gap is mounted in front of a parabolic reflector, and the reflector, spray nozzle, and microscope are placed in line so that the photomicrographs are silhouettes. A glass tube was slipped over the spark-gap points, to confine the spark discharge to a relatively narrow path.

The nozzles were used in an automatic injection valve and also as open nozzles. Figure 2 shows a

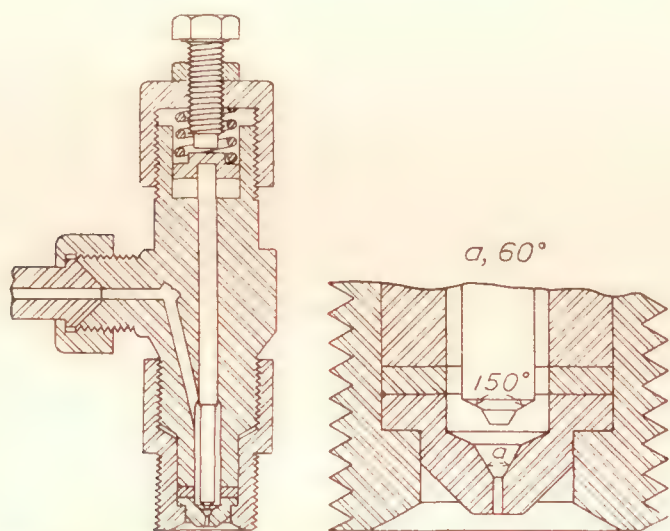


FIGURE 2.—Sketch of automatic injection valve, and enlarged view of nozzle assembled in valve

sketch of the injection valve and an enlarged view of a nozzle assembled in the valve. The injection valve was operated by the common-rail fuel-injection system of the N. A. C. A. spray photographic apparatus. (Reference 8.) Synchronization of the spark with the spray from the valve was accomplished by a rotary disk switch on the shaft with the cams that control the injection. The spark could be made to occur at any desired stage in the development of the spray by changing the phasing of the disk switch with respect to the cam shaft. The sprays from the open nozzles were continuous, the fuel being supplied from a reservoir arranged to maintain a constant pressure for several seconds. In this case the timing of the spark was manually controlled. It has been shown by Rothrock in reference 8 that with the common-rail injection system used there are pronounced fluctuations in the instantaneous pressures at the nozzle during the injection period. Therefore, in order that the data might be strictly comparable, continuous sprays from open nozzles were used whenever possible.

For experiments at other than atmospheric air density, the sprays were injected into a glass-walled chamber in which the air density could be raised by admitting compressed air from an air bottle or lowered by exhausting the chamber with a vacuum pump.

Except where otherwise noted, the fuel used in the tests was a Diesel fuel oil having, at atmospheric pressure and a temperature of 22° C., a viscosity of 0.022 poise, and a specific gravity of 0.837.

RESULTS AND DISCUSSION

The fact that the photomicrographs are silhouettes must be kept in mind while studying them, because frequently the core of the spray was the only part dense enough to register on the films. Most of the minute drops in the envelope of the spray surrounding the core could not be photographed. At high injection pressures or high air densities the surrounding cloud of drops became so dense that all details were obscured. Therefore, in order to study the process of fuel spray formation to the best advantage, the majority of the photomicrographs were taken at low injection pressures and low air densities. As the conditions were altered progressively until engine conditions were approached, the changes in the spray were carefully studied, and from these observations there have been drawn a number of general conclusions about the formation of fuel sprays.

A certain amount of discretion had to be used in selecting representative photomicrographs for illustration. Variations and irregularities, probably caused by fluctuations in the flow through the nozzle, were often present in the fuel jets. Only a relatively small portion of the jet could be photographed, and it sometimes happened that one of these irregularities was in front of the lens when the illuminating spark occurred. Therefore, several photomicrographs were always taken at each test condition, and pictures representative of the general trend were selected. The conclusions presented in this report are based on the study of about 2,800 fuel-spray photomicrographs.

TERMINOLOGY

Many different terms have been used by various investigators in describing the process by which liquid fuel is transformed into fuel sprays. "Jet disintegration", "disruption", "collapse", "decay", and "break-up" have been used, as well as the word "atomization." In this report, the recommendations of Castleman (reference 5) concerning the terminology of fuel-spray formation have been adopted whenever possible. He proposed that the word "atomization" be limited to the last stage of the process, during which the fuel particles attain their final size and form, and that the word "disintegration" be used in connection with that part of the process preceding atomization. The term "dispersion" has quite generally been accepted as denoting the ratio

of spray volume to fuel volume. In this investigation, dispersion was estimated qualitatively from the photomicrographs.

DIFFERENCES BETWEEN CONTINUOUS AND INTERMITTENT SPRAYS

As has been mentioned, both continuous sprays from open nozzles and intermittent sprays from an automatic injection valve were photographed. The first portions of sprays from the valve were considerably more dispersed than the later portions; however, when the sprays were fully developed, their appearance was the same as that of continuous sprays. The difference in dispersion between the early and late portions of a spray from the valve was most noticeable when the injection occurred in a vacuum, where the restricting influence of the air was much reduced. As the air

seat and the sudden surge when the fuel under pressure is released contribute to this turbulence. With the exception of Figures 3 and 4, all photomicrographs of sprays from an injection valve, shown in this report, were made when the spray was fully developed.

THEORIES OF SPRAY FORMATION

Among recent works on the phenomena of spray formation, the contributions of Haenlein, Castleman, and Schweitzer are the most directly related to the work that has been done at this laboratory.

Haenlein (reference 3) took spark photographs of jets of liquids having a wide range of physical properties and obtained very definite information concerning the nature of the disintegration of a liquid jet up to injection velocities of about 230 feet per second. He described four characteristic disintegration phenomena,

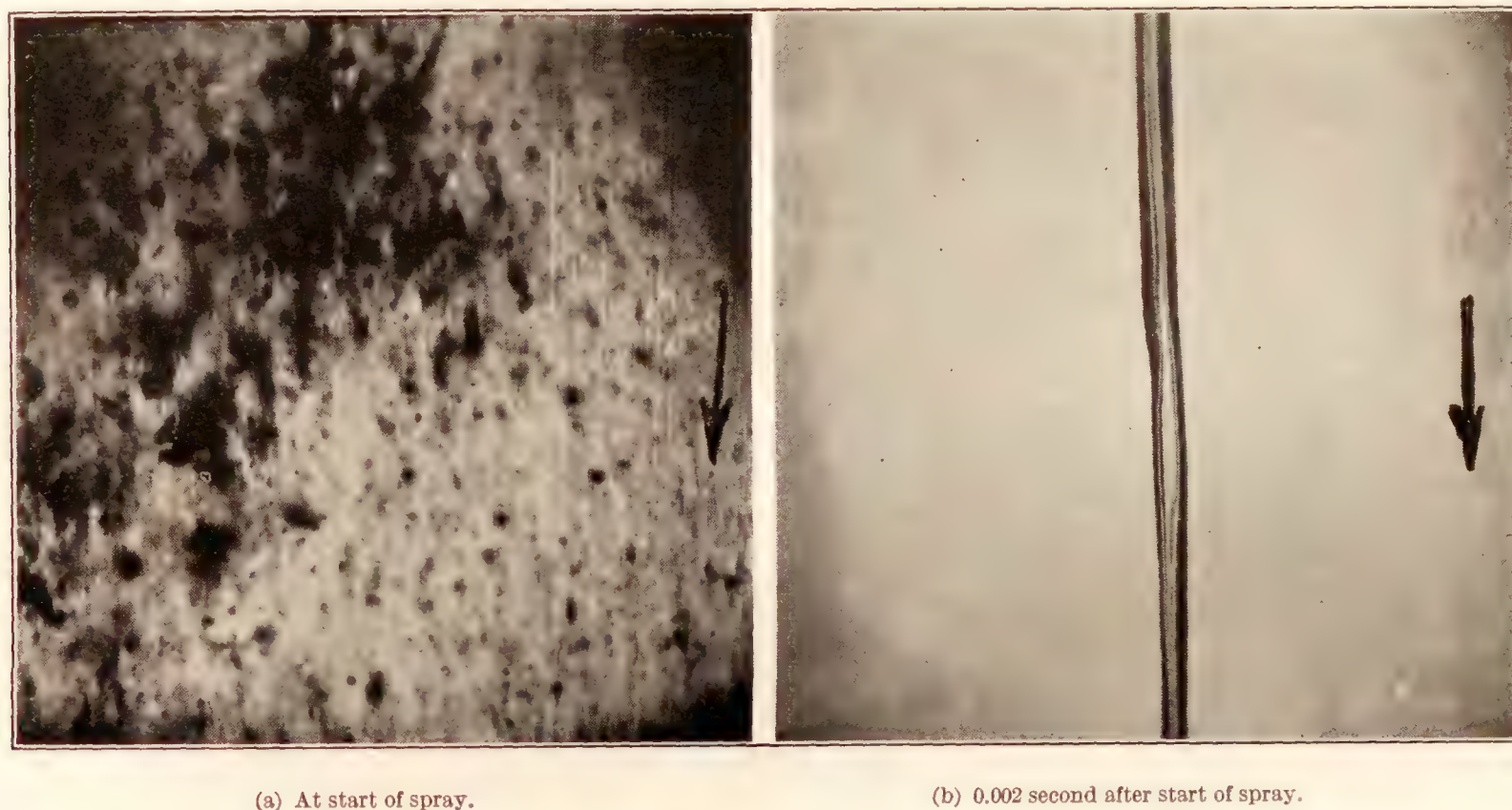


FIGURE 3.—Two stages of similar intermittent sprays in a vacuum, $\times 10$. Injection pressure, 2,000 pounds per square inch; orifice diameter, 0.014 inch; air density, 0.0026 atmosphere (pressure = 2 mm Hg, absolute); distance from nozzle, 3 inches

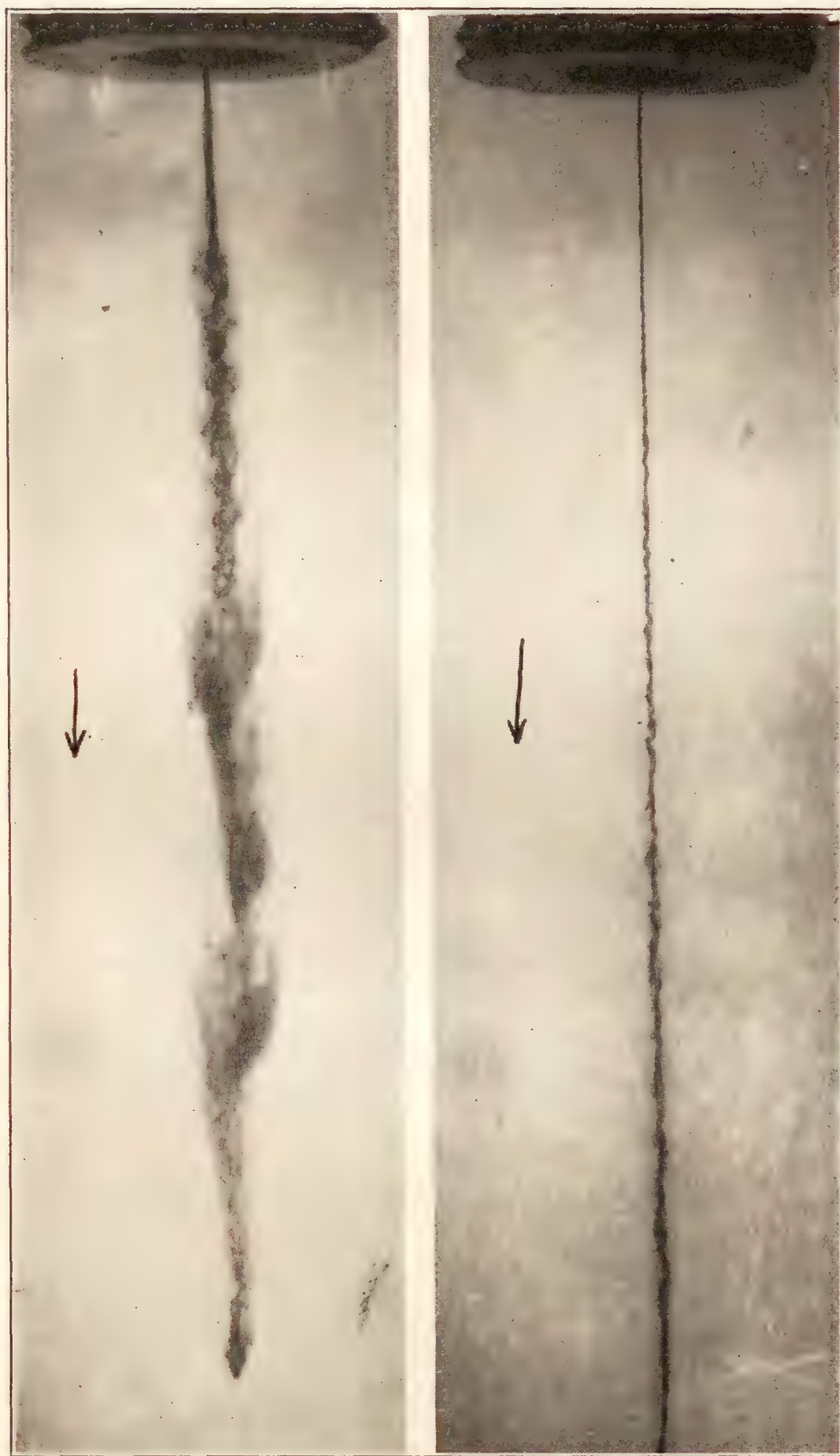
density was increased, this difference in dispersion decreased until at high air densities it was relatively slight. This initial dispersion effect is shown quite strikingly by Figure 3, which shows two stages in the development of similar intermittent sprays injected into a vacuum. The first part of the spray is dispersed very greatly, although the individual drops are relatively large. However, 0.002 second after the start the jet appears as an unbroken column. The general appearance of the first and later portions of intermittent sprays injected into air at atmospheric density is shown by Figure 4. As the dispersion of the early part of the spray is most apparent at low air densities when the air has the least restricting effect, it seems probable that the flow conditions at the start of injection are such as to produce considerable turbulence. The momentary throttling as the valve stem leaves its

which are dependent upon the velocity of injection: (1) Drop formation accomplished solely by the surface tension of the liquid; (2) drop formation where the surface tension is reenforced by air action; (3) wave formation by the air; (4) sudden and complete disintegration of the jet. No explanation was offered for the last phenomenon.

In references 4 and 5, Castleman has expressed a very reasonable explanation of the atomization of liquids. He says, in reference 4:

The actual process of atomization in an air stream seems rather simple: A portion of the large mass is caught up (say, at a point where its surface is ruffled) by the air stream and, being anchored at the other end, is drawn out into a fine ligament. This ligament is quickly cut off by the rapid growth of a dent in its surface, and the detached mass, being quite small, is swiftly drawn up into a spherical drop. (A quite similar phenomenon occurs when a large drop is detached from a tube.

The chief difference is that the ligament connecting the small drop to the main mass is much finer than that connecting the large drop to the liquid in the tube, and, hence, the time of detachment is enormously less.) The higher the air speed, the finer the ligaments, the shorter



At start of spray.

0.002 second after start of spray.

FIGURE 4.—Two stages of similar intermittent sprays in the atmosphere, $\times 2.5$. Injection pressure, 1,500 pounds per square inch; orifice diameter, 0.008 inch; air density, 1 atmosphere

their lives, and the smaller the drops formed, within the limits discussed above.

He also compares airless injection of fuel to air-stream atomization, and concludes that the atomization process is the same

in each case, the formation of ligaments being controlled by the relative velocity between the air and the fuel.

Schweitzer discusses the mechanism of jet disintegration in reference 2. He emphasizes the fact that rotationally symmetric disturbances and wavelike disturbances caused by the air can not possibly cause such extremely fine atomization as occurs in ordinary fuel injection, and gives particular attention to the influence of turbulent flow in the nozzle. Experiments are cited in which fuel was injected into a vacuum, and a distinct dispersion was noted at Reynolds Numbers of about 3,500 and above.

TYPES OF JET DISINTEGRATION

The forms of jet disintegration analyzed by Haenlein, caused by rotationally symmetric and wavelike disturbances, are illustrated in Figure 5. In photograph (a) of this figure the jet velocity is so low that the air plays no part, and the fuel column is separated into drops solely by the forces of surface tension. The beginning of enlargements and contractions in the stream is visible at some distance above the point of jet collapse. These inequalities in the fuel column increase slowly at first, then quite rapidly until the column is broken into elongated fragments. These fragments as they are falling through the air continue to be acted upon by surface tension. They therefore shorten themselves and, after a series of oscillations in which they become alternately elongated and flattened, settle down in the form of spherical drops.

In Figure 5(b), which was taken at a higher magnifying power than 5(a), the jet velocity has been increased until the aerodynamic forces also play a part in the disintegration of the jet. The action of the air on the fuel column may be similar to that of the wind on the surface of a body of water. If the relative velocity between the liquid and the layer of air close to its surface increases at the wave crests and decreases in the troughs, the result will be a decrease in pressure at the crests and an increase in pressure at the troughs. These pressure differences will increase the amplitude of the waves, and, in the case of the fuel jet accelerate its disintegration. (See reference 3.)

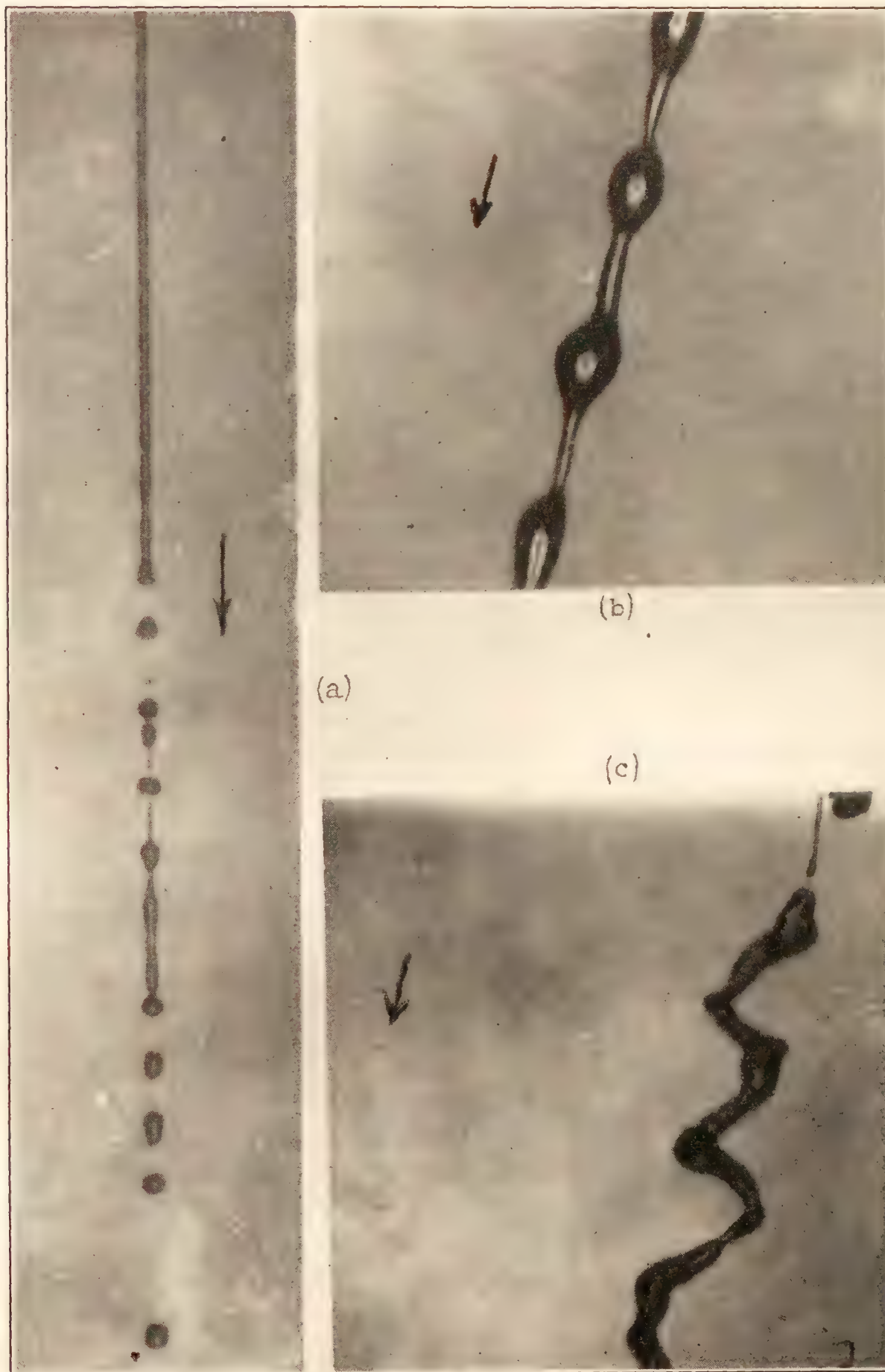


FIGURE 5.—Types of jet disintegration. Orifice diameter, 0.020 inch; air density, 1 atmosphere

(a) Rotationally symmetric disturbances without air influence, $\times 3.25$. Injection pressure less than 10 pounds per square inch.

(b) Rotationally symmetric disturbances with air influence, $\times 10$. Injection pressure, 50 pounds per square inch.

(c) Wave formation, $\times 10$. Injection pressure, 100 pounds per square inch.

In Figure 5(c) the jet velocity is still greater, and waves have been formed in addition to the rotationally symmetric disturbances. These waves are also the result of aerodynamic forces, and at the higher velocities they develop more rapidly than do the rotationally symmetric disturbances so that the jet is broken into many irregular parts.

LIGAMENT FORMATION

The formation of ligaments and their collapse into drops are shown in Figure 6. Virtually all photographs, except those at very low or very high pressures, show such ligaments. At very low pressures the relative velocity of the fuel and air is not sufficient for ligament formation, and at very high pressures the velocity is so high and the ligaments so small and so obscured by the fuel particles in the spray envelope that they are not distinguishable. The collapse of the ligaments is seen to be very similar to the collapse of a larger column, as described in connection with Figure 5.

The similarity between the photomicrographs of Figure 6 and the photographs made by Scheubel of air-stream atomization in a model carburetor (reference 9) indicates that the two methods of atomizing fuel are fundamentally the same.

EFFECT OF TURBULENT FUEL FLOW

The question of fuel turbulence is associated both with nozzle conditions and with Reynolds Number as determined by the injection velocity, the orifice diameter, and the kinematic viscosity of the fuel. If the Reynolds Number is below a certain critical value, any turbulence caused by nozzle irregularities will tend to damp out, but if it is above the critical value, an initial disturbance will persist. From experiments with fluid flow in long, uniform tubes, this critical value has been determined to be about 2,300. As the ratio of the length to the diameter of the nozzle bores was usually 2.5 or less, the use of Reynolds Numbers to determine whether the flow was turbulent or not is somewhat questionable. However, the appearance of fuel jets injected into an evacuated chamber, where the influence of air forces must be negligible, indicates that the Reynolds Number criterion may be applied in most cases.

Figures 7 and 8 show a series of fuel jets in vacuum, for which the Reynolds Number was varied from 1,500 to 9,000 by increasing the injection velocity. In these photographs, and in most of the others taken of injections into a vacuum, the nature of the flow seems to be controlled by the Reynolds Number, appearing to be laminar at values below the critical and turbulent above it.

The disintegration of the fuel jets in vacuum was much slower than in air. Sheets of fuel were thrown out from the higher velocity jets, and these later split

into parts and were then drawn up into relatively large drops by the force of surface tension. In no case were any extremely fine drops formed in a vacuum, such as were observed when fuel was injected into air.

PHOTOMICROGRAPHS AT VARIOUS DISTANCES FROM THE NOZZLE

The progressive effect of the various forces acting on the fuel jet may be shown quite distinctly by photographing a jet at increasing distances from the nozzle, other conditions being kept constant. The photomicrographs in Figure 9 show the disintegration of a low-velocity jet at various stages of the process. The jet issuing from the orifice contains slight irregularities, which may be caused by fuel turbulence or by vibrations of the nozzle. These irregularities are accentuated by the action of the air until the jet consists of many irregular parts, which are then drawn out into ligaments by further action of the air, and the ligaments collapse to form drops. Here, at low velocity, are found in modified forms the types of jet disintegration previously described.

Photomicrographs of a high-velocity spray at different distances from the nozzle are shown in Figure 10. In this case, the relative air velocity is high enough to draw ligaments away from the jet as soon as it has been slightly ruffled.

In Figure 11, the velocity of the jet was about the same as that in Figure 10, but the viscosity of the fuel was 0.102 poise instead of 0.022. As was expected from the observations of other investigators, jets of this fuel did not disintegrate as quickly as jets of the less viscous fuel. Wavelike disturbances were very prominent with the more viscous fuel, and the ligaments were long, and slow to collapse into drops.

It is apparent from these photomicrographs that the disintegration of a jet is a progressive affair; as the distance from the nozzle increases so does the degree of disintegration, until the relative velocity of the fuel and air has become so low that interaction no longer takes place.

EFFECT OF AIR DENSITY

If the theory of atomization by ligament formation holds, there will be little tendency toward the formation of extremely fine drops when sprays are injected into a vacuum. The photomicrographs show that although there is sometimes considerable disintegration of fuel jets injected into a vacuum, in all such cases the jet is merely broken up into relatively large parts, or extended into wide sheets, and the drops are always larger than in sprays injected into air. (See figs. 3 and 12). As the air density is increased (fig. 12) the degree of disintegration of the jet at a given distance from the nozzle becomes greater, and the sizes of the fuel particles are apparently reduced.



Injection pressure, 250 lb./sq. in.
Orifice diameter, 0.014 inch.
Distance from nozzle, 5 inches.
Fuel viscosity, 0.022 poise at 22° C.



Injection pressure, 550 lb./sq. in.
Orifice diameter, 0.020 inch.
Distance from nozzle, 5 inches.
Fuel viscosity, 0.022 poise at 22° C.



Injection pressure, 120 lb./sq. in.
Orifice diameter, 0.020 inch.
Distance from nozzle, 7.5 inches.
Fuel viscosity, 0.022 poise at 22° C.



Injection pressure, 700 lb./sq. in.
Orifice diameter, 0.020 inch.
Distance from nozzle, 1.5 inches.
Fuel viscosity, 0.102 poise at 22° C.

FIGURE 6.—Photomicrographs of fuel sprays showing the formation and collapse of ligaments, $\times 10$. All sprays continuous, injected into air at atmospheric density

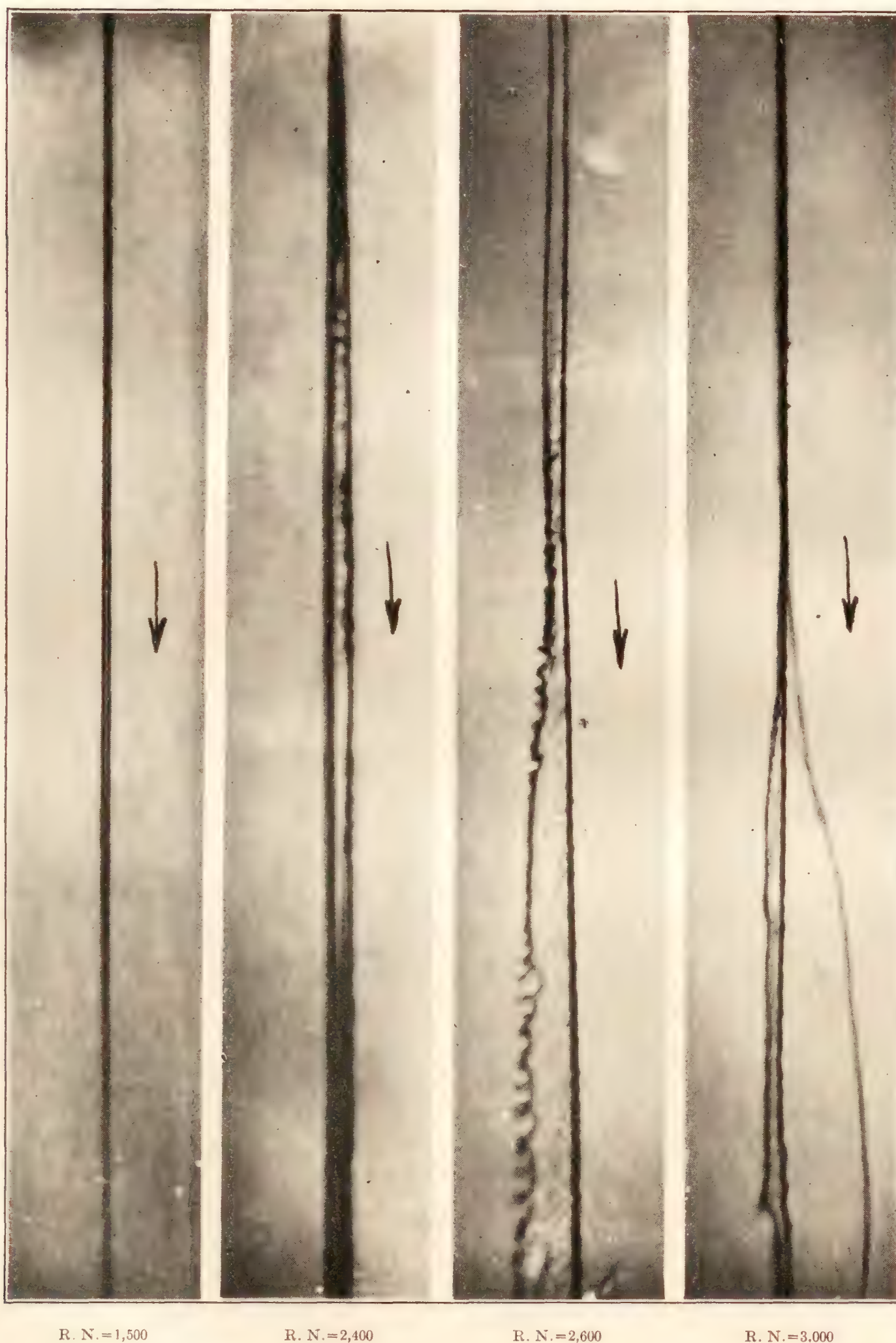


FIGURE 7.—Fuel jets at various Reynolds Numbers, in vacuum, $\times 2.5$. Orifice diameter, 0.020 inch; air density, 0.0013 atmosphere (pressure=1 mm Hg, absolute); fuel viscosity, 0.102 poise at 22° C.; photographs taken just beyond the orifice



R. N.=3,500

R. N.=5,000

R. N.=7,000

R. N.=9,000

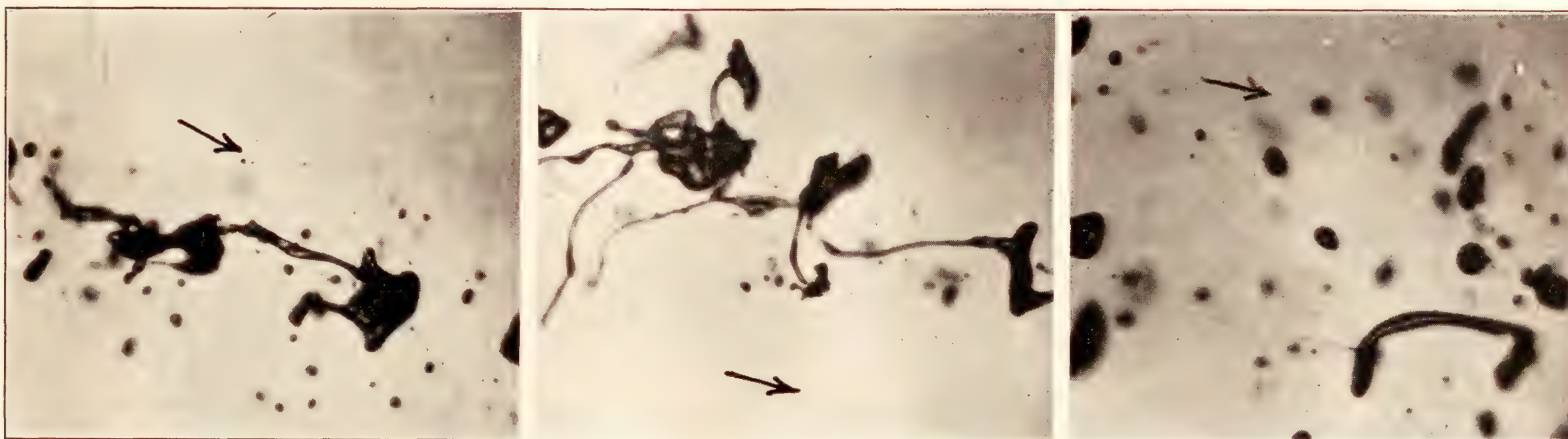
FIGURE 8.—Fuel jets at various Reynolds Numbers, in vacuum, $\times 2.5$. Orifice diameter, 0.020 inch; air density, 0.0013 atmosphere (pressure=1 mm Hg, absolute); fuel viscosity, 0.102 poise at 22° C.; photographs taken just beyond the orifice



At the nozzle.

1 inch from nozzle.

3 inches from nozzle.



5 inches from nozzle.

7.5 inches from nozzle.

10 inches from nozzle.

FIGURE 9.—Photomicrographs of a low-velocity fuel jet at different distances from the nozzle, $\times 10$. Injection pressure, 100 pounds per square inch; orifice diameter, 0.020 inch; air density, 1 atmosphere

The 2.5-power photographs in Figure 13 show the general effect of increasing the air density. The effective injection pressure in this case was maintained at 250 pounds per square inch above the chamber pressure, and even at this low injection pressure the cloud of fine drops in the envelope becomes very dense when the chamber-air density reaches values corresponding to those in compression-ignition engines at the time of fuel injection.

An examination of the photomicrographs taken at different air densities and at different distances from the nozzle, shows that, at a given injection pressure and distance from the nozzle, an increase in air density causes a very decided increase in the degree of disintegration of a jet. Substantially the same results may be obtained, however, by keeping the air density constant and increasing the distance from the nozzle. Thus it is seen that the disintegrating process is not completed immediately, but continues as long as the fuel retains enough velocity for the air to act upon it. In dense air, the process is more quickly carried to the limits obtainable with the jet velocity being used, but in air at low density the jet loses velocity more slowly and travels farther, and the final effect is the same, as shown in reference 10.

EFFECT OF THE CONDITION AND DIMENSIONS OF NOZZLE ORIFICES

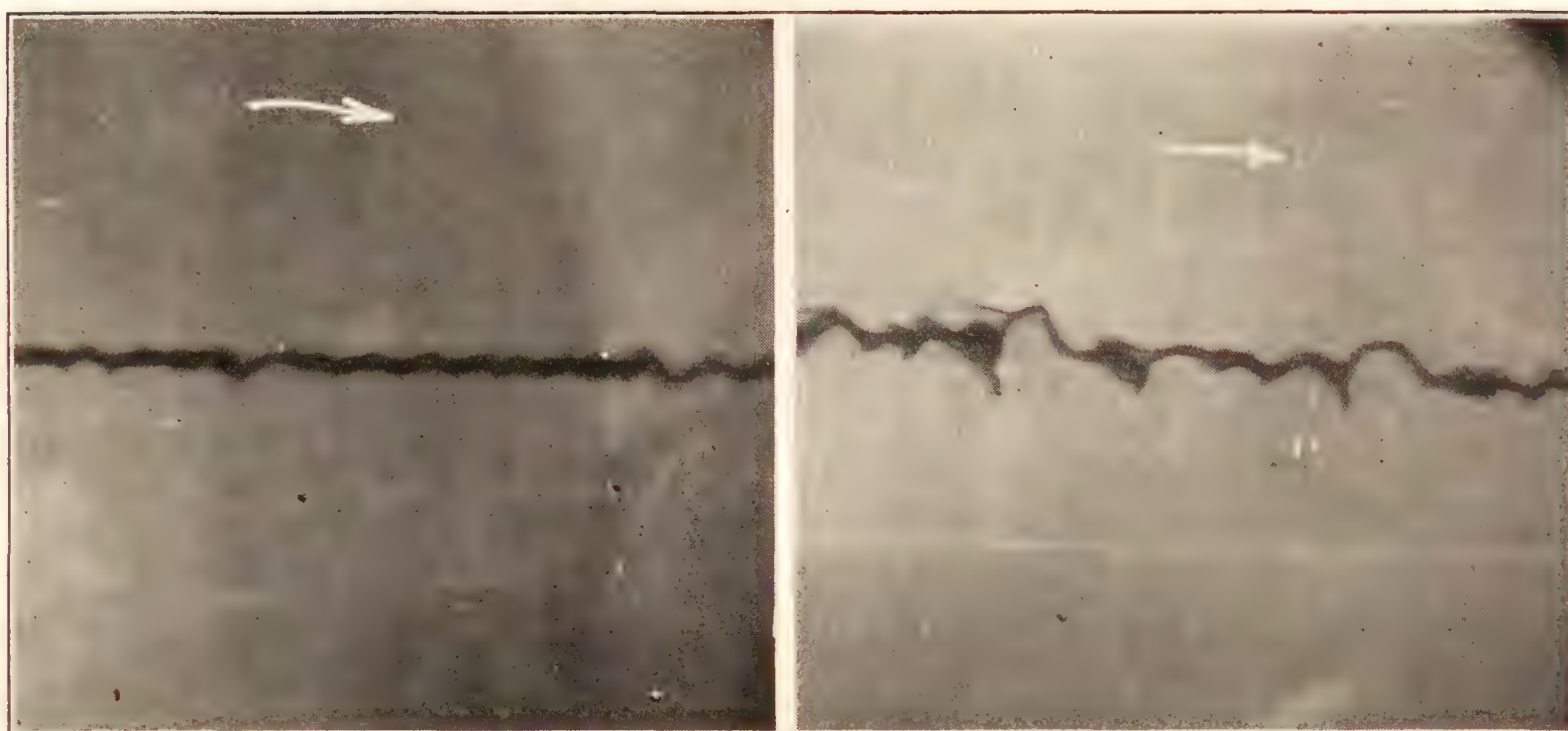
It is a well-known fact that fuel jets from large orifices penetrate farther than jets from small orifices. In air whose density is atmospheric or greater, air forces predominate in the disintegration of the jet, so that small jets with their high surface/volume ratio are disintegrated sooner than large jets. Most of the photomicrographs showed this faster disintegration of small jets, other conditions being the same. As deceleration of the jet increases with its degree of disintegration, the reason for the greater penetrating power of large jets is apparent.

As will be noted when inspecting the various photographs of sprays in a vacuum, different nozzles may give greatly different dispersions at low air densities. As this difference in dispersion decreases rapidly with increasing air density, it is of little importance with respect to compression-ignition engines. In fuel-injection spark-ignition engines requiring injection during the intake stroke or early in the compression stroke, the air density is low enough for this change in dispersion to be effective.

Figure 12 showed the effect of air density on the dispersion of sprays from two nozzles, each having an orifice diameter of 0.008 inch but with different orifice lengths. In this case the spray from the orifice having a length/diameter ratio of 2.5 was more widely dispersed than that from the orifice having a ratio of 0.5. When two nozzles having orifice diameters of

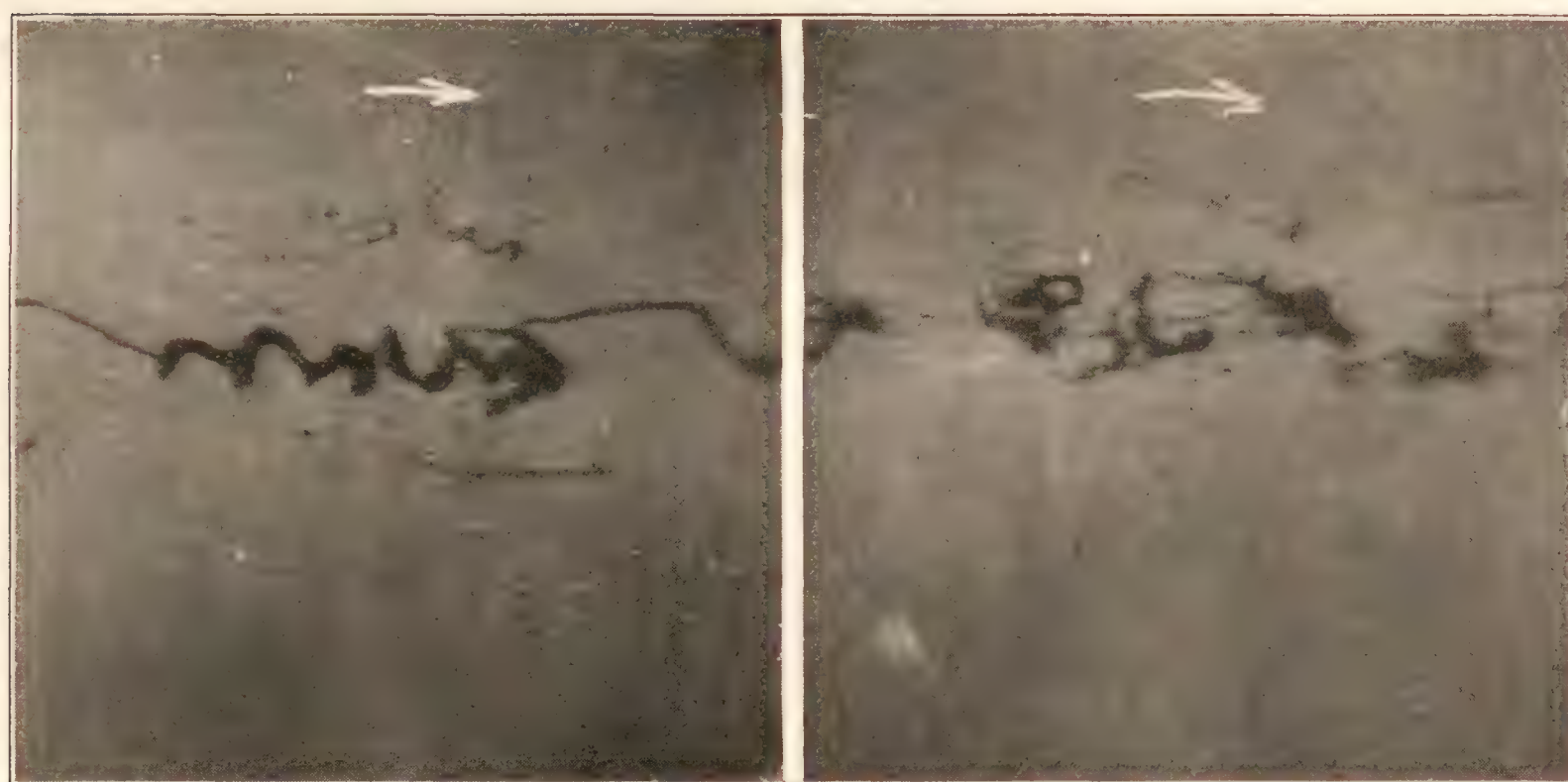


FIGURE 10. Photomicrographs of a high-velocity fuel jet at different distances from the nozzle, $\times 10$. Injection pressure, 1,000 pounds per square inch; orifice diameter, 0.014 inch; air density, 1 atmosphere



3.5 inches from nozzle.

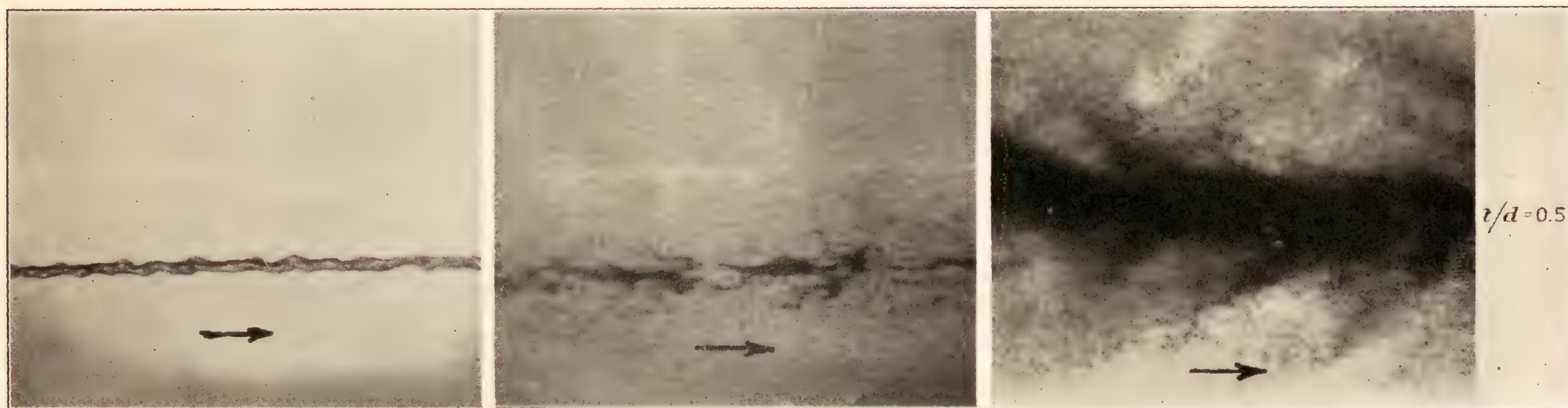
5 inches from nozzle.



5.5 inches from nozzle.

6 inches from nozzle.

FIGURE 11.—Jet disintegration at different distances from the nozzle, $\times 10$. Injection pressure, 1,000 pounds per square inch; orifice diameter, 0.008 inch; air density, 1 atmosphere; fuel viscosity, 0.102 poise at 22° C.



Air density, 0.0052 atmosphere (pressure=4 mm Hg, absolute).

Air density, 1 atmosphere.

Air density, 13 atmospheres.



Air density, 0.0052 atmosphere (pressure=4 mm Hg, absolute).

Air density, 1 atmosphere.

Air density, 13 atmospheres.

FIGURE 12.—Effect of air density on fuel jets from nozzles having orifice length/diameter ratios of 0.5 and 2.5, $\times 10$. Injection pressure, 1,000 pounds per square inch; orifice diameters, 0.008 inch; distance from nozzle, 1.5 inches

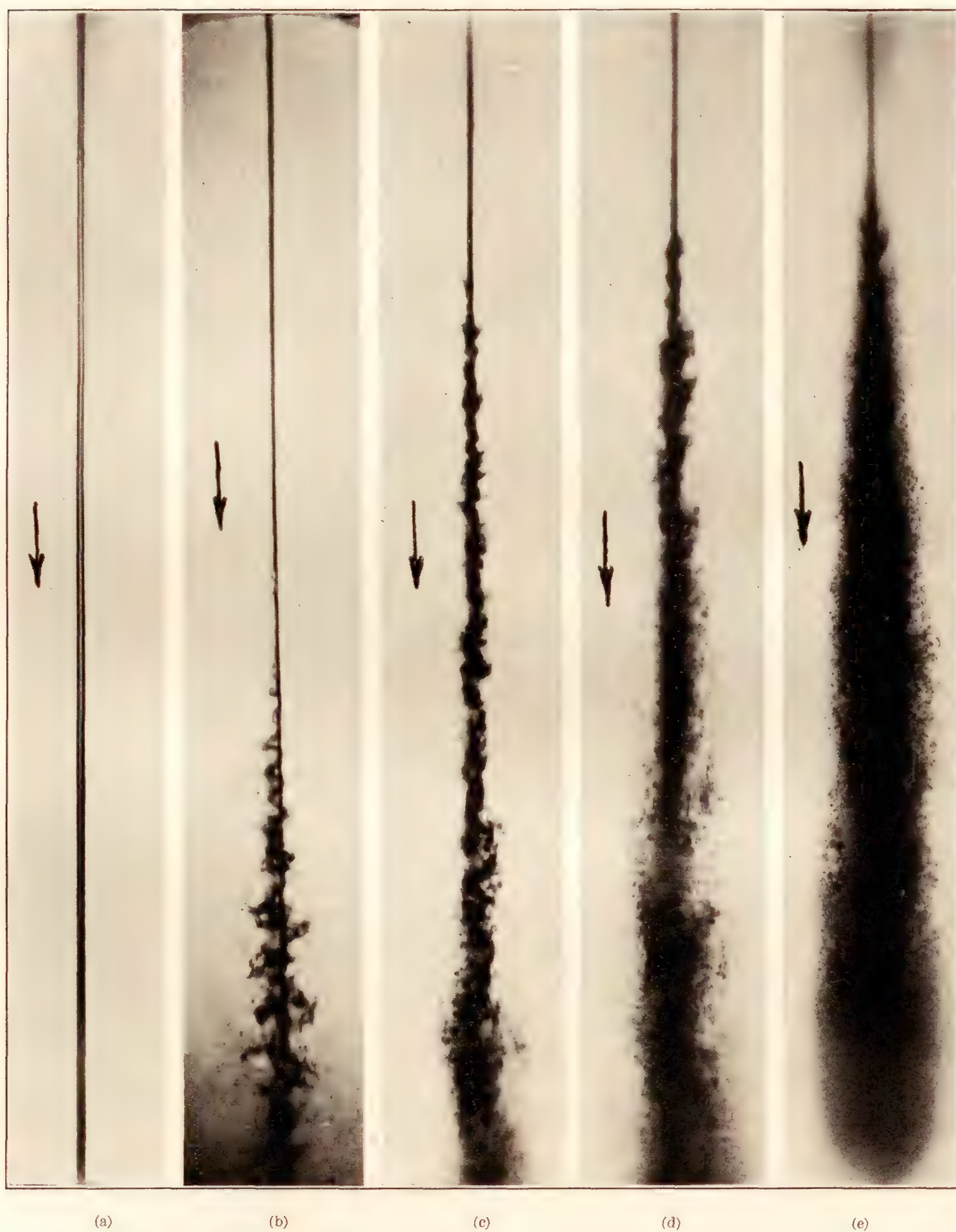


FIGURE 13.—Effect of air density on fuel jets, $\times 2.5$. Effective injection pressure, 250 pounds per square inch; orifice diameter, 0.020 inch; fuel viscosity, 0.130 poise at 22° C.

Air densities:

(a) 0.0013 atmosphere. (b) 1 atmosphere. (c) 4.4 atmospheres. (d) 7.8 atmospheres. (e) 14.5 atmospheres.



FIGURE 14.—Jets from orifices having the same dimensions, in vacuum, $\times 2.5$. Injection pressure, 3,000 pounds per square inch; orifices, 0.014 inch in diameter and 0.028 inch long; air density, 0.0013 atmosphere (pressure=1 mm Hg, absolute)

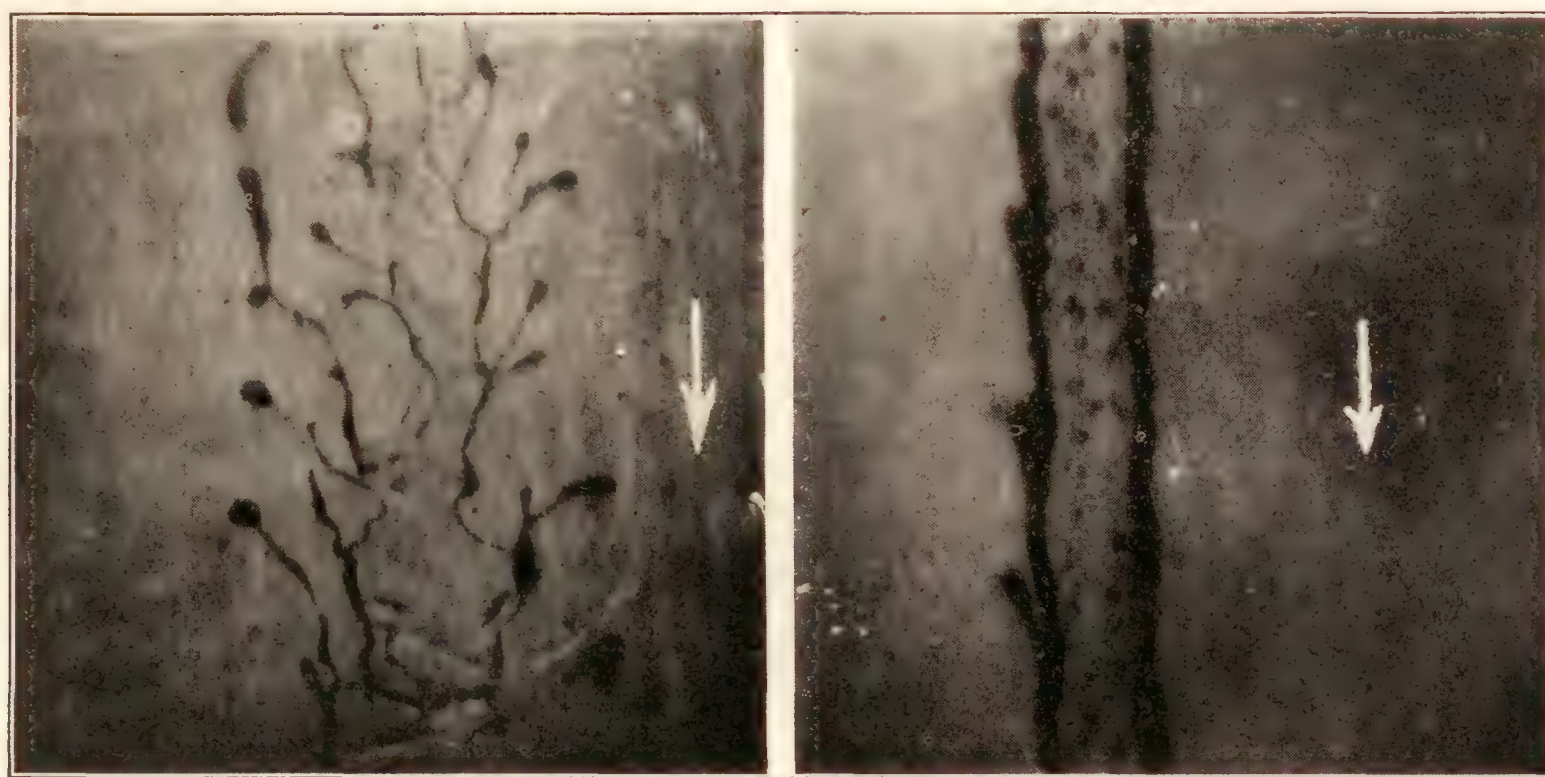
Nozzles:

(a) straight hole in thin steel plate. (b) conventional nozzle, polished. (c) conventional nozzle, unpolished.

0.014 inch and lengths of 0.006 and 0.028 inch were tried, it was found that the shorter orifice produced the greater dispersion. Four nozzles having orifice diameters of 0.020 inch and lengths of 0.010, 0.040, 0.100, and 0.200 inch were also tried. In this case the 0.040-inch-long orifice produced the widest spray. Nozzles similar to the ones used in the present experiments were used by Gelalles in his measurements of spray-tip penetration. (Reference 11.) He found that the spray-tip penetration was least with orifice length/diameter ratios of 2 or 3, and greatest with a ratio of about 6.

Photographs taken of jets from three nozzles having identical orifice lengths and diameters, but differing in other respects, are shown in Figure 14. The nozzle for Figure 14 (a) was a straight hole in the

the entire jet may be seen in the various characteristic forms of jet disintegration. At higher injection velocities the jet issues from the orifice in a turbulent condition, and the irregular surface is accentuated by air action. The fuel is divided into smaller and smaller parts until the air forces can no longer overcome the resisting forces due to the surface tension and viscosity of the fuel. These smallest parts then collapse to form drops. Ligaments may be drawn directly from the unbroken column soon after it has been ruffled, but the majority are formed after the jet has been disintegrated into parts. At very high velocities the ligaments are so small that most of them will probably not be visible in the photomicrographs when they are reproduced for publication. Ligaments have been observed on the original negatives of sprays



(a) Orifice pitted by rust.

(b) Orifice polished.

FIGURE 15.—Change in dispersion when disturbing influences are present in the orifice, $\times 10$. Injection pressure, 1,000 pounds per square inch; orifice diameter, 0.038 inch; air density, 0.0352 atmosphere (pressure=4 mm Hg, absolute); distance from nozzle, 3 inches

center of a steel disk. The nozzles for (b) and (c) were of the type shown in Figure 2, the difference being that for (b) the orifice was polished after it was drilled out, but for (c) the orifice was left rough.

Another example of the effect of small irregularities in the nozzle on spray dispersion is shown in Figure 15. Photograph (a) shows a spray from a slightly corroded nozzle, and (b) shows a spray from the same nozzle after it had been carefully polished.

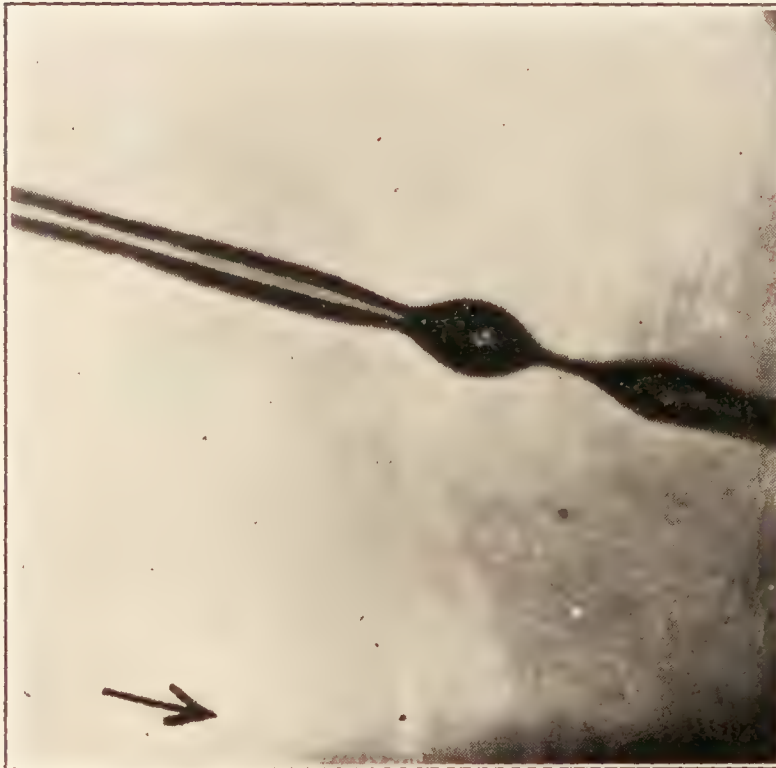
EFFECT OF INJECTION VELOCITY

The effect of injection velocity on the disintegration of fuel jets is shown by the photomicrographs of Figures 16, 17, and 18. As the injection velocity is increased, the disintegrating forces which result from air action and from fuel turbulence increase. At very low injection velocities, when these forces are slight,

the entire jet may be seen in the various characteristic forms of jet disintegration. At higher injection velocities the jet issues from the orifice in a turbulent condition, and the irregular surface is accentuated by air action. The fuel is divided into smaller and smaller parts until the air forces can no longer overcome the resisting forces due to the surface tension and viscosity of the fuel. These smallest parts then collapse to form drops. Ligaments may be drawn directly from the unbroken column soon after it has been ruffled, but the majority are formed after the jet has been disintegrated into parts. At very high velocities the ligaments are so small that most of them will probably not be visible in the photomicrographs when they are reproduced for publication. Ligaments have been observed on the original negatives of sprays

HIGH DISPERSION NOZZLES

Nozzles intended to give great dispersion are generally designed to produce a jet of fuel that has as large a surface as possible exposed to the action of the air. Flow conditions in such nozzles usually produce considerable turbulence, and the combination of turbulence and large surface exposed to the air causes very rapid jet disintegration. Figures 19 and 20 show the flow conditions at the exit of some nozzles of this type. For clearness the injection velocities were kept below 130 feet per second and the sprays injected into the atmosphere. Figure 19(a) shows the pronounced whirling of the fuel as it leaves a nozzle equipped with a helically grooved stem. Figure 19(b)



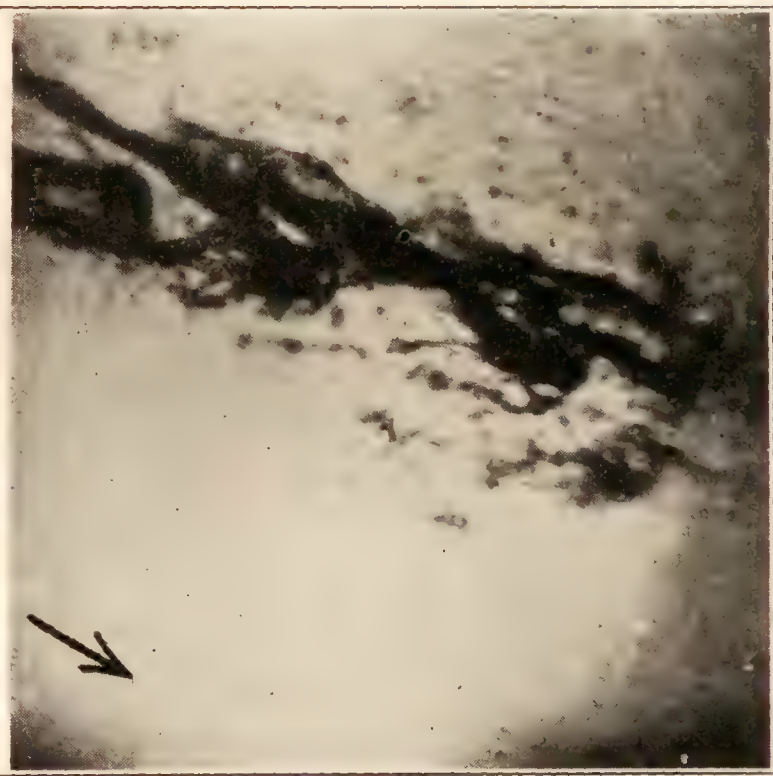
20 pounds per square inch.



200 pounds per square inch.

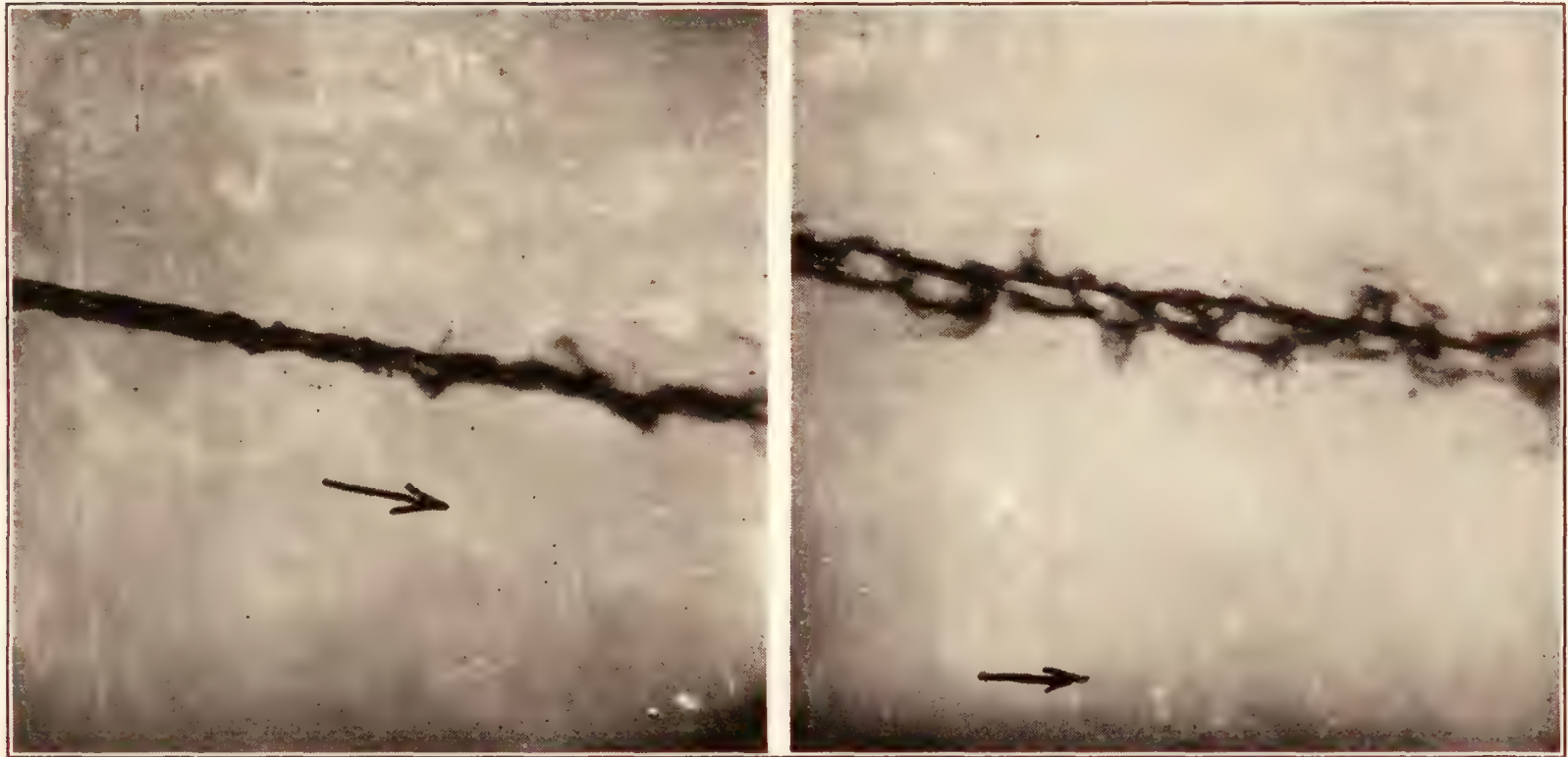


300 pounds per square inch.



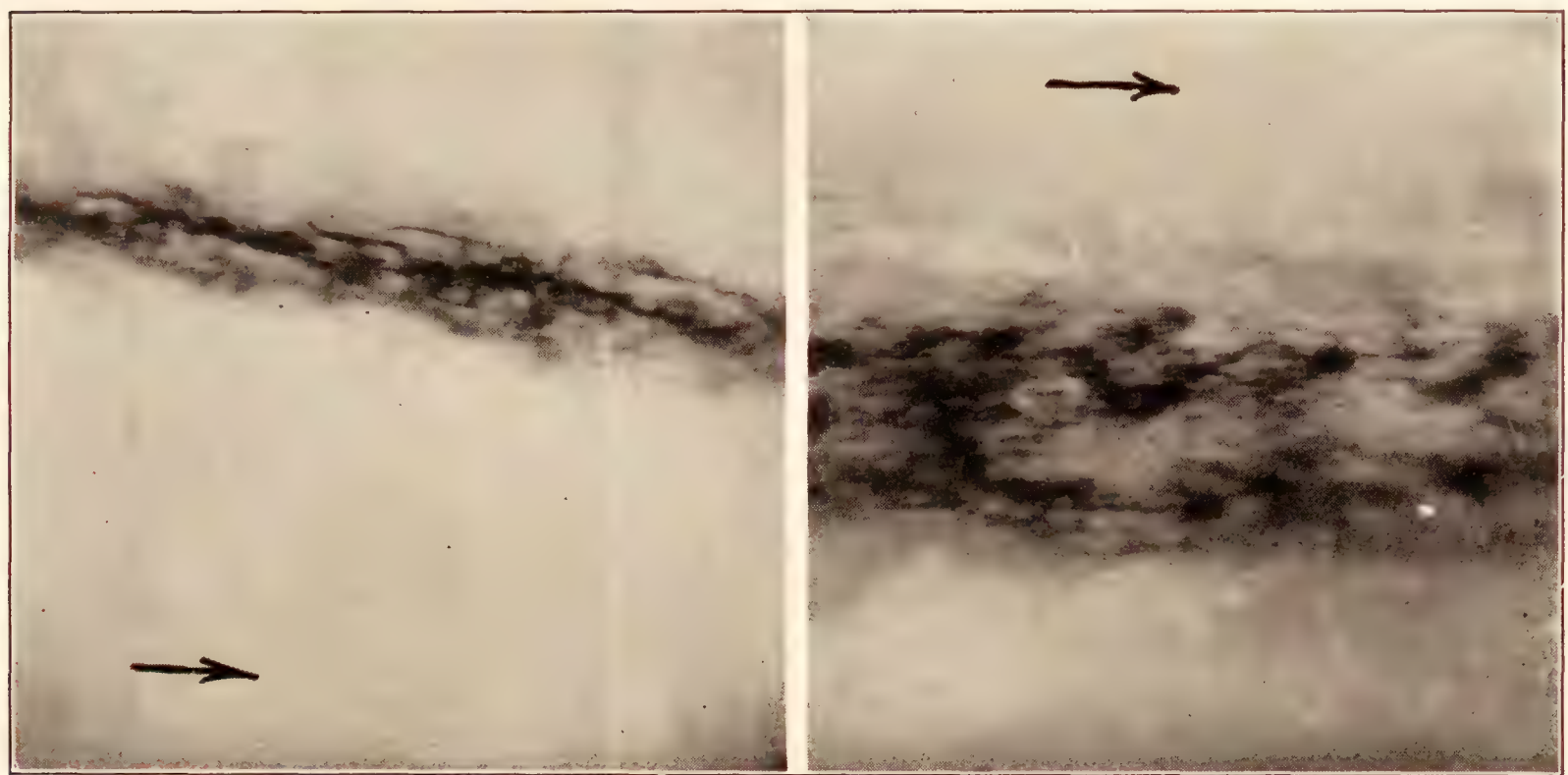
900 pounds per square inch.

FIGURE 16.—Effect of injection pressure on jet disintegration, $\times 10$. Orifice diameter, 0.020 inch; air density, 1 atmosphere; distance from nozzle, 4.75 inches



100 pounds per square inch.

250 pounds per square inch.



1,000 pounds per square inch.

4,000 pounds per square inch.

FIGURE 17.—Effect of injection pressure on jet disintegration, $\times 10$. Orifice diameter, 0.008 inch; air density, 1 atmosphere; distance from nozzle, 2.5 inches



50 pounds per square inch.

250 pounds per square inch.

550 pounds per square inch.

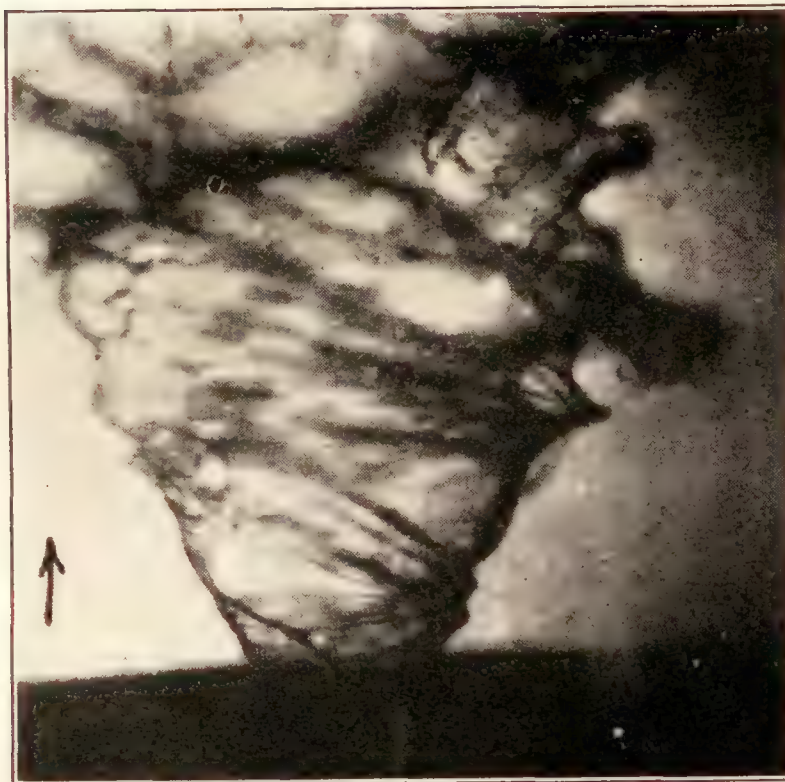


1,000 pounds per square inch.

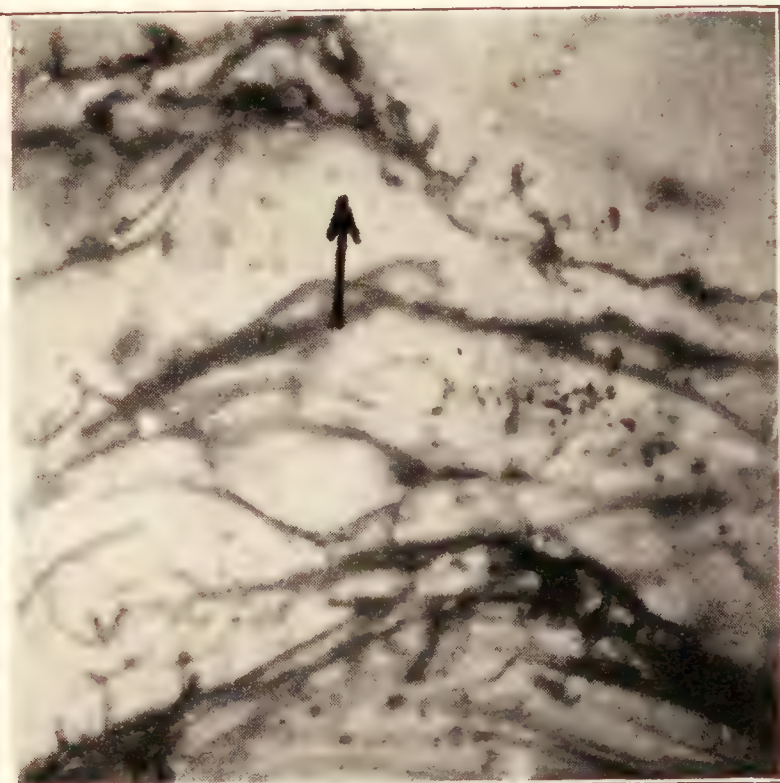
1,500 pounds per square inch.

2,000 pounds per square inch.

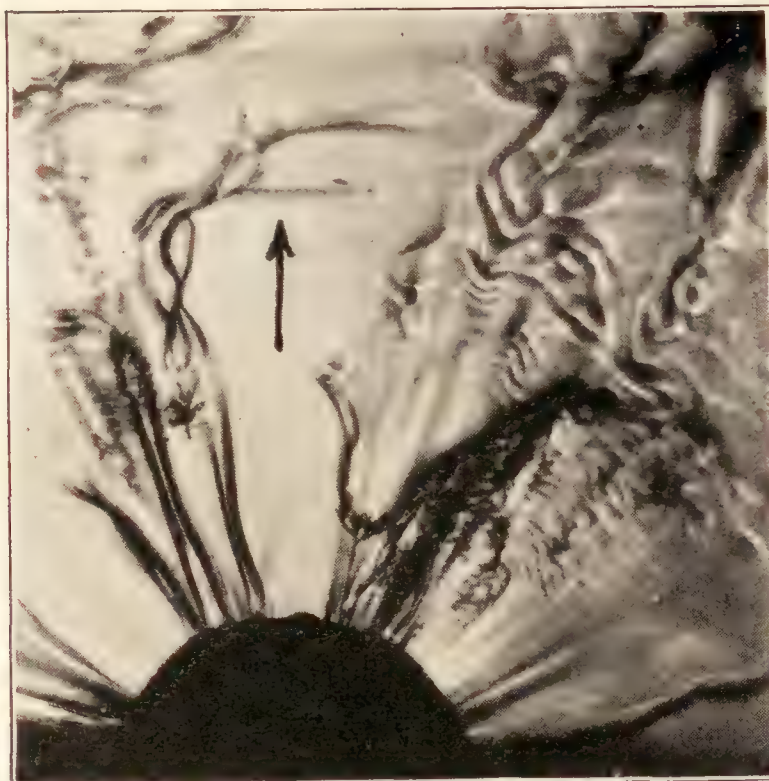
FIGURE 18.—Effect of injection pressure on jet disintegration, $\times 10$. Orifice diameter, 0.020 inch; air density, 1 atmosphere; distance from nozzle, 5 inches



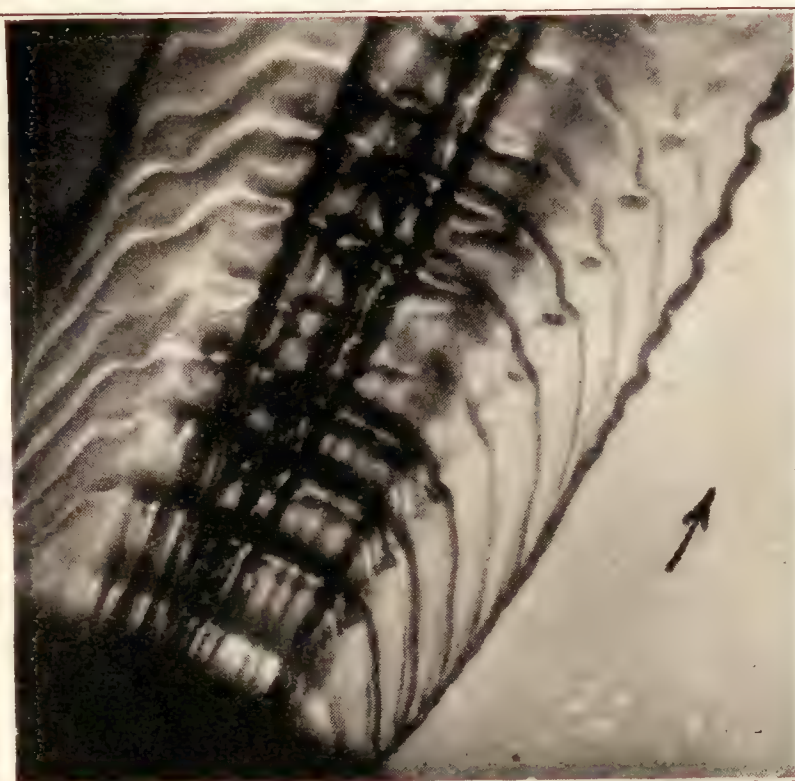
(a) Centrifugal-type spray.



(b) Spray from impinging-jets nozzle.



(c) Slit nozzle.



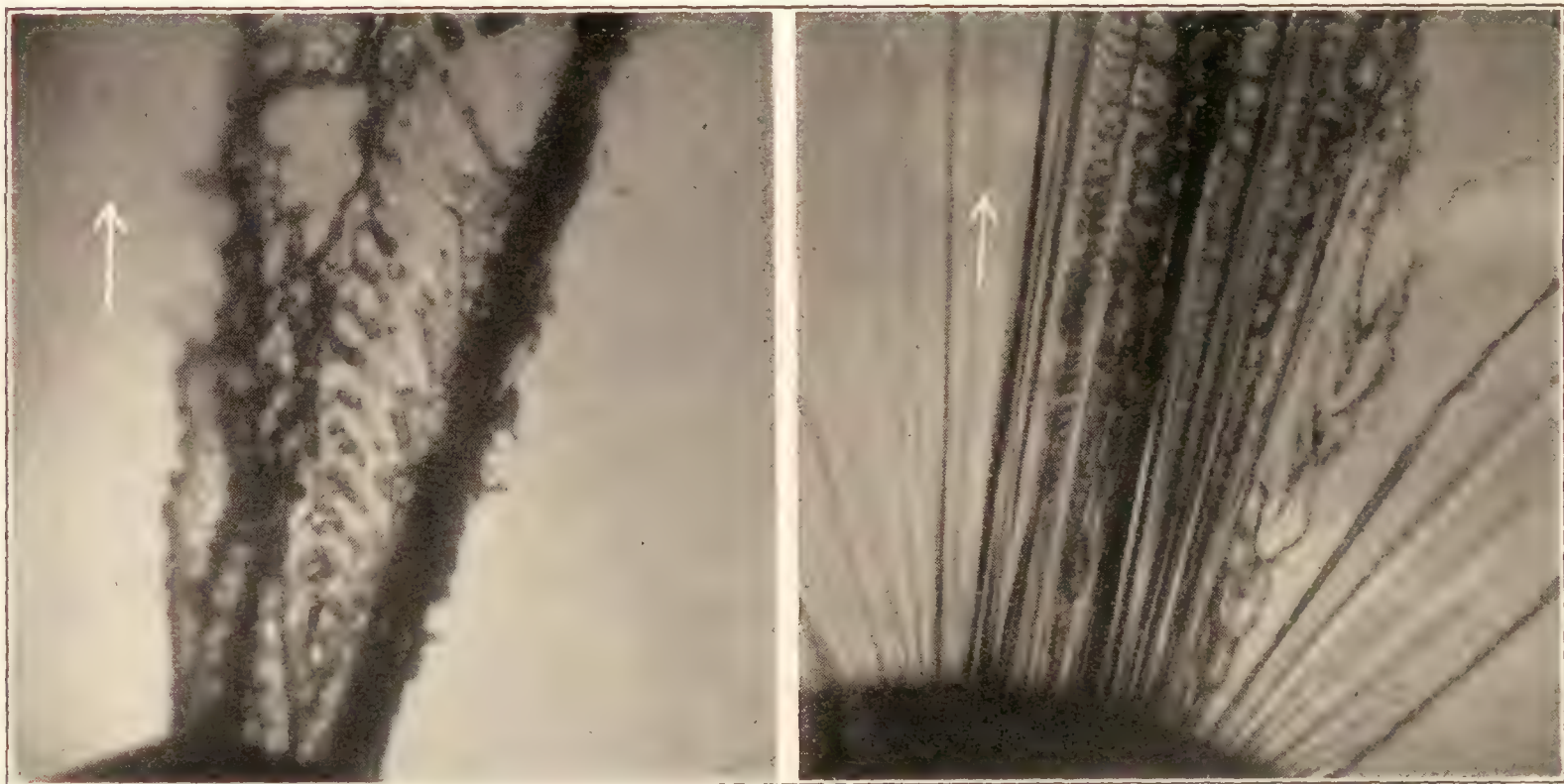
(d) Slit nozzle.

FIGURE 19.—Flow conditions at exit of some high-dispersion nozzles, $\times 10$. Injection pressure, 100 pounds per square inch or less; air density, 1 atmosphere



(a)

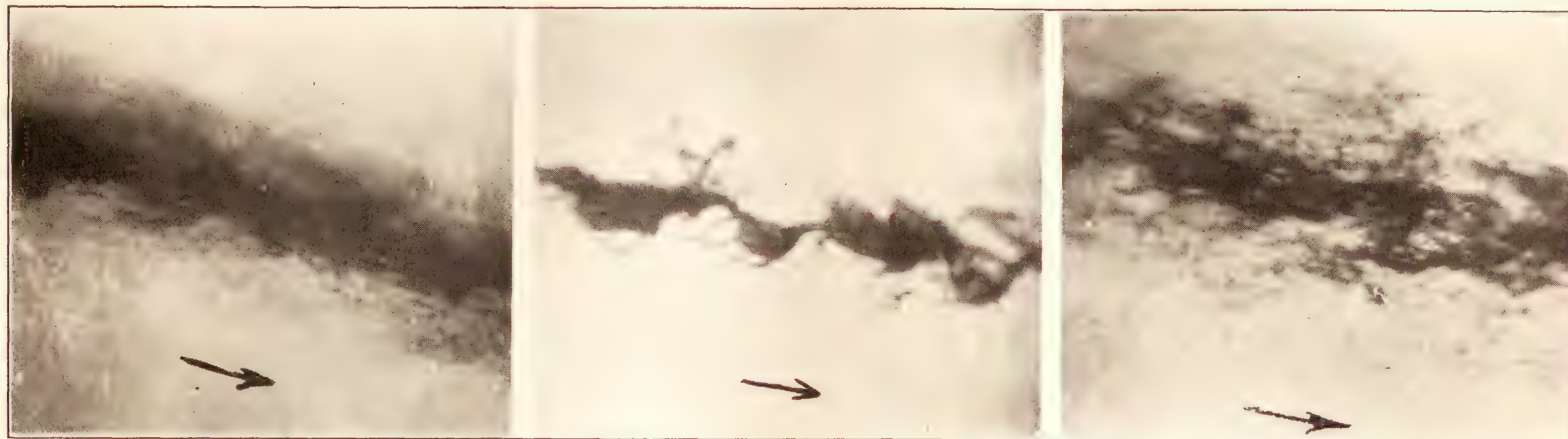
(b)



(c)

(d)

FIGURE 20.—Flow conditions at exit of some high-dispersion nozzles, $\times 10$. Injection pressure, 100 pounds per square inch or less; air density, 1 atmosphere; all sprays from slit nozzles



Gasoline.

Water.

Ethyl alcohol.



Diesel fuel No. 1.

Diesel fuel No. 2.

Lubricating oil.

FIGURE 21.—Jets of various liquids, $\times 10$. Injection pressure, 1,500 pounds per square inch; orifice diameter, 0.020 inch; air density, 1 atmosphere; distance from nozzle, 5 inches

shows the flat side of the spray from an impinging-jets nozzle, just beyond the point of impingement. Figure 19(c) shows the flat side of a sheet of fuel injected from a slit orifice in a hemispherically shaped nozzle. The irregular waves were probably the result of air forces. In Figure 19(d) the flat side of a sheet of fuel from a rectangular slit is shown. The regularity of the waves and the fact that they seem to possess their full amplitude as they leave the nozzle suggest that they are the result of nozzle vibrations.

The low-velocity jets shown in Figure 20 were all from slit nozzles. The turbulence of the flow shown in photographs (a) and (b) was of such a nature that a few large drops were thrown off at right angles to the main jet. The peculiar flow conditions shown in (c) were caused by a slight obstruction in the slit orifice. Photograph (d) shows examples of laminar flow, forced vibrations, and turbulent flow in different parts of a fan-shaped sheet of fuel.

EFFECT OF DIFFERENT LIQUIDS

Sass (reference 12) took 10-power photomicrographs of sprays of fuels having different viscosities and concluded that the atomization improved as the viscosity was decreased.

A number of photomicrographs were taken at this laboratory using different liquids to determine qualitatively the effects of viscosity and surface tension on spray formation. For convenience the viscosities and surface tensions of the various liquids are listed in Table I. All values were determined at temperatures as near as possible to those prevailing in the laboratory at the time the photomicrographs were taken.

TABLE I
PROPERTIES OF LIQUIDS USED

[Temperature, 22° C.; pressure, atmospheric]

Liquid	Viscosity, poises	Surface tension, dynes per cm
Gasoline.....	0.0042	21
Water.....	.0096	68
Ethyl alcohol.....	.0115	24
Diesel fuel No. 1.....	.022	27
Diesel fuel No. 2.....	.102	28
Lubricating oil.....	3.07	31

Representative photographs taken at 1,500 pounds per square inch injection pressure were selected and are shown in Figure 21. At higher injection pressures the differences in behavior become more evident, but at such high pressures and under these particular conditions the photographs are blurred and unsuitable for reproduction.

Examination of the photomicrographs of Figure 21 and the values given in Table I shows that for any one set of conditions the degree of disintegration of the jet decreases as the viscosity is increased. In the case of water, a decided effect of the increased surface tension

in reducing the degree of jet disintegration is noticeable. However, for such differences in surface tension as are found among the various fuels the effect is negligible.

ATOMIZATION MEASUREMENTS

Most of the photomicrographs were entirely unsuitable for quantitative measurements of the fineness of the atomization. In the atmosphere the atomization process was usually not completed in the region photographed, and in dense air the photomicrographs

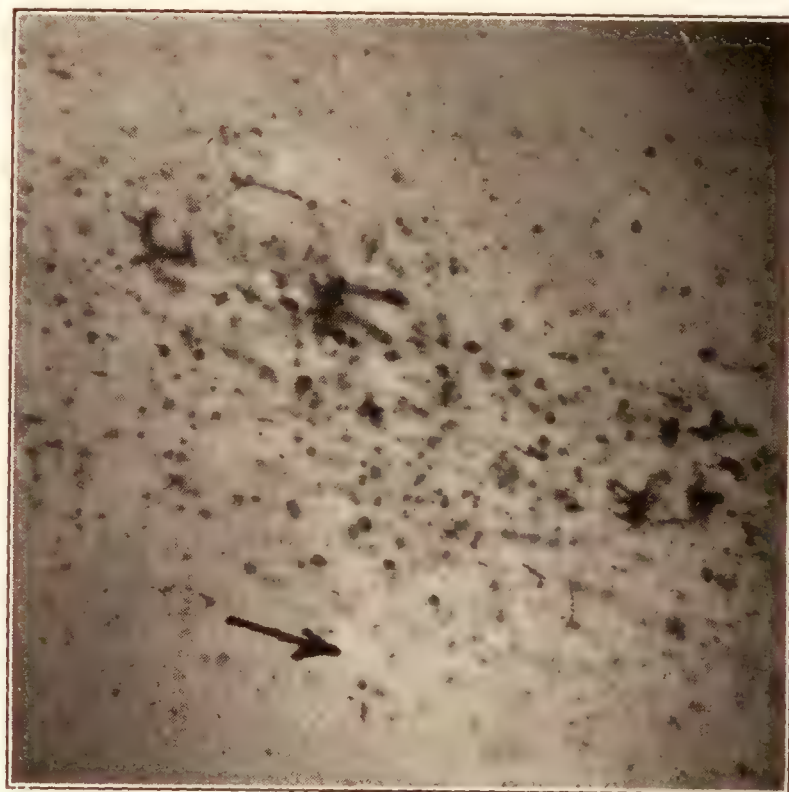


FIGURE 22.—Photomicrograph used to measure drop sizes for the Diesel fuel No. 1 curve of Figure 24

were not clear. In a few cases, however, it was possible to measure the sizes of the fuel particles from the photomicrographs. An example of such a photomicrograph is shown in Figure 22. Only a very small part of the spray was included in the field of the microscope, and many of the fuel particles were irregular or out of focus, so that the results may not be truly representative of the entire spray. The atomization measurements are included in this report because they support some of the conclusions reached from a study of all the photomicrographs.

In Figures 23 to 25 the ordinates of the curves show what percentage of the fuel volume was broken up into drops having diameters between zero and the value of the abscissa. In Figure 23 curves obtained by measuring photomicrographs of sprays injected into the atmosphere from an orifice 0.008 inch in diameter and 0.020 inch long are compared with curves for carburetor atomization (from Scheubel, reference 9) and with curves for fuel injections into dense air (data from Lee, reference 10). Each curve is identified by the relative velocity between the fuel and the air. For the carburetor sprays this is the air velocity at the Venturi throat, and for the injected sprays it is the initial fuel-jet velocity. A strict comparison of these

different sets of curves is impossible because of the different fuels, nozzles, and air densities used, but the fact that the curves arrange themselves according to their relative fuel-air velocities shows that it is this factor which predominates. Moreover, the close agreement between Scheubel's curves for alcohol and those obtained from photomicrographs of alcohol sprays injected into the atmosphere supports Castleman's conclusion that the atomization process in injected sprays is the same as that in carburetors.

The curves in Figure 24 give atomization data for four different liquids at low fuel-air velocities. They supplement the conclusions derived from a study of the photomicrographs as to the effects of the surface tension and viscosity of the fuel on jet disintegration. At these low injection velocities the atomization of Diesel fuel No. 2 and lubricating oil had not begun at 5 inches from the nozzle, the distance at which all the atomization measurements were made.

As a supplement to the above experiments, atomization measurements were made with Diesel fuels Nos. 1 and 2 at an injection velocity of 765 feet per second (pressure=4,000 pounds per square inch) and an air density of 1.01 pounds per cubic foot. The sprays were caught on smoked-glass plates and the impressions made there by the fuel drops were counted and measured. For a complete description of this method, see reference 10. The results of these measurements

and forces resulting from the relative motion between the fuel and the air. Atomization is accomplished by

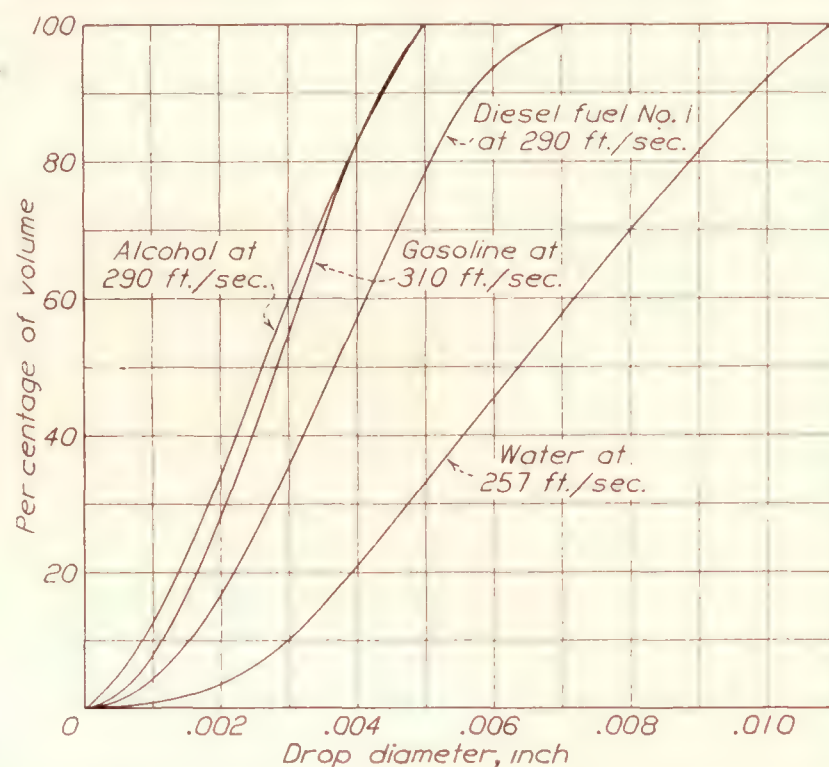


FIGURE 24.—Atomization data for different liquids. Orifice diameter, 0.008 inch; air density, 1 atmosphere

air acting upon the fuel column and the detached parts, tearing off fine, irregular threads or ligaments, which subsequently collapse into drops because of the surface tension of the fuel. The observations of

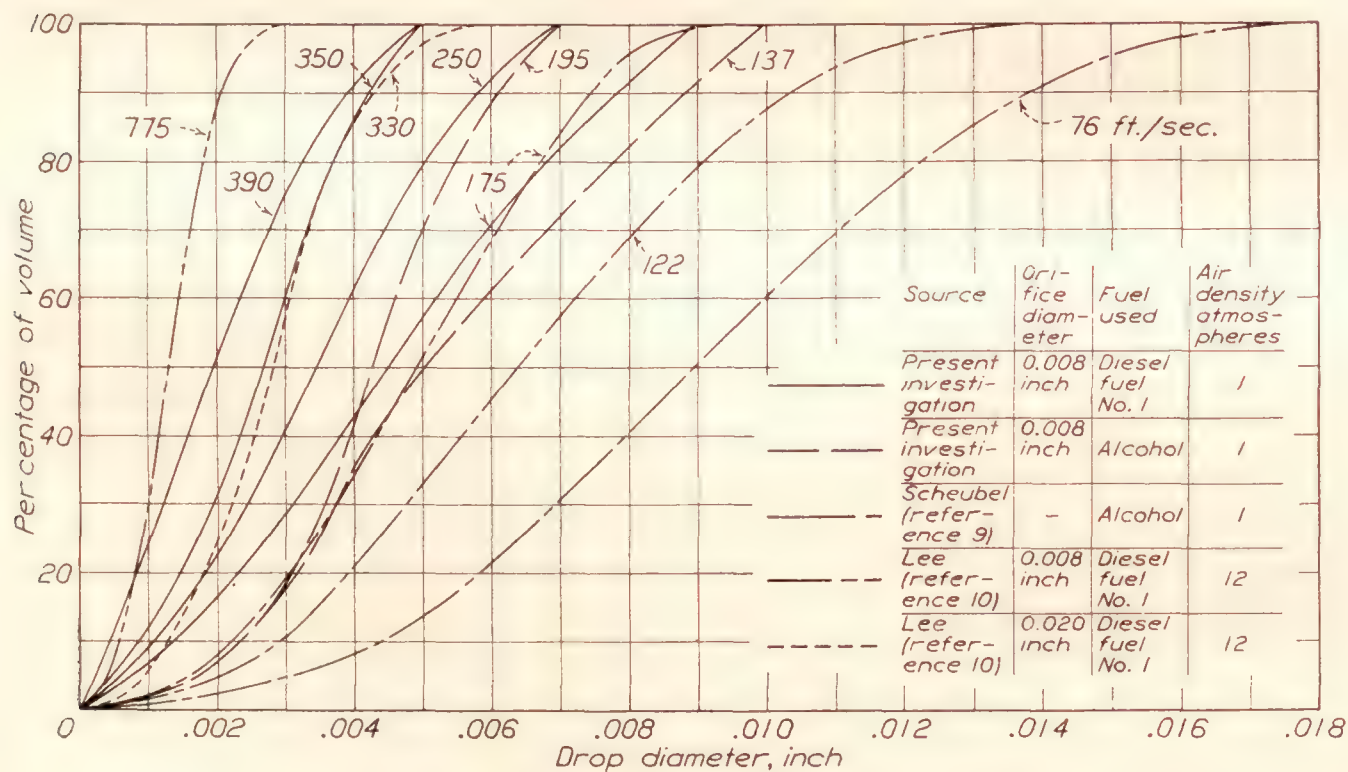


FIGURE 23.—Comparison of atomization data from different sources

are shown in Figure 25. The atomization was finer for the less viscous fuel, but the effect of fuel viscosity was less pronounced under these conditions than it was at low injection velocities and low air densities.

CONCLUSIONS

This photomicrographic study of fuel sprays has shown that the fuel leaves the nozzle as an unbroken column, but is quickly disintegrated into many irregular parts by a combination of fuel-stream turbulence

ligament formation and the results of drop size measurements, within the range investigated, support the conclusion of Dr. R. A. Castleman, jr., that the atomization process in injected sprays is the same as that in carburetors.

When other variables are held constant, the degree of disintegration of the jet:

(a) Increases with distance from the nozzle, until the disintegrating forces due to the relative velocity between the air and the fuel are no longer sufficient

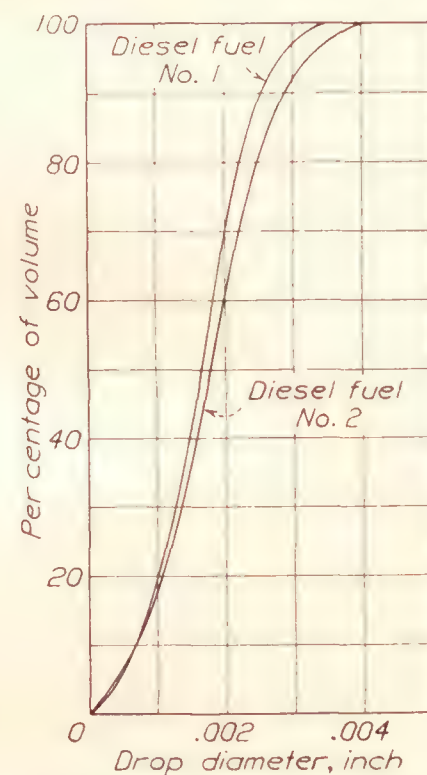


FIGURE 25.—Effect of fuel viscosity on the fineness of the atomization. Injection pressure, 4,000 pounds per square inch (initial jet velocity about 785 feet per second); orifice diameter, 0.020 inch; air density, 13 atmospheres.

to overcome the resisting forces due to the surface tension and viscosity of the fuel.

- (b) Increases with increase of air density.
- (c) Increases with increase of jet velocity.
- (d) Decreases with increase of orifice diameter.
- (e) Decreases with increase of fuel viscosity.
- (f) Decreases with increase of fuel surface tension.
- (g) Increases with increase of fuel turbulence. Fuel

turbulence accelerates the disintegration of the fuel jet by ruffling its surface close to the orifice, but it has relatively little disintegrating force in itself.

At atmospheric and subatmospheric air densities there may be wide differences in the dispersion of sprays from geometrically similar nozzles, because of different degrees of turbulence caused by slight irregularities in the nozzles. This difference is also shown between the early and late parts of sprays from nozzles used with automatic injection valves. At air densities corresponding to those in compression-ignition engines at the time of fuel injection the differences are slight.

LANGLEY MEMORIAL AERONAUTICAL LABORATORY,
NATIONAL ADVISORY COMMITTEE FOR AERONAUTICS,
LANGLEY FIELD, VA., *December 15, 1932.*

REFERENCES

1. Kuehn, R.: Atomization of Liquid Fuels, Part II. T. M. No. 330, N. A. C. A., 1925.
2. DeJuhasz, Kalman J., Zahn, O. F., jr., and Schweitzer, P. H.: On the Formation and Dispersion of Oil Sprays. Bulletin No. 40 of the Pennsylvania State College Engineering Experiment Station, 1932, pp. 63-68.
3. Haenlein, A.: Disintegration of a Liquid Jet. T. M. No. 659, N. A. C. A., 1932.
4. Castleman, R. A., jr.: The Mechanism of the Atomization of Liquids. Bur. Standards Jour. Research, March, 1931, pp. 369-376.
5. Castleman, R. A., jr.: The Mechanism of Atomization Accompanying Solid Injection. T. R. No. 440, N. A. C. A., 1932.
6. Triebnigg, Heinrich: Der Einblase und Einspritzvorgang bei Dieselmotoren. Julius Springer (Vienna), 1925.
7. Conrady, A. E., and others: Photography as a Scientific Implement. Blackie and Son, Ltd. (London), pp. 266-267, 1923.
8. Rothrock, A. M.: Pressure Fluctuations in a Common-Rail Fuel Injection System. T. R. No. 363, N. A. C. A., 1930.
9. Scheubel, F. N.: On Atomization in Carburetors. T. M. No. 644, N. A. C. A., 1931.
10. Lee, Dana W.: The Effect of Nozzle Design and Operating Conditions on the Atomization and Distribution of Fuel Sprays. T. R. No. 425, N. A. C. A., 1932.
11. Gelalles, A. G.: Effect of Orifice Length-Diameter Ratio on Fuel Sprays for Compression-Ignition Engines. T. R. No. 402, N. A. C. A., 1931.
12. Sass, F.: Probleme der Neuzeitlichen Ölmaschine. Forschung und Technik, Allgemeine Elektrizitäts-Gesellschaft, 1930.

REPORT No. 455

PENETRATION AND DURATION OF FUEL SPRAYS FROM A PUMP INJECTION SYSTEM

By A. M. ROTHROCK and E. T. MARSH

SUMMARY

High-speed motion pictures were taken of individual fuel sprays from a pump injection system. The changes in the spray-tip penetration with changes in the pump speed, injection-valve opening and closing pressures, discharge-orifice area, injection-tube length and diameter, and pump throttle setting were measured. The pump was used with and without a check valve. The results show that the penetration of the spray tip can be controlled by the dimensions of the injection tube, the area of the discharge orifice, and the injection-valve opening and closing pressures.

INTRODUCTION

In order to determine the suitability of a given type of injection system for high-speed compression-ignition engines, it is necessary to know the operating characteristics of the system. One of the most important characteristics to be investigated is the formation and the development of the fuel spray. During the last five years the National Advisory Committee for Aeronautics has published considerable information on the effects of the various factors which control the formation and the development of the fuel spray. Investigations have been conducted with a mechanically operated injection valve and with automatic injection valves. In these investigations it was necessary to operate the injection system from a constant source of pressure because the purpose of the tests was to investigate the effects of such variables as the injection pressure, the spray-chamber density, and the discharge-orifice design.

With pump injection systems, however, the injection pressure varies with pump speed and in some cases with the fuel quantity delivered. Tests already conducted (reference 1) have shown that the injection pressures affect the penetration of the fuel spray during the first few thousandths of a second. As this is the time available for injection in a high-speed compression-ignition engine, it is important to know how the pressure variations in a pump injection system will affect the fuel-spray penetration and dispersion. It is also advantageous to know the effects of such variables as the injection-tube length, the injection-tube diameter, the discharge-orifice diameter, and the

injection-valve opening and closing pressures on the penetration and dispersion of the fuel spray.

This report presents the results obtained from an investigation made at the Langley Memorial Aeronautical Laboratory, Langley Field, Va., to determine the effect of pump speed, the dimensions of the injection tube, the pump throttle setting, the discharge-orifice diameter, and the adjustment of the injection valve on the penetration and dispersion of the fuel spray. As far as was practicable the test conditions were the same as those used by Rothrock in his investigation of the hydraulics of fuel-pump injection sys-

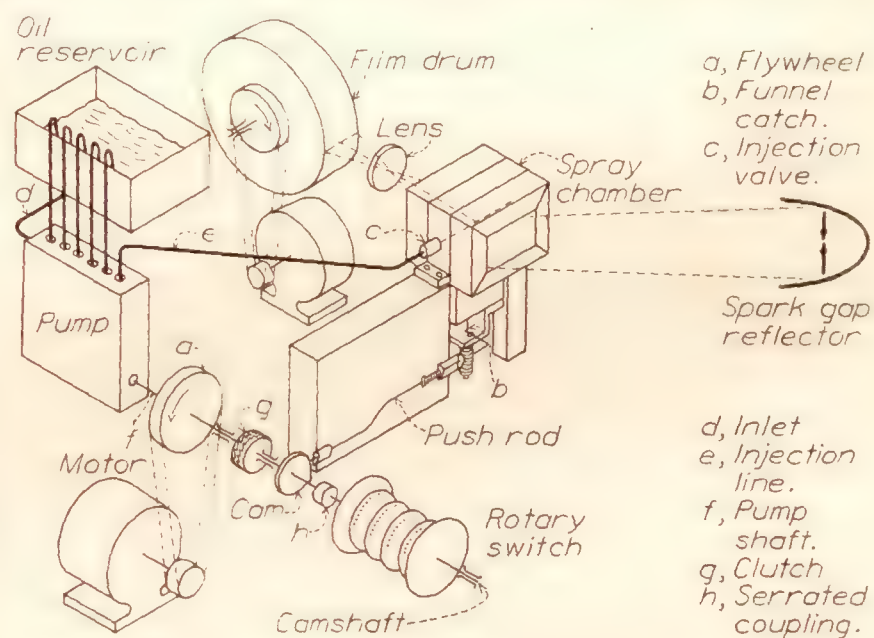


FIGURE 1.—Diagrammatic arrangement of N. A. C. A. spray photographic equipment for use with fuel pumps

tems. (See reference 2.) The injection valve and the fuel pump were the same as those described in reference 2. The pump was tested with and without a check valve.

APPARATUS AND METHODS

A diagrammatic arrangement of the apparatus used in this investigation is shown in Figure 1. This apparatus is a modification of the N. A. C. A. spray photographic equipment (reference 3) used in taking high-speed motion pictures of a single spray discharge from a common-rail system. Two modifications have been made: a change from the common-rail system to the pump system of injection, and a change in the

spray chamber so that continuous injections from a fuel pump into the compressed air would not fog the chamber and prevent photographs from being taken of a single spray.

In the modified spray chamber (fig. 2) a funnel was arranged in front of the nozzle to deflect the sprays

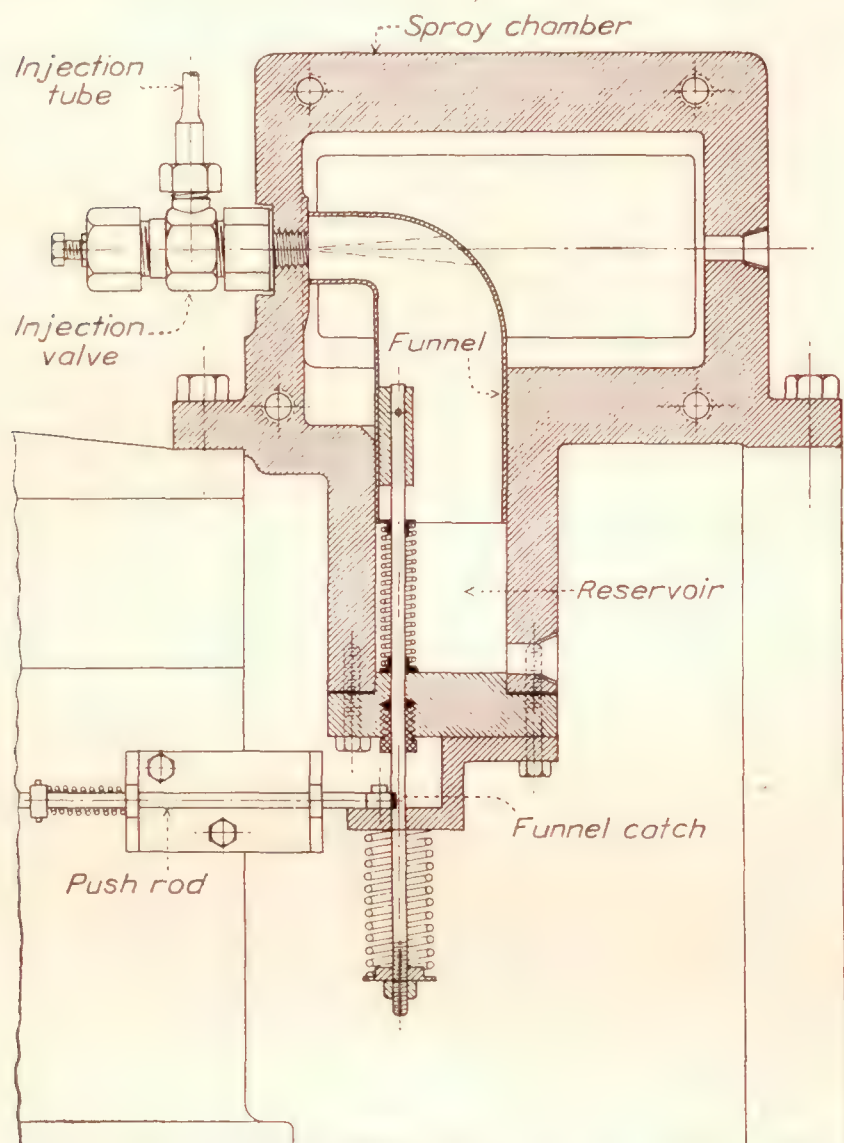


FIGURE 2.—Spray chamber for use with fuel pumps

into a reservoir. Releasing the funnel catch allowed the funnel to drop below the nozzle and permitted the spray to enter the spray chamber. With the proper timing the funnel uncovered the valve nozzle between pump discharges so that there was no interference between the spray and the funnel.

The pump tested was a 6-cylinder commercial fuel pump. A cross section through one of the cylinders of the pump (fig. 3) shows its construction. The outlets from five of the pump plungers were by-passed to the oil reservoir and the sixth was connected to the injection valve with a seamless steel tube having an outside diameter approximately twice the inside diameter.

The injection pump was rotated by a variable-speed electric motor and was connected to the camshaft through a jaw clutch. The camshaft remained stationary until engaged by this clutch. It then made one revolution with the pump shaft. During this revolution of the camshaft, the funnel catch was released; the rotary switch completed the electric circuit between the condensers and the spark gap.

The rotary switch and the pump were timed with the serrated coupling so that the spray was synchronized with the discharges of the condensers. The injection-valve closing pressure instead of opening pressure was measured because of the greater accuracy of this measurement. (See reference 2.) The injection-valve opening pressure was approximately 1.4 times the closing pressure.

The fuel oil used had a specific gravity of 0.83 and an absolute viscosity of 0.022 poise at 100° F.

Unless otherwise stated, all tests were made with a 0.020-inch diameter orifice and a 34-inch injection tube. The discharge orifice length/diameter ratio was 6:1 in all tests.

The procedure for taking a spray photograph was the same for all tests. The pump was brought up to the desired speed and the throttle opened for a few revolutions to expel all air from the injection tube. Air was then blown through the spray chamber to clear the glass walls and to remove suspended oil particles. The air pressure, unless otherwise stated, was raised to 200 pounds per square inch, a density of 1.1 pounds per cubic foot, which is equivalent to the density in the combustion chamber of an engine operating at a compression ratio of 14, and the funnel was raised and latched in position. When the desired film-drum

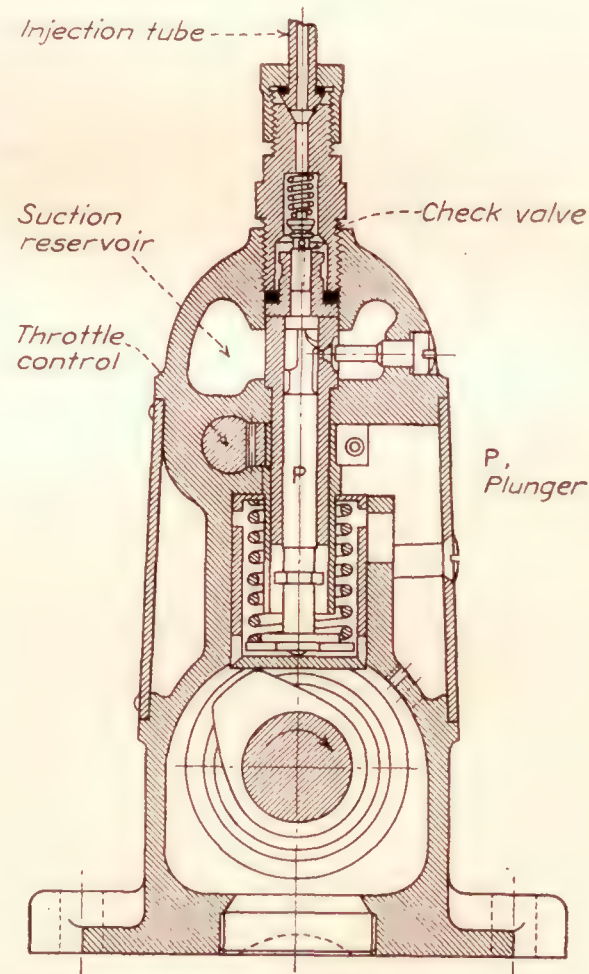


FIGURE 3.—Diagrammatic sketch of fuel pump used in tests

speed was reached, the pump throttle was again opened, and after several revolutions of the pump the clutch was engaged. A progressive series of photographs was thus recorded of the spray development. From these records the spray-tip penetration curves were obtained.

Stem-lift records of the injection-valve stem were also taken in a few cases to determine the movement of the valve stem under the pressure conditions in the injection valve. The method was the same as described in reference 2.

TEST RESULTS AND DISCUSSION

SPRAY-TIP PENETRATION

The results of the tests are shown by graphs on which the penetration of the fuel spray-tip in the spray

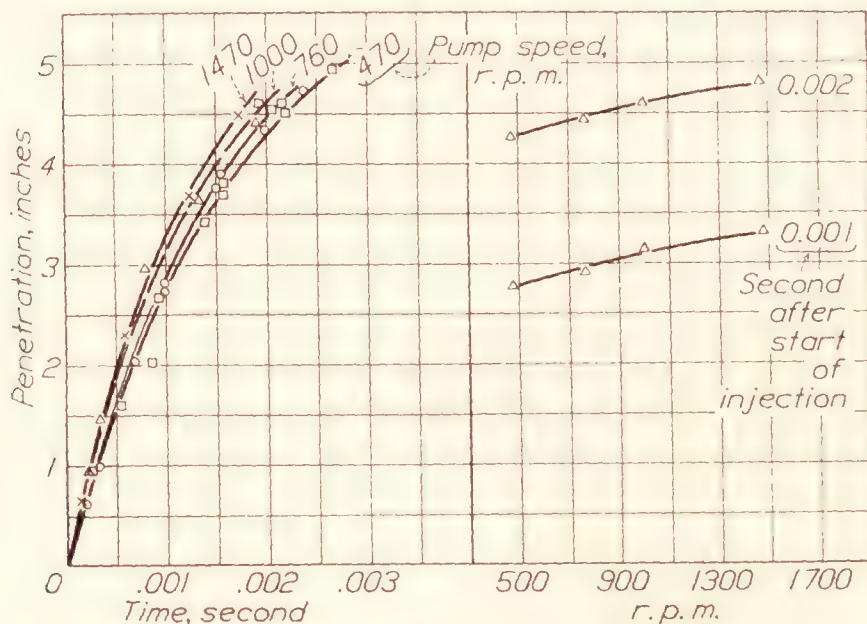


FIGURE 4.—Effect of pump speed on penetration. Valve closing pressure, 2,000 lb./sq. in. Tube length, 34 in. Injection tube inside diameter, 0.125 in. Orifice diameter, 0.020 in.

chamber is plotted against time. Tangents to these curves indicate the rate of penetration of the spray tip. A separate curve is plotted for each variable and the effect of the variable on spray-tip penetration is noted. Each curve is plotted from two or three tests under the same conditions. Additional checks were made when large variations appeared. Zero time on the graphs refers to the start of the spray from the orifice.

Effect of pump speed.—In reference 2 it was shown that varying the pump speed added to the initial pressure (approximately the valve-closing pressure) in the injection tube instantaneous values of pressure proportional to the velocity of the pump plunger. As the initial pressure was increased the ratio of the pressures created by the motion of the pump plunger to the total pressure at any instant decreased. It has also been shown in references 1 and 4 that both the maximum injection pressures and the injection-valve opening pressure affect the spray-tip velocity. However, as the rate-of-pressure rise, after the injection valve opens, decreases or as the ratio of the maximum pressure to the injection-valve opening pressure decreases it can be expected that the effect of the injection-valve opening pressure on the spray-tip penetration will increase and the effect of the maximum pressure will decrease. We can therefore expect that, in general, as the injection-valve opening pressure

is increased the effect of pump speed on spray-tip penetration will decrease.

In reference 2 it has also been shown that as the pump speed is decreased a speed is reached below which the pressure waves originating at the fuel pump are not sufficient to hold the injection-valve stem from the seat. This value of speed depends on the injection-pump plunger diameter, the pump-cam contour, the injection-tube diameter, the initial pressure in the injection tube, the injection-valve opening and closing pressures, and the pressure into which the discharge takes place. It is, within practical limits, independent of the injection-tube length. For speeds below this value the injection-valve stem will tend to oscillate, thereby opening and closing the injection valve. The phenomenon is sometimes accompanied by a chattering of the injection-valve stem against its seat during the injection period. When this phenomenon occurs the fuel discharge instead of consisting of a single spray will consist of two or more individual sprays following each other, generally in quick succession. Under certain circumstances the stem may not lift sufficiently to expose a flow area greater than the discharge-orifice area. In this case the stem and seat together act as a variable-area orifice. Owing to restriction to flow the spray will not have the penetrating ability possible were the stem fully lifted.

The effect of pump speed on the spray-tip penetration at an injection-valve closing pressure of 2,000 pounds per square inch is shown in Figure 4. In no

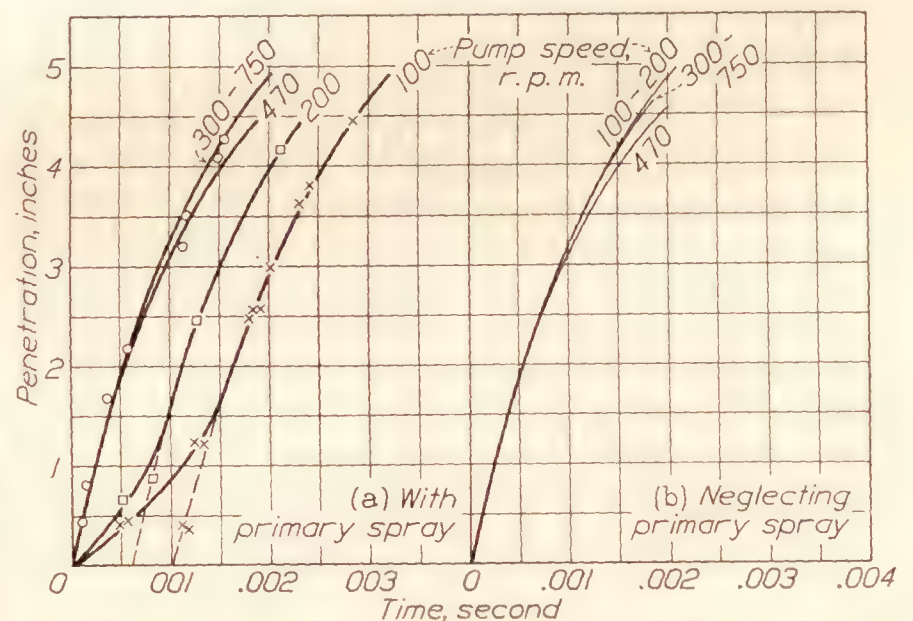


FIGURE 5.—Effect of pump speed on spray-tip penetration at high injection-valve closing pressure. Injection-valve closing pressure, 2,500 lb./sq. in. Tube length, 34 in. Injection tube inside diameter, 0.125 in. Orifice diameter, 0.020 in.

case was there evidence of primary sprays before the main spray at pump speeds above 760 r. p. m. The variation in maximum pressures and in the rate-of-pressure rise was sufficient to cause the spray-tip penetration to increase with pump speed.

Figure 5 shows the effect of low pump speeds on the spray-tip penetration at an injection-valve closing pressure of 2,500 pounds per square inch. The figure

shows that at the two lower speeds primary sprays appeared before the main spray. These primary sprays were caused by the seating of the injection-valve stem after the initial opening. After the second lifting of the stem the pressure was sufficient to keep the injection-valve stem off its seat. If the main sprays at the two lower speeds are compared with those at the higher speeds (fig. 5(b)) it is seen that the penetration of the main spray is not appreciably affected by the pump speed. It may be concluded that in this case the injection-valve closing pressure was sufficiently high so that the effect of the rate-of-pressure rise and maximum pressures had no appreciable effect on the spray-tip penetration of the main sprays.

At low pump speeds and with an injection-valve closing pressure of 500 pounds per square inch, the rate-of-pressure rise and the maximum pressures

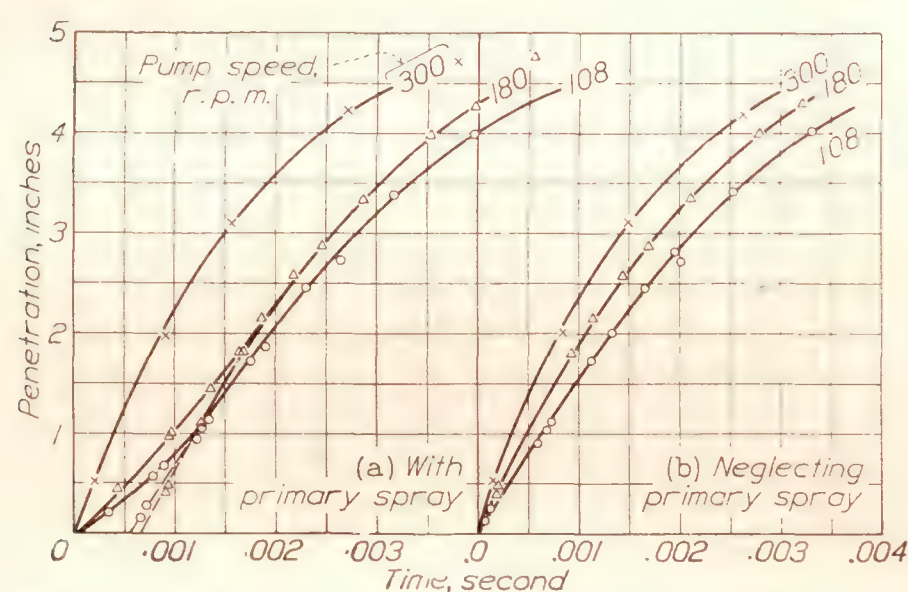


FIGURE 6.—Effect of pump speed on spray-tip penetration at low injection-valve closing pressure. Injection-valve closing pressure, 500 lb./sq. in. Injection tube inside diameter, 0.125 in. Tube length, 34 in. Orifice diameter, 0.020 in.

materially influenced the penetration. (Fig. 6.) At the two lower speeds primary sprays occurred.

Figure 7 shows a spray photograph and stem-lift record taken at a pump speed of 190 r. p. m. with atmospheric pressure in the spray chamber. The small lines at the top of the stem-lift record were caused by a spark gap placed in series with the main gap for taking the photographs. Consequently, each line corresponds to a spray photograph. Because the stem record extended for more than a single revolution of the film drum, the spray photographs and the stem record are not synchronized. The injection-valve stem oscillated, thus opening and closing the injection valve and causing a series of sprays. The bouncing of the stem was eliminated when the chamber pressure was increased to 200 pounds per square inch, because of the additional force on the stem. However, when the pump speed was decreased to 108 r. p. m. (fig. 8) the bouncing of the stem during the whole injection period again occurred though the chamber pressure was 200 pounds per square inch. Comparison of Figures 7 and 8 shows that in the

former the stem lift and consequently the pressures were higher than in the latter.

Effect of injection-valve closing pressure.—Figure 9 shows the effect of the injection-valve closing pressure on the penetration of the tip of the main spray for a pump speed of 470 r. p. m. The records showed that there were primary sprays with injection-valve closing pressures of 1,500 pounds per square inch or greater. The figure shows that the penetration of the main spray increases as the injection-valve closing pressure was increased until a value of 1,500 pounds per square inch is reached. For this pressure the spray-tip penetration decreased. As the injection-valve closing pressure was further increased the penetration again increased. The decrease in the penetration at the injection-valve closing pressure of 1,500 pounds per square inch was probably caused by the injection-valve stem throttling the flow of fuel past the valve seat. Above this injection-valve closing pressure, although throttling still occurred as has been shown in reference 2, the pressure at the start of injection was sufficient to give the spray the increased penetration.

The penetration of both the primary and main sprays for the injection-valve closing pressures of 1,500 and 2,000 pounds per square inch is shown in Figure 10. It is seen that the primary spray as well as the main spray penetrated at a faster rate as the injection-valve closing pressure was increased.

Figure 11 shows the effect of the injection-valve closing pressure on the spray-tip penetration for a pump speed of 760 r. p. m. No primary sprays were observed at this speed. However, as was the case with 470 r. p. m. a minimum penetration occurred at a particular injection-valve closing pressure, 2,000 pounds per square inch.

At low injection-valve closing pressures and a pump speed of 760 r. p. m., it was shown in reference 2 that the pressure-wave phenomenon caused secondary discharge after cut-off occurred at the fuel pump. Secondary discharges did not occur with the higher injection-valve closing pressures. The photographs showed these secondary discharges with the low valve closing pressures, but because of the fogging of the chamber the photographs were not clear enough to reproduce on a half-tone photo-engraving.

Effect of injection-tube diameter.—As shown in reference 2, it is advisable to use an injection-tube diameter equal to or slightly greater than the critical tube diameter so that the flow through the injection tube will be laminar with a resultant small pressure loss caused by friction. Figure 12 (a) shows that the penetration at a pump speed of 760 r. p. m. was nearly the same for all injection-tube diameters even when diameters considerably less than the critical diameter (0.098 inch) were employed. For the conditions shown in Figure 12 (a) it may be concluded that the

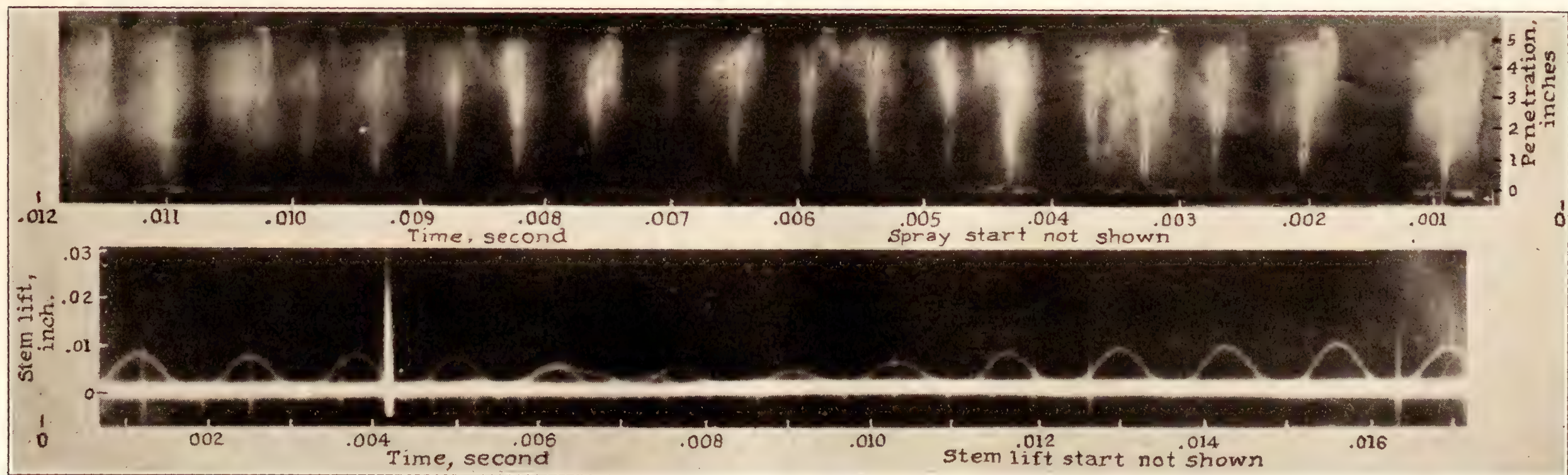


FIGURE 7.—Spray photograph and stem-lift record at low pump speed. Pump speed, 190 r. p. m. Injection-valve closing pressure, 500 lb./sq. in. Injection tube inside diameter, 0.125 in. Tube length, 34 in. Spray chamber density, 0.0765 lb./cu. ft.

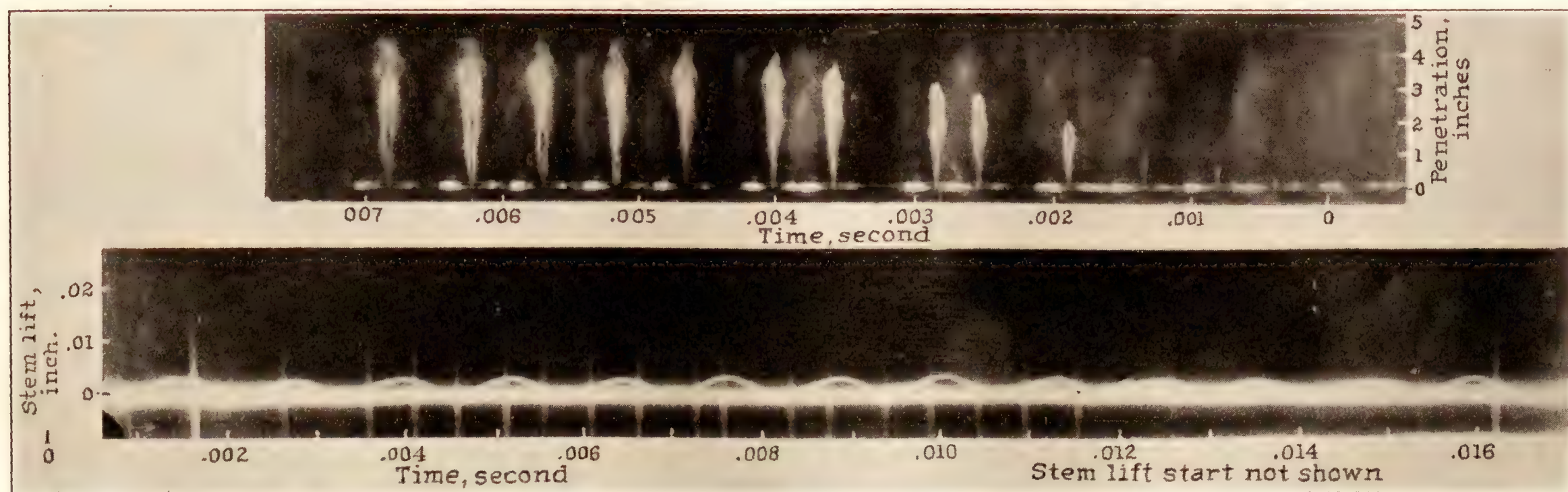


FIGURE 8.—Spray photograph and stem-lift record at low pump speed. Pump speed, 108 r. p. m. Injection-valve closing pressure, 500 lb./sq. in. Injection-tube inside diameter, 0.125 in. Tube length, 34 in. Spray chamber density, 1.11 lb./cu. ft.

injection-valve opening and closing pressure controlled the spray-tip penetration.

For the pump speed of 470 r. p. m. (fig. 12 (b)) the smaller tube gave the lower spray-tip penetration. As the test conditions caused primary starts at the begin-

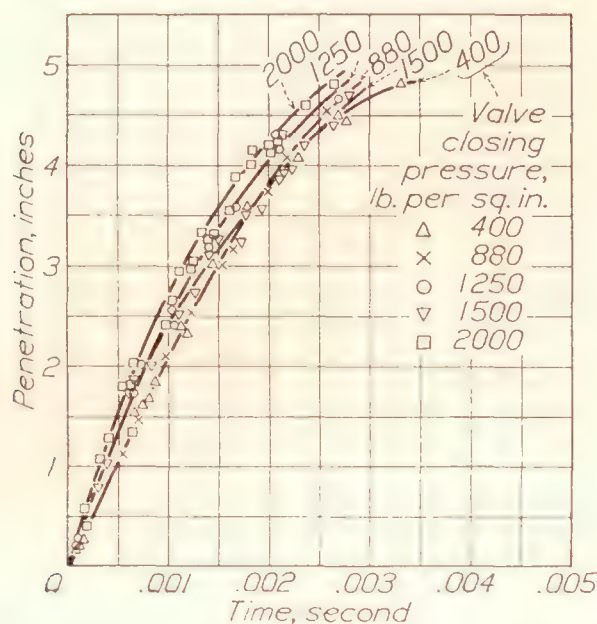


FIGURE 9.—Effect of injection-valve closing pressure on spray-tip penetration. Pump speed, 470 r. p. m. Injection-tube inside diameter, 0.076 in. Tube length, 34 in. Orifice diameter, 0.020 in.

ning of the spray (fig. 10) the drop in rate of penetration was probably due to their formation.

In order to illustrate the influence of these primary sprays in this instance, a comparison of Figure 10 with Figure 12 (b) shows that the primary spray penetration for the 0.076-inch tube falls below the curve for the primaries of the 0.041 and 0.059 inch diameter tubes, indicating lower penetration for the 0.076-inch tube.

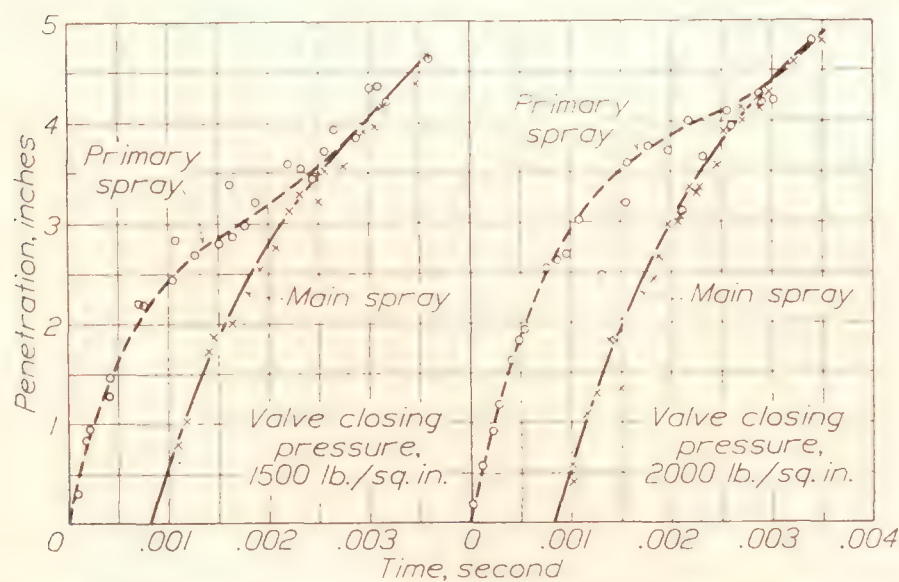


FIGURE 10.—Effect of injection-valve closing pressure on spray-tip penetration of primary and main sprays. Pump speed, 470 r. p. m. Injection-tube inside diameter, 0.076 in. Tube length 34 in. Orifice diameter, 0.020 in.

However, the main spray for the 0.076-inch tube shows greater penetration. The spray photographs for the 0.041 and 0.059 inch diameter tubes show primaries but the main sprays are not clear enough to be measured directly. Measurement of the clearest main spray (0.059-inch tube) shows the main spray penetration to be the same as that for the 0.076-inch tube.

The increase in penetration for the 0.125-inch tube (470 r. p. m.) is due to laminar flow which exists in the tube. As shown in reference 2, turbulent flow in a

tube results in friction and pressure losses which give a low initial stem lift and a slow rise in pressure at the injection valve. Both conditions aid the formation of primary sprays. With laminar flow these conditions

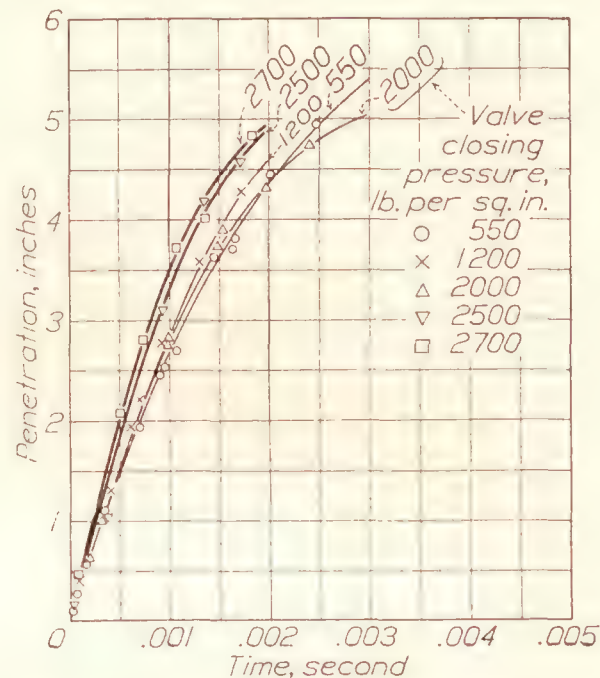


FIGURE 11.—Effect of injection-valve closing pressure on spray-tip penetration. Pump speed, 760 r. p. m. Injection-tube inside diameter, 0.125 in. Tube length, 34 in. Orifice diameter, 0.020 in.

are lacking and a faster rate-of-pressure rise results which increases the penetration.

Effect of injection-tube length.—Figure 13 shows the effect of the injection-tube length on the spray-tip penetration. The results show that there was little variation in the spray-tip penetration for tube lengths

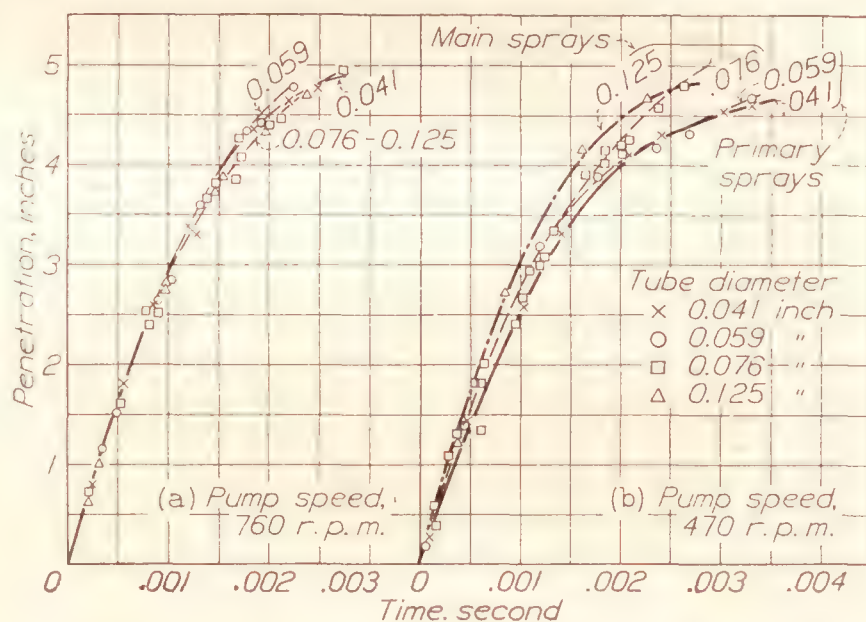


FIGURE 12.—Effect of injection-tube inside diameter on spray-tip penetration. Injection-valve closing pressure, 2,000 lb./sq. in. Tube length, 34 in. Orifice diameter, 0.020 in.

between 34 and 70 inches. Because of the limitations of the apparatus it was not possible to test injection-tube lengths of less than 34 inches. However, it was shown in reference 2 that the instantaneous pressures showed little variation with injection-tube lengths of from 4 to 34 inches. Consequently, it may be assumed that the injection-tube length does not have an appreciable effect on the penetration of the fuel spray.

Effect of pump-throttle setting.—Increase in the pump-throttle setting (fig. 14) gave decreased penetration. The injection periods for low throttle settings

were short, but the spray reached the maximum penetration that could be measured before cut-off occurred. The effect of the initial pressure rise with early cut-off should have a determining effect on the action of the spray. From stem-lift records (reference 2, fig. 17) the pressure rise as the valve stem is first lifting is more rapid at the lower throttle setting. The

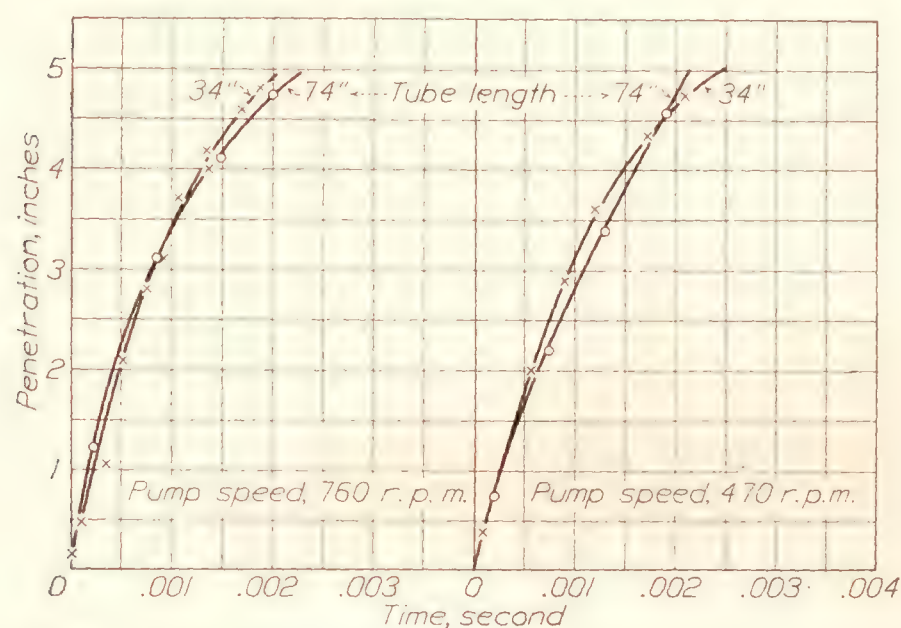


FIGURE 13.—Effect of injection-tube length on spray-tip penetration. Injection-valve closing pressure, 2,500 lb./sq. in. Injection-tube inside diameter, 0.125 in. Orifice diameter, 0.020 in.

higher initial velocity of the spray gives, therefore, an increased rate of penetration for the lower throttle settings.

Effect of check valve in pump.—With no check valve in the pump there was a slight increase in the rate of penetration over that obtained by using a check valve, as is shown by Figure 15. The results

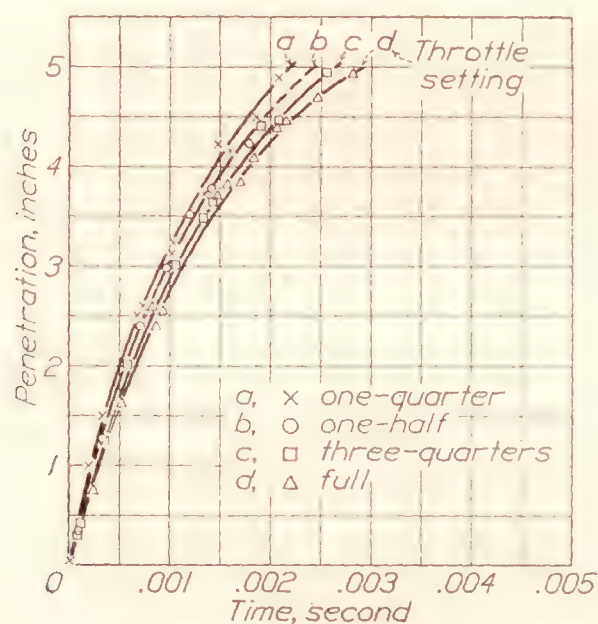


FIGURE 14.—Effect of pump throttle setting on spray-tip penetration. Pump speed, 760 r. p. m. Injection-valve closing pressure, 2,000 lb./sq. in. Injection-tube inside diameter, 0.076 in. Tube length, 34 in. Orifice diameter, 0.020 in.

without the check valve were erratic. In reference 2, Figure 19, the stem-lift curve obtained without a check valve in the pump shows a faster rate of stem lift than with a check valve, indicating a greater pressure rise and greater initial spray-tip velocity than that obtained with a check valve in the pump, but the injection period was materially decreased. How-

ever, later results have shown that removing the check valve also decreases the total fuel quantity discharged.

With no check valve between the pump and the injection tube, the tube often became air locked causing a pulsating flow in the injection tube, but no injection. The air lock was probably caused by air leakage from the spray chamber past the injection-valve seat. This air lock persisted even after the

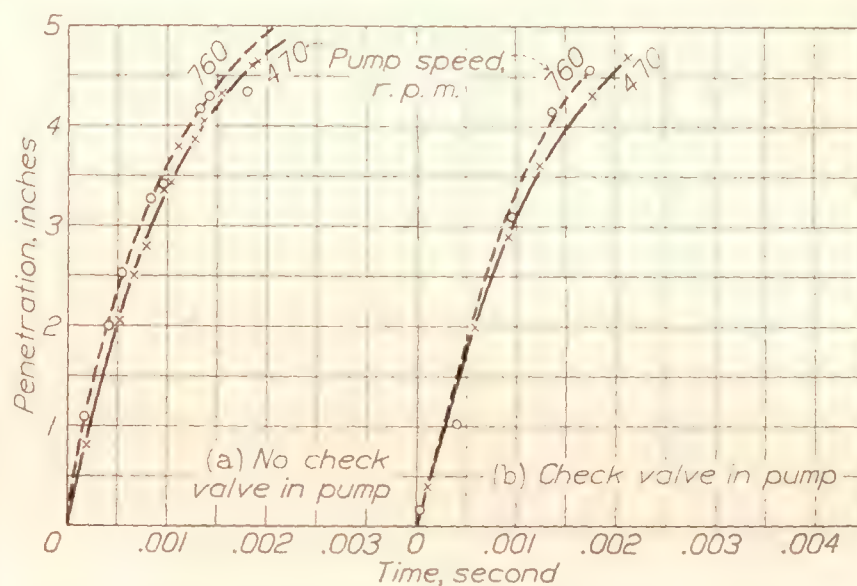


FIGURE 15.—Effect of check valve on spray-tip penetration. Injection-valve closing pressure, 2,500 lb./sq. in. Injection-tube inside diameter, 0.125 in. Tube length, 34 in. Orifice diameter, 0.020 in.

injection-valve closing pressure had been raised to 4,500 pounds per square inch. The other five plungers would discharge regularly into the oil reservoir. With the check valve in the pump, any air in the tube was forced out during the first few revolutions.

Effect of open nozzle.—The open nozzle used in these tests was fitted with a ball-check valve close to

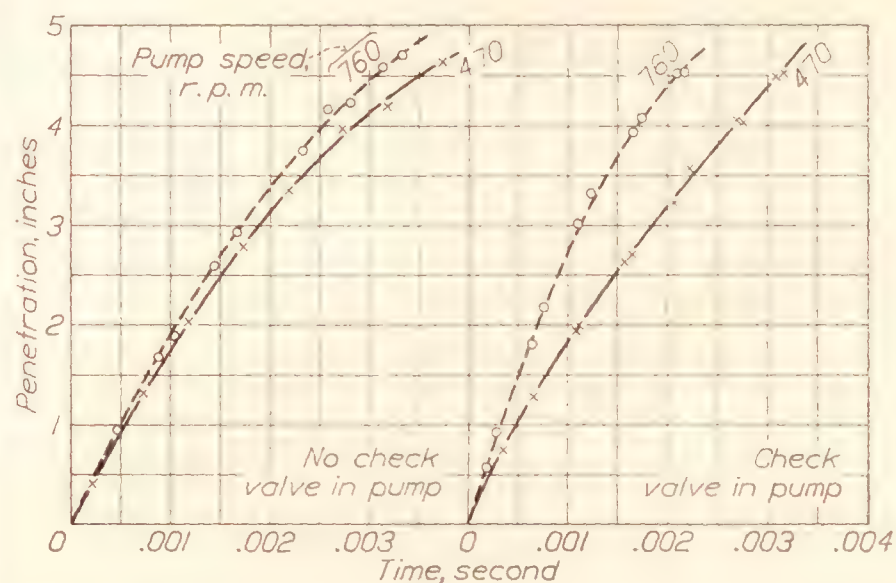


FIGURE 16.—Effect of check valve and open nozzle on spray-tip penetration. Open nozzle. Injection-tube inside diameter, 0.125 in. Tube length, 34 in. Orifice diameter, 0.020 in.

the nozzle to prevent leakage of air into the injection line, as recommended in reference 5. With the check valve in the pump a marked increase in the rate of penetration was noted at 760 r. p. m. (fig. 16) over that obtained without the check valve. The increase at 470 r. p. m. was not so noticeable. The increase in rate of penetration was due to the fact that the closing of the check valve trapped an initial pressure in the

injection tube equal to the spray-chamber pressure. This initial pressure aided in building up higher pressures in the injection tube. Furthermore, the check valve lessened the probability of the formation of an air pocket in the injection tube.

The penetration obtained with the open nozzle with and without the check valve at the pump was less than

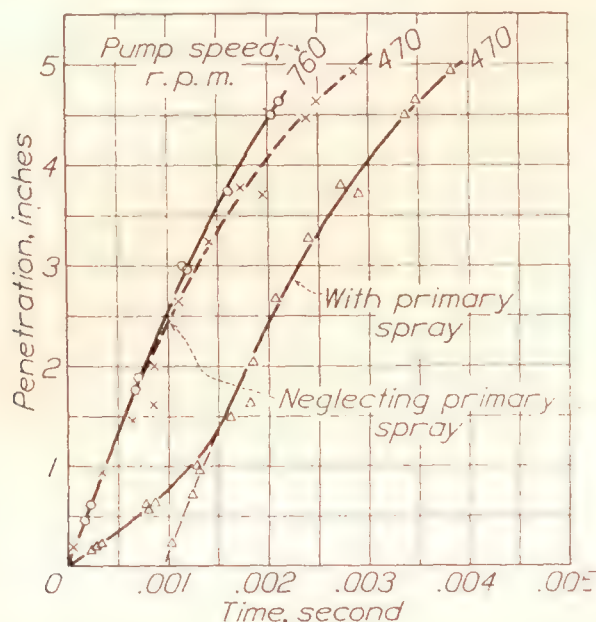


FIGURE 17.—Spray-tip penetration with 0.030 in. orifice. Injection-valve closing pressure, 2,500 lb./sq. in. Injection-tube inside diameter, 0.125 in. Tube length, 34 in. Orifice diameter, 0.030 in.

that obtained with the closed nozzle under the same conditions.

Effect of orifice diameter.—Figure 17 shows the results obtained with an 0.030-inch diameter orifice at pump speeds of 470 and 760 r. p. m. These curves show a lower rate of penetration than the corresponding series for the 0.020-inch orifice (fig. 15(b)) and the

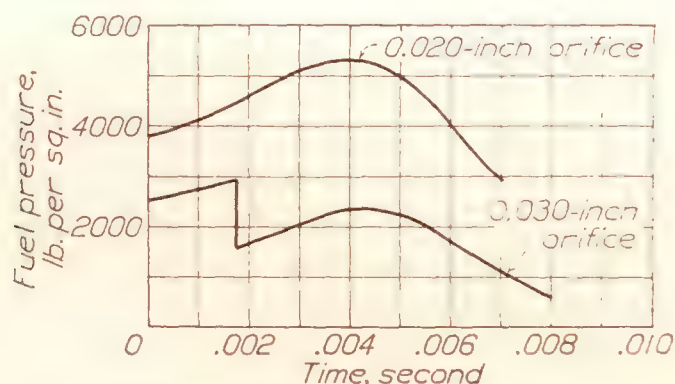


FIGURE 18.—Computed instantaneous pressure at discharge orifice. Pump speed, 760 r. p. m. Injection-valve closing pressure, 2,500 lb./sq. in. Injection-tube inside diameter, 0.125 in. Tube length, 34 in.

photographic record shows a decreased injection period.

Values for the instantaneous pressures (fig. 18) at the orifice, computed by the method presented in reference 2, show that with the 0.020-inch orifice the instantaneous pressures were much higher than with

the 0.030-inch orifice. These higher pressures resulted in a higher rate of penetration for the smaller orifice.

CONCLUSIONS

1. The test results presented show that fuel-injection pumps designed for high-speed compression-ignition engines have satisfactory operating characteristics over the speed range which is encountered under load in ordinary practice. At low speeds, such as are used for starting and idling, the fuel injection takes place as a series of sprays, because the fuel pressures originating at the pump are not sufficient to maintain high injection pressures at the discharge orifice of the injection valve. The results also show that the fuel-spray characteristics are affected by the injection-tube diameter, the discharge-orifice area, the pump throttle setting, and check valves placed in the system.

2. Increasing the injection-valve opening and closing pressure increases the spray-tip penetration, decreases the duration of the injection, and increases the tendency for primary sprays to appear before the start of injection.

3. Increasing the pump speed increases the spray-tip penetration with low injection-valve opening and closing pressures, but has little effect on the penetration for high injection-valve opening and closing pressures; decreases the injection lag; increases the duration of the injection in pump degrees; and decreases the tendency for primary discharge to occur.

LANGLEY MEMORIAL AERONAUTICAL LABORATORY,
NATIONAL ADVISORY COMMITTEE FOR AERONAUTICS,
LANGLEY FIELD, VA., August 24, 1931.

REFERENCES

1. Gelalles, A. G.: Effect of Orifice Length-Diameter Ratio on Fuel Sprays for Compression-Ignition Engines. N. A. C. A. Technical Report No. 402, 1931.
2. Rothrock, A. M.: Hydraulics of Fuel Injection Pumps for Compression-Ignition Engines. N. A. C. A. Technical Report No. 396, 1931.
3. Beardsley, E. G.: The N. A. C. A. Photographic Apparatus for Studying Fuel Sprays from Oil Engine Injection Valves and Test Results from Several Researches. N. A. C. A. Technical Report No. 274, 1927.
4. Rothrock, A. M., and Marsh, E. T.: The Effect of Injection-Valve Opening Pressure on Spray-Tip Penetration. N. A. C. A. Technical Note No. 384, 1931.
5. Rothrock, A. M., and Lee, D. W.: Some Characteristics of Fuel Sprays from Open Nozzles. N. A. C. A. Technical Note No. 356, 1930.

REPORT No. 456

THE AERODYNAMIC FORCES AND MOMENTS EXERTED ON A SPINNING MODEL OF THE NY-1 AIRPLANE AS MEASURED BY THE SPINNING BALANCE

By M. J. BAMBER and C. H. ZIMMERMAN

SUMMARY

A preliminary investigation of the effects of changes in the elevator and rudder settings and of small changes in attitude upon the aerodynamic forces and moments exerted upon a spinning airplane was undertaken with the spinning balance in the 5-foot vertical tunnel of the National Advisory Committee for Aeronautics. The tests were made on a $\frac{1}{12}$ -scale model of the "NY-1" airplane.

Data by which to fix the attitude, the radius of spin, and the rotational and air velocities were taken from recorded spins of the full-scale airplane. Two spinning conditions were investigated. All six components of the aerodynamic reaction were measured and are presented in coefficient form referred to airplane axes.

The results show that, except for pitching and yawing moments, the changes in forces and moments introduced by elevator and rudder movements were small and of the same order of magnitude as those introduced by small changes in attitude. The pitching moment was approximately doubled by movement of the elevator from 33° up to 27° down but was little affected by rudder movement regardless of the elevator position. A large yawing moment opposing the spin was introduced when the rudder was moved from full with the spin to full against the spin with the elevator up. When the elevator was down the yawing moment given by full rudder movement was reduced to approximately one fourth its former value.

The results indicate that the change in yawing moment produced by the rudder with the elevator up was the only component of force or moment produced by the elevator and rudder that could not have been balanced in an actual spin by small changes in attitude and angular velocity.

INTRODUCTION

Spinning of airplanes has been the subject of a great amount of research in recent years but the problem is far from a solution at the present time. When considering possible solutions airplanes may be classified under two headings; namely, those which should never be spun and those which should be controllable in the spin.

For the first class, which includes most commercial airplanes as well as bombers and transports for military

and naval use, the problem is open to three lines of attack: (1) To make the airplane incapable of attaining a stalled attitude; (2) to so proportion and limit the movement of the stabilizing and control surfaces for a given wing combination that there will always be an aerodynamic diving moment when the airplane is stalled and it will not be possible for any rotation to persist that will give an inertia stalling moment great enough to overcome the aerodynamic diving moment even with all controls set for a spin; or (3) to use a wing and stabilizing surface combination which will be stable in rectilinear flight when the airplane is stalled. Prevention of the stall is undoubtedly a complete solution, but unfortunately it is probable that adverse weather conditions, coupled with improper use of the controls, will cause any airplane to stall if it has good performance and maneuverability characteristics.

The solution of the problem by making the airplane incapable either of maintaining a stall or of maintaining rotation when stalled is closely related to the solution of the problem of making airplanes of the second class, such as pursuit, fighter, or commercial stunting airplanes, readily controllable in the spin. The difference is one of magnitudes of pitching, autorotation, and damping moments. The whole spinning problem therefore reduces to a study of the balance of moments and forces when the airplane is rotating and stalled, and of the nature and magnitude of the changes of those moments and forces with changes in the motion.

The conditions for equilibrium are that for any axis the sum of the moments due to aerodynamic reactions upon the lifting and the control surfaces must equal and oppose the inertia moments, and that the aerodynamic forces must equal and oppose the components of gravity and of centrifugal force. It is possible to calculate the inertia forces and moments for all spinning conditions, but present knowledge of the directions and magnitudes of the forces and moments exerted by the air upon the parts of a rotating airplane is so limited that the engineer has no certain way of knowing whether or not the airplane he is designing will balance in a spin. Consequently, a great amount of time and money which could be saved if sufficient data were available is spent trying to correct the spinning characteristics of airplanes after they are built.



FIGURE 1.—The NY-1 airplane model mounted in a spinning attitude in the downward flowing air stream. The 6-component balance (shown with cover removed to display mechanism) revolves with the model.

Data upon the aerodynamic characteristics of a spinning airplane may be obtained in several ways; namely, flight tests with full-scale airplanes, flight tests with balanced models, strip-method analysis of wind-tunnel force and moment tests, and wind-tunnel tests of rotating models. A brief discussion of these methods will be given here.

Spinning tests of full-scale airplanes have been made from time to time over a period of years. (See references 1, 2, 3, 4, and 5.) Such tests have revealed the range of attitudes and conditions in which airplanes will spin, they have contributed much to the knowledge of the aerodynamics of the spin, and they undoubtedly must be continued to verify the results obtained by more convenient methods. Because of the expense of making full-scale tests, the danger to equipment and personnel, the difficulty of studying the forces and moments upon the component parts of the airplane, and the fact that the spinning range that can be investigated with a particular airplane is limited, it is desirable that other methods be used for a general investigation of the problem.

Flight tests with balanced models have also been a valuable source of information concerning the spin, and the most notable effort along this line is the series of tests being conducted in England in a vertical tunnel built especially for such purposes. (See references 6 and 7.) Model tests are much less expensive and are not subject to the dangers of full-scale tests. Balanced models, however, are relatively expensive and troublesome to build and use as compared with ordinary models, the tests must be made at very low Reynolds Number, the determination of the aerodynamic forces and moments is difficult and tedious, it is nearly impossible to secure complete data of the effects of small changes in attitude, and it is not possible to determine the aerodynamic reactions upon the component parts.

Strip-method analysis is useful chiefly as a means of studying the effects of certain changes in the aerodynamic characteristics of wings upon the balance in the spin, it being postulated that the results of tests of wings which have all sections at the same angle of attack can be used to predict the characteristics of the same wings when the angle of attack varies along the span. Such analyses are very laborious and of doubtful value in determining the spinning characteristics of a particular airplane.

Several forms of rolling balances have been used for testing the autorotation characteristics of airfoil and airplane models. (See references 8, 9, and 10.) Data from rolling-balance tests are subject to errors because of tunnel-wall, blocking, and scale effects. Much greater velocities may be used in wind-tunnel tests where the model is restrained than in dropping tests, and it is possible to vary the air speed to study the effect of scale. Rolling balances make it possible to

measure the forces and moments supplied by the component parts of the airplane. In the past, attempts have been made to use tail moments of a yawed model obtained in straight force tests, but it has been found that such data are likely to lead to erroneous conclusions when applied to the spinning condition. (See reference 11.) Rolling-balance data have been of limited value because it has not been possible to measure all six force and moment components or to reproduce a true spinning condition. The spinning balance used in this investigation is a 6-component rotating balance from which it is possible to obtain wind-tunnel data for any of a wide range of possible spinning conditions.

The present series of tests was undertaken as a preliminary investigation of the effects of changes in Reynolds Number (within the range obtainable), of attitude, and of elevator and rudder settings upon the aerodynamic forces and moments upon a model when spinning. A model of the NY-1 airplane was used in order that a comparison of the data might be made with those obtained from full-scale spins of the airplane. (See reference 5.)

APPARATUS AND MODEL

Apparatus.—The tests were made on the spinning balance that has been developed for use in the 5-foot vertical wind tunnel of the National Advisory Committee for Aeronautics. The wind tunnel, which is of the open-jet type, is described in reference 12. The spinning balance (fig. 1) consists of a balance head that supports the model and contains the force-measuring units, a horizontal turntable supported by streamline struts in the center of the jet and, outside the tunnel, a direct-current driving motor, a liquid tachometer, an air compressor, a mercury manometer, a pair of indicating lamps, and the necessary controls. The balance head is mounted on the turntable and it may be set to give any radius of spin between 0 and 8 inches.

The balance head contains a vertical spindle to the upper end of which the model is rigidly attached. The spindle has six degrees of freedom, except as restrained by a linkage system which connects it to six measuring units. A line diagram of the force system is shown in figure 2. The lower two thirds of the spindle, the linkage system, the measuring units, and the supporting framework are enclosed by a duralumin case one half of which is shown removed in figure 1.

A diagrammatic sketch of one of the force-measuring units is shown in figure 3. A force of tension or compression in the connecting link is transmitted through the self-aligning ball bearings and becomes a moment in the beam about the Emery knife-edge. This moment and a constant moment produced by the spring attached to the beam are balanced by the

pressure of air behind the rubber diaphragm. Air pressure is admitted to the rotating parts of the balance through an oil-sealed slip joint at the bottom of the turntable shaft. The air pressure is regulated

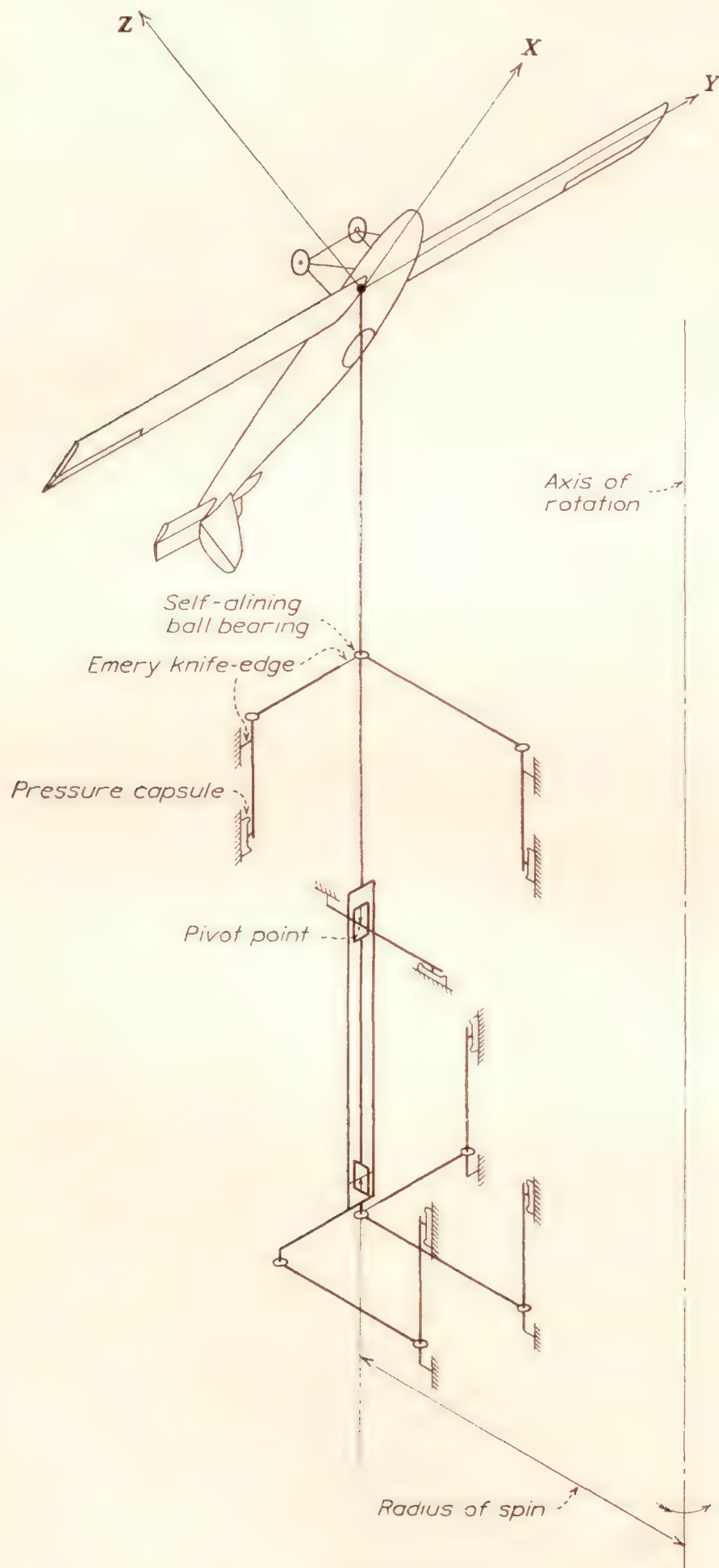


FIGURE 2.—Line diagram of spinning-balance force system

by valves and indicated by a mercury manometer. Balance is indicated by neon lamps connected through slip rings to the contact points. Since there is but one air-pressure tube leading to the balance, only one reading can be made at a time. Each of the measuring units is fitted with a small glycerin-filled

dashpot which serves to damp the oscillations of the beam.

In order that the balance reading might be easily corrected for forces introduced by the weights and the moments of inertia of the model and balance parts, tare readings were made for each spinning condition with the balance head and the model completely enclosed by a shield which was attached to the turntable and rotated with the balance.

Model.—The model, which had been built by the Navy Department for wind-tunnel tests, was a $\frac{1}{12}$ -scale mahogany reproduction of the NY-1 airplane (fig. 1). Originally it differed from the full-scale airplane in the following particulars: There were no landing or flying wires; the landing gear and wing struts were $\frac{3}{32}$ -inch rods of circular cross section; a pair of N struts a short distance out from the fuselage were used

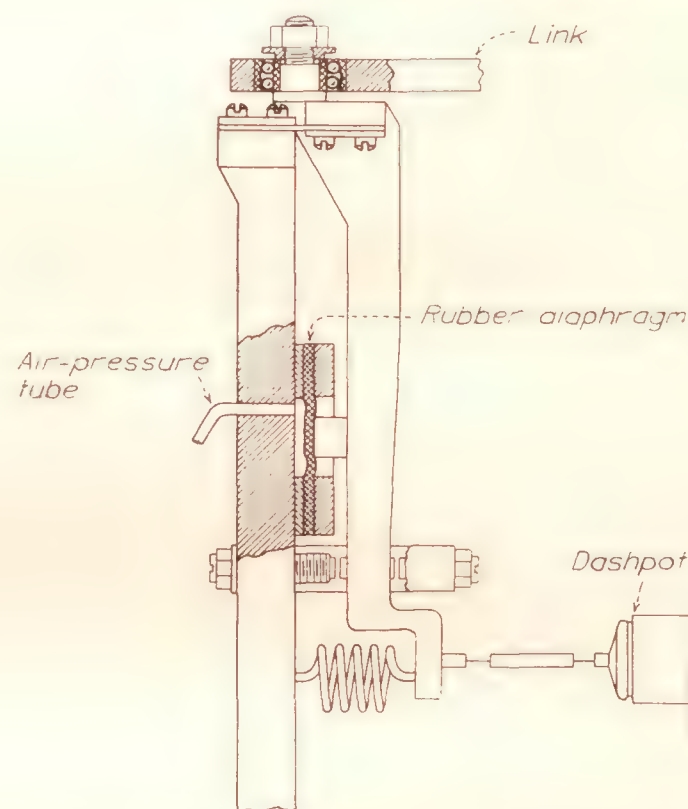


FIGURE 3.—Diagram of a measuring unit of spinning balance.

in place of the cabane struts. The model was equipped with movable elevator and rudder but it had no ailerons. It was rigged with no washin or washout ($\pm 0.1^\circ$) and the fin was set parallel to the plane of symmetry.

For this investigation the original wooden fin and rudder, which were of a thin symmetrical section, were replaced with a $\frac{1}{16}$ -inch duralumin flat plate fin and rudder of the same plan form. Additional bracing struts were added between the fuselage and the upper wing. The fuselage was cut out for installation of a ball clamp for attachment to the balance.

TESTS

The direction and velocity of the flow about the balance head were determined in the positions to be occupied by the wings and tail surfaces of the model. These surveys were made with the balance rotating at a speed corresponding to a normal spin and at a radius of 5 inches. The air stream was found to have a

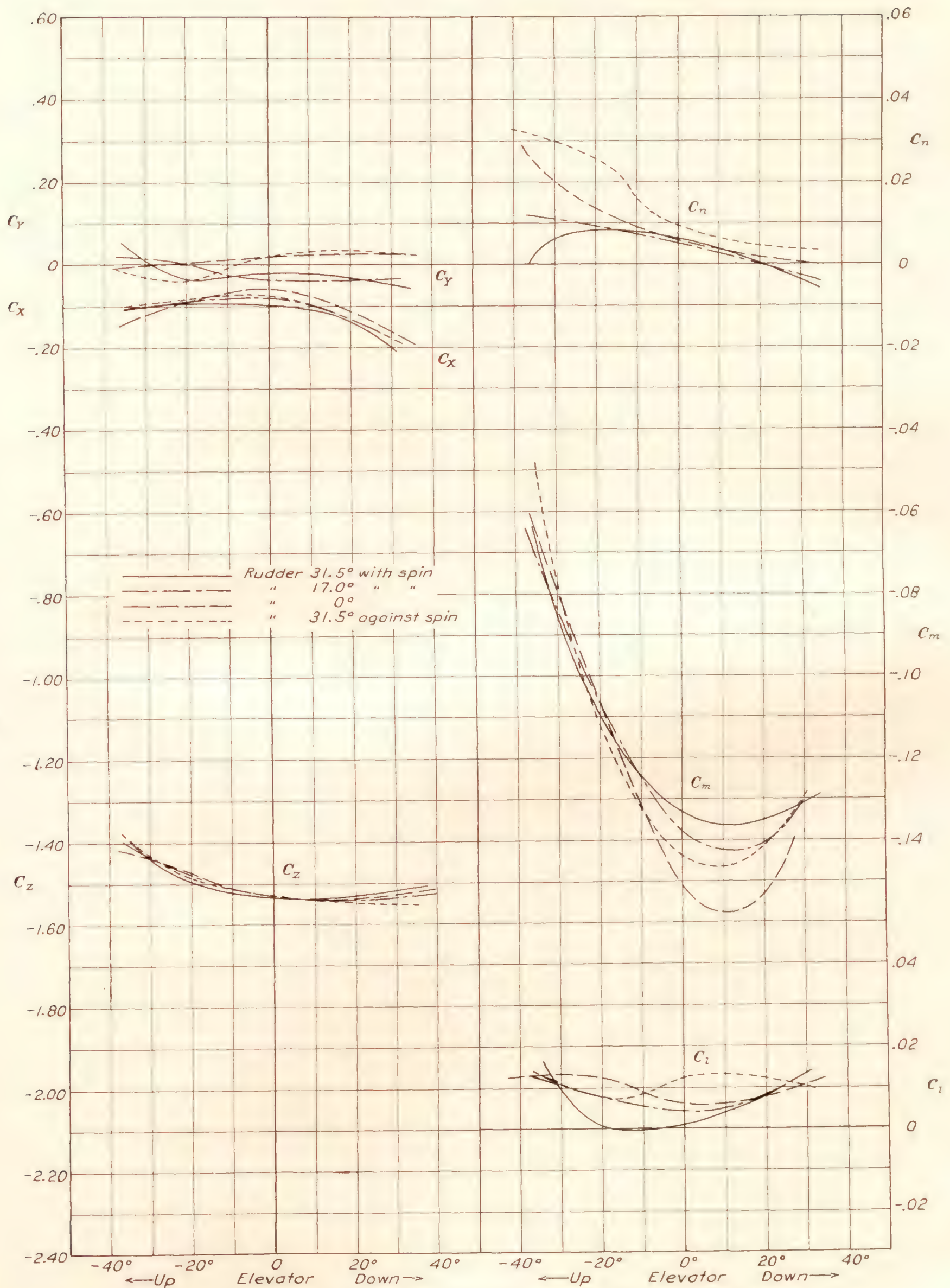


FIGURE 4.—Effect of elevator setting upon aerodynamic characteristics of NY-1 airplane model in spin of 3.4-inch radius.

twist of 0.4° , which was corrected for by increasing the rotational speed of the balance. In the region to be occupied by the tail there was an outflow of about 1° and an increase in velocity of about 2.5 percent caused by the blocking effect of the balance head and turntable. Since these parts were partly shielded by the model when force tests were being made it is unlikely that they then affected the air flow to the extent the survey indicated.

For the force and moment tests two left spinning conditions were chosen from uncorrected data obtained in a series of full-scale spins of the NY-1 airplane. (The corrected data appear in reference 5 as test nos. 30L and 19L. It may be noted that the actual differences are small.) The principal characteristics of the spins, the difference being due to changes in moments of inertia, are given in the following table:

Radius, feet	α	β	$(90^\circ - \sigma)$	Ω rad./sec.	V ft./sec.	δ_R	δ_H	δ_A	φ_1	θ_1	ψ_1
3.4	50°	$-30'$	$5^\circ 54'$	2.76	91.4	33°	34°	0°	$-7^\circ 17'$	$-38^\circ 17'$	$18^\circ 58'$
6.2	$46^\circ 20'$	$1^\circ 42'$	$8^\circ 30'$	2.20	92.4	33°	34°	0°	$-6^\circ 44'$	$-42^\circ 17'$	$13^\circ 53'$

where $+\beta$ is sideslip outward and φ_1 , θ_1 , and ψ_1 are angles defining the attitude. As here used, φ_1 is the vertical angle between the Y (span) axis and the horizontal, positive when the right wing tip is the lower; θ_1 is the vertical angle between the X (fuselage) axis and the horizontal, negative when the tail is above the horizontal; and ψ_1 is the angle between the spin radius and the projection of the X axis upon the horizontal, positive when the airplane has been rotated in a clockwise direction (viewed from above) about a vertical axis, from a position in which the X axis intersects the spin axis. For the attitudes defined, small changes of θ_1 give negligible changes of β and nearly equal changes of α (α approximately $= 90^\circ + \theta_1$), small changes of φ_1 give negligible changes of α and nearly equal changes of β (β approximately $= \sigma + \varphi_1$), and small changes of ψ_1 give negligible changes of both α and β .

A preliminary series of tests was made in each of the spinning conditions with tunnel air speeds of 45, 50, 60, 65, 70, 75, and 80 feet per second to determine the scale effect. The scale effect over this range was found to be negligible and all further tests were made at 65 feet per second (Reynolds Number approximately 153,000) at which speed the operation of the balance was most satisfactory. The control settings and attitudes for the remainder of the tests are given in the following tables:

Radius=3.4 inches. $\Omega=23.7$ radians per second. $V=65$ feet per second (tunnel velocity)

δ_R	δ_H	φ_1	θ_1	ψ_1
$33^\circ, 18^\circ, 3^\circ, -27^\circ$	$31^\circ 30'$	$-7^\circ 17'$	$-38^\circ 17'$	$18^\circ 58'$
$33^\circ, 18^\circ, 3^\circ, -27^\circ$	17°	$-7^\circ 17'$	$-38^\circ 17'$	$18^\circ 58'$
$33^\circ, 18^\circ, 3^\circ, -27^\circ$	0°	$-7^\circ 17'$	$-38^\circ 17'$	$18^\circ 58'$
$33^\circ, 18^\circ, 3^\circ, -27^\circ$	$-31^\circ 30'$	$-7^\circ 17'$	$-38^\circ 17'$	$18^\circ 58'$
33°	$31^\circ 30'$	$-3^\circ, -5^\circ, -9^\circ$	$-38^\circ 17'$	$18^\circ 58'$
33°	$31^\circ 30'$	$-7^\circ 17'$	$-36^\circ, -40^\circ, -42^\circ$	$18^\circ 58'$
33°	$31^\circ 30'$	$-7^\circ 17'$	$-38^\circ 17'$	$15^\circ, 17^\circ, 21^\circ$

Radius=6.2 inches. $\Omega=18.77$ radians per second. $V=65$ feet per second (tunnel velocity)

δ_R	δ_H	φ_1	θ_1	ψ_1
$33^\circ, 18^\circ, 3^\circ, -27^\circ$	$31^\circ 30'$	$-6^\circ 44'$	$-42^\circ 17'$	$13^\circ 53'$
$33^\circ, 18^\circ, 3^\circ, -27^\circ$	17°	$-6^\circ 44'$	$-42^\circ 17'$	$13^\circ 53'$
$33^\circ, 18^\circ, 3^\circ, -27^\circ$	0°	$-6^\circ 44'$	$-42^\circ 17'$	$13^\circ 53'$
$33^\circ, 18^\circ, 3^\circ, -27^\circ$	$-31^\circ 30'$	$-6^\circ 30'$	$-42^\circ 17'$	$13^\circ 53'$
33°	$31^\circ 30'$	$-5^\circ, -9^\circ, -11^\circ$	$-42^\circ 17'$	$13^\circ 53'$
33°	$31^\circ 30'$	$-6^\circ 44'$	$-38^\circ, -40^\circ, -44^\circ$	$13^\circ 53'$
33°	$31^\circ 30'$	$-6^\circ 44'$	$-42^\circ 17'$	$12^\circ, 16^\circ, 18^\circ$

RESULTS

The forces measured by the balance units for the various test conditions were plotted and data for the calculations of the forces and moments about the body axes were taken from the charts, it being assumed that these values should follow smooth curves. The forces and moments so obtained were reduced to coefficient form by the relations:

$$C_x = \frac{X}{qS} \quad C_Y = \frac{Y}{qS} \quad C_Z = \frac{Z}{qS}$$

$$C_l = \frac{L}{qbS} \quad C_m = \frac{M}{qbS} \quad C_n = \frac{N}{qbS}$$

where the symbols X , Y , Z , L , M , N , q , b , and S have their usual significance. The lower wing was considered as extending through the fuselage in computing wing area. It should be noted that the span was taken as the fundamental length in all the moment equations to facilitate the transfer from one set of axes to another and to make the moments appear in their proper magnitude with respect to each other ($b/c=7.66$). The results, in absolute coefficient form, are presented as curves in figures 4 to 10, inclusive.

At least one repeat test was made for each test condition and differences in balance readings were found, in general, to be within 5 percent. A comparison of the force and moment values computed from the flight tests and those obtained from the spinning-balance measurements is given in the discussion.

No corrections were made for tunnel-wall or blocking effects.

DISCUSSION

Changes in control settings.—The effects of changes in elevator and rudder settings are shown in figures 4 to 7, inclusive. The changes in C_x , C_Y , C_Z , and C_l are small and will be discussed in connection with attitude changes.

The pitching-moment coefficient, C_m , was approximately doubled as the elevator was moved from full with the spin to neutral. Further movement against the spin had a comparatively small effect. The curves are similar to those for an airfoil when passing through

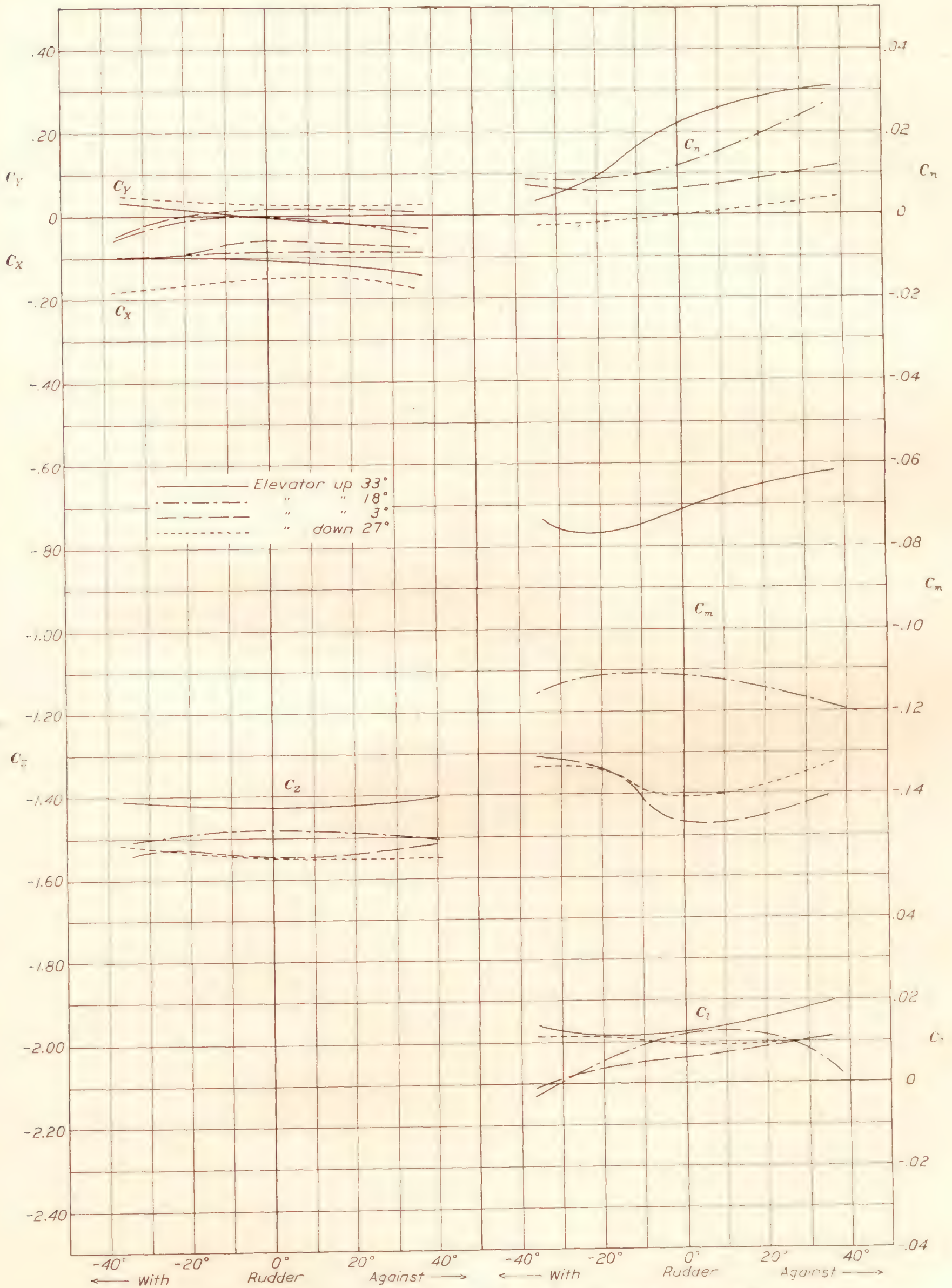


FIGURE 5.—Effect of rudder setting upon aerodynamic characteristics of NY-1 airplane model in spin of 3 1/4-inch radius.

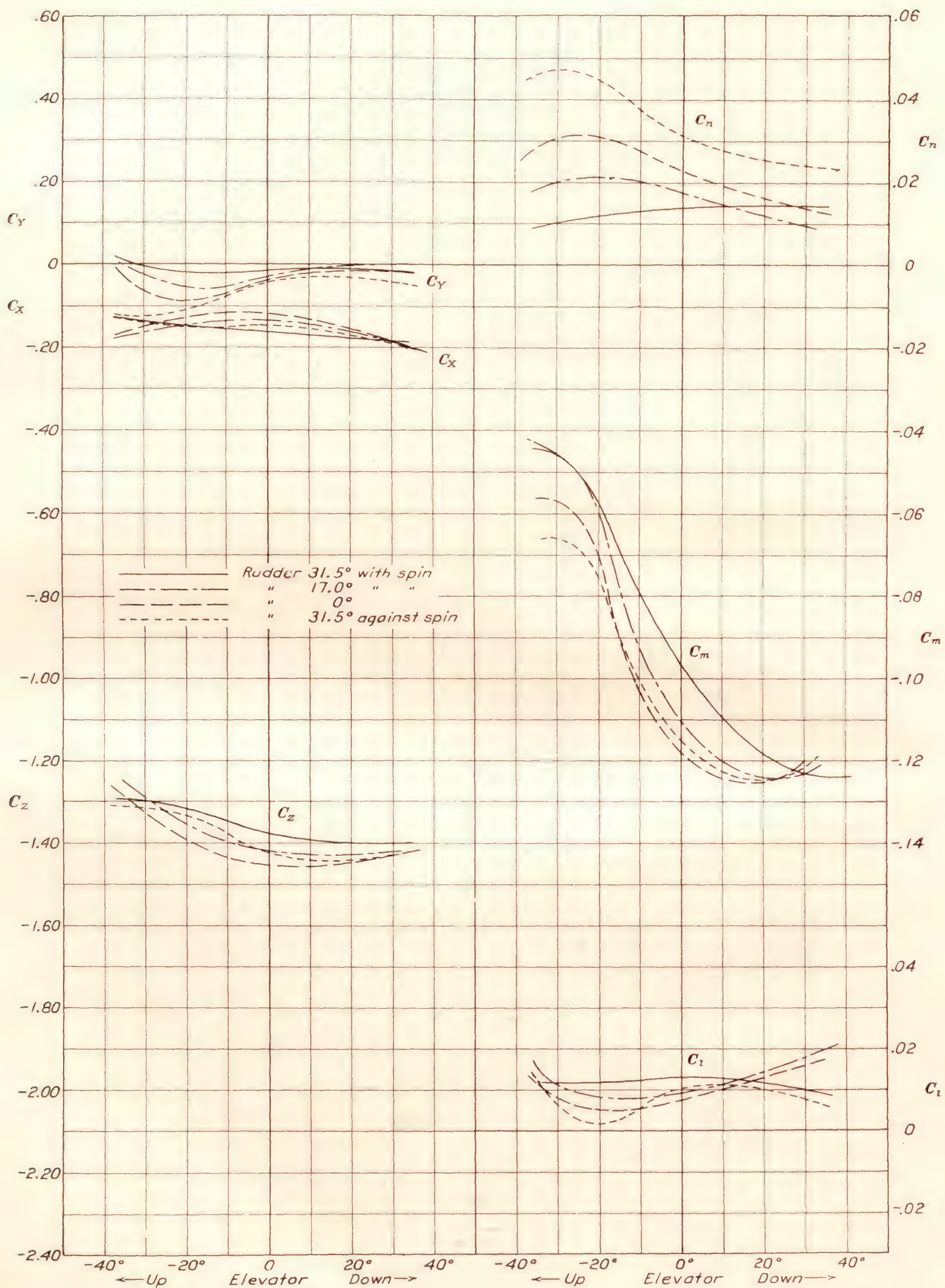


FIGURE 6.—Effect of elevator setting upon aerodynamic characteristics of NY-1 airplane model in spin of 6.2-inch radius.

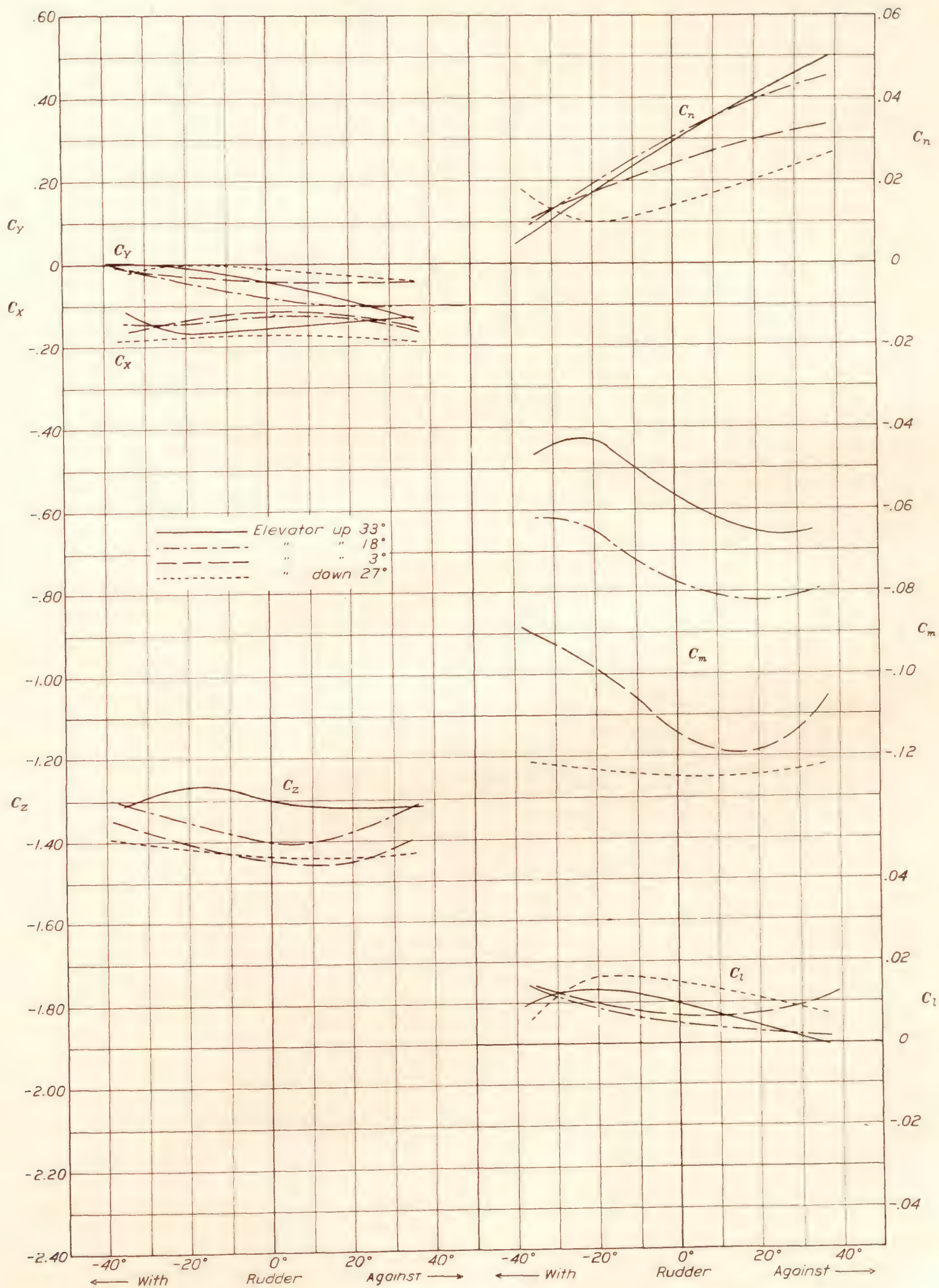


FIGURE 7.—Effect of rudder setting upon aerodynamic characteristics of NY-1 airplane model in spin of 6.2-inch radius.

the stall. Movement of the rudder gave small changes of C_m but no general tendency was revealed.

When the elevator was up the value of C_n was increased, in the sense to oppose the spin, as the rudder was moved from full with the spin to full against it. The change of moment was approximately proportional

shielded when the elevator was down. They confirm the deductions from smoke-flow tests (reference 13) and are similar to the results obtained in tests of various stabilizer locations (references 14 and 15).

Changes in attitude.—Small changes in attitude (see figs. 8, 9, and 10) gave changes in C_x , C_y , C_z , and C_l

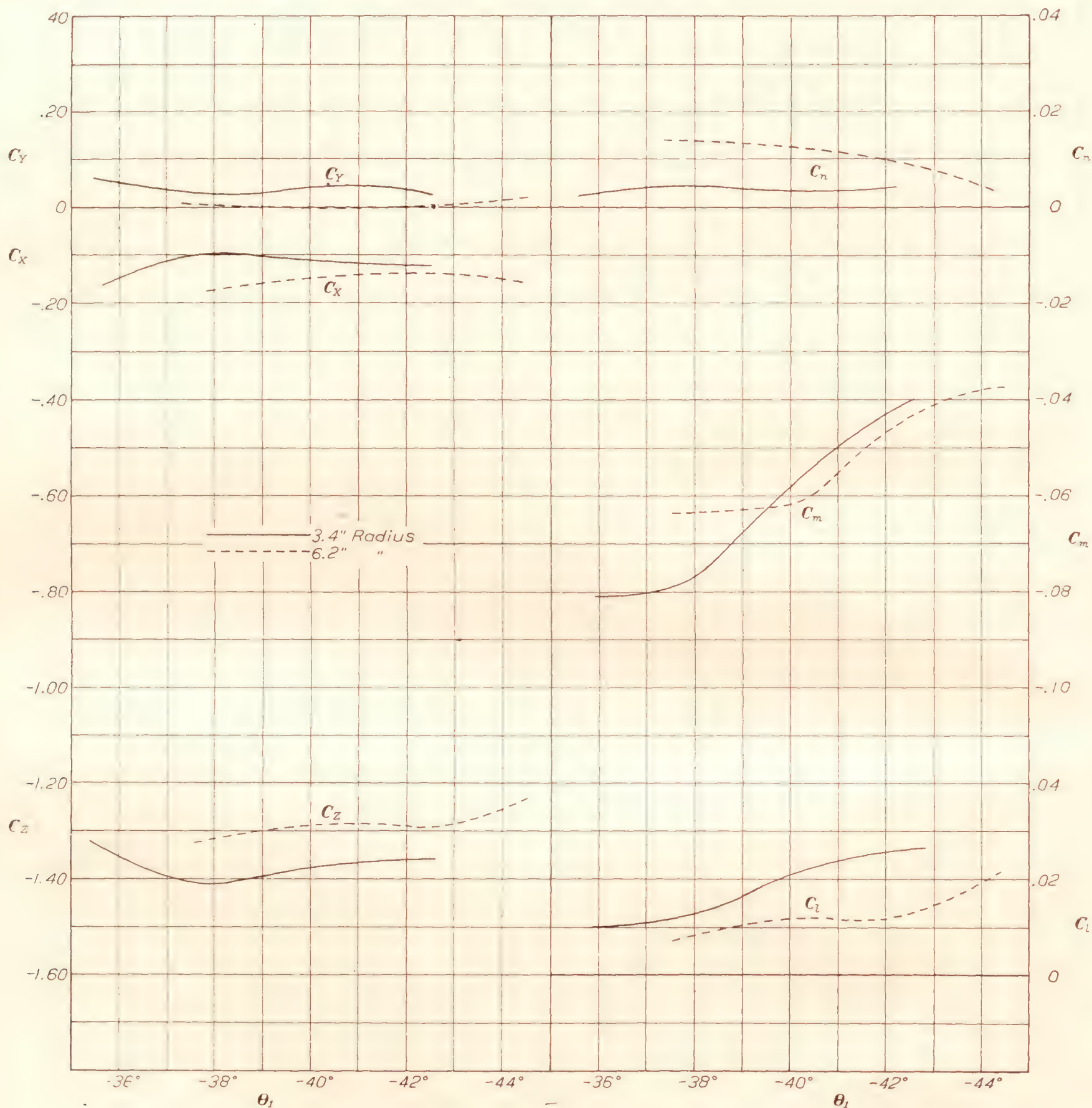


FIGURE 8.—Effect of inclination of thrust axis to horizontal (θ_t) upon aerodynamic characteristics of NY-1 airplane model when spinning.

to the change of rudder position. When the elevator was down (against the spin) rudder movement had practically no effect in producing a yawing moment opposing the spin, this being especially true in the case of the spin of small radius. These results might have been predicted because a considerable portion of the rudder was exposed to the undisturbed air when the elevator was up but the rudder was almost entirely

of the same order of magnitude as those given by full movement of the elevator and/or rudder. Within the range of attitudes tested, the changes in C_n were not sufficient to balance those obtained with elevator movement. It is apparent that small changes in attitude coupled with a small increase in rotational velocity, and hence inertia stalling moment, might lead to a balance with elevators down. Since changes in

C_n produced by small changes in attitude were of the same order of magnitude as those given by elevator movement when the rudder was with the spin, it appears that it would be quite possible for the airplane to continue the spin with very little change in attitude if the elevators were down.

The results indicate that, with the elevators up, relatively large changes of attitude would be necessary to balance the change of C_n due to rudder movement. It is likely that if a large change in attitude would give a balance of C_n , balance of the other forces and moments would be disturbed and the spin would not con-

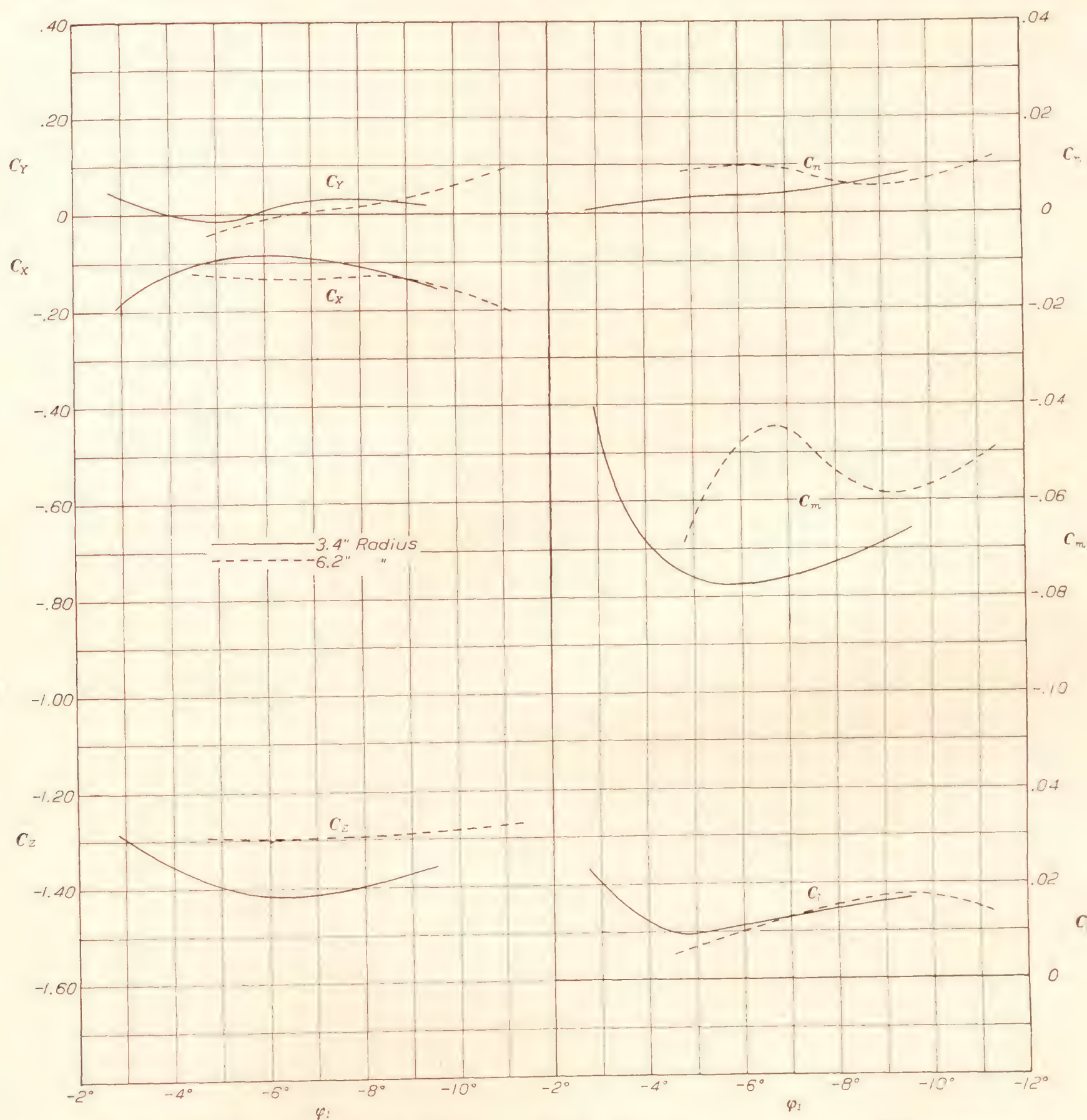


FIGURE 9.—Effect of inclination of span axis to horizontal (ϕ_1) upon aerodynamic characteristics of NY-1 airplane model when spinning.

Full-scale tests confirm these deductions. In a spin made with the elevator down (no. 54L, reference 5) the only definite changes revealed were a decrease in radius, a decrease in resultant air velocity, and an increase in rotational speed. The sideslip, the flight path, and the angles of attack at the center section were intermediate between those for the spins described under Tests.

This conclusion is confirmed by flight results, which showed the impossibility of maintaining balance with the rudder against the spin and with the elevators up.

With the elevators down, the changes in C_n due to rudder movement were small and it appears that the airplane might continue to spin in this condition regardless of rudder position. This possibility was not thor-

oughly investigated in flight but in the few cases tried recovery was effected with little increase in the number of turns necessary.

Comparison between full-scale and model data.— A comparison between the full-scale and the model data for the steady spin is given in the following table:

Radius, inches	Test	C_R	C_Q	C_n''
3.4	Full scale.....	1.414	0.0759	0.0015
	Model.....	1.415	.0765	.027
6.2	Full scale.....	1.466	.0674	.0010
	Model.....	1.301	.0619	.023

The limits of error in the full-scale measurements (reference 5) are given as 7 percent for the vertical velocity and 3 percent for the rotational velocity, and since the squares of both of these quantities enter into the computation of the coefficients it is evident that the tunnel measurements are well within the limits of accuracy of the flight tests.

There is one important difference which is as yet not explained. The fundamental relations of mechanics show that the aerodynamic moment about the vertical axis through the center of gravity of the airplane (C_n'')

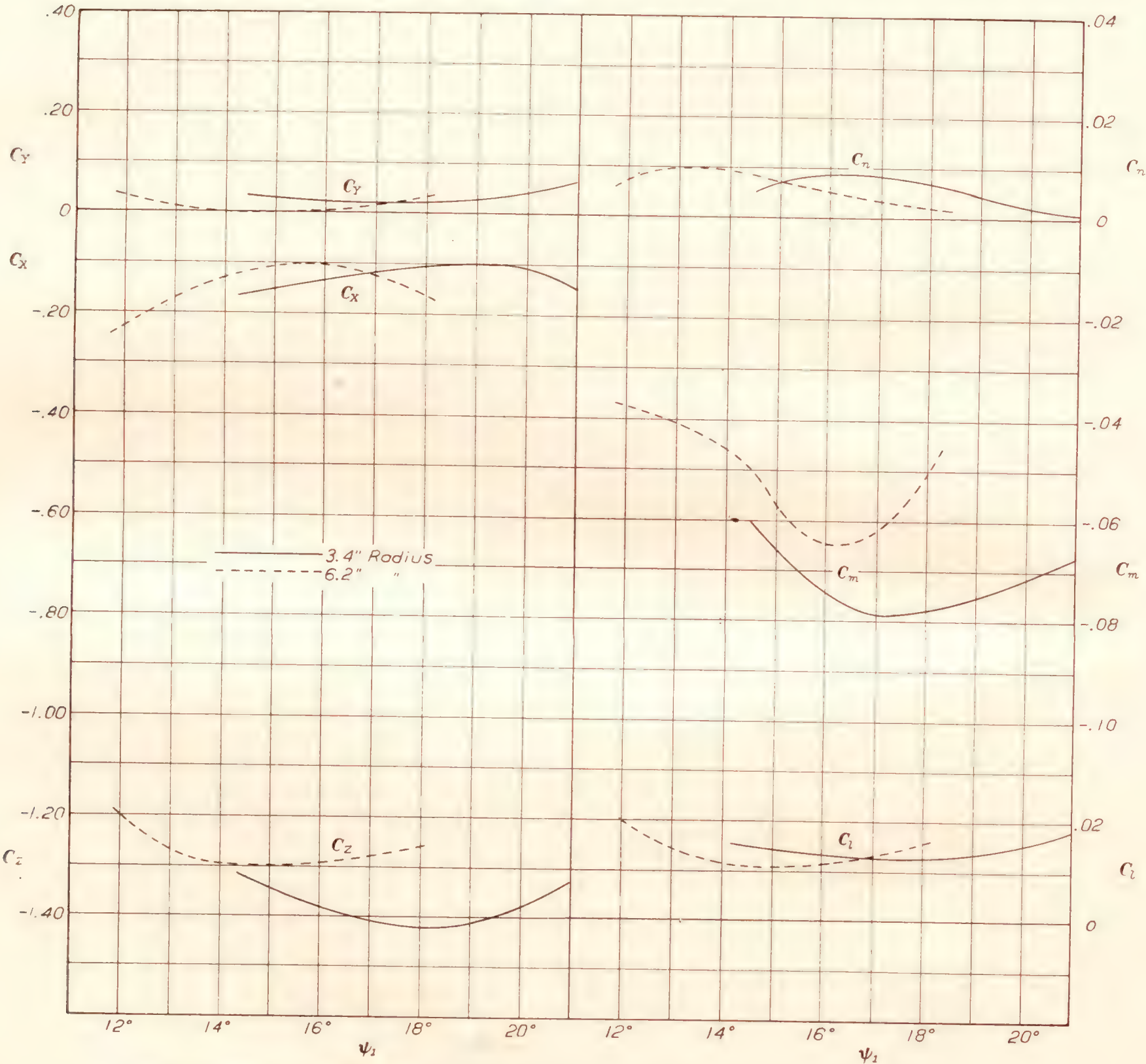


FIGURE 10.—Effect of yaw about vertical axis (ψ_1) upon aerodynamic characteristics of NY-1 airplane model when spinning.

The resultant force and moment coefficients (C_R and C_Q) are in good agreement for the case of the spin with the smaller radius but the values from model tests are about 10 percent lower than the values computed from the full-scale spin of 6.2-foot radius.

is very small, being equal to the gyroscopic moment of the propeller about that axis. A yawing moment opposing the spin and equal in magnitude to about one third the resultant moment was found in the tunnel measurements.

An attempt was made to explain this discrepancy on the basis that there was washin of the left wing and that the fin was set at an angle to the plane of symmetry on the full-scale airplane while both washin and fin angle were zero for the model. Accordingly, the lower left wing of the model was given $1^{\circ}15'$ washin and an additional test made, but no appreciable change in moment about the vertical axis was obtained. No tests were made with different fin settings but rudder-moment curves indicate that a change in fin setting could have produced only a small change in C_n'' . It was found possible to reduce C_n'' to zero by giving the model about 12° of outward sideslip.

It is believed that the differences revealed between the full-scale and the tunnel results are not such as to change the slopes or configurations of the curves of figures 4 to 10, and that they do not affect the analysis given in the preceding discussion or the conclusions to which it points.

CONCLUSIONS

1. A rudder may be rendered ineffective as a source of yawing moments in the spin by the shielding effect of the stabilizer and elevator.
2. Small changes in attitude coupled with changes in rotational velocity may be sufficient to balance force and moment changes given by changes in elevator setting or by changes in rudder setting with the elevators down.
3. Large changes in attitude are necessary to produce moments sufficient to balance the yawing moment about the body axis given by movement of an unshielded rudder.
4. The spinning balance is a practical and economical means of obtaining valuable data upon the aerodynamic forces and moments given by a spinning model and its component parts.

LANGLEY MEMORIAL AERONAUTICAL LABORATORY,
NATIONAL ADVISORY COMMITTEE FOR AERONAUTICS,
LANGLEY FIELD, VA., February 7, 1933.

REFERENCES

1. Gates, S. B., and Bryant, L. W.: The Spinning of Aeroplanes. R. & M. No. 1001, British A.R.C., 1926.
2. Soulé, Hartley A., and Scudder, Nathan F.: A Method of Flight Measurement of Spins. T.R. No. 377, N.A.C.A., 1931.
3. Irving, H. B., and Stephens, A. V.: Safety in Spinning. Roy. Aero. Soc. Jour., March 1932.
4. Allen, Edmund T.: Spin Flight Testing of Three Similar Airplanes. Paper presented at the Pacific Coast Aeronautic Meeting of the A.S.M.E., June 9-10, 1932.
5. Scudder, Nathan F.: A Flight Investigation of the Spinning of the NY-1 Airplane with Varied Mass Distribution and Other Modifications, and an Analysis Based on Wind-Tunnel Tests. T.R. No. 441, N.A.C.A., 1932.
6. Stephens, A. V.: Free-Flight Spinning Experiments with Several Models. R. & M. No. 1404, British A.R.C., 1931.
7. Stephens, A. V.: Free Model Spinning Researches. Aircraft Eng., vol. 3, no. 31, September 1931.
8. Lavender, T.: A Continuous Rotation Balance for the Measurement of Pitching and Yawing Moments Due to Angular Velocity of Roll (M_p and N_p). R. & M. No. 936, British A.R.C., 1925.
9. Knight, Montgomery, and Wenzinger, Carl J.: Rolling Moments Due to Rolling and Yaw for Four Wing Models in Rotation. T.R. No. 379, N.A.C.A., 1931.
10. Harris, Thomas A.: The 7 by 10 Foot Wind Tunnel of the National Advisory Committee for Aeronautics. T.R. No. 412, N.A.C.A., 1932.
11. Irving, H. B., and Batson, A. S.: Experiments on a Model of a Single Seater Fighter Aeroplane in Connection with Spinning. R. & M. No. 1184, British A.R.C., 1928.
12. Wenzinger, Carl J., and Harris, Thomas A.: The Vertical Wind Tunnel of the National Advisory Committee for Aeronautics. T.R. No. 387, N.A.C.A., 1931.
13. Scudder, N. F., and Miller, M. P.: The Nature of Air Flow About the Tail of an Airplane in a Spin. T.N. No. 421, N.A.C.A., 1932.
14. Irving, H. B., and Batson, A. S.: Spinning of a Model of the Fairey IIIF Seaplane. R. & M. No. 1356, British A.R.C., 1931.
15. Irving, H. B., Batson, A. S., and Stephens, A. V.: Spinning Experiments on a Single Seater Fighter with Deepened Body and Raised Tailplane. Part I. Model Experiments. Part II. Full Scale Spinning Tests. R. & M. No. 1421, British A.R.C., 1932.

REPORT No. 457

MANEUVERABILITY INVESTIGATION OF AN O3U-1 OBSERVATION AIRPLANE

By F. L. THOMPSON and H. W. KIRSCHBAUM

SUMMARY

This report presents the results obtained in maneuverability tests conducted by the National Advisory Committee for Aeronautics with an O3U-1 observation airplane. This investigation is the third in a series of similar investigations requested by the Bureau of Aeronautics, Navy Department, for the purpose of comparing the maneuverability of different airplane types and to provide quantitative data for use in establishing a criterion or method for rating the maneuverability of any airplane. The two former investigations were conducted with the fighter types designated F6C-3 and F6C-4 and have been reported previously.

Measurements of the air speed, the angular velocity, the linear acceleration, and the positions of the controls were made during abrupt single-control maneuvers with three stop positions for each control, during steady horizontal turns for the determination of minimum radius, and during 180° turns by various methods. Flight-path coordinates in two dimensions were determined for the 180° turns by means of a special camera obscura designed for the previous investigation of the F6C-4 airplane. All maneuvers were performed at an altitude of approximately 3,000 feet.

The results of the abrupt single-control maneuvers are presented by curves showing the variation of the measured quantities with respect to air speed and control movement. The results of the 180° turns are shown by time histories of the measured quantities for one maneuver of each type and by a table giving principal flight-path dimensions, altitude change, speed change, time required for completion, and maximum values of recorded quantities for all turns. The minimum radius of turn for steady horizontal flight at an altitude of 3,000 feet was found to be 322 feet at 74 miles per hour as compared with 155 feet at 76 miles per hour and 135 feet at 62 miles per hour for the F6C-3 and F6C-4 airplanes, respectively.

INTRODUCTION

A series of three investigations of the maneuverability of military airplanes has been conducted by the National Advisory Committee for Aeronautics at the request of the Bureau of Aeronautics, Navy Department. The results of the first two of these investigations pertain to the single-seat fighter airplanes, F6C-3 and F6C-4, and are given in references 1 and 2. The results of the third investigation, which was conducted on an O3U-1 observation airplane, are presented herein. These investigations have been made for the purpose of obtaining data that will facilitate the rating of military airplanes according to their maneuvering qualities.

The general procedure followed in this investigation was similar to that used in the two previous ones. Maneuvers were chosen so as to show as well as possible the separate and combined effectiveness of various elements that influence the ability of the airplane to maneuver. The maneuvers chosen can be divided into three principal groups: Abrupt single-control maneuvers, 180° turns by various methods, and steady horizontal turns for the determination of minimum radius of turn. Recording instruments within the airplane were used to determine air speed, linear acceleration, angular velocity, and position of controls. Angular accelerations were deduced from angular-velocity records. A camera obscura on the ground was used to record flight paths during 180° turns. Various items pertaining to the performance of the airplane were determined in a series of preliminary tests.

The tests with this airplane complete the contemplated series of investigations. The data obtained from the complete series of tests are now being studied for the purpose of developing a satisfactory criterion or method of rating airplanes according to their ability to maneuver. This study has not been completed and will be reported at a later date.

APPARATUS AND METHODS

APPARATUS

In this investigation tests were made on an O3U-1 airplane (fig. 1) equipped with a 450-hp. air-cooled engine. The principal specifications pertaining to the dimensions and arrangement of this airplane are shown in the appendix. The gross weight for the tests was

The recording instruments in the airplane consisted of a control-position recorder (reference 3), three angular-velocity recorders (reference 4), a 3-component accelerometer (reference 5), an inclinometer, and a performance recorder containing an air-speed unit (reference 6) and an aneroid unit. All these instruments give continuous photographic records. An



FIGURE 1.—The O3U-1 airplane.

4,055 pounds and the center of gravity was located 16.54 inches back of the leading edge of the lower wing. This weight and center-of-gravity location correspond

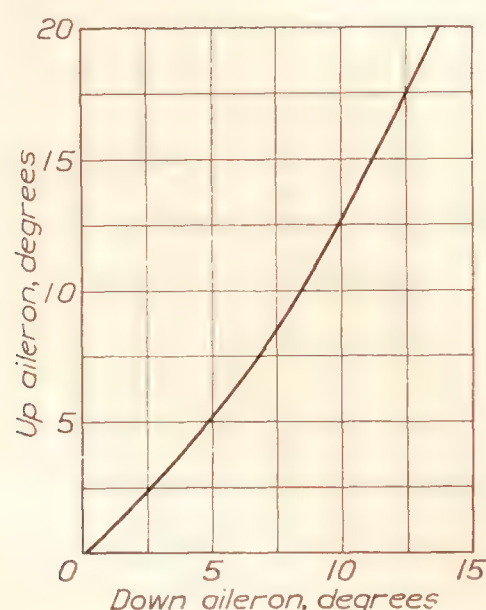


FIGURE 2.—Differential aileron action on O3U-1 airplane.

to the conditions specified for the normal full load. The ailerons on this airplane have a differential movement as shown in figure 2.

electrically driven timer was used in conjunction with these instruments to synchronize the records.

The accelerometer was located in the rear cockpit as near to the center of gravity as possible. The control-position recorder was connected to the three controls in the front cockpit. The air-speed recorder was connected to the swiveling pitot-static head mounted on a boom extending forward 1.1 chord lengths from the upper wing (fig. 1) to eliminate the errors caused by interference. A liquid-in-glass thermometer was mounted on the interplane wires to permit observation of air temperatures during flight.

As previously mentioned, a camera obscura was used to record flight paths during 180° turns. This apparatus and its accessories are described and illustrated in reference 2.

A system of one-way radiotelephone communication from the ground to the airplane was used in conjunction with the camera obscura to coordinate flight and ground operations. The microphone was located near the camera for use by a ground observer. An aircraft radio receiver designated "Type BC-SA-167" by the

Signal Corps, United States Army, was installed in the airplane.

METHOD

Preliminary tests.—Preliminary tests were made with the airplane in the full-scale wind tunnel and in flight. The data obtained in these tests served several purposes but particularly permitted the calculation of the minimum radius of turn. In the wind-tunnel tests the propeller-thrust curve was determined with the airplane at 0° angle of attack. In the flight tests several level runs and full-throttle climbs were made from which numerous data were obtained. A calibration of the swiveling air-speed head was determined by obtaining simultaneous records of the air speed indicated by this head and that indicated by another head suspended 60 feet below the airplane. The angle of attack for the level runs was obtained from records of the attitude of the airplane. The air temperature and engine speed were noted and the barometric pressure of the air recorded so that the true air speed and thrust horsepower could be computed. The level runs were made at an air density corresponding approximately to a standard altitude of 3,000 feet ($\rho/\rho_0=0.915$) and the climb data were obtained at about the same density. An additional item obtained during the preliminary tests was the stabilizer position required for balance with zero stick force at each speed, hence at each angle of attack.

From the wind-tunnel and flight data, lift and drag characteristics for the power-on condition and curves of horsepower required and horsepower available at a standard altitude of 3,000 feet were computed. When making these computations it was assumed that the thrust was directed along the thrust axis and that the thrust coefficients were not influenced by the angle of attack. The computations involved in determining the desired quantities are as follows:

For level flight

$$C_L = \frac{2(W - T \sin \alpha_T)}{\rho S V^2} \quad (1)$$

and

$$C_D = \frac{2T \cos \alpha_T}{\rho S V^2} \quad (2)$$

where W is the weight of the airplane

$T = C_T \rho n^2 D^4$ is the effective thrust

α_T is the angle of attack of the thrust line, and the other symbols have their usual significance. For a given flight condition the thrust coefficient C_T was found from the observed V/nD and the thrust curve obtained from the wind tunnel.

Although all the preliminary flights were made at approximately the same air density, there was sufficient variation in the test conditions to influence appreciably the calculated values of horsepower required and horsepower available. Consequently, the procedure followed in finding the horsepower curves

for the altitude of 3,000 feet entailed corrections necessary to reduce observed results to the common altitude. The forms of expressions used in finding horsepower were:

$$\text{hp}_{\text{reqd}} = \frac{\text{drag} \times V}{550 \cos \alpha_T} \quad (\text{level flight}) \quad (3)$$

and

$$\text{hp}_{\text{avail}} = \frac{TV}{550} \quad (\text{full-throttle climbs}) \quad (4)$$

The flight data for the level runs give the lift and drag coefficients and angle of attack for a given velocity at the air density of the flight. The lift coefficient required for flight at the same velocity and at the desired standard density was found from the relation

$$C_L' = C_L \frac{\rho}{\rho'} \quad (\text{the prime refers to the value at the required standard altitude}) \quad (5)$$

and the corresponding angle of attack was found from the lift-coefficient curve. The drag coefficient corresponding to this required angle of attack was then found and the horsepower required calculated by means of the expression

$$\text{hp}_{\text{reqd}} = \frac{C_D' \rho' V^3 S}{1,100 \cos \alpha_T'} \quad (6)$$

The corrections to thrust horsepower available were made in accordance with the average variations with altitude given by Diehl in reference 7.

Principal tests.—The flight program of the principal tests included single-control maneuvers requiring the abrupt use of elevator, ailerons, and rudder; 180° turns in vertical and horizontal planes; some special slow rolls; and steady horizontal turns for the determination of minimum radius of turn. The tests were performed in an air density corresponding approximately to that at a standard altitude of 3,000 feet and, in general, were started from steady level flight at various speeds with the stabilizer adjusted for zero stick force. As the procedure during the tests was essentially the same as that described in references 1 and 2, it will be described very briefly herein.

The single-control maneuvers, except those involving the ailerons, were made at various indicated air speeds up to the maximum level-flight indicated air speed of 124 miles per hour. A limit of 97 miles per hour was placed on the speed for abrupt aileron maneuvers to prevent undue stress of the airplane. The single control involved in each test was moved as quickly as possible and great care was taken to prevent the movement of any other control during the initial stage of the subsequent motion. Tests were made with the normal full movement and with two intermediate stop positions for each control, corresponding roughly to one half and three fourths of the full movement. The control movements were as follows: Elevator up 30.3° , 22.6° , and 18.0° ; left aileron down 13.0° , 10.4° , and 6.4° ; rudder right 27.0° , 19.5° , and

13.9°. A test for each condition was performed by each of two pilots.

The various types of 180° turns are classified as wing-over, horizontal turn, half aileron roll—half loop, half kick roll—half loop, and Immelman turn. The maneuvers were performed in the field of the camera obscura so that the flight paths could be recorded. When it was possible to do so, the maneuvers were started from various speeds up to the maximum indicated air speed of 124 miles per hour. For the Immelman turn the starting speed was raised to 132 miles per hour by diving slightly at the start. Several special slow rolls were made in which the pilot attempted to produce rotation solely about the *X* axis. After many attempts the desired motion was approximately attained. The steady horizontal turns used to determine the minimum radius of turn were started with full throttle and gradually tightened up until the desired air speed was attained without changing the throttle. Records were taken after steady conditions were attained at this air speed. This procedure was repeated for several speeds in the lower part of the normal speed range. In each case the stabilizer was set for high-speed level-flight balance.

Values of control position, angular velocity, and linear accelerations were obtained directly from the instrument records. Angular accelerations were derived from the recorded angular velocity by graphical differentiation. True air speed was derived from the air-speed records, barometric-pressure records, and observed temperature. Flight paths for the 180° turns were determined from the camera-obscura records in accordance with the method described in reference 2.

PRECISION

Lag in the angular-velocity recorders influenced the records obtained by these instruments considerably in the abrupt single-control maneuvers. Lag tests were made with these instruments and the results were used in applying corrections to the flight data. The validity of the corrections is not entirely assured, however, so that the angular accelerations obtained from the flight records are not regarded as satisfactorily precise except as regards their use in indicating similarity or difference in the manner in which the controls were applied by the two pilots in the abrupt single-control maneuvers. The precision of the various measurements is estimated to lie within the following limits:

Linear accelerations,	$\pm 0.05 g$
Air speed,	± 2 percent
Control position,	$\pm 1^\circ$
Angular velocities,	± 2 percent for fairly steady motion
Angular velocities,	± 7 percent for maximum values in abrupt maneuvers
Flight-path dimensions,	± 4 per cent

RESULTS

PRELIMINARY TESTS

The results of the preliminary tests are shown in figures 3 to 7, inclusive. The variations of stabilizer position with indicated air speed (fig. 3) can be used in determining the stabilizer setting during each maneuver performed in the principal tests by reference to the indicated air speed at which the maneuver was performed. In a similar manner the curves in figure 4 indicate the initial angle of attack and propeller speed in each maneuver. The effective thrust coefficients shown in figure 5 were used in a manner previously described for the calculation of forces during steady turns and in determining the lift, drag, and horsepower curves shown in figures 6 and 7. Attention is called to the fact that the lift and drag characteristics pertain to the power-on condition rather than the power-off condition as would be obtained in glide tests. The lines of constant angle of attack on the horsepower curves are utilized in calculations described later regarding the minimum radius of turn.

SINGLE-CONTROL MANEUVERS

Elevator maneuvers.—The data obtained in abrupt pull-ups are shown in figures 8, 9, and 10 where maximum normal acceleration, maximum pitching velocity, and maximum pitching acceleration are plotted against initial indicated air speed. Noteworthy features of the results for full elevator movement are that the values for normal accelerations are not proportional to the second power of the velocity, that the curves of maximum pitching velocity flatten at high speed, and that the flattening is different for the two pilots. These peculiarities are attributed chiefly to the large force required to operate the elevators. A study of the records obtained in these pull-ups shows that the time required to operate the elevators increased with speed and was such as to permit a considerable decrease in air speed during the period required to operate the elevators. The decrease in air speed permitted the maximum normal accelerations to attain smaller values than would have occurred if the change in angle of attack could have been accomplished rapidly. In this connection it should be mentioned that in the tests reported in references 1 and 2 the normal accelerations were found to vary as the second power of the initial air speed. The difference in the curves of maximum pitching velocity attained by the two pilots is attributed to the fact that Pilot A did not actually attain the nominal full elevator movement at high speeds and utilized rather more time during the latter stage of the elevator movement than did Pilot B. Differences in piloting are also reflected in the difference between the curves of maximum pitching accelerations for the same nominal control movement.

The average effect of elevator movement on maximum pitching velocity and acceleration is shown in figure 11 for three indicated air speeds. These curves

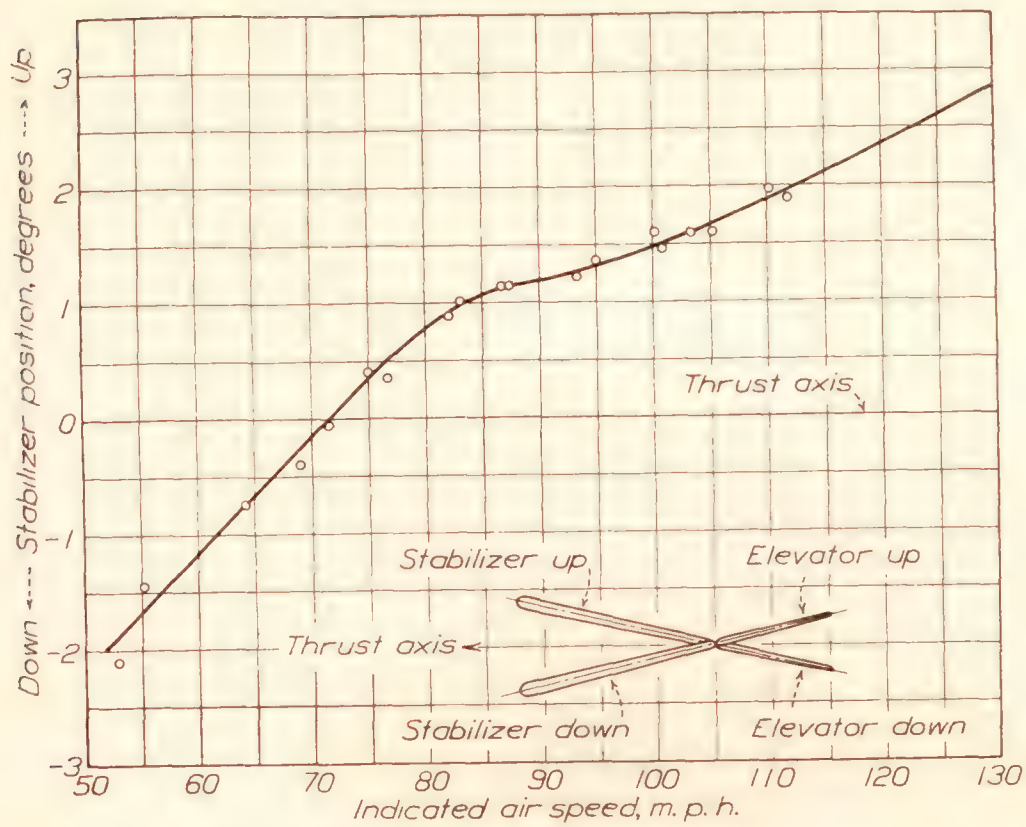


FIGURE 3.—Stabilizer setting for zero stick force in steady level flight (O3U-1 airplane).

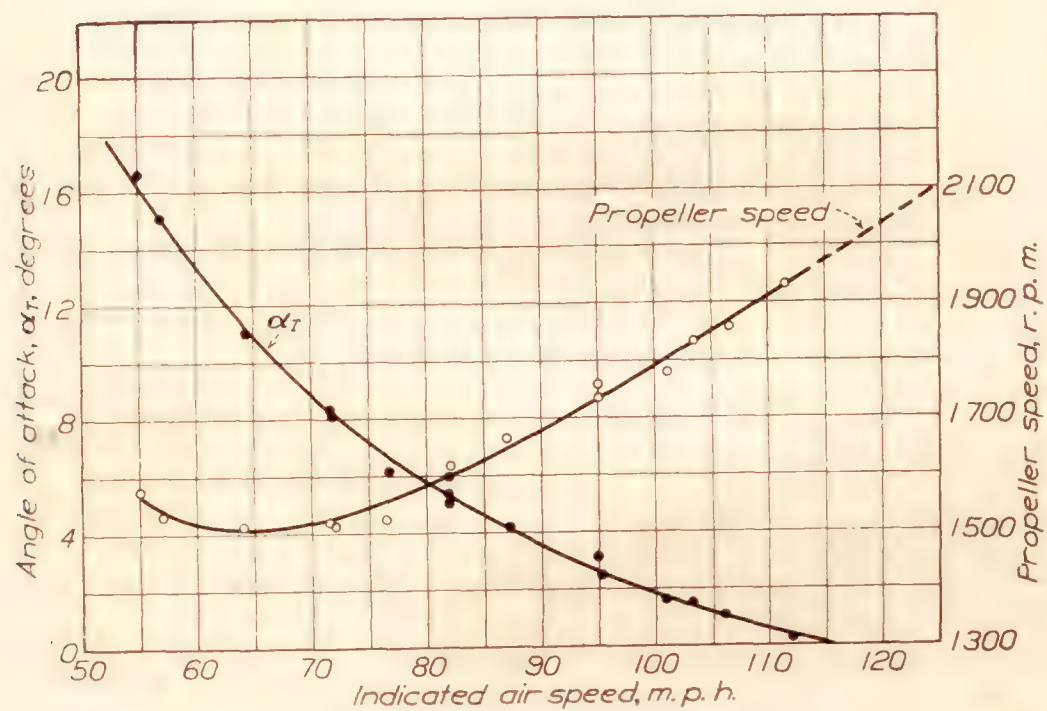


FIGURE 4.—Variation of angle of attack and propeller speed with indicated air speed for steady level flight at altitude of 3,000 feet (O3U-1 airplane).

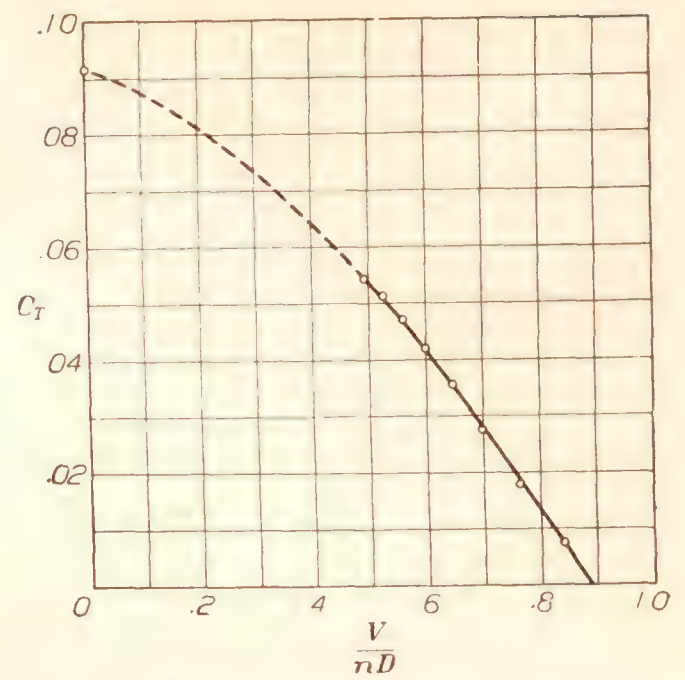


FIGURE 5.—Effective thrust coefficients for O3U-1 airplane at zero angle of attack.

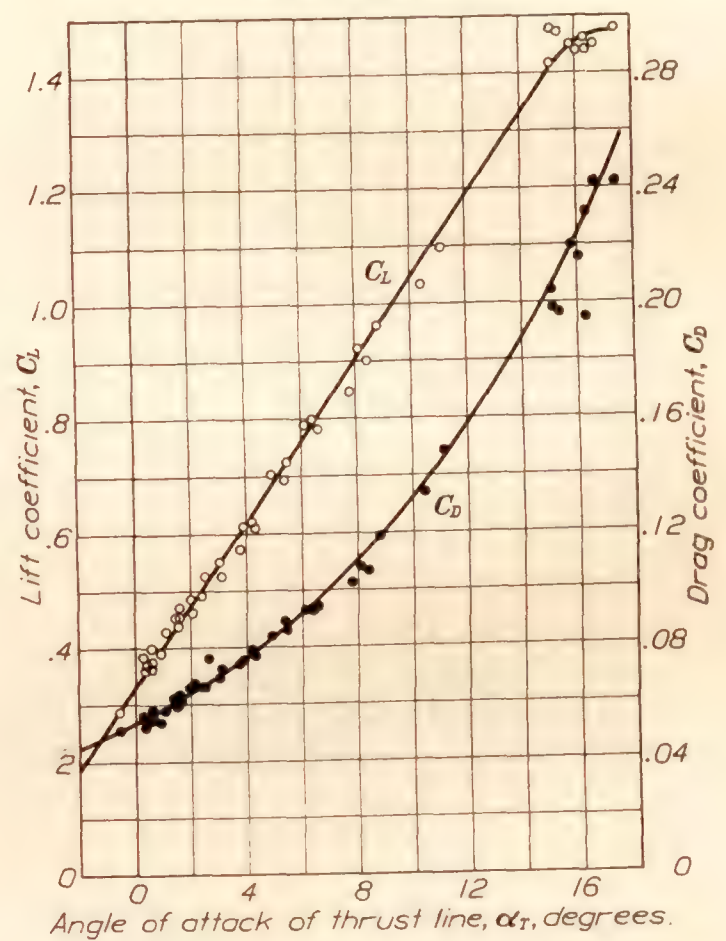


FIGURE 6.—Lift and drag coefficients calculated from level-flight data (O3U-1 airplane).

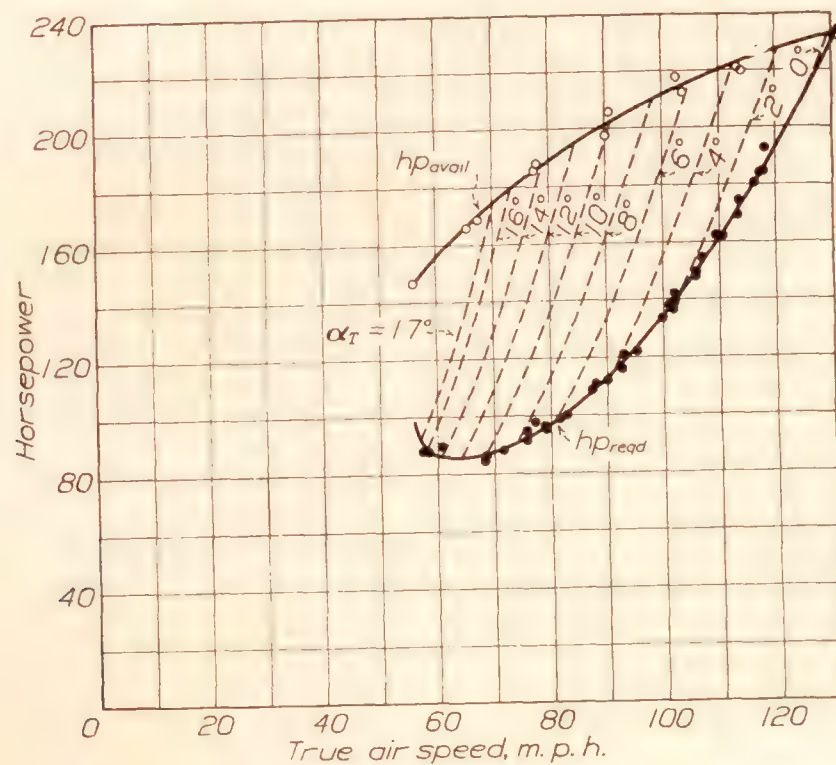


FIGURE 7.—Horsepower curves for flight at altitude of 3,000 feet (O3U-1 airplane).

were obtained from the average curves of the preceding figures. The slopes of these curves show that increasing the elevator movement would increase the elevator effectiveness during the initial stage of the rotation, but that the final rate of rotation would not be appreciably increased.

Aileron maneuvers.—The data obtained in the tests involving abrupt aileron movements are shown in

rapidity than did Pilot B. As this difference exists in spite of repeated attempts by Pilot B to obtain values equaling those obtained by Pilot A, the values obtained by Pilot A should probably be regarded as exceptional. Thus, as in the case of the elevator maneuvers, the force required to operate the controls apparently had some influence on the maneuver. In this case, however, the maximum angular velocities

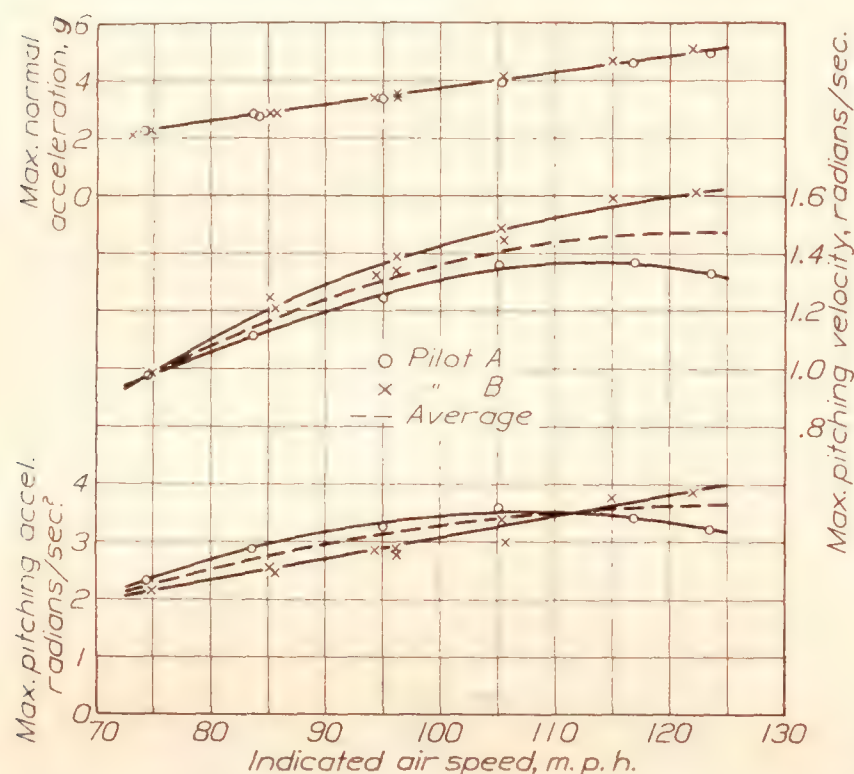


FIGURE 8.—Maximum values of normal acceleration, pitching velocity, and pitching acceleration for abrupt pull-ups with 30.3° (full) elevator movement (O3U-1 airplane).

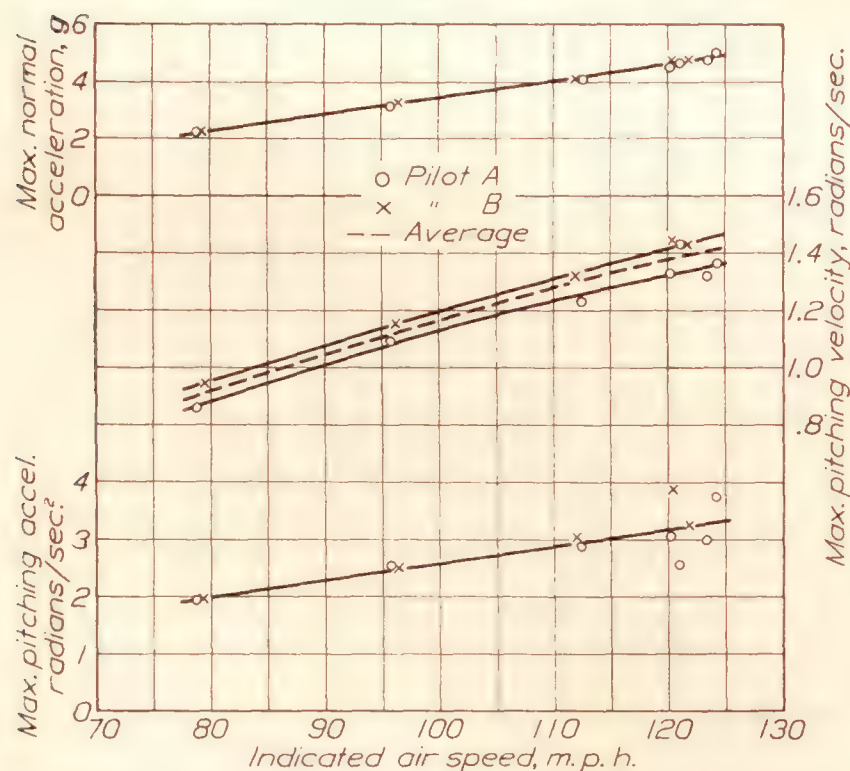


FIGURE 9.—Maximum values of normal acceleration, pitching velocity, and pitching acceleration for abrupt pull-ups with 22.6° elevator movement (O3U-1 airplane).

figures 12, 13, and 14 where maximum rolling velocity and acceleration are plotted against indicated air speed. The difference between the maximum rolling accelerations attained by the two pilots with full aileron movement indicates that Pilot A exerted a greater stick force and thereby moved the ailerons with greater

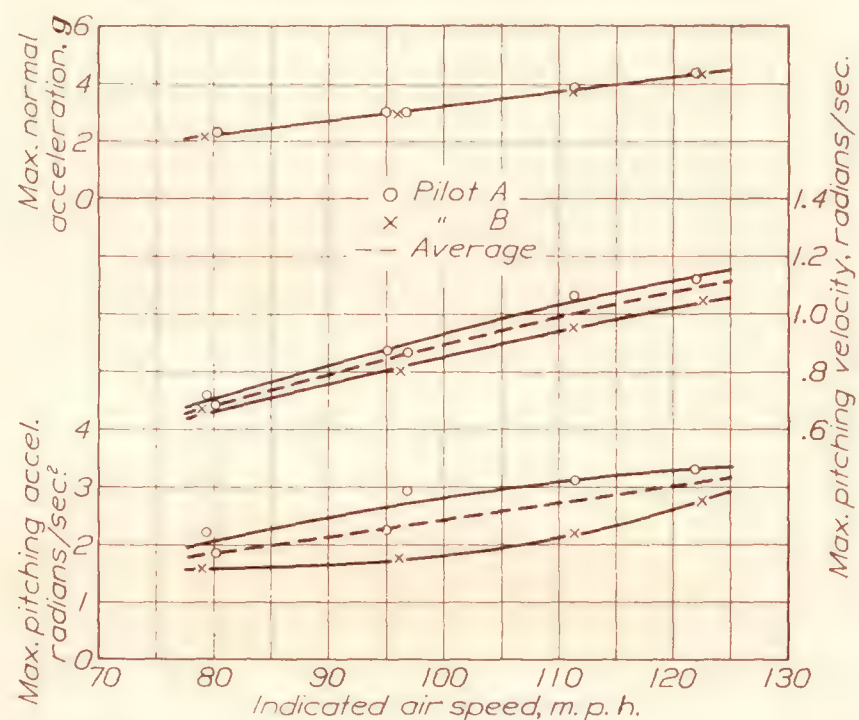


FIGURE 10.—Maximum values of normal acceleration, pitching velocity, and pitching acceleration for abrupt pull-ups with 18.0° elevator movement (O3U-1 airplane).

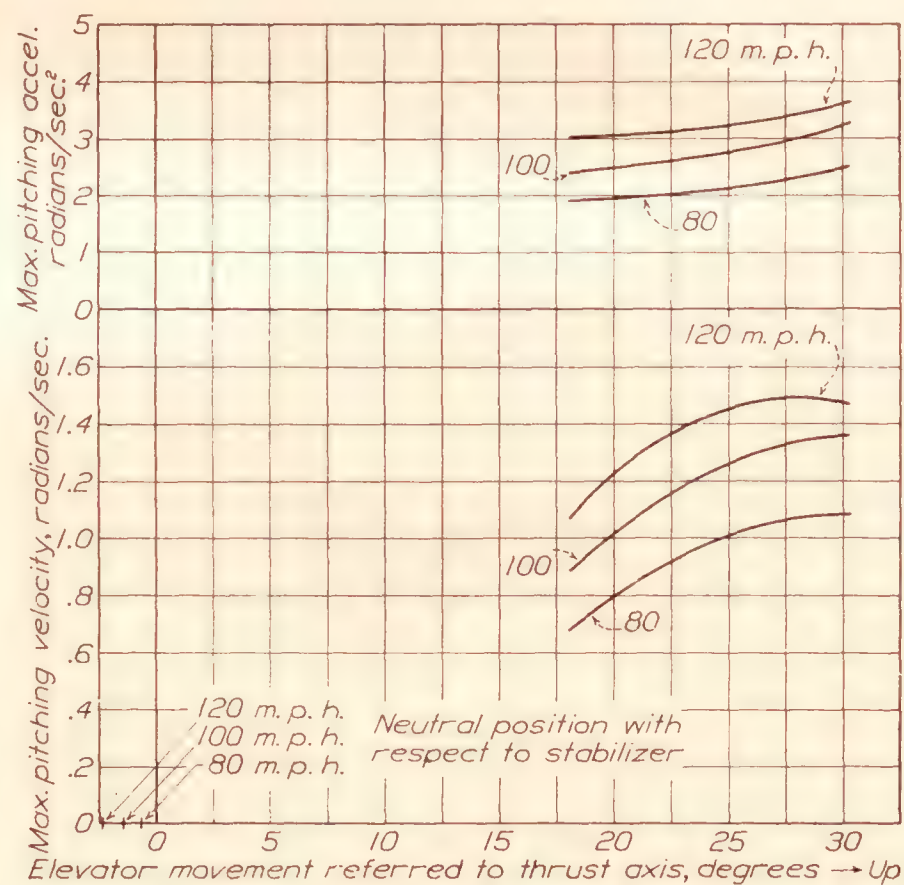


FIGURE 11.—Variation of maximum pitching velocity and maximum pitching acceleration with elevator movement (O3U-1 airplane).

show no consistent differences. As the period during which the high acceleration acts is very short the large stick force in this case apparently has no appreciable influence on the pilot's ability to roll the airplane. The large force required may be important, however, in complicated maneuvers where the pilot is unable

to concentrate his energy on the operation of the ailerons.

The curves in figure 15 show maximum rolling velocity and acceleration against aileron movement. The

by Pilot A are considered to be exceptional. The positive slope of all the curves in this figure indicates that the effectiveness of the aileron will be increased by increasing the movement.

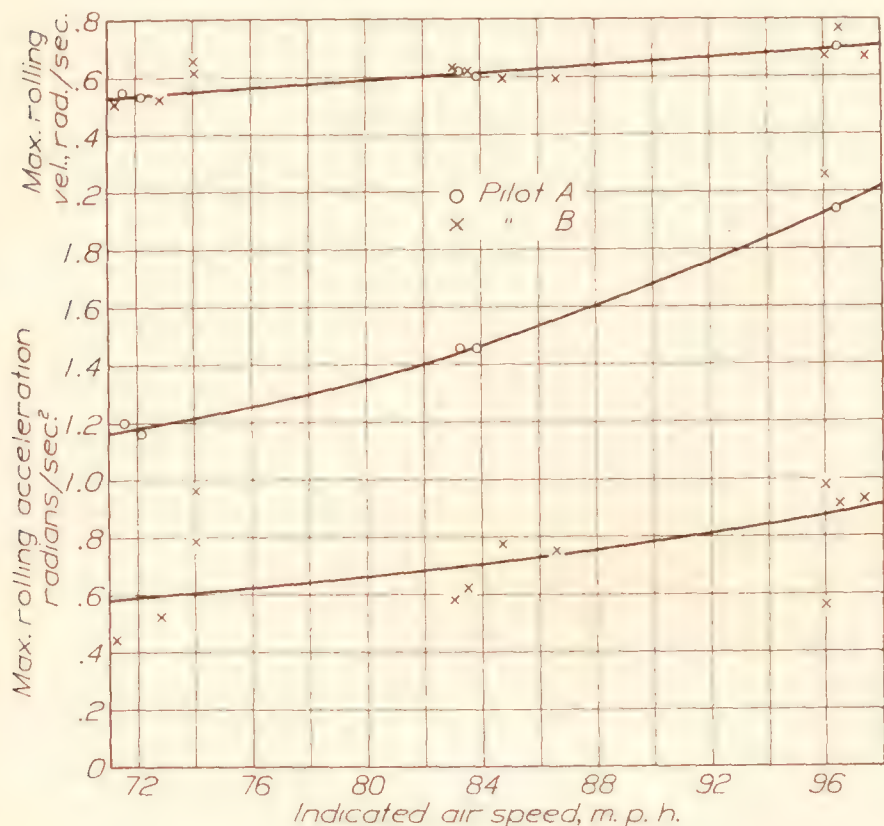


FIGURE 12.—Maximum values of rolling velocity and acceleration for abrupt aileron movement, left aileron down 13.0°, full movement (O3U-1 airplane)

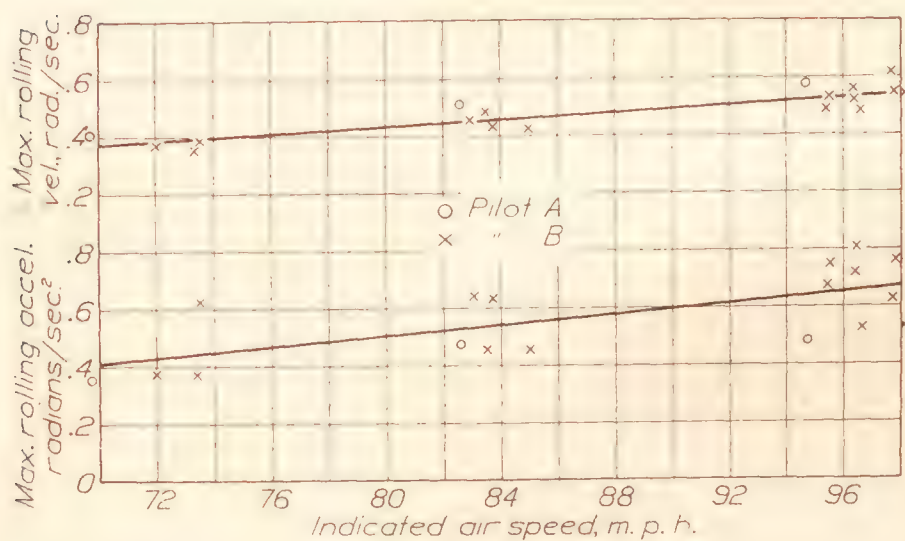


FIGURE 13.—Maximum values of rolling velocity and acceleration for abrupt aileron movement, left aileron down 10.4° (O3U-1 airplane).

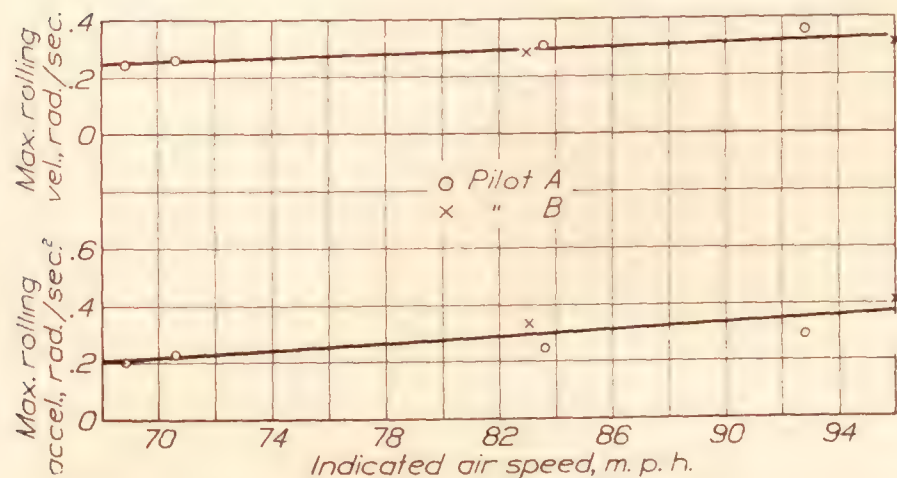


FIGURE 14.—Maximum values of rolling velocity and acceleration for abrupt aileron movement, left aileron down 6.4° (O3U-1 airplane).

values of acceleration for full movement were taken from the results obtained by Pilot B, as those obtained

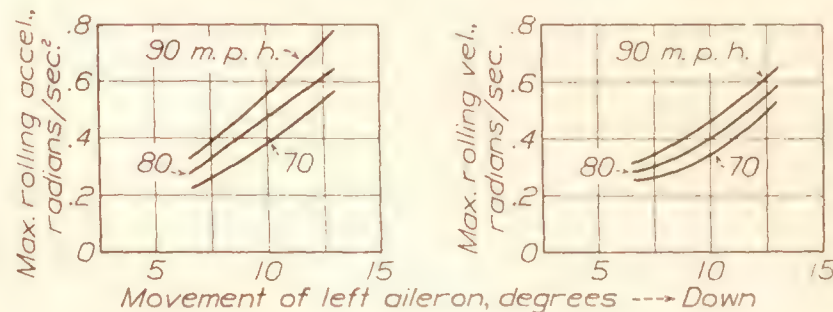


FIGURE 15.—Variation of maximum rolling velocity and maximum rolling acceleration with aileron movement (O3U-1 airplane).

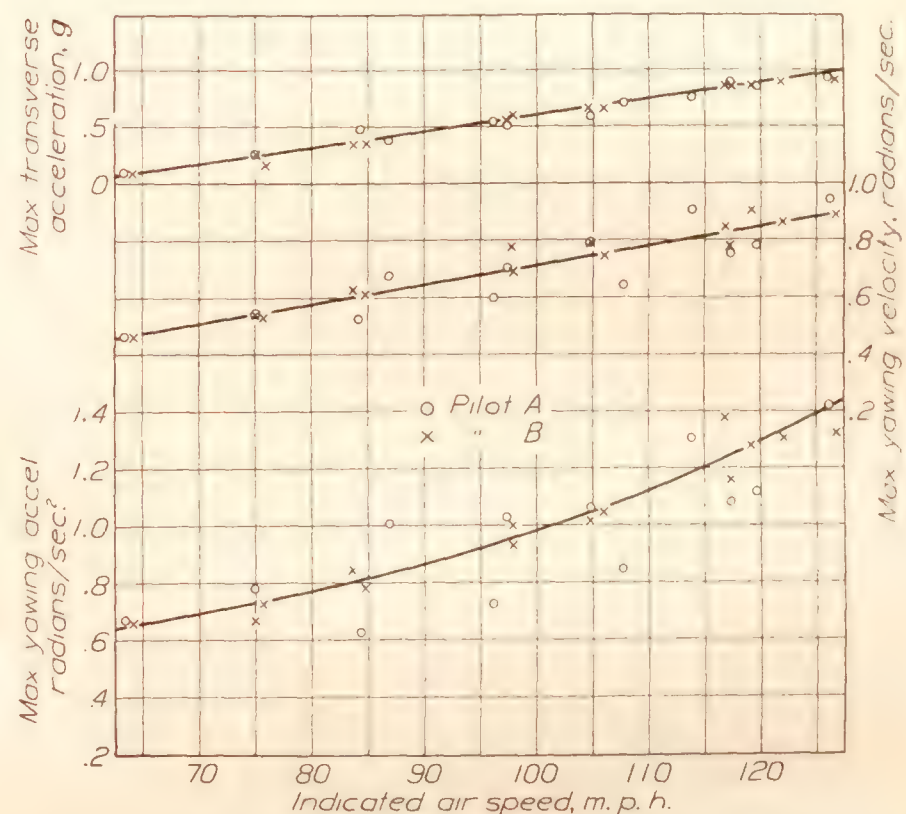


FIGURE 16.—Maximum values of transverse acceleration, yawing velocity, and yawing acceleration for abrupt rudder movement, right 27.0°, full movement (O3U-1 airplane).

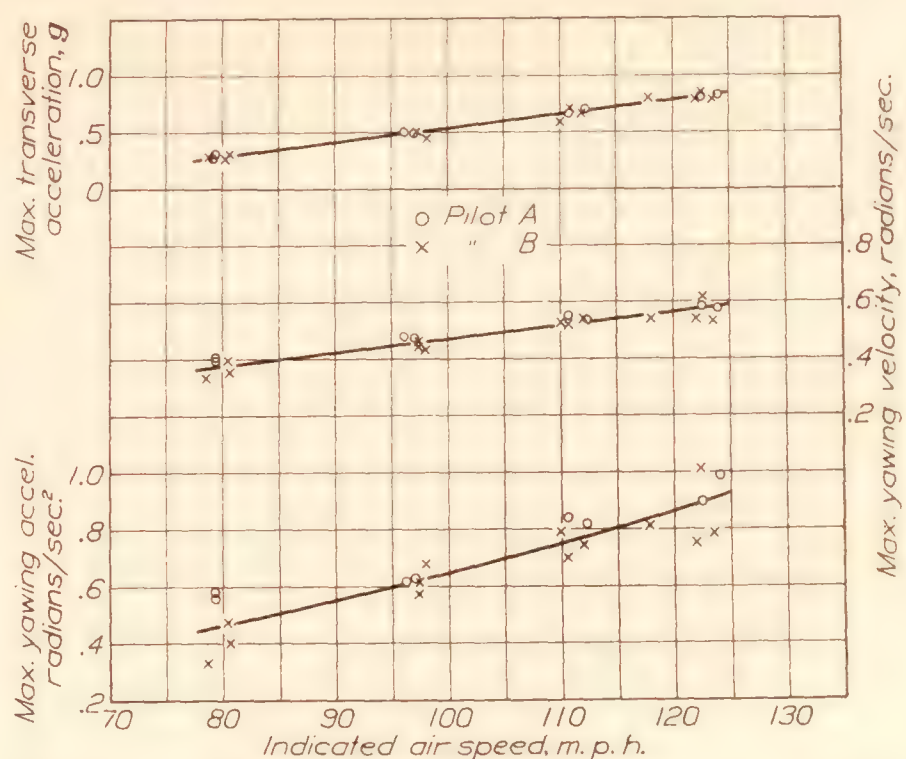


FIGURE 17.—Maximum values of transverse acceleration, yawing velocity, and yawing acceleration for abrupt rudder movement, right 19.5° (O3U-1 airplane).

Rudder maneuvers.—Maximum values of transverse acceleration, yawing velocity, and yawing acceleration

obtained in the maneuvers involving the abrupt use of the rudder are shown in figures 16, 17, and 18. In contrast to the results obtained with the two other controls, there is no evidence of a consistent difference due to difference in piloting. The curves of figure 19

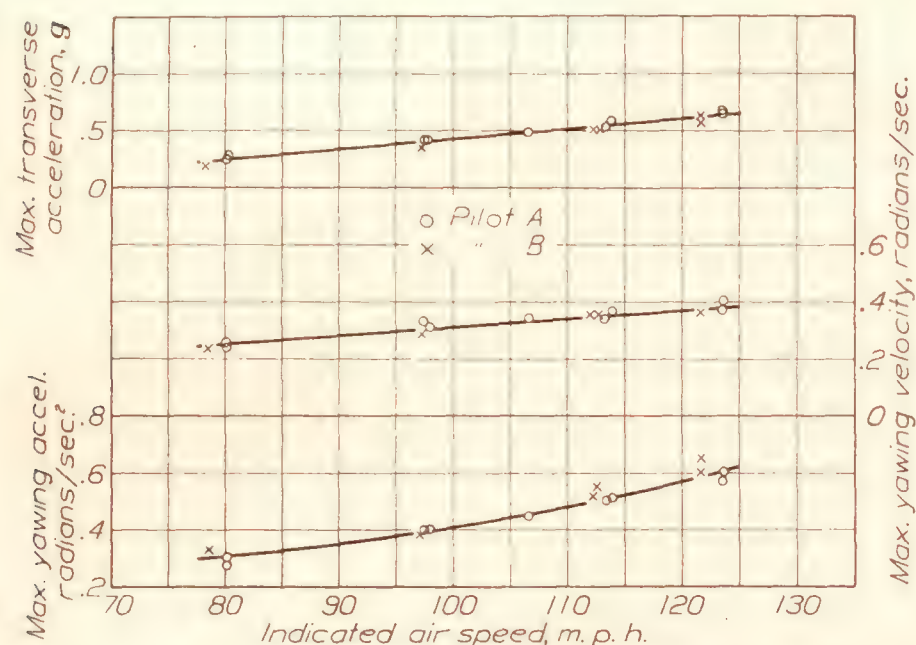


FIGURE 18.—Maximum values of transverse acceleration, yawing velocity, and yawing acceleration for abrupt rudder movement, right 13.9° (O3U-1 airplane).

showing the variation of maximum yawing velocity and acceleration with control movement indicate a practically constant increase of rudder effectiveness with increased movement.

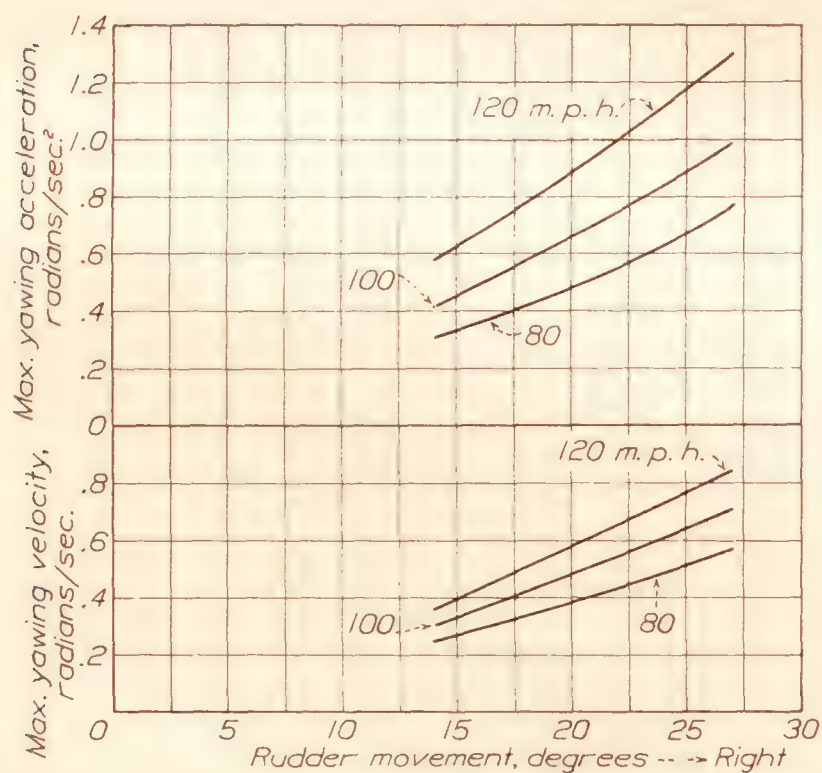


FIGURE 19.—Variation of maximum yawing velocity and maximum yawing acceleration with rudder movement (O3U-1 airplane).

Special slow rolls.—These maneuvers have been regarded as a good indication of the control effectiveness. It was concluded, however, that the performance of these maneuvers is so closely related to the pilot's skill that the results are of small value where quantitative data are required. The results obtained in one of these maneuvers are shown in figure 20.

These results illustrate the most nearly successful attempt to produce rotation solely about the X axis.

Turns of 180°.—The results for the 180° turns are shown principally in table I. Time histories of data obtained in each type of turn are given in figures 21 to 25, inclusive. The data shown in these figures are representative of each type of maneuver. Table I gives a complete summary of significant quantities determined in these maneuvers. The flight-path dimensions given in this table apply to the projection of the flight path in either a vertical or horizontal plane. The wing-over is regarded as a horizontal-plane maneuver in which there is no resultant change of altitude. Data from the horizontal-plane maneuvers in which the airplane did not return to approximately the initial altitude were excluded. The Immelman turn, the half kick roll—half loop, and the half aileron roll—half loop are regarded as vertical-plane maneuvers although the actual motion was not strictly limited to a vertical plane. The maneuvers were regarded as complete when the starting point had been passed after reversing the direction of flight. In several cases the flight-path records were terminated slightly before completion of maneuvers. The extrapolation of the flight paths to determine the time required for completion in those cases results in no appreciable error.

The relative merits of the various maneuvers can be judged by a comparison of the data given in table I. Owing to the violence of the half kick roll—half loop, this maneuver was not performed at speeds greater than 102 miles per hour, but for the range of speed in which it was performed it required the least time for completion, the time being about 10 seconds. The time required to complete the horizontal turns decreased rapidly with increased speed until at 123 miles per hour, the time required was only 8.3 seconds. The wing-over turns required the greatest time for completion, the time being about 21 seconds at all speeds. The least horizontal displacement required for turning was about 500 feet and occurred in the half kick roll—half loop at 84 miles per hour and the horizontal turn at 123 miles per hour. The greatest horizontal displacement required was 1,390 feet and occurred in the half aileron roll—half loop at 117 miles per hour. As previously noted, the Immelman turn was performed with a slight initial dive to gain speed for the performance of the maneuver. The speeds that have been tabulated for the above cases are indicated air speeds and are about 4 percent less than the true air speeds.

Steady horizontal turns.—The results of the tests to determine the minimum radius of steady horizontal turn are shown in figure 26. Experimental points obtained from the same tests by two methods of calculation are given. The most direct method involved

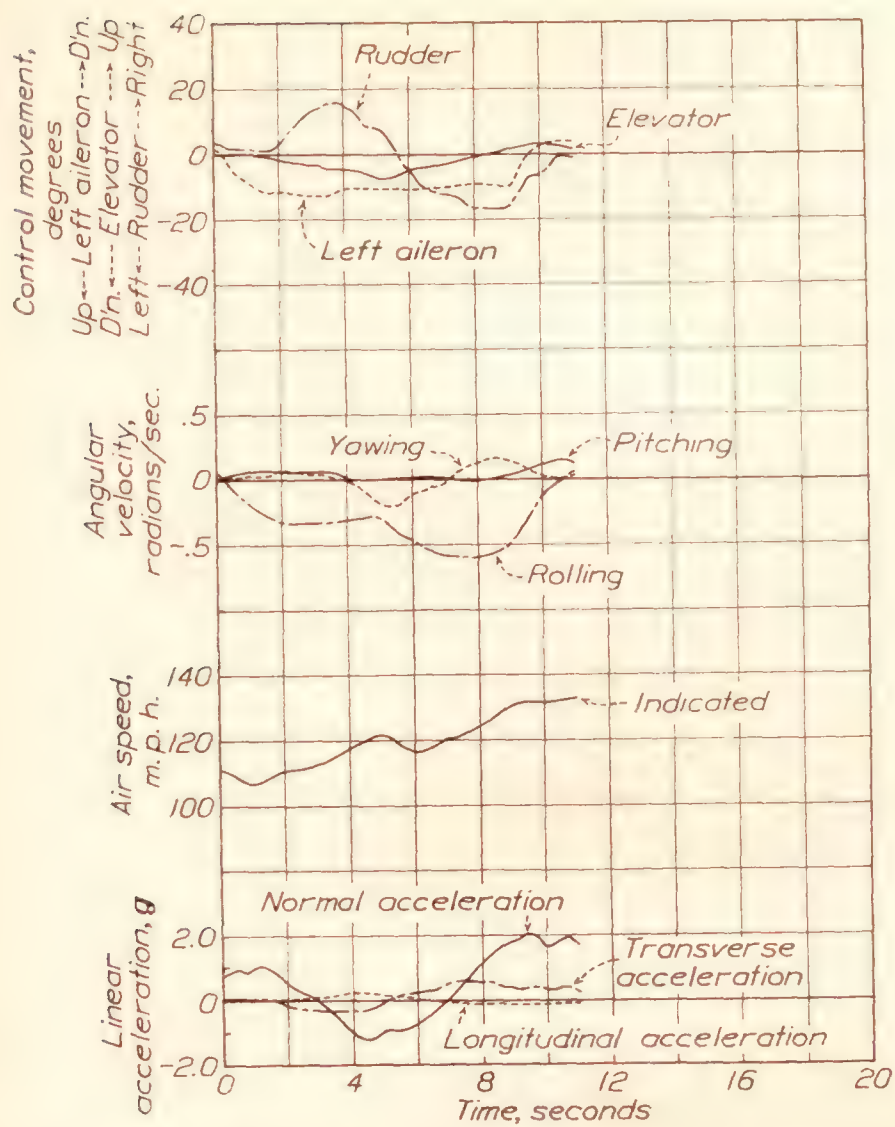


FIGURE 20.—Slow roll, attempting roll about X axis only (O3U-1 airplane).

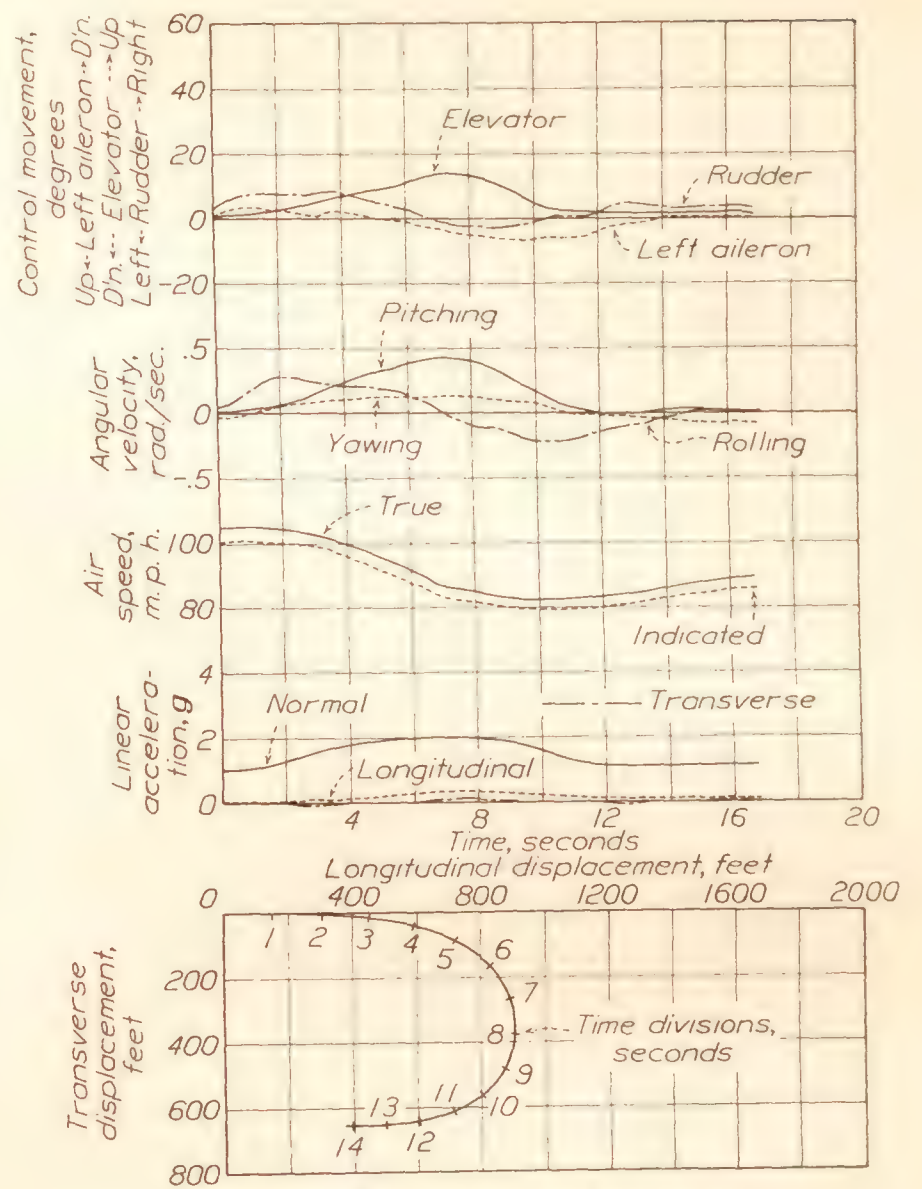


FIGURE 22.—Horizontal turn (O3U-1 airplane).

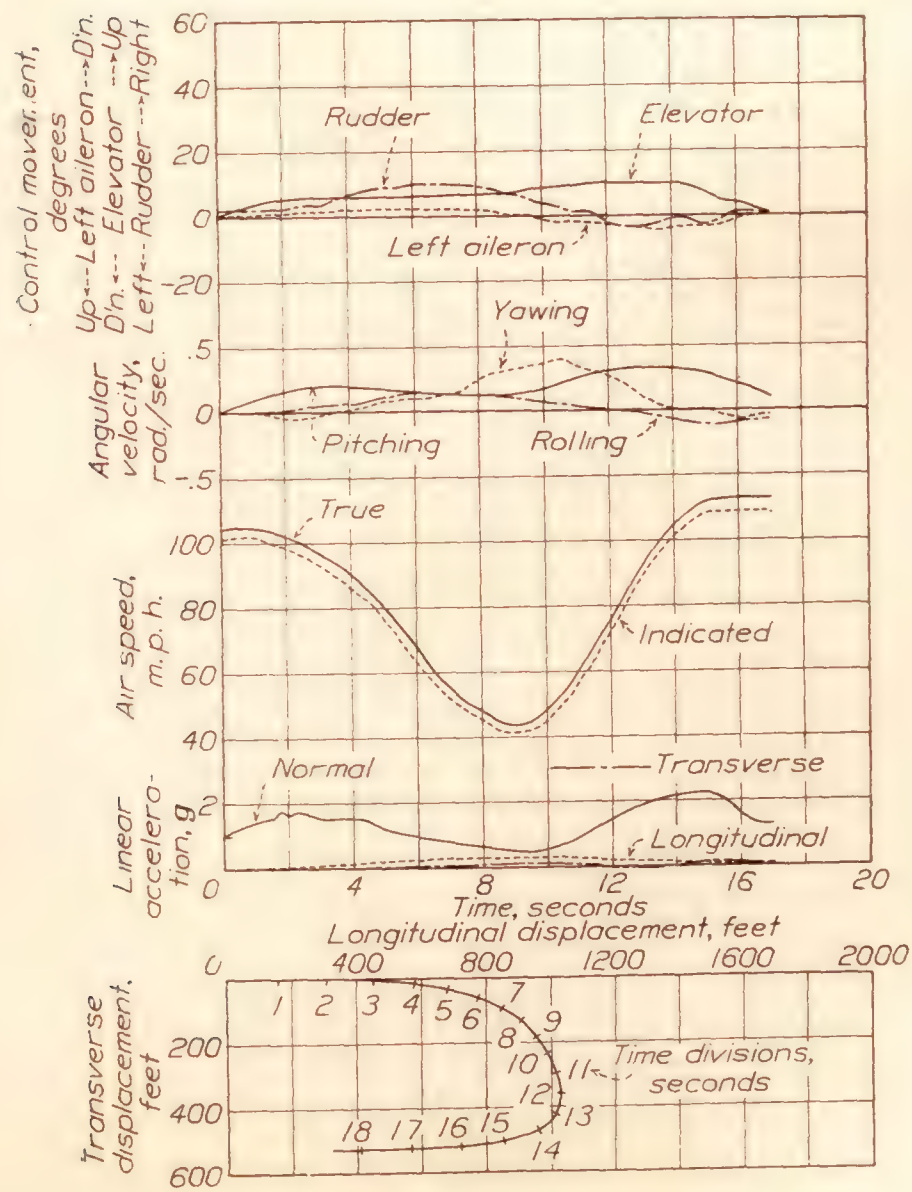


FIGURE 21.—Wing-over turn (O3U-1 airplane).

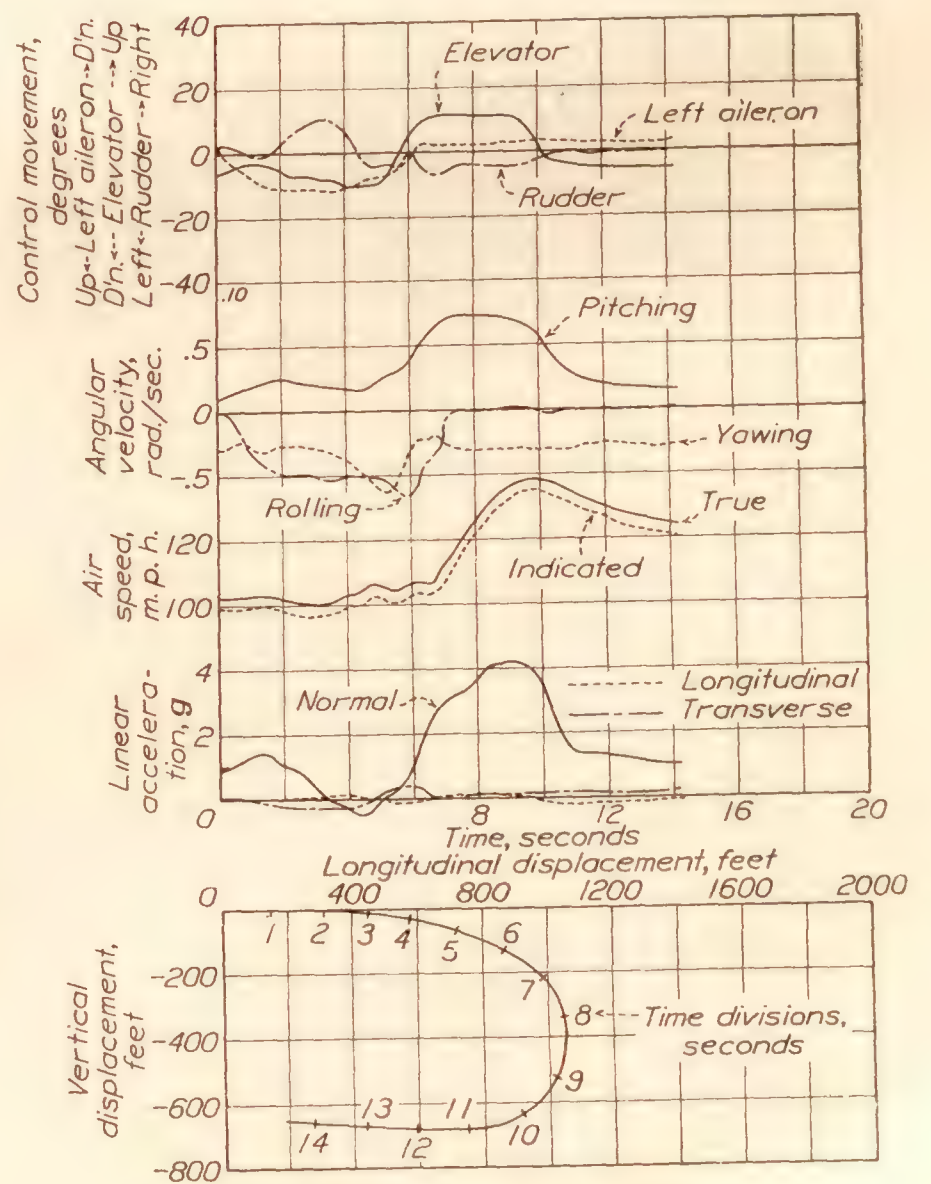


FIGURE 23.—Half aileron roll—half loop (O3U-1 airplane).

only the recorded air speed and acceleration, from which the radii were calculated by means of the equation

$$r = \frac{V^2}{(a_R^2 - g^2)^{1/2}} \quad (7)$$

where r is the radius of turn

a_R , the resultant accelerometer reading

V , the true air speed.

The results obtained by this method were erratic, possibly because the airplane was traveling in its own wake.

For the second method the data required from the steady turns were air speed and corresponding engine speed. The thrust was calculated by means of these flight data and the thrust curve of figure 5. The angle

by the previous method. This curve shows the minimum radius of turn to be 322 feet at 74 miles per hour.

The usual method of calculating minimum radius of turn where flight data are not available is to use curves of horsepower available and required. (See reference 8, p. 217.) This method utilizes the expression

$$r = \frac{V^2}{g \tan \theta} \quad (9)$$

where θ is the angle of bank, given by the expression

$$\theta = \cos^{-1} \left(\frac{V_i}{V} \right)^2 \quad (10)$$

and V_i/V is the ratio of the speed in level flight to the speed in a steady turn at the same angle of attack.

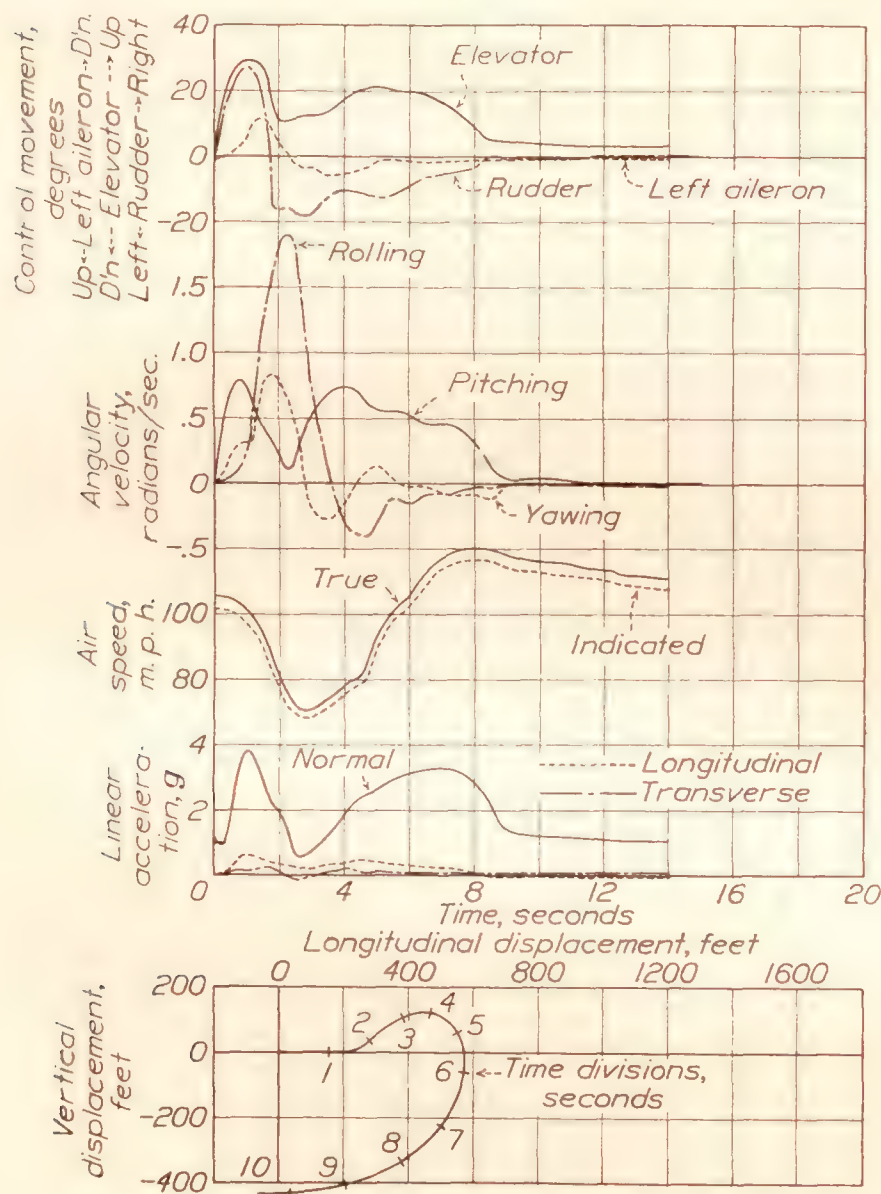


FIGURE 24.—Half kick roll—half loop (O3U-1 airplane).

of attack and corresponding lift coefficient were then found by utilizing first and second approximate solutions of equation (2) and the curves of figure 6. The resultant acceleration was calculated by means of the expression

$$a_R = \frac{g(C_L \rho S V^2 + 2T \sin \alpha_T)}{2W} \quad (8)$$

and r was found from equation (7). The values obtained by this method lie close to a smooth curve that represents fairly well an average of the points obtained

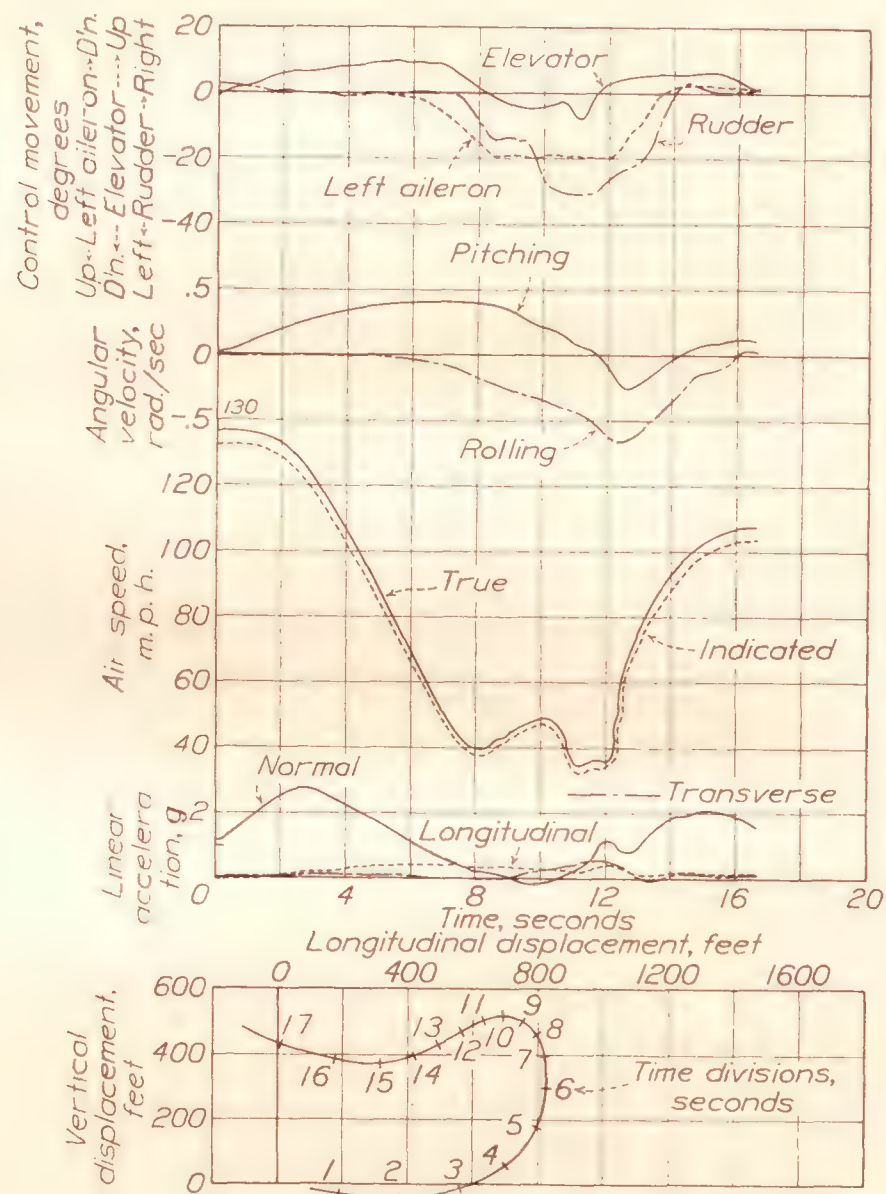


FIGURE 25.—Immelman turn (O3U-1 airplane).

Radii calculated by this method using the horsepower curves of figure 7 are shown by the broken curve in figure 26. The corresponding values of V and V_i are found from the curves of horsepower required and horsepower available by having these curves intersected by other curves representing the variation of horsepower required with speed at constant angles of attack, that is, at constant drag coefficients. Such curves for various angles of attack are shown by dotted lines in figure 7. The results obtained by this method give a minimum radius of 295 feet, which is

about 8 percent less than the probably more nearly correct value shown by the previous curve and which lies within the region covered by the scattered points obtained by the most direct method. Consideration

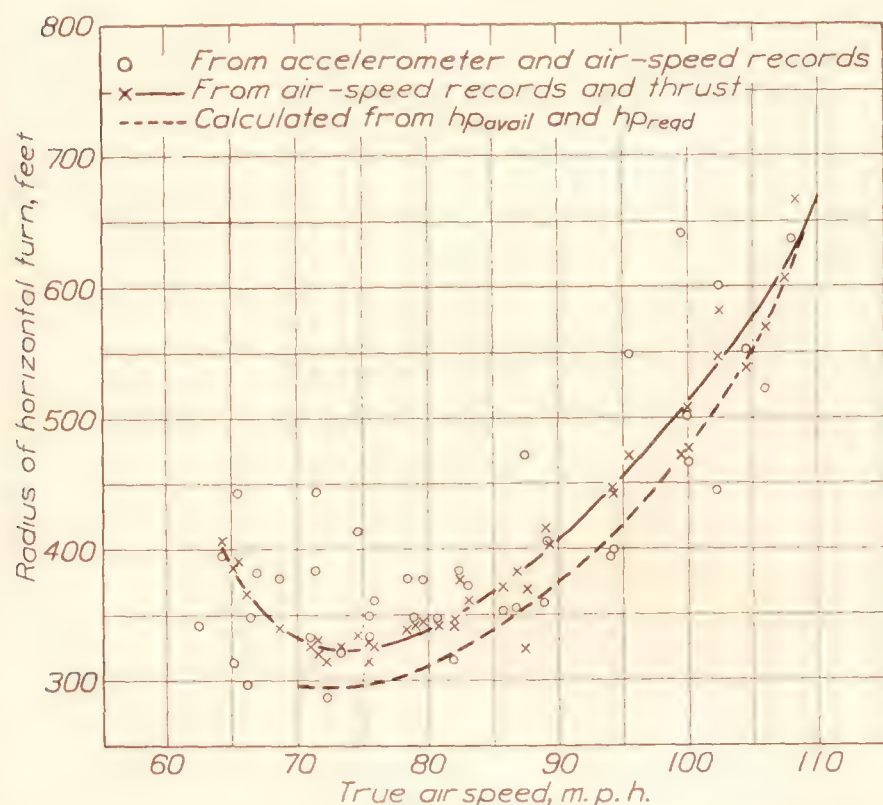


FIGURE 26.—Radius of steady horizontal turn with full throttle at altitude of 3,000 feet (O3U-1 airplane).

of the change of horsepower required and horsepower available with altitude indicates that the minimum radius at sea level would be about 18 percent less than the value at 3,000 feet.

SUMMARY OF RESULTS

With full elevator movement (up 30.3°) maximum angular velocities in pitch as obtained by either pilot varied from 0.98 radian per second at 75 miles per hour to 1.61 radians per second at 122 miles per hour. These values agree closely with the data obtained with the F6C-4 airplane. Considerable time was required to move the elevator at high speed, apparently because of the large force required, so that there was a considerable decrease in speed before the angle of attack for maximum lift was attained. No appreciable increase in pitching velocities would have been attained by increasing the allowable elevator movement above 30.3° .

With the full aileron movement (left aileron down 13.0° , right aileron up 18.5°) the maximum rolling velocities varied from 0.53 radian per second at 71 miles per hour to 0.70 radian per second at 97 miles per hour. At the same indicated air speeds with the F6C-4 airplane the maximum rolling velocities attained were 0.61 and 0.75 radian per second, respectively, but at 140 miles per hour the F6C-4 airplane attained a rolling velocity of 0.90 radian per second. Although the large force required to operate the ailerons apparently affected the maximum rolling accelerations as attained by the two pilots, maximum angular

velocities were not affected. An increase in the allowable aileron movement above 13.0° would have increased the maximum rolling velocity attainable.

With full rudder movement (right 27.0°) maximum yawing velocities varied from 0.46 radian per second at 64 miles per hour to 0.90 radian per second at 127 miles per hour. At corresponding speeds with the F6C-4 airplane the values obtained were about 0.10 radian per second greater than those obtained with the O3U-1 airplane. No effect of the force required to operate the rudder was indicated in either the angular acceleration or angular velocity attained. The variation of angular velocity with control movement indicated that greater angular velocity would have been attained with an increase in the allowable rudder movement.

In the 180° turns the half kick roll—half loop in general required the least time (about 10 seconds) for completion. The violence of this maneuver excluded it from test at speeds greater than about 100 miles per hour. At full speed the horizontal turns required the least time for completion (about 8 seconds). Wing-over turns required the greatest time for completion (about 21 seconds at all speeds). An Immelman turn was performed in which the altitude gained was 430 feet and the time required for completion was 17 seconds. In this particular maneuver, however, sufficient momentum was acquired by diving slightly at the start. Similar maneuvers were made with the F6C-4 airplane at generally higher speeds and in generally less time than was required for the O3U-1 airplane. An exception is noted in the case of the horizontal turns, however, in which the F6C-4 with an initial speed of 128 miles per hour, required about 9 seconds and a horizontal displacement of 565 feet, and the O3U-1, with an initial speed of 123 miles per hour, required about 8 seconds and a horizontal displacement of 490 feet. The one maneuver of this class that provides the most definite indication of superior maneuverability of the F6C-4 airplane over the O3U-1 airplane is the Immelman turn. With the F6C-4 airplane this maneuver was performed without diving at the start, required 11 seconds for completion, and resulted in a gain of 550 feet of altitude.

The minimum radius of turn at an altitude of 3,000 feet was found to be 322 feet at a true air speed of 74 miles per hour. The minimum radius calculated from horsepower curves was 8 percent less than that value. The estimated minimum radius at sea level is 265 feet. The minimum radii for the F6C-3 and F6C-4 airplanes were 155 feet at 76 miles per hour and 135 feet at 62 miles per hour, respectively, for an altitude of about 2,500 feet, which is sufficiently close to 3,000 feet to make the test results comparable.

The tests with the O3U-1 airplane complete the contemplated series of investigations. Consideration is now being given to the problem of developing a

suitable criterion or method for rating airplanes according to their ability to maneuver. The results of this study will be reported at a later date. An important factor to be considered is that the method of rating should be based on items that are independent of the personal characteristics of a particular pilot, and that, as far as is possible, can be determined readily. Maximum speed, control effectiveness as shown by the results of abrupt single-control maneuvers, and minimum radius of steady horizontal turn are regarded as items of particular importance. The fact that the excess energy required for maneuvering is largely acquired through loss of speed suggests the possibility that the maximum kinetic energy that an airplane can surrender without varying the speed beyond the range of normal level-flight speeds may prove to be a particularly useful and convenient item.

LANGLEY MEMORIAL AERONAUTICAL LABORATORY,
NATIONAL ADVISORY COMMITTEE FOR AERONAUTICS,
LANGLEY FIELD, VA., *January 19, 1933.*

APPENDIX

SPECIFICATIONS OF O3U-1 AIRPLANE ^a

Type.....	Tractor biplane, landplane.
Engine.....	Pratt and Whitney, R-1340-C.
Horsepower.....	450 at 2,100 r.p.m.
Full load.....	4,057 lb.
Weight per square foot.....	12.5 lb.
Weight per horsepower.....	9.02 lb.
Maximum speed.....	138 m.p.h. ^b
Distance from leading edge of lower wing to rudder post..	17 ft. 9 ⁵ / ₈ in.

^a From Table of Characteristics, Weights, and Performance of U.S. Navy Observation and Training Planes. Bureau of Aeronautics, Navy Department, January 1931.
^b Maximum speed as flown during tests, 132 m.p.h.

Service ceiling.....	16,300 ft.
Wing area including ailerons....	325.6 sq. ft.
Aileron area.....	32.6 sq. ft.
Stabilizer area.....	23.6 sq. ft.
Elevator area.....	18.5 sq. ft.
Fin area.....	4.4 sq. ft.
Rudder area.....	14.1 sq. ft.
Airfoil section.....	Upper N-22, lower G-398.
Wing span.....	36 ft.
Length.....	26 ft. ¾ in.
Height.....	10 ft. 8 in.
Gap.....	5 ft. 5 in.
Chord.....	Upper 5 ft. 5 in., lower 4 ft. 9 in.
Angle of incidence.....	0°.
Stagger.....	17.5 in.
Dihedral.....	Upper 2°, lower 1.75°.
Sweepback.....	4.75°.
Distance back from leading edge lower wing to c.g.....	16.27 in.

REFERENCES

1. Dearborn, C. H., and Kirschbaum, H. W.: Maneuverability Investigation of the F6C-3 Airplane with Special Flight Instruments. T.R. No. 369, N.A.C.A., 1930.
2. Dearborn, C. H., and Kirschbaum, H. W.: Maneuverability Investigation of an F6C-4 Fighting Airplane. T.R. No. 386, N.A.C.A., 1931.
3. Ronan, K. M.: An Instrument for Recording the Position of Airplane Control Surfaces. T.N. No. 154, N.A.C.A., 1923.
4. Reid, H. J. E.: A Study of Airplane Maneuvers with Special Reference to Angular Velocities. T.R. No. 155, N.A.C.A., 1922.
5. Reid, H. J. E.: The N.A.C.A. Three-Component Accelerometer. T.N. No. 112, N.A.C.A., 1922.
6. Norton, F. H.: N.A.C.A. Recording Air Speed Meter. T.N. No. 64, N.A.C.A., 1921.
7. Diehl, Walter S.: The Reduction of Observed Airplane Performance to Standard Conditions. T.R. No. 297, N.A.C.A., 1928.
8. Diehl, Walter S.: Engineering Aerodynamics. Ronald Aeronautic Library. The Ronald Press Co., New York, 1928.

TABLE I
SUMMARY OF SIGNIFICANT QUANTITIES MEASURED IN VARIOUS MANEUVERS WITH
THE "O3U-1" AIRPLANE

Maneuver	Indicated air speed, m.p.h.		Altitude, feet		Longi- tudinal displace- ment, feet	Time to com- plete maneu- ver, seconds	Maxi- mum normal accelera- tion, g	Maximum angular veloc- ities, radians/second			Maximum control movement, degrees		
	Start	End	Maxi- mum varia- tion (+) gain, (-) loss	Result- ant (+) gain, (-) loss				X axis	Y axis	Z axis	Elevator ¹	Aileron ²	Rudder ³
Wing-over turn.....	84	94			980	21.0	2.20	0.17	0.34	0.36	12	-6	7, -5
	100	108			1,025	20.8	2.25	.15	.32	.38	9	2, -4	10, -4
	116	111			970	20.5	2.10	.41	.25	-.22	7	2, -6	6, -4
Horizontal turn.....	84	79			820	19.5	1.55	.24	.29	.18	10	4, -7	9
	100	87			900	17.5	2.00	.27	.41	.12	13	2, -7	8, -3
	115	93			670	11.6	2.60	.42	.57	.16	16	5, -11	11, -3
	123	99			490	8.3	3.00	.44	.58	.22	16	7, -6	13, -4
Half aileron roll—half loop.....	84	109	-630	-600	750	15.0	3.64	-.73	.69	-.73	-12, 11	-14, 5	3, -10
	99	119	-680	-675	1,050	16.0	4.20	-.66	.72	-.64	-11, 11	-12, 2	10, -7
	117		-660	-470	1,390	18.0	4.25	-.56	.66	-.29	-15, 4	-8, 4	8
	122	141	-560	-340	1,290	16.7	4.10	-.62	.63		-7, 14	-15	8, -7
Half kick roll—half loop.....	84	108	-665	-575	495	10.2	3.10	1.50	.66	.88	31.5	7, -4	31, -16
	102	112	-560	-440	570	10.2	3.80	1.88	.77	.82	28.5	11, -6	27, -19
Immelman turn.....	132	104	550	430	830	17.0	2.70	-.66	.39		9, -8	-20	-31

¹ Elevator up, +.
² Left aileron down, +.
³ Rudder right, +.

REPORT No. 458

RELATIVE LOADING ON BIPLANE WINGS

By WALTER S. DIEHL

SUMMARY

It is shown that the lift coefficients of the individual wings of a biplane are given by

$$C_{LU} = C_L + \Delta C_{LU}$$

and

$$C_{LL} = C_L - \Delta C_{LL}$$

Where C_{LU} , C_{LL} , and C_L are the lift coefficients for the upper wing, lower wing, and biplane, respectively.

For the upper wing it is shown that

$$\Delta C_{LU} = K_1 + K_2 C_L$$

K_1 and K_2 being functions of gap/chord, stagger, aspect ratio, decalage, overhang and wing thickness. The combination of existing biplane theory and experimental data supply curves from which K_1 and K_2 can easily be determined for any biplane. This enables the designer to calculate with reasonable accuracy the relative loading for any condition of flight.

INTRODUCTION

The accuracy of a biplane stress analysis depends greatly on the accuracy with which the loads on each wing can be determined. The division of the load between biplane wings has usually been determined in the current stress analysis methods from a chart giving the "relative efficiency" as a function of gap/chord ratio and stagger. This "relative efficiency" or ratio of the lift coefficient of the upper wing to lift coefficient of the lower wing has been based on the average values at high lift coefficients and therefore does not necessarily hold true for all lift coefficients. Recent improvements in stress analysis methods have made it necessary to revise and to extend the loading curves to cover all conditions of flight. This paper is concerned with a study of existing biplane data in connection with such a revision.

A survey of theoretical biplane data, in which numerous comparisons were made between observed and calculated lift curves, showed that while the agreement between theory and experiment is reasonably close, the theoretical methods do not appear entirely satisfactory except at moderate lift coefficients. By combining the experimental and theoretical data, however,

it is possible to derive a series of curves from which the lift curves of the individual wings of a biplane may be obtained.

BIPLANE THEORY

The first important contribution to biplane theory was due to Betz (reference 1). This theory was elaborated by Fuchs (reference 3), and is given in its final form by Fuchs and Hopf in chapter IV of their book *Aerodynamik* (reference 4). Denoting the upper and lower wing by the subscripts U and L , respectively, the lift equations are

$$\Delta C_{LL} = -\frac{\mu}{2\pi} \frac{S_U}{b_U b_L} C_{LU} C_{LL} - \frac{57.3}{4\pi} (\nu + \kappa) \frac{S_U}{b_U b_L} C_{LU} \left(\frac{dC_{LL}}{d\alpha} \right) \quad (1)$$

$$\Delta C_{LU} = +\frac{\mu}{2\pi} \frac{S_L}{b_U b_L} C_{LL} C_{LU} + \frac{57.3}{4\pi} (\nu - \kappa) \frac{S_L}{b_U b_L} C_{LL} \left(\frac{dC_{LU}}{d\alpha} \right) \quad (2)$$

Where S is area and b the span. μ , ν , and κ are functions of gap G , wing span and stagger β . If we let

$$\lambda_1 = \frac{b_U + b_L}{2G} \text{ and } \lambda_2 = \frac{b_U - b_L}{2G}$$

Then

$$\mu = \mu(\lambda_1) - \mu(\lambda_2) \quad (3)$$

$$\nu = \nu(\lambda_1) - \nu(\lambda_2) \quad (4)$$

and

$$\kappa = \kappa(\lambda_1) - \kappa(\lambda_2) \quad (5)$$

That is, the value of μ , ν or κ for a given biplane is the difference between the values for λ_1 and λ_2 .

The variations of μ , ν , and κ with λ are given by the relations

$$\mu(\lambda) = \cos \beta [(1 + \lambda^2 \cos^2 \beta)^{1/2} - 1] \quad (6)$$

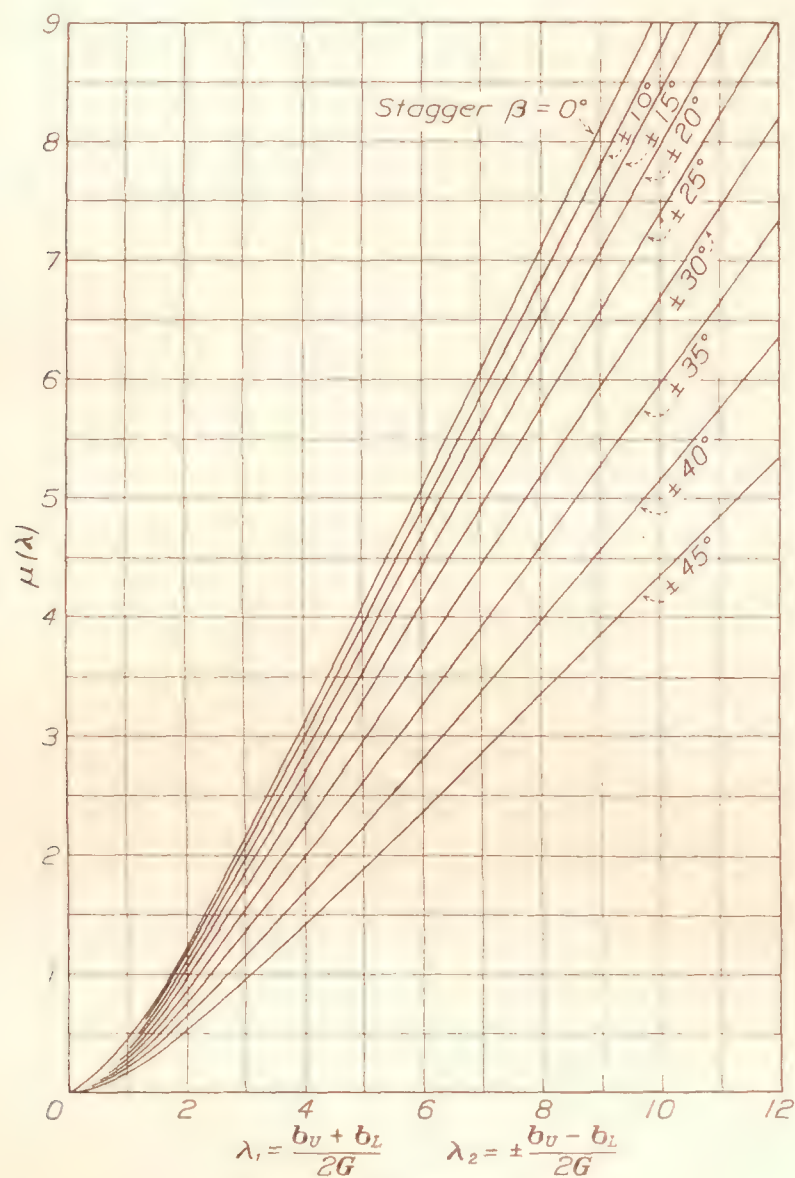
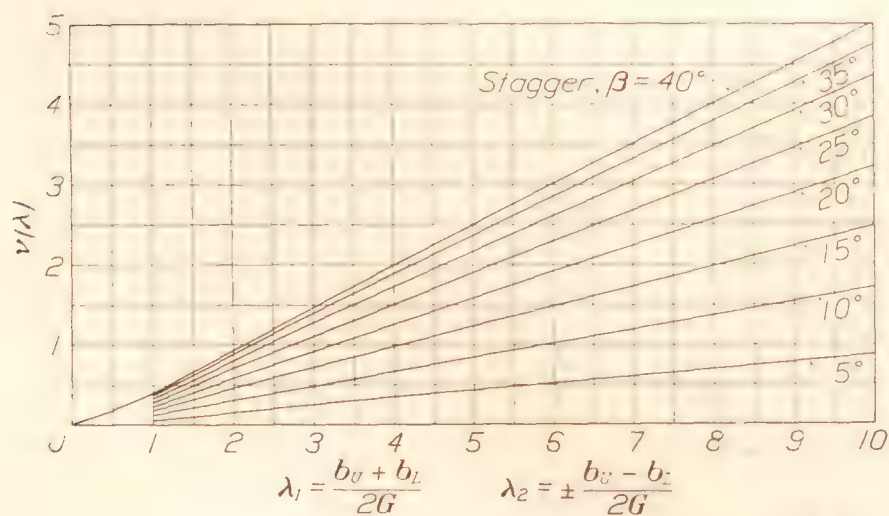
$$\nu(\lambda) = \sin \beta [(1 + \lambda^2 \cos^2 \beta)^{1/2} - 1]$$

$$+ \log_e \frac{(1 + \sin \beta) \sqrt{1 + \lambda^2}}{\sin \beta + \sqrt{1 + \lambda^2 \cos^2 \beta}} \quad (7)$$

$$\kappa(\lambda) = \frac{1}{2} \log_e (1 + \lambda^2) \quad (8)$$

Values of $\mu(\lambda)$, $\nu(\lambda)$ and $\kappa(\lambda)$ from the above equations are plotted in figures 1, 2, and 3. $\mu(\lambda)$ and $\nu(\lambda)$ vary with stagger but $\kappa(\lambda)$ is independent of stagger. Since stagger varies with angle of attack it will be found more convenient and more accurate to read values of $\mu(\lambda)$ and $\nu(\lambda)$ at some particular stagger and

then apply a correction for the stagger corresponding to each angle of attack. Figure 4 gives the variation of $\mu(\lambda)$ with stagger in terms of the value of $\mu(\lambda)$ for zero stagger. Figure 5 gives the variation of $\mu(\lambda)$ with stagger in terms of the value of $\nu(\lambda)$ for 30° stagger. The angle of stagger is to be measured between the lift direction and the line connecting the one third chord points (measured from the leading

FIGURE 1.—Values of $\mu(\lambda)$.FIGURE 2.— $\nu(\lambda)$ for $-\beta^\circ = -\nu(\lambda)$ for $+\beta^\circ$.

edge) of the upper and lower wings. Stagger is positive when the third point in the upper wing is ahead of the lower wing.

Physically, $\mu(\lambda)$ is a factor which takes care of the velocity change due to the presence of each wing, while $\nu(\lambda)$ and $\kappa(\lambda)$ factors which allow for change in angle of attack due to the deflection of the air flow in the neighborhood of each wing.

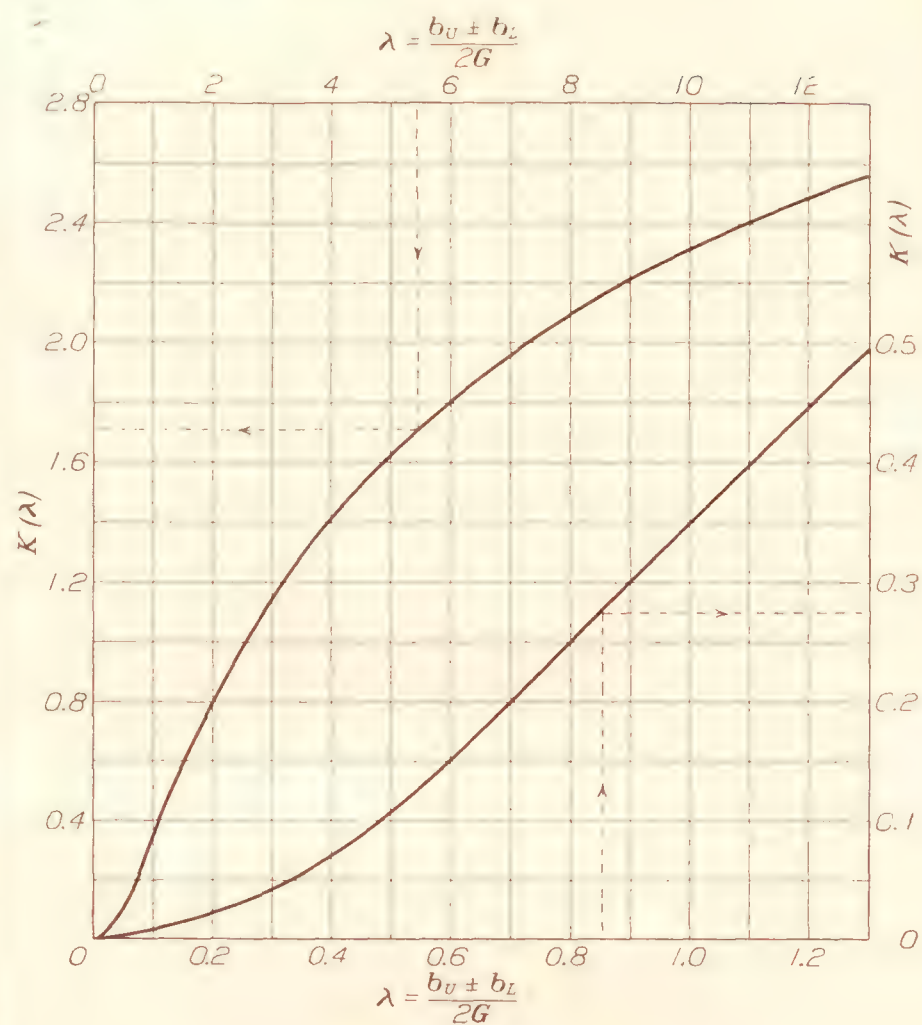


FIGURE 3.

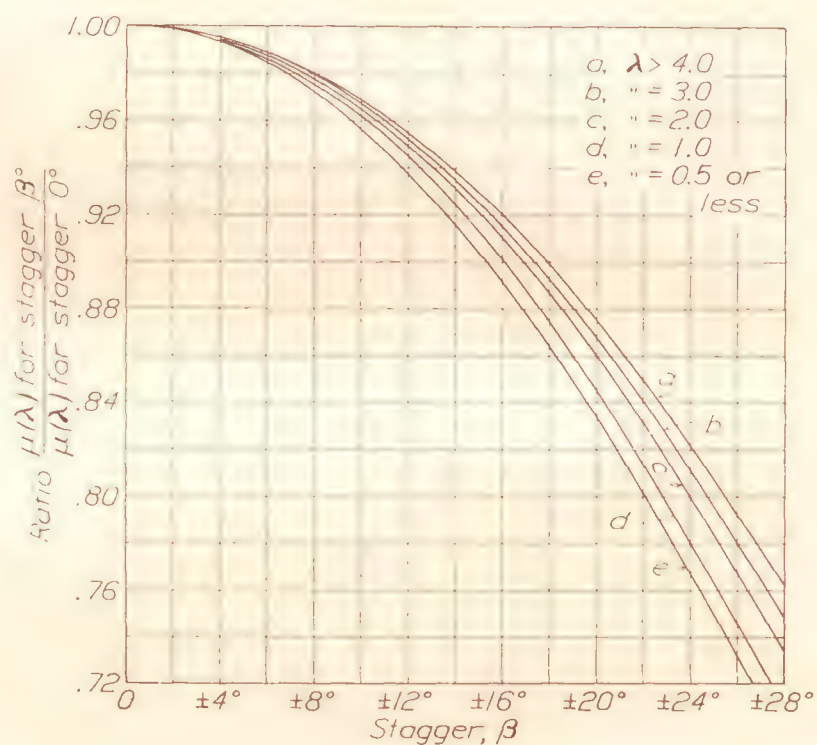
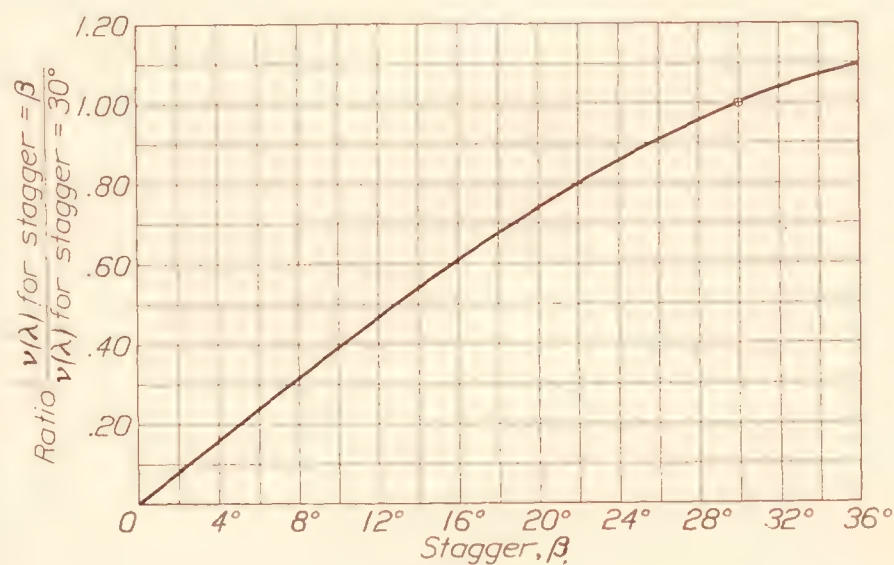
FIGURE 4.— $\lambda = \frac{b_u + b_l}{2G}$.

FIGURE 5.

Equation (1) gives the change in the lift coefficient of the lower wing due to the presence of the upper wing. Equation (2) gives the change in the lift coefficient of the upper wing to the presence of the lower wing. Similar equations for the change in drag coefficients are given in reference 4, as follows:

$$\Delta C_{DL} = -\frac{\mu}{2\pi} \frac{S_U}{b_U b_L} C_{LU} C_{DL} - \frac{\nu + \kappa}{4\pi} \frac{S_U C_{LU}}{b_U b_L} \left[57.3 \frac{dC_{DL}}{d\alpha} - C_{LL} \right] \quad (9)$$

$$\Delta C_{DU} = \frac{\mu}{2\pi} \frac{S_L}{b_U b_L} C_{LU} C_{DU} + \frac{\nu - \kappa}{4\pi} \frac{S_L C_{LU}}{b_U b_L} \left[57.3 \frac{dC_{DU}}{d\alpha} - C_{LU} \right] \quad (10)$$

Munk also finds the additional lift coefficient due to decalage of $\pm \delta$ as:

$$\Delta C_L = \pm 2\pi \frac{S}{2} B_o(1+2d)\delta \quad (12)$$

where $B_o(1+2d)$ is a factor obtained in his integration of the flow components. $B_o(1+2d)$ is given as a function of gap/chord ratio as follows:

G/c	2.02	1.46	1.11	.98	.79	.64	.56	.46	.39
$B_o(1+2d)$	1.03	1.06	1.10	1.12	1.19	1.25	1.30	1.38	1.48

These values are plotted in figure 7.

Millikan's treatment of the biplane theory (reference 7), is along lines very similar to that used in reference 4, but extending the theory. The resulting equations appear to give somewhat better agreement with test data than is obtained with the previous methods, but

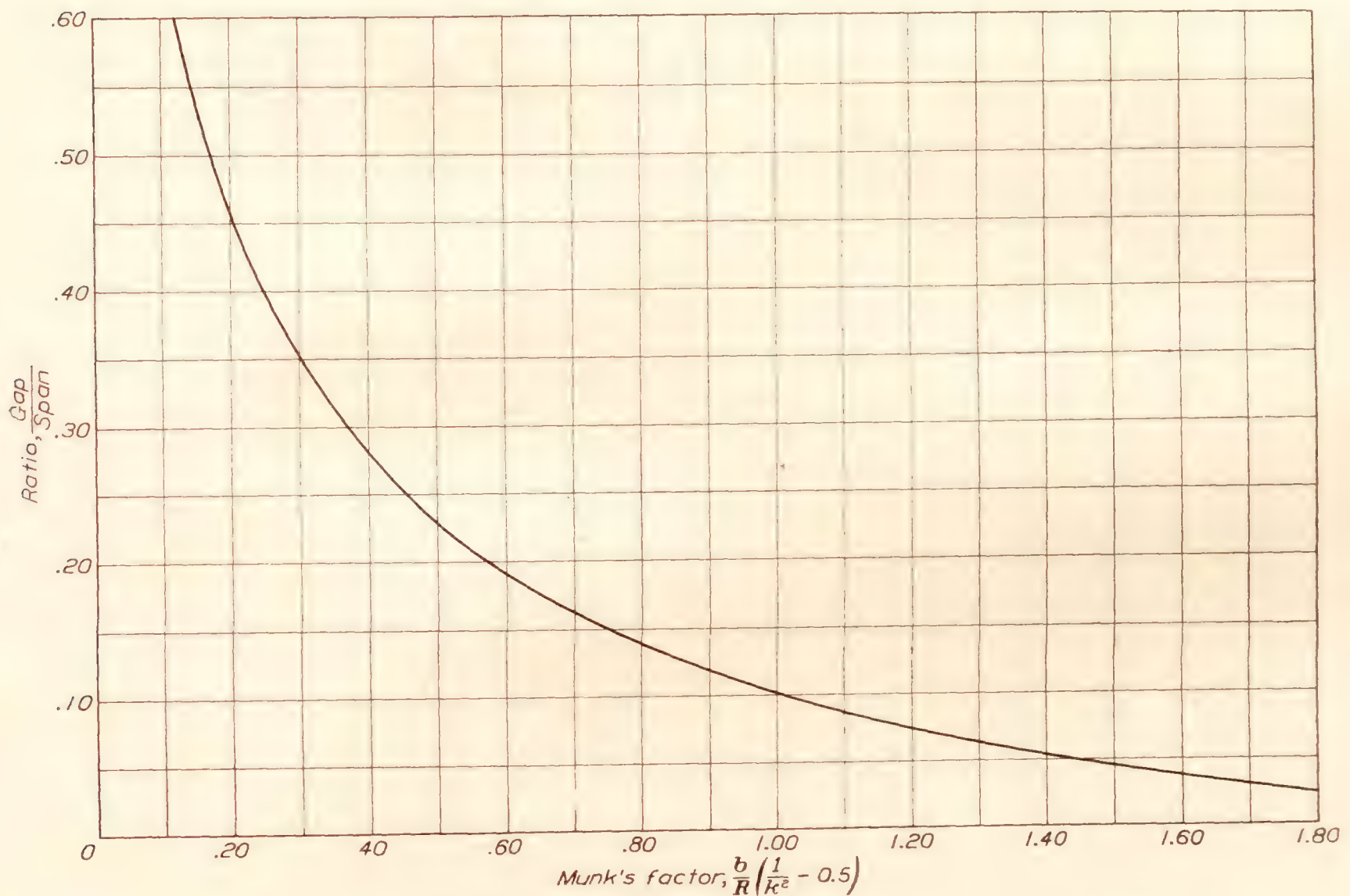


FIGURE 6.

Munk, in reference 5, derives comparatively simple formulas for the biplane. He finds that the additional lift coefficient of staggered wings is

$$\Delta C_L = \pm 2C_L \frac{S}{b^2} \left(\frac{1}{k^2} - 0.5 \right) \frac{b}{R} \frac{s}{c} \frac{c}{b} \quad (11)$$

where S is the total area, s the stagger, b the span, c the chord, k the equivalent monoplane span factor, and R a distance used in calculating the induced

downwash. Munk gives $\frac{b}{R} \left(\frac{1}{k^2} - 0.5 \right)$ as a function of the ratio of gap to span G/b . His tabulated values have been plotted in figure 6.

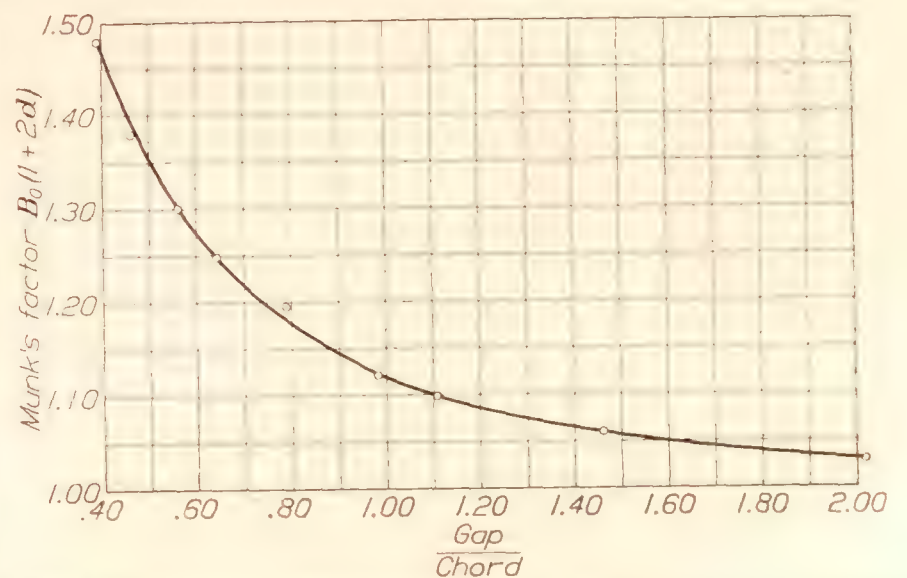


FIGURE 7.—Effect of decalage on lift distribution. Table I, N.A.C.A. T.R. No. 151

it is very difficult for an engineer to follow the steps required in a typical calculation.

It is proposed to show how the foregoing theory may be used with test data in the derivation of working charts for routine use.

I. SIMPLE BIPLANES

It is desirable for the present to consider the simplest form of biplane in which the wings are of same chord and span, and to study the effect of stagger. The effect of unequal chords, decalage, and overhang can be considered later.

Equation (11) is equivalent to a statement that the lift coefficient of the upper wing (or lower wing) differs from that of the biplane by an amount depending directly on the biplane lift coefficient. That is,

$$C_{LU} = C_L \pm \Delta C_L \quad (13)$$

or

$$C_{LL} = C_L \mp \Delta C_L \quad (13a)$$

ΔC_L varying with stagger and gap/span ratio as indicated by equation (11) and figure 6.

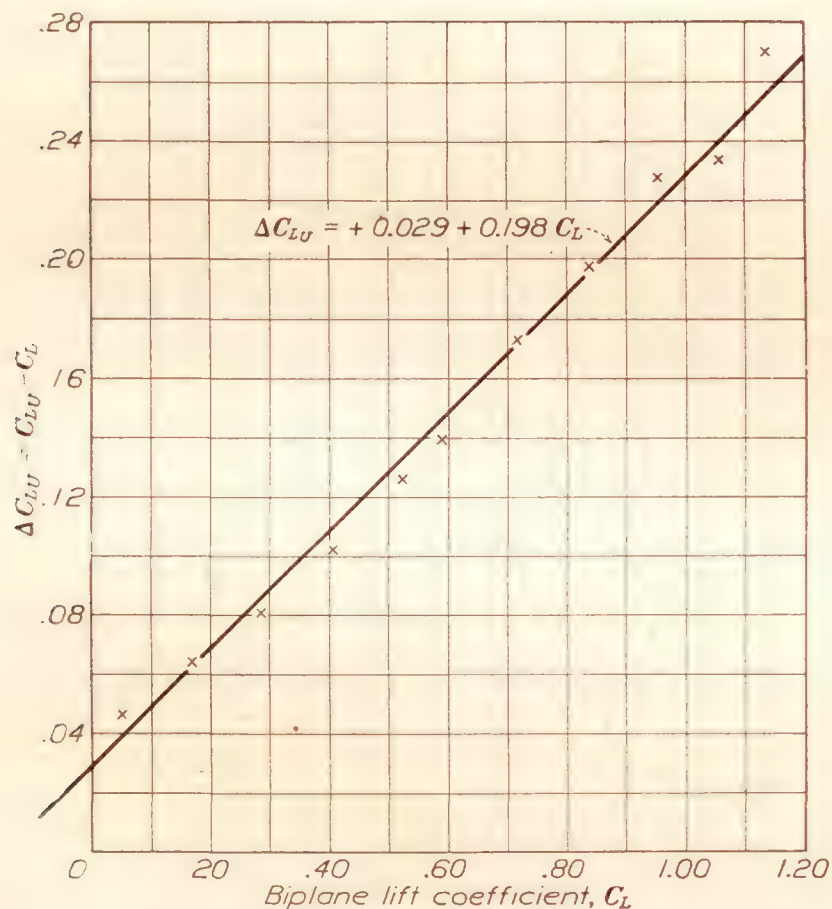


FIGURE 8.—U.S.A. TS-5 biplane $\frac{\text{gap}}{\text{chord}} = 0.9$. Stagger 30° . Effective stagger = 0.64 c. Data from N.A.C.A. T.R. No. 256.

In order to verify the relation of equation (13), data from a number of biplane tests have been analyzed by the method illustrated in table I. The values of ΔC_{LU} so obtained have been plotted against the biplane lift coefficient as in figure 8. In all cases the values of ΔC_{LU} have shown a linear relation with C_L . The test data and calculations are too extensive for inclusion in this report but the equations of the lines are given in tables II to V inclusive. An inspection of these equations shows several outstanding facts, the most important of which is that the value of ΔC_{LU} has the general form

$$\Delta C_{LU} = K_1 + K_2 C_L \quad (14)$$

K_1 and K_2 being functions of gap/chord, stagger, decalage, overhang and wing thickness. The observed variation of K_2 with these factors is in surprisingly good agreement with the wing theory and in particular with the values given by Munk's equations, as will be shown later. The presence of the constant K_1 for biplanes *without* decalage is not indicated by existing theory but these data have been shown to Dr. Munk, who suggests that K_1 is due to the Venturi effect between the wings. In the case of the orthogonal biplane a simple integration of the flow between the wings on this basis gives a reduction in pressure of the order required by the average value of K_1 .

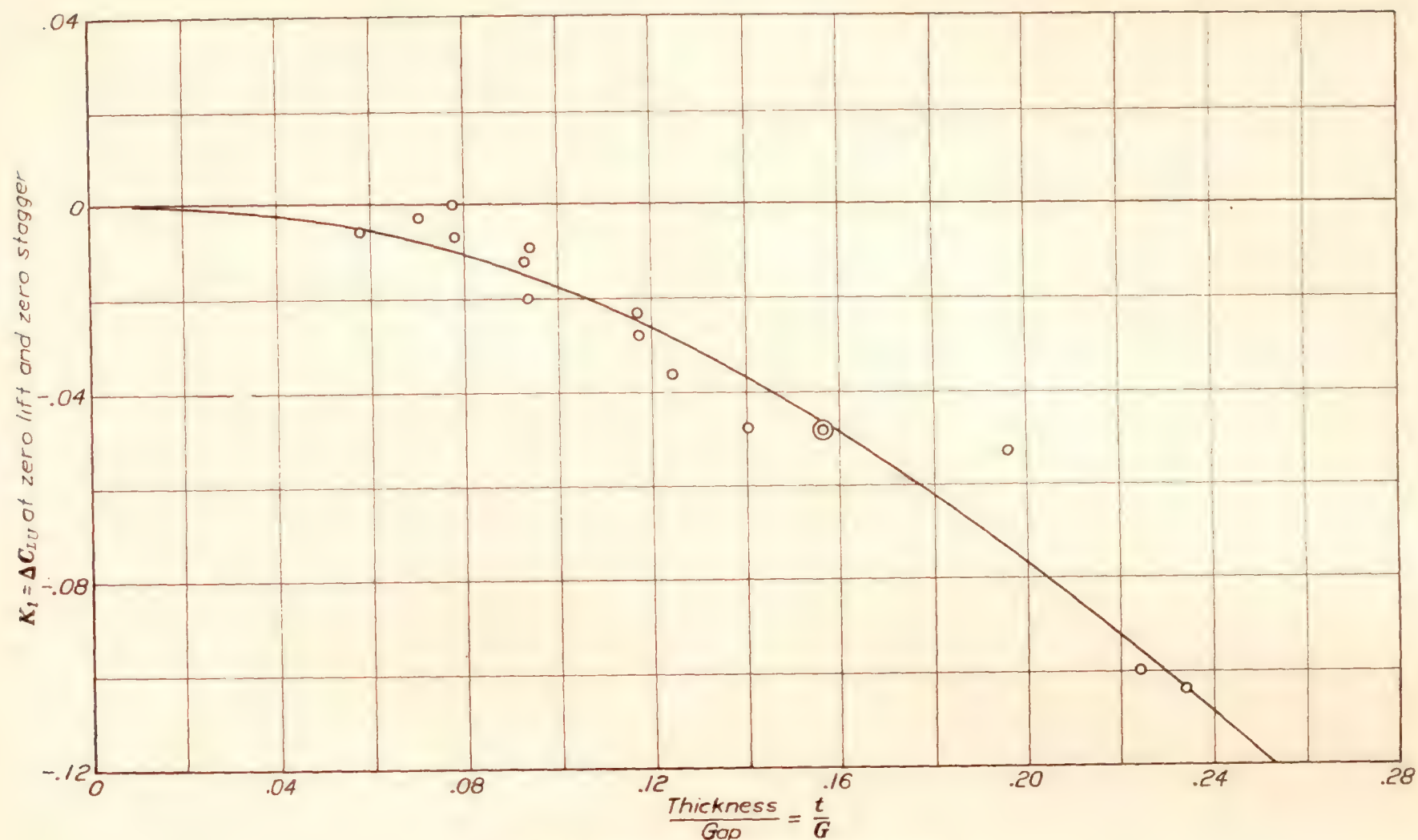
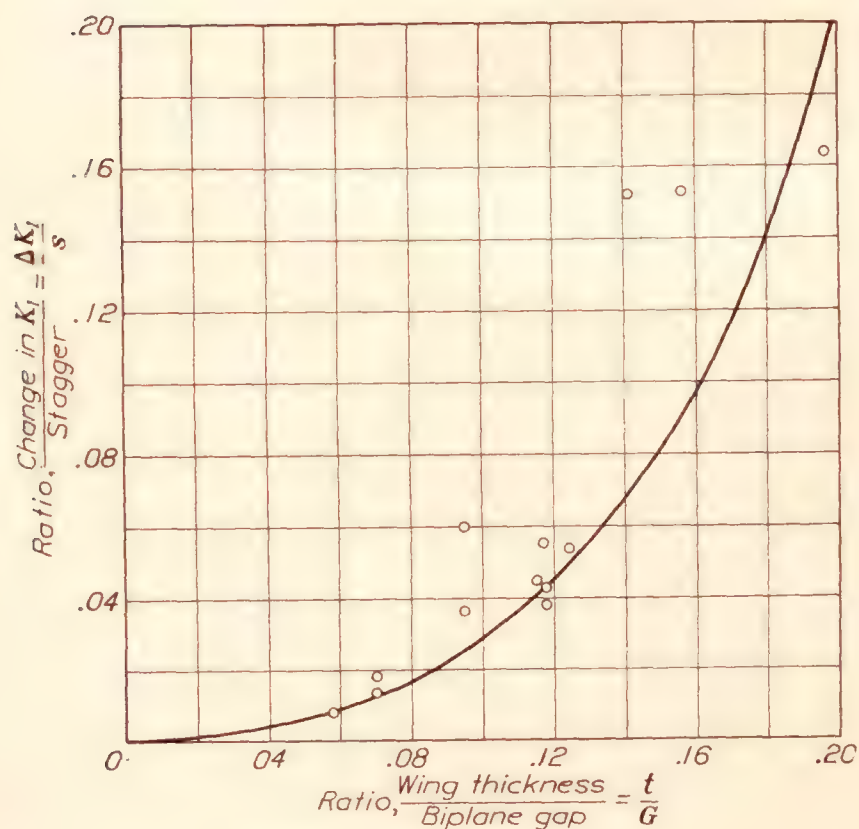
Assuming that K_1 is due to the Venturi effect it should vary with the restriction, or the ratio of wing thickness to gap t/G , and with stagger. Table VI contains the results of an analysis on this basis of test data in which the stagger was varied with gap/chord constant. The fifth column of this table is the value of K_1 for zero stagger and the sixth column is the slope of K_1 when plotted against stagger. The values of K_1 for zero stagger are plotted in figure 9 and a probable curve is drawn through the points which are fairly consistent. Values of $\Delta K_1/\Delta s$ from column 6 of table VI are plotted on figure 10. As might be expected, the scattering of the points is greater here than in figure 9 since the difficulty of eliminating decalage is greater when stagger is present. It should be noted that the values of K_1 are quite small and correspond to an angular change of less than one half a degree, so that the usual error in measuring the alignment may become a relatively large item. The value of K_1 is greatly affected by decalage, as will be shown later. It would be highly desirable to determine the curve of figure 10 accurately by special wind-tunnel tests.

EFFECT OF GAP/CHORD ON THE COEFFICIENT K_2

Munk's relation, equation (11), indicates that K_2 varies with the ratios of gap/span and stagger/chord. Although the ratio of gap/span offers some advantages with no difficulties, the ratio of gap/chord is easier to visualize and the latter will, therefore, be used to study the effect of stagger. Table VII contains calculations for a set of typical curves showing the variation of K_2 with gap/chord. These curves are plotted as solid lines on figure 11. They are obtained

by taking the values of $\frac{b}{R} \left(\frac{1}{k^2} - 0.5 \right)$ relative to the value

for gap/chord = 1.00 and assuming values of K_2 for this condition. Observed values of K_2 for varying gap/chord with constant stagger, from tables II to V, are connected by broken lines in each series in the plotting on figure 11. The observed variation of K_2 with gap/chord is seen to be in excellent agreement with Munk's theoretical analysis. A set of correction curves may now be prepared from figure 6 and table VII for use in reducing observed values of K_2 to

FIGURE 9.—Effect of wing thickness and gap on K_1 .FIGURE 10.—Effect of stagger on K_1 .

gap/chord = 1.00 and thereby separating the effect of gap/chord and stagger. The calculations are given in table VIII. For each assumed ratio of span to chord, the values of gap/span are calculated from the first column values of gap/chord. The factor $F = \frac{b}{R} \left(\frac{1}{k} - 0.5 \right)$ is then read from figure 6. These values are then taken relative to the value for $b = 6c$ and gap/chord = 1.00, for which $F_0 = 0.675$ from figure 6. The ratios are then multiplied by $\frac{36}{\left(\frac{b}{c} \right)^2}$ as required by

equation (11). The resulting values which are plotted on figure 12, show the relative variation of K_2 with gap/chord.

EFFECT OF STAGGER ON THE COEFFICIENT K_2

Stagger may be given in terms of its ratio to either gap or chord, or in degrees. It should be measured from the line connecting the forward third points on the chords and in a fore and aft vertical plane. The true stagger varies with angle of attack but that given in the tabulation of data is usually measured from the zero angle of attack. In plotting up test data on widely different sections it was found that very much better agreement was obtained by using the stagger measured at the zero lift attitude. This may be called the "effective stagger." The effective stagger will therefore be used.

Observed values of K_2 from the tests with varying stagger listed in tables II to V have been collected in table IX and corrected to gap/chord = 1.00 by use of the curves of figure 12. The corrected values have been plotted on figure 13. With the exception of points at negative stagger and for low gap/chord ratios, the value of K_2 for gap/chord = 1.00 is given satisfactorily by the linear relation

$$K_2 = 0.050 + 0.17 \frac{s}{c} \quad (15)$$

where s/c is the basic stagger measured at zero lift. The deviations of the points from this line are due partially to experimental errors and partially to the difficulty in determining the direction of the lines from which K_2 is read on the original plots of ΔC_{L_U}

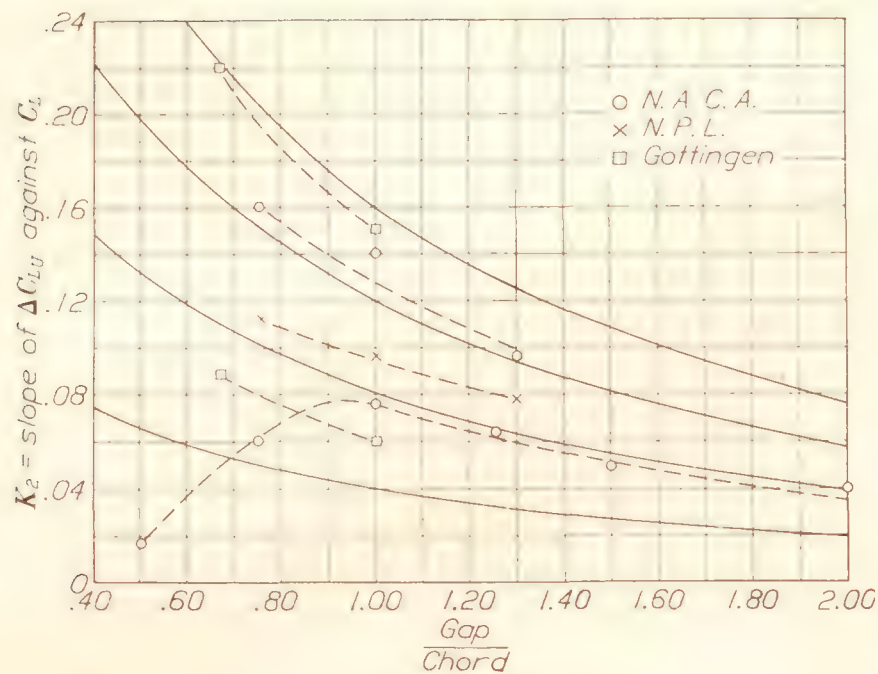


FIGURE 11.—Variation of K_2 with $\frac{\text{gap}}{\text{chord}}$ for constant stagger.

second case, the agreement is exact from 0.75 to 1.50, but the results for gap/chord ratio 0.5 deviate from the general curve. The theory can therefore be regarded as quite satisfactory in all practical applications. The deviation at the smallest gap implies that the theory must be examined more accurately in this case. In developing the theory it has been assumed that one wing may be treated as a lifting line as regards its influence on the other wing, and this assumption probably breaks down when the gap becomes as small as one half of the chord." Glauert also states in reference 6, "It will be noticed that the calculated values are in good agreement with the observed values for positive angles of stagger, but that there is a definite discrepancy in the case of negative stagger, for which no explanation has been found as yet."

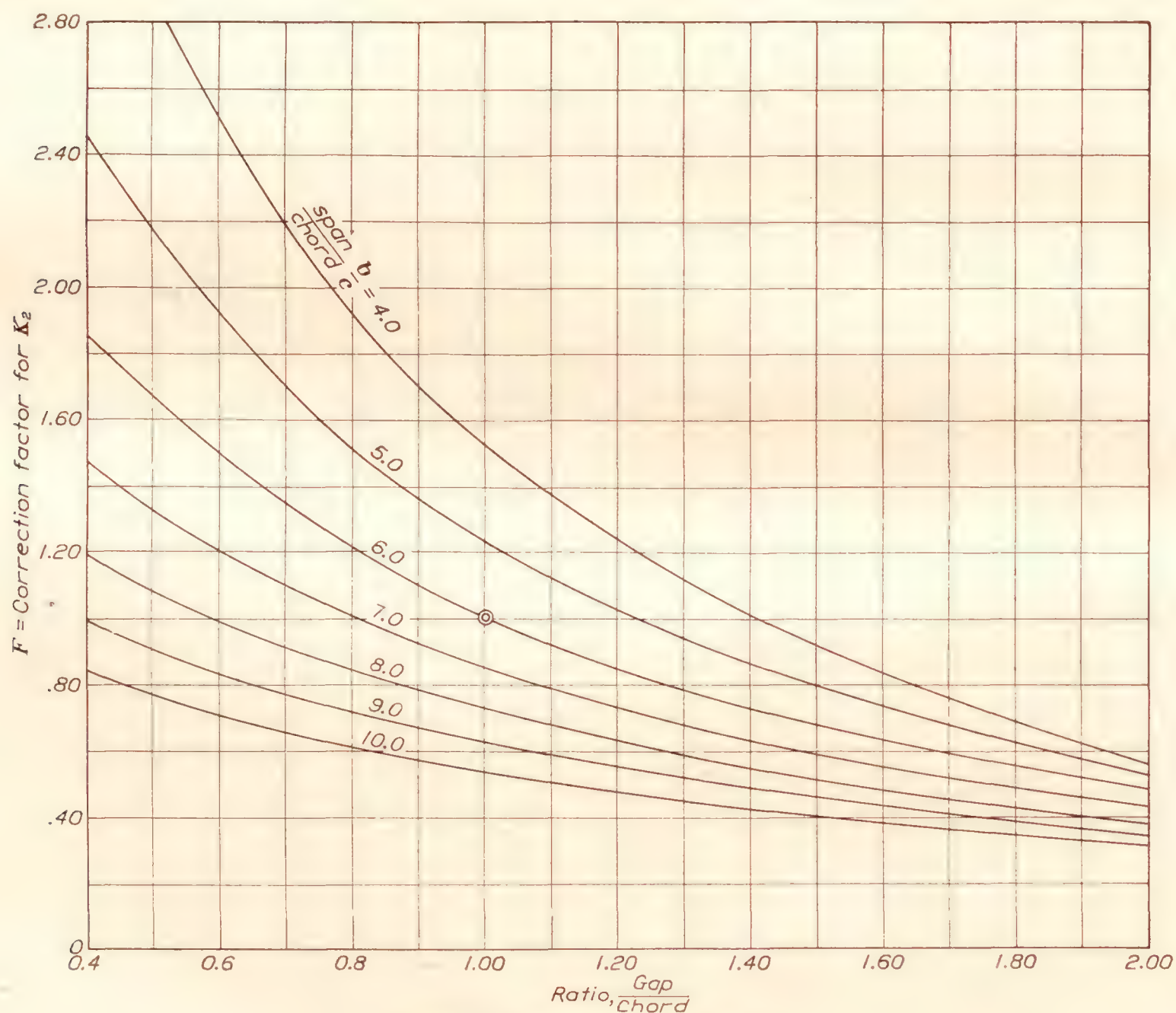


FIGURE 12.—Variation of K_2 with gap/chord.

against C_L , of which figure 8 has been given as an example. This uncertainty is, in general, of the order of 0.01 in the value of K_2 . With this in mind the agreement is quite satisfactory.

In connection with the scattering of the points for low ratios of gap/chord, Glauert states in reference 6, "In the first case, exact agreement is obtained for gap/chord ratios ranging from 0.67 to 2.33. In the

It is fortunate that the interest in low gap/chord values and negative stagger is academic at present. There is some question, however, as to whether a biplane with small stagger at positive lifts acts like a biplane with negative stagger at negative lifts. No biplane tests covering the negative range are available to decide this point. Most of the available data, condensed in tables II to V, are not carried very far below

zero lift. Those that do extend to, say, $C_L = -0.30$ show no change in the value of K_2 . Figure 13 indicates that there should be no change for small negative staggers, but this point cannot be determined without a revision of the theory and special tests.

II. BIPLANES WITH DECALAGE

Decalage has been defined as the acute angle between the wing chords of a biplane. This is equivalent to the

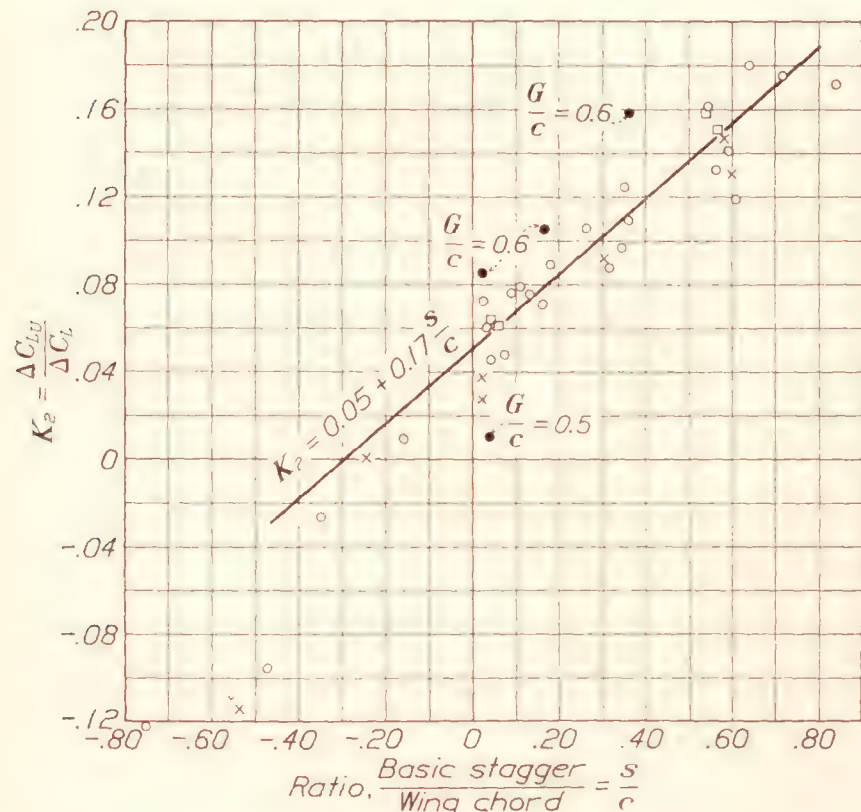


FIGURE 13.—Variation of K_2 with stagger for $\frac{\text{gap}}{\text{chord}} = 1.00$. Based on the effective stagger at zero lift.

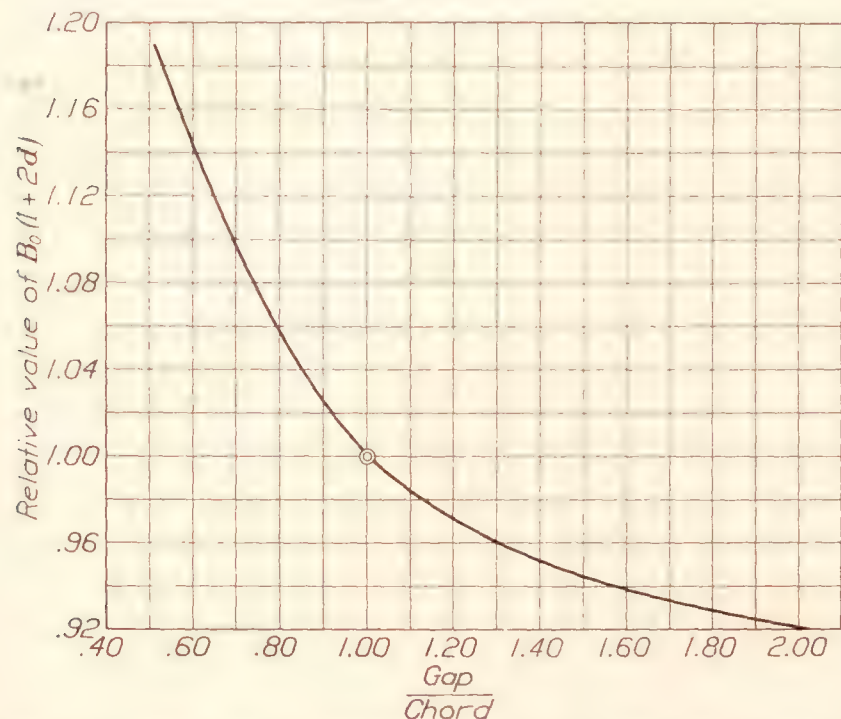


FIGURE 14.—Relative value of Munk's factor $B_0(1+2d)$. From table I, N.A.C.A. No. 151.

difference between the angles of incidence of the upper and lower wings. There is some confusion regarding the sign of the decalage, but the weight of authority and usage favors the definition of positive decalage for the lower wing at a positive angle with respect to the upper wing so that the chord lines of the upper and lower wings intersect forward of the leading edge.

The great influence of decalage on lift distribution and stability has not been fully appreciated by air-

plane designers. The definitions have been based on geometrical angles, which may be misleading. For the purpose of this study it is necessary to use aerodynamic decalage measured from the zero lift directions in the upper and lower wing, and not from the chord lines. The decalage will be considered positive when the zero lift direction lines intersect forward of the leading edge. The zero lift direction for each wing is further defined as the direction of the relative wind for zero lift on that wing.

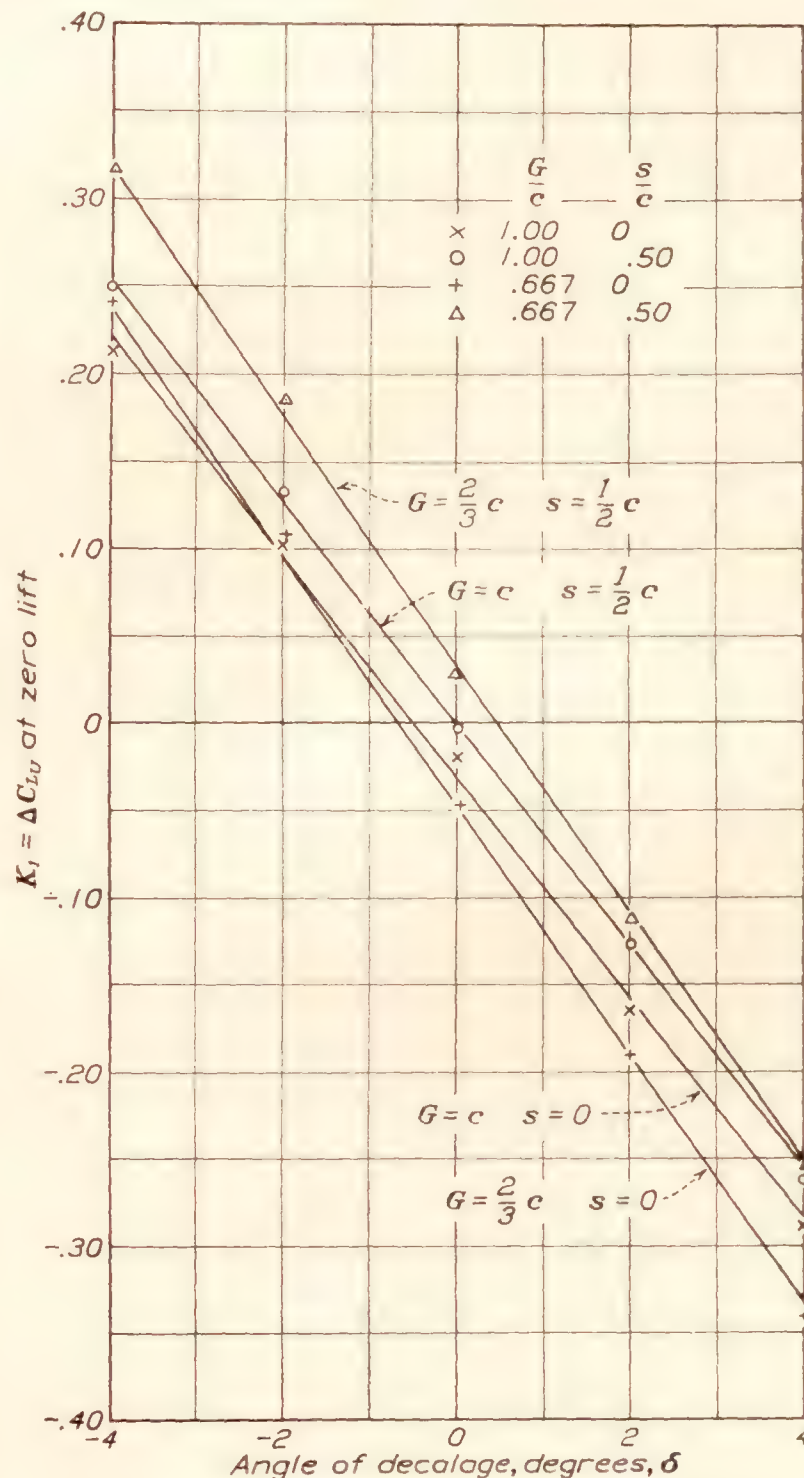


FIGURE 15.—Effect of decalage on K_1 . From Munk's tests (reference 8).

According to Munk, equation (12), the effect of decalage is to change the lift coefficients of the individual wings by an equal and opposite increment which is a function of the gap/chord ratio and directly proportional to the decalage angle. That is, the chief effect of decalage is to change the value of K_1 in equation (14).

The factor $B_0(1+2d)$ in equation (12) has been given in figure 7. This may be replotted to give values of $B_0(1+2d)$ relative to the value for gap/chord = 1.00, as in figure 14. This form is convenient for comparing the theoretical and the observed variation in K_1 .

Figure 15 is a plot of the values of K_1 against decalage from Munk's tests abstracted in table V. Data from Mock's tests (reference 14) are plotted on figure 16. In figure 15 the slope of the lines are as follows:

Gap Chord	Stagger	$\frac{\Delta K_1}{\Delta \delta}$
1.00	0	-.0635
1.00	.50	-.0635
.67	0	-.071
.67	.50	-.071

Mock's tests (fig. 16) give $\frac{\Delta K_1}{\Delta \delta} = -.063$ for gap/chord = 1.00. Munk's test data show that stagger does not affect the value of $\frac{\Delta K_1}{\Delta \delta}$.

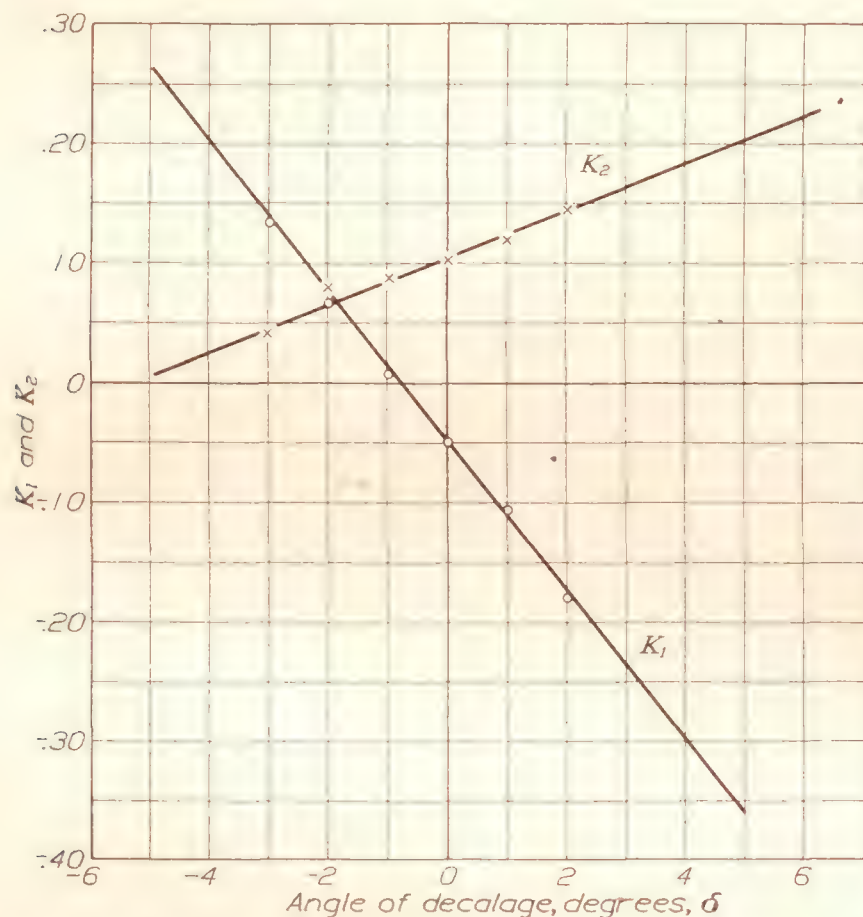


FIGURE 16.—Effect of decalage on K_1 and K_2 . From Mock's tests (reference 14).

Figure 17 shows a curve similar to figure 14 derived by assuming $\frac{\Delta K_1}{\Delta \delta} = -.063$ at gap/chord = 1.00. Munk's points obviously lie on a similar curve passing through $\frac{\Delta K_1}{\Delta \delta} = -.0635$ at gap/chord = 1.00. The observed effect of decalage appears to follow very closely the theoretical effect predicted by Munk's equation.

The effect of decalage on K_2 is not covered by the theory but it is too great to be neglected. Values of K_2 for various decalage angles, as obtained from Mock's tests in reference 14, have been given on figure 16. A similar plot from Munk's data in table V is given on figure 18. The effect appears independent of gap/chord

and stagger and is linear with decalage, the uniform slopes giving

$$\frac{\Delta K_2}{\Delta \delta} = 0.0186 \quad (16)$$

Decalage therefore affects both K_1 and K_2 in equation (14), the effect on K_1 being given by figure 17 and the effect on K_2 by equation (16).

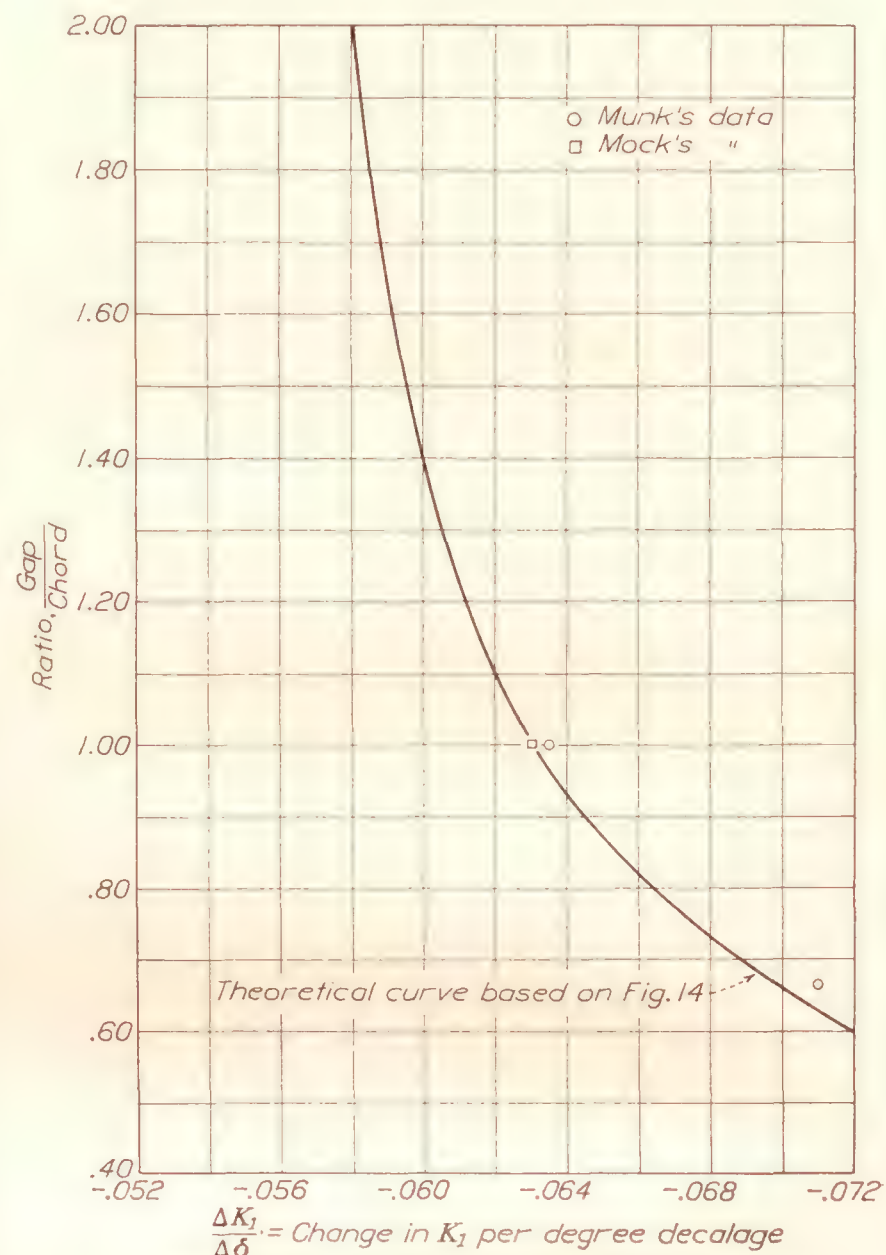


FIGURE 17.—Effect of decalage and gap/chord on K_1 .

III. BIPLANES WITH OVERHANG

Overhang is defined as the ratio of the difference in wing spans to the span of the upper wing and is positive when the upper span is the greater. Overhang is usually given in percent of the upper wing span, or

$$\text{Overhang percent} = 100 \frac{b_U - b_L}{b_U}$$

where b_U and b_L are the spans of the upper and lower wings, respectively.

Limited tests on the effect of overhang are given in reference 13. These data are abstracted in table X and plotted on figure 19. The effect is surprisingly large. Calculations have been made by equations (1)

and (2) in order to check this point. These calculations are too long to be given in full, but the following results were obtained:

Overhang percent	K_1	K_2
-20	-0.025	+0.092
0	-0.017	+0.101
+20	-0.017	+0.100
+40	-0.014	+0.081
50	-0.012	+0.074
67	-0.007	+0.054

These are compared with the observed values of K_1 and K_2 on figure 20. The agreement is not entirely

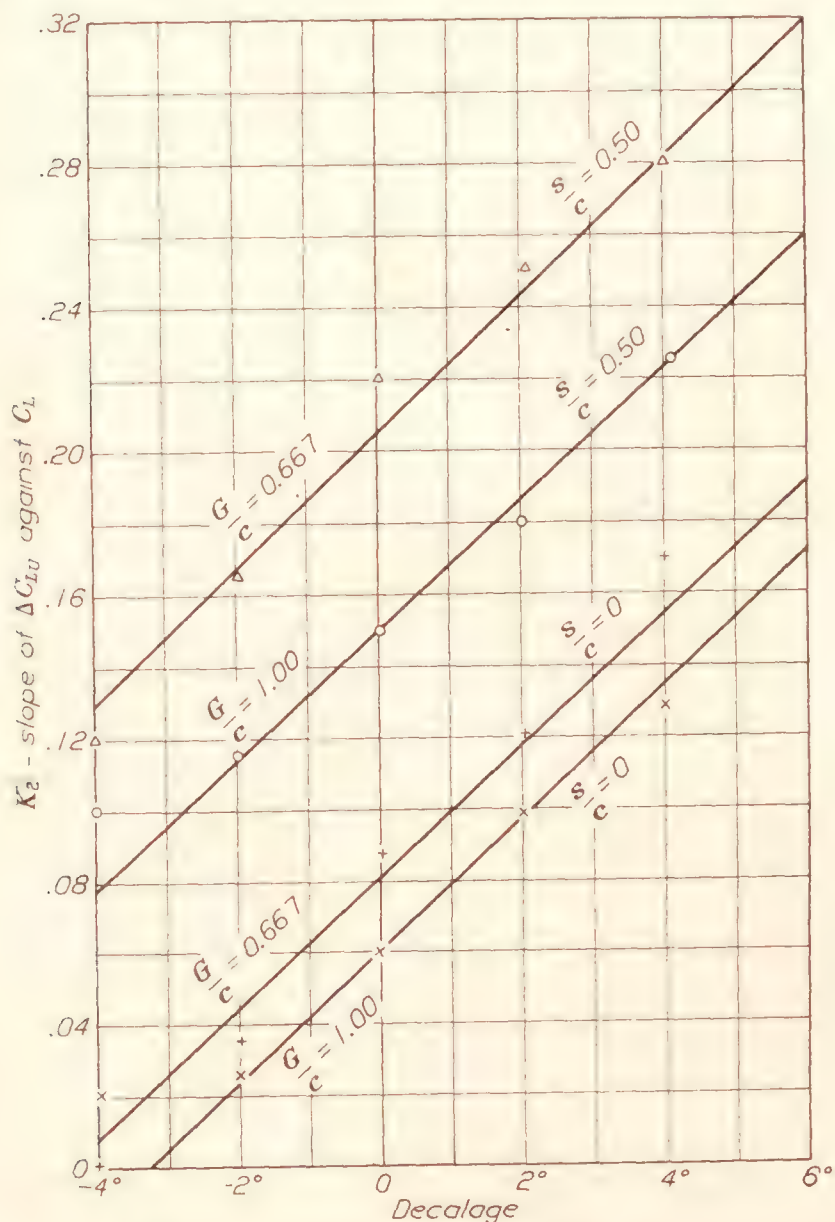


FIGURE 18.—Effect of decalage on K_2 . From Munk's tests (reference 8).

satisfactory, although there is less difference than appears from a casual inspection of the curves. In the first place, the existence of the term K_1 is not predicted directly by the theory, equations (1) and (2) or (11). The values of K_1 given above have been obtained by extrapolating the lift curves through zero lift. Consequently, the fact that the values of K_1 so found are of the order obtained by wind-tunnel test is about all that can be expected. On the other hand, K_2 can be determined with better accuracy than K_1 , so that the difference between theory and experiment is here of more importance. It appears highly desirable that special tests be made on biplanes with overhang to investigate these differences. In the

meanwhile, the values of K_1 and K_2 for biplanes with overhang are probably best obtained from a contour plotting as in figure 21, which is based on the experimental values in table X. In using this plot the values

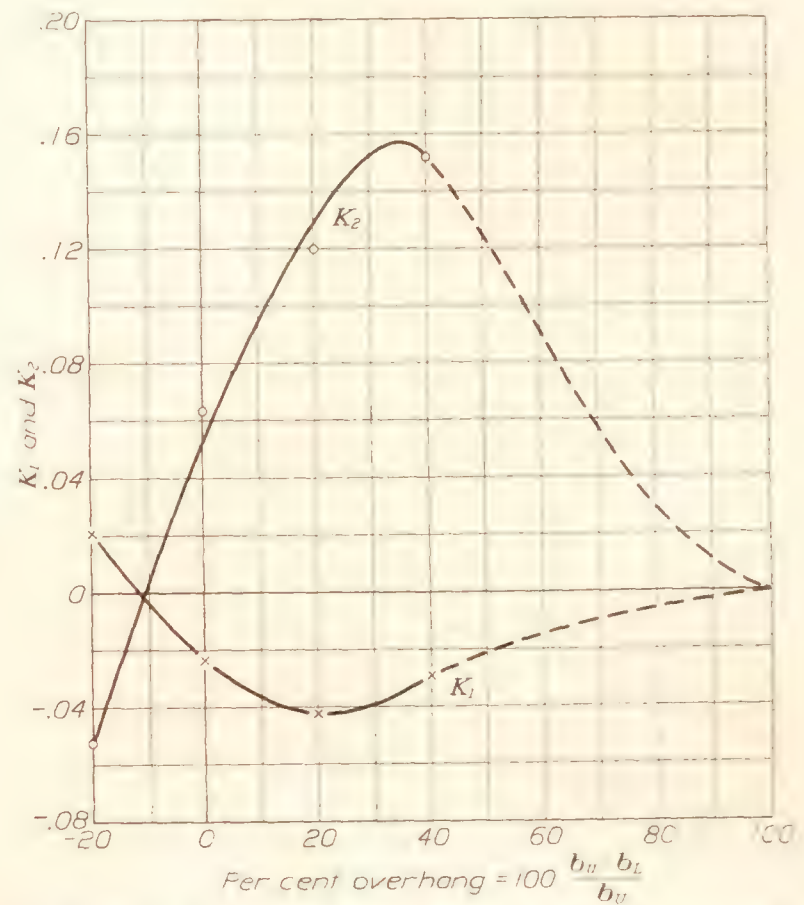


FIGURE 19.—Effect of overhang on K_1 and K_2 . From data in reference 13. (See table X.)

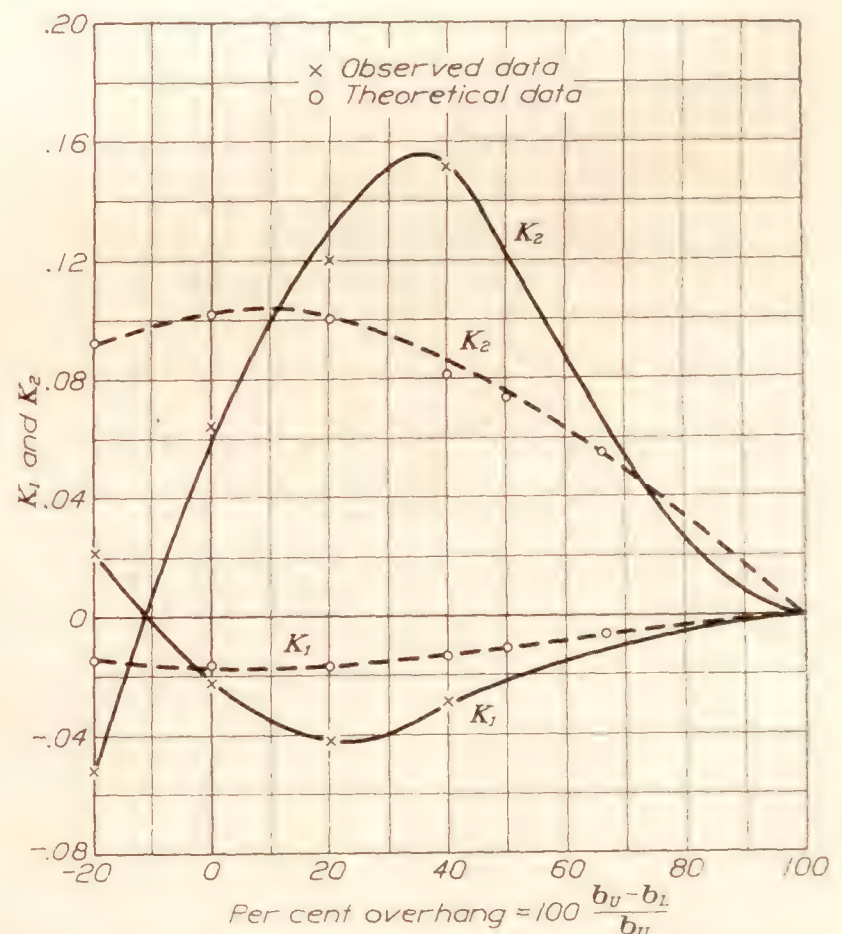


TABLE 20.—Effect of overhang on K_1 and K_2 as found by observation and by calculation from theoretical curves.

of K_1 and K_2 are determined first for a biplane without overhang but with the same stagger, gap and decalage as for the biplane in question. Spotting these points at zero overhang on figure 21, the corresponding point at the desired overhang will lie on curve similar to those given.

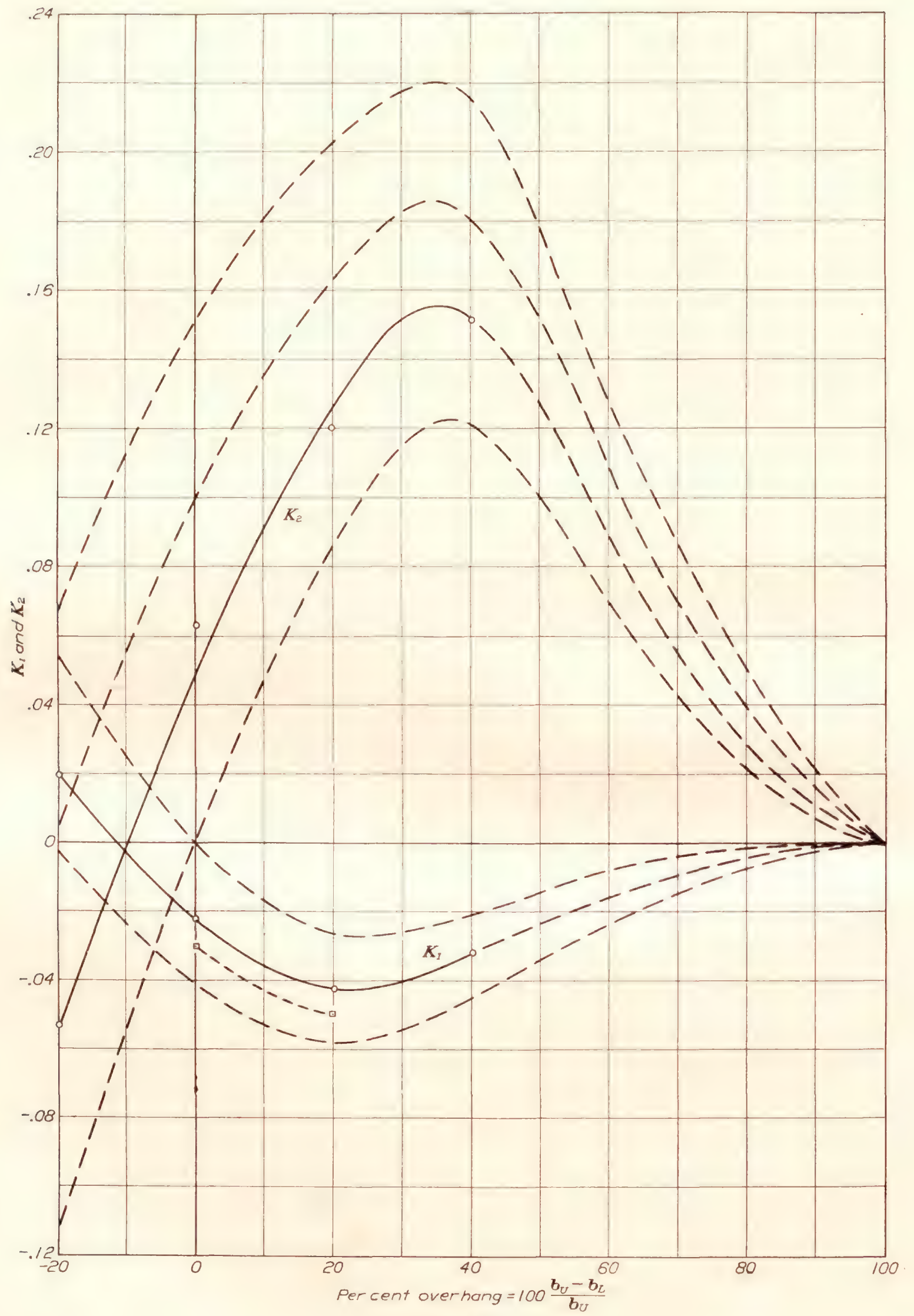


FIGURE 21.

PRACTICAL APPLICATION

The relative lift of the wings of any biplane may now be calculated from

$$C_{LU} = C_L \pm \Delta C_{LU} \quad (17)$$

$$C_{LL} = C_L \mp \Delta C_{LL} \quad (17a)$$

where C_L , C_{LU} , and C_{LL} are the lift coefficients for the biplane, the upper wing, and the lower wing, respectively.

It has been shown that

$$\Delta C_{LU} = K_1 + K_2 C_L \quad (14)$$

where K_1 and K_2 are functions of gap/chord, stagger, decalage, overhang, and wing thickness. K_1 is numerically the lift coefficient on the upper wing when the biplane lift is zero, while K_2 determines the slope of the lift curve of the upper wing relative to that of the biplane. When the upper and lower wings are of equal area, the increments ΔC_{LU} and ΔC_{LL} are equal and of opposite sign. When the areas are unequal the increments are inversely proportional to the relative areas and of opposite sign. In any case:

$$\Delta C_{LL} = -\Delta C_{LU} \frac{S_U}{S_L} \quad (18)$$

where S_U and S_L are the areas of the upper and lower wings. It should be noted that ΔC_{LL} is usually negative in equation (17a).

A convenient procedure for calculating ΔC_{LU} is as follows:

1. Tabulate the average values of the ratios;

$$\frac{\text{maximum wing thickness}}{\text{chord}} = \frac{t}{c}$$

$$\frac{\text{gap}}{\text{chord}} = \frac{G}{c}$$

$$\frac{\text{stagger}}{\text{chord}} = \frac{s}{c}$$

Use the average gap and average stagger with an average chord defined by

$$c = \frac{1}{2} \left[\frac{S_U C_U + S_L C_L}{S_U + S_L} \right] \text{ where } C_U \text{ and } C_L \text{ are the chords of the upper and lower wings.}$$

With tapered wings the weighted average chord of each wing should be used.

The effective stagger measured at zero lift from the third chord points must be used.

2. Calculate the ratio

$$\frac{\text{maximum wing thickness}}{\text{gap}} = \frac{t}{G} = \frac{t}{c} \div \frac{G}{c}$$

3. Calculate the overhang if present by

$$\text{overhang} = 100 \left[\frac{b_U - b_L}{b_U} \right]$$

where b_U and b_L are the actual spans of the upper and lower wings without reduction for fuselage or nacelle blanketing.

4. Calculate K_1 from $K_1 = K_{10} + K_{11} + K_{12} + K_{13}$ (19)

Where K_{10} is the value of K_1 for the equal wing orthogonal arrangement without decalage or overhang

as read from figure 9, K_{11} is the change in K_1 due to stagger, K_{12} is the change in K_1 due to decalage and K_{13} is the change in K_1 due to overhang. The actual value of K_{13} is not determined directly since it is easier to pass from the value of K_1 with no overhang to the value of K_1 with overhang as will be explained later. The values of K_{10} , K_{11} , and K_{12} are determined as follows:

K_{10} : This is plotted as a function of t/G in figure 9;

K_{11} : This is obtained from figure 10 where $\Delta K_1/s$ is plotted against t/G and

$$K_{11} = \frac{\Delta K_1}{s} s \quad (20)$$

K_{11} is negative with negative stagger.

K_{12} : The effect of decalage is to change K_1 in a linear relation:

$$K_{12} = \left(\frac{\Delta K_1}{\delta} \right) \delta^\circ \quad (21)$$

$\left(\frac{\Delta K_1}{\delta} \right)$ varies with gap/chord as shown on figure 17. It has an average value of about -0.063 , so that negative decalage, where the incidence of the lower wing is less than the incidence of the upper wing, gives a positive K_{12} which increases K_1 .

K_{13} : The actual value of K_{13} need not be obtained, since it is more convenient to correct for overhang by the use of figure 21, and pass directly from the value of K_1 with no overhang to the value of K_1 with overhang. The value of K_1 with no overhang is the sum of $K_{10} + K_{11} + K_{12}$. This value may be spotted at zero overhang on the lower set of curves on figure 21. A curve similar to those given and passing through this point gives the value of K_1 at any other overhang as desired. It is unnecessary to draw the curve since the interpolation may be made visually with sufficient accuracy. For example, assume that without overhang $K_1 = K_{10} + K_{11} + K_{12} = -0.030$, then for $+20$ percent overhang $K_1 = -0.050$ as indicated on the lightly dotted curve.

5. Calculate K_2 from

$$K_2 = (K_{20}) F + K_{21} + K_{22} \quad (22)$$

Where K_{20} is the value of K_2 for the desired stagger at gap/chord = 1.00, F is a correction factor for gap/chord and aspect ratio, K_{21} is the change in K_2 due to decalage and K_{22} is the change in K_2 due to overhang. The values of these factors are determined as follows:

K_{20} : The effect of stagger, is either read from figure 13 or obtained from the equation

$$K_{20} = 0.050 + 0.17 \frac{S}{c} \quad (15a)$$

F , the effect of gap/chord and aspect ratio

on K_2 , is obtained from figure 12. In using this figure, the average aspect ratio of the two wings must be used, and not the effective aspect ratio of the combination.

K_{21} : The effect of decalage is obtained from equation (16) in the form

$$K_{21} = +0.0186\delta^0 \quad (16a)$$

where δ is the angle of decalage in degrees with its positive or negative sign. Positive decalage increases K_2 , negative decalage decreases K_2 .

K_{22} : The effect of overhang. This is obtained indirectly by the same procedure used for K_{13} . The value of K_2 without overhang is $K_2 = (K_{20}) F + K_{21}$. This value is spotted at zero overhang on figure 21 and a line traced through it following the trend of the upper set of curves. This line gives the corrected value of K_2 at the desired overhang.

The relative unit lift or efficiency of the upper and lower wings of a biplane is defined by the ratio

$$e = \frac{C_{LU}}{C_{LL}} = \frac{C_L \pm \Delta C_{LU}}{C_L \pm \Delta C_{LL}} \quad (23)$$

which is now readily calculated. Obviously, e will vary over wide limits and in general it will become infinite at or near zero lift for the cellule. Any method that works directly with the ratio e must become unmanageable in the region of zero lift. The method here developed gives definite lift coefficients for any condition.

For the normal biplane, upper and lower wing of equal areas, with moderate stagger but without decalage, the values of K_1 and K_2 in equation (14) may be of the order of -0.020 and $+0.120$, respectively. That is,

$$\Delta C_{LU} = -0.020 + 0.120 C_L$$

$$\text{and } \Delta C_{LL} = -\Delta C_{LU} = +0.020 - 0.120 C_L$$

so that equations (17) and (17a) would be

$$C_{LU} = 1.12 C_L - 0.020$$

$$\text{and } C_{LL} = 0.88 C_L + 0.020$$

$$\text{When } C_L = 0 \text{ for this biplane } C_{LU} = -0.020,$$

$$\text{and } C_{LL} = +0.020 \text{ giving } e = -1.00.$$

$$\text{If } C_L = +0.01785, C_{LU} = 0 \text{ and } C_{LL} = +0.0357$$

giving $e = 0$. If $C_L = -0.0228$, $C_{LU} = -0.0456$ and $C_{LL} = 0$ giving $e = -\infty$. At negative values of C_L below -0.0228 , e will again be positive. Since the vertical location of the aerodynamic mean chord depends on the value of e , it is obvious that the vertical location of the mean chord is a function of the lift coefficient. It therefore follows that biplane arrangements having positive or very small negative values of K_1 tend to give a high location for the mean chord at low lift coefficients, which tends to improve the static

longitudinal stability. This is one method of explaining the improvement in longitudinal stability due to negative decalage.

The steps involved in the calculation of C_{LU} and C_{LL} may perhaps be clarified by a numerical example. Assume a biplane with the following characteristics:

Upper wing: span $b_U = 40$ feet, chord = 6 feet, area $S_U = 230$ square feet.

Lower wing: span $b_L = 36$ feet, chord = 5 feet, area $S_L = 170$ square feet.

Mean gap: $G = 70$ inches.

Chord (weighted average) $c = 67$ inches.

Stagger measured on leading edge at zero lift = 34 inches.

Stagger measured on the $\frac{1}{3}$ chord points at zero lift $s = 30$ inches.

No decalage $\delta = 0^\circ$.

Wing section Clark Y.

Then

$$\frac{t}{c} = 0.117 \text{ for Clark Y}$$

$$\frac{\text{gap}}{\text{chord}} = \frac{G}{c} = \frac{70}{67} = 1.045$$

$$\frac{\text{wing thickness}}{\text{gap}} = \frac{t}{G} = \frac{0.117}{1.045} = 0.112$$

$$\frac{\text{stagger}}{\text{chord}} = \frac{s}{c} = \frac{30}{68} = 0.44$$

$$\text{overhang} = 100 \frac{b_U - b_L}{b_U} = +10 \text{ percent}$$

K_1 is now found as follows:

From figure 9, $K_{10} = -0.023$.

From figure 10, $\frac{\Delta K_1}{S} = 0.038$, hence,

$$K_{11} = 0.038 \times 0.44 = +0.017$$

$$K_{12} = 0 \text{ since } \delta = 0^\circ$$

$$\therefore K_{10} + K_{11} + K_{12} = -0.023 + 0.017 = -0.006$$

From figure 21, a value of $K_1 = -0.006$ for zero overhang gives $K_1 = -0.022$ for 10 percent overhang.

Hence $K_1 = -0.022$.

K_2 is now found as follows:

From figure 13, or equation (15a)

$$K_{20} = 0.050 + 0.17 \times 0.44 = 0.125$$

Since the average aspect ratio of the two wings is

$$\frac{1}{2} \left[\frac{(40)^2}{230} + \frac{(36)^2}{170} \right] = \frac{1}{2} [6.95 + 7.62] = 7.3,$$

the value of F from figure 12 is $F = 0.82$, so that $K_{20}F = 0.125 \times 0.82 = 0.103$. For zero decalage $K_{21} = 0$. Hence $(K_{20}F) + K_{21} = 0.103$. From figure 21 a value of $K_2 = 0.103$ for zero overhang gives $K_2 = 0.138$ for 10 percent overhang.

The lift increment for the upper wing is

$$\Delta C_{LU} = -0.022 + 0.138 C_L$$

and for the lower wing it is $\Delta C_{LL} = -\Delta C_{LU} \frac{S_U}{S_L}$

$$= -[-0.022 + 0.138 C_L] \frac{230}{170}$$

$$= +0.030 - 0.187 C_L$$

Hence

$$C_{LU} = C_L - 0.022 + 0.138 C_L \\ = 1.138 C_L - 0.022$$

and
$$C_{LL} = C_L + 0.030 - 0.187 C_L \\ = 0.813 C_L + 0.030$$

The relative lift is

$$e = \frac{C_{LU}}{C_{LL}} = \frac{1.138 C_L - 0.022}{0.813 C_L + 0.030}$$

CONCLUSIONS

The method here outlined for calculating the lift coefficients of the individual wings of a biplane has been based on a combination of theoretical and experimental data. In some respects there is excellent general agreement between theory and experiment, as follows:

1a. The effect of gap/chord stagger and aspect ratio on K_2 as shown by figure 11, table IX, and figure 13. (See equation 11.)

2a. The effect of decalage on K_1 as shown by figure 17. (See equation 12.)

The experimental data are consistent and fairly complete in other items such as:

1b. The effect of wing thickness and gap/chord ratio on K_1 with zero stagger as shown by figure 9.

2b. The effect of decalage on K_2 as shown by figures 16 and 18.

The remaining factors that need further investigation are:

1c. The effect of stagger on K_1 . Special tests to obtain greater accuracy in figure 10 are highly desirable.

2c. The effect of overhang on K_1 and K_2 . Special tests to obtain greater accuracy in figure 21 are required.

3c. The extension of test data to maximum negative lifts. Available test data indicate no appreciable change in K_2 at zero lift. Special tests should be made to investigate this effect.

Several conclusions may be drawn from a study of the method developed in this report, in the light of the foregoing summary.

1. The calculation of the individual wing lift coefficients is the only practical method of determining the ratio e at low lift coefficients.

2. The method here presented is not difficult to use.

3. In general, the existing biplane theory is verified by experiment, but further investigation is desirable to cover the interaction at zero lift and the effects of overhang.

4. Special biplane tests to cover the items listed under 1c, 2c, and 3c above should be made in order to eliminate the present uncertainty in these items.

BUREAU OF AERONAUTICS,

NAVY DEPARTMENT,

WASHINGTON, D.C., February 15, 1933.

REFERENCES

1. Betz, A.: Die gegenseitige Beeinflussung zweier Tragflächen. Z.F.M., Oct. 17, 1914, pp. 253-258.
2. Betz, A.: Berechnung der Luftkräfte auf eine Doppeldeckerzelle aus den entsprechenden Werten für Eindeckertragflächen. T.B., vol. I, no. 4, 1917, pp. 103-107.
3. Fuchs, R.: Systematic Rechnung über Auftrieb und Widerstand beim Doppeldecker. T.B., vol. II, no. 2, 1918, pp. 177-185.
4. Fuchs, R., and Hopf, L.: Aerodynamik. Richard Carl Schmidt & Co., 1922.
5. Munk, Max M.: General Biplane Theory. T.R. no. 151, N.A.C.A., 1922.
6. Glauert, H.: Theoretical Relationships for a Biplane. R. & M. no. 901, British A.R.C., 1923.
7. Millikan, Clark B.: An Extended Theory of Thin Airfoils and Its Application to the Biplane Problem. T.R. no. 362, N.A.C.A., 1930.
8. Munk, Max M.: Beitrag zur Aerodynamik der Flugzeugtragorgane. T.B., vol. II, no. 2, 1918, pp. 187-273.
9. Cowley, W. L., and Levy, H.: The Contribution of the Separate Planes to the Forces on a Biplane (R.A.F.-15 Section). R. & M. no. 589, British A.C.A., 1919.
10. Cowley, W. L., and Lock, C. N. H.: Biplane Investigation with R.A.F.-15 section. R. & M. no. 774, British A.R.C., 1921.
11. Cowley, W. L., and Jones, L. J.: Biplane Investigation with R.A.F.-15 section. Part II. R. & M. no. 857, British A.R.C., 1922.
12. Munk, Max M.: The Air Forces on a Systematic Series of Biplane and Triplane Cellule Models. T.R. no. 256, N.A.C.A., 1927.
13. Noyes, Richard W.: Pressure Distribution Tests on a Series of Clark Y Biplane Cellules with Special Reference to Stability. T.R. no. 417, N.A.C.A., 1932.
14. Mock, Richard M.: The Distribution of Loads between the Wings of a Biplane Having Decalage. T.N. no. 269, N.A.C.A., 1927.
15. Kuhn, Paul: Working Charts for the Determination of the Lift Distribution between Biplane Wings. T.R. no. 445, N.A.C.A., 1932.

TABLE I
LIFT COEFFICIENTS FOR U.S.A. TS-5 BIPLANE ¹

Gap
chord=0.9 Stagger=+30°=+0.69 c

Angle of attack	Lower wing C_{L_L}	Upper wing C_{L_U}	Biplane C_L	$\Delta C'_{L_U}$ = $C'_{L_U}-C'_L$
-9	+0.003	+0.097	+0.050	+0.047
-7	.102	.229	.165	.064
-5	.203	.363	.283	.080
-3	.300	.504	.402	.102
-1	.395	.646	.520	.126
0	.447	.724	.585	.139
2	.544	.890	.717	.173
4	.635	1.030	.833	.197
6	.725	1.180	.952	.228
8	.823	1.290	1.057	.233
10	.921	1.340	1.130	.210

¹ Data from N.A.C.A. Technical Report No. 256.

TABLE II
DIFFERENCE BETWEEN LIFT COEFFICIENT OF UPPER WING AND BIPLANE ¹ NO DECALAGE

Gap chord	Stagger chord		$\Delta C'_{L_U}$	Section
	Nominal	Effective		
0.9	-0.51	-0.47	-0.007-0.104 C_L	R.A.F.-15.
1.2	-.69	-.74	+.011- .104 C_L	Do.
.6	0	+.02	-.028+ .127 C_L	Do.
.8	0	+.02	-.010+ .088 C_L	Do.
1.0	0	+.03	-.004+ .060 C_L	Do.
1.2	0	+.04	-.006+ .038 C_L	Do.
.6	.16	.17	-.034+ .157 C_L	Do.
.9	.24	.26	-.008+ .116 C_L	Do.
1.2	.31	.35	-.005+ .104 C_L	Do.
.6	.35	.36	-.014+ .236 C_L	Do.
.9	.52	.54	-.005+ .178 C_L	Do.
1.2	.69	.72	-.001+ .147 C_L	Do.
.9	-.51	-.35	-.036- .030 C_L	U.S.A. TS-5.
.9	0	+.16	-.053+ .077 C_L	Do.
.9	+.51	+.64	-.051+ .198 C_L	Do.

¹ From N.A.C.A. Technical Report No. 256.

TABLE III
DIFFERENCE BETWEEN NORMAL FORCE COEFFICIENT OF UPPER WING AND BIPLANE

From N.A.C.A. Pressure Distribution Tests
Clark Y Section—Circular Tips ¹

Gap chord	Stagger chord		ΔC_{NF_U}
	Nominal	Effective	
0.50	0	+0.04	-0.104+0.017 C_{NF}
.75	0	.07	-.048+ .060 C_{NF}
.75	.25	.31	0 + .111 C_{NF}
.75	.50	.56	+.047+ .160 C_{NF}
1.00	-.25	-.16	-.024+ .009 C_{NF}
1.00	0	+.09	-.027+ .076 C_{NF}
1.00	+.25	.34	-.007+ .096 C_{NF}
1.00	.50	.59	+.001+ .141 C_{NF}
1.00	.75	.84	+.006+ .172 C_{NF}
1.25	0	+.11	-.011+ .064 C_{NF}
1.25	.25	.36	+.010+ .088 C_{NF}
1.25	.50	.61	+.023+ .096 C_{NF}
1.50	0	.13	0 + .050 C_{NF}
2.00	0	.18	+.033+ .040 C_{NF}

¹ N.A.C.A. Technical Report No. 417.

TABLE IV
DIFFERENCE BETWEEN LIFT COEFFICIENT OF UPPER WING AND BIPLANE ¹

R.A.F.-15 Section—No Decalage

Gap chord	Stagger chord		$\Delta C'_{L_U}$	Reference
	Nominal	Effective		
1.00	+0.57	0.60	+0.015+0.130 C_L	R. & M. 589.
1.00	0	+.02	+.002+ .027 C_L	R. & M. 589.
1.00	-.57	-.54	-.005- .115 C_L	R. & M. 589.
1.00	0	+.02	-.008+ .036 C_L	R. & M. 774.
1.00	.56	.58	+.006+ .146 C_L	R. & M. 857.
1.00	.27	.30	-.005+ .091 C_L	R. & M. 857.
1.00	-.28	-.25	-.004+0	R. & M. 857.

¹ From British A.R.C. Reports and Memoranda as indicated.

TABLE V
DIFFERENCE BETWEEN LIFT COEFFICIENT OF UPPER WING AND BIPLANE ¹ GÖTTINGEN 133 SECTION

Gap chord	Stagger chord		Decalage degrees	$\Delta C'_{L_U}$
	Nominal	Effective		
1.00	0	0.06	-4	+0.213+0.020 C_L .
			-2	+.103+ .025 C_L .
			0	-.020+ .060 C_L .
			+2	-.165+ .120 C_L .
			+4	-.290+ .130 C_L .
1.00	.50	.56	-4	+.250+ .100 C_L .
			-2	+.132+ .115 C_L .
			0	-.002+ .150 C_L .
			+2	-.125+ .180 C_L .
			+4	-.262+ .225 C_L .
.667	0	.04	-4	+.240+0
			-2	+.105+ .035 C_L .
			0	-.048+ .088 C_L .
			+2	-.192+ .120 C_L .
			+4	-.342+ .170 C_L .
.667	.50	.54	-4	+.315+ .120 C_L .
			-2	+.185+ .165 C_L .
			0	+.028+ .220 C_L .
			+2	-.113+ .250 C_L .
			+4	-.243+ .280 C_L .

¹ From Technische Berichte II-2.

TABLE VI
VARIATION OF $K_1=\Delta C_{L_U}$ AT ZERO LIFT AS A FUNCTION OF CHORD, GAP, STAGGER AND WING THICKNESS

Gap chord $\frac{G}{c}$	Wing sec- tion	Wing thick- ness $\frac{t}{c}$	Thickness $\frac{\text{gap}}{t}$ $\frac{t}{G}$	K_1	Change in K_1 with stagger $\frac{\Delta K_1}{\Delta S}$	Reference
0.50	Clark Y	0.117	0.234	-0.104	-----	N.A.C.A. T.R. 417.
.60	RAF-15	.070	.117	-.028	0.045	N.A.C.A. T.R. 256.
.67	G-133	.094	.140	-.048	.152	T.B. II-2.
.75	Clark Y	.117	.156	-.053	.153	N.A.C.A. T.R. 417.
.90	USA TS-5	.174	.196	-.053	.164	N.A.C.A. TR. 256.
1.00	G-133	.094	.094	-.020	.036	T.B. II-2.
1.00	Clark Y	.117	.117	-.027	.055	N.A.C.A. T.R. 417.
1.00	RAF-15	.070	.070	-.008	.014	R. & M. 589.
1.00	do	.070	.070	+.002	.018	R. & M. 774 and 857.
1.20	do	.070	.058	-.006	.008	N.A.C.A. T.R. 256.
1.25	Clark Y	.117	.094	-.011	.060	N.A.C.A. T.R. 417.
1.50	do	.117	.078	0	-----	Do.

TABLE VII
EFFECT OF $\frac{\text{GAP}}{\text{CHORD}}$ RATIO ON K_2

Gap chord	Gap span for $b=6c$	$\frac{b}{c} \left(\frac{1}{k^2} - 0.5 \right)$ Munk's factor	Relative values of Munk's factor		Typical curves			
			As cal- culated	Faired				
0.4	0.067	1.25	1.850	1.850	0.074	0.148	0.222	0.296
.6	.100	1.00	1.482	1.490	.059	.118	.178	.239
.8	.133	.825	1.223	1.210	.048	.097	.145	.194
1.0	.167	.675	1.000	1.000	.040	.080	.120	.160
1.2	.200	.570	.845	.845	.034	.068	.101	.135
1.4	.233	.490	.726	.725	.029	.058	.087	.116
1.6	.267	.425	.630	.630	.025	.050	.076	.101
1.8	.300	.370	.548	.550	.022	.044	.066	.088
2.0	.333	.320	.474	.475	.019	.038	.057	.076

NOTE.—The typical curves are based on assumed values of K_2 for gap/chord=1.00

TABLE VIII
CALCULATIONS FOR CORRECTION CURVES GIVING
EFFECT OF GAP/CHORD ON K_2

Gap chord $\frac{G}{c}$	$b=4c$				$b=5c$				$b=8c$				$b=10c$			
	Gap span $\frac{G}{b}$	F	$\frac{F}{F_0}$ $\times \frac{36}{16}$		Gap span $\frac{G}{b}$	F	$\frac{F}{F_0}$ $\times \frac{36}{25}$		Gap span $\frac{G}{b}$	F	$\frac{F}{F_0}$ $\times \frac{36}{64}$		Gap span $\frac{G}{b}$	F	$\frac{F}{F_0}$ $\times \frac{36}{100}$	
0.4	0.100	1.00	3.33		0.080	1.145	2.45		0.050	1.435	1.196		0.040	1.555	0.829	
.6	.150	.750	2.50		.120	.892	1.91		.075	1.185	.988		.060	1.325	.706	
.8	.200	.574	1.910		.160	.706	1.51		.100	1.00	.833		.080	1.145	.610	
1.00	.250	.455	1.52		.200	.574	1.227		.125	.865	.721		.100	1.00	.533	
1.2	.300	.368	1.226		.240	.473	1.012		.150	.750	.625		.120	.892	.476	
1.4	.350	.298	.993		.280	.400	.855		.175	.655	.546		.140	.793	.422	
1.6	.400	.245	.817		.320	.338	.723		.200	.574	.479		.160	.706	.376	
1.8	.450	.202	.673		.360	.287	.613		.225	.505	.421		.180	.638	.340	
2.0	.500	.167	.557		.400	.245	.524		.250	.455	.379		.200	.574	.306	

$F_0=0.675=F$ for $\frac{b}{c}=6$ and $\frac{G}{c}=1.0$.

TABLE IX
VARIATION OF K_2 WITH STAGGER

Stagger chord		Gap chord	Munk's factor F from figure 12	$K_2 = \frac{\Delta C_{L U}}{\Delta C_L}$		Reference
Nomi- nal	Basic			Ob- served	Cor- rected to $\frac{G}{c}=1$	
0	0.04	0.50	1.66	0.017	0.010	N.A.C.A. T.R. 417.
0	.07	.75	1.27	.060	.047	Do.
.25	.31	.75	1.27	.111	.087	Do.
.50	+.56	.75	1.27	.160	.126	Do.
-.25	-.16	1.00	1.00	.009	.009	Do.
0	+.09	1.00	1.00	.076	.076	Do.
.25	.34	1.00	1.00	.096	.096	Do.
.50	.59	1.00	1.00	.141	.141	Do.
.75	.84	1.00	1.00	.172	.172	Do.
0	.11	1.25	.81	.064	.079	Do.
.25	.36	1.25	.81	.088	.109	Do.
.50	.61	1.25	.81	.096	.119	Do.
0	.13	1.50	.67	.050	.075	Do.
0	.18	2.00	.47	.042	.089	Do.
0	.06	1.00	1.00	.060	.060	T.B. II-2.
.50	.56	1.00	1.00	.150	.150	Do.
0	.04	.67	1.39	.088	.063	Do.
.50	.54	.67	1.39	.220	.158	Do.
-.51	-.47	0.9	1.10	-.104	-.095	N.A.C.A. T.R. 256.
-.69	-.66	1.2	.84	-.112	-.133	Do.
0	+.02	0.6	1.49	+.127	+.085	Do.
0	.02	0.8	1.21	.088	.072	Do.
0	.03	1.0	1.00	.060	.060	Do.
0	.04	1.2	.84	.038	.045	Do.
+.16	.17	0.6	1.49	.157	.105	Do.
.24	.26	0.9	1.10	.116	.105	Do.
.31	.35	1.2	.84	.104	.124	Do.
.35	.36	0.6	1.49	.236	.158	Do.
.52	.54	0.9	1.10	.178	.161	Do.
.69	+.72	1.2	.84	+.147	+.175	Do.
-.51	-.35	0.9	1.10	-.030	-.027	Do.
0	+.16	0.9	1.10	+.077	+.070	Do.
+.51	+.64	0.9	1.10	.198	.180	Do.
.57	.60	1.00	1.00	.130	.130	R. & M. 589.
0	+.02	1.00	1.00	.027	.027	Do.
-.57	-.54	1.00	1.00	-.115	-.115	Do.
0	+.02	1.00	1.00	.036	.036	R. & M. 774.
+.56	.58	1.00	1.00	.146	.146	R. & M. 857.
+.27	+.30	1.00	1.00	.091	.091	Do.
-.28	-.25	1.00	1.00	0	0	Do.

TABLE X
EFFECT OF OVERHANG ON LIFT DISTRIBUTION

Overhang percent	Gap chord	Stagger chord	Decalage	$\Delta C_{L U} =$
-20	1.00	0	0	+0.020-0.053 C_{NF}
0	1.00	0	0	-.023+ .063 C_{NF}
+20	1.00	0	0	-.043+ .120 C_{NF}
+40	1.00	0	0	-.030+ .152 C_{NF}

Overhang percent = $100 \frac{b_U - b_L}{b_U}$

REPORT No. 459

THE N.A.C.A. FULL-SCALE WIND TUNNEL

By SMITH J. DE FRANCE

SUMMARY

This report gives a complete description of the full-scale wind tunnel of the National Advisory Committee for Aeronautics. The tunnel is of the double-return flow type with a 30 by 60 foot open jet at the test section. The air is circulated by two propellers 35 feet 5 inches in diameter, located side by side, and each directly connected to a 4,000-horsepower slip-ring induction motor. The motor control equipment permits varying the speed in 24 steps between 25 and 118 miles per hour. The tunnel is equipped with a 6-component balance for obtaining the forces in 3 directions and the moments about the 3 axes of an airplane. All seven dial scales of the balance system are of the recording type, which permits simultaneous records to be made of all forces.

The tunnel has been calibrated and surveys have shown that the dynamic-pressure distribution over that portion of the jet which would be occupied by an airplane having a wing span of 45 feet is within $\pm 1\frac{1}{2}$ percent of a mean value. Based on the mean velocity of 118 miles per hour at the jet, the ratio of the kinetic energy per second to the energy input to the propellers per second is 2.84. Since it is generally recognized that a long open jet is a source of energy loss, the above figure is considered very satisfactory.

Comparative tests on several airplanes have given results which are in good agreement with those obtained on the same airplanes in flight. This fact, together with information obtained in the tunnel on Clark Y airfoils, indicates that the flow in the tunnel is satisfactory and that the air stream has a very small amount of turbulence.

INTRODUCTION

It is a generally accepted fact that the aerodynamic characteristics of a small model cannot be directly applied to a full-sized airplane without using an empirical correction factor to compensate for the lack of dynamic similarity. Two methods have been used to overcome this difficulty. One is to compress the working fluid and vary the kinematic viscosity to compen-

sate for the reduction in the size of the model. This method is used in the variable-density wind tunnel where tests can be conducted at the same Reynolds Number as would be experienced in flight. The other method is to conduct tests on the full-scale airplane.

The variable-density wind tunnel offers a satisfactory means for testing the component parts of an airplane and is particularly suitable for conducting fundamental research on airfoil sections and streamline bodies. However, this equipment has its limitations when the aerodynamic characteristics of a complete airplane are desired, especially if the effect of the slipstream is to be considered. It is practically impossible to build a model of the required size that is a true reproduction of a complete airplane. This difficulty is increased by the requirement that the model withstand large forces.

It is apparent that the most satisfactory method of obtaining aerodynamic characteristics of a complete airplane is to conduct a full-scale investigation. Heretofore such investigations have been conducted only in flight. Because of the variation in atmospheric conditions, it has been necessary to make a large number of check flights to obtain enough data to average out the discrepancies. Furthermore, in flight testing the scope of experiments is often limited by the fact that the possible alterations that can be made are restricted to those that do not seriously affect the weight or airworthiness of the airplane. In order to provide a means of full-scale investigation by which the conditions can be controlled and alterations made without serious limitations, the full-scale wind tunnel has been erected. Of course, only the steady-flight conditions can be readily investigated in the wind tunnel, but the execution of this work in the tunnel will facilitate full-scale testing and allow the flight-research personnel of the laboratory to concentrate on those problems possible of solution only in flight.

The full-scale wind tunnel may be used to determine the lift and drag characteristics of a complete airplane, to study the control and stability characteristics both

with and without the slipstream, and to study body interference. In addition, equipment has been installed to determine the direction and velocity of the flow at any point around an airplane. Aircraft engine cooling and cowling problems can also be investigated under conditions similar to those in flight.

The design of the full-scale wind tunnel was started in 1929. Since this was to be the first wind tunnel

tunnel was started in the spring of 1930; it was completed and operated for the first time in the spring of 1931.

DESCRIPTION OF TUNNEL

The general arrangement of the tunnel is shown in figure 1 and an external view of the building is given in figure 2. The tunnel is of the double-return flow

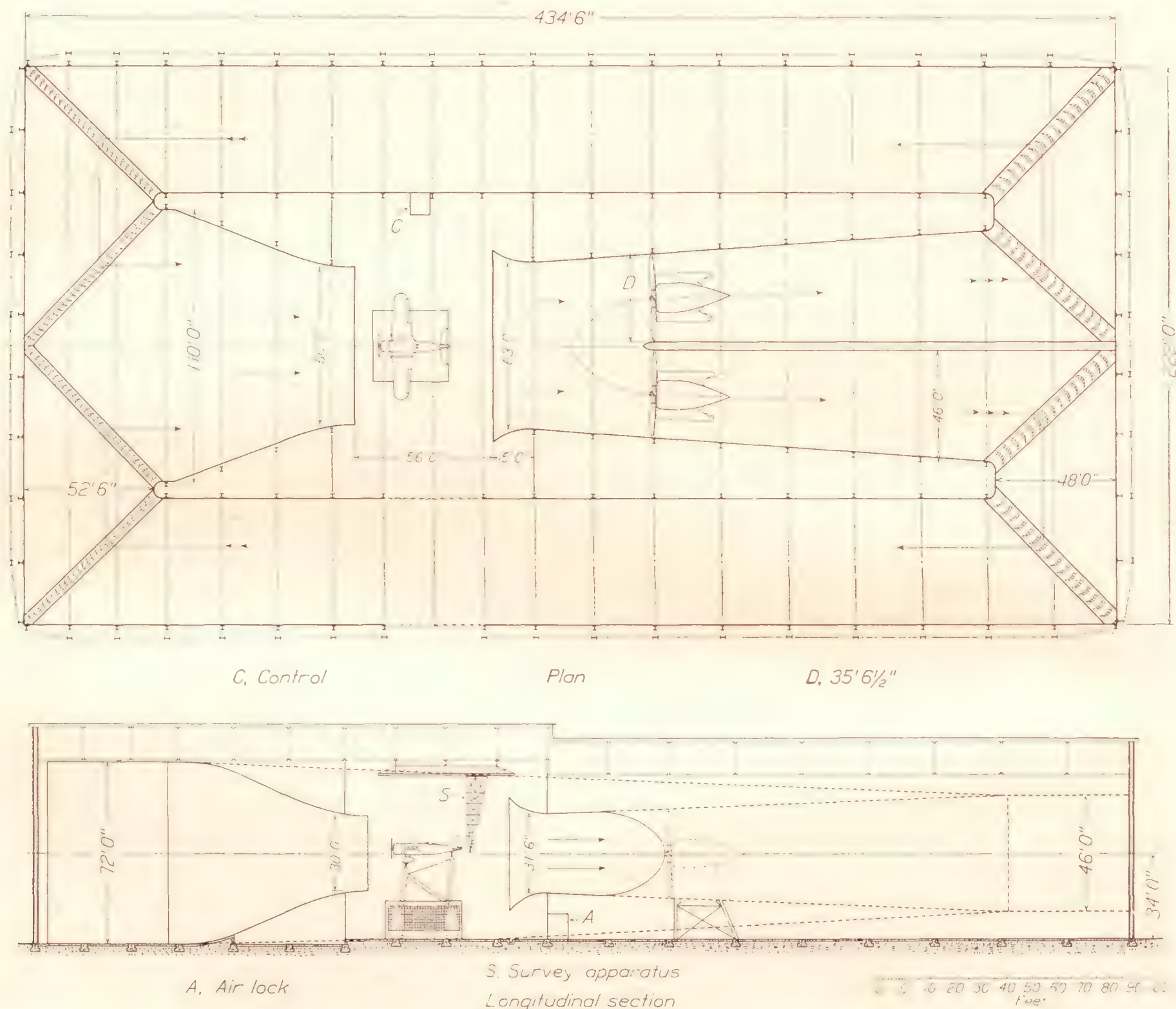


FIGURE 1.—Plan and elevation of the tunnel.

constructed with an elliptic throat and with two propellers mounted side by side, a $\frac{1}{15}$ -scale model was constructed to study the flow problems. Very satisfactory flow conditions were obtained in the model tunnel. This piece of equipment is now being used for small-scale testing. Construction of the full-scale wind

type with an open throat having a horizontal dimension of 60 feet and a vertical dimension of 30 feet. On either side of the test chamber is a return passage 50 feet wide, with the height varying from 46 to 72 feet. The entire equipment is housed in a structure, the outside walls of which serve as the outer walls of the

return passages. The over-all length of the tunnel is 434 feet 6 inches, the width 222 feet, and the maximum height 97 feet. The framework is of structural steel and the walls and roof are of $\frac{5}{16}$ -inch corrugated cement asbestos sheets. The entrance and exit cones are constructed of 2-inch wood planking, attached to a steel frame and covered on the inside with galvanized sheet metal as a protection against fire.

Entrance cone.—The entrance cone is 75 feet in length and in this distance the cross section changes from a rectangle 72 by 110 feet to a 30 by 60 foot elliptic section. The area reduction in the entrance

is approximately 30 by 40 feet, which provide excellent lighting conditions for daytime operation; eight 1,000-watt flood lights provide adequate artificial illumination for night operation. Attached to the roof trusses and running across the test chamber at right angles to the air stream and also in the direction of the air stream are tracks for an electric crane which lifts the airplanes onto the balance.

Exit cone.—Forward of the propellers and located on the center line of the tunnel is a smooth fairing which transforms the somewhat elliptic section of the single passage into two circular ones at the propellers.



FIGURE 2.—Exterior view of the tunnel.

cone is slightly less than 5:1. The shape of the entrance cone was chosen to give as far as possible a constant acceleration to the air stream and to retain a 9-foot length of nozzle for directing the flow.

Test chamber.—The test chamber, in which is located the working section of the jet, is 80 by 122 feet. The length of the jet, or the distance between the end of the entrance cone and the smallest cross section of the exit-cone collector, is 71 feet. Doors 20 by 40 feet located in the walls of the return passage on one side provide access for airplanes. In the roof of the test chamber are two skylights, each approxi-

From the propellers aft, the exit cone is divided into two passages and each transforms in the length of 132 feet from a 35-foot $6\frac{1}{2}$ -inch circular section to a 46-foot square. The included angle between the sides of each passage is 6° .

Propellers.—The propellers are located side by side and 48 feet aft of the throat of the exit-cone bell. The propellers are 35 feet 5 inches in diameter and each consists of four cast aluminum alloy blades screwed into a cast-steel hub.

Motors.—The most commonly used power plant for operating a wind tunnel is a direct-current motor and

motor-generator set with Ward Leonard control system. For the full-scale wind tunnel it was found that alternating current slip-ring induction motors, together with satisfactory control equipment, could be purchased for

of speed one pole change was provided and the other variations are obtained by the introduction of resistance in the rotor circuit. This control permits a variation in air speed from 25 to 118 miles per hour. The two

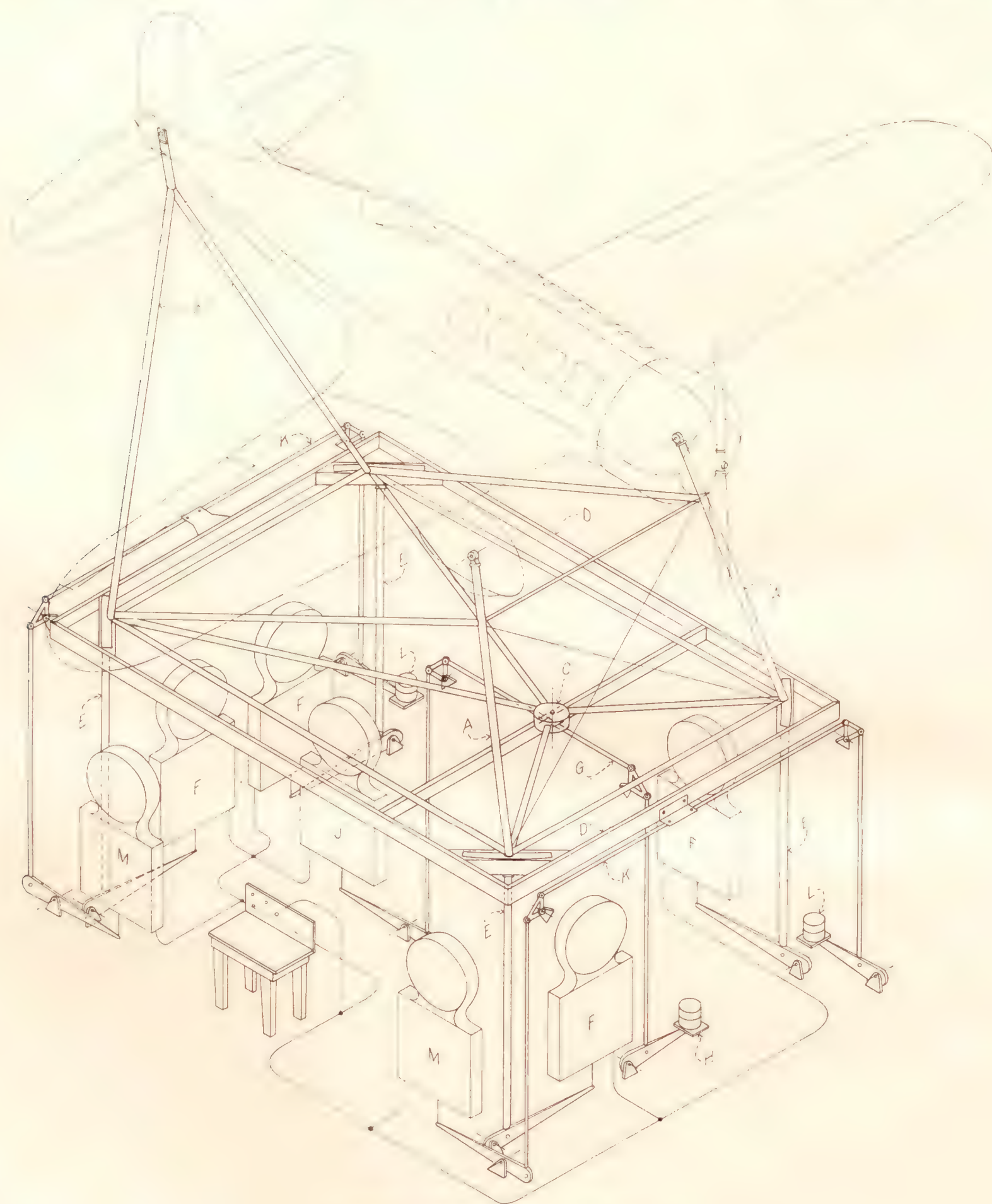


FIGURE 3.—Schematic drawing of the balance.

approximately 30 percent less than the direct-current equipment. Two 4,000-horsepower slip-ring induction motors with 24 steps of speed between 75 and 300 r.p.m. were therefore installed. In order to obtain the range

motors are connected through an automatic switchboard to one drum-type controller located in the test chamber. All the control equipment is interlocked and connected through time-limit relays, so that regardless

of how fast the controller handle is moved the motors will increase in speed at regular intervals.

The motors are provided with ball and roller bearings, which reduce the friction losses to a minimum. Roller bearings of 8.5- and 11.8-inch bores are provided at the slip-ring and propeller ends respectively, while the thrust of the propellers is taken on a ball bearing at the rear end of each motor shaft. The motors are mounted with the rotor shafts centered in the exit-cone passages. The motors and supporting structure are

opposite end of the tunnel have chords of 3 feet 6 inches and are spaced at 0.41 of a chord length. By a proper adjustment of the angular setting of the vanes, a satisfactory velocity distribution has been obtained and no honeycomb has been found necessary.

Balance.—The balance, which is of the 6-component type, is shown diagrammatically in figure 3. Ball and socket fittings at the top of each of the struts **A** hold the axles of the airplane to be tested; the tail is attached to the triangular frame **B**. These struts are secured to

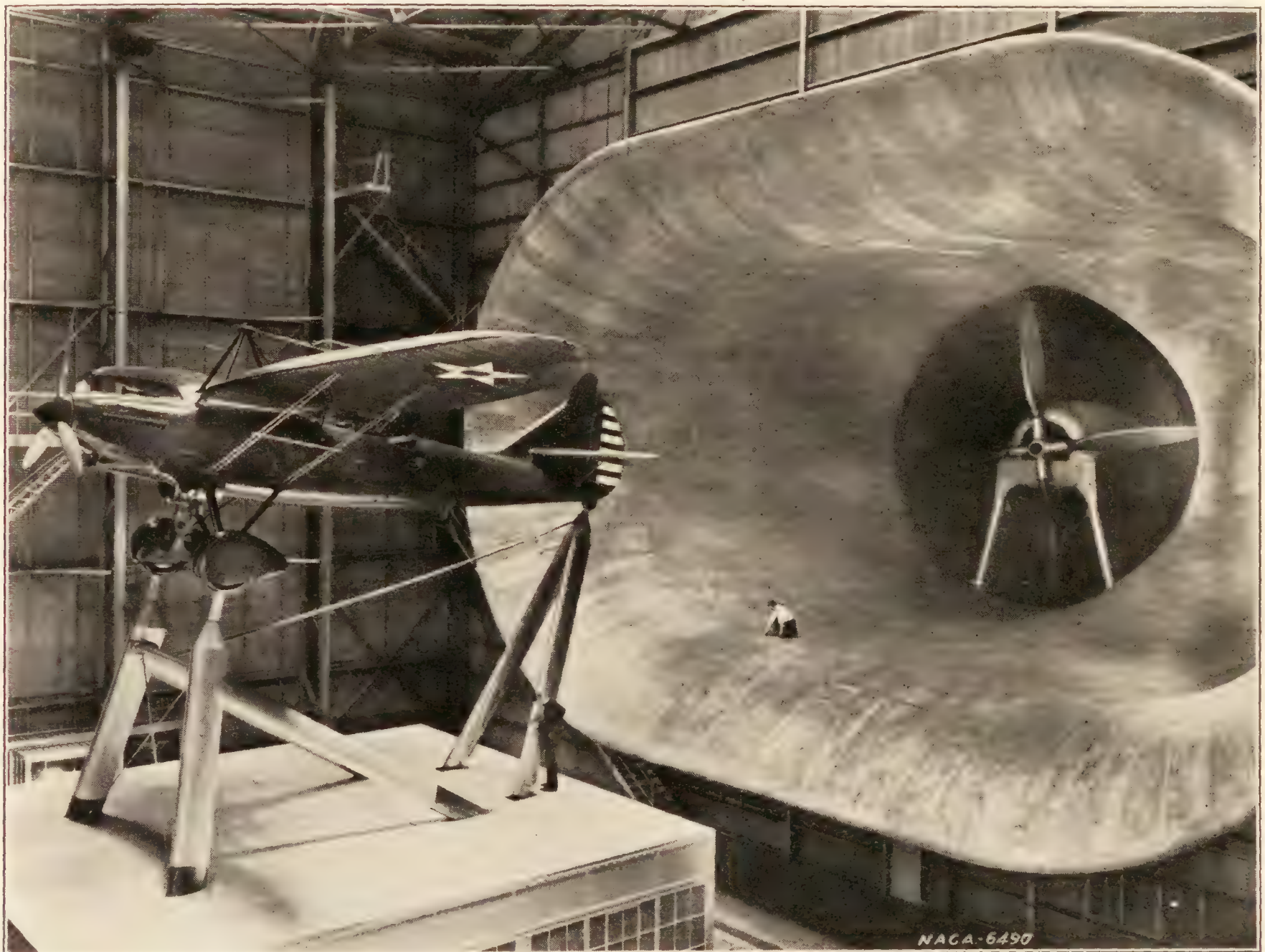


FIGURE 4.—The YO-31A airplane ready for test in the tunnel.

enclosed in fairings so that they offer a minimum resistance to the air flow.

Guide vanes.—The air is turned at the four corners of each return passage by guide vanes. The vanes are of the curved-airfoil type formed by two intersecting arcs with a rounded nose. The arcs were so chosen as to give a practically constant area through the vanes.

The vanes at the first two corners back of the propellers have chords of 7 feet and are spaced at 0.45 and 0.47 of a chord length, respectively. Those at the

the turntable **C**, which is attached to the floating frame **D**. This frame rests on the struts **E**, which transmit the lift forces to the scales **F**. The drag linkage **G** is attached to the floating frame on the center line and, working against a known counterweight **H**, transmits the drag force to the scale **J**. The cross-wind force linkages **K** are attached to the floating frame on the front and rear sides at the center line. These linkages, working against known counterweights **L**, transmit the cross-wind force to scales **M**. In the above manner the

forces in three directions are measured and by combining the forces and the proper lever arms, the pitching, rolling, and yawing moments can be computed.

The scales are of the dial type and are provided with solenoid-operated printing devices. When the proper test condition is obtained, a push-button switch is momentarily closed and the readings on all seven scales are recorded simultaneously, eliminating the possibility of personal errors.

free from the balance. In figure 4 it can be seen that a very limited amount of the supporting structure is exposed to the air stream. The tare-drag measurements are therefore reduced to a minimum.

Survey equipment.—Attached to the bottom chord of the roof trusses is a 55-foot structural steel bridge (fig. 5), which can be rolled across the full width of the test chamber; mounted on this bridge is a car which can be rolled along the entire length. Suspended

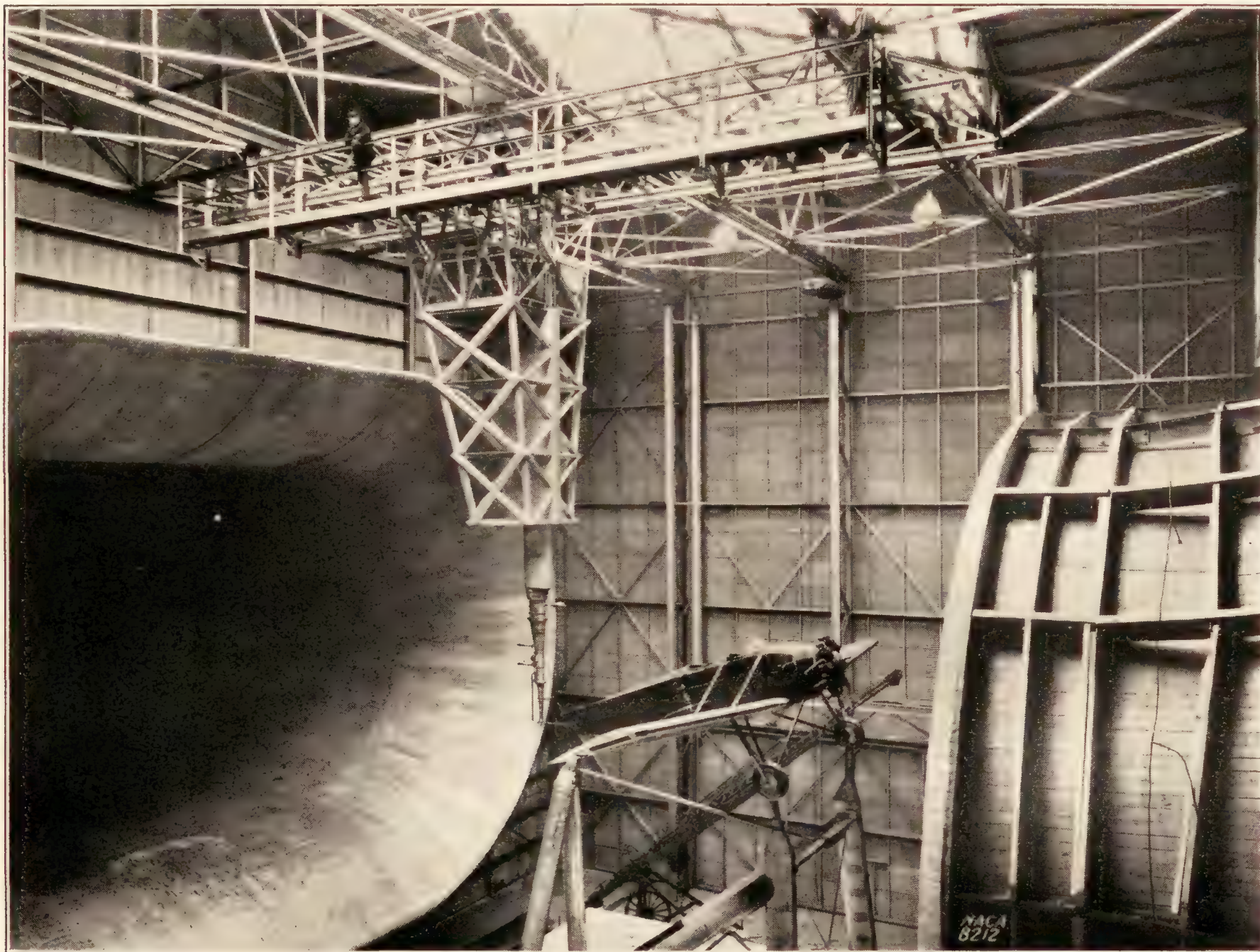


FIGURE 5.—Yaw, pitch, and pitot survey apparatus in position for survey at tail of airplane.

The triangular frame **B** is caused to telescope by electrically operated screws which raises and lowers the tail of the airplane and thereby varies the angle of attack. By a similar mechanism the turntable **C** can be moved so as to yaw the airplane from 20° left to 20° right.

The entire floating frame and scale assembly is enclosed in a room for protection from air currents and the supporting struts are shielded by streamlined fairings which are secured to the roof of the balance room and

below the car is a combined pitot, pitch, and yaw tube which can be raised or lowered and pitched or yawed by gearing with electrical control on the car. This arrangement permits the alinement of the tube with the air flow at any point around an airplane. The alinement of the tube is indicated by null readings on the alcohol manometers connected to the pitch and yaw openings in the head and the angle of pitch or yaw is read from calibrated Veeder counters connected to the electric operating motors. This equipment is very

valuable for studying the downwash behind wings and the flow around the tail surfaces of an airplane.

CALIBRATIONS AND TESTS

The velocity distribution has been measured over several planes at right angles to the jet, but the plane representing approximately the location of the wings of an airplane during tests was most completely explored. The dynamic-pressure distribution over the area that would be occupied during tests by an airplane with a wing span of 45 feet is within $\pm 1\frac{1}{2}$ percent

static pressure is within ± 1 percent of the mean dynamic pressure at the test section.

Two wall plates with static orifices are located in each return passage just ahead of the guide vanes at the entrance-cone end of the tunnel. The orifices are connected by a common pressure line, which is led to a micromanometer on the control desk in the test chamber. The other side of the manometer is left open to the test-chamber pressure. This installation has been calibrated against the average dynamic pressure determined by pitot surveys of the jet at the test

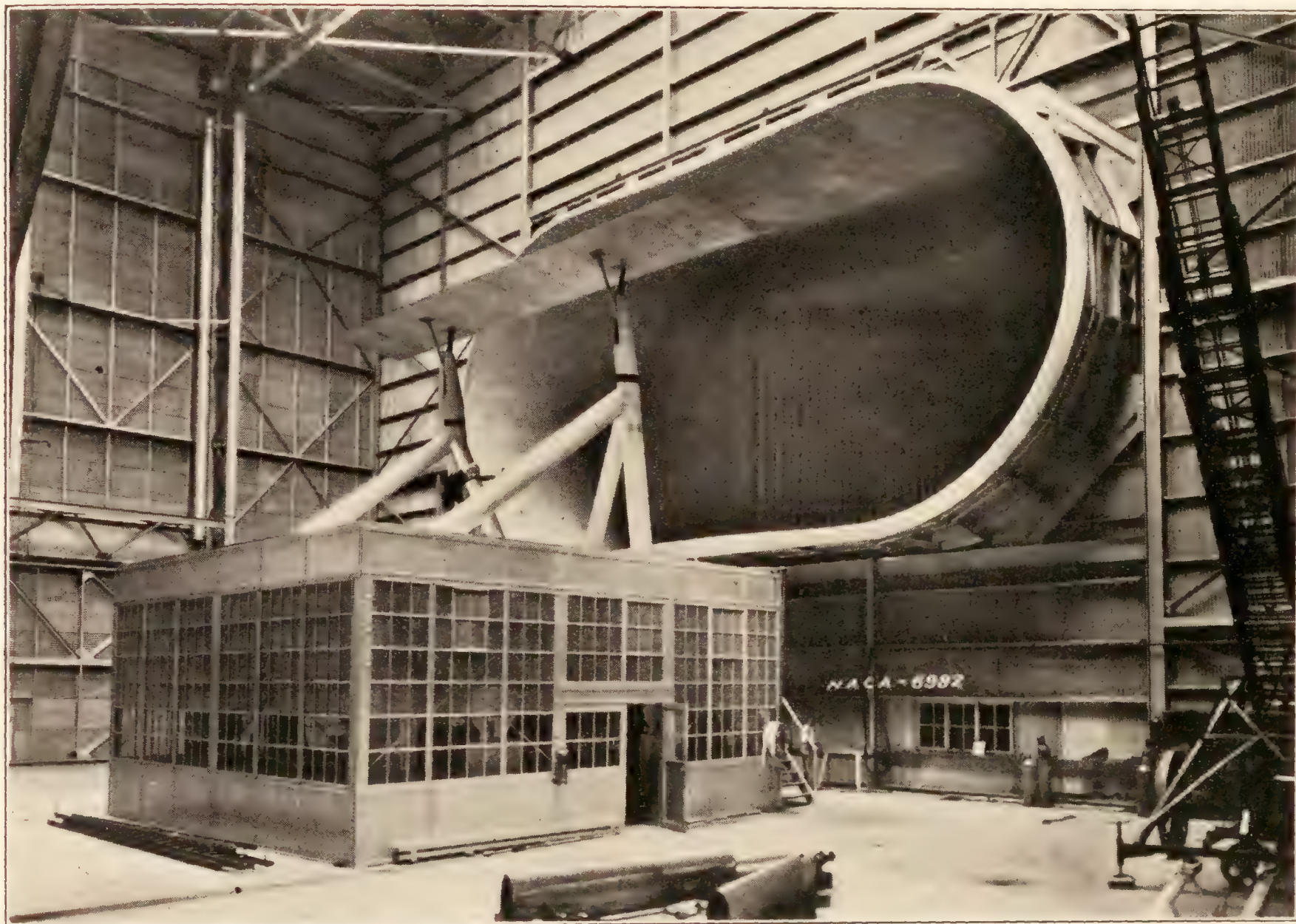


FIGURE 6.—A 6 by 36 foot Clark Y airfoil mounted in the tunnel.

of a mean value. It is possible to improve the distribution by further adjustment of the guide vanes. However, tests already conducted in the tunnel indicate that the present distribution does not detrimentally affect the results. This fact has been shown by the excellent agreement which has been obtained between the tunnel and flight results.

A survey of the static pressure along the axis of the tunnel showed that the longitudinal pressure gradient is small, as evidenced by the fact that between 11 and 36 feet from the entrance cone the variation of the

location and it is used to determine the dynamic head during tests.

A series of Clark Y airfoils of the same aspect ratio, but with spans of 12, 24, 36, and 48 feet, have been tested at the same Reynolds Number to determine the jet-boundary correction. Tests have also been made to determine the blocking effect of an airplane in the jet. The results of the complete investigation will be presented in a separate report.

Using the mean velocity across the jet of 118 miles per hour for computing the kinetic energy per second

at the working section and dividing this by the energy input to the propellers per second

$$\frac{\frac{1}{2} \rho A V^3}{550 \times \text{b.hp. input}}$$

gives an energy ratio for the tunnel of 2.84. This ratio, considering the length of the open jet, compares

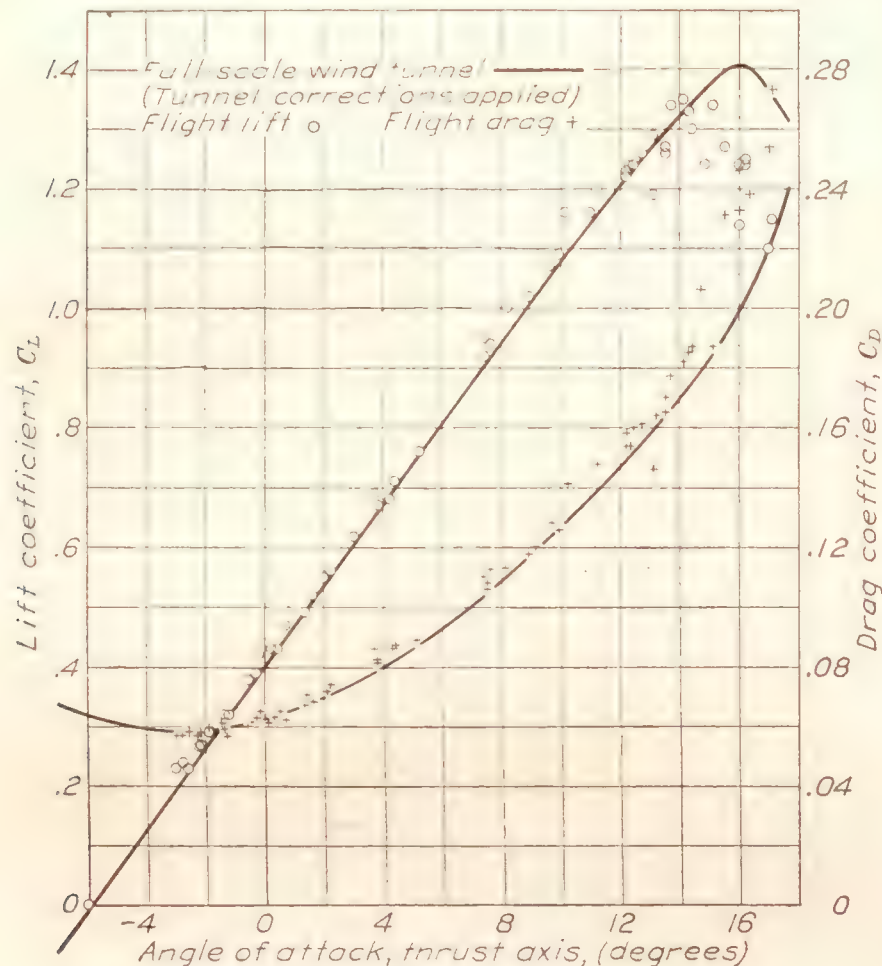


FIGURE 7.—Lift and drag characteristics of the F-22 airplane.

very favorably with the most efficient open-throat tunnels now in operation and exceeds the efficiency expected when the tunnel was designed.

Before force measurements are made on an airplane, the airplane is suspended from the roof trusses by cables and held within one half inch from the balance supports

while the tare forces are measured. The tare-drag coefficient determined in the above manner has been of the order of 25 percent of the minimum drag coefficient of the airplanes tested.

When testing airfoils the airplane supports are replaced by those shown in figure 6. The angle of attack is changed by displacing the rear support arms and rotating the airfoil about pins in the top of the main supports. The rear support arms are moved by linkages, which are connected to long screws on the back of the main supports, and the screws are operated by hand cranks inside the balance house. The tare drag of this support system is exceptionally small and amounts to only 3 percent of the minimum drag of a 6 by 36 foot Clark Y airfoil.

The lift and drag characteristics have been measured in the tunnel on several airplanes which had been previously tested in flight and their polars determined. These tests were conducted to obtain a check between the tunnel results and those from flight tests. A comparison of the results from the two methods of testing for one of the airplanes, the Fairchild F-22, is shown in figure 7. The wind-tunnel results are shown by the solid lines and the flight results are presented by the experimental points. These curves are representative of the results obtained with the different airplanes.

The agreement that has been obtained between the flight and full-scale tunnel results, together with the consistent manner in which measurements can be repeated when check tests are made, has demonstrated the accuracy and value of the equipment for aeronautical research.

LANGLEY MEMORIAL AERONAUTICAL LABORATORY,
NATIONAL ADVISORY COMMITTEE FOR AERONAUTICS,
LANGLEY FIELD, VA., March 13, 1933.

REPORT No. 460

THE CHARACTERISTICS OF 78 RELATED AIRFOIL SECTIONS FROM TESTS IN THE VARIABLE-DENSITY WIND TUNNEL

By EASTMAN N. JACOBS, KENNETH E. WARD, and ROBERT M. PINKERTON

SUMMARY

An investigation of a large group of related airfoils was made in the N.A.C.A. variable-density wind tunnel at a large value of the Reynolds Number. The tests were made to provide data that may be directly employed for a rational choice of the most suitable airfoil section for a given application. The variation of the aerodynamic characteristics with variations in thickness and mean-line form were therefore systematically studied.

The related airfoil profiles for this investigation were developed by combining certain profile thickness forms, obtained by varying the maximum thickness of a basic distribution, with certain mean lines, obtained by varying the length and the position of the maximum mean-line ordinate. A number of values of these shape variables were used to derive a family of airfoils. For the purposes of this investigation the construction and tests were limited to 68 airfoils of this family. In addition to these, several supplementary airfoils have been included in order to study the effects of certain other changes in the form of the mean line and in the thickness distribution.

The results are presented in the standard graphic form representing the airfoil characteristics for infinite aspect ratio and for aspect ratio 6. A table is also given by means of which the important characteristics of all the airfoils may be conveniently compared. The variation of the aerodynamic characteristics with changes in shape is shown by additional curves and tables. A comparison is made, where possible, with thin-airfoil theory, a summary of which is presented in an appendix.

INTRODUCTION

The forms of the airfoil sections that are in common use today are, directly or indirectly, the result of investigations made at Göttingen of a large number of airfoils. Previously, airfoils such as the R.A.F. 15 and the U.S.A. 27, developed from airfoil profiles investigated in England, were widely used. All these investigations, however, were made at low values of the Reynolds Number; therefore, the airfoils developed may not be the optimum ones for full-scale application. More recently a number of airfoils have been tested in the variable-density wind tunnel at values of the Reynolds Number approaching those of flight (refer-

ence 1) but, with the exception of the M-series and a series of propeller sections, the airfoils have not been systematically derived in such a way that the results could be satisfactorily correlated.

The design of an efficient airplane entails the careful balancing of many conflicting requirements. This statement is particularly true of the choice of the wing. Without a knowledge of the variations of the aerodynamic characteristics of the airfoil sections with the variations of shape that affect the weight of the structure, the designer cannot reach a satisfactory balance between the many conflicting requirements.

The purpose of the investigation reported herein was to obtain the characteristics at a large value of the Reynolds Number of a wide variety of related airfoils. The benefits of such a systematic investigation are evident. The results will greatly facilitate the choice of the most satisfactory airfoil for a given application and should eliminate much routine airfoil testing. Finally, because the results may be correlated to indicate the trends of the aerodynamic characteristics with changes of shape, they may point the way to the design of new shapes having better characteristics.

Airfoil profiles may be considered as made up of certain profile-thickness forms disposed about certain mean lines. The major shape variables then become two, the thickness form and the mean-line form. The thickness form is of particular importance from a structural standpoint. On the other hand, the form of the mean line determines almost independently some of the most important aerodynamic properties of the airfoil section, e.g., the angle of zero lift and the pitching-moment characteristics.

The related airfoil profiles for this investigation were derived by changing systematically these shape variables. The symmetrical profiles were defined in terms of a basic thickness variation, symmetrical airfoils of varying thickness being obtained by the application of factors to the basic ordinates. The cambered profiles were then developed by combining these thickness forms with various mean lines. The mean lines were obtained by varying the camber and by varying the shape of the mean line to alter the position of the maximum mean-line ordinate. *The maximum ordinate*

of the mean line is referred to throughout this report as the camber of the airfoil and the position of the maximum ordinate of the mean line as the position of the camber. An airfoil, produced as described above, is designated by a number of four digits: the first indicates the camber in percent of the chord; the second, the position of the camber in tenths of the chord from the leading edge; and the last two, the maximum thickness in percent of the chord. Thus the N.A.C.A. 2315 airfoil has a maximum camber of 2 percent of the chord at a position 0.3 of the chord from the leading edge, and a maximum thickness of 15 percent of the chord; the N.A.C.A. 0012 airfoil is a symmetrical airfoil having a maximum thickness of 12 percent of the chord.

In addition to the systematic series of airfoils, several supplementary airfoils have been included in order to study the effects of a few changes in the form of the mean line and in the thickness distribution.

Preliminary results which have been published include those for 12 symmetrical N.A.C.A. airfoils, the 00 series (reference 2) and other sections having different nose shapes (reference 3); and those for 42 cambered airfoils, the 43 and 63 series (reference 4), the 45 and 65 series (reference 5), the 44 and 64 series (reference 6), and the 24 series (reference 7).

If the chord is taken along the x axis from 0 to 1, the ordinates y are given by an equation of the form

$$\pm y = a_0\sqrt{x} + a_1x + a_2x^2 + a_3x^3 + a_4x^4$$

The equation was adjusted to give the desired shape by imposing the following conditions to determine the constants:

- (1) Maximum ordinate 0.1 at 0.3 chord

$$x = 0.3 \quad \begin{matrix} y = 0.1 \\ dy/dx = 0 \end{matrix}$$

- (2) Ordinate at trailing edge

$$x = 1 \quad y = 0.002$$

- (3) Trailing-edge angle

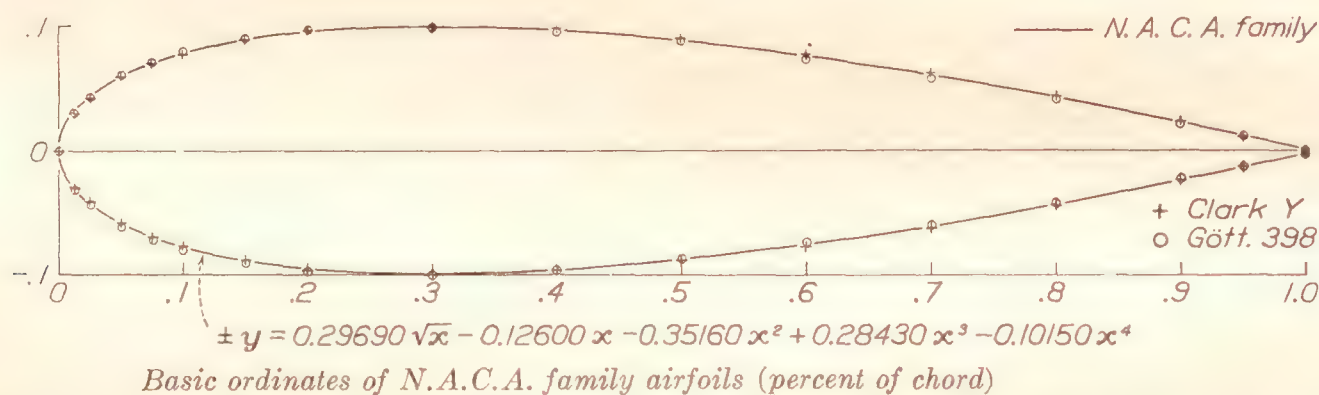
$$x = 1 \quad dy/dx = -0.234$$

- (4) Nose shape

$$x = 0.1 \quad y = 0.078$$

The following equation satisfying approximately the above-mentioned conditions represents a profile having a thickness of approximately 20 percent of the chord.

$$\pm y = 0.29690\sqrt{x} - 0.12600x - 0.35160x^2 + 0.28430x^3 - 0.10150x^4$$



Sta.....	0	1.25	2.5	5.0	7.5	10	15	20	25	30	40	50	60	70	80	90	95	100
Ord.....	0	3.157	4.358	5.925	7.000	7.805	8.909	9.563	9.902	10.003	9.672	8.823	7.606	6.107	4.372	2.413	1.344	0.210

L.E. radius, 4.40.

FIGURE 1.—Thickness variation.

The tests were made in the variable-density wind tunnel of the National Advisory Committee for Aeronautics during the period from April 1931 to February 1932.

DESCRIPTION OF AIRFOILS

Well-known airfoils of a certain class including the Göttingen 398 and the Clark Y, which have proved to be efficient, are nearly alike when their camber is removed (mean line straightened) and they are reduced to the same maximum thickness. A thickness variation similar to that of these airfoils was therefore chosen for the development of the N.A.C.A. airfoils. An equation defining the shape was used as a method of producing fair profiles.

This equation was taken to define the basic section. The basic profile and a table of ordinates are given in figure 1. Points obtained by removing the camber from the Göttingen 398 and the Clark Y sections, and applying a factor to the ordinates of the resulting thickness curves to bring them to the same maximum thickness, are plotted on the above figure for comparison. Sections having any desired maximum thickness were obtained by multiplying the basic ordinates by the proper factor; that is

$$\pm y_t = \frac{t}{0.20} (0.29690\sqrt{x} - 0.12600x - 0.35160x^2 + 0.28430x^3 - 0.10150x^4)$$

where t is the maximum thickness. The leading-edge radius is found to be

$$r_l = \frac{1}{2} \left(\frac{t}{0.20} a_0 \right)^2 = 1.10 t^2$$

When the mean lines of certain airfoils in common use were reduced to the same maximum ordinate and compared it was found that their shapes were quite different. It was observed, however, that the range of shapes could be well covered by assuming some simple shape and varying the maximum ordinate and its position along the chord. The mean line was, therefore, arbitrarily defined by two parabolic equations of the form

$$y_c = b_0 + b_1 x + b_2 x^2$$

where the leading end of the mean line is at the origin and the trailing end is on the x axis at $x=1$. The values of the constants for both equations were then expressed in terms of the above variables; namely,

(1) Mean-line extremities

$$x=0 \quad y_c=0$$

$$x=1 \quad y_c=0$$

(2) Maximum ordinate of mean line

$$x=p \text{ (position of maximum ordinate)}$$

and

$$y_c = \frac{m}{(1-p)^2} [(1-2p) + 2px - x^2]$$

(aft of maximum ordinate)

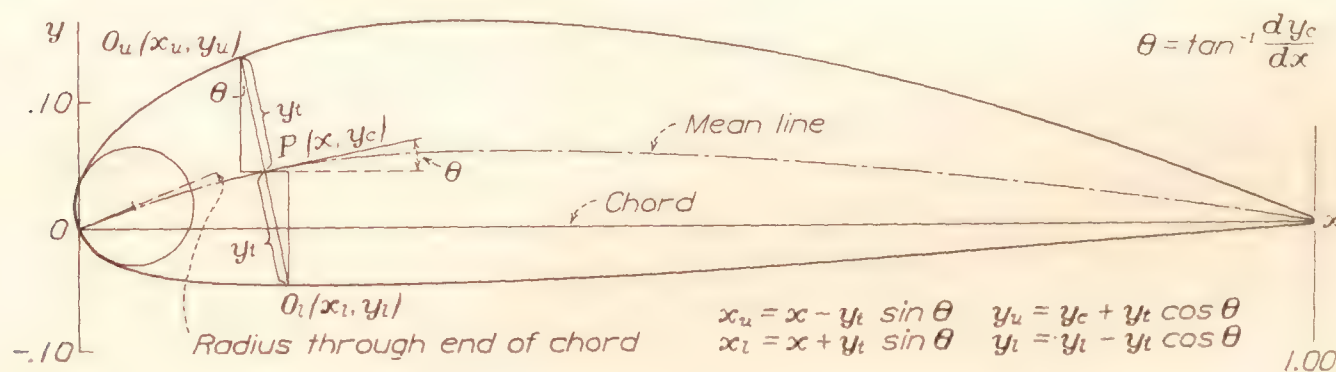
The method of combining the thickness forms with the mean-line forms is best described by means of the diagram in figure 2. The line joining the extremities of the mean line is chosen as the chord. Referring to the diagram, the ordinate y_t of the thickness form is measured along the perpendicular to the mean line from a point on the mean line at the station along the chord corresponding to the value of x for which y_t was computed. The resulting upper and lower surface points are then designated:

Stations x_u and x_l

Ordinates y_u and y_l

where the subscripts u and l refer to upper and lower surfaces, respectively. In addition to these symbols, the symbol θ is employed to designate the angle between the tangent to the mean line and the x axis. This angle is given by

$$\theta = \tan^{-1} \frac{dy_c}{dx}$$



Sample calculations for derivation of N.A.C.A. 6321

x	y_t	y_c	$\tan \theta$	$\sin \theta$	$\cos \theta$	$y_t \sin \theta$	$y_t \cos \theta$	x_u	y_u	x_l	y_l
0	0	0	0.40000	0.37140	0.92840	0	0	0.00064	0.03583	0	0
0.01250	0.03314	0.00489	.38333	.35793	.93375	0.01186	0.03094	.30000	.16503	.30000	-.04503
.30000	.10503	.06000	0	0	1	0	.10503	.60585	.12863	.59415	-.03067
.60000	.07986	.04898	-.07347	-.07327	.99731	-.00585	.07965	1.00037	.00218	.99963	-.00218
1	.00221	0	-.17143	-.16897	.98562	-.00037	.00218				

Slope of radius through end of chord.

FIGURE 2.—Method of calculating ordinates of N.A.C.A. cambered airfoils.

$$y_c = m(\text{maximum ordinate})$$

$$dy_c/dx = 0$$

The resulting equations defining the mean line then became

$$y_c = \frac{m}{p^2} [2px - x^2]$$

(forward of maximum ordinate)

The following formulas for calculating the ordinates may now be derived from the diagram:

$$x_u = x - y_t \sin \theta$$

$$y_u = y_c + y_t \cos \theta$$

$$x_l = x + y_t \sin \theta$$

$$y_l = y_c - y_t \cos \theta$$

Sample calculations are given in figure 2. The center for the leading-edge radius is placed on the tangent to the mean line at the leading edge.

A family of related airfoils was derived in the manner described. Seven values of the maximum thickness, 0.06, 0.09, 0.12, 0.15, 0.18, 0.21, and 0.25; four values of the camber, 0.00, 0.02, 0.04, and 0.06; and six values of the position of the camber, 0.2, 0.3, 0.4, 0.5, 0.6, and 0.7 were used to derive the related sections of this family. The profiles of the airfoils derived are shown collectively in figure 3.

For the purposes of this investigation the construction and tests were limited to 68 of the airfoils. Tables of ordinates at the standard stations are given in the figures presenting the aerodynamic characteristics. These ordinates were obtained graphically from the computed ordinates for all but the symmetrical sec-

models, which are made of duralumin, have a chord of 5 inches and a span of 30 inches. They were constructed from the computed ordinates by the method described in reference 8.

Routine measurements of lift, drag, and pitching moment about a point on the chord one quarter of the chord behind its forward end were made at a Reynolds Number of approximately 3,000,000 (tank pressure, approximately 20 atmospheres). Groups of airfoils were first tested to study the variations with thickness, each group containing airfoils of different thicknesses but having the same mean line. Finally, all airfoils having a thickness of 12 percent of the chord were

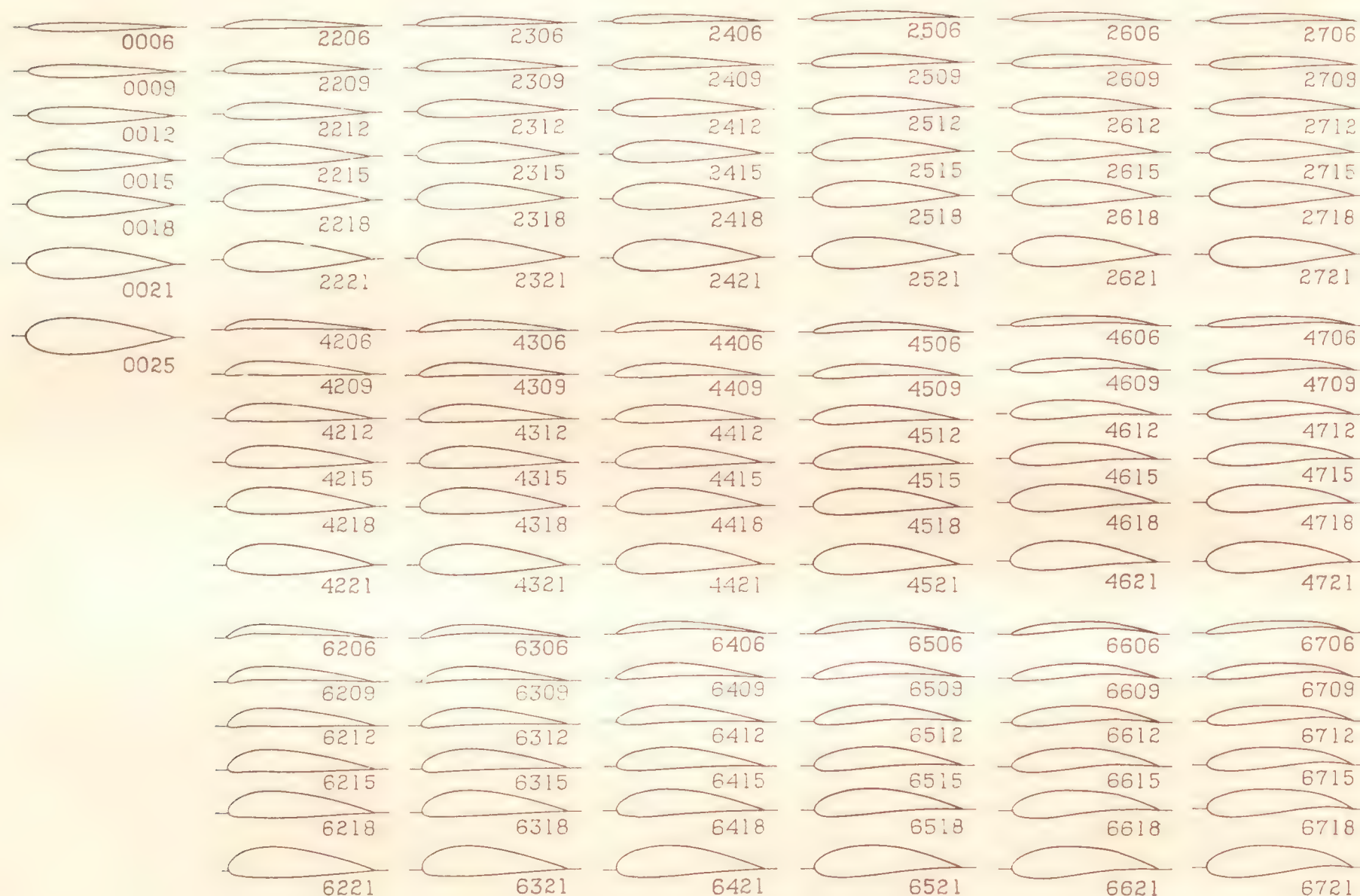


FIGURE 3.—N.A.C.A. airfoil profiles.

tions. Two sets of trailing-edge ordinates are given. Those inclosed by parentheses, which are given to facilitate construction, represent ordinates to which the surfaces are faired. In the construction of the models the trailing edges were rounded off.

Three groups of supplementary airfoils were also constructed and tested. The derivation of these airfoils will be considered later with the discussion.

APPARATUS AND METHODS

A description of the variable-density wind tunnel and the method of testing is given in reference 8. The

tested to study the variations with changes in the mean line.

RESULTS

The results are presented in the standard graphic form (figs. 4 to 80) as coefficients corrected after the method of reference 8 to give airfoil characteristics for infinite aspect ratio and aspect ratio 6. Where more than one test has been used for the analysis, the infinite aspect ratio characteristics from the earlier test have been indicated by additional points on the figure. Table I gives the important characteristics of all the airfoils.

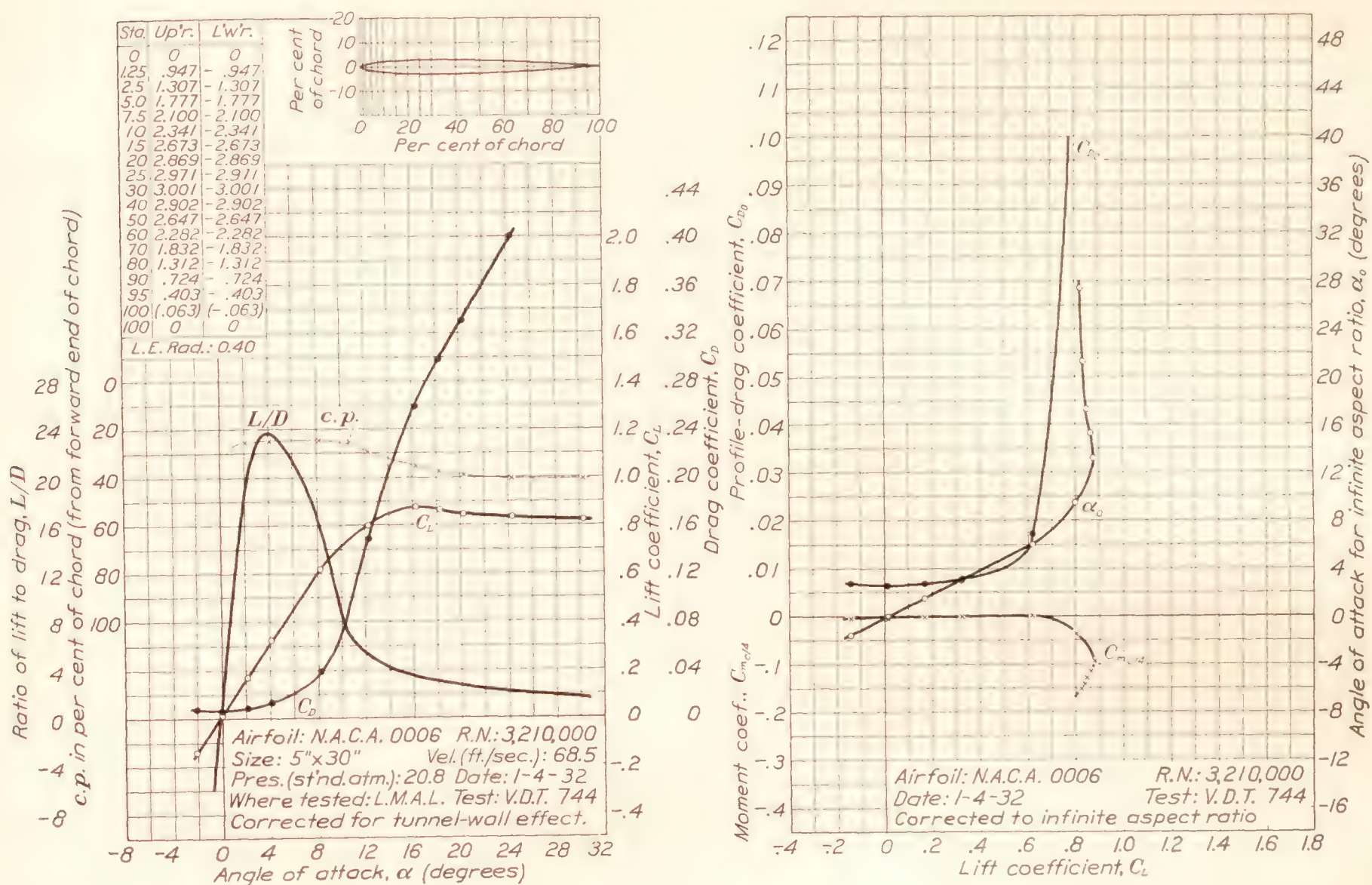


FIGURE 4.—N.A.C.A. 0006 airfoil.

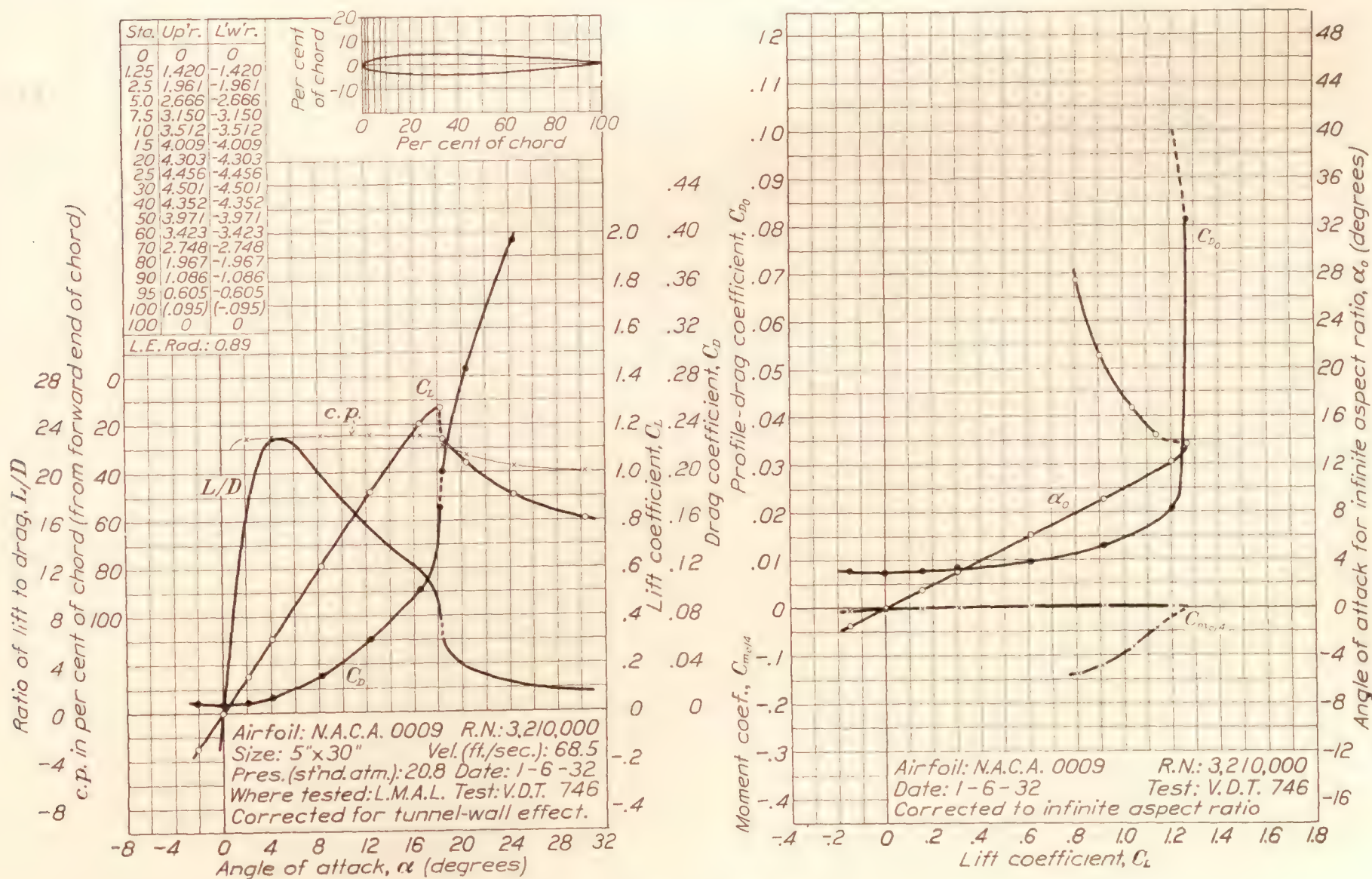


FIGURE 5.—N.A.C.A. 0009 airfoil.

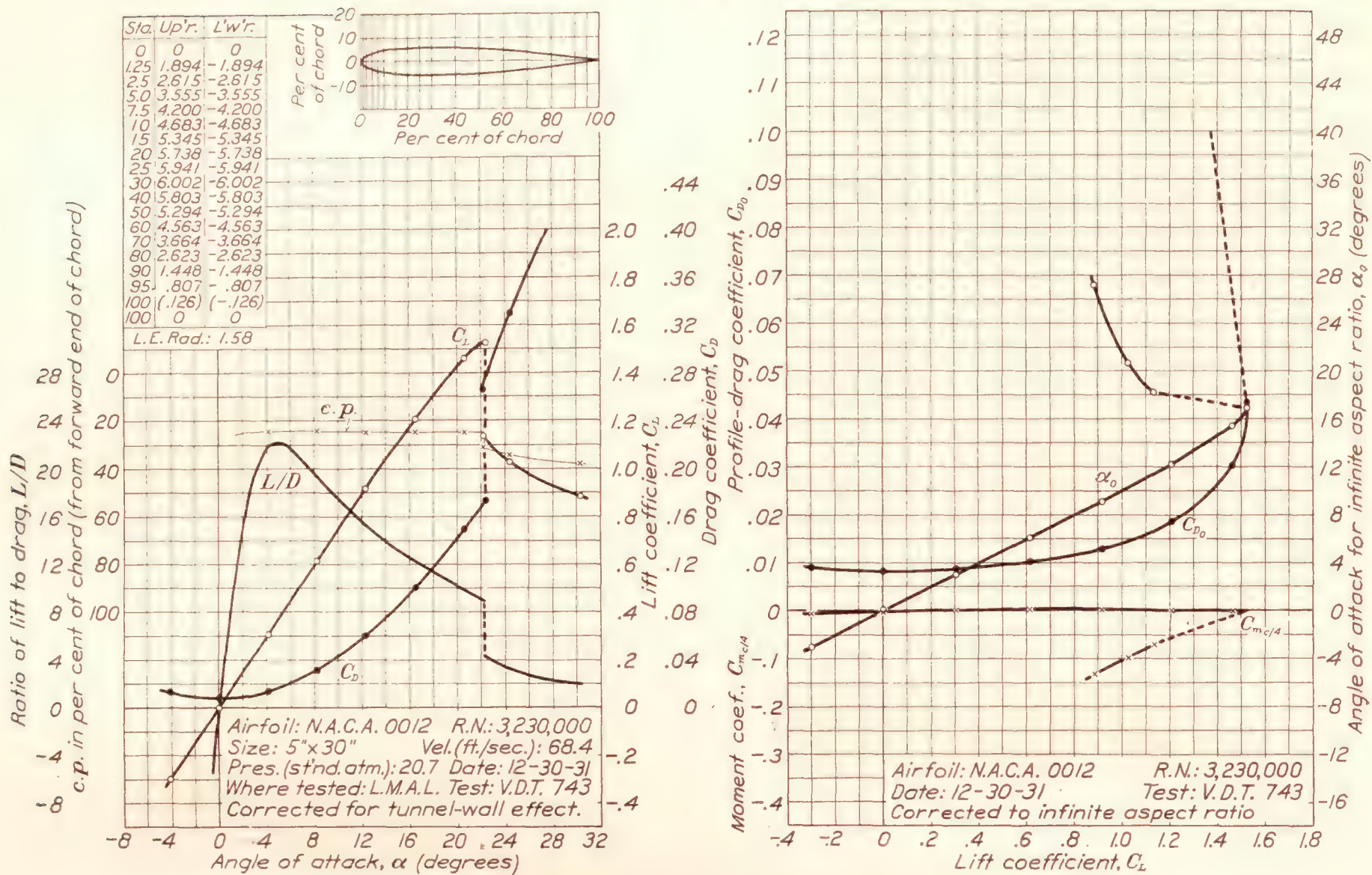


FIGURE 6.—N.A.C.A. 0012 airfoil.

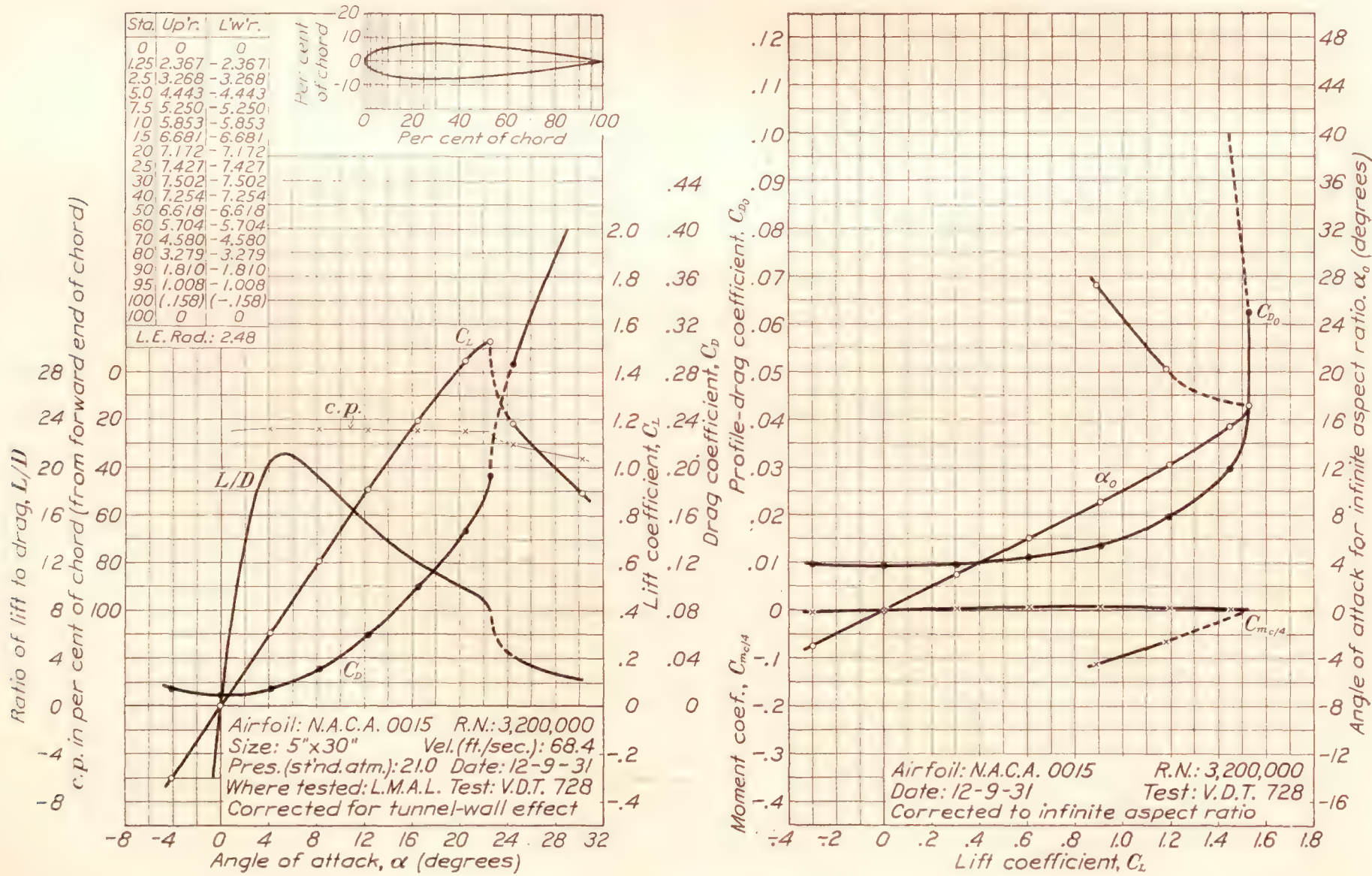


FIGURE 7.—N.A.C.A. 0015 airfoil.

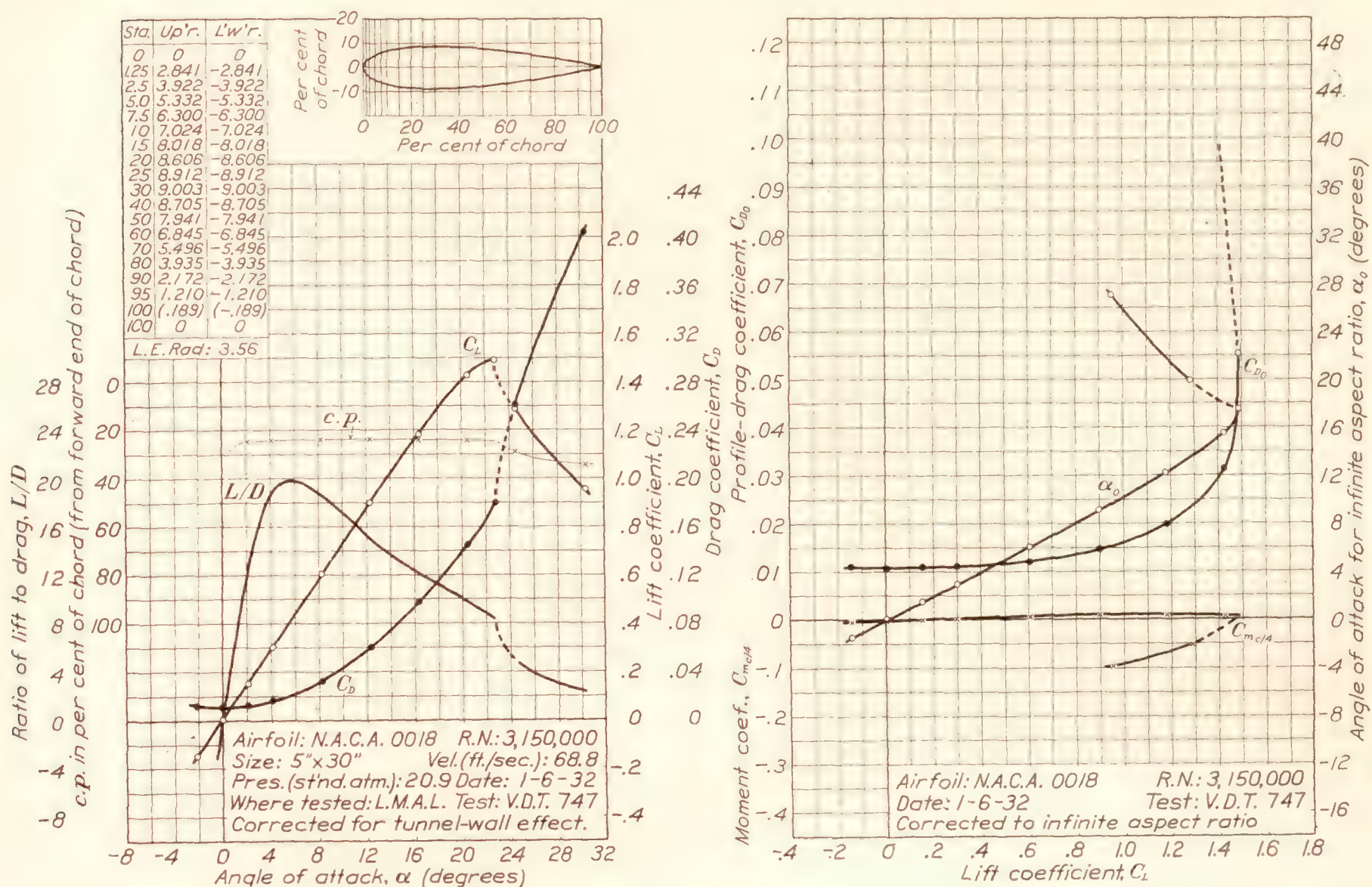


FIGURE 8.—N.A.C.A. 0018 airfoil.

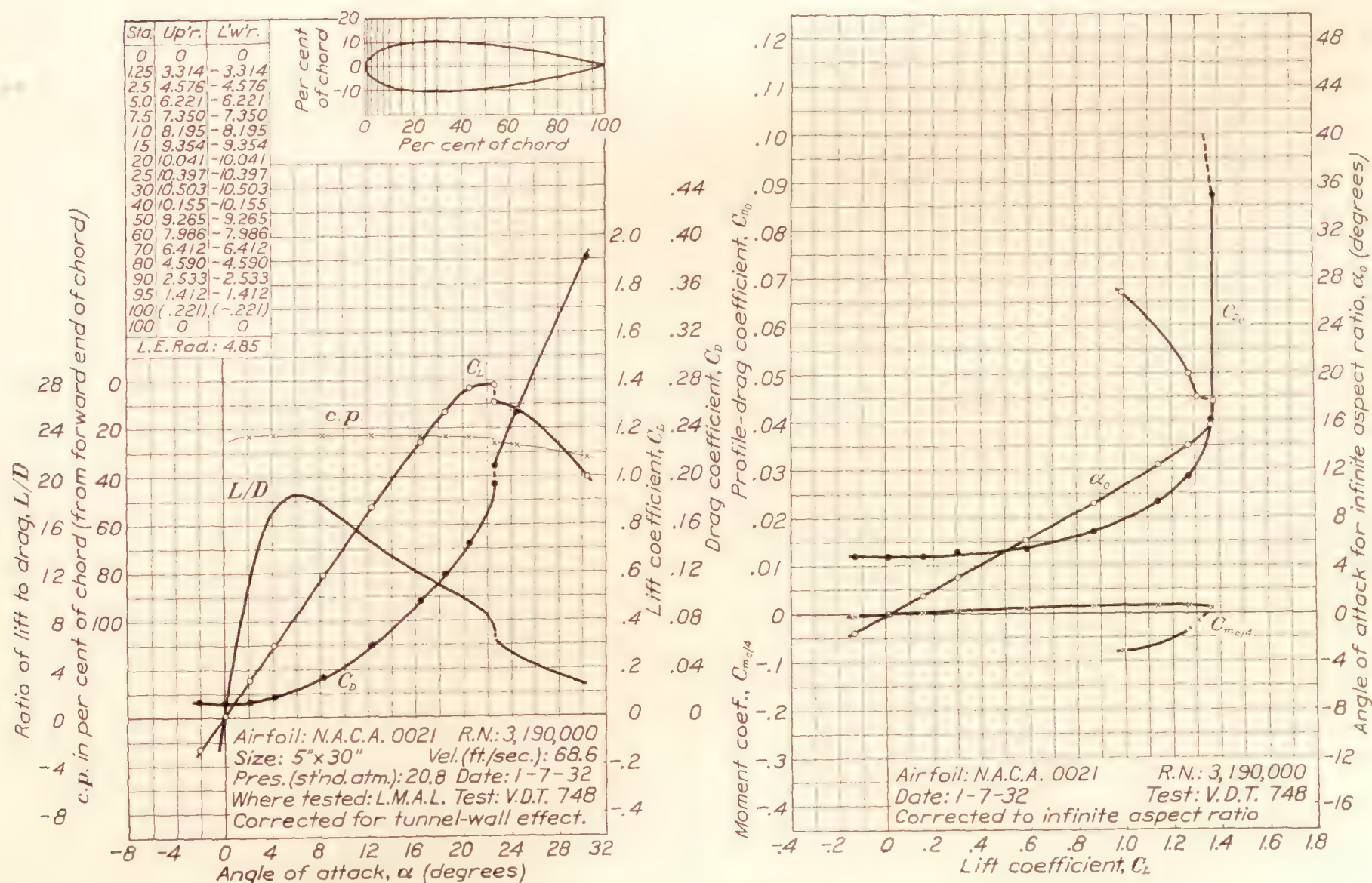


FIGURE 9.—N.A.C.A. 0021 airfoil.

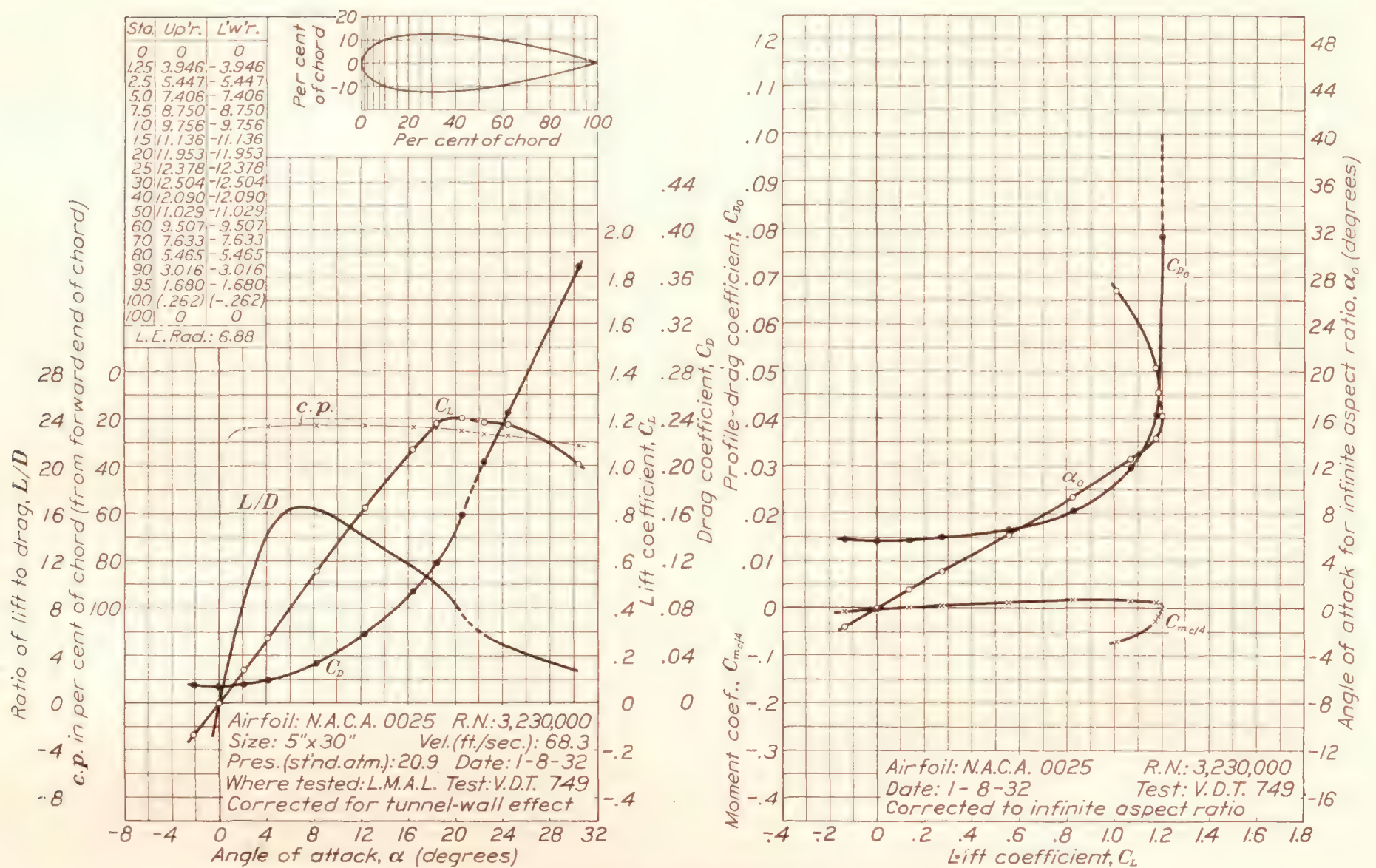


FIGURE 10.—N.A.C.A. 0025 airfoil.

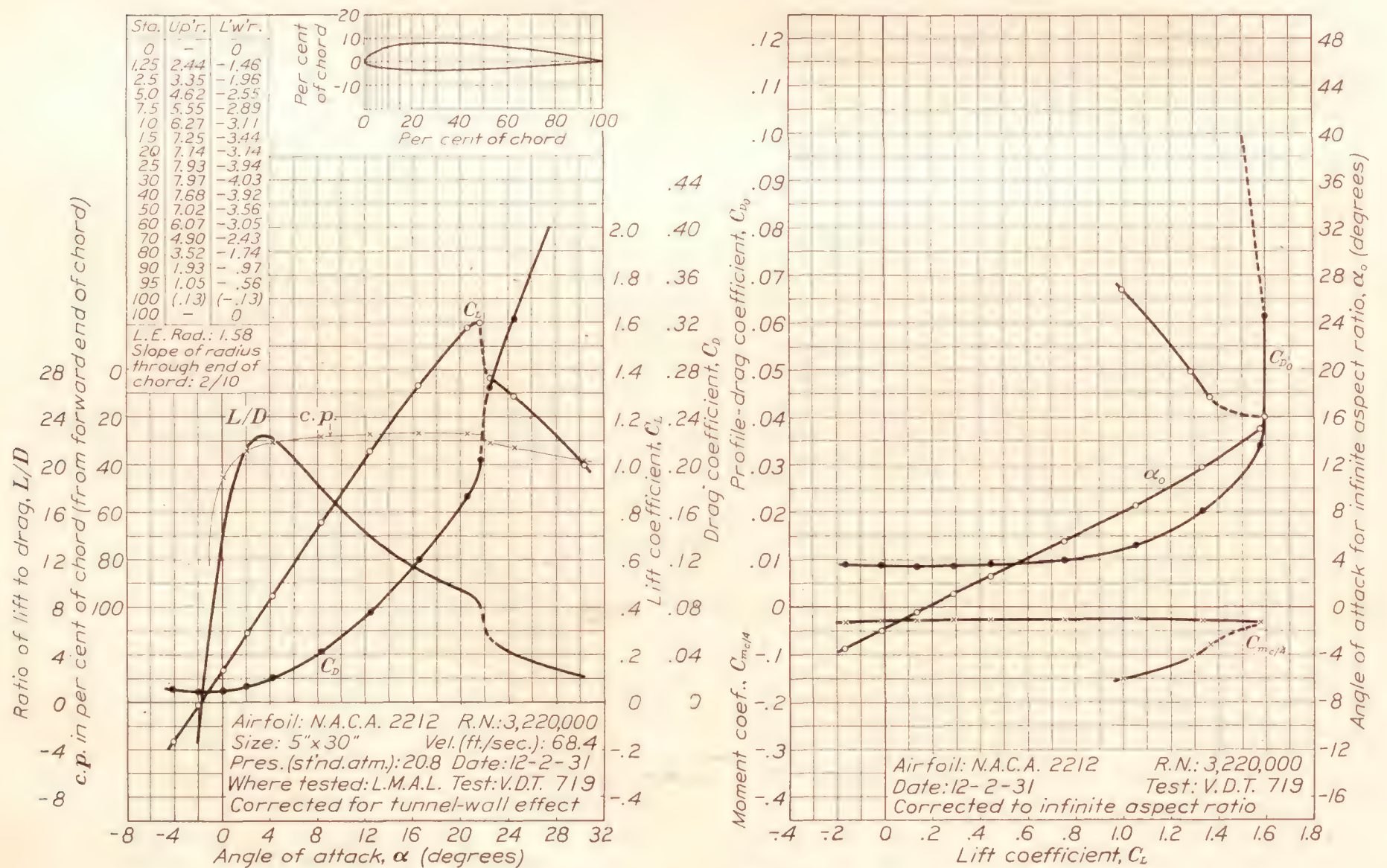


FIGURE 11.—N.A.C.A. 2212 airfoil.

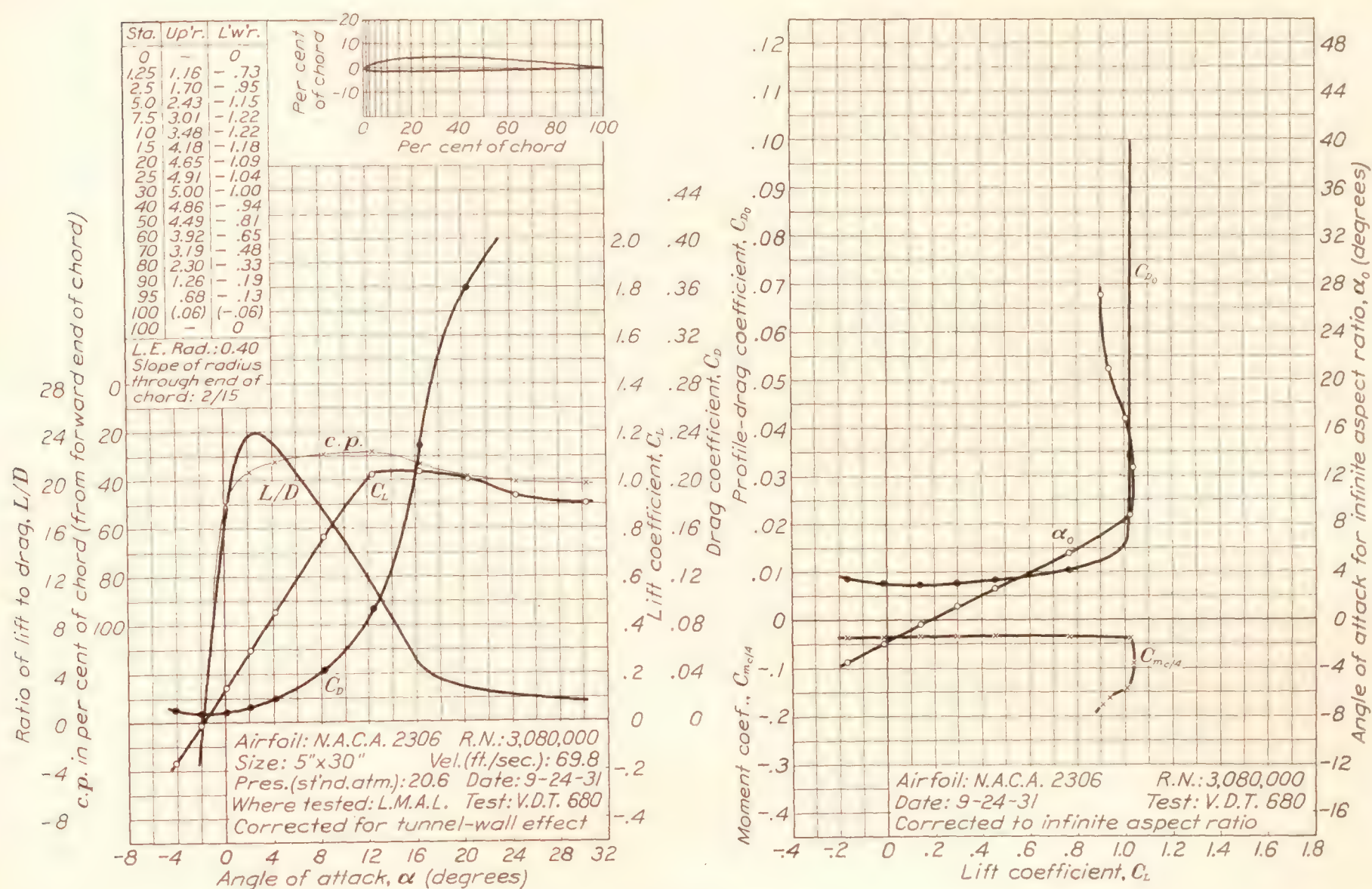


FIGURE 12.—N.A.C.A. 2306 airfoil.

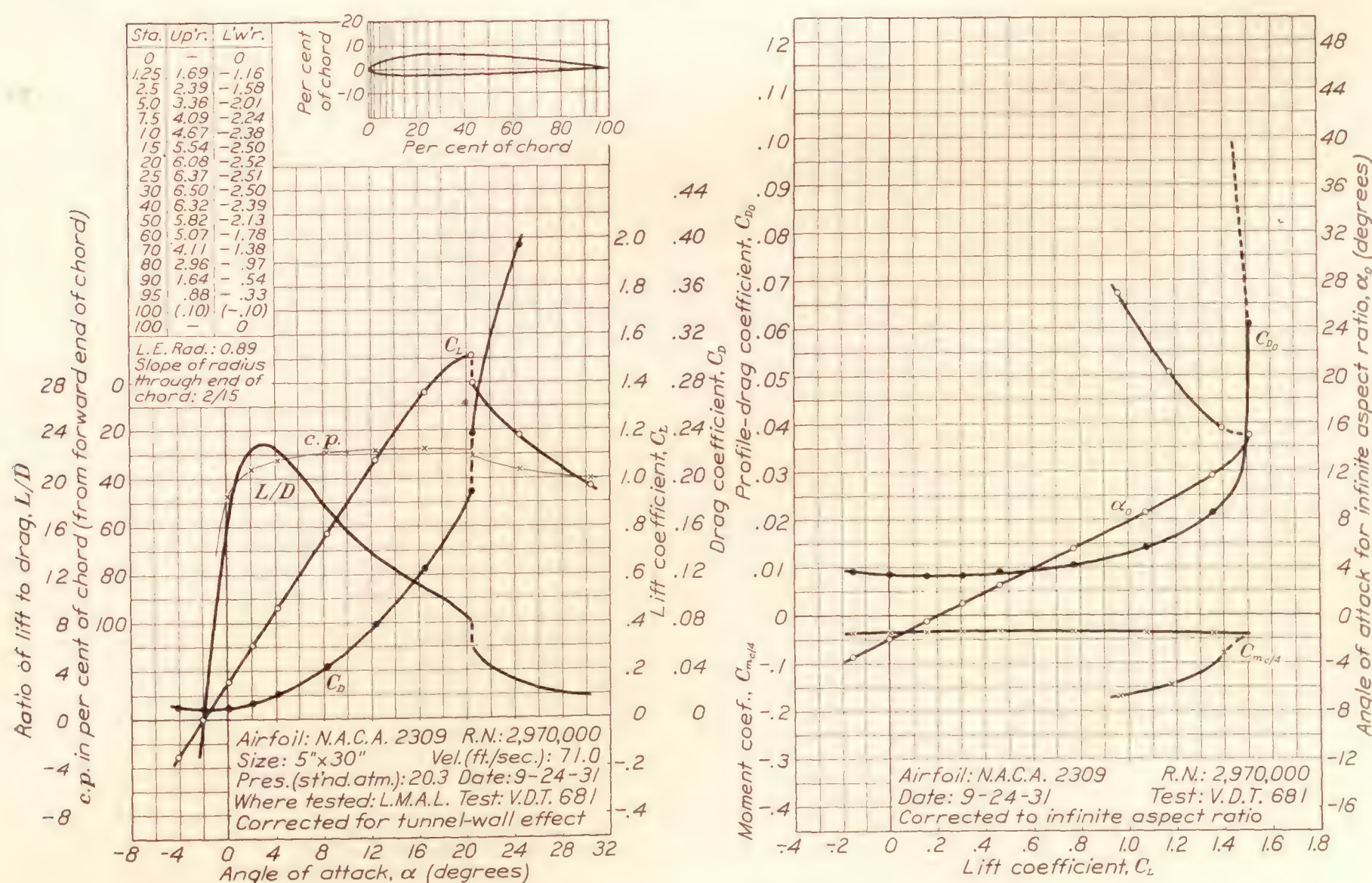


FIGURE 13.—N.A.C.A. 2309 airfoil.

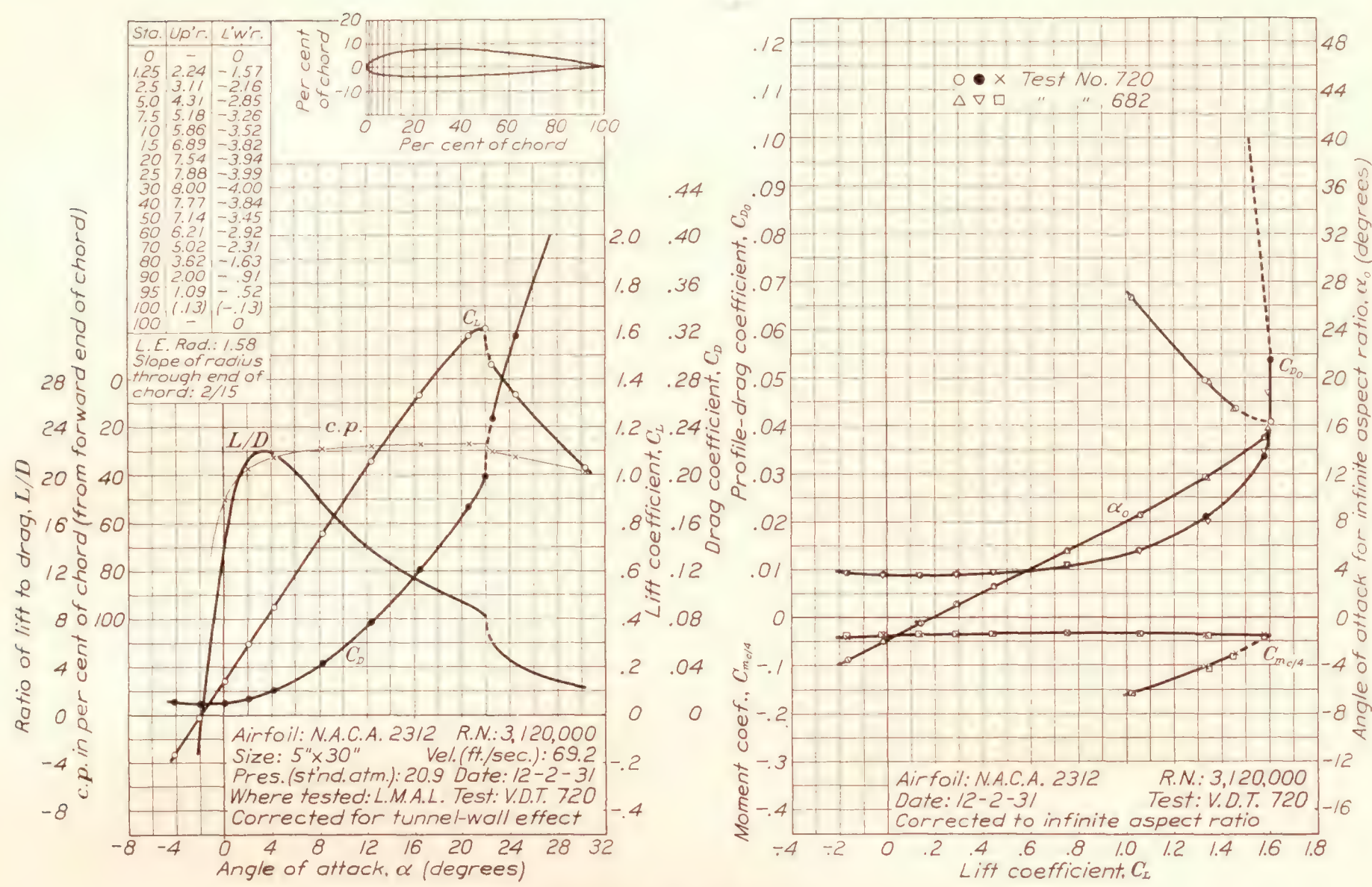


FIGURE 14.—N.A.C.A. 2312 airfoil.

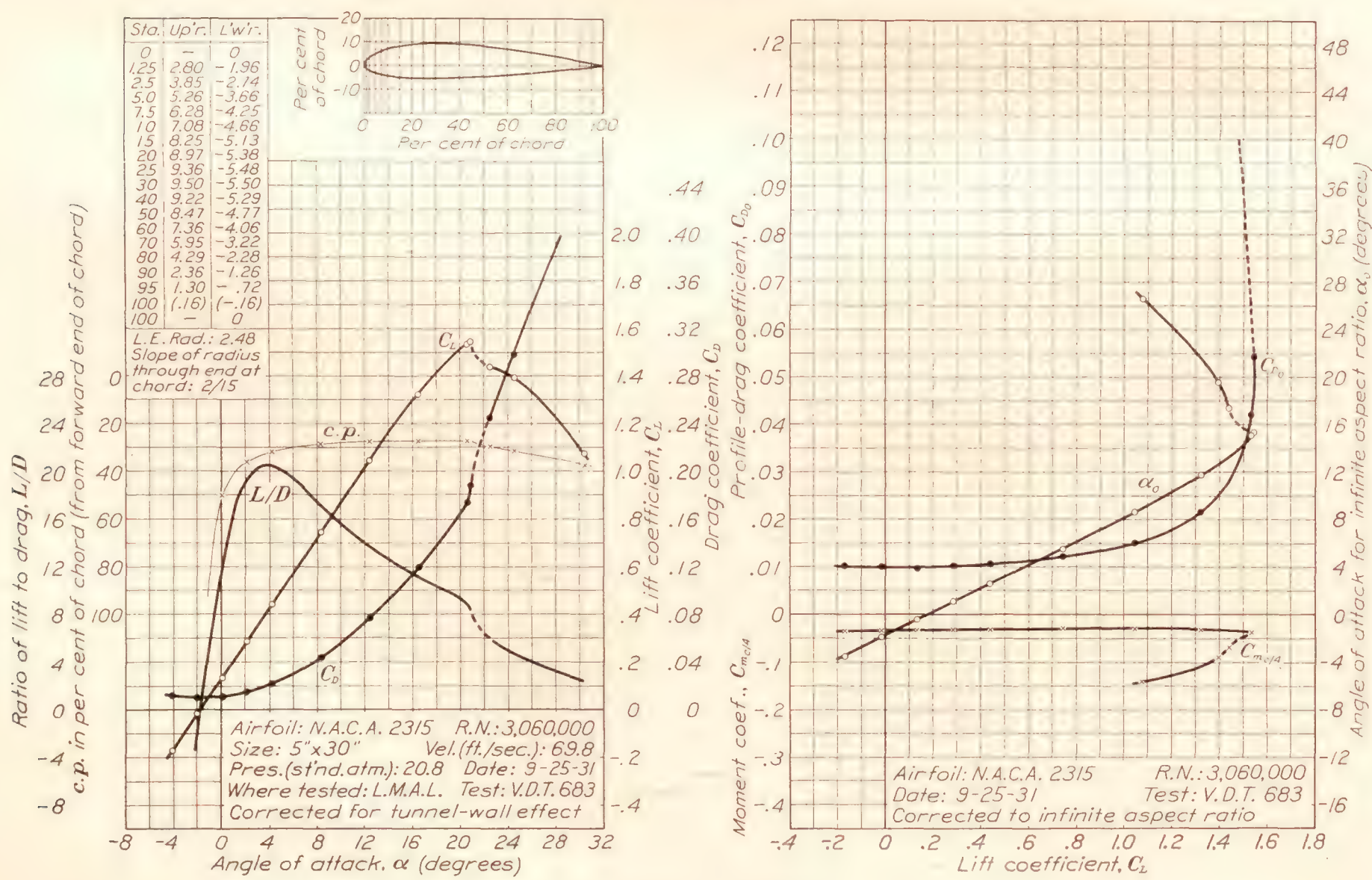


FIGURE 15.—N.A.C.A. 2315 airfoil.

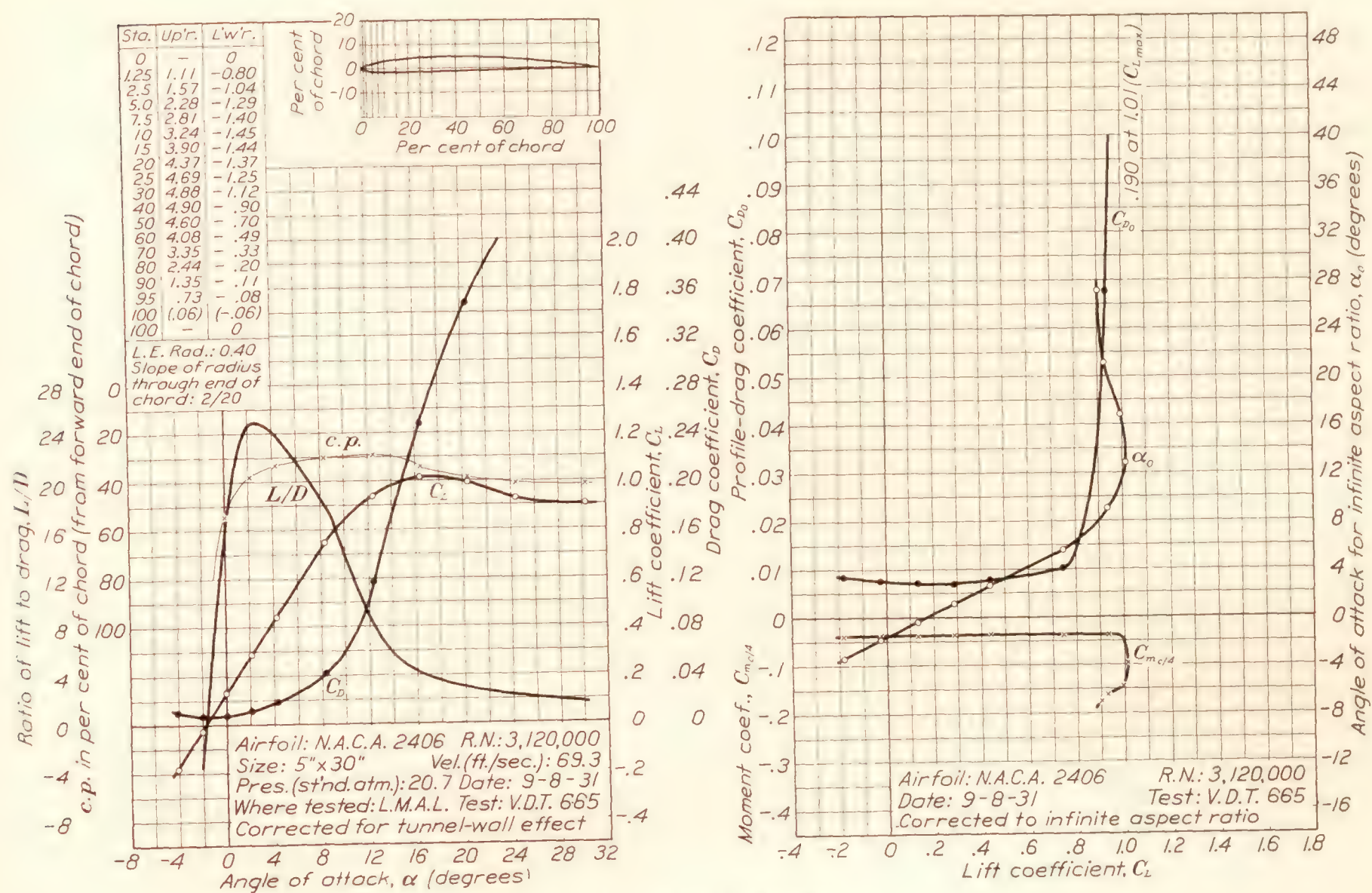


FIGURE 16.—N.A.C.A. 2406 airfoil.

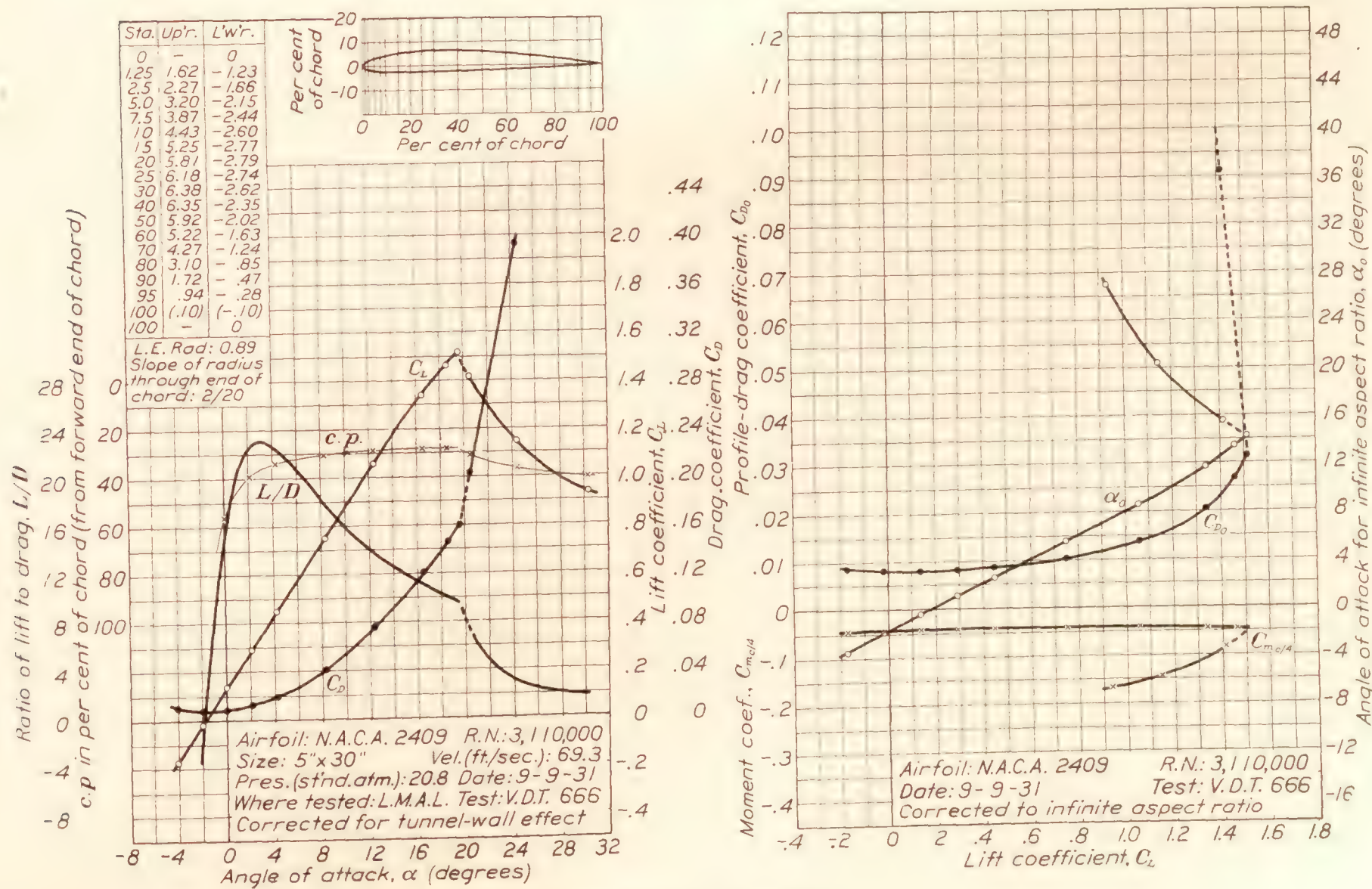


FIGURE 17.—N.A.C.A. 2409 airfoil.

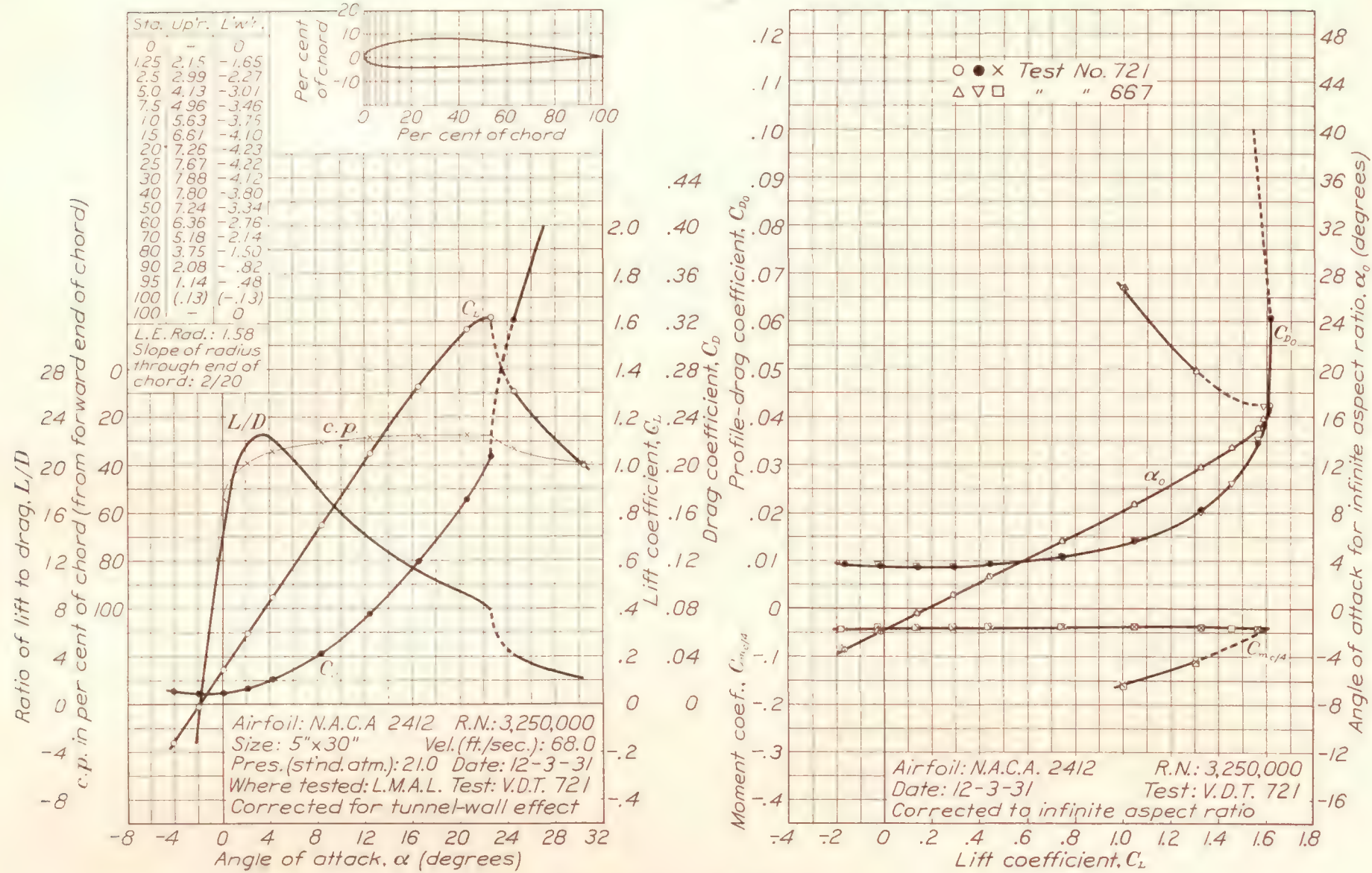


FIGURE 18.—N.A.C.A. 2412 airfoil.

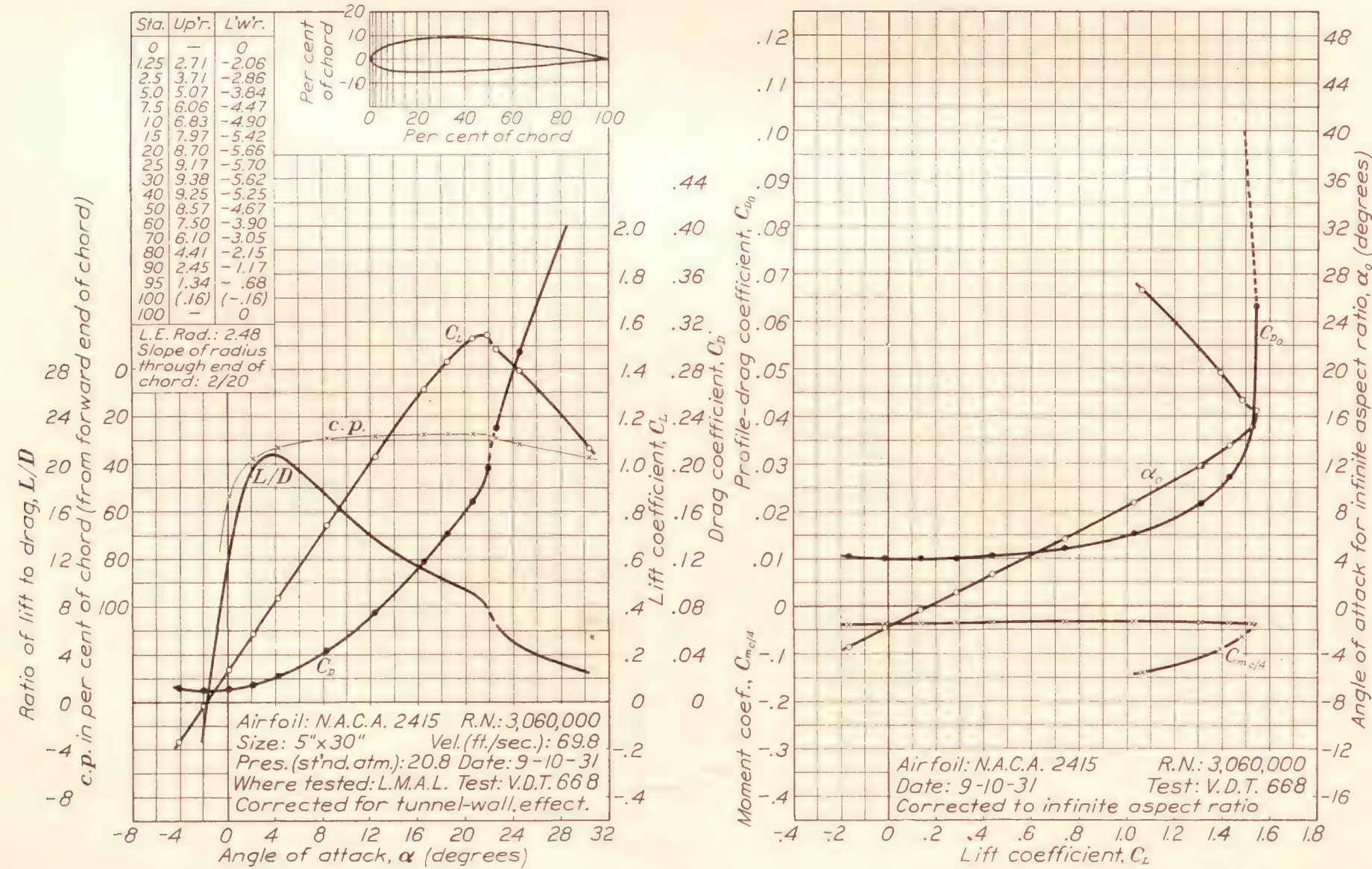


FIGURE 19.—N.A.C.A. 2415 airfoil.

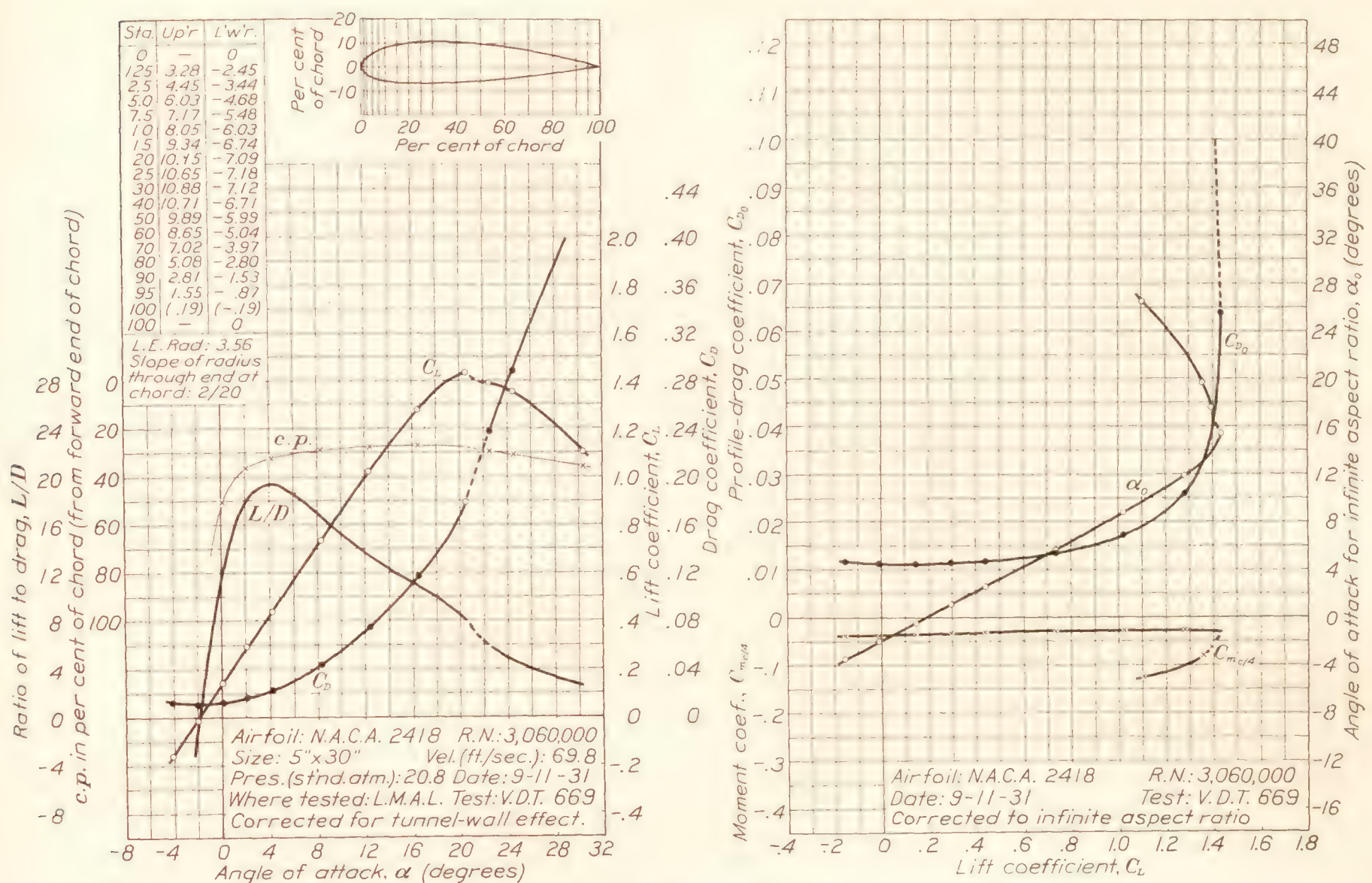


FIGURE 20.—N.A.C.A. 2418 airfoil.

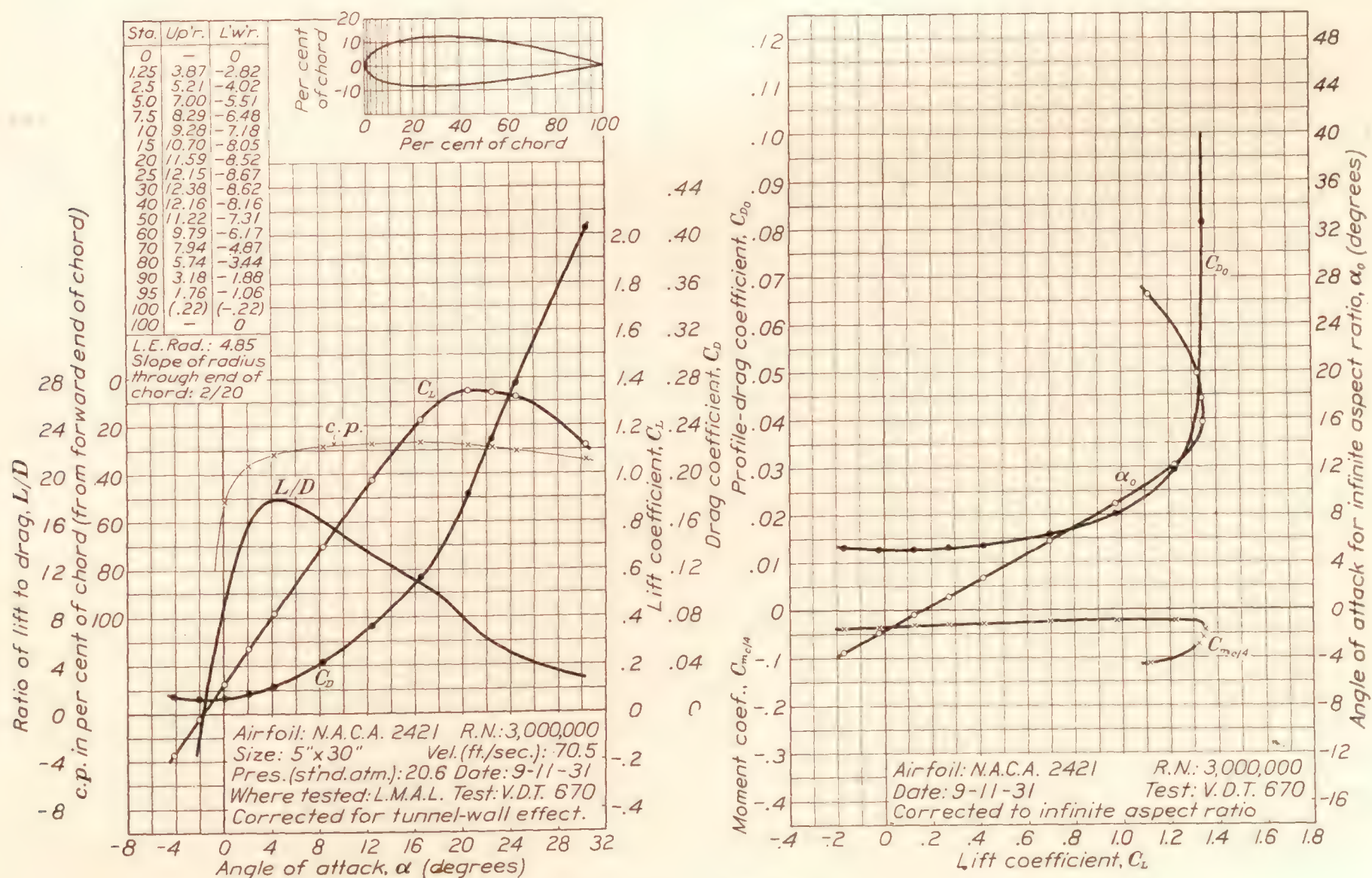


FIGURE 21.—N.A.C.A. 2421 airfoil.

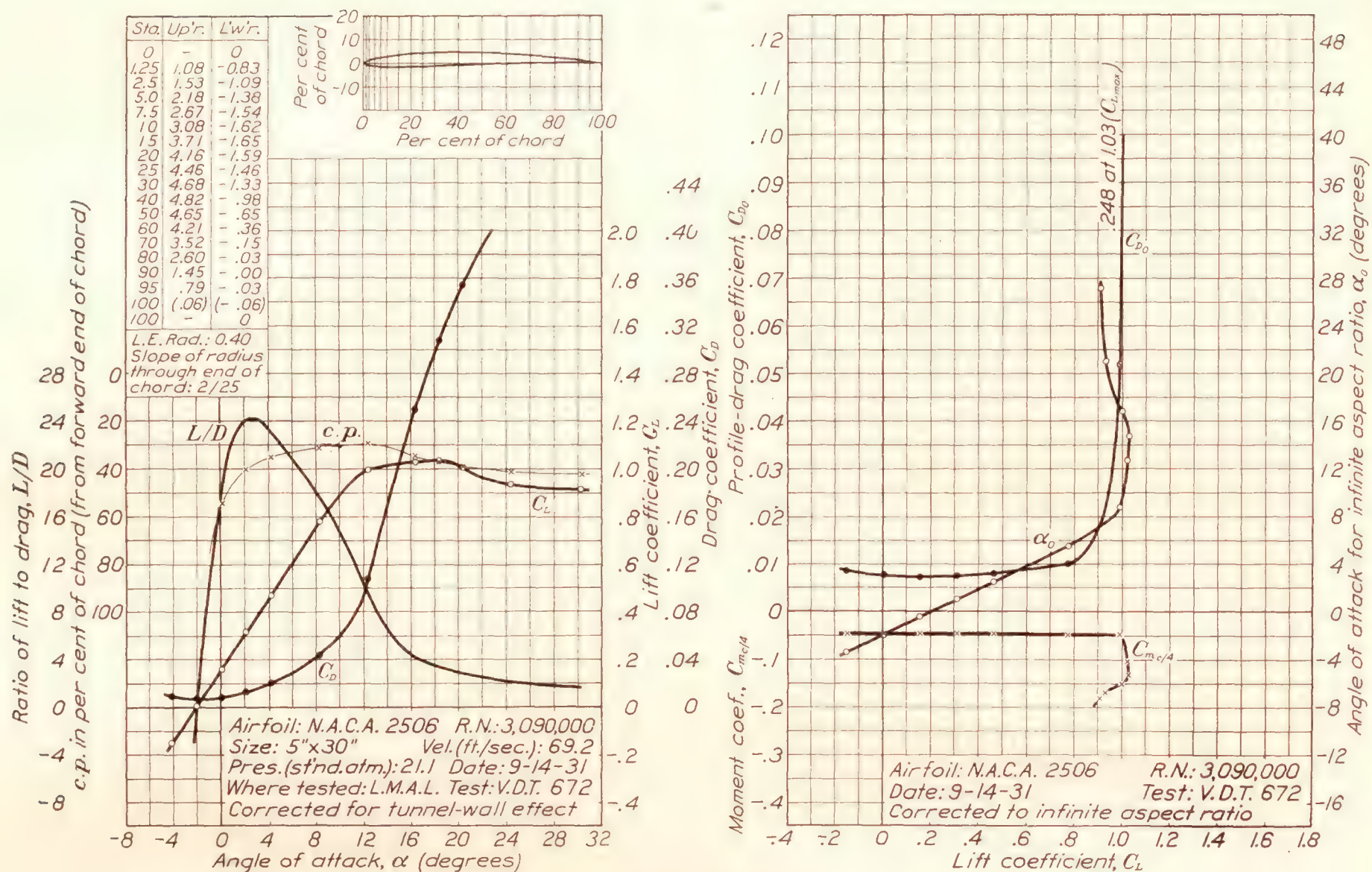


FIGURE 22.—N.A.C.A. 2506 airfoil.

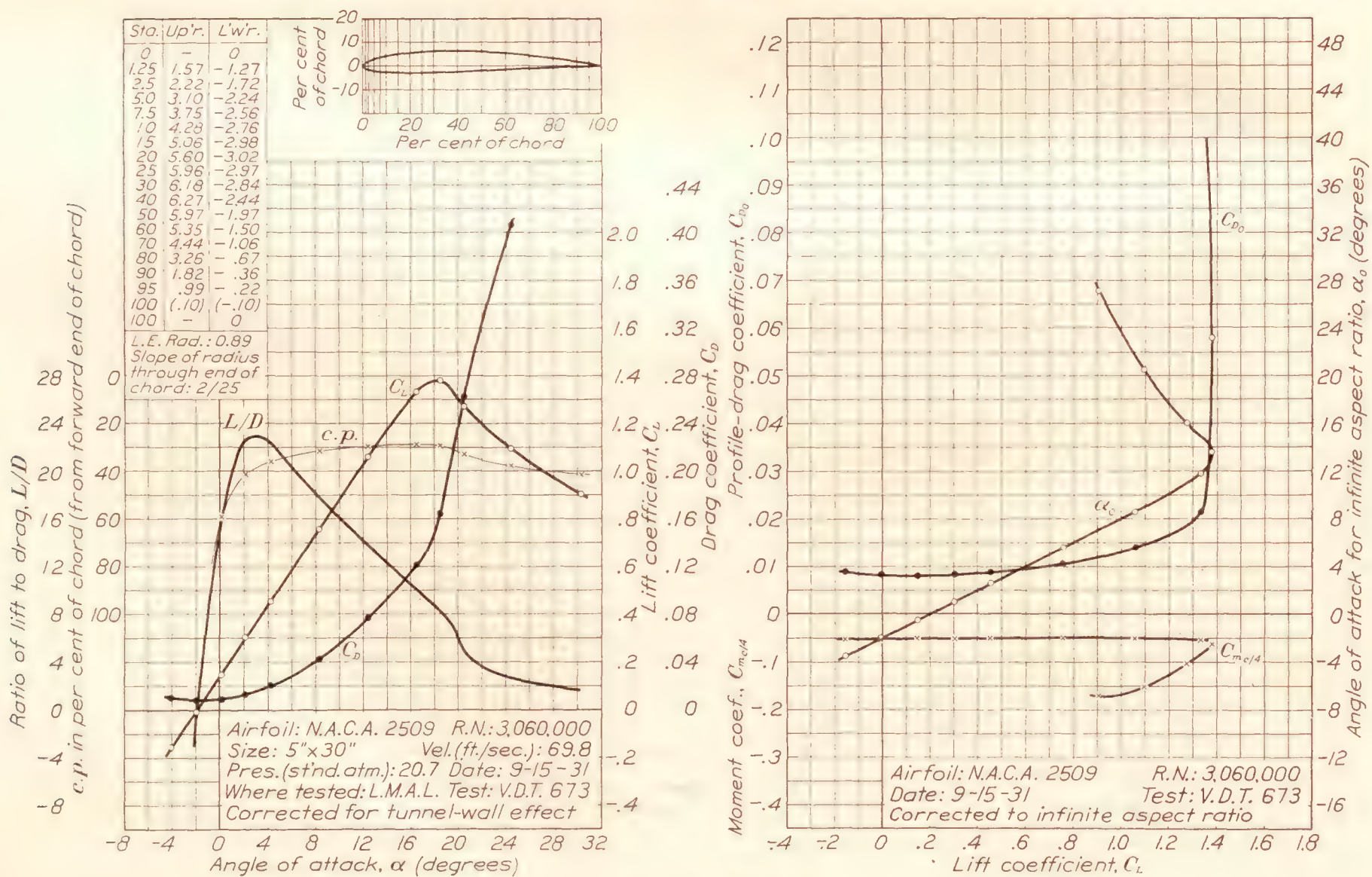


FIGURE 23.—N.A.C.A. 2509 airfoil.

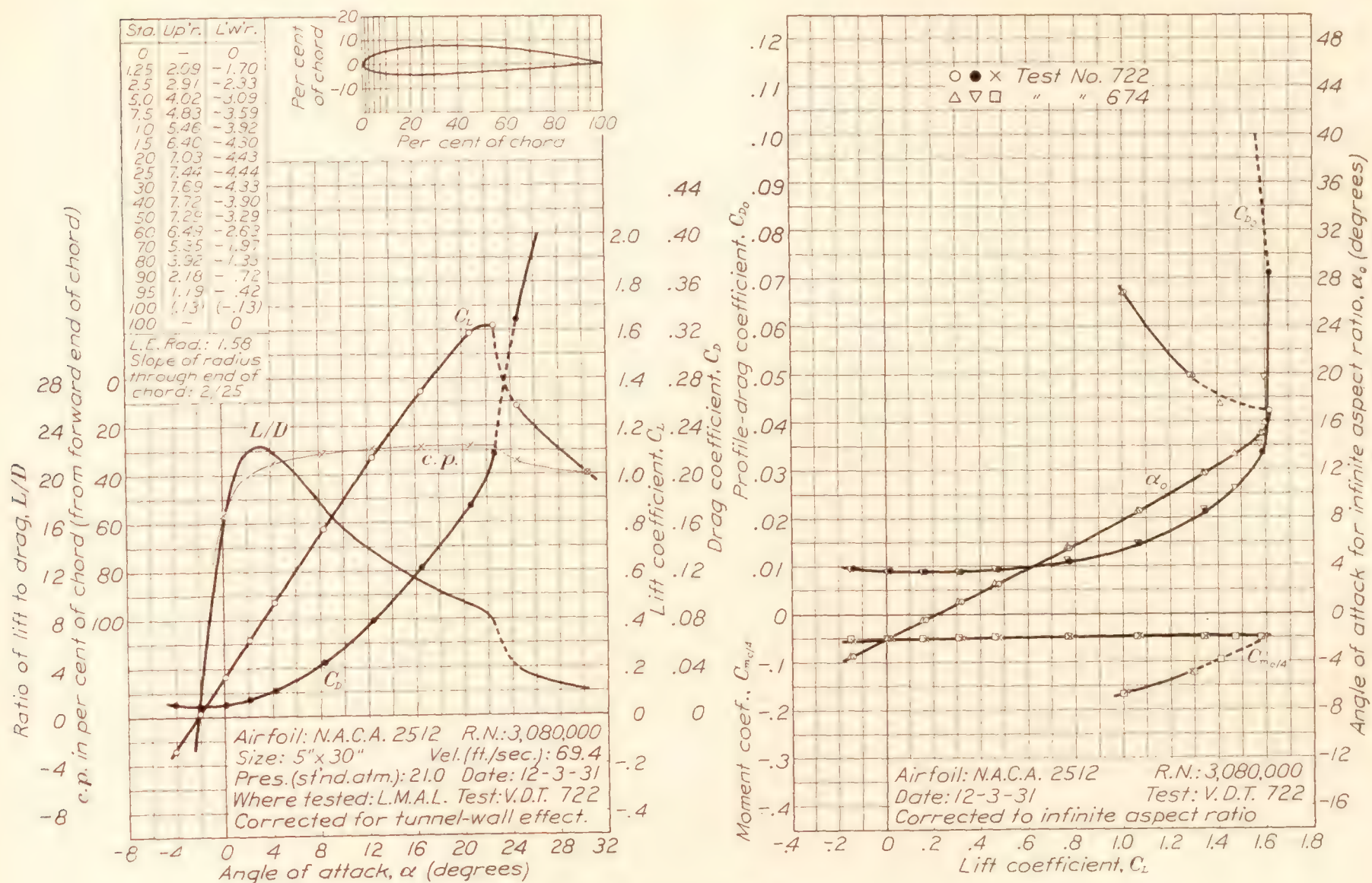


FIGURE 24.—N.A.C.A. 2512 airfoil.

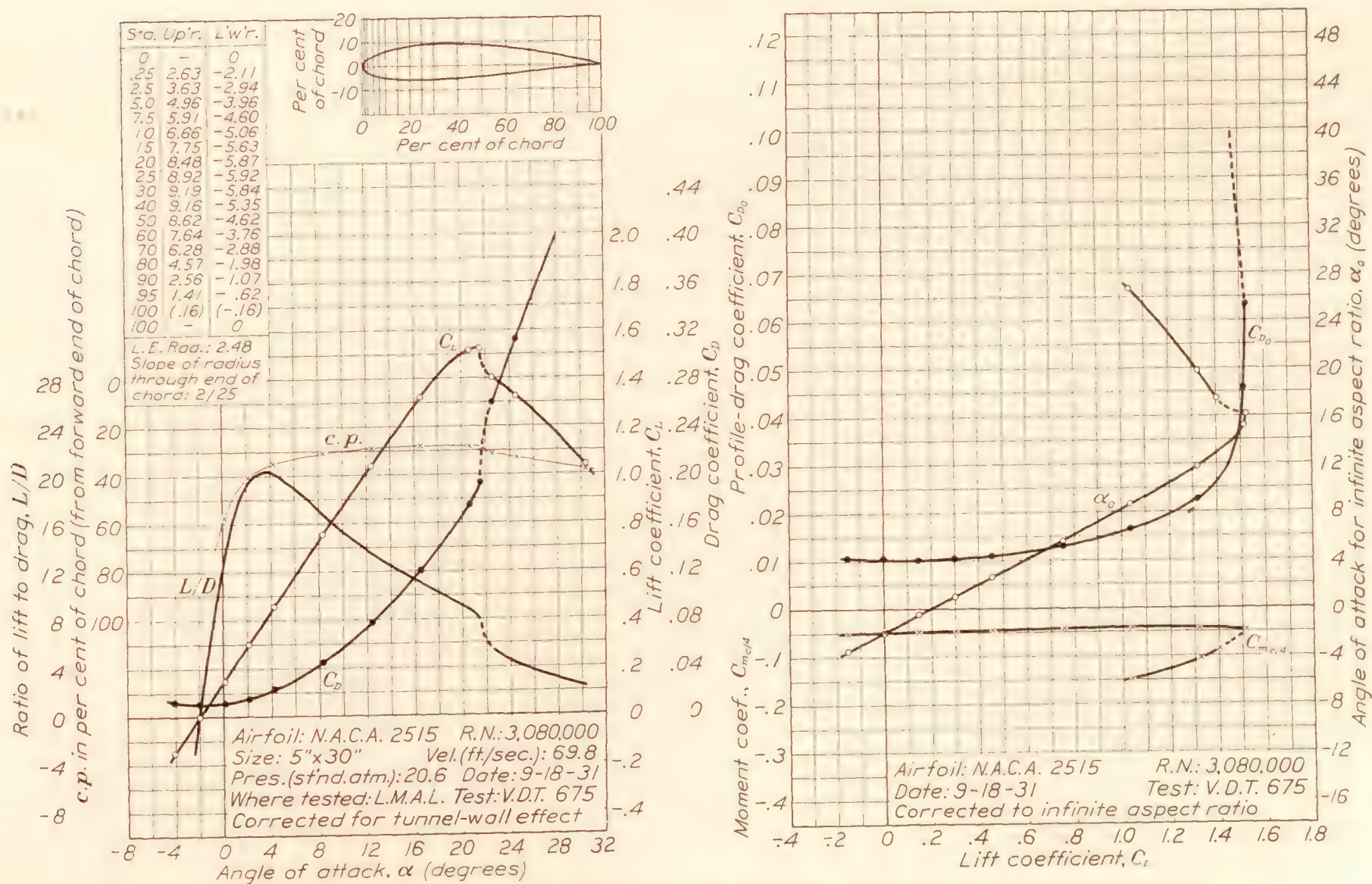


FIGURE 25.—N.A.C.A. 2515 airfoil.

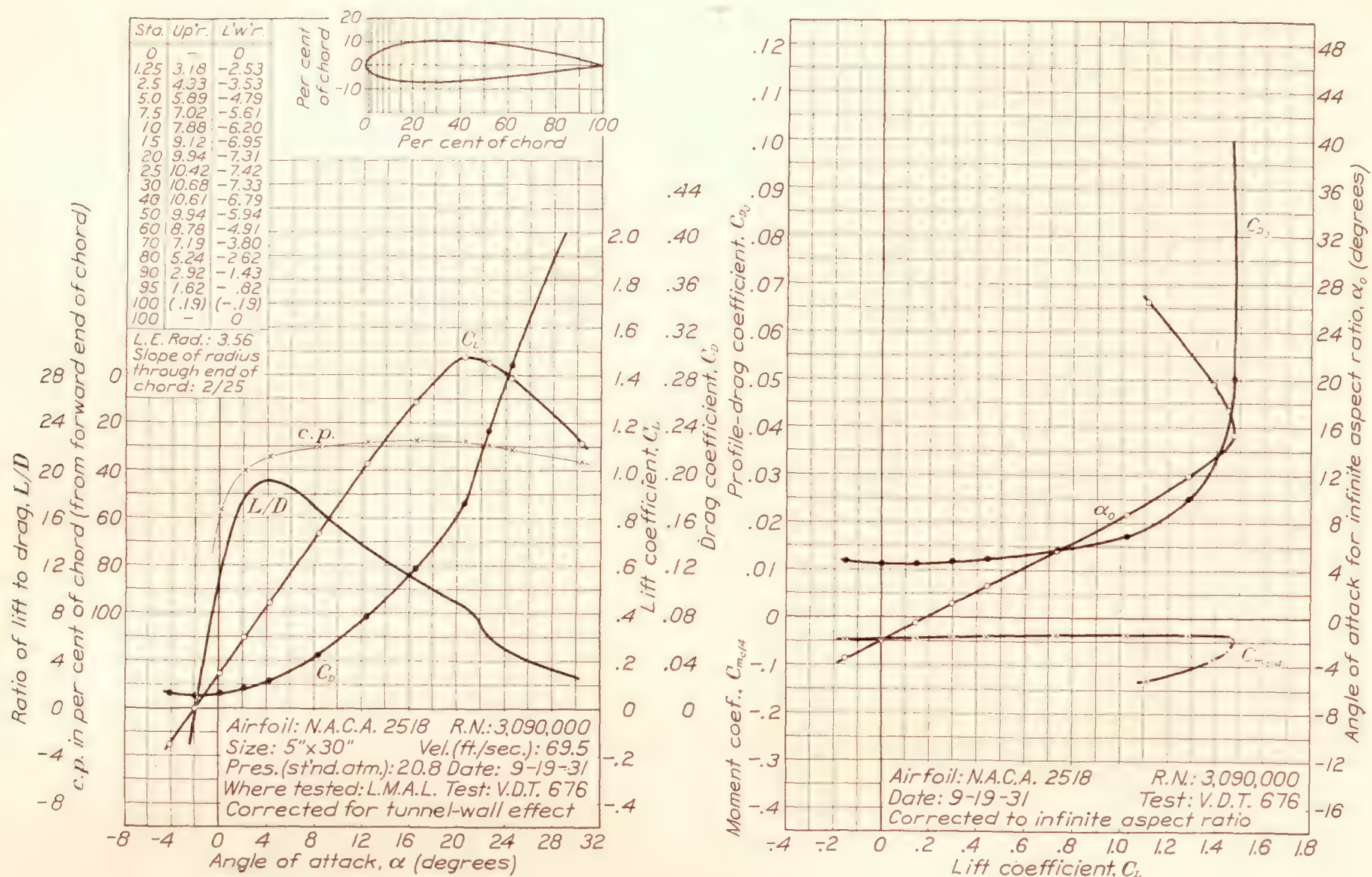


FIGURE 26.—N.A.C.A. 2518 airfoil.

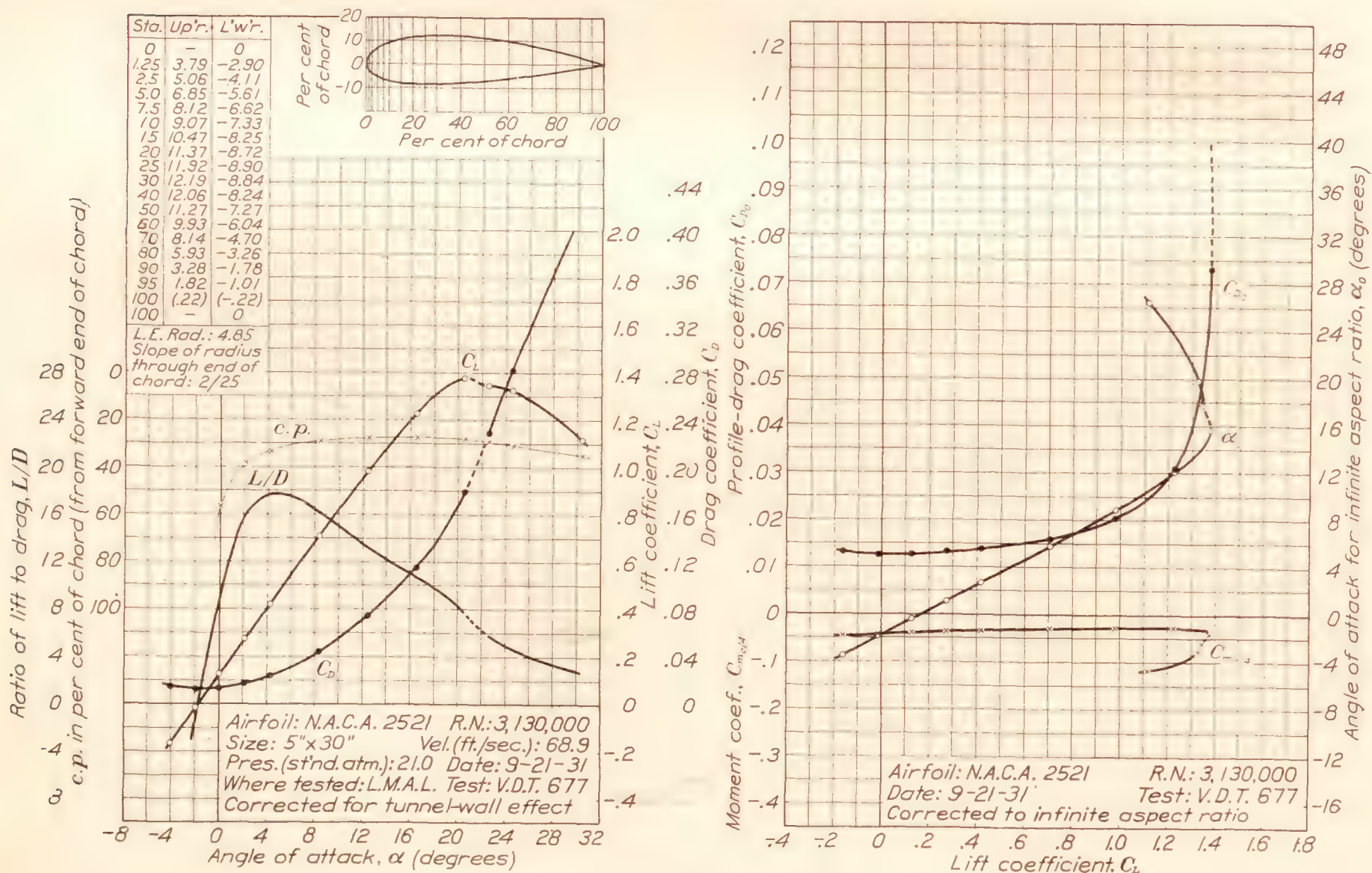


FIGURE 27.—N.A.C.A. 2521 airfoil.

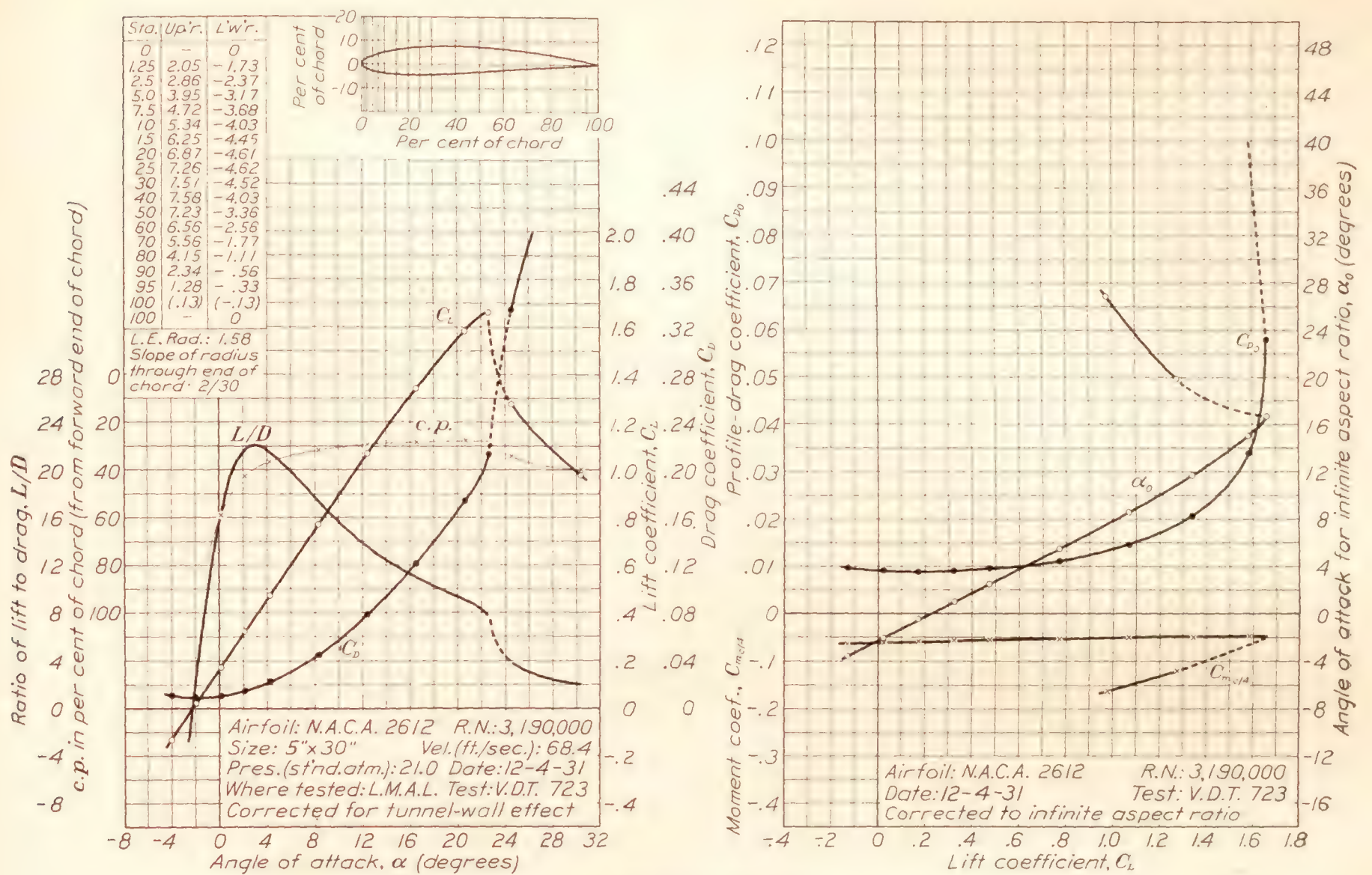


FIGURE 28.—N.A.C.A. 2612 airfoil.

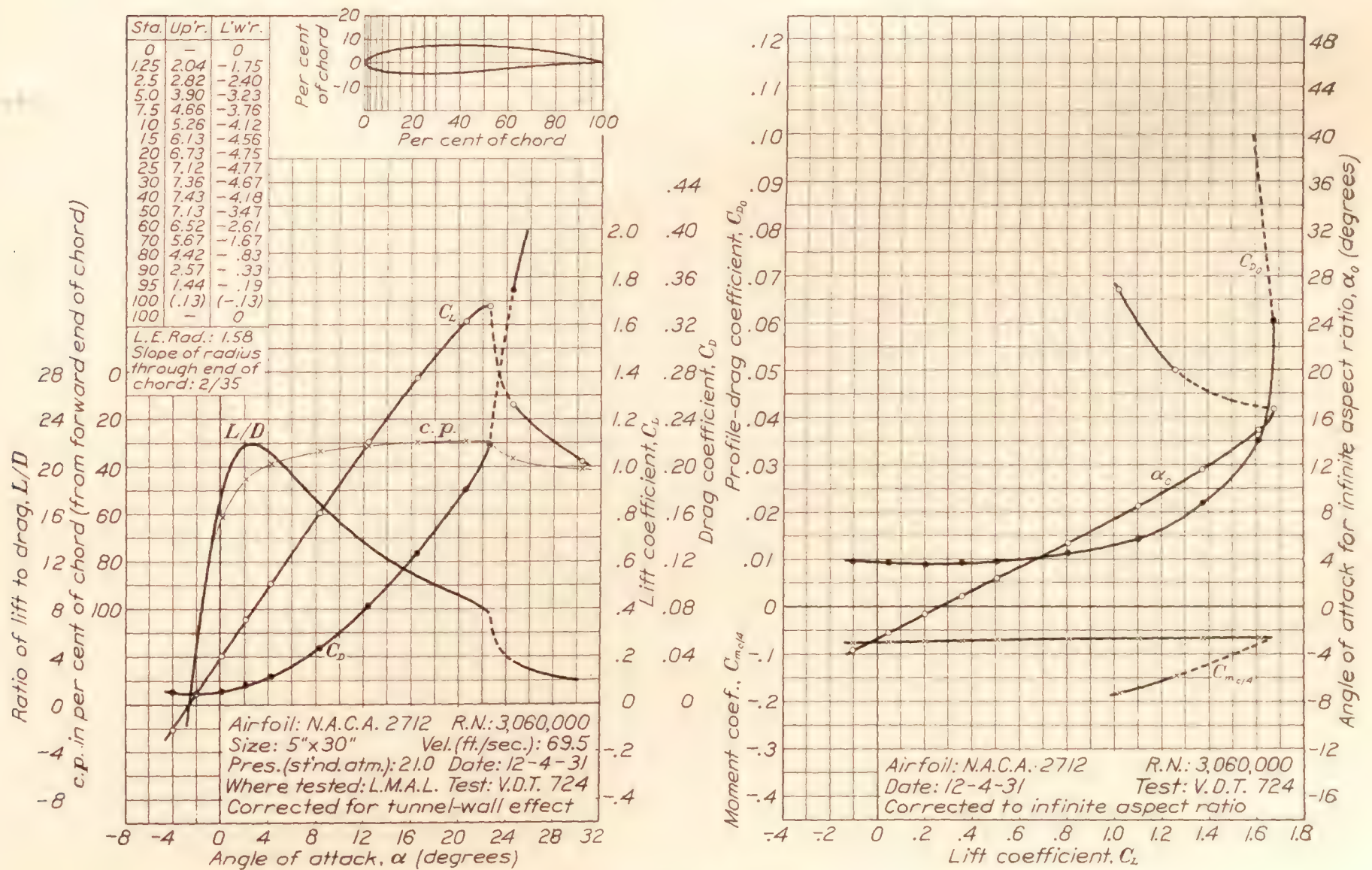


FIGURE 29.—N.A.C.A. 2712 airfoil.

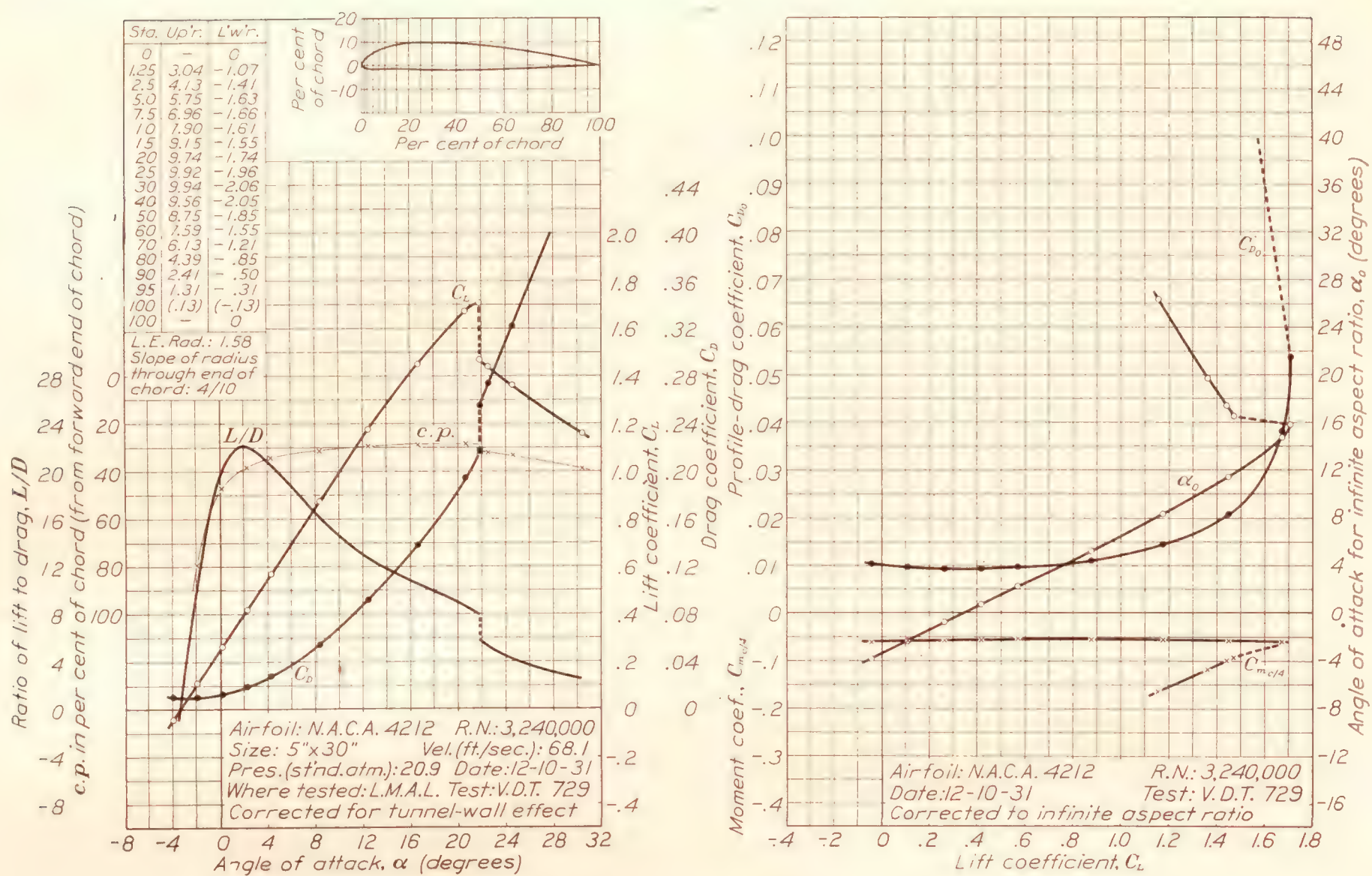


FIGURE 30.—N.A.C.A. 4212 airfoil.

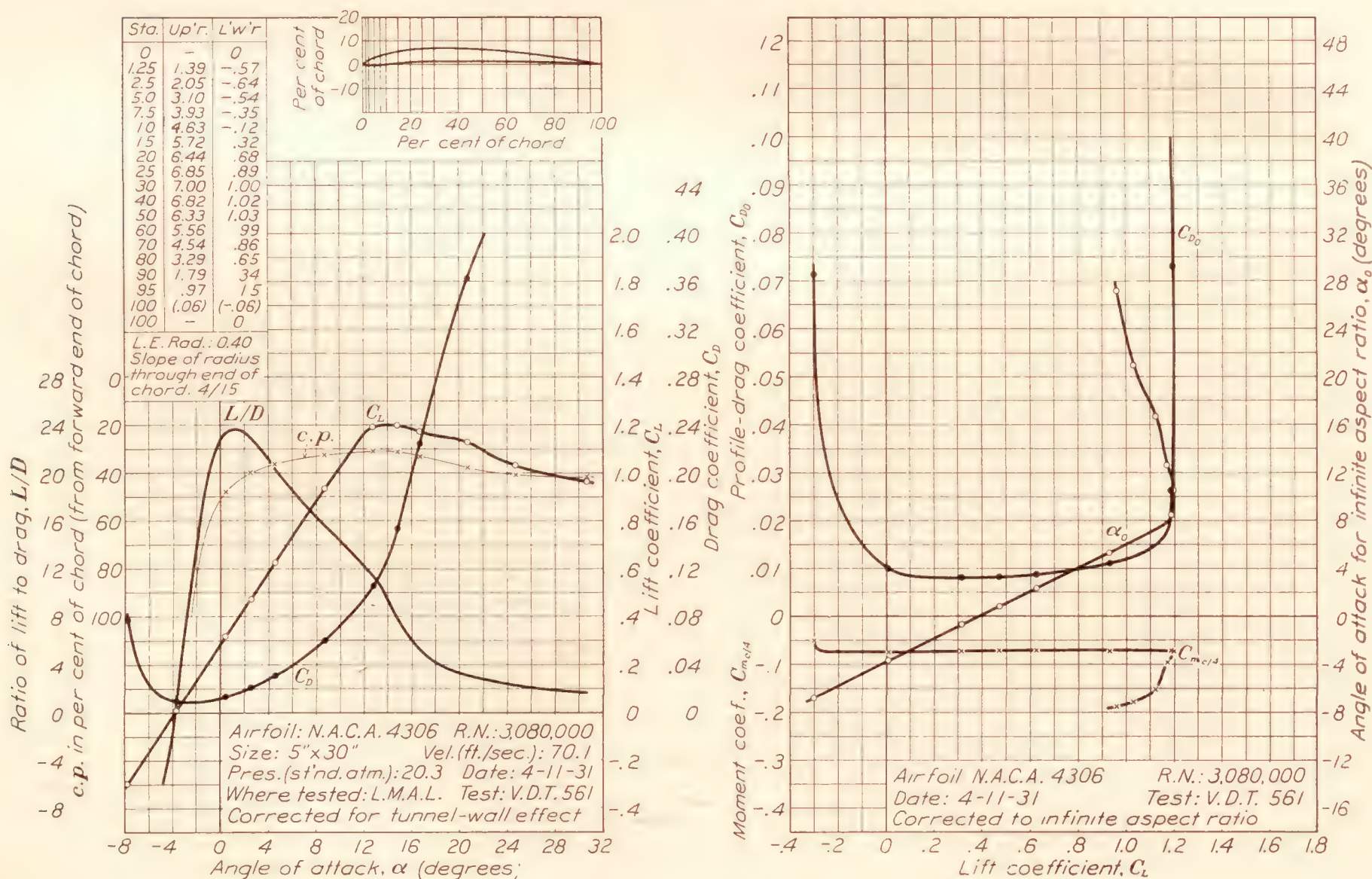


FIGURE 31.—N.A.C.A. 4306 airfoil.

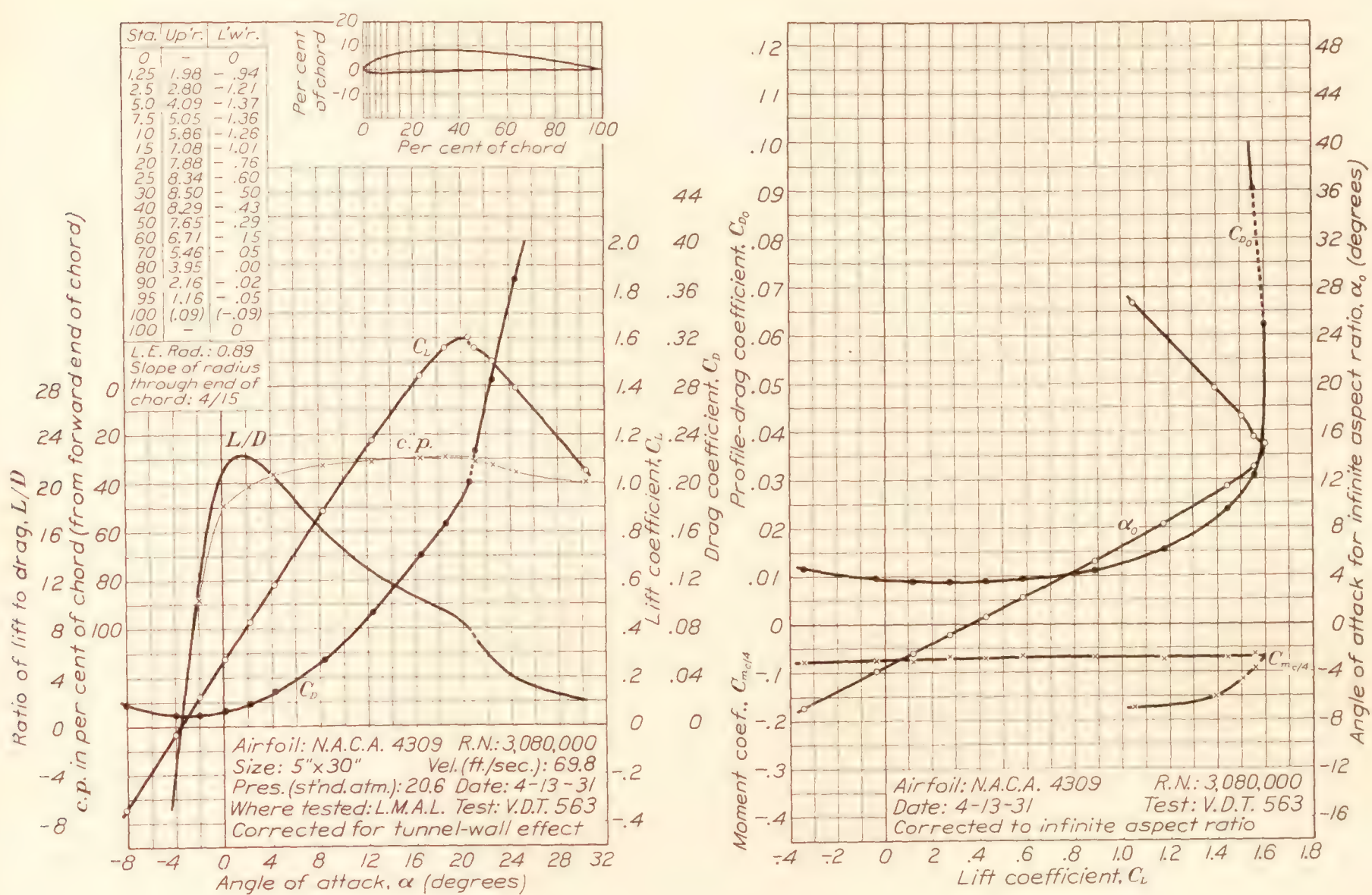


FIGURE 32.—N.A.C.A. 4309 airfoil.

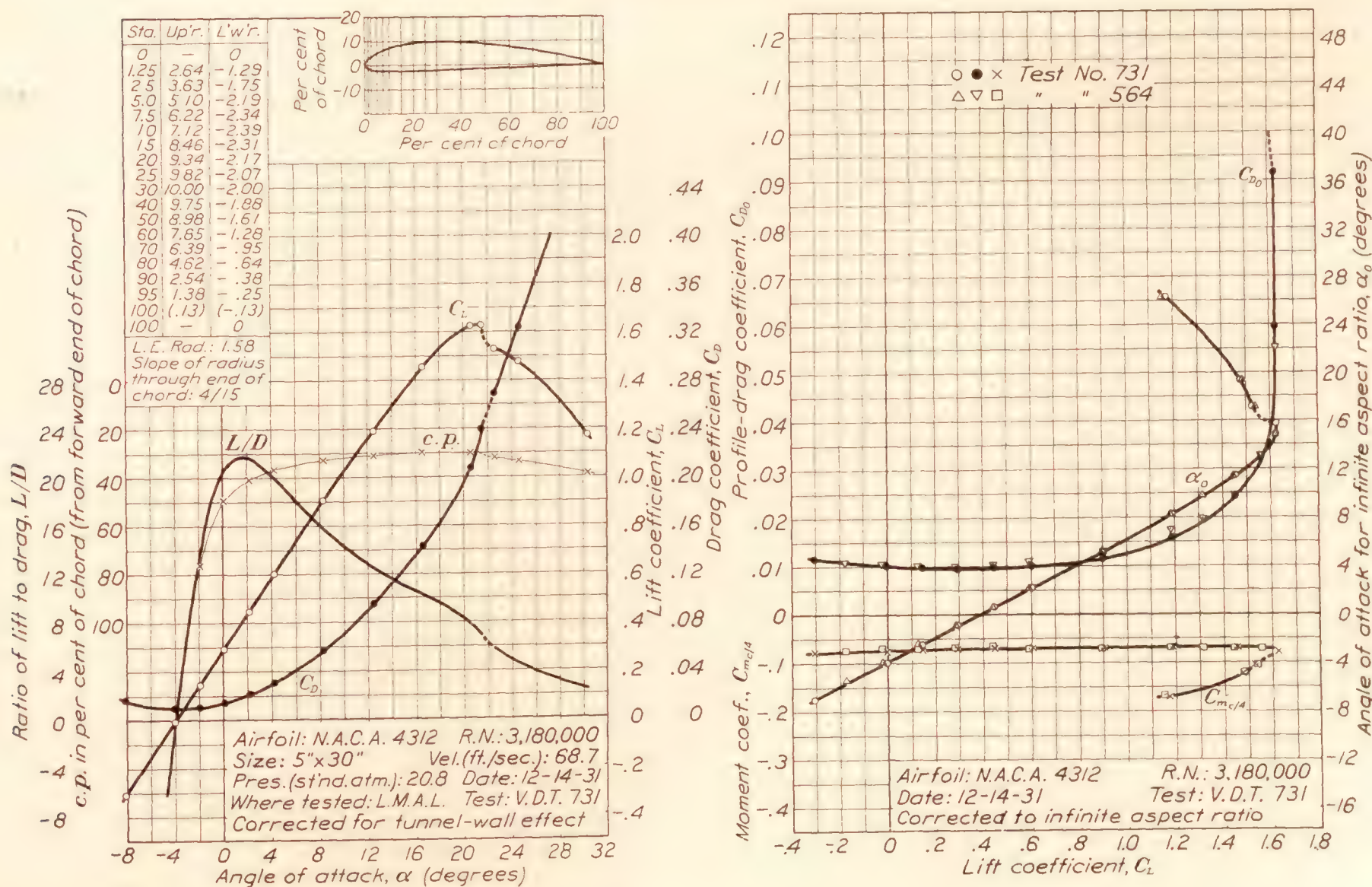


FIGURE 33.—N.A.C.A. 4312 airfoil.

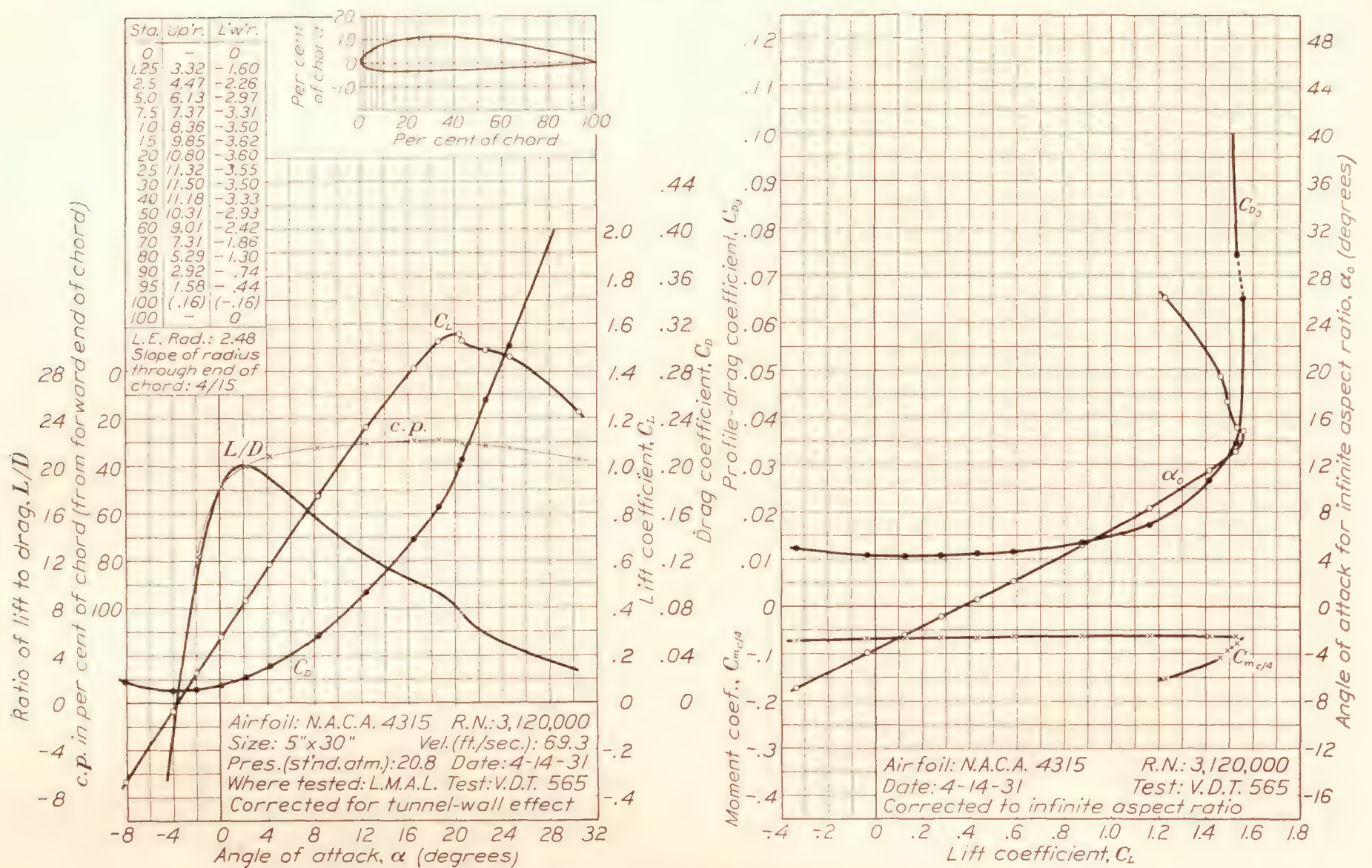


FIGURE 34.—N.A.C.A. 4315 airfoil.

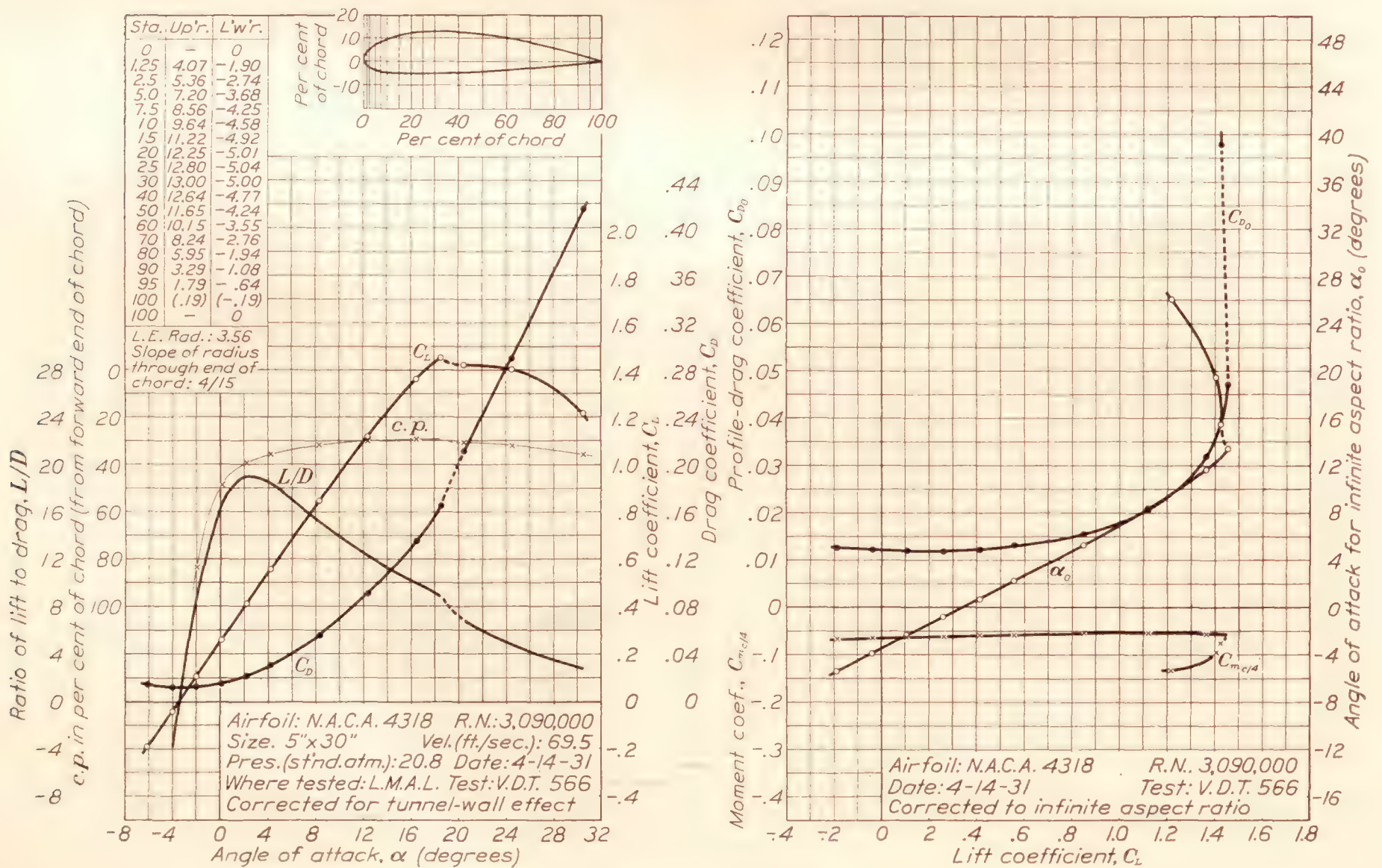


FIGURE 35.—N.A.C.A. 4318 airfoil.

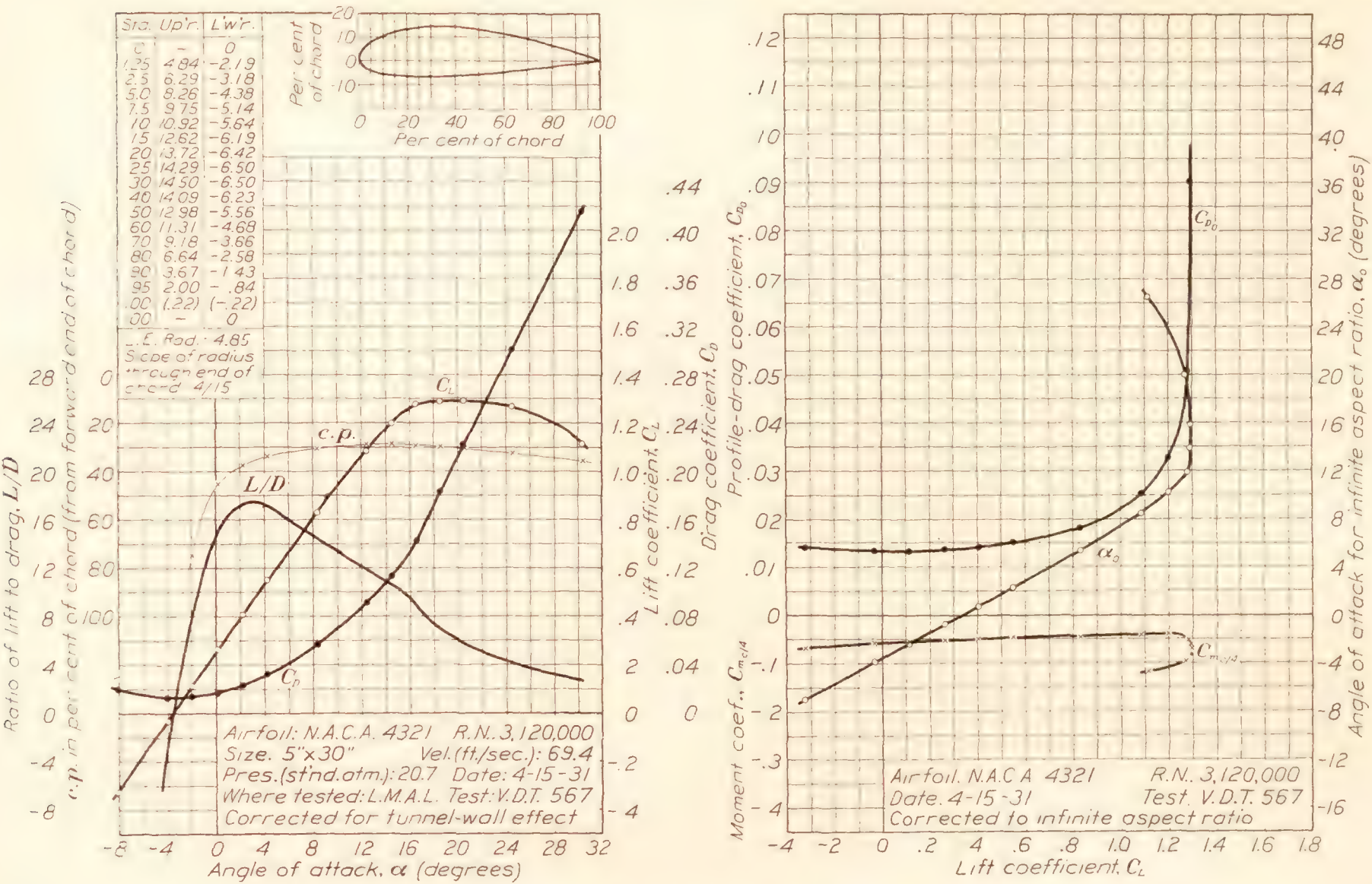


FIGURE 36.—N.A.C.A. 4321 airfoil.

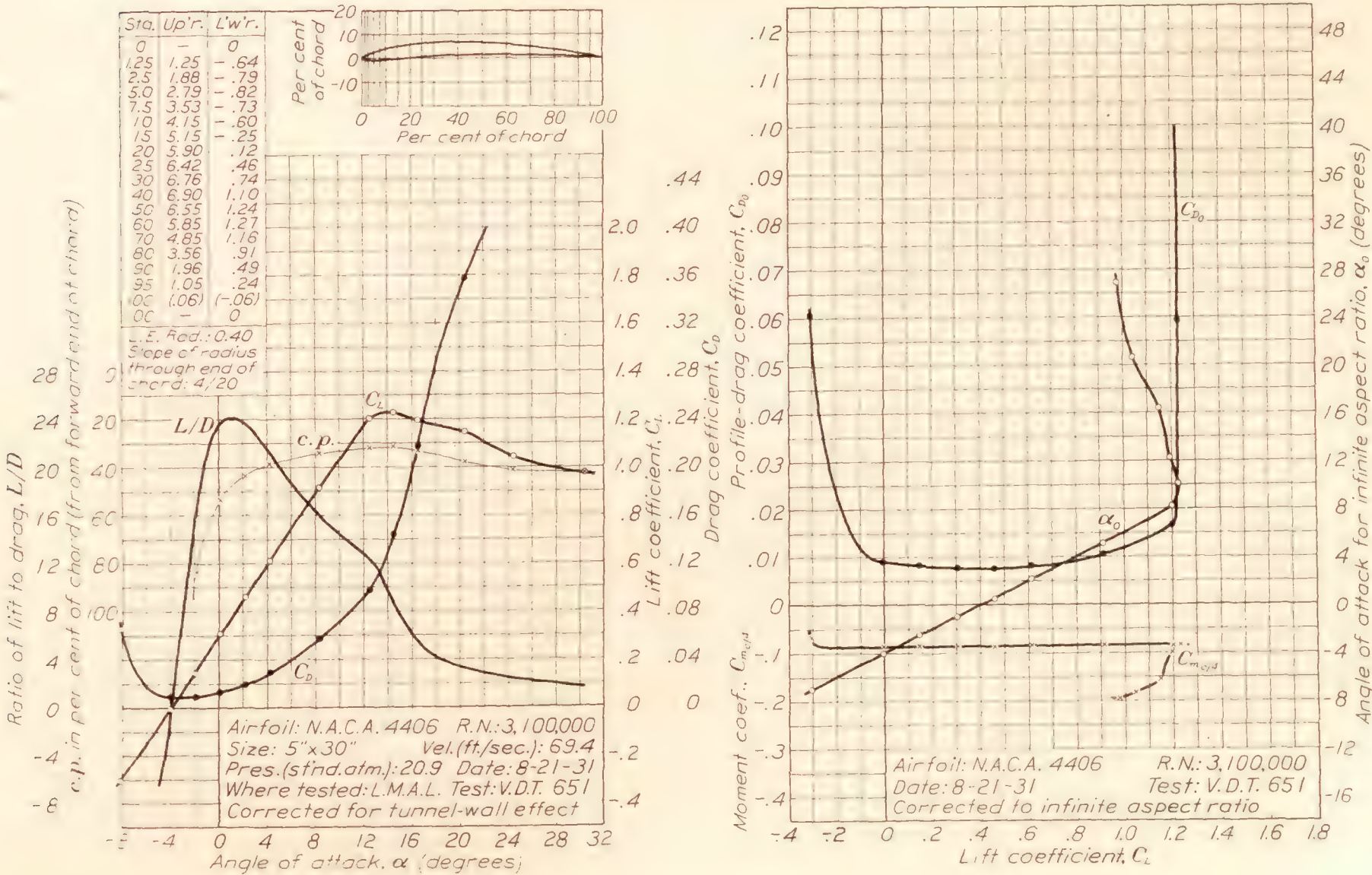


FIGURE 37.—N.A.C.A. 4406 airfoil.

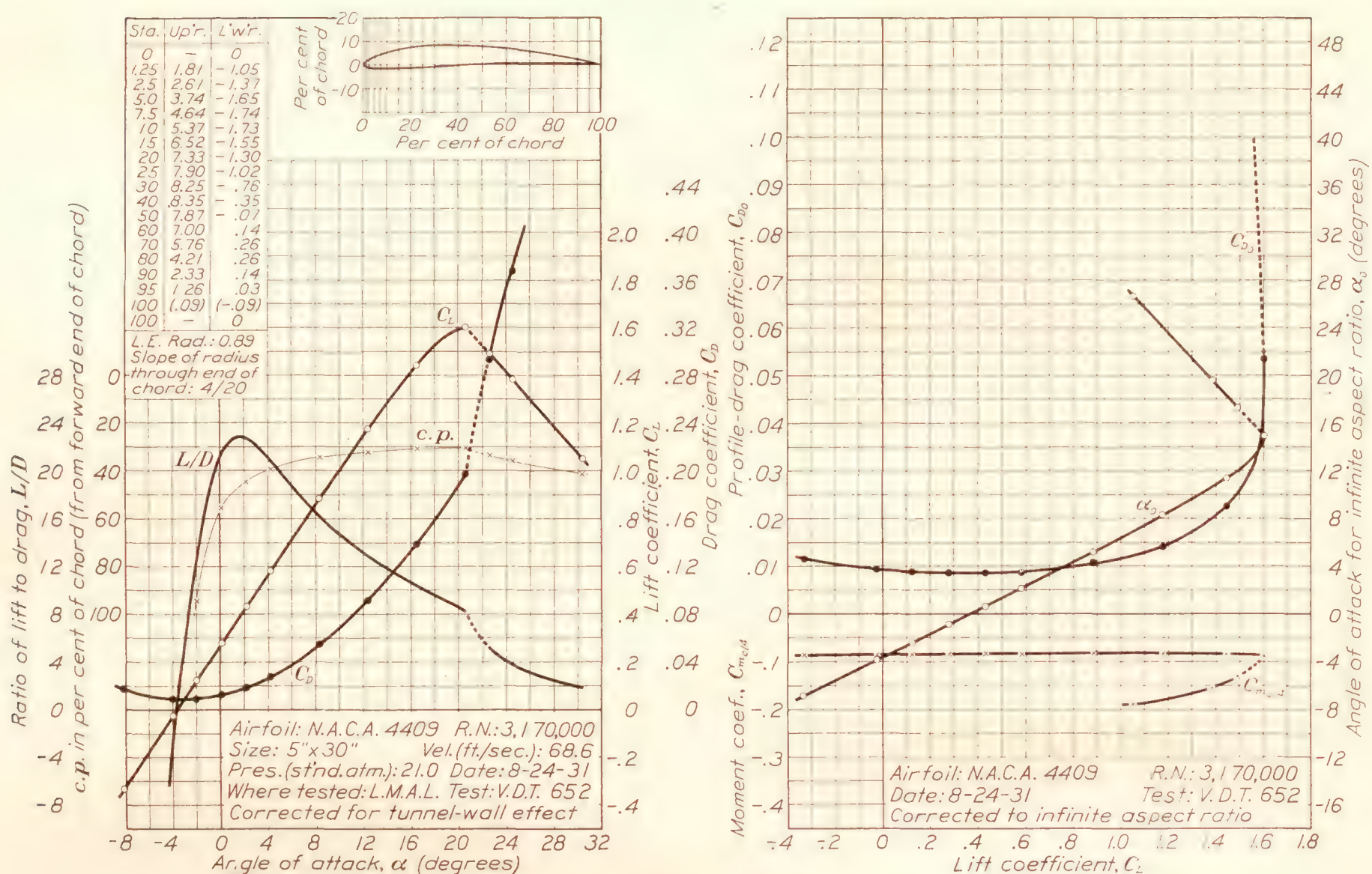


FIGURE 38.—N.A.C.A. 4409 airfoil.

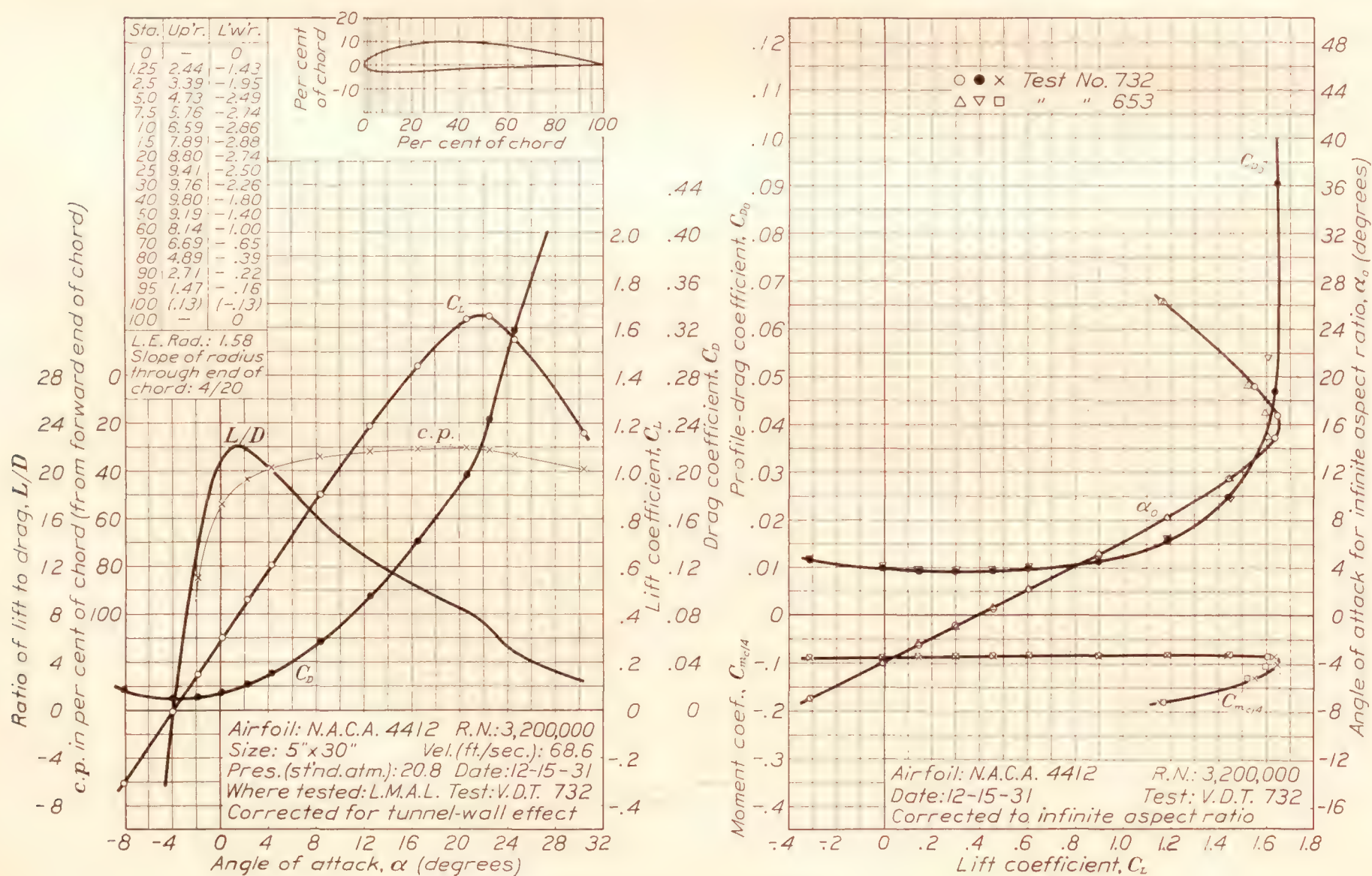
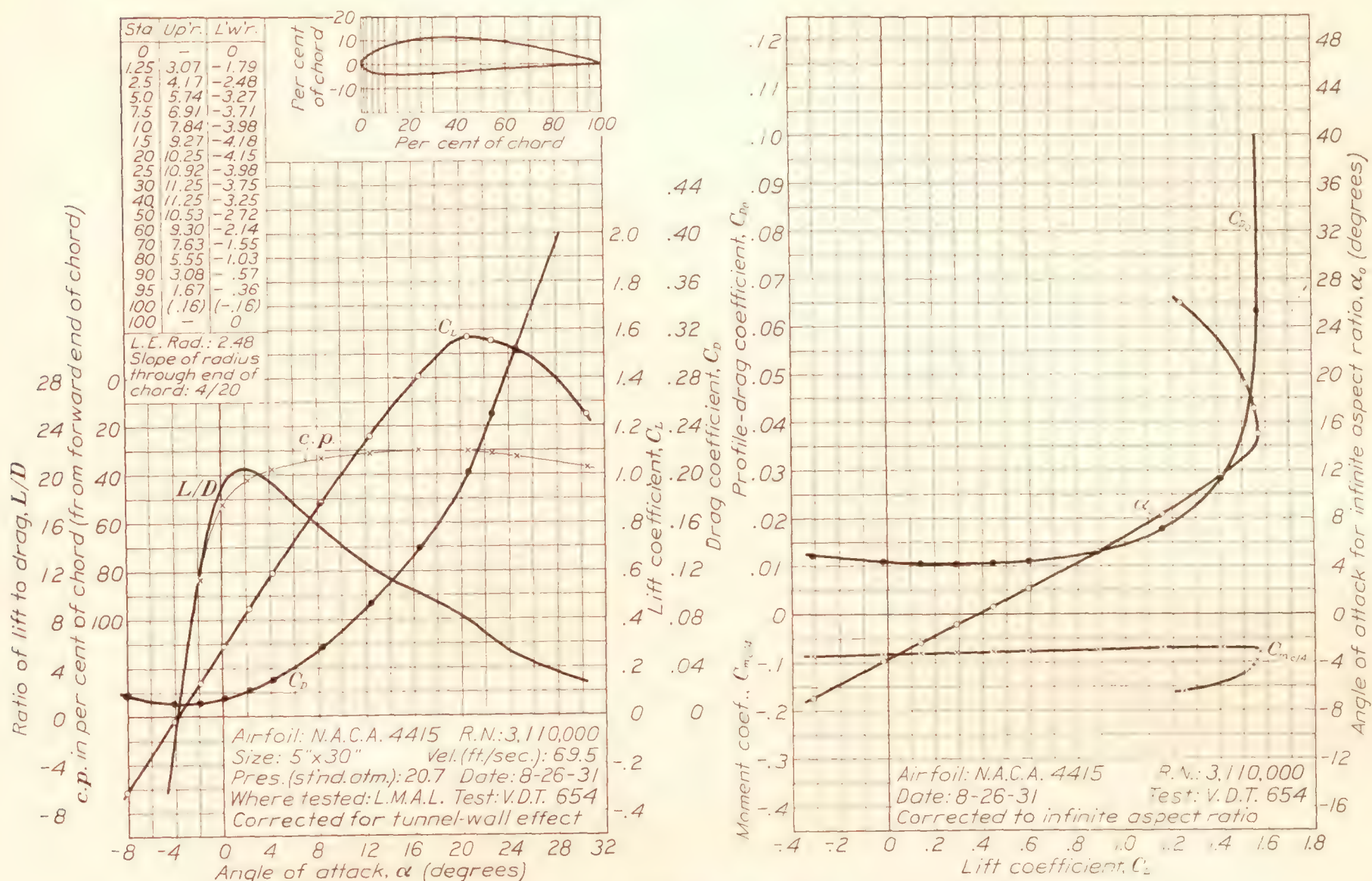


FIGURE 39.—N.A.C.A. 4412 airfoil.



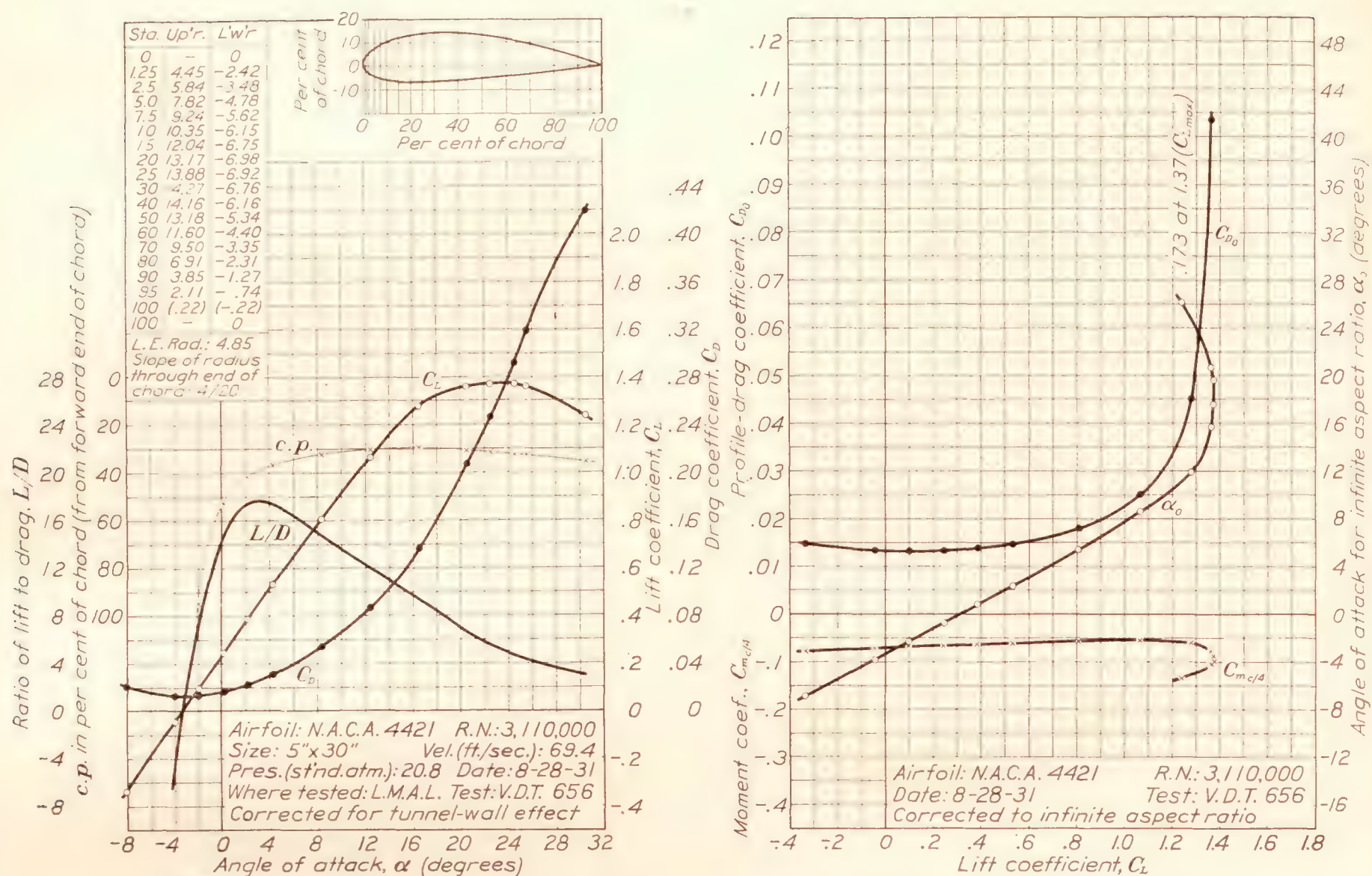


FIGURE 42.—N.A.C.A. 4421 airfoil.

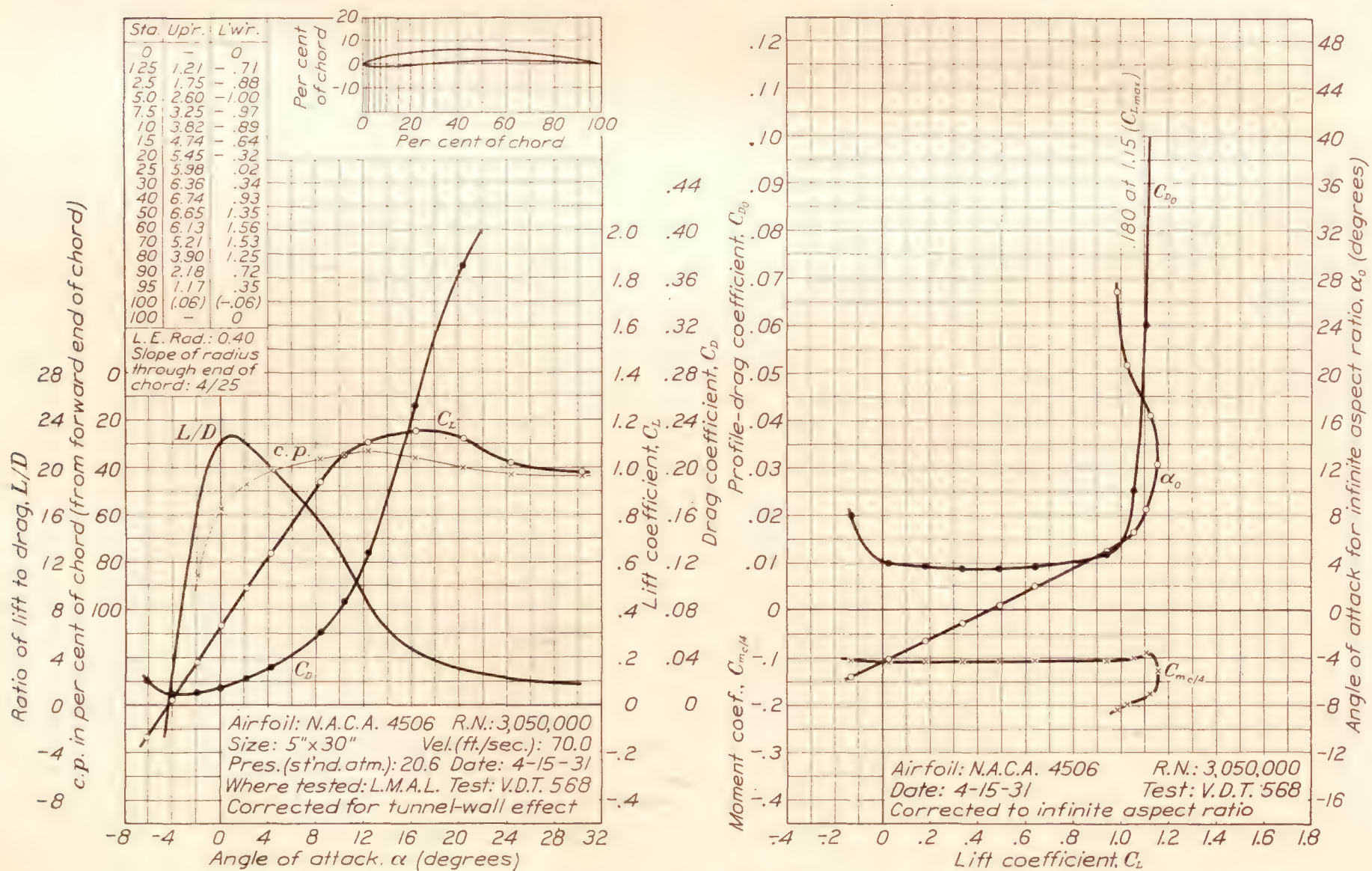


FIGURE 43.—N.A.C.A. 4506 airfoil.

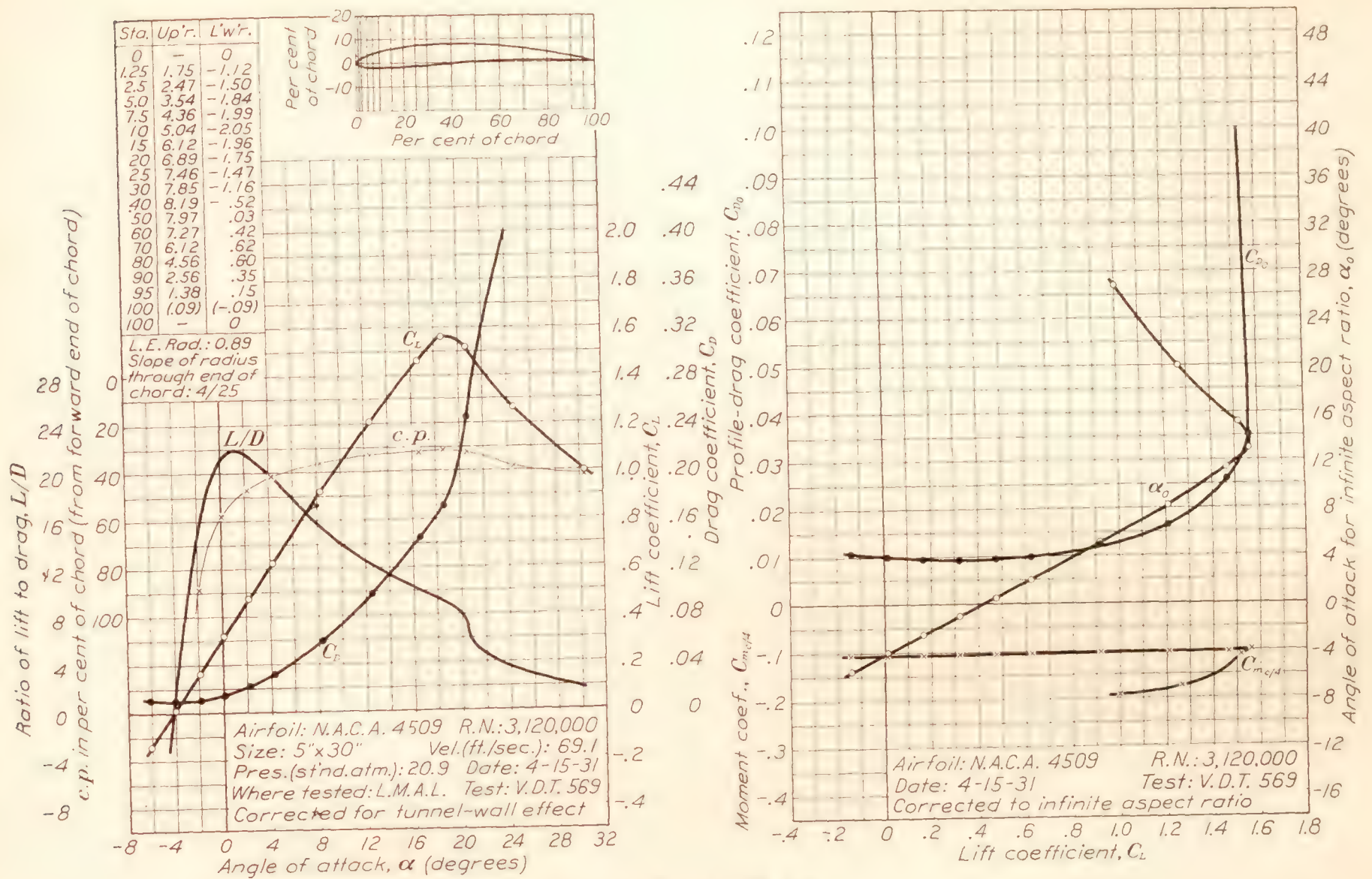


FIGURE 44.—N.A.C.A. 4509 airfoil.

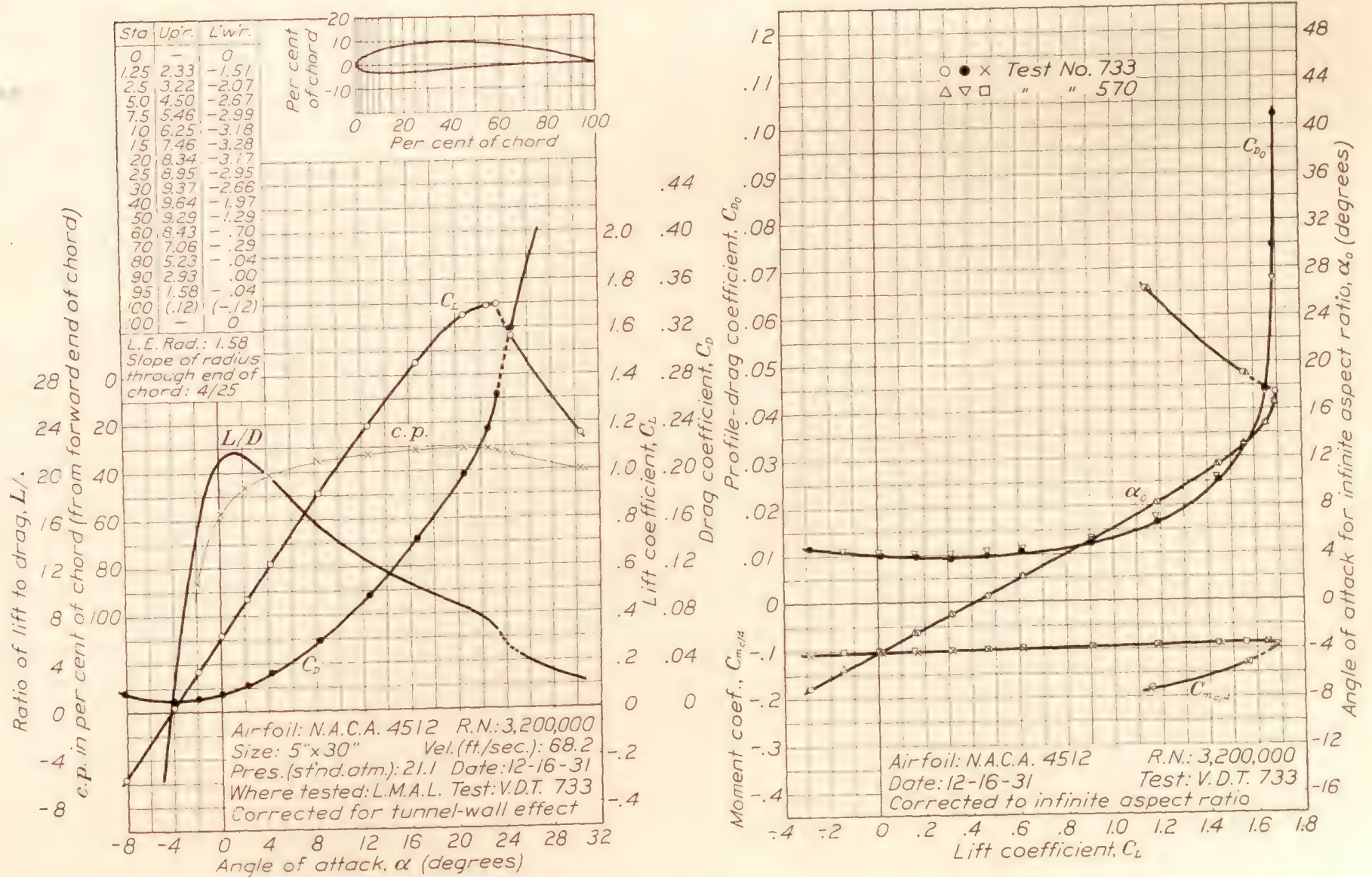


FIGURE 45.—N.A.C.A. 4512 airfoil.

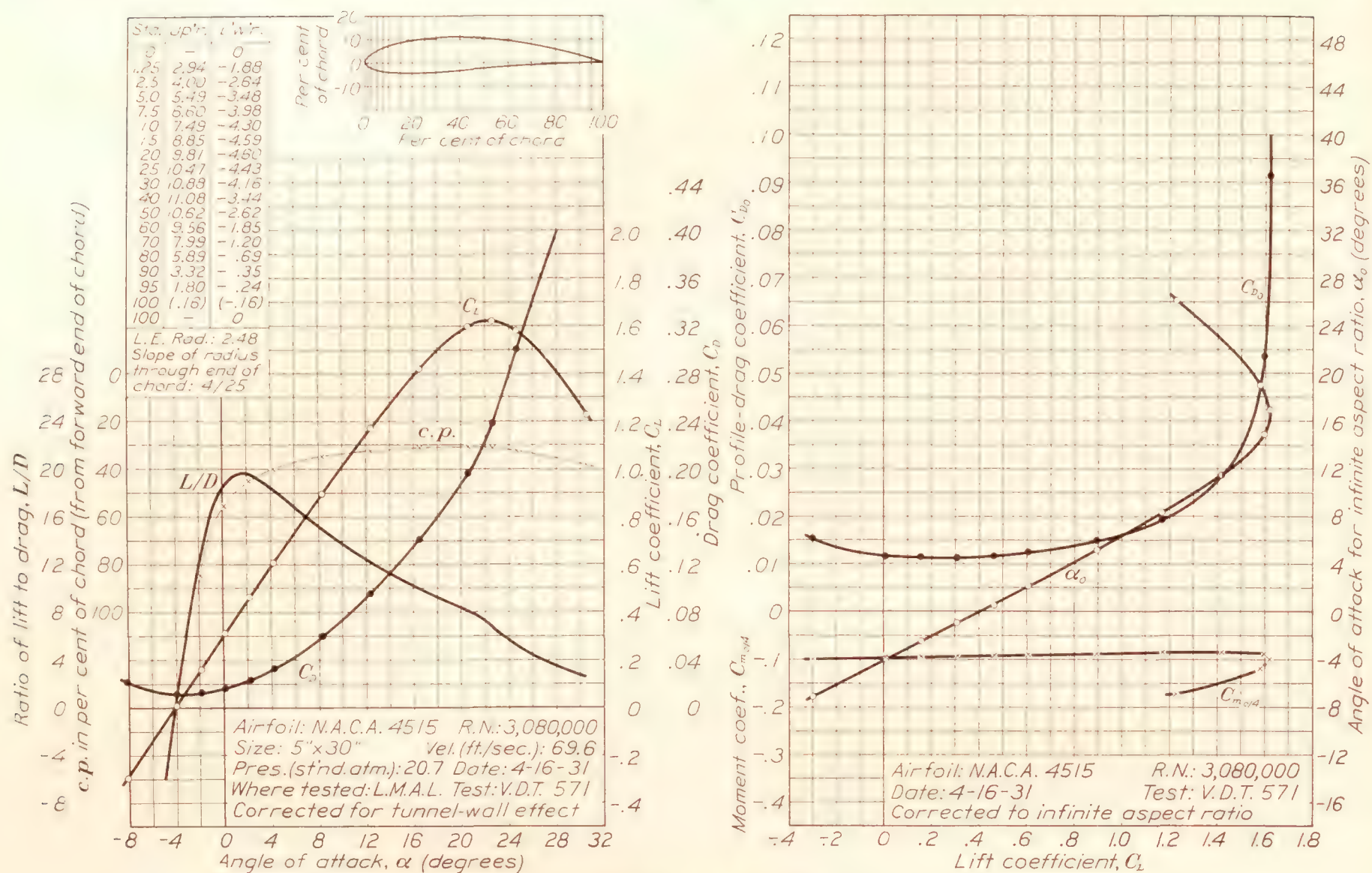


FIGURE 46.—N.A.C.A. 4515 airfoil.

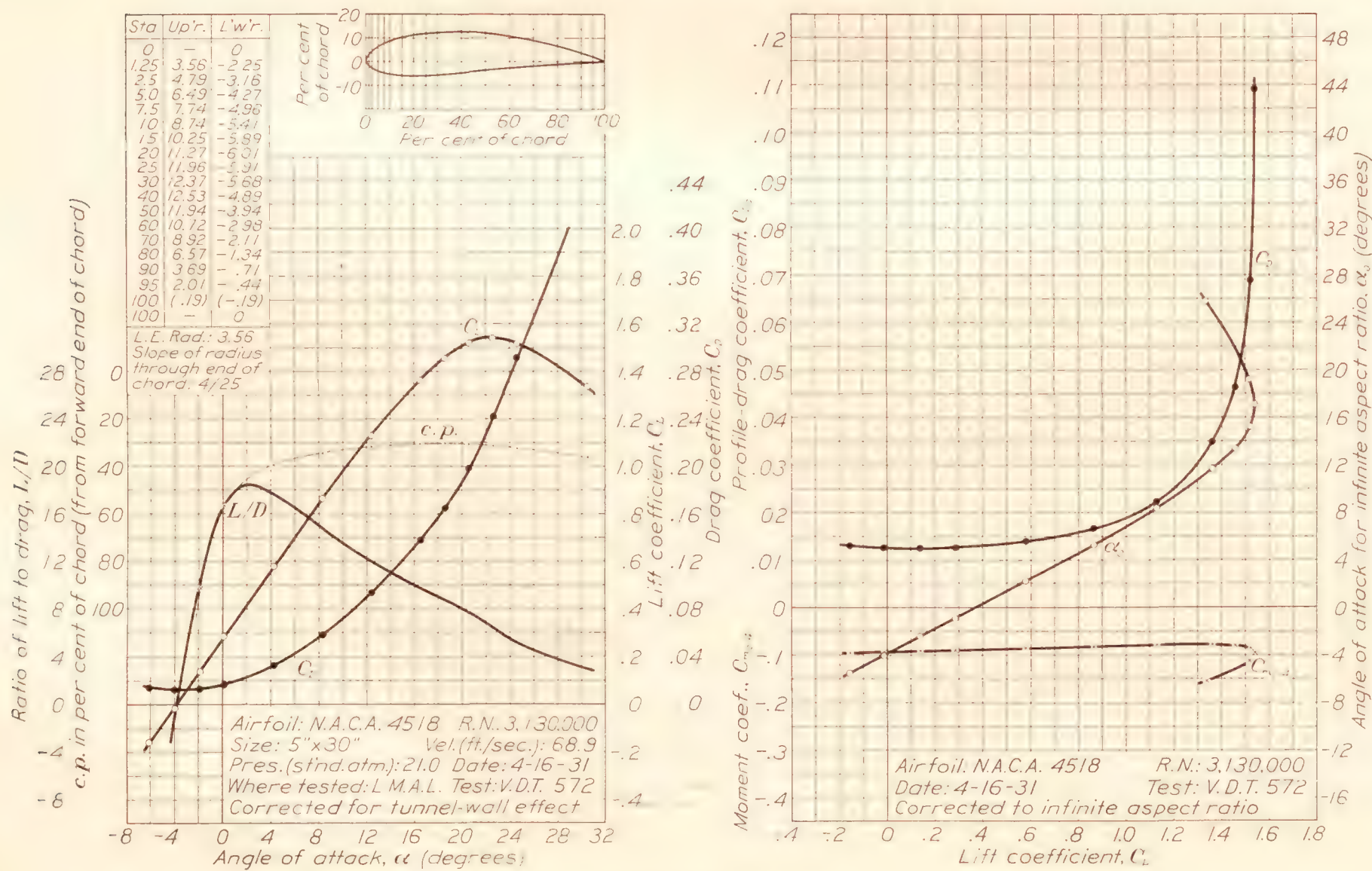


FIGURE 47.—N.A.C.A. 4518 airfoil.

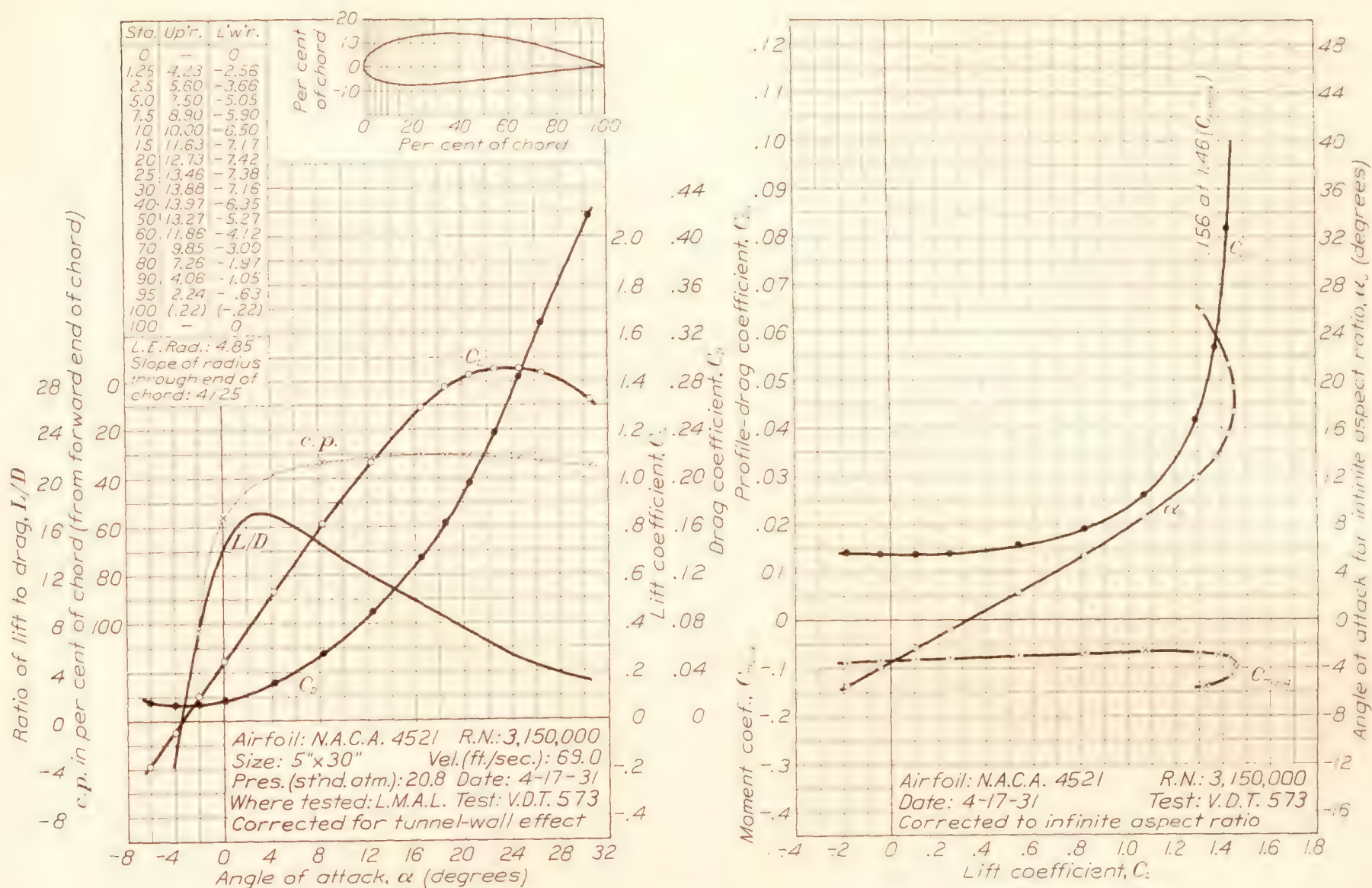


FIGURE 48.—N.A.C.A. 4521 airfoil.

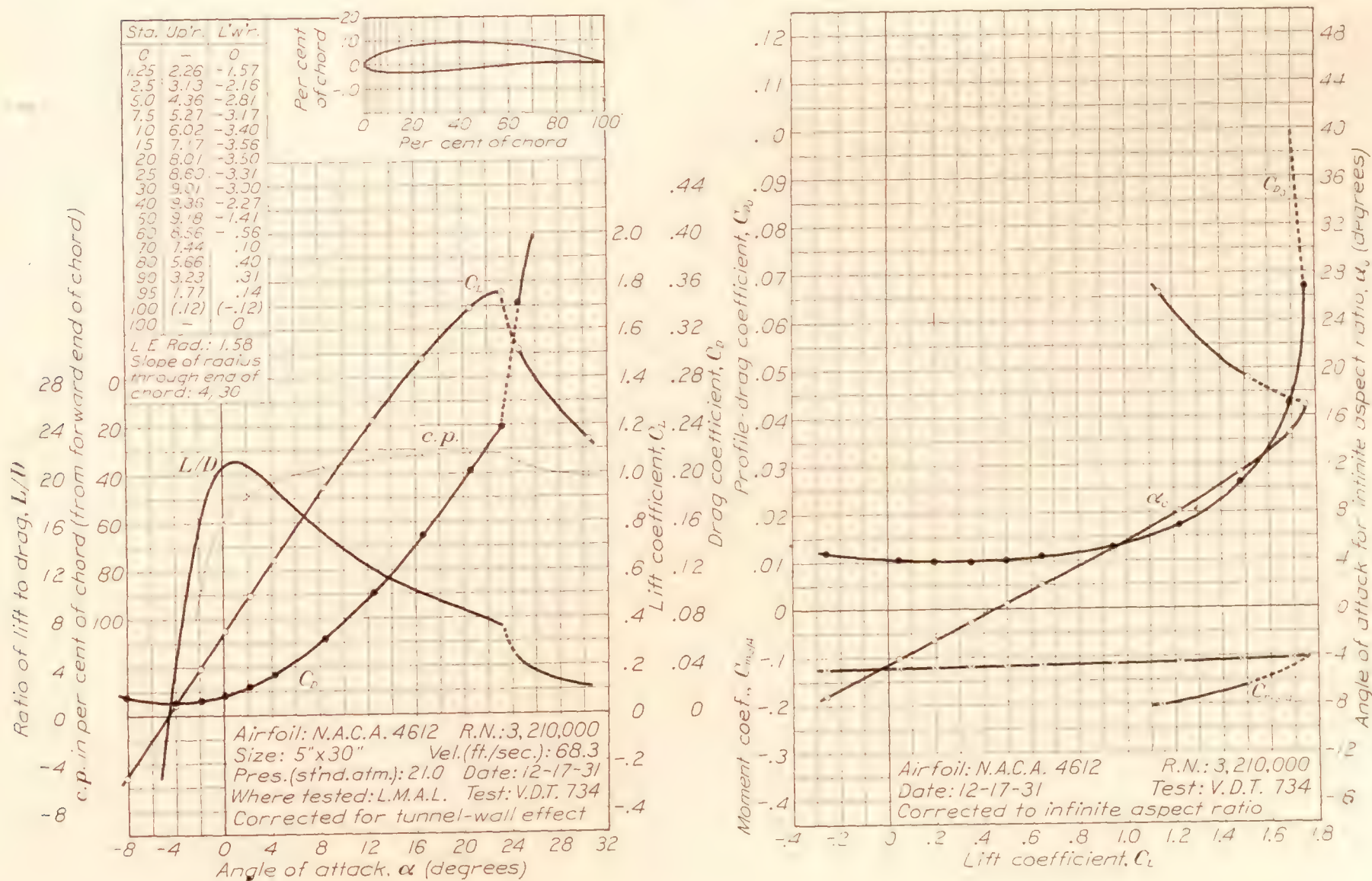


FIGURE 49.—N.A.C.A. 4612 airfoil.

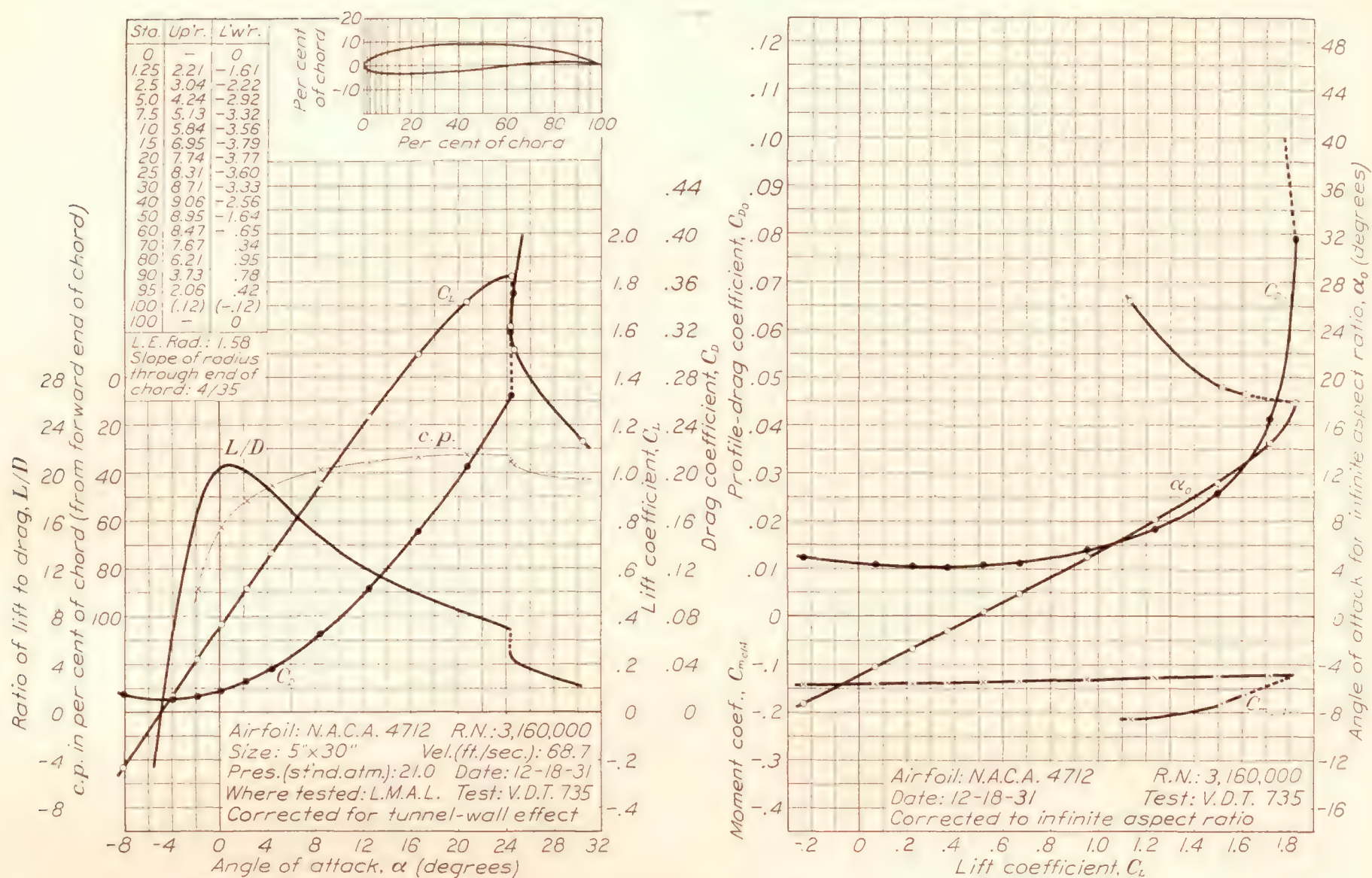


FIGURE 50.—N.A.C.A. 4712 airfoil.

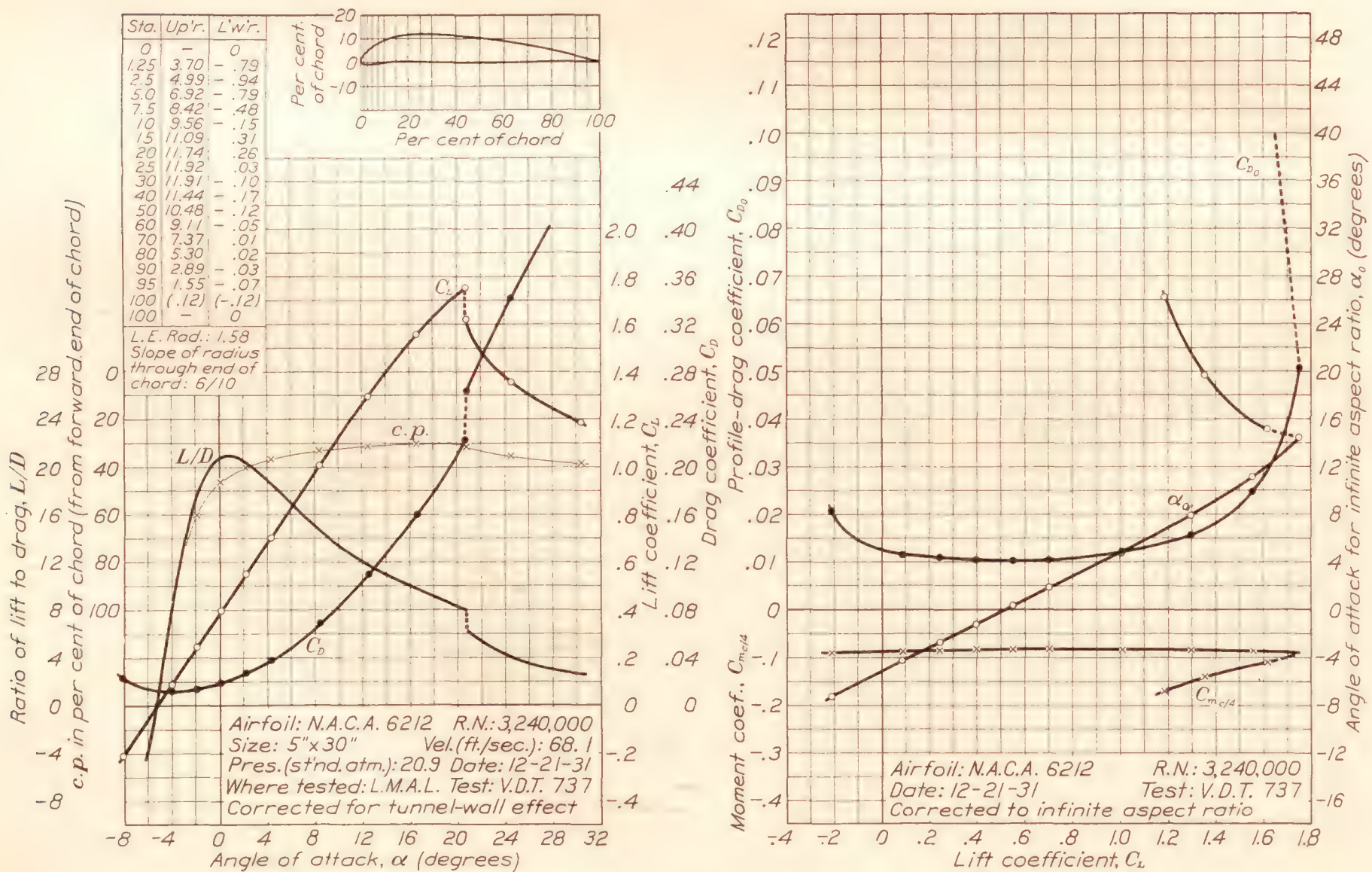


FIGURE 51.—N.A.C.A. 6212 airfoil.

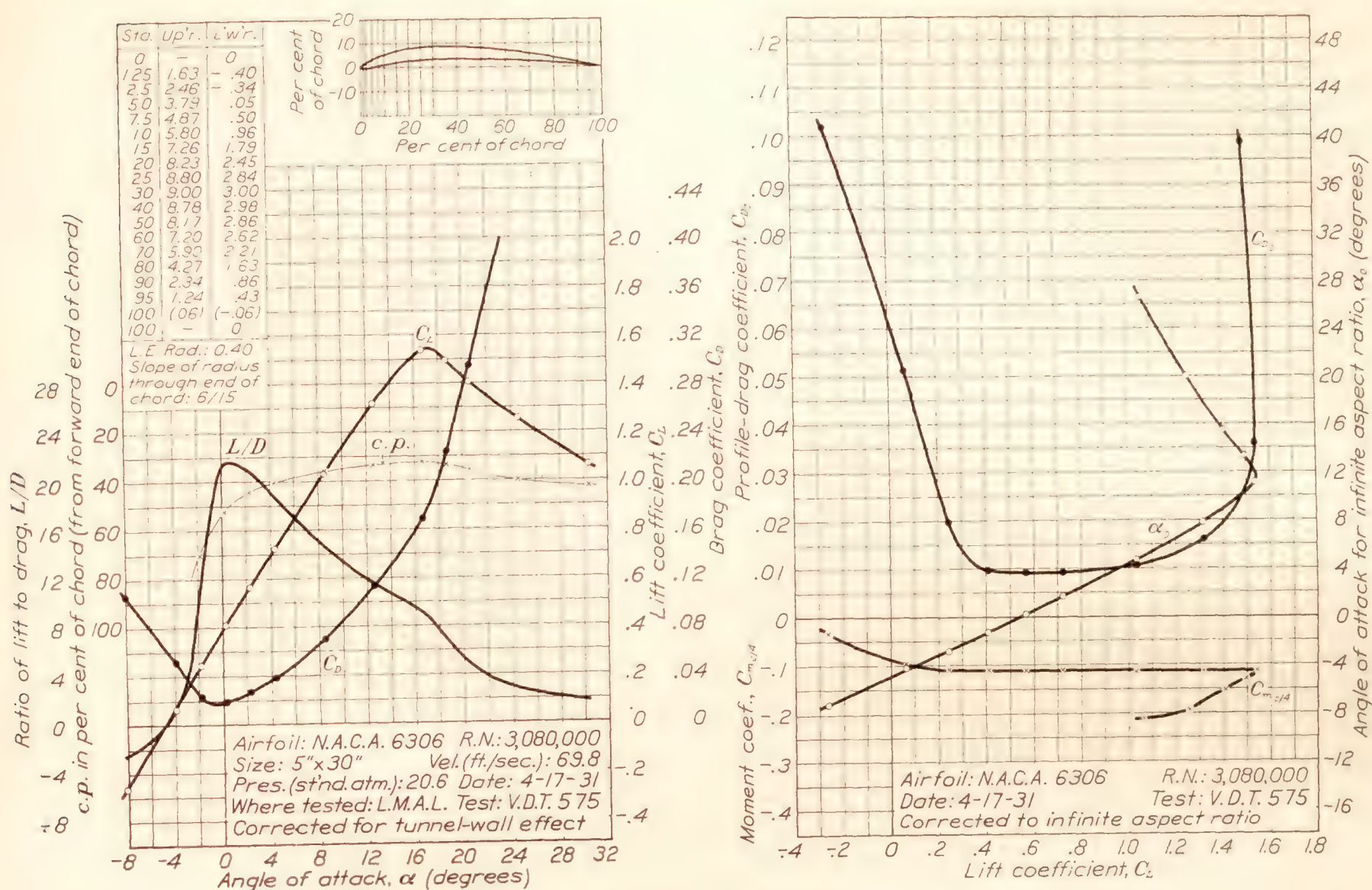


FIGURE 52.—N.A.C.A. 6306 airfoil.

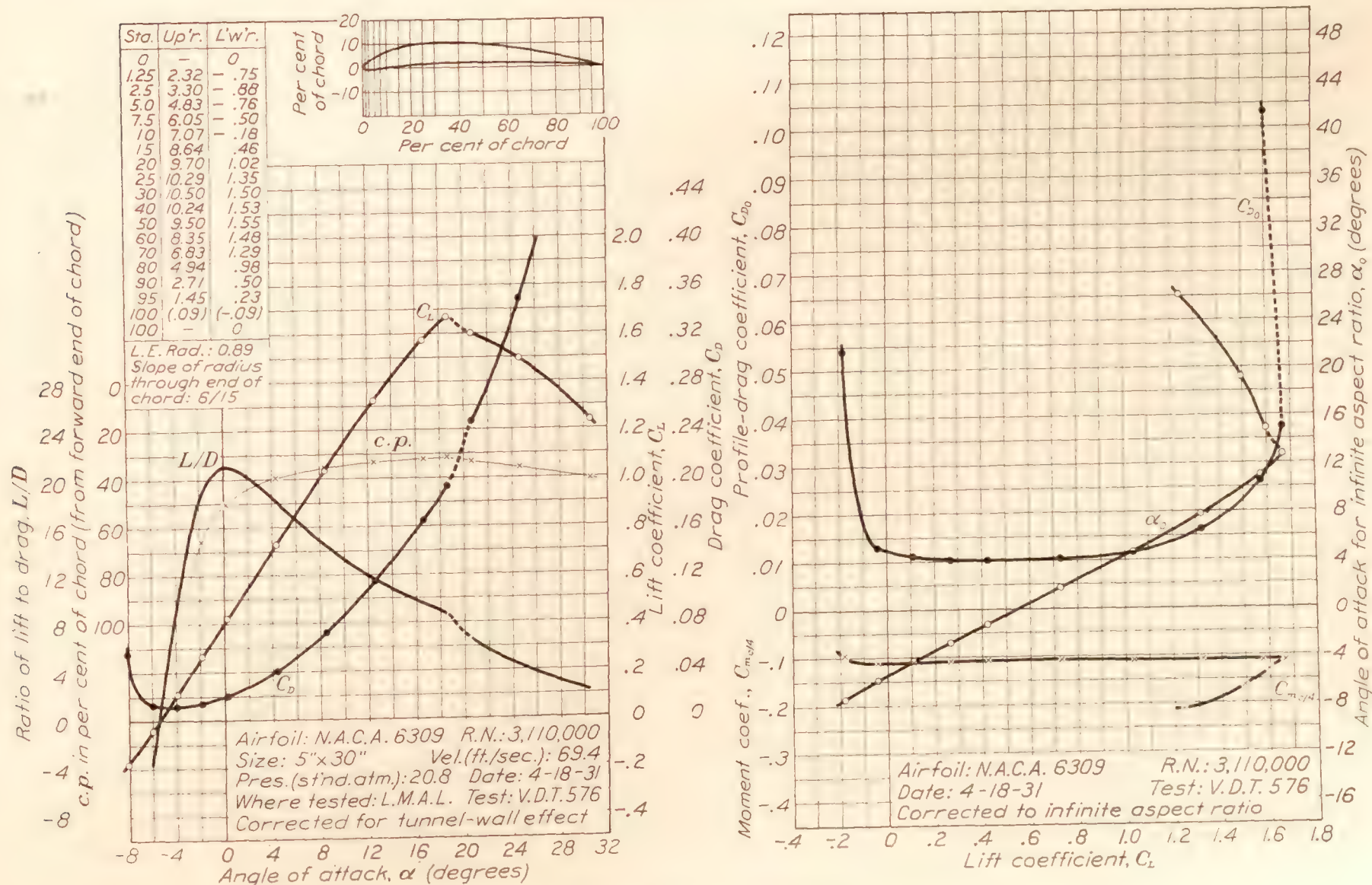


FIGURE 53.—N.A.C.A. 6309 airfoil.

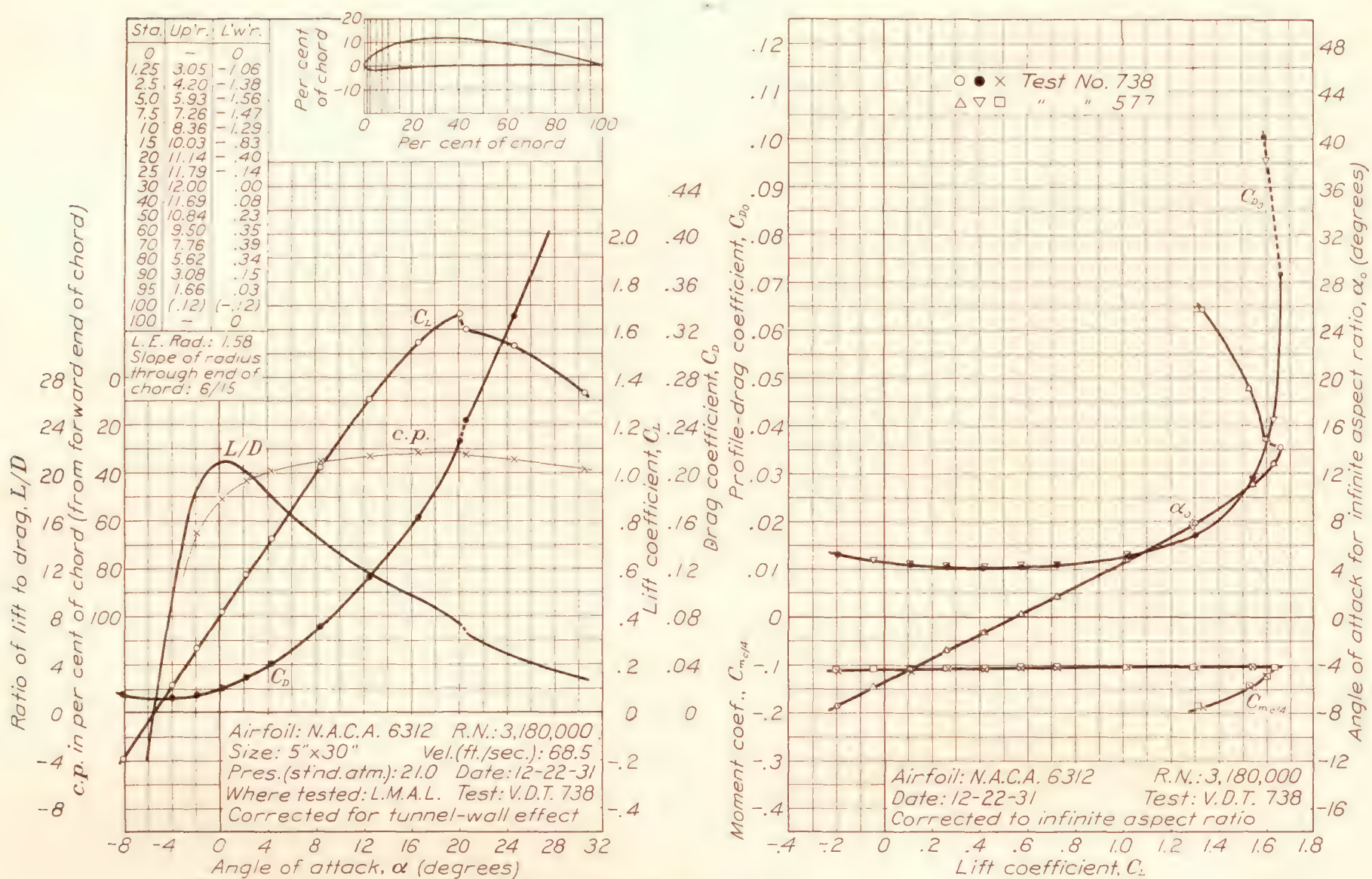


FIGURE 54.—N.A.C.A. 6312 airfoil.

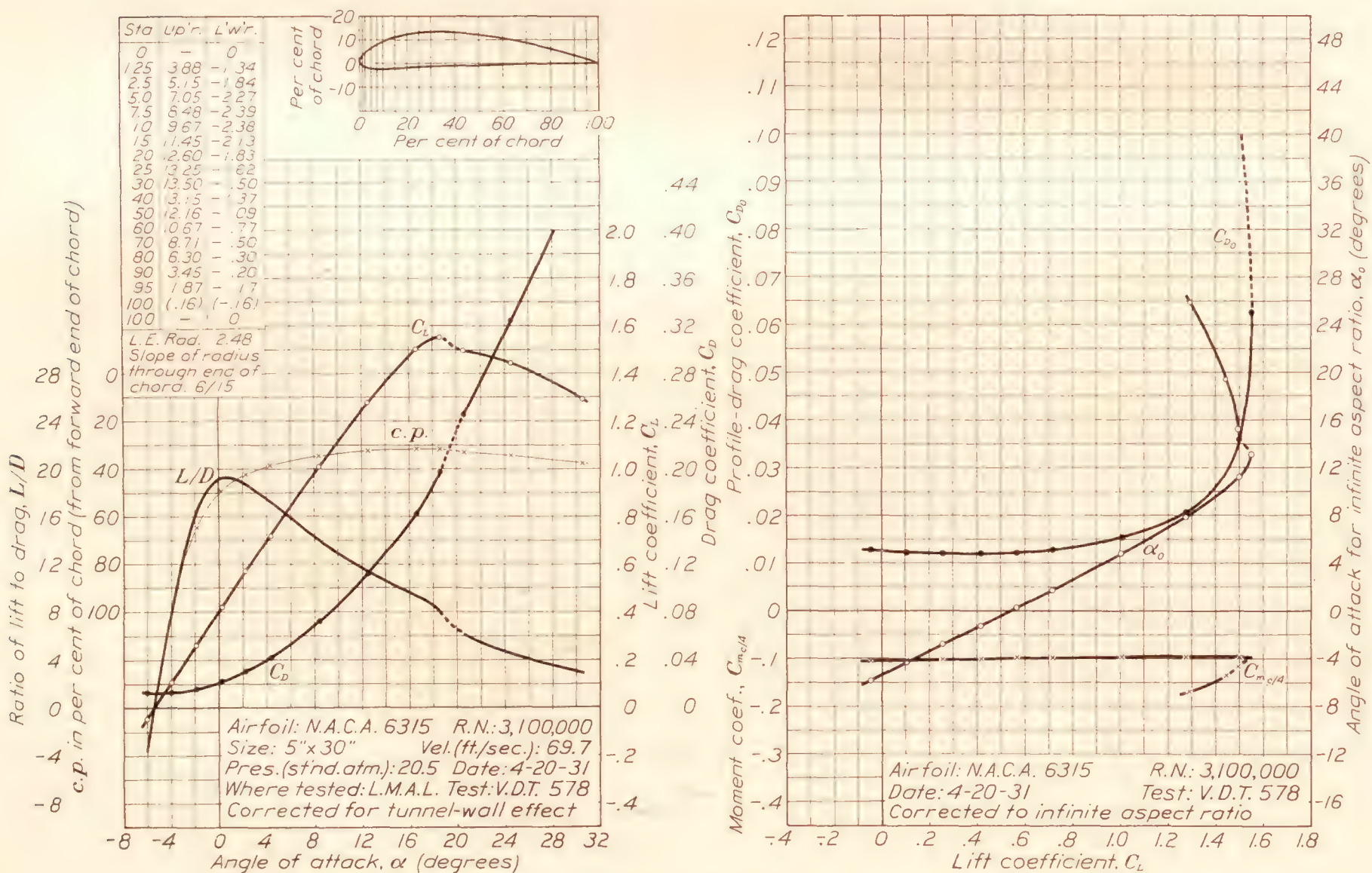


FIGURE 55.—N.A.C.A. 6315 airfoil.

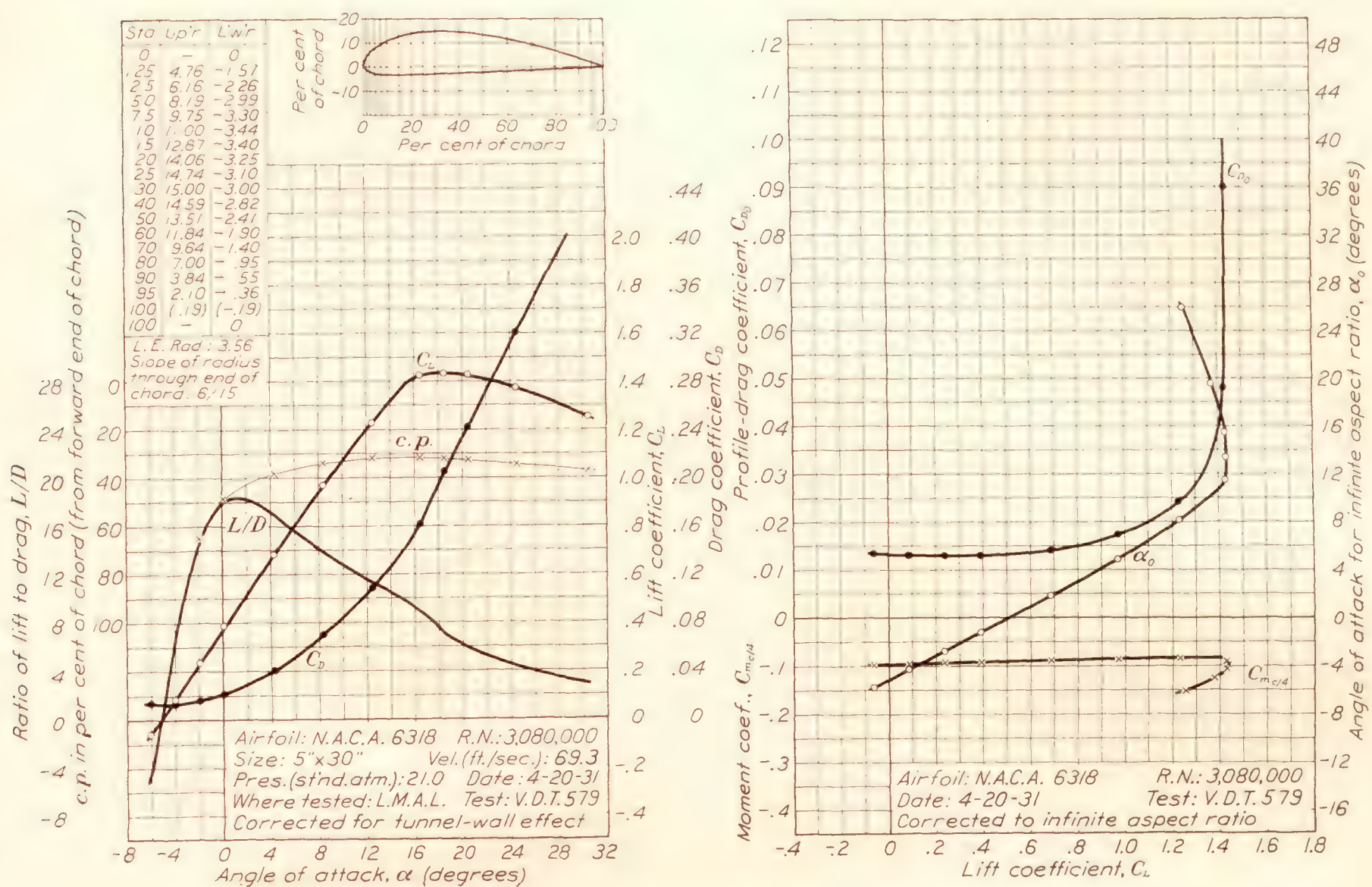


FIGURE 56.—N.A.C.A. 6318 airfoil.

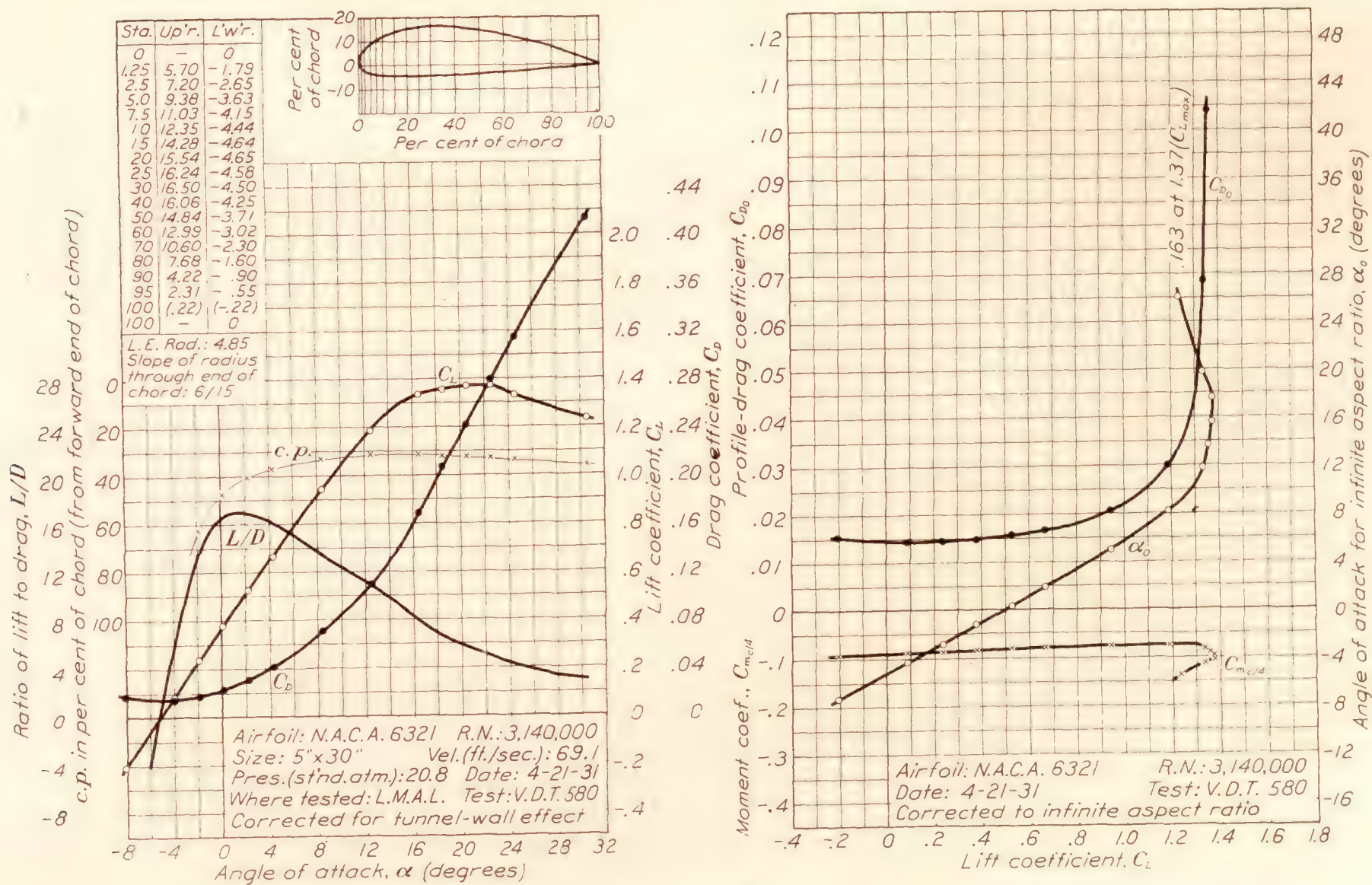


FIGURE 57.—N.A.C.A. 6321 airfoil.

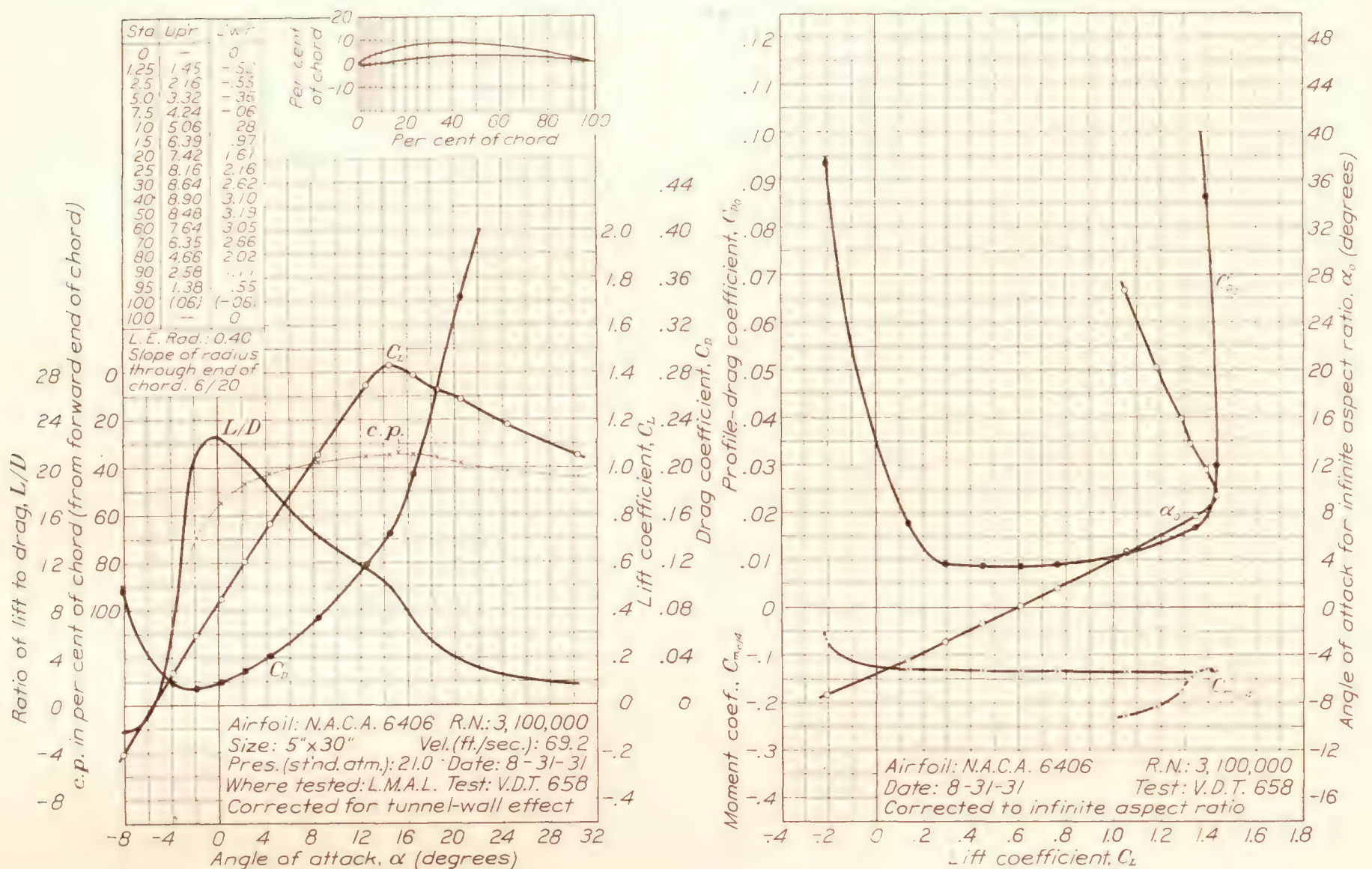


FIGURE 58.—N.A.C.A. 6406 airfoil.

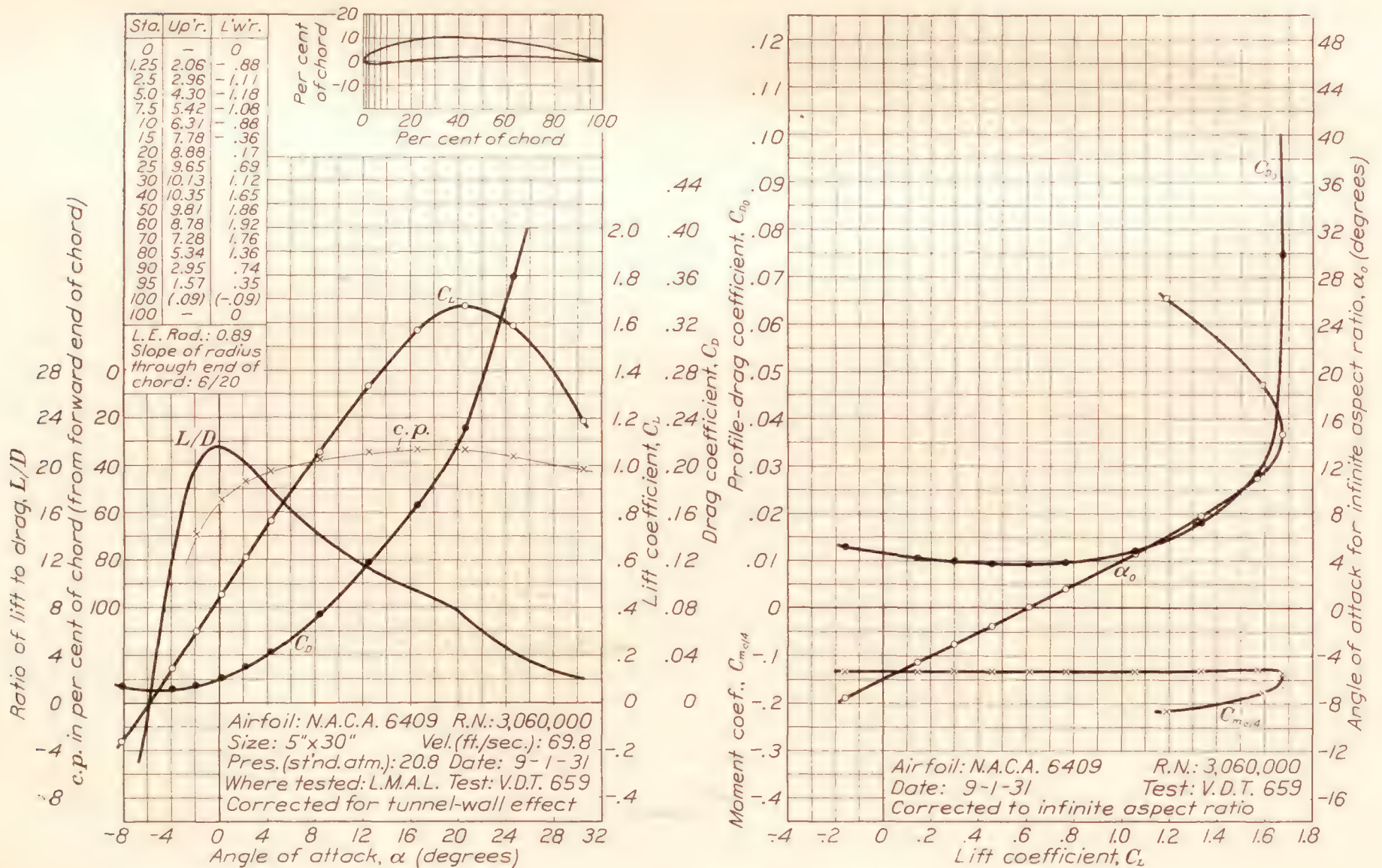


FIGURE 59.—N.A.C.A. 6409 airfoil.

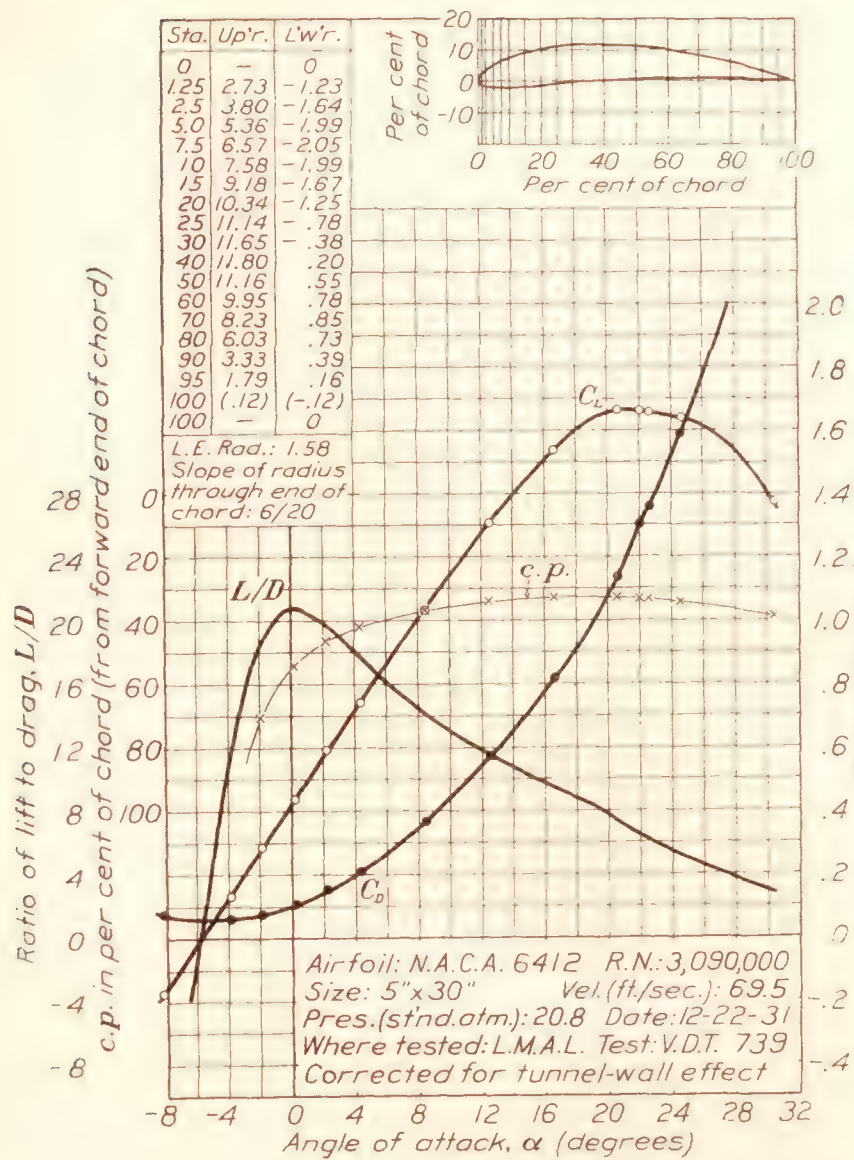


FIGURE 60.—N.A.C.A. 6412 airfoil.

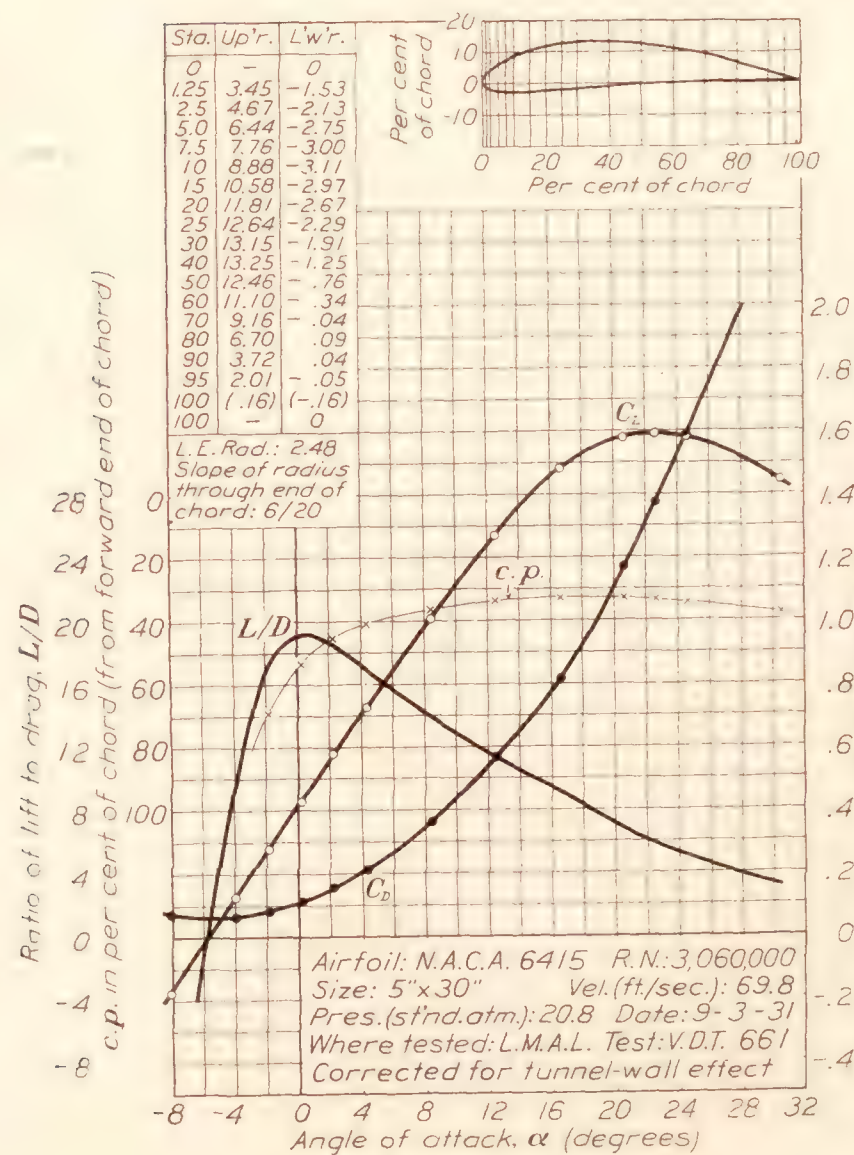
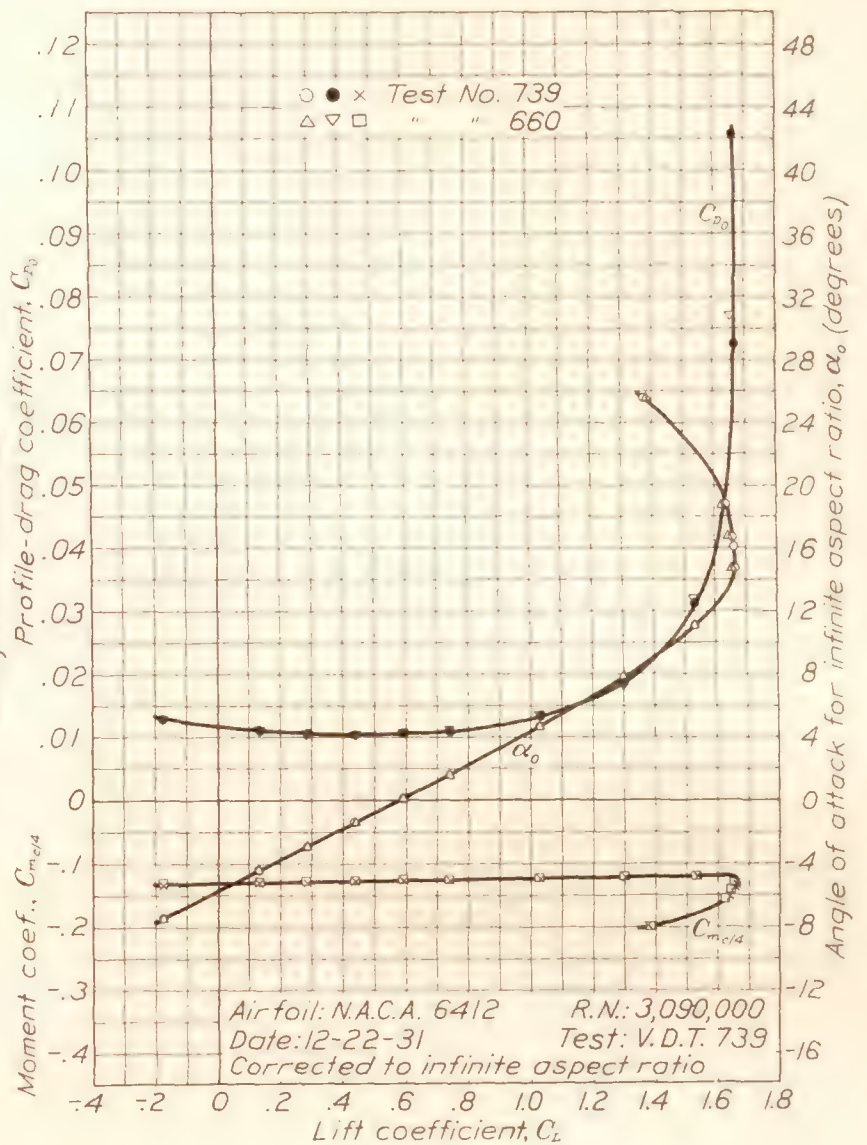
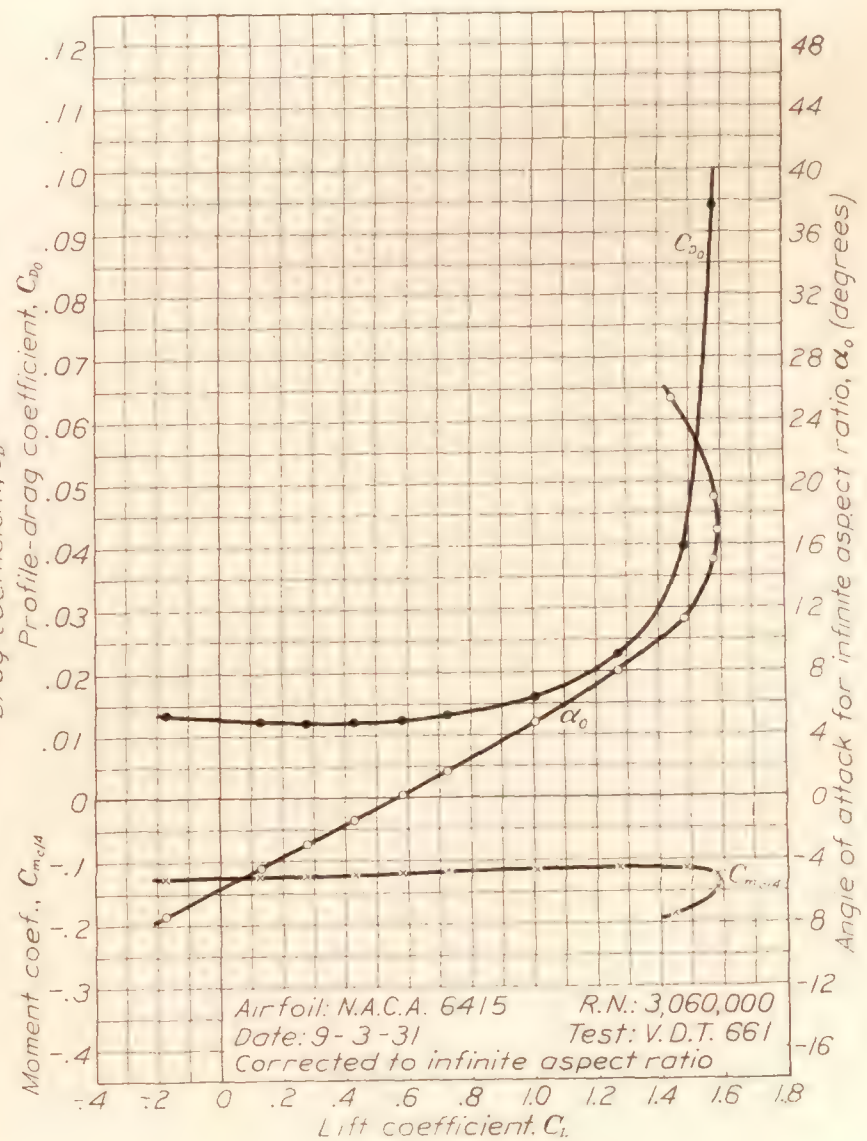


FIGURE 61.—N.A.C.A. 6415 airfoil.



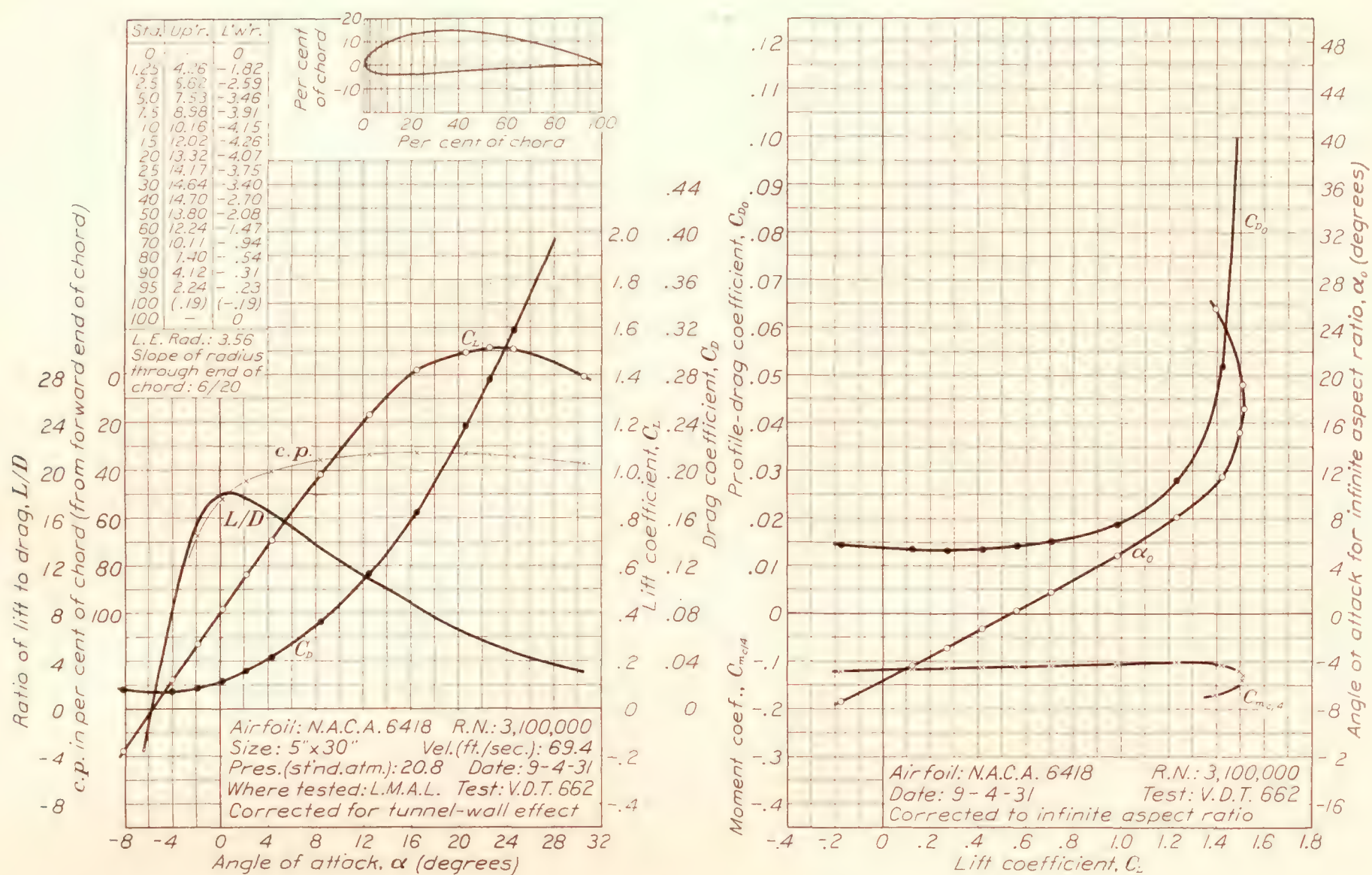


FIGURE 62.—N.A.C.A. 6418 airfoil.

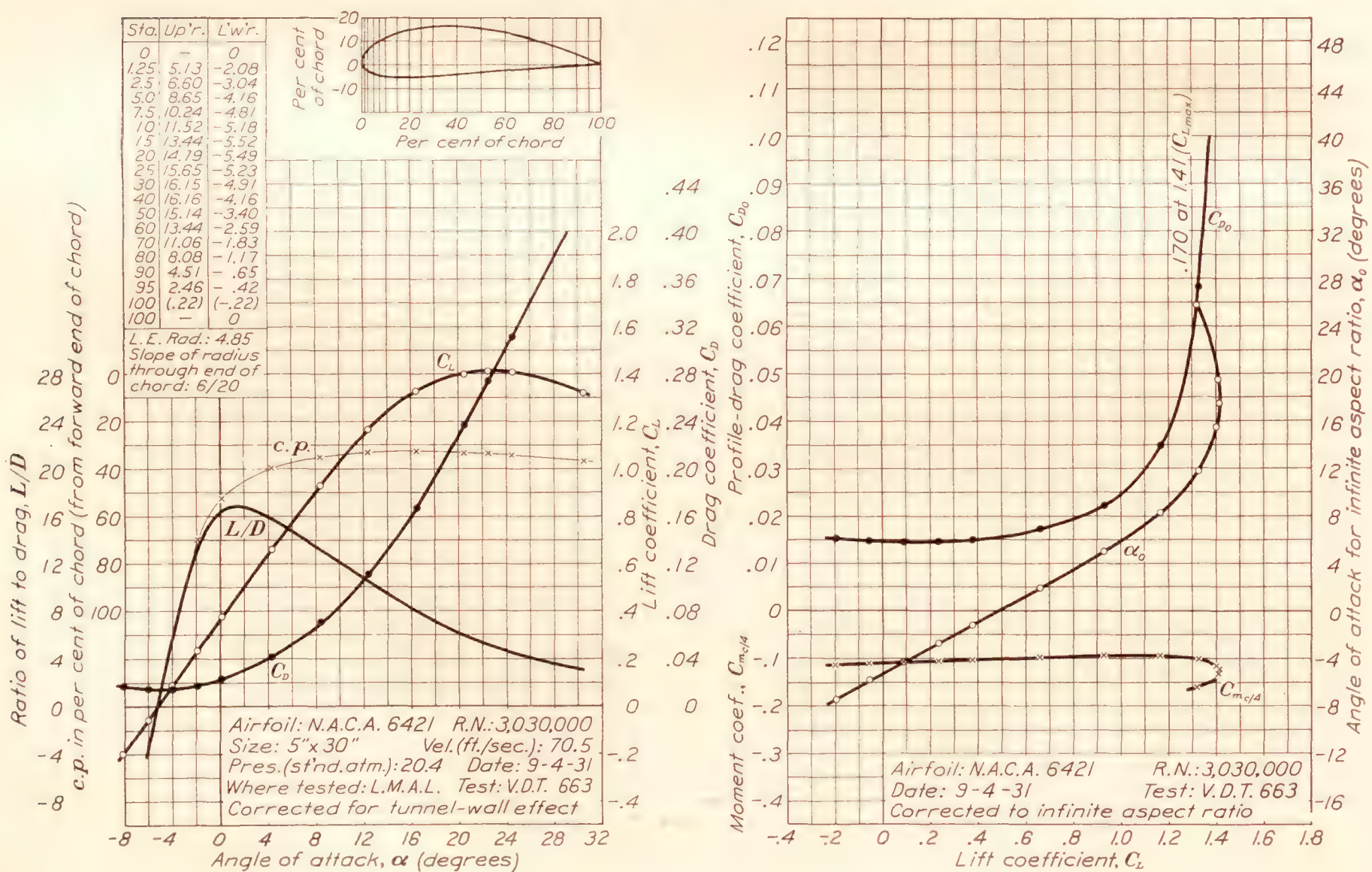


FIGURE 63.—N.A.C.A. 6421 airfoil.

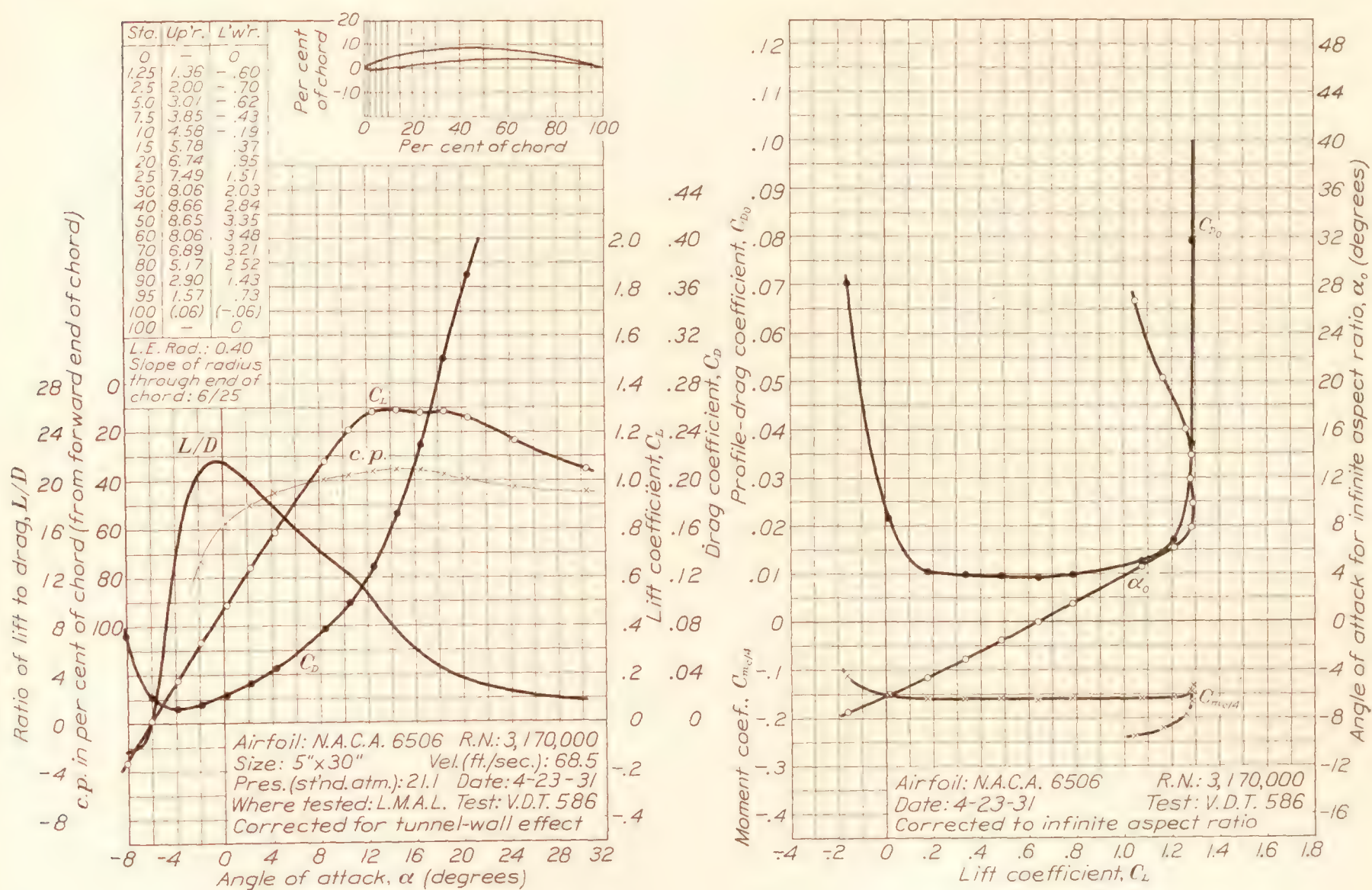


FIGURE 64.—N.A.C.A. 6506 airfoil.

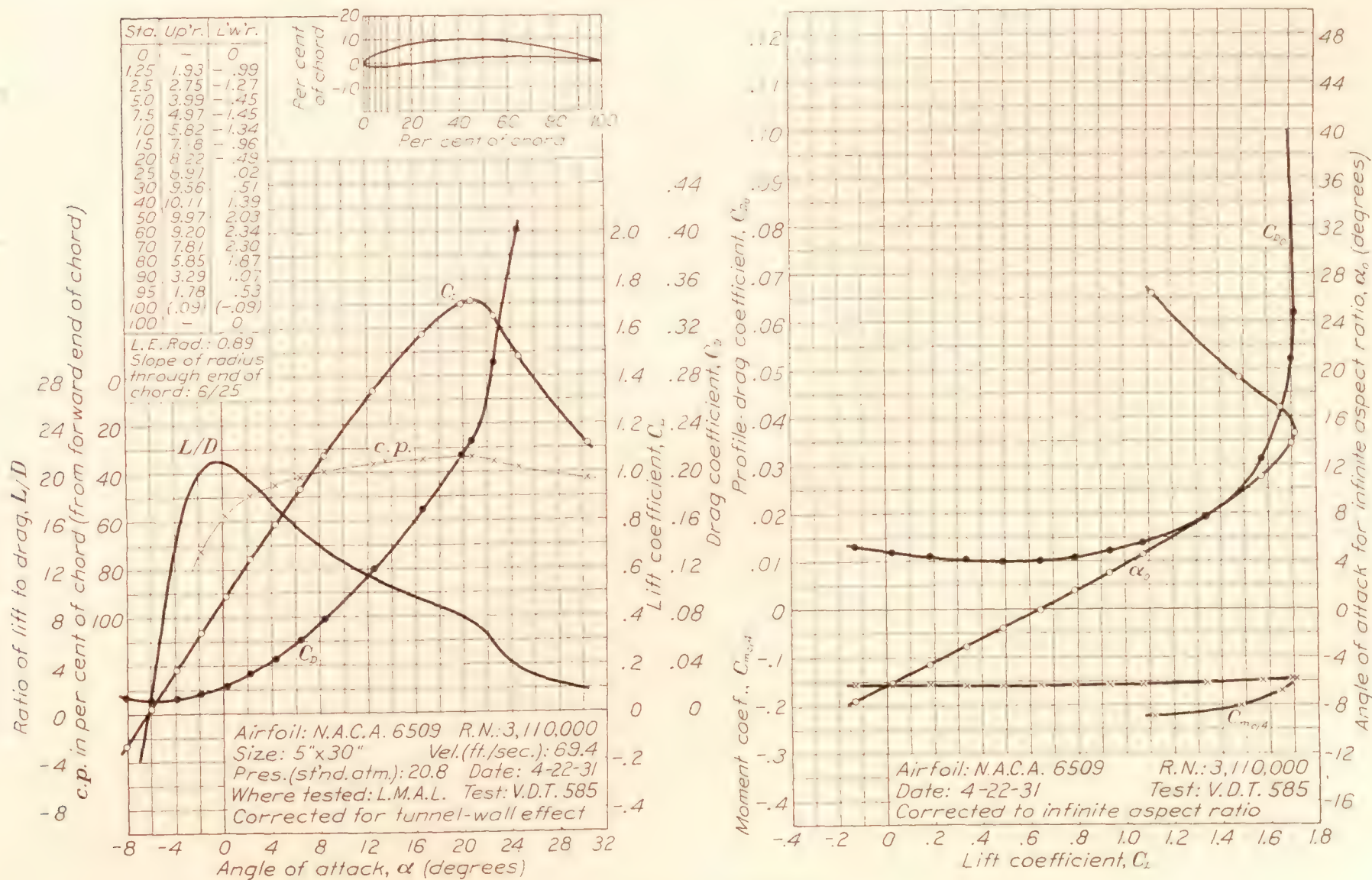


FIGURE 65.—N.A.C.A. 6509 airfoil.

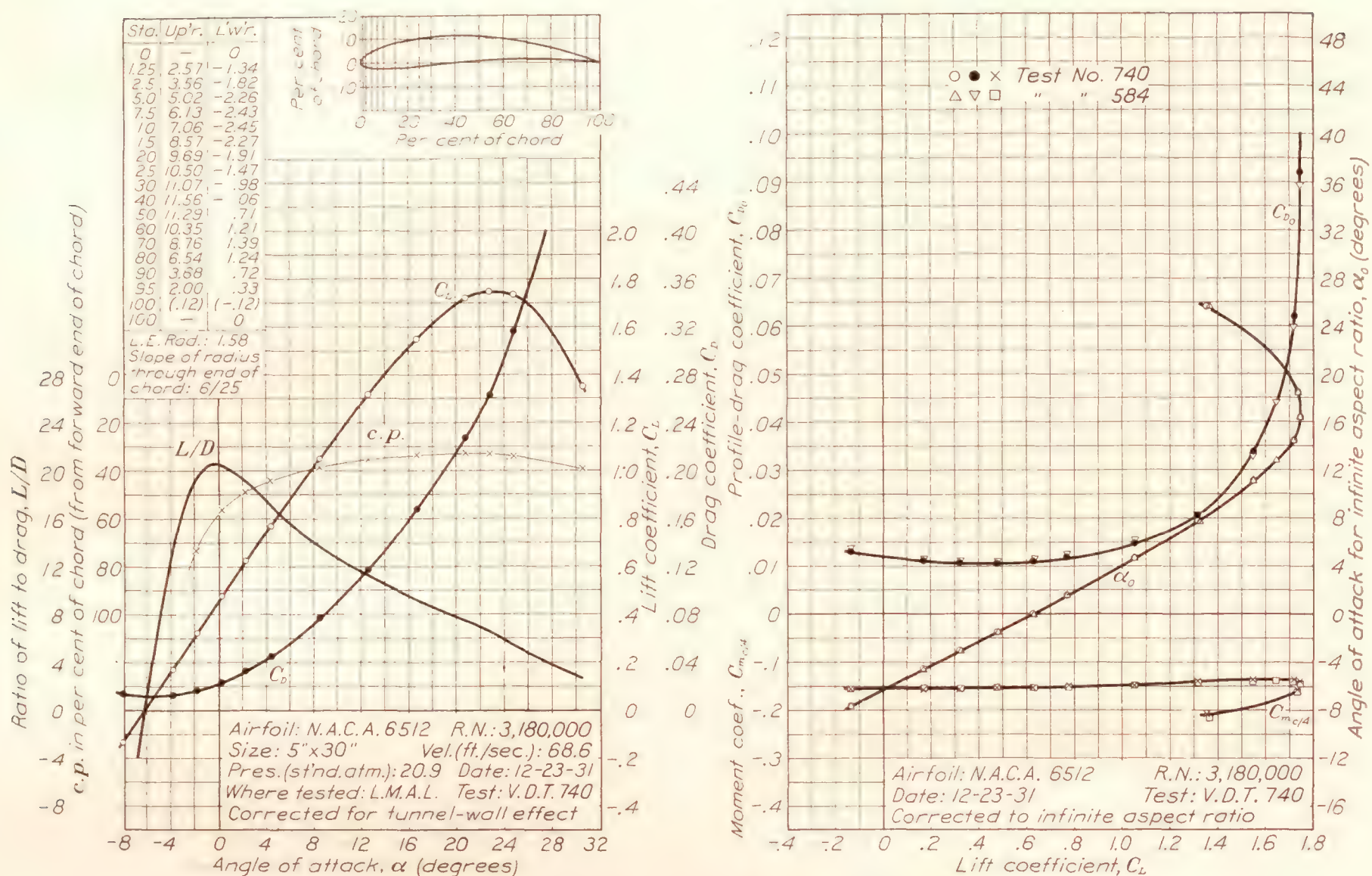


FIGURE 66.—N.A.C.A. 6512 airfoil.

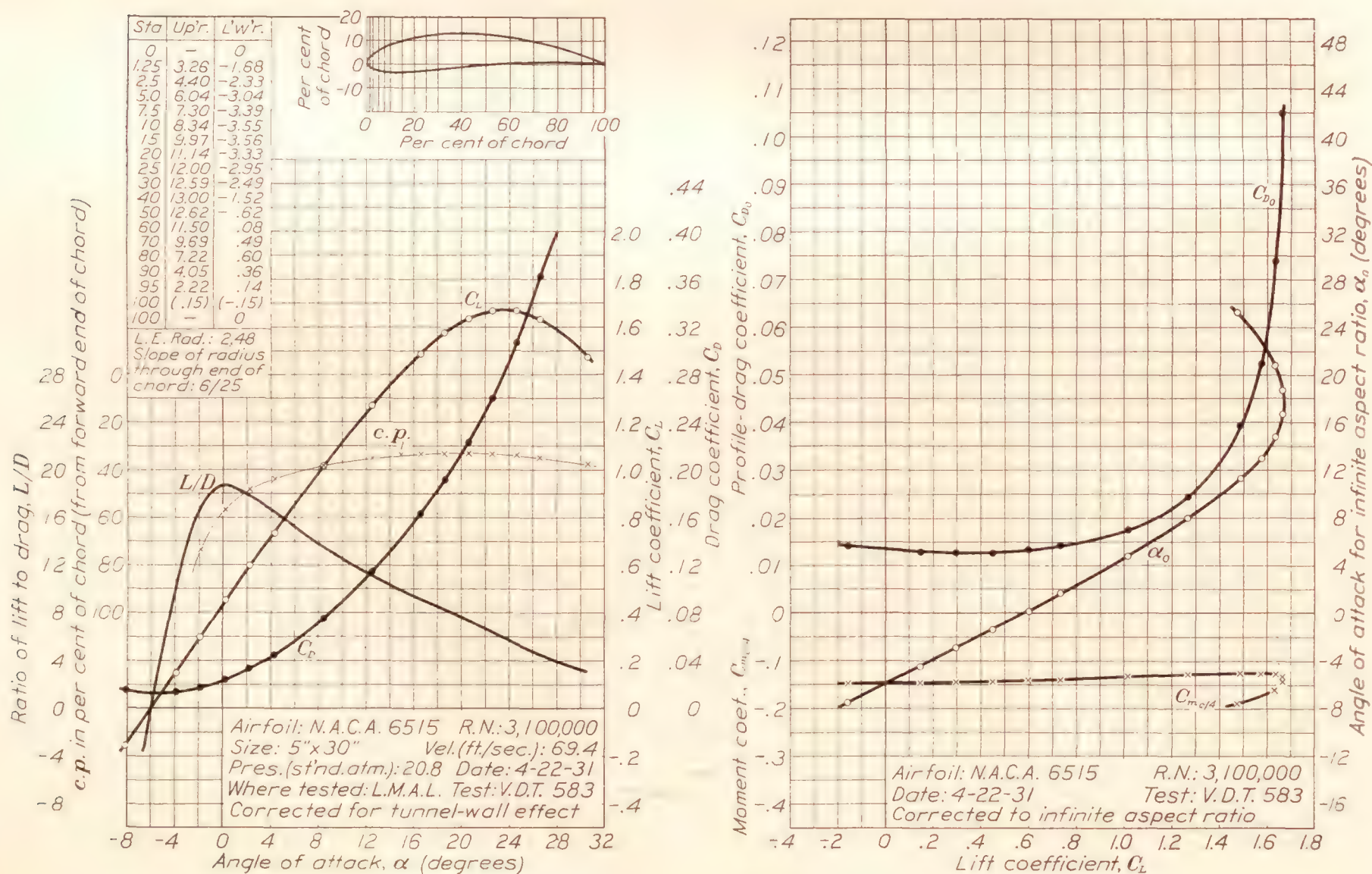


FIGURE 67.—N.A.C.A. 6515 airfoil.

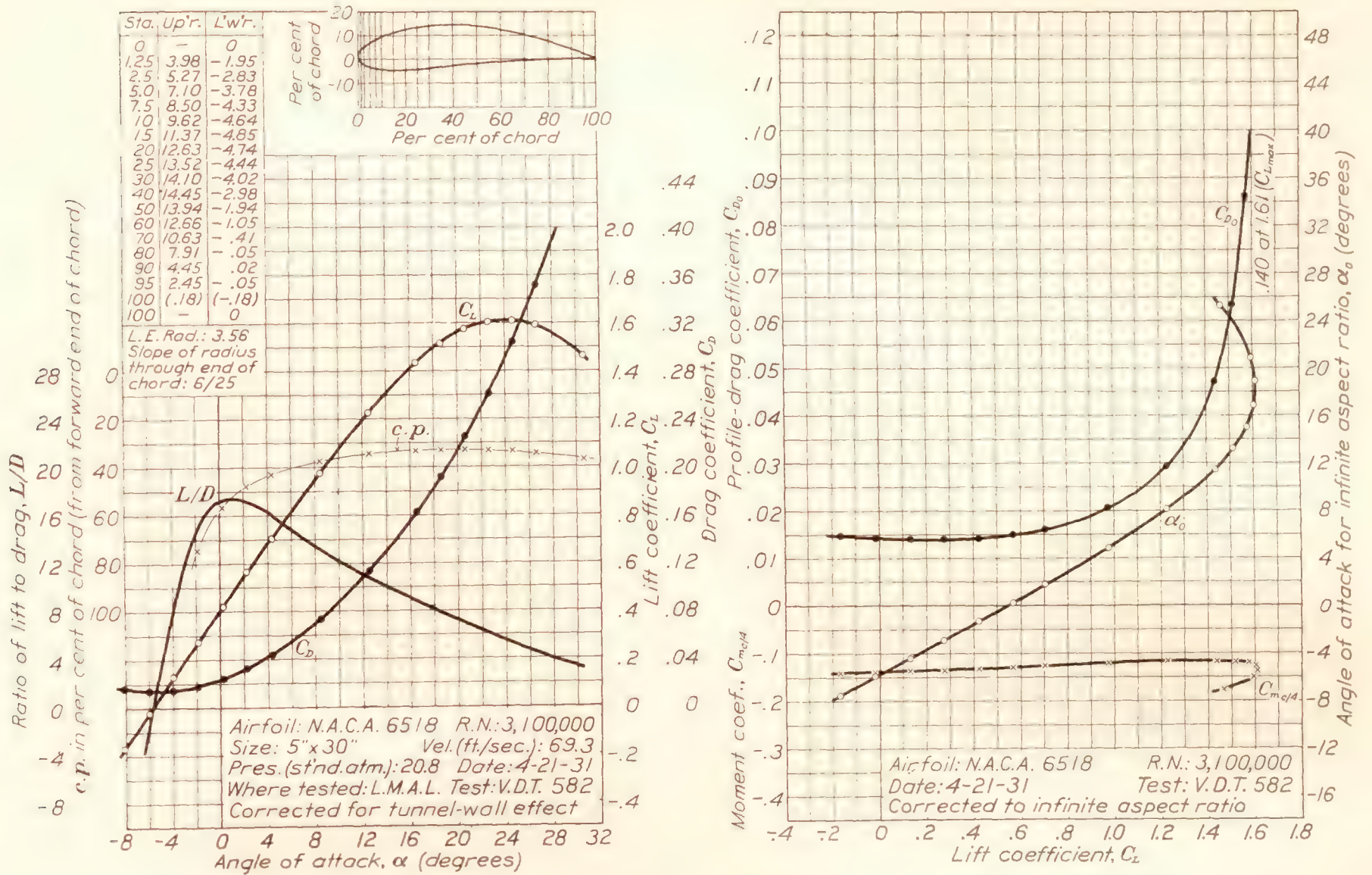


FIGURE 68.—N.A.C.A. 6518 airfoil.

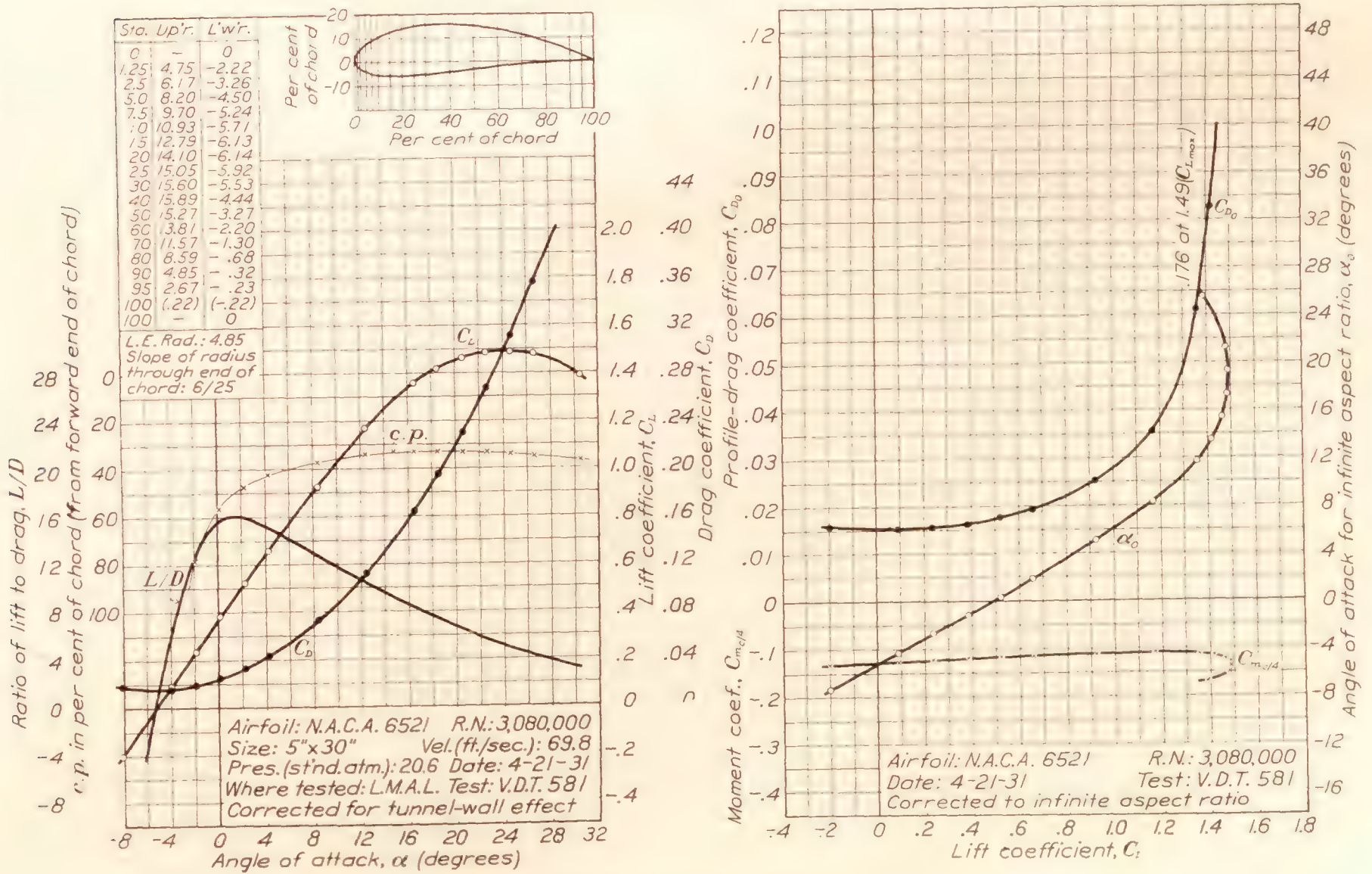


FIGURE 69.—N.A.C.A. 6521 airfoil.

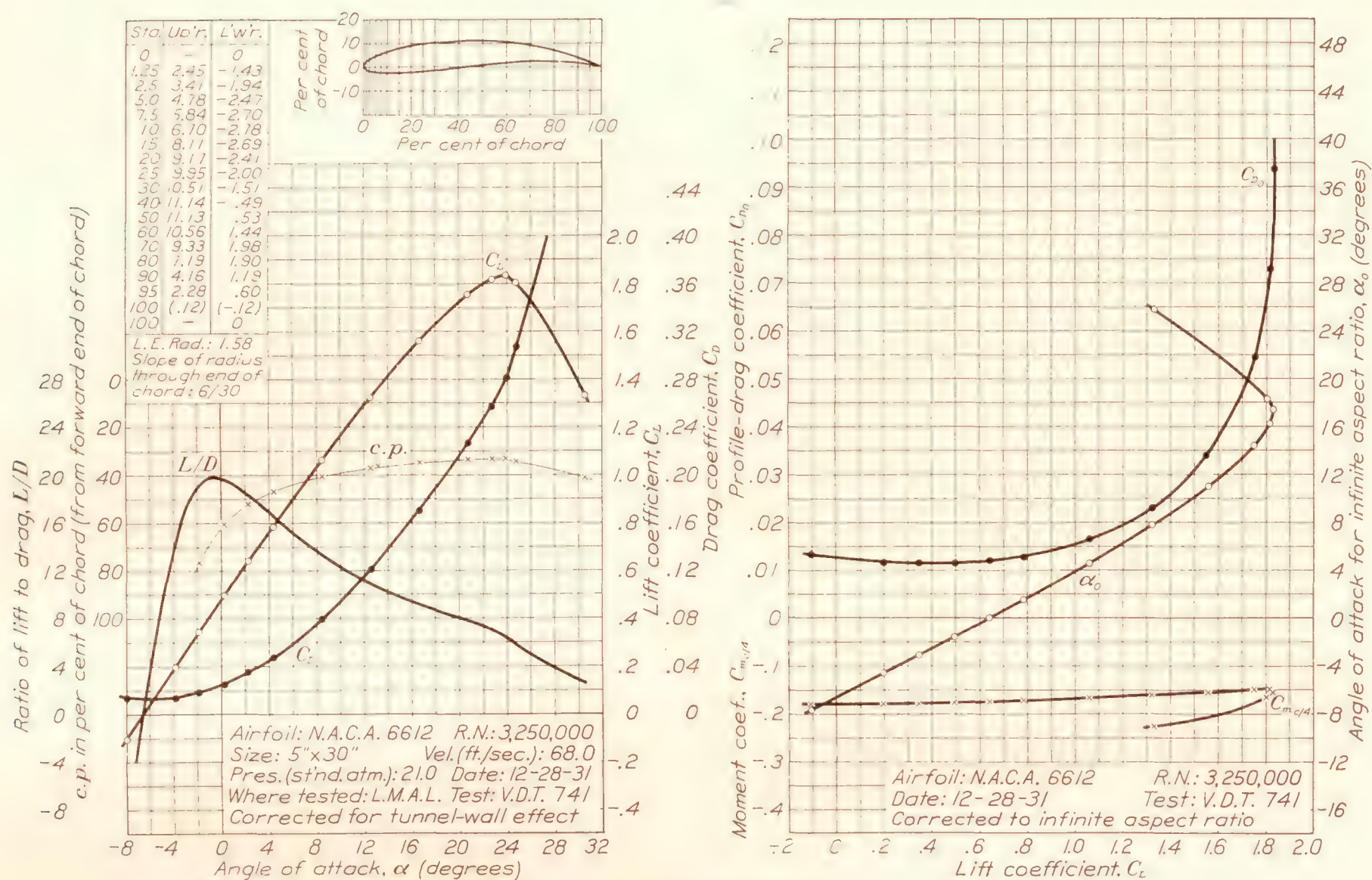


FIGURE 70.—N.A.C.A. 6612 airfoil.

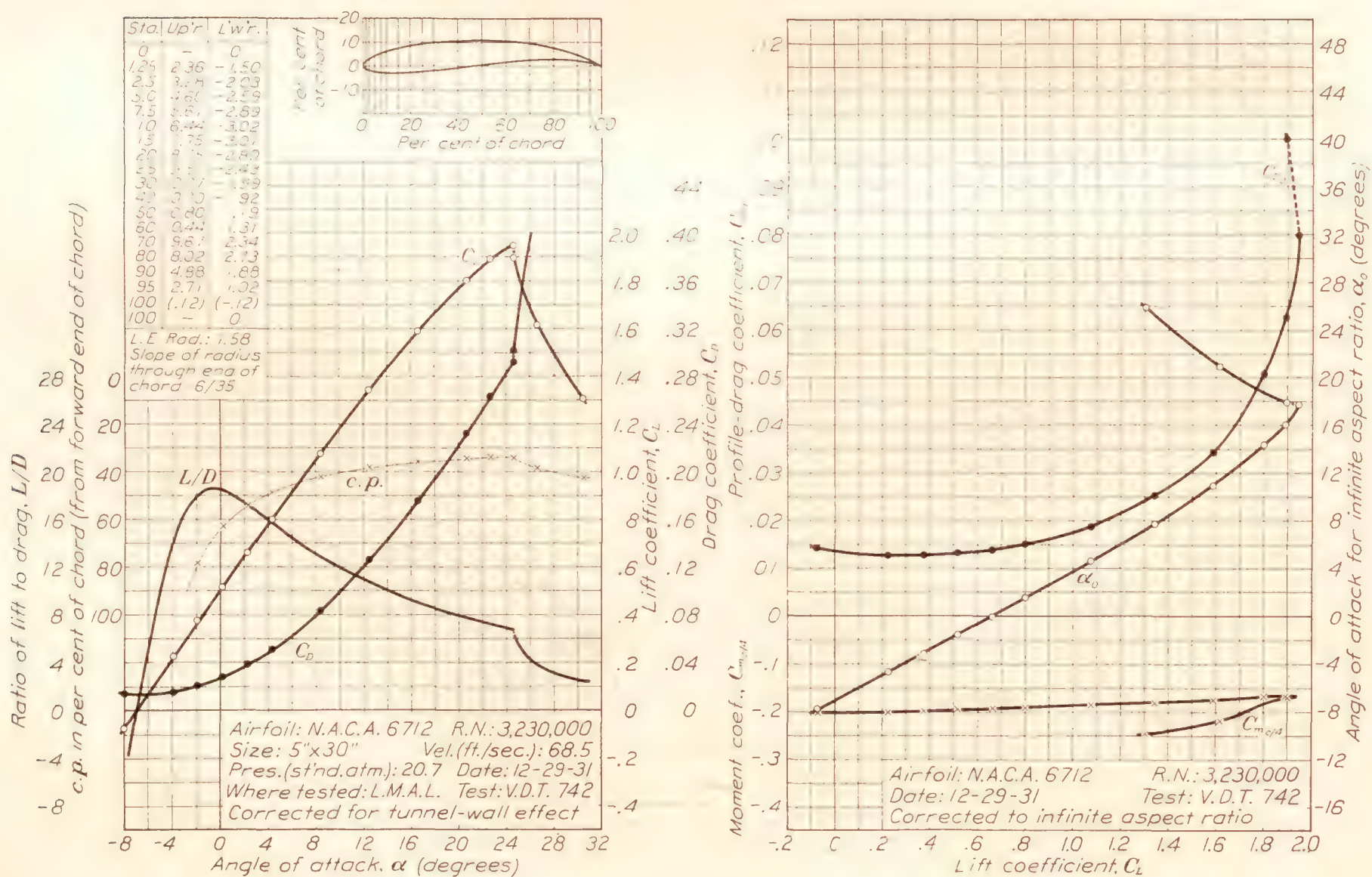


FIGURE 71.—N.A.C.A. 6712 airfoil.

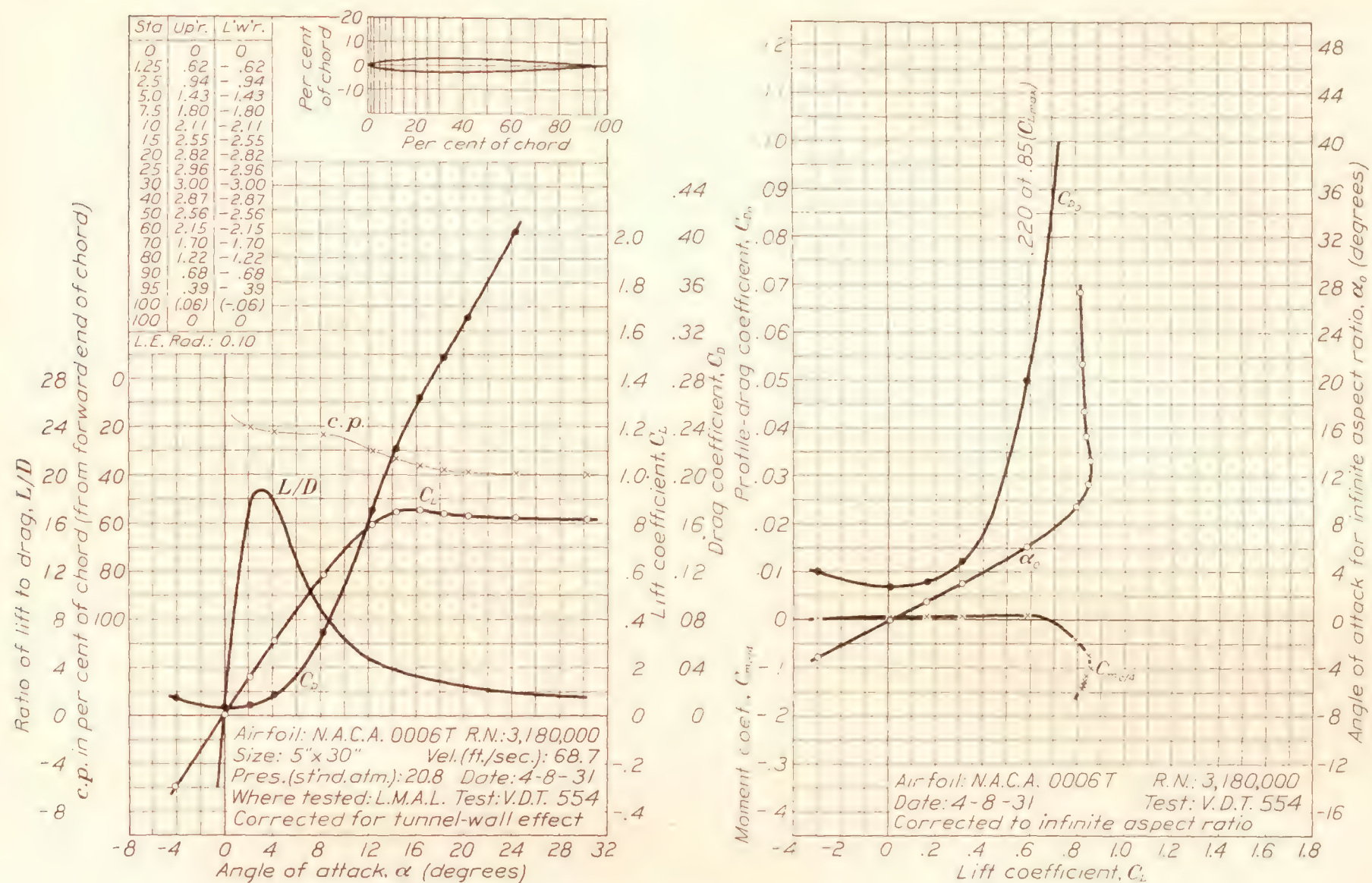


FIGURE 72.—N.A.C.A. 0006T airfoil.

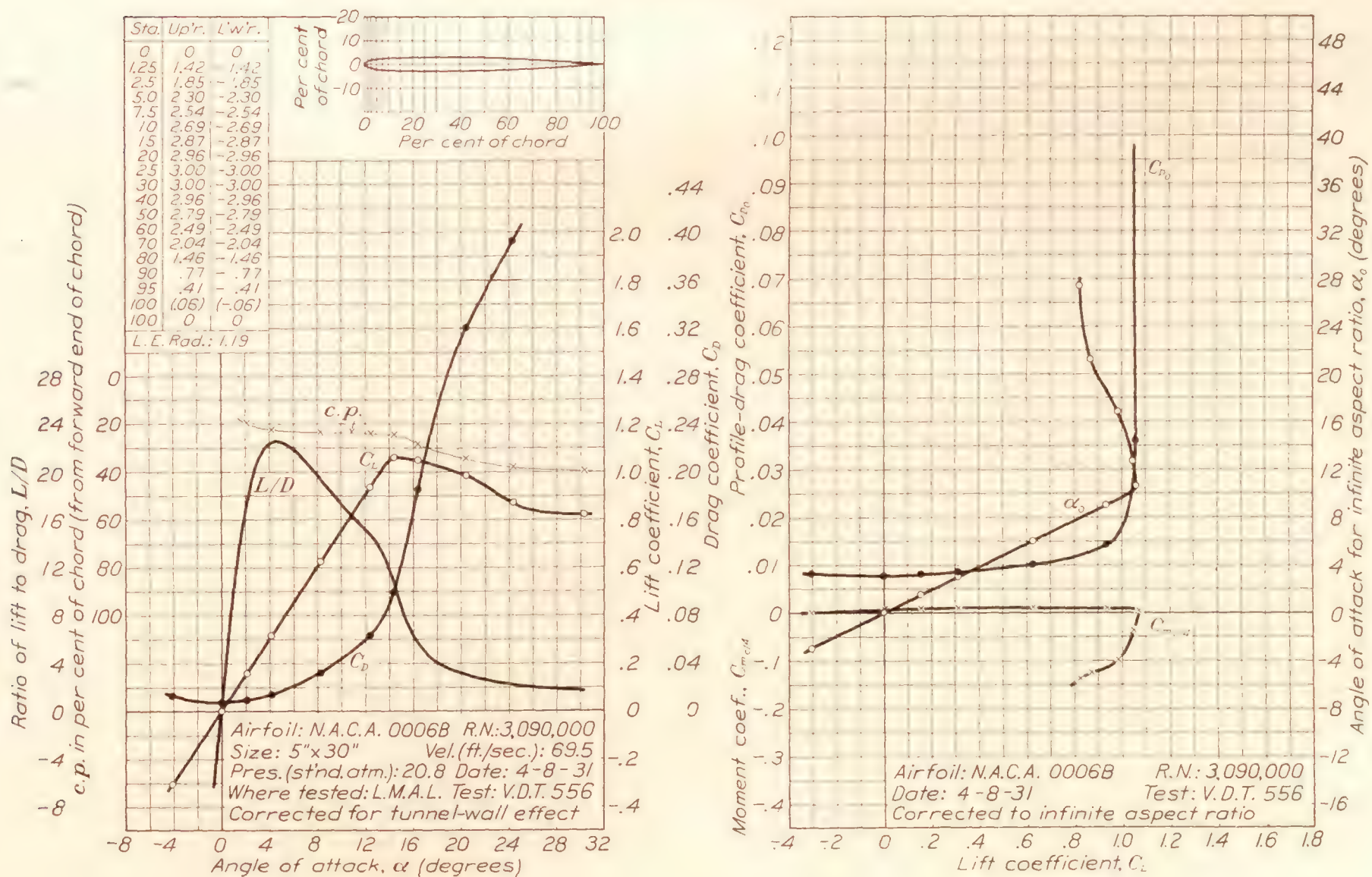


FIGURE 73.—N.A.C.A. 0006B airfoil.

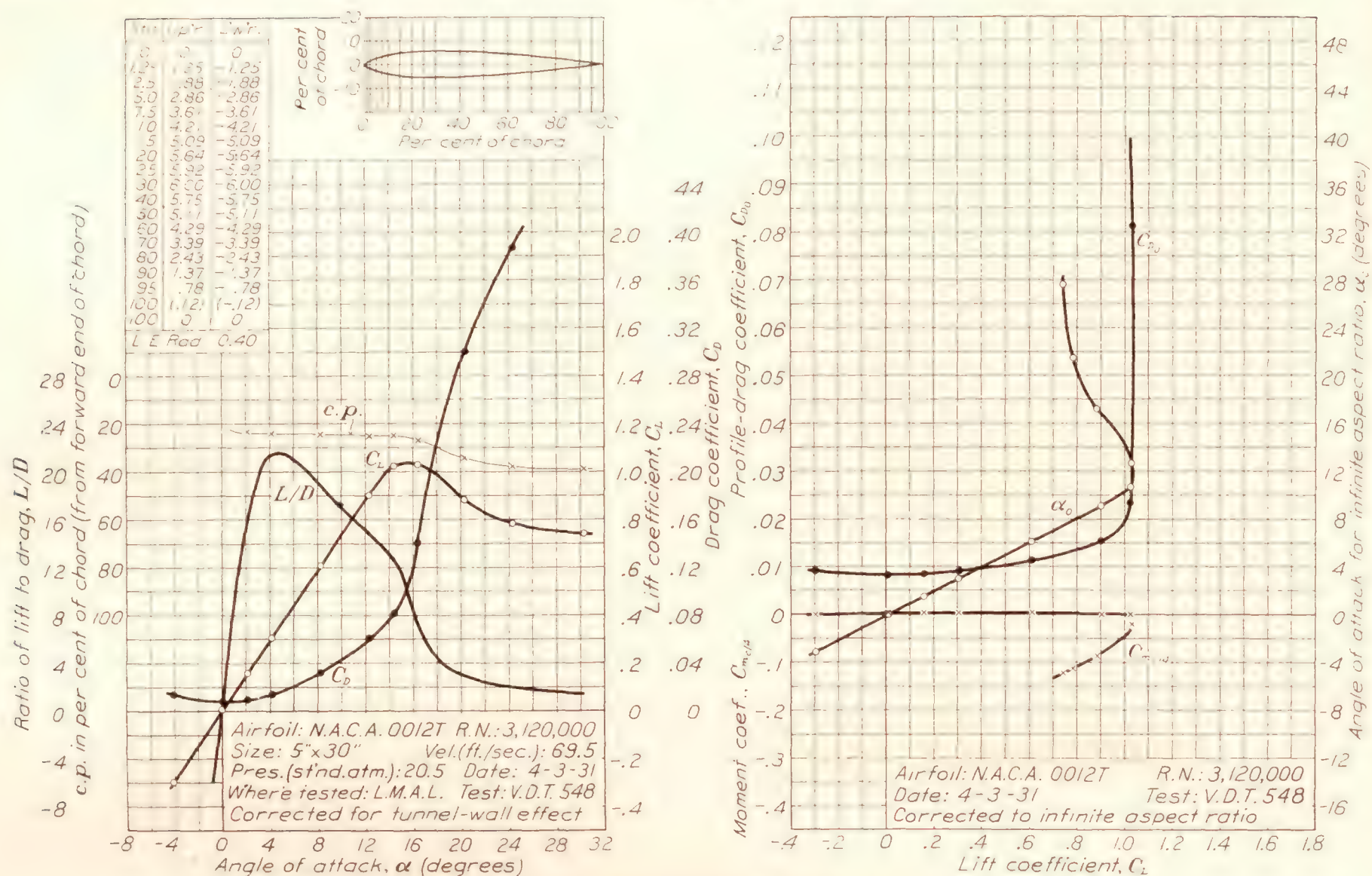


FIGURE 74.—N.A.C.A. 0012T airfoil.

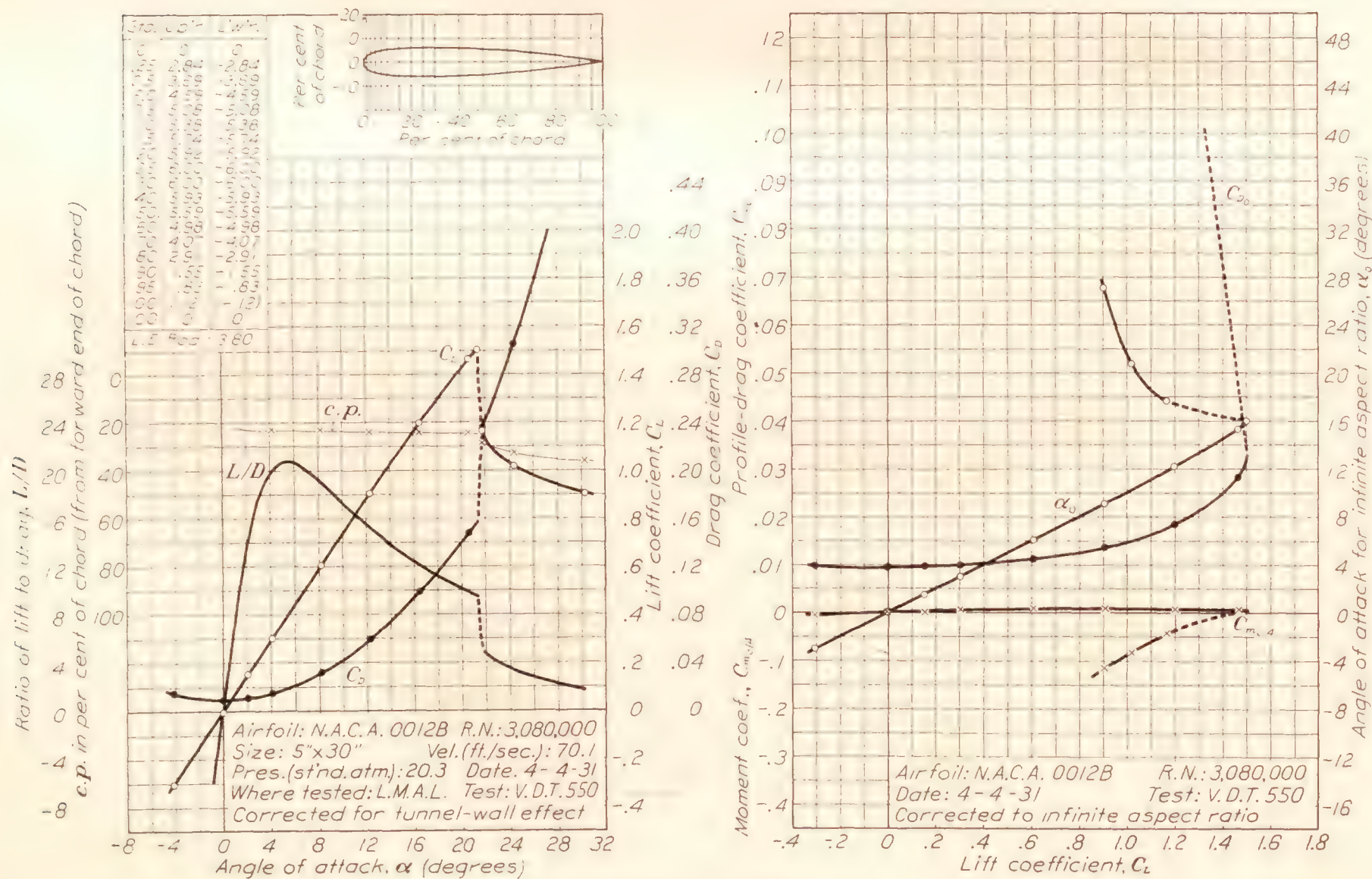


FIGURE 75.—N.A.C.A. 0012B airfoil.

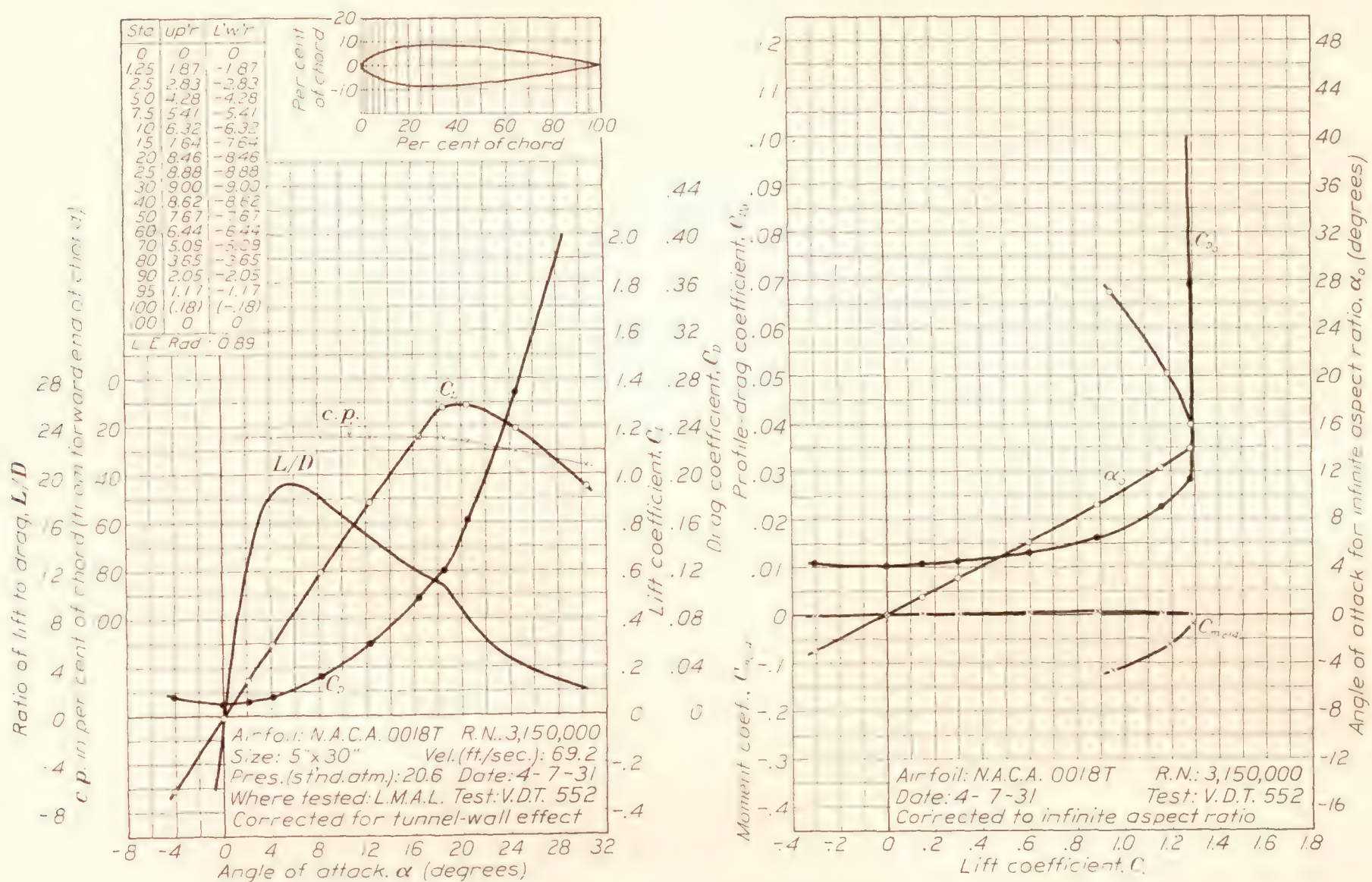


FIGURE 76.—N.A.C.A. 0018T airfoil.

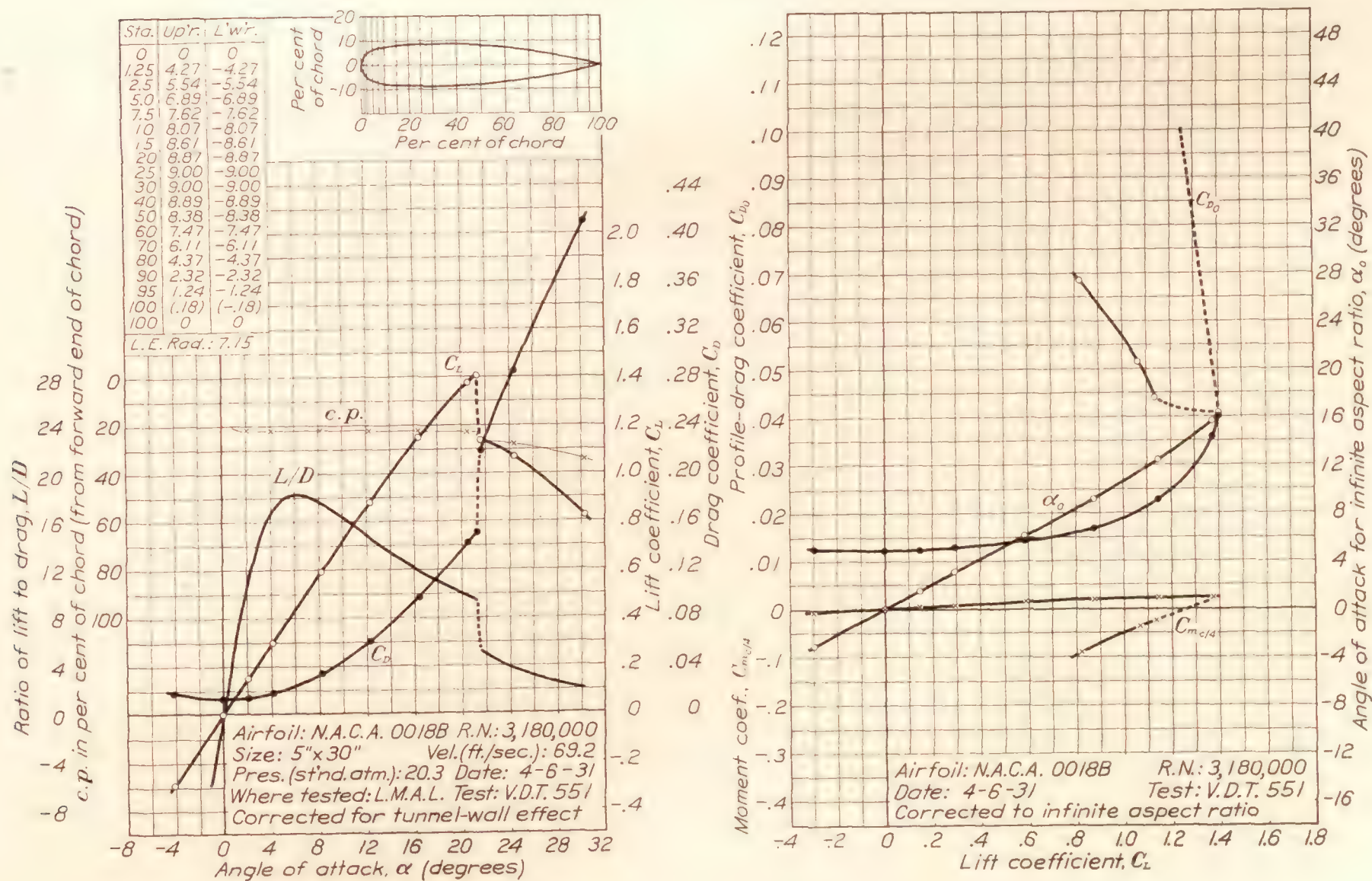


FIGURE 77.—N.A.C.A. 0018B airfoil.

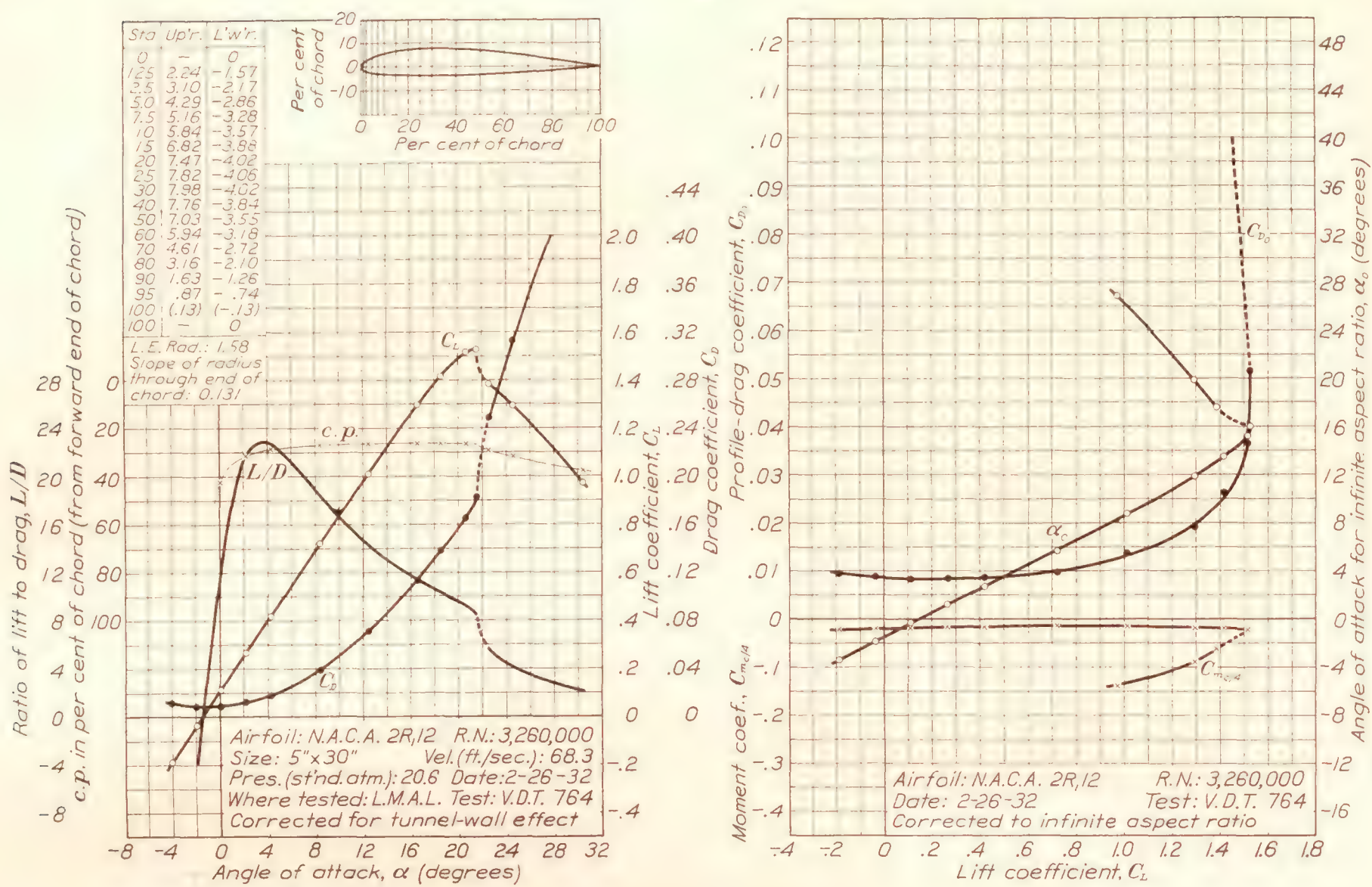


FIGURE 78.—N.A.C.A. 2R12 airfoil.

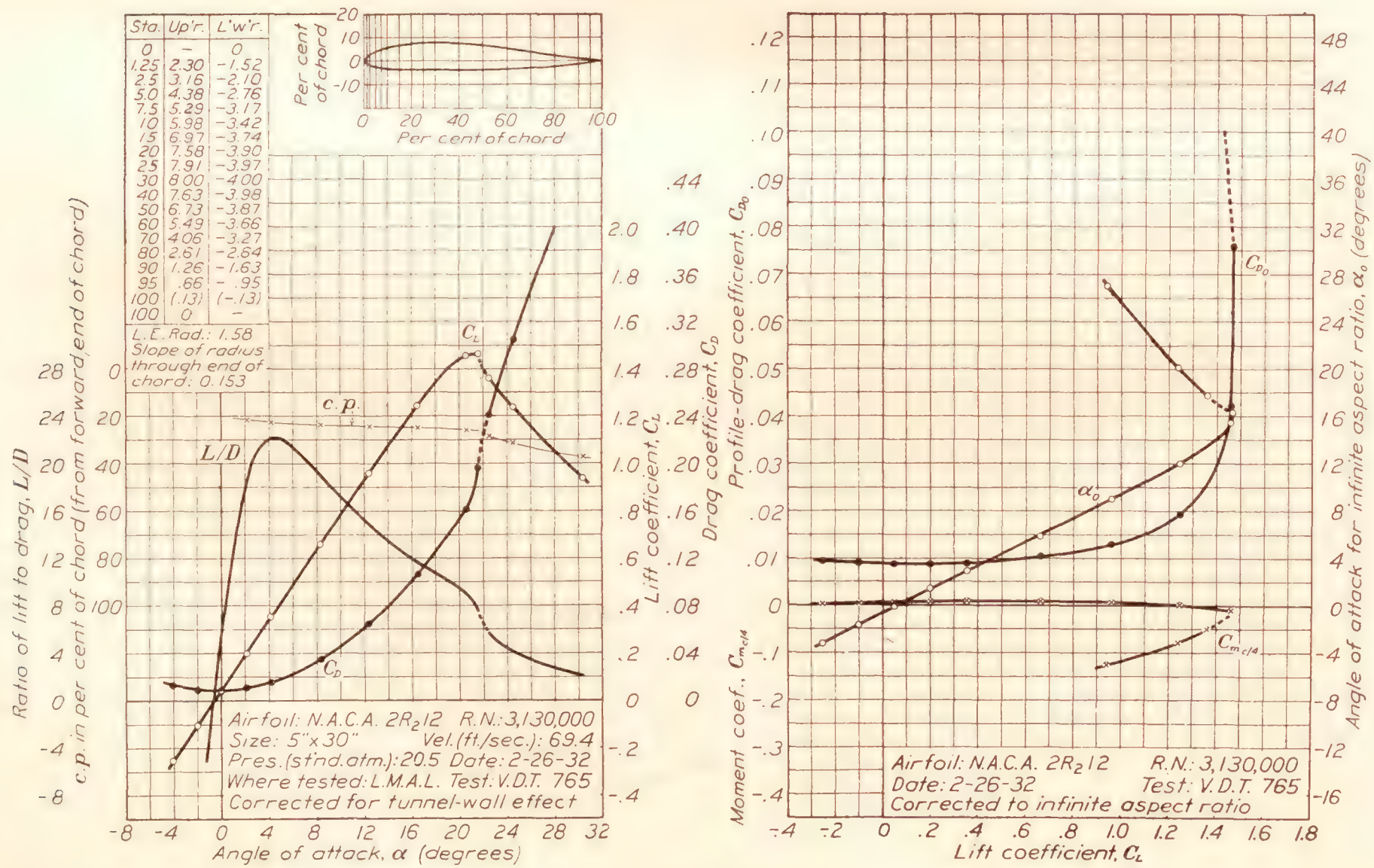
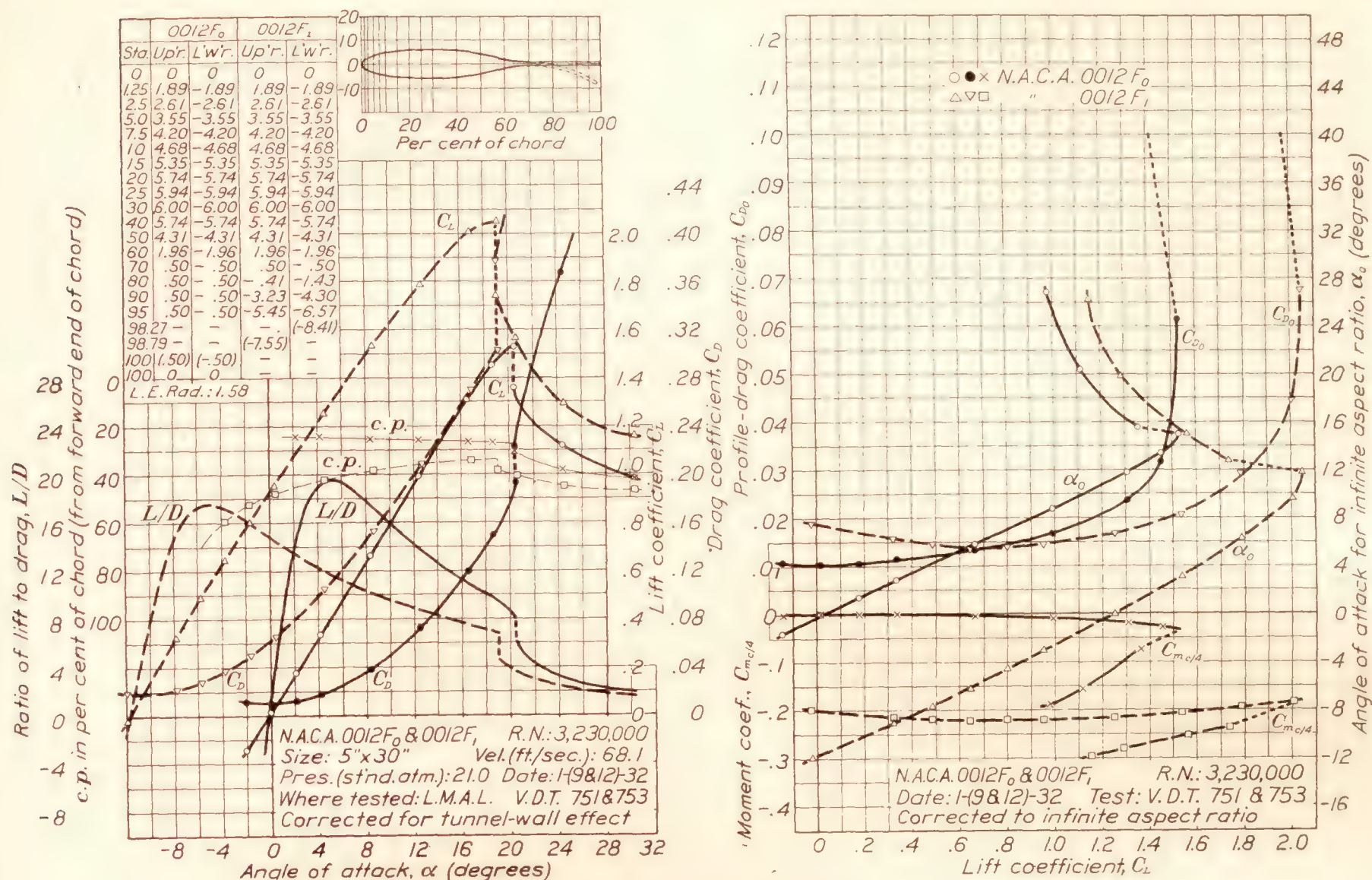


FIGURE 79.—N.A.C.A. 2R212 airfoil.

FIGURE 80.—N.A.C.A. 0012F₀ and 0012F₁ airfoils.

PRECISION

A general discussion of the errors and corrections involved in airfoil testing in the variable-density tunnel is included in reference 8. In connection with this report, it was hoped that a more specific discussion of the various sources of error and separate estimates of the various errors might be given. However, after a careful study of all the measurements it became apparent that practically all the errors may be regarded as accidental; that is, of the type the magnitude of which may best be estimated from the dispersion of the results of independent repeat measurements. The major portion of these errors is caused by insufficient sensitivity of the balance and manometers, by the personal error involved in reading mean values of slightly fluctuating quantities, and by the error due to slight surface imperfections in the model. The last is perhaps the most serious source of error. The models were carefully finished before each test, but the presence of particles of hard foreign matter in the air stream tended to cause a slight pitting of the leading edge of the model during each test. This pitting was probably the major source of error in connection with the earlier tests, but it was reduced for the later tests when the necessity of a more careful inspection of each model was appreciated. After a considerable period of running the particles in the tunnel were found to become lodged, permitting this source of error to be

largely eliminated during the later tests. For this report, however, the effect of the error from this source has been minimized by repeating the tests of many of the airfoils, including all of the symmetrical series originally reported in reference 2.

The magnitude of all such accidental errors was judged from the results of repeat tests of many airfoils, and from the results of approximately 25 tests of one airfoil that were made periodically throughout the investigation to check the consistency of the measurements. The accidental errors in the results presented in this report are believed to be within the limits indicated in the following table:

α	$\pm 0.15^\circ$
C_{Lmax}	$\begin{cases} 0.01 \\ -0.03 \end{cases}$
$C_{m_{c/4}}$	± 0.003
$C_{D_0}(C_L=0)$	$\begin{cases} 0.0006 \\ -0.0002 \end{cases}$
$C_{D_0}(C_L=1)$	$\begin{cases} 0.0015 \\ -0.0008 \end{cases}$

In addition to the consideration of the accidental errors, all measurements were carefully analyzed to consider possible sources of errors of the type that would not be apparent from the dispersion of the results of repeat tests. A rather large (approximately 1.5 percent) error of this type is present in all the air-

velocity measurements resulting from a reduction in the apparent weight of the manometer liquid when the density of the air in the tunnel is raised to that corresponding to a pressure of 20 atmospheres. The effects of this error, however, are reduced by the presence of another error in the air-velocity measurements due to the blocking effects of the model in the tunnel. The measured coefficients, obtained by dividing the measured forces by $\frac{1}{2}\rho V^2$, as well as the derived coefficients are, of course, affected by errors in the air-velocity measurement. Aside from this source of error, it is believed that only two other sources need be considered: first, the deflection of the model and supports under the air load; and second, the interference of the airfoil supports on the airfoil. The angle of attack and the moment coefficient are affected by the deflection of the airfoil and supports. The error in angle of attack, which is proportional to $C_{m_{c/4}}$, was found to be approximately -0.1° for an

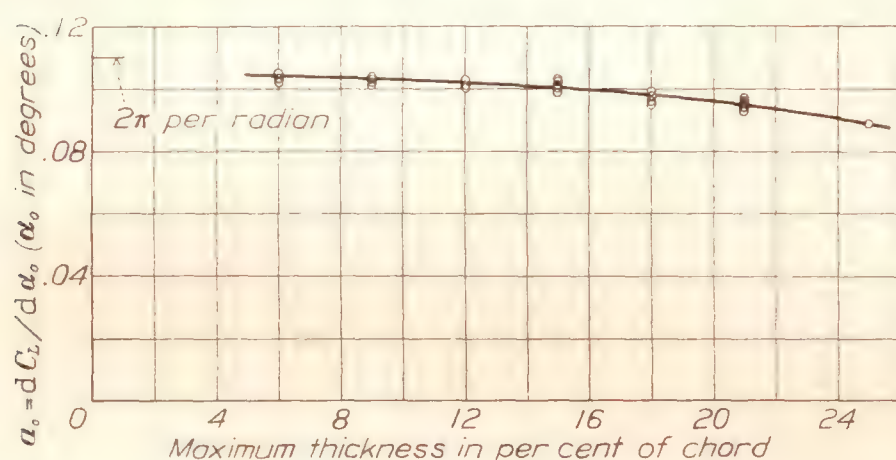


FIGURE 81.—Variation of lift-curve slope with thickness.

airfoil having a moment coefficient of -0.075 . The error from this source in the moment coefficient is inappreciable at zero lift, but at a lift coefficient of 1 may amount to -0.001 . The errors resulting from the support interference are more difficult to evaluate, but tests of airfoils with different support arrangements lead to the belief that they are within the limits indicated in the following table:

α	$\pm 0.05^\circ$
$C_{L_{max}}$	$\begin{cases} 0.00 \\ -0.02 \end{cases}$
$C_{m_{c/4}}$	± 0.001
$C_{D_0}(C_L=0)$	$\begin{cases} 0.0002 \\ 0.0000 \end{cases}$
$C_{D_0}(C_L=1)$	± 0.0010

The tunnel-wall and induced-drag corrections applied to obtain the airfoil section characteristics might also be treated as sources of systematic errors. Such errors need not be considered, however, if the section characteristics are defined as the measured characteristics with certain calculated corrections applied. Errors in the tunnel-wall corrections, however, should be considered when the results from different wind tunnels are compared. For consideration of these errors, the reader is referred to references 9 and 10.

For the purpose of comparing the results from different wind tunnels and of applying these results to airplanes in flight, it is also necessary to consider the effects of air-stream turbulence. In air streams having different degrees of turbulence, the value of the Reynolds Number cannot be considered as a sufficient measure of the effective dynamic scale of the flow. The airfoil characteristics presented in this report were obtained at a value of the Reynolds Number of approximately 3,000,000, which corresponds roughly to the Reynolds Number attained in flight by a medium-sized airplane flying near its stalling speed. Consideration of the effects of the turbulence present in the variable-density tunnel (see references 11 and 12) leads, however, to the belief that these results are more nearly directly applicable to the characteristics that would be obtained in flight at larger values of the Reynolds Number.

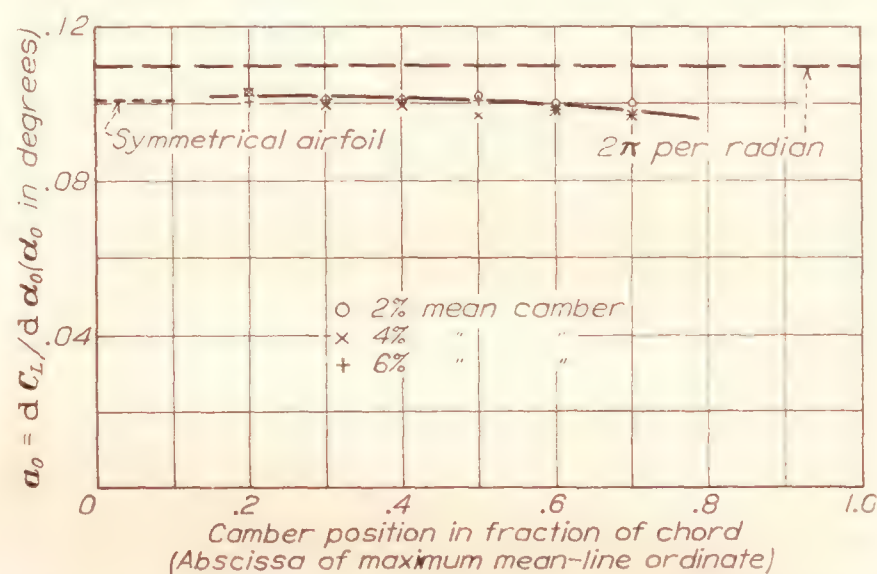


FIGURE 82.—Variation of lift-curve slope with camber. Results for 12 percent thick airfoils.

DISCUSSION

The results of this investigation are here discussed and analyzed to indicate the variation of the aerodynamic characteristics with variations in thickness and in mean-line form. For the analysis of the effect of thickness, test data from consecutive tests of airfoils having different thicknesses and the same mean-line form are used. The analysis of the effect of the mean-line form is made with respect to consecutive tests of airfoils of the same thickness (12 percent of the chord) and related mean-line forms. The results are compared, where possible, with the results predicted by thin-airfoil theory, a summary of which is presented in the appendix.

LIFT

Lift curve.—In the usual working range of an airfoil section the lift coefficient may be expressed as a linear function of the angle of attack

$$C_L = a_0 (\alpha_0 - \alpha_{L_0})$$

where a_0 is the slope of the lift curve for the wing of infinite aspect ratio and α_{L_0} is the angle of attack at zero lift.

The variation of the lift-curve slope with thickness is shown in figure 81. The points on the figure represent the deduced slopes as measured in the angular range of low profile drag. These results confirm previous results (reference 1) in that they show the lift-curve slope to decrease with increasing thickness. The camber has very little effect on the slope, as indicated in figure 82, although a rearward movement of the position of the camber tends to decrease the

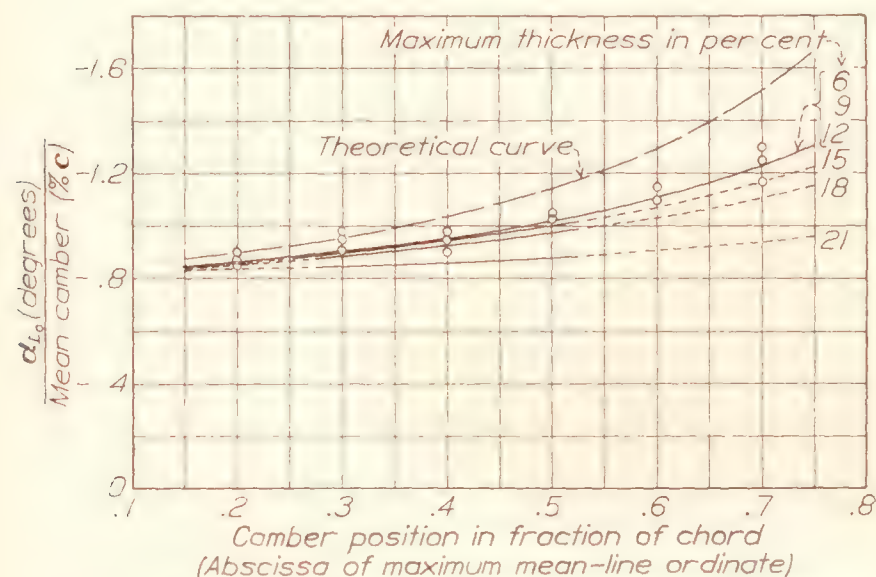


FIGURE 83.—Variation of angle of zero lift with camber. Points shown are for 12 percent thick airfoils. Curves indicate general trends for the different thicknesses.

given mean line without altering the camber position. The theory also predicts an increased negative angle as the position of the camber moves back along the chord. The experimental values are compared with the theoretical values in figures 83 and 84. The ex-

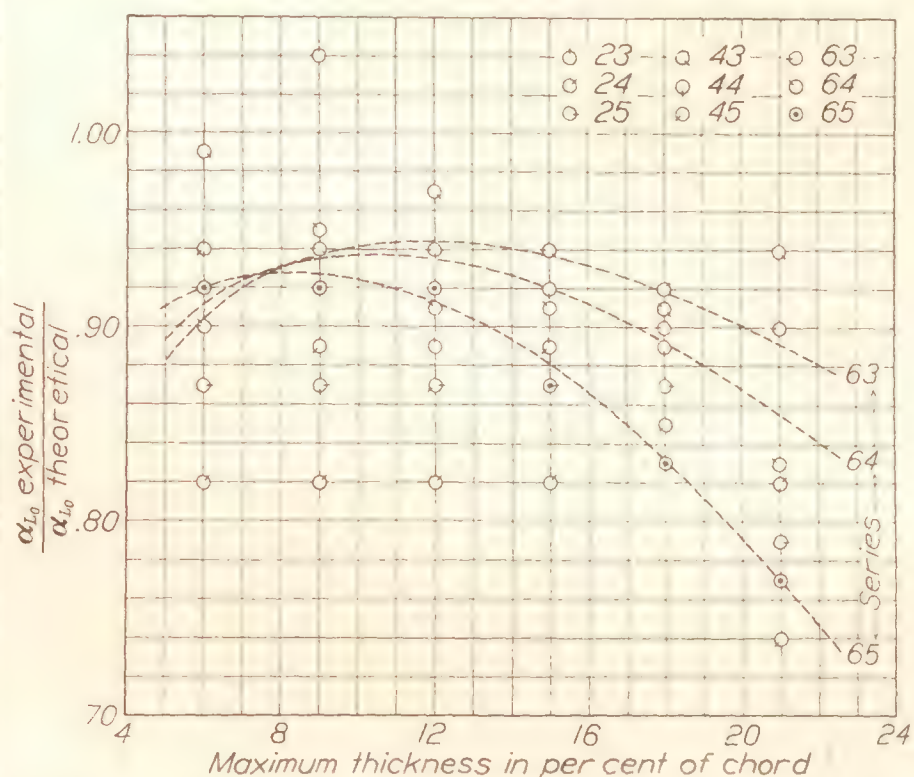


FIGURE 84.—Variation of angle of zero lift with thickness. Numbers refer to mean-camber designation.

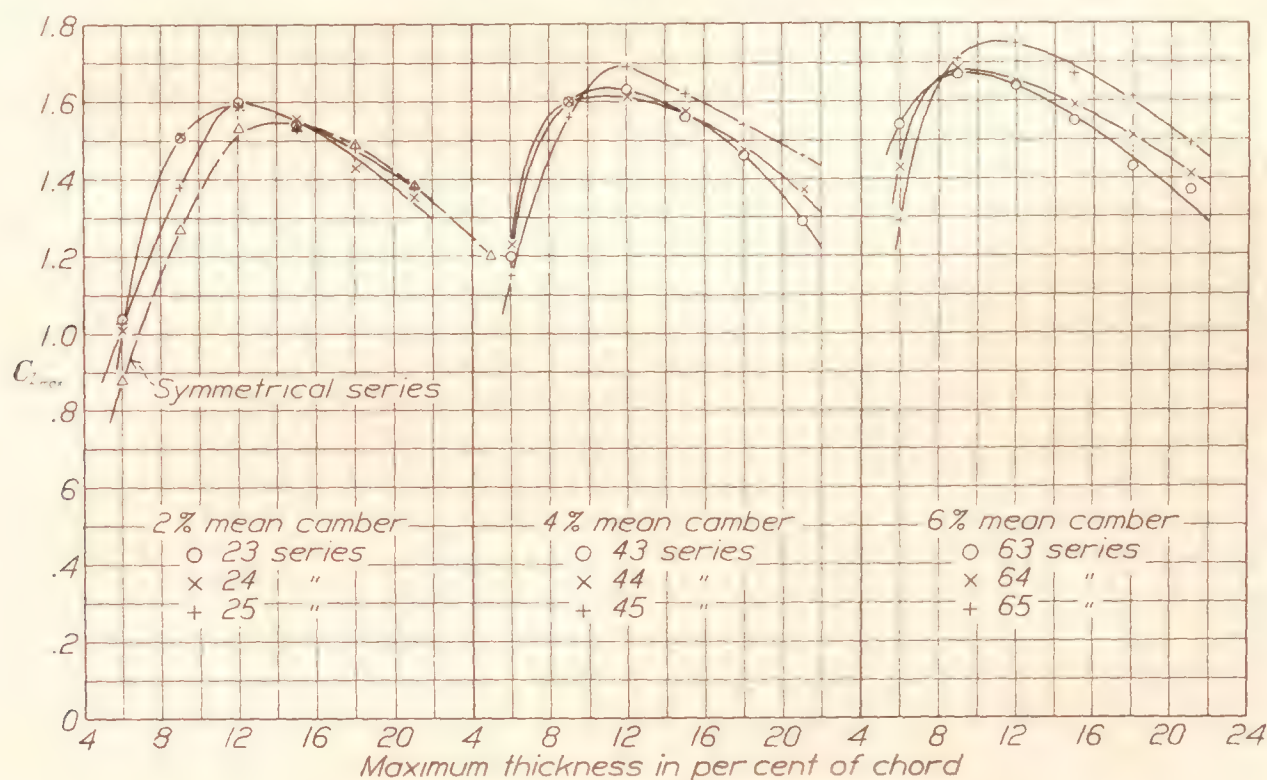


FIGURE 85.—Variation of maximum lift with thickness.

slope slightly. Table II gives the numerical values of the slope in convenient form for noting the general trends with respect to variations in thickness and in camber. It will be noted that all values of the slope lie below the approximate theoretical value for thin wings, 2π per radian; the measured values lie between 95 and 81 percent, approximately, of the theoretical.

The angle of zero lift is best analyzed by means of a comparison with that predicted by the theory. Thin-airfoil theory states that the angle of zero lift is proportional to the camber if the camber is varied, as with these related airfoils, by scaling the ordinates of a

perimental values lie between 100 and 75 percent, approximately, of the theoretical values, the departure becoming greater with a rearward movement of the position of the camber and with increased thickness (above 9 to 12 percent of the chord). Numerical values of the angle of zero lift are given in table III.

Maximum lift.—The variation of the maximum lift coefficient with thickness is shown in figure 85. It will be noted that the highest values are obtained with moderately thick sections (9 to 12 percent of the chord thick, except for the symmetrical sections for which the highest values are obtained with somewhat thicker

sections). The variation with camber, shown in figure 86, confirms the expected increase in maximum lift with camber. The gain is small, however, for the normal positions of the camber, but becomes larger as the camber moves either rearward or forward. It will be seen by reference to figure 85 that the camber becomes less effective as the thickness is increased. This reduced effectiveness of the camber is in agreement with a conclusion reached in reference 13 that for airfoils having a thickness ratio of approximately 20 percent of the chord, camber is of questionable value. Numerical values of the maximum lift coefficient are given in table IV.

Air-flow discontinuities.—These and other wind-tunnel tests indicate that at the attitude of maximum

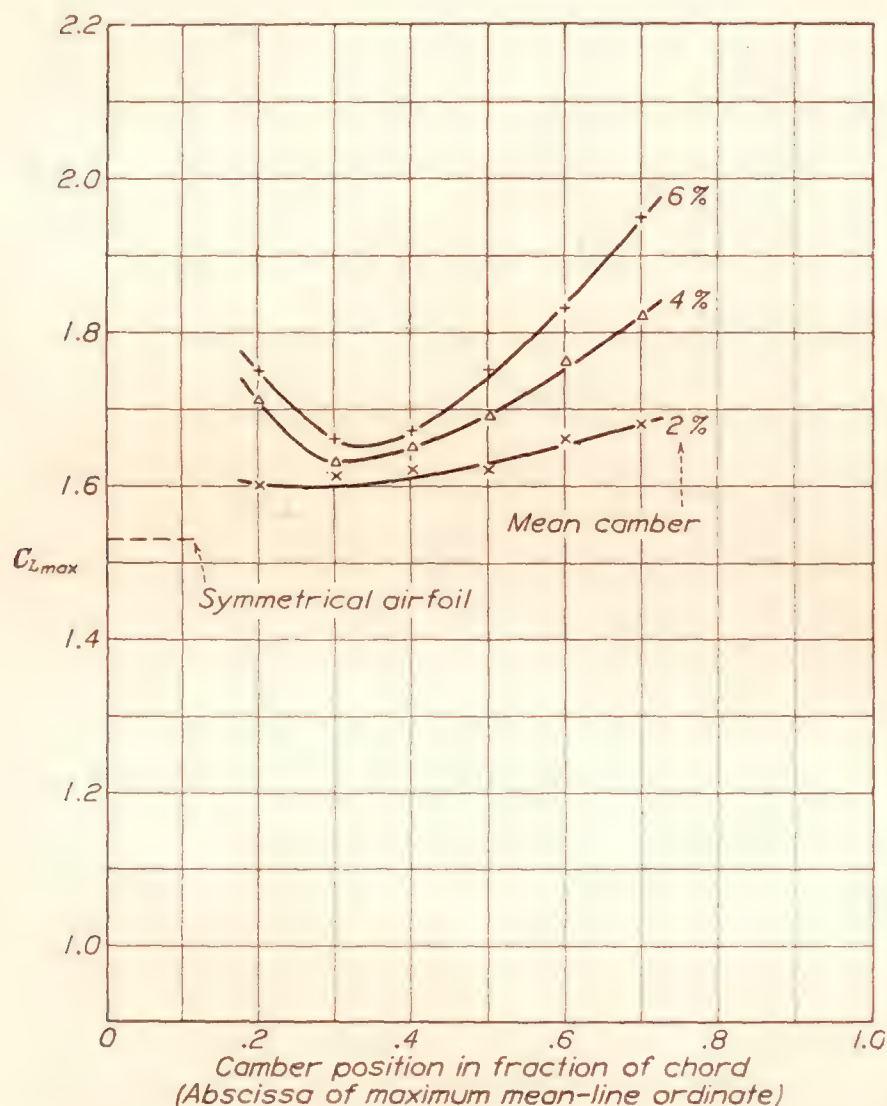


FIGURE 86.—Variation of maximum lift with camber. Results for 12 percent thick airfoils.

lift the air forces on certain airfoils exhibit sudden changes which in many instances result in a serious loss of lift. The probable cause of these air-flow discontinuities is discussed briefly in reference 13. The stability or instability of the air flow at maximum lift may be judged by the character of the lift-curve peaks indicated for the various airfoils. The curves are classified into three general types as noted in table IV, but the degree of stability is difficult to judge. It may be generally concluded that improved stability may be obtained by (1) having a small leading-edge radius, which causes an early breakdown of the flow with a consequent low value of the maximum lift, (2) increasing the thickness (beyond the normal thickness ratios), or (3) increasing the cam-

ber (for airfoils having normal camber positions; i.e., $0.3c$ to $0.5c$).

MOMENT

Thin-airfoil theory separates the air forces acting on any airfoil into two parts: First, the forces that produce a couple but no lift (they are dependent only on the shape of the mean line); second, the forces that produce the lift only, the resultant of which acts at

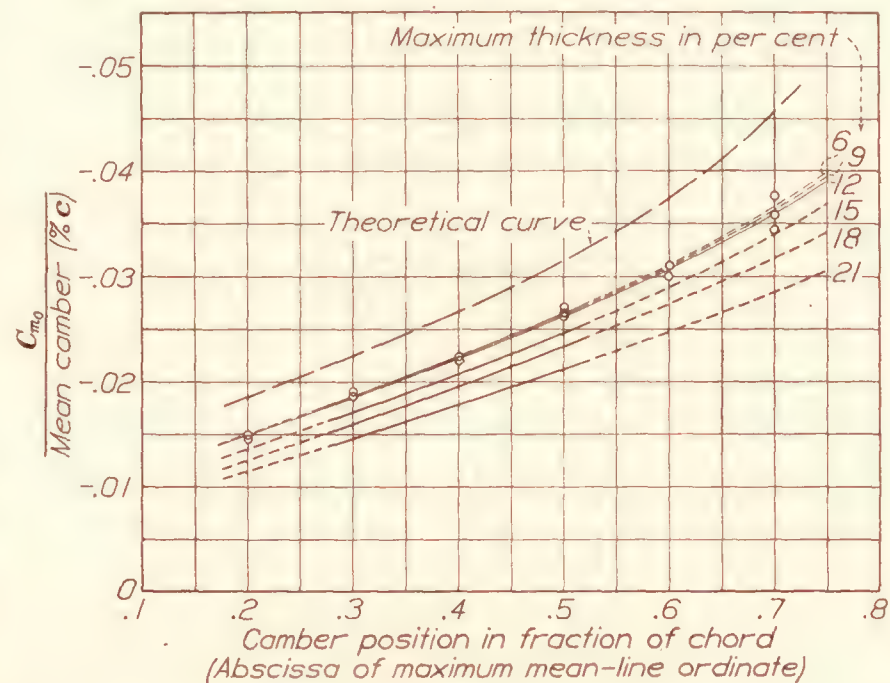


FIGURE 87.—Variation of moment at zero lift with camber. Points shown are for 12 percent thick airfoils. Curves indicate general trends for the different thicknesses.

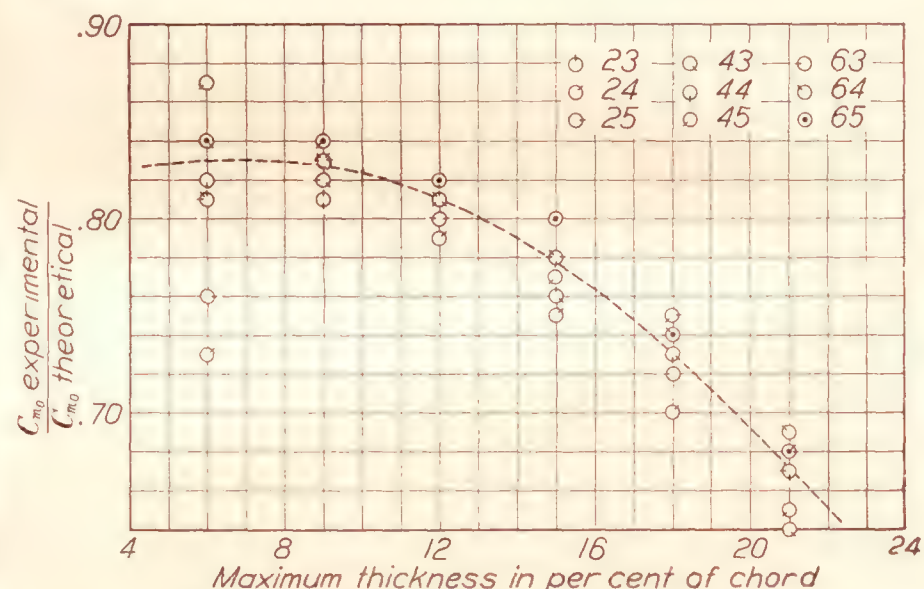


FIGURE 88.—Variation of moment at zero lift with thickness. Numbers refer to mean-camber designation.

a fixed point. We then have in the working range an expression for the total moment taken about any point

$$C_m = C_{m0} + nC_L$$

where C_{m0} is the moment coefficient at zero lift and nC_L is the additional moment due to lift.

As with the angle of zero lift, the theory states that the moment at zero lift is proportional to the camber and predicts an increase in the magnitude of the moment as the camber moves back along the chord. Figures 87 and 88 show the values of the moment coefficient as affected by variations of camber and thickness compared with the theoretical values. Referring to figure 87, the plotted data indicate that the

moment coefficients are nearly proportional to the camber. It will also be noted that the curves representing the ratios of the experimental coefficients to the camber are nearly parallel to the equivalent curve representing the theoretical ratios except that the curves tend to diverge for positions of the camber well back. Figure 88 shows that the experimental values lie between 87 and 64 percent, approximately, of the theoretical. Numerical values of the moment coefficient at zero lift are given in table V.

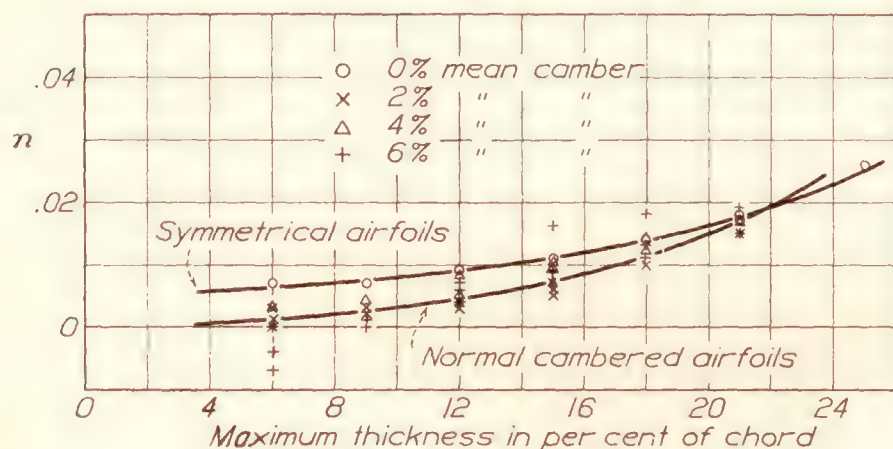


FIGURE 89.—Variation of position of constant moment with thickness. Values of n for equation $C_{m_{c/4}} = C_{m_0} + nC_L$. Results for airfoils having normal camber positions (0.3c to 0.5c).

If the resultant of the lift forces acted exactly through the quarter-chord point, as predicted by the theory of thin airfoils, there would be no additional moment due to the lift when the moments are taken about this point. The curves of $C_{m_{c/4}}$ against C_L , however, show a slope in the working range which indicates that the axis of constant moment is displaced somewhat from the quarter-chord point. The factor n represents the amount of this displacement as obtained from the deduced slopes of the moment curves in the

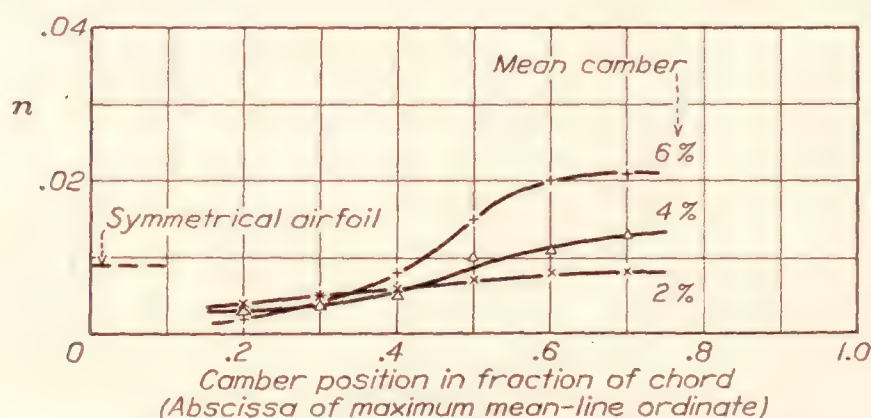


FIGURE 90.—Variation of position of constant moment with camber. Values of n for equation $C_{m_{c/4}} = C_{m_0} + nC_L$. Results for 12 percent thick airfoils.

normal working range. The variation of this displacement with thickness and with camber is shown in figures 89 and 90. Table VI gives the numerical values. Beyond the stall all the airfoils show a sharp increase in the magnitude of the pitching moment. The suddenness of this increase follows the degree of stability at the stall as indicated by the type of the lift-curve peak.

DRAG

The total drag of an airfoil is considered as made up of the induced drag and the profile drag. Considering

the profile drag as the minimum value plus an additional drag dependent upon the attitude of the airfoil, we have in coefficient form

$$C_D = C_{D_i} + (C_{D_{0min}} + \Delta C_{D_0})$$

The induced-drag coefficient C_{D_i} , which is computed by means of the formula given in reference 8, is considered to be independent of the airfoil section. The variation of the profile-drag coefficient with the shape variables of the airfoil section is analyzed with respect

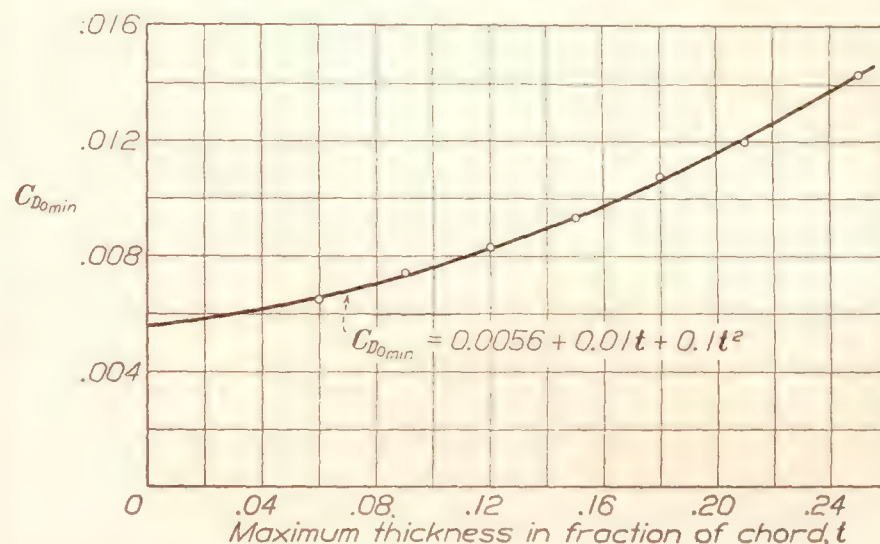


FIGURE 91.—Variation of minimum profile drag with thickness for the symmetrical airfoils.

to the variations of the two components of the profile drag.

Minimum profile drag.—The variation of the minimum profile-drag coefficient with thickness for the symmetrical sections is shown in figure 91. The cambered sections show the same general variation with thickness but, to avoid confusion, the results are not plotted. The variation of the minimum profile-drag

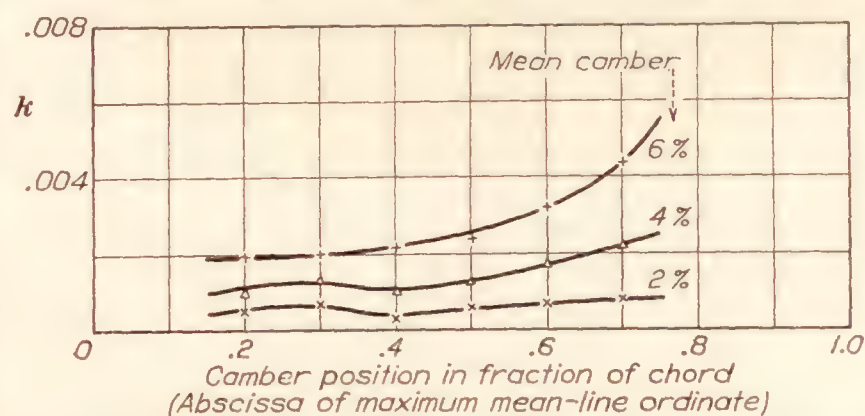


FIGURE 92.—Increase in minimum profile drag due to camber. Results for 12 percent thick airfoils. Values of k for equation $C_{D_{0min}} = k + 0.0056 + 0.01t + 0.1t^2$, where k is the increase in $C_{D_{0min}}$ due to camber and t is the maximum thickness in fraction of chord.

coefficient with the profile thickness may be expressed by the empirical relation

$$C_{D_{0min}} = k + 0.0056 + 0.01t + 0.1t^2$$

where t is the thickness ratio and k (which is approximately constant for sections having the same mean line) represents the increase in $C_{D_{0min}}$ above that computed for the symmetrical section of corresponding thickness. The variation of $C_{D_{0min}}$ with camber is indicated by the variation of k as shown in figure 92.

The effect of camber is small except for the highly cambered sections having the maximum camber well back. Numerical values of C_{D0min} are given in table VII.

Additional profile drag.—The additional profile drag, which is dependent upon the attitude of the airfoil, has previously been expressed as a function of the lift (reference 4) by the equation

$$\Delta C_{D0} = C_{D0} - C_{D0min} = 0.0062 (C_L - C_{Lopt})^2$$

where C_{Lopt} may be called the optimum lift coefficient; that is, the lift coefficient corresponding to the minimum profile-drag coefficient. This equation holds

This function is represented in figure 93 as the curve determined from the results for the symmetrical airfoils and for the airfoils having a camber of 2 percent of the chord. As the camber is increased, the dispersion of the plotted points from the curve becomes greater. In general the points above the curve correspond to thick sections and sections in which the maximum camber is well back. The departure from the curve becomes greater with increased thickness and with a rearward movement of the maximum-camber position. The points well below the curve correspond to the thin airfoils.

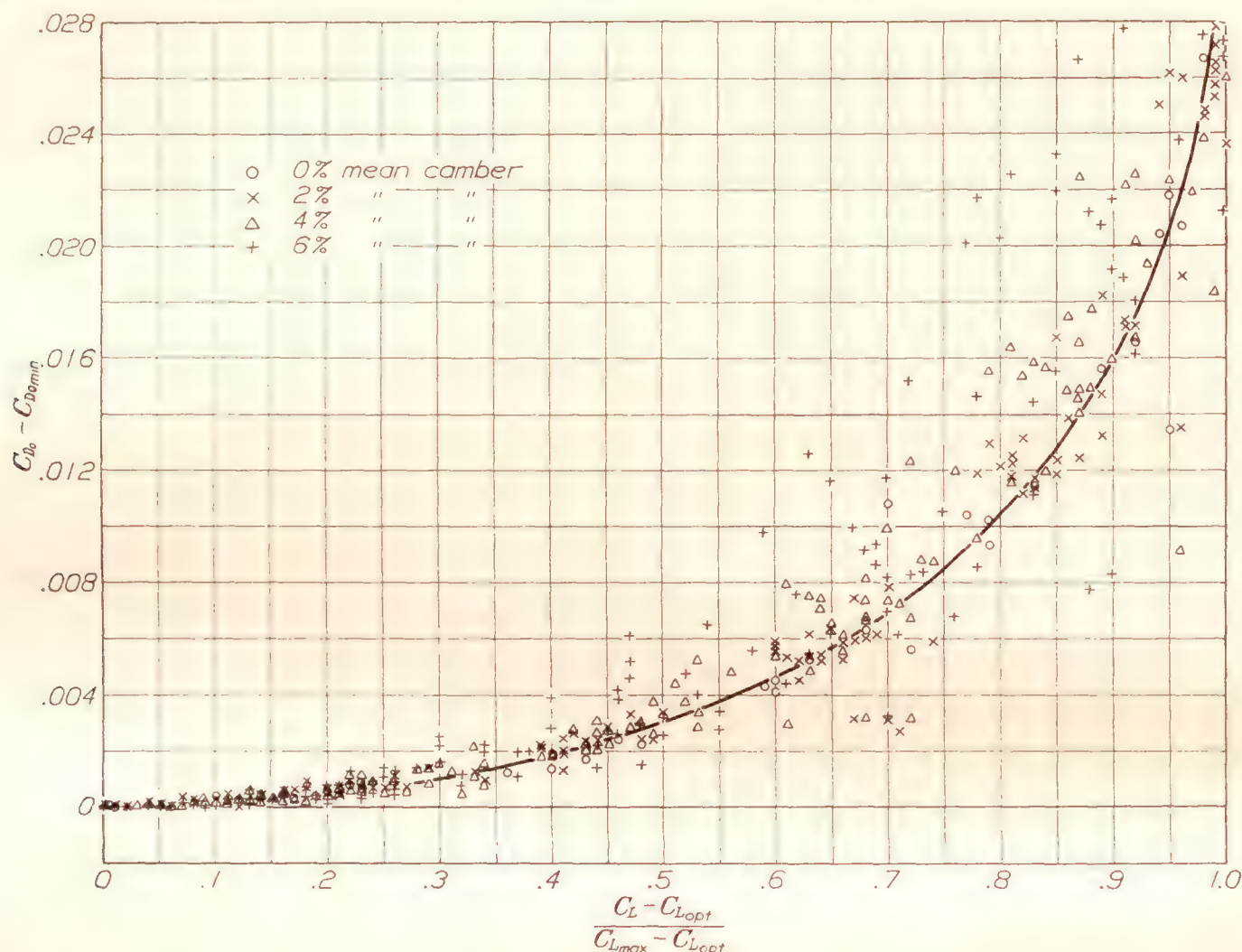


FIGURE 93.—Additional profile drag.

reasonably well for the normally shaped airfoils at values of the lift coefficient below unity.

A convenient practical method of allowing for the increased values of C_{D0} at moderately high values of the lift coefficient is to include the additional profile drag with the induced drag, as suggested in reference 2. For the symmetrical airfoils of moderate thickness the term to be added to the induced-drag coefficient was given as $0.0062 C_L^2$. The relative importance of this term may be better appreciated by considering that it represents 11.7 percent of the induced drag of an elliptical airfoil of aspect ratio 6. The same method may also be applied to other airfoils if the value of the optimum lift is not too large.

Andrews (reference 14), using the part of these data published in references 2, 4, and 5, suggests for the additional profile drag the form

$$\Delta C_{D0} = f \left(\frac{C_L - C_{Lopt}}{C_{Lmax} - C_{Lopt}} \right)$$

Because the additional profile drag is not a simple function of the lift, and also because the results as presented in figure 93 are difficult to follow, generalized curves for the relation

$$\Delta C_{D0} = f(C_L - C_{Lopt})$$

are given in figure 94. These curves are given to represent more accurately the additional profile drag for the normally shaped sections.

Optimum lift.—The optimum lift, as defined above, is the value of the lift corresponding to the minimum profile drag. As the determination of this value of the lift is largely dependent upon the fairing of the profile-drag curves, special curves were faired for this purpose on enlarged-scale plots corresponding to certain related airfoils grouped together. The values of the optimum lift coefficients obtained in this manner are given in table VIII. It may be noted by reference to this table that the optimum lift coefficient increases with camber

and for the highly cambered sections a definite increase accompanies a forward movement of the camber.

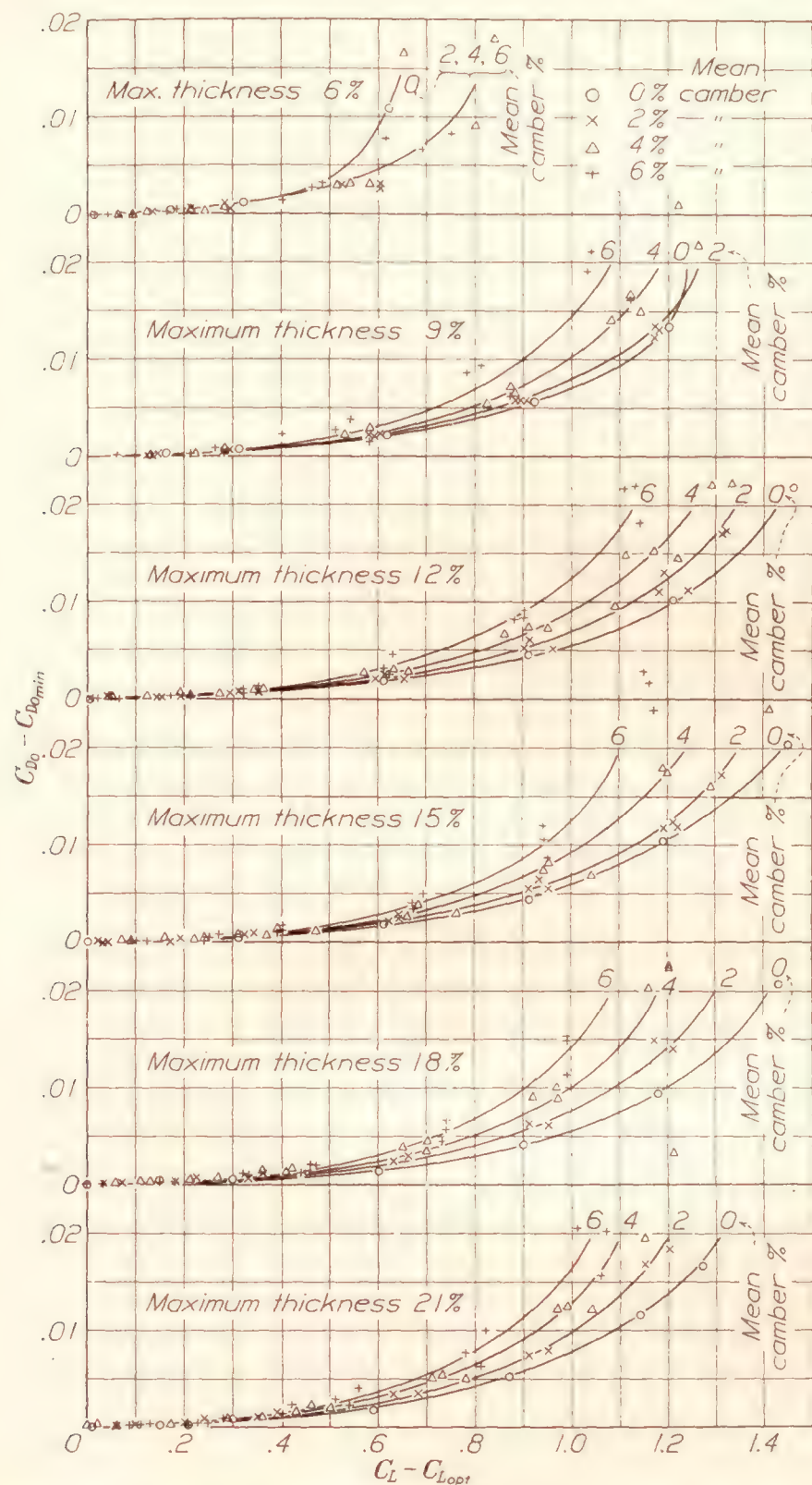


FIGURE 94.—Additional profile drag as a function of $C_L - C_{L_{opt}}$. Results are for airfoils having normal camber positions (0.3c to 0.5c).

it is not primarily dependent upon the shape of the mean line. Nevertheless it is interesting to compare the optimum lift coefficients with the values included in table VIII representing the theoretical lift coefficients at the "ideal" angle of attack for the mean line; i.e., the angle of attack for which the thin-airfoil theory gives a finite velocity at the nose. (See the appendix.)

GENERAL EFFICIENCY

The general efficiency of an airfoil cannot be expressed by means of a single number. The ratio of

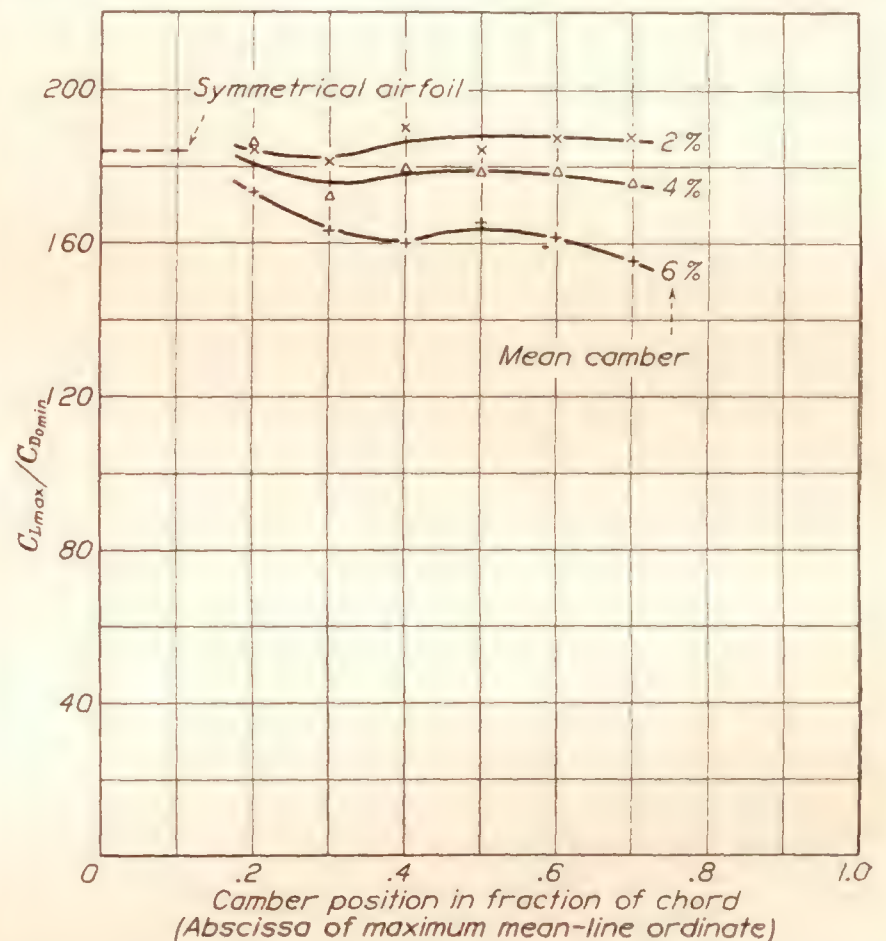


FIGURE 96.—Variation of $C_{L_{max}}/C_{D_{0min}}$ with camber. Results are for 12 percent thick airfoils.

the maximum lift to the minimum profile drag is, however, of some value as the measure of the efficiency of an airfoil section. The variation of this ratio with thickness is shown in figure 95. The curves of this figure indicate that the highest values of the ratio are

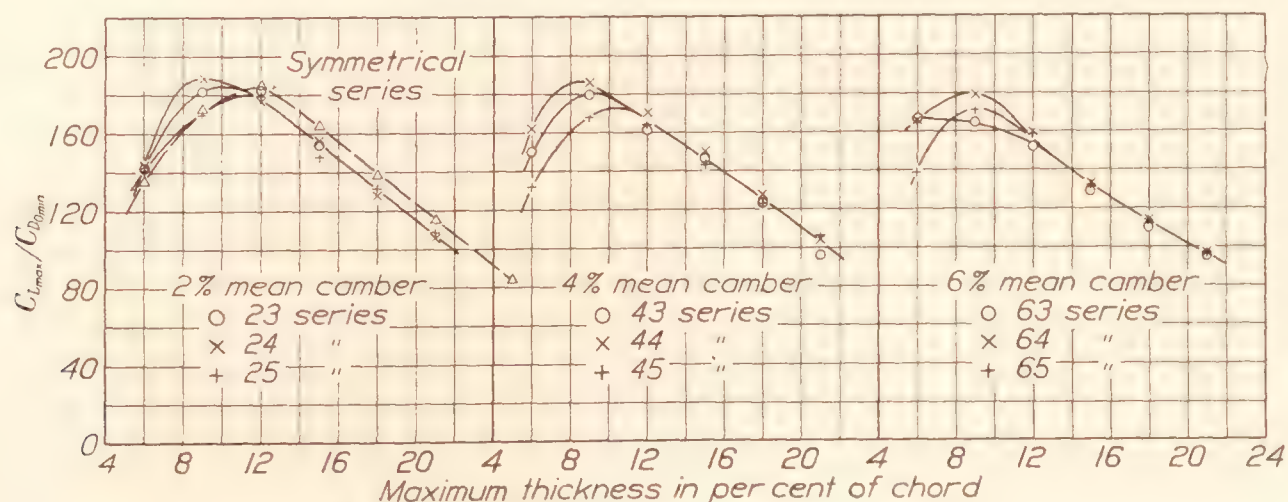


FIGURE 95.—Variation of $C_{L_{max}}/C_{D_{0min}}$ with thickness.

More important than these variations, however, is the variation with thickness. The rapid decrease in the optimum lift with increased thickness indicates that

given by the sections between 9 and 12 percent of the chord thick. The variation with camber, shown in figure 96, is less important. An increase in the camber

above 2 percent of the chord and a rearward movement of the camber (for the highly cambered sections) tend to decrease the value of $C_{L_{max}}/C_{D_{0min}}$. The numerical values of the ratio are given in table IX.

SUPPLEMENTARY AIRFOILS

For the purpose of investigating briefly the effects of certain shape variables other than those discussed in the main body of the report, 10 supplementary airfoils were tested. The airfoil sections were as follows: 6 symmetrical sections with modified nose shapes, 2 sections with reflexed mean lines, and 2 sections simulating those of a wing having a flexible trailing edge.

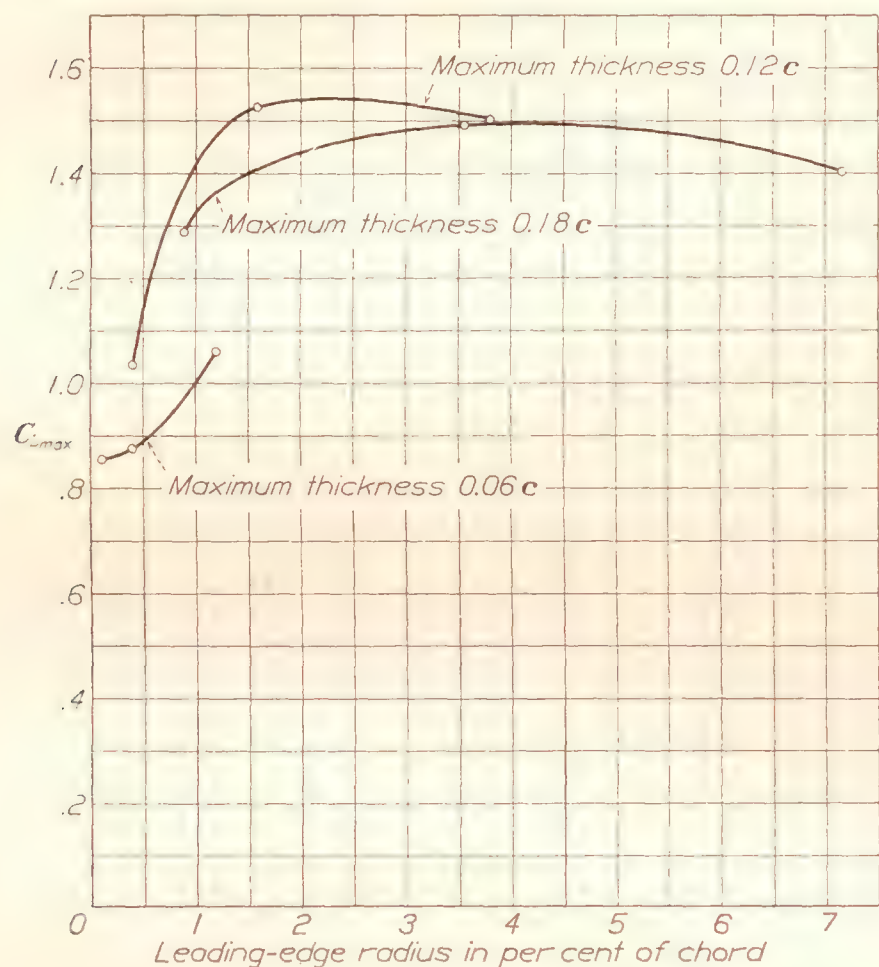


FIGURE 97.—Variation of maximum lift with nose radius.

Airfoils with modified nose shapes.—The airfoils of the first supplementary group investigated were developed from three of the symmetrical N.A.C.A. family airfoils: The N.A.C.A. 0006, the N.A.C.A. 0012, and the N.A.C.A. 0018. For each of these basic (or normal) sections one thinner-nosed section, denoted by the suffix T, and one blunter-nosed section, denoted by the suffix B, were developed and tested. The derivation of each modified section was similar to that of the normal section and was accomplished by a systematic change in the equation that defines the normal section. This change is principally a change in the nose radius, but it also results in modifications to the profile throughout its length, except at the maximum ordinate and at the trailing edge. The nose radii of the sections in percent of the chord are as follows:

Section	T series	Normal	B series
0006	0.10	0.40	1.19
0012	.40	1.58	3.80
0018	.89	3.56	7.15

The aerodynamic characteristics of the modified sections are given in figures 72 to 77. These may be compared with the characteristics of the normal sections given in figures 4, 6, and 8. The maximum lift coefficients of the modified and the normal sections are plotted against the leading-edge radii in figure 97. It is interesting to note that the leading-edge radius is very critical in its effect on the maximum lift when the radius is small. This critical effect is also indicated by the rapid increase in the maximum lift with increasing thickness for the thin sections as shown in figure 85.

Airfoils with reflexed mean lines.—Previous investigations have shown that the pitching moment of cambered airfoils can be reduced by altering the form of the mean line toward the trailing edge, with a consequent loss of maximum lift but only a small reduction in drag. In order to compare the characteristics of sections of this type with those of the related sections of normal form, two airfoils were developed with the basic thickness distribution of the N.A.C.A. 0012 disposed about certain mean lines of the form given in reference 15

$$y_c = hx(1-x)(1-\lambda x)$$

The values of h in this equation were chosen to give a camber of 0.02 and the values of λ were chosen to give the airfoil designated the N.A.C.A. 2R₁12 a small negative moment and the airfoil designated the N.A.C.A. 2R₂12 a small positive moment. Characteristic curves for the two airfoils are given in figures 78 and 79. The principal characteristics of the sections may be conveniently compared with those of the related symmetrical section, the N.A.C.A. 0012, and a related normal section having a camber of 2 percent of the chord, the N.A.C.A. 2412, by means of the following table arranged in the order of increasing pitching-moment coefficients.

Section	$C_{L_{max}}$	$C_{D_{0min}}$	$\frac{C_{L_{max}}}{C_{D_{0min}}}$	C_{m_0}
2R ₂ 12	1.47	0.0086	171	0.004
0012	1.53	.0083	184	-.002
2R ₁ 12	1.53	.0083	184	-.020
2412	1.62	.0085	190	-.044

These results indicate that airfoils having reflexed mean lines may be of questionable value because of the adverse effect of this mean-line shape on the maximum lift coefficient.

Thickness and camber modifications near the trailing edge.—Two airfoils were developed to simulate an airfoil having a flexible trailing edge in a straight and in a given deflected position. The thickness distribution is composed of three parts: the forward portion (0 to $0.3c$) having the same distribution as the N.A.C.A. 0012, the rear portion (from $0.7c$ to the trailing edge) having a thin, uniform value, and the central portion joining these two with fair curves. As shown in figure 80, the two airfoils differ only in the rear portion, the section designated N.A.C.A. 0012F₀ simulating that of a wing having the trailing edge deformed for the high-speed condition, and the section designated N.A.C.A. 0012F₁ simulating that of the same wing with the trailing edge bent down in a circular arc. Curves of the aerodynamic characteristics for both conditions are compared in figure 80. Considering the results given by both airfoils as two conditions for one airfoil, a very high maximum lift with a reasonably low minimum drag is obtained.

On this assumption the ratio $\frac{C_{L_{max}}}{C_{D_{min}}}$ is 197, slightly higher than the value of this ratio given by the N.A.C.A. 2412.

In order to study the effects of an extreme change in the thickness distribution, the principal characteristics of the two sections may be compared with those of the related normal sections, the N.A.C.A. 0012 and the N.A.C.A. 6712. The maximum lift coefficient is little affected by the change in the thickness distribution, but it is of interest to note (table I) that the slope of the lift curve of the N.A.C.A. 0012F₀ is slightly greater than 2π per radian, as compared with an appreciably lower slope for the N.A.C.A. 0012. The profile drag is also affected by the change in the thickness distribution. Of the two symmetrical sections, the profile drag of the N.A.C.A. 0012F₀ is much higher than that of the N.A.C.A. 0012 over the entire lift range. This is not true, however, for the two cambered sections. Comparing the characteristics of the N.A.C.A. 0012F₁ with those of the N.A.C.A. 6712, we find that at low values of the lift the profile drag of the former is much higher, but as the lift increases this difference becomes less, and in the high-lift range the profile drag of the N.A.C.A. 0012F₁ is considerably less than that of the N.A.C.A. 6712.

CONCLUSIONS

The variation of the aerodynamic characteristics of the related airfoils with the geometric characteristics investigated may be summarized as follows:

Variation with thickness ratio:

1. The slope of the lift curve in the normal working range decreases with increased thickness, varying from 95 to 81 percent, approximately, of the theoretical slope for thin airfoils (2π per radian).

2. The angle of zero lift moves toward zero with increased thickness (above 9 to 12 percent of the chord thickness ratios).

3. The highest values of the maximum lift are obtained with sections of normal thickness ratios (9 to 15 percent).

4. The greatest instability of the air flow at maximum lift is encountered with the moderately thick, low-cambered sections.

5. The magnitude of the moment at zero lift decreases with increased thickness, varying from 87 to 64 percent, approximately (for normally shaped airfoils), of the values obtained by thin-airfoil theory.

6. The axis of constant moment usually passes slightly forward of the quarter-chord point, the displacement increasing with increased thickness.

7. The minimum profile drag varies with thickness approximately in accordance with the expression

$$C_{D_{min}} = k + 0.0056 + 0.01t + 0.1t^2$$

where the value of k depends upon the camber and t is the ratio of the maximum thickness to the chord.

8. The optimum lift coefficient (the lift coefficient corresponding to the minimum profile-drag coefficient) approaches zero as the thickness is increased.

9. The ratio of the maximum lift to the minimum profile drag is highest for airfoils of medium thickness ratios (9 to 12 percent).

Variation with camber:

1. The slope of the lift curve in the normal working range is little affected by the camber; a slight decrease in the slope is indicated as the position of the camber moves back.

2. The angle of zero lift is between 100 and 75 percent, approximately, of the value given by thin-airfoil theory, the smaller departures being for airfoils with the normal camber positions.

3. The maximum lift increases with increased camber, the increase being more rapid as the camber moves forward or back from a point near the $0.3c$ position.

4. Greater stability of the air flow at maximum lift is obtained with increased camber if the camber is in the normal positions ($0.3c$ to $0.5c$).

5. The moment at zero lift is nearly proportional to the camber. For any given thickness, the difference between the experimental value of the constant of proportionality and the value predicted by thin-airfoil theory is not appreciably affected by the position of the camber except for the sections having the maximum camber well back, where the difference becomes slightly greater.

6. The axis of constant moment moves forward as the camber moves back.

7. The minimum profile drag increases with increased camber, and also with a rearward movement of the camber.

8. The optimum lift coefficient increases with the camber and for the highly cambered sections a definite increase accompanies a forward movement of the camber.

9. The ratio of the maximum lift to the minimum profile drag tends to decrease with increased camber (above 2 percent of the chord) and with a rearward movement of the camber (for the highly cambered sections).

LANGLEY MEMORIAL AERONAUTICAL LABORATORY,
NATIONAL ADVISORY COMMITTEE FOR AERONAUTICS,
LANGLEY FIELD, VA., December 20, 1932.

APPENDIX

It is proposed in this section of the report to present, briefly, a summary of the results of the existing thin-airfoil theory (based on the section mean line) as applied to the prediction of certain section characteristics. Such a summary is desirable because at present the results must be obtained from several different sources which give them in a form not easily applied. Three characteristics are considered; namely, (1) the angle of zero lift α_{L_0} , (2) the pitching-moment coefficient $C_{m_{c/4}}$, and (3) the "ideal" angle of attack α_I , or the corresponding lift coefficient C_{L_I} , that is, values corresponding to the unique condition for which the theory gives a finite velocity at the nose of the airfoil. (See reference 16.)

Expressions for lift and moment coefficients may be written as follows if the angles are measured in radians:

$$C_L = 2\pi(\alpha - \alpha_{L_0}) \quad (1)$$

$$C_{L_I} = 2\pi(\alpha_I - \alpha_{L_0}) \quad (2)$$

$$C_{m_{c/4}} = \frac{\pi}{2}(\beta + \alpha_{L_0}) \quad (3)$$

If the leading end of the mean line is chosen as the origin of coordinates and the trailing end is taken on the x axis at $x=1$, then the parameters α_{L_0} , α_I , and β are given by the following integrals

$$\alpha_{L_0} = \int_0^1 y f_1(x) dx \quad (4)$$

$$\alpha_I = \int_0^1 y f_2(x) dx \quad (5)$$

$$\beta = \int_0^1 y f_3(x) dx \quad (6)$$

where

$$f_1(x) = \frac{-1}{\pi(1-x)[x(1-x)]^{1/2}} \quad (7)$$

$$f_2(x) = \frac{(1-2x)}{2\pi[x(1-x)]^{3/2}} \quad (8)$$

$$f_3(x) = \frac{4(1-2x)}{\pi[x(1-x)]^{1/2}} \quad (9)$$

and y is the ordinate of the mean line at a given abscissa x . The integrals (4) and (6) may be shown to be identical with the corresponding integrals given by Glauert (reference 15) and by Munk (reference 17), and integral (5) is given by Theodorsen (reference 16).

The evaluation of these integrals for the N.A.C.A. airfoil sections given in this report was accomplished analytically. The values of α_{L_0} (changed from radians to degrees), $C_{m_{c/4}}$ and C_{L_I} , so computed, are given in tables III, V, and VIII, respectively, in the main body of the report. This method of evaluation, however, cannot be applied to many of the commonly used sections because they do not have analytically defined mean lines; hence, an approximate method must be used. A graphical determination gives good results and for convenience the values of the three functions, (7), (8), and (9), at several values of x , are given in the following table:

x	$f_1(x)$	$f_2(x)$	$f_3(x)$	x	$f_1(x)$	$f_2(x)$	$f_3(x)$
0	$-\infty$	∞	∞	0.30	-0.992	0.662	1.111
0.0125	-2.901	113.15	11.17	.40	-1.083	.271	.520
.0250	-2.091	39.73	7.747	.50	-1.273	0	0
.0500	-1.537	13.84	5.258	.60	-1.624	-.271	-.520
.0750	-1.306	7.403	4.109	.70	-2.315	-.662	-1.111
.1000	-1.179	4.716	3.395	.80	-3.979	-1.492	-1.910
.15	-1.049	2.447	2.496	.90	-10.61	-4.716	-3.395
.20	-.995	1.492	1.910	.95	-29.21	-13.84	-5.258
.25	-.980	.980	1.470	1.00	$-\infty$	$-\infty$	$-\infty$

In general, some difficulty would be expected with the graphical method because the values of the above functions tend to infinity at the leading and trailing edges. Actually, because the ordinates of the mean-line extremities are zero, the integrand may approach zero, and does at the leading edge for the integral (4), and at the leading and trailing edges for the integral (6). Difficulty, however, is encountered at the trailing edge for the integral (4) and at the leading and trailing edges for the integral (5). In order to avoid this difficulty, integral (4) is evaluated graphically from $x=0$ to $x=0.95$, and the increment contributed by the portion from $x=0.95$ to $x=1$ is determined analytically. Likewise, integral (5) is evaluated graphically from $x=0.05$ to $x=0.95$ and analytically for the extremities. The analytical determination of the increments is accomplished by assuming the mean line near the ends to be of the form

$$y = a + bx + cx^2$$

Evaluating the integrals gives

$$\Delta\alpha_{L_0} = -0.964y_{0.95} + 0.0954y'_1 \quad (x=0.95 \text{ to } x=1)$$

$$\Delta\alpha_I = \begin{cases} +0.467y_{0.05} + 0.0472y'_0 & (x=0 \text{ to } x=0.05) \\ -0.467y_{0.95} + 0.0472y'_1 & (x=0.95 \text{ to } x=1) \end{cases}$$

where y_0 and y'_1 are the mean-line slopes at the leading and trailing edges, respectively.

REFERENCES

1. Jacobs, Eastman N., and Anderson, Raymond F.: Large-Scale Aerodynamic Characteristics of Airfoils as Tested in the Variable-Density Wind Tunnel. T.R. No. 352, N.A.C.A., 1930.
2. Jacobs, Eastman N.: Tests of Six Symmetrical Airfoils in the Variable-Density Wind Tunnel. T.N. No. 385, N.A.C.A., 1931.
3. Pinkerton, Robert M.: Effect of Nose Shape on the Characteristics of Symmetrical Airfoils. T.N. No. 386, N.A.C.A., 1931.
4. Jacobs, Eastman N., and Pinkerton, Robert M.: Tests of N.A.C.A. Airfoils in the Variable-Density Wind Tunnel. Series 43 and 63. T.N. No. 391, N.A.C.A., 1931.
5. Jacobs, Eastman N., and Pinkerton, Robert M.: Tests of N.A.C.A. Airfoils in the Variable-Density Wind Tunnel. Series 45 and 65. T.N. No. 392, N.A.C.A., 1931.
6. Jacobs, Eastman N., and Pinkerton, Robert M.: Tests of N.A.C.A. Airfoils in the Variable-Density Wind Tunnel. Series 44 and 64. T.N. No. 401, N.A.C.A., 1931.
7. Jacobs, Eastman N., and Ward, Kenneth E.: Tests of N.A.C.A. Airfoils in the Variable-Density Wind Tunnel. Series 24. T.N. No. 404, N.A.C.A., 1932.
8. Jacobs, Eastman N., and Abbott, Ira H.: The N.A.C.A. Variable-Density Wind Tunnel. T.R. No. 416, N.A.C.A., 1932.
9. Higgins, George J.: The Prediction of Airfoil Characteristics. T.R. No. 312, N.A.C.A., 1929.
10. Knight, Montgomery, and Harris, Thomas A.: Experimental Determination of Jet Boundary Corrections for Airfoil Tests in Four Open Wind Tunnel Jets of Different Shapes. T.R. No. 361, N.A.C.A., 1930.
11. Stack, John: Tests in the Variable-Density Wind Tunnel to Investigate the Effects of Scale and Turbulence on Airfoil Characteristics. T.N. No. 364, N.A.C.A., 1931.
12. Dryden, H. L., and Kuethe, A. M.: Effect of Turbulence in Wind Tunnel Measurements. T.R. No. 342, N.A.C.A., 1930.
13. Jacobs, Eastman N.: The Aerodynamic Characteristics of Eight Very Thick Airfoils from Tests in the Variable-Density Wind Tunnel. T.R. No. 391, N.A.C.A., 1931.
14. Andrews, W. R.: The Estimation of Profile Drag. *Flight*, vol. XXIV, no. 25, pp. 530a-530d, 1932 and no. 31, pp. 710a-710c, 1932.
15. Glauert, H.: *The Elements of Aerofoil and Aircrew Theory*. Cambridge University Press (London), 1926.
16. Theodorsen, Theodore: *On the Theory of Wing Sections with Particular Reference to the Lift Distribution*. T.R. No. 383, N.A.C.A., 1931.
17. Munk, Max M.: *Elements of the Wing Section Theory and of the Wing Theory*. T.R. No. 191, N.A.C.A., 1924.

TABLE I.—IMPORTANT CHARACTERISTICS

Airfoil	Page	Section characteristics							Wing characteristics A.R. 6			Thickness at		c.p. at		$^{1/4}(C/B)_0$
		$C_{L_{max}}$	α_0 at $C_{L_{max}}$ (deg.)	α_{L_0} (deg.)	$a_0 = \frac{dC_L}{d\alpha_0}$ (per deg.)	$C_{D_{0min}}$	$\frac{C_{L_{max}}}{C_{D_{0min}}}$	C_{m_0}	$C_{D_{min}}$	$(L/D)_{max}$	C_L at $(L/D)_{max}$	0.15 chord	0.65 chord	Maxi- mum forward position	$\frac{1}{4} C_{L_{max}}$	
												Percent chord	Percent chord			
0006	303	0.88	13	-0.1	0.102	0.0065	135	-0.002	0.0065	23.8	0.31	5.35	4.13	25	25	-0.082
0009	303	1.27	14	.0	.101	.0074	172	-.003	.0074	22.9	.36	8.02	6.20	25	25	-.213
0012	304	1.53	17	.0	.101	.0083	184	-.002	.0083	22.2	.37	10.69	8.27	25	25	-.285
0015	304	1.53	17	.0	.100	.0093	164	.000	.0093	21.2	.40	13.36	10.33	24	24	-.279
0018	305	1.49	17	.0	.098	.0108	138	-.002	.0108	19.8	.40	16.04	12.40	24	24	-.285
0021	305	1.38	17	-1	.094	.0120	115	-.001	.0120	18.5	.44	18.71	14.46	23	23	-.270
0025	306	1.20	16	.0	.089	.0143	84	-.003	.0143	16.5	.47	22.27	17.22	23	23	-.233
2212	306	1.60	16	-1.8	.103	.0087	184	-.029	.0088	22.4	.40	10.69	8.25	27	32	-.262
2306	307	1.04	11	-1.8	.104	.0073	142	-.036	.0075	23.9	.33	5.36	4.14	29	38	-.130
2309	307	1.51	15	-2.0	.103	.0083	182	-.036	.0085	22.9	.39	8.04	6.21	28	34	-.236
2312	308	1.61	16	-1.9	.101	.0089	181	-.038	.0090	22.1	.39	10.71	8.27	27	34	-.268
2315	308	1.54	15	-1.7	.102	.0100	154	-.034	.0100	20.5	.41	13.38	10.36	27	34	-.251
2406	308	1.01	13	-1.7	.103	.0070	144	-.039	.0074	24.9	.32	5.34	4.14	29	40	-.103
2409	309	1.51	14	-1.7	.103	.0080	189	-.044	.0082	23.1	.36	8.02	6.20	28	36	-.242
2412	310	1.62	17	-1.8	.101	.0085	190	-.044	.0087	22.5	.39	10.71	8.27	28	35	-.274
2415	310	1.55	16	-1.7	.101	.0099	156	-.040	.0100	20.8	.40	13.39	10.34	28	35	-.262
2418	311	1.43	15	-1.9	.098	.0112	128	-.037	.0113	19.4	.42	16.08	12.39	27	34	-.238
2421	311	1.35	16	-1.7	.097	.0127	106	-.036	.0128	17.9	.43	18.75	14.46	27	34	-.229
2506	312	1.03	15	-2.0	.103	.0073	141	-.048	.0076	24.2	.36	5.36	4.13	30	44	-.116
2509	312	1.38	13	-2.0	.102	.0081	170	-.052	.0083	22.9	.37	8.04	6.21	29	40	-.207
2512	313	1.62	17	-2.1	.102	.0088	184	-.054	.0091	22.3	.39	10.70	8.27	28	37	-.270
2515	313	1.53	16	-2.0	.099	.0103	148	-.049	.0104	20.4	.41	13.38	10.33	28	37	-.255
2518	314	1.48	16	-2.0	.096	.0112	132	-.047	.0113	19.1	.42	16.07	12.41	28	36	-.255
2521	314	1.38	16	-1.8	.095	.0126	109	-.043	.0126	17.7	.44	18.72	14.47	28	36	-.233
2612	315	1.66	17	-2.3	.100	.0089	187	-.060	.0091	22.1	.38	10.70	8.26	28	38	-.274
2712	315	1.68	17	-2.6	.100	.0090	187	-.075	.0093	22.0	.38	10.69	8.25	29	41	-.272
4212	316	1.71	16	-3.4	.102	.0092	186	-.059	.0100	22.1	.40	10.70	8.27	29	38	-.260
4306	316	1.20	10	-3.8	.103	.0080	150	-.075	.0094	23.7	.38	5.40	4.14	31	49	-.141
4309	317	1.60	15	-3.6	.103	.0089	180	-.073	.0094	22.3	.39	8.09	6.21	29	43	-.236
4312	317	1.63	16	-3.9	.100	.0095	172	-.075	.0100	21.7	.40	10.77	8.27	30	43	-.236
4315	318	1.56	15	-3.6	.103	.0107	146	-.068	.0108	20.2	.42	13.47	10.34	29	42	-.233
4318	318	1.46	14	-3.5	.099	.0119	123	-.065	.0121	19.0	.43	16.14	12.41	29	41	-.225
4321	319	1.29	15	-3.6	.095	.0134	96	-.057	.0134	17.4	.45	18.81	14.46	29	41	-.196
4406	319	1.23	10	-3.9	.104	.0076	162	-.087	.0089	24.2	.38	5.40	4.16	32	53	-.144
4409	320	1.60	15	-3.6	.103	.0086	186	-.086	.0092	22.9	.40	8.07	6.21	31	46	-.242
4412	320	1.65	16	-3.9	.100	.0092	179	-.089	.0096	22.1	.40	10.77	8.28	31	45	-.253
4415	321	1.57	15	-3.8	.101	.0105	150	-.083	.0108	20.5	.42	13.45	10.34	30	45	-.242
4418	321	1.47	17	-3.7	.096	.0116	127	-.078	.0120	19.2	.43	16.15	12.40	30	44	-.231
4421	322	1.37	19	-3.4	.093	.0132	104	-.071	.0133	17.7	.44	18.79	14.48	30	44	-.222
4506	322	1.15	13	-4.3	.104	.0087	132	-.109	.0098	22.7	.40	5.38	4.14	33	63	-.103
4509	323	1.56	13	-4.1	.103	.0093	168	-.106	.0099	22.0	.40	8.08	6.21	32	52	-.229
4512	323	1.69	17	-4.2	.097	.0095	178	-.105	.0099	21.7	.40	10.74	8.28	31	49	-.262
4515	324	1.62	17	-4.1	.101	.0113	143	-.097	.0116	19.6	.43	13.44	10.35	31	48	-.253
4518	324	1.54	17	-3.9	.096	.0125	123	-.094	.0126	18.4	.43	16.14	12.41	31	48	-.244
4521	325	1.46	19	-3.4	.095	.0138	106	-.082	.0138	17.2	.45	18.80	14.47	30	46	-.244
4612	325	1.76	17	-4.6	.098	.0099	178	-.124	.0105	21.1	.41	10.73	8.27	31	52	-.275
4712	326	1.82	18	-5.0	.097	.0104	175	-.143	.0110	20.7	.41	10.74	8.26	32	55	-.290
6212	326	1.75	14	-5.2	.100	.0101	173	-.087	.0117	20.9	.44	10.78	8.29	30	44	-.240
6306	327	1.54	12	-5.2	.105	.0092	167	-.109	.0177	21.6	.42	5.47	4.15	32	54	-.187
6309	327	1.67	13	-5.4	.104	.0101	165	-.110	.0116	21.1	.42	8.18	6.23	32	51	-.213
6312	328	1.66	14	-5.5	.101	.0102	163	-.110	.0115	20.9	.44	10.86	8.29	31	51	-.218
6315	328	1.55	13	-5.4	.101	.0120	129	-.105	.0125	19.3	.45	13.58	10.37	32	52	-.214
6318	329	1.43	13	-5.2	.098	.0130	110	-.097	.0133	18.4	.45	16.27	12.44	32	50	-.209
6321	329	1.37	17	-5.2	.096	.0144	95	-.090	.0145	17.0	.47	18.92	14.51	31	50	-.214
6406	330	1.43	9	-5.6	.104	.0086	166	-.129	.0139	22.6	.42	5.42	4.15	34	62	-.157
6409	330	1.68	15	-5.9	.101	.0094	179	-.133	.0113	21.6	.42	8.14	6.21	33	57	-.225
6412	331	1.67	15	-5.7	.101	.0104	160	-.132	.0117	20.8	.42	10.85	8.29	33	56	-.242
6415	331	1.59	17	-5.7	.099	.0120	133	-.125	.0127	19.2	.45	13.55	10.36	33	56	-.238
6418	332	1.51	18	-5.7	.099	.0132	114	-.118	.0137	18.1	.4					

TABLE II.—SLOPE OF LIFT CURVE, $a_0=\frac{dC_L}{d\alpha_0}$ (PER DEG.)

Thickness designa- tion Camber des- ignation	06	09	12	15	18	21	25	12
00	0.102	0.101	0.101	0.100	0.098	0.094	0.089	0.101
22								.103
23	.104	.103	.102	.102				.101
24	.103	.103	.103	.101	.098	.097		.101
25	.103	.102	.102	.099	.096	.095		.102
26								.100
27								.100
42								.102
43	.103	.103	.102	.103	.099	.095		.100
44	.104	.103	.100	.101	.096	.093		.100
45	.104	.103	.101	.101	.096	.095		.097
46								.098
47								.097
62								.100
63	.105	.104	.102	.101	.098	.096		.101
64	.104	.101	.102	.099	.099	.096		.101
65	.101	.103	.101	.099	.095	.094		.101
66								.099
67								.097

¹ Additional tests to determine variation with camber.

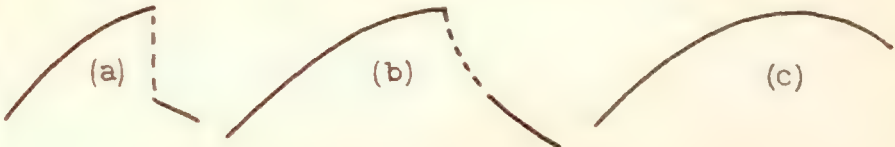
TABLE III.—ANGLE OF ZERO LIFT, α_{L_0} (DEGREES)

Thickness designa- tion Camber des- ignation	06	09	12	15	18	21	25	12	Theor.
00	-0.1	0.0	0.0	0.0	0.0	-0.1	0.0	0.0	0
22								-1.8	-1.80
23	-1.8	-2.0	-1.7	-1.7				-1.9	-1.92
24	-1.7	-1.7	-1.7	-1.7	-1.9	-1.7		-1.8	-2.08
25	-2.0	-2.0	-2.0	-2.0	-2.0	-1.8		-2.1	-2.29
26								-2.3	-2.59
27								-2.6	-3.04
42								-3.4	-3.60
43	-3.8	-3.6	-3.7	-3.6	-3.5	-3.6		-3.9	-3.84
44	-3.9	-3.6	-3.9	-3.8	-3.7	-3.4		-3.9	-4.15
45	-4.3	-4.1	-4.0	-4.1	-3.9	-3.4		-4.2	-4.58
46								-4.6	-5.18
47								-5.0	-6.09
62								-5.2	-5.40
63	¹ -5.2	-5.4	-5.4	-5.4	-5.2	-5.2		-5.5	-5.75
64	-5.6	-5.9	-5.7	-5.7	-5.7	-5.2		-5.7	-6.23
65	¹ -6.3	-6.3	-6.3	-6.0	-5.7	-5.3		-6.2	-6.88
66								-6.6	-7.78
67								-7.0	-9.13

¹ Based on straight portion of lift curve extended. See curve for actual value.

TABLE IV.—MAXIMUM LIFT COEFFICIENT, $C_{L_{max}}$

Thickness designa- tion Camber des- ignation	06	09	12	15	18	21	25	12
00	c 0.88	b 1.27	a 1.53	b 1.53	b 1.49	a 1.38	b 1.20	a 1.53
22								b 1.60
23	c 1.04	a 1.51	b 1.60	b 1.54				b 1.61
24	c 1.01	b 1.51	b 1.59	b 1.55	b 1.43	c 1.35		b 1.62
25	c 1.03	c 1.38	b 1.60	b 1.53	c 1.48	b 1.38		b 1.62
26								b 1.66
27								b 1.68
42								a 1.71
43	c 1.20	b 1.60	b 1.63	b 1.56	b 1.46	c 1.29		b 1.63
44	c 1.23	b 1.60	c 1.61	c 1.57	c 1.47	c 1.37		a 1.65
45	c 1.15	c 1.56	b 1.69	c 1.62	c 1.54	c 1.46		b 1.69
46								b 1.76
47								a 1.82
62								b 1.75
63	a 1.54	b 1.67	b 1.64	b 1.55	c 1.43	c 1.37		b 1.66
64	c 1.43	c 1.68	c 1.65	c 1.59	c 1.51	c 1.41		c 1.67
65	c 1.29	c 1.71	c 1.75	c 1.67	c 1.61	c 1.49		c 1.75
66								c 1.83
67								a 1.95



NOTE.—Letter indicates type of lift curve peak.

TABLE V.—MOMENT COEFFICIENT AT ZERO LIFT, C_{m_0}

Thickness designa- tion Cam- ber des- ignation	06	09	12	15	18	21	25	12	Theor.
00.....	-0.002	-0.003	-0.002	0.000	-0.002	-0.001	-0.003	-0.002	0
22.....								-0.029	-0.0370
23.....	-.036	-.036	-.036	-.034				-.038	-.0447
24.....	-.039	-.044	-.042	-.040	-.037	-.036		-.044	-.0531
25.....	-.048	-.052	-.050	-.049	-.047	-.043		-.054	-.0628
26.....								-.060	-.0749
27.....								-.075	-.0912
42.....								-.059	-.0739
43.....	-.075	-.073	-.072	-.068	-.065	-.057		-.075	-.0894
44.....	-.087	-.086	-.087	-.083	-.078	-.071		-.089	-.1062
45.....	-.109	-.106	-.102	-.097	-.094	-.082		-.105	-.1257
46.....								-.124	-.1497
47.....								-.143	-.1825
62.....								¹ -.087	-.1109
63.....	¹ -.109	-.110	-.108	-.105	-.097	-.090		-.110	-.1342
64.....	¹ -.129	-.133	-.129	-.125	-.118	-.110		-.132	-.1594
65.....	¹ -.159	-.158	-.154	¹ -.150	-.139	-.129		¹ -.159	-.1885
66.....								¹ -.186	-.2246
67.....								¹ -.206	-.2737

¹ Based on straight portion of moment curve extended. See curve for actual value.

TABLE VI.—DISPLACEMENT OF CONSTANT MOMENT POSITION IN PERCENT CHORD AHEAD OF QUARTER-CHORD POINT (100 TIMES VALUES OF n FOR EQUATION $C_{m_{c/4}} = C_{m_0} + nC_L$)

Thickness designa- tion Cam- ber des- ignation	06	09	12	15	18	21	25	12
00.....	0.7	0.7	0.9	1.1	1.4	1.8	2.6	0.9
22.....								.4
23.....	.3	.3	.3	.5				.5
24.....	.1	.3	.4	.7	1.0	1.5		.6
25.....	.0	.2	.3	.6	1.0	1.7		.7
26.....								.8
27.....								.8
42.....								.3
43.....	.3	.4	.5	.7	1.2	1.6		.4
44.....	.3	.3	.5	1.0	1.4	1.7		.5
45.....	.3	.3	.8	.9	1.4	1.7		1.0
46.....								1.1
47.....								1.3
62.....								.2
63.....	-.4	.1	.4	.9	1.1	1.5		.5
64.....	-.7	.0	.6	.9	1.3	1.7		.8
65.....	.0	.0	.7	1.6	1.8	1.9		1.5
66.....								2.0
67.....								2.1

TABLE VII.—MINIMUM PROFILE-DRAG COEFFICIENT, $C_{D_{0min}}$

Thickness designa- tion Cam- ber des- ignation	06	09	12	15	18	21	25	12
00.....	0.0065	0.0074	0.0083	0.0093	0.0108	0.0120	0.0143	0.0083
22.....								.0087
23.....	.0073	.0083	.0088	.0100				.0089
24.....	.0070	.0080	.0090	.0099	.0112	.0127		.0085
25.....	.0073	.0081	.0089	.0103	.0112	.0126		.0088
26.....								.0089
27.....								.0090
42.....								.0092
43.....	.0080	.0089	.0101	.0107	.0119	.0134		.0095
44.....	.0076	.0086	.0095	.0105	.0116	.0132		.0092
45.....	.0087	.0093	.0103	.0113	.0125	.0138		.0095
46.....								.0099
47.....								.0104
62.....								.0101
63.....	.0092	.0101	.0108	.0120	.0130	.0144		.0102
64.....	.0086	.0094	.0104	.0120	.0132	.0146		.0104
65.....	.0093	.0100	.0111	.0127	.0141	.0154		.0106
66.....								.0114
67.....								.0126

TABLE VIII.—OPTIMUM LIFT COEFFICIENT, $C_{L_{opt}}$

Thickness designa- tion Cam- ber des- ignation	06	09	12	15	18	21	25	12	¹ C_{L_I}
00.....	0.00	0.00	0.00	0.00	0.00	0.00	0.00	0.00	0
22.....								.17	0.308
23.....	.17	.18	.10	.10				.15	.272
24.....	.23	.17	.15	.12	.11	.07		.20	.256
25.....	.18	.16	.15	.11	.08	.03		.23	.251
26.....								.20	.256
27.....								.20	.272
42.....								.35	.616
43.....	.35	.30	.23	.12	.20	.05		.34	.544
44.....	.40	.36	.33	.22	.16	.10		.32	.512
45.....	.40	.34	.27	.22	.16	.08		.30	.502
46.....								.30	.512
47.....								.33	.544
62.....								.55	.923
63.....	.63	.45	.40	.33	.24	.13		.47	.816
64.....	.60	.55	.42	.33	.24	.15		.45	.767
65.....	.60	.53	.42	.33	.24	.10		.45	.754
66.....								.38	.767
67.....								.30	.816

¹ Theoretical lift coefficient at "ideal" angle of attack.

TABLE IX.—RATIO OF MAXIMUM LIFT COEFFICIENT TO MINIMUM PROFILE-DRAG COEFFICIENT, $C_{L_{max}}/C_{D_{0min}}$

Thickness designa- tion Cam- ber des- ignation	06	09	12	15	18	21	25	12
00.....	135	172	184	164	138	115	84	184
22.....								184
23.....	142	182	182	154				181
24.....	144	189	177	156	128	106		190
25.....	141	170	180	148	132	109		184
26.....								187
27.....								187
42.....								186
43.....	150	180	161	146	123	96		172
44.....	162	186	170	150	127	104		179
45.....	132	168	164	143	123	106		178
46.....								178
47.....								175
62.....								173
63.....	167	165	152	129	110	95		163
64.....	166	179	159	133	114	97		160
65.....	139	171	158	132	114	97		165
66.....								161
67.....								155

REPORT No. 461

INTERFERENCE ON AN AIRFOIL OF FINITE SPAN IN AN OPEN RECTANGULAR WIND TUNNEL

By THEODORE THEODORSEN

SUMMARY

The wall interference on an airfoil of finite span in an open-throat rectangular section has been treated theoretically and the result is presented in a convenient formula. Numerical results are given in tables and diagrams.

INTRODUCTION

Recently a number of investigators have been engaged in the study of wind-tunnel wall interference. Until a short time ago the only results available were the interference in a circular section by Prandtl (reference 1) and the closed rectangular section by Glauert (reference 2) with the latter result valid for small spans. The author (reference 3) then added the general theory for rectangular sections. Of particular interest was the interference in an open rectangular section.

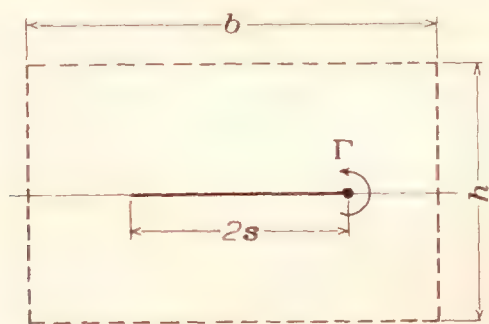


FIGURE 1.

These results were also restricted to small spans. Some time ago Terazawa (reference 4) and subsequently Rosenhead (reference 5) solved the problem of the interference on an airfoil of finite span in a closed rectangular tunnel. It remained for Glauert to bring the result into a form more suitable for calculation; the results are given in reference 6. A very interesting paper by Sanuki and Tani (reference 7) then produced the interference for the elliptic tunnels both open and closed and for airfoils of any span. In the meantime Glauert (reference 8) had already solved the particular case of small spans. It thus appears that the only case not available is the interference on an airfoil of finite span in an open rectangular tunnel. This problem will be studied in the following.

THE WALL INTERFERENCE ON AN AIRFOIL OF FINITE SPAN IN AN OPEN RECTANGULAR TUNNEL

In figure 1, Γ represents one of the semi-infinite trailing vortices of an airfoil. The airfoil is located

symmetrically in the tunnel which is of the open, or free-jet, type.

Mathematically the problem is now to find a stream function, regular in the interior of the rectangle, and satisfying the boundary condition of zero tangential velocity. The problem leads to elliptic functions due to the double periodicity. It is fortunately possible to obtain the result directly by locating a number of singular points in the exterior region. The arrangement of

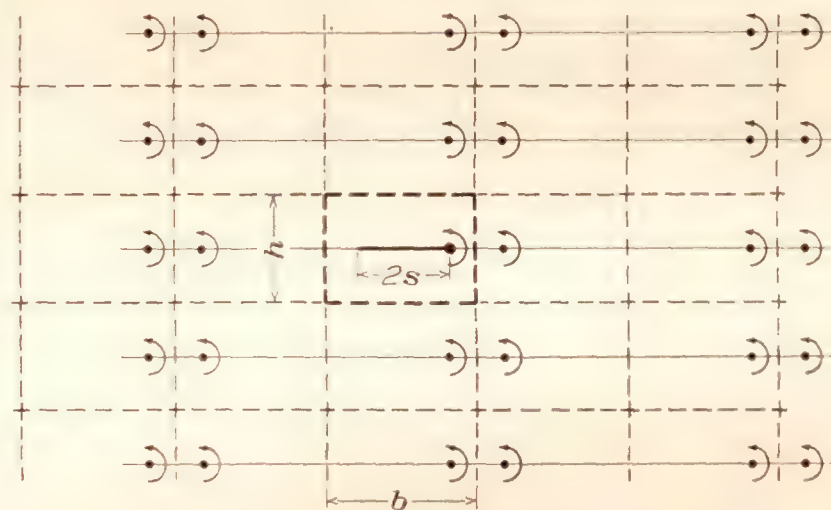


FIGURE 2.

these singular points is shown in figure 2. The singular points are obviously vortices of strength Γ . The tangential velocity is seen to be zero along all bound-

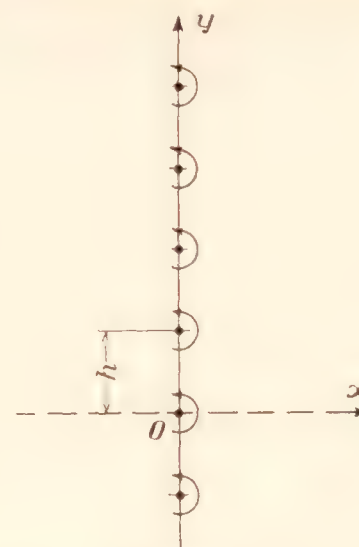


FIGURE 3.

aries of the section by virtue of the existing complete symmetry with respect to each and all boundaries.

We can therefore proceed to consider the stream function due to the external vortex filaments. This function is known for a single infinite row of equidistant vortices. (See reference 9, p. 207.) We shall put down the velocity function for an infinite vertical row

of semi-infinite vortex filaments at $x=0$ and with a spacing of h (fig. 3). This is

$$v = \frac{\Gamma}{4h} \frac{\sinh \frac{2\pi x}{h}}{\cosh \frac{2\pi x}{h} - \cos \frac{2\pi y}{h}}$$

where v is the vertical velocity.

We simplify the result by putting the x axis through the vortex representing the airfoil. This permits us to put $y=0$ in the formula, which becomes

$$v = \frac{\Gamma}{4h} \frac{\sinh \frac{2\pi x}{h}}{\cosh \frac{2\pi x}{h} - 1} \text{ or } \frac{\Gamma}{4h} \coth \frac{\pi x}{h}$$

Following Terazawa, we shall now find the total downflow due to this row of vortex filaments by integrating along the x axis. Thus

$$D = \int v dx = \int \frac{\Gamma}{4h} \coth \frac{\pi x}{h} dx = \frac{\Gamma}{4\pi} \log \sinh \frac{\pi x}{h}$$

We shall now extend the result to include *two* vertical rows as in figure 4. Both rows extend from minus to

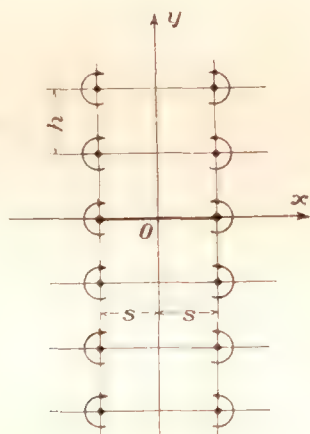


FIGURE 4.

plus infinity; the second row contains filaments of negative sign. The distance between the rows is $2s$. Let the original row be located at $+s$ and the negative one at $-s$, respectively, so that the middle point is located at the origin. The stream function now becomes

$$\begin{aligned} D &= \frac{\Gamma}{4\pi} \log \sinh \pi \frac{(x-s)}{h} - \frac{\Gamma}{4\pi} \log \sinh \pi \frac{(x+s)}{h} \\ &= -\frac{\Gamma}{4\pi} \log \frac{\sinh \pi \frac{(x+s)}{h}}{\sinh \pi \frac{(x-s)}{h}} \end{aligned} \quad (1)$$

We may now complete figure 1 by adding the negative vortex filaments as in figure 5. The boundary condition is, of course, still satisfied in proper manner. Notice that we have a number of double rows like the one just considered. We expect to calculate the total downflow between $-s$ and $+s$ at the location of the airfoil, $y=0$. Because of the right-left symmetry, it is only necessary to determine the downflow between

$x=-s$ and $x=+s$ due to all vortex rows located on one side of the y axis. Now, however, the contribution to this downflow due to a certain double row, say the n th, is numerically the same as the downflow at the location of the n th row caused by the double row at the origin. It is therefore only necessary to calculate the downflow of this double row located at the origin between the limits $x=nb-s$ and $x=nb+s$.

To obtain the actual downflow due to the first exterior double row at $x=b$, we simply put in the

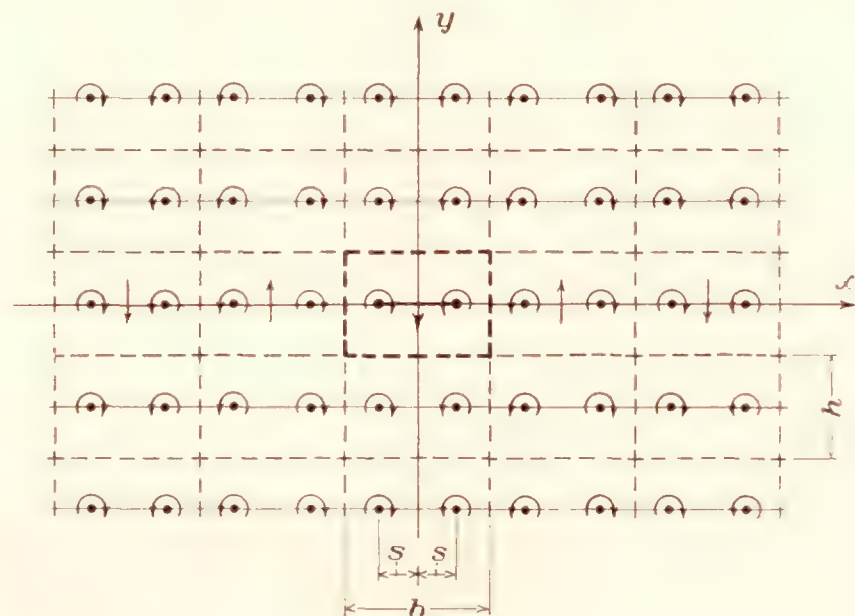


FIGURE 5.

limits $x=b-s$ and $x=b+s$ in our equation (1). This gives as the downflow due to this row

$$\begin{aligned} D &= \frac{\Gamma}{4\pi} \left(\log \frac{\sinh \pi \frac{b+2s}{h}}{\sinh \pi \frac{b}{h}} - \log \frac{\sinh \pi \frac{b}{h}}{\sinh \pi \frac{b-2s}{h}} \right) \\ D &= \frac{\Gamma}{4\pi} \log \frac{\sinh \pi \frac{b+2s}{h} \sinh \pi \frac{b-2s}{h}}{\sinh^2 \pi \frac{b}{h}} \\ D &= \frac{\Gamma}{4\pi} \log \left(1 - \frac{\sinh^2 \pi \frac{2s}{h}}{\sinh^2 \pi \frac{b}{h}} \right) \end{aligned}$$

For the n th double row consequently

$$D = \frac{\Gamma}{4\pi} (-1)^n \log \left(1 - \frac{\sinh^2 \pi \frac{2s}{h}}{\sinh^2 \pi \frac{nb}{h}} \right)$$

and for the entire downflow due to all rows from $x=-\infty$ to $x=+\infty$, except the one at the origin,

$$D = -\frac{\Gamma}{2\pi} \sum_{n=1}^{\infty} (-1)^n \log \left(1 - \frac{\sinh^2 \pi \frac{2s}{h}}{\sinh^2 \pi \frac{nb}{h}} \right) \quad (2)$$

The double row located at the origin requires a separate treatment. We desire to find the effect of the exterior vortices only; we must therefore eliminate the effect of the vortex pair representing the airfoil at $y=0$.

The vertical-flow velocity of one semi-infinite vortex at the origin is $\frac{\Gamma}{4\pi} \frac{1}{x}$. Integrated, this gives the downflow

$$D = \frac{\Gamma}{4\pi} \log x$$

Putting a positive vortex at $-s$ and a negative vortex at $+s$ leads to a total downflow

$$D = \frac{\Gamma}{4\pi} \log \frac{x+s}{x-s}$$

By adding this expression to (1) we obtain the desired result

$$D_1 = -\frac{\Gamma}{4\pi} \log \frac{\frac{\sinh \pi \frac{x+s}{h}}{\pi \frac{x+s}{h}}}{\frac{\sinh \pi \frac{x-s}{h}}{\pi \frac{x-s}{h}}}$$

We may now put in the limits $x=-s$ to $x=+s$, which gives the downflow of the zero double row

$$D_1 = -\frac{\Gamma}{2\pi} \log \frac{\sinh \pi \frac{2s}{h}}{\pi \frac{2s}{h}}$$

By adding the equations (2) and (3) we obtain finally:

$$D = -\frac{\Gamma}{2\pi} \left(\log \frac{\sinh \pi \frac{2s}{h}}{\pi \frac{2s}{h}} + \sum_{n=1}^{\infty} (-1)^n \log \left(1 - \frac{\sinh^2 \pi \frac{2s}{h}}{\sinh^2 \pi \frac{nb}{h}} \right) \right) = \frac{\Gamma}{2\pi} \psi$$

where ψ represents the negative of the quantity in the brackets.

By means of the relation

$$\Gamma 2s \rho V = \frac{1}{2} C_L \rho V^2 S$$

where V is the velocity, ρ the density of the medium, and S the area of the airfoil, we obtain

$$\Gamma = \frac{C_L V S}{4s}$$

The angle of deflection of the air stream is given by

$$\epsilon = \frac{v}{V} = \frac{D}{2sV} = \frac{C_L S}{16s^2 \pi} \psi$$

or, with $bh=C$, the cross-sectional area of the jet, and $\frac{b}{h}=r$, the ratio of tunnel width to tunnel height,

$$\epsilon = \frac{C_L S}{C} \frac{\psi}{4\pi \left(\frac{2s}{b} \right)^2 r} = \frac{C_L S}{C} \delta$$

where δ is the wall correction factor as conventionally defined.

Introducing $\sigma = \frac{2s}{b}$, the ratio of the span of the airfoil

to the width of the tunnel, we obtain the final result

$$\delta = -\frac{1}{4\pi r \sigma^2} \left\{ \log \frac{\sinh \pi r \sigma}{\pi r \sigma} + \sum_{n=1}^{\infty} (-1)^n \log \left(1 - \frac{\sinh^2 \pi r \sigma}{\sinh^2 \pi n r} \right) \right\} \quad (4)$$

Table I and figure 6 give the numerical results of the boundary correction factor δ for various spans σ for the height-width ratios of practical importance. The series converges so rapidly that the third term already is negligible. Notice that the correction in the

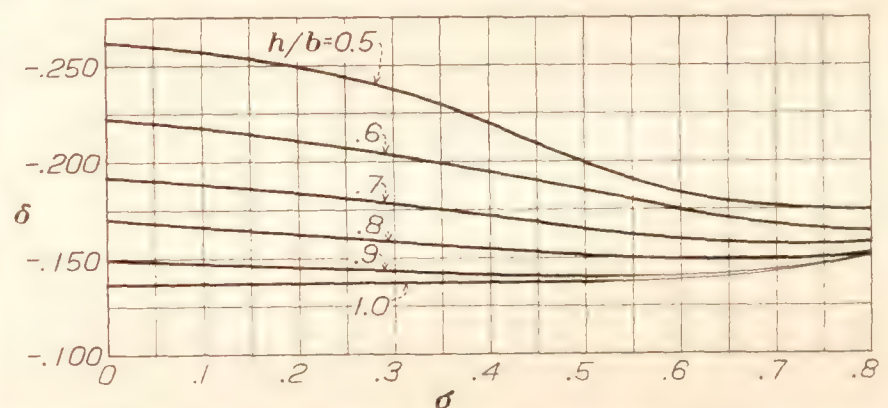


FIGURE 6.—Boundary correction factor δ against the span ratio σ for open rectangular wind tunnels of various height-width ratios, h/b .

square tunnel remains practically constant while the 2:1 tunnel shows a considerable change with the span. The results are strictly true for a constant span loading; however, the vortices Γ may be considered to represent the centers of the trailing tip-vortex systems and the results thus be extended to include any normal span loading with an accuracy sufficient for all practical purposes.

It is interesting to determine the above expression for $s \rightarrow 0$.

It appears in the form

$$\delta = \frac{\pi r}{4} \left(-\frac{1}{6} + \sum_{n=1}^{\infty} (-1)^n \frac{1}{\sinh^2 \pi n b} \right)$$

or exactly as given for this case by the formula (VIII) on page 6 and by case II on page 8 of a previous report (reference 3) by the author.

REFERENCES

1. Prandtl, L.: Tragflügeltheorie. II C, Göttingen Nachrichten, 1919.

2. Glauert, H.: The Elements of Aerofoil and Airscrew Theory. Chap. XIV. Cambridge University Press, 1930.

3. Theodorsen, Theodore: The Theory of Wind-Tunnel Wall Interference. T.R. No. 410, N.A.C.A., 1931.

4. Terazawa, Kwan-ichi: On the Interference of Wind Tunnel Walls of Rectangular Cross-Section on the Aerodynamical Characteristics of a Wing. Report No. 44, Aero. Res. Inst., Tokyo Imperial University, 1928.

5. Rosenhead, L.: The Effect of Wind Tunnel Interference on the Characteristics of an Airfoil. Roy. Soc. Proc. (A) 1929, p. 135, 1930.

6. Glauert, H.: Interference on Characteristics of an Aerofoil in a Wind Tunnel of Rectangular Section. R. & M. No. 1459, British A.R.C., 1932.

7. Sanuki, Matao, and Tani, Itiro: The Wall Interference of a Wind Tunnel of Elliptic Cross-Section. Proc. of the Physico-Mathematical Society of Japan, 3d ser., vol. 14, no. 10, November 1932.

8. Glauert, H.: Some General Theorems Concerning Wind Tunnel Interference on Aerofoils. R. & M. No. 1470, British A.R.C., 1932.

9. Lamb, Horace: Hydrodynamics. Fifth Edition, Cambridge University Press, 1924.

TABLE I.—CORRECTION FACTOR δ IN OPEN-THROAT RECTANGULAR WIND TUNNELS

$\lambda=\frac{h}{b}$	$\sigma=\frac{2s}{b}$	δ
1.0	0	0.137
	.2	.137
	.4	.1375
	.6	.139
	.8	.151
.9	0	0.149
	.2	.145
	.4	.142
	.6	.141
	.8	.1515
.8	0	0.171
	.2	.162
	.4	.156
	.6	.149
	.8	.152
.7	0	0.192
	.2	.183
	.4	.172
	.6	.160
	.8	.158
.6	0	0.222
	.2	.211
	.4	.194
	.6	.175
	.8	.164
.5	0	0.262
	.2	.249
	.4	.222
	.6	.183
	.8	.1745

REPORT No. 462

TESTS OF NACELLE-PROPELLER COMBINATIONS IN VARIOUS POSITIONS WITH REFERENCE TO WINGS. III—CLARK Y WING—VARIOUS RADIAL-ENGINE COWLINGS—TRACTOR PROPELLER

By DONALD H. WOOD

SUMMARY

This report is the third of a series giving the results obtained in the 20-foot wind tunnel of the National Advisory Committee for Aeronautics on the interference drag and propulsive efficiency of nacelle-propeller-wing combinations. The first report gave the results of the tests of an N.A.C.A. cowled air-cooled engine nacelle with tractor propeller located in 21 positions with reference to a thick wing. The second report gave the results for several engine cowlings and nacelles with tractor propeller located in four positions with reference to the same wing. The present report gives results of tests of the same nacelles and cowlings in the same positions with reference to a smaller wing of Clark Y section.

The wing had a 38-inch chord and a 15-foot-10-inch span. The engine was a 4/9-scale model of a Wright J-5 radial air-cooled engine. Tests were made with a small nacelle with exposed engine cylinders, with a narrow variable-angle cowling ring, and with a hood taken from an N.A.C.A. cowled nacelle. Tests were also made with the N.A.C.A. cowled nacelle complete and with a smooth body forming the nacelle. The propeller was a 4-foot-diameter model of the Navy No. 4412 adjustable-pitch metal propeller.

The lift, drag, and propulsive efficiency were determined at several angles of attack for each cowling and in each nacelle location. The net efficiency was computed by the methods of N.A.C.A. Report 415, and the results are compared with those of that report and of N.A.C.A. Report 436.

The results of the tests with the Clark Y wing are in general agreement with those obtained using a thick wing. The N.A.C.A. cowled nacelle located directly ahead of the wing is the best tractor-nacelle arrangement. Analysis of the results shows that the net efficiency is but little affected by the airfoil section of the wing if the nacelles are located the same fraction of the chord from the leading edge. The gain in efficiency due to cowl the engine is so much greater than the gain due to proper nacelle location that it is advisable to cowl radial engines carefully before attempting to take advantage of the favorable effects of locating the nacelle ahead of the wing. The proper location of nacelles and careful cowl are important in the high-speed range of flight, but in the lower

speed ranges there is little advantage of one nacelle position or cowling over another.

INTRODUCTION

This report is the third of a series giving the results of a general investigation of the mutual effects of wings, nacelles, and propellers. The program, originally presented at the Fourth Annual Aircraft Engineering Research Conference in May 1929, has been modified and extended from time to time, and now includes nacelles with tractor, pusher, and tandem propellers, and biplane as well as monoplane wings. Tests have been made with several propeller pitch settings and with numerous types of air-cooled engine cowlings. Later tests will give results on nacelles and cowlings for liquid-cooled engines.

The first report (reference 1) gave the results obtained with an N.A.C.A. cowled air-cooled engine nacelle and tractor propeller located in 21 positions with reference to a thick monoplane wing. The second report (reference 2) gave the results for several engine cowlings and nacelles with tractor propeller located in four positions with respect to the same wing.

The thick wing used in the early tests was designed to be comparable to the portion of the wing where the nacelles are located on unbraced monoplanes. In many installations thinner wings are used and it was considered advisable to determine in a general way the effect of using a smaller wing.

This third report therefore presents the results obtained with the same engine nacelles that were used on the thick wing and with several of the same variations in cowling. The nacelles were so located that the propeller was the same distances from the wing as in the tests of reference 2. The wing had a Clark Y section of considerably narrower chord than the thick wing. Additional results were also obtained with a smooth body located in the 4 positions previously mentioned, and in 3 other positions farther from the wing. These latter results are useful in indicating the effect of body shape on the nacelle-propeller performance.

As pointed out in the previous reports, the nacelle positions tested represent the best location, directly

ahead of the wing, and three other positions which have been quite commonly used in airplanes in the past. The number of positions was limited to some extent by the necessity of reducing the number of tests because of the time required. In any event, actual airplanes employ nacelle and wing arrangements which, because of practical considerations, will differ from those tested however detailed the program may be.

In all the reports of the investigation the same system of presenting the results is being used. Detailed information is included in the tables in the event that the reader may wish to reduce the results by other methods. This report completes the presentation of the information obtained on tractor propellers with radial engines and cowlings.

APPARATUS AND METHODS

The propeller-research tunnel, in which the tests were made, is described in reference 3. Standard

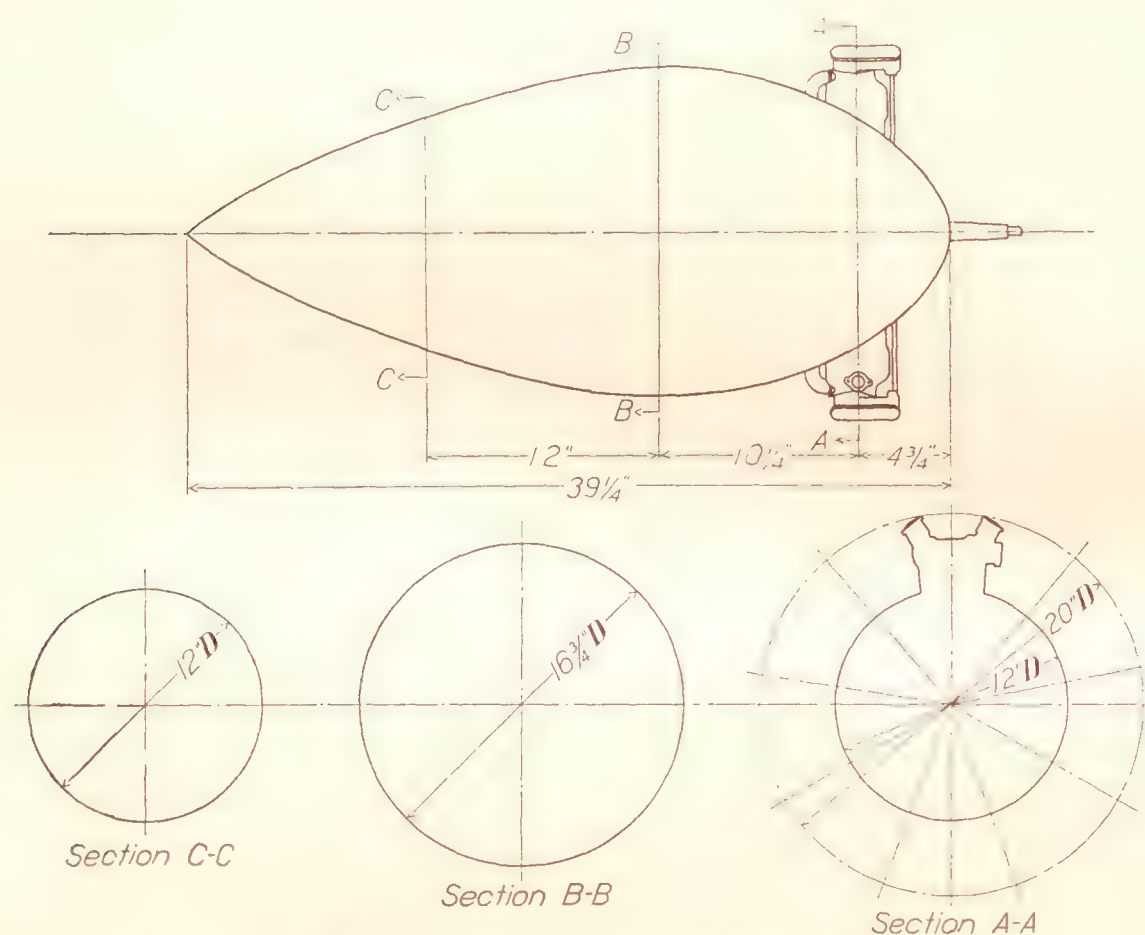


FIGURE 1.—Small nacelle and engine assembly.

apparatus and test methods were used, with certain exceptions mentioned later.

The wing was constructed of wood with a 38-inch chord and a 15-foot 10-inch span (aspect ratio 5). This span was the largest that could be conveniently accommodated in the wind tunnel. The airfoil section was the Clark Y, which has a maximum thickness of 11.68 percent of the chord. The ordinates of this section are so well known that they are not repeated here. The central portion of the wing was provided with suitable metal ribs and plates for the connection of the struts required in attaching the nacelle to the wing.

The engine nacelles, constructed of sheet duralumin, were similar to nacelles required for a Wright J-5

radial engine, and were four-ninths (0.445) full scale. A detailed wooden model of this engine was installed in the proper position in the nacelles. One nacelle, constructed with the dimensions given in figure 1 and called "small nacelle", represents a normal nacelle such as is employed when the engine is uncowled. A larger nacelle fitted with a hood, the nacelle and hood constituting an N.A.C.A. cowled nacelle, was also used in some of the tests. The principal dimensions of this nacelle and the hood are given in figure 2. A third nacelle, called a "smooth body", was also used in some tests. The dimensions of this body are given in figure 3. It may be mentioned that the small nacelle and the N.A.C.A. cowled nacelle are identical with those used in the tests of references 1 and 2.

Tests were also made with the small nacelle fitted with the N.A.C.A. hood mentioned previously, and with a variable-angle ring. The ring was so constructed that the angle of its inner surface with reference to the thrust axis could be adjusted, and in these tests this angle was made -8° . This ring is identical with that used in tests of reference 2; its dimensions are given in figure 4. In all the tests with the variable-angle ring the leading edge was located $5\frac{3}{4}$ inches ahead of the center line of the engine cylinders.

The propeller, which is 4 feet in diameter, is geometrically similar to the Navy No. 4412, 9-foot-diameter aluminum alloy propeller. A number of full-scale tests of this propeller have been made and are described in reference 4. The blades may be turned in the hub to give different pitch settings. In the tests discussed here the pitch setting was 17° at $0.75 R$, which is about average for usual operating conditions. This is the same pitch used in the tests of references 1 and 2, and the results of the propeller

tests are therefore directly comparable.

For driving this propeller, a 25-horsepower 220-volt direct-current motor was mounted within the nacelle. Wires were led from the motor down the struts into the wing and along the supporting members to the control equipment on the floor below. The wires were carefully taped to the struts, and subsequent tests indicated a negligible effect on the tare drag. In a few of the first tests the wires were carried to the nacelle through a separate streamline strut. A Prony brake was used for calibrating the motor, and curves were obtained giving armature current against torque for several values of the field current. During the tests the field current was held at one of these calibrated values. Revolution speed was indicated by

a condenser-type electric tachometer connected by wires to an indicating instrument on the control board.

The wing-nacelle-propeller combinations with the various cowlings were tested with the nacelle and wing

in the tests of reference 1. The nacelle positions are designated by the system of letters shown.

The wing and nacelle combinations were mounted on the balance by means of standard supports, which have

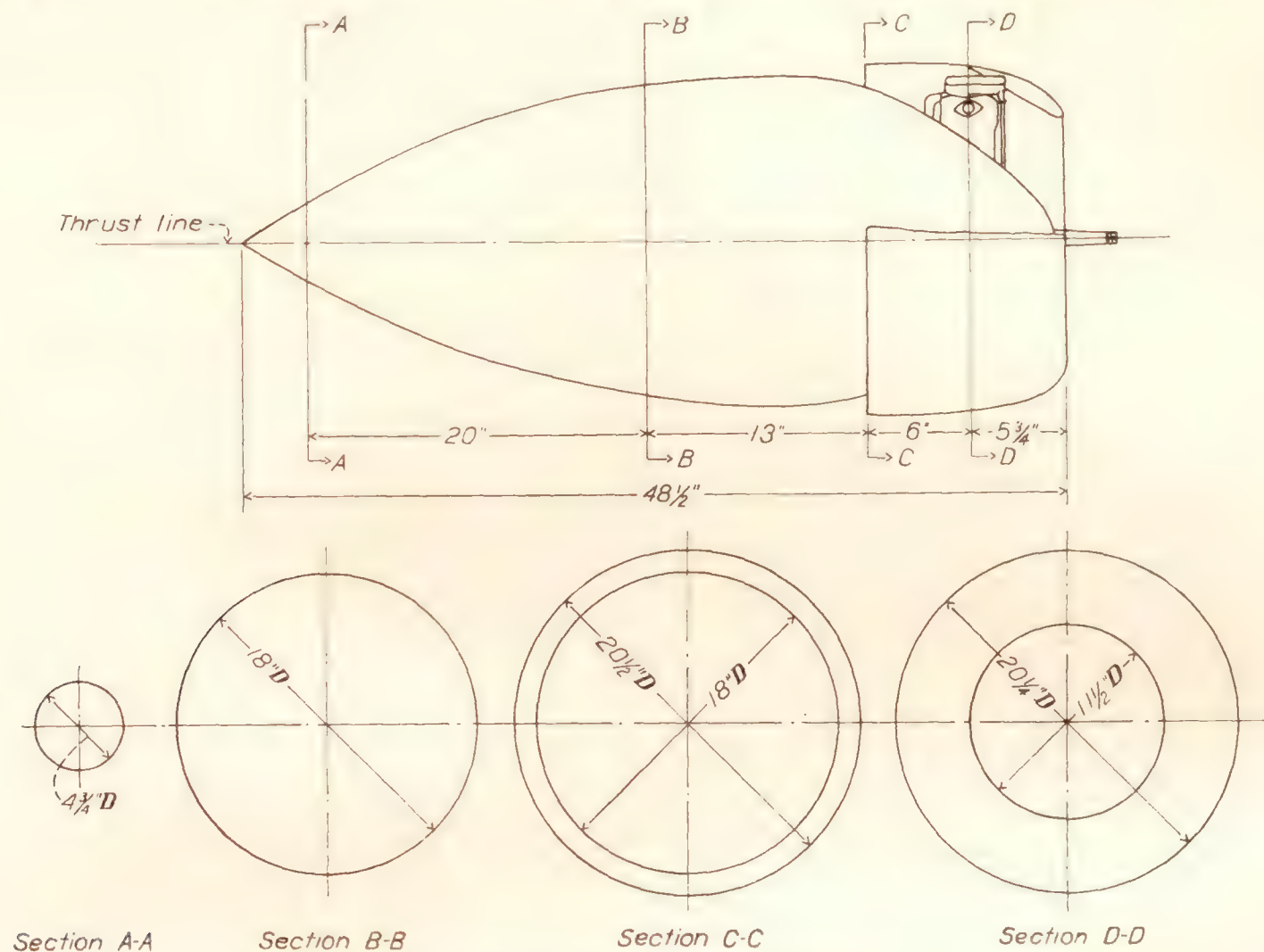


FIGURE 2.—N.A.C.A. cowled nacelle and engine assembly.

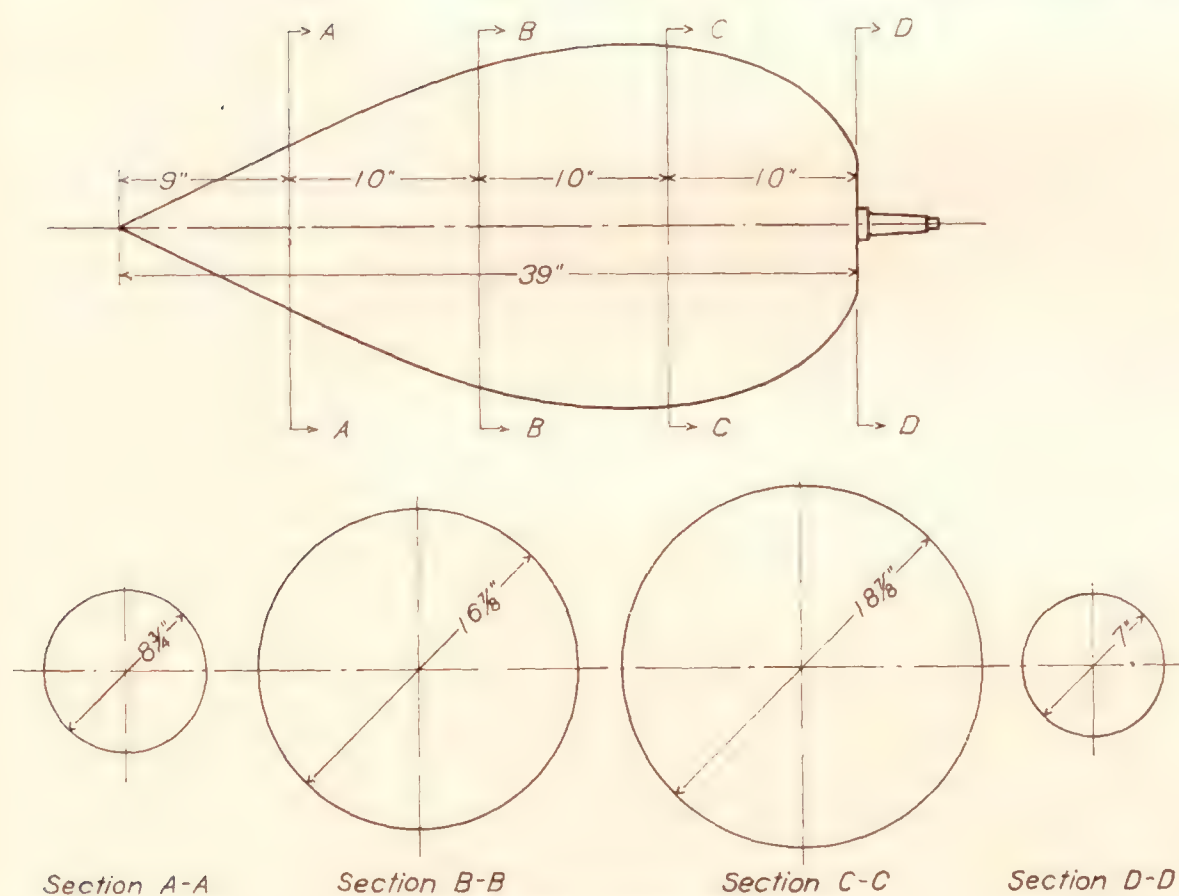


FIGURE 3.—Smooth body.

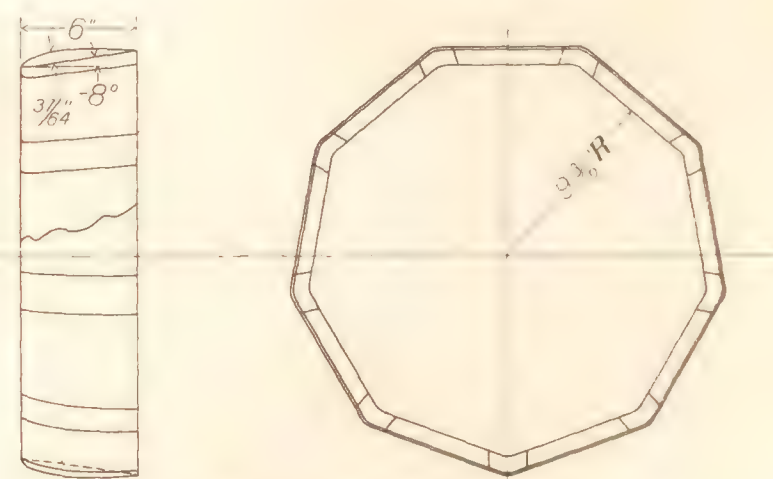


FIGURE 4.—Variable-angle ring.

in the relative positions marked in figure 5. In the figure the crosses and circles indicate the positions of the center line of the propeller hub in the present tests. The crosses alone indicate other nacelle locations used

been described in reference 5. With these supports the airfoil pivots about a line near the lower surface 25 percent of the chord back from the leading edge, and the angle of attack is adjusted by a crank operating a

post connected with a sting on the airfoil. The airfoil and nacelle mounted in one test position are shown in figure 6. Figures 7, 8, 9, 10, and 11 are photographs of the other wing-nacelle set-ups. In all cases the thrust line of the propeller was parallel to the wing chord. The lift and drag forces were measured simultaneously by balances on the floor below. The Reynolds Number varied from about 1,350,000 at the lowest air speed (50 miles per hour) to 2,750,000 at the highest speed (100 miles per hour).

For use in subsequent analyses, a series of tests at various air speeds was made with the wing alone at angles of attack of -5° , 0° , 5° , 10° , and 15° . Similar tests had been previously made with the nacelles alone (reference 6).

With each combination a run was made at several air speeds with the propeller removed. The lift, drag, and

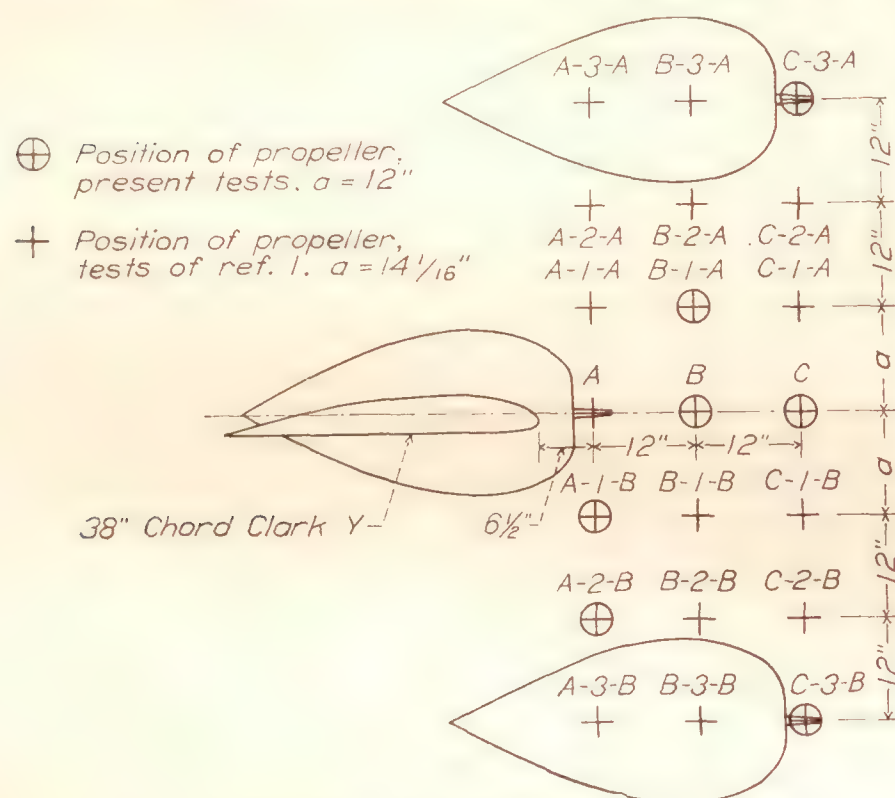


FIGURE 5.—Wing-nacelle test locations.

air speed were measured. A second test was then made with the propeller in place, and with the tunnel operating at several air speeds. In this test the lift, drag (or thrust), torque, propeller revolutions, and air speed were measured. Separate tests were made at angles of attack of -5° , 0° , 5° , and 10° .

Tare-drag measurements were made with the wing supported free of the supports. Other tests indicated that the propeller had a negligible effect on the tare drag.

Previous results (references 1 and 2) had shown that there was an advantage in fairing the nacelle into the wing when the two were close together and, accordingly, in these tests with the nacelle in positions B-1-A and A-1-B, the space between the nacelle and wing was filled with a fairing. Previous results had also shown a peculiar effect of the side brackets used for mounting the nacelles when the nacelle was located

ahead of the wing. Tests were made on the small nacelle both with a fairing surrounding these side brackets and with the brackets removed. The fairings required over the brackets on the N.A.C.A. cowled nacelle were very small and no tests were made with them removed. The fairings and side brackets are shown in the photographs of figure 8 and in figures 13 and 14. When the nacelles were located in positions C-3-A, C-3-B, and A-2-B, they were supported on struts and no fairings were used.

RESULTS

The measured lift and drag were reduced to the usual coefficients

$$C_L = \frac{\text{lift}}{qS}$$

$$C_D = \frac{\text{drag}}{qS}$$

$$C_m = \frac{\text{moment}}{qSc}$$

where

q , the dynamic pressure ($\frac{1}{2} \rho V^2$).

ρ , mass density of the air.

V , velocity.

S , area of the wing.

c , chord of the wing.

(All moments are taken about the quarter-chord point of the wing.)

These coefficients were first plotted against the dynamic pressure q and then cross-plotted as C_L , C_D , and C_m against α (angle of attack) at values of the dynamic pressure corresponding to 50, 75, and 100 miles per hour.

The lift and drag coefficients have been plotted as polar diagrams arranged to facilitate comparison of the results with various cowlings in the different nacelle positions. Figure 12 shows the results for position B-1-A with various cowlings; figure 13 shows the results for position B with side bracket fairing in place; figure 14 shows the results for position B with side brackets removed; figure 15 shows the results for position A-1-B; and figure 16 shows the results for position A-2-B. Figure 17 shows the comparative results for the small nacelle without cowling in four nacelle positions, and figure 18 shows similar results with the N.A.C.A. cowled nacelle. Figure 19 shows the comparative results obtained with the smooth body in various positions. In all these diagrams the polar of the wing alone is also given. All the polars are plotted from the data obtained at an air speed of 100 miles per hour. The results are also given in tables I and II, together with those for two other air speeds, 50 and 75 miles per hour. The values of the moment coefficients, which were found to be the same for all air speeds, are given in table III.

The results with propeller operating are reduced to the usual coefficients

$$C_T = \frac{T - \Delta D}{\rho n^2 D^4} \quad C_P = \frac{P}{\rho n^3 D^5}$$

and η = propulsive efficiency

$$= \frac{\text{effective thrust} \times \text{velocity of advance}}{\text{motor power}}$$

$$= \frac{(T - \Delta D) V}{P}$$

$$= \frac{C_T}{C_P} \frac{V}{nD}$$

(C_{LP}) Table VIII, Moment Coefficient with Propeller Operating (C_{mP}). Since only individual values of the above coefficients are used in later comparisons, no curves are reproduced here. The reader is referred to reference 1 for a typical set of such curves.

ACCURACY

All readings were taken on scales and instruments that were calibrated frequently during the tests. The angles of attack of the airfoil were set within 5' of the desired angles with an inclinometer. The motor calibration showed a scattering of points repre-



FIGURE 6.—Photograph of wing-nacelle combination in position B mounted for test.

where T , thrust of propeller operating in front of body (tension in crank shaft).

ΔD , change in drag of body due to action of propeller.

$T - \Delta D$, effective thrust (discussed in reference 4) and C_L and C_m are computed as before but are now called C_{LP} and C_{mP} .

The coefficients for all nacelle positions and cowlings at various values of V/nD and different angles of attack are given in tables IV to VIII, inclusive: Table IV, Thrust Coefficient (C_T); Table V, Power Coefficient (C_P); Table VI, Propulsive Efficiency (η); Table VII, Lift Coefficient with Propeller Operating

senting a maximum error of 1 percent. Tachometer readings were accurate within 10 revolutions per minute. The lift and drag were measured to the nearest pound.

In certain cases at high angles of attack the forces fluctuated rapidly and the above accuracy could not be obtained. These fluctuations occurred mainly near the burble point of the airfoil. The major portion of the faired results are believed to be correct within ± 2 percent.

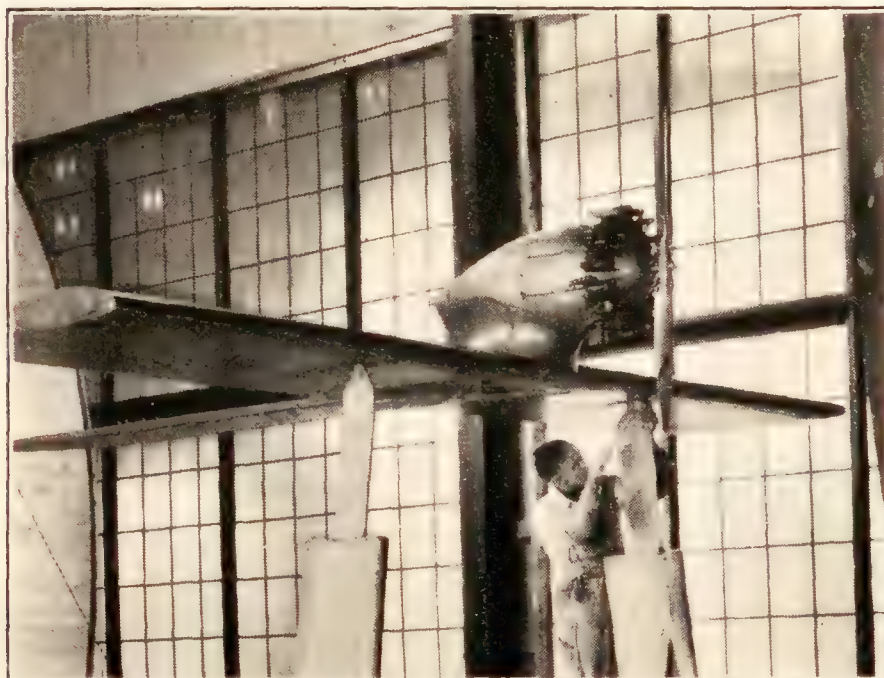
DISCUSSION

In a general consideration of the problem of a nacelle and a propeller operating near a wing, several factors must be considered. The nacelle and wing have mu-

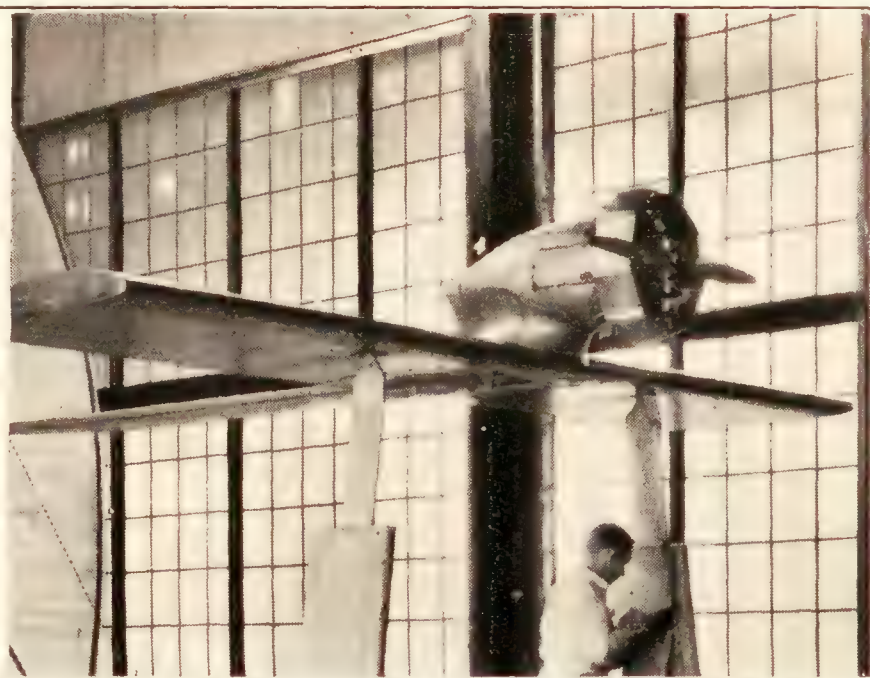
tual interferences which appear as changes in the lift and drag, the propeller characteristics are influenced by the presence of wing and nacelle, and the slipstream in turn changes the forces on the wing and nacelle. A detailed discussion of these questions is given in reference 1, and it is concluded there that a comparison of the relative merits of wing-nacelle-propeller combinations must include propulsive efficiency, interference-drag effects, and lift effects. A net efficiency

arrangements in a fairly narrow range so that the predominating factor in the determination of the net efficiency is the nacelle drag and interference. A comparison of the relative drags of the various combinations is then a first approximation to their relative merits.

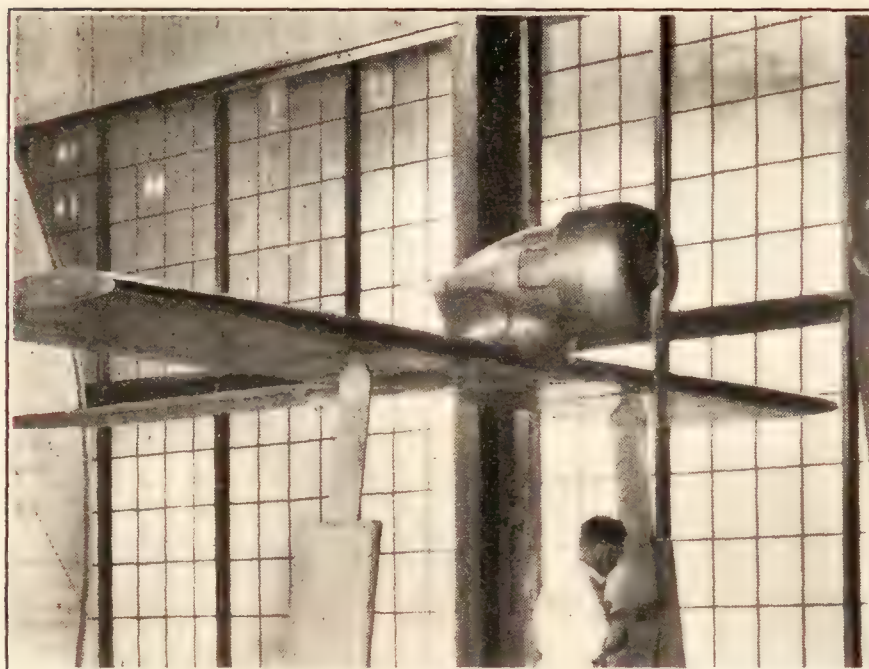
Accordingly, the drag results are first discussed and later the propeller effects are included. Besides simplifying the discussion, a somewhat clearer picture



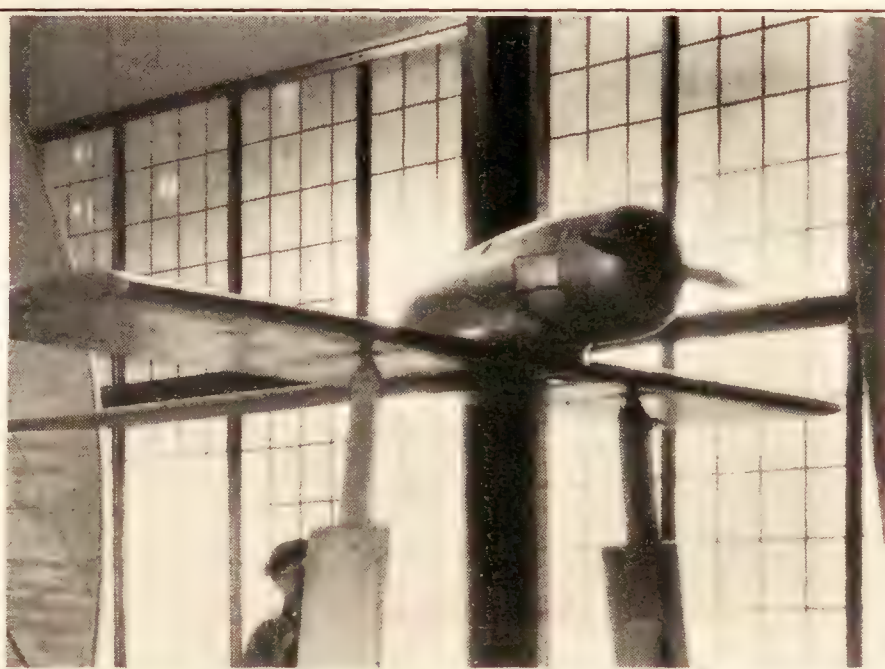
Small nacelle, exposed cylinders, faired into wing.



Small nacelle, variable-angle ring set -8° , faired into wing.



Small nacelle, N.A.C.A. hood, faired into wing.



N.A.C.A. cowled nacelle, faired into wing.

FIGURE 7.—Nacelles in position B-1-A.

is derived therein which includes the above factors in a rational and simple manner. The same methods are employed here. The method is perfectly general and the results can be compared directly with those previously given.

INTERFERENCE LIFT AND DRAG

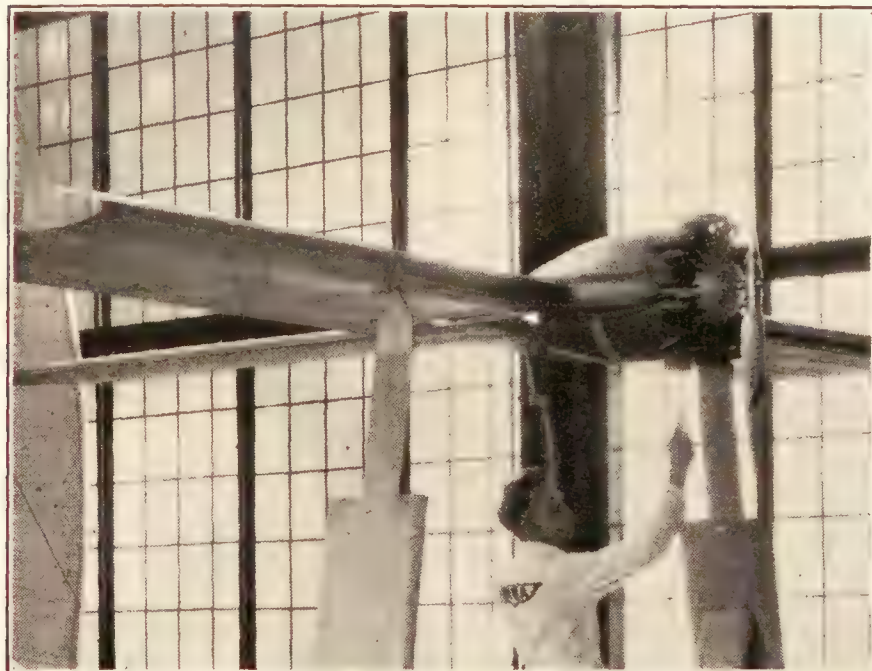
The largest item in the net efficiency is the propulsive efficiency, but all test results point to the fact that the propulsive efficiency varies with different

of the phenomena is perhaps thus obtained. In figures 12 to 19, inclusive, each line represents a different combination of nacelle, wing, and cowling. The abscissa intercept between the wing-alone polar and that for any wing-nacelle cowling combination represents the drag added by the nacelle; i.e., the nacelle drag plus wing-nacelle-interference drag. Similarly, the ordinate intercept represents the lift change due to the nacelle and cowling. These intercepts are of first importance because the arrangement that

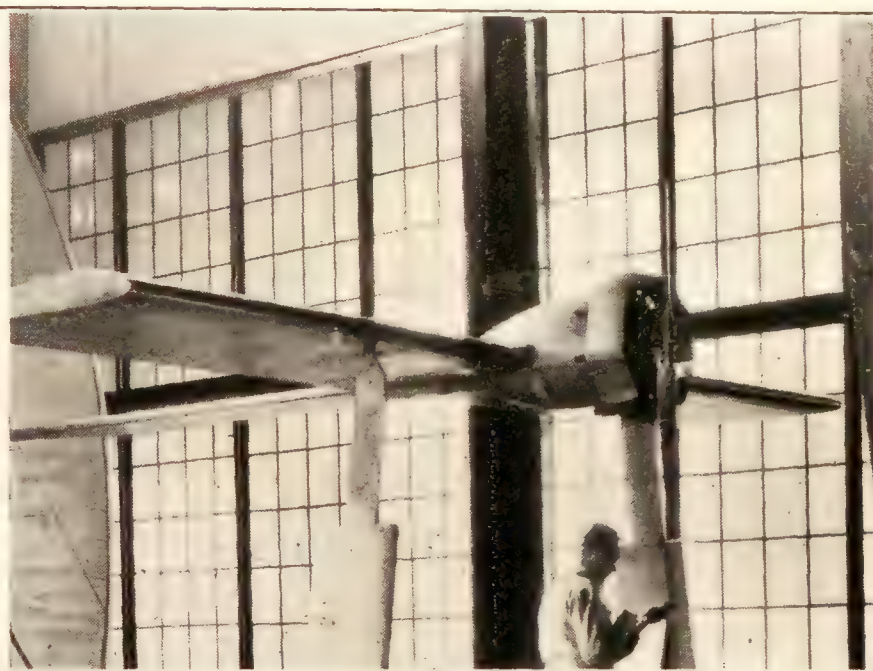
develops the least increase of drag and the least loss of lift (that polar closest to the wing-alone polar) is the best, considering only the lift and drag.

In figure 12, which shows the results with nacelles and cowlings in position B-1-A, at a lift coefficient of 0.35 corresponding to about 0° for the wing alone, the drag added by the small nacelle with exposed engine cylinders is about $2\frac{1}{2}$ times that added by the N.A.C.A. cowled nacelle; that added by the N.A.C.A. hood or

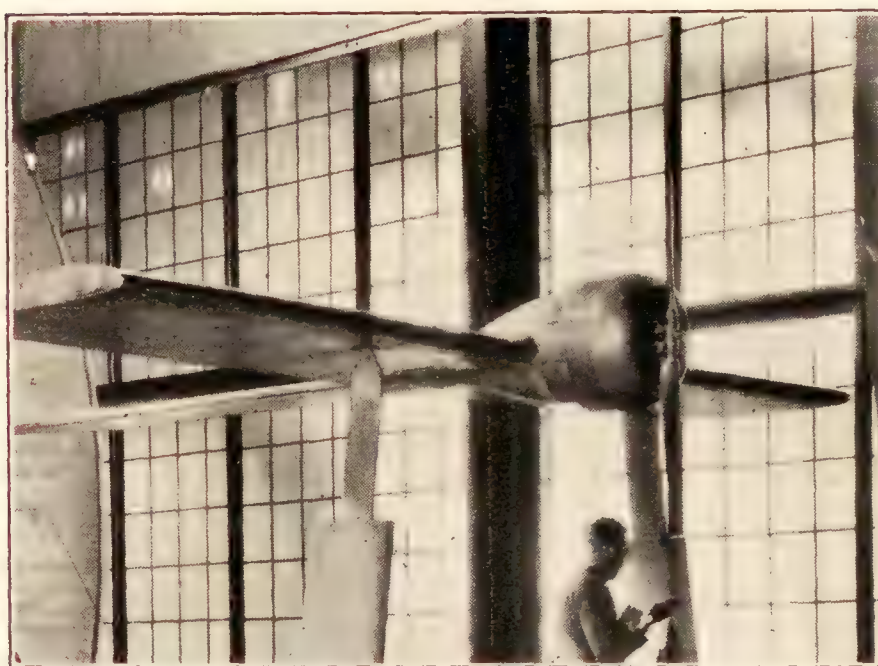
added is very much less. Nevertheless, the nacelle with exposed engine cylinders adds about three times as much drag as the N.A.C.A. cowled nacelle, and the hood on the small nacelle adds about twice as much drag as the N.A.C.A. cowled nacelle. The smooth body is only slightly better than the N.A.C.A. cowled nacelle. The loss of lift is not as great as with the nacelles in the previous position except in the case of the small nacelle with exposed engine cylinders. These



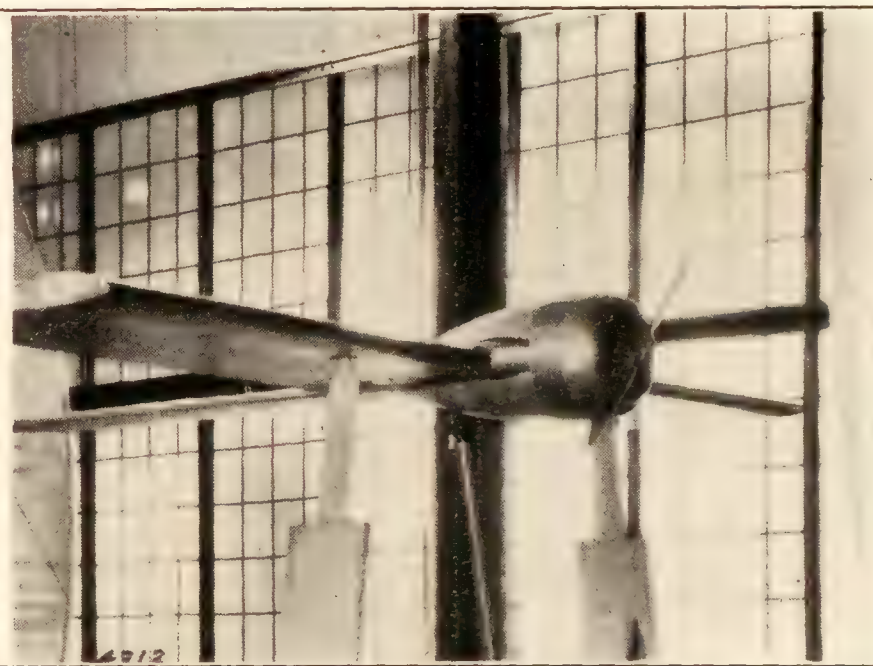
Small nacelle, exposed cylinders, with side bracket fairing.



Small nacelle, variable-angle ring set -8° .



Small nacelle, N.A.C.A. hood.



N.A.C.A. cowled nacelle.

FIGURE 8.—Nacelles in position B.

the variable-angle ring and the small nacelle is about $1\frac{1}{2}$ times that added by the N.A.C.A. cowled nacelle. These proportions hold approximately at the other lower angles of attack. The large loss of lift at high angles of attack from the nacelle installation in this position is to be noted, particularly in the case of the small nacelle with exposed engine cylinders. The advantage of cowling is amply evident.

In figure 13, showing the results for position B, similar conclusions may be drawn. In this position the nacelle is partly within the wing so that the drag

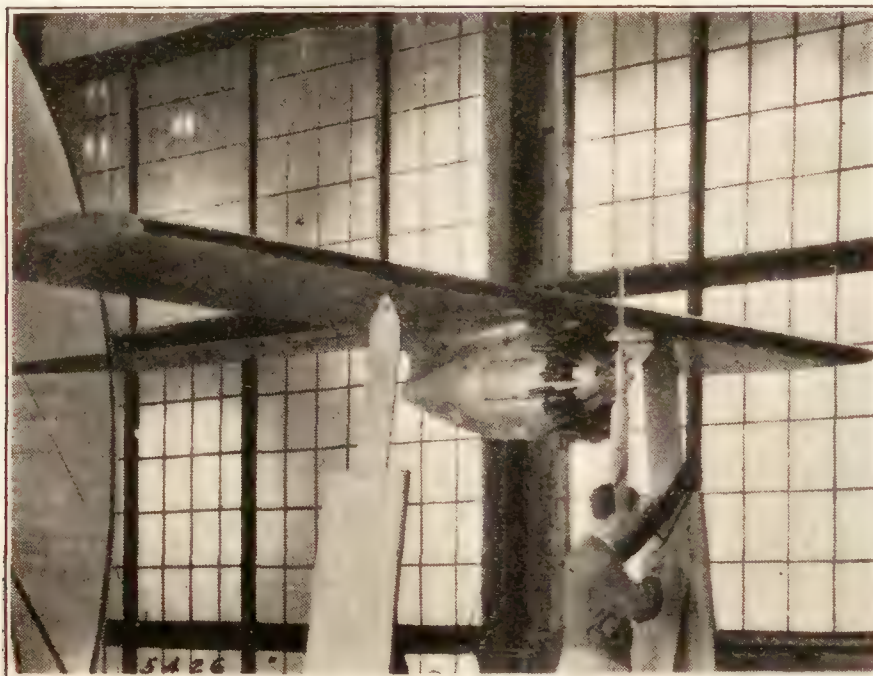
results were obtained with fairings surrounding the side brackets supporting the nacelle.

In figure 14 some of the results are shown for the case with these side brackets completely removed. It will be noted that the drag added is about 17 percent greater than when the brackets were in place. This result is in contrast to that of reference 2, in which the removal of the side brackets was shown to reduce the drag. In the case of the thick wing, the brackets were only a fraction of the wing thickness in depth; whereas in the present case they were practically as deep as

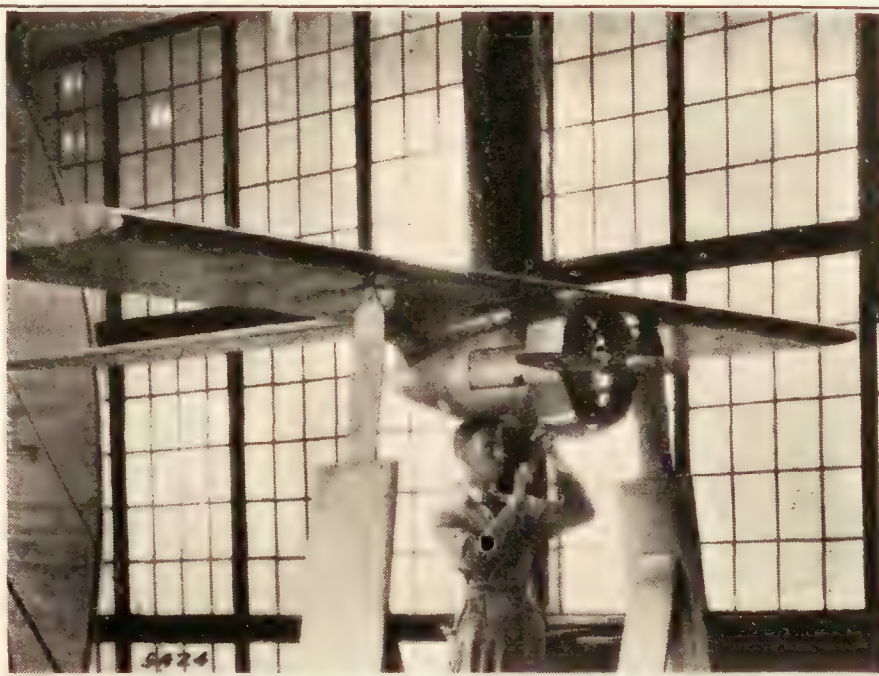
the wing and may have constituted a partial fairing of the nacelle into the wing. The nacelle with the exposed engine cylinders is still poor, particularly with reference to the lift at high angles of attack.

In figure 15, showing the results in position A-1-B, the small nacelle with the exposed engine cylinders adds about twice as much drag as the N.A.C.A. cowled nacelle. The peculiar result with the variable-angle ring in this instance is to be noted. The drag, except

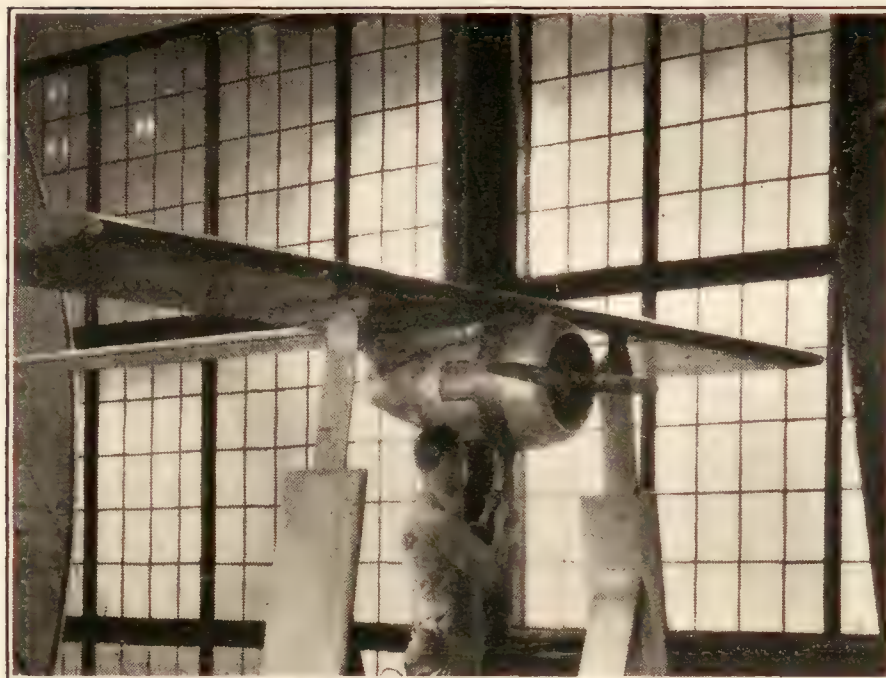
N.A.C.A. hood or the variable-angle ring adds about twice as much. This result indicates that its interference drag must be slightly less than that of the N.A.C.A. cowled nacelle, because when tested alone its drag was slightly greater. (See reference 6.) The drag with the nacelle located directly ahead of the wing is considerably less than that in other locations, and the result therefore confirms previous tests indicating this location as the best.



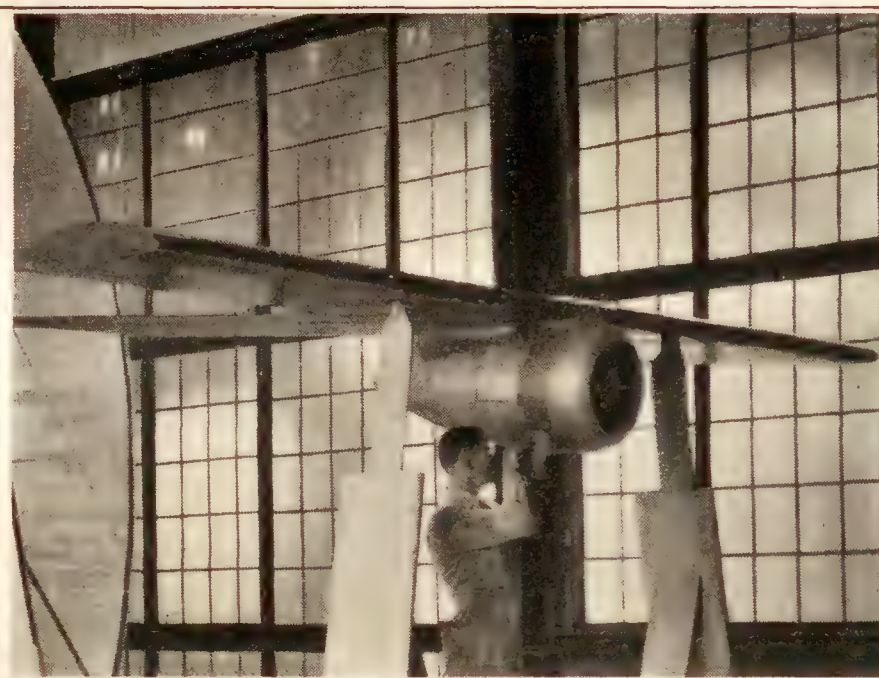
Small nacelle, exposed cylinders, faired into wing.



Small nacelle, variable-angle ring set -8° , faired into wing.



Small nacelle, N.A.C.A. hood, faired into wing.



N.A.C.A. cowled nacelle, faired into wing.

FIGURE 9.—Nacelles in position A-1-B.

at the very low angles of attack, is considerably higher than that of the nacelle without cowling, and a very large loss of lift occurs at the higher angles of attack. This result points to some peculiar interference effect created by this particular cowling. At the high angles of attack the other cowlings seem to be of about equal merit.

In figure 16, showing the results for position A-2-B, the small nacelle with exposed engine cylinders adds about three times as much drag as the N.A.C.A. cowled nacelle; the small nacelle with either the

From the diagrams, it appears that at the higher angles of attack there is no great advantage of one cowling over another. An exception is the nacelle with exposed engine cylinders, which shows very detrimental lift effects at the high angles in all except the position far below the wing.

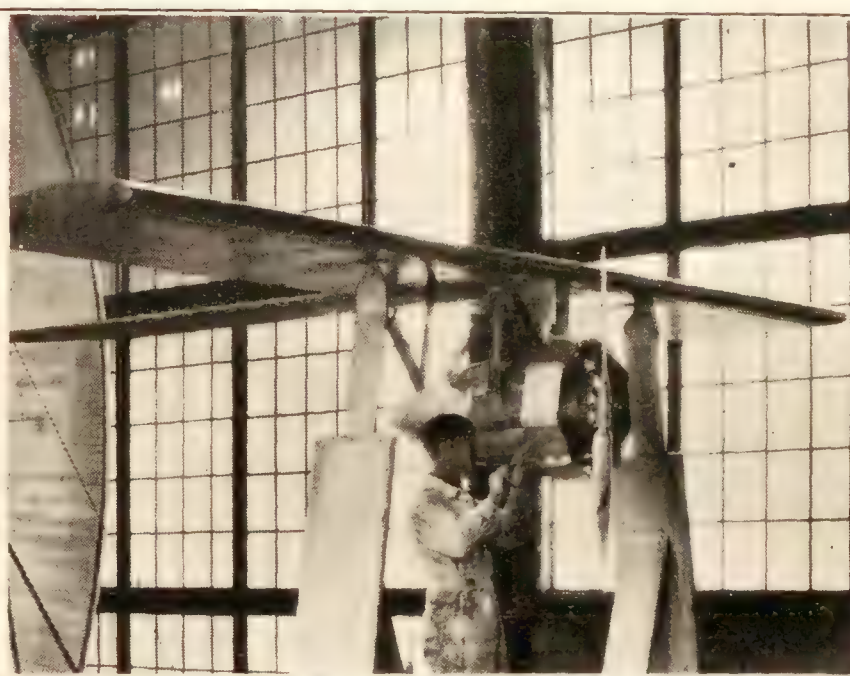
An easier comparison of the effect of position can be obtained from figures 17, 18, and 19. In figure 17, the results are shown for the small nacelle with exposed engine cylinders, and in figure 18 the results for the N.A.C.A. cowled nacelle in the four locations. The

location directly ahead of the wing is the best in both cases at the high-speed angles of attack, and in the case of the N.A.C.A. cowled nacelle it is only at the highest angles that it is inferior to locations below the wing. In figure 19, the results of the smooth-body tests in five positions are shown. The position directly ahead of the wing is superior to the others, but the variation is considerably less than with other types of cowlings. This body is only a hypothetical shape and

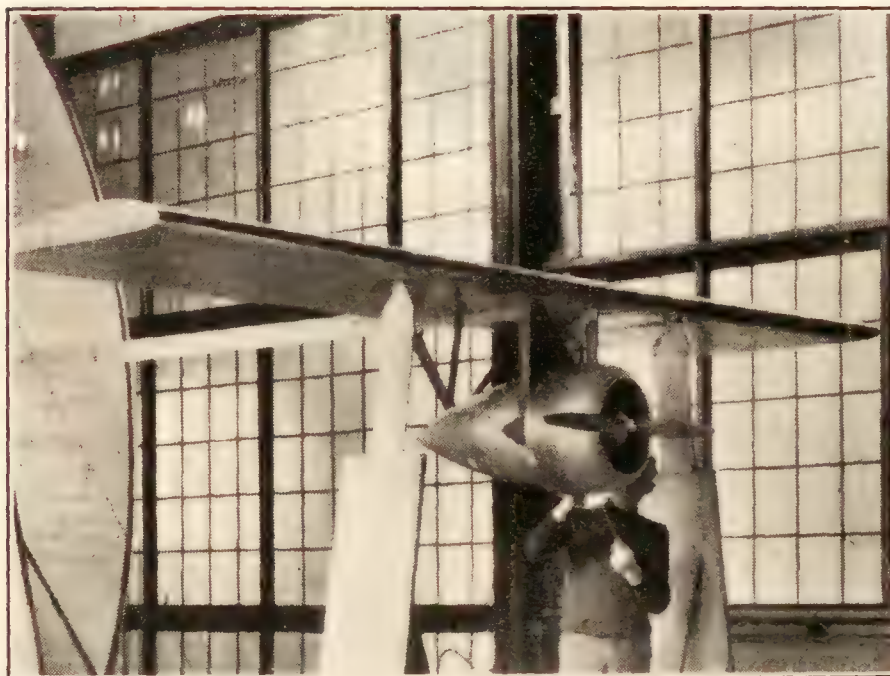
tests where only the nacelle and wing were present. One of the principal advantages of the present tests, however, is the opportunity for studying the effects of the operating propeller. The propeller supplies the thrust necessary to move the airplane through the air, and a proper determination of the thrust available under any given conditions for the different nacelle-propeller-wing combinations is a measure of the relative merits of the different arrangements. The varia-



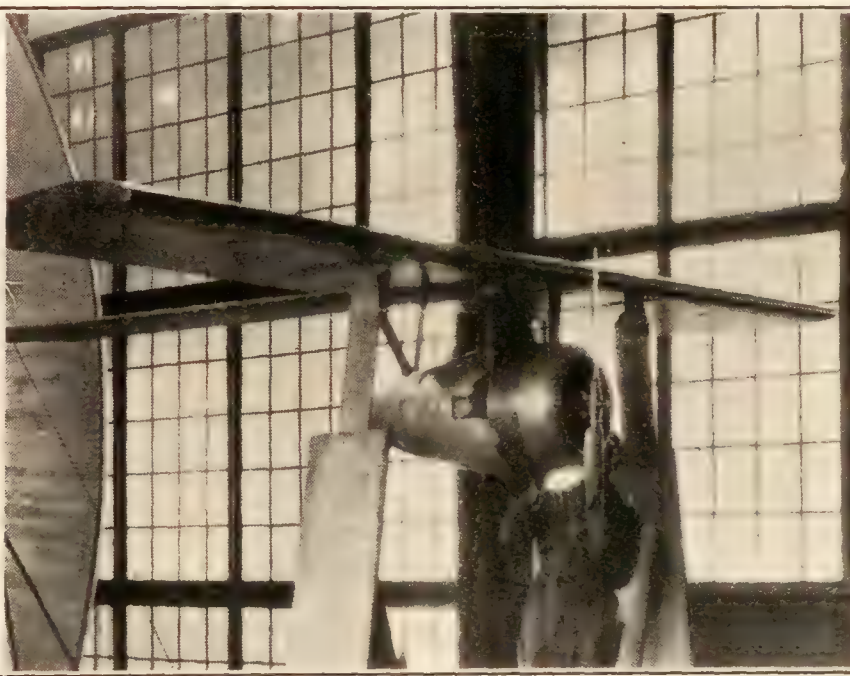
Small nacelle, exposed cylinders.



Small nacelle, variable-angle ring set -8° .



Small nacelle, N.A.C.A. hood.



N.A.C.A. cowled nacelle.

FIGURE 10.—Nacelles in position A-2-B.

could not be used in practice without modification, but the results indicate that careful shaping of the body may result in material reduction in drag. Even though its drag is not particularly low, the fact that it was of smooth contour seems to have had an appreciable effect in reducing the interference drag.

NET EFFICIENCY

The preceding discussion and conclusions have been made without considering the propeller. The conclusions are similar to what would result from any model

tion in lift and drag without propeller has just been examined in detail. When the propeller is operating further changes occur, and in addition the propeller is affected by the presence of the nacelle and wing.

In the detailed discussion in reference 1, two factors are developed which are summed up to give the net efficiency, a measure of the real merit of any wing-nacelle-propeller combination. These factors are:

(1) The propulsive efficiency, representing the ratio of the effective thrust power to the motor power. Effective thrust power is defined as the propeller

thrust minus the increase of drag due to slipstream, so that the effects of the body on the propeller and the propeller on the body are accounted for.

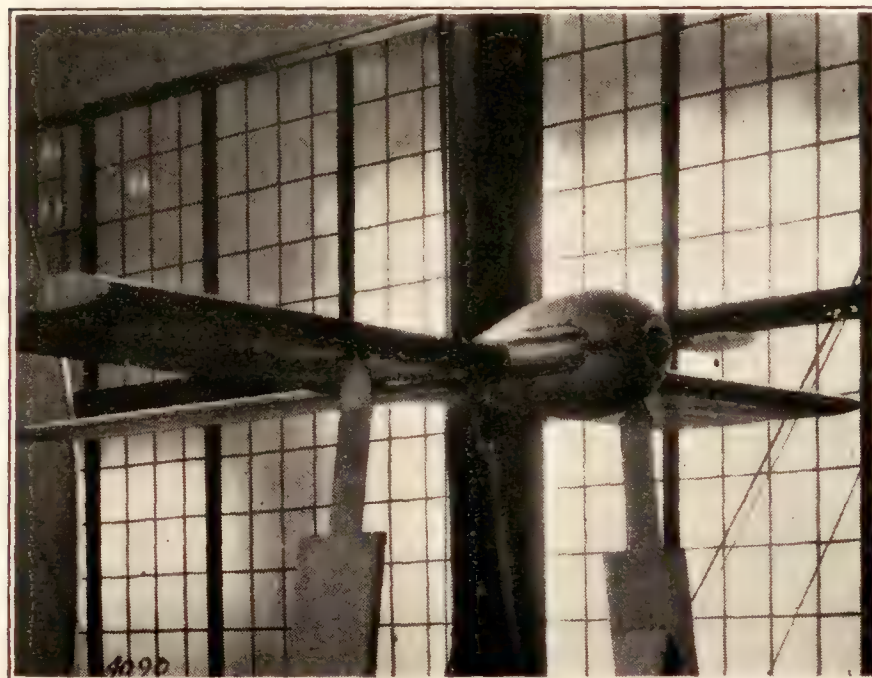
(2) The nacelle drag efficiency factor, representing the fraction of the motor power which is used in overcoming the drag and interference of the nacelle.

The net efficiency, (1) minus (2), represents the fraction of the total motor power that is available for overcoming the drag of the other parts of the airplane

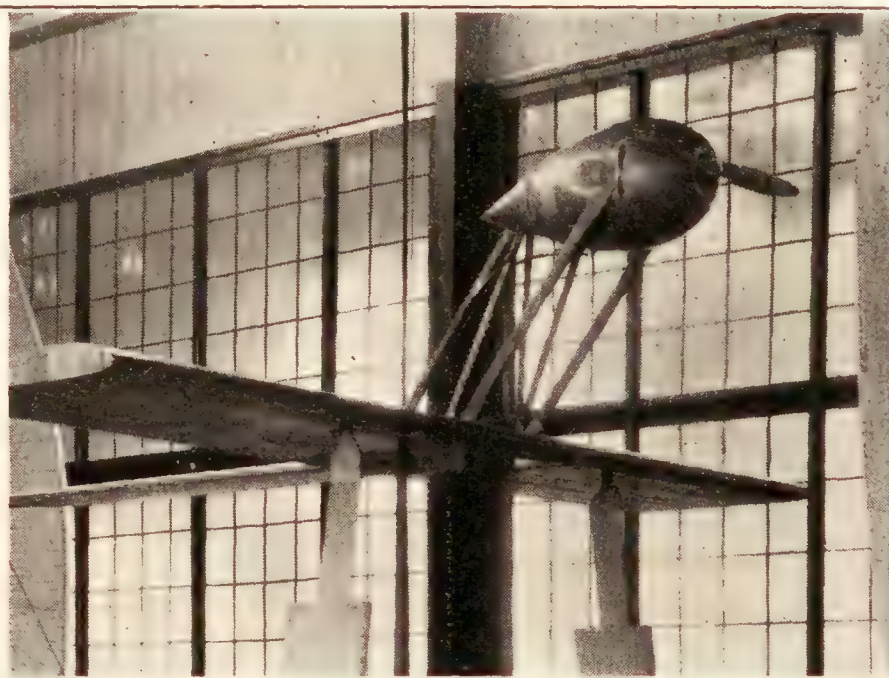
$$\text{Net efficiency} = \frac{C_T}{C_P} \frac{V}{nD} - \frac{C_{DC} - C_{DW}}{C_P} \frac{S}{2D^2} \left(\frac{V}{nD} \right)^3$$

where C_{DW} , drag coefficient of the wing at a given angle of attack.

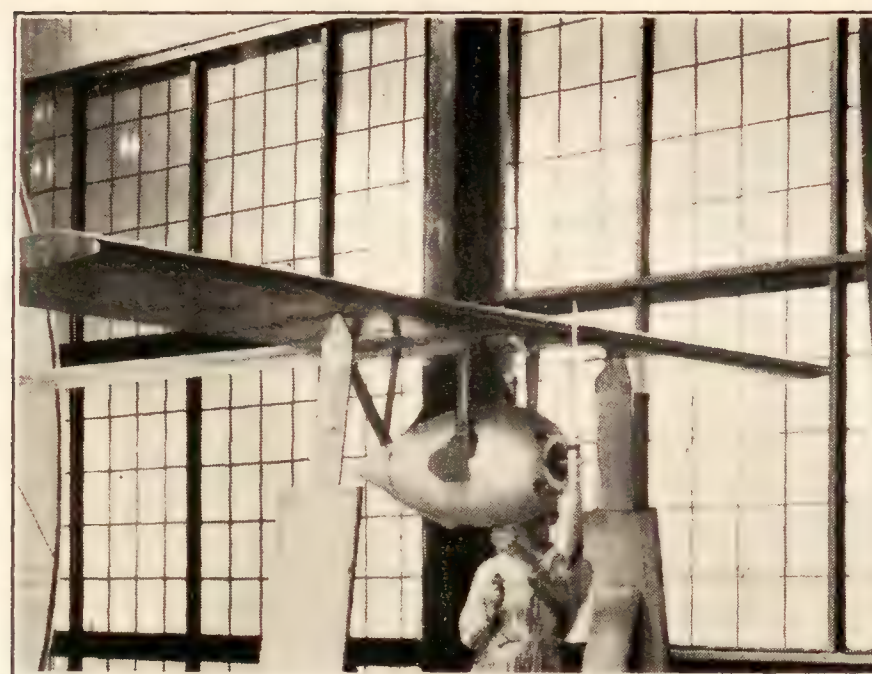
C_{DC} , drag coefficient of the wing-nacelle combination at the same lift coefficient with propeller operating as the wing alone, and the other symbols as previously defined.



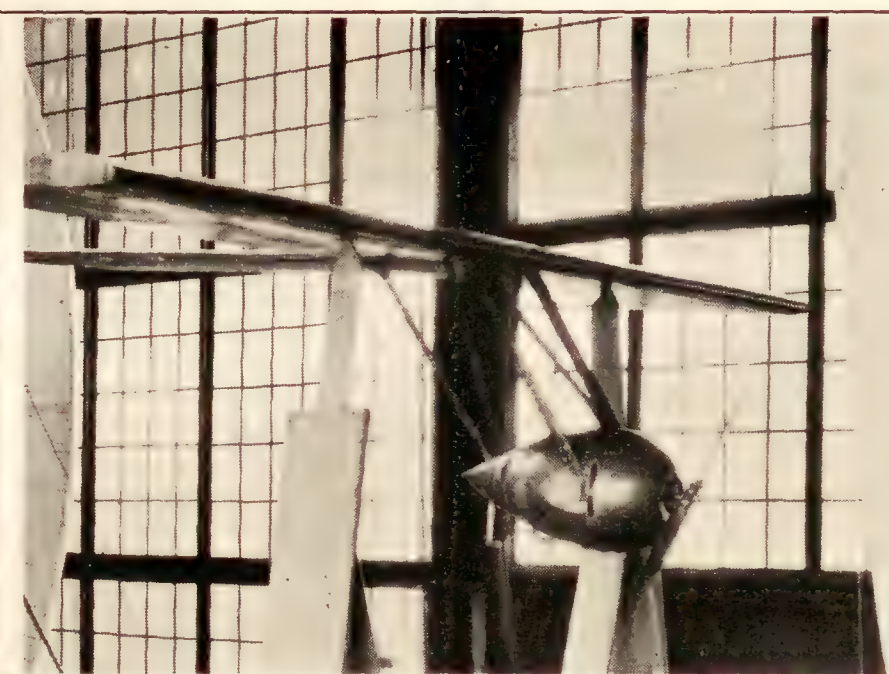
Position B.



Position C-3-A.



Position A-2-B.



Position C-3-B.

FIGURE 11.—Smooth body in several positions.

exclusive of the nacelle. A high value of net efficiency indicates a high propulsive efficiency or low nacelle drag efficiency factor, or both. In any case, the higher the value the better the arrangement.

The details of the derivation of these factors are given in reference 1, and only the resulting formulas are repeated here.

$$\text{Propulsive efficiency} = \eta = \frac{(T - \Delta D)V}{P} = \frac{C_T}{C_P} \frac{V}{nD}$$

$$\text{Nacelle drag efficiency factor} = \frac{C_{DC} - C_{DW}}{C_P} \frac{S}{2D^2} \left(\frac{V}{nD} \right)^3$$

These formulas may be applied to any operating condition, and if the conditions are fixed for all nacelle-propeller-wing combinations a direct comparison may be made. Following the method of reference 1, the factors have been computed for an angle of attack of the wing alone of 0° ($C_L = 0.347$) and a propeller $V/nD = 0.65$, corresponding to an assumed high-speed operating condition, and also for an angle of attack of the wing alone of 5° ($C_L = 0.635$) and $V/nD = 0.42$, corresponding to climb. The high-speed V/nD is the average value at which the propeller operated at peak

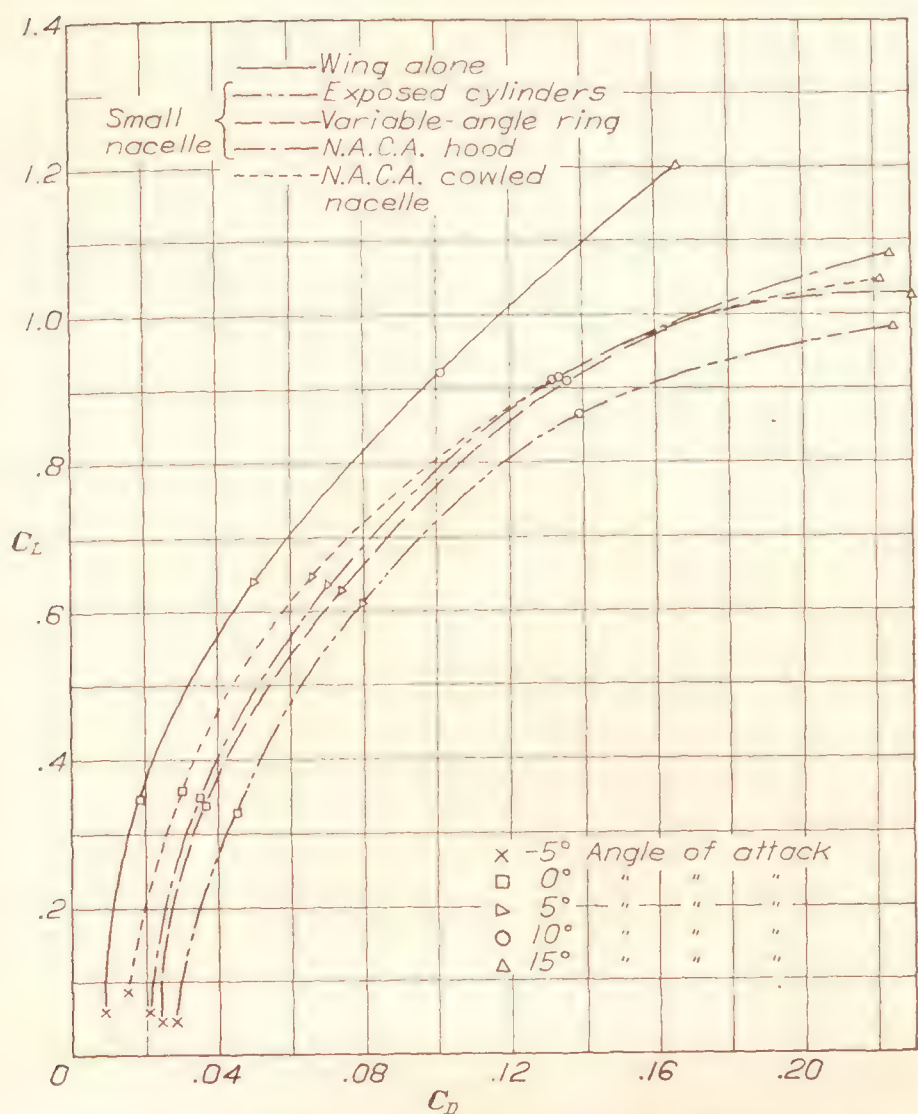


FIGURE 12.—Comparison of lift and drag characteristics of wing alone and nacelle combinations in position B-1-A faired into the wing.

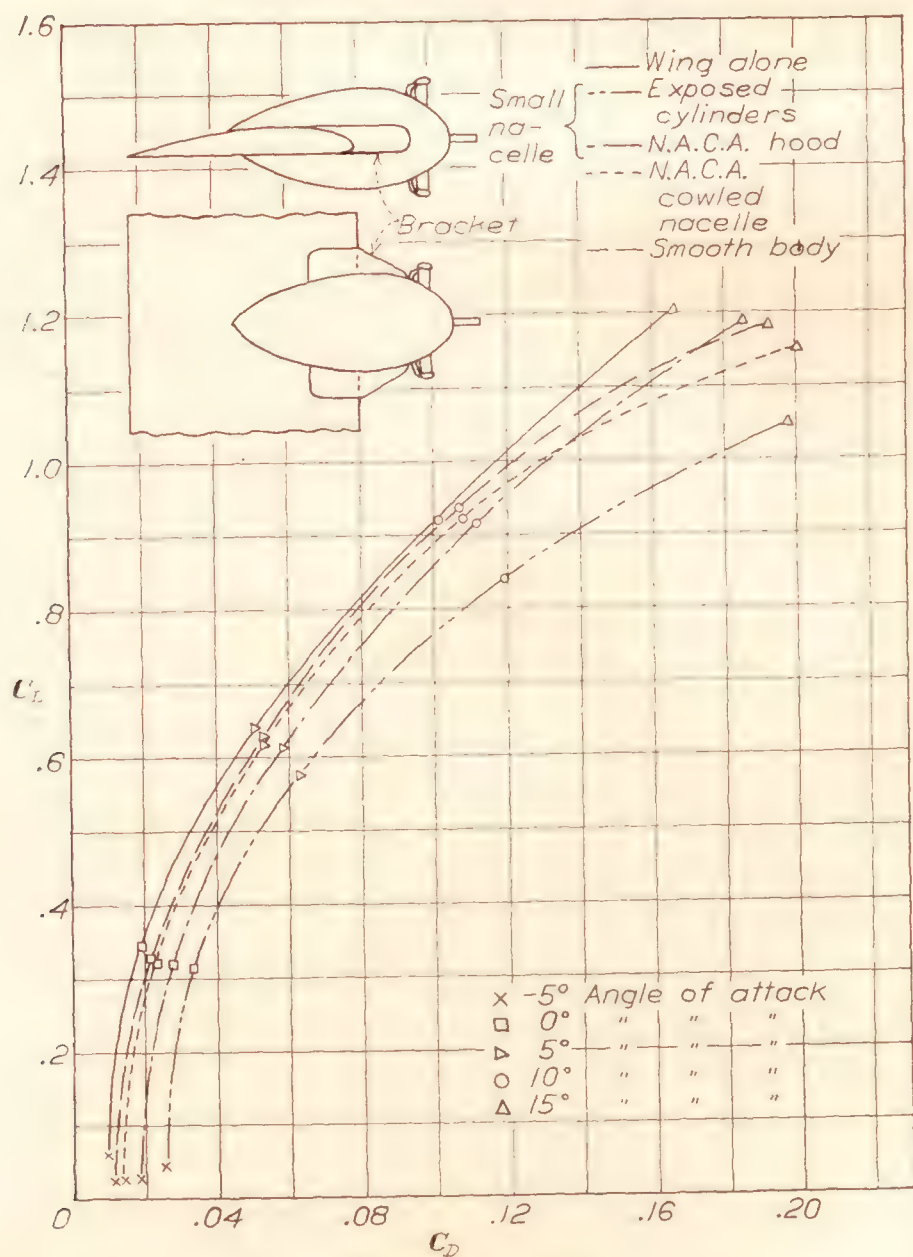


FIGURE 13.—Comparison of lift and drag characteristics of wing alone and nacelle combinations in position B with side bracket fairing.

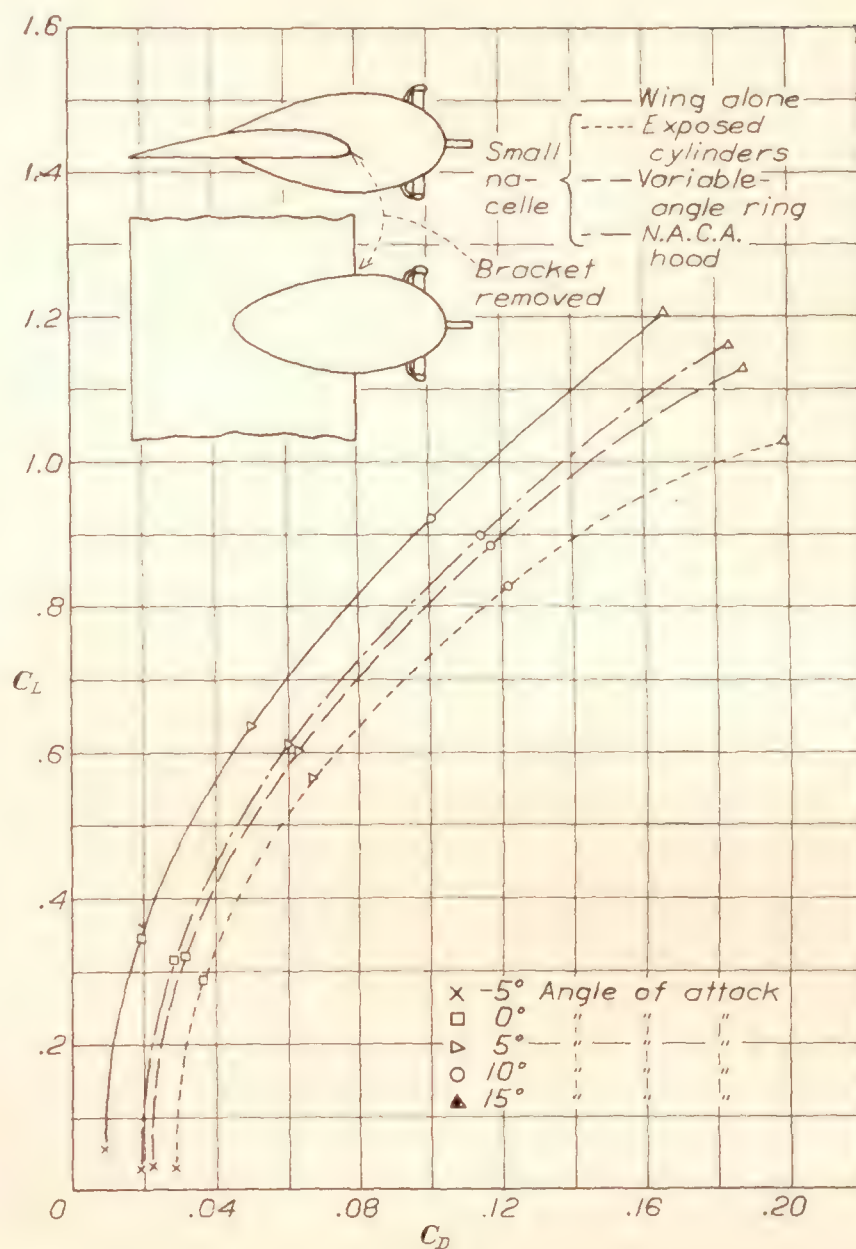


FIGURE 14.—Comparison of lift and drag characteristics of wing alone and nacelle combinations in position B without side brackets.

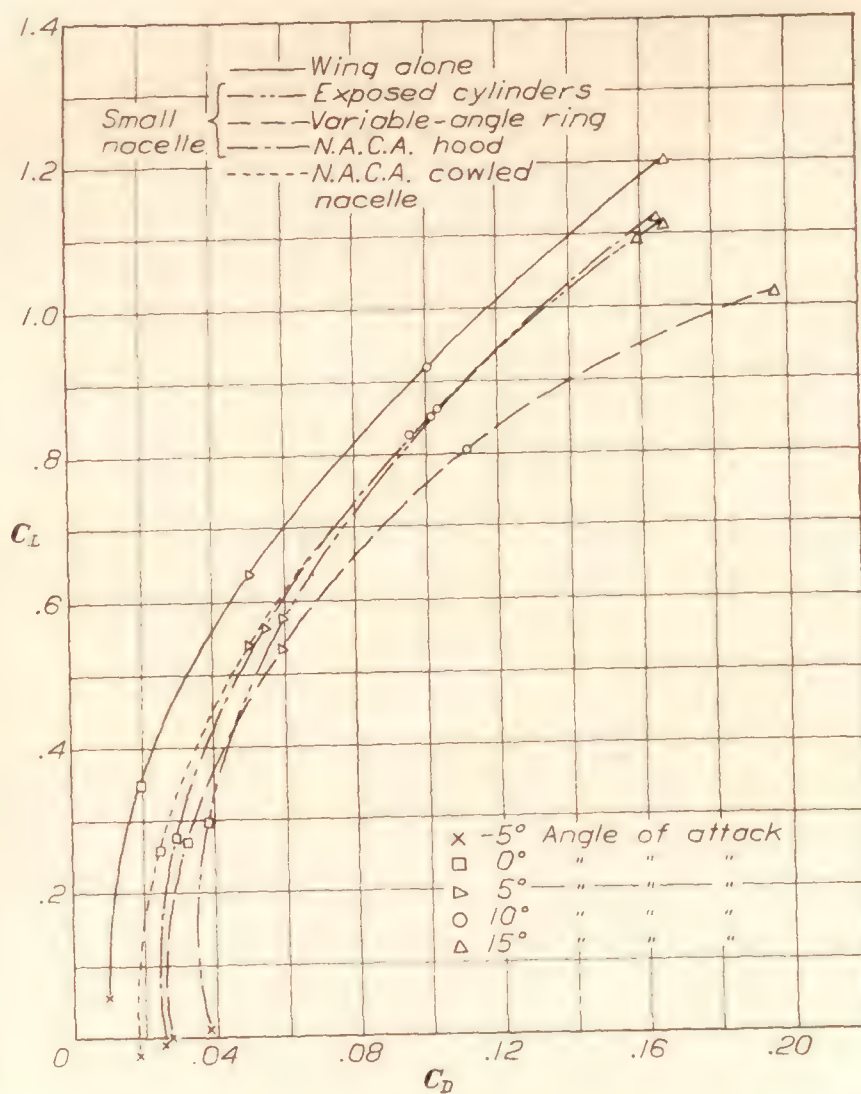


FIGURE 15.—Comparison of lift and drag characteristics of wing alone and nacelle combinations in position A-1-B faired into wing.

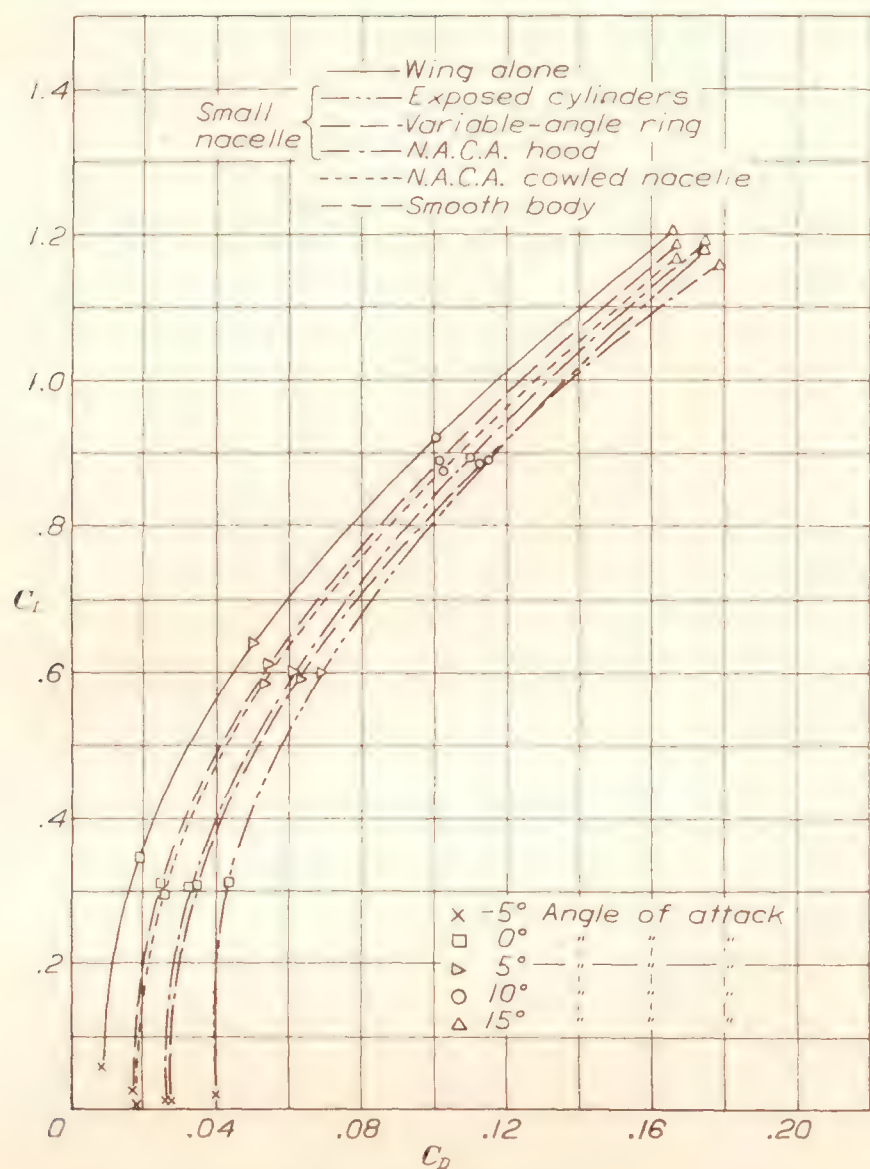


FIGURE 16.—Comparison of lift and drag characteristics of wing alone and nacelle combinations in position A-2-B.

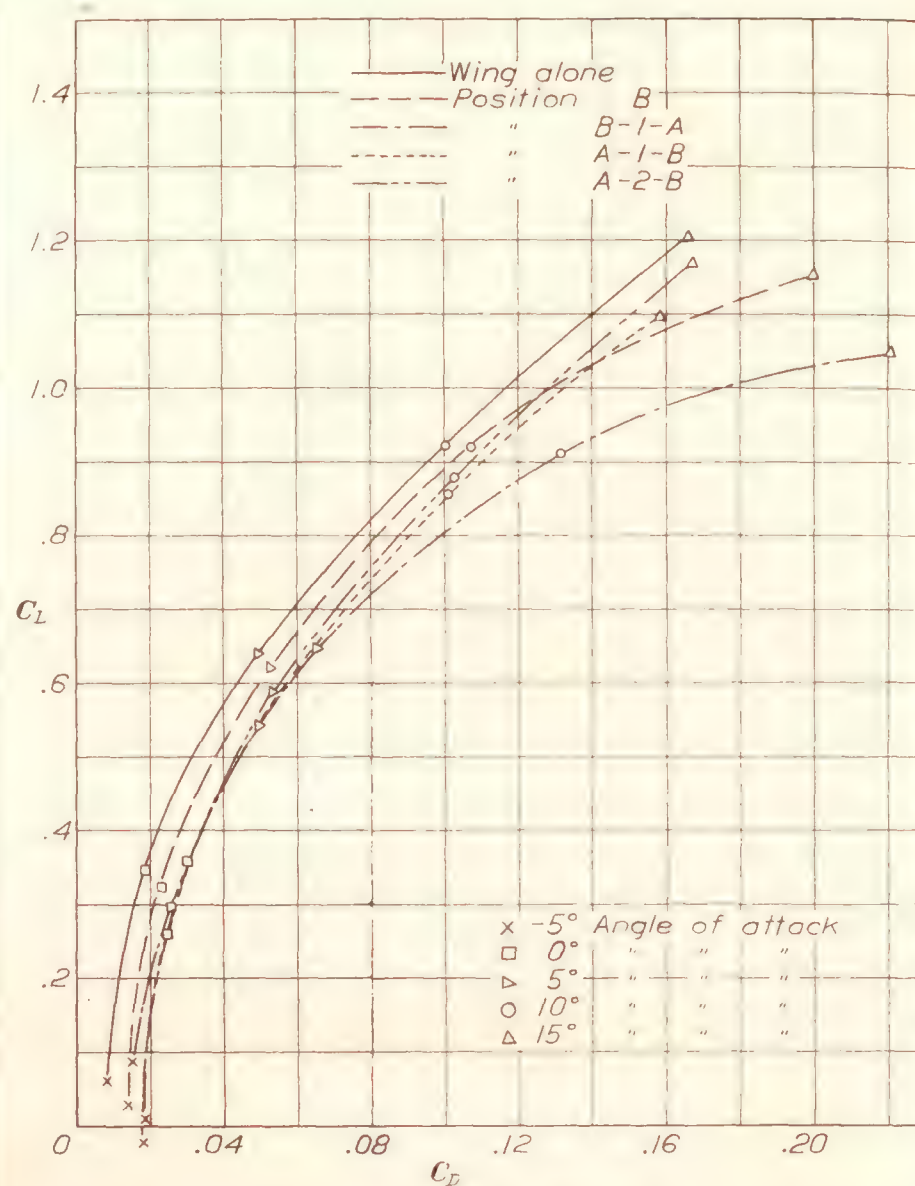


FIGURE 18.—Comparison of lift and drag characteristics of wing alone and N.A.C.A. cowled nacelle combination in four positions.

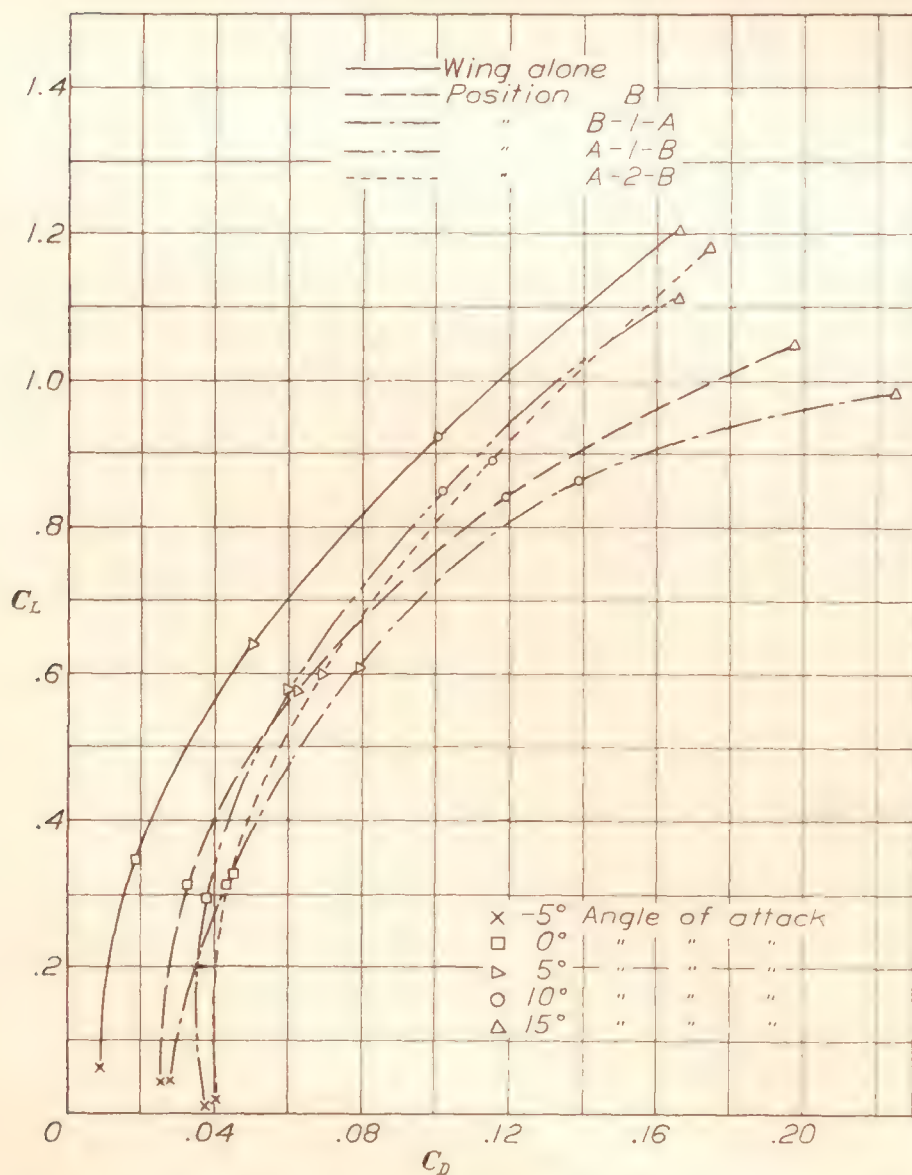


FIGURE 17.—Comparison of lift and drag characteristics of wing alone and exposed-cylinder nacelle combination in four positions.

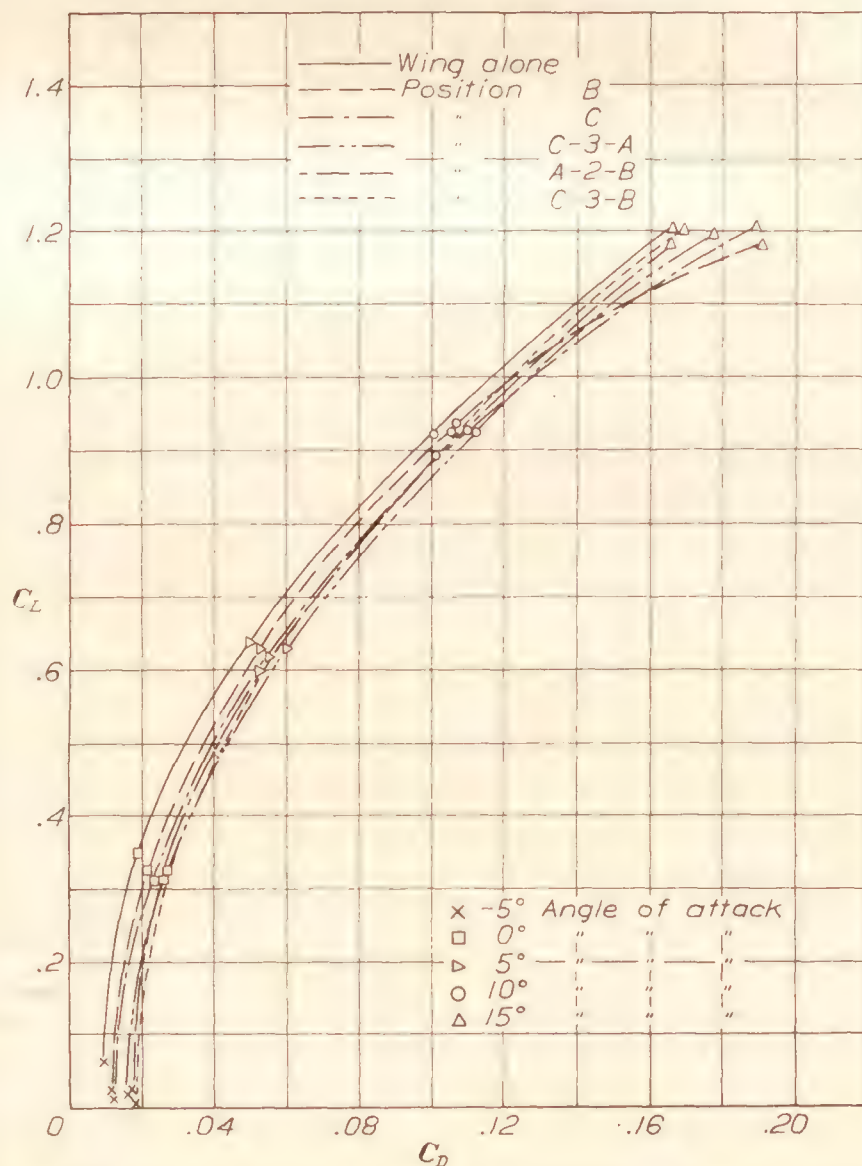


FIGURE 19.—Comparison of lift and drag characteristics of wing alone and smooth-body combination in five positions.

efficiency in the tests. The climb V/nD is the corresponding average value obtained by assuming a climbing speed equal to 60 percent of the high speed and the motor power reduced in proportion to the engine speed, that is, the engine developing constant torque, which is substantially true for airplane engines. The lift effect of the propeller is accounted for by adjusting the angle of attack to give the same lift as the wing alone, as noted in the definition of C_{DC} , so that the comparisons are essentially for the same speed although the actual speed is undetermined.

The method may be illustrated by the following example. In figure 20 are plotted the lift and drag coefficients for the wing alone and the drag coefficient for the small nacelle with exposed cylinders on the wing in position B-1-A. The plotted values are taken from tables I and II. The lift coefficients with propeller operating at $V/nD=0.65$ and at $V/nD=0.42$ are obtained by interpolating between values in table VII and plotted for several angles of attack.

For the high-speed condition ($C_L=0.347$, $V/nD=0.65$) the lift with propeller operating is only slightly greater than that of the wing alone for this particular combination. Projecting down from the lift-coefficient curves at $C_L=0.347$ to the drag-coefficient curves, the drag coefficient added by the nacelle, taking into account the lift due to the propeller, is obtained as indicated on the figure.

The nacelle drag efficiency factor is

$$\text{N.D.F.} = \frac{C_{DC} - C_{DW}}{C_P} \frac{S}{2D^2} \left(\frac{V}{nD} \right)^3$$

Reading C_P from table V and substituting the above values, there results

$$\text{N.D.F.} = \frac{0.0250}{0.0337} \times \frac{50}{2 \times 4^2} \times (0.65)^3 = 0.318$$

Reading η from table VI

$$\text{Net efficiency} = \eta - \text{N.D.F.}$$

$$= 0.853 - 0.318 = 0.535$$

as given in table IX.

For the climbing condition ($C_L=0.635$, $V/nD=0.42$) the lift coefficient with propeller operating is considerably greater than that of the wing alone. The drag coefficient chargeable to the nacelle is reduced accordingly because the same lift can be obtained at a lower angle of attack.

The nacelle drag efficiency factor becomes, substituting C_P from table V,

$$\text{N.D.F.} = \frac{0.0127}{0.0421} \times \frac{50}{2 \times 4^2} (0.42)^3 = 0.035$$

$$\text{The net efficiency} = \eta - \text{N.D.F.}$$

$$= 0.675 - 0.035 = 0.640$$

as given in table X.

The factors thus derived for the nacelles and cowlings in the different positions are given in tables IX and X. The values given here are based on different lift coefficients than the corresponding values in references 1 and 2. It is evident that the factors assume different values depending on what operating conditions are assumed and although there may be some question as to the possibilities of comparing the results directly it is felt that no material discrepancies result from such a comparison. In order to be strictly correct, all comparisons should be made at a constant value of the lift which, in general, means different values of the lift coefficient because of variations in airfoil section and area.

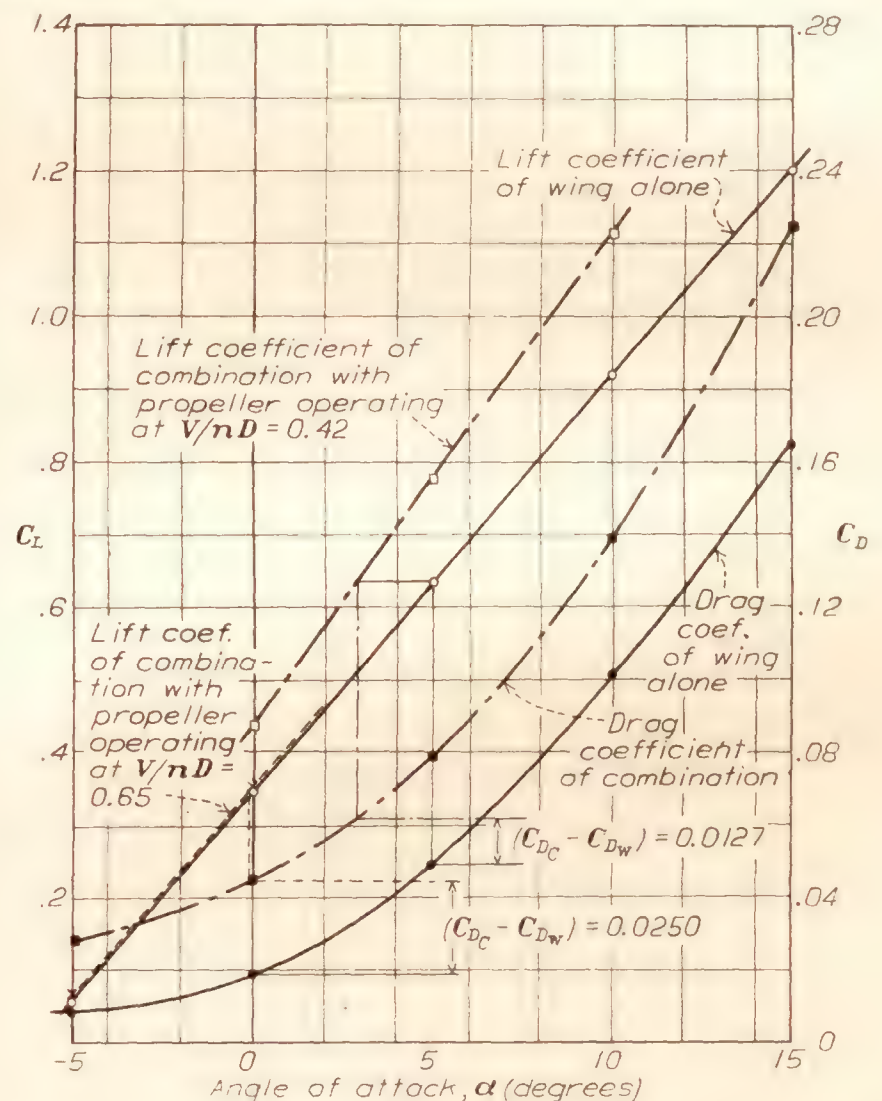


FIGURE 20.—Method of obtaining nacelle drag used in computing nacelle drag efficiency factor.

(Small nacelle with exposed engine cylinders in position B-1-A.)

An examination of table IX indicates that the propulsive efficiency is highest in the high-speed condition with the nacelle with exposed engine cylinders. The N.A.C.A. cowled nacelle and the smooth body give the lowest propulsive efficiencies. These results are in agreement with those of other tests on propellers with smooth and with poorly stream-lined bodies.

The high propulsive efficiency with the uncowed engine nacelle does not mean high net efficiency, however. The nacelle-drag factor is very high and the net efficiency is correspondingly reduced. In almost every case, the order of the net efficiencies is in the inverse order of the drags of the various com-

binations, so that the N.A.C.A. cowled nacelle and wing combination has the highest net efficiency. There does not seem to be much choice between the various intermediate cowlings, although they are all better than the uncowed nacelle arrangement.

In the climb condition (table X) the differences are, as expected, less marked. The propeller adds appreciably to the lift, however, owing to the considerable vertical component of thrust and increase of velocity over the wing. This results in the nacelle drag efficiency factor becoming negative in most instances, indicating that the angle of attack is reduced sufficiently below the angle selected for the climbing condition to make the net drag less than that of the wing alone. Because the nacelle drag is a much smaller proportion of the total drag at the high angles of attack, the differences in net efficiencies are less marked although the cowled nacelle still is the best. The differences, in general, are so slight that the performance of any arrangement in the climbing range would not be greatly affected by the choice of nacelle location or cowling.

The conclusion in the preceding section on the difference in drag in favor of the nacelle with side bracket fairing does not seem to hold true when the propeller effects are considered. There is enough gain in propulsive efficiency by removing the side brackets to overcome the greater drag and the conclusion of reference 2 that side brackets are detrimental remains true. An exception will be noted in the case of the nacelle with exposed engine cylinders in the high-speed condition.

COMPARISON WITH PREVIOUS RESULTS

In the preceding discussion no attempt has been made to compare the results of these tests with those of reference 2. The present tests were made for the specific purpose of comparison, the same nacelles and cowlings being used in both sets of tests. The purpose of the tests with different wings is to show whether the shape and size of the wing has a great influence on the nacelle drag and interference, and also to indicate, if possible, general rules for applying the results to various wings. In the two sets of tests the nacelles were located with the propellers the same actual distances¹ above, below, and forward of the leading edge of the wing. If the efficiency factors with the two wings are in agreement, it must be concluded that the relative spacings are not the predominating factor but that the results are determined by the absolute location of nacelle, propeller, and wing. If the results are not in agreement, then some other explanation is required.

In order to compare the results without omitting any of the factors, it seems best to consider the efficiency factors obtained with some of the arrangements located in the same positions on the two wings. In the following table these are listed for the N.A.C.A.

cowled nacelle located in four positions on both the thick wing and the Clark Y wing. The differences between the factors in the two cases are also indicated.

COMPARISON OF EFFICIENCY FACTORS FOR CLARK Y WING AND THICK WING WITH PROPELLER LOCATED THE SAME ACTUAL DISTANCES FROM THE LEADING EDGE OF THE WING IN EACH CASE

N.A.C.A. COWLED NACELLE

	(1) Clark Y wing.	(2) Thick wing.	(1) - (2)
Nacelle in position B-1-A ¹			
Propulsive efficiency.....	0.788	0.732	0.056
Nacelle drag efficiency factor.....	.125	.072	.053
Net efficiency.....	.663	.660	.003
Nacelle in position B			
Propulsive efficiency.....	0.760	0.761	-0.001
Nacelle drag efficiency factor.....	.046	.009	.037
Net efficiency.....	.714	.752	-.038
Nacelle in position A-1-B ¹			
Propulsive efficiency.....	0.793	0.719	0.074
Nacelle drag efficiency factor.....	.151	.079	.072
Net efficiency.....	.642	.640	.002
Nacelle in position A-2-B			
Propulsive efficiency.....	0.773	0.770	0.003
Nacelle drag efficiency factor.....	.135	.161	-.026
Net efficiency.....	.638	.609	.029

¹ Nacelle faired into wing.

It appears from an examination of this table that the net efficiencies are not greatly different in the two cases, the maximum variation being 3.8 percent. There are, however, considerably greater discrepancies in the propulsive efficiency and nacelle drag efficiency factors. In 3 of the 4 cases, the net efficiency is higher for the Clark Y wing arrangement. The agreement does not seem to be close enough to establish the fact that the net efficiency is purely a function of the actual distance from nacelle and propeller to the wing, or that the net efficiency is independent of the wing section used.

There is some indication that the net efficiencies are more a function of the relative distance between nacelle, propeller, and wing than of the absolute distance. By making use of the contours in reference 1, it is possible to select values of the efficiency factors for conditions for the thick wing where the propeller is located the same relative distance in fractions of the chord from the leading edge of the wing as it is on the Clark Y wing of these tests.

In the following table are listed the efficiency factors for the Clark Y wing, and also for the thick wing propeller-nacelle combinations with the nacelle and propeller located the same fractions of the chord above, below, and forward of the wing as in the Clark Y tests.

¹ This is not strictly correct. (See fig. 5.)

COMPARISON OF EFFICIENCY FACTORS FOR CLARK Y WING AND THICK WING WITH PROPELLER LOCATED THE SAME FRACTION OF THE CHORD FROM THE LEADING EDGE OF THE WING IN EACH CASE

N.A.C.A. COWLED NACELLE

	(1) Clark Y wing, these tests.	(2) Thick wing, figs. 14, 15, 16 of reference 1.	(1) - (2)
Nacelle on Clark Y wing in position B-1-A ¹			
Propulsive efficiency.....	0.788	0.756	0.032
Nacelle drag efficiency factor.....	.125	.096	.029
Net efficiency.....	.663	.660	.003
Nacelle on Clark Y wing in position B			
Propulsive efficiency.....	0.760	0.753	0.007
Nacelle drag efficiency factor.....	.046	.060	-.014
Net efficiency.....	.714	.693	.021
Nacelle on Clark Y wing in position A-1-B ¹			
Propulsive efficiency.....	0.793	0.749	0.044
Nacelle drag efficiency factor.....	.151	.107	.044
Net efficiency.....	.642	.642	.000
Nacelle on Clark Y wing in position A-2-B			
Propulsive efficiency.....	0.773	0.783	-0.010
Nacelle drag efficiency factor.....	.135	.150	-.015
Net efficiency.....	.638	.633	.005

¹ Nacelle faired into wing.

It will be noted from this table that the differences between the results are less marked, and that only in the position A-1-B immediately below the wing is the difference of any factor over 3 percent. The difference in this case is perhaps accounted for by the fact that in the tests with the thick wing the hood of the N.A.C.A. cowled nacelle was faired into the leading edge of the wing, whereas in the tests with the Clark Y wing the hood was not faired in. The mean difference in all the factors is 2 percent, and in the net efficiencies 1 percent.

The agreement of these results lends strength to the theory that the relative location of the propeller, nacelle, and wing is the main factor in determining the net efficiencies, at least for cowled engine nacelles. With so many variables operating and considering the unknown separate effects of small changes in the nacelle and wing and propeller, the agreement is rather surprising. It may be safely said then that, to a first approximation, the location of the propeller and the nacelle with reference to different wings should be determined in fractions of the wing chord if the efficiency of the arrangement is to be estimated from results of these tests. With a wing of wide chord the nacelle should then be located a correspondingly greater actual distance ahead of the wing for the best results. By analogy it would seem that if a larger engine is used the propeller and nacelle should be

moved forward in proportion to the relative sizes of the engine, enlarging all dimensions of the nacelle in proportion. These statements are equivalent to saying that the geometrical proportions of the nacelle and the wing, both as to size and location of elements, should be kept the same for comparable results. It should be stated that this is not conclusively established as a fact by the test results, but it is true that in a few recent airplanes using larger engines it has been necessary to place the propeller farther ahead of the wing than the 25 percent of the chord recommended as the result of the earlier tests. Besides showing a lower speed, the nacelle located with the propeller too close to the wing indicated a considerable loss of lift at high angles of attack, the possibility of which has previously been pointed out. (See reference 7.) It would seem preferable, therefore, to err in the direction of placing the nacelle too far ahead of the wing than too close.

There may also be some interest in comparing the actual drags and interferences obtained with the two wing arrangements. If this is done it is pointed out that the values of the coefficients C_L and C_D given in this report should be multiplied by two thirds to give coefficients that can be compared directly with the results of references 1 and 2. This is due to the difference in the wing areas of the Clark Y and the thick wing. In most instances, however, designers will probably wish to compute the actual drag, and if the results are computed independently no confusion should arise between the two reports. It is also to be noted that the lift and drag coefficients of the wing alone are of no value in themselves because the wings used in the tests do not represent complete airplane wings.

Finally, it may be said that, despite many minor deviations, the interference of nacelles is largely a function of the relative location of wing and nacelle, and that it is not greatly affected by the cross-sectional shape of the wing. The N.A.C.A. cowled nacelle located directly ahead of the wing is the best arrangement of an air-cooled engine so far found. With uncowed engines there is no great advantage of one nacelle location over another. The advantage of cowling, however, is so much greater than any advantage resulting from nacelle locations that it would seem reasonable to cowl the engine properly before attempting to take advantage of the additional gains resulting from the proper location of the nacelle.

CONCLUSIONS

The following general conclusions may be drawn. Of these, the first five are in agreement with those of reference 2. The last two conclusions result from a comparison of the present data with those previously obtained.

REFERENCES

1. The drag and interference of nacelles are reduced by cowlings the nacelle. Cowled nacelles located near the wing, however, should be carefully faired into the wing rather than supported by struts only.

2. The propulsive efficiency of propellers on wing-nacelle combinations is reduced by adding cowlings to the nacelle.

3. The net efficiency is greatest for a smooth body or an N.A.C.A. cowled nacelle.

4. The best location for a tractor propeller and nacelle is directly ahead of the leading edge of the wing, the distance being determined by the engine size (25 percent chord minimum).

5. The location of the nacelle and the type of cowling are of importance at high speed but are of relatively little importance at climbing speeds.

6. The net efficiency of a wing-nacelle-propeller combination is but little affected by the airfoil section of the wing. Nacelles with propellers located at the same fractions of the chord from the wing give about the same results for different wing sections.

7. The advantage of cowling is greater than any advantage resulting from nacelle location. Air-cooled engines should be carefully cowled before attempting to take advantage of the additional gains resulting from the proper location of the nacelle.

1. Wood, Donald H.: Tests of Nacelle-Propeller Combinations in Various Positions with Reference to Wings. Part I. Thick Wing—N.A.C.A. Cowled Nacelle—Tractor Propeller. T.R. No. 415, N.A.C.A., 1932.
2. Wood, Donald H.: Tests of Nacelle-Propeller Combinations in Various Positions with Reference to Wings. II—Thick Wing—Various Radial-Engine Cowlings—Tractor Propeller. T.R. No. 436, N.A.C.A., 1932.
3. Weick, Fred E., and Wood, Donald H.: The Twenty-Foot Propeller Research Tunnel of the National Advisory Committee for Aeronautics. T.R. No. 300, N.A.C.A., 1928.
4. Weick, Fred E.: Working Charts for the Selection of Aluminum Alloy Propellers of a Standard Form to Operate with Various Aircraft Engines and Bodies. T.R. No. 350, N.A.C.A., 1930.
5. Wood, Donald H.: Tests of Large Airfoils in the Propeller Research Tunnel, Including Two with Corrugated Surfaces. T.R. No. 336, N.A.C.A., 1929.
6. Windler, Ray: Drag Tests of 4/9-Scale Model Engine Nacelles with Various Cowlings. T.N. No. 432, N.A.C.A., 1932.
7. Windler, Ray: The Effect of Propellers and Nacelles on the Landing Speeds of Tractor Monoplanes. T.N. No. 420, N.A.C.A., 1932.

LANGLEY MEMORIAL AERONAUTICAL LABORATORY,
NATIONAL ADVISORY COMMITTEE FOR AERONAUTICS,
LANGLEY FIELD, VA., *April 20, 1933*

TABLE I
LIFT COEFFICIENT WITHOUT PROPELLER

$C_L = \frac{\text{lift}}{qS}$

Type of nacelle	50 m.p.h.				75 m.p.h.				100 m.p.h.				
	R.N.=1,360,000				R.N.=2,040,000				R.N.=2,720,000				
Angle of attack.....	−5°	0°	5°	10°	−5°	0°	5°	10°	−5°	0°	5°	10°	15°
Nacelle position B, with side brackets													
Smooth body.....	0.025	0.327	0.630	0.935	0.025	0.327	0.630	0.935	0.025	0.327	0.630	0.935	1.180
Exposed cylinders ¹052	.312	.575	.855	.052	.312	.575	.842	.052	.312	.575	.840	1.045
N.A.C.A. hood ¹033	.330	.626	.920	.033	.327	.619	.915	.033	.323	.613	.902	1.195
N.A.C.A. cowled nacelle.....	.033	.330	.630	.930	.027	.325	.627	.927	.020	.317	.620	.920	1.202
Nacelle position B, without side brackets													
Exposed cylinders ¹	0.045	0.307	0.570	0.830	0.037	0.301	0.567	0.830	0.025	0.293	0.563	0.830	1.027
N.A.C.A. hood ¹027	.317	.605	.900	.027	.317	.605	.900	.027	.317	.605	.900	1.163
Variable ring −8° ¹030	.315	.600	.886	.030	.315	.600	.886	.030	.315	.600	.886	1.123
Nacelle position C													
Smooth body.....	0.030	0.330	0.633	0.936	0.022	0.321	0.628	0.931	0.010	0.312	0.617	0.925	1.210
Nacelle position B-1-A, faired into wing													
Exposed cylinders ¹	0.060	0.341	0.625	0.878	0.056	0.337	0.619	0.871	0.050	0.330	0.610	0.864	0.983
N.A.C.A. hood ¹058	.348	.637	.910	.058	.348	.637	.910	.058	.348	.637	.910	1.080
N.A.C.A. cowled nacelle.....	.092	.373	.652	.915	.085	.368	.649	.915	.075	.360	.645	.915	1.043
Variable ring −8° ¹048	.336	.627	.908	.048	.336	.627	.908	.048	.336	.627	.908	1.027
Nacelle position C-3-A													
Smooth body.....	0.035	0.333	0.630	0.930	0.030	0.328	0.627	0.928	0.020	0.320	0.623	0.925	1.197
Nacelle position A-1-B, faired into wing													
Exposed cylinders ¹	0.015	0.295	0.578	0.860	0.015	0.295	0.578	0.860	0.015	0.295	0.578	0.860	1.113
N.A.C.A. hood ¹000	.286	.575	.860	−.004	.283	.571	.858	−.010	.278	.565	.855	1.125
Variable ring −8° ¹010	.275	.545	.815	.006	.271	.541	.811	.000	.265	.535	.805	1.020
N.A.C.A. cowled nacelle.....	−.026	.257	.540	.827	−.026	.257	.540	.827	−.026	.257	.540	.827	1.093
Nacelle position A-2-B													
Smooth body.....	0.030	0.322	0.610	0.902	0.028	0.319	0.606	0.897	0.023	0.310	0.600	0.890	1.182
Exposed cylinders ¹055	.342	.628	.915	.042	.332	.620	.905	.024	.313	.600	.890	1.182
N.A.C.A. hood ¹020	.312	.605	.900	.018	.309	.603	.899	.015	.305	.600	.897	1.192
Variable ring −8° ¹020	.310	.595	.885	.020	.310	.595	.885	.020	.310	.595	.885	1.160
N.A.C.A. cowled nacelle.....	.020	.312	.602	.890	.015	.305	.595	.885	.005	.295	.585	.873	1.167
Nacelle position C-3-B													
Smooth body.....	0.005	0.313	0.619	0.923	0.005	0.313	0.619	0.923	0.005	0.313	0.619	0.923	1.205
Wing alone													
	0.070	0.359	0.646	0.934	0.065	0.354	0.642	0.928	0.059	0.348	0.637	0.920	1.205

¹ Small nacelle.

TABLE II
DRAG COEFFICIENT WITHOUT PROPELLER

$$C_D = \frac{\text{drag}}{qS}$$

Type of nacelle	50 m.p.h. R.N.=1,350,000				75 m.p.h. R.N.=2,040,000				100 m.p.h. R.N.=2,720,000				
Angle of attack.....	-5°	0°	5°	10°	-5°	0°	5°	10°	-5°	0°	5°	10°	15°
Nacelle position B, with side brackets													
Smooth body.....	0.0120	0.0220	0.0525	0.1070	0.0118	0.0216	0.0525	0.1070	0.0115	0.0210	0.0525	0.1070	0.1910
Exposed cylinders ¹0320	.0400	.0680	.1230	.0390	.0375	.0660	.1210	.0250	.0325	.0620	.1185	.1970
N.A.C.A. hood ¹0180	.0270	.0575	.1100	.0180	.0270	.0578	.1108	.0180	.0270	.0585	.1120	.1840
N.A.C.A. cowled nacelle.....	.0125	.0230	.0545	.1080	.0125	.0225	.0541	.1077	.0125	.0215	.0535	.1070	.1800
Nacelle position B, without side brackets													
Exposed cylinders ¹	0.0320	0.0390	0.0695	0.1260	0.0310	0.0383	0.0685	0.1240	0.0290	0.0370	0.0670	0.1210	0.1990
N.A.C.A. hood ¹0215	.0320	.0625	.1140	.0207	.0312	.0615	.1140	.0190	.0290	.0600	.1140	.1840
Variable ring -8° ¹0235	.0335	.0640	.1200	.0227	.0325	.0635	.1192	.0215	.0310	.0625	.1180	.1870
Nacelle position C													
Smooth body.....	0.0120	0.0230	0.0550	0.1100	0.0120	0.0230	0.0550	0.1100	0.0120	0.0230	0.0550	0.1100	0.1890
Nacelle position B-1-A, faired into wing													
Exposed cylinders ¹	0.0320	0.0475	0.0810	0.1430	0.0305	0.0465	0.0802	0.1415	0.0280	0.0445	0.0790	0.1390	0.2250
N.A.C.A. hood ¹0230	.0375	.0735	.1330	.0222	.0365	.0725	.1326	.0210	.0350	.0705	.1320	.2250
N.A.C.A. cowled nacelle.....	.0185	.0330	.0690	.1365	.0170	.0320	.0680	.1350	.0155	.0300	.0660	.1330	.2220
Variable ring -8° ¹0260	.0400	.0785	.1370	.0253	.0385	.0770	.1363	.0240	.0360	.0740	.1350	.2290
Nacelle position C-3-A													
Smooth body.....	0.0201	0.0325	0.0630	0.1150	0.0185	0.0305	0.0615	0.1135	0.0160	0.0270	0.0595	0.1115	0.1770
Nacelle position A-1-B, faired into wing													
Exposed cylinders ¹	0.0400	0.0400	0.0630	0.1070	0.0390	0.0390	0.0620	0.1060	0.0375	0.0375	0.0600	0.1040	0.1670
N.A.C.A. hood ¹0270	.0315	.0555	.1010	.0263	.0305	.0553	.1010	.0250	.0290	.0550	.1010	.1640
Variable ring -8° ¹0310	.0340	.0590	.1110	.0295	.0333	.0590	.1110	.0270	.0320	.0590	.1110	.1970
N.A.C.A. cowled nacelle.....	.0215	.0275	.0520	.0960	.0200	.0260	.0513	.0958	.0180	.0240	.0500	.0955	.1585
Nacelle position A-2-B													
Smooth body.....	0.0201	0.0270	0.0565	0.1035	0.0190	0.0263	0.0555	0.1025	0.0175	0.0250	0.0540	0.1010	0.1655
Exposed cylinders ¹0425	.0450	.0700	.1165	.0415	.0442	.0696	.1160	.0400	.0430	.0690	.1150	.1750
N.A.C.A. hood ¹0300	.0345	.0630	.1100	.0285	.0340	.0622	.1100	.0260	.0330	.0610	.1100	.1750
Variable ring -8° ¹0300	.0350	.0625	.1125	.0290	.0348	.0625	.1125	.0275	.0345	.0625	.1125	.1790
N.A.C.A. cowled nacelle.....	.0215	.0275	.0555	.1025	.0200	.0268	.0550	.1027	.0180	.0255	.0540	.1030	.1670
Nacelle position C-3-B													
Smooth body.....	0.0220	0.0305	0.0585	0.1070	0.0205	0.0295	0.0570	0.1066	0.0180	0.0270	0.0550	0.1060	0.1710
Wing alone													
	0.0096	0.0210	0.0522	0.1011	0.0092	0.0202	0.0509	0.1012	0.0086	0.0192	0.0492	0.1013	0.1656

¹ Small nacelle.

TABLE III
MOMENT COEFFICIENT WITHOUT PROPELLER

$C_m = \frac{\text{moment}}{qSc}$

Type of nacelle	Angle of attack				
	−5°	0°	5°	10°	15°
Nacelle position B, with side brackets					
Smooth body.....	−0.079	−0.063	−0.043	−0.039	−0.050
Exposed cylinders ¹	−.062	−.058	−.049	−.040	−.051
N.A.C.A. hood ¹	−.071	−.049	−.034	−.031	−.031
N.A.C.A. cowled nacelle.....	−.071	−.053	−.041	−.034	−.039
Nacelle position B, without side brackets					
Exposed cylinders ¹	−0.072	−0.064	−0.053	−0.047	−0.054
N.A.C.A. hood ¹	−.074	−.060	−.048	−.034	−.035
Variable ring −8° ¹	−.075	−.060	−.045	−.035	−.030
Nacelle position C					
Smooth body.....	−0.078	−0.058	−0.038	−0.023	−0.016
Nacelle position B-1-A, faired into wing					
Exposed cylinders ¹	−0.057	−0.054	−0.043	−0.038	−0.068
N.A.C.A. hood ¹	−.064	−.039	−.030	−.034	−.060
N.A.C.A. cowled nacelle.....	−.061	−.046	−.030	−.037	−.071
Variable ring −8° ¹	−.062	−.050	−.034	−.026	−.051
Nacelle position C-3-A					
Smooth body.....	−0.060	−0.043	−0.037	−0.039	−0.031
Nacelle position A-1-B, faired into wing					
Exposed cylinders ¹	−0.078	−0.075	−0.068	−0.056	−0.062
N.A.C.A. hood ¹	−.086	−.078	−.065	−.064	−.056
Variable ring −8° ¹	−.078	−.070	−.061	−.058	−.071
N.A.C.A. cowled nacelle.....	−.071	−.069	−.060	−.055	−.056
Nacelle position A-2-B					
Smooth body.....	−0.079	−0.068	−0.064	−0.064	−0.067
Exposed cylinders ¹	−.079	−.077	−.070	−.060	−.063
N.A.C.A. hood ¹	−.082	−.071	−.069	−.064	−.062
Variable ring −8° ¹	−.085	−.074	−.068	−.066	−.063
N.A.C.A. cowled nacelle.....	−.079	−.067	−.067	−.063	−.058
Nacelle position C-3-B					
Smooth body.....	−0.085	−0.088	−0.073	−0.064	−0.066

¹ Small nacelle.

TABLE IV
THRUST COEFFICIENT

$$C_T = \frac{(T - \Delta D)}{\rho n^2 D^4}$$

Propeller No. 4412-4 feet. Set 17° at 0.75 R. Angle of attack = -5°

Type of nacelle	$\frac{V}{n D}$									
	0.1	0.2	0.3	0.4	0.5	0.6	0.7	0.8	0.9	1.0
Nacelle position B, with side brackets										
Smooth body	0.0828	0.0778	0.0712	0.0628	0.0524	0.0405	0.0272	0.0125	-0.0042	-0.0217
Exposed cylinders ¹	.0863	.0821	.0761	.0680	.0584	.0467	.0337	.0193	.0037	-.0125
N.A.C.A. hood	.0862	.0815	.0749	.0667	.0567	.0450	.0313	.0154	-.0013	-.0198
N.A.C.A. cowled nacelle	.0862	.0811	.0743	.0661	.0564	.0452	.0319	.0165	-.0001	-.0189
Nacelle position B, without side brackets										
Exposed cylinders ¹	0.0920	0.0871	0.0805	0.0723	0.0623	0.0509	0.0380	0.0227	0.0065	-0.0111
N.A.C.A. hood ¹	.0902	.0854	.0788	.0706	.0605	.0487	.0355	.0201	.0035	-.0146
Variable ring -8° ¹	.0900	.0851	.0787	.0704	.0603	.0489	.0356	.0212	.0050	-.0129
Nacelle position C										
Smooth body	0.0836	0.0788	0.0720	0.0637	0.0531	0.0412	0.0275	0.0120	-0.0052	-0.0245
Nacelle position B-1-A, faired into wing										
Exposed cylinders ¹	0.0908	0.0865	0.0806	0.0728	0.0629	0.0510	0.0376	0.0224	0.0058	-0.0110
N.A.C.A. hood ¹	.0891	.0853	.0790	.0711	.0611	.0493	.0360	.0212	.0056	-.0103
N.A.C.A. cowled nacelle	.0899	.0850	.0786	.0709	.0605	.0492	.0365	.0220	.0065	-.0102
Variable ring -8° ¹	.0891	.0848	.0789	.0710	.0611	.0497	.0369	.0230	.0072	-.0100
Nacelle position C-3-A										
Smooth body	0.0833	0.0788	0.0723	0.0639	0.0537	0.0414	0.0275	0.0125	-0.0025	-0.0210
Nacelle position A-1-B, faired into wing										
Exposed cylinders ¹	0.0880	0.0834	0.0772	0.0696	0.0600	0.0490	0.0367	0.0234	0.0097	-0.0050
N.A.C.A. hood ¹	.0852	.0805	.0741	.0660	.0565	.0450	.0320	.0188	.0040	-.0106
Variable ring -8° ¹	.0860	.0817	.0751	.0668	.0569	.0451	.0320	.0180	.0030	-.0130
N.A.C.A. cowled nacelle	.0865	.0814	.0747	.0664	.0565	.0458	.0329	.0185	.0035	-.0125
Nacelle position A-2-B										
Smooth body	0.0879	0.0831	0.0765	0.0680	0.0572	0.0445	0.0300	0.0140	-0.0028	-0.0209
Exposed cylinders ¹	.0890	.0845	.0782	.0701	.0603	.0485	.0350	.0201	.0045	-.0121
N.A.C.A. hood ¹	.0867	.0818	.0751	.0668	.0566	.0444	.0309	.0161	.0006	-.0170
Variable ring -8° ¹	.0893	.0849	.0787	.0702	.0601	.0480	.0344	.0195	.0032	-.0144
N.A.C.A. cowled nacelle	.0872	.0823	.0757	.0672	.0570	.0451	.0312	.0155	-.0012	-.0193
Nacelle position C-3-B										
Smooth body	0.0859	0.0804	0.0733	0.0645	0.0538	0.0415	0.0278	0.0130	-0.0030	-0.0195

¹ Small nacelle.

TABLE IV—Continued
THRUST COEFFICIENT

$$C_T = \frac{(T - \Delta D)}{\rho n^2 D^4}$$

Propeller No. 4412—4 feet. Set 17° at 0.75 R. Angle of attack = 0°

Type of nacelle	$\frac{V}{n D}$									
	0.1	0.2	0.3	0.4	0.5	0.6	0.7	0.8	0.9	1.0
Nacelle position B, with side brackets										
Smooth body.....	0.0827	0.0777	0.0712	0.0628	0.0527	0.0403	0.0268	0.0125	-0.0036	-0.0211
Exposed cylinders ¹0861	.0814	.0751	.0673	.0576	.0465	.0336	.0193	.0037	-.0126
N.A.C.A. hood ¹0862	.0815	.0750	.0665	.0564	.0446	.0312	.0162	.0000	-.0169
N.A.C.A. cowled nacelle.....	.0852	.0804	.0740	.0660	.0562	.0447	.0310	.0152	-.0014	-.0291
Nacelle position B, without side brackets										
Exposed cylinders ¹	0.0903	0.0856	0.0792	0.0711	0.0613	0.0500	0.0372	0.0225	0.0064	-0.0112
N.A.C.A. hood ¹0896	.0847	.0781	.0698	.0595	.0477	.0344	.0192	.0028	-.0151
Variable ring—8° ¹0907	.0856	.0788	.0704	.0601	.0484	.0353	.0200	.0039	-.0140
Nacelle position C										
Smooth body.....	0.0827	0.0780	0.0714	0.0630	0.0525	0.0405	0.0267	0.0105	-0.0068	-0.0261
Nacelle position B-1-A, faired into wing										
Exposed cylinders ¹	0.0908	0.0862	0.0800	0.0718	0.0618	0.0499	0.0371	0.0202	0.0058	-0.0108
N.A.C.A. hood ¹0893	.0842	.0776	.0690	.0588	.0480	.0350	.0197	.0035	-.0128
N.A.C.A. cowled nacelle.....	.0895	.0842	.0772	.0686	.0584	.0469	.0340	.0195	.0032	-.0145
Variable ring—8° ¹0884	.0837	.0772	.0690	.0589	.0468	.0336	.0185	.0018	-.0165
Nacelle position C-3-A										
Smooth body.....	0.0833	0.0787	0.0722	0.0640	0.0535	0.0412	0.0273	0.0120	-0.0040	-0.0212
Nacelle position A-1-B, faired into wing										
Exposed cylinders ¹	0.0882	0.0840	0.0780	0.0700	0.0601	0.0495	0.0362	0.0223	0.0081	-0.0070
N.A.C.A. hood ¹0860	.0820	.0760	.0680	.0581	.0463	.0330	.0194	.0045	-.0112
Variable ring—8° ¹0868	.0820	.0759	.0678	.0580	.0465	.0340	.0204	.0062	-.0085
N.A.C.A. cowled nacelle.....	.0870	.0820	.0760	.0675	.0580	.0460	.0337	.0200	.0059	-.0090
Nacelle position A-2-B										
Smooth body.....	0.0879	0.0831	0.0764	0.0680	0.0575	0.0451	0.0314	0.0157	-0.0010	-0.0181
Exposed cylinders ¹0890	.0844	.0781	.0701	.0604	.0490	.0357	.0215	.0066	-.0096
N.A.C.A. hood ¹0864	.0817	.0751	.0670	.0572	.0458	.0329	.0186	.0036	-.0149
Variable ring—8° ¹0898	.0853	.0790	.0710	.0610	.0496	.0366	.0225	.0067	-.0105
N.A.C.A. cowled nacelle.....	.0873	.0822	.0756	.0672	.0571	.0457	.0330	.0183	.0022	-.0161
Nacelle position C-3-B										
Smooth body.....	0.0857	0.0802	0.0733	0.0647	0.0540	0.0425	0.0285	0.0128	-0.0040	-0.0220

¹ Small nacelle.

TABLE IV—Continued
THRUST COEFFICIENT

$$C_T = \frac{(T - \Delta D)}{\rho n^2 D^4}$$

Propeller No. 4412—4 feet. Set 17° at 0.75 R. Angle of attack = 5°

Type of nacelle.....	$\frac{V}{n D}$									
	0.1	0.2	0.3	0.4	0.5	0.6	0.7	0.8	0.8	1.0
Nacelle position B, with side brackets										
Smooth body.....	0.0808	0.0757	0.0690	0.0604	0.0503	0.0388	0.0265	0.0125	−0.0028	−0.0186
Exposed cylinders ¹0857	.0807	.0741	.0660	.0560	.0448	.0322	.0188	.0034	−.0145
N.A.C.A. hood ¹0854	.0800	.0730	.0645	.0545	.0435	.0312	.0172	.0010	−.0172
N.A.C.A. cowled nacelle.....	.0834	.0784	.0719	.0637	.0540	.0428	.0297	.0144	−.0021	−.0201
Nacelle position B, without side brackets										
Exposed cylinders ¹	0.0899	0.0850	0.0781	0.0696	0.0598	0.0487	0.0358	0.0216	0.0065	−0.0095
N.A.C.A. hood ¹0888	.0840	.0774	.0690	.0585	.0467	.0333	.0187	.0030	−.0139
Variable ring −8° ¹0900	.0850	.0781	.0695	.0592	.0473	.0340	.0200	.0046	−.0118
Nacelle position C										
Smooth body.....	0.0838	0.0781	0.0708	0.0621	0.0518	0.0398	0.0263	0.0110	−0.0063	−0.0255
Nacelle position B-1-A, faired into wing										
Exposed cylinders ¹	0.0880	0.0832	0.0770	0.0685	0.0585	0.0467	0.0335	0.0197	0.0050	−0.0105
N.A.C.A. hood ¹0874	.0826	.0762	.0679	.0573	.0450	.0310	.0167	.0013	−.0152
N.A.C.A. cowled nacelle.....	.0875	.0823	.0758	.0672	.0570	.0453	.0320	.0172	.0014	−.0155
Variable ring −8° ¹0867	.0820	.0757	.0676	.0579	.0465	.0336	.0195	.0042	−.0120
Nacelle position C-3-A										
Smooth body.....	0.0833	0.0788	0.0723	0.0640	0.0537	0.0415	0.0275	0.0122	−0.0044	−0.0220
Nacelle position A-1-B, faired into wing										
Exposed cylinders ¹	0.0890	0.0840	0.0780	0.0699	0.0600	0.0489	0.0362	0.0226	0.0080	−0.0075
N.A.C.A. hood ¹0862	.0817	.0750	.0668	.0570	.0458	.0332	.0200	.0060	−.0090
Variable ring −8° ¹0870	.0820	.0760	.0677	.0582	.0472	.0351	.0225	.0095	−.0041
N.A.C.A. cowled nacelle.....	.0870	.0825	.0760	.0681	.0585	.0470	.0349	.0219	.0078	−.0065
Nacelle position A-2-B										
Smooth body.....	0.0870	0.0821	0.0755	0.0675	0.0576	0.0457	0.0329	0.0195	0.0055	−0.0083
Exposed cylinders ¹0882	.0831	.0764	.0684	.0590	.0483	.0369	.0242	.0103	−.0044
N.A.C.A. hood ¹0864	.0816	.0752	.0671	.0575	.0463	.0343	.0216	.0081	−.0070
Variable ring −8° ¹0892	.0845	.0782	.0703	.0608	.0498	.0375	.0244	.0105	−.0121
N.A.C.A. cowled nacelle.....	.0871	.0821	.0753	.0671	.0572	.0460	.0339	.0205	.0064	−.0090
Nacelle position C-3-B										
Smooth body.....	0.0852	0.0800	0.0731	0.0646	0.0540	0.0423	0.0290	0.0146	−0.0005	−0.0170

¹ Small nacelle.

TABLE IV—Continued
THRUST COEFFICIENT

$$C_T = \frac{(T - \Delta D)}{\rho n^2 D^4}$$

Propeller No. 4412—4 feet. Set 17° at 0.75 R. Angle of attack = 10°

Type of Nacelle	$\frac{V}{n D}$									
	0.1	0.2	0.3	0.4	0.5	0.6	0.7	0.8	0.9	1.0
Nacelle position B, with side brackets										
Smooth body	0.0787	0.0732	0.0664	0.0578	0.0478	0.0365	0.0244	0.0115	−0.0021	−0.0166
Exposed cylinders ¹0835	.0786	.0720	.0639	.0540	.0430	.0303	.0172	.0015	−.0151
N.A.C.A. hood ¹0830	.0770	.0696	.0607	.0505	.0395	.0275	.0152	.0019	−.0121
N.A.C.A. cowled nacelle0821	.0770	.0700	.0614	.0513	.0401	.0274	.0135	−.0015	−.0173
Nacelle position B, without side brackets										
Exposed cylinders ¹	0.0880	0.0827	0.0758	0.0673	0.0577	0.0468	0.0350	0.0219	0.0077	−0.0075
N.A.C.A. hood ¹0872	.0813	.0737	.0646	.0545	.0430	.0308	.0173	.0028	−.0127
Variable ring −8° ¹0873	.0814	.0742	.0655	.0557	.0448	.0325	.0197	.0056	−.0086
Nacelle position C										
Smooth body	0.0800	0.0749	0.0678	0.0591	0.0486	0.0370	0.0235	0.0090	−0.0065	−0.0234
Nacelle position B-1-A, faired into wing										
Exposed cylinders ¹	0.0859	0.0811	0.0755	0.0678	0.0580	0.0464	0.0332	0.0189	0.0038	−0.0121
N.A.C.A. hood ¹0852	.0800	.0730	.0640	.0540	.0434	.0313	.0180	.0041	−.0100
N.A.C.A. cowled nacelle0853	.0798	.0725	.0637	.0535	.0421	.0297	.0157	.0010	−.0151
Variable ring −8° ¹0851	.0796	.0725	.0640	.0543	.0436	.0318	.0188	.0050	−.0095
Nacelle position C-3-A										
Smooth body	0.0820	0.0775	0.0711	0.0628	0.0524	0.0403	0.0266	0.0117	−.0045	−0.0218
Nacelle position A-1-B, faired into wing										
Exposed cylinders ¹	0.0875	0.0825	0.0760	0.0677	0.0580	0.0468	0.0348	0.0220	0.0085	−0.0055
N.A.C.A. hood ¹0850	.0800	.0740	.0658	.0562	.0455	.0341	.0220	.0095	−.0040
Variable ring −8° ¹0855	.0808	.0745	.0670	.0581	.0482	.0377	.0266	.0152	.0030
N.A.C.A. cowled nacelle0860	.0810	.0740	.0660	.0565	.0461	.0347	.0229	.0106	−.0023
Nacelle position A-2-B										
Smooth body	0.0858	0.0806	0.0740	0.0660	0.0565	0.0457	0.0339	0.0212	0.0079	−0.0059
Exposed cylinders ¹0870	.0816	.0748	.0665	.0571	.0464	.0351	.0230	.0104	−.0023
N.A.C.A. hood ¹0854	.0800	.0730	.0650	.0558	.0452	.0340	.0221	.0096	−.0037
Variable ring −8° ¹0885	.0836	.0770	.0691	.0599	.0495	.0382	.0263	.0140	.0015
N.A.C.A. cowled nacelle0860	.0817	.0738	.0654	.0558	.0448	.0332	.0213	.0092	−.0026
Nacelle position C-3-B										
Smooth body	0.0850	0.0803	0.0735	0.0648	0.0542	0.0423	0.0296	0.0160	0.0020	−0.0125

¹ Small nacelle.

TABLE V
POWER COEFFICIENT

$C_P = \frac{P}{\rho n^3 D^5}$

Propeller No. 4412—4 feet. Set 17° at 0.75 R. Angle of attack = -5°

Type of nacelle	$\frac{V}{n D}$									
	0.1	0.2	0.3	0.4	0.5	0.6	0.7	0.8	0.9	1.0
Nacelle position B, with side brackets										
Smooth body.....	0.0407	0.0407	0.0403	0.0393	0.0370	0.0320	0.0254	0.0165	0.0054
Exposed cylinders ¹0448	.0449	.0441	.0426	.0399	.0355	.0290	.0205	.0101
N.A.C.A. hood ¹0448	.0450	.0445	.0432	.0406	.0360	.0292	.0200	.0095
N.A.C.A. cowled nacelle.....	.0450	.0447	.0438	.0420	.0393	.0351	.0290	.0205	.0100
Nacelle position B, without side brackets										
Exposed cylinders ¹	0.0443	0.0441	0.0435	.00420	0.0397	0.0363	0.0311	0.0231	0.0124
N.A.C.A. hood ¹0430	.0431	.0425	.0413	.0390	.0355	.0300	.0219	.0110
Variable ring -8° ¹0438	.0437	.0430	.0417	.0393	.0356	.0300	.0220	.0115
Nacelle position C										
Smooth body.....	0.0397	0.0397	0.0390	0.0375	0.0349	0.0310	0.0245	0.0153	0.0033
Nacelle position B-1-A, faired into wing										
Exposed cylinders ¹	0.0443	0.0442	0.0435	0.0420	0.0398	0.0361	0.0306	0.0226	0.0120
N.A.C.A. hood ¹0452	.0449	.0441	.0426	.0400	.0361	.0306	.0229	.0124
N.A.C.A. cowled nacelle.....	.0450	.0447	.0438	.0423	.0399	.0364	.0311	.0230	.0127
Variable ring -8° ¹0456	.0453	.0445	.0428	.0400	.0360	.0304	.0226	.0118
Nacelle position C-3-A										
Smooth body.....	0.0407	0.0406	0.0403	0.0391	0.0362	0.0315	0.0249	0.0160	0.0051
Nacelle position A-1-B, faired into wing										
Exposed cylinders ¹	0.0435	0.0435	0.0430	0.0416	0.0390	0.0355	0.0306	0.0230	0.0135	0.0020
N.A.C.A. hood ¹0430	.0429	.0420	.0403	.0380	.0346	.0294	.0217	.0110
Variable ring -8° ¹0429	.0426	.0420	.0408	.0382	.0345	.0287	.0209	.0108
N.A.C.A. cowled nacelle.....	.0420	.0422	.0420	.0409	.0387	.0352	.0297	.0218	.0115
Nacelle position A-2-B										
Smooth body.....	0.0427	0.0435	0.0428	0.0411	0.0382	0.0339	0.0272	0.0180	0.0061
Exposed cylinders ¹0439	.0440	.0434	.0420	.0396	.0356	.0294	.0209	.0102
N.A.C.A. hood ¹0443	.0441	.0432	.0416	.0388	.0343	.0280	.0195	.0078
Variable ring -8° ¹0445	.0443	.0436	.0420	.0395	.0355	.0298	.0212	.0102
N.A.C.A. cowled nacelle.....	.0443	.0442	.0433	.0417	.0390	.0348	.0284	.0200	.0084
Nacelle position C-3-B										
Smooth body.....	0.0416	0.0416	0.0409	0.0395	0.0366	0.0320	0.0251	0.0164	0.0051

¹ Small nacelle.

TABLE V—Continued
POWER COEFFICIENT

$C_P = \frac{P}{\rho n^3 D^5}$

Propeller No. 4412—4 feet. Set 17° at 0.75 R. Angle of attack=0°

Type of nacelle	$\frac{V}{nD}$									
	0.1	0.2	0.3	0.4	0.5	0.6	0.7	0.8	0.9	1.0
Nacelle position B, with side brackets										
Smooth body	0.0415	0.0413	0.0405	0.0393	0.0368	0.0320	0.0252	0.0165	0.0054
Exposed cylinders ¹0447	.0445	.0436	.0421	.0395	.0354	.0289	.0203	.0095
N.A.C.A. hood ¹0447	.0449	.0442	.0427	.0400	.0359	.0290	.0204	.0096
N.A.C.A. cowled nacelle0450	.0449	.0442	.0425	.0397	.0355	.0290	.0202	.0095
Nacelle position B, without side brackets										
Exposed cylinders ¹	0.0446	0.0445	0.0439	0.0426	0.0404	0.0369	0.0312	0.0231	0.0123
N.A.C.A. hood ¹0430	.0431	.0426	.0413	.0390	.0353	.0296	.0213	.0106
Variable ring—8° ¹0436	.0435	.0428	.0414	.0391	.0356	.0300	.0218	.0110
Nacelle position C										
Smooth body	0.0402	0.0404	0.0397	0.0381	0.0351	0.0306	0.0238	0.0144	0.0015
Nacelle position B-1-A, faired into wing										
Exposed cylinders ¹	0.0443	0.0441	0.0439	0.0421	0.0398	0.0360	0.0302	0.0203	0.0119
N.A.C.A. hood ¹0450	.0447	.0440	.0426	.0399	.0365	.0306	.0220	.0110
N.A.C.A. cowled nacelle0454	.0451	.0443	.0427	.0403	.0363	.0303	.0221	.0114
Variable ring—8° ¹0453	.0450	.0442	.0425	.0399	.0360	.0303	.0222	.0111
Nacelle position C-3-A										
Smooth body	0.0416	0.0417	0.0409	0.0393	0.0364	0.0319	0.0251	0.0161	0.0050
Nacelle position A-1-B, faired into wing										
Exposed cylinders ¹	0.0434	0.0435	0.0430	0.0419	0.0390	0.0358	0.0302	0.0224	0.0135	0.0023
N.A.C.A. hood ¹0430	.0430	.0424	.0410	.0389	.0354	.0300	.0224	.0128
Variable ring—8° ¹0426	.0428	.0421	.0410	.0390	.0351	.0299	.0220	.0127
N.A.C.A. cowled nacelle0420	.0420	.0418	.0410	.0385	.0351	.0298	.0220	.0125	.0008
Nacelle position A-2-B										
Smooth body	0.0437	0.0435	0.0428	0.0411	0.0384	0.0343	0.0284	0.0198	0.0089
Exposed cylinders ¹0438	.0438	.0433	.0420	.0395	.0359	.0300	.0221	.0122
N.A.C.A. hood ¹0446	.0444	.0438	.0419	.0394	.0356	.0296	.0217	.0110
Variable ring—8° ¹0447	.0447	.0441	.0427	.0403	.0365	.0310	.0233	.0130
N.A.C.A. cowled nacelle0443	.0442	.0435	.0419	.0393	.0356	.0299	.0215	.0110
Nacelle position C-3-B										
Smooth body	0.0408	0.0412	0.0410	0.0397	0.0373	0.0330	0.0262	0.0171	0.0058

¹ Small nacelle.

TABLE V—Continued
POWER COEFFICIENT

$$C_P = \frac{P}{\rho n^3 D^5}$$

Propeller No. 4412—4 feet. Set 17° at 0.75 *R*. Angle of attack=5°

Type of nacelle	$\frac{V}{n D}$									
	0.1	0.2	0.3	0.4	0.5	0.6	0.7	0.8	0.9	1.0
Nacelle position B, with side brackets										
Smooth body	0.0418	0.0415	0.0407	0.0392	0.0367	0.0320	0.0252	0.0164	0.0051	
Exposed cylinders ¹	.0458	.0457	.0446	.0428	.0400	.0360	.0295	.0206	.0095	
N.A.C.A. hood ¹	.0447	.0448	.0440	.0425	.0399	.0355	.0290	.0203	.0098	
N.A.C.A. cowled nacelle	.0451	.0450	.0442	.0427	.0399	.0355	.0292	.0205	.0100	
Nacelle position B, without side brackets										
Exposed cylinders ¹	0.0444	0.0444	0.0439	0.0427	0.0404	0.0366	0.0310	0.0232	0.0123	
N.A.C.A. hood ¹	.0438	.0438	.0432	.0420	.0398	.0359	.0299	.0215	.0112	
Variable ring —8° ¹	.0446	.0445	.0439	.0425	.0402	.0363	.0301	.0217	.0109	
Nacelle position C										
Smooth body	0.0415	0.0411	0.0403	0.0390	0.0363	0.0322	0.0254	0.0160	0.0038	
Nacelle position B-1-A, faired into wing										
Exposed cylinders ¹	0.0455	0.0450	0.0442	0.0427	0.0400	0.0357	0.0299	0.0219	0.0110	
N.A.C.A. hood ¹	.0447	.0446	.0440	.0425	.0399	.0367	.0292	.0216	.0110	
N.A.C.A. cowled nacelle	.0445	.0445	.0440	.0427	.0401	.0363	.0301	.0219	.0110	
Variable ring —8° ¹	.0450	.0448	.0439	.0423	.0399	.0360	.0300	.0217	.0105	
Nacelle position C-3-A										
Smooth body	0.0424	0.0420	0.0413	0.0400	0.0371	0.0323	0.0255	0.0165	0.0052	
Nacelle position A-1-B, faired into wing										
Exposed cylinders ¹	0.0430	0.0430	0.0427	0.0416	0.0391	0.0359	0.0305	0.0229	0.0140	0.0030
N.A.C.A. hood ¹	.0440	.0438	.0430	.0418	.0394	.0360	.0306	.0231	.0136	.0020
Variable ring —8° ¹	.0426	.0430	.0423	.0415	.0394	.0361	.0310	.0237	.0140	.0025
N.A.C.A. cowled nacelle	.0420	.0426	.0421	.0411	.0392	.0360	.0309	.0237	.0146	.0033
Nacelle position A-2-B										
Smooth body	0.0443	0.0441	0.0433	0.0418	0.0393	0.0355	0.0300	0.0221	0.0123	
Exposed cylinders ¹	.0436	.0436	.0430	.0418	.0397	.0365	.0316	.0243	.0150	0.0031
N.A.C.A. hood ¹	.0451	.0448	.0438	.0421	.0397	.0359	.0308	.0240	.0138	.0013
Variable ring —8° ¹	.0448	.0445	.0439	.0425	.0402	.0369	.0318	.0244	.0152	.0036
N.A.C.A. cowled nacelle	.0442	.0443	.0438	.0425	.0403	.0368	.0315	.0240	.0142	.0018
Nacelle position C-3-B										
Smooth body	0.0412	0.0420	0.0419	0.0405	0.0377	0.0328	0.0267	0.0180	0.0071	

¹ Small nacelle

TABLE V.—Continued
POWER COEFFICIENT

$C_P = \frac{P}{\rho n^3 D^5}$

Propeller No. 4412—4 feet. Set 17° at 0.75 R. Angle of attack=10°

Type of nacelle	$\frac{V}{nD}$									
	0.1	0.2	0.3	0.4	0.5	0.6	0.7	0.8	0.9	1.0
Nacelle position B, with side brackets										
Smooth body	0.0417	0.0413	0.0405	0.0393	0.0368	0.0320	0.0257	0.0173	0.0071	-----
Exposed cylinders ¹0460	.0461	.0452	.0434	.0404	.0361	.0305	.0230	.0122	-----
N.A.C.A. hood ¹0447	.0450	.0444	.0431	.0403	.0357	.0288	.0202	.0095	-----
N.A.C.A. cowled nacelle0453	.0452	.0443	.0427	.0400	.0358	.0295	.0212	.0110	-----
Nacelle position B, without side brackets										
Exposed cylinders ¹	0.0443	0.0443	0.0438	0.0424	0.0403	0.0369	0.0318	0.0242	0.0141	-----
N.A.C.A. hood ¹0440	.0441	.0437	.0423	.0401	.0365	.0310	.0228	.0127	-----
Variable ring —8° ¹0445	.0445	.0440	.0427	.0404	.0368	.0310	.0233	.0135	-----
Nacelle position C										
Smooth body	0.0405	0.0410	0.0405	0.0393	0.0366	0.0320	0.0248	0.0149	0.0018	-----
Nacelle position B-1-A, faired into wing										
Exposed cylinders ¹	0.0455	0.0453	0.0450	0.0430	0.0410	0.0372	0.0314	0.0230	0.0125	-----
N.A.C.A. hood ¹0446	.0449	.0442	.0430	.0400	.0361	.0300	.0211	.0107	-----
N.A.C.A. cowled nacelle0442	.0447	.0444	.0431	.0408	.0366	.0306	.0223	.0113	-----
Variable ring —8° ¹0444	.0448	.0444	.0431	.0407	.0369	.0308	.0224	.0115	-----
Nacelle position C-3-A										
Smooth body	0.0427	0.0422	0.0412	0.0392	0.0367	0.0319	0.0250	0.0160	0.0044	-----
Nacelle position A-1-B, faired into wing										
Exposed cylinders ¹	0.0420	0.0420	0.0420	0.0412	0.0396	0.0370	0.0326	0.0260	0.0172	0.0066
N.A.C.A. hood ¹0434	.0440	.0438	.0429	.0408	.0372	.0325	.0258	.0170	.0060
Variable ring —8° ¹0430	.0430	.0425	.0419	.0400	.0370	.0326	.0260	.0170	.0058
N.A.C.A. cowled nacelle0420	.0421	.0420	.0415	.0401	.0380	.0331	.0265	.0175	.0070
Nacelle position A-2-B										
Smooth body	0.0446	0.0444	0.0438	0.0425	0.0403	0.0372	0.0324	0.0255	0.0164	-----
Exposed cylinders ¹0442	.0442	.0439	.0429	.0408	.0377	.0332	.0269	.0180	0.0069
N.A.C.A. hood ¹0452	.0450	.0442	.0435	.0416	.0382	.0335	.0269	.0180	.0065
Variable ring —8° ¹0446	.0445	.0441	.0429	.0410	.0380	.0338	.0277	.0196	.0093
N.A.C.A. cowled nacelle0443	.0442	.0437	.0424	.0401	.0367	.0320	.0256	.0170	.0059
Nacelle position C-3-B										
Smooth body	0.0411	0.0417	0.0417	0.0405	0.0376	0.0332	0.0271	0.0189	0.0082	-----

¹ Small nacelle.

TABLE VI
PROPULSIVE EFFICIENCY

$$\eta = \frac{(T - \Delta D) V}{P}$$

Propeller No. 4412—4 feet. Set 17° at 0.75 R. Angle of attack = -5°

Type of nacelle	$\frac{V}{nD}$									
	0.1	0.2	0.3	0.4	0.5	0.6	0.7	0.8	0.9	1.0
Nacelle position B, with side brackets										
Smooth body	0.204	0.383	0.530	0.640	0.709	0.760	0.750	0.607		
Exposed cylinders ¹193	.366	.518	.640	.732	.790	.814	.754	0.348	
N.A.C.A. hood ¹193	.362	.505	.618	.698	.750	.751	.617		
N.A.C.A. cowled nacelle192	.363	.508	.630	.717	.772	.770	.644		
Nacelle position B, without side brackets										
Exposed cylinders ¹	0.208	0.395	0.555	0.688	0.784	0.841	0.855	0.786	0.472	
N.A.C.A. hood ¹210	.396	.556	.684	.775	.822	.828	.734	.286	
Variable ring -8° ¹205	.389	.549	.675	.767	.823	.831	.771	.391	
Nacelle position C										
Smooth body	0.211	0.397	0.553	0.680	0.761	0.798	0.786	0.628		
Nacelle position B-1-A, faired into wing										
Exposed cylinders ¹	0.206	0.392	0.555	0.692	0.790	0.846	0.860	0.795	0.435	
N.A.C.A. hood ¹197	.380	.538	.667	.764	.819	.824	.742	.417	
N.A.C.A. cowled nacelle200	.381	.538	.665	.758	.811	.821	.765	.460	
Variable ring -8° ¹195	.375	.532	.663	.763	.828	.850	.815	.549	
Nacelle position C-3-A										
Smooth body	0.204	0.388	0.538	0.644	0.742	0.788	0.774	0.625		
Nacelle position A-1-B, faired into wing										
Exposed cylinders ¹	0.202	0.383	0.538	0.670	0.770	0.829	0.841	0.810	0.646	
N.A.C.A. hood ¹199	.375	.529	.656	.744	.781	.762	.692	.327	
Variable ring -8° ¹203	.383	.535	.655	.743	.784	.782	.687	.250	
N.A.C.A. cowled nacelle206	.387	.534	.650	.730	.780	.775	.678	.274	
Nacelle position A-2-B										
Smooth body	0.201	0.382	0.536	0.662	0.749	0.787	0.772	0.622		
Exposed cylinders ¹203	.384	.540	.667	.761	.817	.833	.770	.397	
N.A.C.A. hood ¹196	.371	.521	.642	.730	.777	.772	.660	.100	
Variable ring -8° ¹201	.383	.542	.668	.761	.811	.808	.736	.282	
N.A.C.A. cowled nacelle197	.372	.524	.645	.731	.777	.769	.620		
Nacelle position C-3-B										
Smooth body	0.206	0.387	0.538	0.653	0.736	0.778	0.775	0.634		

¹ Small nacelle.

TABLE VI—Continued
PROPULSIVE EFFICIENCY

$$\eta = \frac{(T - \Delta D) V}{P}$$

Propeller No. 4412—4 feet. Set 17° at 0.75 R. Angle of attack=0°

Type of nacelle	$\frac{V}{nD}$									
	0.1	0.2	0.3	0.4	0.5	0.6	0.7	0.8	0.9	1.0
Nacelle position B, with side brackets										
Smooth body	0.199	0.373	0.528	0.640	0.717	0.756	0.745	0.607		
Exposed cylinders ¹	.192	.366	.516	.639	.730	.790	.815	.760	0.350	
N.A.C.A. hood ¹	.193	.363	.510	.622	.706	.746	.753	.636		
N.A.C.A. cowled nacelle	.189	.358	.502	.621	.709	.756	.750	.603		
Nacelle position B, without side brackets										
Exposed cylinders ¹	0.202	0.385	0.541	0.667	0.758	0.812	0.834	0.780	0.468	
N.A.C.A. hood ¹	.208	.393	.550	.676	.762	.811	.813	.721	.238	
Variable ring —8° ¹	.208	.393	.552	.680	.768	.816	.823	.734	.319	
Nacelle position C										
Smooth body	0.206	0.387	0.540	0.661	0.748	0.795	0.785	0.583		
Nacelle position B-1-A, faired into wing										
Exposed cylinders ¹	0.205	0.392	0.547	0.682	0.775	0.834	0.859	0.799	0.439	
N.A.C.A. hood ¹	.198	.377	.529	.647	.738	.790	.800	.716	.286	
N.A.C.A. cowled nacelle	.197	.373	.523	.643	.724	.775	.785	.706	.252	
Variable ring —8° ¹	.195	.372	.524	.650	.738	.780	.777	.667	.146	
Nacelle position C-3-A										
Smooth body	0.200	0.377	0.530	0.652	0.736	0.775	0.761	0.596		
Nacelle position A-1-B, faired into wing										
Exposed cylinders ¹	0.203	0.386	0.545	0.671	0.770	0.828	0.840	0.790	0.540	
N.A.C.A. hood ¹	.200	.381	.538	.665	.748	.783	.770	.694	.317	
Variable ring —8° ¹	.202	.382	.540	.662	.745	.795	.795	.740	.440	
N.A.C.A. cowled nacelle	.207	.391	.544	.660	.752	.787	.790	.728	.425	
Nacelle position A-2-B										
Smooth body	0.201	0.382	0.535	0.662	0.749	0.788	0.774	0.631		
Exposed cylinders ¹	.203	.385	.541	.668	.764	.819	.833	.778	0.486	
N.A.C.A. hood ¹	.194	.368	.515	.640	.727	.773	.777	.686	.294	
Variable ring —8° ¹	.201	.381	.538	.665	.757	.815	.827	.773	.464	
N.A.C.A. cowled nacelle	.197	.372	.522	.642	.727	.771	.773	.680	.245	
Nacelle position C-3-B										
Smooth body	0.210	0.389	0.536	0.652	0.724	0.772	0.763	0.600		

¹ Small nacelle.

TABLE VI—Continued
PROPULSIVE EFFICIENCY

$$\eta = \frac{(T - \Delta D) V}{P}$$

Propeller No. 4412—4 feet. Set 17° at 0.75 R. Angle of attack=5°

Type of nacelle	$\frac{V}{nD}$									
	0.1	0.2	0.3	0.4	0.5	0.6	0.7	0.8	0.9	1.0
Nacelle position B, with side brackets										
Smooth body.....	0.193	0.365	0.509	0.616	0.686	0.728	0.736	0.610	0.322	-----
Exposed cylinders ¹187	.354	.498	.617	.700	.748	.764	.730	.170	-----
N.A.C.A. hood ¹191	.357	.498	.607	.683	.736	.753	.678	-----	-----
N.A.C.A. cowled nacelle.....	.185	.348	.487	.596	.677	.724	.712	.562	-----	-----
Nacelle position B, without side brackets										
Exposed cylinders ¹	0.202	0.383	0.533	0.652	0.740	0.698	0.808	0.745	0.475	-----
N.A.C.A. hood ¹203	.383	.537	.657	.735	.781	.780	.695	.241	-----
Variable ring —8° ¹202	.382	.534	.654	.736	.782	.791	.736	.380	-----
Nacelle position C										
Smooth body.....	0.201	0.381	0.527	0.638	0.713	0.741	0.723	0.549	-----	-----
Nacelle position B-1-A, faired into wing										
Exposed cylinders ¹	0.193	0.370	0.524	0.641	0.730	0.785	0.785	0.720	0.410	-----
N.A.C.A. hood ¹196	.371	.519	.640	.719	.757	.743	.618	.106	-----
N.A.C.A. cowled nacelle.....	.197	.370	.517	.630	.711	.749	.744	.628	.115	-----
Variable ring —8° ¹193	.366	.517	.639	.725	.775	.784	.719	.360	-----
Nacelle position C-3-A										
Smooth body.....	0.196	0.375	0.525	0.640	0.724	0.771	0.755	0.592	-----	-----
Nacelle position A-1-B, faired into wing										
Exposed cylinders ¹	0.205	0.390	0.549	0.673	0.763	0.818	0.830	0.790	0.514	-----
N.A.C.A. hood ¹196	.372	.523	.640	.722	.765	.758	.693	.397	-----
Variable ring —8° ¹204	.382	.540	.654	.736	.785	.792	.760	.610	-----
N.A.C.A. cowled nacelle.....	.207	.388	.542	.664	.745	.785	.790	.740	.482	-----
Nacelle position A-2-B										
Smooth body.....	0.196	0.372	0.523	0.645	0.732	0.772	0.768	0.706	0.402	-----
Exposed cylinders ¹202	.381	.533	.654	.743	.794	.818	.795	.618	-----
N.A.C.A. hood ¹192	.364	.515	.637	.723	.775	.780	.720	.528	-----
Variable ring —8° ¹199	.380	.534	.662	.756	.810	.825	.800	.621	-----
N.A.C.A. cowled nacelle.....	.197	.371	.515	.632	.710	.750	.753	.683	.406	-----
Nacelle position C-3-B										
Smooth body.....	0.207	0.381	0.524	0.638	0.716	0.774	0.760	0.650	-----	-----

¹ Small nacelle.

TABLE VI—Continued
PROPULSIVE EFFICIENCY

$$\eta = \frac{(T - \Delta D) V}{P}$$

Propeller No. 4412—4 feet. Set 17° at 0.75 R. Angle of attack=10°

Type of nacelle	$\frac{V}{n D}$									
	0.1	0.2	0.3	0.4	0.5	0.6	0.7	0.8	0.9	1.0
Nacelle position B, with side brackets										
Smooth body.....	0.189	0.355	0.491	0.589	0.649	0.685	0.665	0.532		
Exposed cylinders ¹181	.341	.478	.589	.668	.715	.695	.599	0.111	
N.A.C.A. hood ¹186	.342	.470	.563	.627	.664	.670	.602	.210	
N.A.C.A. cowled nacelle.....	.182	.340	.475	.575	.640	.672	.650	.510		
Nacelle position B, without side brackets										
Exposed cylinders ¹	0.199	0.373	0.518	0.635	0.716	0.761	0.770	0.724	0.491	
N.A.C.A. hood ¹198	.369	.506	.611	.680	.706	.695	.607	.199	
Variable ring —8° ¹196	.366	.506	.613	.689	.730	.734	.676	.373	
Nacelle position C										
Smooth body.....	0.198	0.365	0.502	0.602	0.663	0.694	0.663	0.483		
Nacelle position B-1-A, faired into wing										
Exposed cylinders ¹	0.188	0.358	0.505	0.630	0.706	0.747	0.740	0.656	0.273	
N.A.C.A. hood ¹191	.356	.497	.595	.675	.720	.730	.656	.345	
N.A.C.A. cowled nacelle.....	.193	.357	.490	.592	.655	.690	.679	.563	.060	
Variable ring —8° ¹192	.355	.490	.594	.667	.710	.723	.672	.391	
Nacelle position C-3-A										
Smooth body.....	0.192	0.367	0.518	0.640	0.714	0.758	0.745	0.585		
Nacelle position A-1-B, faired into wing										
Exposed cylinders ¹	0.208	0.392	0.542	0.657	0.730	0.760	0.747	0.675	0.445	
N.A.C.A. hood ¹197	.363	.508	.614	.690	.735	.735	.682	.503	
Variable ring —8° ¹197	.376	.526	.638	.725	.780	.810	.820	.805	0.518
N.A.C.A. cowled nacelle.....	.204	.385	.530	.636	.705	.729	.733	.691	.545	
Nacelle position A-2-B										
Smooth body.....	0.193	0.363	0.506	0.621	0.701	0.738	0.733	0.665	0.433	
Exposed cylinders ¹197	.369	.512	.620	.700	.738	.740	.684	.520	
N.A.C.A. hood ¹189	.356	.495	.597	.670	.710	.710	.657	.480	
Variable ring —8° ¹198	.376	.524	.644	.730	.782	.792	.760	.643	0.197
N.A.C.A. cowled nacelle.....	.194	.370	.506	.617	.695	.733	.727	.665	.487	
Nacelle position C-3-B										
Smooth body.....	0.207	0.385	0.530	0.640	0.720	0.766	0.765	0.678	0.245	

¹ Small nacelle.

TABLE VII
LIFT COEFFICIENT WITH PROPELLER OPERATING

$C_{LP} = \frac{L_P}{qS}$

Propeller No 4412—4 feet. Set 17° at 0.75 R. Angle of attack = -5°

Type of nacelle	$\frac{V}{nD}$									
	0.1	0.2	0.3	0.4	0.5	0.6	0.7	0.8	0.9	1.0
Nacelle position B, with side brackets										
Smooth body.....				0.017	0.029	0.036	0.041	0.044	0.046	0.047
Exposed cylinders ¹041	.039	.034	.030	.028	.023	.020
N.A.C.A. hood ¹023	.022	.021	.020	.020	.019	.018
N.A.C.A. cowled nacelle.....				.031	.030	.030	.030	.030	.029	.029
Nacelle position B, without side brackets										
Exposed cylinders ¹				0.013	0.013	0.015	0.020	0.023	0.029	0.032
N.A.C.A. hood ¹059	.041	.031	.023	.020	.021	.026
Variable ring -8° ¹031	.023	.020	.019	.018	.019	.020
Nacelle position C										
Smooth body.....				0.040	0.038	0.034	0.033	0.034	0.036	0.038
Nacelle position B-1-A, faired into wing										
Exposed cylinders ¹				0.091	0.072	0.060	0.050	0.043	0.040	0.037
N.A.C.A. hood ¹140	.100	.075	.058	.044	.039	.037
N.A.C.A. cowled nacelle.....				.092	.088	.081	.078	.074	.071	.070
Variable ring -8° ¹058	.051	.050	.049	.050	.051	.058
Nacelle position C-3-A										
Smooth body.....				0.055	0.049	0.042	0.039	0.035	0.032	0.030
Nacelle position A-1-B, faired into wing										
Exposed cylinders ¹				-0.042	-0.022	-0.009	0.005	0.013	0.021	0.030
N.A.C.A. hood ¹010	.005	.001	-.001	-.002	-.004	-.005
Variable ring -8° ¹				-.072	-.039	-.018	-.005	.000	.000	-.003
N.A.C.A. cowled nacelle.....				-.081	-.065	-.051	-.040	-.032	-.025	-.020
Nacelle position A-2-B										
Smooth body.....				-0.024	-0.010	0.001	0.011	0.019	0.027	0.030
Exposed cylinders ¹				-.002	.000	.004	.011	.021	.039	.060
N.A.C.A. hood ¹				-.020	-.011	-.004	.000	.002	.004	.004
Variable ring -8° ¹				-.059	-.051	-.041	-.029	-.010	.009	.029
N.A.C.A. cowled nacelle.....				-.043	-.022	-.009	.000	.006	.008	.008
Nacelle position C-3-B										
Smooth body.....				-0.038	0.000	0.010	0.011	0.011	0.011	0.011

¹ Small nacelle.

TABLE VII—Continued
LIFT COEFFICIENT WITH PROPELLER OPERATING

$C_{LP} = \frac{L_P}{qS}$

Propeller No. 4412—4 feet. Set 17° at 0.75 R. Angle of attack=0°

Type of nacelle	$\frac{V}{n D}$									
	0.1	0.2	0.3	0.4	0.5	0.6	0.7	0.8	0.9	1.0
Nacelle position B, with side brackets										
Smooth body				0.353	0.350	0.344	0.340	0.334	0.330	0.324
Exposed cylinders ¹				.362	.350	.339	.328	.316	.304	.292
N.A.C.A. hood ¹				.386	.350	.330	.321	.316	.312	.311
N.A.C.A. cowled nacelle				.339	.337	.333	.330	.328	.324	.321
Nacelle position B, without side brackets										
Exposed cylinders ¹				0.364	0.331	0.311	0.303	0.303	0.302	0.301
N.A.C.A. hood ¹				.360	.333	.318	.308	.301	.300	.306
Variable ring -8° ¹				.339	.329	.320	.313	.311	.310	.310
Nacelle position C										
Smooth body				0.390	0.362	0.342	.0329	0.319	0.311	0.308
Nacelle position B-1-A, faired into wing										
Exposed cylinders ¹				0.450	0.397	0.364	0.340	0.328	0.320	0.313
N.A.C.A. hood ¹				.430	.387	.361	.346	.341	.339	.338
N.A.C.A. cowled nacelle				.475	.416	.375	.358	.360	.365	.370
Variable ring -8° ¹				.452	.400	.370	.352	.345	.345	.350
Nacelle position C-3-A										
Smooth body				0.352	0.340	0.330	0.325	0.321	0.320	0.320
Nacelle position A-1-B, faired into wing										
Exposed cylinders ¹				0.291	0.282	0.279	0.275	0.272	0.270	0.270
N.A.C.A. hood ¹				.301	.290	.281	.275	.271	.270	.267
Variable ring -8° ¹				.278	.272	.270	.268	.267	.264	.263
N.A.C.A. cowled nacelle				.243	.245	.249	.250	.250	.249	.248
Nacelle position A-2-B										
Smooth body				0.276	0.283	0.290	0.296	0.298	0.299	0.298
Exposed cylinders ¹				.302	.303	.303	.304	.306	.309	.311
N.A.C.A. hood ¹				.267	.280	.290	.299	.302	.304	.305
Variable ring -8° ¹				.249	.261	.270	.276	.280	.282	.282
N.A.C.A. cowled nacelle				.273	.279	.281	.285	.290	.292	.298
Nacelle position C-3-B										
Smooth body				0.320	0.320	0.320	0.320	0.320	0.320	0.320

¹ Small nacelle.

TABLE VII—Continued
LIFT COEFFICIENT WITH PROPELLER OPERATING

$C_{LP} = \frac{L_P}{qS}$

Propeller No. 4412—4 feet. Set 17° at 0.75 R. Angle of attack=5°

Type of nacelle	$\frac{V}{nD}$									
	0.1	0.2	0.3	0.4	0.5	0.6	0.7	0.8	0.9	1.0
Nacelle position B, with side brackets										
Smooth body.....				0.715	0.682	0.659	0.643	0.634	0.631	0.630
Exposed cylinders ¹680	.647	.621	.601	.588	.573	.562
N.A.C.A. hood ¹721	.680	.650	.630	.616	.609	.602
N.A.C.A. cowled nacelle.....				.721	.679	.650	.631	.620	.618	.618
Nacelle position B, without side brackets										
Exposed cylinders ¹				0.710	0.657	0.617	0.594	0.581	0.572	0.567
N.A.C.A. hood ¹686	.653	.630	.611	.599	.590	.582
Variable ring —8° ¹699	.652	.622	.600	.583	.574	.570
Nacelle position C										
Smooth body.....				0.732	0.677	0.642	0.625	0.616	0.614	0.612
Nacelle position B-1-A, faired into wing										
Exposed cylinders ¹				0.795	0.724	0.675	0.643	0.625	0.616	0.609
N.A.C.A. hood ¹764	.704	.666	.642	.630	.628	.627
N.A.C.A. cowled nacelle.....				.813	.733	.692	.670	.660	.655	.652
Variable ring —8° ¹825	.721	.678	.658	.650	.643	.638
Nacelle position C-3-A										
Smooth body.....				0.640	0.627	0.617	0.610	0.606	0.602	0.601
Nacelle position A-1-B, faired into wing										
Exposed cylinders ¹				0.605	0.588	0.578	0.570	0.562	0.558	0.550
N.A.C.A. hood ¹620	.595	.578	.563	.553	.547	.541
Variable ring —8° ¹584	.572	.565	.560	.559	.556	.553
N.A.C.A. cowled nacelle.....				.563	.557	.550	.542	.538	.532	.528
Nacelle position A-2-B										
Smooth body.....				0.594	0.599	0.601	0.604	0.609	0.610	0.613
Exposed cylinders ¹600	.603	.609	.611	.613	.619	.621
N.A.C.A. hood ¹589	.590	.592	.595	.598	.600	.601
Variable ring —8° ¹601	.600	.595	.590	.589	.584	.581
N.A.C.A. cowled nacelle.....				.619	.601	.592	.590	.592	.600	.609
Nacelle position C-3-B										
Smooth body.....				0.600	0.600	0.599	0.598	0.597	0.595	0.592

¹ Small nacelle.

TABLE VII—Continued
LIFT COEFFICIENT WITH PROPELLER OPERATING

$$C_{LP} = \frac{L_P}{qS}$$

Propeller No. 4412—4 feet. Set 17° at 0.75 *R*. Angle of attack = 10°

Type of nacelle	$\frac{V}{nD}$									
	0.1	0.2	0.3	0.4	0.5	0.6	0.7	0.8	0.9	1.0
Nacelle position B, with side brackets										
Smooth body				1.080	1.026	0.989	0.963	0.946	0.937	0.931
Exposed cylinders ¹				1.101	.991	.930	.887	.859	.839	.828
N.A.C.A. hood ¹				1.072	1.003	.971	.949	.931	.919	.910
N.A.C.A. cowled nacelle				1.078	1.006	.976	.956	.940	.929	.919
Nacelle position B, without side brackets										
Exposed cylinders ¹				1.060	0.988	0.934	0.898	0.871	0.853	0.840
N.A.C.A. hood ¹				1.042	.990	.952	.927	.910	.900	.893
Variable ring —8° ¹				1.041	.997	.960	.933	.913	.900	.892
Nacelle position C										
Smooth body				1.080	1.021	0.981	0.957	0.940	0.930	0.928
Nacelle position B-1-A, faired into wing										
Exposed cylinders ¹				1.121	1.041	0.981	0.941	0.915	0.895	0.880
N.A.C.A. hood ¹				1.111	1.042	.996	.966	.946	.933	.926
N.A.C.A. cowled nacelle				1.140	1.050	.989	.961	.955	.952	.950
Variable ring —8° ¹				1.135	1.040	.992	.970	.951	.939	.926
Nacelle position C-3-A										
Smooth body				0.945	0.930	0.919	0.910	0.908	0.905	0.908
Nacelle position A-1-B, faired into wing										
Exposed cylinders				0.930	0.908	0.890	0.875	0.860	0.848	0.835
N.A.C.A. hood ¹				.971	.930	.900	.881	.870	.861	.855
Variable ring —8° ¹				.968	.922	.893	.872	.861	.853	.850
N.A.C.A. cowled nacelle				.914	.890	.873	.860	.850	.838	.833
Nacelle position A-2-B										
Smooth body				0.950	0.941	0.934	0.930	0.922	0.918	0.911
Exposed cylinders ¹				.969	.944	.929	.918	.911	.910	.910
N.A.C.A. hood ¹				.963	.942	.929	.921	.915	.910	.909
Variable ring —8° ¹				.896	.893	.891	.889	.888	.883	.880
N.A.C.A. cowled nacelle				.936	.930	.924	.921	.920	.919	.919
Nacelle position C-3-B										
Smooth body				0.930	0.920	0.910	0.900	0.890	0.881	0.872

¹ Small nacelle.

TABLE VIII
MOMENT COEFFICIENT WITH PROPELLER OPERATING

$$C_{mP} = \frac{M_P}{qSc}$$

Propeller No. 4412—4 feet. Set 17° at 0.75 *R*. Angle of attack = -5°

Type of nacelle	$\frac{V}{nD}$									
	0.1	0.2	0.3	0.4	0.5	0.6	0.7	0.8	0.9	1.0
Nacelle position B, with side brackets										
Smooth body				-0.123	-0.100	-0.086	-0.080	-0.076	-0.075	-0.075
Exposed cylinders ¹				-.098	-.084	-.073	-.065	-.060	-.057	-.055
N.A.C.A. hood ¹				-.104	-.091	-.082	-.075	-.071	-.068	-.066
N.A.C.A. cowled nacelle				-.110	-.100	-.092	-.088	-.085	-.084	-.084
Nacelle position B, without side brackets										
Exposed cylinders ¹				-0.104	-0.093	-0.083	-0.074	-0.069	-0.065	-0.065
N.A.C.A. hood ¹				-.104	-.093	-.086	-.081	-.078	-.077	-.076
Variable ring -8° ¹				-.095	-.088	-.083	-.078	-.075	-.072	-.071
Nacelle position C										
Smooth body				-0.105	-0.089	-0.079	-0.075	-0.071	-0.069	-0.067
Nacelle position B-1-A, faired into wing										
Exposed cylinders ¹				-0.162	-0.118	-0.092	-0.077	-0.067	-0.060	-0.054
N.A.C.A. hood ¹				-.142	-.114	-.092	-.076	-.066	-.060	-.056
N.A.C.A. cowled nacelle				-.187	-.130	-.095	-.079	-.069	-.063	-.060
Variable ring -8° ¹				-.185	-.127	-.096	-.079	-.068	-.062	-.061
Nacelle position C-3-A										
Smooth body				-0.340	-0.202	-0.135	-0.100	-0.074	-0.056	-0.042
Nacelle position A-1-B, faired into wing										
Exposed cylinders ¹				-0.026	-0.043	-0.055	-0.063	-0.067	-0.071	-0.072
N.A.C.A. hood ¹				-.024	-.040	-.052	-.059	-.063	-.065	-.066
Variable ring -8° ¹				-.015	-.039	-.055	-.065	-.073	-.079	-.083
N.A.C.A. cowled nacelle				-.027	-.042	-.054	-.062	-.069	-.074	-.077
Nacelle position A-2-B										
Smooth body				0.031	-0.010	-0.036	-0.056	-0.070	-0.080	-0.085
Exposed cylinders ¹				.050	-.007	-.040	-.061	-.075	-.085	-.092
N.A.C.A. hood ¹				.045	-.012	-.043	-.062	-.075	-.083	-.088
Variable ring -8° ¹				.060	.010	-.029	-.056	-.072	-.082	-.085
N.A.C.A. cowled nacelle				.044	-.001	-.031	-.052	-.067	-.077	-.084
Nacelle position C-3-B										
Smooth body				0.144	0.034	-0.020	-0.054	-0.076	-0.090	-0.100

¹ Small nacelle.

TABLE VIII—Continued
MOMENT COEFFICIENT WITH PROPELLER OPERATING

$C_{mP} = \frac{M_P}{qSc}$

Propeller No. 4412—4 feet. Set 17° at 0.75 R. Angle of attack = 0°

Type of nacelle	$\frac{V}{nD}$									
	0.1	0.2	0.3	0.4	0.5	0.6	0.7	0.8	0.9	1.0
Nacelle position B, with side brackets										
Smooth body				−0.096	−0.078	−0.066	−0.059	−0.055	−0.055	−0.055
Exposed cylinders ¹				−.085	−.072	−.062	−.055	−.052	−.050	−.049
N.A.C.A. hood ¹				−.084	−.065	−.054	−.047	−.045	−.044	−.044
N.A.C.A. cowled nacelle				−.079	−.071	−.066	−.063	−.060	−.059	−.058
Nacelle position B, without side brackets										
Exposed cylinders ¹				−0.077	−0.072	−0.067	−0.063	−0.060	−0.058	−0.056
N.A.C.A. hood ¹				−.083	−.072	−.065	−.059	−.056	−.055	−.054
Variable ring −8° ¹				−.075	−.070	−.065	−.062	−.060	−.059	−.058
Nacelle position C										
Smooth body				−0.081	−0.064	−0.054	−0.050	−0.049	−0.048	−0.046
Nacelle position B-1-A, faired into wing										
Exposed cylinders ¹				−0.134	−0.100	−0.076	−0.060	−0.051	−0.047	−0.044
N.A.C.A. hood ¹				−.157	−.107	−.079	−.062	−.052	−.046	−.041
N.A.C.A. cowled nacelle				−.145	−.104	−.075	−.058	−.048	−.044	−.040
Variable ring −8° ¹				−.145	−.105	−.078	−.062	−.050	−.042	−.037
Nacelle position C-3-A										
Smooth body				−0.322	−0.180	−0.118	−0.083	−0.058	−0.043	−0.031
Nacelle position A-1-B, faired into wing										
Exposed cylinders ¹				−0.008	−0.033	−0.050	−0.060	−0.067	−0.070	−0.072
N.A.C.A. hood ¹				.003	−.030	−.051	−.066	−.077	−.085	−.092
Variable ring −8° ¹				.009	−.024	−.045	−.059	−.067	−.072	−.074
N.A.C.A. cowled nacelle				−.022	−.035	−.045	−.053	−.060	−.065	−.067
Nacelle position A-2-B										
Smooth body				0.052	0.002	−0.028	−0.050	−0.065	−0.075	−0.078
Exposed cylinders ¹				.068	.009	−.029	−.050	−.065	−.074	−.078
N.A.C.A. hood ¹				.061	.000	−.030	−.050	−.063	−.073	−.079
Variable ring −8° ¹				.063	.008	−.023	−.045	−.061	−.072	−.079
N.A.C.A. cowled nacelle				.065	.010	−.021	−.045	−.060	−.071	−.079
Nacelle position C-3-B										
Smooth body				0.147	0.040	−0.012	−0.044	−0.066	−0.082	−0.094

¹ Small nacelle.

TABLE VIII—Continued
MOMENT COEFFICIENT WITH PROPELLER OPERATING

$C_{m_P} = \frac{M_P}{qSc}$

Propeller No. 4412—4 feet. Set 17° at 0.75 R. Angle of attack=5°

Type of nacelle	$\frac{V}{nD}$									
	0.1	0.2	0.3	0.4	0.5	0.6	0.7	0.8	0.9	1.0
Nacelle position B, with side brackets										
Smooth body.....				−0.074	−0.057	−0.050	−0.045	−0.040	−0.039	−0.039
Exposed cylinders [†]				−.064	−.054	−.046	−.042	−.039	−.037	−.036
N.A.C.A. hood [†]				−.058	−.044	−.035	−.030	−.026	−.023	−.023
N.A.C.A. cowled nacelle.....				−.068	−.061	−.056	−.052	−.050	−.048	−.047
Nacelle position B, without side brackets										
Exposed cylinders [†]				−0.060	−0.055	−0.051	−0.048	−0.045	−0.042	−0.040
N.A.C.A. hood [†]				−.059	−.054	−.050	−.046	−.044	−.043	−.041
Variable ring −8° [†]				−.059	−.055	−.051	−.048	−.046	−.045	−.044
Nacelle position C										
Smooth body.....				−0.056	−0.045	−0.036	−0.030	−0.027	−0.026	−0.025
Nacelle position B-1-A, faired into wing										
Exposed cylinders [†]				−0.117	−0.092	−0.072	−0.058	−0.048	−0.041	−0.036
N.A.C.A. hood [†]				−.142	−.083	−.058	−.047	−.039	−.034	−.030
N.A.C.A. cowled nacelle.....				−.115	−.080	−.056	−.042	−.035	−.031	−.027
Variable ring −8° [†]				−.115	−.082	−.058	−.043	−.032	−.026	−.023
Nacelle position C-3-A										
Smooth body.....				−0.295	−0.172	−0.105	−0.066	−0.043	−0.030	−0.021
Nacelle position A-1-B, faired into wing										
Exposed cylinders [†]				0.026	−0.010	−0.033	−0.047	−0.055	−0.060	−0.061
N.A.C.A. hood [†]014	−.022	−.045	−.059	−.061	−.060	−.060
Variable ring −8° [†]025	−.009	−.033	−.049	−.058	−.064	−.066
N.A.C.A. cowled nacelle.....				.004	−.022	−.038	−.048	−.055	−.059	−.061
Nacelle position A-2-B										
Smooth body.....				0.075	0.017	−0.019	−0.039	−0.052	−0.061	−0.066
Exposed cylinders [†]056	.005	−.028	−.046	−.059	−.068	−.074
N.A.C.A. hood [†]066	.013	−.023	−.043	−.054	−.063	−.069
Variable ring −8° [†]060	.016	−.018	−.045	−.064	−.075	−.081
N.A.C.A. cowled nacelle.....				.071	.020	−.012	−.035	−.050	−.061	−.069
Nacelle position C-3-B										
Smooth body.....				0.159	0.057	0.005	−0.028	−0.050	−0.064	−0.075

[†] Small nacelle.

TABLE VIII—Continued
MOMENT COEFFICIENT WITH PROPELLER OPERATING

$$C_{mP} = \frac{M_P}{qSc}$$

Propeller No. 4412—4 feet. Set 17° at 0.75 R. Angle of attack = 10°

Type of nacelle	$\frac{V}{nD}$									
	0.1	0.2	0.3	0.4	0.5	0.6	0.7	0.8	0.9	1.0
Nacelle position B, with side brackets										
Smooth body				−0.053	−0.042	−0.035	−0.031	−0.028	−0.028	−0.028
Exposed cylinders ¹				−.041	−.038	−.036	−.035	−.035	−.035	−.035
N.A.C.A. hood ¹				−.033	−.028	−.025	−.023	−.021	−.020	−.020
N.A.C.A. cowled nacelle				−.045	−.042	−.040	−.038	−.036	−.035	−.035
Nacelle position B, without side brackets										
Exposed cylinders ¹				−0.065	−0.054	−0.046	−0.042	−0.039	−0.038	−0.038
N.A.C.A. hood ¹				−.030	−.030	−.030	−.030	−.030	−.030	−.030
Variable ring −8°				−.030	−.030	−.030	−.030	−.030	−.030	−.030
Nacelle position C										
Smooth body				−0.020	−0.015	−0.012	−0.010	−0.008	−0.007	−0.007
Nacelle position B-1-A, faired into wing										
Exposed cylinders ¹				−0.143	−0.100	−0.069	−0.053	−0.045	−0.040	−0.038
N.A.C.A. hood ¹				−.112	−.068	−.048	−.035	−.027	−.023	−.021
N.A.C.A. cowled nacelle				−.104	−.078	−.058	−.042	−.033	−.027	−.024
Variable ring −8° ¹				−.107	−.073	−.050	−.035	−.025	−.019	−.017
Nacelle position C-3-A										
Smooth body				−0.285	−0.152	−0.096	−0.063	−0.041	−0.026	−0.016
Nacelle position A-1-B, faired into wing										
Exposed cylinders ¹				0.000	−0.015	−0.031	−0.043	−0.051	−0.056	−0.060
N.A.C.A. hood ¹				.020	−.010	−.031	−.043	−.050	−.055	−.057
Variable ring −8° ¹				.026	−.005	−.026	−.039	−.047	−.052	−.056
N.A.C.A. cowled nacelle				.025	−.005	−.027	−.042	−.050	−.055	−.058
Nacelle position A-2-B										
Smooth body				0.093	0.019	−0.017	−0.027	−0.049	−0.057	−0.062
Exposed cylinders ¹				.057	.010	−.023	−.044	−.058	−.066	−.071
N.A.C.A. hood ¹				.088	.018	−.020	−.039	−.049	−.056	−.062
Variable ring −8° ¹				.082	.032	−.013	−.040	−.054	−.061	−.066
N.A.C.A. cowled nacelle				.091	.024	−.020	−.040	−.049	−.054	−.057
Nacelle position C-3-B										
Smooth body				0.185	0.066	0.009	−0.024	−0.045	−0.061	−0.072

¹ Small nacelle.

TABLE IX
RELATIVE MERITS OF VARIOUS COWLINGS FOR DIFFERENT NACELLE LOCATIONS
HIGH AND CRUISING SPEED CONDITION

Propeller No. 4412—4 feet. Set. 17° at 0.75 R. $\frac{V}{nD}=0.65$ $C_L=0.347$

Nacelle location.....	B	B ²	C	B-1-A ³	C-3-A	A-1-B ³	A-2-B	C-3-B
Propulsive efficiency (η)								
Smooth body.....	0.760		0.793		0.778		0.788	0.775
Exposed cylinders ¹805	0.832		0.853		0.840	.829	
Variable ring —8° ¹823		.783		.800	.829	
N.A.C.A. hood ¹758	.816		.803		.782	.783	
N.A.C.A. cowled nacelle.....	.760			.788		.793	.773	
Nacelle drag efficiency factor (N.D.F.)								
Smooth body.....	0.037		0.070		0.141		0.128	0.143
Exposed cylinders ¹185	0.262		0.318		0.283	.335	
Variable ring —8° ¹177		.211		.242	.259	
N.A.C.A. hood ¹122	.170		.195		.180	.227	
N.A.C.A. cowled nacelle.....	.046			.125		.151	.135	
Net efficiency (η —N.D.F.)								
Smooth body.....	0.723		0.723		0.637		0.660	0.632
Exposed cylinders ¹620	0.570		0.535		0.557	.494	
Variable ring —8° ¹646		.572		.558	.570	
N.A.C.A. hood ¹636	.646		.608		.602	.556	
N.A.C.A. cowled nacelle.....	.714			.663		.642	.638	

¹ Small nacelle.
² Side brackets removed.
³ Nacelle faired into wing.

TABLE X
RELATIVE MERITS OF VARIOUS COWLINGS FOR DIFFERENT NACELLE LOCATIONS
CLIMBING CONDITION

Propeller No. 4412—4 feet. Set 17° at 0.75 R. $\frac{V}{nD}=0.42$ $C_L=0.635$

Nacelle location.....	B	B ²	C	B-1-A ³	C-3-A	A-1-B ³	A-2-B	C-3-B
Propulsive efficiency at climbing speed								
Smooth body.....	0.640		0.650		0.665		0.662	0.652
Exposed cylinder ¹638	0.672		0.675		0.692	.670	
Variable ring —8° ¹679		.665		.670	.680	
N.A.C.A. hood ¹627	.678		.662		.658	.652	
N.A.C.A. cowled nacelle.....	.618			.658		.670	.647	
Nacelle drag efficiency factor (N.D.F.)								
Smooth body.....	—0.016		—0.014		0.030		0.027	0.031
Exposed cylinders ¹021	0.026		0.035		0.039	.065	
Variable ring —8° ¹021		.013		.044	.051	
N.A.C.A. hood ¹000	.018		.020		.024	.049	
N.A.C.A. cowled nacelle.....	— .013			— .010		.027	.019	
Net efficiency (η —N.D.F.)								
Smooth body.....	0.656		0.674		0.635		0.635	0.621
Exposed cylinders ¹617	0.646		0.640		0.653	.605	
Variable ring —8° ¹658		.652		.626	.629	
N.A.C.A. hood ¹627	.660		.642		.634	.603	
N.A.C.A. cowled nacelle.....	.631			.668		.643	.628	

¹ Small nacelle.
² Side brackets removed.
³ Nacelle faired into wing.

REPORT No. 463

THE N.A.C.A. HIGH-SPEED WIND TUNNEL AND TESTS OF SIX PROPELLER SECTIONS

BY JOHN STACK

SUMMARY

This report gives a description of the high-speed wind tunnel of the National Advisory Committee for Aeronautics. The operation of the tunnel is also described and the method of presenting the data is given. An account of an investigation of the aerodynamic properties of six propeller sections is included.

The tunnel is operated on the induction-jet principle. Compressed air discharged through an annular nozzle surrounding the tunnel downstream from the test section induces a flow of air from the atmosphere through the test section of the tunnel where the models are placed. The forces on the model are measured by a 3-component photo-recording balance.

The test results included herein comprise measurements of the lift, drag, and pitching moments of six airfoils. The sections chosen for tests have thickness ratios of 0.06, 0.08, and 0.10; three are based on the Clark Y profile and three on the R.A.F. 6 profile. The tests were made over a wide speed range and for several angles of attack, varying from that of zero lift to 12° , in order to investigate the effects of compressibility on the airfoil characteristics.

The data obtained indicate that the Clark Y airfoils are superior to the R.A.F. 6 airfoils for propeller applications except for high-pitch propellers operating at low values of V/nD . The effects of compressibility on the airfoil characteristics are large and important. As the speed of the air flowing past an airfoil is increased the lift, drag, and moment coefficients undergo a small numerical increase which continues until a compressibility burble occurs. As the speed is increased further, the breakdown of the flow corresponding to the compressibility burble is evidenced by a marked decrease in the lift coefficient and a rapid increase in the drag coefficient. The speed at which the compressibility burble occurs is dependent on the angle of attack and the airfoil thickness; increasing either causes the compressibility burble to occur at lower speeds. A comparison of these data with the theoretical work of Glauert and Ackeret as regards the nature and amount of the effects of compressibility on the lift-curve slope substantiates the theory for speeds below that at which the compressibility burble occurs.

A computation of propeller characteristics based on these results is compared with the experimental results on a full-scale propeller. The reasons for differences are discussed and recommendations for future work are given.

INTRODUCTION

The advantages of model testing as an aid to the solution of full-scale problems are often neutralized by the inaccurate reproduction of the full-scale flow in the model test. The conditions which must be fulfilled in the model test so that the results may be directly applicable to the full-scale problem are twofold. First, the model must be geometrically similar to the full-scale object—a condition usually obtained—and second, the model flow pattern must be similar to the full-scale flow pattern—a condition generally not fulfilled. The principal factors that determine flow similarity are the Reynolds Number $\rho V l / \mu$ and the compressibility factor V/V_c where V_c is the velocity of sound in the gas. The first of these two factors, the Reynolds Number, expresses the ratio of the mass forces to the viscous forces in the gas. It is essential that this ratio have the same value for the model flow as for the full-scale flow. The second factor, the ratio of the velocity of the body to the velocity of sound in the gas V/V_c , indicates to what extent the flow is affected by the compressibility of the gas. For most applications the effects of variations in the value of this ratio are neglected because the velocities of the air streams in most wind tunnels are of the same order of magnitude as the velocities of most aircraft and the effect of the differences in the value of this factor between the model flow and the full-scale flow is therefore small. In addition, the speeds common to most aircraft are low with respect to the velocity of sound in air and the corresponding pressure differences are likewise small.

A knowledge of the compressibility phenomenon is essential, however, because the tip speeds of propellers now in use are commonly in the neighborhood of the velocity of sound. Further, the speeds that have been attained by racing airplanes are as high as half the velocity of sound. Even at ordinary airplane speeds the effects of compressibility should not be disregarded if accurate measurements are desired.

Some data on the effects of compressibility are already available. Experiments on propellers rotated at very high speeds have demonstrated that large detrimental effects are to be expected as the tip speed approaches the speed of sound. These experiments, although of immediate practical value, are not well suited for a study of the compressibility phenomena. Efforts to provide more suitable data have also been made. Airfoils have been tested at high speeds, but the experiments have been conducted under unfavorable circumstances. The large amount of power required to drive a stream of air at very high speeds has necessitated the use of small wind tunnels, the characteristics of which were often unknown. Furthermore, the size of the models being large in relation to the size of the wind tunnels, the test results are subject to large corrections which are in themselves problematical.

In order to provide more suitable means for studying compressibility phenomena, the National Advisory Committee for Aeronautics has constructed a comparatively large closed-throat high-speed wind tunnel. The tunnel, which was designed to utilize compressed air from the N.A.C.A. variable-density wind tunnel as a source of motive power, was the outgrowth of experiments dealing with thrust augmentors for jet propulsion (reference 1). High-velocity compressed-air jets were employed to induce a flow of the surrounding air through the augmenting devices. The results indicated that it was possible to apply the principles of the induction jet to the development of a high-speed wind tunnel. The calculations leading to the preliminary design were started in July 1927. After a series of model tests, a 12-inch diameter open-throat high-speed tunnel was constructed in April 1928. Further developments were carried out with this tunnel from which the present closed-throat tunnel was finally evolved.

The N.A.C.A. high-speed wind tunnel has several advantages over previous devices. The diameter of the tunnel is large compared to previous tunnels in which high-speed tests have been made. The flow past the model is relatively nonturbulent, since the air stream in the tunnel throat is composed entirely of air taken directly from the atmosphere. Moreover, the models extend through the walls and are supported outside the air stream, thus eliminating the effects of support interference. Several airfoils have been tested in this tunnel and this report presents a description of the tunnel, together with the results of tests on six airfoils having commonly used propeller sections. The data presented comprise the results of tests made over a wide speed range and these data have been analyzed with a view toward demonstrating the compressibility effects and their relation to design problems.

I. DESCRIPTION OF TUNNEL

The high-speed wind tunnel is similar in form to most venturi-type wind tunnels. There are, however, important differences in its characteristics and equipment, which arise in part from its purpose and in part from the method of operation. The novel features are the large speed range which extends up to the velocity of sound when there is no model in the tunnel, the drive system, and the automatic-recording balance used to measure the forces.

Arrangement.—The general arrangement of the tunnel is shown in figures 1 and 2. Compressed air from the variable-density wind tunnel is piped to the high-pressure chamber and discharged through the annular nozzle shown in figure 2. The jet from this nozzle induces a flow of air from the atmosphere through the lower portion of the tunnel, where the model is placed on a photo-recording balance as shown in figure 2. The atmospheric air mixes with the high-pressure air in the diffuser which conducts the air outside through the roof of the building.

The balance and the lower portion of the tunnel are enclosed in an airtight wooden chamber which is supported by a metal framework fastened to the floor of the building as shown in figure 1. Access to the tunnel and balance is obtained by removing two opposite sides of the chamber. One half of the test section is also removable in order to facilitate mounting the model.

Tunnel air passages.—The entrance cone is 17.67 inches long and 11 inches in diameter at its junction with the test section. Six vanes, which extend from the floor to the plane of the mouth of the entrance cone, are provided to prevent twisting of the air stream at the entrance cone. The test section is 7 inches long, and is made slightly divergent to reduce the axial static-pressure gradient. The included angle between the walls of the exit cone is 4.6° ; the portion tapered at this angle is $13\frac{5}{16}$ inches and ends in an abrupt step just below the annular nozzle. The diffuser is 19 feet 10 inches long and the included angle between diametrically opposite elements is 4.8° .

Power supply.—The motive power for the air stream is provided by compressed air from the variable-density wind tunnel. At the end of a test at high values of the Reynolds Number in this tunnel a relatively large supply of air at high pressure is available. The compressed air is piped to the chamber surrounding the annular nozzle shown in figure 2 and discharged through the nozzle. The high-pressure chamber and the nozzle are of cast steel. The nozzle has a minimum annular opening of 0.06 inch and a divergent portion $1\frac{5}{16}$ inches long. The total angle of divergence is 11.1° .

TUNNEL CHARACTERISTICS

Velocity and pressure distribution.—Figure 3 indicates the dynamic-pressure variation across the tunnel along the quarter-chord position of the model. The variation is less than ± 0.5 percent. The directional variation of the air flow is believed to be less

ratio is therefore defined as the quotient of the kinetic energy of the air passing through the test section in a unit time divided by the power due to adiabatic expansion of the high-pressure air. The value for the tunnel as operated varies considerably over the speed range but at a speed $0.5 V_c$ the value is 1.6.

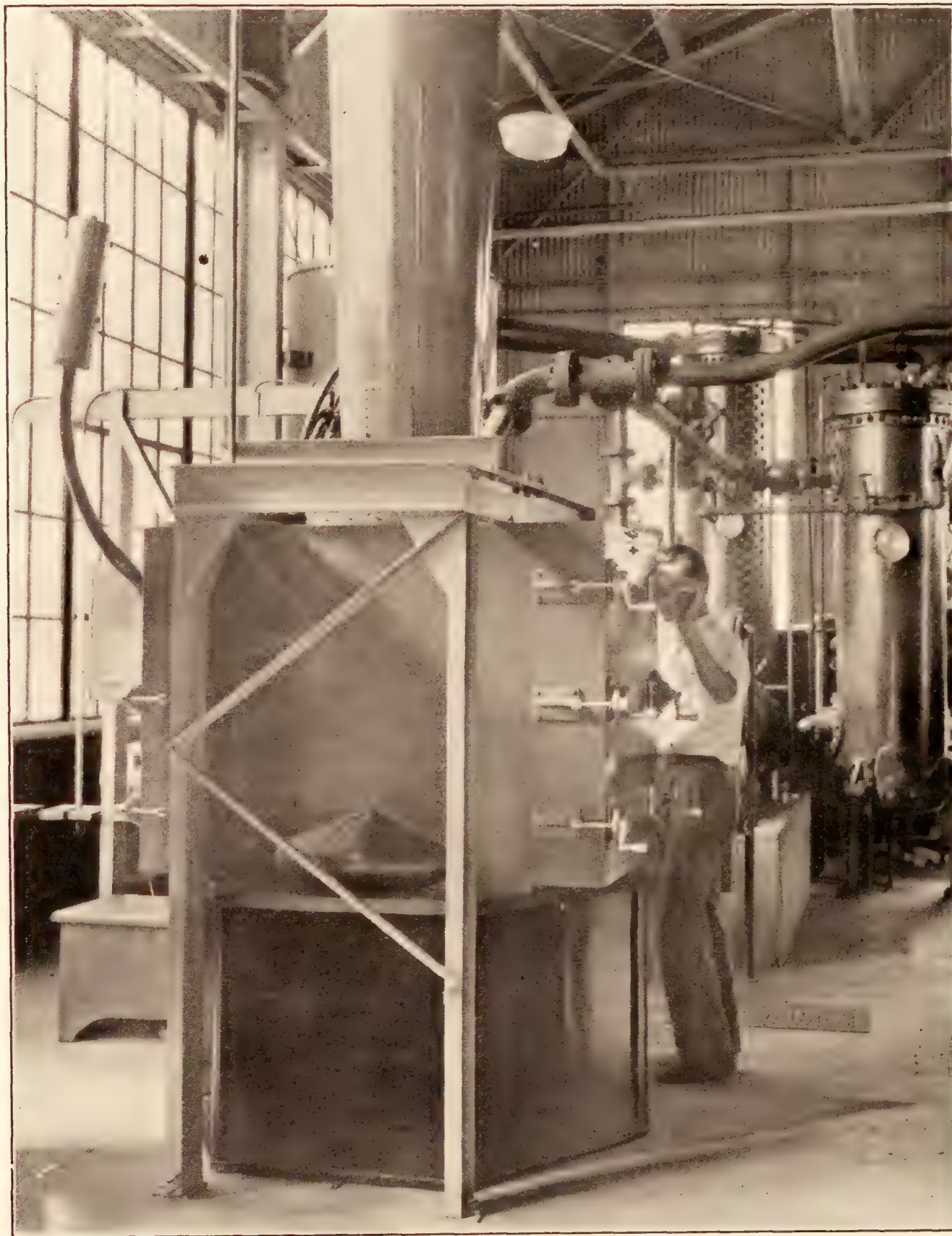


FIGURE 1.—General view of the high-speed wind tunnel.

than $\pm \frac{1}{4}^\circ$. Figure 4 shows the small static-pressure gradient.

Energy ratio.—The energy ratio is difficult to determine for this type of tunnel because of the uncertainty of the value of the power input. For comparative purposes, however, the power input is taken as the rate of work due to an adiabatic expansion of the high-pressure air from the pressure in the reservoir to atmospheric pressure. The energy

DESCRIPTION OF THE BALANCE

General.—The balance must measure the large range of forces resulting from the wide speed range over which tests are made, and it must be automatic recording because the allowable time for observations is short. The balance measures the lift, drag, and pitching moment by multiplying and recording the deflection of steel springs (cantilever beam type) to which the forces are transmitted. The essential parts

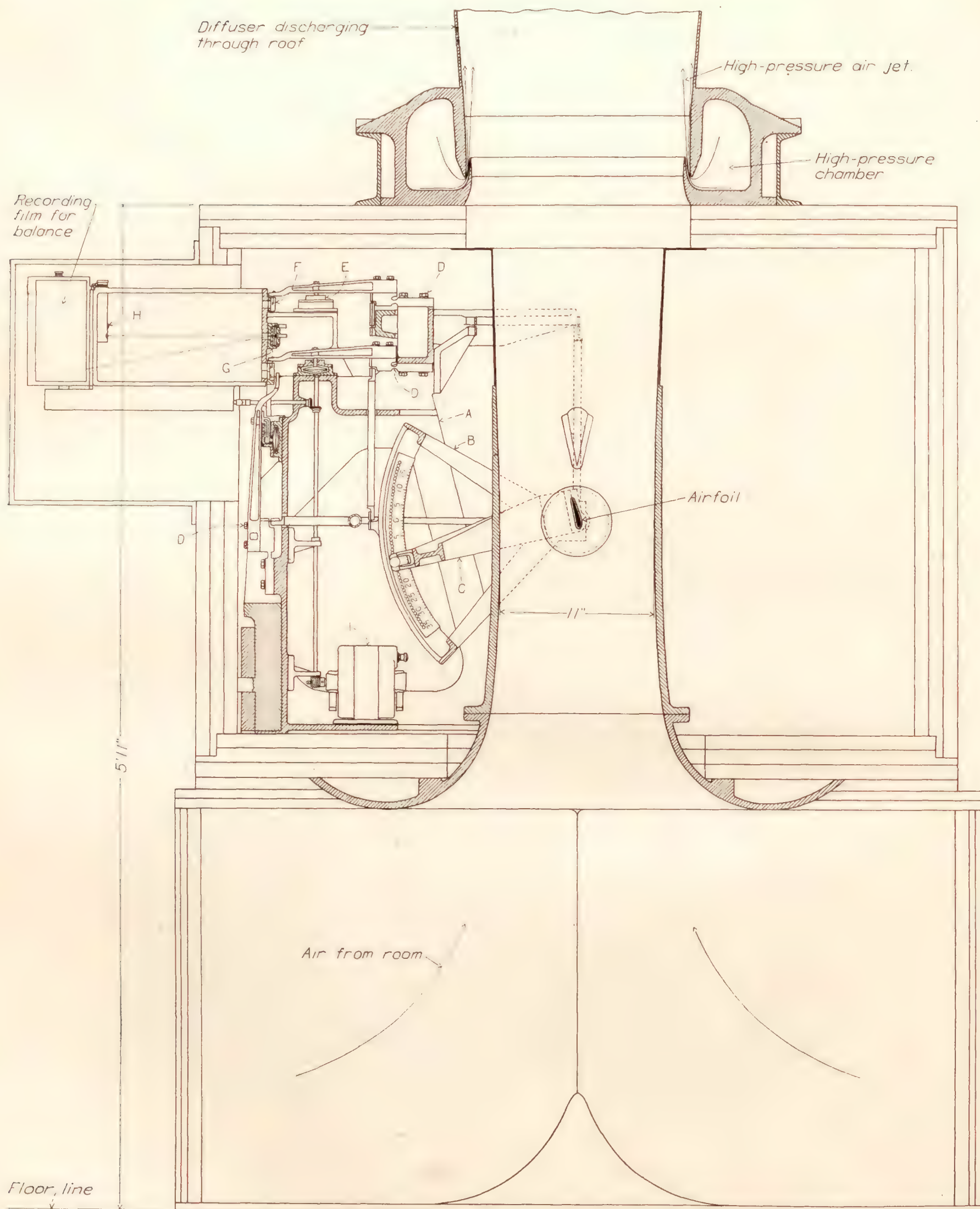


FIGURE 2.—Diagrammatic section of the high-speed wind tunnel.

- A, balance frame
- B, cradle
- C, rotatable yoke for changing angle of attack
- D, springs
- E, dashpot
- F, lens and mirror container
- G, N.A.C.A. pressure cell
- H, source light
- I, film drive motor

consist of a cast-iron cradle in which is mounted a yoke to which the model is attached, the linkages necessary to transmit the forces to the steel springs, and a camera for multiplying and recording the deflections of the springs.

Linkages and knife-edges.—The balance is shown in figures 2 and 5. The cradle extends around one half of the tunnel and contains a rotatable yoke to which the model is secured. The cradle supports consist of three vertical rods, one of which is directly connected to one of the balance springs. The other two rods are connected to ends of a fork-shaped lever above the cradle. The lever is supported at its center and the other end is connected to another of the balance springs. Horizontal movement is constrained by two

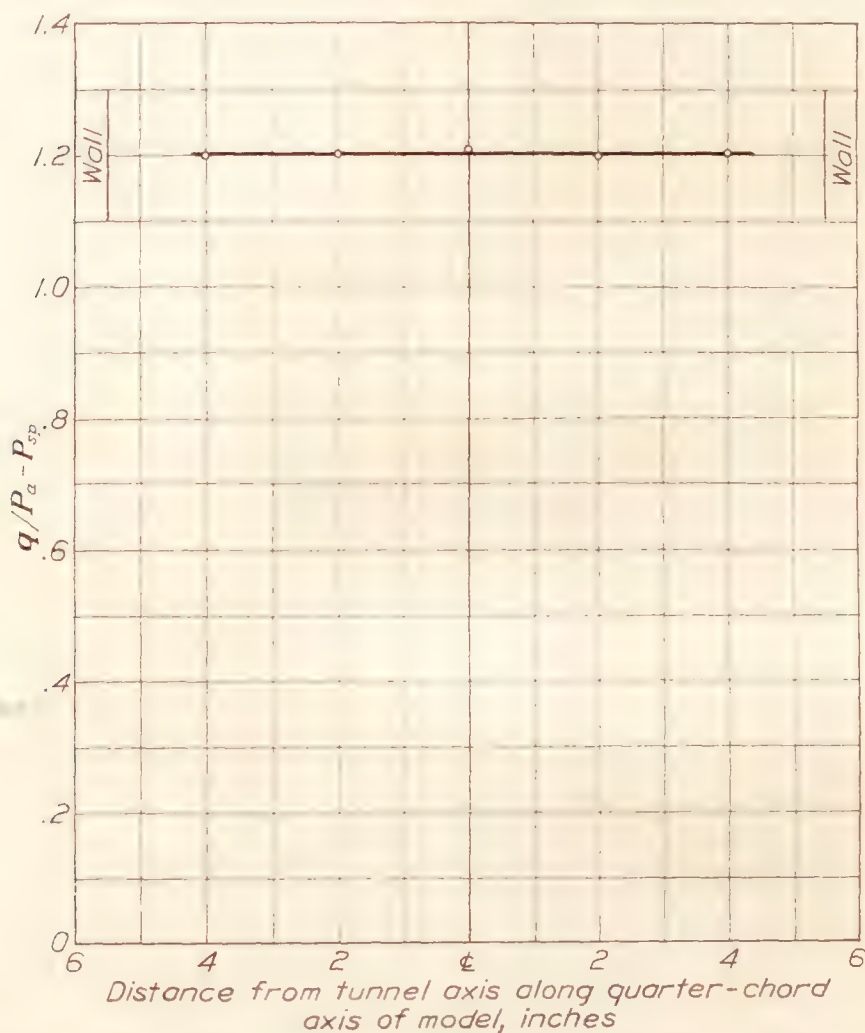


FIGURE 3.—Ratio of dynamic pressure at the test section to the difference between the atmospheric pressure and the pressure at the static-pressure orifices for velocity equal to $0.8 V_c$.

rods, one on either side of the cradle, which are connected through a truss to the third balance spring.

The lift linkage transmits the horizontal or lift forces from the balance cradle to the spring at the rear of the balance. The drag and moment linkages are interacting. The drag is the algebraic sum of the forces in the three vertical supports. The forward supports are parallel to the tunnel axis and their axes are in a vertical plane which passes through the axis of the tunnel and the quarter-chord line of the models. The forces in these supports are transmitted through a fork, which is mounted on the balance frame above the cradle, to the deflecting spring shown at the top of the diagram (fig. 2). Therefore, if moments are taken about the line joining the intersection of the horizontal

and vertical linkages on either side of the tunnel, the forces in these linkages will not contribute to the moment. The force in the rear support, which is connected to another deflecting spring, gives the moment directly.

Instead of the usual knife-edges, the balance linkages are connected by means of Emery knife-edges which are actually thin steel deflecting strips joining the members (figs. 2 and 5).

Springs.—All three balance springs are of the same general form, varying principally in their size, which is determined by the magnitude of the forces to be measured. They are cantilever beams of rectangular cross section, constructed of heat-treated steel, and have a short length of reduced thickness to localize the deflections. They are mounted on heavily reinforced pedestals on the rigid balance frame and are held in place by dowels and screws. The thickness of the springs is such that the deflections corresponding to the largest forces encountered are of the order of 0.005 inch.

Recording system.—Owing to the small deflections of the balance springs, the recording system must provide a large multiplication. A further requirement

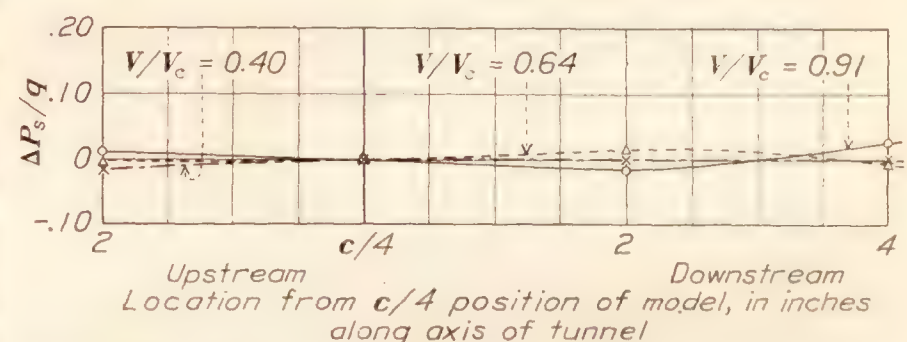


FIGURE 4.—Ratio of the change in the absolute static pressure from that at the model position to the dynamic pressure.

is the provision for sensitivity control; that is, some easy means of increasing the multiplication so that good accuracy may be maintained when the forces are comparatively small, such as those encountered at very low speeds and low angles of attack. In addition, it is necessary to record the forces automatically because of the short time during which observations must be made.

The general arrangement of the recording system is shown in figures 2 and 5. Long arms are fastened to the balance springs. At the ends of these arms a bushing is mounted in which a stylus is eccentrically fitted. By rotation of the bushing the multiplication of the beam movement can be altered. The stylus is in contact with a pivoted mirror which is thus actuated by the movement of the balance springs. Suitable damping is provided by means of dashpots connected to the spring arms. A source of light and suitable lenses are provided so that light is reflected by the mirrors to a moving film. The film is driven by a small electric motor through a train of gears which permits three speed variations. The source light and the film drive are controlled from the exterior of the balance and tunnel chamber.

Model support.—The model is mounted in jaws at the ends of the yoke. It is located by means of dowels so that the line joining the intersections of the horizontal and vertical linkages coincides with the quarter-chord axis of the model. The angle of attack is changed by rotating the yoke, which is arranged to turn about an axis through the intersection of the horizontal and vertical linkages. The yoke is fixed at various angles by means of a pin which projects from the yoke into holes in the graduated quadrant shown in figure 2.

The model extends across the tunnel and through holes in the tunnel wall. In order to reduce the flow into the tunnel from the dead-air space and to reduce interference with the air flow, these holes are covered with specially designed end plates shown in figure 6. The end plates are made of thin brass and are circular in form. They fit into recesses cut in the tunnel wall

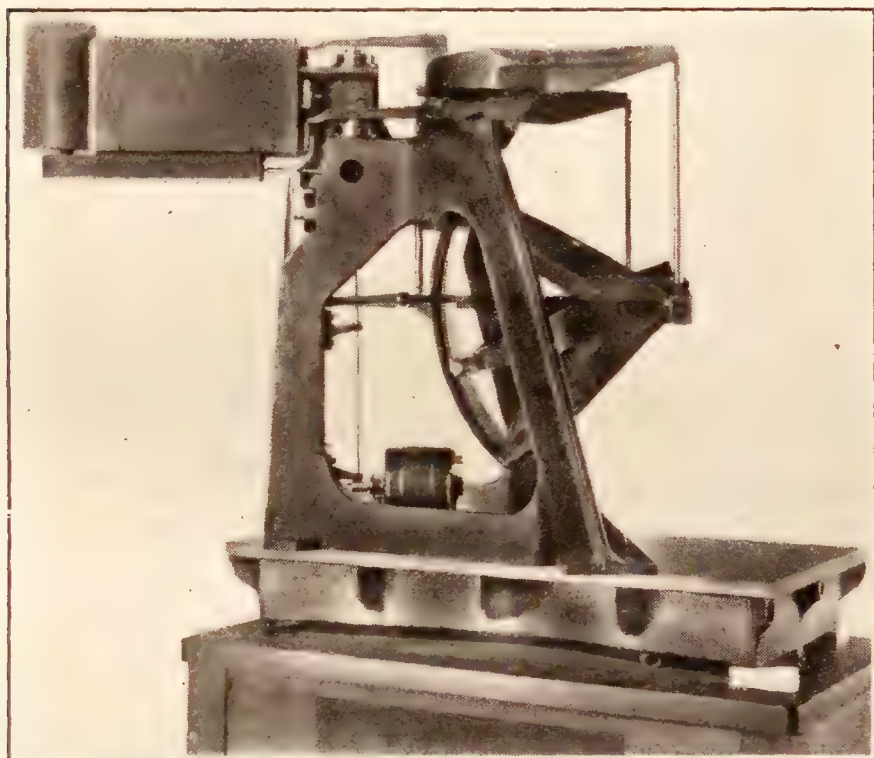


FIGURE 5.—The high-speed wind tunnel balance.

around the edges of the holes and are sufficiently flexible so that they can bend as the angle of attack is changed and thus maintain the contour of the walls. Holes of the same shape as the airfoil section but slightly larger are cut in the end plates to provide $\frac{1}{16}$ -inch clearance so that the model and the end plates cannot touch. The end plates are held in position by six U-shaped pieces. One side of each piece is soldered to the end plate and the other side carries a screw which is turned down against a ledge on the outside wall of the tunnel as shown in figure 6. The end plates can be turned with the model as the angle of attack is changed by loosening the screws in the U-shaped pieces. A telltale lamp is provided which lights if the model makes contact with the end plates during a test.

TUNNEL CALIBRATIONS

Dynamic pressure and velocity determination.—The dynamic pressure and velocity are computed from Bernoulli's equation for a compressible fluid. The equation is

$$P_a = P_s \left[1 + \frac{k-1}{2} \left(\frac{V_s}{V_c} \right)^2 \right]^{\frac{k}{k-1}}$$

where the subscript *a* denotes atmospheric conditions, the subscript *s* denotes conditions at the test section of the tunnel, *P* denotes the pressure in the fluid, *V_c* is the velocity of sound in the fluid for the conditions at the test section, and *k* is the ratio of the specific heats for air, numerically equal to 1.4. The formula is derived by substituting the pressure-density relation for adiabatic flow in the general form of the Bernoulli equation. A detailed derivation of this formula is given in reference 2 (p. 15). A more convenient form

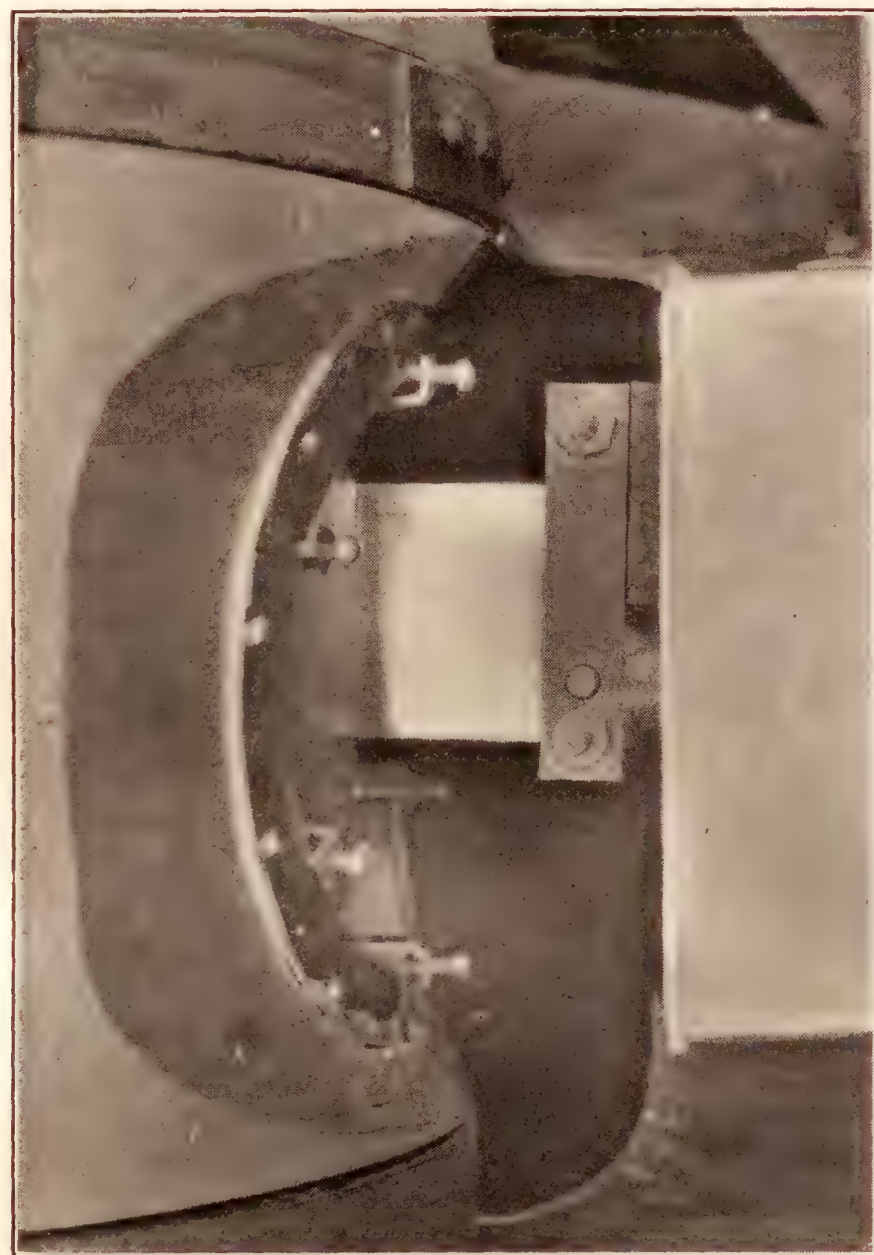


FIGURE 6.—View showing tunnel-wall fitting and airfoil mounting.

of the foregoing equation for use when V_s/V_c is less than unity is obtained by expanding in the series

$$P_a = P_s + \frac{1}{2} \rho_s V_s^2 \left[1 + \frac{1}{4} \left(\frac{V_s}{V_c} \right)^2 + \frac{1}{40} \left(\frac{V_s}{V_c} \right)^4 + \frac{1}{1600} \left(\frac{V_s}{V_c} \right)^6 \dots \right]$$

This is the form used to compute the dynamic pressure, which is therefore

$$q = \frac{1}{2} \rho_s V_s^2 = \frac{P_a - P_s}{1 + \frac{1}{4} \left(\frac{V_s}{V_c} \right)^2 + \frac{1}{40} \left(\frac{V_s}{V_c} \right)^4 + \frac{1}{1600} \left(\frac{V_s}{V_c} \right)^6 \dots}$$

The values of V_s/V_c are computed from the first form

of the equation. Solving this equation for V_s/V_c gives

$$\frac{V_s}{V_c} = \sqrt{\frac{2}{k-1} \left[\left(\frac{P_a}{P_s} \right)^{\frac{k-1}{k}} - 1 \right]}$$

The validity of these formulas is dependent primarily upon the existence of true adiabatic flow and the absence of losses due to friction. The errors induced by the first of these assumptions are probably small because of the rapidity with which the heat energy of the air is converted to kinetic energy. In order to check the validity of the formulas, the total pressure at the test section has been measured and it was found that its value differed from the atmospheric pressure by less than 0.02 percent of the dynamic pressure, except for a very small core at the center and a relatively thin layer adjacent to the wall.

The difference between the static pressure at the test section and the atmospheric pressure cannot be reliably determined from a direct measurement during a test because of the presence of the model. Accordingly, calibrated static-pressure orifices are used for this purpose. Four small holes in the tunnel wall 10 inches below the location of the quarter-chord axis of the model are connected to a manifold which is in turn connected to pressure-measuring devices. The calibration factor is determined from simultaneous measurements of the quantities $(P_a - P_s)$ and $(P_a - P_{sp})$, where the subscript *sp* denotes conditions at the static-pressure orifices. The static pressure at the test section is taken as the value registered by four holes in a tube located along the axis of the tunnel. The holes in the tube are 90° apart and are in the horizontal plane which passes through the quarter-chord position of the airfoil model. In order to avoid end interferences the tube extends from the relatively low velocity region at the mouth of the entrance cone to a point 20¼ inches above the model location. The calibration factor as computed from these measurements is

$$F = \frac{q}{P_a - P_{sp}}$$

For use in computing test results both this factor and V/V_c are plotted against $P_a - P_{sp}$. The variation of these quantities with atmospheric pressure for constant values of $P_a - P_{sp}$ is negligible except at speeds in the immediate neighborhood of the velocity of sound.

The only pressure measured during a test is the difference between the atmospheric pressure and the pressure at the static-pressure orifices. Two pressure-measuring devices are connected to the orifices. A single-tube mercury manometer is mounted outside the tunnel to provide the operator with means for adjusting the speed and measuring the pressure difference; a standard N.A.C.A. pressure cell (reference 3) mounted on the camera records the pressure difference on the film on which the forces are registered. The pressure cell serves to check the values observed by the

operator and, in addition, gives a record of the air-flow steadiness while the observations are being taken.

Balance alinement and calibration.—The alinement of the balance linkages with respect to each other is fixed by the construction of the balance. Alinement of the balance with respect to the air-flow direction is obtained by applying an external force in the horizontal or lift direction and adjusting the height of the rear base of the balance until the drag balance indicates zero force. The air-flow alinement has been checked by testing an airfoil in the normal and inverted positions

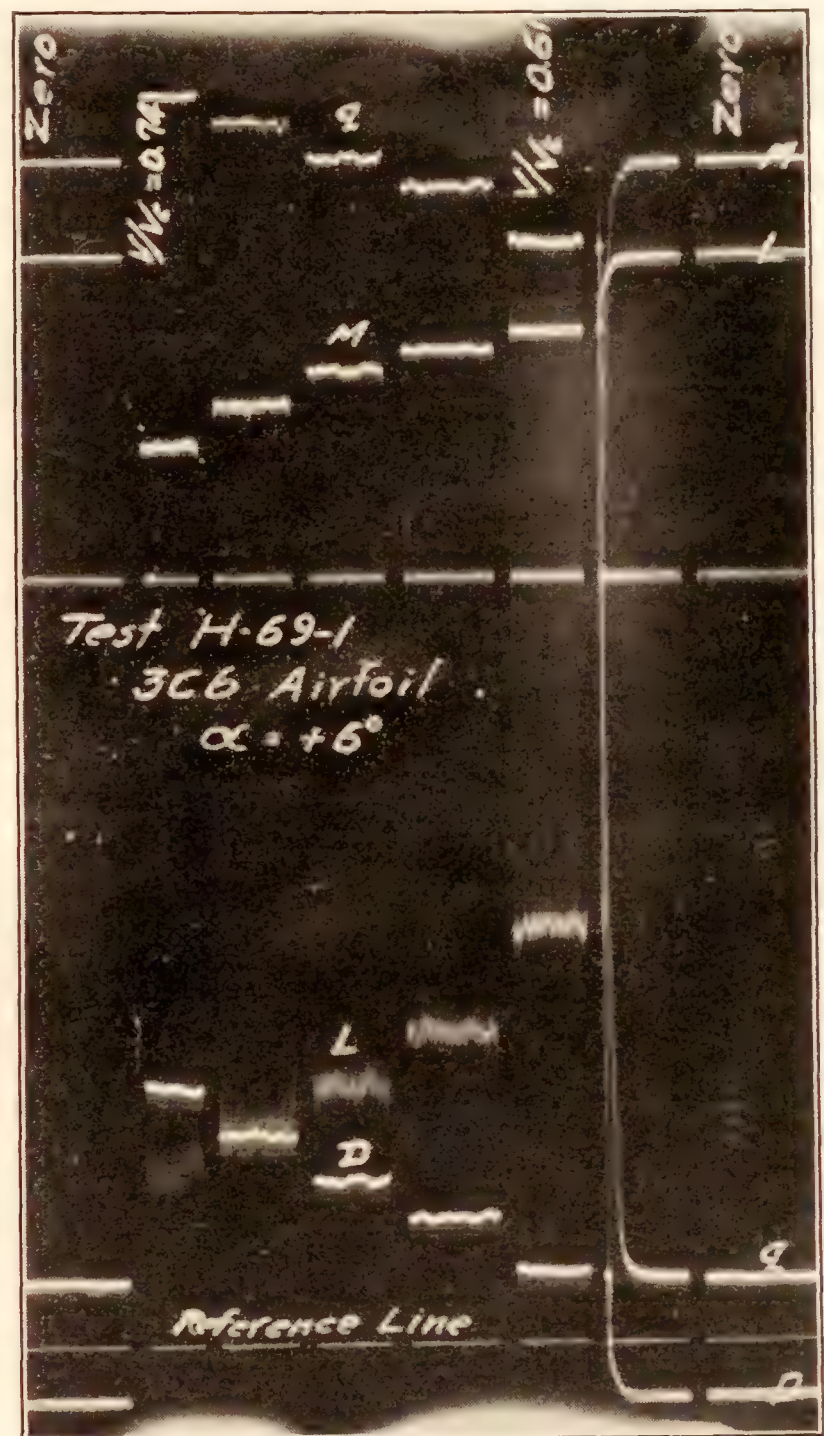


FIGURE 7.—Section of photographic record taken from balance.

and also by tests of a symmetrical airfoil at positive and negative angles of attack.

The balance calibration is obtained by applying known loads in the direction of the various forces by means of a specially designed system of levers. The deflections corresponding to these loads are recorded on the film and from these data calibration charts are constructed. Errors due to misalignment of the various levers which comprise the calibrating fixture are less than 1 part in 3,000 and the errors in the weights used in calibrating are of the order of 1 part in 700.

A TYPICAL AIRFOIL TEST

The standard airfoils, 2-inch chord, are made of metal, usually steel. They are constructed by a generating machine which works from a sixfold templet. The method of construction is described in reference 4. The extremities of the airfoil are machined flat and drilled from a jig to insure accurate mounting on the balance.

The airfoil is mounted in the balance and the angle of attack is set by means of the pivoted yoke. The chamber doors are then clamped in place. The valve in the high-pressure air duct is opened wide and when conditions become steady, as indicated by the mercury manometer, observations are taken. Lower speeds are obtained by throttling. The run is continued, with interruptions for recording zeros, until the entire speed range is covered. The chamber is then opened and the angle of attack is changed and the procedure as outlined above is repeated. The number of angles of attack for which tests can be obtained from one tank of air is dependent on the number of speeds for which observations are made. Even when a relatively large number of observations for various speeds are taken, complete observations for two angles of attack can be made. The tunnel operating time required for testing an airfoil at one angle of attack over the entire speed range is approximately 12 minutes.

The forces and moments are evaluated from the photographic record (fig. 7). The deflections indicated on the film are measured by means of a special device and the forces corresponding to these deflections are read from the calibration charts. The data are then reduced to the standard nondimensional coefficient form.

PRESENTATION OF DATA

The effect of the tunnel walls on the aerodynamic characteristics of airfoils tested in this tunnel is not definitely known or understood. The effect of variations in the form and clearance of the end plates is known to be critical and, accordingly, the end plates are very carefully adjusted. Some preliminary tests with airfoils having different chords indicate that no correction need be applied to these data to obtain characteristics for infinite aspect ratio. In other words, it is believed that the data may be directly applied in practical design problems as airfoil data for infinite aspect ratio.

The data are presented in two graphic forms. The first form, which shows directly the effects of compressibility, consists of plots of the various coefficients for a given angle of attack against V/V_c . The other form consists of plots of the lift coefficient and the drag coefficient against angle of attack for several speeds.

II TESTS OF SIX COMMONLY USED PROPELLER AIRFOILS AT HIGH SPEEDS

The prediction of propeller performance is dependent to a large extent on an accurate determination of the aerodynamic characteristics of the airfoil sections which are used as the propeller blade sections. Here-tofore, it has been common practice to adopt the results of airfoil tests at low speeds in conventional wind tunnels for this purpose. The effects of compressibility have usually been neglected, because of the lack of the information necessary to establish a valid correction for this effect. The first series of tests in the high-speed wind tunnel was performed to provide more accurate data on which the design of propellers could be based.

TESTS

Models.—Of the 6 airfoils tested, 3 have sections based on the R.A.F. 6 section and 3 on the Clark Y section. In each group of three, the airfoil thickness is the major variable. The thickness ratios chosen are 0.06, 0.08, and 0.10, and the airfoil profiles were obtained by scaling the ordinates of the original airfoil, measured from the chord line, in the ratio of the desired thickness to the thickness of the basic section. The ordinates are given in table I. The airfoils are designated as in reference 5 by a system of numbers and a letter. Thus, the designation 3C6 is applied to the 6 percent thick Clark Y airfoil. The first number gives the location of the maximum thickness in tenths of the chord, the letter indicates the basic section from which the airfoil is derived, C for the Clark Y and R for the R.A.F. 6, and the last numbers give the maximum thickness of the airfoil in percent of the chord. The six airfoils are then the 3C6, 3C8, 3C10, 3R6, 3R8, and 3R10.

All of the airfoils were of 2-inch chord. Four were made of duralumin. The two thinnest airfoils, however, were made of steel in order to reduce the deflections of the models under high lift loads. A detailed description of the method of constructing the airfoils is given in reference 4.

Method of testing.—Because of the large range of forces involved in testing the airfoils over a wide angle-of-attack range and a wide speed range, the tests were performed in two parts. The lift and drag balances were set for maximum sensitivity and the airfoils were tested at low angles of attack; that is, up to 4° . Then, in order to permit recording the larger forces for the higher angles of attack, the sensitivities of the lift and drag balances were reduced and the high angle-of-attack tests were performed. Because of the small clearance between the airfoil and the hole in the end plates through which the airfoil protrudes, additional end plates were required for the high angle-

of-attack tests. The holes in the end plates were kept the same size as formerly but were moved slightly to one side to prevent the airfoil from touching and to keep the clearance as uniform as possible throughout the tests as the airfoil deflected under the high loads encountered at high angles of attack.

The tests in each part were made in pairs, airfoils of the same thickness being tested consecutively. The operating procedure was identical in other respects with the description previously given.

PRECISION

The various factors contributing to inaccuracy in these experiments may, in general, be classified under two major divisions. The first consists of errors in measurements made to determine the dynamic pressure and the second consists of errors in the evaluation of the actual forces and moments.

Inaccuracies arising from the dynamic-pressure variation across the throat are insignificant. The value of the static-pressure calibration factor was checked over the speed range three times while the tests were in progress. The maximum differences found were approximately 1 percent. Determinations of this factor may, however, have a consistent error due to a constriction effect at the throat when the airfoil is in position. The magnitude of this error is unknown, and because of the difficult nature of the problem, a satisfactory solution has not yet been obtained. Accordingly, no correction has been applied.

Balance calibrations before and after each group of tests agreed very closely. The lift calibrations agreed to within 1.5 percent and the drag calibrations agreed to within 1 percent. The differences in the moment calibrations were less than either of the above and may be considered negligible. The evaluation of tare corrections resulting from air leakage where the model passes through the tunnel wall was not feasible. However, tests made with no model in place and with the holes in the tunnel wall closed indicated the presence of small tare readings of uncertain origin for which the data have been corrected. The magnitudes of these corrections are -0.020 for the lift coefficient, 0.0005 for the drag coefficient, and 0.020 for the moment coefficient. These corrections have been checked by repeat tests to within 0.001 for the lift, 0.0003 for the drag, and 0.005 for the moment. A few repeat tests of these airfoils at various angles of attack indicated that the results could be reproduced to within 3 percent except for high angles of attack at high speeds, when the flow was unsteady.

RESULTS

The results of the tests are presented in figures 8 to 13, inclusive. These figures show the variation in the force and moment coefficients with speed for a given angle of attack. Complete data for one airfoil are presented in each figure, each curve showing the variation of one of the three coefficients over the

speed range for one angle of attack. In the presentation of the moment-coefficient data, the origin of the axes for each angle of attack has been raised above that for the previous angle of attack so that the moment curve for any angle may be easily distinguished.

Additional figures are presented to show the aerodynamic characteristics of the airfoils in more familiar form and also to illustrate further the effects of compressibility on the important characteristics. Figures 14 to 19, inclusive, are plots of the lift and drag coefficients against angle of attack. These curves are presented for several speeds to provide an easy comparison with previous work. Figure 20 shows the variation of the drag coefficients of all six airfoils with speed for three values of the lift coefficient and, in addition, the variation of the minimum drag with speed is shown. Figure 21 illustrates the effect of compressibility on the slope of the lift curve. Figures 22 and 23 illustrate an application of these data to the computation of propeller characteristics.

DISCUSSION

Comparison of airfoils.—The comparison of these airfoils should be made on the basis of lowest profile-drag coefficient for any fixed value of the lift coefficient because this characteristic is generally of paramount importance in the selection of airfoil sections for propellers. If airfoils of like thickness are compared, it is apparent from figure 20 that the C airfoils have lower profile-drag coefficients than the corresponding R airfoils except at high values of the lift coefficient. However, the differences at high values of the lift coefficient are slight except for the thinnest sections at low speeds. The reason for the advantage of the 3R6 airfoil over the 3C6 airfoil is apparent from an examination of figures 14 and 17. The maximum lift coefficient of the 3C6 airfoil is lower than that for the 3R6 airfoil and the consequent earlier burble of the C airfoil causes its efficiency to drop sooner than the efficiency for the corresponding R airfoil. Further examination of figures 14 to 19 indicates that all the C airfoils burble at somewhat lower lift coefficients than the corresponding R airfoils.

It is apparent from this comparison that C airfoils are, in general, superior to corresponding R sections for propeller applications except for very high-pitch propellers operating at low values of V/nD where the angles of attack of the propeller blade sections are in the region of maximum lift. This conclusion is in substantial agreement with previous propeller tests (reference 6).

The differences between the moment coefficients for corresponding airfoils of the two families are relatively unimportant for propeller application, but it is to be noted that the differences over the entire speed range are in accord with the results of previous low-speed tests. The lift-curve slopes (taken as the slope of the

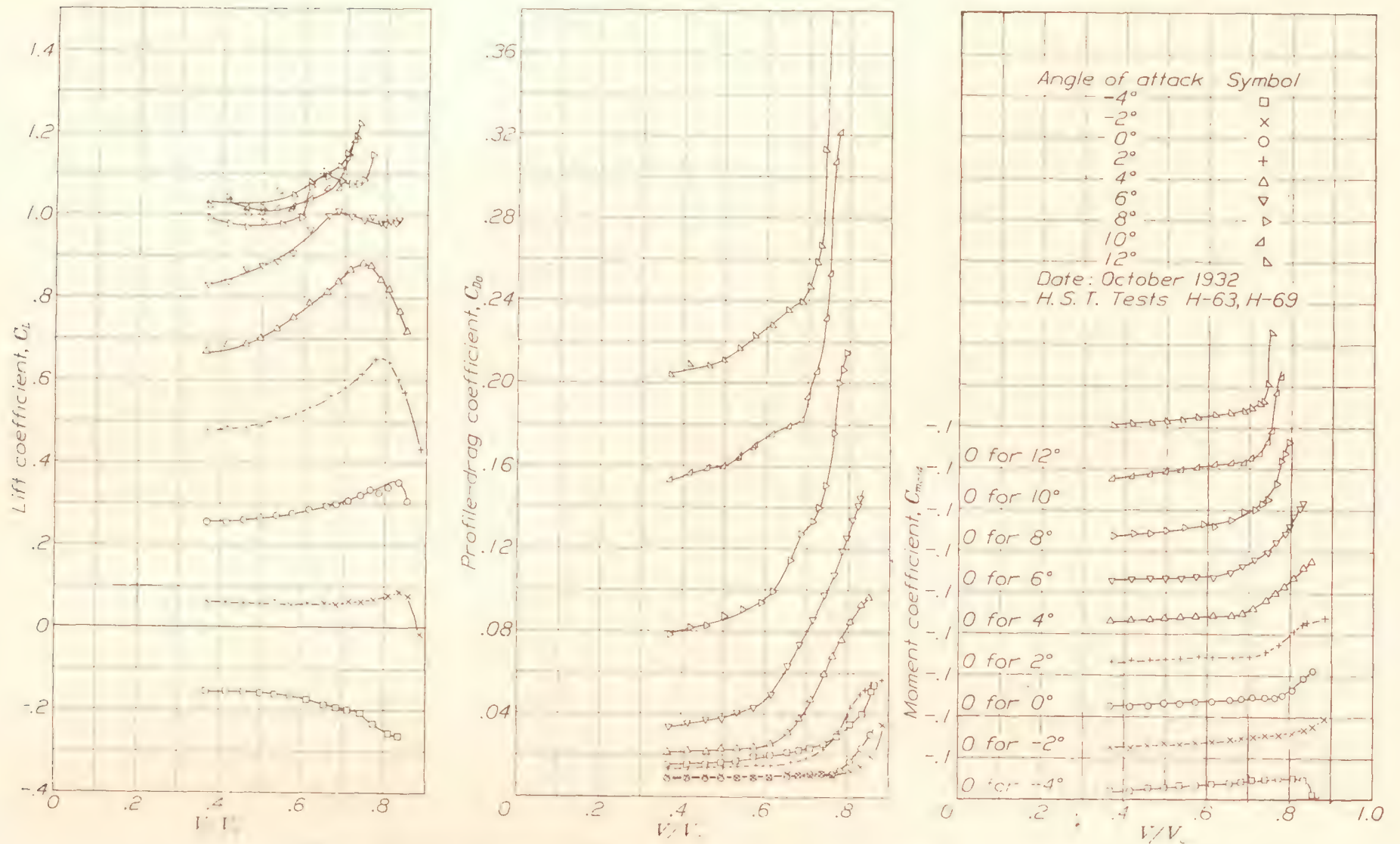


FIGURE 8.—Effects of compressibility on the aerodynamic characteristics of the 3C6 airfoil.

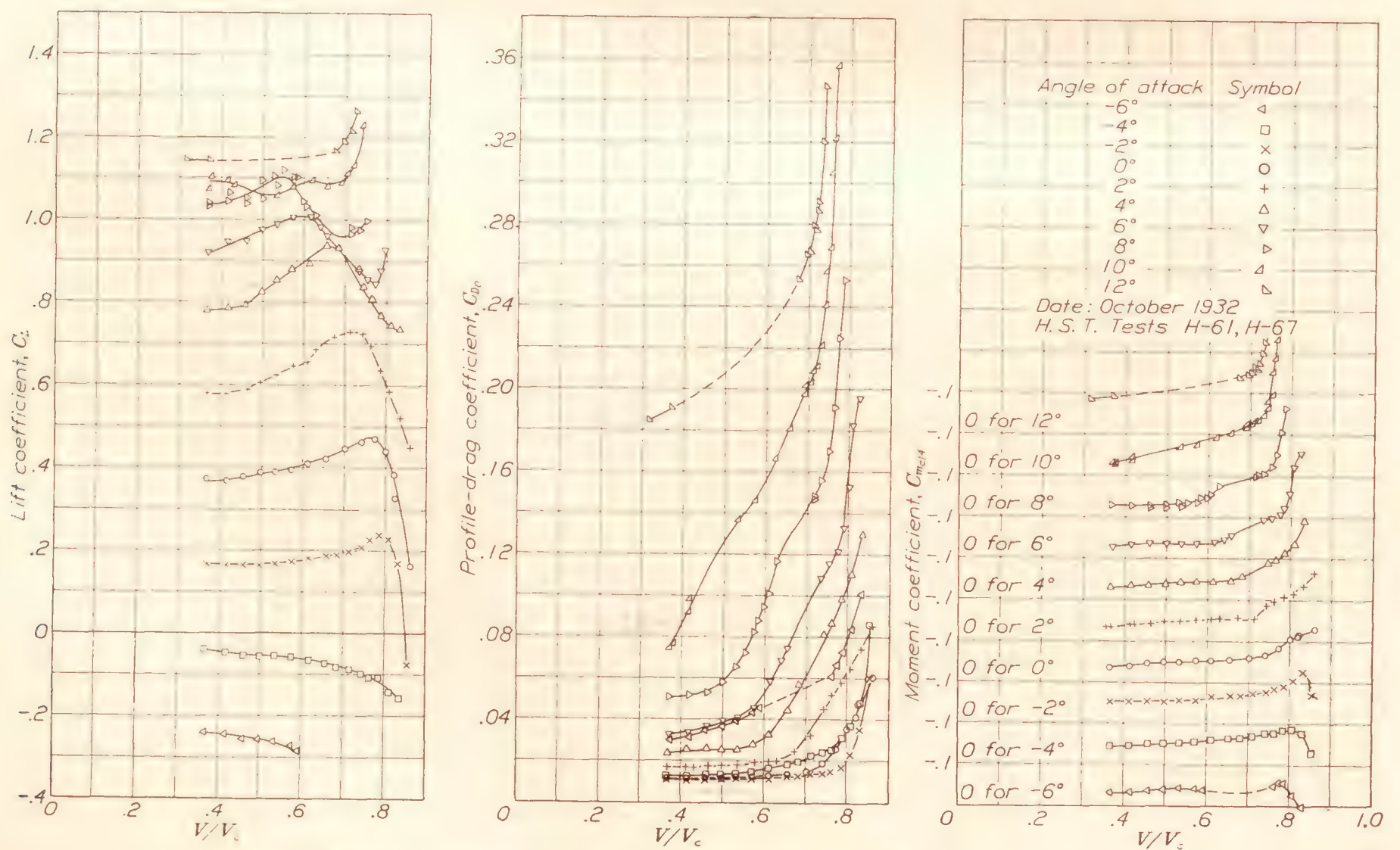


FIGURE 9.—Effects of compressibility on the aerodynamic characteristics of the 3C8 airfoil.

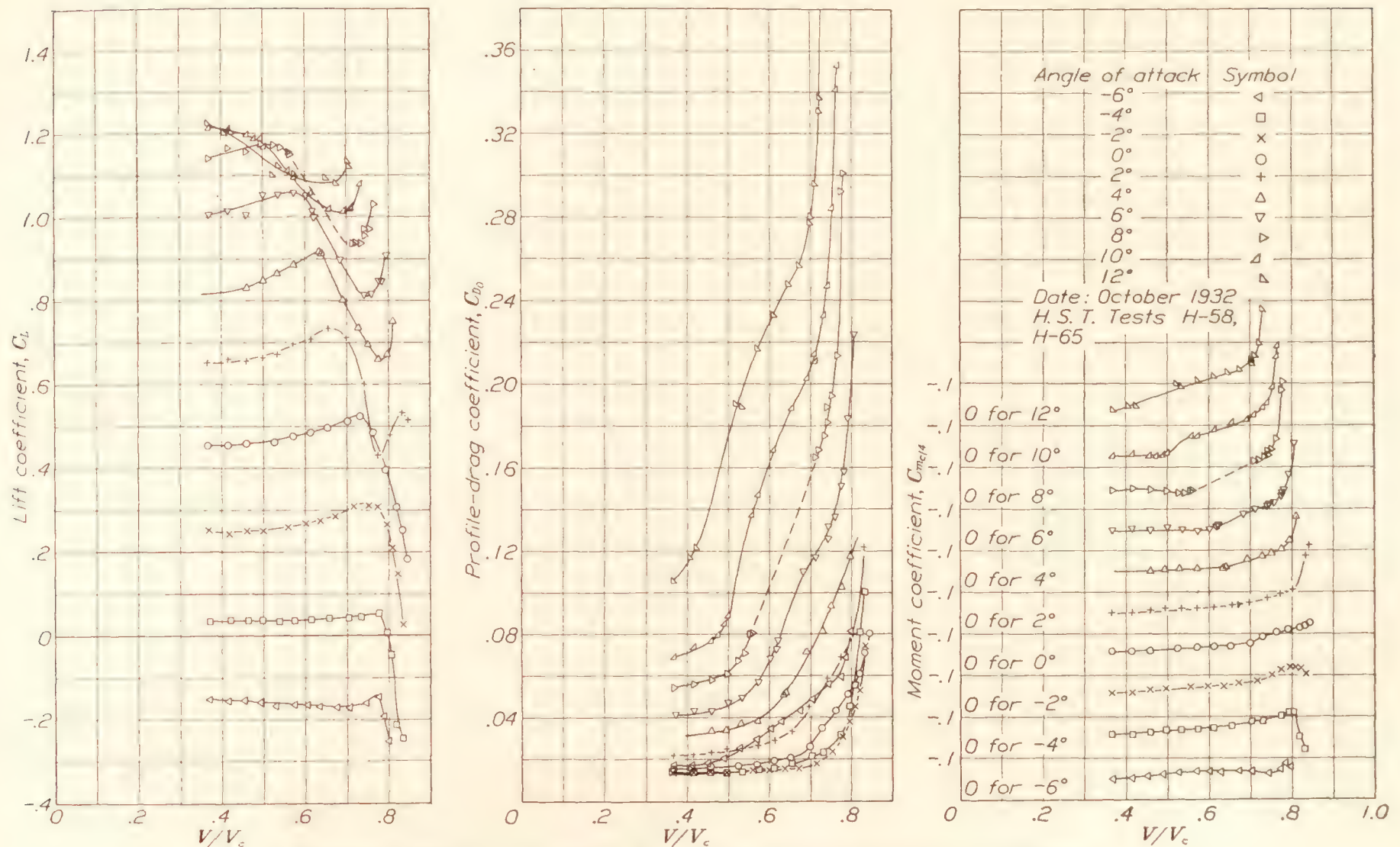


FIGURE 10.—Effects of compressibility on the aerodynamic characteristics of the 3C10 airfoil.

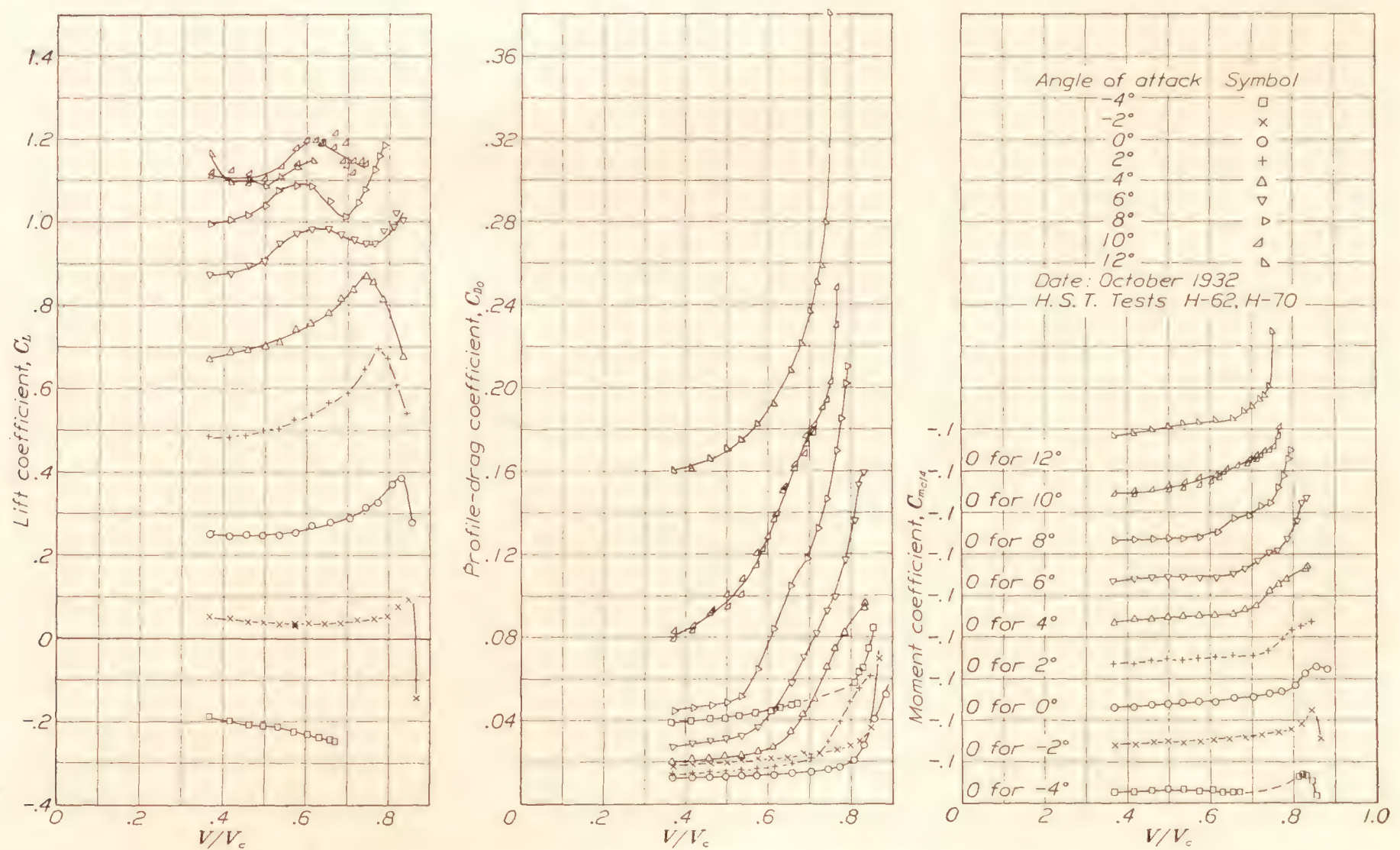


FIGURE 11.—Effects of compressibility on the aerodynamic characteristics of the 3R6 airfoil.

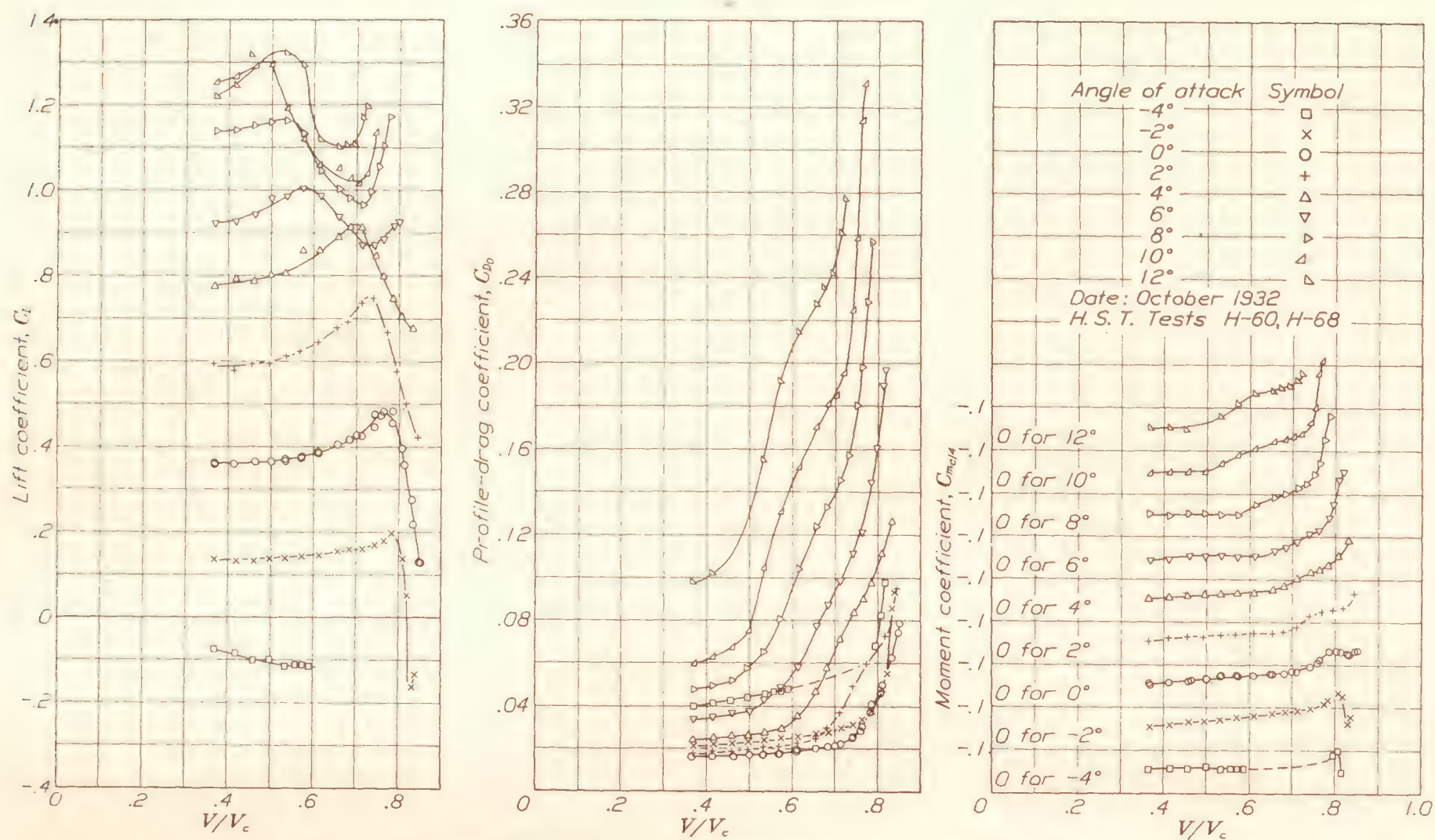


FIGURE 12.—Effects of compressibility on the aerodynamic characteristics of the 3R8 airfoil.

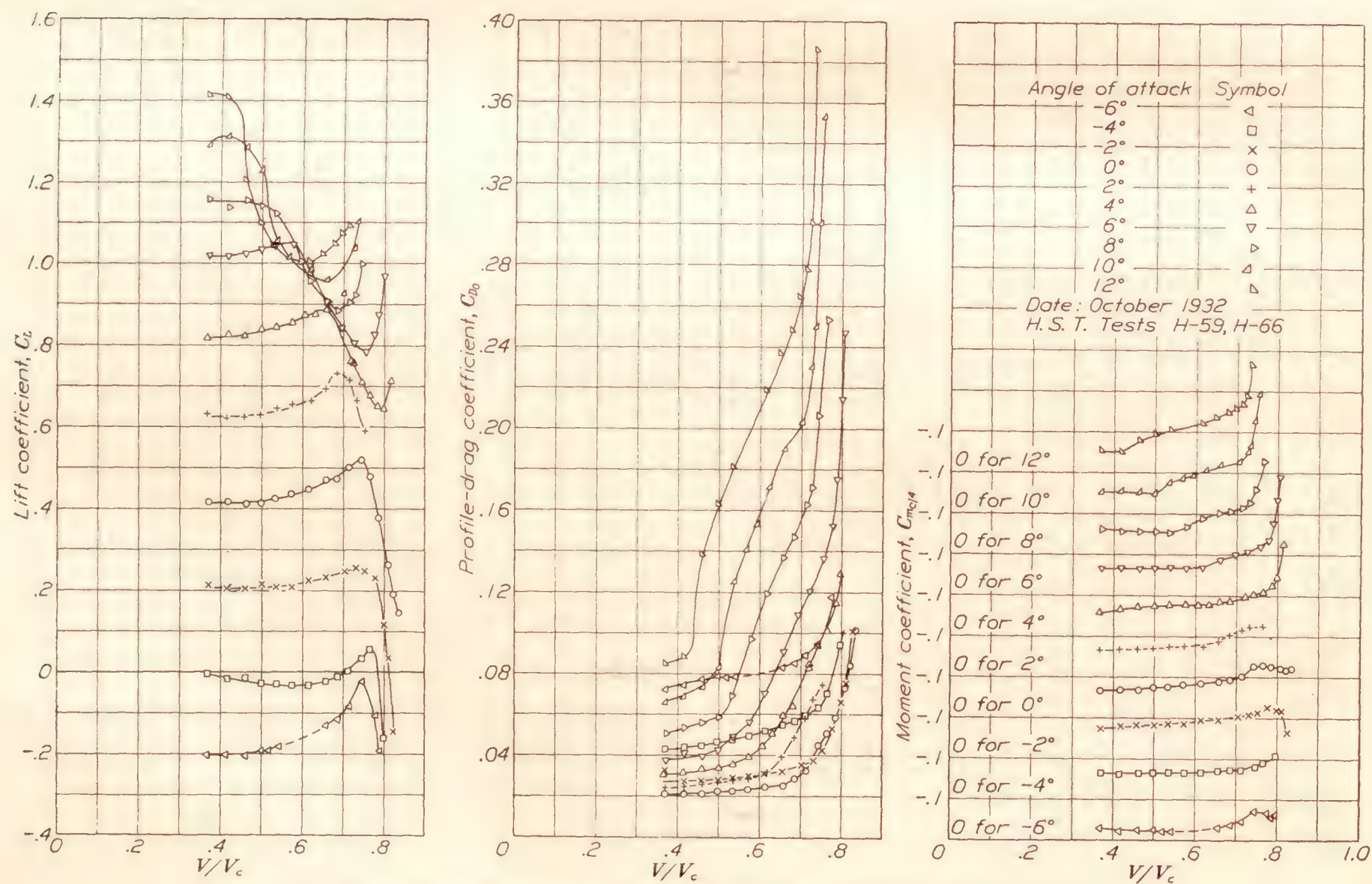


FIGURE 13.—Effects of compressibility on the aerodynamic characteristics of the 3R10 airfoil.

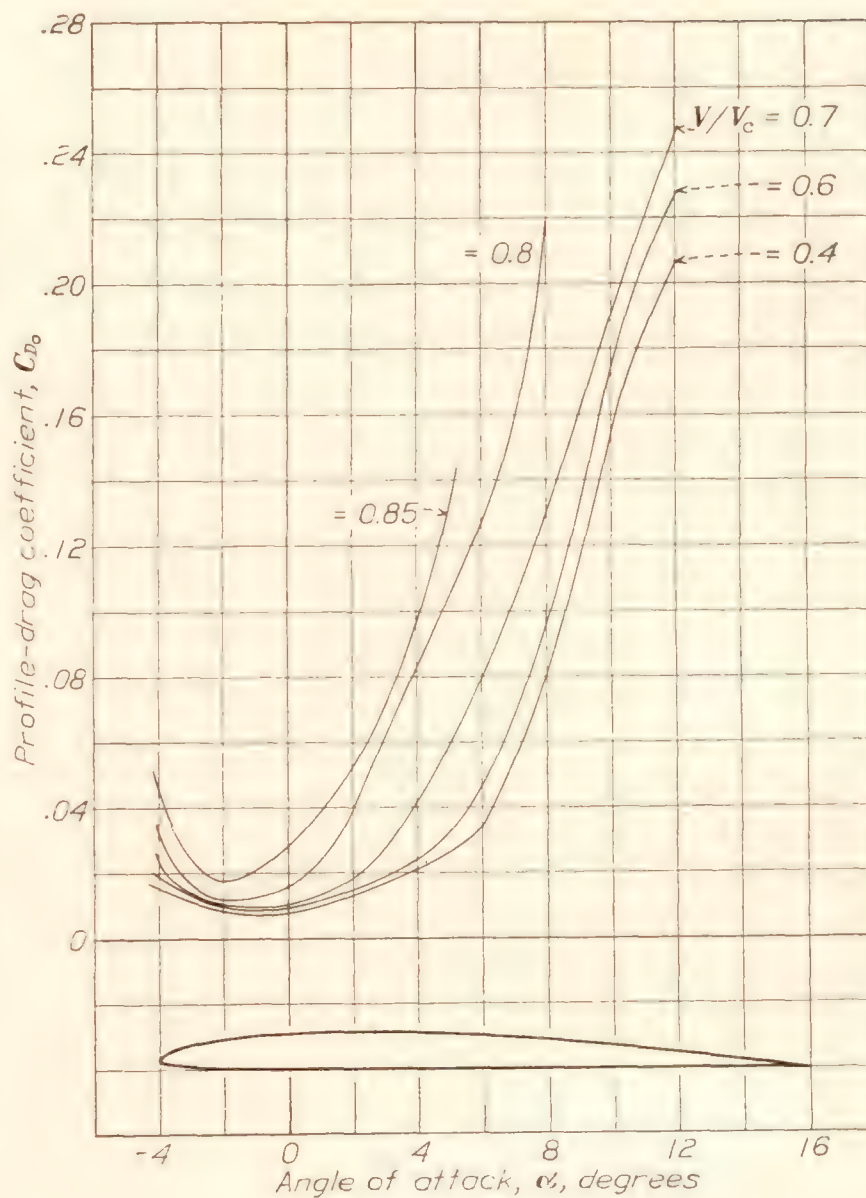
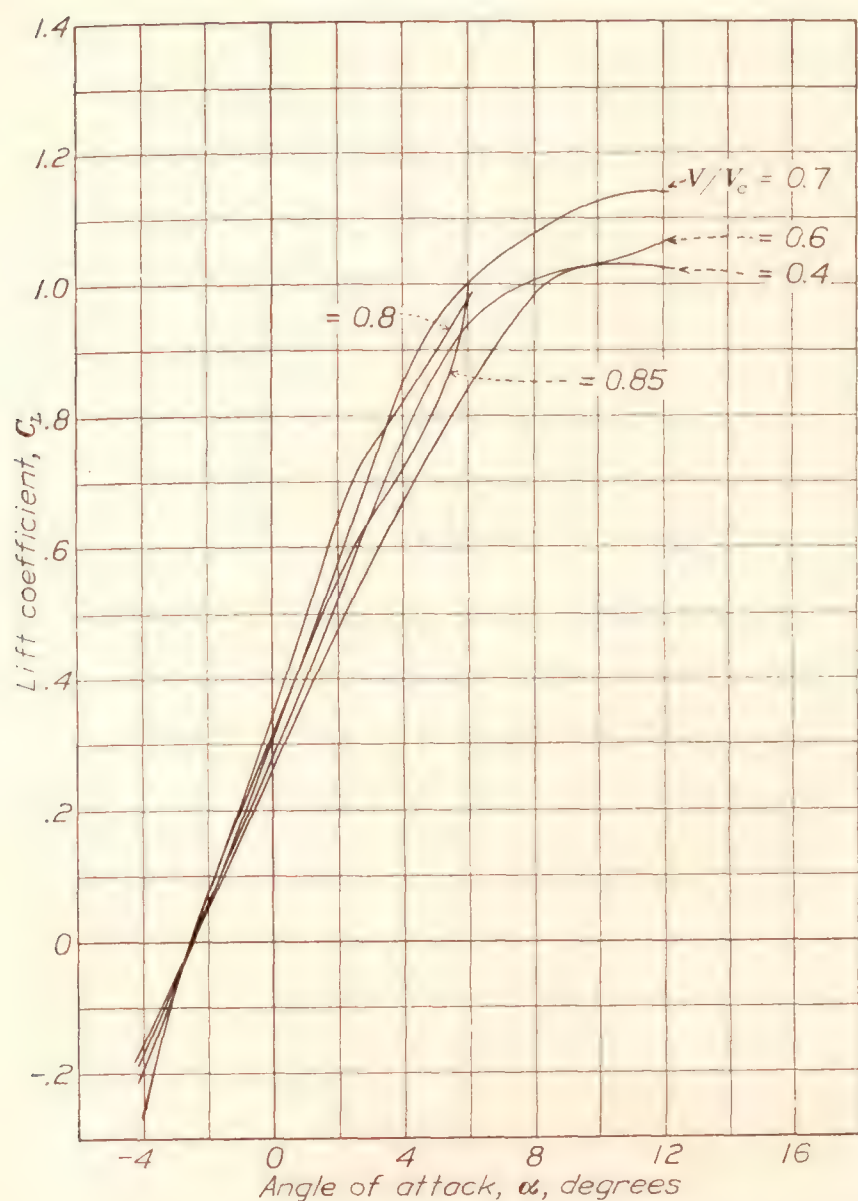


FIGURE 14.—Aerodynamic characteristics of the 3C6 airfoil for various speeds.

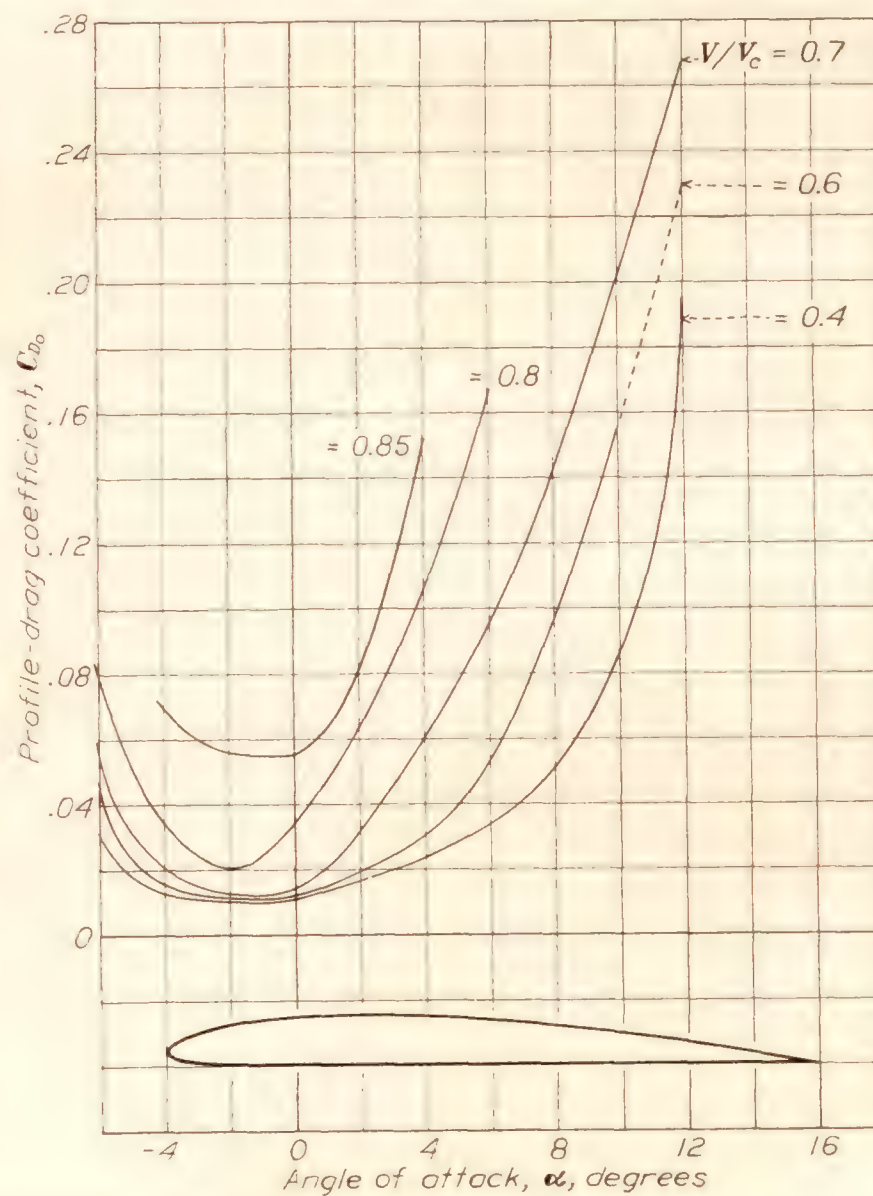
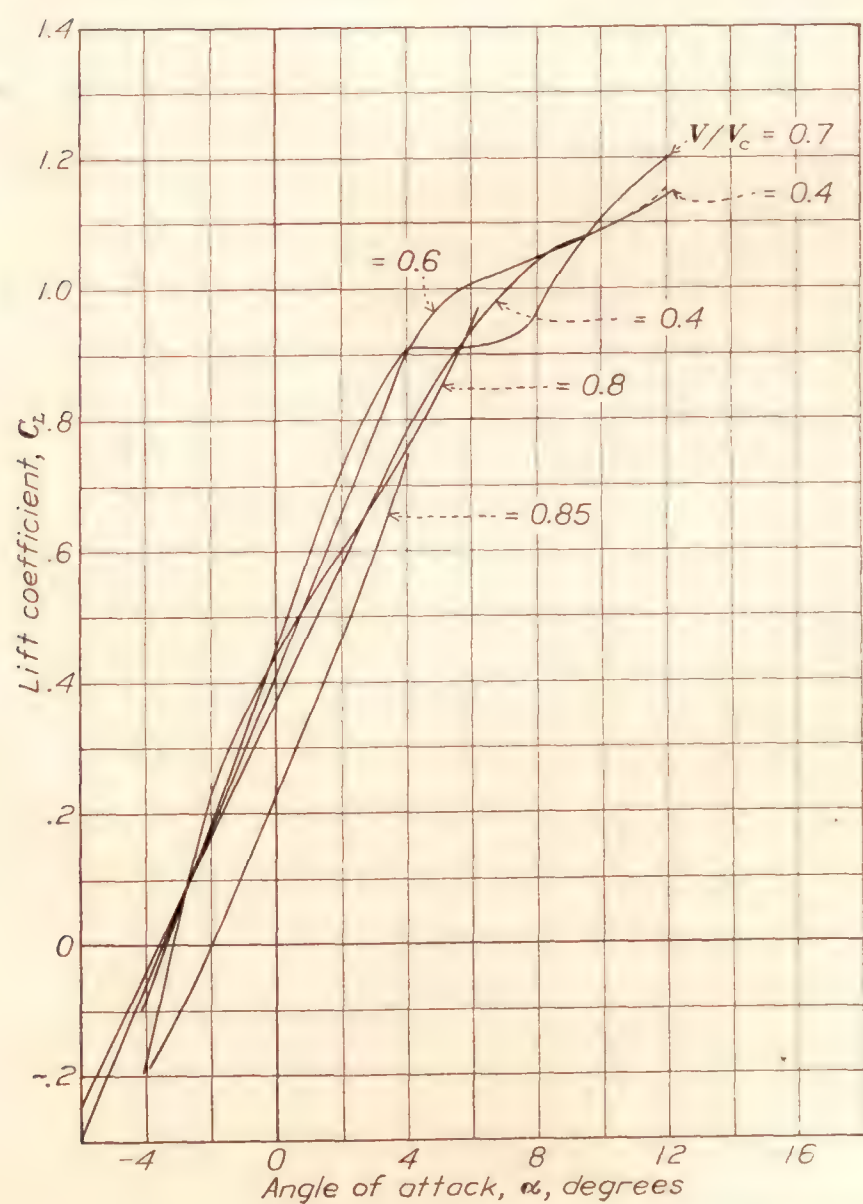


FIGURE 15.—Aerodynamic characteristics of the 3C8 airfoil for various speeds.

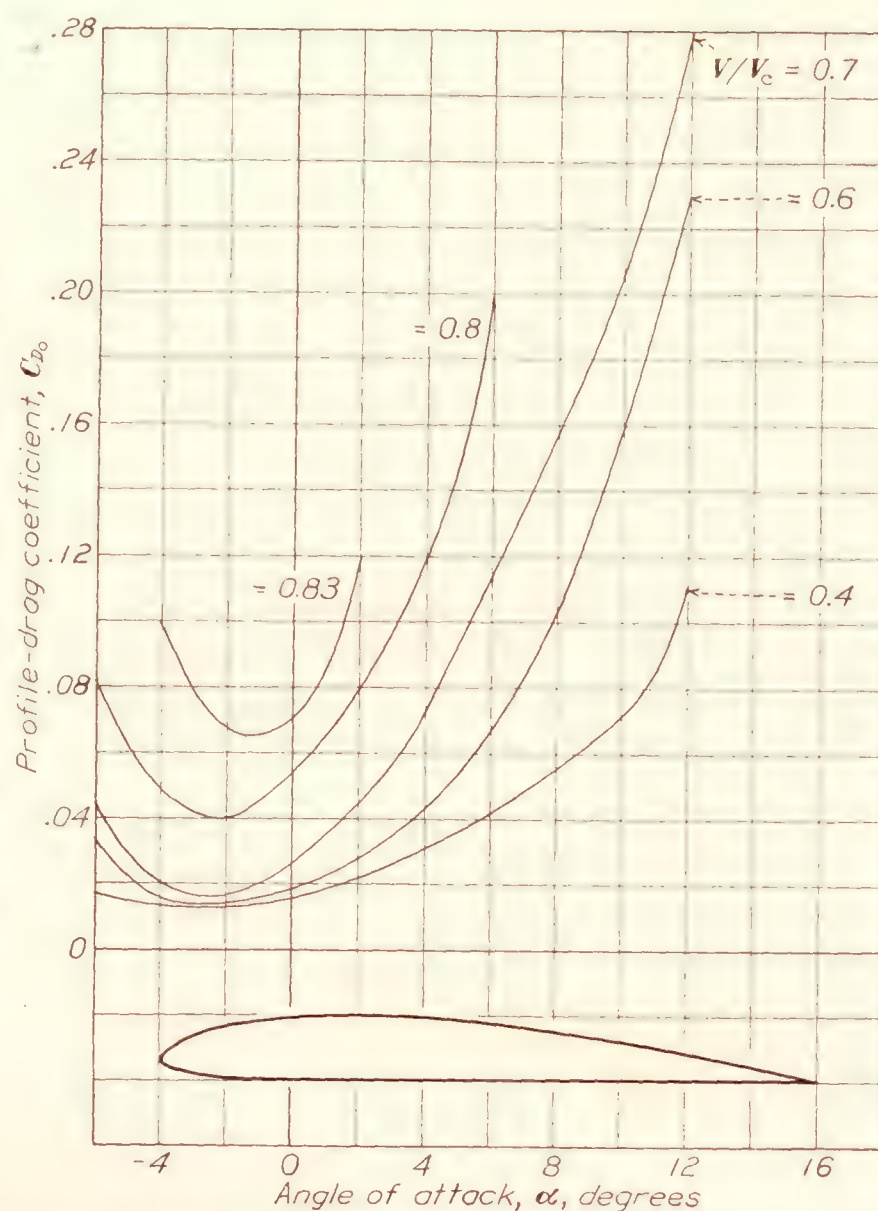
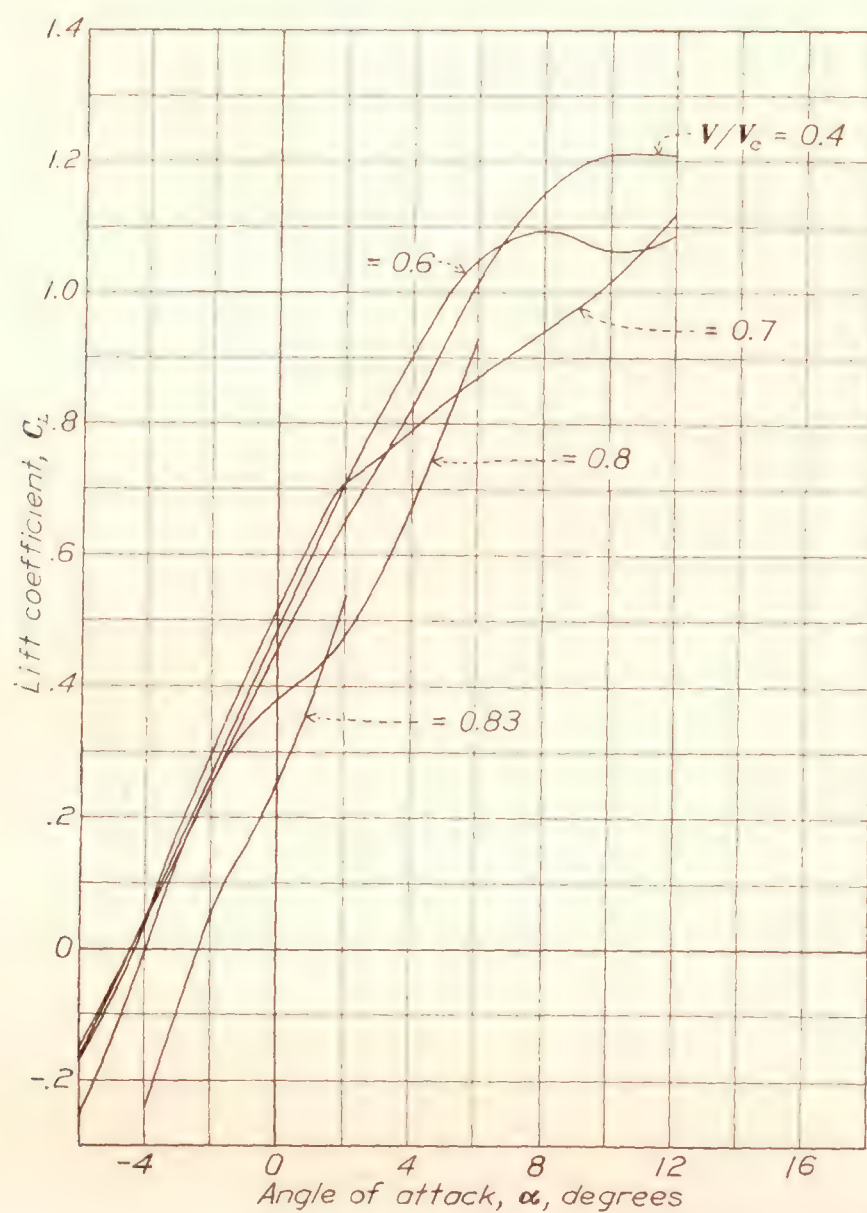


FIGURE 16.—Aerodynamic characteristics of the 3C10 airfoil for various speeds.

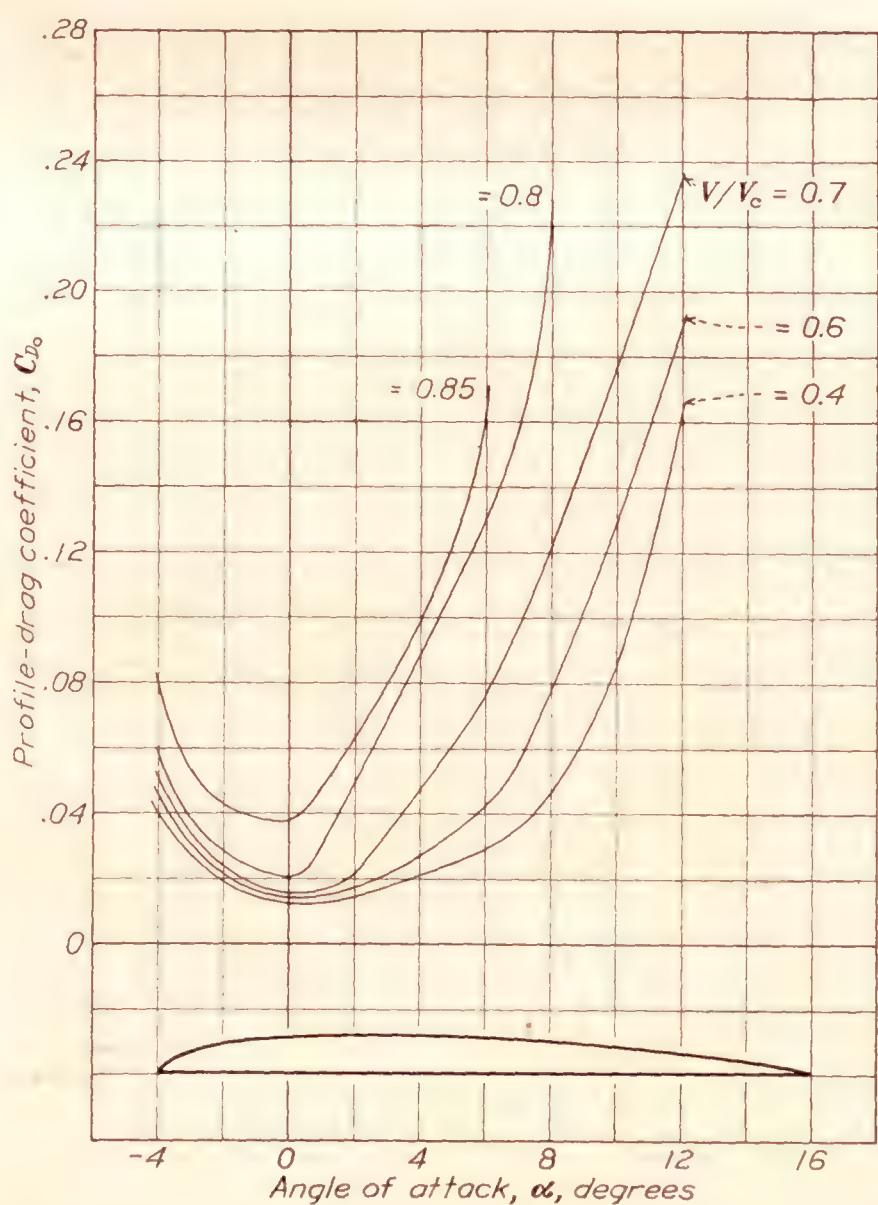
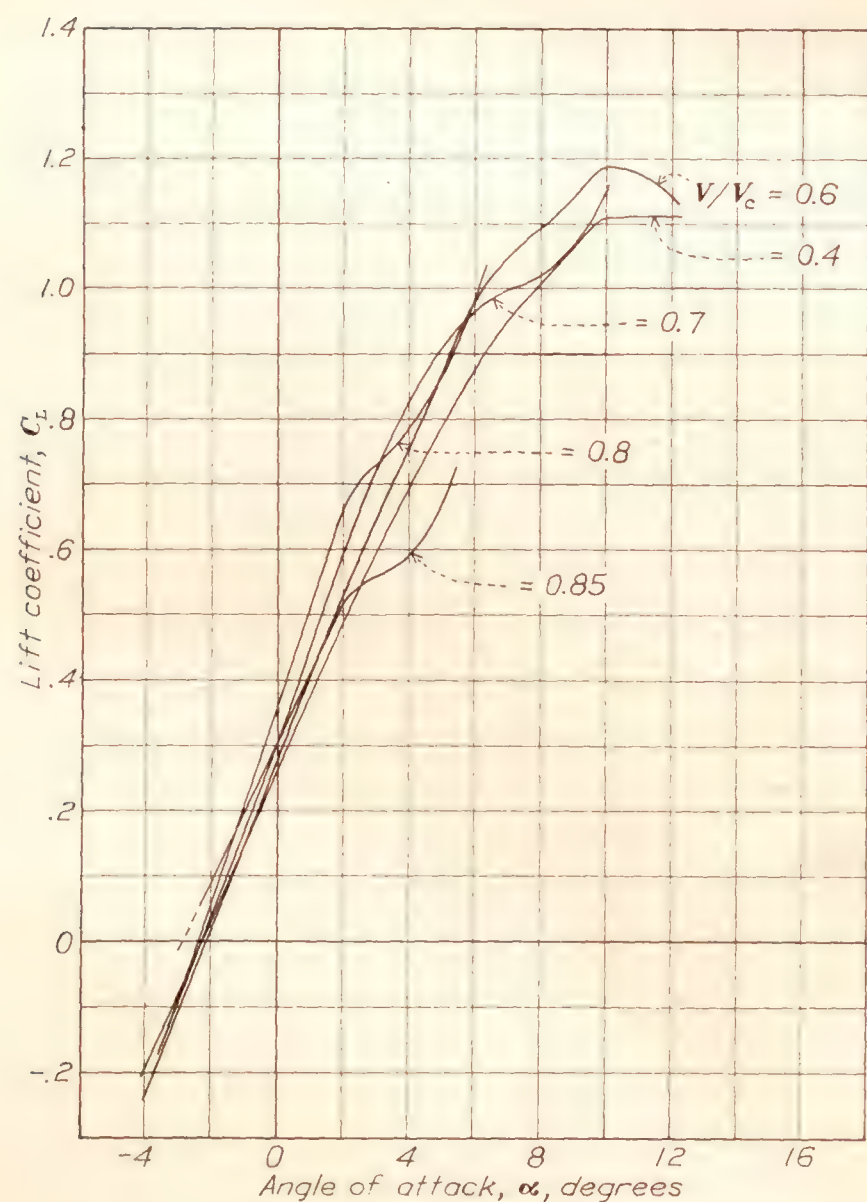


FIGURE 17.—Aerodynamic characteristics of the 3R6 airfoil for various speeds.

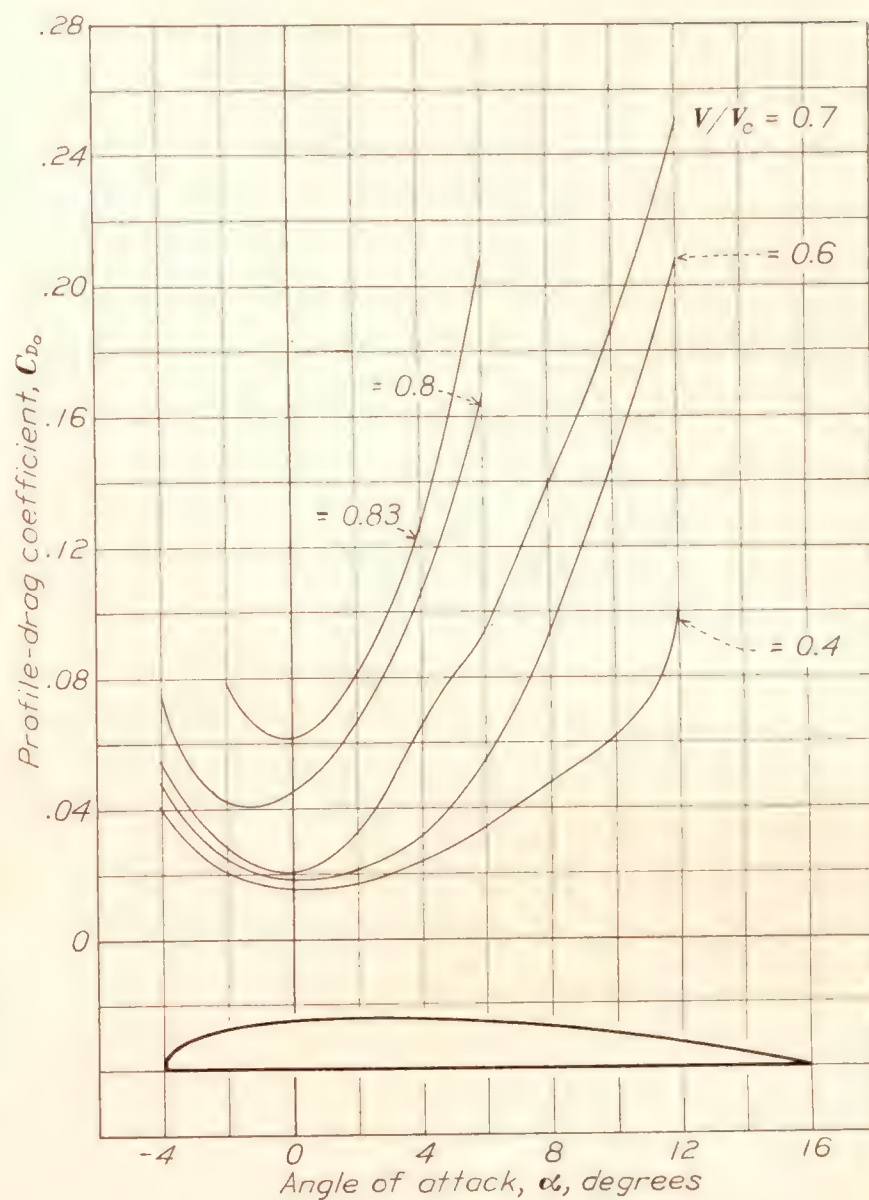
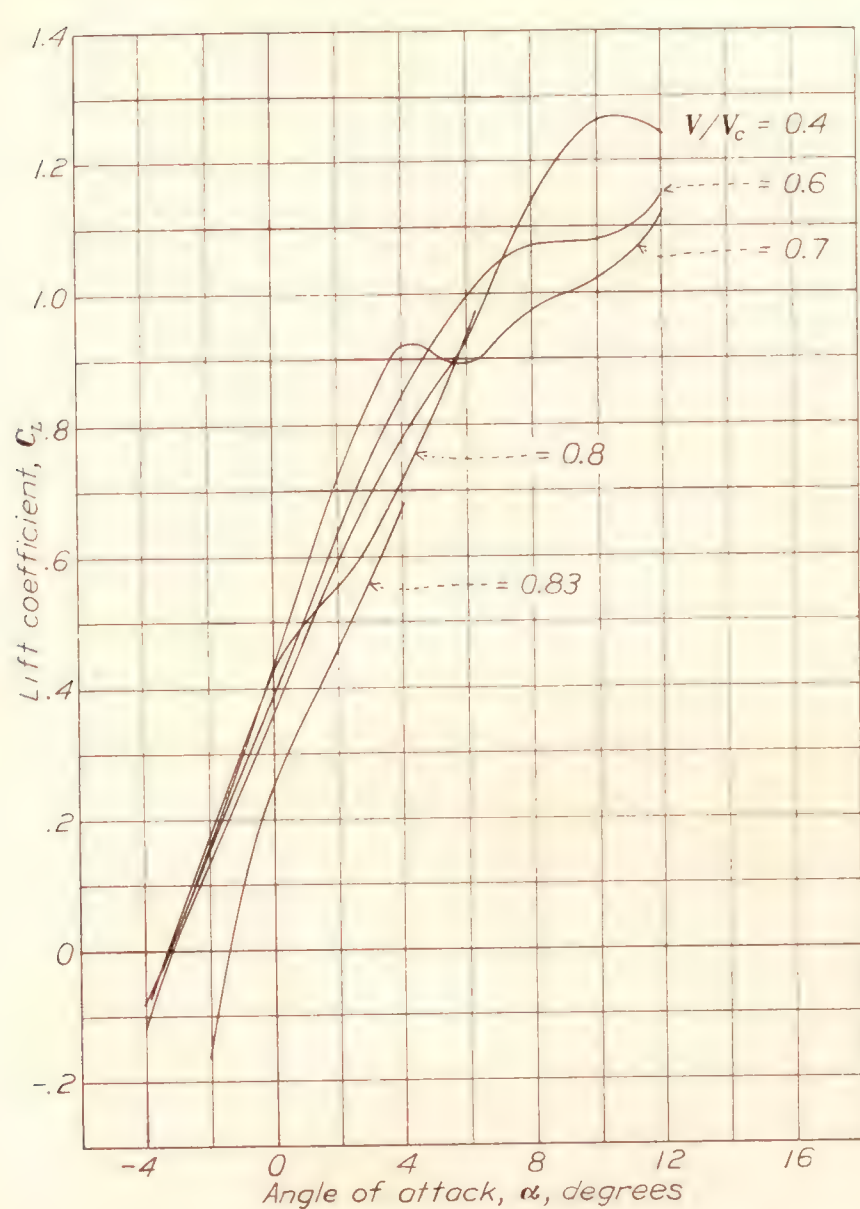


FIGURE 18.—Aerodynamic characteristics of the 3R8 airfoil for various speeds.

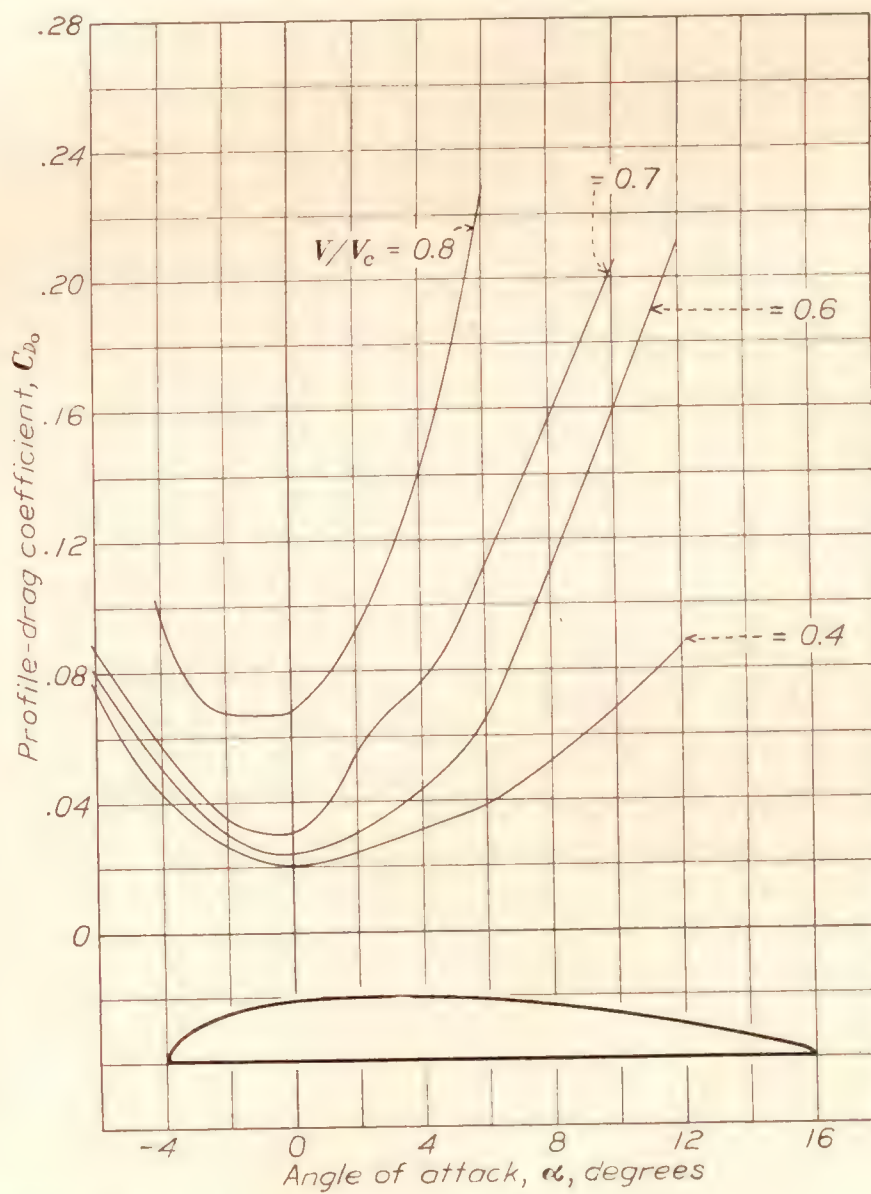
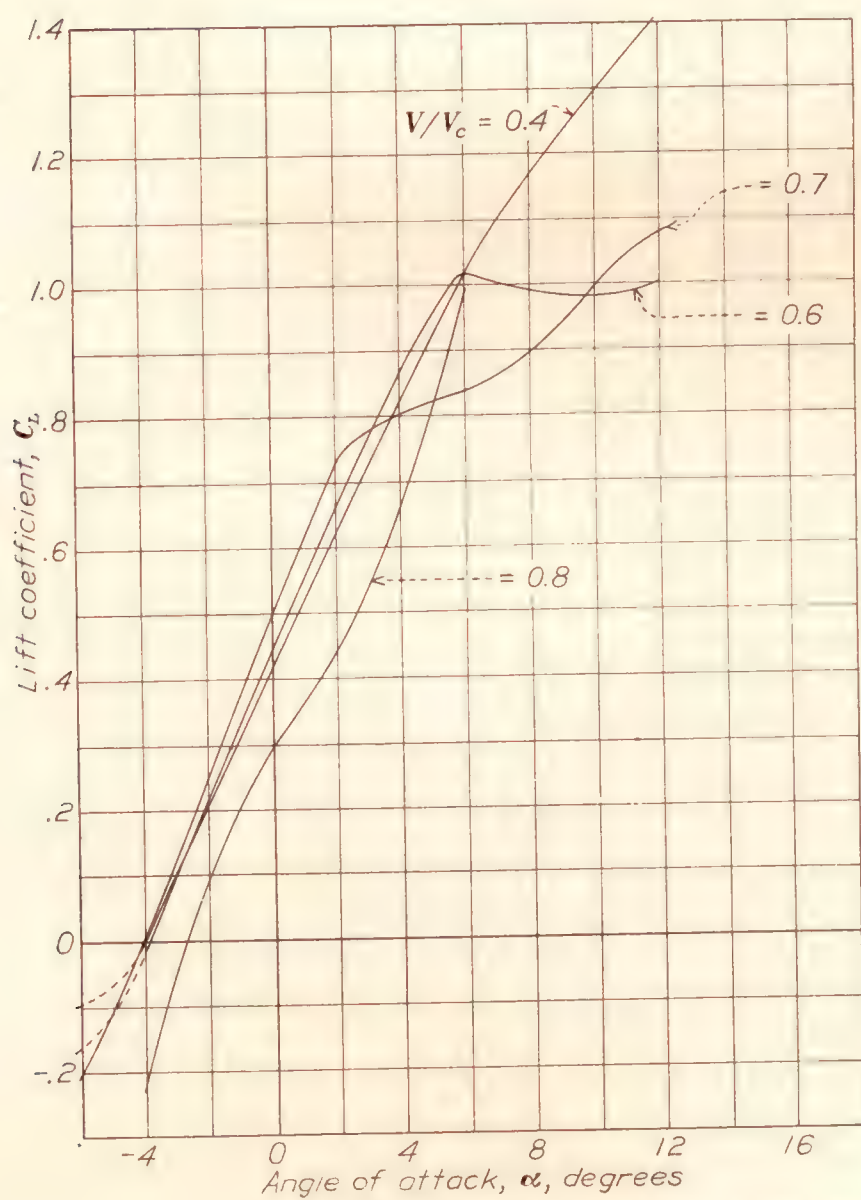


FIGURE 19.—Aerodynamic characteristics of the 3R10 airfoil for various speeds.

lift curve in the low-drag range) of the R airfoils are slightly higher than the lift-curve slopes for the corresponding C airfoils except for the thickest airfoils. However, the differences are not very great, and, in view of the difficulty of accurately measuring this quantity, no definite conclusions should be drawn.

Variation of the airfoil characteristics with thickness.—Figure 20 shows a uniform increase of minimum-drag coefficients with increasing thickness and, in addition, shows with one exception a like change for the drag coefficient at various values of the lift coefficient. At lower speeds the drag coefficient of the 3C6 airfoil for a lift coefficient of 0.8 is higher than might be

reduction of the lift-curve slope. The maximum lift variations have not been studied in detail because the values of this characteristic are not definite at high speeds.

Effects of compressibility.—As the velocity of the air past the model is increased, pronounced changes occur in the aerodynamic characteristics of the airfoil. These changes are best studied by referring to figures 8 to 13, inclusive. The lift coefficients increase as the speed is increased, slowly as the speed is increased over the lower portion of the range, then more rapidly as speeds above half the velocity of sound are exceeded, and finally at higher speeds, depending on the airfoil

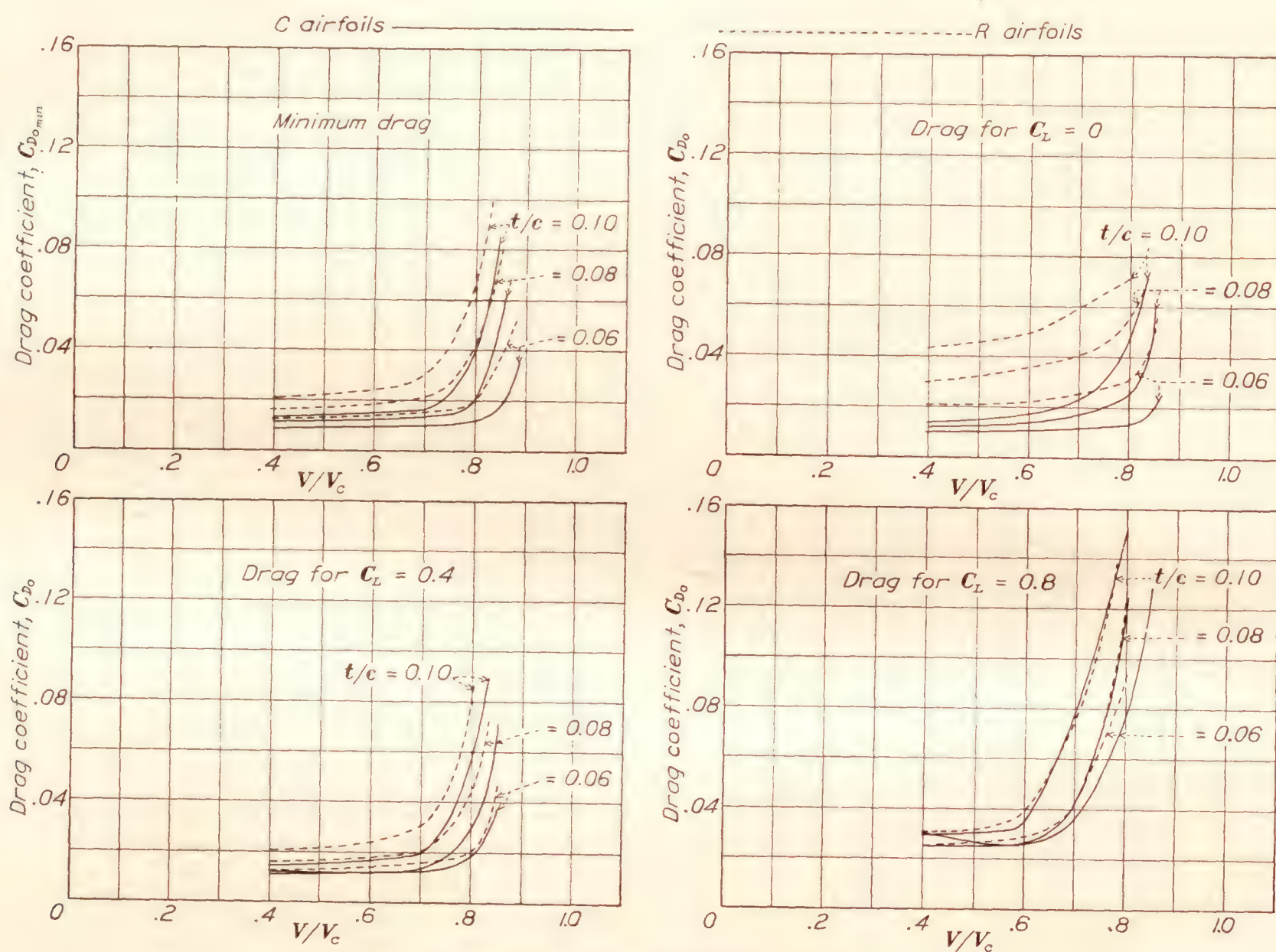


FIGURE 20.—Effect of compressibility on drag.

expected, which as previously noted is due to the early burble of this C airfoil. The moment coefficient and the angle of zero lift show uniform changes with thickness. These quantities, although not primarily dependent on thickness changes, may be expected to change in a systematic manner because the method employed for varying the airfoil thickness also varies the mean camber. An examination of figures 8 to 13 shows the moment variation with increasing thickness and figures 14 to 19 show the angle of zero-lift variation. The effect of thickness variation on lift-curve slope is not as uniform as the changes of the other aerodynamic properties. However, it is shown in figure 21 that increased thickness, in general, causes a

section and the angle of attack, the flow breaks down as shown by a drop in the lift coefficient. This breakdown of the flow, hereinafter called the compressibility burble, occurs at lower speeds as the lift is increased by changing the angle of attack of the model. At the highest lift coefficients, which are in the region of the normal burble, the breakdown of the flow occurs at low speeds and, because of the unsteadiness of the flow, the curves of lift coefficient plotted against speed become irregular. The drag coefficient behaves in a similar manner. A small but steady increase in drag as the speed is increased is observed, which continues until the compressibility burble is reached. At this point the drag coefficients rise rapidly to values several

times as large as the low-speed values. As with the lift coefficient, the rapid rise in the drag coefficient occurs at lower speeds as the angle of attack is increased until finally, at angles of attack in the neighborhood of

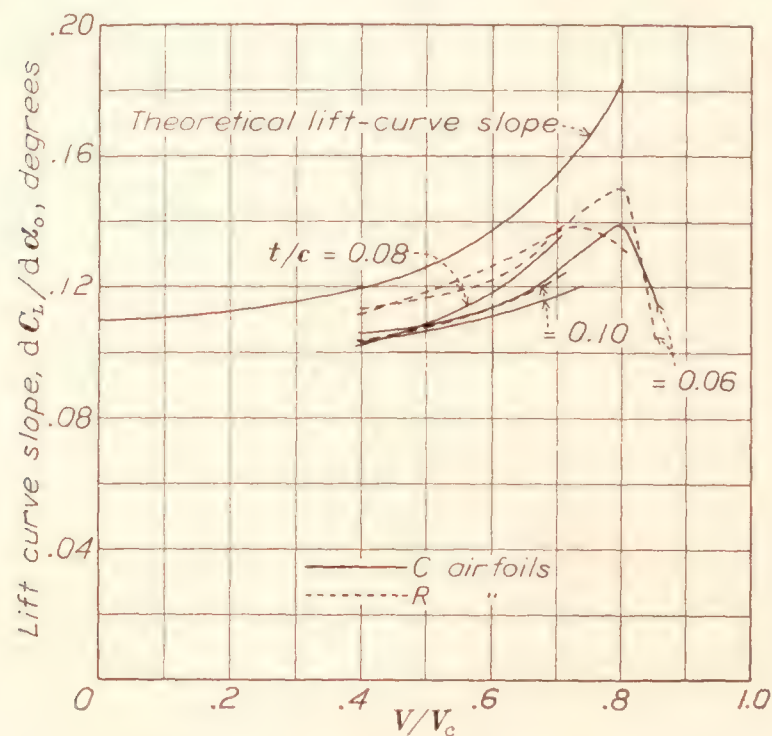


FIGURE 21.—Effect of compressibility on lift.

the normal stall at low speeds, the drag rises rapidly at velocities of the order of 0.4 the velocity of sound. The variation of the moment coefficient is similar to the variation of the lift and drag coefficients. The

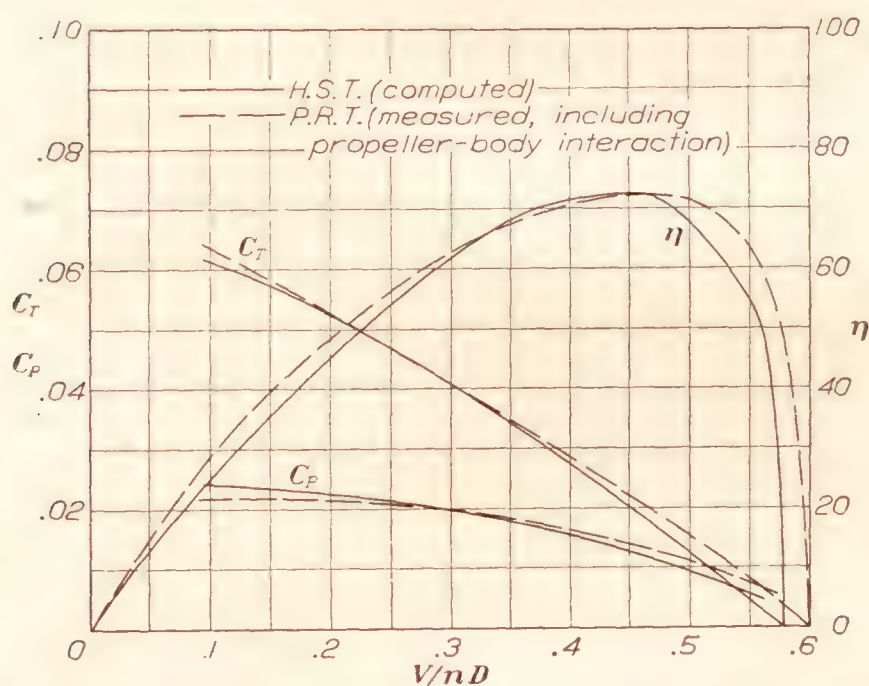


FIGURE 22.—Comparison of computed and measured propeller characteristics—tip speed 0.75 V_c , C-10 propeller.

moment increases numerically as the speed is increased, this change continuing until the compressibility burble is reached. At this point rapid changes in the moment occur.

The effect of compressibility on the moment coefficient is of considerable importance in the structural design of fast-diving airplanes. Speeds in the neighborhood of half the velocity of sound are commonly attained by most airplanes of this type when in a dive, and if low-speed moment data are applied to the design of the spars large errors in the estimation of the distribution of load between the spars may be introduced.

Further changes in the aerodynamic characteristics occur as the speed is increased. The lift-curve slope increases with the speed until a speed corresponding to the general breakdown of the flow is reached. Above this speed the lift curves show either discontinuities or irregularities of form. (See figs. 14 to 19 and fig. 21.) Figures 14 to 19 also show large changes in the angle of zero lift at high speeds. The value is but little affected by speed changes until the compressibility burble occurs. At higher speeds the zero-lift attitude approaches zero angle of attack. The changes are shown in the following table, which has been compiled from figures 14 to 19.

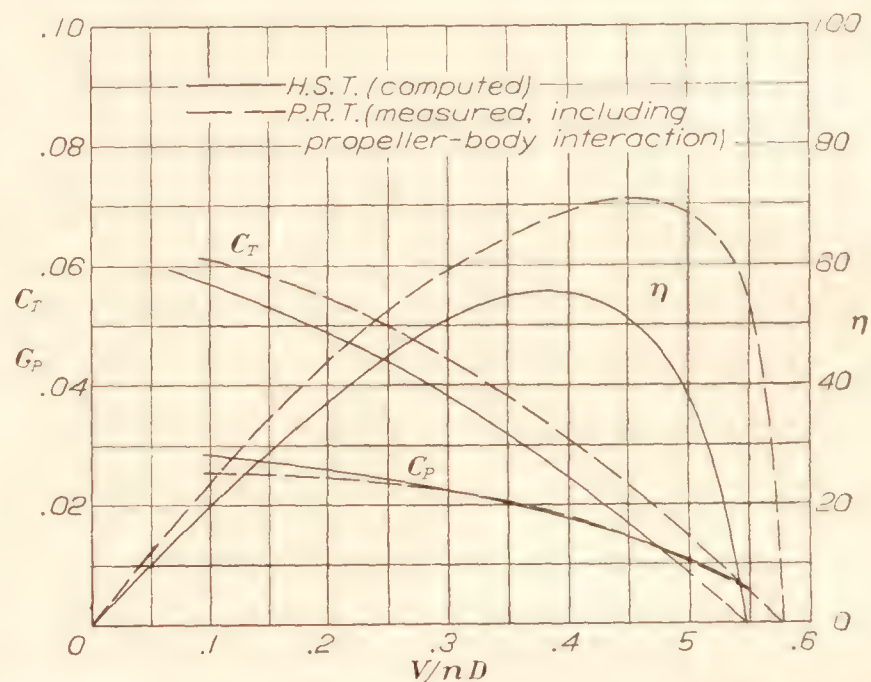


FIGURE 23.—Comparison of computed and measured propeller characteristics—tip speed 0.9 V_c , C-10 propeller.

V/V_c	0.4	0.6	0.7	0.8	0.83	0.85
Airfoil	Angle of zero lift					
3C6	-2.5°	-2.45°	-2.45°	-2.5°	-----	-2.55°
3R6	-2.3°	-2.2°	-2.3°	-2.4°	-----	-----
3C8	-3.55°	-3.5°	-3.4°	-3.1°	-----	-1.95°
3R8	-3.2°	-3.2°	-3.25°	-3.3°	-1.45°	-----
3C10	-4.35°	-4.35°	-4.35°	-3.9°	-2.4°	-----
3R10	-4.0°	-3.85°	-4.0°	-2.7°	-----	-----

The shift of the angle of zero lift is not shown by the thinnest airfoils because the compressibility burble at low lifts takes place at speeds slightly higher than those recorded in the table. The results shown in the table, as well as the results shown by figures 20 and 21, lead to the conclusion that the speed at which the compressibility burble occurs is a function of the airfoil thickness. The table shows no change in the angle of zero lift at 85 percent of sound velocity for the thinnest airfoils. The 8 percent thick airfoils show a change in angle of zero lift in the neighborhood of 0.8 V_c and the thickest airfoils show this change occurring at speeds slightly in excess of 0.7 V_c . An examination of the profile-drag coefficient curves for zero lift coefficient (fig. 20) shows the rapid rise in drag occurring at substantially the same values as those previously noted for the angle-of-zero-lift changes.

All the data indicate that the flow breakdown occurs at speeds well below the velocity of sound. The early breakdown of flow is probably due (references 7 and 8) to the fact that the induced velocities over the airfoil are higher than the main-stream velocity and so reach the velocity of sound when the main-stream velocity is much lower than the speed of sound. There are some reasons to believe that the attainment of sound velocity at any point in the field of flow causes a marked change in the type of flow and is probably responsible for the compressibility burble. The experimental data tend to substantiate this deduction. The compressibility burble, as indicated by the peaks of the curves of the lift coefficient plotted against V/V_c for various angles of attack (figs. 8 to 13), occurs at lower speeds as the angle of attack or the lift is increased. The shift of the angle of zero lift following the compressibility burble is attributed to the reduction in lift over the upper surface of the airfoil which occurs concurrently with the flow breakdown.

Theoretical investigations of the effects of compressibility have so far yielded but little information regarding the actual flow phenomena, principally because of mathematical complications arising in the analysis. Rayleigh and Bryan (references 9, 10, and 11) have attempted solutions but the mathematical complication involved in the application of their work seems to have virtually prohibited the solution of any practical problem. More recently Taylor, Glauert, and Ackeret (references 12, 13, and 14) have attempted solutions and have to some extent succeeded in predicting some of the effects that have been observed experimentally. The mechanical method for solving fluid flow as devised by Taylor (reference 12) indicates that a change in the type of flow occurs when the velocity at any place in the field of flow, and not necessarily the velocity of the main stream, attains the velocity of sound. This work is of importance in that it points to definite limitations in the theoretical analysis of Glauert and Ackeret. The success of the mechanical method for solving fluid flows depends on an analogy between the equations for the irrotational motion of a fluid and the equations for the flow of electric current in a sheet of conducting substance of variable depth, an electrolyte in Taylor's experiments. As the experiments with the electric analogy progressed, it became apparent that no solution could be obtained if the velocity of the fluid at any point in the field of flow equaled or exceeded the velocity of sound. This fact leads to the inference that irrotational motion, the type of flow postulated by Glauert and Ackeret, does not exist if sound speed is reached at any point in the field of flow. Taylor's experiments on the 12¼ percent thick R.A.F. 31a airfoil indicate a change in type of flow at a main-stream velocity between $0.5 V_c$ and $0.65 V_c$ when the attitude of the airfoil is such that the low-speed lift coefficient is in the neighborhood of 0.8. The present work indi-

cates that a breakdown of the flow occurs at a speed of approximately $0.64 V_c$ for the thicker airfoils when their attitude is the same as that of the R.A.F. 31a in Taylor's experiments. It would seem, therefore, in view of the agreement of the direct experimental and mechanical methods of measurement regarding the breakdown in flow, that any theoretical analysis of the effect of compressibility postulated on irrotational motion is inapplicable at relatively high speeds.

This limitation is imposed on the theoretical work of Glauert and Ackeret. In addition, Glauert's work is further restricted because it assumes that the velocity at the surface of the airfoil does not differ appreciably from the main-stream velocity. Ackeret's method of analysis differs somewhat from Glauert's, but it also is subject to the same restrictions. Both agree, however, on the change which might be expected in the early stages. The important conclusion reached by both is that the lift-curve slope may be expected to vary proportionately with the factor $(1 - (V/V_c)^2)^{-1/2}$. In order to verify this prediction the theoretical lift-curve slope variation has been plotted against V/V_c with the experimental results in figure 21. The similarity of the experimental curves to the theoretical curve is striking and leads to the conclusion that at speeds below that at which the compressibility burble occurs, the application of the factor to the known experimental lift-curve slope at low speeds is justified for practical purposes.

Glauert's work also indicates that the chord of the airfoil in a compressible flow is effectively shorter than the chord of the airfoil in an incompressible flow. The effect of compressibility is then to increase the effective camber of the airfoil and as a result the moment coefficient may be expected to increase numerically. The moment-coefficient curves (figs. 8 to 13) show a change in the same direction as that predicted.

Comparison with previous work.—Airfoils similar to those studied in this investigation, as well as other airfoils, have been tested previously over a wide speed range but the results of the earlier investigations are not directly comparable with these results because of different test conditions. The earliest experimental investigation of airfoil characteristics as affected by compressibility is described in reference 15. Similar airfoils were later tested (reference 16) over a wider speed range in a different form of wind tunnel. Pressure-distribution tests of these airfoils were also made (reference 7) but quantitative correlation with previous results was again impossible because of different test conditions. The latest measurements are those given in reference 5. None of the foregoing investigations, however, affords a quantitative comparison with the present investigation. The tests of reference 15 consisted only of lift measurements of six airfoils of 1-inch chord and 6-inch span mounted on a central support in a 14-inch diameter wind tunnel. The results are

of limited value because of the small speed range and the low Reynolds Number. The tests described in reference 16 were made in an open-jet wind tunnel. The models were of 3-inch chord; they extended across a jet of air issuing from a 12.24-inch nozzle and projected into the still-air region on either side of the jet. The air mixed directly with the atmosphere. The tests described in references 5 and 7 were made in a similar tunnel but the diameter of the air jet was 2 inches and the chord of the models was 1 inch. These results are, of course, subject to large aspect-ratio corrections and because of the unknown influence of the jet boundaries and model end conditions, these corrections are unknown. The results are therefore comparable only qualitatively with the results of this investigation. Some tests of other airfoils have been made in England under approximately infinite aspect-ratio conditions in a small wind tunnel so that although the tunnel-boundary conditions are satisfactory the Reynolds Number for the tests is much smaller than that obtained in the present investigation.

An examination of the effects of compressibility on airfoil characteristics as demonstrated by the earlier investigations does show good agreement, qualitatively, with the results of the present investigation. The existence of a definite compressibility burble has been shown and the speed at which this occurs has been shown to be influenced by the airfoil thickness and the angle of attack of the airfoil (reference 16). The marked drag increase has also been demonstrated. The gradual change in the moment coefficients for speed changes below the speed at which the compressibility burble occurs has not been shown previously. This difference may be explained by the inherent inaccuracy of the methods previously used for measuring this quantity (reference 16). The systematic change in the lift-curve slope has been shown by the British tests (reference 17), but not by previous American tests, which is undoubtedly due to the large influences of the boundaries of the air jet used in the American tests on the character of the flow over the airfoil. An important difference between the present tests and those of reference 5 concerns the relative advantages of C and R airfoils. The results of reference 5 indicate that for airfoil thicknesses less than 0.1c the R airfoils are superior to the C airfoils at high angles of attack. For thickness ratios of 0.08 or larger the difference between the C and R airfoils at high angles of attack is shown by these tests to be small, but the C airfoils are, in general, slightly better. Because the differences are small, it may be that the relatively large effects of the jet boundaries in the earlier tests influenced the results. Another difference in the results of these and previous tests which may be attributed to jet-boundary phenomena is found in the speeds at which the compressibility burble occurs. The shift of the angle of zero lift at very high speeds is substan-

tiated and the advantages of using thin sections in preference to thick sections at high speeds are also substantiated.

Computation of propeller characteristics.—The six airfoils tested in this investigation are used chiefly as propeller blade sections, and one of the purposes of this investigation was to provide better data than have heretofore been available on the aerodynamic properties of these sections. In order to demonstrate the extent to which the results of this investigation may be directly applied to practical propeller design, the characteristics of a propeller on which tests for a wide range of tip speeds are available have been computed from these data.

The propeller chosen is the C-10 propeller of reference 18. The blade sections of this propeller are 3C10 sections. The pitch of the propeller is 9.6° at the 0.75 radius. The propeller characteristics have been computed from the section data by means of the improved vortex theory of Goldstein (reference 19). The equations used have been taken from this reference and modified so that the standard nondimensional coefficients in use in this country may be used directly in the formulas. The expression for the differential thrust is

$$R \frac{dC_T}{dr} = \frac{1}{4} \left(\frac{r}{R} \right)^3 \pi^3 \delta (1 - a_2)^2 \lambda_1 \sec^2 \varphi \quad (1)$$

The differential torque is obtained from the formula

$$R \frac{dC_Q}{dr} = \frac{1}{8} \left(\frac{r}{R} \right)^4 \pi^3 \delta (1 - a_2)^2 \lambda_2 \sec^2 \varphi \quad (2)$$

The rate of advance is given by

$$V/nD = \pi \left(\frac{r}{R} \right) (1 - a_2) (1 - F) \tan \varphi \quad (3)$$

where the factors F and a_2 are obtained from the following expressions

$$F = \frac{\cos^2 \varphi}{K} \frac{\delta}{4} \frac{\lambda_1}{\sin^2 \varphi} \quad (4)$$

$$\frac{a_2}{1 - a_2} = \frac{\cos^2 \varphi}{K} \frac{\delta}{2} \frac{\lambda_2}{\sin 2 \varphi} \quad (5)$$

and the following are the symbols used:

φ , the angle between the path of a blade element and the plane of rotation

$$\delta = \frac{Bc}{2\pi r}$$

R , tip radius

r , section radius

B , number of blades

c , chord of blade section

$\lambda_1 = C_L \cos \varphi - C_D \sin \varphi$

$\lambda_2 = C_L \sin \varphi + C_D \cos \varphi$

K , a coefficient dependent on r/R , B , and φ

These expressions are identical with those given by the vortex theory with the exception of the factor

$\cos^2\phi/K$ in the expressions for a_2 and F . In order to facilitate application of the foregoing equations a chart giving values of $K/\cos^2\phi$ for 2-bladed propellers plotted against $\tan\phi$ is given as figure 24. This chart has been taken from reference 19. It is worth noting in passing that the factor $\cos^2\phi/K$ becomes unity if the number of blades is infinite. The vortex theory assumes that the number of blades is infinite and the agreement of the new theory with the vortex theory is complete for this condition.

The actual calculation was carried out in the usual manner. The differential thrust and torque coefficients and rate of advance were computed from the foregoing formulas. The coefficients were plotted against V/nD and from these plots the thrust and torque grading curves were constructed for various values of V/nD . The grading curves were integrated mechanically to obtain the over-all coefficients of the propeller. The computation was carried out for two tip speeds, $0.75V/V_c$ and $0.9V/V_c$. The airfoil coefficients were taken from figure 10. Calculations

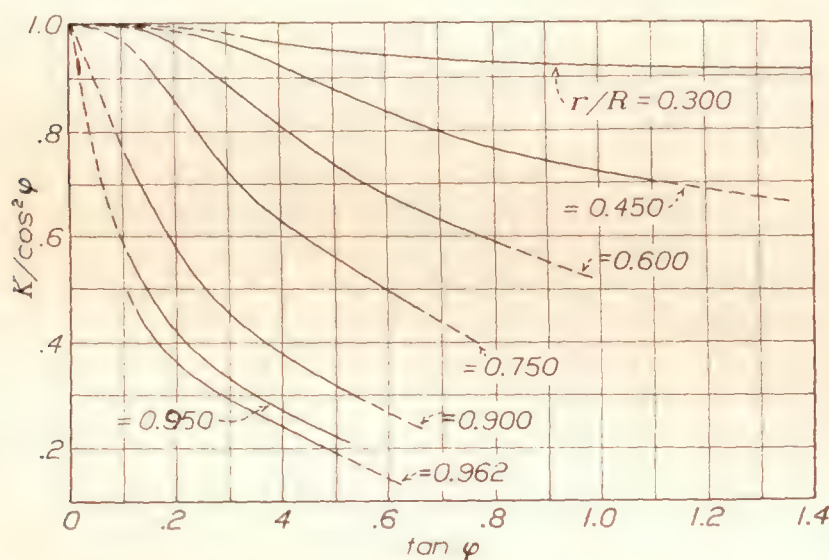


FIGURE 24.—Goldstein factor for correcting the vortex theory for 2-bladed propellers (reproduced from British R. & M. No. 1377).

were made for even 2° intervals of angle of attack. The speed of the various propeller sections was taken as the product of the tip speed and the ratio of the section radius to the tip radius. A slight error is introduced in this way because the resultant speed at any section is not exactly proportional to the radius, owing to the forward speed. The error is small, however, for low pitches; in the present instances it is of the order of 1.3 percent for the highest rates of advance.

The propeller characteristics as computed from these data and the measured propeller characteristics, taken from reference 18, are plotted in figures 22 and 23. In view of the fact that the measured propeller characteristics are influenced by the effects of the hub drag and the propeller-body interaction, exact agreement cannot be expected. Previous experience, however, indicates that the net interference effect is small because the effects of the hub drag and the additional drag of the body due to slipstream tend to compensate the effects of the body on the propeller characteristics, so that a

comparison of the computed and the measured propeller characteristics may be expected to yield information of some value.

The important difference between the computed and the measured characteristics is in the value of the thrust coefficient when the tip speed is equal to $0.9V_c$. This difference causes a marked reduction in the propeller efficiency as deduced from the airfoil data. Apparently, the maximum efficiency from the computed characteristics begins to fall off at lower tip speeds than the corresponding efficiency from the measured characteristics.

There are several possible causes for the disagreement at the high tip speed. The most important factors contributing to the difference are probably Reynolds Number differences and a constriction at the test section of the high-speed tunnel when the model is in position. Tests made in England of model propellers have shown a drop in efficiency at speeds lower than that shown by the full-scale tests. This difference between the model and full-scale tests has been attributed to Reynolds Number differences. The Reynolds Number of both the present tests and the British model propeller tests giving similar results is in the neighborhood of half that attained in the full-scale propeller tests of reference 18.

A constriction effect at the test section due to the presence of the model would also tend to cause a difference in the same direction as that shown in figure 23. In substance, the velocity and q as determined from the static-plate measurements would be lower than the effective velocity and q at the throat. As a result, the observations plotted in figures 8 to 13 would be plotted at speeds slightly lower than the correct values and the coefficients would be somewhat larger than the true values. The magnitude of the constriction or blocking correction would probably be greater for high speeds and high angles of attack than for low speeds and low angles of attack.

A thorough investigation of the causes of the discrepancy would require considerable additional experiment. The variation of the maximum efficiency of a propeller with tip speed should first be studied by means of flight tests to verify or disprove the results of the tests in the propeller-research tunnel. The effects of the body behind the propeller (a fuselage housing a D-12 engine in the tests of reference 18) should be investigated by means of tests of the propeller without a body. The effects of Reynolds Number should be investigated by means of tests of a geometrically similar model in the propeller-research tunnel. The blocking or constriction correction for the high-speed tunnel results cannot be investigated with the equipment now available. The method of determining this correction consists of testing geometrically similar airfoils of different chord. If this were to be done in the equipment now available the Reynolds Number would vary

as well as the constriction at the throat. A method suitable for establishing this correction is the construction of a high-speed wind tunnel similar to the present tunnel, but different in size, and the testing in both tunnels of airfoils of the same chord. The Reynolds Number would then be the same for the tests in each tunnel but the effects of constriction would depend on the sizes of the tunnels. One additional recommendation, but one which at present seems to offer but little possibility of success, is a theoretical analysis of the flow in the tunnel with a view to determining the constriction correction. The analysis should include an examination of the effects of compressibility. This stipulation is important but, because of the mathematical difficulty involved, a solution by this means seems improbable.

CONCLUSIONS

1. Clark Y airfoil sections are superior to R.A.F. 6 airfoil sections for propeller applications except for high-pitch propellers operating at low values of V/nD .

2. For propellers rotating at very high speeds, thin sections are better than thick sections.

3. As the speed of the air flowing past an airfoil is increased the lift, drag, and moment coefficients undergo a small numerical increase which continues until a compressibility burble occurs.

4. As the speed is further increased the breakdown of the flow corresponding to the compressibility burble is evidenced by a drop in the lift coefficient and a rapid increase in the drag coefficient.

5. The speed at which the compressibility burble occurs is dependent on the angle of attack and the thickness of the airfoil; increasing either of these causes the compressibility burble to occur at lower speeds.

6. Although the Reynolds Numbers at which these tests were conducted are low the results indicate that errors may be expected in the estimated design loads for airplanes which attain speeds such as those attained by diving bombers when in a dive if the effects of compressibility on the wing moment coefficient are neglected.

7. These results indicate that the limited theory available may be applied with sufficient accuracy for most practical purposes only for speeds below the compressibility burble.

LANGLEY MEMORIAL AERONAUTICAL LABORATORY,
NATIONAL ADVISORY COMMITTEE FOR AERONAUTICS,
LANGLEY FIELD, March 28, 1933.

REFERENCES

1. Jacobs, Eastman N., and Shoemaker, James M.: Tests on Thrust Augmentors for Jet Propulsion. T.N. No. 431, N.A.C.A., 1932.
2. Glauert, H.: The Elements of Aerofoil and Airscrew Theory. Cambridge University Press, 1926.
3. Norton, F. H.: N.A.C.A. Recording Air Speed Meter. T.N. No. 64, N.A.C.A., 1921.
4. Jacobs, Eastman N., and Abbott, Ira H.: The N.A.C.A. Variable-Density Wind Tunnel. T.R. No. 416, N.A.C.A., 1932.
5. Briggs, L. J., and Dryden, H. L.: Aerodynamic Characteristics of Twenty-Four Airfoils at High Speeds. T.R. No. 319, N.A.C.A., 1929.
6. Freeman, Hugh B.: Comparison of Full-Scale Propellers Having R.A.F. 6 and Clark Y Airfoil Sections. T.R. No. 378, N.A.C.A., 1931.
7. Briggs, L. J., and Dryden, H. L.: Pressure Distribution over Airfoils at High Speeds. T.R. No. 255, N.A.C.A., 1927.
8. Taylor, G. I.: Report on Progress during 1927-28 in Calculation of Flow of Compressible Fluid, and Suggestions for Further Work. R. & M. No. 1196, British A.R.C., 1929.
9. Rayleigh, Lord: On the Flow of Compressible Fluid Past an Obstacle. Philosophical Magazine, vol. 32, July 1916, pp. 1-6.
10. Bryan, G. H.: The Effect of Compressibility on Stream Line Motions. R. & M. No. 555, British A.C.A., 1918.
11. Bryan, G. H.: The Effect of Compressibility on High Speed Stream Line Motions. Part II. R. & M. No. 640, British A.C.A., 1919.
12. Taylor, G. I., and Sharman, C. F.: A Mechanical Method for Solving Problems of Flow in Compressible Fluids. R. & M. No. 1195, British A.R.C., 1928.
13. Glauert, H.: The Effect of Compressibility on the Lift of an Aerofoil. R. & M. No. 1135, British A.R.C., 1927.
14. Ackeret, J.: Über Luftkräfte bei sehr grossen Geschwindigkeiten insbesondere bei ebenen Strömungen. Helvetica Physica Acta, vol. I, Fasciculus Quintus, 1928.
15. Caldwell, F. W., and Fales, E. N.: Wind Tunnel Studies in Aerodynamic Phenomena at High Speed. T.R. No. 83, N.A.C.A., 1920.
16. Briggs, L. J., Hull, G. F., and Dryden, H. L.: Aerodynamic Characteristics of Airfoils at High Speeds. T.R. No. 207, N.A.C.A., 1925.
17. Stanton, T. E.: A High Speed Wind Channel for Tests on Aerofoils. R. & M. No. 1130, British A.R.C., 1928.
18. Wood, Donald H.: Full-Scale Tests of Metal Propellers at High Tip Speeds. T.R. No. 375, N.A.C.A., 1931.
19. Lock, C. N. H.: Application of Goldstein's Airscrew Theory to Design. R. & M. No. 1377, British A.R.C., 1932.

TABLE I
AIRFOIL ORDINATES
[NOTE.—All values in percent of chord]

Station	3C6		3C8		3C10		3R6		3R8		3R10	
	Upper surface	Lower surface	Upper surface	Lower surface	Upper surface	Lower surface	Upper surface	Lower surface	Upper surface	Lower surface	Upper surface	Lower surface
0	1.79	1.79	2.39	2.39	2.99	2.99						
1.25	2.80	.99	3.73	1.32	4.66	1.65						
2.5	3.33	.75	4.44	1.00	5.56	1.26	2.46	0.00	3.28	0.00	4.10	0.00
5	4.05	.48	5.40	.64	6.75	.80	3.54	.00	4.72	.00	5.90	.00
7.5	4.54	.32	6.05	.43	7.56	.54	4.23	.00	5.66	.00	7.08	.00
10	4.92	.22	6.56	.29	8.20	.36	4.74	.00	6.32	.00	7.90	.00
15	5.48	.08	7.31	.10	9.14	.13	5.37	.00	7.16	.00	8.95	.00
20	5.82	.02	7.77	.02	9.72	.03	5.70	.00	7.60	.00	9.50	.00
30	6.00	.00	8.00	.00	10.00	.00	5.99	.00	7.98	.00	9.98	.00
40	5.85	.00	7.80	.00	9.75	.00	5.94	.00	7.92	.00	9.90	.00
50	5.40	.00	7.20	.00	9.00	.00	5.70	.00	7.60	.00	9.50	.00
60	4.69	.00	6.26	.00	7.82	.00	5.22	.00	6.96	.00	8.70	.00
70	3.77	.00	5.03	.00	6.28	.00	4.44	.00	5.92	.00	7.40	.00
80	2.68	.00	3.57	.00	4.46	.00	3.36	.00	4.48	.00	5.60	.00
90	1.44	.00	1.91	.00	2.39	.00	2.11	.00	2.82	.00	3.52	.00
95	.76	.00	1.02	.00	1.27	.00	1.48	.00	1.97	.00	2.46	.00
100	.06	.00	.08	.00	.10	.00						
L. E. Rad.							.60		.80		1.00	
T. E. Rad.							.46		.62		.92	

REPORT No. 464

NEGATIVE THRUST AND TORQUE CHARACTERISTICS OF AN ADJUSTABLE-PITCH METAL PROPELLER

By EDWIN P. HARTMAN

SUMMARY

This paper presents the results of a series of negative thrust and torque measurements made with a 4 foot diameter model of a conventional aluminum-alloy propeller. The tests were made in the 20-foot propeller-research tunnel of the National Advisory Committee for Aeronautics.

The propeller was tested for thrust and torque through a blade-angle range from 22° to -23° at 0.75 radius and a V/nD range from zero to infinity, while mounted in front of a cowled radial-engine nacelle. With this arrangement the drag of the propeller was also measured through a blade-angle range from 0° to 90° while locked in a vertical position. Additional tests were made with the propeller and nacelle located in two positions with respect to both a monoplane wing and a biplane cellule, in which smaller ranges of blade angles and values of V/nD were covered.

The results show that the negative thrust is considerably affected by the shape and size of the body behind the propeller, that the maximum negative thrust increases with decrease in blade-angle setting, and that the drag of a locked propeller may be greatly reduced by feathering it into the wind. Several examples of possible applications of the data are given.

INTRODUCTION

Wind-tunnel tests of both model and full-scale propellers through the ordinary ranges of air velocity and revolution speed have been quite extensive. Very few tests of propellers operating under conditions of negative thrust and torque have been made, however, because conditions of negative thrust and torque are encountered only in dives and fast glides and these maneuvers in nonmilitary airplanes are relatively unimportant. The recent development of the controllable-pitch propeller has broadened the field of use for negative propeller thrust and has therefore created new interest in the subject.

In 1920, as part of a rather extensive research program on wooden propellers, Durand and Lesley ob-

tained the negative-thrust characteristics of a series of 12 wooden propellers of varying pitch, blade width, and plan form. The details of these tests may be found in reference 1. More recently the British have obtained the negative thrust and torque characteristics of a 4-bladed wooden propeller (reference 2).

Both of the above studies were narrowly limited in range of blade angles and were made without a body. Their results are therefore only indirectly applicable to flight problems.

In view of the trend in recent years toward the use of metal propellers, it seemed advisable to obtain some data on the negative thrust and torque of a conventional aluminum-alloy propeller. As the propeller is usually mounted close to a fuselage and engine, it was considered necessary to include tests with bodies comparable to those found in actual practice.

This report gives the thrust and torque characteristics of a conventional adjustable-pitch metal propeller throughout the complete V/nD range from $V=0$ to $n=0$, and through a range of blade-angle settings from 22° to -23° at 0.75 radius. The drag of a locked propeller through a blade-angle range of 0° to 90° at 0.75 radius is also given.

The greater part of this research comprises a series of tests with the propeller mounted ahead of a dummy radial-engine nacelle without wings or fuselage. Other tests, not so complete, were made with the propeller and nacelle mounted in various positions with respect to a monoplane wing and also to a biplane cellule.

Although the study is confined to one propeller and relatively few body shapes, it is believed that the data given are sufficient to enable designers to make fairly accurate calculations in most cases.

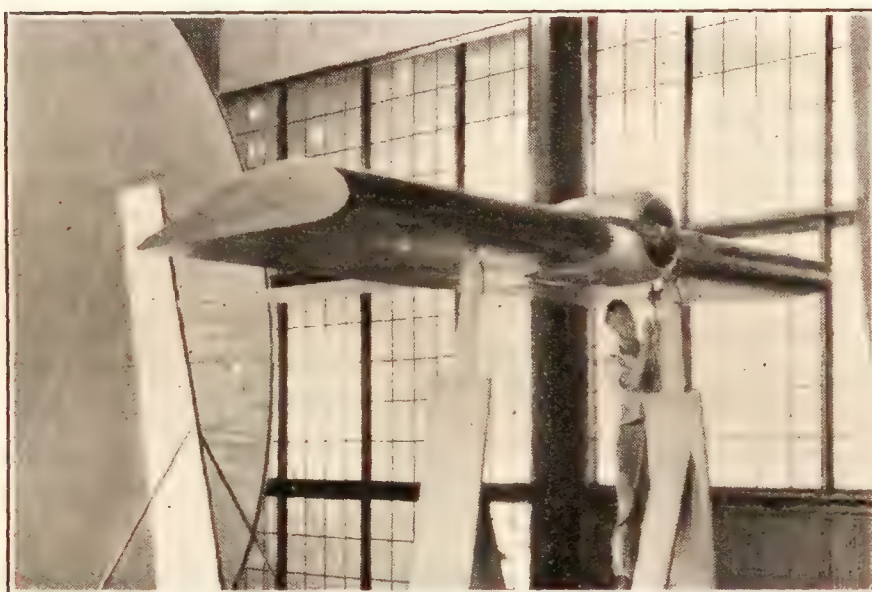
APPARATUS AND METHODS

The tests were made in the 20-foot propeller-research tunnel of the National Advisory Committee for Aeronautics. Details of the construction and characteristics of this tunnel are given in reference 3.

The engine-nacelle unit was composed of a 25-horsepower direct-current motor enclosed in a sheet-metal nacelle with a 4/9-scale wooden model of a Wright J-5 9-cylinder engine mounted outside at the front.



(a) Cowled engine nacelle with propeller.



(b) Nacelle mounted on monoplane wing in position A.



(c) Nacelle mounted on biplane cellule in position 9.

FIGURE 1.—Nacelle arrangements.

The motor shaft projected through the nose of the nacelle and drove a tractor propeller. In most of the tests an N.A.C.A. cowled nacelle was used. Figure 1(a) is a photograph of this nacelle mounted in testing position. Full details and dimensions may be obtained from reference 4.

The propeller-nacelle unit was tested in two positions with respect to a monoplane wing having a 15-foot span, a 5-foot chord, and a maximum thickness of 1 foot. Reference 4 gives a table of ordinates for this wing section, as well as photographs of these two monoplane-nacelle arrangements which are therein designated positions "A" and "C." The same designations will be used in this report. Figure 1(b) shows the monoplane wing with nacelle in position A.

Two biplane-nacelle arrangements, designated positions "5" and "9", were also tested. The biplane cellule had the following dimensions: Span, both wings, 15 feet 10 inches; chord, both wings, 3 feet 2 inches; gap, 3 feet; stagger, none; airfoil section, Clark Y. Figure 1(c) shows the position 9 arrangement.

The aluminum-alloy propeller used in these tests was similar to a Navy 4412 9-foot propeller, and was 4 feet in diameter, corresponding in scale to the engine and nacelle. Detailed dimensions of this propeller are given in reference 5.

The motor was made to act as an electrical brake through the negative-torque range, by means of a variable resistance in the armature circuit, the amount of resistance determining the speed of revolution. The field current was held constant at a predetermined value and the armature current measured. The motor having been previously calibrated both as a motor and as a generator, the input or output power was easily calculated.

The revolution speed of the propeller was measured by a condenser-type electrical tachometer mounted on the rear of the motor housing and connected by wires to an indicating instrument on the floor below.

For the purpose of obtaining test points throughout the full V/nD range, both the tunnel air speed and the propeller revolution speed were varied through wide ranges. The propeller speed varied from 0 to 3,500 r.p.m., and the tunnel air speed from 0 to 100 miles per hour. As previously mentioned, the more complete tests in this program were made with the cowled nacelle alone, in which propeller blade-angle ranges of 22° to -23° with propeller free and 0° to 90° with propeller locked were covered. Tests were also made at two blade-angle settings with the hood of the N.A.C.A. cowling removed and the engine cylinders exposed. In all the tests made with the nacelle alone the thrust line was parallel to the wind direction.

The propeller was tested at four blade angles, 22° , 17° , 12° , and 7° at 0.75 radius, with the nacelle in position A, and at two blade angles, 22° and 17° at 0.75 radius, with the nacelle in positions C, 5, and 9. The latter three tests were made at two angles of attack, -5° and 0° , whereas all of the other tests in this report were made at 0° only. The monoplane and biplane tests were limited to the negative thrust and torque range.

In each test the drag or thrust, torque, propeller revolution speed, and air speed were determined over

the desired range from readings of the balances, ammeters, and manometer.

RESULTS

Two forms of coefficients were used in plotting these data. In the majority of the tests the coefficients $T_c = \frac{T_e}{\rho V^2 D^2}$ and $Q_c = \frac{Q}{\rho V^2 D^3}$ were used; since they are better adapted to plotting in the range of high V/nD values, where negative propeller thrust usually occurs. In the tests with the nacelle alone, however, where the full range of V/nD was covered, it was found necessary to use the coefficients $C_T = \frac{T_e}{\rho n^2 D^4}$ and $C_Q = \frac{Q}{\rho n^2 D^5}$ in the range of low V/nD values.

The significance of the units in these coefficient forms is as follows:

T , thrust of propeller (tension in propeller shaft)

ΔD , change in drag of the airplane due to propeller slipstream

T_e , effective thrust $= T - \Delta D$

Q , aerodynamic torque. Negative torque is defined as an air reaction upon the propeller tending to assist the rotation. Positive torque, which is the reaction occurring in normal flight, tends to resist rotation.

D , propeller diameter

n , revolutions per unit of time

ρ , mass density of the air

all values being expressed in consistent units.

It is clear that one form of the coefficients given may be changed to the other by multiplying or dividing by $(V/nD)^2$.

Figures 2 and 3 represent the performance of a propeller throughout the complete V/nD range and through a large range of blade angles. The use of both forms of the coefficient keeps the charts within reasonable dimensions. A V/nD value of unity was used as the point of transition from one form of coefficient to the other because both have equal values at that point.

Figure 4 was obtained by cross-plotting some of the curves from figures 2 and 3, and replotting. It was designed primarily as a working chart and covers what might at this time be called the usable negative-thrust range of blade angles and V/nD ratios. The coefficients T_c and Q_c were used exclusively in this figure since their similarity to a drag coefficient renders them suitable for use in performance calculations.

Figures 5 and 6 present the results of the tests with the monoplane wing, and figures 7 and 8 those with the biplane cellule. Figure 9 shows the curves for the propeller mounted on the nacelle alone both with and without the engine cowl; and in figures 10 and 11 composite curves show the comparative

performances of the propeller with various wing-nacelle combinations. The drag coefficient for a locked propeller set at any blade angle between 0° and 90° is given in figure 12.

DISCUSSION

The negative-thrust curves in this report are very similar in shape to those given in references 1 and 2. On account of the small amount of available data on negative propeller thrust, all comparisons are confined to the data given in this report.

The curves in figures 2 and 3 cover every condition that an airplane would ever encounter in flight. On the left halves of the charts in their normal positions are plotted C_T and C_Q , respectively, and on the right halves the alternative coefficients T_c and Q_c , respectively. If it be desired to extend either set of coefficients beyond the center line, it is only necessary to divide by the square of the abscissa.

The curves in figure 4 are taken from figures 2 and 3. From them it appears that in the range of blade angles covered in these tests, the maximum negative thrust coefficient increases with a decrease in blade angle. Inasmuch as the drag of an idling propeller depends upon its speed of revolution, which in turn depends upon the torque of the engine, it is essential that curves of torque coefficients should be included in any working chart. Congestion is avoided in this chart by limiting the range of blade angles and nD/V to that portion which is most likely to be of use.

The curves in figures 5 and 6, for the nacelle mounted on the monoplane wing, have the same general shape as those for the nacelle alone, but show somewhat lower values. Figure 6 indicates that small changes in angle of attack have but slight effect on the propeller drag.

The results of the tests with the biplane arrangements in figures 7 and 8 show no material differences from the other test results. The effect of removing the cowl is indicated in figure 9. The curves show that this effect is not large, and also show that a difference in negative thrust coefficients is not always accompanied by a difference in the corresponding torque coefficients.

Figures 10 and 11 present a composite of curves taken from the previous plots for the purpose of comparing the results from various wing-nacelle arrangements. These curves indicate that, in general, the larger the obstruction and the closer its position behind the propeller the less the negative thrust of the propeller. The thrust and torque curves vary in approximately the same manner. Considerable variation in the V/nD for zero thrust is noted. It is evident from these charts that body effect must be considered for accurate performance calculation.

The curve in figure 12 shows that a remarkable saving in drag may be effected by feathering the

blade of a locked propeller into the wind. The drag coefficient T_c drops from 0.0227 at 22° to 0.0014 at 88° .

APPLICATIONS

Only recently has any attempt been made to put negative propeller thrust to use. The development and more general use of the controllable-pitch propeller have brought about a new interest in this subject, and

tude rapidly, the dive speeds of modern airplanes have reached such high values as to make it difficult for the pilot to maintain satisfactory control of his airplane. In such cases it is desirable to provide a means by which the pilot, if he wishes, may reduce its terminal velocity.

It has been proposed that the high drag of a propeller set at low blade angles be used to reduce terminal

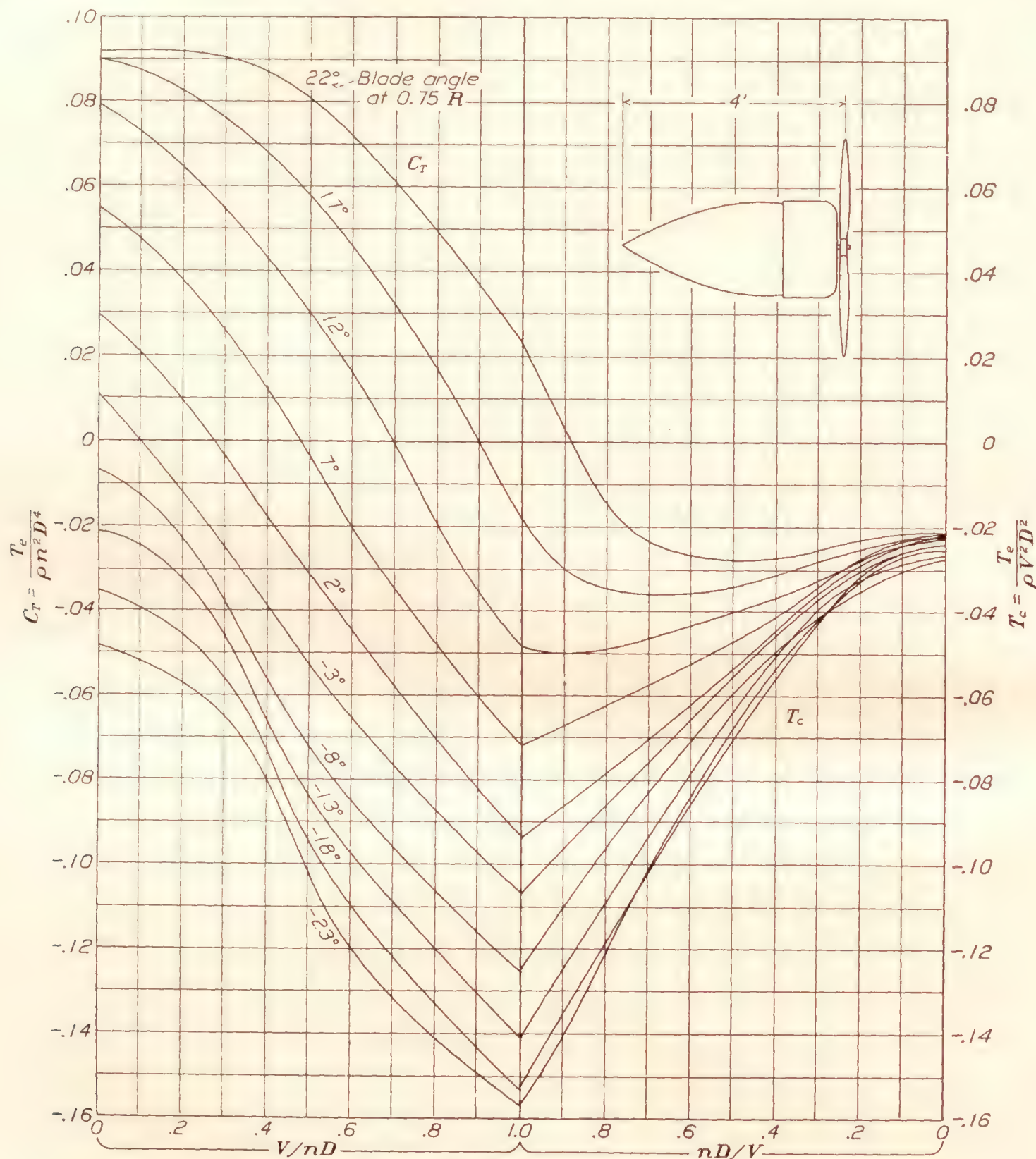


FIGURE 2.—Thrust coefficients for propeller with nacelle alone.

requests for negative-thrust data for aluminum-alloy propellers have become more frequent. Some of the applications of the data are discussed in the following paragraphs.

REDUCTION OF TERMINAL VELOCITY

Airplanes, particularly those used by the military services, are frequently required to dive to terminal velocity in order to carry out their specified missions. Although the purpose of this maneuver is to lose alti-

velocities, both to provide better control in the dive and to lessen the strain on both airplane and pilot in the dive and the subsequent pull-out. This procedure, of course, requires the use of a controllable-pitch propeller.

Figure 13 presents graphically the results of terminal-velocity calculations for a conventional biplane. The calculations were made using the data in figure 4; as body or high-tip-speed effects were not considered no pretension to great accuracy is made. The short

portions of the curves were calculated for the condition where engine power was used to maintain the propeller revolution speed at 2,200 r.p.m. In this way the terminal velocity is reduced much more than when the engine is fully throttled.

In making these calculations the equation used to compute the terminal velocity was

V_T , terminal velocity in feet per second

ρ , air density in slugs per cubic foot.

A curve of friction torque plotted against revolution speed of the engine is necessary for these calculations.

An approximate method of making terminal-velocity calculations is as follows:

1. Select a propeller-blade angle and diameter

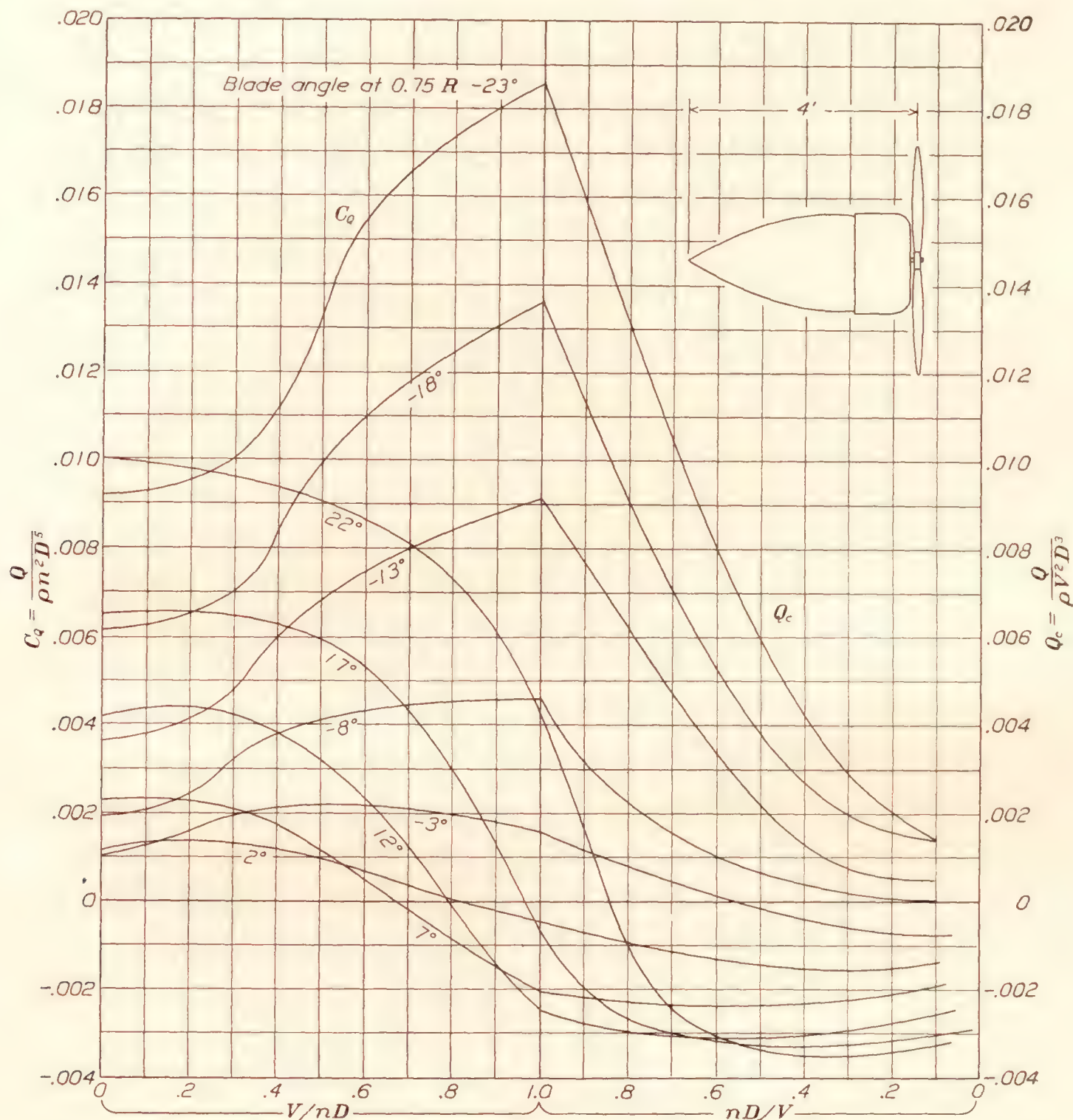


FIGURE 3.—Torque coefficients for propeller with nacelle alone.

$$V_T = \sqrt{\frac{W}{\frac{\rho}{2} A + K T_c}}$$

where

W , the weight of the airplane

$A = \frac{\text{parasite drag of airplane}}{\frac{\rho}{2} V^2}$, an equivalent para-

site area

T_c , the propeller-thrust coefficient taken from the charts

$K = \rho D^2$

D , propeller diameter in feet

2. Estimate V_T and propeller speed at V_T .

3. Using estimated propeller speed, obtain friction torque from curve of friction torque against propeller speed, which is assumed to be available.

4. Calculate Q_c from known values of friction torque and V_T .

5. Project down from value of Q_c on curves and obtain T_c and nD/V .

6. Substitute value of T_c in equation and calculate V_T .

7. Knowing D and nD/V , calculate propeller speed using calculated value of V_T .

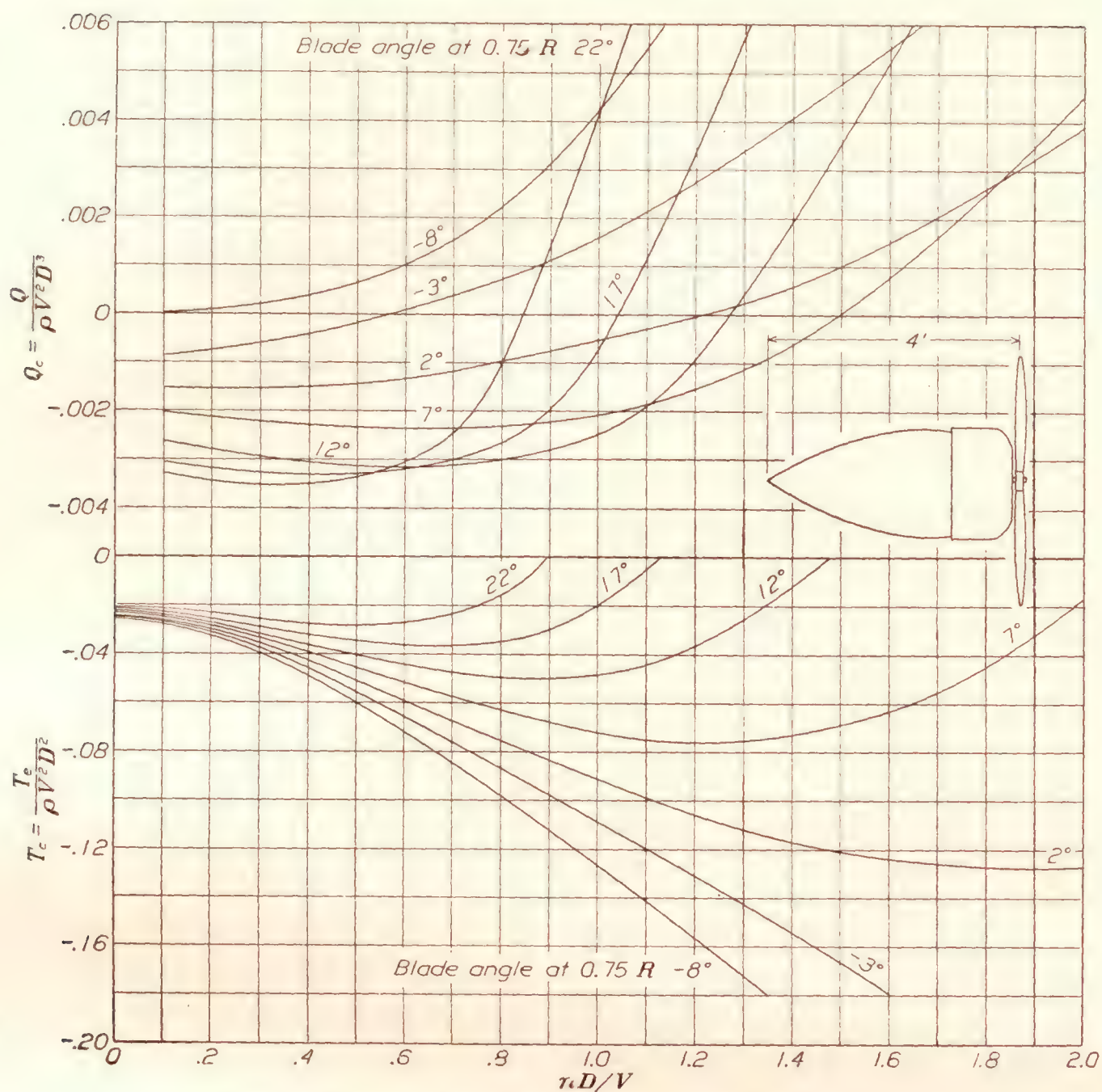


FIGURE 4.—Negative thrust and torque coefficients with nacelle alone.

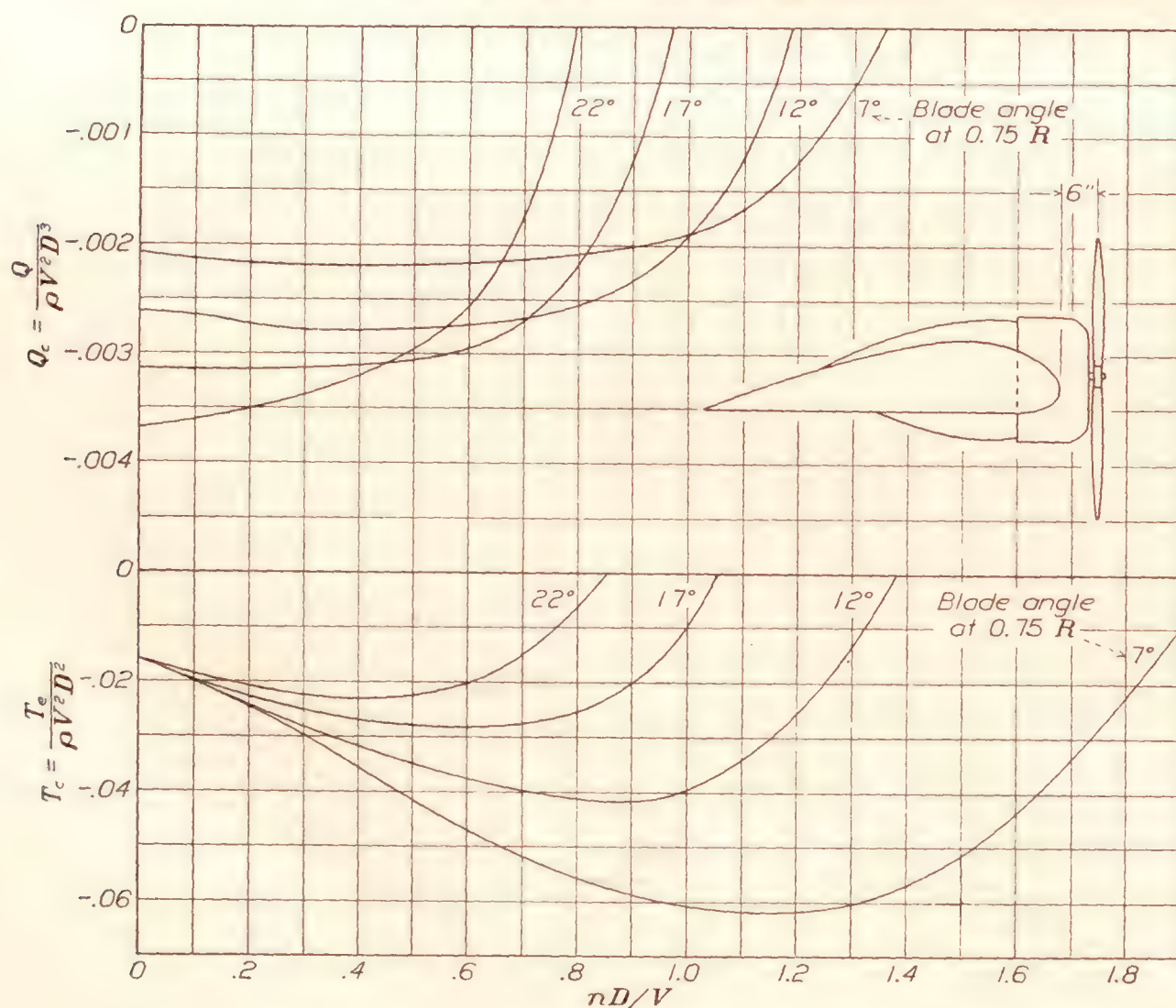


FIGURE 5.—Negative thrust and torque coefficients with monoplane wing, nacelle in position A.

8. If the calculated values of V_T and propeller speed are not the same as the estimated values, a new estimate must be made and the process repeated.

If the propeller is not of the same form as the one used in these tests, an adjustment of the data will of course be necessary. For greater accuracy high-tip-speed and body effects must also be considered. The effect of high tip speeds may be determined from data given in reference 6.

The results of the terminal-velocity calculations given in figure 13 show that as the propeller pitch is

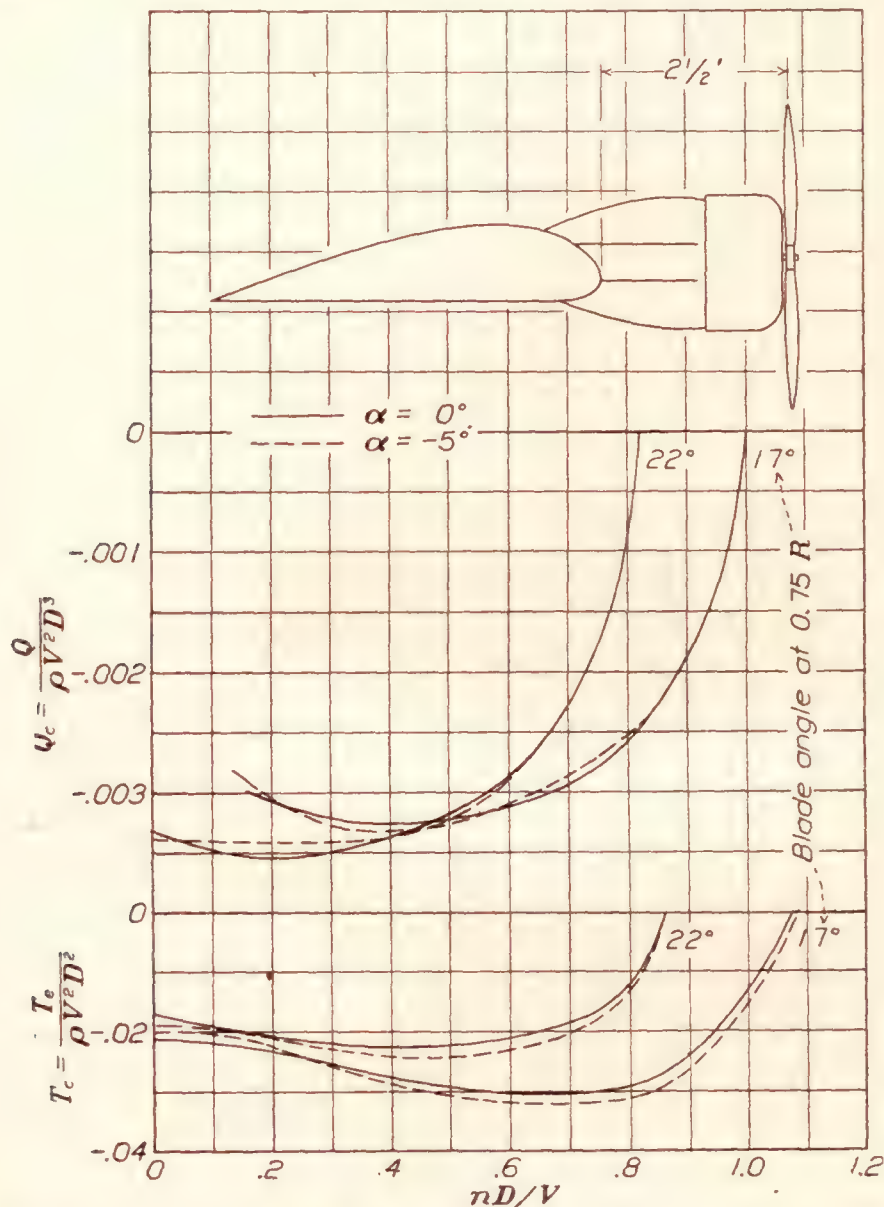


FIGURE 6.—Negative thrust and torque coefficients with monoplane wing, nacelle in position C.

reduced the terminal velocity drops rapidly to a point where the blade angle is about 4° at 0.75 radius, after which, with further decrease of pitch, it rises unless the revolution speed of the propeller is maintained by the use of engine power.

The flight-research section of the National Advisory Committee for Aeronautics has recently completed a series of terminal-velocity dive tests upon a military airplane equipped with a Hamilton Standard controllable-pitch propeller. The results of these tests when published will give more exact information concerning the effect of propeller-blade angle upon diving velocities.

BRAKING EFFECT

The braking effect of the propeller may be used to reduce the landing distance required by an airplane in the following ways:

1. To increase the angle of descent.
2. To counteract the floating tendency of clean airplanes.
3. To reduce the landing run.

In landing, a high-pitch propeller produces considerable thrust even at low engine revolution speeds. The thrust may be greatly reduced by decreasing the blade angle and the extreme braking effect may be

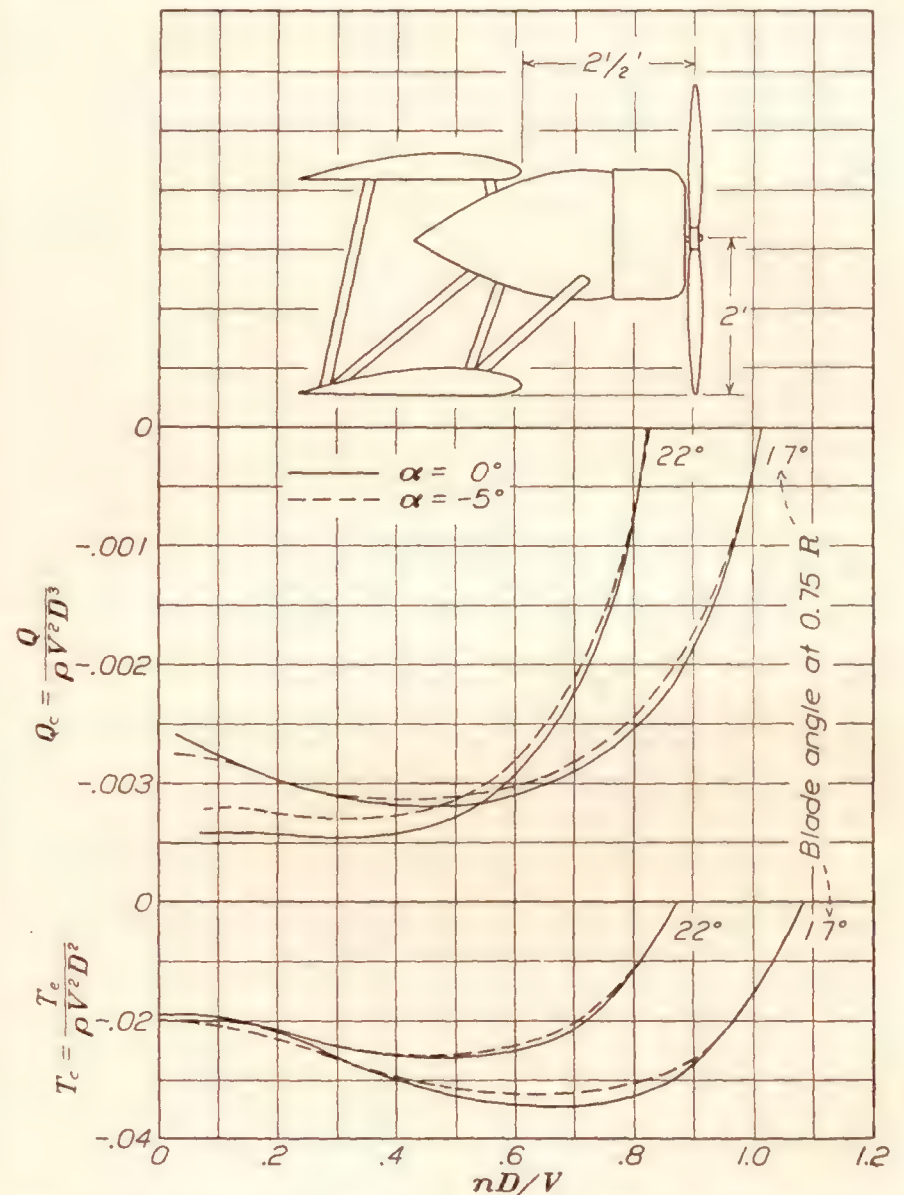


FIGURE 7.—Negative thrust and torque coefficients with biplane cellule, nacelle in position 9.

obtained by reducing the blade angle to a high negative value and applying engine power to maintain a V/nD giving the greatest negative thrust. In actual practice this might be a dangerous procedure if the airplane were not safely on the ground. In the glide before landing it would hardly be safe to reduce the blade angle below a value giving sufficient performance to enable the airplane to pull off the field again in case of an emergency.

The accurate calculation of the effect of propeller braking upon the landing run is altogether too lengthy to be of practical use; however, an estimate may be

made using the landing-run formula for still air given by Glauert (reference 7):

$$\text{Landing run in feet, } S = \frac{V_L^2}{2g\left(\frac{D}{L} - \mu\right)} \log_e \left(\frac{D}{L} \right)$$

where V_L is the landing speed in feet per second; $\frac{D}{L} = \frac{C_D}{C_L}$ is the value of these ratios in the landing attitude; and μ is the coefficient of friction between the landing gear and the ground.

Assuming a given reduction in blade angle, an equivalent additional ΔC_D may be calculated using

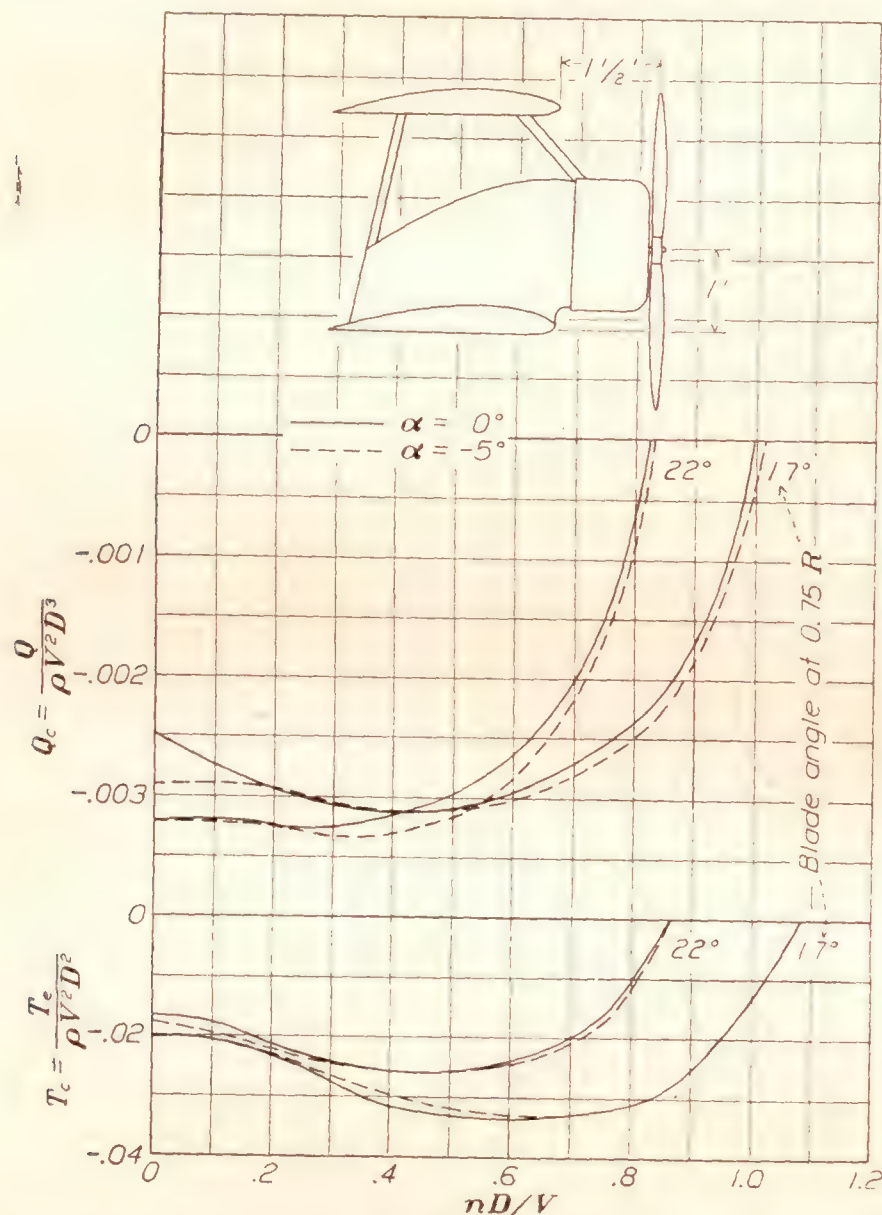


FIGURE 8.—Negative thrust and torque coefficients with biplane cellule, nacelle in position 5.

curves in figure 2 and the known characteristics of the airplane. The new value of D/L is $\frac{C_D + \Delta C_D}{C_L}$. It is then easy to calculate the length of landing run for each blade angle using the two values of D/L .

The additional-drag coefficient ΔC_D varies considerably with V/nD , which makes it necessary to use an average value to avoid a lengthy integration. The use of an average coefficient may involve some error but it is believed that a close approximation to the correct results may be obtained if the ΔC_D used is calculated for the V/nD that exists at the beginning of the landing run. The calculation of ΔC_D is merely a transformation from T_c .

As an illustration, consider the example of an airplane with the following characteristics: Landing speed, 88 feet per second; a 9-foot diameter controllable-pitch propeller with a normal high-speed setting of 22° ; wing area of 250 square feet; a D/L or C_D/C_L ratio in the landing position of 0.125. For convenience a value of μ of 0.10 will be used.

The lift coefficient C_L in the landing position will be about 1.4, so that $C_D = 1.4 \times 0.125 = 0.175$. If it is assumed that the blade angle for landing has been reduced to 7° , the average additional-drag coefficient ΔT_c is about 0.125.

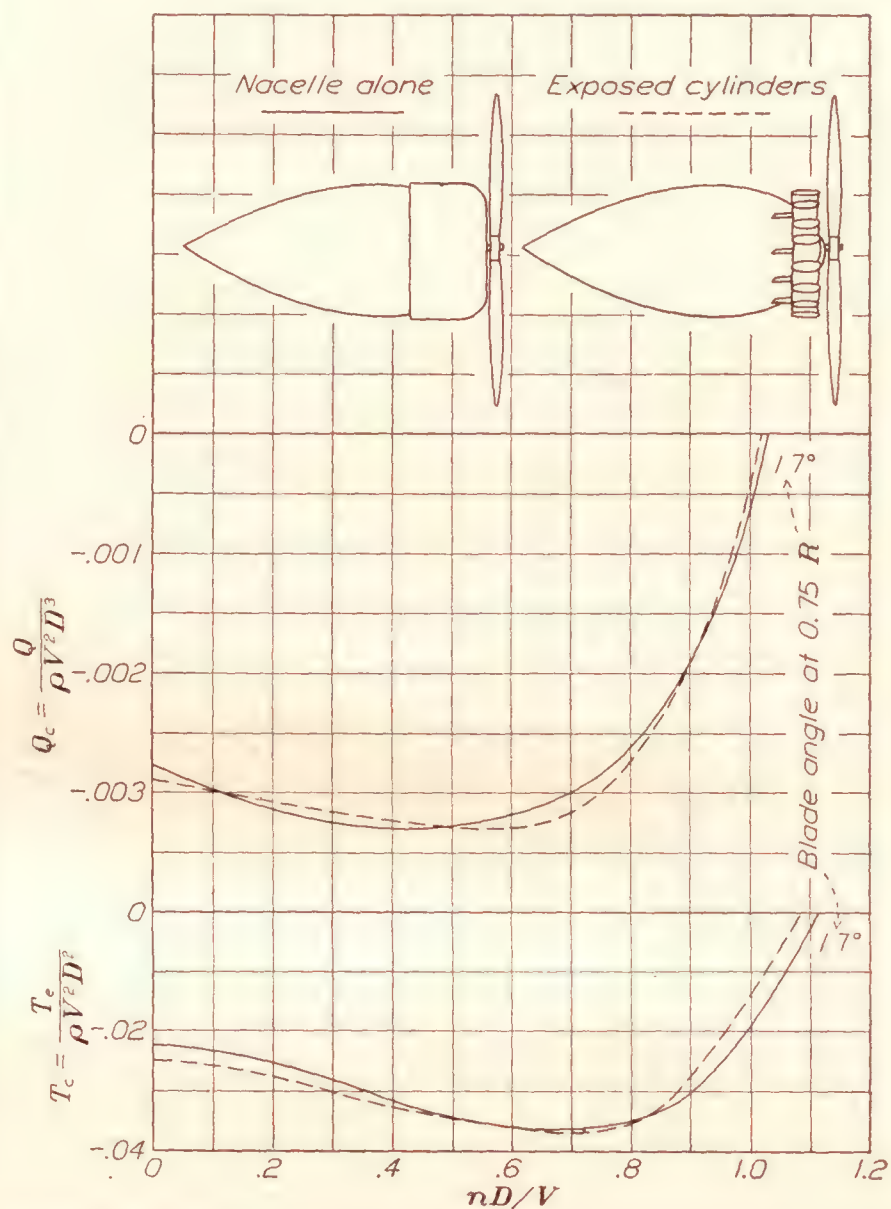


FIGURE 9.—Negative thrust and torque coefficients with nacelle alone, both with and without the engine cowl.

The relation between C_D and T_c is:

$$\frac{C_D}{T_c} = \frac{2D^2}{S_w} = \frac{2 \times 9^2}{250} = 0.648$$

The drag coefficient ΔC_D corresponding to the additional-drag coefficient ΔT_c is $0.648 \times 0.125 = 0.081$. The total drag coefficient in the 7° position will be $0.175 + 0.081 = 0.256$. The D/L ratio for the 7° condition will be $\frac{0.256}{1.4} = 0.183$.

If we consider that Glauert's formula using the original value of D/L gives the correct landing run with the blade at 22° , then the landing run with a 7° blade setting may be obtained by using the new value of D/L .

The solution for each blade angle gives 1,080 feet for the 22° setting and 880 feet for the 7° setting, the ratio of the two landing runs being 0.82. The reduction in landing run is perhaps a trifle optimistic because of the low D/L assumed for the 22° blade setting, for it is evident that the cleaner the airplane the greater will be the benefit derived from a reduction in blade angle.

The ratio of the L/D ratios in the landing position for the two blade settings is then $\frac{0.125}{0.183} = 0.68$. It is evident that the reduction in the L/D ratio will not only increase the glide angle but should also effectively eliminate any floating tendency. The combination of these effects should materially reduce the length of runway required. The fact that any air-

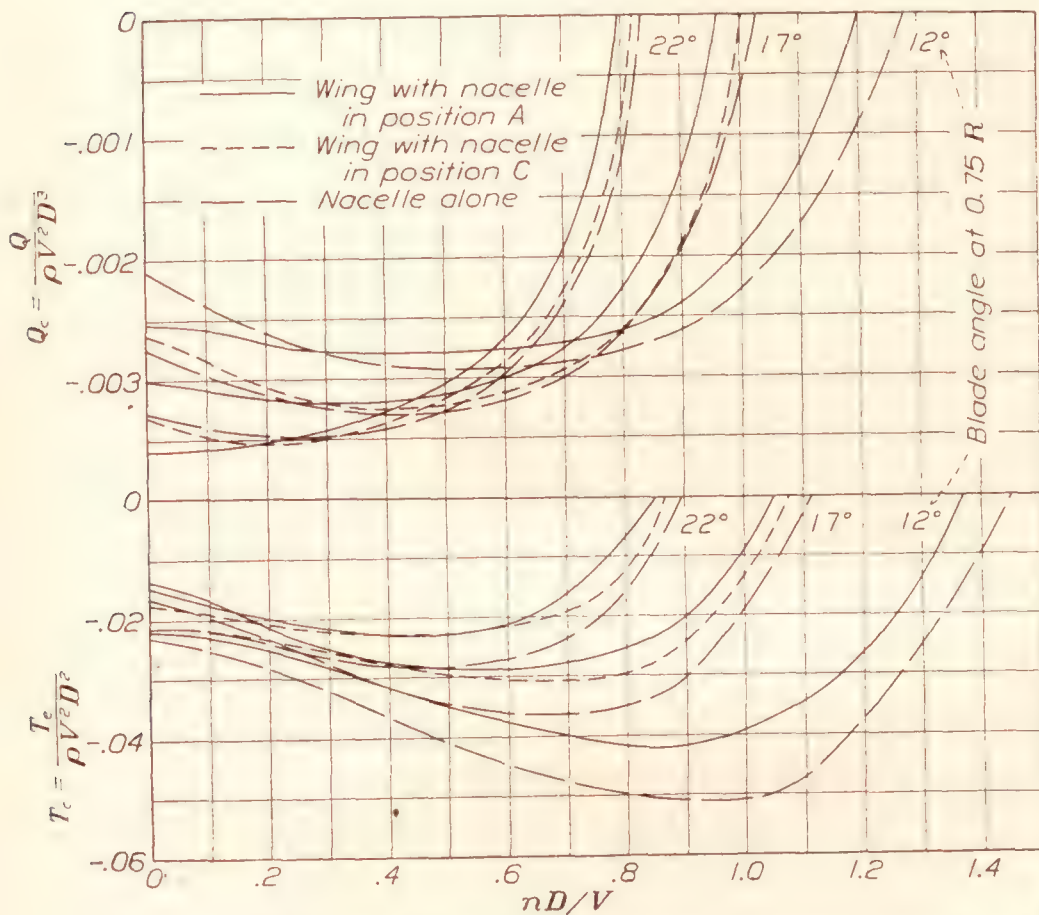


FIGURE 10.—Negative thrust and torque coefficients, nacelle mounted on monoplane wing—composite curves.

plane with a controllable-pitch propeller is very probably equipped with brakes tends to minimize the value of the propeller braking effect in shortening the landing run.

DRAG OF LOCKED, IDLING, AND FREE-WHEELING PROPELLERS

For the purpose of reducing the drag of an idling propeller it has often been proposed that a "free-wheeling" clutch be placed upon the propeller shaft so that the propeller might be disengaged from the engine while the engine is not in operation. Using such a device a multi-engine airplane after reaching its cruising altitude could, it has been proposed, have one or more engines stopped and could cruise more economically under reduced power. It has also been proposed that in case controllable-pitch propellers were being used the dead-engine propellers might be feathered into the wind and locked, thus effecting an

additional saving. There has been some doubt as to whether a free-wheeling propeller actually has less drag than a locked or idling propeller.

Using the data in figure 4, such problems may be solved. The drag of a locked propeller is easily found, since the drag coefficient remains constant and is equal to the thrust coefficient at $\frac{nD}{V} = 0$. The coefficient may be quickly found from figure 12. The drag

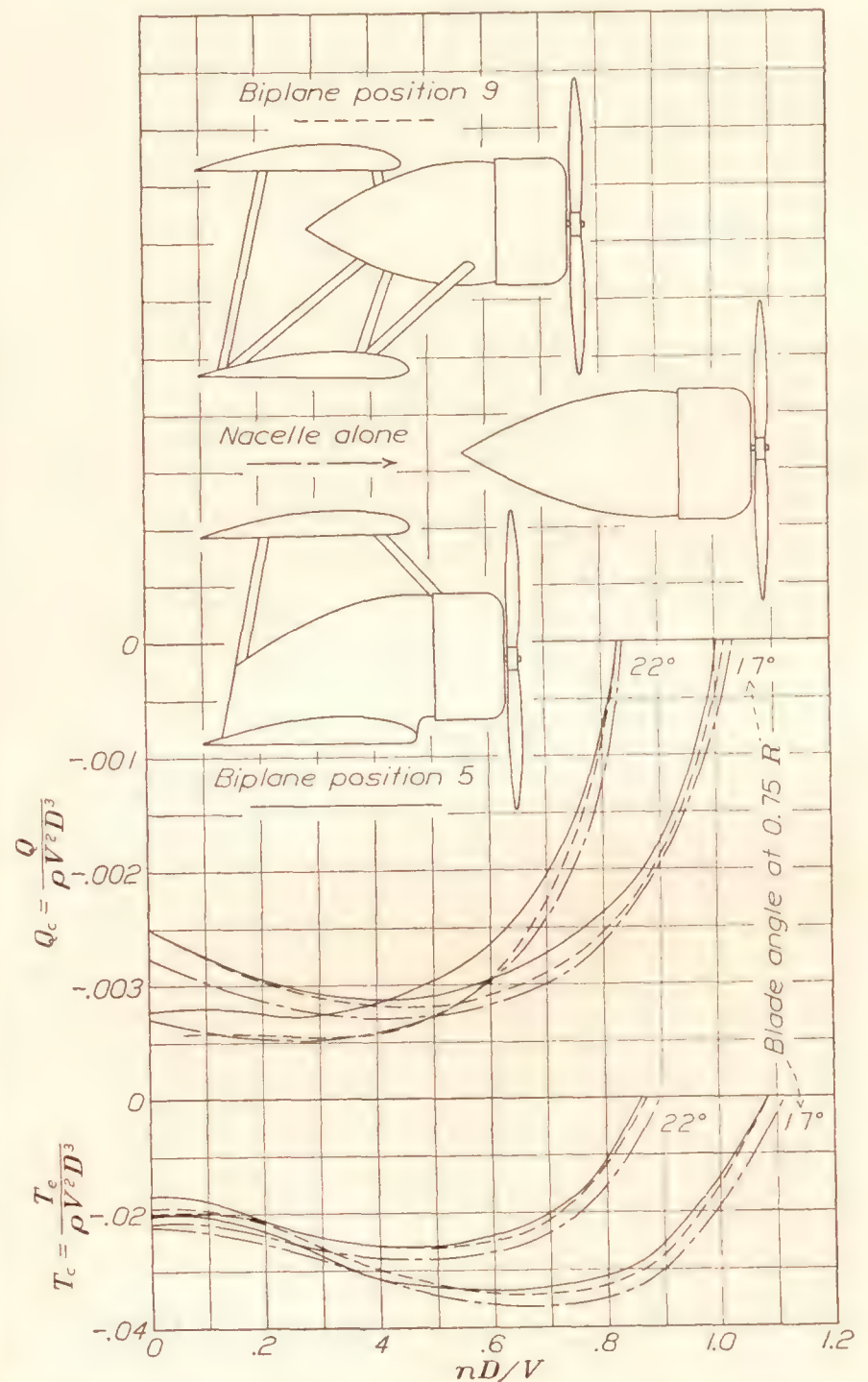


FIGURE 11.—Negative thrust and torque coefficients, nacelle mounted on biplane cell—composite curves.

coefficient of a free-wheeling propeller also remains constant since the propeller is operating at nearly zero torque. It may be found by projecting down from the point of zero torque to the appropriate thrust curve. From an observation of the free-wheeling propeller-thrust coefficients for various blade angles in figure 4, it is noted that, for blade angles of more than 15° at 0.75 radius, the drag of a free-wheeling propeller is slightly less than the drag of a locked propeller, whereas for blade angles less than 15° the drag of a free-wheeling propeller is more than that of a locked propeller.

The drags of dead-engine idling and throttled-engine idling propellers are much more difficult to calculate

because the thrust coefficient is different for each velocity. A friction-torque curve for the engine must be at hand because the speed of rotation of the propeller, therefore the thrust coefficient, depends upon the friction in the engine. In addition to the friction-torque curve a throttled-power curve must be had for the calculation of the drag of a throttled-engine idling propeller. These data being available, the determination of propeller drag for the idling propellers resolves itself into a cut-and-try process.

The results of calculations for a typical example follow. The airplane in this example is assumed to have a 250-horsepower engine. Friction-torque and throttled-power curves for this engine were assumed but will not be shown here.

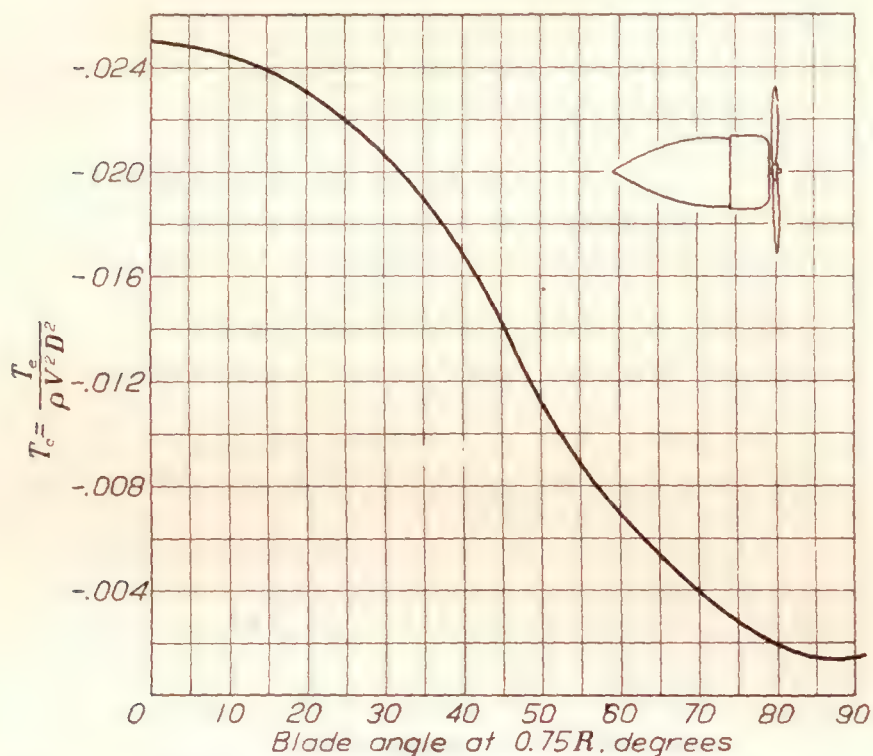


FIGURE 12.—Variation of negative-thrust coefficient with blade-angle setting for a locked propeller.

DRAG OF LOCKED, FREE-WHEELING, AND IDLING PROPELLERS

Propeller No. 4412—Diameter, 9 feet

Drag in pounds

Velocity, m.p.h.	Locked propeller set 17°	Locked propeller set 88°	Free- wheeling propeller set 17°	Dead-en- gine propeller set 17°	Throttled- engine propeller set 17°
25	5.9	0.36	3.7	5.9	-22
50	23.6	1.5	15.0	37.2	22
75	53.0	3.3	33.7	68.6	60
100	94.4	5.8	60.1	101.0	100

The throttled engine was assumed to be throttled to a point giving 350 r.p.m. at zero velocity. From this table it appears that in most cases a free-wheeling propeller would have some advantage over a locked or an idling propeller, except where the blade of the locked propeller has been feathered into the wind.

In this example the dead-engine idling propeller absorbs 27 horsepower at 100 miles per hour; the free-wheeling propeller, 16 horsepower; and the locked propeller set 88°, only 1½ horsepower.

At some speed between 25 and 50 miles per hour the aerodynamic torque of the dead-engine propeller becomes insufficient to overcome the friction torque of the engine, and the propeller stops. Below this speed the drag is the same as that for a locked propeller.

Although the number of uses for negative propeller thrust has been greatly increased by the development of the controllable-pitch propeller, the uses are still relatively few. An attempt has been made in the preceding paragraphs to indicate some of the problems in this field and to show how the data in this report may be used in their solution.

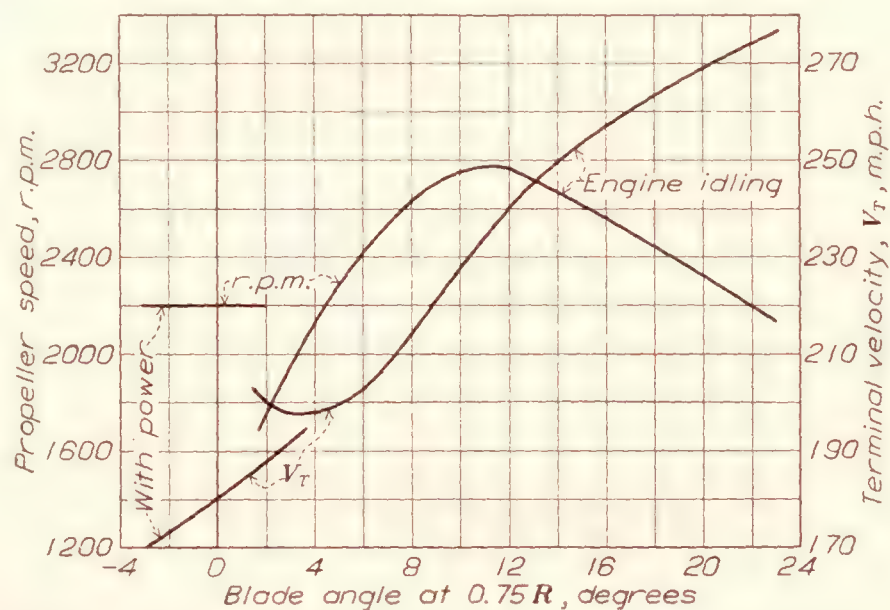


FIGURE 13.—The performance in a terminal-velocity dive of an airplane having the following characteristics: Gross weight, 2,580 pounds; engine, 420 horsepower at 2,200 r.p.m.; propeller, 4412, diameter 9 feet. Equivalent parasite area (D_p/q) 11.4 square feet.

CONCLUSIONS

1. The negative thrust of a propeller is considerably affected by the shape and size of the body behind it.
2. Through the range of blade angles covered in these tests, the maximum negative-thrust coefficient increases with decrease in blade angle.
3. For blade angles below 7° it is necessary to use engine power to obtain the greatest negative thrust.
4. The drag of a free-wheeling propeller is slightly less than that of a locked propeller in the normal range of blade-angle settings.
5. The drag of a locked propeller may be greatly reduced by feathering it into the wind.

LANGLEY MEMORIAL AERONAUTICAL LABORATORY,
NATIONAL ADVISORY COMMITTEE FOR AERONAUTICS,
LANGLEY FIELD, VA., May 23, 1933.

REFERENCES

1. Durand, William F., and Lesley, E. P.: Experimental Research on Air Propellers, II. T.R. No. 30, N.A.C.A., 1920.
2. Lock, C. N. H., and Bateman, H.: Airscrews at Negative Torque. R. & M. No. 1397, British A.R.C., 1931.

3. Weick, Fred E., and Wood, Donald H.: The Twenty-Foot Propeller Research Tunnel of the National Advisory Committee for Aeronautics. T.R. No. 300, N.A.C.A., 1928.
4. Wood, Donald H.: Tests of Nacelle-Propeller Combinations in Various Positions with Reference to Wings. Part I. Thick Wing—N.A.C.A. Cowled Nacelle—Tractor Propeller. T.R. No. 415, N.A.C.A., 1932.
5. Weick, Fred E.: Working Charts for the Selection of Aluminum Alloy Propellers of a Standard Form to Operate with Various Aircraft Engines and Bodies. T.R. No. 350, N.A.C.A., 1930.
6. Wood, Donald H.: Full-Scale Tests of Metal Propellers at High Tip Speeds. T.R. No. 375, N.A.C.A., 1931.
7. Glauert, H.: The Landing of Aeroplanes (Part I). R. and M. No. 666 British A.C.A., 1920.

REPORT No. 465

DETERMINATION OF THE THEORETICAL PRESSURE DISTRIBUTION FOR TWENTY AIRFOILS

By I. E. GARRICK

SUMMARY

This report gives the theoretical distribution of pressure at lift coefficients of 0, 0.5, 1.0, and 1.5 for 20 airfoils, calculated on the basis of a rigorous potential theory of arbitrary airfoils. It also provides tables from which the characteristics of the airfoils for any angle of attack in 2-dimensional potential flow are readily calculable. The theoretical values of the angles of zero lift, the lift and moment coefficients, and the ideal angles of attack are listed and some comparisons with experiment are indicated. Some of the well-known characteristics and properties of airfoils are accounted for in terms of the theoretical pressure-distribution curves. Qualitative deductions are made concerning the causes of breakdown of potential flow and the efficiency of the airfoil in viscous flow. The results presented may be of value in predicting structural loads and also in a correlation of theoretical pressure gradients with profile resistance.

INTRODUCTION

Until recently the theoretical distribution of pressure around airfoils could be determined only for the so-called "theoretical" airfoils. Indeed, only in the particular case of the Joukowski airfoils is the calculation not unduly laborious. (See references 1 and 2.) The theoretical airfoils, which are defined by special mathematical transformations, have, however, seldom been employed in practice. Their use in a precise study of pressure distribution has in fact been due more to necessity than to desire. The distribution of pressure for mathematically "thin" airfoils (i.e., the airfoil is represented by the mean-camber line) can be obtained, at least approximately, by the processes given by Munk, Glauert, and Theodorsen (references 3, 4, and 5). In another report (reference 6) Theodorsen developed a theory readily applicable to arbitrary airfoils. This theory was extended by Theodorsen and Garrick in reference 7, in a report which gives a unified treatment of the 2-dimensional potential flow around airfoils of *any* shape. The treatments given in references 6 and 7 avoid approximations in the anal-

ysis, and are referred to for details of the underlying theory of the results of the present paper.

The differences exhibited by airfoils in potential flow, as well as the differences between the actual and ideal cases for a particular airfoil, can, of course, be critically studied only if the ideal case is known. Furthermore, it is only on this basis that the assumptions of the theory itself can be critically analyzed and modified. It is therefore believed that an existing gap in aerodynamical literature will be, to some extent, bridged by the publishing in the present paper of convenient tables and curves of the theoretical results for a number of commonly used and related airfoils.

A knowledge of the theoretical distribution of pressure for an airfoil is, undoubtedly, a major factor in making it ultimately possible to predict accurately the behavior and efficiency of the airfoil under actual conditions, for the theoretical changes along the surface from pressure to velocity and from velocity to pressure are very significant in the determination of the drag characteristics. Knowledge of the theoretical results is of considerable value, too, for guiding experimental work whenever the measurements are rather critical, and such information also directs attention to the significance and interpretation of differences between theory and experiment.

Unfortunately, because of lack of sufficient accurate experimental data, comparison cannot be made directly with wind-tunnel results except in a few cases. In reference 7 an interesting comparison was given between theory and experiment of the pressure distribution around the N.A.C.A.-M6 airfoil at 12 different angles of attack. Reference 8 may be referred to for qualitative experimental results for five additional airfoils. A more accurate experimental study of pressure distributions is in progress at the present time at the N.A.C.A. laboratories.

A part of the following work was undertaken at the request of the Bureau of Aeronautics, Navy Department, for use in work on structural loads.

In making the calculations the author was ably assisted by Miss Alyce V. Rudeen, of the Committee's staff.

SUMMARY OF FORMULAS USED

The formulas used to obtain the results presented in the tables and curves are developed in references 6 and 7. A sample calculation for the N.A.C.A.-M6 airfoil with a comparison with experimental results, as well as explanatory figures and diagrams illustrating the use of the formulas, is given in reference 7. The following list presents the symbols employed and their definitions:

SYMBOL	DEFINITION
(1) (x, y)	See discussion of the choice of axes in a following paragraph.
(2) θ	$2 \sin^2 \theta = p + \sqrt{p^2 + y^2}$ where $p = 1 - \left(\frac{x}{2}\right)^2 - \left(\frac{y}{2}\right)^2$
(3) ψ	$2 \sinh^2 \psi = -p + \sqrt{p^2 + y^2}$. Since y is generally small for airfoils, the following equation may be preferable: $\sinh \psi = \frac{y}{2 \sin \theta}$. Near the leading (or trailing) edge ψ is given approximately by $\psi = \sqrt{\frac{\sigma}{2}}$ where σ is the radius of curvature at the leading (or trailing ¹) edge.
(4) ϵ	$\epsilon(\phi') = -\frac{1}{2\pi} \int_0^{2\pi} \psi(\phi) \cot \frac{\phi - \phi'}{2} d\phi$ See appendix ² of reference 7 for method of evaluation.
(5) ϵ'	Obtained graphically from the ϵ, θ curve. (Denoted $\frac{d\epsilon}{d\theta}$ in reference 7.)
(6) ψ'	Obtained graphically from the ψ, θ curve. (Denoted $\frac{d\psi}{d\theta}$ in reference 7.)
(7) ϕ	$\phi = \theta + \epsilon$.
(8) ψ_0	A constant: $\psi_0 = \frac{1}{2\pi} \int_0^{2\pi} \psi(\phi) d\phi$
(9) α	Angle of attack with respect to the x axis.
(10) β	The angle of zero lift, given by the value of ϵ for $\theta = \pi$.
(11) k	$k = \frac{e^{\psi_0} (1 + \epsilon')}{\sqrt{(\sinh^2 \psi + \sin^2 \theta) (1 + \psi'^2)}}$ Note: k is independent of the angle of attack.
(12) $\frac{v}{V}$	The ratio of the local velocity at the airfoil surface to the uniform stream velocity:

¹ For airfoils whose trailing edges are not uniquely defined, it is convenient to consider the trailing edge as formed by an arc of very small radius of curvature, and to fair in the ψ, θ curve near $\theta = \pi$.

² A convenient 20-point method is given here which in practice is quite sufficient. However, any number may be used, or any interval which appears to be critical may be subdivided and treated separately.

$$\frac{v}{V} = k[\sin(\alpha + \phi) + \sin(\alpha + \beta)].$$

(13) $\frac{p}{q}$

The ratio of the local superstream pressure to the dynamic pressure (the term "superstream pressure" is used to designate the difference of the local pressure and the static pressure in the undisturbed uniform stream):

$$\frac{p}{q} = 1 - \left(\frac{v}{V}\right)^2 \text{ and } q = \frac{1}{2} \rho V^2.$$

(14) c

The segment of the x axis intercepted by the airfoil boundary.

(15) C_L

The lift coefficient

$$C_L = \frac{L}{\frac{1}{2} \rho c V^2} = \frac{8 \pi e^{\psi_0}}{c} \sin(\alpha + \beta)$$

(16) F

A point designated the "focus" of the airfoil. We may first define the complex constants c_1 and c_2 as

$$\begin{aligned} c_1 &= m e^{i\delta} = A_1 + i B_1 \\ &= \frac{e^{\psi_0}}{\pi} \int_0^{2\pi} \psi(\phi) (\cos \phi + i \sin \phi) d\phi \\ c_2 &= A_2 + i B_2 \\ &= \frac{e^{2\psi_0}}{\pi} \int_0^{2\pi} \psi(\phi) (\cos 2\phi + i \sin 2\phi) d\phi \end{aligned}$$

Then writing

$$b^2 c^{2i\gamma} = 1 + \frac{c_1^2}{2} + c_2$$

we have

$$b^4 = \left(1 + \frac{A_1^2 - B_1^2}{2} + A_2\right)^2 + (A_1 B_1 + B_2)^2$$

$$\text{and } \gamma = \frac{1}{2} \tan^{-1} \frac{A_1 B_1 + B_2}{1 + \frac{A_1^2 - B_1^2}{2} + A_2}$$

Then the complex coordinate of F is

$$z_F = (x + iy)_F = m e^{i\delta} + \frac{b^2}{e^{\psi_0}} e^{i(2\gamma - \beta)}$$

(17) M_F

The moment at F is constant for all angles of attack:

$$M_F = 2\pi \rho b^2 V^2 \sin 2(\gamma - \beta)$$

(18) C_{MF}

The moment coefficient referred to the point F :

$$C_{MF} = \frac{M_F}{c^2 q} = 4\pi \frac{b^2}{c^2} \sin 2(\gamma - \beta)$$

(19) α_I

The "ideal" angle of attack:

$$\alpha_I = -\frac{\epsilon_N + \epsilon_T}{2}$$

where ϵ_N and ϵ_T denote, respectively, the values of ϵ at the nose and tail; i.e., for $\theta = 0$ and $\theta = \pi$, respectively.

The ideal angle of attack for thin airfoils has been defined by Theodorsen (reference 5) as that angle for which the front stagnation point is at the leading edge.

At this angle of attack large velocity gradients at the leading edge are avoided and the profile drag is at, or very near, its minimum value. The definition can be naturally extended to actual airfoils to designate that angle of attack for which the front stagnation point is at the foremost edge of the mean-camber line. However, as pointed out by Theodorsen, the effective mean-camber line of a thick airfoil actually alters with change of angle of attack, and the ideal angle of attack for a thick airfoil represents an average of a range of angles for which the profile drag is very near its minimum.

PROCEDURE AND ACCURACY OF THE CALCULATIONS

In order to avoid possible confusion it may be well to state beforehand that the term "chord" is used in this paper as synonymous with the segment of the x axis intercepted by the airfoil. The "standard chord" in terms of which the airfoil is usually empirically defined does not, in general, coincide with this above-defined chord. The angle between the x axis as chosen and the standard chord is designated λ and is listed in table I. (See also fig. 1.)

In the procedure of the calculations, the axes of coordinates are first chosen in a definite convenient way, since the ease and rapidity of convergence of further evaluations depend considerably on the choice of axes (references 6 and 7). This choice may be made as follows: If the distance between the leading edge of the airfoil and the center of curvature of the leading edge is bisected at E (the coordinates of E are $(2, 0)$), and the same is done for the trailing edge at E' (the coordinates of E' are $(-2, 0)$), then the x axis should pass through EE' and the origin bisects the distance EE' . However, small variations from this particular choice of axis and origin do not noticeably influence the ease of calculation.³ The quantities given in the headings of table II are directly calculated in terms of x and y by means of the formulas previously listed. The angle of attack corresponding to a given value of the lift coefficient may be obtained from (15), in which c is $X_N - X_T$, where X_N and X_T denote the abscissas of the leading edge and trailing edge, respectively. The moment coefficient C_{MF} may be obtained from (18), in which the constants b^2 and γ are obtained from (16) by graphical integration of the $\psi \sin \phi$, $\psi \cos \phi$, $\psi \sin 2\phi$, and $\psi \cos 2\phi$ curves.

The ordinates of the airfoil are given empirically to hundredths of a percent of the standard chord for 16 stations of the upper and lower surfaces respectively. The quantities x , y , ψ , and θ are defined to the same degree of accuracy. The ψ , θ curve is thus a faired curve through 32 points and $\epsilon(\theta)$ is estimated to be of the same order of accuracy as $\psi(\theta)$. The deriva-

tives ϵ' and ψ' , being determined graphically, admit of a possible small error which, however, causes an error in k of probably less than 2 percent. The angle of zero lift, or the value of ϵ for $\theta = \pi$, may perhaps be in error as much as $15'$, but the influence of this possible error on the theoretical pressure-distribution curves for fixed values of C_L is negligible.

The numerical data for the Clark Y airfoil are presented in table II. The distribution of velocity and pressure for any angle of attack or at any lift coefficient, as well as other theoretical characteristics, are obtained with a minimum of effort from this table. Similar tables for the remaining airfoils are omitted here for reasons of economy in printing and also because it is not known how general the interest in them will be. They are available on request from the National Advisory Committee for Aeronautics.

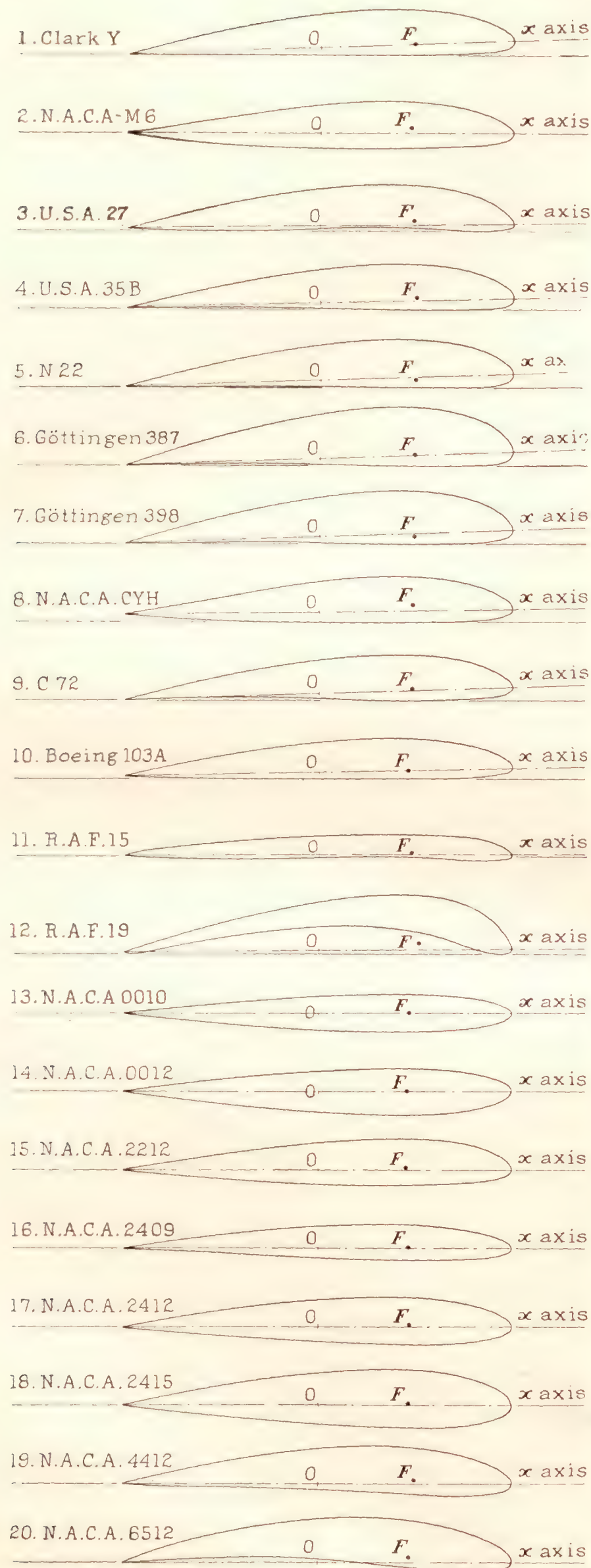
DISCUSSION

Although the airfoils chosen in this paper are mainly conventional airfoils (fig. 1) and not extremely radical types, it is nevertheless possible to isolate some of the individual effects of change of shape and compare these with experimental results. It is believed, however, that future experimental work on radical and less conventional shapes, for which the theoretical results are readily available (see, for example, reference 7, p. 31), will enable the isolation and analysis of effects which are probably masked and unemphasized in conventional types.

We may first make some general comments regarding the curves of theoretical pressure distribution given in the following pages. In each figure the abscissa represents the location of a point of the airfoil surface in percent chord and the ordinate gives the quantity p/q , the ratio of the local superstream pressure to the dynamic pressure q . It may be noted that negative values of p/q are plotted upwards. This is an arbitrary convention and is made because it is more readily associated with the upper surface of the airfoil, which for ordinary angles of attack is the surface of suction or negative pressure. In figures 2 to 21, inclusive, it may be noted that the points of the curves above the zero, or normal pressure, line represent suction; that is, velocities, greater than V . Positive values of p/q denote pressures greater than normal static pressure; i.e., $v < V$. The stagnation points at which $v = 0$ correspond to $\frac{p}{q} = 1$.

Effect of compressibility.—In figure 22 there is shown for convenience a curve of the dynamic pressure q in inches of water and in pounds of force per square foot against velocity in miles per hour. The values given correspond to atmospheric conditions at 2,000 feet altitude and 0° C. For the ordinary velocity range of aircraft, say from 45 to 200 miles per hour, q varies from about 1 to 20 inches of water. For very great velocities the effect of compressibility of the air

³ Notice, however, that we have chosen the rear stagnation point on the x axis at $\theta = \pi$, thus fixing the calculation by the Kutta condition. Strictly speaking, then, the x axis should be chosen in the unique manner indicated above (this has been done for the airfoils treated here), for, if another axis is chosen, the rear stagnation point must be properly relocated with respect to it, causing a change in the angle of zero lift with respect to the new axis.

FIGURE 1.—The 20 airfoils chosen, showing axes and location of F .

becomes significant and the potential-theory characteristics based on an assumption of incompressibility may be considerably altered. However, as is pointed out by Glauert (reference 10), the compressibility of air has minor influence for velocities under 0.5 the velocity of sound, or ordinarily about 350 miles per hour. However, it should be noted that at certain angles of attack the local velocity may be as much as two or more times the stream velocity. Thus, for very great velocities, the strong suction in the region of the peak pressures may introduce radical changes in the flow, as the compressibility properties of the fluid become important. This effect is associated with Mach's Number (v/c , where c is the velocity of sound in the medium), and the ordinary Reynolds Number alone is not a safe criterion for scale effect. The potential theory yet remains to be properly modified for the effect of compressibility. Reference 9 gives some experimental results of the distribution of pressure over airfoils for very high speeds. The maximum negative pressure (or suction) obtained in this reference was 37 cm of mercury.

Pressure gradients.—From the concept of the ideal angle of attack we are led to expect that the thinner the airfoil at the leading edge the greater the velocities near the leading edge for angles different from α_L . This expectation is confirmed by the large negative values of p/q attained by the R.A.F. 15 and the N.A.C.A. 0010, 0012, and 2409 airfoils. In particular, the pressure on the N.A.C.A. 0010 reaches $-11q$ for lift coefficient $C_L=1.5$, whereas the somewhat thicker N.A.C.A. 0012 reaches $-7q$ at the same lift coefficient. In practice, the value of C_{Lmax} for the N.A.C.A. 0012 is somewhat greater than that for the N.A.C.A. 0010. Results of force tests of the airfoils treated in this paper are presented in references 11, 12, and 13.

The large gradient of pressure behind the negative peak pressure is very significant for the breakdown of potential flow. The deceleration of fluid becomes so rapid that fluid is piled up at the trailing edge and the flow no longer separates precisely at the trailing edge but breaks off along the upper surface. The flow along the lower surface undergoes but little change at high angles of attack except that, after the breakdown of potential flow has occurred, the pressure at the trailing edge may be somewhat negative instead of positive.

The change from the front stagnation point to maximum velocity occurs within a very small space interval, and all indications are that frictional losses are practically negligible while the fluid is accelerating, as compared with losses when deceleration occurs. The fluid follows the surface boundary more easily in the change from pressure energy to kinetic energy than vice versa. This fact is also abundantly confirmed by experiments with nozzles and venturi tubes. For

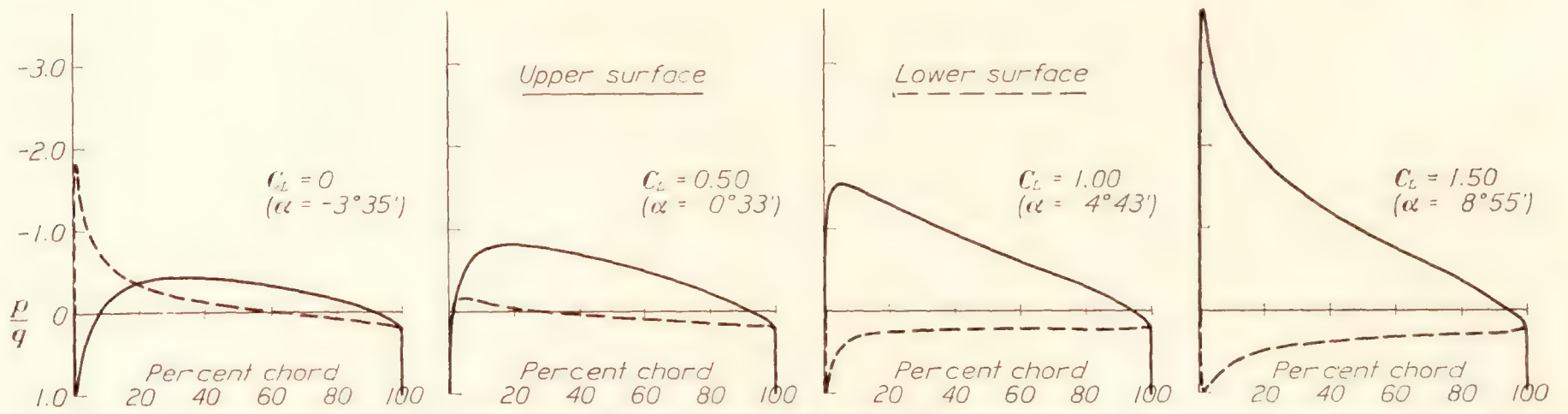


FIGURE 2.—Theoretical pressure distribution for the Clark Y airfoil.

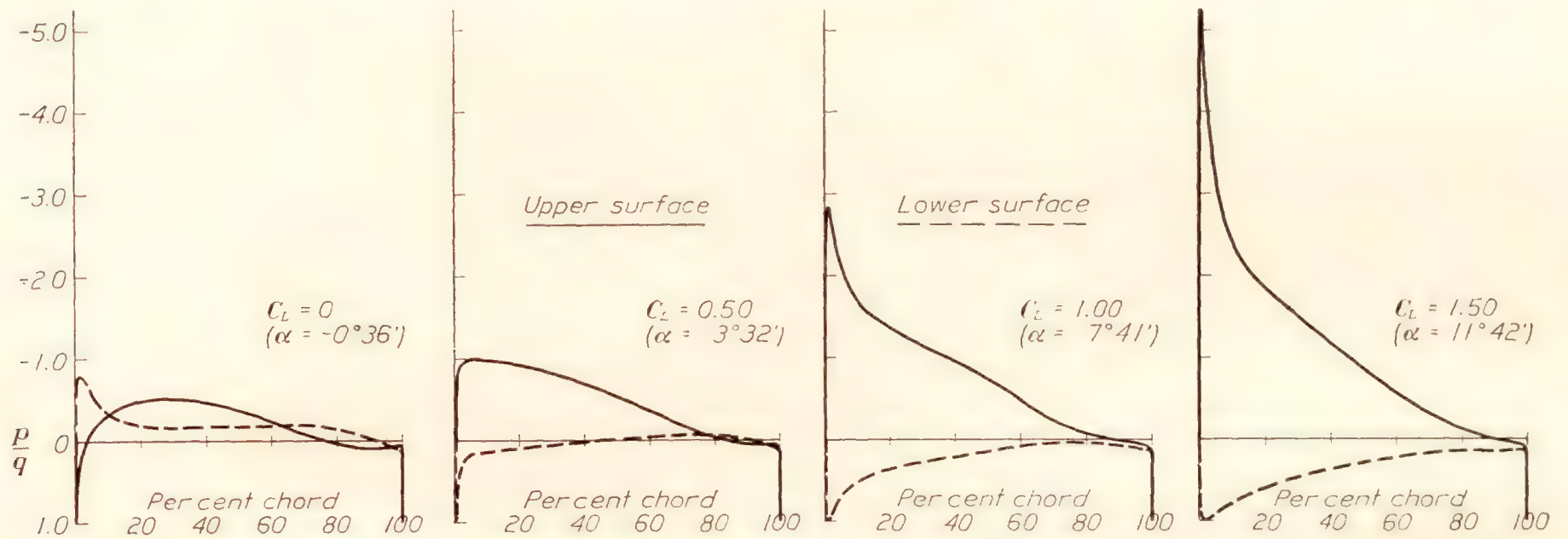


FIGURE 3.—Theoretical pressure distribution for the N.A.C.A.-M6 airfoil.

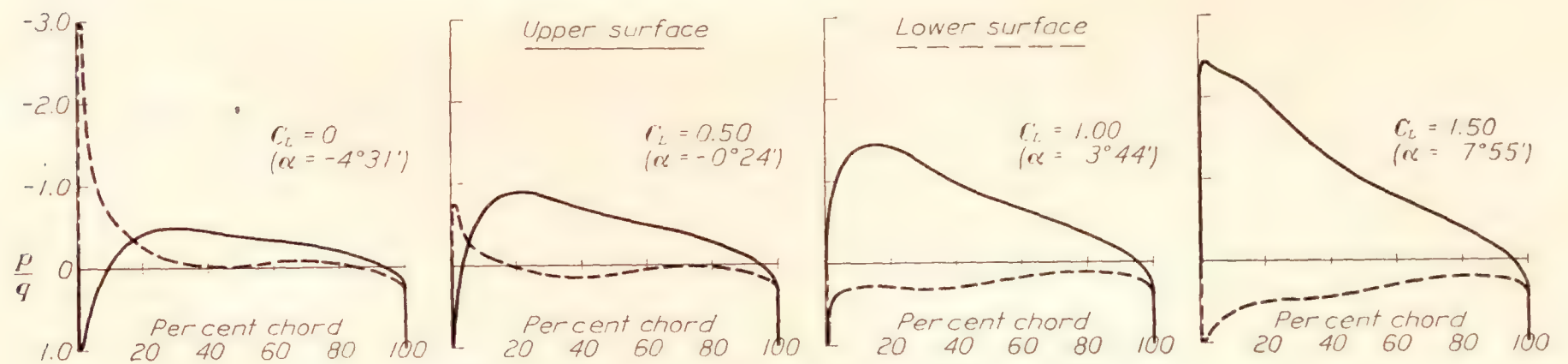


FIGURE 4.—Theoretical pressure distribution for the U.S.A. 27 airfoil.

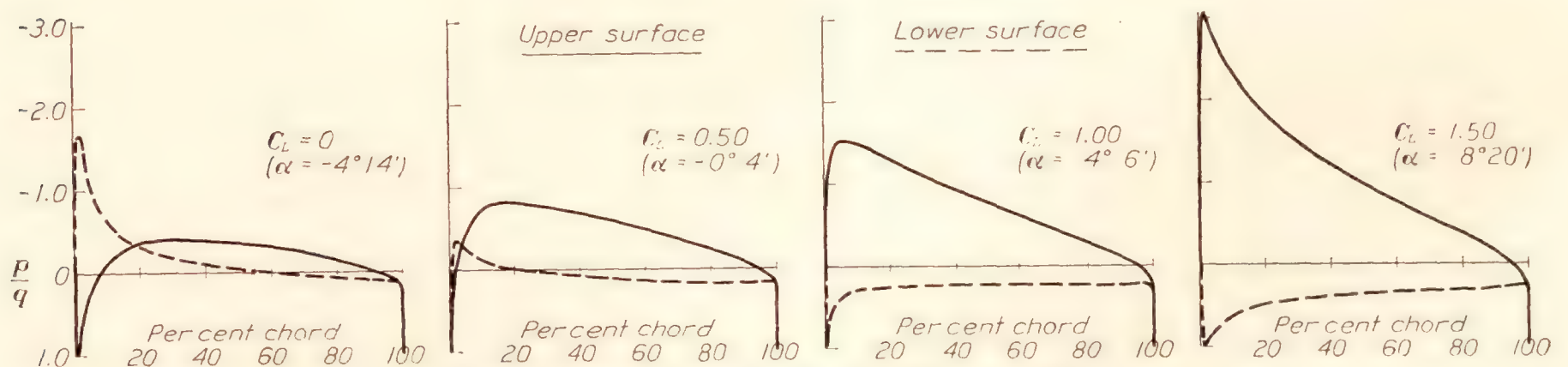


FIGURE 5.—Theoretical pressure distribution for the U.S.A. 35B airfoil.

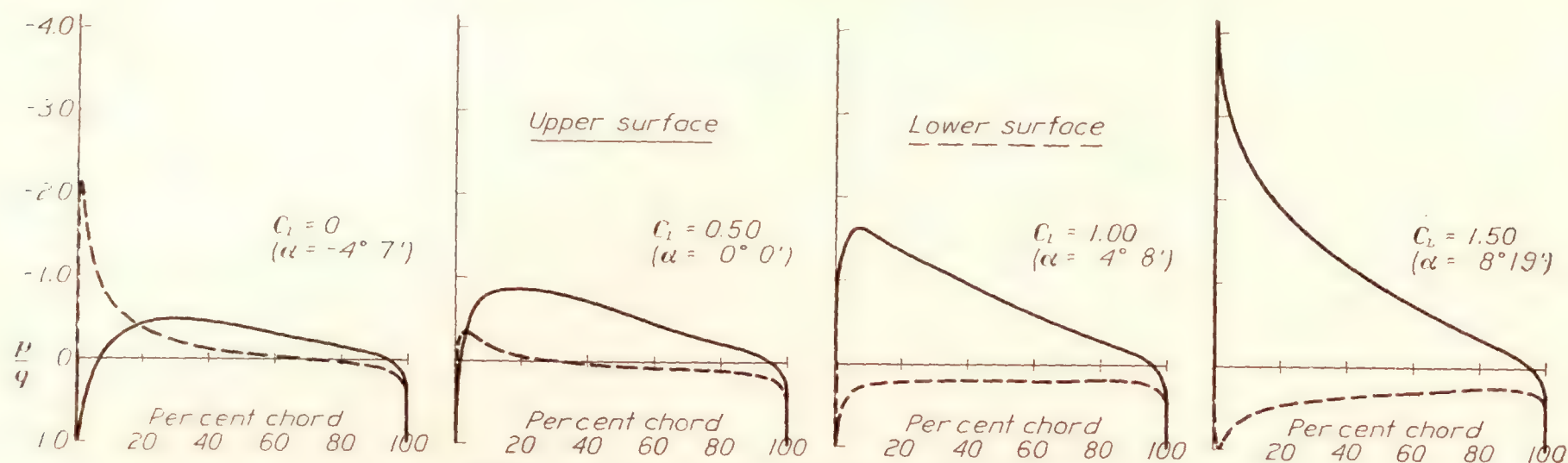


FIGURE 6.—Theoretical pressure distribution for the N 22 airfoil.

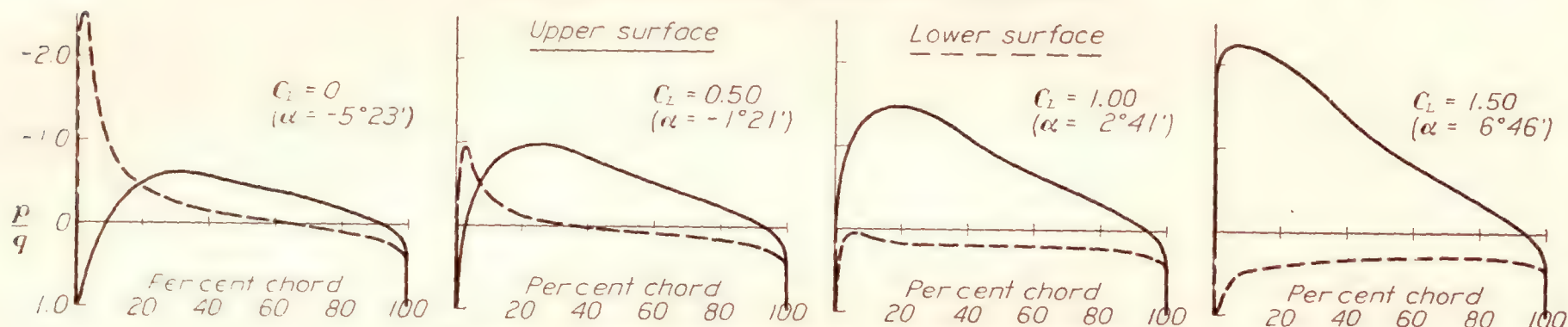


FIGURE 7.—Theoretical pressure distribution for the Göttingen 387 airfoil.

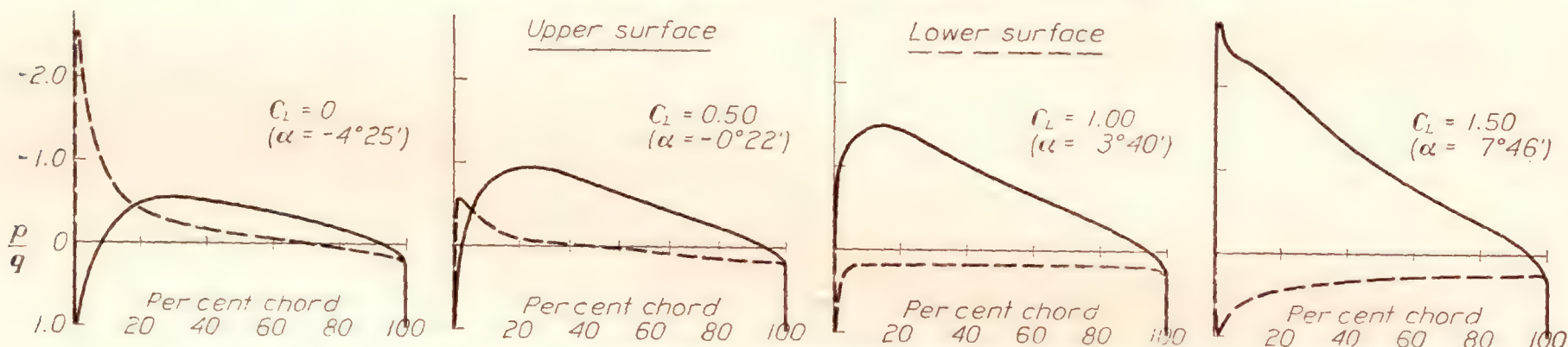


FIGURE 8.—Theoretical pressure distribution for the Göttingen 398 airfoil.

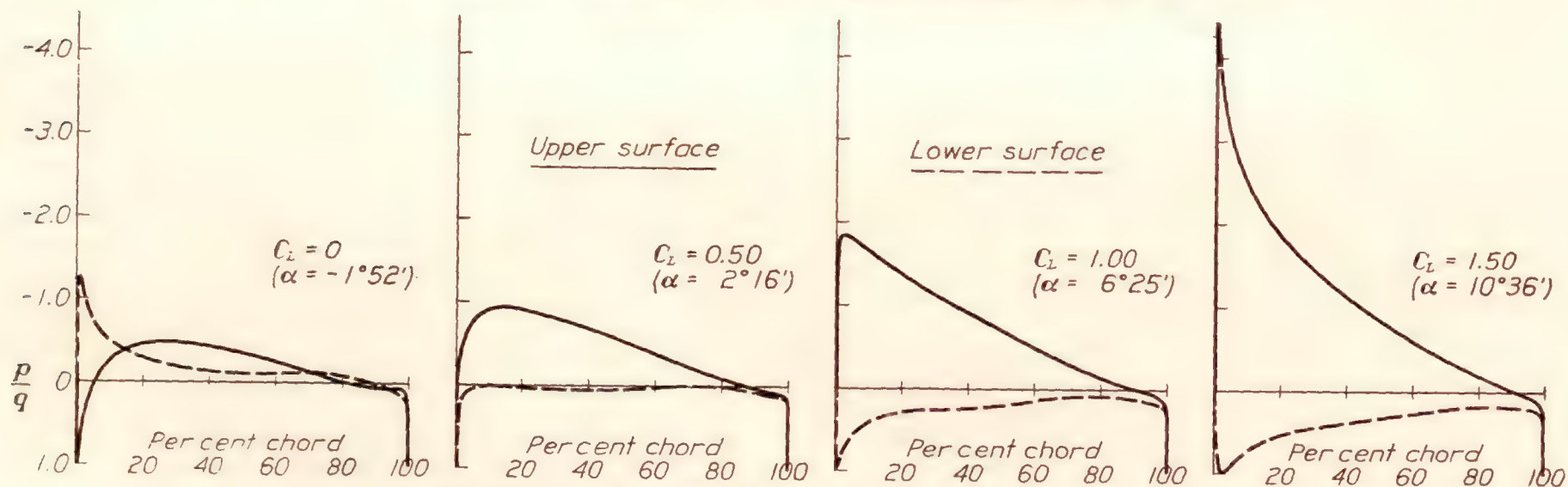


FIGURE 9.—Theoretical pressure distribution for the N.A.C.A.-CYH airfoil.

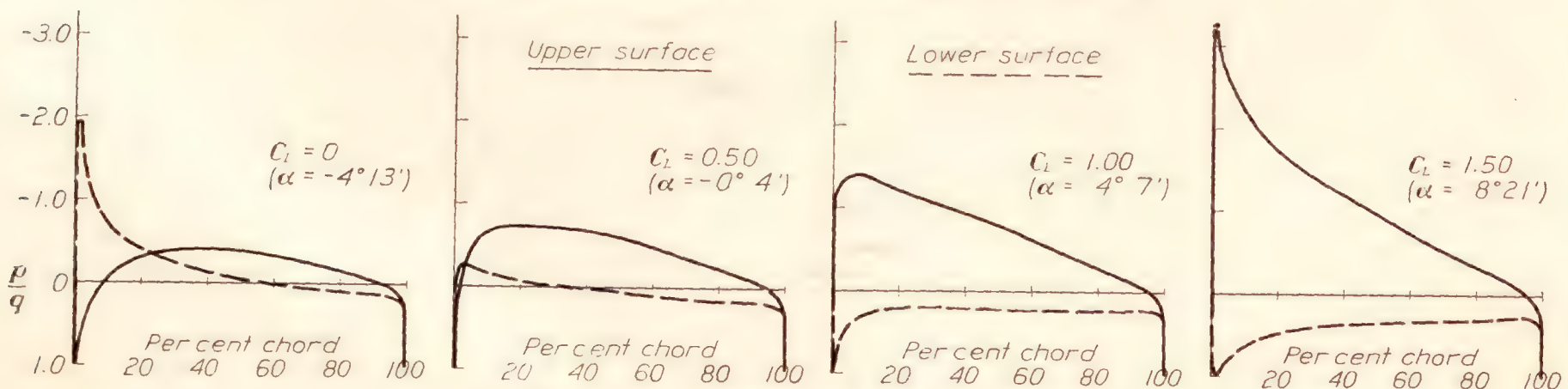


FIGURE 10.—Theoretical pressure distribution for the C 72 airfoil.

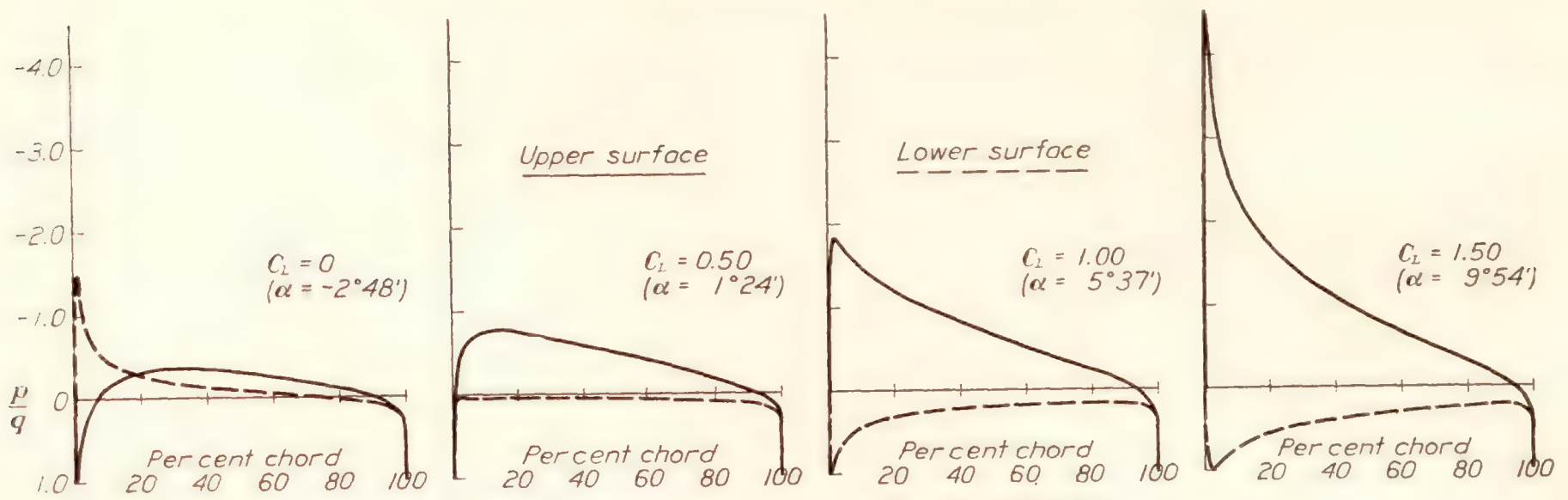


FIGURE 11.—Theoretical pressure distribution for the Boeing 103-A airfoil.

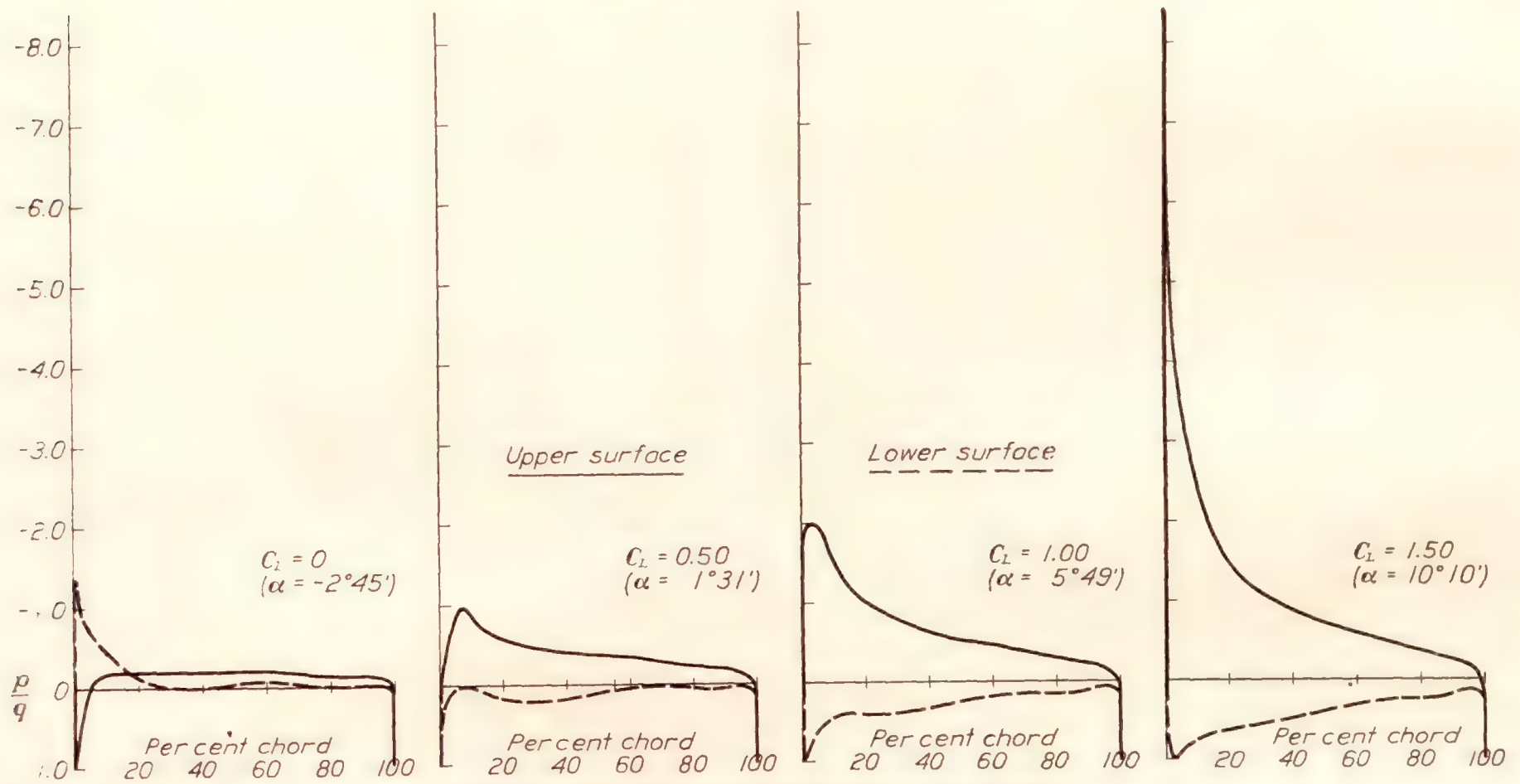


FIGURE 12.—Theoretical pressure distribution for the R.A.F. 15 airfoil.

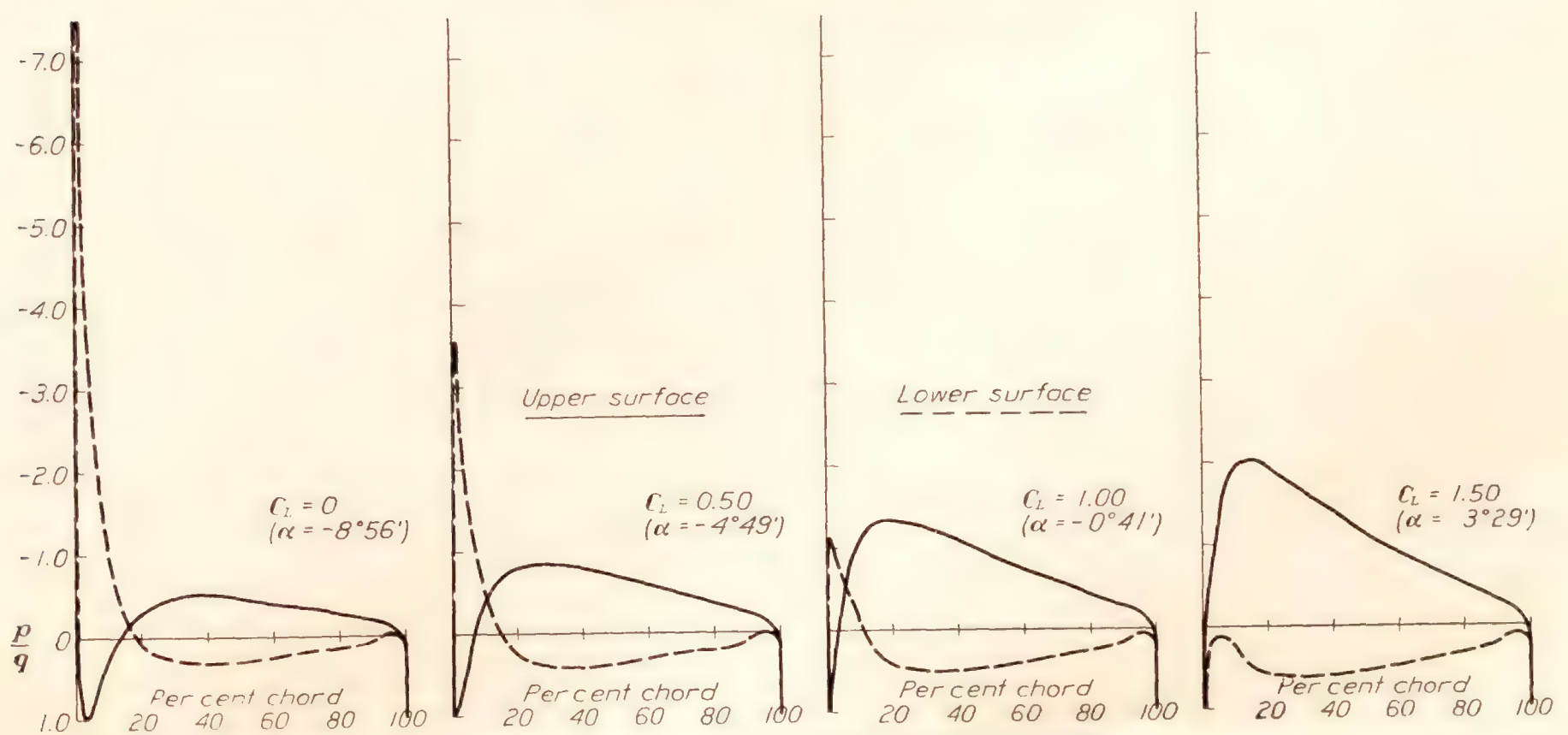


FIGURE 13.—Theoretical pressure distribution for the R.A.F. 19 airfoil.

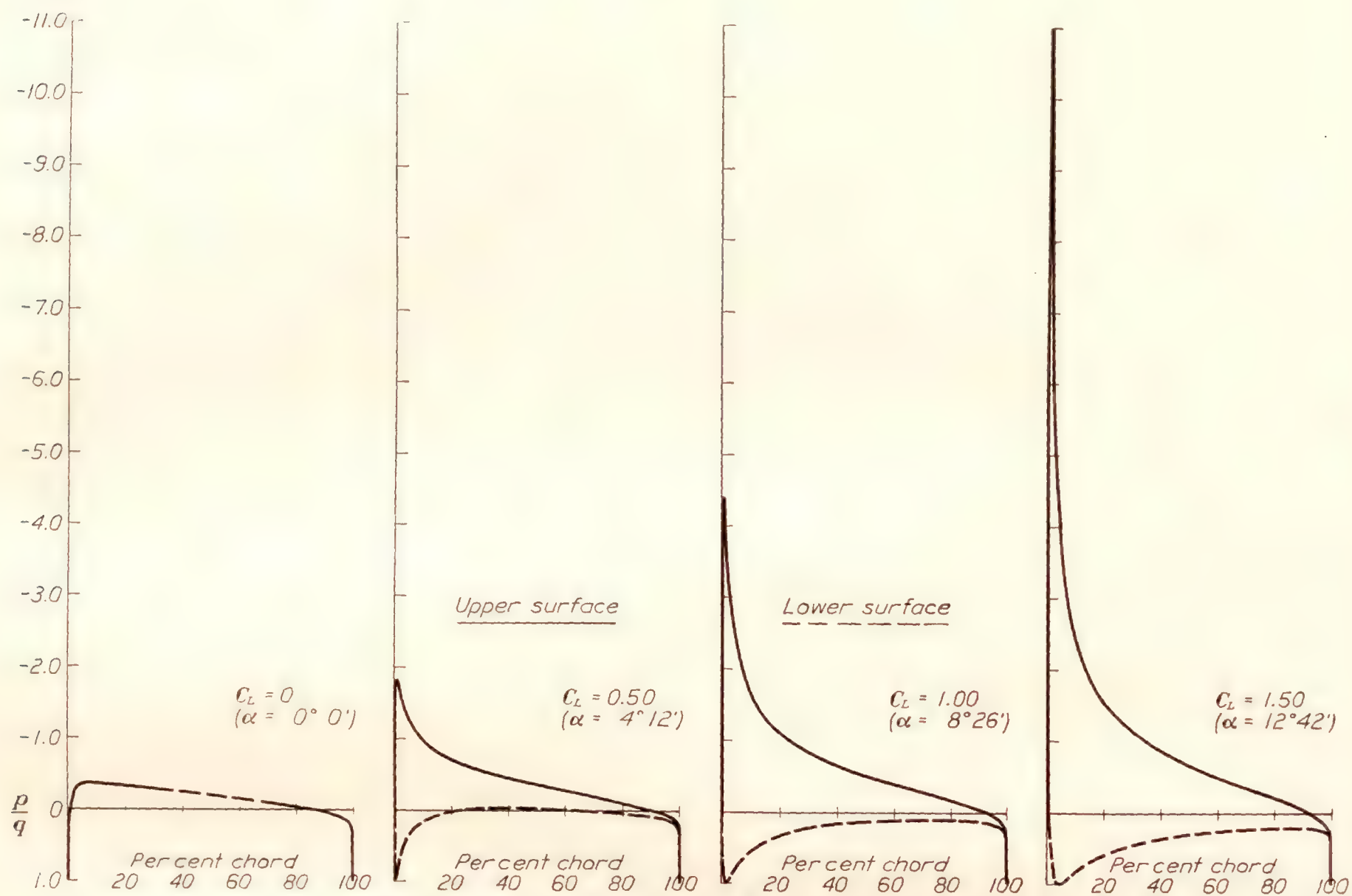


FIGURE 14.—Theoretical pressure distribution for the N.A.C.A. 0010 airfoil.

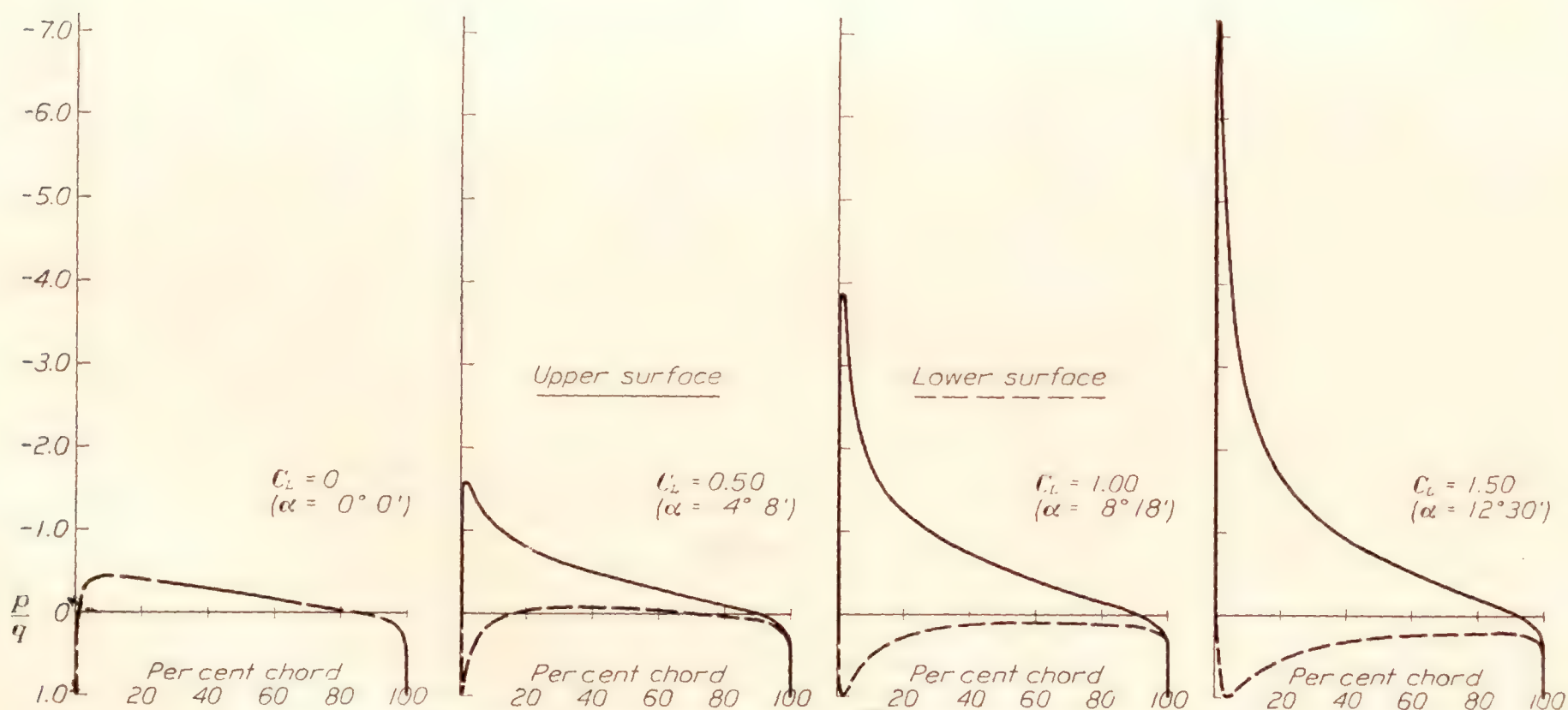


FIGURE 15.—Theoretical pressure distribution for the N.A.C.A. 0012 airfoil.

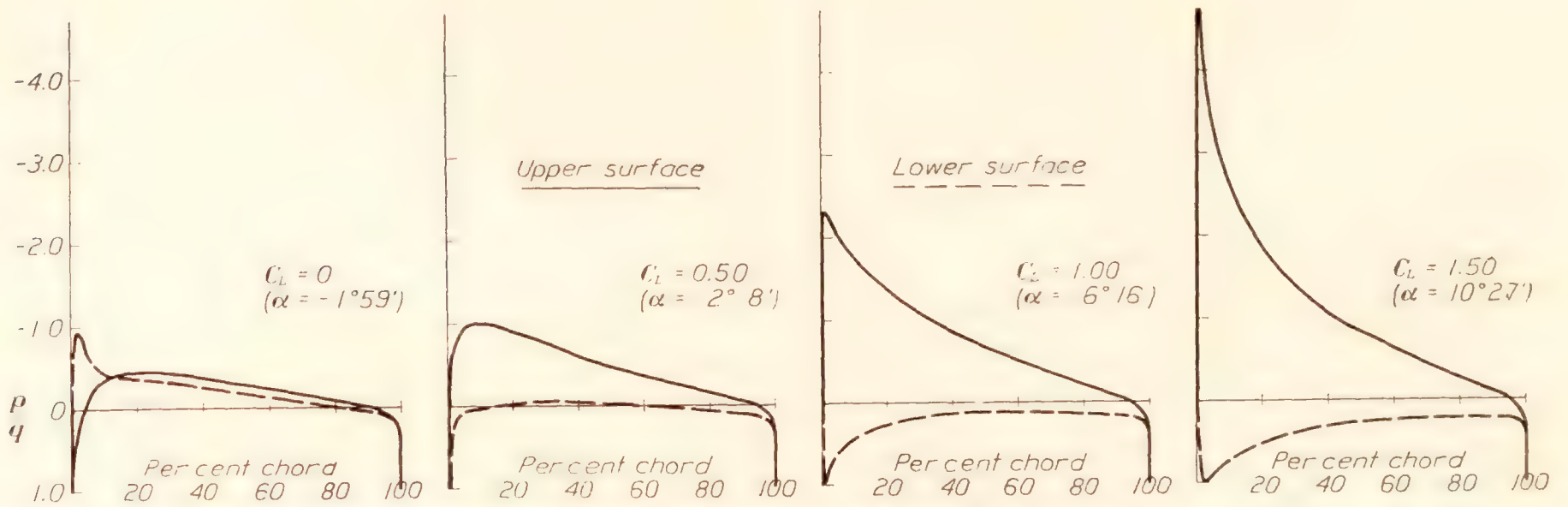


FIGURE 16. Theoretical pressure distribution for the N.A.C.A. 2212 airfoil.

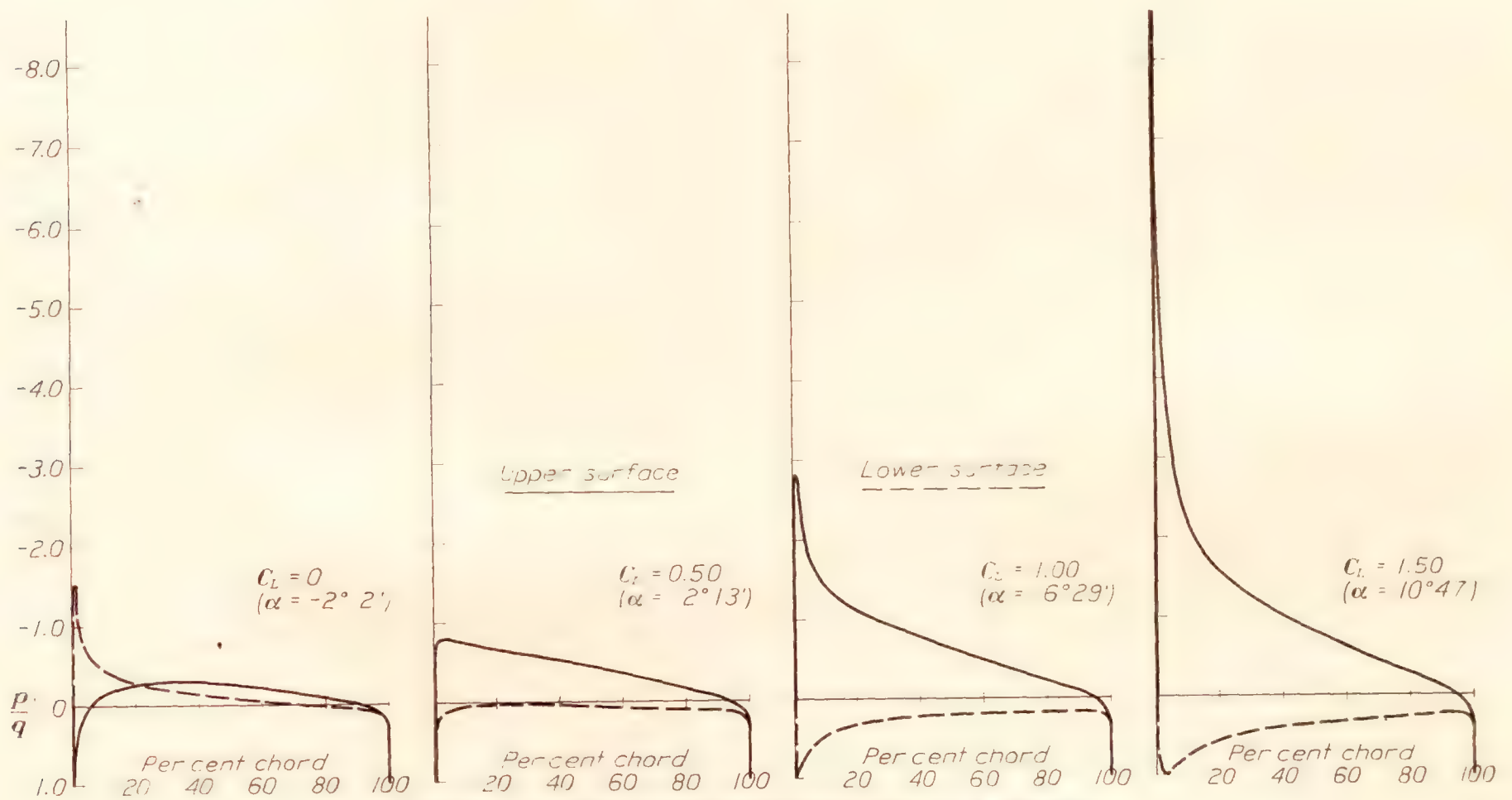


FIGURE 17. Theoretical pressure distribution for the N.A.C.A. 2409 airfoil.

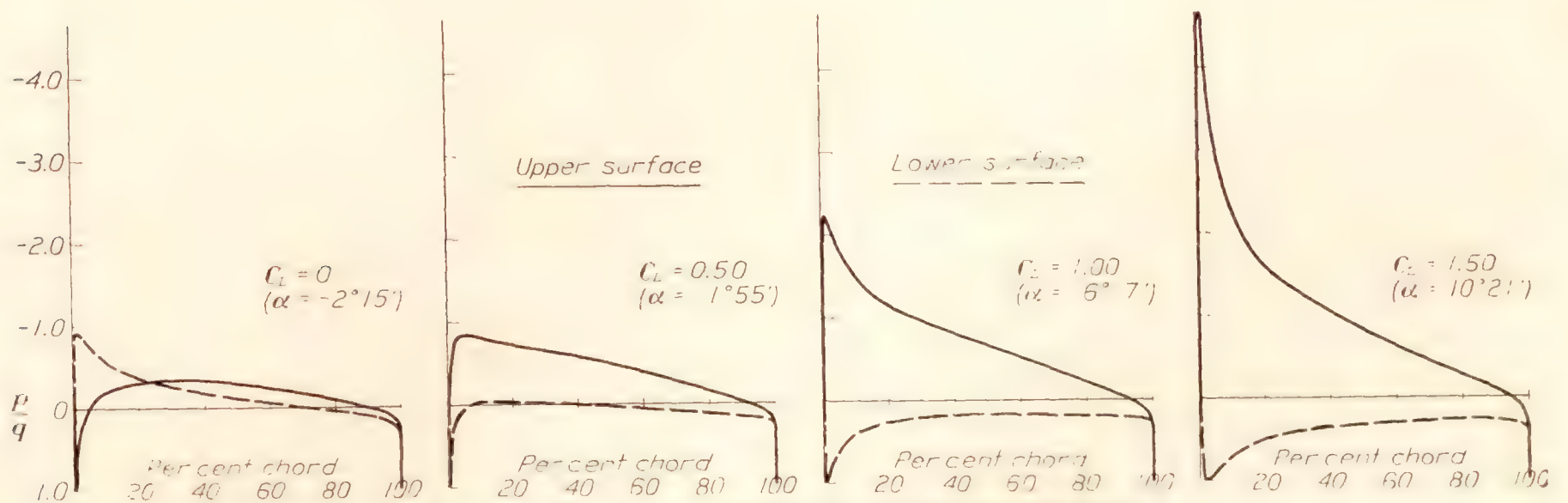


FIGURE 18. Theoretical pressure distribution for the N.A.C.A. 2412 airfoil.

airfoils used in practice without auxiliary devices, a pressure ratio p/q of about -3 or -4 is the maximum attained. It may be observed here that since the leading edge of the airfoil and the upper surface near the leading edge experience very large pressure gradients, they are critical regions, to be especially kept free from unnecessary protuberances and roughness.

It may be noted in the figures that very large pressure gradients exist in the region near the rear

Some effects of camber.—It may be observed that a property common to all airfoils is that the negative values of p/q mount rapidly near the leading edge on the upper surface after $C_L=1.00$ is exceeded. However, for the highly cambered airfoils, as the R.A.F. 19 and N.A.C.A. 6512, it may be noted that even for $C_L=1.50$ the p/q negative peak is but slightly above -2 . These airfoils are high-lift airfoils, and the lift is well distributed over the whole chord. However, they have

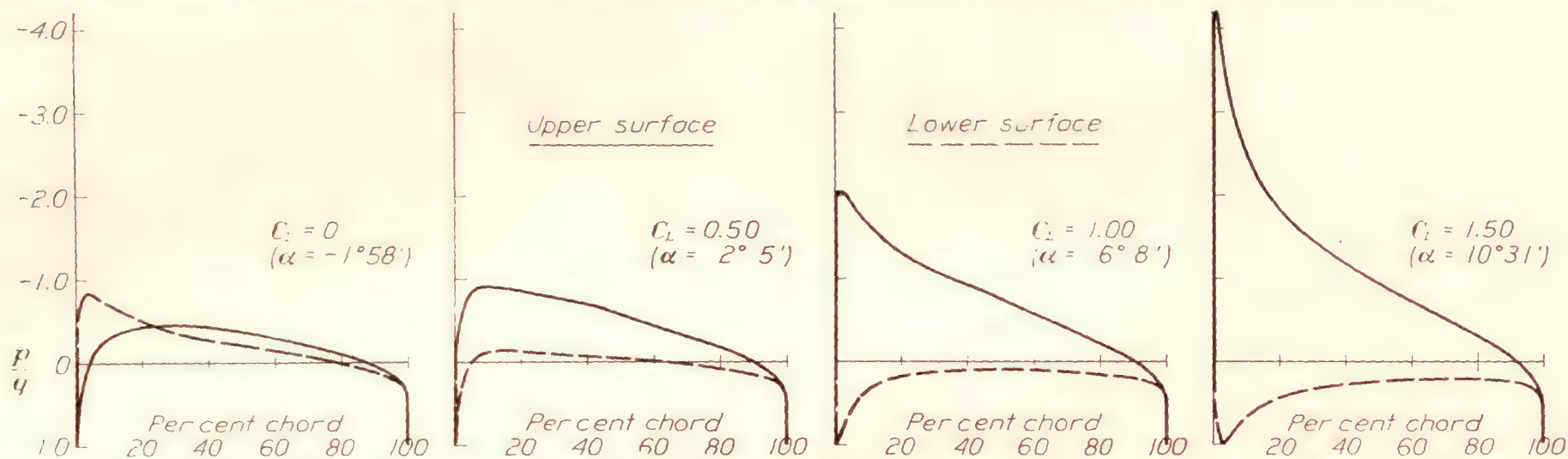


FIGURE 19.—Theoretical pressure distribution for the N.A.C.A. 2415 airfoil.

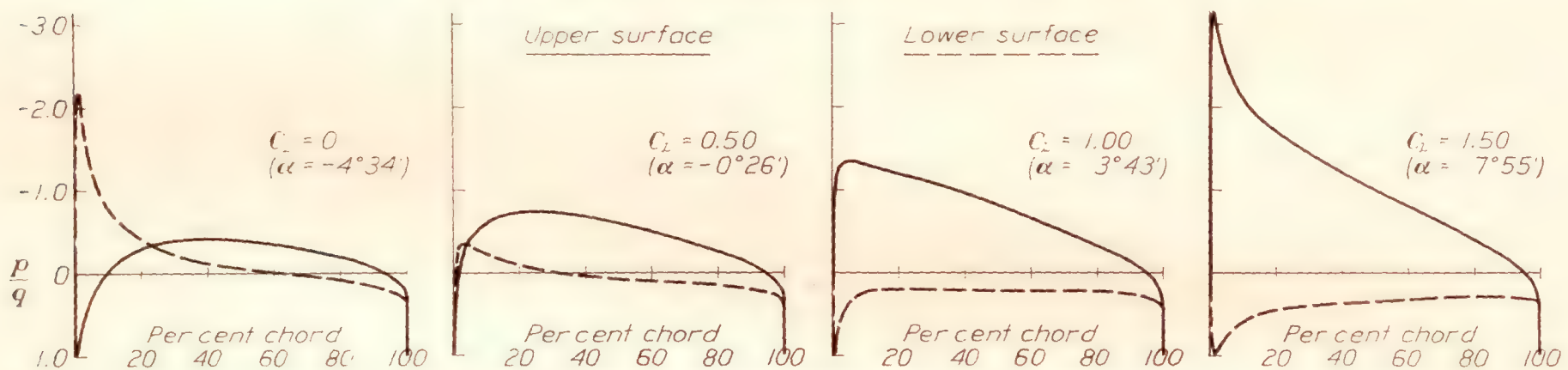


FIGURE 20.—Theoretical pressure distribution for the N.A.C.A. 4412 airfoil.

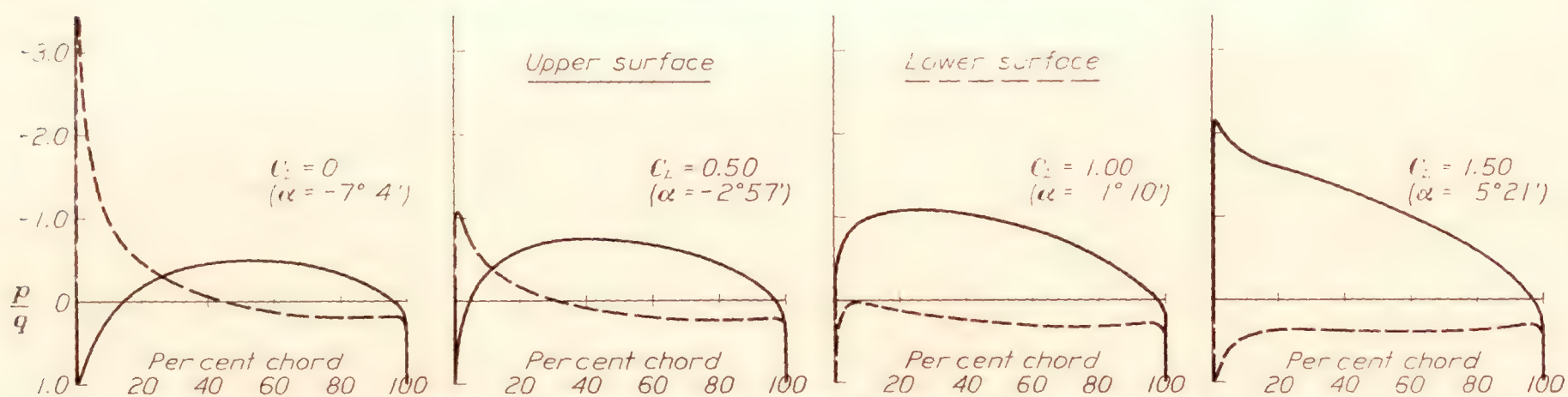


FIGURE 21.—Theoretical pressure distribution for the N.A.C.A. 6512 airfoil.

stagnation point, within the shadow of the 100 percent chord line. The rapid deceleration of fluid as thus shown to exist theoretically at the trailing edge most probably does not occur to any such extent in practice. The flow probably recombines at the trailing edge at velocities not much below normal, and the pressure curves are rounded off at a small positive pressure as shown in the figures. There is in this fact no essential violation of the Kutta condition for fixing the circulation, the primary purpose of which is only to avoid infinite velocities at the trailing edge.

usually unfavorable pitching moments and rather wide travel of the center of pressure, as evidenced by the theoretical moment coefficients at zero lift, which are respectively -0.210 and -0.185 .

Further effects of camber may be observed in figures 15, 18, 20, and 21 for the N.A.C.A. 0012, 2412, 4412, and 6512 airfoils, where in every case the maximum thickness is 12 percent of the chord and the maximum mean cambers are, respectively, 0, 2, 4, and 6 percent of the chord. The theoretical moment coefficients C_{MF} are, respectively, 0, -0.055 , -0.110 , and -0.185 .

The ideal angle, also, increases with camber and, hence, the optimum lift coefficient increases in general with camber. We may observe that the high-cambered airfoils, and more especially thin high-cambered airfoils, are not efficient at low values of the lift coefficient, as is evidenced by the high negative peaks in the pressure distribution for zero lift. In fact, the flow around many high-cambered airfoils (for example, the R.A.F. 19) is known to burble on the under surface at low lift coefficients. Indeed, large gradients of deceleration of fluid may everywhere be associated with decreased efficiency. The bringing of pressure gradients and profile resistance into a precise correlation is a significant problem for further investigation. A uniform gradual change from velocity to pressure, as in figure 2 for the Clark Y airfoil at $C_L=0.5$, gives probably the optimum lift distribution and occurs very nearly at the ideal angle of attack.

The experimental curves of lift coefficient against angle of attack for high-cambered airfoils like the R.A.F. 19 and N.A.C.A. 6512 are well rounded near maximum lift, whereas for airfoils like the N.A.C.A. 0010 and R.A.F. 15 they are likely to be sharp and jagged (reference 12). The former airfoils lose their lift rather gradually after maximum lift is attained, while for the latter airfoils this effect is likely to occur suddenly.

Effects of thickness.—In figures 17, 18, and 19 we may note some effects of the airfoil thickness. The N.A.C.A. 2409, 2412, and 2415 airfoils have a common mean-camber line and maximum thicknesses, respectively, of 9, 12, and 15 percent of the chord. For the N.A.C.A. 2415 it may be noted that the pressure on the under surface is generally less positive than for the 2412 and 2409. Also, we may observe that at lift coefficients $C_L=1.00$ and $C_L=1.50$ the down gradient of pressure along the first 15 percent of the chord is greatest for the 2409, while for the rest of the chord it is greatest for the 2415, indicating that an optimum effect for thickness lies perhaps between the extremes listed. The theoretical slope of the lift curve increases somewhat with thickness, and for the above airfoils has values of 6.75, 6.90, and 7.10, respectively. An experimental result that merits closer investigation is the fact that after a maximum thickness of about 12 percent is attained, $\frac{dC_L}{d\alpha}$ decreases somewhat with further increase in thickness (reference 12). A partial explanation lies in the fact that, in general, a thicker boundary layer exists on thick airfoils, decreasing their aerodynamic efficiency. It has, indeed, puzzled some observers employing various schemes for removing the boundary layer that the experimental slope of the lift curve for infinite aspect ratio often exceeds 2π , which is the value given by the approximate thin-airfoil theory. The average theoretical slope of the curves of lift against angle of attack for the airfoils listed in

this report is approximately 6.90 or about $1.10 \times 2\pi$. This value is about 15 to 20 percent greater than the experimental value of the slope of the lift curve for infinite aspect ratio, and indicates that the airfoil is in general from about 80 to 85 percent efficient with regard to lift.

Moment properties.—The theoretical moment M_F is, in most of the cases studied in this paper, from about 10 to 20 percent greater than the experimental value of the moment for zero lift. (See references 12 and 13.) On the basis of (16), the position of the focus F , at which the theoretical moment is constant for all angles of attack, was calculated and is shown in the figures of the airfoils. (See fig. 1 and also table I.) In every case its abscissa is very nearly at 25 percent of the chord from the leading edge, the maximum for

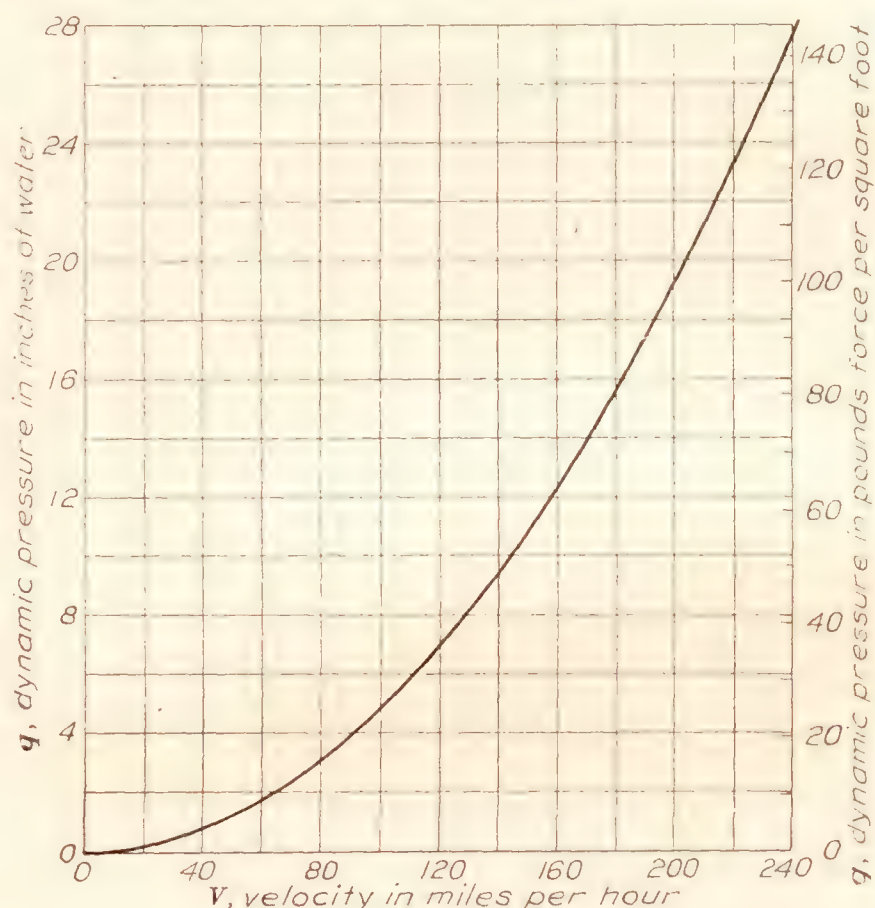


FIGURE 22.—Velocity V against dynamic pressure q .

the airfoils considered being near 27 percent and the minimum near 24 percent of the chord line. However, it is important to note that, in general, the ordinate of F does not fall on the chord line but is usually located at a small distance from it.

The tendency for more constant center-of-pressure properties may be observed in figure 4 for the U.S.A. 27, where the lower-surface pressure curve has a small inflection or bend. For the N.A.C.A.-M6 (fig. 3), which theoretically has practically zero travel of the center of pressure, the double bend on the pressure curves at zero lift may be observed. Alternate regions of suction and pressure thus exist on each surface. The N.A.C.A.-CYH shows the same tendencies to a lesser degree. The double bend in the pressure-distribution curves is probably common to most reflexed airfoils.

Experimental results on the angles of zero lift show considerable discrepancies and indicate a change with the Reynolds Number. In general, the consistent experimental result is obtained that the angle of zero lift increases (algebraically) with increase in the Reynolds Number. For this reason we may only indicate a comparison with experimental values. The values listed in table I of this paper consistently fall within the range of values obtained by experiment and seem to agree more closely with experimental results obtained at moderate Reynolds Numbers (about 2×10^6) than with those taken at very large Reynolds Numbers. This fact should be investigated further.

CONCLUSIONS

The preceding discussion shows that, to a large extent, the general properties and characteristics of airfoils, such as effects due to camber, thickness, or change of shape, may be accounted for by the theoretical pressure-distribution curves. The theoretical pressure-distribution curves at definite lift coefficients may be safely used for structural-load considerations. A correlation between pressure gradients and profile resistance, affecting the efficiency of the airfoil, has been qualitatively indicated. Further theoretical and experimental investigations should be concerned with the significance of the differences between theory and experiment.

LANGLEY MEMORIAL AERONAUTICAL LABORATORY,
NATIONAL ADVISORY COMMITTEE FOR AERONAUTICS,
LANGLEY FIELD, VA., *June 2, 1933.*

REFERENCES

1. Blumenthal, Otto, and Trefftz, E.: Pressure Distribution on Joukowski Wings and Graphic Construction of Joukowski Wings. T.M. No. 336, N.A.C.A., 1925.

2. Perring, W. G. A.: The Theoretical Pressure Distribution around Joukowski Aerofoils. R. & M. No. 1106, British A.R.C., 1927.
3. Munk, Max M.: General Theory of Thin Wing Sections. T.R. No. 142, N.A.C.A., 1922.
4. Glauert, H.: A Theory of Thin Aerofoils. R. & M. No. 910, British A.R.C., 1924.
5. Theodorsen, Theodore: On the Theory of Wing Sections with Particular Reference to the Lift Distribution. T.R. No. 383, N.A.C.A., 1931.
6. Theodorsen, Theodore: Theory of Wing Sections of Arbitrary Shape. T.R. No. 411, N.A.C.A., 1931.
7. Theodorsen, T., and Garrick, I. E.: General Potential Theory of Arbitrary Wing Sections. T.R. No. 452, N.A.C.A., 1933.
8. Jacobs, Eastman N., Stack, John, and Pinkerton, Robert M.: Airfoil Pressure Distribution Investigation in the Variable Density Wind Tunnel. T.R. No. 353, N.A.C.A. 1930.
9. Briggs, L. J., and Dryden, H. L.: Pressure Distribution over Airfoils at High Speeds. T.R. No. 255, N.A.C.A., 1927.
10. Glauert, H.: The Effect of Compressibility on the Lift of an Aerofoil. R. & M. No. 1135, British A.R.C., 1928.
11. Anderson, Raymond F.: The Aerodynamic Characteristics of Airfoils at Negative Angles of Attack. T.N. No. 412, N.A.C.A., 1932.
12. Jacobs, Eastman N., Ward, Kenneth E., and Pinkerton, Robert M.: The Characteristics of 78 Related Airfoil Sections from Tests in the Variable Density Wind Tunnel. T.R. No. 460, N.A.C.A., 1933.
13. Jacobs, Eastman N., and Anderson, Raymond F.: Large-Scale Aerodynamic Characteristics of Airfoils as Tested in the Variable Density Wind Tunnel. T.R. No. 352, N.A.C.A., 1930.

TABLE I
THEORETICAL CONSTANTS FOR THE TWENTY AIRFOILS

Airfoil	$e\psi_0$	c	$\frac{d C_L}{d \sin(\alpha+\beta)}$	β	γ	b^2	$\frac{b^2}{e\psi_0}$	C_{MP}	α_I	C_{aI}	m	δ	λ
				$^\circ$	$^\circ$				$^\circ$			$^\circ$	$^\circ$
Clark Y.....	1.112	4.031	6.93	3 35	0 24	0.995	0.894	-0.085	0 38	0.51	0.110	46 50	1 59
N.A.C.A.—M6.....	1.117	4.040	6.95	0 36	0 42	.966	.864	.003	1 0	.19	.079	29 0	0 0
U.S.A. 27.....	1.115	4.024	6.96	4 31	0 57	.990	.888	-.095	1 16	.69	.117	58 0	0 38
U.S.A. 35B.....	1.109	4.038	6.90	4 14	0 29	1.000	.900	-.100	0 49	.60	.127	47 10	1 36
N. 22.....	1.118	4.036	6.96	4 7	0 18	1.000	.894	-.102	0 35	.56	.125	48 0	1 50
Göttingen 387.....	1.153	4.064	7.12	5 23	0 39	1.000	.867	-.125	0 55	.77	.173	46 10	2 0
Göttingen 398.....	1.142	4.040	7.09	4 25	0 37	1.002	.878	-.102	0 35	.61	.140	48 30	2 3
N.A.C.A.—CYH.....	1.114	4.029	6.95	1 52	0 44	1.000	.897	-.017	1 0	.34	.094	40 0	0 52
C 72.....	1.107	4.029	6.91	4 13	0 11	.990	.900	-.107	0 25	.55	.113	47 30	2 0
Boeing 103 A.....	1.093	4.022	6.84	2 48	0 13	.985	.900	-.075	1 17	.48	.092	49 20	1 11
R.A.F. 15.....	1.071	4.012	6.71	2 35	0 37	1.017	.950	-.052	1 18	.47	.068	63 10	0 0
R.A.F. 19.....	1.116	4.022	6.97	8 56	1 26	1.053	.944	-.210	2 0	1.30	.200	68 30	0 24
N.A.C.A. 0010.....	1.092	4.023	6.82	0 0	0 0	.990	.910	.000	0 0	.00	.051	0 0	0 0
N.A.C.A. 0012.....	1.112	4.033	6.93	0 0	0 0	.995	.900	.000	0 0	.00	.080	0 0	0 0
N.A.C.A. 2212.....	1.119	4.034	6.97	1 59	0 30	.997	.892	-.039	1 12	.38	.057	60 10	0 0
N.A.C.A. 2409.....	1.083	4.019	6.78	2 2	0 6	1.000	.922	-.052	0 22	.28	.065	45 50	0 0
N.A.C.A. 2412.....	1.103	4.034	6.87	2 15	0 13	.998	.905	-.055	0 20	.30	.085	28 30	0 0
N.A.C.A. 2415.....	1.142	4.052	7.10	1 58	0 6	.997	.875	-.050	0 32	.30	.116	25 20	0 0
N.A.C.A. 4412.....	1.114	4.034	6.94	4 34	0 21	.995	.895	-.110	0 38	.62	.128	49 50	0 0
N.A.C.A. 6512.....	1.119	4.034	6.98	7 4	0 0	.993	.887	-.185	0 19	.89	.148	65 30	0 0

NOTE.—The values of the angles listed in table I with respect to the x axis may be converted to values with respect to the standard chord by the addition of λ .

TABLE II
CLARK Y AIRFOIL
UPPER SURFACE

Percent <i>c</i>	<i>y</i> in per- cent <i>c</i>	<i>x</i>	<i>y</i>	$\sin^2 \theta$	$\sinh^2 \psi$	θ	ψ	ϵ	ψ'	ϵ'	<i>k</i>	$\phi = \theta + \epsilon$	
												radians	° /
0	0	2.030	0	0	0.0302	0	0.173	−0.0846	0.035	0.070	6.842	−0.085	−4 51
1.25	1.99	1.983	.0802	.0486	.0331	.222	.182	−.0735	.067	.080	4.192	.1485	8 31
2.50	3.09	1.933	.1246	.1007	.0386	.323	.195	−.0640	.110	.114	3.299	.259	14 50
5.0	4.57	1.834	.184	.194	.0436	.456	.207	−.0501	.067	.133	2.578	.406	23 17
7.5	5.61	1.736	.226	.280	.0457	.557	.212	−.0362	.044	.150	2.240	.521	29 51
10	6.45	1.636	.260	.361	.0468	.644	.215	−.0225	.021	.145	1.993	.622	35 38
15	7.70	1.436	.310	.508	.0474	.793	.216	−.0005	.008	.133	1.691	.793	45 25
20	8.55	1.236	.345	.635	.0467	.922	.214	.0163	−.017	.133	1.525	.939	53 47
30	9.23	.834	.372	.833	.0415	1.150	.202	.0430	−.067	.111	1.318	1.193	68 20
40	9.28	.430	.374	.955	.0366	1.358	.190	.0635	−.067	.086	1.210	1.422	81 29
50	8.74	.0263	.352	.998	.0311	1.530	.175	.0772	−.080	.073	1.172	1.607	92 6
60	7.72	−.378	.311	.965	.0251	1.759	.158	.0918	−.089	.050	1.169	1.850	106 2
70	6.26	−.783	.252	.850	.0187	1.969	.136	.101	−.100	.040	1.235	2.070	118 37
80	4.47	−1.189	.180	.651	.0125	2.203	.112	.106	−.114	.013	1.374	2.309	132 18
90	2.40	−1.595	.0968	.338	.0063	2.489	.0793	.105	−.114	−.022	1.766	2.594	148 39
95	1.26	−1.798	.0508	.1945	.0032	2.685	.0566	.0961	−.100	−.057	2.346	2.781	159 20
100	0	−2.001	0	0	.0010	3.142	.0310	.0626	−.044	−.077	large	3.204	183 36

LOWER SURFACE

0	0	2.030	0	0	0.0302	6.283	0.173	−0.0846	0.035	0.070	6.842	6.199	−4 51
1.25	−1.53	1.983	−.0617	.0429	.0221	6.074	.148	−.108	.171	.055	4.535	5.966	−18 8
2.50	−1.94	1.933	−.0782	.0885	.0173	5.981	.131	−.110	.149	−.011	3.344	5.871	−23 35
5.0	−2.40	1.834	−.0968	.178	.0131	5.847	.114	−.108	.123	−.024	2.463	5.739	−31 10
7.5	−2.61	1.736	−.105	.265	.0104	5.743	.102	−.106	.100	−.031	2.044	5.637	−37 1
10	−2.73	1.636	−.110	.347	.0087	5.653	.0932	−.103	.092	−.033	1.795	5.550	−41 59
15	−2.83	1.436	−.114	.498	.0055	5.499	.0805	−.0975	.080	−.044	1.491	5.402	−50 29
20	−2.78	1.236	−.112	.630	.0049	5.366	.0699	−.0918	.073	−.044	1.331	5.275	−57 46
30	−2.47	.834	−.0996	.833	.0030	5.133	.0548	−.0809	.057	−.057	1.145	5.053	−70 27
40	−2.12	.430	−.0855	.957	.0019	4.920	.0436	−.0670	.044	−.080	1.066	4.853	−81 55
50	−1.78	.0263	−.0718	1.000	.0013	4.712	.0361	−.0538	.040	−.037	1.036	4.659	−93 4
60	−1.43	−.378	−.0576	.962	.0008	4.516	.0283	−.0425	.031	−.067	1.057	4.473	−103 41
70	−1.09	−.783	−.0439	.842	.0005	4.304	.0224	−.0282	.025	−.067	1.130	4.276	−114 58
80	−.75	−1.189	−.0302	.643	.0003	4.030	.0173	−.0080	.014	−.080	1.276	4.022	−129 31
90	−.40	−1.595	−.0161	.361	.0002	3.786	.0141	.0083	.017	−.095	1.674	3.794	−142 36
95	−.23	−1.798	−.0093	.190	.0001	3.593	.0100	.0255	.000	−.100	2.295	3.618	−152 40
100	0	−2.001	0	0	.0010	3.142	.0310	.0626	−.044	−.077	large	3.204	−176 24

REPORT No. 466

AIRCRAFT POWER-PLANT INSTRUMENTS

By HARCOURT SONTAG and W. G. BROMBACHER

SUMMARY

This report supersedes that on aircraft power-plant instruments, published in 1921 as N.A.C.A. Technical Report No. 129, which is now, on the whole, obsolete. Aircraft power-plant instruments include tachometers, engine thermometers, pressure gages, fuel-quantity gages, fuel flow meters and indicators, and manifold pressure gages. The report includes a description of the commonly used types and some others, the underlying principle utilized in the design, and some design data. The inherent errors of the instruments, the methods of making laboratory tests, descriptions of the test apparatus, and data in considerable detail on the performance of commonly used instruments are presented. Standard instruments and, in cases where it appears to be of interest, those used as secondary standards are described. A bibliography of important articles is included.

INTRODUCTION

PREFATORY NOTE

A general report on power-plant instruments was prepared at the Bureau of Standards in 1921 for the National Advisory Committee for Aeronautics (reference 5), which dealt mainly with instruments developed during the war. During the last 10 years aircraft instruments, including power-plant instruments, have undergone intensive development. This report covers the present status of power-plant instruments and was prepared at the Bureau of Standards with the approval and financial assistance of the National Advisory Committee for Aeronautics. A large amount of the material presented was obtained during the course of cooperative work with the Bureau of Aeronautics of the Navy Department.

TYPES AND FUNCTIONS OF POWER-PLANT INSTRUMENTS

Power-plant instruments are taken to include all types of instruments which are used on aircraft to indicate or record the performance of aircraft engines in flight. The instruments and the quantities measured are listed below:

Instruments	Quantity measured
Tachometers.....	Engine speed.
Recording tachometers.....	Do.
Running-time meters.....	Service time of engine.
Engine thermometers.....	Temperature of lubricant, cooling liquid, or cylinder.
Pressure gages.....	Pressure of lubricant or fuel.
Fuel quantity gages.....	Quantity of fuel available.
Fuel flow meters.....	Rate of fuel consumption.
Fuel consumed meters.....	Quantity of fuel consumed.
Combustion indicators.....	Degree of fuel combustion.
Manifold pressure gages.....	Absolute pressure in intake manifold.

While power-plant instruments are of value to the pilot in connection with the normal operation of the engine, their function is also to assist him in detecting and locating the first sign of trouble. Their dependability thus becomes a matter of prime importance.

SCOPE OF THE REPORT

The discussion of each type of power-plant instrument includes a statement of the underlying principle used in making the measurement, a description of the instruments commonly used, the methods of making laboratory tests and data on the performance of typical instruments. In addition the standard instruments used in making the laboratory tests are described in most cases and, where it appears to be of interest, secondary standard instruments also. Instruments and methods not commonly used in aircraft but which are either of interest in this connection or have possible application in the future are briefly described.

RECENT GENERAL DEVELOPMENTS

Many developments during the past decade have affected aircraft instruments as a class. These have included the design of instruments having a linear vertical scale (now largely obsolescent), the standardization (and decrease) of the diameter of the dials of the commonly used instruments, a general improvement in over-all performance, and the adoption of a clockwise direction of rotation of the pointers for increasing values of the quantities measured. There has been a

number of other developments relating to power-plant instruments alone; and of these, two are mentioned as noteworthy—first, the improvement in the design and development of new types of distant-indicating electrical instruments and, second, the gradual development of various types of fuel flow meters.

A. VERTICAL SCALE INSTRUMENTS

Instruments having linear vertical scales were developed primarily in order to conserve the area of the instrument panel. Examples of power-plant instruments of this type are shown in figures 6 and 40. The design is particularly desirable in aircraft powered by more than one engine, since the several instruments can be mounted side by side, and synchronization is indicated when the pointers all lie in a horizontal line. Owing to the limited length of scale, the necessity for complicating the mechanism in order to obtain a motion of the pointer sufficiently linear, and the relatively high cost of manufacture, the vertical scale instrument is rapidly becoming obsolete.

B. STANDARDIZATION OF CASE SIZES

Largely through the initiative of the Bureau of Aeronautics of the Navy Department, experimental air-speed meters, altimeters, and tachometers were constructed by manufacturers in 1928, the diameter of the dials of which was reduced to $2\frac{3}{4}$ inches and the cases made uniform as regards mounting dimensions. Further, engine thermometers and fuel- and oil-pressure gages were made with uniform cases but with a smaller dial ($1\frac{7}{8}$ inches in diameter). These new dial and case dimensions were adopted as a standard by the Army and Navy Standards Conference of February 1929. Since then practically all service instruments have been standardized in one or the other of these two dial sizes with the corresponding mounting dimensions. In addition to the military air services, the Society of Automotive Engineers has also adopted the two new sizes as standard. The reduction in size is noteworthy. The dial of the tachometer previously considered standard was $3\frac{3}{4}$ inches in diameter and that of the pressure gage and thermometer 2 inches. The reduced size permits a reduction of the center to center distance between two tachometers mounted side by side from $4\frac{7}{8}$ to $3\frac{1}{4}$ inches. Examples of instruments with the new dial sizes are shown in figures 5 and 32.

C. UNIFORM DIRECTION OF POINTER ROTATION

Uniformity in the direction of rotation of the pointers (clockwise) with increasing values of the quantity measured, the advantages of which are obvious, is now an accepted requirement. As an example the pointer of the altimeter formerly rotated counterclockwise with increasing altitude while that of the tachometer rotated clockwise with increasing speed.

D. FITTINGS

The connections of the flexible shaft to the tachometer and to the engine have been standardized. Details are given later in the subsection on "Flexible drive shafts." The fittings on fuel quantity gages and manifold pressure gages for connecting to the lines of copper tubing have also been standardized both as to type and size. This fitting is described on page 26 of reference 20. A similar but different size fitting is used on fuel and oil pressure gages. Aluminum tubing and fittings are coming into use where practicable.

E. DISTANT INDICATING ELECTRICAL INSTRUMENTS

In multi-engined aircraft and in lighter-than-aircraft of the dirigible type, remote indicating instruments are required. This has led to improvement in the design and performance of electrical tachometers and the development of new types. As a result an electrical tachometer of the direct-current type with much improved performance and weighing less than 3 pounds, complete, is now available. Its indicator has a range of deflection of the pointer of nearly 300° of arc. (See fig. 12.) Tachometers of the alternating-current type have been developed by manufacturers. An electrical tachometer depending for its operation on the charge and discharge of a condenser has been developed, although it is not commercially available at the present time.

The thermocouple, the unbalanced Wheatstone bridge, and ohmmeters have been adapted for making measurements of temperature and other quantities on aircraft. Oil-pressure gages and thermometers utilizing an ohmmeter and thermometers of the thermocouple type are available. Types of electrical instruments which are independent of an outside source of electrical energy are preferred, other qualities being equal.

F. IMPROVEMENTS IN PERFORMANCE

The performance of most of the existing types of instruments has been slowly and steadily improved by minor modifications in design and more careful selection of the materials used in fabrication. This has been brought about in large part by the stimulus of changes made from time to time in military specifications. For example, a decided improvement followed the introduction of a definite vibration test, and poor performance at low temperatures was largely eliminated by requiring that tests be made at -35°C . instead of at -10°C . or -20°C . Further improvement in tachometers appears to be desirable with respect to the scale errors, the ability of the instruments to withstand vibration and to operate successfully under conditions of extreme low temperature. The trend has been toward more rigid inspection and tests on the part of both the instrument manufacturer and the buyer.

G. ILLUMINATION

The primary numerals and graduations, and the tips of the pointers of most service instruments are coated with luminous radium paint. This procedure has continued in spite of the development of methods of indirect electric illumination of the instrument board. The radium paint has the definite advantage of simplicity and the disadvantage of being more expensive.

Radium paint becomes brown with age and loses its luster which is stated to be caused by the use of poor oil in the adhesive. No short-time test for determining the quality of radium paint is known. Exposure of both good and poor radium paint to ultra-violet light and to temperatures up to 100° C. have failed to show any marked difference in behavior.

TACHOMETERS

USEFULNESS OF TACHOMETERS

A tachometer is an instrument which indicates speed of rotation and is used in aircraft to indicate continuously the speed of the engine crankshaft. The instrument is usually actuated by the camshaft, which on the conventional four-stroke cycle engine rotates at one half the speed of the crankshaft. The dial of the instrument is commonly graduated in revolutions per minute of the crankshaft.

It is desirable to know the rotational speed of the aircraft engine during, first, the course of normal operation; second, the flight testing of aircraft; and, third, the choice or adjustment of the propeller.

During the course of normal operation a knowledge of the speed is required before taking off in order (a) to determine that approximately the maximum power is available, and during flight (b) to detect engine trouble; (c) to maintain any desired speed in the case of a single engine or to synchronize approximately all engines at a given speed in multi-engine installations (in the latter case the final adjustment of the speed is normally made by listening to the beats in the sound produced by the propellers); (d) in emergencies, in combination with an air-speed meter, to indicate the deviations from level flight.

(a) Before taking off, the speed of the engine is observed while it is operating at full throttle. Under these conditions the maximum speed attained by the engine is somewhat lower than when the aircraft is in level flight at full throttle at a low altitude. Any drop from the usual value of this speed indicates improper functioning of the engine and the procedure is thus a simple test of the operating condition of the engine.

(b) Complete or even partial failure of a few engine parts results in a change in the operating speed, the indication of which should be of value to the pilot.

(c) It is generally assumed that all engines give service freer from trouble when operated somewhat below the normal maximum rated speed. This

reduced speed referred to as the "cruising speed" is determined by a number of factors such as smoothness of operation, rate of fuel consumption, etc. The tachometer indicates whether or not this desired speed is being maintained.

(d) Descent or climb of an aircraft is always accompanied by an increase or decrease, respectively, in the rotational speed of the engine together with an increase or decrease in the air speed, provided the engine controls remain in the same position. It follows therefore that a combined knowledge of the engine speed and the air speed may aid in indicating deviations from level flight.

In normal operation it is also desirable to synchronize the speed of engines on multi-engined airplanes. The tachometer is too insensitive to do this accurately. When the speeds are nearly the same, beats are distinctly heard which afford a measure of the difference in the speeds and a guide to synchronizing.

In the flight testing of aircraft it is necessary that certain conditions of operation remain constant, one of which is the rotational speed of the engine, while changes in other conditions of operation are measured.

A knowledge of the rotational speed of the engine is necessary when determining the suitability of the propeller or propeller setting. The use of a propeller whose pitch angle may be varied during flight requires a knowledge of the engine speed in order that the pitch setting may be adjusted properly.

CLASSIFICATION

It is obvious that the indication of the speed must be at a distance from the aircraft engine, and this involves the use of instruments commonly called distant-indicating. Tachometers are classified here on the basis of the particular means used to connect the indicator to the engine or the actuating element at the engine. Common methods of making this connection are by means of (a) a flexible shaft rotating at a speed proportional to that of the engine (b) an electrical current controlled by an element rotated by the engine and (c) an air pressure dependent on engine speed. Instruments with these respective methods of transmission will be called the mechanical, electrical, and pneumatic types.

The mechanical type includes the centrifugal, chronometric, magnetic drag, viscous drag, inertia and a number of other tachometers.

The electrical type includes the direct current, the alternating current, the solenoid-operated chronometric, and the commutator-condenser instruments.

The various pneumatic instruments are the same in principle and differ only in design details.

Other types of tachometers are essentially unsuited for use on aircraft. These instruments include the tachiscope, the various forms of stroboscopes, and the electrical type utilizing synchronous motors. The resonance or vibrating reed instrument has not been

used on aircraft up to the present but may be of possible use in the future.

MECHANICAL TACHOMETERS

Instruments of the mechanical type are used more extensively on aircraft than the others due to their

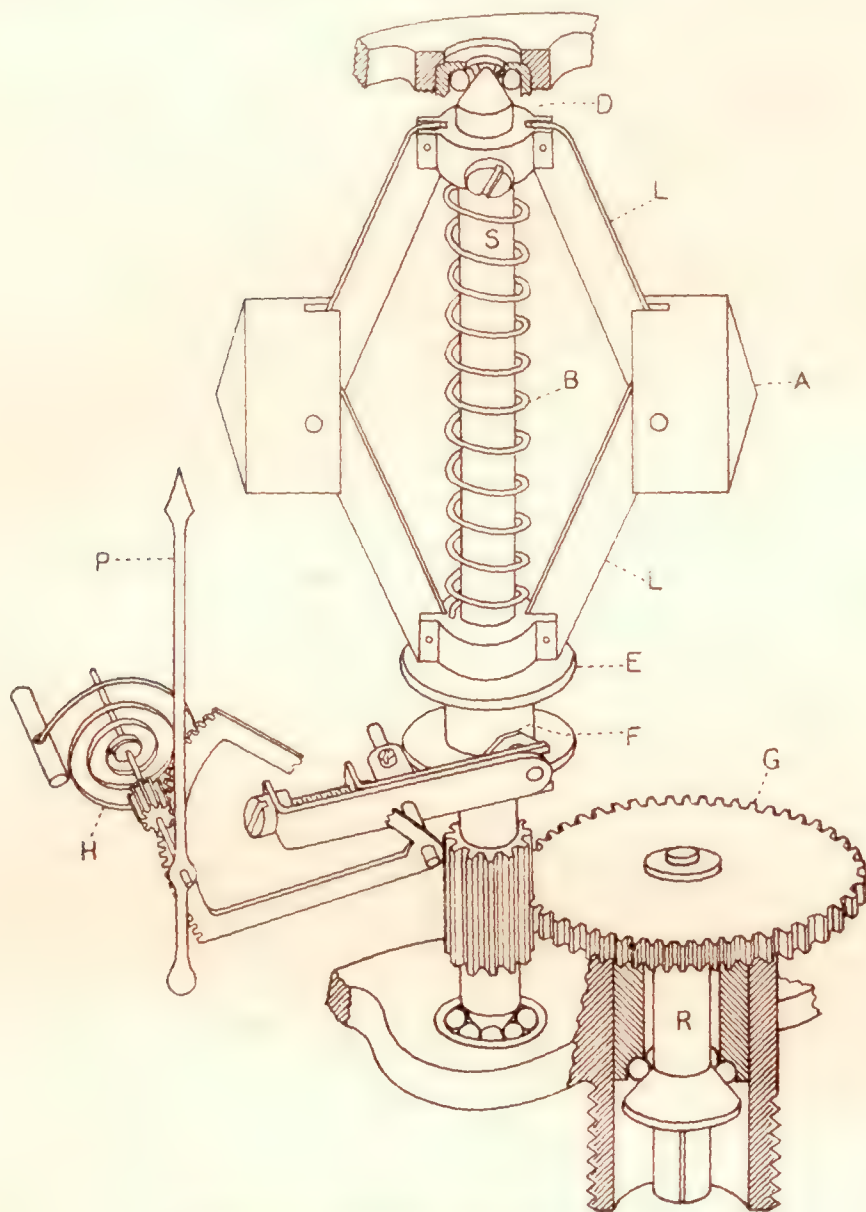


FIGURE 1.—Diagram of centrifugal tachometer.

relatively low cost and their reliability of operation. These tachometers are operated by means of a flexible drive shaft extending from the engine to the tachometer. The latter is usually installed on the instrument board.

The practical impossibility of obtaining smooth performance from the long drive shaft needed to connect most outboard engines to the tachometer on the instrument panel has led to the practice in such cases of attaching the tachometer to the engine mount in such a position that the dial may be readily observed from the cockpit. Obviously this arrangement is unsatisfactory and especially so when the weather is unfavorable for good visibility.

A. CENTRIFUGAL TACHOMETERS

Principle of operation.—In this instrument the centrifugal force produced by the rotation of weights is balanced by a spring. The deflection of this spring is a measure of the speed of rotation and is indicated by a pointer after magnification by means of a suitable mechanism. A diagram of a typical mechanism is

shown in figure 1. The centrifugal element is similar to that of the fly-ball governor, and usually consists of 2 or 3 brass weights A (fig. 1), each pinned to 2 links L. The upper links are attached to sleeve D which is clamped to shaft S, and the lower links to sleeve E, which is free to slide along the shaft. The two sleeves are held apart by the helical spring B. The flexible drive shaft is connected to shaft R and drives shaft S through gear G. As the speed of rotation of the weights is increased, they fly outward and draw sleeve E upward, thus compressing spring B until the centrifugal force is balanced by the force exerted by the spring. A pin or shoe F held in bearing on the sleeve E by the hairspring H is deflected upward as the spring is compressed. This deflection is amplified and transmitted to the pointer through the sector and pinion as shown in the figure.

Elementary theory.—An expression for the deflection of the sliding sleeve E is easily obtained for the simple form of mechanism shown in figure 2. Since it is obvious that the expression to be derived will be independent of the number of revolving masses and links, the sum of the masses and the sum of the tensions in the links only will be considered. It is assumed that each of the masses is pivoted at its center of gravity and that when the speed of rotation is zero the main-

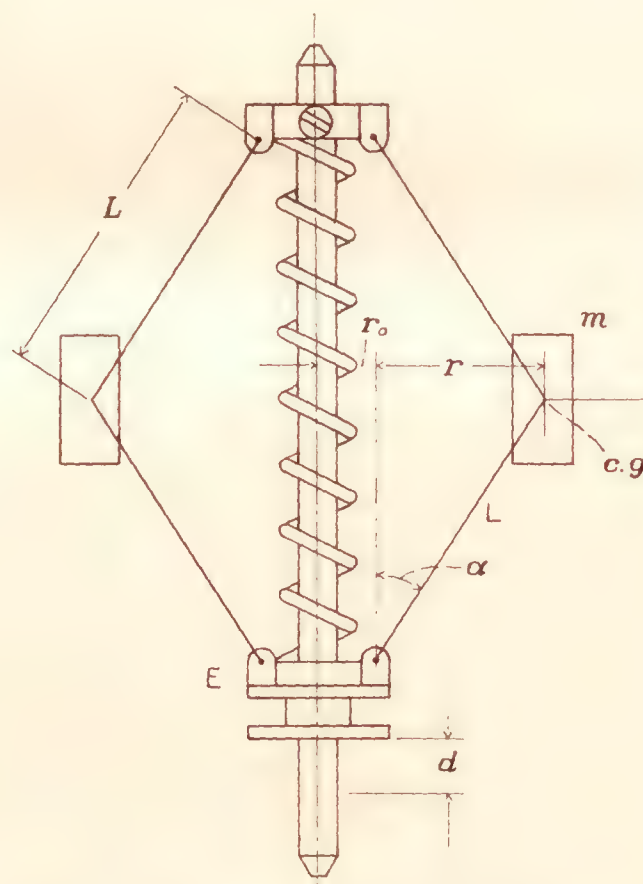


FIGURE 2.—Diagram of centrifugal element of tachometer.

spring is under a compressional stress and the effective radius of the masses is not zero. The sum of the tensions T in the lower links of the mechanism due to the centrifugal force acting on the sum of the revolving masses m is equal to

$$T = \frac{m(r + r_o)\omega^2}{2 \sin \alpha} \quad (1)$$

where r_o is the distance of the center of gravity of mass m from the axis of rotation when the speed is zero, $(r+r_o)$ is the distance when the angular velocity is ω , and α is the angle between the link L and the axis of rotation. This tension is balanced by that due to the compressive force F exerted by the spring and the gravitational weight of mass m . Therefore

$$T = \frac{F}{\cos \alpha} + \frac{mg}{2 \cos \alpha} \quad (2)$$

where g is the acceleration of gravity.

The compressive force $F = sd + sd'$ where d is the deflection of both the sliding sleeve and of the spring, d' the initial deflection of the spring, and s the stiffness of the spring. The stiffness is defined as the load required to produce unit deflection.

Substituting $sd + sd'$ for F in equation (2) and equating the identities of equations (1) and (2) there results

$$\frac{s(d+d')}{\cos \alpha} = \frac{m\omega^2}{2 \sin \alpha} (r+r_o) - \frac{mg}{2 \cos \alpha} \quad (3)$$

The first term on the right-hand side of equation (3) is usually large compared to the second term so that the latter is dropped.

From the geometry of the linkage the following relations are obtained:

$$r = \frac{\sqrt{4Ld - d^2}}{2} \quad (4)$$

$$\sin \alpha = \frac{r}{L} = \frac{\sqrt{4Ld - d^2}}{2L} \quad (5)$$

and

$$\cos \alpha = \frac{\sqrt{L^2 - r^2}}{L} = \frac{2L - d}{2L} \quad (6)$$

L here represents the length of one of the links.

Substituting these values of $\sin \alpha$ and $\cos \alpha$ in equation (3) there is obtained:

$$\omega^2 = \frac{2s(d+d')}{(2L-d) \left(\frac{m}{2} + \frac{mr_o}{\sqrt{4Ld - d^2}} \right)} \quad (7)$$

It is convenient to express the deflections d and d' as percentages of the length of the link L . Thus $d = KL$ and $d' = ML$. Also more convenient units are

obtained by using the relations $\omega = \frac{2\pi N}{60}$ and $m = \frac{w}{g}$

where N is the number of revolutions per minute and w is the weight of mass m . Substituting these values for d , d' , ω , and m in equation (7) and taking the square root of both sides of the equation there results:

$$N = \frac{60}{2\pi} \sqrt{\frac{2s(K+M)}{\frac{w}{g}(2-K) \left(\frac{1}{2} + \frac{r_o}{L\sqrt{4K-K^2}} \right)}} \quad (8)$$

If r_o and L in the above equation are in inches and s is in pounds per inch, g must be expressed in inches per second per second.

The relation between K , the relative deflection of the sliding sleeve, and N , the speed of rotation of the weights, given by formula (8) was computed for the case when $M=0$, $w=0.054$ pound, $g=386.4$ inches per second per second, $s=10.8$ pounds per inch, and $r_o/L=0.625$ and is given in figure 3. These values were obtained by measurements made on a Jones tachometer. The graph shows that for values of K from 0.2 to 1.0 the relation between K and N is sufficiently linear for practical purposes and that the curve is concave upward for lower values of K and concave downward for large values. It can be further shown that when $M=0$, only r_o/L need be considered as a factor in affecting the extent of the linear portion of the curve. As the values of r_o/L are increased up to 1.0, the approximately linear portion of the curve is extended

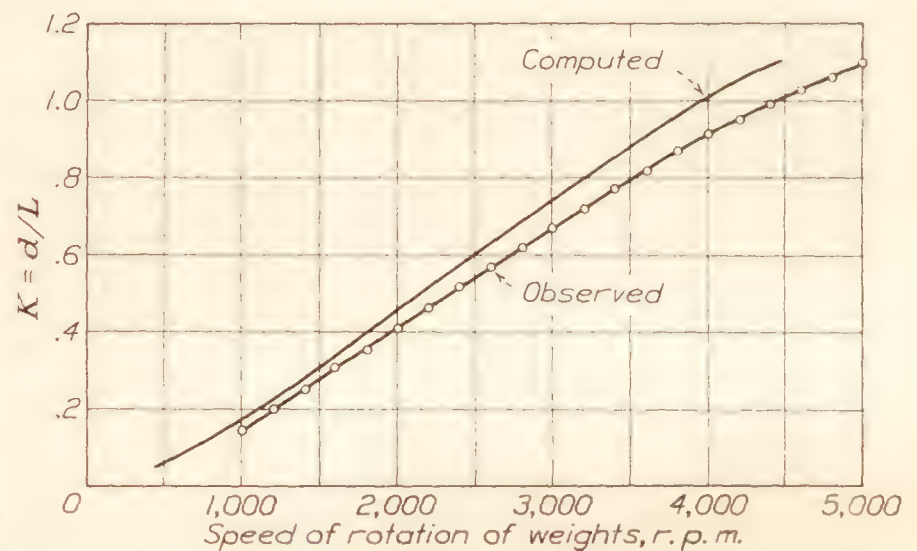


FIGURE 3.—Computed and experimental values of the ratio of the deflection d of the sliding collar to the length L of the link for various speeds of rotation of the weights of a Jones centrifugal tachometer.

but slightly beyond the limiting values of K given above but the rate of change of curvature is much less for the values of K beyond these limits.

The deflection of the sliding sleeve corresponding to the rate of rotation of the Jones tachometer was also measured and is given in figure 3 by the curve marked "observed." The agreement is not good with respect to coincidence which is probably due to the fact that the initial tension M in the spring was not zero, as assumed in the computation, and that r_o was taken as the distance from the axis of rotation to the pin instead of to the center of gravity of the weight. No attempt was made to eliminate the discrepancy by additional measurements since the formula is sufficiently established for use in obtaining first-order accuracy.

Description of centrifugal instruments.—A number of centrifugal tachometers are made in this country. The Stewart-Warner tachometer is shown in figure 4, the Pioneer in figure 5, and a Pioneer experimental vertical scale instrument in figure 6. In the latter instrument the two links holding the weights also act as the main spring.

The principal difference between the various makes of aircraft centrifugal tachometers lies in the method of transferring the deflection of the sliding sleeve to the multiplying mechanism. This is the point at which practically all of the wear affecting the calibration of the instrument occurs. In the Pioneer tachometer (fig. 6) the contact point is on the axis of the main shaft which has been bored to permit the insertion of a plunger the outer end of which is connected with the multiplying mechanism. In the Friez tachometer a

attached to the pointer shaft. In order to reduce the pressure of contact between the pin and the rotating flange to the allowable minimum it is the practice to employ a hair spring as light and as flexible as possible.

The maximum deflection of the main spring of a centrifugal tachometer is usually large. Thus for the instrument for which data are given in figure 3 the deflection at the highest speed is over one half of the original length of the helical spring. Due to limitations of space it is practically impossible to de-

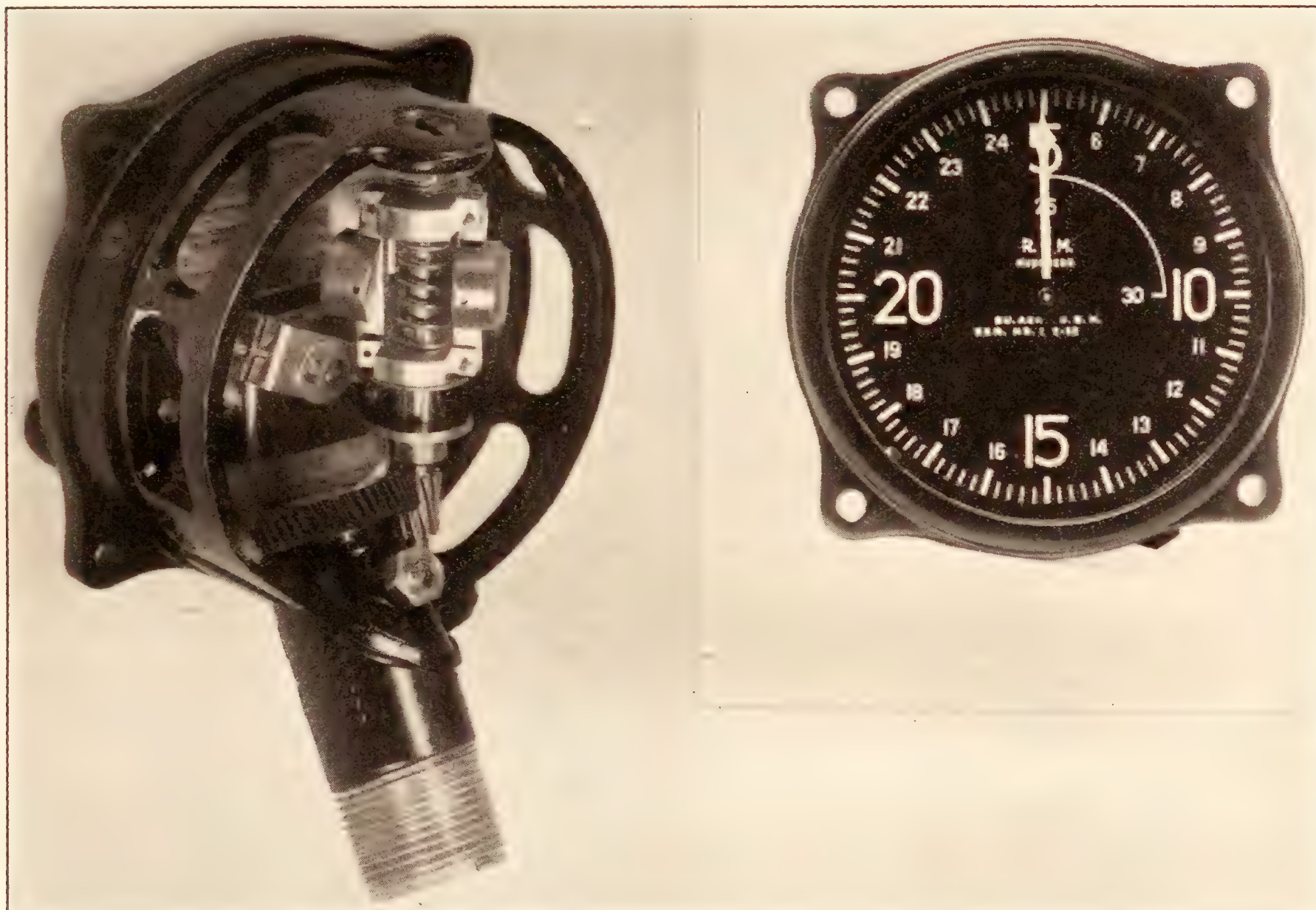


FIGURE 4.—Mechanism and dial of the Stewart-Warner centrifugal tachometer.

sapphire pin attached to the primary lever of the multiplying mechanism bears against a flange on the sliding sleeve. In the Stewart-Warner tachometer, shown in figure 4, a shoe made of wear-resisting alloy is pivoted to the primary lever of the multiplying mechanism and bears against a hardened steel flange which has been forced onto the sliding sleeve.

When a sapphire is used to transmit the deflection of the sliding sleeve, it should be provided with metallic reinforcement. Experience has shown that the accelerative force accompanying a sudden opening of the throttle is in some instances great enough to fracture the jewel.

In all of the mechanisms described the force exerted on the sliding sleeve by the multiplying mechanism at the contact point is that imposed by the hair spring

sign a spring suitable for the purpose that is not highly stressed at the higher speeds of the range of the instrument without at the same time requiring an excessive magnification of the deflection of the sliding sleeve. It is essential therefore that the main spring be made of a material having a high elastic limit.

It is the practice in this country to operate the governor elements of aircraft centrifugal tachometers at a speed four times that of the drive shaft (twice the speed of the engine crankshaft) which is accomplished by means of suitable gearing. (See fig. 1.) This greater speed permits the use of smaller rotating masses and a reduction of the dimensions of the instrument. The error introduced by tipping the instrument is greatly minimized by operating the governor elements at the higher speeds. An exception to this practice,

however, is found in one model of the Reliance tachometer in which the gearing is eliminated and the governor element is rotated at the speed of the camshaft.

The standard range of tachometers used in the military air services is now 500 to 3,000 r.p.m. corresponding to a pointer motion of $1\frac{1}{4}$ revolutions (fig. 4). The graduations are usually evenly divided. The graduations below 500 r.p.m. are not needed and are omitted since it is not practical to obtain accurate indications owing to the much smaller deflection of the spring

peratures largely due to congealing of the lubricant, but this disadvantage would be obviated by the development of a more suitable lubricant.

CHRONOMETRIC TACHOMETER

Principle of operation.—The chronometric tachometer is essentially a revolution-counting device, the operation of which is automatically governed by an escapement mechanism so as to integrate and indicate periodically the number of revolutions of the drive shaft.

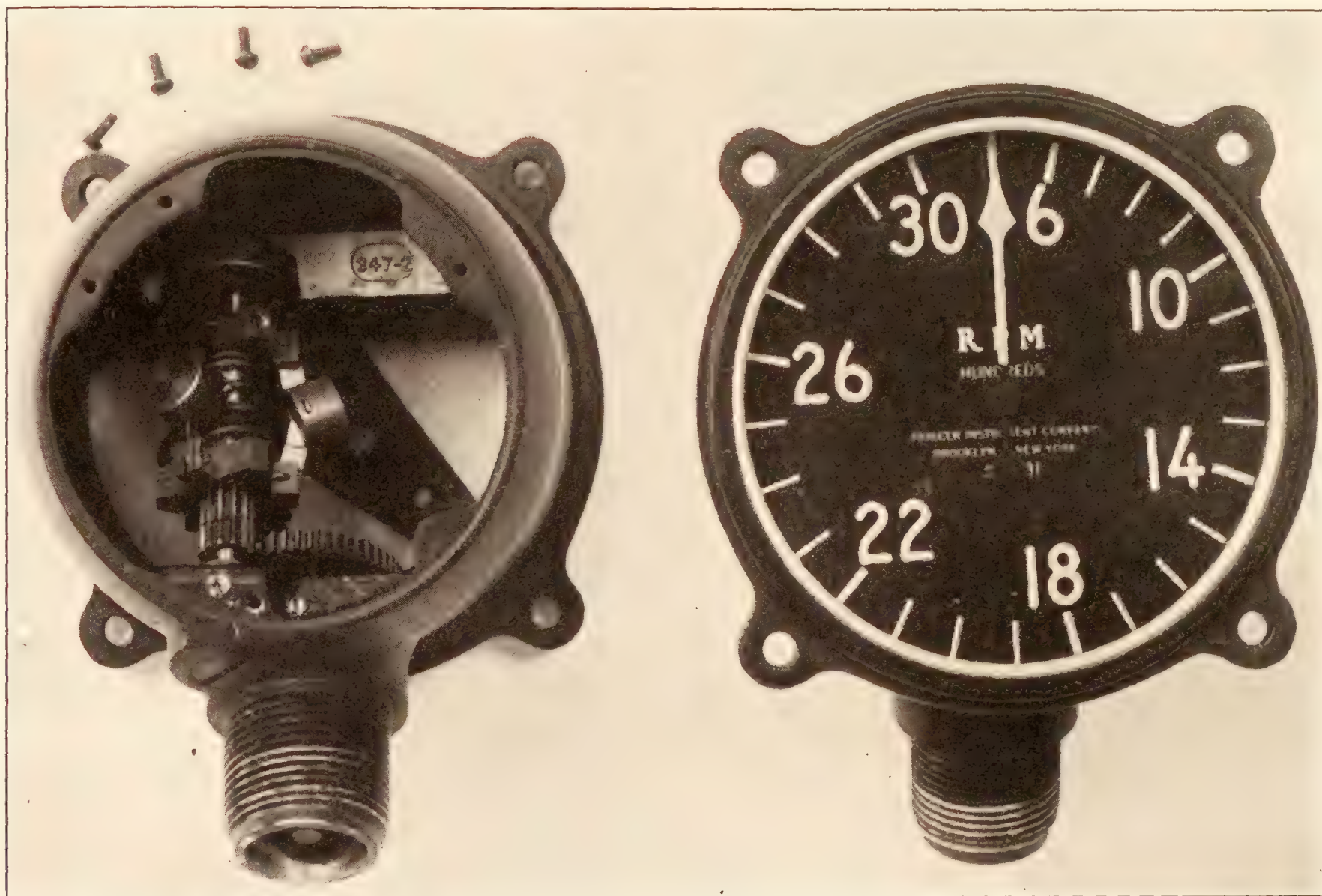


FIGURE 5.—Dial and mechanism of the Pioneer centrifugal tachometer.

per unit change in velocity. Thus in figure 3 the change in deflection measured when the speed of the weights (two times engine speed) is changed from 0 to 1,000 is only about one half of that when the speed is changed from 1,000 to 2,000 r.p.m.

Characteristics of centrifugal tachometers.—The centrifugal tachometer is simple in design and inherently rugged. It indicates the instantaneous speed with but negligible time lag and independently of the direction of rotation of the drive shaft. Its mechanism is easily adjusted to correct small errors in indication, which is an advantage in manufacture and maintenance. On the other hand, the centrifugal tachometer is difficult to lubricate after installation and of course requires the use of a flexible drive shaft. The frictional drag of the latter increases greatly at low tem-

The essential parts of the mechanism of the ordinary chronometric tachometer are (a) driving mechanism, (b) escapement mechanism, (c) power supply for the escapement mechanism, and (d) counting mechanism.

Van Sicklen.—Referring to figure 7, which is a diagram of the Elgin-Van Sicklen tachometer, the driving mechanism is identified by the letters A and B and includes a mechanism to rectify the motion of the drive shaft, whether clockwise or counterclockwise, into a unidirectional motion of rotation. The escapement mechanism, shown in the figure at C, governs the speed of rotation of the cams, one of which is shown at J. The power supply for the escapement mechanism is contained in drum M and consists of a spiral spring, the inner coil of which is fastened to the shaft connected with the driving mechanism, while the outer

coil normally bears with some friction against the inner cylindrical surface of the drum. This mechanism

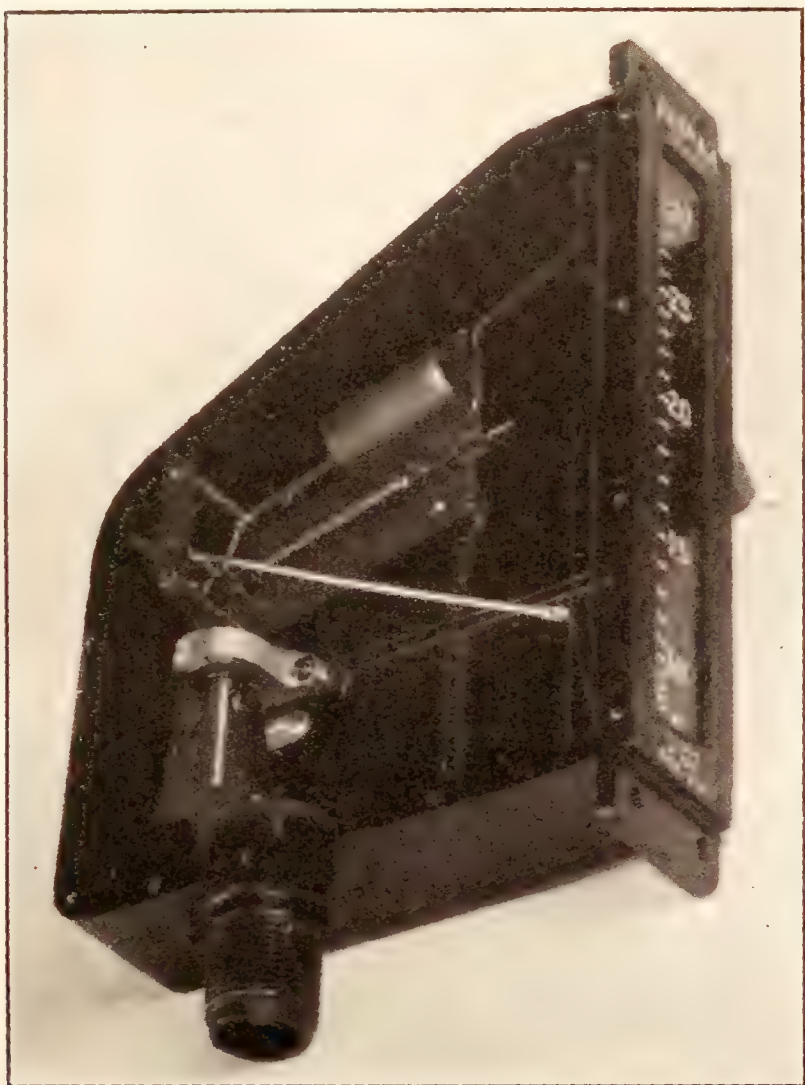


FIGURE 6.—Pioneer centrifugal tachometer with linear scale.

transmits a torque sufficient for rotating the cams, slippage occurring when the torque becomes excessive. The counting mechanism is identified in the figure by

counting gear *D* is first placed in mesh for a period of one second with gear *F* which is actuated by the drive shaft. The engagement of the two gears *D* and *F* is produced through the intermediate gear *E* actuated by a cam, one lobe of which is shown at *J*. By means of a pin and floating link mechanism shown at *G*, gear *H* and the pointer which is rigidly fastened to the same shaft as gear *H*, are caused to rotate through an angle proportional to the total number of revolutions over a period of one second. Gear *H* is essentially a ratchet gear and is provided with a pawl which is also actuated by a cam (not shown in the figure). At the end of the one second period the pointer remains stationary while the counting gear *D* is disengaged and, by means of the hair spring *K*, returned to its initial position. At the end of the following second the cycle is repeated. If the speed of the drive shaft has increased, the pointer is caused to increase its reading to correspond with the new average speed. If the speed has decreased, the pointer is released by the aforementioned pawl and under the influence of hairspring *L* returned to a position corresponding to the decreased speed.

The complete cycle of operation requires 2 seconds of time. When the speed varies greatly, the resulting periodic fluctuation of the pointer is disconcerting. When the speed varies only slightly, the pointer will change its position at the end of every 2-second interval by steps of 10 r.p.m. due to the fact that the number of teeth on gear *H* is 250 while one revolution of the pointer corresponds to a speed range of 0 to 2,500 r.p.m.

Shortly after the introduction of this instrument by the manufacturer its mechanism was greatly improved by substituting the double-roller type for the single-

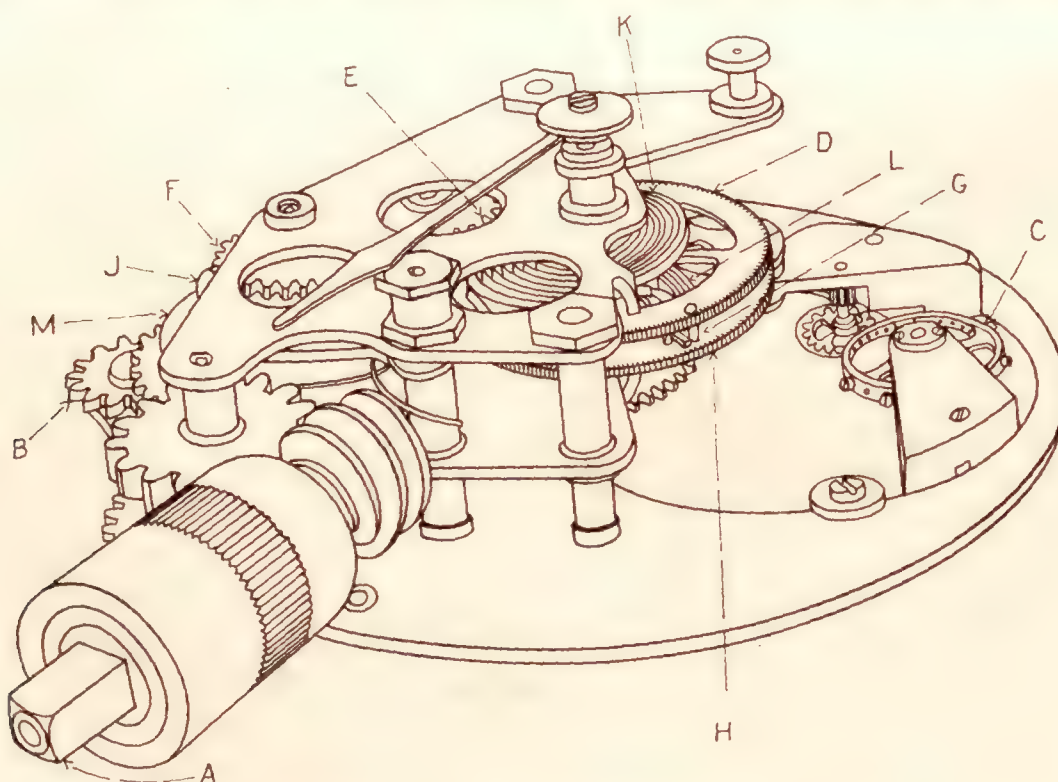


FIGURE 7.—Diaphragm of Van Sicklen (Elgin) chronometric tachometer.

gears *D* and *H*. Its function is to produce a deflection of the pointer corresponding to the speed of the driving mechanism.

The operation of the instrument (reference 29) may be understood by again referring to figure 7. A

roller type of escapement. See figure 8 and reference 23. This has resulted in more certain starting and longer life. The balance wheel of this escapement is of the bimetallic form commonly used to secure temperature compensation.

Hasler and Jaeger tachometers.—Two additional makes of chronometric tachometers, the Hasler "Tel" (reference 25) and the Jaeger, both of which are imported, are being used to some extent. All of the chronometric tachometers are fundamentally similar with regard to the principle of operation. The chief differences between them lie for the most part in the details of design and arrangement of their component parts. The following table gives a few of the principal characteristics of recent models of each of three makes of tachometers.

Make	Weight	Usual range	Period of cycle	Pointer deflection
	Ounces	R.p.m.	Seconds	Degrees
Van Sicklen.....	13	0-3500	2	504
Hasler Tel.....	21	0-2500	1	360
Jaeger.....	20	0-3500	1	504

Comparison of centrifugal and chronometric tachometers.—The chronometric tachometer has many of the characteristics which are desirable in an instrument designed for use on aircraft. In comparison with the centrifugal tachometer three favorable characteristics are outstanding: (a) Low speeds in the range 0 to 500 r.p.m. are indicated; (b) the indications have an equal or greater initial accuracy and maintain this accuracy throughout the life of the instrument; and (c) the indications are free from lag due to friction in the mechanism. In addition to these comparative advantages the chronometric instrument has (d) a scale uniformly divided in units of r.p.m. and is (e) easy to adjust for minor deviations from the proper calibration which is done by adjusting the period of the balance wheel.

The instrument suffers by comparison with the centrifugal tachometer in that (a) the indication follows changes in speed at intervals of 1 or 2 seconds, depending upon the design, which experience shows is troublesome in estimating the average speed during minor fluctuations, and (b) the average speed of the previous interval of time is indicated, not as is more desirable, that at the instant of observation. The centrifugal tachometer indicates the instantaneous speed with a lag caused by the inertia of the mechanism, which has, however, the practical advantage of smoothing out the minor rapid fluctuations in speed, thus aiding the observer in determining the average speed. A further point against the chronometric instrument which is perhaps secondary is (c) that the mechanism is inherently complicated and, in a number of designs, not sufficiently rugged for aircraft use.

C. OTHER MECHANICAL TACHOMETERS

Other ingenious mechanisms have been designed for measuring speed of rotation by direct coupling to the rotating body. Most of these have no advantage over the centrifugal or chronometric tachometer for aircraft

use. A few of these mechanisms will be briefly described.

Magnetic tachometer.—*Principle and description:* The magnetic tachometer designed for use on aircraft is similar in principle to the magnetic speedometer commonly used on automobiles (references 1 and 21). The instrument consists of a permanent magnet which is mechanically connected with, and rotated by, the engine through a length of flexible shafting. A metallic disk or cylinder, usually of aluminum, is mounted axially in close proximity with the rotating magnet and is restrained from revolving by a hair spring. As the permanent magnet is rotated, eddy currents are

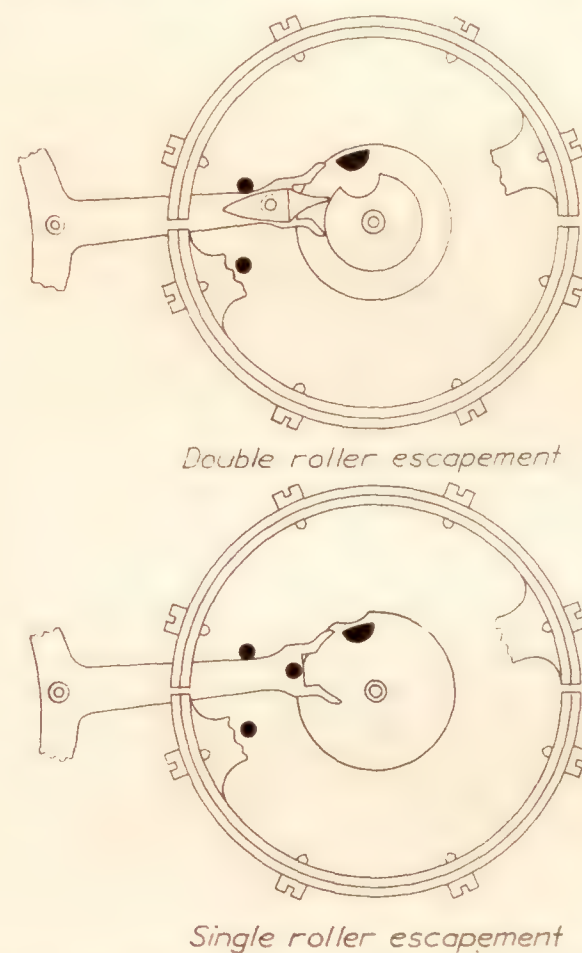


FIGURE 8.—Diagram of double and single roller escapements.

induced in the disk, the magnetic field of which interacts with the field of the permanent magnet so that the disk is subject to a couple tending to rotate it with the magnet. In short the principle of operation is that of Arago's disk, which is described in most text books of physics. Since the induced torque is a function of the speed of rotation of the magnet, the angular deflection of the disk is a measure of the speed. For use in aircraft a pointer is attached to the disk, and a dial graduated in r.p.m. is provided.

An attempt was made to adapt the instrument to aircraft use in 1918. The Warner instrument is described in reference 1, and 3 German types in reference 7. A later development is the A C instrument (reference 38), which has not come into any extended use. The weight of the latter instrument is 20 ounces.

Characteristics.—The magnetic drag tachometer is simple in design and construction and has a smooth pointer motion. Mechanical wear of the parts affects

the clearance between the disk and rotating magnet, giving rise to relatively large changes in calibration. In the latter respect the performance of the instrument appears to be more dependent on wear than that of the centrifugal tachometer. It is also necessary to shield the instrument magnetically in order to avoid interfering with the indications of the magnetic compass. The indicating disk has a free period of vibration, quite large in comparison with that of commonly used tachometers, which gives rise to a relatively large time lag in indicating a varying speed.

Inherently the instrument indications are excessively affected by temperature, but methods of compensation have been developed which are sufficiently effective for automobile speedometers and perhaps promising for aircraft tachometers.

The earlier methods of temperature compensation depended upon changing the air gap in the magnetic

for friction sufficient to hold a given position, and has attached to it a rigid strip (not shown in the figure) which overhangs the brass disk C, almost touching the gear A.

At the start of a cycle of operation, the pin on arm B engages lever E and disk C moves with the rotating gear A, winding up hair spring D. The motion in common of A and C is interrupted once every revolution of A by a pin fixed to the case which disengages E from B. The tension in the hair spring D causes disk C to reverse its motion and rotate to the position where E and B again come into contact. At the time E and B are disengaged a pawl on arm B catches on the strip attached to the pointer shaft so that the pointer shaft moves with gear A. At the point where the lever E, carried by the returning disk C, and the pin on B of the advancing gear A meet, the pointer is released by a cam action of arm E and holds this posi-

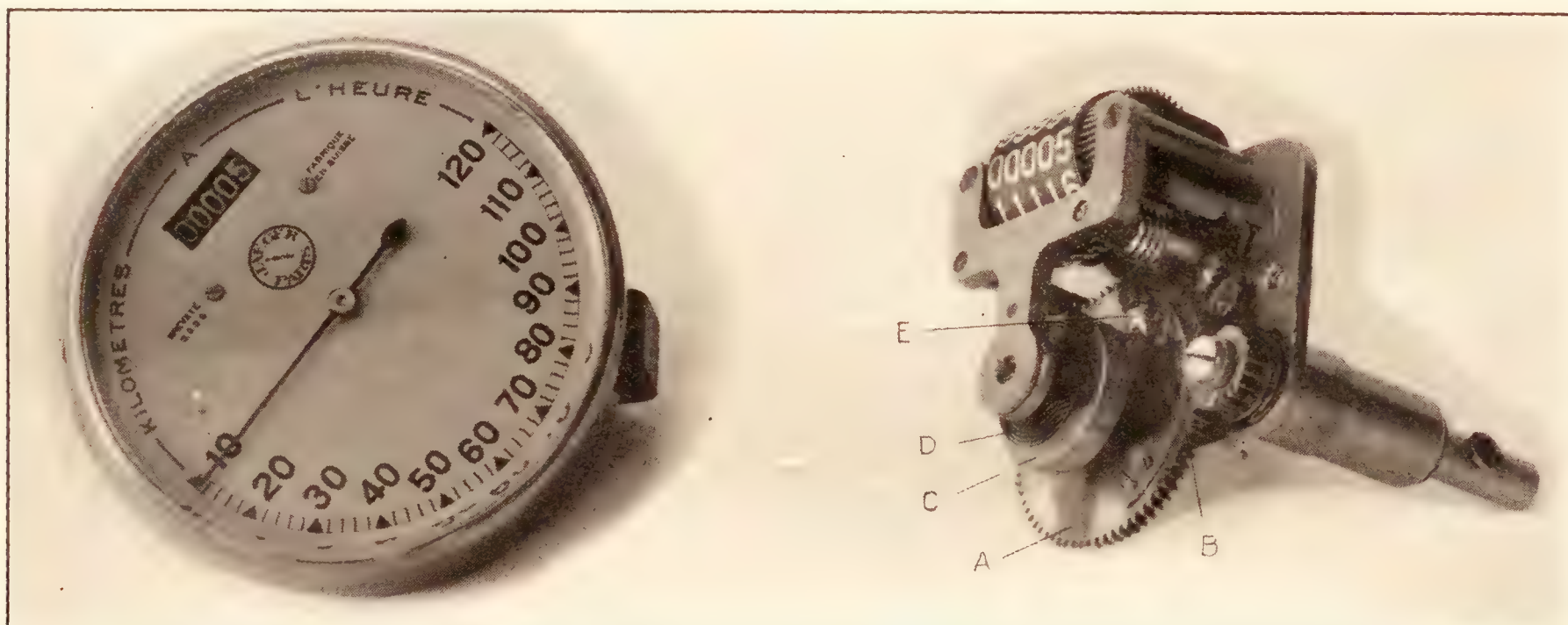


FIGURE 9.—Inertia tachometer.

circuit with temperature by means of a bimetallic strip (Warner, reference 5) or by a liquid-filled capsule (Ihle, reference 7). Later methods depend upon the use of a magnetic shunt of copper-nickel-iron alloy in the manner described in the section on "Electric Tachometers." Difficulties arise in this method, due to the fact that the effect of temperature on the uncompensated instrument is not the same function of temperature as that of the effect on the compensator.

Inertia tachometer.—The inertia tachometer of Swiss manufacture (Jaeger) in use abroad for many years as an automobile speedometer is very simple and interesting. A comparatively heavy brass gear A (figure 9) carrying an arm B very close to its periphery is rotated by a pinion at a speed proportional to the engine speed. A heavy disk C is mounted concentrically with the gear but on an independent shaft. A hair spring D is attached to the shaft of C and to a member fixed with respect to the case. Lever E is integral with disk C. The pointer shaft is free, except

tion until the above cycle is again repeated. The deflection of the pointer is thus nearly proportional to the speed of rotation. If a subsequent speed is lower, the pointer is moved backwards by E on disk C engaging the strip on the pointer.

The average speed for the previous interval of time is indicated as in a chronometric tachometer, with the difference that the time interval is variable, being short for high speeds and long for low speeds. The condition for obtaining an evenly divided scale is that the inertia disk C should have a constant velocity. This is achieved in large measure by making the scale short — 180° of arc in figure 9. This inherently short length of scale is a serious disadvantage to its use in aircraft. Variation in the temperature of the instrument will affect the stiffness of the hairspring and may vary the friction in the pivots of the inertia disk.

Other types.—The viscous drag tachometer using either air, mercury or other fluid for operation has entirely disappeared from use in aircraft. Instru-

ments of this type which have been constructed for aircraft use include the American Waltham (reference 5), the French Atmo (reference 5), and a German instrument by Lehmbeck (reference 7). The first mentioned instrument used air and the other two used mercury as the fluid.

A differential drive tachometer of unique design has been proposed by A.E.G. (German), but has apparently not been used on aircraft (reference 7).

Liquid centrifugal tachometer.—The liquid Veeder instrument described in the section on "Testing Equipment" in a design with a much shortened scale was used to a slight extent in the early days of airplanes. The measurement of pressure, as is here necessary, by means of a liquid column involves, compared to instruments of other types, (a) an excessive position error, (b) lack of sensitivity in a small bulk, and (c) difficulty in retaining the liquid.

The mechanism of the friction disk tachometer designed by Behrens (French) (references 17 and 7) consists of two disks, one driven at constant speed and the other at a speed proportional to that of the engine. The axes of rotation are at right angles and the edge of the variable speed disk is in frictional contact with the constant speed disk. The variable speed disk moves along its shaft, which is essentially a worm gear, until the peripheral speeds of the points of contact are equal. The position of the disk, and thus the speed, is indicated by a pointer connected to the disk by a pinion and rack. The constant speed disk is also driven by the engine, a frictional clutch controlled by a centrifugal governor in a cylindrical barrel serving to obtain constant speed. The instrument indicates rotation in either direction, two pinions driven differentially being used with an automatic clutch so as to drive the disks in a uniform direction.

In a later design, known as the Delta tachometer and described by Aera (1926), a cone is used instead of the constant speed disk.

The performance of the instrument is not as satisfactory as other types (reference 17), which, as might be expected, is due to the difficulty of maintaining the necessary constancy of friction under the conditions of use.

D. FLEXIBLE DRIVE SHAFTS

The flexible drive shaft used with the tachometer consists of a torsionally stiff but otherwise flexible driving element and a casing capable of guiding and protecting it and retaining without leakage a suitable lubricant. The flexible driving element is composed of a single strand core of tempered steel wire on which several layers of steel music wire are wound alternately in right and left hand helices. See figure 10. The direction of pitch, whether right or left, of the final

helix is made such that it tends to coil tighter when the shaft is in use. The casing consists of an inner flexible steel tube and an outer one of whip cord braiding.

The tachometer shaft adopted as standard by the Army and Navy air services has a shaft diameter of 0.150 inch and an over-all diameter of the shaft casing of $\frac{27}{64}$ inch, and a specified design for the connections to the engine and to the tachometer. The standard for aircraft (not for marine use) adopted by the Society of Automotive Engineers (see S.A.E. Handbook) is the same except for slight differences in the end connections. Shafts according to either standard are interchangeable. The standard shaft as ordinarily constructed will transmit safely a torque of not more than 8 pound-inches when the shaft is straight and a torque decreasing from this value as the curvature is increased.

Steel driving elements and other steel parts become magnetized and in this condition are a source of troublesome error in the indications of the magnetic compass. For this reason nonmagnetic flexible shafting is very desirable and is under development.

The length of flexible shafts in service is limited to about 35 feet and rarely exceeds 25 feet. They must be installed without sharp bends; the radius of curvature should not be less than about 12 inches. Operation at low temperatures causes failure in many instances owing to the stiffening of the lubricant in the drive shaft casing and in the tachometer.

ELECTRIC TACHOMETERS

Tachometers of the electrical type developed for aircraft use consist either (a) of a voltage-generating element rotated by the engine through a very short connecting shaft and a distant indicator of this voltage or (b) of a commutator rotated by and at the engine and of some device either mechanical or electrical in nature for counting the number of electrical impulses per unit of time.

The electric tachometer is particularly suited, in contrast with the mechanical tachometer, for securing an indication on the instrument board of the speed of the outboard engines of multi-engined aircraft. There is also the possible advantage that two or more indicators may be connected to the same generator. However, the cost of the electrical type is greater than that of the mechanical tachometer of equal accuracy.

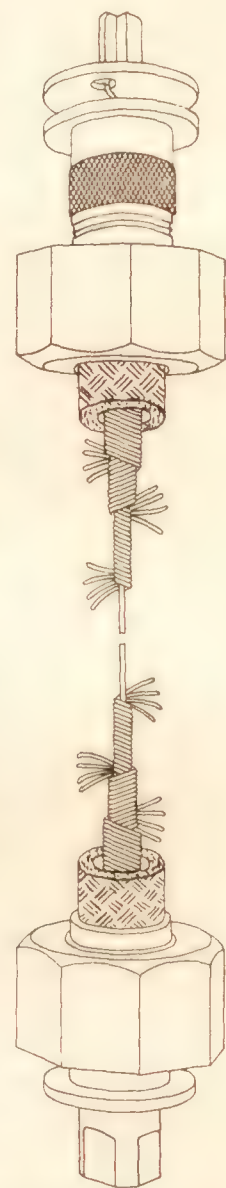


FIGURE 10. — Diagram of a flexible drive shaft.

A. DIRECT CURRENT TACHOMETERS

Essential parts.—This tachometer consists of a generator attached to the engine at the point usually provided for the tachometer connection, and a volt-

about 270° of arc. The indicator first mentioned is installed in a fan-shaped case (fig. 11) which is awkward to mount on an instrument panel, while the latter is in a case (fig. 12) the size and shape of which conforms to that adopted as standard for aircraft

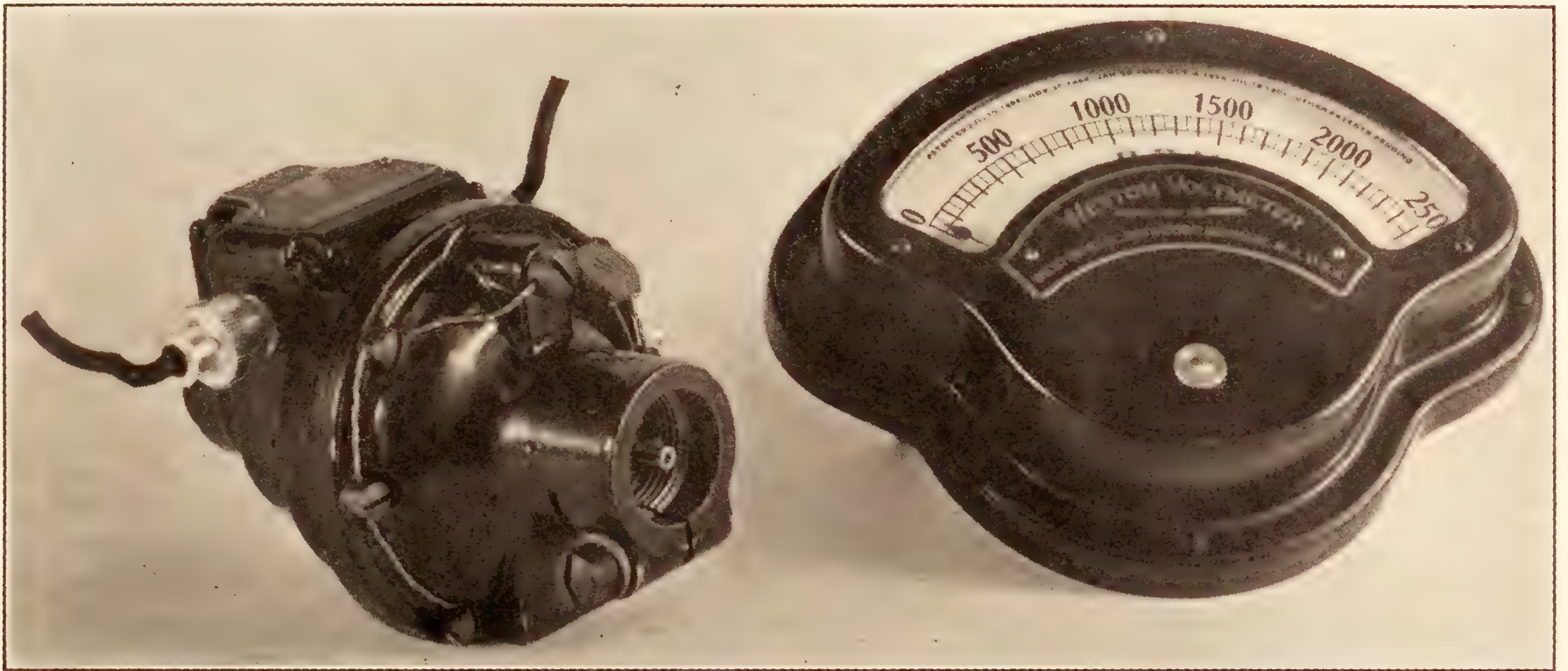


FIGURE 11.—Generator and fan type indicator of Weston d.c. electric tachometer.

meter of the moving coil type for indicating the speed. The field of the generator is obtained from a permanent magnet, usually of cobalt steel. The generator and

instruments. The fan-shaped indicator weighs 22 ounces, the other, 20 ounces. The generator develops 3 volts per 1,000 r.p.m. It weighs 20 ounces and is designed to fasten directly to the tachometer fitting of the engine. The instrument is furnished with both the generator and indicator individually compensated for temperature.

Tetco.—A photograph of the Tetco tachometer is shown in figure 13. The indicator of this instrument weighs 20 ounces, has a pointer deflection of 270° and conforms in size and shape to the new standard for the cases of aircraft instruments. The generator develops 4.5 volts per 1,000 r.p.m., weighs 18 ounces, and is designed to fasten directly to the tachometer fitting of the engine.

Horn.—The Horn electric tachometer shown in figure 14 is of German manufacture and is not particularly suitable for use on aircraft, as is evident from the fact that the magneto weighs $4\frac{3}{4}$ pounds. It develops 25.6 volts per 1,000 r.p.m. and is designed to be connected with the engine by means of a short length of flexible shafting. The indicator has a maximum deflection of the pointer of 300° , a resistance of approximately 2,400 ohms, and weighs 26 ounces.

Characteristics of d.c. tachometer.—In general the lag in indication of these instruments is negligible. Some difficulty is experienced in maintaining a given calibration due to a weakening with time of the permanent magnets in the generator and indicator, and to a zero shift of the hairspring in the indicator. These possible defects are well known and can be avoided by careful technique in manufacture.

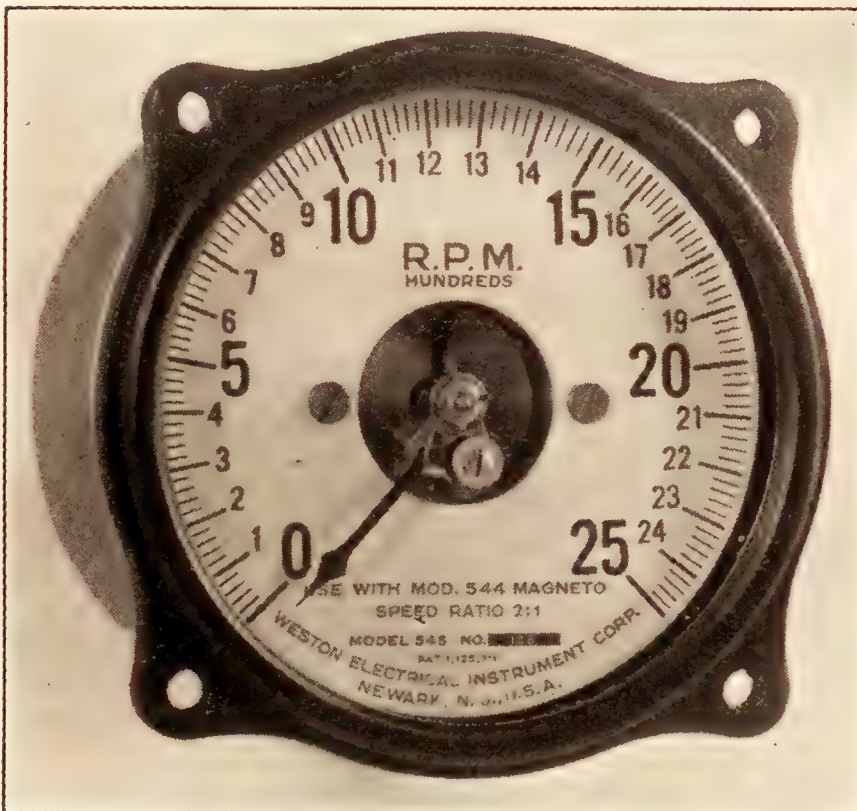


FIGURE 12.—Indicator of the Weston d.c. electric tachometer with 270° pointer motion.

the indicator are connected by means of two insulated electrical conductors.

Weston.—A photograph of the Weston tachometer is reproduced in figure 11. Either of two types of indicators are available for use with this instrument, one having a pointer deflection of 120° and the other

The d.c. instrument has long been available, but has not been used extensively on aircraft until quite recently. In order to be satisfactory for such use the requirements special to such operation had to be met by modifications in existing designs. These are outlined below.

(a) *Weight*.—The general requirement of low weight for aircraft parts has led to the development of generators of light weight with essentially the same voltage output as that of heavier generators previously available. However, the weight of complete instruments at present available is inherently greater than that of mechanical tachometers. The difference is not so considerable when the weight of a long line of flexible shafting is included with that of the mechanical tachometer.

(b) *Long scale indicator*.—In order to conserve space on the instrument board and at the same time secure an adequate length of scale, an indicator with a much greater pointer motion is required than the 120° of arc of the ordinary fan type voltmeter. Several methods for increasing the range of pointer motion are now being employed. A sector and pinion mechanism is used in the indicator of the Horn tachometer shown in figure 14, by means of which an angular deflection of the pointer of about 300° is secured.

A pointer motion of approximately 270° of arc has been obtained in the Cirscale indicator by a unique arrangement of the pole faces of the permanent magnet, one of which is split to permit the insertion of the pointer shaft and moving coil (reference 8). A diagram of the mechanism is shown in figure 15 and a photograph of a commercially manufactured instrument in figure 12. Securing the necessary scale length by a greater angular deflection of the pointer has obvious advantages. A disadvantage, however, of this indicator is its lack of sufficient ruggedness to endure the vibration to which it is ordinarily subjected on an instrument board.

(c) *Compensation for temperature*.—The indicator and the generator must be individually compensated for temperature, first, because of the range of temperature to which the instruments are subjected and second, because the temperature of the indicator on the instrument board may be widely different from that of the generator installed close to the engine. Compensation is necessary because of the effect of temperature on the resistance of the windings, on the permeability of the magnets of both the generator and indicator, and on the stiffness of the hairspring of the indicator (reference 2).

A commercial instrument was compensated at the Bureau of Standards in 1928 by the following method. The air gap of the permanent magnet of the generator was provided with a magnetic shunt of "thermalloy"

(reference 10). This material is a copper-nickel-iron alloy, the magnetic permeability of which is low compared with that of ferrous materials, and decreases almost linearly with increase in temperature. In the uncompensated generator the voltage decreases with rise in temperature which, in the generator provided with the thermalloy shunt, is prevented by an increase

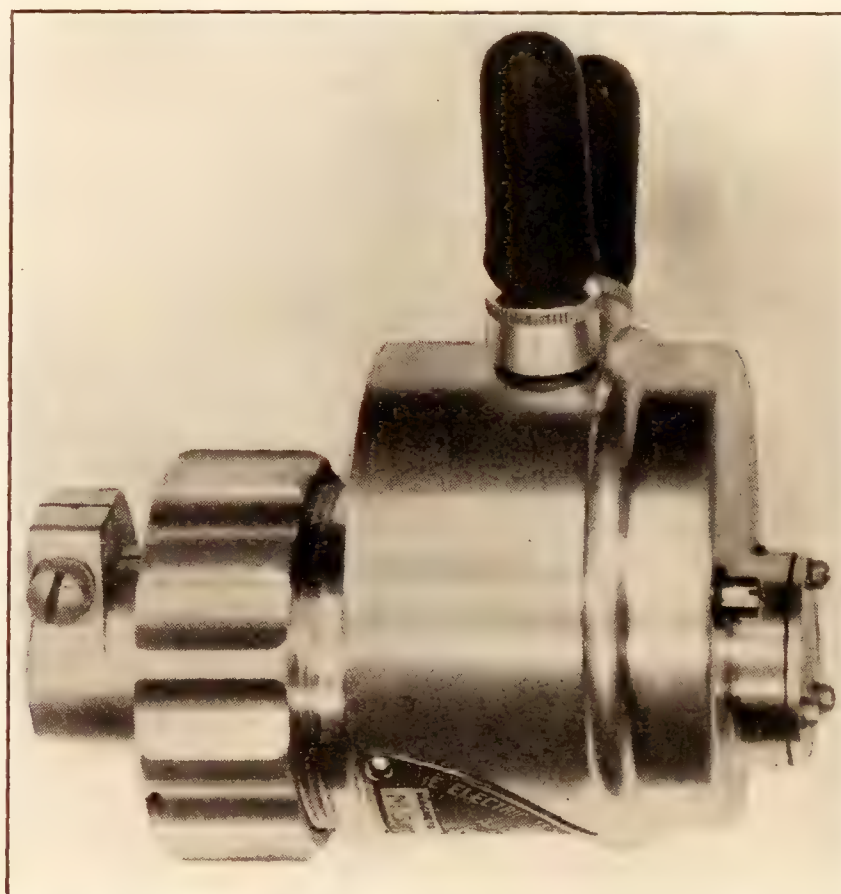
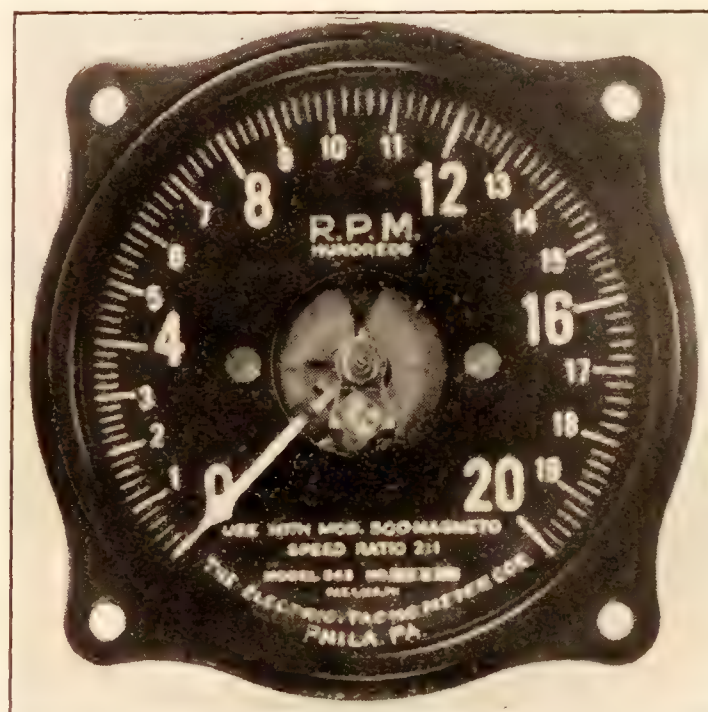


FIGURE 13.—Indicator and generator of Tetco d.c. electric tachometer.

in magnetic flux across the air gaps due to a decrease in flux across the shunt.

The temperature coefficient of the uncompensated indicator may be in general either positive or negative, depending upon the design. Compensation was effected in the indicator of the above-mentioned instrument by adding a series-parallel combination of electrical resistances of copper and constantan.

(d) *Rugged indicator*.—It is common experience that delicate electrical instruments will not withstand vibration of the severity found on instrument boards unless mounted in some sort of shock-absorbing ma-

B. ALTERNATING CURRENT TACHOMETER

This instrument consists of an alternating current generator and a suitable indicator. The field of the generator consists of one or more permanent magnets,

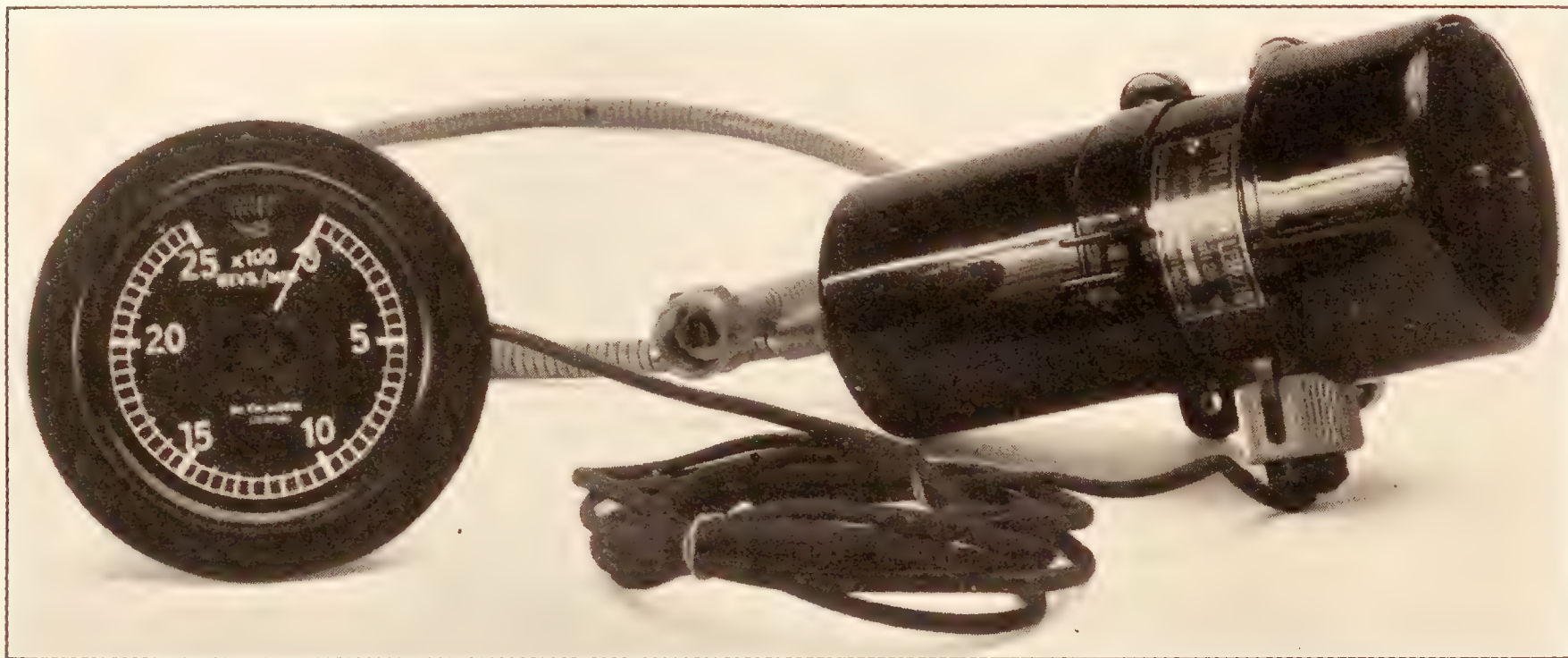


FIGURE 14.—Horn d.c. electric tachometer.

terial. In general, the ruggedness of an instrument of a given design decreases with increase in its sensitivity. It is therefore important that the generator produce as large a voltage as possible consistent with low weight, not only to avoid the effect of variation in brush and

usually of cobalt steel. As the rotor of the generator revolves there is induced in the stator windings an alternating voltage the frequency of which is proportional to the speed of the engine. The windings of the stator may be connected to secure either 1-, 2-, or 3-phase current, depending upon the type of indicator used.

If the generator is of the single-phase type, the induced voltage is measured, after rectification by a copper oxide rectifier, by a direct current voltmeter calibrated in units of speed of rotation.

If the generator is of the polyphase type, the indicator contains either a stator winding or a combination of electromagnets, and a metal disk or cylinder restrained from rotation by means of a hairspring. The combination of electromagnets and a disk is similar to that in watt-hour meters. The stator or electromagnets are wound so that a revolving magnetic field is produced. The resulting torque tending to rotate the disk is balanced by the hairspring. The angular deflection of the disk, or attached pointer, is a measure of the rate of rotation of the generator.

General Electric.—This instrument is of the single-phase type and consists of an a.c. generator, d.c. indicator, a saturation transformer, and a copper oxide rectifier. The saturation transformer gives a voltage output proportional to the frequency alone. The generator is of the polar inductor type and has stator windings which are coiled around a nonrotating, permanent magnet. A soft iron spider is the only rotating part. The indicator is supported within another case on a layer of sponge rubber so that it is shielded from the effects of severe vibration. The outer case con-

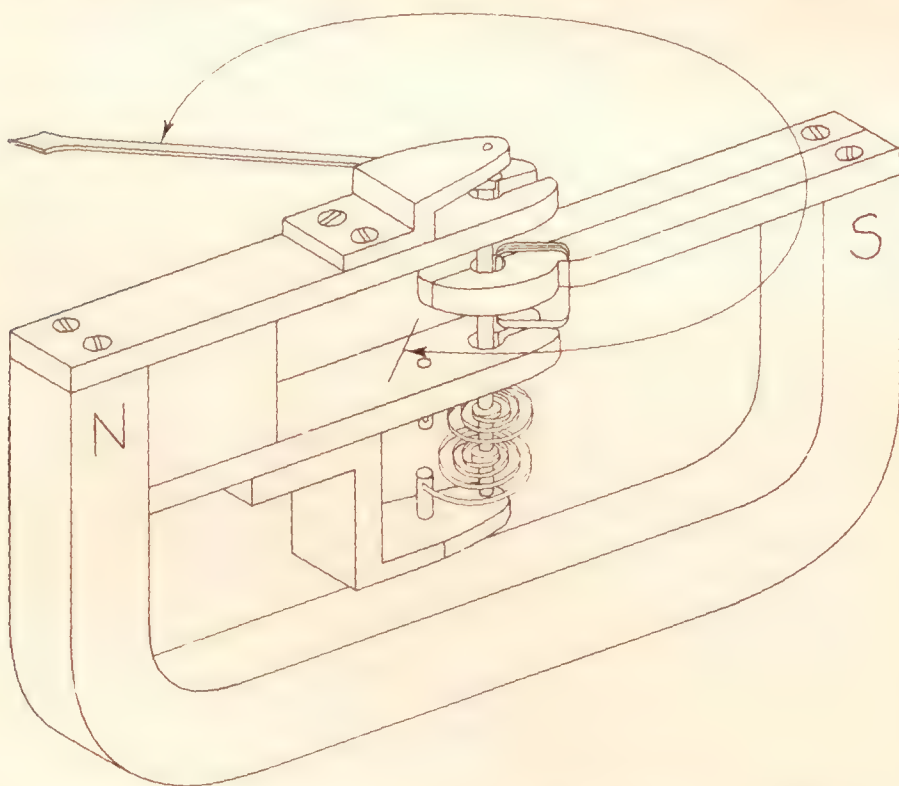


FIGURE 15.—Diagram of mechanism of Cirscale moving coil instrument

commutator resistance but also to permit the use of a less sensitive indicator.

(e) *Magnetic shielding*.—The indicators of electrical tachometers usually contain permanent magnets, or electromagnets, which makes it essential to provide magnetic shielding in order to avoid an effect on the indications of magnetic compasses mounted in their proximity.

forms in dimensions to the standard 2 $\frac{3}{4}$ -inch dial size case. The total weight of the instrument is approximately 4 $\frac{1}{2}$ pounds.

Pioneer.—This instrument is of the 2-phase type and consists of an a.c. generator and an a.c. indicator. A photograph of the instrument is shown in figure 16.

The rotor of the generator is a permanent magnet

about its axis against the torque of a hairspring. A pointer on the disk shaft indicates its position relative to the dial. Damping of the disk is obtained by means of a permanent magnet, the use of which requires shielding so as to avoid affecting the compass. Temperature compensation is obtained by shunting a resistance of the proper temperature coefficient across the

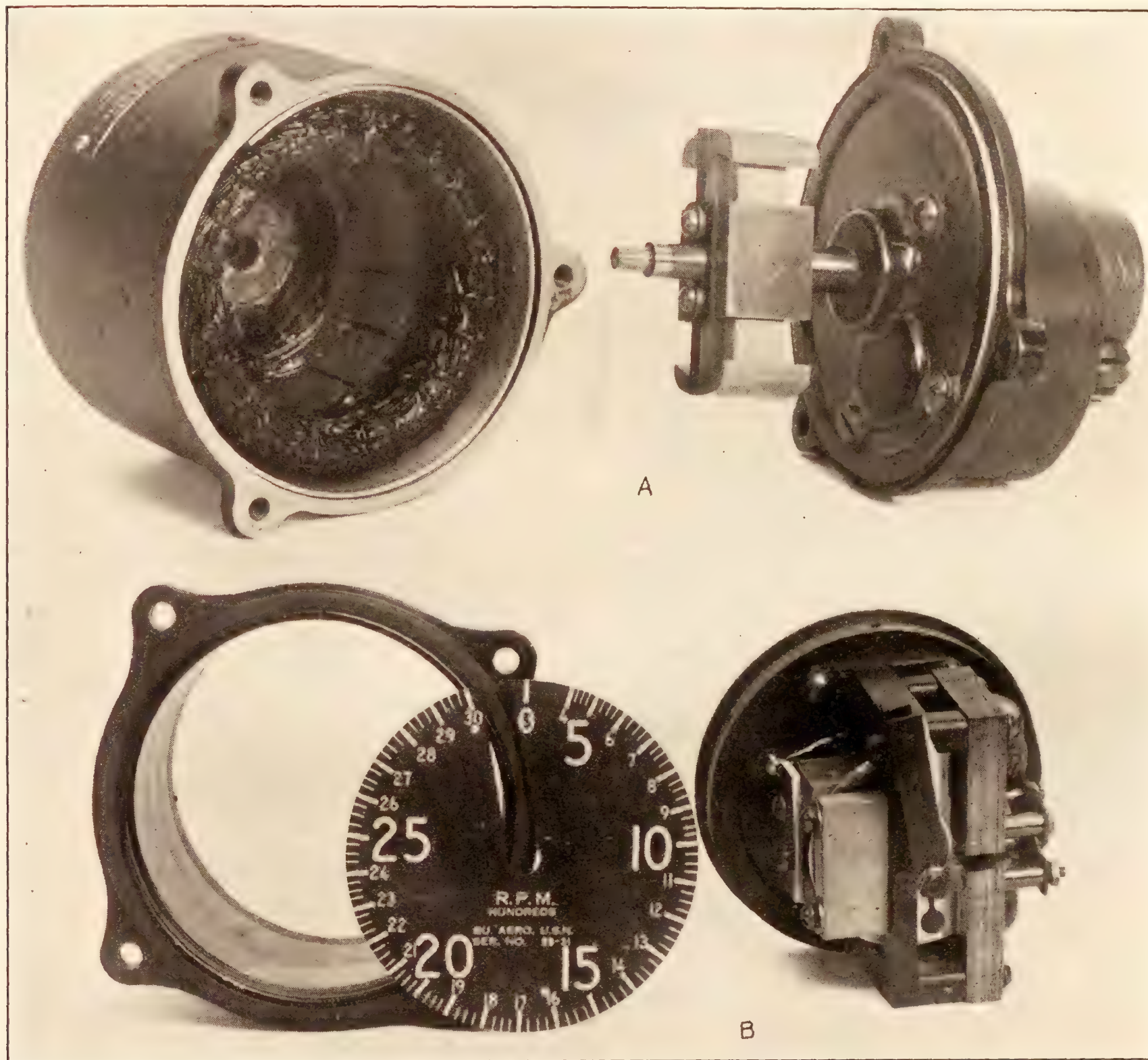


FIGURE 16.—Pioneer a.c. electric tachometer. A, generator; B, indicator.

and the stator is of the 2-phase 3-wire, wound type. A swamping resistance is added so as to obtain an indication independent of the usual variation in the length of leads used in service. Temperature compensation is obtained by means of a magnetic shunt. The rotor makes 13,500 r.p.m. when the generator is connected to a shaft having a speed of 1,500 r.p.m.

The indicator contains two stationary coils electrically connected to the output side of the generator. The revolving magnetic field thus set up produces eddy currents in an aluminum disk which is free to turn

coils. The pointer moves 345° of arc for the range 400 to 3,000 r.p.m.

The weights of the generator and the indicator are 2.4 and 1.2 pounds respectively.

Comparative advantages and disadvantages.—The principal advantage of the alternating current tachometer lies in the elimination of the errors caused by variation in the resistance between the commutator and the brushes. The alternating current tachometer, however, has the disadvantage of weighing more than the direct current instrument.

C. SOLENOID-OPERATED CHRONOMETRIC TACHOMETERS

Stover-Lang.—The Stover-Lang tachometer, as developed for aircraft use, consists of a chronometric tachometer, a solenoid, an electric contactor, and a battery of 12 volts or other source of direct current. The solenoid is mounted within the indicator and the contactor is fastened to the tachometer adapter of the engine. The battery, electric contactor, and solenoid

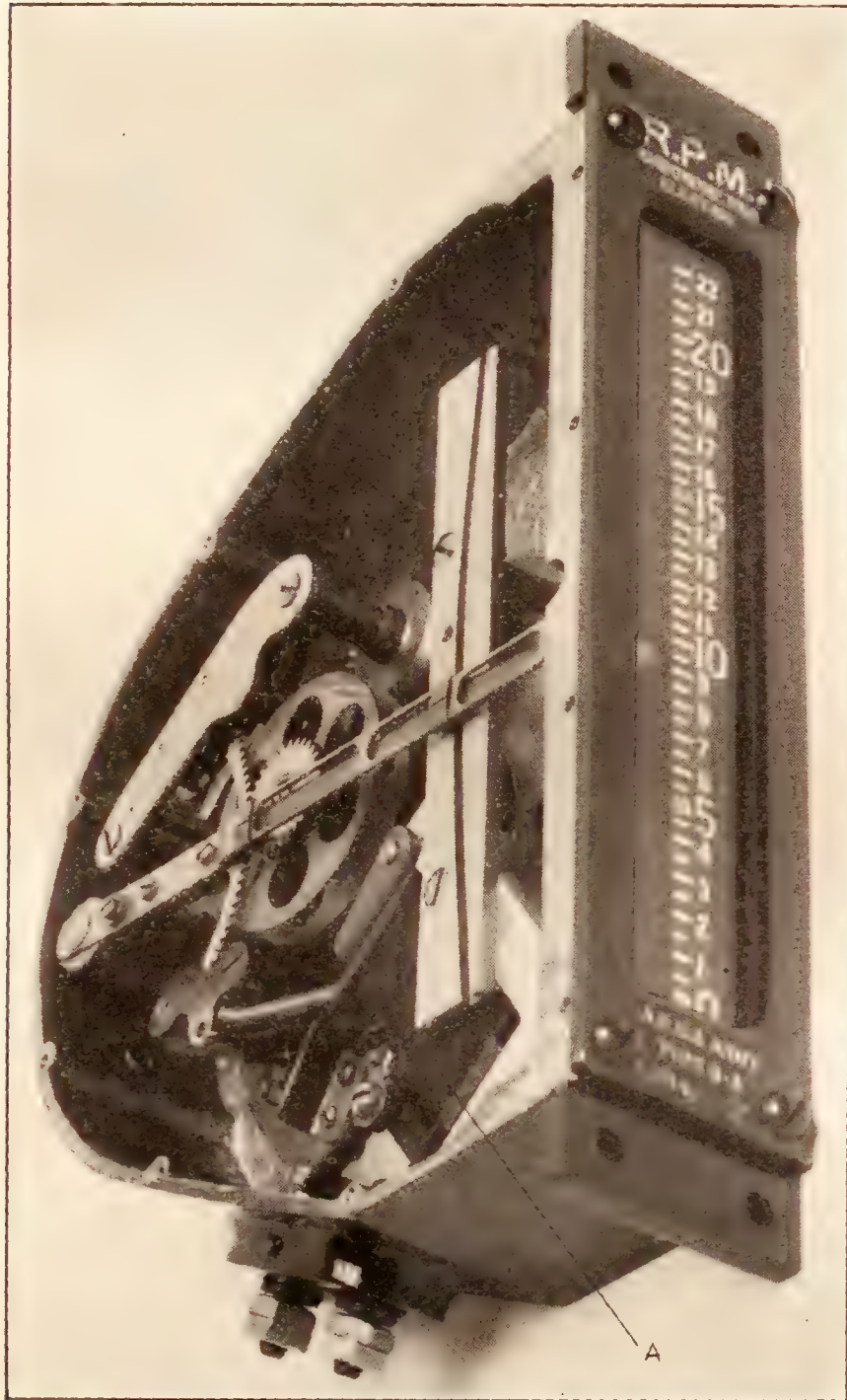


FIGURE 17.—Stover Lang chronometric-electric tachometer.

are connected in series. A photograph of the indicator of this instrument is shown in figure 17, in which **A** is the solenoid. For aircraft use the indicator has been developed only in the vertical-scale type. The contact in the contactor unit is made and broken by means of a cam, which is rotated by the engine. During each revolution of the cam of the contactor (two revolutions of the engine crankshaft) the circuit is opened and closed two times, and thus intermittently energizes the solenoid in the indicator. The solenoid operates a pawl and ratchet mechanism which

drives the chronometric tachometer at a rate proportional to the speed of the engine.

Comparative advantages and disadvantages.—The instrument suffers in comparison with the d.c. and a.c. tachometers in that (a) an outside source of current is required, (b) it is an integrating instrument and thus in general has inherent defects of a relatively long period between indications and of not indicating the instantaneous speed. To avoid the possibility of draining the battery, it is essential that the electrical circuit be broken when the instrument is not in use. Up to the present (1932) the cost of this instrument has been greater than that of the d.c. or a.c. types.

This instrument compares favorably with the d.c. and a.c. types in that (a) a sufficiently long scale can be obtained without loss of ruggedness or accuracy. Although the instrument is available only in the vertical scale type, there is no inherent difficulty in modifying it for installation in a round dial type case and in securing a pointer motion of one revolution or greater. (b) The indication is independent of changes in the temperature of the mechanism, provided that a lubricant of the proper grade is used and that the escapement is compensated, which is a well-understood and common procedure. (c) The accuracy is ordinarily maintained for the operating life of the instrument, while with the direct or alternating current tachometers there is possibility of changes in the magnetism of the permanent magnet and the effect of mechanical wear in the generators and indicators. (d) The scale is inherently evenly divided in speed units as contrasted with some of the designs of a.c. instruments.

In common with the chronometric types the instrument is easily adjusted to a desired calibration by varying the periodicity of the escapement. There is no position error.

On the whole the inherent disadvantages of the instrument preclude its extensive use.

D. COMMUTATOR-CONDENSER TACHOMETERS

Principle of operation.—In this instrument an electrical condenser is alternately charged and discharged at a rate proportional to the rotational speed which is to be measured.

A number of electrical circuits, of which one of the most efficient will be described, have been devised to utilize this principle (reference 36). The essential parts consist of a commutator **A** (fig. 18) designed for attachment to the engine at the tachometer connection, an electrical condenser **B** of fixed capacity, a milliammeter **C** (graduated in r.p.m.), and a source of direct current **D**. The part of the circuit marked **E** in figure 18 is a voltage regulator which will be discussed later. Each terminal of the condenser is

connected to alternate segments of the commutator through a slip ring. As the commutator is rotated from one segment to next, the condenser is discharged and again charged with electricity of the opposite sign, all of which quantity of charge passes through the milliammeter *C*.

The indication depends upon the voltage impressed upon the condenser. This voltage is measured by the milliammeter *C* upon completing the circuit through resistance *G* by means of switch *F* (fig. 18).

Theory.—Neglecting the inductance in the circuit shown in figure 18, which is largely that of the moving coil of the indicator, the charge passing through the indicator during the time the brushes remain in contact

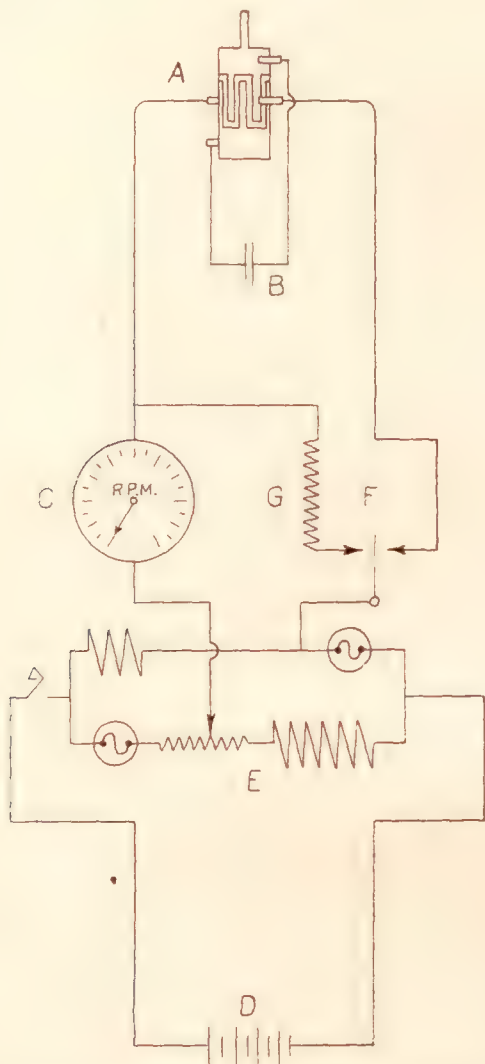


FIGURE 18.—Electric circuit of commutator-condenser type tachometer.

with a given segment of the commutator is given by the expression:

$$Q = CE \left(1 - e^{-\frac{t}{Cr}} \right) \quad (9)$$

Here *Q* is the charge transferred in the circuit in the time *t*, *C* is capacity of the condenser, *r* is the resistance in the circuit, and *E* is the voltage applied at the instant from which time *t* starts. If *t* is the time interval of contact on the commutator, *Q* is the charge passing through the indicator per contact. It should be noted that the effective voltage *E* applied to the condenser is twice the voltage output from the voltage regulator as the polarity of the condenser is changed from complete charge for one direction to complete charge in the opposite direction of flow.

The total charge passing through the indicator per second, or the current *I* is

$$I = NQ \quad (10)$$

where *N* is the product of the number of commutator segments and the rate of rotation. Substituting for *Q* from equation (9) it is seen that

$$I = CEN \left(1 - e^{-\frac{t}{Cr}} \right) \quad (11)$$

This equation shows that the current *I* is directly proportional to the rate of rotation of the commutator provided that a constant voltage *E* is maintained and that the quantity $e^{-\frac{t}{Cr}}$ be small. The value of the latter quantity depends upon the design of the circuit, and its constancy upon keeping the variation of the brush-commutator resistance within reasonable limits.

Automatic voltage regulator.—The automatic voltage regulator (reference 1) consists of a parallel circuit of equal resistances (*E*, fig. 18), both of the two legs of the circuit being composed of a fixed resistance and a tungsten lamp but in reversed order. The resistance of the tungsten lamps varies approximately with the impressed voltage. The output voltage for the instrument is taken from the junction point of the two resistances in each leg of the circuit. Its constancy depends upon the characteristics of the lamps, the current required and the variation in the voltage supplied. In one circuit the output voltage remained constant within 0.3 percent for values of the voltage supplied from 10.5 to 13.5 volts. The efficiency, defined as the power output divided by power input, is very low in the circuits thus far devised, not exceeding 2 percent.

Instruments constructed.—These instruments have not been used extensively in aircraft for measuring the speed of the engine. A tachometer of this type was constructed in 1921 at the Bureau of Standards for the Army Air Service (reference 34). The electrical circuit differs from that described (fig. 18) in that the differential voltage on the condenser was that of the supply battery and not twice its value.

Instruments operating on this principle are used to measure the air speed of airships in which case the commutator has been driven by a propeller or in one case by Robinson cups (reference 20).

Advantages and disadvantages.—The commutator-condenser tachometer is not excessive in size and is relatively light in weight. The lag in indication is negligible and aircraft accelerations have comparatively little effect on its indications. It is easily compensated for temperature errors. On the other hand there is the necessity for an external source of direct current, the necessity for operating a switch when the instrument is not in use if a voltage regulator

is used, and the difficulty of securing satisfactory performance from the inherently sensitive indicator when it is subject to airplane vibration. Its simplicity of design and other characteristics render this instrument of possible use on multi-engined aircraft.

STROBOSCOPIC TACHOMETER

This instrument consists of two parts, a device for interrupting at an adjustable rate the rays of light reflected from a propeller, or other rotating part, and

rotate the distance between two of the holes. The speed of the propeller is obtained from the following equation,

$$S = Nh$$

where S is the speed of the propeller, N the speed of the disk, and h the number of holes in the disk.

Many forms of stroboscopic instruments have been developed (references 32, 33, 35, 40, 42, 43, and 44).

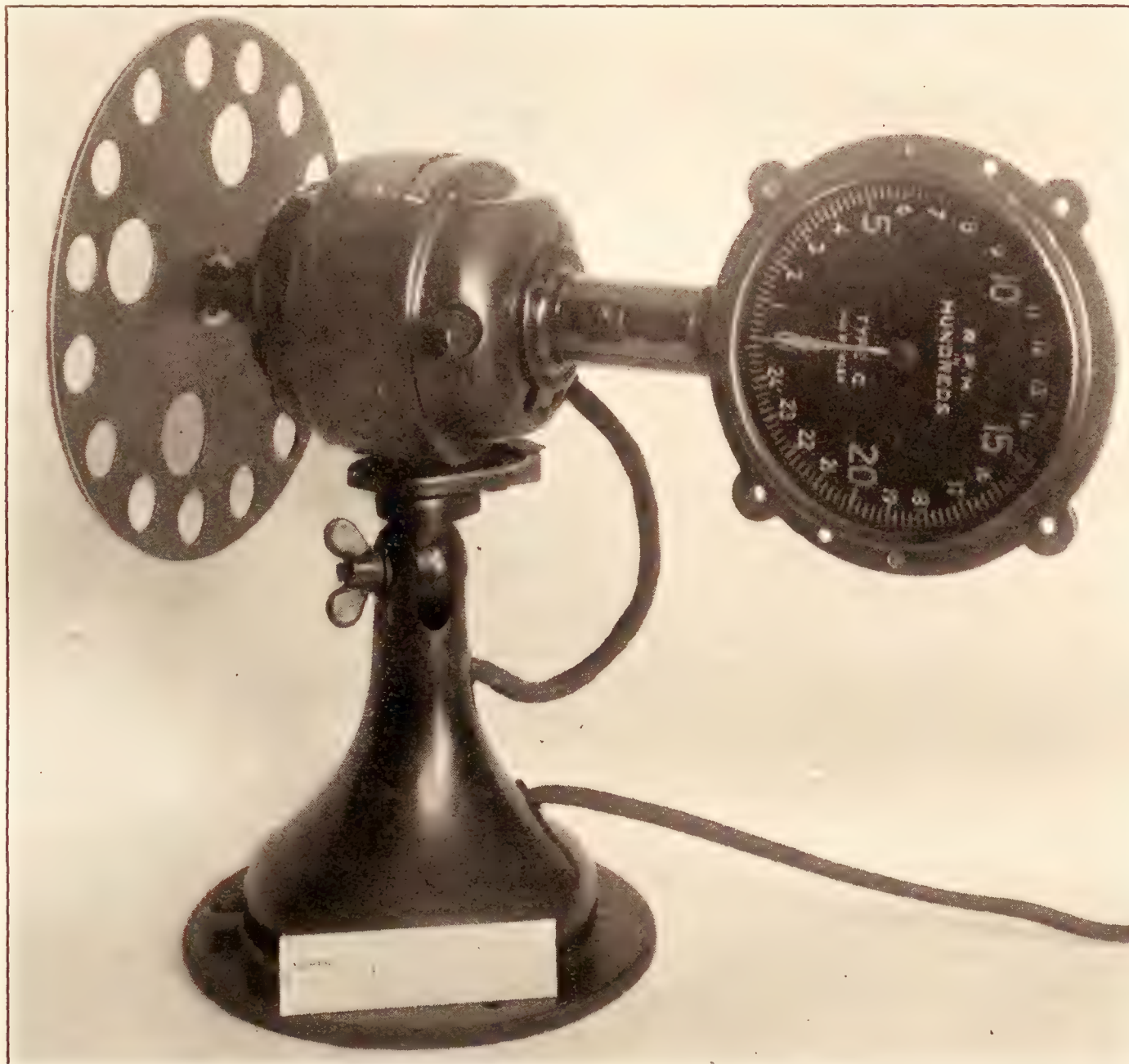


FIGURE 19.—Stroboscopic tachometer.

a tachometer. Figure 19 shows a simple form of stroboscopic tachometer utilizing a small fan motor. In this apparatus a motor-driven disk, in which uniformly spaced holes were drilled on a circle concentric with the disk, serves as the interrupter. The speed of the disk is controlled by a rheostat mounted within the base of the motor and is indicated by the tachometer connected to the opposite end of the shaft.

If all of the blades of the propeller except one have been blackened and the speed of the tachometer is adjusted so that the image of the propeller, as seen through the holes of the stroboscopic disk, appears to remain stationary, then the propeller makes one complete revolution in the time required for the disk to

The stroboscopic tachometer is useful in determining the speed of any revolving object to which it is inconvenient or undesirable to connect mechanically a tachometer. It has been used on lighter-than-aircraft of the larger size as a means for determining at a central point the speed of the individual propellers.

MISCELLANEOUS TACHOMETERS

Two instruments, the pneumatic and the resonance, have thus far not come into any extended use on aircraft, but may have future possibilities.

A. PNEUMATIC TACHOMETERS

The pneumatic tachometer consists of an air pump and a pressure gage. The pump is attached directly

to the tachometer adapter and develops a pressure depending upon the speed of the engine. It is connected by means of copper tubing with a pressure gage which is graduated in speed units.

The pneumatic method of measuring rotational speeds has been used to some extent in automotive service (Van Sicklen speedometer, reference 5) in which form the pump was contained within the case of the pressure gage and was driven by a flexible drive shaft. New designs, however, have recently been developed abroad.

Askania.—As shown schematically in figure 20, this instrument as designed for aircraft use has two units, consisting of (a) a centrifugal element and an air pump, attached to the tachometer adapter of the engine, and (b) of an indicator installed in the cockpit. The indicator and engine unit are connected by means of a length of air tight metallic tubing. The centrifugal element A controls the position of piston B operating in a cylinder provided with ports located at one point along its axis. As the centrifugal element is revolved by the engine it moves the piston so as to cover the port openings. The pressure of the air delivered by the pump to the cylinder thus closed off is sufficient to overbalance the centrifugal force and to move the piston back so as to open the ports sufficiently to relieve the air pressure in excess of that needed for balancing. The pressure of the air required to balance the piston varies with the speed of rotation of the centrifugal element and is measured by the indicating instrument. Since large port openings are uncovered by a small displacement of the piston the position of the latter is essentially constant at all speeds, and therefore the balancing pressure depends only on the speed.

The weight of the pump unit of the Askania pneumatic tachometer is approximately 22 ounces.

Amyot-Le Prieur.—This instrument consists of an oleo centrifugal pump and a pressure gage. The pump is mounted on the engine and is driven by a short length of flexible shafting. In one form of the instrument the air above the oil in the pump is compressed an amount depending upon the speed of the rotor. The pressure is then transmitted pneumatically through copper tubing to the indicator, which is graduated in terms of the speed of the engine. In another form, the pump when operating is entirely filled with oil and a line filled partly with air and partly with oil connects the pump with the indicator.

Neither form of the instrument appears to give satisfactory performance owing to the effect of pitch of the aircraft on the indication of the oil-filled instrument and the effect of temperature on the pneumatic transmission type.

B. RESONANCE TACHOMETERS

Resonance tachometers (reference 24) have not been developed for aircraft, but may possibly be of use in measuring engine speed in view of the fact that instrument boards in most airplanes with a single engine vibrate with the same frequency as the engine. The instrument contains a graduated series of tuned metal reeds, the natural frequencies of which vary uniformly in the range of the instrument. When the instrument is brought into contact with the frame of a vibrating or rotating body at any given frequency of vibration, or rate of rotation with even slight unbalance, one or a group of the reeds vibrates in resonance, and thus indicates the input frequency. Extraneous vibrations

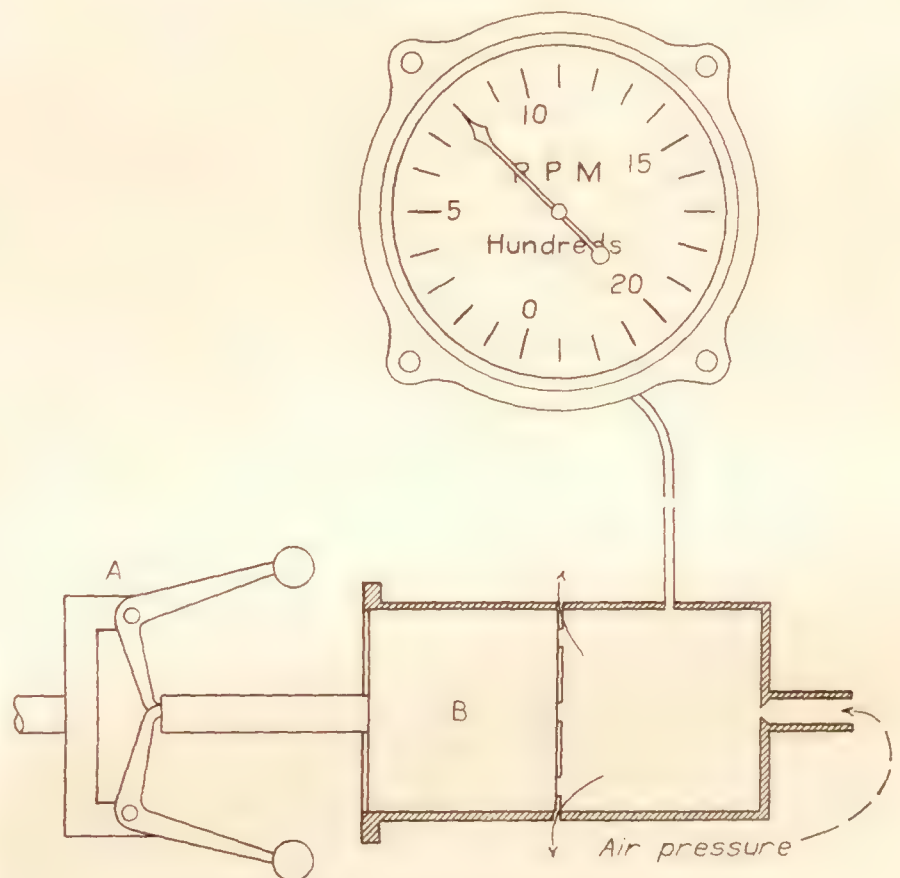


FIGURE 20.—Diagram of Askania pneumatic tachometer.

and harmonics of the fundamental frequency may cause ambiguity in the indications.

LABORATORY TESTING OF TACHOMETERS

A. APPARATUS

It is more convenient in practically all cases to determine the errors of tachometers by means of laboratory tests. The calibration apparatus consists of a standard instrument and means for driving at variable speeds both the standard and the tachometer under test.

Calibration apparatus—(a) *With d.c. motor.*—The tachometer calibration apparatus used at the Bureau of Standards is shown in figure 21. A liquid centrifugal tachometer, T in the figure, is used as the master instrument. The instrument under test is connected

to the apparatus through the chuck C. A quarter horsepower direct-current motor having a rated speed of 1,160 r.p.m. at full load is used to operate the instruments. The flywheel shown in the figure serves the twofold purpose of preventing rapid fluctuations of the speed and of supplying a convenient means of regulating the speed which is accomplished by a pressure of the hand on the rim. A rheostat R mounted on the base of the apparatus forms part of the electrical circuit of the motor and is used to obtain a coarse adjustment of the speed. Switches are provided (a)

spring to absorb the jars incident to a gear-driven operating device. It has been found that centrifugal tachometers, which are the most susceptible to unevenness in operation of the driving shaft, may be operated with this device without any perceptible flicker of the pointers. It should be pointed out that when tests at low temperatures are made a lubricant must be chosen which in the temperature range remains in the liquid state.

(b) *With a.c. motor.*—If an a.c. motor is used to drive the test apparatus, the speeds at the various test

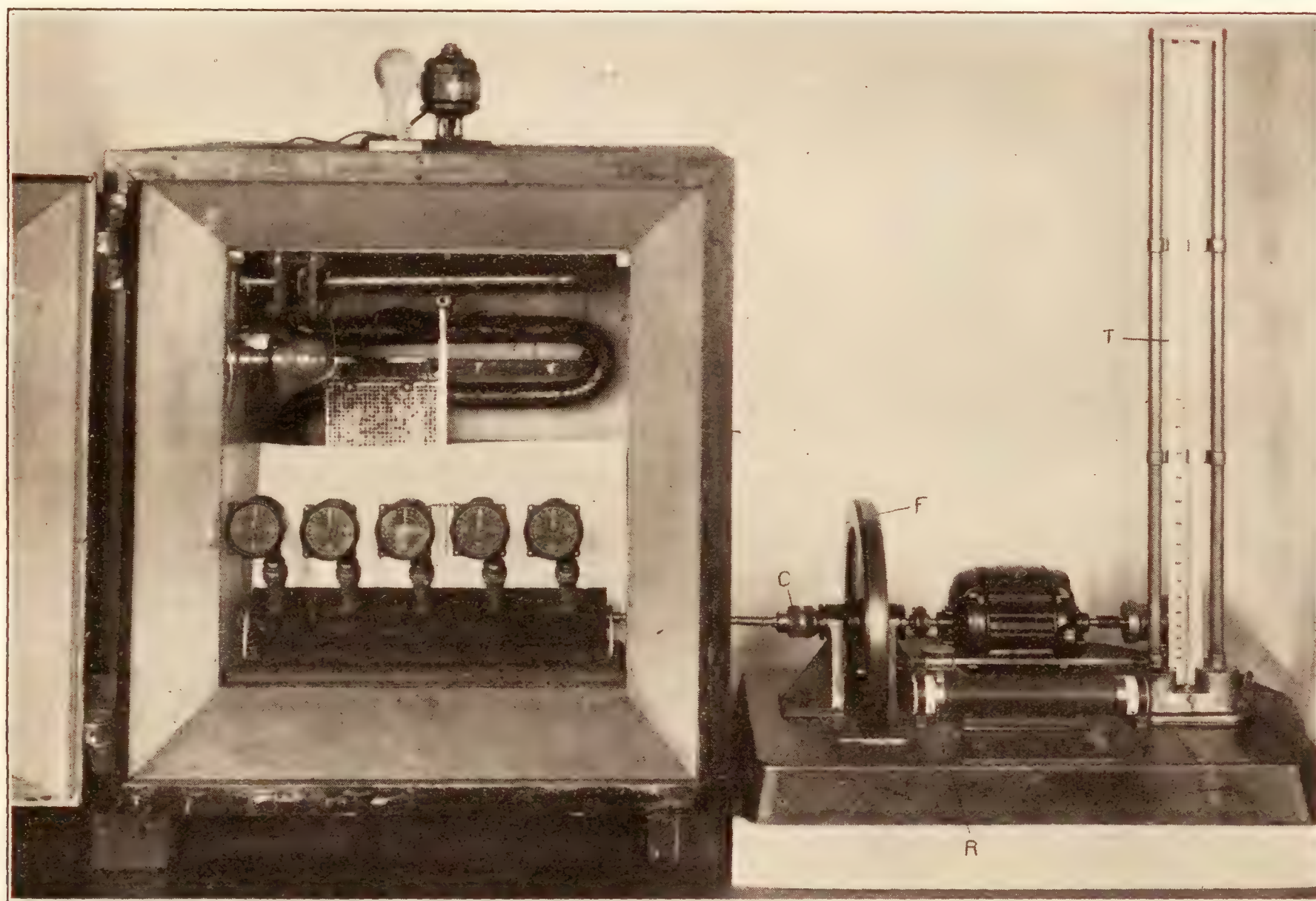


FIGURE 21.—Tachometer test stand and temperature control chamber.

between the motor and the power supply, (b) for reversing the direction of rotation of the motor, and (c) for inserting the rheostat either in the armature or field circuit of the motor. The instrument drive shafts are connected to the motor shaft through flexible couplings. See reference 30 for a more detailed description.

A test stand such as shown in figure 21 is used when it is desired to test more than one instrument at a time. The stand consists of a horizontal main shaft which is directly connected with the driving motor and five vertical counter shafts which are coupled to the main shaft by means of spiral bevel gearing. These parts are all enclosed in an oil-tight housing. Each tachometer is driven through a flexible helical

points must be obtained by mechanical means since the motor speed cannot be sufficiently varied. The main drive shaft of the tachometers and the master instrument is connected to the motor shaft by a friction disk and wheel. The variation in the speed of the instruments is obtained by varying the point of contact of the wheel along the radius of the disk.

A cone can be used instead of the disk, the wheel being arranged to make contact at any desired radius of the cone. This gives a much closer speed adjustment.

In some cases tests are desired only at a few fixed speeds. In such cases a gear box arranged so as to have outlets rotating at the desired speeds has been found to be more convenient than the use of the friction disk.

(c) *With motor-generator set.*—With only alternating current available there is the alternative possibility of obtaining variable speed by using an a.c. motor-d.c. generator set which may be preferable to the use of the friction disk and wheel described above. Two generators would give the ideal solution, one to maintain constant voltage on the field of the driving motor and the other to furnish a variable voltage on its armature. This variable voltage can be obtained by adjusting a rheostat connected in series with the field of the generator.

(d) *With synchronous motor.*—In calibrating instruments at a factory it is in some cases advantageous to use a synchronous motor to drive the tachometers. In order to obtain the chief advantage of this type of apparatus which is the elimination of the master tachometer, it is necessary that the frequency of the electric current be controlled at the source so that the fluctuations in speed are within desired tolerances. A gear box is used to obtain a number of values of the speed within the range of the tachometers to be adjusted so that each outlet of the gear box can be used as the source of a definite constant speed. A distinct limitation of the apparatus is the fact that only a limited number of speeds can be obtained.

Liquid veeder master tachometer.—The master tachometer (T, fig. 21) is essentially a liquid centrifugal pump. The pressure developed is measured by a manometer in which the liquid customarily used is kerosene colored red with an aniline dye. The rotor of the pump, which is at all times completely immersed in the liquid, is equipped with radial blades and is mounted in its housing with small clearances. The use of radial blades obviously enables the instrument to hold its calibration for either direction of rotation of the pump. The instrument is provided with two knobs, one for adjusting the height of the liquid in the reservoir to the proper level and the other for adjusting the damping of the liquid column. The first adjustment is obtained by raising or lowering a partly submerged sink in the reservoir. The second adjustment is produced by controlling the area of a restriction at the entrance to the manometer tube.

The pressure developed in the liquid due to centrifugal force at any point along the axis of rotation is

$$dP = w^2 D r dr \quad (12)$$

Where P is the pressure developed,

w is the angular velocity,

r is the radius of rotation at the point at which

P is measured,

and D is the density of the liquid.

In the instrument the pressure caused by centrifugal force is balanced by a head of liquid in the manometer tube so that

$$P = g D h$$

where h is the head of liquid and g is the acceleration of gravity.

It follows that

$$dh = \frac{w^2 r dr}{g} \quad (13)$$

Integrating both sides of this equation we have

$$h = \frac{w^2 R^2}{2g} + c \quad (14)$$

where c is the constant of integration and R is the radius of the radial blades.

Since $h = 0$ when $w = 0$, $c = 0$ and it follows that

$$h = \frac{w^2 R^2}{2g} \quad (15)$$

It is obvious from this equation that the scale of a manometer calibrated in speed units is unequally divided, being progressively more open from low to high speed. The scale of an instrument having a range of 1,500 r.p.m. and a scale 36 inches long is rarely graduated in the range from 0 to 250 r.p.m.

For testing service instruments it has been found convenient to have the master tachometer equipped with two scales, one graduated to indicate the speed, and the other twice the speed. The latter scale is used when testing aircraft tachometers which are operated in service by the cam shaft (one half the speed of the crankshaft). Gear boxes are used either between the master tachometer and the driving motor shaft or between the instrument under test and the driving motor shaft, in order to drive the instrument under test at the proper speeds and at the same time to obtain indications on the sensitive part of the scale of the master instrument.

Methods of testing master tachometers.—(a) *Revolution counter and clock.*—A fundamental method of calibrating master tachometers consists of counting the number of revolutions for a measured period of time while the speed is maintained constant. The revolutions per unit time give the speed. This method is simple and requires no special or expensive apparatus. A stop watch, or a watch with a second's hand, and a revolution counter comprise the needed apparatus.

The sources of the largest error are in the difficulty of making the observations and in holding the speed of the master instrument constant.

(b) *Semiautomatic timing apparatus.*—A semiautomatic apparatus is used at the Bureau of Standards for determining the total number of revolutions in a given time interval. It has the advantage of eliminating in large measure the errors due to the personal equation.

The apparatus consists of a bicycle counter, a clutch, two solenoids, and a relay. A diagram of the electrical connections is shown in figure 22 and a photograph of

the apparatus in figure 23. Contact A, figure 22, is controlled by the relay R which is actuated by the time signals from a master clock. Switches B and C are hand operated by means of push buttons. When contacts A and B are made, solenoid S_1 is energized attracting lever D, and thus causing clutch L to engage the shaft M of the master tachometer. The counter is then recording the number of revolutions of the shaft

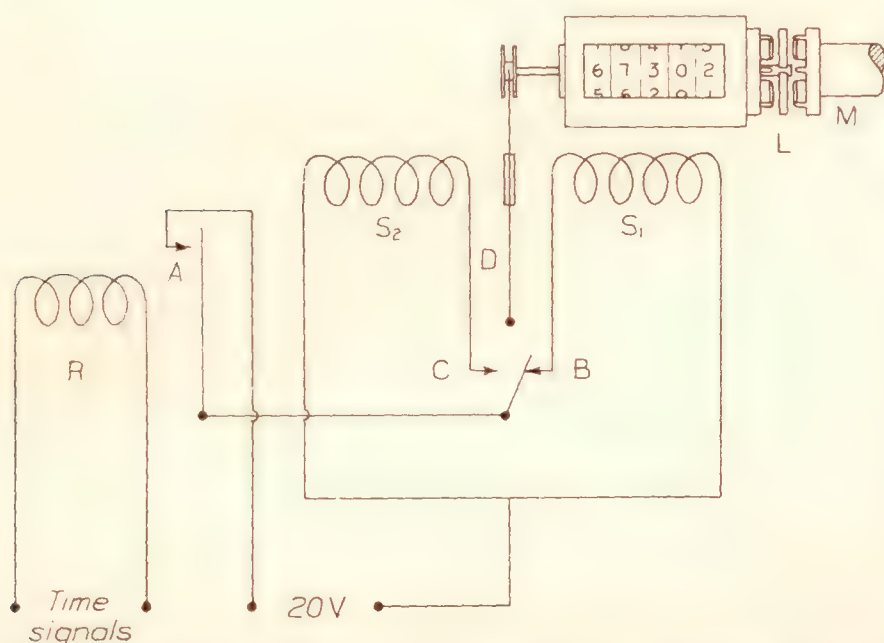


FIGURE 22.—Diagram of the apparatus used to calibrate the master tachometer.

M. When contacts A and C are made, lever D is pulled from a position in contact with solenoid S_1 toward solenoid S_2 , which disengages the clutch at L.

The signals from the master clock are received every second, except the fifty-ninth second, of each minute. This makes 1 minute a convenient timing interval. Just before the sixtieth second signal, the observer makes the contact at B until the clutch is engaged by the following time signal. One minute later, just before the sixtieth second, he makes the contact at C and the clutch is disengaged by the sixtieth second signal. The difference in the two readings of the counter gives the speed in revolutions per minute, it being assumed, of course, that the speed of the master tachometer has been held constant during the time interval.

In order that no coasting or slipping of the revolution counter exist either when being connected with, or disconnected from, the main shaft of the calibrating apparatus the revolution counter spindle is equipped with a fly which engages either the fins attached to the main shaft of the calibrating apparatus or to the revolution counter housing. The fins are designed so that a maximum error of 0.1 revolution may result when either connecting or disconnecting the counter. A total error of 0.2 revolution may therefore occur in the determination of the speed. The speed of the master tachometer calibrating apparatus cannot be adjusted to a constant value with an error less than one revolution per minute, so that the accuracy of the method of calibration is commensurate with that of the apparatus used for the purpose.

(c) *Speed indicator*.—In many cases a speed indicator of the chronometric type is adequate for determining the errors of a master tachometer. It consists of a timing element or escapement, a revolution indicator, and a mechanism whereby the revolution indicator is connected to the rotating spindle of the instrument for a definite interval of time, which is usually between 3 and 6 seconds. The deflection of the pointer is thus proportional to the number of revolutions for this time interval. The error of these instruments does not ordinarily exceed 0.3 percent. One instrument of this type weighs 5 ounces and is 2 inches in diameter and less than 1 inch in depth.

Field test set.—An inexpensive and simple apparatus is required for testing tachometers at airports and other field service stations. A simple form of apparatus which has proven suitable is that consisting of the mechanism of a hand-driven high-speed grinding wheel in which a small flywheel has been substituted for the grinding wheel. A chronometric or other tachometer of good quality, the errors of which are small or known, is mounted on the spindle shaft and serves as the master instrument. The tachometer to be tested is connected with the same shaft by means of a two-way adapter.

Temperature control apparatus.—The apparatus used at the Bureau of Standards for controlling the temperature of tachometers and other instruments consists of an insulated chamber in which the instruments are installed and which is designed so that suitable

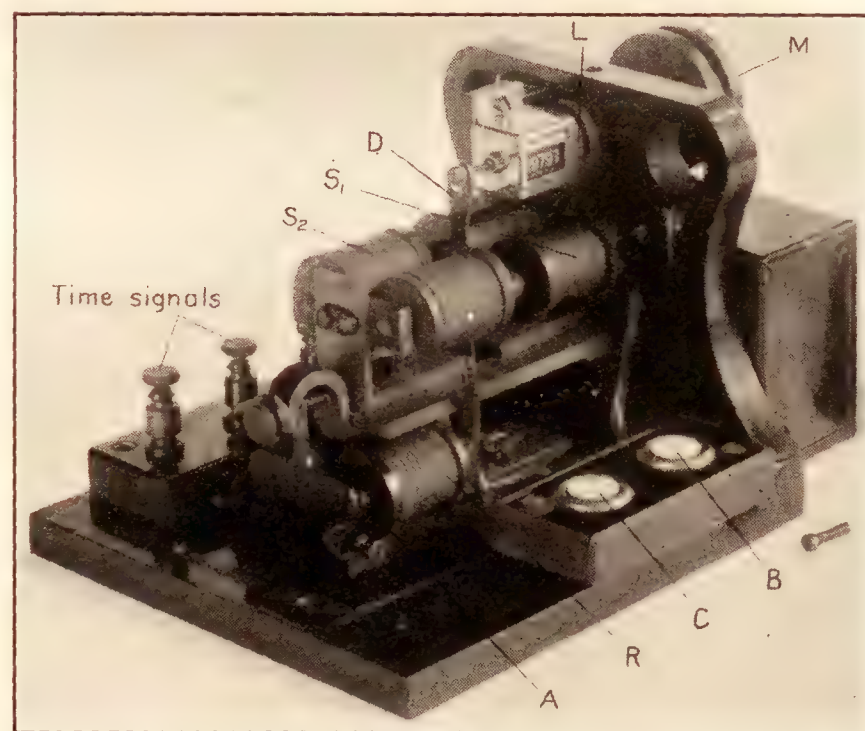


FIGURE 23.—Apparatus used to calibrate the master tachometer.

connections can be inserted through its walls to permit the master instrument to remain outside at room temperature. See figure 21. The chamber is conveniently heated above room temperature by means of an electrical heater which is thermostatically controlled. Temperatures below room temperature are obtained by means of an ammonia-refrigeration system. The apparatus is designed so that the ammonia is expanded

directly into coils located within the chamber itself. In order to obtain more quickly the temperature of -35°C . within the chamber, which is standard for routine tests, as well as to obtain the somewhat lower temperatures which may be required for special tests, a rotary compressor is installed to operate on the low pressure side of the ammonia compressor. The arrangement is such that the operation is either one or two stage as desired. It has been found that temperatures of -40°C . can be obtained easily with both compressors of the system operating simultaneously.

A temperature chamber in which solid carbon dioxide (dry ice) is used as a refrigerant is both convenient

tween the bearings. One end of the shaft is cut to form an eccentric. An aluminum plate is mounted normal to the axis of the shaft and connected with its eccentric by means of a ball bearing. Parallel ball-bearing guides located at the four corners of this plate restrict its motion to one of reciprocation in its own plane and along the ordinate of displacement. The outer races of the guides are mounted on an intermediate aluminum plate, at the four corners of which are again located parallel ball-bearing guides which restrict its motion to one of reciprocation in its own plane and along the abscissa of displacement. The outer races of the latter guides are mounted directly on the brass

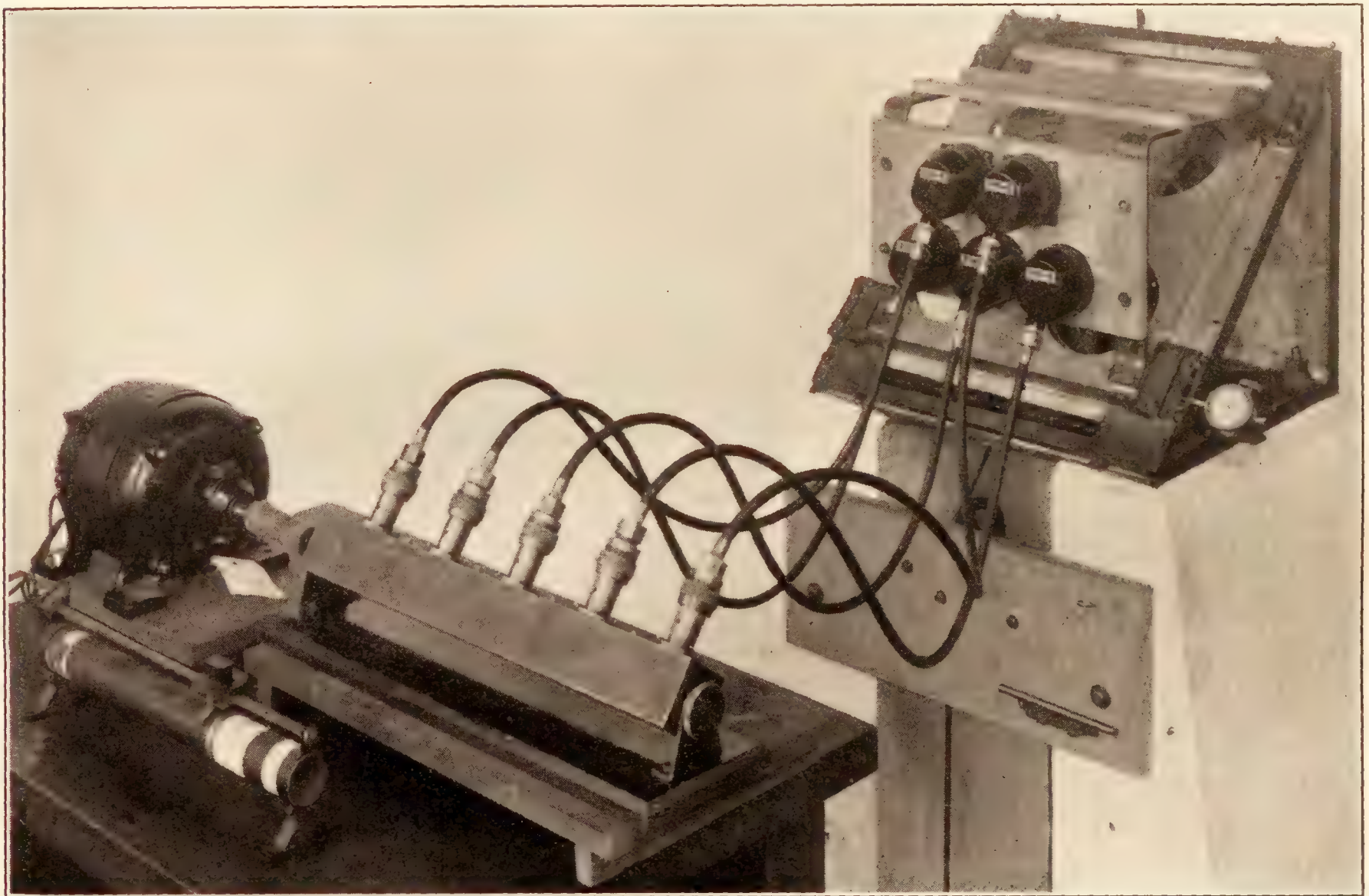


FIGURE 24.—Vibration board for testing aircraft instruments. Five centrifugal tachometers are shown under test.

and economical in many cases. Such chambers are used at Wright Field for testing aircraft instruments. See reference 20 for details.

Vibration apparatus.—The standard vibration to which aircraft instruments are subjected in the laboratory is a translational motion in a circular path one thirty-second inch in diameter in a plane inclined 45° with the horizontal plane. The frequency range of the vibration is from 1,000 to 2,000 cycles per minute.

The apparatus constructed at the Bureau of Standards for subjecting instruments to this standard vibration consists of a brass supporting frame (see fig. 24) in which a shaft is mounted on ball bearings. The shaft is rotated by means of a belt and pulley mounted be-

supporting frame which is designed to support the plate in the plane inclined 45° to the horizontal. The instruments under test are mounted with the plane of the dials vertical on a bracket attached to the first-mentioned plate of the vibration board. The equipment is arranged so as to secure any desired scale reading of the instrument undergoing vibration.

Speed acceleration apparatus.—An apparatus is required by means of which the instrument can be brought a selected number of times to a definite speed in 1 second. The apparatus used at the Bureau of Standards consists of an electric motor of sufficient power to bring the tachometer up to the selected speed in 1 second and a rotary switch which by

means of electrical signals from a standard clock periodically operates the motor. The use of this automatic switch is justified by reason of its greater convenience.

B. METHODS OF TEST

The nature of the tests made at the Bureau of Standards and the sequence with which they are made have been arranged in order that, first, the conditions encountered in service are simulated as nearly as possible; and second, the effect of any preceding test does not influence the results of the tests that follow. In general, but with some modifications and additions to suit the individual requirements of the various types of tachometers, tests are made for the following factors in the order given:

Factor	Test
Scale errors at room temperature (+20° C.)	Scale error test.
Lag in indication	Lag test.
Friction in the mechanism	Friction test.
Static balance of the mechanism	Position error test.
Effect of vibration	Vibration test.
Effect of exceeding the range of the instrument.	Overspeed test.
Temperature effects	Temperature tests.
Seasoning and speed acceleration effects.	Speed acceleration test.
Endurance	Endurance test.
Effect of electrical indicator on compass.	Shielding test.

These tests are substantially the same as those required for acceptance in the purchase specifications issued individually and jointly by the Army Air Corps and the Bureau of Aeronautics of the Navy Department. In these specifications the tests are conveniently divided into three classes—individual tests, routine type tests, and special type tests. The individual tests are made on each instrument and include the scale error and friction tests. The routine type tests include, in addition to the individual tests, the vibration, overspeed, and temperature tests, and are made on not less than 5 percent of the instruments of a given lot, selected at random. It is assumed that the performance of the instruments chosen for the tests is representative of the performance of all of the instruments of the lot. The position error, acceleration, and endurance tests are designated as special type tests, and are made, in addition to the individual and routine type tests, on a small number of instruments of a new design. The special type tests are made to determine that part of the performance which is a function of the design of an instrument and not carelessness in adjustment.

Scale error test.—In the manufacture of instruments in quantity lots the dials are usually standardized so that the spacing of the graduations is uniform. The mechanism of each instrument must therefore

be adjusted so that the deflection of the pointer of the instrument for a given speed is that required by the corresponding graduations on the dial. The error in indication is designated the scale error. The difficulty of avoiding scale errors is more fully appreciated when it is realized that the deflection of the sensitive element in many cases does not depend directly upon the quantity measured.

In the scale error test the tachometer at room temperature (+20° C.) is connected to the master tachometer. The readings of the two instruments are obtained at any desired number of points in the range with the speed increasing up to the highest speed of the range. In careful tests the instrument is brought up to but not above the speed at the desired test point. The instrument is then lightly tapped or vibrated just before taking a reading. The scale error is the difference between the true speed and the speed indicated by the instrument, and is positive when the instrument reads high, and negative when low.

Lag.—Instruments in which the indications depend upon the elastic elements in general differ in indication for increasing and decreasing values of the measured quantity. In pressure-measuring instruments the difference, in a special sense, is called the elastic hysteresis or lag. This difference in indication is also present in tachometers, but is in part due to mechanical imperfections in the mechanism.

In testing for the lag, scale errors are determined for speeds decreasing after attaining the highest speed of the range in the scale error test. At each test point the speed is brought down to but not below the desired value. The lag is the difference in the errors of the instrument at any one speed.

Friction.—Friction in the pivots and bearings of the instrument mechanism causes a lag in indication, which is considerably reduced if not entirely eliminated by vibration.

Since instruments installed on aircraft are ordinarily subjected to vibration, a small amount of friction in the mechanism of tachometers can be tolerated and is perhaps advantageous in damping out the indication of minor fluctuations. Excessive friction, however, results in a jerky motion of the pointer and often renders the instrument practically worthless.

The effect of the friction is determined by noting at the various test points the reading of the instrument before and after tapping. The difference is defined as the error due to friction.

Position errors.—Error arising from a change in orientation or position of an instrument are those resulting from lack of static balance of the mechanism. This is inherent in a centrifugal instrument since the sliding collar and the rotating weights are unbalanced and vary in their effect on the indication as the instrument is rotated. The effect is usually small.

Dynamic balance in the mechanisms of tachometers is desirable but not absolutely required except in the case of the centrifugal tachometer where a lack of dynamic balance of the governor element results in excessive vibration.

The effect of change in the orientation of tachometers, or the position error, is obtained by determining the difference in the errors of the instrument in two scale error tests, one with the instrument in the normal operating position and the other with the instrument in any other desired orientation. In the test specified by the Army and Navy Air Services the instrument is mounted so that, with the plane of the dial remaining vertical, the zero on the dial is 90° of arc from its position during normal operation (see fig. 25). This orientation is chosen because frequently due to interference between the flexible drive shaft and the other

a period of 3 hours while the instrument is operated at an indicated speed of 2,000 r.p.m. The apparatus with five instruments undergoing test is shown in figure 24. Further, the amplitude of oscillation of the pointer is noted in the frequency range 1,000 to 2,000 c.p.m. After being subjected to the vibration the instrument is given a scale error test the results of which are compared with those of a test previous to the vibration. The mechanical condition is determined by inspection for loosened screws or parts.

Overspeed.—In service the instrument may be momentarily subjected to a speed in excess of its range which should not affect the accuracy.

The overspeed test consists of subjecting the instrument for a period of 5 minutes to a speed 500 r.p.m. greater than the maximum indication on its dial. The maximum range of the commonly used instru-

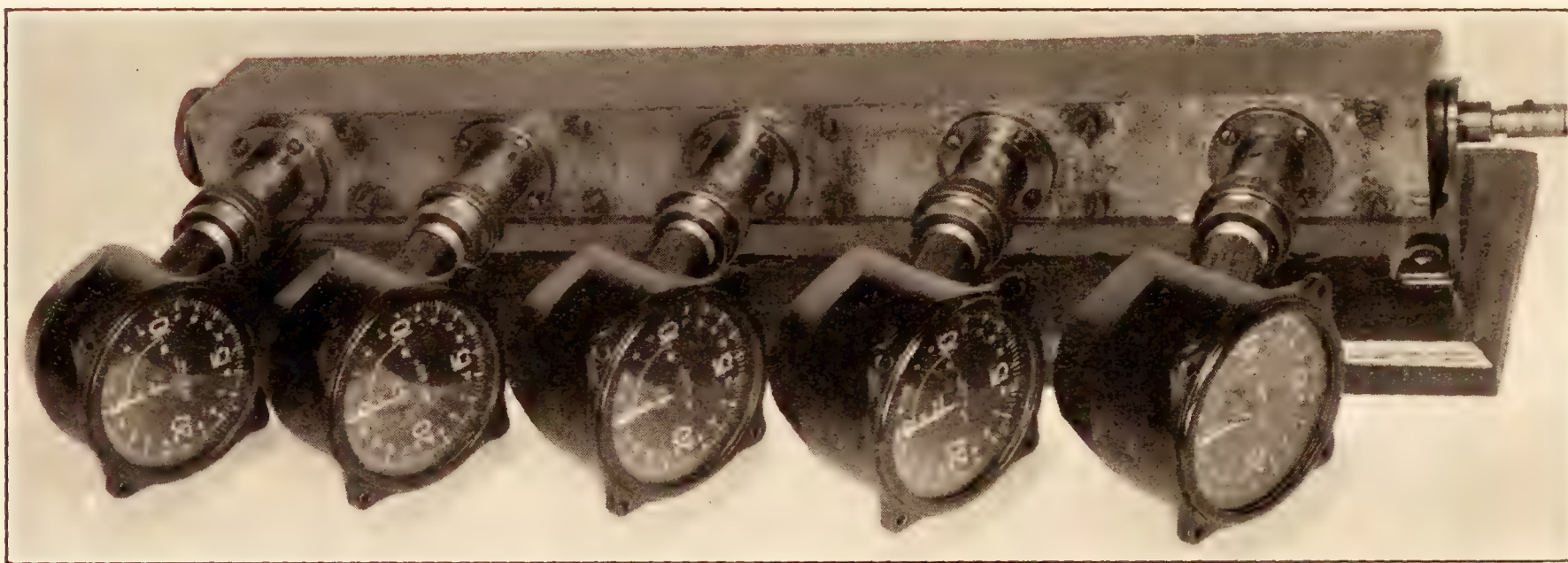


FIGURE 25.—Centrifugal tachometers undergoing test for position error. The instruments have been deflected 90° laterally with the dials remaining vertical.

equipment usually present behind the instrument panel it is necessary so to mount the tachometer.

Vibration.—Instruments must ordinarily withstand considerable vibration in service. This vibration has been measured by Zand by means of an instrument which photographically records the frequency and the amplitude of the vibration of the instrument board (reference 19). Its size is such that it can be installed on the instrument board in place of any of the $2\frac{3}{4}$ -inch standard dial size instruments. The results of tests show that in general the instrument board vibrates with a frequency equal to the speed of the engine and that the amplitude of vibration is by far the greatest in the fore and aft direction, with a magnitude depending upon the type of airplane and the number and location of the instruments on the panel.

Tachometers are tested for two effects—(a) the effect of vibration for a certain period of time on the scale errors and mechanical condition and (b) for excessive pointer oscillation. The instrument is subjected to the standard vibration at a frequency in the range 1,500 to 2,000 cycles per minute (c.p.m.) for

ments is 3,000 r.p.m., so that the indicated test speed is 3,500 r.p.m. The effects of the overspeed are determined by a comparison of the scale errors obtained before and after the overspeed.

Temperature errors.—Changes in temperature produce a change in the physical dimensions of the parts of the mechanism and a change in the stiffness of the elastic elements. There may be difficulty in securing satisfactory operation at low temperatures if congealing of the lubricant occurs. Unless a differential effect is present, the first effect is of minor importance. The second effect requires compensation if extreme accuracy is required.

The standard temperature at which aircraft instruments are tested are $+45^\circ$ and -35° centigrade. At these two temperatures tachometers are subjected to scale error tests, the differences between the results of which is used as a measure of the effect.

For electrical tachometers additional temperature tests are frequently found desirable since the temperature effects are not necessarily proportional to the temperature. These consist of, first, varying the tem-

perature of the generator while that of the indicator is held constant at the desired value, and, second, varying the temperature of the indicator while that of the generator is held constant.

Seasoning and speed acceleration test.—Tachometers are subjected in service to rapid changes in speed which requires ruggedness in the instrument. Further, since the indication of most types of tachometers depends upon the deflection of an elastic element, the calibration may change due to imperfect seasoning. Seasoning may be defined as the process of relieving internal stresses in the elastic members to such a degree that no further relief takes place in service.

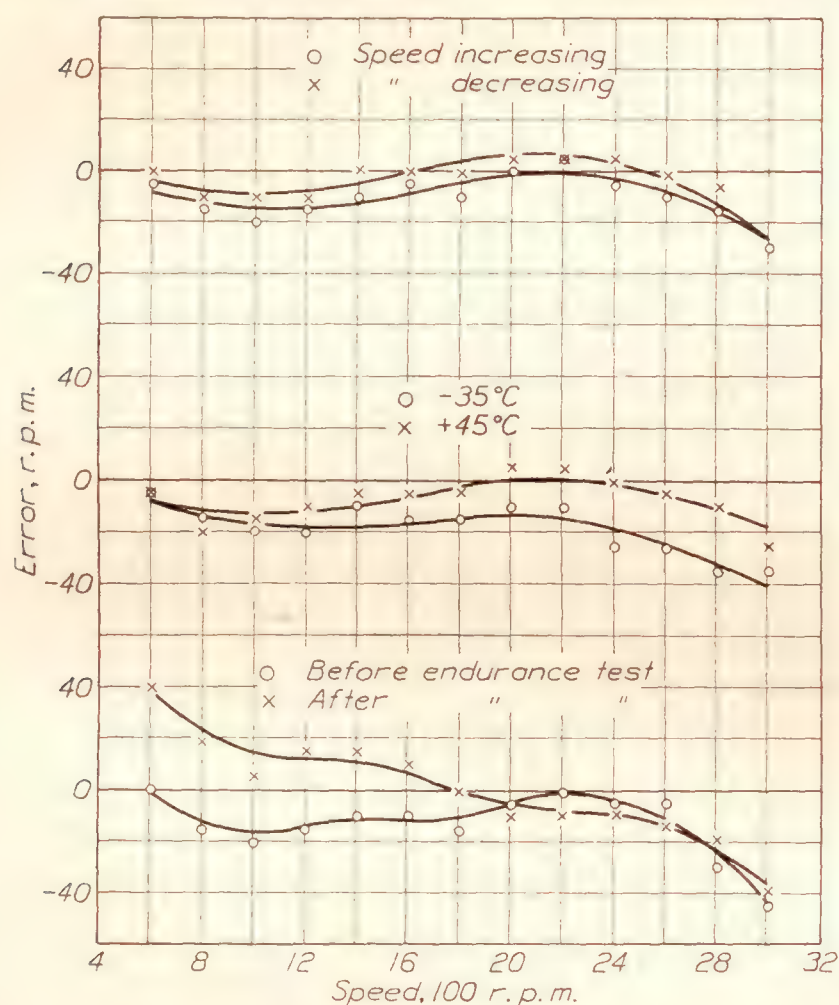


FIGURE 26.—Errors of a well-adjusted centrifugal tachometer. The curves show the scale errors, the lag, the effect of temperature, and the effect of a 300-hour endurance test.

The speed-acceleration test is a method of measuring the performance in both of these respects.

The test consists of the application of 500 successive accelerations by changing the indicated speed from 0 to 1,500 r.p.m. within a period of 1 second. In this test mechanical tachometers are connected to the motor through an 8-foot length of flexible shafting, in order to approximate more closely service conditions. The scale errors determined before and afterwards are compared in order to measure the effect.

Endurance.—Tachometers are likely to change their calibration or to fail entirely owing to the effects of wear in service. Their endurance characteristics are determined by operating them at an indicated speed of 2,000 r.p.m. for a period of 300 hours. Following this run, usually 1 hour after its completion, the instruments are given a scale error test, the results of which

are compared with a scale error test made just previously to the endurance run.

It should be noted that a change in calibration also occurs, due to another effect. If an elastic body is subjected to a change in load, which is then maintained constant, the deflection of the elastic body gradually increases with time. This increase is known as drift or creep. Drift in the spring, and thus in the indication, of centrifugal tachometers takes place during the endurance test. If desired to separate the drift from the effect of wear, the instrument should be calibrated immediately after and also about 24 hours or more after the endurance run. The difference in the errors in these two tests affords a measure of the effect of the drift, while the difference between the last test and the one just before the endurance run is a measure of the effect of wear.

Magnetic shielding.—In common with other electrical indicators, the indicator of electrical tachometers must in general be shielded magnetically in order to eliminate as far as possible the effect on the magnetic compass. The degree of this shielding is determined by noting the deflection of a standard type compass when the centers of the two instruments are 8 inches apart. The compass must be in a horizontal magnetic field 0.18 gauss in strength.

PERFORMANCE OF TACHOMETERS

The data on performance given in this section are for the best grade of instrument which is at the present time available commercially. It is of course obvious that selection is necessary in order to obtain an instrument of this performance, since an individual instrument of any given design may have, for one cause or another, an inferior performance.

A. CENTRIFUGAL TYPE

The scale errors of a well-adjusted instrument are shown in figure 26 by the points marked "Speed increasing." The tolerance in the current specifications of the air services is a scale error not to exceed 10 r.p.m. in the middle range of the indicated speeds and an error less than about 1 percent of the maximum indicated speed at other speeds.

The lag typical of a first-class instrument is shown in the two upper curves of figure 26. It does not exceed 10 r.p.m.

The position error, determined for the two positions given in the description of the test, usually has an average value of about 10 r.p.m. It varies considerably with speed, however, in one design of tachometer ordinarily varying from 5 to 20 r.p.m.

Under vibration the total deflection of the pointer with reference to the dial of a centrifugal instrument does not ordinarily exceed an amount equivalent to an indication of 20 r.p.m. (2.4° of arc). The average

change in error of an instrument before and after being subjected to the standard vibration at a frequency of about 1,500 c.p.m. for 3 hours is less than 10 r.p.m. for good quality instruments.

An overspeed of 500 r.p.m. on tachometers properly designed to meet this requirement causes substantially no average change in the errors. Usually a stop is provided so that the spring is prevented from deflecting beyond the amount obtained at an indicated speed slightly in excess of the rated range of the tachometer. In figure 4 such a stop is shown attached to the fixed upper sleeve.

The effect of changes in instrument temperature is shown in figure 26 for a good quality tachometer. Assuming that the effect is due to the change in the elastic modulus of the steel spring which balances the centrifugal force and that the deflection of this spring is proportional to the speed, the difference in the slopes of the best straight lines through the curves should be of the order of 2 percent (reference 14). Actually the temperature errors of centrifugal instruments are much smaller which is partly due to compensating changes in dimensions in the centrifugal element and to the lack of direct proportionality in the relation between speed and deflection of the spring. Thus in figure 26 the difference in the slopes, or the change in the scale value, of straight lines through the curves for $+45^{\circ}$ and -35° C. is about 1.2 percent. The instruments are ordinarily not compensated for temperature.

The average change in error before and after subjecting instruments 500 times to a change in indicated speed from 0 to 1,500 r.p.m. in 1 second is less than 10 r.p.m. for a representative instrument of high quality. Since the seasoning effect usually results in a stiffening of the elastic elements, the reading at a given speed is usually lower after the test.

The effect of an endurance run on a good quality instrument is shown in figure 26. The results of two scale error tests are given, one before the endurance run and one immediately afterwards. The difference between the two curves is a combined measure of the drift of the elastic element and wear in the mechanism. In tests made 24 hours after the completion of the endurance test, instruments of this type usually show a recovery from the drift effect to the extent of about 5 r.p.m. Ordinarily the results of the tests made just before and about 1 hour after the endurance run are compared. The average change in the errors in these two tests does not exceed 20 r.p.m. for good quality instruments.

B. CHRONOMETRIC TACHOMETERS

The scale errors of chronometric tachometers of the best quality can be reduced to an average value less than the inherent sensitivity of its mechanism which

may be defined as the speed range divided by the number of teeth in the ratchet gear. (See H in fig. 7.) This is of the order of 10 r.p.m. in most designs. Scale errors are those caused by improper adjustment of the escapement mechanism for the correct periodicity of vibration. When improperly adjusted, the scale errors are directly proportional to the speed.

Laboratory tests show that for properly designed instruments the average change in scale errors due to vibration, overspeed, angular acceleration, and seasoning are of the order of ± 5 r.p.m.; in other words, negligible. The lag is likewise small.

The percentage change in scale errors due to change in temperature from -35° to $+45^{\circ}$ C. does not exceed 0.5 percent if the instrument is designed to operate at temperatures as low as -35° C. An important cause of failure to operate is due to the use of a lubricant in the drum of the main spring which freezes at a temperature above -35° C. The use of a mixture of deflocculated graphite and oil with a pour point of -40° C. or lower has been found to be satisfactory.

Errors arising from a change in temperature are caused by insufficient or overcompensation of the escapement mechanism. The change in stiffness with temperature of the hairspring controlling the motion of the balance wheel is compensated by using a balance wheel with a bimetallic rim designed so as to expand with increase in the stiffness of the hairspring and to increase its moment of inertia correspondingly. The congealing of the lubricant of the balance staff of the escapement tends to decrease the amplitude of vibration of the balance wheel, causing it to vibrate at a higher frequency which results in a lower indication of a given speed.

Chronometric tachometers do not have a progressive change in their scale errors with continued operation. Wear of the mechanism due to continued operation or to repeatedly subjecting the instrument to rapid accelerations of speed is indicated by a slipping back of the pointer during the time interval in which the indication ordinarily remains constant. This, strictly speaking, is a failure to operate rather than an error in indication and is caused by wear between the teeth of the ratchet wheel (gear H, fig. 7) and its pawl. An instrument of the best grade should on the average withstand 500 hours of operation in service before requiring repair.

C. MAGNETIC TACHOMETERS

Data on the performance of very few magnetic tachometers designed for aircraft use are available. This type is very little used and rarely considered when accuracy is desired.

The errors of the instrument which are commonly small or are dependent only on care in adjustment are scale errors, lag, and overspeed. Temperature errors

and, in common designs, the effect of endurance running are both inherently large. Magnetic shielding of the instrument is necessary to avoid affecting the compass.

The temperature error is caused by the increase in electrical resistance of the indicating disk and the decrease in field strength of the permanent magnet as the temperature increases. The two effects are additive and introduce relatively large errors. The methods of compensation have been described in the section in which magnetic tachometers are described. The

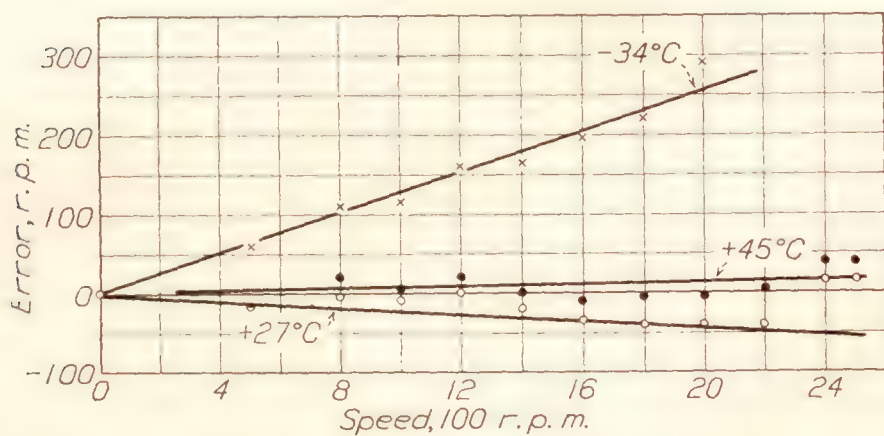


FIGURE 27.—Change in scale error with temperature of a magnetic tachometer.

effect of temperature on an instrument which has not been properly compensated is shown in figure 27.

Wear in the pivots or bearings of magnetic tachometers is, in the common designs, likely to affect the gap between the disk and magnet, a small change in which causes a large change in the calibration. Vibration greatly accelerates this process.

D. DIRECT CURRENT TACHOMETERS

The scale errors of a well-adjusted instrument will not exceed twice its least reading, which in an instrument with a pointer motion of 270° of arc is 10 r.p.m. The lag is of negligible amount. The position error of the indicator of instruments thus far tested does not exceed, on the average, twice the least reading.

Indicators which operate on a low-power input will not withstand the effect of airplane vibration and therefore must be mounted in a vibration-absorbing case. In designs in which the generator has a relatively large power output, the indicator is more rugged and in general will withstand a moderate amount of vibration. The vibration causes wear in the pivots of the indicator. It should be noted that the free frequency of the coil, spring and pointer combination is much lower than that of the vibration usually experienced. The case vibrates but the elastic system tends to remain fixed. The resulting relative motion is electromagnetically damped.

The temperature errors for an uncompensated instrument are shown in figure 28. The average change in the errors in the temperature range -35° to $+45^\circ$ C. of a compensated instrument should not exceed 20 r.p.m. and may be as low as 10 r.p.m. See the section

on "Characteristics of d.c. Tachometers" for discussion of the methods of compensation.

The effect of an endurance test on the best instruments causes an average decrease in the indication which will not exceed 20 r.p.m. The indicated speed is always decreased because in general the strength of the permanent magnets tends to decrease with time and the brush resistance to increase, due to the accumulation of dirt on the commutator of the generator.

The unshielded indicator will cause deflections upward of 10° on a magnetic compass in its vicinity. The addition of a soft-iron case around the indicator reduces this effect to a maximum of 4° when the two instruments are 8 inches from center to center.

E. ALTERNATING CURRENT TACHOMETERS

The performance of these instruments in tests for scale error, lag, position error and vibration is about the same as that of the d.c. type. There is also the same necessity for magnetic shielding.

(a) *Single-phase type.*—The errors due to change in instrument temperature are due to the effect on the field strength of the permanent magnets and on the resistance of the windings of the generator and of the indicator. There is also an effect on the output of the rectifier. Temperature compensation is essential.

The performance of the generator in an endurance test will be inherently better than that of a d.c. instrument, due to the absence of the commutator brushes.

No test data are available on these instruments.

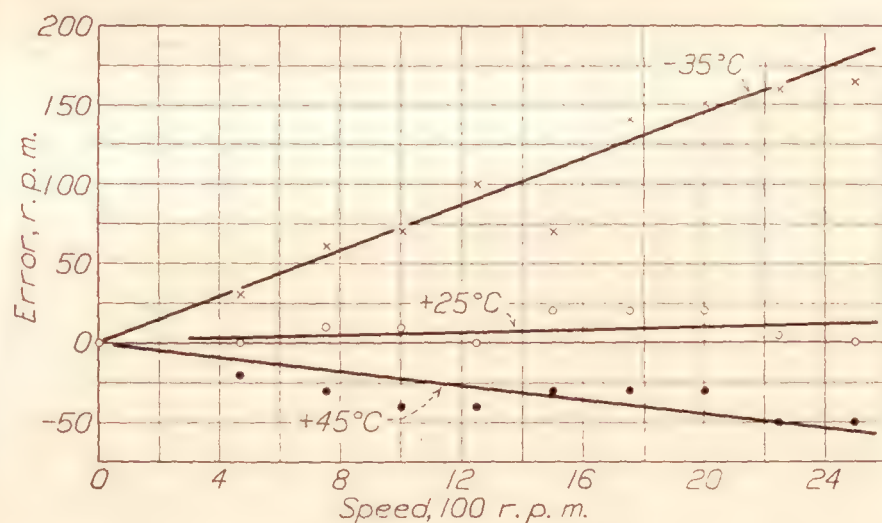


FIGURE 28.—Changes in scale error with temperature of a Horn electric tachometer.

(b) *Two-phase type.*—The output of the generator is affected by temperature changes for the causes stated above. Changes in temperature affect the indicator in a very complex manner. The satisfactory compensation of instruments of this type is a recent and outstanding development. The average change in the errors for the two conditions, one in which the generator is at -10° C. and the indicator at -35° C. and the other in which the generator is at $+60^\circ$ C. and the indicator at $+45^\circ$ C., does not exceed 20 r.p.m. for well compensated instruments. The compensation is as good at intermediate temperatures.

An endurance run of 300 hours on the generator of one model of this type of instrument shows that the resulting average change in reading is within 20 r.p.m.

In the larger number of instruments the effect of vibration is manifested by an excessive increase in reading over the central portion of the range in indication. The effect is probably due to wear in the pivots of the indicator. A more adequate measurement of the effect of wear in the pivots of the indicator is obtained in the speed-acceleration test. The effect on the small number of instruments tested was an average change in reading of approximately 10 r.p.m.

(c) *Three-phase type*.—No test data on this type of instrument are available.

F. SOLENOID OPERATED CHRONOMETRIC TACHOMETERS

In general this instrument is subject to the same errors as a chronometric tachometer. Special difficulty is experienced in obtaining satisfactory operation at low temperatures because of the additional power required to operate the chronometric mechanism owing to congealing of the lubricant. All of this power is obtained from the solenoid which, on account of limitations of space, is designed so as to require nearly full voltage during room temperature

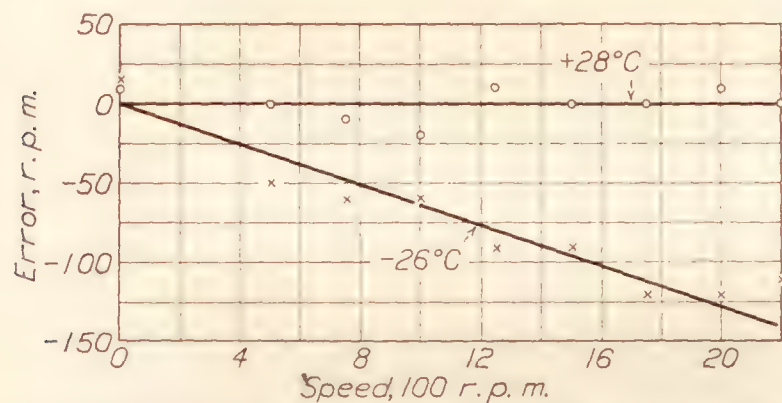


FIGURE 29.—Changes in scale error with temperature of solenoid-operated chronometric tachometer.

operation. The scale errors of an instrument at $+28^{\circ}\text{C}$. and -26°C . are shown in figure 29.

G. COMMUTATOR-CONDENSER TACHOMETERS

The errors of the commutator-condenser type tachometer may be conveniently divided into scale errors, temperature errors, and errors due to variation in voltage supplied.

The scale errors can be reduced to a value as low as the least reading of the indicator, since the scale divisions are approximately equally divided for speed.

Temperature errors are caused by the effect of temperature on the capacity of the condenser and on the performance of the indicator. The capacity of a well-designed mica condenser is affected by variations in temperature only by the change in the physical dimensions which is negligible. The indication of speed is independent of the resistance of the circuit

within the limits previously discussed, but depends upon the strength of the permanent magnet and the stiffness of the spring of the indicator, both of which are affected by temperature changes. If the indicator is compensated for the effect of temperature on its resistance and is also used to indicate the proper voltage, the effect of temperature on the voltage indication is the same as the effect on the speed indication. In this case the temperature error is compensated by a proportional change in the voltage.

The indications of the instrument are directly proportional to the voltage supplied, which can be maintained constant for long intervals of time by means of the automatic voltage regulator previously described.

H. ASKANIA PNEUMATIC TACHOMETER

The differential pressure developed by the pump unit is practically independent of the density of the air and of the temperature of the instrument. The pressure developed by the pump unit is pulsating and requires damping by means of a capillary tube in the line. In aircraft an indicator of the aneroid type would be used which would be subject to errors of the same type and amount as those of pitot-static airspeed indicators as described in reference 20.

ENGINE LOG INSTRUMENTS

In the flight testing of aircraft, in the operation of aircraft, and in special installations in connection with research problems, a record of the engine speed during flight and of the total number of hours of operation may be desired. In operating aircraft a record of the speed of the engine is useful in indicating any abuse to which the engine may have been subjected during flight and in determining its operating characteristics. A knowledge of the total number of hours of operation is of value in indicating when it is necessary to overhaul the engine. In order to coordinate the results of flight test data a record of the engine speed obtained automatically may be preferable to the recording of such information at frequent intervals by an observer.

There are three classes of engine log instruments which are in use, viz, the recording tachometer, the running-time meter, and the revolution counter, all of which are of the mechanical type. Both the recording tachometer and the running-time meter are driven from the engine by means of a flexible drive shaft. The revolution counter is usually designed to be attached to the engine by means of a two-way adapter directly at the connector provided for operating the tachometer drive shaft. In one make of recording tachometer the revolution counter is included as an integral part of the instrument.

RECORDING TACHOMETERS

The recording tachometer both indicates and records continuously the speed of the engine during the total operating period. The instrument consists of, first, a speed-measuring element and, second, a recording mechanism containing several rollers, one of which, the feed roll, rotates at constant speed. A strip of

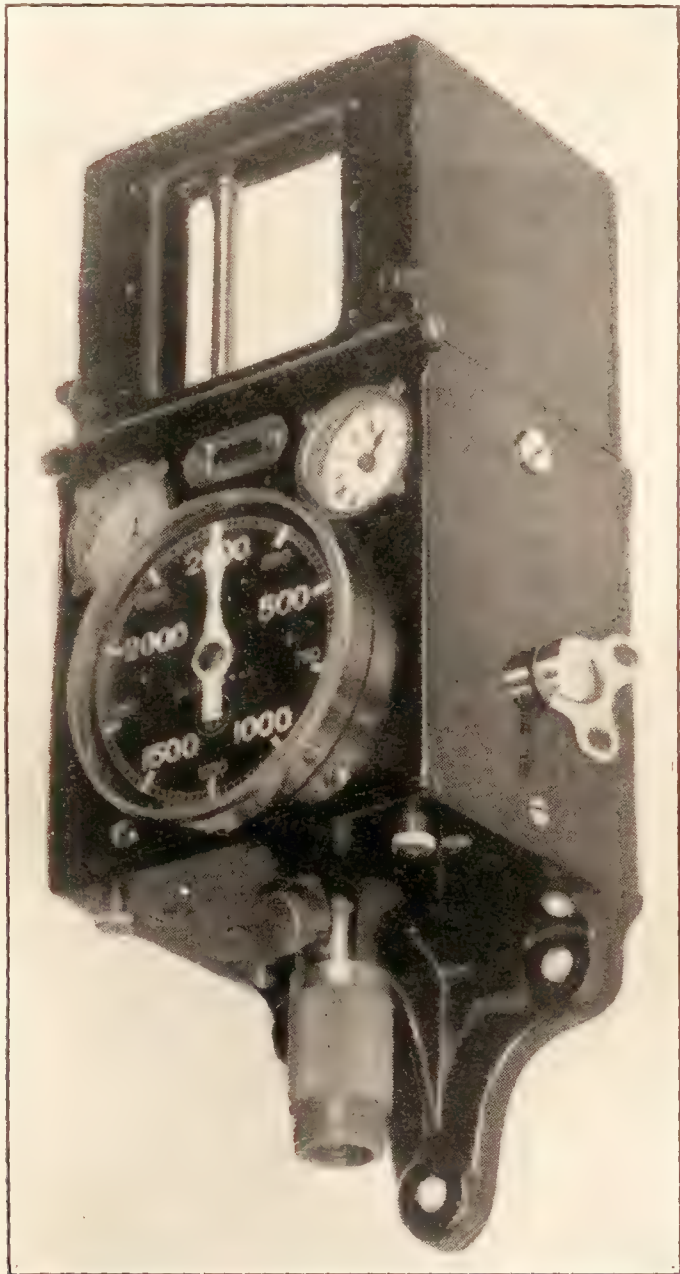


FIGURE 30.—Hasler "Tel" chronometric recording tachometer.

paper is fed from a magazine roll to the feed roll and thence to a receiving roll. A stylus actuated by the speed-measuring element bears lightly on the surface of the paper and traces a record of the speed. The abscissa and ordinate of this form of chart represent time and engine speed, respectively.

A record of the engine speed is sometimes made by photographing at intervals the face of a tachometer together with that of other instruments (references 31 and 41). An arrangement of this kind is known as a "dummy observer."

Hasler "Tel."—A photograph of the Hasler "Tel" recording tachometer is shown in figure 30. The instrument is of the chronometric type and is designed to record, first, a continuous trace of the engine speed; second, the time and duration of a flight; and, third, the trip revolutions of the engine. The surface of the recording paper is chemically prepared and is white in

color so that a practically black trace is described by a brass stylus. The recording rollers are designed for a capacity of 20 feet of paper, which length is sufficient for 30 hours of operation.

A spring-wound clock is provided as an integral part of the instrument. The weight complete is 10½ pounds and the dimensions 11½ by 4 by 3¾ inches. Its size is such as to preclude its mounting on the instrument panel in place of the tachometer already installed. (See references 37 and 39.)

B.S. recording tachometer.—A recording tachometer which may be installed on the instrument panel in place of the 3¾ inch round dial instrument has been constructed at the Bureau of Standards for the Bureau of Aeronautics of the Navy Department. It is a Van Sicklen chronometric tachometer modified to include a recording element. (See fig. 31.) The recording element is similar in general design to that of the Hasler "Tel" recording tachometer with the exception that it is built on the rear of the instrument so that it increases the dimension of the case in depth only. A commercial recording paper which is dark in color and is coated on one side with finely divided white wax particles is used with this instrument. As the paper is fed over the rolls a line of the wax particles is removed by the stylus, thus leaving a clearly defined trace.



FIGURE 31.—Bureau of Standards-Van Sicklen recording tachometer.

The trace becomes less well defined with decrease in temperature, becoming indefinable at about -20°C .

In order to facilitate the interpretation of the record, speed reference lines representing the even 100 r.p.m. speed intervals are automatically traced as the paper is fed through the recording mechanism. The weight of the instrument is approximately 3 pounds.

RUNNING TIME METER

This instrument registers the elapsed time during which the engine is in operation. The mechanism of the instrument is similar to that of a chronometric tachometer excepting that the speed-indicating mechanism of the latter instrument is replaced by a dial-type device for counting the beats of the escapement. Combinations of a chronometric tachometer and a



FIGURE 32.—Vapor-pressure type aircraft engine thermometer.

running-time meter are available, as in the Hasler Telmot Flight-O-Meter. The running-time meter may also be obtained as a complete instrument by itself, in which case it is usually driven by a flexible drive shaft connected with the tachometer drive shaft by means of a 2-way adapter.

ENGINE THERMOMETERS

USEFULNESS AND TYPES

Aircraft engines operate most efficiently when the temperatures of the lubricant and cylinders each remain within a limited range. Ordinarily the temperature of the lubricating oil of air-cooled engines and of the cooling liquid of liquid-cooled engines is measured. The practice is growing of measuring in addition the cylinder-head temperature of air-cooled engines. An indication of the temperature of the lubricant is of value when means for its control are provided, and similarly a knowledge of the temperature of the cooling liquid is essential in the control of manually operated radiator shutters. The temperature of the cylinders of air-cooled engines cannot normally be controlled, but is of primary interest as an indicator of trouble. One of the precautions always observed by a pilot before taking off is to ascertain that the temperature of the lubricant or cooling liquid has risen to and remains at the normal operating value.

Thermometers used in aircraft to indicate the temperature of various parts of the engine are of three types—(a) vapor pressure, (b) liquid expansion, and (c) electrical. All the instruments are distant indicating.

The temperature of the cooling liquid of liquid-cooled engines and of the lubricating oil has been measured

almost exclusively for a number of years by vapor-pressure instruments. They are standardized with regard to the sizes of the cases and dials ($1\frac{1}{8}$ inches in diameter) and are used in either of the two ranges, 0° to 100° C. (32° to 212° F.) or 30° to 200° C. (86° to 392° F.). The lower range instrument is used in measuring the temperature of the oil or of the cooling water. The thermometer having the higher range is used when the cooling medium is a liquid such as ethylene-glycol, since the engine then normally operates at a higher temperature. The pointer has a motion of 300° of arc for both ranges of the instrument.

The liquid expansion thermometer is little used on aircraft, owing principally to the greater cost of its manufacture to have a performance equal to that of the vapor-pressure type.

The electrical instruments include the resistance and the thermocouple types. The resistance thermometer has been designed to measure the temperature of either the cooling water or oil. Thermocouples are particularly useful in measuring the temperature of metal parts of the engine, as, for example, the temperature at some point of the cylinder wall of air-cooled engines.

A. VAPOR-PRESSURE THERMOMETERS

The vapor-pressure thermometer indicates in terms of temperature the vapor pressure of a liquid contained within the instrument. The instrument (see fig. 32) is a closed system consisting of an elongated

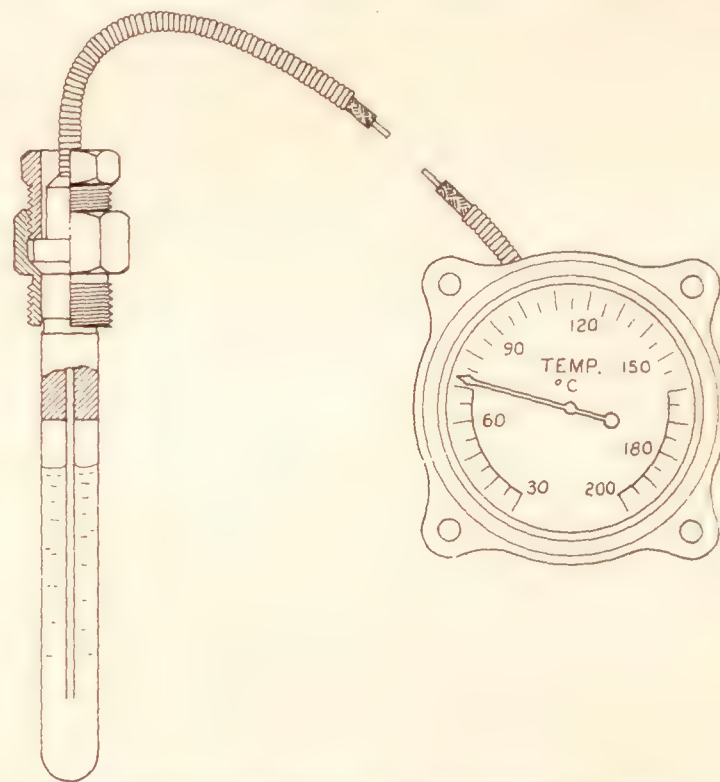


FIGURE 33.—Diagram of vapor-pressure thermometer.

bulb, a capillary tube, and a pressure gage, and is partially filled with a liquid having a vapor pressure conveniently measurable in the desired temperature range. The bulb is installed on the engine at a point where a knowledge of the temperature is desired. The capillary tube connects the bulb with the indicator mounted on the instrument panel.

A diagram of the vapor-pressure thermometer is shown in figure 33. The pressure element within the

indicator is a Bourdon tube, the internal volume of which is relatively small. The end of the capillary tube extends into the liquid in the bulb so that the Bourdon tube fills with liquid by flowing, and not by condensing, when the temperature of the bulb is changing from a condition where it is colder than the indicator to one where it is hotter. By this arrangement the time lag of the thermometer at the transition point is greatly reduced.

The temperature of the free surface of the constrained liquid is indicated, and thus in order that the temperature at the desired point be indicated it is necessary that the design be such that the free surface of the liquid is always within the bulb. In order to obtain this under the normal conditions of operation, during which the bulb is at a temperature higher than that of the indicator, the volume of the bulb is made larger than that of the combined volumes of the capillary and Bourdon tubes. In this case the liquid completely fills the Bourdon and capillary tubes, and partially fills the bulb.

The vapor pressures of liquids do not vary uniformly with temperature, but a scale approximately evenly divided is obtained in instruments by means of a suitably designed multiplying mechanism. The development of an instrument with an equally divided scale has been a big factor in its adoption for general use on aircraft. Table I gives the vapor pressure and the rate of change of vapor pressure with temperature for the commonly used liquids. The wide variation in the rate of change of vapor pressure for the various liquids is a measure of the difficulty in obtaining an equally divided temperature scale.

TABLE I

[Vapor pressure and rate of change of vapor pressure at various temperatures]

Liquid	Vapor pressure in atmospheres				Rate of change in atmospheres per ° C.			
	Temperature ° C.							
	0	50	100	193.8	0	50	100	196
Sulphur dioxide (SO ₂)	1.53	8.18	28.8		0.073		0.55	
Methyl ether (C ₂ H ₆ O)	2.54	11.25	32.6		.10		.57	
Methyl chloride (CH ₃ Cl)	2.50	10.7	31.4		.10		.55	
Ether (C ₄ H ₁₀ O)	.24	1.68	6.39	35.5		0.053	.29	0.51

Installation precautions.—The vapor-pressure thermometer should be installed so as to avoid breakage of the capillary tube, due to excessive vibration, chafing, or straining where it joins with the bulb. Breakage at the bulb due to vibration can be greatly reduced by taping the tube, just above the reinforcement, to the part vibrating with the engine. This appears to distribute the deflection of the tubing over a short length. Local overheating at any point along the tube may produce large errors in the indications of the instrument. Wherever possible the excess

length of tubing should be coiled and securely fastened to a structural member of the aircraft at a point which is comparatively free from vibration.

B. LIQUID-FILLED THERMOMETERS

The liquid filled thermometer is actuated by the thermal expansion of a liquid contained within the instrument and has essentially the same parts as the vapor-pressure thermometer. The increase in volume of the contained liquid (usually alcohol or ethyl ether, or in some instances mercury) with increase in temperature is linear for all practical purposes within the range of temperature from 0° to 100° C. The scale is therefore divided evenly and equally positive indications are obtained at either end of the scale. Usually the instrument is filled so that the contained liquid is at a considerable pressure (100 pounds per square inch) when its temperature is 0° C. This is necessary so that the Bourdon tube will remain under tension while the liquid in it and in the capillary contracts as the temperature is lowered to -35° C. At 100° C. the internal pressure may amount to 700 or 800 pounds per square inch depending upon the thermal coefficient of expansion of the liquid used and the stiffness of the Bourdon tube.

The indications of instruments are affected considerably by variations in the temperature of the liquid in the Bourdon and capillary tube. The effect of change in temperature of the Bourdon tube is readily eliminated by means of a bimetallic strip, properly inserted in the indicator. Considerable difficulty is experienced in compensating at reasonable cost for the effect of temperature changes in the capillary tube. The simplest method depends upon the use of capillary tubing having a bore so small that a change in the volume of the liquid contained within it produces an inconsequential error in indication.

C. ELECTRIC THERMOMETERS

General Electric resistance thermometer.—An electrical resistance thermometer for use in measuring the temperature of the engine oil or cooling liquid has been developed recently (reference 18). The instrument consists of a temperature sensitive resistance **A**, figure 34, in series with one of the coils of part **C**, and a fixed resistance **B** in series with the other coil of part **C** of the indicator. A 12-volt source of electrical current is connected in series with each resistance. Part **A** is in the field of a permanent magnet and is free to rotate to a position of equilibrium under the action of the opposing torques of a hairspring and of the interaction of the magnetic fields of the differential currents in the coils and the magnet. The indication is independent of the voltage within wide limits. Resistance element **A** is mounted within a sealed cartridge which is installed

on the engine at the point at which the temperature is required. The case of the indicator floats on sponge rubber within an outer case the dimensions of which conform to the standard for the 1½-inch dial size. The indicator mechanism is magnetically shielded. The pointer has a motion of 90° of arc for the temperature range.

This instrument is adaptable for use in measuring free-air temperature, in which case the cartridge is ven-

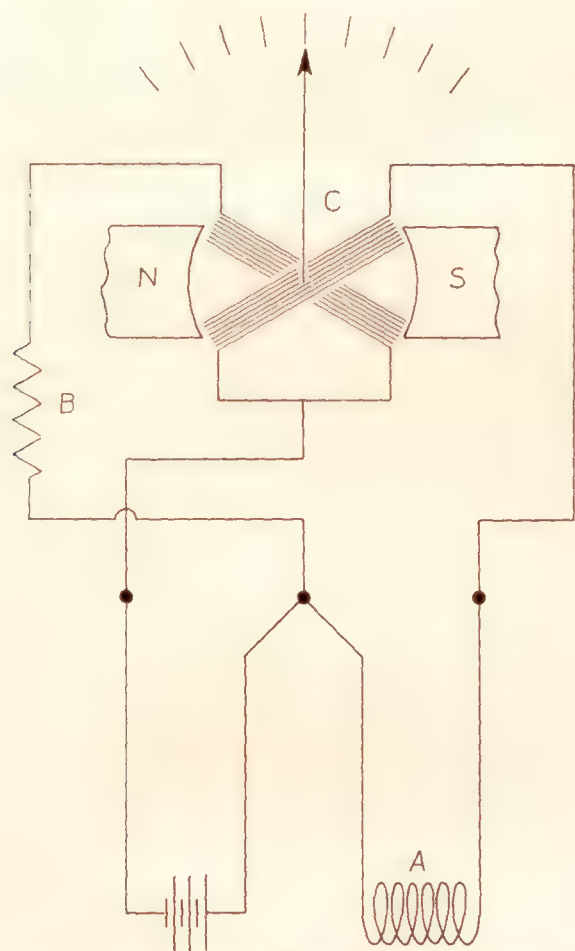


FIGURE 34.—Electric circuit of G.E. resistance thermometer.

tilated and is mounted on a strut in a position removed from the blast of the hot exhaust gases of the engine.

Thermocouple thermometers.—When one junction point of a loop composed of two dissimilar metals such as copper and constantan is at a temperature differing from that of the other junction point, an electrical current will flow through the circuit. The magnitude of the current depends upon the difference in the temperatures of the two junction points. In thermocouple thermometers for aircraft a suitable millimeter calibrated in units of temperature is used as the indicator. One of the junctions, the cold junction, is installed within the case of the indicator and the other, the hot junction, is constructed in the form of a spark-plug gasket, or attached to an expanding rivet which is forced into a hole in the engine cylinder at the point at which the temperature is desired. In order to obtain indications of the actual temperature of the hot junction, rather than the difference in the temperature between the two junction points, a compensation is usually provided for the effect of variation in the temperature of the cold junction. When this compensator is within the indicator, as is usually the case, compensation is also

obtained automatically for most of the effect of changes in the temperature of the indicator.

The instruments available differ mainly in the method of compensation. One of these methods is illustrated by the Brown thermometer, a diagram of the indicator of which is shown in figure 35. The compensation is obtained with a bimetallic strip B, one end of which is mounted directly on a pole piece at A and the other end of which is fastened at C to the outer coil of one of the hairsprings attached to the pointer shaft. If the bimetallic strip is of proper design, any tendency of the pointer to deflect due to a change in the temperature of the indicator and cold junction is very nearly balanced.

The indicator of the Weston aircraft engine thermometer contains the bimetallic type of compensation. Its internal resistance is 13.5 ohms, part of which is swamping resistance for temperature compensation. Copper-constantan thermocouples are used. The pointer has a motion of 120° of arc for the range from 0° to 600° F. (−18° to 317° C.) or 0° to 350° C. The case is the standard 2¼-inch dial size. The leads of various lengths, including the engine thermocouple, have in all cases the same resistance of 2 ohms and are of stranded wire. The instrument is unique in the use of cover glasses of nonshatterable glass.

In the General Electric thermocouple thermometer (reference 54) a magnetic shunt, the permeability of which decreases with increase in temperature, is added to the magnet of the indicator. This controls the magnetic flux through the moving coils so as to

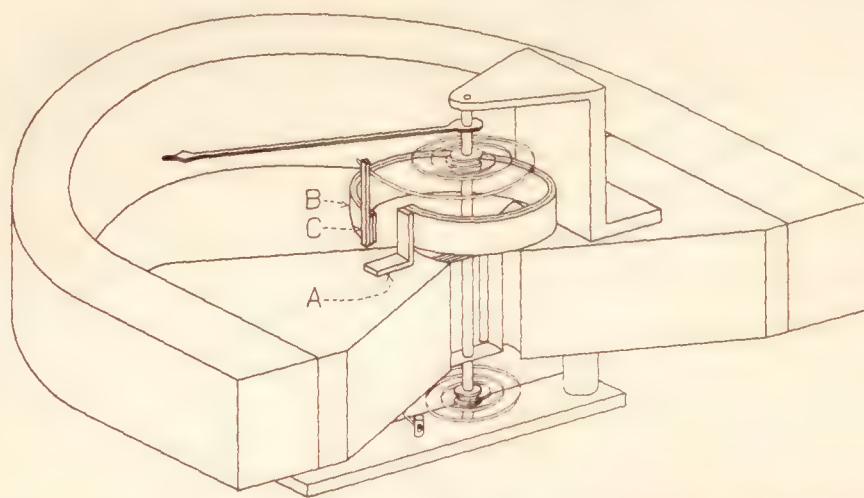


FIGURE 35.—Electric indicator showing the Brown cold junction compensator for thermocouple thermometers. B is the bimetallic strip, one end of which is fastened to the pole piece at A and the other to the hairspring at C.

compensate for the effect of change in the temperature of the cold junction and of the indicator, insofar as possible. Iron-constantan thermocouples are used.

In one type of thermocouple thermometer nine hot junctions are provided which may be installed in various locations on the engine. A selector switch and an indicator containing one cold junction are included with each instrument. With this equipment an indication of the temperature at any one of nine points on the engine may be conveniently obtained.

APPARATUS FOR TESTING ENGINE THERMOMETERS

Apparatus for scale-error tests.—The scale errors of an engine thermometer are determined in the laboratory by comparing its readings at a number of points within its range with those of a calibrated thermometer of the mercury-in-glass type or with those of a calibrated thermocouple. The testing apparatus consists of an insulated liquid bath in which are immersed the standard thermometer, the temperature sensitive elements of the instruments under test, and a stirrer driven by a small motor. The temperature of the bath is reduced by adding cracked ice or raised by means of an electric immersion heater.

Water is the most suitable liquid in calibrating instruments of the range 0° to 100° C. A cylinder oil with a pour point slightly below 0° C. which gives off relatively little vapor at 200° C., has been found particularly serviceable for testing instruments in the

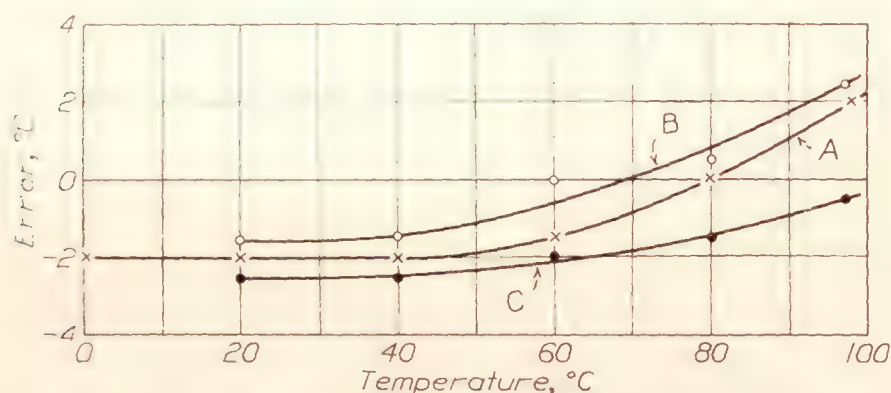


FIGURE 36.—Errors of a vapor pressure thermometer of good quality. Curve a was obtained with the gage and capillary at $+26^{\circ}$ C, b at $+45^{\circ}$ C, and c at -35° C.

range from $+30^{\circ}$ to 200° C. Tempering lavite, a compound of salts commercially available for tempering metals, can be used in the range above 125° C., and down to 30° C. when dissolved in water. The excessive length of time necessary to evaporate the water at about 125° C. makes it impractical to use the water-lavite solution.

For tests at airports and other field stations similar liquid baths are required. The test points can all be at or above the ambient temperature, so that a means for raising the temperature is all that is required. Calibrated mercury-in-glass thermometers are used as a standard.

Vibration and temperature control apparatus.—Engine thermometers are tested for the effects of vibration by mounting them on the apparatus described in the section on "Laboratory Testing of Tachometers-Apparatus" and subjecting them to the standard vibration. Temperature chambers suitable for controlling the temperature of the indicators are also described in the section just referred to.

Pressure-control apparatus.—Vapor-pressure thermometers, and to a smaller extent liquid filled thermometers, are subject to errors resulting from extraneous deflections of the Bourdon tube of the indicator due to variations in the air pressure. An apparatus

consisting of a chamber capable of withstanding a partial vacuum and large enough to receive the entire calibrating apparatus described above is used in determining these errors. The pressure within the chamber is reduced by means of a vacuum pump. A mercurial barometer connected with the chamber indicates the absolute pressure.

PERFORMANCE OF ENGINE THERMOMETERS

A. VAPOR-PRESSURE THERMOMETERS

The tests described below for vapor-pressure thermometers are substantially those required for acceptance in the purchase specifications issued jointly by the Army Air Corps and the Bureau of Aeronautics of the Navy Department.

The same tests are made on both the 100° C. and the 200° C. instruments except for obvious differences due to the difference in the ranges. The performance of the two types is essentially the same if expressed in terms of pointer motion in degrees of arc; in terms of temperature the errors of the 200° C. instrument are from $1\frac{1}{2}$ to 2 times those of the 100° C. instrument.

Scale errors.—Each thermometer is subjected to the scale error test in order to determine that it is in operating condition and to evaluate the error at any desired number of points over the range of indication. The test is made by comparing the reading of the thermometer with that of a standard instrument when the bulbs of both instruments are immersed in a liquid bath the temperature of which is under control. During the test the capillary tube and the indicator are maintained at room temperature.

The scale errors of a well-adjusted thermometer with a range of 100° C. are shown in curve (A) of figure 36. The indication of the instrument is not as reliable at temperatures below, as it is above, 20° C. owing to relatively small rate of change of vapor pressure with temperature in this range and the consequent greater effect of friction in the mechanism.

Excess temperature.—Engine thermometers which are graduated in the range 0 to 100° C. are likely to be subjected in service to temperatures exceeding the range in indication. Within limits the accuracy in indication should not be affected by this treatment. The excess temperature test is made by comparing the readings of the instrument corresponding to a bulb temperature of 100° C. obtained before and after a 10-minute period during which the temperature of the bulb has been raised to approximately 110° C. The change in reading should not exceed 3° C. No data on the effect of excess temperature on the 200° C. instrument are available.

Drift.—Drift is manifested in a thermometer of the liquid-filled or vapor-pressure type by a gradual increase in indication after the temperature of the bulb has been raised to, and while it is being maintained

at, a value higher than that at which it was previously subjected. The drift test is made by subjecting the bulb of an instrument to approximately the maximum temperature of the range for a period of 1 hour. The increase in indication obtained during this time is a measure of the drift.

In good quality instruments of either range the drift does not exceed 2° C.

Temperature errors.—The errors caused by a variation in the temperature of the capillary tube and indicator are determined by repeating the scale error test with the temperature of the capillary tube and indicator, first at plus 45° C. and then at minus 35° C. The difference between the scale errors as obtained in these tests is a measure of the temperature effect.

Failure to function at the low temperature is in general due to insufficient liquid in the bulb or perhaps to freezing of an impurity in the liquid. These conditions are detected by a failure of the instrument to change its indication as the bulb temperature is varied. Insufficient filling may often be definitely demonstrated by the fact that progressively greater lengths of the capillary tubing must be immersed in the temperature bath as its temperature is increased in order to secure the indication of the bath temperature. In order to detect freezing of an impurity it is the practice in the low temperature test to reduce the temperature of the entire instrument to -20° C., so that it may freeze solid in the tubing undisturbed by the flow caused by differential temperatures in the parts of the instrument.

The temperature errors of a representative 100° C. instrument are shown in figure 36 in which curve (B) shows the errors with the gage and capillary tubing held at +45° C. and curve (C) with their temperature held at -35° C. The temperature effect is usually obtained by averaging the differences in the error at each test point, irrespective of algebraic sign. This average difference for curves (B) and (C) is 1.8° C. and should not exceed 3° C. for instruments of either range.

Vibration.—In the vibration test the indicator alone is subjected to the standard vibration for a period of 3 hours. It is also subjected to vibrations varying in frequency from 1,000 to 2,000 c.p.m. and the amplitude of the pointer vibration relative to the dial observed. During the latter test the thermometer bulb is maintained at a specified temperature within the usual range of temperatures to be measured on aircraft. The amplitude of the pointer vibration should not be such as to indicate a free period of the mechanism in the above range of frequencies nor should the functioning or performance of the instrument be affected. The latter requirements are determined by an examination of the instrument for loose parts and a comparison of the difference in the scale errors usually at 100° C. or 200° C. of the instrument obtained before and after the vibration.

The oscillation of the pointer during vibration is usually within 2° C. for 100° C. instruments and 3° C. for the 200° C. type.

If the natural frequency of vibration of the mechanism of an instrument coincides with that to which it is subjected, an excessive amplitude of vibration of the pointer may occur. The natural frequency may be shifted outside of the frequency range of vibration by redesigning the mechanism, which means in effect a change in the stiffness of the elastic element, or by addition of an inertia disk or a damping device. The inertia disk in the form of a flywheel is attached to the pointer shaft and in effect constitutes an inertial force opposing that of the vibrating elastic element, reducing both the natural frequency and amplitude of vibration. The use of the inertia disk does not interfere with the pointer assuming the true mean position of indication.

Chief among the damping devices for reducing the effect of vibration are the well-known magnetic drag and the air-drag mechanisms. The retarding force of the magnetic drag mechanism is proportional to the relative velocity of the parts, and therefore a true mean reading of the pointer is obtained. The retarding force of the air-drag mechanism is proportional to the square of the velocity in some instruments, and tends to produce a reading of the pointer slightly in error from the true mean reading. (See reference 17.)

Capillary temperature.—The capillary tube of an engine thermometer is likely to be subjected in service to localized heating, a condition which usually occurs when a portion of the capillary is attached to a frame member which is too close to the oil line or exhaust pipe. The effect of local heating ordinarily experienced is negligible in properly designed vapor pressure thermometers but not in liquid filled instruments. A capillary temperature test is made by subjecting a short length of the capillary tubing to a temperature of 100° C. while the indicator, bulb, and remainder of the tubing is maintained at room temperature. The change in indication obtained indicates the capillary temperature effect.

Reduced pressure.—The actuating elements of the indicators of both the vapor pressure and liquid filled thermometers are subjected externally to the pressure of the surrounding atmosphere. The indications of the instruments are affected as a consequence by variations in the altitude by an amount equal to

$$\frac{(P_o - P)}{R}$$

where $P_o - P$ is the change in atmospheric pressure and R is the rate of change of the vapor pressure with temperature at the temperature of the bulb. It follows that the effect depends upon the choice of the filling liquid and that it varies with the temperature of the bulb, decreasing as its temperature increases.

A test at reduced pressure is made by subjecting the entire instrument to an absolute pressure of approximately 12 inches of mercury. With the indicator and capillary maintained at room temperature ($+20^{\circ}\text{C.}$), the temperature of the bulb is then raised to 60°C. , or about 150°C. for instruments having a range extending up to 200°C. The reading of the instrument at this temperature and at the reduced pressure is compared with that at room pressure and the same temperature in order to obtain the effect of the reduced pressure. In instruments now available the effect is less than 3°C. for 100°C. instruments and 4°C. for 200°C. instruments.

Capillary strain.—The mechanical strength of the capillary tubing is determined by means of the capillary bending and strain tests. The bending test is made by flexing the capillary 20 times at one point through an angle of 90° around a cylindrical core of $\frac{1}{2}$ -inch radius. The strain test is made by clamping the capillary at a point approximately 6 inches from the indicator and suspending a weight of 25 pounds from the free end of the tubing for a period of 1 minute. This test is also made with the capillary clamped at a point approximately 6 inches from the bulb. Possible failure of the tubing is indicated by a large difference between the readings at a given bulb temperature taken before and after the tests.

B. LIQUID-FILLED TYPE

Except for the effect of reduced pressure and capillary temperature, the performance of liquid-filled instruments does not differ essentially from the vapor-pressure type (reference 5). The effect of reduced pressure is ordinarily negligible. As has been stated the effect of local changes in the temperature of the capillary tubing is excessive in the ordinary instrument.

C. ELECTRICAL THERMOMETERS

Electrical thermometers are tested for scale errors, temperature errors, and vibration in essentially the same manner as described for vapor-pressure thermometers. The indicator is tested for the degree to which it affects the magnetic compass exactly as described in the section on the methods of testing tachometers. In addition if the instrument requires a voltage supply, tests are made for the effect of its variation.

The time lag (reference 15) in indication of aircraft-engine thermometers is in general not a factor under the conditions of their use.

Resistance thermometer.—The instrument should be tested (a) for scale errors, (b) drift, (c) for the effect of changes in temperature of the indicator, (d) vibration, and (e) magnetic shielding. No laboratory data have been obtained at the Bureau of Standards. The performance should be substantially equal to that of

vapor-pressure thermometers if any advantage from its use is to be realized.

Thermocouple thermometers.—These instruments are at present made with a deflection of the tip of the pointer of approximately $2\frac{1}{2}$ inches for a range of temperature of 350°C. , which means the temperature can be read at best not closer than 1°C. and in flight under average conditions not closer than about 3°C. Tests show that the scale errors of instruments can be reasonably expected not to exceed 7°C. at any point on the scale.

Laboratory tests show that electrical indicators of the sensitivity used in the thermocouple thermometers do not ordinarily withstand vibration in that the calibration slowly changes, due to wear of the pivots.

The change in indication with change in temperature of the indicator is far larger than expected in the few instruments thus far tested, amounting to about one half of the change in temperature of the indicator. The results are probably not typical of well-adjusted instruments. It is believed that instruments now available will have errors not exceeding 17.5°C. when the temperature of the indicator varies from -25° to 45°C.

An additional error in service use, not determined by the laboratory tests, is the effect of the uncertainty in the temperature, and thus the resistance, of the copper or iron connecting wires. This effect is probably negligible in most instruments now available, in view of the relatively high resistance of the other parts of the circuit.

The indicator, as in the case of electrical tachometers, must be magnetically shielded. As a practical minimum the effect on a compass should not exceed 4° when 8 inches distant from its center.

PRESSURE GAGES

Aircraft engines are equipped with pumps for circulating the lubricating oil under pressure to the bearings. A pressure gage which indicates the pressure developed by the oil pump is used to determine its satisfactory operation.

In addition to oil pumps most aircraft engines are provided with fuel pumps for delivering the fuel to the carburetor. Information on the operation of the pump is obtained by measurement of the pressure developed.

Pressure gages may be conveniently grouped into two general classes—mechanical and electrical.

MECHANICAL PRESSURE GAGES

General design characteristics.—A diagram of a typical mechanical pressure gage is shown in figure 37. A Bourdon tube **B** is used as the pressure-sensitive element. It is of interest that the Bourdon tube is reported to have originated with Schinz in Germany in 1845. (See reference 48.) It is formed by

bending into the arc of a circle a length of thin walled metallic tubing which has been previously shaped to have in section the contour of an ellipse. One end of the tube is mounted on the base of the instrument so as to communicate with a threaded fitting. The other end is sealed off and connects with the multiplying mechanism through a suitable linkage. An increase in the pressure within the tube is accompanied by an increase in the cross-sectional area which gives

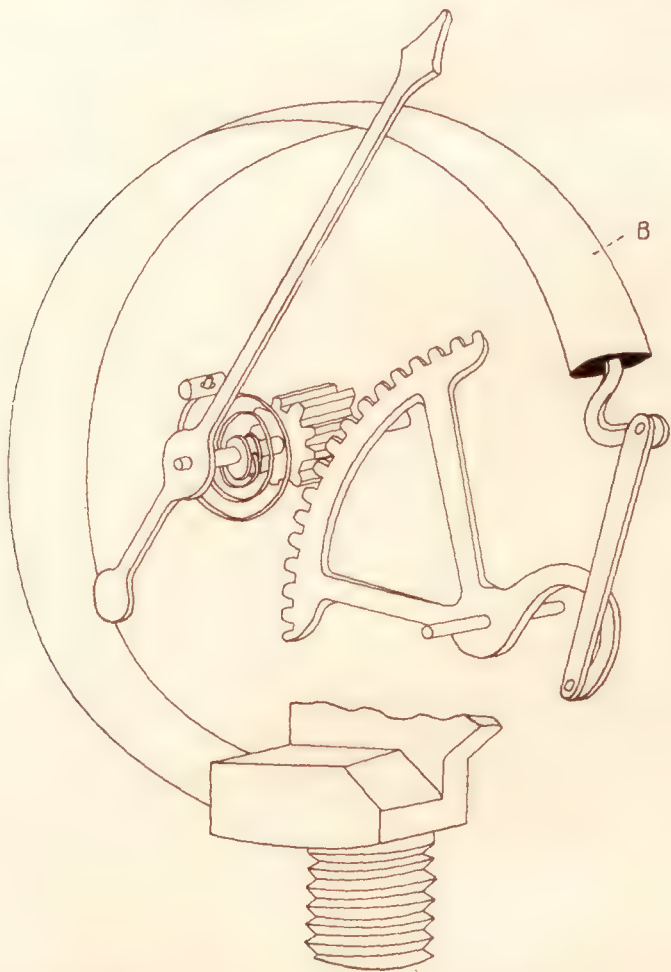


FIGURE 37.—Diagram of pressure gage of the Bourdon tube type.

rise to a force tending to straighten the tube and consequently to a displacement of the free end.

A deflection formula derived by Lorenz (reference 51) is stated by Rolnick (reference 59) to be reasonably accurate for tubes with a small ratio of thickness to width of cross section, and is given below.

$$\frac{A}{A_0} = \frac{1.16PR_0^2}{hbE}$$

Here A is the angular rotation of the Bourdon tube produced by the differential pressure P ; A_0 , the angular length of the tube; R_0 , the radius of the tube; h , the wall thickness; b , the thickness of the tube from center to center of the walls; and E , the modulus of elasticity.

For additional theory and data on Bourdon tubes see references 46 to 52, inclusive, and 58.

The multiplying mechanism of the gage consists of a link, a sector, and a pinion arranged as shown in figure 37. For convenience in calibrating, the point of connection of the link to the sector is made adjustable.

The gage is usually mounted on the instrument panel and is connected to the pump by means of copper tubing. The connection to the indicator and to the

point at which the pressure is measured is made by a fitting, such as is shown in figure 18 of reference 20.

Oil-pressure gage.—Oil-pressure gages are graduated in either of the two ranges, 0 to 120 and 0 to 200 pounds per square inch. As stated in the "Introduction" the diameter of the dials of oil-pressure gages is now fixed at $1\frac{1}{8}$ inches and the spacing between the mounting holes is standardized, so that instruments of the various manufacturers may be interchanged. The weight of the instrument is approximately 6 ounces.

The design of the Bourdon tube depends upon the range of indication. In one instrument having a range of 0 to 120 pounds per square inch the tube is of hard-drawn brass and has an outside diameter of $1\frac{3}{4}$ inches, an elliptical section of $\frac{1}{2}$ by $\frac{3}{32}$ inch, and a wall thickness of 0.011 inch.

Fuel-pressure gage.—The general appearance and the construction of the fuel-pressure gage are similar to those of the oil-pressure gage. The Bourdon tube, however, is constructed of much thinner metal, so that its stiffness is approximately one tenth that of the oil-pressure gage. The fuel-pressure gage is usually graduated in the range 0 to 10 pounds per square inch and weighs approximately 5 ounces.

Diaphragm type relay.—In order to conserve the supply of lubricant in case of breakage of the copper

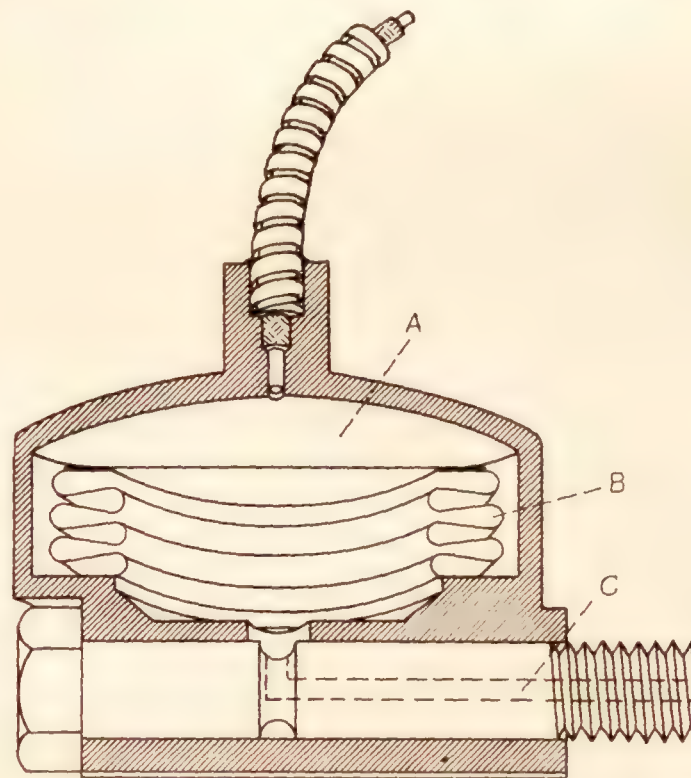


FIGURE 38.—Diagram of diaphragm relay for oil-pressure gages. The metal bellows B intervenes between the lubricating oil and the liquid in A which transmits the pressure to the gage.

tube connecting the oil-pressure gage with the engine and to decrease the lag in indication at low temperatures due to congealing of the oil within the connecting tube, pressure relay devices have been developed both here and abroad (references 16 and 17). A cross-sectional diagram of the essential features of such a device is shown in figure 38. The relay is mounted on the engine at the oil-line fitting and contains a diaphragm or metal bellows B. The space A outside of

the diaphragm, the connecting tubing, and the Bourdon tube in the indicator are completely filled with a liquid which has a low freezing point, a low viscosity, and a relatively low thermal coefficient of expansion. Mineral spirits (varnolene) has been found satisfactory. The pressure of the lubricating oil which connects to

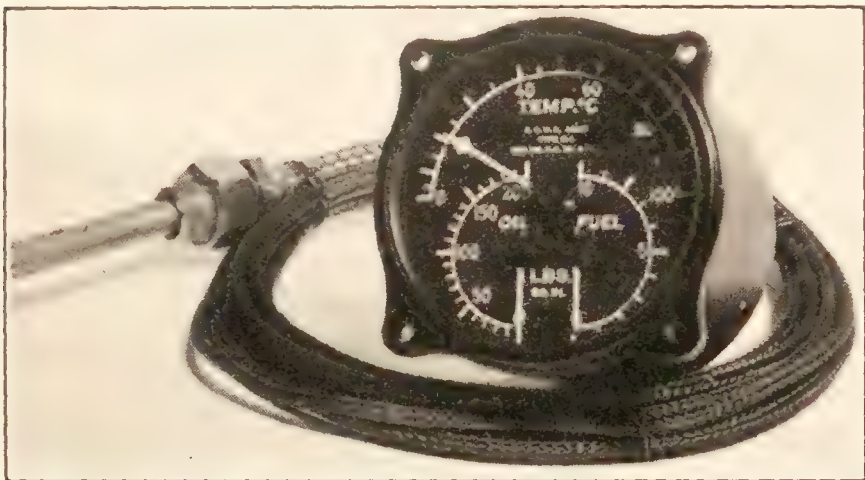


FIGURE 39.—Engine gage unit.

the inside of the diaphragm through hole **C** is transmitted through the diaphragm to the liquid and thence to the pressure gage.

Engine gage unit.—The oil and fuel pressure gage and the oil or cooling liquid thermometer are sometimes installed within a single case. The combination is known as the engine gage unit. The latest form is



FIGURE 40.—Engine gage unit with approximately linear scale.

shown in figure 39, and an older form, in which the individual instruments are arranged vertically in tandem within a case, is shown in figure 40.

The instrument shown in figure 39 is mounted in a case which conforms to the standard 2 $\frac{3}{4}$ -inch dial size. Contrary to general practice the pointer of the fuel pressure gage moves counter-clockwise with increase in pressure. Its weight with a 22-foot capillary tube averages 1.9 pounds.

ELECTRICAL PRESSURE GAGES

The electrical circuit of the G.E. electrical oil or fuel pressure gage is the same as that of the thermometer shown in figure 34. The resistance **A** is made to vary with pressure by means of the deflection of a metal bellows the combination of which is mounted in a cartridge type container suitable for installation on the engine at either the oil- or fuel-line fitting. The indicator is of the same type as that used with the thermometer and similarly is magnetically shielded and is protected from the effects of shocks and vibration. The instrument operates on 12 volts and is stated to draw normally 50 milliamperes of current. The combined weight of the pressure element and indicator is 12 ounces.

APPARATUS FOR TESTING PRESSURE GAGES

The scale errors of oil-pressure gages are determined by means of a deadweight gage tester. The tester

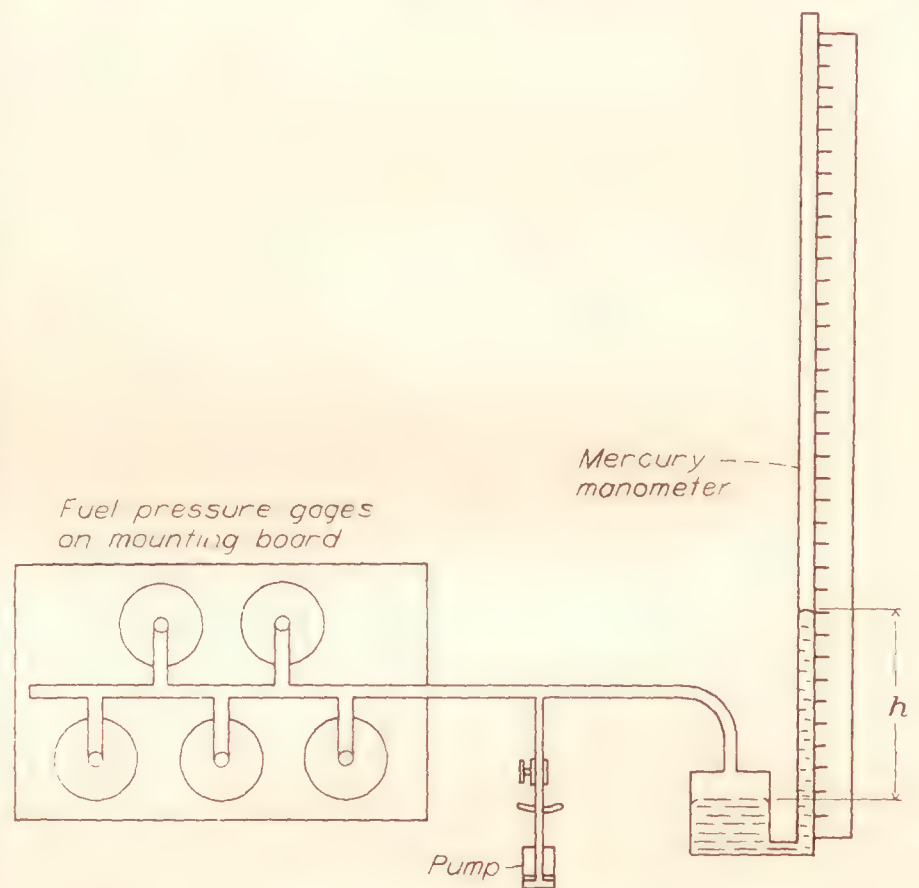


FIGURE 41.—Diagram of apparatus for testing fuel-pressure gages.

consists essentially of a vertical cylinder, a closely fitting piston provided with a pan for weights and a pump. The instrument to be tested is connected to the cylinder by means of suitable fittings and a connecting tube. The cylinder is filled with a light mineral oil. To obtain a desired pressure, a weight equal to the product of this pressure by the area of the cylinder is placed on the pan of the piston and the pump operated until the piston is supported by hydrostatic pressure. The effect of friction between the weighted piston and the wall of its cylinder is usually eliminated by spinning the piston before reading the instrument.

It has been found possible to operate the deadweight gage tester with a mineral oil with a pour point of

-40°C . This has made it possible to test oil-pressure gages at -35°C . without danger of the oil freezing in the tubing connecting the gage to the tester.

The arrangement of apparatus used in determining the scale errors of fuel-pressure gages is shown in figure 41. A mercurial manometer is used as the standard, which may be of the reservoir type as shown or of the U-tube type. In either case it should be noted that the pressure is determined by the difference in height. The required pressures are obtained by means of a hand pump.

Apparatus for controlling the temperature of the instruments during test and for subjecting them to vibration are described in the section, Testing of Tachometers.

For determining scale errors of both fuel and oil pressure gages at instrument repair stations a dead-weight gage tester designed for both ranges is most convenient. It is also feasible to use a calibrated gage as the standard, in which case a suitable pump is required.

PERFORMANCE OF PRESSURE GAGES

A. MECHANICAL TYPE

Mechanical pressure gages are subjected to tests for (a) scale errors, (b) friction, (c) vibration effect, (d) seasoning, (e) drift, (f) effect of suction and over-pressure, and (g) the effect of temperature.

A general discussion of most of the above tests is given in the section on Tachometers under "Methods of Test."

It should be noted that the construction of aircraft pressure gages to the accuracy needed offers in general no particular problem. This follows from the fact that the least reading of these gages is about 1 percent of the maximum range, for example 0.1 pound per square inch in the gage with a range from 0 to 10 pounds per square inch, and that an accuracy of at least 1 percent in most respects is usual in pressure gages used in engineering work.

Scale errors.—The scale errors of the pressure gage are determined by subjecting the instrument at the pressure connection to a number of specified pressures over its range and obtaining the corresponding instrument readings. The error is $R-S$, where R is the reading of the gage and S is the true pressure.

The scale errors of both fuel and oil pressure gages of good quality do not exceed 2 percent of the maximum range. Those of a typical oil pressure gage of good quality are given in curve A, figure 42.

Friction.—The effect of friction is found by subjecting the instrument to a given pressure and comparing the readings of the instrument before and after it has been tapped. The difference in the two readings indicates the effect of friction. The friction is usually obtained at a number of pressures over the range of

the instrument and amounts on the average to about 1 percent of the maximum range.

Vibration.—The effects of vibration are determined by subjecting the instrument to the standard vibration with a frequency between 1,500 and 2,000 c.p.m. for a period of 3 hours, during 2 hours of which time the instrument is subjected to a pressure equal to 50 percent of its range. The amplitude of vibration of the pointer with respect to the dial is observed in the frequency range 1,000 to 2,000 c.p.m., while the instrument indicates the pressure of 50 percent of its range. Immediately following the vibration the scale errors are determined and compared with those previous to the vibration.

The total amplitude of vibration of the pointers of the pressure gages should not exceed 2 percent of the maximum range.

It appears that the Bourdon tube in a number of designs of fuel-pressure gages has a free frequency between 1,000 and 2,000 c.p.m., and consequently the

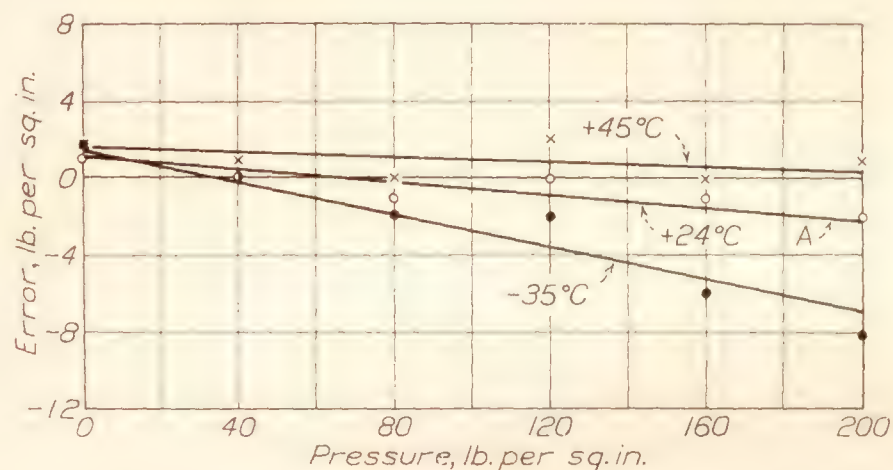


FIGURE 42.—Errors of oil-pressure gages at temperatures of $+24^{\circ}$, $+45^{\circ}$, and -35°C

pointers vibrate with an amplitude so large that fatigue failure of the Bourdon tube may be anticipated in service. This condition may be most easily remedied by the addition of an inertia disk to the pointer shaft, which, as pointed out in the section on Performance of Vapor Pressure Thermometers, reduces the free frequency and greatly reduces the amplitude of vibration at this frequency.

The average change in the scale errors due to a vibration of 3 hours should be negligible; that is, less than 1 percent of the maximum range.

Seasoning.—The seasoning test is made by subjecting the instrument to 100 applications of the pressure required to produce a deflection of the pointer corresponding to 50 percent of the range of indication. The scale errors before and afterwards are compared in order to determine the effects of seasoning.

The average change in the scale errors of good quality instrument should not exceed about 1 percent of the range, and are usually of the order of the least reading.

Drift.—In this test increase in reading of an instrument in a period of 1 hour is observed after it is suddenly subjected to, and held at, a pressure equal to 50

percent of its range in indication. This increase in reading is the drift, and in satisfactory instruments does not exceed 1 percent of the maximum range.

Suction and overpressure.—Pressure gages are likely to be subjected in service to pressures which are either below atmospheric pressure or exceed the range in indication. Their ability to withstand such treatment is determined in the suction and overpressure tests. The tests are made by subjecting an instrument first to a suction of 10 pounds per square inch for the oil pressure gage and 3 pounds per square inch for the fuel pressure gage, for a period of 1 minute, and, second, to a pressure 50 percent greater than the range in indication for a period of 10 minutes. The scale errors before and after the excess differential pressures are compared in order to determine the effect on the performance of suction and overpressure.

The average change in scale errors as a result of suction and overpressure does not usually exceed 1 percent of the maximum range.

Temperature errors.—The scale errors of the instrument are obtained with its temperature first at -35° and then at $+45^{\circ}$ C. The difference in the errors at these two temperatures is the effect of temperature.

The results of temperature tests on the typical oil pressure gage are also given in figure 42. The effect of temperature can be expressed as the difference in the slopes of the best straight lines for the data, divided by the temperature difference. This is the change in scale value per degree centigrade and is 0.044 percent for the temperature interval -35° to $+45^{\circ}$ C. for the instrument for which data is given in figure 42. The effect is due to the change in the modulus of elasticity of the Bourdon tube and the hair spring since the instruments are ordinarily uncompensated, and in poorly seasoned instruments due to unreleased internal stresses in the Bourdon tube. The temperature coefficient of the modulus of elasticity of bronze is about 0.040 percent per degree centigrade.

The effect of temperature may also be expressed in terms of the average of the change in error at each test point, which is 3.7 pounds per square inch for the data in figure 42.

B. ELECTRICAL PRESSURE GAGES

The performance of electrical pressure gages is determined by tests which are, in general, the same as those listed for mechanical pressure gages. In addition the resistance element should be subjected to vibration. The temperature test of the electrical pressure gage should include a scale error test in which the indicator is at room temperature and the pressure element is at the maximum temperature experienced in service.

Also the indicators must be tested for adequacy of magnetic shielding which should be such that an

aircraft compass is not deflected in excess of 4° when the distance between the two is 8 inches from center to center.

FUEL QUANTITY GAGES

The fuel quantity gage is used in aircraft to indicate the quantity of fuel available for continuing flight and is commonly installed in every modern aircraft. Although the amount of fuel remaining in the tank can be estimated from a knowledge of the rate of fuel consumption and the elapsed time, the possibility always remains that, due to leakage, less than this amount is available.

Fuel quantity gages are essentially of two types, one in which the position of a float in the liquid is indicated and the other in which the hydrostatic pressure of the head of the fuel is measured. In most cases a distant indicating instrument is essential.

Acceleration of the aircraft and deviation from the normal flying attitude of airplanes with shallow wing tanks cause errors equally in the two types.

The float-type gage is preferred when an indication at the tank is easily visible to the pilot. In the latter case the instrument is called a simple float type. The indicators are generally mechanically connected to the float, although in one design the coupling is made magnetically. The float type of instrument is relatively easy to install and reliable in operation.

The distant indicating float type is available in a great variety of designs (references 5 and 17) most of which have been produced in an effort to secure an instrument which is at the same time simple in design and dependable and accurate in operation. Distant indication has been secured (a) by a variety of mechanical connections, (b) electrically, and (c) by a hydrostatic device.

In the common design of the hydrostatic fuel quantity gage the head of the fuel is balanced by an air pressure which is measured by a suitable gage. The instrument is distant indicating. Other designs have been proposed in which the indication depends upon the pressure of the head of fuel, but these for various reasons have not proved practical.

SIMPLE FLOAT TYPE

In fuel quantity gages of this type the indication is obtained at the tank either below or above the float, whichever may be the most easily accessible to the pilot. The instrument consists of some form of indicating device connected to a cork or metal float resting on the surface of the fuel. A number of the designs which have been developed, are described below.

(a) The method of indication shown in figure 43 is especially useful in aircraft equipped with a fuel tank which is centrally located in the upper wing. As shown in the figure, the float is fastened to a disk by

means of a rod. The disk is visible through a glass tube graduated in terms of the quantity of fuel. One objection to this design is the possibility and consequences of breakage of the glass tube, which, however, has not been as frequent as might be expected.

(b) In the instrument shown in figure 44 the float is attached to the end of a long rod which rotates as the float falls with the level of the fuel. As is obvious from the figure, the rotation of the rod also causes rotation of the indicating drum by means of the sector and pinion mechanism.

(c) In a third type the float is mounted between guides which permit vertical movement but prevent rotation. A twisted metallic strip extends through a slot in the center of the float and is rotated by the float as the level of the fuel changes. A pointer attached to the twisted strip indicates on a suitable dial the quantity of fuel.

(d) In still another type, of which many are in use, the displacement of the float is transmitted to the

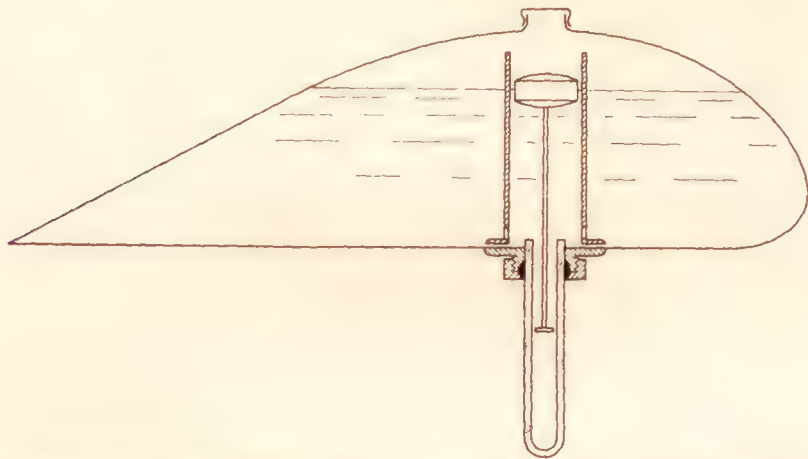


FIGURE 43.—Float type fuel quantity gage with indicator below tank.

indicator by means of a braided silk cord. One end of the cord is connected to the float and the other end is secured to a sheave mounted within the indicator. The cord is kept taut by means of a light spring mounted within the sheave. As the float drops with the level of the fuel the sheave is caused to rotate by the unwinding of the cord. Through a suitable gear and pinion the sheave operates a pointer which indicates the fuel quantity on a suitably engraved dial.

(e) **Boston gage.**—Stuffing boxes or similar shaft glands are eliminated by means of the magnetic method of indication which is used in the Boston gage. In this instrument a bar magnet is rotated by the float as it changes its level. The magnet is mounted inside and, coaxially, a magnetized pointer outside of the tank. Due to the magnetic force between the pointer and magnet the pointer aligns itself with the magnet and thus indicates the quantity of fuel.

DISTANT INDICATING FLOAT TYPE

Mechanical types.—The only distant indicating float type instrument with a mechanical transmission used in this country is the one in which a braided silk cord is used to connect the float with an indicating sheave,

similarly as described under (d) above. Outside of the tank the cord runs in tubing in which a roller is installed at each bend. In this instrument the number of bends in the line and the distance between the indicator and float must be kept to a minimum, as otherwise the friction is likely to be excessive. Further, it is difficult to design a stuffing box at the point where the cord comes through the tank so as to eliminate wetting part of the cord which passes through the tubing. When the cord is wet the friction is greatly augmented.

Considerable attention has been given abroad to the perfection of the mechanical transmission type. In

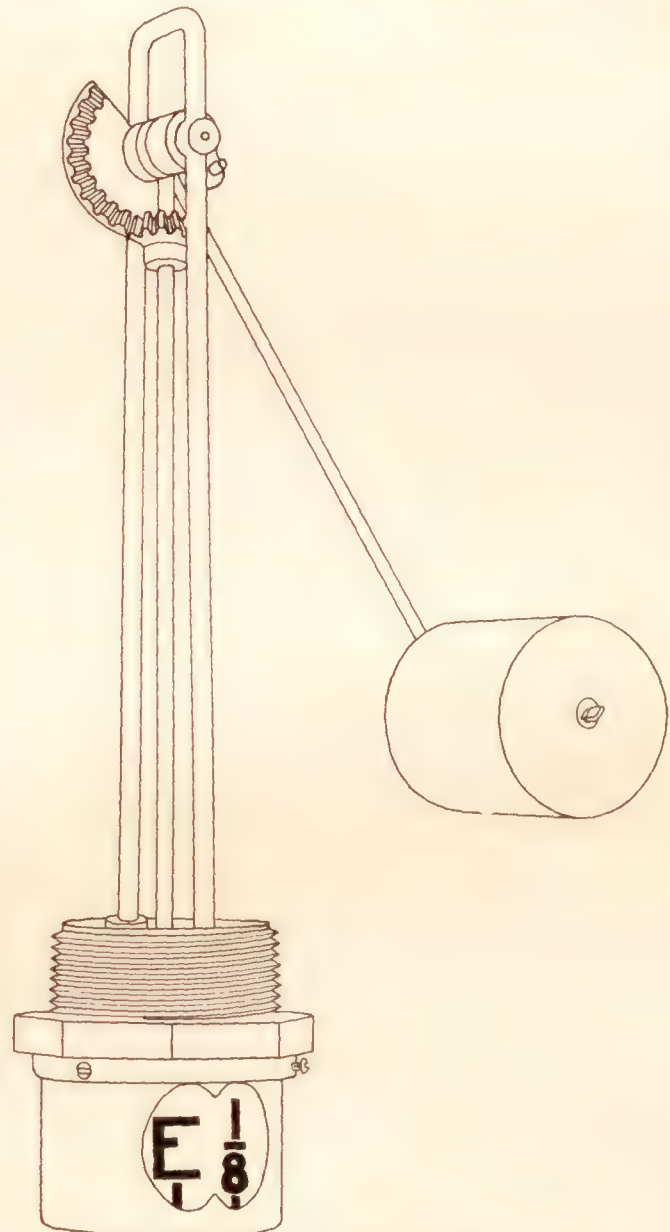


FIGURE 44.—Float and rod type fuel quantity gage.

one instrument (the Corset) the motion of the float causes longitudinal motion in the connecting line to the indicator, which consists of a series of short push rods connected to each other by means of a ball and cup arrangement. In two other instruments, the Televel and Spirobloc gages, the power to operate the indicator is furnished by the pilot. When a reading is desired, the pilot, by means of a wire connection to the tank element, either rotates or raises the float until a stop is encountered, which operation at the same time correspondingly varies the reading on an indicator. The point at which the stop is encountered, and thus the reading, depends on the level of the fuel. (See reference 17.)

Nagel gage.—An electrical transmission system is used in the Nagel gage. The float, mounted as shown in figure 44, governs the position of contact *S*, figure 45, which divides a resistance into two parts R_1 and R_2 .

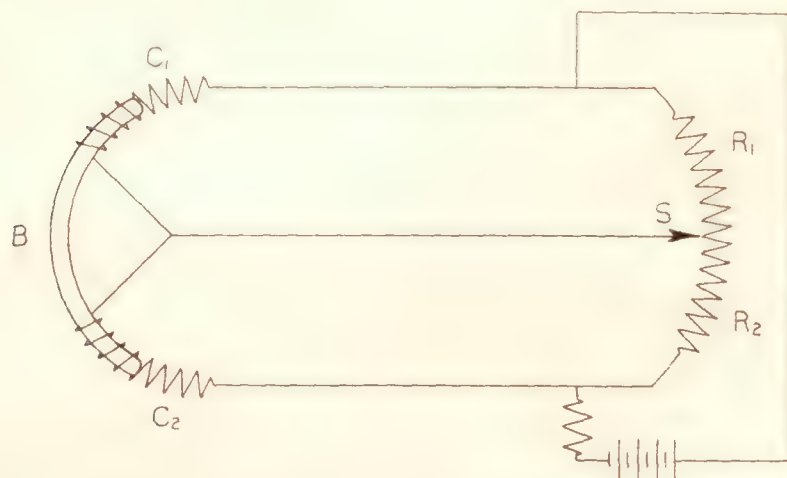


FIGURE 45.—Diagram of electric circuit of Nagel fuel quantity gage. The contact *S* is operated by a float, and the resulting change in current in C_1 and C_2 changes the position of equilibrium of the iron armature *B*.

Changes in resistance R_1 and R_2 affect the relative amount of current through the two coils C_1 and C_2 in the indicator. The pointer is attached through a suitable mechanism to a circular iron vane *B*, the posi-

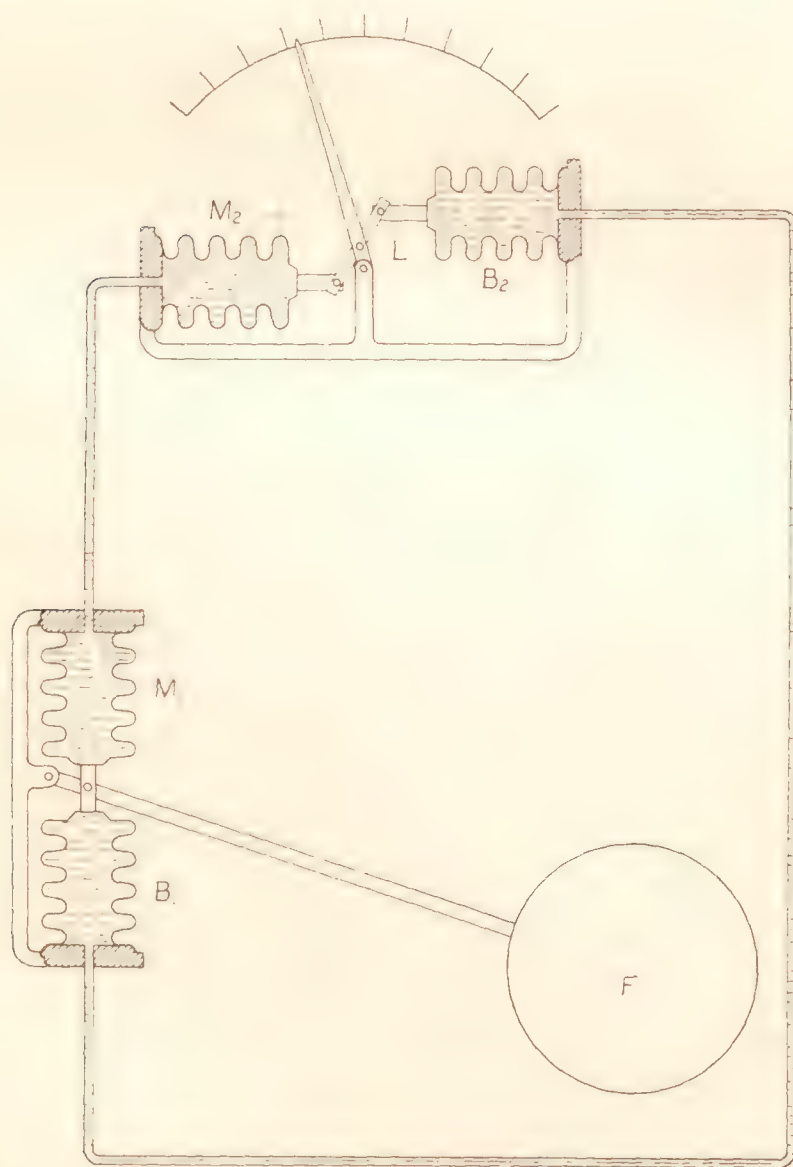


FIGURE 46.—Liquidometer fuel quantity gage.

tion of which varies with the relative amounts of the current through C_1 and C_2 . Since the indicator is in effect an ohmmeter, its indication is independent of the impressed voltage within a wide range. Although considerable attention has been given to the design of

a fireproof stuffing box between the resistances R_1 and R_2 and the fuel, a possible fire hazard remains.

Liquidometer.—In this fuel-quantity gage the deflections of the float are transmitted hydraulically through any desired length of line to the indicator. Referring to figure 46, float *F* is mechanically connected with two metallic bellows M_1 and B_1 each of which is in communication by means of copper tubing with another bellows, M_2 and B_2 , respectively, contained within the indicator. The two closed hydraulic systems thus formed are of approximately equal volumes and are filled with a suitable liquid having a low freezing point. The bellows M_2 and B_2 are connected together by means of link *L* which is pivoted at its center to the pointer. As the float falls, due to fall in the fuel level in the tank, B_1 is compressed and M_1 expanded, the resulting differential displacement of the liquid expanding B_2 and compressing M_2 , thus deflecting the pointer to the left. The design of link *L* permits

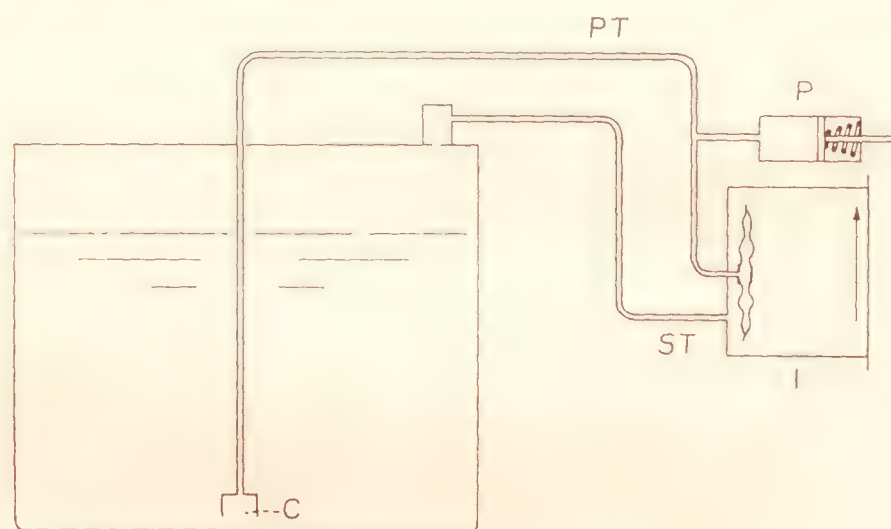


FIGURE 47.—Diagram of hydrostatic type fuel quantity gage.

changes in volume of the liquid due to changes in temperature without affecting the indication.

HYDROSTATIC FUEL-QUANTITY GAGE

Common type.—The essential parts of this instrument consist of an airtight pressure gage *I*, figure 47, a pump *P*, a pressure line *PT* leading from the interior of the diaphragm capsule to a cell *C* at the bottom of the fuel tank and a static pressure line *ST* leading from the case of the indicator to the top or the vent of the tank.

When the pump handle is pulled out against the action of a spring and permitted to return, the return stroke of the pump clears the entire line *PT* of liquid, the excess air passing into the liquid through openings in the cell *C*. The head of liquid *H* is now balanced at the cell *C* by the air pressure at this point, that is, by the air pressure in the line *PT* and the interior of the diaphragm. The static tube *ST* serves to maintain the interior of the indicator case at the pressure of the air above the fuel. The gage thus indicates the difference in these two air pressures or the pressure of the head of the fuel.

The indicator is made in a number of convenient ranges for use with tanks of differing depths. The cases are ordinarily of bakelite and are the standard 2 $\frac{3}{4}$ -inch dial size. The dials are calibrated after installation, as is almost necessarily the case with all fuel quantity gages. For test purposes temporary dials graduated in degrees of arc are usually furnished. The indicator has a restriction in the line to the diaphragm capsule in order to dampen out the effect of surges in the fuel. The weights of the pump and the indicating gage are 4 and 9 ounces, respectively. Connecting tubing of copper is commonly used.

The accuracy of the instrument is not affected by changes in the temperature of the air in the lines if the pump is operated before making a reading.

It is essential that the fuel be prevented from getting into the line insofar as possible. Fuel in the line **PT** up to the point where the pump is installed can be removed by means of the pump. Fuel in the line beyond this point and in the line **ST** or in the case of the indicator make the instrument inoperative until removed. Check valves at the point where the tubing connects to the tank may be desirable to prevent the fuel from entering the lines during maneuvers. A float-operated check valve is desirable in the line to the bottom of the tank. In the rare case when the indicator is colder than the fuel, condensation may occur in the indicator. This is difficult to prevent.

The fuel tank is sometimes vented to a modified pitot head which is mounted in the air stream, in which case the line **ST** is connected in such manner as to prevent fuel getting into it.

SUBMERGED CAPSULE TYPE

This instrument differs from the common hydrostatic gage in that the line **PT** connects to a diaphragm capsule in place of the cell **C**, figure 47, and in that the pump **P** is eliminated. In order to take care of changes in air pressure with altitude, and changes in temperature, the diaphragm capsule must be perfectly flexible so that the resulting volume changes in the contained air do not affect the indication. As in the case of the common type instrument the pressure of the air within the capsule differs from that above the liquid by that of the head of the liquid. A serviceable instrument has not as yet been obtained owing to the difficulty of obtaining a diaphragm material which has the required degree of flexibility and is at the same time dependable in operation.

G.E. ELECTRIC GAGE

An electrically operated hydrostatic fuel quantity gage which has been developed is of interest (reference 56), although it is not at present being manufactured. In the instrument, shown diagrammatically in figure 48, the head of the fuel is for the most part balanced

magnetically by a solenoid which is energized by means of a storage battery. The pressure of the head of the fuel is transmitted through a diaphragm to the plunger of the solenoid and a carbon-pile rheostat. The solenoid is connected in series with the carbon pile. As the load on the diaphragm decreases, with decrease in the fuel supply, the resistance of the carbon pile increases, which in turn decreases the current through the solenoid until the force exerted by the plunger and carbon pile just balances the load on the diaphragm. Thus the current varies with the force required to secure equilibrium. An ammeter gradu-

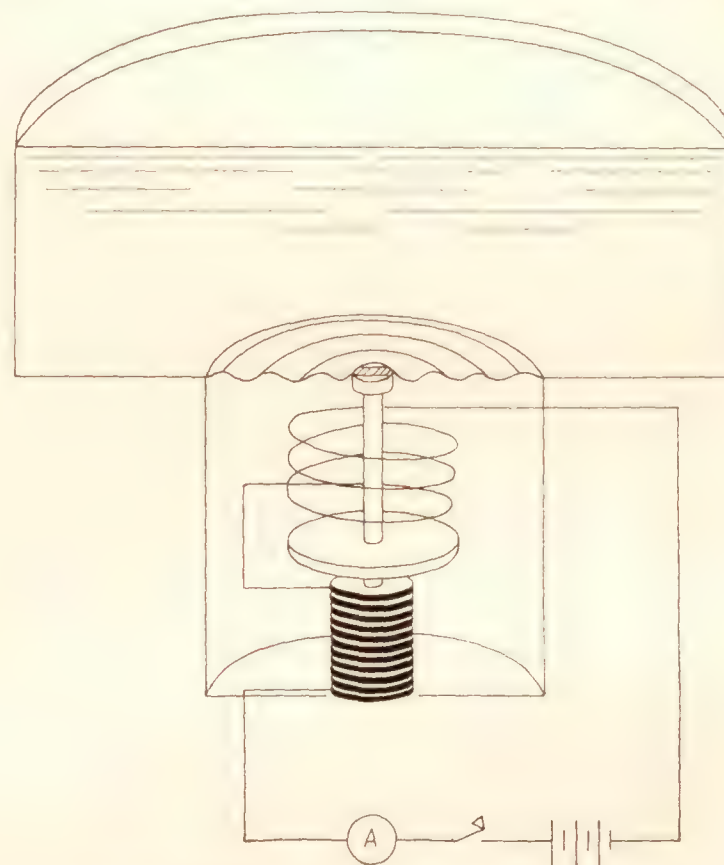


FIGURE 48.—Electric balance type fuel quantity gage.

ated in terms of fullness of the fuel tank serves as the indicator.

PERFORMANCE OF FUEL QUANTITY GAGES

TEST APPARATUS

No special apparatus is required to test instruments of the float type.

The indicator of the hydrostatic gage is tested for its accuracy as a pressure gage, and for this purpose a water manometer such as is used for testing air-speed indicators (reference 20), a vibration board and temperature-control apparatus as described in the section, Laboratory Testing of Tachometers, and a small hand pump are required. To test the pump a tank is needed which is merely a 4-inch pipe about 45 inches long, closed at one end. Water is used to fill it.

Although the submerged capsule and electric gage types have not been tested at the Bureau of Standards, it appears that the only special test equipment required in addition to that noted above is a tank of somewhat larger cross-section and perhaps a little deeper.

SIMPLE FLOAT TYPE

In the cases where this type of gage can be used, no trouble is experienced in securing sufficient accuracy and dependability of operation. It is a simple matter to determine whether or not the pointer motion is sufficient for the range of motion of the float and that excessive friction is not present in the mechanism.

DISTANT INDICATING FLOAT TYPE

(a) *Mechanical transmission*.—The presence of excessive friction and the scale errors can be determined by operating the instruments in a laboratory. Service tests are necessary to determine performance factors such as reliability in operation, ease of installation, and ease of repair.

(b) *Performance of Nagel gage*.—Laboratory tests show that the reading of the instrument is unchanged for variations in the rated applied voltage of about 20 percent; that the indications are affected on the average less than 4 percent for a change in temperature of 50° C. of either the indicator or resistance unit; that, for one unit tested, an explosive mixture of acetylene and air maintained on the tank side of the tank unit was not ignited. The latter test indicated that either the stuffing box prevented the gas from getting into the housing of the resistance unit or, if it did, that sparking sufficient to ignite it did not take place. Due to the possible fire hazard it is recommended, however, that the instrument be connected to the battery only when a reading is desired.

(c) *Liquidometer*.—No data are available on the performance of this instrument. It is just being adapted for aircraft use.

HYDROSTATIC GAGE

Common type.—The indicator of this fuel quantity gage is given tests to determine its accuracy as a pressure gage similar to those given air-speed indicators. The tests for the latter are described in reference 20 and will not be described in detail here. The mechanism of these indicators is similar and the range of pressures for which they indicate are of the same order of magnitude. Test results for a typical indicator show that the effect of friction in the mechanism, the drift, and changes in calibration due to seasoning are negligible. Tipping the instrument 90° from the normal operating position causes a change of about 2° of arc; the total amplitude of vibration of the pointer when the instrument is subjected to the standard vibration, and the change in scale errors afterwards, does not exceed 2° of arc; and the maximum difference in reading at any point on the scale for a temperature change from +45° to -35° C. does not exceed about 6° of arc.

The case of the indicators must be leak tight against pressure differences which are estimated not to exceed 10 inches of water.

It is essential that the capacity of the pump be sufficient, under the most unfavorable conditions, to clear the pressure line and the hydrostatic cell of fuel. To test its capacity, the pump is connected by 20 feet of standard tubing to a hydrostatic cell, having an internal volume approximately equivalent to that of the cell C, figure 47. The cell, but not the excess tubing, is submerged in a tank of water to a depth of 40 inches. The pump capacity is deemed ample when one stroke is sufficient to clear the cell and 40 inches of tubing of water which is made evident by bubbles of air rising to the surface. The design of the pump must be such that the forward stroke causes but little suction in the tubing and a forcible return does not give rise to a pressure great enough to harm the indicator.

FUEL-FLOW INDICATORS

Fuel-flow indicators may be classified as follows:

(a) Flow meters which indicate the rate at which the fuel is flowing to the carburetor.

(b) Fuel consumed meters which indicate primarily the quantity of fuel consumed. The rate of fuel consumption can be determined with the use of a stop watch.

(c) Combustion indicators which indicate the extent to which all of the available energy is being obtained from the fuel.

A fuel-flow meter or a combustion meter is useful in adjusting the air-fuel mixture ratio so as to obtain the most economical rate of fuel consumption. A reduction in operating costs and an increase in the cruising radius are two of the advantages gained. Tests have shown that in some cases with the aid of a fuel-flow meter as much as one third of the total amount of fuel consumed may be saved if the mixture ratio is carefully adjusted (reference 55). Due to the fact that an entirely satisfactory instrument has not as yet been developed, the instrument has not come into general use.

The fuel-consumed meter is used in flight tests to measure rate of fuel consumption under various conditions. As time must be measured to determine the rate of flow, the instrument finds little favor in general service.

The first two types can be used with engines in which free-flowing fuels, such as aviation gasoline, are used. The combustion indicator is suitable for use with any type of fuel, including heavy oil.

Fuel-flow meters are either of the venturi or the variable-orifice type. The venturi instrument is an adaptation of the venturi flow meter commonly employed in hydraulic engineering work. The variable-orifice types have been developed in England, the most promising of which is a refinement of the well-known sink and tube type flow meter.

Flow meters for service use on aircraft, and also fuel-consumed meters insofar as they are useful, should have the following ideal characteristics:

(a) They should be designed to have the minimum interference with the fuel supply to the engine. An easily operated bypass, preferably automatic, should be provided for use either in case of failure of the instrument in service or stoppage of the line in case all the fuel flows through the flow meter.

(b) The indicator should be on the instrument panel and be of a type such that no fuel lines need be brought up to the instrument panel. The method of distant indication should be such that the flow meter can be used on multi-engined aircraft.

(c) If possible, the indicator should conform in size and shape to existing service instruments.

(d) The instrument should not add to the fire hazard.

(e) The instrument should not require frequent priming to eliminate air or other gases from the lines leading to the indicator. This procedure is necessary in the ordinary venturi type.

(f) If other requirements are met, an over-all error as great as 5 percent may be tolerated in flow meters for general service use.

FUEL-FLOW METERS

VENTURI TYPE

A diagram of the venturi fuel-flow meter is shown in figure 49. The parts consist of a venturi tube, a differential pressure gage, and connecting tubing. The venturi tube is inserted in the fuel line leading to the carburetor and, as is shown in the figure, is connected with the indicator by means of two copper tubes of small bore.

One tube connects the throat section of the Venturi tube with one side of the diaphragm, or, more exactly, to the interior of a diaphragm capsule, and the other connects the entrance section of the Venturi to the case of the indicator. When fuel flows the fuel pressure is less at the throat section than at the entrance, which difference is indicated by the gauge.

The differential pressure developed by the Venturi tube (reference 53) can be obtained by means of Bernoulli's theorem, which may be stated as follows: The total energy of a liquid flowing in a pipe is equal at one point, if frictional effects are neglected, to the total energy at any other point. If the pipe is horizontal, the theorem may be expressed mathematically as follows:

$$\frac{P_1}{D} + \frac{V_1^2}{2g} = \frac{P_2}{D} + \frac{V_2^2}{2g} \quad (16)$$

where P_1 and P_2 are the static pressures, and V_1 and V_2 the velocities at the points 1 and 2, respectively. D is the density of the liquid and g the acceleration of gravity.

Substituting $\frac{Q}{a_1}$ for V_1 , $\frac{Q}{a_2}$ for V_2 , and P for $P_1 - P_2$ in the above expression there is obtained

$$Q = \sqrt{\frac{2gP}{D}} \frac{a_1 a_2}{\sqrt{a_1^2 - a_2^2}} \quad (17)$$

Here Q is the average volume rate of flow, and a_1 and a_2 the cross-sectional areas of the pipe at points 1 and 2 respectively.

Applying equation (17) to the Venturi tube, the last term, designated M , is called the geometrical constant of the Venturi tube since it depends only upon the areas of the entrance and throat sections. Rearranging

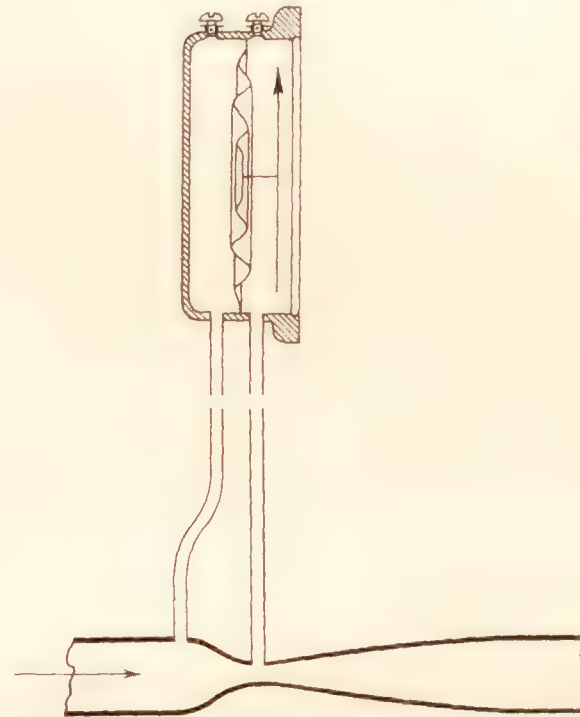


FIGURE 49.—Venturi type fuel-flow meter.

equation (17) and substituting M for its equivalent there results

$$P = \left(\frac{Q}{M} \right)^2 \frac{D}{2g} \quad (18)$$

Inspection of equation (18) shows that the differential pressure P increases as the geometrical constant M decreases. A large value of P is desirable in order to permit the use of as rugged an indicator as possible. A small value of M is obtained when the area a_2 of the throat section is small compared with the area a_1 of the entrance section. Referring again to equation (18) it may be seen that an error in indication is introduced by deviations of the density of the fuel from the value used in calibrating the instrument. For small changes in the density of the fuel the reading of the instrument at a given volume rate of flow increases one half percent for each 1 percent increase in the density.

There is considerable objection from the viewpoint of safety of the pilot in an accident to having fuel at the instrument board. In the ordinary instrument the case

is completely filled with fuel and the cover glass is required to retain it under the pressure of the fuel pump. As a further safeguard the Bureau of Standards has recently developed for the Bureau of Aeronautics of the Navy Department an indicator which contains two pressure-sensitive capsules. The venturi tube is connected to the interior of the capsules, and fuel therefore does not fill the case of the indicator. The arrangement of the mechanism is such that it is prac-

tically insensitive to variations in the pressure developed by the fuel pump, but is responsive to variations in the differential pressure developed by the venturi tube.

A primary difficulty with venturi flow meters of the conventional type is the necessity that the lines to the indicator and the pressure capsules be entirely filled with liquid. The presence of air or gas in the lines causes errors so large as to make the indication worthless. Each of the lines can be vented to the atmosphere at the indicator end, but this is not a safe procedure under all conditions. Connecting the lines to each other at their highest points through a valve has been suggested, thus utilizing the differential pressure of the venturi tube to clear the lines of gas. This arrangement works only when the installation is such that the head of gas in the lines to the indicator is less than

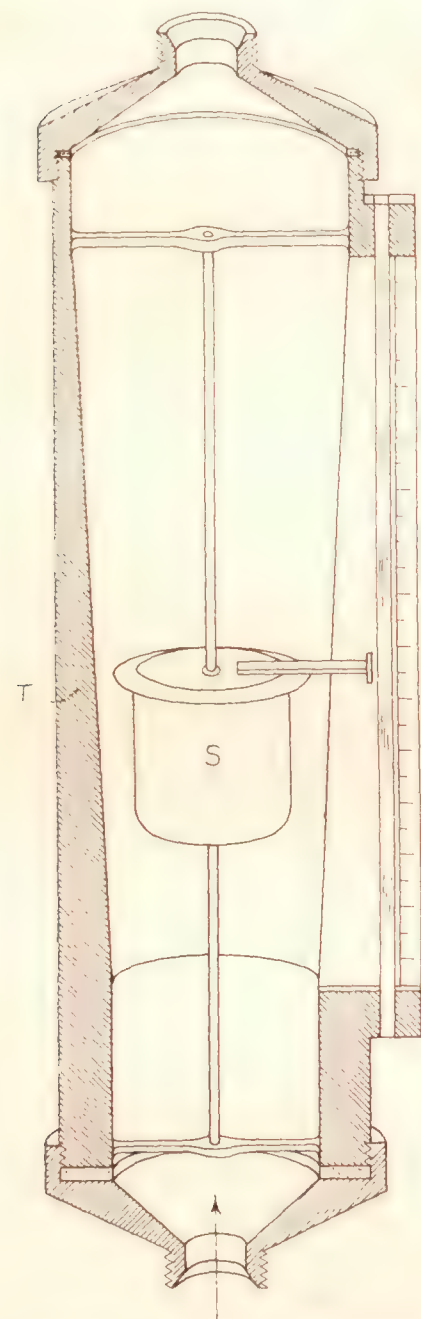


FIGURE 50.—Orifice and sink type fuel-flow meter.

the differential pressure developed by the venturi tube.

VARIABLE ORIFICE FLOW METER

A diagram of the variable orifice fuel-flow meter as modified by Griffith (reference 55) is shown in figure 50. Referring to the figure, a sink *S* having a knifed-edge disk for its upper surface, is free to move vertically along the axis of a tapered tube, *T*, being guided in its movement by a central post. The sink carries a pointer to indicate its position with reference to a scale graduated in weight of fuel per hour and affixed to the body of the tube. Fuel entering the lower end of the instrument raises the sink until its weight is balanced by the dynamic pressure of the fuel against it. The fuel passes through the annular orifice between

the edge of the disk and the tapered tube and then out through the upper end of the instrument to the carburetor. It follows that the drop in pressure across the instrument is constant.

When the rate of flow of fuel is constant the sink is suspended in equilibrium by a system of forces related as follows:

$$\frac{1}{2} D_f V^2 = \frac{W_a}{A} \quad (19)$$

where D_f is the density of the fuel, V the velocity of the fuel through the orifice, W_a the weight of the sink when submerged in the fuel and A the area of the disk. In this equation the left-hand member represents the dynamic pressure exerted upward against the under side of the sink. The right-hand member represents the downward pressure due to the weight of the submerged sink

However,

$$W_a = gv(D_s - D_f) \quad (20)$$

where v is the volume and D_s the density of the sink. Substituting this value of W_a in equation (19) and solving for V ,

$$V = \sqrt{\frac{2gv(D_s - D_f)}{AD_f}} \quad (21)$$

The equation for the mass rate of flow through an orifice is as follows:

$$M = KaVD_f \quad (22)$$

where M is the mass rate of flow of the fuel, K the discharge coefficient, and a the area of the orifice.

Substituting for V from equation (21)

$$M = Ka\sqrt{\frac{2gv(D_s - D_f)D_f}{A}} \quad (23)$$

Since the vertical displacement of the sink determines a , the area of the orifice, it is also a measure of the mass rate of flow M .

Inspection of equation (23) shows that, for a given mass rate of flow the reading of the instrument, which is proportional to a , and the densities of the fuel and sink have the following relation:

$$\frac{1}{a} \propto \sqrt{(D_s - D_f)D_f} \quad (24)$$

In order that there be a minimum change in the reading with variations in D_f , it is necessary that the derivative with respect to D_f of the right-hand member of equation (24) equal zero. This is the case when $D_s = 2D_f$; that is, when the density of the sink is twice the density of the fuel. If this relation holds for one density of the fuel, the error in indication is only 0.8 percent for a variation of 12 percent in the fuel density.

Up to the present the instrument is stated to be useful only in flight testing. It is not used on service airplanes mainly because of the added complication in installing and maintaining the fuel lines and partly

because of the difficulty of finding a suitable place to install an instrument of such an unusual shape. In common with other types of flow meters, all of the fuel must pass through the instrument and therefore close to the pilot, which, in view of the window entails an extra hazard in case of accident. The fuel just ahead of the instrument must be filtered, since it is sensitive to minor obstructions in the flow. A bypass is usually provided.

VANE TYPE FLOW METER

In the R.A.E. (British) vane type flow meter, the pressure of the flowing fuel upon a rotatable vane is balanced by the action of a spring (references 5, 11, and 17). The axis of the vane is offset from that of its case, so that the space between the case and the vane, or orifice, varies with the position of the vane. In effect it is a variable orifice, variable pressure drop type instrument.

Difficulties are experienced in obtaining the same state of turbulent flow under all conditions of use.

charge of the fuel to the individual cylinders. Some form of revolution counter is attached either directly to the wobble plate shaft or indirectly by means of a flexible drive shaft.

The fuel-consumed meter is highly accurate (in instruments available the error does not exceed 0.01 gallon per gallon of fuel delivered). It is readily installed by inserting it at any convenient point in the fuel line between the fuel pump and the carburetor. Since the total quantity of fuel used is indicated it may be used as an independent, although not certain, means of determining the quantity of fuel remaining in the tank. Average rates of flow may be obtained by measuring the time with a stop watch for a selected volume of flow, but this procedure is unsatisfactory in general service. An objectionable feature is the danger of restriction to the flow of the fuel which necessitates the installation of a manually operated bypass. There is the further disadvantage in the necessity for tight stuffing boxes in the instrument with a mechanical method of transmission, and the fire

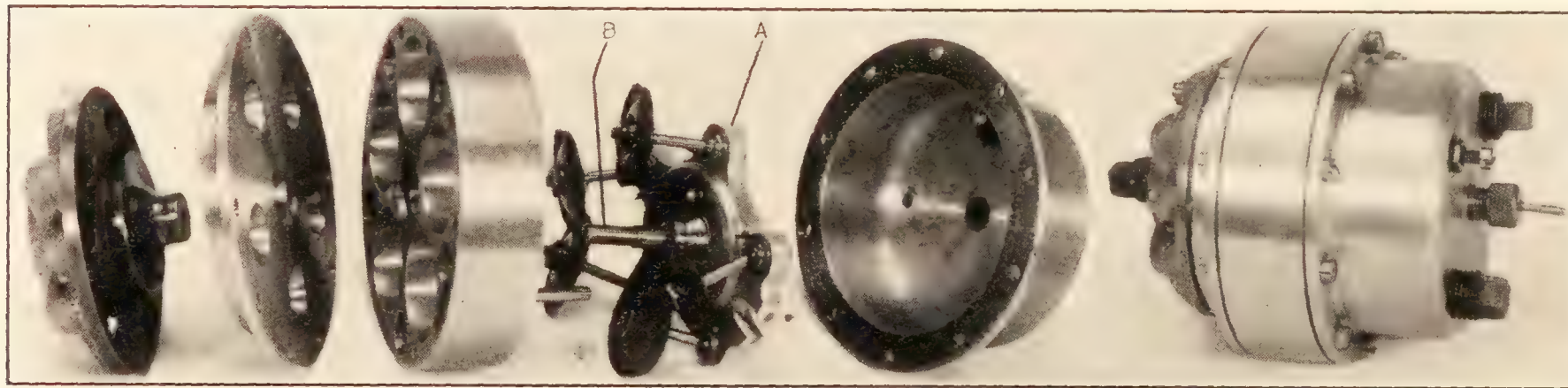


FIGURE 51.—“Western” fuel-consumed meter.

Bubbles of gas in the fuel, which appear with increase in the altitude of flight, affect the readings. The above two difficulties appear to be inherent so that the instrument remains an experimental type. As the force on the spring varies as the square of the rate of flow, the force decreases rapidly with the rate of flow, so that low rates cannot be measured.

FUEL-CONSUMED METERS

The fuel-consumed meter is essentially a displacement pump equipped with a counting device for integrating the revolutions of the pump shaft. The counting device is usually graduated in terms of volume of fuel flowing through the pump. Pump units usually have five cylinders with their axes parallel and arranged symmetrically around the shaft.

A design typical of the fuel-consumed meter is shown in figure 51. The five pistons are connected to wobble plate **A** which is pivoted to shaft **B** by means of a large ball bearing set at an angle to the shaft. With this arrangement the reciprocating motion of the pistons causes the shaft, to rotate. A valve plate which is rotated by the shaft controls the delivery and dis-

charge of the fuel to the individual cylinders. Some form of revolution counter is attached either directly to the wobble plate shaft or indirectly by means of a flexible drive shaft.

BOWSER

The Bowser fuel consumed meter is distant indicating. The pump unit includes an electrical make-and-break mechanism which is connected to the wobble plate shaft and is submerged in transformer oil in order to eliminate the danger from sparking. The indicator unit consists of a counter operated by a solenoid the electrical circuit of which is interrupted by the make-and-break mechanism. The power is furnished by a 12-volt battery or its equivalent. The pump capacity is such that every time the solenoid is energized, which is twice in every revolution of the wobble plate shaft, 0.01 gallon of fuel is delivered. One hand of the counter makes one revolution for each gallon of fuel consumed and indicates by steps of 0.01 gallon. Another hand is provided which rotates once for each 10 gallons. A pressure varying from 0.25 to 0.50 pounds per square inch is required to operate the pump unit. The weights of the pump unit and revolution counter are 9 $\frac{3}{8}$ and 1 $\frac{3}{8}$ pounds, respectively.

WESTERN

In this instrument, which is shown in figure 51, the pistons are made of leather cup washers. The indication is secured by means of a small revolution counter attached to the wobble plate shaft. The weight of the pump unit is $2\frac{1}{4}$ pounds.

COMBUSTION INDICATOR

It is obvious that the most economical functioning of the engine is obtained when the amount of the combustible gases in the exhaust is relatively small. The Moto Vita combustion meter (reference 57) indicates the energy available in the unburned gaseous products in the exhaust of the engine.

The instrument is based upon the catalytic property of heated platinum to cause chemical combination, or combustion, upon its surface of a mixture of combusti-

regulator is used to compensate for variations in the voltage supply.

The exhaust gases consist principally of methane (CH_4), carbon monoxide (CO), hydrogen (H_2), and more complex compounds. In burning, these gases liberate widely varying amounts of energy per molecule and thus the heating of the exposed wires depends upon the composition as well as the amount of the combustible gases. The instrument therefore indicates only the latent calorific value of the energy remaining in the exhaust.

The combustion indicator indicates the efficiency of combustion without regard to any design characteristics of the engine, viz, speed, power, etc., is distant indicating, requires no modification of the fuel line for its installation, and is applicable to heavy-oil engines as well as those burning lighter fuels.

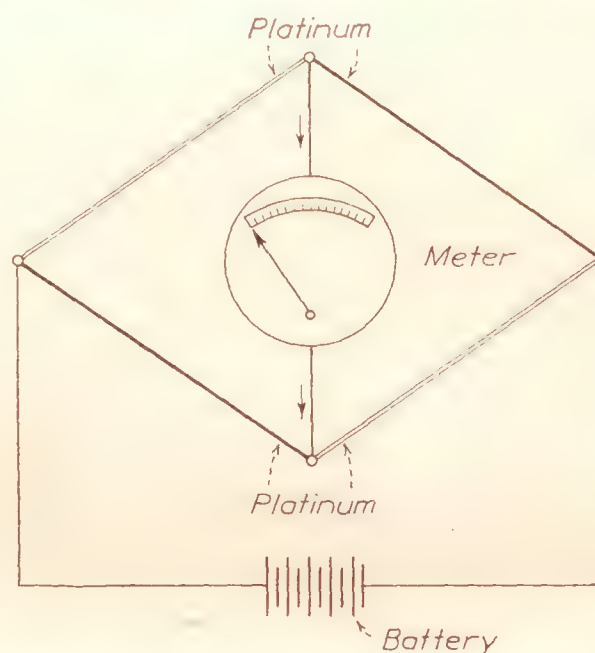
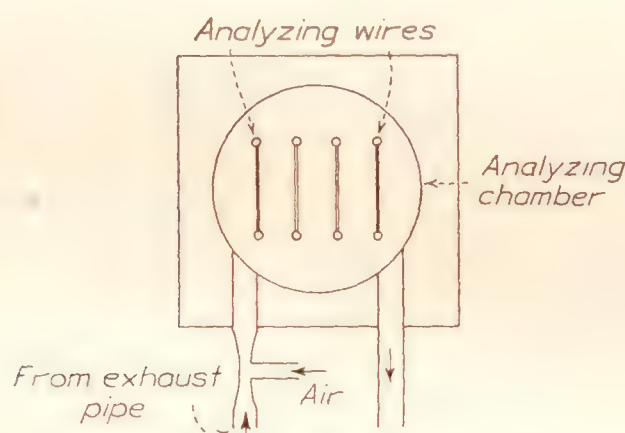


FIGURE 52.—Diagram of combustion indicator.

ble vapors and oxygen. It is essentially an unbalanced Wheatstone bridge an electrical diagram of which is shown in figure 52. It has three parts—the combustion element, the indicator, and a battery. The four platinum wire resistances of the Wheatstone bridge are mounted in the combustion element, or analyzing chamber, so that a constant-ratio mixture of exhaust gas and air passes over them. Two of the wires are protected from the exhaust gases by means of tubing, presumably glass. All of the wires are heated electrically, including the nonactive wires, in order to avoid errors due to differences in temperatures. Since all four legs of the bridge are mounted in the analyzing chamber and are therefore at the same temperature, as long as only noncombustible gases are present, their resistances increase equally and the circuit remains in balance. Upon the admission of a mixture of a combustible gas and air, combustion occurs only on the surface of the bare wires, which increases their temperature, and consequently their resistance, over that of the covered wires of the bridge. A ballast type voltage

LABORATORY TESTING OF FUEL-FLOW INDICATORS

APPARATUS

The apparatus used in the calibration of fuel-flow meters and fuel consumed meters consists of an elevated tank, a graduated flask, a supply tank, and a return pump driven by an induction motor. The instrument is connected at a point in the copper tube line from the elevated tank to the graduated flask so as to be subjected to the desired head of liquid. The fuel flows under gravity from the elevated tank, through the instrument being tested, and then into the graduated flask from which it is dumped into the supply tank. The pump then returns the fuel to the reservoir. In practice the pump is operated continuously, so that, regardless of the rate at which the fuel is passing through the instrument, practically a constant head of fuel is maintained in the reservoir, the excess fuel being conducted to the supply tank through an overflow pipe. At each test point the average volume rate of flow of fuel is obtained by measuring with a stop watch the

time required for a definite quantity of fuel to flow into the measuring flask. The rate of flow is controlled by means of a variable orifice.

TESTS

Up to the present, tests on flow meters, fuel-consumed meters, and combustion meters have not been standardized, nor have they been developed so as to determine the performance of the instruments under all of the conditions of use on aircraft. Development of these tests for flow meters has not been justified in view of (a) the large gap between the ideal characteristics and the actual performance and (b) the consequent fact that the instruments are used but little. Fuel-consumed meters have a fine performance in most respects but are little used on aircraft mainly because they do not indicate directly either the fuel flow or fuel quantity available, and partly owing to the somewhat unsatisfactory design of the mechanism for securing distant indication. Combustion indicators are highly experimental with respect to their usefulness and appear, in the present design, to be insufficiently rugged for service use on airplanes.

Only the primary tests on flow meters and fuel-consumed meters will be described.

Scale error.—The scale errors of both fuel flow meters and fuel-consumed meters are determined by means of the apparatus described above. The scale error of the instrument under test is the difference between its reading and the average rate of flow. The liquid used should have very nearly the density of that used as the standard in calibrating the instrument, otherwise a correction must be made based on the experimentally determined effect of the variation from this density.

Density effect.—The effect of variation in the density of the fuel is determined by scale error tests in which two or three fuels, or equivalent liquids of various densities, are used successively. Since the effect of changes in density is predicted theoretically for most available types of flow meter, and is presumably zero for the fuel-consumed meter, the test needs to be made only once on each type in order to establish the validity of the predicted effect.

Pressure error.—The effect of variation of fuel pressure on the reading of an instrument is obtained from scale error tests in each of which the instrument is subjected to a different head of liquid. These heads are within the extremes of pressure which may occur in service. It is obvious that the effect should be negligible within small limits for both flow meters and fuel-consumed meters.

Other tests.—The power to operate, or the pressure drop across, fuel-consumed meters must be reasonably small in comparison with the ordinary value of fuel

pressure. Further their reading should be independent, within reasonable limits, of the rate of flow.

In addition to the above tests, flow meters and fuel-consumed meters should conform to the usual requirements for aircraft instruments relative to (a) freedom from position error, (b) vibration effects and (c) operation in the temperature range which may be experienced. The tests for these errors are similar in nature to those described for pressure gages or tachometers.

MANIFOLD PRESSURE GAGES

Supercharging is accomplished either (a) by increasing the pressure of the air entering the carburetor or, more commonly, (b) by increasing the pressure of the fuel-air mixture after it leaves the carburetor and before it reaches the engine. In order to control the amount of supercharging it is necessary for the pilot to know the absolute pressure of the air or fuel-air mixture after leaving the supercharger. The instrument used to indicate this pressure is now known as a "manifold pressure gage", but until 1933 was called a "supercharger pressure gage."

In case method (a) is used, the fuel pressure must be in excess of the supercharger outlet pressure and the installation of the fuel pressure gage must be such that this excess is indicated. This is accomplished by making the case of the fuel pressure gage airtight and connecting it to the carburetor. This type of fuel pressure gage and the supercharger gage are sometimes combined to form a unit known as a "supercharger gage unit."

DESCRIPTION OF GAGE

The manifold pressure gage is essentially an aneroid altimeter with a leak-tight case. As shown in figure 53, the instrument contains a diaphragm capsule, which is evacuated, and a suitable mechanism for multiplying its deflections. As is now the usual practice in this country, the diaphragm capsule is without a restraining spring, except for the hairspring. The range of the latest instrument is from 10 to 50 inches of mercury of absolute pressure. Instruments constructed before 1933 were calibrated in altitude units with a range, as shown in figure 53, from $-10,000$ to $+20,000$ feet (13.75 to 42.45 inches of mercury). As knowledge of the absolute pressure is required, the dial is nonadjustable, in contrast with that of the altimeter. In the latest design an adjustable dial, visible through a circumferential slot in the main dial, is provided in order to indicate permanently the allowable degree of supercharging for the particular engine. The inside of the case is connected by means of metal tubing to the intake manifold of those engines in which the fuel-air mixture is compressed and to the carburetor of those in which only the air passes through the supercharger.

Since the accuracy required of the manifold pressure gage is not as great as in the case of the altimeter, its construction from this angle presents no great difficulty. The case is specified to be leak tight and strong enough to withstand a pressure above atmospheric of



FIGURE 53.—Manifold or supercharger pressure gage.

20 pounds per square inch. Cover glasses one eighth inch thick and of the diameter required have been found on the average to withstand a differential pressure of over 25 pounds per square inch. It is further necessary to design the diaphragm capsule and mechanism to withstand reasonable pressures above and below the range. Surges in the pressure within the instrument case are greatly minimized by the insertion of a capillary tube in the fitting attached to the case. This is accomplished most simply by threading the hole in the fitting and inserting a machine screw to the proper depth.

The case of the instrument is of the standard $2\frac{3}{4}$ inch dial size and is usually made of a phenol condensation product. The instrument weighs 9 ounces.

APPARATUS FOR TESTING GAGES

The apparatus required to make the scale error test is shown diagrammatically in figure 54. A hand

pump **P** is used to obtain pressures above atmospheric and a vacuum pump **S** to obtain those below atmospheric. The difference in height of the mercury columns of the manometer is measured at each test point. To obtain the absolute pressure requires in addition the value of the atmospheric pressure which requires reading a mercurial barometer.

The heights of the mercury column of the manometer and barometer must be corrected for scale error and reduced to the standard conditions of temperature and acceleration of gravity. It is assumed that the scale errors are either negligible or known. The reduction to standard temperature can be made by subtracting 16×10^{-5} mm per mm (or inch per inch) of height of column for every degree centigrade the manometer or barometer is above 0° C. The reduction to the standard value of the acceleration of gravity can be made by subtracting 8×10^{-5} mm per mm (or inch per inch) of height of column, for each degree of latitude the station is below 45 degrees. Similarly when the latitude exceeds 45 degrees this amount is added. The above constants are first order approximations which are sufficiently accurate for use in testing supercharger pressure gages. The absolute pressure when above atmospheric, is obtained by adding the corrected height of the manometer mercury column to the corrected barometer reading, and when below atmospheric, by subtracting it from the barometer reading.

For gages calibrated in altitude units the altitude in the standard atmosphere corresponding to the pressure is then obtained from convenient tables. The

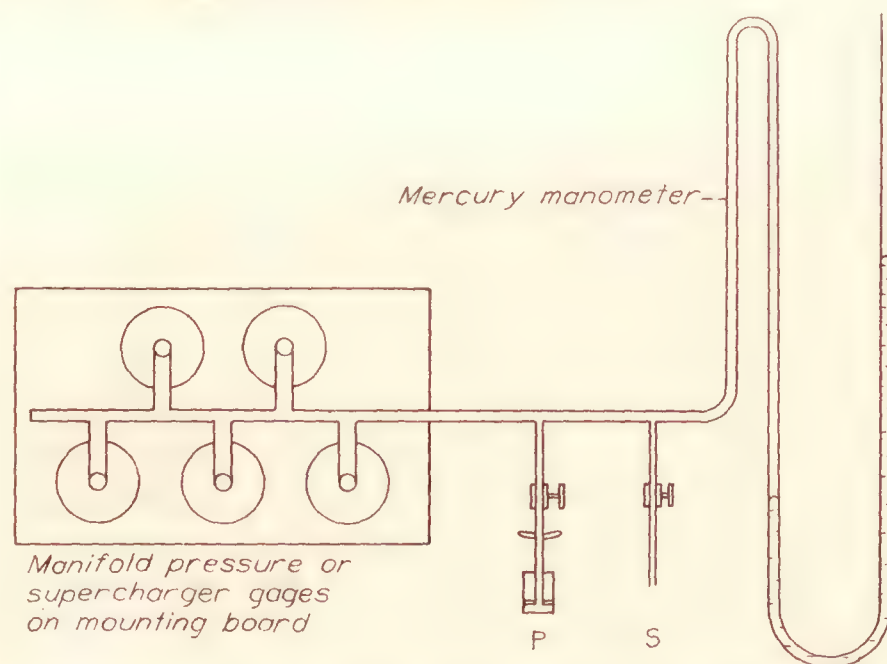


FIGURE 54.—Apparatus for testing manifold or supercharger pressure gages.

standard altitude-pressure table (reference 9) is given in table II.

It should be noted that other procedures may be followed in reducing the column heights to those under standard conditions. Tables of the corrections such as those given in the Smithsonian Meteorological Tables are preferred by most observers.

TABLE II
ALTITUDE-PRESSURE TABLE FOR CALIBRATING
MANIFOLD PRESSURE GAGES

Altitude, feet	Pressure		Altitude, feet	Pressure	
	Mm of mercury	Inches of mercury		Mm of mercury	Inches of mercury
-10,000	1,078.1	42.44	6,000	609.9	23.98
-9,000	1,042.2	41.03	7,000	586.4	23.09
-8,000	1,007.2	39.65	8,000	564.4	22.22
-7,000	973.1	38.31	9,000	543.2	21.38
-6,000	940.0	37.01			
-5,000	907.8	35.74	10,000	522.6	20.58
-4,000	876.6	34.51	11,000	502.6	19.79
-3,000	846.1	33.31	12,000	483.3	19.03
-2,000	816.6	32.15	13,000	464.5	18.29
-1,000	787.9	31.02	14,000	446.4	17.57
0	760.0	29.92	15,000	428.8	16.88
1,000	732.9	28.86	16,000	411.8	16.21
2,000	706.6	27.82	17,000	395.3	15.56
3,000	681.1	26.81	18,000	379.4	14.94
4,000	656.3	25.84	19,000	364.0	14.33
5,000	632.3	24.89	20,000	349.1	13.75

A standard for measuring the pressure more convenient and logical than the manometer and barometer combination is an altitude mercurial barometer in which the tube and scale are made long enough to measure also the pressures above atmospheric.

For determining the scale errors at airports or other field stations, apparatus similar to that shown in figure 54 is required except that the mercury manometer is eliminated. A calibrated supercharger or manifold pressure gage is used as the standard and is installed on the mounting board together with the instruments under test.

The temperature chambers and vibration board for testing the gages for the effect of temperature and vibration are similar to those described in section A of Laboratory Testing of Tachometers.

PERFORMANCE OF GAGES

The scale errors of a manifold pressure gage are determined by comparing its reading at a number of points over the range of indication with the pressures determined by means of a mercury monometer and barometer or its equivalent. The readings are made while the pressure is held constant both for decreasing and increasing pressures.

GAGE CALIBRATED IN ALTITUDE UNITS

The results of a scale error test made on a high quality instrument calibrated in altitude units as shown in figure 53 are given in table III, in which a positive sign means that the instrument reads too high and a negative sign, too low. It should be noted that the least reading of the instrument is 50 feet and that the highest accuracy is required at and near zero altitude, at which point a reasonable tolerance is an error of 250 feet.

The effect of changes in temperature of the gage upon the scale errors is obtained in tests made at +45° C. and -35° C. The scale errors at these tempera-

tures of the instrument referred to above are given in table III. The average change in reading in this temperature interval is 310 feet, for which a reasonable tolerance is 350 feet. The change in reading at zero altitude should be small, not exceeding about 200 feet.

TABLE III
SCALE ERRORS OF A MANIFOLD PRESSURE GAGE

Standard altitude, feet	Scale errors, in feet, at—		
	+30° C.	+45° C.	-35° C.
-10,000	-150	-100	-100
-6,000	0	+100	-50
-4,000	0	+150	-100
-2,000	0	+150	-150
-1,000	-50	+50	-100
0	0	+50	-100
1,000	+50	+50	-150
2,000	0	0	-150
4,000	0	0	-250
6,000	-50	+50	-300
8,000	0	+150	-250
10,000	0	+50	-300
12,000	+100	+200	-300
16,000	+50	+300	-400
20,000	0	+200	-600

The instrument is tested on the vibration apparatus for the amount of pointer oscillation in the frequency range 1,000 to 2,000 c.p.m. and for change in zero reading resulting from 3 hours' vibration. No parts should work loose. The pointer should not oscillate with respect to the dial more than an amount equal to about 200 feet. The change in reading at zero altitude of good quality instruments does not exceed 100 feet, or twice the least reading.

The damping of the instruments has been found to be satisfactory if the time for the reading to change from 20,000 to 5,000 feet, when the inside of the case initially at a pressure corresponding to 20,000 feet of altitude is suddenly opened to the atmosphere, is between 1 and 2 seconds.

The instruments may be subjected in service to differential pressures equal on one hand to those of the maximum altitude of flight of the aircraft and on the other hand to positive pressures, owing to surges, in excess of that corresponding to -10,000 feet of altitude. Their effect on the calibration should be negligible. As outside practical limits, absolute pressures of 7 and 25 pounds per square inch are selected. The instrument is given scale-error tests before and after being subjected to these pressures and has been found to have average changes in scale errors within the least reading or 50 feet.

The position error is the change in reading of the instrument when it is oriented from the normal position of dial vertical and pointer vertical to any other position. This change does not exceed the least reading, or 50 feet, in well-balanced instruments.

The case of the instrument must be leak tight against the difference in pressures corresponding to that between altitudes of -10,000 and +20,000 feet.

The instrument case should, as a safety provision, withstand a differential pressure greatly in excess of that corresponding to the pressure range of the instrument. The cases are made to withstand while subjected to vibration a pressure of 20 pounds per square inch. Sample cases without the mechanism are tested and are considered satisfactory if leak tight after the application of the pressure.

GAGE CALIBRATED TO READ PRESSURE

The manifold pressure gage calibrated to read in units of pressure from 10 to 50 inches of mercury for a pointer motion of about 320° of arc is given the tests described for the gage calibrated in altitude. No test results are available on the pressure-indicating instrument. On the basis of the results on altitude-reading gages reasonable tolerances are as follows: Scale error, 0.25 inch of mercury; average change in reading due to temperature, 0.5 inch of mercury; change in reading at 30 inches of mercury due to temperature, 0.2 inch of mercury; pointer oscillation under vibration, 0.2 inch of mercury; change in reading due to vibration, 0.15 inch of mercury; and position error, 0.1 inch of mercury.

BUREAU OF STANDARDS,
WASHINGTON, D.C., May 31, 1933.

REFERENCES

GENERAL

1. Campbell, Albert: On Test-Room Methods of Alternate Current Measurements. *Journ. Institution Elect. Eng.*, v. 30, p. 889, 1901.
2. Brooks, H. B.: The Accuracy of Commercial Electrical Instruments. *Journ. Amer. Inst. Elect. Eng.*, v. 39, p. 117, 1920.
3. Mendenhall, C. E.: Aeronautic Instruments. *Journ. Franklin Institute*, v. 191, p. 57, 1921.
4. Griffiths, E. A.: Engineering Instruments and Meters. D. Van Nostrand Co., 1921.
5. Bureau of Standards: Power Plant Instruments. N.A.C.A. Technical Report No. 129, 1921.
6. Keinath, G.: Die Technik der elektrischen Messgeräte. R. Oldenbourg, 1922.
7. Bennowitz, Kurt: Flugzeuginstrumente. R. C. Schmidt & Co., Berlin, 1922.
8. Drysdale, C. V., and Jolley, A. C.: Electrical Measuring Instruments. Ernest Benn, Ltd., 1924.
9. Diehl, W. S.: Standard Atmosphere Tables and Data. N.A.C.A. Technical Report No. 218, 1925.
10. Kinnard, I. F., and Faus, H. T.: Temperature Errors in Induction Watt-Hour Meters. *Jour. Amer. Inst. Elect. Eng.*, v. 44, p. 241, 1925.
11. Eaton, H. N., and others: Aircraft Instruments. Ronald Press, 1926.
12. Brombacher, W. G.: Recent Development in Aircraft Instruments, *Trans. A.S.M.E. Aero. Eng.*, v. 51, p. 119, 1929.
13. Air Corps: Aircraft Instruments. Pamphlet No. 1170-50, 1929.

14. Brombacher, W. G., and Melton, E. R.: Temperature Coefficient of the Modulus of Rigidity of Aircraft Instrument Diaphragm and Spring Materials. N.A.C.A. Technical Report No. 358, 1930.
15. Henrickson, H. B.: Thermometric Lag of Aircraft Thermometers, Thermographs and Barographs. *Bureau of Standards Journal of Research*, v. 5, p. 695, 1930.
16. Subcommittee on Instruments: Present Status of Aircraft Instruments. N.A.C.A. Technical Report No. 371, 1930.
17. Stewart, C. J.: Aircraft Instruments. Chapman & Hall, Ltd., 1930.
18. General Electric Co.: New Aircraft Indicating Instruments. *Instruments*, v. 4, p. 129, 1931.
19. Zand, S. J.: A study of Airplane and Instrument Board Vibration. *S.A.E. Trans.*, v. 26, p. 513, 1931.
20. Beij, K. Hilding: Aircraft Speed Instruments. N.A.C.A. Technical Report No. 420, 1932.

TACHOMETERS

21. Boudon, Alfred: Les Tachymetres Electromagnetiques (Magnetic Tachometer) *La Revue Technique*, v. 18, p. 388, 1897.
22. Benischke, G.: Elektrische Geschwindigkeitsmessapparate. *Electrotechnische Zts.*, v. 24, p. 401, 1903.
23. Watch and Clock Escapements. *The Keystone*, 1904 (Organ of the Jewelry and Optical Trades) 19th and Brown Sts., Philadelphia, Pa.
24. Lux, F.: Frahm's Geschwindigkeitsmesser. *Zt. des Vereines Deutschen Ingenieure*, v. 48 II, p. 1580, 1904.
25. The Tel Revolution Indicator for Aircraft. *Flight*, v. 4, p. 943, 1912.
26. Esterline Electric Speed Indicator (d.c. generator type). *Elect. Rev. and West. Eng.*, v. 66, p. 829, 1915.
27. Wilke, W.: Drehzahl-und Fahrt Fernzeiger für Flugzeuge und Luftschiffe. *Der Motorwagen*, v. 21, pp. 461 and 492, 1918.
28. Wilke, W.: Untersuchung über Fliehkraft Tachometer nach dem Drehpendel Prinzip. *Zt. des Vereines Deutschen Ingenieure*, v. 62, pp. 801-809, pp. 829-835, 1918.
29. Feely, F. J.: The Van Sicklen Chronometric Tachometer. *Aviation*, v. 8, p. 138, 1919.
30. Bureau of Standards: Testing of Airplane Tachometers, *Air Service Information Circular*, v. 1, No. 61, 1920.
31. Hunt, F. L.: Recent Developments and Outstanding Problems. N.A.C.A. Technical Report No. 132, 1921.
32. Pritschow, K.: Gerät zur Beobachtung umlaufender Teile in Scheinbarer Ruhe. *Werkstattstechnik*, v. 19, p. 246, 1925.
33. Seguin, L. and A.: A New Stroboscopic Method of Great Intensity. *Comptes Rendus*, v. 181, p. 539, 1925.
34. Hunt, F. L.: New Types of Aircraft Instruments. *Jour. Opt. Soc. Am. and Rev. Sci. Inst.*, v. 12, p. 227, 1926.
35. Lenckh, H. E., and Vieweg, R.: Über Stroboskopische Beobachtungen. *Archiv f Elektrotechnik*, v. 15, p. 509, 1926.
36. Huey, C.: Tachometers, Revolution Indicators, Speed Indicators, and Revolution Counters. Types and Principles of Operation. *Journ. Am. Soc. Naval Eng.*, v. 39, p. 30, 1927.
37. Engine Revolution Indicator and Recorder for Aeroplanes. (Hasler-Tel Recorder) *Engineering (London)*, v. 124, p. 168, 1927. *Aero Digest*, v. 12, p. 196, 1928.
38. A C Airplane Tachometer. *Aviation*, v. 25, p. 281, 1928.
39. Stocks, C. W.: Motor-Vehicle Performance: Indicating and Recording Devices. (Hasler-Tel Recorder) *S.A.E. Journ.*, v. 27, p. 534, 1930.

40. Standerwick, R. G.: A New Form of Stroboscope. *Gen. Elect. Review*, v. 33, p. 566, 1930.
41. Jones, D. A.: The R.A.E. Automatic Observer Mark IA. *Brit. Aero. Res. Com. Reports and Memo. No. 1405*, 1931.
42. Speed-Measuring Instrument (Ashdown rotoscope). *Electrical Review (London)*, v. 109, p. 708, 1931.
43. Hoff, W.: Research Work of the D.V.L. *Jour. Roy. Aero. Soc.*, v. 35, p. 778, 1931.
44. Bartlett, B. W.: The Rotating Sector Disc. *Rev. Sci. Inst.*, v. 2, p. 96, 1931.
45. Electric Speedometer (Stewart-Warner) Automotive Ind., v. 64, p. 557, 1931.
46. Lord Rayleigh: On the Bending and Vibration of Thin Elastic Shells. No. 152, *Scientific Papers*, vol. III, p. 230, 1887-92.
47. Mauerer, L.: Deformation gekrümmter elastischer Platten. *Archiv. d. Math. und Physik*, Leipzig (3), v. 6, p. 1 and 260, 1903.
48. Lemkes, C. R. L.: Pressure Gauges, Their Construction and Use. *Mechanical World*, Nov. 23, 1894.
49. Wagner, E.: Metall Manometer als Hochdruckpräzisionsmeter. *Ann. d. Physik* (4), v. 15, p. 906, 1904.
50. Klein, G.: Untersuchung und Kritik von Hochdruckmessen. Dissertation, Königl. Tech. Hochschule, Berlin, Sept. 1908.
51. Lorenz, H.: Theorie der Röhrenfedermanometer. *V.D.I.*, v. 54, p. 1865, 1910.
52. Sunatani, Chido. The Theory of a Bourdon Tube Pressure Gauge and an Improvement in its Mechanism. *Sendai Univ. (Japan) Technologic Reports*, v. 4, p. 69, 1924.
53. Fluid Meters, Their Theory and Application. Report of the A.S.M.E. Special Research Committee on Fluid Meters, part 1, second edition, 1927.
54. Engine Temperature Indicator for Aircraft. *Instruments*, v. 2, p. 476, 1929.
55. Kerr, P. S.: Fuel Flowmeters Designed to Measure Mass Flow. *Brit. Aero. Res. Com. Reports and Memo.*, No. 1245, 1929.
56. New Airplane Gasoline Gauge. *Instruments*, v. 2, p. 467, 1929.
57. Measuring Unconsumed Gases in Exhaust. *Aviation*, v. 30, p. 57, 1931. Also, Brochure by Motometer Gauge & Equipment Corp.
58. Susa, Chas.: Determining Range of Helical Bourdon Springs. *Instruments*, v. 5, p. 85, 1932.
59. Rolnik, H. A.: Deflection of Bourdon Tubes. *Instruments*, v. 6, p. 52, 1933.

REPORT No. 467

THE EXPERIMENTAL DETERMINATION OF THE MOMENTS OF INERTIA OF AIRPLANES

By HARTLEY A. SOULÉ and MARVEL P. MILLER

SUMMARY

The application of the pendulum method to the experimental determination of the moments of inertia of airplanes is discussed in this report. Particular reference is made to the effects of the air, in which the airplane is immersed, on the swinging tests and to the procedure by which these effects are taken into account.

Consideration of the effects of the ambient air has shown that the virtual moment of inertia of the airplane about any given axis of oscillation must be regarded as made up of three distinct parts; namely, that of the structure, that of the air entrapped within the structure, and that of the apparent additional mass of external air influenced by the airplane's motion. As the true moment of inertia consists only of the moments of inertia of the structure and the entrapped air, the apparent additional moment of inertia due to the influence of the external air is determined and deducted from the virtual moment of inertia. The apparent additional moment of inertia is obtained by computations utilizing the results of experiments made to determine the additional-mass effect for plates of various aspect ratios.

The procedure described in this report has been used for some time, and the data on several airplanes for which the moments of inertia have been found are included. The precision is believed to be within limits of ± 2.5 percent, ± 1.3 percent, and ± 0.8 percent for the X, Y, and Z axes, respectively.

INTRODUCTION

The necessity for precise values of moments of inertia of airplanes has arisen, particularly in connection with the study of spinning. Because of the demands of this problem, the National Advisory Committee for Aeronautics has developed apparatus and procedure for adapting for airplanes the familiar pendulum method of determining the moments of inertia of small dense bodies. Two major difficulties were encountered in the application of this method to the determination of the moments of inertia of airplanes. The first concerned the development of a system of suspension whereby the suspended body could be made to oscillate solely about a single well-defined axis. Essential features of the apparatus eventually found to be suitable and data

obtained by swinging tests with this apparatus have been previously reported in references 1 and 2. The second difficulty concerned the effect of the medium in which the experiments were performed, an effect which was large because of the low mass density of the airplane and hard to determine because of its irregular shape.

The purpose of the present paper is to give a complete discussion of the determination of the moments of inertia of airplanes by the pendulum method, with particular reference to the effects of the ambient air on the moments of inertia, and the procedure by which these effects are taken into account. A description of the apparatus and test procedure used by the N.A.C.A. and the data for several airplanes for which the moments of inertia have been found are included.

During the preparation of the paper, Mr. Miller, who performed most of the experimental work, died, and the paper was completed by Mr. Soulé.

APPLICATION OF PENDULUM METHOD TO AIRPLANES

BASIC EQUATIONS

For an undamped pendulum oscillating with small amplitude in a vacuum, the equation of motion is

$$I \frac{d^2\theta}{dt^2} + b\theta = 0 \quad (1)$$

where I is the moment of inertia about the axis of oscillation

b is a constant depending on the dimensions and weight of the pendulum

and θ is the angular displacement of the pendulum. From the solution of this equation, the period of oscillation is found

$$T = \frac{2\pi}{\sqrt{b/I}} \quad (2)$$

so that

$$I = \frac{T^2 b}{4\pi^2} \quad (3)$$

The constant b depends upon different dimensions for different types of pendulums.

When determining the moments of inertia the bifilar torsion type of pendulum is used for the Z axis and the

compound type for the remainder of the axes (figs. 1 and 2). For the bifilar torsion pendulum, the axis of oscillation is vertical, lies midway between the two vertical filaments, and passes through the center of gravity of the system. For the compound pendulum, the axis of oscillation is horizontal and passes through

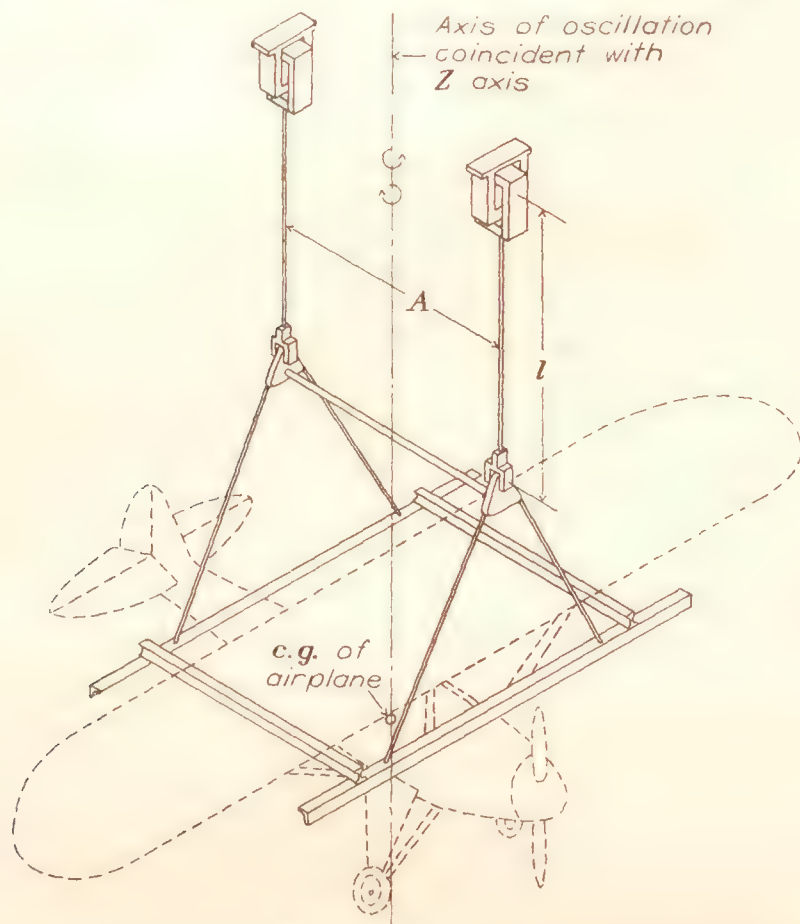


FIGURE 1.—Airplane and swinging gear arranged for the determination of the moment of inertia about the Z axis by the bifilar torsion pendulum method.

the points of support but not through the center of gravity of the pendulum.

For the bifilar torsion pendulum

$$b = \frac{WA^2}{4l}$$

and consequently

$$I = \frac{T^2 WA^2}{16\pi^2 l} \quad (4)$$

where W is the weight of the pendulum

A is the distance between the vertical filaments

and l is the length of the filaments.

For the compound pendulum

$$b = WL$$

and

$$I = \frac{T^2 WL}{4\pi^2} \quad (5)$$

where L is the distance between the center of gravity and the axis of oscillation. When the compound pendulum is used, the moment of inertia about an axis passing through the center of gravity is given by the equation

$$I_{cg} = \frac{T^2 WL}{4\pi^2} - ML^2 \quad (6)$$

where M is the mass of the pendulum.

DAMPING

In any practical case the motion of a pendulum will be damped by friction, whereas the theoretical case assumes no damping. Damping has the effect of increasing the period over the theoretical value. It can be shown that the effect of damping on the period can be determined by the observation of the decrease in amplitude during the first oscillation. Observations during the swinging experiments have shown that the decrease of amplitude during the first oscillation never exceeds one tenth the original amplitude. For this amount of damping the error in the moment of inertia will be less than 0.02 percent, and consequently can be neglected.

AMBIENT AIR

Equations (4) and (6), though derived for the motion of a pendulum in a vacuum, apply to the case of the pendulum oscillating in air but in this case I , W , and M refer to the virtual values of the moment of inertia, weight, and mass of the pendulum when immersed in air. The differences between the values of I , W , and M for motion in a vacuum and the case where the pendulum is immersed in air arise from three effects: the buoyancy of the structure, the air entrapped within the structure, and the *additional-mass* effect. A discussion of these effects follows.

Buoyancy and entrapped air.—The weight W in equations (4) and (6) equals the true weight of the

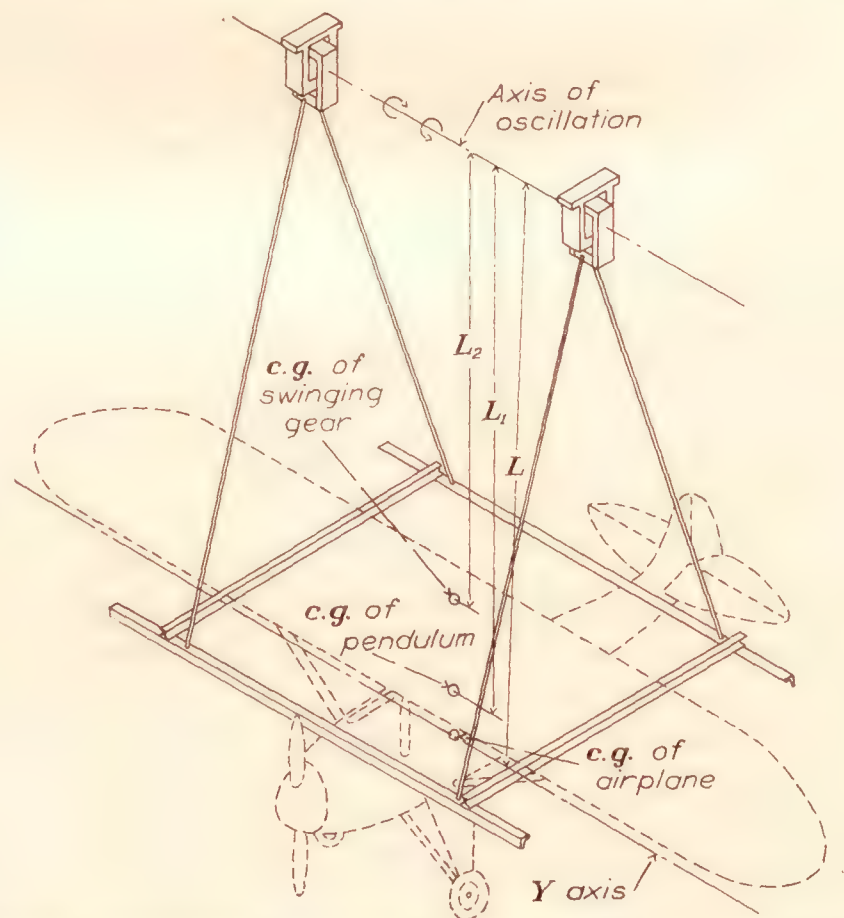


FIGURE 2.—Airplane and swinging gear arranged for the determination of the moment of inertia about the Y axis by the compound-pendulum method.

pendulum only for the case where the swinging is done in a vacuum. In the practical case where the pendulum is surrounded by a fluid medium, air, W equals the virtual weight; that is, the true weight minus the buoyancy of the structure. Weighing the pendulum

in air gives the virtual weight so that the weighing results can be applied directly for the determination of the moments of inertia about the axis of oscillation. From the virtual weight, the mass of the structure, for use in equation (6), can be found by the equation

$$M_s = \frac{W}{g} + V_s \rho \quad (7)$$

where M_s is the mass of the structure
 V_s is the volume of the structure
 and ρ is the density of the air.

The total volume enclosed within the external covering of the airplane, with the exception of the volume taken up by the structure, is filled with air of the same density as the surrounding air. This mass of air should be considered as part of the airplane because the major portion of it moves with the airplane, although there is some leakage through the openings in the fuselage and wings. Thus, the true mass of the pendulum

$$M = \frac{W}{g} + V_s \rho + (V - V_s) \rho$$

or

$$M = \frac{W}{g} + V \rho \quad (8)$$

Where V is the total volume of the airplane. Similarly, the true moment of inertia of the pendulum about its gravity axis is made up of two parts, a constant part I_s representing the moment of inertia of the structure, and a part I_E representing the moment of inertia of the entrapped air and varying with the density of the air; that is,

$$I = I_s + I_E$$

where

$$I_E \propto \rho \quad (9)$$

Additional mass.—When a body is put in motion in a fluid a flow about the body is immediately created. The momentum of this flow is imparted by the body, so it must be considered in determining the motion of the body. Hence, the period of a pendulum vibrating in air is to some extent dependent on the momentum imparted to the air by its motion through the air, a fact noted and discussed by Green in 1836 (reference 3). The momentum imparted to the air is proportional to the momentum of the body. As the additional momentum depends on the density of the air as well as on the size of the body and its shape relative to the direction of motion, the extent to which the period of a pendulum is affected by the surrounding air depends on the relative densities of the air and the pendulum. The late Mr. K. V. Wright (reference 4) first demonstrated that, because of the relatively low mass density of the airplane, it is necessary to consider the additional-mass effect when determining its moments

of inertia by the pendulum method. It is well to note that although the effect of the surrounding medium is commonly called the additional-mass effect, the theory actually deals with the additional momentum, and it is only because the additional momentum remains proportional to the momentum of the body for a given motion that an equivalent additional mass may be used.

The effective moment of inertia of the additional mass of a pendulum about its axis of oscillation may be represented as

$$I_A + M_A L^2$$

where I_A is the additional moment of inertia about the center of gravity and M_A is the additional mass for the conditions under consideration, if the center of the additional mass is assumed to coincide with that of the pendulum. Thus, equations (4) and (6) may be expanded to the following forms

$$I_v = I_s + I_E + I_A = \frac{T^2 W A^2}{16 \pi^2 l} \quad (10)$$

for the bifilar torsion pendulum, and

$$I_v = I_s + I_E + I_A = \frac{T^2 W L}{4 \pi^2} - \left(\frac{W}{g} + V \rho + M_A \right) L^2 \quad (11)$$

for the compound pendulum, where I_v is the virtual moment of inertia about the center of gravity.

VIRTUAL MOMENTS OF INERTIA

Assuming that I_E , I_A , $V \rho$, and M_A can all be evaluated, three different moments of inertia for each axis of the airplane can be determined by swinging the airplane in air. These are: the virtual moment of inertia, the true moment of inertia of the airplane consisting of the moments of inertia of the structure and the air entrapped within the airplane, and the moment of inertia of the structure.

The virtual moments of inertia are obtained directly with the bifilar pendulum. With the compound pendulum they can be obtained either by evaluating $V \rho$ and M_A or by swinging tests with two pendulum lengths. The term $V \rho$ can be readily calculated from consideration of the airplane dimensions. The method for calculating the term M_A is discussed later in connection with the general subject of determining additional mass characteristics. The method for determining I_v experimentally will be apparent from consideration of equation (11), in which the unknown terms are I_v and $(V \rho + M_A)$. Thus, by swinging with two different pendulum lengths, two simultaneous equations in two unknowns are obtained.

TRUE MOMENTS OF INERTIA

The true moments of inertia are obtained by computing I_A for each of the body axes and subtracting the

values thus found from the virtual moments of inertia. The method of computing I_A is explained in the section on additional mass. The true moments of inertia vary slightly with altitude owing to the fact that I_E is dependent on density. The term I_E is very small, however, so that its variation with altitude can be neglected.

SUPPORTING MECHANISM

Thus far the discussion has assumed a pendulum made up solely of the airplane. In general, however, the total mass of the pendulum includes the mass of additional equipment required for supporting the airplane in the desired manner. Experience in swinging airplanes has shown that it is practically impossible to reduce the weight of the additional structure to a negligible amount. The use of a strong rigid swinging gear has been found to be the best means of handling the airplane. This gear is integral in itself and is handled and swung as an independent pendulum. The moment of inertia of this gear as an independent unit is found so that it can be subtracted from the moment of inertia of the complete assembly consisting of swinging gear and airplane. The equations when the gear is used become, for the bifilar torsion pendulum,

$$I_V = \frac{T_1^2 W_1 A^2}{16\pi^2 l} - \frac{T_2^2 W_2 A^2}{16\pi^2 l} \quad (12)$$

and, for the compound pendulum

$$I_V = \frac{T_1^2 W_1 L_1}{4\pi^2} - \frac{T_2^2 W_2 L_2}{4\pi^2} - \left(\frac{W}{g} + V\rho + M_A \right) L^2 \quad (13)$$

where the subscripts ¹ and ² refer to the total pendulum and gear, respectively.

ELLIPSOIDS OF INERTIA

In the study of spinning it is necessary that the ellipsoid of inertia of the airplane be known for the determination of the gyroscopic couples acting on the airplane during a spin. It has been noted in practice that the principal axes of the ellipsoid nearly coincide with the body axes of the airplane. For every airplane swung, however, it is well to determine the position of the principal axes of the ellipsoid with respect to the body axes and, if there is an appreciable displacement between them, to compute the moments of inertia about the principal axes.

As the airplane is symmetrical about the XZ plane, the Y body axis coincides with the Y principal axis and it is only necessary to determine the positions of the principal axes in the XZ plane. The orientation of the principal axes in the XZ plane is found by determining the moment of inertia about a third axis in this plane at a known angle from the body axes. With these data the product of inertia, D , about the X and Z body axes can be computed by the formula,

$$D = \frac{A \cos^2 \theta + C \sin^2 \theta - I_{xz}}{\sin 2\theta} \quad (14)$$

where A is the moment of inertia about the X body axis

C is the moment of inertia about the Z body axis

I_{xz} is the moment of inertia about the third axis in the XZ plane

and θ is the angle between the X and the XZ axes. The angle τ between the X body axis and the X principal axis can then be found

$$\tau = \frac{1}{2} \tan^{-1} \frac{2D}{C-A} \quad (15)$$

The moments of inertia about the principal axes are given by the following equations:

$$\begin{aligned} A^{IV} &= A \cos^2 \tau + C \sin^2 \tau + D \sin 2\tau \\ B^{IV} &= B \\ C^{IV} &= A \sin^2 \tau + C \cos^2 \tau - D \sin 2\tau \end{aligned} \quad (16)$$

DETERMINATION AND DISCUSSION OF ADDITIONAL MASS CHARACTERISTICS

An analogy with the momentum imparted to the air by the motion of flat plates provides a basis for the determination of the additional mass effect of the airplane. For a flat plate (or circular cylinder) of infinite span moving with velocity V normal to its surface in air, assumed to be an incompressible and frictionless fluid, aerodynamic theory gives the momentum of the air per unit span as

$$\frac{\rho c^2 \pi V}{4} \quad (17)$$

where ρ is the density of the air and c is the chord of the plate (or diameter of the cylinder).

For finite plates with end flow, the total momentum of the air for this type of motion can be expressed as

$$\frac{k \rho c^2 \pi b V}{4} \quad (18)$$

where k is the coefficient of additional momentum for motion normal to the plate and b is the span of the plate. The value of k depends on the aspect ratio of the plate. For motion parallel to the plane of the plate, the additional momentum is zero.

For rotation of the plate about an axis passing through its center the additional angular momentum can be expressed by the introduction of a coefficient k' . Thus, for rotation about the mid chord, the angular momentum of the additional mass is

$$\frac{k' \rho \pi c^2 b^3 \Omega}{48} \quad (19)$$

where k is the coefficient for rotation about the mid chord of a plate of aspect ratio b/c , and Ω is the angular velocity.

A similar expression with a different coefficient k'' may be written for rotation about an axis parallel to the span and passing through the center of the plate.

If b and c are still regarded as the major and minor dimensions of the plate respectively, the corresponding expression for this type of motion becomes

$$\frac{k'' \rho \pi c^3 b^2 \Omega}{48} \quad (20)$$

and the aspect ratio to which k'' applies is c/b .

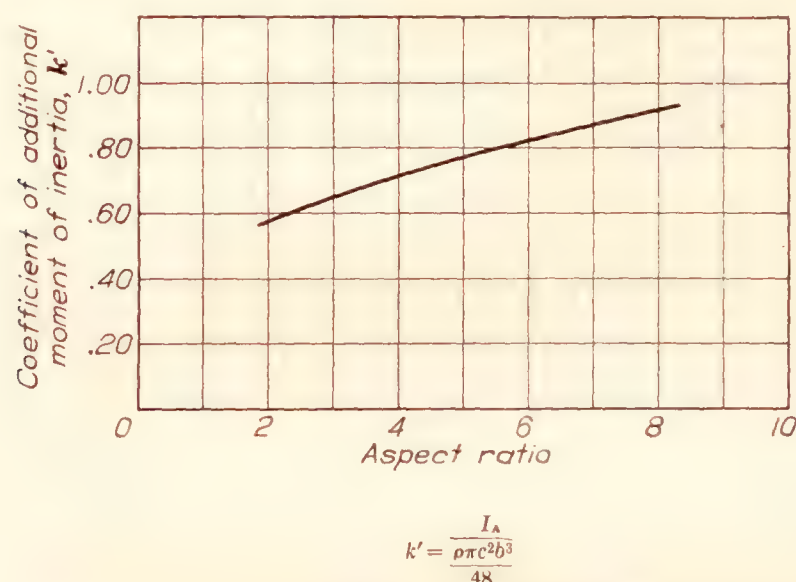
When the rotation is about an axis in the plane of the plate parallel to either the chord or the span but not passing through the center of the plate, the additional angular momentum may be expressed as

$$\frac{k' \rho \pi c^2 b^3 \Omega}{48} + \frac{k \rho c^2 \pi b \Omega l^2}{4} \quad (21)$$

or

$$\frac{k'' \rho \pi c^3 b^2 \Omega}{48} + \frac{k \rho c^2 \pi b \Omega l^2}{4} \quad (22)$$

respectively, where l is the distance from the center of the plate to the axis of rotation. It is worth noting that, in general, the first term of equation (22) can be neglected owing to the small effective aspect ratio.



The coefficients k and k' for use in equations (23) and (24) are given in figure 3. The values for k were obtained from experimental data given by Pabst (reference 5) for plates of aspect ratios up to 4. The extrapolation to aspect ratio 10 was made through the use of the approximate empirical formula for the curve

$$k = l - \frac{0.537}{A. R.} \quad (25)$$

As Pabst's experiments were performed with small plates in water, it was desirable to check at least one value of k under conditions similar to those met in the swinging tests of the airplane. For this purpose a plate 20 by 5 feet was constructed of a wooden framework covered with doped fabric. The plate was swung with its plane vertical about an axis parallel to the span and $1\frac{1}{2}$ chord lengths above the center of the plate and its virtual moment of inertia about the axis of oscillation was determined. The moment of inertia

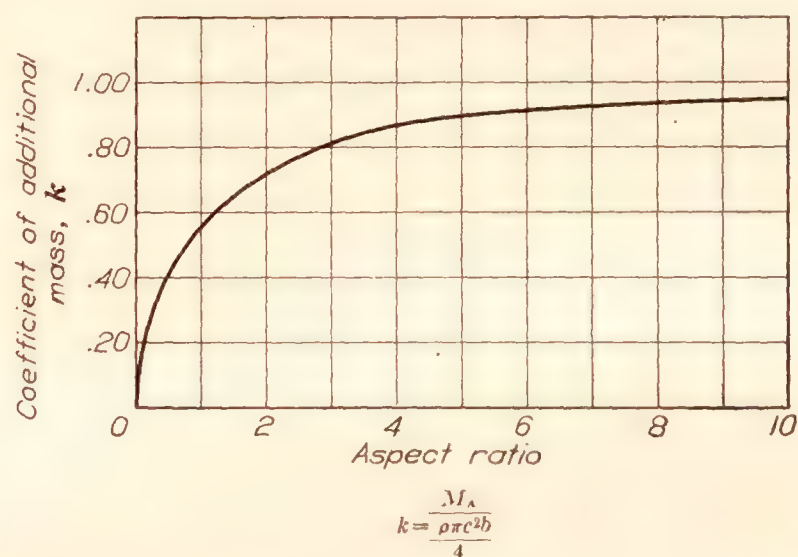


FIGURE 3.—Coefficients of additional mass and additional moments of inertia for flat plates.

It is further apparent that the above expressions, equations (21) and (22), also apply to the case in which the axis of rotation lies outside the plane of the plate. In that case, the displacement of the axis from the plate results only in an additional component of motion parallel to the plane of the plate, which imparts no additional momentum to the air. Thus it can be stated that the additional angular momentum is independent of the distance of the plane of the plate from the axis of rotation. The additional moment of inertia is found by eliminating Ω . Then, if the first term of equation (22) is neglected, additional moments of inertia become

$$\frac{k' \rho \pi c^2 b^3}{48} + \frac{k \rho \pi c^2 b l^2}{4} \quad (23)$$

for rotation about any axis parallel to the chord and

$$\frac{k \rho \pi c^2 b l^2}{4} \quad (24)$$

for rotation about any axis parallel to the span, where l is the distance in the plane of the plate from the center of the plate to the axis of rotation.

of the structure was found by swinging the uncovered framework, and adding to the moment thus obtained the computed moment of inertia of the fabric. The additional moment of inertia of the plate, the difference between the virtual moment of inertia and the moment of inertia of the structure, was divided by the square of the pendulum length to find the additional mass. From the additional mass, k was computed. The value of k obtained in this manner agreed within 1 percent of the value given by the curve for aspect ratio 4.

As the additional mass of the fuselage is the most important additional-mass item in determining the virtual moments of inertia about the center of gravity from the swinging-test results, and as the fuselage obviously is not similar to a flat plate, an attempt was made to obtain a satisfactory value of k for fuselages. A box 20 by 5 by 5 feet was constructed and the coefficient k found by swinging tests for motion normal to one of the faces, k being based only on the dimensions of the face. The value obtained was 1.20, whereas, as shown in figure 3, the value of k for a

plate of aspect ratio 4 is 0.9. As fuselages usually have a depth greater than their width, k will have a value between 0.9 and 1.20. In practice it was decided to use 1.0.

The values for k' were found by experiment. The program for the experiments was arranged in such a manner that it was possible, when obtaining check observations, to verify the assumption that the additional moment of inertia of a plate about a given axis

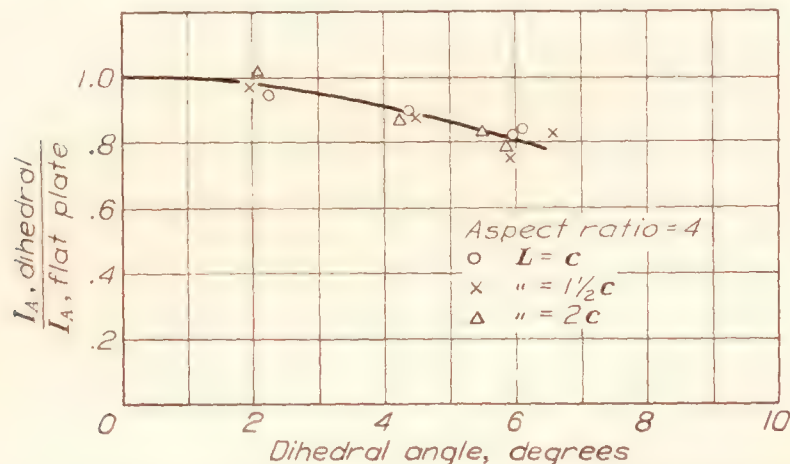


FIGURE 4.—Variation of the additional moment of inertia of a single plate with dihedral.

is independent of the distance from the axis to the plane of the plate. Four plates having aspect ratios of 2, 4, 6, and 8 were used in the experiments. These plates had a span of 4 feet and a thickness of one-fourth inch, and consisted of light wooden frameworks covered on both sides with paper. Each plate was swung at four pendulum lengths with its plane horizontal and its chord parallel to the axis of oscillation. In terms of the chord the pendulum lengths were 1, 1½, 2, and 2½. The additional moments of inertia were found

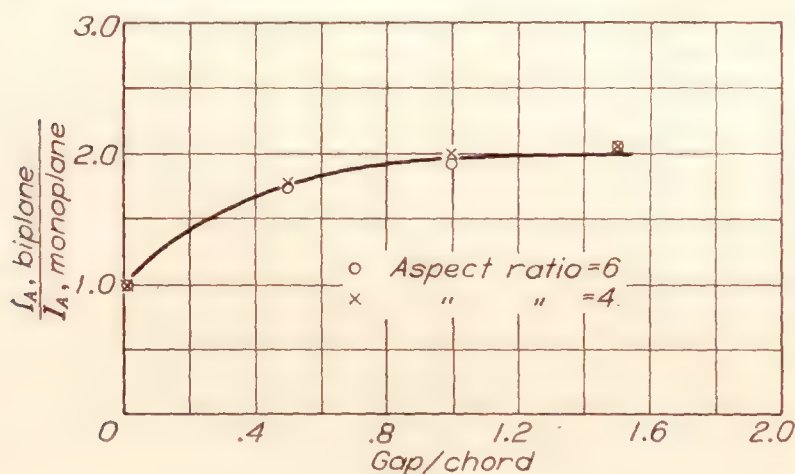


FIGURE 5.—Variation of additional moment of inertia with gap-chord ratio for orthogonal biplanes.

by deducting the computed moments of inertia of the structure of the plate and of the entrapped air from the virtual moments of inertia determined from the swinging tests. The values of the additional moments of inertia found in this manner for each plate showed a slight amount of dispersion for the different lengths, but the variation was not consistent with pendulum length and was within the precision of the experiments. The curve for coefficient k' (fig. 3) represents the average values of the additional

moments of inertia obtained for the different aspect ratios.

Additional experiments were performed to determine the effect of dihedral on the coefficient k' and the manner of treating biplanes. The value of k' was found to decrease with dihedral, as shown in figure 4, the decrease being in the order of 10 percent for 4° dihedral. In the biplane experiments gap-chord ratios of ½, 1, and 1½ were investigated for orthogonal biplane cellules consisting of plates having aspect ratios of 4 and 6. The results are given in figure 5. From these results it is concluded that for normal gap-chord ratios each wing of a biplane may be treated as an independent plate.

In the application of the general expressions for the additional moments of inertia of flat plates (equations (23) and (24)) to the airplane, the principal parts of the airplane are considered independently on the basis of their projected area in the XY , XZ , and YZ planes. Thus, in the determination of the additional moments of inertia of the airplane about an axis of oscillation parallel to the X body axis, the fuselage with length b and depth c and $L-z$ feet below the axis of oscillation will contribute an amount

$$\frac{k\rho c^2\pi b(L-z)^2}{4} \quad (26)$$

to the total moments of inertia, where z is the distance in the XZ plane from the X body axis to the center of the additional mass of the fuselage and is positive when the center of the fuselage is above the center of gravity. The distance z , however, is usually small and can be neglected and the equation written

$$\frac{k\rho c^2\pi bL^2}{4} \quad (27)$$

The vertical tail surface of the airplane can be treated similarly. The axis of oscillation lies in the plane of symmetry of both the wings and the horizontal tail surface so their additional moments of inertia are independent of L .

In general it is necessary to consider only these items. Thus, the total additional moment of inertia about the axis of oscillation equals

$$\frac{k_w'\rho c_w^2\pi b_w^3}{48} + \frac{k_{ht}'\rho c_{ht}^2\pi b_{ht}^3}{48} + \frac{k_f\rho c_f^2\pi b_fL^2}{4} + \frac{k_{vt}\rho c_{vt}^2\pi b_{vt}L^2}{4} \quad (28)$$

where the subscripts w , ht , f , and vt refer to the wings, horizontal tail surface, fuselage, and vertical tail surface, respectively, or

$$I_A + M_A L^2 \quad (29)$$

where I_A is the additional moment of inertia about the X axis and M_A , the additional mass for translation along the Y axis. Similar treatment may be applied

to the Y axis and Z axis. For the Y axis, M_A may be neglected and for the Z axis L is, of course, zero.

It should be noted that in special cases, as for float seaplanes, it may be necessary to consider other items than those mentioned and that z may not always be neglected.

APPARATUS AND PROCEDURE FOR SWINGING TESTS

SWINGING GEAR

The swinging gear is the apparatus used for supporting the airplanes during the swinging experiments. It has been constructed so as to be adaptable for airplanes up to 6,000 pounds. When used for a compound pendulum it consists of a cradle, tie rods, and knife-edges assembled as shown in figure 2. The cradle is a rectangular frame made of two I-beams for supporting the airplane and two light angle irons for spacers. The spacers are drilled to permit the distance between the I-beams to be changed to suit airplanes of different sizes. The knife-edges (fig. 6) provide a definite axis about which the pendulum oscillates with very little friction. They are mounted on a track so that their spacing can be varied when necessary. The tie rods are used to join the cradle to the knife-edges. The length and arrangement of the pendulum are varied by use of different combinations of the tie rods.

When used as a bifilar torsion pendulum, the swinging gear consists of the same essential parts as before, with the addition of two universal joints (fig. 7) and a spacer at the lower ends of the vertical members, assembled as shown in figure 1. The universal joints provide definite points of oscillation at the lower ends of the filaments. The spacer between these joints prevents a change in distance between the lower end of the vertical members when the pendulum is oscillating.

The weight, length, and center-of-gravity location of every part of the swinging gear are known so that no matter what arrangement is used it is a relatively simple process to compute the weight and center-of-gravity location of the assembly. The moment of inertia of the gear is found by swinging it as an individual pendulum.

DETERMINATION OF THE CENTER OF GRAVITY

As the center of gravity of the airplane is the origin of the axes about which the moments of inertia are to be found its location is determined before any swinging is done. The method used for locating the center of gravity is based on the principle that the center of gravity of a body suspended from a single pivot lies on a vertical line through the point of suspension. In its simplest form the method consists of suspending the airplane from two successive points in the XZ plane, and projecting a plumb line from each point of suspension on the side of the fuselage by means of a transit set up with its optical axis in a plane contain-

ing the point of suspension and perpendicular to the XZ plane of the airplane. The intersection of the two lines locates the vertical and longitudinal position of the center of gravity. Its lateral position is assumed to be in the plane of symmetry.

In practice it is not usually convenient to follow the simple method outlined above, because of the

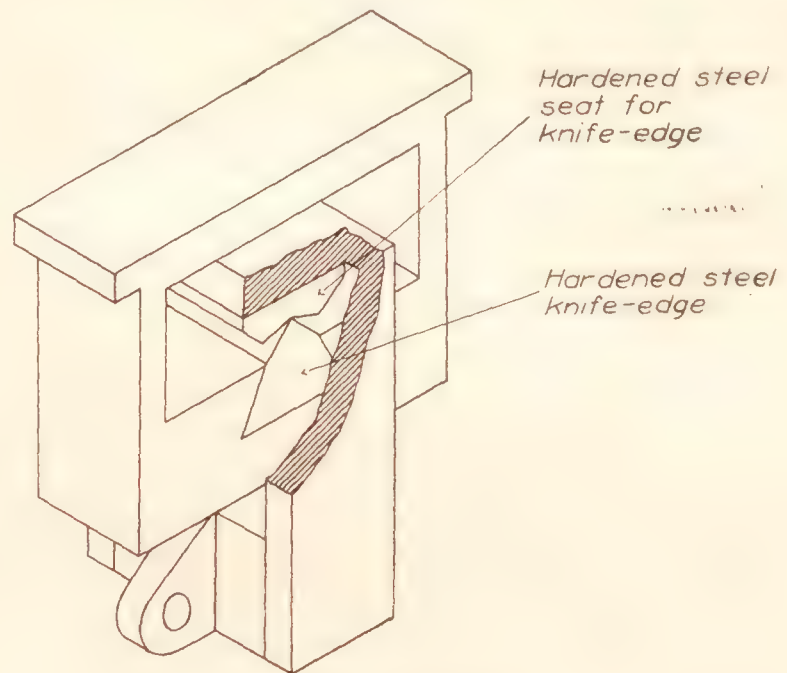


FIGURE 6.—Knife-edge.

difficulty in finding points of attachment on the airplane that do not endanger the structure. A satisfactory method employing the use of the swinging gear assembled as a compound pendulum is therefore usually followed.

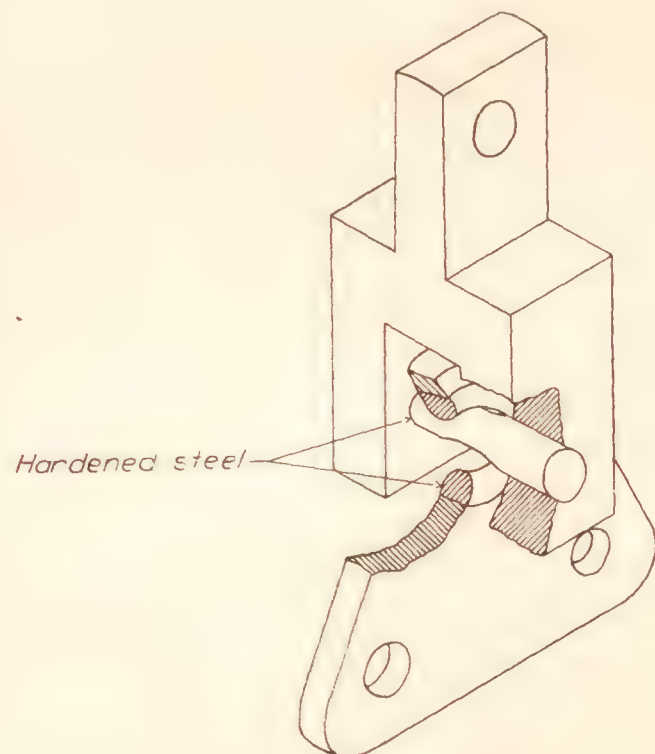


FIGURE 7.—Universal joint.

When the latter method is used the plumb line for the entire mass, airplane and swinging gear, is found as previously described and a correction is made for the effect of the swinging gear. Before the airplane is placed on the gear the variation of angle of the cradle with applied moment is determined by hanging known weights on one side of the cradle. By this procedure a calibration showing the moment corresponding to

any position of the gear is obtained. The airplane is then weighed and mounted on the gear with the X axis parallel to and equidistant from the I-beams, and in such a position that the angle assumed by the cradle is about 12° to 15° . The moment of the gear about the knife-edge axis is then found from the calibration and, since the moments of the gear and airplane are equal in magnitude, the moment of the airplane is thus obtained. The horizontal distance between the center of gravity of the entire mass and the center of gravity of the airplane is found by dividing this moment by the weight of the airplane. A vertical line drawn on the side of the fuselage at the above-calculated distance from the plumb line will then pass through the center of gravity. The fore-and-aft position of the airplane relative to the gear is then changed so that the inclination of the cradle is approximately as great as before, but in the opposite direction, and a second vertical line is drawn through the center of gravity. As by the first method, the intersection of these two lines locates the vertical and longitudinal position of the center of gravity of the airplane. A check is obtained by moving the airplane until the gear is level. A plumb line through the knife-edge axis should then pass through the intersection of the two lines previously established.

DETERMINATION OF PENDULUM CHARACTERISTICS

The second method of determining the center of gravity just described leaves the airplane suspended level and in position for swinging about an axis parallel to the Y axis. Thus, it is usually convenient to make this swinging test the next step in the procedure. The characteristics of the compound pendulum that must be measured are the weight, pendulum length, and period. The weight equals the sum of the weights of the airplane and the gear. The pendulum length is determined by measuring the difference in elevation of the center of gravity of the airplane and the knife-edges by means of a transit. The center-of-gravity location of the gear relative to the knife-edges, as previously mentioned, is computed from a knowledge of the constituents of the gear. From the center-of-gravity locations and weights of the airplane and gear, the center of gravity of the system is found. The period is found by timing 50 or more oscillations. The change of length for the check swinging is obtained by adding an additional length of tie rod in each of the four supports. When making this and other changes the weight of the airplane is never taken off the cradle, the cradle being temporarily supported by a chain hoist. The determination of the moment of inertia of the gear is, for convenience, left until all swingings with the airplane in place have been completed.

In order to place the airplane in position for the X -axis swinging, the cradle is disconnected from the tie rods, turned 90° , and again fastened to the tie rods.

The spacing of the knife-edges is changed, if necessary. For the XZ axis, additional tie rods are added to either the two front or the two rear supports.

For the Z -axis swinging test the gear is assembled as shown in figure 1. The filaments are made vertical by proper spacing of the knife-edges. With the bifilar torsion pendulum the necessary measurements are the weight, the spacing and length of the filaments, and the period. Care must be taken in starting the motion to obtain an oscillation about a vertical axis, half-way between the filaments. The weight and period are obtained as before. The spacing and length of the filaments are measured directly.

COMPUTATIONS

The virtual moment of inertia about the Z axis is found by direct substitution of the pendulum characteristics in equation (12). When computing the virtual moments of inertia about the XY and XZ axes the buoyancy and additional mass are first calculated and substitution is made in equation (13). The check computation is made by substituting the values obtained from the swinging experiments for the two pendulum lengths in equation (13) and solving simultaneously for I_v . Computation of I_A is made on the basis of the equations given in the section on additional mass. Sample computations for the VE-7 airplane are given in the appendix.

PRECISION

The precision with which the moments about the body axes of an airplane can be found depends upon three items. The first item is the precision with which the virtual moments of inertia about the axis of oscillation can be found with the swinging gear and by the procedure outlined. The second item is the precision with which account is taken of the buoyancy and additional mass in transposing the compound pendulum results from the axis of oscillation to the body axes. The third item is the precision of the computation of I_A , the additional moment of inertia.

The precision with which the moments of inertia about the axis of oscillation can be found was checked by swinging a railroad rail at the pendulum lengths usually used for airplanes. The rail was a dense homogeneous body of regular dimensions, for which the moment of inertia could be calculated and the buoyancy and additional mass neglected. The moment of inertia of the rail was comparable to that of a small airplane. The magnitude of the disagreement between the calculated and experimental values of the moments about the axis of oscillation for either type of pendulum never exceeded an amount equal to 1 percent of the moment of inertia of the rail about its center of gravity. Recent improvements in the swinging gear have tended to improve the precision

so that it seems permissible to assume that the error in determining the virtual moment of inertia about the knife-edge is less than 0.5 percent of the true moment of inertia about the center of gravity.

As no transposition is necessary for the bifilar suspension, the discussion of the second item refers only to the determination of the moments of inertia about the X and Y axes. The magnitude of the combined effects of buoyancy and additional mass that must be considered in determining the virtual moments of inertia about the body axes of the compound pendulum is small in relation to the desired moments of inertia. Consequently, fairly large errors in determining these effects lead to but small errors in the final results. Experience has shown that the correction attributable to the buoyancy is about 3 percent of the moment of inertia about the center of gravity. If reasonable care is taken in computing the volume, the buoyancy can be obtained with an error of less than 10 percent. Such an error will introduce an error of 0.3 percent in the final result. For the X axis, the effect of the additional mass amounts to about 5 percent of the desired result; for the Y axis it is negligible. Although the effects of some parts of the airplane are neglected in computing the additional mass, it is believed that the error in the computation is not greater than 10 percent, hence that the error in the final results attributable to the computation of the additional mass is less than 0.5 percent. The maximum resultant error attributable to these two causes would then be 0.8 percent.

Consideration of the above-enumerated items concerning the precision with which the virtual moments of inertia about the body axes are obtained leads to the conclusion that for the X and Y body axes the precision is within ± 1.3 percent and for the Z body axis is within ± 0.5 percent, the greater precision for the Z axis arising from the fact that no transposition of axes is required. In practice it is customary to obtain check values by swinging the airplane at two different pendulum lengths and to average the results if there is a discrepancy. On the basis of the small magnitude of the discrepancies experienced it is assumed that the precision thereby obtained, particularly for the compound pendulum, is slightly improved so that the final error for the X and Y axes is less than ± 1 percent.

One remaining source of error in determining the true moments of inertia arises from the possibility of error in determining I_A , the additional moment of inertia. For the X body axis, owing to the influence of the wings, this term has been found to be as great as 20 percent of the true moment of inertia in one case but has an average value of 15 percent for the remaining cases. For the Y and Z body axes this term amounts to only about 3 percent. The values of I_A are believed to be precise to within ± 10 percent. In

terms of the true moments of inertia, an error of this magnitude for the average case would amount to ± 1.5 percent for the X axis and ± 0.3 percent for the Y and Z axes. Consideration of these possible errors and those that may be incurred in determining the virtual moments of inertia leads to the conclusion that errors in the true moments of inertia are less than ± 2.5 percent for the X axis, ± 1.3 percent for the Y axis, and ± 0.8 percent for the Z axis.

Because of the nature of the airplane, the principal axes of the ellipsoid of inertia are never more than a few degrees from the body axes, and the product of inertia is only a small percentage of $C-A$. Consideration of these facts and the possible error in virtual moments of inertia leads to the conclusion that the limits of the precision with which the angle of the principal axes can be determined are $\pm 1^\circ$.

There are several practical considerations in the construction and operation of the swinging gear that have been found by experience to have considerable bearing upon the precision of the results obtained with it. In the construction of the gear, care should be exercised in making absolutely certain that the oscillations take place about the pivots provided for that purpose. The knife-edge supports should be rigidly placed, and for the compound pendulum the tie rods from the corners of the cradle should be carried directly to the knife-edges. The importance of the latter requirement was brought out during development of the gear, when an arrangement similar to that for the bifilar torsion pendulum, but with no universal joints at the lower ends of the vertical members, was tried for the compound pendulum. This arrangement gave erratic results and inspection showed that the vertical members were flexing for a short distance from both ends. Similarly for the bifilar torsion pendulum, the universal joints and spacer bar are necessary to obtain the motion desired.

Although the pendulum dimensions are governed somewhat by the size and type of airplane to be swung, it has been found by tests that they should also be governed as far as possible by other considerations. The compound pendulum should be kept short so that the moment of inertia about an axis through its center of gravity will be a large percentage of the total moment of inertia of the pendulum about the axis of oscillation. Pendulum lengths of approximately 4 to 10 feet have given satisfactory results with airplanes weighing up to 5,000 pounds. In tests of the bifilar torsion pendulum with varied lengths of the vertical filaments and with a fixed distance between them, it was found that the most satisfactory results were obtained when the length of the filaments was greater than the distance between them. It has been found satisfactory and convenient in swinging various airplanes to place the vertical filaments about 8 feet apart.

The oscillations of both the compound and bifilar pendulums should have a small amplitude because the

pendulum formulas used apply only when the assumption $\sin \theta = \tan \theta = \theta$ (where θ equals one half the angle of oscillation) is valid. In practice, this angle need not exceed 2° .

The precision of the measurement of length of the compound pendulum depends primarily upon the accurate location of the center of gravity of the airplane. If it is not located accurately, the pendulum dimensions will be in error even though subsequent measurements are very precise.

Swinging the airplane at two pendulum lengths about each axis, not only is useful in checking the additional-mass effect, but also provides a check on the swinging tests themselves. Similarly, it is a good practice to swing the airplane in both the nose-up and nose-down attitudes to afford a check on the position of the principal inertia axes of the airplane.

RESULTS OBTAINED FOR SEVERAL AIRPLANES

The method given in this report for the determination of the moments of inertia has been used regularly by the Committee and, in all, the moments of inertia have been found for 13 airplanes. These results are listed in table I. The angle between the X body and the X principal axis, being small, is omitted. The additional moments of inertia about the three axes are given.

DETERMINATION OF MOMENTS OF INERTIA BY CALCULATION

There are times when it is desired to estimate the moments of inertia of airplanes not available for swinging tests. It is usual in these cases to compute the

moments of inertia by a summation of the moments of inertia of the constituent parts. As the accuracy of the results of such computations has been questioned, it was decided to check the results by computing the moments of inertia for an airplane for which the moments of inertia have been found experimentally. The computations were made carefully; a balance diagram was used to locate the parts relative to the center of gravity, and the true weights of each part were found by weighing the individual parts for the airplane in question. On comparison of the computed with the experimental values of true moments of inertia, it was found that the computed value was in error by 6 percent for the X axis. For the other axes the error was less.

CONCLUSIONS

1. The pendulum method for finding moments of inertia can be successfully applied to airplanes.
2. Owing to the effect of the ambient air, the virtual moments of inertia obtained directly through application of the pendulum formulas are considerably greater than the desired true moments of inertia.
3. The effects of the ambient air can be determined with sufficient precision so that the true moments of inertia may be obtained from swinging experiments with an error of less than ± 2.5 percent, ± 1.3 percent, and ± 0.8 percent for the X , Y , and Z axes, respectively.

LANGLEY MEMORIAL AERONAUTICAL LABORATORY,
NATIONAL ADVISORY COMMITTEE FOR AERONAUTICS
LANGLEY FIELD, VA., *June 8, 1933.*

APPENDIX

SAMPLE COMPUTATIONS

The following are sample data and computations for determining the ellipsoid of inertia for the VE-7 airplane.

VIRTUAL MOMENTS OF INERTIA

For the X body axis the compound pendulum is used and the equation for the virtual moment of inertia about the axis is

$$I_{vX} = \frac{W_1 T_1^2 L_1}{4\pi^2} - \frac{W_2 T_2^2 L_2}{4\pi^2} - \left(\frac{W}{g} + V\rho + M_A \right) L^2$$

The experimental data obtained by swinging the airplane about axes parallel to the X axis are:

	Short suspension	Long suspension
W	2,208 pounds.....	2,208 pounds.
W_1	2,591 pounds.....	2,584 pounds
W_2	383.3 pounds.....	376.1 pounds.
L_1	9.050 feet.....	13.81 feet.
L	9.513 feet.....	14.32 feet.
L_2	6.382 feet.....	10.84 feet.
T_1	3.759 seconds.....	4.378 seconds.
T_2	3.209 seconds.....	3.931 seconds.

The volume V is computed from the dimensions of the airplane. Only the fuselage and wings are considered. The fuselage is treated in three sections:

Section	Length	Average cross-section	Volume
	Feet	Square feet	Cubic feet
1.....	7.5	7.95	59.7
2.....	7.0	6.51	45.5
3.....	7.0	2.08	14.6
Total volume of fuselage, V_f			119.8

The volume of the wings is determined by the equation

$$V_w = 0.74St$$

where S is the wing area = 312 square feet
and t is the maximum ordinate of the wing = 0.298 feet from which

$$V_w = 0.74 \times 312 \times 0.298 = 69 \text{ cubic feet}$$

then

$$V = V_f + V_w = 119.8 + 69 = 188.8 \text{ cubic feet}$$

The tests were made at sea level under approximately standard conditions so that

$$\rho = 0.00238 \text{ slug per cubic feet}$$

The additional mass is computed only for the fuselage and vertical tail surface. The fuselage is again divided

into three sections. The coefficient k is assumed to be unity, so

$$M_{Af} = \frac{\rho c_1^2 \pi (\Delta b)_1}{4} + \frac{\rho c_2^2 \pi (\Delta b)_2}{4} + \frac{\rho c_3^2 \pi (\Delta b)_3}{4}$$

where c_1^2 , c_2^2 , and c_3^2 are the mean values of the squares of the fuselage depths for each of the three sections.

Section	Δb	c^2	ΔM_A
	Feet	Sq. ft.	Slug
1.....	7.5	9.50	0.133
2.....	7.0	9.00	.118
3.....	7.0	5.14	.067
Total additional mass for fuselage M_{Af}318

The vertical tail area of this airplane may be considered of circular shape and its additional mass as

$$M_{At} = \frac{\pi D^3 \rho}{6}$$

where $D = 4$ feet

$$\text{so } M_{At} = \frac{\pi \times (4)^3 \times 0.00238}{6} = 0.079 \text{ slug}$$

$$\text{and } M_A = M_{Af} + M_{At} = 0.318 + 0.079 = 0.397 \text{ slug.}$$

Substituting in the compound-pendulum formula:
Short suspension

$$I_{vX} = \frac{2591 \times (3.759)^2 \times 9.05}{39.48} - \frac{383.3 \times (3.209)^2 \times 6.382}{39.48} - \left[\frac{2208}{32.147} + (188.8 \times 0.00238) + 0.397 \right] (9.513)^2 = 1463 \text{ slug feet}^2$$

Long suspension

$$I_{vX} = \frac{2584 \times (4.378)^2 \times 13.81}{39.48} - \frac{376.1 \times (3.931)^2 \times 10.84}{39.48} - \left[\frac{2208}{32.147} + (188.8 \times 0.00238) + 0.397 \right] (14.32)^2 = 1474 \text{ slug feet}^2$$

The average value of I_{vX} is 1469 slug feet².

I_{vX} is checked by solving the equations for the two suspensions simultaneously, I_{vX} and $V\rho + M_A$ being the unknowns.

$$I_{vX} = 1545 + (V\rho + M_A) (9.513)^2$$

$$I_{vX} = 1649 + (V\rho + M_A) (14.32)^2$$

$$I_{vX} = 1462 \text{ slug feet}^2$$

The agreement is within 0.5 percent.

The virtual moments of inertia about the Y axis and the XZ axis are calculated in a similar manner from the data obtained with the compound pendulum. In the case of the Y axis, the additional mass is very small, and therefore neglected. In the case of the XZ axes, the additional mass is the same as for the X axis.

The equation for the bifilar pendulum which is used for a determination of the virtual moments of inertia about the Z axis is

$$I_{VZ} = \frac{W_1 T_1^2 A^2}{16\pi^2 l} - \frac{W_2 T_2^2 A^2}{16\pi^2 l}$$

The experimental data obtained by swinging are

	Short suspension	Long suspension
W_1	2,575 pounds.....	2,575 pounds.
W_2	367 pounds.....	367 pounds.
T_1	2.622 seconds.....	3.808 seconds.
T_2	3.238 seconds.....	3.398 seconds.
A	9.917 feet.....	9.917 feet.
l	7.412 feet.....	8.237 feet.

From which is obtained:

Short suspension

$$I_{VZ} = \frac{2575 \times (3.622)^2 \times (9.917)^2}{157.92 \times 7.412} - \frac{367 \times (3.238)^2 \times (9.917)^2}{157.92 \times 7.412} = 2515 \text{ slug feet}^2$$

Long suspension

$$I_{VZ} = \frac{2575 \times (3.808)^2 \times (9.917)^2}{157.92 \times 8.237} - \frac{367 \times (3.398)^2 \times (9.917)^2}{157.92 \times 8.237} = 2505 \text{ slug feet}^2$$

the average of which is 2,510 slug feet².

The average value of the moment of inertia about each axis is as follows:

$$I_{VX} = 1469 \text{ slug feet}^2$$

$$I_{VY} = 1498 \text{ slug feet}^2$$

$$I_{VZ} = 2510 \text{ slug feet}^2$$

$$I_{VXZ} = 1546 \text{ slug feet}^2 \text{ (from nose-up swinging, } X \text{ axis inclined } 13.4^\circ)$$

$$I_{VXZ} = 1490 \text{ slug feet}^2 \text{ (from nose-down swinging, } X \text{ axis inclined } 13^\circ)$$

ADDITIONAL MOMENTS OF INERTIA

The additional moment of inertia about the X axis is assumed to be contributed only by the wings and the horizontal tail surface. The X axis is in the plane of symmetry of both the wings and the tail surface. The equation for the additional moment of inertia for this case is

$$I_A = \frac{k' \rho c^2 \pi b^3}{48}$$

For the wings

$$c = 4.62 \text{ feet} \quad b = 34.33 \text{ feet} \quad \text{aspect ratio} = 7.4$$

then, from figure 3,

$$k' = 0.89$$

and

$$I_{Aw} = \frac{2 \times 0.89 \times 0.00238 \times (4.62)^2 \times \pi \times (34.33)^3}{48} = 241 \text{ slug feet}^2$$

For the horizontal tail

$$c = 4.08 \text{ feet} \quad b = 9.50 \text{ feet} \quad \text{aspect ratio} = 2.5$$

then

$$k' = 0.62$$

and

$$I_{At} = \frac{0.62 \times 0.00238 \times (4.08)^2 \times \pi \times (9.50)^3}{48} = 1.3 \text{ slug feet}^2$$

so that for the X axis

$$I_{AX} = I_{Aw} + I_{At} = 241.0 + 1.3 = 242.3 \text{ slug feet}^2$$

The principal items that contribute to the additional moment of inertia about the Y axis are the fuselage and horizontal tail surface. For the horizontal area of the fuselage an equivalent rectangle is considered, with length equal to that of the fuselage, and width equal to the square root of the mean square of the fuselage width. The dimensions are

$$b = 18.3 \text{ feet} \quad c = 2.07 \text{ feet} \quad \text{aspect ratio} = 8.8$$

for which

$$k' = 0.95$$

As the Y axis is parallel to the chord but is displaced from the center of the additional mass of the fuselage by a distance l ,

$$I_{Af} = \frac{k' \rho c^2 \pi b^3}{48} + \frac{k \rho c^2 \pi b l^2}{4}$$

The constant k is assumed to be 1.0 and

$$l = 4.1 \text{ feet}$$

Thus

$$I_{Af} = \frac{0.95 \times 0.00238 \times (2.07)^2 \times \pi \times (18.3)^3}{48} + \frac{1.0 \times 0.00238 \times (2.07)^2 \times \pi \times 18.3 \times (4.1)^2}{4} = 6.3 \text{ slug feet}^2$$

The Y axis is parallel to the span of the horizontal tail, so that

$$I_{At} = \frac{k \rho c^2 \pi b l^2}{4}$$

where $k = 0.78$ and $l = 15.8$ feet and

$$I_{At} = \frac{0.78 \times 0.00238 \times (4.08)^2 \times \pi \times 9.50 \times (15.8)^2}{4} = 57.6 \text{ slug feet}^2$$

Then for the Y axis

$$I_{AY} = I_{Af} + I_{At} = 6.3 + 57.6 = 63.9 \text{ slug feet}^2$$

The determination of I_{AZ} is similar to that for I_{AY} with the difference that the vertical fuselage and tail areas are considered;

$$I_{AZ} = 31.6 \text{ slug feet}^2$$

TRUE MOMENTS OF INERTIA

The true moment of inertia about any axis is the difference between the virtual moment of inertia and the moment of inertia of the additional mass about that axis. Thus

$$A = I_{VX} - I_{AX} = 1469 - 242 = 1227 \text{ slug feet}^2$$

$$B = I_{VY} - I_{AY} = 1498 - 64 = 1434 \text{ slug feet}^2$$

$$C = I_{VZ} - I_{AZ} = 2510 - 32 = 2478 \text{ slug feet}^2$$

$$I_{XZ}(\text{nose-up}) = I_{VXZ}(\text{nose-up}) - I_{AX} = 1546 - 242 = 1304 \text{ slug feet}^2$$

$$I_{XZ}(\text{nose-down}) = I_{VXZ}(\text{nose-down}) - I_{AX} = 1490 - 242 = 1248 \text{ slug feet}^2$$

Location of Principal Axes:

The product of inertia about the body axis is given by

$$D = \frac{A \cos^2 \theta + C \sin^2 \theta - I_{XZ}}{\sin 2\theta}$$

where

	Nose-up	Nose-down
$\theta =$	-13.4°	13.0°
$\sin \theta =$	-0.2317	0.2250
$\cos \theta =$	$.9728$	$.9744$
$\sin 2\theta =$	$-.4509$	$.4384$

and the moments of inertia are as given above.

From the nose-up swinging

$$D = \frac{1227 \times (0.9728)^2 + 2478 \times (-0.2317)^2 - 1304}{-0.4509} = 21.5$$

From the nose-down swinging

$$D = \frac{1227 \times (0.9744)^2 + 2478 \times (0.2250)^2 - 1248}{0.4384} = 96.7$$

the average of which is $D = 59.1$

The tangent of twice the angle between the principal axis and the X axis is given by

$$\tan 2\tau = \frac{2D}{C-A}$$

$$\tan 2\tau = \frac{2 \times 59.1}{2478 - 1227} = 0.0941$$

$$\tau = 2^\circ 42'$$

Principal Moments of Inertia:

The principal moments of inertia are given by

$$A^{IV} = A \cos^2 \tau + C \sin^2 \tau + D \sin 2\tau$$

$$B^{IV} = B$$

$$C^{IV} = A \sin^2 \tau + C \cos^2 \tau - D \sin 2\tau$$

then, since

$$\tau = 2^\circ 42'$$

$$\sin \tau = 0.0471$$

$$\cos \tau = 0.9989$$

$$\sin 2\tau = 0.0941$$

and the other quantities are as previously determined, it follows that

$$A^{IV} = 1227 \times (0.9989)^2 + 2478 \times (0.0471)^2 + 59.1 \times 0.0941 = 1236 \text{ slug feet}^2$$

$$B^{IV} = 1434 \text{ slug feet}^2$$

$$C^{IV} = 1227 \times (0.0471)^2 + 2478 \times (0.9989)^2 - 59.1 \times 0.0941 = 2471 \text{ slug feet}^2$$

REFERENCES

1. Miller, M. P.: An Accurate Method of Measuring the Moments of Inertia of Airplanes. T.N. No. 351, N.A.C.A., 1930.
2. Miller, Marvel P., and Soulé, Hartley A.: Moments of Inertia of Several Airplanes. T.N. No. 375, N.A.C.A., 1931.
3. Green, George: Researches on the Vibration of Pendulums in Fluid Media. Trans. of the Roy. Soc. of Edinburgh, pp. 54-62, vol. 13, 1836.
4. Gates, S. B.: Moments of Inertia of Aeroplanes. R. & M. No. 1415, British A.R.C., 1932.
5. Pabst, Wilhelm: Theory of the Landing Impact of Seaplanes. T.M. No. 580, N.A.C.A., 1930.

TABLE I.—MOMENTS OF INERTIA OF SEVERAL AIRPLANES

Airplane	Type	Weight (lb.)	A (slug ft. ²)	B (slug ft. ²)	C (slug ft. ²)	I_{AX} (slug ft. ²)	I_{AY} (slug ft. ²)	I_{AZ} (slug ft. ²)
VE-7	Naval training, biplane landplane	2,208	1,227	1,434	2,478	242	64	32
PT-1	Army training, biplane landplane	2,512	1,967	2,088	3,289	238	80	54
PW-9	Army pursuit, biplane landplane	2,885	1,299	1,888	2,648	101	42	25
NY-1	Naval training, biplane landplane	2,622	2,098	2,450	3,807	238	80	80
Doyle O-2	Commercial monoplane, landplane	1,388	596	659	971	97	14	9
O2U-3	Naval observation, biplane landplane	3,550	2,482	2,796	4,481	335	84	49
F4B-1	Naval fighter, biplane landplane	2,540	1,023	1,560	2,077	124	30	15
O-11	Army observation, biplane landplane	4,558	2,507	4,133	6,231	370	105	59
NB-1	Naval training, biplane landplane	2,544	2,409	2,239	4,099	347	67	44
XN2Y-1	Naval training, biplane landplane	1,567	732	922	1,299	86	22	17
O3U-1	Naval observation, biplane landplane	4,057	2,740	3,283	5,112	335	84	49
F4B-2	Naval fighter, biplane landplane	2,816	1,063	1,795	2,378	124	30	15
McDonnell	Experimental low-wing monoplane equipped with slots and flaps.	1,708	1,345	1,101	2,279	157	42	26

REPORT No. 468

THE INTERFERENCE BETWEEN STRUTS IN VARIOUS COMBINATIONS

By DAVID BIERMANN and WILLIAM H. HERRNSTEIN, Jr.

SUMMARY

This report presents the results of tests made in the N.A.C.A. 7- by 10-foot wind tunnel to determine the interference drag arising from various arrangements of streamline struts and round struts, or cylinders. Determinations were made of the interference drag of struts spaced side by side, struts in tandem, tandem struts encased in a single fairing, a strut intersecting a plane, and struts intersecting to form a V. Three sizes of struts were used for most of the tests.

These tests show that the interference drag arising from struts in close proximity may be of considerable magnitude, in some instances amounting to more than the drag of the struts themselves.

INTRODUCTION

With the increasing demand for higher speeds in flight, attention has been focused on all possible methods of reducing the drag of aircraft. Considerable coordinated information has been compiled on the drag of component parts of airplanes, but relatively little is known about the interference resulting from combining these parts into an airplane. Until recently not much systematic work has been done on the general subject of interference.

The investigation reported in this paper has been confined to the determination of interference drag arising from various combinations of struts, both streamline and round. Struts were tested, side by side, in tandem, and intersecting at various angles to form V's. Tests were made on a streamline strut intersecting plane surfaces of various chords. The drag of tandem struts encased in a single fairing was determined for two types of fairings. Incidental tests were made to determine the drag of struts of various sizes and fineness ratios. Three sizes of struts were used throughout the program, with some exceptions, to determine if possible to what extent the rules of dynamic similarity may be applied to interference tests in wind tunnels.

Many of the tests herein reported have direct applications in airplane design. Although there has been an attempt to cover the subject of strut interference in a systematic fashion, the limitations of time and equipment have necessitated curtailing the program. Further tests on interference between struts and wheels are being made in connection with a study of landing gears, and will be reported at a later date.

APPARATUS AND METHODS

The N.A.C.A. 7- by 10-foot wind tunnel in which these tests were made is completely described with its equipment in reference 1. The standard force-test model support was used throughout these tests.

The streamline strut models were made from Navy no. 1 strut-section offsets given in table I. With a few exceptions to be discussed later, the tests were made on struts of three section sizes: 1 by 3 inches, 1.75 by 5.25 inches, and 2.5 by 7.5 inches. The models were made of white pine, sanded smooth and shellacked. The surface was not highly polished, but was sufficiently smooth to be comparable with good commercial practice. All model dimensions were held to ± 0.010 inch. The round struts (cylinders) were made from seamless steel tubing, accurate to ± 0.004 inch. The surface was finished bright but not highly polished. The diameters of tubing used were 1, 1.75, and 2.5 inches.

STRUT ARRANGEMENTS

Struts alone, streamline and round.—Preliminary to the interference tests each different size of strut was tested for drag. An 8-foot length of strut was mounted horizontally at its center on the force-test support. At each tip independently supported struts were mounted and extended through the tunnel jet boundary, in an attempt to simulate infinite-length conditions. A gap of one thirty-second inch was left between the active strut and each dummy extension.

Side-by-side struts, streamline and round.—In order to determine the interference drag arising from two

parallel struts located side by side, a 12-foot length of strut was mounted independently above the active strut previously described. (See fig. 1.) Drag was measured only on the active lower strut, the assumption being that the drag of the two struts was equal. The spacing between the struts was varied by moving the fixed 12-foot length of strut away from the active strut in small increments until the effects were no longer noticeable.

Struts in tandem, streamline and round.—The set-up to measure interference drag of tandem struts was identical to the one used for side-to-side spacings ex-

fabric around the pair and doping it. In order to simulate this condition a special model was built. A 1.75- by 5.25-inch strut was sawed lengthwise along the plane of maximum thickness. The leading-edge portion was separated from the trailing-edge portion by a distance of 20 inches and this intervening space was filled up with five 4- by 1.75-inch boards. This unit was bolted together, forming a flat-sided section 1.75 inches thick with a 25.25-inch chord and an 8-foot span. Two dummy tip extensions of the same section were also made. This model, representing streamline struts faired together with a flat-sided section, was

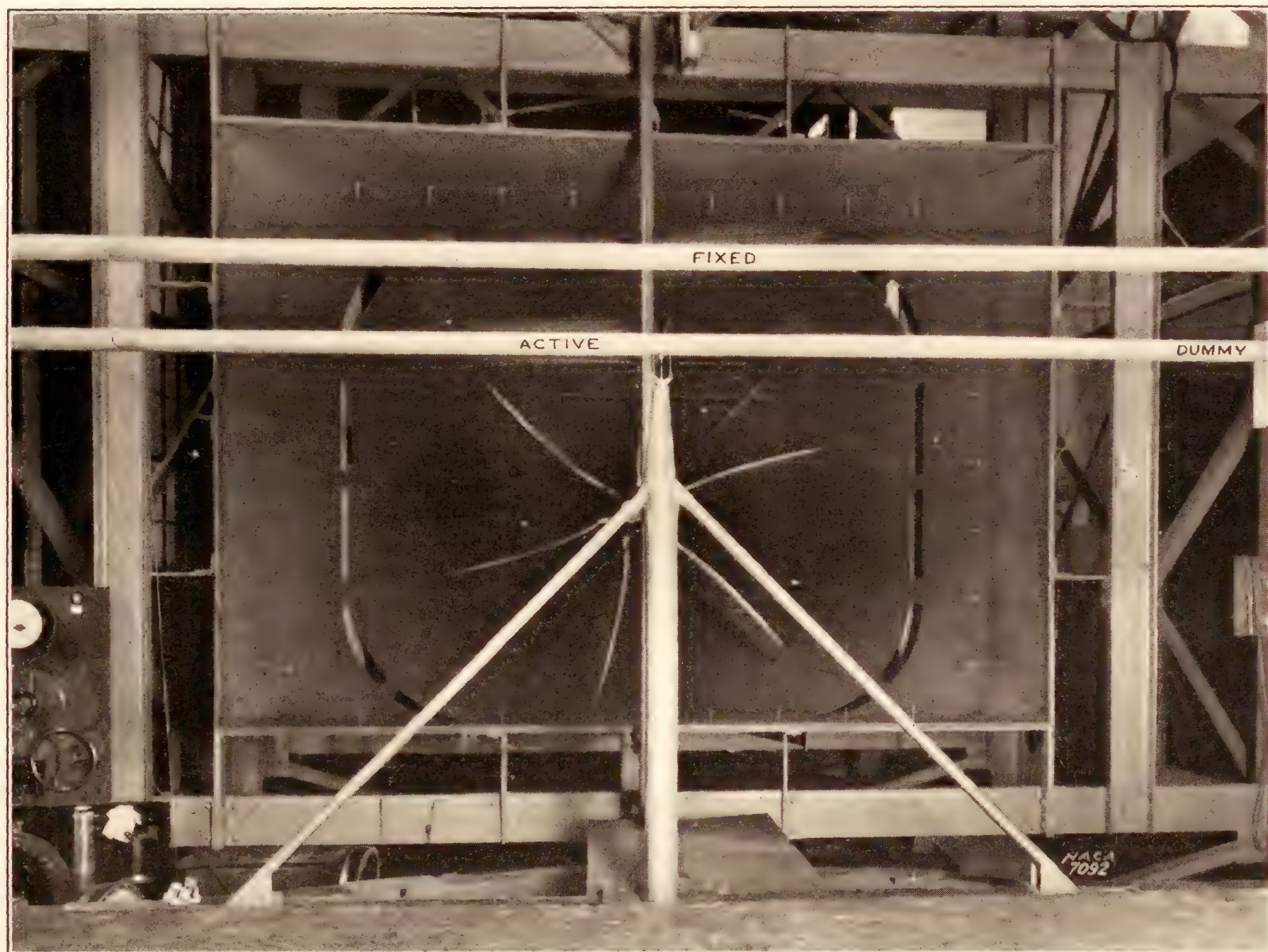


FIGURE 1.—Streamline struts spaced side by side, showing method of support and dummy tip extensions.

cept that the fixed strut was located first at different spacings to the rear of the active strut and then located at different spacings in front of the active strut. The tunnel balance thus measured the drag of a strut plus the interference effect of a strut behind it or in front of it, as the case might be. By simple addition the interference effect of either strut on the other as well as the total interference, may be computed.

Tandem struts faired together, streamline and round.—Tandem streamline struts are sometimes faired together by the simple procedure of wrapping

mounted in the tunnel in the same manner as were the struts alone in previous tests. The spacing of these hypothetical struts was reduced in increments of 4 inches by successive removal of the intervening boards. Only one strut size was used for these tests.

Obviously the best and most practicable method of fairing tandem cylinders that are relatively close together is to encase them in a single streamline fairing. In order to accomplish this it is necessary to decide on the fairing form to use; the form for minimum drag will vary, of course, with the ratio of cylinder

diameter to spacing. Since the Navy no. 1 strut section has both good aerodynamic and good geometric properties for housing tandem struts, it was selected as a basic section for housing tandem cylinders. The fairing dimensions to give the least drag for any cylinder size and spacing may be calculated from tests on struts of various fineness ratios. Tests were made on Navy no. 1 struts of four fineness ratios: 3, 4, 6.25, and 8.34. The variation was made in thickness only, the chord being held constant at 7.5 inches. These struts, 8 feet long, were mounted in the tunnel in the same manner as in previous tests.

A strut intersecting a plane.—Tests were made to determine the interference drag arising from a 2.25-by 6.75-inch strut, 23 inches long, intersecting the surface of the flat-sided section previously used for fairing tandem struts. The strut was mounted at the center of the plane with a hinge-type fitting in such a manner that the angle between the strut and the plane, measured in a plane perpendicular to the tunnel axis, could be varied through the range from 20° to 90° . This test was made with planes of three chord sizes: 25.25 inches, 17.25 inches, and 9.25 inches. Several sizes of fillets were also used at the intersection of strut and plane.

Intersecting struts.—Struts intersecting to form a V in which the included angle could be varied from 15° to 180° were mounted in the tunnel on the regular force-test support. One leg of the V was supported at its midpoint, the other leg being allowed to swing in a plane perpendicular to the tunnel axis. Each strut was 32 inches long. No dummy tip extensions were considered necessary for this set-up, inasmuch as the interference did not extend to the tips to an appreciable extent. Several sizes of fillets were used for a number of angular settings of the struts.

General considerations.—Although most of the results were obtained at an air speed of 80 miles per hour, many of the tests were run at several lower speeds also. These additional test points were taken in order to increase the accuracy of the single test point by determining a curve, and also to show whether the drag coefficient changed with air speed for any given set-up. The tare drag was measured for all struts alone by suspending them independent of the balance support, providing only a small clearance. The forces on streamline struts alone were measured to within ± 0.03 pound; but for cylinders and for models in which unsteady flow conditions prevailed to an appreciable extent they were measured to ± 0.1 pound.

RESULTS AND DISCUSSION

The observed data and computed nondimensional coefficients of drag and interference drag are presented in tables II and III and in figures 2 to 14, inclusive. The terms and coefficients used are defined as follows:

Drag coefficient,

$$C_D = \frac{\text{drag}}{q d l}$$

Interference drag = drag of the bodies in combination
— the sum of the drags of the bodies tested separately

Interference-drag coefficient,

$$C_{D_{int}} = \frac{\text{interference drag}}{q d l}$$

Length of strut equivalent to interference drag

$$= \frac{\text{interference drag}}{\text{drag per unit length of strut}}$$

where q , dynamic pressure in pounds per square foot.

d , diameter or maximum cross-wind dimension of strut in feet.

l , length of strut in feet.

NOTE.—Interference-drag coefficients are based on d and l of one strut only.

The drag coefficients are corrected for tare drag and for static-pressure variation in the tunnel by the usual methods.

STRUTS ALONE

Streamline struts.—The results for streamline struts tested alone are given in figures 2 and 3. Figure 2 shows the variation of C_D with Reynolds Number for the three sizes of struts tested, all of fineness ratio 3.

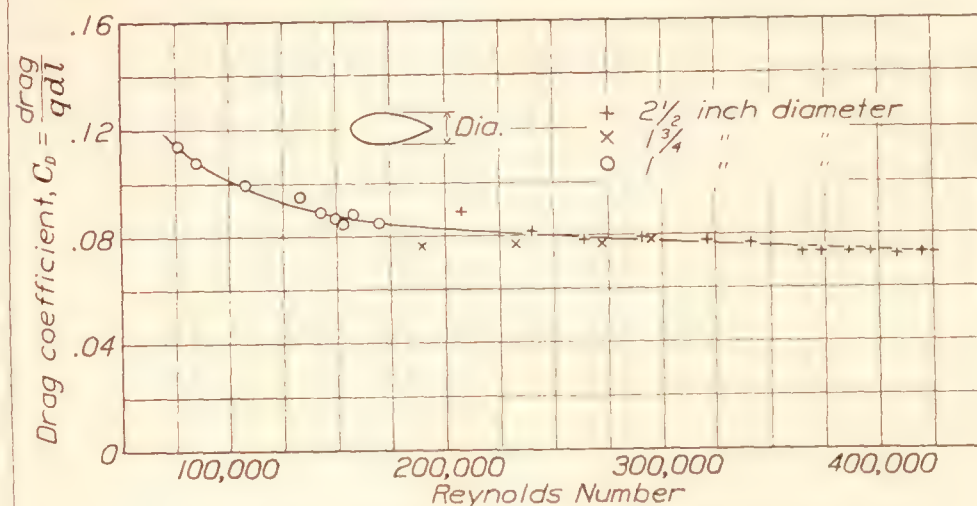


FIGURE 2.—Variation of drag of streamline struts with Reynolds Number. Navy no. 1 strut section, fineness ratio, 3.

The drag coefficients are consistently higher than those obtained from an early test (reference 2), but later

tests (reference 3) agree more closely with the present results and indicate that the results of reference 2 were influenced by the presence of a support strut.

Figure 3, which is only incidental to the present report, shows the relation between C_D and fineness ratio for Navy no. 1 struts. These results, too, differ somewhat from those of previous tests in that minimum drag occurs at a fineness ratio of about 5 instead of at 3 or 4 as observed for other tests. Furthermore, the

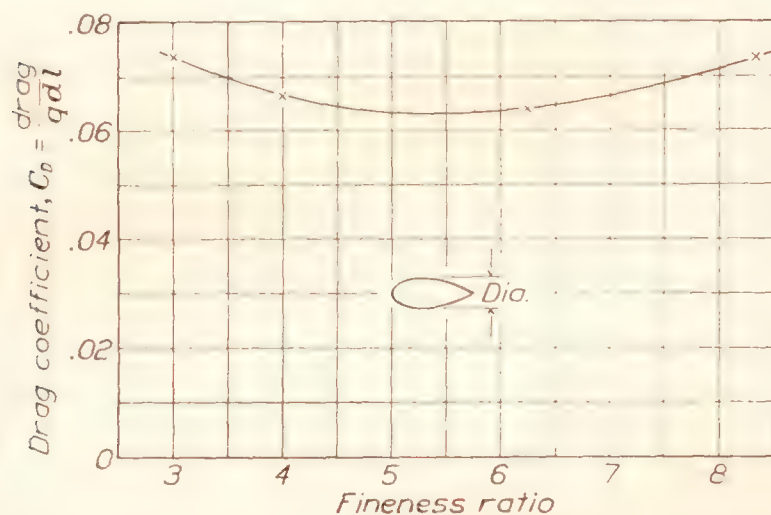


FIGURE 3.—Drag of Navy no. 1 struts of various fineness ratios. Air speed, 80 m.p.h. Reynolds Number, 420,000.

drag coefficient does not change as greatly with small changes of fineness ratio as the other tests show it to have done. Results from recent N.A.C.A. tests on symmetrical airfoils (reference 4) agree, however, fairly well with these results, in that the drag coefficient does not change rapidly with changes in fineness ratio within the range from 3 to 7. In view of the differences between these results and those of former tests, it is suggested that further investigation be made of the subject.

Round struts (cylinders) alone.—The variation of C_D with Reynolds Number for three sizes of cylinders is given in figure 4. In general, these results check previous tests of cylinders fairly well. It is noted that each size of cylinder defines a slightly different C_D for a

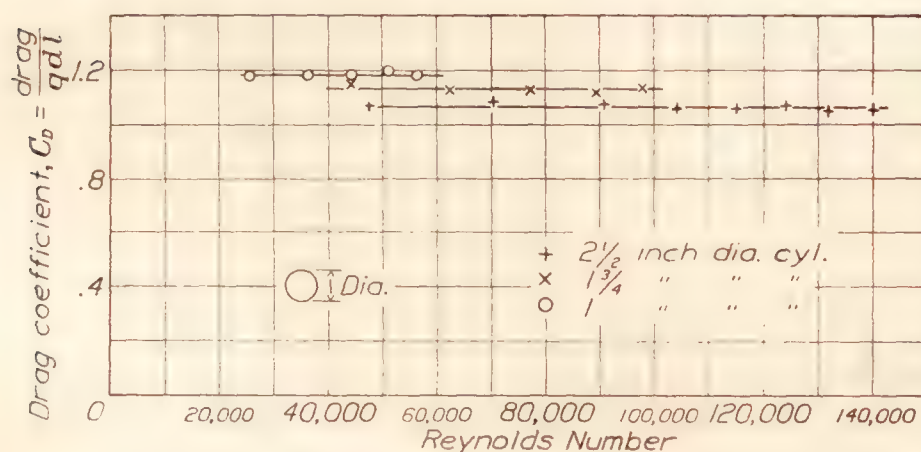


FIGURE 4.—Variation of drag of cylinders with Reynolds Number.

given Reynolds Number. The reason for this is not readily apparent, inasmuch as several factors pertinent to wind tunnels might possibly account for the effect. More detailed work on this subject would probably disclose information concerning this effect.

STRUTS SIDE BY SIDE

Streamline struts.—Streamline struts spaced side by side 6 diameters or more have little or no interference effect (fig. 5). For smaller spacings the interference drag increases gradually with decreases in spacing down to a spacing of about 2.5 diameters. For spacings less than 2.5 diameters the interference increases rapidly with reduction in spacing to a maximum value not determined in these tests because of excessive vibration. The magnitude of the interference drag at these small spacings may be ten or more times the drag of a single strut. Another significant fact is that each size of strut defines a separate curve, suggesting a Reynolds Number effect; but with the exception of struts spaced very close together, the drag coefficient is constant for all air speeds for each strut size, indicating the reason for the difference to be elsewhere. Wind-tunnel conditions influencing the results on cylinders as previously noted may possibly be responsible for these discrepancies.

Probably the most reasonable explanation for the cause of interference between two streamline struts

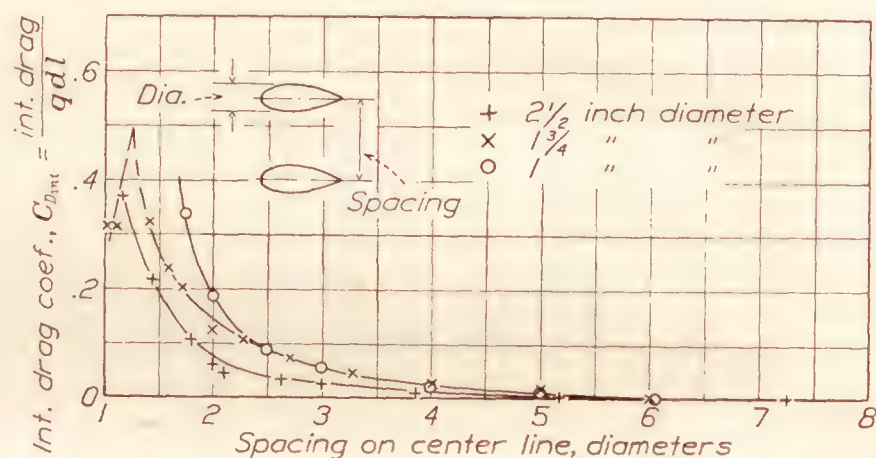


FIGURE 5.—Effect of side-by-side spacing on interference drag of streamline struts. Navy no. 1 strut section, fineness ratio, 3. Air speed, 80 m.p.h.

spaced side by side is that the flow cannot follow the contour of the adjacent strut surfaces. Streamline struts spaced relatively close together form an effective venturi having a high degree of divergence. Upon passing the throat of the venturi the air flow does not expand sufficiently to fill the diverging passage. Owing to losses in the boundary layer, sufficient kinetic energy is lacking in the air stream to overcome the increasing pressure in the expanding jet.

Cylinders.—As is the case for streamline struts, the interference drag of cylinders side by side increases gradually with reduction of spacing for intervals less than 5 or 6 diameters (fig. 5); but instead of rapidly increasing for spacings less than 2.5 diameters, the interference drag varies between wide ranges of positive and negative values. For 2.5- and 1.75-inch cylinders a critical region exists at about 1.75-diameter spacing, where the interference drag may be either positive or negative, depending, of course, on the flow pattern existing at the time. Apparently the type of flow changes rapidly with a change in spacing; it may even change while the spacing is held constant. The

rapid decreases in drag are probably due to the fact that the trailing vortices behind the two cylinders join or interlock for certain spacings to form only a single path, resulting in a decreased amount of disturbed air. For spacings less than 1.25 diameters the interference drag increases very rapidly with decreases in spacing.

STRUTS IN TANDEM

Streamline struts.—Figure 7 shows the interference drag resulting from spacing streamline struts in tandem. Since separate measurements were made on each strut, a more general picture was obtained of the flow conditions than if the struts had been combined in one unit. Several noteworthy results were obtained from these tests. First, the drag of the rear strut is increased to some extent by the presence of the front strut for all spacings tested, the magnitude being much greater for small spacings. Second, the drag of the front strut is reduced an almost equal amount by the presence of the rear strut. For spacings less than 4.5 diameters the net front-strut reaction is actually in an upstream direction. Third, considering the two struts as a unit, the drag is increased a small amount throughout the range, reaching a maximum at about 4 diameters. Fourth, the agreement of results is excellent for all sizes of struts tested.

The probable reason for the relatively high upstream force on the front strut and the downstream force on the rear strut is the presence of a region of increased pressure head between the struts, gained at the expense of velocity head.

Cylinders.—The results of tandem-cylinder tests are somewhat different from those of tandem streamline struts (fig. 8), in that the drag of the rear cylinder is decreased in the presence of the front cylinder, while the drag of the front cylinder is not greatly affected by the presence of the rear cylinder. The magnitude of interference does not change appreciably for spacings greater than 4 diameters. For smaller spacings the drag of the rear cylinder decreases rapidly with decreases in spacing. For spacings less than 3 diameters the rear-cylinder reaction is forward. For spacings less than 3.5 diameters the net drag of both cylinders is less than the drag of one cylinder.

The probable reason for the reduction of drag of the rear cylinder is its presence in the turbulent wake of the front cylinder. The effect of turbulent flow on the drag of cylinders is well known (reference 5). However, turbulence alone will not explain the decrease in drag for small spacings. For these spacings the vortices produced by the front cylinder probably partly encircle the rear cylinder, impinging on the back surface with sufficient force to produce a forward reaction.

TANDEM STRUTS FAIRED TOGETHER

Streamline struts.—The drag of tandem streamline struts is materially reduced for spacings less than 10 diameters by fairing them with the flat-sided fairing (fig. 9). Throughout the practical range the drag is proportional to the spacing of the struts. For spacings greater than 10 diameters it is impractical to fair struts by this method.

Cylinders.—Although an additional decrease in drag may be obtained for tandem streamline struts by enclosing them in a streamline fairing, this method of fairing was confined to cylinders. However, for most cases the same streamline fairing used for cylinders will also fit streamline struts. Hence, the curve (fig. 9) illustrating the variation of drag with spacing for cylinders faired together with a streamline section also applies, in general, to tandem streamline struts. It is noteworthy that this type of fairing is materially better than the flat-sided type in that the drag is considerably lower throughout the range and the maximum practical spacing is increased to about 12 diameters.

The method of obtaining this curve was not direct because it was impossible to determine the dimensions of the minimum-drag fairing for each strut spacing without first testing a series of different thickness sections. The drag of a complete series of fairings, covering the practical range of cylinder diameter-spacing ratios, was calculated from the data of tests on Navy no. 1 struts of different fineness ratios (fig. 3). Figure 10 shows the fairing fineness ratio at which minimum drag occurs for different cylinder spacings.

Figure 11 is a working chart for the determination of dimensions for tandem-cylinder fairings having minimum drag. To use the chart one need know only the cylinder or tube spacing in terms of cylinder diameter. The fairing chord may be read directly from the opposite side of the chart and the section thickness from the abscissa. With these dimensions the section ordinates may be calculated from table I. In case the cylinders are of unequal size the average should be taken. This method works out fairly well for cylinders of nearly the same size but may err somewhat for great differences in size. The chart is also applicable to streamline struts, providing that the diameters of the struts be assumed as slightly larger than they are. This modification will allow the necessary clearance for the nose and tail of the struts.

A STREAMLINE STRUT INTERSECTING A FLAT SURFACE

The results of tests on a streamline strut intersecting a flat surface at various angles are given in figure 12. Interference drag is given in terms of the equivalent drag of a length of strut. Drag or interference-drag

coefficients are not applicable because of the lack of a length dimension. With the strut perpendicular to the 25.25-inch chord plane the interference drag is zero, but it increases gradually with decreases in angle between strut and plane. For an angle of 20° the interference drag is equal to the drag of a strut 14 diameters long, or in this case 31.5 inches.

tion in plane chord. Any direct application of these results to design should be tempered with judgment. These tests are probably more valuable for demonstrating flow conditions than for any general application.

Table II shows the results from some tests on fairing the intersection between plane and strut. For the

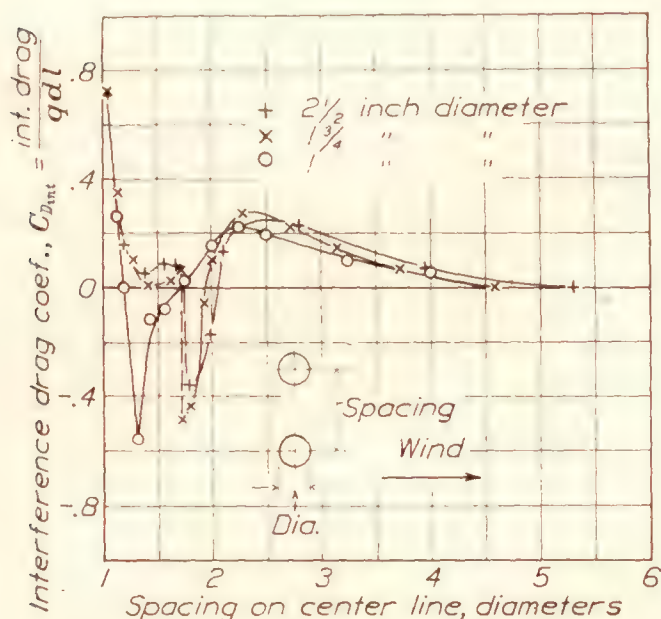
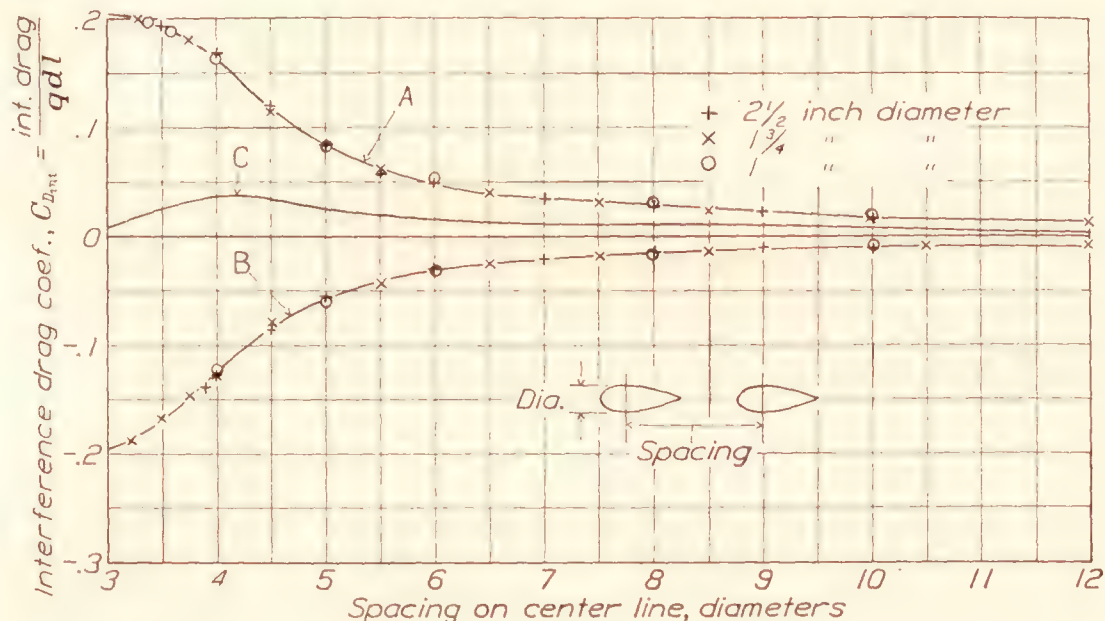
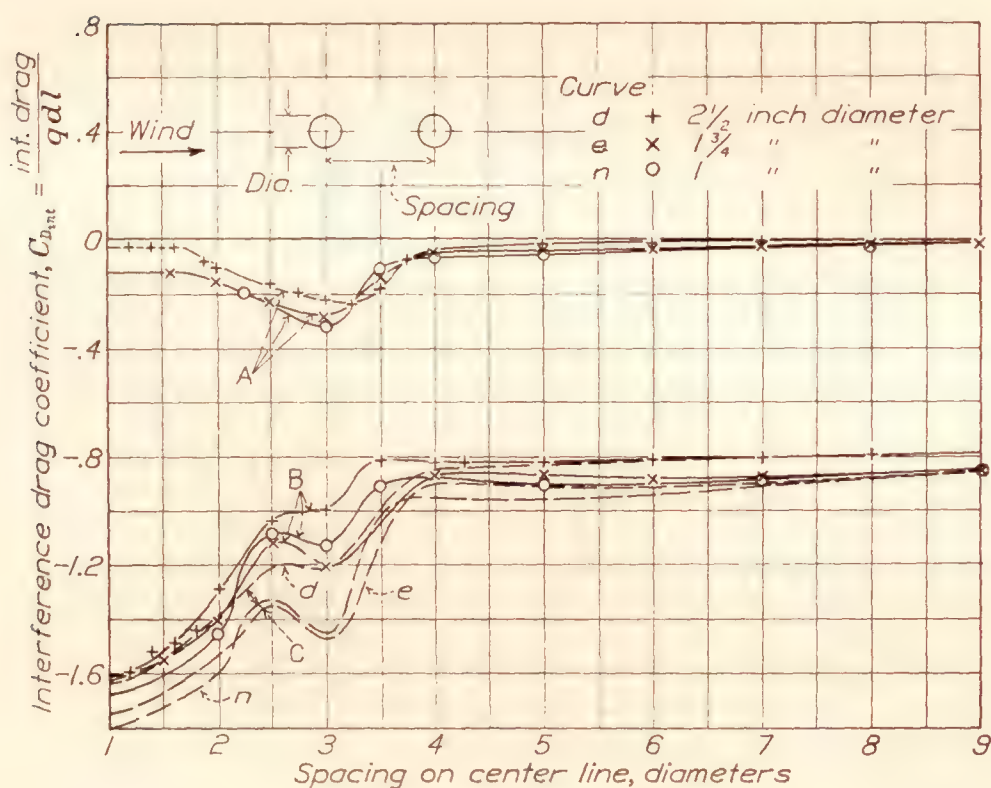


FIGURE 6.—Effect of side-by-side spacing on interference drag of cylinders. Air speed, 80 m.p.h.



Curve A, rear strut in presence of front strut.
Curve B, front strut in presence of rear strut.
Curve C, total interference drag.

FIGURE 7.—Effect of tandem spacing on interference drag of streamline struts. Navy no. 1 strut section, fineness ratio, 3. Air speed 80 m.p.h.



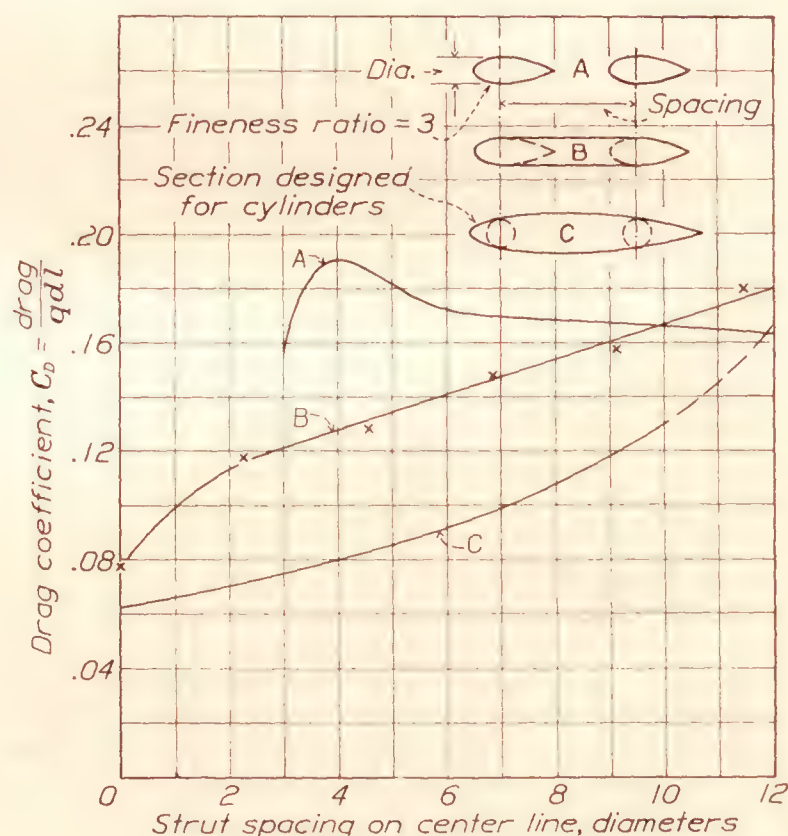
Curve A, front cylinder in presence of rear cylinder.
Curve B, rear cylinder in presence of front cylinder.
Curve C, total interference drag.

FIGURE 8.—Effect of tandem spacing on interference drag of cylinders. Air speed, 80 m.p.h.

It is interesting to note the increases in interference with decreases in the chord of the plane. For the 17.25-inch plane with a strut setting of 90° the interference drag is equal to the drag of a strut about 3 diameters long, and for the 9.25-inch plane to one of 9 diameters. Evidently the chord of the plane materially affects the flow, increasing the interference with reduc-

strut mounted perpendicular to the 25.25-inch plane the interference drag is shown to be zero if the fitting is not exposed. Fillets of the usual type failed to reduce the drag, and even increased the drag for the fillet of largest radius.

With the strut inclined 20° to the 25.25-inch plane, the attempt to reduce the interference by modifying



Curve A, streamline struts in tandem.
Curve B, struts faired together with parallel-sided fairing.
Curve C, drag of Navy no. 1 strut of optimum fineness ratio for enclosing cylinders.

FIGURE 9.—Effect of fairing together tandem struts.

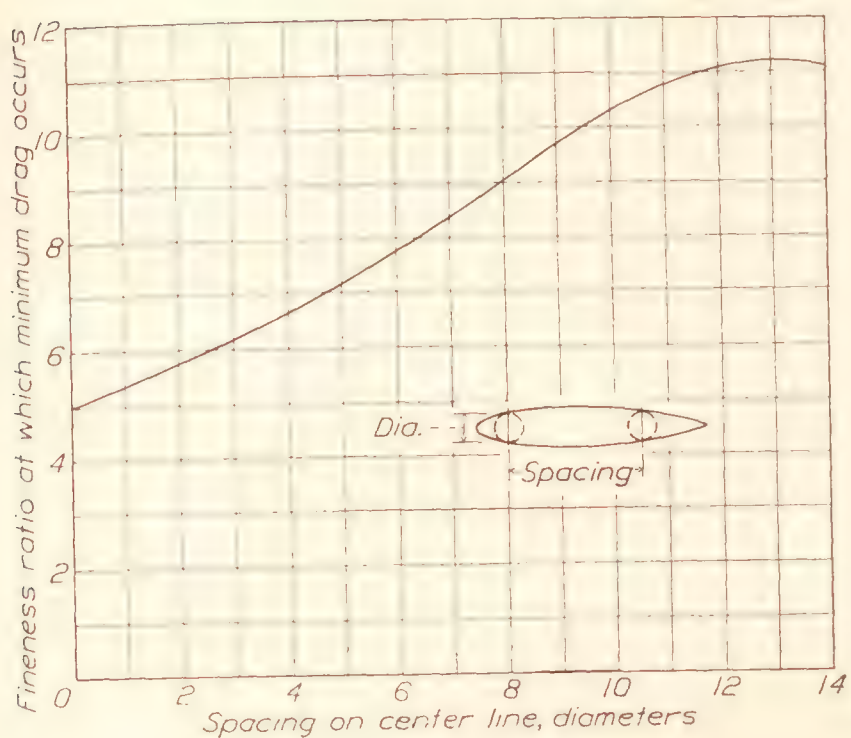


FIGURE 10.—Best fineness ratio for Navy no. 1 strut section used for fairing tandem cylinders.

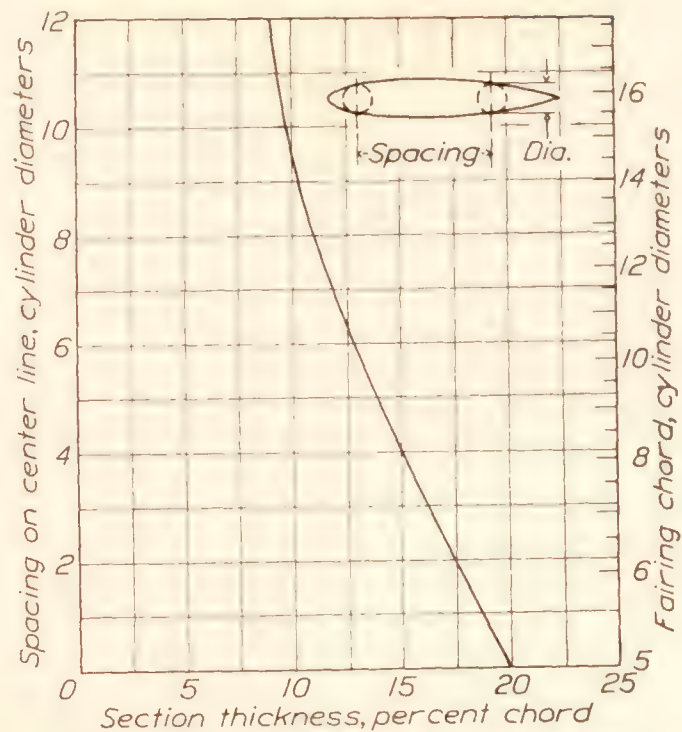


FIGURE 11.—Working chart for determining dimensions of tandem-strut fairings of minimum drag. Navy no. 1 strut section.

NOTE.—For tubes of unequal size, use average.

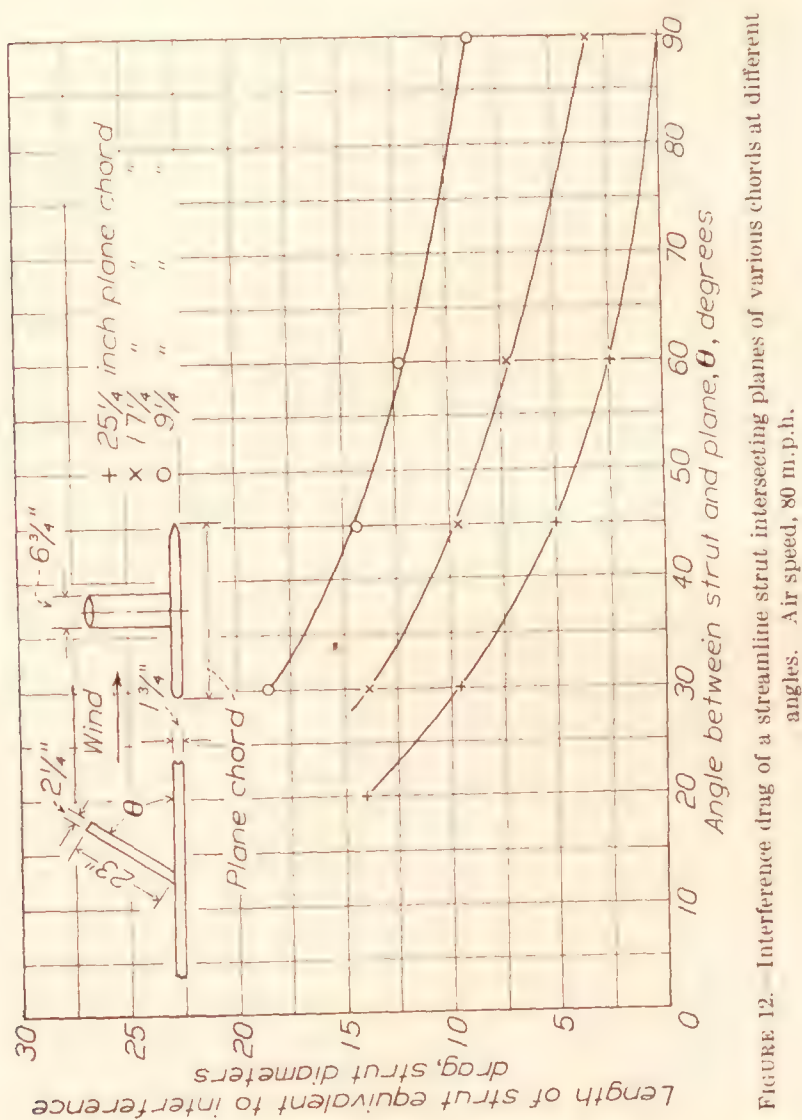


FIGURE 12.—Interference drag of a streamline strut intersecting planes of various chords at different angles. Air speed, 80 m.p.h.

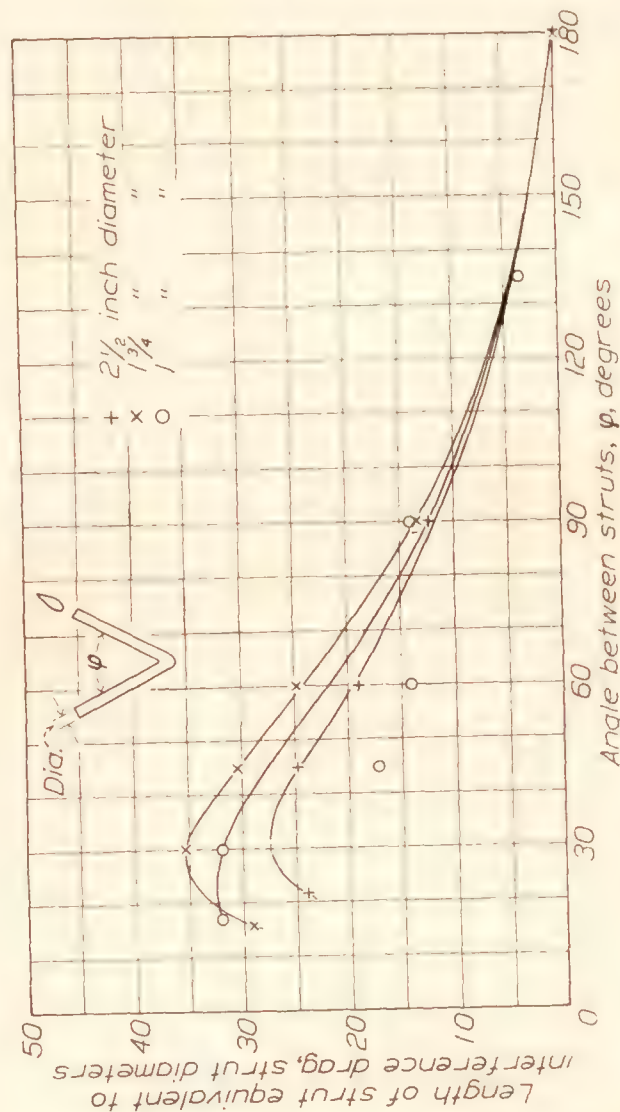


FIGURE 13.—Interference drag of streamline struts intersecting at various angles. Navy no. 1 strut section, fineness ratio, 3. Wind axis perpendicular to plane of struts. Air speed, 80 m.p.h.

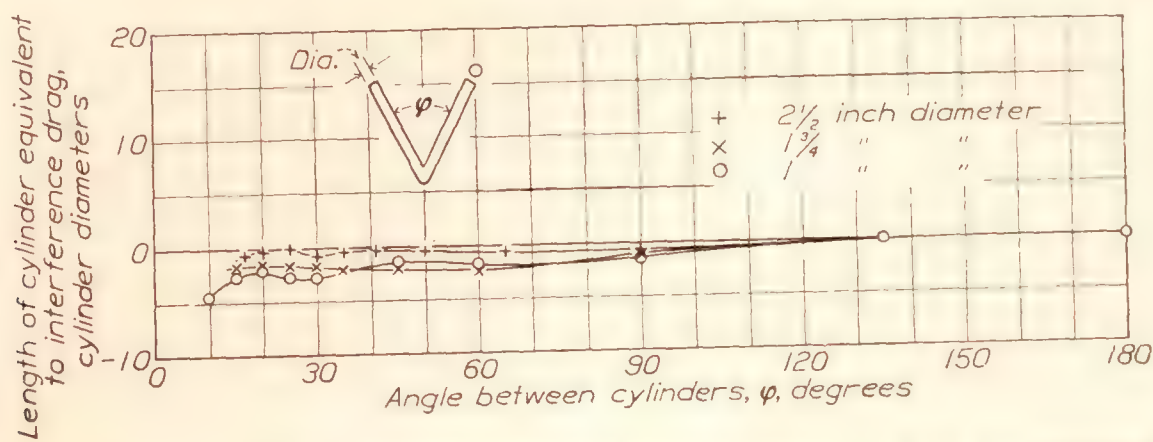


FIGURE 14.—Interference drag of cylinders intersecting at various angles. Wind axis perpendicular to plane of cylinders. Air speed, 80 m.p.h.

the effect of the acute angle with the usual type of constant-radius fillets failed. However, the interference drag was reduced 31 percent by the modification designated "1" on the sketch. This modification was considered to be of practical value because the strut fitting is often relatively small in comparison to the strut diameter, allowing a modification of this type to be made. Modification 1 also reduced the interference drag for the strut inclined 30° to the 17.25-inch plane. Furthermore, fillets reduced the drag even more, amounting to a total reduction of interference drag of 50 percent. With the strut inclined 30° to the 9.25-inch plane modification 1 reduced the interference drag 15 percent. A fillet failed to decrease the drag further.

STRUTS INTERSECTING TO FORM A V

Streamline struts.—Figure 13 shows the interference resulting from streamline struts intersecting at various angles to form V's. The interference was assumed to be equal to zero when the struts were placed end to end, forming one continuous strut. With reduction of the angle between the struts the interference increases fairly uniformly for all three sizes of models tested, reaching a maximum at about 30° . The probable reason for the reduction in interference for angles less than 30° is the rapid overlapping of the struts near the hinge point, inasmuch as the axis of rotation lies on the strut center lines. The maximum value of interference is equal to the drag of a strut from 27 to 35 diameters long, depending upon the size of the strut. For the 2.5-inch strut, this amounts to an equivalent strut length of 80 inches.

The conditions in these tests that give rise to interference are very similar to those encountered for struts spaced side by side, in that the surfaces of the struts which face each other are divergent. However, in these tests there is the additional effect of the acute angle, which probably increases the interference.

Table III shows the results of some miscellaneous fillet tests made on intersecting streamline struts. Because of the small differences in forces it was impossible to obtain very satisfactory results. For the 1 by 3 inch strut, fillets were found to have detrimental effects, increasing the interference as much as 51 percent. For the larger struts, fillets consistently reduced the interference for all angular settings of the struts tested.

Cylinders.—The interference drag of cylinders intersecting at various angles is negligible, as can be seen from figure 14.

GENERAL REMARKS

Although these tests furnish some interesting and usable data on the interference of struts in various combinations, this particular branch of the study of interference deserves much more consideration. There are other basic strut combinations which could be

tested to advantage, and the relationships between interference, turbulence, tunnel speed, and model size could be more fully studied with profit.

CONCLUSIONS

The results of this investigation indicate the following:

1. Streamline struts spaced side by side 5 diameters apart or more have little or no interference. For closer spacings the interference drag increases rapidly with reduction of the interval.
2. Cylinders spaced side by side 5 diameters apart or more have practically no interference; for spacings less than 5 diameters the interference may be highly favorable or unfavorable, depending upon the size and spacing of the cylinders.
3. When streamline struts are placed in tandem the drag of the front strut is decreased by the presence of the rear one, while the drag of the rear strut is increased by the presence of the front one. This effect exists for all spacings tested, but the magnitude increases rapidly for spacings less than six times the strut thickness. The resultant interference drag for the combination is unfavorable throughout the range.
4. When cylinders are placed in tandem the drag of the front cylinder is but little affected by the presence of the rear one, while the drag of the rear cylinder is greatly reduced by the presence of the front one. The resultant interference is highly favorable for all spacings tested.
5. Tandem streamline struts spaced less than 10 diameters apart may be faired together to advantage with a flat-sided section, and to a greater advantage by encasing the struts in a streamline fairing.
6. The interference drag of a streamline strut intersecting a plane of finite thickness increases with a decrease in the chord of the plane, within the range tested, and also with a decrease in the angle between strut and plane.
7. For streamline struts intersecting to form a V and lying in a plane perpendicular to the air stream the interference drag increases with decreasing included angle, reaching a maximum value at about 30° . For angles less than 30° the interference decreases with decreasing included angle.
8. For cylinders intersecting to form a V and lying in a plane perpendicular to the air stream the interference drag is negligible for all values of the included angle.

LANGLEY MEMORIAL AERONAUTICAL LABORATORY,
NATIONAL ADVISORY COMMITTEE FOR AERONAUTICS,
LANGLEY FIELD, VA., June 5, 1933.

REFERENCES

1. Harris, Thomas A.: The 7- by 10-Foot Wind Tunnel of the National Advisory Committee for Aeronautics. T.R. No. 412, N.A.C.A., 1931.

2. Zahm, A. F.; Smith, R. H.; and Hill, G. C.: Point Drag and Total Drag of Navy Struts No. 1 Modified. T.R. No. 137, N.A.C.A., 1922.

3. Smith, R. H.: Air Forces on Three Series of Navy No. 1 Struts. Report No. 406, Construction Dept., Washington Navy Yard, 1929.

4. Jacobs, Eastman N.; Ward, Kenneth E.; and Pinkerton, Robert, M.: The Characteristics of 78 Related Airfoil Sections from Tests in the Variable-Density Tunnel. T.R. No. 460, N.A.C.A., 1932.

5. Dryden, H. L., and Heald, R. H.: Investigation of Turbulence in Wind Tunnels by a Study of the Flow about Cylinders. T.R. No. 231, N.A.C.A., 1926.

TABLE I

NAVY NO. 1 STRUT OFFSETS

% c	% d	% c	% d
1.25	26.0	35	100.0
2.5	37.1	40	99.5
5	52.5	50	95.0
7.5	63.6	60	86.1
10	72.0	70	73.2
12.5	78.5	80	56.2
15	83.6	90	33.8
20	91.1	95	19.0
25	95.9	98	7.8
30	98.8	100	0.0

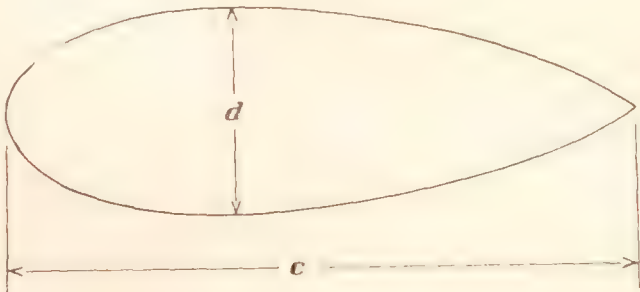
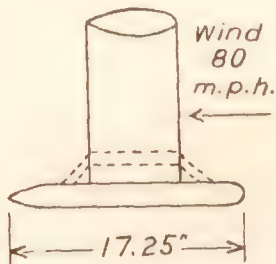
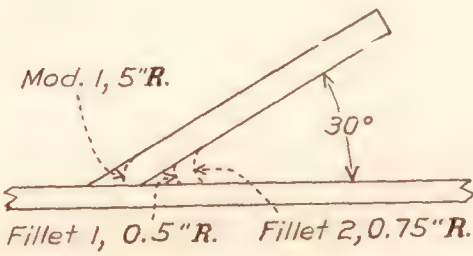
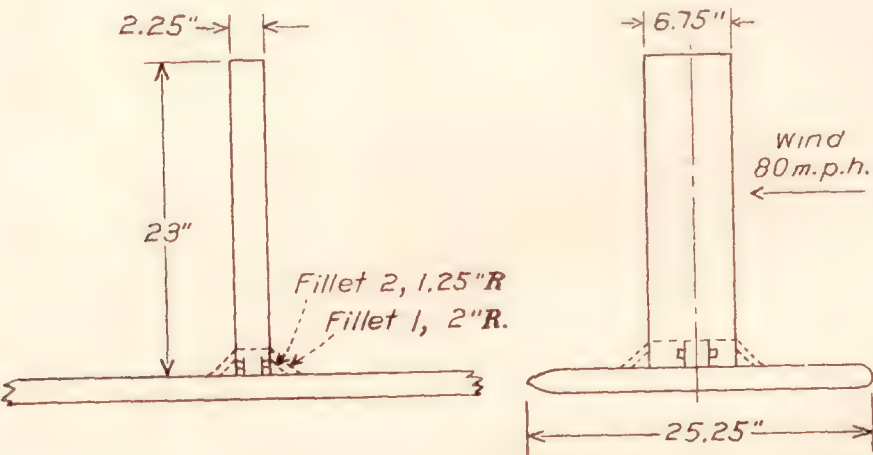


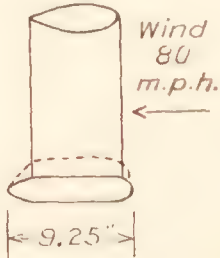
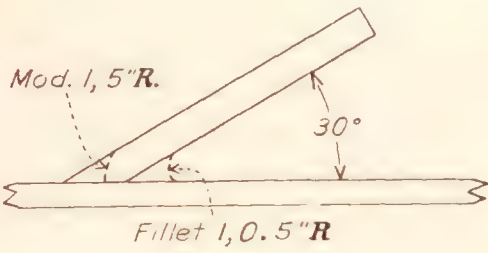
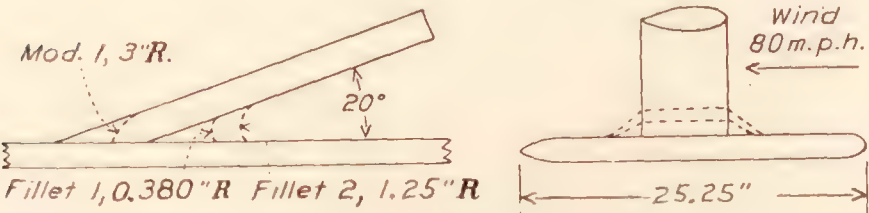
TABLE II

MISCELLANEOUS FAIRING TESTS ON INTERSECTION BETWEEN STREAMLINE STRUT AND PLANE



Nature of intersection	Interference drag (pound)	Equivalent strut length (diameters)	Percentage reduction by modification
Unmodified	0	0	
Bare fitting	.34	6.4	
Fillet 1	0	0	0
Fillet 2	.06	1.1	

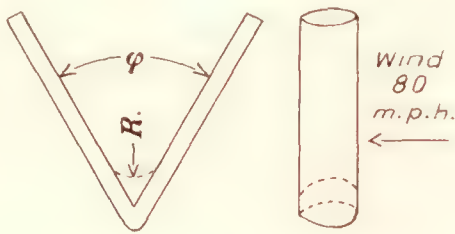
Nature of intersection	Interference drag (pound)	Equivalent strut length (diameters)	Percentage reduction by modification
Unmodified	0.74	13.9	
Modification 1	.60	11.3	19
Modification 1 and fillet 1	.47	8.8	37
Modification 1 and fillet 2	.37	7.0	50



Nature of intersection	Interference drag (pound)	Equivalent strut length (diameters)	Percentage reduction by modification
Unmodified	0.75	14.1	
Modification 1	.51	9.6	31
Modification 1 and fillet 1	.51	9.6	31
Modification 1 and fillet 2	.51	9.6	31

Nature of intersection	Interference drag (pound)	Equivalent strut length (diameters)	Percentage reduction by modification
Unmodified	0.98	18.5	
Modification 1	.83	15.6	15
Modification 1 and fillet 1	.83	15.6	15

TABLE III
MISCELLANEOUS FILLET TESTS ON STREAMLINE
STRUTS INTERSECTING AT VARIOUS ANGLES



Strut dimen- sions (inches)	ϕ	Fillet radius (inches)	Interfer- ence drag (pounds)	Equiva- lent length (diameter)	Percent- age re- duction with fillet
1 by 3-----	90°	0	0.136	14.2	24
1.75 by 5.25---		.50	.103	10.7	
2.5 by 7.5-----		0	.368	13.4	22
		1.00	.648 .505	12.3 9.6	
1 by 3-----	60°	0	.136	14.2	-51
		.375	.205	21.4	
		.50	.205	21.4	
1.75 by 5.25---		0	.682	24.9	40
		.50	.410	14.9	
		.75	.321	11.7	
2.5 by 7.5-----		1.00	.286	10.4	58
		0	1.000	19.0	
		1.00	.730	13.9	27
1 by 3-----	45°	0	.171	17.8	-31
		.25	.225	23.4	
1.75 by 5.25---		0	.832	30.4	26
		.50	.613	22.4	
		.75	.737	26.9	11
2.5 by 7.5-----		0	1.310	24.9	
		1.00	1.140	21.7	13
1 by 3-----	30°	0	.307	32.0	0
		.187	.307	32.0	
		.25	.341	35.5	
1.75 by 5.25---		0	.968	35.3	25
		.375	.730	26.6	
		.625	.750	27.4	
2.5 by 7.5-----		0	1.445	27.5	16
		.75	1.210	23.0	
		1.00	1.410	26.8	2
1 by 3-----	17.3°	0	.307	32.0	-18
		.187	.362	37.7	
1.75 by 5.25---	15.5°	0	.797	29.1	6
		.25	.750	27.4	
		.50	.845	30.8	-6
2.5 by 7.5-----	21.5°	0	1.275	24.2	3
		.50	1.240	23.6	

REPORT No. 469

INCREASING THE AIR CHARGE AND SCAVENGING THE CLEARANCE VOLUME OF A COMPRESSION-IGNITION ENGINE

By J. A. SPANOGLE, C. W. HICKS, and H. H. FOSTER

SUMMARY

The object of the investigation presented in this report was to determine the effects of increasing the air charge and scavenging the clearance volume of a 4-stroke-cycle compression-ignition engine having a vertical-disk form of combustion chamber.

Boosting the inlet-air pressure with normal valve timing increased the indicated engine power in proportion to the additional air inducted and resulted in smoother engine operation with less combustion shock.

Scavenging the clearance volume by using a valve overlap of 145° and an inlet-air boost pressure of approximately $2\frac{1}{2}$ inches of mercury produced a net increase in performance for clear exhaust operation of 33 percent over that obtained with normal valve timing and the same boost pressure. The engine tests indicate that, with a large valve overlap, $2\frac{1}{2}$ inches of mercury boost pressure is sufficient to scavenge completely the clearance volume, and that the increase in engine power effected by scavenging the clearance volume, for a constant fuel quantity, is more than twice what could be obtained from the additional air charge alone. The improved combustion characteristics result in lower specific fuel consumption, and a clearer exhaust. The starting and idling characteristics were not affected by variation in boost pressure or by the use of scavenging with a large valve overlap.

Analysis of the exhaust of several compression-ignition engines showed the carbon monoxide gas content to be less than one half of 1 percent when operating with a clear exhaust.

INTRODUCTION

The work of the National Advisory Committee for Aeronautics in developing the 4-stroke-cycle compression-ignition engine for aircraft use has been carried on chiefly with two different types of these engines. The one type utilizes high velocity of air flow to obtain the necessary mixing of the air and fuel in the combustion chamber, while the other type has no effective air flow at the time of the injection of the fuel and the fuel itself must be distributed as uniformly as possible to obtain the required mixture of air and fuel.

The latter type of engine with its quiescent combustion chamber has been used for a series of tests which led to the development of multiple-orifice nozzles and verified the proportional-area principle for the design of these nozzles as reported in references 1 and 2. After this work had been completed, attention was turned toward increasing the amount of air available for combustion as a means for increasing the power developed.

It has become accepted practice to increase the power output of the spark-ignition aircraft engine by boosting the inlet-air pressure so that the engine will induct more charge than would be inducted under atmospheric pressure. The work of Schey and Young (reference 3) with a spark-ignition engine has shown the additional increase in engine power that may be obtained by boosting when using a large valve overlap to effect better scavenging of the clearance volume. They have pointed out that the ratio of the power with complete scavenging to that with normal scavenging should be equal to the ratio of the volumes of the charge $r/(r-1)$ where r is the compression ratio. This formula shows that with an increase in compression ratio the increase in power to be obtained decreases; therefore, it does not seem to offer much advantage for the compression-ignition engine on a comparative basis with the spark-ignition engine. However, boosting the air charge in a compression-ignition engine showed better net fuel economy and caused the engine to operate with less combustion shock (reference 4).

Boosting a 4-stroke compression-ignition engine not only introduces more air per cycle for supporting combustion, but it also reduces the proportional amount of residual gases in the air charge, because the amount of residual gases carried over is practically constant depending upon the exhaust back pressure. As the amount of residual gases left in the combustion chamber is affected by a change of valve timing, the engine performance was investigated both with normal valve timing and boosting and also with a large valve overlap and boost pressures to effect better scavenging of the clearance volume.

This investigation was conducted during 1931 and 1932 in the power plants laboratory of the National Advisory Committee for Aeronautics at Langley Field, Va.

APPARATUS AND METHODS

The engine and combustion chamber used in these tests are described in references 1 and 2. The combustion chamber (fig. 1) is a vertical disk-shaped space formed between the valve heads and has a smooth, flared orifice connecting this space to the main cylinder. The piston runs within mechanical clearance of the cylinder head, insuring the displacement of the air charge into the combustion chamber. For all the test data presented in this report the compression ratio was held constant at 12.6. Unless engine speed

from the individual orifices in a container with a long neck shown in figure 2. The sum of the weights of the sprays from the individual orifices caught in this way was within ± 1 percent of the weight of the sprays from all orifices caught simultaneously under the same conditions. The areas of the orifices discharging insufficient fuel were increased until all spray discharges were in the proper ratio. The nozzle as finally used had two main orifices of 0.020-inch diameter, two intermediate orifices of 0.011-inch diameter, and two outside orifices of 0.007-inch diameter. The orifices were arranged symmetrically about the center line of the nozzle with an angle of 25° between adjacent axes.

With the injection system used for these tests the duration of injection for a fuel quantity of 0.000325 pound per cycle was 24 crank degrees at 1,500 engine

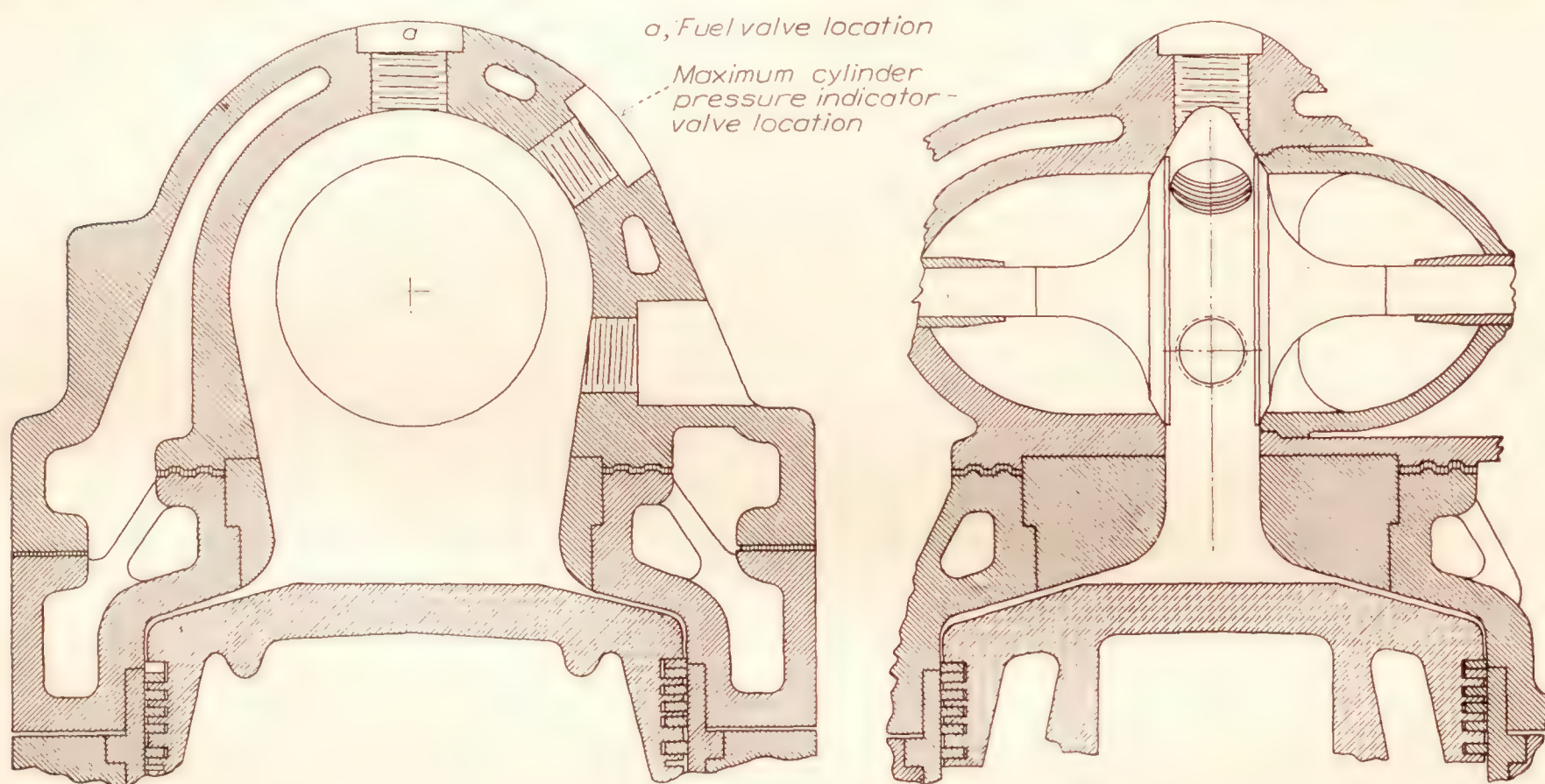


FIGURE 1.—Combustion chamber.

was the variable the speed was held constant at 1,500 r.p.m.

The fuel pump used for the tests was a cam-operated plunger pump with a poppet by-pass control. A spring-loaded automatic injection valve, set to open at 3,000 pounds per square inch, was installed in the top hole of the combustion chamber. The fuel-injection valve nozzle used had six round-hole orifices arranged in a plane parallel to the heads of the exhaust and inlet valves.

Observation of the fuel spray in the atmosphere indicated that, as the areas of the orifices were increased for the greater discharge area required for boosted operation, the flow of fuel from the large main orifices reduced the effective pressure on the other orifices and therefore the fuel distribution did not fulfill the requirements outlined in reference 2. This lack of proportion was verified by catching sprays

r.p.m. The fuels used were conventional Diesel-engine fuels described in reference 5 as fuels no. 1 and no. 2. The injection advance angle was determined by noting, with the aid of a Stroborama, the start of fuel spray while injecting into the atmosphere.

Figure 3 shows a flow-area diagram both for the normal valve timing and for the valve-overlap timing used for the engine tests. The ordinate represents the area exposed to gas flow at the inner valve seat diameters. For the valve-overlap setting the valve heads were allowed to run within 0.016 inch of each other at the point of closest travel. This condition allowed as nearly as practicable a free path for the scavenging air through the combustion chamber.

Figure 4 is a schematic diagram of the apparatus used in conducting the tests. A Roots-type blower was separately driven at the required speeds for supplying air at pressures up to 10 inches of mercury. A 16-

cubic-foot tank was connected in the air duct between the blower and the engine for damping pulsations. A mercury manometer was installed on the tank for measuring the effective air-charging pressure. The

in boost pressure, but the variation for comparative tests was negligible.

Gas samples were taken at a point approximately 5 inches from the exhaust-valve port under conditions

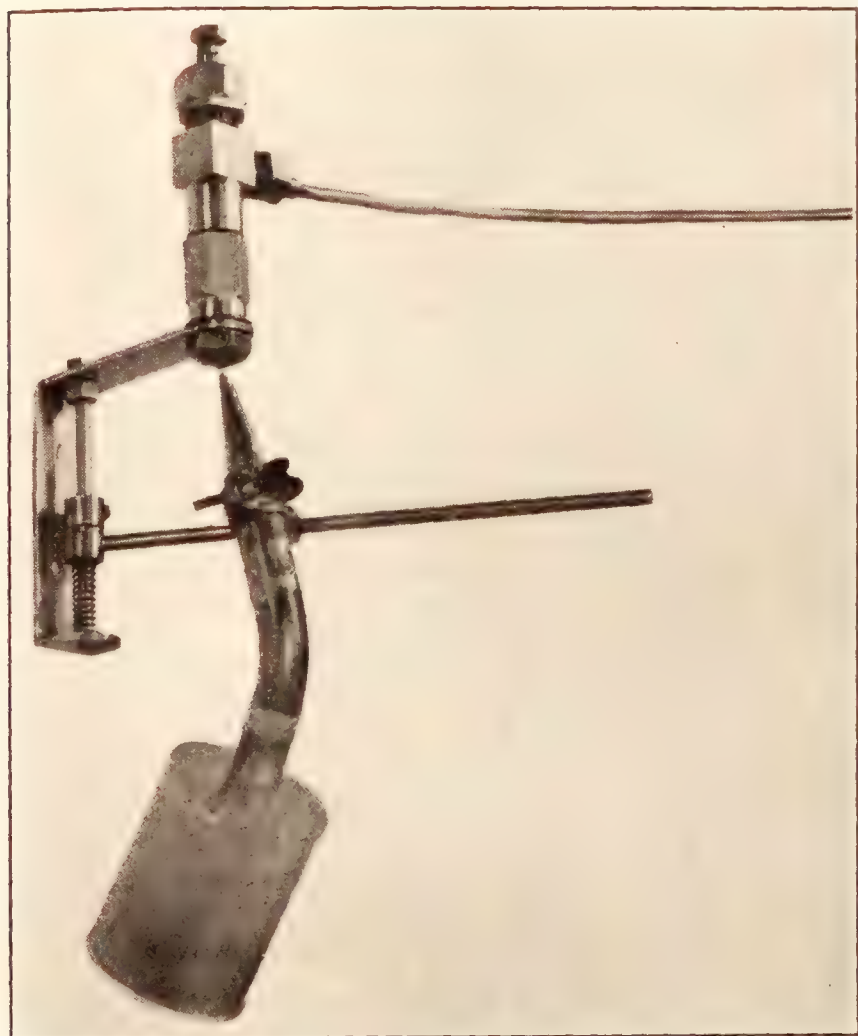


FIGURE 2.—Apparatus for catching sprays from individual orifices of a multiorifice nozzle.

length of the air duct between the tank and the engine was reduced to 15 inches to minimize the induction-wave effect. A revolution counter operated through an electro-magnetic clutch was used to record the blower

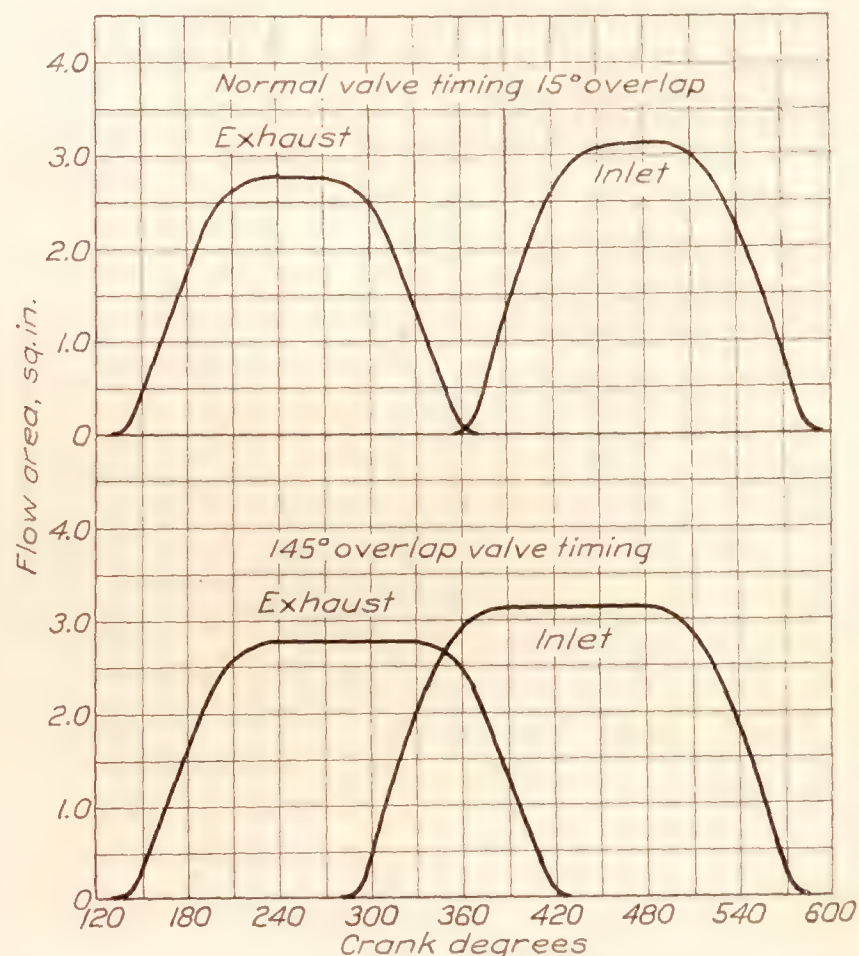


FIGURE 3.—Comparison of valve time-area diagrams with overlaps of 15° and 145°.

of variable-fuel quantity, with and without valve overlap and with and without boost pressure. A steel tube was used for conducting the gases to a sampling bottle. A modified Orsat gas-analysis apparatus

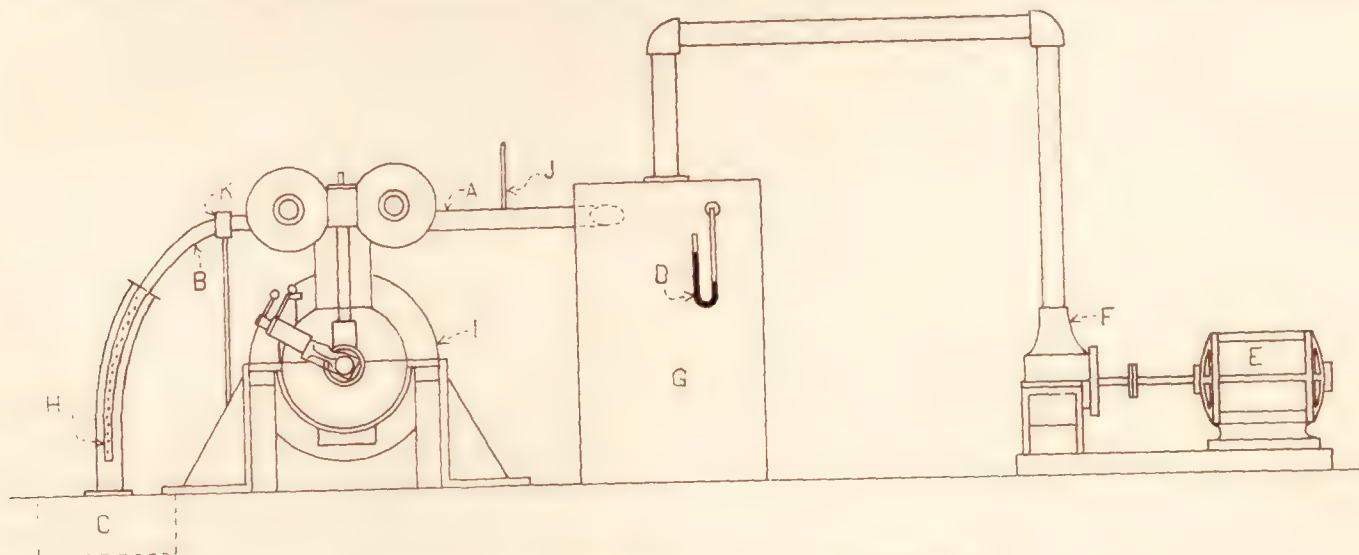


FIGURE 4.—Diagrammatic representation of air system.

A, Air duct 5" diameter, 15" long. B, Exhaust stack, 5' long: 3" diameter section, 2' 8"; Section 2' 4" tapers to 1 3/4" diameter. C, Exhaust trench. D, Manometer. E, Motor. F, Roots-type blower. G, Surge tank, 16 cu. ft. capacity. H, Tapered section, perforated. I, Test engine. J, Thermometer. K, Water sprayer.

revolutions during a test run. Slip-speed data taken over a range of speeds enabled calculations to be made for determining the air quantities delivered to the engine. The air temperature and barometric pressure were used for determining air weights. The air temperatures were not controllable and the temperature increased approximately 40° F. for a maximum increase

(reference 6) was used for analyzing the samples of exhaust gas.

For all conditions of engine operation the injection advance angle was increased until a light permissible knock was heard or until the maximum cylinder pressure reached 900 pounds per square inch as recorded by a modified Farnboro indicator. The limit of al-

lowable injection advance angle as judged from the sound of the engine was usually about 2° or 3° greater than the earliest advance angle at which no knock could be heard.

The exhaust gases were observed during the engine tests through a peephole located in the exhaust manifold about 11 inches from the exhaust-valve port. The limit of the clear-exhaust range, as used in the discussion, was that marked by the first appearance of short flashes of flame or of a slight haze.

The maximum cylinder pressures were obtained from the readings of a trapped-pressure indicator and

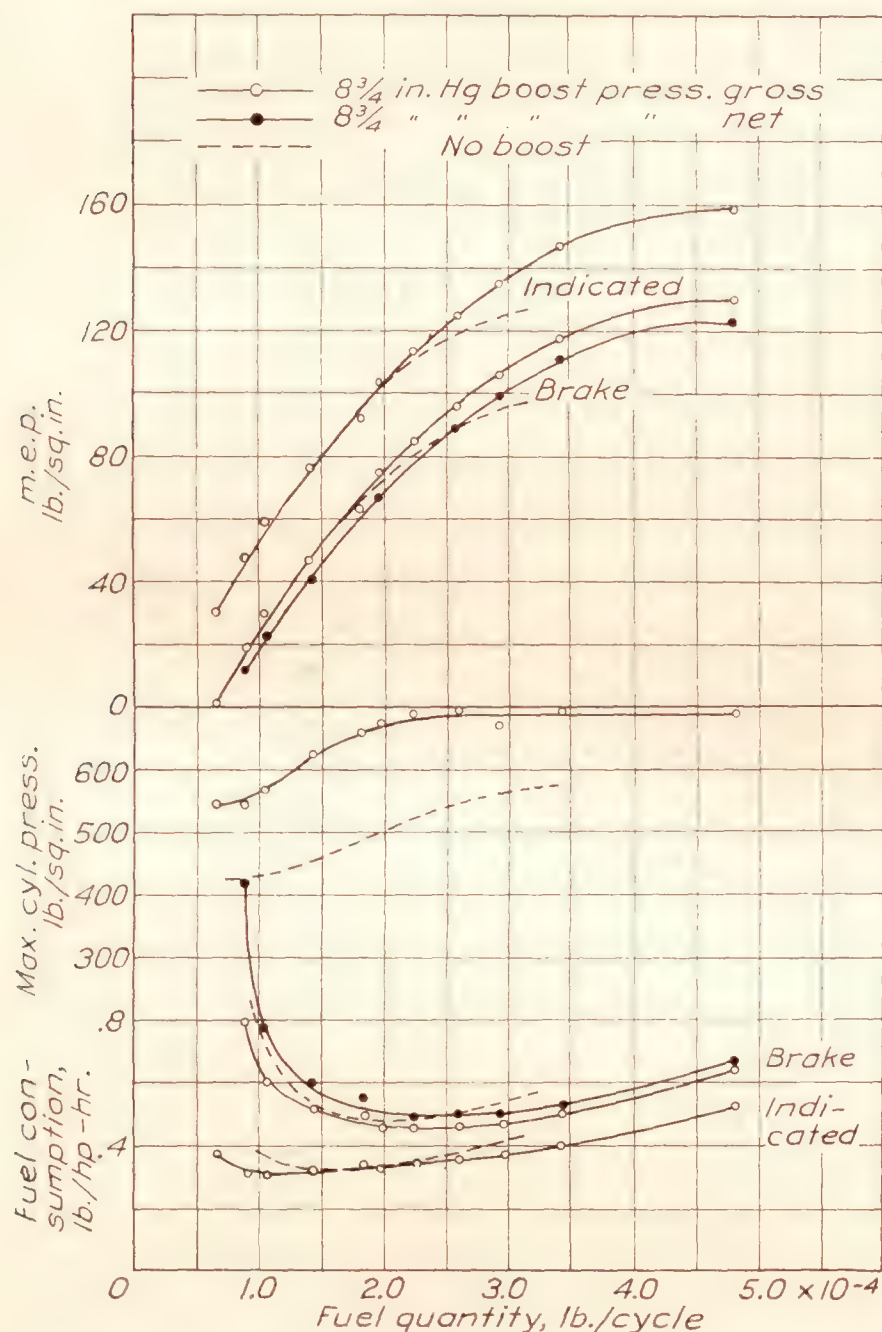


FIGURE 5.—Performance obtained with and without boost pressure (normal valve timing, speed 1,500 r.p.m.).

checked at intervals by a modified Farnboro indicator. The trapped-pressure readings are 10 to 70 pounds per square inch lower than the Farnboro readings.

All performance data shown in this paper are presented on a net basis by subtracting the power required by the blower. Unless otherwise stated, all comparative data were obtained under comparable engine operating conditions.

RESULTS AND DISCUSSION

Because of the accessory equipment driven by this single-cylinder test unit, the mechanical efficiency is

less than that obtained by a multicylinder engine. The mechanical efficiency of this engine calculated for full-load operation with no excess air is as follows: 77.0 percent for no boost and no valve overlap, 77.6 percent net for $8\frac{3}{4}$ inches of mercury boost and no valve overlap, 78.6 percent for no boost and with valve overlap, and 82.0 percent for $6\frac{1}{4}$ inches of mercury boost and with valve overlap.

Figure 5 shows the effect of boosting a compression-ignition engine with normal valve timing. The curves show that the gross brake mean effective pressure when boosting is equal to the unboosted value for the small fuel quantities. The net brake mean effective pressure, when boosting, is less than when unboosted for small fuel quantities but greater for all fuel quantities above 0.00025 pound per cycle. This fuel quantity corresponds to an excess air quantity of 30 percent for the normal engine. It has been found from the results of many tests that additional air increases the brake performance of the normal engine only when the engine is operated over a range of excess air from 0 to 30 percent. Excess fuel does not improve engine performance but may decrease the rate-of-pressure rise. It would appear from the data for indicated mean effective pressure that boosting an engine using normal valve timing increases the capacity of the engine and that the increase in indicated engine power is proportional to the additional amount of air inducted for a condition of approximately full-load operation. The balanced-diaphragm maximum-cylinder-pressure indicator shows that the difference in maximum cylinder pressure between individual cycles becomes considerably less when the engine is boosted. The engine operation becomes smoother with less combustion shock for boosted conditions. Although these results were obtained from tests at a compression ratio of 12.6, they should be true for other compression ratios except where other factors may have a greater influence on the engine operation. When boosting the air charge of a normally timed engine the proportional amount of residual gases in the fresh charge decreases and, as will be discussed later, these gases have an effect on the combustion characteristics.

Figure 6 shows the increase in engine performance with clear exhaust obtained by scavenging the combustion chamber. At zero boost pressure there is an increase in brake mean effective pressure and a decrease in fuel consumption when scavenging, even though the weight of air received by the engine is less than when using normal valve timing. This increase in brake mean effective pressure shows that the combustion characteristics are improved by the removal of the residual gases. The clear-exhaust performance for the large valve overlap increases very rapidly up to $2\frac{1}{2}$ inches of mercury boost pressure and then increases very slowly for further boost pressure. Thus it may be concluded that at $2\frac{1}{2}$ inches of mercury boost pressure the combustion chamber is

practically completely scavenged of residual gases and any further increase in performance is due to the additional air that can be trapped in the cylinder as the induction pressure is increased. The recorded compression pressures for scavenging operation show

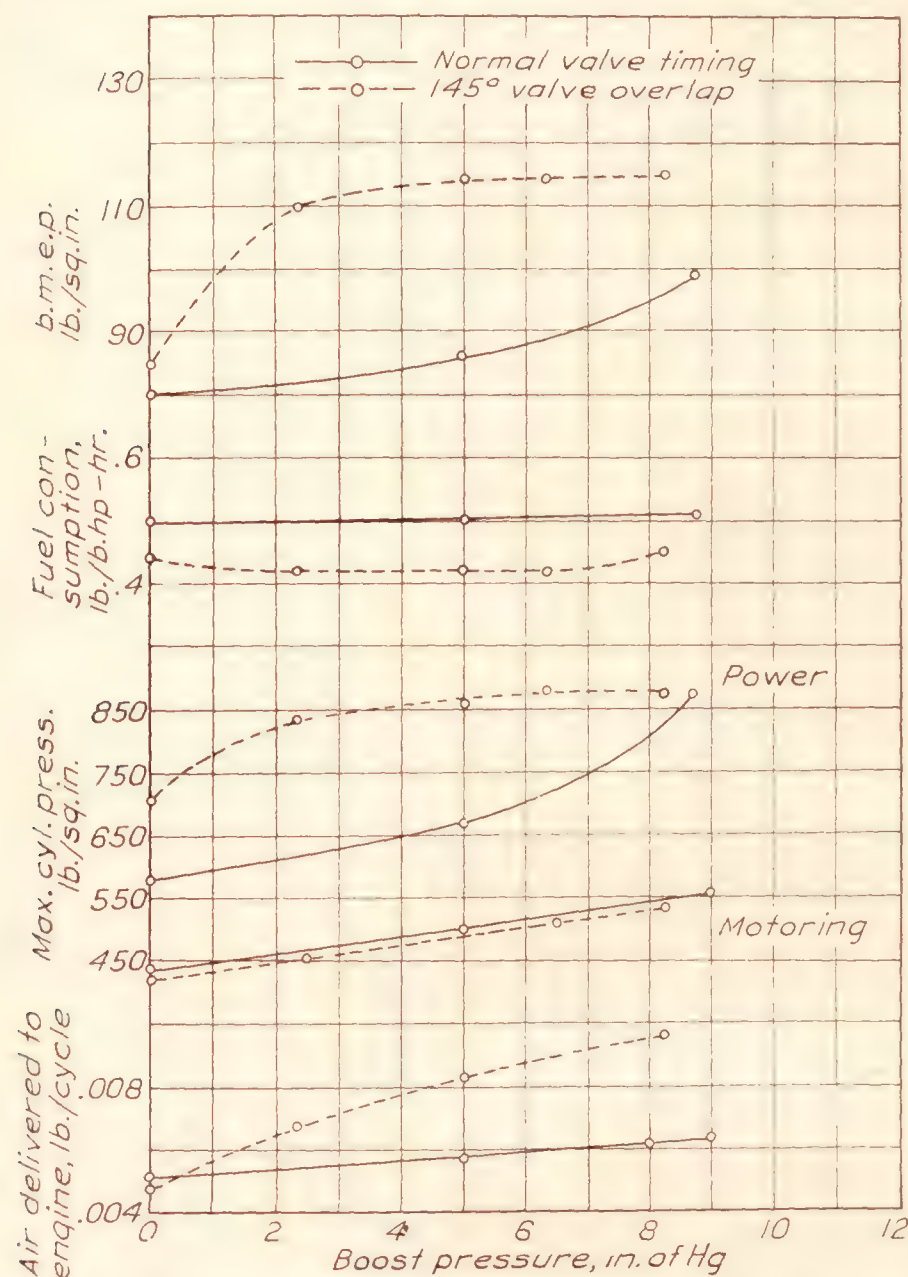


FIGURE 6.—Effect of scavenging on engine performance (clear exhaust, 1,500 r.p.m.).

lower values than for normal operation for all boost pressures, probably as a result of a decrease in the air retained in the cylinder and of a loss of the heat carried by the residual gases.

It should be noted that as the boost pressure is increased the brake mean effective pressure with clear exhaust and normal valve timing approaches that obtained with valve overlap, and at some high boost pressure would probably equal the brake mean effective pressure with valve overlap. This condition is brought about mainly by the improved combustion characteristics caused by the decreasing proportional amount of residual gases. As the boost pressure increases, there is inducted an increasingly greater air charge, and as the weight of residual gases is dependent upon the exhaust back pressure, they remain practically constant and become a proportionally smaller part of the new charge in the cylinder. This decreased effect of the residual gases for a boost condition is probably responsible to a

large degree for the smoother engine operation noted in the previous discussion.

The compression-ignition engine always has a large excess of air available when starting or idling and the use of valve overlap does not require any special arrangements or apparatus for maintaining a proper mixture ratio. In the course of these tests the starting and idling characteristics of the engine were quite satisfactory and no difference could be detected between starting or idling with normal valve timing and with valve overlap. The variation in boost pressure, as could be expected, had no effect on either starting or idling.

Exhaust-gas analysis has shown that with clear exhaust operation and normal valve timing the compression-ignition engine has less than one half of 1 percent carbon monoxide gas in the exhaust. During a test with the large valve overlap and a

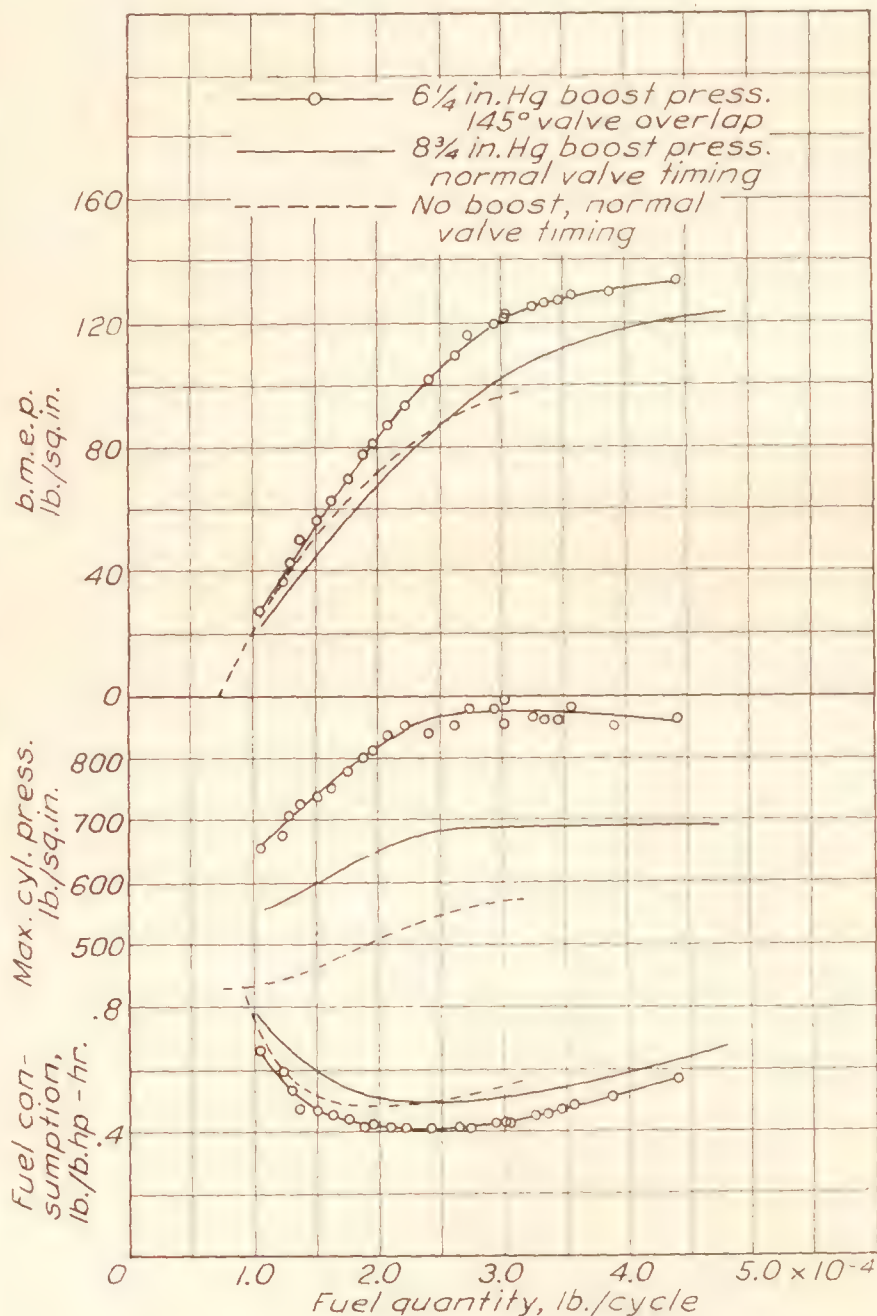


FIGURE 7.—Effect of scavenging on engine performance—variable fuel quantity (1,500 r.p.m., net results).

medium boost pressure enough excess fuel was injected to show excessive smoke and flame in the exhaust, but the exhaust-gas analysis showed only three quarters of 1 percent carbon monoxide gas.

Figure 7 shows the effect of scavenging the combustion chamber by using 145° valve overlap and

6¼ inches of boost pressure for variable fuel quantity. The unboosted performance and the net performance for 8¾ inches of boost pressure obtained with normal valve timing are shown in comparison with the scavenged net performance. It should be noted that the scavenged performance is better than the un-

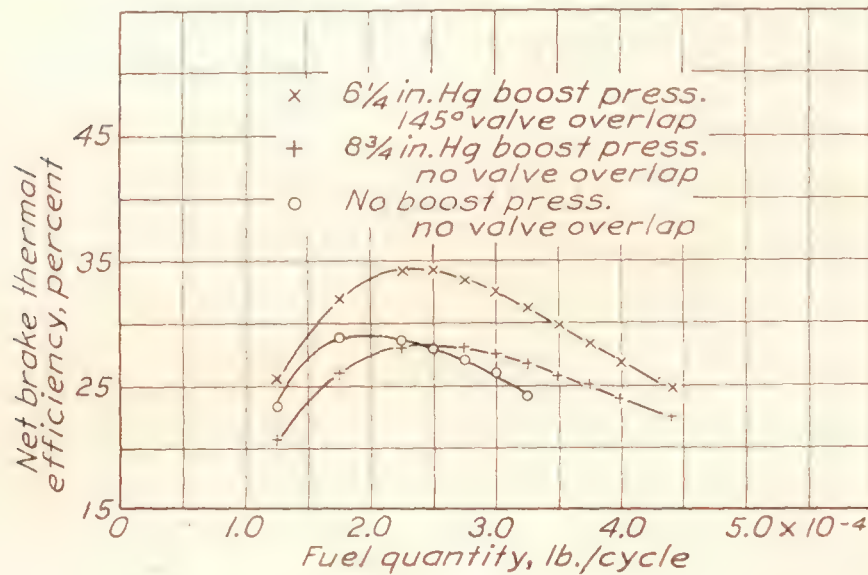


FIGURE 8.—Effect of fuel quantity at different boost pressures on thermal efficiency (speed 1,500 r.p.m.).

scavenged performance for all fuel quantities. Figure 8 shows the net brake thermal efficiencies for these data.

Figure 9 shows the comparative engine performance for variable fuel quantity both for normal valve timing and valve-overlap timing when no boost pressure is used. The increase in engine performance for a scavenged condition is effective over the entire fuel range even though there is less air trapped in the cylinder when using valve overlap as shown by the data for zero boost pressure in figure 8. The increase in the indicated mean effective pressure for all points, including the small fuel quantities where the excess air in the combustion chamber is more than 30 percent, indicates quite definitely that the combustion characteristics are improved when some of the residual gases are removed. The injection advance angle used was 18° for both the normal valve timing and for the valve-overlap data shown on this figure.

Figure 10 shows the effect of speed on engine performance with a boost pressure of 3 inches of mercury, a valve overlap of 145°, and clear exhaust. For each speed the maximum injection advance angle for smooth operation was used, and this limitation made it necessary to retard the advance angle as the speed of the engine was reduced. The fuel quantity was increased to the maximum that would allow clear exhaust for each engine speed and the fuel quantity varied from 0.000256 to 0.000280 pound per cycle. For all practical purposes the fuel quantity could have been held constant and then the brake-horsepower curve would have been practically a straight line. The brake mean effective pressure remained fairly constant over the range of speeds, as did the fuel economy. The brake

thermal efficiency of this engine for the entire speed range was between 29 and 33 percent and the indicated thermal efficiency varied from 33.7 to 40.2 percent.

In figure 11 are shown data taken under conditions simulating propeller load when operating the engine with the large valve overlap and a boost pressure comparable with the pressure from a Roots-type blower driven directly from the engine. The blower used was oversize for the single-cylinder engine and it was only necessary to drive it at one third engine speed. In accordance with the output of a suitably sized and geared blower the boost pressures were increased linearly from 3½ inches of mercury at an engine speed of 900 r.p.m. to 6⅝ inches of mercury at 1,700 r.p.m. When making the propeller-load run, the full-load rating of the engine was arbitrarily taken to be 38 brake horsepower at 1,700 r.p.m. At this rating there was a small amount of smoke and flame present in the exhaust. The exhaust was clear for the speeds less than 1,600 r.p.m., which indicates efficient operation in the cruising range. For a range of speeds

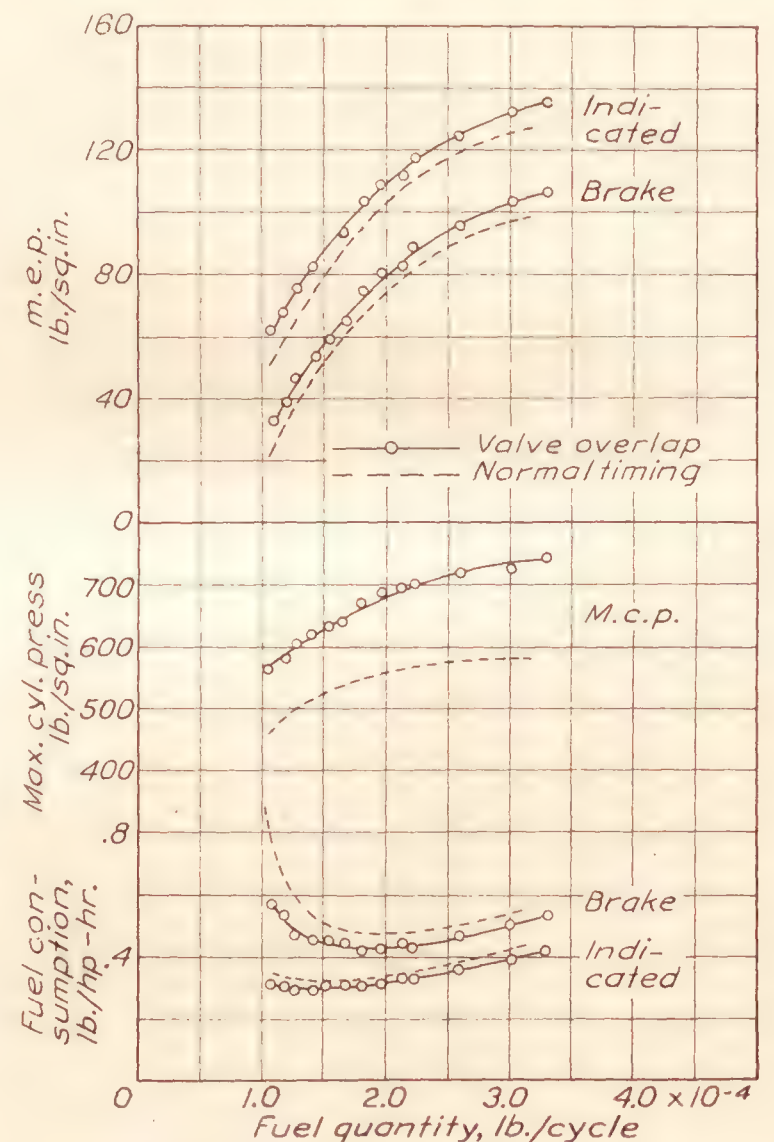


FIGURE 9.—Comparison of engine performance using normal valve timing and 145° valve overlap (no boost, 1,500 r.p.m.).

from 1,600 r.p.m. to 1,100 r.p.m the fuel consumption is between 0.47 and 0.435 pound per brake horsepower per hour. The flatness of the fuel-economy curve for variable speed indicates the desirability of this type of engine operation for aircraft. In order not to exceed an allowable knock, it was necessary to retard the

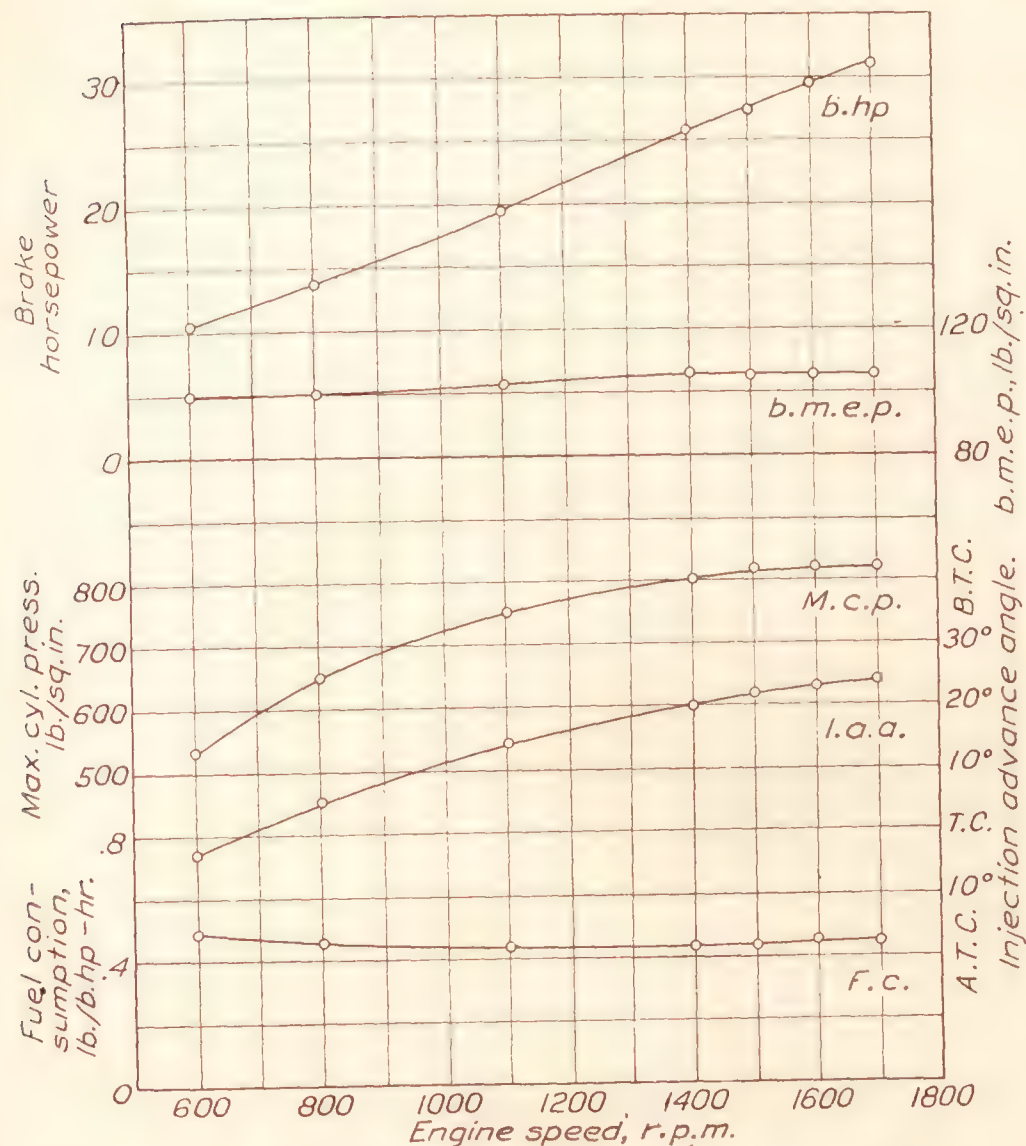


FIGURE 10.—Effect of engine speed on performance with clear exhaust (145° valve overlap, 3 inches Hg boost pressure).

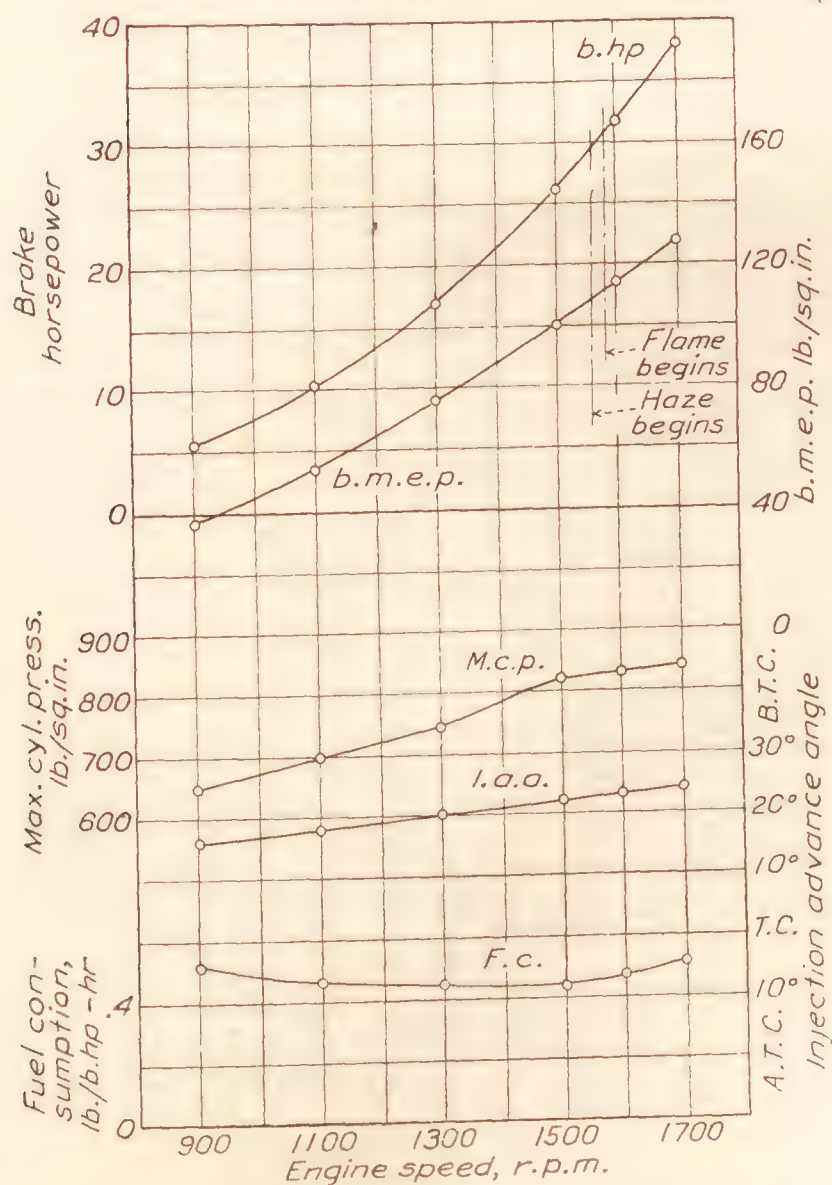


FIGURE 11.—Effect of propeller loading on engine performance (145° valve overlap boost pressure: $3\frac{1}{2}$ inches Hg at 900 r.p.m. to $6\frac{1}{2}$ inches Hg at 1,700 r.p.m.).

injection advance angle for reduced speeds as in the other variable-speed tests, but to a lesser degree, owing to the reduction in fuel quantity for the reduced speeds.

The friction mean effective pressures as affected by speed, boost pressures, and valve overlap are shown in figure 12. The values shown are for the engine alone, as the blower was separately driven. Practically no difference is observable between the friction mean effective pressures for normal valve timing and for the large valve overlap. Boosting the inlet pressure decreases the friction mean effective pressure because the induction air does work on the piston. If the blower were geared directly to the engine shaft, the values shown would of course be increased by the amount of mean effective pressure required to drive the blower. For example, at 1,500 r.p.m. and $8\frac{3}{4}$ inches of mercury boost, the friction mean effective pressure would be 36 pounds per square inch instead of 27.

Figure 13 shows an indicator card taken with the Farnboro indicator while obtaining the data for figure 6. The performance values are 143.5 pounds per square inch indicated mean effective pressure, 111 pounds per square inch net brake mean effective pressure, and a net specific fuel consumption of 0.407 pound per brake horsepower per hour with a clear exhaust. The boost pressure was $6\frac{1}{4}$ inches of mercury and the valve overlap 145° . The

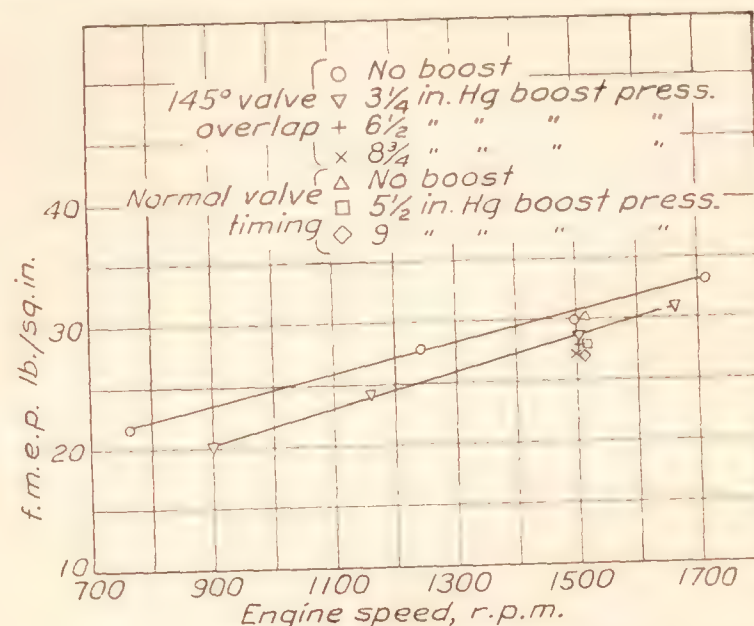


FIGURE 12.—Effect of speed, boost pressure, and valve timing on f.m.e.p.

multiplicity of points on the indicator card shows the large number of engine cycles used for recording this pressure-time diagram and the small dispersion of the points indicates the regularity and consistency with which the pressure cycle repeated itself when the engine was operating with boosting and valve overlap.

It may be noted that for 3 inches of boost pressure and 1,500 r.p.m. the brake mean effective pressure on figure 10 is 106 pounds per square inch; whereas for the same boost pressure and speed, 112 pounds per

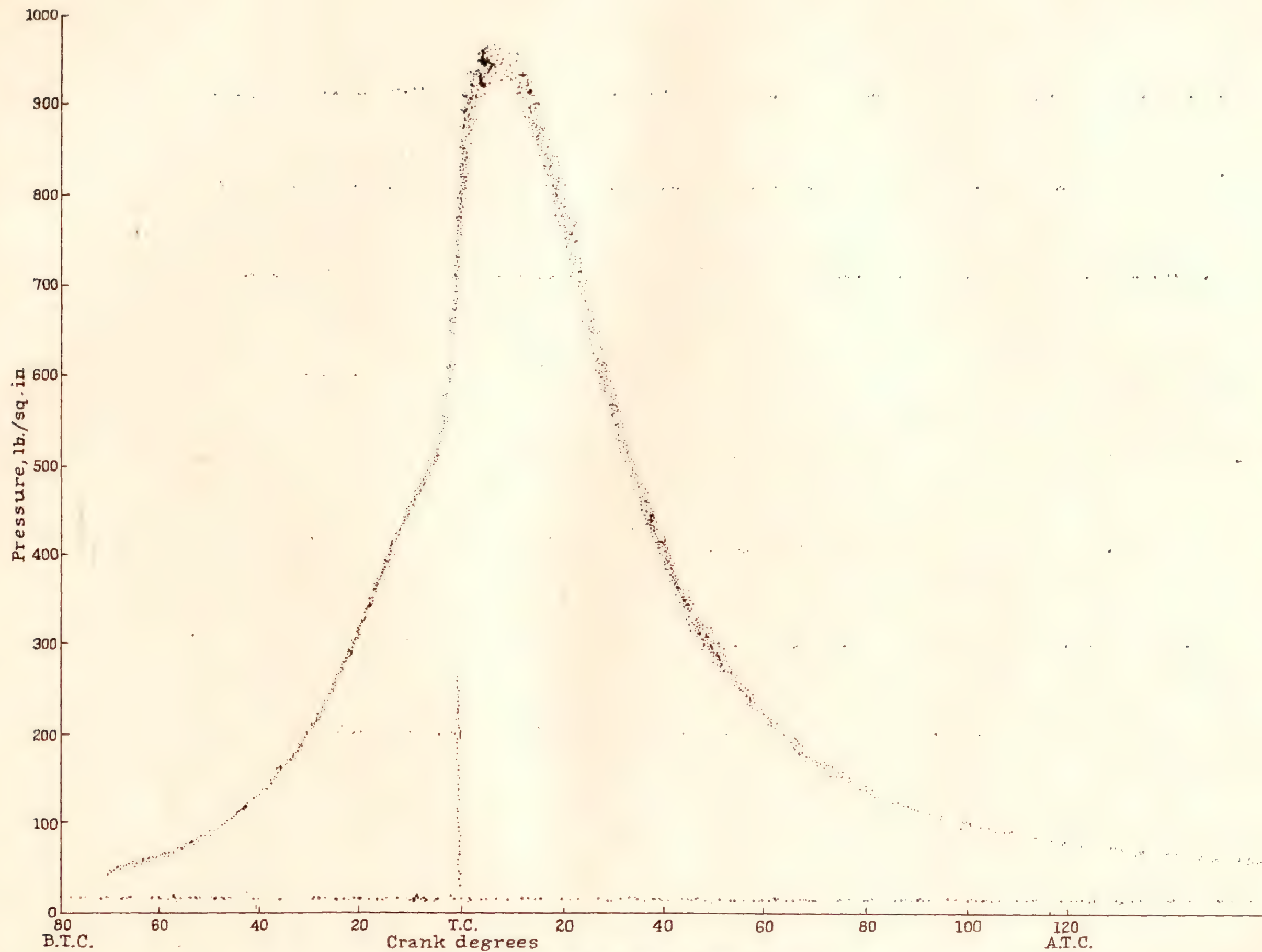


FIGURE 13.—Indicator card taken with Farnboro indicator.

square inch is shown on figure 6. The difference is due principally to the use of two different fuels and the different fuel quantities considered to give clear exhaust. The fuels are noted as no. 1 and no. 2 in reference 5. Fuel no. 1 has a longer ignition lag and therefore a faster rate-of-pressure rise and a greater tendency to knock than fuel no. 2. Observations of engine power and inspection of the exhaust show that both fuels will carry the same load with practically clear exhaust up to flame start, but with fuel no. 2 a haze precedes the start of flame as shown in figure 11. The appearance of this haze may be accounted for by the shorter ignition lag of the fuel and the correspondingly earlier occurrence of high temperatures due to combustion, which would cause some of the fuel from the latter part of the injection to pass through regions of high temperature, and probably cause the formation of free carbon particles. This early occurrence of high temperatures would also tend to reduce the penetration and prevent some fuel from reaching sufficient air for combustion.

Indicator cards taken during the variable-speed tests showed that the rate-of-pressure rise in pounds per degree of crank travel decreased as the engine speed was increased. At 1,700 r.p.m. there was practically no audible knock. Although it was not deemed advisable to operate the single-cylinder test engine at higher speeds, there was nothing in the fuel system or engine combustion characteristics to indicate that speeds higher than 1,700 r.p.m. could not be used to advantage.

In view of the cooling effects that result from scavenging the combustion chamber with fresh air and the improved combustion characteristics resulting from the removal of the residual gases, it was considered advisable to investigate the heat loss to the cooling system under conditions of normal valve timing and for scavenging conditions when using valve overlap. It was found that with normal valve timing the heat loss to the coolant was 17.0 percent of the total heat of the fuel, and by using the large valve overlap and a scavenging pressure of $3\frac{1}{4}$ inches of mercury this heat loss was not materially reduced.

All the test data herein reported were obtained at a compression ratio of 12.6 but, for purposes of determining the optimum available compression ratio, comparative tests were made at a compression ratio of 15.0. It was found that at the high compression ratio it was not practicable to boost with normal valve timing, for the reduction in ignition lag reduced the permissible injection advance angle to a point where good distribution of the fuel throughout the air charge was not possible in the time available, and the exhaust became hazy for reasons previously stated. The use of a large

valve overlap allowed smoother boosted operation at the high compression ratio than the normal valve timing but, with either, the high compression pressures caused the maximum cylinder pressures to be raised from 150 to 200 pounds per square inch higher than at the lower compression ratio, and the resultant engine performance was not as good. For best engine operation the injection advance angle was increased to a point where the indicator card showed the cylinder pressure breaking away from the compression line ahead of top center. For the compression ratio of 15.0 the injection advance angle was necessarily retarded below that used at the lower compression ratio and, for a full-load fuel quantity and with optimum injection advance angle, the maximum cylinder pressure for the compression ratio was 1,000 pounds per square inch.

The better engine performance at the 12.6 compression ratio indicates that a range of compression ratios should be investigated so as to establish the most advantageous balance between the requirements for favorable combustion characteristics and the requirements for proper formation of the necessary mixture of fuel and air.

CONCLUSIONS

Boosting the air charge of a high-speed 4-stroke-cycle compression-ignition engine without removing the residual gases tends to make the engine operation smoother, and for a vertical-disk form of combustion chamber operated at a compression ratio of 12.6 the indicated mean effective pressure is increased in proportion to the additional air inducted.

Removing the residual gases from the clearance volume of a compression-ignition engine improves the combustion characteristics, results in decreased specific fuel consumption, and permits operating at higher fuel quantities with a clear exhaust.

The residual gases can be removed efficiently from the clearance volume of a high-speed, 4-stroke-cycle compression-ignition engine by using a valve overlap of 145° and a pressure difference of from 2 to 5 inches of mercury across the inlet and exhaust ports.

The increase in engine power effected by scavenging the combustion chamber of a compression-ignition engine is greater than the increase that can theoretically be obtained by adding additional air equivalent to the replacement volume of exhaust gases.

The starting and idling characteristics of a compression-ignition engine are not affected either by boosting or by scavenging with a large valve overlap.

The operation of this engine at a compression ratio of 15 at high scavenging pressures was unsatisfactory because of inferior performance and higher maximum cylinder pressures.

The percentage of carbon monoxide gas in the exhaust of a compression-ignition engine when operating with a clear exhaust is less than one half of 1 percent.

LANGLEY MEMORIAL AERONAUTICAL LABORATORY,
NATIONAL ADVISORY COMMITTEE FOR AERONAUTICS,
LANGLEY FIELD, VA., *June 10, 1933.*

REFERENCES

1. Spanogle, J. A., and Foster, H. H.: Performance of a High-Speed Compression-Ignition Engine Using Multiple Orifice Fuel Injection Nozzles. T.N. No. 344, N.A.C.A., 1930.
2. Spanogle, J. A., and Foster, H. H.: Basic Requirements of Fuel-Injection Nozzles for Quiescent Combustion Chambers. T.N. No. 382, N.A.C.A., 1931.
3. Schey, Oscar W., and Young, Alfred W.: The Use of Large Valve Overlap in Scavenging a Supercharged Spark-Ignition Engine Using Fuel Injection. T.N. No. 406, N.A.C.A., 1932.
4. Spanogle, J. A.: The Quiescent Combustion Chamber. Trans. A.S.M.E., Oil and Gas Power, vol. 53, no. 17, Sept.-Dec. 1931, pp. 123-129.
5. Spanogle, J. A.: Compression-Ignition Engine Tests of Several Fuels. T.N. No. 418, N.A.C.A., 1932.
6. Burrell, Geo. A., and Seibert, Frank M.: Sampling and Examination of Mine Gases and Natural Gas. Revised by G. W. Jones. U.S. Dept. of Com., Bu. of Mines, Bull. No. 197, 1926.

BIBLIOGRAPHY

- Cameron, J. G.: Supercharging, A Statement of the Fundamental Principles. The Automobile Engineer, August 1925, pp. 244-7.
- Hunter, Harry: The Super-Atmospheric Oil Engine. Trans. North-East Coast Institution of Engineers and Shipbuilders, England. Part 4, vol. XLVIII, 1932, pp. 135-8. Discussion, part 5, vol. XLVIII, pp. D-62-74.
- Oppitz, Dr.: Increasing the Output of Four-Cycle Engines. The British Motor Ship, April 1932, pp. 24-7.
- Rothrock, A. M.: Combustion in a High-Speed Compression-Ignition Engine. T.R. No. 401, N.A.C.A., 1931.
- Taylor, Edward S.: Valve Timing of Engines Having Intake Pressures Higher Than Exhaust. T.N. No. 405, N.A.C.A., 1932.

REPORT No. 470

THE N.A.C.A. TANK

A HIGH-SPEED TOWING BASIN FOR TESTING MODELS OF SEAPLANE FLOATS

By STARR TRUSCOTT

SUMMARY

This report describes the high-speed model towing basin of the National Advisory Committee for Aeronautics, usually referred to as the N.A.C.A. tank. The purpose of this piece of equipment is to enable the Committee to provide information and data regarding the performance of seaplanes on the water analogous to the information furnished concerning the performance of airplanes in the air.

The tank and its equipment, together with the method of operation, are described, and the type of work done in it is illustrated by data from two typical tests. The one was to determine the effect on the take-off performance of a model of the hull of a flying boat of fitting the step with "hooks" of three different heights, and the second to determine the effect on the take-off performance of the same model of fitting the bottom just forward of the main step successively with two and three flutes of two different depths. In each case the performance with the alterations is compared with the performance of the model with a plain bottom. The distinctive discontinuities found in the speed-resistance curves at hump speed are a notable feature of the results of these tests.

INTRODUCTION

HISTORICAL—GENERAL CONSIDERATIONS

A survey of the information available regarding the application of the results of tests of models in towing basins to the design of floats for seaplanes was made by the National Advisory Committee for Aeronautics in 1929. It was found that the development of flying boats and seaplanes had been assisted very much in the United States, and possibly more in other countries, by tests of models in towing basins or tanks (references 1 and 2). Some tanks already existed which were designed especially for testing models of seaplane floats and the construction of other tanks for this special purpose was projected (references 3 and 4). There was no such tank in the United States; in fact, there were only two tanks, both constructed before the appearance of the seaplane and designed originally to test models of ships. The construction in the United States of a special towing basin that

could be devoted to tests of models of seaplane floats and hulls might reasonably be expected to be of great assistance in the further development of this type of aircraft, the importance of which appeared to be increasing.

In considering the construction of such a piece of equipment it was necessary to evaluate many features, and in the case of the N.A.C.A. tank the decisions arrived at led to the incorporation of certain novel features which appeared to be more suitable for their respective purposes than the constructions used in other tanks. The reasons for these decisions are of general interest and discussions of them will be found later in the report.

CHARACTERISTICS OF SEAPLANE FLOATS

The desirable characteristics of the float supporting a seaplane are many, but among them may safely be included the following:

1. Low resistance to propulsion on the water.
2. Freedom from tendencies to trim or pitch violently while being propelled on the water.
3. Freedom from excessive moments, about the center of gravity of the whole craft, of the hydrodynamic forces arising from propulsion on the water.
4. Freedom from excessive spray or from throwing solid water upward or outward to excessive distances while being propelled on the water.
5. As great stability as is compatible with other properties.
6. Low drag in the air.

The combination of these characteristics, with others which have not been mentioned, in a single form presents a problem which has been solved in widely different ways by different designers. The forms adopted have changed as experience dictated and with the demands of the respective users until they have taken the distinctive shapes now associated with certain designers, and even with certain nations. This process has been influenced also by the results of tests made in model towing basins to determine the hydrodynamic properties of models of the various forms proposed or adopted.

TESTS OF MODELS IN MODEL BASINS

When the development of the seaplane began, model towing basins had been in regular use for about forty years for the purpose of obtaining information as to the performance of surface vessels of all types, and it was only natural to turn to the towing basins for assistance in designing seaplane floats. Although much valuable information was obtained from the ship-model towing basins, it was soon perceived that tests of models of seaplane floats in such model basins suffered from serious disadvantages because of the relatively low speeds of the towing carriages (reference 1). These disadvantages become apparent from a consideration of the method of applying the results from such tests, which generally is as follows:

The total resistance of the model, and of the ship, is assumed to be made up of two parts: frictional or viscous resistance, and wave-making resistance. The former is computed for the model by the use of generally accepted formulas and coefficients, and is deducted from the total measured resistance. The remainder, the wave-making resistance, is assumed to follow that particular one of the Laws of Mechanical Similitude, usually called Froude's Law, which may be expressed as follows: If V and v are corresponding speeds of ship and model, of lengths L and l , respectively, and R_w and r_w are the respective wave-making resistances at those speeds, then at the corresponding speeds of ship and model

$$\frac{V}{\sqrt{L}} = \frac{v}{\sqrt{l}}$$

and

$$r_w = \left(\frac{L}{l}\right)^3$$

or

$$R_w = r_w \left(\frac{L}{l}\right)^3$$

The total resistance of the ship is then obtained for each corresponding speed by adding to the wave-making resistance determined from the tests of the model the frictional resistance computed anew from the dimensions of the ship and its speed.

SIZES OF MODEL AND EFFECTS OF SCALE

The expression for corresponding speeds shows that no matter how large the tank may be the maximum size of the model that can be towed at the speed corresponding to a given speed of the full-size craft is fixed by the maximum speed of the towing carriage. If the get-away speed V of a full-size seaplane is 60 miles per hour, the full-size length L 64 feet, and the maximum speed of the towing carriage v 15 miles per hour, then

$$\frac{60}{\sqrt{64}} = \frac{15}{\sqrt{l}}$$

and the length of the longest model of the seaplane that can be towed at a speed corresponding to get-away speed will be 4 feet. As the get-away speed of the craft increases for a given length of hull, or as the length of the hull decreases for a given get-away speed, the length of the model that may be towed to get-away speed decreases.

It must also be remembered that, in contrast with the smooth fair form found in a ship, the form of the hull of a seaplane or flying boat includes definite discontinuities, as the chines and steps. At high speeds, irregularities and inaccuracies in a model may be expected to produce serious disturbances in the results of tests. If the models of the hulls of seaplanes must be made to very small scale, the accuracy of the models to dimensions must be most carefully maintained, otherwise doubt may be thrown on the conclusions.

Difficulties of even more serious character appear with the demonstration that there is a scale effect on the resistance and other quantities measured that increases as the size of the model is reduced (references 5 and 6), and that the difference between the waves and spray produced by a model and those of the full size at the corresponding speed increases as the size of the model decreases (reference 6). As it has been the general practice to consider the observed resistance of models of seaplane floats as all wave-making resistance, and to obtain the resistance of the full-size craft by converting the whole according to Froude's method, these scale effects may explain some of the observed discrepancies.

ADVANTAGES OF A LARGE TANK

In view of the disadvantages found in the use of small models at low speeds, a new tank, to be of the greatest service, should be equipped to tow large models at high speeds so that the similarity of phenomena between full size and model might be greater, the accuracy of construction of the models need not be so great, and the conclusions drawn should therefore be more trustworthy. The nearer the approach to full-scale size and speed the more accurate and satisfactory would be the conclusions drawn from the tests. However, it had to be remembered that excessively large models meant a correspondingly large tank and high speed of the towing carriage. The cost of such equipment would be more than correspondingly high.

The circumstances just outlined were given careful consideration by the National Advisory Committee for Aeronautics, and it was decided to construct a tank which should represent an attempt to balance the various factors involved against one another.

The construction of the tank was approved in 1929, and plans and specifications were prepared by the Committee in that year. Construction began in 1930 and was completed in 1931. The new tank was offi-

cially dedicated at the time of the Sixth Annual Aircraft Engineering Conference, May 27, 1931, by Dr. D. W. Taylor, Vice Chairman of the Committee, who supervised the construction of the first modern experimental model basin in this country, at the Washington Navy Yard, and whose work in that basin is known the world over.

DESCRIPTION

Type.—The N.A.C.A. tank is of the Froude type; that is, the model which is being tested is towed through still water at successive constant speeds from a carriage spanning the tank. At each constant speed the towing pull is measured, the trim and the rise, or change of draft, are recorded and, if the model is being towed at a fixed trim, the moment required to hold it there is measured and recorded.

Location.—The N.A.C.A. tank is located at Langley Field, Va., and extends about north and south along the west bank of the Southwest Branch of Back River, the distance from the shore varying from about 75 to 150 feet. (See fig. 1.)

Dimensions.—The reinforced concrete basin containing the water has the following dimensions:

	<i>Feet</i>
(1) Length on water, extreme.....	2, 020
(2) Normal width of water surface.....	24
(3) Normal depth of water.....	12
(4) Length of 12-foot depth.....	1, 980

The sides of the tank are coved in above the water line in order to bring the rails closer together and thus reduce the width of the car, and also to assist in suppressing the waves which are produced by the models. The appearance of the empty tank is shown in figure 2.

The salt water with which the tank is filled is supplied from Back River by a centrifugal pump driven by an electric motor. The tank contains approximately 4,000,000 gallons of water which can be pumped in or out in about 40 hours.

At the south end of the basin there is an annex containing the shop and offices, together with the pumping plant and the electrical equipment, including motor generator set, switchboards, etc., for the supply of current to the carriage.

Shelter.—The whole tank is covered by a shelter intended more to protect the surface of the water from the effect of wind and weather than to maintain a temperature within the building. This shelter consists of a simple building 2,060 feet long and 28 feet wide having a steel frame of ordinary construction covered with corrugated sheets of an asbestos-cement composition. The trusses and columns supporting the roof are spaced at 20-foot centers, and a small window is placed in the middle of each 20-foot bay on each side and as high up as is feasible. These windows are glazed with light-diffusing glass to reduce the amount of direct sunlight falling on the

water of the tank. The general arrangement of the tank may be seen in figure 3.

Rails.—The rails on which the towing carriage runs are heavy H-beams set with the web vertical. They are supported on cross ties, or chairs, made of short lengths of steel tie section. The rails are laid in 60-foot lengths with staggered joints. The joints are not welded or scarfed, but are simply butted with sufficient clearance to permit the ends to come together at a temperature of about 80° F.

The rails are leveled to the same height above the water surface and the east rail is alined with extreme care. Leveling of the top surfaces of the rails is done by measuring from the surface of the water in the tank while it is perfectly still, using an electrical contact point on the extended spindle of a micrometer head. In this manner the rails are made to follow the curvature of the earth taken by the surface of the water. Careful checking of the measurements indicates that the rails are within ± 0.015 inch of parallel to the water surface. The alinement of the east rail is done by means of a special transit and reference points placed in the concrete of the tank. This rail is used to hold the car on the rails and in a straight line by means of guide wheels which bear on both sides of the web. There are no guide wheels on the west rail.

Towing carriage.—The structure of the towing carriage is of carbon-steel tube, with all joints welded. In order to insure accuracy of alinement in the girders forming the car structure, the ends of all the tubes meeting at a joint were milled to fit snugly before welding and all welding was done with the structure in a massive jig. The gear cases also are of welded construction.

The structure of the car may be divided into a center-line girder, two side girders, and two transverse girders. The center-line girder is of sufficient depth to carry the dynamometer and to permit persons to stand within it. The other girders are shallower and are proportioned solely by the strength requirements and the necessity for securing other parts of the carriage, such as the electric motors and the reduction gears between the motors and the wheels. A general view of the towing carriage is shown in figure 4.

Wheels and tires.—The carriage runs on four wheels fitted with pneumatic tires. These wheels are mounted on stub axles, and are not connected by cross axles. They are each driven by an independent electric motor through a single-reduction herringbone pinion and gear. The pneumatic tires are high-speed bus or truck tires, with smooth treads. The guide wheels which hold the carriage in alinement on the east rail have grooved solid rubber tires of a medium soft composition. It is planned to try small pneumatic tires later, although the present tires are very satisfactory.



FIGURE 1.—Airplane view showing the location of the N.A.C.A. tank with respect to other equipment of the Committee at Langley Field, Va.
1. The tank. 2. The full-scale tunnel. 3. The propeller-research tunnel. 4. The administration building.



FIGURE 2.—Looking north in the empty basin of the N.A.C.A. tank.

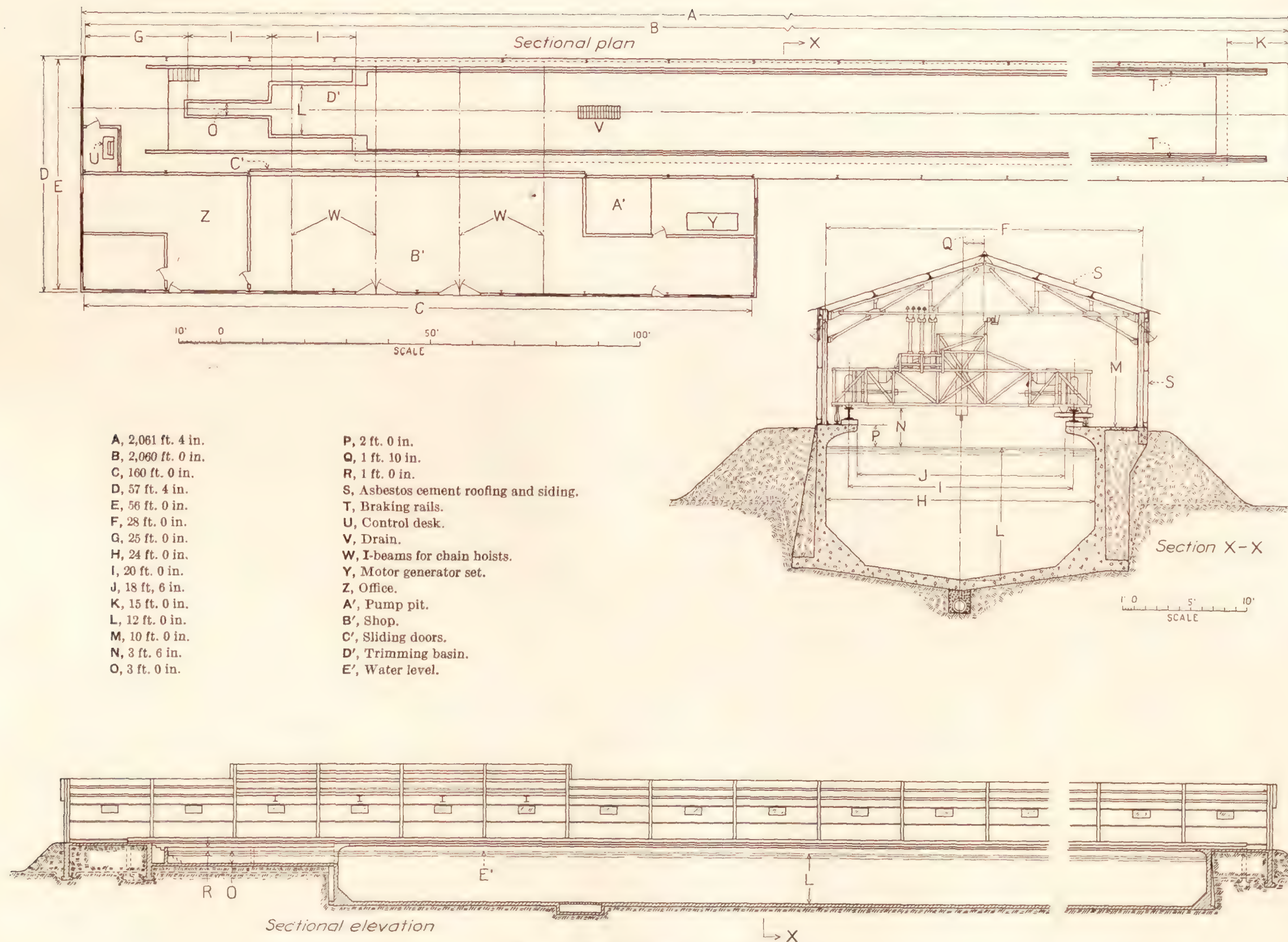


FIGURE 3.—Plan and section of the N.A.C.A. tank.

Propelling motors.—The four electric motors propelling the car are each nominally of 75 horsepower, but for short periods they may be safely called upon to deliver 220 horsepower each. They are direct-current motors having two field windings. One of the fields is excited separately, and the other is excited by the armature current from one of the other motors. The wiring is so arranged that the armature current from the front pair of motors passes through the field windings of the rear pair of motors, and vice versa. The shunt field current is held at a constant voltage and the speed of the car is varied by varying the voltage of the armature current. The increase of the armature current during acceleration is controlled automatically to suit the rate of acceleration desired; the change to constant speed conditions is also made automatically.

the carriage at definite positions easier. This brake is of the automotive type with internal-expanding shoes which are carried in brake drums fitted on the wheels.

If the other braking systems should all fail the carriage would be stopped by the emergency brakes at the end of the tank. These are continuous rail friction brakes consisting of two heavy T-bars securely anchored to the concrete, one just outside each running rail. The stem of each projects vertically upward and forcibly sandwiches itself between two spring brake plates secured to the carriage. Four pairs of these brake plates are fitted on each side of the carriage. Instead of using coil springs to control the grip of the brake plates, the plates themselves are designed as flat-plate springs and the intensity of the braking action is controlled by the width of the initial opening between them.

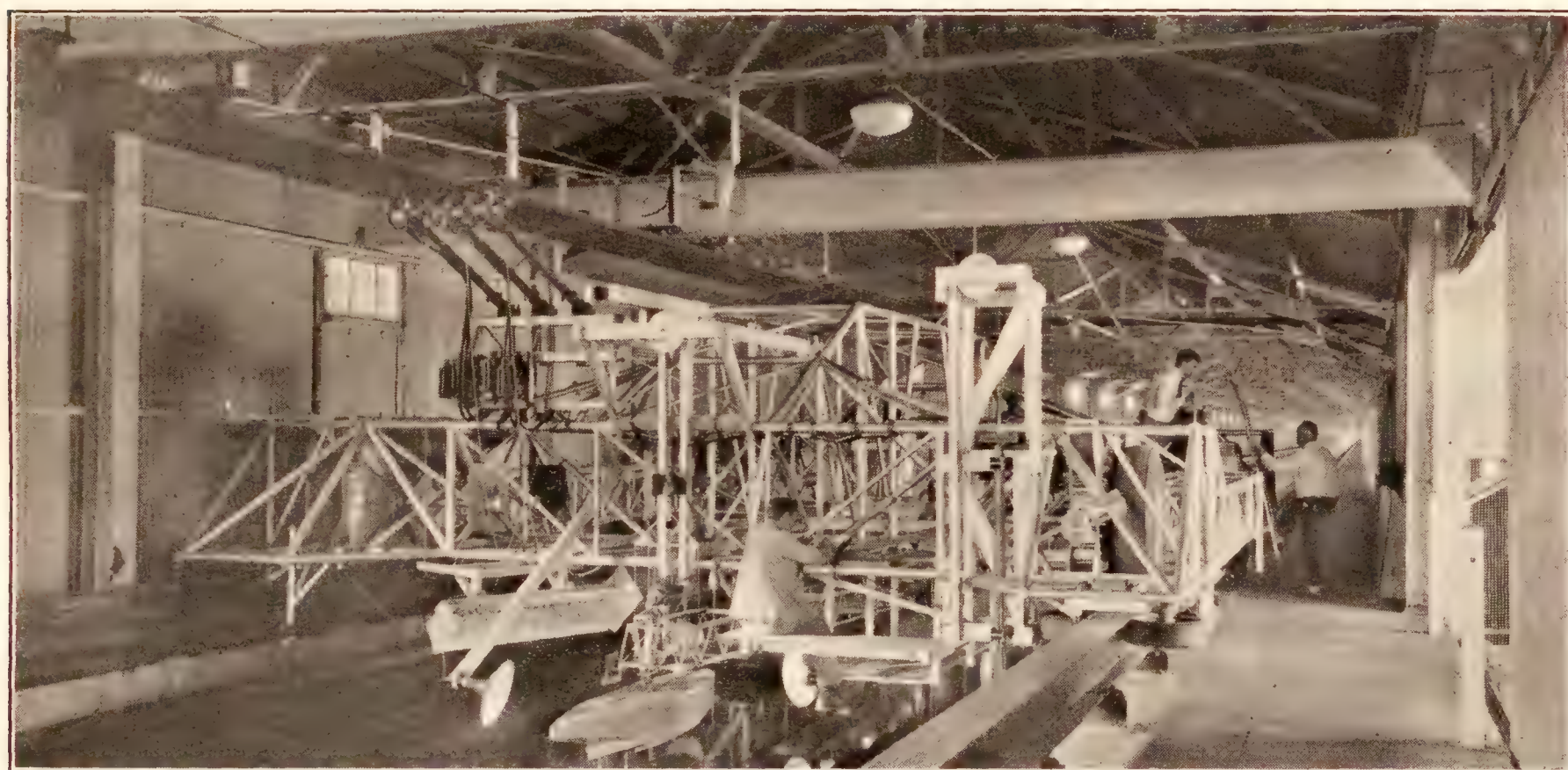


FIGURE 4.—The towing carriage of the N.A.C.A. tank.

Electrical braking.—Current for propulsion is supplied to the car by four overhead trolley wires on which travel two armature trolleys and two field trolleys. In addition there are two trolley wires and trolleys providing two circuits for the control of the electrical braking of the carriage. Opening one of these circuits sets into operation automatically controlled regenerative braking, opening the other dynamic braking. By means of a switch located at the control desk the operator can select either of two points along the tank at which the circuit controlling the regenerative braking will be opened and braking produced. If the incoming line voltage fails the braking automatically changes to dynamic.

The electrical braking can also be applied at will by either the operator at the control desk or the personnel on the towing carriage. A hand-operated brake is also provided to assist in the final stop and to make spotting

All the braking systems have been thoroughly tested and found to operate satisfactorily in service. The emergency brakes have been used but once. The carriage was moving at less than 5 miles per hour and was stopped in less than 3 inches. The deceleration was violent but without shock.

Control of operation.—The control of the whole propelling system is concentrated at a control desk located at the south end of the tank. Here are the rheostats controlling the acceleration and determining the constant speed at which the carriage is to be propelled. Switches control the field and armature currents, and a selector switch controls the points at which the electrical braking is to be applied. A voltmeter and an ammeter are fitted to indicate the voltage and current in the armature circuit. The whole is mounted on a metal desk with the rheostats concealed within it.

The personnel carried on the car have no control of the speed of the car other than the ability to stop it at any time. They are free to give all their attention to taking the readings and to watching the behavior of the model being towed.

Time and distance gear.—The speed at which the carriage has been propelled on any run is determined from the time and distance traveled. A special clock is mounted on the carriage and so arranged as to send an electrical impulse to the dynamometer every second. The distance traveled is given by an indication in the dynamometer corresponding to every 5 feet of travel. A steel tape extends the entire length of the tank, and is supported by brackets projecting down from the bottom chords of the roof trusses. This tape has an accurately located hole through it every 5 feet. As the carriage moves along the length of the tank the tape is picked up by a set of rollers on the carriage and passes through a slot in a box placed between the rollers which contains a source of light and a photoelectric cell. The path of the light to the cell is interrupted by the solid tape, but when one of the holes in the tape passes through the box the light beam slips through and falls on the cell. The electrical impulse which this produces is amplified by a radio-type amplifier and is sent to the recording device of the dynamometer as a relatively powerful impulse.

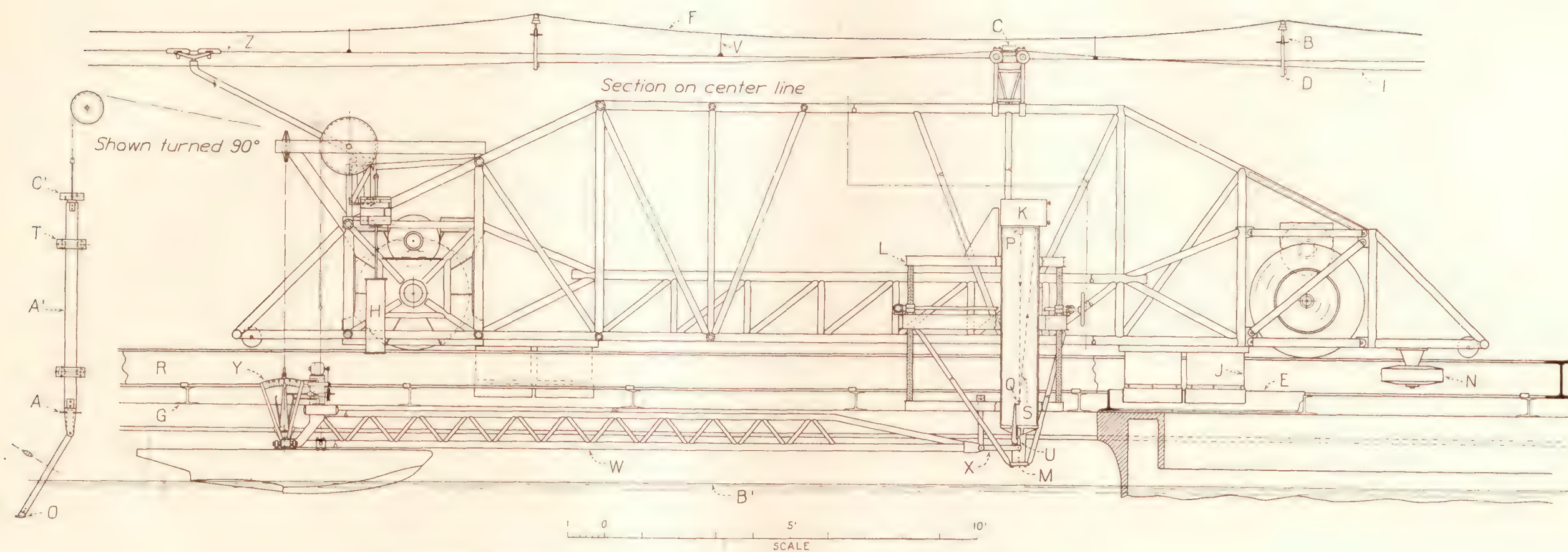
Motor-generator set.—The direct current for operating the carriage is obtained from a motor-generator set located in the shop section of the building. This set consists of a 350-horsepower alternating-current motor, taking current at 2,200 volts, driving a 300-kilowatt direct-current generator and two direct-current exciters. One exciter provides current for the shunt fields of the motors on the car; the other provides exciting current for the alternating-current motor and the fields of the direct-current generator.

The towing gear.—The arrangement of the towing gear is shown on figure 5. The model being towed is attached to the after end of a stiff latticed girder, or "towing gate." The forward end of this girder is attached to the dynamometer proper which weighs and records the pull of the model as it passes through the water. The length of the towing girder is as great as is feasible in order to reduce the obliquity of the pull as the model rises or sinks. The towing pull is applied to the model at a point corresponding to the center of gravity of the full-size craft and about this point the model can swing freely, when tests are made free to trim, or it can be held at any desired trim, and the moment required to hold it thus can be measured. A pointer moving with the model swings over a graduated scale and indicates the trim, while the deflection of a spring through which the constraining force is applied indicates the magnitude of the force and the moment which must be applied to constrain the trim.

Two sizes of towing gates are available, each with its own gear for measuring the trim and moments. The lighter and smaller one is made of duralumin structural sections and is used with models up to about 10 feet in length; the "heavy" one, used with models up to 16 feet in length, is made of steel tubing and has exceptionally heavy gear for measuring the trim and moments. The weight of the gate is counterbalanced by weights on the end of a flexible wire rope suspended over a sheave. A large damping cylinder, fitted on the lower end of the rod carrying the weights, reduces any tendency to vibrate vertically.

Through the point of suspension of the model is applied a vertical lift to simulate the lift derived from the wings of the full-sized craft. This lift is obtained from a flexible wire rope which passes over two sheaves to the upper end of a steel bar that is free to move vertically in roller guides. The upper end of the bar is fitted to receive weights to counterbalance any overweight of the model. At the lower end of the bar there is fitted a bronze blade that projects downward into the water. The immersed end of the blade is fitted to receive any one of several bronze hydrofoils, or hydrovanes, which can be firmly secured to it. The size of the hydrovane is selected to suit the model that is being tested and the angle of attack may be adjusted by changing the angle of the blade. The selection and adjustment of the hydrovane are so made that at the speed corresponding to the get-away speed of the full-sized craft the downward pull exerted by the hydrovane will equal the weight corresponding to the gross weight of the full size and, if the model is balanced to that weight, it will be just lifted from the water. At any other speed the lift produced by the hydrovane will be to the lift at get-away as the square of the speed is to the square of the get-away speed and will correspond to the lift of the wings at that speed. The blade and the hydrovane are placed as far to one side of the model as is feasible to avoid any interference with the flow around the model.

This method of supplying the lift corresponding to the wing lift implies that the lift coefficient of the wings does not change during the take-off. This assumption is contrary to the fact, but devices intended to provide a lift that will be varied automatically to correspond with the variation in angle of attack due to change in trim introduce complications and do not seem to be sufficiently trustworthy to warrant their use at present. Devices similar to the present one have been used for years with reasonably good results. It should also be remembered that if a large range of trim angles is involved the get-away speed can be varied to suit the change in angle of attack of the wings. In general, the difference in the values of Δ/R obtained is not great. The provision of a suitable device providing automatic variation of the lift with



- A, Adjustment of hydrovane.
 B, Bottom chord of roof truss.
 C, Box containing light source and photoelectric cell.
 D, Bracket for distance tape.
 E, Braking rail.
 F, Catenary.
 G, Chair.
 H, Damping cylinder.
 I, Distance tape
 J, Emergency brake.
 K, Film box.
 L, Frame for adjusting height of towing point.
 M, Guide.
 N, Guide wheel.
 O, Hydrovane.

- P, Light source.
 Q, Mirror.
 R, Rail.
 S, Reflecting ray.
 T, Rollers.
 U, Spring.
 V, Suspender.
 W, Towing gate.
 X, Towing link.
 Y, Trim and moment indicator
 Z, Trolley wire.
 A', Vertical bar.
 B', Water level.
 C', Weights to counterbalance model.

FIGURE 5.—Elevation and sections of the carriage and towing gear of the N.A.C.A. tank.

the trim is contemplated but its development has not begun.

The rise of the model is indicated by a pointer, attached to the wire providing the lift, which traverses a vertical scale attached to the carriage.

At the forward end of the towing gate are two vertical suspension links which support a part of the weight of the gate and any reaction from the trimming moments. There are thus no vertical forces applied to the weighing device of the dynamometer. A single horizontal link connects the beam to the weighing device, which consists of a stiff spring in the form of a single flat plate of steel. The magnitude of the pull exerted by the model is obtained by measuring the deflection of the spring.

The upper end of the spring is rigidly attached to a massive tube supported in the center girder of the carriage and is presumed to have no deflection. The deflection of the lower end of the spring is magnified by an arm attached to it and extending up into the tube. The upper end of this arm carries a stylus, the point of which bears against a vertical plate mounted on a horizontal staff that also carries a horizontal mirror. The plate on the mirror staff is held against the stylus by a small hairspring.

A beam of light projected against the mirror from a light source at the top of the tube is reflected back against a slit in the top plate of the tube. When a sheet of sensitized paper is moved at constant speed across the slit the reflected spot of light traces a curve that becomes visible on development. In addition to the curve from the movable mirror, a series of parallel straight lines are ruled on the record by light rays from six fixed mirrors. These are so adjusted as to provide a convenient series of reference lines.

In order that the operator may be informed as to the magnitude of the pull exerted by the model during the run, a second beam of light is projected against the measuring mirror at such an angle that as it returns to the top of the tube it may be intercepted by a horizontal mirror set to reflect the beam against a translucent screen. This screen is suitably graduated and the gross pull exerted by the model may be read from the position of the spot of light coming from the measuring mirror.

The speed of the car is determined from the records of time and distance traveled. The time is indicated by successive dots produced by flashes of a lamp lighted every second by the timing clock. The distance is indicated by the breaks in a line traced on the sensitive paper by the light reflected from a galvanometer mirror mounted inside the tube. The deflection of this galvanometer is produced by the amplified impulse coming from the photoelectric tube which is illuminated every 5 feet as the car progresses along the track.

The record thus obtained includes a curve showing the pull exerted by the model, a series of dots which

indicate the time in seconds, and a broken line the deflections from which indicate 5-foot intervals of progress. The speed may be computed from the time required to cover a given distance, or the distance covered in a given time.

The recording part of the dynamometer is mounted on a frame that can be moved vertically to bring the point at which the pull is applied to the spring to any desired height from the water. The movable frame is carried on four lead screws in a fixed frame, but two vertical guides on the fixed frame relieve the lead screws of any side load.

PRELIMINARY TESTS

The first task, after the work of construction was finished, was to assemble and test the equipment to demonstrate the accuracy of operation and the ability to reproduce results on successive runs. A number of novel features, referred to in the introduction, required especial attention.

The designed maximum speed of the towing carriage had been set at 60 miles per hour for three reasons: First, to be sure that there would be ample acceleration for any speeds that might ordinarily be required (40 miles per hour as the get-away speed of a $\frac{1}{4}$ -size model of a seaplane having an 80-mile get-away was easily foreseen); second, to make it possible to determine the properties of details of bottoms, or of planing surfaces, at speeds at or near actual get-away speeds; and third, to make it possible to study the phenomena of fluid friction on surfaces moving at high speeds and the effects of roughnesses such as rivet heads and plate butts. High speeds meant high accelerations of the carriage and great length of run so that conditions might settle down before readings were taken, at a constant speed.

The towing carriages of all previous tanks had run on wheels with iron or steel tires, usually of hardened steel carefully ground to perfectly circular form. These were used with steel rails which had been carefully machined to give the greatest practicable smoothness and straightness to the surfaces. Such an arrangement appeared certain to be extremely costly if used on the very long tank that was contemplated. It also appeared to include a promise of trouble. At the high accelerations, which were necessary if the already long tank were not to be longer, the torques transmitted to the wheels in starting the carriage might cause them to slip. Furthermore, in braking at the end of the testing run the brakes might lock and slide the wheels. Either event would spoil the truly circular form of the tires and might also spoil the smooth surface of the rails. At the high speeds which were contemplated the slightest irregularities in the rail or in the wheel, no matter how produced, would surely produce violent shocks and erratic motion of the carriage. One method of avoiding the

high starting and braking tractions was to provide a catapult for accelerating and a reversed one for braking. These meant considerable increases in the cost and unknown difficulties in operation.

A simple solution was to abandon the steel tires and substitute pneumatic rubber tires running on wide flat surfaces. Such tires could be made and kept very close to truly circular at no great expense. They would have much greater adhesion than steel tires and accelerating and braking torques could be correspondingly increased. There would also be less necessity for a fine finish on the rails for the tires would absorb slight irregularities and even provide damping for any vertical vibrations.

Coupled with these advantages was a possible disadvantage in that a pneumatic tire always has a flat surface in contact with the rail and the loaded radius, or axle height, is not the radius of the unloaded tire. Variations in this height might produce tramping or magnify vertical motions.

The advantages appeared to outweigh the possible disadvantages and it was decided to use the pneumatic tires. It was realized that this was a radical departure from well-established practice and the testing and breaking in of the new equipment was carefully watched to determine exactly how the tires affected the operation of the towing carriage.

During the trial period the carriage was operated through a wide range of speeds and accelerations. The maximum speed attained was $58\frac{1}{2}$ miles per hour. A still higher speed can be reached if required, probably more than the designed 60 miles per hour, but it was thought unwise to attempt it with equipment that was still new and not completely broken in. The carriage has since been operated at speeds of about 50 miles per hour several times in connection with actual tests and the operation is even smoother than it was during the trial period.

The tests during the trial period showed very plainly that the pneumatic tires did not produce tramping, that they did damp out threatened vibrations and absorb the effects of slight irregularities, and also that for a given air pressure in the tires the axle height remained constant as nearly as could be determined.

Because of the use of the pneumatic tires it had been decided to omit the planing of the top surface of the H-beams that were used as rails, and to install them as they came from the mill, depending on the tires to absorb any irregularities. The rails were laid with plain butt joints and no special arrangements were fitted to avoid shocks as the wheels crossed the rail joints. Steel tires would have hammered the open butt joints into violently distorted forms; pneumatic tires promised to leave them unharmed. The tests demonstrated that these anticipations were fulfilled.

However, the heavy H-beam rails were of surprising rigidity, and leveling and alining them so that the two

top surfaces should be parallel to the water surface and the web of one should be straight from end to end proved a time-consuming operation. About 2,000 feet of rail had to be leveled on each side of the tank. Weather conditions sometimes produced surges in the water which stopped measurements for days. Some of these could be explained only by the theory that the barometric pressures at the ends of the tank sometimes differed by amounts sufficient to depress bodily the whole mass of water at one end and to permit it to rise correspondingly at the other. The change in level would be small but it would exceed the allowable error in leveling the rails.

METHODS OF TESTING

Tests of models of hulls or floats may be made in either of two ways. The earlier method was originally developed to obtain information regarding an aircraft for which most of the essential data are known. A second, or general, method does not require this information, and at the same time gives much more complete information than the earlier method. Both methods are susceptible of some modification, and may even be partially combined.

Earlier, or specific, method.—The model is presumed to be of a hull or float for a specific aircraft of which the gross weight, initial trim, position of center of gravity, and get-away speed are known. If the dimensions of the model are $\frac{1}{\lambda}$ times those of the full size, then according to Froude's Law,

L , length of full size.

$l = \frac{1}{\lambda} L$, length of model.

W , gross weight of full size.

$w = \frac{1}{\lambda^3} W$, gross weight of model.

V_g , get-away speed of full size.

$v_g = \sqrt{\frac{1}{\lambda}} V_g$, get-away speed of model.

M , trimming moment of full size.

$m = \frac{1}{\lambda^4} M$, trimming moment of model.

The initial trim of the model will be the same as that of the full size and the position of the center of gravity of the model, which is the point at which the towing pull is applied, will be the same as that of the full size to scale.

The weight of the model as constructed will rarely be that determined from the relations given above; usually it will be considerably heavier. Accordingly, counterweights are fitted on the top of the vertical bar carrying the hydrovane until the weight of the model which remains waterborne is exactly that corresponding to the gross weight of the full size.

The setting of the hydrovane device is then adjusted to give a downward pull, and an upward lift at the model, of w at speed v_0 . This is obtained approximately from curves previously prepared and is checked and adjusted to the proper setting by trial runs. There is also prepared a curve showing the air drag produced by windage on the parts of the towing gear exposed to the air stream.

The model is towed at a succession of constant speeds. Usually the first runs are made with the model free to trim. These are followed by other series of runs at various fixed trims. If no fixed trims have been specified these usually are 4° , 6° , and 8° . The speeds used vary with the size and type of model. The free-to-trim runs usually begin at about 5 feet per second and extend by intervals of 1 foot per second to about 75 percent of the get-away speed.

to-trim runs. In most cases the trend of the curve governs the speeds selected and the range covered, and additional runs are made at critical points in the curves.

During the runs the resistance, time, and distance are recorded automatically, while the trim angle and rise, for free-to-trim runs, or trimming moment and rise for fixed-trim runs, must be read by an observer stationed at the rear of the carriage. For fixed-trim runs it is also his task to operate the control of the electric motor that drives the device to apply the proper moment to hold the trim at the constant value which has been previously selected.

Photographs of the model are taken at each speed at which the wave system or spray will be of interest. Two cameras are used and are located to give a record of those features of the wave system which show

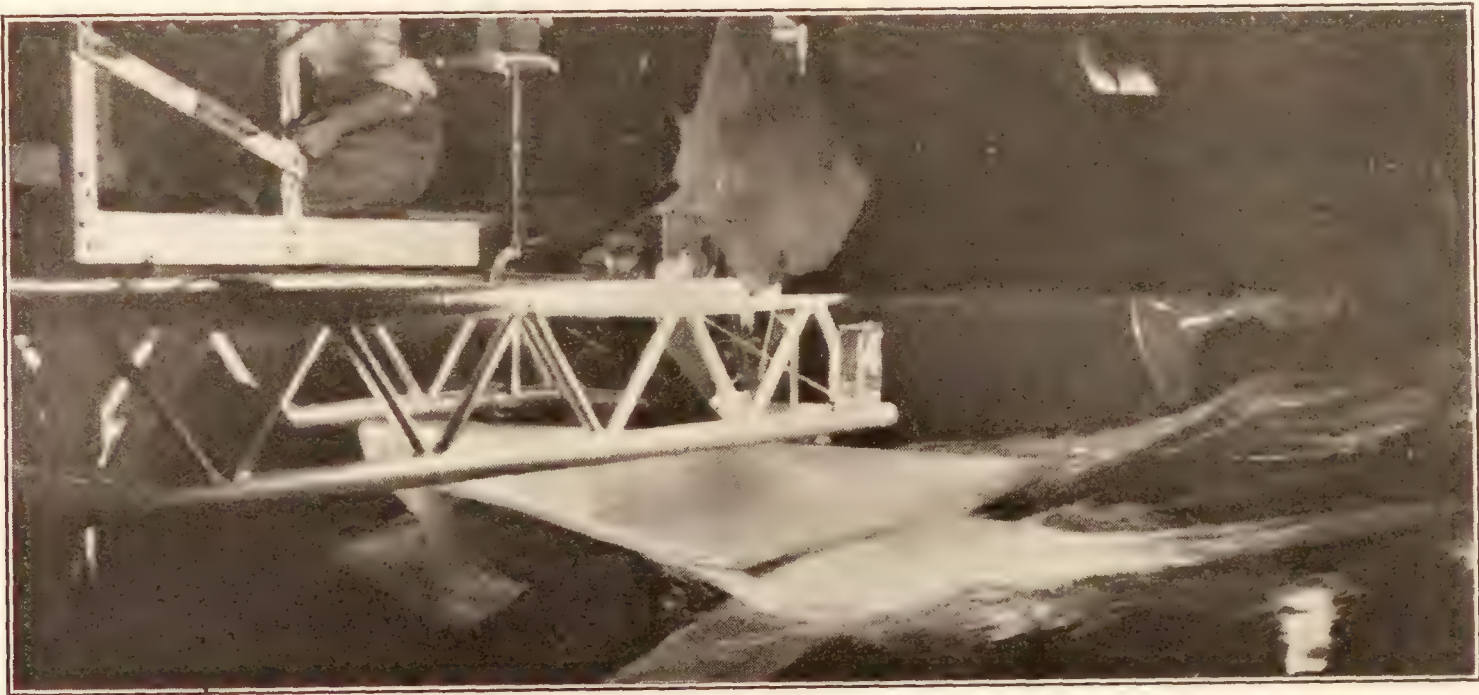


FIGURE 6.—Bow view of model of PH-1 flying-boat hull at 14 f.p.s., free to trim.

At this speed the trim usually is back close to the initial trim and there would be danger of putting the bow of the model into the water if the speeds were carried higher with the model free to trim, which might result in the wreck of the gear and the breaking of the model. At such speeds the aerodynamic control of the full size should be sufficiently effective to control the attitude, which will be a considerably larger trim, and usually there seems no need to investigate a condition which does not ordinarily occur. It is possible, however, to carry the free-to-trim runs further if necessary, but in such runs substantial stops must be fitted to the model to keep it from suddenly trimming too far down by the bow, with possibly disastrous consequences.

The aerodynamic controls have little effect at speeds much below 50 percent of get-away speed, so the fixed-trim runs usually begin at about 35 percent get-away speed and are carried up to, or very near to, get-away speed. Usually speeds are selected at somewhat larger intervals for these runs than for the free-

the properties of the model most plainly. Two typical and simultaneous pictures are shown as figures 6 and 7.

After the runs have been completed the sensitized paper on which the various points of light have been projected is developed and dried. Points giving a curve of gross resistance against speed have been made on a rough plot from readings of the repeater made by an observer, but the accurate readings of resistance and speed can be obtained only after the record has been developed.

The resistance record appears as a wavy line through which a mean line can be drawn by eye, using a straightedge. Experience in drawing this mean line soon makes it possible to draw it so accurately that usually only one attempt is necessary. The height of the mean line above the line representing zero resistance is multiplied by the instrument constant and gives the gross resistance in pounds. The true speed of the run is determined by the distance traveled in a given number of seconds, as recorded by the time and distance indicators.

Corrections.—The gross resistance is corrected for the error introduced by the obliquity of the towing gear, which is determined from the rise of the model as read by the observer, and for the windage drag at the true speed. Both are obtained from curves previously prepared. If the trimming moment has been observed it is corrected to take account of the fact that the vertical position of the center of gravity of the model is not at the towing point, where it was assumed to be, and that the weight of the model is not the true weight corresponding to that of the aircraft. These figures are obtained by weighing the model and determining the gravity moments it exerts about the point of suspension.

No correction is made for windage on the model itself. This part of the resistance probably varies as

account of the effect of variations in the temperature of the water on the viscosity.

The mean specific gravity of the water in the tank is very nearly that of normal sea water. If correction of the results of tests is desired it may be made on the basis of a mean specific gravity of 1.018.

After the computations have been completed there remain for entering in a table of values for each speed the weight on the water (Δ), the resistance (R), the weight on water divided by the resistance (Δ/R), the trim, the trimming moment if recorded, and the rise. The plots of these respective values as they vary with the speed provide the curves that indicate the behavior and properties of a design.

General, or "complete", method.—This method gives more general information than the specific



FIGURE 7.—Beam view of model of PH-1 flying-boat hull at 14 f.p.s., free to trim.

the wave-making resistance, or so nearly so as to cause an insignificant error in the conversion to full scale. No correction is made for interference between model and gear. This is believed to be of relatively small importance, and there appears to be no reasonably simple method of determining the actual amount in each case.

It has been found that testing can be done without serious difficulty at any temperature ordinarily met with, although the tank is unheated and consequently the air temperature varies with the outside conditions. However, extremely low temperatures last for such short periods that no serious delay has been noted from stopping work when operation becomes uncomfortable to those on the carriage.

The change in temperature of the water in the tank is very slow and the maximum range so far has been from 44° F. in mid March to 63° F. in mid October. No attempt is made, at least for the present, to take

method, and is especially useful if no data are at hand as to the complete airplane with which the float is to be used. It is the same as the method of testing described by P. Schröder in reference 7. In this method the model is towed at a number of fixed weights on the water with fixed trims and at various constant speeds, and the resistance, trimming moment, and rise are determined for each of these as in the earlier method. This method requires more runs but gives information which can be applied to more widely varying conditions of load, get-away speed, position of center of gravity, etc. The data obtained from the individual test runs are the same and the methods of deriving them are identical. In view of the more complete information obtained, this is usually referred to as the "complete" method. A full description of this method, with an example of its application, will form a later report.

ACCURACY

The accuracy of the readings from the various parts of the dynamometer and towing gear has been checked by frequent calibration and it is believed that the values used in preparing the curves are correct within the following limits:

Speed.....	± 0.1 ft. per sec.
Resistance.....	± 0.1 lb.
Rise.....	± 0.10 in.
Trim.....	$\pm 0^\circ 6'$.
Trimming moment.....	± 1.0 lb.-ft.

While the possible errors may seem large, particularly the 1.0 lb.-ft. in the trimming moment, it will be seen by reference to the curves which appear later that they are relatively small percentages of the magnitudes involved.

TYPICAL TEST DATA

COMPARISON OF TAKE-OFF OF LANDPLANE AND SEAPLANE

The special importance of reductions in the resistance to motion on the water of a flying-boat hull or a seaplane float becomes apparent from an examination of the contrast found in the curves of figure 8. This figure presents the curves of resistance on the water and land and in the air which might be expected of a large amphibian flying boat. On land this machine runs up to take-off speed on wheels like any landplane. On water it runs to get-away like any flying boat. For simplicity it is assumed that the aerodynamic resistance is the same in both cases.

The total resistance of the machine as a landplane before it leaves the ground consists of the sum of the aerodynamic resistance and the resistances due to friction and rolling along the ground. The sum of the last two is a maximum at the moment of beginning to move and becomes steadily less until it becomes zero at take-off. Compared to the resistance at take-off the initial value of the total resistance is not very large and at no time before take-off does it exceed that at take-off.

The case is far otherwise when operating as a seaplane. Here the total resistance before the craft leaves the water is the sum of the aerodynamic resistance and the hydrodynamic resistance. The course of the former is the same as for the landplane but the hydrodynamic resistance shows a violent difference. From zero at the start it rises rapidly until at "hump" speed it may be double the total resistance at get-away. It then decreases, first sharply and then more slowly, until it becomes zero at get-away. The total resistance at hump speed often comes surprisingly close to equaling the thrust at that speed. Should there be any decrease in thrust or increase in resistance at this speed the margin of thrust available for acceleration might easily disappear and the craft would not be

able to reach a speed above the hump speed and could not leave the water.

That hump of resistance menacing the propeller thrust stands out as a most obvious point to be attacked if we desire to improve the performance of seaplanes. Every reduction in its height and extent will be repaid by a decrease in the time and distance run to get-away and the margin for contingencies between the thrust and resistance will be correspondingly increased.

In the case of the landplane very little can be done to reduce the already low rolling and frictional resistance while on the ground and it is mainly the aerodynamic qualities that determine the time and length of take-off run. In the seaplane the hydrodynamic resistance is preponderant throughout almost the whole run on the water and reductions in the time and length of run to get-away must come almost solely from reductions in that resistance.

The effect of small changes in the form or dimensions of the hull of a seaplane on the hydrodynamic resistance may be surprisingly large. On small models the effects of almost microscopic changes are correspondingly difficult to perceive and interpret. When larger models can be used, as in the N.A.C.A. tank, the changes themselves may be of a substantial nature; their effects are much more apparent and relatively easier to interpret. As illustrating this, we may consider the two following cases:

THE EFFECT OF A "HOOK" ON THE STEP

Designers sometimes introduce a hook, or sharp downward drop of the bottom, at the step of a flying-boat hull. Usually the depth of the addition is small and it is of very small extent fore and aft. On a small model the addition is hardly perceptible.

Test of Navy PH-1 with hook.—In order to obtain information as to the effect of such hooks on the performance on the water of a typical flying boat, the step of a $\frac{1}{8}$ full-size model of the hull of a Navy PH-1 flying boat that was known to have a good performance on the water and in the air was fitted successively with hooks of three different sizes. A general plan of this model with the principal dimensions appears in figure 9. The model was made of pine and finished with several coats of enamel. The model was carefully checked on a surface plate for closeness to dimensions and it was found that the underwater body was within ± 0.01 inch of the designed dimensions.

The dimensions of the hooks appear on figure 10. As fitted on the model these dimensions were held to within ± 0.002 inch. A photograph of the model with the various pieces which were inserted at the step to form the hooks is reproduced as figure 11.

The model was tested with no hook on the step and with the three hooks as shown. Test runs were made

both free to trim and at fixed trims of 4° , 6° , and 8° . For each run the resistance and speed were recorded and the rise and trim, or trimming moment at fixed trim, were observed and recorded. After the proper corrections had been made for windage and rise of

curves in which the irregularities were so great as to cast doubt on the tests. Careful checking and additional points confirmed the original points and showed that there existed a real discontinuity which appeared in all four curves, but to a degree which was much

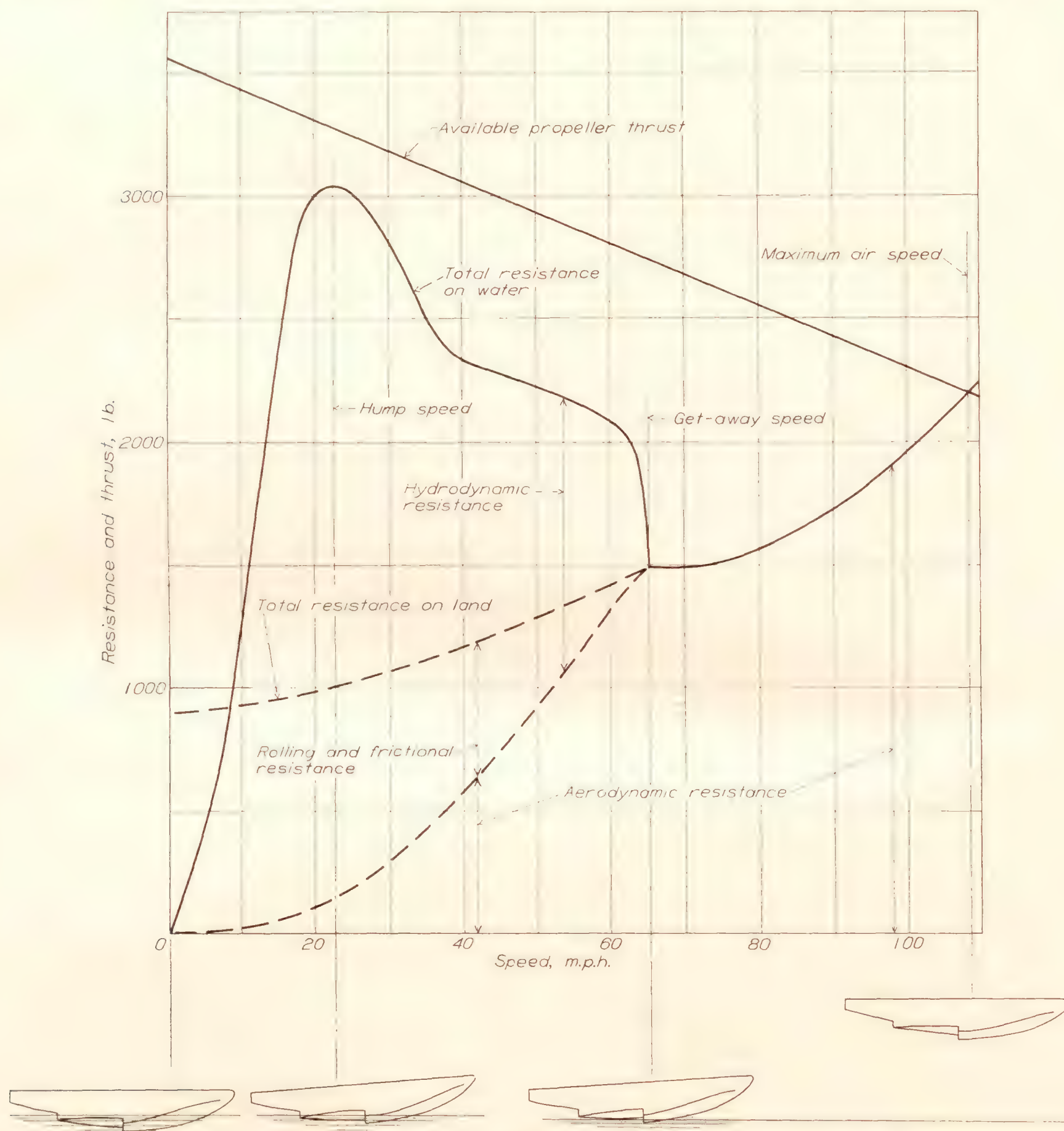


FIGURE 8. —Comparison of the resistances of an amphibian flying boat taking off from water and from land.

towing gear the results were set forth as the curves forming figures 12 (a) to (e).

Discussion of results.—A conspicuous feature of these curves is that the speed-resistance curve, free to trim, shows a sharp break, or discontinuity at the hump speed, 10 to 12 feet per second. This discontinuity was faired out in some of the earlier plots and led to

influenced by the depth of the hook. A search was made of the published results of tests of boat and float models and it was found that such a discontinuity had been mentioned in reference 8 and shown in figure 4 of that paper. This peculiarity has been found in curves from other models tested in the N.A.C.A. tank and is now regularly looked for. The speed-resistance

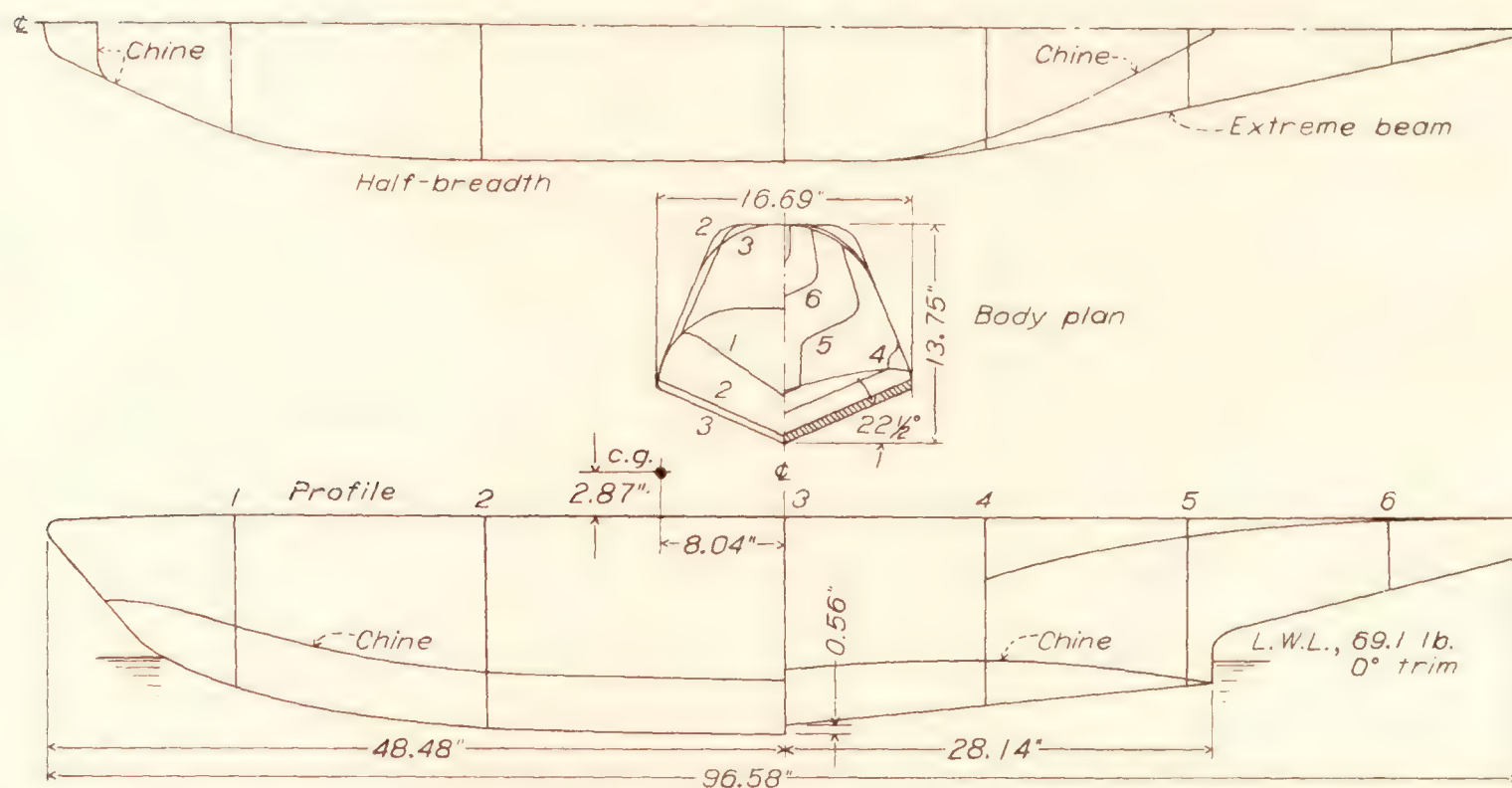


FIGURE 9.—Principal dimensions of the model of the hull of the PH-1 flying boat used in tests in the N.A.C.A. tank.

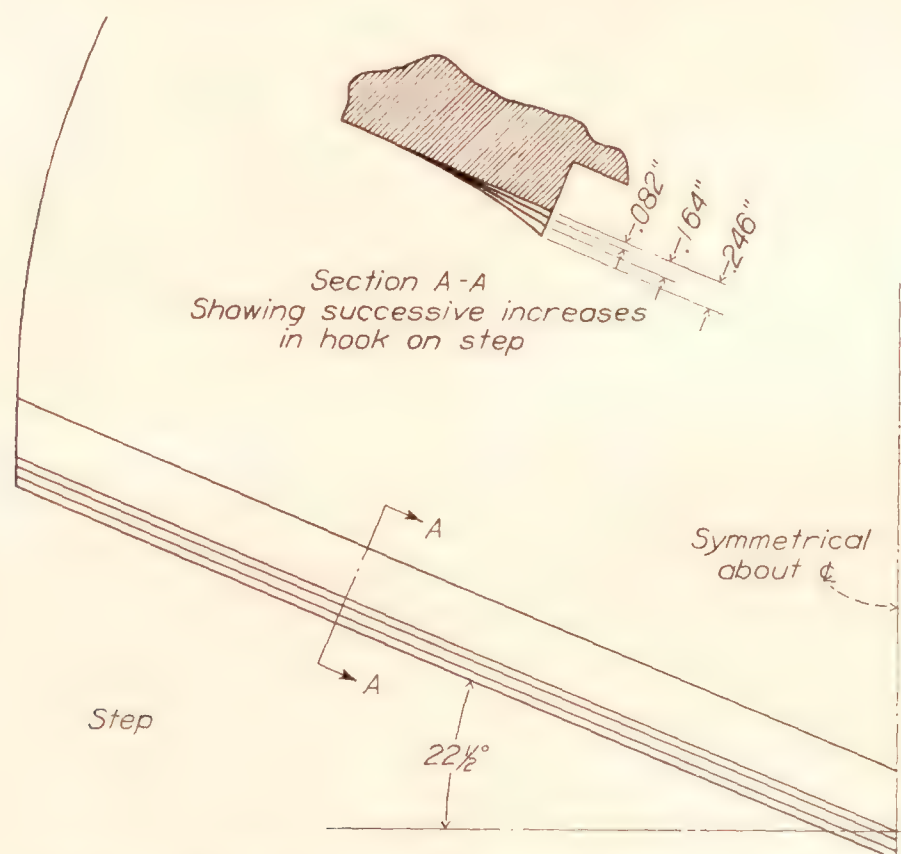


FIGURE 10.—Dimensions of the hooks fitted on the step of the model of the PH-1.

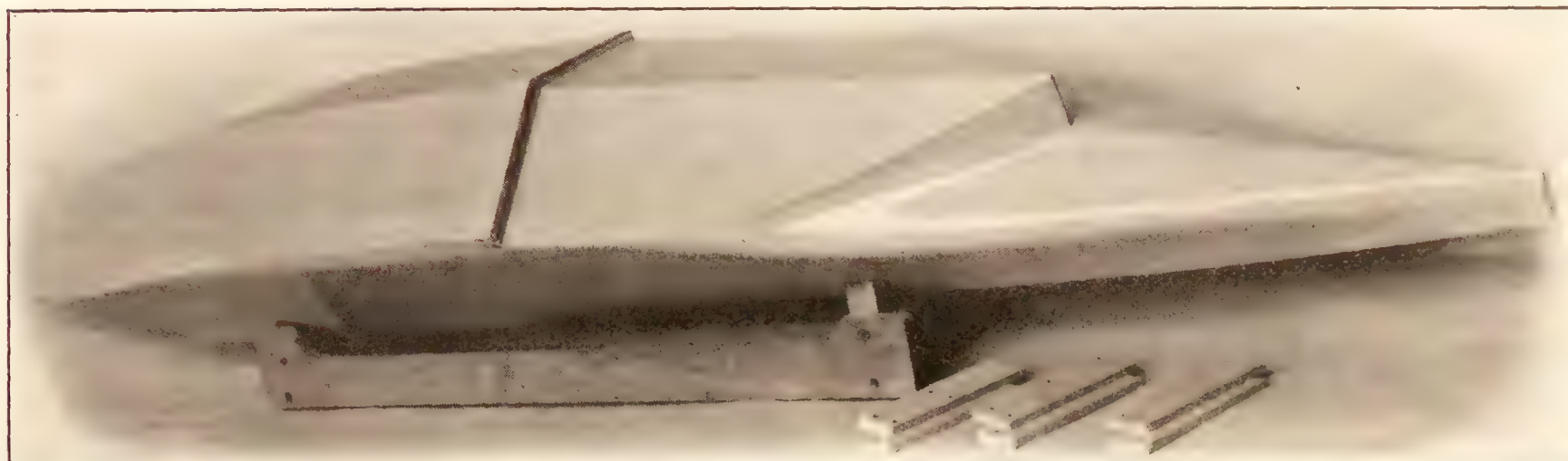


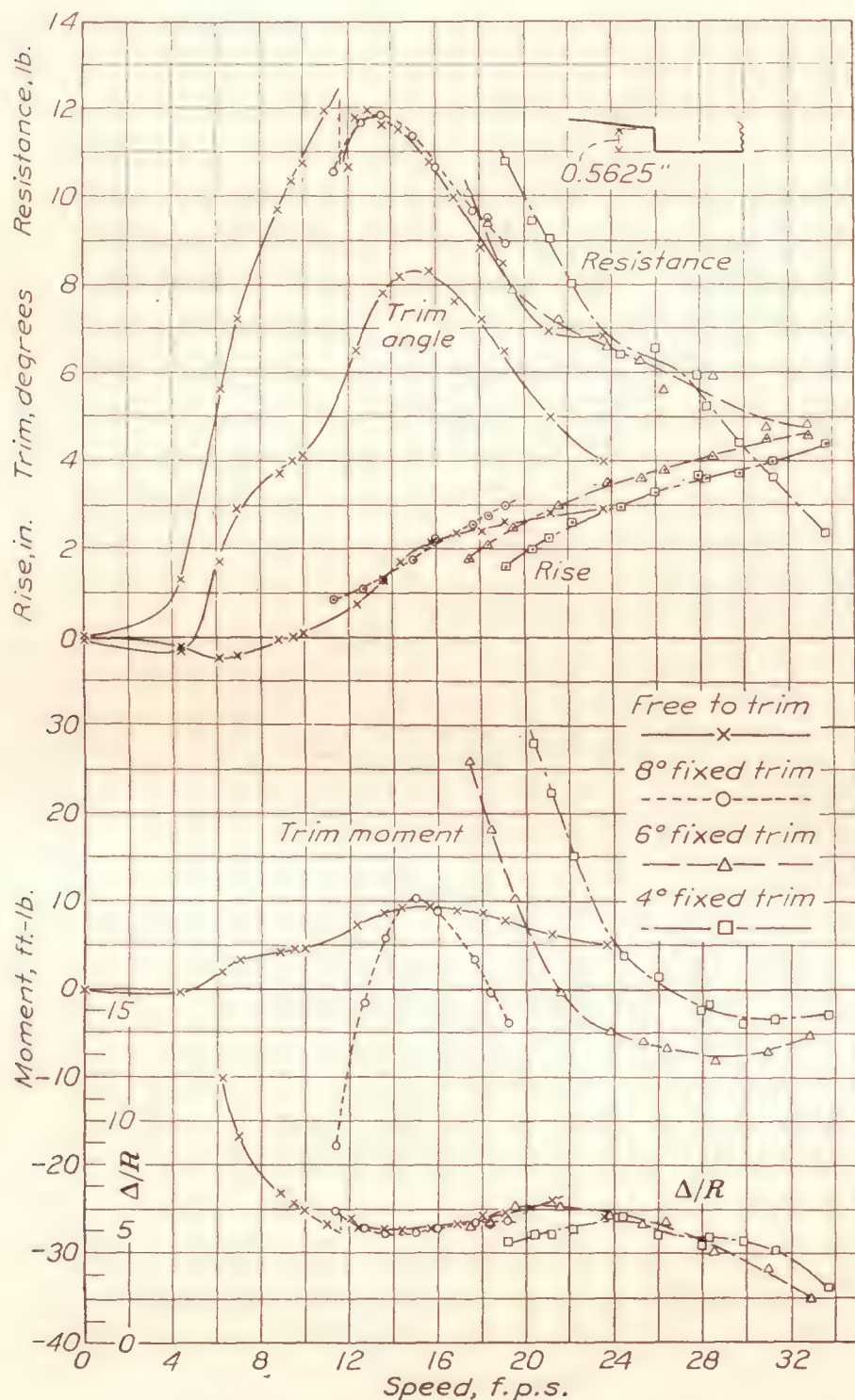
FIGURE 11.—The model of the PH-1 showing the blocks for fitting the hooks on the step.

curve for a model with a stepped bottom is drawn as a smooth curve only after check tests have shown that the expected discontinuity does not exist.

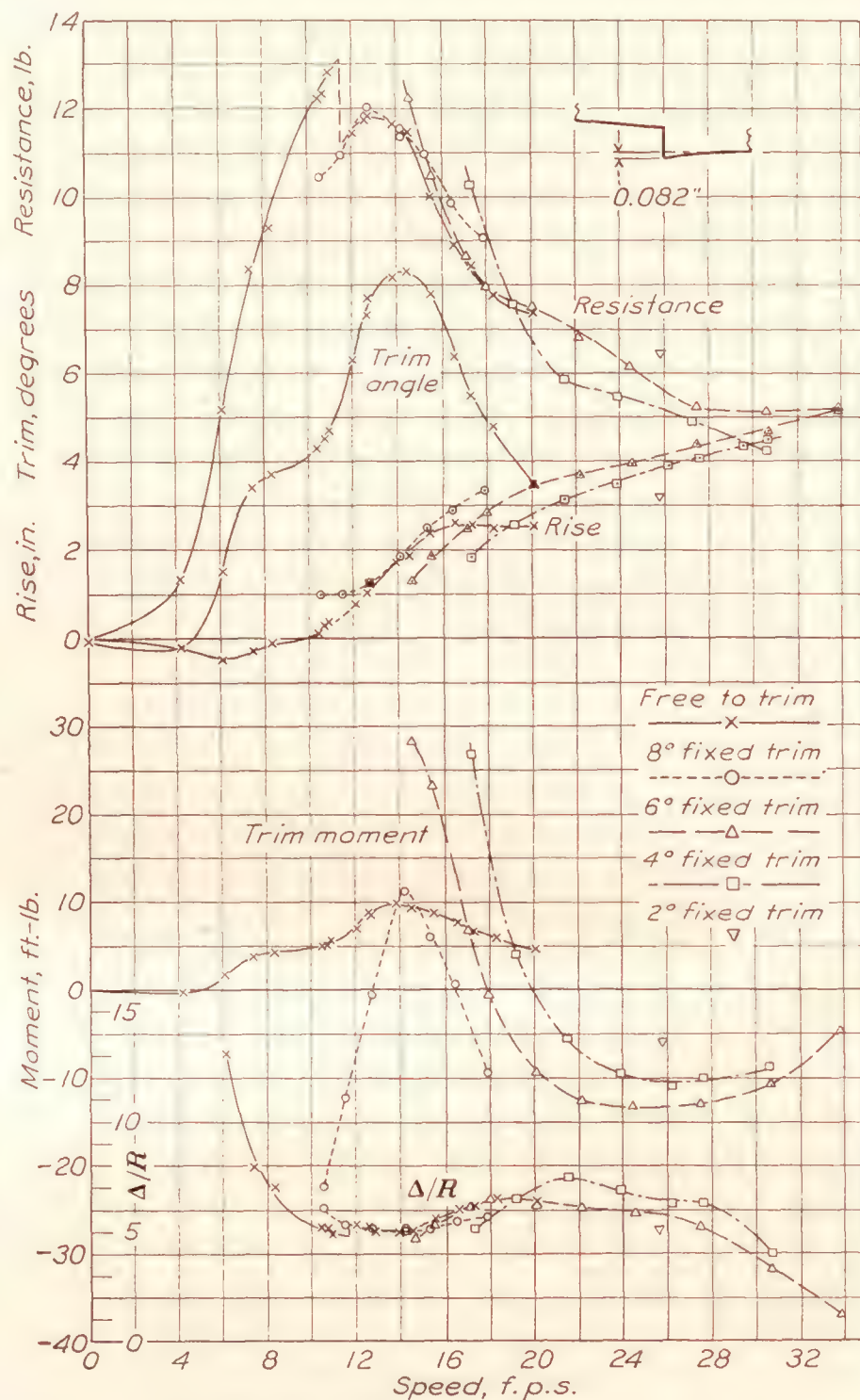
The discontinuity appears at about the speed where the model changes from a condition where buoyant support predominates to one where hydrodynamic support becomes predominant. The change can be seen in the waves and spray thrown by the model, where it appears as the point where the flow from the step

model are extended to meet and this point is indicated by a circle. The manner in which this point travels toward a lower speed and a higher resistance as the depth of the hook increases suggests the possibility of a systematic connection between depth of step, depth of hook, and resistance. This possibility has been noted for future investigation.

From the present curves we may draw the conclusion that the second hook, 0.164 inch high, is somewhat



(a) Performance curves of model with no hook.



(b) Performance curves of model with 0.082-inch hook.

FIGURE 12.—The effect of fitting hooks on the step of the model of the PH-1 flying-boat hull.

cleans up and the step ventilates properly. At that point the character of the resistance probably changes from predominantly wave making to predominantly viscous.

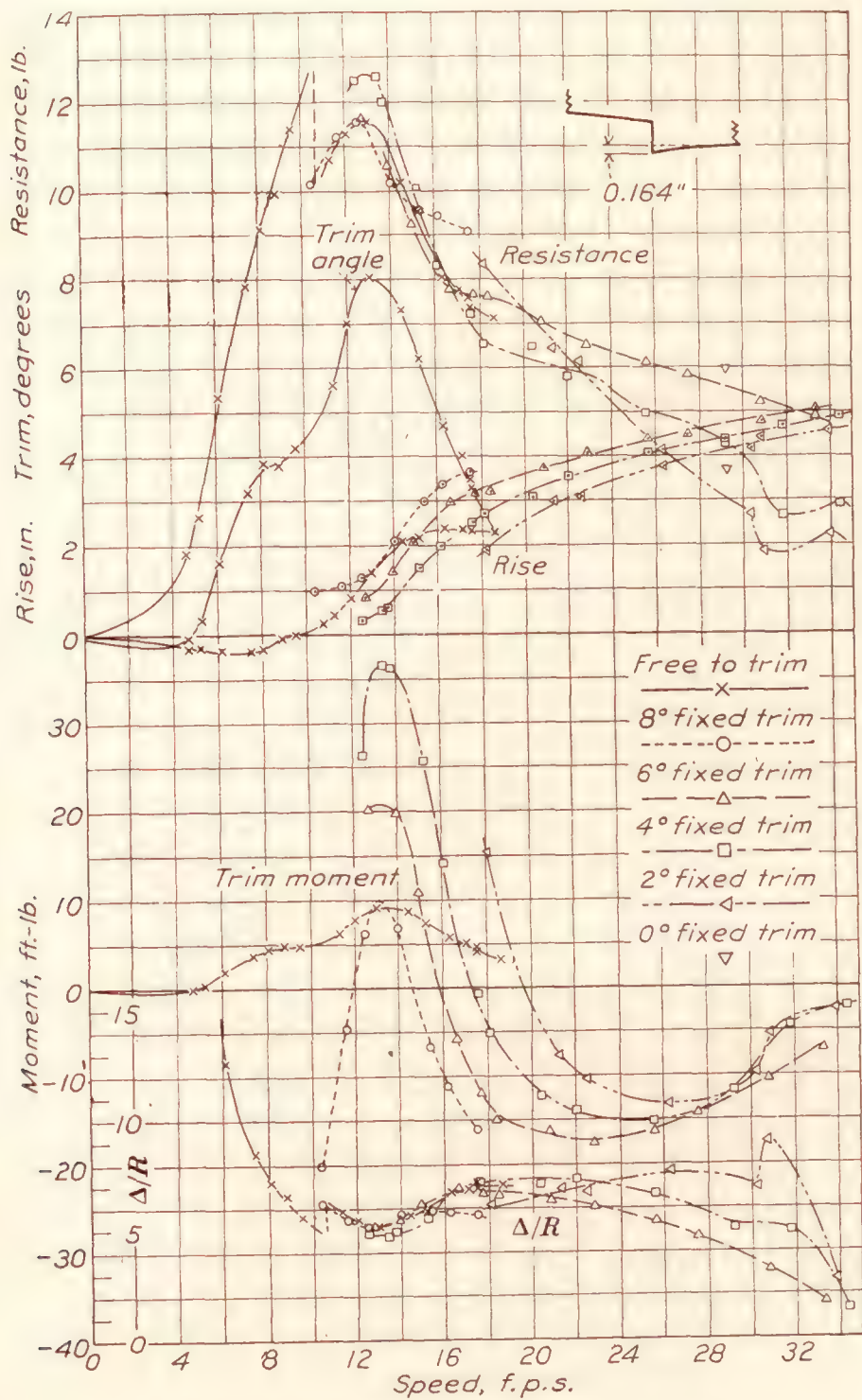
It is believed that the use of large models in the N.A.C.A. tank makes it possible to detect this discontinuity; it probably does not appear as plainly with small models.

In figure 12 (e) the comparison of the curves of resistance free to trim and at 4° fixed trim is facilitated by plotting them together. The two curves for each

the better. It gave a slight reduction in maximum resistance, made the maximum resistance come at a lower speed, and caused a general lowering of resistance from maximum resistance on.

The highest hook was most unfavorable for it produced an increase in resistance at the hump of more than 20 percent above that for the model with no hook. In all probability this would exceed the thrust at that speed and if allowed to run along freely the craft with this hook on the step probably would fail to accelerate and could not get off.

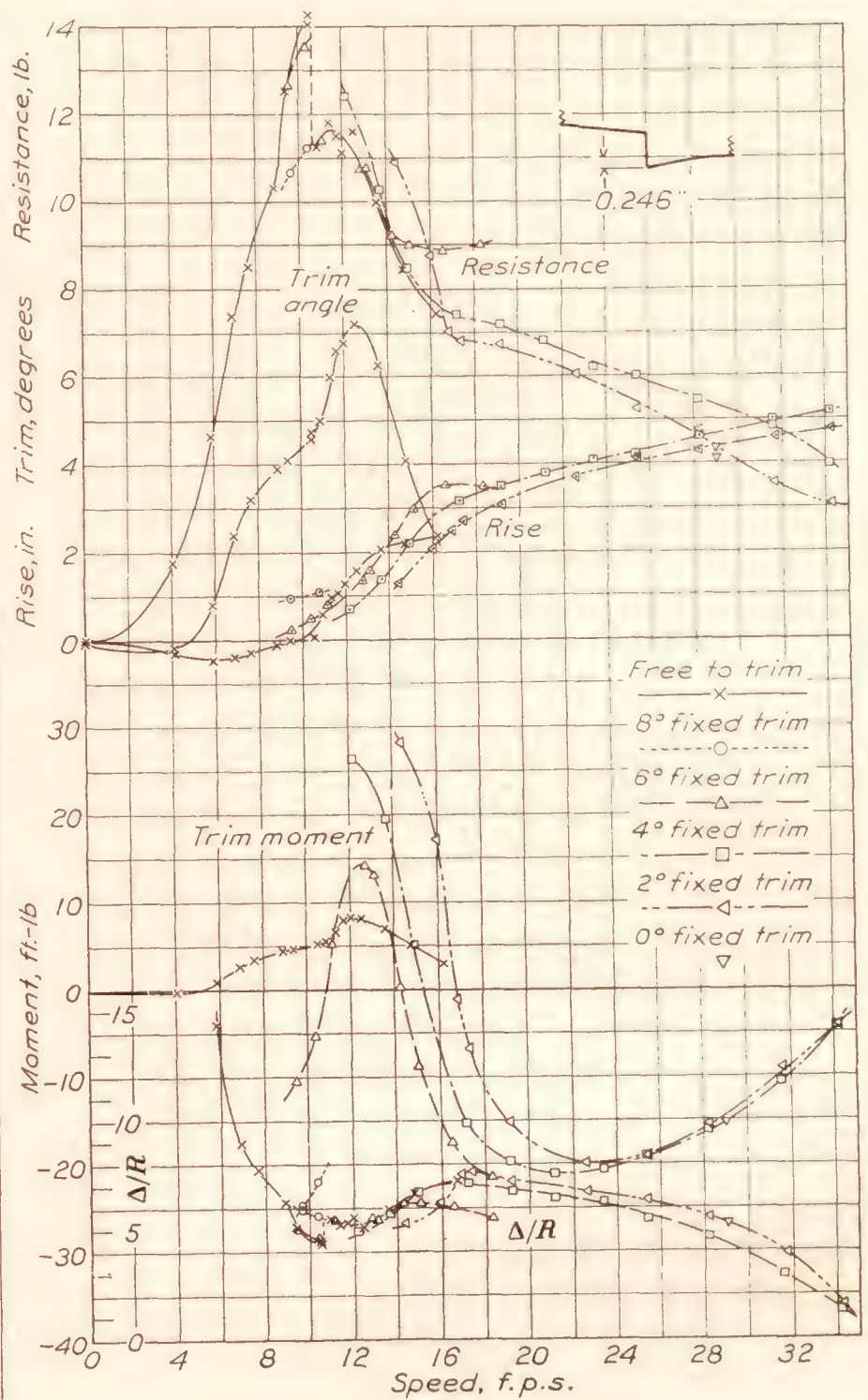
From these curves it can be seen why "rocking" a flying boat sometimes helps it to get off. If by rocking back and forth a regime can be found which will even momentarily have a lower resistance, the speed may be increased enough to pass through the narrow peak of the discontinuity and permit further running to be done on the rapidly decreasing second part of the curve. It would appear that the real purpose of the rocking,



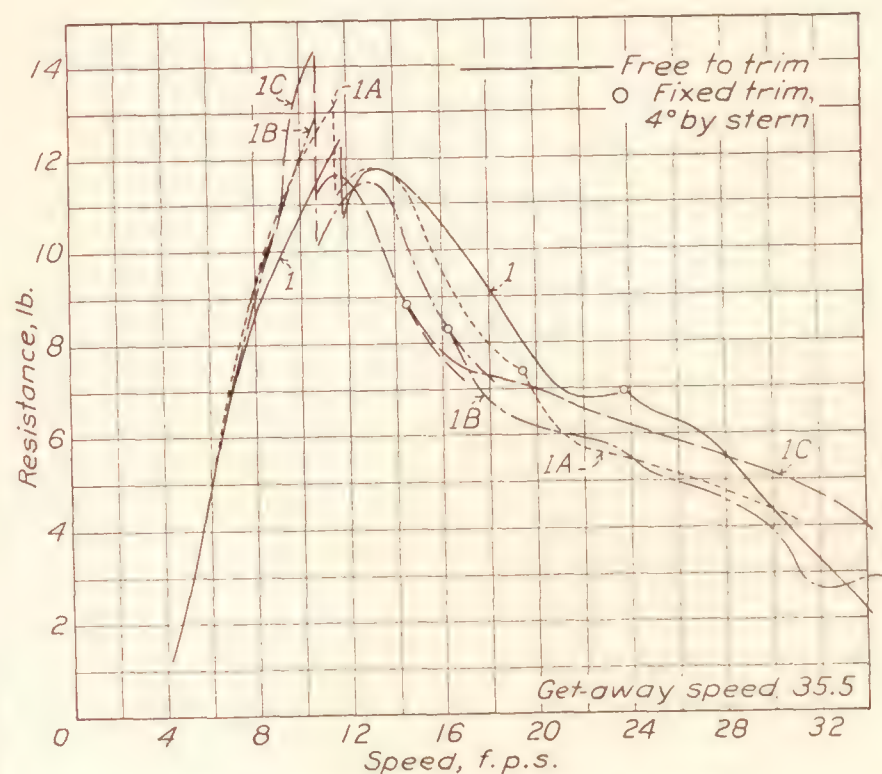
(c) Performance curves of model with 0.164-inch hook.

which frequently proves effective, is to find by trial the regime which momentarily permits the jumping from one part of the resistance curve to the other. This change in regime of course involves a change in many elements, not in the resistance alone.

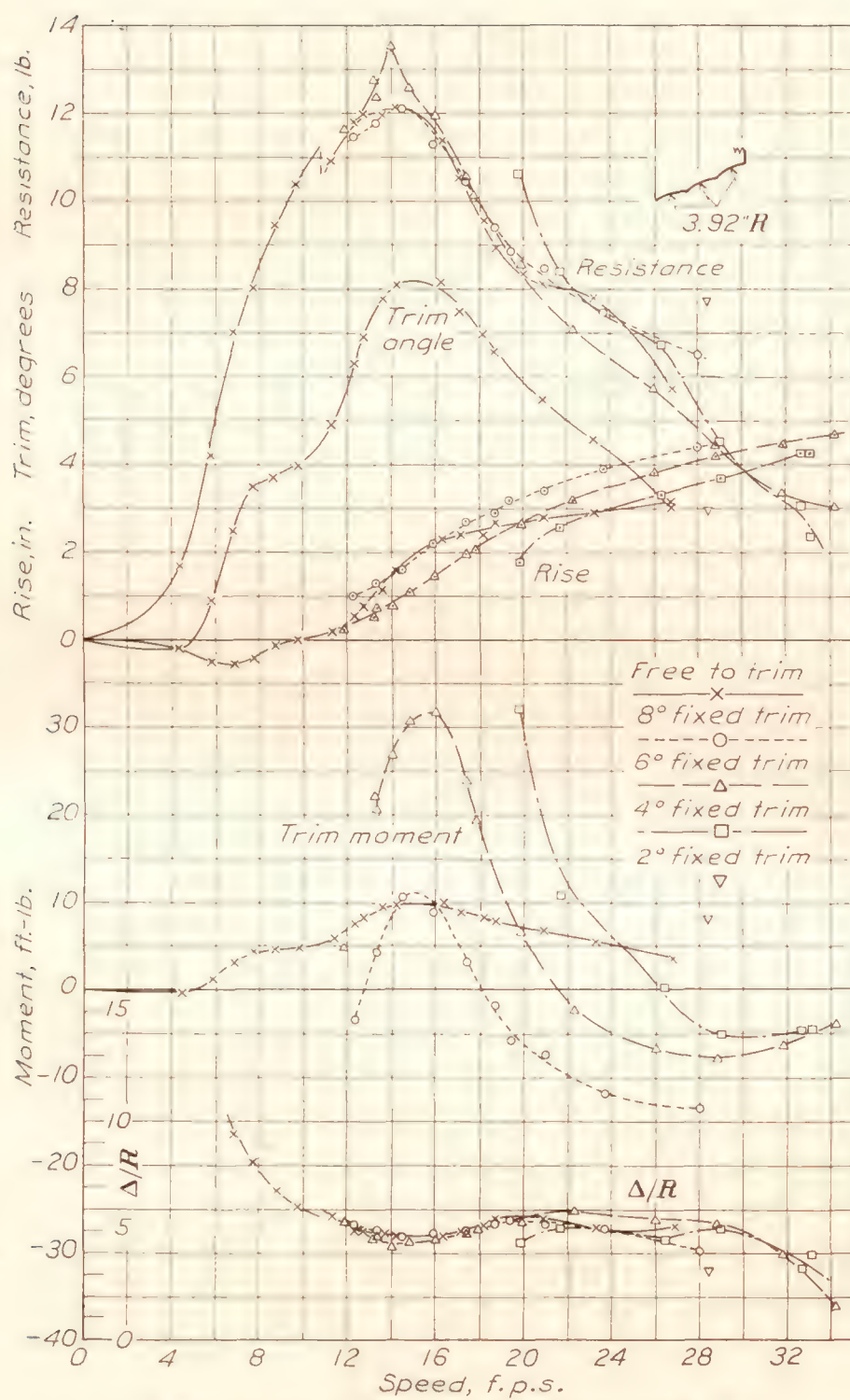
A further general conclusion is that a moderate hook on the step is an advantage. The present data are insufficient to formulate a rule. However, the proportions which gave the best result in these tests should hold for generally similar forms and applications.



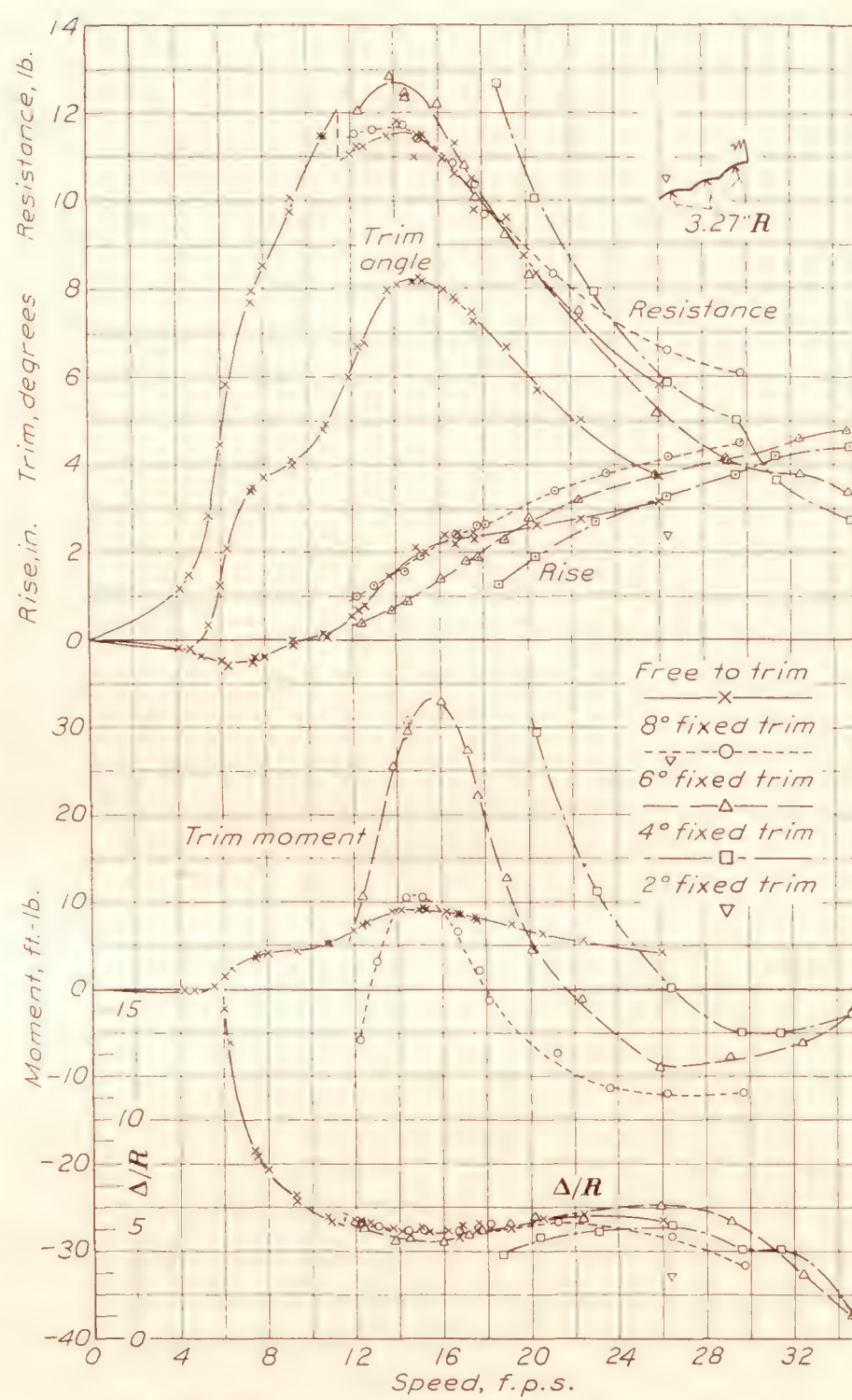
(d) Performance curves of model with 0.246-inch hook.



(e) Comparison of four speed-resistance curves.

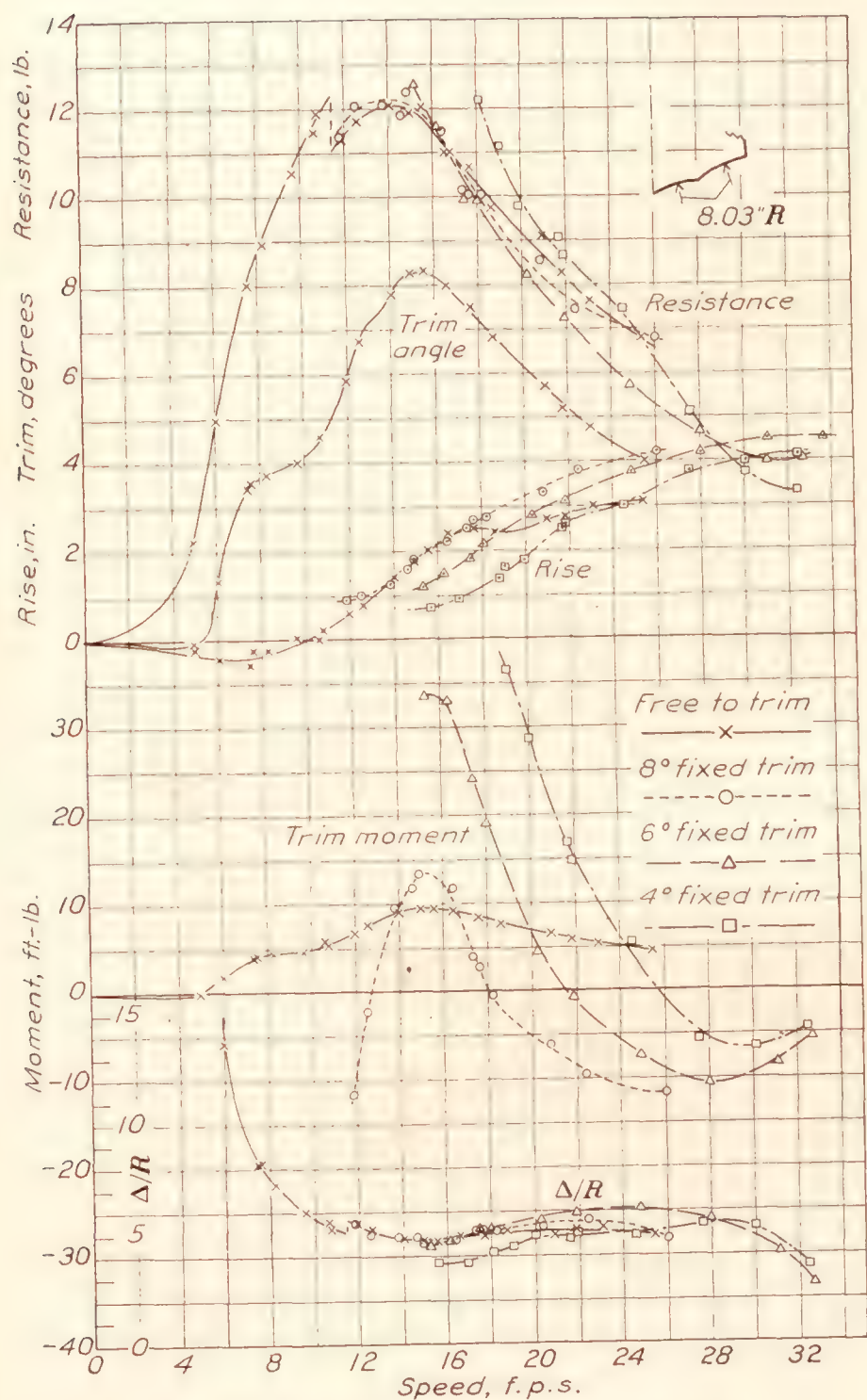


(a) Performance curves of model with three shallow flutes.

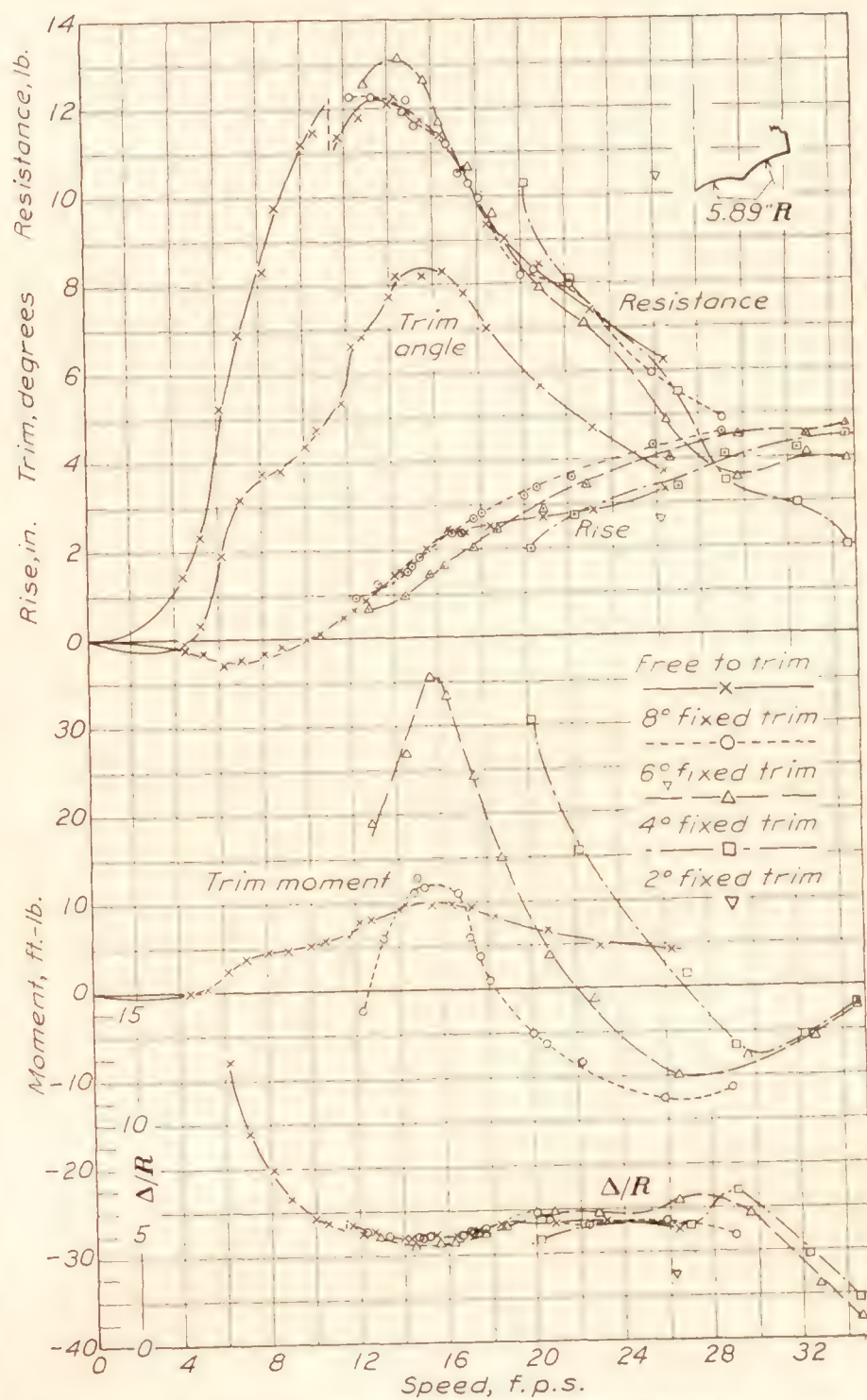


(b) Performance curves of model with three deep flutes.

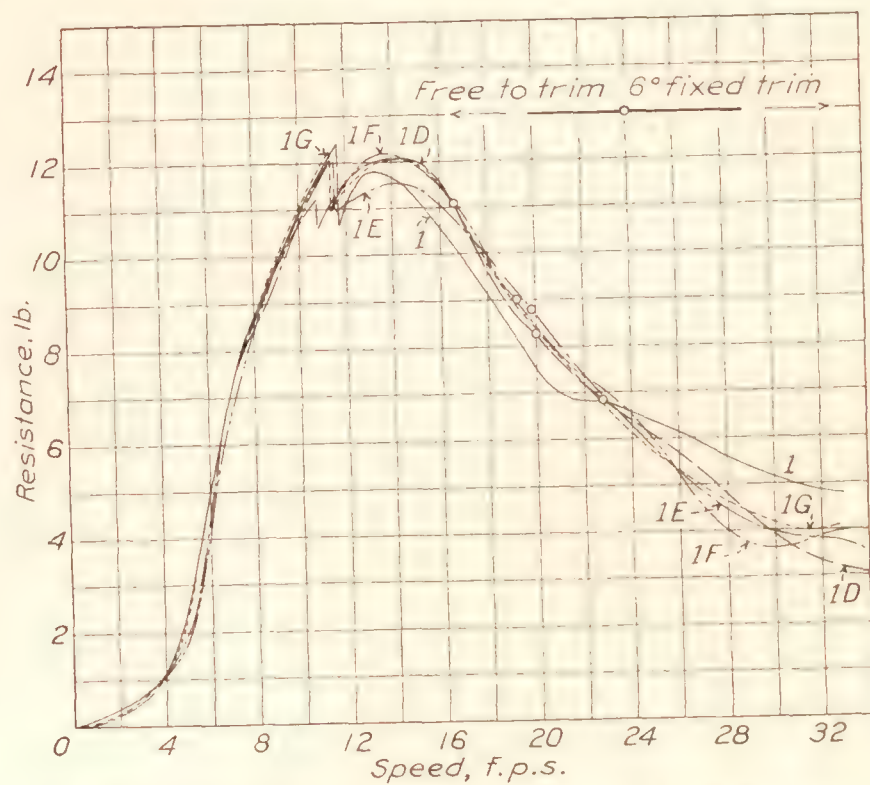
FIGURE 15.—The effect of fitting flutes in the forward bottom of the model of the PH-1 flying-boat hull.



(c) Performance curves of model with two shallow flutes.



(d) Performance curves of model with two deep flutes.



(e) Comparison of four speed-resistance curves with that of original model.

THE EFFECT OF FLUTED BOTTOMS

Longitudinal flutes have been fitted in the planing bottom of a float by several designers. The flutes usually produce a reduction in the spray thrown and as the craft rises on the step it would appear that they should give

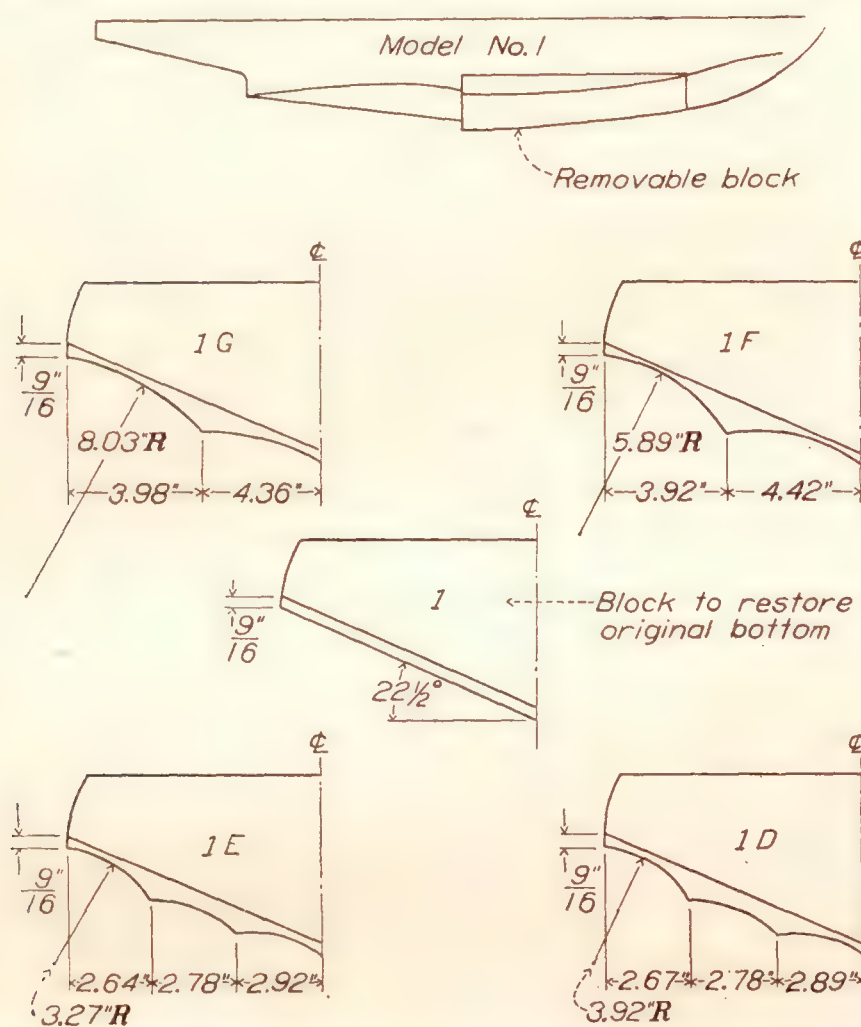


FIGURE 13.—Cross sections at the step of the model of the PH-1 flying-boat hull showing the original and the fluted forward bottoms.

a reduction in the area of bottom wetted by the rising sheet of water and thus reduce the frictional resistance.

Test of Navy PH-1 with flutes.—In order to obtain an idea of the effect of a relatively simple set of flutes

will be seen that there are two shallow and two deep and three shallow and three deep flutes. The extent of the block containing the flutes is shown on the same figure. The appearance of the original model and the fluted blocks can be seen in figure 14.

The model was tested with the four modifications both free to trim and at fixed trims. During each test run the resistance and speed were recorded and the rise and trim, or trimming moment if at fixed trim, were observed and recorded. After the proper corrections had been made for windage and rise of towing gear the results were set forth as the curves forming figure 15 (a) to (e). The curves obtained from tests in the original form, with no hook on the step, are included for comparison.

Discussion of results.—In figure 15 (e) are shown the assembled curves for the resistance free to trim and at 6° fixed trim. The curves for the two conditions have been extended until they intersect and this point of intersection is indicated by a circle.

An examination of the curves shows that the fitting of the fluted bottom has had little effect on the resistances. All the curves have the same general character with a discontinuity at a speed of about 11 feet per second. Before this discontinuity appears the model is running as a displacement craft and the change produced by the flutes is small. After the discontinuity has been passed the model is more nearly a planing craft but the resistance is held up by the interference in the flows from the respective flutes. When the model has risen to where it is running on a single flute on each side the flow cleans up and the area of bottom wetted is sharply reduced below that wetted with the plain bottom. From this point the resistance of the fluted bottoms lies below that of the plain bottom.



FIGURE 14.—Model of the PH-1 flying-boat hull showing the original form and the blocks to be inserted to give the four fluted forward bottoms.

in the bottom of a flying-boat hull the model of the PH-1 which was used in the tests just described was modified, by fitting portable blocks in the bottom, to have successively four different types of flutes. The original cross section at the step and those produced by the four modifications are shown in figure 13. It

As is usually the case, observation of the flow around the bottom gave many interesting hints. At the hump and at certain stages after the hump was passed the number of flutes in the bottom could be told by the number of clearly marked separate jets in which the water issued from under the bottom.

In general, the fluted bottoms threw less spray than the plain bottom. However, a spray strip at the chine on the original model made the spray from the plain bottom as little as from the fluted bottom. A report on the effect of spray strips on the performance of this model is in preparation.

From the results of this test it may be concluded that fluting the bottom of a flying-boat hull of a good design, such as was used in this case, will probably give no very large changes in performance. Any improvement in spray thrown can probably be equaled by a proper spray strip on the original model.

LANGLEY MEMORIAL AERONAUTICAL LABORATORY,
NATIONAL ADVISORY COMMITTEE FOR AERONAUTICS,
LANGLEY FIELD, VA., *June 9, 1933.*

REFERENCES

1. Sallé: Les Essais de Modèles en Hydraviation. Bull. de l'Association Technique Maritime et Aeronautique, vol. 32, 1928, pp. 281-329.
2. Hunsaker, J. C.: Naval Architecture in Aeronautics. Aero. Jour., vol. 24, no. 115, July 1920, pp. 321-405.
3. British A.R.C.: Aeronautics. Report of the Aeronautical Research Committee for the year 1925-26, pp. 11-12.
4. Relf, Ernest F.: Research Progress 1928. Aircraft Engineering, March 1929, pp. 7-8.
5. Herrmann, H., Kempf, G., and Kloess, H.: Tank Tests of Twin Seaplane Floats. T.M. No. 486, N.A.C.A., 1928.
6. Sottorf, W.: Scale Effect of Model in Seaplane-Float Investigations. T.M. No. 704, N.A.C.A., 1933.
7. Schröder, P.: Towing Tests of Models as an Aid in the Design of Seaplanes. T.M. No. 676, N.A.C.A., 1932.
8. Sottorf, W.: Experiments with Planing Surfaces. T.M. No. 661, N.A.C.A., 1932.

REPORT No. 471

PERFORMANCE OF A FUEL-INJECTION SPARK-IGNITION ENGINE USING A HYDROGENATED SAFETY FUEL

By OSCAR W. SCHEY and ALFRED W. YOUNG

SUMMARY

This report presents the performance of a single-cylinder test engine using a hydrogenated safety fuel. The safety fuel has a flash point of 125° F. (Cleveland open-cup method), which is high enough to remove most of the fire hazard, and an octane number of 95, which permits higher compression ratios to be used than are permissible with most undoped gasolines. The fuel was injected into the engine cylinder, except for a few comparative runs with gasoline, when a carburetor was used. The tests were made with compression ratios of 5.85 and 7.0, valve timings giving 30° and 130° overlap, inlet pressures from atmospheric to 6 inches of mercury boost, and engine speeds from 1,250 to 2,200 r.p.m. Under similar conditions the power obtained with the safety fuel was the same as that obtained with gasoline, whereas the fuel consumption was from 5 to 10 percent higher. With a compression ratio of 7.0, a valve overlap of 130 crankshaft degrees, and a boost pressure of 2 inches of mercury, the safety fuel gave a brake mean effective pressure of 175 pounds per square inch with a fuel consumption of 0.50 pound per brake horsepower hour.

INTRODUCTION

The importance of replacing gasoline with a fuel that would reduce or eliminate the fire hazard in aircraft has long been recognized. The use of gasoline is a fire hazard because inflammable vapors are given off in nearly all climates and seasons. Aviation gasoline has a flash point of about -30° F. Those acquainted with the problem of fire prevention in airplanes agree that the highly inflammable gasoline should be replaced by a fuel having a higher flash point, preferably over 105° F. as determined by the closed-cup method.

One of the advantages of the compression-ignition engine is that it uses a fuel of such a high flash point (approximately 175° F.) that no inflammable vapors are given off even in the warmest climate. Aircraft-engine operators, however, have considered the advantage of reducing the fire hazard by using compression-ignition engines to be insufficient to offset the disadvantage of the decreased power per unit of weight and displacement obtained with this type engine.

In France, Sabatier has reported an investigation on the use of fuels having flash points of 100° F. and 77° F., obtained from coal-tar and petroleum derivatives, respectively (reference 1). The commercial use of these fuels was restricted, if not entirely prevented, by their poor performance as compared with gasoline: the power was reduced, the fuel consumption was increased, starting was difficult, and increased heating of the carburetor was necessary.

The National Advisory Committee for Aeronautics has conducted tests with safety fuels manufactured by the hydrogenation process (reference 2). Because of the low volatility of the fuel it has been injected into the engine cylinder instead of being introduced through a carburetor. The first fuel investigated had a flash point of 137° F. as determined by the Cleveland open-cup method. The full-throttle power obtained with this fuel was lower than with gasoline, and the fuel consumption was considerably higher. The second fuel tested had a flash point of 115° F. With this fuel the power was as high as that with gasoline, but the fuel consumption was from 25 to 30 percent higher (reference 3).

The results obtained from an investigation conducted with a third fuel, which had a flash point of 125° F., are presented in this report. The object of this investigation was to determine the performance obtained with a spark-ignition engine when operating with a hydrogenated safety fuel injected into the engine cylinder. As a basis for comparison the performance was obtained for several comparable conditions with gasoline. The tests were conducted at Langley Field, Va., in December 1932 and January 1933.

APPARATUS AND METHOD

Figure 1 shows the set-up of the test equipment. A single-cylinder 4-stroke-cycle water-cooled test engine of 5½-inch bore and 6-inch stroke was used. The engine could be operated with either a fuel-injection system or a carburetor. A commercial fuel-injection pump was driven from the engine crankshaft through a reduction gear which permitted the phase of the injection to be changed at will. A spring-loaded automatic injection valve and a multi-orifice nozzle of

N.A.C.A. design were used (fig. 2). When the injection system was used the carburetor was left in place and the throttle valves were used to control the air supply for starting.

The engine was directly connected to an electric dynamometer. A small weighing tank suspended from a sensitive beam balance was used to measure the fuel during a run, the length of the run being the time required to consume one-half pound of fuel. The engine coolant was piped to a radiator, which was cooled by

valve location gave the best performance; however, the performance was only slightly better than with the valve located in the center hole. Two spark plugs were located in opposite sides of the combustion chamber.

Two different pistons and two different sets of valve cams were used. These pistons gave compression ratios of 5.85 and 7.0. The set of cams that gave normal valve timing caused the inlet valves to open 15° before top center and close 55° after bottom center,

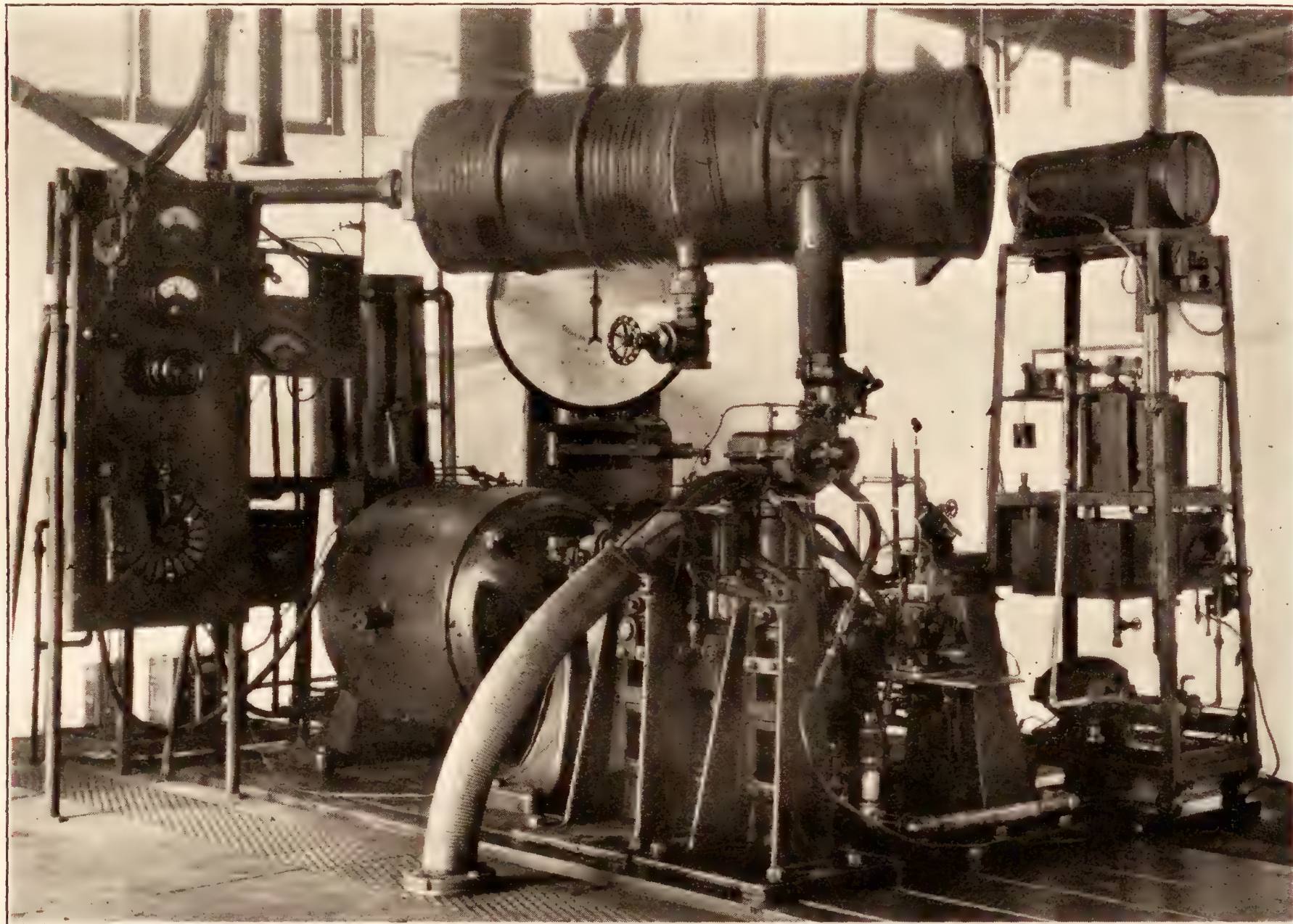


FIGURE 1.—Set-up of test equipment.

a water spray when necessary. The small volume of liquid necessary to fill this cooling system made it feasible to use Prestone and operate at high coolant temperatures when desired. Temperatures up to 280° F. at the engine outlet could be obtained.

This engine has a pent-roof form of combustion chamber, with two inlet and two exhaust valves (fig. 3). The inlet-valve ports are $1\frac{13}{16}$ inches and the exhaust-valve ports $1\frac{5}{8}$ inches in diameter. There are five tapped holes in the head, permitting some choice in locating the spark plugs and injection valve. The injection valve was located between the exhaust valves, and directed the spray horizontally across the combustion chamber toward the inlet valves. This injection-

while the exhaust valves opened 55° before bottom center and closed 15° after top center. The other set of cams did not change the events at the bottom of the stroke, except to advance the inlet closing 10° , but caused the inlet valves to open 70° before top center and the exhaust valves to close 60° after top center. This valve timing results in an overlap of the open periods of the exhaust and inlet valves of 130° , giving improved scavenging of the clearance volume, particularly when some boosting is used (reference 4). Figure 4 shows the amount of valve opening during the period of overlap. A separately driven Roots blower was connected to the inlet system through a large surge tank placed near the carburetor.

The results obtained from runs in which the length of the exhaust pipe was varied caused the adoption of a length of 2 feet for these tests. Shorter pipes caused lower torque at all speeds and more variation of torque over the useful speed range, unless boosting was used. The length of inlet pipe to the point of attachment at the surge tank was $2\frac{1}{2}$ feet, but this length was not critical. With a large valve overlap the effect of pressure waves in the exhaust and inlet pipes becomes negligible when a supercharging pressure of several inches of mercury is used.

The engine performance with the hydrogenated safety fuel using fuel injection was obtained for speeds

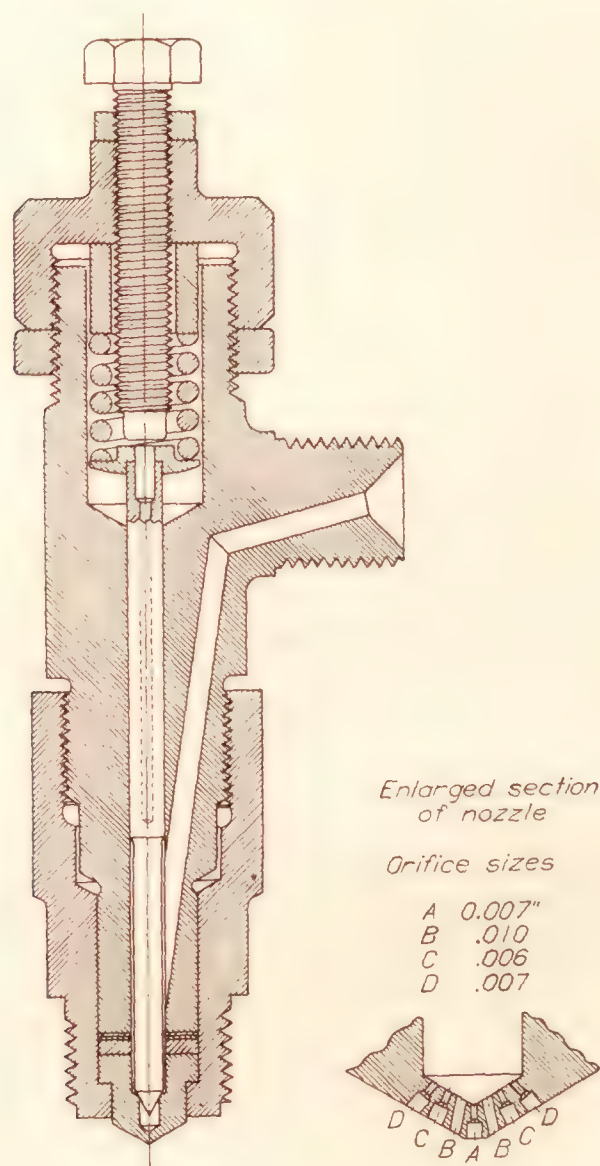


FIGURE 2.—Fuel-injection valve and nozzle.

from 1,250 to 2,200 r.p.m., compression ratios of 5.85 and 7.0, valve timings giving 30° overlap and 130° overlap, and boost pressures up to 6 inches of mercury. A sufficient number of these tests using fuel injection were repeated with aviation gasoline as fuel to furnish a reliable comparison of the safety fuel and the gasoline. A few runs were made with gasoline using the carburetor.

The procedure for each test condition was to make three or four full-throttle runs using fuel quantities that gave mixtures ranging from one richer than necessary for maximum power to a very lean one. The engine torque and fuel consumption were measured for each run. The brake power was corrected to an atmospheric pressure of 29.92 inches of mercury and a

temperature of 59° F. on the assumption that it varied directly as the pressure and inversely as the square root of the absolute temperature. No correction was made for humidity or for the power required to drive

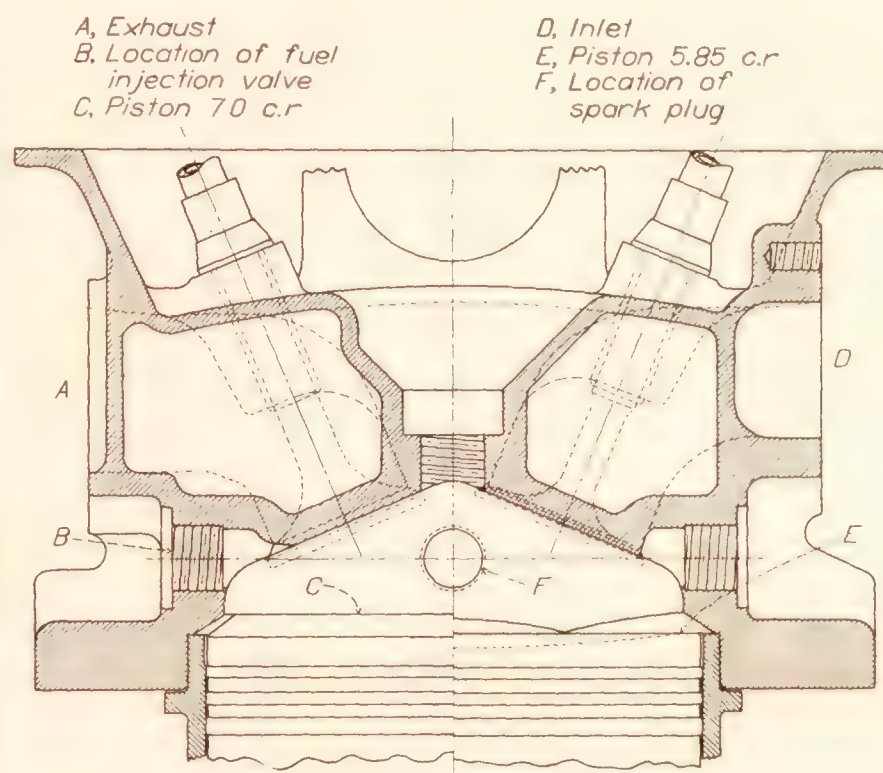


FIGURE 3.—Combustion chamber form.

the supercharger. The correction for power required to drive the supercharger, when used, would not be over 3 percent of the engine power at 6 inches of mercury boost pressure.

Some additional data were obtained with special equipment. Where maximum cylinder pressures were

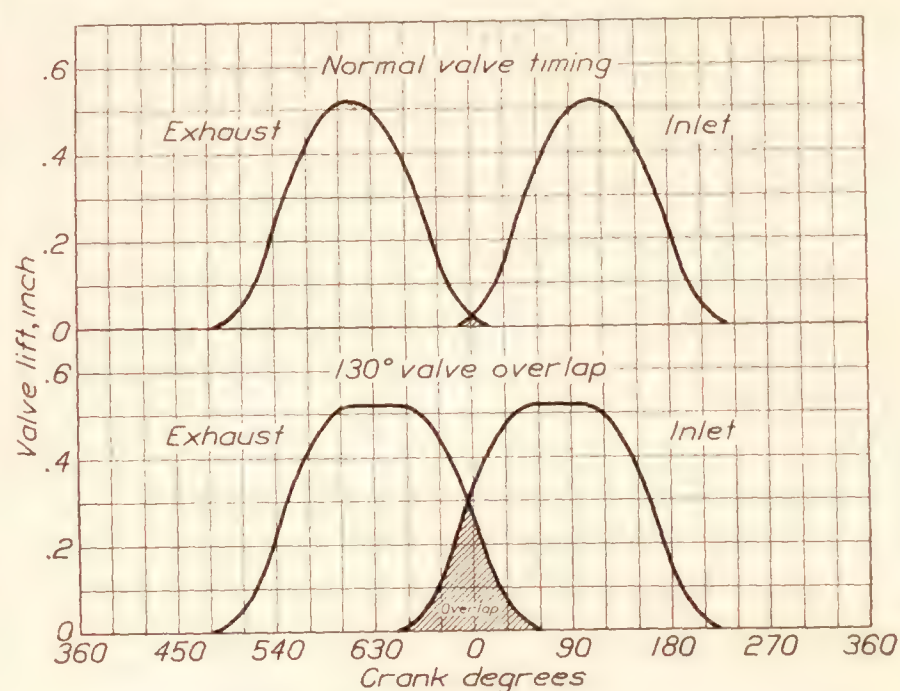


FIGURE 4.—Valve motion with normal valve timing and with 130° overlap.

taken a trapped-pressure valve was used. A reduced back pressure on the exhaust of the engine was obtained for a few tests by discharging the exhaust into a large tank, the outlet of which was connected to the section side of a supercharger. With the same equipment the outlet of the tank was throttled to produce increased exhaust back pressure. Data on the characteristics of the fuel-injection system were obtained

with the N.A.C.A. rate-of-discharge apparatus, which is described in reference 5.

FUELS

Distillation curves for the gasoline and the hydrogenated safety fuel are given in figure 5. The flash

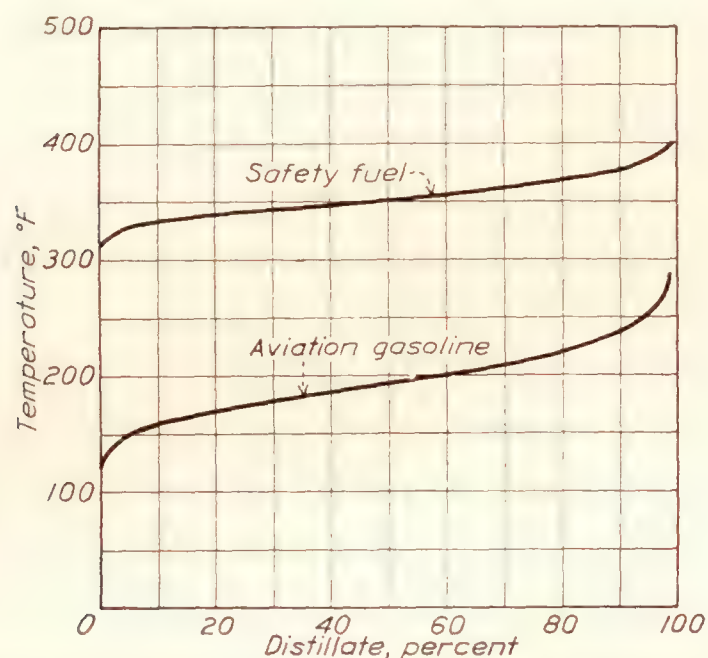


FIGURE 5.—Distillation curves for the gasoline and safety fuel.

point of gasoline is below ordinary atmospheric temperatures even in winter, while that of the safety fuel (125°F . by the Cleveland open-cup method or 106°F . by the Abel closed-cup method) is well above the highest operating temperatures usually encountered. Besides reduced fire hazard, the hydrogenated safety fuel has excellent antidetonating qualities, so that the fuel may be used at high compression ratios without the use of fuel dopes such as tetraethyl lead. The hydrogenated safety fuel has an octane number of 95 as determined by the manufacturer using a series 30 Ethyl Gasoline Corporation test engine operated at a speed of 600 r.p.m. and with a coolant temperature of 300°F . Sufficient ethyl fluid was added to the aviation gasoline to prevent detonation under any of the test conditions, thereby placing the engine performance with the two fuels on a comparative basis that is independent of antiknock characteristics. A study of the behavior of the hydrogenated fuel at low temperatures showed satisfactory characteristics. At a temperature of -25°F . a few solid particles appeared in the fuel, but at temperatures as low as -100°F . there was no tendency for all of the fuel to solidify.

RESULTS AND DISCUSSION

EFFECT ON BRAKE MEAN EFFECTIVE PRESSURE AND FUEL CONSUMPTION

Compression ratio, scavenging, fuel, and fuel system.—Figure 6 presents the comparative performance obtained at a compression ratio of 5.85 with gasoline and safety fuel and with the fuel-injection system and the carburetor. The performance curves with gasoline show that the maximum brake mean effective pressure obtained with the fuel-injection system is greater than

that obtained with the carburetor. The difference in brake mean effective pressure decreases as the quantity of fuel per cycle is decreased, indicating that the volumetric efficiency was probably slightly higher with the use of injection into the cylinder than with the use of the carburetor.

In most of these tests no air measurements were made because the use of the air-measuring system caused a small reduction in power. A few runs were made, however, in which measurements of air consumption were obtained. The first set of these air measurements was made to determine the difference in volumetric efficiency obtained when operating with the fuel-injection system and when operating with the carburetor. The results showed that the volumetric efficiency was from 1 to 3 percent higher with the injection system than with the carburetor, depending on the engine speed. As the carburetor was left in place when operating with the injection system, any gain in volumetric efficiency must be attributed to the difference between external and internal carburetion.

A comparison of the brake mean effective pressure and the economy obtained with safety fuel and gasoline when operating with the fuel-injection system shows

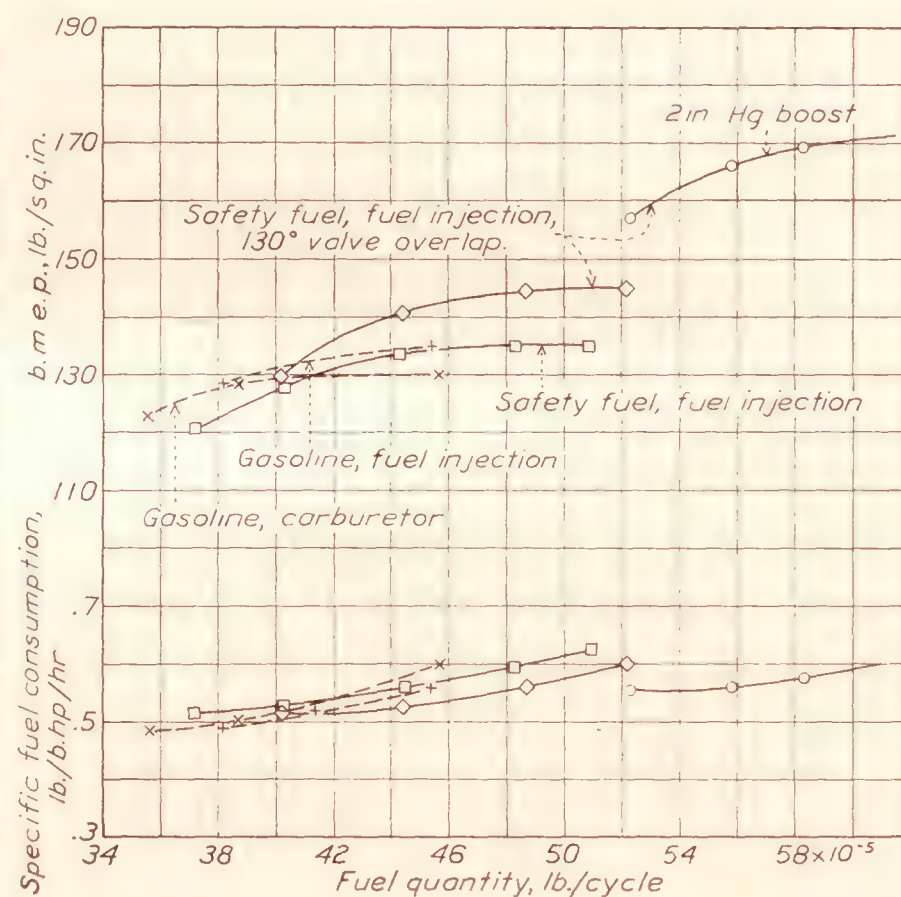


FIGURE 6.—B.m.e.p. and fuel consumption obtained when operating at a compression ratio of 5.85 and an engine speed of 1,750 r.p.m. with gasoline and with safety fuel.

that the maximum power is the same for the two fuels, and that the fuel consumption is 5 to 10 percent lower with gasoline.

There were more exhaust odors and fumes present when operating with the safety fuel than when operating with the gasoline. However, the exhaust fumes were not so noticeable that the operating conditions could be considered disagreeable or unsatisfactory.

The results that have been discussed so far are for standard valve-timing conditions. In figure 6 there are also shown performance curves for valve timing giving 130 crankshaft degrees overlap. When operating with atmospheric pressure at the intake with this valve overlap a maximum brake mean effective pressure of 145 pounds per square inch is obtained and when

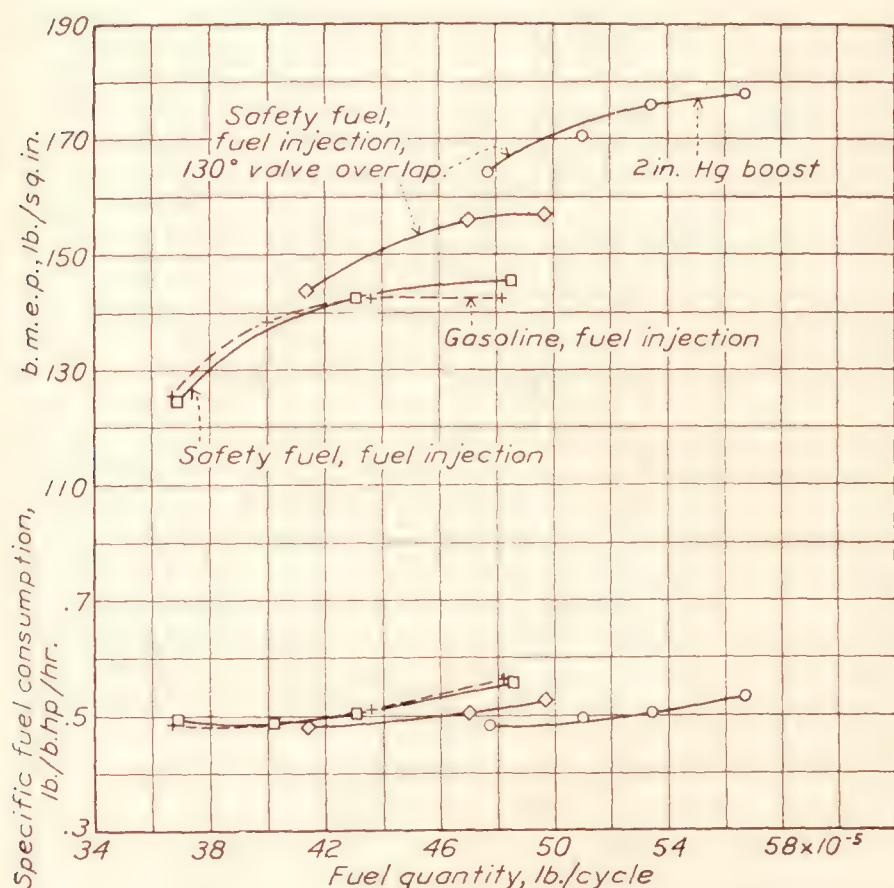


FIGURE 7.—B.m.e.p. and fuel consumption obtained when operating at a compression ratio of 7.0 and an engine speed of 1,750 r.p.m. with gasoline and with safety fuel.

operating with 2 inches of mercury boost pressure a maximum brake mean effective pressure of 170 pounds per square inch is obtained. The large increase in maximum brake mean effective pressure obtained with a small boost pressure is caused principally by the scavenging of the clearance volume. In these tests with safety fuel at a compression ratio of 5.85 there was a small increase in fuel consumption for the scavenged condition, whereas in earlier tests with gasoline on another engine there was a slight decrease in fuel consumption when scavenging (reference 4).

The curves in figure 7 for a compression ratio of 7.0 and no boost pressure show that with safety fuel the brake mean effective pressure is approximately 10 pounds per square inch greater and the specific fuel consumption is 7 to 8 percent lower than for the 5.85 compression ratio. The compression ratio could probably be further increased without the addition of fuel dope to the safety fuel, for there was no indication of detonation in these tests. When operating with a valve overlap of 130 crankshaft degrees and 2 inches of mercury boost, a brake mean effective pressure of 175 pounds per square inch was obtained with a fuel consumption of 0.50 pound per brake horsepower hour. The specific fuel consumption was the same for the

scavenged condition as for the condition with no scavenging.

In the comparison of the curves for these two compression ratios it should be borne in mind that a constant fuel quantity per cycle does not mean a constant mixture ratio, because the volume of air inducted per cycle depends on the valve overlap and the boost pressure. A charge that is excessively lean may not give as much power as a smaller charge of about the right proportion of fuel and air for maximum power.

Boost pressure.—Figure 8 shows the comparative brake mean effective pressure and fuel consumption obtained when operating at compression ratios of 5.85 and 7.0 with boost pressures varying from 0 to 6 inches of mercury. Increasing the compression ratio from 5.85 to 7.0 resulted in a reduction of fuel consumption of 10 to 13 percent over this range of boost pressures and an increase in power of 8 percent at no boost pressure and 3 percent at 6 inches of mercury boost pressure. It might be well to mention here that the uni-

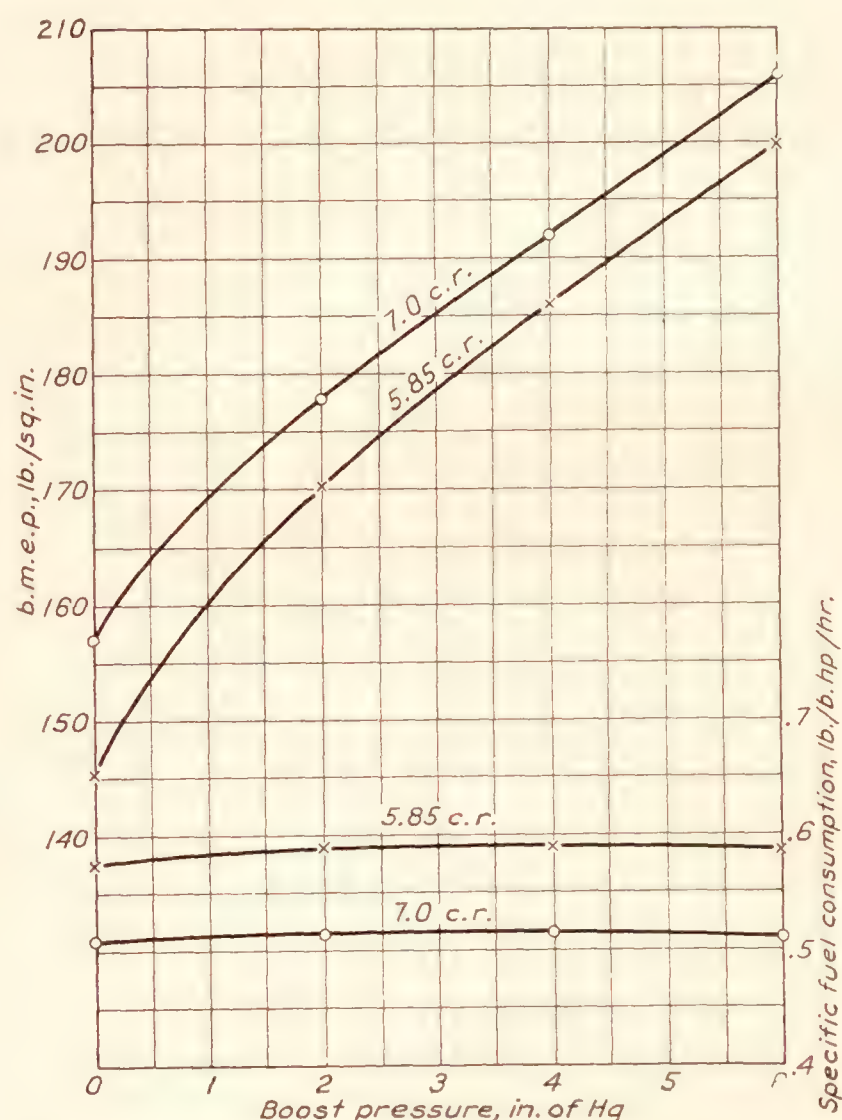


FIGURE 8.—Effect of boost pressure on b.m.e.p. and fuel consumption. Safety fuel; fuel injection; 130° valve overlap; 1,750 r.p.m.

versal test engine, an engine of practically the same design, has been operated with no boost pressure at a compression ratio of 9.0 with this fuel. In the tests with the universal test engine an increase in maximum brake mean effective pressure of 12 pounds per square inch was obtained by increasing the compression ratio from 7.0 to 9.0, even though, to avoid detonation, the

spark was retarded 16 crankshaft degrees from the optimum spark setting at a compression ratio of 7.0.

Speed.—Figure 9 shows the fuel consumption and the power obtained at speeds from 1,250 r.p.m. to 2,200 r.p.m. The maximum brake mean effective pressure on this engine is obtained at speeds from 1,700 to 1,900 r.p.m. and there is very little falling off in the brake mean effective pressure at speeds up to 2,200 r.p.m.

Table I is included for a convenient comparison of the power and economy obtained with gasoline and safety fuel and the friction mean effective pressure at each compression ratio for several speeds with normal valve timing. The values given in this table have been taken for the lowest fuel quantities per cycle at which the maximum brake mean effective pressure is ob-

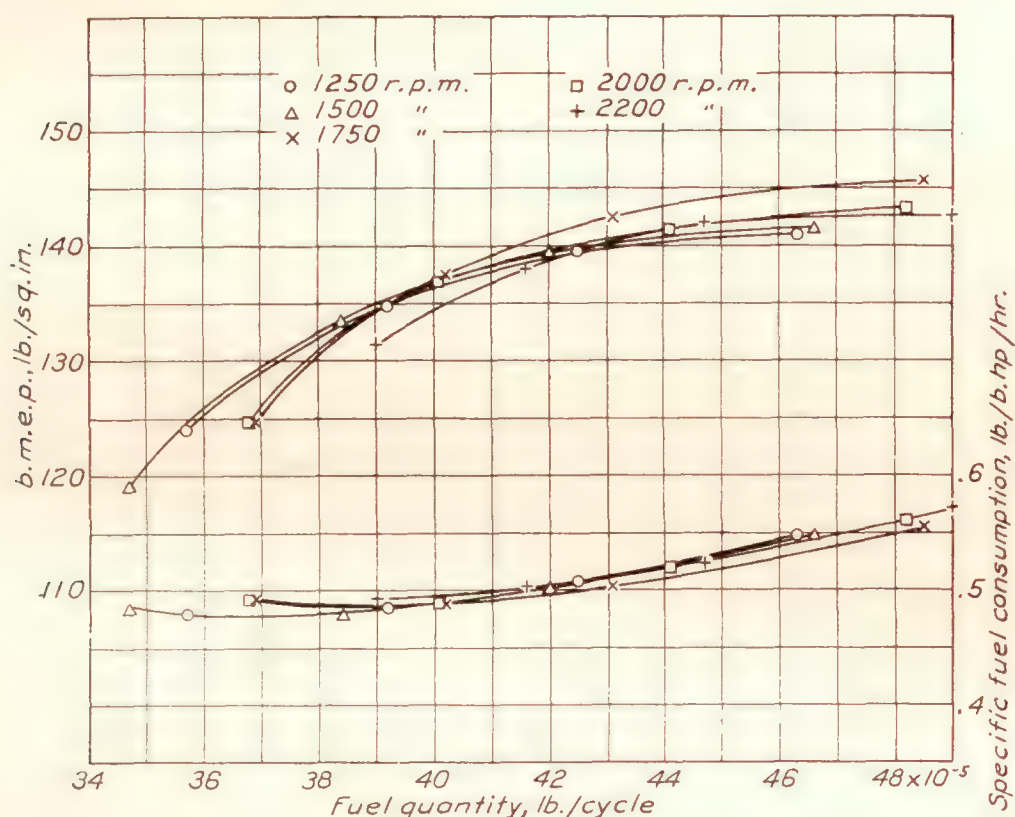


FIGURE 9.—B.m.e.p. and fuel consumption obtained for various engine speeds. 7.0 compression ratio; safety fuel; fuel injection; normal valve timing; no boost pressure.

tained. These tabulated results show that the brake mean effective pressure obtained with safety fuel is equal to that obtained with gasoline and that the fuel consumption obtained with safety fuel is only from 5 to 10 percent higher than that with gasoline. As the calculated lower heating value of the safety fuel of 17,560 B.t.u. per pound is 7 to 8 percent lower than that of gasoline, the thermal efficiency for the two fuels would be practically the same. It is believed that the fuel economy obtained with safety fuel as compared with that obtained with gasoline cannot be appreciably improved.

Coolant temperature.—The tests so far discussed were conducted at coolant temperatures of 150° F. Other tests made at coolant temperatures of 200, 250, and 280° F. showed that no improvement in the brake mean effective pressure or the fuel consumption could be obtained by operating at high coolant temperatures.

Some time ago, when operating the universal test engine with another hydrogenated safety fuel, a large improvement in the economy was obtained by operating at high coolant temperatures (reference 3). In those tests the fuel consumption was high at coolant temperatures of 150° F., whereas in the present tests the fuel consumption was normal. High coolant temperatures apparently result in improved economy where the economy is poor at low temperatures, but increasing the coolant temperatures when the economy is already good results in no improvement. When operating with safety fuel, low coolant temperatures (150° F.) are to be preferred because high coolant temperatures impair the antiknock properties of the safety fuel. From the results obtained on the universal test engine with a different safety fuel it is believed that since this safety fuel can be used at 7.0 compression ratio with coolant temperatures of 250° F., it can be used at a compression ratio of 8.5 with coolant temperatures of 150° F.

IDLING AND STARTING

The idling of the engine with normal valve timing when operating with safety fuel is entirely satisfactory. When operating with a large valve overlap the idling is poor with the usual throttle arrangement, because some of the exhaust gases flow into the intake manifold whenever the engine is throttled. The idling with a large valve overlap will be satisfactory if the throttle is placed close to the inlet valve so as to reduce to a minimum the volume between the throttle valve and the intake valves. The universal test engine operating with a valve overlap of 112° would idle at an engine speed of 150 r.p.m. when the throttle valve was close to the intake valve.

Starting with safety fuel was difficult when the engine was cold; that is, when it had been standing overnight at a temperature of 50°–60° F. It has been started cold when motoring at 700 r.p.m. with a compression ratio of 5.85, but starting under these conditions is not satisfactory. In later tests satisfactory starting was obtained by injecting a small quantity of gasoline into the intake manifold while the engine was being motored at speeds as low as 120 r.p.m. and while safety fuel was being injected into the cylinder. Immediately after the engine was started on gasoline it would continue to run on safety fuel. This method of starting requires only the addition of a small gasoline tank, as the priming system is identical with the present priming system used on aircraft engines. On engines equipped with air starters the fuel might be mixed with the starting air just before it is inducted. Both of these methods would require the use of two fuels, but the supply of gasoline carried for starting would be very small.

The engine could be started on safety fuel if the intake air, the fuel, or both were heated. The curve in figure 10 shows approximately the minimum air temperature at which the engine will start with different fuel temperatures. The engine would start

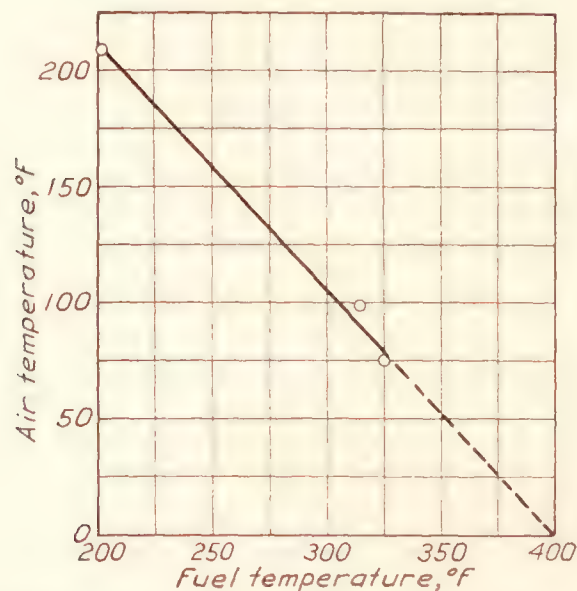


FIGURE 10.—Minimum fuel and air temperatures required for starting at a compression ratio of 7.0 when motored at 350 r.p.m.

consistently at a speed of 350 r.p.m. with air and fuel temperatures as shown in this figure.

THE INJECTION SYSTEM

In these tests the fuel consumption and the brake mean effective pressure were not critically sensitive to the timing of the start of the injection period, the duration of the injection period, the injection pressure, or the valve-opening pressure. The effect of the timing of the start of the injection period on the brake mean effective pressure is shown by the curve in figure 11. With the injection system used in these tests, the best results were obtained when the start of injection was from 70 to 90 crankshaft degrees after top center on the suction stroke.

The curves in figures 12 and 13 show the characteristics of the injection system used. For these tests the pump setting gave a fuel quantity of approximately 0.00058 pound per cycle at an engine speed of 1,750 r.p.m. It will be noted from figure 7 that this is the fuel quantity giving maximum power with a compression ratio of 7.0 and 2 inches of mercury boost pressure. Although the rate of injection shown in figure 12 gave the best performance of the several rates tried, it is believed that some deviation from these rates will not appreciably impair the performance. The length of the injection period increased from 74 to 93 crankshaft degrees with an increase in pump speed from 750 to 1,100 r.p.m. In other tests on the same engine with the injection period varying from 150 to 200 crankshaft degrees the fuel consumption was higher and the power lower. An injection period of approximately 30 crankshaft degrees has

been tried on the universal test engine. The results of all these tests indicated that better economy and power could be obtained when the length of the injection period was from approximately 60 to 90 crankshaft degrees.

All data submitted in this report were obtained with a commercial fuel pump, an injection-valve opening pressure of 2,000 pounds per square inch, and injection pressures as shown in figure 13. A few tests, however, have been conducted with other fuel pumps and with gasoline as a fuel. In some of these tests a valve-opening pressure of 800 pounds per square inch and an injection pressure of 1,200 pounds per square inch were used. The results obtained with these low injection pressures were, for practically all conditions, equal to those obtained with high injection pressures. It is believed that an injection system operating with injection pressures as low as 500 pounds per square inch or lower would be satisfactory.

MECHANICAL CONSIDERATIONS

The use of a large valve overlap requires a consideration of several mechanical problems. The overlap must be sufficiently large to give the desired scavenging at sea level with a pressure difference across the valves of from 2 to 5 inches of mercury, but not so large that an appreciable amount of the air is wasted at moderate or high altitudes, when the pressure difference across the valves may be 10 to 15 inches of mercury. The

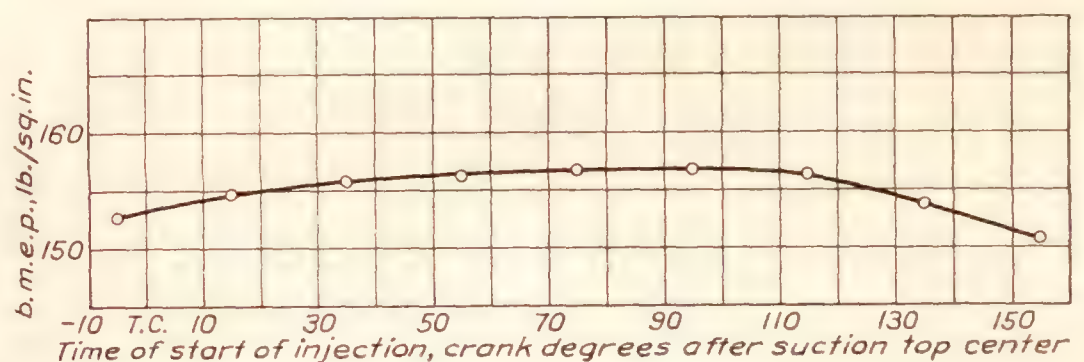


FIGURE 11.—Effect of start of injection period on b.m.e.p.

pressure difference across the valves on a supercharged engine increases with the altitude of operation because the pressure at the intake is usually kept constant up to some definite altitude, whereas the atmospheric pressure at the exhaust decreases with altitude. Under these conditions the importance of scavenging the clearance volume decreases with altitude. For instance, the gain obtained by scavenging the clearance volume of an engine at 18,000 feet is only 50 percent of that obtained at sea level because the reduced exhaust pressure permits more of the exhaust gas to escape.

Exhaust back pressure.—A few tests were made to determine the effect of reduced exhaust back pressures on the volumetric efficiency and the power when operating with a large valve overlap. The results of these tests showed that the air supplied to an engine oper-

ating with a valve overlap of 130 crankshaft degrees corresponds to volumetric efficiencies of 110, 117, and 122 percent at engine speeds of 2,200, 1,800, and

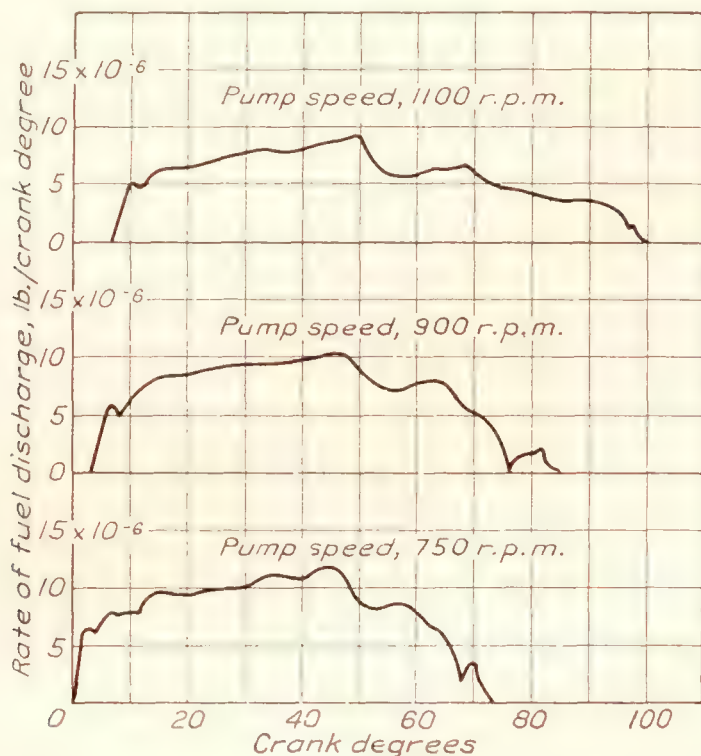


FIGURE 12.—Effect of pump speed on the length of the injection period and the rate of discharge. 12-millimeter plunger diameter; 0.125-inch tube diameter; 32-inch tube length; 2,000 pounds per square inch valve-opening pressure.

1,500 r.p.m., respectively, when operating with atmospheric pressure at the intake and a pressure 8 inches of mercury less than atmospheric at the exhaust. For these conditions the volumetric efficiency increased at

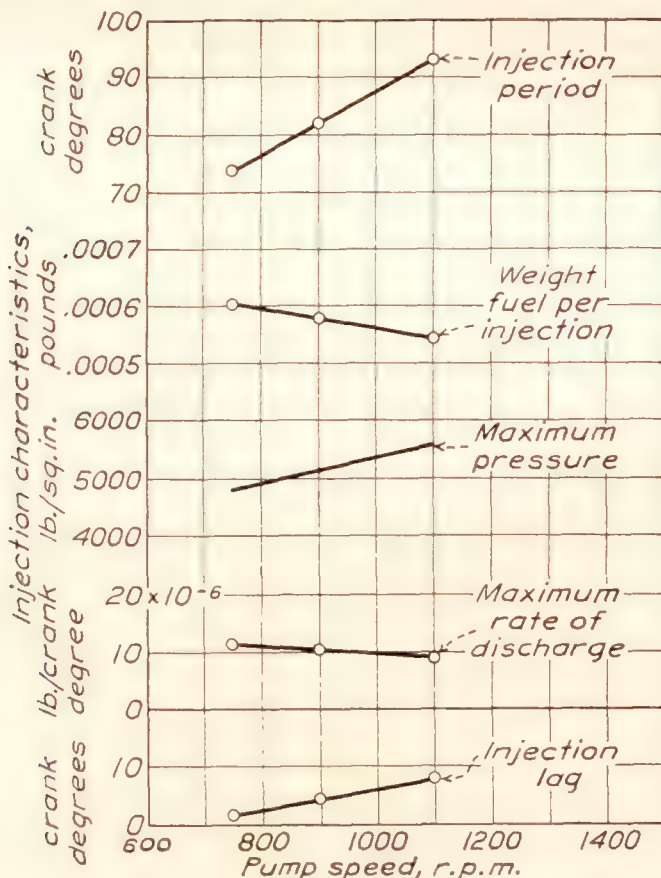


FIGURE 13.—Effect of pump speed on injection characteristics. 12-millimeter plunger diameter; 0.125-inch tube diameter; 32-inch tube length; 2,000 pounds per square inch valve-opening pressure.

a greater rate than the power, indicating that a large amount of the fresh air escaped during the scavenging process. With the exhaust pressure from 3 to 5 inches of mercury lower than the intake, the increase in volumetric efficiency was practically equal to the

increase in power, indicating that very little of the fresh air was wasted.

Some tests were also made to determine the effect of exhaust back pressure of $3\frac{1}{2}$ inches of mercury on the maximum brake mean effective pressure when operating with a valve overlap of 130 crankshaft degrees and intake pressures varying from 0 to 10 inches of mercury boost. The results of these tests are shown in figure 14. Note that when the intake pressure is 7 inches of mercury and the exhaust pressure is increased from 0 to $3\frac{1}{2}$ inches of mercury the power decreases 4 percent as compared to 20 percent when the

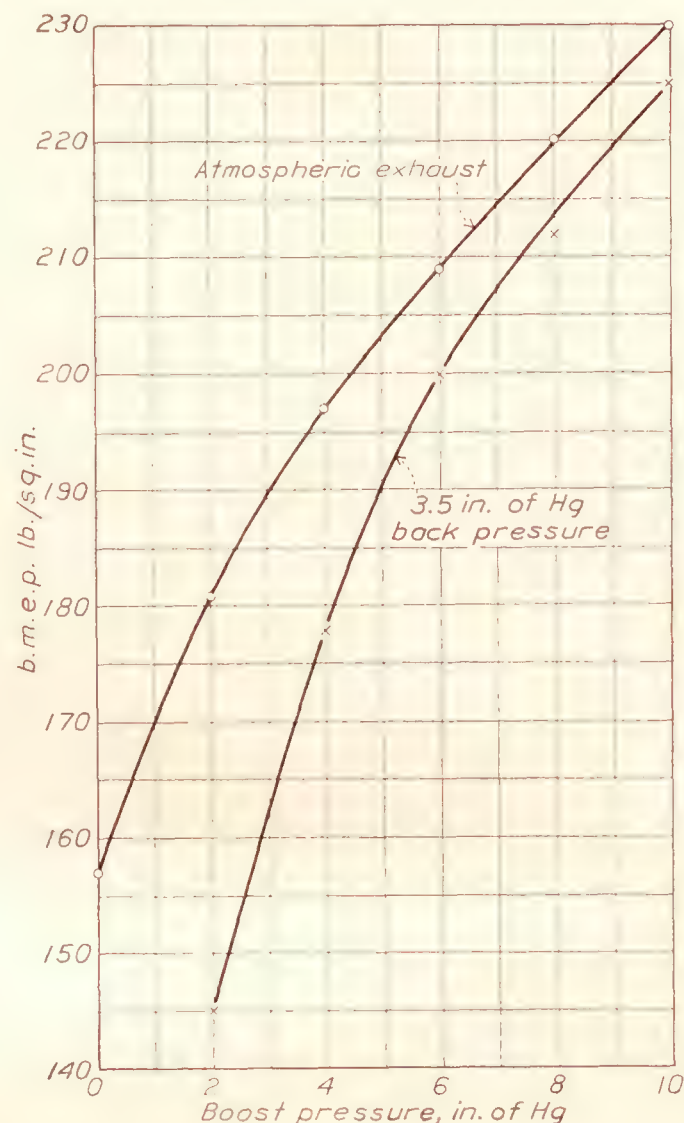


FIGURE 14.—Effect of $3\frac{1}{2}$ inches of mercury exhaust back pressure on the power with the boost pressure varying from 0 to 10 inches of mercury. 1,750 r.p.m.; 7.0 compression ratio; safety fuel.

intake pressure is 2 inches. It is very important that the intake pressure be greater than the exhaust pressure when operating with a valve overlap. If the exhaust back pressure is higher than the inlet pressure the gas flow may be reversed during part of the cycle, and exhaust gas may fill part of the displacement volume and induction pipes.

Air and fuel control.—When applying fuel injection to a spark-ignition engine for aircraft service the air throttle and fuel-quantity control should be interconnected so that the engine will receive air and fuel in the proper proportions over the entire range of loads and speeds. This problem may require the working out of a complicated linkage, particularly if an accurate proportioning of fuel and air is attempted.

Spark setting.—The maximum cylinder pressures were determined for the most severe operating condition tried and are plotted in figure 15. With the spark at 30° before top center, the setting for maximum power, the maximum pressure recorded was 890 pounds per square inch. This pressure could be reduced to 800 pounds per square inch by setting the spark for 22° before top center—a reduction of 10

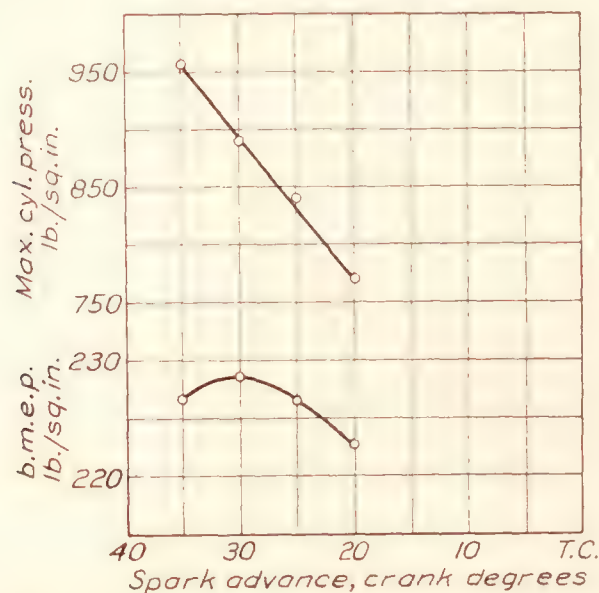


FIGURE 15.—Effect of spark advance on b.m.e.p. and maximum cylinder pressure: 1,750 r.p.m.; 7.0 compression ratio; safety fuel; 10 inches of Hg boost pressure; 3.5 inches of Hg back pressure.

percent in maximum cylinder pressure with a sacrifice of 2½ percent in brake mean effective pressure.

CONCLUSIONS

1. The hydrogenated safety fuel manufactured primarily to eliminate fire hazard in aircraft gives a maximum brake mean effective pressure equal to that with gasoline when using the fuel-injection system, and the fuel consumption is from 5 to 10 percent higher.
2. The high antiknock value of the hydrogenated safety fuel permits a higher compression ratio to be

used than can be used with most gasolines without the addition of fuel dope, thus improving both the power and the economy.

3. At present the hydrogenated safety fuel can be used to best advantage by employing fuel injection, and the use of fuel injection makes scavenging by the use of large valve overlap and moderate supercharging feasible.

4. The results of the test with 130 crankshaft degrees overlap show that so long as the pressure difference between the intake and the exhaust is not greater than 5 inches of mercury practically no air is wasted in the scavenging process.

5. Additional measures must be taken to insure starting when using safety fuel. Priming with gasoline is a simple and practical way of solving this problem.

LANGLEY MEMORIAL AERONAUTICAL LABORATORY,
NATIONAL ADVISORY COMMITTEE FOR AERONAUTICS,
LANGLEY FIELD, VA., June 13, 1933.

REFERENCES

1. Sabatier, J.: Fire Prevention on Airplanes. Parts I and II. T. M. Nos. 536 and 537, N.A.C.A., 1929.
2. Haslam, R. T., and Russell, R. P.: Hydrogenation of Petroleum. Indus. Eng. Chem., vol. XXII, pp. 1030–1050, October 1930.
3. Schey, Oscar W., and Young, Alfred W.: Engine Performance with a Hydrogenated Safety Fuel. T.N. No. 466, N.A.C.A. 1933.
4. Schey, Oscar W., and Young, Alfred W.: The Use of Large Valve Overlap in Scavenging a Supercharged Spark-Ignition Engine Using Fuel Injection. T.N. No. 406, N.A.C.A., 1932.
5. Gelalles, A. G., and Marsh, E. T.: Rates of Fuel Discharge as Affected by the Design of Fuel-Injection Systems for Internal-Combustion Engines. T.R. No. 433, N.A.C.A., 1932.

TABLE I
ENGINE PERFORMANCE WITH GASOLINE AND HYDROGENATED SAFETY FUEL

(Best Setting for Maximum Power; Normal Valve Timing; No Boost)

Engine speed, r.p.m.	5.85 compression ratio							7.0 compression ratio				
	Carburetor with gasoline		Fuel injection				f.m.e.p., lb./sq. in.	Fuel injection				f.m.e.p., lb./sq. in.
			Gasoline		Safety fuel			Gasoline		Safety fuel		
	b.m.e.p., lb./sq. in.	s.f.c., lb./b.hp./hr.	b.m.e.p., lb./sq. in.	s.f.c., lb./b.hp./hr.	b.m.e.p., lb./sq. in.	s.f.c., lb./b.hp./hr.		b.m.e.p., lb./sq. in.	s.f.c., lb./b.hp./hr.	b.m.e.p., lb./sq. in.	s.f.c., lb./b.hp./hr.	
1, 250	128	0. 485	130	0. 550	131	0. 575	17. 8	139	0. 485	140. 5	0. 535	18. 1
1, 500	129	. 490	132	. 550	131	. 570	21. 7	141	. 500	141. 5	. 535	22. 4
1, 750	129	. 515	133	. 530	{ 135	. 595	25. 4	142. 5	. 510	145. 5	. 540	26. 5
					{ 132. 5	. 550						
2, 000	129	. 490	132	. 530	132	. 560	28. 9	141	. 525	143. 0	. 550	32. 4
2, 200	127	. 490	132	. 530	-----		33. 9	139	. 520	142. 5	. 550	37. 4

¹ 2 percent less than maximum power.

REPORT No. 472

WIND-TUNNEL TESTS ON COMBINATIONS OF A WING WITH FIXED AUXILIARY AIRFOILS HAVING VARIOUS CHORDS AND PROFILES

BY FRED E. WEICK and ROBERT SANDERS

SUMMARY

Various auxiliary airfoils having three different airfoil sections and several different chord lengths were tested in combination with a Clark Y model wing in a sufficient number of relative positions to determine the optimum with regard to certain criterions of aerodynamic performance. The airfoil sections included a symmetrical profile, one of medium camber, and a highly cambered one. The chord sizes of the auxiliary airfoils ranged from 7.5 to 25 percent of the chord of the main wing, and the span was equal to that of the main wing. The tests were made in the N.A.C.A. 5-foot vertical wind tunnel.

It was found that each of the auxiliary airfoil combinations tested, regardless of size or airfoil section, had, when located at its best position, substantially higher values of the maximum lift coefficient and of the ratio C_{Lmax}^2/C_{Dmin} than the main wing alone. The maximum values of the lift coefficient obtained, based on the total area, were very nearly the same with all the auxiliary airfoils tested. The symmetrical airfoils gave lower values of the minimum drag coefficient and higher values of the ratio C_{Lmax}^2/C_{Dmin} than the cambered auxiliary airfoils. The highest value of the ratio C_{Lmax}^2/C_{Dmin} was obtained with the symmetrical auxiliary having a chord length 14.5 percent of the main wing chord. The positions giving the highest values of this ratio did not vary greatly for the different auxiliary airfoils tested, except for the narrowest ones, which gave higher values in lower positions.

Additional tests, in which the auxiliary airfoils were supported separately, were made to determine the division of air load between the auxiliary and the main wing for two representative cases. The results showed that the auxiliary airfoil took a relatively large proportion of the total load, particularly in the case of the highly cambered auxiliary at low angles of attack.

INTRODUCTION

In a previous investigation (reference 1) it was found that with an auxiliary airfoil fixed in a certain position ahead of the main wing the combination had a sub-

stantially higher value of the maximum lift coefficient (based on total area) and of the speed-range criterion, C_{Lmax}/C_{Dmin} , than either of the airfoils alone. These earlier tests were made with a single form of auxiliary airfoil now referred to as the N.A.C.A. 22. The chord was 14.5 percent of the main wing chord, and the profile was highly cambered and of medium thickness. This auxiliary airfoil was tested in a large number of positions near the front of the main wing in order to find the best location.

The tests described in the present report continue the investigation of fixed auxiliary airfoils to include the effect of variations in size and in airfoil section. Four sizes were tested having the original N.A.C.A. 22 section, four having a symmetrical section (N.A.C.A. 0012), and one having the Clark Y section. The lift and drag of the combinations were measured with each of the auxiliary airfoils in a sufficient number of positions ahead of the main wing to determine the optimum location. Pitching moments were then measured with each auxiliary airfoil in one or two of the best positions. Finally, the air force on the auxiliary airfoil was found for two representative combinations.

APPARATUS AND METHODS

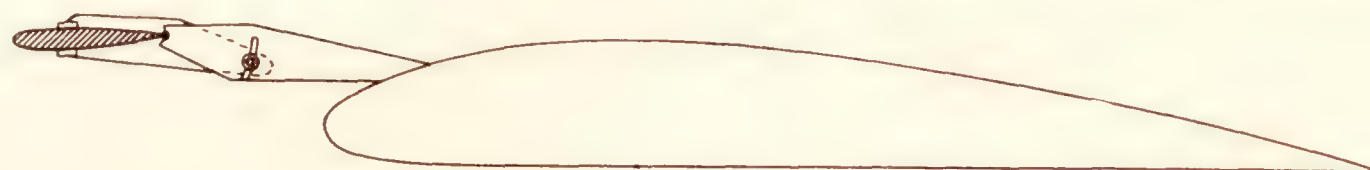
Wind tunnel.—The tests were made in the 5-foot vertical wind tunnel under essentially the same conditions as those of the original portion of the investigation (reference 1). The wind tunnel is described in detail in reference 2. A "reflection plane" and half-span model were used to permit as high a Reynolds Number as possible.

Models.—The main wing was a rectangular Clark Y airfoil, constructed of mahogany, with a 10-inch chord and a 30-inch semispan. The auxiliary airfoils, whose semispans were also 30 inches, were constructed of aluminum alloy. The chords of the auxiliary airfoils were varied until the tests indicated that the optimum range had been covered. The original highly cambered section (N.A.C.A. 22) was tested with chords of 7.5, 11, 14.5 (check on original in optimum position only), and 25 percent of the main

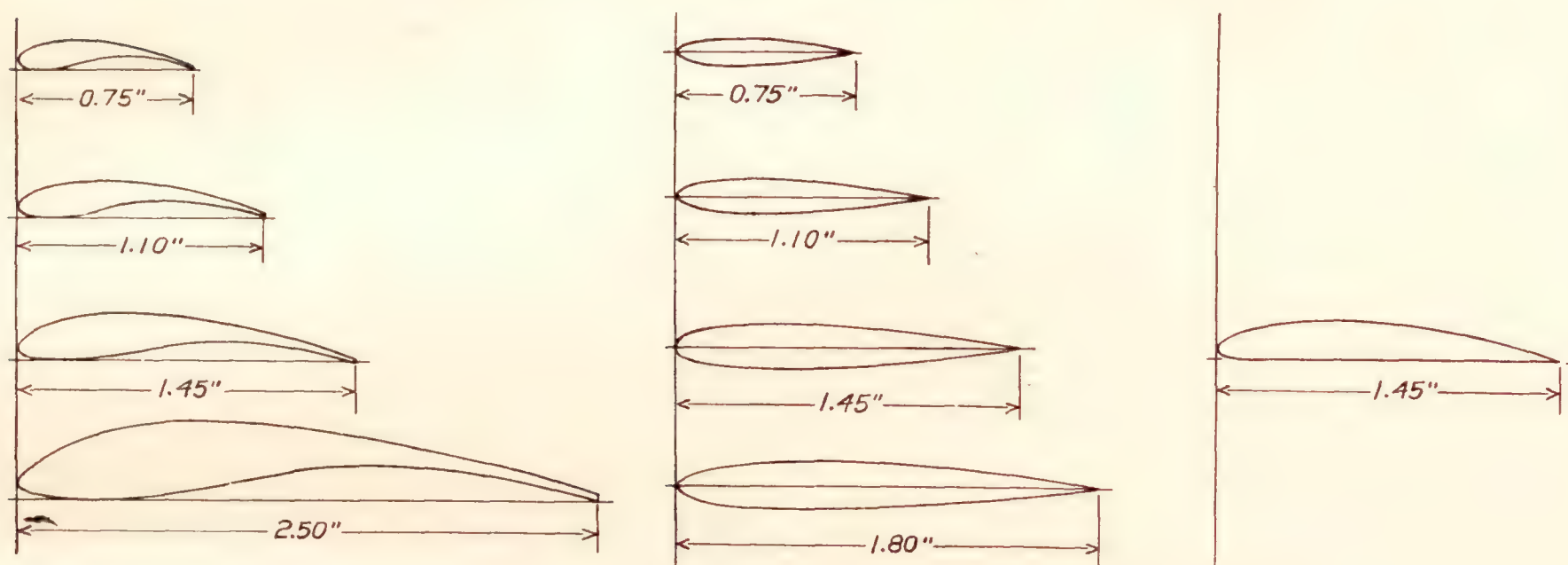
wing chord. The symmetrical section, which was the next tested, was the N.A.C.A. 0012. This section was tested with chords of 7.5, 11, 14.5, and 18 percent of the main wing chord, the 25 percent size having been indicated as definitely too large by the tests with the original N.A.C.A. 22 section. The Clark Y section was tested with the 14.5 percent chord only.

independently of the main wing. The air force on the main wing was measured in the presence of the auxiliary and subtracted from the total force to give the force on the auxiliary alone.

Tests.—The lift and drag over a range of angles of attack were measured with each of the auxiliary airfoils in a sufficient number of positions with respect



Main wing with 14.5 percent symmetrical auxiliary airfoil



ORDINATES OF AUXILIARIES

N.A.C.A. 22		
Stations, percent chord	Upper, percent chord	Lower, percent chord
0	2.88	2.88
1.25	5.40	1.09
2.5	6.48	.65
5	8.02	.28
7.5	9.11	.08
10	9.96	.00
15	11.34	.12
20	12.29	.44
30	13.35	1.46
40	13.42	3.08
50	12.60	4.78
60	11.12	5.63
70	9.15	5.79
80	6.68	4.68
90	3.95	2.67
95	2.51	1.32
100	1.13	0.00
L. E. Radius=2.00		

N.A.C.A. 0012		
Stations, percent chord	Upper, percent chord	Lower, percent chord
0	0.00	0.00
1.25	1.89	1.89
2.5	2.62	2.62
5	3.56	3.56
7.5	4.20	4.20
10	4.68	4.68
15	5.35	5.35
20	5.74	5.74
30	6.00	6.00
40	5.80	5.80
50	5.29	5.29
60	4.56	4.56
70	3.66	3.66
80	2.62	2.62
90	1.45	1.45
95	.81	.81
100	.13	.13
L. E. Radius=1.58		

CLARK Y		
Stations, percent chord	Upper, percent chord	Lower, percent chord
0	3.50	3.50
1.25	5.45	1.93
2.5	6.50	1.47
5	7.90	.93
7.5	8.85	.63
10	9.60	.42
15	10.69	.15
20	11.36	.03
30	11.70	0
40	11.40	0
50	10.52	0
60	9.15	0
70	7.35	0
80	5.22	0
90	2.80	0
95	1.49	0
100	.12	0
L. E. Radius=1.50		

FIGURE 1.—Sections of auxiliary airfoils tested.

All three sections have approximately the same thickness and form except for the camber, which varies through a large range. The cross-sectional views of the various auxiliary airfoils are shown together with a table of ordinates in figure 1. The auxiliary airfoils were supported at each end and at two intermediate positions by metal fittings, as shown in figure 2.

For obtaining the force on the auxiliary airfoil separately, fixtures were made to support the auxiliary

to the main wing to determine the optimum location according to the criterion C_{Lmax}^2/C_{Dmin} , which was used in reference 1. The variations in position were made in the following manner. The angle δ between the chord line of the auxiliary and that of the main wing was changed about an axis through the trailing edge of the auxiliary until the angle giving the highest value of the ratio C_{Lmax}^2/C_{Dmin} was determined. This procedure was repeated for various trailing-edge

locations until closed contour charts of the maximum value of the ratio C_{Lmax}^2/C_{Dmin} obtained at each trailing-edge location could be drawn, showing that the position giving the highest value had been determined.

The 14.5 percent N.A.C.A. 22 auxiliary airfoil, which was the one tested in various positions in reference 1, was retested only at the best position, as a check. The results are slightly different from those of the previous tests, which is partly due to a change of the fittings supporting the auxiliary airfoil and partly to the normal experimental error. The new fittings, designed to increase the rigidity of the set-up, caused an interference effect resulting in a reduction of the maximum lift coefficient of about 3 percent (reference 3).

The pitching moments, which were obtained with a slight change in the balance arrangement, were measured for the best positions of each auxiliary airfoil.

The tests to determine the distribution of load between the auxiliary airfoil and the main wing were made with two representative auxiliary airfoils. One had the highly cambered N.A.C.A. 22 section and the other the symmetrical N.A.C.A. 0012 section, both being 14.5 percent of the main wing chord. Each of the auxiliary airfoils was tested at two different settings of the angle δ . The values of the air loads on the auxiliary airfoils must be considered as approximate, for they were obtained as the difference between two relatively large forces and the accuracy was therefore not high.

RESULTS AND DISCUSSION

The results of the simple lift and drag tests are given in tables I to IX in terms of several critical values, or criteria, of the aerodynamic characteristics. The lift and drag coefficients are based on the area of the main wing plus that of the auxiliary, and for this reason the various combinations must be compared as complete units.

CONTOURS OF PERFORMANCE CRITERIONS

The variations of four of the criteria with changes in the locations of the various auxiliary airfoils are shown by means of contour charts which serve as convenient aids to the selection of the optimum locations (figs. 3 to 10). The values on the contour charts are those obtained with the auxiliary airfoil set at the angles giving the highest value of C_{Lmax}^2/C_{Dmin} for each trailing-edge location; where two angles gave the same value within the experimental error, the choice was based on the other criteria. The values for the different angles are given in tables I to IX. The four sets of contours shown on each of the figures are for the following criteria:

a. C_{Lmax}^2/C_{Dmin} , which is the main criterion in selecting the optimum position. This is an arbitrary

criterion which gives equal weight to the maximum lift coefficient and the speed-range ratio C_{Lmax}/C_{Dmin} .

b. C_{Lmax} .

c. L/D at $C_L = 0.7$, which is used as a criterion of the effectiveness in climbing flight.

d. L/D at C_{Lmax} , which gives an indication of the steepest gliding angle obtainable in unstalled flight. An examination of the contour charts shows that no single auxiliary airfoil had the best characteristics on the basis of all the criteria. The variation of the characteristics with size, profile, and location of the

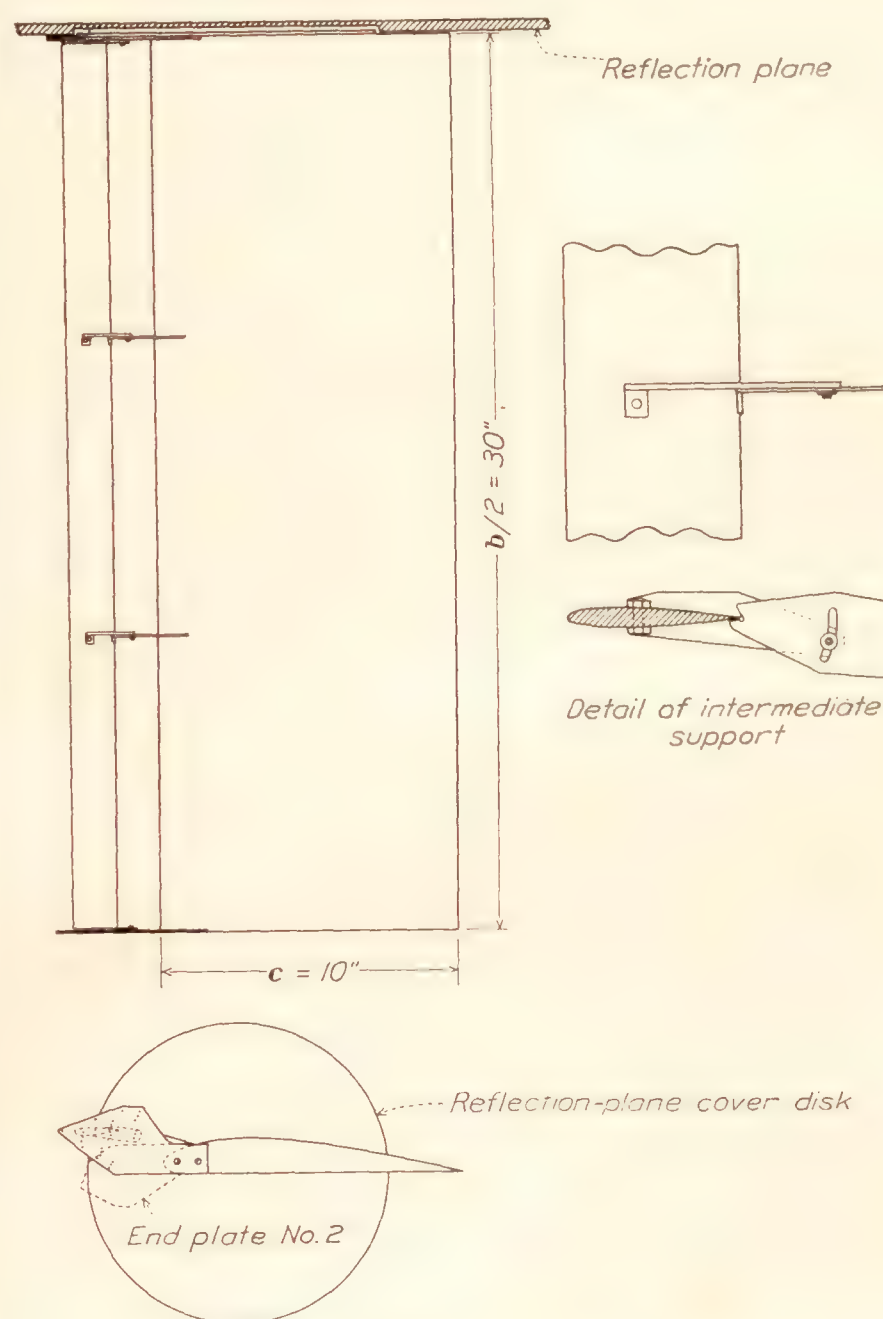
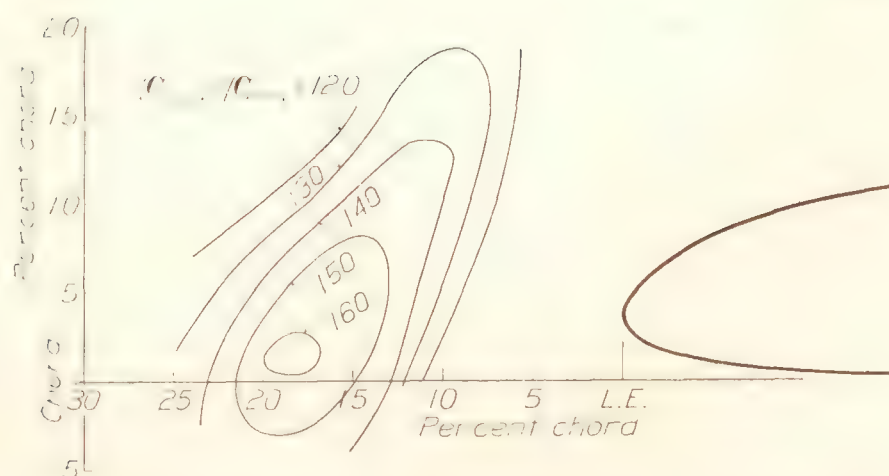


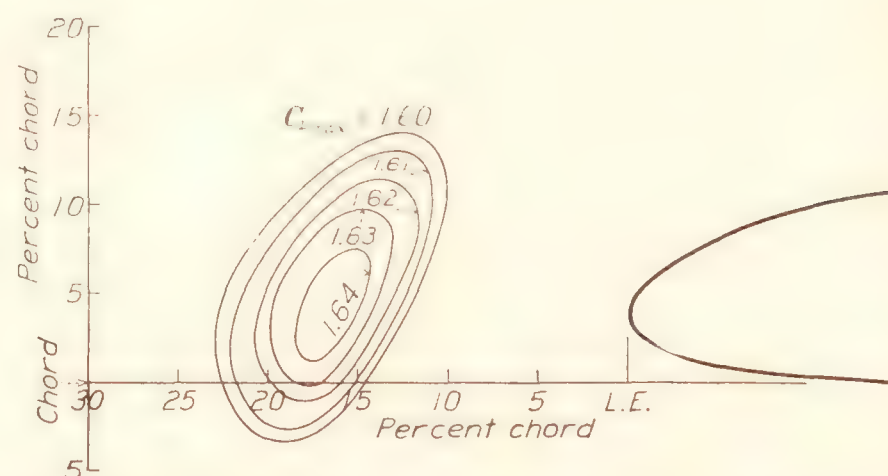
FIGURE 2.—Method of supporting auxiliary airfoils.

auxiliary is complex and requires that the data be studied in detail in order to select the best auxiliary airfoil to fulfill the requirements of any particular set of operating conditions.

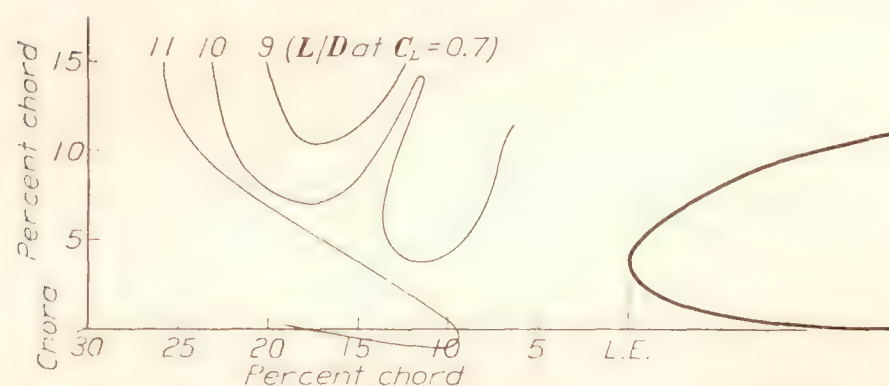
Effect of location.—In general, the location giving the highest value of the ratio C_{Lmax}^2/C_{Dmin} for any of the auxiliary airfoils was not greatly different from that giving the highest value of C_{Lmax} , being in most cases slightly lower and farther forward. The positions giving the highest values of C_{Lmax}^2/C_{Dmin} did not vary greatly with airfoil section or with size of auxiliary, except for the smallest size, which required a lower position for both the airfoil sections tested. In fact, for each size



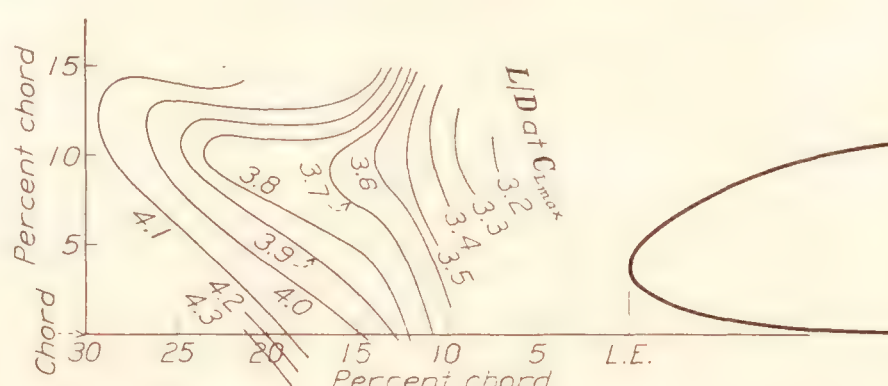
Loci of trailing-edge positions for equal values of $C_{L_{max}}^2/C_{D_{min}}$ obtained with a 7.5 percent c N.A.C.A. 22 auxiliary airfoil set at the optimum angle for each position.



Loci of trailing-edge positions for equal values of $C_{L_{max}}$ obtained with a 7.5 percent c N.A.C.A. 22 auxiliary airfoil set at the optimum angle for each position.

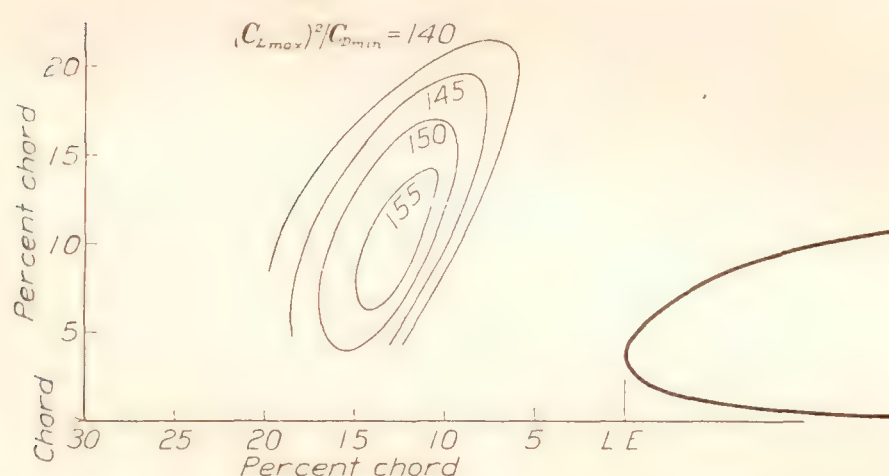


Loci of trailing-edge positions for equal values of L/D at $C_L=0.7$ obtained with a 7.5 percent c N.A.C.A. 22 auxiliary airfoil set at the optimum angle for each position.

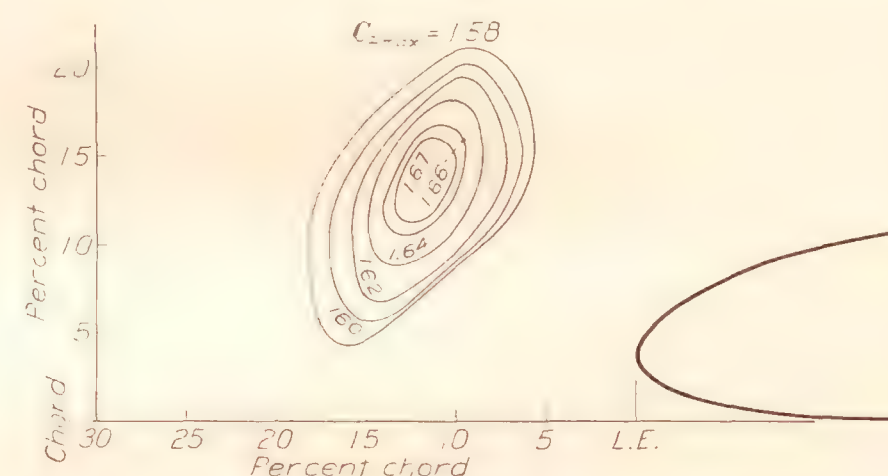


Loci of trailing-edge positions for equal values of L/D at $C_{L_{max}}$ obtained with a 7.5 percent c N.A.C.A. 22 auxiliary airfoil set at the optimum angle for each position.

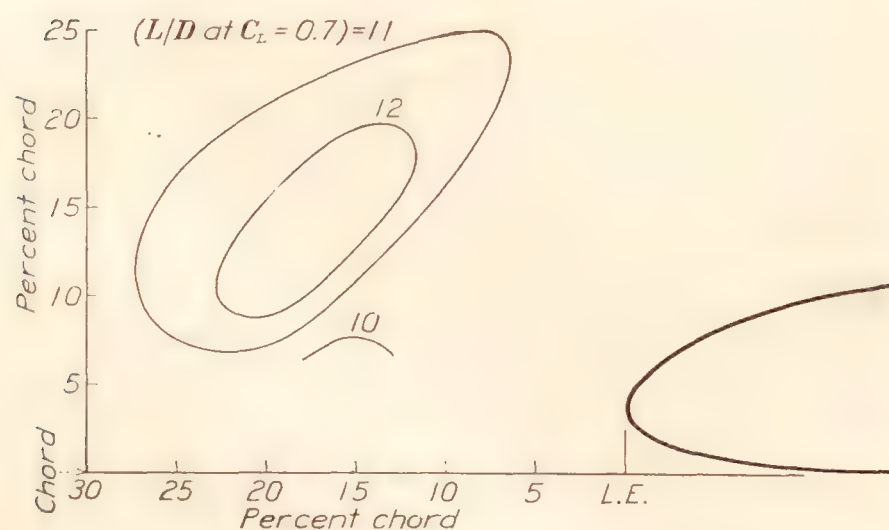
FIGURE 3.



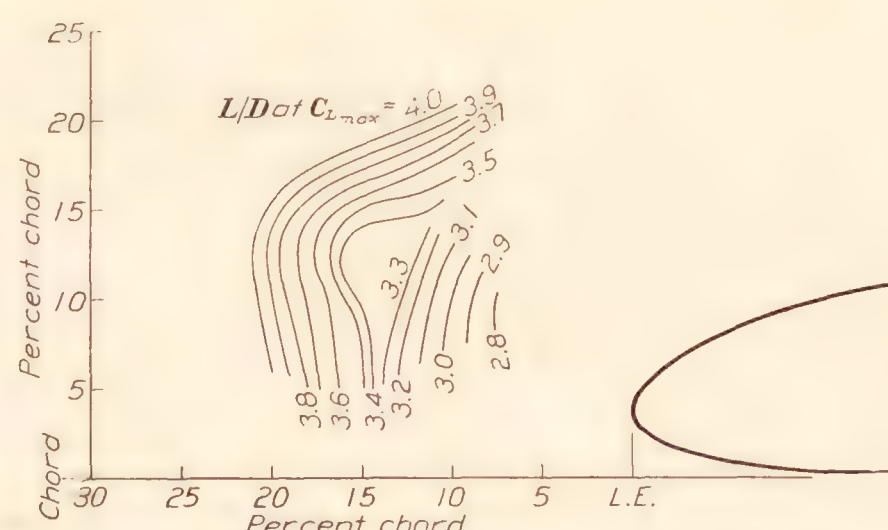
Loci of trailing-edge positions for equal values of $C_{L_{max}}^2/C_{D_{min}}$ obtained with an 11.0 percent c N.A.C.A. 22 auxiliary airfoil set at the optimum angle for each position.



Loci of trailing-edge positions for equal values of $C_{L_{max}}$ obtained with an 11.0 percent c N.A.C.A. auxiliary airfoil set at the optimum angle for each position.

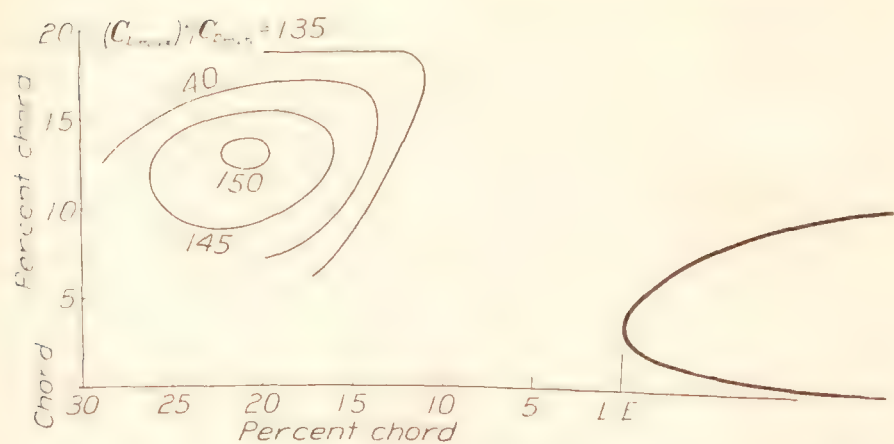


Loci of trailing-edge positions for equal values of L/D at $C_L=0.7$ obtained with an 11.0 percent c N.A.C.A. 22 auxiliary airfoil set at the optimum angle for each position.

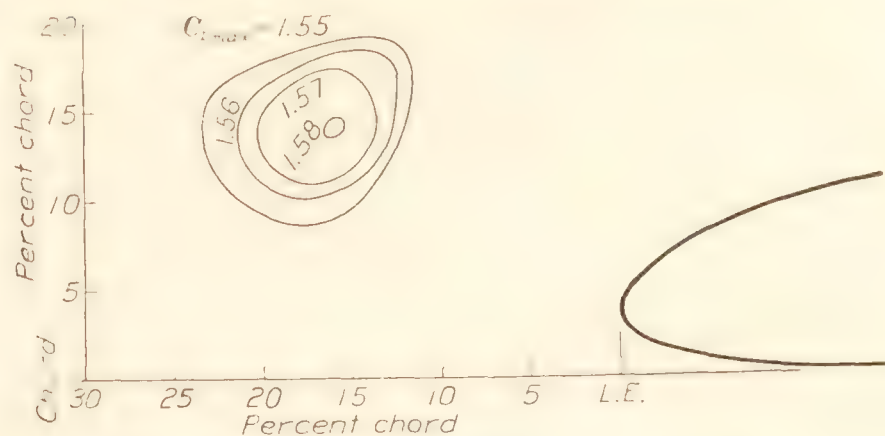


Loci of trailing-edge positions for equal values of L/D at $C_{L_{max}}$ obtained with an 11.0 percent c N.A.C.A. 22 auxiliary airfoil set at the optimum angle for each position.

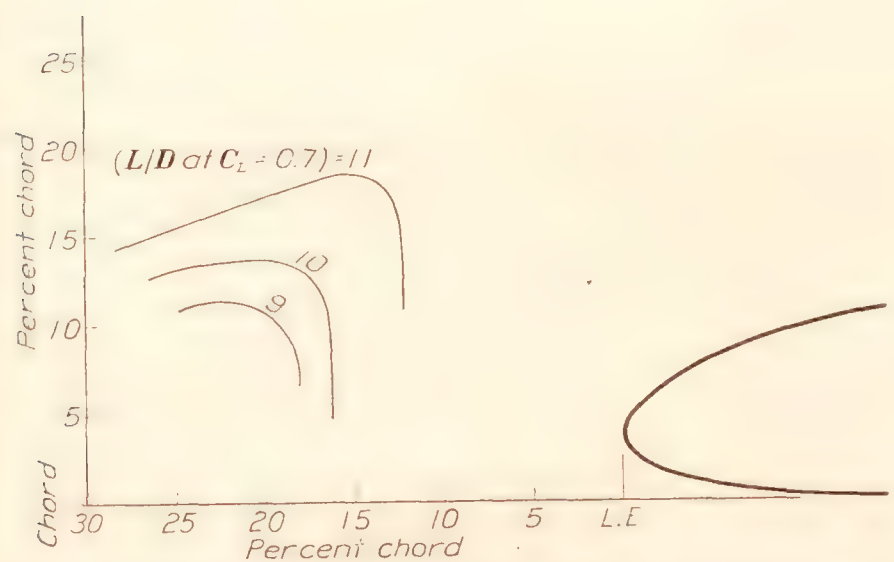
FIGURE 4.



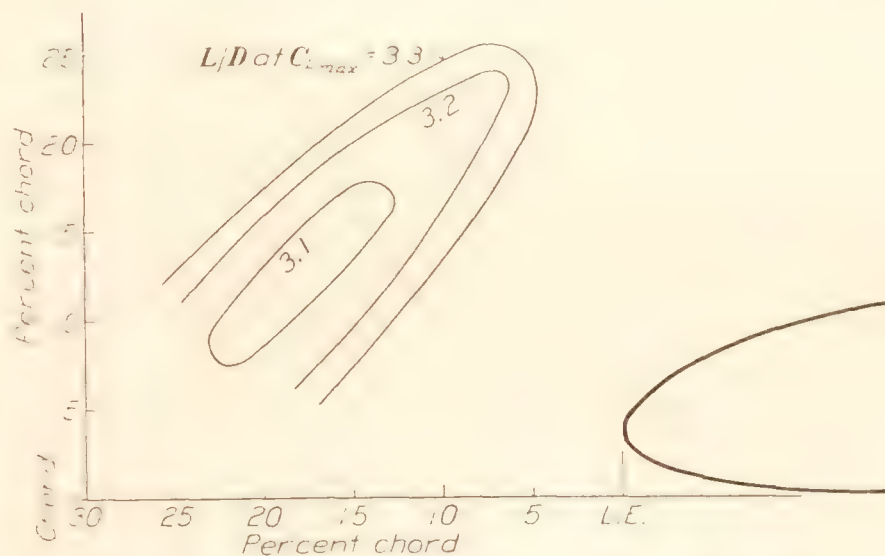
Loci of trailing-edge positions for equal values of C_{Lmax}^2/C_{Dmin} obtained with a 25.0 percent *c* N.A.C.A. 22 auxiliary airfoil set at the optimum angle for each position.



Loci of trailing-edge positions for equal values of C_{Lmax} obtained with a 25.0 percent *c* N.A.C.A. 22 auxiliary airfoil set at the optimum angle for each position.

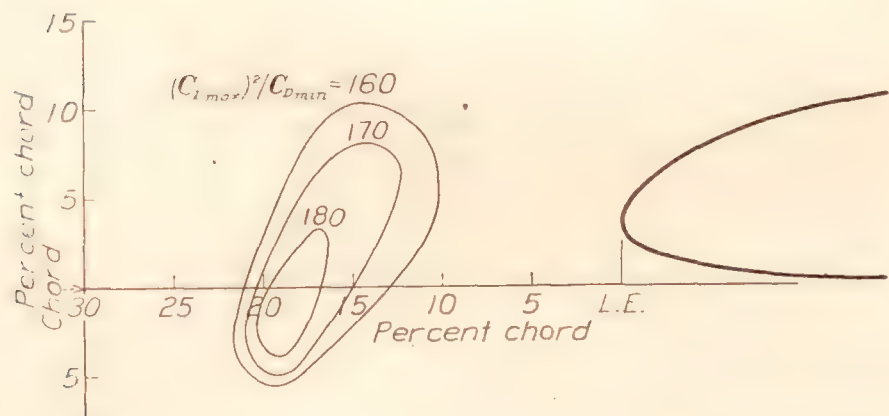


Loci of trailing-edge positions for equal values of L/D at $C_L=0.7$ obtained with a 25.0 percent *c* N.A.C.A. 22 auxiliary airfoil set at the optimum angle for each position.

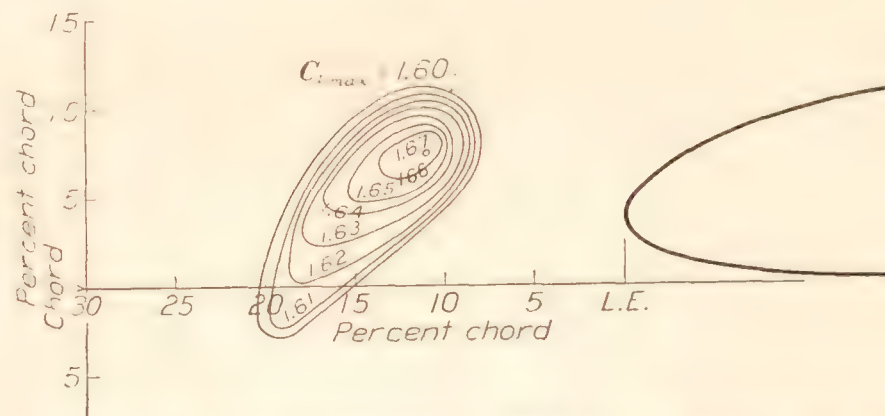


Loci of trailing-edge positions for equal values of L/D at C_{Lmax} obtained with a 25.0 percent *c* N.A.C.A. 22 auxiliary airfoil set at the optimum angle for each position.

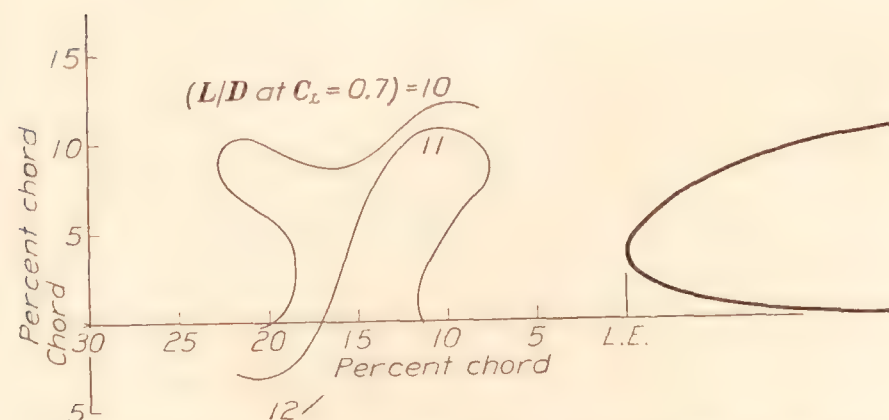
FIGURE 5.



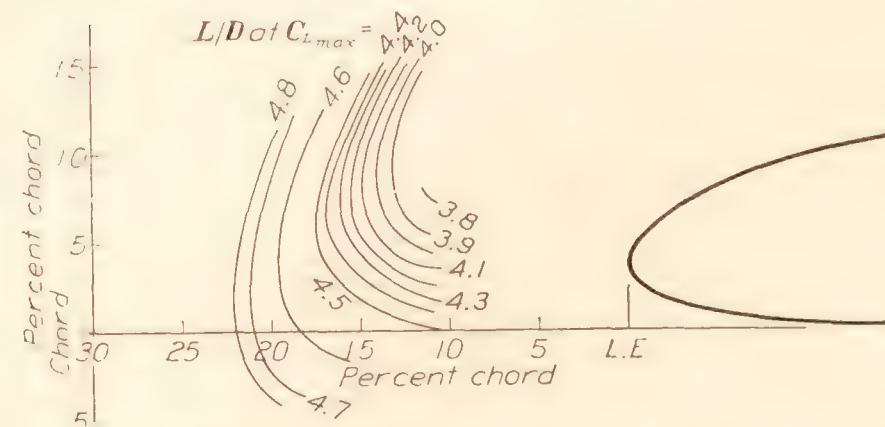
Loci of trailing-edge positions for equal values of C_{Lmax}^2/C_{Dmin} obtained with a 7.5 percent *c* N.A.C.A. 0012 auxiliary airfoil set at the optimum angle for each position.



Loci of trailing-edge positions for equal values of C_{Lmax} obtained with a 7.5 percent *c* N.A.C.A. 0012 auxiliary airfoil set at the optimum angle for each position.

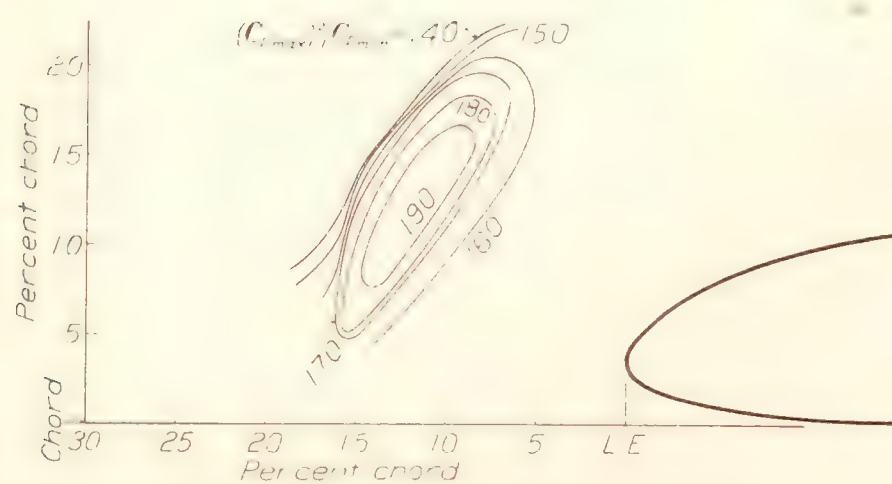


Loci of trailing-edge positions for equal values of L/D at $C_L=0.7$ obtained with a 7.5 percent *c* N.A.C.A. 0012 auxiliary airfoil set at the optimum angle for each position.

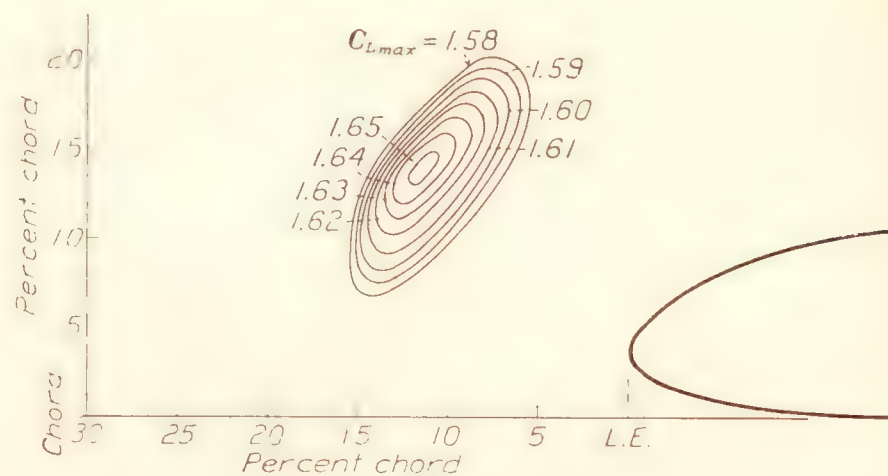


Loci of trailing-edge positions for equal values of L/D at C_{Lmax} obtained with a 7.5 percent *c* N.A.C.A. 0012 auxiliary airfoil set at the optimum angle for each position.

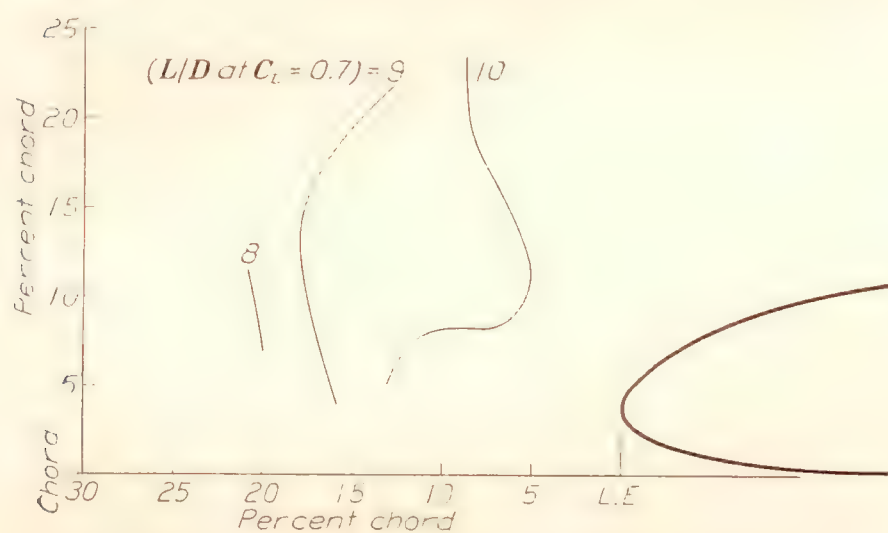
FIGURE 6.



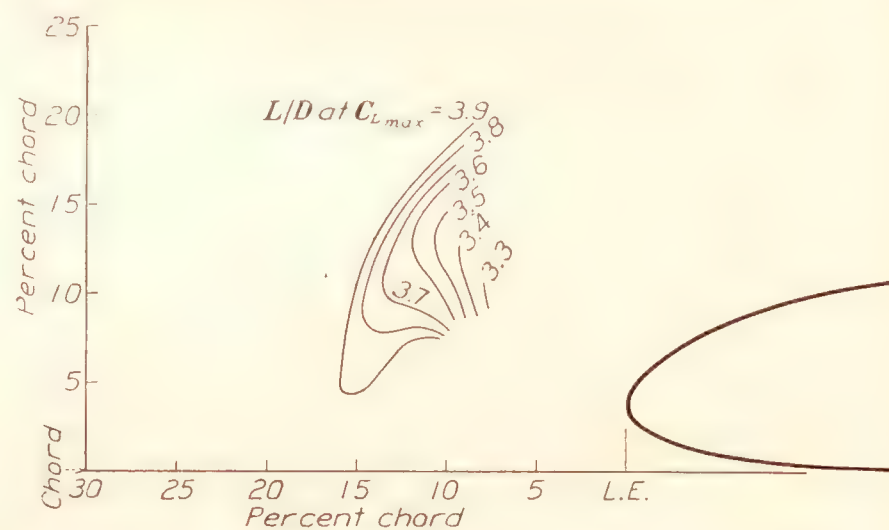
Loci of trailing-edge positions for equal values of $C_{L_{max}}^2/C_{D_{min}}$ obtained with an 11.0 percent c N.A.C.A. 0012 auxiliary airfoil set at the optimum angle for each position.



Loci of trailing-edge positions for equal values of $C_{L_{max}}$ obtained with an 11.0 percent c N.A.C.A. 0012 auxiliary airfoil set at the optimum angle for each position.

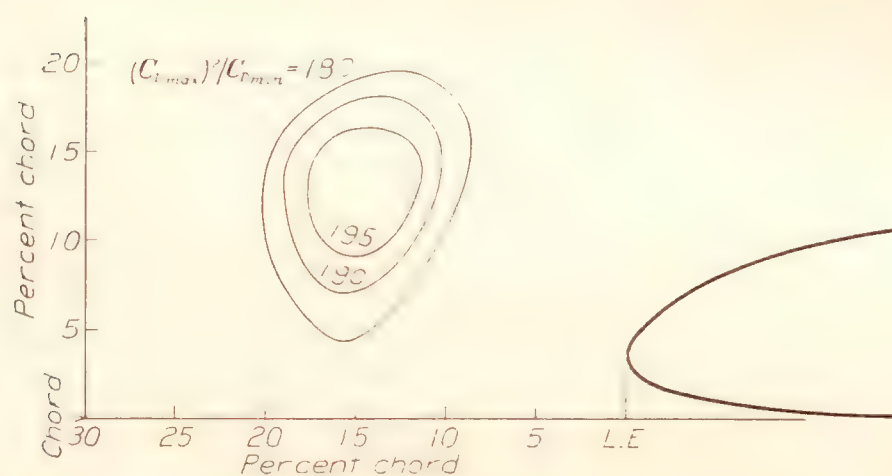


Loci of trailing-edge positions for equal values of L/D at $C_L = 0.7$ obtained with an 11.0 percent c N.A.C.A. 0012 auxiliary airfoil set at the optimum angle for each position.

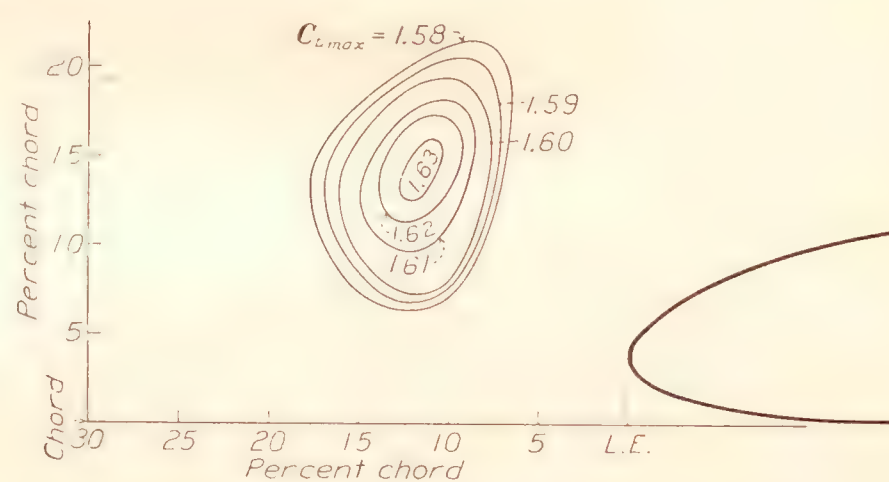


Loci of trailing-edge positions for equal values of L/D at $C_{L_{max}}$ obtained with an 11.0 percent c N.A.C.A. 0012 auxiliary airfoil set at the optimum angle for each position.

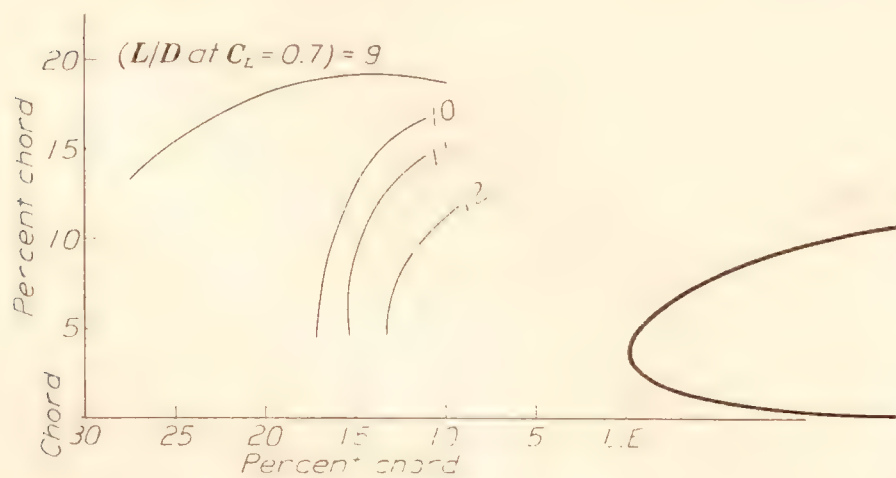
FIGURE 7.



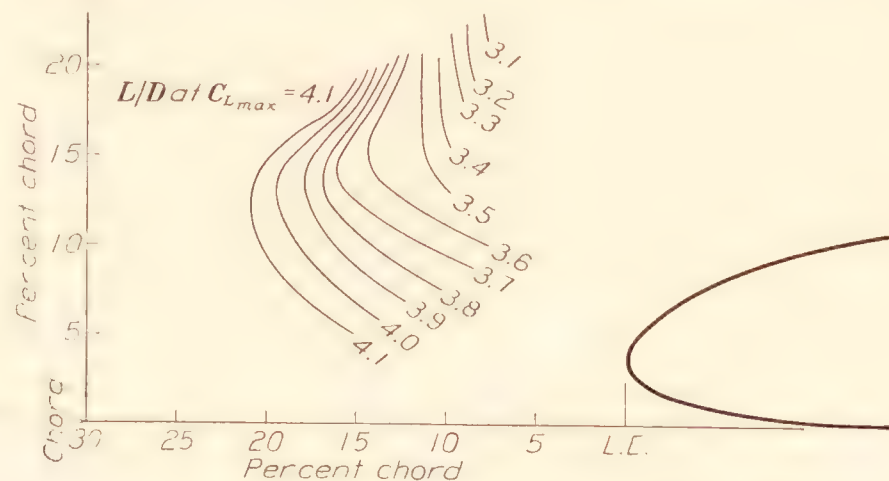
Loci of trailing-edge positions for equal values of $C_{L_{max}}^2/C_{D_{min}}$ obtained with a 14.5 percent c N.A.C.A. 0012 auxiliary airfoil set at the optimum angle for each position.



Loci of trailing-edge positions for equal values of $C_{L_{max}}$ obtained with a 14.5 percent c N.A.C.A. 0012 auxiliary airfoil set at the optimum angle for each position.

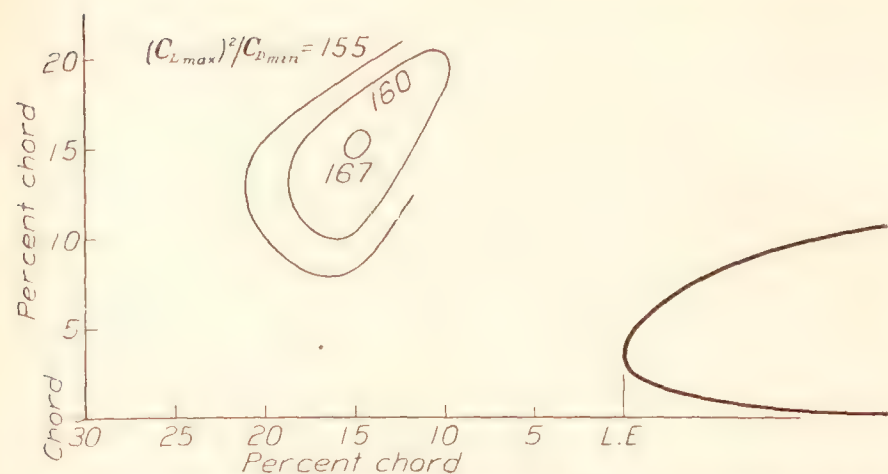


Loci of trailing-edge positions for equal values of L/D at $C_L = 0.7$ obtained with a 14.5 percent c N.A.C.A. 0012 auxiliary airfoil set at the optimum angle for each position.

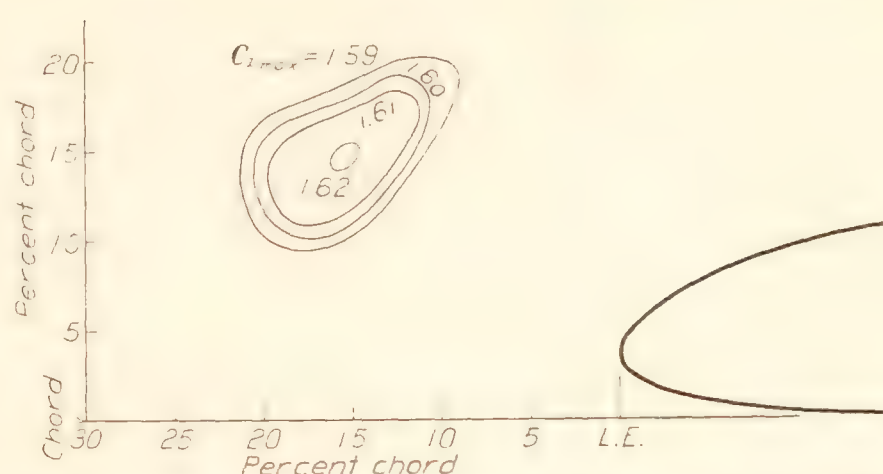


Loci of trailing-edge positions for equal values of L/D at $C_{L_{max}}$ obtained with a 14.5 percent c N.A.C.A. 0012 auxiliary airfoil set at the optimum angle for each position.

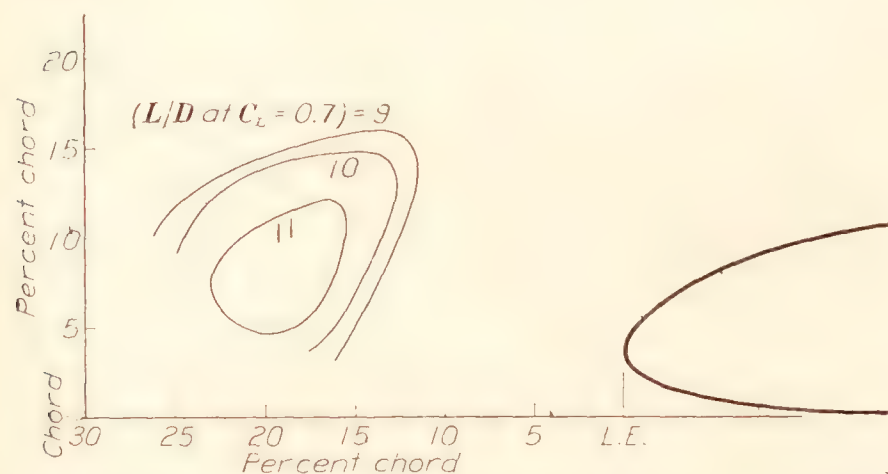
FIGURE 8.



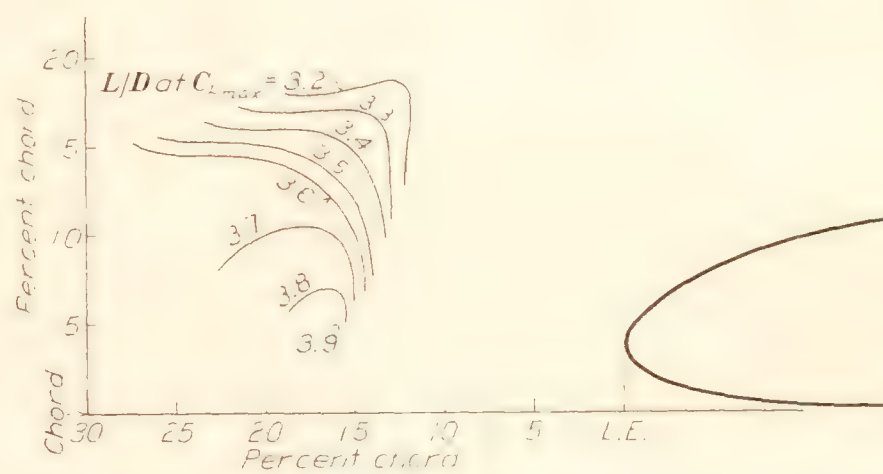
Loci of trailing-edge positions for equal values of C_{Lmax}^2/C_{Dmin} obtained with an 18.0 percent c N.A.C.A. 0012 auxiliary airfoil set at the optimum angle for each position.



Loci of trailing-edge positions for equal values of C_{Lmax} obtained with an 18.0 percent c N.A.C.A. 0012 auxiliary airfoil set at the optimum angle for each position.

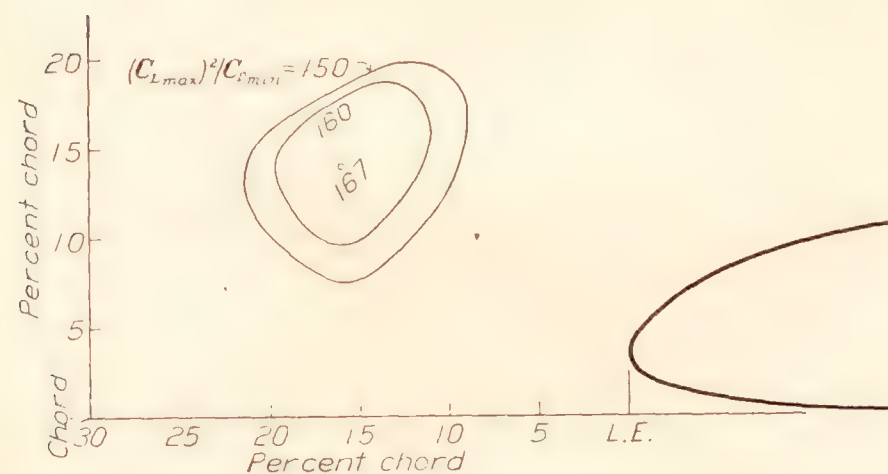


Loci of trailing-edge positions for equal values of L/D at $C_L=0.7$ obtained with an 18.0 percent c N.A.C.A. 0012 auxiliary airfoil set at the optimum angle for each position.

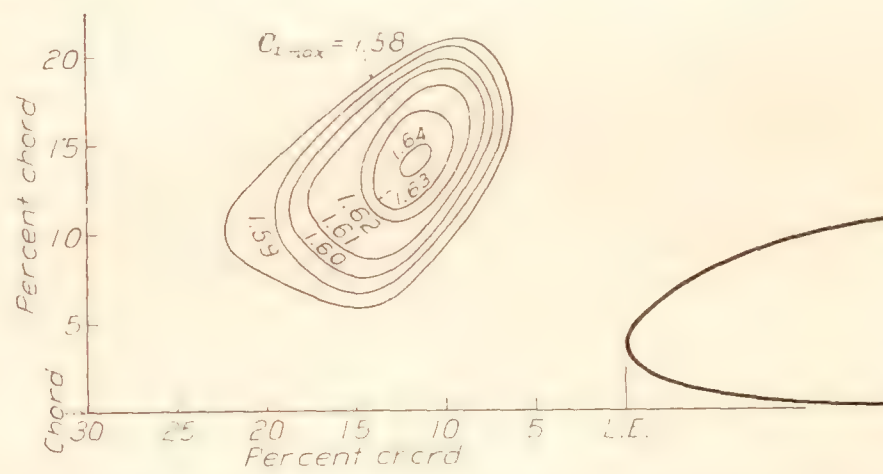


Loci of trailing-edge positions for equal values of L/D at C_{Lmax} obtained with an 18.0 percent c N.A.C.A. 0012 auxiliary airfoil set at the optimum angle for each position.

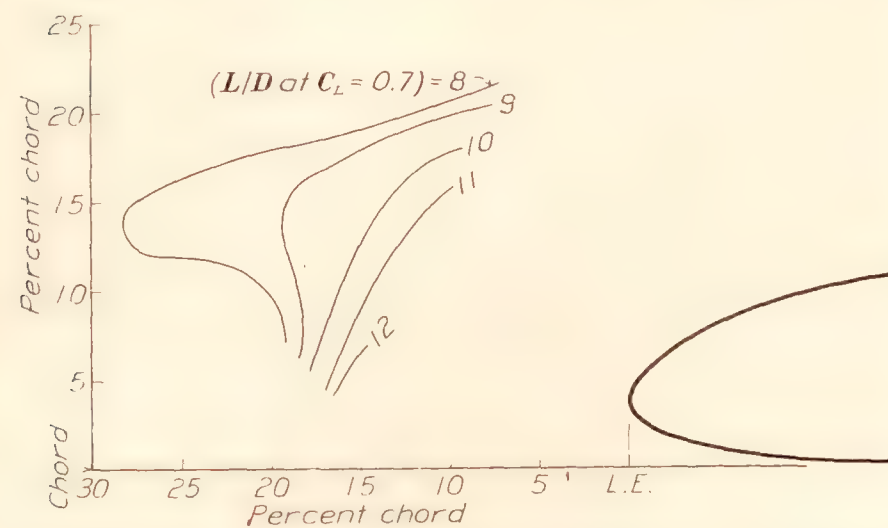
FIGURE 9



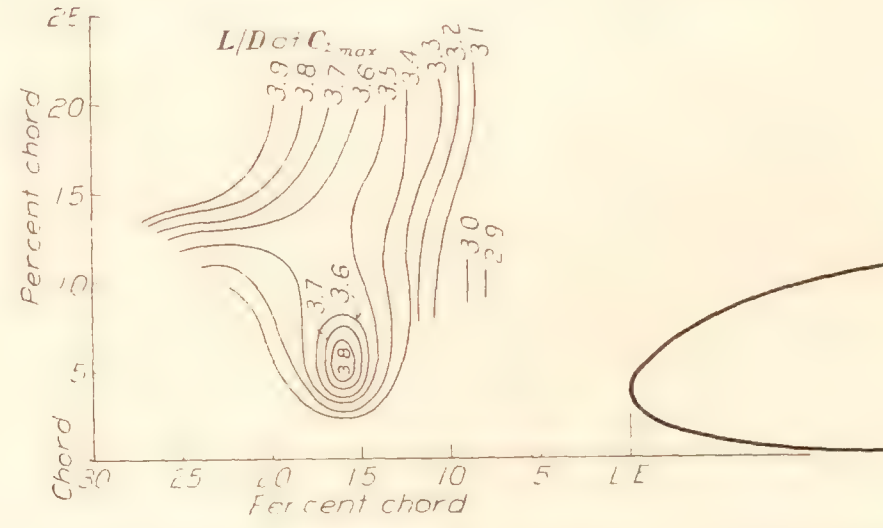
Loci of trailing-edge positions for equal values of C_{Lmax}^2/C_{Dmin} obtained with a 14.5 percent c Clark Y auxiliary airfoil set at the optimum angle for each position.



Loci of trailing-edge positions for equal values of C_{Lmax} obtained with a 14.5 percent c Clark Y auxiliary airfoil set at the optimum angle for each position.



Loci of trailing-edge positions for equal values of L/D at $C_L=0.7$ obtained with a 14.5 percent c Clark Y auxiliary airfoil set at the optimum angle for each position.



Loci of trailing-edge positions for equal values of L/D at C_{Lmax} obtained with a 14.5 percent c Clark Y auxiliary airfoil set at the optimum angle for each position.

FIGURE 10.

of auxiliary airfoil except the extreme 7.5 and 25 percent sizes, and for each of the three airfoil sections, a position with the trailing edge 14 percent ahead of the nose and 12 percent above the chord line of the main wing gave a value of C_{Lmax} within 2 percent and a value of the ratio C_{Lmax}^2/C_{Dmin} within 5 percent of the maximum value obtained for the particular auxiliary airfoil at any position. The best angle δ was within 3° of zero for all medium-sized auxiliary airfoils, regardless of section.

In most cases, moving the auxiliary airfoil closer to the main wing than the position giving the highest value of the ratio C_{Lmax}^2/C_{Dmin} gave a slight increase in the value of L/D in the climbing range and at the same time a decrease in the value of L/D near maximum lift, both of which result in an increase in the range of possible gliding angles. Considering this fact, together with the similar condition in regard to the maximum lift coefficient, and also the structural requirements, the optimum position would seem to be somewhat closer to the main wing than the position giving the highest ratio of C_{Lmax}^2/C_{Dmin} . No rigid general rule can be drawn, however, for the details of each case must be considered separately.

Effect of size.—A comparison of the results for the different sized auxiliary airfoils as given on the contour charts shows that for any one airfoil section there was no great change in the values of the criteria with change in size within the range covered, if the values taken are for each size in its best position. The maximum lift coefficients obtained with the auxiliary airfoils of all sizes and sections, set at the value of δ which gave the highest value of the ratio C_{Lmax}^2/C_{Dmin} , were all within 2 percent (or approximately within the experimental error) of the value 1.64, except for the value with the 25 percent auxiliary airfoil, which was within 4 percent. With the highly cambered N.A.C.A. 22 section the smaller auxiliary airfoils had slightly higher values of the ratio C_{Lmax}^2/C_{Dmin} than the larger ones, but the entire range was only 7 percent. With the symmetrical section the variation of the maximum value of the ratio C_{Lmax}^2/C_{Dmin} with size was about twice as great, the highest value being obtained with the medium size and the lowest values with the extreme sizes.

The values of the climb criterion, L/D at $C_L=0.7$, were nearly the same for all sizes, but were slightly greater for the smallest size than for the others. The smallest sized auxiliary airfoils, unfortunately, also gave definitely higher values of the criterion of steep glides, L/D at C_{Lmax} , than the others. The variation among the larger sizes was very small.

Effect of auxiliary airfoil section.—Although the auxiliary airfoils of all sizes and sections gave approximately the same values of the maximum lift coefficient, the minimum drag coefficients were found to be decidedly lower with the auxiliary airfoils of symmetrical section than with the cambered ones, so that higher values

of the ratio C_{Lmax}^2/C_{Dmin} were obtained with them. The cross plots for the three different sections with the 14.5 percent chord indicated that the highest values of the ratio obtained with each varied consistently with the camber, the value with the symmetrical N.A.C.A. 0012 auxiliary airfoil being 199, that for the Clark Y being 166, and that for the highly cambered N.A.C.A. 22, being 154. The value of 199 obtained with the 14.5 percent symmetrical auxiliary airfoil was the highest found in the investigation.

The values of L/D at $C_L=0.7$ were approximately the same for the symmetrical and for the highly cambered sections, but the values of L/D at C_{Lmax} were slightly lower with the highly cambered sections.

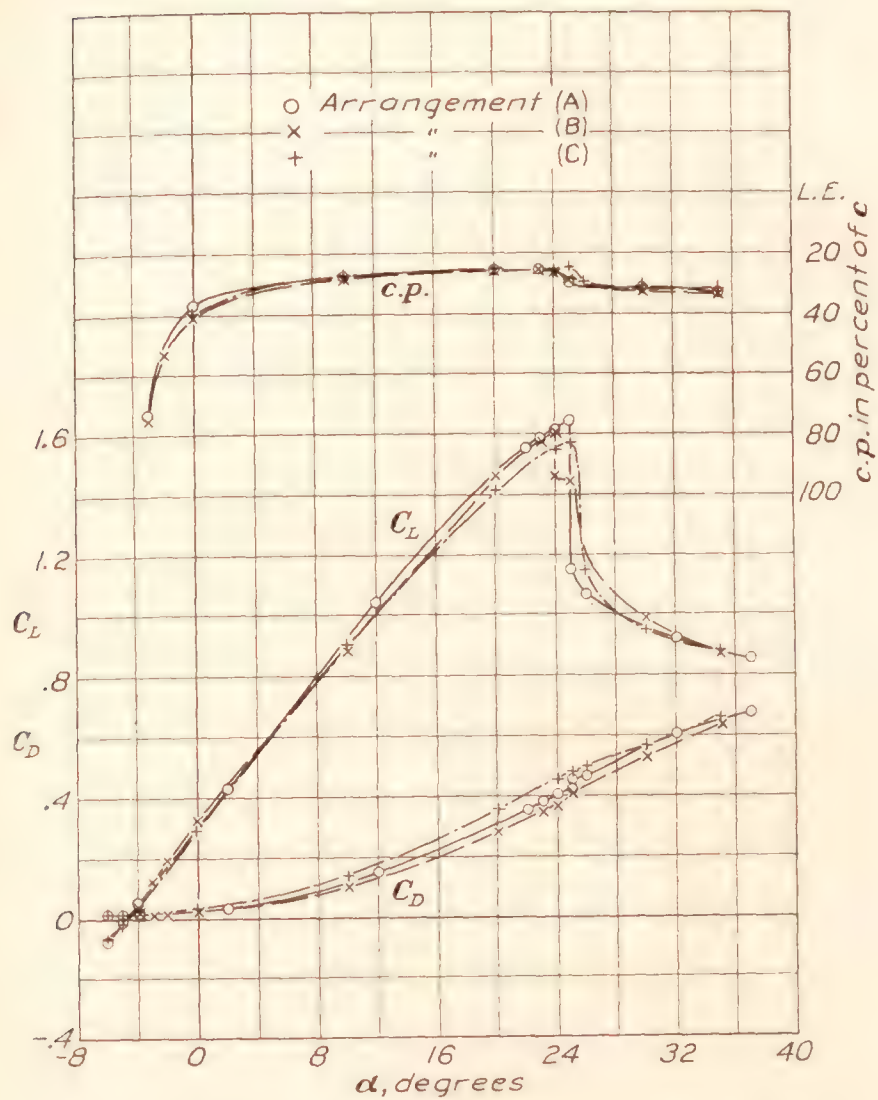
LIFT, DRAG, AND CENTER-OF-PRESSURE CURVES FOR OPTIMUM POSITIONS

Curves of lift, drag, and center-of-pressure coefficients against angle of attack are given in figures 11 to 19 for each of the auxiliary airfoils in one or more of the optimum positions, selected mainly on the basis of the ratio C_{Lmax}^2/C_{Dmin} . In addition, values of the pitching-moment coefficients for all the angles of attack measured are given in table X. The values of center-of-pressure positions were computed on the basis of the main wing chord and the values of C_m on the basis of the main wing chord and the combined area.

The numerical value of C_m at zero lift for the combination with the 14.5 percent Clark Y auxiliary airfoil was found to be 14 percent less than the value for the plain Clark Y wing alone. With the symmetrical auxiliary airfoil having the 11 percent chord the value was the same as for the plain wing, but it became greater if the size of the auxiliary was either increased or decreased from the 11 percent point. The highly cambered N.A.C.A. 22 auxiliary airfoils gave somewhat smaller negative values than the plain Clark Y wing, the values decreasing as the size of the auxiliary was increased. If C_m is plotted against C_L the curve will not in any case be a straight line, but will have a definite bend in the neighborhood of the 5° angle of attack.

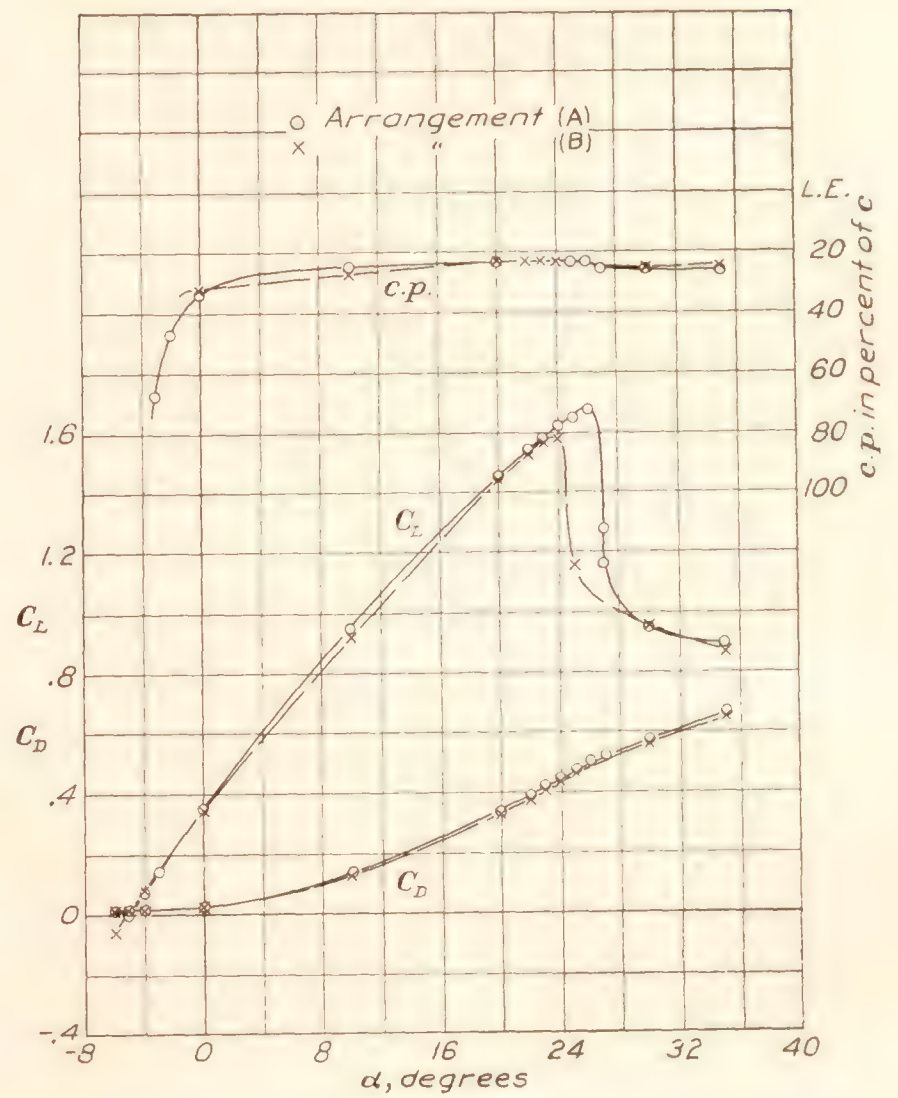
DIVISION OF AIR LOAD BETWEEN MAIN WING AND AUXILIARY AIRFOIL

The results of the tests to show the division of the air load between the main wing and the two selected auxiliary airfoils are shown in figure 20. The load on the auxiliaries is divided into normal and chord components and these are given in terms of the total lift on the main wing plus the auxiliary. The auxiliary airfoil having the symmetrical section sustained in the neighborhood of one fifth of the total load throughout the entire angle-of-attack range tested. The highly cambered N.A.C.A. 22 auxiliary airfoil sustained about the same portion of the total load at the high lift coefficients, but a higher proportion if the angle of attack was reduced. At $\alpha=0^\circ$ the lowest angle of attack which could be obtained with the set-up



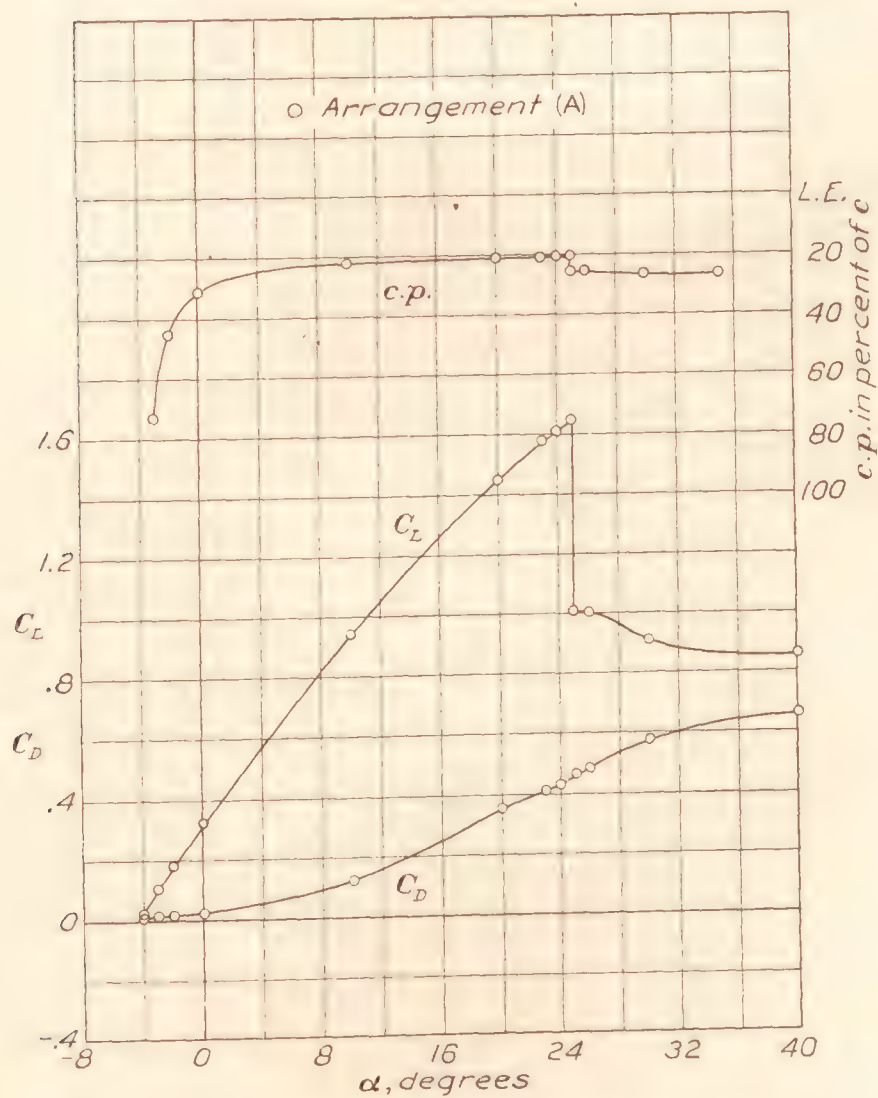
(A) Aux. T.E. 16.0 percent ahead of L.E., 4.5 percent above chord, $\delta=5^\circ$.
 (B) Aux. T.E. 19.3 percent ahead of L.E., 2.5 percent above chord, $\delta=2\frac{1}{2}^\circ$.
 (C) Aux. T.E. 11.1 percent ahead of L.E., 7.4 percent above chord, $\delta=10^\circ$.

FIGURE 11.—Characteristics with N.A.C.A. 22, 7.5 percent chord auxiliary.



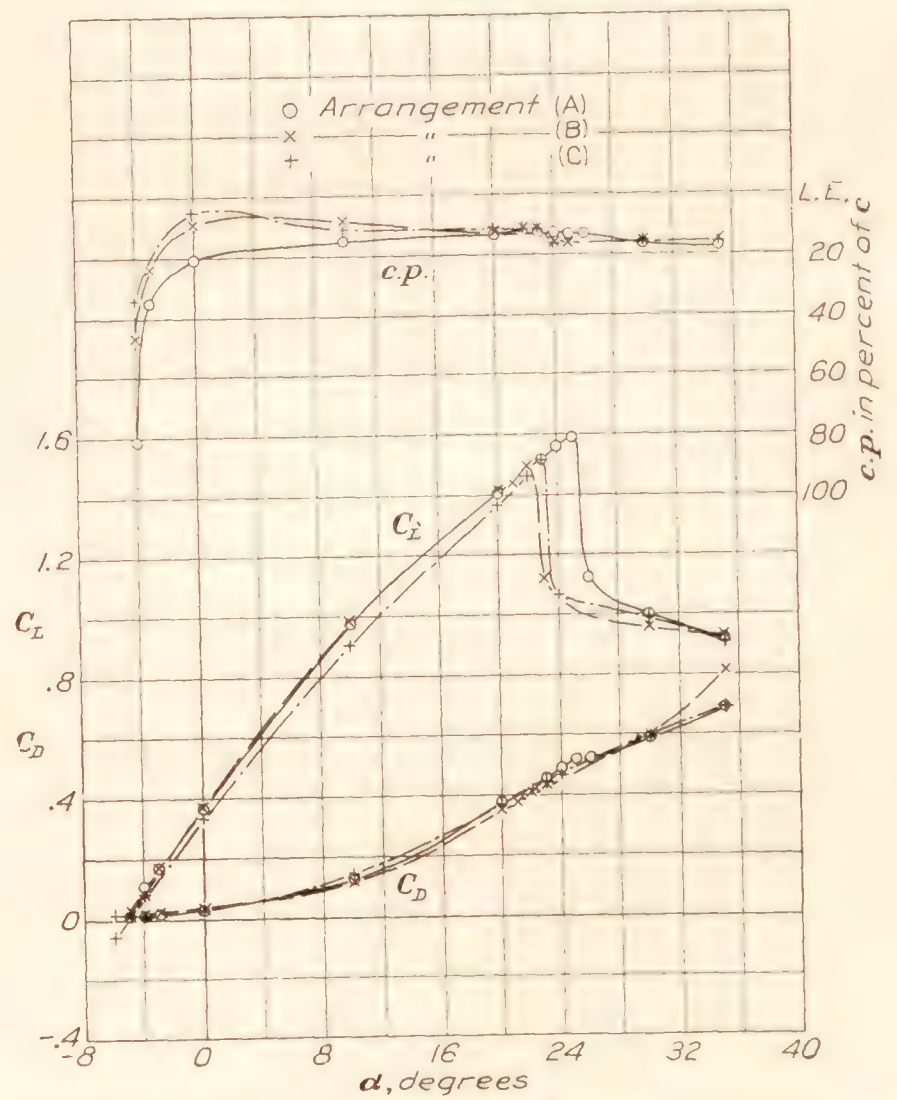
(A) Aux. T.E. 11.5 percent ahead of L.E., 14.0 percent above chord, $\delta=0^\circ$.
 (B) Aux. T.E. 16.0 percent ahead of L.E., 4.5 percent above chord, $\delta=2\frac{1}{2}^\circ$.

FIGURE 12.—Characteristics with N.A.C.A. 22, 11.0 percent chord auxiliary.



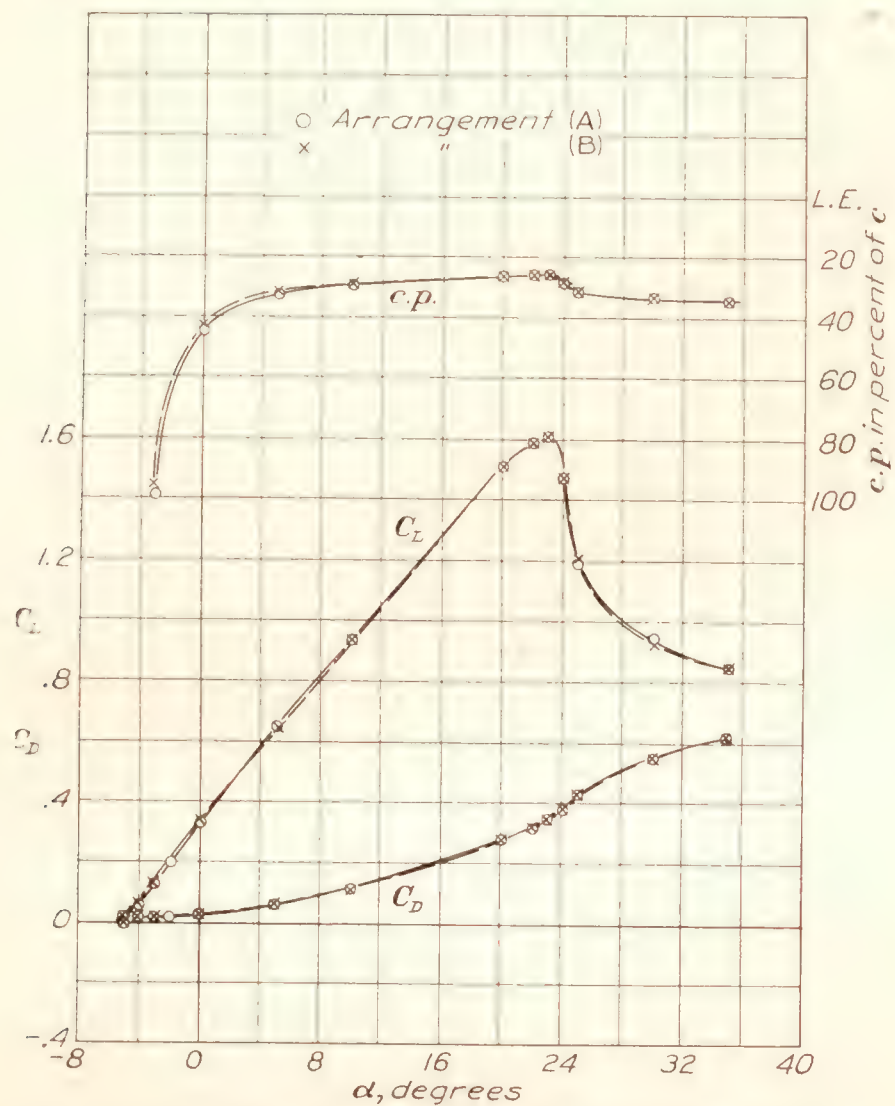
(A) Aux. T.E. 15.2 percent ahead of L.E., 12.0 percent above chord, $\delta=0^\circ$.

FIGURE 13.—Characteristics with N.A.C.A. 22, 14.5 percent chord auxiliary.



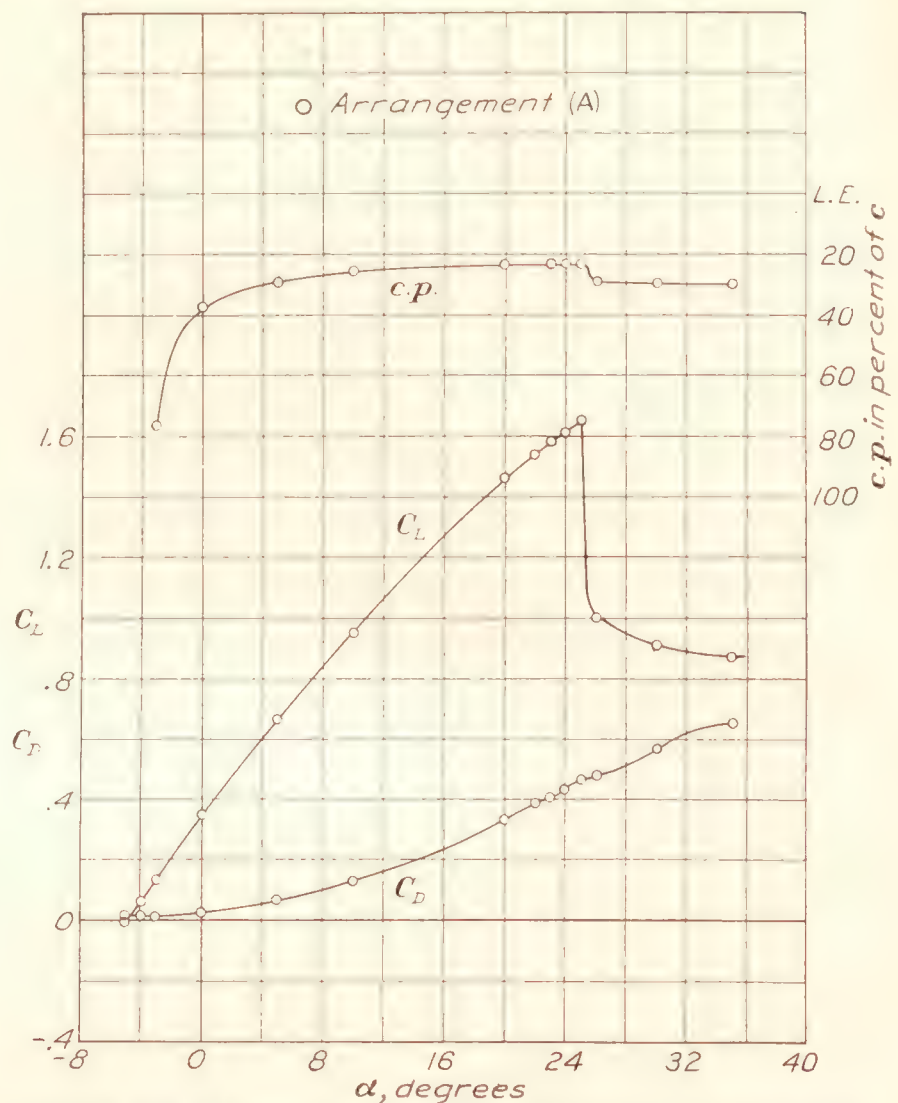
(A) Aux. T.E. 16.0 percent ahead of L.E., 14.0 percent above chord, $\delta=0^\circ$.
 (B) Aux. T.E. 27.5 percent ahead of L.E., 14.0 percent above chord, $\delta=0^\circ$.
 (C) Aux. T.E. 21.2 percent ahead of L.E., 8.8 percent above chord, $\delta=2\frac{1}{2}^\circ$.

FIGURE 14.—Characteristics with N.A.C.A. 22, 25.0 percent chord auxiliary.



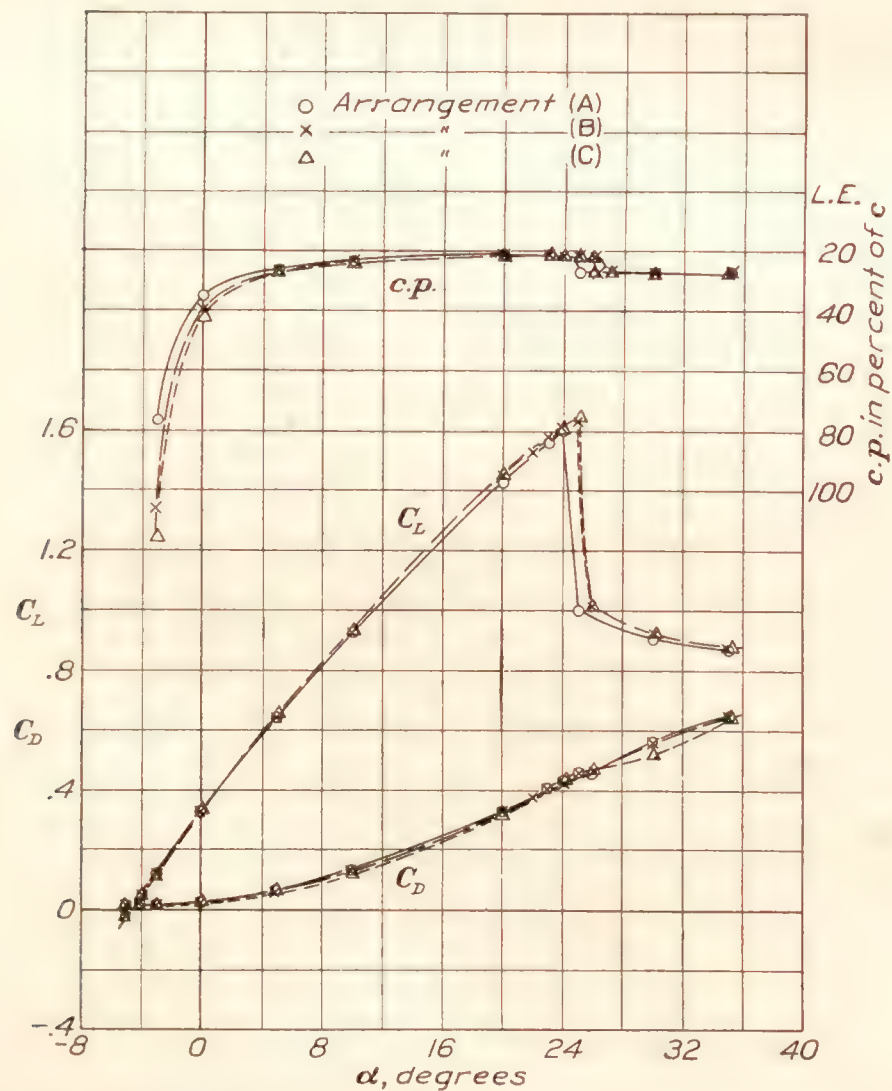
(A) Aux. T.E. 19.3 percent ahead of L.E., 2.5 percent below chord, $\delta=0^\circ$.
 (B) Aux. T.E. 19.3 percent ahead of L.E., 2.5 percent below chord, $\delta=2\frac{1}{2}^\circ$.

FIGURE 15.—Characteristics with N.A.C.A. 0012, 7.5 percent chord auxiliary.



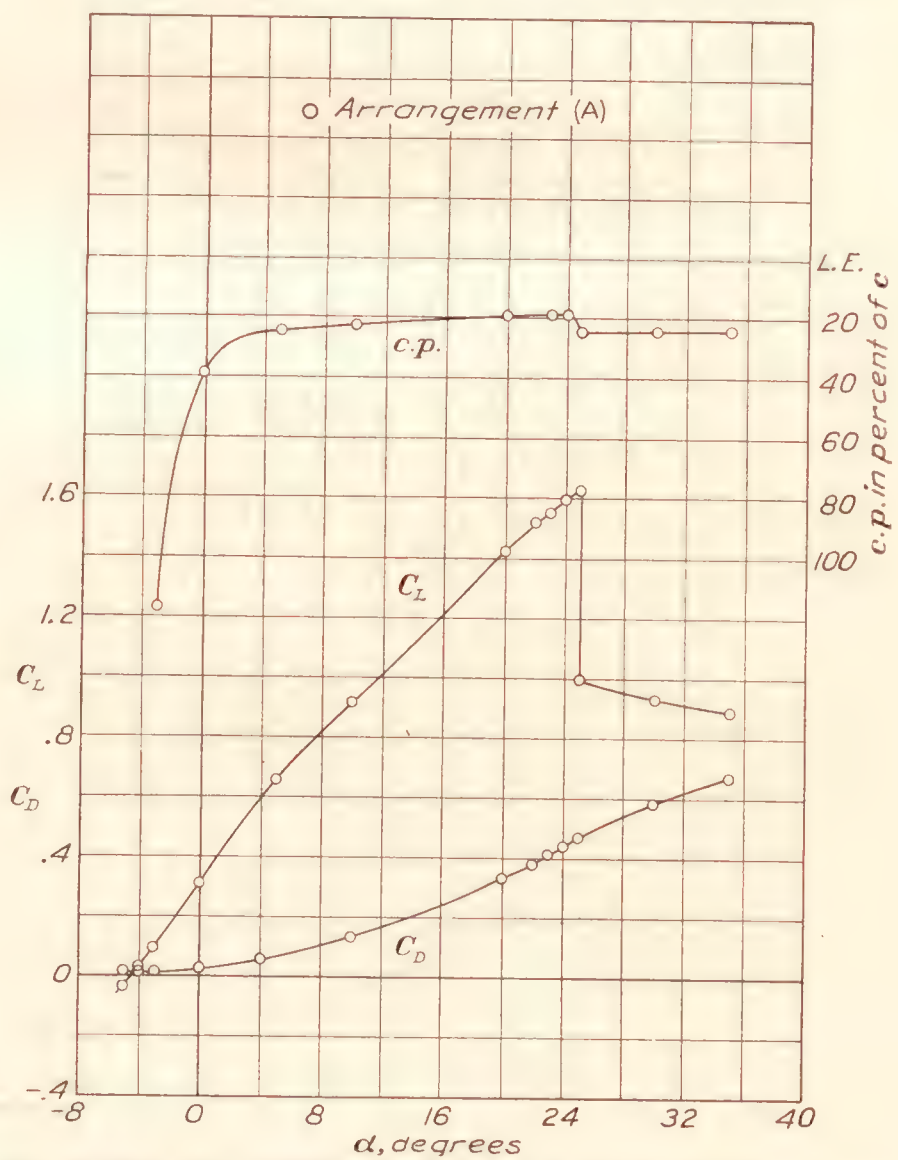
(A) Aux. T.E. 11.5 percent ahead of L.E., 14.0 percent above chord, $\delta=2\frac{1}{2}^\circ$.

FIGURE 16.—Characteristics with N.A.C.A. 0012, 11.0 percent chord auxiliary.



(A) Aux. T.E. 16.0 percent ahead of L.E., 14.0 percent above chord, $\delta=2\frac{1}{2}^\circ$.
 (B) Aux. T.E. 11.5 percent ahead of L.E., 14.0 percent above chord, $\delta=0^\circ$.
 (C) Aux. T.E. 11.5 percent ahead of L.E., 14.0 percent above chord, $\delta=-2\frac{1}{2}^\circ$.

FIGURE 17.—Characteristics with N.A.C.A. 0012, 14.5 percent chord auxiliary.



(A) Aux. T.E. 16.0 percent ahead of L.E., 14.0 percent above chord, $\delta=0^\circ$.

FIGURE 18.—Characteristics with N.A.C.A. 0012, 18 percent chord auxiliary.

used, approximately half the total load was taken by the N.A.C.A. 22 auxiliary airfoil.

CONCLUSIONS

1. Each of the auxiliary airfoil combinations tested, regardless of size or airfoil section, gave, in the best positions, substantially higher values of C_{Lmax} and of the ratio C_{Lmax}^2/C_{Dmin} than the main wing alone.

2. The maximum values of C_L obtained, based on the total area, were very nearly the same with all the auxiliary airfoils tested.

3. The symmetrical auxiliary airfoils gave lower values of the minimum drag coefficient and higher values of the ratio C_{Lmax}^2/C_{Dmin} than the auxiliary airfoils having other sections, the highest value of the ratio C_{Lmax}^2/C_{Dmin} being obtained with the 14.5 percent symmetrical auxiliary airfoil.

4. The positions giving the highest values of the ratio C_{Lmax}^2/C_{Dmin} did not vary greatly for the auxiliary airfoils of different sizes and sections tested, except for the smallest size, which required a lower position.

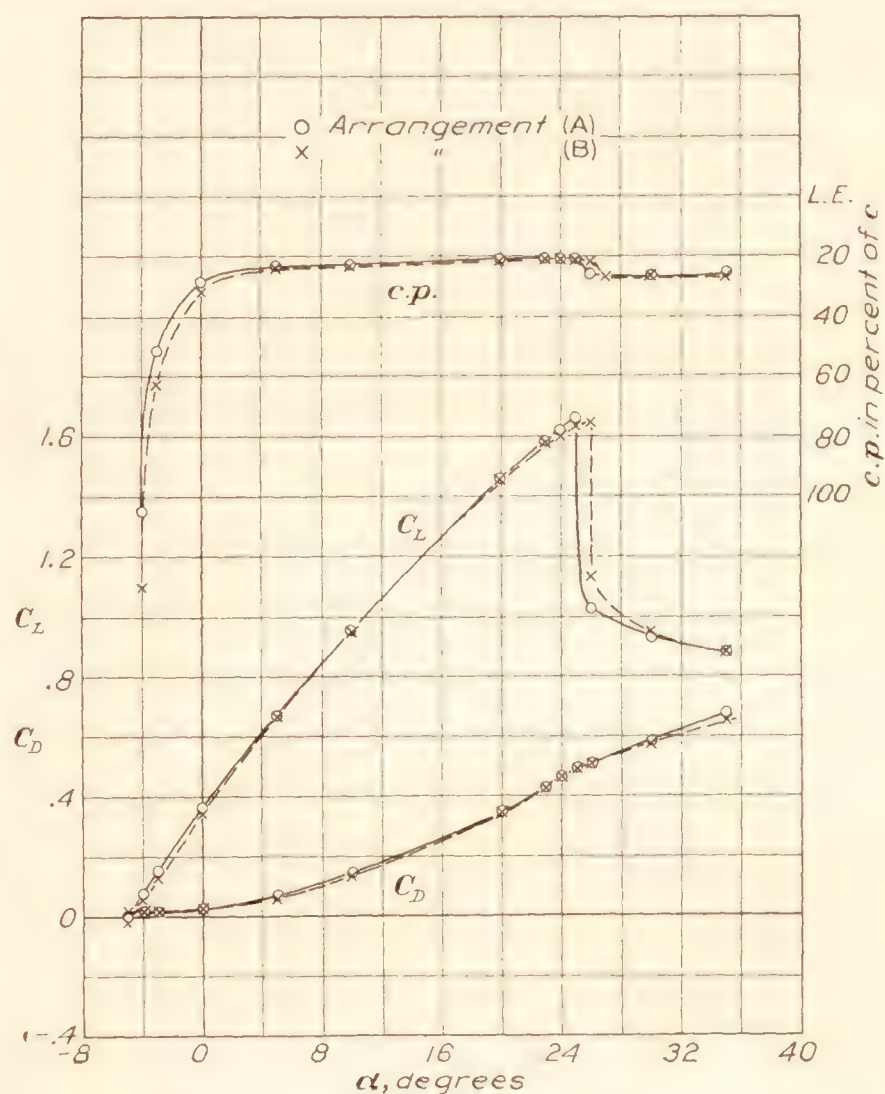
5. In most cases within the range of the tests, moving the auxiliary airfoil closer to the main wing than the position giving the highest value of the ratio C_{Lmax}^2/C_{Dmin} gave a slight increase in the value of L/D in the climbing range and a decrease in the value of L/D near maximum lift, thus giving a dual increase in the range of possible flight angles.

6. The air load on the 14.5 percent symmetrical auxiliary airfoil was about one fifth the total air load on the combination at all angles of attack; the proportional air load on the highly cambered auxiliary airfoil was about the same at the high values of the lift coefficient, but approximately half the total air load at low values of the lift coefficient.

LANGLEY MEMORIAL AERONAUTICAL LABORATORY,
NATIONAL ADVISORY COMMITTEE FOR AERONAUTICS,
LANGLEY FIELD, VA., June 10, 1933.

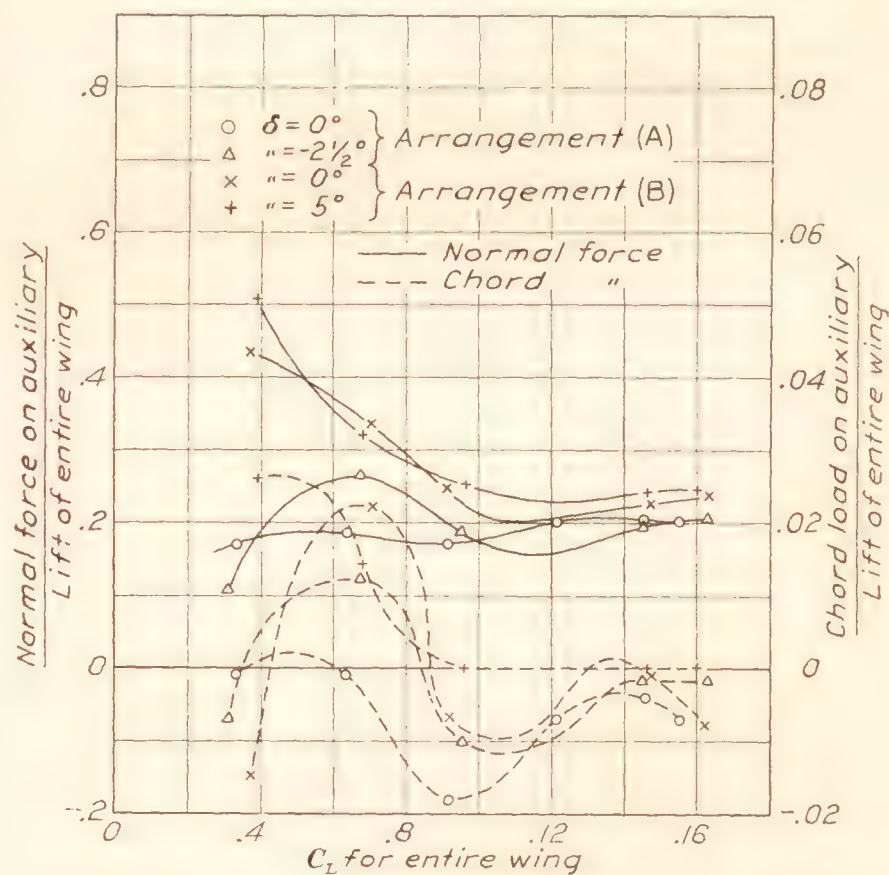
REFERENCES

1. Weick, Fred E., and Bamber, Millard J.: Wind-Tunnel Tests of a Clark Y Wing with a Narrow Auxiliary Airfoil in Different Positions. T.R. No. 428, N.A.C.A., 1932.
2. Wenzinger, Carl J., and Harris, Thomas A.: The Vertical Wind Tunnel of the National Advisory Committee for Aeronautics. T.R. No. 387, N.A.C.A., 1931.
3. Weick, Fred E., and Noyes, Richard W.: Wind-Tunnel Research Comparing Lateral Control Devices, Particularly at High Angles of Attack. X. Various Control Devices on a Wing with a Fixed Auxiliary Airfoil. T.N. No. 451, N.A.C.A., 1933.



(A) Aux. T.E. 16.0 percent ahead of L.E., 14.0 percent above chord, $\delta=2\frac{1}{2}^\circ$.
(B) Aux. T.E. 11.5 percent ahead of L.E., 14.0 percent above chord, $\delta=0^\circ$.

FIGURE 19.—Characteristics with Clark Y, 14.5 percent chord auxiliary.



(A) N.A.C.A. 0012, T.E. 11.5 percent ahead of L.E., 14.0 percent above chord.
(B) N.A.C.A. 22, T.E. 15.2 percent ahead of L.E., 12.0 percent above chord.

FIGURE 20.—Normal and chord components of the force on 14.5 percent chord auxiliary airfoils.

TABLE I.—CHARACTERISTICS AND CRITERIONS FOR AN N.A.C.A. 22, 7.5 PERCENT AUXILIARY WITH A CLARK Y WING

Position of T.E. of auxiliary airfoil		δ	C_{Dmin}	C_{Lmax}	$\alpha_{C_{Lmax}}$	$\frac{C_{Lmax}}{C_{Dmin}}$	$\frac{(C_{Lmax})^2}{C_{Dmin}}$	$\frac{L}{\bar{D}}$ for $C_L=0.7$	$\frac{L}{\bar{D}}$ for C_{Lmax}
Ahead	Above								
Percent c	Percent c	Degrees			Degrees				
16.0	14.0	5	0.0187	1.458	21	78	114	11.1	4.42
		7½	.0185	1.462	21	79	116	10.0	4.27
		12½	.0185	1.478	21	80	118	7.6	4.06
11.5	14.0	2½	.0188	1.560	24	84	130	10.4	3.84
		5	.0188	1.602	25	85	137	10.4	3.61
		7½	.0185	1.602	25	87	139	10.1	3.54
		10	.0196	1.620	25	83	134	8.9	3.47
		12½	.0199	1.602	25	81	129	8.6	3.37
27.5	14.0	0	.0184	1.400	20	76	107	10.8	5.19
		2½	.0170	1.374	22	79	109	13.0	4.07
		5	.0187	1.390	20	74	103	11.7	4.81
21.2	8.8	0	.0201	1.415	23	70	100	12.1	3.94
		2½	.0185	1.420	23	77	109	14.0	3.86
		5	.0180	1.415	23	79	111	12.1	3.74
		7½	.0191	1.510	22	79	119	10.8	4.18
		10	.0201	1.563	23	78	122	10.0	3.74
		12½	.0199	1.551	23	78	121	18.4	3.96
16.0	4.5	2½	.0160	1.523	21	95	145	12.1	4.62
		5	.0174	1.646	25	95	157	10.9	3.85
		7½	.0168	1.605	24	96	153	10.0	3.96
7.5	9.6	0	.0204	1.563	25	77	120	10.0	3.45
		2½	.0199	1.563	26	79	123	9.9	3.21
		5	.0204	1.522	25	75	114	9.9	3.24
10.7	0.0	0	.0185	1.401	24	76	106	11.3	3.80
		5	.0157	1.340	23	86	114	11.3	3.79
		7½	.0163	1.380	24	85	117	11.3	3.69
		12½	.0166	1.323	23	80	106	11.3	3.66
19.3	-2.5	-5	.0218	1.628	23	75	121	14.0	4.92
		0	.0177	1.620	24	92	149	11.1	4.33
		2½	.0171	1.615	24	94	153	10.6	4.39
		5	.0177	1.598	24	91	145	10.6	4.19
11.1	7.4	0	.0196	1.640	25	84	137	9.7	3.82
		5	.0185	1.618	25	87	141	10.3	3.58
		7½	.0182	1.605	25	88	142	9.3	3.48
		10	.0191	1.575	25	83	130	8.9	3.26

TABLE II. CHARACTERISTICS AND CRITERIONS FOR AN N.A.C.A. 22, 11.0 PERCENT AUXILIARY WITH A CLARK Y WING

Position of T.E. of auxiliary airfoil		δ	C_{Dmin}	C_{Lmax}	$\alpha_{C_{Lmax}}$	$\frac{C_{Lmax}}{C_{Dmin}}$	$\frac{(C_{Lmax})^2}{C_{Dmin}}$	$\frac{L}{\bar{D}}$ for $C_L=0.7$	$\frac{L}{\bar{D}}$ for C_{Lmax}
Ahead	Above								
Percent c	Percent c	Degrees			Degrees				
7.50	22.5	-5	0.0172	1.470	22	85	126	12.5	4.26
		-2½	.0161	1.480	22	92	136	11.5	4.08
		0	.0172	1.492	22	87	129	10.8	3.94
16.0	18.9	-5	.0203	1.435	21	71	102	12.3	4.60
		0	.0169	1.452	21	86	124	12.5	4.27
		2½	.0169	1.465	21	87	128		4.30
		5	.0185	1.474	21	80	117	11.9	3.97
16.0	14.0	-5	.0201	1.481	22	74	109	14.0	4.32
		0	.0172	1.532	22	89	136	13.5	4.14
		2½	.0172	1.571	23	91	143	13.7	3.79
		5	.0183	1.610	24	88	142	12.7	3.41
11.5	14.0	-5	.0209	1.650	25	79	130	10.9	3.69
		0	.0183	1.678	26	92	154	10.9	3.34
		2½	.0183	1.660	26	91	151	10.9	3.22
		5	.0191	1.610	25	84	136	10.9	3.20
27.5	14.0	-5	.0211	1.395	20	66	93	13.5	5.03
		0	.0185	1.410	20	76	107	10.9	4.70
		2½	.0182	1.420	20	78	111	10.8	4.44
		5	.0185	1.426	20	77	111	10.9	4.34
21.2	8.8	0	.0180	1.510	21	84	127	13.7	4.47
		2½	.0182	1.558	22	86	134	12.3	4.15
		5	.0180	1.545	22	86	132	13.2	3.99
16.0	4.5	-5	.0225	1.605	23	72	115	15.9	4.34
		0	.0175	1.580	23	90	143	8.9	3.97
		2½	.0167	1.584	24	95	150	9.0	3.56
		5	.0178	1.571	24	88	138	9.0	3.58
7.5	9.6	-5	.0215	1.542	25	72	111	10.1	3.20
		-2½	.0201	1.525	25	76	116	9.7	3.27
		0	.0191	1.480	27	78	115		2.79
		5	.0209	1.425	25	68	97	13.7	2.85
11.1	7.4	-5	.0225	1.648	25	73	121	12.7	3.77
		0	.0190	1.597	25	84	134	12.1	3.47
		5	.0172	1.558	26	91	141	10.9	3.03
		7½	.0175	1.520	25	87	132	10.9	3.07

TABLE III. CHARACTERISTICS AND CRITERIONS FOR AN N.A.C.A. 22, 14.5 PERCENT AUXILIARY WITH A CLARK Y WING

Position of T.E. of auxiliary airfoil		δ	C_{Dmin}	C_{Lmax}	$\alpha_{C_{Lmax}}$	$\frac{C_{Lmax}}{C_{Dmin}}$	$\frac{(C_{Lmax})^2}{C_{Dmin}}$	$\frac{L}{\bar{D}}$ $C_L=0.7$	$\frac{L}{\bar{D}}$ C_{Lmax}
Ahead	Above								
Percent c 15.2	Percent c 12.0	Degrees 0	0.0177	1.650	Degrees 25	93	154	8.0	3.56

TABLE IV. CHARACTERISTICS AND CRITERIONS WITH N.A.C.A. 22, 25 PERCENT AUXILIARY FOR EACH POSITION TESTED

Position of T.E. of auxiliary airfoil		δ	C_{Dmin}	C_{Lmax}	$\alpha_{C_{Lmax}}$	$\frac{C_{Lmax}}{C_{Dmin}}$	$\frac{(C_{Lmax})^2}{C_{Dmin}}$	$\frac{L}{\bar{D}}$ $C_L=0.7$	$\frac{L}{\bar{D}}$ C_{Lmax}
Ahead	Above								
Percent c 7.5	Percent c 22.5	Degrees			Degrees				
		-7½	0.0238	1.575	25	66	105	11.9	3.24
		-5	.0186	1.504	24	81	122	11.3	3.12
		0	.0163	1.416	21	87	124	10.0	3.25
16.0	18.9	-5	.0209	1.562	24	75	117	11.7	3.55
		-2½	.0188	1.574	24	84	133	12.3	3.42
		0	.0180	1.550	24	86	133	11.1	3.19
		5	.0180	1.527	24	85	130	9.6	2.85
16.0	14.0	-5	.0207	1.656	26	80	133	10.4	3.27
		-2½	.0185	1.620	25	87	141	11.3	3.30
		0	.0162	1.592	25	98	156	10.4	3.07
		2½	.0178	1.568	25	88	138	9.5	2.98
		5	.0178	1.510	24	85	128	8.1	2.87
11.5	14.0	-5	.0206	1.576	25	77	121	13.2	3.21
		-2½	.0176	1.528	24	87	133	11.5	3.19
		0	.0169	1.470	23	87	128	9.9	3.11
		5	.0169	1.365	21	81	111	8.6	3.05
27.5	14.0	-5	.0200	1.510	23	75	114	-----	3.85
		0	.0156	1.498	22	96	144	10.9	3.71
		2½	.0179	1.534	23	86	131	12.1	3.75
		5	.0179	1.487	22	83	124	11.1	3.39
21.2	8.8	-5	.0211	1.603	25	76	122	10.8	3.49
		0	.0182	1.556	24	86	134	12.1	3.34
		2½	.0168	1.516	23	90	137	9.0	3.41
		5	.0168	1.480	23	98	144	8.3	3.08
16.0	4.5	-5	.0207	1.516	25	73	112	11.1	3.43
		-2½	.0169	1.470	24	87	128	10.1	3.46
		0	.0155	1.405	23	90	127	10.3	3.44
		5	.0155	1.281	20	83	106	9.5	3.55

TABLE V. CHARACTERISTICS AND CRITERIONS FOR AN N.A.C.A. 0012, 7.5 PERCENT AUXILIARY WITH A CLARK Y WING

Position of T.E. of auxiliary airfoil		δ	C_{lmin}	C_{lmax}	$\alpha_{C_{lmax}}$	$\frac{C_{lmax}}{C_{Dmin}}$	$\frac{(C_{lmax})^2}{C_{lmin}}$	$\frac{L}{D}$ for $C_L=0.7$	$\frac{L}{D}$ for C_{Lmax}
Ahead	Above								
Percent c	Percent c	Degrees			Degrees				
16.0	14.0	0	0.0163	1.402	20	86	121	10.8	4.93
		5	.0155	1.418	20	91	130	11.3	4.80
		7½	.0152	1.428	20	94	134	9.2	4.65
		12½	.0166	1.434	20	84	120	8.3	4.35
11.5	14.	0	.0161	1.438	21	89	129	10.6	4.57
		5	.0166	1.500	22	90	136	9.5	4.17
		7½	.0164	1.520	22	93	141	8.9	4.12
		10	.0169	1.545	23	91	141	8.4	3.84
		12½	.0180	1.590	24	88	140	7.4	3.53
21.2	8.8	-2½	.0169	1.401	20	81	114	10.3	4.90
		0	.0150	1.383	19	92	128	11.5	5.47
		2½	.0152	1.390	20	91	127	10.6	4.83
		5	.0161	1.420	20	88	125	10.4	4.91
16.0	4.5	0	.0155	1.646	24	106	175	10.9	4.35
		2½	.0149	1.621	23	109	176	10.4	4.45
		5	.0152	1.609	23	106	170	9.9	4.36
		7½	.0160	1.637	24	102	167	9.5	4.07
7.5	9.6	-2½	.0153	1.580	24	103	163	10.9	3.85
		0	.0147	1.545	23	105	162	10.1	3.89
		5	.0158	1.582	25	100	158	8.9	3.35
10.7	0.0	-2½	.0146	1.475	22	101	149	11.9	4.71
		0	.0138	1.470	22	106	157	10.6	4.50
		2½	.0133	1.403	22	105	148	9.5	4.28
		5	.0133	1.407	21	106	149	9.7	4.53
19.3	-2.5	-2½	.0158	1.622	23	103	166	13.0	4.88
		0	.0141	1.610	23	114	184	11.7	4.74
		2½	.0139	1.610	23	116	186	10.9	4.68
		5	.0144	1.600	23	111	178	10.1	4.57
11.1	7.4	-5	.0182	1.660	25	91	151	11.9	4.17
		-2½	.0172	1.670	25	97	162	11.5	3.80
		0	.0172	1.636	25	95	156	10.6	3.67
		5	.0172	1.608	24	94	150	10.4	3.91
20.0	2.1	0	.0160	1.540	22	96	147	11.3	4.87
		5	.0155	1.570	22	101	159	10.0	4.68
		7½	.0155	1.570	22	101	159	9.6	4.61
16.0	-1.5	-2½	.0163	1.602	23	98	157	11.9	4.75
		0	.0152	1.590	23	105	166	11.3	4.65
		2½	.0152	1.582	23	104	165	10.1	4.54
		5	.0152	1.570	23	103	162	9.9	4.41
18.6	-7.1	-2½	.0169	1.570	23	93	146	12.5	4.85
		0	.0163	1.571	23	96	152	12.1	4.82
		2½	.0163	1.512	23	93	140	10.9	4.61
		5	.0163	1.482	22	91	135	10.6	4.72
21.8	-2.8	-2½	.0172	1.570	22	91	143	12.3	5.06
		0	.0161	1.573	22	98	154	11.1	4.97
		2½	.0169	1.570	22	93	146	10.1	4.86
		5	.0169	1.590	23	94	150	9.5	4.49

TABLE VI. CHARACTERISTICS AND CRITERIONS FOR AN N.A.C.A. 0012, 11.0 PERCENT AUXILIARY WITH A CLARK Y WING

Positions of T.E. of auxiliary airfoil		δ	C_{Dmin}	C_{Lmax}	$\alpha_{C_{Lmax}}$	$\frac{C_{Lmax}}{C_{Dmin}}$	$\frac{(C_{Lmax})^2}{C_{Dmin}}$	$\frac{L}{D}$ for $C_L=0.7$	$\frac{L}{D}$ for C_{Lmax}
Ahead	Above								
Percent c 7.5	Percent c 22.5	Degrees			Degrees				
		-5	0.0153	1.400	20	91	128	12.5	4.98
		0	.0151	1.413	20	94	132	10.1	4.67
		5	.0158	1.426	20	90	129	8.4	4.26
16.0	18.9	0	.0151	1.392	20	92	128	10.8	4.73
		5	.0153	1.408	20	92	130	8.9	4.46
		10	.0151	1.395	20	92	129	9.1	4.42
16.0	14.0	0	.0157	1.413	20	90	127	10.4	4.74
		2½	.0148	1.410	21	95	134	9.7	4.47
		5	.0159	1.461	20	91	130	8.9	4.41
11.5	14.0	0	.0143	1.568	23	110	172	10.0	3.95
		2½	.0143	1.656	25	116	192	9.5	3.58
		5	.0143	1.618	25	113	183	8.6	3.60
		10	.0162	1.614	25	100	161	7.9	3.22
21.2	8.8	0	.0156	1.432	20	92	132	11.1	4.92
		5	.0169	1.508	21	89	135	9.1	4.42
		10	.0164	1.531	22	93	143	8.1	3.89
		12½	.0164	1.536	22	94	144	7.9	3.83
16.0	4.5	0	.0143	1.560	22	109	170	11.3	4.46
		2½	.0140	1.562	22	112	174	9.3	4.27
		5	.0136	1.558	23	114	178	9.0	3.90
		7½	.0144	1.527	22	106	162	8.5	4.00
7.5	9.6	-5	.0157	1.546	24	99	152	12.5	3.65
		-2½	.0154	1.540	24	100	154	10.4	3.53
		0	.0152	1.535	25	101	155	9.3	3.25
		5	.0152	1.468	24	97	142	7.8	3.14
11.1	7.4	-5	.0172	1.610	23	94	151	11.7	4.25
		-2½	.0164	1.598	23	97	156	11.7	4.13
		0	.0156	1.571	23	101	159	10.1	3.96
		5	.0172	1.561	24	91	142	8.4	3.48

TABLE VII. CHARACTERISTICS AND CRITERIONS FOR AN N.A.C.A. 0012, 14.5 PERCENT AUXILIARY WITH A CLARK Y WING

Positions of T.E. of auxiliary airfoil		δ	C_{Dmin}	C_{Lmax}	$\alpha_{C_{Lmax}}$	$\frac{C_{Lmax}}{C_{Dmin}}$	$\frac{(C_{Lmax})^2}{C_{Dmin}}$	$\frac{L}{D}$ for $C_L=0.7$	$\frac{L}{D}$ for C_{Lmax}
Ahead	Above								
Percent c 7.5	Percent c 22.5	Degrees			Degrees				
		0	0.0151	1.443	21	96	138	10.0	4.23
		5	.0149	1.556	24	104	162	7.6	3.34
		7½	.0154	1.575	25	102	161	6.9	3.08
16.0	18.9	-5	.0159	1.390	20	87	122	12.3	4.90
		-2½	.0149	1.400	21	94	132	12.1	4.42
		0	.0141	1.408	21	100	140	10.6	4.27
		2½	.0149	1.443	21	97	140	9.2	4.13
		5	.0146	1.460	21	97	139	8.3	4.07
16.0	14.0	0	.0129	1.501	22	116	175	11.5	4.15
		2½	.0129	1.603	24	124	199	9.2	3.67
		5	.0131	1.603	24	122	196	8.8	3.58
		7½	.0134	1.593	24	119	190	7.9	3.38
11.5	14.0	-2½	.0139	1.651	25	119	196	11.7	3.65
		0	.0137	1.639	25	120	196	11.1	3.53
		5	.0137	1.613	25	118	190	8.1	3.26
27.5	14.0	0	.0149	1.333	19	89	119	11.5	5.02
		5	.0146	1.370	20	94	129	8.9	4.32
		7½	.0164	1.434	21	87	125	7.9	3.96
21.2	8.8	-5	.0164	1.408	20	86	121	12.5	5.12
		0	.0149	1.485	21	100	148	11.1	4.54
		2½	.0157	1.540	22	98	151	9.5	4.17
		5	.0167	1.534	22	92	141	8.5	4.02
16.0	4.5	-5	.0159	1.550	22	97	151	12.5	4.56
		-2½	.0129	1.537	22	119	183	12.7	4.38
		0	.0126	1.520	22	121	184	10.8	4.15
		5	.0126	1.490	22	118	176	8.3	3.92
7.5	9.6	-7½	.0159	1.504	23	94	142	13.0	3.90
		-5	.0146	1.513	24	103	156	12.3	3.61
		-2½	.0146	1.466	23	100	147	10.9	3.58
		0	.0152	1.440	25	95	137	8.8	3.00
		5	.0156	1.400	25	90	126	7.3	2.79
11.1	7.4	-5	.0154	1.605	24	104	167	12.5	3.91
		-2½	.0142	1.542	23	109	167	11.9	3.96
		0	.0142	1.518	23	107	162	9.9	3.73
		5	.0144	1.480	23	103	153	8.2	3.51

TABLE VIII. CHARACTERISTICS AND CRITERIONS FOR AN N.A.C.A 0012, 18 PERCENT AUXILIARY WITH CLARK Y WING

Position of T.E. of auxiliary airfoil		δ	C_{Dmin}	C_{Lmax}	$\alpha_{C_{Lmax}}$	$\frac{C_{Lmax}}{C_{Dmin}}$	$\frac{(C_{Lmax})^2}{C_{Dmin}}$	$\frac{L}{D}$ for $C_L=0.7$	$\frac{L}{D}$ for C_{Lmax}
Ahead	Above								
Percent c 7.5	Percent c 22.5	Degrees			Degrees				
		0	0.0159	1.473	22	93	136	9.5	3.77
		2½	.0159	1.578	25	99	157	8.0	3.14
		5	.0159	1.565	25	98	154	7.1	3.09
		7½	.0161	1.531	24	95	146	6.5	2.96
16.0	18.9	0	.0152	1.440	21	95	136	10.8	4.09
		2½	.0161	1.485	22	92	136	8.5	3.75
		5	.0161	1.488	22	92	137	8.2	3.65
		7½	.0166	1.580	24	95	150	6.6	3.15
		10	.0169	1.530	23	89	139	6.2	3.87
		12½	.0174	1.552	24	88	137	6.1	2.91
16.0	14.0	-2½	.0157	1.560	23	99	155	11.7	4.05
		0	.0155	1.621	25	104	169	11.1	3.48
		2½	.0152	1.550	23	102	158	8.3	3.59
		5	.0157	1.575	24	100	158	7.8	3.32
11.5	14.0	0	.0164	1.600	25	98	156	10.4	3.33
		2½	.0162	1.590	25	98	156	8.0	3.15
		5	.0164	1.580	26	96	152	7.4	3.01
27.5	14.0	0	.0156	1.337	19	86	114	11.3	4.82
		5	.0156	1.395	20	89	125	8.0	4.21
		7½	.0164	1.426	21	87	124	7.4	3.69
21.2	8.8	-2½	.0166	1.470	21	89	130	11.7	4.51
		0	.0156	1.544	22	99	153	11.3	3.71
		2½	.0166	1.513	22	91	138	9.2	3.99
		5	.0176	1.510	22	86	130	7.5	3.83
16.0	4.5	-2½	.0157	1.488	22	95	141	12.1	4.21
		0	.0149	1.488	22	100	149	11.1	4.02
		2½	.0142	1.468	22	103	152	8.8	3.91
		5	.0144	1.418	21	99	140	11.9	3.92

TABLE IX. CHARACTERISTICS AND CRITERIONS FOR A CLARK Y, 14.5 PERCENT AUXILIARY WITH A CLARK Y WING

Position of T.E. of auxiliary airfoil		δ	C_{Dmin}	C_{Lmax}	$\alpha_{C_{Lmax}}$	$\frac{C_{Lmax}}{C_{Dmin}}$	$\frac{(C_{Lmax})^2}{C_{Dmin}}$	$\frac{L}{D}$ for $C_L=0.7$	$\frac{L}{D}$ for C_{Lmax}
Ahead	Above								
Percent c 7.5	Percent c 22.5	Degrees			Degrees				
		0	0.0156	1.460	25	94	137	11.7	3.06
		2½	.0164	1.470	25	90	132	10.1	2.91
		5	.0174	1.571	25	90	142	7.3	3.05
		7½	.0179	1.555	24	87	135	6.7	3.08
16.0	18.9	0	.0164	1.446	21	88	128	11.7	4.14
		5	.0172	1.502	22	87	131	8.0	3.65
		7½	.0182	1.532	23	84	129	7.2	3.38
16.0	14.0	0	.0159	1.612	24	101	163	11.7	3.73
		2½	.0157	1.616	24	103	166	9.6	3.51
		5	.0162	1.622	25	100	163	8.2	3.23
11.5	14.0	-2½	.0178	1.665	26	93	156	11.7	3.35
		0	.0170	1.647	26	97	159	11.1	3.27
		2½	.0170	1.631	26	96	157	9.2	3.21
		5	.0165	1.608	26	97	157	7.6	2.96
27.5	14.0	0	.0169	1.390	20	82	114	11.9	4.51
		5	.0172	1.443	21	84	121	8.4	3.99
		7½	.0182	1.475	21	81	120	7.7	3.91
21.2	8.8	0	.0182	1.542	22	85	131	11.7	4.27
		5	.0180	1.578	23	88	138	8.5	3.71
		7½	.0180	1.565	23	87	136	7.4	3.57
		10	.0178	1.587	24	89	141	6.9	3.30
		12½	.0193	1.536	23	79	122	6.5	3.25
		-2½	.0177	1.562	23	88	138	12.1	4.06
16.0	4.5	0	.0167	1.548	23	93	144	11.5	3.81
		2½	.0159	1.502	22	94	142	9.3	3.94
		5	.0159	1.480	22	93	138	7.4	3.77
		-5	.0218	1.500	26	69	103	11.9	2.99
7.5	9.6	-2½	.0192	1.470	26	77	113	11.3	2.84
		0	.0192	1.443	26	75	108	11.1	2.75
		5	.0192	1.400	24	73	102	6.7	2.84

TABLE X. CHARACTERISTICS OF A CLARK Y WING WITH VARIOUS AUXILIARIES IN THEIR MOST PROMISING POSITIONS

NO AUXILIARY

α (degrees)	C_L	C_D	C_m 0.25c of main wing
-4	0.047	0.016	-0.077
-3	.111	.015	-.076
-2	.188	.017	-.076
0	.331	.022	-.076
10	.984	.092	-.067
13	1.169	.127	-.065
14	1.222	.140	-.064
15	1.260	.150	-.064
16	1.295	.162	-.064
17	1.333	.180	-.069
18	1.319	.204	-.078
19	1.295	.224	-.086
20	1.275	.250	-.094
30	.911	.552	-.168

N.A.C.A. 22, 25.0 PERCENT AUXILIARY

T.E. of auxiliary 0.16c ahead, 0.14c above, $\delta=0^\circ$

α (degrees)	C_L	C_D	C_m 0.25c of main wing
-5	-0.032	0.024	-0.047
-4	.061	.017	-.033
-3	.145	.018	-.015
0	.363	.038	.016
10	1.015	.129	.100
20	1.412	.370	.165
23	1.521	.444	.194
24	1.555	.476	.196
25	1.590	.507	.199
26	1.114	.535	.147
30	.995	.582	.100
35	.935	.685	.089

N.A.C.A. 0012, 14.5 PERCENT AUXILIARY

T.E. of auxiliary 0.115c ahead, 0.14c above, $\delta=0^\circ$

α (degrees)	C_L	C_D	C_m 0.25c of main wing
-5	-0.040	0.017	-0.094
-4	.035	.016	-.089
-3	.100	.017	-.081
0	.310	.022	-.046
5	.664	.061	-.013
10	.954	.132	.004
20	1.468	.333	.045
23	1.578	.411	.051
24	1.630	.439	.053
25	1.660	.469	.055
26	1.685	.495	.058
27	1.000	.496	-.025
30	.937	.554	-.026
35	.889	.642	-.026

N.A.C.A. 22, 7.5 PERCENT AUXILIARY

T.E. of auxiliary 0.150c ahead, 0.045c above, $\delta=5^\circ$

α (degrees)	C_L	C_D	C_m 0.25c of main wing
-6	-0.084	0.020	-0.071
-5	-.019	.018	-.064
-4	.046	.018	-.059
-3	.117	.019	-.055
0	.305	.029	-.036
10	.916	.121	-.025
20	1.474	.311	-.004
23	1.578	.381	-.001
24	1.632	.405	.000
25	1.191	.444	-.056
30	.968	.553	-.072
35	.876	.647	-.088

T.E. of auxiliary 0.212c ahead, 0.088c above,
 $\delta=2\frac{1}{2}^\circ$

α (degrees)	C_L	C_D	C_m 0.25c of main wing
-6	-0.061	0.020	-0.051
-5	.023	.017	-.028
-4	.091	.017	-.008
0	.332	.028	.065
10	.903	.144	.126
20	1.361	.367	.193
22	1.463	.417	.205
23	1.518	.445	.213
24	1.064	.464	.114
30	.989	.595	.114
35	.903	.695	.107

T.E. of auxiliary 0.115c ahead, 0.14c above,
 $\delta=-2\frac{1}{2}^\circ$

α (degrees)	C_L	C_D	C_m 0.25c of main wing
-5	-0.039	0.018	-0.097
-4	.031	.017	-.093
-3	.095	.017	-.086
0	.306	.023	-.054
5	.664	.055	-.016
10	.955	.128	-.001
20	1.461	.322	.042
24	1.631	.429	.051
25	1.660	.457	.049
26	1.696	.484	.052
26	1.010	.464	-.029
30	.929	.551	-.033
35	.894	.637	-.030

T.E. of auxiliary 0.123c ahead, 0.025c below, $\delta=2\frac{1}{2}^\circ$

α	C_L	C_D	C_m 0.25c of main wing
<i>Degrees</i>			
-4	0.054	0.017	-0.068
-3	.122	.017	-.061
-2	.196	.019	-.056
0	.321	.024	-.050
10	.887	.106	-.028
20	1.469	.288	-.012
23	1.585	.350	-.010
24	1.618	.374	-.018
24	1.450		-.015
25	1.418	.415	-.040
30	.993	.534	-.080
35	.870	.629	-.096

T.E. of auxiliary 0.275c ahead, 0.14c above, $\delta=0^\circ$

α	C_L	C_D	C_m 0.25c of main wing
<i>Degrees</i>			
-5	-0.009	0.019	-0.035
-4	.061	.017	-.013
-3	.145	.017	-.002
0	.349	.026	.055
10	.965	.114	.164
20	1.397	.343	.190
22	1.480	.391	.203
23	1.516	.415	.207
24	1.111	.447	.113
25	1.043	.474	.110
30	.960	.585	.109
35	.934	.691	.115

T.E. of auxiliary 0.16c ahead, 0.14c above, $\delta=2\frac{1}{2}^\circ$

α	C_L	C_D	C_m 0.25c of main wing
<i>Degrees</i>			
-5	-0.023	0.016	-0.090
-4	.049	.016	-.079
-3	.127	.017	-.065
0	.335	.024	-.033
5	.660	.069	-.011
10	.960	.137	.010
20	1.460	.335	.054
23	1.590	.410	.061
24	1.620	.442	.063
25	1.048	.469	-.021
30	.931	.572	-.021
35	.882	.656	-.019

TABLE X. CHARACTERISTICS OF A CLARK Y WING WITH VARIOUS AUXILIARIES IN THEIR MOST PROMISING POSITIONS—Continued

N.A.C.A. 22, 11.0 PERCENT AUXILIARY
T.E. of auxiliary 0.115c ahead, 0.14c above, $\delta=0^\circ$

α	C_L	C_D	C_m 0.25c of main wing
<i>Degrees</i>			
-5	-0.050	0.023	-0.062
-4	.045	.019	-.054
-3	.111	.018	-.047
-2	.185	.019	-.041
0	.320	.025	-.027
10	.929	.133	.004
20	1.460	.331	.032
25	1.653	.466	.036
26	1.682	.496	.035
27	1.072	.509	-.041
30	.997	.564	-.041
35	.903	.655	-.050

N.A.C.A. 0012, 7.5 PERCENT AUXILIARY
T.E. of auxiliary 0.193c ahead, 0.025c below, $\delta=0^\circ$

α	C_L	C_D	C_m 0.25c of main wing
<i>Degrees</i>			
-5	-0.027	0.017	-0.093
-4	.044	.016	-.084
-3	.112	.016	-.083
0	.325	.023	-.062
5	.633	.052	-.042
10	.920	.103	-.040
20	1.498	.277	-.034
22	1.577	.316	-.027
23	1.605	.341	-.025
24	1.381	.365	-.056
25	1.210	.431	-.088
30	.944	.530	-.095
35	.856	.617	-.109

N.A.C.A. 0012, 18.0 PERCENT AUXILIARY
T.E. of auxiliary 0.16c ahead, 0.14c above, $\delta=0^\circ$

α	C_L	C_D	C_m 0.25c of main wing
<i>Degrees</i>			
-5	-0.040	0.016	-0.108
-4	.030	.015	-.097
-3	.093	.015	-.085
0	.312	.022	-.043
5	.670	.057	.005
10	.933	.134	.023
20	1.446	.333	.079
23	1.565	.406	.088
24	1.590	.439	.091
25	.973	.458	.000
30	.910	.573	.004
35	.870	.659	.009

T.E. of auxiliary 0.16c ahead, 0.045c above, $\delta=2\frac{1}{2}^\circ$

α	C_L	C_D	C_m 0.25c of main wing
<i>Degrees</i>			
-6	-0.063	0.023	-0.075
-5	-.018	.017	-.062
-4	.048	.017	-.052
0	.327	.027	-.024
10	.900	.127	.000
20	1.436	.322	.030
22	1.529	.374	.036
23	1.568	.399	.037
24	1.591	.433	.031
30	.963	.559	.035
35	.945	.643	.043

T.E. of auxiliary 0.193c ahead, 0.025c below, $\delta=2\frac{1}{2}^\circ$

α	C_L	C_D	C_m 0.25c of main wing
<i>Degrees</i>			
-5	-0.022	0.016	-0.089
-4	.048	.015	-.085
-3	.112	.016	-.078
0	.324	.022	-.059
5	.626	.055	-.041
10	.920	.106	-.040
20	1.492	.284	-.030
22	1.592	.323	-.028
23	1.616	.344	-.026
24	1.558	.376	-.035
25	1.200	.425	-.076
30	.950	.534	-.093
35	.862	.615	-.103

CLARK Y, 14.5 PERCENT AUXILIARY
T.E. of auxiliary 0.115c ahead, 0.14c above, $\delta=0^\circ$

α	C_L	C_D	C_m 0.25c of main wing
<i>Degrees</i>			
-5	-0.010	0.018	-0.071
-4	.059	.017	-.062
-3	.135	.017	-.051
0	.357	.025	-.024
5	.705	.058	.008
10	.973	.141	.016
20	1.473	.352	.056
24	1.619	.458	.063
25	1.654	.490	.064
26	1.680	.522	.064
27	1.042	.516	-.014
30	.967	.567	-.018
35	.896	.663	-.019

N.A.C.A. 22, 14.5 PERCENT AUXILIARY
T.E. of auxiliary 0.15c ahead, 0.12c above, $\delta=0^\circ$

α	C_L	C_D	C_m 0.25c of main wing
<i>Degrees</i>			
-4	0.010	0.024	-0.051
-3	.105	.018	-.050
-2	.182	.019	-.040
0	.325	.023	-.021
10	.942	.124	.026
20	1.450	.356	.063
23	1.582	.407	.073
24	1.610	.434	.076
25	1.650	.465	.079
25	1.080	.466	-.003
26	1.014	.484	-.009
30	.909	.574	-.013
35	.861	.661	-.013

N.A.C.A. 0012, 11.0 PERCENT AUXILIARY
T.E. of auxiliary 0.115c ahead, 0.14c above, $\delta=2\frac{1}{2}^\circ$

α	C_L	C_D	C_m 0.25c of main wing
<i>Degrees</i>			
-5	-0.020	0.015	-0.079
-4	.055	.015	-.071
-3	.120	.015	-.061
0	.331	.023	-.042
5	.654	.067	-.028
10	.963	.135	-.008
20	1.480	.335	.023
23	1.594	.413	.025
24	1.630	.438	.027
25	1.660	.466	.027
26	1.013	.483	-.048
30	.920	.566	-.054
35	.875	.654	-.055

T.E. of auxiliary 0.16c ahead, 0.14c above, $\delta=2\frac{1}{2}^\circ$

α	C_L	C_D	C_m 0.25c of main wing
<i>Degrees</i>			
-5	-0.003	0.017	-0.061
-4	.065	.017	-.051
-3	.151	.018	-.041
0	.369	.027	-.012
5	.690	.069	.011
10	.965	.146	.021
20	1.471	.351	.063
23	1.590	.432	.072
24	1.630	.460	.073
25	1.656	.490	.074
26	1.018	.503	-.010
30	.944	.593	-.013
35	.944	.680	-.009

REPORT No. 473

STRENGTH TESTS OF THIN-WALLED DURALUMIN CYLINDERS IN COMPRESSION

By EUGENE E. LUNDQUIST

SUMMARY

This report is the second of a series presenting the results of strength tests of thin-walled duralumin cylinders and truncated cones of circular and elliptic section. It contains the results obtained from compression tests on 45 thin-walled duralumin cylinders of circular section with ends clamped to rigid bulkheads. In addition to the tests on duralumin cylinders, there are included the results of numerous tests on rubber, celluloid, steel, and brass cylinders obtained from various sources.

The results of all tests are presented in nondimensional form and are discussed in connection with existing theory. In the theoretical discussion, it is shown that the buckling of the walls of a thin-walled cylinder in compression can be correlated with the buckling of flat plates under edge compression in an elastic medium, and that perhaps many solutions for problems in the buckling of plates can, with the proper factors, be applied to similar problems in the buckling of cylinders and curved sheets.

INTRODUCTION

In a stressed-skin or monocoque structure, the strength and stability of the curved skin are closely related to the strength and stability of the walls of a thin-walled cylinder, not only for compression but for other types of loading as well. The National Advisory Committee for Aeronautics, in cooperation with the Army Air Corps; the Bureau of Aeronautics, Navy Department; the Bureau of Standards; and the Aeronautics Branch of the Department of Commerce, made an extensive series of tests on thin-walled cylinders and on truncated cones of circular and elliptic section at Langley Field, Va. In these tests the absolute and relative dimensions of the specimens were varied in order to study the types of failure and to establish useful quantitative data in the following loading conditions: Torsion, compression, bending, and combined loading.

The first report of this series (reference 1) presents the results obtained in the torsion (pure shear) tests on cylinders of circular section. The present report is the second of the series and presents the results obtained in the compression tests on cylinders of circular section.

In addition to the results of the N.A.C.A. compression tests on duralumin cylinders, there are presented, through the courtesy of Dr. L. H. Donnell of the California Institute of Technology, the unpublished results of 40 compression tests on steel and brass cylinders. There are also included the results of numerous compression tests on rubber, celluloid, and steel cylinders reported in references 2, 3, and 4. The latter two of these references came to the attention of the author after the experiments of the present report had been completed. It is suggested that they be read in conjunction with the present report. The first is largely theoretical; the second, experimental.

By way of introduction to the detailed discussion of the test data herein presented, it may be said that secondary, or local, failure in thin-walled cylinders of circular section under uniform compression seems to have been first investigated by Lilly (1905-07). Since that time Timoshenko, Lorenz, Southwell, and others have studied the problem theoretically. The first theoretical studies were confined to the case of deformation symmetrical with respect to the axis (fig. 1). Later the theory was extended to include the case of deformation not symmetrical with respect to the axis (figs. 2 and 6), but the results of the extensions did not always lead to the same conclusions.

Perhaps the best known of the early treatises on the subject of the stability of thin-walled cylinders in compression is that by Southwell (reference 5), but unfortunately his interpretation of the general equation is incomplete. In reference 2, Robertson shows that Southwell's final equations are invalid for certain cases, and he derives new equations for these cases. In the present report it is shown that Southwell's general equation contains the equations for the buckling of flat and curved plates subjected to edge compression.¹

Until Robertson made the tests reported in reference 2, there seem to have been no comprehensive tests made to verify the theory. Robertson found that failure occurred by the formation of a multilobed wrinkle

¹ In reference 3 Flügge has presented the general equation in graphical form and has recognized that the buckling of flat plates is a special case of the buckling of a cylinder of infinite radius. Timoshenko also seems to have recognized the same fact in some of his early work, 1914-16.

pattern, as predicted by his modification of Southwell's final equations, but that both the number of wrinkles, or lobes, forming in the circumference of the cylinder and the stress at failure were less than the theoretical values. The stress at failure was slightly less than the critical stress for the 2-lobed failure predicted by Southwell.



FIGURE 1.—Buckling symmetrical with respect to the axis. (Tubes tested by the Bureau of Standards.)

The results of the N.A.C.A tests herein reported confirm, quantitatively, the results obtained by Robertson. Consequently, in the present report detailed consideration is given to the lack of agreement between theory and experiment.

As an introduction to a study of the strength and behavior of curved sheet and stiffener combinations, a general discussion of the buckling of flat and curved plates under edge compression is given in an appendix.

TESTS ON DURALUMIN CYLINDERS

Material.—The duralumin (Al. Co. of Am. 17ST) used in the N.A.C.A. tests was obtained from the manufacturer in sheet form with nominal thicknesses of 0.011, 0.016, and 0.022 inch. The properties of the

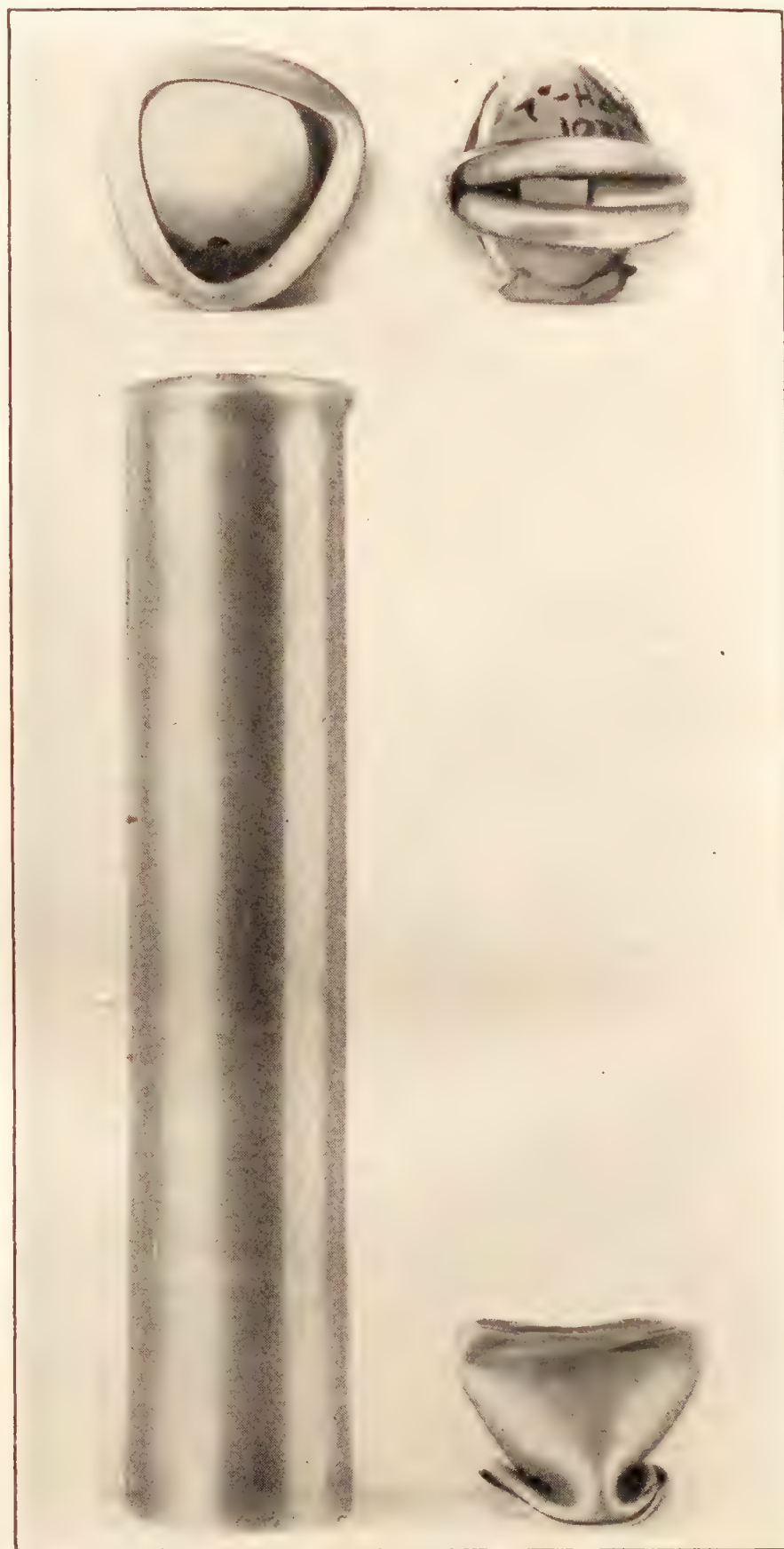


FIGURE 2.—Buckling not symmetrical with respect to the axis. (Tubes tested by the Bureau of Standards.)

material, as determined by the Bureau of Standards from specimens selected at random, are given in table I. Typical stress-strain curves taken parallel and normal to the direction of rolling are given in figures 3 and 4, respectively.

In table I and figures 3 and 4, it will be observed that the modulus of elasticity is substantially the same in the two directions of the sheet but that the ultimate strength and yield point are considerably lower normal

to than parallel to the direction of rolling. However, as all the cylinders tested failed at stresses considerably below the yield-point stress, the difference in the strength properties in the two directions has no bearing on the results.

Specimens.—The test specimens consisted of right circular cylinders of 7.5- and 15.0-inch radius with lengths ranging from 3.6 to 22.5 inches. The cylinders were constructed in the following manner: First, a duralumin sheet was cut to the dimensions of the

for the bulkheads of 7.5-inch radius, and $3\frac{1}{2}$ inches thick for the bulkheads of 15.0-inch radius. These parts were bolted together and turned to the specified outside diameter. Steel bands approximately one fourth inch thick were used to clamp the duralumin sheet to the bulkheads. These bands were bored to the same diameter as the bulkheads.

Apparatus and method.—The thickness of each sheet was measured to an estimated precision of ± 0.0003 inch at a large number of stations, by means of a dial

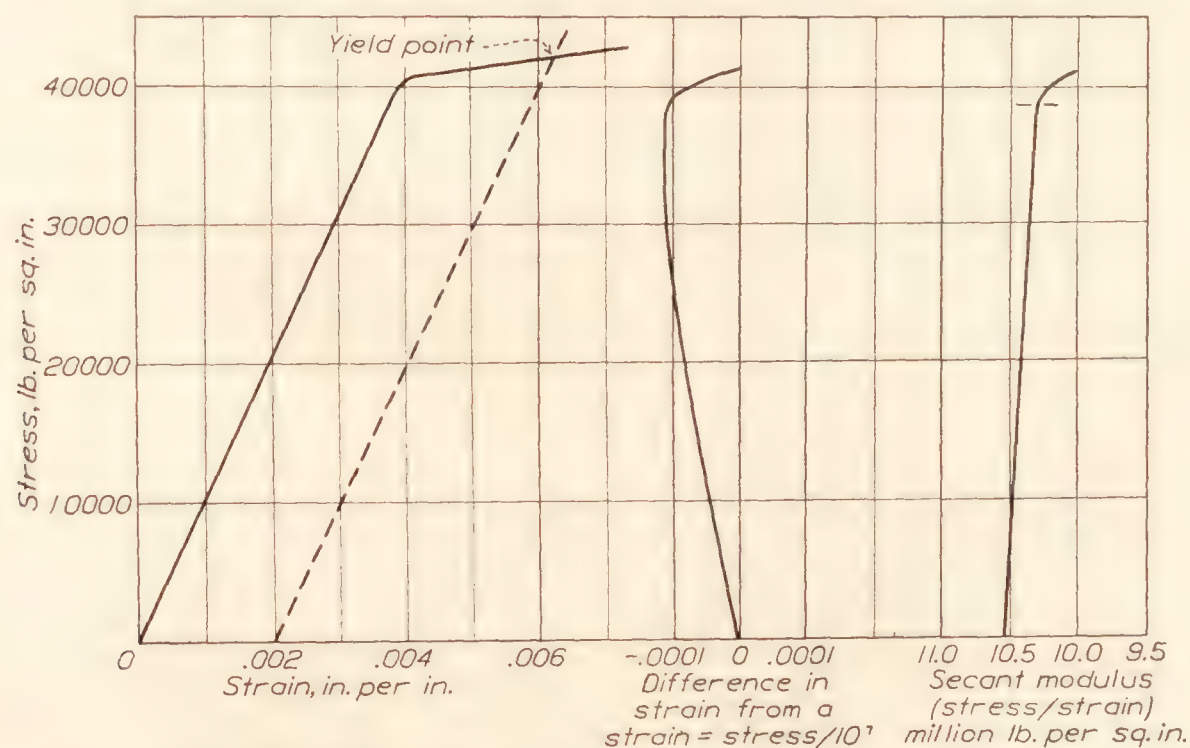


FIGURE 3.—Stress-strain diagram for sheet duralumin 0.011 inch thick, parallel to the direction of rolling.

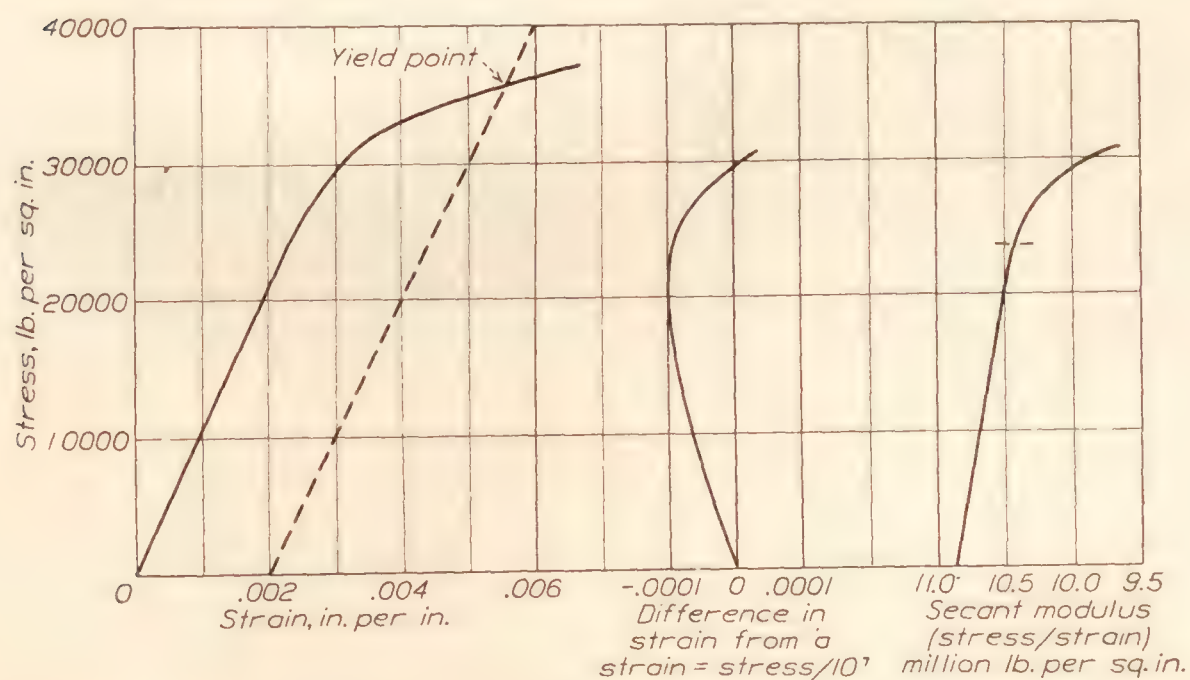


FIGURE 4.—Stress-strain diagram for sheet duralumin 0.011 inch thick, normal to the direction of rolling.

developed surface. The sheet was then wrapped about and clamped to the end bulkheads. (See figs. 5 and 6.) With the cylinder thus assembled, a butt strap 1 inch wide and of the same thickness as the sheet was fitted, drilled, and bolted in place to close the seam. In the assembly of the specimen, care was taken to avoid having either a looseness of the skin (soft spots), or wrinkles in the walls when finally constructed.

The end bulkheads, to which the loads were applied, were each constructed of two steel plates one fourth inch thick, separated by a plywood core $1\frac{1}{2}$ inches thick

gauge mounted in a special jig. In general, the variation in thickness throughout a given sheet was not more than 2 percent of the average thickness. The average thicknesses of the sheets were used in all calculations of radius/thickness ratio and stress.

A photograph of the loading apparatus used in the compression tests is shown in figure 5. Loads were applied by the jack in increments of about 1 percent of the estimated load at failure. At first wrinkling, which usually occurred prior to failure, diamond-shaped wrinkles began to form and grew steadily in size and

sometimes in number with increase in load until failure occurred by a sudden formation of wrinkles in several circumferential rows. (See fig. 6.) Failure was always accompanied by a loud report and by a reduction in load, which continued with deformation of the cylinder after failure. In all the tests, 5 to 10 minutes elapsed from the time that load was first applied to the specimen until failure occurred.



FIGURE 5.—Loading apparatus used in N.A.C.A. compression tests.

With the cylinder loaded at the axis, the 1-inch butt strap at the seam caused a slight eccentricity on all specimens. The effect of this eccentricity was small, however, as there was no tendency for failure to occur consistently on one side of the cylinder.

TESTS ON RUBBER, CELLULOID, STEEL, AND BRASS CYLINDERS

In the compression tests made by Donnell, brass and steel shim stock were used. The sheet that formed the walls of the cylinder was first cut to size and then wrapped about a mandrel and soldered at the seam. In order to stiffen the ends for bearing against the heads of the testing machine, a light metal ring was soldered in place at each end of the cylinder. All the cylinders were tested in a special machine constructed at the California Institute of Technology. For more

complete information concerning the material, specimens, and method of testing, the reader is referred to a report by Donnell on the strength of cylinders in torsion (reference 6). The compression cylinders were constructed in the same manner as the torsion cylinders and were tested in the same machine as the medium-length torsion specimens.

For detailed information concerning the tests on rubber, celluloid, and steel cylinders, the reader is referred to the original sources (references 2, 3, and 4). It should be mentioned, however, that the size and type of specimen and the method of testing differed greatly among the various groups of cylinders tested and that some of these differences were responsible for differences in the strengths obtained. These factors are considered in the discussion of the results.

The results of all the test data considered in this report are given in tables II to VI, inclusive, and in figures 7, 8, and 9.

THEORY AND DISCUSSION OF RESULTS

BRIEF RÉSUMÉ OF GENERAL THEORY

By use of the theory of thin shells as applied to a cylinder of infinite length, Southwell derived an equation (equation 98 of reference 5) relating the critical stress, the properties of the material, and the phenomenon of failure. This equation as given by Prescott in a more simplified form (equation (17.126) of reference 7, p. 553) is

$$-q^2 \frac{S}{E} [(k^2 + q^2)^2 + k^2 + 2q^2 + 2\sigma q^2] + A \left[(k^2 + q^2)^4 + k^4 + 3k^2 q^2 + 2(1 - \sigma)q^4 - 2k^6 - 7k^4 q^2 - (7 + \sigma - 2\sigma^2)k^2 q^4 - \sigma q^6 \right] + q^4 = 0 \quad (1)$$

where

$$A = \frac{t^2}{12(1 - \sigma^2)r^2}$$

$$q = \frac{2\pi r}{\lambda_a}$$

$$k = \frac{2\pi r}{\lambda_c}, \text{ an integer}$$

r , radius of cylinder

t , thickness of cylinder wall

σ , Poisson's ratio

E , modulus of elasticity

S , critical stress

λ_a and λ_c , wave lengths of the wrinkles in the direction of the axis and circumference of the cylinder, respectively.

In his interpretation of the general equation, Southwell reasoned that for a lobed type of failure ($k > 1$) q must be small if S/E is to have a value possible in practice. Upon the basis of this assumption, Southwell wrote as an approximation for equation (1):

$$\frac{S}{E} = \frac{q^2}{k^2(k^2 + 1)} + \frac{Ak^2(k^2 - 1)^2}{(k^2 + 1)q^2} \quad (2)$$

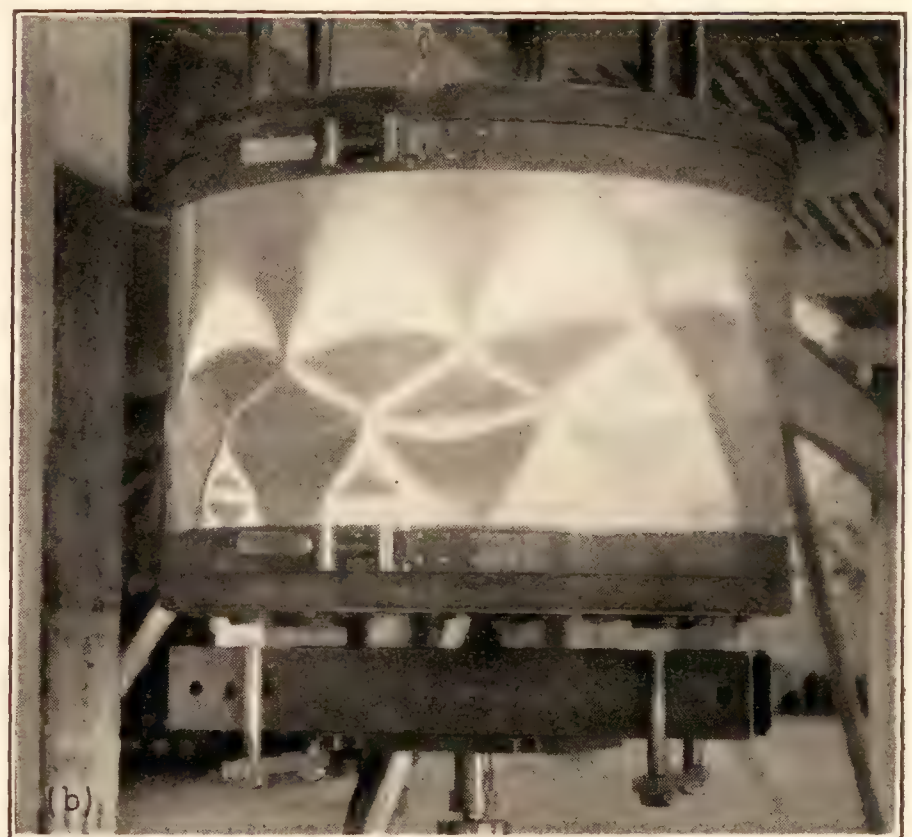
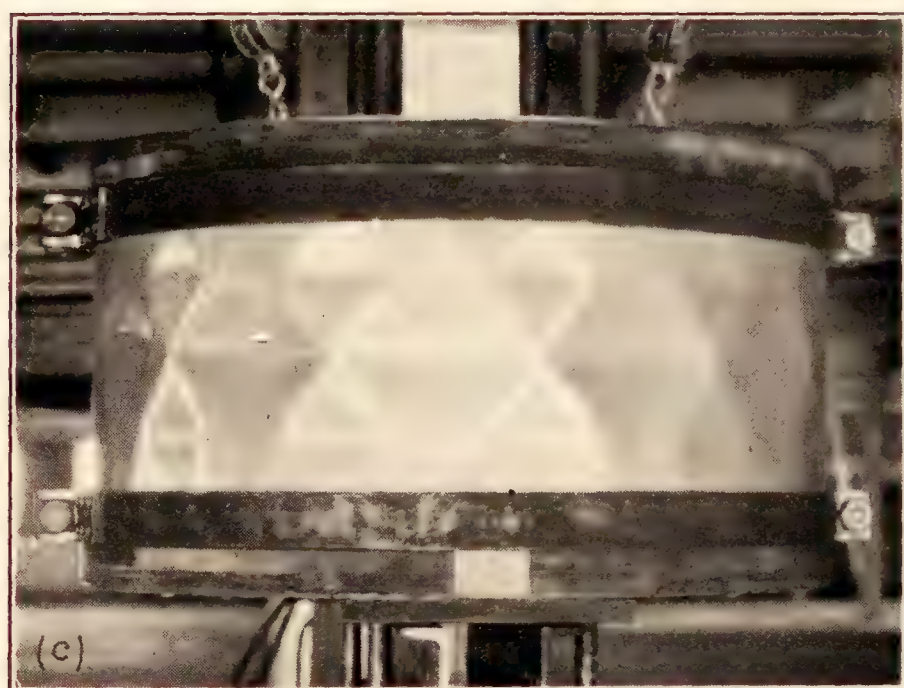
(a) $r=7.5$ in.; $\frac{l}{r}=2.50$; $\frac{r}{t}=646$ (b) $r=15.0$ in.; $\frac{l}{r}=1.00$; $\frac{r}{t}=920$ (c) $r=15.0$ in.; $\frac{l}{r}=0.63$; $\frac{r}{t}=1,415$ (d) $r=15.0$ in.; $\frac{l}{r}=0.50$; $\frac{r}{t}=711$

FIGURE 6.—Cylinders after failure, N.A.C.A. tests on duralumin cylinders.

In reference 2, Robertson shows Southwell's reasoning to be in error, and that for a lobed type of failure, a possible value of S/E may occur with a large value of q . Upon the assumption that q is large, Robertson wrote as an approximation for equation (1):

$$\frac{S}{E} = \frac{1}{\alpha^2} + A\alpha^2 \quad (3)$$

where

$$\alpha = \frac{k^2 + q^2}{q}$$

In references 2 and 5 it is not clear as to which absolute values of q may be regarded as small and which

as large. An inspection of equation (1) reveals that any given value of q may be regarded as small or large, depending upon the value of k . From equation (3) it is evident that Robertson regarded values of q approximately equal to k as large. It would therefore seem better to say that equation (2) is an approximation for equation (1) when q/k is small, and that equation (3) is an approximation for it when q/k is not small. In any event it is desirable to examine the accuracy and limitations of equations (2) and (3).

If $q = \epsilon k$ and $\sigma = 0.3$, the quantities in the brackets in the first and second terms of equation (1), together

with the Southwell and Robertson approximations for them, became

C, correct values

$$\text{First term} \quad [k^4(1+\epsilon^2)^2 + k^2(1+2.6\epsilon^2)]$$

$$\text{Second term} \quad \left[k^8(1+\epsilon^2)^4 + k^4(1+3\epsilon^2+1.4\epsilon^4) \right. \\ \left. - k^6(2+7\epsilon^2+7.1\epsilon^4+0.3\epsilon^6) \right]$$

S, Southwell approximation ($\epsilon = \frac{q}{k}$, small)

$$\text{First term} \quad [k^4 + k^2]$$

$$\text{Second term} \quad [k^8 + k^4 - 2k^6]$$

R, Robertson approximation ($\epsilon = \frac{q}{k}$, not small)

$$\text{First term} \quad [k^4(1+\epsilon^2)^2]$$

$$\text{Second term} \quad [k^8(1+\epsilon^2)^4]$$

In table VII numerical values of the preceding quantities are tabulated for values of ϵ ranging from 0.01 to 10 and values of k from 1 to 25, the case $k=0$ being omitted in the table because when $k=0$, q is infinitely large with respect to k . Robertson's approximation, which includes only the highest powers of q in each term of equation (1), is therefore valid for $k=0$.²

From table VII, it is evident that for each value of ϵ there is a value of k that cannot be exceeded if q/k is to be regarded as small. For values of k given above the horizontal lines in table VII, Southwell's approximation (q/k small) is preferable to Robertson's approximation (q/k not small). For values of k given below the horizontal lines, Robertson's approximation is equally as good as, or preferable to, Southwell's.

PRIMARY FAILURE OR COLUMN ACTION ($k=1$)

According to the theory (reference 5 or 7), the case $k=1$ corresponds to a buckling of the cylinder as a whole in a manner similar to primary failure in columns. This type of failure is characteristic only of a long slender tube where the wave length λ_a is large compared to the circumference ($2\pi r$). It therefore follows that for $k=1$, both q and the ratio q/k must be small and Southwell's approximation applies. Thus, putting $k=1$ in equation (2) leads to the Euler column formula,

$$\frac{S}{E} = \frac{q^2}{2} = \frac{1}{2} \left(\frac{2\pi r}{\lambda_a} \right)^2$$

Since $\frac{\lambda_a}{2} = l$, the length of a pin-ended column, and

$\frac{r}{\sqrt{2}} = \rho$, the radius of gyration of a thin-walled tube,

$$S = \frac{\pi^2 E}{\left(\frac{l}{\rho} \right)^2}$$

In terms of the total load this latter equation becomes

$$P = \frac{\pi^2 EI}{l^2}$$

² The statement that Robertson's approximation is valid for $k=0$, is made on the assumption that $q>1$. In the end it can be shown that when $k=0$ all practical values of q are greater than 1.

SECONDARY FAILURE OR LOCAL BUCKLING

[All values of k other than $k=1$]

All values of k other than 1 correspond to failure by local buckling of the cylinder walls. Figure 1 shows the type of failure for $k=0$. Figures 2 and 6 show failures that correspond to $k>1$.

It will be recalled that equations (2) and (3) are merely approximations for the general equation relating the critical stress, the properties of the material, and the phenomenon of failure. For a test cylinder that is free to buckle into any wrinkle pattern, instability will occur at the minimum value of the critical stress. Thus differentiating S with respect to q as the independent variable in equation (2), it is found that Southwell's approximation gives:

$$\frac{S_{min}}{E} = \frac{k^2-1}{k^2+1} 2\sqrt{A} = \frac{k^2-1}{k^2+1} \sqrt{\frac{1}{3(1-\sigma^2)}} \frac{t}{r} \quad (4)$$

when

$$q^4 = k^4(k^2-1)^2 A = \frac{k^4(k^2-1)^2 t^2}{12(1-\sigma^2)r^2} \quad (5)$$

In a similar manner, differentiating S with respect to α in equation (3), the corresponding equations for Robertson's approximation are:

$$\frac{S_{min}}{E} = 2\sqrt{A} = \sqrt{\frac{1}{3(1-\sigma^2)}} \frac{t}{r} \quad (6)$$

when

$$\alpha = \frac{k^2+q^2}{q} = \sqrt[4]{\frac{1}{A}} = \sqrt[4]{12(1-\sigma^2)} \sqrt{\frac{r}{t}} \quad (7)$$

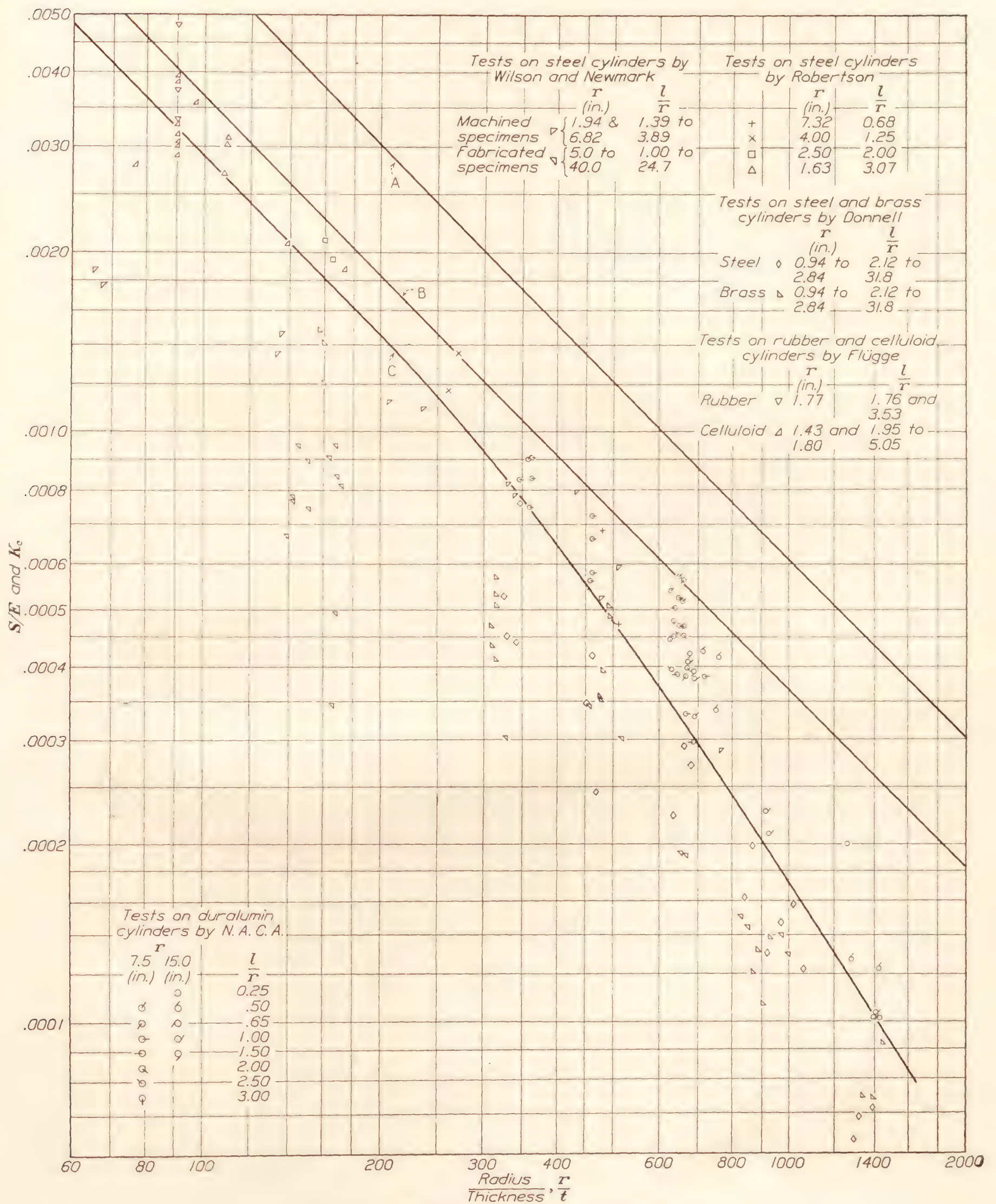
It will be noted from equations (4) and (6) that when q/k is small, the critical stress is $\frac{k^2-1}{k^2+1}$ times the critical stress when q/k is not small. As the ratio $\frac{k^2-1}{k^2+1}$ is always less than unity for $k>1$, the critical stress for the formation of lobes as given by Southwell is always less than the critical stress given by Robertson. Consequently, failure should occur in the manner predicted by Southwell unless the dimensions of the test cylinder are such that it is physically impossible for q/k to be small.

For a cylinder of infinite length in which failure of the Euler type is prevented it is certainly possible for q/k to be small. In such a cylinder, buckling should occur at a stress equal to the smallest value of S_{min} given by equation (4) or when $k=2$, the minimum value of k for Southwell's approximation (table VII).

For $k=2$, the ratio $\frac{k^2-1}{k^2+1} = 0.6$, and equation (4) becomes

$$\frac{S_{min}}{E} = 0.6 \sqrt{\frac{1}{3(1-\sigma^2)}} \frac{t}{r} \quad (8)$$

From Southwell's treatment of the buckling of a cylinder of infinite length, a section of length $\lambda_a/2$ may be regarded as equivalent to a cylinder of finite

*FIGURE 7—Logarithmic plot of S/E and K_c against r/t .

length with hinged ends. Thus for a test cylinder with hinged ends and of such length that the Euler type of failure does not occur, $\lambda_a/2$ may approach the length of the cylinder and q may be as small as $\pi r/l$, where l is the length of the cylinder. If the value of k in equation (5) that corresponds to this value of q is greater than the value of k given by the horizontal line in table VII for the ratio of q/k obtained from equation (5), it is physically impossible for q/k to be small, as Southwell assumed; therefore Robertson's equations based on q/k not small, apply. In this report a cylinder of such dimensions that it is impossible for q/k to be small is designated a "Robertson" cylinder, in contrast to a "Southwell" cylinder in which it is possible for q/k to be small.

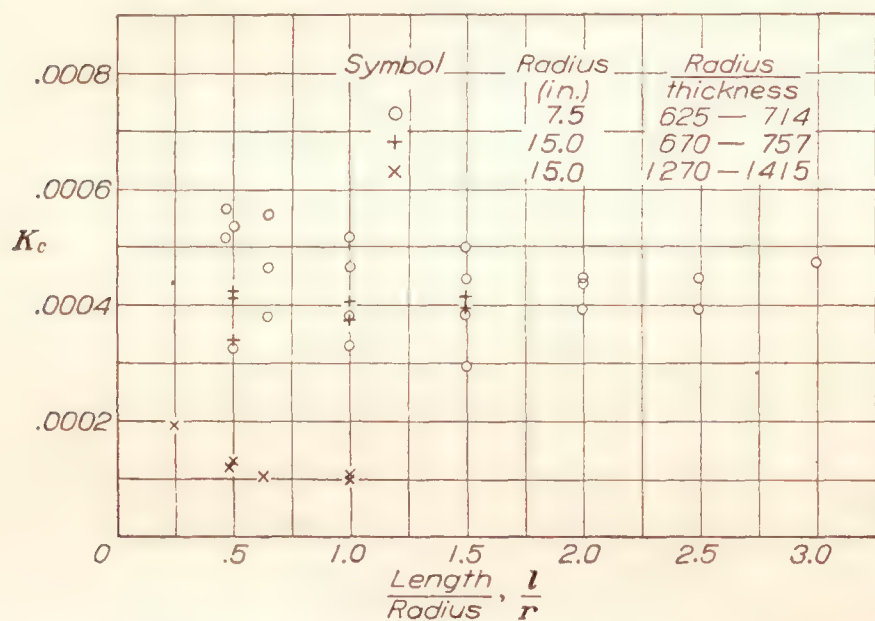


FIGURE 8.—Plot of K_c against length/radius ratio, N.A.C.A. tests on duralumin cylinders.

Although Southwell's theory does not apply to a cylinder with ends clamped to rigid bulkheads, it is reasonable to assume that for such a cylinder the effective value of $\lambda_a/2$ is less than l . Consequently, if it be assumed that $\lambda_a/2 = l$ and the test cylinder under consideration comes within the range of Robertson's approximation as outlined in the preceding paragraph, it may certainly be classed as a Robertson cylinder.

For the duralumin cylinders tested by the N.A.C.A. and the steel cylinders tested by Robertson and reported in reference 2, the lengths ranged from approximately $0.25r$ to $3.0r$. Consequently, the smallest value of q that could occur in these cylinders is $\frac{\pi r}{3r}$ or 1, approximately. From figure 10, where equation (5) is presented in graphical form, it is found that for $q=1$ and $\frac{r}{t}=100$, $k=4$, approximately, and hence $\frac{q}{k} = \frac{1}{4}$, approximately. Since 4 is below the horizontal lines in table VII for $\frac{q}{k}=0.2$ and 0.4 , it is impossible for $\frac{q}{k}$ to be small in this cylinder; hence, it is

classed as a Robertson cylinder. In a similar manner, it can be shown that all the test cylinders of these two groups are classed as Robertson cylinders and, so far as stressed-skin or monocoque structures are concerned, the radius, thickness, and spacing of bulkheads are such that any part of the structure is always a part of a Robertson cylinder. Consequently, the significance of Robertson's equations will be discussed in considerable detail.

CLOSE RELATION BETWEEN THE BUCKLING OF A ROBERTSON CYLINDER AND THE BUCKLING OF A FLAT PLATE

Multiplication of the right-hand side of equation (6) by $\alpha^2 \sqrt{A}$ (which is equal to unity, by equation (7)) gives

$$\frac{S_{min}}{E} = 2A \left[\frac{k^2 + q^2}{q} \right]^2$$

from which

$$S_{min} = \frac{8\pi^2 Et^2}{12(1-\sigma^2)\lambda_c^2} \left[\frac{\lambda_a}{\lambda_c} + \frac{\lambda_c}{\lambda_a} \right]^2$$

On putting $\lambda_a = 2a$ and $\lambda_c = 2b$

$$S_{min} = \frac{2\pi^2 Et^2}{12(1-\sigma^2)b^2} \left[\frac{a}{b} + \frac{b}{a} \right]^2 \quad (9)$$

Inspection of equation (9) reveals that the critical stress for a Robertson cylinder is twice the critical stress for a flat plate that buckles to form waves or wrinkles of the same size as form in the cylinder (reference 8). In reference 9 it is shown that the critical load or stress for a long strut that buckles in an elastic medium³ is also twice the critical load or stress for the same type of buckling without the lateral support of the medium. Consequently, by analogy, the buckling of a Robertson cylinder may be regarded as equivalent to the buckling of a flat plate under edge compression in an elastic medium.

PHENOMENON OF FAILURE

It will be noted that for a Robertson cylinder, equation (7) does not define a particular wrinkle pattern, but rather a family of wrinkle patterns. For $k=0$ ($\lambda_c = \infty$), the walls of the cylinder form circumferential bulges or corrugations (fig. 1). For $k \geq 2$, diamond-shaped or wavelike wrinkles of various dimensions form. (See figs. 2 and 6.) If equation (7) is solved for q it will be found that two values of q are associated with each value of k , one smaller and the other larger than k (reference 2, p. 598). In order to determine which of the many wrinkle patterns described by equation (7) is most likely to occur, it is necessary to examine the condition of buckling for each.

Although equation (7) shows that buckling may occur by the formation of circumferential corrugations, this type of failure is not likely to occur in preference

³ An elastic medium is assumed to provide lateral resistance to buckling. The resistance is distributed along the length of the column and is proportional to the lateral deflection.

to the formation of diamond-shaped or wavelike wrinkles. When buckling begins, circumferential tensions and compressions that are set up in the crests and troughs of the corrugations reinforce the longitudinally stressed elements and prevent complete fail-

axis", has ever occurred except in tubes of small radius/thickness ratio where the stresses have equaled or exceeded the yield point. (See reference 2.)

If failure occurs by the formation of diamond-shaped or wavelike wrinkles, it might be expected, by analogy

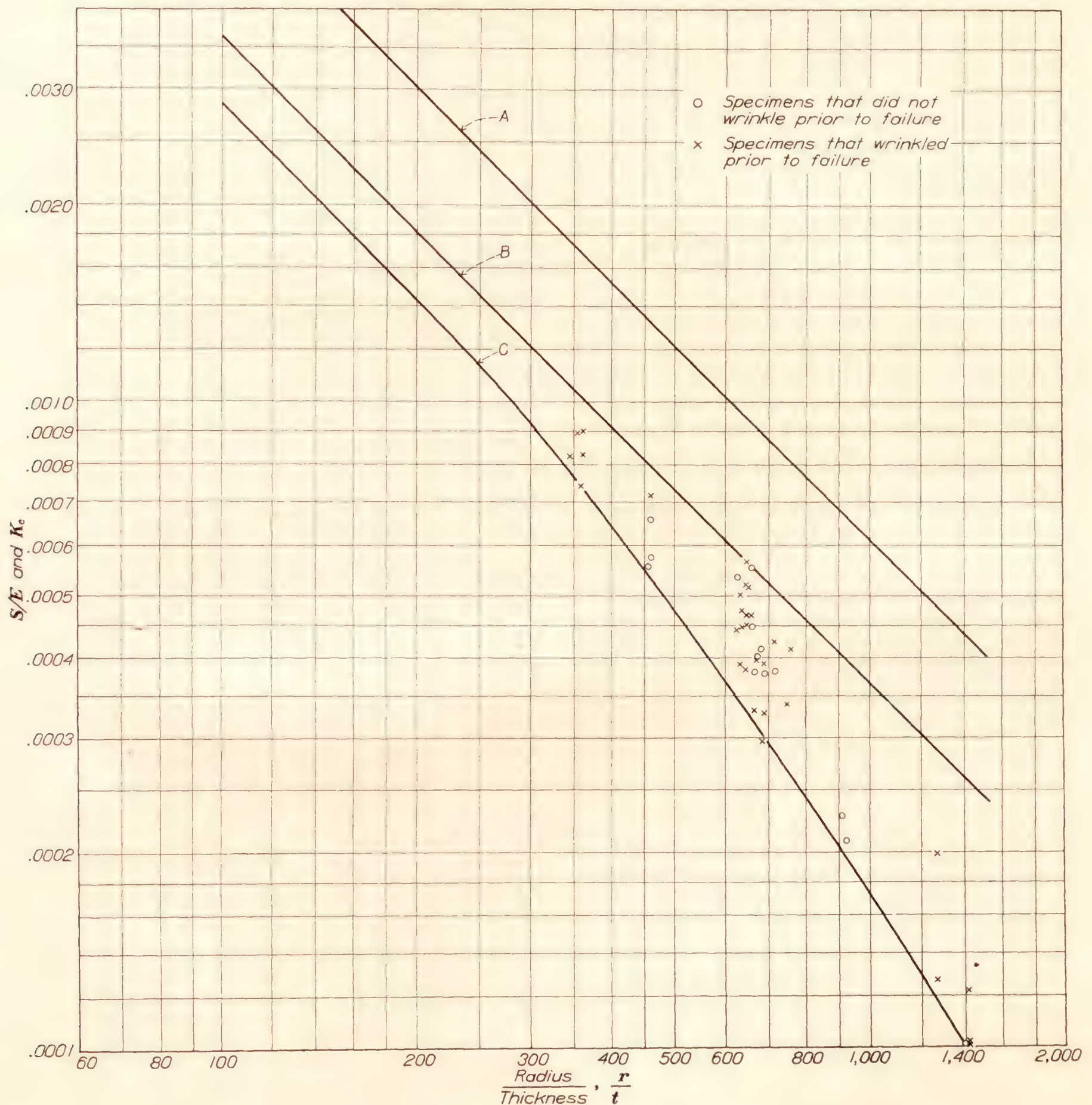


FIGURE 9.—Effect of wrinkling prior to failure on the strength of thin-walled cylinders in compression. Tests by N.A.C.A. Curves A, B, and C obtained from figure 7.

ure until the yield point of the material is reached or exceeded. In fact, it is doubtful if this type of failure, known in the theoretical literature by the name "deformation symmetrical with respect to the

to the buckling of flat plates, that the wave lengths of the buckles in the direction of the axis and circumference of the cylinder will be equal. Differentiation of k with respect to q in equation (7) shows that the maximum

value of k is obtained when $k=q$ or $\lambda_a=\lambda_c$. Thus, if $\lambda_a=\lambda_c$, equation (7) gives

$$k_{max} = \frac{1}{2} \sqrt{\frac{1}{A}} = \sqrt{\frac{3}{4} (1 - \sigma^2)} \sqrt{\frac{r}{t}} \quad (10)$$

Examination of the graphical presentation of the general equation relating the critical stress with the properties of the material and the phenomenon of failure as given in figure 16 of reference 3 shows a gradual reduction of S_{min} and k with a decrease in q . Thus for both Southwell and Robertson cylinders it might be expected that the number of wrinkles will be given by equations (5) and (7), respectively, if q has the smallest ($\lambda_a/2$ the largest) value consistent with the length and end conditions of the test cylinder.

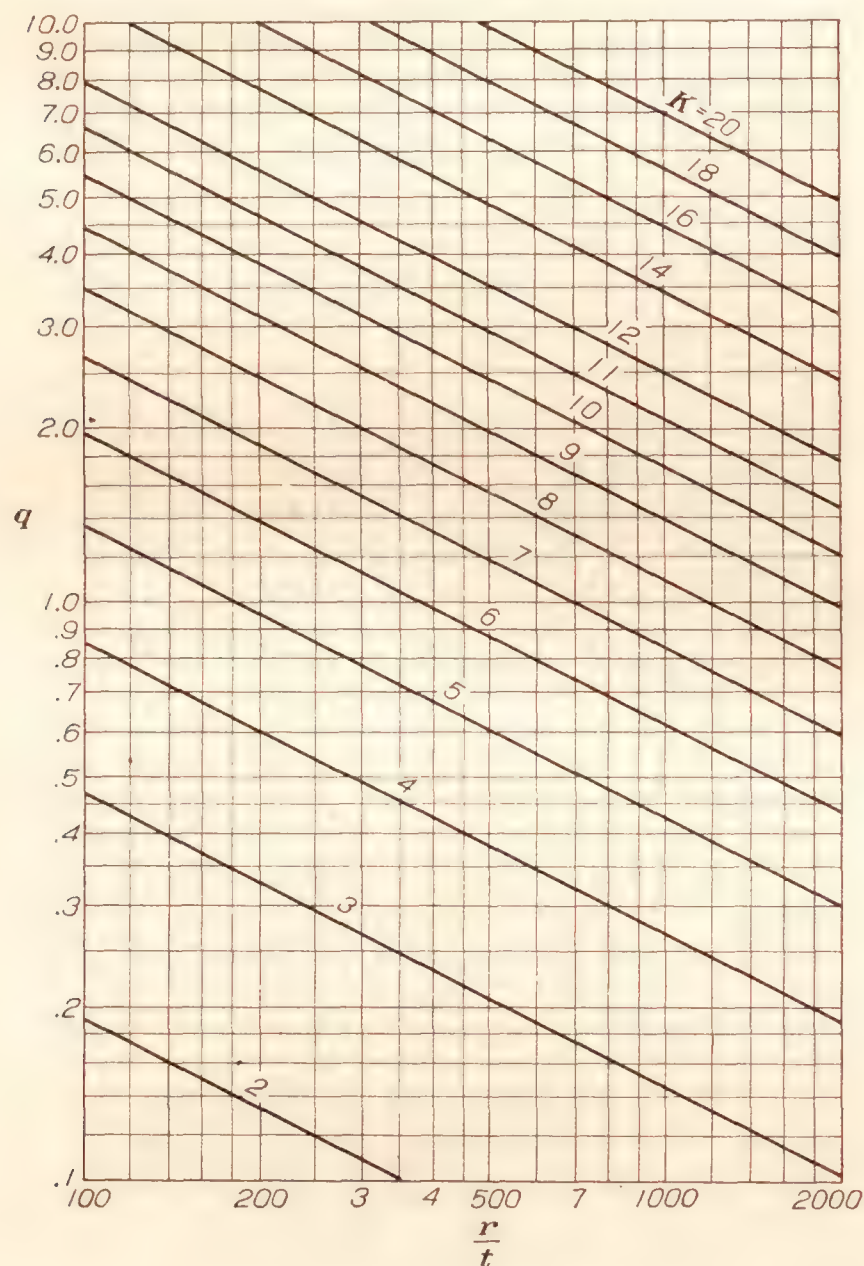


FIGURE 10.—Graphical solution of equation (5),

$$q^4 = \frac{k^4(k^2 - 1)2t^2}{12(1 - \sigma^2)r^2}$$

(curves drawn for $\sigma=0.3$)

From the photographs of cylinders after failure (fig. 6), it is evident that λ_a tends to be equal to λ_c . However, upon reference to tables II to VI inclusive, where calculated and experimental values of k are tabulated for comparison, it is observed that the number of wrinkles that form in the circumference of the cylinder is always less than k_{max} . Except for short cylinders ($l/r < 1.0$), the experimental values are generally greater

than the smallest values of k calculated when assuming $\lambda_a/2 = l/2$ and $\lambda_a/2 = l$ in equation (5) or (7). For cylinders of a given radius/thickness ratio, the experimental values of k vary inversely with l/r and approach a constant value for the larger values of l/r . These observed facts are explained as follows:

When buckling occurs by the formation of diamond-shaped or wavelike wrinkles, the walls of the cylinder subdivide into a series of curved plates of length a and width b simply supported along the adjacent edges. According to the equations of the deflected surface (equation (56), reference 5; or equation (17.116), reference 7), these edges do not move out of the plane of the cylinder wall. However, when buckling begins there is no positive support provided to prevent a displacement normal to the cylinder wall. Consequently, the edges of the curved plates behave like Euler columns and buckle, with the result that the cylinder collapses. If the type of buckling predicted by the theory actually took place so that the edges of the curved plates remained in the plane of the cylinder wall, a collapse of the cylinder would not occur and the curved plates would buckle in a manner similar to the corresponding flat plate simply supported at the edges. The load carried by the cylinder would then increase to a maximum value that is dependent upon the properties of the material in the same manner as the load for a flat plate increases to a maximum. (See references 8 and 10.)

From the preceding description of the behavior of a test cylinder during the process of failure, it is evident that the wrinkle pattern assumed by the cylinder when it collapses is dependent upon a type of buckling not described by the equations of the theory. It is, therefore, to be expected that the number of wrinkles that actually form may differ from the theoretical number, although the two values may be related in some manner.

For example, in a few of the N.A.C.A. tests where preliminary wrinkles formed prior to failure, the wave lengths were very nearly equal to $\frac{2\pi r}{k_{max}}$. However, upon continued loading the wrinkles grew steadily in size until failure occurred.

In another case a tube ($r=0.607$ in.; $r/t=15.7$; $l/r=10.6$) was observed that developed what would correspond to a 2-lobed deformation of the Southwell type, but failure occurred at one end by the formation of three or four lobes of the Robertson type.

STRESS AT FAILURE IN TEST CYLINDERS

In figure 7 the results of all the tests are plotted logarithmically, S/E against r/t , together with the graphs of equations (6) and (8). It will be observed from this figure that except for a few of the tests made by Flügge, all of the tests made by Flügge, Robertson, and the N.A.C.A. plot between curves B and C. It will also be observed that for these tests,

the stress at failure approaches as a maximum the critical stress for a cylinder of infinite length, and that the results of the tests scatter widely and depart from the theoretical straight line at large values of the radius/thickness ratio. This departure from the theoretical stress relation is caused by imperfections and eccentricities in the elements of the cylinder which, relatively speaking, increase with increase in the radius/thickness ratio.

The results of the tests on machined cylinders by Wilson and Newmark (reference 4) plotted in figure 7 are in agreement with the results discussed in the preceding paragraph, except for radius/thickness ratios less than 235 where the stresses obviously approached or exceeded the proportional limit and yield point of the material. In fact, there were additional tests made by Wilson and Newmark on machined specimens, the results of which are not included in the present report because the stresses developed were so high that yielding of the material must have occurred.

The results of the tests made by Wilson and Newmark on fabricated steel cylinders and the results of the tests made by Donnell on steel and brass cylinders plot below curve C in figure 7. In the tests by Wilson and Newmark the cylinders were loaded directly between the heads of a testing machine. The ends of the cylinder were held circular by means of either a steel angle or a wood ring, but contact with the heads of the machine was made by the shell alone. This fact, together with the fact that fabricated cylinders with riveted or welded seams are inherently less perfect than machined cylinders, may possibly account for the reduced strength of the Wilson and Newmark cylinders.

In the case of Donnell's tests, the reduced strength may possibly have been caused by imperfect cylinders. Obviously, in the construction of cylinders with shim stock of the small dimensions used by Donnell, greater skill is required to obtain a given degree of perfection than would be required for larger cylinders of thicker material.

Upon reference to the tests on the large fabricated cylinders of series E in table VI, it will be observed that a change from welded to riveted seams has but little effect upon the stress at failure.

It should be mentioned here that the fabricated cylinders tested by Wilson and Newmark were built of structural material such as might be used in bridges, buildings, or ships, whereas the cylinders tested by Donnell were built of material much thinner than that used even in aircraft structures. As a consequence, the test data should have a wide range of usefulness in various fields of engineering, particularly in view of the fact that the results are in agreement when plotted nondimensionally.

In view of the wide differences between the results of the various tests, it is concluded that for design purposes the compressive stress at failure is best given by an equation of the most general form

$$S_c = K_c E \quad (11)$$

where K_c is a nondimensional coefficient that varies with the dimensions and imperfections of the cylinder. Except for very short cylinders the radius and thickness as expressed by the ratio r/t are the only dimensions of the cylinder that need be considered because the large effect of slight imperfections and eccentricities in the elements of the cylinder completely overshadow the small effect of length. (See fig. 8.) Consequently, the designer who uses these data must estimate the degree of perfectness of his particular design by a proper choice of the value of K_c from figure 7. In general, design values for K_c will be less than the values given by curve C which represents the lower limit of the results obtained with the most perfect laboratory test specimens.

The results of the N.A.C.A. tests plotted in figure 7 are replotted in figure 9, where distinction is made regarding those points representing cylinders in which wrinkling occurred prior to failure. From this figure it is concluded that preliminary wrinkling did not apparently reduce the stress at failure.

Why the critical stress for the Robertson cylinders tested approached as a maximum, but did not exceed, the critical stress for a cylinder of infinite length, is difficult to explain. It may be that the type of buckling for a collapse of the cylinder is associated with the lower stress, or that when the stress given by equation (8) is reached a condition of instability is obtained and the cylinder deforms slightly as a part of a cylinder of infinite length. Then, since the cylinder is so sensitive to slight imperfections and eccentricities, failure is precipitated at the critical stress for a cylinder of infinite length, and the wrinkles assume a pattern consistent with the dimensions of the cylinder. This latter explanation of the inability to develop stresses greater than the critical stress for a cylinder of infinite length seems reasonable because it is impossible to construct a mathematically perfect cylinder. Thus, a slight deformation of the test cylinder may be expected at the critical stress for a cylinder of infinite length, and the upper limit of perfectness is established by this fact.

EFFECT OF END BULKHEADS

In view of the fact that the stress at failure is independent of length ($l/r > 0.5$, fig. 8) and approaches but does not exceed the critical stress for a cylinder of infinite length (fig. 7), it is concluded that the end bulkheads contribute little, if any, toward the stability of the cylinder walls. This conclusion appears reasonable so long as the length of the cylinder is greater

than several times the smallest value of $\lambda_a/2$ likely to be associated with the type of failure characteristic of the cylinder under consideration. For the test cylinders considered in this report, the smallest value of $\lambda_a/2$ is not likely to exceed the value corresponding to the condition $k=q$ in equation (7) or

$$\frac{\lambda_a}{2} = \frac{\pi r}{k_{max}} = \frac{\pi r}{\sqrt[4]{\frac{3}{4}(1-\sigma^2)} \sqrt{r/t}} \quad (12)$$

In table VIII values of $\lambda_a/2r$ obtained from equation (12) are tabulated for comparison with the smallest length/radius ratios of the test cylinders considered in this report. An examination of this table in connection with figures 7 and 8 shows that for practical purposes, if l/r is greater than three to five times the value of $\lambda_a/2r$ obtained from equation (12), bulkheads have no effect upon the stress at failure.

EFFECT OF LONGITUDINAL STIFFENERS

From consideration of the effect of bulkheads on the strength of thin-walled cylinders in compression, it follows by parallel reasoning that longitudinal stiffeners will contribute little toward the stability of the cylinder walls if spaced at a distance greater than several times the smallest value of $\lambda_c/2$ likely to be associated with elastic buckling of the walls. Since the smallest values of $\lambda_c/2$ are obtained when $k=q$ in equation (7), this minimum value of $\lambda_c/2$ is equal to the value of $\lambda_a/2$ given by equation (12). With longitudinal stiffeners, however, failure as characterized by a collapse of the cylinder is delayed until the stiffeners fail. The ultimate load supported by a cylinder with longitudinal stiffeners may therefore greatly exceed the load at which buckling begins.

CONCLUSIONS

1. For thin-walled cylinders in which failure occurs by elastic buckling of the walls, the stress at failure (collapse of the cylinder) is best given by an equation of the form

$$S_c = K_c E$$

where K_c is a nondimensional coefficient that varies with the dimensions and imperfections of the cylinder. Except for very short cylinders, the radius and thickness as expressed by the ratio r/t are the only dimensions that need be considered.

2. Wrinkling prior to failure does not apparently reduce the stress at failure.

3. For large fabricated cylinders, a change from welded to riveted seams has but little effect upon the stress at failure.

4. After the cylinder has failed, the wave lengths of the wrinkles in the direction of the axis and circumference are equal. The number of wrinkles that form in the circumference varies inversely with the length/radius ratio and for a given radius/thickness ratio seems to approach a constant value at the larger values of l/r .

5. The compressive stress at failure is independent of length so long as the length of the cylinder is greater than three to five times the value of $\lambda_a/2$ given by the equation

$$\frac{\lambda_a}{2} = \frac{\pi r}{k_{max}} = \frac{\pi r}{0.91 \sqrt{r/t}}$$

In the preceding conclusions, a cylinder whose length is less than from three to five times the value of $\lambda_a/2$ given by the above equation is designated "a very short cylinder."

6. Bulkheads, or transverse stiffeners, to be effective in preventing failure by elastic buckling of the walls, hence in strengthening the walls, should be spaced at a distance less than from three to five times the value of $\lambda_a/2$ given by the above equation. The same conclusion applies for longitudinal stiffeners, except that failure as characterized by a collapse of the cylinder would be delayed until the stiffeners failed.

LANGLEY MEMORIAL AERONAUTICAL LABORATORY,
NATIONAL ADVISORY COMMITTEE FOR AERONAUTICS.
LANGLEY FIELD, VA., June 10, 1933.

APPENDIX

GENERAL DISCUSSION OF THE BUCKLING OF FLAT AND CURVED PLATES UNDER EDGE COMPRESSION

EQUATIONS FOR THE BUCKLING OF A FLAT PLATE UNDER EDGE COMPRESSION IN AN ELASTIC MEDIUM

The critical stress for a flat plate under edge compression without the support of an elastic medium is equal to the critical stress for a pin-ended plate column of the same thickness with a length equal to

$$\frac{b}{\frac{a}{b} + \frac{b}{a}}$$

where b is the half-wave length of a buckle normal to the direction of loading, and a is the half-wave length of the same buckle parallel to the direction of loading. Equation (11) of reference 9 gives the critical load for a column under compression in an elastic medium. Consequently, if

$$\frac{b}{\frac{a}{b} + \frac{b}{a}}$$

is substituted for l in this equation and both sides divided by bt , the area of a strip of plate of width b , the following general expression is obtained for the critical stress in a flat plate under edge compression in an elastic medium:

$$S = \frac{P_{cr}}{bt} = \frac{E'I\pi^2}{bt\beta^2} \left[1 + \frac{K\beta^4}{E'I\pi^4} \right] \\ = \frac{\pi^2 Et^2}{12(1-\sigma^2)\beta^2} \left[1 + \frac{12(1-\sigma^2)K\beta^4}{Ebt^3\pi^4} \right] \quad (13)$$

where

P_{cr} , critical load for a strip of plate of width b , pounds.

t , thickness of plate, inches.

S , critical stress, pounds per square inch.

$E' = \frac{E}{1-\sigma^2}$, bending modulus for a plate as contrasted with E , the bending modulus of a beam or column, pounds per square inch.

$I = \frac{1}{12}bt^3$, moment of inertia of a strip of plate of width b , inches⁴.

K , modulus of the elastic medium taken in such a way that $\frac{K}{b}$ times the deflection represents the reaction of the medium per unit area of the plate, pounds per square inch.

σ , Poisson's ratio.

$$\beta = \frac{b}{\frac{a}{b} + \frac{b}{a}}$$

If the plate is large and free to buckle in any manner, β will assume such a value that S is a minimum. Consequently, differentiation of S with respect to β in equation (13) gives

$$S_{min} = 2\sqrt{\frac{KEt}{12(1-\sigma^2)b}} \quad (14)$$

when

$$\beta = \sqrt[4]{\frac{Ebt^3\pi^4}{12(1-\sigma^2)K}} \quad (15)$$

EQUIVALENT ELASTIC MEDIUM FOR A ROBERTSON CYLINDER

When buckling begins in a Robertson cylinder, the effect of curvature is such as to set up forces that oppose buckling. For small deflections, these forces are proportional to the deflections, hence they may be regarded as analogous to the lateral reactions of an elastic medium in the previous discussion of the buckling of flat plates. The modulus of an equivalent elastic medium for a Robertson cylinder may therefore be obtained by equating S_{min} in equations (6) and (14) and solving for K . Thus,

$$\sqrt{\frac{1}{3(1-\sigma^2)} \frac{Et}{r}} = 2\sqrt{\frac{KEt}{12(1-\sigma^2)b}}$$

from which

$$K = \frac{Ebt}{r^2} \quad (16)$$

Substitution of this value of K in equation (13) gives the following general expression for the critical compressive stress in a Robertson cylinder

$$S = \frac{\pi^2 Et^2}{12(1-\sigma^2)\beta^2} \left[1 + \frac{12(1-\sigma^2)\beta^4}{t^2 r^2 \pi^4} \right] \quad (17)$$

Equation (17), while different in form, is in substance the same as equation (3). This fact will be shown by the following derivation: According to equation (3),

$$\frac{S}{E} = \frac{1}{\alpha^2} + A\alpha^2$$

and

$$S = E\alpha^2 A \left[1 + \frac{1}{\alpha^4 A} \right] \quad (18)$$

By definition

$$\alpha = \frac{\pi r}{\beta} \quad (19)$$

Consequently, substitution of the values that define α and A in equation (18) gives equation (17).

BRIEF DISCUSSION OF FORCED FAILURE

From the form of equation (17), it may be concluded that Southwell's general equation (equation (1) of this report) contains the solutions for the buckling of both flat and curved plates subjected to edge compression. The second term in the brackets represents the effect of curvature on the critical stress. If $r = \infty$, this term becomes zero and equation (17) gives the critical compressive stress for a flat plate simply supported at the four edges. In a similar manner, if t and r have fixed values such as correspond to the dimensions of a particular cylinder and β is forced with stiffeners to be less than the value that causes S to be a minimum

$$\beta = \sqrt[4]{\frac{t^2 r^2 \pi^4}{12(1 - \sigma^2)}} \quad (20)$$

the second term in the brackets rapidly becomes a small fraction and the critical stress approaches that for a flat plate. If values of β less than half the value given by equation (20) are forced, the portion of the curved sheet under consideration may be regarded as flat with an error not greater than 6.3 percent.

Further consideration of the subject of forced failure is beyond the scope of the present report. However, in view of the correlation of the buckling of thin-walled cylinders with the buckling of plates, it would appear that perhaps many solutions obtained for problems in the buckling of plates can, with the proper factors, be applied to similar problems in the buckling of cylinders and curved sheets. It is therefore recommended that theoretical and experimental research be conducted to explore this field, particularly as regards the compressive strength of curved sheet and stiffener combinations.

REFERENCES

1. Lundquist, Eugene E.: Strength Tests on Thin-Walled Duralumin Cylinders in Torsion. T.N. No. 427, N.A.C.A., 1932.
2. Robertson, Andrew: The Strength of Tubular Struts. R. & M. No. 1185, British A.R.C., 1929.
3. Flügge, W.: Die Stabilität der Kreiszyinderschale. Ingenieur-Archiv, Band III, no. 5, pp. 463-506, December 1932.
4. Wilson, Wilbur M., and Newmark, Nathan M.: The Strength of Thin Cylindrical Shells as Columns. Bull. No. 255, Eng. Exp. Sta., Univ. Ill., Feb. 28, 1933.
5. Southwell, R. V.: On the General Theory of Elastic Stability. Phil. Trans. Roy. Soc. (London), vol. 213, series A, 1914, pp. 187-244.
6. Donnell, L. H.: Stability of Thin-Walled Tubes under Torsion. T.R. No. 479, N.A.C.A., 1933.
7. Prescott, John: Applied Elasticity. Longmans, Green and Co., London, 1924, chap. XVII.

8. Schuman, Louis, and Back, Goldie: Strength of Rectangular Flat Plates under Edge Compression. T.R. No. 356, N.A.C.A., 1930.
9. Timoshenko, S.: Problems Concerning Elastic Stability in Structures. Trans. Amer. Soc. Civ. Eng., vol. 94, 1930, pp. 1,000-1,035.
10. von Kármán, Theodor, Sechler, Ernest E., and Donnell, L. H.: The Strength of Thin Plates in Compression. Applied Mechanics Section of Trans. A.S.M.E., Jan. 30, 1932, p. 53.

BIBLIOGRAPHY

1905. Lilly, W. E.: The Strength of Columns. Proc. Inst. Mech. Eng., London, Parts 3 and 4, June 1905, p. 697.
1907. Lilly, W. E.: The Economic Design of Columns. Proc. Inst. Civ. Eng. of Ireland (Dublin), vol. 33, March 1907, p. 57.
1908. Lilly, W. E.: The Design of Struts. Engineering, Jan. 10, 1908.
1908. Mallock, A.: Note on the Instability of Tubes Subjected to End Pressure, and on the Folds in a Flexible Material. Proc. Roy. Soc. (London), series A, vol. 81, 1908, p. 388.
1908. Lorenz, Rudolph: Achsensymmetrische Verzerrungen in Dünnwandigen Hohlzylindern. Z.V.D.I., Oct. 24, 1908, vol. 52, pp. 1706-13.
1910. Timoshenko, S.: Einige Stabilitätsprobleme der Elastizitätstheorie. Z.f. Math. u. Physik, vol. 58, p. 337. (Abstract of a paper published in 1907 in the Bull. of the Polytechnical Institute at Kiew.)
1911. Lorenz, Rudolph: Die Nicht Achsensymmetrische Knickung Dünnwandiger Hohlzylinder. Physik. Zeits. Leipzig. Jahrg. 12, pp. 241-260.
1914. Timoshenko, S.: (Buckling of Cylinders—Title Unknown). Bull. Electrotechnical Inst., St. Petersburg, vol. XI.
1916. Timoshenko, S.: Theory of Elasticity. Vol. II, St. Petersburg.
1922. Westergaard, H. M.: Buckling of Elastic Structures. Trans. Amer. Soc. of Civ. Eng., pp. 576-676. Paper No. 1490. (Including discussions by George Paaswell, Eugene E. Halmos, and Edward Godfrey.)
1925. Dean, W. R.: On the Theory of Elastic Stability. Proc. Roy. Soc. (London) vol. 107, series A, pp. 734-59.
1928. Geckeler, J. W.: Plastisches Knicken der Wandung von Hohlzylindern und einige andere Faltungerscheinungen an Schalen und Blechen. Z.f.a.M.M., October 1928, vol. 8, pp. 341-52.
1928. Geckeler, J. W.: Elastostatics. Handbuch der Physik. H. Geiger und Karl Scheel, bearb. Band VI, Kapitel III, pp. 298-302. Julius Springer (Berlin) 1928.
1930. Timoshenko, S.: Stability and Strength of Thin-Walled Constructions. Proc. Third International Congress for Applied Mechanics, Stockholm, vol. III, 1930.
1931. Timoshenko, S.: Stabilitätsprobleme der Elasticität. Handbuch der Physikalischen und Technischen Mechanik. F. Auerbach und W. Hort, bearb. Band IV, I. J. A. Barth, Leipzig, 1931, pp. 81-145.
1932. von Sanden, K. V., and Tölke, F.: Über Stabilitätsprobleme dünner, Kreiszyindrischer Schalen. Ingenieur-Archiv, vol. 3, no. 1, March 1932, pp. 24-66.

TABLE I.—PROPERTIES OF SHEET DURALUMIN USED IN STRENGTH TESTS ON THIN-WALLED CYLINDERS

[Longitudinal and transverse refer to specimens taken parallel and normal to the direction of rolling, respectively]

Material		Ultimate tensile strength (pounds per square inch)		Tensile yield point (pounds per square inch)		Elongation in 2 inches (percent)		Modulus of elasticity			
								Secant modulus at a stress of 5,000 pounds per square inch (pounds per square inch)		Secant modulus at a stress of 20,000 pounds per square inch (pounds per square inch)	
Lot	Specimen no.	Longitudinal	Transverse	Longitudinal	Transverse	Longitudinal	Transverse	Longitudinal	Transverse	Longitudinal	Transverse
1	17	58,500	55,500	41,400	36,500	18	16.5	10,620,000	10,720,000	10,510,000	10,520,000
1	34	59,400	56,600	42,500	37,100	15	16.5	10,720,000	10,770,000	10,580,000	10,570,000
2	48		57,300		36,800		16.5		10,570,000		10,340,000
2	50		56,800		35,800		13.0		10,550,000		10,380,000
2	55		58,200		36,500		18.0		10,470,000		10,270,000
2	70		57,800		35,800		16.0		10,560,000		10,440,000
3	2A		62,850		33,750		19.3		10,270,000		10,130,000
3	14A		62,800		41,000		14.0		10,410,000		10,190,000
3	46A		61,550		38,750		19.0		10,550,000		10,350,000
3	63A		61,400		39,050		18.5		10,110,000		10,060,000
3	68A		61,400		37,900		18.5		10,410,000		10,070,000

TABLE II.—CALCULATED AND EXPERIMENTAL VALUES OF k FOR N.A.C.A. TESTS ON DURALUMIN CYLINDERS

$\frac{l}{r}$	Radius=7.5 inches												Radius=15.0 inches													
	$\frac{r}{t}=333-362$				$\frac{r}{t}=455-460$				$\frac{r}{t}=625-714$				$\frac{r}{t}=670-757$				$\frac{r}{t}=909-920$				$\frac{r}{t}=1270-1415$					
	k_{max}	$k\left(\frac{\lambda_a}{2}=\frac{l}{2}\right)$	$k\left(\frac{\lambda_a}{2}=l\right)$	$k\text{ (exp.)}$	k_{max}	$k\left(\frac{\lambda_a}{2}=\frac{l}{2}\right)$	$k\left(\frac{\lambda_a}{2}=l\right)$	$k\text{ (exp.)}$	k_{max}	$k\left(\frac{\lambda_a}{2}=\frac{l}{2}\right)$	$k\left(\frac{\lambda_a}{2}=l\right)$	$k\text{ (exp.)}$	k_{max}	$k\left(\frac{\lambda_a}{2}=\frac{l}{2}\right)$	$k\left(\frac{\lambda_a}{2}=l\right)$	$k\text{ (exp.)}$	k_{max}	$k\left(\frac{\lambda_a}{2}=\frac{l}{2}\right)$	$k\left(\frac{\lambda_a}{2}=l\right)$	$k\text{ (exp.)}$	k_{max}	$k\left(\frac{\lambda_a}{2}=\frac{l}{2}\right)$	$k\left(\frac{\lambda_a}{2}=l\right)$	$k\text{ (exp.)}$		
0.25																		32.7	31.8	25.8	16					
.50	17.2	16.6	3.3	12					23.2 23.3 23.9 22.8	21.0 21.1 21.0 20.4	16.3 16.3 16.1 15.7	13-17	24.4 25.2 25.0	21.3 21.8 21.7	16.3 16.6 16.6	12			32.7 34.5	25.8 27.0	10.3 20.2	13-14				
.65									23.4 23.4 23.5	18.9 18.9 19.0	14.2 14.2 14.3	13-15						34.5	24.3	17.9	12-13					
1.00	16.9 17.2 17.3 17.3	13.1 13.3 13.4 13.4	9.8 9.9 10.0 10.0	9-10	19.5 19.5 19.5 19.4	14.5 14.5 14.3 14.3	10.8 10.8 10.6 10.6	10	24.4 23.5 23.2 23.2	16.3 16.0 15.9 15.9	12.0 11.7 11.7 11.7	10-13	23.6 23.9	16.0 16.1	11.8 11.8	11	27.5 27.7	17.5 17.6	12.8 12.8	11-13	34.2 34.4	19.8 19.8	14.3 14.4	12-15		
1.50									23.8 23.1 23.0 23.0	13.5 13.3 13.2 13.2	9.8 9.7 9.6 9.6	8-12	23.8 23.8	13.5 13.5	9.8 9.8	10										
2.00									23.4 23.6 22.8	11.7 11.8 11.5	8.4 8.5 8.3	8-10														
2.50									22.9 23.2	10.4 10.5	7.5 7.5	7-10														
3.00									23.0	9.6	6.8	8-10														

TABLE III.—CALCULATED AND EXPERIMENTAL VALUES OF k FOR TESTS ON STEEL CYLINDERS REPORTED BY ROBERTSON IN REFERENCE 2

$\frac{l}{r}$	r (in.)	$\frac{r}{t}$ (approx.)	k_{max}	$k\left(\frac{\lambda_a}{2}=\frac{l}{2}\right)$	$k\left(\frac{\lambda_a}{2}=l\right)$	$k\text{ (exp.)}$
0.68	7.32	500	20.3	17.0	12.9	12
1.25	4.00	263	14.7	11.1	8.2	8
2.00	2.50	164	11.6	7.9	5.8	8
3.07	1.63	110	9.5	5.9	4.3	7

TABLE IV.—CALCULATED AND EXPERIMENTAL VALUES OF *k* FOR TESTS ON STEEL AND BRASS CYLINDERS BY DONNELL

Material	$\frac{l}{r}$	$\frac{r}{t}$	Radius=0.943				Radius=1.88				Radius=2.84				$\frac{S_c}{E}$
			k_{max}	$\left(\frac{k}{\frac{\lambda_a}{2}=\frac{l}{2}}\right)$	$\left(\frac{k}{\frac{\lambda_a}{2}=l}\right)$	<i>k</i> (exp.)	k_{max}	$\left(\frac{k}{\frac{\lambda_a}{2}=\frac{l}{2}}\right)$	$\left(\frac{k}{\frac{\lambda_a}{2}=l}\right)$	<i>k</i> (exp.)	k_{max}	$\left(\frac{k}{\frac{\lambda_a}{2}=\frac{l}{2}}\right)$	$\left(\frac{k}{\frac{\lambda_a}{2}=l}\right)$	<i>k</i> (exp.)	
Brass.....	2.12	483									20.0	10.5	7.5	10.0	0.000393
Do.....		923									27.6	12.4	8.9	10.0	.000138
Steel.....		971									28.4	12.6	9.0	11.4	.000146
Do.....		1,013									29.0	12.8	9.1	11.4	.000157
Do.....		1,284									32.6	13.6	9.7	12.0	.000062
Do.....		1,307									32.9	13.6	9.8	12.0	.000068
Brass.....		1,331									33.2	13.7	9.8	11.0	.000074
Do.....		1,383									33.8	13.8	9.9	10.5	.000073
Brass.....	3.20	311					16.0	7.7	5.5	8.8					.000435
Do.....		314					16.1	7.7	5.5	8.0					.000414
Steel.....		633					22.9	9.3	6.6	10.0					.000224
Do.....		660					23.4	9.4	6.7	9.6					.000292
Do.....		837					26.3	10.0	7.1	10.4					.000161
Do.....		864					26.7	10.1	7.2	10.0					.000198
Brass.....		864					26.7	10.1	7.2	9.7					.000120
Do.....		897					27.3	10.2	7.3	10.0					.000106
Brass.....	4.22	476									19.9	7.5	5.4	9.0	.000358
Do.....		490									20.1	7.6	5.4	9.0	.000508
Do.....		490									20.1	7.6	5.4	9.2	.000484
Steel.....		1,058									29.6	9.3	6.6	10.0	.000121
Do.....		1,383									33.8	9.9	7.0	10.0	.000071
Brass.....		1,440									34.5	10.0	7.1	10.0	.000091
Brass.....	6.38	160	11.5	4.7	3.3	8.0									.001200
Do.....		315	16.1	5.6	4.0	6.9									.000511
Do.....		315	16.1	5.6	4.0	7.4									.000572
Steel.....		328	16.5	5.6	4.0	6.7									.000530
Do.....		347	16.9	5.7	4.1	9.2									.000758
Do.....		451	19.3	6.1	4.3	6.7									.000348
Do.....		460	19.5	6.1	4.4	7.5									.000420
Do.....															
Brass.....	6.38	311					16.0	5.5	3.9	7.2					.000472
Steel.....		679					23.7	6.8	4.8	8.7					.000272
Brass.....		880					27.0	7.2	5.1	10.0					.000131
Steel.....		915					27.5	7.3	5.2	8.9					.000129
Brass.....	10.6	474									19.8	4.9	3.5	6.8	.000352
Brass.....	12.7	160	11.5	3.5	2.6	7.9									.001410
Steel.....		342	16.8	4.2	3.0	7.3									.000437
Brass.....	16.0	315					16.1	3.7	2.7	7.4					.000535
Steel.....	25.5	332	16.6	3.0	2.2	5.0									.000045
Brass.....	31.8	158	11.4	2.3	2—	8.3									.001472
Steel.....		469	19.7	2.9	2—	7.2									.000245

NOTE.—In calculating *k* for this table cylinders with $\frac{l}{r} > 6.38$ were considered as Southwell cylinders.

TABLE V.—CALCULATED AND EXPERIMENTAL VALUES OF *k* FOR TESTS ON RUBBER AND CELLULOID CYLINDERS REPORTED BY FLÜGGE IN REFERENCE 3

Material	$\frac{l}{r}$	$\frac{r}{t}$ (in.)	$\frac{r}{t}$ (approx.)	k_{max}	$\left(\frac{k}{\frac{\lambda_a}{2}=\frac{l}{2}}\right)$	$\left(\frac{k}{\frac{\lambda_a}{2}=l}\right)$	<i>k</i> (exp.)	$\frac{S_c}{E}$
Rubber.....	1.76	1.77	90.0	8.6	7.0	5.3	5	0.00479
Celluloid.....	1.95	1.80	90.2	8.6	6.7	5.0	5	.00386
Rubber.....	3.53	1.77	90.0	8.6	5.3	3.8	2	.00374
Do.....	3.53	1.77	90.0	8.6	5.3	3.8	4	.00333
Celluloid.....	3.97	1.80	174.1	12.0	6.0	4.3	4	.00187
Do.....	4.01	1.80	90.2	8.6	5.0	3.6	—	.00317
Do.....	4.01	1.80	90.2	8.6	5.0	3.6	—	.00328
Do.....	4.01	1.80	90.2	8.6	5.0	3.6	4	.00317
Do.....	4.02	1.80	96.4	8.9	5.0	3.6	4	.00357
Do.....	4.02	1.80	90.2	8.6	5.0	3.6	4	.00394
Do.....	4.02	1.80	90.2	8.6	5.0	3.6	3	.00306
Do.....	4.02	1.80	90.2	8.6	5.0	3.6	4	.00317
Do.....	4.02	1.80	90.2	8.6	5.0	3.6	3	.00302
Do.....	4.02	1.80	90.2	8.6	5.0	3.6	4	.00291
Do.....	5.02	1.43	138.0	10.7	5.0	3.6	4	.00207
Do.....	5.05	1.43	76.6	8.0	4.3	3.1	4	.00281

TABLE VI.—CALCULATED AND EXPERIMENTAL VALUES OF k FOR TESTS ON STEEL CYLINDERS REPORTED BY WILSON AND NEWMARK IN REFERENCE 4

Types of construction	Test series	Specimen no.	$\frac{l}{r}$	r (in.)	$\frac{r}{t}$	k_{max}	$\left(\frac{\lambda_a k}{2} = \frac{l}{2}\right)$	$\left(\frac{k}{2} = l\right)$	k (exp.)	$\frac{S_e}{E}$ calculated from data given in reference 4
Machined cylinders with no seams	1	110	3.86	1.94	66.5	7.4	4.6	3.4	5	0.00186
		111	3.89	1.94	133.0	10.5	5.6	4.0	8	.00135
		112	3.89	1.94	67.5	7.5	4.7	3.4	5	.00176
		113	3.88	1.94	136.0	10.6	5.6	4.1	8	.00146
	6	610	1.39	6.82	478	19.9	12.6	9.2	10	.000525
		611	1.41	6.82	206	13.1	9.8	7.3	8	.00112
		612	1.39	6.82	330	16.5	11.4	8.3	10	.000822
		613	1.39	6.82	435	19.0	12.3	9.0	12	.000792
		614	1.40	6.82	763	25.1	14.3	10.4	12	.000286
		615	1.35	6.82	510	20.6	13.0	9.5	12	.000593
		616	1.39	6.82	340	16.8	11.5	8.4	10	.000777
		617	1.39	6.82	235	14.0	10.3	7.6	11	.00109
Fabricated cylinders with either riveted or welded seams—R denotes riveted seams.	E	816R	1.80	40.0	167	11.8	8.4	6.2	8	.000836
		817R	1.80	40.0	172	11.9	8.4	6.2	8	.000812
		114	1.80	40.0	165	11.7	8.4	6.1	8	.000900
		86	1.80	40.0	167	11.8	8.4	6.2	8	.000944
	7	710	6.00	5.0	166	11.7	4.8	3.5	8	.000346
		711	6.00	5.0	168	11.8	4.9	3.5	8-9	.000493
		721	3.00	10.0	329	16.5	8.0	5.8	11-12	.000302
		730	2.00	15.0	518	20.7	11.0	7.9	10-12	.000299
		731	2.00	15.0	450	19.3	10.5	7.6	10-12	.000339
		740	1.50	20.0	667	23.5	13.4	9.7	10	.000191
		741	1.50	20.0	654	23.3	13.3	9.6	10	.000192
		750	1.20	25.0	825	26.1	15.7	11.4	13	.000148
		751	1.20	25.0	848	26.5	15.8	11.5	10-13	.000143
		760	1.00	30.0	971	28.4	17.8	13.0	10	.000139
		761	1.00	30.0	990	28.6	18.0	13.0	10	.000129
	8	810	24.7	17.0	139	11.7	2.5	2-	(1)	.000666
		811	24.7	17.0	151	11.2	2.5	2-	7	.000741
		820	14.1	17.0	142	10.8	3.2	2.3	6-7	.000772
		821	14.1	17.0	142	10.8	3.2	2.3	7	.000778
		830	4.24	17.0	151	11.2	5.6	4.0	8	.000894
		831	4.24	17.0	145	11.0	5.5	4.0	7	.000941

¹ Irregular.NOTE.—In calculating k for this table cylinders with $\frac{l}{r} > 6.00$ were considered as Southwell cylinders.

TABLE VII.—TABLE FOR DIFFERENTIATION BETWEEN SOUTHWELL AND ROBERTSON CYLINDERS

k	Term	Multiplying factor	$\epsilon = q/k = 0.01$			$q/k = 0.05$			$q/k = 0.1$			$q/k = 0.2$			$q/k = 0.4$			$q/k = 1.0$			$q/k = 10.0$		
			S	C	R	S	C	R	S	C	R	S	C	R	S	C	R	S	C	R	S	C	R
1	1	10^{-2}	200	200	100	200	201	101	200	205	102	200	218	108	200	277	135	200	760	400	200	104	102
	2	10^{-2}	000	000	100	000	000	101	000	000	104	000	1	117	000	17	181	000	500	1,600	000	104	104
2	1	10^{-1}	200	200	160	200	201	161	200	204	163	200	217	173	200	273	216	200	784	640	200	164	163
	2	1	144	144	256	144	146	259	144	150	266	144	172	300	144	287	463	144	3,132	4,096	144	266	266
3	1	10^{-1}	900	900	810	900	905	814	900	918	826	900	973	874	900	1,220	1,094	900	3,560	3,240	900	828	826
	2	10	518	519	656	518	524	663	518	539	682	518	610	768	518	961	1,189	518	9,348	10,500	518	683	682
4	1	1	272	272	256	272	273	257	272	277	261	272	295	277	272	369	346	272	1,082	1,024	272	261	262
	2	10^2	576	576	656	576	582	662	576	599	682	576	676	767	576	1,056	1,186	576	9,832	10,490	576	682	682
5	1	1	650	650	625	650	653	628	650	664	638	650	703	675	650	879	844	650	2,590	2,500	650	638	638
	2	10^3	360	360	391	360	364	394	360	374	406	360	421	457	360	657	707	360	5,997	6,250	360	407	407
6	1	10	133	133	130	133	134	130	133	136	132	133	144	140	133	180	175	133	531	518	133	132	132
	2	10^4	159	159	168	159	160	170	159	165	175	159	186	197	159	289	304	159	2,611	2,687	159	176	176
7	1	10	245	245	240	245	246	241	245	250	245	245	265	259	245	331	324	245	978	960	245	245	245
	2	10^5	553	554	577	553	559	582	553	576	600	553	648	675	553	101	105	553	904	923	553	60	60
8	1	10	416	416	410	416	418	412	416	424	418	416	449	442	416	562	553	416	1,661	1,638	-----	-----	-----
	1	10^5	163	163	168	163	164	169	163	169	175	163	190	196	163	296	304	163	2,642	2,685	-----	-----	-----
9	1	10^2	664	664	656	664	668	659	664	678	669	664	717	708	664	898	886	664	265	262	-----	-----	-----
	2	10^5	420	420	431	420	424	435	420	437	448	420	492	504	420	762	779	420	6,800	6,887	-----	-----	-----
10	1	10^2	101	101	100	101	102	101	101	103	102	101	109	108	101	136	135	101	404	400	-----	-----	-----
	2	10^5	980	980	1,000	980	990	1,010	980	1,019	1,040	980	1,147	1,170	980	1,778	1,810	980	15,840	16,000	-----	-----	-----
15	1	10^2	509	509	506	509	511	509	509	519	516	509	549	547	509	687	684	-----	-----	-----	-----	-----	-----
	2	10^7	254	254	256	254	257	259	254	264	267	254	297	300	254	460	464	-----	-----	-----	-----	-----	-----
20	1	10^3	160	160	160	160	161	161	160	164	163	160	173	173	160	217	216	-----	-----	-----	-----	-----	-----
	2	10^8	255	255	256	255	257	259	255	265	266	255	298	300	255	461	463	-----	-----	-----	-----	-----	-----
25	1	10^3	391	391	391	391	393	393	391	399	398	391	423	422	391	528	528	-----	-----	-----	-----	-----	-----
	2	10^9	152	152	153	152	154	154	152	158	159	152	178	179	152	276	276	-----	-----	-----	-----	-----	-----

¹ Multiplying factor = $10^4 \times$ values given in third column.

TABLE VIII.—CALCULATED VALUES OF $\frac{\lambda_a}{2r}$ AND SMALLEST VALUES OF $\frac{l}{r}$

r (inches)	$\frac{r}{t}$ (average)	$\frac{\lambda_a}{2r}$ (equation 12)	$\frac{l}{r}$ smallest in tests	Remarks
1.63	110	0.33	3.07	Tests on steel cylinders by Robertson.
2.50	165	.27	2.00	
4.00	260	.21	1.25	
7.32	500	.15	.68	
7.5	350	.18	.50	
7.5	460	.16	1.00	Tests on duralumin cyl- inders by N.A.C.A.
7.5	670	.13	.50	
15.0	715	.13	.50	
15.0	915	.11	1.00	
15.0	1,340	.094	.25	

REPORT No. 474

NOMENCLATURE FOR AERONAUTICS

By the NATIONAL ADVISORY COMMITTEE FOR AERONAUTICS

INTRODUCTION

The nomenclature for aeronautics presented in this Report No. 474 is a revision of the last previous report on this subject (Report No. 240), which was issued in 1926.

This nomenclature was prepared by a special con-

ference on aeronautical nomenclature authorized by the executive committee of the National Advisory Committee for Aeronautics. The organization of the conference was as follows:

CONFERENCE ON AERONAUTICAL NOMENCLATURE

Dr. JOSEPH S. AMES, *Chairman*

NATIONAL ADVISORY COMMITTEE FOR AERONAUTICS:

Mr. Charles H. Helms
Mr. Carlton Kemper
Mr. G. W. Lewis
Mr. H. J. E. Reid
Hon. Edward P. Warner

AIR CORPS, U.S.A.:

Capt. Karl S. Axtater, U.S.A.
Capt. Albert C. Foulk, U.S.A.
Capt. A. F. Hegenberger, U.S.A.
Maj. C. W. Howard, U.S.A.
Maj. William E. Kepner, U.S.A.
Capt. Clements MacMullen, U.S.A.
Capt. E. R. Page, U.S.A.

BUREAU OF AERONAUTICS, NAVY DEPARTMENT:

Lt. Comdr. W. S. Diehl (C.C.), U.S.N.
Commander Garland Fulton (C.C.), U.S.N.
Lt. Comdr. R. D. MacCart (C.C.), U.S.N.
Commander C. A. Pownall, U.S.N.
Commander R. D. Weyerbacher (C.C.), U.S.N.

BUREAU OF STANDARDS:

Dr. L. J. Briggs
Dr. W. G. Brombacher
Dr. H. C. Dickinson
Dr. H. L. Dryden

AERONAUTICS BRANCH, DEPARTMENT OF COMMERCE:

Col. Harry H. Blee
Mr. Richard C. Gazley
Capt. F. C. Hingsburg

The members of the conference were engaged in the preparation of the report from the time of the

appointment of the members August 11, 1931, to the date of approval of the report for publication by the executive committee of the National Advisory Committee for Aeronautics on November 14, 1933.

This report supersedes all previous publications of the Committee on this subject. The entire text has been thoroughly revised and new sketches have been inserted to replace obsolete photographs. The arrangement is alphabetical throughout and not by subjects, but the complete cross-indexing will, it is expected, make each term easily found. The definitions have been made as brief and as general as possible except in the cases where use of the term is restricted to a small specialized group. In cases where uncertainty or ambiguity is known to exist, the complete definition given herein represents the meaning ascribed to the term in the official publications of the National Advisory Committee for Aeronautics.

This report is published for the purpose of encouraging greater uniformity and precision in the use of terms relating to aeronautics, both in official documents of the Government and in commercial publications. Terms in general use in other branches of engineering have been included only where they have some special significance in aeronautics, or form an integral part of its terminology.

REPORT No. 474

NOMENCLATURE FOR AERONAUTICS

By the NATIONAL ADVISORY COMMITTEE FOR AERONAUTICS

absolute altitude—See ALTITUDE, ABSOLUTE.

absolute ceiling—See CEILING, ABSOLUTE.

accelerometer—An instrument that measures the accelerations of an aircraft in a defined direction.

acrobatics—Evolutions voluntarily performed with an aircraft other than those required for normal flight.

adjustable propeller—See PROPELLER, ADJUSTABLE.

aerodynamic center, wing section—A point located on or near the chord of the mean line approximately one quarter of the chord length aft of the leading edge and about which the moment coefficient is practically constant. (See fig. 2.)

aerodynamics—The branch of dynamics that treats of the motion of air and other gaseous fluids and of the forces acting on solids in motion relative to such fluids.

aerodynamic volume (or air volume)—The total volume of an aerostat, including its projecting parts.

aerodyne—A generic term for aircraft that derive their lift in flight chiefly from aerodynamic forces.

aerograph—Same as METEOROGRAPH.

aeronaut—The pilot of an aerostat.

aeronautics—The science and art of flight.

aerostat—(a) A generic term for an aircraft whose support is chiefly due to buoyancy derived from aerostatic forces. The immersed body consists of one or more containers filled with a gas that is lighter than air. (b) A balloon or airship.

aerostatics—The science that treats of the equilibrium of gaseous fluids and of bodies immersed in them.

aerostation—The art of operating aerostats.

aileron—A hinged or movable portion of an airplane wing, the primary function of which is to impress a rolling motion on the airplane. It is usually part of the trailing edge of a wing. (See fig. 5.)

external aileron—A separate airfoil mounted clear of the wing surfaces of an airplane but usually attached to them and deflected for lateral control.

Frise aileron—An aileron having the nose portion projecting ahead of the hinge axis, the lower surface being in line with the lower surface of the wing. When the trailing edge of the aileron is raised, the nose portion protrudes below the lower surface of the wing, increasing the drag. (See fig. 1.)

aileron—continued.

slotted aileron—An aileron having a nose and axis arrangement somewhat similar to a Frise aileron but having a smooth air passage between the nose portion of the aileron and the wing for the purpose of maintaining a smooth air flow over the upper surface of the aileron when its trailing edge is deflected downward. (See fig. 1.)

upper-surface aileron—A split flap forming the rear upper surface of a wing, deflected for lateral control.

aileron angle—See ANGLE, AILERON.

aileron linkage arrangements:

differential aileron linkage arrangement—Ailerons so interconnected that a given movement of the control stick results in the upward displacement of one aileron being greater than the downward displacement of the other.

floating aileron linkage arrangement—Ailerons so linked together and to the control stick as to "float" freely in the air stream except when displaced by the lateral motion of the control stick.

aircraft—Any weight-carrying device designed to be supported by the air, either by buoyancy or by dynamic action.

aircraft carrier—A ship designed to carry aircraft and to permit their landing and take-off.

air duct—A tube, usually of fabric, supplying air for filling or for maintaining pressure in the air-filled parts of an aerostat. (See fig. 4.)

airfoil—Any surface, such as an airplane wing, aileron, or rudder, designed to obtain reaction from the air through which it moves.

airfoil profile—The outline of an airfoil section (fig. 2).

airfoil section—A cross section of an airfoil parallel to the plane of symmetry or to a specified reference plane.

airline—The great circle route between two points.

air line—An established system of aerial transportation, its equipment, or the company owning or operating it.

airplane—A mechanically driven fixed-wing aircraft, heavier than air, which is supported by the dynamic reaction of the air against its wings (fig. 5).

canard airplane—A type of airplane having the horizontal stabilizing and control surfaces in front of the main supporting surfaces.

airplane—continued.

pusher airplane—An airplane with the propeller or propellers aft of the main supporting surfaces.

tailless airplane—An airplane in which the devices used to obtain stability and control are incorporated in the wing.

tractor airplane—An airplane with the propeller or propellers forward of the main supporting surfaces.

airport—A tract of land or water which is adapted for the landing and take-off of aircraft and which provides facilities for their shelter, supply, and repair; a place used regularly for receiving or discharging passengers or cargo by air.

air scoop—A scoop or hood designed to catch the air and maintain the air pressure in ballonets, internal-combustion engines, ventilators, etc. (See fig. 3.)

airship—An aerostat provided with a propelling system and with means of controlling the direction of motion.

nonrigid airship—An airship whose form is maintained by the internal pressure in the gas bags and ballonets (fig. 3).

pressure-rigid airship—An airship combining the principles used in both rigid and nonrigid airships to maintain shape and skin tautness.

rigid airship—An airship whose form is maintained by a rigid structure (fig. 6).

semirigid airship—An airship whose shape is maintained by means of a rigid or jointed keel in conjunction with internal pressure in the gas containers and ballonets (fig. 4).

airship shed—See DOCK.

airship station—(1) The complete assembly of sheds, masts, gas plants, shops, landing fields, and other equipment required to operate airships and supply their needs. (2) The base from which airships are operated.

air speed—The speed of an aircraft relative to the air.

air-speed head—An instrument which, in combination with a gage, is used to measure the speed of an aircraft relative to the air. It usually consists of a pitot-static tube or a pitot-venturi tube.

air volume—See AERODYNAMIC VOLUME.

airway—An air route along which aids to air navigation, such as landing fields, beacon lights, radio direction-finding facilities, intermediate fields, etc., are maintained.

airworthiness—The quality of an aircraft denoting its fitness and safety for operation in the air under normal flying conditions.

altigraph—A recording altimeter.

altimeter—An instrument that measures the elevation of an aircraft above a given datum plane.

altitude:

absolute altitude—The height of an aircraft above the earth.

altitude—continued.

critical altitude—The maximum altitude at which a supercharger can maintain a pressure in the intake manifold of an engine equal to that existing during normal operation at rated power and speed at sea level.

density altitude—The altitude corresponding to a given density in a standard atmosphere.

pressure altitude—(1) The altitude corresponding to a given pressure in a standard atmosphere. (2) The altitude at which the gas bags of an airship become full.

altitude mixture control—See MIXTURE CONTROL, ALTITUDE.

amphibian—An airplane designed to rise from and alight on either land or water.

angle:

aileron angle—The angular displacement of an aileron from its neutral position. It is positive when the trailing edge of the aileron is below the neutral position.

blade angle—The acute angle between the chord of a section of a propeller, or of a rotary wing system, and a plane perpendicular to the axis of rotation.

coning angle—The average angle between the span axis of a blade or wing of a rotary wing system and a plane perpendicular to the axis of rotation.

dihedral angle—The acute angle between a line perpendicular to the plane of symmetry and the projection of the wing axis on a plane perpendicular to the longitudinal axis of the airplane. If the wing axis is not approximately a straight line, the angle is measured from the projection of a line joining the intersection of the wing axis with the plane of symmetry and the aerodynamic center of the half-wing on either side of the plane of symmetry. (See fig. 5.)

downwash angle—The angle through which an air stream is deflected by any lifting surface. It is measured in a plane parallel to the plane of symmetry.

drift angle—The horizontal angle between the longitudinal axis of an aircraft and its path relative to the ground.

effective helix angle—The angle of the helix described by a particular point on a propeller blade as the airplane moves forward through air otherwise undisturbed.

elevator angle—The angular displacement of the elevator from its neutral position. It is positive when the trailing edge of the elevator is below the neutral position.

flapping angle—The difference between the coning angle and the instantaneous angle of the span axis of a blade of a rotary wing system relative to the plane perpendicular to the axis of rotation.

angle—continued.

flight-path angle—The angle between the flight path of the aircraft and the horizontal.

gliding angle—The angle between the flight path during a glide and a horizontal axis fixed relative to the air.

landing angle—The acute angle between the wing chord and the horizontal when the airplane is resting on level ground in its normal position; also called "ground angle."

minimum gliding angle—The acute angle between the horizontal and the most nearly horizontal path along which an airplane can descend steadily in still air when the propeller is producing no thrust.

rudder angle—The acute angle between the rudder and the plane of symmetry of the aircraft. It is positive when the trailing edge has moved to the left with reference to the normal position of the pilot.

trim angle—The angle between the horizontal and the longitudinal base line of a seaplane float or flying-boat hull. It is positive when the bow is higher than the stern.

zero-lift angle—The angle of attack of an airfoil when its lift is zero.

angle of attack—The acute angle between a reference line in a body and the line of the relative wind direction projected on a plane containing the reference line and parallel to the plane of symmetry. (See fig. 9.)

absolute angle of attack—The angle of attack of an airfoil, measured from the attitude of zero lift.

critical angle of attack—The angle of attack at which the flow about an airfoil changes abruptly as shown by corresponding abrupt changes in the lift and drag.

effective angle of attack—See ANGLE OF ATTACK FOR INFINITE ASPECT RATIO.

induced angle of attack—The difference between the actual angle of attack and the angle of attack for infinite aspect ratio of an airfoil for the same lift coefficient.

angle of attack for infinite aspect ratio—The angle of attack at which an airfoil produces a given lift coefficient in a two-dimensional flow. Also called "effective angle of attack."

angle of dead rise—The angle with the horizontal made by a transverse line joining the keel of a hull with the chine.

angle of heel—The angle between a horizontal plane and the lateral axis of a seaplane on the water.

angle of incidence—Same as ANGLE OF WING SETTING. In British terminology the angle of incidence is equivalent to the American term "angle of attack."

angle of pitch (aircraft)—The acute angle between two planes defined as follows: One plane includes the lateral axis of the aircraft and the direction of

the relative wind; the other plane includes the lateral axis and the longitudinal axis. The angle is positive when the nose of the aircraft is above the direction of the relative wind. (In normal flight the angle of pitch is the angle between the longitudinal axis and the direction of the relative wind.)

angle of pitch (propeller)—Same as ANGLE, BLADE.

angle of roll (or angle of bank)—The angle through which an aircraft must be rotated about its longitudinal axis in order to bring its lateral axis into the horizontal plane. The angle is positive when the left side is higher than the right.

angle of stabilizer setting—The acute angle between the longitudinal axis of an airplane and the chord of the stabilizer. The angle is positive when the leading edge is higher than the trailing edge. (See fig. 5.)

angle of wing setting—The acute angle between the plane of the wing chord and the longitudinal axis of the airplane. The angle is positive when the leading edge is higher than the trailing edge. (See fig. 5.)

angle of yaw—The acute angle between the direction of the relative wind and the plane of symmetry of an aircraft. The angle is positive when the aircraft turns to the right.

antidrag wire—See WIRE (AIRPLANE), ANTIDRAG.

appendix—The tube, usually located at the bottom of a balloon, used primarily for inflation and deflation. In the case of a free balloon it may also serve as an automatic-discharge opening. The term should be restricted to the various types of balloons and should not be applied to airships.

approach light—See LIGHT, APPROACH.

area, equivalent flat-plate—The area of a square flat plate, normal to the direction of motion, which offers the same amount of resistance to motion as the body or combination of bodies under consideration.

area, measurement of (performance calculations):

control-surface area, trailing—The area of a trailing control surface is the area of the actual outline projected on the plane of the surface, except that any portion of the movable surface lying forward of the hinge axis and within the fixed surface is included in the fixed surface. Auxiliary or paddle-type balance surfaces shielded by and lying outside of the fixed surface are not included in the area of either the fixed or the movable surfaces.

horizontal tail area—The horizontal tail area is measured in the same manner as the wing area, that is, with no deduction for the area blanketed by the fuselage, such blanketed area being bounded within the fuselage by lateral straight lines that connect the intersections of the leading and trailing edges of the stabilizer with the sides of the fuselage, the fairings and fillets being ignored.

area, measurement of—continued.

vertical tail area—The area of the actual outline of the rudder and the fin projected in the vertical plane, the fairings and fillets being ignored.

wing area—Wing area is measured from the projection of the actual outline on the plane of the chords, without deduction for area blanketed by fuselage or nacelles. That part of the area, so determined, which lies within the fuselage or nacelles is bounded by two lateral lines that connect the intersections of the leading and trailing edges with the fuselage or nacelle, ignoring fairings and fillets. For the purpose of calculating area, a wing is considered to extend without interruption through the fuselage and nacelles. Unless otherwise stated, wing area always refers to total area including ailerons.

area, projected propeller—Projected blade area times the number of blades.

area, projected propeller-blade—The projection of the propeller-blade area on a plane perpendicular to the axis of rotation of the propeller.

area, propeller—Blade area times the number of blades.

area, propeller-blade—The developed area of the blade face exclusive of the boss and the root; i.e., exclusive of that portion the thrust of which is negligible in comparison with the total thrust of the blade.

area, propeller-disk—The total area swept by a propeller; i.e., the area of a circle having the same diameter as the propeller.

arresting gear—The gear incorporated in aircraft and in the landing area to facilitate landing in a limited space.

artificial horizon—(1) A device that indicates the attitude of an aircraft with respect to the true horizon. (2) A substitute for a natural horizon, such as a liquid level, pendulum, or gyroscope, incorporated in a navigating instrument.

aspect ratio—The ratio of the span to the mean chord of an airfoil; i.e., the ratio of the square of the span to the total area of an airfoil.

effective aspect ratio—The aspect ratio of an airfoil of elliptical plan form that, for the same lift coefficient, has the same induced-drag coefficient as the airfoil, or the combination of airfoils, in question.

aspect ratio, propeller-blade—The ratio of the tip radius to the maximum blade width. (Obsolete.)

atmosphere:

altimeter-calibration standard atmosphere—A standard atmosphere used in calibrating aeronautic instruments. The standard now in use in the United States is completely defined in N.A.C.A. Report No. 246.

atmosphere—continued.

standard atmosphere—An arbitrary atmosphere used in comparing the performance of aircraft. The standard atmosphere in use in the United States at present represents very nearly the average conditions found at latitude 40° and is completely defined in N.A.C.A. Report No. 218.

standard international atmosphere—The atmosphere used as an international standard presumes for mean sea level and a temperature of 15° C., a pressure of 1,013.2 millibars, lapse rate of 6.5° C. per kilometer from sea level to 11 kilometers, and thereafter a constant temperature of -56.5° C.

attack, angle of—See ANGLE OF ATTACK.

attitude—The position of an aircraft as determined by the inclination of its axes to some frame of reference. If not otherwise specified, this frame of reference is fixed to the earth.

attitude of flight—Inclination of the three principal airplane axes to the relative wind.

autogiro—A type of rotor plane whose support in the air is chiefly derived from airfoils rotated about an approximately vertical axis by aerodynamic forces, and in which the lift on opposite sides of the plane of symmetry is equalized by the vertical oscillation of the blades.

automatic pilot—An automatic control mechanism for keeping an aircraft in level flight and on a set course. Sometimes called "gyro pilot," "mechanical pilot," or "robot pilot."

automatic propeller—See PROPELLER, AUTOMATIC.

aviation—The operation of aircraft heavier than air.

aviator—The pilot of an aircraft heavier than air.

axes of an aircraft—Three fixed lines of reference, usually centroidal and mutually perpendicular. The horizontal axis in the plane of symmetry, usually parallel to the axis of the propeller, is called the longitudinal axis; the axis perpendicular to this in the plane of symmetry is called the normal axis; and the third axis perpendicular to the other two is called the lateral axis. In mathematical discussions, the first of these axes, drawn from rear to front, is called the *X* axis; the second, drawn downward, the *Z* axis; and the third, running from left to right, the *Y* axis. (See page 32.)

axial cone—See CONE, AXIAL.

axis, elastic (stress analysis)—The locus of all points through which a force may be applied to a structure without causing torsional deflection.

axis, wing—The locus of the aerodynamic centers of all the wing sections.

backswept—See SWEEPBACK.

balance—A condition of steady flight in which the resultant force and moment on the airplane are zero.

balanced surface:

aerodynamic balanced surface—A control surface that extends on both sides of the axis of the hinge or pivot or that has auxiliary devices or extensions connected with it in such a manner as to effect a small or zero resultant moment of the air forces about the hinge axis.

static balanced surface—A control surface whose center of mass is in the hinge axis.

ballonet—A gas-tight compartment of variable volume constructed of fabric and placed within a balloon or airship. It is usually partly inflated with air to compensate for changes of volume in the gas contained in the envelope. (See figs. 3 and 4.)

ballonet ceiling—See CEILING, BALLONET.

balloon—An aerostat without a propelling system.

captive balloon—A balloon restrained from free flight by means of a cable attaching it to the earth.

ceiling balloon—A small free balloon, whose rate of ascent is known, used to determine the ceiling.

free balloon—A balloon, usually spherical, whose ascent and descent may be controlled by releasing ballast or gas and whose direction of flight is determined by the wind.

kite balloon—An elongated form of captive balloon, fitted with lobes to keep it headed into the wind; it usually derives increased lift from the inclination of its axis to the wind.

pilot balloon—A small balloon sent up to show the direction and speed of the wind.

sounding balloon—A small balloon used to send up a meteorograph.

balloon fabric—See FABRIC, BALLOON.

band:

mooring band—A band of tape or webbing, over the top of a kite balloon, to which the mooring ropes are attached. It forms part of the mooring harness.

suspension band—A horizontal fabric band, securely fastened to the envelope of a balloon or airship, to which are attached the main suspension lines of the basket or car, or the captive cable of a kite balloon.

trajectory band—A band of webbing carried in a special curve over the surface of the envelope of an airship to distribute the stresses due to the suspension of the car.

bank—The position of an airplane when its lateral axis is inclined to the horizontal. A right bank is the position with the lateral axis inclined downward to the right.

bank—To incline an airplane laterally; i.e., to rotate it about its longitudinal axis.

bank (or banking) indicator—See TURN-AND-BANK INDICATOR.

bar, rudder—See RUDDER BAR.

basic load—See LOAD, BASIC.

basin, towing—See TANK, SEAPLANE.

basket—The car suspended beneath a balloon for carrying passengers, ballast, etc.

basket suspension—See SUSPENSION BASKET.

beaching gear—An arrangement of wheels to be attached to the hull of a seaplane to permit handling ashore.

beacon—A light, group of lights, or other signaling device, indicating a location or direction.

airport beacon—A beacon light of high candlepower located at or near an airport for the purpose of indicating the general or specific location of the airport.

airway beacon—A beacon light of high candlepower, other than an airport or landmark beacon, located on or near an airway for the purpose of indicating the location of the airway.

auxiliary airport beacon—A beacon light, usually of lower candlepower than the main airport beacon light, located on the airport site to indicate the specific location of an airport that has a separate airport beacon visible at a greater distance to indicate the general location of the airport.

auxiliary airway beacon—A beacon light, usually of lower candlepower than the principal airway beacon lights, used to mark special features of the terrain along an airway or otherwise to supplement the principal airway beacons.

code beacon—A flashing beacon light having a recognizable characteristic of dots and/or dashes by which its individual identity can be established.

landmark beacon—A beacon light, other than an airport beacon or an airway beacon, that serves to indicate a definite geographical location.

beacon, radio-marker—See RADIO-DIRECTIVE DEVICES.

beacon, radio-range—See RADIO-DIRECTIVE DEVICES.

beam direction (stress analysis)—The direction parallel to the plane of the spar web and the plane of symmetry of an airplane (cf. *chord*, *drag*, *lift*, and *side directions*).

beam force or component (stress analysis)—A force, or component, in the beam direction; i.e., parallel to the plane of the spar web and the plane of symmetry of an airplane (cf. *chord*, *drag*, *lift*, and *side forces*).

bearing projector—A fixed directional projector used in conjunction with a landmark beacon to indicate the direction toward a landing area by means of the direction of its beam.

biplane—An airplane with two main supporting surfaces placed one above the other.

blade angle—See ANGLE, BLADE.

blade back—The side of a propeller blade that corresponds to the upper surface of an airfoil.

- blade element**—A portion of a propeller blade contained between the surfaces of two cylinders coaxial with the propeller cutting the propeller blades.
- blade face**—The surface of a propeller blade that corresponds to the lower surface of an airfoil. Sometimes called "thrust face" or "driving face."
- blade section**—A cross section of a propeller blade made at any point by a plane parallel to the axis of rotation of the propeller and tangent at the centroid of the section to an arc drawn with the axis of rotation as its center.
- blade-width ratio**—The ratio of the chord of a propeller blade section to the diameter of the propeller.
- mean blade-width ratio**—The ratio of the mean blade width to the diameter of the propeller.
- blast gate (supercharger)**—A device for controlling the pressure in the nozzle box of a turbosupercharger by discharging into the free atmosphere a portion of the exhaust gases that would otherwise pass through the turbine wheel.
- blimp**—A colloquial term for a nonrigid airship.
- blind flying**—See INSTRUMENT FLYING.
- blinker light**—See LIGHT, BLINKER.
- blister**—A sheet of clear water raised by the motion of a float or hull and separated from the free-water surface by an air space.
- boat, flying**—See FLYING BOAT.
- boom, tail**—See TAIL BOOM.
- boost**—To supply an engine with more air or mixture than it would normally induct at sea level.
- boost control, automatic**—An automatic regulator of boost pressure.
- booster magneto**—See MAGNETO, BOOSTER.
- boundary layer**—A layer of fluid, close to the surface of a body placed in a moving stream, in which the impact pressure is reduced as a result of the viscosity of the fluid.
- boundary light**—See LIGHT, BOUNDARY.
- bow cap**—See CAP, BOW.
- bowheavy**—The condition in which, in normal flight, the forward end of an airship tends to sink, and which requires correction by means of the horizontal controls. It may be due to either aerodynamic or static conditions, or to both (cf. *sternheavy*).
- bow-weighing device**—An instrument for measuring the horizontal and vertical forces between an airship and its mooring mast (cf. *stern-weighing device*).
- box girder**—See GIRDER, BOX.
- breathing**—The passage of air into or out of an aerostat, due to changing volume.
- bridle**—(a) A sling of cordage or cable which has its ends fixed at two different points, to the bight of which a single line may be attached, either movable or fixed, thus distributing the pull of the single line to two points or more in the case of a multiple bridle. (b) A towing or mooring line having two legs and intended to reduce yawing when towing or mooring.
- buffeting**—The repeated aerodynamic forces experienced by any part of an aircraft, caused and maintained by unsteady flow arising from a disturbance set up by any other part of the aircraft (cf. *flutter*).
- bump**—A sudden acceleration of an aircraft caused by a region of unstable atmosphere characterized by marked local vertical components in the air currents.
- bumper bag**—A cushion secured to the bottom of an airship to prevent damage when in contact with the ground. (See figs. 4 and 6.)
- buoyancy**:
- center of buoyancy (aerostat)**—The center of gravity of the air displaced by a balloon or airship. It is approximately the center of gravity of the contained gas.
- center of buoyancy (seaplane)**—The center of gravity of the fluid displaced.
- reserve buoyancy (excess buoyancy)**—The difference between the buoyancy of a completely submerged float and the buoyancy of the float when submerged to the normal-load water line, usually expressed as a percentage of the normal-load buoyancy.
- burble**—A term designating the breakdown of the streamline flow about a body.
- cabane**—An arrangement of struts used for bracing on an aircraft.
- cable**:
- axial cable**—The axial member sometimes fitted in a rigid airship. It is attached to the central fitting of the radial or diametral wires of each main transverse and to the hull structure at bow and stern.
- control cable**—The line of wire or stranded cable leading from the control levers to the control surfaces or interconnecting the control surfaces. (See fig. 5.)
- main mooring cable**—The wire cable by which an airship is hauled in to a mooring mast.
- camber**—The rise of the curve of an airfoil section, usually expressed as the ratio of the departure of the curve from a straight line joining the extremities of the curve to the length of this straight line. "Upper camber" refers to the upper surface; "lower camber" to the lower surface; and "mean camber" to the mean line of the section. Camber is positive when the departure is upward, and negative when it is downward. (See fig. 2.)
- canard airplane**—See AIRPLANE, CANARD.
- canopy, parachute**—The main supporting surface of a parachute.
- cap, bow**—(1) A cap of metal or fabric used to reinforce the extreme forward end of a bow stiffener of a nonrigid or semirigid airship. (See figs. 3 and 4.) (2) The conical or cap-shaped structure at the extreme bow of a rigid airship to which the longi-

tudinal girders are attached and which supports the bow mooring spindle. (See fig. 6.)

capacity—The volume of the gas cell or cells of an aerostat.

nominal gas capacity—The volume of the gas cell or cells of an aerostat under certain definite conditions of pressure and inflation.

cap-strip—A continuous member on the outer edge of a wing rib.

captive balloon—See BALLOON, CAPTIVE.

car—A structure in, or suspended from, the hull or envelope of an airship for carrying crew, engineers, passengers, etc. (See figs. 3 and 4.)

side car—A car suspended off the center line of an airship; also called "wing car."

car, subcloud—An observation car which may be lowered from an airship to a position below the clouds.

card compass—See COMPASS, CARD.

catapult—A device by which an airplane can be launched at flying speed.

cat walk—A narrow footway along the keel of a rigid airship.

ceiling—Height of the lower level of a bank of clouds above the ground.

ceiling:

absolute ceiling—The maximum height above sea level at which a given airplane would be able to maintain horizontal flight under standard air conditions.

ballonet ceiling—The altitude from which a pressure airship with empty ballonets can return to sea level without loss of operating pressure.

service ceiling—The height above sea level, under standard air conditions, at which a given airplane is unable to climb faster than a small specified rate (100 feet per minute in the United States and England). This specified rate may differ in different countries.

static ceiling—The altitude in standard atmosphere, at which an aerostat is in static equilibrium after removal of all dischargeable weight.

ceiling balloon—See BALLOON, CEILING.

ceiling-height indicator—A device that measures the height from the horizontal to the illuminated spot produced by a ceiling projector as seen from a fixed position.

ceiling projector—A projector that produces an illuminated region on the under side of a cloud for the purpose of determining the height of that part of the cloud above the indicator.

cell, gas—In an airship, one of the bags containing the aerostatic gas. (See figs. 4 and 6.)

cellule (or cell)—In an airplane, the entire structure of the wings and wing trussing of the whole airplane on one side of the fuselage, or between fuselages or nacelles, where there are more than one.

center, aerodynamic—See AERODYNAMIC CENTER, WING SECTION.

center, elastic (stress analysis)—A point within the wing section at which the application of a single concentrated load will cause the wing to deflect without rotation and, conversely, a point within the wing section about which rotation occurs when the wing is subjected to rotational deflection.

center of buoyancy—See BUOYANCY, CENTER OF.

center of pressure of an airfoil—The point in the chord of an airfoil, prolonged if necessary, which is at the intersection of the chord and the line of action of the resultant air force.

center-of-pressure coefficient—The ratio of the distance of the center of pressure from the leading edge to the chord length.

center section—The central panel of a wing; in the case of a continuous wing or any wing having no central panel, the limits of the center section are arbitrarily defined by the location of points of attachment to the cabane struts or fuselage.

centrifugal-type supercharger—See SUPERCHARGER, CENTRIFUGAL-TYPE.

chandelle—An abrupt climbing turn to approximately a stall in which the momentum of the airplane is used to obtain a higher rate of climb than would be possible in unaccelerated flight. The purpose of this maneuver is to gain altitude at the same time that the direction of flight is changed (fig. 8).

chine—The intersection of the bottom with the sides or deck of a seaplane float.

chord—An arbitrary datum line from which the ordinates and angles of an airfoil are measured. It is usually the straight line tangent to the lower surface at two points, the straight line joining the ends of the mean line, or the straight line between the leading and trailing edges. (See figs. 2 and 5.)

chord, mean aerodynamic—The chord of an imaginary airfoil which would have force vectors throughout the flight range identical with those of the actual wing or wings.

chord, mean, of a wing—The quotient obtained by dividing the wing area by the span.

chord direction (stress analysis)—The direction parallel to the intersection of the plane of the internal wing truss with the plane of symmetry of the airplane. When a wing has two internal trusses in nonparallel planes, the plane bisecting the dihedral angle between those two planes should be used (cf. *beam, drag, lift, and side directions*).

chord force, or component (stress analysis)—A force, or component, in the chord direction; i.e., parallel to the intersection of the plane of the internal wing truss with the plane of symmetry of the airplane (cf. *beam, drag, lift, and side forces*).

chord length—The length of the projection of the airfoil profile on its chord.

cockpit—An open space in an airplane for the accommodation of pilots or passengers. When completely enclosed, such a space is usually called a cabin. (See fig. 5.)

column, control—See CONTROL COLUMN.

compass:

card (or card magnetic) compass—A magnetic compass in which the magnets are attached to a pivoted card on which the directions are marked.

earth-inductor (or induction) compass—A compass the indications of which depend on the current generated in a coil revolving in the earth's magnetic field.

sun compass—A compass in which the direction of the sun is utilized instead of the direction of the magnetic north or south pole.

compression-ignition engine—See ENGINE, COMPRESSION-IGNITION.

compression ratio—The ratio of the volume of the gas in an engine cylinder at the beginning of the compression stroke to its volume at the end of the stroke.

cone:

axial cone—(1) The cone-shaped fabric fitting, in the end of a gas cell of a rigid airship, which provides a gas-tight connection of the cell to the axial cable and yet permits the cell some degree of freedom in its movements. (2) A special form of conical sleeve.

danger cone—A pennant or a hollow cone of light cloth on the wire cable of a captive balloon to warn aircraft of its presence.

entrance cone—That portion of a wind tunnel from which the air flows to the experiment chamber. (See fig. 7.)

exit cone—That portion of a wind tunnel into which the air flows from the experiment chamber. (See fig. 7.)

mooring cone—The grooved conical member at the extreme bow of an airship which engages with a hollow cone at the top of the mooring mast and provides the coupling between the airship and the mooring mast. (See fig. 6.)

wind cone—A tapered fabric sleeve pivoted on a standard to indicate the wind direction.

coning angle—See ANGLE, CONING.

control cable—See CABLE, CONTROL.

control column—A lever having a rotatable wheel mounted at its upper end for operating the longitudinal and lateral control surfaces of an airplane. This type of control is called "wheel control."

control, servo—A control devised to reinforce the pilot's effort by an aerodynamic or mechanical relay.

controllability—The quality of an aircraft that determines the ease of operating its controls and/or the effectiveness of displacement of the controls in producing change in its attitude in flight.

controllable propeller—See PROPELLER, CONTROLLABLE.

controls—A general term applied to the means provided to enable the pilot to control the speed, direction of flight, attitude, power, etc., of an aircraft.

control stick—The vertical lever by means of which the longitudinal and lateral control surfaces of an airplane are operated. The elevator is operated by a fore-and-aft movement of the stick; the ailerons, by a side-to-side movement. (See fig. 5.)

control surface—A movable airfoil designed to be rotated or otherwise moved by the pilot in order to change the attitude of the aircraft.

control-surface area, trailing—See AREA, MEASUREMENT OF.

cord, rip—See RIP CORD.

course light—See LIGHT, COURSE.

cove—The line of intersection between two surfaces of a hull, the vertex of the angle of intersection pointing inward.

cowling—A removable covering.

cockpit cowling—A metal or plywood cowling placed around a cockpit.

engine cowling—A removable covering placed around all or part of an airplane engine.

N.A.C.A. cowling—A cowling enclosing a radial air-cooled engine, consisting of a hood, or ring, and a portion of the body behind the engine so arranged that the cooling air smoothly enters the hood at the front and leaves through a smooth annular slot between the body and the rear of the hood; the whole forming a relatively low-drag body with a passage through a portion of it for the cooling air.

cowling, ring—See RING COWLING.

cradle:

building cradle—A support provided for the frame of a rigid airship or the keel of a semi-rigid airship during construction.

docking cradle—A support for the car of an airship while it is being inflated in the shed; mostly used with rigid airships.

crew, landing (or ground)—A detail of men necessary for the landing and handling of an airship on the ground.

critical altitude—See ALTITUDE, CRITICAL.

critical angle of attack—See ANGLE OF ATTACK, CRITICAL.

cross-wind force—The component perpendicular to the lift and to the drag of the total air force on a body.

crowsfoot—(1) A system of diverging short ropes for distributing the pull of a single rope. (2) An arrangement in which the strands of a cord are opened out so that they can be effectively cemented to a fabric surface.

cyclogiro—A type of rotor plane whose support in the air is normally derived from airfoils mechanically rotated about an axis perpendicular to the plane of symmetry of the aircraft, the angle of attack of the

- airfoils being always less than the angle at which the airfoils stall.
- dead rise**—In a cross section of a float or flying-boat hull, the amount by which the height of the chine differs from that of the keel.
- dead rise, angle of**—See **ANGLE OF DEAD RISE**.
- decalage**—The difference between the angular settings of the wings of a biplane or multiplane. The decalage is measured by the acute angle between the chords in a plane parallel to the plane of symmetry. The decalage is considered positive if the upper wing is set at the larger angle. (See fig. 5.)
- deflation sleeve**—See **SLEEVE, DEFLATION**.
- density altitude**—See **ALTITUDE, DENSITY**.
- derivatives, resistance**—Quantities expressing the variation of the forces and moments on aircraft due to disturbance of steady motion. They form the experimental basis of the theory of stability, and from them the periods and damping factors of aircraft can be calculated. In the general case there are 18 translatory and 18 rotary derivatives.
- lateral resistance derivatives**—Resistance derivatives expressing the variation of moments and forces due to small changes in the lateral, yawing, and rolling velocities.
- longitudinal resistance derivatives**—Resistance derivatives expressing the variation of moments and forces due to small changes in the longitudinal, normal, and pitching velocities.
- rotary resistance derivatives**—Resistance derivatives expressing the variation of moments and forces due to small changes in the rotational velocities of the aircraft.
- translatory resistance derivatives**—Resistance derivatives expressing the variation of moments and forces due to small changes in the translational velocities of the aircraft.
- design load**—See **LOAD, DESIGN**.
- diaphragm, ballonnet**—The fabric partition between the gas and air compartments of the envelope of a nonrigid or semirigid airship or kite balloon.
- differential aileron linkage arrangement**—See **AILERON LINKAGE ARRANGEMENTS**.
- dihedral angle**—See **ANGLE, DIHEDRAL**.
- directional gyro**—A gyroscopic instrument for indicating direction, containing a free gyroscope which holds its position in azimuth and thus indicates angular deviation from the course.
- directional stability**—See **STABILITY, DIRECTIONAL**.
- discharge header**—The duct through which the air is conducted from the supercharger to the engine.
- displacement, engine**—The total volume swept by the pistons of all the cylinders during one complete stroke of each piston.
- displacement, float or hull**—The total volume, or total weight, of water displaced by a seaplane float or hull.
- dive**—A steep descent, with or without power, in which the air speed is greater than the maximum speed in horizontal flight.
- dive (stress analysis)**—A design condition for the wings representing a steady state of flight characterized by high speed and an angle of attack approximately that of zero lift (cf. *inverted flight* and *pull-up, sudden*).
- dock**—A large shed used for housing airships.
- dock**—To haul an airship into its dock.
- dope**:
- airplane dope**—The liquid material applied to the fabric surfaces of airplanes to increase their strength, to produce tautness by shrinking, and to act as a filler for maintaining airtightness.
- fuel dope**—Any material added to the fuel in small quantities for the purpose of preventing detonation.
- downwash**—The air deflected perpendicular to the direction of motion of an airfoil.
- downwash angle**—See **ANGLE, DOWNWASH**.
- drag**—The component of the total air force on a body parallel to the relative wind. (See fig. 9.)
- induced drag**—That part of the drag induced by the lift.
- parasite drag**—That portion of the drag of an aircraft exclusive of the induced drag of the wings.
- profile drag**—The difference between the total wing drag and the induced drag.
- profile drag, effective**—The difference between the total wing drag and the induced drag of a wing with the same geometric aspect ratio but elliptically loaded.
- drag direction (stress analysis)**—The direction of the relative wind (cf. *beam, chord, lift, and side directions*).
- drag force, or component (stress analysis)**—A force, or component, in the drag direction; i.e., parallel to the relative wind (cf. *beam, chord, lift, and side forces*).
- drag rope**—A long rope which can be hung overboard from a balloon so as to act as a brake and a variable ballast in making a landing. Sometimes called "trail rope" or "guide rope."
- drag strut**—A fore-and-aft compression member of the internal bracing system of an aircraft. (See fig. 5.)
- drift angle**—See **ANGLE, DRIFT**.
- drip flap**—A strip of fabric attached by one edge to the envelope of an aerostat so that rain runs off its free edge instead of dripping into the basket or car. It also assists in keeping the suspension ropes dry and nonconducting. Also called "drip band" or "drip strip."
- dry weight of an engine**—See **ENGINE, DRY WEIGHT OF**.
- dynamic factor (stress analysis)**—The ratio between the load carried by any part of an aircraft when accelerating and the corresponding basic load.

dynamic load—See **LOAD, DYNAMIC**.

dynamic pressure—The product $\frac{1}{2} \rho V^2$, where ρ is the density of the air and V is the relative speed of the air.

dynamic stability—See **STABILITY, DYNAMIC**.

dynamometer, hub—A device built into a propeller hub for measuring the engine thrust and/or torque.

earth-inductor compass—See **COMPASS, EARTH-INDUCTOR**.

edge, leading—See **LEADING EDGE**.

edge, trailing—See **TRAILING EDGE**.

efficiency, propeller—See **PROPELLER EFFICIENCY**.

efficiency, propulsive—See **PROPULSIVE EFFICIENCY**.

elastic center—See **CENTER, ELASTIC**.

elevator—A movable auxiliary airfoil, the function of which is to impress a pitching moment on the aircraft. It is usually hinged to the stabilizer. (See figs. 3, 4, 5, and 6.)

elevator angle—See **ANGLE, ELEVATOR**.

emergency flotation gear—A device attached to a landplane to provide buoyancy in case of an emergency landing on the water.

empennage—See **TAIL, AIRPLANE**.

engine:

axial-type engine—An engine having its cylinders equidistant from and parallel to the main shaft. Power is transmitted to the shaft through a wobble plate, swash plate, or gears.

cam engine—A type of engine in which the pistons are reciprocated by means of a cam-and-roller mechanism.

compression-ignition engine—A type of engine in which the fuel is sprayed into the cylinder and ignited by the heat of compression of the air charge.

double-row radial engine—An engine having two rows of cylinders arranged radially around a common crankshaft. The corresponding front and rear cylinders may or may not be in line.

left-hand engine—An engine whose propeller shaft, to an observer facing the propeller from the engine end of the shaft, rotates in a counter-clockwise direction.

right-hand engine—An engine whose propeller shaft, to an observer facing the propeller from the engine end of the shaft, rotates in a clockwise direction.

supercharged engine—An engine with a compressor for increasing the air or mixture charge taken into the cylinder beyond that inducted normally at the existing atmospheric pressure.

engine, dry weight of an—The weight of an engine exclusive of fuel, oil, and liquid coolant.

engine weight per horsepower—The dry weight of an engine divided by the rated horsepower.

entrance cone—See **CONE, ENTRANCE**.

envelope—(1) The outer covering of an aerostat, usually of fabric. (2) The bag containing the aerostatic gas of a free balloon, kite balloon, or non-rigid airship. (See fig. 3.)

equivalent monoplane—A monoplane wing equivalent as to its lift and drag properties to any combination of two or more wings.

exhaust-collector ring—A circular duct into which the exhaust gases from the cylinders of a radial engine are discharged.

exit cone—See **CONE, EXIT**.

experiment (or test) chamber—The central portion of a wind tunnel, where aircraft models or other objects are tested.

fabric:

balloon fabric—The finished material, usually rubberized, of which balloon or airship envelopes are made.

gas-cell fabric—The fabric used in making gas cells for rigid airships.

goldbeaters-skin fabric—A fabric consisting of a layer of light, fine, strong cloth, usually cotton, to which one or more layers of goldbeaters skin have been cemented.

factor, dynamic—See **DYNAMIC FACTOR**.

factor, load—See **LOAD FACTOR**.

factor of safety (stress analysis)—The ratio of the ultimate load to any applied load. This term usually refers to the probable minimum factor of safety, which is the ratio of the ultimate load to the probable maximum applied load.

fairing—An auxiliary member or structure whose primary function is to reduce the drag of the part to which it is fitted.

feather—In rotary wing systems, to periodically increase and decrease the incidence of a blade or wing by oscillating the blade or wing about its span axis.

fin—A fixed or adjustable airfoil, attached to an aircraft approximately parallel to the plane of symmetry, to afford directional stability; for example, tail fin, skid fin, etc. (See figs. 3, 4, and 5.)

fin carrier—A frame to which the inboard edge of the fin of a nonrigid or semirigid airship is attached, so as to prevent the edge of the fin from sinking into the envelope.

fineness ratio—The ratio of the length to the maximum diameter of a streamline body, as an airship hull.

fishtail—A colloquial term describing the motion made when the tail of an airplane is swung from side to side to reduce speed in approaching the ground for a landing.

fitting—A generic term for any small part used in the structure of an airplane or airship. If without qualification, a metal part is usually understood. It may refer to other parts, such as fabric fittings.

fixed light—See LIGHT, FIXED.

flap—A hinged or pivoted airfoil forming the rear portion of an airfoil, used to vary the effective camber.

split flap—A hinged plate forming the rear upper or lower portion of an airfoil. The lower portion may be deflected downward to give increased lift and drag; the upper portion may be raised over a portion of the wing for the purpose of lateral control (cf. *upper-surface aileron*).

flap, drip—See DRIP FLAP.

flap, pressure—See PRESSURE FLAP.

flapping angle—See ANGLE, FLAPPING.

flare:

parachute flare—A pyrotechnic device attached to a parachute and designed to illuminate a large area when released from an aircraft at an altitude.

signal flare—A pyrotechnic signaling device of distinctive color and characteristics.

wing-tip flare—A pyrotechnic device attached to an aircraft for illuminating the ground while landing.

flat-plate area, equivalent—See AREA, EQUIVALENT FLAT-PLATE.

flat spin—See SPIN, FLAT.

flight path—The flight path of the center of gravity of an aircraft with reference to the earth, or with reference to a frame fixed relative to the air. (See fig. 9.)

flight-path angle—See ANGLE, FLIGHT-PATH.

float—A completely enclosed watertight structure attached to an aircraft to give it buoyancy and stability when in contact with water.

float, inboard stabilizing—A stabilizing float placed relatively close to the main float or hull.

float, outboard (or wing-tip) stabilizing—A stabilizing float placed relatively far out from the main float or hull, usually at or very near the tip of the wing.

float, single—A single central float fitted under a seaplane and usually requiring two stabilizing floats to give adequate stability and complete the float system.

float, stabilizing (or side)—A float used in addition to a single float or hull and intended to provide lateral stability while the seaplane or flying boat is at rest on the water.

float system—The complete system of permanent floats, used to give buoyancy and stability to a seaplane or a flying boat while it is at rest on the water, and to provide hydrodynamic lift while it is taking off.

floating aileron linkage arrangement—See AILERON LINKAGE ARRANGEMENTS.

floodlight, landing-area—A device designed to illuminate the surface of a landing area.

floodlight system, landing-area—A complete installation of floodlighting equipment designed to illuminate a landing area.

flotation gear—See EMERGENCY FLOTATION GEAR.

flow:

laminar flow—A particular type of streamline flow. The term is usually applied to the flow of a viscous liquid near solid boundaries, when the flow is not turbulent.

streamline flow—A fluid flow in which the streamlines, except those very near a body and in a narrow wake, do not change with time.

turbulent flow—Any part of a fluid flow in which the velocity at a given point varies more or less rapidly in magnitude and direction with time.

flutter—An oscillation of definite period but unstable character set up in any part of an aircraft by a momentary disturbance, and maintained by a combination of the aerodynamic, inertial, and elastic characteristics of the member itself (cf. *buffeting*).

fly—(1) To operate an aircraft in flight. (2) To ride as a passenger in an aircraft.

flying boat—A form of seaplane whose main body or hull provides flotation.

frame, field handling—A portable frame which may be attached to an airship when it is on the ground and which is intended to provide a hold for more men than could grasp the handling rails of the cars. (See fig. 6.)

framing, stern—All framework, aft of the cruciform girder, necessary to complete the shape and contour of a rigid airship.

free balloon—See BALLOON, FREE.

free-balloon net—See NET, FREE-BALLOON.

Frise aileron—See AILERON, FRISE.

fuel bypass regulator—See REGULATOR, FUEL BYPASS.

fuselage—The body, of approximately streamline form, to which the wings and tail unit of an airplane are attached. (See fig. 5.)

monocoque fuselage—A fuselage construction which relies on the strength of the skin or shell to carry either the shear or the load due to bending moments. Monocoques may be divided into three classes (reinforced shell, semi-monocoque, and monocoque), and different portions of the same fuselage may belong to any one of these classes. The reinforced shell has the skin reinforced by a complete framework of structural members. The semimonocoque has the skin reinforced by longerons and vertical bulkheads, but has no diagonal web members. The monocoque has as its only reinforcement vertical bulkheads formed of structural members.

gap—The distance separating two adjacent wings of a multiplane. (See fig. 5.)

gas—To replenish a balloon with fresh gas, in order to increase the purity, or to make up for a loss of gas.

gas-cell fabric—See FABRIC, GAS-CELL.

gas-cell net—See NET, GAS-CELL.

gassing factor—The quantity of aerostatic gas required to maintain an aerostat for one year. It is ordinarily expressed as a percentage of the gas volume.

geared propeller—See PROPELLER, GEARED.

geometrical pitch of a propeller—See PITCH OF A PROPELLER, GEOMETRICAL.

get-away speed—See SPEED, GET-AWAY.

girder:

box girder—Any built-up girder of rectangular section. Frequently used for the rectangular longitudinal members in the keel of a rigid airship from which the fuel tanks and gas cells are suspended.

cruciform girder—The structure, consisting of vertical and horizontal transverse girders, fitted at the stern of a rigid airship for the purpose of supporting the inboard ends of the sternposts of the fins or of the rudder posts.

walkway girder—A girder supporting a walkway along the keel or other part of a rigid or semi-rigid airship.

gland—A short tube fitted to an envelope or gas bag so that a rope or line may slip through it without leakage of gas or air. (See fig. 4.)

glide—To descend at a normal angle of attack with little or no thrust.

glide landing—See LANDING, GLIDE.

glider—An aircraft heavier than air, similar to an airplane but without a power plant.

primary-type glider—A ruggedly built glider designed for use in elementary training of student glider pilots.

secondary-type glider—A glider designed to have better aerodynamic performance than the primary type, but rugged enough for the use of pilots with limited training.

performance-type glider—A glider having a high degree of aerodynamic refinement and low minimum sinking speed.

gliding angle—See ANGLE, GLIDING.

goldbeaters-skin fabric—See FABRIC, GOLDBEATERS-SKIN.

ground angle—Same as LANDING ANGLE.

ground gear—The gear, or equipment, necessary for the landing and handling of an airship on the ground.

ground loop—An uncontrollable violent turn of an airplane while taxiing, or during the landing or take-off run.

ground speed—See SPEED, GROUND.

guide rope—See DRAG ROPE.

gyro, directional—See DIRECTIONAL GYRO.

gyro horizon—A gyroscopic instrument that indicates the lateral and longitudinal attitude of the airplane by simulating the natural horizon.

gyro pilot—See AUTOMATIC PILOT.

gyroplane—A type of rotor plane whose support in the air is chiefly derived from airfoils rotated about an approximately vertical axis by aerodynamic forces, and in which the lift on opposite sides of the plane of symmetry is equalized by rotation of the blades about the blades' axes.

hangar—A shelter for housing airplanes.

head, air-speed—See AIR-SPEED HEAD.

heaviness, nose—See NOSEHEAVY.

heaviness, stern—See STERNHEAVY.

heaviness, tail—See TAILHEAVY.

heaviness, wing—See WINGHEAVY.

height, pressure—The altitude at which the gas cells of a rigid airship or the gas bag of a nonrigid airship are completely full of gas.

helicopter—A type of rotor plane whose support in the air is normally derived from airfoils mechanically rotated about an approximately vertical axis.

honeycomb—A grid of intersecting surfaces used to check lateral disturbances in a fluid stream. (See fig. 7.)

hood:

gas-shaft hood—A hood, or cowl, located on the outer cover of a rigid airship at the outer end of a gas shaft.

maneuvering-valve hood—A hood, or cowl, located on the outer cover of a rigid airship just over a maneuvering valve. It is usually made of light wood or fabric and is faced to facilitate the escape of gas.

valve hood—The appliance, having the form of a hood or parasol, which protects the valve of an airship or balloon against rain; also called "valve cover" or "bonnet." (See fig. 4.)

hood, N.A.C.A.—The ring portion of an N.A.C.A. cowling.

hook, arresting—A hook attached to an airplane which engages the arresting gear in landing.

horizon, artificial—See ARTIFICIAL HORIZON.

horn—A short lever attached to a control surface of an aircraft, to which the operating wire or rod is connected. (See fig. 5.)

horsepower of an engine, rated—The average horsepower developed by a given type of engine at the rated speed when operating at full throttle, or at a specified altitude or manifold pressure.

hub dynamometer—See DYNAMOMETER, HUB.

hull:

airship hull—The main structure of a rigid airship, consisting of a covered elongated framework which incloses the gas cells and supports the cars and other equipment.

seaplane hull—That portion of a flying boat which furnishes buoyancy when in contact with the

- surface of the water. It contains accommodations for the crew and passengers, usually combining the functions of both float and fuselage.
- hump speed**—See SPEED, HUMP.
- hydrofoil (or hydrovane)**—Any surface designed to obtain reaction from the water through which it moves.
- hydroplane**—See PLANE.
- identification light**—See LIGHT, IDENTIFICATION.
- Immelman turn, normal**—A maneuver made by completing the first half of a normal loop; from the inverted position at the top of the loop, half-rolling the airplane to the level position, thus obtaining a 180° change in direction simultaneously with a gain in altitude. (See fig. 8.)
- impact pressure**—The pressure acting at the forward stagnation point of a body, such as a pitot tube, placed in an air current. Impact pressure may be measured from an arbitrary datum pressure.
- incidence, angle of**—See ANGLE OF WING SETTING.
- inclinometer**—An instrument that measures the attitude of an aircraft with respect to the horizontal.
- induced drag**—See DRAG, INDUCED.
- induction compass**—See COMPASS, EARTH-INDUCTOR.
- induction system, rotary**—A carburetor induction system used on radial engines, in which a rotary fan assists in distributing the fuel charge to the cylinders.
- inflation net**—See NET, INFLATION.
- inflation sleeve**—See SLEEVE, INFLATION.
- inflow**—The flow of air into a propeller.
- instability, spiral**—A type of instability, inherent in certain airplanes, which becomes evident when the airplane assumes too great a bank and sideslips; the bank continues to increase and the radius of the turn to decrease.
- instrument flying**—The art of controlling an aircraft solely by the use of instruments; sometimes called "blind flying."
- intake header**—A short duct extending from outside the engine cowl to the supercharger intake.
- interceptor**—A lateral-control device consisting of a small plate placed just back of a wing slot to spoil the effect of the slot at high angles of attack. (See fig. 1.) (Cf. *spoiler*.)
- interference**—The aerodynamic influence of two or more bodies on one another.
- inverted flight (stress analysis)**—A loading condition for the wings simulating the conditions of flying upside down and of commencing a dive (cf. *dive (stress analysis)*.)
- jackstay**—A longitudinal rigging provided to maintain the correct distance between various parts in the fittings of an aerostat.
- keel, airship**—The assembly of members at the bottom of the hull of a semirigid or rigid airship, which provides special strength to resist hogging and sagging and also serves to distribute the effect of concentrated loads along the hull. (See fig. 4.)
- kite balloon**—See BALLOON, KITE.
- laminar flow**—See FLOW, LAMINAR.
- landing**—The act of terminating flight in which the aircraft is made to descend, lose flying speed, establish contact with the ground, and finally come to rest.
- glide landing**—A landing in which a steady glide is maintained to the landing surface without the usual leveling-off before contact.
- level landing (stress analysis)**—A loading condition for the fuselage and landing gear, representing a two-point landing with the fuselage horizontal.
- normal (or three-point) landing**—A landing in which a path tangential to the landing surface and the loss in flying speed are attained at approximately the instant of contact.
- pancake landing**—A landing in which the leveling-off process is carried out several feet above the ground, as a result of which the airplane settles rapidly on a steep flight path in a normal attitude.
- three-point landing (stress analysis)**—A loading condition for the fuselage and landing gear, representing landing with the wheels and tail skid touching the ground simultaneously (cf. *level landing*).
- landing angle**—See ANGLE, LANDING.
- landing area, effective**—That portion of the landing area, with approaches clear within the allowable safe climbing and gliding angle, available for the take-off and landing of aircraft.
- landing-direction light**—See LIGHT, LANDING-DIRECTION.
- landing field**—Any area of land designed for the take-off and landing of aircraft. It may or may not be part of an airport.
- landing gear**—The understructure which supports the weight of an aircraft when in contact with the land or water and which usually contains a mechanism for reducing the shock of landing. Also called "undercarriage." (See fig. 5.)
- retractable landing gear**—A type of landing gear which may be withdrawn into the body or wings of an airplane while it is in flight, in order to reduce the parasite drag.
- landing light**—See LIGHT, LANDING.
- landing strip**—A narrow and comparatively long area forming part of a landplane airport or of an intermediate or auxiliary field, which is suitable for the landing and take-off of airplanes under ordinary weather conditions.
- landplane**—An airplane designed to rise from and alight on the land.
- lateral axis**—See AXES OF AN AIRPLANE.
- leading edge**—The foremost edge of an airfoil or propeller blade.
- length, chord**—See CHORD LENGTH.

level landing—See **LANDING, LEVEL**.

level-off—To make the flight path of an airplane horizontal after a climb, glide, or dive.

lift:

aerostatic lift—The difference between the weight of a volume of air and of an equal volume of a gas lighter than air under given conditions.

dynamic lift—The component of the total aerodynamic force on a body perpendicular to the relative wind. (See fig. 9.)

gross lift (aerostat)—The buoyancy under standard conditions of density, purity, and fullness.

useful lift (aerostat)—The lift available for carrying passengers, fuel, oil, supplies, cargo, etc. It is the difference between the gross lift and the fixed weight of an aerostat.

lift direction (stress analysis)—The direction in the plane of symmetry perpendicular to the relative wind (cf. *beam*, *chord*, *drag*, and *side directions*).

lift/drag ratio—The ratio of the lift to the drag of any body.

lift force, or component (stress analysis)—A force, or component, in the lift direction (cf. *beam*, *chord*, *drag*, and *side forces*).

light:

anchor light—A light, or group of clear lights carried on an aircraft to indicate its position at night while at anchor.

approach light—A light, usually green, designed to indicate a favorable direction of approach for landing an aircraft.

blinker light—A flashing light giving more than 20 flashes per minute.

boundary light—Any one of the lights designed to indicate the limits of the landing area of an airport or landing field.

ceiling light—Same as **CEILING PROJECTOR**.

course light—A light projected along the course of an airway so as to be visible chiefly from points on or near the airway.

fixed light—A light which is constant in luminous intensity with respect to both time and direction.

flashing light—A light which is intermittent as viewed from a single direction.

identification light—A group of lights, clear and colored, carried on the rear part of an airplane for identification at night.

landing-direction light—A light designed to indicate, either by itself or in conjunction with other lights, the direction in which landings are to be made.

landing light—A light carried by an aircraft to illuminate the ground while landing.

navigation light—Same as **POSITION LIGHT**.

obstruction light—A red light designed to indicate the position and height of an object hazardous to the operation of aircraft.

light—continued.

position light—Any one of a group of lights—red, green, and clear—used aboard an aircraft to indicate its position and direction of motion.

line:

control line—One of the lines leading from the control car or compartment to the various parts of an airship and operating (either through mechanisms or directly) the rudders, valves, etc., which control the speed, altitude, etc., of the airship.

handling line (aerostat)—A line attached to the side of an airship or balloon for use by the ground crew in handling the aerostat. (See fig. 3.)

handling line (airplane)—Two lines of steel strand attached to the upper wings of a seaplane for steadying it when hauled out of the water aboard ship.

main mooring line—The line dropped from the bow of an airship to be coupled to the main mooring-mast line.

main mooring-mast line—A line leading from the main winch of a mooring mast through the mooring attachment at the top of the mast for the purpose of attaching the main mooring line of an airship.

mast yaw line—One of the two lines leading from the winches at the base of the mooring mast through snatch blocks and carried to the leeward of the mast 60° from the wind direction. The airship's yaw lines are coupled to these lines. The snatch blocks are fixed to anchorages selected so that the joined lines tend to keep the bow of the airship into the wind and prevent its overriding the mast. These lines are sometimes called "mast yaw guys" or "mast bow-steadying lines." (The main mooring line and the yaw guys, when taut, establish a fixed point in space.)

mooring line—A line attached near the bow of an aircraft for securing it to the ground, buoy, anchor, or to a mooring mast.

sandbag line—A rope extending along the line of suspension ropes or bridles of a kite balloon to which are hooked the sandbags used in mooring the balloon. The purpose is to prevent wear on the suspension cordage.

shroud line—The suspension cords of a parachute which attach the harness to the canopy.

suspension line—A line attached to the hull or envelope of an airship for supporting an appendage, such as a car or fin.

yaw line—A line dropped from the bow of an airship, when mooring to the mast, to be coupled to the mast yaw line and act as a steadying line to prevent yawing and overriding the mast.

load:

basic load (stress analysis)—The load on a structural member or part in any condition of static equilibrium of an airplane. When a specific basic load is meant, the particular condition of equilibrium must be indicated in the context.

design load (stress analysis)—A specified load below which a structural member or part should not fail. It is the probable maximum applied load multiplied by the factor of safety. Also, in many cases, an appropriate basic load multiplied by a design load factor.

full load—Weight empty plus useful load; also called *gross weight*.

normal load (stress analysis)—The load on that part of a wing assumed to be unaffected by tip losses or similar corrections. In any given case, it may be a basic, design, gross, net, or ultimate load, depending on the context.

pay load—That part of the useful load from which revenue is derived, viz, passengers and freight.

ultimate load (stress analysis)—The load that causes destructive failure in a member during a strength test, or the load that, according to computations, should cause destructive failure in the member.

useful load—The crew and passengers, oil and fuel, ballast other than emergency, ordnance, and portable equipment.

load factor (stress analysis)—The ratio of two loads (the second being a basic load) that have the same relative distribution. The first load may be the load applied during some special maneuver, the maximum probable load on the airplane or part, the design load, or the ultimate load. Whenever a load factor is mentioned, the context should indicate clearly what load is being compared with the basic load. If the context does not so indicate, the load factor is usually the ratio of the design load to the weight of the airplane.

loading:

power loading—The gross weight of an airplane divided by the rated horsepower of the engine computed for air of standard density, unless otherwise stated.

span loading—The ratio of the weight of an airplane to its equivalent monoplane span.

unsymmetrical loading (stress analysis)—A design loading condition for the wings and connecting members, representing the conditions as in a roll.

wing loading—The gross weight of an airplane divided by the wing area.

longeron—A principal longitudinal member of the framing of an airplane fuselage or nacelle, usually continuous across a number of points of support. (See fig. 5.)

longitudinal:

intermediate longitudinal—A light longitudinal girder between main longitudinals of a rigid airship, primarily intended for support of the outer cover.

main longitudinal—A main longitudinal strength member of a rigid airship, which connects the various transverse frames. (See fig. 6.)

loop—A maneuver executed in such a manner that the airplane follows a closed curve approximately in a vertical plane.

inverted normal loop—A loop starting from inverted flight and passing successively through a dive, normal flight, climb, and back to inverted flight.

inverted outside loop—An outside loop starting from inverted flight and passing successively through a climb, normal flight, dive, and back to inverted flight.

normal loop—A loop starting from normal flight and passing successively through a climb, inverted flight, dive, and back to normal flight. (See fig. 8.)

outside loop—A loop starting from normal flight and passing successively through a dive, inverted flight, climb, and back to normal flight, the pilot being on the outside of the flight path.

loop, ground—See GROUND LOOP.

loop, radio—A specified number of turns of wire located in the wings or wound around the fuselage of an airplane. Small portable loops on a rectangular frame are also used.

loop, safety—A loop formed in a rip cord of an aerostat and attached to a securing patch by a breakable cord or a spring clip.

loop, sandbag—A system of cordage loops on the envelope of a balloon for suspending sandbags.

magneto, booster—An auxiliary magneto used for starting.

maneuver—(a) To operate an aircraft in a skillful manner, so as to cause it to perform evolutions out of the ordinary. (b) To perform tactical or acrobatic evolutions with aircraft.

maneuverability—That quality in an aircraft which determines the rate at which its attitude and direction of flight can be changed.

maneuvering valve—See VALVE, MANEUVERING.

manhole, appendix—A short appendix of large diameter used for access to the interior of the envelope of an aerostat.

manometer pressure (aerostat)—See PRESSURE, MANOMETER.

margin of safety (stress analysis)—The difference between the ultimate load and any applied load.

marker, boundary—A painted cone, solid circle, disk, or other device used to mark the boundary of the available landing area on an airport or landing field.

marker, circle—A circular band marking the approximate center of the landing area or the intersection of the principal landing strips on an airport or landing field.

mast, mooring—See **MOORING MAST**.

mast, radio—See **RADIO MAST**.

mean line (of an airfoil profile)—An intermediate line between the upper and lower contours of the profile. (See fig. 2.)

mechanical pilot—See **AUTOMATIC PILOT**.

meteorograph—A recording instrument for obtaining meteorological information above the earth's surface. It contains elements to record temperature, pressure, and humidity. (Also called *aerograph*.)

mixture control, altitude—A device on the carburetor for regulating the weight proportions of air and fuel supplied to the engine at different altitudes.

moment, trimming—See **TRIMMING MOMENT**.

monocoque fuselage—See **FUSELAGE, MONOCOQUE**.

monoplane—An airplane with but one main supporting surface, sometimes divided into two parts by the fuselage.

high-wing monoplane—A monoplane in which the wing is located at, or near, the top of the fuselage.

low-wing monoplane—A monoplane in which the wing is located at, or near, the bottom of the fuselage.

midwing monoplane—A monoplane in which the wing is located approximately midway between the top and bottom of the fuselage.

parasol monoplane—A monoplane in which the wing is above the fuselage.

monoplane, equivalent—See **EQUIVALENT MONOPLANE**.

mooring band—See **BAND, MOORING**.

mooring cone—See **CONE, MOORING**.

mooring-cone outrigger—See **OUTRIGGER, MOORING-CONE**.

mooring drag—Same as **TAIL DRAG**.

mooring harness—A system of webbing bands, fitted over the top of a balloon, to which the mooring ropes are attached; usually found only on kite or observation balloons.

mooring mast—A mast or tower at the top of which there is a fitting to which the bow of an airship may be secured.

multiplane—An airplane with two or more main supporting surfaces placed one above another.

nacelle—An enclosed shelter for personnel or for a power plant. A nacelle is usually shorter than a fuselage, and does not carry the tail unit.

navigation light—See **LIGHT, NAVIGATION**.

net:

free-balloon net—A rigging made of ropes and twine shaped to fit the upper surface of the envelope, which supports the weight of the basket, etc., and distributes the load over the entire upper surface of the envelope.

gas-cell net (rigid airship)—A small-mesh netting of cord, intended to assist the fabric of the gas

net—continued.

cells in transmitting the gas force to a wire netting of coarser mesh and to the longitudinals both being fitted between the longitudinals. It may be compared to the net of a free balloon. Sometimes called "gas-cell netting" or "cord netting." (See fig. 6.)

inflation net—A rectangular net of cordage, used to restrain the envelope of a kite balloon or nonrigid airship during inflation. Also applied to a free-balloon net designed to be removed after inflation.

net weight—See **WEIGHT, NET**.

nonrigid airship—See **AIRSHIP, NONRIGID**.

nose-down—To depress the nose of an airplane in flight.

noseheavy—The condition of an airplane in which the nose tends to sink when the longitudinal control is released in any given attitude of normal flight (cf. *tailheavy*).

nose-over—A colloquial expression referring to the accidental turning over of an airplane on its nose when landing.

nose-up—To elevate the nose of an airplane in flight.

Number, Reynolds—See **REYNOLDS NUMBER**.

obstruction light—See **LIGHT, OBSTRUCTION**.

octant—A variation of the aircraft sextant which measures angles up to 90°. Its artificial horizon is usually the bubble type.

oleo gear—A type of oil-damping device that depends on the flow of oil through an orifice for its shock-absorbing effect in a landing gear.

ornithopter—A form of aircraft heavier than air, deriving its chief support and propelling force from flapping wings.

oscillation:

phugoid oscillation—A long-period oscillation characteristic of the disturbed longitudinal motion of an aircraft.

stable oscillation—An oscillation whose amplitude does not increase.

unstable oscillation—An oscillation whose amplitude increases continuously until an attitude is reached from which there is no tendency to return toward the original attitude, the motion becoming a steady divergence.

outrigger, mooring-cone—The member, usually tubular, which supports the mooring cone at the bow of an airship; sometimes referred to as the "mooring spindle." (See fig. 6.)

over-all length—The distance from the extreme front to the extreme rear of an aircraft, including the propeller and the tail unit.

overhang—(1) One half the difference in span of any two main supporting surfaces of an airplane. The overhang is positive when the upper of the two main supporting surfaces has the larger span. (See fig. 5.) (2) The distance from the outer strut attachment to the tip of a wing.

overshoot—To fly beyond a designated mark or area, such as a landing field, while attempting to land on the mark or within the area.

pancake landing—See **LANDING, PANCAKE**.

panel (aerostat)—(1) The unit piece of fabric of which the envelope or outer cover of an aerostat is made. (2) In rigid airships, the area bounded by two consecutive longitudinals and two consecutive transverses.

panel (airplane)—A portion of an airplane wing constructed separately from the rest of the wing to which it is attached.

panel, rip—A strip of fabric, inserted or fitted in the upper part of the envelope of a balloon or semirigid or nonrigid airship, which is torn or ripped open when immediate deflation is desired. (See fig. 3.)

parachute—An umbrella-like device used to retard the descent of a falling body by offering resistance to its motion through the air.

pilot parachute—A small auxiliary parachute attached to the apex of the main parachute, designed to pull the latter out of its pack when the rip cord is pulled.

parachute flare—See **FLARE, PARACHUTE**.

parachute harness—A combination of straps, buckles, and fastenings used to attach a parachute to the wearer.

parachute pack—A parachute and its container.

parachute rigger—A person who packs, repairs, and inspects parachutes.

parasite drag—See **DRAG, PARASITE**.

parasol monoplane—See **MONOPLANE, PARASOL**.

patch—A strengthened or reinforced flap of fabric of special shape and construction cemented to the envelope or gas cell of an aerostat. It usually forms an anchorage by which some portion of the structure may be attached to the envelope, or by which the positioning lines controlling the gas cell may be attached to the cell.

channel patch—A channel-shaped fabric fitting secured to the envelope of an aerostat to allow a rod or spar to be laced to the envelope.

finger patch—A special form of patch having "fingers" extending from the central portion to distribute the load more widely to the fabric of an envelope or gas cell.

suspension patch—A patch, secured to the envelope or to a gas cell of an aerostat, to which a suspension line may be attached.

path, flight—See **FLIGHT PATH**.

pay load—See **LOAD, PAY**.

pendant, sighting—A vertical wire on the center line and forward of the control car of an airship, used as a guide in steering and to assist in determining the direction of the wind.

permeability—The measure of the rate of diffusion of a gas per unit area of any material used in the construction of a gas container.

pilot—One who operates the controls of an aircraft in flight.

pilot, automatic—See **AUTOMATIC PILOT**.

pilot balloon—See **BALLOON, PILOT**.

pilot parachute—See **PARACHUTE, PILOT**.

pilot plane—An auxiliary airfoil pivoted near the leading edge of a main airfoil and free to take up a position in line with the wind.

pitch—An angular displacement about an axis parallel to the lateral axis of an aircraft.

pitch, angle of—See **ANGLE OF PITCH**.

pitching—Angular motion about the lateral axis (fig. 12).

pitch (or pitching) indicator—An instrument for indicating the existence and approximate magnitude of the angular velocity about the lateral axis of an aircraft.

pitch of a propeller:

effective pitch—The distance an aircraft advances along its flight path for one revolution of the propeller.

geometrical pitch—The distance an element of a propeller would advance in one revolution if it were moving along a helix having an angle equal to its blade angle.

zero-thrust pitch—The distance a propeller would have to advance in one revolution to give no thrust. Also called "experimental mean pitch."

pitch ratio (propeller)—The ratio of the pitch to the diameter.

pitot-static tube—A parallel or coaxial combination of a pitot and a static tube. The difference between the impact pressure and the static pressure is a function of the velocity of flow past the tube.

pitot tube—A cylindrical tube with an open end pointed upstream, used in measuring impact pressure.

pitot-venturi tube—A combination of a pitot and a venturi tube.

plane (or hydroplane)—To move through the water at such a speed that the support derived is due to hydrodynamic and aerodynamic rather than to hydrostatic forces.

plan form, developed—The plan of an airfoil as drawn with the chord lines at each section rotated about the airfoil axis into a plane parallel to the plane of projection and with the airfoil axis rotated or developed and projected into the plane of projection.

plan form, projected—The contour as viewed from above.

platform, observation—A small deck fitted on the top of an airship for a lookout and defense or for making observations used in navigating the airship.

plowing—Taxying a seaplane at low speed before rising on the step.

pontoon—Obsolete as applied to aircraft. (See **FLOAT**.)

porpoising—An undulatory movement of a seaplane consisting of a combination of a vertical oscillation and an oscillation about its transverse axis, which occurs at certain stages of planing.

position light—See LIGHT, POSITION.

power loading—See LOADING, POWER.

pressure, altitude—See ALTITUDE, PRESSURE.

pressure, dynamic—See DYNAMIC PRESSURE.

pressure, impact—See IMPACT PRESSURE.

pressure, manometer (aerostat)—The excess pressure inside the envelope of an aerostat over the atmospheric pressure at a standard reference point. The point of reference for the excess pressure is usually the bottom of the envelope or gas cell on airships and the level of the basket on kite balloons.

pressure flap—A flap valve fitted in the outer cover or envelope of a rigid airship and arranged to permit the rapid flow of air in and out—particularly inward. The purpose is to facilitate the rapid equalization of the pressure of the air in the envelope with that of the surrounding air.

pressure height—See HEIGHT, PRESSURE.

primary structure (stress analysis)—The main framework, including fittings and attachments. Any structural member, the failure of which would seriously impair the safety of the airplane, is a part of the primary structure.

profile drag—See DRAG, PROFILE.

profile thickness—The maximum distance between the upper and lower contours of an airfoil, measured perpendicularly to the mean line of the profile. (See fig. 2.)

projected propeller-blade area—See AREA, PROJECTED PROPELLER-BLADE.

projector—A device for projecting a beam of light, as a searchlight projector.

projector, bearing—See BEARING PROJECTOR.

projector, ceiling—See CEILING PROJECTOR.

projector, traffic-control—See TRAFFIC-CONTROL PROJECTOR.

propeller—Any device for propelling a craft through a fluid, such as water or air; especially a device having blades which, when mounted on a power-driven shaft, produce a thrust by their action on the fluid.

adjustable propeller—A propeller whose blades are so attached to the hub that the pitch may be changed while the propeller is at rest.

automatic propeller—A propeller whose blades are attached to a mechanism that automatically sets them at their optimum pitch for various flight conditions.

controllable propeller—A propeller whose blades are so mounted that the pitch may be changed while the propeller is rotating.

geared propeller—A propeller driven through gearing, generally at some speed other than the engine speed.

pusher propeller—A propeller mounted on the rear end of the engine or propeller shaft.

tractor propeller—A propeller mounted on the forward end of the engine or propeller shaft.

propeller area—See AREA, PROPELLER.

propeller-blade area—See AREA, PROPELLER-BLADE.

propeller-disk area—See AREA, PROPELLER-DISK.

propeller efficiency—The ratio of the thrust power to the input power of a propeller.

propeller radius—See TIP RADIUS.

propeller rake—The mean angle which the line joining the centroids of the sections of a propeller blade makes with a plane perpendicular to the axis.

propeller root—That part of the propeller blade near the hub. (See fig. 5.)

propeller thrust—The component of the total air force on the propeller which is parallel to the direction of advance.

propeller thrust, effective—The net driving force developed by a propeller when mounted on an aircraft, i.e., the actual thrust exerted by the propeller, as mounted on an airplane, minus any increase in the resistance of the airplane due to the action of the propeller.

propeller thrust, static—The thrust developed by a propeller when rotating without translation.

propeller tipping—A protective covering of the blade of a propeller near the tip. (See fig. 5.)

propulsive efficiency—The ratio of the product of the effective thrust and flight speed to the actual power input into the propeller as mounted on the airplane.

pull-out—The maneuver of transition from a dive to horizontal flight.

pull-up—A maneuver, in the vertical plane, in which the airplane is forced into a short climb, usually from approximately level flight. (cf. *zoom*).

sudden pull-up (or sudden pull-out) (stress analysis)—A loading condition for the tail surfaces resulting from a sudden application of up-elevator (cf. *dive*).

purity (of gas)—The ratio of the partial pressure of the aerostatic gas in the container to the total pressure of all the contained gases.

push-down—The opposite of *pull-up*.

pusher airplane—See AIRPLANE, PUSHER.

pusher propeller—See PROPELLER, PUSHER.

radial engine—See ENGINE, RADIAL.

radio-directive devices:

landing beam—A beam projected from the field to indicate to the pilot his height above the ground and the position of the airplane on the proper path for a glide landing.

radio-marker beacon—A radio transmitter of low power emitting a characteristic aural signal to indicate course positions with respect to a landing field or an airway.

radio-range beacon—A radio transmitter supplying directive radio waves that provide a means of keeping an aircraft on its proper course.

runway localizing beacon—A small radio-range beacon giving accurate lateral direction along the runway of an airport or landing field and a few miles beyond.

radio loop—See LOOP, RADIO.

radio mast—A mast attached to an aircraft which serves as part of the radio-antenna structure.

rail, docking—A rail or guide, installed on the landing field and extending into the shed, which affords a means for resisting the lateral pull of an airship's docking or handling lines.

rake, propeller—See PROPELLER RAKE.

ram—The combination of tubes and springs mounted in gimbals at the top of a mooring mast to ease the shock when the moor is made.

ramming—The effect obtained when the air intake to the engine is placed in the slipstream in such a manner as to take advantage of the difference in velocity of this air intake and the slipstream, in order to increase the pressure in the induction system.

range, maximum—The maximum distance a given aircraft can cover under given conditions, by flying at the economical speed and altitude at all stages of the flight.

range at maximum speed—The maximum distance a given aircraft can fly at full speed at the altitude for maximum speed under given conditions.

rated horsepower of an engine—See HORSEPOWER OF AN ENGINE, RATED.

rate-of-climb indicator—An instrument that indicates the rate of ascent or descent of an aircraft.

recovery, water—See WATER RECOVERY.

reference area—The area used in the equations defining the coefficient of the air force acting upon a body or the coefficients of the components of the air force. This area is logically or conveniently chosen in different manners for different types of bodies.

regulator, fuel bypass—A device placed in the fuel line of a supercharged engine for regulating the fuel pressure in the carburetor float chamber so that it will be a fixed amount above the carburetor air pressure.

relative efficiency of biplane wings (stress analysis)—The ratio of the normal load per square foot on the upper wing to that on the lower.

relative wind—See WIND, RELATIVE.

renversement—A maneuver consisting of a half roll and a half loop in the order named.

resistance derivatives—See DERIVATIVES, RESISTANCE.

retractable landing gear—See LANDING GEAR, RETRACTABLE.

Reynolds Number—A nondimensional coefficient used as a measure of the dynamic scale of a flow. Its usual form is the fraction $\rho \frac{Vl}{\mu}$ in which ρ is the density of the fluid, V is the velocity of the fluid, l is a linear dimension of a body in the fluid, and μ is the coefficient of viscosity of the fluid (cf. *scale effect*).

rib, wing—See WING RIB.

rig:

(aerostat)—To attach and adjust the car, rudders, valves, controls, etc., of an airship, i.e., to erect.

(airplane)—To assemble, adjust, and aline the parts of an airplane.

rigger—One who rigs aircraft.

righting or restoring moment—A moment that tends to restore an aircraft to its previous attitude after any small rotational displacement.

rigid airship—See AIRSHIP, RIGID.

ring, concentration:

airship concentration ring—A ring to which several rigging lines are led from the envelope and from which one or more lines also lead to the car.

free-balloon concentration ring—A ring to which are attached the ropes suspending the basket and to which the net is also secured; sometimes called "load ring."

ring, exhaust-collector—See EXHAUST-COLLECTOR RING.

ring cowl—A ring-shaped cowl placed around a radial air-cooled engine to reduce its drag and improve cooling.

rip cord—(1) The rope running from the rip panel to the car or basket, the pulling of which tears off or rips the panel and causes immediate deflation of a balloon or a nonrigid airship. (See fig. 3.) (2) The cord, together with the handle and fastening pins, which, when pulled, releases a parachute from its container.

roach—A heavy jet or vertical sheet of water thrown above the water surface behind a seaplane float.

roll—A maneuver in which a complete revolution about the longitudinal axis is made, the horizontal direction of flight being approximately maintained.

aileron roll—A roll in which the motion is largely maintained by forces arising from the displacement of the aileron (fig. 8).

outside roll—A roll executed while flying in the negative angle-of-attack range.

snap roll—A roll executed by a quick movement of the controls, in which the motion is largely maintained by autorotational couples on the wings (fig. 8).

roll—An angular displacement about an axis parallel to the longitudinal axis of an aircraft.

rolling—Angular motion about the longitudinal axis (fig. 10).

root, propeller—See PROPELLER ROOT.

Roots-type supercharger—See SUPERCHARGER, ROOTS-TYPE.

rotor—The complete rotating portion of a rotary wing system.

rotor plane—A form of aircraft whose support in the air is chiefly derived from the vertical component of the force produced by rotating airfoils.

rudder—A hinged or movable auxiliary airfoil on an aircraft, the function of which is to impress a yawing moment on the aircraft. (See figs. 3, 4, 5, and 6.)

rudder angle—See **ANGLE, RUDDER**.

rudder bar—The foot bar by means of which the control cables leading to the rudder are operated. (See fig. 5.)

rudder pedals—The foot pedals by means of which the controls leading to the rudder are operated.

runway—An artificial landing strip permitting the landing and take-off of airplanes under all weather conditions.

safety, factor of—See **FACTOR OF SAFETY**.

sailplane—A performance-type glider.

scale effect—The change in any force coefficient, such as the drag coefficient, due to a change in the value of Reynolds Number.

school, ground—A school in which instruction is given to a student undergoing flight training.

scoop, air—See **AIR SCOOP**.

seaplane—An airplane designed to rise from and alight on the water.

semirigid airship—See **AIRSHIP, SEMIRIGID**.

separation—The phenomenon in which the flow past a body placed in a moving stream of fluid separates from the surface of the body.

separation point—The point at which the separation of the boundary layer begins.

service ceiling—See **CEILING, SERVICE**.

servo control—See **CONTROL, SERVO**.

sesquiplane—A form of biplane in which the area of one wing is less than half the area of the other.

shaft:

climbing shaft—A shaft, fitted with a ladder, which leads from the bottom to the top of an airship hull to provide access to the upper portion. (See fig. 4.)

gas shaft—A passageway between the gas cells of an airship to permit the escape of gas which has been discharged from the cells.

shed, airship—See **DOCK**.

shipboard plane—A landplane designed to rise from and alight on the deck of a ship.

side direction (stress analysis)—The direction perpendicular to the plane of symmetry.

side force or component (stress analysis)—A force, or component, perpendicular to the plane of symmetry.

sideslipping—Motion of an aircraft relative to the air, in which the lateral axis is inclined and the airplane has a velocity component along the lateral axis. When it occurs in connection with a turn, it is the opposite of *skidding*. (See fig. 11.)

signal flare—See **FLARE, SIGNAL**.

sinking speed—The vertical downward component of velocity that an aircraft would have while descending in still air under given conditions of equilibrium.

skid, tail—See **TAIL SKID**.

skid, wing—See **WING SKID**.

skidding—Sliding sidewise away from the center of curvature when turning. It is caused by banking insufficiently, and is the opposite of *sideslipping*.

skid fin—A longitudinal vertical surface, usually placed above the upper wing to increase the lateral stability.

skin friction—The tangential component of the fluid force at a point on a surface.

sky writing—The act of emitting from an aircraft a trail of smoke or other visible substance, the flight of the aircraft being so directed as to cause the trail to assume the form of letters or symbols.

slat—A movable auxiliary airfoil, attached to the leading edge of a wing, which when closed falls within the original contour of the main wing and which when opened forms a slot. (See fig. 1.)

sleeve:

deflation sleeve—(1) A sleeve or appendix made of fabric provided for the special purpose of facilitating the deflation of an aerostat. (2) The sleeve or appendix fitted in the lower lobe of a kite balloon and used to permit the rapid escape of the air in the lobes when the balloon is hauled down.

inflation sleeve—A tubular fabric attachment to an envelope or gas bag, serving as a lead for the inflation tube. (See figs. 3 and 4.)

towing sleeve—A tubular fabric envelope towed by an aircraft and used as a target.

slip—The difference between the geometrical pitch and the effective pitch of a propeller. Slip may be expressed as a percentage of the mean geometrical pitch, or as a linear dimension.

slip function—The ratio of the speed of advance through the undisturbed air to the product of the propeller diameter and the number of revolutions per unit time; i.e., V/nD .

slipstream—The current of air driven astern by a propeller.

slot—The nozzle-shaped passage through a wing whose primary object is to improve the flow conditions at high angles of attack. It is usually near the leading edge and formed by a main and an auxiliary airfoil, or *slat*. (See fig. 1.) (Cf. *slat*.)

slotted aileron—See **AILERON, SLOTTED**.

soar—To fly without engine power and without loss of altitude, as does a glider in ascending air currents.

solidity—The ratio of the total blade area of a rotor to the area of the disk swept by the blades.

sounding balloon—See **BALLOON, SOUNDING**.

span—The maximum distance, measured parallel to the lateral axis, from tip to tip of an airfoil, of an airplane wing inclusive of ailerons, or of a stabilizer inclusive of elevator. (See fig. 5.)

effective span—The true span of a wing less corrections for tip loss.

span loading—See **LOADING, SPAN**.

spar, wing—See **WING SPAR**.

speed:

air speed—See **AIR SPEED**.

get-away speed—The air speed at which a seaplane becomes entirely air-borne.

ground speed—The horizontal component of the velocity of an aircraft relative to the ground.

hump speed—The speed of a seaplane during take-off at which the float resistance reaches a maximum.

landing speed—The minimum speed of an airplane at the instant of contact with the landing area in a normal landing.

minimum flying speed—The lowest steady speed that can be maintained, with any throttle setting whatsoever, by an airplane in level flight at an altitude above the ground greater than the span of the wings.

operating speed—The speed in level flight corresponding to 87.5 percent of the rated speed of the engine.

pitch speed—The product of the mean geometrical pitch and the number of revolutions of the propeller in unit time.

rated engine speed—The rotative speed of an engine at which its reliability has been determined for continuous performance.

sinking speed—See **SINKING SPEED**.

slip speed (supercharger)—The supercharger speed necessary to maintain a given pressure difference between intake and discharge when there is no air delivery.

stalling speed—The speed of an airplane in steady flight at its maximum coefficient of lift.

take-off speed—The air speed at which an airplane becomes entirely air-borne.

terminal speed—See **VELOCITY, TERMINAL**.

spin—A maneuver in which an airplane descends along a helical path of large pitch and small radius while flying at a mean angle of attack greater than the angle of attack at maximum lift (cf. *spiral*).

flat spin—A spin in which the longitudinal axis is less than 45° from the horizontal.

inverted spin—A maneuver having the characteristics of a normal spin except that the airplane is in an inverted attitude.

normal spin—A spin which is continued by reason of the voluntary position of the control surfaces, recovery from which can be effected within two turns by neutralizing or reversing all the controls. Sometimes called "controlled spin" (fig. 8).

uncontrolled spin—A spin in which the controls are of little or no use in effecting a recovery.

spinner—A fairing of approximately conical or paraboloidal shape, which is fitted coaxially with the

propeller hub and revolves with the propeller. (See fig. 5.)

spiral—A maneuver in which an airplane descends in a helix of small pitch and large radius, the angle of attack being within the normal range of flight angles (fig. 8) (cf. *spin*).

split S—A maneuver consisting of a half snap roll followed by a pull-out to normal flight, thus obtaining a 180° change in direction accompanied by a loss of altitude (fig. 8).

spoiler—A small plate arranged to project above the upper surface of a wing to disturb the smooth air flow, with consequent loss of lift and increase of drag. (See fig. 1.) (Cf. *interceptor*.)

squat—A downward, or negative, displacement of the center of gravity of a seaplane while running on the water.

spray strip—A strip projecting from the hull of a seaplane to change the manner in which the spray is thrown.

sponson—A protuberance from a seaplane hull designed to increase the beam or give lateral stability at rest.

stability—That property of a body which causes it, when its equilibrium is disturbed, to develop forces or moments tending to restore the original condition.

automatic stability—Stability dependent upon movable control surfaces automatically operated by mechanical means.

directional stability—Stability with reference to disturbances about the normal axis of an aircraft, i.e., disturbances which tend to cause yawing.

dynamic stability—That property of an aircraft which causes it, when its state of steady flight is disturbed, to damp the oscillations set up by the restoring forces and moments and gradually return to its original state.

inherent stability—Stability of an aircraft due solely to the disposition and arrangement of its fixed parts; i.e., that property which causes it, when disturbed, to return to its normal attitude of flight without the use of the controls or the interposition of any mechanical device.

lateral stability—Stability with reference to disturbances about the longitudinal axis; i.e., disturbances involving rolling or sideslipping. The term lateral stability is sometimes used to include both directional and lateral stability, since these cannot be entirely separated in flight.

longitudinal stability—Stability with reference to disturbances in the plane of symmetry, i.e., disturbances involving pitching and variation of the longitudinal and normal velocities.

static stability—That property of an aircraft which causes it, when its state of steady flight is disturbed, to develop forces and moments tending to restore its original condition.

- stabilizer (airplane)**—Any airfoil whose primary function is to increase the stability of an aircraft. It usually refers to the fixed horizontal tail surface of an airplane, as distinguished from the fixed vertical surface. (See fig. 5.)
- stabilizer (aerostat)**—Same as FIN.
- stabilizer, stub-wing**—A projection from the side of the central hull of a flying boat intended to increase the buoyancy and stability of a flying boat while the boat is at rest and to increase the hydrodynamic lift during the take-off. It is an integral part of the hull, and usually takes the form of a stumpy airfoil or a stub wing.
- stagger**—A term referring to the longitudinal position of the axes of two wings of an airplane. Stagger of any section is measured by the acute angle between a line joining the wing axes and a line perpendicular to the upper wing chord, both lines lying in a plane parallel to the plane of symmetry. The stagger is positive when the upper wing is in advance of the lower. (See fig. 5.)
- stall**—The condition of an airfoil or airplane in which it is operating at an angle of attack greater than the angle of attack of maximum lift.
- stalling speed**—See SPEED, STALLING.
- standard atmosphere**—See ATMOSPHERE, STANDARD.
- static ceiling**—See CEILING, STATIC.
- static pressure**—The force per unit area exerted by a fluid on a surface at rest relative to the fluid.
- static stability**—See STABILITY, STATIC.
- static tube**—A cylindrical tube with a closed end and a number of small openings normal to the axis, pointed upstream, used to measure static pressure.
- station, airship**—See AIRSHIP STATION.
- step**—A break in the form of the bottom of a float or hull, designed to diminish resistance, to lessen the suction effects, and to improve control over longitudinal attitude.
- stern-droop**—A deformation of an airship in which its longitudinal axis bends downward at the after end.
- sternheavy**—The condition in which, in normal flight, the after end of an airship tends to sink and which requires correction by means of the horizontal controls. It may be due to either aerodynamic or static conditions, or to both (cf. *bowheavy*).
- stern-weighing device**—An instrument located near the stern of an airship for measuring its buoyancy (cf. *bow-weighing device*).
- stiffener, bow**—A rigid member attached to the bow of a nonrigid or semirigid envelope to reinforce it against the pressure caused by the motion of the airship. (See figs. 3 and 4.)
- sting**—A light rod attached to and extending backward from a body for convenience of mounting when testing in a wind tunnel.
- streamline**—The path of a particle of a fluid, supposedly continuous, commonly taken relative to a solid body past which the fluid is moving; generally used only of such flows as are not eddying.
- streamline flow**—See FLOW, STREAMLINE.
- streamline form**—The form of a body so shaped that the flow about it tends to be a streamline flow.
- stresses, breathing**—Stresses produced in an aerostat by breathing. They are of importance in the envelope and keel of a semirigid airship, due to the interaction of the envelope and keel when the envelope breathes.
- strut**—A compression member of a truss frame. (See fig. 5.)
- oleo strut**—A shock-absorbing telescopic strut in which an oleo gear is incorporated.
- stub plane**—See STABILIZER, STUB-WING.
- sun compass**—See COMPASS, SUN.
- supercharge**—To supply an engine with more air or mixture than would be inducted normally at the prevailing atmospheric pressure. The term supercharged is generally used to refer to conditions at altitudes where the pressure in the intake manifold is partly or completely restored to that existing under normal operation at sea level (cf. *boost*).
- supercharger**—A pump for supplying the engine with a greater weight of air or mixture than would normally be inducted at the prevailing atmospheric pressure.
- centrifugal-type supercharger**—A high-speed rotary blower equipped with one or more multi-blade impellers which, through centrifugal action, compress the air or mixture in the induction system.
- positive-driven-type supercharger**—A supercharger driven at a fixed speed ratio from the engine shaft by gears or other positive means.
- reciprocating-type supercharger**—A positive-displacement reciprocating pump in which the air or mixture is compressed by a piston working in a cylinder.
- Roots-type supercharger**—A positive-displacement rotary blower consisting of two double-lobed impellers turning in opposite directions on parallel shafts within a housing, the impellers rolling together except for a small clearance, meanwhile alternately trapping incoming air or mixture in the ends of the housing and sweeping it through to the outlet.
- vane-type supercharger**—A positive-displacement rotary blower having an eccentrically located rotor provided with one or more vanes.
- supercharger control: bypassing (Roots)**—Regulating the pressure of the air supplied to the carburetor by discharging into the free atmosphere the excess delivered by the supercharger.

superheat—The amount by which the temperature of the gas in the envelope or gas cells of an aerostat exceeds the temperature of the surrounding air. If the gas has a lower temperature, the superheat is said to be negative.

superpressure—The excess of pressure at the bottom of an airship gas cell or envelope over the outside atmospheric pressure.

suspension band—See **BAND, SUSPENSION**.

suspension bar (or ring)—A bar to which the suspension ropes of the balloon basket are secured. It is also fitted with ropes and toggles for attachment to the basket suspensions from the envelope or net; also called "trapeze bar."

suspension, basket—The suspension by means of which the basket of a kite balloon is supported beneath the balloon body proper. It is independent of the winch suspension.

suspension, winch—The rigging by means of which the lift and drag of a kite balloon are transmitted from the envelope to the towing or traction cable.

sweepback—The acute angle between a line perpendicular to the plane of symmetry and the plan projection of a reference line in the wing. (See fig. 5.)

tab—An auxiliary airfoil attached to a control surface for the purpose of reducing the control force or trimming the aircraft.

tachometer—An instrument that measures in revolutions per minute the rate at which the crankshaft of an engine turns.

tail, airplane—The rear part of an airplane, usually consisting of a group of stabilizing planes, or fins, to which are attached certain controlling surfaces such as elevators and rudders; also called "empennage."

tail area—See **AREA, MEASUREMENT OF**.

tail boom—A spar or outrigger connecting the tail surfaces and the main supporting surfaces.

tail drag—A movable or variable weight suspended from the after part of an airship moored to a mast, to aid in restraining the vertical and lateral motions of the stern of the airship.

tailheavy—The condition of an airplane in which the tail tends to sink when the longitudinal control is released in any given attitude of normal flight (cf. *noseheavy*).

tail skid—A skid for supporting the tail of an airplane on the ground. (See fig. 5.)

tailless airplane—See **AIRPLANE, TAILLESS**.

tail slide—Rearward motion, relative to the air, of an aircraft in flight.

tail surface—A stabilizing or control surface in the tail of an aircraft.

tail wheel—See **WHEEL, TAIL**.

take-off—The act of beginning flight in which an airplane is accelerated from a state of rest to that of normal flight. In a more restricted sense, the final breaking of contact with the land or water.

take-off distance—The distance in which an airplane will finally break contact with the land or water, starting from zero speed. Take-off distance is considered in a calm or at a specified wind velocity.

tank, seaplane—An elongated tank filled with water through which models of seaplane floats, boat hulls, hydrovanes, etc., are towed, and the forces and moments on the model are measured.

tank, service—A fixed fuel tank near each power unit, into which fuel from other tanks is pumped and from which the fuel supplying the engine is drawn.

taper in plan only—A gradual change (usually a decrease) in the chord length along the wing span from the root to the tip, with the wing sections remaining geometrically similar.

taper in thickness ratio only—A gradual change in the thickness ratio along the wing span with the chord remaining constant.

taxi—To operate an airplane under its own power, either on land or on water, except as necessarily involved in take-off or landing.

taxiway—A specially prepared area over which airplanes may taxi to and from the landing area of a landing field.

tee, wind—See **WIND TEE**.

terminal velocity—See **VELOCITY, TERMINAL**.

test chamber—See **EXPERIMENT CHAMBER**.

thickness ratio—The ratio of the maximum thickness of an airfoil section to its chord.

three-point landing—See **LANDING, THREE-POINT**.

thrust, effective propeller—See **PROPELLER THRUST, EFFECTIVE**.

thrust, propeller—See **PROPELLER THRUST**.

thrust, static propeller—See **PROPELLER THRUST, STATIC**.

tip radius (or propeller radius)—The distance of the outermost point of a propeller blade from the axis of rotation.

torque stand—A test stand on which the engine torque is measured.

towing sleeve—See **SLEEVE, TOWING**.

tractor airplane—See **AIRPLANE, TRACTOR**.

traffic-control projector—A projector designed to give light signals to an aircraft pilot.

trailing edge—The rearmost edge of an airfoil or of a propeller blade.

trail rope—See **DRAG ROPE**.

trajectory band—See **BAND, TRAJECTORY**.

transition strip—A section of the landing area adjacent to a runway or other hard-surfaced area, constructed of crushed stone, or other suitable material, properly bound, to insure the safe landing and taxiing of airplanes across such a runway or area in any direction.

transverse:

intermediate transverse—An open unbraced transverse frame of a rigid airship between two main or braced transverse frames.

transverse—continued.

main transverse—One of the main transverse strengthening frames of a rigid airship provided with wire or girder bracing and spaced at regular intervals throughout the length of the airship.

trim:

(airplane) trim—The attitude with respect to wind axes at which balance occurs in rectilinear flight with free controls.

(airship) trim—The attitude of the longitudinal axis of an airship with respect to the horizontal.

(seaplane) trim—The angle with the horizontal surface of the water assumed by the float or hull under given conditions.

trimming moment—The moment about a reference point, usually the center of gravity, exerted by the seaplane hull or float when held at a fixed trim angle.

It is considered positive when the bow tends to rise.

tunnel, water—See WATER TUNNEL.

tunnel, wind—See WIND TUNNEL.

turbulent flow—See FLOW, TURBULENT.

turn, Immelman—See IMMELMAN TURN.

turn-and-bank indicator—An instrument combining in one case a turn indicator and a lateral inclinometer.

turn indicator—An instrument for indicating the existence and approximate magnitude of angular velocity about the normal axis of an aircraft.

turnmeter—An instrument that measures the rate of turn of an aircraft about any predetermined axis.

ultimate load—See LOAD, ULTIMATE.

undercarriage—See LANDING GEAR.

undock—To remove an airship from its dock.

useful load—See LOAD, USEFUL.

valve—To release air or supporting gas from an aerostat into the atmosphere.

valve:

automatic valve—(1) A spring-loaded relief valve fitted to the envelope, ballonnet, or gas cell of an aerostat and set to open at a predetermined pressure for the purpose of preventing excessive internal pressure. (See figs. 4 and 6.)

(2) A type of valve, used on some aerostats, which opens at a predetermined volume or hull dimension.

maneuvering valve—A manually operated valve fitted to the envelope, ballonnet, or gas cell of an aerostat for the purpose of releasing gas or air from within the envelope or gas cell as desired.

valve petticoat—A special sleeve between the valve and gas container making it possible to tie off the sleeve and change valves without loss of gas.

valve seal—A fabric cover used to seal the automatic valves of a rigid airship while it is docked.

vane-type supercharger—See SUPERCHARGER, VANE-TYPE.

velocity, terminal—The hypothetical maximum speed that an airplane could attain along a specified straight flight path under given conditions of weight

and propeller operation, if diving an unlimited distance in air of specified uniform density. If the term is not qualified, a vertical path angle, normal gross weight, zero thrust, and standard sea-level air density are assumed.

vent:

fuel-tank vent—A small tube used to conduct surplus fuel from a fuel tank, overboard clear of the airplane, and to equalize pressures.

oil-tank vent—A large tube used to conduct oil vapors from the engine to the oil tank.

parachute vent—A distendable opening in the apex of the canopy of a parachute designed to relieve excess pressure and to stabilize the parachute in descent.

venturi tube (or venturi)—A short tube of varying cross section. The flow through the venturi causes a pressure drop in the smallest section, the amount of the drop being a function of the velocity of flow.

visibility—The greatest distance at which conspicuous objects can be seen and identified.

volume, aerodynamic—See AERODYNAMIC VOLUME.

volume, gas (airship)—The volume of the contained gas (cf. *capacity*).

walkway girder—See GIRDER, WALKWAY.

warp—To change the form of a wing by twisting it. Warping was formerly used to perform the function now performed by ailerons.

wash—The disturbance in the air produced by the passage of an airfoil. Also called the "wake" in the general case for any solid body.

washin—A warp of an airplane wing giving an increase of the angle of attack toward the tip.

washout—A warp of an airplane wing giving a decrease of the angle of attack toward the tip.

water recovery—The process and the equipment used on an airship for condensing and recovering the water contained in the exhaust gases of internal-combustion engines, in order to avoid the valving of gas as the fuel is consumed.

water tunnel—A device similar to a wind tunnel, but using water as the working fluid.

weight:

dischargeable (or consumable) weight (airship)—All weight that can be consumed or discharged and still leave the airship in safe operating condition with a specified reserve of fuel, oil, water ballast, and provisions, and with the normal crew.

empty weight—The structure, power plant, and fixed equipment of an aircraft. Included in this fixed equipment are the water in the radiator and cooling system, all essential instruments and furnishings, fixed electric wiring for lighting, heating, etc. In the case of an aerostat, it also includes the amount of ballast that must be carried to assist in making a safe landing.

weight—continued.

fixed weight (airship)—The weight of the machinery and all equipment and parts that are fixed in position and nonconsumable. Liquids in the cooling systems of the engines are included.

fixed power plant weight for a given airplane weight—The weight of the power plant and its accessories, exclusive of fuel and oil and their tanks.

gross weight (airplane)—The total weight of an airplane when fully loaded. (Cf. *load, full*.)

net weight (stress analysis)—The gross weight, less some specific partial weight. Very often the partial weight is the dead weight of the wings, but it may be the useful load. The partial weight in question should always be clearly indicated by the context.

wheel control—See CONTROL COLUMN.

wheel, tail—A wheel used to support the tail of an airplane when on the ground. It may be steerable or nonsteerable, fixed or swiveling.

winch suspension—See SUSPENSION, WINCH.

wind cone—See CONE, WIND.

wind indicator—A device that indicates the direction and velocity of the surface wind.

wind, relative—The velocity of the air with reference to a body in it. It is usually determined from measurements made at such a distance from the body that the disturbing effect of the body upon the air is negligible.

window, inspection—A small transparent window fitted in the envelope of a balloon or airship, or in the wing or fuselage of an airplane, to allow inspection of the interior. (See figs. 3 and 5.)

wind tee—A large T-shaped weather vane located on a landing field or on the top of an adjacent structure to indicate the direction of the wind. It may have the form of an airplane and may be illuminated for night landings. Also called "landing tee."

wind tunnel—An apparatus producing an artificial wind or air stream, in which objects are placed for investigating the air flow about them and the aerodynamic forces exerted on them (fig. 7).

wing—A general term applied to the airfoil, or one of the airfoils, designed to develop a major part of the lift of a heavier-than-air craft.

equivalent wing (stress analysis)—A wing of the same span as the actual wing, but with the chord at each section reduced in proportion to the ratio of the average beam load at that section to the average beam load at the section taken as the standard.

wing area—See AREA, MEASUREMENT OF.

wing axis—See AXIS, WING.

wing heavy, right or left—The condition of an airplane whose right or left wing tends to sink when the lateral control is released in any given attitude of normal flight.

wing loading—See LOADING, WING.

wing-over—A maneuver in which the airplane is put into a climbing turn until nearly stalled, at which point the nose is allowed to fall while continuing the turn, then returned to normal flight from the ensuing dive or glide in a direction approximately 180° from that at the start of the evolution (fig. 8).

wing profile—The outline of a wing section.

wing rib—A chordwise member of the wing structure of an airplane, used to give the wing section its form and to transmit the load from the fabric to the spars.

compression wing rib—A heavy rib designed to perform the function of an ordinary wing rib and also to act as a strut opposing the pull of the wires in the internal drag truss.

former (or false) wing rib—An incomplete rib, frequently consisting only of a strip of wood extending from the leading edge to the front spar, which is used to assist in maintaining the form of the wing where the curvature of the airfoil section is sharpest. (See fig. 5.)

wing section—A cross section of a wing parallel to the plane of symmetry or to a specified reference plane.

wing section, aerodynamic center of—See AERODYNAMIC CENTER.

wing skid—A skid placed near the wing tip to protect the wing from contact with the ground.

wing spar—A principal spanwise member of the wing structure of an airplane. (See fig. 5.)

wing tip—The outer end of an airplane wing.

wing-tip flare—See FLARE, WING-TIP.

wing-tip rake—A term referring to the shape of the tip of the wing when the tip edge is sensibly straight in plan but is not parallel to the plane of symmetry. The amount of rake is measured by the acute angle between the straight portion of the wing tip and the plane of symmetry. The rake is positive when the trailing edge is longer than the leading edge.

wire (airplane):

antidrag wire—A wire intended primarily to resist the forces acting forward in the chord direction. It is generally enclosed in the wing. (See fig. 5.)

drag wire—A wire intended primarily to resist the forces acting backward in the chord direction. It is generally enclosed in the wing. (See fig. 5.)

landing wire—A wire or cable which braces the wing against the forces opposite to the normal direction of the lift. (See fig. 5.)

lift wire—A wire or cable which braces the wings against the lift force; sometimes called "flying wire." (See fig. 5.)

stagger wire—A wire connecting the upper and lower wings of an airplane and lying in a plane substantially parallel to the plane of symmetry; also called "incidence wire." (See fig. 5.)

wire (airship):

antiflutter wire—A wire in the plane of the outer cover for local reinforcement and for reducing flutter due to variations in air pressure or propeller wash.

chord wire—A wire joining the vertices of a main transverse frame.

diametral wire—A chord wire that passes through or near the center of a main transverse frame. It is usually attached to the axial fitting.

fairing wire—A wire provided as a point of attachment for the outer cover to maintain the contour lines of the envelope of an airship.

main shear wire—A diagonal wire taking up main shear loads in the structure of a rigid airship.

netting wire—Diagonal or circumferential wire netting fitted between the longitudinals over the entire hull of a rigid airship to transmit the lift of the gas cells to the structure.

wire—continued.

radial wire—A wire that extends from an axial fitting at the center of a transverse frame of a rigid airship to one of the vertices of the frame.

secondary shear wire—An additional reinforcing shear wire.

yaw—An angular displacement about an axis parallel to the normal axis of an aircraft.

yawing—Angular motion about the normal axis (fig. 13.)

yaw line—See **LINE, YAW**.

yawmeter—An instrument that measures the angle of yaw of an aircraft.

zero-lift angle—See **ANGLE, ZERO-LIFT**.

zoom—To climb for a short time at an angle greater than the normal climbing angle, the airplane being carried upward at the expense of kinetic energy.

AERONAUTIC SYMBOLS

1. FUNDAMENTAL AND DERIVED UNITS

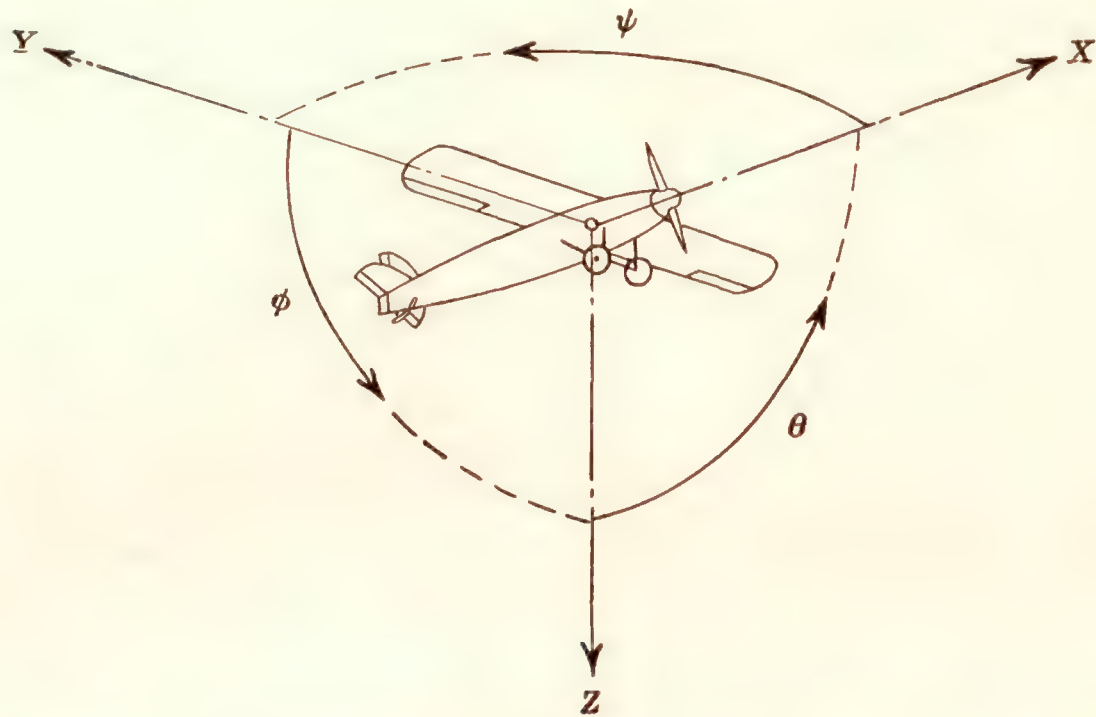
	Symbol	Metric		English	
		Unit	Abbrevia- tion	Unit	Abbrevia- tion
Length.....	l	meter.....	m	foot (or mile).....	ft. (or mi.)
Time.....	t	second.....	s	second (or hour).....	sec. (or hr.)
Force.....	F	weight of 1 kilogram.....	kg	weight of 1 pound.....	lb.
Power.....	P	horsepower (metric).....	-----	horsepower.....	hp.
Speed.....	V	{kilometers per hour.....	k.p.h.	miles per hour.....	m.p.h.
		{meters per second.....	m.p.s.	feet per second.....	f.p.s.

2. GENERAL SYMBOLS

W ,	Weight = mg	ν ,	Kinematic viscosity
g ,	Standard acceleration of gravity = 9.80665 m/s ² or 32.1740 ft./sec. ²	ρ ,	Density (mass per unit volume)
m ,	Mass = $\frac{W}{g}$		Standard density of dry air, 0.12497 kg-m ⁻⁴ -s ² at 15° C. and 760 mm; or 0.002378 lb.-ft. ⁻⁴ -sec. ²
I ,	Moment of inertia = mk^2 . (Indicate axis of radius of gyration k by proper subscript.)		Specific weight of "standard" air, 1.2255 kg/m ³ or 0.07651 lb./cu.ft.
μ ,	Coefficient of viscosity		

3. AERODYNAMIC SYMBOLS

S ,	Area	i_w ,	Angle of setting of wings (relative to thrust line)
S_w ,	Area of wing	i_t ,	Angle of stabilizer setting (relative to thrust line)
G ,	Gap	Q ,	Resultant moment
b ,	Span	Ω ,	Resultant angular velocity
c ,	Chord	$\frac{Vl}{\mu}$,	Reynolds Number, where l is a linear dimension (e.g., for a model airfoil 3 in. chord, 100 m.p.h. normal pressure at 15° C., the corresponding number is 234,000; or for a model of 10 cm chord, 40 m.p.s. the corresponding number is 274,000)
$\frac{b^2}{S}$,	Aspect ratio	C_p ,	Center-of-pressure coefficient (ratio of distance of c.p. from leading edge to chord length)
V ,	True air speed	α ,	Angle of attack
q ,	Dynamic pressure = $\frac{1}{2}\rho V^2$	ϵ ,	Angle of downwash
L ,	Lift, absolute coefficient $C_L = \frac{L}{qS}$	α_o ,	Angle of attack, infinite aspect ratio
D ,	Drag, absolute coefficient $C_D = \frac{D}{qS}$	α_i ,	Angle of attack, induced
D_o ,	Profile drag, absolute coefficient $C_{D_o} = \frac{D_o}{qS}$	α_a ,	Angle of attack, absolute (measured from zero-lift position)
D_i ,	Induced drag, absolute coefficient $C_{D_i} = \frac{D_i}{qS}$	γ ,	Flight-path angle
D_p ,	Parasite drag, absolute coefficient $C_{D_p} = \frac{D_p}{qS}$		
C ,	Cross-wind force, absolute coefficient $C_C = \frac{C}{qS}$		
R ,	Resultant force		



Positive directions of axes and angles (forces and moments) are shown by arrows

Axis		Force (parallel to axis) symbol	Moment about axis			Angle		Velocities	
Designation	Sym- bol		Designation	Sym- bol	Positive direction	Designa- tion	Sym- bol	Linear (compo- nent along axis)	Angular
Longitudinal	X	X	Rolling	L	Y→Z	Roll	ϕ	u	p
Lateral	Y	Y	Pitching	M	Z→X	Pitch	θ	v	q
Normal	Z	Z	Yawing	N	X→Y	Yaw	ψ	w	r

Absolute coefficients of moment

$$C_l = \frac{L}{qbS}$$

(rolling)

$$C_m = \frac{M}{qcS}$$

(pitching)

$$C_n = \frac{N}{qbS}$$

(yawing)

Angle of set of control surface (relative to neutral position), δ . (Indicate surface by proper subscript.)

4. PROPELLER SYMBOLS

- D, Diameter
- p, Geometric pitch
- p/D, Pitch ratio
- V', Inflow velocity
- V_s, Slipstream velocity

$$T, \text{ Thrust, absolute coefficient } C_T = \frac{T}{\rho n^2 D^4}$$

$$Q, \text{ Torque, absolute coefficient } C_Q = \frac{Q}{\rho n^2 D^5}$$

$$P, \text{ Power, absolute coefficient } C_P = \frac{P}{\rho n^3 D^5}$$

$$C_s, \text{ Speed-power coefficient } = \sqrt[5]{\frac{\rho V^5}{P n^2}}$$

$$\eta, \text{ Efficiency}$$

$$n, \text{ Revolutions per second, r.p.s.}$$

$$\Phi, \text{ Effective helix angle } = \tan^{-1} \left(\frac{V}{2\pi r n} \right)$$

5. NUMERICAL RELATIONS

- 1 hp. = 76.04 kg-m/s = 550 ft-lb./sec.
- 1 metric horsepower = 1.0132 hp.
- 1 m.p.h. = 0.4470 m.p.s.
- 1 m.p.s. = 2.2369 m.p.h.

- 1 lb. = 0.4536 kg
- 1 kg = 2.2046 lb.
- 1 mi. = 1,609.35 m = 5,280 ft.
- 1 m = 3.2808 ft.

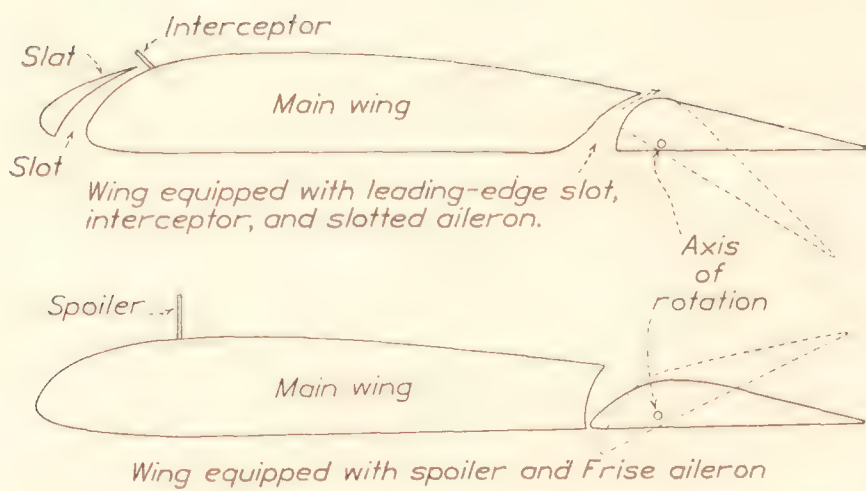


FIGURE 1.—Wing equipped with special control devices

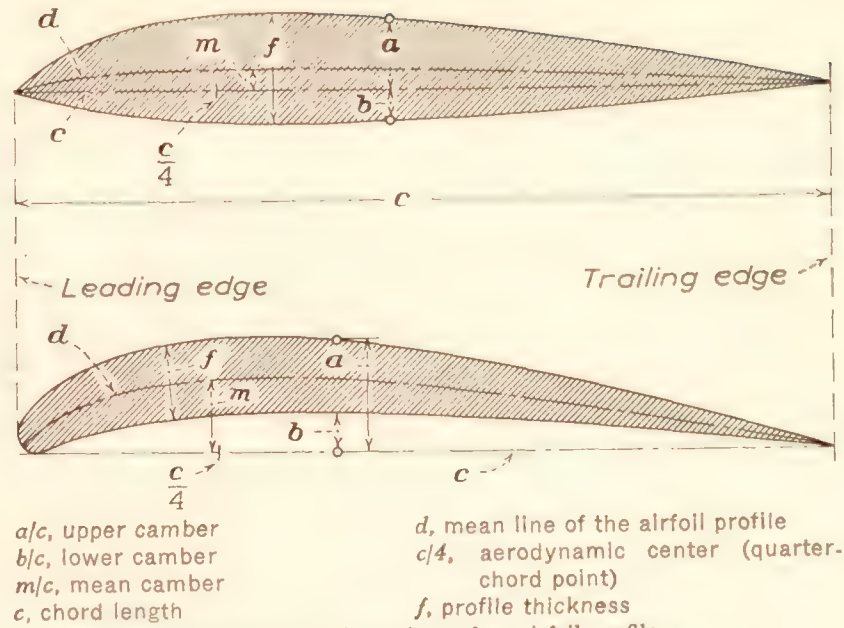
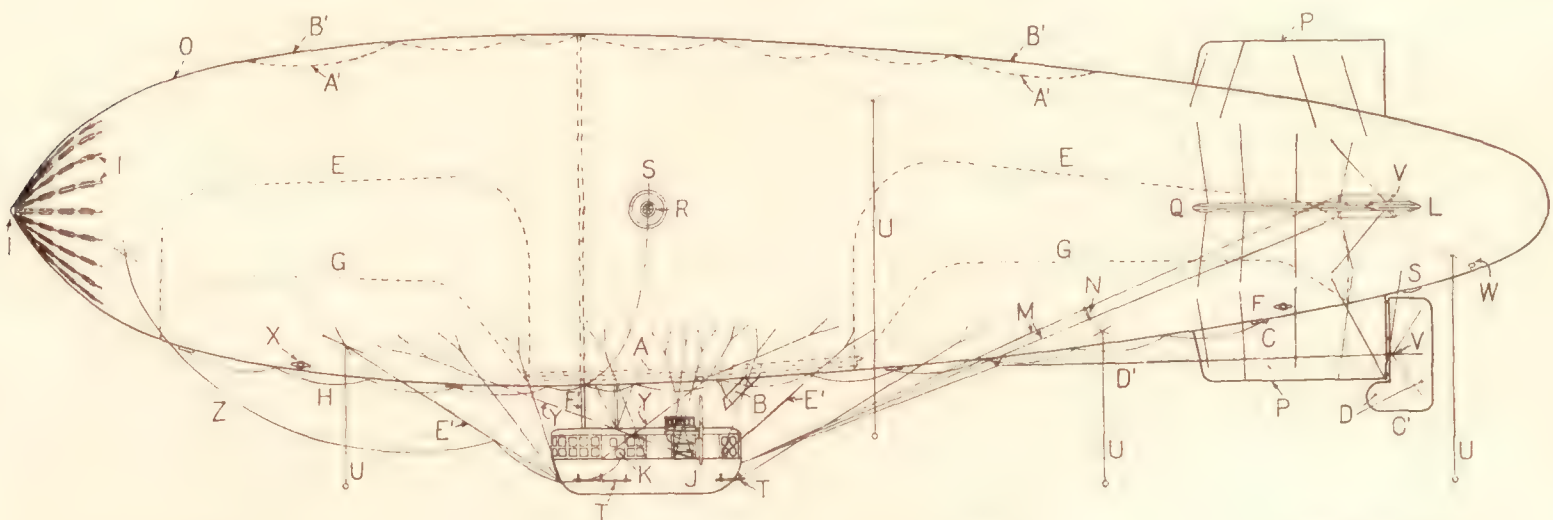


FIGURE 2.—Dimensions of an airfoil profile.



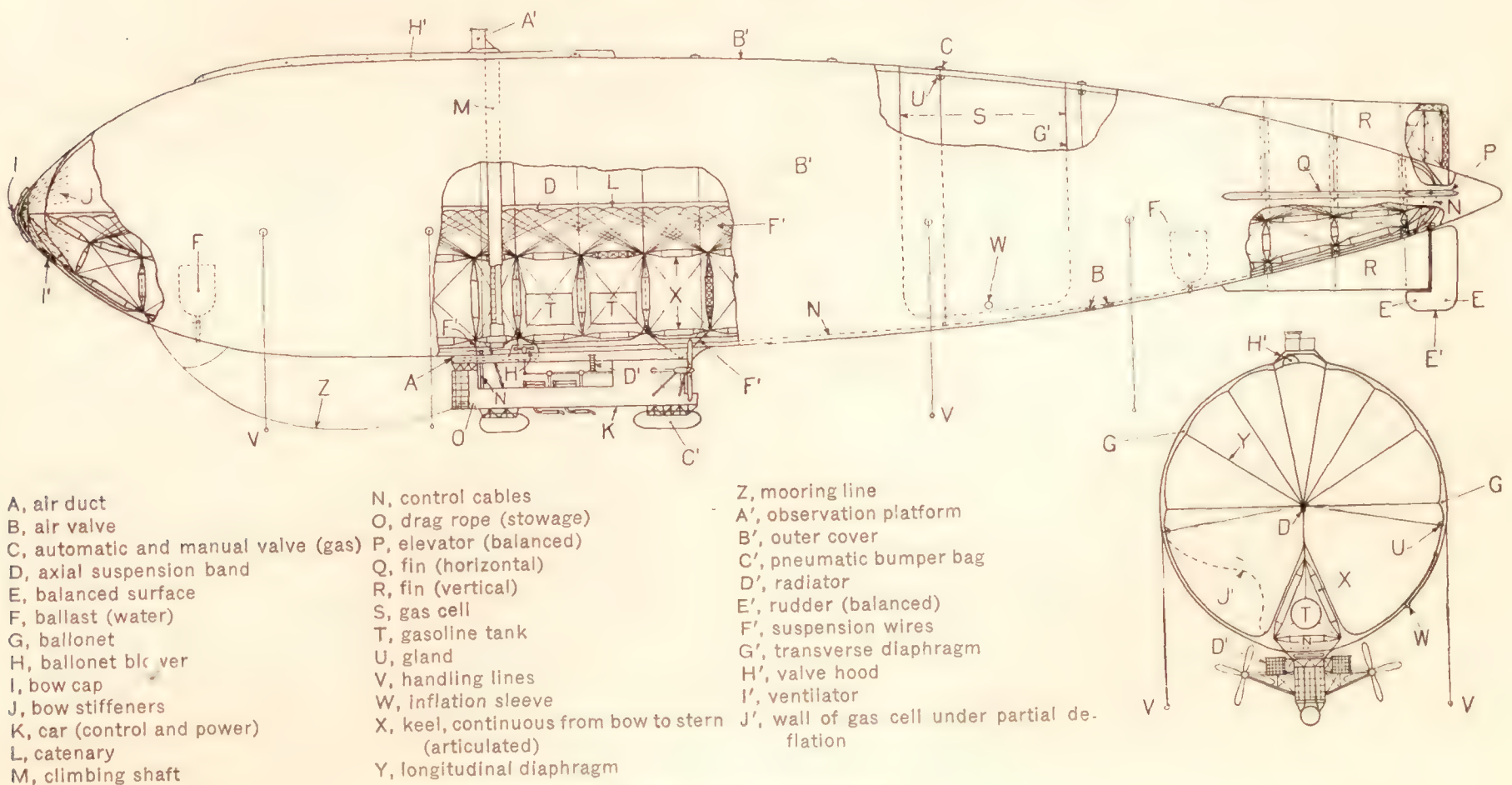
A, air pipe to ballonet
 B, air scoop
 C, air valve
 D, balanced surface
 E, ballonet
 F, ballonet manhole
 G, ballonet seam
 H, ballonet valve cord

I, bow cap and stiffeners
 J, car
 K, drag rope stowage
 L, elevator (balanced)
 M, elevator controls
 N, elevator-control fairlead
 O, envelope
 P, fin, vertical

Q, fin, horizontal
 R, gas manhole
 S, gas valve
 T, hand rail
 U, handling lines
 V, horn (rudder, elevator)
 W, inflation sleeve
 X, inspection window

Y, martingales
 Z, mooring line
 A', rip cord
 B', rip panel
 C', rudder (balanced)
 D', rudder controls
 E', suspension wires, car
 F', valve controls

FIGURE 3.—A nonrigid airship.



A, air duct
 B, air valve
 C, automatic and manual valve (gas)
 D, axial suspension band
 E, balanced surface
 F, ballast (water)
 G, ballonet
 H, ballonet blower
 I, bow cap
 J, bow stiffeners
 K, car (control and power)
 L, catenary
 M, climbing shaft

N, control cables
 O, drag rope (stowage)
 P, elevator (balanced)
 Q, fin (horizontal)
 R, fin (vertical)
 S, gas cell
 T, gasoline tank
 U, gland
 V, handling lines
 W, inflation sleeve
 X, keel, continuous from bow to stern (articulated)
 Y, longitudinal diaphragm

Z, mooring line
 A', observation platform
 B', outer cover
 C', pneumatic bumper bag
 D', radiator
 E', rudder (balanced)
 F', suspension wires
 G', transverse diaphragm
 H', valve hood
 I', ventilator
 J', wall of gas cell under partial deflation

FIGURE 4.—A semirigid airship.

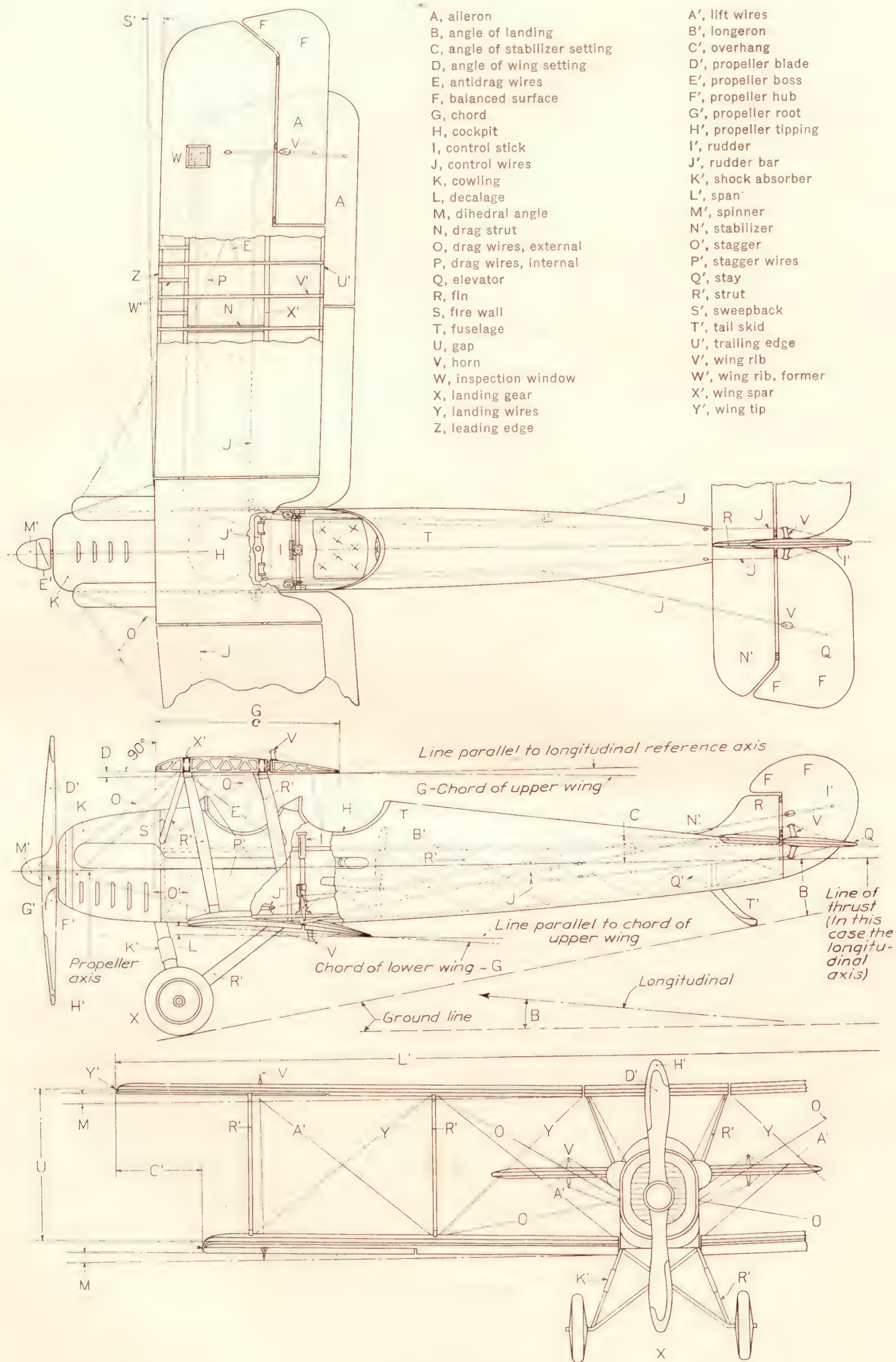


FIGURE 5.—An airplane.

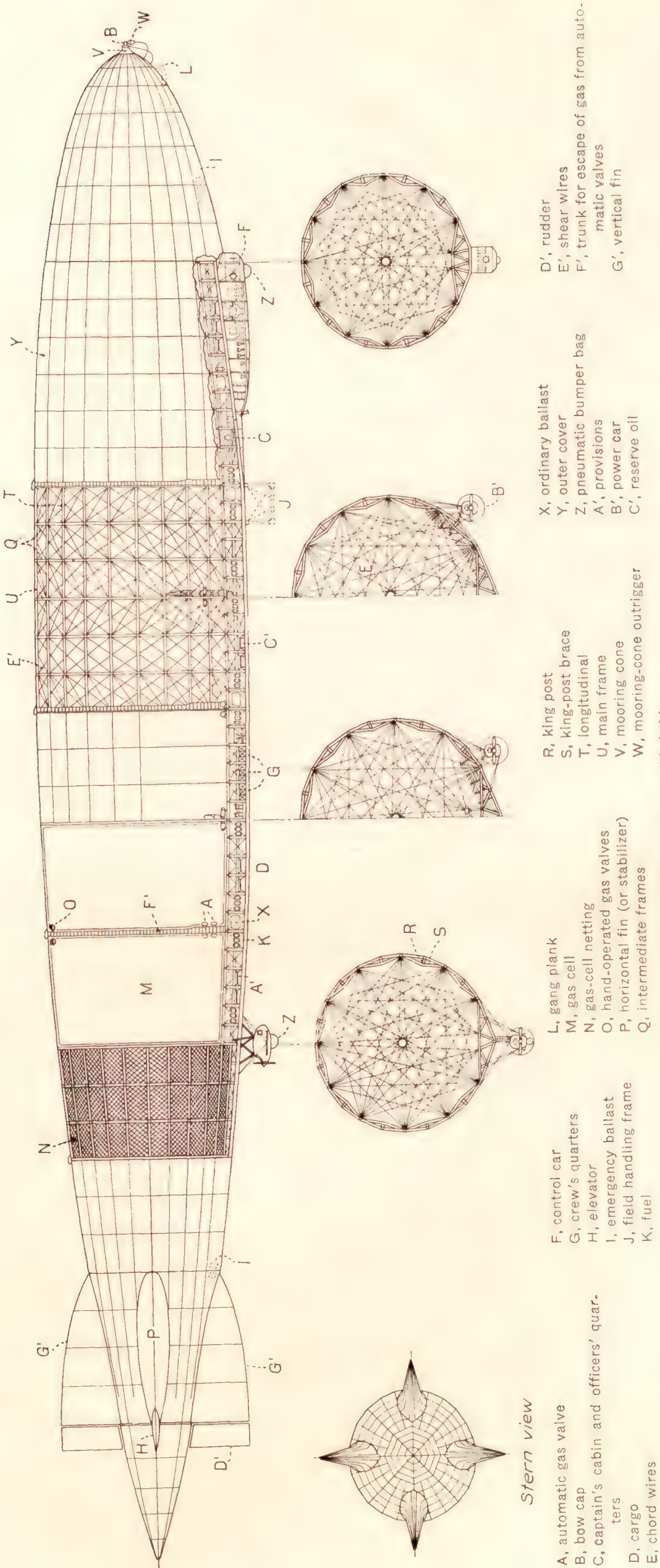


FIGURE 6.—A rigid airship.

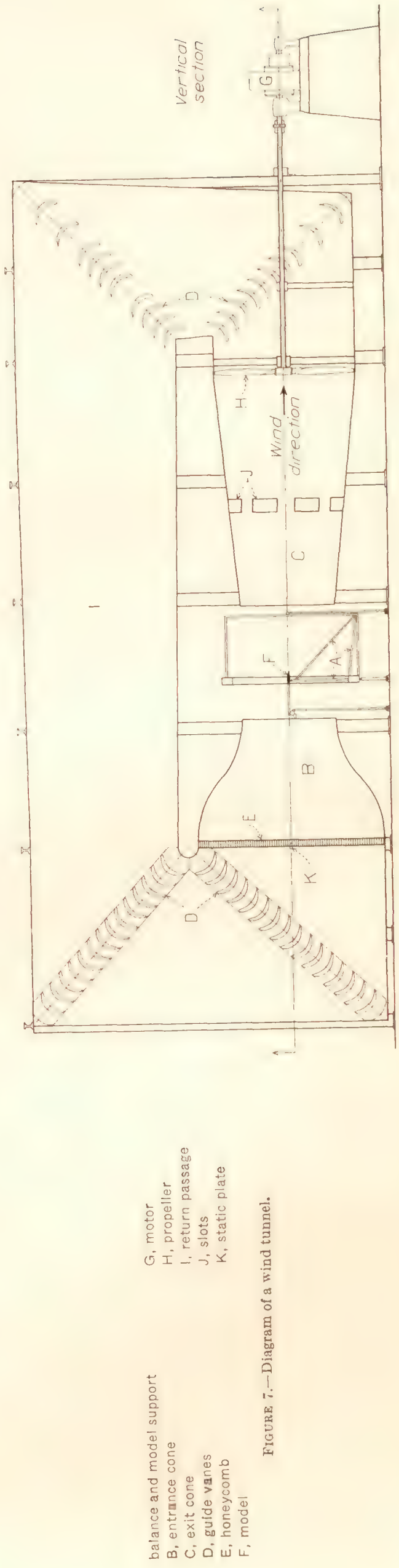


FIGURE 7.—Diagram of a wind tunnel.

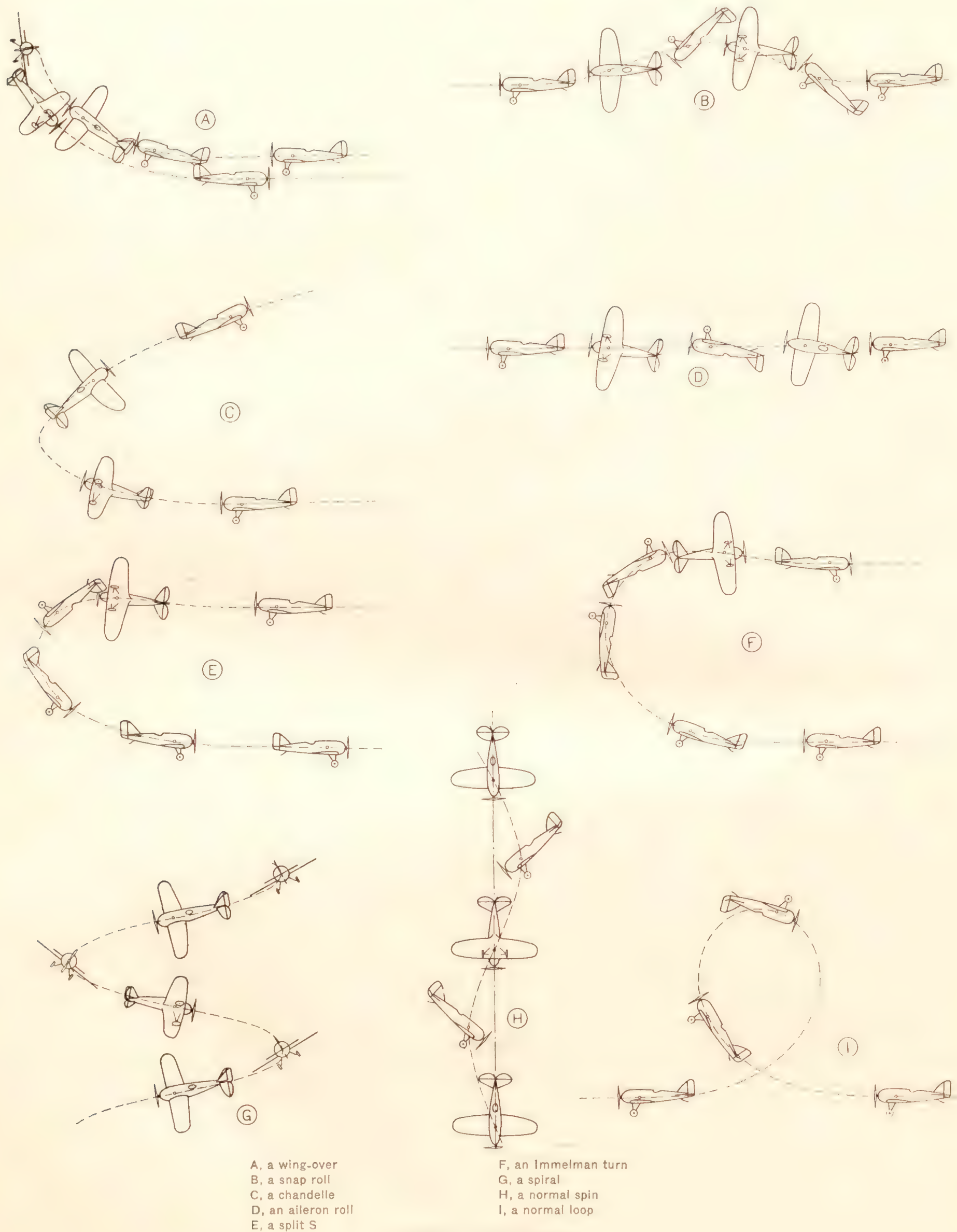
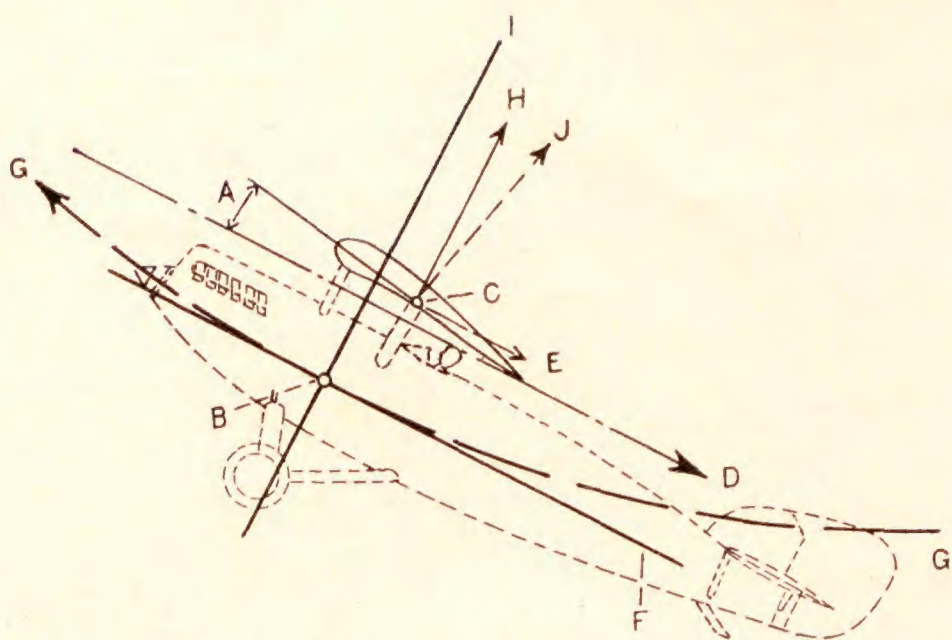
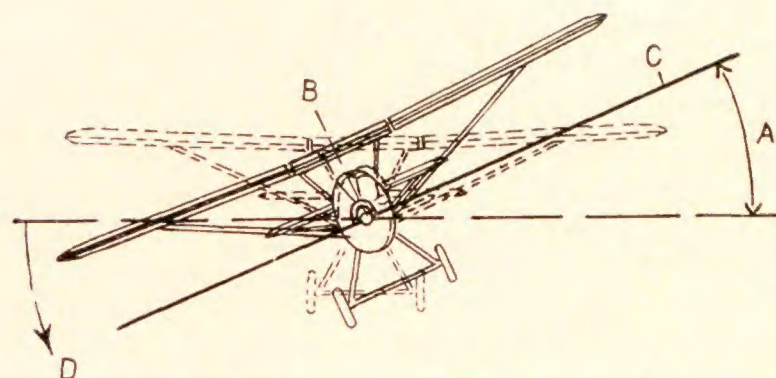


FIGURE 8.—Airplane maneuvers.



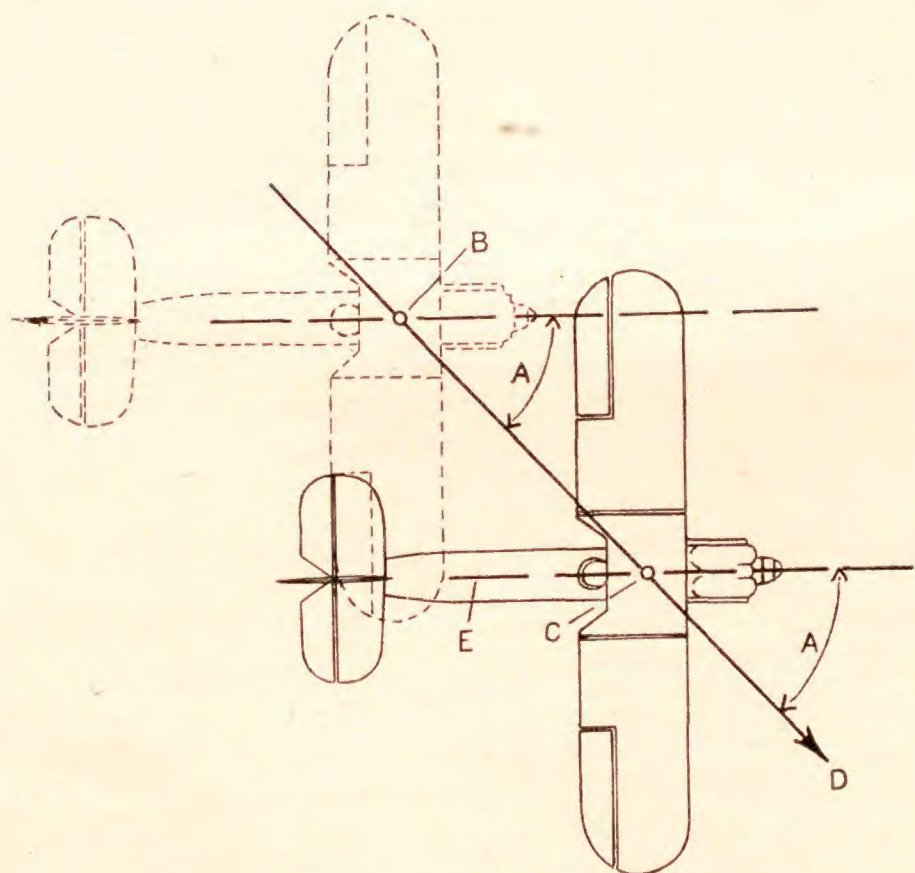
- A, angle of attack
B, center of gravity
C, center of pressure
D, direction of relative wind
E, drag
F, drag axis
G, flight path
H, lift, dynamic
I, positive lift axis
J, resultant force

FIGURE 9.—Lift and drag axes.



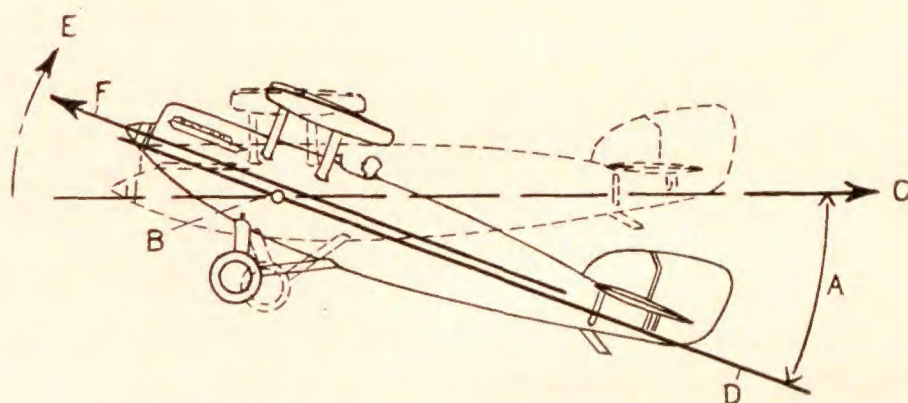
- A, angle of roll
B, c.g. and longitudinal axis
C, lateral axis
D, positive direction of roll

FIGURE 10.—Rolling.



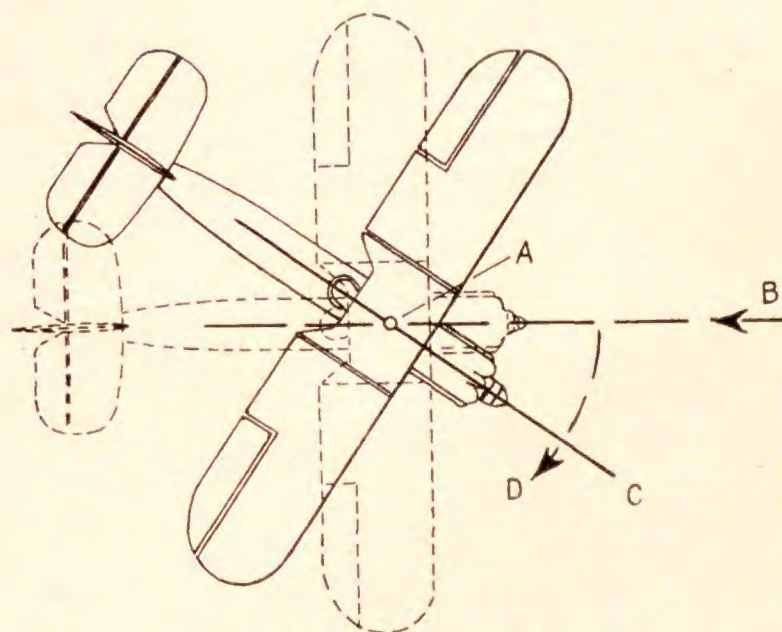
- A, angle of sideslip
B, center of gravity
C, c.g. and normal axis
D, direction of motion of aircraft
E, longitudinal axis

FIGURE 11.—Sideslipping.



- A, angle of pitch
B, c.g. and lateral axis
C, direction of relative wind
D, longitudinal axis
E, positive direction of pitch
F, propeller thrust

FIGURE 12.—Pitching.



- A, c.g. and normal axis
B, direction of relative wind
C, longitudinal axis
D, positive direction of yaw

FIGURE 13.—Yawing.

BB

W

SMITHSONIAN LIBRARIES



3 9088 01800 8540